

Technical Basis for Revision of Regulatory Guidance on Design Ground Motions: Hazard- and Risk-consistent Ground Motion Spectra Guidelines

Risk Engineering, Inc.

**U.S. Nuclear Regulatory Commission
Office of Nuclear Regulatory Research
Washington, DC 20555-0001**



AVAILABILITY OF REFERENCE MATERIALS IN NRC PUBLICATIONS

NRC Reference Material

As of November 1999, you may electronically access NUREG-series publications and other NRC records at NRC's Public Electronic Reading Room at www.nrc.gov/NRC/ADAMS/index.html.

Publicly released records include, to name a few, NUREG-series publications; *Federal Register* notices; applicant, licensee, and vendor documents and correspondence; NRC correspondence and internal memoranda; bulletins and information notices; inspection and investigative reports; licensee event reports; and Commission papers and their attachments.

NRC publications in the NUREG series, NRC regulations, and *Title 10, Energy*, in the Code of *Federal Regulations* may also be purchased from one of these two sources.

1. The Superintendent of Documents
U.S. Government Printing Office
Mail Stop SSOP
Washington, DC 20402-0001
Internet: bookstore.gpo.gov
Telephone: 202-512-1800
Fax: 202-512-2250
2. The National Technical Information Service
Springfield, VA 22161-0002
www.ntis.gov
1-800-553-6847 or, locally, 703-605-6000

A single copy of each NRC draft report for comment is available free, to the extent of supply, upon written request as follows:

Address: Office of the Chief Information Officer,
Reproduction and Distribution
Services Section
U.S. Nuclear Regulatory Commission
Washington, DC 20555-0001
E-mail: DISTRIBUTION@nrc.gov
Facsimile: 301-415-2289

Some publications in the NUREG series that are posted at NRC's Web site address www.nrc.gov/NRC/NUREGS/indexnum.html are updated periodically and may differ from the last printed version. Although references to material found on a Web site bear the date the material was accessed, the material available on the date cited may subsequently be removed from the site.

Non-NRC Reference Material

Documents available from public and special technical libraries include all open literature items, such as books, journal articles, and transactions, *Federal Register* notices, Federal and State legislation, and congressional reports. Such documents as theses, dissertations, foreign reports and translations, and non-NRC conference proceedings may be purchased from their sponsoring organization.

Copies of industry codes and standards used in a substantive manner in the NRC regulatory process are maintained at—

The NRC Technical Library
Two White Flint North
11545 Rockville Pike
Rockville, MD 20852-2738

These standards are available in the library for reference use by the public. Codes and standards are usually copyrighted and may be purchased from the originating organization or, if they are American National Standards, from—

American National Standards Institute
11 West 42nd Street
New York, NY 10036-8002
www.ansi.org
212-642-4900

Legally binding regulatory requirements are stated only in laws; NRC regulations; licenses, including technical specifications; or orders, not in NUREG-series publications. The views expressed in contractor-prepared publications in this series are not necessarily those of the NRC.

The NUREG series comprises (1) technical and administrative reports and books prepared by the staff (NUREG-XXXX) or agency contractors (NUREG/CR-XXXX), (2) proceedings of conferences (NUREG/CP-XXXX), (3) reports resulting from international agreements (NUREG/IA-XXXX), (4) brochures (NUREG/BR-XXXX), and (5) compilations of legal decisions and orders of the Commission and Atomic and Safety Licensing Boards and of Directors' decisions under Section 2.206 of NRC's regulations (NUREG-0750).

DISCLAIMER: This report was prepared as an account of work sponsored by an agency of the U.S. Government. Neither the U.S. Government nor any agency thereof, nor any employee, makes any warranty, expressed or implied, or assumes any legal liability or responsibility for any third party's use, or the results of such use, of any information, apparatus, product, or process disclosed in this publication, or represents that its use by such third party would not infringe privately owned rights.

Technical Basis for Revision of Regulatory Guidance on Design Ground Motions: Hazard- and Risk-consistent Ground Motion Spectra Guidelines

Manuscript Completed: May 2001

Date Published: October 2001

Prepared by

R. K. McGuire¹

W. J. Silva²

C. J. Costantino³

¹Risk Engineering, Inc., Principal Contractor
4155 Darley Avenue, Suite A
Boulder, CO 80305

Subcontractor:

²Pacific Engineering & Analysis
311 Pomona Avenue
El Cerrito, CA 94530

³Carl J. Costantino, Consultant
4 Rockingham Road
Spring Valley, NY 10977

R. M. Kenneally, NRC Project Manager

Prepared for
Division of Engineering Technology
Office of Nuclear Regulatory Research
U.S. Nuclear Regulatory Commission
Washington, DC 20555-0001
NRC Job Code W6248



**NUREG/CR-6728 has been reproduced
from the best available copy.**

Abstract

Recommendations for seismic design ground motions for nuclear facilities require a consistency with both observed strong motion data and with seismological theory on the characteristics of strong shaking. Different recommendations are appropriate for various regions of the US, because both earthquake source characteristics differ and the earth's crustal properties vary with region.

A database of recorded time histories forms the foundation of empirical recommendations for spectral shapes. This database includes motions recorded as recently as the 1999 Turkey and Taiwan earthquakes. Empirical attenuation equations derived primarily from California strong motion data form the basis for spectral shape recommendations for western US (WUS) sites on rock, and these spectral shape recommendations are confirmed and supported by the empirical database.

For the central and eastern US (CEUS), a well-validated, simple model of strong motion allows quantification of the difference between WUS and CEUS motions, accounting for differences in both the seismic source and in path and site attenuation. This model adjusts the WUS empirical soft-rock spectral shapes to CEUS hard-rock conditions. These spectral shape recommendations are made for both the 1-corner and 2-corner seismic source model for the CEUS, which are competing models that imply different spectral shapes for design.

Selecting the appropriate design spectrum or spectra requires a probabilistic seismic hazard analysis (PSHA) at the site for rock conditions. The seismic hazard is deaggregated at 10 and 1 Hz to determine the dominant magnitudes and distances at those frequencies. Two sets of spectral shapes are developed for those magnitudes and distances: one from the recommended functions, and a second from the attenuation equations used in the PSHA. In the CEUS, the designer will use both the 1- and 2-corner earthquake source models to develop weighted spectral shapes, both from the recommended functions and from the PSHA attenuation equations. The spectral shapes are scaled to match the uniform hazard spectrum (UHS) amplitudes at 10 and 1 Hz, typically at the 10^{-4} annual frequency of exceedence level. The two sets of spectral shapes provide a consistency check with the UHS.

For design recommendations, the UHS is modified by a scale factor to a Uniform Reliability Spectrum (URS). This scale factor achieves a relatively consistent annual frequency of plant component failure across the range of plant locations and structural frequencies. It does this by accounting for the slope of the seismic hazard curve, which changes with structural frequency and site location. For some sites and natural frequencies the URS exceeds the UHS, and at other sites and frequencies it lies below the UHS.

For design purposes the spectral shapes determined from the attenuation equations are scaled to the 10 Hz and 1 Hz URS amplitudes. The URS must be matched within certain tolerances by the scaled spectral shapes, but the use of two (or more) design shapes allows a more accurate representation of the seismic threat, for example when a broad-banded spectrum is unlikely.

The database of recorded time histories on rock is divided into magnitude and distance bins, and three component records (two horizontals and one vertical) are archived on a CD-ROM for both the WUS and CEUS. We augmented available recorded rock motions for the CEUS by modifying WUS rock records to account for differences in seismic source and crustal properties between the two regions. This database allows designers to select one or a set of records from the appropriate magnitude and distance range and to adjust those records to match a rock design spectrum, for the derivation of detailed input motions.

For these artificial motions, we recommend criteria for matching their spectra to the target (scaled) spectra. The matching criteria lead to mean-based fits, with half of the spectral values above the target and half below, within specified limits. The matching is done with the response spectrum at 5% of critical damping, obviating the need to meet a minimum power spectral density requirement or to match at multiple dampings. However, checks are required of peak motion parameters, duration of shaking, and directional correlation.

For soil sites, a PSHA is conducted for rock conditions to determine spectra scaled to the 10 Hz and 1 Hz UHS amplitudes, as discussed above. These spectra represent control motions input to a soil model that calculates soil response and that accounts for uncertainties in soil properties. The soil analysis gives the mean soil amplification, its uncertainty, and its slope with increasing rock amplitude. These factors allow the engineer to estimate the soil UHS at 10^{-4} and 10^{-5} annual frequencies of exceedence, from which the 10^{-4} URS can be determined for that soil. Generic soil spectral shapes are not derived here because the soil spectra should be obtained from a site-specific analysis. The site-specific soil amplification studies yield spectral shapes that are scaled to the UHS (for a consistency check) and to the URS (for design purposes).

The database of recorded time histories includes motions at WUS and CEUS soil sites, divided into magnitude and distance bins, and these three-component motions are archived on a CD-ROM. The CEUS soil site motions were derived from WUS soil motions by modeling differences in seismic sources and crustal properties between the two regions. These archived records allow designers to select one or a set of records from the appropriate magnitude and distance range and to adjust those records to match a soil design spectrum, for the derivation of detailed input motions.

We demonstrate the procedures for developing design spectra for rock conditions and for four soil profiles in the WUS and in the CEUS, using as example sites a location in the Mojave desert, California, and Columbia, South Carolina. To demonstrate that the URS gives reliability-consistent design amplitudes, we examine eleven sites across the US and use three ground motion parameters at each. These results indicate that the URS, as calculated here, provides reliability-consistent designs over a range of site locations and structural frequencies.

REVISION OF REGULATORY GUIDANCE ON DESIGN GROUND MOTION

TABLE OF CONTENTS

Abstract	iii
Contents	v
List of Figures	x
List of Tables	xlii
Acknowledgments	xlvi
List of Terms	xlvi
1. Introduction	1-1
1.1 Historical Perspective	1-1
1.2 Objectives and Scope	1-5
1.3 Development of Recommended Spectral Shapes	1-7
1.4 Time History Database for Analysis	1-8
1.5 Site Specific Soil Motions	1-8
1.6 Development of Uniform Reliability Spectra (URS)	1-9
1.7 Contents of Report	1-9
2. Characteristics of WUS and CEUS Strong Ground Motions at Rock Sites	2-1
2.1 Differences between CEUS and WUS Rock Site Strong Ground Motions	2-1
2.1.1 Effects of Shallow Crustal Damping	2-2
2.1.2 Effects of Crustal Amplification	2-3
2.1.3 Effects of Source Processes	2-4
3. Time History Database for Analyses	3-1
3.1 Site Conditions for Time Histories	3-2
3.2 Magnitude and Distance Bins for Time Histories	3-2
3.3 WUS to CEUS Scaling	3-4
3.3.1 WUS to CEUS Transfer Functions	3-4
3.3.2 Example Case: M 6.5, $R = 0$ to 10 km, Rock Bin	3-4
3.4 Matching WUS Time History to CEUS Spectrum	3-5
4. Development of Design Response Spectral Shapes	4-1
4.1 Approach	4-2
4.2 WUS Statistical Spectral Shapes	4-3
4.2.1 Magnitude and Distance bins for WUS Spectral Shapes	4-3
4.2.2 Development of WUS Statistical Spectral Shapes	4-4
4.3 Ground Motion Model for Spectral Shapes	4-4
4.3.1 Point Source Model	4-5
4.3.2 Comparison of Model Shapes to WUS Statistical Shapes	4-6
4.3.3 WUS to CEUS Transfer Functions	4-7

4.4	Design Response Spectra	4-7
4.4.1	Western US Spectral Shapes	4-7
4.4.2	Development of Weighted Empirical Spectral Shapes	4-8
4.4.3	Magnitude and Distance Dependencies of Weighted Empirical Spectral Shapes	4-10
4.4.4	Model for Central and Eastern US Spectral Shapes	4-11
4.4.4.1	Scaling of WUS Weighted Empirical Spectral Shapes to CEUS Conditions	4-11
4.4.4.2	Modeling the Effect of Magnitude and Distance on CEUS Spectral Shapes	4-11
4.5	Comparison of Recommended Shapes to Current Regulatory Guidance	4-12
4.6	Effects of Source Mechanism and Near-Fault Conditions on Response Spectral Shapes	4-12
4.6.1	Effects of Source Mechanism	4-13
4.6.2	Subduction Zone Spectral Shapes	4-14
4.7	Vertical Motions	4-15
4.7.1	V/H Ratios for WUS Rock Site Conditions	4-15
4.7.2	V/H Ratios for CEUS Rock Site Conditions	4-17
4.8	Intermediate Rock Site Conditions	4-19
4.9	Estimation of Spectra For Other Dampings	4-19
4.9.1	Random Vibration Methods	4-19
4.9.2	Empirical Methods	4-20
5.	Criteria for Evaluation of Ground Motions for the Analysis of Nuclear Facilities	5-1
5.1	Introduction	5-1
5.2	Current Regulatory Criteria	5-1
5.3	Recommended Regulatory Criteria	5-3
5.4	Description of Analyses	5-5
5.4.1	Generation of Artificial Enveloping Time Histories, Segmented Target	5-7
5.4.2	Generation of Artificial Enveloping Time Histories, Smooth Target	5-8
5.4.3	Comparison of Fourier Amplitude Spectra with Bin Averages	5-9
5.4.4	Influence of Gaps in the Fourier Spectrum	5-10
5.4.5	Limitations on Exceedences of Response Spectra	5-10
5.5	Other Important Ground Motion Characteristics	5-11
5.5.1	Peak Velocity and Displacement Parameters	5-11
5.5.2	Duration Parameter	5-11
5.5.3	Component Correlation Characteristics	5-12
5.6	Example Application of Spectral Matching Criteria	5-13
5.7	Conclusions	5-15
6.	Procedures for Developing Hazard-consistent Spectra on Soil	6-1
6.1	Approaches	6-1

6.2	Development of WUS and CEUS Attenuation Relations	6-5
6.2.1	Point Source Model Parameters	6-6
6.2.2	Soil Profiles and Nonlinear Properties	6-8
6.2.3	Attenuation Relations	6-10
6.2.3.1	Attenuation Relations for WUS and CEUS Rock Site Conditions	6-10
6.2.3.2	Attenuation Relations for WUS and CEUS Soil Site Conditions	6-11
6.2.3.3	Uncertainty Estimates for Soil Sites	6-13
6.3	Seismic Hazard at CEUS and WUS Example Sites	6-13
6.3.1	Introduction	6-13
6.3.2	Seismic Hazard Environment, CEUS Example Site	6-14
6.3.3	Calculated Spectra, CEUS	6-16
6.3.4	Seismic Hazard Environment, WUS Example Site	6-17
6.3.5	Calculated Spectra, WUS	6-18
6.4	Evaluation of Procedures to Develop Site-specific Soil Hazard Spectra	6-18
6.4.1	Site-specific Soil UHS	6-19
6.4.2	Approaches to Developing Hazard-Consistent Site-Specific Soil Motions Incorporating Profile Uncertainties	6-20
6.4.3	Control Motions	6-21
6.4.4	Example Case 1: Intermediate Depth Very Stiff Profile, Rinaldi	6-22
6.4.4.1	CEUS Conditions	6-22
6.4.4.2	WUS Conditions	6-23
6.4.5	Example Case 2: Deep Stiff Profile, Gilroy 2	6-25
6.4.5.1	CEUS Conditions	6-25
6.4.5.2	WUS Conditions	6-26
6.4.6	Example Case 3: Deep Firm Profile, Savannah River Generic	6-27
6.4.6.1	CEUS Conditions	6-27
6.4.6.2	WUS Conditions	6-28
6.4.7	Example Case 4: Deep Soft Profile: Meloland	6-29
6.4.7.1	CEUS Conditions	6-29
6.4.7.2	WUS Conditions	6-29
6.4.8	Baserock Motions	6-30
6.4.8.1	Development of Outcrop-to-Basement Spectral Correction Factors	6-31
6.4.8.2	Effects of Baserock Motions on the WUS Soil Motions	6-31
6.5	Conclusions and Recommendations	6-32
7.	Procedure for the Development of Risk Consistent Spectra	7-1
7.1	Introduction	7-1
7.2	Methodology	7-2
7.2.1	Concepts and Goals for Seismic Risk Consistency Across Sites	7-2

	7.2.2	Factors Affecting Seismic Risk	7-5
	7.2.3	Risk Equation	7-6
	7.2.4	Accounting for Soil Amplification	7-9
7.3		Examples of Risk-consistent Spectral Amplitudes	7-10
	7.3.1	Example Sites	7-10
	7.3.2	Scaling Factor for Hazard Curve Slopes	7-12
	7.3.3	Results for Example Sites	7-13
	7.3.4	Alternative Representations	7-14
7.4		Summary	7-15
8.		Conclusions and Recommendations	8-1
	8.1	Response Spectral Shapes	8-1
	8.2	Time History Database	8-1
	8.3	Development of Artificial Time Histories	8-2
	8.4	Hazard-consistent Spectra on Soil	8-2
	8.5	Risk-consistent Spectra	8-3
Appendix A		Strong Motion Catalog (WUS)	A-1
Appendix B		Catalog of Time Histories for Analyses	B-1
Appendix C		WUS Statistical Response Spectral Shapes (SA/PGA, 5% Damping) for Rock and Deep Soil Site Conditions	C-1
Appendix D		Stochastic Point Source Ground Motion Model	D-1
	D.1	Background	D-1
	D.2	Point Source Model Description	D-3
	D.3	Site Effects Model	D-6
	D.4	Partition and Assessment of Ground Motion Variability	D-6
		D.4.1 Assessment of Modeling Variability	D-8
		D.4.2 Assessment of Parametric Variability	D-8
		D.4.3 Model Bias And Variance Estimates for The Point Source Model	D-9
Appendix E		Fourier Amplitude Spectra for WUS Empirical Motions	E-1
Appendix F		Plots of Empirical Data from WUS Records	F-1
Appendix G		Plots of Arias Intensity and Cumulative Absolute Velocity from WUS Records	G-1
Appendix H		Duration Relations for WUS Strong Ground Motion	H-1
	H.1	Introduction	H-1
	H.2	Approach	H-1

H.3	Duration Model	H-5
H.4	Model Predictions	H-5
Appendix I	Site- and Soil-Specific PSHA for Nonlinear Soil Sites	I-1
I.1	Introduction	I-1
I.2	Methodology	I-1
I.3	Applications	I-2
I.3.1	Ground Motion Database	I-3
I.3.2	Soil Amplification Software and Soil Modeling	I-3
I.3.3	Amplification Study Results	I-4
I.3.4	PSHA Results	I-4
I.4	Summary and Conclusions	I-5
Appendix J	Characteristics of Vertical Strong Ground Motions for Applications to Engineering Design	J-1
J.1	Introduction	J-1
J.2	Effects of Site Conditions on the Characteristics of Vertical and Horizontal Strong Ground Motions	J-1
J.3	Generic Rock and Soil Site Velocity Profiles	J-1
J.4	Short-Period Time Domain Characteristics of Vertical Motions	J-3
J.5	Response Spectral Characteristics of Vertical Motions	J-5
J.6	Magnitude, Site, and Distance Dependencies of Horizontal and Vertical Component Response Spectral Shapes	J-6
J.7	Empirical and Numerical Model Estimates of the Vertical-to-Horizontal Response Spectral Ratios	J-8
J.8	Applications to WUS Rock and Deep Soil Sites	J-8
J.9	Applications to CEUS Rock and Deep Soil Sites	J-9
J.10	Computational Model	J-9
J.11	Treatment of Soil Response for Vertical Motions	J-10
J.12	Conclusions	J-12
Appendix K	Comparison of WUS Recommended Response Spectral Shapes to Recordings of the Chi-Chi, Taiwan and Turkey Earthquakes	K-1

List of Figures

<u>Figure #</u>		<u>Page</u>
Figure 1-1	Flowchart of design ground motion procedure and application to rock sites. S3, S4, etc. refer to Sections of this report, TH = time history.	1-14
Figure 1-2	Flowchart of design ground motion procedure and application to soil sites. S3, S4, etc. refer to Sections of this report, TH = time history.	1-15
Figure 2-1	Comparison of response spectral shapes (SA/PGA, 5% damping) between CEUS and WUS crustal conditions for earthquakes recorded at rock sites: M 6 3/4 (upper) M 5 3/4 (lower)	2-14
Figure 2-2	Comparison of generic compression (P) and shear (S) wave velocity profiles for WUS and CEUS crustal conditions.	2-15
Figure 2-3	Crustal amplifications factors (smoothed) for Fourier amplitude spectra computed for the crustal models shown in Figure 2-2 (10 km to the surface).	2-16
Figure 2-4	Response spectral shapes (SA/PGA, 5% damping) computed for M 6.5 at a distance of 25 km for a suite of kappa values using WUS parameters (Table 2-2). The lowest kappa value shows the highest high-frequency amplification, the highest kappa value shows the highest low-frequency amplification.	2-17
Figure 2-5	Response spectra (5% damping) computed for an M 6.5 earthquake at a distance of 25 km for a suite of kappa values using WUS parameters (Table 2-2). The lowest K value shows the highest spectral amplitudes and the highest K value shows the lowest spectral amplitudes.	2-18
Figure 2-6	Response spectral shapes (SA/PGA, 5% of critical damping) computed for M 6.5 at a distance of 25 km for a suite of stress drop values using WUS parameters (Table 2-2). Spectral shapes reduce with increasing stress drop, beginning with 32 bars.	2-19
Figure 2-7	Response spectra (5% of critical damping) computed for M 6.5 at a distance of 25 km for a suite of stress drop values using WUS parameters (Table 2-2). Spectral shapes increase with increasing stress drop, beginning with 32 bars.	2-20
Figure 2-8	Response spectral shapes (5% of critical damping) computed for M = 6.5 at $R = 25$ km using both single- and double-corner frequency source spectra for WUS and CEUS conditions (Table 2-2).	2-21
Figure 2-9	Absolute response spectra (5% of critical damping) computed for M = 6.5 at $R = 25$ km using both single- and double-corner frequency source spectra for WUS and CEUS conditions (Table 2-2).	2-22

Figure 2-10	Comparison of 5% damped statistical shapes computed for WUS recordings ($M 6 \frac{3}{4}$) to single- and double-corner model predictions using the parameters listed in Table 2-2.	2-23
Figure 2-11	Comparison of 5% damped statistical shapes computed for CEUS recordings ($M 6 \frac{3}{4}$) to single- and double-corner model predictions using the parameters listed in Table 2-2.	2-24
Figure 2-12	Comparison of 5% damped statistical shapes computed for WUS recordings ($M 5 \frac{1}{4}$) to single- and double-corner model predictions using the parameters listed in Table 2-2.	2-25
Figure 2-13	Comparison of 5% damped statistical shapes computed for CEUS recordings ($M 5 \frac{1}{4}$) to single- and double-corner model predictions using the parameters listed in Table 2-2.	2-26
Figure 3-1	Example of duration bin criteria for $M 5.5$ bin and rock site conditions. Solid line is WUS empirical relation for 5 to 75% Arias Intensity (Appendix I) and X's reflect $\pm 1 \sigma$ fractiles. Boxes represent $\pm 50\%$ duration bin (horizontal dashes) and distance bins of 0 to 10 km, 10 to 50 km, 50 to 100 km, and 100 to 200 km (vertical dashes).	3-16
Figure 3-2	Example of duration bin criteria for $M 6.5$ bin and rock site conditions. Solid line is WUS empirical relation for 5 to 75% Arias Intensity (Appendix I) and X's reflect $\pm 1 \sigma$ fractiles. Boxes represent $\pm 50\%$ duration bin (horizontal dashes) and distance bins of 0 to 10 km, 10 to 50 km, 50 to 100km and 100 to 200 km (vertical dashes).	3-17
Figure 3-3	Example of duration bin criteria for $M 7.5$ bin and rock site conditions. Solid line is WUS empirical relation for 5 to 75% Arias Intensity (Appendix I) and X's reflect $\pm 1 \sigma$ fractiles. Boxes represent $\pm 50\%$ duration bin (horizontal dashes) and distance bins of 0 to 10 km, 10 to 50 km, 50 to 100 km, 100 to 200 km (vertical dashes).	3-18
Figure 3-4	Example of rock and deep soil WUS-to-CEUS transfer functions (5% damped response spectra) computed for $M = 6.5$ and a suite of distances.	3-19
Figure 3-5	Acceleration, velocity, and displacement time histories from the 1989 $M 6.9$ Loma Prieta earthquake recorded at the Los Gatos Presentation Center site (component 000), rupture distance of 6.1 km.	3-20
Figure 3-6	Response spectra (5% damping) for the motions recorded at site LGPC from the 1989 $M 6.9$ Loma Prieta earthquake.	3-21
Figure 3-7	Acceleration, velocity, and displacement time histories from the 1989 $M 6.9$ Loma Prieta earthquake (Figure 3-5) scaled to CEUS hard rock site conditions.	3-22
Figure 3-8	Response spectra (5% damping) for the recorded motions from the 1989 $M 6.9$ Loma Prieta earthquake (Figure 3-7) scaled to CEUS hard rock conditions	3-23

Figure 3-9	Acceleration, velocity, and displacement time histories from the 1989 M 6.9 Loma Prieta earthquake (Figure 3.5) scaled to CEUS hard rock site conditions, acausal high-pass filter.	3-24
Figure 3-10	Comparison of 5% damped response spectra computed from scaled CEUS records to causal and acausal high-pass filters with 0.1 Hz corner frequencies. Corresponding time histories are shown in Figures 3-7 and 3-9 respectively.	3-25
Figure 3-11	Comparison of 5% damped rock outcrop UHS spectra for CEUS and WUS conditions.	3-26
Figure 3-12	Spectral match of WUS record to WUS target: 10^{-4} rock UHS (Figure 3-11).	3-27
Figure 3-13	Acceleration, velocity, and displacement time histories resulting from match of WUS record to WUS target (Figure 3-11).	3-28
Figure 3-14	Spectral match of WUS record to CEUS target: 10^{-4} rock UHS using two sample intervals, 0.02 sec and 0.005 sec.	3-29
Figure 3-15	Acceleration, velocity, and displacement time histories resulting from match of WUS record to CEUS target, sample interval of 0.02 sec.	3-30
Figure 3-16	Acceleration, velocity, and displacement time histories resulting from match of WUS record to CEUS target, sample interval of 0.005 sec.	3-31
Figure 3-17	Fourier amplitude spectra resulting from fitting WUS record to WUS and CEUS targets (Figure 3-4). Fit to CEUS target used two sample intervals, 0.02 sec and 0.005 sec.	3-32
Figure 4-1	Response spectral shapes (5% damping) for the M 6.5, $R = 10$ to 50 km bins normalized by spectral ordinates at a suite of frequencies (0.5 to 100.0 Hz)	4-40
Figure 4-2	Response spectral shapes (5% damping) for the M 6.5, $R = 10$ to 50 km bins from Figure 1 renormalized by their respective 100 Hz values.	4-41
Figure 4-3	Response spectral shapes (5% damping) computed for the M = 5.5 magnitude bin for WUS soft rock site conditions.	4-42
Figure 4-4	Response spectral shapes (5% damping) computed for the M = 6.5 magnitude bin for WUS soft rock site conditions.	4-43
Figure 4-5	Response spectral shapes (5% damping) computed for the M = 7.5 magnitude bins for WUS soft rock site conditions.	4-44
Figure 4-6	Response to spectral shapes (5% damping) computed for the M = 5.5 magnitude bins for WUS deep soil site conditions.	4-45
Figure 4-7	Response spectral shapes (5% damping) computed for the M = 6.5 magnitude bin for WUS deep soil conditions.	4-46
Figure 4-8	Response spectral shapes (5% damping) computed for the M = 7.5 magnitude bin for WUS deep soil conditions.	4-47

Figure 4-9	Response spectral shapes (5% damping) computed for $M = 6.5$ at $R=25$ km using both single and double corner frequency source spectra for WUS and CEUS conditions.	4-48
Figure 4-10	Absolute response spectra (5% damping) computed for $M = 6.5$ at $R=25$ km using both single and double corner frequency source spectra for WUS and CEUS conditions.	4-49
Figure 4-11	Comparison of WUS statistical response spectral shapes (5% damping) for the M 6.5, $R = 10$ to 50 km bins for rock and deep soil site conditions.	4-50
Figure 4-12	Response spectral shapes (5% damping) computed for the $M = 5.5$ to 7.5, $R = 10$ to 50 km bins for WUS rock site conditions.	4-51
Figure 4-13	WUS to CEUS transfer functions. Top, magnitude dependencies at a distance of 25 km; bottom, distance dependencies for M 6.5.	4-52
Figure 4-14	Comparison of the statistical shapes from Figures 3 to 5 with spectral shapes predicted by the attenuation relationships of Abrahamson and Silva	4-53
Figure 4-14b	(1997) [A&S 97], Boore and others (1997) [Bao 97], Campbell (1997)	4-54
Figure 4-14c	[C 97], Idriss (1991) [I 91], and Sadigh and others (1997) [Sao 97].	4-55
Figure 4-15	Mean residuals and their 90% confidence intervals for the five attenuation relationships.	4-56
Figure 4-15b		4-57
Figure 4-15c	(Continued)	4-58
Figure 4-15d	(Continued)	4-59
Figure 4-16	Relative bias (“ T ”) weights (left column) and relative likelihood (“ L ”) weights (right column) for M 6-7 and R 10-50 km magnitude distance bins. Top plot in each column shows weights computed using Equations (4-4) and (4-6). The remaining plots show the smoothed weights obtained using Equation (4-7) with values of h from 0.25 to 1.0.	4-60
Figure 4-17	Example comparisons of the statistical spectral shapes from Figure 4-5 with spectral shapes predicted by the weighted combination of the five attenuation relationships. Weighted empirical spectral shapes are shown for smoothed “ T ” and “ L ” weights and values of h from 0.25 to 1.0.	4-61
Figure 4-18	Relative weights used to obtain weighted empirical attenuation spectral shapes. The weights are the average of the smoothed “ T ” and “ L ” weights with $h = 1.0$.	4-62
Figure 4-19	Weighted empirical attenuation response spectral shapes obtained using the relative weights shown on Figure 4-18.	4-63
Figure 4-20	Example of a fit of Equation (4-8) to an individual spectral shape.	4-64
Figure 4-21	Example WUS response spectral shapes predicted by Equation (4-8) with parameters listed in table 4-3 compared to the weighted empirical spectral shape data used in the fit.	4-65
Figure 4-22	Example EUS response spectral shapes obtained by scaling weighted empirical WUS response spectral shapes.	4-66

Figure 4-23	Examples of adjustments to scaled EUS response spectral shapes to remove valley near 10 Hz.	4-67
Figure 4-24	Example EUS single-corner response spectral shapes predicted by Equation (4-9) with parameters listed in Table 4-3 compared to the scaled and adjusted EUS spectral shape data used in the fit.	4-68
Figure 4-25	Example EUS double-corner response spectral shapes predicted by Equation (4-9) with parameters listed in Table 4-3 compared to the scaled and adjusted EUS spectral shape data used in the fit.	4-69
Figure Set 4-26	Comparison of recommended WUS shapes (solid line) to current regulatory guidance R.G. 1.60 and Newmark-Hall shapes for the distance bin 0 to 50 km and for mean magnitudes 5.6, 4.4, and 7.3. Peak parameters are taken from Table 4-1 for the Newmark-Hall shapes.	4-70
Figure Set 4-27	Comparison of recommended CEUS shapes (solid line) to current regulatory guidance R.G. 1.60 and Newmark-Hall shapes for the distance bin 0 to 50 km and for mean magnitudes 5.6, 6.4, and 7.3. Peak parameters are taken from Table 4-1 for the Newmark-Hall shapes.	4-73
Figure 4-28	Predicted effects of source mechanism on spectral shapes for empirical WUS attenuation relations. For the Abrahamson and Silva, 1997 empirical relation, the frequency dependence differs for small and large magnitudes.	4-76
Figure 4-29	Predicted effects of site location (hanging wall vs. foot wall) for oblique-slip source mechanisms on spectral shapes compared to strike-slip spectral shapes for an empirical WUS attenuation relation (Abrahamson and Silva, 1997).	4-77
Figure 4-30	Comparison of recommended shapes for M 8.0 at $R = 25$ km to empirical subduction zone shapes for M 9.0 at a suite of distances (Youngs et al., 1997).	4-78
Figure 4-31	V/H ratio for 5% damped response spectra implied by the R.G. 1.60 design motions.	4-79
Figure 4-32	Average V/H ratio (5% damped) magnitude dependencies based on the Abrahamson and Silva, 1997; Campbell, 1997; and Sadigh et al., 1997 empirical WUS rock attenuation relations for a suite of magnitudes.	4-80
Figure 4-33	Average V/H ratio (5% damped) distance dependencies based on Abrahamson and Silva, 1997; Campbell, 1997; and Sadigh et al., 1997 empirical WUS rock attenuation relations for a suite of magnitudes.	4-81
Figure 4-34	Magnitude dependence of 5% damped horizontal component response spectral acceleration at a rupture distance of 10 km for a WUS rock empirical attenuation relation (Abrahamson and Silva, 1997).	4-82
Figure 4-35	Magnitude dependence of 5% damped vertical component response spectral acceleration at a rupture distance of 10 km for a WUS rock empirical attenuation relation (Abrahamson and Silva, 1997).	4-83

Figure 4-36	Recommended V/H ratios (5% damped) for WUS soft rock site conditions for ranges in horizontal component peak accelerations.	4-84
Figure 4-37	V/H ratios (5% damped) computed from recordings of the M 5.9 1988 Saguenay, and M 6.8 1976 Gazli, and 1985 Nahanni earthquakes. The Gazli and Nahanni earthquakes are considered to represent CEUS source, path, and site conditions.	4-85
Figure 4-38	V/H ratios (5% damped) for CEUS rock site conditions computed with the simple point-source model.	4-86
Figure 4-39	Recommended V/H ratios (5% damped) for CEUS hard rock site conditions for ranges in horizontal component peak accelerations.	4-87
Figure 4-40	WUS vertical component response spectra (5% damped) based on the M 6.4, $R = 27.4$ km horizontal shape (Figure Set 4-26) and recommended V/H ratios (Table 4-4).	4-88
Figure 4-41	CEUS vertical component response spectra (5% damped) based on the M 6.4, $R = 27.4$ km single corner horizontal shape (Figure Set 4-27) and recommended V/H ratios (Table 4-5).	4-89
Figure 4-42	CEUS vertical component response spectra based on the M 6.4, $R = 27.4$ km double corner horizontal shape (Figure Set 4-26) and recommended V/H ratios (Table 4-5).	4-90
Figure 5-1A	Average smoothed Fourier amplitude spectra, distance 0-10 km, rock sites.	5-25
Figure 5-1B	Average smoothed Fourier amplitude spectra, horizontal motions, distance 10-50 km, soil sites.	5-26
Figure 5-2	5% damped spectrum for distance bin D2, rock sites, magnitude bin M55, horizontal motion.	5-27
Figure 5-3A	5% damped spectrum, trial 1	5-28
Figure 5-3B	5% damped spectrum, trial 2	5-29
Figure 5-3C	5% damped spectrum, trial 3	5-30
Figure 5-3D	5% damped spectrum, trial 4	5-31
Figure 5-3E	5% damped spectrum, trial 4S (shorter duration)	5-32
Figure 5-3F	5% damped spectrum, trial 4L (longer duration)	5-33
Figure 5-3G	5% damped spectrum, trial 5	5-34
Figure 5-3H	5% damped spectrum, trial 1S	5-35
Figure 5-4A	5% damped spectrum, trial SM01	5-36
Figure 5-4B	5% damped spectrum, trial SM02	5-37
Figure 5-5	Spectral acceleration shapes for $\bar{M} = 5.57, \bar{R} = 21.8$ rock horizontal motion bin D2RM55H	5-38

Figure 5-6A	5% damped spectrum, trial SM01, WUS spectrum, $\bar{M} = 5.57$, $\bar{R} = 21.8$ km (random phase spectrum)	5-39
Figure 5-6B	5% damped spectrum, trial SM02, WUS spectrum, $\bar{M} = 5.57$, $\bar{R} = 21.8$ km (record phase spectrum 1)	5-40
Figure 5-6C	5% damped spectrum, trial SM03, WUS spectrum, $\bar{M} = 5.57$, $\bar{R} = 21.8$ km (record phase spectrum 2)	5-41
Figure 5-6D	5% damped spectrum, trial SM04, WUS spectrum, $\bar{M} = 5.57$, $\bar{R} = 21.8$ km (record phase spectrum 3)	5-42
Figure 5-7A	5% damped spectrum, trial SM01, CEUS 1-corner spectrum, $\bar{M} = 5.57$, $\bar{R} = 21.8$ km (random phase spectrum)	5-43
Figure 5-7B	5% damped spectrum, trial SM02, CEUS 1-corner spectrum, $\bar{M} = 5.57$, $\bar{R} = 21.8$ km (random phase spectrum 1)	5-44
Figure 5-7C	5% damped spectrum, trial SM03, CEUS 1-corner spectrum, $\bar{M} = 5.57$, $\bar{R} = 21.8$ km (random phase spectrum 2)	5-45
Figure 5-7D	5% damped spectrum, trial SM04, CEUS 1-corner spectrum, $\bar{M} = 5.57$, $\bar{R} = 21.8$ km (random phase spectrum 3)	5-46
Figure 5-8A	Arias Intensity ratios for trial records used to envelop WUS bin spectrum of Figure 5-6.	5-47
Figure 5-8B	Arias Intensity ratios for WUS records scaled to maximum time duration.	5-48
Figure 5-9A	Arias Intensity ratios for trial records used to envelop CEUS 1-corner spectrum of Figure 5-7.	5-49
Figure 5-9B	Arias Intensity ratios for CEUS records scaled to maximum time duration.	5-50
Figure 5-10A	Fourier amplitude spectra of envelope fits to 5% damped segmented target spectrum.	5-51
Figure 5-10B	Fourier amplitude spectra of envelope fits to 5% damped smooth target spectrum.	5-52
Figure 5-10C	Fourier amplitude spectra of envelope fits to 5% damped smooth WUS target spectrum.	5-53
Figure 5-10D	Fourier amplitude spectra of enveloping fits to 5% damped segmented WUS target spectrum (bin D2RM55H)	5-54
Figure 5-11A	Influence of gap in Fourier amplitudes at 0.5 Hz on 5% damped response spectra. Left: change in original Fourier amplitudes; center: change in smoothed Fourier amplitudes; right: change in 5% damped response spectrum.	5-55
Figure 5-11B	Influence of gap in Fourier amplitude at 1 Hz on 5% damped response spectra. Left: change in original Fourier amplitudes; Center: change in smoothed Fourier amplitudes; Right: change in 5% damped response spectrum.	5-56

Figure 5-11C	Influence of gap in Fourier amplitudes at 2.5 Hz on 5% damped response spectra. Left: change in original Fourier amplitudes; Center: change in smoothed Fourier amplitudes; Right: change in 5% damped response spectrum.	5-57
Figure 5-11D	Influence of gap in Fourier amplitudes at 6 Hz on 5% damped response spectra. Left: change in original Fourier amplitudes; Center: change in smoothed Fourier amplitudes; Right: change in 5% damped response spectrum.	5-58
Figure 5-11F	Influence of gap in Fourier amplitudes at 15 Hz on 5% damped response spectra. Left: change in original Fourier amplitudes; Center: change in smoothed Fourier amplitudes; Right: change in 5% damped response spectrum.	5-59
Figure 5-11G	Influence of gap in Fourier amplitudes at 25 Hz on 5% damped response spectra. Left: change in original Fourier amplitudes; Center: change in smoothed Fourier amplitudes; Right: change in 5% damped response spectrum.	5-60
Figure 5-11H	Influence of narrower gap in Fourier amplitudes at 2.5 Hz on 5% damped response spectra. Left: change in original Fourier amplitudes; Center: change in smoothed Fourier amplitudes; Right: change in 5% damped response spectrum.	5-61
Figure 5-12	Influence of gaps in the Fourier amplitude spectrum on reduction of 5% damped response spectra, record "trial 03".	5-62
Figure 5-13A	5% damped response spectra for 1g sine pulse at 5 Hz.	5-63
Figure 5-13B	Fourier spectra for 1g sine pulse with a frequency of 5 Hz.	5-64
Figure 5-13C	5% damped response spectra for 1g pulse consisting of three frequencies (2.5, 5, and 10 Hz).	5-65
Figure 5-13D	Fourier spectra for 1g sine pulse consisting of three frequencies (2.5, 5, and 10 Hz).	5-66
Figure 5-14A	Duration times from 5% - 75% Arias intensity, empirical WUS data for rock sites, M 5-6, horizontal motions.	5-67
Figure 5-14B	Duration times from 5% - 75% Arias intensity, empirical WUS data for rock sites, M 6-7, horizontal motions.	5-68
Figure 5-14C	Duration times from 5% - 75% Arias intensity, empirical WUS data for rock sites, M 7+, horizontal motions.	5-69
Figure 5-15A	Statistics of Arias intensity ratio vs. time scaled by record times for empirical WUS records in bin D1RM55H.	5-70
Figure 5-15B	Statistics of Arias intensity ratio vs. time scaled by Arias T_{95} for empirical WUS records in bin D1RM55H.	5-71
Figure 5-15C	Statistics of Arias intensity ratio vs. time scaled by Arias $T_{5,95}$ for empirical WUS records in bin D1RM55H.	5-72

Figure 5-16A	Statistics for cumulative absolute velocity vs. time scaled by record times for empirical WUS records in bin D1RM55H.	5-73
Figure 5-16B	Statistics of cumulative absolute velocity vs. time scaled by Arias $T_{5.95}$ for empirical WUS records in bin D1RM55H.	5-74
Figure 5-17A	Correlations of H1-H2 acceleration pairs, WUS rock sites.	5-75
Figure 5-17B	Comparison of correlations of vertical-horizontal acceleration pairs at WUS rock sites.	5-76
Figure 5-18A	Example of uniform hazard spectrum and scaled deaggregated spectra at low and high frequencies.	5-77
Figure 5-18B	Recommended upper- and lower-bound spectral limits to target UHS spectrum for time history designed to envelop UHS.	5-78
Figure 5-18C	Recommended upper- and lower-bound spectral limits to target low-frequency deaggregated spectrum.	5-79
Figure 5-18D	Recommended upper- and lower-bound spectral limits to target high-frequency deaggregated spectrum.	5-80
Figure 6-1	Integrations to calculate soil hazard, for known soil properties and aleatory variability on soil response.	6-40
Figure 6-2	Integration to calculate soil hazard with uncertain soil properties.	6-41
Figure 6-3	Integration to calculate soil hazard using distribution of AF at a' .	6-42
Figure 6-4	Scaling soil UHS from rock UHS, single magnitude.	6-43
Figure 6-5	Scaling soil UHS from rock UHS with magnitude dependence.	6-44
Figure 6-6	Comparison of generic shear-wave velocity profiles for WUS (Los Angeles) and CEUS crustal conditions.	6-45
Figure 6-7	Variations in base case shallow crustal velocities. Solid lines are median estimates from a suite of randomly generated profiles (30) using base-case profiles (Figure 6-6) as input. Ranges reflect $\pm 1\sigma$ estimates.	6-46
Figure 6-8	Generic G/G_{\max} and hysteretic damping curves for soft rock.	6-47
Figure 6-9	Base case shear-wave velocity profiles based on suspension logging measurements. Placed on top of Wald and Heaton (1994) crustal model (Table 6-4).	6-48
Figure 6-10	Variation in base case shear-wave velocity, generic Savannah River profile (Figure 6-9) based on thirty realizations. Median estimate along with $\pm\sigma$ values.	6-49
Figure 6-11	Generic G/G_{\max} and hysteretic damping curves used for Northern California cohesionless soil site Gilroy 2 (EPRI, 1993).	6-50
Figure 6-12	Generic G/G_{\max} and hysteretic damping curves for Peninsular Range deep cohesionless soils. Used for soil sites Rinaldi and Savannah River Generic.	6-51

Figure 6-13	Generic G/G_{max} and hysteretic damping curves for Imperial Valley soils. Used for soil site Meloland.	6-52
Figure 6-14	Generic G/G_{max} and hysteretic damping curves from SHAKE (Idriss and Sun, 1992).	6-53
Figure 6-15	Generic G/G_{max} and hysteretic damping curves for cohesive soils (Vucetic and Dobry, 1991).	6-54
Figure 6-16	Peak acceleration estimates and regression fit at M 7.5 for WUS rock site conditions.	6-55
Figure 6-17	Peak acceleration estimates and regression fit at M7.5 for CEUS rock site conditions.	6-56
Figure 6-18	Attenuation of median peak horizontal acceleration at M 5.5, 6.5, and 7.5 for WUS rock site conditions.	6-57
Figure 6-19	Attenuation of median peak horizontal acceleration at M 5.5, 6.5, and 7.5 for CEUS rock site conditions.	6-58
Figure 6-20	Median response spectra (5% damping) at a distance of 10 km for magnitudes M 5.5, 6.5, and 7.5 : WUS rock site.	6-59
Figure 6-21	Response spectra (5% damping) at a distance of 10 km for M 6.5 showing median and $\pm 1\sigma$ estimates (parametric and regression uncertainty): WUS rock site.	6-60
Figure 6-22	Median response spectra (5% damping) at a distance of 10 km for magnitudes M 5.5, 6.5, and 7.6 : CEUS rock site.	6-61
Figure 6-23	Response spectra (5% damping) at a distance of 10 km for M 6.5 showing median and $\pm 1\sigma$ estimates (parametric and regression uncertainty): CEUS rock site.	6-62
Figure 6-24	Variability in response spectral ordinates at WUS and CEUS rock sites resulting from parametric variability and regression fit over all magnitudes and distances (Tables 6-2 and 6-3).	6-63
Figure 6-25	Attenuation of median peak horizontal acceleration at M 5.5, 6.5, and 7.5 for soil profile Gilroy 2 and WUS conditions.	6-64
Figure 6-26	Median response spectra (5% damping) at a distance of 10 km for M 5.5, 6.5, and 7.5 for soil profile Gilroy 2 and WUS conditions.	6-65
Figure 6-27	Attenuation of median peak horizontal acceleration at M 5.5, 6.5, and 7.5 for soil profile Gilroy 2 and CEUS conditions.	6-66
Figure 6-28	Median response spectra (5% damping) at a distance of 10 km for M 5.5, 6.5, and 7.5 for soil profile Gilroy 2 and CEUS conditions.	6-67
Figure 6-29	Attenuation of median peak horizontal acceleration at M 5.5, 6.5, and 7.5 for soil profile Meloland and WUS conditions.	6-68
Figure 6-30	Median response spectra (5% damping) at a distance of 10 km for M 5.5, 6.5, and 7.5 for soil profile Meloland and WUS conditions.	6-69

Figure 6-31	Attenuation of median peak horizontal acceleration at M 5.5, 6.5, and 7.5 for soil profile Meloland and CEUS conditions.	6-70
Figure 6-32	Median response spectra (5% damping) at a distance of 10 km for M 5.5, 6.5, and 7.5 for soil profile Meloland and CEUS conditions.	6-71
Figure 6-33	Attenuation of median peak horizontal acceleration at M 5.5, 6.5, and 7.5 for soil profile Rinaldi and WUS conditions.	6-72
Figure 6-34	Median response spectra (5% damping) at a distance of 10 km for M 5.5, 6.5, and 7.5 for soil response Rinaldi and WUS conditions.	6-73
Figure 6-35	Attenuation of median peak horizontal acceleration at M 5.5, 6.5, and 7.5 for soil profile Rinaldi and CEUS conditions.	6-74
Figure 6-36	Median response spectra (5% damping) at a distance of 10 km for M 5.5, 6.5, and 7.5 for soil profile Rinaldi and CEUS conditions.	6-75
Figure 6-37	Attenuation of median peak horizontal acceleration at M 5.5, 6.5, and 7.5 for soil profile Savannah River Generic and WUS conditions.	6-76
Figure 6-38	Median response spectra (5% damping) at a distance of 10 km for M 5.5, 6.5, and 7.5 for soil profile Savannah River Generic and WUS conditions.	6-77
Figure 6-39	Attenuation of median peak horizontal acceleration at M 5.5, 6.5, and 7.5 for soil profile Savannah River Generic and CEUS conditions.	6-78
Figure 6-40	Median response spectra (5% damping) at a distance of 10 km for M 5.5, 6.5, and 7.5 for soil profile Savannah River Generic and CEUS conditions.	6-79
Figure 6-41	Variability in response spectral ordinates for WUS soil sites resulting from parametric variability and regression fit over all magnitudes and distances (Table 6-2 and 6-3).	6-80
Figure 6-42	Variability in response spectral ordinates for CEUS soil sites resulting from parametric variability and regression fit over all magnitudes and distances (Tables 6-2 and 6-3).	6-81
Figure 6-43	Configuration of background source and Charleston fault affecting CEUS example site (Columbia, South Carolina).	6-82
Figure 6-44	Contribution to seismic hazard by source for 10 Hz spectral acceleration, Columbia site.	6-83
Figure 6-45	Contribution to seismic hazard by source for 1 Hz spectral acceleration, Columbia site.	6-84
Figure 6-46	Deaggregation of seismic hazard by M , R , and a for 10 Hz SA at 0.38g, Columbia site.	6-85
Figure 6-47	Deaggregation of seismic hazard by M and R for 10 Hz SA at 0.38g, Columbia site.	6-86
Figure 6-48	Deaggregation of seismic hazard by M , R , and a for 1 Hz SA at 0.067g, Columbia site.	6-87

Figure 6-49	Deaggregation of seismic hazard by M and R for 1 Hz SA at 0.067g, Columbia site.	6-88
Figure 6-50	10 ⁻⁴ UHS for rock, Columbia site, with spectra from deaggregation earthquakes.	6-89
Figure 6-51	Variable σ and constant σ vs. frequency for Savannah profile.	6-90
Figure 6-52	Variable σ and constant σ vs. frequency for Gilroy profile.	6-91
Figure 6-53	Variable σ and constant σ vs. frequency for Meloland profile.	6-92
Figure 6-54	Variable σ and constant σ vs. frequency for Rinaldi profile.	6-93
Figure 6-55	10 ⁻⁴ UHS for rock, Columbia site, for constant σ and variable σ assumptions.	6-94
Figure 6-56	10 ⁻⁴ UHS for CEUS rock and four soils, Gilroy profile.	6-95
Figure 6-57	10 ⁻⁴ UHS for CEUS rock and Meloland profile.	6-96
Figure 6-58	10 ⁻⁴ UHS for CEUS rock and Savannah profile.	6-97
Figure 6-59	10 ⁻⁴ UHS for CEUS rock and Rinaldi profile.	6-98
Figure 6-60	Configuration of background source and Mojave fault affecting WUS example site (Mojave, California).	6-99
Figure 6-61	Contribution to seismic hazard by source for 10 Hz spectral acceleration, Mojave site.	6-100
Figure 6-62	Contribution to seismic hazard by source for 1 Hz spectral acceleration, Mojave site.	6-101
Figure 6-63	Deaggregation of seismicity hazard by M , R and ϵ for 10 Hz SA at 1.92g, Mojave site.	6-102
Figure 6-64	Deaggregation of seismic hazard by M and R for 10 Hz SA at 1.92g, Mojave.	6-103
Figure 6-65	Deaggregation of seismic hazard by M , R and ϵ for 1 Hz SA at 0.65g, Mojave site.	6-104
Figure 6-66	Deaggregation of seismic hazard by M and R for 1 Hz SA at 0.65g, Mojave site.	6-105
Figure 6-67	10 ⁻⁴ UHS for rock, Columbia site, with spectra from deaggregation earthquakes.	6-106
Figure 6-68	10 ⁻⁴ UHS for rock, Mojave site, for constant σ and variable σ assumptions.	6-107
Figure 6-69	10 ⁻⁴ UHS for WUS rock and Savannah site.	6-108
Figure 6-70	10 ⁻⁴ UHS for WUS rock and Gilroy profile.	6-109
Figure 6-71	10 ⁻⁴ UHS for WUS rock and Meloland profile.	6-110
Figure 6-72	10 ⁻⁴ UHS for WUS rock and Rinaldi profile.	6-111
Figure 6-73	10 ⁻⁴ UHS for CEUS site (Columbia) and WUS site (Mojave).	6-112

Figure 6-74	Comparison of spectral match (dotted line) to median spectrum computed for $M = 7.5$ at a distance of 1 km (solid line): CEUS rock outcrop.	6-113
Figure 6-75	Median and $\pm\sigma$ spectra computed for $M = 7.5$ at a distance of 1 km using the Savannah River generic profile with site variations only (profile, G/G_{max} , and hysteretic damping): CEUS conditions.	6-114
Figure 6-76	Median and $\pm\sigma$ spectra computed for $M=7.5$ at an epicentral distance of 12 km using the Savannah River Generic profile with source, path and site variations: CEUS conditions.	6-115
Figure 6-77	Comparison of median spectral estimates computed for $M=7.5$ at an epicentral distance of 1 km using the Savannah River Generic profile: varying site properties only (solid line) and varying source, path, and site properties (dashed line); CEUS conditions.	6-116
Figure 6-78	Comparison of Approaches 1, 2B, and 4 10^{-4} UHS on soil for profile Rinaldi: CEUS conditions.	6-117
Figure 6-79	Median and $\pm\sigma$ effective strains for soil profile Rinaldi using Approach 1: CEUS conditions.	6-118
Figure 6-80	Comparison of transfer functions computed for the scaled 1 Hz design earthquake; soil profile Rinaldi, CEUS conditions.	6-119
Figure 6-81	Comparison of transfer functions computed for the scaled 10 Hz design earthquake, soil profile Rinaldi, CEUS conditions.	6-120
Figure 6-82	Comparison of mean transfer functions computed for the scaled 1 Hz and 10 Hz design earthquakes; soil profile Rinaldi, CEUS conditions.	6-121
Figure 6-83	Comparison of soil spectra for Approaches 1, 2A, and 2B; soil profile Rinaldi, CEUS conditions.	6-122
Figure 6-84	Comparison of soil spectra for Approach 2B with base case profile and deterministic profile variations (\pm factor of 2 on shear modulus); soil profile Rinaldi, CEUS conditions.	6-123
Figure 6-85	Comparison of soil spectra for Approach 2B with mean and $\pm 1\sigma$ variations of base case (\pm factor of 2 on shear modulus), soil profile Rinaldi, CEUS conditions.	6-124
Figure 6-86	Comparison of Approaches 1, 2B, and 4 10^{-4} UHS on soil for profile Rinaldi: WUS conditions.	6-125
Figure 6-87	Median and $\pm 1 \sigma$ effective strains for soil profile Rinaldi using Approach 1: WUS conditions.	6-126
Figure 6-88	Comparison of transfer functions computed for the scaled 1 Hz design earthquake; soil profile Rinaldi, WUS conditions.	6-127
Figure 6-89	Comparison of transfer functions computed for the scaled 10 Hz design earthquake; soil profile Rinaldi, WUS conditions.	6-128
Figure 6-90	Comparison of mean transfer functions computed for the scaled 1 Hz and 10 Hz design earthquakes; soil profile Rinaldi, WUS conditions.	6-129

Figure 6-91	Comparison of soil spectra for Approaches 1, 2A, and 2B; soil profile Rinaldi, WUS conditions.	6-130
Figure 6-92	Comparison of soil spectra for Approach 2B with base case profile and deterministic profile variations (\pm factor of 2 on shear modulus); soil profile Rinaldi, WUS conditions.	6-131
Figure 6-93	Comparison of soil spectra for Approach 2B with mean and $\pm 1\sigma$ variations of base case (\pm factor of 2 on shear modulus), soil profile Rinaldi, WUS conditions.	6-132
Figure 6-94	Comparison of Approaches 1, 2B, and $4 \cdot 10^{-4}$ UHS on soil for profile Gilroy 2: CEUS conditions.	6-133
Figure 6-95	Median and $\pm 1 \sigma$ effective strains for soil profile Gilroy 2 using Approach 1: CEUS conditions.	6-134
Figure 6-96	Comparison of transfer functions computed for the scaled 1 Hz design earthquake, soil profile Gilroy 2, CEUS conditions.	6-135
Figure 6-97	Comparison of transfer functions computed for the scaled 10 Hz design earthquake: soil profile Gilroy 2, CEUS conditions.	6-136
Figure 6-98	Comparison of mean transfer functions computed for the scaled 1 Hz and 10 Hz design earthquakes; soil profile Gilroy 2, CEUS conditions.	6-137
Figure 6-99	Comparison of soil spectra for Approaches 1, 2A, and 2B; soil profile Gilroy 2, CEUS conditions.	6-138
Figure 6-100	Comparison of soil spectra for Approach 2B with base case profile and deterministic profile variations (\pm factor of 2 on shear modulus); soil profile Gilroy 2, CEUS conditions.	6-139
Figure 6-101	Comparison of soil spectra for Approach 2B with mean and $\pm 1\sigma$ variations of base case (\pm factor of 2 on shear modulus), soil profile Gilroy 2, CEUS conditions.	6-140
Figure 6-102	Comparison of soil spectra for Approach 2B (full profile) with base case profile and deterministic profile variations (\pm factor of 2 on shear modulus) with profile truncated at 150m; soil profile Gilroy 2, CEUS conditions.	6-141
Figure 6-103	Comparison of soil spectra for Approach 2B (full profile) with mean and $\pm 1\sigma$ profile variations with profile truncated at 150m. Soil profile Gilroy 2, CEUS conditions.	6-142
Figure 6-104	Comparison of soil spectra for Approach 2B (full profile) with base case profile and deterministic profile variations (\pm factor of 2 on shear modulus) with profile truncated at 90m; soil profile Gilroy 2, CEUS conditions.	6-143
Figure 6-105	Comparison of soil spectra for Approach 2B (full profile) with mean and $\pm 1\sigma$ profile variations with profile truncated at 90m. Soil profile Gilroy 2, CEUS conditions.	6-144

Figure 6-106	Comparison of Approaches 1, 2B, and 4 10^{-4} UHS on soil for profile Gilroy 2: WUS conditions.	6-145
Figure 6-107	Median and $\pm 1\sigma$ effective strain for soil profile Gilroy 2 using Approach 1: WUS conditions.	6-146
Figure 6-108	Comparison of transfer functions computed for the scaled 1 Hz design earthquake: soil profile Gilroy 2, WUS conditions.	6-147
Figure 6-109	Comparison of transfer functions computed for the scaled 10 Hz design earthquake; soil profile Gilroy 2, WUS conditions.	6-148
Figure 6-110	Comparison of mean transfer functions computed for the scaled 1 Hz and 10 Hz design earthquakes; soil profile Gilroy 2, WUS conditions.	6-149
Figure 6-111	Comparison of soil spectra for Approaches 1, 2A, and 2B; soil profile Gilroy 2, WUS conditions.	6-150
Figure 6-112	Comparison of soil spectra for Approach 2B with base case profile and deterministic profile variations (\pm factor of 2 on shear modulus); soil profile Gilroy 2, WUS conditions.	6-151
Figure 6-113	Comparison of soil spectra for Approach 2B with mean and $\pm 1\sigma$ variations of base case (\pm factor of 2 on shear modulus), soil profile Gilroy 2, WUS conditions.	6-152
Figure 6-114	Comparison of soil spectra for Approach 2B (full profile) with base case profile and deterministic profile variations (\pm factor of 2 on shear modulus) with profile truncated at 150m; soil profile Gilroy 2, WUS conditions.	6-153
Figure 6-115	Comparison of soil spectra for Approach 2B (full profile) with mean and $\pm 1\sigma$ profile variations with profile truncated at 150m; soil profile Gilroy 2, WUS conditions.	6-154
Figure 6-116	Comparison of soil spectra for Approach 2B (full profile) with base case profile and deterministic profile variations (\pm factor of 2 on shear modulus) with profile truncated at 90m; soil profile Gilroy 2, WUS conditions.	6-155
Figure 6-117	Comparison of soil spectra for Approach 2B (full profile) with mean and $\pm 1\sigma$ profile variations with profile truncated at 90m. Soil profile Gilroy 2, WUS conditions.	6-156
Figure 6-118	Comparison of Approaches 1, 2B, and 4, 10^{-4} UHS on soil for profile Savannah River Generic: CEUS conditions.	6-157
Figure 6-119	Median and $\pm 1\sigma$ effective strains for soil profile Savannah River Generic using Approach 1: CEUS conditions.	6-158
Figure 6-120	Comparison of transfer functions computed for the scaled 1 Hz design earthquake; soil profile Savannah River Generic, CEUS conditions.	6-159
Figure 6-121	Comparison of transfer functions computed for the scaled 10 Hz design earthquake; soil profile Savannah River Generic, CEUS conditions.	6-160

Figure 6-122	Comparison of mean transfer functions computed for the scaled 1 Hz and 10 Hz design earthquakes; soil profile Savannah River Generic, CEUS conditions.	6-161
Figure 6-123	Comparison of soil spectra for Approaches 1, 2A, and 2B; soil profile Savannah River Generic, CEUS conditions.	6-162
Figure 6-124	Comparison of soil spectra for Approach 2B with base case profile and deterministic profile variations (\pm factor of 2 on shear modulus); soil profile Savannah River Generic, CEUS conditions.	6-163
Figure 6-125	Comparison of soil spectra for Approach 2B with mean and $\pm 1\sigma$ variations of base case (\pm factor of 2 on shear modulus), soil profile Savannah River Generic, CEUS conditions.	6-164
Figure 6-126	Comparison of soil spectra for Approach 2B (full profile) with base case profile and deterministic profile variations (\pm factor of 2 on shear modulus) with profile truncated at 150m; soil profile Savannah River Generic, CEUS conditions.	6-165
Figure 6-127	Comparison of soil spectra for Approach 2B (full profile) with mean and $\pm 1\sigma$ profile variations with profile truncated at 150m. Soil profile Savannah River Generic; CEUS conditions.	6-166
Figure 6-128	Comparison of soil spectra for Approach 2B (full profile) with base case profile and deterministic profile variations (\pm factor of 2 on shear modulus) with profile truncated at 90m; soil profile Savannah River Generic, CEUS conditions.	6-167
Figure 6-129	Comparison of soil spectra for Approach 2B (full profile) with mean and $\pm 1\sigma$ profile variations with profile truncated at 90m. Soil profile Savannah River Generic, CEUS conditions.	6-168
Figure 6-130	Comparison of Approaches 1, 2B, and 4 soil spectra for profile Savannah River Generic: WUS conditions.	6-169
Figure 6-131	Median and $\pm 1\sigma$ effective strains for soil profile Savannah River Generic using Approach 1: WUS conditions.	6-170
Figure 6-132	Comparison of transfer functions computed for the scaled 1 Hz design earthquake; soil profile Savannah River Generic, WUS conditions.	6-171
Figure 6-133	Comparison of transfer functions computed for the scaled 10 Hz design earthquake; soil profile Savannah River Generic, WUS conditions.	6-172
Figure 6-134	Comparison of mean transfer functions computed for the scaled 1 Hz and 10 Hz design earthquakes; soil profile Savannah River Generic, WUS conditions.	6-173
Figure 6-135	Comparison of soil spectra for Approaches 1, 2A, and 2B; soil profile Savannah River Generic, WUS conditions.	6-174

Figure 6-136	Comparison of soil spectra for Approach 2B with base case profile and deterministic profile variations (\pm factor of 2 on shear modulus); soil profile Savannah River Generic, WUS conditions.	6-175
Figure 6-137	Comparison of soil spectra for Approach 2B with mean and $\pm 1\sigma$ variations of base case (\pm factor of 2 on shear modulus), soil profile Savannah River Generic, WUS conditions.	6-176
Figure 6-138	Comparison of soil spectra for Approach 2b (full profile) with base case profile and deterministic profile variations (\pm factor of 2 on shear modulus) with profile truncated at 150m; soil profile Savannah River Generic, WUS conditions.	6-177
Figure 6-139	Comparison of soil spectra for Approach 2B (full profile) with mean and $\pm 1\sigma$ profile variation with profile truncated at 150m. Soil profile Savannah River Generic, WUS conditions.	6-178
Figure 6-140	Comparison of soil spectra for Approach 2B (full profile) with base case profile and deterministic profile variations (\pm factor of 2 on shear modulus) with profile truncated at 90m; soil profile Savannah River Generic, WUS conditions.	6-179
Figure 6-141	Comparison of soil spectra for Approach 2B (full profile) with mean and $\pm 1\sigma$ profile variations with profile truncated at 90m. Soil profile Savannah River Generic, WUS conditions.	6-180
Figure 6-142	Comparison of Approaches 1, 2B, and 4 soil spectra for profile Meloland; CEUS conditions.	6-181
Figure 6-143	Median and $\pm 1\sigma$ effective strains for soil profile Meloland using Approach 1; CEUS conditions.	6-182
Figure 6-144	Comparison of transfer functions computed for the scaled 1 Hz design earthquake; soil profile Meloland, CEUS conditions.	6-183
Figure 6-145	Comparison of transfer functions computed for the scaled 10 Hz design earthquake; soil profile Meloland, CEUS conditions.	6-184
Figure 6-146	Comparison of mean transfer functions computed for the scaled 1 Hz and 10 Hz design earthquakes; soil profile Meloland, CEUS conditions.	6-185
Figure 6-147	Comparison of soil spectra for Approaches 1, 2A, and 2B; soil profile Meloland, CEUS conditions.	6-186
Figure 6-148	Comparison of soil spectra for Approach 2B with base case profile and deterministic profile variations (\pm factor of 2 on shear modulus); soil profile Meloland, CEUS conditions.	6-187
Figure 6-149	Comparison of soil spectra for Approach 2B with mean and $\pm 1\sigma$ variations of base case (\pm factor of 2 on shear modulus); soil profile Meloland, CEUS conditions.	6-188

Figure 6-150	Comparison of soil spectra for Approach 2B (full profile) with base case profile and deterministic profile variations (\pm factor of 2 on shear modulus) with profile truncated at 150m; soil profile Meloland, CEUS conditions.	6-189
Figure 6-151	Comparison of soil spectra for Approach 2B (full profile) with mean and $\pm 1\sigma$ profile variations with profile truncated at 150m. Soil profile Meloland, CEUS conditions.	6-190
Figure 6-152	Comparison of soil spectra for Approach 2B (full profile) with base case profile and deterministic profile variations (\pm factor of 2 on shear modulus) with profile truncated at 90m; soil profile Meloland; CEUS conditions.	6-191
Figure 6-153	Comparison of soil spectra for Approach 2B (full profile) with mean and $\pm 1\sigma$ profile variations with profile truncated at 90m. Soil profile Meloland, CEUS conditions.	6-192
Figure 6-154	Comparison of Approaches 1, 2B, and 4 soil spectra for profile Meloland: WUS conditions.	6-193
Figure 6-155	Median and $\pm 1\sigma$ effective strains for soil profile Meloland using Approach 1 WUS conditions.	6-194
Figure 6-156	Comparison of transfer functions computed for the scaled 1 Hz design earthquake; soil profile Meloland, WUS conditions.	6-195
Figure 6-157	Comparison of transfer functions computed for the scaled 10 Hz design earthquake; soil profile Meloland, WUS conditions.	6-196
Figure 6-158	Comparison of mean transfer functions computed for the scaled 1 Hz and 10 Hz design earthquakes; soil profile Meloland, WUS conditions.	6-197
Figure 6-159	Comparison of soil spectra for Approaches 1, 2A, and 2B; soil profile Meloland, WUS conditions.	6-198
Figure 6-160	Comparison of soil spectra for Approach 2B with base case profile and deterministic profile variations (\pm factor of 2 on shear modulus); soil profile Meloland, WUS conditions.	6-199
Figure 6-161	Comparison of soil spectra for Approach 2B with mean and $\pm 1\sigma$ variations of base case (\pm factor of 2 on shear modulus), soil profile Meloland, WUS conditions.	6-200
Figure 6-162	Comparison of soil spectra for Approach 2B (full profile) with base case profile and deterministic profile variations (\pm factor of 2 on shear modulus) with profile truncated at 150m; soil profile Meloland, WUS conditions.	6-201
Figure 6-163	Comparison of soil spectra for Approach 2B (full profile) with mean and $\pm 1\sigma$ deterministic profile variations with profile truncated at 150m. Soil profile Meloland, WUS conditions.	6-202

Figure 6-164	Comparison of soil spectra for Approach 2B (full profile) with base case profile and deterministic profile variations (\pm factor of 2 on shear modulus) with profile truncated at 90m; soil profile Meloland, WUS conditions.	6-203
Figure 6-165	Comparison of soil spectra for Approach 2B (full profile) with mean and $\pm 1\sigma$ profile variations with profile truncated at 90m. Soil profile Meloland, WUS conditions.	6-204
Figure 6-166	Median and $\pm 1\sigma$ shear-wave velocities based on measurements at WUS rock strong motion sites. Geomatrix categories A and B (Appendix A) assumed to reflect rock site conditions. Dashed line is smooth model used in analyses.	6-205
Figure 6-167	Median WUS rock response spectra (5% damping) computed for $M = 6.5$ at a distance of 25 km using the soft rock profile (Figure 6-166) and the point source model (Appendix D). Suite of depths (shear-wave velocities) reflect depth to which overlying materials are removed.	6-206
Figure 6-168	Depth-to-surface response spectral ratios (median estimates) computed for the suite of spectra shown on Figure 6-167.	6-207
Figure 6-169	Depth-to-surface response spectral ratios (median estimates) computed for $M=6.5$ at a distance of 10 km.	6-208
Figure 6-170	Depth-to-surface response spectral ratios (median estimates) computed for $M=6.5$ at a distance of 1 km.	6-209
Figure 6-171	Comparison of WUS UHS at surface of rock site (solid line) and UHS at free surface with a shear-wave velocity of 914m/sec (3,000 ft/sec) using transfer function corresponding to surface acceleration of 0.483g (Figure 6-170). Modified spectrum represents modification of surface soft rock motions to base-of-soil motions.	6-210
Figure 6-172	Comparison of WUS soil motions using rock UHS and modified rock (base-of-soil) UHS soil profile Rinaldi.	6-211
Figure 6-173	Comparison of WUS soil motions using rock UHS and modified rock (base-of-soil) UHS soil profile Gilroy 2.	6-212
Figure 6-174	Comparison of WUS soil motions using rock UHS and modified rock (base-of-soil) UHS soil profile Savannah River Generic.	6-213
Figure 6-175	Comparison of WUS soil motions using rock UHS and modified rock (base-of-soil) UHS soil profile Meloland.	6-214
Figure 7-1	Steps to designate required component capacity.	7-17
Figure 7-2	Graphical representation of curves for failure calculation.	7-18
Figure 7-3	Alternative capacity distribution with same CAP_{10} .	7-19
Figure 7-4	Hazard curve with different slopes.	7-20
Figure 7-5	Comparison of hazard curves with different slopes to capacity curve.	7-21

Figure 7-6	PGA hazard curves for the eleven test sites: (top) as calculated, (bottom) normalized by the acceleration value corresponding to 10^{-4} annual probability.	7-22
Figure 7-7	SA (10 Hz) hazard curves for the eleven test sites: (top) as calculated, (bottom) normalized by the acceleration value corresponding to 10^{-4} annual probability.	7-23
Figure 7-8	SA (1 Hz) hazard curves for the eleven test sites: (top) as calculated, (bottom) normalized by the acceleration value corresponding to 10^{-4} annual probability.	7-24
Figure 7-9	Maine Yankee PGA seismic hazard curve (top), fragility curve for $\beta = 0.3$ (middle), and contributions to P_F by PGA (bottom).	7-25
Figure 7-10	Maine Yankee PGA seismic hazard curve (top), fragility curve for $\beta=0.6$ (middle), and contributions to P_F by PGA (bottom).	7-26
Figure 7-11	UHS for Columbia site, with URS calculated from seismic hazard analysis.	7-27
Figure 7-12	UHS for Columbia site, with URS calculated from seismic hazard analysis using background source only.	7-28
Figure 7-13	UHS for Mojave site with URS calculated from seismic hazard analysis.	7-29
Figure 7-14	R_p calculated from risk equation for 11 test sites and 3 parameters, using $\alpha = 1.67$ (top) and using $\alpha = 1.67 \times SF$ (bottom).	7-30
Figure 7-15	Ratio of approximate to exact P_F using $\alpha = 1.67$ (top), and using $\alpha = 1.67 \times SF$ (bottom).	7-31
Figure 7-16	R_p calculated from direct integration for 11 test sites and 3 parameters, using $\alpha = 1.67$ (top) and using $\alpha = 1.67 \times SF$ (bottom).	7-32
Figure 7-17	R_p calculated from direct integration for 11 test sites and 3 parameters, using median hazard curves.	7-33
Figure 7-18	Ratio of approximate to exact P_F using $\alpha = 1.67$ (top) and using median hazard curves.	7-34
Figure C-1	Median 1σ spectral shapes for $M \approx 5.5$, $R = 0-10$ km, horizontal WUS rock.	C-8
Figure C-2	Median 1σ spectral shapes for $M \approx 6.5$, $R = 0-10$ km, horizontal WUS rock.	C-9
Figure C-3	Median 1σ spectral shapes for $M \approx 7.5$, $R = 0-10$ km, horizontal WUS rock.	C-10
Figure C-4	Median 1σ spectral shapes for $M \approx 5.5$, $R = 0-10$ km, horizontal WUS soil.	C-11
Figure C-5	Median 1σ spectral shapes for $M \approx 6.5$, $R = 0-10$ km, horizontal WUS soil.	C-12

Figure C-6	Median 1σ spectral shapes for $M \approx 7.5$, $R = 0-10$ km, horizontal WUS soil.	C-13
Figure C-7	Median 1σ spectral shapes for $M \approx 5.5$, $R = 10-50$ km, horizontal WUS rock.	C-14
Figure C-8	Median 1σ spectral shapes for $M \approx 6.5$, $R = 10-50$ km, horizontal WUS rock.	C-15
Figure C-9	Median 1σ spectral shapes for $M \approx 7.5$, $R = 10-50$ km, horizontal WUS rock.	C-16
Figure C-10	Median 1σ spectral shapes for $M \approx 5.5$, $R = 10-50$ km, horizontal WUS soil.	C-17
Figure C-11	Median 1σ spectral shapes for $M \approx 6.5$, $R = 10-50$ km, horizontal WUS soil.	C-18
Figure C-12	Median 1σ spectral shapes for $M \approx 7.5$, $R = 10-50$ km, horizontal WUS soil.	C-19
Figure C-13	Median 1σ spectral shapes for $M \approx 5.5$, $R = 50-100$ km, horizontal, WUS rock.	C-20
Figure C-14	Median 1σ spectral shapes for $M \approx 6.5$, $R = 50-100$ km, horizontal, WUS rock.	C-21
Figure C-15	Median 1σ spectral shapes for $M \approx 7.5$, $R = 50-100$ km, horizontal, WUS rock.	C-22
Figure C-16	Median 1σ spectral shapes for $M \approx 5.5$, $R = 50-100$ km, horizontal, WUS soil.	C-23
Figure C-17	Median 1σ spectral shapes for $M \approx 6.5$, $R = 50-100$ km, horizontal, WUS soil.	C-24
Figure C-18	Median 1σ spectral shapes for $M \approx 7.5$, $R = 50-100$ km, horizontal, WUS soil.	C-25
Figure C-19	Median 1σ spectral shapes for $M \approx 5.5$, $R = 100-200$ km, horizontal, WUS rock.	C-26
Figure C-20	Median 1σ spectral shapes for $M \approx 6.5$, $R = 100-200$ km, horizontal, WUS rock.	C-27
Figure C-21	Median 1σ spectral shapes for $M \approx 7.5$, $R = 100-200$ km, horizontal, WUS rock.	C-28
Figure C-22	Median 1σ spectral shapes for $M \approx 5.5$, $R = 100-200$ km, horizontal, WUS soil.	C-29
Figure C-23	Median 1σ spectral shapes for $M \approx 6.5$, $R = 100-200$ km, horizontal, WUS soil.	C-30
Figure C-24	Median 1σ spectral shapes for $M \approx 7.5$, $R = 100-200$ km, horizontal, WUS soil.	C-31

Figure C-25	Median 1 σ spectral shapes for $M \approx 5.5$, $R = 0-50$ km, horizontal, WUS rock.	C-32
Figure C-26	Median 1 σ spectral shapes for $M \approx 6.5$, $R = 0-50$ km, horizontal, WUS rock.	C-33
Figure C-27	Median 1 σ spectral shapes for $M \approx 7.5$, $R = 0-50$ km, horizontal, WUS rock.	C-34
Figure C-28	Median 1 σ spectral shapes for $M \approx 5.5$, $R = 0-50$ km, horizontal, WUS soil.	C-35
Figure C-29	Median 1 σ spectral shapes for $M \approx 6.5$, $R = 0-50$ km, horizontal, WUS soil.	C-36
Figure C-30	Median 1 σ spectral shapes for $M \approx 7.5$, $R = 0-50$ km, horizontal, WUS soil.	C-37
Figure C-31	Median 1 σ spectral shapes for $M \approx 5.5$, $R = 0-10$ km, vertical, WUS rock.	C-38
Figure C-32	Median 1 σ spectral shapes for $M \approx 6.5$, $R = 0-10$ km, vertical, WUS rock.	C-39
Figure C-33	Median 1 σ spectral shapes for $M \approx 7.5$, $R = 0-10$ km, vertical, WUS rock.	C-40
Figure C-34	Median 1 σ spectral shapes for $M \approx 5.5$, $R = 0-10$ km, vertical, WUS soil.	C-41
Figure C-35	Median 1 σ spectral shapes for $M \approx 6.5$, $R = 0-10$ km, vertical, WUS soil.	C-42
Figure C-36	Median 1 σ spectral shapes for $M \approx 7.5$, $R = 0-10$ km, vertical, WUS soil.	C-43
Figure C-37	Median 1 σ spectral shapes for $M \approx 5.5$, $R = 10-50$ km, vertical, WUS rock.	C-44
Figure C-38	Median 1 σ spectral shapes for $M \approx 6.5$, $R = 10-50$ km, vertical, WUS rock.	C-45
Figure C-39	Median 1 σ spectral shapes for $M \approx 7.5$, $R = 10-50$ km, vertical, WUS rock.	C-46
Figure C-40	Median 1 σ spectral shapes for $M \approx 5.5$, $R = 10-50$ km, vertical, WUS soil.	C-47
Figure C-41	Median 1 σ spectral shapes for $M \approx 6.5$, $R = 10-50$ km, vertical, WUS soil.	C-48
Figure C-42	Median 1 σ spectral shapes for $M \approx 7.5$, $R = 10-50$ km, vertical, WUS soil.	C-49
Figure C-43	Median 1 σ spectral shapes for $M \approx 5.5$, $R = 50-100$ km, vertical, WUS rock.	C-50

Figure C-44	Median 1σ spectral shapes for $M \approx 6.5$, $R = 50-100$ km, vertical, WUS rock.	C-51
Figure C-45	Median 1σ spectral shapes for $M \approx 7.5$, $R = 50-100$ km, vertical, WUS rock.	C-52
Figure C-46	Median 1σ spectral shapes for $M \approx 5.5$, $R = 50-100$ km, vertical, WUS soil.	C-53
Figure C-47	Median 1σ spectral shapes for $M \approx 6.5$, $R = 50-100$ km, vertical, WUS soil.	C-54
Figure C-48	Median 1σ spectral shapes for $M \approx 7.5$, $R = 50-100$ km, vertical, WUS soil.	C-55
Figure C-49	Median 1σ spectral shapes for $M \approx 5.5$, $R = 100-200$ km, vertical, WUS rock.	C-56
Figure C-50	Median 1σ spectral shapes for $M \approx 6.5$, $R = 100-200$ km, vertical, WUS rock.	C-57
Figure C-51	Median 1σ spectral shapes for $M \approx 7.5$, $R = 100-200$ km, vertical, WUS rock.	C-58
Figure C-52	Median 1σ spectral shapes for $M \approx 5.5$, $R = 100-200$ km, vertical, WUS soil.	C-59
Figure C-53	Median 1σ spectral shapes for $M \approx 6.5$, $R = 100-200$ km, vertical, WUS soil.	C-60
Figure C-54	Median 1σ spectral shapes for $M \approx 7.5$, $R = 100-200$ km, vertical, WUS soil.	C-61
Figure C-55	Median 1σ spectral shapes for $M \approx 5.5$, $R = 0-50$ km, vertical, WUS rock.	C-62
Figure C-56	Median 1σ spectral shapes for $M \approx 6.5$, $R = 0-50$ km, vertical, WUS rock.	C-63
Figure C-57	Median 1σ spectral shapes for $M \approx 7.5$, $R = 0-50$ km, vertical, WUS rock.	C-64
Figure C-58	Median 1σ spectral shapes for $M \approx 5.5$, $R = 0-50$ km, vertical, WUS soil.	C-65
Figure C-59	Median 1σ spectral shapes for $M \approx 6.5$, $R = 0-50$ km, vertical, WUS soil.	C-66
Figure C-60	Median 1σ spectral shapes for $M \approx 7.5$, $R = 0-50$ km, vertical, WUS soil.	C-67
Figure D-1	Model bias and variability estimates for all earthquakes computed over all 503 sites for the point-source model.	D-15

Figure D-2	Model bias and variability estimates for all earthquakes computed over all 344 soil sites for the point-source model.	D-16
Figure D-3	Model bias and variability estimates for all earthquakes computed over all 159 rock sites for the point-source model.	D-17
Figure E-1	Mean Fourier spectra for distance 0-10km, rock sites, M5-6	E-2
Figure E-2	Mean Fourier spectra for distance 0-10km, rock sites, M6-7	E-3
Figure E-3	Mean Fourier spectra for distance 0-10km, rock sites, M7+. Note: discontinuity at 25 Hz is caused by few records available above that frequency.	E-4
Figure E-4	Mean Fourier spectra for distance 10-50km, rock sites, M5-6	E-5
Figure E-5	Mean Fourier spectra for distance 10-50km, rock sites, M6-7	E-6
Figure E-6	Mean Fourier spectra for distance 10-50km, rock sites, M7+	E-7
Figure E-7	Mean Fourier spectra for distance 50-100km, rock sites, M5-6	E-8
Figure E-8	Mean Fourier spectra for distance 50-100km, rock sites, M6-7	E-9
Figure E-9	Mean Fourier spectra for distance 50-100km, rock sites, M7+	E-10
Figure E-10	Mean Fourier spectra for distance 100-200km, rock sites, M5-6	E-11
Figure E-11	Mean Fourier spectra for distance 100-200km, rock sites, M6-7	E-12
Figure E-12	Mean Fourier spectra for distance 10-200km, rock sites, M7+	E-13
Figure E-13	Mean Fourier spectra for distance 0-10km, soil sites, M5-6	E-14
Figure E-14	Mean Fourier spectra for distance 0-10km, soil sites, M6-7	E-15
Figure E-15	Mean Fourier spectra for distance 0-10km, soil sites, M7+	E-16
Figure E-16	Mean Fourier spectra for distance 10-50km, soil sites, M5-6	E-17
Figure E-17	Mean Fourier spectra for distance 10-50km, soil sites, M6-7	E-18
Figure E-18	Mean Fourier spectra for distance 10-50km, soil sites, M7+. Note: discontinuity at 25 Hz is caused by few records available above that frequency.	E-19
Figure E-19	Mean Fourier spectra for distance 50-100km, soil sites, M5-6	E-20
Figure E-20	Mean Fourier spectra for distance 50-100km, soil sites, M6-7. Note: discontinuity at 50 Hz is caused by few records available above that frequency.	E-21
Figure E-21	Mean Fourier spectra for distance 50-100km, soil sites, M7+. Note: discontinuity at 25 Hz is caused by few records available above that frequency.	E-22
Figure E-22	Mean Fourier spectra for distance 100-200km, soil sites, M5-6	E-23
Figure E-23	Mean Fourier spectra for distance 100-200km, soil sites, M6-7. Note: discontinuity at 50 Hz is caused by few records available above that frequency.	E-24

Figure E-24	Mean Fourier spectra for distance 100-200km, soil sites, M7+. Note: discontinuity at 25 and 50 Hz is caused by few records available above that frequency.	E-25
Figure E-25	Mean Fourier spectra for distance 0-10km, rock sites, horizontal motions. Note: discontinuity at 25 and 50 Hz is caused by few records available above that frequency.	E-26
Figure E-26	Mean Fourier spectra for distance 0-10km, rock sites, vertical motions. Note: discontinuity at 25 Hz is caused by few records available above that frequency.	E-27
Figure E-27	Mean Fourier spectra for distance 0-10km, soil sites, horizontal motions. Note: discontinuity at 25 and 50 Hz is caused by few records available above that frequency.	E-28
Figure E-28	Mean Fourier spectra for distance 0-10km, soil sites, vertical motions. Note: discontinuity at 25 and 50 Hz is caused by few records available above that frequency.	E-29
Figure E-29	Mean Fourier spectra for distance 10-50km, rock sites, horizontal motions.	E-30
Figure E-30	Mean Fourier spectra for distance 10-50km, rock sites, vertical motions.	E-31
Figure E-31	Mean Fourier spectra for distance 10-50km, soil sites, horizontal motions. Note: discontinuity at 25 and 50 Hz is caused by few records available above that frequency.	E-32
Figure E-32	Mean Fourier spectra for distance 10-50km, soil sites, vertical motions. Note: discontinuity at 25 and 50 Hz is caused by few records available above that frequency.	E-33
Figure E-33	Mean Fourier spectra for distance 50-100km, rock sites, horizontal motions.	E-34
Figure E-34	Mean Fourier spectra for distance 50-100km, rock sites, vertical motions.	E-35
Figure E-35	Mean Fourier spectra for distance 50-100km, soil sites, horizontal motions. Note: discontinuity at 25 and 50 Hz is caused by few records available above that frequency.	E-36
Figure E-36	Mean Fourier spectra for distance 50-100km, rock sites, vertical motions. Note: discontinuity at 25 and 50 Hz is caused by few records available above that frequency.	E-37
Figure E-37	Mean Fourier spectra for distance 100-200km, rock sites, horizontal motions.	E-38
Figure E-38	Mean Fourier spectra for distance 100-200km, rock sites, vertical motions.	E-39
Figure E-39	Mean Fourier spectra for distance 100-200km, soil sites, horizontal motions. Note: discontinuity at 25 and 50 Hz is caused by few records available above that frequency.	E-40

Figure E-40	Mean Fourier spectra for distance 100-200km, soil sites, vertical motions. Note: discontinuity at 25 and 50 Hz is caused by few records available above that frequency.	E-41
Figure F-1	PGD/PGA (cm/g) for horizontal motion, rock sites.	F-2
Figure F-2	PGV/PGA (cm/s/g) for horizontal motion, rock sites.	F-3
Figure F-3	PGA•PGA/PGV ² for horizontal motion, rock sites.	F-4
Figure F-4	PGD/PGA (cm/g) for vertical motion, rock sites	F-5
Figure F-5	PGV/PGA (cm/s/g) for vertical motion, rock sites.	F-6
Figure F-6	PGA•PGD/PGV ² for vertical motion, rock sites.	F-7
Figure F-7	PGD/PGA (cm/g) for horizontal motion, soil sites.	F-8
Figure F-8	PGV/PGA (cm/s/g) for horizontal motion, soil sites.	F-9
Figure F-9	PGA•PGD/PGV ² for horizontal motion, soil sites.	F-10
Figure F-10	PGD/PGA (cm/g) for vertical motions, soil sites.	F-11
Figure F-11	PGV/PGA (cm/s/g) for vertical motion, soil sites.	F-12
Figure F-12	PGA•PGD/PGV ² for vertical motion, soil sites.	F-13
Figure F-13	Duration calculated as 5%-75% of Arias intensity, rock sites, horizontal motion.	F-14
Figure F-14	Duration calculated as 5-75% of Arias intensity, rock sites, vertical motion.	F-15
Figure F-15	Duration calculated as 5-75% of Arias intensity, soil sites, horizontal motion.	F-16
Figure F-16	Duration calculated as 5-75% of Arias intensity, soil sites, vertical motion.	F-17
Figure F-17	Duration calculated as 5-95% of Arias intensity, rock sites, horizontal motion.	F-18
Figure F-18	Duration calculated as 5-95% of Arias intensity, rock sites, vertical motion.	F-19
Figure F-19	Duration calculated as 5-95% of Arias intensity, soil sites, horizontal motion.	F-20
Figure F-20	Duration calculated as 5-95% of Arias intensity, soil sites, vertical motion.	F-21
Figure F-21	Correlations of H1/H2 acceleration pairs, WUS rock sites.	F-22
Figure F-22	Correlations of H1/H2 acceleration pairs, WUS soil sites.	F-23
Figure F-23	Correlations of H1/H2 velocity pairs, WUS rock sites.	F-24
Figure F-24	Correlations of H1/H2 velocity pairs, WUS soil sites.	F-25
Figure F-25	Correlations of H1/H2 displacement pairs, WUS rock sites.	F-26
Figure F-26	Correlations of H1/H2 displacement pairs, WUS soil sites.	F-27

Figure F-27	Comparison of correlations of vertical/horizontal acceleration pairs at WUS rock sites.	F-28
Figure F-28	Comparison of correlations of vertical/horizontal acceleration pairs at WUS soil sites.	F-29
Figure F-29	Comparison of correlations of vertical/horizontal velocity pairs at WUS rock sites.	F-30
Figure F-30	Comparison of correlations of vertical/horizontal velocity pairs at WUS soil sites.	F-31
Figure F-31	Comparison of correlations of vertical/horizontal displacement pairs at WUS rock sites.	F-32
Figure F-32	Comparison of correlations of vertical/horizontal displacement pairs at WUS soil sites.	F-33
Figure G-1	Arias intensity, WUS horizontal motions, rock sites.	G-2
Figure G-2	Arias intensity, WUS vertical motions, rock sites.	G-3
Figure G-3	Arias intensity, WUS horizontal motions, soil sites.	G-4
Figure G-4	Arias intensity, WUS vertical motions, soil sites.	G-5
Figure G-5	CAV, WUS horizontal motions, rock sites.	G-6
Figure G-6	CAV, WUS vertical motions, rock sites.	G-7
Figure G-7	CAV, WUS horizontal motions, soil sites.	G-8
Figure G-8	CAV, WUS vertical motions, soil sites.	G-9
Figure H-1a	Distance dependence of the horizontal duration for the 5-75% intensity for rock site conditions.	H-8
Figure H-1b	Distance dependence of the horizontal duration for the 5-75% intensity for soil site conditions.	H-9
Figure H-2a	Distance dependence of the vertical duration for the 5-75% intensity for rock site conditions.	H-10
Figure H-2b	Distance dependence of the vertical duration for the 5-75% intensity for soil site conditions.	H-11
Figure H-3a	Distribution of the horizontal 5-75% intensity model (Equation H-9).	H-12
Figure H-3b	Distribution of the vertical 5-75% intensity model (Equation H-9).	H-13
Figure H-4a	Distribution of the horizontal 5-75% intensity model (Equation H-9).	H-14
Figure H-4b	Distribution of the vertical 5-75% intensity model (Equation H-9).	H-15
Figure H-5a	Stress drop estimates and model for the horizontal component.	H-16
Figure H-6	Horizontal residuals for magnitudes between $6.5 < \mathbf{M} < 7.0$.	H-17
Figure H-7	Vertical residuals for magnitudes between $6.5 < \mathbf{M} < 7.0$.	H-18

Figure H-8a	Horizontal 5-75% intensity duration model for rock site conditions.	H-19
Figure H-8b	Horizontal 5-75% intensity duration model for soil site conditions.	H-20
Figure H-8c	Vertical 5-75% intensity duration model for rock site conditions.	H-21
Figure H-8d	Vertical 5-75% intensity duration model for rock site conditions.	H-22
Figure H-9	Mean normalized durations averaged over distance bins for the horizontal component for rock site conditions and $6.5 < M < 7.0$.	H-23
Figure H-10	Mean normalized durations averaged over magnitude bins for the horizontal component for rock site conditions and distance = 30-60 km..	H-24
Figure H-11a	Mean predicted model (Equation H-11) compared to the mean of the data for the horizontal component.	H-25
Figure H-11b	Mean predicted model (Equation H-11) compared to the mean of the data for the vertical component.	H-26
Figure H-12	Standard errors for the horizontal and vertical duration models.	H-27
Figure H-13	Duration model for horizontal component for rock site conditions and distance of 30 km.	H-28
Figure H-14	Duration model for horizontal component for soil site conditions and distance of 30 km.	H-29
Figure H-15	Duration model for vertical component for rock site conditions and distance of 30 km.	H-30
Figure H-16	Duration model for vertical component for soil site conditions and distance of 30 km.	H-31
Figure I-1	Response spectra for 5% of damping of the selected records.	I-7
Figure I-2	Amplification function for both soil deposits	I-7
Figure I-3	Regression of $AF(f)$ on $S_a^r(f)$ at different f values for both soil deposits	I-8
Figure I-4	Regression of $AF(f)$ on M , R , $S_a^r(f)$, and PGA	I-9
Figure I-5	Location of the site in the Santa Barbara channel.	I-9
Figure I-6	Uniform Hazard Spectra (UHS) for the SBC site. (PE=Probability of Exceedence; MRP=Mean Return Period.)	I-10
Figure J-1	Median and 1σ compression- and shear-wave velocity profiles for Geomatrix site class A plus B (soft rock, Table J-1).	J-17
Figure J-2	Median and 1σ compression- and shear-wave velocity profiles for Geomatrix site class C plus D (deep soil, Table J-1).	J-18
Figure J-3	Median and 1σ Poisson's ratio profiles for Geomatrix site class A plus B (soft rock, Table J-1).	J-19
Figure J-4	Median and 1σ Poisson's ratio profiles for Geomatrix site class C plus D (deep soil, Table J-1).	J-20

Figure J-5	Poisson's ratio profiles for Geomatrix site class A plus B and C plus D (soft rock, Table J-1).	J-21
Figure J-6	Horizontal and vertical component acceleration time histories recorded at rock sites Pacoima Downstream for the 1994 M 6.7 Northridge earthquake (top) and Corralitos for the 1989 M 6.9 Loma Prieta earthquake (bottom). (Source: CDMG initial data reports).	J-22
Figure J-7	Horizontal and vertical component acceleration time histories recorded at soil sites Sylmar (top) and Arleta (bottom) for the 1994 M 6.7 Northridge earthquake. (Source: CDMG initial data reports).	J-23
Figure J-8	Horizontal and vertical component acceleration time histories recorded at rock sites Gilroy 6,7 and 1 (top, middle and bottom) for the 1989 M 6.9 Loma Prieta earthquake. (Source: CDMG initial data reports).	J-24
Figure J-9	Horizontal and vertical component acceleration time histories recorded at "rock" site Pacoima Kagel for the 1994 M 6.7 Northridge earthquake. (Source: CDMG initial data reports).	J-25
Figure J-10	Horizontal and vertical component acceleration time histories recorded at soil sites Gilroy 2,3 and 4 (top, middle and bottom) for the 1989 M 6.9 Loma Prieta earthquake (source: CDMG initial data reports).	J-26
Figure J-11	5% damped psuedo absolute response spectra at the SCE rock site Lucerne for the 1992 M 7.2 Landers earthquake. Fault distance is about 2 km.	J-27
Figure J-12	Acceleration, velocity and displacement time histories at the SCE rock site Lucerne for the 1992 M 7.2 Landers earthquake. Fault distance is about 2 km.	J-28
Figure J-13	5% damped psuedo absolute response spectra at the soil site Arleta for the 1994 M 6.7 Northridge earthquake. Fault distance is about 9 km.	J-29
Figure J-14	Acceleration, velocity and displacement time histories at the soil site Arleta for the 1994 M 6.7 Northridge earthquake. Fault distance is about 9 km.	J-30
Figure J-15	5% damped psuedo absolute response spectra at the rock site Gilroy 6 for the 1989 M 6.9 Loma Prieta earthquake. Fault distance is about 19 km.	J-31
Figure J-16	Acceleration, velocity and displacement time histories at the rock site Gilroy 6 for the 1989 M 6.9 Loma Prieta earthquake. Fault distance is about 19 km.	J-32
Figure J-17	5% damped psuedo absolute response spectra at the soil site Gilroy 4 for the 1989 M 6.9 Loma Prieta earthquake. Fault distance is about 16 km.	J-33
Figure J-18	Acceleration, velocity and displacement time histories at the soil site Gilroy 4 for the 1989 M 6.9 Loma Prieta earthquake. Fault distance is about 16 km.	J-34

Figure J-19	Median statistical response spectral shapes (5% damping) computed from WUS data recorded at rock sites in the magnitude range of M 5 to M 6. Rupture distances range from 0 to 10 km and 10 to 50 km.	J-35
Figure J-20	The effects of kappa on 5% damped response spectral shapes computed for a M 6.5 earthquake at 10 km using WNA parameters. As kappa increases, the peak shifts to longer periods and remains essentially constant in amplitude.	J-36
Figure J-21	Median statistical response spectral shapes (5% damping) computed from WUS data recorded at rock sites in the magnitude range of M 6 to M 7+. Rupture distances range from 0 to 10 km and 10 to 50 km.	J-37
Figure J-22	Median statistical response spectral shapes (5% damping) computed from WUS data recorded at soil sites in the magnitude range of M 5 to M 6. Rupture distances range from 0 to 10 km and 10 to 50 km.	J-38
Figure J-23	Median statistical response spectral shapes (5% damping) computed from WUS data recorded at soil sites in the magnitude range of M 6 to M 7+. Rupture distances range from 0 to 10 km and 10 to 50 km.	J-39
Figure J-24	Average 5% damping response spectral shapes (SA/PGA) computed from motions recorded on rock sites at close distances to M = 6.4 earthquakes (top figure) and M = 4.0 earthquakes (bottom figure). In each figure the solid line corresponds to motions recorded in WNA, dashed line to motions recorded in ENA.	J-40
Figure J-25	Median empirical response spectra (5% damped) computed at rock and soil sites for M 6.5 at fault distance of 5 km.	J-41
Figure J-26	Distance to fault dependency of response spectral ratios (V/H) for M 6.5 at rock and soil sites. Line at 0.66 indicates the constant ratio of 2/3. The R=1 km line is the highest on each plot at 0.05 sec.	J-42
Figure J-27	Magnitude dependency of response spectral ratios (V/H) at fault distances 1 and 20 km. M 7.5 shows the highest amplification at 0.05 sec., M 5.5 shows the lowest.	J-43
Figure J-28	Comparison of simulations to recorded motions for vertical and horizontal (average) components at the SCE rock site Lucerne for the 1992 M 7.2 Landers earthquake. The site is at a fault distance of about 2 km. A point-source model is used with the generic rock compression- and shear-wave velocity profiles (Figure J-1) over the regional crustal model (Wald and Heaton, 1994).	J-44
Figure J-29	Comparison of generic compression- and shear-wave velocity profiles for WUS and CEUS crustal conditions.	J-45
Figure J-30	Comparison of empirical and model response spectral ratios (V/H) at rock sites for M 6.5. The R=1 km line is the highest on each plot at 0.05sec.	J-46
Figure J-31	Comparison of empirical and model response spectral ratios (V/H) at soil sites for M 6.5. The R=1 km line is the highest on each plot at 0.05 sec.	J-47

Figure J-32	Response spectral ratios (V/H) computed for CEUS rock and soil sites for M 6.5 at a suite of distances. The CEUS crustal model (Figure J-29) is used for rock sites with the generic soil profile (Figure J-2) placed on top to model soil sites.	J-48
Figure K-1	Comparison of statistical response spectral shapes computed for the Chi Chi, Taiwan and Turkey earthquakes with recommended shape: bin M 7+ and $D = 0$ to 10 km.	K-26
Figure K-2	Comparison of statistical response spectral shapes computed for the Chi Chi, Taiwan and Turkey earthquakes with recommended shape: bin M 7+ and $D = 10$ to 50 km.	K-27
Figure K-3	Comparison of statistical response spectral shapes computed for the Chi Chi, Taiwan and Turkey earthquakes with recommended shape: bin M 7+ and $D = 50$ to 100 km.	K-28
Figure K-4	Comparison of statistical response spectral shapes computed for the Chi Chi, Taiwan and Turkey earthquakes with recommended shape: bin M 7+ and $D = 100$ to 200 km.	K-29
Figure K-5	Comparison of statistical response spectral shapes computed for the Chi Chi, Taiwan and Turkey earthquakes with recommended shape: bin M 7+ and $D = 0$ to 50 km.	K-30
Figure K-6	Response spectral shapes computed for M 6.5 at a distance of 25 km for a suite of kappa values using WUS parameters.	K-31
Figure K-7	Comparison of statistical response spectral shapes computed for the Chi Chi, Taiwan earthquake with recommended shape: bin M 7+ and $D = 0$ to 10 km.	K-32
Figure K-8	Comparison of statistical response spectral shapes computed for the Chi Chi, Taiwan earthquake with recommended shape: bin M 7+ and $D = 10$ to 50 km.	K-33
Figure K-9	Comparison of statistical response spectral shapes computed for the Chi Chi, Taiwan earthquake with recommended shape: bin M 7+ and $D = 50$ to 100 km.	K-34
Figure K-10	Comparison of statistical response spectral shapes computed for the Chi Chi, Taiwan earthquake with recommended shape: bin M 7+ and $D = 100$ to 200 km.	K-35
Figure K-11	Comparison of statistical response spectral shapes computed for the Chi Chi, Taiwan earthquake with recommended shape: bin M 7+ and $D = 0$ to 50 km.	K-36
Figure K-12	Comparison of statistical response spectral shapes computed for the Turkey earthquakes with recommended shape: bin M 7+ and $D = 0$ to 10 km.	K-37

Figure K-13	Comparison of statistical response spectral shapes computed for the Turkey earthquakes with recommended shape: bin M 7+ and $D = 10$ to 50 km.	K-38
Figure K-14	Comparison of statistical response spectral shapes computed for the Turkey earthquakes with recommended shape: bin M 7+ and $D = 50$ to 100 km.	K-39
Figure K-15	Comparison of statistical response spectral shapes computed for the Turkey earthquakes with recommended shape: bin M 7+ and $D = 0$ to 50 km.	K-40

List of Tables

<u>Table #</u>		<u>Page</u>
Table 1-1	WUS, CEUS M and <i>D</i> bins	1-13
Table 2-1	Kappa Values for “Average” Site Conditions in WUS and CEUS	2-12
Table 2-2	Point-Source Parameters	2-13
Table 3-1	Geotechnical Subsurface Characteristics	3-8
Table 3-2	Magnitude and Distance Bins and Duration Criteria	3-9
Table 3-3	WUS Time History Bins	3-10
Table 3-4	CEUS Time History Bins	3-11
Table 3-5	WUS Analysis Time History Statistics	3-12
Table 3-6	CEUS Analysis Time History Statistics	3-14
Table 4-1	WUS Statistical Shape Bins	4-26
Table 4-2	Point-source Parameters	4-29
Table 4-3	Response Spectral Shape Coefficients for 5% Damping	4-30
Table 4-4	Recommended V/H Ratios for WUS Rock Site Conditions	4-31
Table 4-5	Recommended V/H Ratios for CEUS Rock Site Conditions	4-32
Table 4-6a	Horizontal c_1 values for separate damping levels for equation (4.12), Abrahamson and Silva (1996)	4-33
Table 4-6b	Vertical c_1 values for separate damping levels for equation (4.12), Abrahamson and Silva (1996)	4-34
Table 4-7a	Horizontal g_2 values for separate damping levels for equation (4.12), Abrahamson and Silva (1996)	4-35
Table 4-7b	Vertical g_2 values for separate damping levels for equation (4.12), Abrahamson and Silva (1996)	4-36

Table 4-8a	Horizontal g_3 values for separate damping levels for equation (4.12), Abrahamson and Silva (1996)	4-37
Table 4-8b	Vertical g_3 values for separate damping levels for equation (4.12), Abrahamson and Silva (1996)	4-38
Table 4-9	Coefficients for Equation (4.13), Idriss (1993)	4-39
Table 5-1	Magnitude and Distance Bins for Record Library WUS Empirical Motions	5-17
Table 5-2	Characteristics of Generated Artificial Records	5-18
Table 5-3	Percent Reduction in 5% Damped Response Spectrum	5-18
Table 5-4	Bin Cross Correlation Statistics for WUS Rock Site Conditions	5-19
Table 5-5	Bin Cross Correlation Statistics for WUS Soil Site Conditions	5-22
Table 6-1	Approaches for Developing Soil UHS	6-36
Table 6-2	Parameters for WUS Rock Outcrop Simulations	6-37
Table 6-3	Parameters for CEUS Rock Outcrop Simulations	6-38
Table 6-4	Southern California Crustal Model	6-39
Table 6-5	CEUS Crustal Model (EPRI, 1993, Midcontinent)	6-39
Table C-1	WUS Statistical Shape Bins (Horizontal Component)	C-2
Table C-2	WUS Statistical Shape Bins (Vertical Component)	C-5
Table D-1	Contributions to Total Variability in Ground Motion Models	D-14
Table H-1	Initial Regression Estimates of Coefficients for T_{5-75} Using $\Delta\sigma$ Independent of Magnitude	H-6
Table H-2	Regression Estimates of Coefficients for T_{5-75} Using Magnitude Dependent $\Delta\sigma$	H-6

Table H-3	Regression Estimates for the Normalized Duration	H-7
Table H-4	Standard Error for Duration (EQ. H-12a,b)	H-7
Table J-1	Strong-Motion Recording Stations Classification System	J-16
Table K-1	WUS Statistical Shape Bins Chi Chi	K-3
Table K-2	WUS Statistical Shape Bins Turkey	K-4
Table K-3	WUS Statistical Shape Bins Chi Chi and Turkey	K-5
Table K-4	Chi-Chi, Taiwan and Turkey Strong-motion Catalog (09/05/00)	K-6

Acknowledgments

This study was sponsored by the US Nuclear Regulatory Commission under Contract NRC-04-96-037. The technical team was assisted by Gabriel Toro of Risk Engineering, Inc., by Robert Darragh, Nick Gregor and Ky Lang of Pacific Engineering and Analysis, by Norman Abrahamson, Consultant (during early planning phases of the work), by Yoshi Moriwaki and Paul Somerville of URS Greiner Woodward-Clyde, and by Robert Youngs of Geomatrix Consultants. The work was reviewed continuously during its development by a Peer Review Panel consisting of Carl Stepp (Chair), David M. Boore, C. Allin Cornell, I.M. Idriss, and Robert P. Kennedy. The insight and direction provided by this Panel were invaluable.

Roger Kenneally of the Nuclear Regulatory Commission was the Contract Monitor for this work, and his support, guidance and reviews of draft reports are gratefully acknowledged. We also acknowledge reviews of draft reports provided by Nilesh C. Chokshi, Andrew J. Murphy, Robert L. Rothman, Clifford G. Munson, and Abou-Bakr K. Ibrahim, of the Nuclear Regulatory Commission. Finally, Katherine Morgan of Risk Engineering, Inc. shepherded the project reports through their many drafts with editorial accuracy and grace, for which we are grateful.

List of Terms

a_1	spectral amplitude on rock at 1 Hz
a_{10}	spectral amplitude on rock at 10 Hz
$A(f)$	crustal amplification
AF	amplification factor, soil amplitude/rock amplitude
A^R, a	ground motion amplitude on rock
A_R	slope parameters on hazard curve
A^S	ground motion amplitude on soil
b_1, b_2	coefficients for magnitude dependence of stress drop
c	constant in stochastic ground motion model
c_1, c_2, \dots, c_9	coefficients used to define spectral shapes for the WUS (eq. 4-8) and the CEUS (eq. 4-9)
C_1	seismic capacity curve 1
C_2	seismic capacity curve 2
CAP_{10}	ground motion or seismic demand with 10% frequency of failure
CAP_{50}	ground motion or seismic demand with 50% frequency of failure
CAV	cumulative absolute velocity
d_1, d_2, d_3	coefficients for distance-dependent duration
D	strong motion duration
DES1	deaggregated spectrum scaled to 1 Hz
DES10	deaggregated spectrum scaled to 10 Hz
DF	frequency window
DRS	design response spectrum
DT	time increment in artificial records
f	frequency in Hz
f_c	interface frequency
f_0	source corner frequency
F_R	factor of safety
$FA(f)$	Fourier amplitude of acceleration
FAS	Fourier amplitude spectrum
FT	scaling factor for Fourier spectra
G/G_{max}	shear modulus behavior of non-linear soils
G_0	elastic shear modulus at low strain levels
$G_z(z)$	complementary cumulative function
h	width of smoothing operator for attenuation equation weights
H	horizontal component of motion
$H(\cdot)$	seismic hazard
H1	one horizontal component of motion
H2	second horizontal component of motion
HCLPF	high confidence of low probability of failure point on fragility curve
$I(t)$	normalized Arias intensity
K_H	slope parameters of hazard curve

List of Terms (continued)

M, m	earthquake magnitude (moment magnitude scale)
m_L, m_M, m_H	low, medium, and high magnitudes used to discretize a magnitude distribution
m_{Lg}	earthquake magnitude (Lg magnitude scale)
M_{\min}	minimum magnitude
M_0	seismic moment
M_x	maximum magnitude
P	compressional waves
P_F	probability of component failure
P(f)	high-frequency truncation filter
PGA	peak ground acceleration
PGD	peak ground displacement
PGV	peak ground velocity
PI	plasticity index
PSD	power spectral density
PSHA	probabilistic seismic hazard analysis
Q_0	frequency-independent component of Q model
Q(f)	deep crustal damping quality factor
R, r	source-to-site distance
r_c	cutoff distance for distance-dependent duration
S	site term coefficient for duration
$S_s^*(f)$	spectral acceleration on soil
$S_r^*(f)$	spectral acceleration on rock
SA	spectral acceleration
SF	scale factor for converting UHS to URS
Syz	effective shear strain
SV	vertical component of shear waves
t	statistic of T distribution
T_{95}	time to reach 95% of total Arias intensity
T_{5-75}	time from 5% to 75% of total Arias intensity
T_{5-95}	time from 5% to 95% of total Arias intensity
t_1	duration distance dependence on rock
t_2	duration distance dependence on site conditions
T_{\max}	maximum duration of artificial records
TBA	average duration of records in bin
TT	strong motion duration of artificial record
T/T_{\max}	fraction of total record duration
UHS	uniform hazard spectrum
URS	uniform reliability spectrum
V	vertical component of motion
v(f)	block diagonal matrix of residuals
V_s	shear-wave velocity
V_p	compressional-wave velocity

List of Terms (continued)

$w(f)_k^T$	weight given to k'th attenuation equation using τ statistics
$w(f)_k^L$	weight given to k'th attenuation equation using likelihood function
$w(f)_k^*$	smoothed weight given to k'th attenuation equation
x_p	number of standard deviates for HCLPF
$z(x)$	normal density function
α	deterministic acceptance criterion
β_C	logarithmic uncertainty in capacity OR logarithmic standard duration of capacity ??
β_0	shear-wave velocity at the source
β_R	logarithmic uncertainty in response
$\gamma_{64\%}$	shear strain at 64% of G_{max}
$\Delta t, dt$	time interval for strong motion records
$\Delta\sigma$	earthquake stress drop
$\varepsilon(f)$	residual of logarithmic deviation of observed SA from predicted value
$\varepsilon_1(f), \varepsilon_2(f)$	residuals in random effects model
ζ	accuracy desired for regression analysis
η	frequency exponent of Q model
κ	shallow crustal damping
κ_0	coefficient of lateral earth pressure
ξ	damping (fraction or percent of critical)
ξ_c	compressional-wave viscous damping
ξ_s	shear-wave damping
σ	standard deviation
σ_m^2	modeling variance
σ_p^2	parametric variance
σ_T^2	total variance
π_0	coefficient of permeability
ρ_0	crustal density at the source
$\tau_1(f), \tau_2(f)$	standard deviations of $\varepsilon_1(f), \varepsilon_2(f)$
$v(\)$	frequency of exceedence
v_i	frequency of earthquake occurrence on fault i
Φ_0	friction angle

1. INTRODUCTION

1.1 Historical Perspective

The regulatory guidance for determination of seismic design basis ground motion at nuclear plant sites emphasizes the essential need for the design ground response spectrum to be a broad-band, smooth spectrum that has adequate energy in all frequencies represented by a plant's structures, systems and components. For this and economic considerations nuclear plants generally have been designed for a site-independent standard broad-band spectrum such as the Regulatory Guide 1.60 spectrum (NRC, 1973), scaled to a site-specific peak ground acceleration value. Regulatory guidance for the determination of Safe Shutdown Earthquake (SSE) ground motion (NRC, 1997a) provides a hazard-consistent approach for determining the seismic design basis ground motion spectrum at a site. The procedure emphasizes site-specific determination of the SSE ground motion. Although a standard site-independent spectrum may still be used as the design basis ground motion spectrum, the procedure requires that this spectrum be scaled to the site-specific average ground motion levels for 5 and 10 Hz, and 1 and 2.5 Hz, representing the controlling earthquake as determined from deaggregation of a probabilistic seismic hazard analysis. These guidelines substantially advance the state of practice for determination of seismic design basis ground motion by including the effects of specific, dominant earthquakes on the frequency content of ground motion. However, it is recognized that additional improvements could be provided with respect to site-specific spectral shape estimation.

Revision 3 of the Standard Review Plan (SRP) 2.5.2 (NRC, 1997b) provides a hierarchy of acceptable approaches for the estimation of seismic ground motion at a site. In descending order of preference these are:

1. The direct use of a sufficiently large number of both horizontal and vertical component strong motion recordings selected to model the site-specific conditions for the controlling earthquakes, including: magnitude, type of faulting, tectonic environment, distance, source depth, regional attenuation and local site wave propagation characteristics;
2. For sites where a large enough ensemble of strong motion recordings is not available representing the site-specific controlling earthquake conditions, the guidance permits scaling strong motion recordings to represent the best estimate of the earthquake source, propagation path and site properties and doing sensitivity studies to evaluate the effects of scaling;
3. For a combination of site and controlling earthquake conditions where representative strong motion recordings are not available, peak motion parameters (peak acceleration, spectral acceleration, velocity and displacement) estimated using state-of-the-art attenuation relationships appropriate for the region of the site and the site geology, may be used to scale site-independent, standard spectral shapes; and
4. The use of theoretical-empirical estimation procedures may be used in a supplemental role when the appropriateness of the model is thoroughly documented.

The development of the SRP ground motion estimation hierarchy attempts to reflect the current state of the profession's uncertainty in ground motion estimation methods together with limitations of available data and to provide reasonable assurance that the ground motion at any site would be conservatively estimated. Recent studies (EPRI, 1993a) have shown however that the uncertainty in ground motion estimates results from the complex interaction of the large number of parameters of the ground motion estimation model. It is difficult to capture the total uncertainty even with the large number of strong motion recordings now available in California. This fact is confirmed by each successive large earthquake, which seems to require modification of the empirically-based ground motion estimation models.

The hierarchy also assumes that ground motion data are transferable from one region to another by matching important source properties such as magnitude, fault type, and tectonic environment; path properties such as distance, hypocenter depth, and attenuation; and site properties such as shear wave velocity. The EPRI (1993a) work has shown that these parameters contain significant random variability and uncertainty and interact in complex ways that are not likely to be adequately captured even by a reasonably large data set, and almost certainly would not be captured by a limited data set that would pass the site-controlling earthquake combination screening. In addition it is now recognized that strong motion recordings at sites in California and other active tectonic regions can not be transferred to continental interior regions. That is, it is not appropriate to use (without proper modification) empirical data from California to represent ground motions in the central and eastern United States (CEUS), and the available data set in the CEUS is too limited to use a direct empirical approach.

For the above reasons it is necessary to use the theoretical-empirical modeling method to estimate ground motions in the eastern United States. The method, described in EPRI (1993a), uses a theoretical model to estimate ground motion amplitudes in the frequency band of interest to engineering analysis and design. The power of the method is that it can be validated using large California data sets that span a wide range of magnitudes. The method develops a *theoretical* estimate of the ground motion spectrum based on parameters of the fault rupture (magnitude, stress drop) and travel path (distance, crustal and surficial rock properties). In regions of few recordings of strong shaking, the parameters can be estimated with *empirical* data from seismograph records. This gives a means to reliably estimate strong ground shaking when records of only weak shaking are available. In addition, site-specific geology and soil information can be quantitatively incorporated directly into the ground motion estimation at any particular site. Thus the method can be applied to any site-controlling earthquake combination to estimate site-specific ground motion and its uncertainty. The method may be applied equally well to develop standardized response spectra for combinations of well-defined site categories, controlling earthquakes and tectonic or regional seismic wave propagation environments.

The Regulatory Guide 1.60 spectrum was derived from a limited set of strong motion recordings primarily at deep alluvial sites in California, beyond 20 km from moderate to large magnitude earthquakes. The data set resulted in relatively high spectral amplification (S_a/A) in the frequency range of primary interest, but spectral amplification for frequencies above 10 Hz was too low even for California sites on rock conditions. Scaling this spectrum at 33 Hz to typical peak acceleration values derived from seismological considerations normally resulted in excessively conservative seismic

demands on plant structures, systems and components (SSCs), particularly for sites located in the eastern United States. This reality stimulated extensive research to develop an “effective acceleration” parameter to scale the standard spectrum so that it would represent the appropriate level of regulatory conservatism (Kennedy et al., 1984; Kennedy et al., 1985; Luco et al., 1986; Power et al., 1986). More recently this work has been extended, taking the somewhat different direction of focusing on the role of inelastic energy absorption in the damaging effectiveness of ground motions (EPRI, 1993b). The results of the EPRI work indicate that high frequency motions above about 20 Hz are not likely damaging, except to brittle components such as relays and ceramic insulators. The work provides the basis for establishing a displacement criterion for conditioning the high frequency amplitudes and developing a damage-consistent ground motion spectrum. This displacement criterion would rely on structural response to condition the ground motion spectral shape and should adequately consider the response of secondary systems. Spatial coherency also has been shown to be an important consideration for establishing ground motion design spectra (Abrahamson et al., 1991). Incoherency increases with increasing frequency. Thus we need a criterion coupling the high frequency amplitude reduction based on inelastic energy absorption with the reduction caused by spatial incoherency is needed. These considerations will be very important in the development of standard response spectra for future application. It would be desirable to develop generic criteria for deriving a damage consistent response spectrum that is fully compatible and easily implemented with ground motion spectral estimates based on geotechnical considerations, either in a site-specific mode or for standardized spectra for different classes of site and regional attenuation conditions.

The limitations in the use of the R.G. 1.60 spectrum involve both the shape of the spectrum and the consequences to structural design and liquefaction analyses. The limitations of the R.G. 1.60 shape fundamentally stem from its early development during the late 1960's and reflect both the limited data available and knowledge base at that time. Approximately 15 earthquakes were available with recordings at about 15 sites. The strong motion data set was comprised of earthquakes of varying magnitudes (M about 5.2 to over 7.5), mixed mechanisms, a large distance range, and poorly known site conditions (mostly deep soil; Newmark et al., 1973).

To develop design spectra two teams (Blume et al., 1972 and Mohraz et al., 1972) separately analyzed almost identical data sets. To develop shapes, different normalization schemes were used by each team. In both studies, amplification or scale factors on peak ground motion parameters were derived from statistical analyses on normalized shapes to construct smooth design spectra for varying fracture and damping levels. In the Blume study, a single normalization parameter, peak ground acceleration (“A”), forms the basis for the shapes with scaling factors specified at fixed anchor points. Although data were partitioned, no clear trends in the shapes based on A level, site condition, or distance were discerned.

In the Newmark study (Mohraz et al., 1972) spectral amplification factors on A, peak ground velocity (“V”), and peak ground displacement (“D”) were developed to construct the design spectrum. The Newmark study led to the scaling of A, V, and D over regions of reasonably constant spectral acceleration, velocity and displacement. Because the variability in strong ground motion data increases with increasing period, normalizing to high, medium, and low frequency parameters over high, medium, and low frequency ranges in the spectra results in scaling factors that reflect more

uniform statistics. Because of this multiparameter scaling based on peak ground motion values and variable anchor points, the shape based on A, V, and D does, to some extent, accommodate site and magnitude dependencies in V/A and AD/V² ratios. (These ratios are often labeled “V/A” and AD/V²,” respectively.)

Based on the two studies, the NRC adopted and formalized a slightly modified form of the single parameter shape (Newmark et al., 1973) as a recommendation in R.G. 1.60.

The single parameter scaling resulted in a shape that was source, path, and site independent. That is, the relative spectral content did not vary and only the absolute levels changed with A (Coats, 1980; Gupta, 1990). A limitation that resulted from the small size of the data set available was that both the fractiles and damping scaling were not well constrained. In addition, due to the normalization to A, the fractiles were not uniform over frequency. The R.G. 1.60 horizontal component shape was generally representative of an 84th percentile for **M** of about 6.75 at a deep soil site and at a distance of about 20-30 km, the 84th percentile representing variability in spectra scaled to the same values of A, V, and D. The scale factors for the vertical component, 1 at high frequency (>3 Hz) and 2/3 at low frequency were reasonable for distances in the 20-40 km range for soil and about the 10-20 km range for rock. The appropriateness of these factors at other distance ranges was questionable, based on recent empirical data.

Later analyses of spectral shapes (Sa/A) with an emphasis on site conditions (Seed et al., 1976; Mohraz, 1976) attempted to resolve strong differences in shapes as well as V/A and AD/V² ratios based primarily on site stiffness. Depending on site conditions, site specific smooth response spectral shapes may significantly depart from these standard spectral shapes.

Recent work shows that the dependence of spectral shapes on source, path, and site conditions is well constrained by both recorded motions and the results of well validated modeling (Silva, 1991; Silva et al., 1997). In general, shapes broaden and show a shifting of the peak spectral amplification to lower frequencies with increasing magnitude due to a decrease in the earthquake source corner frequency (Silva, 1991; Silva and Darragh, 1995). Site dependencies are reflected in an increase in spectral levels at low frequencies and a decrease in levels at high frequencies as site stiffness decreases due to a combination of site amplification and material damping. This site effect also results in a shifting of the peak spectral amplification to lower frequencies, presumably as a result of an increase in material damping with decreasing site stiffness. This is especially evident at very stiff (rock) sites (Silva and Darragh, 1995). An additional observation of site effects is the reduction in maximum spectral amplification with decreasing site stiffness. For rock sites, the maximum spectral amplification is approximately 2.1 to 2.3 and decreases for soil sites. This reduction in peak spectral amplification is directly related to the shear-wave velocity gradient in the relatively shallow (<200 ft) portion of the rock/soil column, and to nonlinear, amplitude-dependent response of the soil itself.

In addition to these far-field dependencies, near-fault effects such as pulse-like motions can dramatically influence spectral content in large earthquakes ($M \geq 6$). Some of these effects are most pronounced within about 10 km: the fault normal component is about 30% larger than the fault parallel component in the frequency range 0.2 to 0.5 sec due primarily to rupture directivity, and the vertical motions can exceed the horizontal at frequencies above about 5 Hz. Directivity effects are

strongest for strike slip motion on vertical faults but can also be significant for cases of updip directivity for sites located near dipping faults. Other factors, perhaps strongest at close distances, include hanging wall/foot wall site location as well as thrust versus strike slip or normal slip mechanisms. These additional factors can have significant impacts on spectral composition.

In summary, the R.G. 1.60 spectral shape given A is very conservative for hard rock sites, at frequencies below 10 Hz and for distances exceeding about 10 km (Reed et al., 1993). For frequencies above 10 Hz the spectral shape is unconservative for these conditions. For soil sites, the degree of conservatism or underconservatism depends upon the particular site soil profile and whether the controlling magnitude differs significantly from about 6.75. The results of systematic SSI analyses (Power et al., 1986) for varying input motions and foundation conditions supported the desirability of site-specific ground motion characterization. The analyses also indicated that the R.G. 1.60 spectral shape provides a generally conservative design basis due to its broad-band nature. Another issue associated with using the R.G. 1.60 spectral shape as the design motion at the ground surface is that it leads to problems when applied at softer soil sites. When using typical deconvolution methodology incorporating strain dependent soil degradation properties, numerical problems are often encountered when generating foundation level motions (EPRI, 1993a). These problems indicate that the broad-band nature of the R.G. 1.60 spectral shape is generally incompatible with the softer soils.

R.G. 1.165, released in March, 1997, looks at the safe shutdown earthquake ground motion as a composite design motion resulting from many possible earthquakes. Two frequency ranges are defined: 5-10 Hz, for a high-frequency controlling earthquake, and 1-2 Hz for a low-frequency controlling earthquake. Deaggregation of seismic hazard is recommended for both frequency ranges, and the dominant magnitudes and distances from a seismic hazard perspective are identified. Spectra from these dominant events are then developed and scaled to probabilistic seismic hazard results for the high- and low-frequency controlling earthquakes. These spectra are smoothed and enveloped to obtain a safe shutdown ground motion.

Several issues are not addressed by R.G. 1.165. Specifically, the spectral shapes to be used for dominant events are not documented, the ground motion time histories for use in dynamic analysis are not described, and the issue of soil response is not addressed in detail in terms of an acceptable procedure. Also, methods for modifying hazard-consistent spectra (with constant annual frequency of exceedence) to achieve *risk*-consistent spectra (with constant annual frequency of component or plant failure) is not addressed. The overall purpose of the current project is to facilitate the R.G. 1.165 methodology by addressing these issues and documenting ground motion records and spectra. The following subsection describes details of the objectives of the current study.

1.2 Objectives and Scope

The overall objectives of this project are to (1) update the standardized design spectra used in the evaluation of nuclear facilities to accommodate the effects of magnitude, site condition, distance, and tectonic environment, (2) assemble a database of strong motion records appropriate for use in design analyses, (3) recommend procedures and requirements for the scaling of ground motion records to be consistent with design spectra, (4) develop recommendations for conducting site response analyses to produce soil motions consistent with rock outcrop hazard results (hazard consistency), and (5)

develop recommendations on how to derive seismic design spectra that provide risk consistency (uniform conservatism) across structural frequency. These objectives support the goal of developing uniform hazard spectra and design spectra that take into account the seismic threat at a site and the response of surficial rock and soil to that threat. Figures 1-1 and 1-2 present flowcharts of the recommended procedure for developing design ground motions on rock and soil, respectively, with references to Sections of this report.

The procedure for rock sites (Figure 1-1) starts with a probabilistic seismic hazard analysis (PSHA) at a site using rock conditions. The hazard results at 10 and 1 Hz are then deaggregated following the method of RG 1.165 described in the previous section, and are scaled to achieve approximate risk-consistency over all sites and frequencies to calculate a Uniform Reliability Spectrum (URS). This deaggregation and scaling is described in Section 7 of this report.

The scaled spectral values at 10 and 1 Hz are then used to scale rock spectral shapes for the appropriate magnitude M and distance R . This procedure is described in Section 4. With the scaled rock spectral shapes, time histories are selected from the appropriate M - R bin, as described in Section 3. The time histories are then scaled to the URS at 10 and 1 Hz, are compared to the scaled spectral shapes, and are adjusted (using procedures described in Section 5) to match the target. For rock sites these adjusted time histories are used to conduct building dynamic analysis.

For soil sites (Figure 1-2) the first five steps are the same as for rock sites, except that the uniform hazard spectrum (UHS) is not scaled to a URS but is used as calculated to define the target spectra. The reason is that the scaling of UHS to URS depends on the slope of the hazard curve, and for soil sites, the slope must be determined by several soil analyses at different amplitudes. Following the adjustment of time histories to match the target spectra, dynamic soil analysis is performed with parameter uncertainty, using the scaled rock time histories as input. Recommendations for this soil analysis are presented in Section 6. The relevant soil spectrum or spectra (depending on the number of dominant earthquakes) are calculated as the average spectrum (or spectra) over earthquake and soil uncertainties. These average spectra themselves become target spectra and are adjusted to a URS to account for the slope of the soil hazard curves, as described in Section 7. Then time histories from soil sites are chosen based on the dominant M and R values (in a similar manner to rock time histories, as described in Section 3). The soil time histories are then spectral matched to the target spectra (as described in Section 5) and are used as input to building dynamic analysis.

Figures 1-1 and 1-2 indicate that one or several time histories may be picked and adjusted to spectral shapes. While it may be possible to conduct a structural analysis with one time history that meets a target spectrum, it is preferable to conduct multiple analyses (perhaps up to 10 or 20) whose spectra on average, meet a target spectrum, so that the natural variability and phasing are peak-to-valley included in the analysis. For these records, a “weak matching” to the target spectrum may be appropriate. Details of these recommendations will be presented in an applications report to be issued at a later date.

This project defines the recommended procedure for developing design ground motions in terms of databases (spectral shapes and time histories) and recommended methods of analysis (deaggregation and scaling of hazard results to achieve risk-consistency, scaling of spectral shapes, spectral matching,

and soil dynamic analysis). Overviews of these databases and procedures are described in the following sections. Using these procedures, design ground motions can be calculated at sites that reflect up-to-date spectral shapes, both for the western US (WUS) and central and eastern US (CEUS). The motions will be approximately risk-consistent across frequency and for different seismic threats. Time histories of motion can be derived consistent with the spectral shapes for dynamic analysis. Finally, motions on soil sites can be derived by a procedure consistent with that for rock sites. None of these features are available in current methods of developing design ground motions.

1.3 Development of Recommended Spectral Shapes

The recommended spectral shapes accommodate continuous M and R scaling as well as potential differences in WUS and CEUS earthquake source processes. They are normalized by peak acceleration, since it is the spectral ordinate with lowest variability (Youngs et al., 1995), and are provided for both soft and hard rock site conditions (defined in Section 4) occurring in either western United States (WUS) or central and eastern United States (CEUS). Shapes for soil categories are not developed since soil response can depend heavily on the characteristics of control motions due to nonlinear dynamic material properties.

The intended use of the revised motions is to provide more realistic spectral shapes for applications of the Regulatory Guide 1.165 (NRC, 1997a) procedure to develop an overall design spectrum. In this procedure, spectral shapes are scaled to the rock outcrop UHS at frequencies near 10 and 1 Hz. For both frequency ranges, shapes are used which reflect the dominant contributions in both magnitude and distance to the UHS. The advantage of this approach, combined with realistic spectral shapes, is that the scaled shapes will represent seismic events that dominate the hazard for different structural frequency ranges as well as distance ranges. The use of rock outcrop control motions avoids the ambiguities in going from soil surface motions to foundation levels and provides for the direct development of site specific motions that accommodate variability in dynamic material properties.

Since the appropriate hazard level is provided by the UHS, which accommodates both epistemic and aleatory variability conditional on M and R , the revised shapes reflect median fractile estimates. Increased broadening of the shapes resulting from applying higher fractile levels is neither warranted nor desired as it can lead to potentially unconservative soil motions due to nonlinearity.

The frequency range of the recommended shapes extends from the lowest frequency that can be reliably obtained from the current strong-motion data set from the WUS (principally California), 0.2 Hz, to 100 Hz. The high frequency limit of 100 Hz permits the ratio of spectral acceleration/ peak ground acceleration to reach nearly 1 for hard rock site conditions. For soft rock conditions, this ratio will reach 1 at about 40-50 Hz. Criteria for spectrum compatible time histories extend to 25 Hz, which captures the range of primary importance to nuclear power plant structures and equipment (0.2 Hz to 25 Hz) for both CEUS and WUS motions.

The development of the spectral shapes for WUS conditions involves the use of empirical attenuation relations. Since these attenuation relations are generally defined over applicable magnitude and

distance ranges, these considerations must also apply to the shapes. In general the shapes are considered valid in the **M** (moment magnitude) range of about 4.75 to 8.0 for both WUS and CEUS conditions. Regarding applicable distances, we consider WUS (soft rock) shapes valid from 0 to about 200 km for crustal earthquakes, with appropriate consideration for near fault effects (Section 4), and out to about 400 km for CEUS conditions. The WUS shapes are considered appropriate for Cascadia subduction zone earthquakes for **M** up to about 9 and closest rupture distances out to about 300 km (Section 4).

1.4 Time History Database For Analysis

An important aspect of this project is the development of a time history database for analyses. The database is parsed into **M** and *R* bins (Table 1-1) which were selected to preserve significant differences in spectral composition and time domain characteristics (e.g. duration). The bins are also appropriate for potential high and low frequency controlling earthquakes in both the WUS and CEUS. The WUS time history bins are the same ones used in developing the WUS spectral shapes, preserving consistency between an average bin shape (Appendix C) and the revised shapes (Section 4) computed for bin average **M** and *R* values.

The bin database is to provide appropriate records for spectral matching as well as scaling. Since each bin contains records reflecting ranges in **M** and *R*, guidelines are given for within bin **M** and *R* adjustments for either constant or narrow band scaling.

For applications to the WUS, the bins are populated largely with recorded motions. Sparse bins have been supplemented with scaled empirical records (from adjoining bins) as well as a few direct finite-fault simulations. For the CEUS, since few recordings exist, the recommendation is to generate motions by scaling WUS records. The scaling procedure is the same as that used to correct the WUS rock shapes to CEUS conditions. While not as desirable as recorded motions, these time histories will be suitable for analyses. They should be replaced as appropriate data become available and as simulation methods improve and become better validated for CEUS conditions.

1.5 Site Specific Soil Motions

The most desirable form of site ground motion design requirements are based on hazard curves appropriate for the soil surface, embedment depth, and any other site conditions upon which category 1 structures are founded. The site-specific hazard curves, from which the required sets of UHS may be obtained, should also accommodate uncertainty in site-specific dynamic material properties as well as local and regional seismicity and attenuation characteristics. This ideal situation of exact consistency among hazard curves for different elevations and soils at a site would then permit the seismic risk to all structures, systems, and components to be evaluated on a consistent basis. One calculation-intensive way to accomplish this is to perform seismic hazard analyses separately for all elevations and site conditions at a site. While this approach has been used on several occasions (for a single rock/soil column), it is not a particularly straightforward task, and involves many assumptions and several limitations. For one thing, a rock PSHA can be performed with regional, not site-specific data, and so can be completed prior to site-specific soil parameters being collected. Also, if multiple distinct soil columns exist at a plant site, or if some critical structures are founded on soil and some

on rock, the same rock PSHA should be used for all. Finally, if new soil data are collected, the effects on design spectra can be determined quickly, without redoing the PSHA. For all of these reasons, it is recommended to perform the PSHA for appropriate rock (rock like) conditions, then modify the rock UHS to reflect the effects of local soils.

There are several approaches to estimate soil UHS given rock outcrop UHS and these are demonstrated in Section 6. These methods are compared to directly computed soil UHS using site specific attenuation relations. Applying these methods at two hazard levels one can then approximate the slope of the soil hazard curve. Also discussed are approximate methods to compute the soil hazard curve given rock UHS and a set of numerical convolutions. The method selected for a particular application will likely depend upon desired accuracy (minimize overconservatism), degree of currently available site information, and computational rigor required.

1.6 Development of Uniform Reliability Spectra (URS)

One of the objectives in developing seismic design spectra is to achieve approximate uniformity of seismic risk for structures, equipment, and components designed to those spectra, across a range of seismic environments, annual probabilities, and structural frequencies. By "seismic risk" we mean the annual frequency of failure of a plant system or of its components, as opposed to "seismic hazard" which is the annual frequency of exceedence of a level of ground motion. By "uniformity," we mean that the procedures should not result in relatively high seismic risk for certain conditions, and relatively low seismic risk for others.

The procedures for developing risk-consistent spectra are illustrated by examining nine existing nuclear plant sites in the central and eastern US, and two hypothetical sites in the western US (California and Washington). Existing seismic hazard curves are used to convolve seismic hazard with component fragility curves to calculate probabilities of failure for a range of structural frequencies. The characteristics of seismic hazard span the range of amplitudes and slopes that can be expected in the US.

A simple modification to the uniform hazard spectrum (UHS) is recommended to achieve a uniform reliability spectrum (URS) consistent across structural frequencies. This modification accounts for the varying slopes of the hazard curves; the UHS is increased where the slope is shallow (e.g., at low frequencies), and is decreased where the slope is steep, so that approximate uniform reliability risks result from choosing a modified UHS with a target annual probability of exceedence.

1.7 Contents of Report

Section 2 of this report presents a background on the differences between WUS and CEUS strong ground motions on rock sites. These are important differences, and they influence many of the procedures used in this project. We do not, for example, develop recommended spectral shapes empirically in the WUS, and apply those to CEUS earthquakes.

One of the fundamental results of this project is a library of strong motion records. For the WUS these are largely empirical records, for the CEUS these are largely synthetic time histories. These databases are described in Section 3.

The design spectral shapes are documented in Section 4. These shapes are presented for the same M and R bins used for the strong motion library but are continuous functions of magnitude and distance, and Section 4 describes the scaling used to obtain the CEUS spectral shapes.

Synthetic motions are often used for time history analysis of structures, and we make recommendations on the spectral characteristics required of such synthetic motions to achieve an acceptable match with target design spectra. Guidelines are also presented for appropriate durations as well as V/A and AD/V^2 ratios for scaled time histories. These recommendations are documented in Section 5.

Section 6 examines several methods for deriving UHS for soil conditions given the rock UHS at the same site. As discussed above, several methods are available, and each is explored and demonstrated in this section.

Finally, recommendations on achieving risk consistency across sites and structural periods are contained in Section 7. These recommendations take into account the absolute level of hazard and the slope of the hazard curve at different sites.

References

- Abrahamson, N.A., J.F. Schneider and J.C. Stepp (1991). "Empirical Spatial Coherency Functions for Application to Soil-Structure Interaction," *Earthquake Spectra*, Vol. 7, Earthquake Engineering Research Institute, Oakland, CA.
- Blume, J.A., R.L. Sharpe and J.S. Dalal (1972). "Recommendations for Shape of Earthquake Response Spectra." John A. Blume and Associates, San Francisco, CA. AEC Report No. 1254.
- Coats, D.W. (1980). "Recommended Revisions to Nuclear Regulatory Commission Seismic Design Criteria." U.S. Nuclear Regulatory Commission Washington, D.C. NRC FIN No. A-0140, NUREG/CR-1161.
- EPRI (1993a). "Guidelines for Determining Design Basis Ground Motions, Volume 1: Method and Guidelines for Estimating Earthquake Ground Motion in Eastern North America," TR-102293, Electric Power Research Institute, Palo Alto, CA.
- EPRI (1993b). "Analysis of High-Frequency Seismic Effects," TR-102470, Electric Power Research Institute, Palo Alto, CA.

- Gupta, A.K. (1990). *“Response Spectrum Method in Seismic Analysis and Design of Structures.”* Foreword by W.J. Hall, Blackwell Scientific Publications, Boston Oxford, London Edinburgh Melbourne.
- Kennedy, R.P., Short, S.A., Merz, K.L., Tokarz, F.J., Idriss, I.M., Power, M.S, and Sadigh, K. (1984). "Engineering characterization of ground motion, Task I: Effects of characteristics of free-field motion on structural response." Prepared for U.S. Nuclear Regulatory Commission. NUREG/CR-3805, vol. 1., Washington, DC.
- Kennedy, R.P., R.H. Kincaid, and S.A. Short. (1985). "Engineering Characterization of Ground Motion, Task II: Effects of Ground Motion Characteristics on Structural Response Considering Localized Structural Nonlinearities and Soil-Structure Interaction Effects," NUREG-3805, Vol. 2, USNRC, Washington, DC.
- Luco, J.E. et al. (1986). "Engineering Characterization of Ground Motion, Task II: Soil-Structure Interaction Effects on Structural Response," NUREG-3805, Vol. 4, USNRC, Washington, DC.
- Mohraz, B. (1976). "A Study of Earthquake Response Spectra for Different Geological Conditions." *Bull. Seism. Soc. Am.*, 66(3) 915-935.
- Mohraz, B., Hall, W.J. and Newmark, N.M. (1972). "A Study of Vertical and Horizontal Earthquake Spectra." Nathan M. Newmark Consulting Engineering Services, Urbana, IL: *AEC Report No. WASH-1255.*
- Newmark, N.M., J.A. Blume and K.K. Kapur (1973). "Seismic Design Criteria for Nuclear Power Plants." *Journal of the Power Division, ASCE* 99, 287-303.
- NRC (1973). "Design Response Spectra for Seismic Design of Nuclear Power Plants," Regulatory Guide 1.60, Revision 1, USNRC, Washington, DC.
- NRC (1997a). "Identification and Characterization of Seismic Sources and Determination of Safe Shutdown Earthquake Ground Motion," Regulatory Guide 1.165, USNRC, Washington, DC.
- NRC (1997b). "Standard Review Plan, 2.5.2 Vibratory Ground Motion," USNRC, Washington, DC, NUREG-0800, Rev. 3, March.
- Power, M.S., C.Y. Chang, I.M. Idriss and R.P. Kennedy (1986). "Engineering Characterization of Ground Motion." U.S. Nuclear Regulatory Commission, Summary R vol. 5, NUREG/CR-3805.
- Reed, J.W., Kennedy, R.P. and Lashkari, B. (1993). "Analysis of High-frequency Seismic Effects." Palo Alto, CA: Electric Power Research Institute, vol. 1-5, EPRI TR-102470.

- Seed, H.B., C. Ugas and J. Lysmer (1976). "Site-dependent Spectra for Earthquake Resistant Design." *Bull. Seism. Soc. Am.*, 66(1), 221-243.
- Silva, W.J., N. Abrahamson, G. Toro, C. Costantino (1997). "Description and validation of the stochastic ground motion model." Report to Brookhaven National Laboratory, Associated Universities, Inc. Upton, New York, Contract 770573.
- Silva, W.J. and R. Darragh (1995). "Engineering Characterization of Earthquake Strong Ground Motion Recorded at Rock Sites." Palo Alto, CA: Electric Power Research Institute, TR-102261.
- Silva, W.J. (1991). "Global Characteristics and Site Geometry." Chapter 6 in *Proc.: NSF/EPRI Workshop on Dynamic Soil Properties and Site Characterization*. Palo Alto, CA: Electric Power Research Institute, NP-7337.
- Youngs, R.R., N.A. Abrahamson, F. Makdisi, and K. Sadigh (1995). "Magnitude dependent dispersion in peak ground acceleration." *Bull. Seism. Soc. Am.*, 85(1), 1161-1176.

Table 1-1

WUS, CEUS M AND D BINS

	Distance (km)				
M	0 - 10	10 - 50	50 - 100	100 - 200	200 - 400
5 - 6	B	B	B	B	-----
6 - 7	B	B	B	B	-----
7+	B	B	B	B	C

B = both WUS and CEUS

C = CEUS only

Overview of Design Ground Motion Procedure and Application to Rock Sites

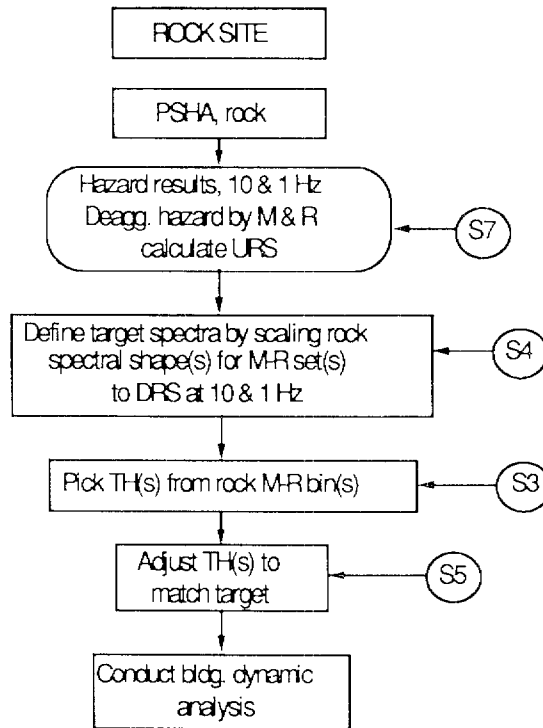


Figure 1-1: Flowchart of design ground motion procedure and application to rock sites. S3, S4, etc. refer to Sections of this report, TH = time history.

Overview of Design Ground Motion Procedure and Application to Soil Sites

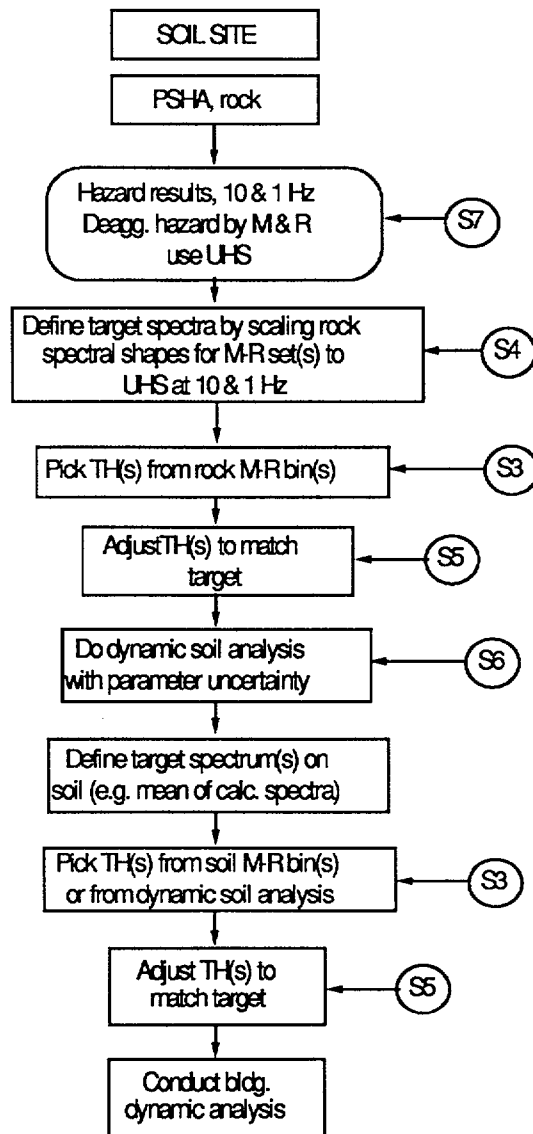


Figure 1-2: Flowchart of design ground motion procedure and application to soil sites. S3, S4, etc. refer to Sections of this report, TH = time history.

2 CHARACTERISTICS OF WUS AND CEUS STRONG GROUND MOTIONS AT ROCK SITES

Ground motion observations of both small and intermediate magnitude earthquakes that have occurred in eastern North America show larger peak ground accelerations as well as higher spectral amplitudes for frequencies > 5 Hz than would be expected based on recordings in western North America, principally California (Brady et al., 1981; Chang, 1983; Borchardt, 1986; Wesson and Nicholson, 1986; Weichert et al., 1982; 1986; Munro and Weichert, 1989; Silva and Darragh, 1995). In addition to these observations at high frequencies, intermediate magnitude ($M \approx 6.2$) earthquakes have shown an opposite trend for frequencies below about 2 Hz, having lower motions than comparable (M , distance, and site condition) WUS recordings would suggest (Boore and Atkinson, 1992; Atkinson, 1993; Silva and Darragh, 1995). This latter observation, in terms of strong ground motions, is principally limited to the 1988 M 5.8 Saguenay, Canada earthquake but is supported by inferences from intensity data (Atkinson, 1993), regional seismograms ($R \approx 1,000$ km) of early instrumental recordings in eastern North America (Atkinson and Chen, 1997), and teleseismic data of worldwide intraplate earthquakes (Boatwright and Choy, 1992).

The differences in high frequency spectral content between WUS and CEUS strong ground motions is pervasive and reasonably well understood (Boore and Atkinson, 1987; Boore et al., 1992; EPRI, 1993; Silva and Darragh, 1995; Atkinson, 1996) especially for very stiff (rock) site conditions. As a result, there is little doubt that future earthquakes occurring in the CEUS will have high frequency spectral characteristics at rock sites distinctly different than the WUS (California) experience. Conversely, the differences in low frequency spectral content between WUS and CEUS strong ground motions is neither well constrained through direct observations nor understood physically. The following discussion illustrates the differences between WUS and CEUS rock site motions and suggests the physical bases for the differences.

2.1 Differences Between CEUS And WUS Rock Site Strong Ground Motions

Observations of strong ground motion due to small magnitude earthquakes occurring in eastern North America, although not causing damage to engineered structures, have shown considerably higher peak accelerations than would have been expected based upon WUS experience (Brady et al., 1981; Chang, 1983; Wesson and Nicholson, 1986; Weichert et al., 1982; 1986; Munro and Weichert, 1989). In addition to the relatively higher peak accelerations associated with these CEUS events, response spectral ordinates appear richer in energy for frequencies exceeding about 5 Hz (Brady et al., 1981; Borchardt, 1986).

It has been known for some time that ground motion for the CEUS attenuates less rapidly with distance than ground motion in the WUS for events of similar moment magnitudes and source depths (Nuttli, 1981; EPRI, 1993; Atkinson and Boore, 1995). The difference in attenuation rate has been attributed to the higher absorptive characteristics generally present in the crust and upper mantle beneath the WUS as compared to the CEUS (Nuttli, 1981; Herrmann and Nuttli, 1982; Singh and Herrmann, 1983; Boore and Atkinson, 1987; Toro and McGuire, 1987; Frankel et al., 1990; Hanks and Johnston, 1992; EPRI, 1993; Frankel, 1994; Benz et al., 1997). This difference is probably a

consequence of active plate margin tectonics in the WUS as opposed to conditions representative of a stable continental interior in the CEUS.

For close-in recordings, where the propagation path is short (< 20 to 30 km), the difference in crustal attenuation between the WUS and CEUS was thought to have a minimal effect, and strong ground motion was expected to be comparable in the two tectonic environments (Campbell, 1981, 1986; Kimball, 1983). However, close-in (< 20 km) strong motion recordings of the 1978 Monticello, South Carolina earthquakes with moment magnitudes of approximately 3 produced a maximum peak-horizontal acceleration of 0.25g (Brady et al., 1981; Mork and Brady, 1981) and the 1986 Painesville, Ohio earthquake with a magnitude of 5.0 (m_{lg}) produced a peak acceleration of nearly 0.20g at an 18 km epicentral distance (Wesson and Nicholson, 1986). Both values are significantly higher than would be expected for earthquakes of similar magnitude and distance in the WUS. Recordings from both of these earthquakes also show unexpected high-frequency energy content in the response spectra compared to similar magnitude WUS recordings (Silva and Darragh, 1995).

Other sources of data also indicate that CEUS ground motions, recorded at rock or very shallow soil sites, are richer in high-frequency energy relative to analogous WUS ground motions. These include aftershocks of the 1982 Miramichi, New Brunswick earthquake (Cranswick et al., 1985), the 1982 Enola, Arkansas swarm (Haar et al., 1984), aftershocks of the 1986 Painesville, Ohio event (Borcherdt, 1986), the 1985 Nahanni earthquakes (Weichert et al., 1986), the 1982 New Hampshire earthquake (Chang, 1983), and the **M** 5.8 1988 Saguenay earthquakes (Boore and Atkinson, 1992). The trends shown in these CEUS data indicate significantly more spectral content at high frequencies compared to WUS rock motion of comparable magnitudes and distances (Fletcher, 1995; Silva and Darragh, 1995).

2.1.1 Effects of Shallow Crustal Damping

The difference in spectral content can perhaps be most easily seen in spectral amplification (spectral acceleration SA/PGA) computed from recordings typical of WUS and CEUS tectonic environments. Figure 2-1 shows average spectral shapes (SA/PGA) computed from recordings made on rock at close distances (≤ 25 km) for **M** = 6 and 5 earthquakes in CEUS and WUS tectonic environments, using records archived for this project. The differences are significant and indicate that CEUS spectral content is higher than that in the WUS for frequencies greater than approximately 10 Hz.

The controlling mechanism for the differences in high frequency spectral content (at close distances) between WUS and CEUS ground motions is thought to be due to differences in damping in the shallow (1 to 2 km) part of the crust (Boore and Atkinson, 1987; Silva et al., 1989a, 1989b; Silva, 1991; Silva and Darragh, 1995). The effects of shallow crustal damping were first pointed out and quantified by Hanks (1982) and Anderson and Hough (1984). The parameter that controls the shallow damping is termed kappa and is defined as the thickness of the zone over which the damping is taking place times the damping and divided by the average velocity over the zone of damping (Appendix D).

In a recent study, kappa values have been estimated by fitting spectral shapes computed from the stochastic ground motion model (Appendix D) to shapes computed from motions recorded at rock sites in eastern North America, WUS, Mexico, Italy (Friuli), USSR (Gazli), and Taiwan (SMART1) (Silva and Darragh, 1995). The kappa values are listed in Table 2-1; they reflect properties in the top 1-2 km of the crust. Results of these analyses indicate that kappa depends strongly on the material properties of the site. Rock sites characterized as soft, such as sedimentary, showed significantly higher kappa values than those characterized as hard, e.g. crystalline basement. Hard and soft rock sites may exist in either the WUS or CEUS; however, on the average, sites in stable cratonic regions such as the CEUS are more likely to be classified as hard in the top 1-2 km (low κ) while those associated with active tectonic regions such as the WUS are more likely to be soft in the top 1-2 km (high κ).

2.1.2 Effects of Crustal Amplification

An example of generic crustal models reflecting typical WUS soft rock and CEUS hard rock crustal conditions is shown in Figure 2-2 for both compression- and shear-wave velocities. The CEUS model is the midcontinent structure from EPRI (1993) and is considered appropriate for strong ground motion propagation in the CEUS except for the Gulf Coast region (Toro et al., 1997). The Gulf Coast region is typified by a crustal structure somewhat intermediate between those of the CEUS and WUS and is predicted to have correspondingly different wave propagation characteristics and strong ground motions (EPRI, 1993; Toro et al., 1997). The WUS model reflects an average of several California crustal models (Silva et al., 1997) representing the most seismically active regions, the north coast and peninsular range areas.

The differences in the shallow crustal velocities between the WUS and CEUS models is striking, particularly over the top 2 to 3 km, and the effects on strong ground motions are profound. In terms of amplification from source regions below about 5 km to the surface, the difference between hard (CEUS) and soft (WUS) crustal conditions is a factor of about 3 in amplification for frequencies exceeding about 5 Hz (Figure 2-3). All else being equal, WUS ground motions above ~5 Hz would then be expected to be nearly three times larger than corresponding CEUS motions. As suggested earlier however, pervasive observations reflect the opposite: high frequency CEUS motions generally exceed comparable WUS motions. Damping in the shallow crust, parameterized through kappa, is much greater in soft crustal rocks resulting in a dramatic loss in high frequency energy content compared to hard rock conditions. The differences in shallow crustal damping, or kappa, between soft and hard crustal conditions is a combined effect of lower velocities (Figure 2-2) as well as larger intrinsic damping. Kappa is defined as:

$$\kappa = \frac{H}{\bar{V}_s \bar{Q}_s}, \quad \bar{Q}_s = \frac{1}{2 \eta_s} \quad (2-1)$$

where H is the thickness of the shallow crustal damping zone (1 to 2 km, Anderson and Hough, 1984; Silva and Darragh, 1995), \bar{V}_s and \bar{Q}_s are the average shear-wave velocities and quality factors over depth H, and η_s is the corresponding critical damping ratio (decimal). For soft rock conditions both the velocities and Q values are lower than hard rock conditions resulting in very large differences in

kappa values and corresponding energy absorption at high frequency. Table 2-1 lists kappa values determined at both WUS and CEUS rock sites (Silva and Darragh, 1995) and shows the strong dependence upon surficial geology in terms of rock quality. Hard and soft conditions can exist in both WUS and CEUS and are reflected in distinct kappa values, increasing as the rock quality degrades. On average, kappa values for the WUS are about 5 times larger than for the CEUS (0.037 sec and 0.008 sec, Table 2-1).

To illustrate the effects of kappa on strong ground motions, Figures 2-4 and 2-5 show response spectral shapes (5% damping) and absolute spectra computed for an **M** 6.5 earthquake occurring at a distance of 25 km for WUS parameters (see Table 2-2, parameter values from Silva et al., 1997) using a range of kappa values from 0.005 sec to 0.160 sec. For the shapes, Figure 2-4, increasing kappa results in a shift in shapes to lower frequencies as the PGA and high frequency spectral amplitudes decrease. For fixed magnitude, the frequency range of maximum spectral amplification is a good estimator of shallow crustal damping (Silva and Darragh, 1995).

The absolute spectra shown in Figure 2-5 further illustrate the effects of kappa on high frequency strong ground motions. A factor-of-two change in kappa results in about a 50% change in peak acceleration. The average difference in WUS and CEUS rock site kappa values of about 5 (Table 2-1) results in a difference of about a factor of four in high frequency ground motions, exceeding the factor of about three in the difference in high frequency (5 Hz) crustal amplification (Figure 2-3). Close-in strong ground motions (that is, at ≤ 50 km; “near-source” is reserved for distances ≤ 10 -15 km), would be expected to be lower at CEUS rock sites than WUS rock sites at low frequencies, because differences in deep crustal properties such as frequency dependent damping ($Q(f)$) and depth to the Moho and Conrad discontinuities do not have large effects (EPRI, 1993). At high frequencies the converse would be expected, providing source processes are similar in both regions. Several lines of evidence suggest that this is not the case however, with CEUS sources generating more high-frequency energy, than WUS sources for the same **M**.

2.1.3 Effects of Source Processes

Another factor regarding the differences in spectral composition between WUS and CEUS strong ground motions at rock sites is the probable differences in earthquake source processes. Prior to the occurrence of the 1988 **M** 5.8 Saguenay earthquake, there was thought to be a difference of about a factor of two in stress drop (the difference in average stress across the rupture surface before and after an earthquake) between WUS and CEUS sources with the CEUS having larger stress drop values, about 100 bars compared to about 50 bars for the WUS (Atkinson, 1984; Boore, 1986). These measures of stress drop, termed Brune stress drops (Brune, 1970; Appendix D), are primarily based on high frequency ground motion levels assuming that in the frequency domain the source can be represented by a single-corner-frequency source model.

An alternative measure of stress drop is based on the ratio of the seismic moment (M_0) to the rupture area and is termed the static stress drop. The stress drop equation for a circular rupture surface is given by

$$\Delta\sigma = \frac{7}{16} \pi \frac{M_o}{(Area/\pi)^{\frac{4}{3}}} \quad (2-2)$$

where *Area* is the area over which rupture occurs. This measure of stress drop was also thought to be higher (by about a factor of two) for earthquakes occurring in the CEUS compared to the WUS (Kanamori and Anderson, 1975; Kanamori and Allen, 1986). For static stress drops, the scaling of strong ground motions is not at all clear. However, since the average slip (fault displacement) is proportional to moment, and strong ground motions increase with slip (for fixed rupture area), strong ground motions must increase with static stress drop, at least at low frequency.

Apart from the differences in stress drops (Brune and static), overall source processes were thought to be similar in both tectonic regimes. The stochastic single-corner-frequency point-source model (Appendix D), originally developed by Hanks and McGuire (1981), provides accurate predictions of WUS strong ground motions using a stress drop of about 50 bars (Boore, 1986; Boore et al., 1992; Silva and Darragh, 1995) although with a tendency to overpredict low frequency (≤ 1 Hz) motions for large magnitude earthquakes (Atkinson and Silva, 1997).

For the CEUS, the simple point-source model with a stress drop of about 100 bars, about double that of the WUS, provided good agreement with existing data (Atkinson, 1984; Boore and Atkinson, 1987; Toro and McGuire, 1987) until the occurrence of the 1988 M 5.8 Saguenay earthquake. Strong ground motions from this earthquake, the largest to have occurred in the CEUS in over 50 years, depart significantly from predictions of the simple 100 bar stress drop model (Boore and Atkinson, 1992). The stress drop required to match high frequency strong ground motions for this earthquake exceed 500 bars, while the intermediate frequency spectral levels are overestimated by a factor of two or more, requiring a significantly lower stress drop (Boore and Atkinson, 1992). Concurrently, Boatwright and Choy (1992) using teleseismic (low frequency, ≤ 2 Hz) data, showed that the source spectra of large intraplate earthquakes differ in general from the simple single-corner-frequency omega-square model, suggesting the presence of a second corner frequency. Based on the limited ground motion data in the CEUS as well as inferences from intensity observations, Atkinson (1993) developed an empirical two-corner source model for CEUS earthquakes. In this model, the high frequency spectral levels are consistent with Brune stress drop of about 150 bars while the equivalent stress drop for the low frequency spectral levels is about 40 to 50 bars (Atkinson, 1993), assuming the crustal model shown in Figure 2-2. This two-corner model currently provides reasonable estimates of recorded CEUS ground motions over the frequency range of the majority of the data, about 10.0 to 0.1 Hz, while the single-corner-frequency model, with stress drops ranging from about 120 to 150 bars, overpredicts ground motions in the frequency range of about 1 Hz to 0.1 Hz but gives a better fit in the 2 to 10 Hz frequency range (Atkinson and Boore, 1998). Both the double and single-corner source models, with stress drops below 200 bars, underpredict ground motions ≥ 2 Hz for the Saguenay earthquake by factors of 2 to 3 suggesting anomalous high frequency levels for this event. While it currently appears that the two-corner source model may be the more appropriate model for CEUS strong ground motions, it is evident that in predicting strong ground motions for engineering design, significantly more variability should be accommodated in applications to the CEUS than to the WUS. This increased variability should accommodate both randomness (aleatory variability) in stress drop above that for the WUS as well as uncertainty

(epistemic variability) in the source model. The larger variability in the CEUS should be represented in the PSHA for a site, and will be reflected in the mean hazard for the site.

For the WUS, recent work has shown some interesting results regarding earthquake source spectra. In the context of the single-corner-frequency model, stress drop appears to be magnitude dependent (Silva and Darragh, 1995; Atkinson and Silva, 1997; Silva et al., 1997), decreasing from about 100 bars for M 5.5 to about 50 bars for M 7.5 with an average value of about 70 bars. Since inferences on stress drop for CEUS sources are based predominantly on small magnitude earthquakes, $M \approx 5.2$ (Atkinson, 1993), scaling of stress drop with magnitude similar to WUS would imply significantly lower stress drops for large magnitude earthquakes. The 150 bar stress drop for CEUS may reflect a value appropriate for M near 5.5. Assuming WUS stress drop scaling with M would result in an average stress drop of about 120 bars for M ranging from 5.5 to 7.5.

A model that appears to be more consistent with WUS source spectra inferred from the strong motion data is similar to the CEUS two corner model but with a less pronounced spectral sag at intermediate frequencies. The two-corner nature of WUS source spectra is filled-in by crustal amplification (Figure 2-3) resulting in a comparatively subtle feature in strong ground motions compared to CEUS data (Atkinson and Silva, 1997). This observation may provide some comforting linkage to CEUS source processes suggesting an appealing underlying similarity. However, CEUS sources, for the same magnitude, do appear to be considerably more energetic at high frequency, and this is reflected in larger Brune stress drops by a factor of about two on average.

To illustrate the effects of stress drop on ground motions, Figures 2-6 and 2-7 show response spectral shapes and absolute spectra (both for 5% of critical damping) computed for M 6.5 at a distance of 25 km using WUS parameters (Table 2-2). For the shapes, Figure 2-6, the effect of stress drop is small, with differences occurring at low frequency below about 1 Hz. Spectral shapes are largely independent of stress drop for ranges of 2 to 3 over most of the frequency band of interest.

The absolute spectra shown in Figure 2-7 illustrate the large effect Brune stress drops have on strong ground motions. The effect is strongest for frequencies exceeding the source corner frequency (Silva, 1993), about 0.2 Hz for a stress drop of 65 bars, and results in about a 70% change in peak acceleration for a factor-of-two change in stress drop. For the single-corner-frequency Brune source model, stress drop is a controlling parameter in absolute levels of strong ground motions.

Comparisons of WUS to CEUS response spectra are shown in Figures 2-8 and 2-9 for shapes and absolute spectra respectively. Also illustrated in the figures are the differences between the single- and double-corner source spectral models. In Figure 2-8, the difference in spectral shapes between the WUS and CEUS at single-corner models (solid and long dash lines) is clearly illustrated in the maximum spectral amplifications at about 5 Hz for the WUS and at about 40 Hz for the CEUS.

The difference between the single- and double-corner source models is also clearly illustrated. For the WUS, the difference is mainly at low frequency and is not large, about 20% near 0.3 Hz. For the CEUS, the single corner source model significantly exceeds the double corner below about 2 Hz. The largest difference occurs near 0.4 Hz and is a factor of over 3 in 5% damped spectral acceleration.

Choices between the two source models for the CEUS, single or double corner, clearly have major impacts on design motions.

The corresponding absolute spectra (not scaled) are shown in Figure 2-9. The WUS and CEUS single-corner spectral estimates are nearly the same for frequencies up to about 5 Hz. This is the result of compensating effects previously discussed, higher stress drop for CEUS (Table 2-2) and larger amplification factors for WUS (Figure 2-3). Beyond about 5 Hz, the differences in kappa values (0.04 sec compared to 0.006 sec, Table 2-2) result in the difference in high frequency spectral estimates.

To see how well the simple point-source models (single and double corner frequency) capture the differences in shapes between the WUS and CEUS rock motions that were illustrated in Figure 2-1, Figures 2-10 and 2-11 compare model predictions to $M 6$ statistical shapes. Figure 2-10 for the WUS compares both the single- and double-corner model predictions to the statistical shape. Both models capture the overall shape reasonably well but overpredict at low frequency (below 1 to 2 Hz). The double-corner model provides a better fit but still shows overprediction in this frequency range.

The comparison to CEUS $M \approx 6$ is shown in Figure 2-11. There is only one earthquake, 1985 Nahanni, with hard rock site recordings (3 stations) in this magnitude and distance range. Both spectral models capture the difference in shape between WUS and CEUS equally well with the single-corner model showing an overprediction at low frequency (≤ 1 Hz) similar to the WUS. Interestingly, the double-corner model shows an underprediction for frequencies below about 2 Hz. Since this is only a single earthquake and variability is large in CEUS strong ground motions, these results should not be interpreted as a potential bias in the model for spectral shapes, but they do emphasize the current state of uncertainty regarding CEUS strong ground motions. Although the data have been processed, the overprediction beyond about 20 Hz may be an artifact of the instruments, which had a cutoff frequency of about 25 Hz.

For a comparison at $M 5$, Figures 2-12 and 2-13 show results for the WUS and CEUS respectively. For the WUS, Figure 2-12 shows reasonable model predictions down to about 1 Hz, below which the number of spectra is greatly reduced because of increasing noise levels. Figure 2-13 shows the corresponding plot for CEUS $M 5$ comparisons. The models capture the shift in shape to higher frequency but overpredict for frequencies above about 20 Hz. As with the $M 6$ comparison, the low frequencies are enveloped by the two models. Since the $M 5$ statistical shape reflects the same Nahanni earthquake sequence with two aftershocks, model departures from observations are not considered particularly significant.

These comparisons to CEUS statistical shapes point out the quandary in estimating strong ground motions in the CEUS. Sufficient recordings at close distances (≤ 50 km) for earthquakes of engineering significance ($M \geq 5$) are not available to unequivocally distinguish between plausible models.

References

- Anderson, J. G. and S. E. Hough (1984). "A Model for the Shape of the Fourier Amplitude Spectrum of Acceleration at High Frequencies." *Bull. Seism. Soc. Am.* 74(5), 1969-1993.
- Atkinson, G.M. (1984). "Attenuation of strong ground motion in Canada from a random vibrations approach." *Bull. Seism. Soc. Am.*, 74(5), 2629-2653.
- Atkinson, G.M. (1993). "Source spectra for earthquakes in eastern North America." *Bull. Seism. Soc. Am.*, 83(6), 1778-1798.
- Atkinson, G.M. (1996). "The high-frequency shape of the source spectrum for earthquakes in eastern and western Canada." *Bull. Seism. Soc. Am.* 86(1A), 106-112.
- Atkinson, G.M. and D.M. Boore (1995). "Ground motion relations for eastern North America." *Bull. Seism. Soc. Am.*, 85(1), 17-30.
- Atkinson, G.M. and D.M. Boore (1998). "Evaluation of models for earthquake source spectra in Eastern North America." *Bull. Seism. Soc. Am.* 88(4), 917-934.
- Atkinson, G.M. and S.Z. Chen (1997). "Regional seismograms from historical earthquakes in southeastern Canada." *Seism. Res. Lett.* 68(5), 797-807.
- Atkinson, G.M. and W.J. Silva (1997). "An empirical study of earthquake source spectra for California earthquakes." *Bull. Seism. Soc. Am.* 87(1), 97-113.
- Benz, H.M., A. Frankel, and D.M. Boore (1997). "Regional L_g attenuation for the continental United States." *Bull. Seism. Soc. of Am.*, 87(3), 606-619.
- Boatwright, J. and G. Choy (1992). "Acceleration source spectra anticipated for large earthquakes in Northeastern North America." *Bull. Seism. Soc. Am.*, 82, 660-682.
- Boore, D.M. (1986). "Short-period P- and S-wave radiation from large earthquakes: implications for spectral scaling relations." *Bull. Seism. Soc. Am.*, 76(1) 43-64.
- Boore, D.M. and G.M. Atkinson (1987). "Stochastic prediction of ground motion and spectral response parameters at hard-rock sites in eastern North America." *Bull. Seism. Soc. Am.*, 77(2), 440-467.
- Boore, D.M. and G.M. Atkinson (1992). "Source spectra for the 1988 Saguenay, Quebec, earthquakes." *Bull. Seism. Soc. Am.*, 82(2), 683-719.
- Boore, D.M., W.B. Joyner, and L. Wennerberg (1992). "Fitting the stochastic ω^2 source model to observed response spectra in western North America: Trade-offs between $\Delta\sigma$ and κ " *Bull. Seism. Soc. Am.*, 82(4), 1956-1963.

- Borcherdt, R. D. (1986). "Preliminary Report on Aftershock Sequence for Earthquake of January 31, 1986 near Painesville, Ohio." U.S. Geological Survey Open File Report 86-181.
- Brady, A.G., P.N. Mork, and J.P. Fletcher (1981). "Processed accelerograms from Monticello Dam, Jenkinsville, South Carolina, August 27, 1978, and two later shocks." *USGS Open-File Rept.* 81-448.
- Brune, J.N. (1970). "Tectonic stress and the spectra of seismic shear waves from earthquakes." *J. Geophys. Res.* 75, 4997-5009.
- Campbell, K. W. (1981). "A Ground Motion Model for the Central United States Based on Near-Source Acceleration Data." In *Proc. of Conf. on Earthquakes and Earthquake Engineering: the Eastern United States.*, edited by J. E. Beavers, Knoxville, Tennessee, September 14-16, Ann Arbor Science Publishers, 1, 213-222.
- Chang, F.K. (1983). "Analysis of strong motion data from the New Hampshire earthquake of 18 January 1982,." US Nuclear Regulatory Commission Rept. NUREG/CR-3327.
- Cranswick, E., R. Wetmiller, and J. Boatwright (1985). "High-frequency observations and source parameters of microearthquakes recorded at hard-rock sites." *Bull. Seism. Soc. Am.*, 75(6), 1535-1567.
- Electric Power Research Institute (1993). "Guidelines for determining design basis ground motions." Palo Alto, Calif: Electric Power Research Institute, vol. 1-5, EPRI TR-102293.
 vol. 1: Methodology and guidelines for estimating earthquake ground motion in eastern North America.
 vol. 2: Appendices for ground motion estimation.
 vol. 3: Appendices for field investigations.
 vol. 4: Appendices for laboratory investigations.
 vol. 5: Quantification of seismic source effects.
- Frankel, A. (1994). "Implications of felt area-magnitude relations for earthquake scaling and the average frequency of perceptible ground motion." *Bull. Seism. Soc. Am.*, 84(2), 462-465.
- Frankel, A., A. McGarr, J. Bicknell, J. Mori, L. Seeber, and E. Cranswick (1990). "Attenuation of high-frequency shear waves in the crust: Measurements from New York State, South Africa, and southern California." *J. Geo. Research*, 95(B11), 17,441-17,457.
- Fletcher, J.B., (1995). "Source parameters and crustal Q for four earthquakes in South Carolina." *Seismol. Research Lett.*, 66(4), 44-58.
- Haar, L. C., J. B. Fletcher, and C. S. Mueller (1984). "The 1982 Enola, Arkansas Swarm and Scaling of Ground Motion in the Eastern United States." *Bull. Seism. Soc. Am.*, 74(6), 2463-2482.

- Hanks, T.C., and A.C. Johnston (1992). "Common features of the excitation and propagation of strong ground motion for north American earthquakes" *Bull. Seism. Soc. Am.*, 82(1), 1-23
- Hanks, T.C. (1982). " f_{\max} ." *Bull. Seism. Soc. Am.*, 72(6), 1867-1879.
- Hanks, T.C., and R.K. McGuire (1981). "The character of high-frequency strong ground motion." *Bull. Seism. Soc. Am.*, 71(6), 2071-2095.
- Herrmann, R.B. and O.W. Nuttli (1982). "Magnitude: the relation of M_L to $m_{bl.g}$." *Bull. Seism. Soc. Am.*, 72(2), 389-397.
- Kanamori, H., and C.R. Allen (1986). "Earthquake repeat time and average stress drop." *Earthquake Source Mech., Am. Geophys. Union Geophys. Monogr.*, S. Das, J. Boatwright, C.H. Scholz, ed., 37, 227-235.
- Kanamori, H., and D.L. Anderson (1975). "Theoretical basis of some empirical relations in seismology." *Bull. Seismol. Soc. Am.*, 65, 1073-1095.
- Kimball, J.K. (1983). "The use of site dependent spectra." *Proc. Workshop on Site-Specific Effects of Soil and Rock on Ground Motion and the Importance for Earthquake-Resistant Design*, Santa Fe, New Mexico, USGS Open-File Rept. 83-845, 410-422.
- Mork, P. and A. G. Brady (1981). "Processed Accelerograms from Monticello Dam, Jenkinsville, South Carolina, October 16, 1979, 0706 UTC." *U.S. Geological Survey Open-File Report* 81-1214.
- Munro, P. S. and D. Weichert. (1989). "The Saguenay earthquake of November 25, 1988: Processed strong motion records." Geological Survey of Canada Open File/Dossier Public 1996.
- Nuttli, O. W. (1981). "Similarities and Differences between Western and Eastern United States Earthquakes, and their Consequences for Earthquake Engineering." In *Proceedings of the Conference on Earthquakes and Earthquake Engineering: the Eastern United States*, ed. J. E. Beavers, vol. 1, Ann Arbor Science Publishers, Inc., Ann Arbor, MI, 25-27.
- Silva, W.J., N.A. Abrahamson, G.R. Toro, and C.J. Costantino (1997). "Description and validation of the stochastic ground motion model." Report to Brookhaven National Laboratory, Associated Universities, Inc. Upton, New York, Contract 770573.
- Silva, W.J. (1991). "Global characteristics and site geometry." Chapter 6 in *Proceedings: NSF/EPRI Workshop on Dynamic Soil Properties and Site Characterization*. Palo Alto, Calif.: Electric Power Research Institute, Rept. NP-7337.

- Silva, W.J. (1993). "Factors controlling strong ground motions and their associated uncertainties." *Seismic and Dynamic Analysis and Design Considerations for High Level Nuclear Waste Repositories*, ASCE 132-161.
- Silva, W.J. and R. Darragh (1995). "Engineering characterization of earthquake strong ground motion recorded at rock sites." Palo Alto, Calif:Electric Power Research Institute, Rept. TR-102261.
- Silva, W.J., R. Darragh, R. Green, and F. Turcotte (1989a). "Spectral characteristics of small magnitude earthquakes with application to western and eastern North American tectonic environments: Surface motions and depth effects." U.S. Army Engineers Waterways Experiment Station Miscellaneous Paper GI-89-16.
- Silva, W.J., R. Darragh, R. Green, and F. Turcotte (1989b). "*Estimated ground motions for a New Madrid event.*" U.S. Army Engineers Waterways Experiment Station Miscellaneous Paper GL-89-17.
- Singh, S. and R.B. Hermann (1983). "Regionalization of crustal coda Q in the continental United States." *J. Geophys. Res.*, 88, 527-538.
- Toro, G.R., N.A. Abrahamson, and J.F. Schneider (1997). "Model of strong ground motions from earthquakes in Central and Eastern North America: Best estimates and uncertainties." *Seismological Research Let.*, 68(1), 41-57.
- Toro, G.R. and R.K. McGuire (1987). "An investigation into earthquake ground motion characteristics in eastern North America." *Bull. Seism. Soc. Am.*, 77(2), 468-489.
- Weichert, D. H., R. J. Wetmiller, R. B. Horner, P. S. Munro, and P. N. Mork (1986). "Strong Motion Records from the 23 December 1985, M_s 6.9 Nahanni, NWT, and Some Associated Earthquakes." *Geological Survey of Canada*, Open-File Report 1330.
- Weichert, D. H., P. W. Pomeroy, P. S. Munro, and P. N. Mork (1982). "Strong motion records from Miramichi, New Brunswick, 1982 aftershocks." *Earth Physics Branch*, Ottawa, Canada, Open File Report 82-31.
- Wesson, R. L. and C. Nicholson (1986). *Studies of the January 31, 1986 Northeastern Ohio Earthquake*. Report submitted to the U.S. NRC, USGS Open-File Report 86-331.

Table 2-1					
KAPPA VALUES FOR "AVERAGE" SITE CONDITIONS IN WUS AND CEUS*					
Tectonic	"Average" Site Condition	N [†]	Median Kappa (sec)	σ_{ln}	Range of Kappa for This Site Condition (sec)
WUS	Hard rock	11	0.026	0.58	0.010 - 0.060
	Weathered hard rock	9	0.035	0.52	0.015 - 0.100
	Soft rock	15	0.045	0.51	0.015 - 0.080
	Sheared rock	4	0.062	0.41	0.040 - 0.120
	Combined	39	0.037	0.59	0.010 - 0.120
CEUS	Hard rock	16	0.007	0.42	0.004 - 0.016
	Soft rock	3	0.017	0.09	0.015 - 0.018
	Sheared rock	1	0.025		0.025
	Combined	20	0.008	0.55	0.004 - 0.025

* Based on template fits using spectral shapes (Silva and Darragh, 1995)

[†] Number of records

"Average" Site Condition is defined as:

Hard Rock: WNA as granite, schist, carbonate, slate
 ENA as granitic pluton, carbonate, sites in Canadian Shield region (Saguenay, New Hampshire).

Weathered hard rock: WNA as weathered granitic rock and tonalite

Soft rock: WNA as sandstone and breccias
 ENA as sandstone and claystone

Sheared rock: WNA as site near fault zone (Gilroy #6) or greenstone site in Franciscan (Redwood City, Hayward).
 ENA as site near fault zone (Nahanni River Site #1)

Table 2-2

POINT-SOURCE PARAMETERS

	WUS	CEUS
$\Delta\sigma$ (bars)	65	120
kappa (sec)	0.040	0.006
Q_0	220	351
η	0.60	0.84
β (km/sec)	3.50	3.52
ρ (g/cc)	2.70	2.60
Amplification	soft rock (Figure 2-3)	hard rock (Figure 2-3)
Double Corner	Atkinson and Silva (1997)	Atkinson (1993)

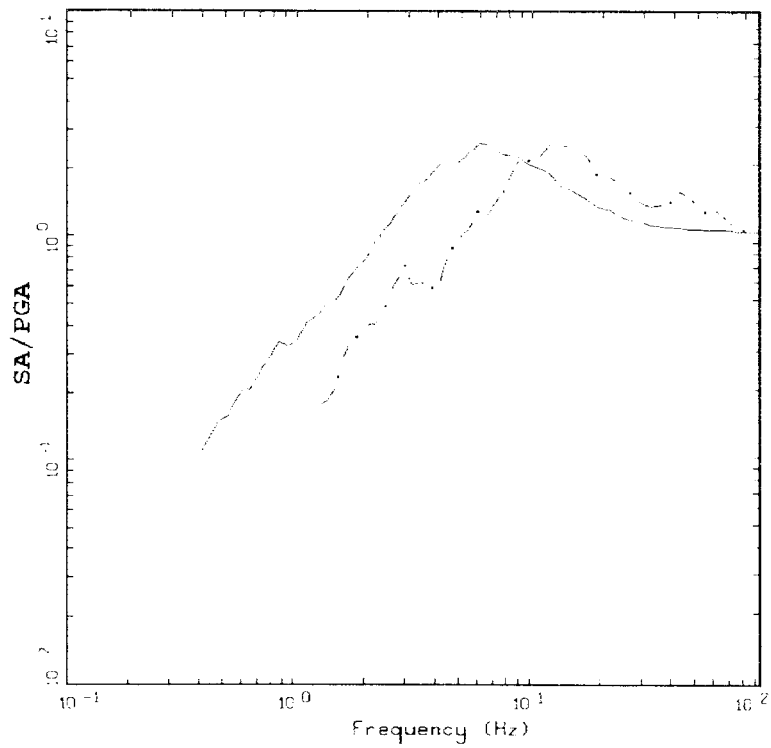
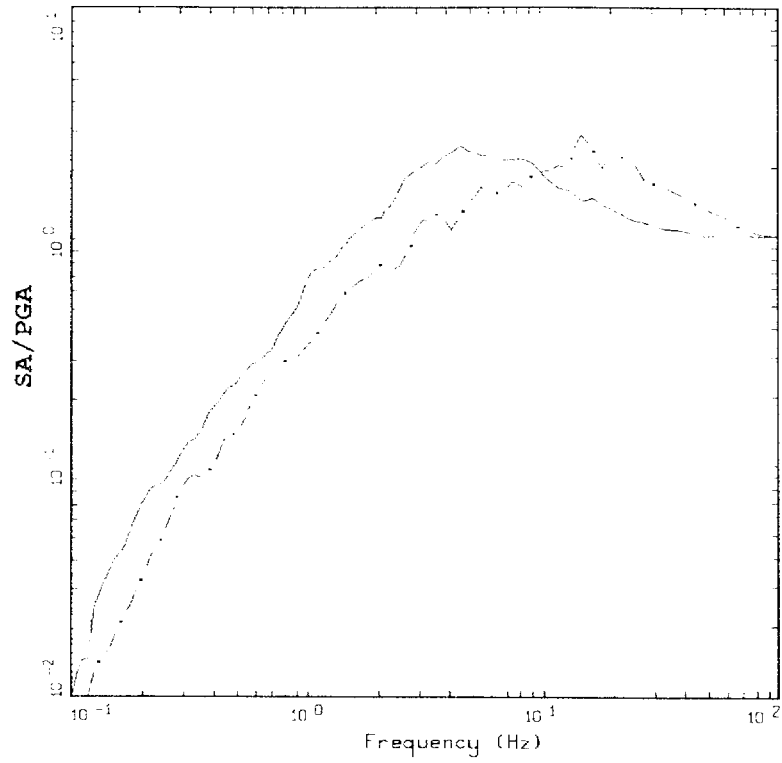
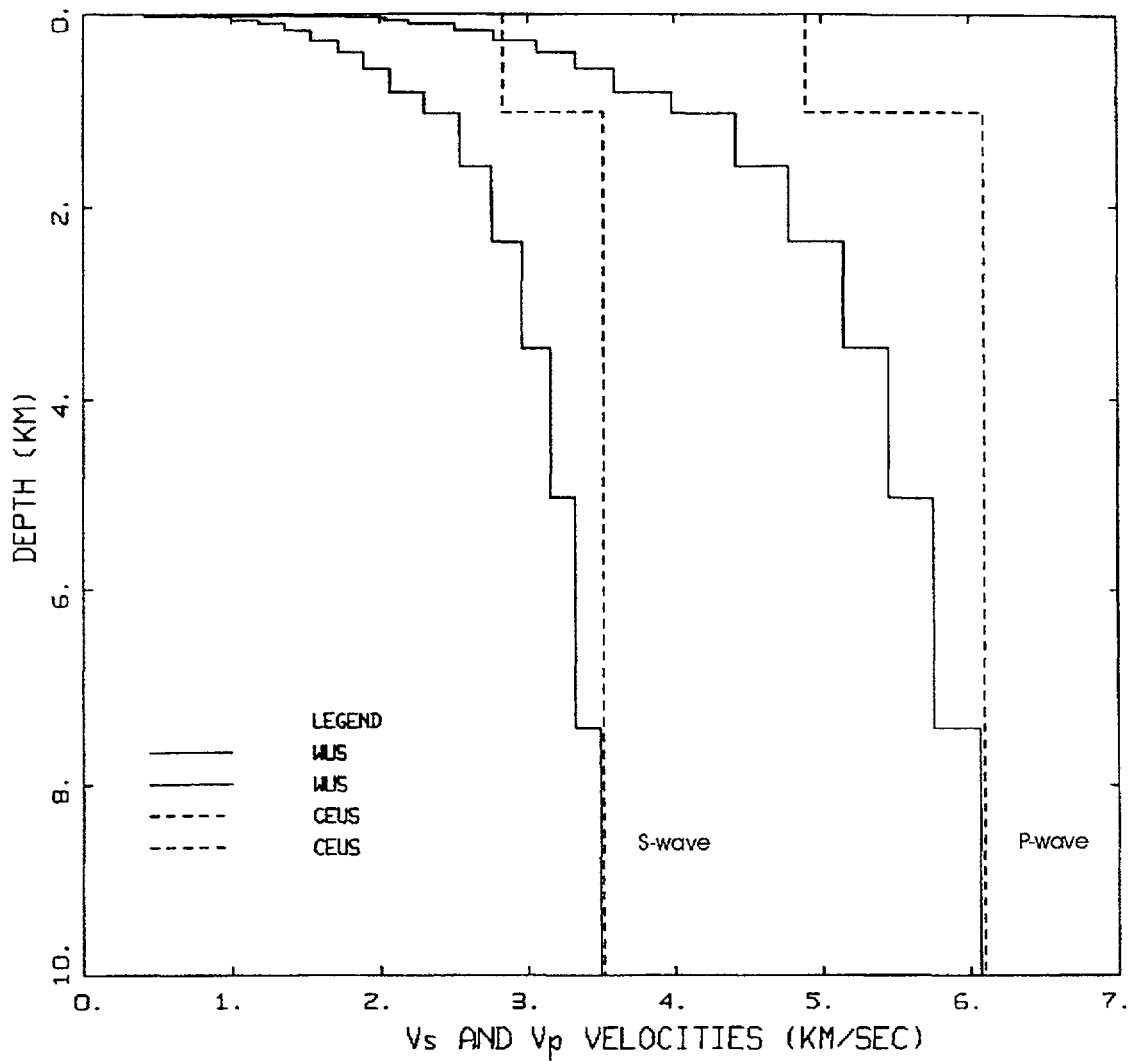
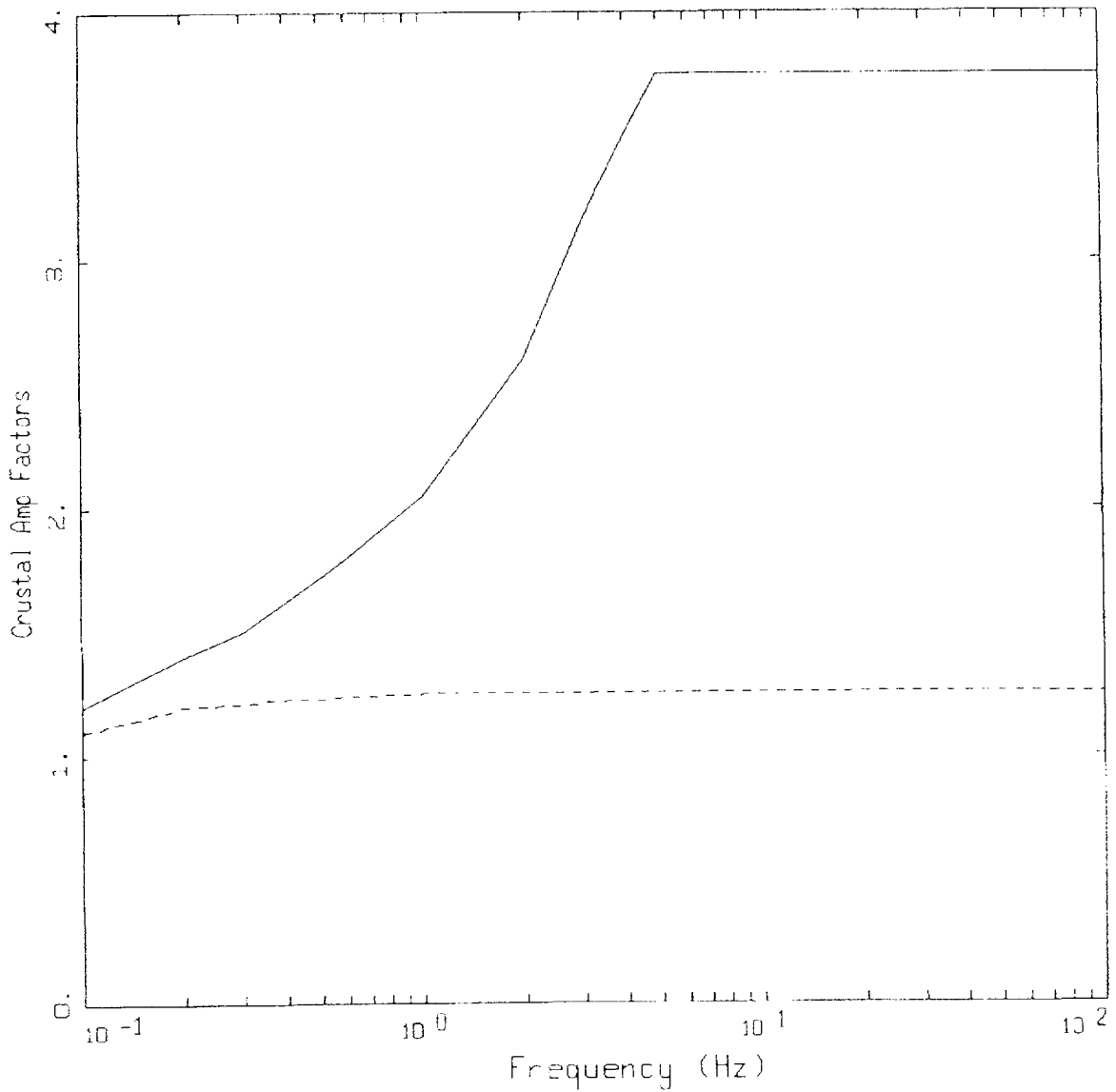


Figure 2-1. Comparison of response spectral shapes (SA/PGA, 5% damping) between CEUS (dashed line), and WUS (solid line) crustal conditions for earthquakes recorded at rock sites: **M** 6³/₄ (upper) and **M** 5³/₄ (lower).



GENERIC WUS AND CEUS
CRUSTAL MODELS

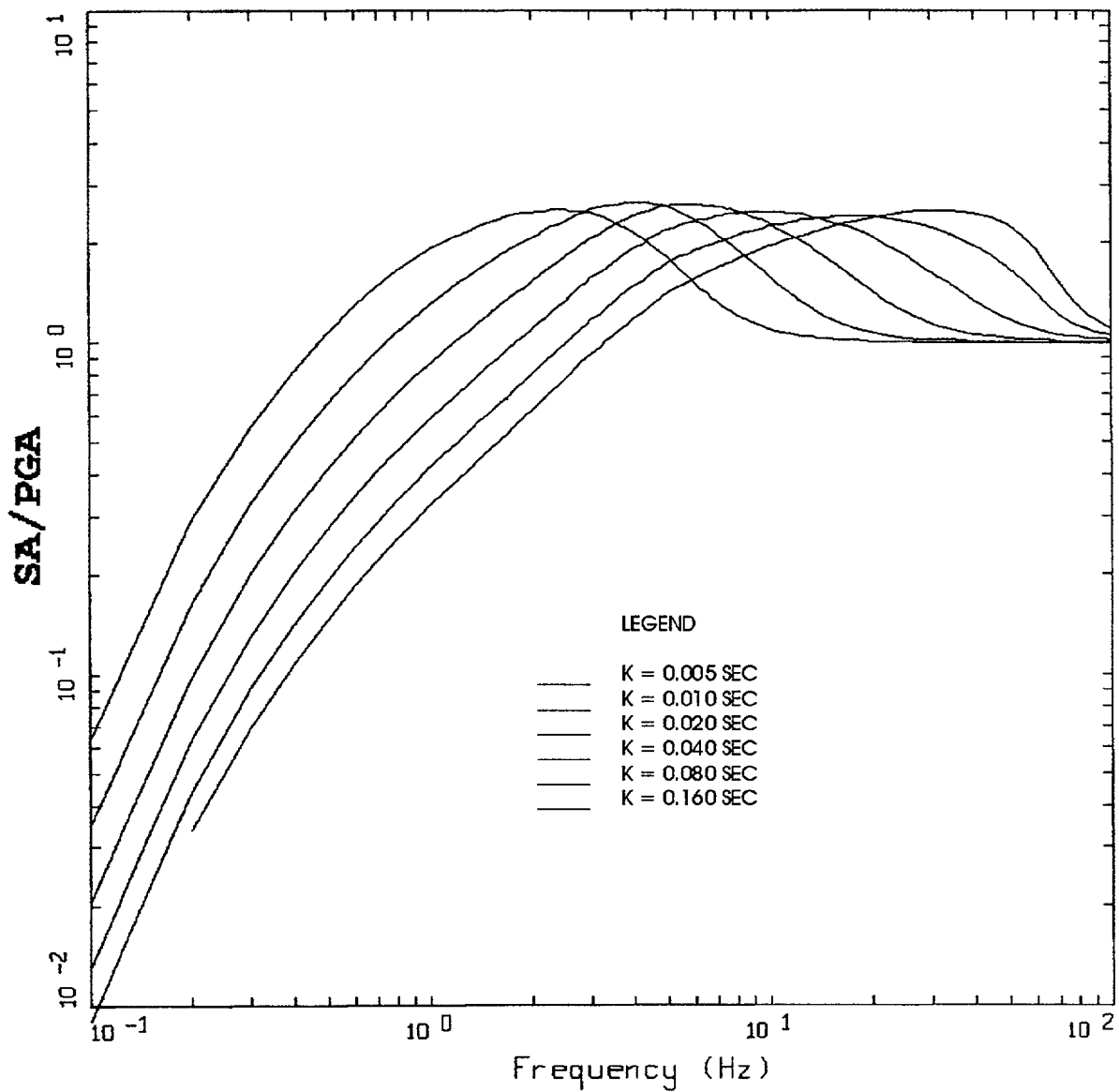
Figure 2-2. Comparison of generic compression (P) and shear (S) wave velocity profiles for WUS and CEUS crustal conditions.



CRUSTAL AMPLIFICATION FACTORS

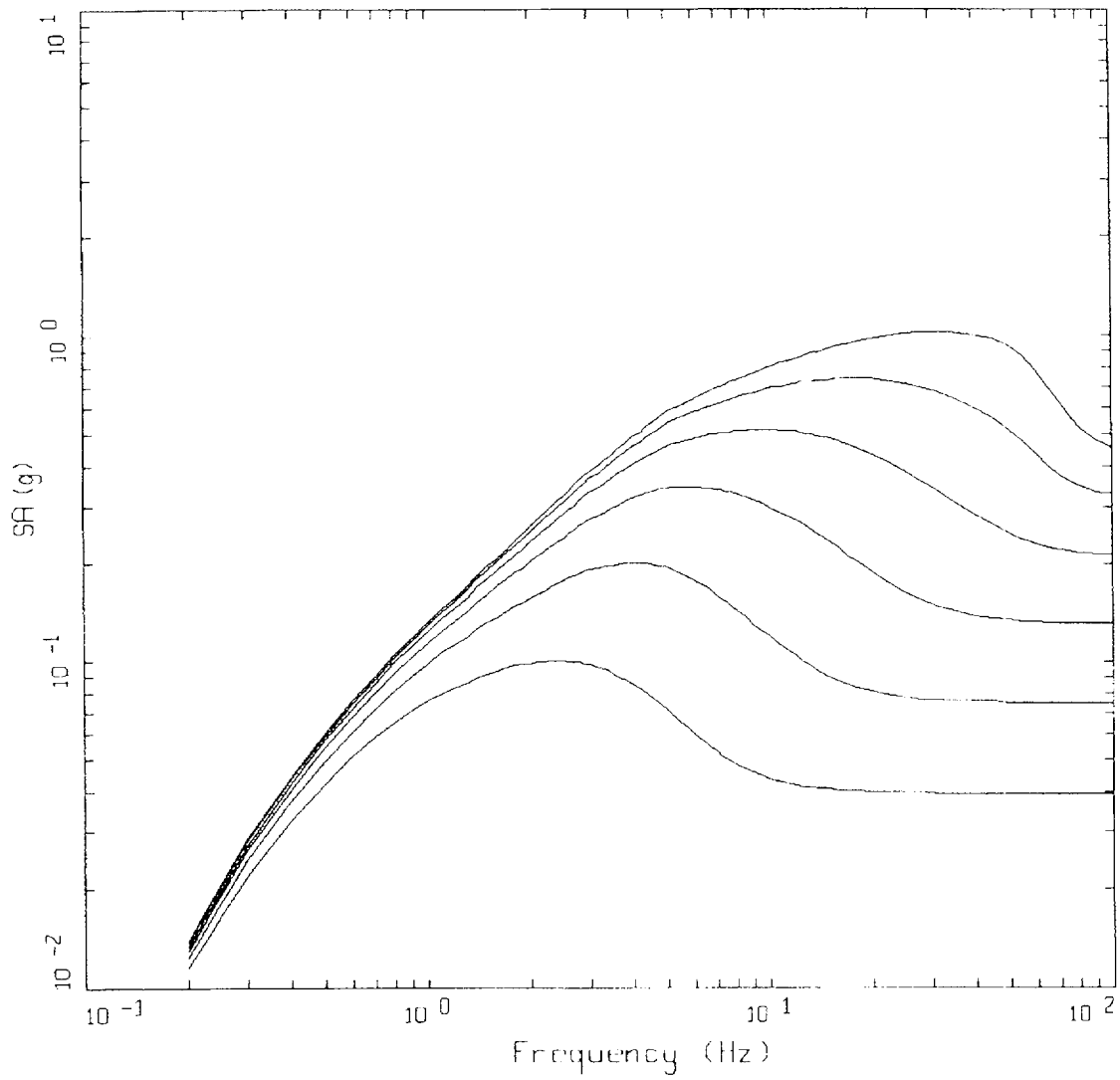
——— WUS, SOFT ROCK
 - - - - CEUS, HARD ROCK

Figure 2-3. Crustal amplification factors (smoothed) for Fourier amplitude spectra computed for the crustal models shown in Figure 2-2 (10 km to the surface).



ROCK
 BASE CASE, WUS, 1-CORNER SOURCE MODEL
 M = 6.5, R = 25 KM, STRESS DROP = 65 BARS

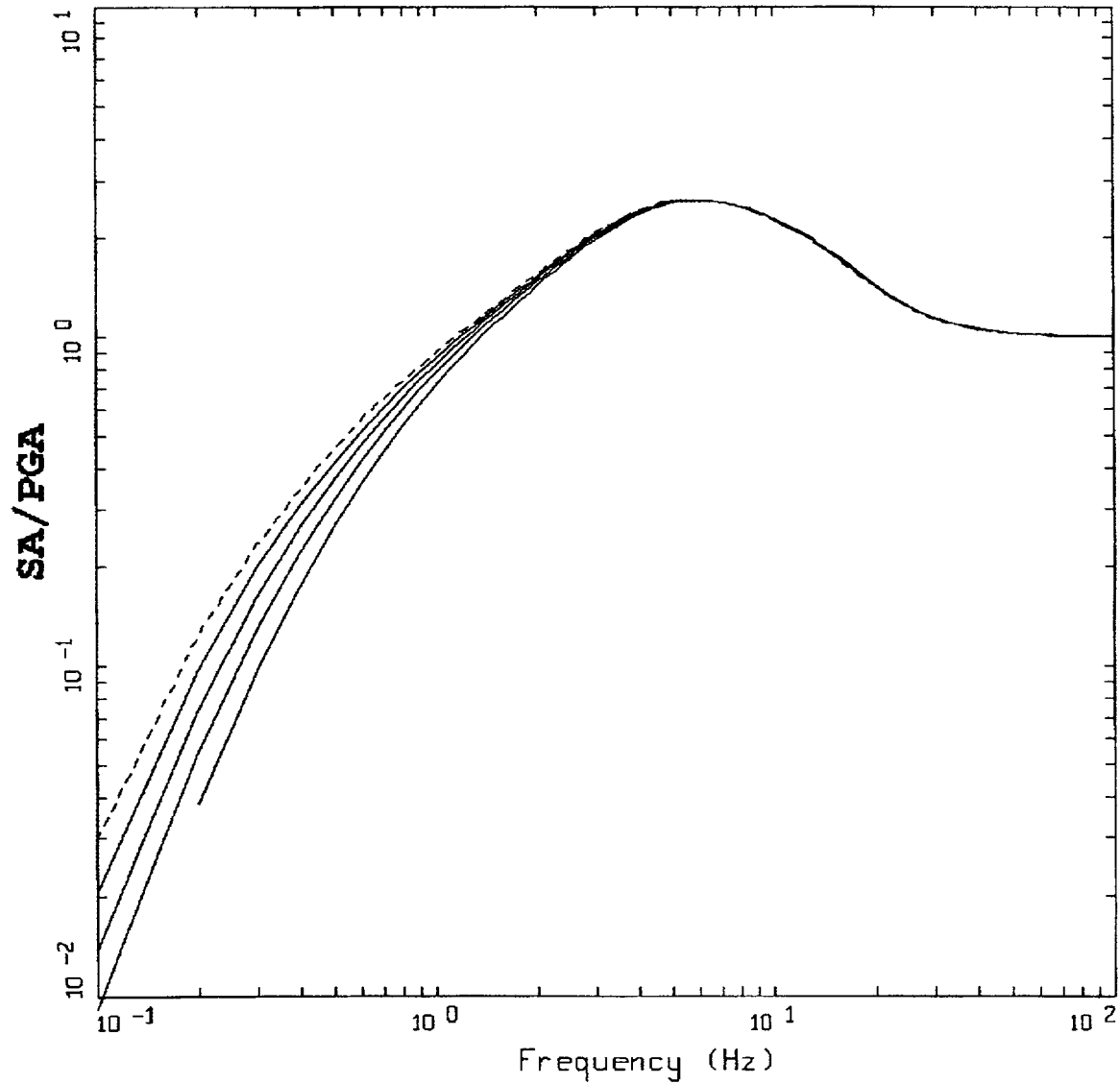
Figure 2-4. Response spectral shapes (SA/PGA, 5% damping) computed for M 6.5 at a distance of 25 km for a suite of kappa values using WUS parameters (Table 2-2). The lowest kappa value shows the highest high-frequency amplification, the highest kappa value shows the highest low-frequency amplification.



ROCK
 BASE CASE, WUS, 1-CORNER SOURCE MODEL
 M = 6.5, R = 25 KM, STRESS DROP = 65 BARS

- LEGEND
- K = 0.005 SEC
 - K = 0.010 SEC
 - K = 0.020 SEC
 - K = 0.040 SEC
 - K = 0.080 SEC
 - K = 0.160 SEC

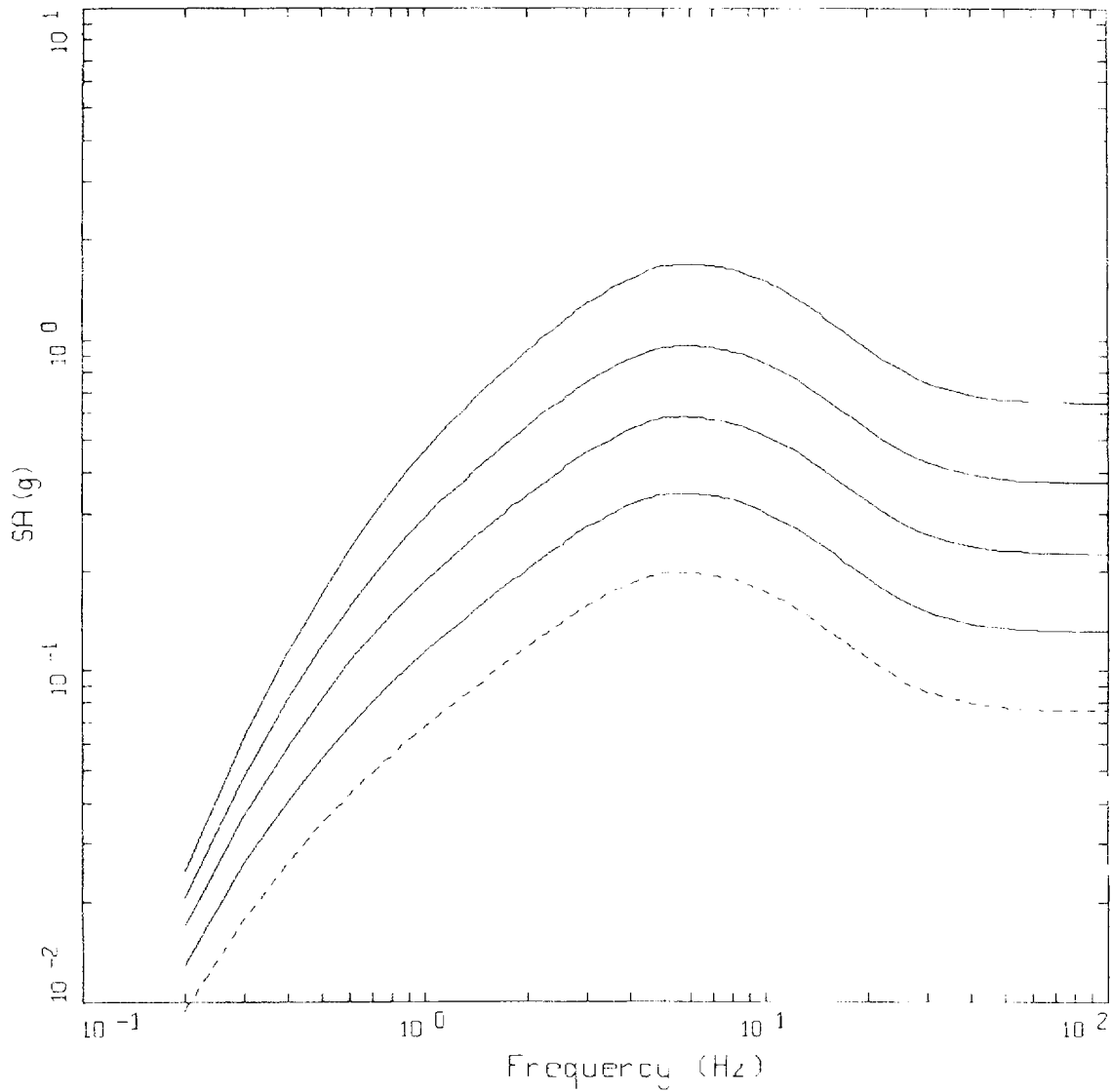
Figure 2-5. Response spectra (5% damping) computed for an M 6.5 earthquake at a distance of 25 km for a suite of kappa values using WUS parameters (Table 2-2). The lowest K value shows the highest spectral amplitudes and the highest K value shows the lowest spectral amplitudes.



ROCK
 BASE CASE, WUS, 1-CORNER SOURCE MODEL
 M = 6.5, R = 25 KM, KAPPA = 0.040 SEC

- LEGEND
- STRESS DROP = 32 BARS
 - STRESS DROP = 65 BARS
 - STRESS DROP = 130 BARS
 - STRESS DROP = 260 BARS
 - STRESS DROP = 520 BARS

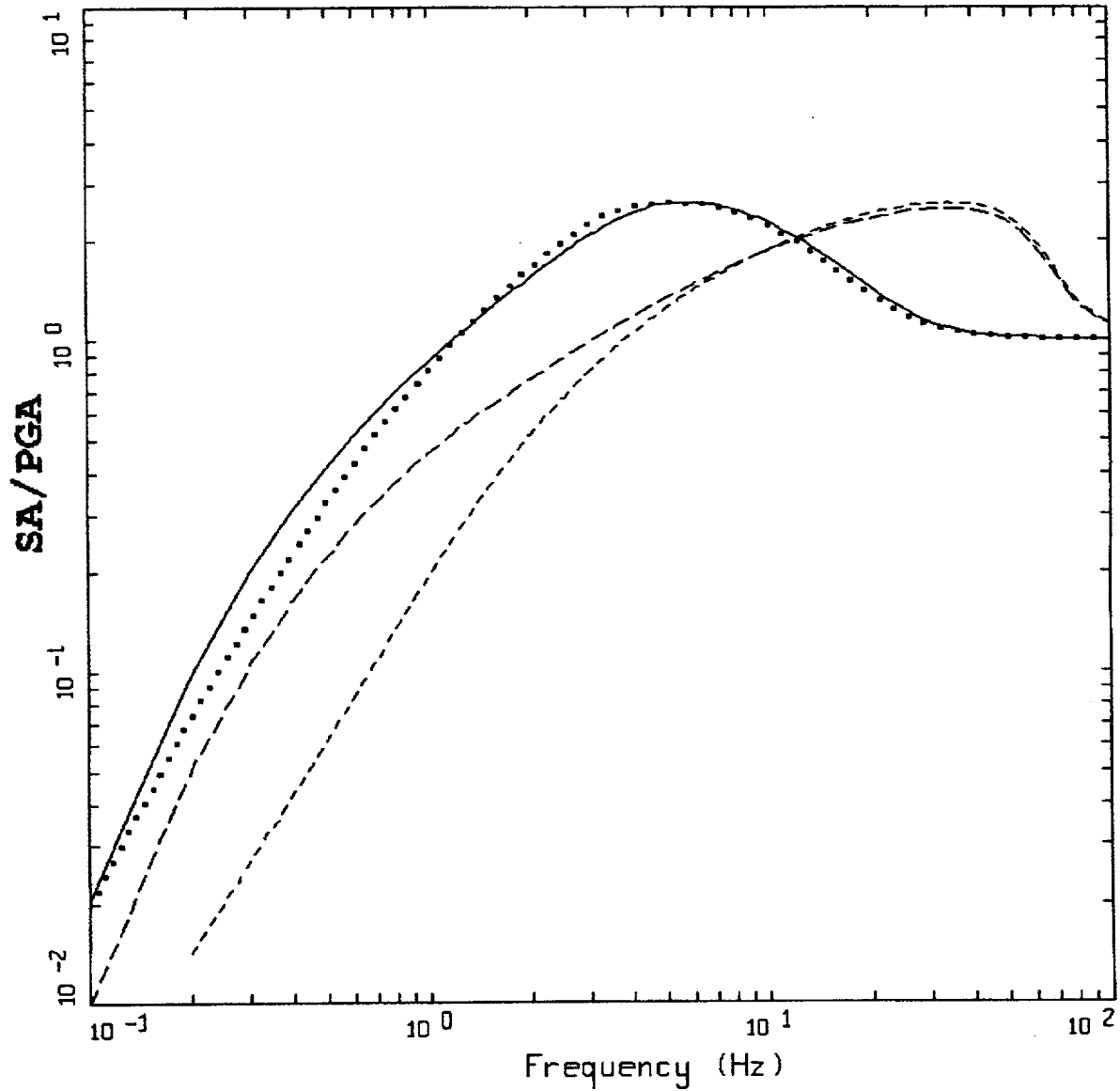
Figure 2-6. Response spectral shapes (SA/PGA, 5% of critical damping) computed for M 6.5 at a distance of 25 km for a suite of stress drop values using WUS parameters (Table 2-2). Spectral shapes reduce with increasing stress drop, beginning with 32 bars.



ROCK
 BASE CASE, WUS, 1-CORNER SOURCE MODEL
 $M = 6.5$, $R = 25$ KM, $KAPPA = 0.040$ SEC

- LEGEND
- STRESS DROP = 32 BARS
 - STRESS DROP = 65 BARS
 - STRESS DROP = 130 BARS
 - STRESS DROP = 260 BARS
 - STRESS DROP = 520 BARS

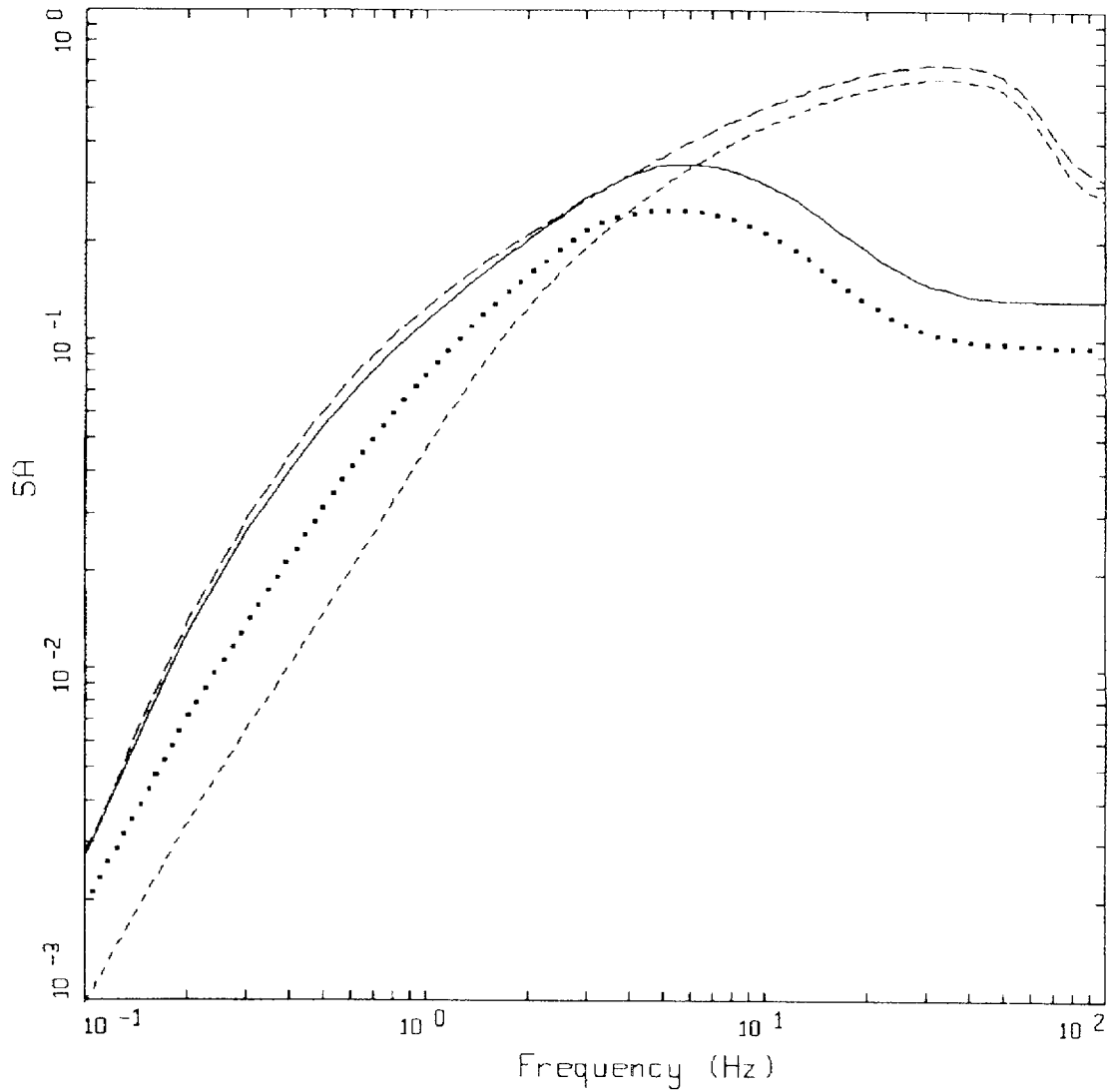
Figure 2-7. Response spectra (5% of critical damping) computed for M 6.5 at a distance of 25 km for a suite of stress drop values using WUS parameters (Table 2-2). Spectral shapes increase with increasing stress drop, beginning with 32 bars.



POINT-SOURCE MODEL
 M = 6.5, R = 25 KM

- LEGEND
- WUS ROCK, SINGLE CORNER
 - WUS ROCK, DOUBLE CORNER
 - - - CEUS ROCK, SINGLE CORNER
 - . - . CEUS ROCK, DOUBLE CORNER

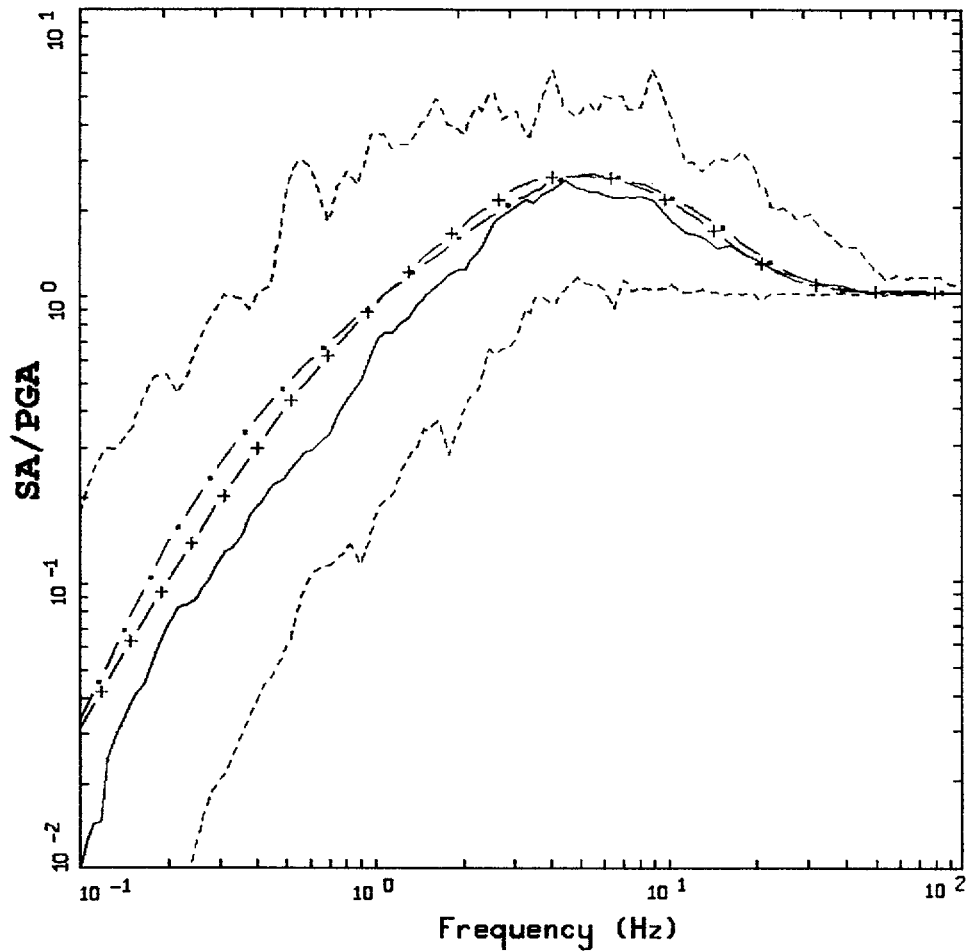
Figure 2-8. Response spectral shapes (5% of critical damping) computed for $M = 6.5$ at $R = 25$ km using both single- and double-corner frequency source spectra for WUS and CEUS conditions (Table 2-2).



POINT-SOURCE MODEL
 $M = 6.5$, $R = 25$ KM

- LEGEND
- WUS ROCK, SINGLE CORNER
 - WUS ROCK, DOUBLE CORNER
 - - - - CEUS ROCK, SINGLE CORNER
 - - - - CEUS ROCK, DOUBLE CORNER

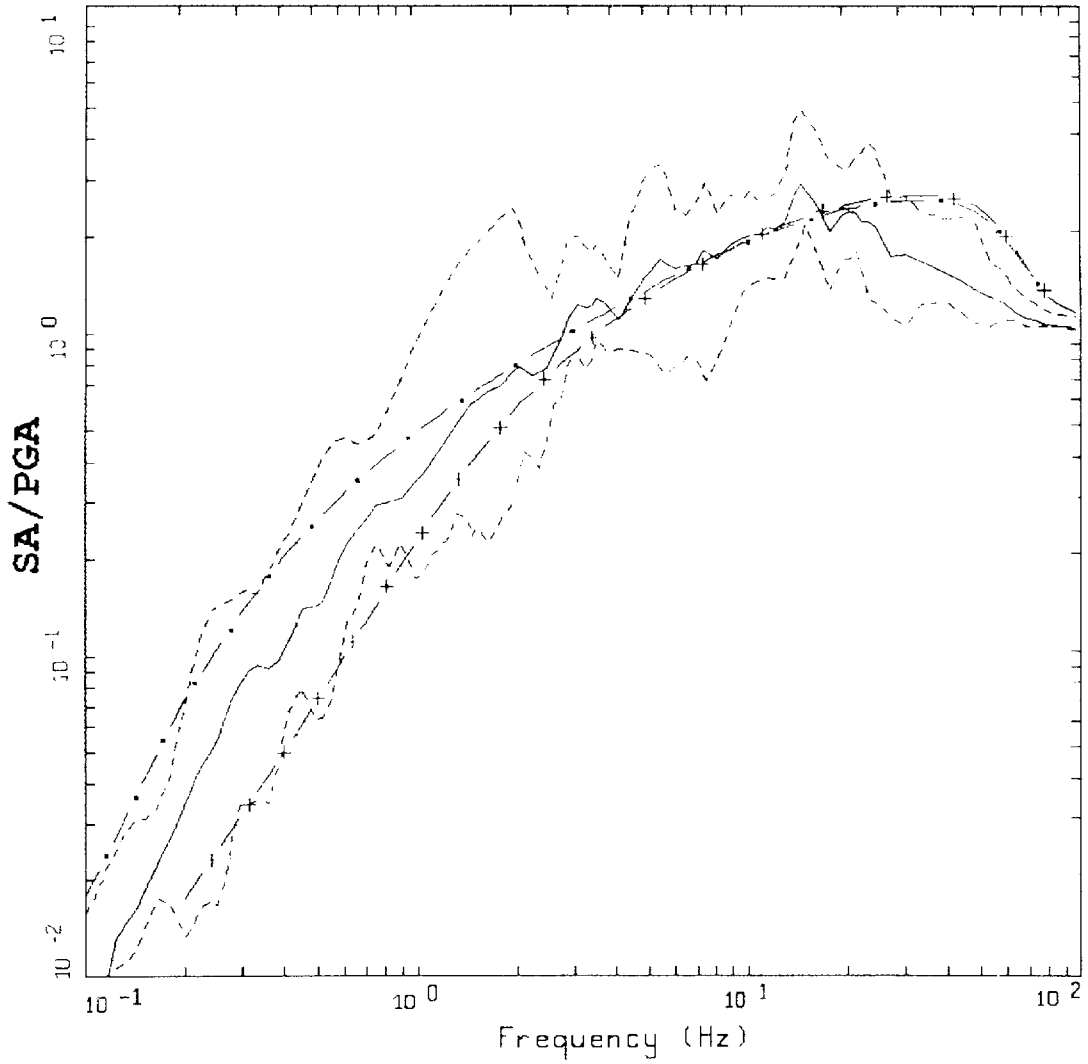
Figure 2-9. Absolute response spectra (5% of critical damping) computed for $M = 6.5$ at $R = 25$ km using both single- and double-corner frequency source spectra for WUS and CEUS conditions (Table 2-2).



AVERAGE HORIZONTAL SPECTRA, WUS
 M=6.75 (6.5-7.0), R=10-50 KM, ROCK
 AVERAGE M = 6.75, AVERAGE DISTANCE = 30.78 KM

- LEGEND
- 50TH PERCENTILE
 - - - MINIMUM ENVELOPE
 - · - MAXIMUM ENVELOPE
 - · · WUS SINGLE CORNER MODEL
 - + - WUS DOUBLE CORNER MODEL

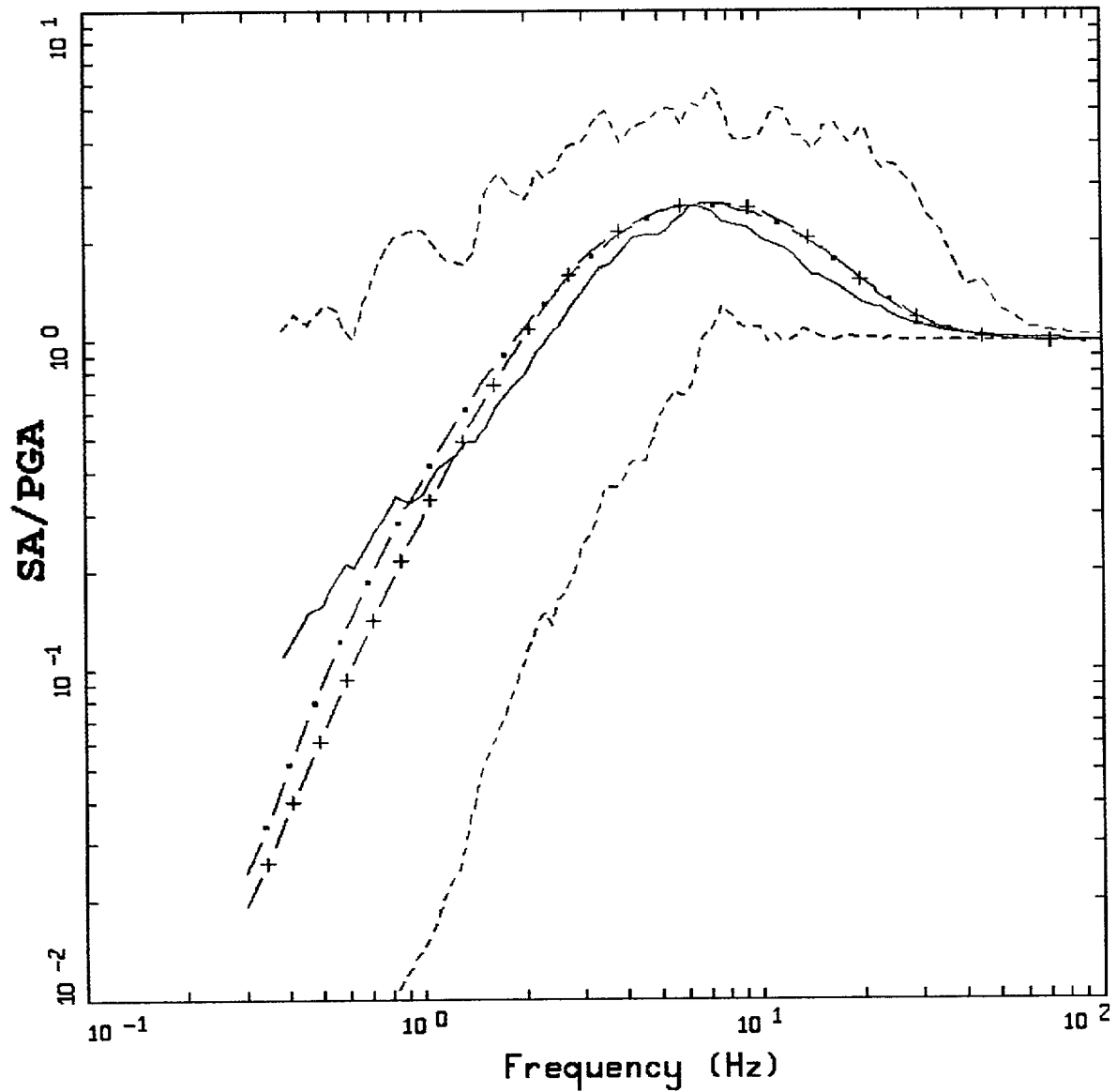
Figure 2-10. Comparison of 5% damped statistical shapes computed for WUS recordings. ($M = 6\frac{3}{4}$) to single- and double-corner model predictions using the parameters listed in Table 2-2.



AVERAGE HORIZONTAL SPECTRA, CEUS
 M=6.75, R=5-50 KM, ROCK

- LEGEND
- 50TH PERCENTILE
 - MINIMUM ENVELOPE
 - MAXIMUM ENVELOPE
 - . - CEUS SINGLE CORNER MODEL
 - + - CEUS DOUBLE CORNER MODEL

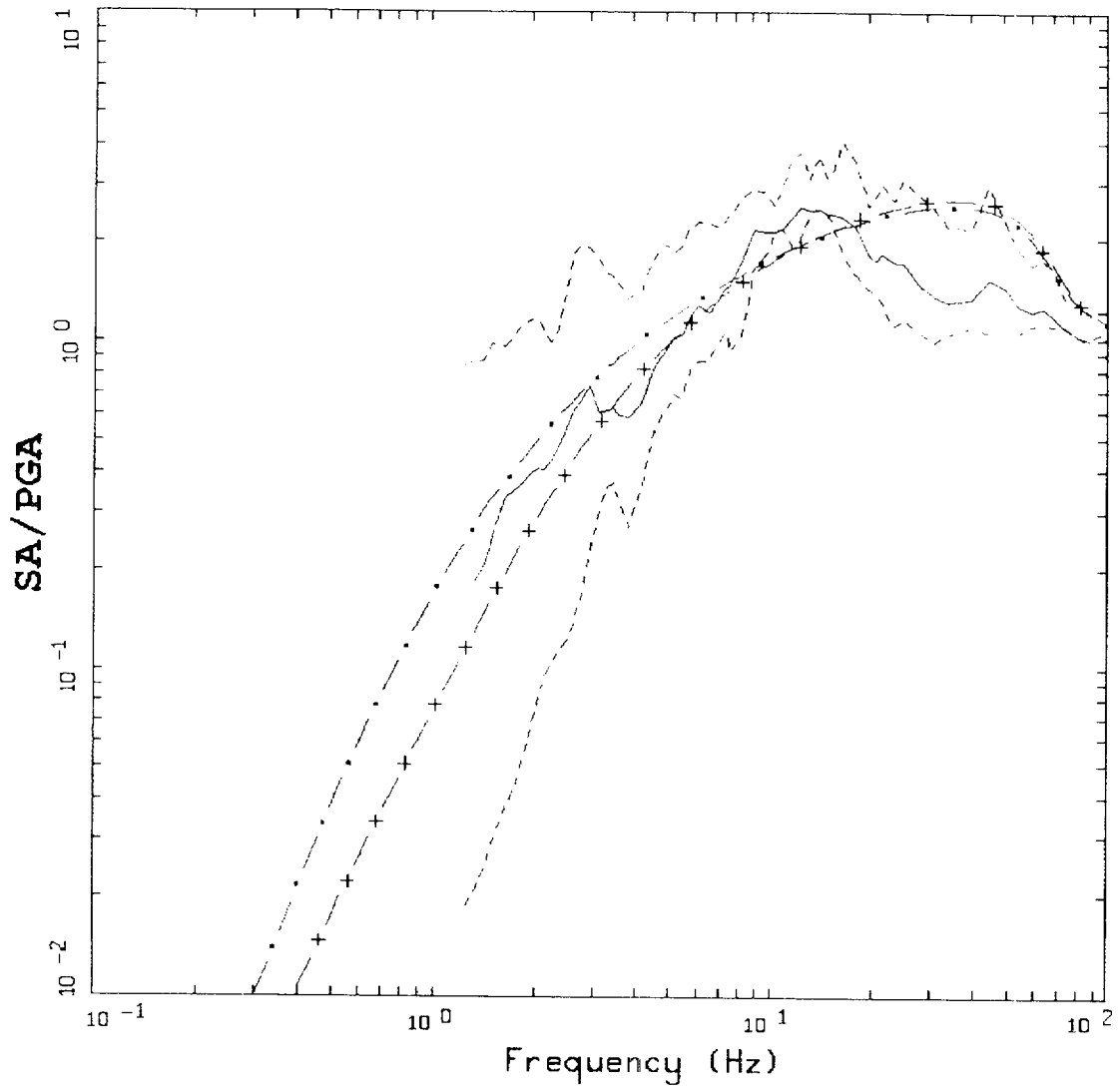
Figure 2-11. Comparison of 5% damped statistical shapes computed for CEUS recordings ($M=6.75$) to single- and double-corner model predictions using the parameters listed in Table 2-2.



AVERAGE HORIZONTAL SPECTRA, WUS
 M=5 1/4 (5.0-5.4), R=0-25 KM, ROCK
 AVERAGE M = 5.18, AVERAGE DISTANCE = 13.57 KM

- LEGEND
- 50TH PERCENTILE
 - - - - MINIMUM ENVELOPE
 - . - . MAXIMUM ENVELOPE
 - . - . CEUS SINGLE CORNER MODEL
 - + - CEUS DOUBLE CORNER MODEL

Figure 2-12. Comparison of 5% damped statistical shapes computed for WUS recordings (M 5¼) to single- and double-corner model predictions using the parameters listed in Table 2-2.



AVERAGE HORIZONTAL SPECTRA, CEUS
 $M=5 \frac{1}{4}$, $R=0-25$ KM, ROCK

- LEGEND
- 50TH PERCENTILE
 - MINIMUM ENVELOPE
 - MAXIMUM ENVELOPE
 - · - CEUS SINGLE CORNER MODEL
 - + - CEUS DOUBLE CORNER MODEL

Figure 2-13. Comparison of 5% damped statistical shapes computed for CEUS recordings ($M=5 \frac{1}{4}$) to single- and double-corner model predictions using the parameters listed in Table 2-2.

3 TIME HISTORY DATABASE FOR ANALYSES

The time history database provides a suite of motions for structural and soil column analyses. For this intended use, it is assumed the motions will undergo a scaling or matching process to the desired hazard levels (Section 5). The parceling of time histories into magnitude and distance bins provides implicit guidelines on the amount of recommended scaling.

In addition to the magnitude and distance bins, an additional screening is done on duration for WUS records. This duration screening results in time histories that are expected to be unbiased in time domain characteristics that affect nonlinear structural or soil column analyses. Since a robust measure of duration that is significant to nonlinear structural analysis eludes quantification, the duration criteria are not imposed in a strict manner. The magnitude and distance bins and the duration criteria are discussed in Section 3-1.

The library of time histories for analysis is intended to rely on recorded motions for WUS conditions. While the field of modeling has progressed significantly in the last few years as a direct result of the increase in the number of recordings and an emphasis on thorough validations (Appendix D), uncertainties remain as to whether purely synthetic records reflect appropriate phasing between components, frequency-to-frequency variations, and effects of rupture directivity. This is a significant issue for the CEUS because that region has not produced many records, particularly for magnitude-distance combinations of relevance to engineering design. To preserve as much of the natural attributes of recorded motions as possible, we recommend using the WUS bin records as inputs to CEUS spectral matching analyses. To assist this process, the CEUS analysis time history bins have been supplemented with scaled WUS recordings taken from the WUS bins. The scaling process involves computing response spectral transfer functions for WUS rock to CEUS rock and for WUS deep soil to CEUS deep soil. The scaling process uses the single-corner-frequency point-source model (Appendices D and K). The transfer functions for horizontal and vertical motions are then applied to the WUS empirical rock and soil bin spectra. This process results in scaled CEUS target spectra, and the WUS bin records are then used as input to a weak spectral matching process (Silva and Lee, 1987). This process results in fully populated CEUS rock and soil bins, supplemented with hybrid empirical records that maintain realistic phase and amplitude relationships between components and realistic frequency-to-frequency variability. The supplemental bin records should be used only as inputs to additional scaling or matching procedures and are not intended to be used to develop CEUS spectral shapes or spectral levels.

For CEUS single-corner-frequency source models, the main difference between WUS and CEUS rock motions is at high frequency (≥ 5 Hz, Figure 4-10) and the issue in fitting CEUS spectra is the ability of the matching process to sufficiently scale up the high frequencies. The double-corner CEUS shapes are similar to the single-corner but incorporate a broad spectral sag. At very low frequency the two shapes are the same because they reflect similar M (or seismic moments). Spectral matching or scaling empirical WUS motions to double-corner CEUS spectra thus presents issues similar to matching CEUS single-corner spectra. Examples of this process are presented in Section 3.2.

An aspect of the resulting CEUS time histories that is largely lost in the scaling approach is the observed general increase in durations over corresponding WUS rock time histories (Atkinson, 1995). Since too few records exist of sufficiently large magnitudes and distances to be of engineering significance, an assessment of differences in durations between WUS and CEUS conditions and their corresponding effects on engineering analyses is currently not available. Users of this time history database in applications to CEUS conditions may wish to select the longer duration records from the bins as a sensitivity analysis. This is the type of test that was envisaged in populating one bin (Table 3-3) with 30 three component sets of time histories. Appendix B contains the WUS and CEUS analysis time history catalog, and separate CD ROMs contain the analysis time histories (acceleration, velocity, and displacement time histories) and the 5% damped response spectra and durations (Section 3.2).

3.1 Site Conditions For Time Histories

Site conditions for the time history database consist of soft rock and firm soil for WUS motions. A convenient site categorization scheme that has been applied to most of the strong motion sites in the US and many abroad is shown in (Table 3-1). Categories A and B are considered appropriate for soft rock and categories C and D for deep firm soil site conditions. The soft rock site conditions for the time histories are consistent with the corresponding site conditions for the response spectral shapes (Section 4).

For CEUS deep (> 300m) soil conditions, the use of corresponding WUS deep soil motions is appropriate because the time histories are intended as inputs to scaling or matching processes. Additionally, deep firm soils (both cohesive and cohesionless) located in the CEUS are not considered to be fundamentally different in dynamic material properties from similar soils located in the WUS. Therefore the CEUS soil motions will be more similar to WUS deep soil motions than corresponding rock motions (Section 6). While the input motions (base of soil and rock outcrop) may be very different between WUS and CEUS conditions, the filtering properties of deep soils significantly reduce the differences. This expectation is strengthened by the observation of possibly similar double corner source spectra in both WUS and CEUS motions that is manifested much more subtly in the WUS due to larger crustal amplification (Section 2).

3.2 Magnitude and Distance Bins for Time Histories

Magnitude and distance bins reflect expected differences in spectral shapes and in time domain characteristics (e.g. duration) that may be of potential significance to engineering analyses. Bin centers and widths control the maximum scaling of records within a bin by a constant factor to adjust for magnitude and distance differences without compensating for changes in spectral shapes. The bin widths also minimize the use of motions with inappropriate time domain characteristics. Continuous scaling approaches would accommodate potential changes in response spectral shapes (Section 3.3; Carballo and Cornell, 1998), particularly for differences in magnitudes (record-to-target) larger than about 1/2 unit in magnitude.

The distance and magnitude bins are listed in Table 3-2. The distance bins are broadly separated into near-source (0 to 10 km fault rupture distance) and beyond (> 10 km). Near-source conditions may

be strongly magnitude (source size) and mechanism dependent and may extend beyond 10 km, particularly for large ($M > 7$) sources. However, the objective here is to capture the overall shorter durations displayed by close-in records and the potential pulse-like low-frequency characteristics of rupture toward a site, both of which are strongly prominent at very small fault distances.

Because duration of shaking may play a significant role in many structural and soil analyses, we apply duration criteria to the magnitude and distance bins. Duration of shaking, expressed as a number of uniform stress cycles, has an influence in the generation of excess pore pressure in soils. This excess pore pressure affects the soil's capacity for failure. The duration definition selected here, which is the time for the cumulative energy (Arias, 1969; Husid, 1969; Dobry et al., 1978) to grow from 5% to 75% of its total value, has been shown to correlate with inelastic structural response for stiff systems (Kennedy et al., 1984). While not being strictly applicable to a duration measure controlling soil deformation, the selected criteria will restrict ranges in time domain characteristics to those that are representative of bin averages.

We use a recently developed empirical relation for WUS strong ground motions to represent the bin average of the 5% to 75% cumulative Arias intensity. The empirical relation is described in Appendix I and is plotted in Figures 3.1 to 3.3 for M 5.5, 6.5, and 7.5, respectively. In the figures, the vertical bars represent ± 1 sigma ranges, with the distance bins (0 to 10 km, 10 to 50 km, 50 to 100 km, 100 to 200 km) spanned by the horizontal dashed lines. Duration ranges for the M and R bins are taken as $\pm 50\%$ (log additions) of the expected median values (solid lines) evaluated at the average (log) bin distance interval (Table 3-2). Liberal duration ranges are considered appropriate because a definitive, causative relationship between strong motion duration and structure and soil response has not yet been quantitatively established. The selected duration criteria for the magnitude and distance bins are represented by the areas enclosed by the dashed lines in Figures 3-1 to 3-3.

To allow a reasonable statistical interpretation of structural and soils analyses, a target number of three-component sets of time histories was set at 15. This number represents a reasonable compromise, allowing the bins to be fully populated with recorded motions (WUS) but not making the bins overly wide in magnitude or distance range. For each of the bins, the numbers of three component recordings are listed in Tables 3-3 and 3-4 for WUS and CEUS respectively, along with bin average magnitudes and distances. The WUS records were selected from the WUS strong motion catalog (Appendix A) by applying the bin criteria and then randomly selecting subsets of 15 (for bins that exceeded 15 three component sets). The duration criteria were applied to the log average duration of the two horizontal components. Since the M 5.5, 0 to 10 km bin was sparsely populated and near-source effects are not considered significant for M 5 to M 6 earthquakes, the 0 to 10 km and 10 to 50 km distance bins were combined into a single 0 to 50 km bin. Also, to provide a bin for assessing the effects of the number of records on the statistical stability of analysis results, the number of three-component sets in the M 6.5, 10 to 50 km rock bin was increased from 15 to 30. For the large-magnitude ($M > 7+$), close distance (0 to 10 km) bin, an effort was made to include sites that recorded both forward and backward directivity. For the soil records, sufficient data are available and the number of sets was increased to 18. Because the magnitude of the 1995 Kobe earthquake is near M 7 (M 6.9), the soil site Takarazuka, at the end of the rupture (maximum directivity), is included in two magnitude bins (M 6 to 7 and M 7+). The large magnitude (M 7+) close distance (0 to 10 km) rock records are dominated by motions obtained during the 1999 Chi Chi earthquake.

To reduce the number of Chi Chi records in this bin and because uncertainty exists regarding site classification, several **M** 6.9 rock site records were added. These include the sites BRN, CLS, and LGPC for the 1989 **M** 6.9 Loma Prieta earthquake, site GAZ for the 1976 **M** 6.8 Gazli earthquake, and sites KBU and KJM for the **M** 6.9 1995 Kobe earthquake. Also, the **M** 6.8 Gazli earthquake is included as both WUS and CEUS. The earthquake was recorded at only one rock site and its horizontal component spectra peak near 10 Hz, so it is considered intermediate between WUS and CEUS rock (Figure 2-8) (Silva and Darragh, 1995).

3.3 WUS to CEUS Scaling

To illustrate the process of scaling the WUS analysis time histories to CEUS conditions, an example is presented for the **M** 6.5, $R = 0$ to 10 km, rock site bin (Table 3-5).

3.3.1 WUS to CEUS Transfer Functions

The WUS to CEUS transfer functions were computed for rock conditions (going from soft rock in the WUS to hard rock in the CEUS, see Figure 2-2) and for deep soil conditions (Silva, 1997), for both horizontal and vertical components of motion. Because of nonlinear site response, the horizontal-component transfer functions are magnitude and distance dependent. A linear site response model (Silva, 1997; EPRI, 1993) was used for vertical components, but the transfer functions still vary with magnitude and distance because of incidence angle variation with both source depth and distance (Tables 2-1 and 2-2 show WUS and CEUS point-source parameters, respectively). For **M** 6.5, an example suite of median transfer functions is shown in Figure 3-4. The transfer functions for rock (both horizontal and vertical) show peaks at high frequency, which are consistent with the expected high frequency peak in CEUS hard rock spectral acceleration. For the horizontal component transfer functions for deep (> 300m) soil sites, Figure 3-4 suggests similar WUS and CEUS response spectra at high loading levels (amplification near unity). Soil nonlinearity evidently masks the differences in frequency content between WUS soft rock and CEUS hard rock control motions (Silva and Darragh, 1995; Silva, 1991). Similar trends are seen in the **M** 5.5 and **M** 7.5 transfer functions, where magnitudes were selected to be equal to the analysis time history bin center magnitudes (Table 3-5). Distances at which the transfer functions were computed (1, 5, 30, 75, and 130 km) span the range of bin mean distances. The transfer function closest to the actual site-to-earthquake rupture distance was used to transform a WUS record to a CEUS record.

3.3.2 Example Case: M 6.5, R = 0 to 10 km, Rock Bin

For this example we selected the north (000) component of the Los Gatos Presentation Center (LGPC) site, which recorded the 1989 **M** 6.9 Loma Prieta earthquake. The site is located at a closest rupture distance of 6.1 km (Appendix A) and reflects WUS rock conditions. The north component acceleration and (processed) velocity and displacement time histories are shown in Figure 3-5, and the response spectra shown in Figure 3-6, for all three components. To scale this recording to CEUS hard rock conditions, the response spectrum is multiplied by the appropriate transfer function (Figure 3-4) to produce a CEUS hard rock target. The original WUS soft rock recording is then used as an input (basis) motion to a weak matching process (1 to 2 iterations). The resulting time history is shown in Figure 3-7, with the scaled CEUS hard rock response spectra shown in Figure 3-8, for all

three components. Comparing the WUS and CEUS time histories in Figures 3-5 and 3-7 respectively, the effects of scaling are mostly apparent in acceleration, dramatically increasing the frequency content and level of motion. The amplitudes and frequency contents of the velocity and displacement time series remain largely unaltered, as most of the amplification is at frequencies exceeding about 3 Hz (Figure 3-4). The scaled response spectra (Figure 3-8) reflect the shift in peaks from about 3 Hz for horizontal components and 10 Hz for the vertical component for WUS soft rock (Figure 3-6) to about 20 Hz and 30 Hz respectively, for CEUS hard rock site conditions. The frequency-to-frequency variation is largely unchanged. The low-frequency (≤ 2 Hz) spectra are essentially unaltered in this process, preserving attributes of near-source records such as differences between fault normal and fault parallel components and the effects of rupture directivity on the average horizontal and vertical components.

Although the low-frequency response spectra remain largely unaffected by the scaling process, high-pass filtering of the scaled records at 0.1 Hz can affect the character of the velocity and displacement time histories. The filters applied to the scaled records consist of causal four-pole Butterworth filters, high-pass at 0.1 Hz and low-pass at 62.5 Hz. The filters are applied to each record and are intended to remove any spurious effects of the scaling and fitting process well outside the general frequency range of interest, 0.5 to 25 Hz. Causal filters are desirable because they minimize the potential effects of distortion due to wraparound of the filter transients. However, there may potentially be undesirable consequences of causal high-pass filters. The character of low-frequency time histories such as velocity and displacement may be altered as a result of the process. Comparing the velocity and displacement time histories for WUS soft rock and CEUS hard rock in Figures 3-5 and 3-7 respectively, differences in characteristics are apparent. Although the amplitudes are nearly the same, the initial peaks have sign reversals in the velocity records, and the largely single-sided WUS displacement time history near 8 sec has become a double sided pulse. While differences in the velocity records are not likely to result in significantly different structural demands at intermediate frequencies, the differences in displacements may be an issue in structural analyses. The double-sided pulse resulting from the causal filters may produce larger demands on long-period structures than the single-sided pulse, because there are more cycles and larger positive-to-negative excursions in displacement. This is only an issue for close-in (near source) short duration records and can be corrected by removing the causal filter and applying an acausal filter. Figure 3-9 illustrates the results of this process and shows both velocity and displacement time histories scaled to CEUS conditions. These records have very similar characteristics to those from the original processing (Figure 3-5). In this case the modulus of the Butterworth filter was applied in the frequency domain. Figure 3-10 compares the response spectra computed from the two time histories, filtered with a causal and with an acausal four-pole Butterworth high-pass filter, showing little difference between the two.

3.4 Matching WUS Time History to CEUS Spectrum

To demonstrate the process of closely matching a WUS motion to a CEUS spectral target, typical 10^{-4} rock UHS are used as targets, and the rock site Ferdows record from the 1978 M 7.4 Tabas earthquake is used as a WUS input motion (bin M 7+, distance 50 to 100 km rock; Table 3-3). The two target spectra are shown Figure 3-11. The spectra illustrate the large differences in WUS and

CEUS spectral amplitudes and shapes, reflecting differences in both hazard environment and in strong motion generation and wave propagation between the two regions.

Figure 3-12 shows the result of matching the WUS record to the WUS UHS, and Figure 3-13 shows the resulting time histories. The fit is acceptably close and the resulting time histories, as expected, are realistic in acceleration as well as integrations to velocity and displacement. Figure 3-14 shows the spectral match for the CEUS. Using the original sample interval of 0.02 sec, with a Nyquist frequency of 25 Hz, results in the low spectral values between 25 and 100 Hz (dashed line in Figure 3-14) and a low peak acceleration of 0.269g (target = 0.298g). Interpolating the record to 200 samples per second results in an improved match beyond 25 Hz and at peak acceleration. The resulting time histories are shown in Figures 3-15 and 3-16 for the two sample intervals (0.02 sec and 0.005 sec). The time histories are nearly identical and are comparable in overall shape to those resulting from the WUS match (Figure 3-13). The comparison of the corresponding Fourier amplitude spectra is shown in Figure 3-17. The result of matching to WUS and CEUS targets largely reflects a broad-band scale factor applied to the Fourier amplitude spectrum of the recorded motion. Decreasing the sample interval actually *lowers* the Fourier amplitude spectrum near 25 Hz as additional energy is available beyond 25 Hz for the higher frequency oscillators. The 25 Hz Fourier amplitude value for the 0.02 sec CEUS spectral match has the largest amplitude of all frequencies, suggesting an aliased record. Although this is not obvious in comparing Figures 3-15 and 3-16, the time history obtained using a higher Nyquist frequency (Figure 3-16) shows overall larger accelerations than the record with a sample interval of 0.02 sec. This may be a consequence of aliasing, however one would normally expect enhanced motions at frequencies below the Nyquist (25 Hz). Overall, these comparisons indicate that WUS motions can be used as inputs to matching CEUS spectra provided the sample interval reflects a Nyquist frequency ($f_N = [2 \Delta t]^{-1}$) of at least 100 Hz. As a corollary, CEUS records could be used as input to matching WUS targets as well.

References

- Arias, A. (1969). "A measure of earthquake intensity." in *Seismic Design for Nuclear Power Plants*, R. Hansen, Editor, Massachusetts Institute of Technology Press, Cambridge.
- Atkinson, G.M. and Boore, D.M. (1998). "Evaluation of models for earthquake source spectra in Eastern North America." *Bull. Seism. Soc. Am.* 88(4), 917-934.
- Atkinson, G.M. (1995). "Attenuation and source parameters of earthquakes in the Cascadia Region." *Bull. Seism. Soc. Am.*, 85(5), 1327-1342.
- Carballo, J.E. and A. Cornell (1998). "Input to nonlinear structural analysis: modification of available accelerograms for different source and site characteristics." *Proceedings, 6th U.S. Nat'l Conference on Earthquake Engineering*, Seattle, Washington.
- Dobry, I. M., I. M. Idriss and E. Ng. (1978). "Duration characteristics of horizontal components of strong motion earthquake records." *Bull. Seis. Soc. Amer.*, 68(5), 1487-1520.

- Electric Power Research Institute (1993). "Guidelines for determining design basis ground motions." Electric Power Research Institute, Palo Alto, CA, Rept. TR-102293, vol. 1-5:
vol. 1: Methodology and guidelines for estimating earthquake ground motion in eastern North America.
vol. 2: Appendices for ground motion estimation.
vol. 3: Appendices for field investigations.
vol. 4: Appendices for laboratory investigations.
vol. 5: Quantification of seismic source effects.
- Husid, R. L. (1969). "Análisis de terremotos." Analisis General, Revista del IDIEM, 8, 21-42, Santiago, Chile.
- Kennedy, R.P., Short, S.A., Merz, K.L., Tokarz, F.J., Idriss, I.M., Power, M.S, and Sadigh, K. (1984). "Engineering characterization of ground motion, Task I: Effects of characteristics of free-field motion on structural response." U.S. Nuclear Regulatory Commission. NUREG/CR-3805, vol. 1.
- Silva, W.J. (1997). "Characteristics of vertical Strong ground motions for applications to engineering design." Proc. Of the FHWA/NCEER Workshop on the Nat'l Representation of Seismic, I.M. Friedland, M.S Power and R. L. Mayes eds., Technical Report NCEER-97-0010.
- Silva, W.J., N. Abrahamson, G. Toro, C. Costantino (1997). "Description and validation of the stochastic ground motion model." Report to Brookhaven National Laboratory, Associated Universities, Inc. Upton, New York, Contract 770573.
- Silva, W.J. and R. Darragh (1995). "Engineering characterization of earthquake strong ground motion recorded at rock sites." Electric Power Research Institute, Palo Alto, CA, Rept. TR-102261.
- Silva, W.J. (1991). "Global characteristics and site geometry." Proceedings: NSF/EPRI Workshop on Dynamic Soil Properties and Site Characterization. Electric Power Res. Inst., EPRI NP-7337.
- Silva, W.J., Lee, K. (1987) "*WES RASCAL code for synthesizing earthquake ground motions*" State-of-the-Art for Assessing Earthquake Hazards in the United States, Report 24, U.S. Army Engineers Waterways Experiment Station, Misc. Paper S-73-1.

Table 3-1

GEOTECHNICAL SUBSURFACE CHARACTERISTICS

- A = Rock. Instrument on rock ($V_s > 600$ mps) or < 5 m of soil over rock.
- B = Shallow (stiff) soil. Instrument on/in soil profile up to 20m thick overlying rock.
- C = Deep narrow soil. Instrument on/in soil profile at least 20m thick overlying rock, in a narrow canyon or valley no more than several km wide.
- D = Deep broad soil. Instrument on/in soil profile at least 20m thick overlying rock, in a broad valley.
- E = Soft deep soil. Instrument on/in deep soil profile with average $V_s < 150$ mps.

Table 3-2
MAGNITUDE AND DISTANCE BINS AND DURATION CRITERIA

M	R (km)	Duration (sec)**	
		Rock	Soil
5.5 (5 - 6)	0 - 50*	1.1 - 3.6*	1.6 - 4.8*
	50 - 100	3.6 - 8.2	2.9 - 6.4
6.5 (6 - 7)	0 - 10	2.6 - 5.8	3.1 - 7.0
	10 - 50	3.1 - 7.0	3.6 - 8.2
	50 - 100	5.1 - 11.6	5.7 - 12.8
	100 - 200	8.1 - 18.3	8.7 - 19.5
	200 - 400***		
7.5 (7+)	0 - 10	6.1 - 13.8	6.6 - 15.0
	10 - 50	6.6 - 14.0	7.2 - 16.1
	50 - 100	8.7 - 19.5	12.2 - 27.5
	100 - 200	11.7 - 26.3	16.2 - 36.5
	200 - 400***		

*For M 5.5 bin, too few records were available for 0-10 km, so distance bins 0-10 km and 10-50 km were combined to 0-50 km

**5% - 75% total cumulative Arias Intensity

***CEUS only

Table 3-3
WUS TIME HISTORY BINS

M	\bar{M}	R (km)	\bar{R} (km)	Number of sets
5 - 6, rock	5.50	0 - 50	17.29	15
	6.00	50 - 100	64.88	15
5 - 6, soil	5.77	0 - 50	16.97	15
	5.75	50 - 100	64.38	15
6 - 7, rock	6.53	0 - 10	6.00	15
	6.39	10 - 50	31.29	30
	6.38	50 - 100	66.12	15
	6.66	100 - 200	89.03	15
6 - 7, soil	6.58	0 - 10	5.74	18
	6.41	10 - 50	27.83	15
	6.57	50 - 100	67.10	15
	6.64	100 - 200	131.53	15
7+, rock	7.25	0 - 10	5.83	15
	7.38	10 - 50	31.48	15
	7.49	50 - 100	76.88	15
	7.49	100 - 200	135.03	15
7+, soil	7.40	0 - 10	4.62	21
	7.47	10 - 50	29.60	15
	7.53	50 - 100	68.79	15
	7.44	100 - 200	134.73	15

Table 3-4
CEUS TIME HISTORY BINS

M	\bar{M}	R (km)	\bar{R} (km)	Number of sets**
4.5* - 6, rock	5.50	0 - 50	17.29	0 (15)
	5.85	50 - 100	78.34	8 (7)
4.5* - 6, soil	5.69	0 - 50	18.81	1 (14)
	5.66	50 - 100	64.99	2 (13)
6 - 7, rock	6.53	0 - 10	6.18	2 (14)
	6.32	10 - 50	28.58	1 (14)
	6.38	50 - 100	66.12	0 (15)
	6.66	100 - 200	89.03	0 (15)
6 - 7, soil	6.58	0 - 10	5.74	0 (18)
	6.41	10 - 50	27.83	0 (15)
	6.57	50 - 100	67.10	0 (15)
	6.64	100 - 200	131.53	0 (15)
7+, rock	7.25	0 - 10	5.83	0 (15)
	7.38	10 - 50	31.48	0 (15)
	7.49	50 - 100	76.88	0 (15)
	7.49	100 - 200	135.03	0 (15)
7+, soil	7.40	0 - 10	4.62	0 (21)
	7.47	10 - 50	29.60	0 (15)
	7.53	50 - 100	68.79	0 (15)
	7.44	100 - 200	134.73	0 (15)

*M range extended to M 4.5

**Supplemented with WUS to CEUS scaled records, first number reflects number of actual CEUS recordings, parentheses show number of scaled WUS to CEUS three component sets.

Table 3-5
WUS ANALYSIS TIME HISTORY STATISTICS

	<u>Magnitude Bins (M)</u>		Number of sets					
	<u>Range</u>			<u>Bin Center</u>				
	5 - 6						5.5	
	6 - 7						6.5	
	7+						7.5	
Distance bin (km)	\bar{M}	\bar{R} (km)		PGA*(g), σ_{ln}	PGV*(cm/sec), σ_{ln}	PGD*(cm), σ_{ln}	$\frac{PGV^*}{PGA} \left(\frac{cm/sec}{g} \right)$, σ_{ln}	$\frac{PGA \cdot PGD^*}{PGV^2}$, σ_{ln}
0 - 10, rock	6.53	6.00	15	0.46, 0.64	36.63, 0.74	7.63, 0.89	79.35, 0.35	2.57, 0.41
	7.25	5.83	15	0.39, 0.73	53.74, 0.73	22.86, 0.65	138.42, 0.58	3.01, 0.52
0 - 10, soil	6.58	5.74	18	0.41, 0.46	54.65, 0.51	19.61, 0.65	132.40, 0.43	2.66, 0.40
	7.40	4.62	21	0.34, 0.50	69.89, 0.44	50.15, 0.70	205.72, 0.44	3.42, 0.42
10 - 50, rock	6.39	31.29	30	0.11, 0.70	7.40, 0.79	1.61, 1.22	68.62, 0.52	3.11, 0.53
	7.38	31.48	15	0.15, 0.90	17.88, 0.88	9.27, 1.37	115.67, 0.68	4.40, 0.58
10 - 50, soil	6.41	27.83	15	0.14, 0.64	10.37, 0.73	2.46, 1.20	71.79, 0.33	3.24, 0.50
	7.47	29.60	15	0.16, 0.58	27.48, 0.74	18.28, 0.78	172.30, 0.27	3.79, 0.51
50 - 100, rock	6.00	64.88	15	0.05, 0.38	2.27, 0.55	0.23, 0.83	42.01, 0.44	2.37, 0.58
	6.38	66.12	15	0.04, 0.54	2.75, 0.61	0.51, 1.02	69.38, 0.41	2.64, 0.51
	7.49	76.88	15	0.06, 0.37	7.18, 0.57	5.68, 0.96	119.02, 0.46	6.52, 0.36
50 - 100, soil	5.75	64.38	15	0.06, 0.78	3.22, 0.70	0.36, 0.87	50.33, 0.22	2.20, 0.40
	6.57	67.10	15	0.06, 0.57	5.72, 0.60	1.33, 0.75	93.72, 0.39	2.44, 0.62
	7.53	68.79	15	0.07, 0.53	12.15, 0.52	7.33, 0.88	178.14, 0.49	3.32, 0.46
100 - 200, rock	6.66	89.03	15	0.03, 0.87	2.86, 0.55	1.05, 0.63	101.82, 0.54	3.55, 0.38

*Median values

Table 3-5 (cont.)

WUS ANALYSIS TIME HISTORY STATISTICS

Magnitude Bins (M)								
Range			Bin Center					
5 - 6			5.5					
6 - 7			6.5					
7+			7.5					
Distance bin (km)	\bar{M}	\bar{R} (km)	Number of sets	PGA*(g), σ_{in}	PGV*(cm/sec), σ_{in}	PGD*(cm), σ_{in}	$\frac{PGV^*}{PGA} \left(\frac{cm/sec}{g} \right)$, σ_{in}	$\frac{PGA \cdot PGD^*}{PGV^2}$, σ_{in}
100 - 200, rock	7.49	135.03	15	0.03, 0.34	5.78, 0.64	3.83, 1.05	177.22, 0.48	3.67, 0.61
100 - 200, soil	6.64	131.53	15	0.03, 0.78	3.22, 0.59	0.92, 0.94	97.91, 0.51	2.86, 0.41
	7.44	134.73	15	0.05, 0.39	7.75, 0.40	4.91, 0.55	166.48, 0.26	3.73, 0.61
0 - 50, rock	5.50	17.29	15	0.16, 0.92	7.52, 0.99	0.76, 1.28	45.92, 0.41	2.17, 0.33
0 - 50, soil	5.77	16.97	15	0.20, 0.43	10.83, 0.54	1.31, 0.79	53.32, 0.26	2.22, 0.25

*Median values

Table 3-6

CEUS ANALYSIS TIME HISTORY STATISTICS

Magnitude Bins (M)									
Range				Bin Center					
5 - 6				5.5					
6 - 7				6.5					
7+				7.5					
Distance bin (km)	\bar{M}	\bar{R} (km)	Number of sets	PGA*(g), σ_{ln}	PGV* (cm/sec), σ_{ln}	PGD*(cm), σ_{ln}	$\frac{PGV^*}{PGA} \left(\frac{cm/sec}{g} \right)$, σ_{ln}	$\frac{PGA \cdot PGD^*}{PGV^2}$, σ_{ln}	
0 - 10, rock	6.53	6.18	2 (14)	1.16, 0.66	39.74, 0.66	7.84, 0.94	34.37, 0.42	5.63, 0.45	
	7.25	5.83	0 (15)	0.89, 0.90	58.40, 0.40	22.33, 0.57	65.84, 0.67	5.70, 0.45	
0 - 10, soil	6.58	5.74	0 (18)	0.61, 0.44	59.36, 0.49	18.56, 0.62	97.46, 0.36	3.15, 0.34	
	7.40	4.62	0 (21)	0.38, 0.54	59.38, 0.42	31.90, 0.59	156.54, 0.39	3.36, 0.36	
10 - 50, rock	6.32	28.58	1 (14)	0.25, 0.78	7.95, 0.62	1.70, 0.99	31.75, 0.51	6.58, 0.70	
	7.38	31.48	0 (15)	0.34, 0.94	19.85, 0.83	9.17, 1.14	58.24, 0.72	7.78, 0.63	
10 - 50, soil	6.41	27.83	0 (15)	0.30, 0.61	15.33, 0.74	2.83, 1.08	51.74, 0.35	3.49, 0.47	
	7.47	29.60	0 (15)	0.23, 0.57	29.58, 0.72	13.86, 0.98	128.74, 0.27	3.57, 0.35	
50 - 100, rock	5.85	78.34	8 (7)	0.06, 1.41	1.24, 1.40	0.10, 1.57	21.28, 0.36	3.61, 0.50	
	6.38	66.12	0 (15)	0.09, 0.55	2.99, 0.53	0.46, 0.83	32.59, 0.33	4.66, 0.52	
	7.49	76.88	0 (15)	0.15, 0.49	7.33, 0.50	3.98, 0.76	50.29, 0.56	10.60, 0.46	
50 - 100, soil	5.66	64.99	2 (13)	0.13, 1.20	4.74, 0.85	0.31, 1.35	37.05, 0.52	1.72, 1.18	
	6.57	67.10	0 (15)	0.15, 0.59	8.35, 0.58	1.43, 0.65	56.04, 0.36	3.01, 0.48	

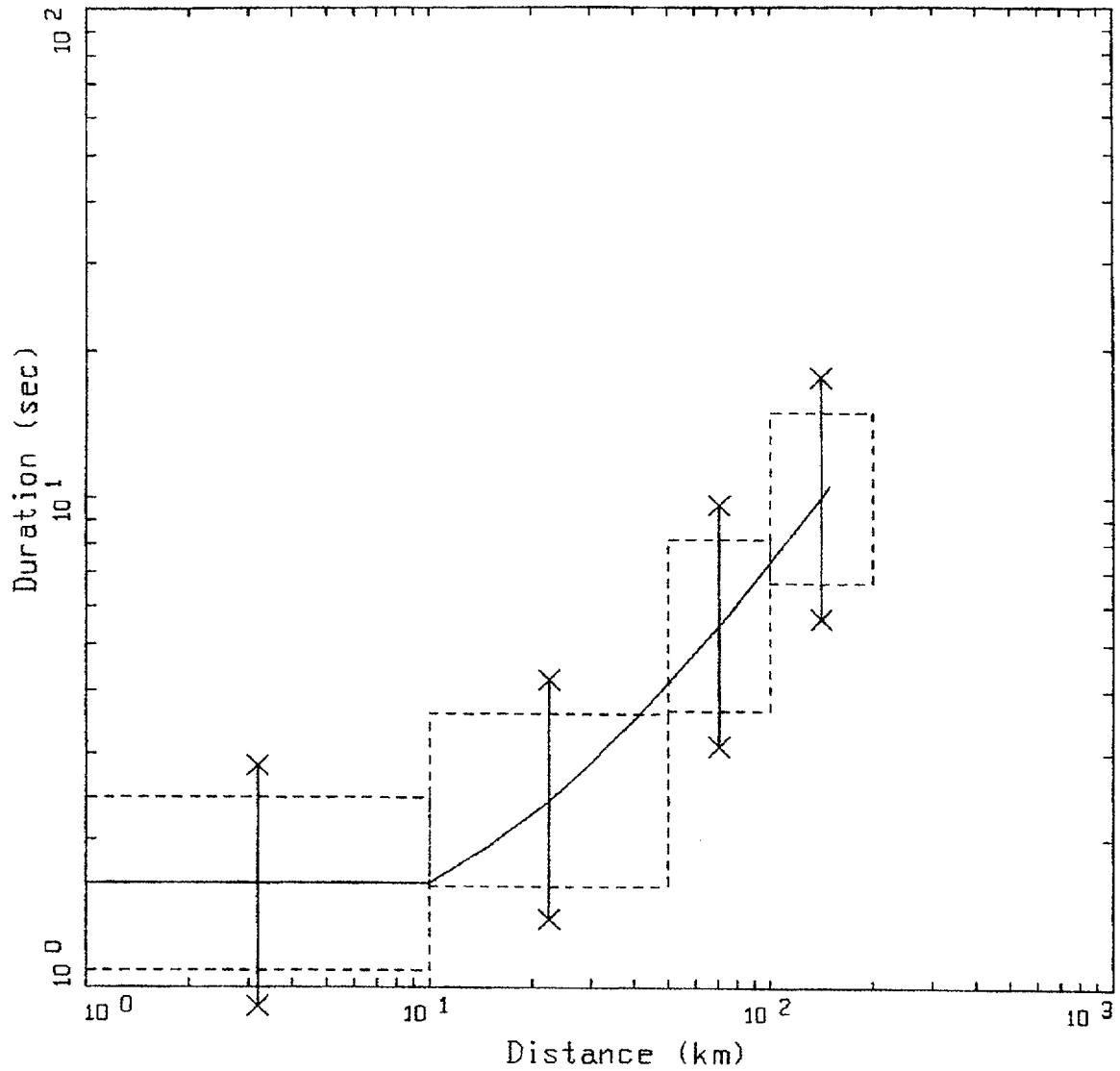
*Median values

Table 3-6 (cont.)

CEUS ANALYSIS TIME HISTORY STATISTICS

Magnitude Bins (M)								
<u>Range</u>				<u>Bin Center</u>				
5 - 6				5.5				
6 - 7				6.5				
7+				7.5				
Distance bin (km)	\bar{M}	\bar{R} (km)	Number of sets	PGA*(g), σ_{ln}	PGV*(cm/sec), σ_{ln}	PGD*(cm), σ_{ln}	$\frac{PGV^*}{PGA} \left(\frac{cm/sec}{g} \right)$, σ_{ln}	$\frac{PGA \cdot PGD^*}{PGV^2}$, σ_{ln}
50 - 100, soil	7.53	68.79	0 (15)	0.12, 0.55	14.41, 0.47	5.54, 0.72	124.27, 0.47	3.03, 0.42
100 - 200, rock	6.66	89.03	0 (15)	0.08, 0.95	3.23, 0.65	0.85, 0.44	41.14, 0.47	6.29, 0.49
	7.49	135.03	0 (15)	0.09, 0.32	6.85, 0.56	3.08, 0.86	72.50, 0.47	6.07, 0.39
100 - 200, soil	6.64	131.53	0 (15)	0.10, 0.80	5.56, 0.66	0.96, 0.70	56.53, 0.40	2.98, 0.45
	7.44	134.73	0 (15)	0.11, 0.43	9.60, 0.44	3.77, 0.42	91.20, 0.37	4.22, 0.56
0 - 50, rock	5.50	17.29	0 (15)	0.29, 0.96	7.24, 0.93	0.59, 1.16	24.86, 0.41	3.20, 0.27
0 - 50, soil	5.69	18.81	1 (14)	0.31, 1.09	11.12, 1.21	1.01, 1.37	36.31, 0.27	2.46, 0.34

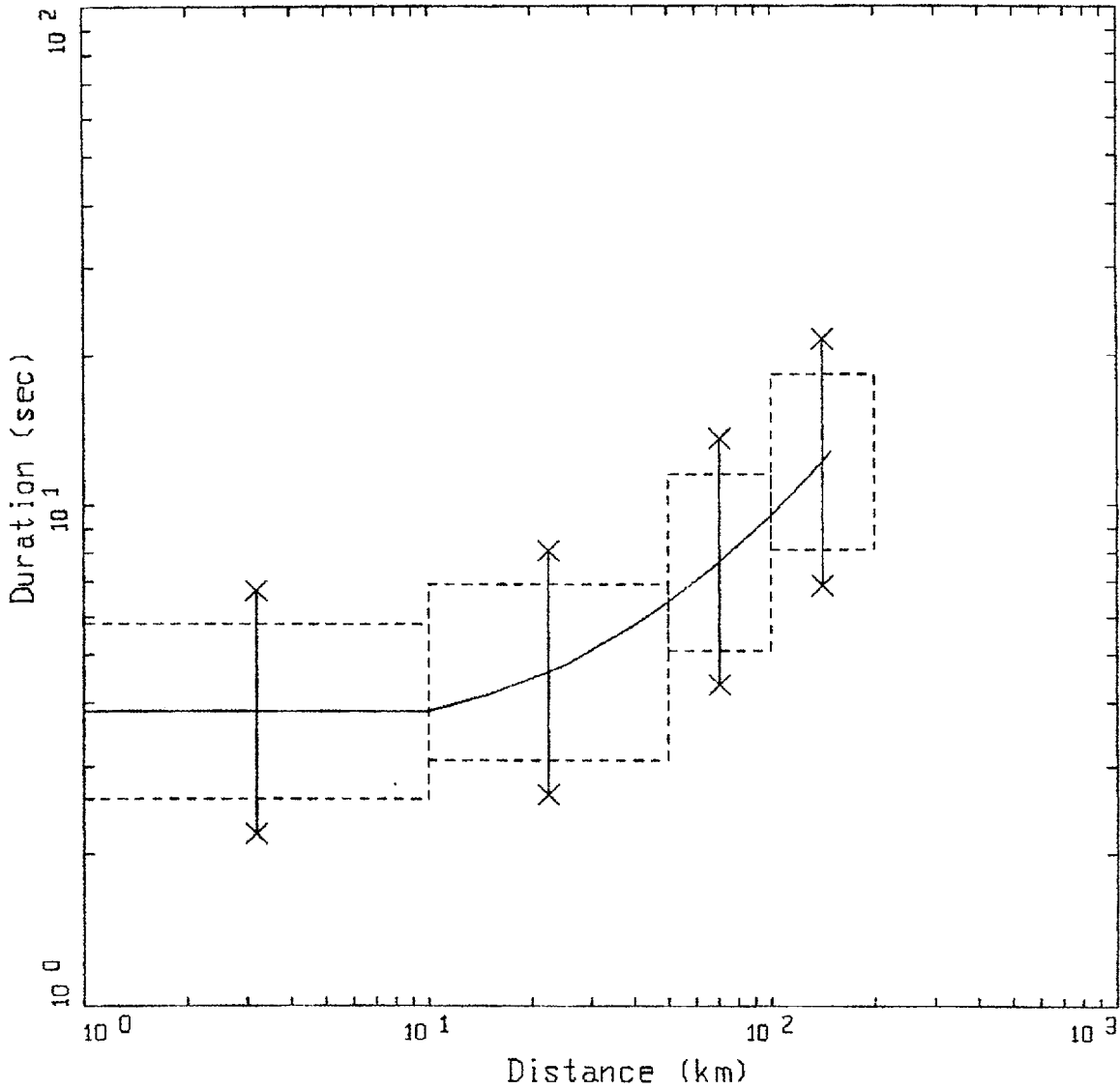
*Median values



5-75% DURATION
 ROCK SITE CONDITIONS, HORIZONTAL, M5.5

LEGEND
 ——— 5-75% DURATION, HORIZONTAL, N=5.5

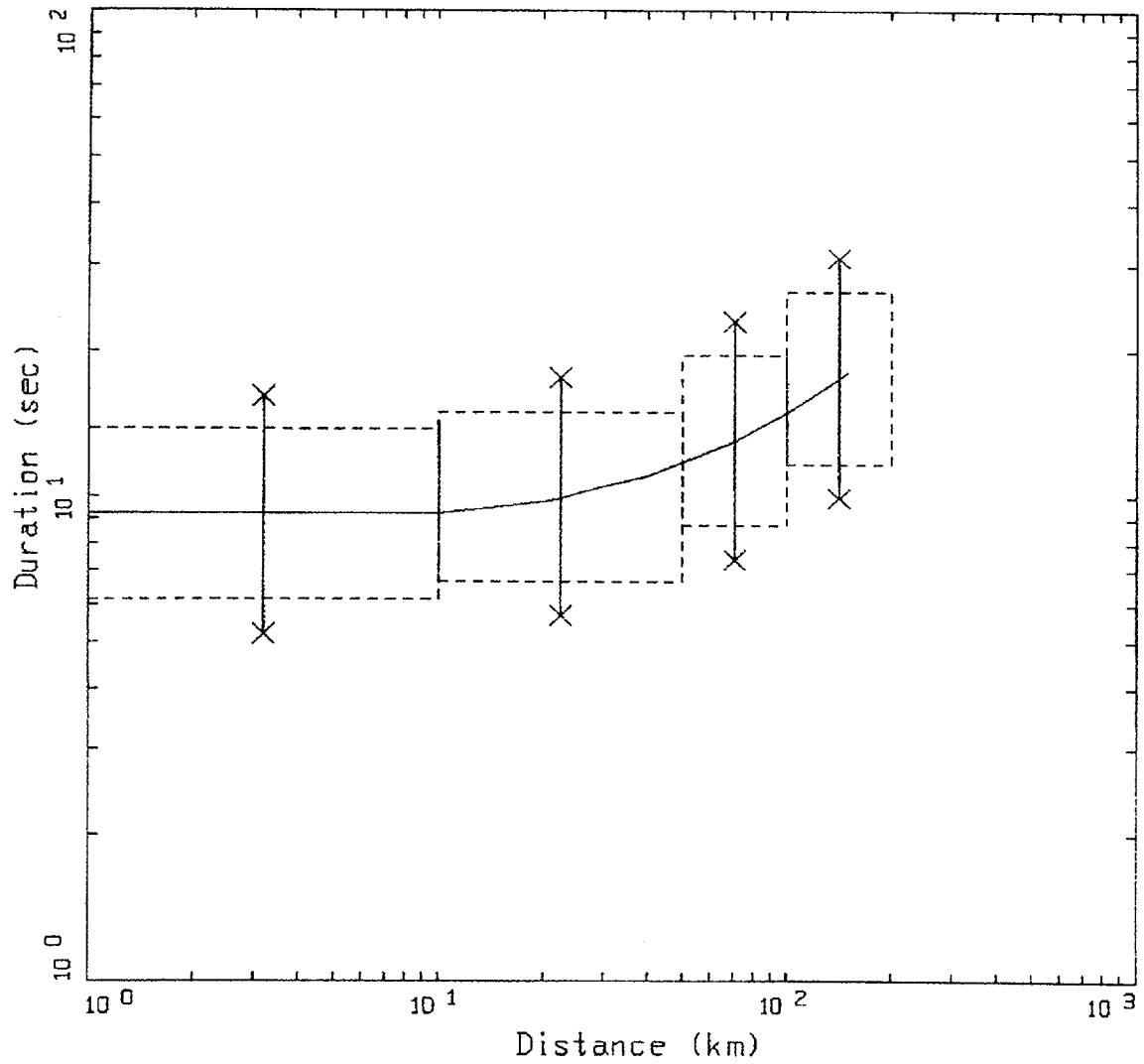
Figure 3-1. Example of duration bin criteria for M 5.5 bin and rock site conditions. Solid line is WUS empirical relation for 5 to 75% Arias Intensity (Appendix I) and X's reflect $\pm 1\sigma$ fractiles. Boxes represent $\pm 50\%$ duration bin (horizontal dashes) and distance bins: 0 to 10 km, 10 to 50 km, 50 to 100 km, 100 to 200 km (vertical dashes).



5-75% DURATION
 ROCK SITE CONDITIONS, HORIZONTAL, M6.5

LEGEND
 ——— 5-75% DURATION, HORIZONTAL, N=6.5

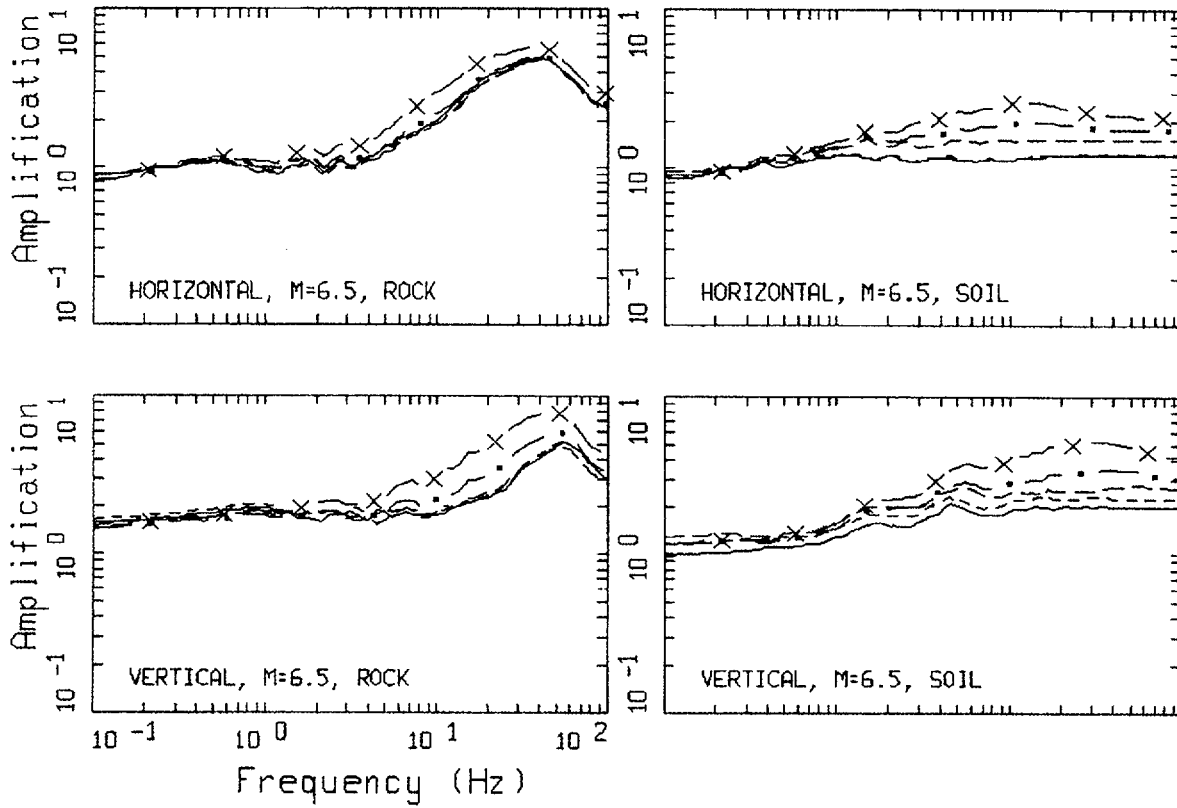
Figure 3-2. Example of duration bin criteria for M 6.5 bin and rock site conditions. Solid line is WUS empirical relation for 5 to 75% Arias Intensity (Appendix I) and X's reflect $\pm 1\sigma$ fractiles. Boxes represent $\pm 50\%$ duration bin (horizontal dashes) and distance bins: 0 to 10 km, 10 to 50 km, 50 to 100 km, 100 to 200 km, (vertical dashes).



5-75% DURATION
 ROCK SITE CONDITIONS, HORIZONTAL, M7.5

LEGEND
 ——— 5-75% DURATION, HORIZONTAL, M=7.5

Figure 3-3. Example of duration bin criteria for **M** 7.5 bin and rock site conditions. Solid line is WUS empirical relation for 5 to 75% Arias Intensity (Appendix I) and X's reflect $\pm 1\sigma$ fractiles. Boxes represent $\pm 50\%$ duration bin (horizontal dashes) and distance bins: 0 to 10 km, 10 to 50 km, 50 to 100 km, 100 to 200 km (vertical dashes).



WUS TO CEUS TRANSFER FUNCTIONS
FOR 5% DAMPING RESPONSE SPECTRA

LEGEND	
————	D = 1 KM
-----	D = 5 KM
- · - · -	D = 30 KM
— · —	D = 75 KM
— x —	D = 130 KM

Figure 3-4. Example of rock and deep soil WUS-to-CEUS transfer functions (5% damped response spectra) computed for $M = 6.5$ and a suite of distances.

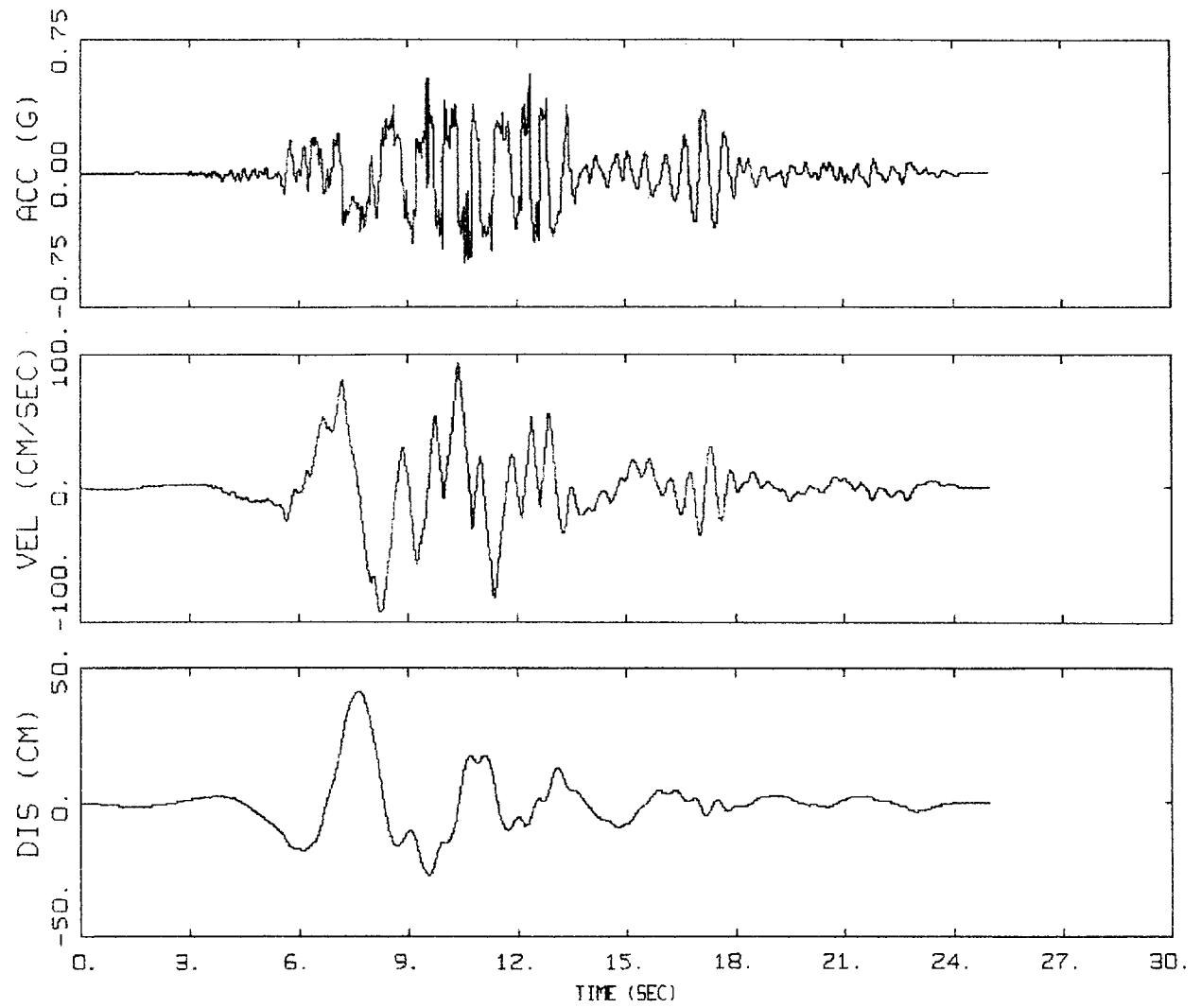
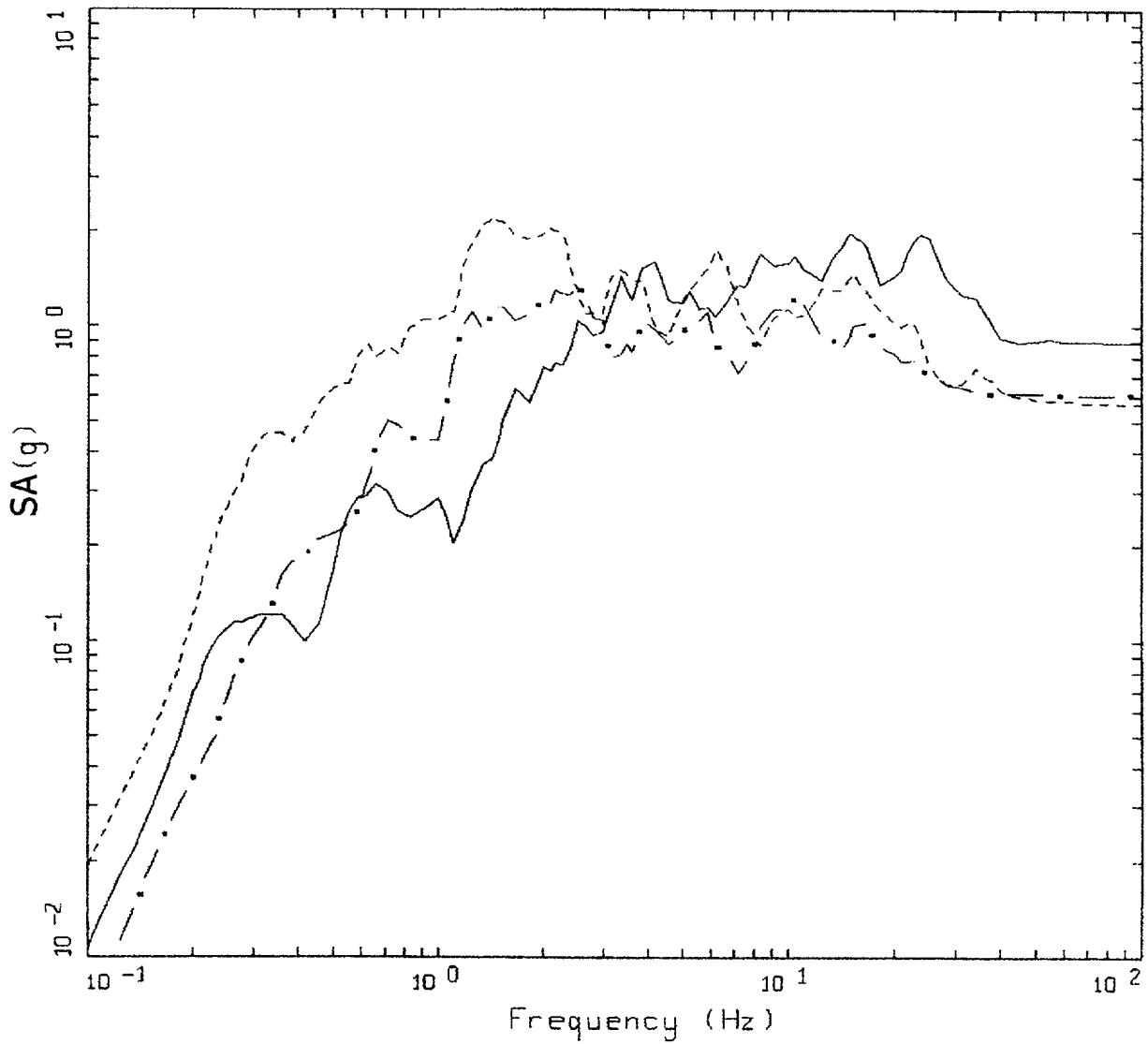


Figure 3-5. Acceleration, velocity, and displacement time histories from the 1989 M Loma Prieta earthquake recorded at the Los Gatos Presentation Center site (component 000), rupture distance of 6.1 km.



LOMA PRIETA EARTHQUAKE

- LEGEND
- 5 %, LGPC, COMP VERT
 - - - 5 %, LGPC, COMP 000
 - . - 5 %, LGPC, COMP 090

Figure 3-6. Response spectra (5% damping) for the motions recorded at site LGPC from the 1989 M 6.9 Loma Prieta earthquake.

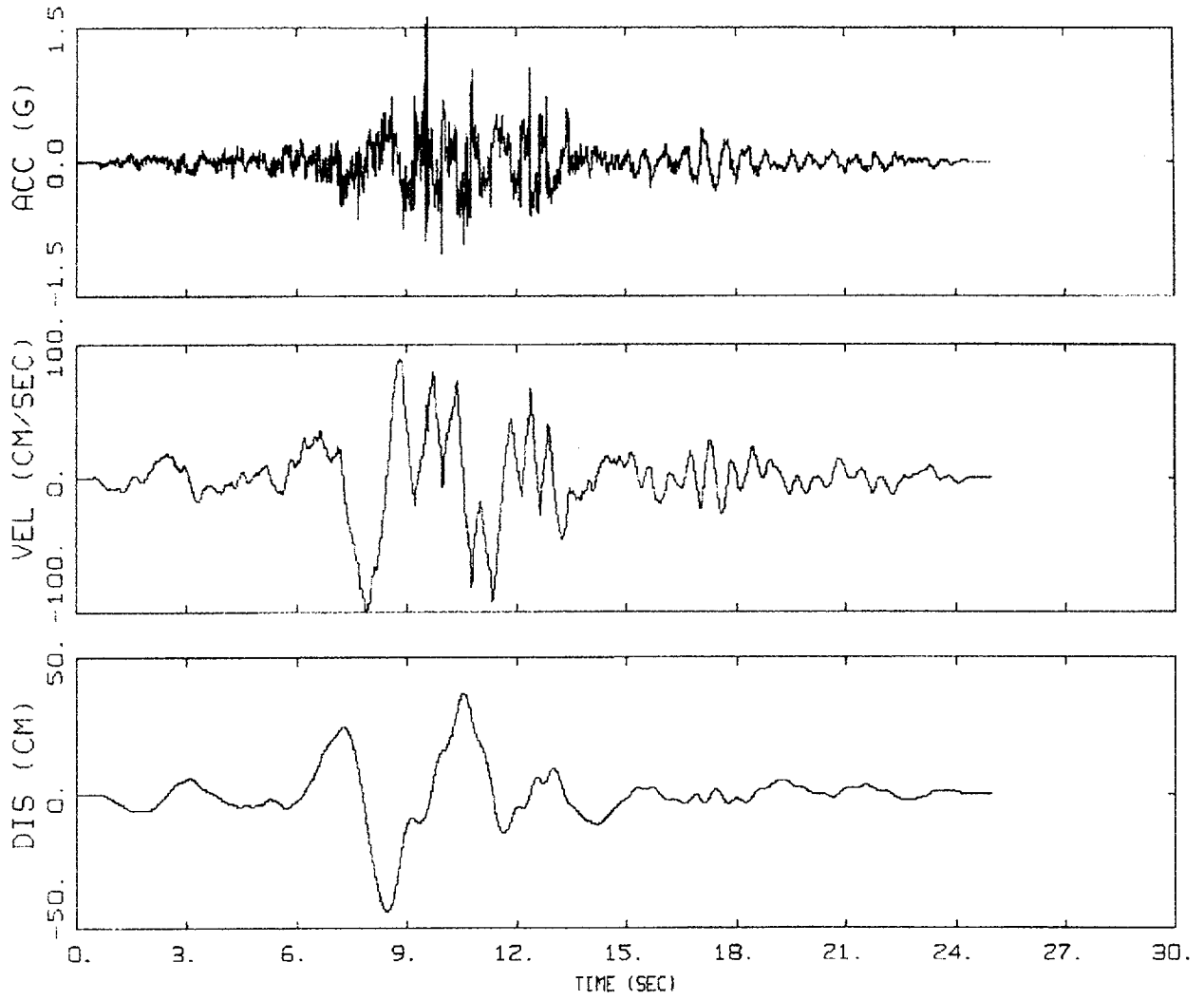
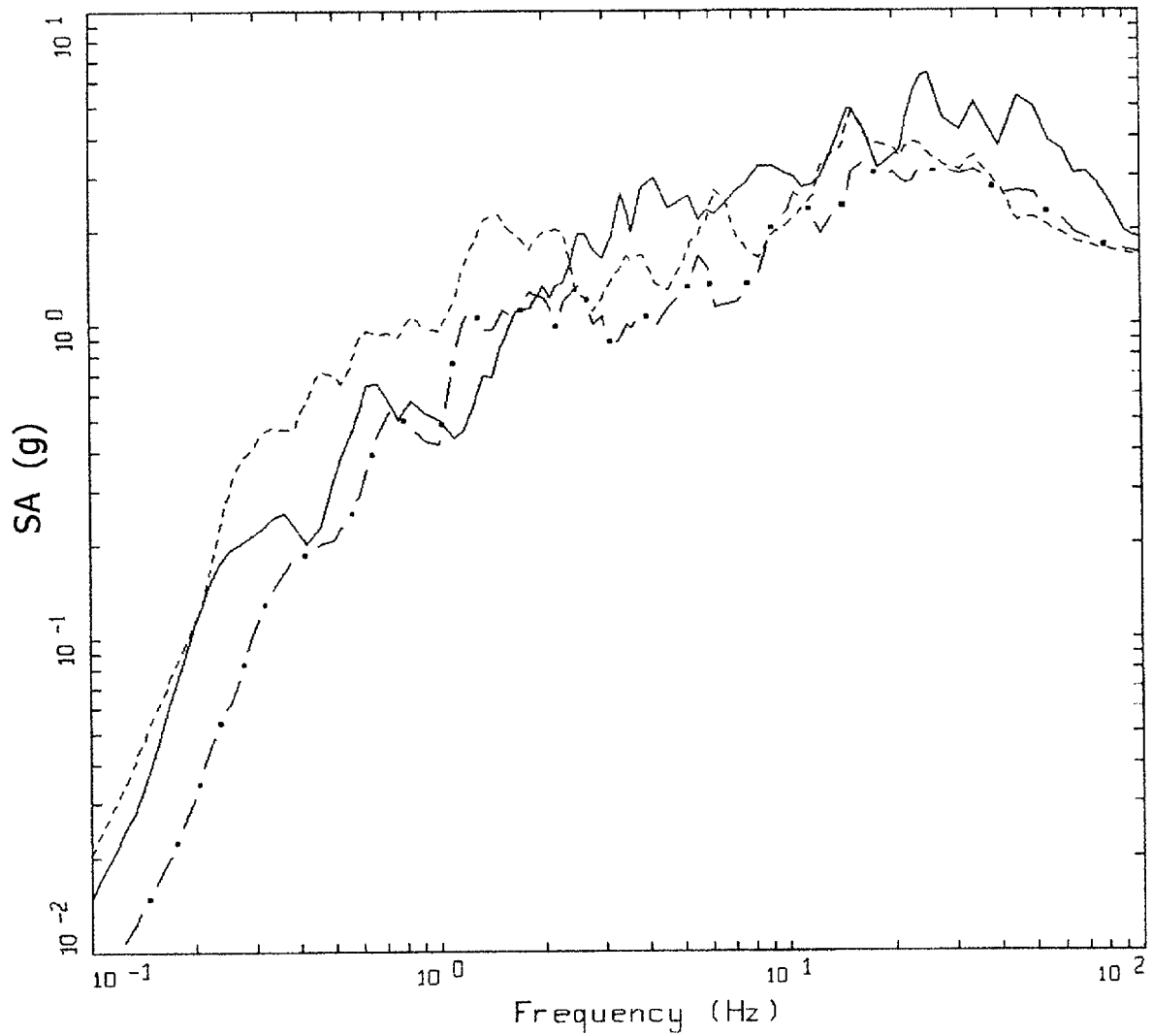


Figure 3-7. Acceleration, velocity, and displacement time histories from the 1989 M 6.9 Loma Prieta earthquake (Figure 3-5) scaled to CEUS hard rock site conditions.



CEUS ROCK

- LEGEND
- 5 %, LGPC, COMP VERT
 - - - 5 %, LGPC, COMP 000
 - . - 5 %, LGPC, COMP 090

Figure 3-8. Response spectra (5% damping) for the recorded motions from the 1989 M 6.9 Loma Prieta earthquake (Figure 3-7) scaled to CEUS hard rock conditions.

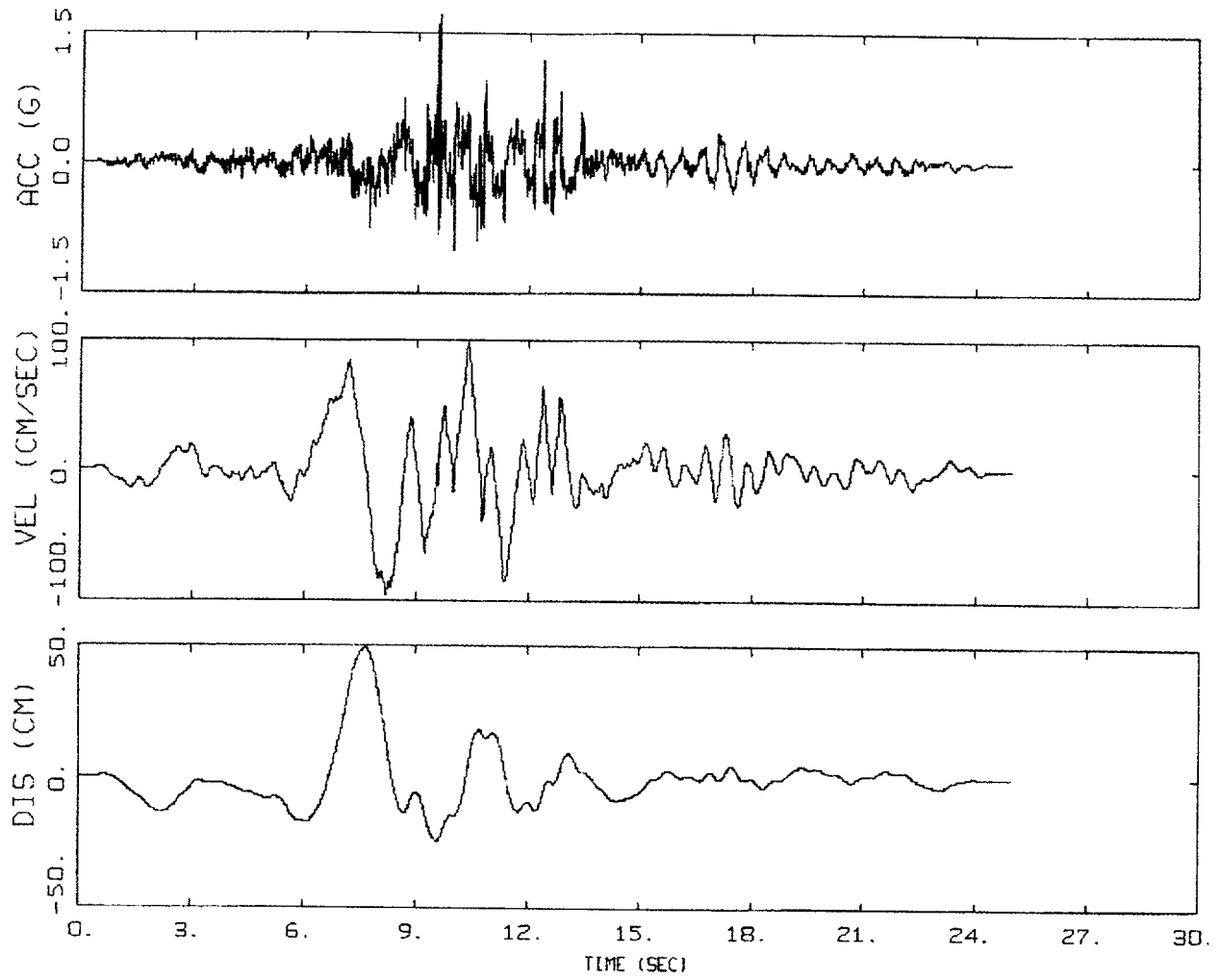
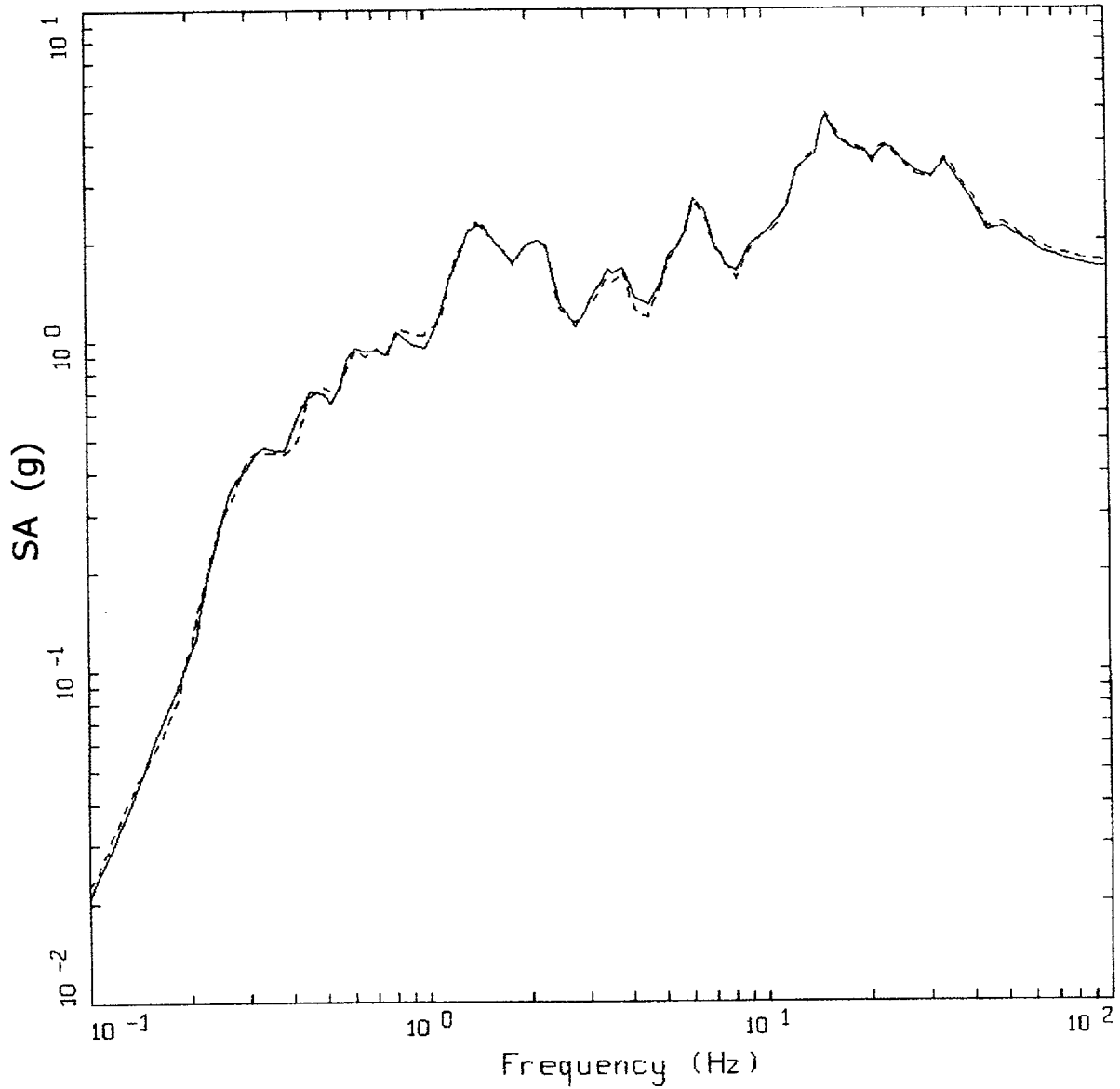


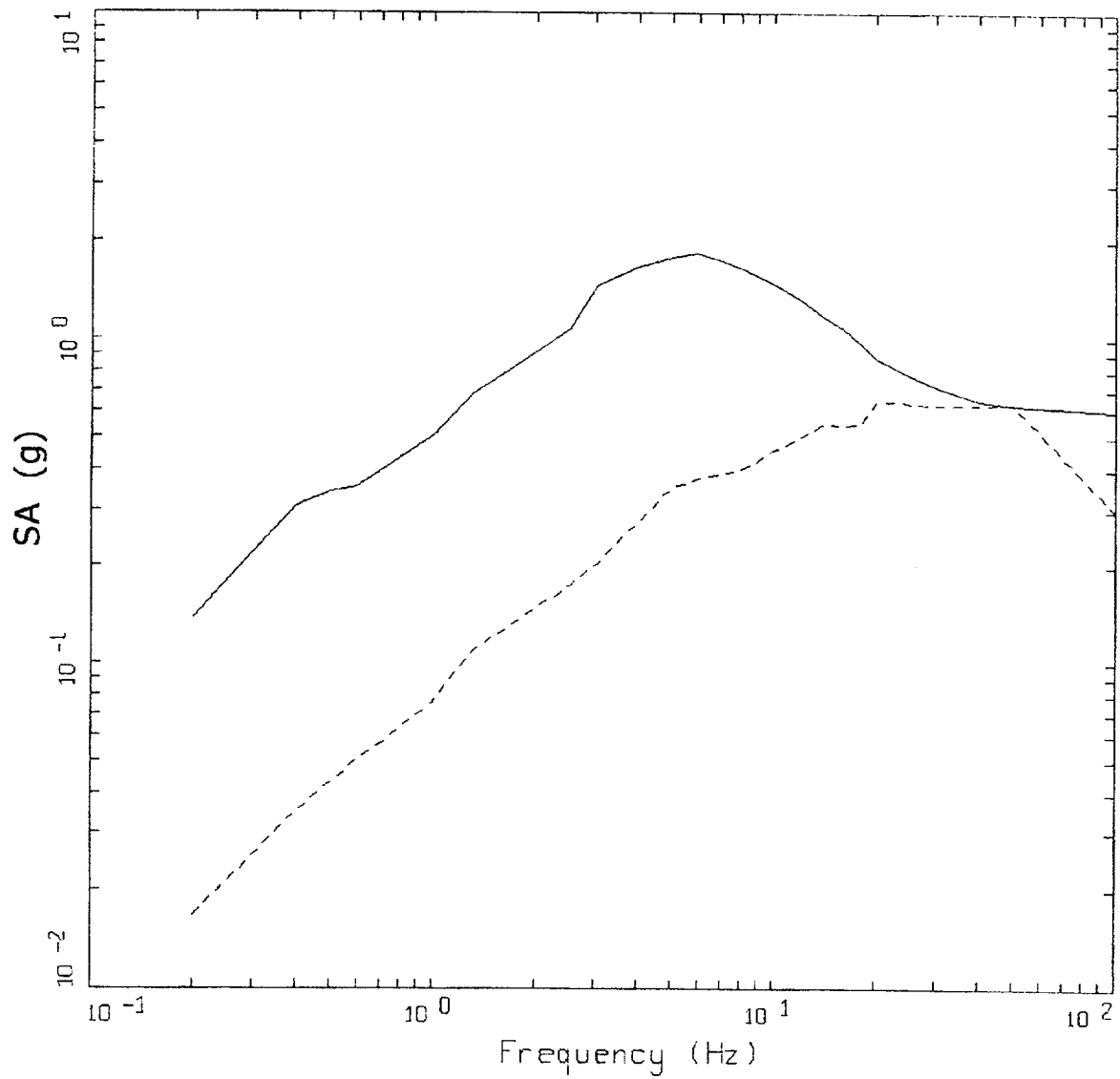
Figure 3-9. Acceleration, velocity, and displacement time histories from the 1989 M 6.9 Loma Prieta earthquake (Figure 3-5) scaled to CEUS hard rock site conditions, acausal high-pass filter.



CEUS ROCK

- LEGEND
- 5 %, LGPC, COMP ODD, CAUSAL FILTER
 - - - 5 %, LGPC, COMP ODD, ACAUSAL FILTER

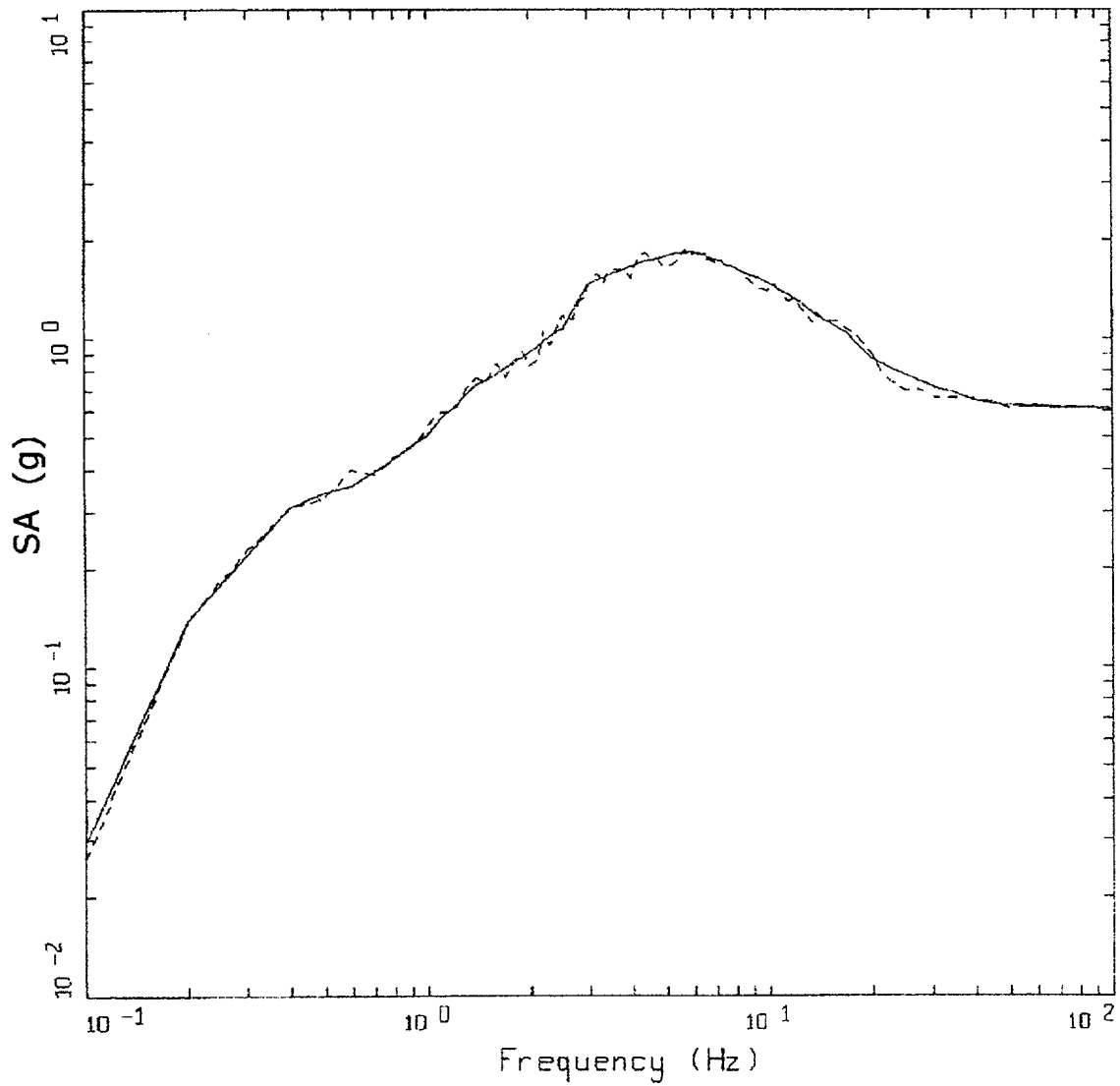
Figure 3-10. Comparison of 5% damped response spectra computed from scaled CEUS records to causal and acausal high-pass filters with 0.1 Hz corner frequencies. Corresponding time histories are shown in Figures 3-7 and 3-9 respectively.



ROCK OUTCROP UHS SPECTRA

- LEGEND
- WUS ROCK UNIFORM HAZARD SPECTRA, PGA=0.6104 g
 - - - CEUS ROCK UNIFORM HAZARD SPECTRA, PGA=0.2984 g

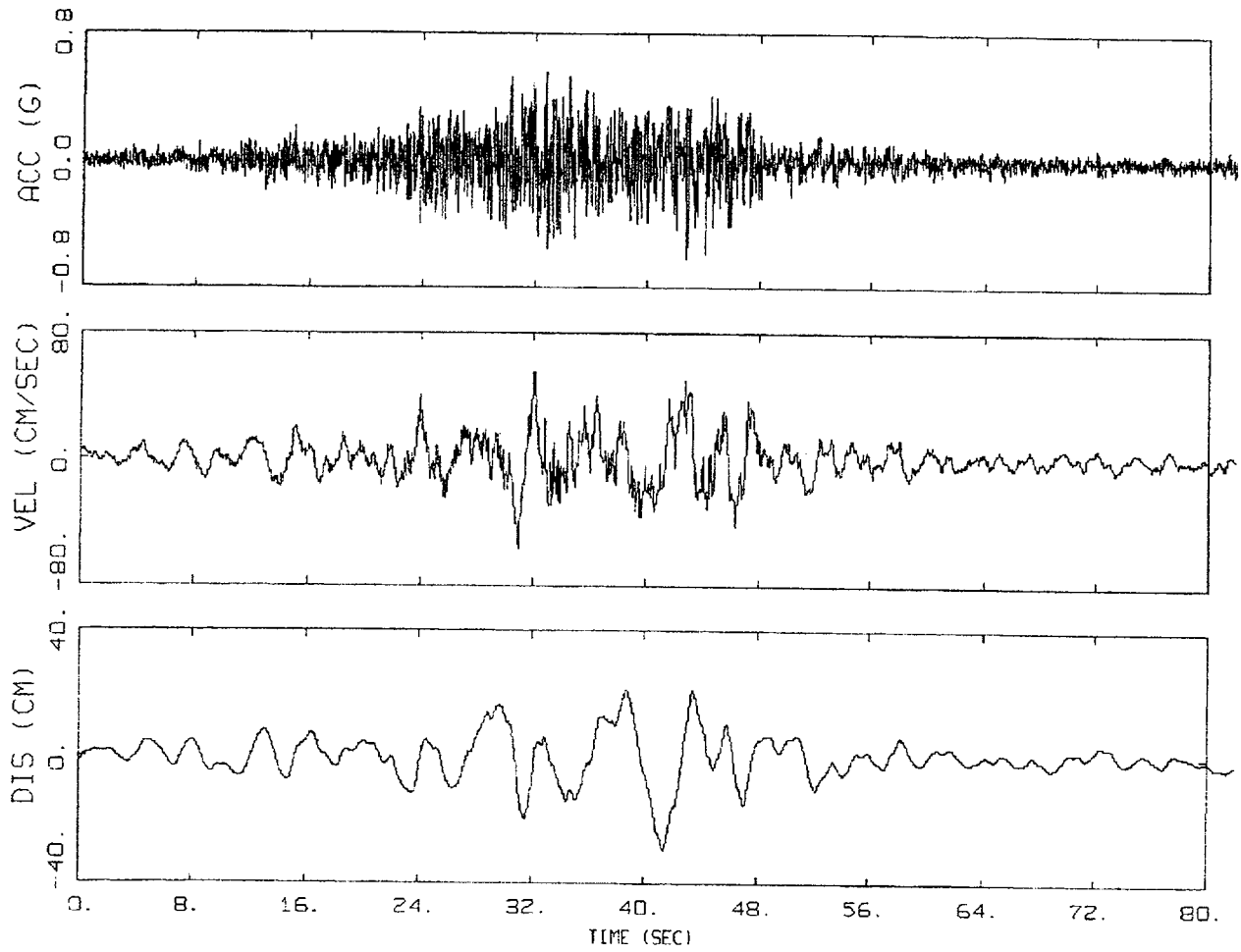
Figure 3-11. Comparison of 5% damped rock outcrop UHS spectra for CEUS and WUS conditions.



WUS SPECTRAL MATCH
10-4, ROCK

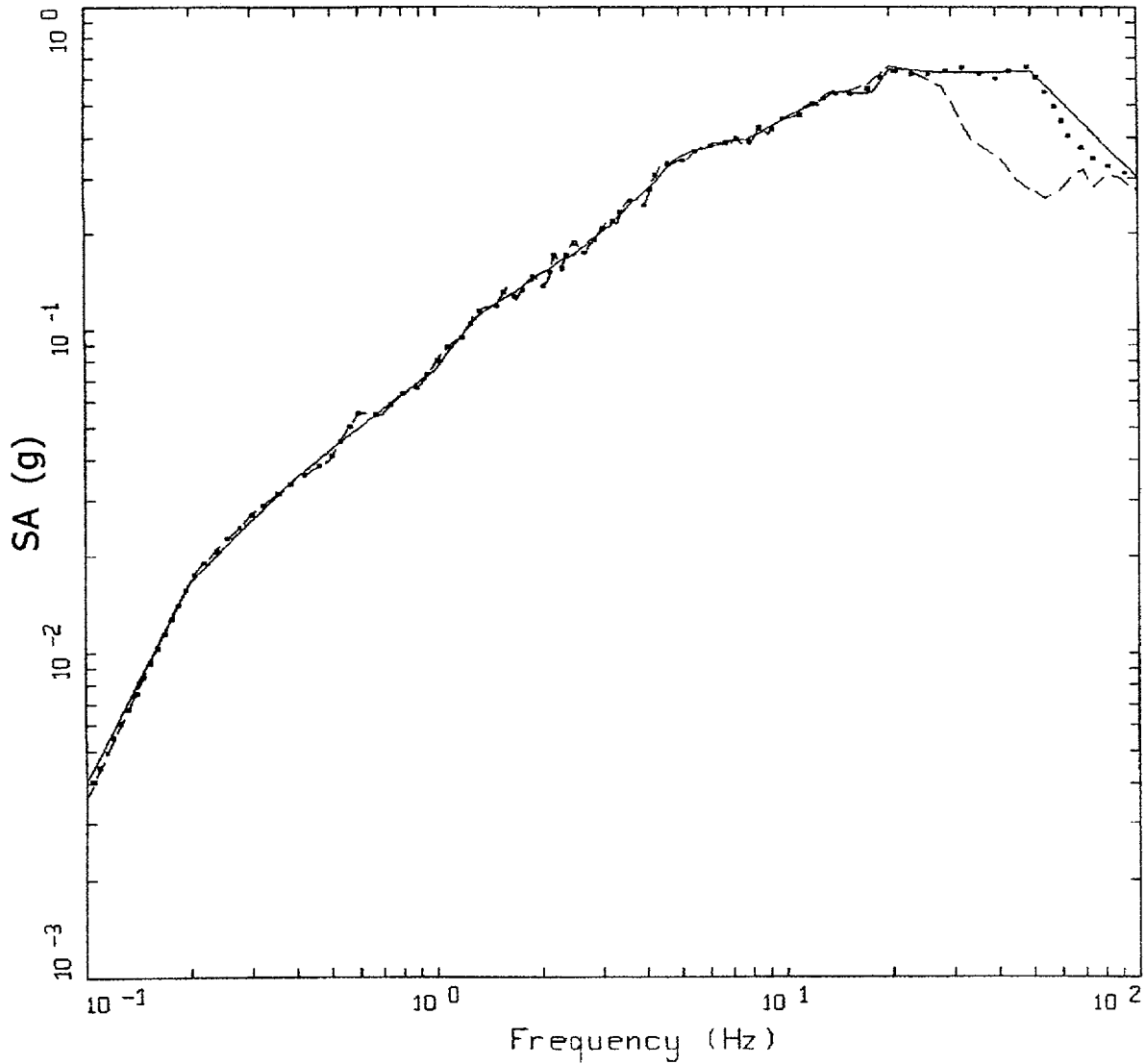
LEGEND
 ——— TARGET; PGA = 0.610 G
 - - - - 5 %, SPECTRAL MATCH; PGA = 0.610 G

Figure 3-12. Spectral match of WUS record to WUS target: 10^4 rock UHS (Figure 3-11).



WUS SPECTRAL MATCH
10-4, ROCK

Figure 3-13. Acceleration, velocity, and displacement time histories resulting from match of WUS record to WUS target (Figure 3-11).



SPECTRAL MATCH
10-4, ROCK

- LEGEND
- TARGET; PGA = 0.298 G
 - 5 %, SPECTRAL MATCH; PGA = 0.298 G, DT = 0.005 SEC
 - - - - - 5 %, SPECTRAL MATCH; PGA = 0.269 G, DT = 0.020 SEC

Figure 3-14. Spectral match of WUS record to CEUS target: 10^{-4} rock UHS using two sample intervals, 0.02 sec and 0.005 sec.

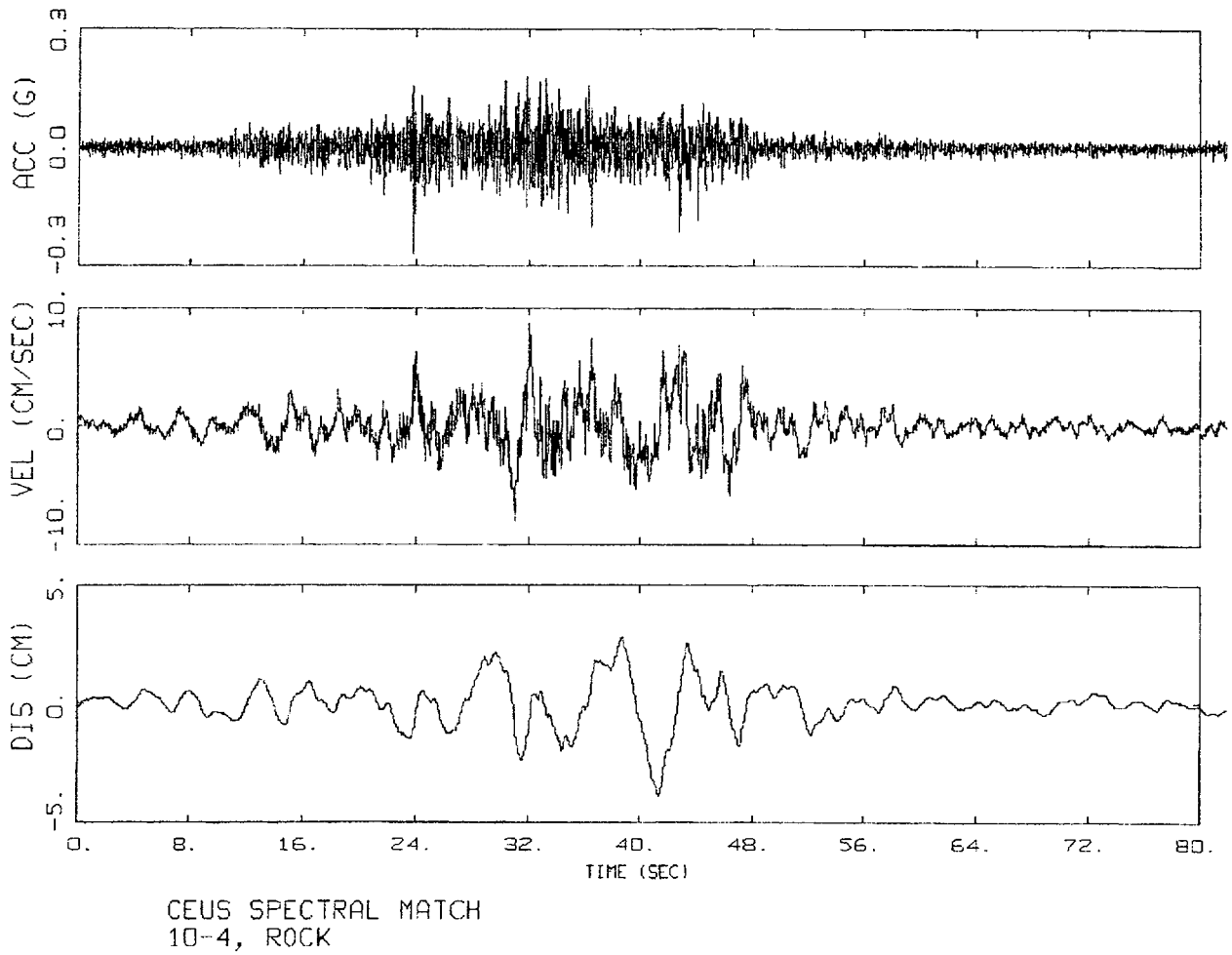
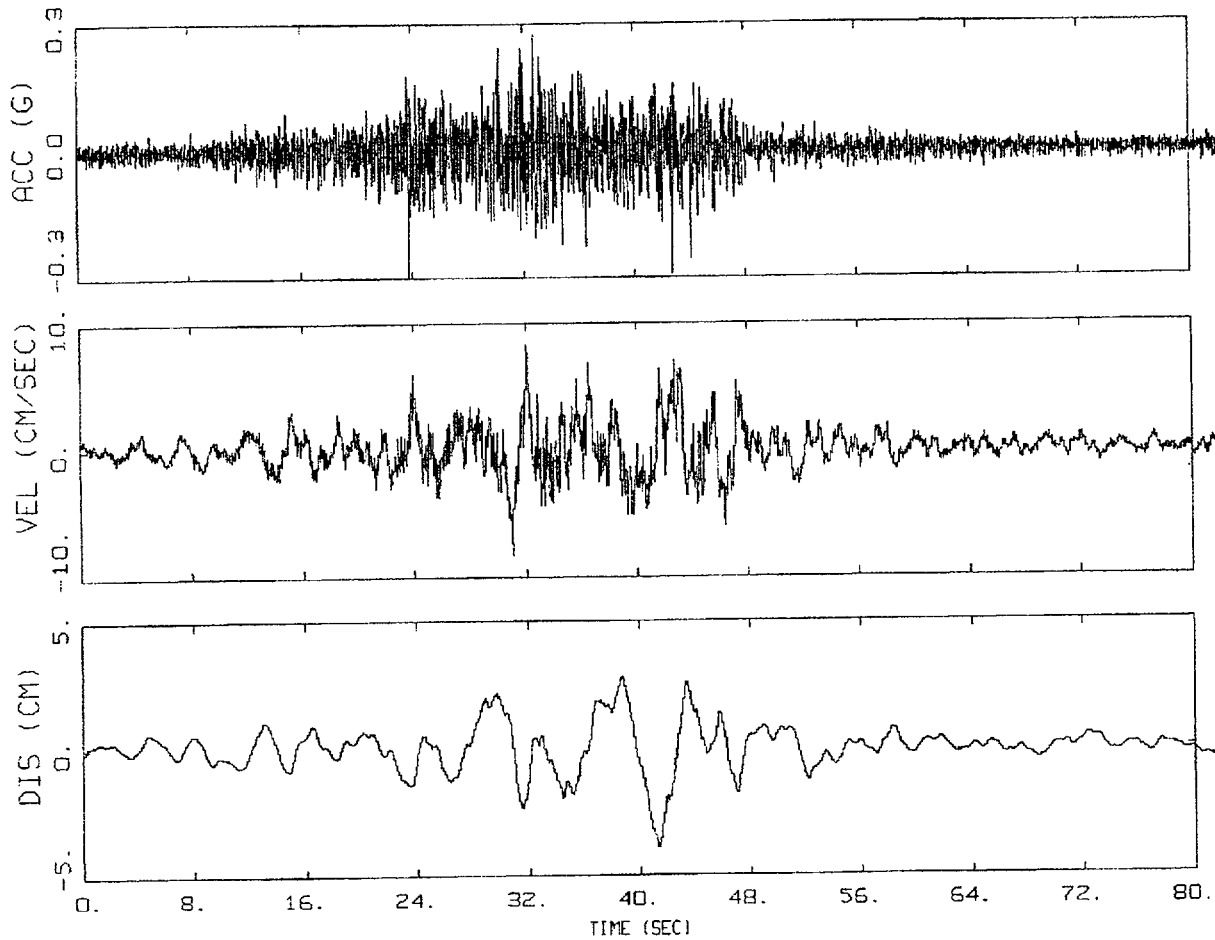
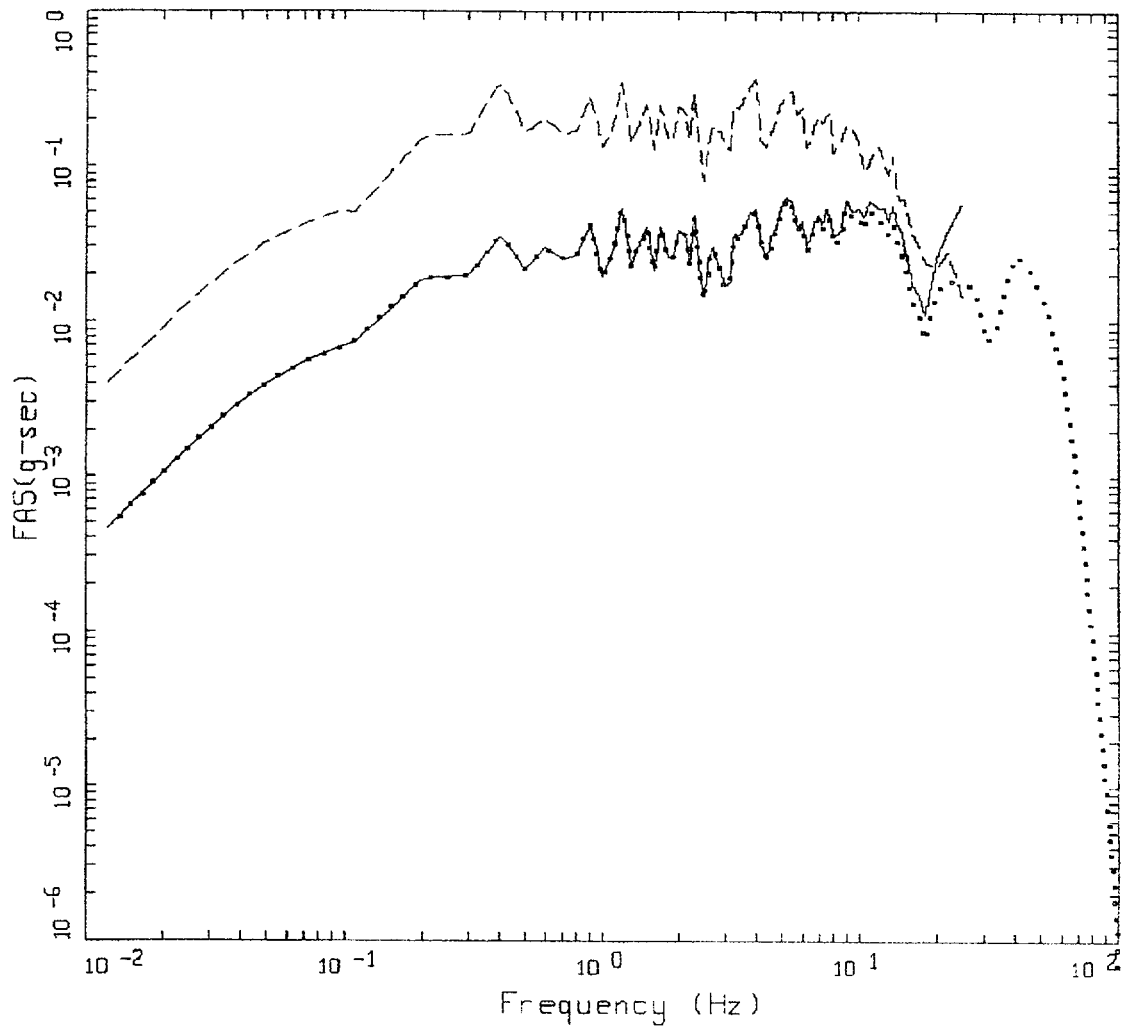


Figure 3-15. Acceleration, velocity, and displacement time histories resulting from match of WUS record to CEUS target, sample interval of 0.02 sec.



CEUS SPECTRAL MATCH
10-4, ROCK

Figure 3-16. Acceleration, velocity, and displacement time histories resulting from match of WUS record to CEUS target, sample interval of 0.005 sec.



SPECTRAL MATCH
10-4 ROCK

- LEGEND
- CEUS, DT = 0.020 SEC
 - CEUS, DT = 0.005 SEC
 - - - WUS, DT = 0.020 SEC

Figure 3-17. Fourier amplitude spectra resulting from fitting WUS record to WUS and CEUS targets (Figure 3-4). Fit to CEUS target used two sample intervals, 0.02 sec and 0.005 sec.

4 DEVELOPMENT OF DESIGN RESPONSE SPECTRAL SHAPES

In this section we document the recommended spectral shapes for both WUS (soft rock) and CEUS (hard rock) for 5% of critical damping. Recommendations for other damping levels are discussed in Section 4.8. For crustal earthquakes, the shapes are valid for moment magnitudes ranging from M 4 to M 8. For applications to subduction zone events (i.e. the Cascadia subduction zone) the shapes are valid up to M 9. The possible effects of mechanism and near-source conditions on the base shapes are discussed in Section 4.6.

In developing spectral shapes, three issues of particular significance arise: (1) selection of an appropriate normalization frequency and fractile level, (2) the paucity of data in the CEUS for $M > 4.5$, and (3) the likelihood that CEUS earthquake source processes for magnitudes larger than about M 6 produce significantly less intermediate frequency energy than corresponding WUS source processes (see Section 2 and Appendix D).

The first issue, selection of an appropriate normalization frequency and fractile level, is complicated somewhat by the desirability of having the fractile level uniform across frequency. This uniformity is highly desirable, as it is implicit in maintaining risk consistency (Section 7) or a constant level of conservatism in design analyses. Unfortunately, strong ground motions in the WUS (the tectonic regime with the most complete database in terms of magnitude and distance ranges) are characterized by a frequency-dependent, as well as magnitude-dependent, variability. Regression analyses on WUS strong ground motion data generally show empirical scatter (variation about the median) that decreases with increasing frequency (Abrahamson and Shedlock, 1997). This variability also decreases with increasing magnitude (Youngs et al., 1995) or ground motion amplitude (Campbell, 1993), particularly for $M \geq 6$. These statistical properties are likely real and stable, not reflecting spurious trends due to a sparse sample size. They are probably related to fundamental physics of earthquake source, path, and site processes and can reasonably be expected to occur in the CEUS as well as the WUS.

The second issue relevant to developing response spectral shapes for the CEUS, the paucity of strong motion data, precludes a purely statistical approach to developing shapes. The direct effect of a small sample size is the necessity of using physical models, resulting in a significantly higher uncertainty in the shapes for applications to CEUS sites.

The third issue is driven largely by the lack of CEUS data for $M \geq 6$ and contributes substantially to the larger uncertainty in CEUS shapes: the possibility that source processes in tectonically stable regions emit less intermediate frequency energy than corresponding sources in active regions (WUS). This difference in spectral content manifests itself seismologically in a second corner frequency (Section 2), which results in response spectral shapes that contain a well-developed spectral sag in a frequency range (near 1 Hz) that varies with magnitude. WUS sources do not show such a well-developed spectral sag, and it is not reflected in empirical attenuation relations. Recent studies, however, suggest that the sag may be present in a much more subtle form, being obscured (filled in) by amplification due to generally softer crustal rocks in the WUS as compared to CEUS crustal conditions. Theoretically this is appealing, suggesting an intrinsic commonality between WUS and CEUS source processes, although there is no compelling argument to prove this should be the case.

The possibility of commonality does not increase our confidence (lower the level of uncertainty) in CEUS shapes because the current state of knowledge does not reflect a high level of confidence in the physical process that produces a stable and predictable spectral sag for large magnitude ($M > 6$) earthquakes. As a result, until more CEUS data become available for $M > 6$ earthquakes, some uncertainty will exist as to the appropriateness and degree of sag in CEUS spectral shapes. The perspective taken in developing shapes for the CEUS is not to attempt resolution of this issue, but to produce spectral shapes using models that reflect both possibilities, i.e., with and without an intermediate-frequency spectral sag.

4.1 Approach

The overall approach taken to define response spectral shapes applicable to WUS and CEUS conditions is to rely as much as possible on recorded strong ground motions. These motions are supplemented, where necessary, by ground motion estimates from well-validated theoretical models. This approach will result both in confidence in the use of the spectral shapes as well as reasonable stability over time because the theoretical estimates will provide a guide where data are sparse, and will avoid fluctuations in empirical approaches caused by many data from one event.

To develop shapes appropriate for the WUS that incorporate magnitude and distance scaling, a suite of empirical attenuation relations were used and their estimates were averaged for a set of magnitude and distance bins. The empirical relations were weighted based on a goodness of fit evaluation (Section 4.4) with statistical shapes (Kimball, 1983). The statistical shapes are computed for the magnitude and distance bins from recorded motions listed in the strong motion catalog (Appendix A). The use of empirical relations rather than the statistical shapes directly (Mohraz et al., 1972; Newmark et al., 1973) provided a formalism for sampling expert opinion in smoothing, interpolation, and extrapolation within the poorly sampled bins and oscillator frequencies. Incorporating a robust weighting scheme based on how well each relation fits statistical shapes reduced bias in the selection of the empirical relations.

The spectral shapes from the weighted empirical relations were then fit to a functional form with magnitude and fault distance as independent variables. This process resulted in an attenuation relation for smooth WUS shapes that was largely driven by recordings and that incorporated the knowledge of a number of researchers of strong ground motions. The approach of producing an attenuation relation for shapes has the advantage of simplicity as well, being a continuous function of magnitude, distance, and frequency (Section 4.4).

For applications to the CEUS, insufficient data preclude a similar empirical approach, necessitating consideration of physical models. In general, reliance on model predictions for regions of sparse data results in increased uncertainty in the shapes. For the CEUS, this is further complicated by observations that strongly suggest the possibility that the spectral content in the intermediate frequency range for large magnitude CEUS sources is significantly different (lower) than corresponding WUS sources (Section 2). Because this issue is currently unresolved, consideration must be given to multiple CEUS spectral models.

To minimize the dependence on models in developing CEUS spectral shapes, we used model predictions in the form of ratios to produce transfer functions. The transfer functions, which are ratios of CEUS model shapes to WUS model shapes, were then applied to the empirical WUS shapes to produce shapes appropriate for CEUS conditions. We then fit an attenuation relation for the CEUS spectral shape.

The use of ratios of model predictions rather than model results directly minimizes the impact of potential model deficiencies. Another advantage of this approach is the emphasis placed on model validations for both WUS and CEUS conditions (Section 4.3).

4.2 WUS Statistical Spectral Shapes

Statistical response spectral shapes (Kimball, 1983) were developed for a suite of magnitude and distance bins by sampling the WUS strong motion data base (Appendix A). Shapes for 5% of critical damping were developed by normalizing each response spectrum by the spectral ordinate at the selected frequency and then averaging the scaled records within each bin. A lognormal distribution was assumed. The resulting suites of normalized spectra provided a basis for choosing the best normalization frequency and fractile level. This choice is illustrated in Section 4.2.2 below.

4.2.1 Magnitude and Distance Bins for WUS Spectral Shapes

Implicit in the selection of appropriate magnitude (M) and distance (fault distance, R) bins is the classic tradeoff of resolution and stability. In this context, resolution refers to the ability to clearly distinguish M and R dependencies in the spectral shapes (which is enhanced by more bins) while stability relates to low variability or statistical stability (which is enhanced by fewer bins, and more data in each bin). In terms of spectral shapes, high stability also results in the desirable feature of smoothness, or less variability from frequency to frequency.

The selection of bin widths and boundaries, in addition to achieving an acceptable compromise between resolution and stability based upon the distribution (in M and R) of data, was also conditioned by knowledge of shape sensitivity to M and R . In general, the distance dependency for WUS spectral shapes is small (less than about 30%) within about 30 to 50 km from the source. For CEUS spectral shapes the corresponding distance is about 50 to 100 km (Silva and Green, 1989). On the other hand, near-source effects are particularly strong for fault distances within about 10 to 15 km, particularly for vertical strike-slip mechanisms (Somerville et al., 1997). Additionally, seismic hazard is generally dominated by sources within about 100 km for WUS (about 200 km for Cascadia subduction zone sources), and within about 300 km for CEUS sources. For response spectral shapes, beyond about 50 km for WUS and 70 to 100 for CEUS, a factor of 2 change in distance results in about a 30% (factor of 1.3) change in spectral shape (Silva, 1991). With these considerations, distance bins of 0 to 10, 10 to 50, 50 to 100, 100 to 200 km for both WUS and CEUS shapes were considered appropriate with an additional bin of 200 to 400 km for CEUS shapes.

Magnitudes of about 5 to about 8 dominate the hazard for both the WUS and CEUS (except for sites affected by the Cascadia subduction zone sources). While a half magnitude change in M results in a 30 to 50% change in PGA normalized shapes (Silva and Green, 1989; Silva, 1991) depending upon

M and frequency, half **M** bins are too sparse at the larger **M** ($M > 6.5$). As a result, unit magnitude wide bins were selected centered on half magnitudes: **M** 5.5, 6.5, and 7.5 with ranges of 5 to 6, 6.01 to 7, and 7.01 and larger. Table 4-1 shows the bins along with summary statistics. For completeness, statistics for soil sites (Geomatrix classifications C and D, Appendix A) were included, in addition to a 0 to 50 km distance bin.

4.2.2 Development of WUS Statistical Spectral Shapes

The first issue to resolve in developing the set of shapes for applications to WUS and CEUS conditions was the appropriate normalization frequency and fractile level. To approach this issue, median bin shapes were computed for a suite of normalization frequencies to determine the degree of similarity between the shapes. Figure 4.1 shows an example for the **M** 6.5 and $D = 10$ to 50 km bin for normalization frequencies of 0.5, 1.0, 5.0, 10.0, 20.0, 34.0, and 100.0 Hz (the last value being equivalent to PGA). The shapes were computed down to frequencies that were 125% (factor of 1.25) of processing corner frequencies (Appendix A). This resulted in an increase in variability at lower frequencies as records dropped out due to noise contamination. For all seven normalization frequencies, the shapes were quite similar, and scaling each shape to unity at 100 Hz (PGA) presented a more convenient display (Figure 4.2). Similar results were obtained for the other bins suggesting a convenient resolution to the issue of selecting an appropriate normalization frequency. Since peak ground acceleration has the lowest variability among response spectral ordinates in the frequency range of 100.0 to 0.2 Hz (Abrahamson and Silva, 1997; Campbell, 1997, Boore et al., 1997; Sadigh et al., 1997), it is an attractive as well as conventional normalization parameter (Seed et al., 1976). Similar results would be obtained if normalization were done using spectral acceleration at any other frequency.

The selection of an appropriate fractile level for spectral shapes must consider the manner in which the shapes are to be used (Section 1). Current regulatory guidance (R.G. 1.165) recommends probabilistic seismic hazard evaluations for rock outcrop (or its equivalent), with coupling to deterministic evaluations using deaggregation of the uniform hazard spectrum (UHS), the deaggregation being done at several frequencies. Deterministic spectra are then scaled to the UHS at the deaggregation frequencies as a check on the suitability of the UHS and to provide control motions for site response evaluations. The deterministic spectra may be computed from the attenuation relations used in the UHS or may be based on the recommended spectral shapes. Additionally, the recommended spectral shapes may be used to evaluate existing design motions at the rock outcrop level. As a result, the development of median shapes is most consistent with intended uses, particularly in the context of UHS, where the desired hazard is appropriately set at the UHS exceedence level.

The bin statistical shapes (median \pm 1 sigma) normalized by peak ground acceleration are shown in Figures 4.3 to 4.5 for rock and Figures 4.6 to 4.8 for soil.

4.3 **Ground Motion Model for Spectral Shapes**

The most desirable feature in a ground motion model for spectral ordinates is the ability to reliably and accurately capture magnitude, distance, and site dependencies with a minimum of parameters.

A necessary aspect of any ground motion model implemented in engineering design practice is a thorough validation with recorded motions. Since all models are mathematical approximations to complicated physical processes, rigorous validation exercises are necessary to assess model accuracy, reveal strengths and shortcomings, and constrain parameter values and their uncertainties (Roblee et al., 1996). Ideally, a ground motion model will be validated over the ranges of magnitudes, distances, site conditions, and tectonic environments for which it is implemented. In this sense, the model is more an interpolative tool that can be used with a confidence level reflected in quantified validation exercises (Abrahamson et al., 1990; EPRI, 1993; Silva et al., 1997). While this is becoming possible for WUS tectonic conditions, it is clearly not the case for the CEUS (Section 2). Because of the paucity of recording in CEUS conditions, thorough validation exercises to assess model accuracy and parameter distributions are not possible. This situation necessarily results in significantly higher uncertainty, which can be assessed only in a qualitative manner (Appendix D).

4.3.1 Point-Source Model

Since response spectral shapes are intended to reflect average horizontal motions at sites distributed at the same fault distance from the source, the effects of source finiteness are expected to be minimal (Silva and Darragh, 1995). The effects of rupture directivity and source mechanism on spectral shapes (Section 4.6) increase the variability associated with spectral shapes at close distances ($R \leq 15$ km) and at low frequency (≤ 1 Hz) but have little effect on the *average* shape. As a result, a point-source model with its attractive simplicity is appropriate. The stochastic point-source model, in the context of strong ground motion simulation, was originally developed by Hanks and McGuire (1981) and refined by Boore (1983; 1986). It has been validated in a comprehensive manner with 18 earthquakes at about 500 sites (Silva et al., 1997) and is described in detail in Appendix D. Table 4-2 lists the parameters used to develop the spectral shapes and transfer functions.

For applications to the CEUS, a single significant set of observations may fundamentally increase uncertainty in model predictions of spectral shapes. This phenomenon was illustrated with ground motions generated by the 1988 M 5.8 Saguenay, Ontario earthquake. Even prior to this earthquake, high frequency (> 5 Hz) motions at hard rock CEUS sites were known to be significantly greater than motions recorded on typical WUS soft rock conditions (Section 2). A number of small earthquake ($M \leq 5$) CEUS data showed this increase in high-frequency content, and less damping in the shallow crust (1 to 2 km) of the CEUS was considered the likely cause for the difference (Silva and Darragh, 1995). This difference was observed for the Saguenay earthquake as well as the M 6.4 1985 Nahanni aftershock earthquakes. However, the Saguenay earthquake also showed anomalously low intermediate-frequency (0.5 to 2 Hz) energy (Boore and Atkinson, 1992; Atkinson, 1993; Silva and Darragh, 1995). This observation along with others (Choy and Boatwright, 1988; Boatwright and Choy, 1992; Atkinson, 1993; Boatwright, 1994) has led to the speculation that CEUS source processes may possess differences from WUS source processes that result in stable and significant differences in intermediate frequency content for earthquakes with magnitude (M) greater than about 5 (Atkinson and Boore, 1995; 1998). Seismologically this spectral sag may be interpreted as the presence of second corner frequency or change in slope of the earthquake source spectrum (Boatwright, 1994; Atkinson and Boore, 1998). Interestingly, recent observations have suggested this may be the case for WUS earthquake source as well (Silva et al., 1997; Atkinson and Silva, 1997), but manifested in a much more subtle effect on response spectra due to differences in crustal

conditions between WUS and CEUS (Appendix C). An example comparison of response spectra computed for M 6.5 at a distance of 25 km using both WUS and CEUS single- and double-corner frequency point-source models is shown in Figure 4.9 for shapes and Figure 4.10 for absolute spectral levels. The two single corner frequency shapes for the WUS and CEUS (solid lines) show large differences over the entire frequency range. The WUS shape exceeds the CEUS for frequencies less than about 10 Hz where the shapes cross. The WUS shape peaks near 5 Hz while the CEUS shape has a maximum amplification in the 30 to 50 Hz frequency range. These trends are very similar to the empirical WUS and CEUS rock site spectra shown in Section 2.

Comparing the single- and double-corner frequency spectra for WUS and CEUS, Figure 4.9 shows the spectral sag significantly more pronounced for the CEUS. At low frequencies (below about 1 Hz) the double corner CEUS spectrum is about a factor of 3 lower than the single corner CEUS spectrum. Over the same frequency range, the difference between single and double corner shapes for the WUS is only about 10 to 20%.

Comparing the absolute levels, Figure 4.10 shows that at low frequencies, the single-corner frequency model (solid lines) predicts similar motions for WUS and CEUS conditions. Peak accelerations for CEUS conditions are predicted to be larger than for WUS conditions, reversing the trends between spectral shapes (normalized by peak acceleration) and absolute spectral levels (Silva, 1991).

Though shifted in frequency, the differences between WUS and CEUS rock site shapes are not unlike the differences in the WUS statistical spectra between soft rock and deep soil shown in Figure 4.11. This is consistent with the explanation that CEUS spectral shapes are caused by the hard crustal conditions found there (Appendix C).

4.3.2 Comparison of Model Shapes to WUS Statistical Shapes

To provide a qualitative evaluation of model performance, Figure 4.12 compares model shapes to WUS statistical shapes in the distance range of 10 to 50 km and for magnitudes near 5.5, 6.5, and 7.5. Model shapes for both single and double corner source spectra are shown illustrating the generally small difference between the alternative source models for WUS conditions. In general, the model shapes reflect the statistical shapes very well for the M 5.5 and M 6.5 bins and over-predict for the M 7.5 statistical shape.

The well developed spectral sag in the M 7.5 $R = 10$ to 50 km statistical shape bin is also not matched by the empirical attenuation equations (Figure 4-14c). Since this magnitude bin is sparsely populated (Table 4-1), the statistical shapes may be biased by sampling only a few earthquakes and rock sites. It is intriguing nonetheless that the statistical shapes for M greater than 7 at rock sites show evidence of a well-developed second corner frequency source spectrum. The developers of the empirical attenuation relations used here have chosen to ignore this observation (Section 4.4), because of the few data on which it is based.

4.3.3 WUS to CEUS Transfer Functions

Using the point-source model, median spectral shapes were computed for single-corner WUS conditions and both double and single corner CEUS conditions using the parameters listed in Table 4-2. Ratios of the shapes, CEUS/WUS, for a dense grid in magnitude and distance were taken to provide transfer functions to apply to the weighted empirical shapes (Section 4.4). An example suite of the transfer functions is shown in Figure 4-13.

4.4 **Design Response Spectra**

4.4.1 Western US Spectral Shapes

The approach used to develop spectral shapes for rock site conditions appropriate for the WUS consisted of the following steps:

1. Use a number of empirical strong ground motion attenuation relationships to compute spectral amplification values, the ratio SA/PGA for the magnitude range ($5 \leq M \leq 8$) and fault distance range ($0.1 \leq R^* \leq 200$ km) of interest.
2. Develop weights to apply to the relationships based on comparisons with a common set of recorded strong motion data.
3. Compute a weighted average of the empirical attenuation relationship spectral shapes for a dense grid of magnitude and distance pairs.
4. Develop a functional form to define spectral amplification over the magnitude and distance range of interest.

Five recently published empirical attenuation relationships were chosen to develop the spectral shapes for the WUS: Abrahamson and Silva (1997), Boore and others (1997), Campbell (1997), Idriss (1991), and Sadigh and others (1997). These relationships are henceforth referred to as A&S 97, Bao 97, C 97, I 91, and Sao 97, respectively. The spectral shapes predicted by these relationships are compared on Figure 4-14 to the statistical spectral shapes developed in Section 4.2. Note that the Bao 97 relationship is limited to $5.5 \leq M \leq 7.5$ and $R \leq 80$ km and the C 97 relationship is limited to $R \leq 60$ km. The selected attenuation relationships have 14 spectral frequencies in common: 0.2, 0.25, 0.333, 0.5, 0.667, 1.0, 2.0, 3.33, 5.0, 6.67, 10.0, 13.33, 20, and 34 Hz. (Note that C 97 does not contain 0.2 Hz and Bao does not contain 0.2, 0.25, and 0.333 Hz. Also, the Bao 97 spectral accelerations for frequencies between 10 and 40 Hz were calculated here by linear interpolation in log-log space as recommended by D. Boore [personal communication, 1998]). Spectral amplifications were computed for each attenuation relationship by dividing the predicted spectral acceleration at each frequency by the predicted peak ground acceleration.

*For each empirical relation the appropriate distance definition is used.

4.4.2 Development of Weighted Empirical Spectral Shapes

The weights to be applied to the spectral shapes defined by the five empirical attenuation relationships were based on the relative ability of the relationships to predict the spectral shapes computed from the strong motion data base described in Section 4.2. To allow for the possibility that the relative prediction ability varies as a function of magnitude and distance, weights were computed for each of the 12 magnitude and distance bins defined in Section 4.2.

We defined the residual $(\epsilon(f)_{ij})_k$ to be the difference between the log of the spectral amplification for frequency f of the j^{th} recorded motion from the i^{th} earthquake, $(SA(f)/PGA)_{ij}^r$ (the geometric mean of the two horizontal components) and the log of the spectral amplification predicted by the k^{th} attenuation relationship for magnitude M_i and source-to-site distance R_{ij} .

$$(\epsilon(f)_{ij})_k = \ln[(SA(f)/PGA)_{ij}^r] - \ln[(SA(f)/PGA)_k] \quad (4-1)$$

These residuals are assumed to be normally distributed with a random effects variance structure (e.g. Brillinger and Preisler 1984, 1985; Youngs and others, 1995):

$$(\epsilon(f)_{ij})_k = \epsilon_1(f)_i + \epsilon_2(f)_{ij} \quad (4-2)$$

where $\epsilon_1(f)_i$ and $\epsilon_2(f)_{ij}$ are independent, normal variates with variances $\tau_1^2(f)$ and $\tau_2^2(f)$, respectively.

Two approaches were used to assign weights to the five attenuation relationships for each spectral frequency within each magnitude and distance bin. The first approach was based on the relative bias of the relationships. For each frequency in each M and R bin, the mean residual for the k^{th} attenuation relationship, $(f)_k$, is found by maximizing the generalized normal distribution likelihood function:

$$L((f)_k, \tau_1(f)_k, \tau_2(f)_k) = \frac{\exp\left[-\frac{[(\epsilon(f)_{ij})_k - (f)_k]^T V(f)_k^{-1} [(\epsilon(f)_{ij})_k - (f)_k]}{2}\right]}{2\pi |V(f)_k|^{1/2}} \quad (4-3)$$

where $V(f)_k$ is the block-diagonal variance matrix of $(\epsilon(f)_{ij})_k - (f)_k$. Figure 4-15 shows the mean residuals and their 90% confidence intervals for the five attenuation relationships and 12 magnitude-distance bins.

The t statistic, $t_k = |(\epsilon(f)_{ij})_k - (f)_k| / \sigma[(\epsilon(f)_{ij})_k - (f)_k]$, together with the cumulative T distribution can be used to compute the probability a sample of size n from a population with zero mean would have a mean residual as large as $|(\epsilon(f)_{ij})_k - (f)_k|$, $P(T \leq t_k | n-1)$. If one considers that the relationships with the higher probability of producing the computed t statistic should be given higher weight, then the relative weight for the k^{th} attenuation relationship, $W(f)_k^T$ can be defined as:

$$W(f)_k^T = \frac{P(T \leq t(f)_k | n-1)}{\sum_k P(T \leq t(f)_k | n-1)} \quad (4-4)$$

These are referred to as "T" weights.

The second weighting approach uses relative likelihoods under the assumption that the mean residual is zero. The likelihood function is given by:

$$L(f)_{k=0, \tau_1(f)_k, \tau_2(f)_k} = \frac{\exp \left[-\frac{(\epsilon(f)_{ij})_k^T V(f)_k^{-1} (\epsilon(f)_{ij})_k}{2} \right]}{2\pi |V(f)_k|^{1/2}} \quad (4-5)$$

where $V(f)_k$ is the block-diagonal variance matrix of $(\epsilon(f)_{ij})_k$. Equation (4-5) gives the probability of observing the sample set of residuals, given that the mean residual is zero. If one considers that the relationships with the higher likelihood should be given higher weight, then the relative weight for the k^{th} attenuation relationship, $W(f)_k^L$ can be defined as:

$$W(f)_k^L = \frac{L(f)_k}{\sum_k L(f)_k} \quad (4-6)$$

These are referred to as "L" weights.

The top plots in the two columns of Figure 4-16 show examples of the "T" and "L" weights for one of the 12 magnitude-distance bins. The weights display a highly irregular pattern, reflecting the variability in the mean residuals shown on Figure 4-15. The approach to developing the response spectral shapes outlined in Section 4.1 is based on the use of the empirical attenuation relationships to provide smoothly varying estimates of response spectral shapes over a magnitude and distance range that extends beyond the bulk of the recorded data. The use of the highly variable weights shown at the top of Figure 4-16, while providing a close match to the recorded data set, would rapidly switch from strongly favoring one attenuation relationship to favoring another over short frequency intervals, and thus tend to defeat the purpose of using the smooth empirical attenuation relationship spectra. In addition, limitations in the band-width of the processed data for the smaller recordings results in no weight estimates for some frequencies. These two issues were addressed by smoothing the weights across frequency with a Gaussian smoothing operator. The smoothed weights are defined by:

$$W(f_i)_k^* = \frac{\sum_{j=1}^J W(f_j)_k \cdot \exp(-\ln(f_j/f_i)^2/h^2)}{\sum_{j=1}^J \exp(-\ln(f_j/f_i)^2/h^2)} \quad (4-7)$$

where $f_j, j = 1$ to J are the 14 common spectral frequencies defined above and h determines the width of the smoothing operator. Larger values of h produce greater smoothing. The remaining plots on Figure 4-16 show smoothed weights for values of h of 0.25, 0.5, and 1.0.

Figure 4-17 shows examples of the weighted average empirical spectral shapes computed for the average magnitude and distance of two of the magnitude-distance bins using smoothed "L" and "T" weights. As indicated on the plot, variations in h have a very minor effect on the computed spectral shapes. Also, the "L" and "T" weights produce very similar spectral shapes. Therefore, the smoothed "L" and "T" weights were averaged to produce the final set of weights. A smoothing parameter of $h = 1.0$ was chosen for the final weights to produce a smoothly varying final set of weights. These are shown on Figure 4-18. Figure 4-19 shows examples of the weighted empirical response spectral shapes for magnitude of M 5 to 8 and distances of 1 to 200 km.

4.4.3 Magnitude and Distance Dependencies of Weighted Empirical Spectral Shapes

The response spectral shapes shown on Figure 4-19 vary with magnitude and distance. In order to provide relationships for specifying a response spectral shape for any magnitude and distance within the specified range of the attenuation relationships, a function form was fit to the weighted empirical spectral shapes. Figure 4-20 shows the statistical spectra for magnitude M 6 to 7 and R 10 to 50 km data. This spectral shape can be closely matched by the ad hoc relationship:

$$\ln[SA(f)/PGA] = \frac{C_1}{\cosh(C_2 f^{C_3})} + C_4 \left[\frac{\exp(C_5 f)}{f^{C_6}} \right] \quad (4-8)$$

The form of Equation (4-8) is not based on a physical model, but is rather designed to fit the general characteristics of the spectral shapes. The first term fits the high frequency portion of the spectrum, decreasing exponentially to zero with increasing frequency. The second term models the low frequency portion of the spectrum. The factor $\exp(C_5 f)$ controls the transition of control from the low frequency to high frequency terms.

Coefficients C_1 through C_6 were defined as functions of magnitude and/or distance by creating a data set of 651 response spectral shapes (31 magnitudes times 21 distances) at 0.1 magnitude units from M5 to M8 and at fault distances (R) of 0.1, 1, 2, 3, 5, 10, 12, 15, 20, 25, 30, 40, 50, 60, 70, 85, 100, 125, 150, 175, and 200 km. Each response spectral shape contained spectral amplifications at the 14 frequencies common to the five empirical attenuation relationships. In addition, fitting time histories to the response spectral shapes requires specification of the spectral amplifications in the frequency range of 0.1 to 100 Hz. The solid diamonds shown on Figure 4-20 indicate the spectral amplifications predicted by an extrapolation of Equation (4-8), which was fit to the frequency range of 0.2 to 34 Hz. As indicated, the functional form provides a good fit in the extrapolated range both for $f > 34$ Hz and $f < 0.2$ Hz. The poorest fit is at 0.1 Hz, where the statistical spectra are becoming somewhat biased due to the exclusion of records with limited band-widths. The 651 weighted empirical spectral shapes were extended from the frequency range of 0.2 to 34 Hz to the frequency range of 0.1 to 100 Hz by fitting Equation (4-8) to each spectral shape and then using the parameters of that fit to predict spectral amplifications in the frequency range of 0.1 to 0.2 Hz and 34 to 100 Hz.

The entire extended data set was then used to obtain expressions for coefficients C_1 through C_6 by nonlinear least squares. The best fit was found by the parameter set listed in Table 4-3. Figure 4-21 shows examples of the response spectral shapes predicted using these relationships.

4.4.4 Model for Central and Eastern US Spectral Shapes

The approach used to develop spectral shapes for rock site conditions appropriate for the CEUS consisted of the following steps:

1. Use numerical modeling to develop scaling relationships between CEUS and WUS response spectral shapes.
2. Use the scaling relationships from step 1 to convert the weighted empirical WUS spectral shapes to CEUS spectral shapes.
3. Develop a functional form to define spectral amplification over the magnitude and distance range of interest.

These steps are discussed in the following subsections.

4.4.4.1 Scaling of WUS Weighted Empirical Spectral Shapes to CEUS Conditions

The scaling relationships for transferring WUS spectral shapes to CEUS spectral shapes are described in Section 4.3 and are shown on Figure 4-13. These scaling relationships were used to scale the extended (0.1 to 100 Hz) weighted empirical WUS response spectral shapes to produce CEUS spectral shapes. As discussed in Section 4.3, two sets of scaling relationships were defined, one based on single corner frequency CEUS earthquake source spectra and one based on double corner frequency CEUS earthquake source spectra. Both scaling relationships assume a single corner frequency WUS earthquake source spectra. Figure 4-22 shows examples of the CEUS response spectral shapes scaled from the weighted empirical WUS spectral shapes using the scaling relationships shown on Figure 4-13.

One problem that was encountered was an inconsistency or flat portion in CEUS spectral shapes around 10 Hz. Close comparison of the model and attenuation-based WUS spectral shapes indicated that the model shapes showed slightly higher spectral amplifications than the attenuation-based spectra around 10 Hz. This over-prediction or bias of WUS model spectral shapes caused an under-prediction of the CEUS/ WUS transfer function. As a result, the transfer function was slightly increased around 10 Hz. Figure 4-23 shows examples of the scaled (before adjustment) and adjusted spectral amplifications, for both the single- and double-corner CEUS spectral models.

4.4.4.2 Modeling the Effect of Magnitude and Distance on CEUS Spectral Shapes

Using the same approach as for WUS response spectral shapes, a functional form was fit to the scaled and adjusted empirical spectral shapes. A modified form of Equation (4-8) was used to model the CEUS shapes. The relationship is:

$$\ln[SA(f)/PGA] = \frac{C_1}{\cosh(C_2 f^{C_3})} + C_4 \left[\frac{\exp(C_5 f)}{f^{C_6}} + \frac{C_7 \exp(C_8 f)}{f^{C_9}} \right]^{1/2} \quad (4-9)$$

A second term was added to the low-frequency portion of the model to provide more flexibility in the shape. Coefficients C_1 through C_9 were defined as functions of magnitude and/or distance using the data set of 651 CEUS response spectral shapes (31 magnitude values times 21 distances) by nonlinear least squares with the spectral amplifications in the frequency range of the adjustment down weighted to reduce their influence on the fitted parameters.

For the single and double corner frequency CEUS earthquake spectra, the resulting coefficients are listed in Table 4-3. Figures 4-24 and 4-25 shows examples of the response spectral shapes predicted using these relationships.

4.5 Comparison of Recommended Shapes to Current Regulatory Guidance

In this section we compare Newmark and Hall (1978) and Regulatory Guide 1.60 (1973) design spectra to both WUS and CEUS recommended design spectra for the most populated distance bin (0 to 50 km) and mean magnitudes of M 5.6, M 6.4, and M 7.3 (Table 4-1). Figure 4-26 shows comparisons to WUS recommended shapes and Figure 4-27 shows analogous comparisons to CEUS shapes. For Newmark and Hall design shapes, WUS bin median values for peak accelerations, velocities, and displacements are used for both WUS and CEUS conditions. Both median and 1-sigma amplification factors are used for the Newmark and Hall design spectra.

For the WUS motions, Figure 4-26 shows a reasonably good comparison between the Newmark and Hall spectra and the recommended shapes. The empirical PGV/PGA ratio is about 60 cm/sec/g for M 6.3 and 7.3. Increasing this ratio to the value recommended by Newmark and Hall (1978) of about 90 cm/sec/g would increase the low frequency levels but result in peak velocities not supported by the data. The dependence of the Newmark and Hall design shapes on peak parameters captures some of the effects of the empirical magnitude dependency and would presumably capture elements of the distance dependency as well. Conversely, the fixed R.G. 1.60 shape is quite conservative even for M 7.3, since it was based on $M \approx 6.7$, used a mixture of rock and soil data, and was derived with 1-sigma amplification factors (Figure 4-26).

For the CEUS, Figure 4-27 shows a similar suite of plots but with recommended shapes for both the single- and double-corner CEUS source models. The Newmark-Hall design shapes use the WUS bin parameters because comparable empirical CEUS data are not available. The expected peak accelerations for CEUS rock motions are larger than corresponding WUS rock motions, so the CEUS shapes (SA/PGA) appear to be lower than WUS shapes at low frequencies. In absolute levels however, single corner WUS and CEUS spectra have comparable spectral levels for frequencies below about 3 Hz (see Figure 4-10). Normalizing at around 1 to 5 Hz would be more indicative of absolute levels and would result in similar comparisons with WUS shapes (Figure 4-26) at frequencies ≤ 5 Hz while showing a larger difference between the R.G. 1.60 and recommended shapes at high frequencies (as illustrated in Figure 4-10).

4.6 Effects of Source Mechanism and Near-Fault Conditions on Response Spectral Shapes

Since both the WUS and CEUS shapes are intended to reflect an average horizontal component for a random source mechanism located at a fixed rupture distance (but at a random azimuth with respect

to a rupture surface), it is important to assess the effects implied by these limitations. Both source mechanism (reverse, oblique, strike-slip, normal) as well as hanging-wall vs. foot-wall site location for dipping faults have frequency-dependent effects (Abrahamson and Shedlock, 1997). Additionally, for potential sites located in the NW Pacific region of WUS, the tectonic environment may include the contribution of large ($M \geq 9$) subduction zone earthquakes. Such sources may dominate the low frequency portion of the UHS requiring appropriate shapes for scaling.

For large magnitude ($M \geq 6.5$) earthquakes, rupture directivity affects both low frequency spectral levels (≤ 1 Hz) and time domain characteristics. Rupture towards a site enhances average spectral levels and reduces durations, while rupture away from a site reduces motions and increases durations, all of these changes being relative to average conditions (Somerville et al., 1997; Boatwright and Seekins, 1997). Differences in fault normal and fault parallel motions are also affected by rupture directivity and can be large at low frequencies (Somerville et al., 1997). Design decisions on whether to incorporate component differences in spectral levels and time domain characteristics should be made on a site-specific basis with consideration of uncertainties and the implications for analyses. Fault normal and fault parallel motions may not define principal directions for design purposes and these implications must be considered in two-dimensional analyses.

These source mechanism and near-fault issues become relevant when a high degree of certainty exists in the nature of the controlling sources as well as the source-site geometry. In calculating the hazard levels for a site, it is assumed that the appropriate degree of seismotectonic knowledge as well as epistemic uncertainty is incorporated in the attenuation relations used in the probabilistic hazard analysis. The UHS levels will then reflect appropriate contributions of source mechanism and site location. The recommended spectral shapes developed here, which are appropriate for average conditions, are scaled to the UHS at selected frequencies and do not reflect either conservatism or unconservatism in the frequency dependence of spectral levels based on source mechanism and site location.

4.6.1 Effects of Source Mechanism

Assessment of the effects of source mechanism, which is taken to include hanging wall vs. foot wall effects, relies on WUS empirical motions and is strictly appropriate for those conditions. Of the five empirical attenuation relations considered in the development of the WUS shapes (Section 4.4.1), two include frequency-dependent source mechanism effects (Abrahamson & Silva, 1997; Boore et al., 1997) and only one includes frequency-dependent hanging wall vs. foot wall effects (Abrahamson & Silva, 1997). To illustrate possible source mechanism effects on the revised WUS shapes, Figure 4-28 shows spectral shapes computed for the two relations for $M 5.5$ and $M 6.5$ earthquakes at a distance of 25 km. When normalizing by peak acceleration, the maximum effect of source mechanism is at low frequency (0.2 Hz) and shows a maximum expected range of about 50%. The shape for the strike-slip mechanism, the base case for the recommended shapes, is highest for frequencies below about 1 Hz, while normal faulting shapes are expected to be slightly higher than strike slip shapes for frequencies in the range of about 1 to 5 Hz. Since the normal faulting shape exceeds the strike-slip shape by less than 10%, use of the recommended shapes for normal faulting conditions is not considered to significantly underestimate design motions.

However, for large magnitude ($M \geq 6.4$) earthquakes occurring on reverse faults, Figure 4-28 shows that the expected shape is lower than the strike-slip shape by about 10% in the 1 to 2 Hz frequency range. Scaling the reverse mechanism shape to a UHS in the 1 to 2 Hz range could then result in larger predicted motions for frequencies above the scaling frequency than scaling the recommended spectral shape. For sites controlled by reverse mechanism sources, care should be taken in evaluating the development of the low frequency design motions for frequencies in the range of the low frequency scaling frequency to the crossover frequency for the next deaggregation frequency (Section 5.5).

To examine the expected effects of site location for dipping faults, Figure 4-29 compares shapes computed for strike-slip mechanism to shapes computed for a dipping fault for both hanging-wall and foot-wall site locations. These site dependencies are strongest in the fault distance range of 8 to 18 km and are based on Somerville and Abrahamson (1995) and included in the Abrahamson and Silva, 1997 relationship. The Boore et al., 1997 relation includes an M , R , and frequency-independent hanging wall vs. foot wall effect implicitly in its distance definition. As a result their shapes are largely site location (hanging wall vs. foot wall) independent.

The hanging-wall vs. foot-wall frequency dependencies illustrated as amplification factors in Figure 4-29 are actually strongest for large magnitude ($M \geq 6.5$) and at high frequency (PGA) and represent a maximum factor of about 1.4 for the horizontal component and about 1.9 for the vertical component (ratio of hanging-wall to “not-hanging-wall” PGA values). Since the hanging-wall shape is lower than the strike-slip shape (the basis mechanism for the recommended spectral shapes) by about 10% in the 1 to 2 Hz frequency range, scaling the hanging-wall shape instead of the strike-slip shape to the UHS in the 1 to 2 Hz frequency range will result in higher spectral levels for frequencies above the scaling frequency. Modifications to the recommended spectral shapes should be made on a site-specific basis, using all relevant records applicable to the site and the fault generating the hazard.

4.6.2 Subduction Zone Spectral Shapes

The possible occurrence of Cascadia subduction zone earthquakes with magnitudes up to M 9.0 can be significant contributors to the low frequency UHS for sites located in the Pacific Northwest (including Northern California), particularly near the Pacific coast. As a result, comparisons of empirical (Youngs et al., 1997) M 9.0 shapes at a suite of distances were made to the recommended shape for M 8.0 (the largest magnitude for which the empirical WUS relations are considered valid). The recommended shape is computed for a distance of 25 km since the dependence on distance is small within about 50 km. The comparisons are shown in Figure 4-30. Interestingly, for the same peak accelerations, the crustal earthquakes for M 8.0 are expected to have larger low frequency (≤ 2 Hz) motions than M 9.0 subduction zone earthquakes. The maximum difference in the 1 to 2 Hz range is about 10% and would be larger for smaller magnitude Cascadia sources. As with the source mechanism comparisons, if large magnitude ($M > 8$) subduction zone earthquakes contribute substantially to the low frequency hazard, appropriate spectral shapes should be developed on a site-specific basis.

4.7 Vertical Motions

Current regulatory guidance for vertical (V) ground motions specifies spectral levels that are equal to the horizontal (H) at frequencies > 3.5 Hz and that are $2/3$ the horizontal for frequencies < 0.25 Hz, with the ratio varying between 1 and $2/3$ between 3.5 Hz and 0.25 Hz (R.G. 1.60). As with the horizontal spectral shape, the implied V/H ratio is independent of magnitude, distance, and site condition and is shown in Figure 4-31. For the Newmark-Hall design motions, the V/H ratio is taken as independent of frequency as well as magnitude, distance, and site condition, having a constant value of $2/3$ (Figure 4-31). With the dramatic increase in strong motion data since the development of these design specifications in the 1970's, the conclusion that the vertical and average horizontal ground motions vary in stable and predictable ways with magnitude, distance, and site condition has become increasingly compelling. In general, vertical motions exceed horizontal (average of both component) motions at high frequency and at close fault distances (within about 10 to 15 km). The amount and frequency range of the exceedence depends on magnitude, distance, and site conditions. For different site conditions, time domain characteristics of vertical motions can be quite different at close distances and may be a consideration in selecting input motions for spectral matching or scaling procedures. Appendix K illustrates the expected differences in vertical and horizontal motions based on magnitude, distance, and site conditions and forms a background for the procedures recommended to develop vertical component spectra that are consistent with the WUS and CEUS revised rock horizontal component shapes.

Because structures, systems, and components have limited capacities for dynamic vertical demands, it is important to accommodate stable and predictable differences in vertical loads based on significant contributors (M and R) to the seismic hazard at a site. Since there are fewer attenuation relations for vertical motions in the WUS and currently none available for the CEUS, the general approach to developing vertical component design spectra is to use a frequency- dependent V/H ratio. It is difficult to capture the appropriate degree of uncertainty in the V/H ratio as well as the corresponding hazard level of the vertical component design spectrum after scaling the horizontal UHS spectrum by the V/H ratio. Thus, the usual assumption is that the derived vertical motions reflect a hazard level consistent with the horizontal UHS. To maintain consistency with the horizontal median shapes developed earlier in this Section, median V/H ratios are developed.

4.7.1 V/H Ratios for WUS Rock Site Conditions

Of the five empirical WUS attenuation relations used in developing the horizontal spectral shapes (Section 4.4.1), three include vertical motions: Abrahamson and Silva, 1997; Campbell, 1997; and Sadigh et al., 1997 (verticals from Sadigh et al., 1993). To develop V/H ratios for WUS rock site conditions, median V/median H ratios for strike slip mechanisms were produced for each relation and averaged assuming equal weights. The resulting V/H dependencies on magnitude and distance are illustrated in Figures 4-32 and 4-33. Figure 4-32 shows expected ratios for M 5.5, M 6.5, and M 7.5 earthquakes for a suite of distances ranging from 1 to 50 km. The ratios are magnitude-dependent, decreasing with decreasing magnitude and with the sensitivity to magnitude decreasing with increasing distance.

These effects are likely driven by the differences in magnitude scaling (change in spectral levels with magnitude) between the horizontal and vertical components. The dependence of the V/H ratios on magnitude decreases with distance (Figure 4-32) as the difference in magnitude scaling between the vertical and horizontal components decreases.

The effects of source mechanism on the V/H ratios (included only in the Abrahamson and Silva, 1997 relation) is small, with strike slip ratios generally exceeding the ratios for oblique, reverse, and normal faulting mechanisms. For hanging wall sites and for fault distances in the 4 to 24 km range, V/H ratios are higher at high frequencies by a maximum of about 30% for M greater than about 6 (Abrahamson and Somerville, 1996; Abrahamson and Silva, 1997). These effects should be considered in developing vertical component spectra for both WUS and CEUS sites, when the geometry of a site with respect to a dominant fault is known.

Figure 4-33 illustrates the distance dependencies for each magnitude, showing a stronger distance effect with increasing magnitude. The peaks in the V/H ratios near 15 Hz are stable with magnitude and distance, and are controlled by the frequency of maximum spectral amplification for the vertical motions. The slight troughs in the ratios in the 1-3 Hz frequency range vary with magnitude (see Figure 4-32) and are controlled by the peaks (maximum spectral amplifications) in the horizontal component spectra. These features, as well as the differences in magnitude scaling between horizontal and vertical spectra, are illustrated in Figures 4-34 and 4-35. These figures show expected median spectra (5% damped) for horizontal and vertical components from the Abrahamson and Silva, 1997 empirical relations for a suite of magnitudes. For the horizontal component spectra, Figure 4-34 shows the strong shift in peak values with increasing magnitude while the vertical spectra (Figure 4-35) show peaks at a constant frequency in the 10-20 Hz range.

The location of peaks in V/H ratios results from peaks in the vertical spectra and are likely controlled by the shallow damping (Figure 2-4 and Appendix K). As a result, these peaks are expected to occur at a higher frequency for CEUS hard rock conditions, which have lower damping values (Appendix K). Additionally, for WUS empirical relations, smaller V/H ratios occur at low frequency (≤ 2 Hz) with soil sites (Appendix K) where the effects of nonlinearity in the horizontal component is small. This suggests that for linear response conditions, the V/H ratio increases with profile stiffness. As a result, V/H ratios for hard rock conditions in the CEUS would be expected to be somewhat higher overall than WUS soft rock conditions.

These trends suggest that magnitude and distance dependencies may be largely captured by the expected peak acceleration of the horizontal motions, with larger V/H ratios associated with higher expected horizontal peak accelerations. The trends in Figures 4-32 and 4-33 clearly show V/H ratios exceeding unity at high frequencies for distances out to about 20 km for M 7.5 earthquakes. The average expected horizontal peak acceleration for M 7.5 at 20 km is about 0.3g suggesting that the current R.G. 1.60 ratio may be appropriate for conditions where the design peak accelerations are less than about 0.3g. The conventional assumption of vertical spectra taken as a constant 2/3 the horizontal is unconservative in the 10 to 30 Hz frequency range even out to 50 km.

To provide for a reasonable accommodation of magnitude and distance dependency in the revised vertical motions for WUS rock site conditions, Figure 4-36 shows recommended V/H ratios for

ranges of expected horizontal peak accelerations. These ratios are simply the averages of the empirical relations. The values are listed in Table 4-4. The ranges in horizontal peak accelerations are intended to capture important M and R dependencies, maintain reasonable conservatism, and result in a procedure that is simple to implement. Direct multiplication of the revised horizontal shapes by these smooth V/H ratios is intended to result in smooth vertical spectra appropriate for design and analyses.

4.7.2 V/H Ratios For CEUS Rock Site Conditions

For applications to CEUS hard rock site conditions, the only numerous empirical V/H ratios available are for small magnitude ($M \leq 5$) earthquakes recorded at distances beyond about 20 km at hard rock sites (Atkinson, 1993). This empirical ratio, computed for Fourier amplitude spectra, is defined only from 1 Hz to 10 Hz and decreases from a value of 0.9 at 1 Hz to 0.7 at 10 Hz. The ratio is independent of distance and is based on recordings at sites in the distance range of about 20 to 1,000 km. This trend of decreasing V/H ratio in the 1 to 10 Hz frequency range, although weak, is opposite to the trend shown in the WUS V/H ratios. This difference may reflect differences in Fourier amplitude and response spectra but the average value of about 0.8 suggests higher V/H ratios at large distance for CEUS rock sites than WUS rock sites. For linear response conditions, this trend is consistent with increasing V/H ratios as profile stiffness increases. This results from less shear-wave (SV) energy being converted from the vertical component to the horizontal component due to wave refraction, for stiffer profiles.

A few V/H ratios are available from recordings at CEUS rock sites (and other intraplate sites) for earthquakes with magnitudes greater than M 5. Figure 4-37 shows results from the M 5.9 Saguenay and M 6.8 Nahanni and Gazli earthquakes. For the Saguenay earthquake, the V/H ratio varies between about 0.7 and 1 suggesting a higher ratio in the CEUS than the WUS at large distances (average distance is 111 km). While the ratio was computed from a large number of sites, it is still a single earthquake that is both deep, with a hypocentral depth of about 30 km, and considered anomalous in its high frequency spectral levels (Boore and Atkinson, 1992). For the larger magnitude data (Gazli and Nahanni earthquakes) only three sites are available for V/H ratios. Sites Karakyr and S1, for the Gazli and Nahanni earthquakes respectively, are located very close to the rupture surfaces at an average distance of about 4.5 km. Site Karakyr is not considered a hard rock site, having about 1.4 km of sedimentary rock (with some clays) overlying a hard schist basement rock (Hartzell, 1980). This geology, with an estimated kappa value of 0.015 sec, may be considered a CEUS soft rock site (Silva and Darragh, 1995). The V/H ratio for the most distant Nahanni site at 16 km (S3, Figure 4-37), shows ratios consistent with those of the Saguenay earthquake, ranging from about 0.6 to about 1 for frequencies above 1 Hz. Interestingly, for frequencies ≤ 0.6 Hz, the V/H ratio is near 2. These V/H ratios from Nahanni are for only a single earthquake, as with Saguenay, and at only a single site but they do suggest the possibility of higher ratios for CEUS sites as well as a high degree of uncertainty in the ratios.

For the near source V/H ratios (distance of 4.5 km), Figure 4-37 shows ratios near unity up to about 5 Hz and values near 2 for frequencies above 10 Hz. These trends are consistent at the two sites for the two earthquakes. Both sites (Karakyr and Site 1) have vertical peak accelerations exceeding 1g (1.3g for Gazli and 2.1g for Nahanni, Appendix A), about double the average horizontal peak

accelerations. These results, reflecting few data for poorly understood earthquakes and largely unknown site conditions, indicate that very large V/H ratios may be likely at very close rupture distances to CEUS earthquakes. Larger than average high frequency (≥ 3 Hz) ratios likely result from both S1 and Karakyr being located on the hanging wall of the fault. As with the more distant Nahanni site, S3, these results suggest higher V/H ratios for CEUS rock sites than WUS sites and show that ratios at near-fault sites can be quite large at high frequencies.

To develop recommended V/H values for applications to CEUS rock sites, the simple point source model (Section 4.3) was extended to consider P-SV waves and was used to estimate vertical component spectra (Appendix K; EPRI, 1993). The model predicts the general trends in the WUS V/H ratios and has been validated at rock sites that recorded the 1989 M 6.9 Loma Prieta earthquake (EPRI, 1993), so V/H ratios computed for the generic CEUS rock site conditions (Figure 2-2) may be used with reasonable confidence to develop guidelines. The V/H ratios predicted by the model for CEUS conditions are illustrated in Figure 4-38. The low frequency peaks (1 to 30 Hz) result from resonances associated with compressional- and shear-wave velocity profiles and would be smoothed out if the velocities were randomized. The peak in the ratios near 60 Hz is associated with the vertical spectra and corresponds to the peak in the WUS ratios (Figures 4-35 and 4-36) but shifted from about 15 to 20 Hz to about 60 Hz because of the lower kappa values for the CEUS vertical motions ($\kappa = 0.003$ sec). The magnitude dependencies in the CEUS ratios are smaller than for the WUS probably because the WUS model currently does not include magnitude saturation, apart from a stress drop that decreases with increasing magnitude (Section 6; Atkinson and Silva, 1997). Since this stress drop scaling affects both vertical and horizontal components equally, the simple model does not show the same trends as the empirical V/H ratios (Figure 4-32). However, the model does show higher ratios at low frequencies (< 3 Hz) than the WUS ratios, consistent with available observations. Based on the trends shown in the model predictions as well as the CEUS recordings, a reasonable approach to defining recommended ratios is to shift the WUS ratios to higher frequencies, so that the peaks correspond to about 60 Hz. Also the low frequency WUS levels should be scaled up by about 50% (factor of 1.5), a proportion reflected in comparing the CEUS and WUS model estimates of the V/H ratios (Appendix K). The recommended ratios are shown in Figure 4-39 and are listed in Table 4-5. Maintaining the same peak acceleration ranges in the horizontal component for the CEUS V/H ratios adds conservatism necessitated by the large uncertainties. For cases where the site is located on the hanging wall of a dipping fault within a rupture distance of about 20 km, the V/H ratio could be significantly larger ($\approx 30\%$) for large magnitude earthquakes, warranting careful site-specific studies.

To illustrate the vertical spectra resulting from the process of scaling the horizontal spectra, Figure 4-40 shows WUS vertical motions while Figures 4-41 and 4-42 show corresponding CEUS vertical motions. Both WUS and CEUS verticals are based on the M 6.4 bin shapes shown in Figures 4-26 and 4-27 and reflect vertical motions relative to 1g horizontal motions. For the WUS verticals, the vertical peak acceleration exceeds the horizontal for horizontal peak accelerations exceeding 0.5g. For peak horizontal accelerations in the 0.2 to 0.5g range, the vertical spectra exceed the horizontal spectra in the frequency range of about 10 to 30 Hz, but the vertical peak accelerations are lower than the horizontal. At low frequency, below about 3 Hz, the verticals spectra are about one half the horizontal. For the CEUS verticals shown in Figures 4-41 and 4-42, both the single and double

corner vertical spectra show trends relative to the horizontals that are similar to the WUS but shifted to higher frequencies, as expected.

In general, both WUS and CEUS V/H ratios provide smooth and reasonable vertical motions when applied to the recommended spectral shapes for horizontal components.

4.8 Intermediate Rock Site Conditions

For rock site conditions intermediate to the CEUS and WUS (which have kappa values of 0.006 sec and 0.04 sec respectively), an appropriate mix of the WUS and CEUS shapes should be based on a site specific kappa value. Weights for the WUS and CEUS rock shapes can easily be determined using the following equations:

$$\kappa_s = \kappa_W W_W + \kappa_E W_E \quad (4-10)$$

$$W_W + W_E = 1 \quad (4-11)$$

where κ_s is the site specific kappa value, W_W and W_E are the WUS and CEUS shape weights, and κ_W and κ_E are the WUS and CEUS rock kappa values. For κ_s values outside κ_W and κ_E , the shape for the closest kappa value should be used.

If a site specific kappa value is not available, a reasonable approach would be to use the inverse of the average shear-wave velocity over the top 30m in Equation 4.10 in lieu of the kappa values (see Equation D5, Appendix D). Appropriate average shear-wave velocity values for the WUS and CEUS rock sites are 520m/sec and 2,800m/sec respectively. The weights used for the CEUS and WUS shapes should also be used for a weighted V/H ratio.

4.9 Estimation of Spectra For Other Dampings

Several methods are available to estimate design response spectra for dampings other than 5%. All are based on scaling the 5% damped spectrum higher or lower. The scaling factors are a function of natural frequency.

4.9.1 Random Vibration Methods

The most theoretically consistent method of accounting for damping is through random vibration theory. The recommended procedure is as follows.

For frequencies $1 \leq f < 5$ Hz, the procedure of Rosenblueth (1980) should be used. This scales the spectral acceleration SA at any frequency f and damping ξ by spectral acceleration at $\xi = 0.05$ by:

$$SA(f, \xi) = SA(f, 0.05) \left[\frac{1 + 4.9 \xi f D}{1 + 4.9 \times 0.05 f D} \right]^{-0.41} \quad (4.12)$$

where D is strong motion duration. For frequencies of 5 Hz and above, the recommended procedure is based on the concept of Vanmarcke (1976) that the response is controlled by a static portion (governed by PGA) and a dynamic portion (governed by equation 4.10). This procedure provides a transition to the peak ground acceleration (PGA)-controlled portion of the spectrum in a realistic way as follows:

$$SA(f, \xi) = \left\{ PGA^2 + [SA(f, 0.05)^2 - PGA^2] \left[\frac{1 + 4.9 \xi f D}{1 + 4.9 \times 0.05 f D} \right]^{-0.82} \right\}^{1/2} \quad (4.13)$$

where the second term on the right-hand-side (involving a subtraction) should not be less than 0.

The strong-motion duration D is distance dependent. For the WUS, D can be estimated from Abrahamson and Silva (1997). For the CEUS, D can be estimated from Atkinson and Boore (1997).

The two equations above allow estimation of dampings in the range of 0.5% to 20% from a design spectrum that is developed for 5% damping. These equations are applicable to both horizontal and vertical motion.

For frequencies below 1 Hz, equation (4.10) can be used as an approximation, but at very low frequencies (0.2 to 0.1 sec) it should be checked to ensure that spectral displacements are approaching the peak ground displacement for all dampings.

4.9.2 Empirical Methods

Several empirical methods have been developed based on recorded motions in California and these can be used to produce spectra at dampings other than 5%.

Abrahamson and Silva (1996) developed a model of the effects of damping based on statistical analyses of strong motion records. Their scaling factor is as follows:

$$\ln \left[\frac{SA(f, \xi)}{SA(f, 5\%)} \right] = \begin{cases} c_1(f, \xi) & \text{for } f > 1.43\text{Hz} \\ c_1(f, \xi) + g_2(f, \xi)(M-6) + g_3(f, \xi)(8.5-M)^2 & \text{for } f < 1.43\text{Hz} \end{cases} \quad (4.14)$$

Coefficients for equation 4.12 are listed in Tables 4-6 through 4-8. Separate coefficients are given for horizontal and vertical motions, and scaling factors are reported for periods of 5 sec to 0.02 sec (0.2 Hz to 50 Hz). They are applicable to damping values between 0.5% and 20%.

Idriss (1993) also developed empirical scale factors for damping based on ground motions during the 1971 San Fernando and 1979 Imperial Valley earthquakes. His scale factor is defined as:

$$\frac{SA(f, \xi)}{SA(f, 5\%)} = \begin{cases} a_1 - b_1 \ln(\xi) & \text{for } \xi \leq 5\% \\ a_2 - b_2 \ln(\xi) & \text{for } \xi > 5\% \end{cases} \quad (4.15)$$

The coefficients a_1 , a_2 , b_1 and b_2 , are listed in Table 4-9 for a range of natural periods from 0.03 sec to 5 sec (33 Hz to 0.2 Hz). These scaling factors are applicable to horizontal motions and to damping values between 1% and 15% (Idriss, personal communication, 1999).

Newmark and Hall (1978) recommended scale factors for different damping values, but these were for different parts of the spectrum controlled by peak acceleration, velocity, and displacement. That is, separate scaling factors were not developed frequency-by-frequency, but were developed for the high-frequency range (3 to 8 Hz), the mid-frequency range (.3 to 3 Hz) and the low-frequency range (below 0.3 Hz). This worked well when scaling spectra from peak values but would leave discontinuities if applied to uniform hazard spectra. For this reason the Newmark and Hall damping factors are not recommended.

References

- Abrahamson, N.A. and W.J. Silva (1996). *Empirical ground motion models*, Rept submitted to Brookhaven Nat'l Lab., May 6.
- Abrahamson, N.A. and W.J. Silva (1997). "Empirical response spectral attenuation relations for shallow crustal earthquakes." *Seism. Soc. Am.*, 68(1), 94-127.
- Abrahamson, N.A. and K.M. Shedlock (1997). "Overview." *Seism. Research Lett.*, 68(1), 9-23.
- Abrahamson, N.A. and P.G. Somerville (1996). "Effects of hanging wall and foot wall on ground motions and recorded during the Northridge earthquake." *Bull. Seism. Soc. Am.* 86(1B), S93-S99.
- Abrahamson, N.A. and P.G. Somerville (1997). "Empirical response spectral attenuation relations for shallow crustal earthquakes." *Seism. Soc. Am.*, 68(1), 94-127.
- Abrahamson, N.A., P.G. Somerville, C.A. Cornell (1990). "Uncertainty in numerical strong motion predictions" *Proc. Fourth U.S. Nat. Conf. Earth. Engin.*, Palm Springs, CA., 1, 407-416.
- Atkinson, G.M. and D.M. Boore (1998). "Evaluation of models for earthquake source spectra in Eastern North America." *Bull. Seism. Soc. Am.* 88(4), 917-934.
- Atkinson, G.M. and D.M. Boore (1997). "Some comparisons between recent ground-motion relations." *Seism. Res. Lett.* 68(1), 24-40.
- Atkinson, G.M. and D.M. Boore (1995). "Ground motion relations for eastern North America." *Bull. Seism. Soc. Am.*, 85(1), 17-30.
- Atkinson, G.M. and W.J. Silva (1997). "An empirical study of earthquake source spectra for California earthquakes." *Bull. Seism. Soc. Am.* 87(1), 97-113.

- Atkinson, G.M. (1993). "Source spectra for earthquakes in eastern North America." *Bull. Seism. Soc. Am.*, 83(6), 1778-1798.
- Boatwright, J. (1994). "Regional propagation characteristics and source parameters of earthquakes in Northeastern North America." *Bull. Seism. Soc. Am.*, 84(1), 1-15.
- Boatwright, J and G. Choy (1992). "Acceleration source spectra anticipated for large earthquakes in Northeastern North America." *Bull. Seism. Soc. Am.*, 82(2), 660-682.
- Boatwright, J. and L. Seekins (1997). "Response spectra from the 1989 Loma Prieta, California, earthquake regressed for site amplification, attenuation, and directivity." USGS Open-File Report 97-858.
- Boore, D.M., W.B. Joyner, and T.E. Fumal (1997). "Equations for estimating horizontal response spectra and peak acceleration from Western North American earthquakes: A summary of recent work." *Seism. Res. Lett.* 68(1), 128-153.
- Boore, D.M., G.M. Atkinson (1992). "Source spectra for the 1988 Saguenay, Quebec, earthquakes." *Bull. Seism. Soc. Am.*, 82(2), 683-719.
- Boore, D.M. (1983). "Stochastic simulation of high-frequency ground motions based on seismological models of the radiated spectra." *Bull. Seism. Soc. Am.*, 73(6), 1865-1894.
- Boore, D.M. (1986). "The effect of finite bandwidth on seismic scaling relationships." in *Earthquake Source Mechanics, Maurice Ewing Ser.*, S.Das, ed., Amer. Geophys. Union, Wash. D.C. vol.6.
- Brillinger, D.R., and H.K. Preisler (1984). An exploratory analysis of the Joyner-Boore attenuation data, *Bull. Seism. Soc. Am.*, 74, 1441-1450.
- Brillinger, D.R., and H.K. Preisler (1985). Further analysis of the Joyner-Boore attenuation data, *Bull. Seism. Soc. Am.*, 75, 611-614.
- Campbell, K W. (1997). "Empirical near-source attenuation relationships for horizontal and vertical components of peak ground acceleration, peak ground velocity, and pseudo-absolute acceleration response spectra." *Bull. Seism. Soc. Am.*, 68(1), 154-176.
- Campbell, K. W. (1993) "Empirical prediction of near-source ground motion from large earthquakes." in V.K. Gaur, ed., *Proceedings, Intern'l Workshop on Earthquake Hazard and Large Dams in the Himalya*. INTACH, New Delhi, p. 93-103.
- Choy, G.L. and J. Boatwright (1988). "Teleseismic and near-field analysis of the Nahanni earthquakes in the Northwest Territories, Canada." *Bull. Seism. Soc. Am.*, 78(5), 1627-1652.

- EPRI (1993). "Guidelines for determining design basis ground motions." Electric Power Research Institute, Palo Alto, CA, Rept. TR-102293, vol 1-5:
 vol. 1: Methodology and guidelines for estimating earthquake ground motion in eastern North America.
 vol. 2: Appendices for ground motion estimation.
 vol. 3: Appendices for field investigations.
 vol. 4: Appendices for laboratory investigations.
 vol. 5: Quantification of seismic source effects.
- Hanks, T.C., and R.K. McGuire (1981). "The character of high-frequency strong ground motion." *Bull. Seism. Soc. Am.*, 71(6), 2071-2095.
- Hartzell, S. (1980). "Faulting Process of the May 17, 1976, Gazli, USSR Earthquake." *Bull. Seism. Soc. Am.*, 70(5), 1715-1736.
- Idriss, I.M. (1991). "Earthquake ground motions at soft soil sites." *Proceedings: 2nd Int'l Confer. on Recent Advances in Geotechnical Earthquake Engineering and Soil Dynamics*, Saint Louis, Missouri, Invited Paper LP01, 2265-2272.
- Idriss, I.M. (1993). "Procedures for selecting earthquake ground motions at rock sites," Nat. Inst. of Stan. And Tech., Rept. NIST GCR 93-625.
- Kimball, J.K. (1983). "The use of site dependent spectra." *Proc. Workshop on Site-Specific Effects of Soil and Rock on Ground Motion and the Importance for Earthquake-Resistant Design*, Santa Fe, New Mexico, USGS Open-File Rept. 83-845, 410-422.
- Mohraz, B., W.J. Hall and N.M. Newmark (1972). "A study of vertical and horizontal earthquake spectra." Nathan M. Newmark Consulting Engineering Services, Urbana, Illinois: *AEC Report No. WASH-1255*.
- Newmark, N.M. and W.J. Hall (1978). "Development of criteria for seismic review of selected nuclear power plants." US Nuc. Reg. Comm., NUREG/CR-0098, May.
- Newmark, N.M., W.J. Hall, and B. Mohraz (1973). *A Study of Vertical and Horizontal Earthquake Spectra*. Directorate of Licensing, U.S. Atomic Energy Commission, Rept. WASH-1255.
- Newmark, N.M., J.A. Blume and K.K. Kapur (1973). "Seismic design criteria for nuclear power plants." *Journal of the Power Division*, ASCE 99, 287-303.
- Regulatory Guide 1.60 (1973). "*Design response spectra for seismic design of nuclear power plants.*" U.S. Atomic Energy Commission, Directorate of Regulatory Standards.
- Roblee, C.J., W.J. Silva, G.R. Toro, and N. Abrahamson (1996). "Variability in Site-Specific Seismic Ground-Motion Predictions." Uncertainty in the Geologic Environment: From Theory to Practice, *Proceedings Uncertainty '96 ASCE Specialty Conference*, Edited by C.D. Shackelford, P.P. Nelson, and M.J.S. Roth, Madison, WI, Aug. 1-3, pp. 1113-1133.

- Rosenblueth, E. (1980) Characteristics of Earthquakes, In E. Rosenblueth, editor, *Design of Earthquake Resistant Structures*, Ch. 1, Wiley.
- Sadigh, K., C.-Y. Chang, J.A. Egan, F. Makdisi, and R.R. Youngs (1997). "Attenuation relationships for shallow crustal earthquakes based on California strong motion data." *Bull. Seism. Soc. Am.*, 68(1), 180-189.
- Sadigh, K., C.-Y. Chang, N.A. Abrahamson, S.J. Chiou, and M.S. Power (1993). "Specification of long-period ground motions: Updated attenuation relationships for rock site conditions and adjustment factors for near-fault effects." in *Proc. ATC-17-1, Seminar on Seismic Isolation, Passive Energy Dissipation, and Active Control, March 11-12, San Francisco, California*, 59-70.
- Silva, W.J., N.A. Abrahamson, G.R. Toro, C.J. Costantino (1997). "Description and validation of the stochastic ground motion model." Report to Brookhaven National Laboratory, Associated Universities, Inc. Upton, New York, Contract 770573.
- Silva, W.J. and R. Darragh (1995). "Engineering characterization of earthquake strong ground motion recorded at rock sites." EPRI, Palo Alto, CA, Rept. TR-102261.
- Silva, W.J. (1991). "Global characteristics and site geometry." Chapter 6 in *Proceedings: NSF/EPRI Workshop on Dynamic Soil Properties and Site Characterization*. Electric Power Research Institute, Palo Alto, CA, Rept. NP-7337.
- Silva, W.J., and R.K. Green (1989). "Magnitude and distance scaling of response spectral shapes for rock sites with applications to North American tectonic environment." *Earthquake Spectra*, 5(3), 591-624.
- Seed, H.B., C. Ugas and J. Lysmer. (1976). "Site-dependent spectra for earthquake resistant design." *Bull. Seism. Soc. Am.*, 66(1), 221-243.
- Somerville, P.G., N.F. Smith, R.W. Graves, and N.A. Abrahamson, (1997). "Modification of empirical strong ground motion attenuation relations to include the amplitude and duration effects of rupture directivity." *Seism. Res. Lett.*, 68(1), 199-222.
- Somerville, P.G. and N.A. Abrahamson (1995). "Ground motion prediction for thrust earthquakes." *Proc. of the SMIP95 Seminar on Seismological and Engineering Implications of Recent Strong Motion Data*, San Francisco, California.
- Vanmarcke, E.H. (1976). Structural response to earthquakes, in *Seismic Risk and Engineering Decisions*, edited by C. Lomnitz and E. Rosenblueth, Elsevier Publishing Co., Amsterdam, London, New York.
- Youngs, R.R., S.J. Chiou, W.J. Silva, and J.R. Humphrey (1997), "Strong ground motion attenuation relationships for subduction zone earthquakes." *Seism. Res. Lett.*, 68(1), 58-73.

Youngs, R.R., N.A. Abrahamson, F. Makdisi, and K. Sadigh (1995). "Magnitude dependent dispersion in peak ground acceleration." *Bull. Seism. Soc. Am.*, 85(1), 1161-1176.

Table 4-1 WUS STATISTICAL SHAPE BINS								
Magnitude Bins (M)								
Range				Bin Center				
5 - 6				5.5				
6 - 7				6.5				
7+				7.5				
Distance Bin (km)	\bar{M}	\bar{R} (km)	Number of Spectra	PGA* (g), σ_{ln}	PGV* (cm/sec), σ_{ln}	PGD* (cm), σ_{ln}	$\frac{PGV^*}{PGA} (\frac{cm/sec}{g}), \sigma_{ln}$	$\frac{PGA \cdot PGD^*}{PGV^2}, \sigma_{ln}$
0 - 10, rock	5.54	7.91	30	0.18, 0.91	8.14, 1.14	0.80, 1.60	44.50, 0.58	2.17, 0.28
	6.53	5.75	32	0.44, 0.76	32.65, 0.93	06.22, 1.26	73.51, 0.40	2.54, 0.42
	7.27	4.20	6	0.93, 0.26	81.73, 0.25	47.42, 0.66	87.94, 0.39	6.47, 0.60
0 - 10, soil	5.76	7.80	24	0.26, 0.65	18.57, 0.56	3.11, 0.46	70.72, 0.33	2.32, 0.35
	6.46	6.00	77	0.38, 0.43	46.88, 0.59	14.79, 0.89	122.00, 0.44	2.54, 0.41
	7.05	8.90	4	0.40, 0.62	44.46, 0.56	21.27, 0.25	110.42, 0.07	4.25, 0.24
10 - 50, rock	5.57	21.80	180	0.11, 0.87	5.08, 0.85	0.54, 1.04	46.96, 0.37	2.24, 0.38
	6.43	30.28	238	0.13, 0.73	8.81, 0.76	1.96, 1.01	70.41, 0.49	3.09, 0.54
	7.27	31.00	6	0.17, 0.85	8.80, 0.88	2.50, 1.56	50.59, 0.37	5.51, 0.90
10 - 50, soil	5.69	21.82	378	0.11, 0.73	6.63, 0.77	0.87, 0.94	59.88, 0.34	2.16, 0.33
	6.35	28.27	542	0.14, 0.63	10.77, 0.74	2.25, 1.04	78.77, 0.41	2.57, 0.41

* median values

Table 4-1 (cont.)
WUS STATISTICAL SHAPE BINS

Magnitude Bins (M)								
Range				Bin Center				
5 - 6				5.5				
6 - 7				6.5				
7+				7.5				
Distance Bin (km)	\bar{M}	\bar{R} (km)	Number of Spectra	PGA*(g), σ_{ln}	PGV*(cm/sec), σ_{ln}	PGD*(cm), σ_{ln}	$\frac{PGV^*}{PGA} (\frac{cm/sec}{g}), \sigma_{ln}$	$\frac{PGA \cdot PGD^*}{PGV^2}, \sigma_{ln}$
10 - 50, soil	7.29	33.46	56	0.16, 0.35	22.38, 0.38	10.46, 0.39	141.17, 0.36	3.25, 0.56
50 - 100, rock	5.91	64.27	34	0.05, 0.40	2.22, 0.53	0.21, 0.83	41.16, 0.43	2.24, 0.57
	6.51	70.35	102	0.06, 0.51	3.87, 0.82	0.79, 1.23	69.89, 0.56	2.88, 0.56
	7.32	81.46	10	0.06, 0.52	5.16, 0.87	2.64, 1.17	80.63, 0.45	6.23, 0.50
50 - 100, soil	5.80	67.22	42	0.06, 0.80	3.12, 0.78	0.38, 0.92	53.20, 0.23	2.28, 0.49
	6.49	67.34	158	0.07, 0.67	6.23, 0.78	1.26, 0.99	88.00, 0.42	2.26, 0.44
	7.31	76.57	14	0.10, 0.12	11.24, 0.34	5.42, 0.60	111.37, 0.35	4.24, 0.50
100 - 200, rock	5.4	107.80	2	0.02, ----	1.16, ----	0.10, ----	49.72, ----	1.74, ----
	6.64	114.57	14	0.02, 0.86	2.03, 0.38	1.09, 0.68	132.54, 0.59	3.98, 0.27
	7.30	152.01	14	0.03, 0.47	5.55, 0.66	2.43, 1.06	184.16, 0.35	2.34, 0.31
100 - 200, soil	6.0	105.00	2	0.03, ----	1.50, ----	0.11, ----	42.92, ----	1.74, ----

* median values

Table 4-1 (cont.)
WUS STATISTICAL SHAPE BINS

Magnitude Bins (M)								
Range				Bin Center				
5 - 6				5.5				
6 - 7				6.5				
7+				7.5				
Distance Bin (km)	\bar{M}	\bar{R} (km)	Number of Spectra	PGA**(g), σ_{ln}	PGV*(cm/sec), σ_{ln}	PGD*(cm), σ_{ln}	$\frac{PGV^*}{PGA} (\frac{cm/sec}{g}), \sigma_{ln}$	$\frac{PGA \cdot PGD^*}{PGV^2}, \sigma_{ln}$
100 - 200, soil	6.64	132.97	28	0.03, 0.78	3.05, 0.58	0.89, 0.97	98.24, 0.53	2.90, 0.42
	7.31	147.07	88	0.04, 0.25	8.09, 0.39	3.50, 0.76	188.64, 0.36	2.25, 0.29
0 - 50, rock	5.57	19.91	208	0.12, 0.89	5.39, 0.91	0.57, 1.14	46.73, 0.40	2.22, 0.37
	6.44	27.39	270	0.15, 0.84	10.27, 0.89	2.24, 1.10	70.77, 0.48	3.02, 0.53
	7.27	17.60	12	0.40, 1.07	26.82, 1.35	10.89, 1.94	66.70, 0.46	5.97, 0.69
0 - 50, soil	5.69	21.10	398	0.12, 0.75	7.02, 0.79	0.93, 0.97	60.48, 0.34	2.16, 0.33
	6.37	25.50	619	0.16, 0.70	12.93, 0.87	2.85, 1.20	83.17, 0.44	2.57, 0.41
	7.27	31.82	60	0.17, 0.42	23.43, 0.42	10.97, 0.42	138.87, 0.36	3.30, 0.55

4-28

**Median values

Table 4-2
POINT-SOURCE PARAMETERS*

	WUS	CEUS
$\Delta\sigma$ (bars)	65	120
kappa (sec)	0.040	0.006
Q_0	220	351
η	0.60	0.84
β (km/sec)	3.50	3.52
ρ (g/cc)	2.70	2.60
Amplification	soft rock (Figure 2-3)	hard rock (Figure 2-3)
Double Corner	Atkinson and Silva (1997)	Atkinson (1993)

* based on Silva et al. (1997)

Table 4-3 RESPONSE SPECTRAL SHAPE COEFFICIENTS FOR 5% DAMPING			
	WUS	CEUS (1C)*	CEUS (2C)*
C_1	1.8197	0.88657	0.97697
C_2	0.30163	$\exp(-10.411)$	$\exp(-9.4827)$
C_3	$0.47498+0.034356M+0.0057204\ln(R+1)$	2.5099	2.3006
C_4	$-12.650+M\cdot[2.4796-0.14732M+0.034605\ln(0.040762R+1)]$	$-7.4408+M[1.5220-0.088588M+0.0073069\ln(0.12639R+1)]$	$-12.665+M[2.4869-0.14562M+0.024477\ln(0.041807R+1)]$
C_5	-0.25746	-0.34965	-0.21002
C_6	$0.29784+0.010723M-0.0000133R$	$-0.31162+0.0019646R$	$0.74361+0.0000671R$
C_7	n.a.	3.7841	$\exp[-13.476+M(4.4007-0.31651M+0.000235R)]$
C_8	n.a.	-0.89019	$0.95259+M(-0.58275+0.000166R)$
C_9	n.a.	$0.39806+0.058832M$	$-3.3534+0.44094M$

Note: Equation (4-8) is used for the WUS; equation (4-9) is used for the CEUS.

M = moment magnitude

R = fault distance

*1C = single corner frequency model

2 C = double corner frequency model

Table 4-4
RECOMMENDED V/H RATIOS FOR WUS ROCK SITE CONDITIONS

Frequency (Hz)	$\leq 0.2g^*$	0.2 - 0.5g*	$> 0.5g^*$
.100+00	.503E+00	.558E+00	.696E+00
.333E+00	.503E+00	.558E+00	.696E+00
.500E+00	.461E+00	.508E+00	.651E+00
.667E+00	.458E+00	.495E+00	.645E+00
.100E+01	.440E+00	.461E+00	.608E+00
.118E+01	.434E+00	.454E+00	.597E+00
.133E+01	.431E+00	.451E+00	.592E+00
.167E+01	.420E+00	.447E+00	.585E+00
.200E+01	.416E+00	.447E+00	.583E+00
.217E+01	.417E+00	.452E+00	.592E+00
.250E+01	.426E+00	.467E+00	.616E+00
.278E+01	.436E+00	.482E+00	.638E+00
.333E+01	.456E+00	.511E+00	.681E+00
.417E+01	.495E+00	.571E+00	.758E+00
.500E+01	.536E+00	.628E+00	.836E+00
.588E+01	.581E+00	.691E+00	.918E+00
.666E+01	.625E+00	.751E+00	.997E+00
.833E+01	.715E+00	.888E+00	.119E+01
.100E+02	.796E+00	.101E+01	.137E+01
.111E+02	.840E+00	.107E+01	.144E+01
.125E+02	.885E+00	.112E+01	.150E+01
.167E+02	.904E+00	.114E+01	.152E+01
.200E+02	.888E+00	.112E+01	.148E+01
.250E+02	.810E+00	.102E+01	.133E+01
.333E+02	.744E+00	.912E+00	.117E+01
.500E+02	.704E+00	.848E+00	.107E+01
.100E+03	.704E+00	.848E+00	.107E+01

*Range in rock outcrop horizontal component peak acceleration

Table 4-5 RECOMMENDED V/H RATIOS FOR CEUS ROCK SITE CONDITIONS			
Frequency (Hz)	$\leq 0.2g^*$	0.2 - 0.5g*	$> 0.5g^*$
0.10	0.67	0.75	0.90
10.00	0.67	0.75	0.90
18.75	0.70	0.81	1.01
22.06	0.73	0.85	1.08
25.00	0.75	0.88	1.12
31.25	0.77	0.95	1.25
37.50	0.81	1.00	1.37
41.67	0.84	1.07	1.44
46.88	0.85	1.12	1.50
62.50	0.90	1.14	1.52
75.00	0.89	1.12	1.48
93.75	0.81	1.02	1.33
100.0	0.78	1.00	1.30

*Range in rock outcrop horizontal component peak acceleration

Table 4-6a
Horizontal c_1 values for separate damping levels
for equation (4.12), Abrahamson and Silva (1996)

Period (sec)	c_1 (0.5%)	c_1 (1.0%)	c_1 (2.0%)	c_1 (3.0%)	c_1 (7.0%)	c_1 (10.0%)	c_1 (15.0%)	c_1 (20.0%)
5.00	0.3698	0.2891	0.1830	0.1084	-0.0812	-0.1763	-0.2964	-0.3899
4.00	0.3955	0.3092	0.1957	0.1159	-0.0869	-0.1886	-0.3171	-0.4170
3.00	0.4233	0.3310	0.2095	0.1241	-0.0930	-0.2018	-0.3393	-0.4463
2.00	0.4526	0.3538	0.2239	0.1326	-0.0994	-0.2157	-0.3628	-0.4471
1.50	0.4667	0.3648	0.2309	0.1368	-0.1025	-0.2225	-0.3741	-0.4920
1.00	0.4780	0.3737	0.2365	0.1401	-0.1050	-0.2279	-0.3832	-0.5040
0.85	0.4801	0.3753	0.2375	0.1407	-0.1054	-0.2289	-0.3848	-0.5061
0.75	0.4808	0.3759	0.2379	0.1409	-0.1056	-0.2292	-0.3854	-0.5069
0.60	0.4808	0.3759	0.2379	0.1409	-0.1056	-0.2292	-0.3854	-0.5069
0.50	0.4808	0.3759	0.2379	0.1409	-0.1056	-0.2292	-0.3854	-0.5069
0.46	0.4808	0.3759	0.2379	0.1409	-0.1056	-0.2292	-0.3854	-0.5069
0.40	0.4808	0.3759	0.2379	0.1409	-0.1056	-0.2292	-0.3854	-0.5069
0.36	0.4808	0.3759	0.2379	0.1409	-0.1056	-0.2292	-0.3854	-0.5069
0.30	0.4808	0.3759	0.2379	0.1409	-0.1056	-0.2292	-0.3854	-0.5069
0.24	0.4808	0.3759	0.2379	0.1409	-0.1056	-0.2292	-0.3854	-0.5069
0.20	0.4808	0.3759	0.2379	0.1409	-0.1056	-0.2292	-0.3854	-0.5069
0.17	0.4808	0.3759	0.2379	0.1409	-0.1056	-0.2292	-0.3854	-0.5069
0.15	0.4616	0.3609	0.2284	0.1353	-0.1014	-0.2200	-0.3700	-0.4866
0.12	0.4327	0.3383	0.2141	0.1268	-0.0950	-0.2063	-0.3469	-0.4562
0.10	0.3885	0.3037	0.1922	0.1138	-0.0853	-0.1852	-0.3114	-0.4096
0.09	0.3630	0.2838	0.1796	0.1064	-0.0797	-0.1730	-0.2910	-0.3827
0.07	0.3193	0.2496	0.1580	0.0936	-0.0701	-0.1522	-0.2559	-0.3366
0.06	0.2654	0.2075	0.1313	0.0778	-0.0583	-0.1265	-0.2127	-0.2798
0.05	0.2212	0.1729	0.1094	0.0648	-0.0486	-0.1054	-0.1773	-0.2332
0.04	0.1673	0.1308	0.0828	0.0490	-0.0367	-0.0798	-0.1341	-0.1764
0.03	0.0933	0.0729	0.0462	0.0273	-0.0205	-0.0445	-0.0748	-0.0983
0.02	0.0000	0.0000	0.0000	0.0000	0.0000	0.0000	0.0000	0.0000

Table 4-6b
Vertical c_1 values for separate damping levels
for equation (4.12), Abrahamson and Silva (1996)

Period (sec)	c_1 (0.5%)	c_1 (1.0%)	c_1 (2.0%)	c_1 (3.0%)	c_1 (7.0%)	c_1 (10.0%)	c_1 (15.0%)	c_1 (20.0%)
5.00	0.4135	0.3230	0.2033	0.1196	-0.0871	-0.1872	-0.3114	-0.4065
4.00	0.4462	0.3485	0.2193	0.1291	-0.0940	-0.2020	-0.3359	-0.4385
3.00	0.4814	0.3760	0.2366	0.1393	-0.1014	-0.2180	-0.3625	-0.4372
2.00	0.5186	0.4050	0.2549	0.1500	-0.1093	-0.2348	-0.3904	-0.5097
1.50	0.5365	0.4190	0.2637	0.1552	-0.1131	-0.2429	-0.4039	-0.5273
1.00	0.5511	0.4304	0.2709	0.1594	-0.1161	-0.2495	-0.4149	-0.5417
0.85	0.5538	0.4325	0.2722	0.1602	-0.1167	-0.2507	-0.4169	-0.5443
0.75	0.5548	0.4333	0.2727	0.1605	-0.1169	-0.2512	-0.4177	-0.5453
0.60	0.5548	0.4333	0.2727	0.1605	-0.1169	-0.2512	-0.4177	-0.5453
0.50	0.5548	0.4333	0.2727	0.1605	-0.1169	-0.2512	-0.4177	-0.5453
0.46	0.5548	0.4333	0.2727	0.1605	-0.1169	-0.2512	-0.4177	-0.5453
0.40	0.5548	0.4333	0.2727	0.1605	-0.1169	-0.2512	-0.4177	-0.5453
0.36	0.5548	0.4333	0.2727	0.1605	-0.1169	-0.2512	-0.4177	-0.5453
0.30	0.5548	0.4333	0.2727	0.1605	-0.1169	-0.2512	-0.4177	-0.5453
0.24	0.5647	0.4411	0.2776	0.1634	-0.1190	-0.2557	-0.4252	-0.5551
0.20	0.5776	0.4511	0.2839	0.1671	-0.1217	-0.2615	-0.4348	-0.5677
0.17	0.5920	0.4623	0.2910	0.1713	-0.1247	-0.2680	-0.4457	-0.5818
0.15	0.5965	0.4658	0.2932	0.1726	-0.1257	-0.2701	-0.4491	-0.5862
0.12	0.5880	0.4593	0.2890	0.1701	-0.1239	-0.2662	-0.4427	-0.5780
0.10	0.5732	0.4477	0.2818	0.1658	-0.1208	-0.2595	-0.4316	-0.5634
0.09	0.5471	0.4273	0.2689	0.1583	-0.1153	-0.2477	-0.4119	-0.5378
0.07	0.5062	0.3954	0.2488	0.1464	-0.1067	-0.2292	-0.3811	-0.4976
0.06	0.4615	0.3604	0.2268	0.1335	-0.0972	-0.2090	-0.3475	-0.4536
0.05	0.4216	0.3293	0.2072	0.1220	-0.0888	-0.1909	-0.3174	-0.4144
0.04	0.3751	0.2930	0.1844	0.1085	-0.0790	-0.1698	-0.2824	-0.3687
0.03	0.2507	0.1958	0.1232	0.0725	-0.0528	-0.1135	-0.1887	-0.2464
0.02	0.0000	0.0000	0.0000	0.0000	0.0000	0.0000	0.0000	0.0000

Table 4-7a
 Horizontal g_2 values for separate damping levels
 for equation (4.12), Abrahamson and Silva (1996)

Period (sec)	g_2 (0.5%)	g_2 (1.0%)	g_2 (2.0%)	g_2 (3.0%)	g_2 (7.0%)	g_2 (10.0%)	g_2 (15.0%)	g_2 (20.0%)
5.00	0.0214	0.0168	0.0106	0.0063	-0.0047	-0.0102	-0.0172	-0.0226
4.00	0.0189	0.0148	0.0094	0.0055	-0.0042	-0.0090	-0.0152	-0.0199
3.00	0.0157	0.0122	0.0078	0.0046	-0.0034	-0.0075	-0.0126	-0.0165
2.00	0.0111	0.0087	0.0055	0.0032	-0.0024	-0.0053	-0.0089	-0.0117
1.50	0.0078	0.0061	0.0039	0.0023	-0.0017	-0.0037	-0.0063	-0.0083
1.00	0.0033	0.0025	0.0016	0.0010	-0.0007	-0.0016	-0.0026	-0.0034
0.85	0.0014	0.0011	0.0007	0.0004	-0.0003	-0.0007	-0.0011	-0.0015
0.75	0.0	0.0	0.0	0.0	0.0	0.0	0.0	0.0
0.60	0.0	0.0	0.0	0.0	0.0	0.0	0.0	0.0
0.50	0.0	0.0	0.0	0.0	0.0	0.0	0.0	0.0
0.46	0.0	0.0	0.0	0.0	0.0	0.0	0.0	0.0
0.40	0.0	0.0	0.0	0.0	0.0	0.0	0.0	0.0
0.36	0.0	0.0	0.0	0.0	0.0	0.0	0.0	0.0
0.30	0.0	0.0	0.0	0.0	0.0	0.0	0.0	0.0
0.24	0.0	0.0	0.0	0.0	0.0	0.0	0.0	0.0
0.20	0.0	0.0	0.0	0.0	0.0	0.0	0.0	0.0
0.17	0.0	0.0	0.0	0.0	0.0	0.0	0.0	0.0
0.15	0.0	0.0	0.0	0.0	0.0	0.0	0.0	0.0
0.12	0.0	0.0	0.0	0.0	0.0	0.0	0.0	0.0
0.10	0.0	0.0	0.0	0.0	0.0	0.0	0.0	0.0
0.09	0.0	0.0	0.0	0.0	0.0	0.0	0.0	0.0
0.07	0.0	0.0	0.0	0.0	0.0	0.0	0.0	0.0
0.06	0.0	0.0	0.0	0.0	0.0	0.0	0.0	0.0
0.05	0.0	0.0	0.0	0.0	0.0	0.0	0.0	0.0
0.04	0.0	0.0	0.0	0.0	0.0	0.0	0.0	0.0
0.03	0.0	0.0	0.0	0.0	0.0	0.0	0.0	0.0
0.02	0.0	0.0	0.0	0.0	0.0	0.0	0.0	0.0

Table 4-7b
 Vertical g_2 values for separate damping levels
 for equation (4.12), Abrahamson and Silva (1996)

Period (sec)	g_2 (0.5%)	g_2 (1.0%)	g_2 (2.0%)	g_2 (3.0%)	g_2 (7.0%)	g_2 (10.0%)	g_2 (15.0%)	g_2 (20.0%)
5.00	0.0247	0.0193	0.0122	0.0072	-0.0052	-0.0112	-0.0186	-0.0243
4.00	0.0218	0.0170	0.0107	0.0063	-0.0046	-0.0099	-0.0164	-0.0215
3.00	0.0181	0.0141	0.0089	0.0052	-0.0038	-0.0082	-0.0136	-0.0178
2.00	0.0128	0.0100	0.0063	0.0037	-0.0027	-0.0058	-0.0096	-0.0126
1.50	0.0090	0.0071	0.0044	0.0026	-0.0019	-0.0041	-0.0068	-0.0089
1.00	0.0038	0.0029	0.0018	0.0011	-0.0008	-0.0017	-0.0028	-0.0037
0.85	0.0016	0.0013	0.0008	0.0005	-0.0003	-0.0007	-0.0012	-0.0016
0.75	0.0	0.0	0.0	0.0	0.0	0.0	0.0	0.0
0.60	0.0	0.0	0.0	0.0	0.0	0.0	0.0	0.0
0.50	0.0	0.0	0.0	0.0	0.0	0.0	0.0	0.0
0.46	0.0	0.0	0.0	0.0	0.0	0.0	0.0	0.0
0.40	0.0	0.0	0.0	0.0	0.0	0.0	0.0	0.0
0.36	0.0	0.0	0.0	0.0	0.0	0.0	0.0	0.0
0.30	0.0	0.0	0.0	0.0	0.0	0.0	0.0	0.0
0.24	0.0	0.0	0.0	0.0	0.0	0.0	0.0	0.0
0.20	0.0	0.0	0.0	0.0	0.0	0.0	0.0	0.0
0.17	0.0	0.0	0.0	0.0	0.0	0.0	0.0	0.0
0.15	0.0	0.0	0.0	0.0	0.0	0.0	0.0	0.0
0.12	0.0	0.0	0.0	0.0	0.0	0.0	0.0	0.0
0.10	0.0	0.0	0.0	0.0	0.0	0.0	0.0	0.0
0.09	0.0	0.0	0.0	0.0	0.0	0.0	0.0	0.0
0.07	0.0	0.0	0.0	0.0	0.0	0.0	0.0	0.0
0.06	0.0	0.0	0.0	0.0	0.0	0.0	0.0	0.0
0.05	0.0	0.0	0.0	0.0	0.0	0.0	0.0	0.0
0.04	0.0	0.0	0.0	0.0	0.0	0.0	0.0	0.0
0.03	0.0	0.0	0.0	0.0	0.0	0.0	0.0	0.0
0.02	0.0	0.0	0.0	0.0	0.0	0.0	0.0	0.0

Table 4-8a
 Horizontal g_3 values for separate damping levels
 for equation (4.12), Abrahamson and Silva (1996)

Period (sec)	g_3 (0.5%)	g_3 (1.0%)	g_3 (2.0%)	g_3 (3.0%)	g_3 (7.0%)	g_3 (10.0%)	g_3 (15.0%)	g_3 (20.0%)
5.00	-0.0166	-0.0130	-0.0082	-0.0049	0.0036	0.0079	0.0133	0.0175
4.00	-0.0146	-0.0114	-0.0072	-0.0043	0.0032	0.0070	0.0117	0.0154
3.00	-0.0121	-0.0095	-0.0060	-0.0036	0.0027	0.0058	0.0097	0.0128
2.00	-0.0086	-0.0067	-0.0042	-0.0025	0.0019	0.0041	0.0069	0.0090
1.50	-0.0061	-0.0047	-0.0030	-0.0018	0.0013	0.0029	0.0049	0.0064
1.00	-0.0025	-0.0020	-0.0012	-0.0007	0.0006	0.0012	0.0020	0.0027
0.85	-0.0011	-0.0009	-0.0005	-0.0003	0.0002	0.0005	0.0009	0.0012
0.75	0.0	0.0	0.0	0.0	0.0	0.0	0.0	0.0
0.60	0.0	0.0	0.0	0.0	0.0	0.0	0.0	0.0
0.50	0.0	0.0	0.0	0.0	0.0	0.0	0.0	0.0
0.46	0.0	0.0	0.0	0.0	0.0	0.0	0.0	0.0
0.40	0.0	0.0	0.0	0.0	0.0	0.0	0.0	0.0
0.36	0.0	0.0	0.0	0.0	0.0	0.0	0.0	0.0
0.30	0.0	0.0	0.0	0.0	0.0	0.0	0.0	0.0
0.24	0.0	0.0	0.0	0.0	0.0	0.0	0.0	0.0
0.20	0.0	0.0	0.0	0.0	0.0	0.0	0.0	0.0
0.17	0.0	0.0	0.0	0.0	0.0	0.0	0.0	0.0
0.15	0.0	0.0	0.0	0.0	0.0	0.0	0.0	0.0
0.12	0.0	0.0	0.0	0.0	0.0	0.0	0.0	0.0
0.10	0.0	0.0	0.0	0.0	0.0	0.0	0.0	0.0
0.09	0.0	0.0	0.0	0.0	0.0	0.0	0.0	0.0
0.07	0.0	0.0	0.0	0.0	0.0	0.0	0.0	0.0
0.06	0.0	0.0	0.0	0.0	0.0	0.0	0.0	0.0
0.05	0.0	0.0	0.0	0.0	0.0	0.0	0.0	0.0
0.04	0.0	0.0	0.0	0.0	0.0	0.0	0.0	0.0
0.03	0.0	0.0	0.0	0.0	0.0	0.0	0.0	0.0
0.02	0.0	0.0	0.0	0.0	0.0	0.0	0.0	0.0

Table 4-8b
 Vertical g_3 values for separate damping levels
 for equation (4.12), Abrahamson and Silva (1996)

Period (sec)	g_3 (0.5%)	g_3 (1.0%)	g_3 (2.0%)	g_3 (3.0%)	g_3 (7.0%)	g_3 (10.0%)	g_3 (15.0%)	g_3 (20.0%)
5.00	-0.0191	-0.0150	-0.0094	-0.0055	0.0040	0.0087	0.0144	0.0188
4.00	-0.0169	-0.0132	-0.0083	-0.0049	0.0036	0.0076	0.0127	0.0166
3.00	-0.0140	-0.0109	-0.0069	-0.0040	0.0029	0.0063	0.0105	0.0138
2.00	-0.0099	-0.0077	-0.0049	-0.0029	0.0021	0.0045	0.0075	0.0097
1.50	-0.0070	-0.0055	-0.0034	-0.0020	0.0015	0.0032	0.0053	0.0069
1.00	-0.0029	-0.0023	-0.0014	-0.0008	0.0006	0.0013	0.0022	0.0029
0.85	-0.0013	-0.0010	-0.0006	-0.0004	0.0003	0.0006	0.0010	0.0012
0.75	0.0	0.0	0.0	0.0	0.0	0.0	0.0	0.0
0.60	0.0	0.0	0.0	0.0	0.0	0.0	0.0	0.0
0.50	0.0	0.0	0.0	0.0	0.0	0.0	0.0	0.0
0.46	0.0	0.0	0.0	0.0	0.0	0.0	0.0	0.0
0.40	0.0	0.0	0.0	0.0	0.0	0.0	0.0	0.0
0.36	0.0	0.0	0.0	0.0	0.0	0.0	0.0	0.0
0.30	0.0	0.0	0.0	0.0	0.0	0.0	0.0	0.0
0.24	0.0	0.0	0.0	0.0	0.0	0.0	0.0	0.0
0.20	0.0	0.0	0.0	0.0	0.0	0.0	0.0	0.0
0.17	0.0	0.0	0.0	0.0	0.0	0.0	0.0	0.0
0.15	0.0	0.0	0.0	0.0	0.0	0.0	0.0	0.0
0.12	0.0	0.0	0.0	0.0	0.0	0.0	0.0	0.0
0.10	0.0	0.0	0.0	0.0	0.0	0.0	0.0	0.0
0.09	0.0	0.0	0.0	0.0	0.0	0.0	0.0	0.0
0.07	0.0	0.0	0.0	0.0	0.0	0.0	0.0	0.0
0.06	0.0	0.0	0.0	0.0	0.0	0.0	0.0	0.0
0.05	0.0	0.0	0.0	0.0	0.0	0.0	0.0	0.0
0.04	0.0	0.0	0.0	0.0	0.0	0.0	0.0	0.0
0.03	0.0	0.0	0.0	0.0	0.0	0.0	0.0	0.0
0.02	0.0	0.0	0.0	0.0	0.0	0.0	0.0	0.0

Table 4-9
Coefficients for Equation (4.13), Idriss (1993)

Period - sec	a_1	b_1	a_2	b_2
0.03	1	0	1	0
0.05	1.1142	0.0709	1.0830	0.0505
0.075	1.3513	0.2183	1.2902	0.1803
0.1	1.4918	0.3056	1.4179	0.2597
0.15	1.5796	0.3601	1.4992	0.3102
0.2	1.6148	0.3820	1.5340	0.3318
0.25	1.6148	0.3820	1.5340	0.3318
0.3	1.6148	0.3820	1.5340	0.3318
0.35	1.6060	0.3765	1.5224	0.3246
0.4	1.5972	0.3711	1.5108	.03174
0.5	1.5796	0.3605	1.4992	0.3102
0.6	1.5445	0.3383	1.4876	0.303
0.7	1.5269	0.3274	1.4876	0.303
0.8	1.5094	0.3165	1.4760	0.2958
0.9	1.4918	0.3056	1.4690	0.2914
1	1.4742	0.2947	1.4644	0.2885
1.5	1.4391	0.2728	1.4644	0.2885
2	1.4216	0.2619	1.4644	0.2885
3	1.4040	0.2510	1.4644	0.2885
4	1.4040	0.2510	1.4644	0.2885
5	1.4040	0.2510	1.4644	0.2885

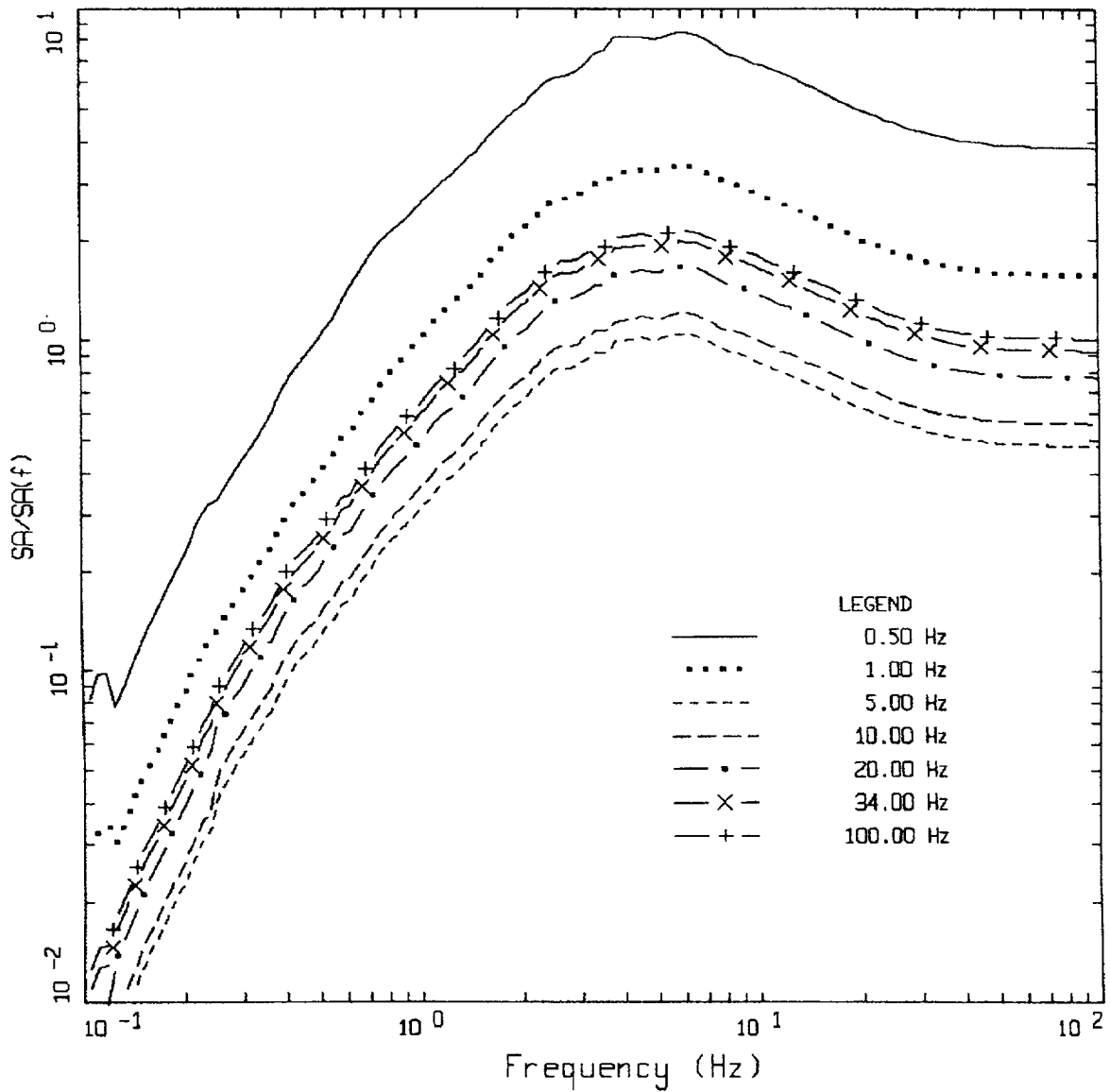
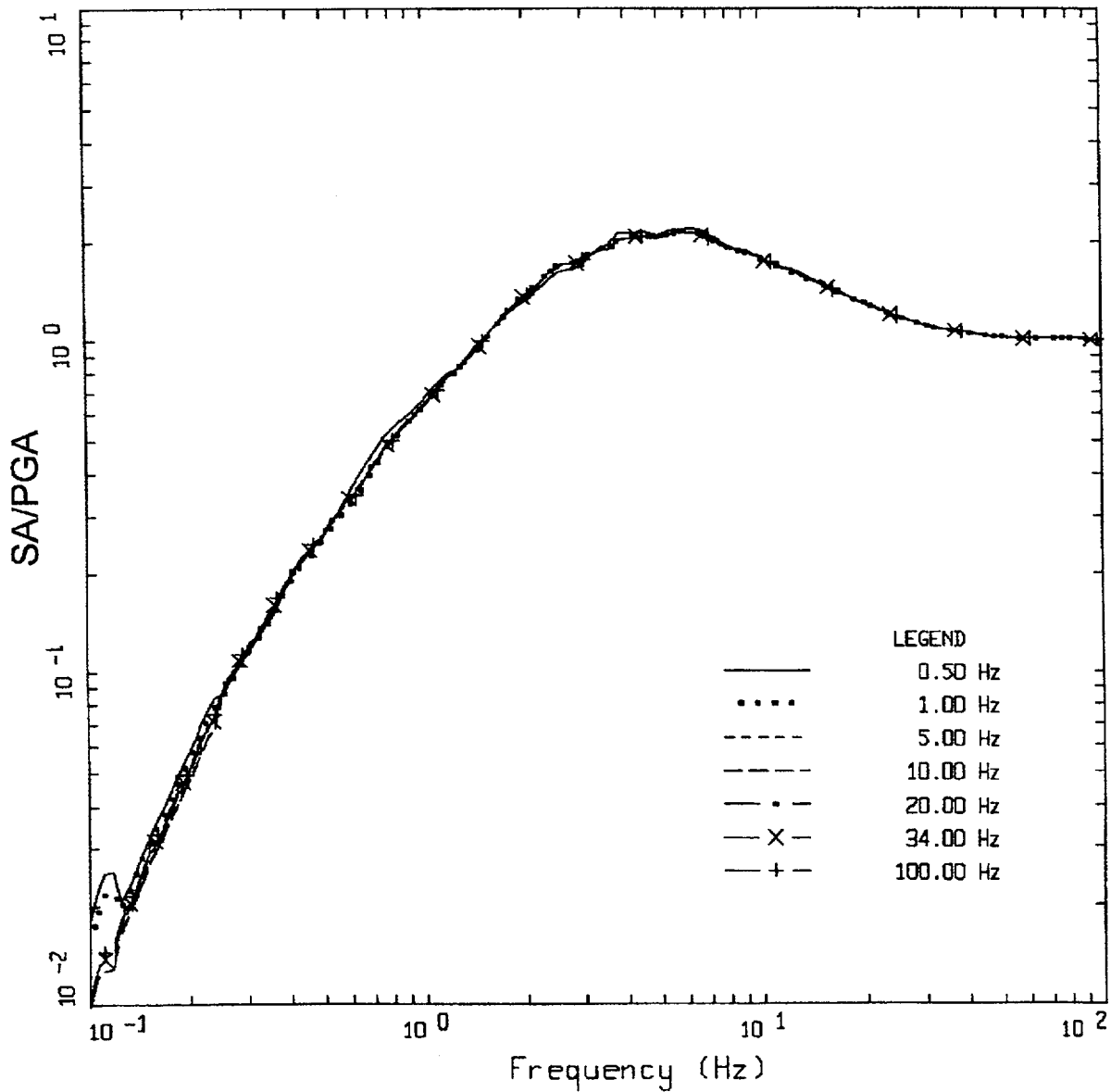
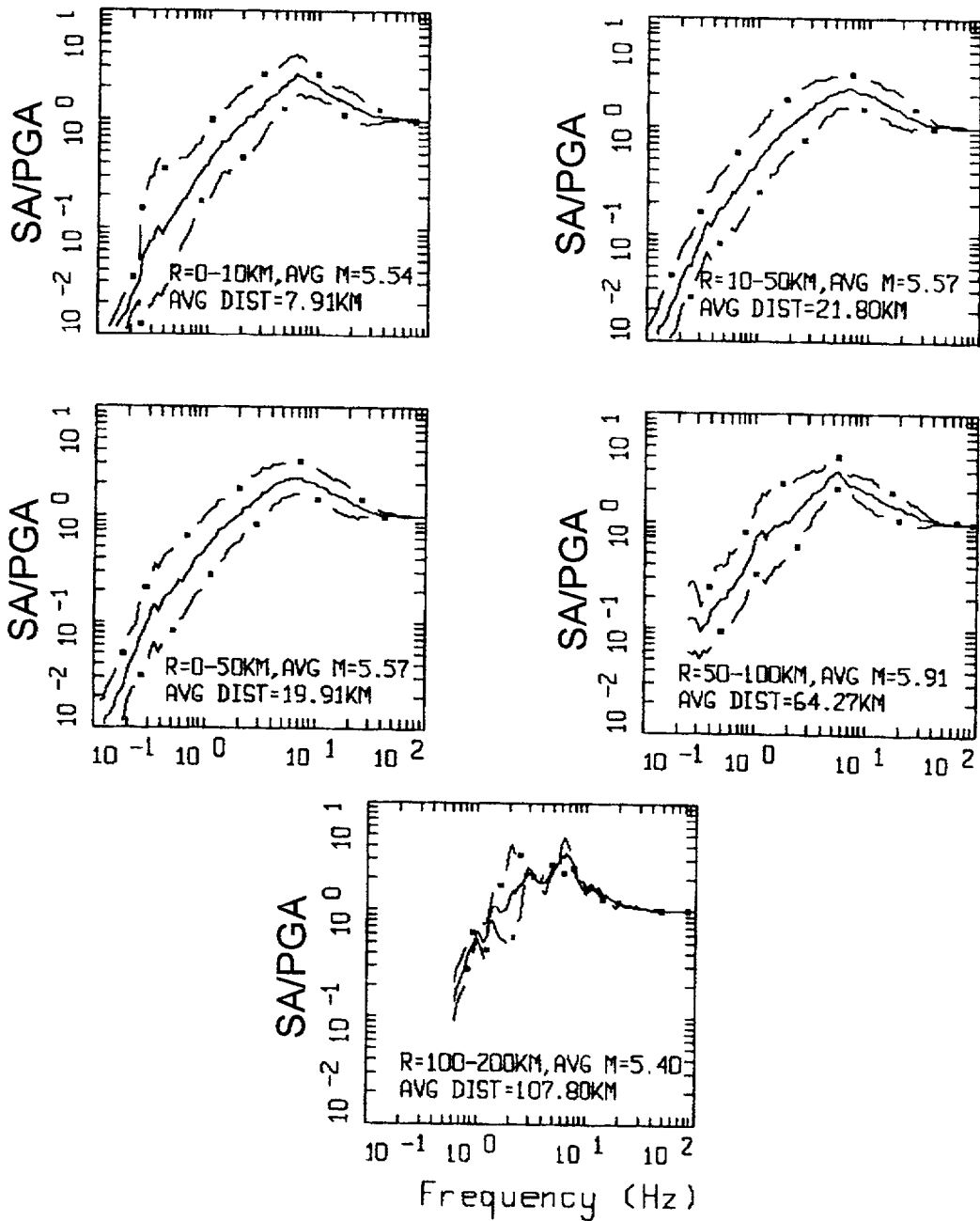


Figure 4-1. Response spectral shapes (5% damping) for the M 6.5, R = 10 to 50 km bins normalized by spectral ordinates at a suite of frequencies (0.5 to 100.0 Hz)



AVERAGE HORIZONTAL SPECTRA, 50TH PERCENTILE
M=6.5 (6.0-7.0), R=10-50 KM, ROCK
AVERAGE M = 6.43, AVERAGE DISTANCE = 30.28 KM

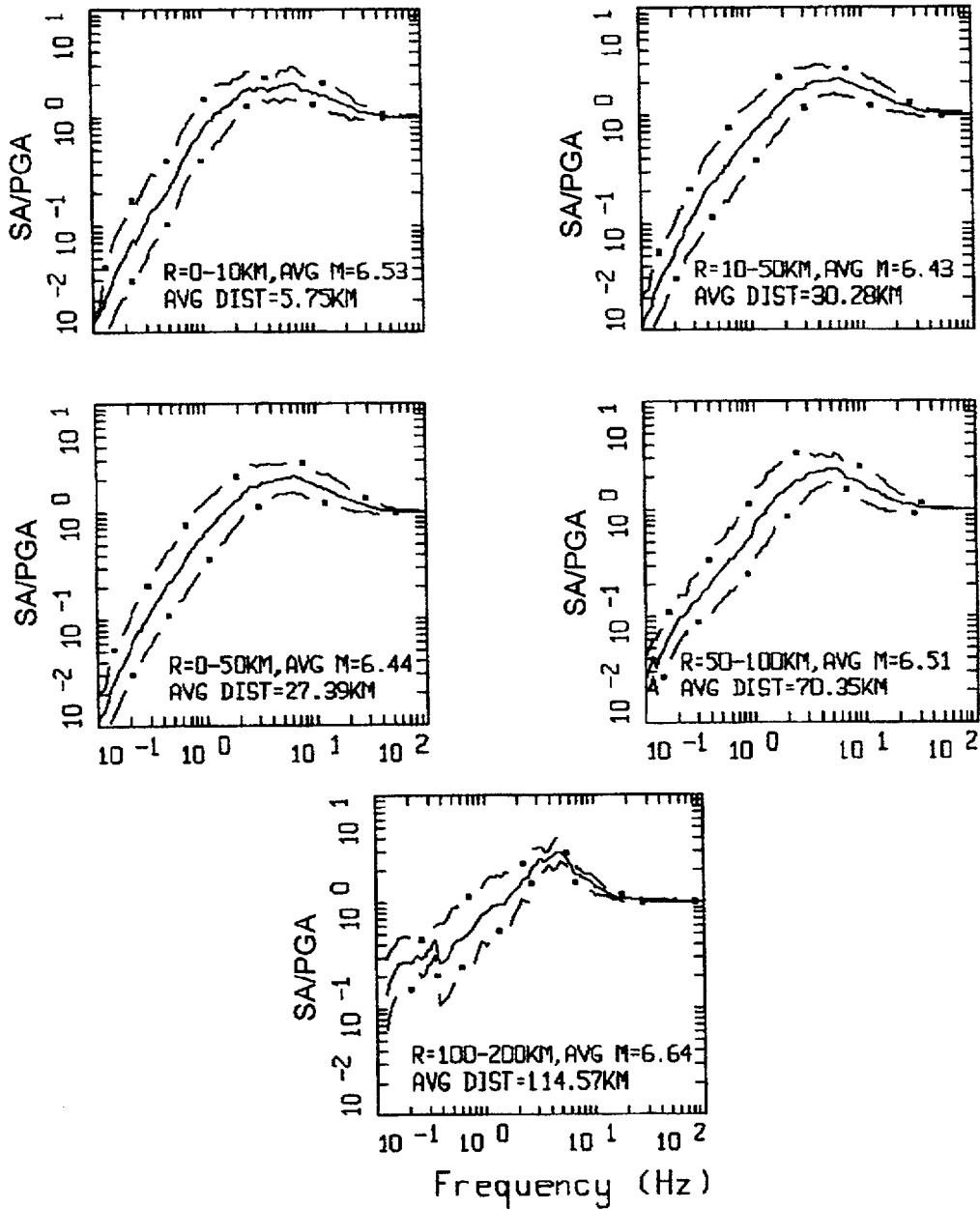
Figure 4-2. Response spectral shapes (5% damping) for the M 6.5, R = 10 to 50 km bins from Figure 1 renormalized by their respective 100 Hz values.



AVERAGE HORIZONTAL SPECTRA, ROCK
 M=5.5 (5.0-6.0)

LEGEND
 — 50TH PERCENTILE
 - . - 84TH PERCENTILE
 - . - 16TH PERCENTILE

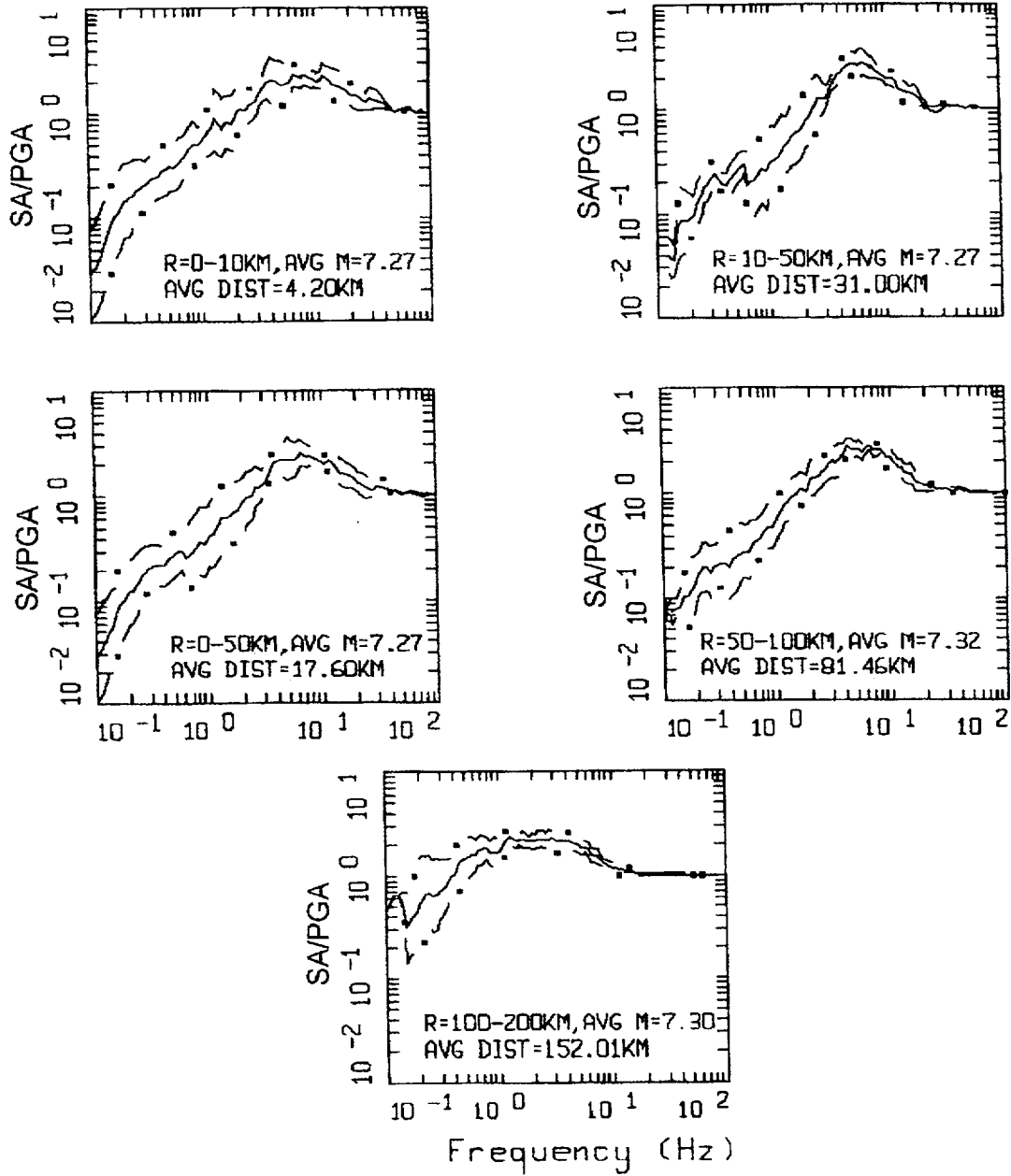
Figure 4-3. Response spectral shapes (5% damping) computed for the $M = 5.5$ magnitude bin for WUS soft rock site conditions.



AVERAGE HORIZONTAL SPECTRA, ROCK
 $M=6.5$ (6.0-7.0)

LEGEND
 ————— 50TH PERCENTILE
 - . - . 84TH PERCENTILE
 - . - . 16TH PERCENTILE

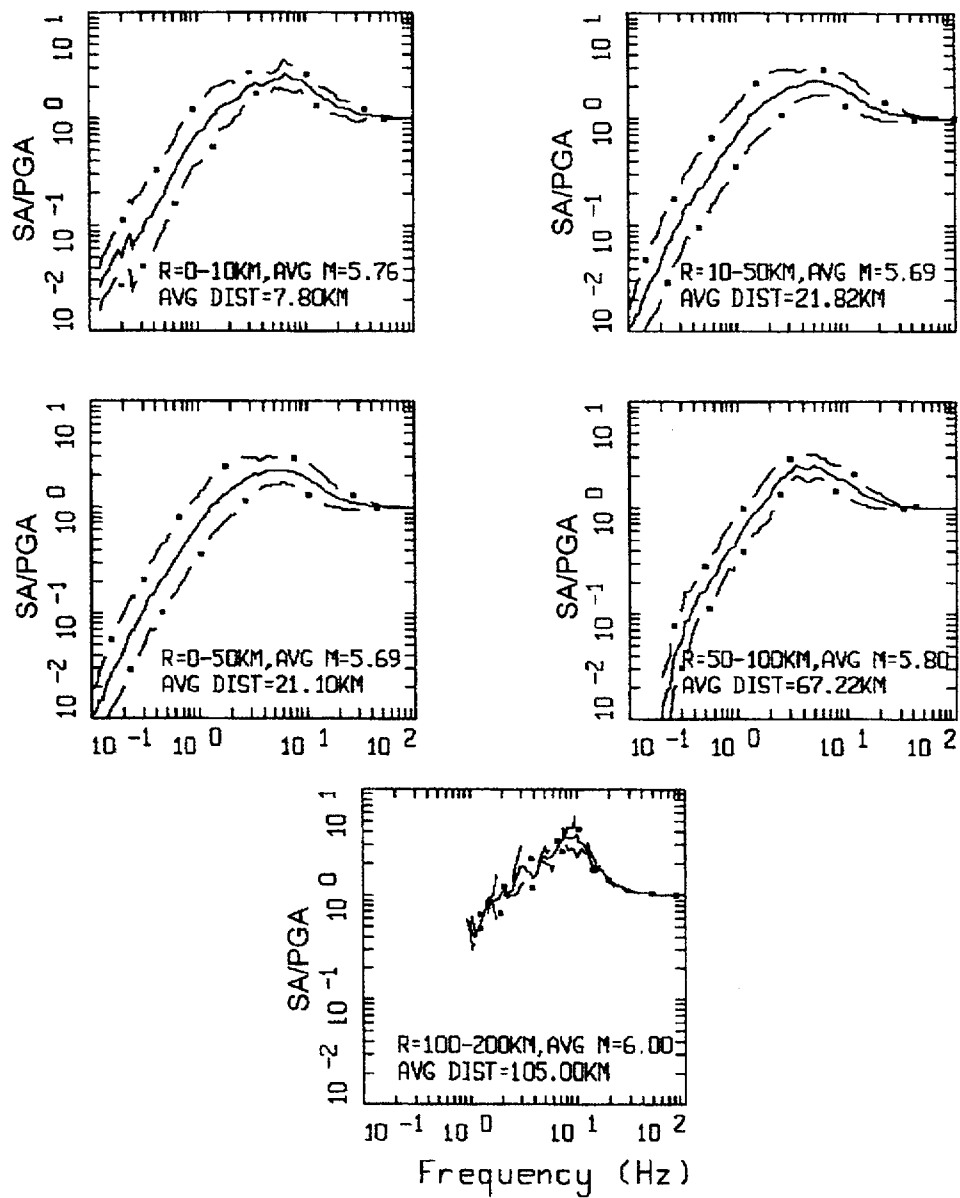
Figure 4-4. Response spectral shapes (5% damping) computed for the $M = 6.5$ magnitude bin for WUS soft rock site conditions.



AVERAGE HORIZONTAL SPECTRA, ROCK
 M=7.5 (7.0-7.0+)

LEGEND
 ————— 50TH PERCENTILE
 — . — 84TH PERCENTILE
 — . — 16TH PERCENTILE

Figure 4-5. Response spectral shapes (5% damping) computed for the $M = 7.5$ magnitude bins for WUS soft rock site conditions.

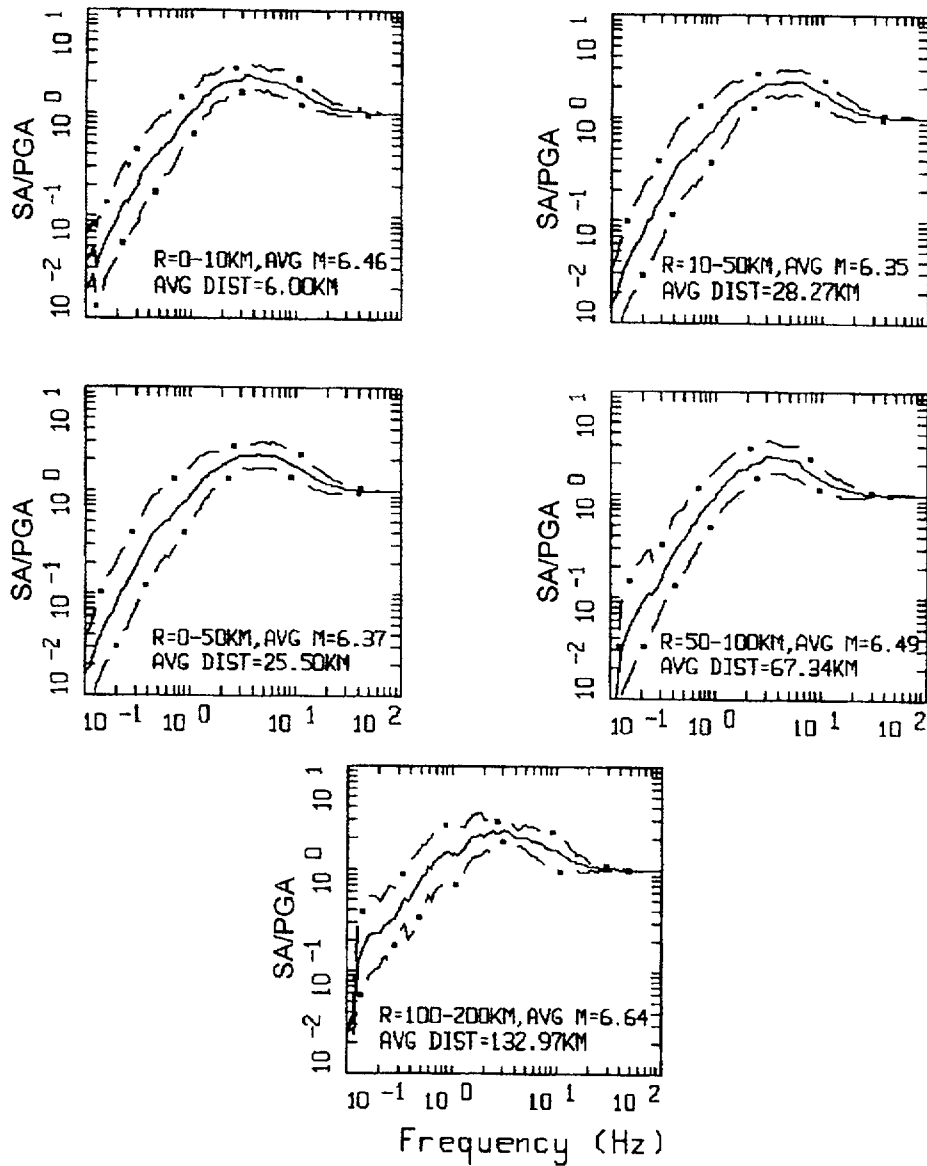


AVERAGE HORIZONTAL SPECTRA, SOIL
 M=5.5 (5.0-6.0)

LEGEND

——— 50TH PERCENTILE
 - · - 84TH PERCENTILE
 - · - 16TH PERCENTILE

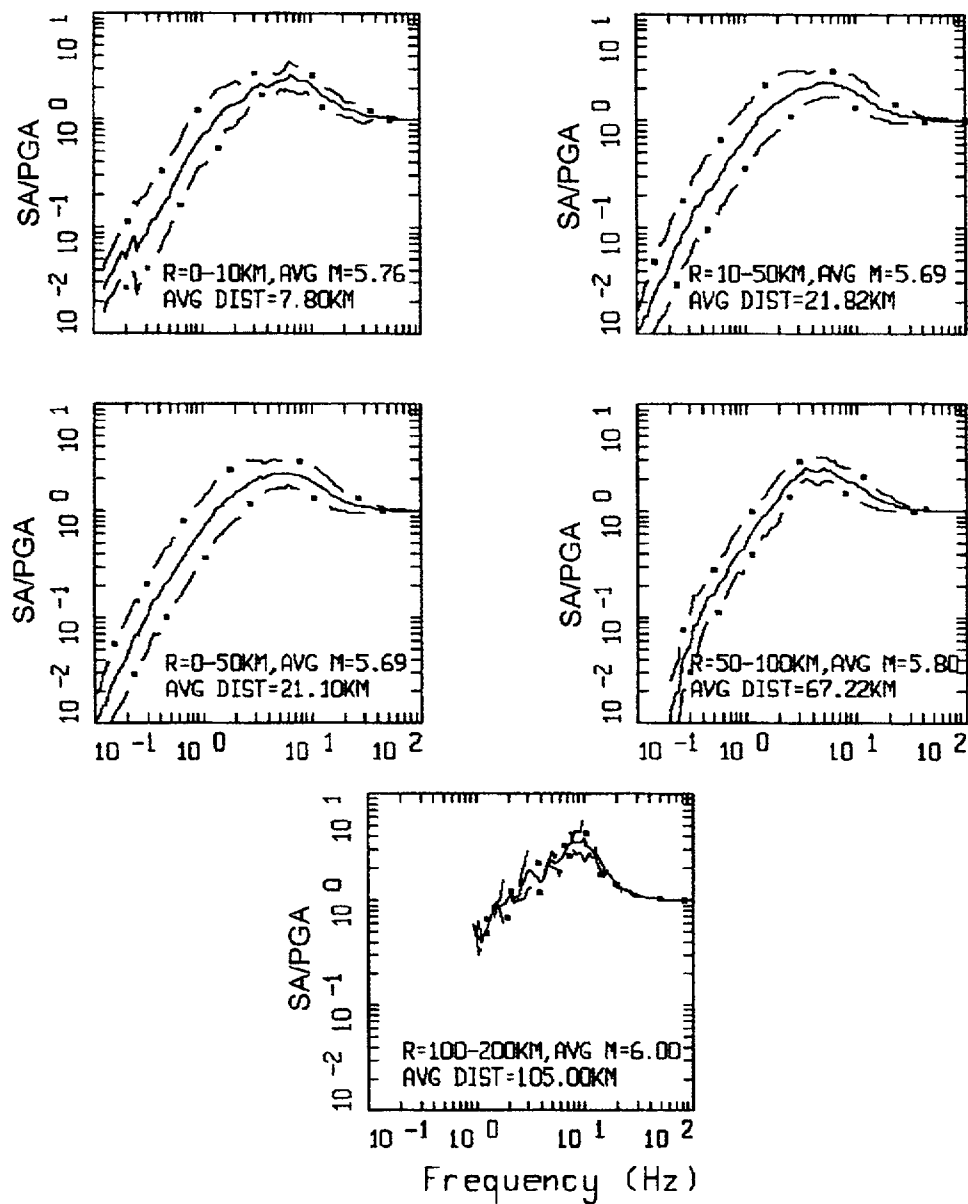
Figure 4-6. Response to spectral shapes (5% damping) computed for the $M = 5.5$ magnitude bins for WUS deep soil site conditions.



AVERAGE HORIZONTAL SPECTRA, SOIL
 M=6.5 (6.0-7.0)

LEGEND
 — 50TH PERCENTILE
 - · - 84TH PERCENTILE
 - · - 16TH PERCENTILE

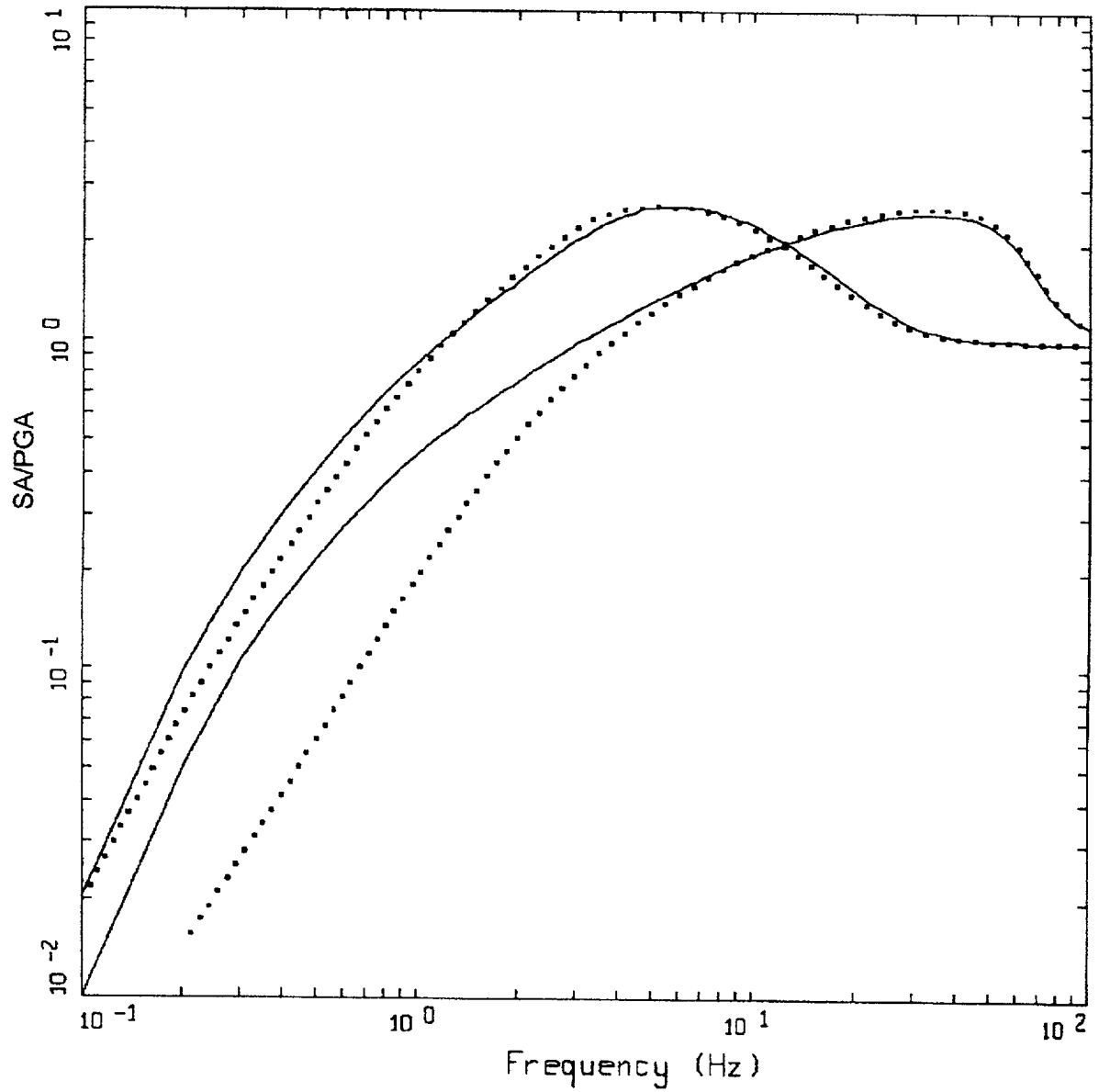
Figure 4-7. Response spectral shapes (5% damping) computed for the $M = 6.5$ magnitude bin for WUS deep soil conditions.



AVERAGE HORIZONTAL SPECTRA, SOIL
 $M=5.5$ (5.0-6.0)

LEGEND
 ————— 50TH PERCENTILE
 - . - . 84TH PERCENTILE
 - . - . 16TH PERCENTILE

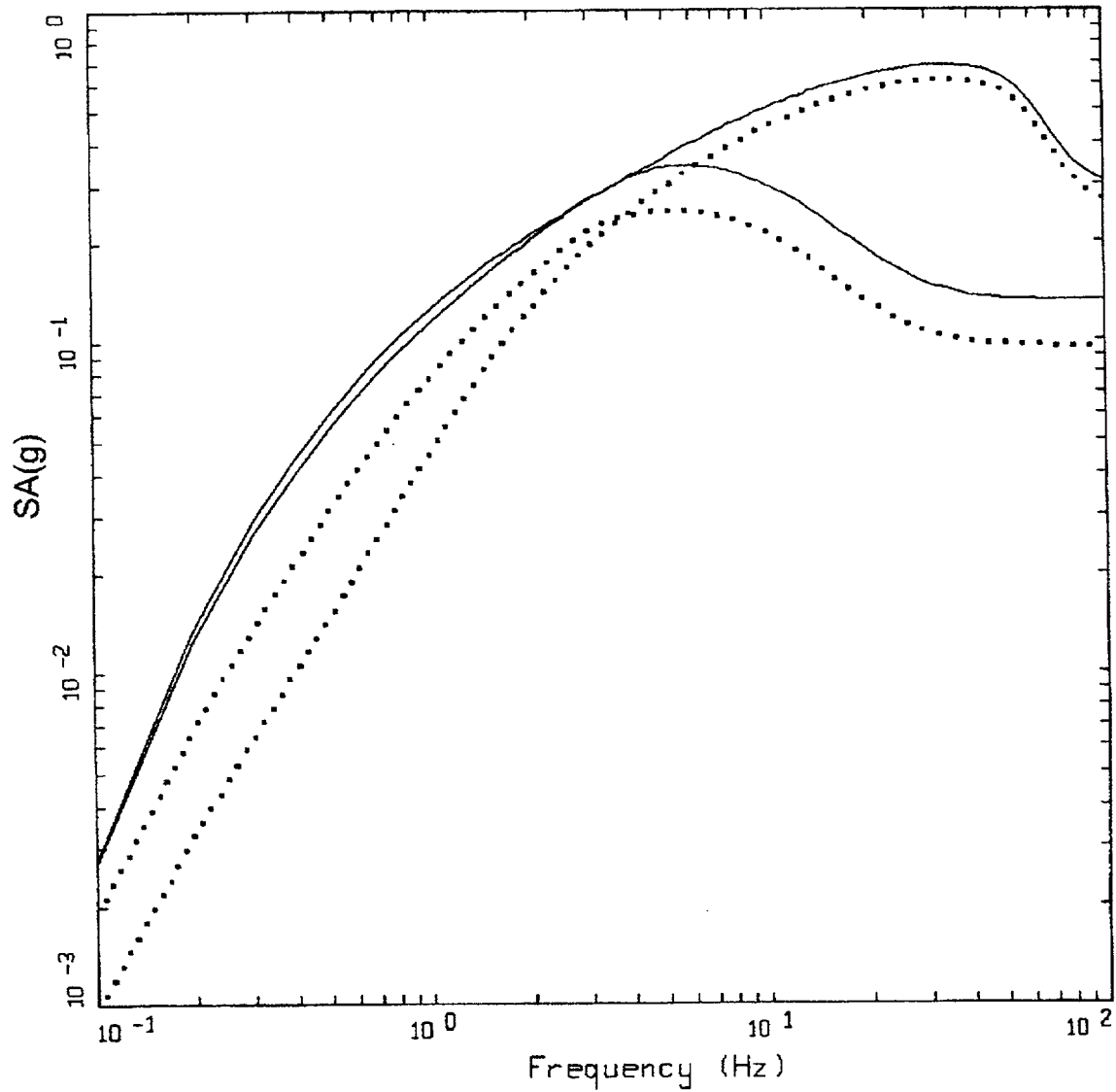
Figure 4-8. Response spectral shapes (5% damping) computed for the $M=7.5$ magnitude bin for WUS deep soil conditions.



POINT-SOURCE MODEL
 $M = 6.5, R = 25 \text{ KM}$

- LEGEND
- WUS ROCK, SINGLE CORNER
 - WUS ROCK, DOUBLE CORNER
 - CEUS ROCK, SINGLE CORNER
 - CEUS ROCK, DOUBLE CORNER

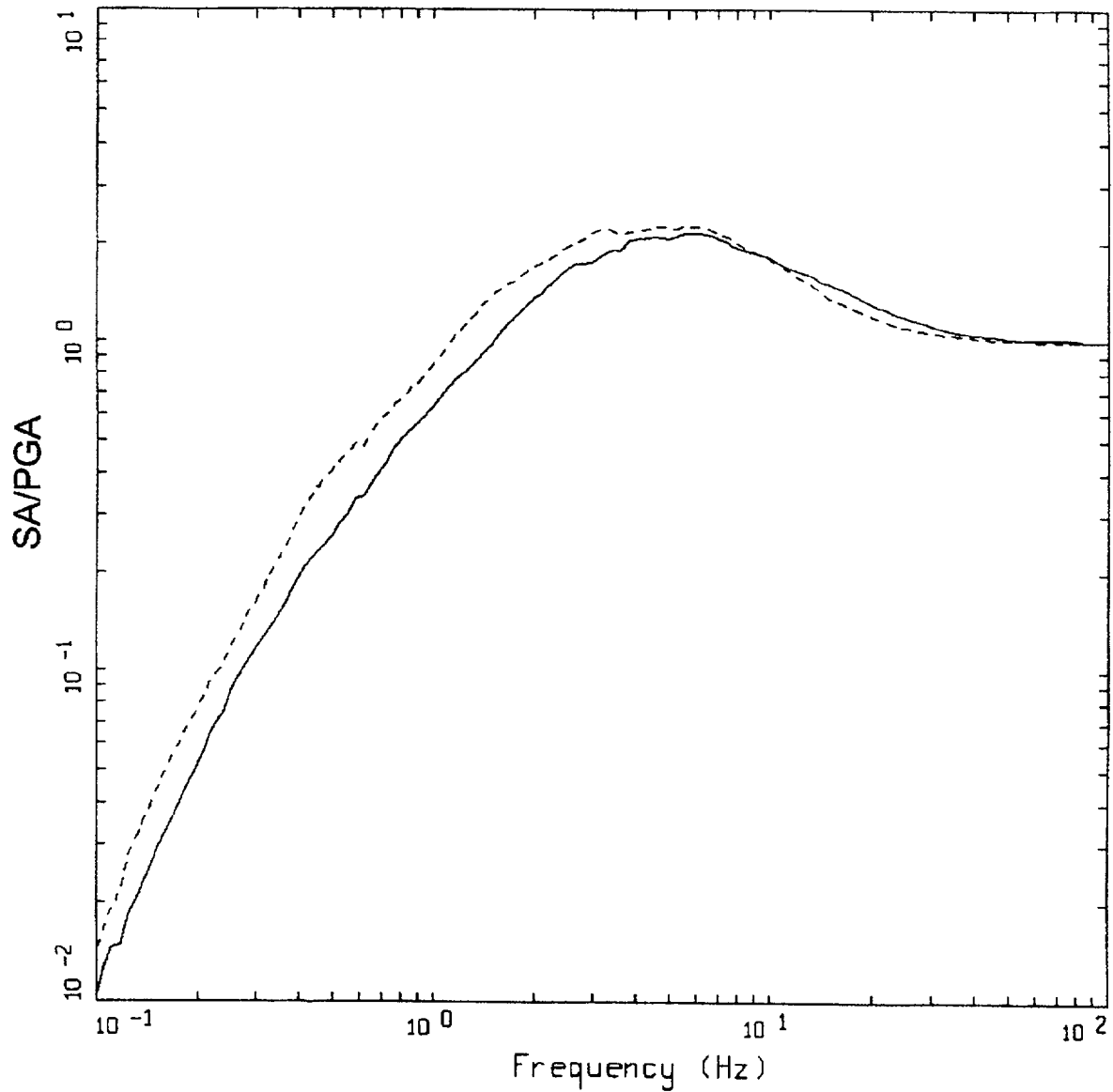
Figure 4-9. Response spectral shapes (5% damping) computed for $M = 6.5$ at $R = 25 \text{ km}$ using both single and double corner frequency source spectra for WUS and CEUS conditions.



POINT-SOURCE MODEL
 M = 6.5, R = 25 KM

- LEGEND
- WUS ROCK, SINGLE CORNER
 - WUS ROCK, DOUBLE CORNER
 - CEUS ROCK, SINGLE CORNER
 - CEUS ROCK, DOUBLE CORNER

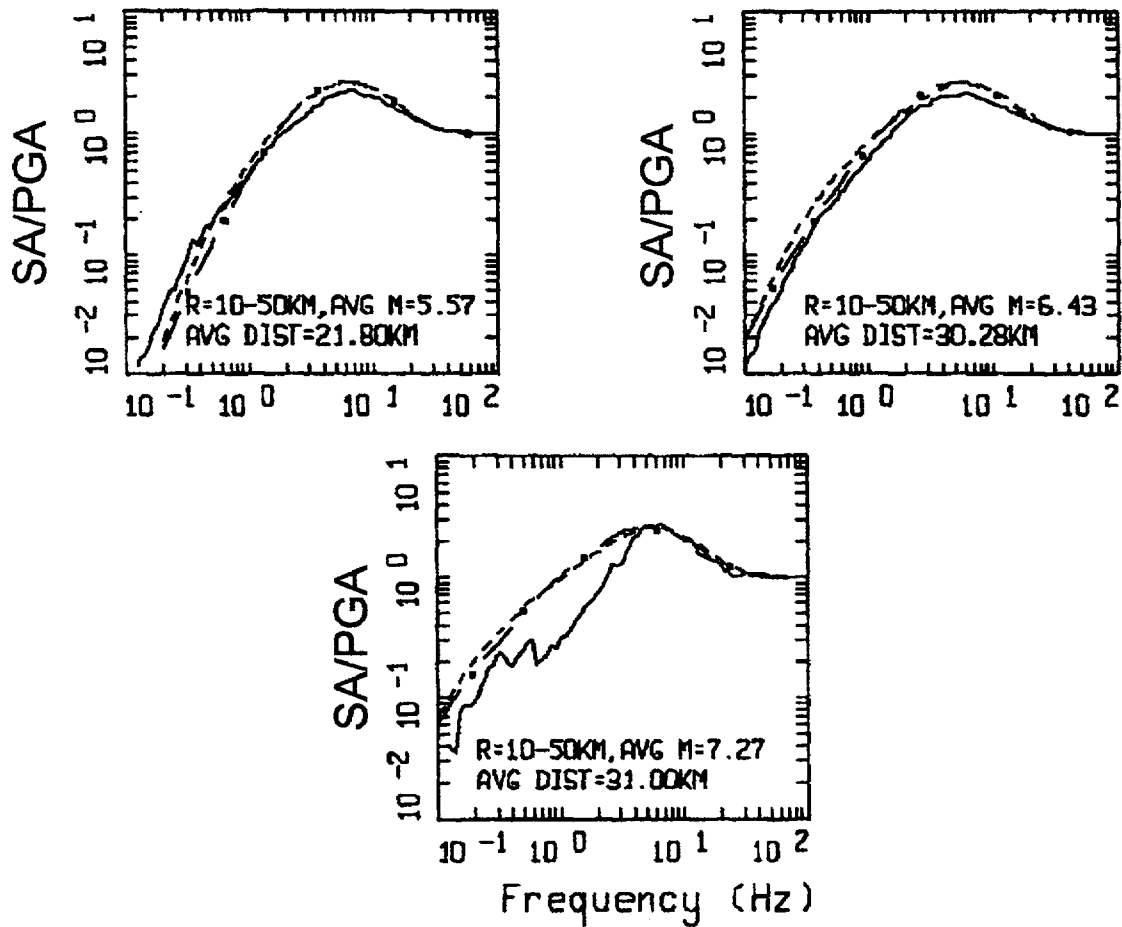
Figure 4-10. Absolute response spectra (5% damping) computed for $M = 6.5$ at $R = 25$ km using both single and double corner frequency source spectra for WUS and CEUS conditions.



AVERAGE HORIZONTAL SPECTRA
 M=6.5 (6.0-7.0), R=10-50 KM,
 ROCK AND SOIL

LEGEND
 ———— ROCK, AVG M = 6.43, AVG DIST = 30.28 KM
 - - - - - SOIL, AVG M = 6.35, AVG DIST = 28.27 KM

Figure 4-11. Comparison of WUS statistical response spectral shapes (5% damping) for the M 6.5, R = 10 to 50 km bins for rock and deep soil site conditions.



AVERAGE HORIZONTAL SPECTRA, WUS ROCK
M=5.5, 6.5, 7.5, R=10-50 KM BINS

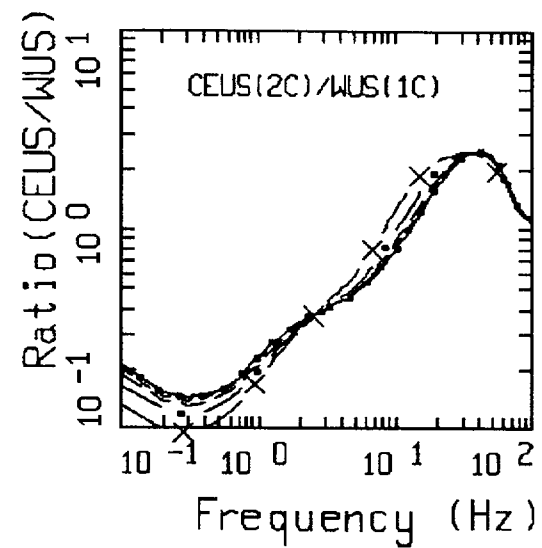
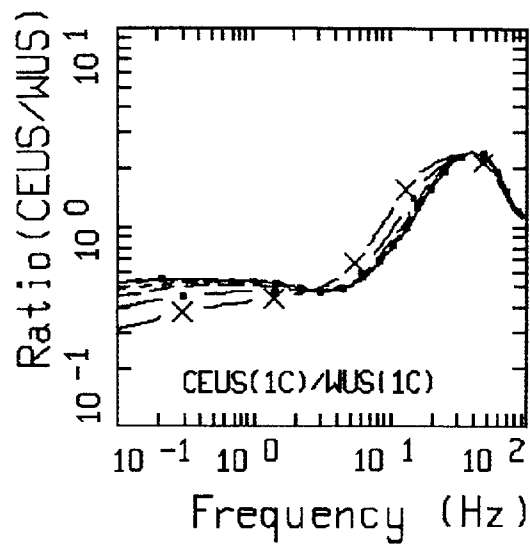
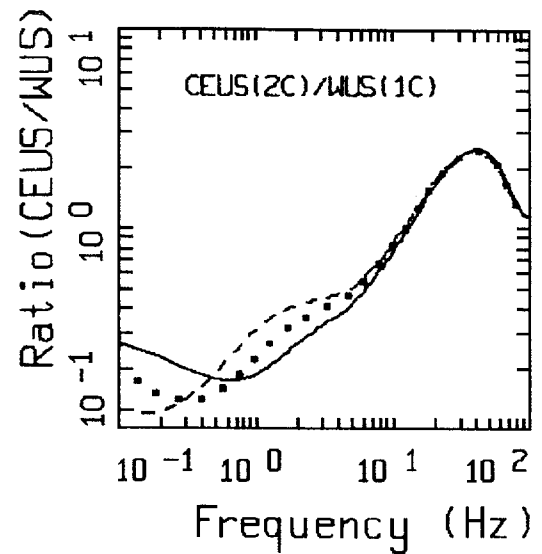
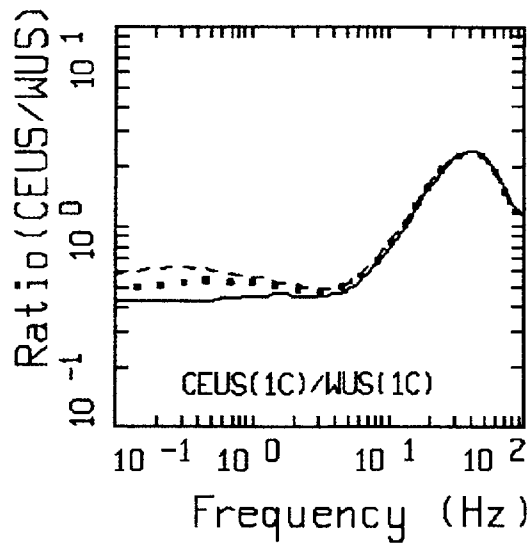
LEGEND

———— STATISTICAL

----- MODEL, SINGLE CORNER FREQUENCY

- . - . MODEL, DOUBLE CORNER FREQUENCY

Figure 4-12. Response spectral shapes (5% damping) computed for the $M = 5.5$ to 7.5 , $R = 10$ to 50 km bins for WUS rock site conditions.



TRANSFER FUNCTIONS
CEUS/WUS

Figure 4-13. WUS to CEUS transfer functions. Top, magnitude dependencies at a distance of 25 km; bottom, distance dependencies for $M 6.5$.

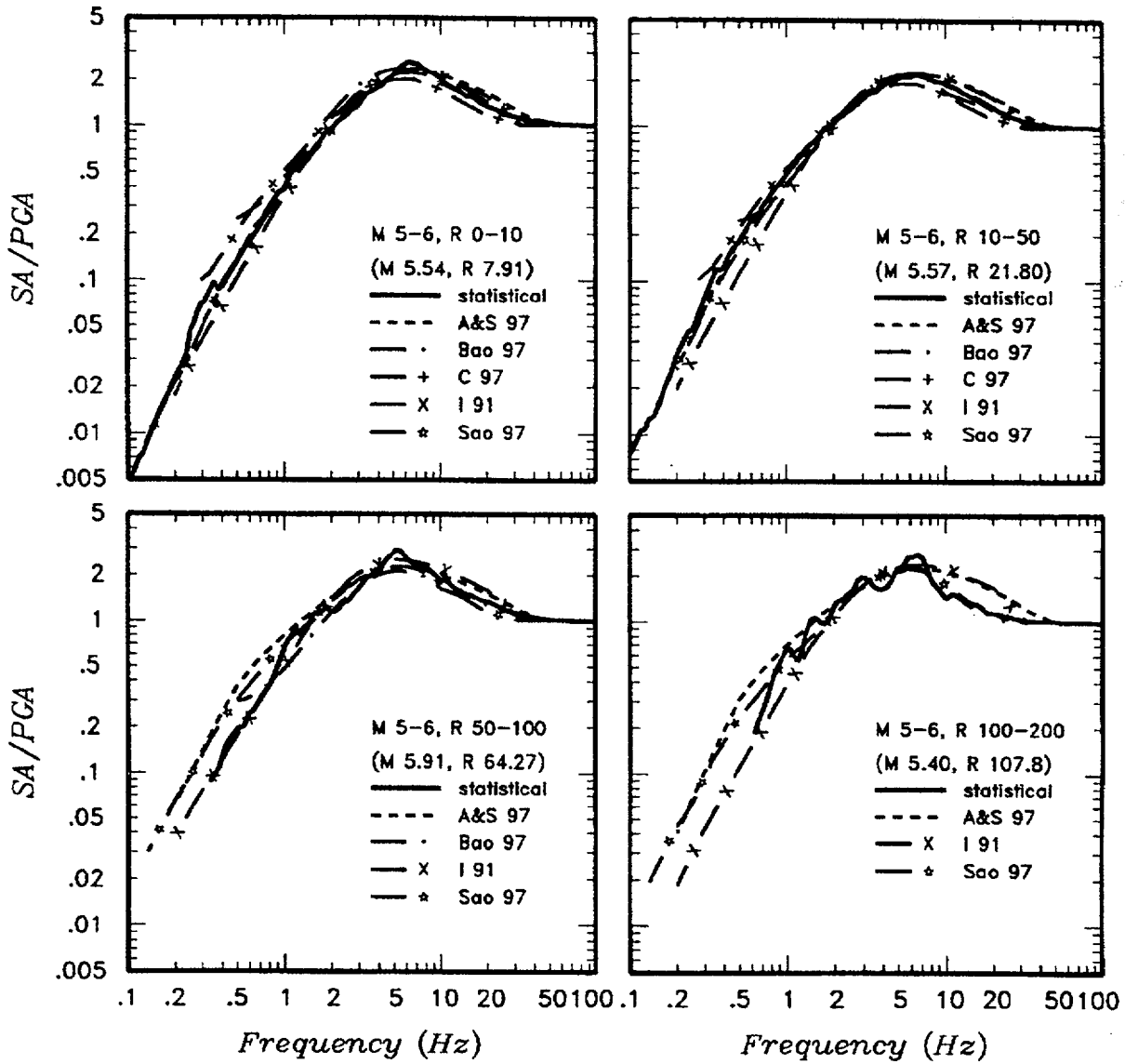


Figure 4-14. Comparison of the statistical shapes from Figures 3 to 5 with spectral shapes predicted by the attenuation relationships of Abrahamson and Silva (1997) [A&S 97], Boore and others (1997) [Bao 97], Campbell (1997) [C 97], Idriss (1991) [I 91], and Sadigh and others (1997) [Sao 97].

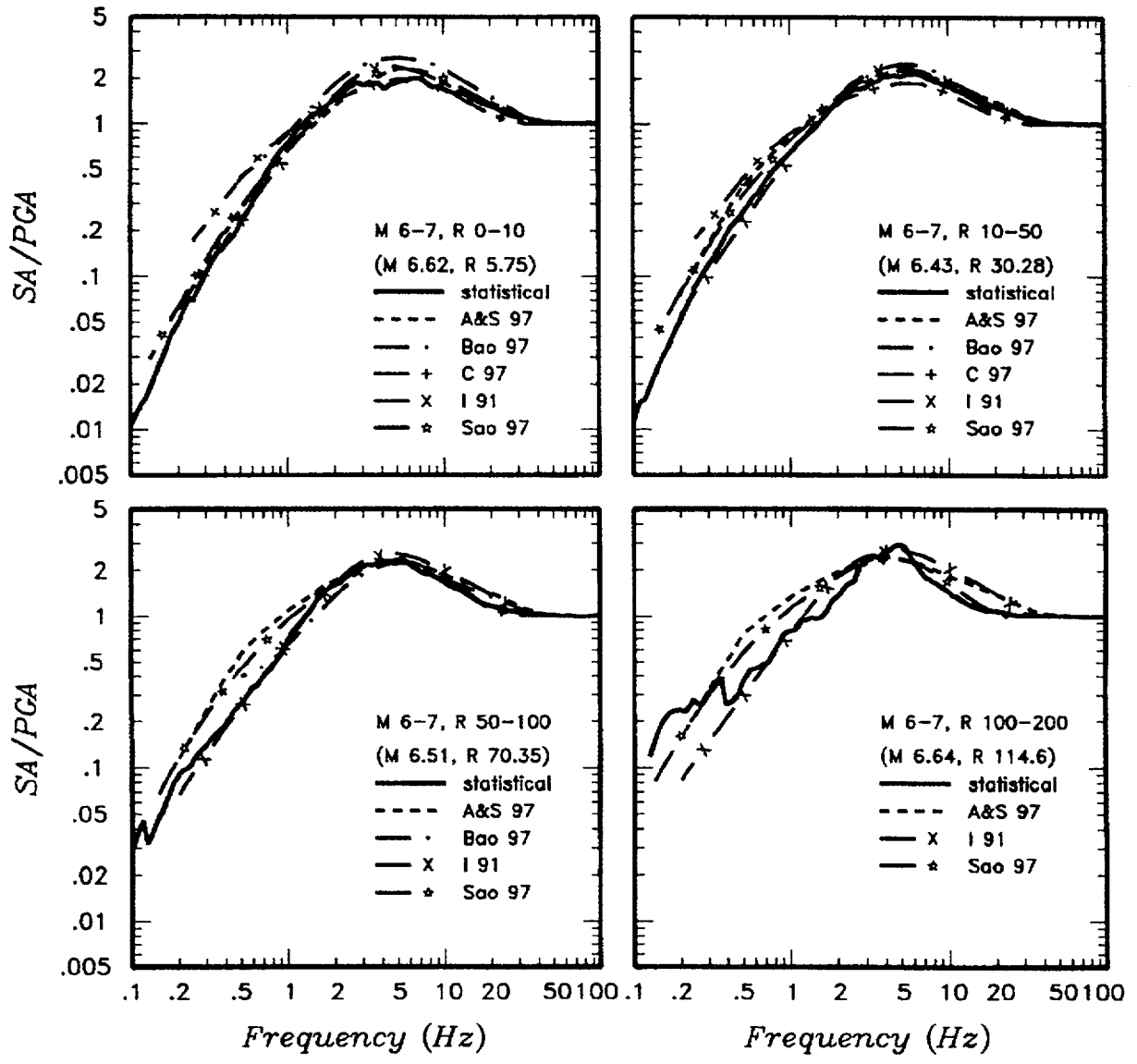


Figure 4-14b. (Continued)

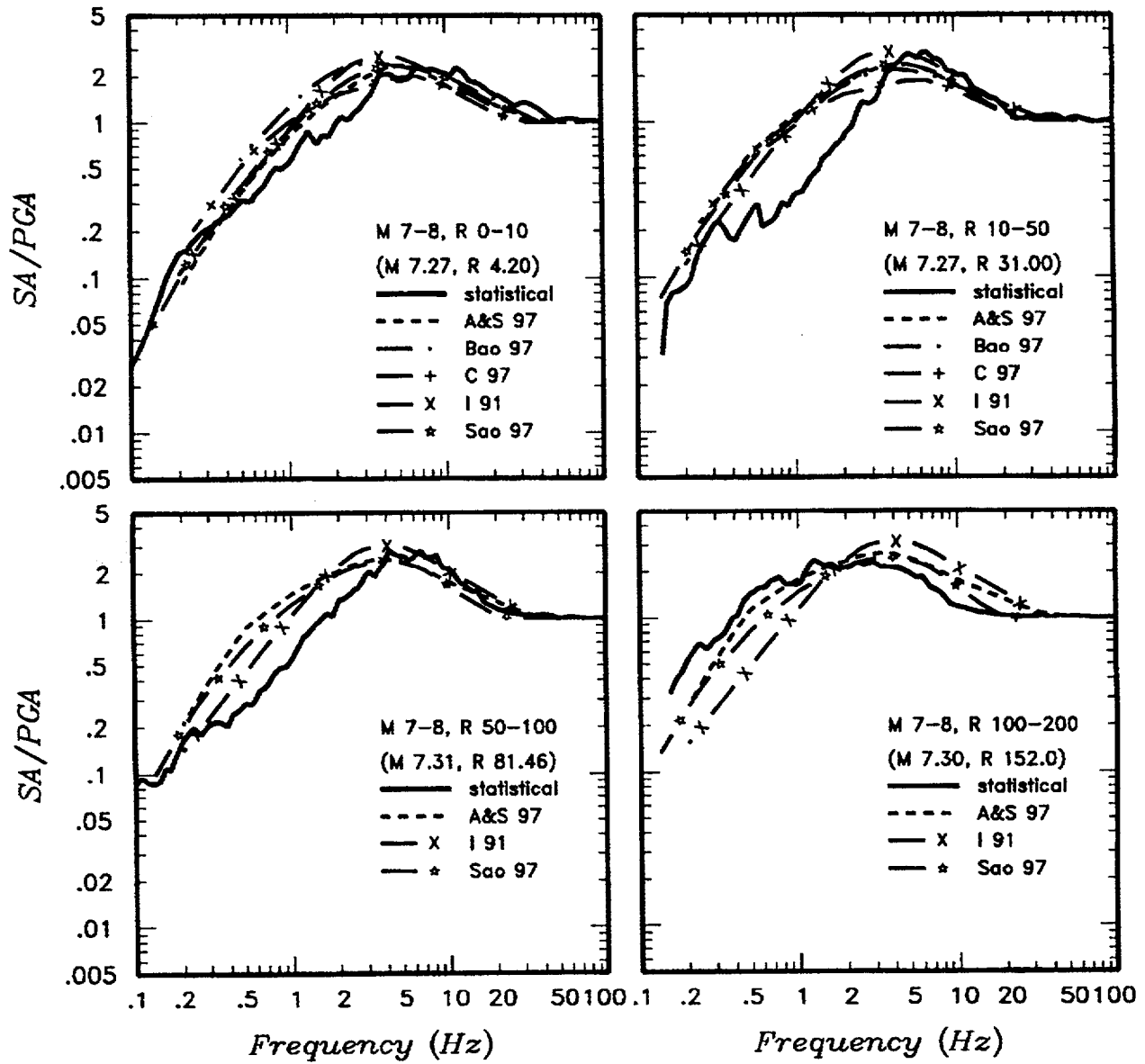


Figure 4-14c. (Continued)

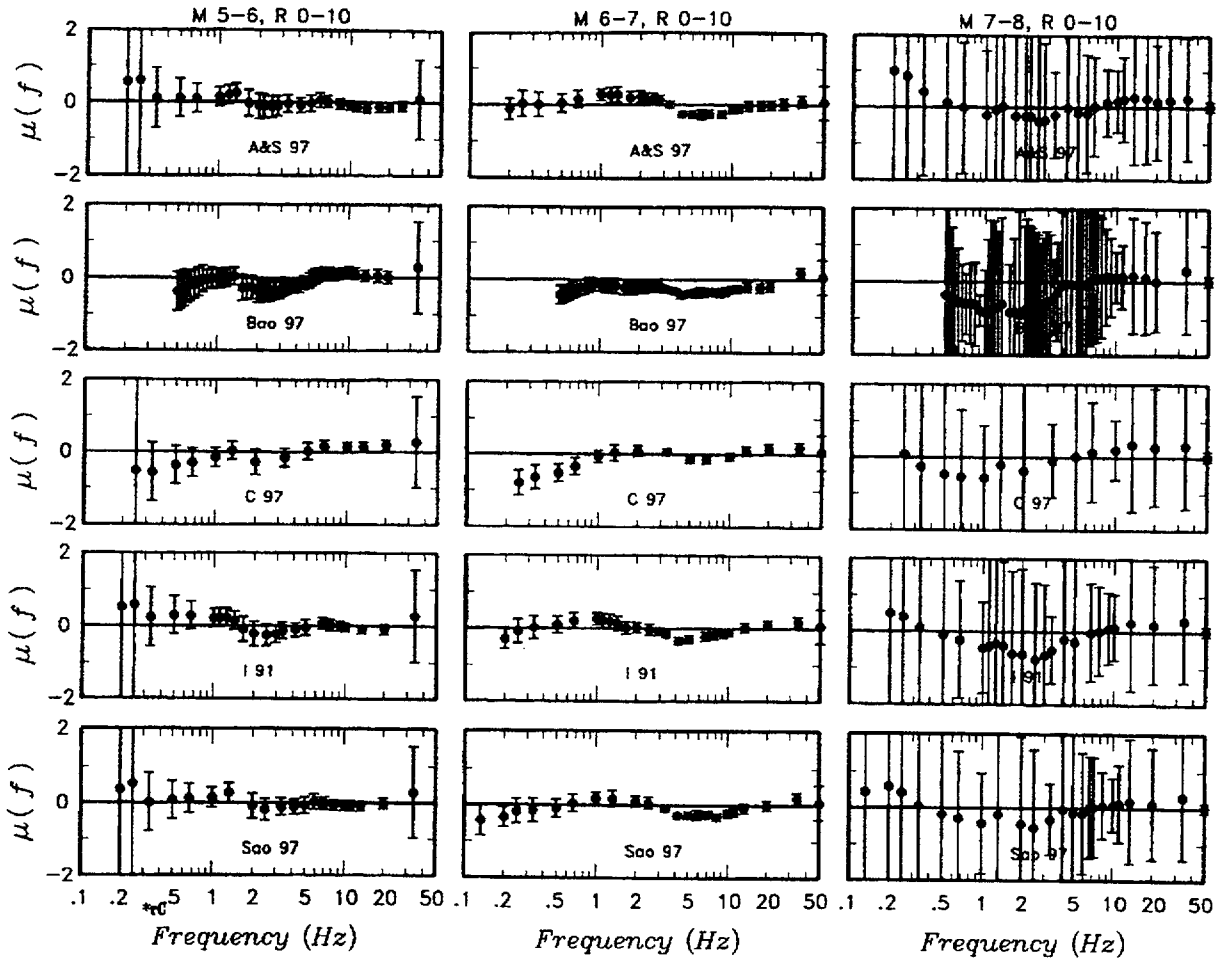


Figure 4-15. Mean residuals and their 90% confidence intervals for the five attenuation relationships.

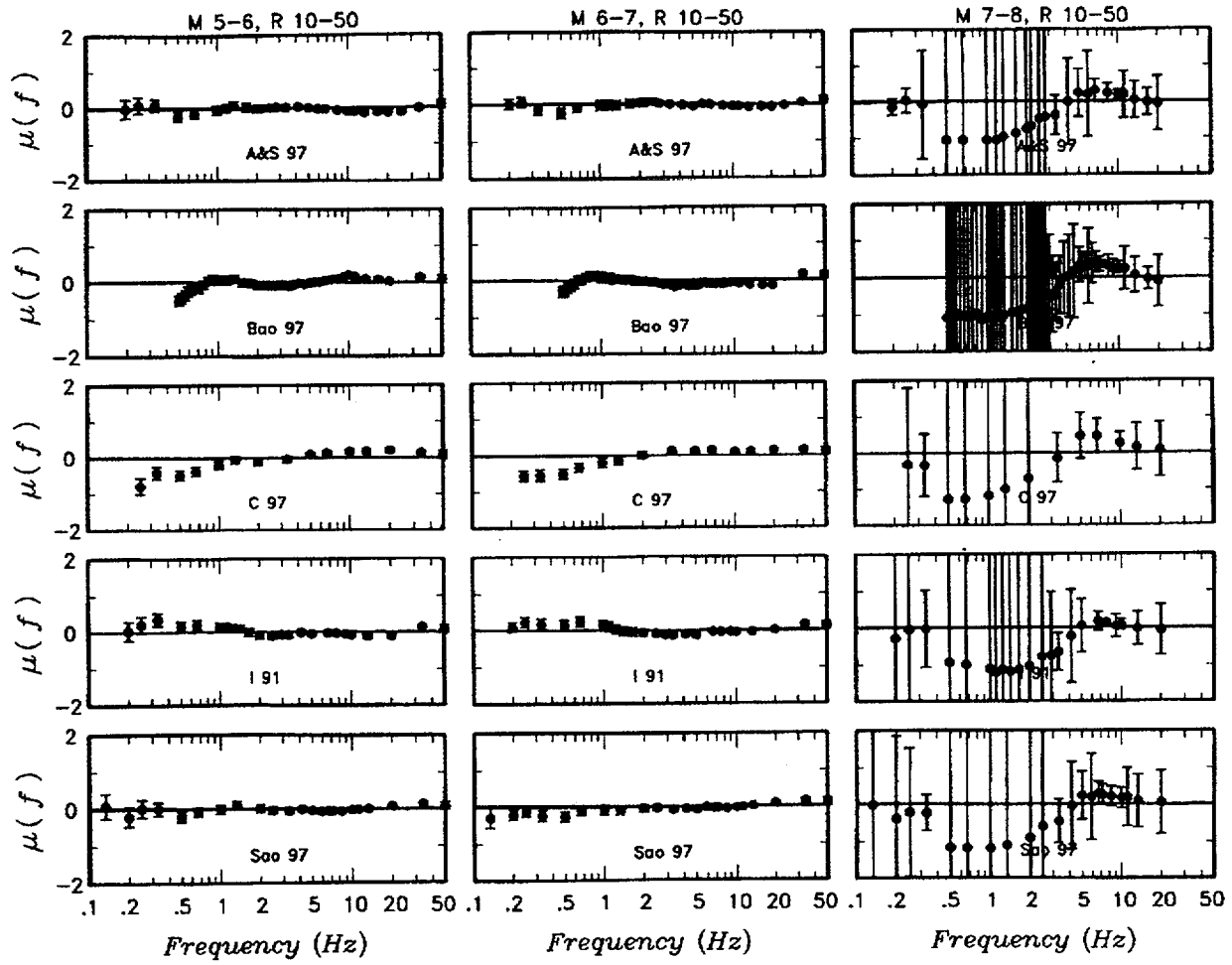


Figure 4-15b. (Continued)

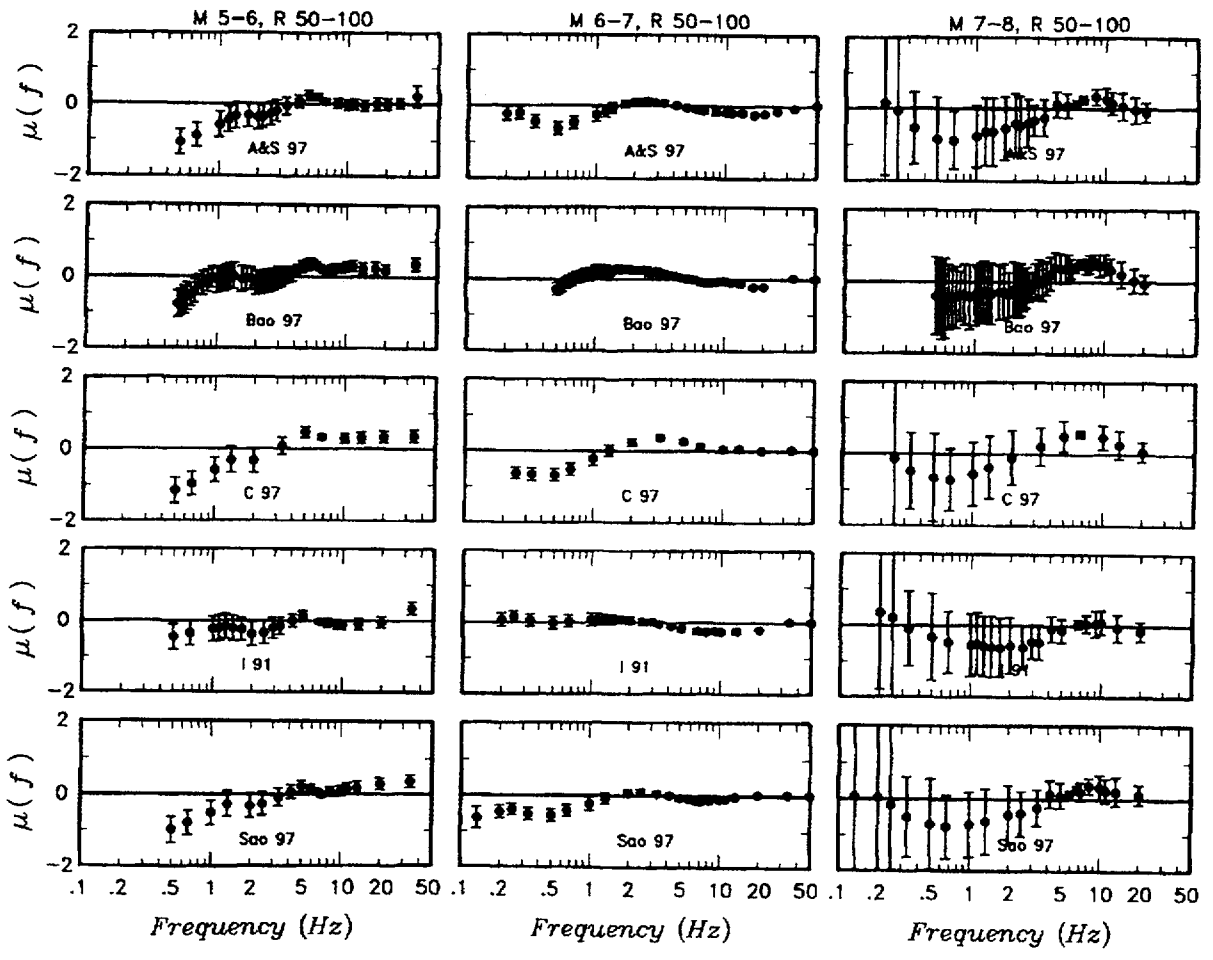


Figure 4-15c. (Continued)

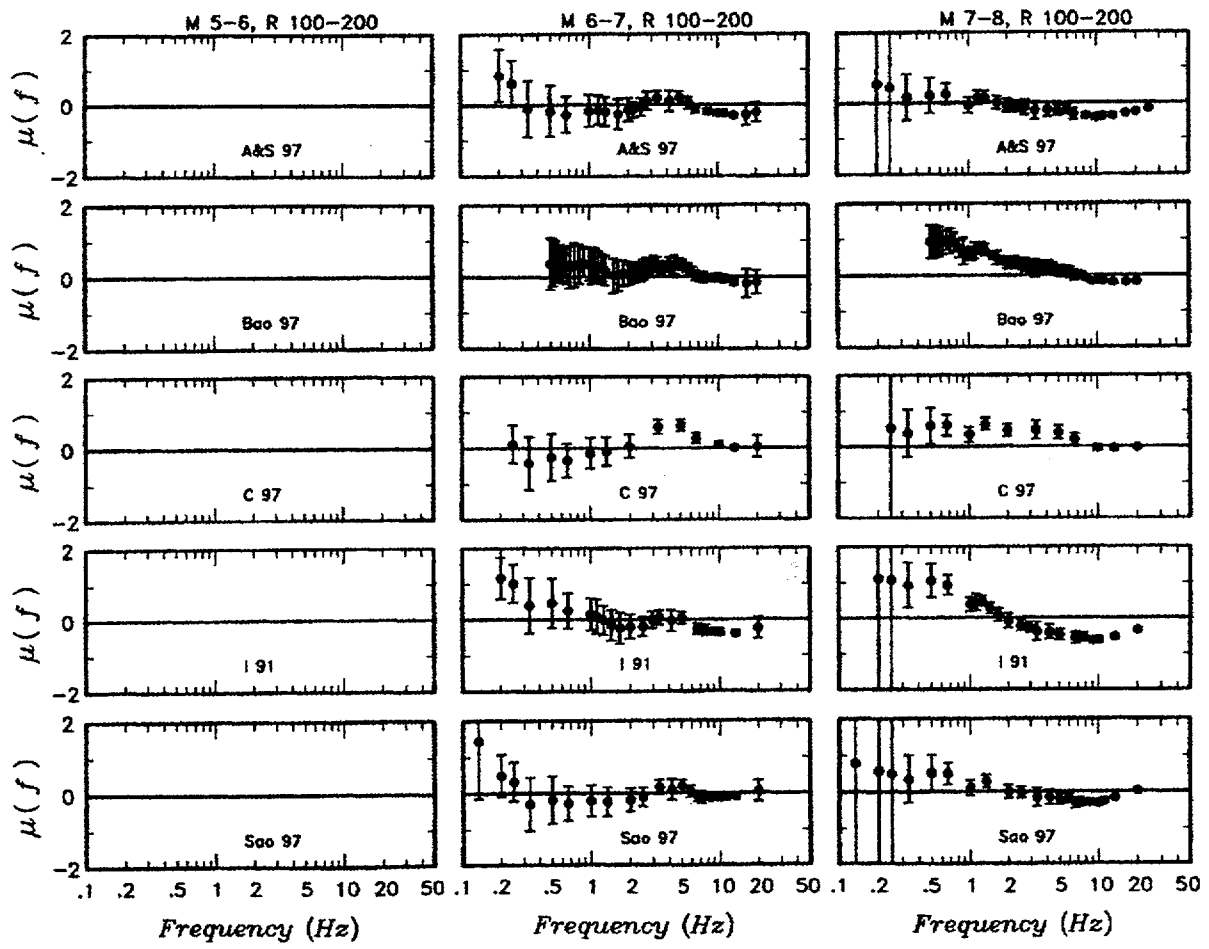


Figure 4-15d. (Continued)

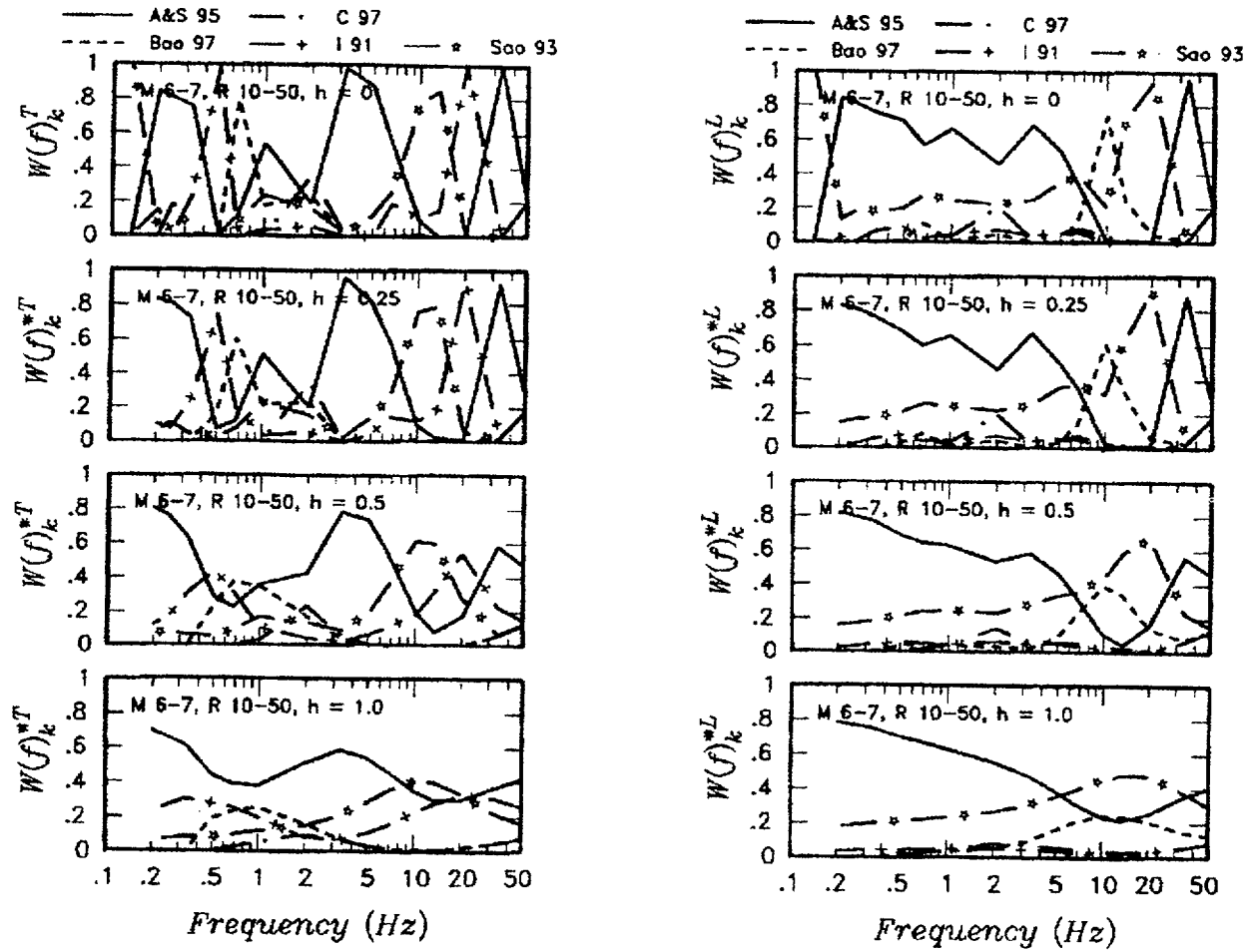


Figure 4-16. Relative bias ("T") weights (left column) and relative likelihood ("L") weights (right column) for M 6-7 and R 10-50 km magnitude distance bins. Top plot in each column shows weights computed using Equations (4-4) and (4-6). The remaining plots show the smoothed weights obtained using Equation (4-7) with values of h from 0.25 to 1.0.

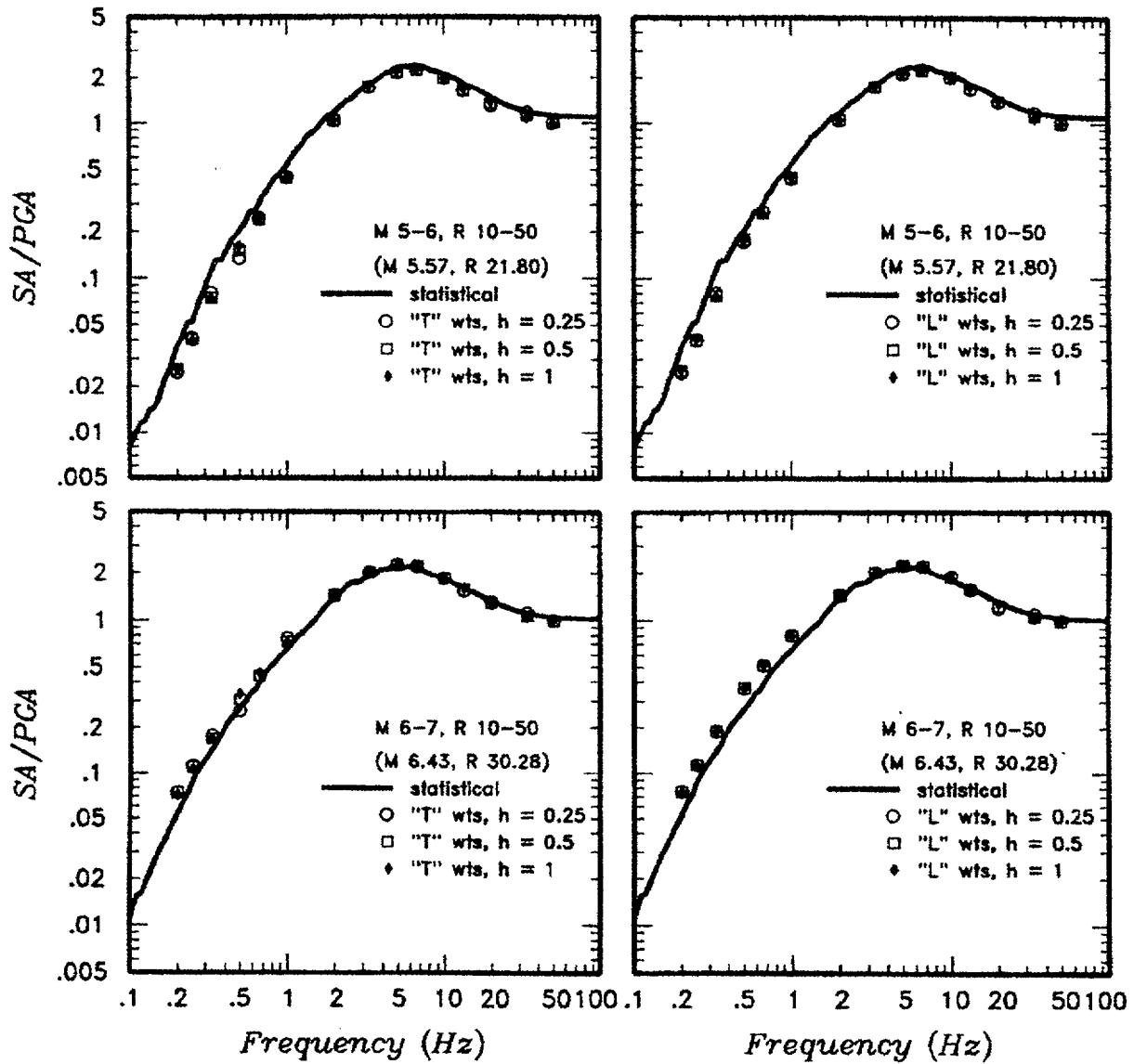


Figure 4-17. Example comparisons of the statistical spectral shapes from Figure 4-5 with spectral shapes predicted by the weighted combination of the five attenuation relationships. Weighted empirical spectral shapes are shown for smoothed "T" and "L" weights and values of h from 0.25 to 1.0.

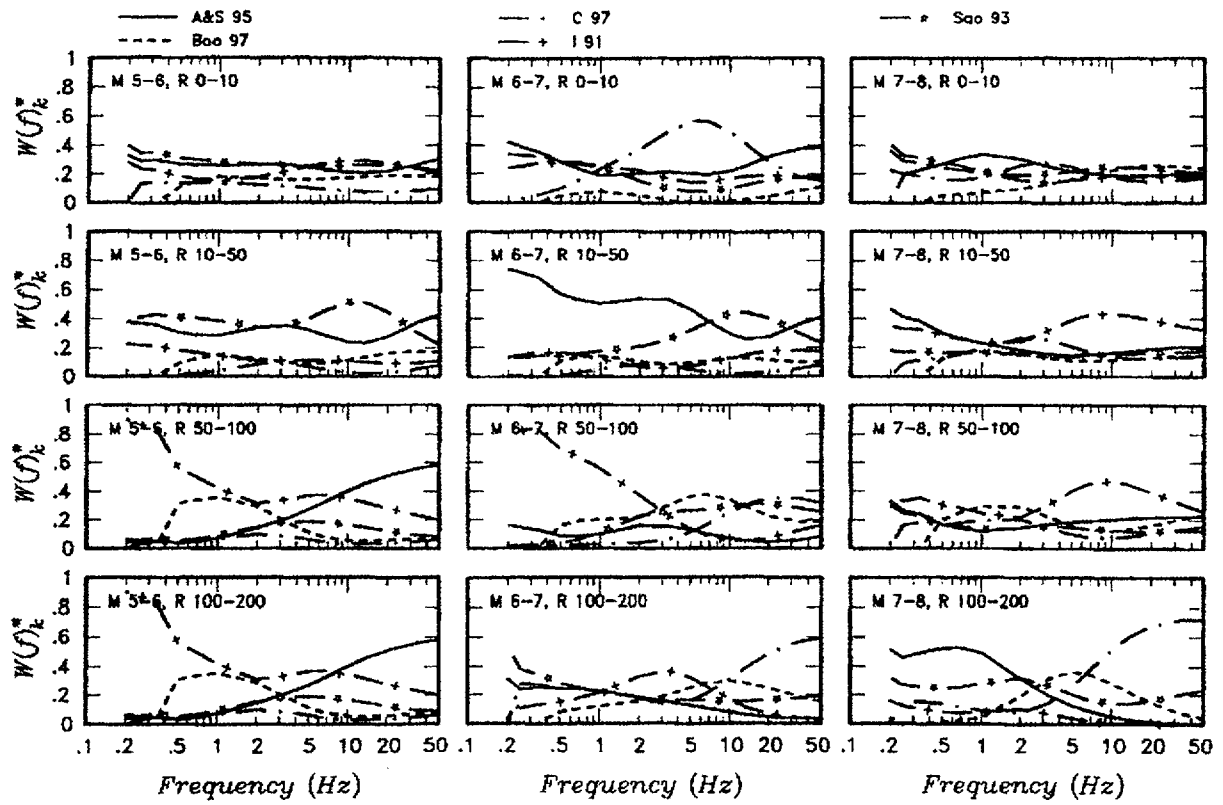


Figure 4-18. Relative weights used to obtain weighted empirical attenuation spectral shapes. The weights are the average of the smoothed "T" and "L" weights with $h = 1.0$.

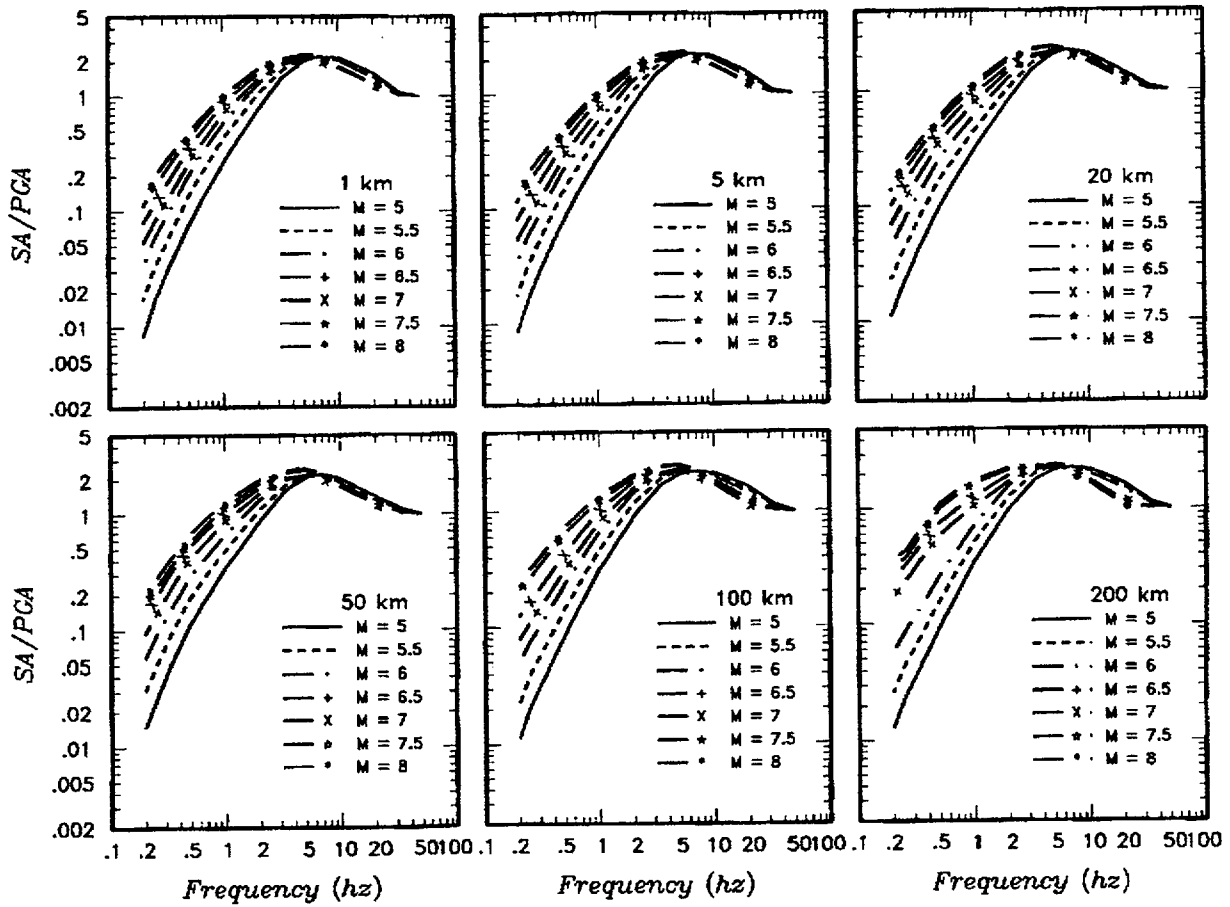


Figure 4-19. Weighted empirical attenuation response spectral shapes obtained using the relative weights shown on Figure 4-18.

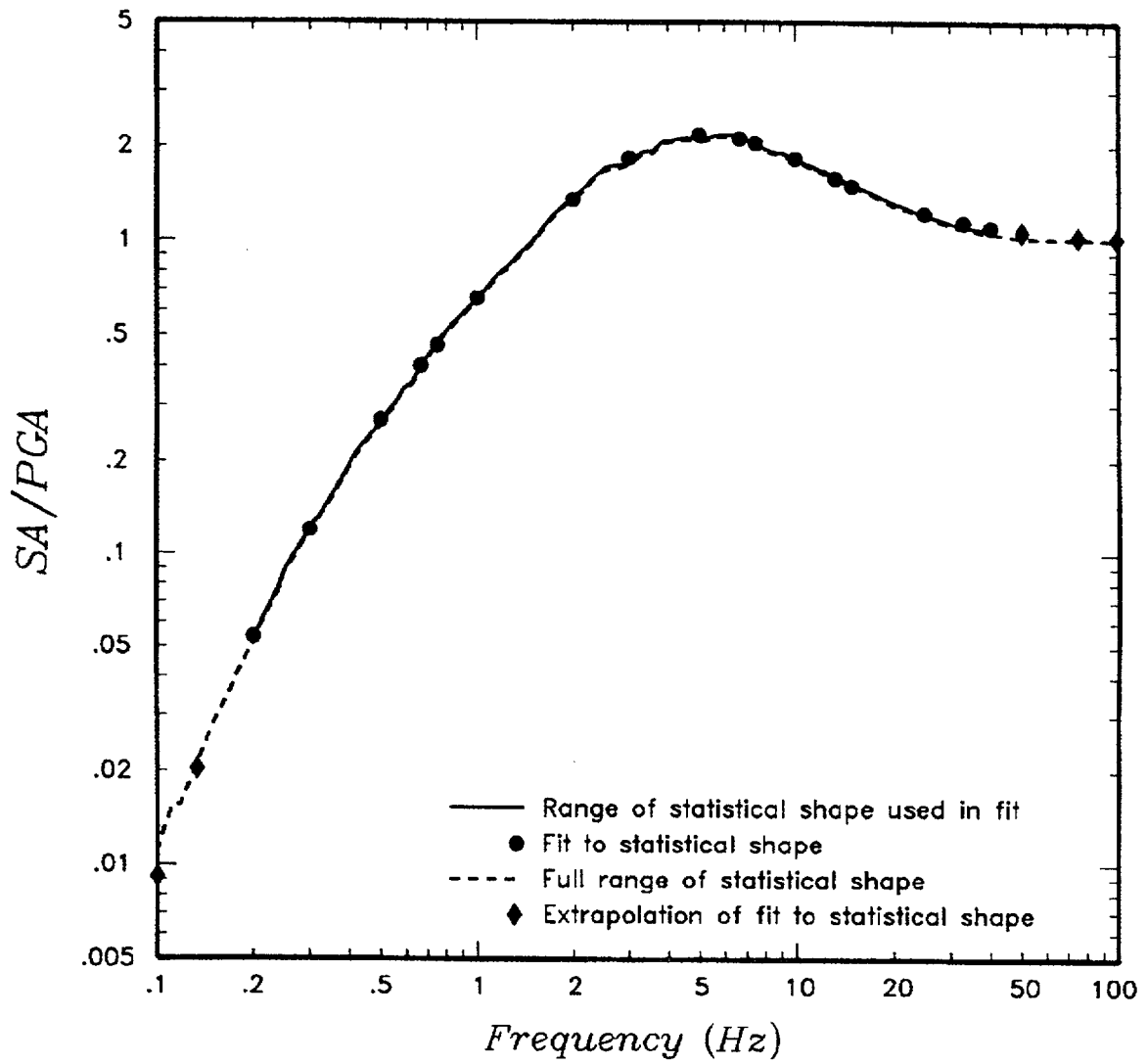


Figure 4-20. Example of a fit of Equation (4-8) to an individual spectral shape.

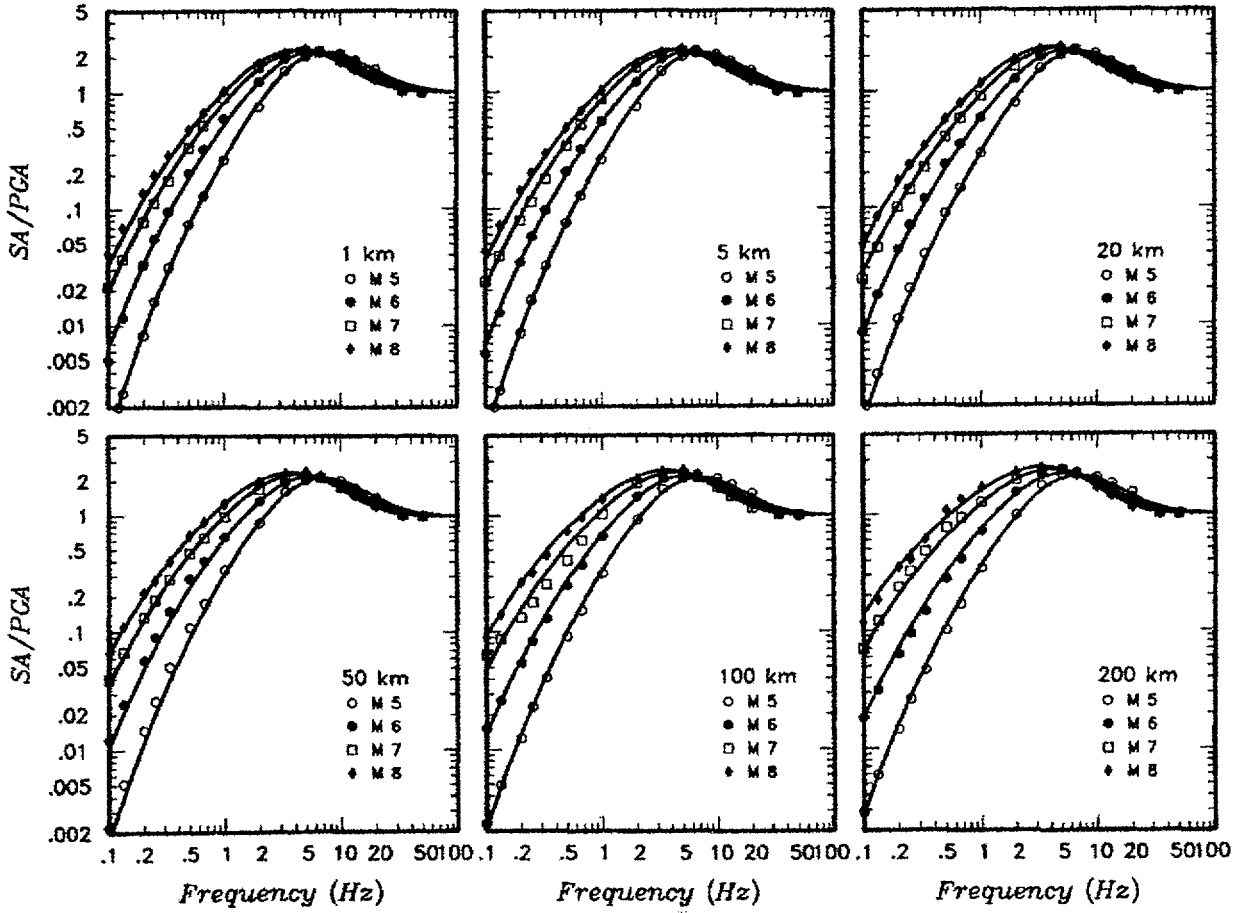


Figure 4-21. Example WUS response spectral shapes predicted by Equation (4-8) with parameters listed in Table 4-3 compared to the weighted empirical spectral shape data used in the fit.

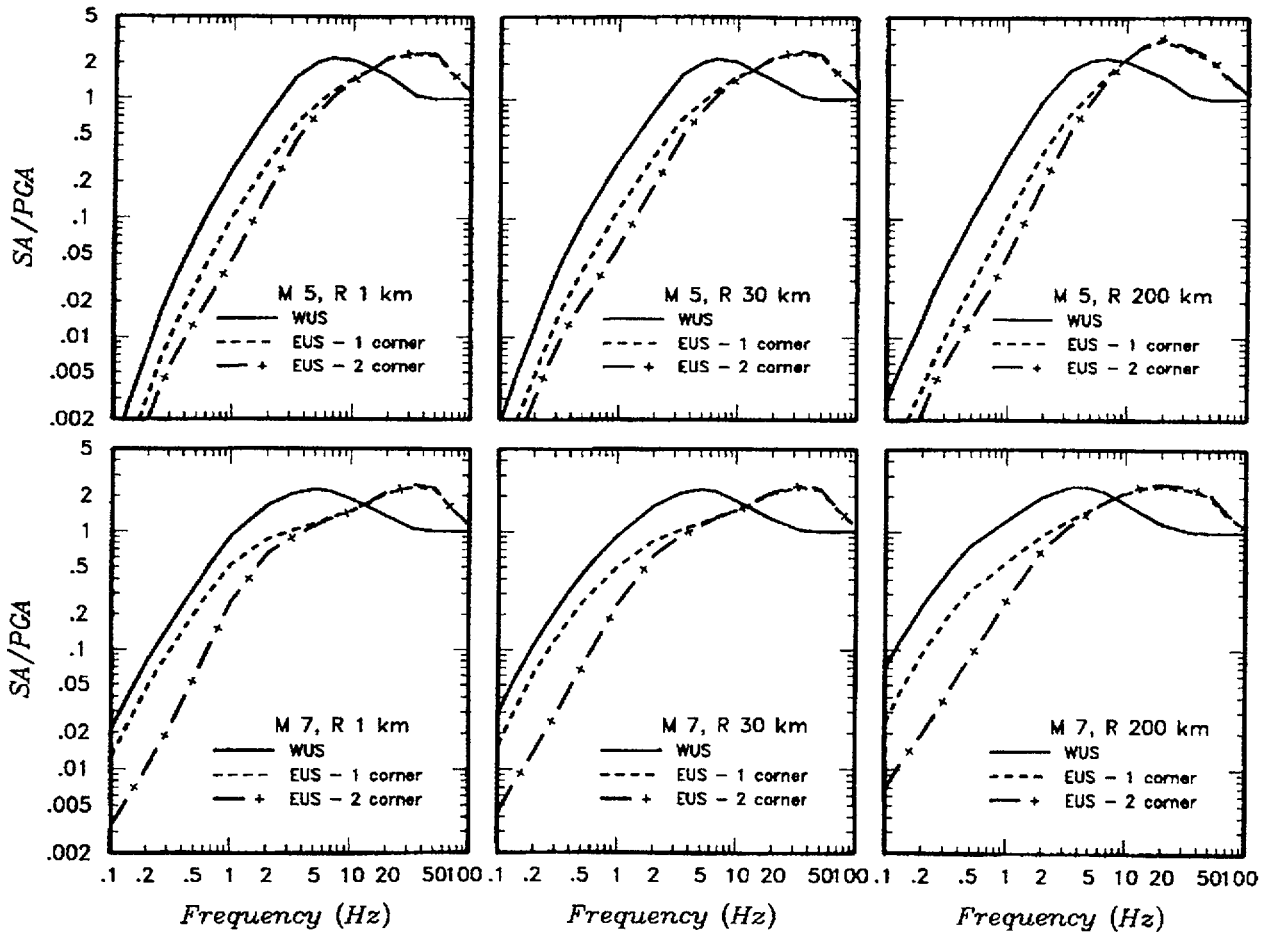


Figure 4-22. Example EUS response spectral shapes obtained by scaling weighted empirical WUS response spectral shapes.

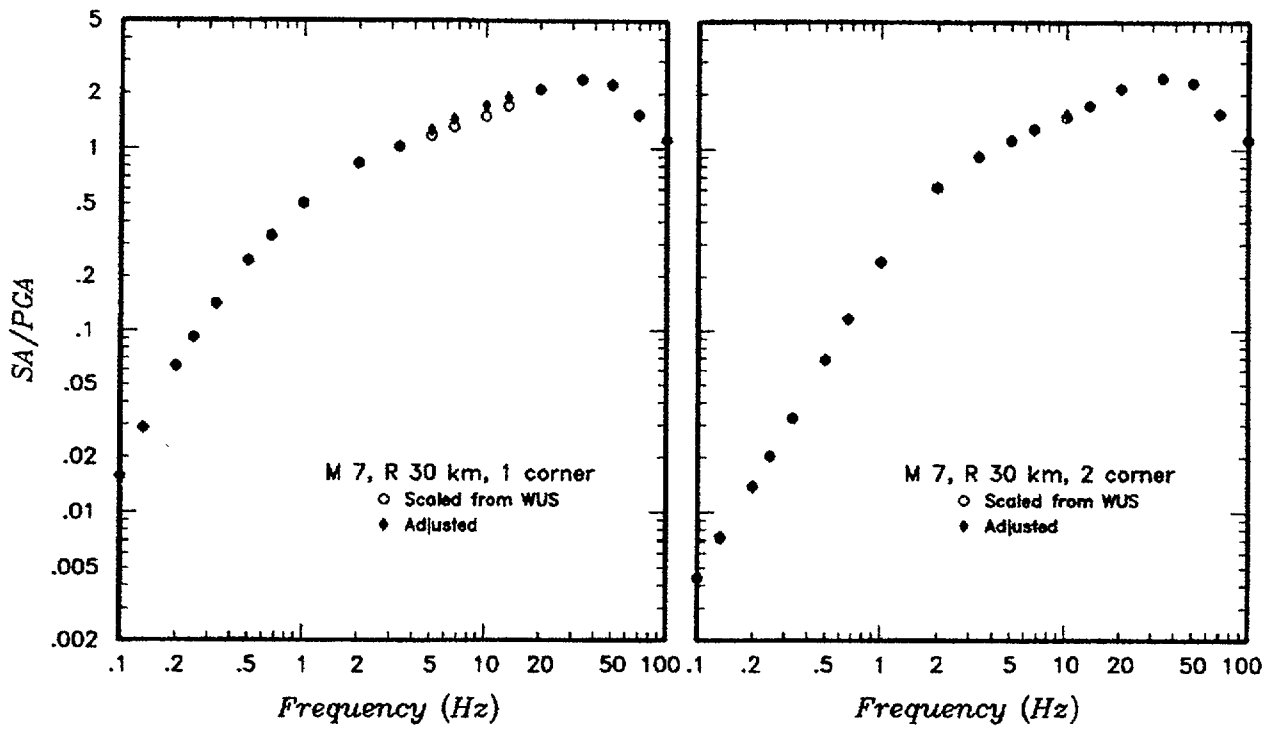


Figure 4-23. Examples of adjustments to scaled EUS response spectral shapes to remove valley near 10 Hz.

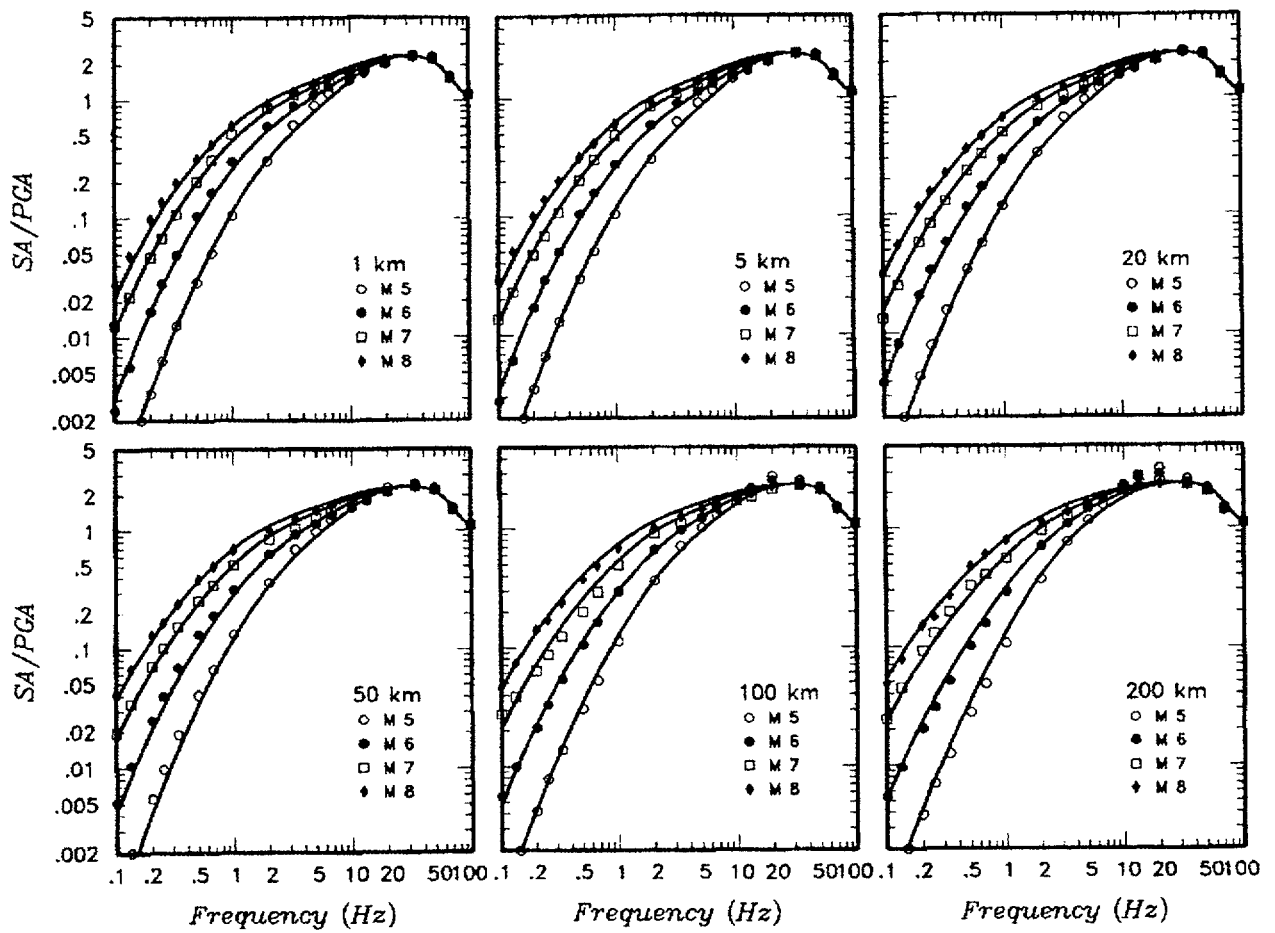


Figure 4-24. Example EUS single-corner response spectral shapes predicted by Equation (4-9) with parameters listed in Table 4-3 compared to the scaled and adjusted EUS spectral shape data used in the fit.

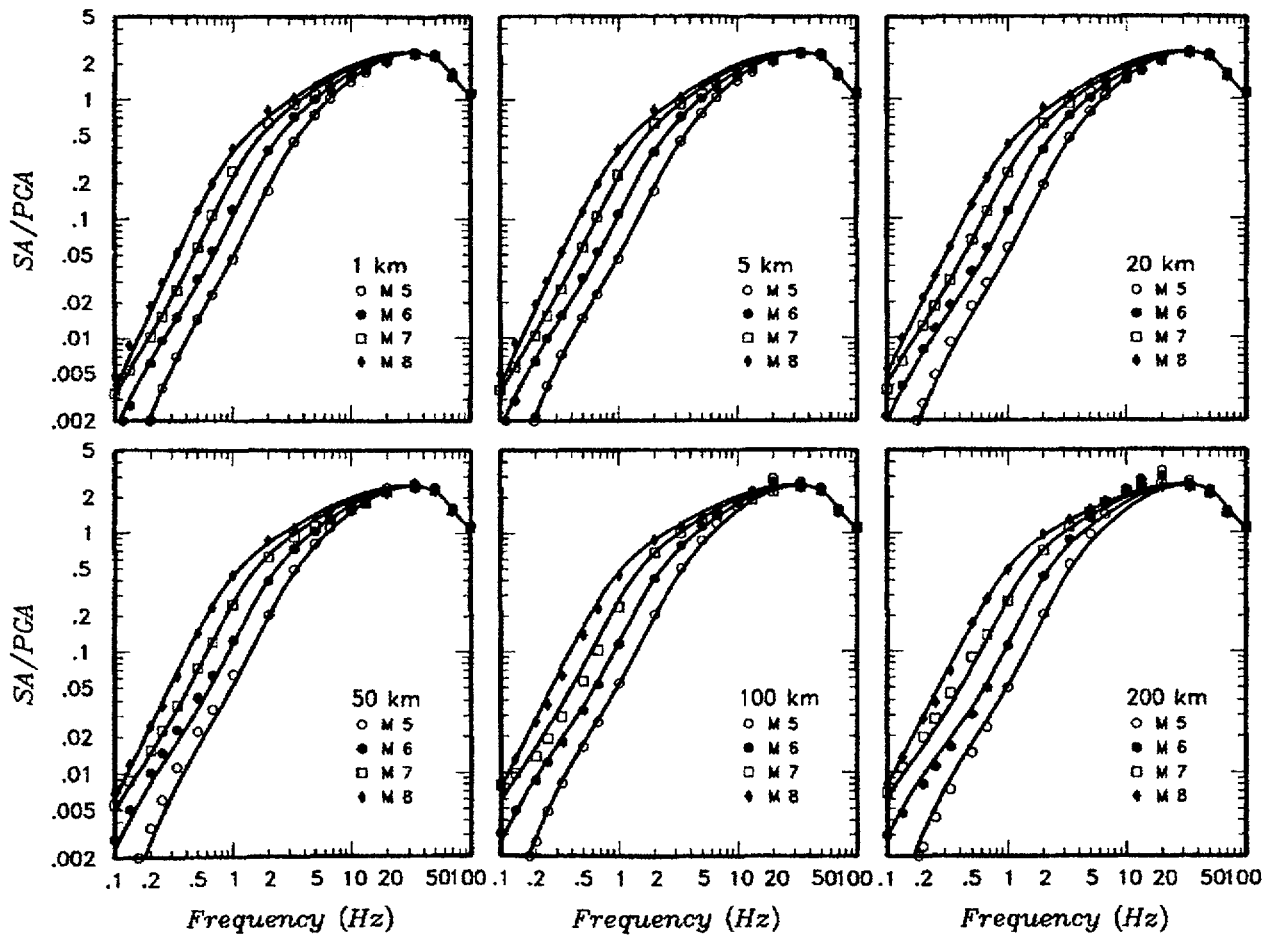
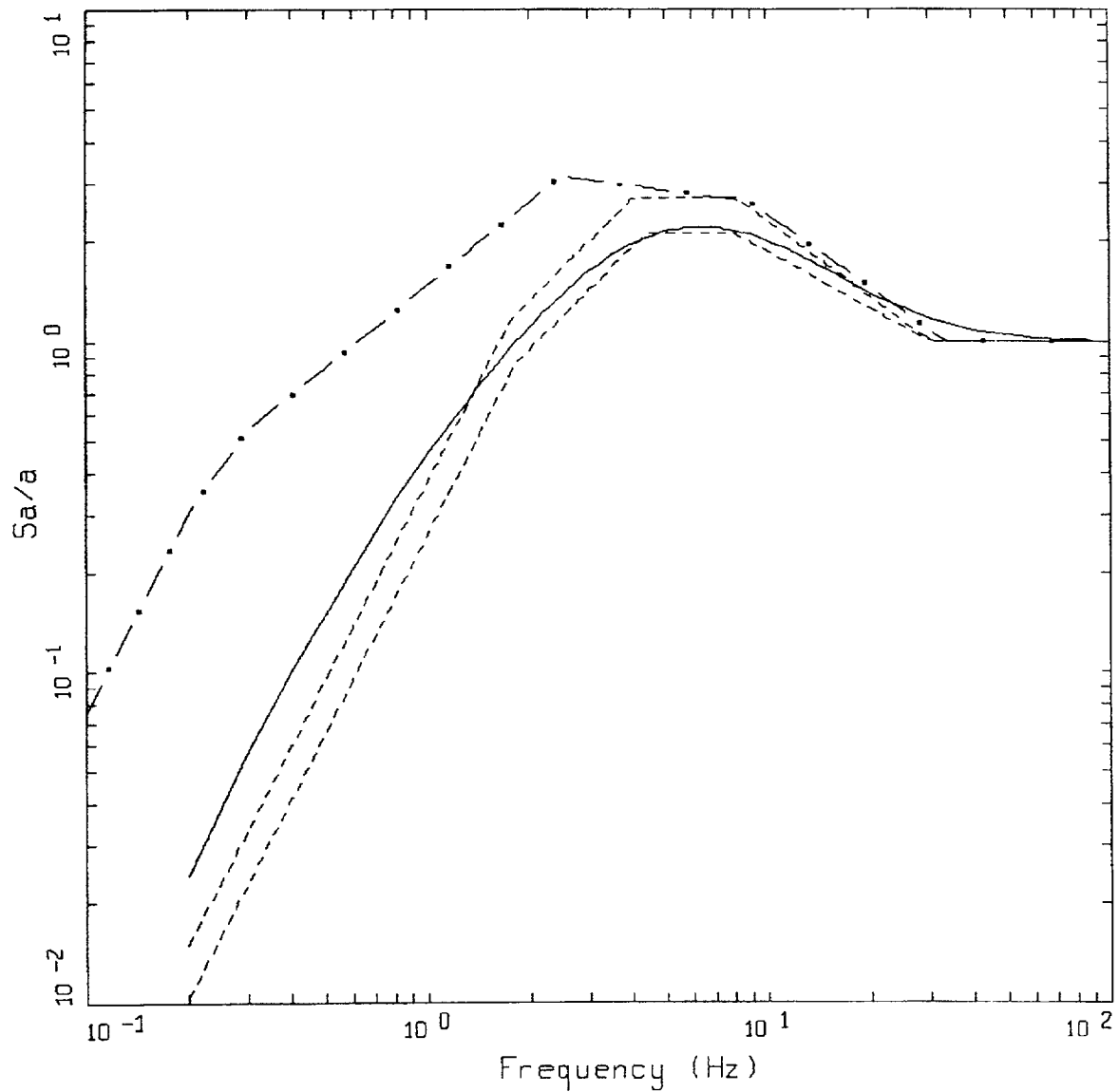


Figure 4-25. Example EUS double-corner response spectral shapes predicted by Equation (4-9) with parameters listed in Table 4-3 compared to the scaled and adjusted EUS spectral shape data used in the fit.

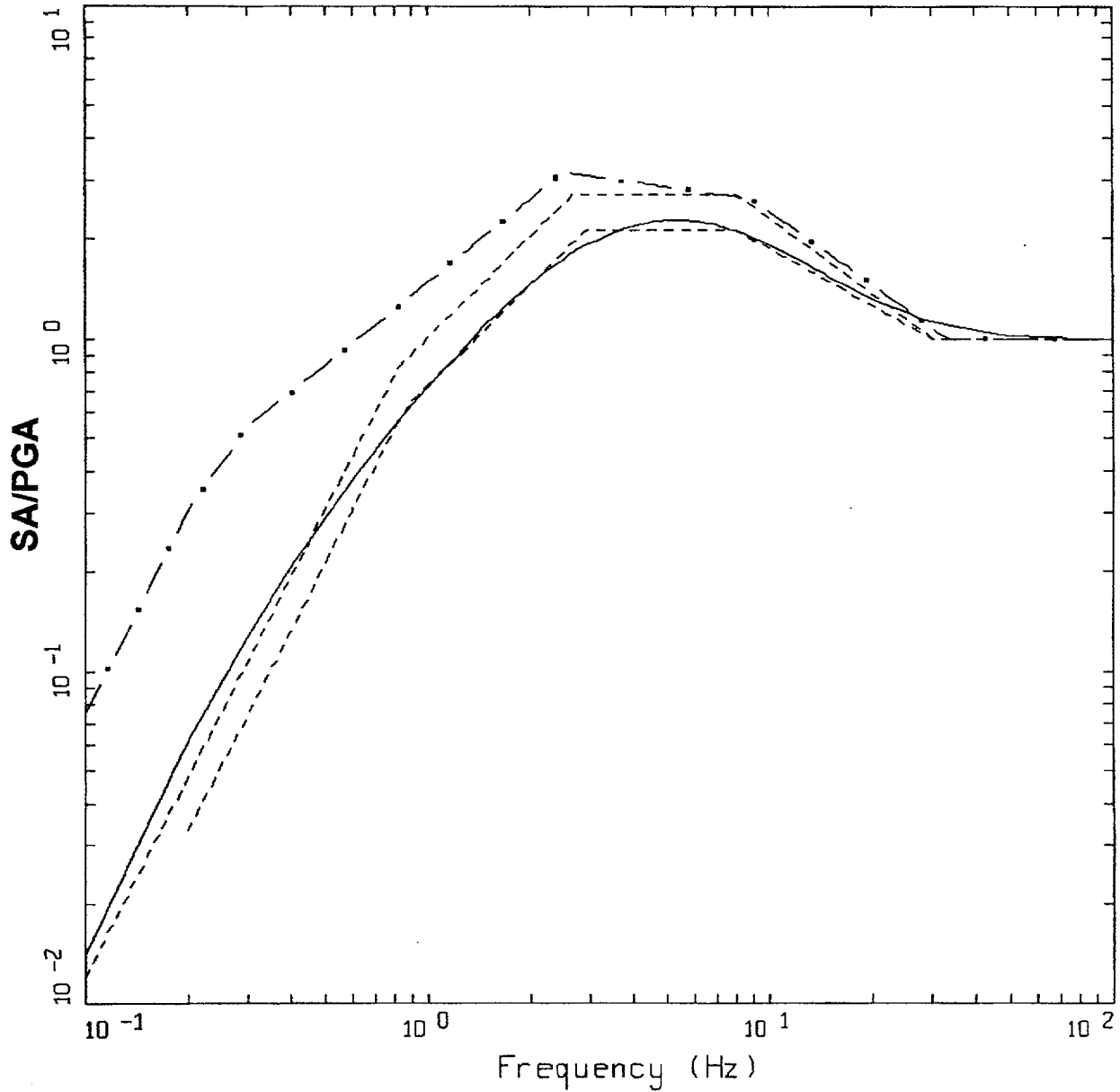


M=5.6, R=19.9 KM, ROCK
 PGA=0.12 G, PGV=5.39 CM/S, PGD=0.57 CM

LEGEND

- 5% DAMPED, REVISED NRC SPECTRA WUS, 50th percentile
- - - 5% DAMPED, NEWMARK&HALL SPECTRA, 50th percentile
- · - 5% DAMPED, NEWMARK&HALL SPECTRA, 84th percentile
- · · 5% DAMPED, REG GUIDE 1.60

Figure Set 4-26. Comparison of recommended WUS shapes (solid line) to current regulatory guidance R.G. 1.60 and Newmark-Hall shapes for the distance bin 0 to 50 km and for mean magnitudes 5.6, 4.4, and 7.3. Peak parameters are taken from Table 4-1 for the Newmark-Hall shapes.

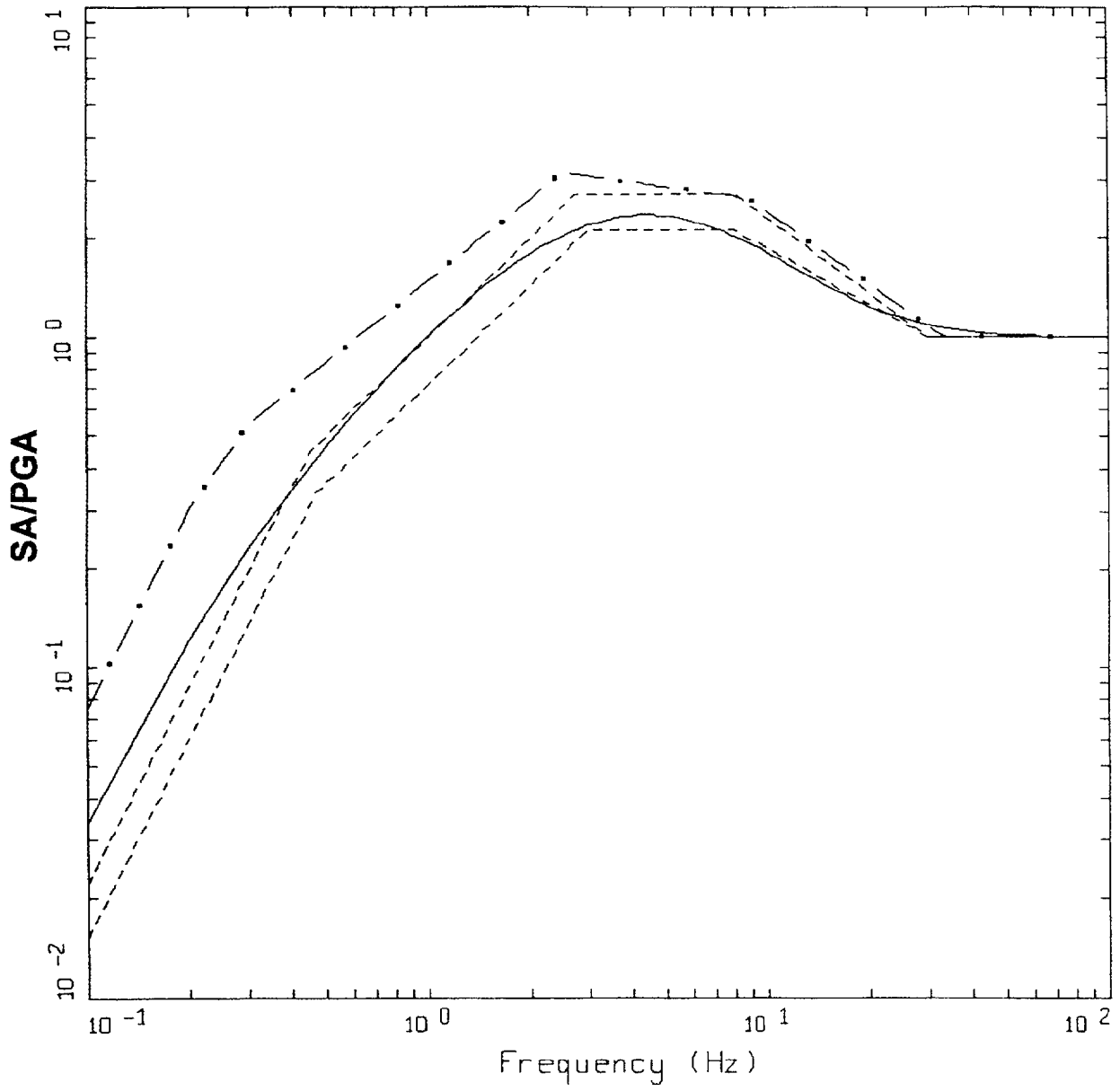


M=6.4, R=27.4 KM, ROCK
 PGA=0.15 G, PGV=10.27 CM/S, PGD=2.24 CM

LEGEND

- 5% DAMPED, RECOMMENDED NRC SPECTRA, 50th percentile
- 5% DAMPED, NEWMARK&HALL SPECTRA WUS, 50th percentile
- 5% DAMPED, NEWMARK&HALL SPECTRA, 84th percentile
- · · · 5% DAMPED, REG GUIDE 1.60

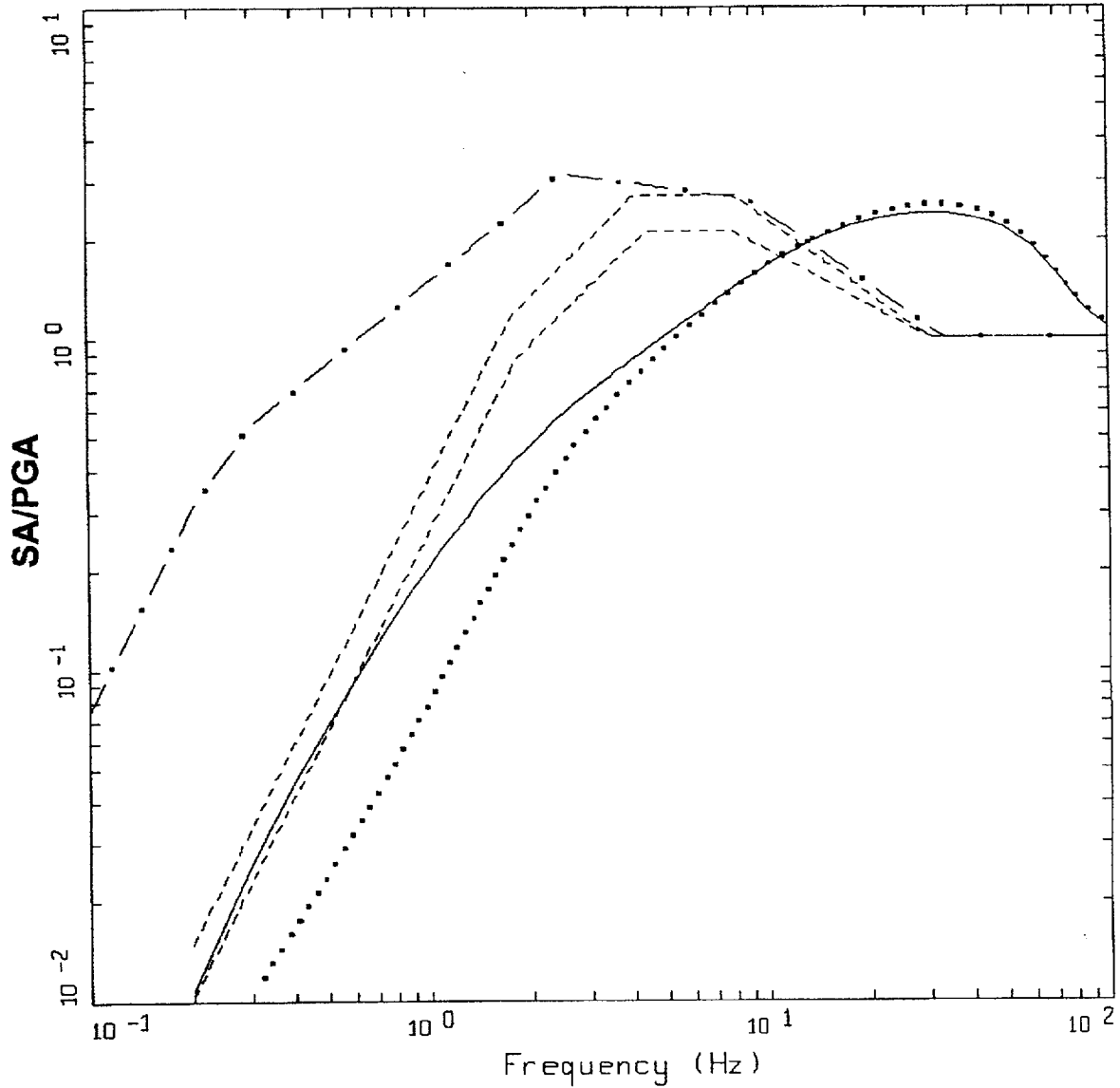
Figure Set 4-26 (Cont'd)



M=7.3, R=17.6 KM, ROCK
 PGA=0.40 G, PGV=26.82 CM/S, PGD=10.89 CM

- LEGEND
- 5% DAMPED, RECOMMENDED NRC SPECTRA, 50th percentile
 - 5% DAMPED, NEWMARK&HALL SPECTRA WUS, 50th percentile
 - 5% DAMPED, NEWMARK&HALL SPECTRA, 84th percentile
 - . - . 5% DAMPED, REG GUIDE 1.60

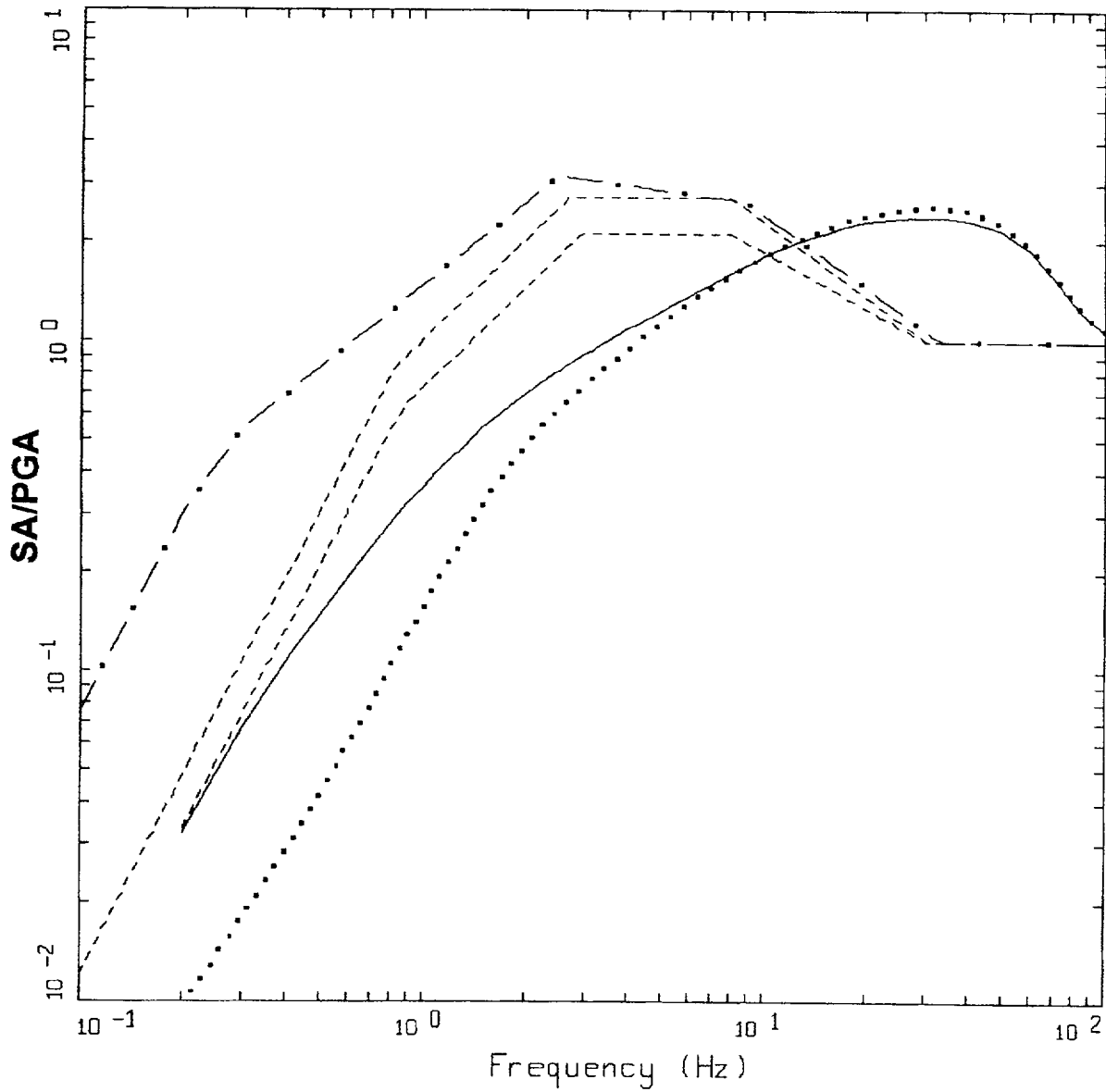
Figure Set 4-26. (Cont'd)



M=5.6, R=19.9 KM, ROCK
 PGA=0.12 G, PGV=5.39 CM/S, PGD=0.57 CM

- LEGEND
- 5% DAMPED, RECOMMENDED NRC SPECTRA CEUS 1 CORNER, 50th percentile
 - 5% DAMPED, RECOMMENDED NRC SPECTRA CEUS 2 CORNER, 50th percentile
 - 5% DAMPED, NEWMARK&HALL SPECTRA, 50th percentile
 - 5% DAMPED, NEWMARK&HALL SPECTRA, 84th percentile
 - . - . 5% DAMPED, REG GUIDE 1.60

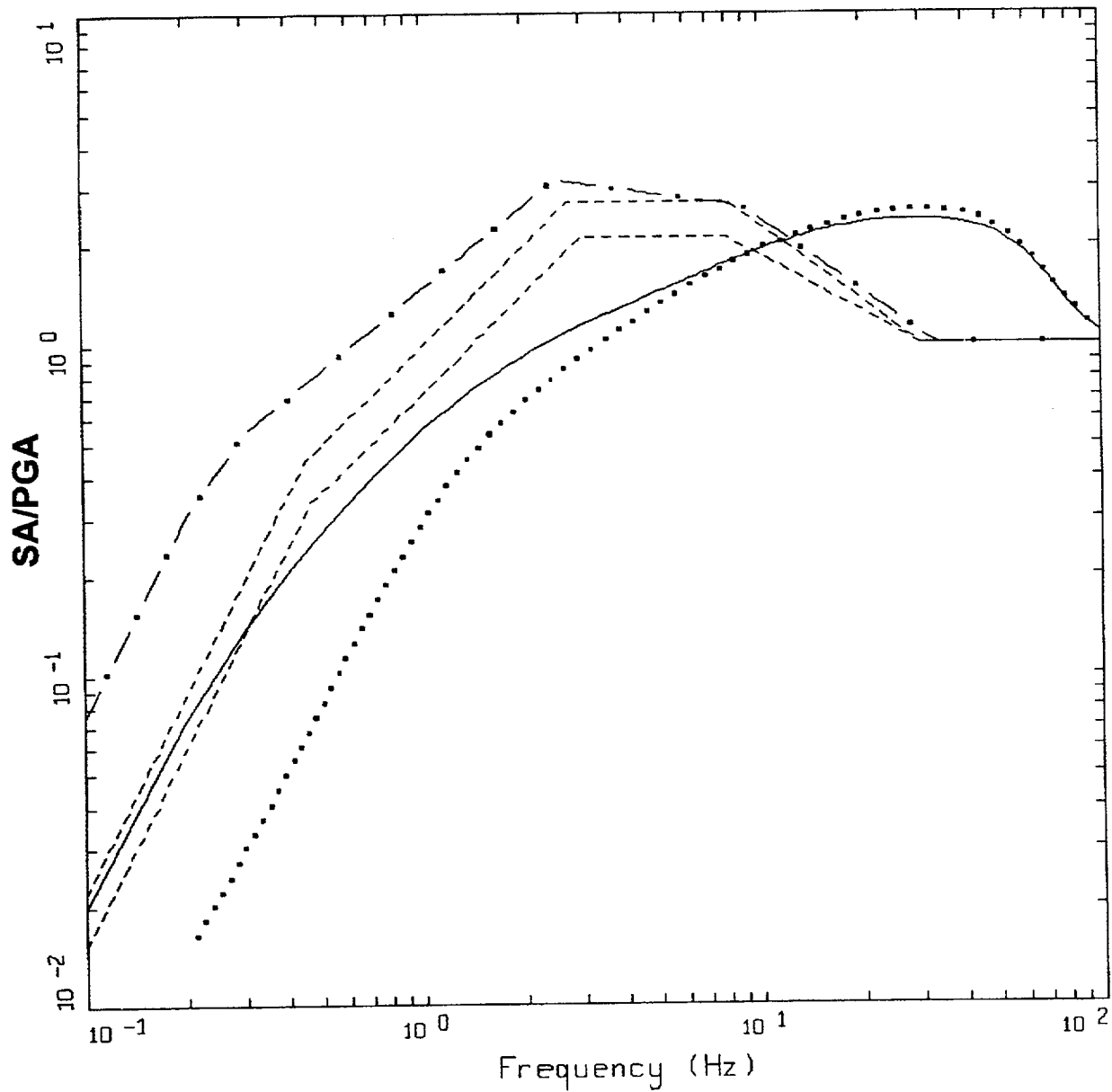
Figure Set 4-27. Comparison of recommended CEUS shapes (solid line) to current regulatory guidance R.G. 1.60 and Newmark-Hall shapes for the distance bin 0 to 50 km and for mean magnitudes 5.6, 6.4, and 7.3. Peak parameters are taken from Table 4-1 for the Newmark-Hall shapes.



M=6.4, R=27.4 KM, ROCK
 PGA=0.15 G, PGV=10.27 CM/S, PGD=2.24 CM

- LEGEND
- 5% DAMPED, RECOMMENDED NRC SPECTRA CEUS 1 CORNER, 50th percentile
 - 5% DAMPED, RECOMMENDED NRC SPECTRA CEUS 2 CORNER, 50th percentile
 - 5% DAMPED, NEWMARK&HALL SPECTRA, 50th percentile
 - - - - - 5% DAMPED, NEWMARK&HALL SPECTRA, 84th percentile
 - . - . - 5% DAMPED, REG GUIDE 1.60

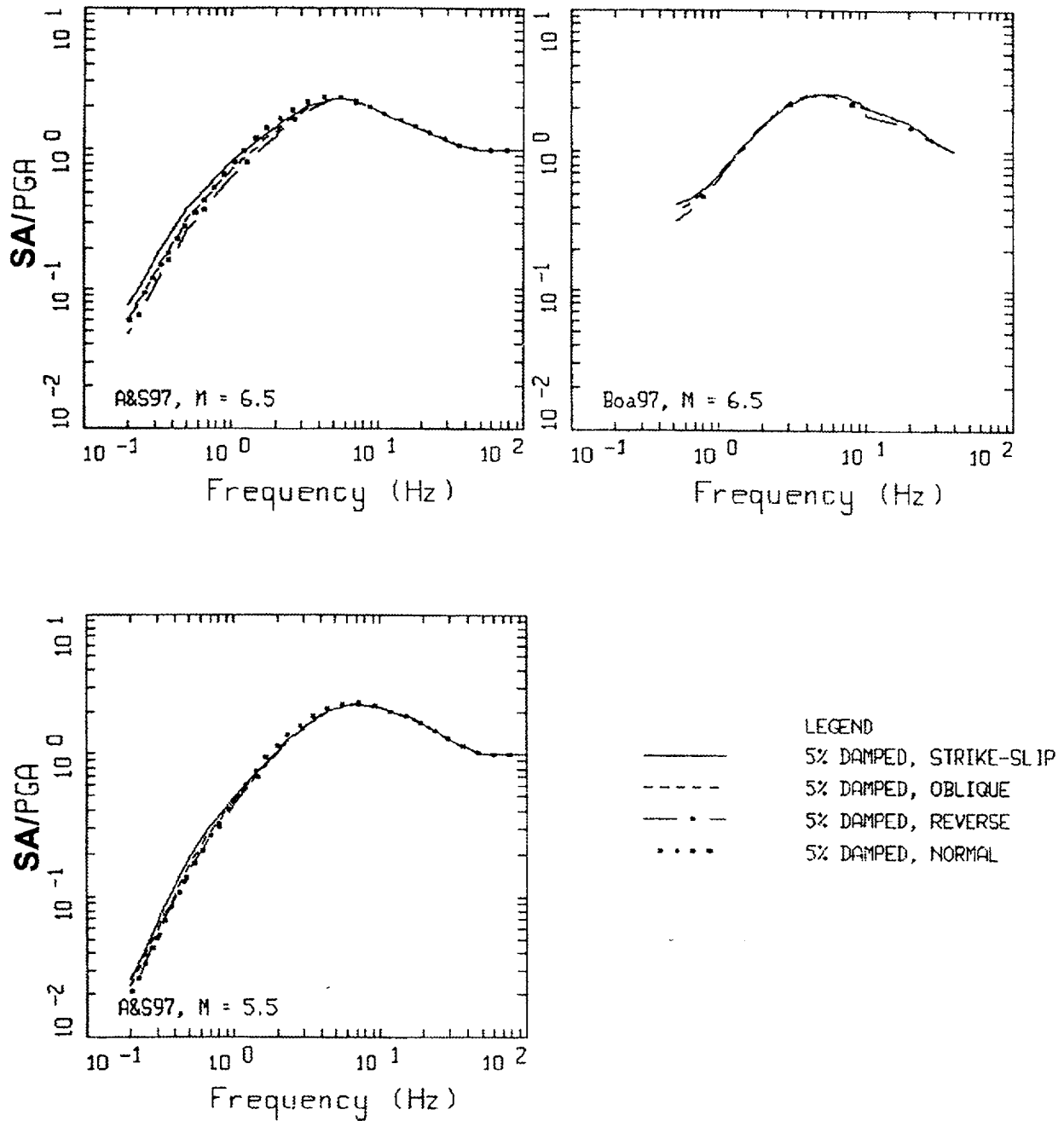
Figure Set 4-27. (Cont'd)



M=7.3, R=17.6 KM, ROCK
 PGA=0.40 G, PGV=26.82 CM/S, PGD=10.89 CM

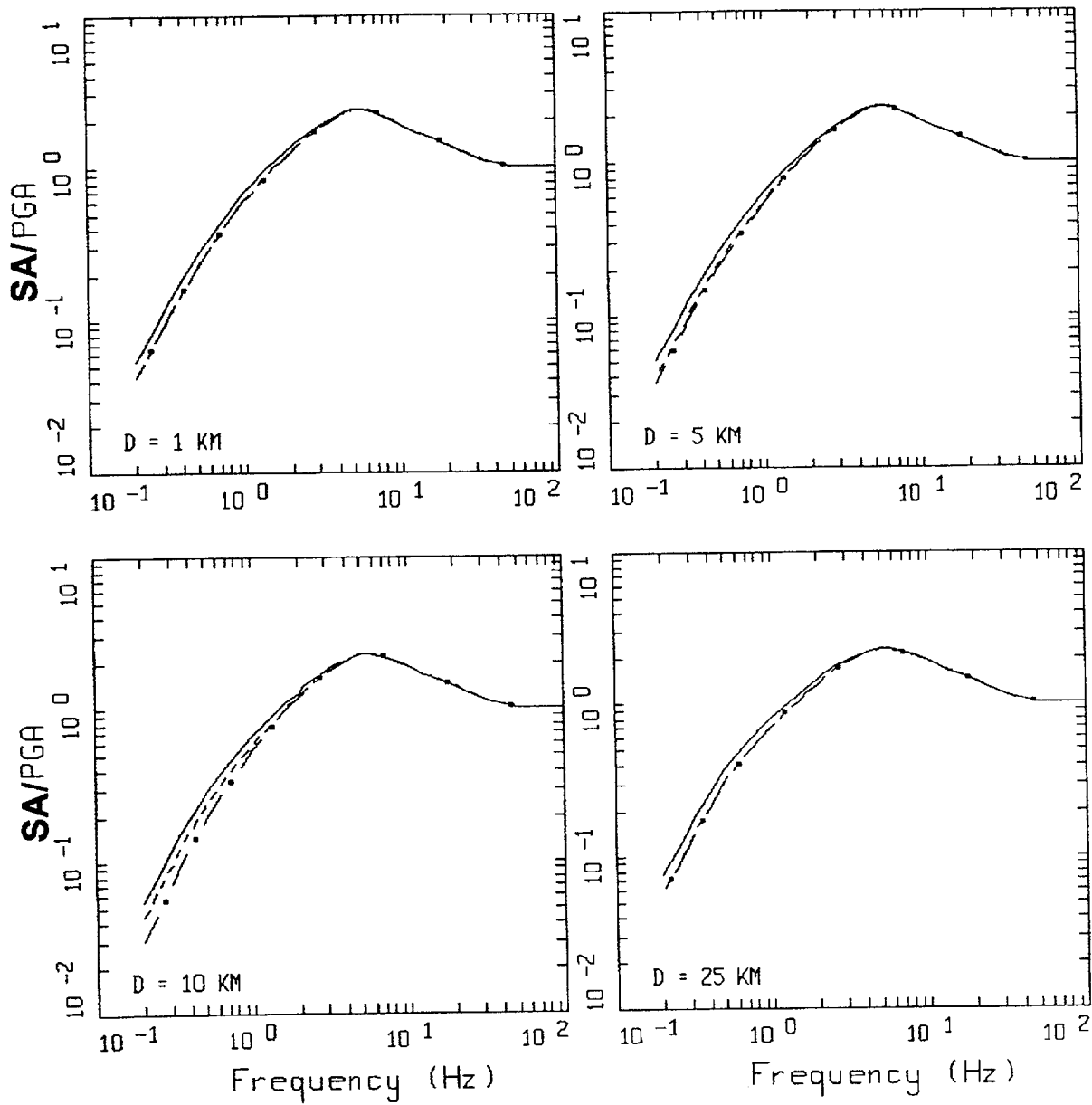
- LEGEND
- 5% DAMPED, RECOMMENDED NRC SPECTRA CEUS 1 CORNER, 50th percentile
 - 5% DAMPED, RECOMMENDED NRC SPECTRA CEUS 2 CORNER, 50th percentile
 - 5% DAMPED, NEWMARK&HALL SPECTRA, 50th percentile
 - - - - 5% DAMPED, NEWMARK&HALL SPECTRA, 84th percentile
 - . - . 5% DAMPED, REG GUIDE 1.60

Figure Set 4-27. (Cont'd)



R = 25 KM, ROCK
EMPIRICAL WUS

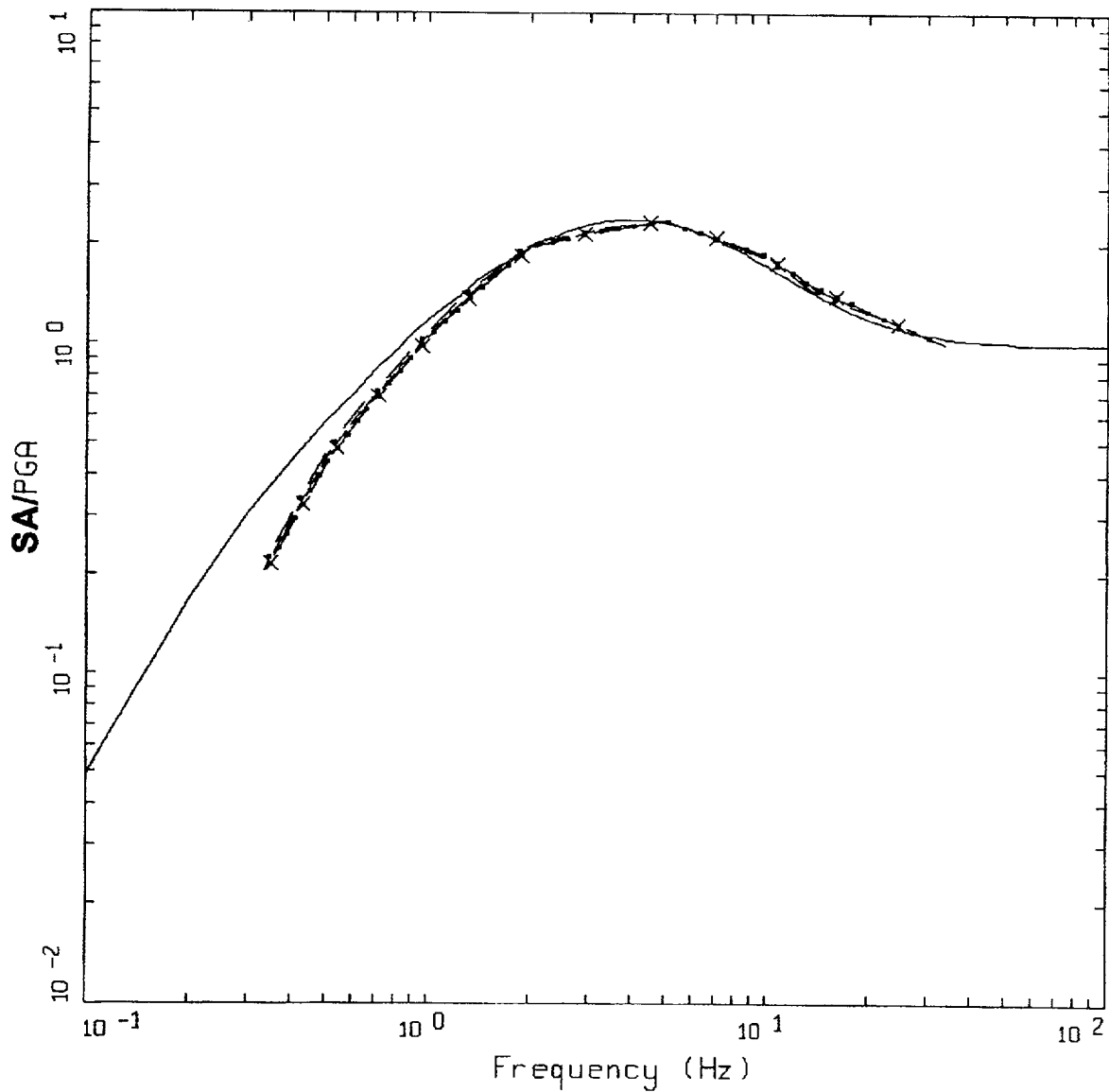
Figure 4-28. Predicted effects of source mechanism on spectral shapes for empirical WUS attenuation relations. For the Abrahamson and Silva, 1997 empirical relation, the frequency dependence differs for small and large magnitudes.



M=6.5, R=25 KM, ROCK
EMPIRICAL WUS

- LEGEND
- 5% DAMPED, STRIKE SLIP
 - 5% DAMPED, OBLIQUE, FOOT WALL
 - · - · 5% DAMPED, OBLIQUE, HANGING WALL

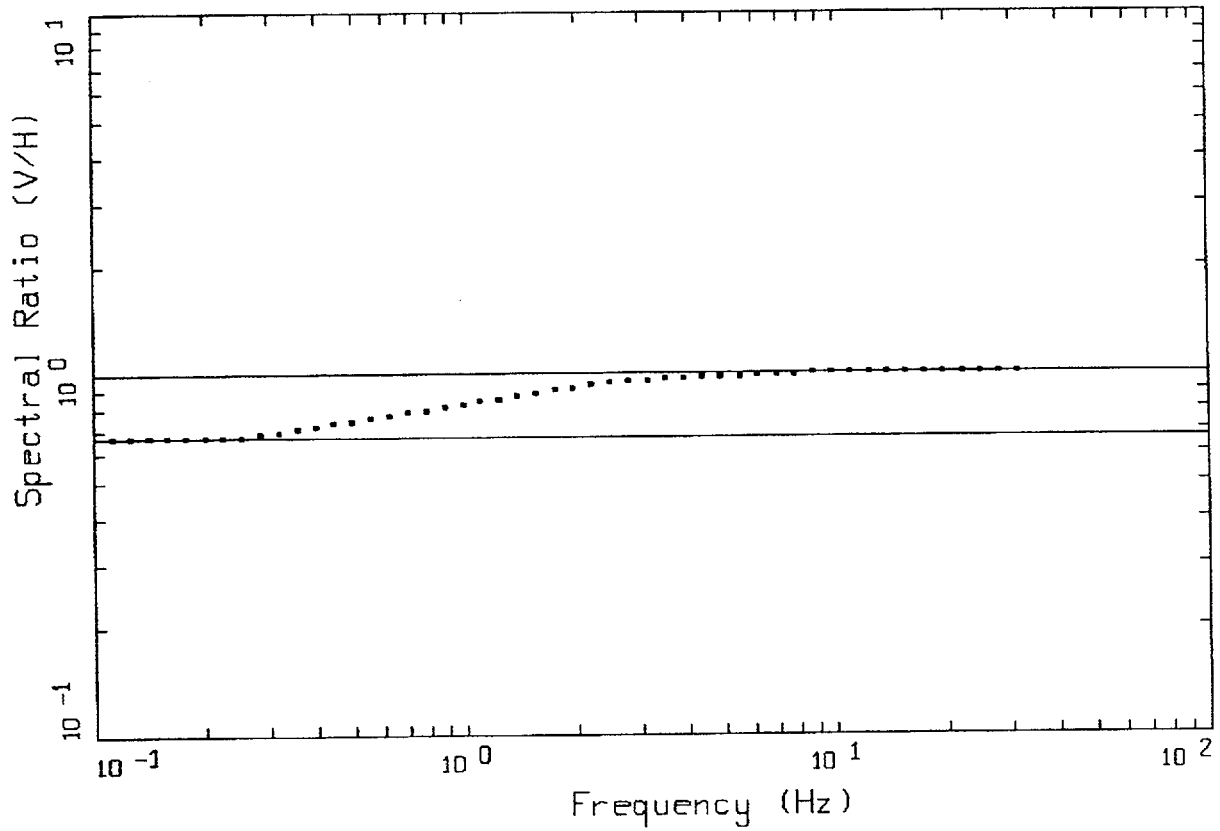
Figure 4-29. Predicted effects of site location (hanging wall vs. foot wall) for oblique-slip source mechanisms on spectral shapes compared to strike-slip spectral shapes for an empirical WUS attenuation relation (Abrahamson and Silva, 1997).



M=9.0, ROCK, H=25 KM, INTERFACE

- LEGEND
- 5% DAMPED, RECOMMENDED NRC SPECTRA WUS, M = 8.0, DISTANCE = 25.0 KM
 - X — 5% DAMPED, M = 9.0, DISTANCE=1 KM, PGA=0.337 g
 - 5% DAMPED, M = 9.0, DISTANCE=5 KM, PGA=0.324 g
 - 5% DAMPED, M = 9.0, DISTANCE=10 KM, PGA=0.309 g
 - 5% DAMPED, M = 9.0, DISTANCE=25 KM, PGA=0.269 g
 - • — 5% DAMPED, M = 9.0, DISTANCE=50 KM, PGA=0.217 g

Figure 4-30. Comparison of recommended shapes for M 8.0 at R = 25 km to empirical subduction zone shapes for M 9.0 at a suite of distances (Youngs et al., 1997).



REGULATORY GUIDE 1.60
 V/H RATIO

LEGEND	
.....	R.G. 1.60
————	1
————	2/3

Figure 4-31. V/H ratio for 5% damped response spectra implied by the R.G. 1.60 design motions.

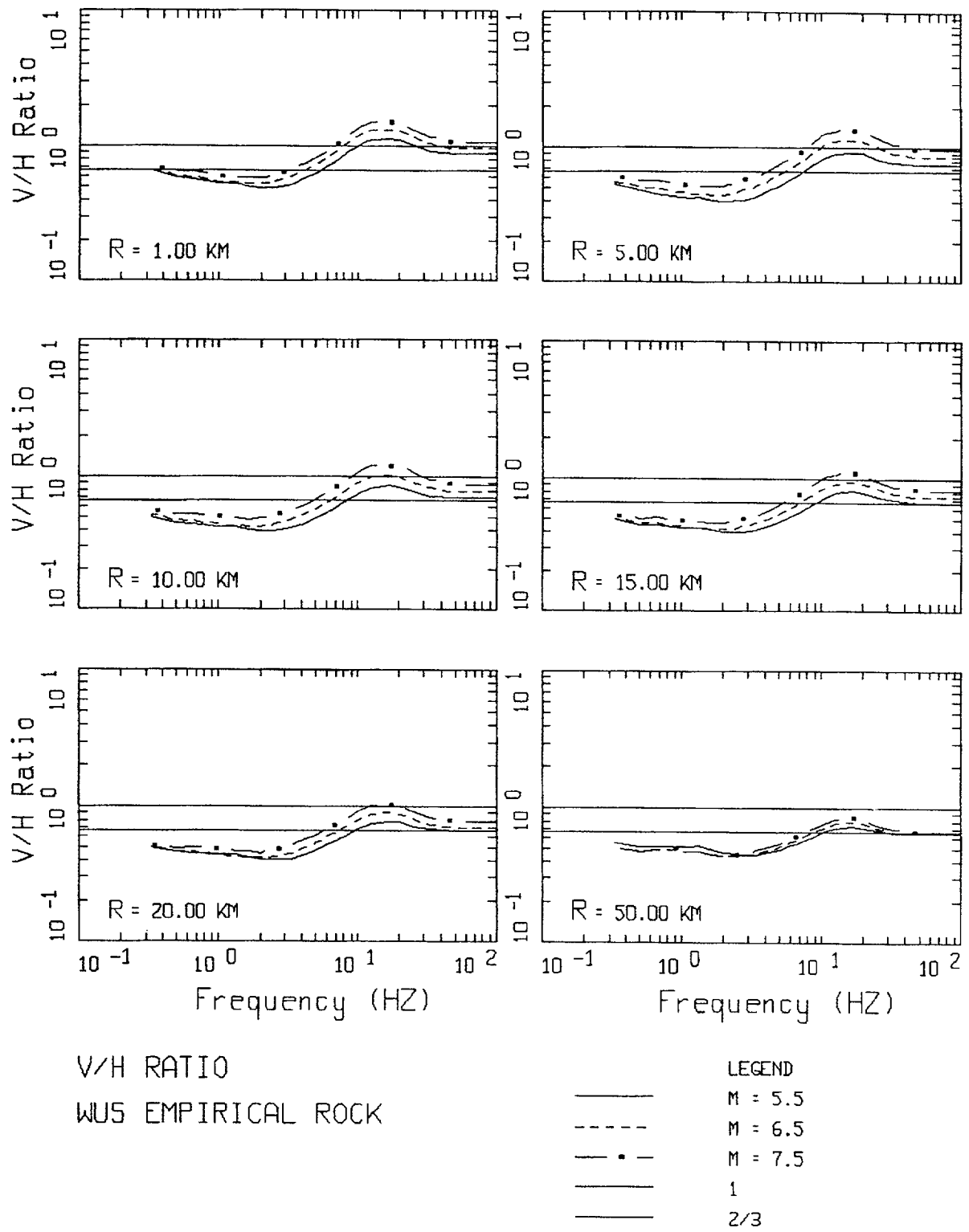
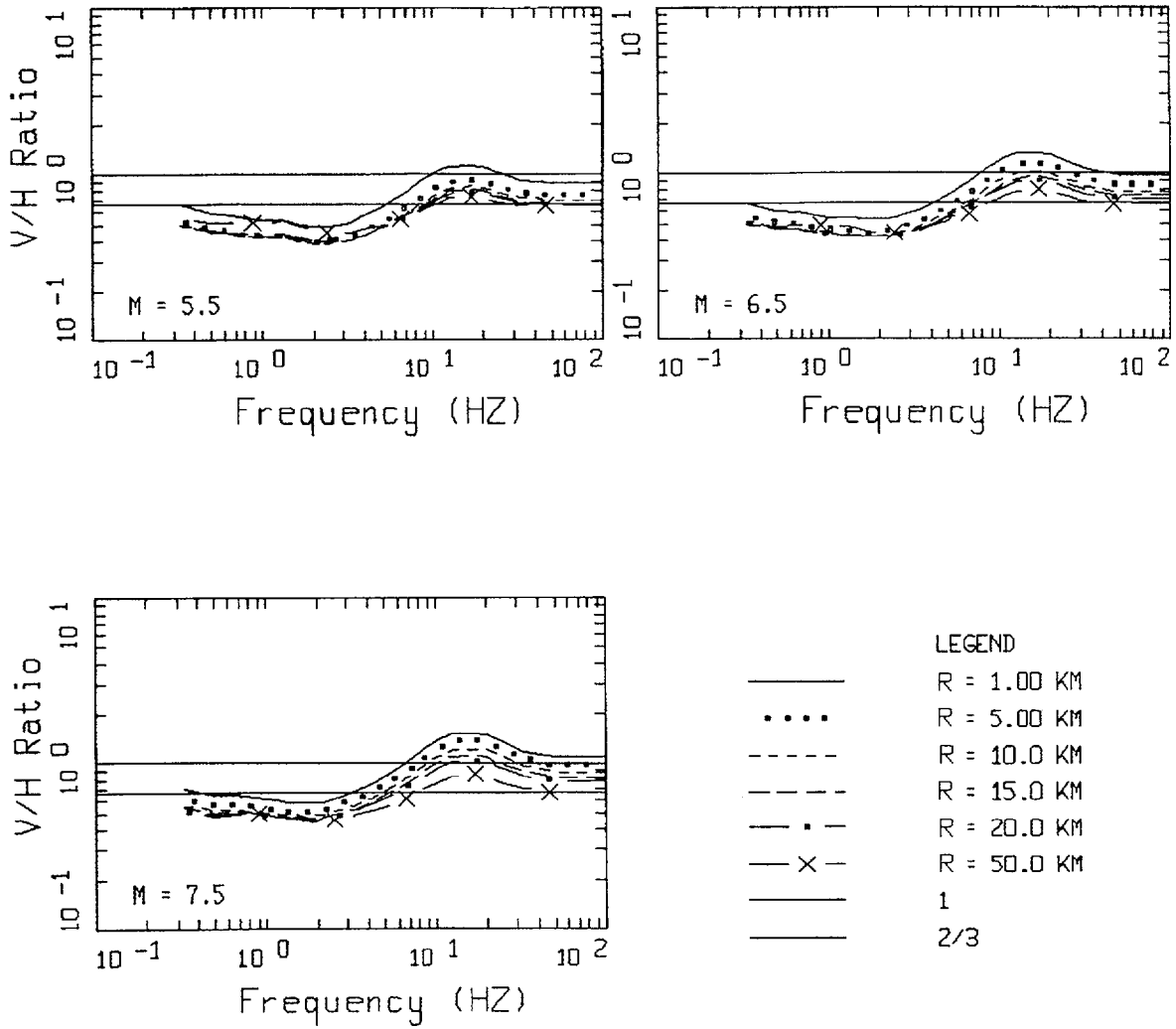
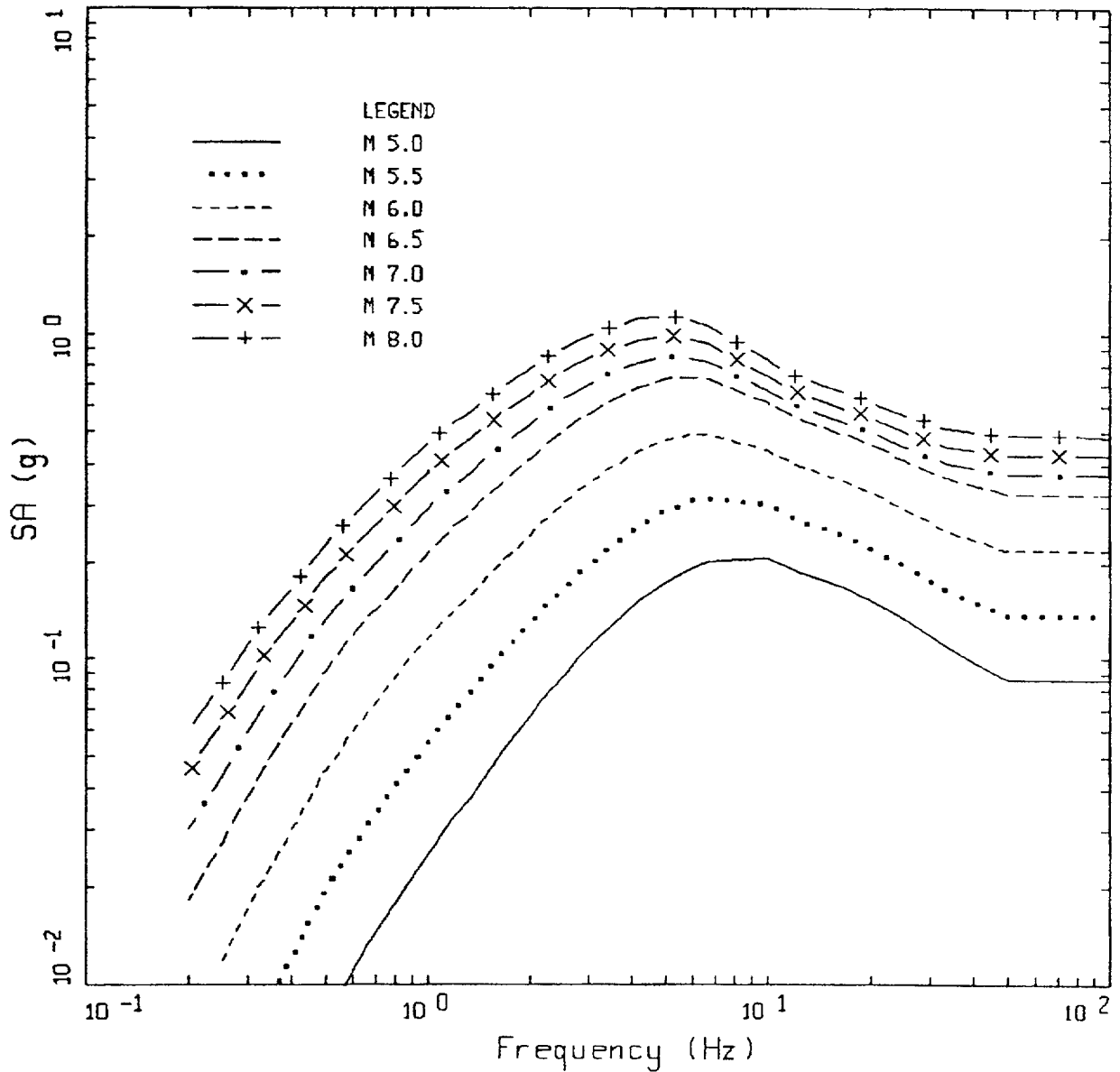


Figure 4-32. Average V/H ratio (5% damped) magnitude dependencies based on the Abrahamson and Silva, 1997; Campbell, 1997; and Sadigh et al., 1997 empirical WUS rock attenuation relations for a suite of magnitudes.



V/H RATIO
WUS EMPIRICAL ROCK

Figure 4-33. Average V/H ratio (5% damped) distance dependencies based on Abrahamson and Silva, 1997; Campbell, 1997; and Sadigh et al., 1997 empirical WUS rock attenuation relations for a suite of magnitudes.



EMPIRICAL, ROCK, HORIZONTAL
R = 10.0

Figure 4-34. Magnitude dependence of 5% damped horizontal component response spectral acceleration at a rupture distance of 10 km for a WUS rock empirical attenuation relation (Abrahamson and Silva, 1997).

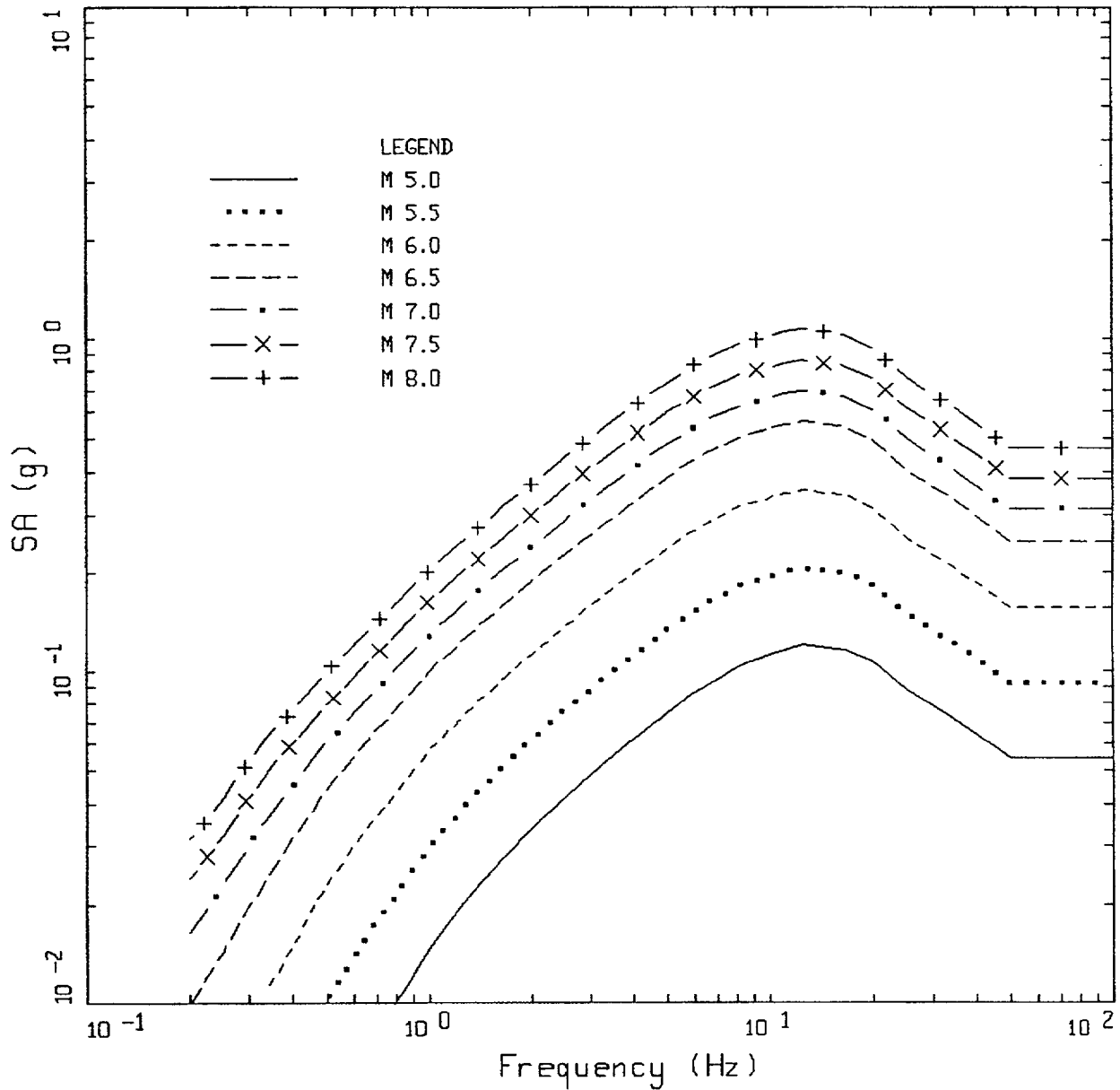
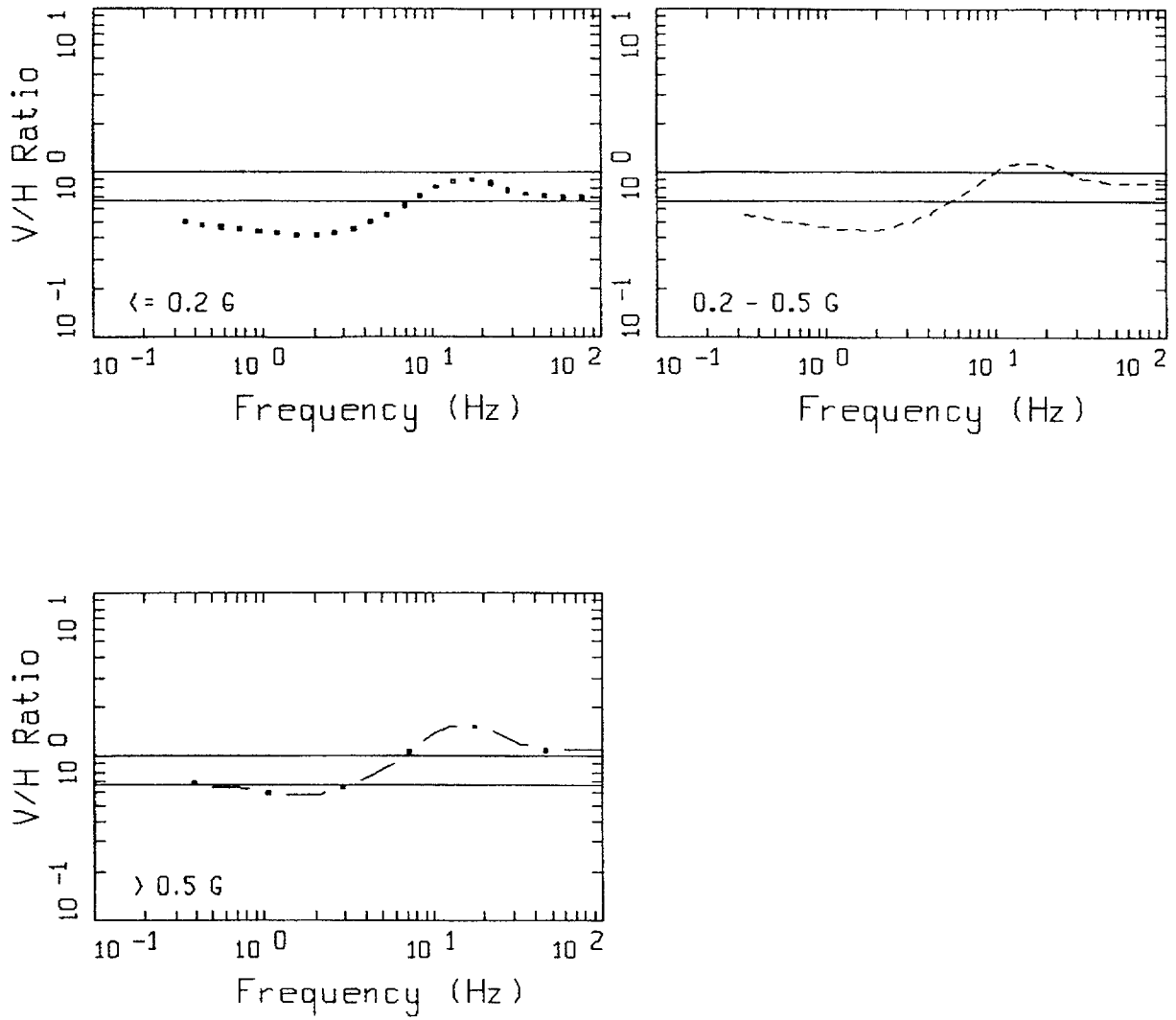


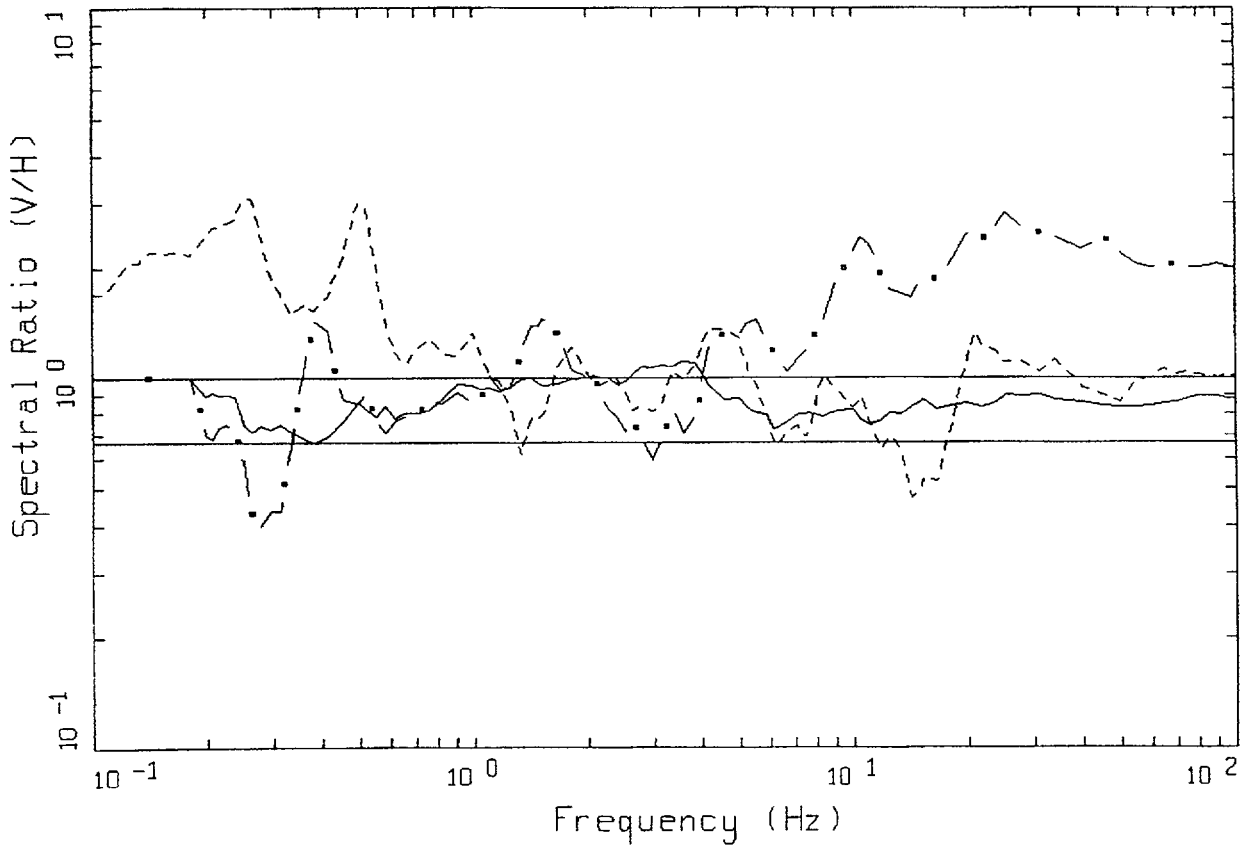
Figure 4-35. Magnitude dependence of 5% damped vertical component response spectral acceleration at a rupture distance of 10 km for a WUS rock empirical attenuation relation (Abrahamson and Silva, 1997).



V/H RATIO
WUS EMPIRICAL ROCK

LEGEND	
— • —	D = 1.00 KM
— — —	1
— — —	2/3

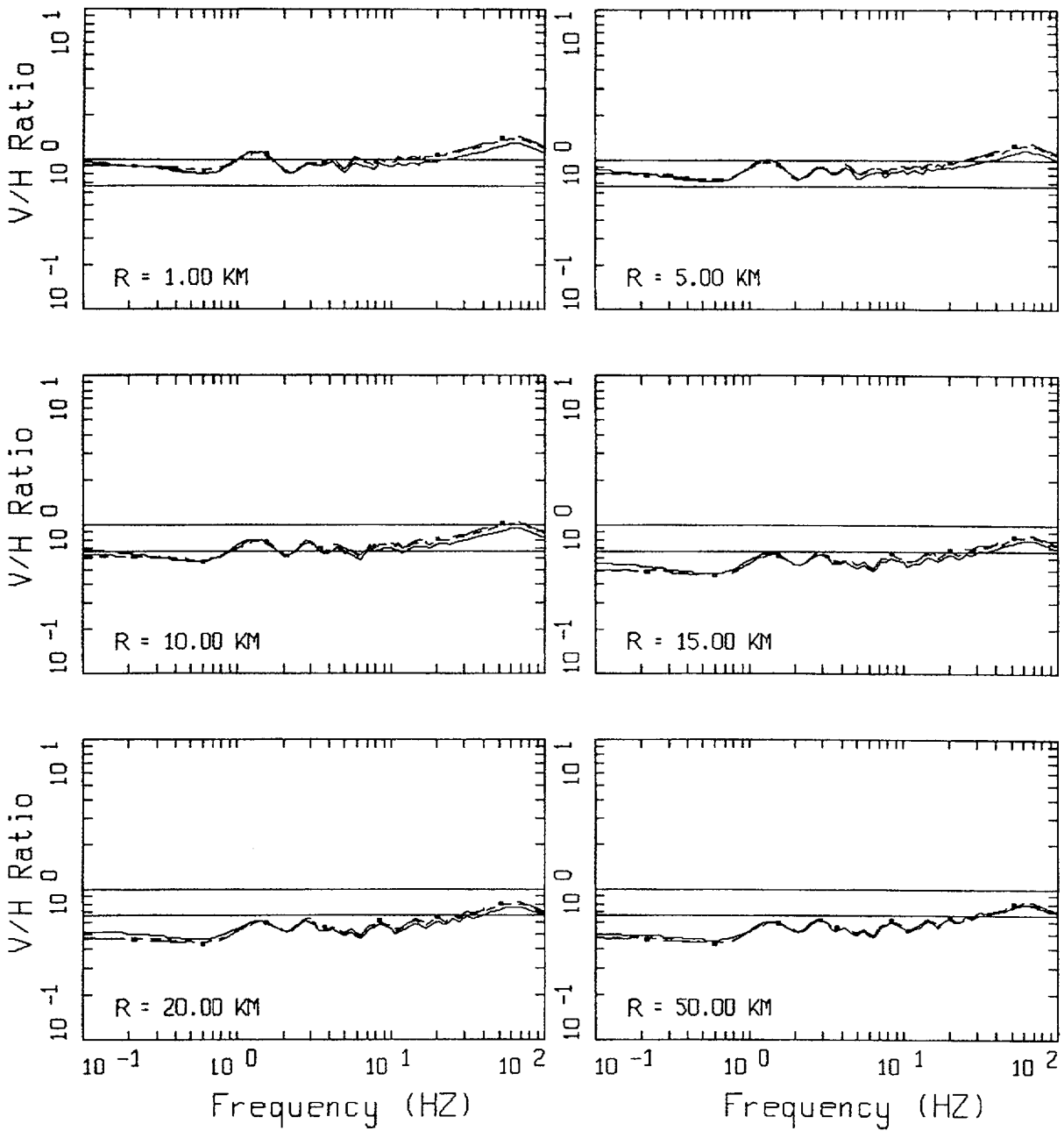
Figure 4-36. Recommended V/H ratios (5% damped) for WUS soft rock site conditions for ranges in horizontal component peak accelerations.



EMPIRICAL CEUS ROCK

LEGEND	
—	SAGUENAY, M=5.9, R=111.22 KM, 18 SITES, 52-200 KM
- · -	GAZLI, NAHANNI, M=6.8, R=4.5 KM, KARAKYR, S1
- - -	NAHANNI, M=6.8, R=16 KM, S3
—	1
—	2/3

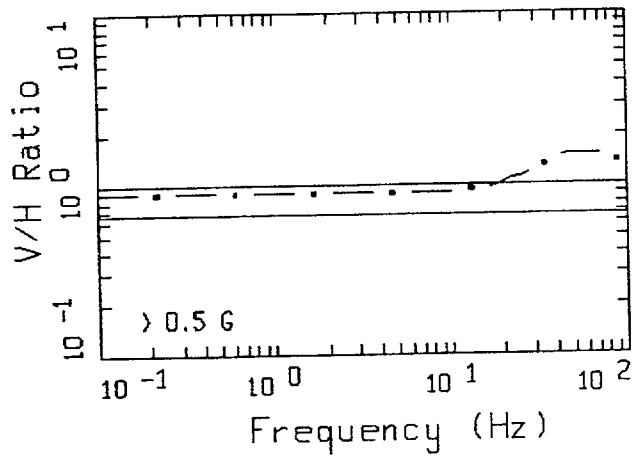
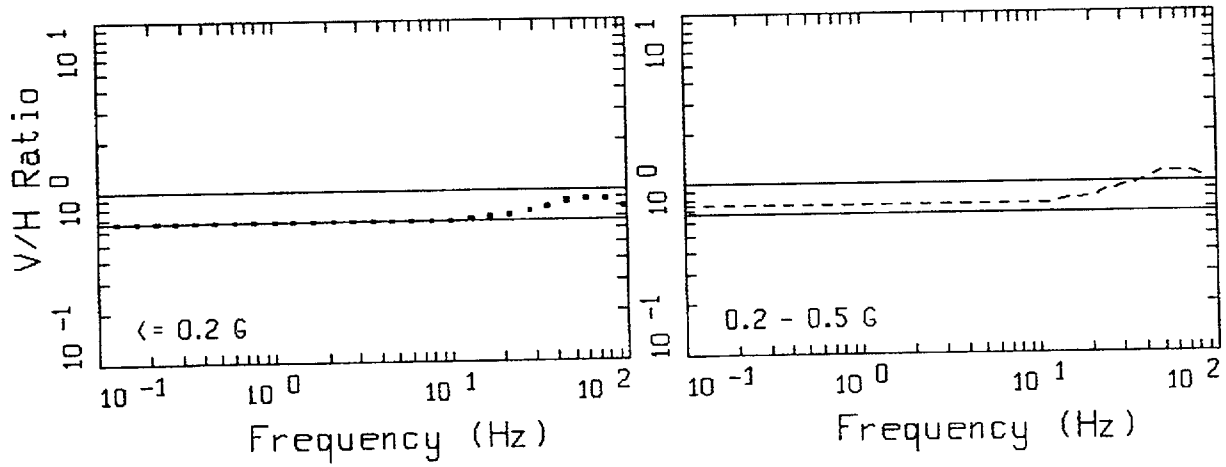
Figure 4-37. V/H ratios (5% damped) computed from recordings of the M 5.9 1988 Saguenay, and M 6.8 1976 Gazlie, and 1985 Nahanni earthquakes. The Gazli and Nahanni earthquakes are considered to represent CEUS source, path, and site conditions.



V/H RATIO
 CEUS MODEL ROCK

————	M = 5.5
-----	M = 6.5
- . - .	M = 7.5
————	1
————	2/3

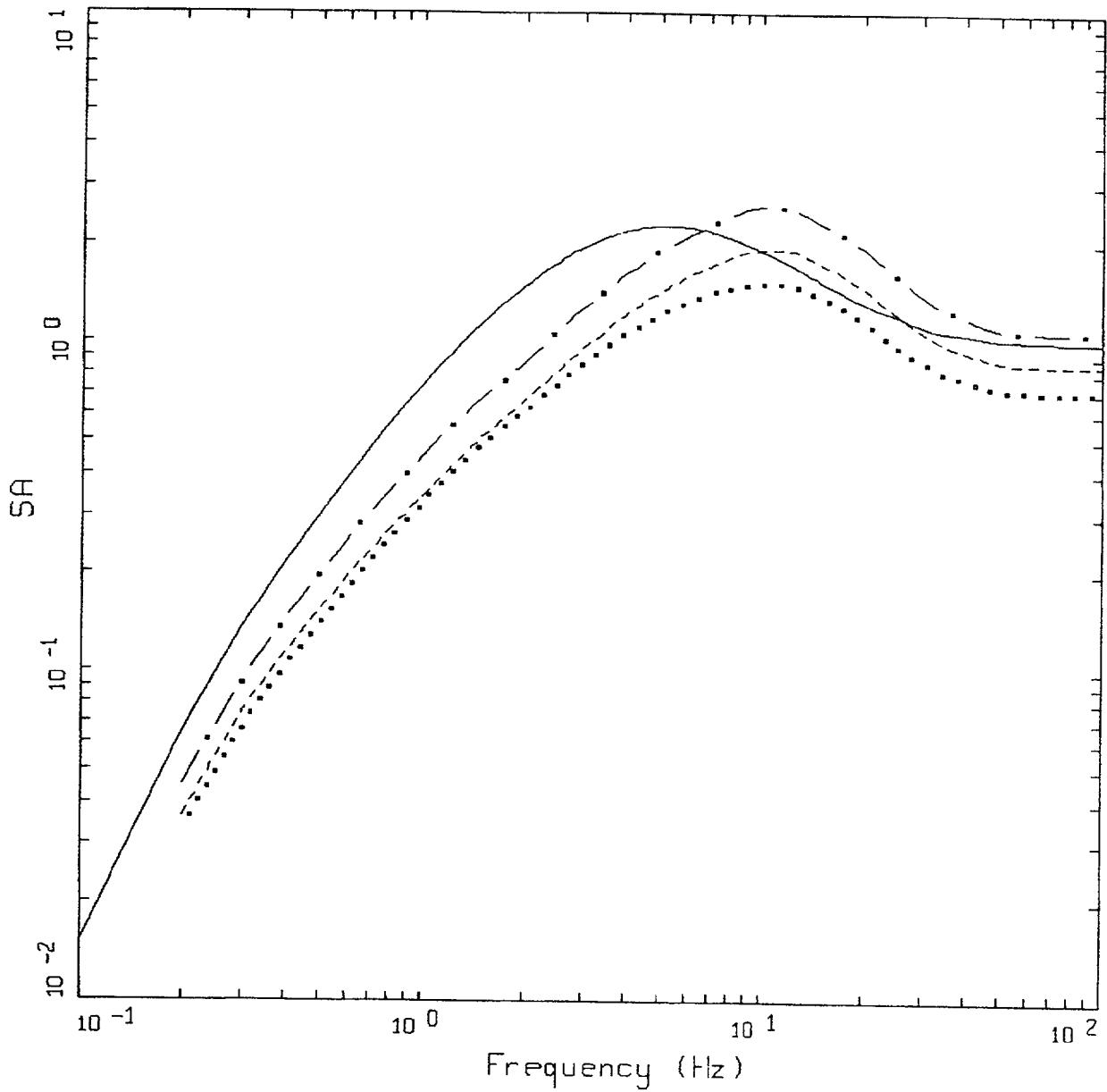
Figure 4-38. V/H ratios (5% damped) for CEUS rock site conditions computed with the simple point-source model.



V/H RATIO
 CEUS RECOMMENDATIONS

- LEGEND
- • — R = 1.00 KM
 - 1
 - 2/3

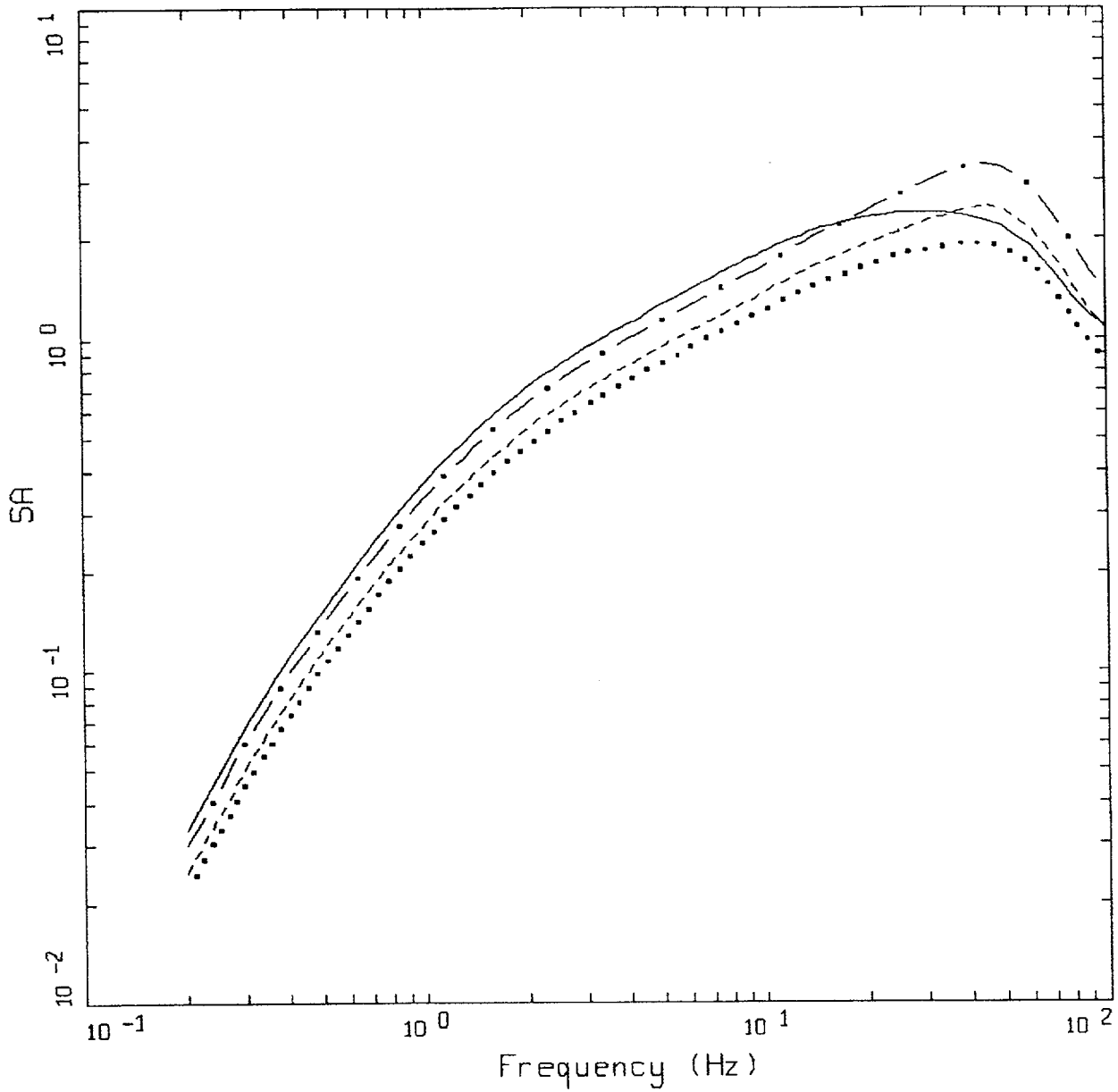
Figure 4-39. Recommended V/H ratios (5% damped) for CEUS hard rock site conditions for ranges in horizontal component peak accelerations.



NRC WUS V/H RATIO * RECOMMENDED NRC SPECTRA

- LEGEND
- 5% DAMPED, RECOMMENDED NRC SHAPE, M6.4, R=27.4 km
 - - - 5% DAMPED VERTICAL > 0.5 G
 - . - . 5% DAMPED VERTICAL 0.2 - 0.5 G
 - 5% DAMPED VERTICAL < 0.2 G

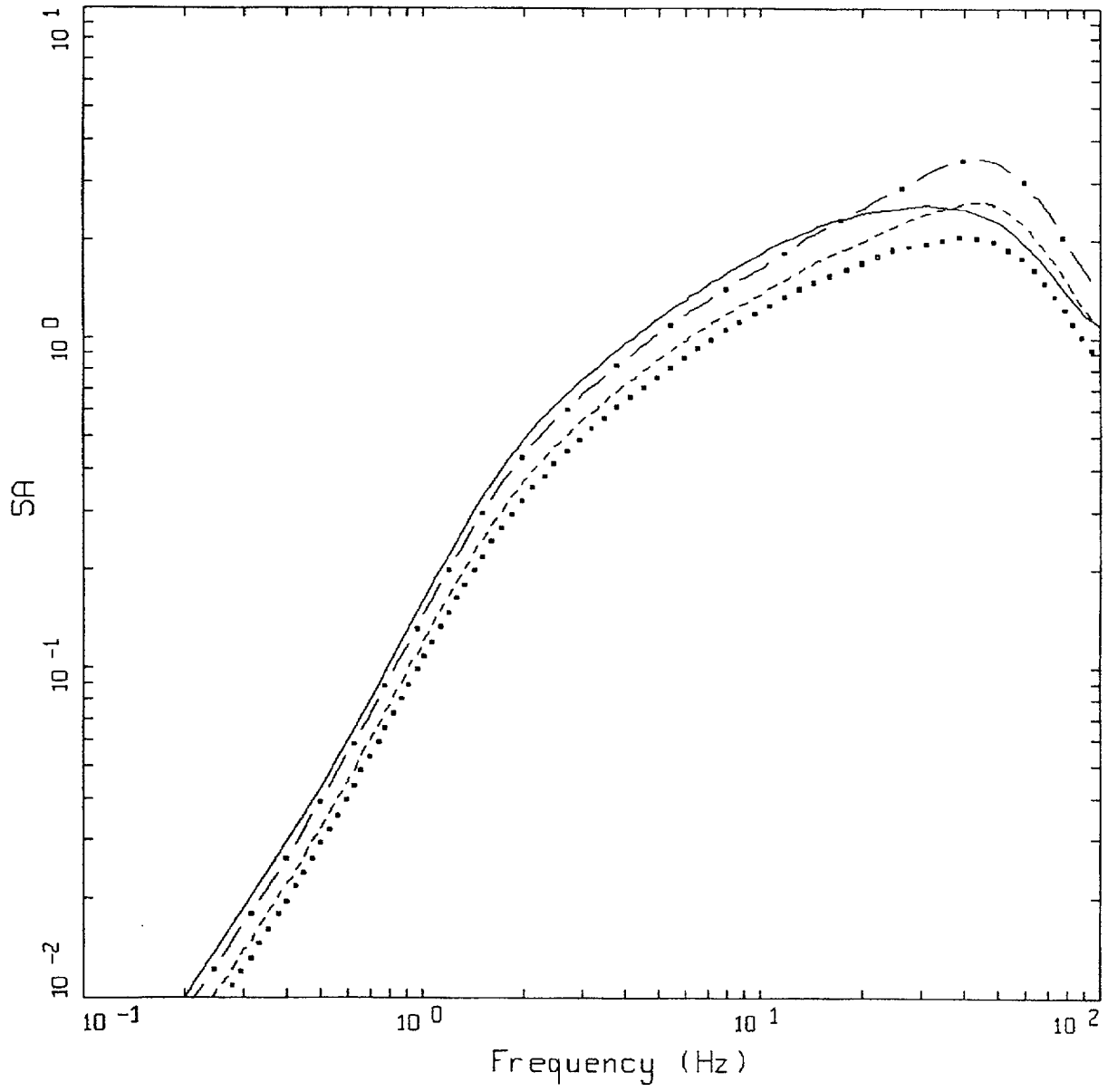
Figure 4-40. WUS vertical component response spectra (5% damped) based on the M 6.4, R = 27.4 km horizontal shape (Figure Set 4-26) and recommended V/H ratios (Table 4-4).



NRC CEUS V/H RATIO * RECOMMENDED NRC SPECTRA
1-CORNER

- LEGEND
- 5% DAMPED, RECOMMENDED NRC SHAPE, M6.4, R=27.4 km
 - - - - > 0.5 G
 - 0.2 - 0.5 G
 - <= 0.2 G

Figure 4-41. CEUS vertical component response spectra (5% damped) based on the M 6.4, R = 27.4 km single corner horizontal shape (Figure Set 4-27) and recommended V/H ratios (Table 4-5).



NRC CEUS V/H RATIO * RECOMMENDED NRC SPECTRA
 2-CORNER

- LEGEND
- 5% DAMPED, RECOMMENDED NRC SHAPE, M6.4, R=27.4 km
 - - - - < 0.5 G
 - 0.2 - 0.5 G
 - <= 0.2 G

Figure 4-42. CEUS vertical component response spectra based on the M 6.4, R = 27.4 km double corner horizontal shape (Figure Set 4-26) and recommended V/H ratios (Table 4-5).

5 CRITERIA FOR EVALUATION OF GROUND MOTIONS FOR THE ANALYSIS OF NUCLEAR FACILITIES

5.1 Introduction

This section summarizes the recommended criteria for developing and evaluating artificial ground motions used to estimate the seismic response of nuclear power plants and other critical nuclear facilities.

The current version (NUREG-0800) of the USNRC Standard Review Plan (SRP) incorporates a specific requirement to consider the minimum Power Spectral Density (PSD) of ground motion records input to building, component, and soil models. Prior to this SRP, ground motion time histories used for such analyses were evaluated based solely upon comparison of their response spectra with the design response spectrum for the site. The response spectrum enveloping criteria was based upon the engineering judgment that if the response spectral input at a given frequency exceeds the corresponding design spectral criteria, the computed system response at that frequency will exceed the response from the criteria input.

However, it was recognized that a design response spectrum could be enveloped by the computed free-field response spectrum across a given frequency range, even though the PSD (or equivalently the Fourier amplitude spectrum) of the input ground motion could possess low levels (gaps) within the same frequency range. For this case, the computed system response may be underpredicted if, for example, the soil-structure interaction (SSI) frequencies fall within those gaps. In addition, the development of large structural response computer codes currently used for system evaluations has made the ability to perform simple checks of computed response more difficult for the reviewer.

Because of the ambiguities in the definition of a PSD as well as the effort involved in developing a minimum PSD requirement for an arbitrary target response spectrum, revised criteria are proposed herein that can be used to evaluate ground motion time histories to be used in the design or evaluation of critical facilities. These revised criteria eliminate the need for a separate PSD check but require that the target 5% damped response spectrum be closely matched both from above and below. The intent of the more stringent matching criteria is to ensure that the developed ground motion does not possess any significant gaps in frequency content. These revised criteria satisfy the general intent of the criteria contained in the SRP, which is currently defined in detail only for the spectral shape embodied by the R.G. 1.60 spectrum.

5.2 Current Regulatory Criteria

In the current regulatory environment, the minimum PSD requirement is included as an additional check on the developed ground motion along with the enveloping criteria of the design response spectra. The PSD criteria was included in the SRP as a result of the studies conducted as part of the resolution of the USI A-40 issues (NUREG/CR 5347, 1989). The detailed specification of the minimum PSD for motions associated with the R.G. 1.60 spectrum was added in an attempt to ensure that no gaps at critical frequencies would occur in the selection of free-field ground motion time histories used in the system response analyses. However, due to the difficulties encountered in

generating time histories that closely match both target response and PSD spectra, it was recommended that a minimum PSD requirement should be included to ensure that the ground motion record had no significant gaps in frequency content. The primary evaluation criteria remains the fit of the calculated response spectrum to the target response spectrum.

To satisfy these recommendations, the following procedure was included in Revision 2 to the SRP when the target response spectrum under consideration is the R.G. 1.60 spectrum:

- The average PSD should exceed 80% of the specified target over the frequency range from 0.3 Hz to 24 Hz.
- At any frequency, the average PSD is computed over a frequency band of $\pm 20\%$ centered on the frequency at which the PSD is being calculated.
- The duration of the ground motion used in the definition of the PSD is the strong motion duration for which the Fourier components of the ground motion are calculated.
- For the case where an ensemble of time histories is used for the generation of spectra, the PSD of the ensemble can be generated at the 84th percentile level and compared to the appropriate target PSD.

The frequency range specified, from 0.3 Hz to 24 Hz, is based on two relatively subjective considerations. First, the power in actual ground motion recordings above 24 Hz was considered negligible so that there is no need to consider spectral content above this value. Secondly, the check below 0.3 Hz was considered unnecessary since most nuclear facilities are relatively stiff and have response frequencies well above this lower bound cutoff. However, since those recommendations were promulgated, several issues have arisen which make these limits potentially problematic. First, at some deep soil sites, it was noted that site response fundamental frequencies extend to values well below 1 Hz. The details of the ground motion at these low frequencies could become important in evaluating site response, requiring more consideration of the frequency content at these lower frequencies of interest. Secondly, at some CEUS rock sites, rock outcrop motions may have significant energy at frequencies as high as 50 Hz (Silva and Darragh, 1995). Thus, even though these motions may not have a significant percentage of their total power at these high frequencies, the Fourier amplitudes of the high frequency components of the motion could become important when these rock outcrop motions are used as input to convolution calculations to determine surface motions at low frequency soil sites.

For design response spectral shapes other than the R.G. 1.60 shape, the SRP does not provide specific guidance but indicates that the procedures used to develop the minimum PSD associated with the R.G. 1.60 shape be used to develop PSD requirements for these other spectral shapes. This is not always a simple task, but generally can require the investment of some significant effort for a given target spectrum. For this study, where spectral shapes are being developed as continuous functions of distance and magnitude (Section 4), such an effort can prove daunting. As a result, guidelines are recommended here that can be used to ensure that artificial design ground motions developed for response analyses satisfy the intent of the SRP.

In addition to the minimum PSD requirement, other characteristics of the developed ground motions are important in judging their adequacy. The strong motion duration, peak velocity and displacement parameters, and correlation among the three component motions of an artificial record set are of interest to ensure that the records are sufficiently "earthquake-like" to satisfy the intent of the SRP. Part of criteria recommended here therefore involve the characteristics of the empirical WUS data base (Appendices A, B, and F).

5.3 Recommended Regulatory Criteria

Based on the results of numerical studies described in the following paragraphs, together with discussions with the project Peer Review Panel, a number of conclusions were reached on recommendations for artificial ground motion records. These artificial records must be generated to "match" or "envelop" given response spectral shapes associated with appropriate magnitude and distance bins (Section 3) and to satisfy other general characteristics associated with these bins. To evaluate the adequacy of artificial records, the following information should be made available with each record. This information can then be used for comparison with bin characteristics.

- Plots of time history and Arias Intensity function;
- Plots of Fourier amplitude and smoothed Fourier amplitude spectra, scaled by the factor FT as discussed in Section 5.4.3 to correlate with bin duration characteristics;
- Comparative plots of 5% damped target response spectrum and spectrum resulting from the ground motion;
- Total duration of the record, time increment, frequency window and Nyquist frequency;
- Strong motion duration of the record as defined by the 5%-75% Arias Intensity;
- Peak motion parameters PGA, PGV and PGD, and ratios PGV/PGA , PGD/PGA and $PGA \cdot PGD/PGV^2$.

Based upon this information the following general criteria are recommended to evaluate the adequacy of the artificially developed ground motions.

- (a) The general objective is to generate an artificial or synthetic accelerogram that achieves approximately a mean-based fit to the target spectrum. That is, the average ratio of the spectral acceleration calculated from the accelerogram to the target, where the ratio is calculated frequency by frequency, is only slightly greater than 1. The aim is to achieve an accelerogram that does not have significant gaps in the Fourier amplitude spectrum but that is not biased high with respect to the target. An accelerogram that exceeds the target may overdrive a site soil column or structure where nonlinear response is of interest.
- (b) Records should have a sufficiently small frequency window and sufficiently high maximum frequency (or alternatively time increment and maximum duration). The total duration of the

record can be increased by zero packing to satisfy these frequency criteria. It is recommended that records have a maximum frequency window of 0.05 Hz with a Nyquist frequency of at least 50 Hz, or a time increment of at most 0.010 seconds for a total duration of 20 seconds. If frequencies higher than 50 Hz are of interest, then the time increment of the record must be suitably reduced to provide a Nyquist frequency above the maximum frequency of interest. Such records can be easily generated with currently available computer power and software. This recommendation is similar to that presented in NUREG/CR-5347.

- (c) Spectral accelerations at 5% damping should be computed at a minimum of 100 points per frequency decade, uniformly spaced over the log frequency scale from 0.1 Hz to 50 Hz or the Nyquist frequency. This results in an increment in \log_{10} frequency of 0.01. If the target response spectrum is assumed to be defined in the frequency range from 0.2 Hz to 25 Hz, the comparison of the artificial motion response spectrum with the target spectrum should be made at each frequency computed above in this frequency range. The number of frequencies at which spectra are computed is therefore increased from 57 (Table 3.7.1-1 of the SRP) to well over 200 from 0.2 Hz to 25 Hz as recommended herein. Again, with current computer power generally available, this requirement should pose no hardship and should result in an accurate representation of the computed spectra.
- (d) The computed 5% damped response spectrum of the accelerogram (if one artificial motion is used for analysis) or of the average of all accelerograms (if a suite of motions is used for analysis) should not fall more than 10% below the target spectrum at any one frequency point. Since the objective is to achieve a mean based fit to the target spectrum, many more points will generally fall below the target spectrum than the 5 point limit mentioned in the current SRP. However, to prevent large frequency ranges falling below the target, no more than 9 adjacent spectral points may be allowed to fall below the target spectrum at any frequency. Using the frequency spacing mentioned above, this corresponds to a moving frequency window of $\pm 10\%$ centered on the frequency.
- (e) The computed 5% damped response spectrum of the artificial ground motion (if one motion is used for analysis) or the mean of the 5% damped response spectra (if a suite of motion is used for analysis) should not exceed the target spectrum at any frequency by more than 30% (a factor of 1.3) in the frequency range between 0.2 Hz and 25 Hz.
- (f) Because of the high variability in time domain characteristics and because few CEUS recordings are available to quantify these characteristics, strict time domain criteria are not recommended. In general, artificial motions should have durations (5%-75% Arias intensity), and ratios PGV/PGA and $PGA \cdot PGD/PGV^2$ that are generally consistent with bin average values. For WUS motions, strong motion durations should generally be within about $\pm 50\%$ of the bin median values (see Section 5.5.2) and PGV/PGA and $PGA \cdot PGD/PGV^2$ values should be within ± 1 sigma of the bin median values. It would be appropriate for CEUS acceleration time histories (excluding the 0 to 10 km distance bin) to have durations on average larger than WUS motions by 20 to 50% with this difference decreasing substantially for velocity and displacement time histories. This recommendation is particularly appropriate for rock outcrop motions.

- (g) Directional correlation coefficients between pairs of records are typically required to be relatively low to ensure that a structure or structural element cannot be oriented in an analysis in such a manner so as to minimize some important directional response quantity of interest. However, if the limiting value is made too low, a significant number of empirical recordings in any earthquake bin may unnecessarily be eliminated from further consideration as a seed for generating design ground motions. Since the response quantity is a function of the structural characteristics and not of the empirical bin data sets, it is recommended that the upper limit for the zero-log cross-correlation coefficient between any two design ground motions be 0.3. For correlation coefficients less than this limit, no significant reduction in response will be attained by orientation of the structure.

If these general criteria are followed, the matching requirements to the 5% damped response spectrum should be adequate to ensure that no gaps in the PSD or Fourier amplitude spectrum will occur over a significant frequency range. There is no special need to evaluate the PSD of the ground motion to compare with minimum PSD targets.

5.4 Description of Analyses

Empirical records appropriate for analyses have been catalogued into magnitude and distance bins (Section 3). These distance and magnitude bins are listed in Table 5.1. The four distance bins selected are labeled "D1" (0-10km), "D2" (10-50km), "D3" (50-100km) and "D4" (100-200km) and the three magnitude bins are labeled "M55" (M5-M6), "M65" (M6-M7) and "M75" (M7+). These magnitude and distance ranges for each bin were selected based upon the judgment of the investigators to arrive at ranges considered to be most significant. If a larger number of bins were selected, for example, the population within each bin would decrease, and this could lead to difficulties in developing average bin characteristics. If fewer bins were selected, then characteristic differences in recordings that were felt to be significant could be lost. The recordings contained within each bin listed in Table 5.1 represent the WUS database (Appendix A). Clearly some bins do not have sufficient empirical data with which to define average characteristics and must be supplemented as described in Section 3.

It should be mentioned that a number of approaches in the open literature are used to develop appropriate artificial time histories. These approaches are based on either time domain or Fourier domain methods that satisfy matching or enveloping criteria of a target response spectrum. It is not the objective of this project to either describe or evaluate these approaches, but rather to describe criteria that can be used to evaluate the appropriateness of given time histories developed by Applicants for use in various system response analyses. As mentioned previously, the primary criterion used to judge the adequacy of such time histories is to ensure that the computed response spectrum closely matches the target response spectrum and ensures that no significant gaps in frequency content exist.

From the outset of this effort, it was recognized that the use of a PSD criterion to evaluate the frequency gap issue has inherent problems with respect to application. First, several different expressions for computation of PSD are available in the open literature. These definitions may not be equivalent to one another. This was also noted in the comments provided by Kennedy (Appendix

A to NUREG/CR-5347), which was the study on which the revision to the current SRP was based. Secondly, it has been noted that there could be a disconnect encountered between the definition of time duration of the ground motion used in the development of the Fourier components of the ground motion and the duration used in computing the PSD as described in the SRP.

For example, in generating artificial time histories, it is usual to extend the initial trial record by zero packing to an integral power of two (2). The record duration used in the Fourier computation with the FFT procedures is then relatively long, consistent with the zero packed record length. In the computation of the PSD, as described in the SRP, the duration mentioned refers to the strong motion duration. Thus, unless one is careful during the review process, the duration used in the FFT and the PSD computations can be different, and can lead to an inconsistency in the computation of the power in the record.

In the work described in the following paragraphs, the average Fourier amplitude spectrum of the empirical records in each bin was computed. Examples of these bin averaged Fourier amplitude spectra are shown in Figures 5-1A and 5-1B and represent some typical results. In these and later figures, the following notation is used to represent a set of strong motion records:

D1RM65H

where D1 is the distance bin as defined above,
R means rock (or S means soil)
M65 is the magnitude bin as defined above,
H means horizontal (or V means vertical).

The Fourier amplitudes for each of the records in the bin, which were first scaled to 1g, were computed and then averaged over the bin without any weighting considered. The shapes plotted in Figure 5-1A compare the horizontal and vertical records in a particular bin (D1RM65) and indicate the general increase in high frequency content of the vertical records with respect to the horizontal records. Figure 5-1B presents a similar comparison of the bin results as a function of magnitude for a given distance bin. Again, the averages show the same general shape with an increase in Fourier amplitude with magnitude. The average Fourier amplitude spectra for all the bins are shown in Appendix E.

In the calculations performed to address the frequency gap issue, the general procedure consisted of (a) selecting target response spectral shapes with different characteristics, (b) generating artificial records that satisfy the enveloping criteria of the SRP, (c) introducing gaps into these artificial records at various frequencies, and (d) determining the influence of these frequency gaps on the recomputed 5% response spectra. In generating appropriate records, the ability to match a given target spectrum reasonably closely is controlled by two characteristics of the spectrum. First, if the target spectrum consists of a series of straight line segments (as plotted, say, on arithmetic spectral acceleration vs. log frequency scales), the discontinuities in the slope of the spectrum can cause difficulties in the iteration process used to generate the artificial time history. Secondly, if the shape of the spectrum is very peaked (relatively large amplification ratio over a narrow frequency band), the iteration

process may again have difficulties in convergence. A number of such spectral shapes were used and the results of some of these computations are presented in the following paragraphs.

5.4.1 Generation of Artificial Enveloping Time Histories, Segmented Target

In generating these trial time histories, a relatively peaked spectral shape of the acceleration spectrum was generated early in the study using the median shape computed for the D2RM55H bin (distance 10-50 km, rock site, magnitudes 5-6, horizontal direction) and shown in Figure 5-2. This spectral shape was computed from all the records (unweighted) in this particular bin and was not modified to match data in adjacent bins. It should be noted that this spectral shape is not necessarily the same as that shown in Section 4 for the given average magnitude and distance, although it is not too different. This smooth bin spectral shape was then enveloped with a series of closely matching straight-line segments. For general interest, a comparison of this segmental shape is made with the NUREG-0098 median rock spectral shape in Figure 5-2. The target spectrum is significantly narrower and more peaked than the generic spectrum.

Eight different time histories were then developed that generate response spectra that envelop this target segmental shape. The computer program CARES, which operates in the frequency domain, was used in these calculations (Costantino et al., 2000). A random phase spectrum was generally used in these computations, as this was simplest to perform and was as appropriate as any other assumption. The enveloping criteria used in each case satisfies the current SRP recommendations (no more than 5 spectral points falling below the target, with no one point falling more than 10% below the target spectrum) over the frequency range from 0.2 Hz to 34 Hz as recommended in Table 3.7.1-1 of the SRP.

The particular characteristics of these artificially generated time histories are listed in Table 5-2. Record 1 has a strong motion duration (Arias Intensity from 5%-75%) of 6.3 seconds. This duration characteristic is long for this particular bin as can be noted from Figure 5-14A, where the bin average is shown to be about 2.5 seconds, with the $\pm 50\%$ variations extending from about 1.6 seconds to about 3.8 seconds. A summary of these bin characteristics is presented in Appendix F. This artificial trial record used the most data points in the calculation by zero padding the record to achieve a total duration of 20 seconds. The frequency increment generated by the one-sided FFT routine is 0.05 Hz with a maximum frequency retained in the calculation of over 200 Hz. Records 2 through 4 have about the same duration as Record 1 but half the number of time steps of the previous record. Record 4S uses a longer zero padded length but with the same total number of time steps as Record 4, while Record 4L uses an increased strong motion duration of 8.4 seconds. Record 5 uses the fewest number of time steps and keeps a total padded duration of 20 seconds. Record 1S has characteristics similar to Record 1 except that the strong motion duration is reduced from 6.3 seconds to 3.4 seconds, which is more in keeping with the average bin characteristic.

Figures 5-3A through 5-3H plot the resulting 5% damped acceleration response spectrum for each generated motion, the segmented target spectrum and the computed error between the two spectra. It should be noted that in the CARES FFT computation, the frequency increment is selected as the inverse of the maximum total padded duration of the record while the maximum frequency is determined from the time increment of the record (defined through the Nyquist frequency). The

spectra computed and shown in the plots of Figure 5-3 are typically cutoff at either 50 Hz or at the Nyquist frequency of the generated motions. Thus for Records 4, 4S, 4L and 5, the cutoff frequency is as low as 12.8 Hz since the time increment selected is relatively large. It should be reiterated that the purpose of these calculations was not to develop closely enveloping records. Rather it was to ensure that records could be generated that yield spectra reasonably close to the target response spectra after only a few iterations, even for this target spectrum, which has relatively poor matching characteristics (segmented and relatively peaked).

The plots of Figures 5-3A through 5-3H indicate that the enveloping of such segmented response spectra can be easily achieved after only a few iterations with resulting errors in spectral amplitude less than 20% over the frequency range from 1 Hz to 25 Hz. This enveloping can be achieved provided that the record uses a sufficiently small frequency increment and sufficiently high cutoff frequency (or alternatively short time increment and long duration of the record). It has been our general experience that enveloping errors increase as frequency ranges approach the Nyquist frequency. The recommendations of NUREG/CR-5347 suggest a maximum frequency window of 0.05 Hz. With a Nyquist frequency of at least 50 Hz, the number of Fourier components computed in the one-sided Fourier computation is then 1024 and number of time steps in the record is 2048. The corresponding time increment of the record is then about 0.01 seconds for a record duration of 20 seconds. During the public comment period associated with the USI A-40 issues, some comments were received that recommended a large frequency window of 0.2 Hz. With today's available computational power on even the most ordinary desktop computer, such a recommendation does not have any real basis.

5.4.2 Generation of Artificial Enveloping Time Histories, Smooth Target

Figures 5-4A and 5-4B indicate similar results but using the smooth shape of the acceleration response spectrum rather than the segmented shape for the same bin (D2RM55H) discussed previously. As can be noted, the calculated artificial motions more closely envelop the smooth target spectrum as compared to the results of Figure 5-3, with errors between 1 Hz and 25 Hz on the order of 5%. This behavior confirms the general experience of the additional convergence difficulties introduced into the fitting process by the use of segmented target spectrum, which has been typical in the past. At low frequencies where the amplitudes of the target spectrum are low, the computed errors become larger although the closeness of the fit (on an absolute basis) is better than in the mid-frequency range. At the high frequency end of the spectrum, the errors in the fitting become larger as the Nyquist frequency is approached, as previously mentioned.

Artificial recordings were also developed using the smooth spectral shape for the same bin (D2RM55H) as used above, but this time using the recommended spectral shapes documented in Section 4. A comparison of the spectral shapes using the recommended WUS, CEUS 1-corner and CEUS 2-corner source models is shown in Figure 5-5 for the average magnitude and distance associated with the empirical bin data. In these calculations, artificial recordings were generated for four different assumed Fourier phase spectra; namely, a random phase and three phase spectra taken from three recordings contained in the empirical bin. Figures 5-6A through 5-6D show the developed spectral comparisons and corresponding error computations for the WUS bin spectral shape. Figures 5-7A through 5-7D show similar results using the CEUS 1-corner model, again using the random

phase spectrum and the phase spectra from the same three recordings used to generate matches to the WUS bin shape.

Figure 5-8A is a plot of the Arias Intensity ratio as a function of time for the four time histories developed to envelop the WUS acceleration spectrum of Figures 5-6A through 5-6D. In addition, the Arias Intensity ratios for the three empirical recordings from which the phase spectra were taken are included on this figure. Figure 5-8B presents the same data, but plotted with respect to the time ratio (T/T_{max}) for each record, since the artificial records were developed for a different duration than the records from which the source spectra were taken. The time characteristics of the Arias Intensity ratios for the artificial records show similar growth rates as those from which the phase spectra were obtained, while the random phase assumption shows a relatively uniform growth in intensity with time, as expected. Figures 5-9A and 5-9B show similar results for the time histories developed to fit the acceleration spectral shape associated with the CEUS 1-corner model used in Figures 5-7A through 5-7D.

5.4.3 Comparison of Fourier Amplitude Spectra with Bin Averages

Figure 5-10A compares the Fourier amplitude spectra for the various generated motions that were developed to envelop the segmented target spectrum (which itself envelops the median response spectrum computed for the bin, Figure 5-3). The Fourier spectra from the artificial records all envelop the bin average spectrum, with the exceedences increasing at the higher frequencies where the fits to the segmented target response spectrum showed high (positive) errors. Similar comparisons are shown Figures 5-10B and 5-10C for those artificial records enveloping the smooth target spectra of Figures 5-4 and 5-6. The same characteristic exceedences can be noted for these two example sets.

One cause of the exceedence of the Fourier amplitude spectra from the generated motions over the bin target amplitude spectrum relates to the response spectra being higher than the target bin response spectrum. However, an additional important cause of this exceedence is the strong motion duration (TT) of the artificial record as compared to the bin average duration (TBA). To correct for this effect in order to make an appropriate comparison of Fourier amplitude spectra with the target bin average Fourier spectrum, either the Fourier amplitude spectrum of the trial motion should be reduced by the factor FT or the target bin average Fourier amplitude spectrum increased by FT, where

$$FT = \sqrt{TT/TBA}$$

As an example, using trial 1 record, the value of TT is equal to 6.3 seconds while the bin average TBA is about 2.5 seconds. The factor FT is then about 1.59. Thus the Fourier amplitude spectrum of the trial motion should be decreased by 1.59 when comparing with the bin average Fourier amplitude spectrum.

To demonstrate this effect more clearly, the Fourier amplitude spectra from Trials 1 and 1S are compared with the bin average in Figure 5-10D. This comparison shows that the Fourier amplitudes for Trial 1S are closer to the bin average values. In addition, the ratio of the Fourier spectra from the two trials is plotted over the frequency range. The strong motion duration for trial 1S is 3.36 seconds

leading to a value of FT of 1.16. The ratio of the factors FT for the two records is then 1.59/1.16 or 1.37. This ratio is a reasonable approximation to the ratio of Fourier amplitudes for the two records. If a Fourier amplitude acceptance criteria is to be added in the future to these recommended criteria, such a scaling of the Fourier spectra is recommended.

5.4.4 Influence of Gaps in the Fourier Spectrum

Following the generation of the artificial ground motions that envelop the 5% target response spectrum for one of the bins, a series of gaps was placed in the Fourier amplitude spectra for the motions. We then determined the influence of these gaps on the 5% damped response spectra. Examples of this process are shown in Figures 5-11A through 5-11G for the record designated "trial03", which was generated to envelop the segmented target spectrum. Gaps in the Fourier spectrum were located at frequencies centered at 0.5 Hz, 1 Hz, 2.5 Hz, 6 Hz, 10 Hz, 15 Hz and 25 Hz, with the width of each gap chosen to be $\pm 20\%$ of the center frequency and the depth of the gap varied by 10%, 20% and 30% of the Fourier amplitude. The phase spectra for these gaps were unchanged. For each revised record, the corresponding smoothed Fourier spectrum and the 5% damped response spectrum were calculated. The smoothing was conducted as described in Appendix A to Section 3.7.1 of the SRP, by computing the average over the frequency band of $\pm 20\%$ of the frequency being evaluated.

The results of this computation indicated that the reduction in the damped response spectrum was similar in magnitude to the reduction in the Fourier spectrum amplitudes at frequencies of 1 Hz, 2.5 Hz, 6 Hz and 10 Hz. The gaps centered at 0.5 Hz and 15 Hz led to a reduction in the response spectrum amplitudes of about one-half the decrease in the Fourier spectrum amplitudes. The gap centered at 25 Hz led to a significantly smaller change in the recomputed response spectrum. Similar changes in response spectra were noted for the case of gaps placed in the "trial01" record described in Table 5-3.

In addition, a similar computation was performed for the case of a gap placed in the Fourier spectrum at 2.5 Hz, but this time using a width of only $\pm 10\%$ in the frequency band. The results of this computation are shown in Figure 5-11H. For this case the error in the computed 5% damped response spectra is of the same order as that in the Fourier spectra. However, the resulting gaps in the smoothed Fourier spectra are now much smaller, as would be expected since the smoothed Fourier spectra are computed using a band width of $\pm 20\%$. Therefore, comparison of smoothed Fourier spectra alone are in general not enough to determine the potential significance of gaps in the input motions. A summary comparison of the magnitudes of change in 5% damped response spectra for a given change in Fourier amplitudes is shown in Figure 5-12, using the results for the "trial03" record shown in Figures 5-11A through 5-11G.

5.4.5 Limitations on Exceedences of Response Spectra

It is well known that the computed 5% damped response spectrum for a time history composed of a single frequency can be made to exceed a given target spectrum if no limitations are placed on the amount of the spectral exceedences that can occur at any one frequency. As an example, a time history was generated using a single frequency sine wave at 5 Hz with a magnitude of 1g. The 5%

damped spectral amplification (SA/PGA) for this motion is shown in Figure 5-13A and is compared to the median spectrum shape obtained from the median empirical (WUS) data for bin D2RM55H. The sine wave record was then uniformly increased in magnitude to either totally envelop the bin target response spectrum or to minimally match at least 90% of the target. It is clear that if large exceedences of the target spectrum were allowed, such a severely gapped motion could satisfy the enveloping criterion alone. However, checking the corresponding Fourier spectrum, illustrated in Figure 5-13B, can uncover the gaps in frequency content in the record. The computed Fourier spectrum is very spiked in appearance although the amplitudes of the spikes depend on the specific details of the digitized record used in the FFT calculation.

Unfortunately, the smoothing process typically used to plot computed Fourier amplitude spectra could serve to severely change the character of even this extreme example, as noted in Figure 5-13B. Care must then be used when judging such smoothed plots. A similar computation was made using a time history generated from three frequencies of 2.5 Hz, 5 Hz and 10 Hz and scaled to a 1g amplitude. Again, the exceedences of the response spectrum are very large as shown in Figure 5-13C. Also, the computed Fourier spectrum shown in Figure 5-13D is very spiked although the smoothing process again tends to hide the spikes. This simple exercise serves to indicate that the acceptance criteria used to judge the adequacy of ground motions must also contain a maximum allowable spectral exceedence criteria as well as a recommendation on the appropriate frequency content of the generated record, as mentioned previously. In addition, reliance on the appearance of smoothed Fourier spectra alone are generally not adequate to judge frequency gaps in such motions.

5.5 Other Important Ground Motion Characteristics

In addition to the two primary acceptance criteria discussed above, other characteristics of artificial ground motions are considered significant when judging acceptability for use in design or evaluation of critical facilities. In Appendices E, F, and G, a number of parameters typically considered of interest in ground motion studies were computed for each record in the WUS empirical database and are summarized in scatter plots for each magnitude and distance bin.

5.5.1 Peak Velocity and Displacement Parameters

The velocity and displacement parameters of interest typically include the peak velocity ratio (PGV/PGA), the peak displacement ratio (PGD/PGA), and the parameter $PGA \cdot PGD / PGV^2$. From the plots in Appendix F, it is evident that the scatter in these data is extremely high, but the data clearly indicate that the parameters are functions of both distance and magnitude as well as site condition (rock vs. soil sites). Average values of these parameters for horizontal motions in each bin of the WUS empirical data are presented in Table 4-1. These bin averages and uncertainties reflect equal weighting for each earthquake within any single bin.

5.5.2 Duration Parameter

In addition to the average parameters of Table 4-1, the recommended duration parameter for each bin has also been defined by an empirical WUS duration model (Appendix I). The results are shown in Figures 5-14A, B and C for horizontal motions in the various magnitude and distance bins for rock

sites. The duration parameter is defined by the 5% - 75% Arias intensity, and is an important characteristic of the ground motion. As described by Kennedy (Appendix A to NUREG/CR-5347, 1989), when an excessively long strong motion duration is selected, the computed combined responses of multimodal systems can be either severely overestimated or underestimated depending upon the details of the Fourier phasing selected in generating the ground motion.

In addition, when using the generated ground motion to evaluate liquefaction potential of a particular soil site, the duration parameter becomes important when using either equivalent linear or nonlinear analyses to estimate soil site responses. It is therefore recommended that the duration of the artificial ground motion approximately satisfy the characteristics shown in Figure 5-14. The solid line in these figures indicates the median bin value, while the dashed limits indicate values 50% higher and lower than these median bin values. Dotted lines forming boxes indicate the \pm one sigma values for the bins. Scatter plots of the duration parameters from the WUS database are contained in Appendix I.

In addition to this duration parameter, the Arias intensity and Cumulative Absolute Velocity (CAV) properties of each record in the empirical bins were evaluated to see if any particular characteristic emerges to differentiate the motions between bins. Figures 5-15A, B and C present plots of the results for a particular bin (D1RM55H). The total Arias intensity was computed for each record, scaled to a total value of unity, and the times associated with the 5% through the 100% Arias intensity ratio were determined in 5% increments. These times were normalized to a value of 1 for the total duration and were ordered. The minimum, 15th, 50th and 85th percentile and maximum time were determined for each Arias intensity level. Figure 5-15A presents the results, with the time parameter for each record scaled by its maximum duration. Results from the majority of the records indicate energy growth at the beginning of the records. This results from the selection of the long time window over which the records in the bin were digitized.

Figure 5-15B shows similar results for the same bin but with the time for each record scaled to the time associated with the 95th percentile Arias intensity ratio (designated " T_{95} "). Figure 5-15C shows a similar comparison for the case where the times for each record are scaled to the time window for the 5% to 95% Arias intensity ratio (designated " $T_{5,95}$ "). The results shown in Figures 5-15B and 5-15C are typical of all bins analyzed. They indicate the large scatter in the data and the different rates of growth in Arias intensity for the records in any one bin. Figures 5-16A and B show the results of similar calculations for CAV. In this case, scatter in the computed data is much less than in the Arias intensity function, which may indicate that the CAV is a more stable indicator of the characteristics of the time details of a given record. Scatter plots of both total Arias Intensity and CAV for the WUS database are contained in Appendix G.

5.5.3 Component Correlation Characteristics

The characteristics of the lag-zero cross-correlation coefficients of the three component data sets in the WUS empirical database were computed and are tabulated in Tables 5-4 and 5-5, with summary plots presented in Appendix F. Table 5-4 summarizes the average component correlations for the rock site bins for acceleration, velocity and displacement. Table 5-5 contains correlations for the soil sites. A typical plot is shown in Figure 5-17A and indicates a relatively wide scatter in the average

values in each bin. In general, the correlation coefficient for acceleration records is somewhat smaller than for integrated velocity and displacement components.

A comparison of the component correlations computed from the vertical and horizontal record pairs is also summarized in Tables 5-4 and 5-5 and a sample plot shown in Figure 5-17B for rock sites. The correlation between the vertical and each horizontal record of the data set is similar. Again, the results indicate higher correlation coefficients for velocity and displacement than with acceleration.

The current NRC staff position limits the correlation between component pairs of artificial acceleration records of a three component enveloping set to a value of 0.16 or less. This is based on some early limited computational results generated by Chen (1975). More complete evaluations were generated by Hadjian (1978, 1981) who included the effect of recorder orientation to estimate maximum values of correlations for a somewhat larger data set. The results of this computation indicated maximum values of acceleration correlation coefficients of 0.32. The data summary of Tables 5-4 and 5-5 do not include the effect of recorder orientation. As mentioned in Section 5.3, a value of 0.3 is recommended for the acceptance criteria.

5.6 Example Application of Spectral Matching Criteria

A further expansion of these general recommendations is provided for the following case in which a typical Uniform Hazard Spectrum (UHS) is defined as the basic target spectrum for the site. The UHS is assumed to be based on studies using the latest ground motion information (source zones and attenuation models) appropriate for the site for which it is defined. The use of older hazard studies based on attenuation models no longer considered appropriate for the site could lead to the definition of target spectra that have deficiencies in certain frequency ranges. Generating appropriate ground motions for such deficient targets requires special considerations that are not incorporated into the following description.

A schematic example of an appropriate UHS is shown in Figure 5-18A. The UHS is defined by spectral ordinates over a given frequency range (shown to be 0.2 Hz to 25 Hz in the figure) and its PGA. To properly generate ground motions that envelop this UHS and satisfy the generic criteria listed above, the spectrum needs to be extrapolated at the low and high frequency ends as shown in Figure 5-18A. As mentioned above, the purpose of these extrapolations is to generate ground motions that have realistic low and high frequency characteristics.

In addition to the UHS, additional spectra are often generated from dominant earthquakes determined from the deaggregated hazard analysis. Such spectra are used to study nonlinear effects (liquefaction assessment, structural damage estimates, etc.). The use of ground motions generated from enveloping the very broad banded UHS spectrum could lead to overdriving systems and incorrectly predicting nonlinear responses. For such cases, ground motions are often generated for separate events that dominate the hazard at low frequency (1 Hz) and high frequency (10 Hz) to attempt to capture the nonlinear characteristics for these dominant events. The low frequency event is typically defined as a large magnitude, distant earthquake while the high frequency deaggregated event is a smaller, close-in earthquake.

The spectra from the deaggregated events are then typically scaled back to the UHS at their corresponding frequencies. It should be noted that an interface frequency, f_c , can then be defined at the intersection of the two deaggregated spectra. For frequencies below f_c , the low frequency deaggregated spectrum is higher than the high frequency spectrum. For frequencies above f_c , the high frequency spectrum governs. In addition, a PGA for each of these two deaggregated spectra is also defined by the scaling process back to the UHS.

Thus three spectra are often defined for a given site, namely the UHS and the two deaggregated scaled spectra. It should be noted that the maximum difference between the UHS and the deaggregated scaled spectra, particularly around the frequency f_c , is assumed to be less than 10%. If this gap between the UHS and the deaggregated spectra exceeds 10%, a third deaggregated spectrum should be defined and scaled back to some intermediate frequency so as to limit the maximum difference between the UHS spectrum and the other deaggregated spectra to less than 10%. Site and structural response analyses can then be performed for either or all of the UHS spectrum and the scaled deaggregated events.

In the following discussion, it is assumed that three such target spectra are defined, requiring that appropriate sets of time histories be generated to envelop each of these spectra. The following recommendations are provided to generate these three sets of time histories, each of which is intended to satisfy the general criteria listed above. If additional spectra are required to fill in areas where gaps exceed the 10% recommendation mentioned above, it should be obvious how to expand the recommendations below for the additional spectra.

If a time history is generated to envelop the UHS, the upper and lower bound enveloping criteria listed above are shown schematically in Figure 5-18B. The PGA of the digitized time history should be at least equal to the PGA defined for the UHS. It is recommended that the strong motion duration associated with this UHS be the longer duration defined for the low frequency deaggregated event. The time step and total zero-packed duration of the motion should satisfy the general criteria mentioned above.

If a time history is generated to envelop the low frequency deaggregated spectrum, the bounding process is similar to that described above, but becomes somewhat more complicated. As evident in Figure 5-18C, below the interface frequency f_c , the bounding criteria should be controlled by the UHS spectrum while above f_c , the bounding criteria should be controlled by the deaggregated spectrum; that is,

$$\begin{aligned} 0.9*UHS < RS < 1.3*UHS & \text{ for frequencies between } 0.2 \text{ Hz} < f < f_c, \text{ and} \\ 0.9*DES1 < RS < 1.3*DES1 & \text{ for frequencies between } f_c < f < 25 \text{ Hz.} \end{aligned}$$

Where RS stands for the Response Spectrum of the artificial record and DES1 is the deaggregated spectrum scaled to 1 Hz. The peak acceleration of the digitized record should equal or exceed the PGA of the low-frequency deaggregated spectrum. The strong-motion duration should be appropriate for the magnitude and distance of the low-frequency deaggregated event.

If a time history is generated to envelop the high-frequency deaggregated spectrum, the bounding process is opposite to that described above; that is, below the interface frequency f_c , the bounding criterion is the deaggregated spectrum while above the interface frequency f_c , the bounding criterion is the UHS. As shown in Figure 5-18D, the criteria

$$\begin{aligned} 0.9 \cdot \text{DES10} < \text{RS} < 1.3 \cdot \text{DES10} & \text{ for frequencies between } 0.2 \text{ Hz} < f < f_c, \text{ and} \\ 0.9 \cdot \text{UHS} < \text{RS} < 1.3 \cdot \text{UHS} & \text{ for frequencies between } f_c < f < 25 \text{ Hz.} \end{aligned}$$

The peak acceleration of the digitized record should equal or exceed the PGA of the high-frequency deaggregated spectrum. The strong motion duration should be appropriate for the magnitude and distance of the high frequency deaggregated event.

5.7 Conclusions

This study has led to recommendations that can be used to generate artificial records that envelop response spectra generated for a particular site and that have sufficient energy content at all frequencies of interest. The conclusions based on these studies are as follows.

1. In the frequency range from 1 Hz to 15 Hz, the 5% damped response spectrum is about as sensitive to gaps in the frequency content of an artificial time history as is the smoothed Fourier amplitude spectrum. There is no need to have additional checks of Fourier spectra or PSD to ensure that no significant gaps in frequency exist.
2. Artificial ground motions can be generated that envelop the target response spectra defined for the project. The artificial records must have small enough time increments and long enough zero packed durations to satisfy the requirements described in this section. These artificial motions should have peak motion characteristics and strong motion durations that are appropriate for the earthquake magnitudes and distances of interest.
3. In general, the artificial record should have a response spectrum that does not fall more than 10% below the target spectrum and does not exceed the target spectrum by more than 30%.

Additionally, time domain characteristics should be generally consistent with bin average values of durations, and the ratios PGV/PGA and $\text{PGA} \cdot \text{PGD}/\text{PGV}^2$. If these criteria are followed, artificial records can be developed that are considered appropriate for analysis of critical facilities.

References

- Chen, C. (1975), "The Definition of Statistically Independent Time Histories", *Journal of the Structures Division*, Amer. Soc. of Civil Engrs, February.
- Hadjian, A.H. (1978), "On the Correlation of the Components of Strong Ground Motion", *Proceedings*, 2nd International Conference on Microzonation, San Francisco.

- Hadjian, A.H. (1981), "On the Correlation of the Components of Strong Ground Motion - Part 2", *Bull. Seism. Soc. Am.*, 71(4), 1323-1331, August.
- Miller, C.A. and C.J. Costantino (2000), "CARES, (Computer Analysis for Rapid Evaluation of Structures)," Version 1.3, Costantino, Miller and Associates for Office of Nuclear Regulatory Research, U. S. Nuclear Regulatory Commission.
- NUREG-0800 (1989) "Standard Review Plan", Office of Nuclear Reactor Regulation, US Nuclear Regulatory Commission, Revision 2.
- NUREG/CR-3805, "Engineering Characterization of Ground Motion," R.P. Kennedy et al., for U.S. Nuclear Regulatory Commission, May 1994.
- Silva, W. J. and R. Darragh (1995), "Engineering Characterization of Earthquake Strong Ground Motion Recorded at Rock Sites", Elec. Power Res. Inst., Palo Alto, CA, Rept. TR-102261.

TABLE 5-1
MAGNITUDE AND DISTANCE BINS FOR RECORD LIBRARY
WUS EMPIRICAL MOTIONS

Magnitude Bins	Range:		Bin Center:	
	5 - 6	6 - 7	5.5	6.5
		7 +	7.5	
<u>Distance (km)</u>	<u>Site Type</u>	<u>Magnitude</u>	<u>Direction</u>	<u>No. of Records</u>
00 - 10	Rock	5.5	H	28
			V	13
		6.5	H	24
			V	10
		7.5	H	6
			V	3
	Soil	5.5	H	24
			V	11
		6.5	H	87
			V	42
		7.5	H	4
			V	2
10 - 50	Rock	5.5	H	184
			V	89
		6.5	H	200
			V	100
		7.5	H	6
			V	3
	Soil	5.5	H	370
			V	182
		6.5	H	504
			V	245
		7.5	H	56
			V	28
50 - 100	Rock	5.5	H	34
			V	15
		6.5	H	76
			V	39
		7.5	H	10
			V	5
	Soil	5.5	H	38
			V	17
		6.5	H	132
			V	61
		7.5	H	12
			V	6
100 - 200	Rock	5.5	H	2
			V	1
		6.5	H	12
			V	-
		7.5	H	16
			V	8
	Soil	5.5	H	2
			V	1
		6.5	H	28
			V	14
		7.5	H	84
			V	42

TABLE 5-2
CHARACTERISTICS OF GENERATED
ARTIFICIAL RECORDS

<u>TRIAL</u>	<u>1</u>	<u>2</u>	<u>3</u>	<u>4</u>	<u>4S</u>	<u>4L</u>	<u>5</u>	<u>1S</u>
Max Duration (secs)	20	20	20	20	40	40	20	20
Time Increment (msec)	2.44	4.88	9.76	19.53	39.06	39.06	39.06	2.44
Frequency Increment (Hz)	0.05	0.05	0.05	0.05	0.025	0.025	0.05	0.05
Max Frequency (Hz)	204.8	102.4	51.2	25.6	12.8	12.8	12.8	204.8
No. of Points in Record	8192	4096	2048	1024	1024	1024	512	8192
No. of Frequency Comps (one-sided FFT)	4096	2048	1024	512	512	512	256	4096
Duration 5%-75% (sec)	6.312	5.83	6.406	6.66	5.703	8.399	6.563	3.356
Duration 5%-95% (sec)	8.464	8.516	8.116	8.144	8.242	11.094	9.063	4.933

TABLE 5-3
PERCENT REDUCTION IN 5% DAMPED RESPONSE SPECTRUM

<u>Trial Time</u> <u>History</u>	<u>Gap Center</u> <u>Frequency (Hz)</u>	<u>% Reduction in Fourier Amplitude</u>		
		<u>10%</u>	<u>20%</u>	<u>30%</u>
Trial01	0.5	1.77	3.85	5.13
	1.0	8.4	16.73	25.03
	2.5	7.55	15.02	22.13
	6.0	7.52	15.04	22.38
	10.0	7.67	15.24	22.85
	15.0	7.73	15.48	22.67
	25.0	5.33	10.51	12.23
Trial03	0.5	4.32	8.7	13.02
	1.0	8.98	17.96	26.19
	2.5	9.22	18.42	27.17
	6.0	7.79	15.61	23.4
	10.0	9.25	18.49	27.14
	15.0	4.97	9.9	14.86
	25.0	1.88	3.77	5.65

TABLE 5-4

BIN CROSS CORRELATION STATISTICS FOR WUS ROCK SITE CONDITIONS*				
M 5 to 6 Distance (km)				
Component	0 - 10	10 - 50	50 - 100	100 - 200
H1 H2 (A)	0.24474	0.19976	0.09709	0.10252
	0.14561	0.16490	0.06540	--
H1 H2 (V)	0.23528	0.23007	0.13299	0.30565
	0.22155	0.17619	0.12378	--
H1 H2 (D)	0.26467	0.23792	0.16215	0.48630
	0.28185	0.18582	0.18043	--
V H1 (A)	0.14208	0.12349	0.11489	0.09163
	0.13028	0.10356	0.07688	--
V H1 (V)	0.20656	0.14220	0.13540	0.08181
	0.16548	0.11067	0.11873	--
V H1 (D)	0.24298	0.14093	0.21570	0.21314
	0.21375	0.13969	0.23893	--
V H2 (A)	0.13294	0.11819	0.12307	0.05975
	0.07192	0.09809	0.07898	--
V H2 (V)	0.13572	0.14827	0.22696	0.08052
	0.11772	0.11696	0.19476	--
V H2 (D)	0.22698	0.16942	0.33728	0.06636
	0.15993	0.15386	0.32475	--

* Averages of absolute cross correlation values

TABLE 5-4 (Cont'd)

BIN CROSS CORRELATION STATISTICS FOR WUS ROCK SITE CONDITIONS*				
M 6.01 to 7.00 Distance (km)				
Component	0 - 10	10 - 50	50 - 100	100 - 200
H1 H2 (A)	0.24003	0.16762	0.11364	0.16388
	0.15214	0.12874	0.10120	0.13329
H1 H2 (V)	0.33729	0.19778	0.21573	0.24105
	0.16690	0.14620	0.19764	0.16954
H1 H2 (D)	0.45990	0.28682	0.36527	0.34095
	0.24497	0.20133	0.26016	0.23319
V H1 (A)	0.11941	0.11436	0.14005	0.12966
	0.10825	0.10694	0.11210	0.08915
V H1 (V)	0.11435	0.16602	0.17746	0.17886
	0.20391	0.13839	0.12075	0.13957
V H1 (D)	0.27504	0.26410	0.26536	0.33865
	0.31230	0.21185	0.19269	0.26241
V H2 (A)	0.15335	0.10497	0.16704	0.11858
	0.13378	0.09000	0.13675	0.12004
V H2 (V)	0.24955	0.16984	0.18455	0.24106
	0.18884	0.13637	0.12658	0.12634
V H2 (D)	0.33334	0.23696	0.25052	0.27682
	0.26913	0.20953	0.19163	0.21686

* Averages of absolute cross correlation values

TABLE 5-4 (Cont'd)

BIN CROSS CORRELATION STATISTICS FOR WUS ROCK SITE CONDITIONS*				
M 7.01 to 9.00 Distance (km)				
Component	0 - 10	10 - 50	50 - 100	100 - 200
H1 H2 (A)	0.18850	0.05462	0.04872	0.12822
	0.12920	0.02904	0.03688	0.10639
H1 H2 (V)	0.14420	0.14262	0.29599	0.19985
	0.13480	0.17780	0.20285	0.08094
H1 H2 (D)	0.42750	0.31014	0.39377	0.20856
	0.48279	0.30137	0.09228	0.17709
V H1 (A)	0.15807	0.11610	0.05123	0.06826
	0.10115	0.10228	0.04747	0.08540
V H1 (V)	0.07071	0.13054	0.14465	0.09808
	0.05992	0.04417	0.12527	0.09805
V H1 (D)	0.30899	0.13038	0.24319	0.11781
	0.15030	0.07088	0.27172	0.07158
V H2 (A)	0.15152	0.07028	0.08265	0.10947
	0.12387	0.00809	0.04978	0.08325
V H2 (V)	0.09780	0.08613	0.14775	0.15762
	0.10510	0.07046	0.12636	0.12961
V H2 (D)	0.28972	0.13716	0.26869	0.18059
	0.10785	0.04979	0.14270	0.13162

*Averages of absolute cross correlation values

TABLE 5-5

BIN CROSS CORRELATION STATISTICS FOR WUS SOIL SITE CONDITIONS*				
M 5 to 6 Distance (km)				
<u>Component</u>	<u>0 - 10</u>	<u>10 - 50</u>	<u>50 - 100</u>	<u>100 - 200</u>
H1 H2 (A)	0.17342	0.15696	0.12166	0.04541
	0.13459	0.12548	0.12533	--
H1 H2 (V)	0.11912	0.20268	0.14745	0.08703
	0.07992	0.16194	0.11952	--
H1 H2 (D)	0.26516	0.22215	0.20062	0.34246
	0.15645	0.16740	0.15146	--
V H1 (A)	0.07054	0.09544	0.08626	0.21234
	0.07015	0.09584	0.08382	--
V H1 (V)	0.15751	0.13181	0.12122	0.07902
	0.10079	0.10267	0.07863	--
V H1 (D)	0.16078	0.15458	0.15456	0.03081
	0.10520	0.13357	0.13590	--
V H2 (A)	0.09258	0.09794	0.10937	0.05739
	0.09860	0.08555	0.09215	--
V H2 (V)	0.14943	0.13624	0.12658	0.12212
	0.13762	0.12026	0.07452	--
V H2 (D)	0.19849	0.15261	0.14552	0.05378
	0.16820	0.14123	0.11392	--

* Averages of absolute cross correlation values

TABLE 5-5 (Cont'd)

BIN CROSS CORRELATION STATISTICS FOR WUS SOIL SITE CONDITIONS*				
M 6.01 to 7.00 Distance (km)				
Component	0 - 10	10 - 50	50 - 100	100 - 200
H1 H2 (A)	0.15101	0.13212	0.12411	0.13606
	0.10475	0.10877	0.09097	0.09504
H1 H2 (V)	0.22037	0.19742	0.16072	0.15680
	0.20010	0.15411	0.13108	0.08728
H1 H2 (D)	0.34518	0.25817	0.20460	0.22099
	0.18472	0.21086	0.16757	0.20771
V H1 (A)	0.06658	0.09266	0.08217	0.08534
	0.04963	0.08532	0.08452	0.09121
V H1 (V)	0.16802	0.13399	0.11214	0.13228
	0.14589	0.11937	0.09121	0.09081
V H1 (D)	0.30871	0.18837	0.16510	0.17180
	0.17399	0.16174	0.17382	0.13845
V H2 (A)	0.10072	0.09171	0.09194	0.12848
	0.09775	0.08664	0.08619	0.09290
V H2 (V)	0.23739	0.14580	0.14041	0.12537
	0.15366	0.11026	0.12639	0.11255
V H2 (D)	0.31197	0.11847	0.19019	0.20311
	0.16903	0.15402	0.16104	0.15927

* Averages of absolute cross correlation values

TABLE 5-5 (Cont'd)

BIN CROSS CORRELATION STATISTICS FOR WUS SOIL SITE CONDITIONS*				
M 7.01 to 9.00 Distance (km)				
<u>Component</u>	<u>0 - 10</u>	<u>10 - 50</u>	<u>50 - 100</u>	<u>100 - 200</u>
H1 H2 (A)	0.11479	0.11722	0.08145	0.15557
	--	0.07127	0.07346	0.08992
H1 H2 (V)	0.29831	0.16527	0.17689	0.28864
	--	0.16624	0.15774	0.21156
H1 H2 (D)	0.12485	0.28326	0.33767	0.36374
	--	0.23762	0.22174	0.24434
V H1 (A)	0.12753	0.06408	0.04877	0.07670
	--	0.04024	0.03418	0.06024
V H1 (V)	0.14516	0.12108	0.16002	0.13618
	--	0.08480	0.11337	0.11040
V H1 (D)	0.75292	0.17739	0.29925	0.13846
	--	0.16239	0.23191	0.13786
V H2 (A)	0.21432	0.09004	0.07420	0.06756
	--	0.09686	0.03698	0.06532
V H2 (V)	0.23649	0.14661	0.13237	0.11420
	--	0.10674	0.15797	0.08882
V H2 (D)	0.2510	0.14113	0.20146	0.12856
	--	0.13691	0.16267	0.12542

* Averages of absolute cross correlation values

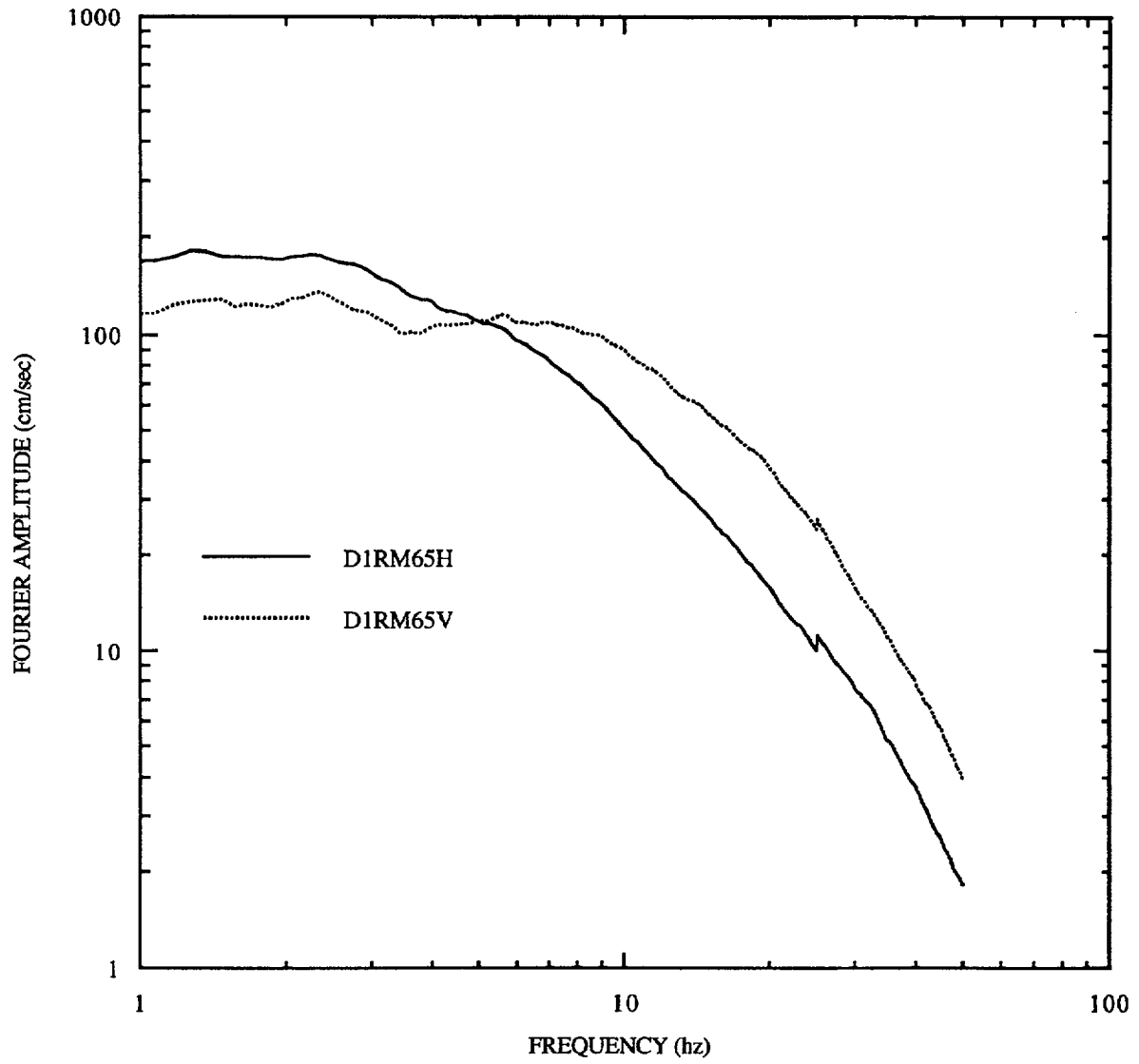


Figure 5-1A. Average smoothed Fourier amplitude spectra, distance 0-10 km, rock sites.

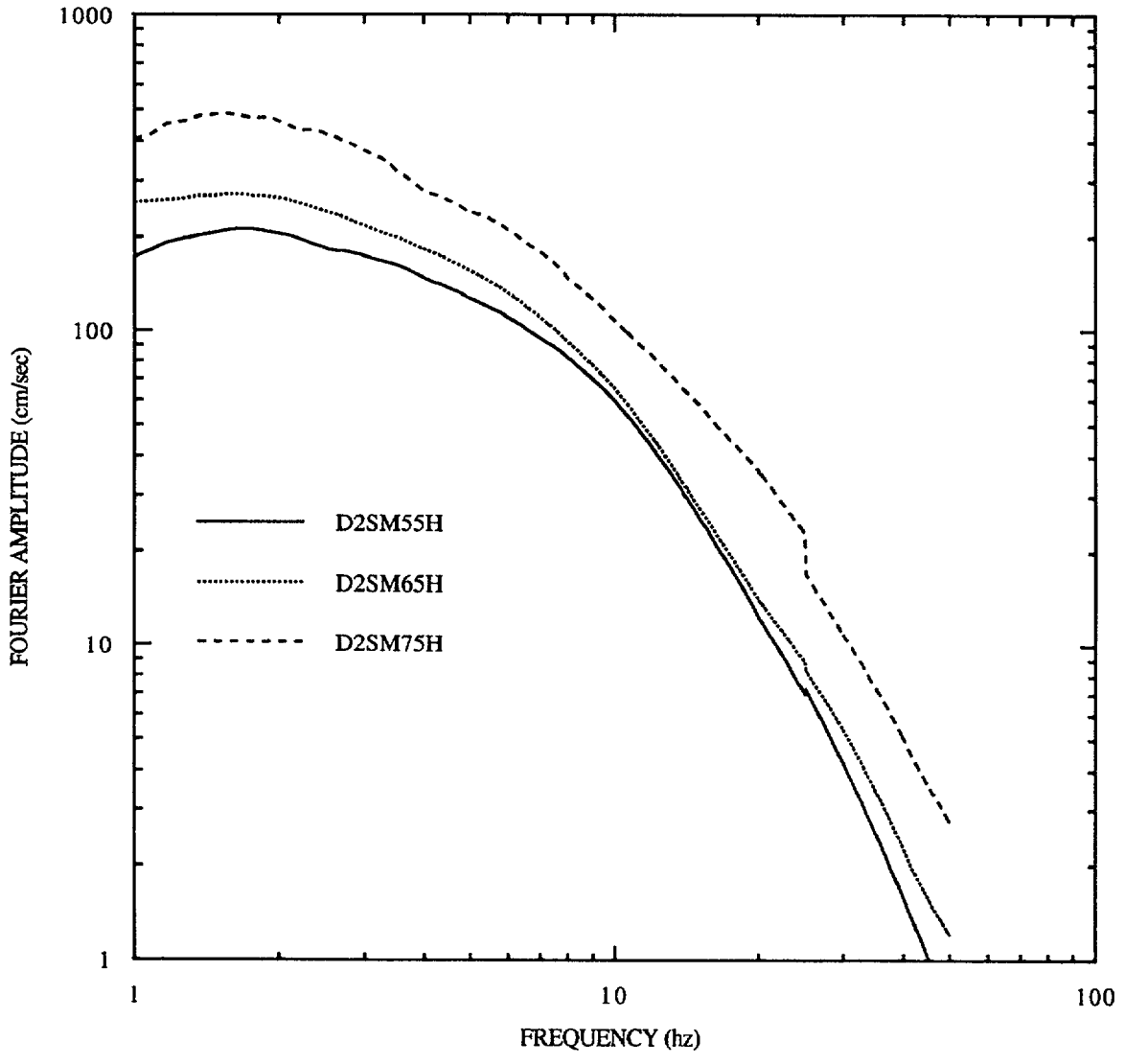


Figure 5-1B. Average smoothed Fourier amplitude spectra, horizontal motions, distance 10-50 km, soil sites.

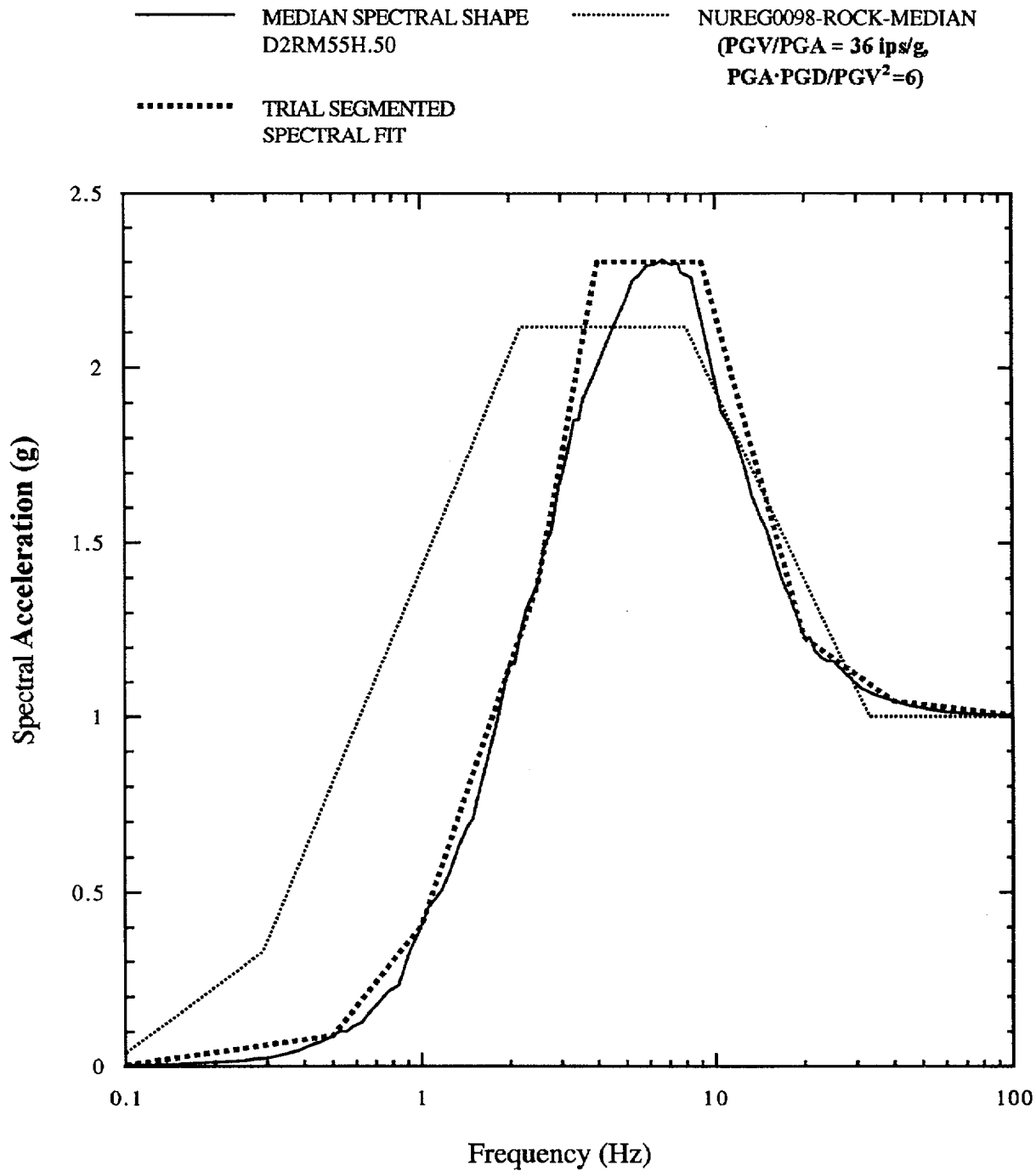


Figure 5-2. 5% damped spectrum for distance bin D2, rock sites, magnitude bin M55, horizontal motion.

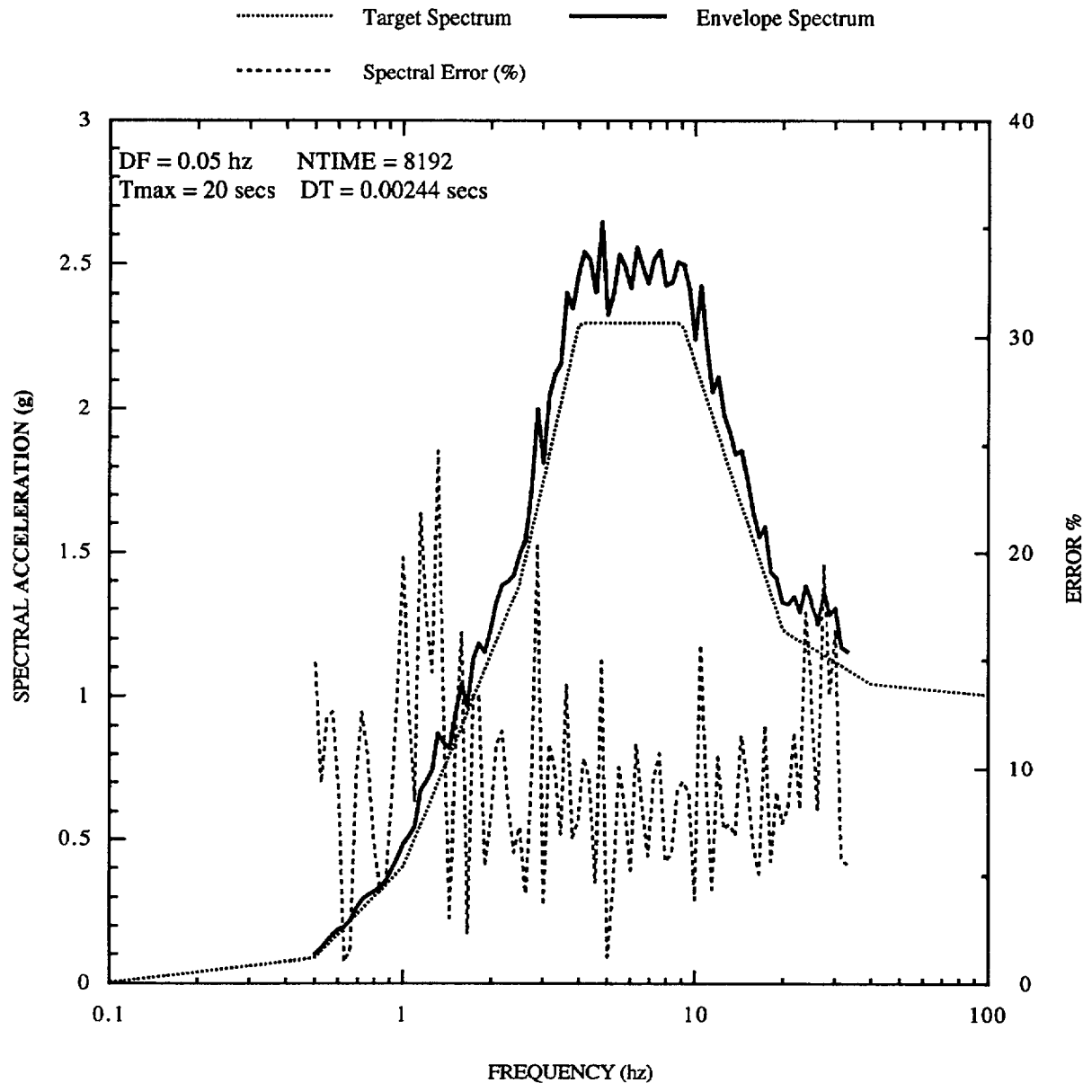


Figure 5-3A. 5% damped spectrum, trial 1

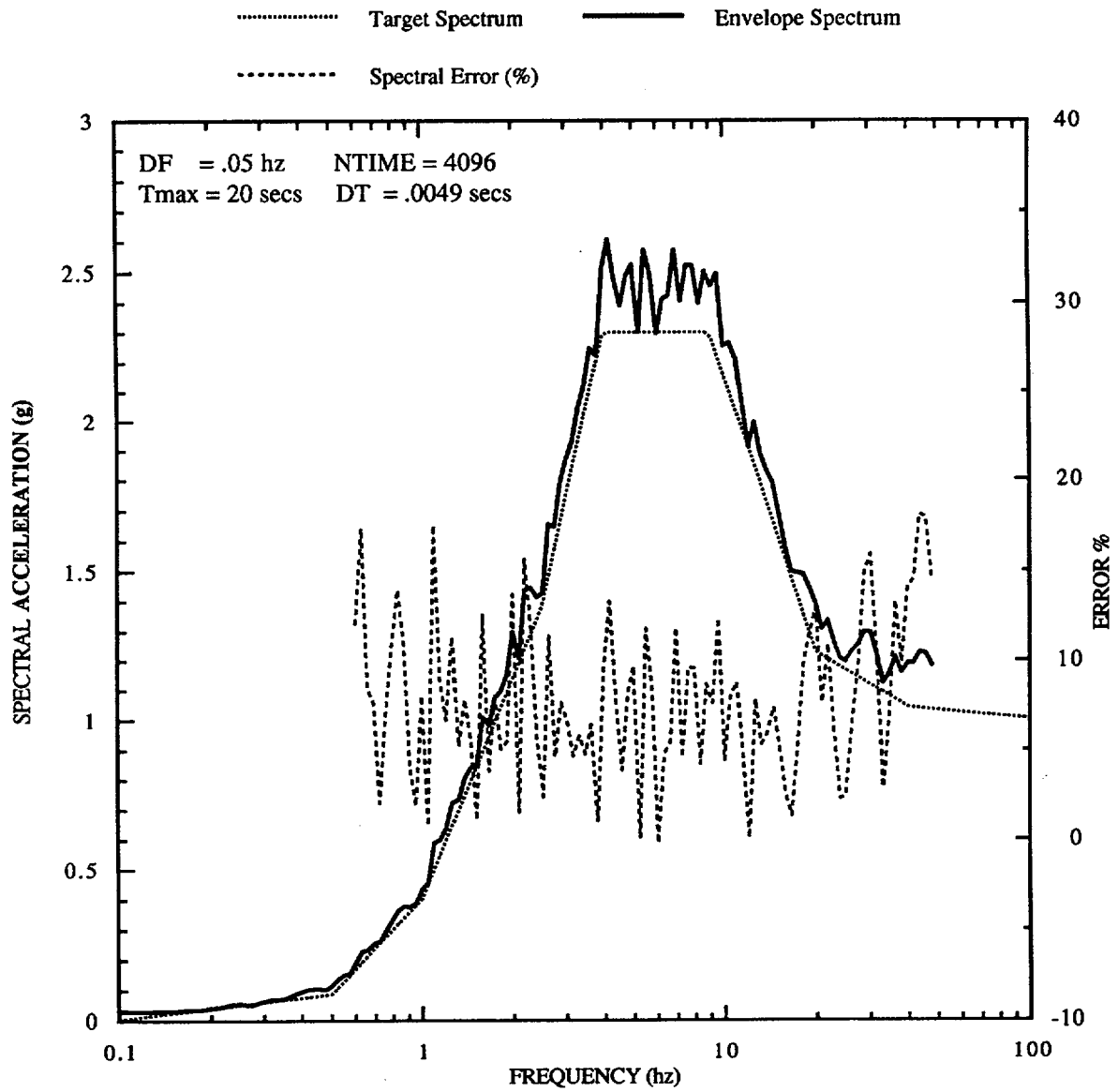


Figure 5-3B. 5% damped spectrum, trial 2

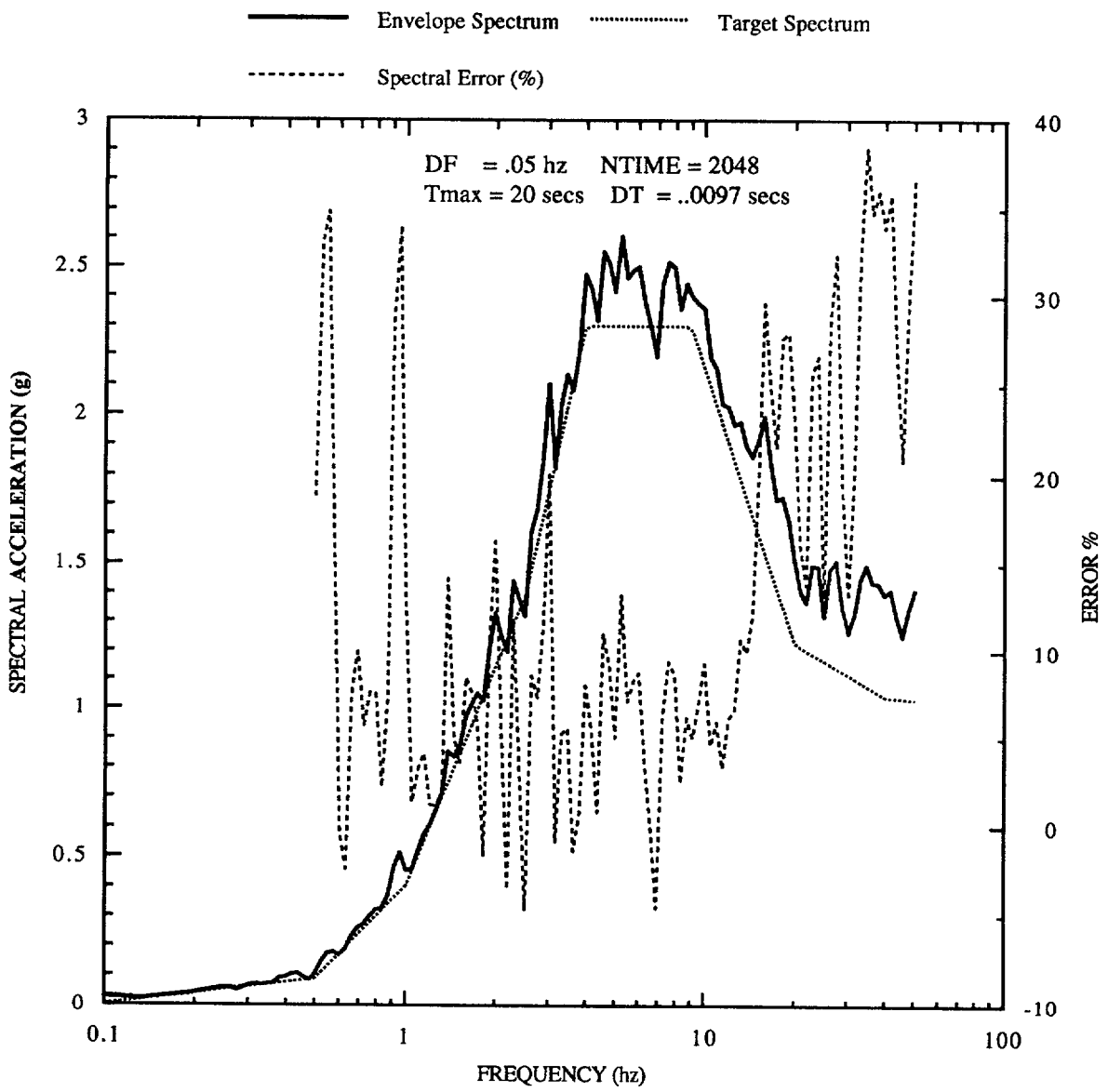


Figure 5-3C. 5% damped spectrum, trial 3

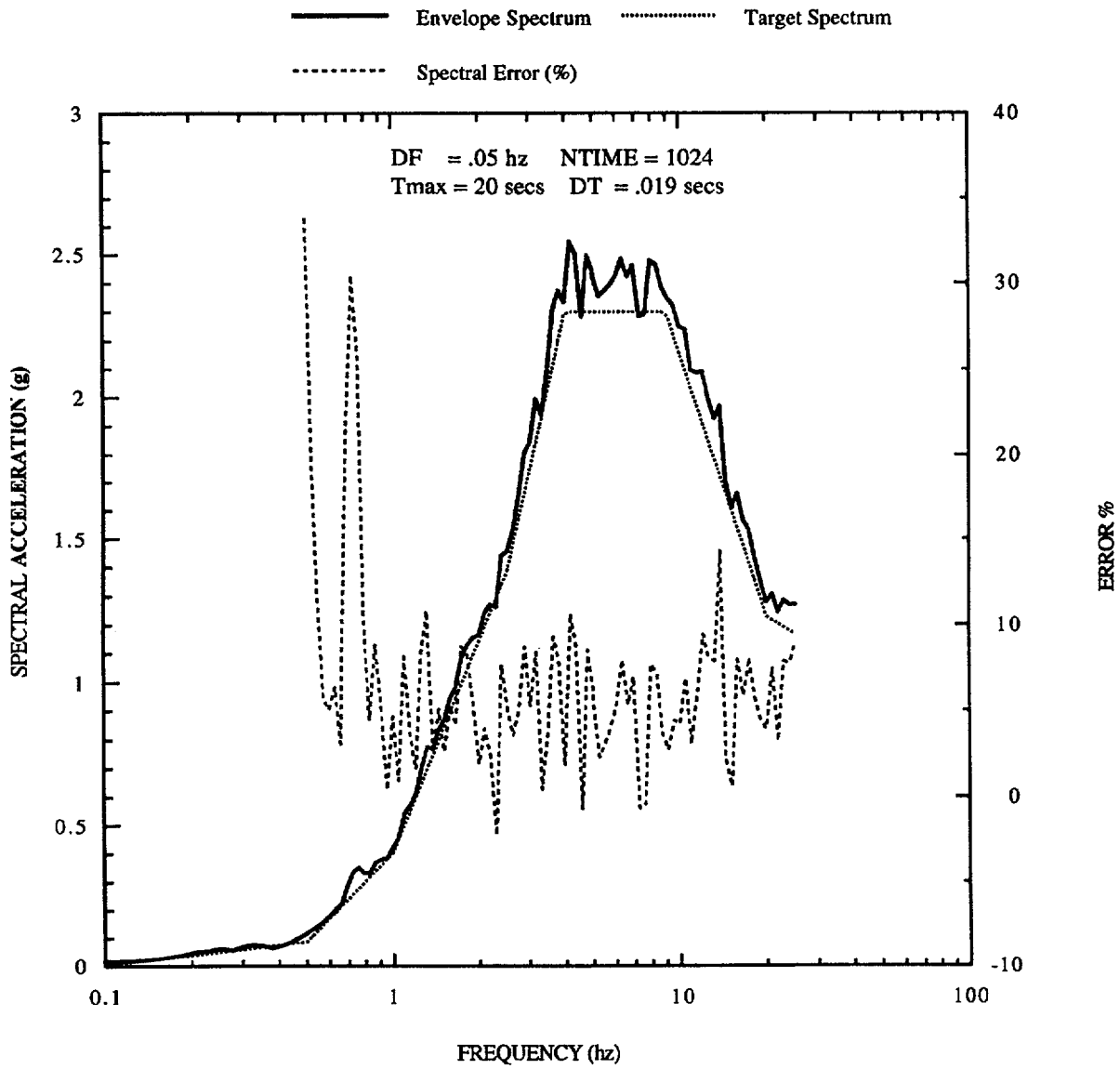


Figure 5-3D. 5% damped spectrum, trial 4

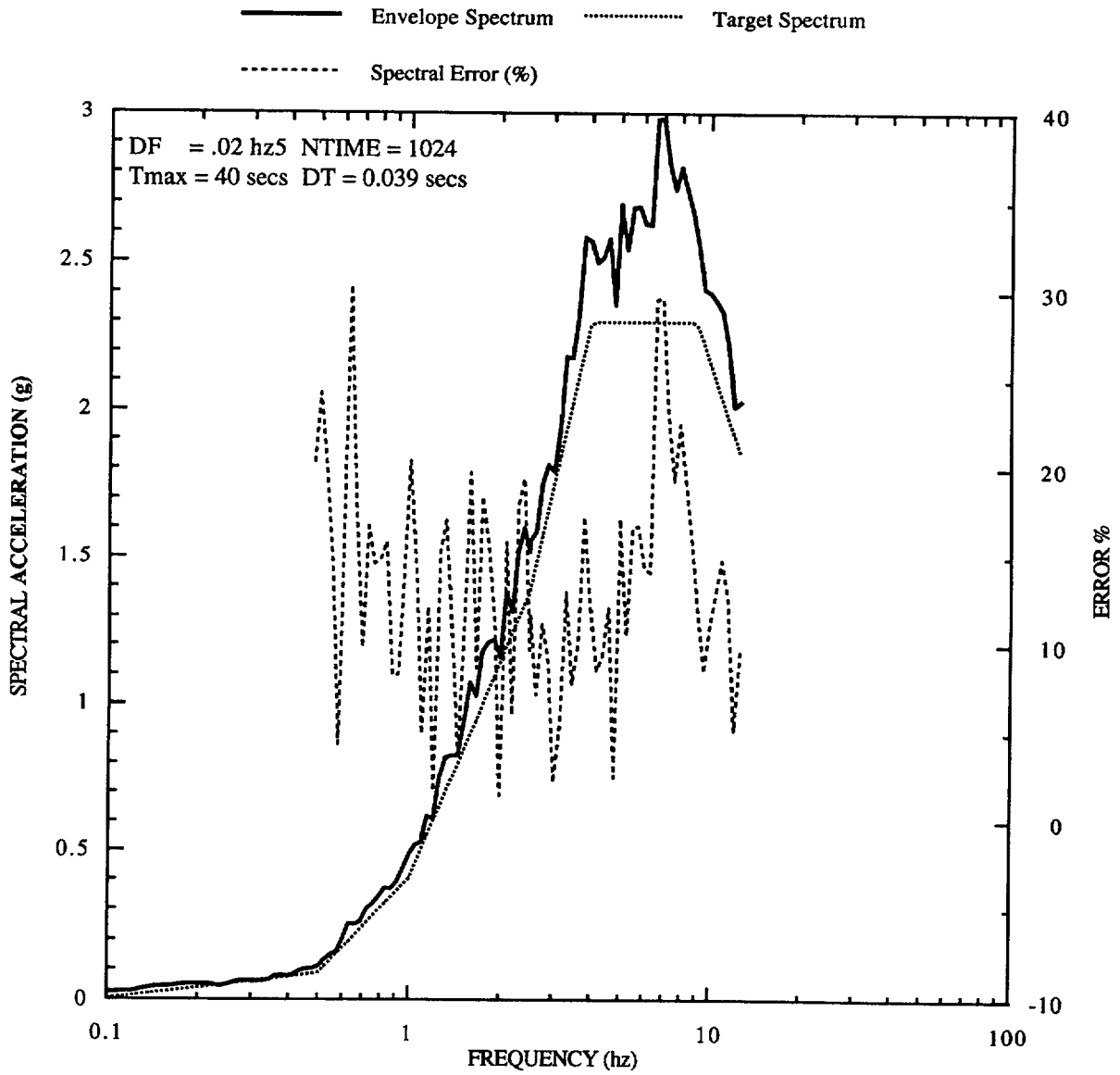


Figure 5-3E. 5% damped spectrum, trial 4S (shorter duration)

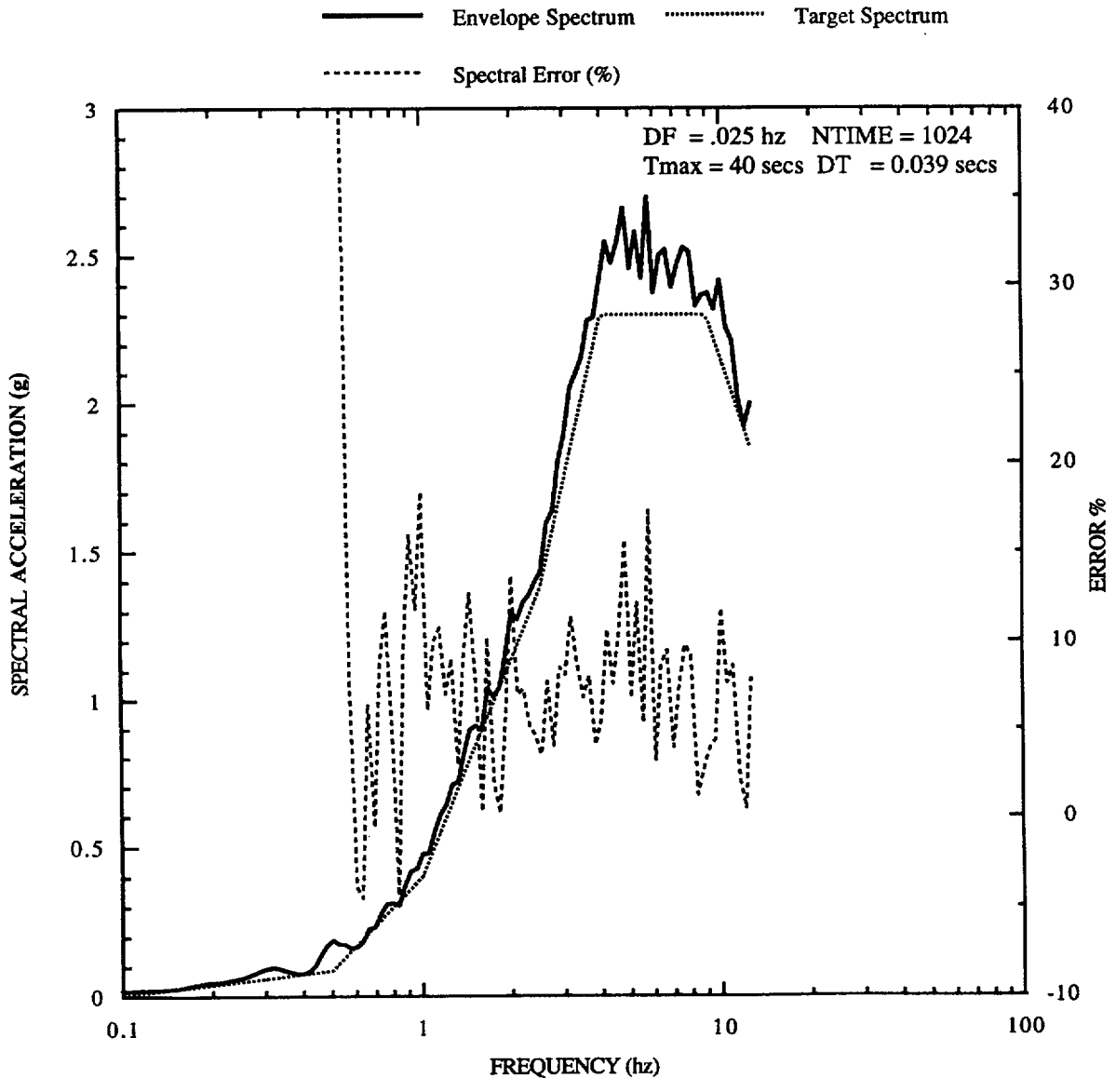


Figure 5-3F. 5% damped spectrum, trial 4L (longer duration)

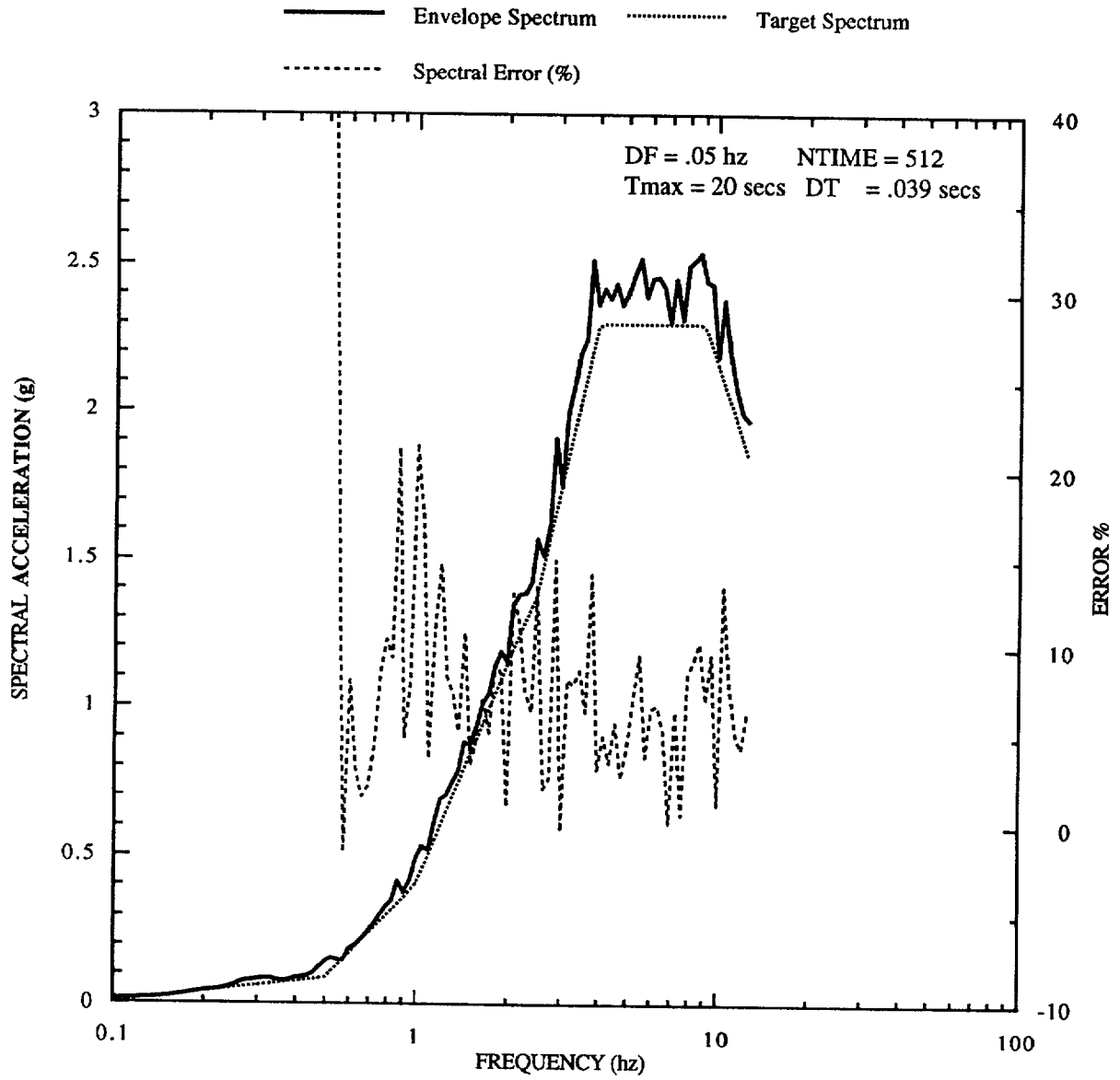


Figure 5-3G. 5% damped spectrum, trial 5

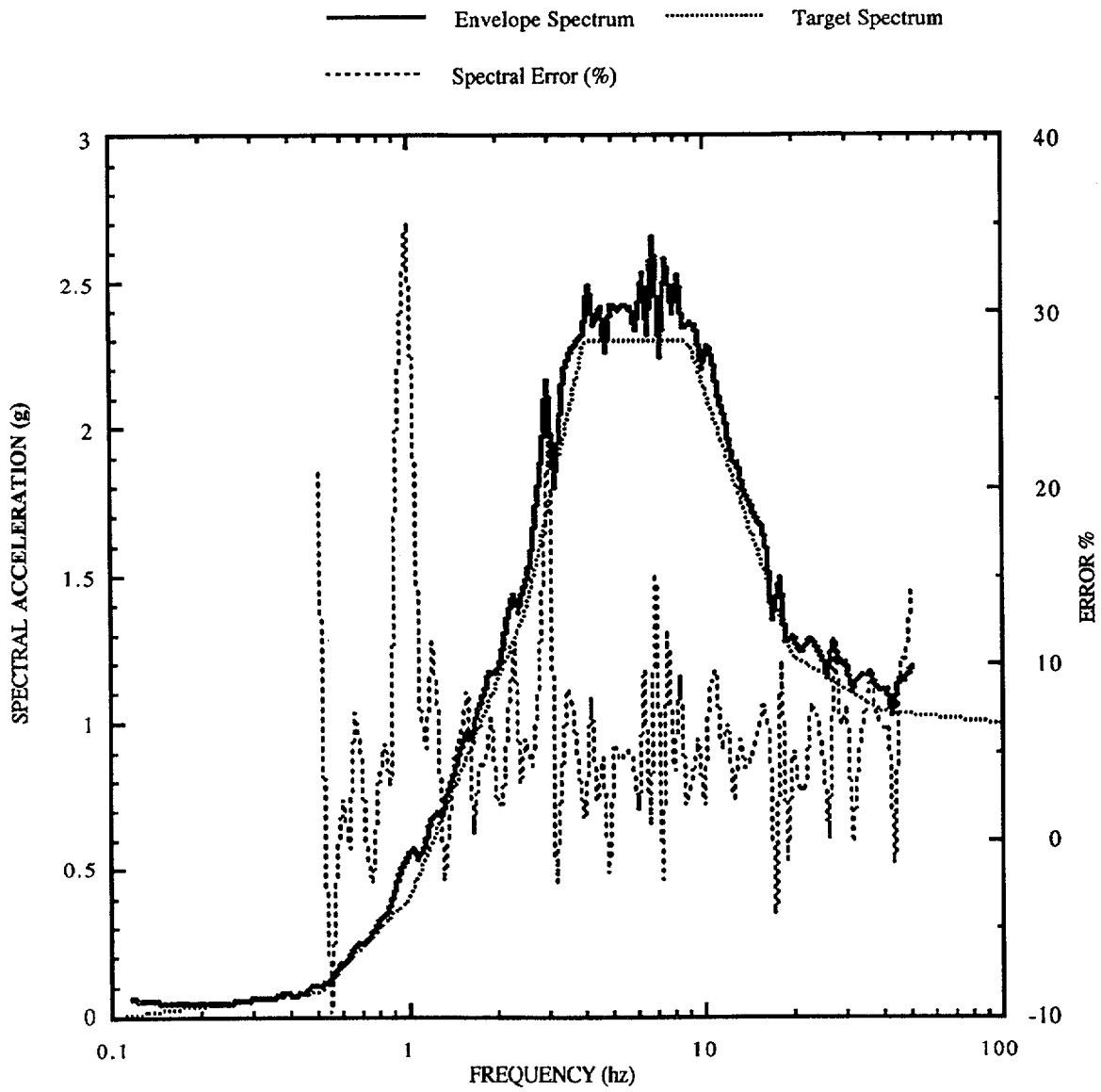


Figure 5-3H. 5% damped spectrum, trial 1S (shorter duration)

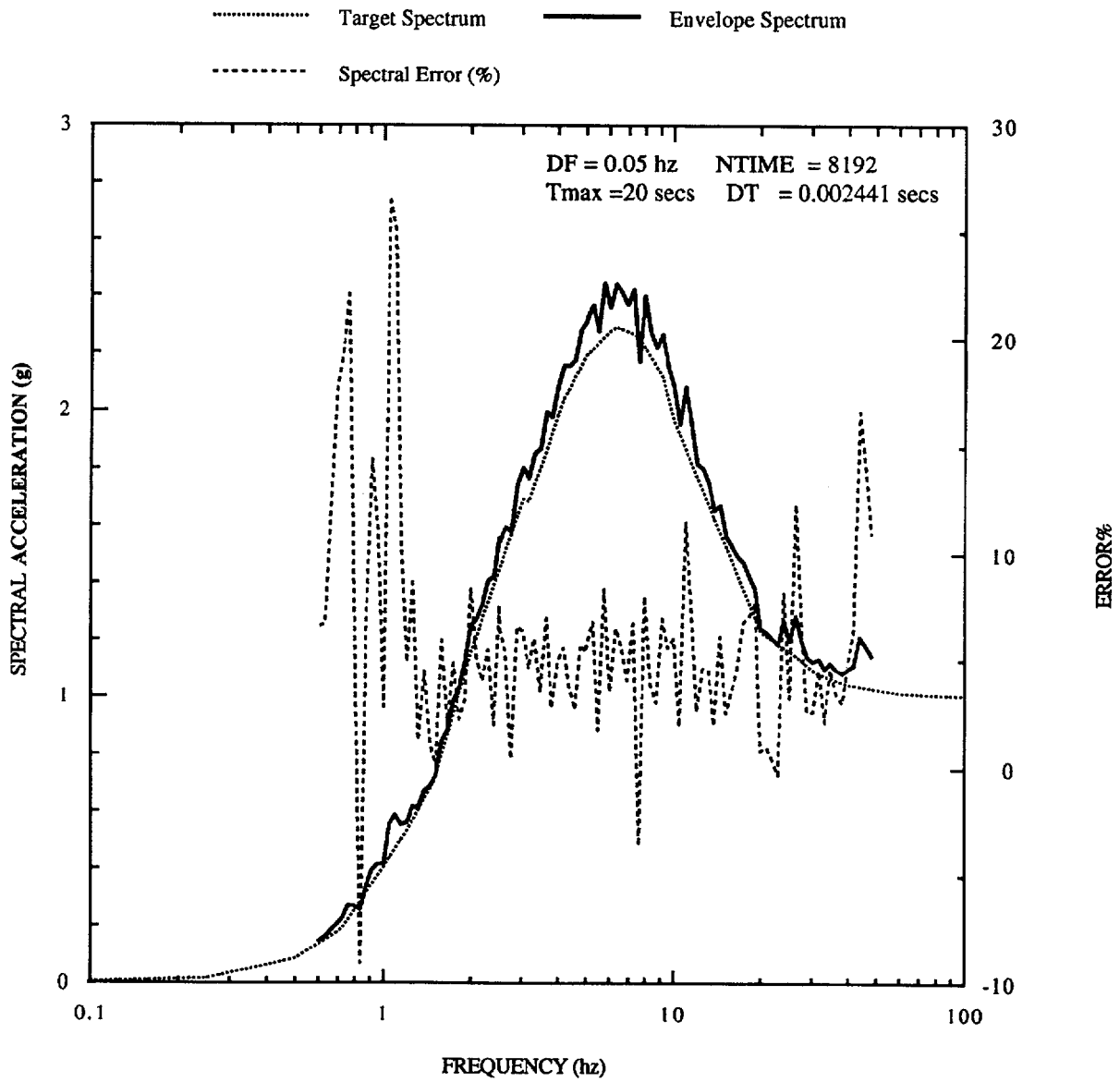


Figure 5-4A. 5% damped spectrum, trial SM01

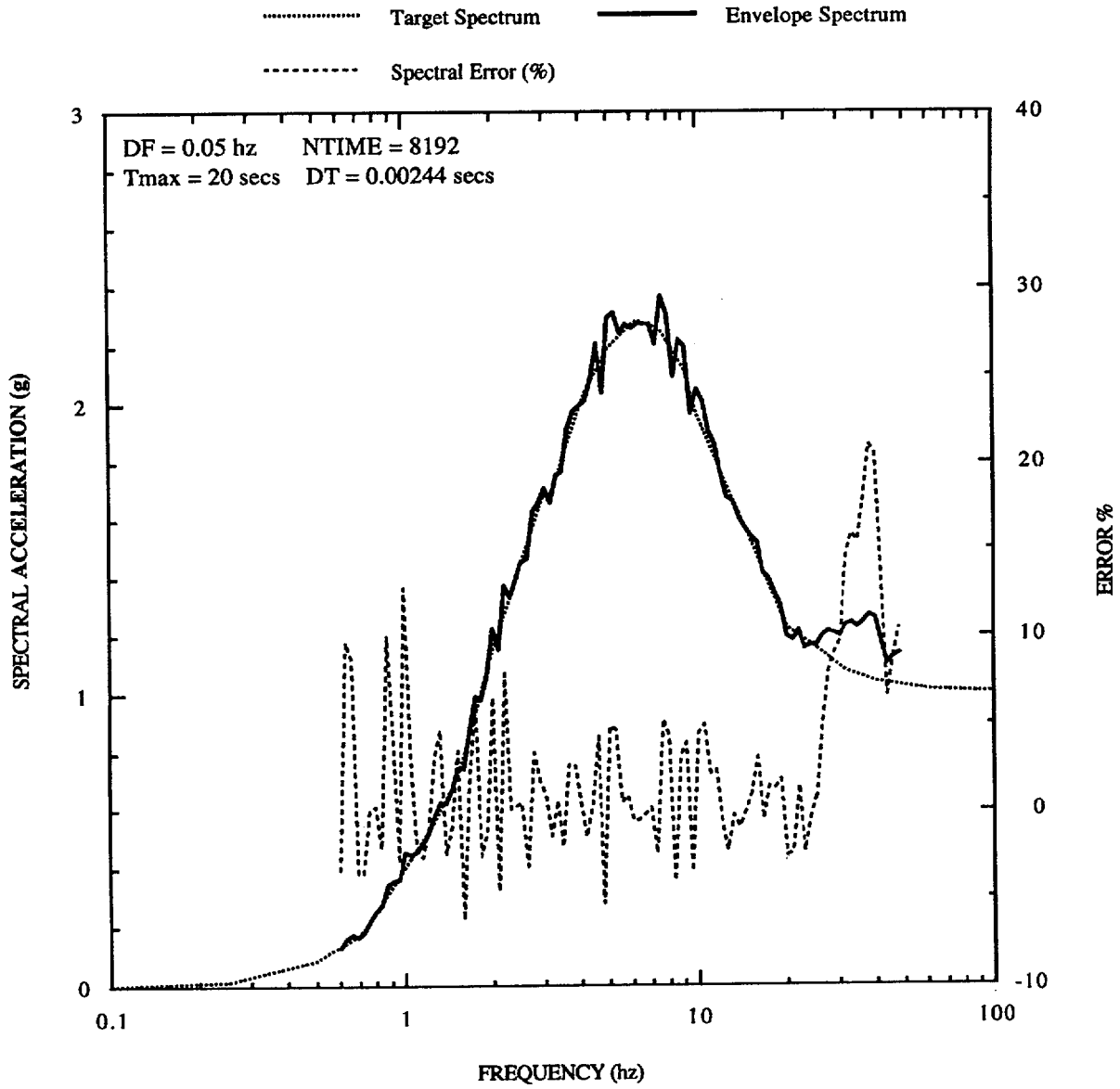


Figure 5-4B. 5% damped spectrum, trial SM02

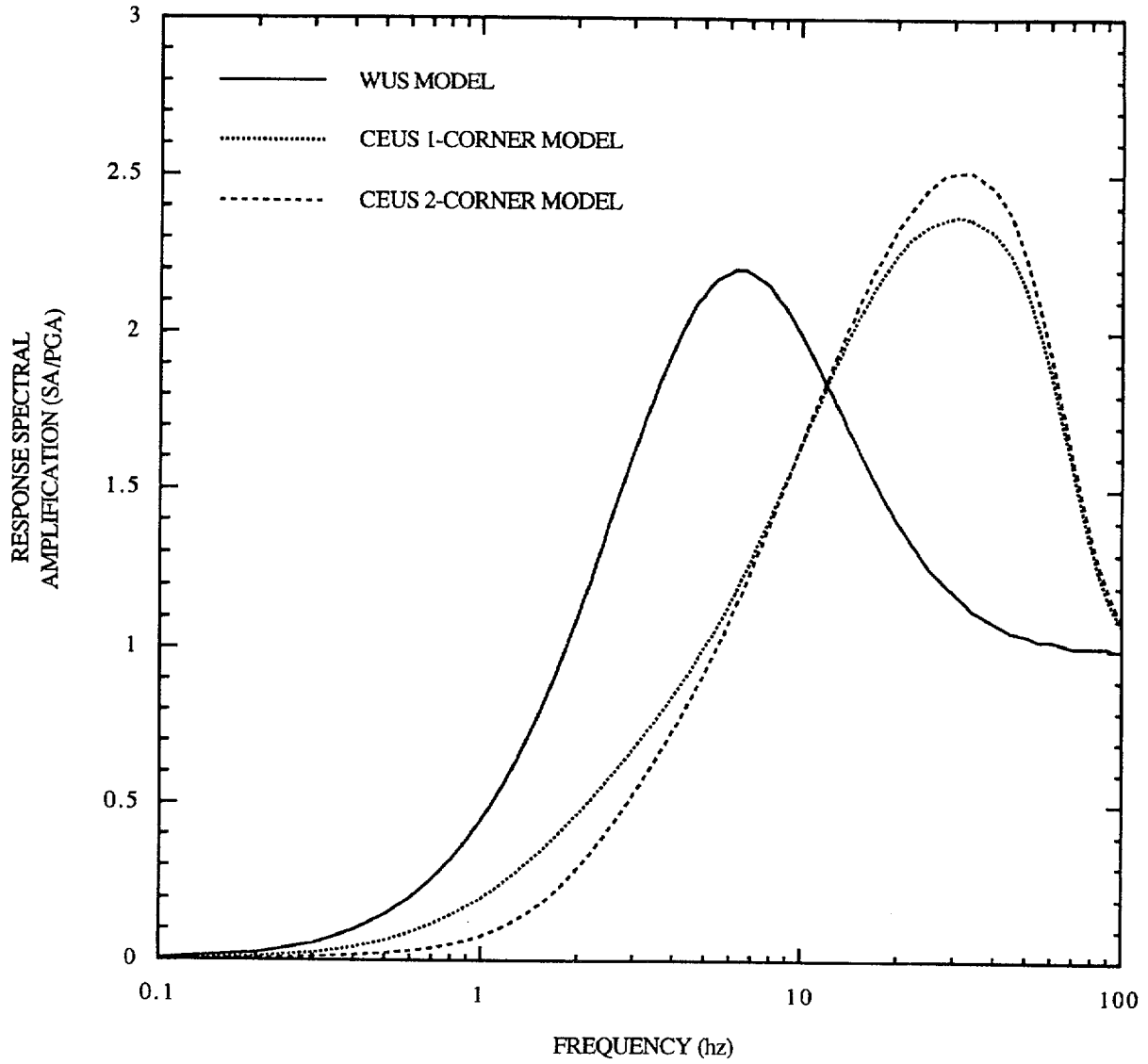


Figure 5-5. Spectral acceleration shapes for $\bar{M} = 5.57, \bar{R} = 21.8$ rock horizontal motion bin D2RM55H

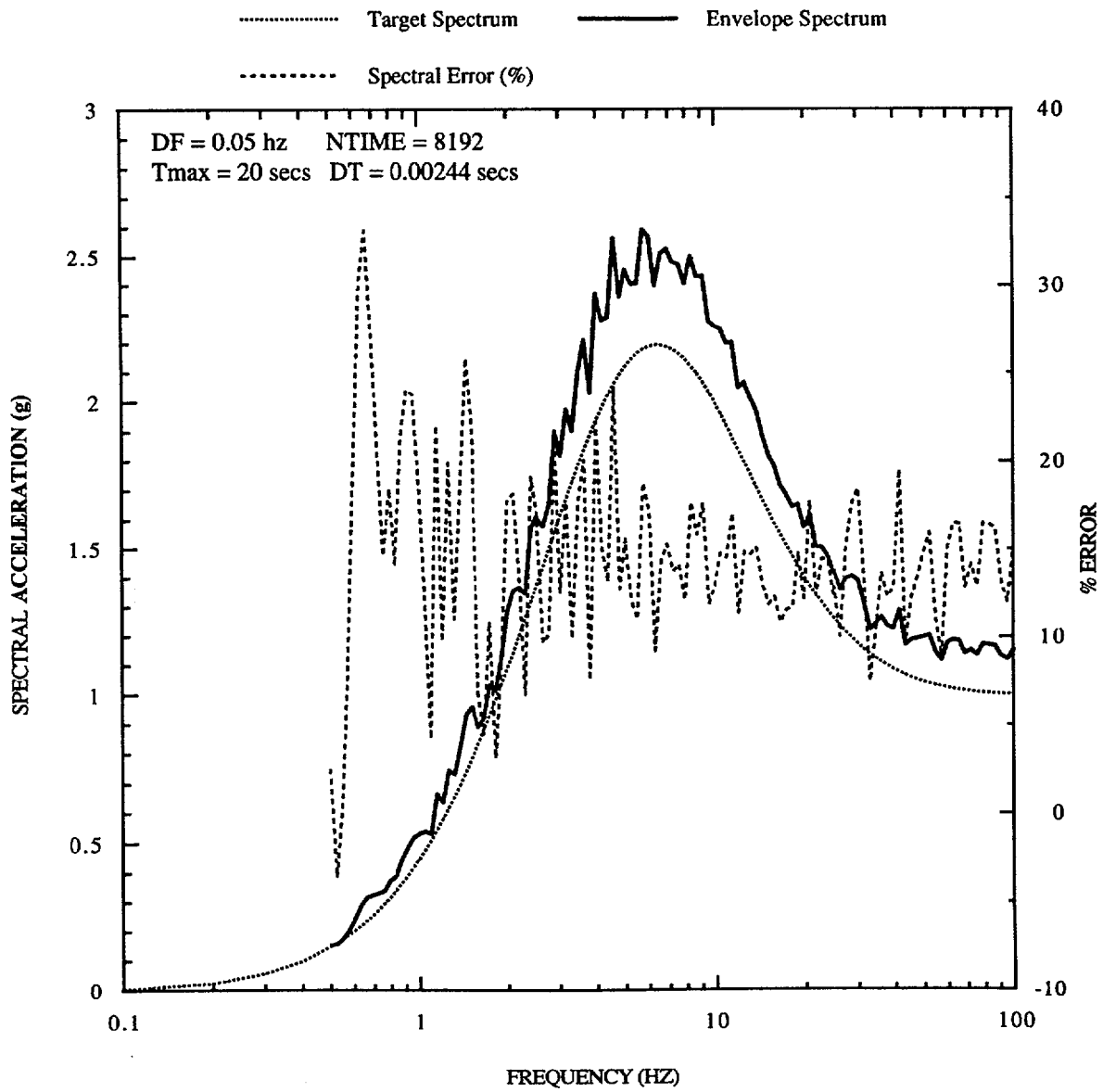


Figure 5-6A. 5% damped spectrum, trial SM01, WUS spectrum, $\bar{M} = 5.57$, $\bar{R} = 21.8$ km (random phase spectrum)

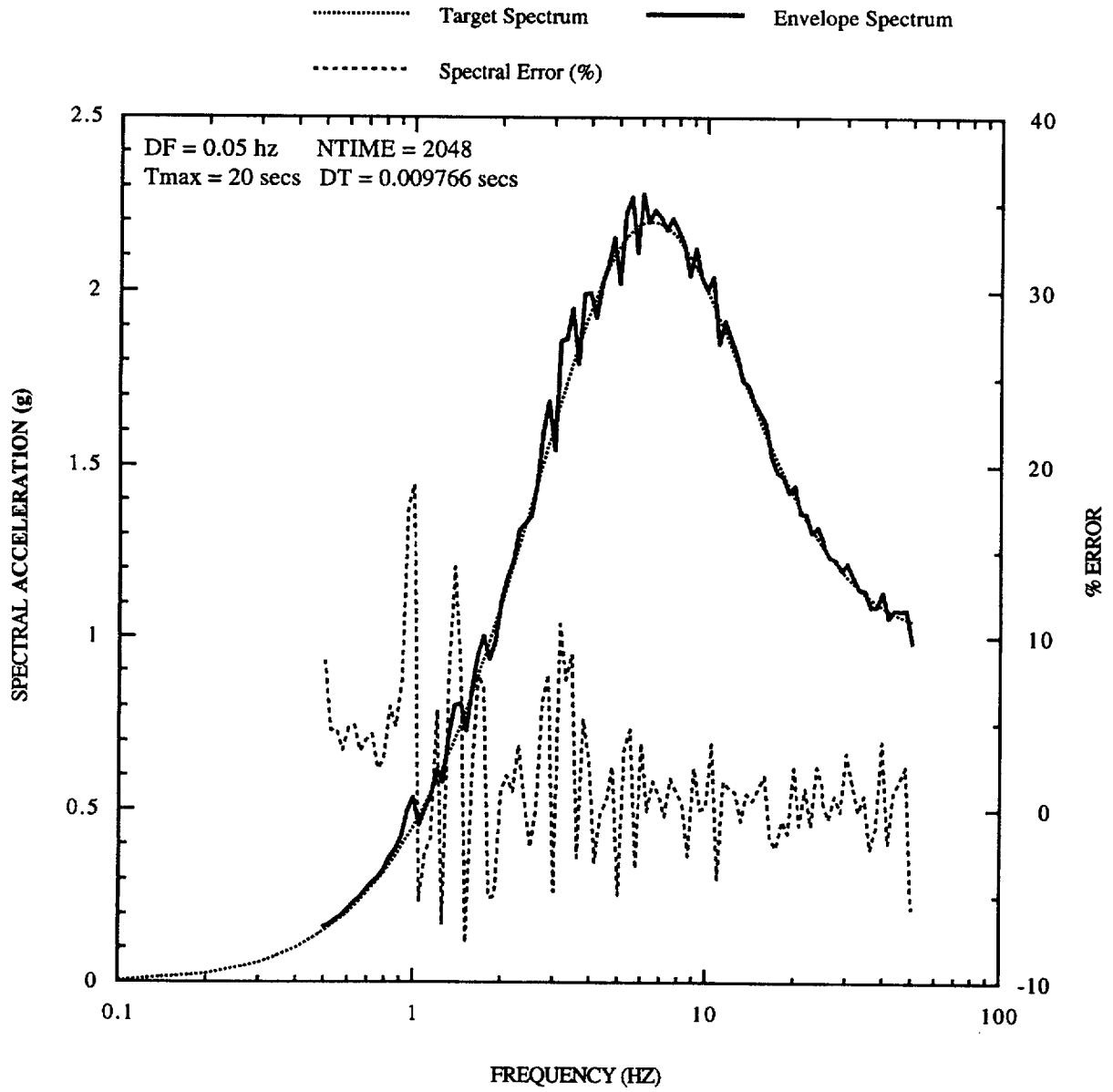


Figure 5-6B. 5% damped spectrum, trial SM02, WUS spectrum, $\bar{M} = 5.57$, $\bar{R} = 21.8$ km (record phase spectrum 1)

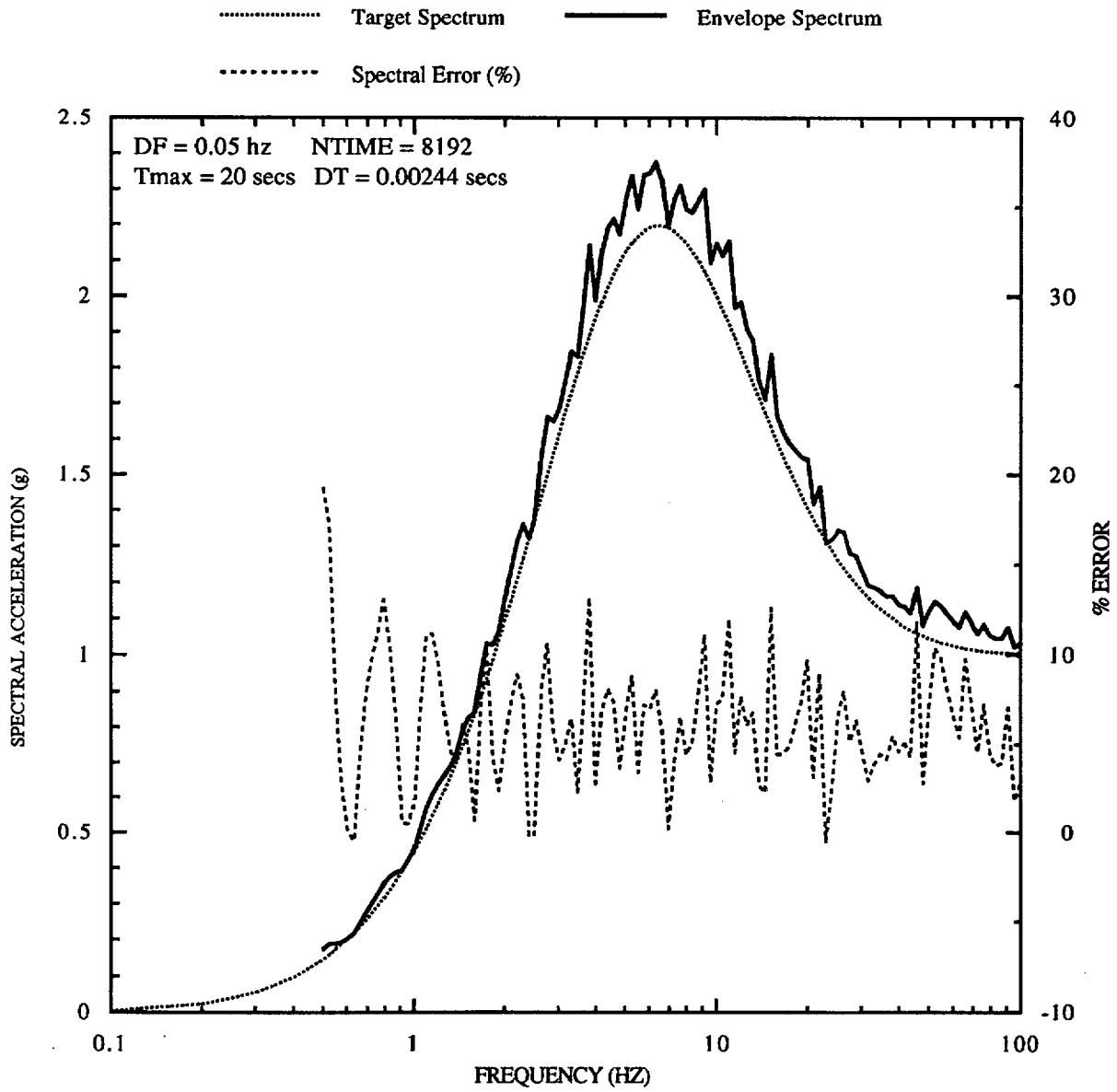


Figure 5-6C. 5% damped spectrum, trial SM03, WUS spectrum, $\bar{M} = 5.57$, $\bar{R} = 21.8$ km (record phase spectrum 2)

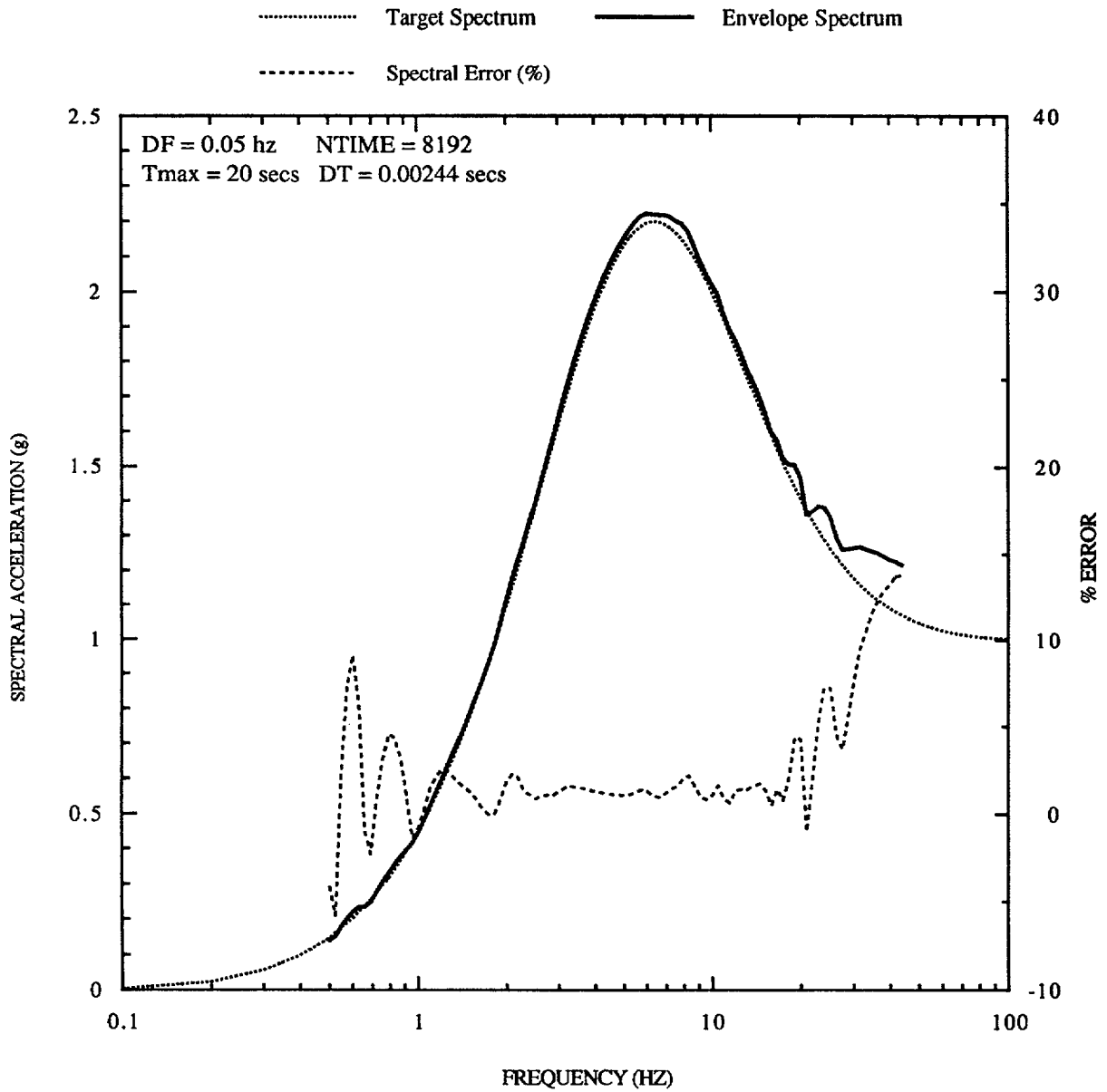


Figure 5-6D. 5% damped spectrum, trial SM04, WUS spectrum, $\bar{M} = 5.57$, $\bar{R} = 21.8$ km (record phase spectrum 3)

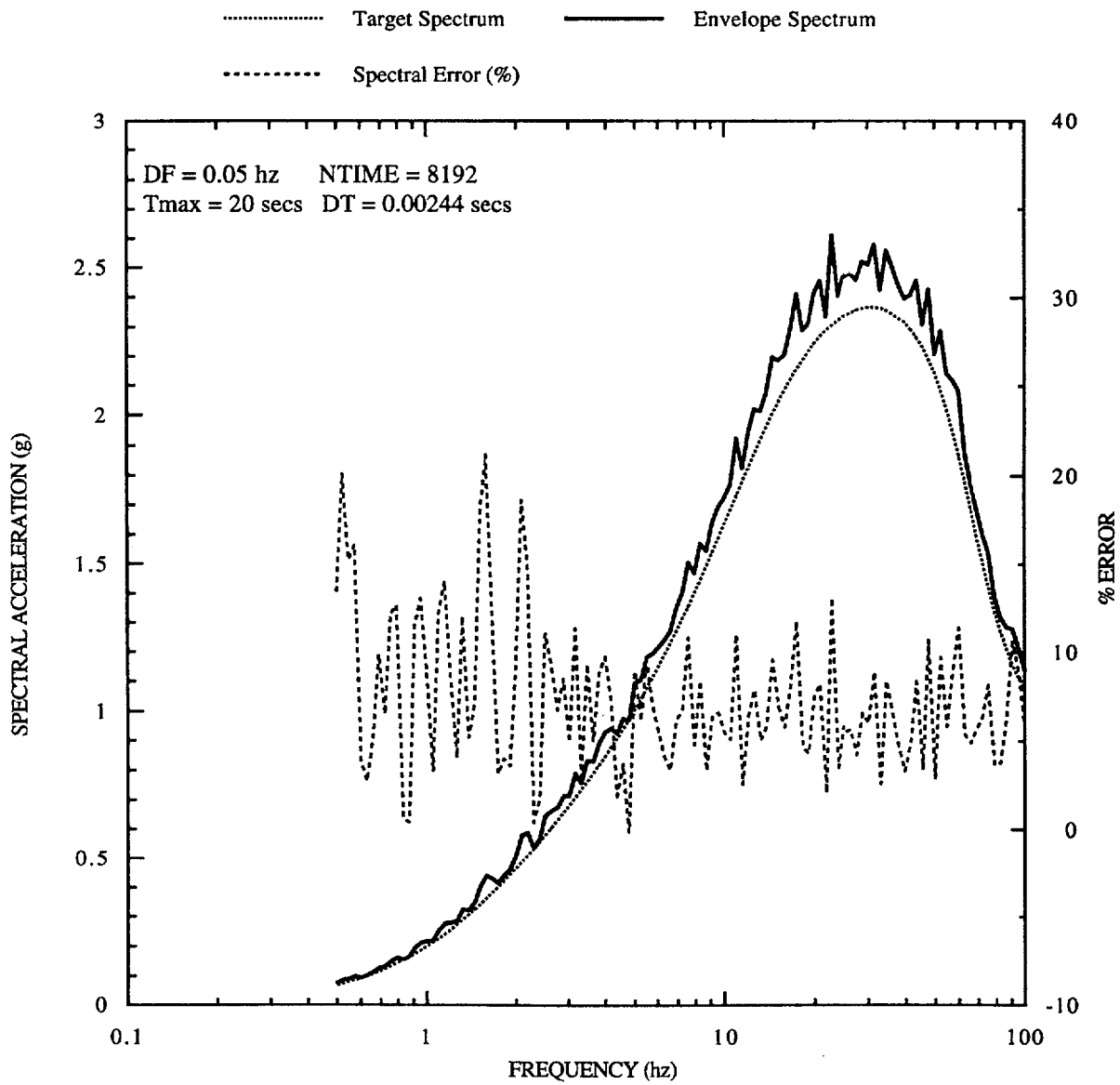


Figure 5-7A. 5% damped spectrum, trial SM01, CEUS 1-corner spectrum, $\bar{M} = 5.57$, $R = 21.8$ km (random phase spectrum)

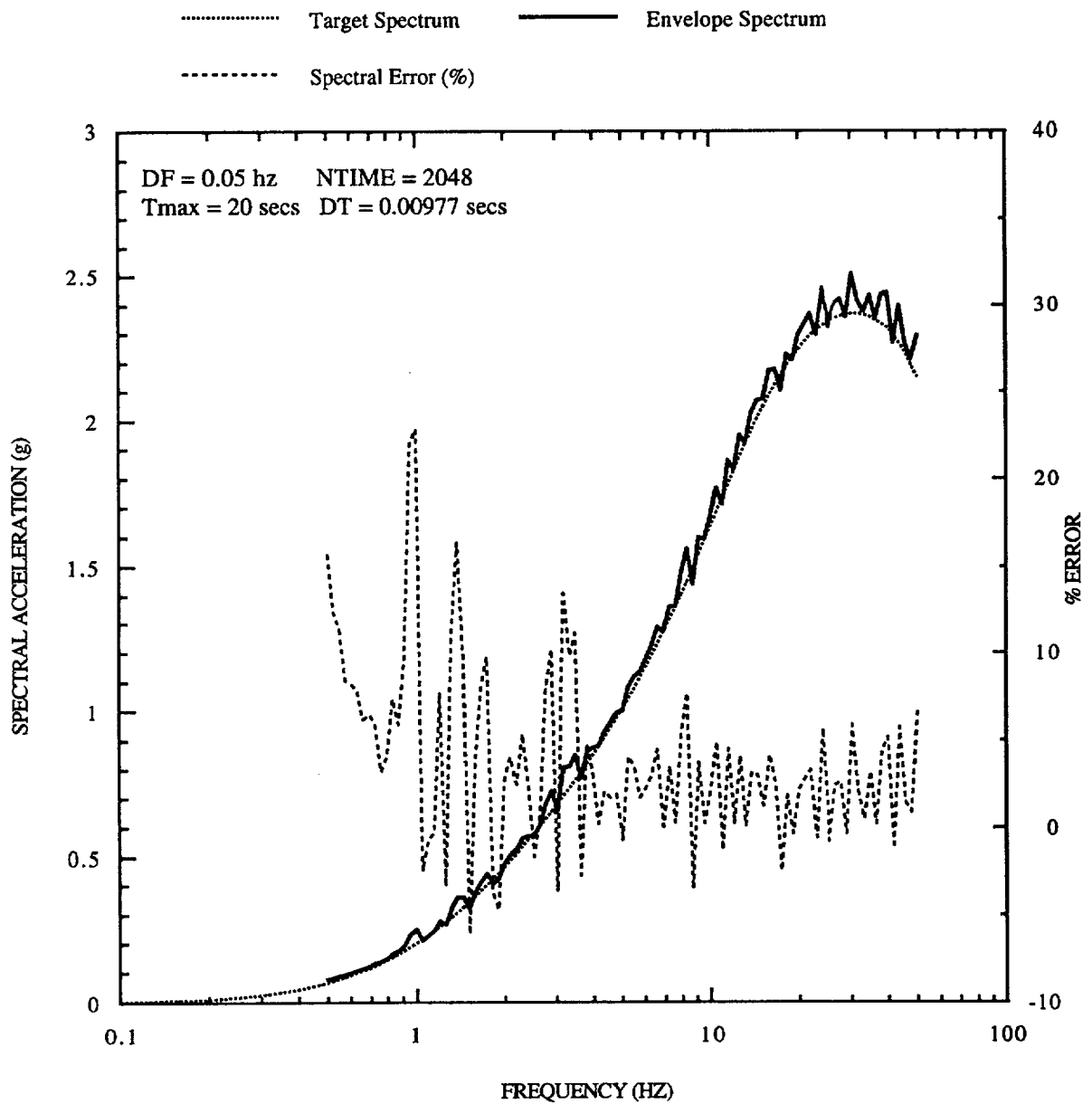


Figure 5-7B. 5% damped spectrum, trial SM02, CEUS 1-corner spectrum, $\bar{M} = 5.57$, $R = 21.8$ km (random phase spectrum 1)

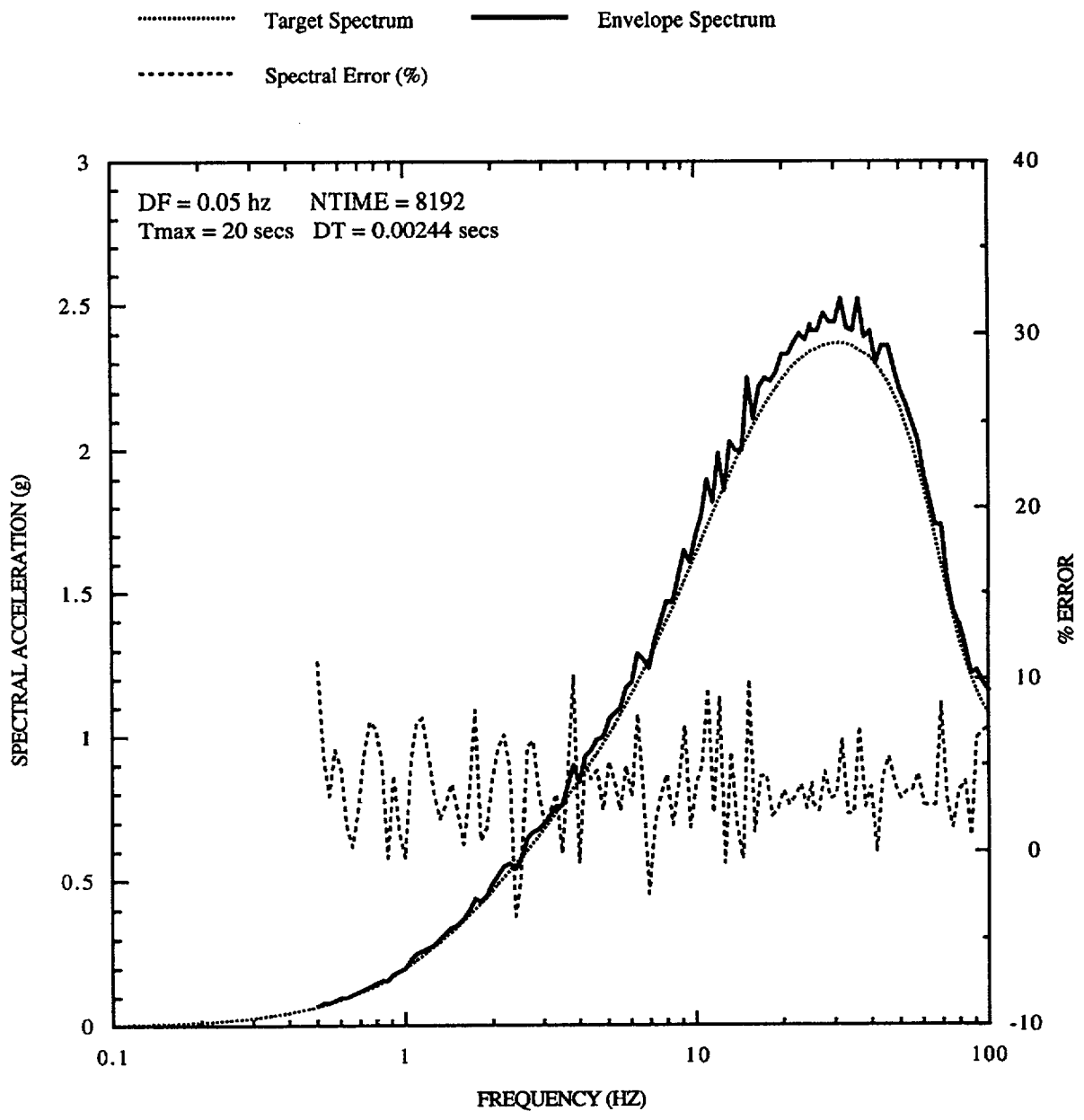


Figure 5-7C. 5% damped spectrum, trial SM03, CEUS 1-corner spectrum, $\bar{M} = 5.57$, $R = 21.8$ km (random phase spectrum 2)

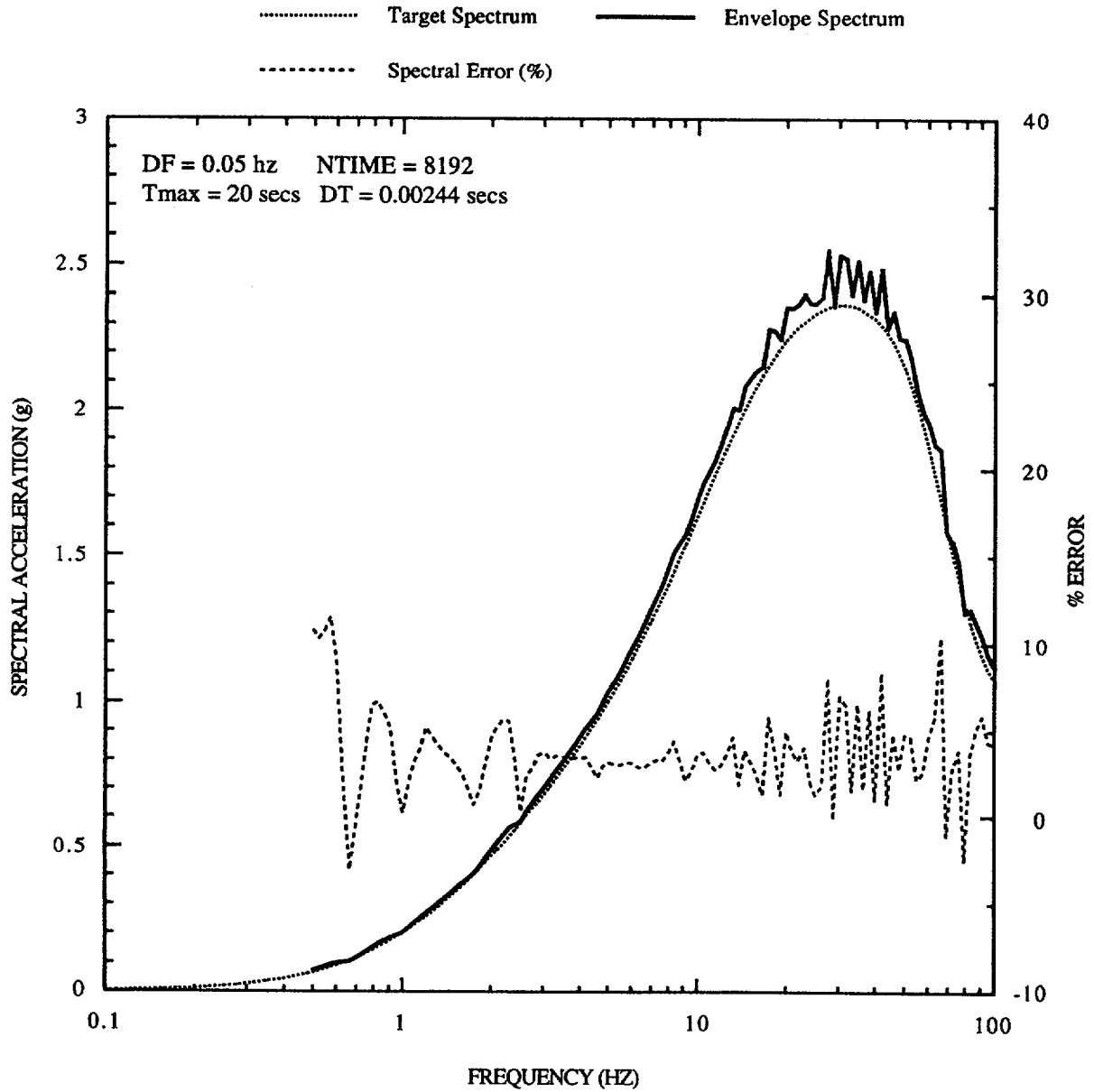


Figure 5-7D. 5% damped spectrum, trial SM04, CEUS 1-corner spectrum, $\bar{M} = 5.57$, $R = 21.8$ km (random phase spectrum 3)

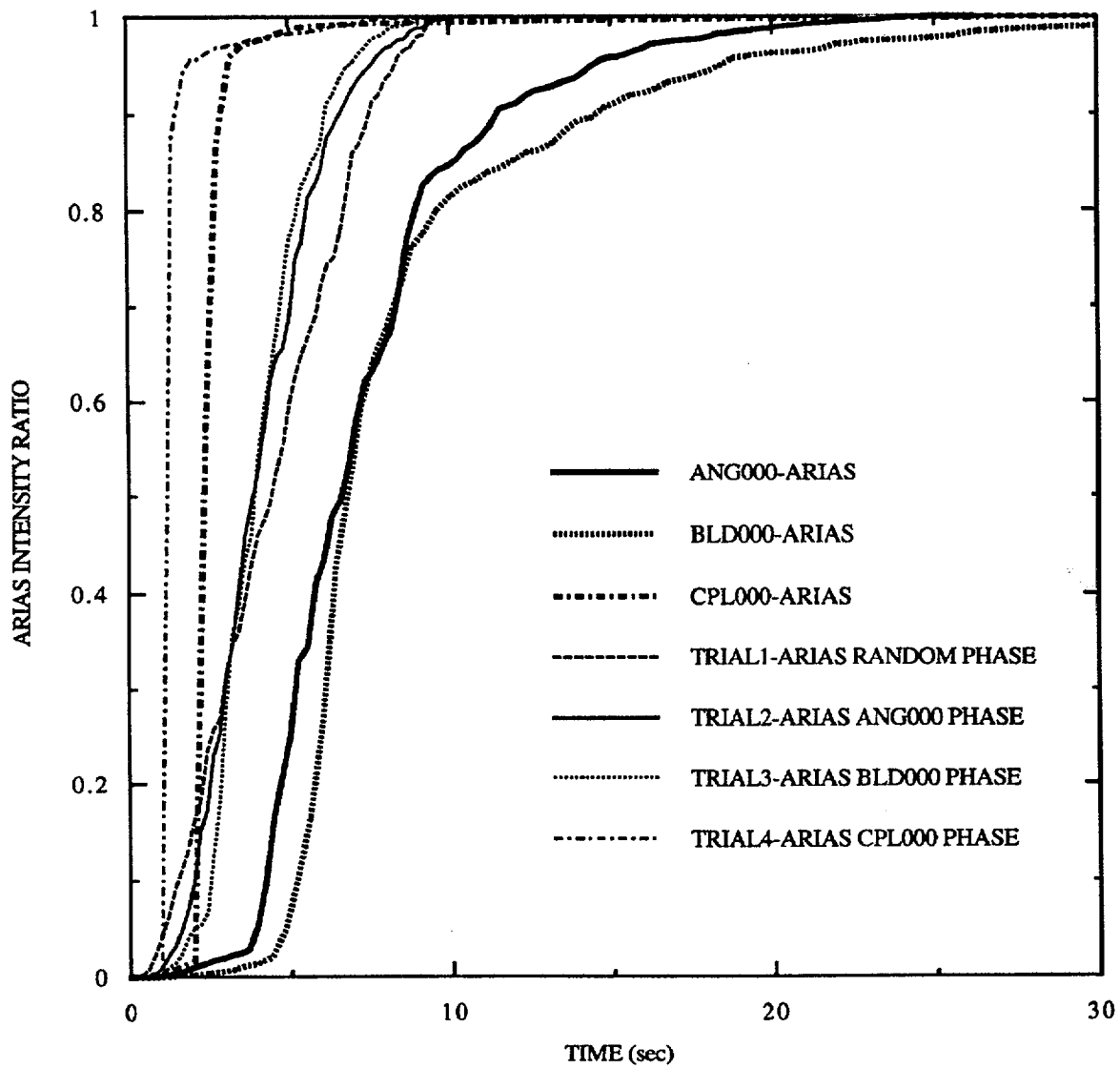


Figure 5-8A. Arias Intensity ratios for trial records used to envelop WUS bin spectrum of Figure 5-6.

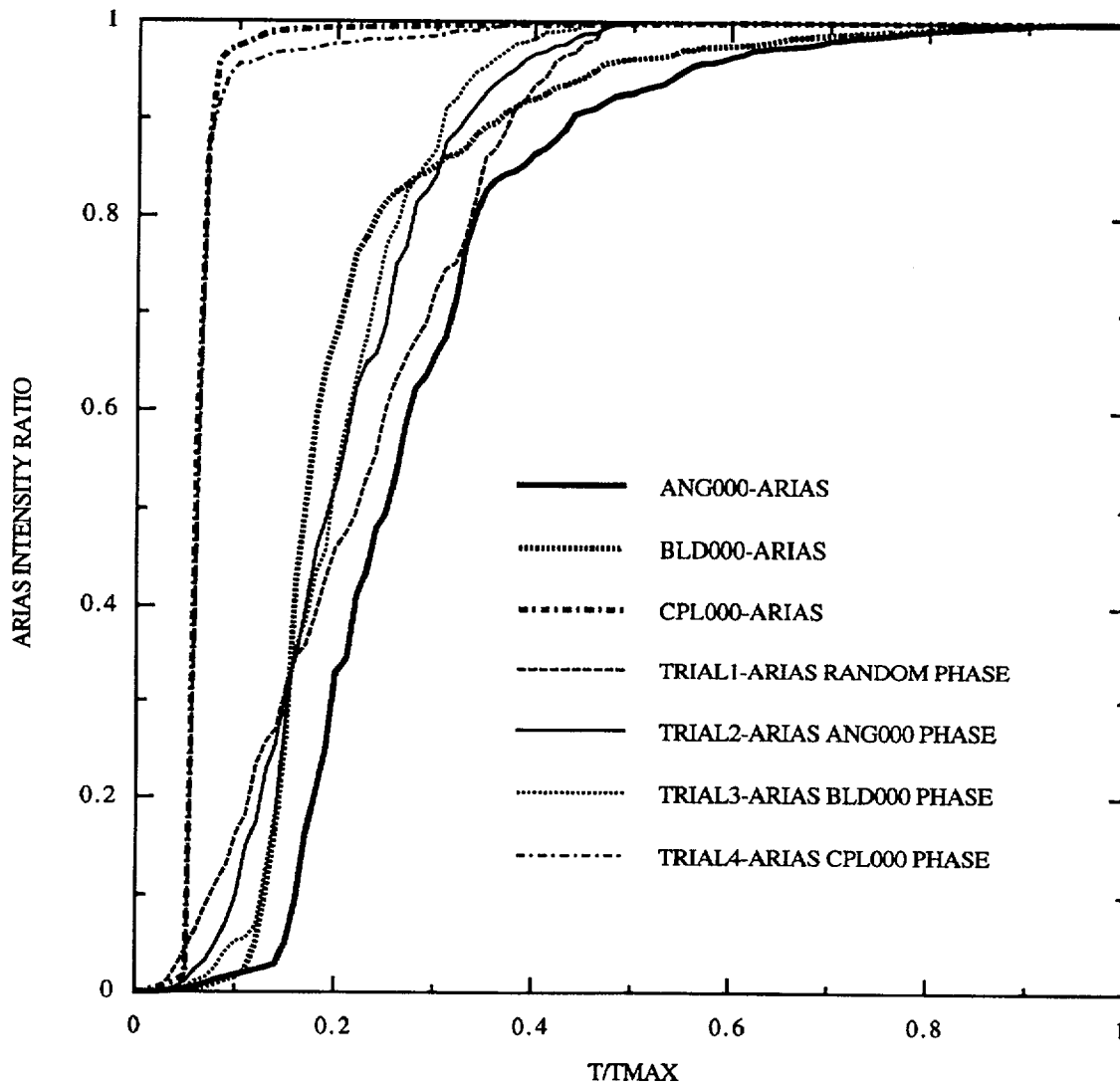


Figure 5-8B. Arias Intensity ratios for WUS records scaled to maximum time duration.

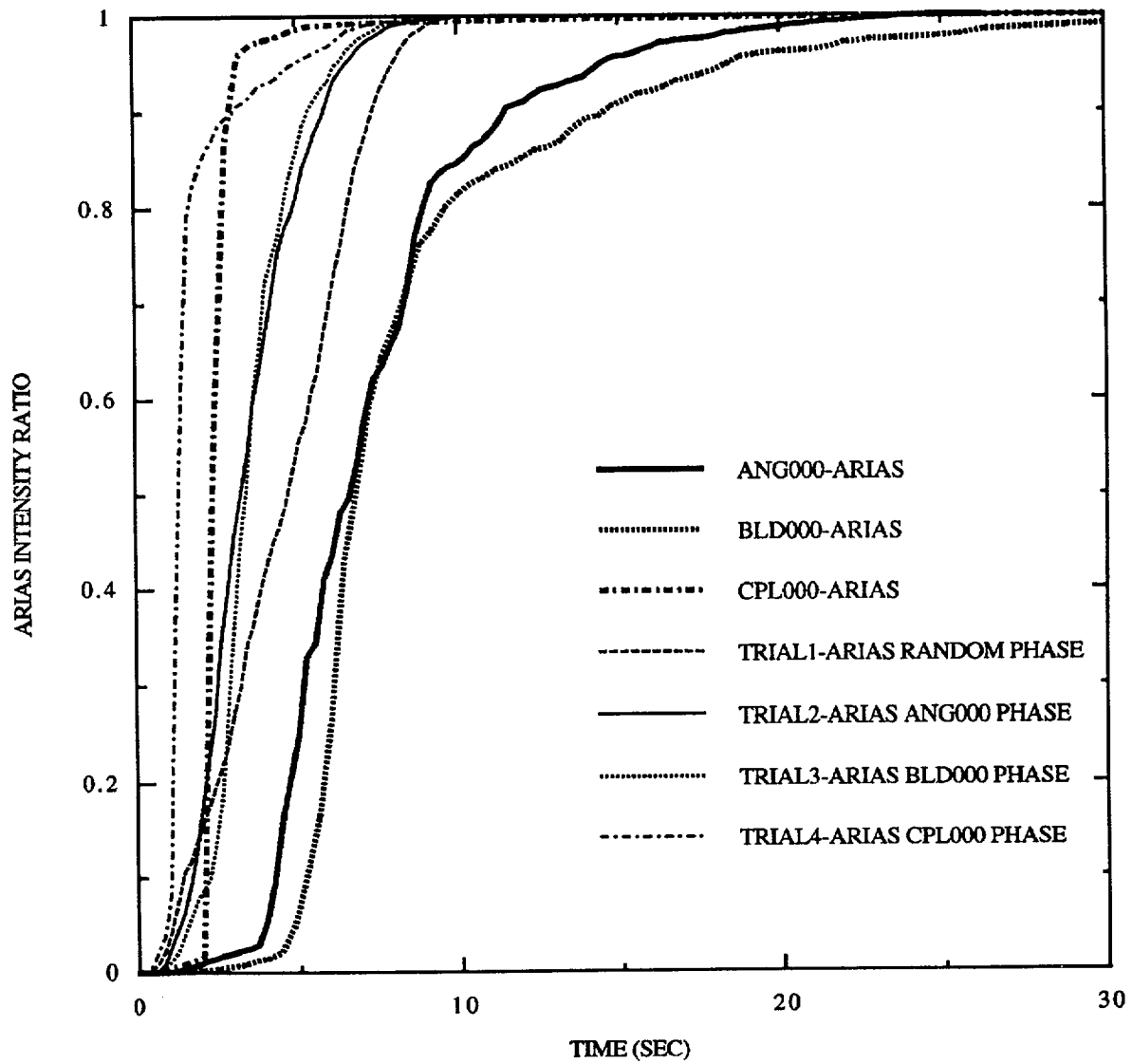


Figure 5-9A. Arias Intensity ratios for trial records used to envelop CEUS 1-corner spectrum of Figure 5-7.

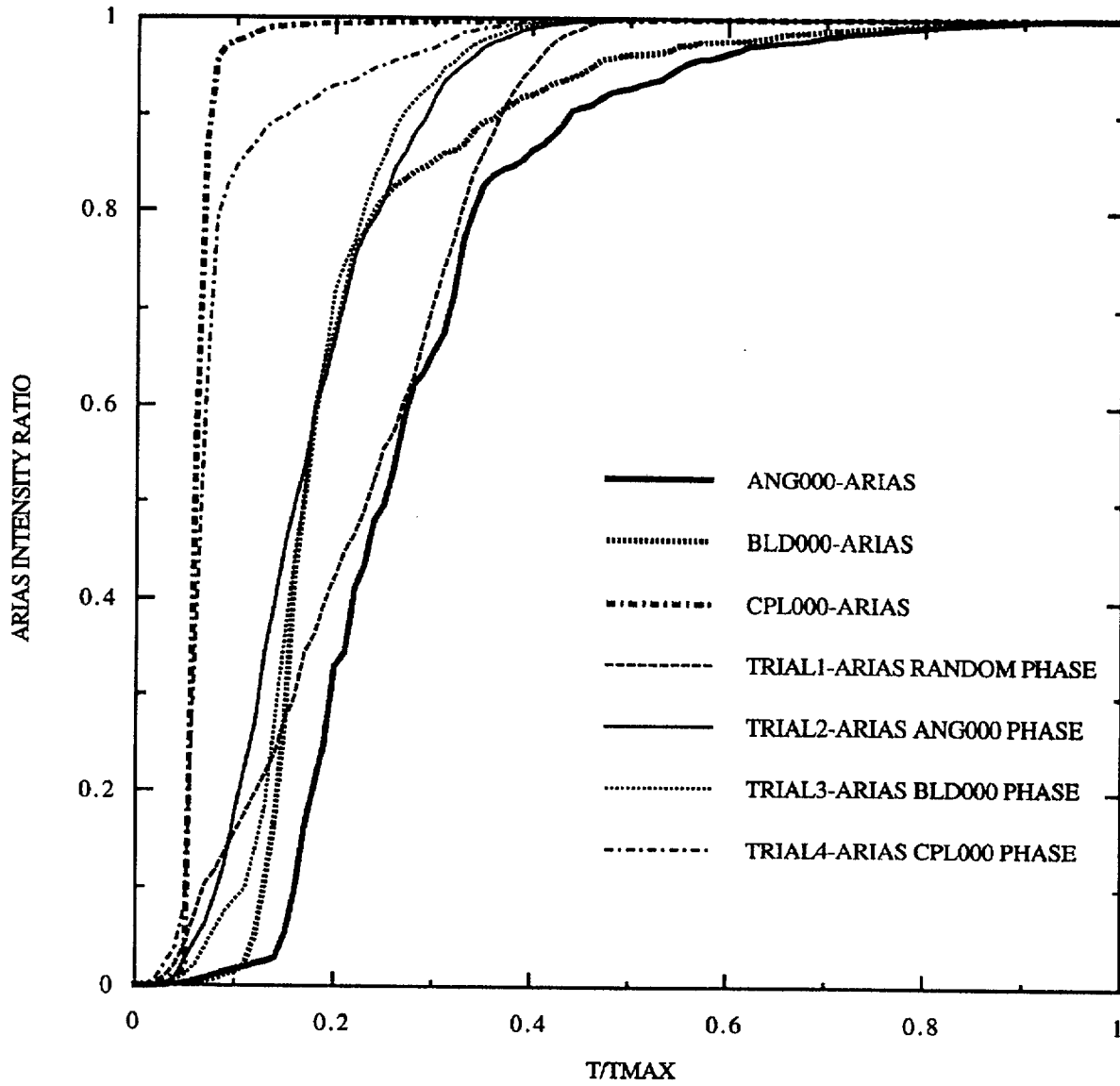


Figure 5-9B. Arias Intensity ratios for CEUS records scaled to maximum time duration.

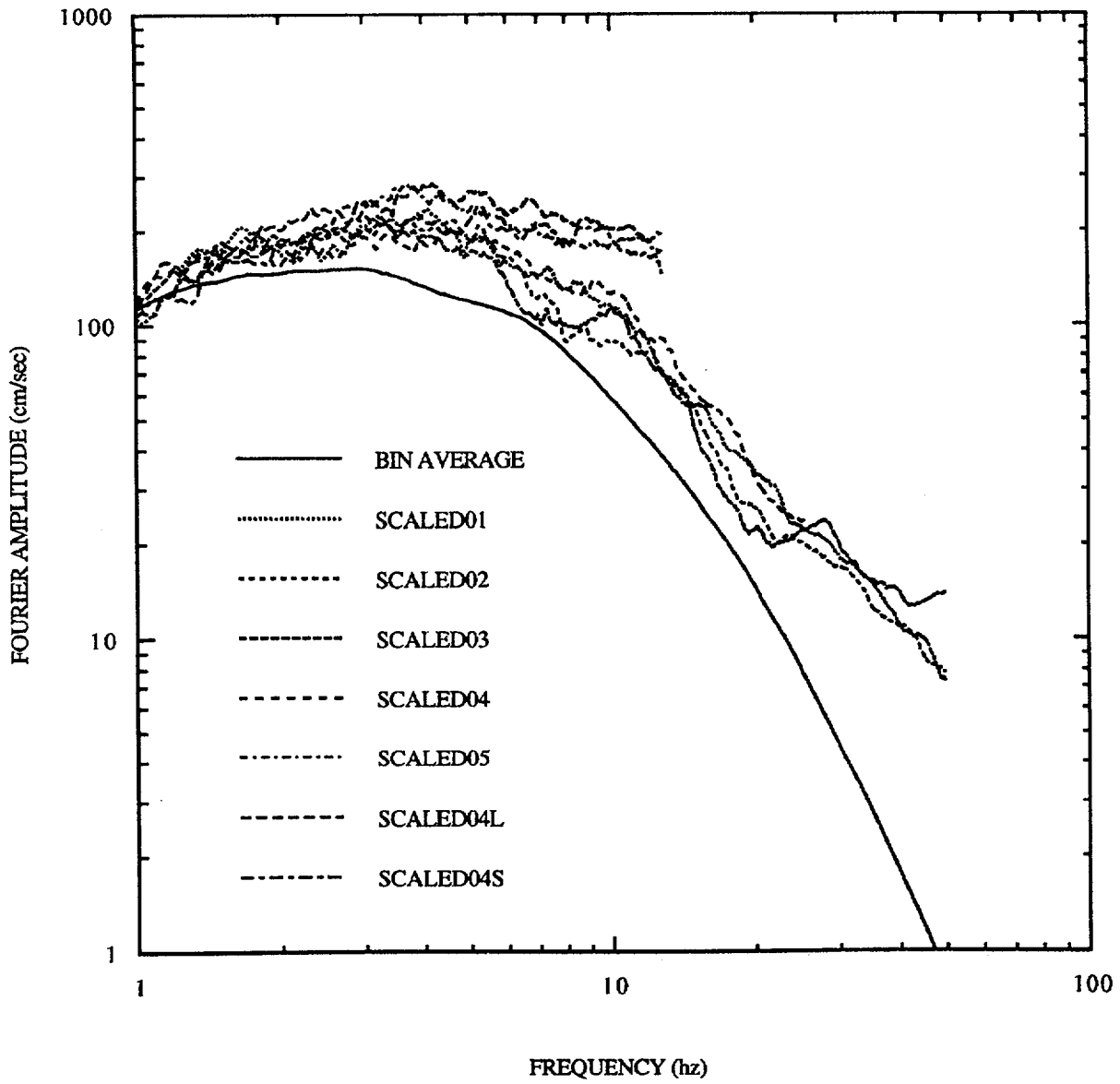


Figure 5-10A. Fourier amplitude spectra of envelope fits to 5% damped segmented target spectrum.

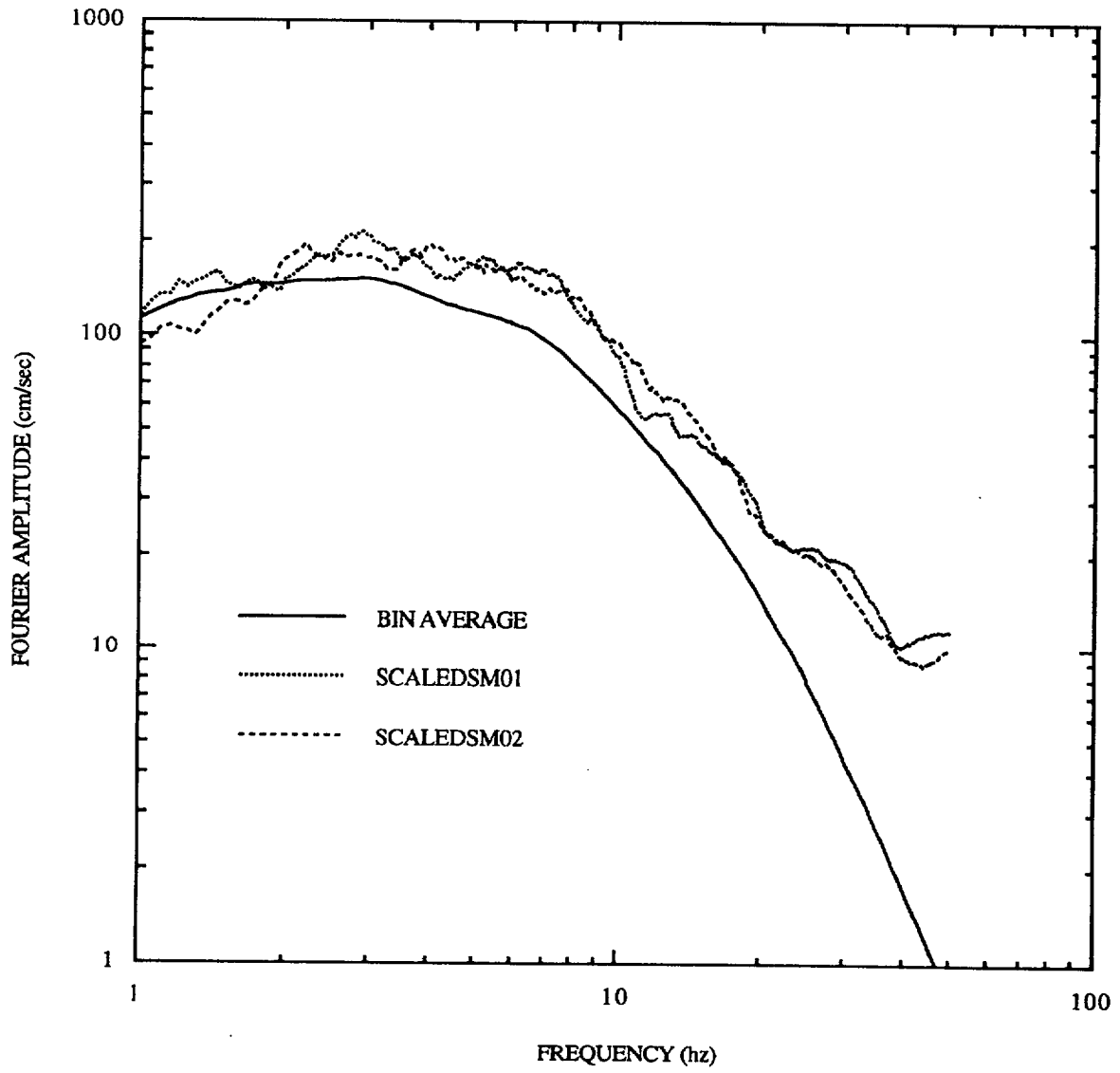


Figure 5-10B. Fourier amplitude spectra of envelope fits to 5% damped smooth target spectrum

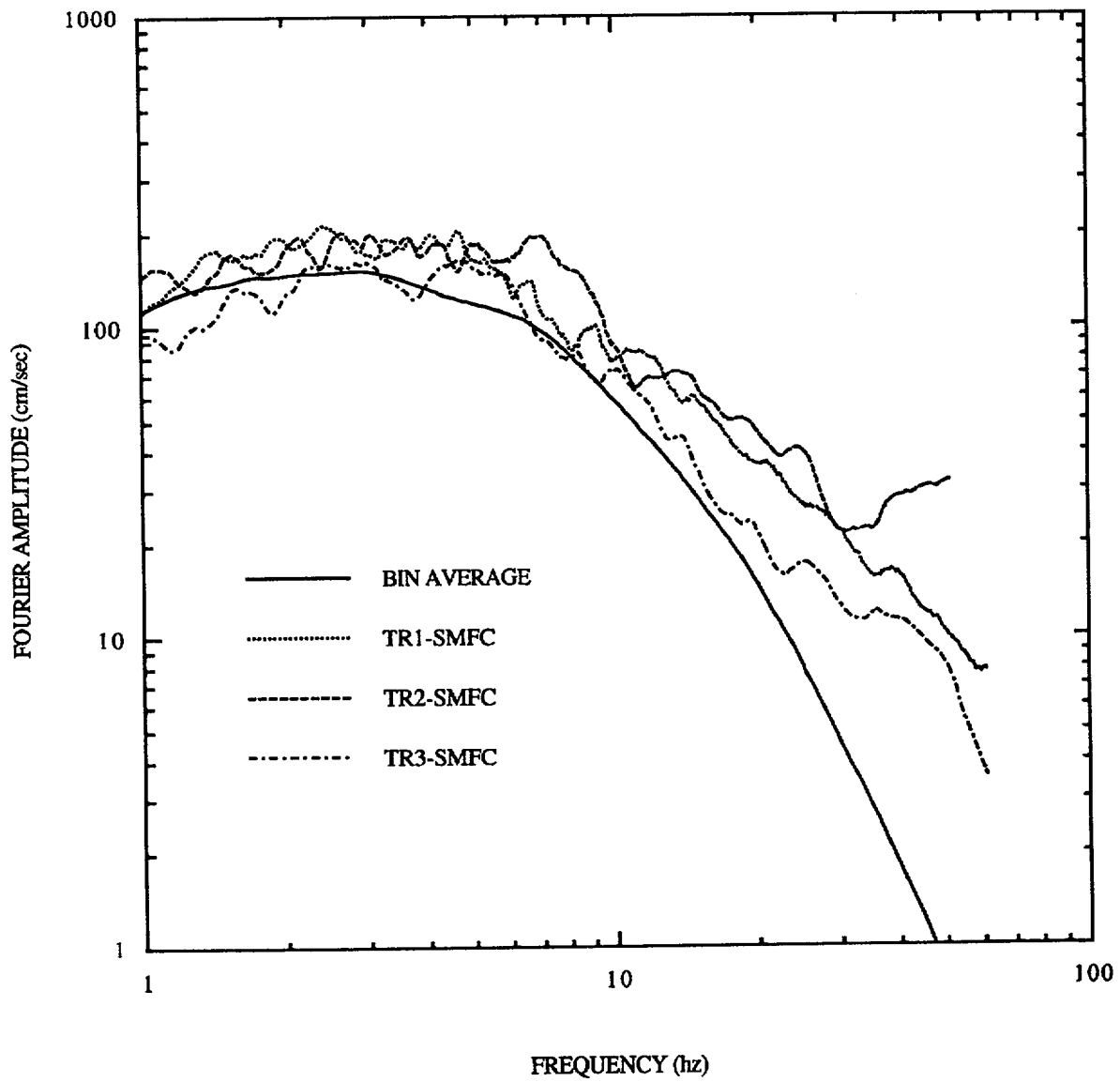


Figure 5-10C. Fourier amplitude spectra of envelope fits to 5% damped smooth WUS target spectrum

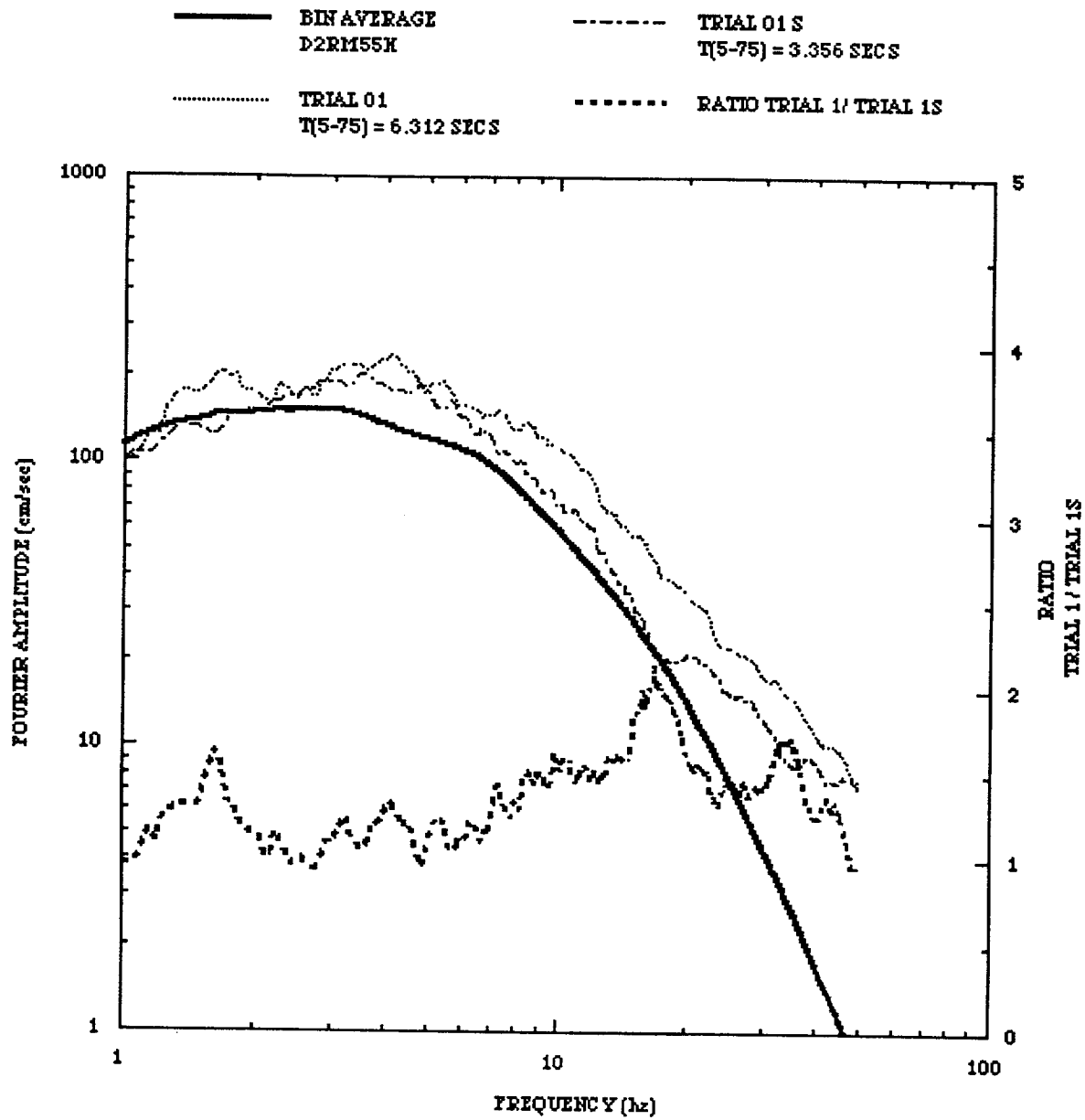


Figure 5-10D. Fourier amplitude spectra of enveloping fits to 5% damped segmented WUS target spectrum (bin D2RM55H)

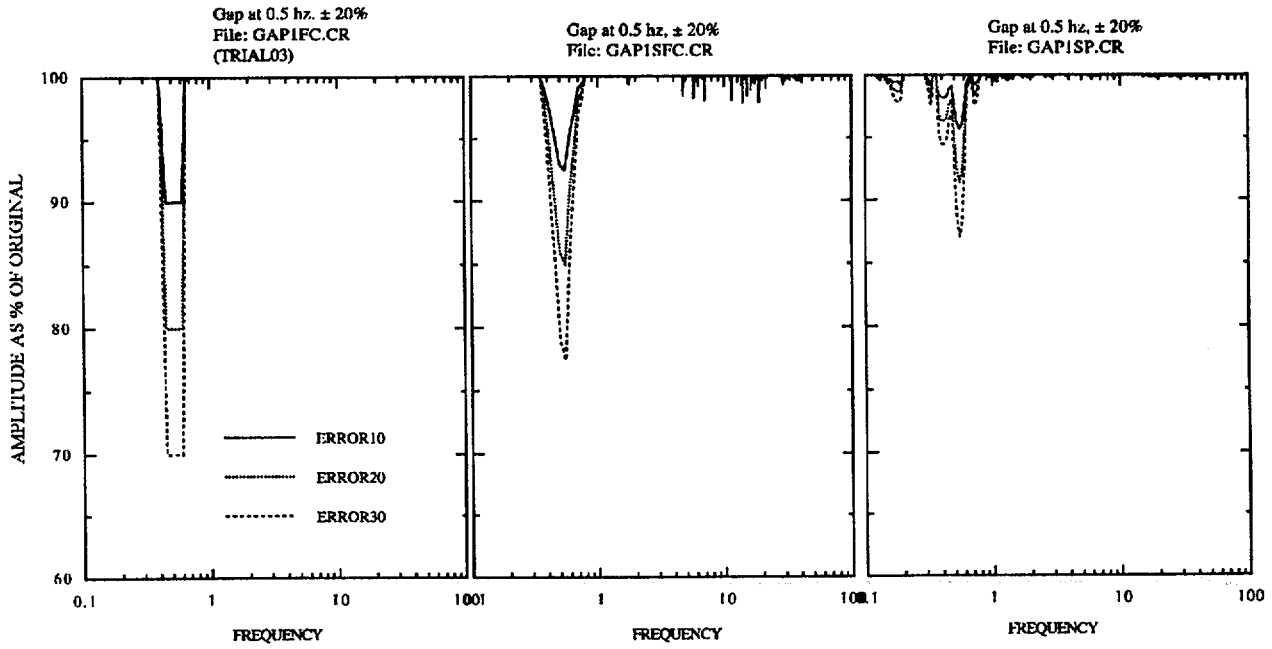


Figure 5-11A. Influence of gap in Fourier amplitudes at 0.5 Hz on 5% damped response spectra. Left: change in original Fourier amplitudes; center: change in smoothed Fourier amplitudes; right: change in 5% damped response spectrum

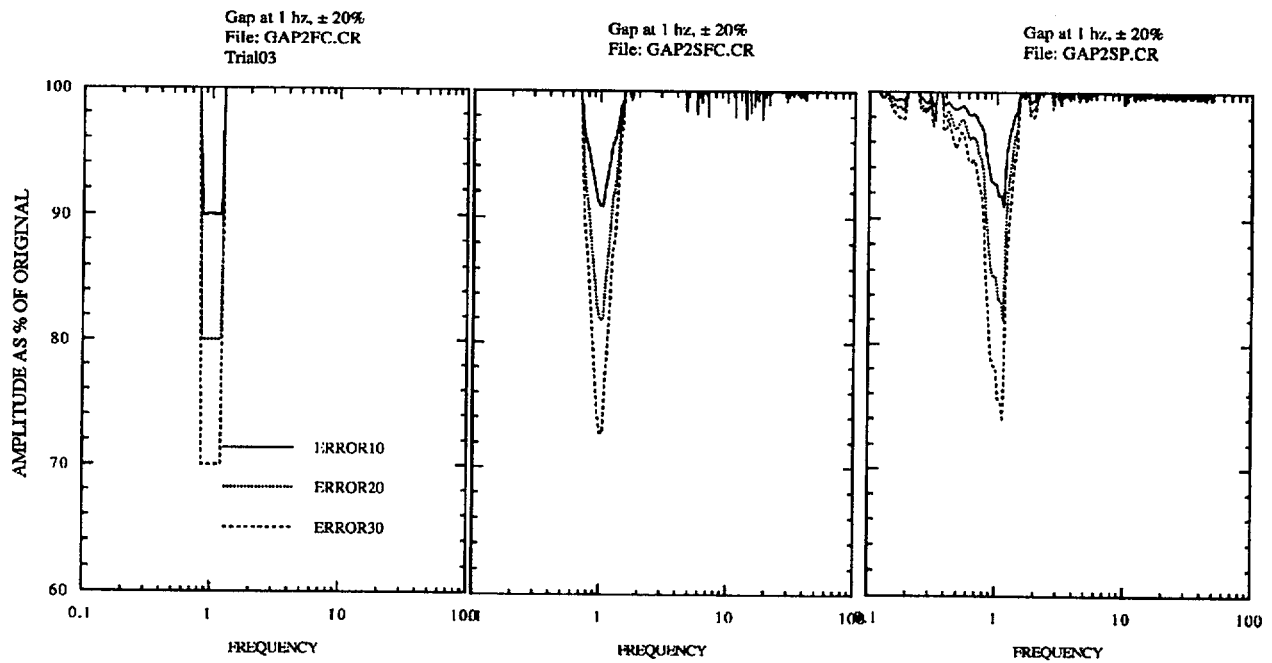


Figure 5-11B. Influence of gap in Fourier amplitude at 1 Hz on 5% damped response spectra. Left: change in original Fourier amplitudes; Center: change in smoothed Fourier amplitudes; Right: change in 5% damped response spectrum.

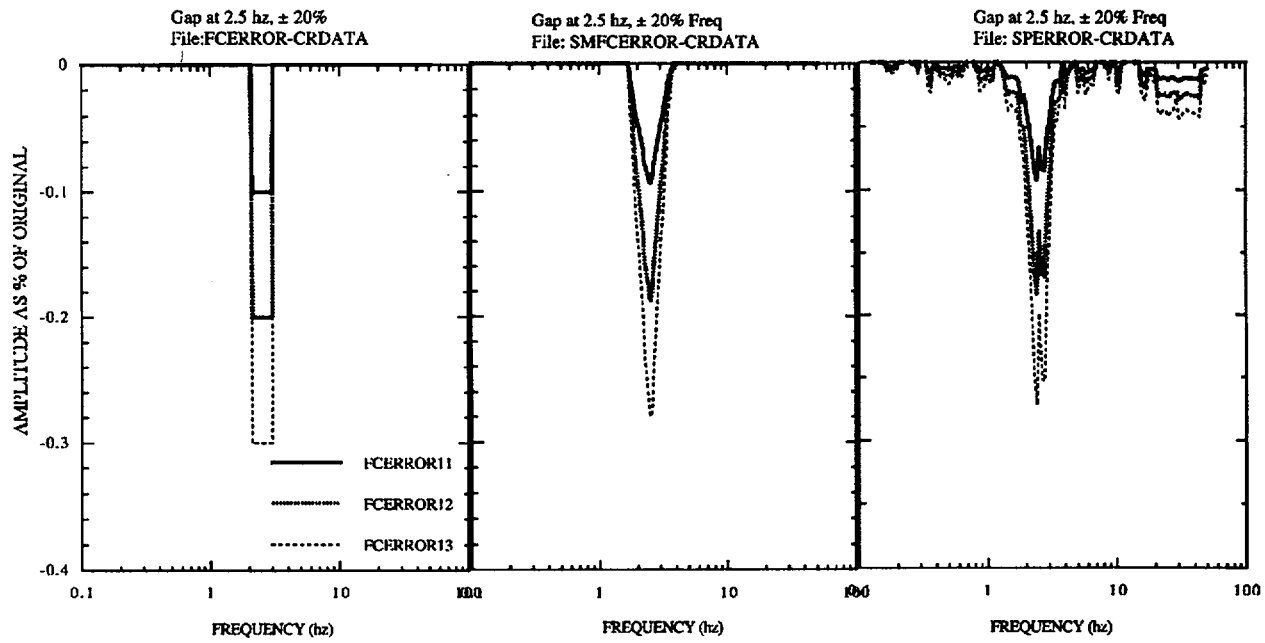


Figure 5-11C. Influence of gap in Fourier amplitudes at 2.5 Hz on 5% damped response spectra. Left: change in original Fourier amplitudes; Center: change in smoothed Fourier amplitudes; Right: change in 5% damped response spectrum.

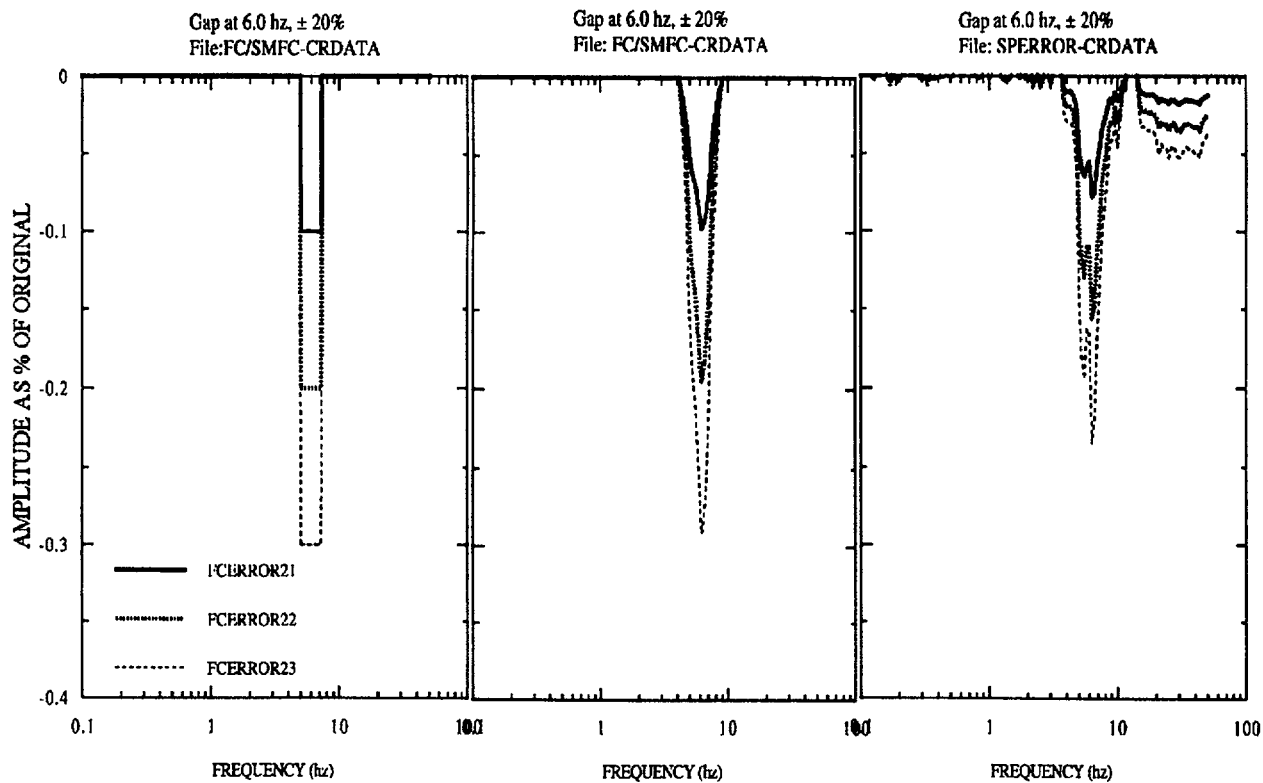


Figure 5-11D. Influence of gap in Fourier amplitudes at 6 Hz on 5% damped response spectra. Left: change in original Fourier amplitudes; Center: change in smoothed Fourier amplitudes; Right: change in 5% damped response spectrum.

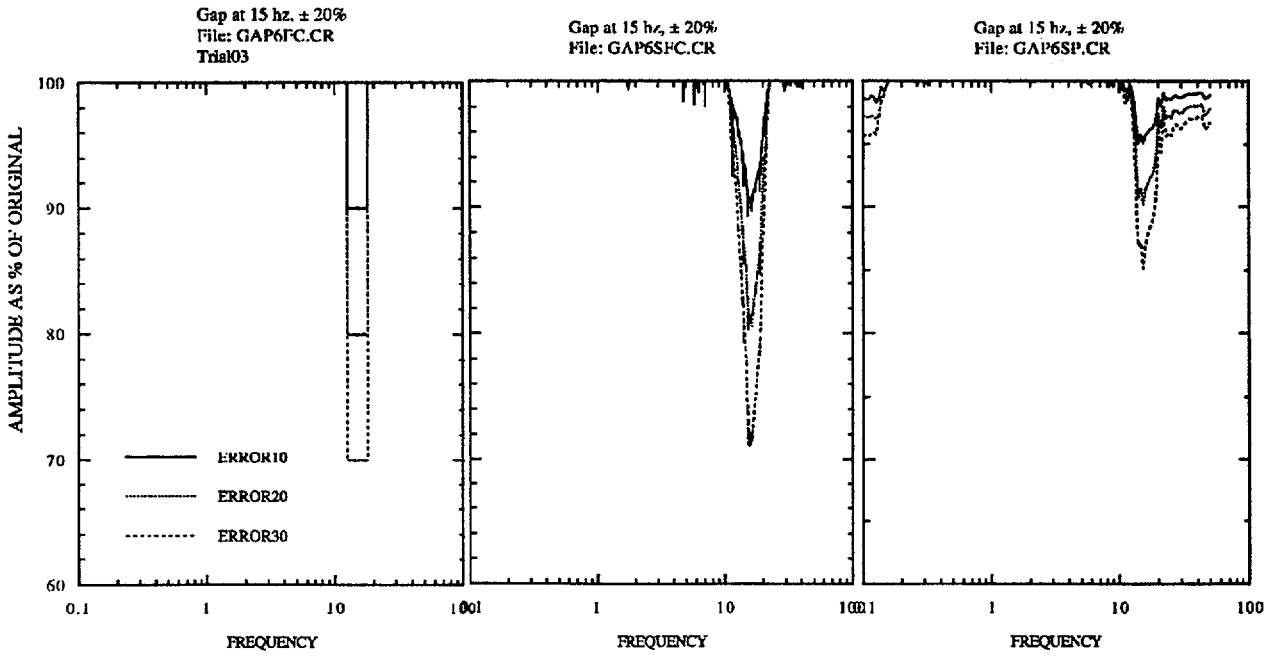


Figure 5-11F. Influence of gap in Fourier amplitudes at 15 Hz on 5% damped response spectra. Left: change in original Fourier amplitudes; Center: change in smoothed Fourier amplitudes; Right: change in 5% damped response spectrum.

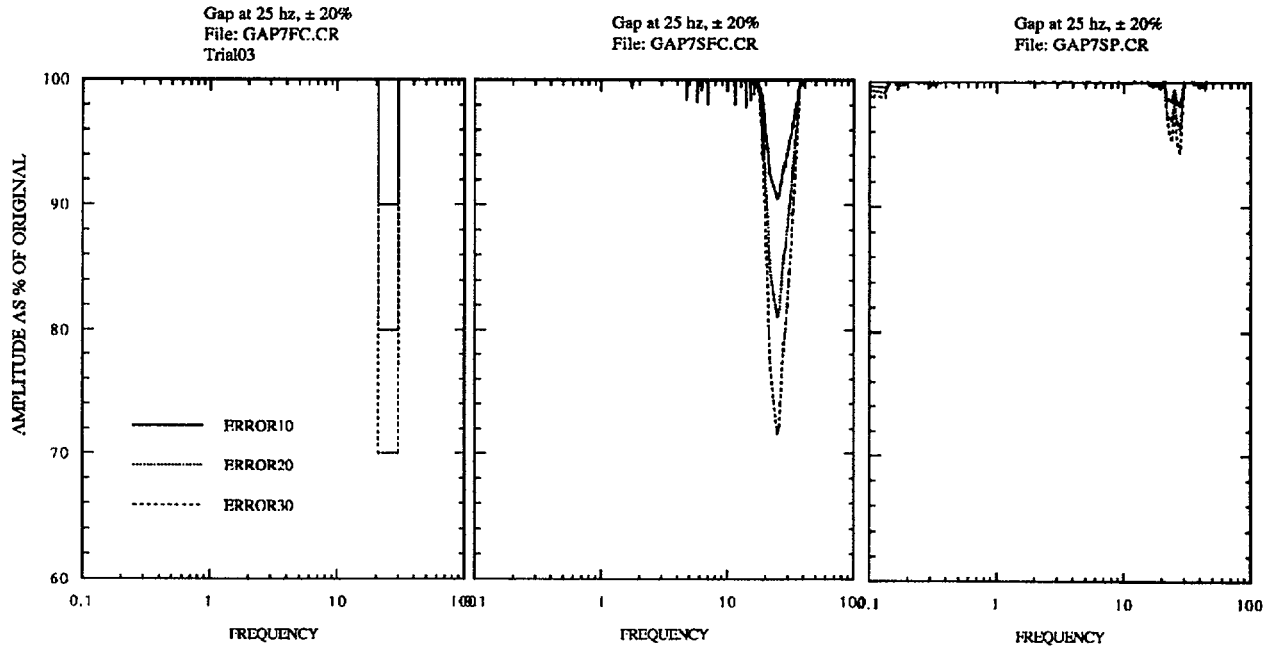


Figure 5-11G. Influence of gap in Fourier amplitudes at 25 Hz on 5% damped response spectra. Left: change in original Fourier amplitudes; Center: change in smoothed Fourier amplitudes; Right: change in 5% damped response spectrum.

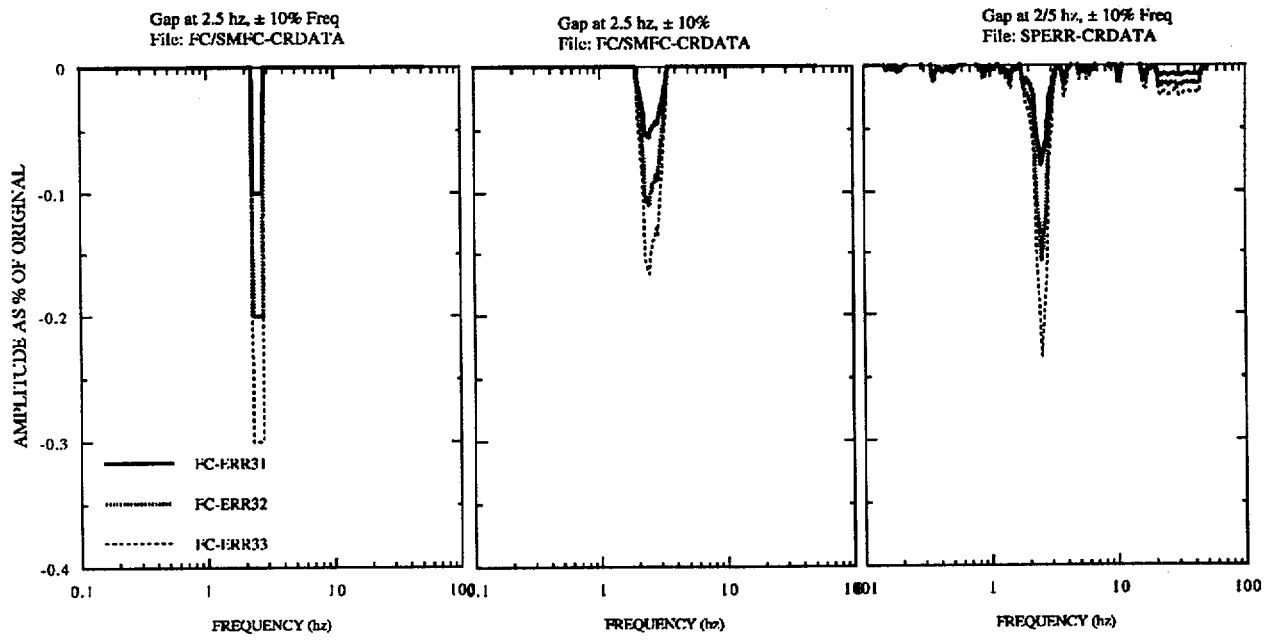


Figure 5-11H. Influence of narrower gap in Fourier amplitudes at 2.5 Hz on 5% damped response spectra. Left: change in original Fourier amplitudes; Center: change in smoothed Fourier amplitudes; Right: change in 5% damped response spectrum.

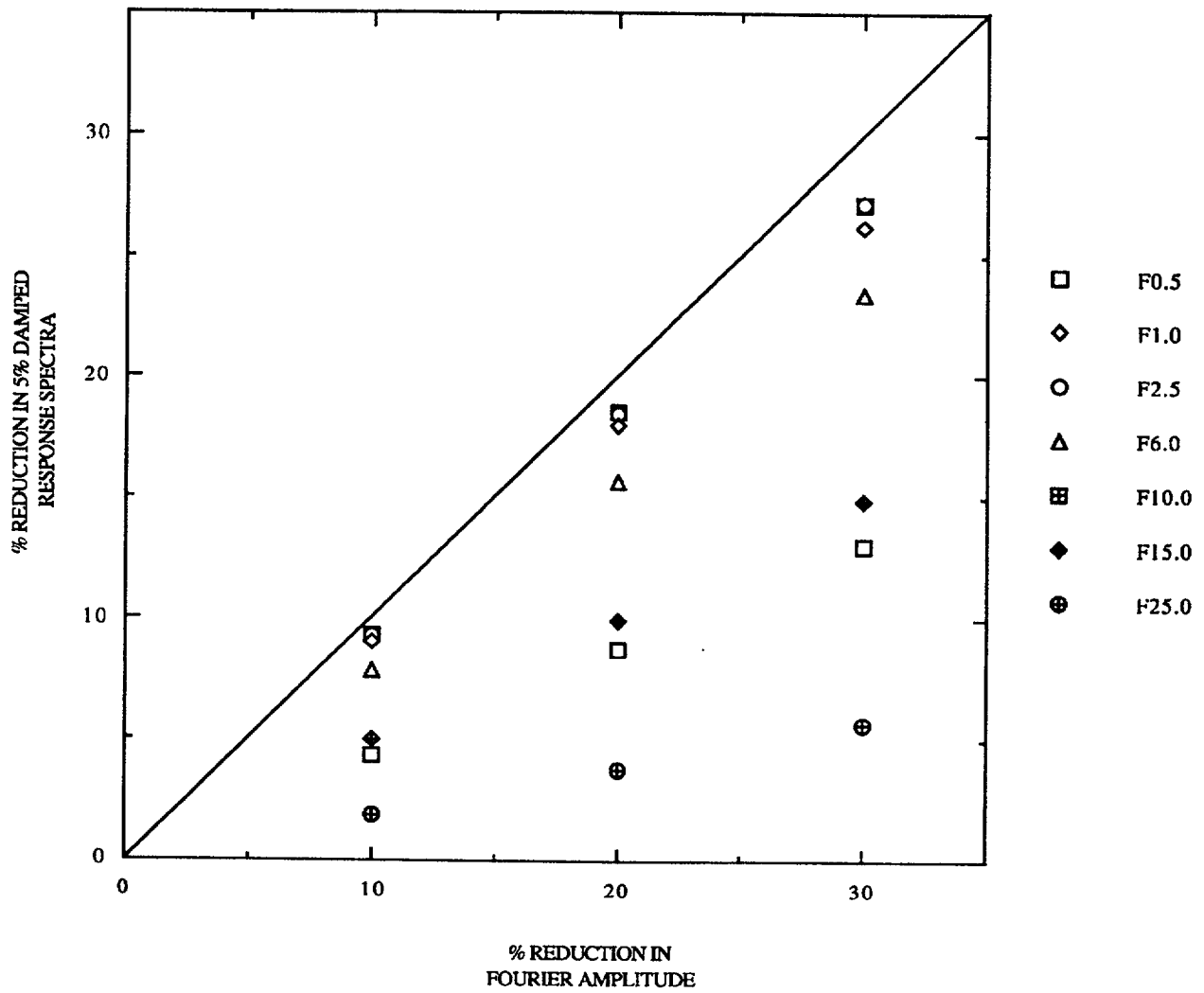


Figure 5-12. Influence of gaps in the Fourier amplitude spectrum on reduction of 5% damped response spectra, record "trial 03".

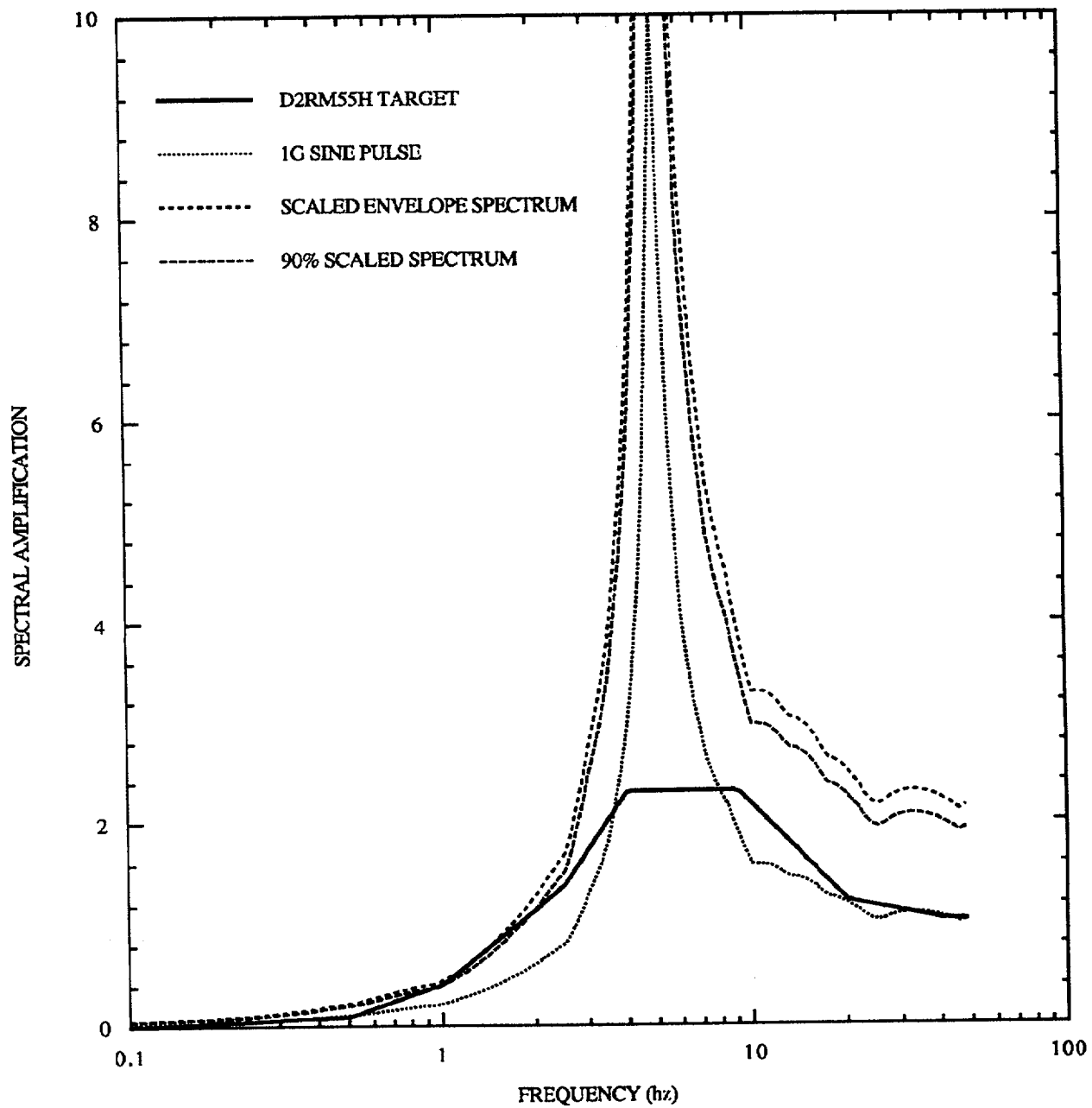


Figure 5-13A. 5% damped response spectra for 1g sine pulse at 5 Hz.

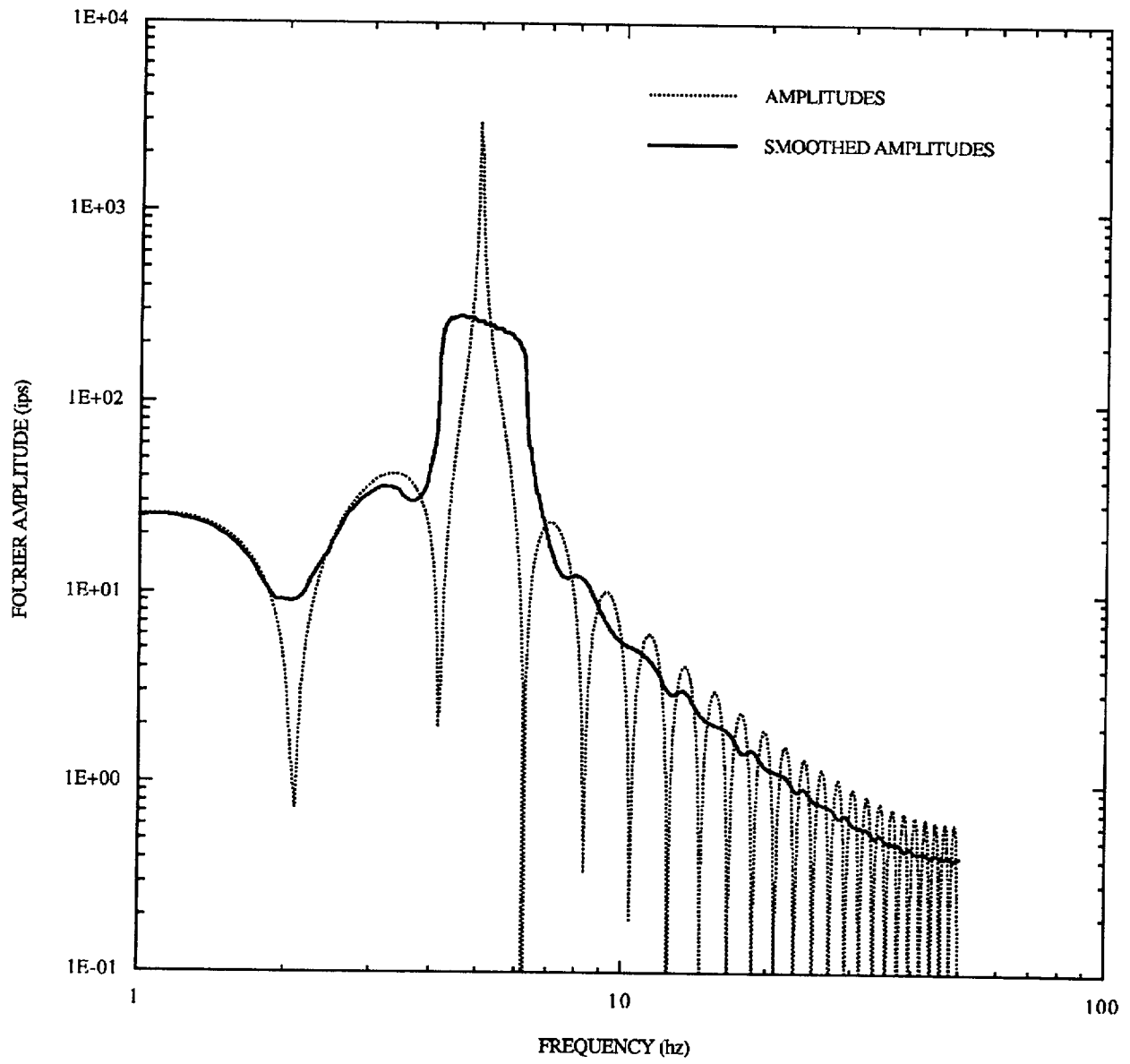


Figure 5-13B. Fourier spectra for 1g sine pulse with a frequency of 5 Hz.

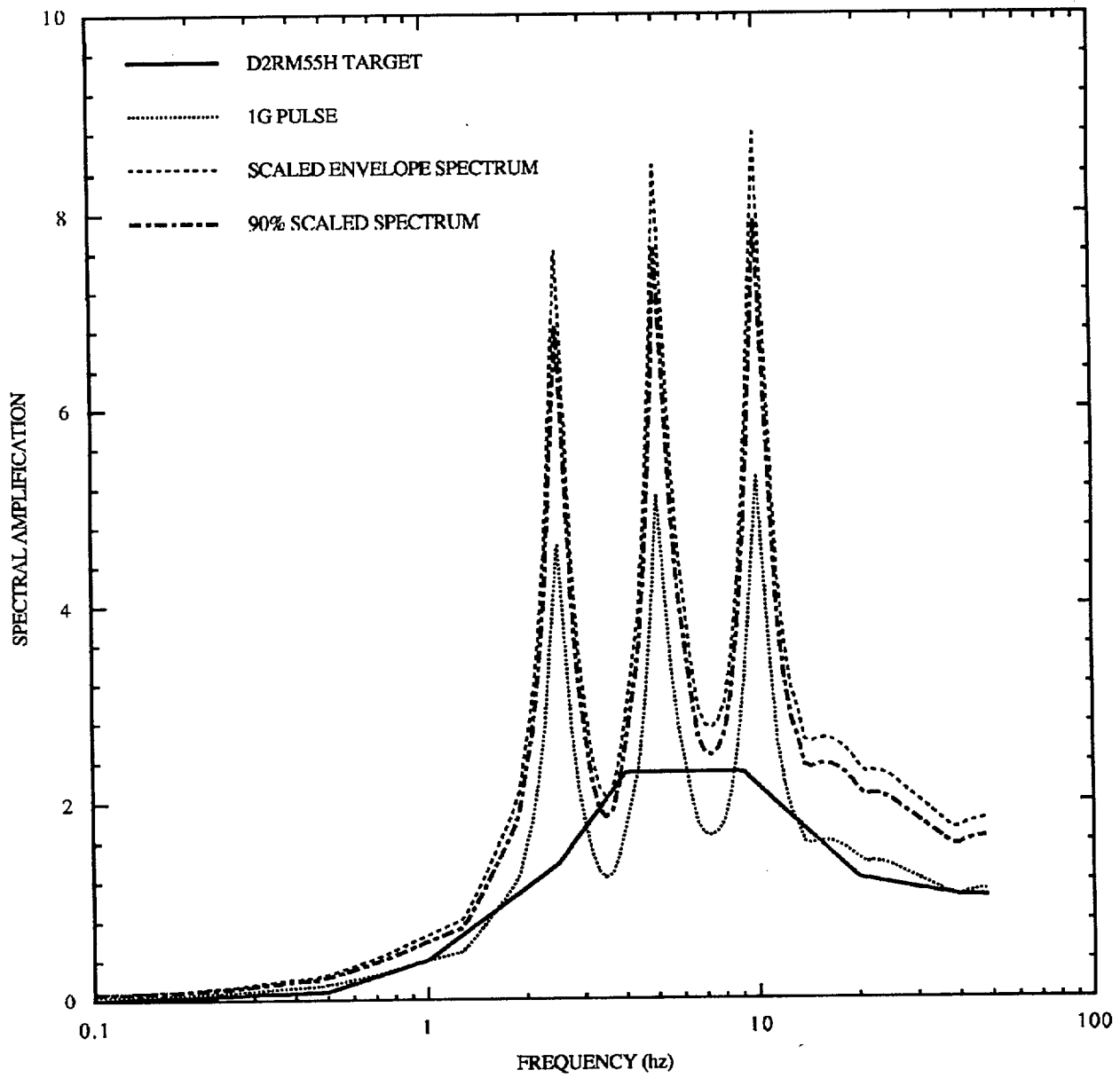


Figure 5-13C. 5% damped response spectra for 1g pulse consisting of three frequencies (2.5, 5, and 10 Hz).

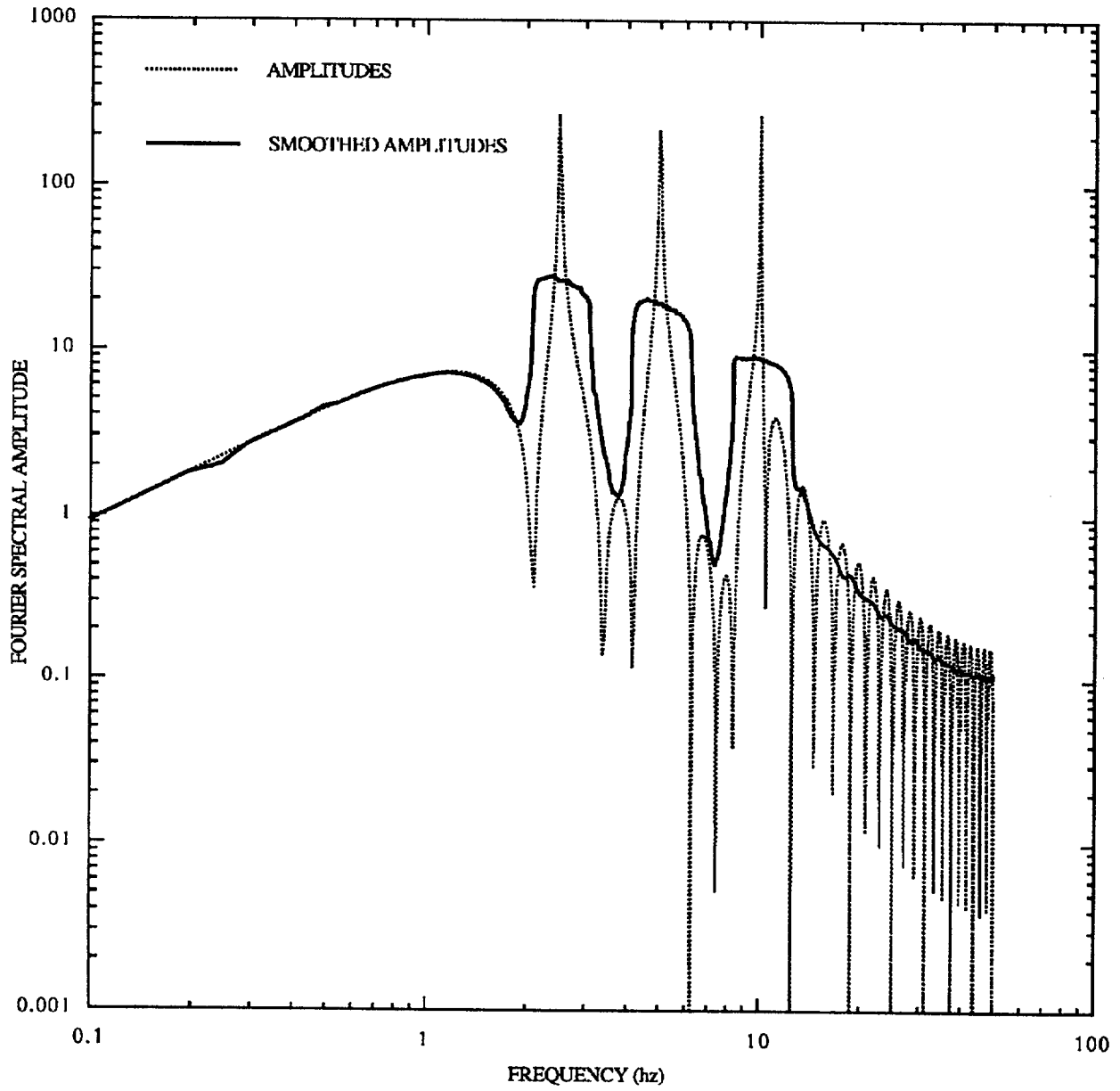


Figure 5-13D. Fourier spectra for 1g sine pulse consisting of three frequencies (2.5, 5, and 10 Hz).

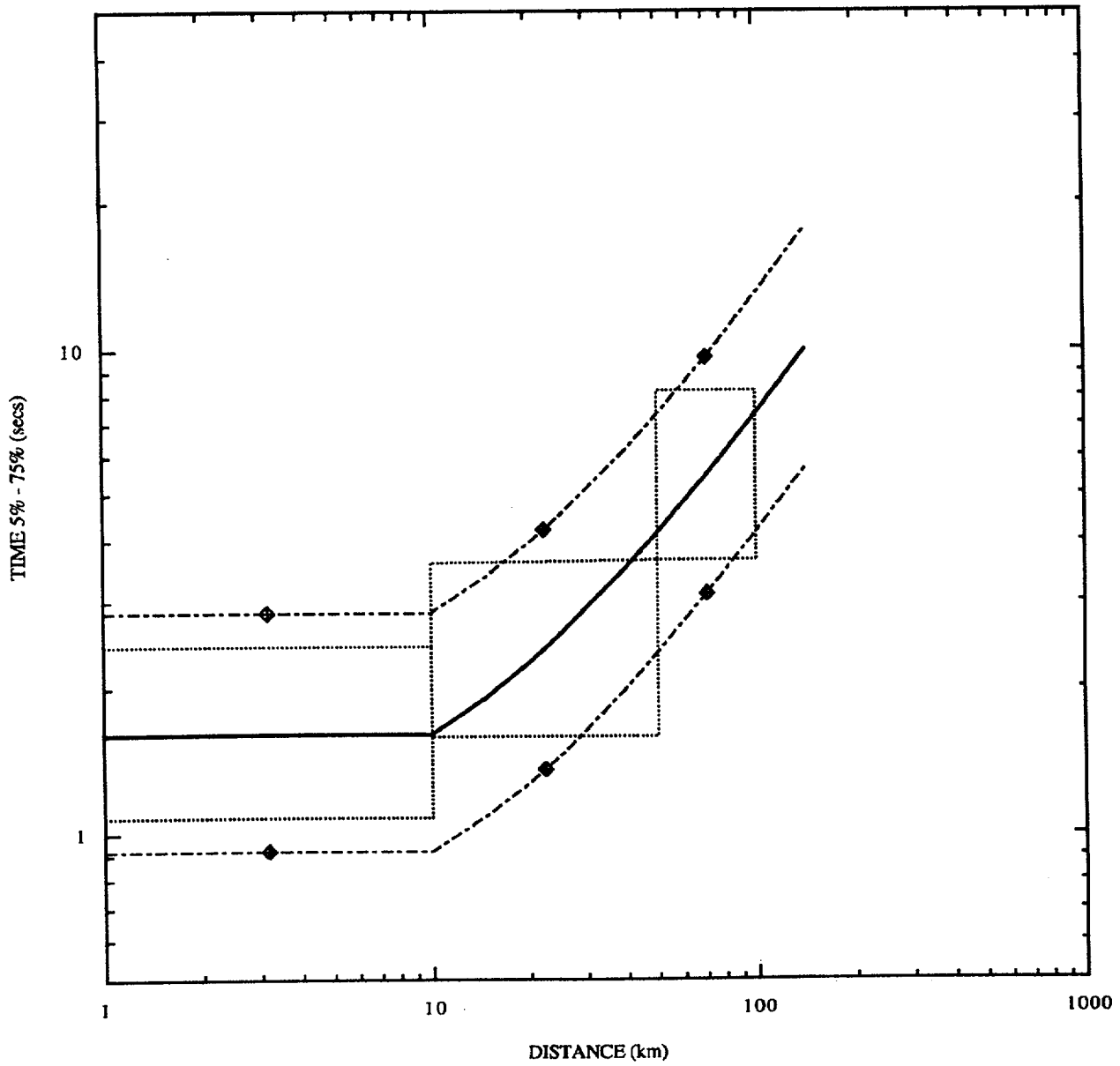


Figure 5-14A. Duration times from 5% - 75% Arias intensity, empirical WUS data for rock sites, M 5-6, horizontal motions.

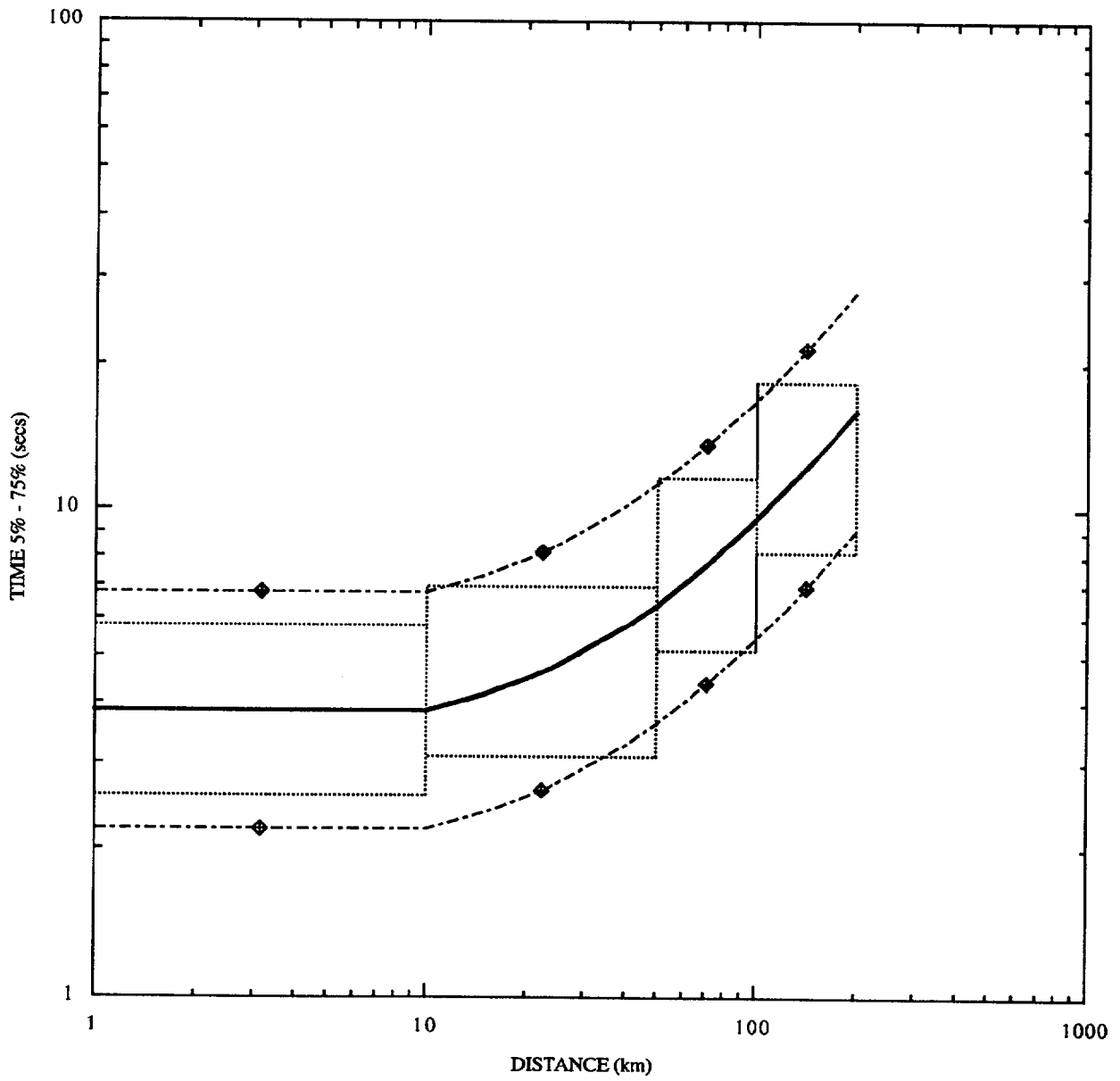


Figure 5-14B. Duration times from 5% - 75% Arias intensity, empirical WUS data for rock sites, M 6-7, horizontal motions.

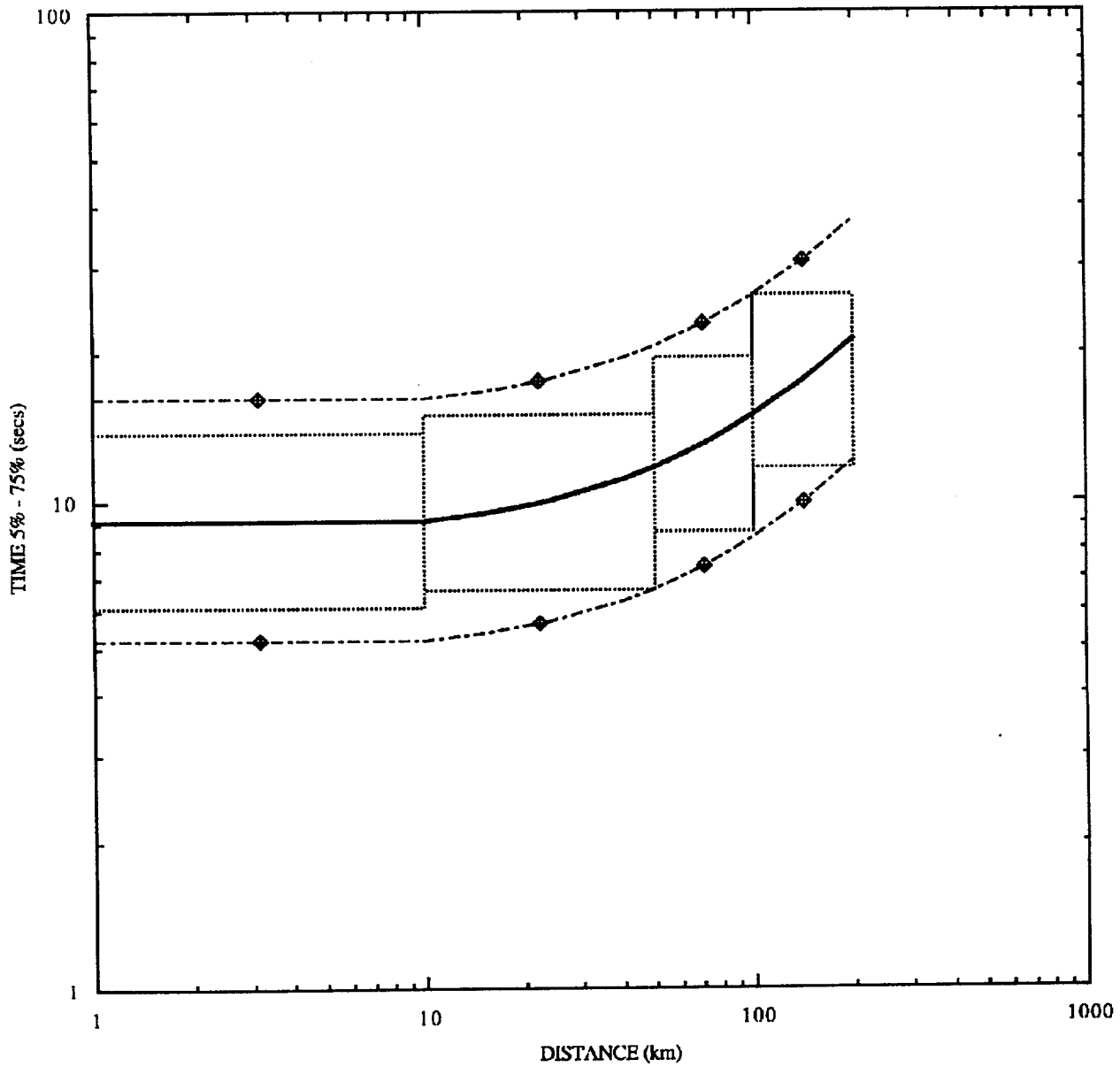


Figure 5-14C. Duration times from 5% - 75% Arias intensity, empirical WUS data for rock sites, M 7+, horizontal motions.

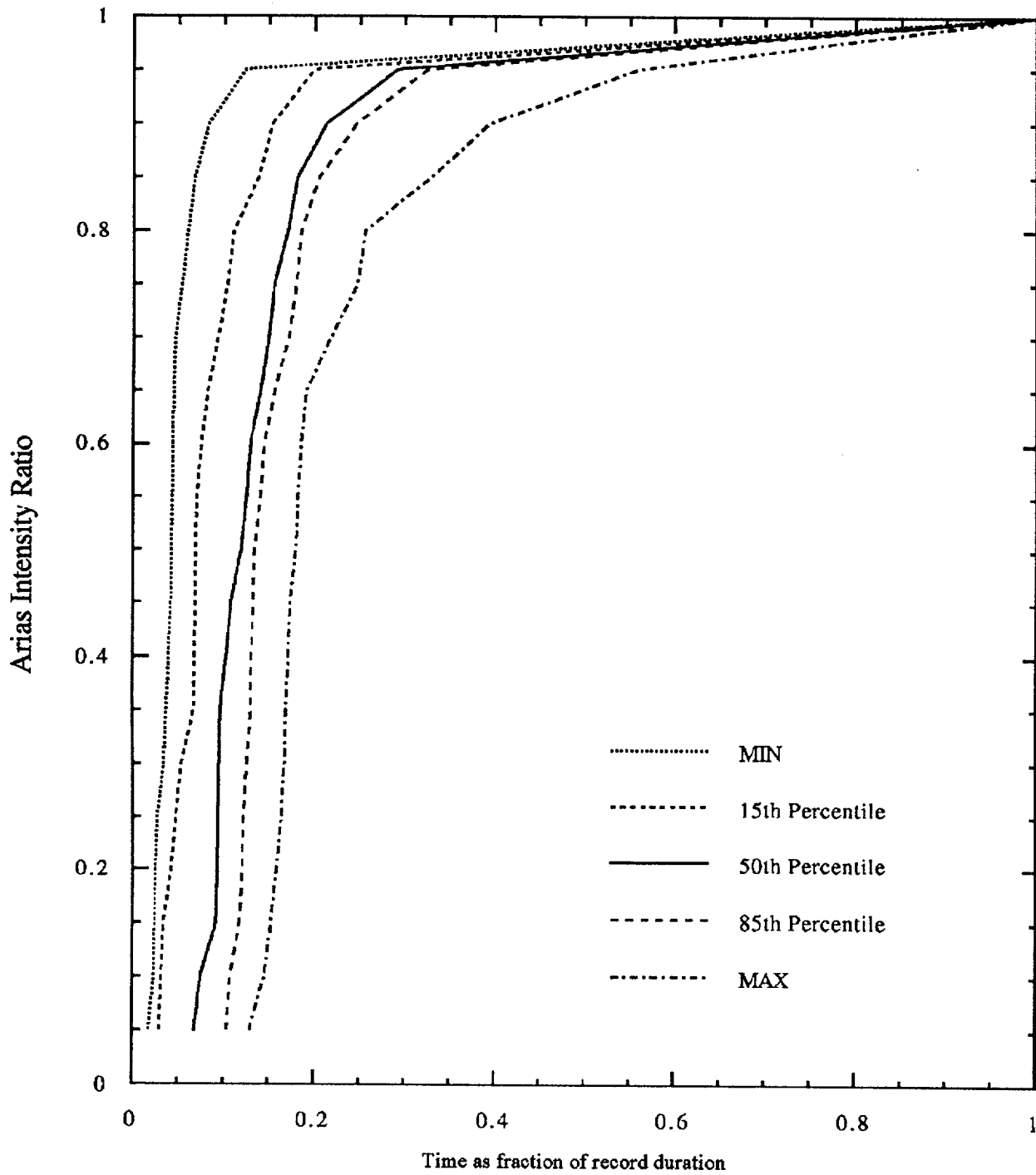


Figure 5-15A. Statistics of Arias intensity ratio vs. time scaled by record times for empirical WUS records in bin D1RM55H.

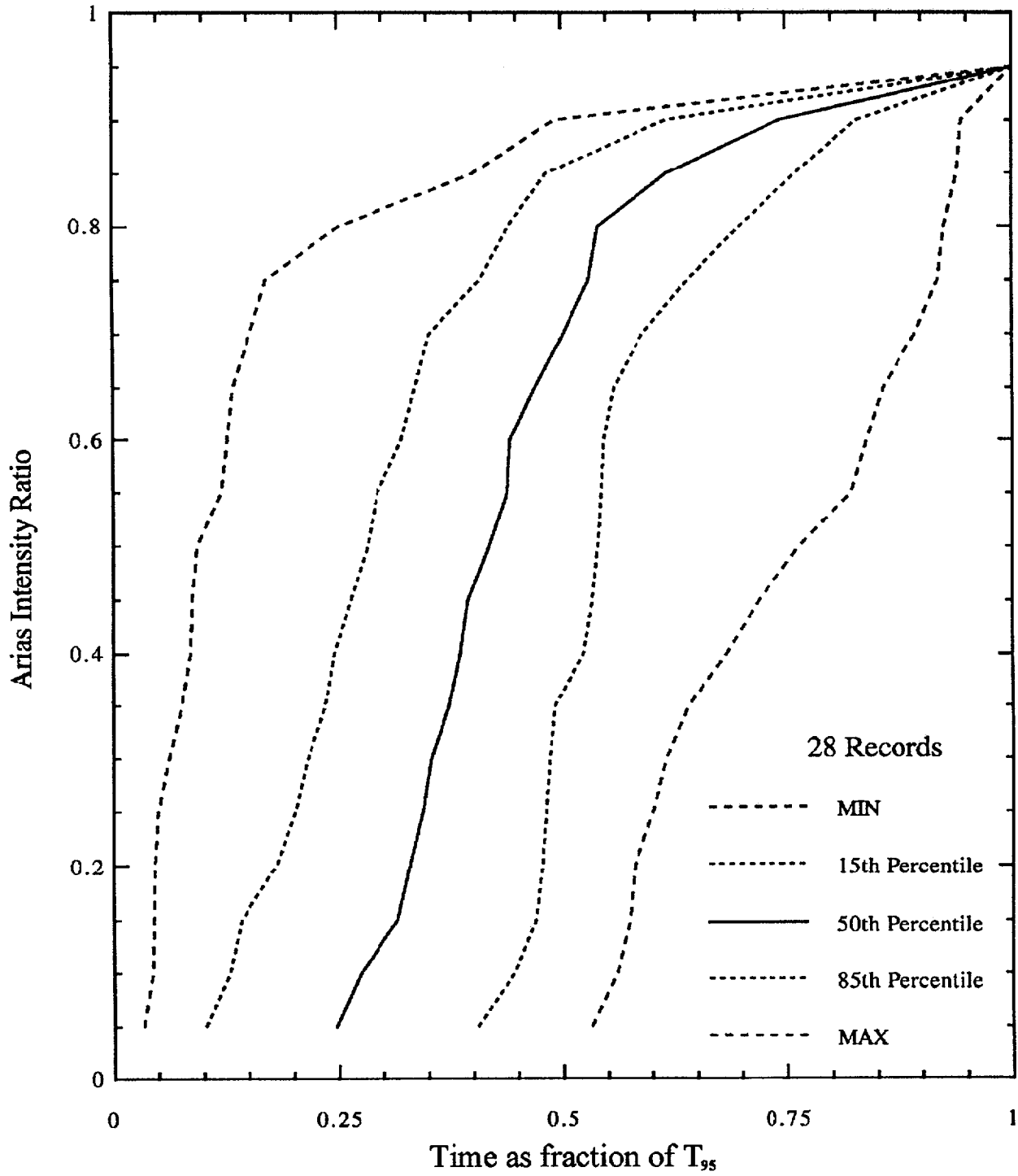


Figure 5-15B. Statistics of Arias intensity ratio vs. time scaled by Arias T_{95} for empirical WUS records in bin D1RM55H.

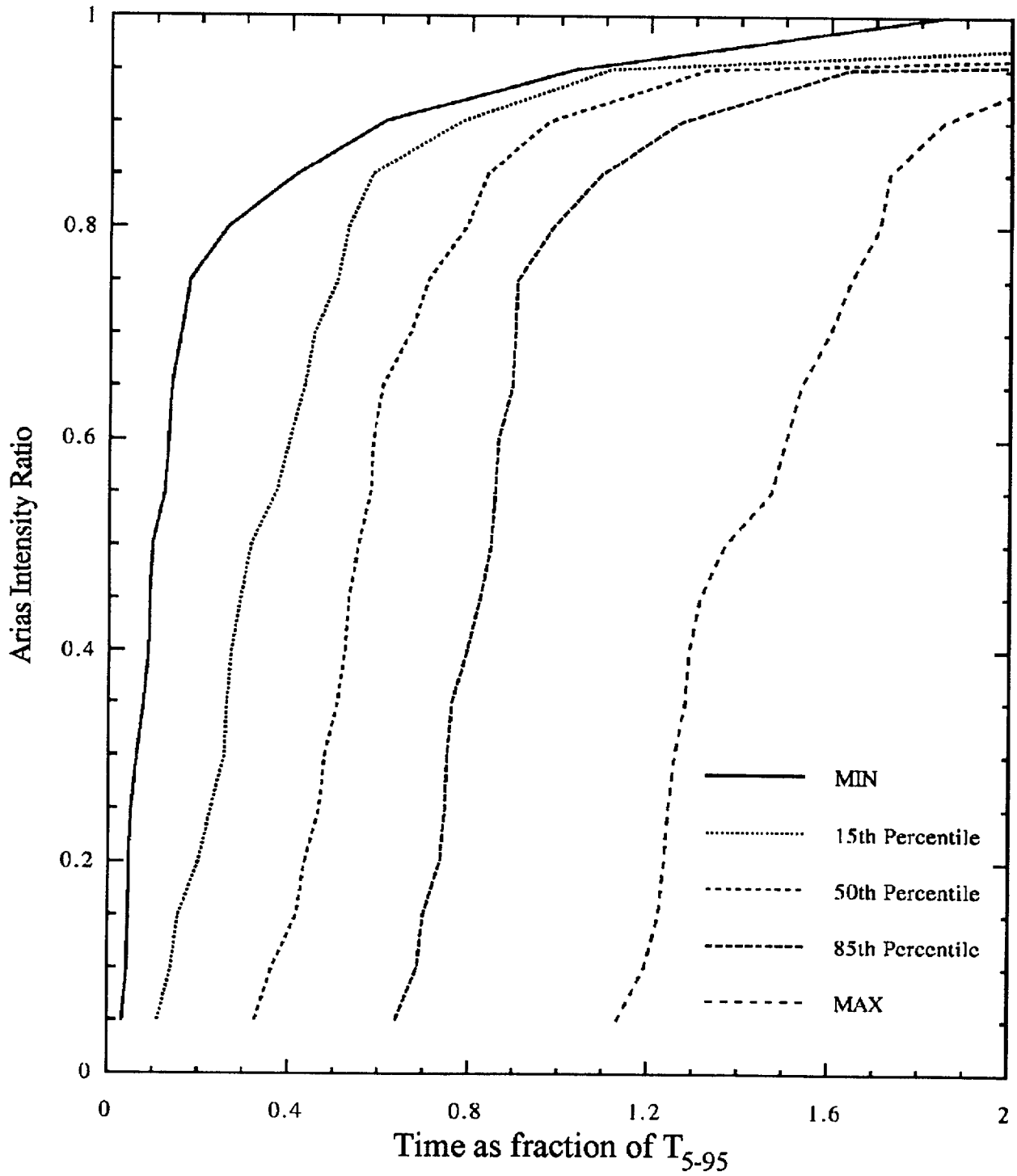


Figure 5-15C. Statistics of Arias intensity ratio vs. time scaled by Arias T_{5-95} for empirical WUS records in bin DIRM55H.

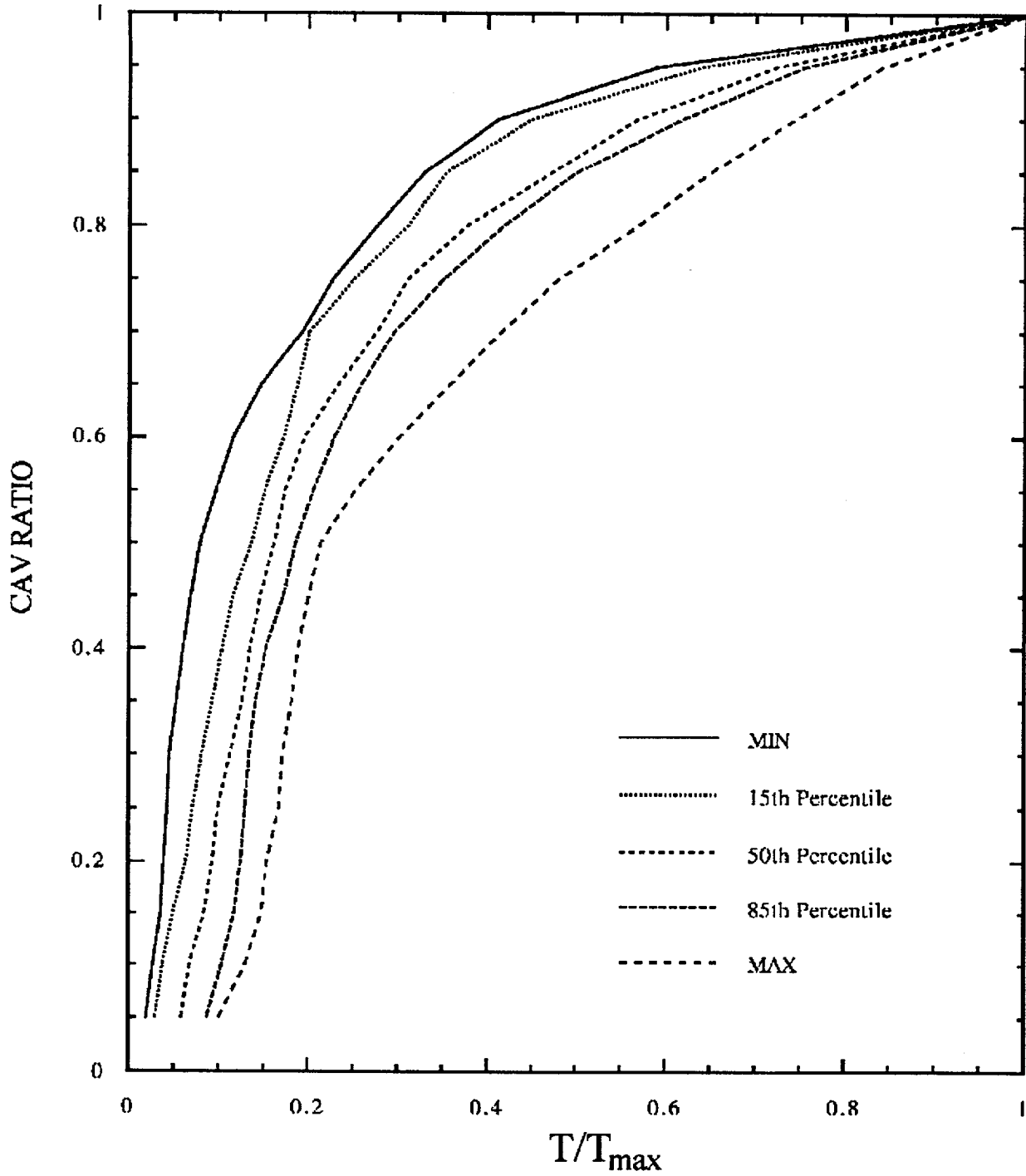


Figure 5-16A. Statistics for cumulative absolute velocity vs. time scaled by record times for empirical WUS records in bin D1RM55H.

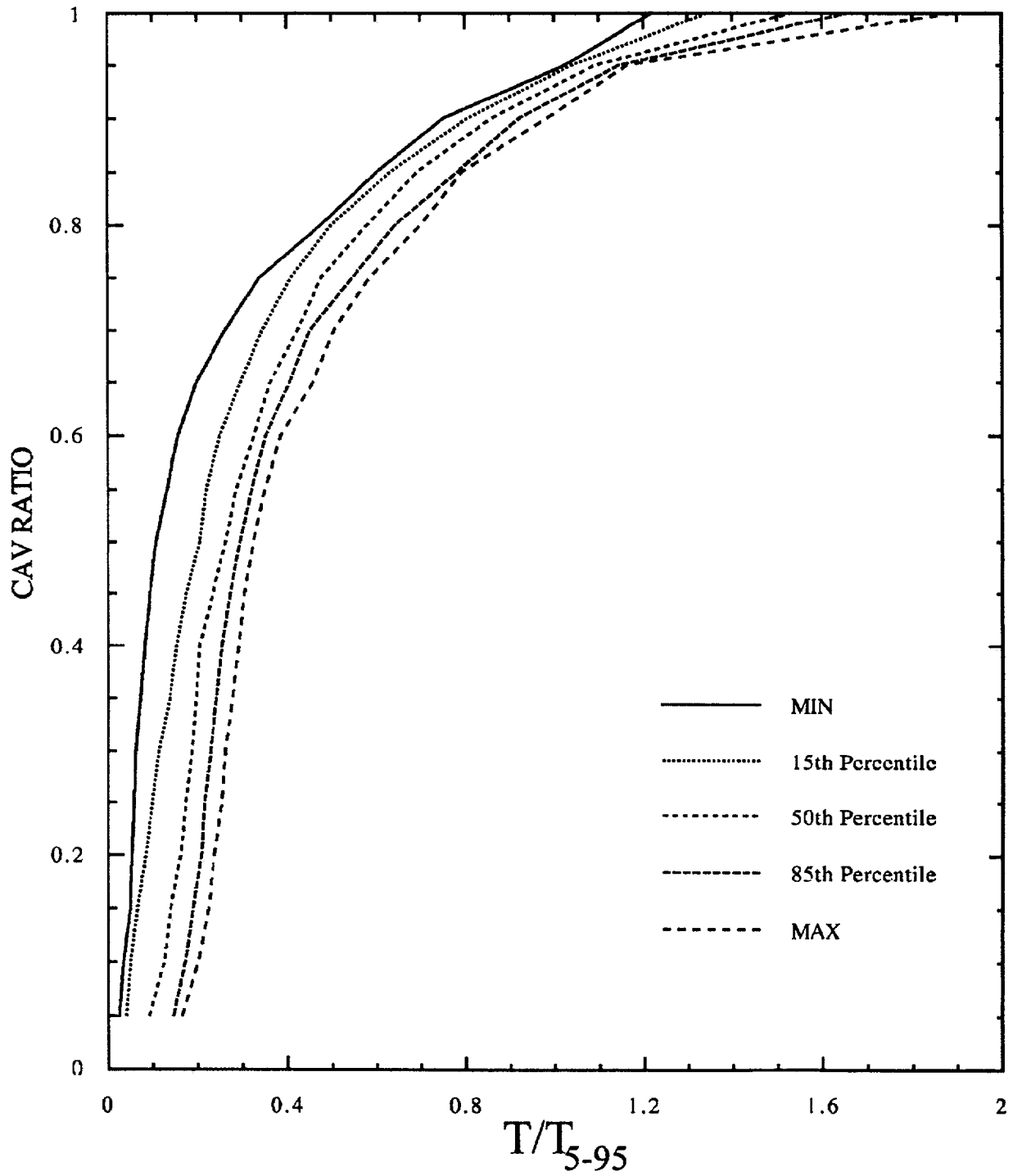


Figure 5-16B. Statistics of cumulative absolute velocity vs. time scaled by Arias T_{5-95} for empirical WUS records in bin D1RM55H.

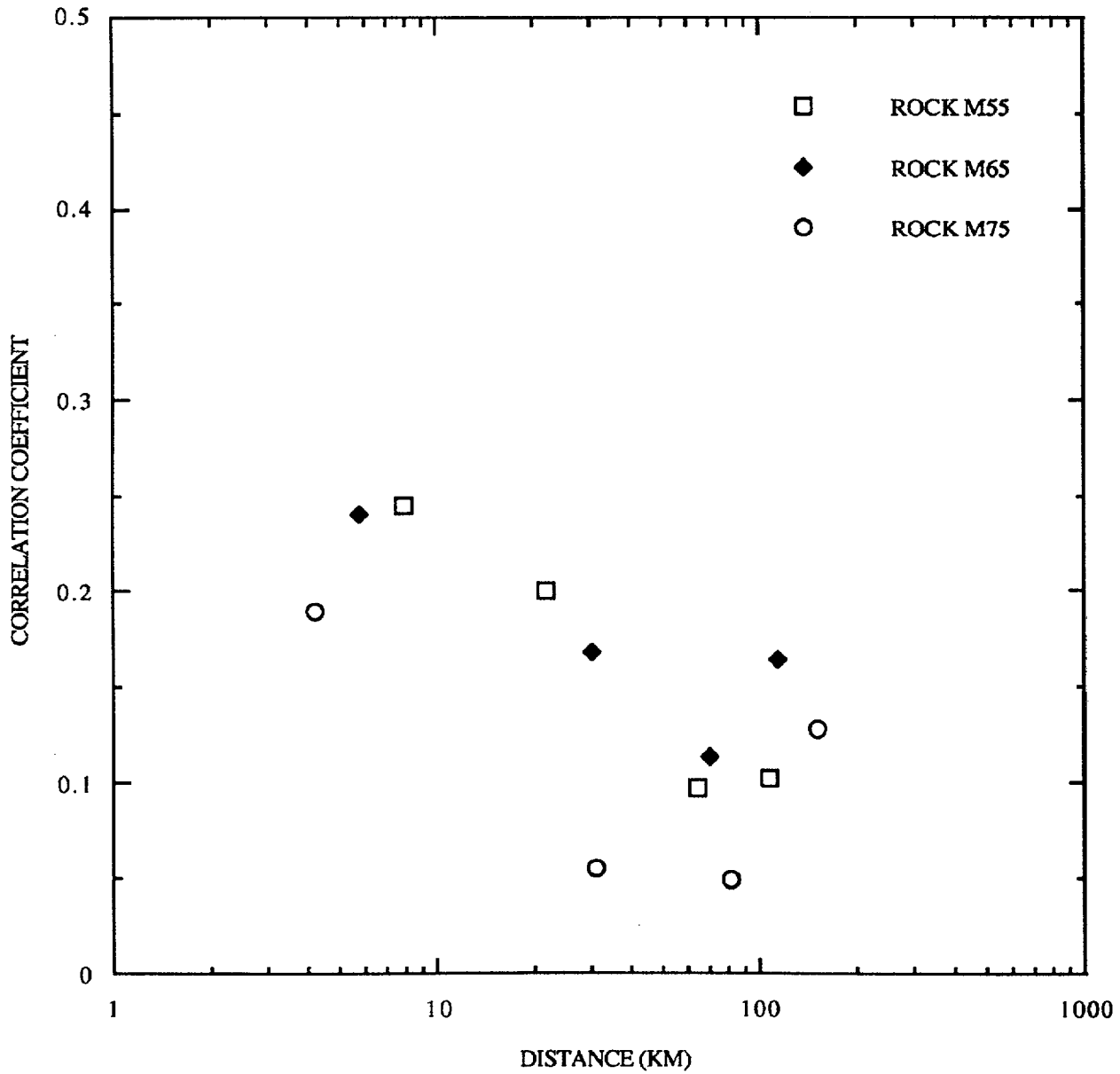


Figure 5-17A. Correlations of H1-H2 acceleration pairs, WUS rock sites.

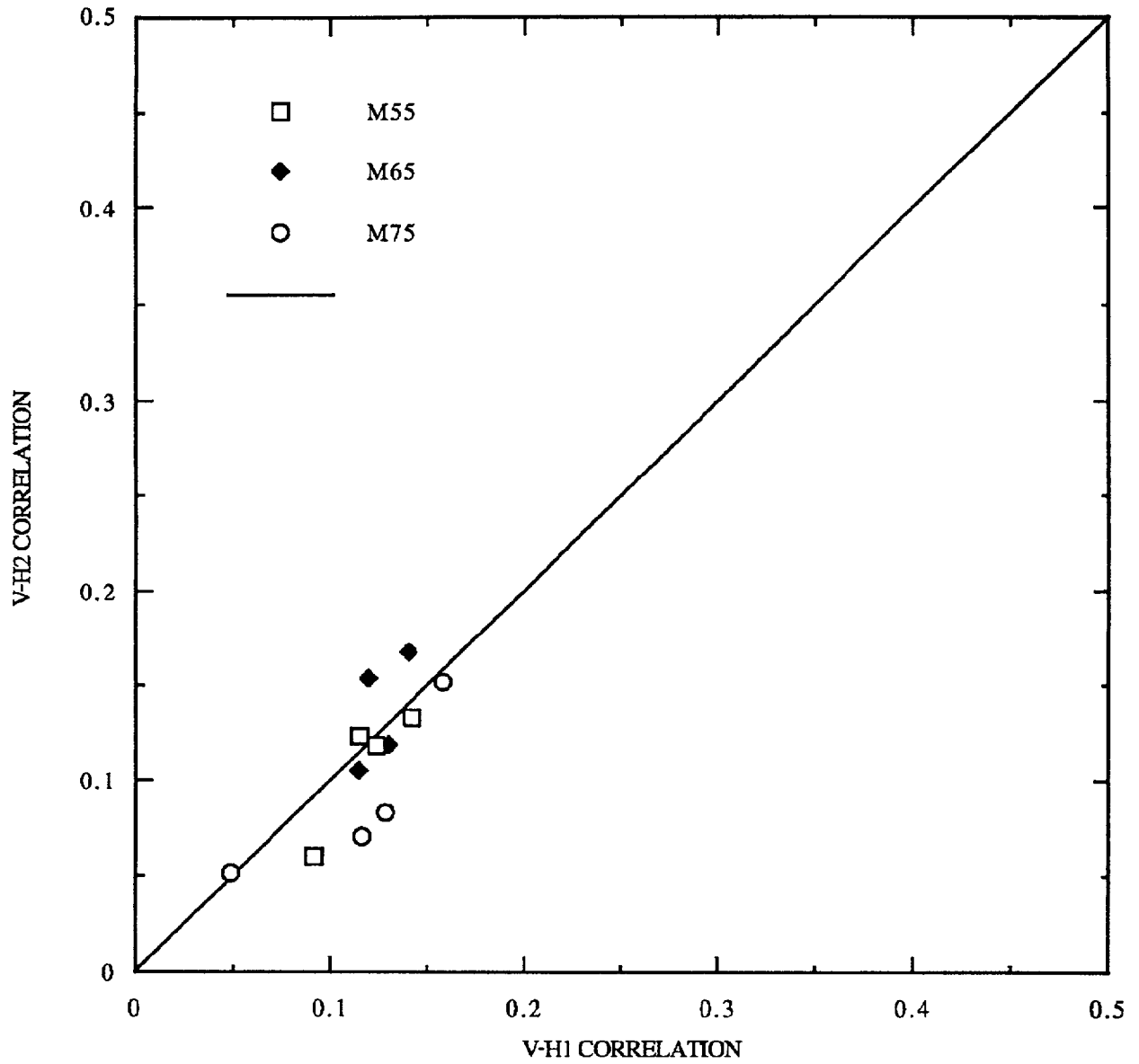


Figure 5-17B. Comparison of correlations of vertical-horizontal acceleration pairs at WUS rock sites.

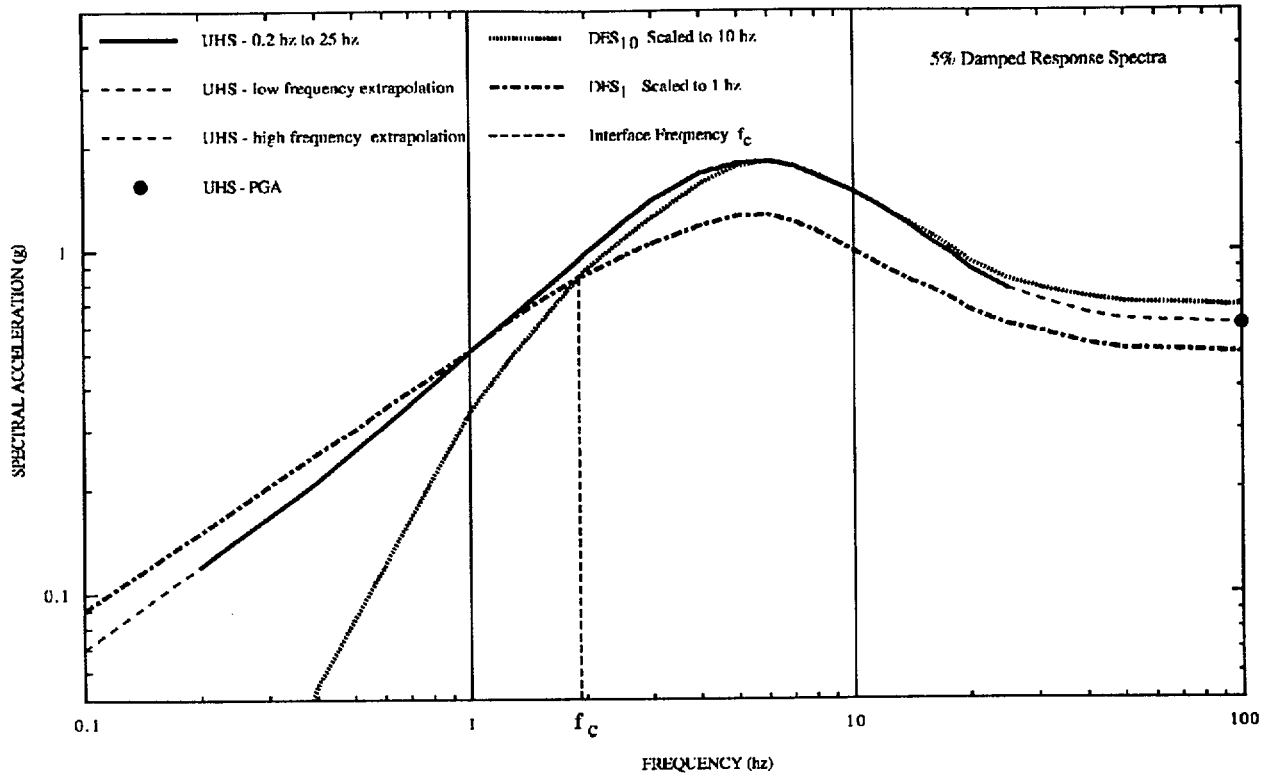


Figure 5-18A. Example of uniform hazard spectrum and scaled deaggregated spectra at low and high frequencies.

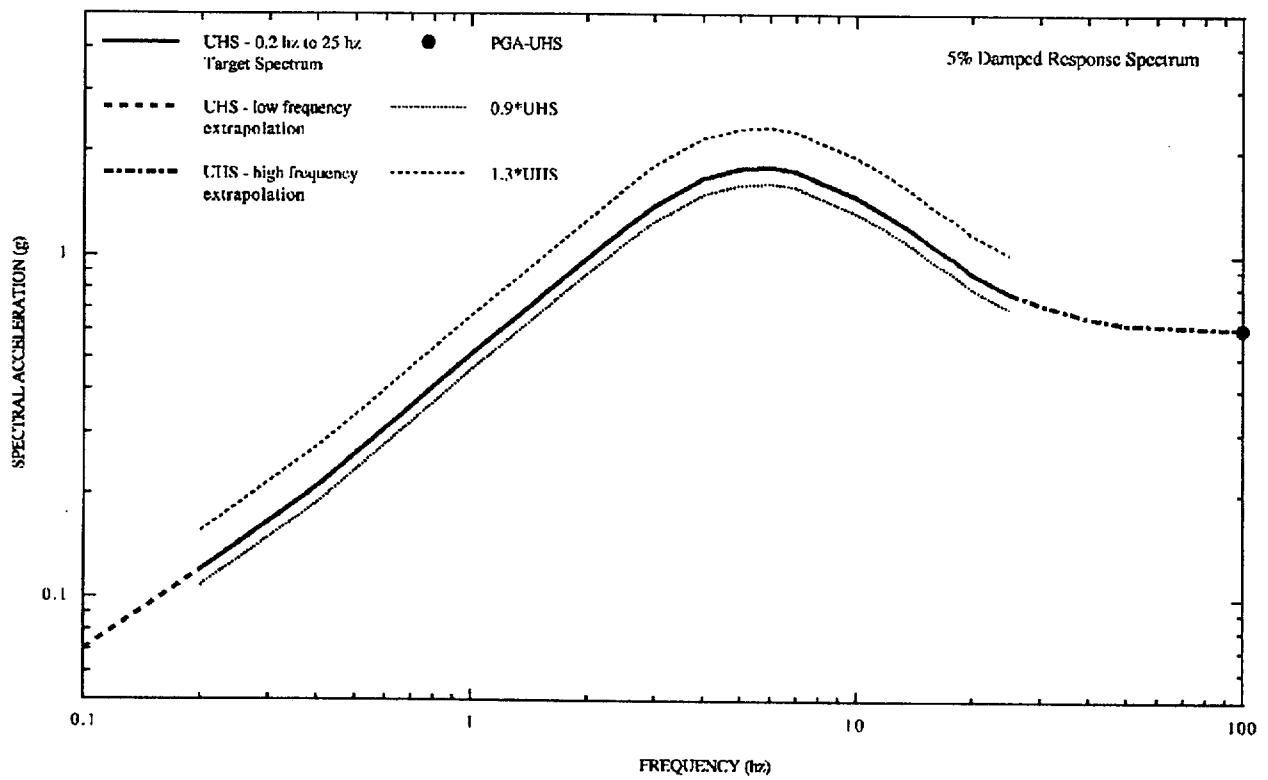


Figure 5-18B. Recommended upper- and lower-bound spectral limits to target UHS spectrum for time history designed to envelop UHS.

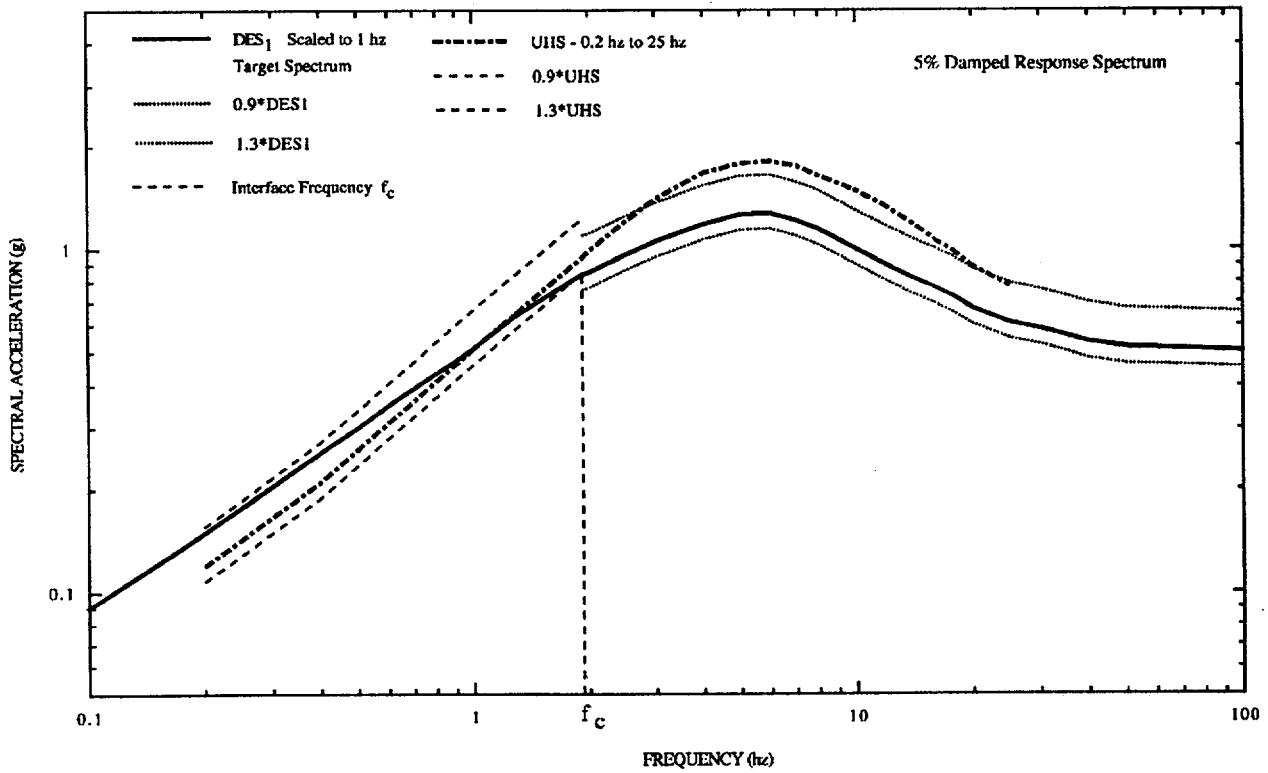


Figure 5-18C. Recommended upper- and lower-bound spectral limits to target low-frequency deaggregated spectrum.

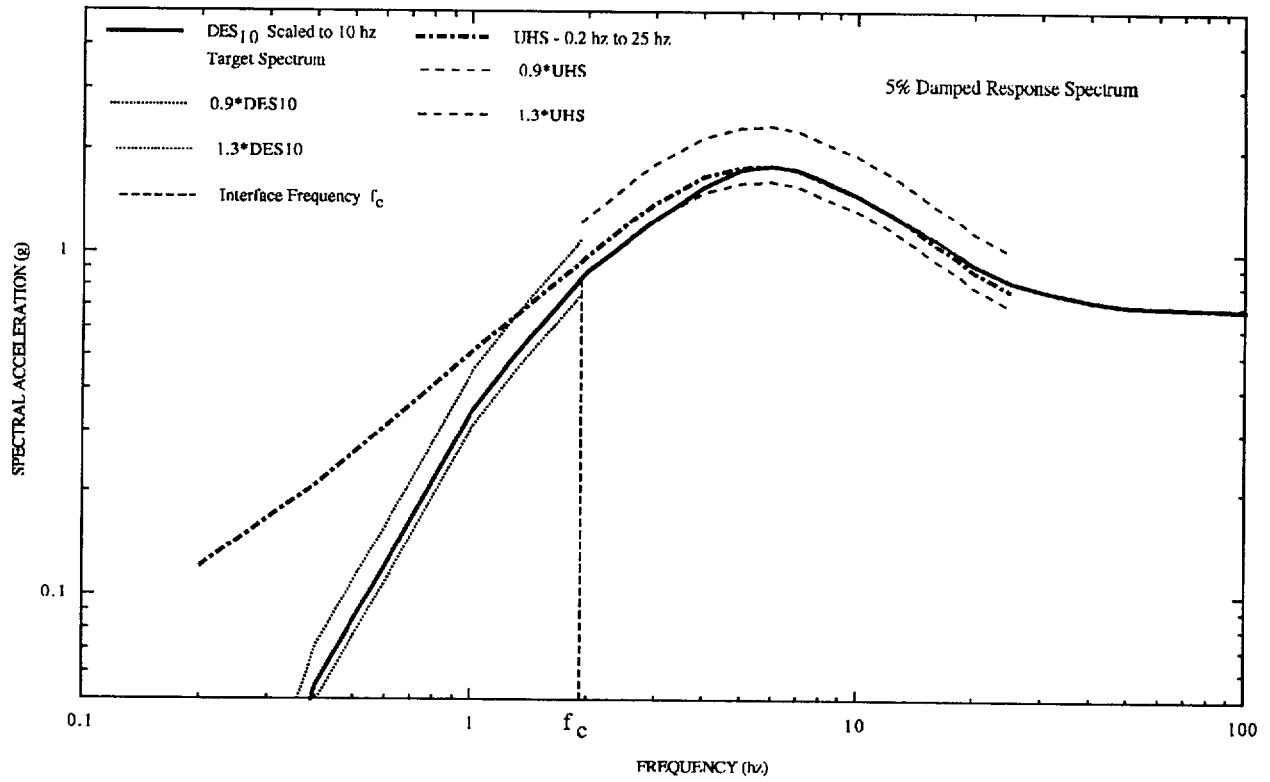


Figure 5-18D. Recommended upper- and lower-bound spectral limits to target high-frequency deaggregated spectrum.

6. PROCEDURES FOR DEVELOPING HAZARD-CONSISTENT SPECTRA ON SOIL

6.1 Approaches

Determining soil uniform hazard spectra (UHS) that are consistent with the underlying rock UHS is a challenging task. There are straightforward methods available, as described below, but they involve either performing a complete PSHA with soil attenuation equations, or extensive deaggregation of the rock hazard at multiple amplitudes and recalculation of soil hazard. For the latter approach the PSHA would not be repeated, per se, but there would be no simple, intuitive link between rock hazard results and soil hazard results. Such an intuitive link is desirable.

Available approaches to estimating soil UHS can be divided into two broad categories. First are those that integrate over multiple rock amplitudes to calculate soil hazard (probability of exceedence vs. amplitude), from which UHS on soil can be derived. Second are approaches that use the rock UHS at a given annual probability to derive a soil UHS at that same probability. Both approaches and their variants are described here, and in subsequent sections, we present examples of applications using soil data from actual sites. Table 6-1 lists these approaches, with a short description and an indication of whether the approach integrates over multiple earthquakes and multiple amplitudes. This table also indicates a label for each approach. The approaches labeled 1, 2A, 2B, and 4 are illustrated in Section 6.4 with quantitative calculations and comparisons for both eastern and western US seismic hazard conditions and multiple soil profiles. In developing these approaches we have benefitted from discussions with C.A. Cornell and P. Bazzurro, who have pursued similar work, most recently documented in Bazzurro (1998) and Bazzurro et al (1999). (Some of the notation below follows what is introduced in these references.)

Approaches Based on Integration. If we define the amplitude on soil at a certain natural frequency to be A^s , then the straightforward approach to calculate soil hazard is through a PSHA:

$$P[A^s > z] = \iint P[A^s > z | m, r] f_{m,r}(m, r) dm dr \quad (6-1)$$

which is the standard PSHA equation in which z is soil amplitude, m is magnitude and r is distance. (Equation (6-1) ignores, for simplicity, rates of occurrence on different faults and is therefore the probability of exceedence for one random earthquake. Rates of occurrence from multiple sources could be incorporated into this and subsequent equations, at the expense of more cumbersome equations.¹) We call this "Approach 4." It can lead to a defensible representation of soil hazard. The

¹The total frequency of exceedence from multiple faults can be written

$$v(A^s > z) = \sum_i v_i P_i[A^s > z]$$

where v_i is the occurrence rate on fault i and P_i is the probability in equation (6-1).

key to making this calculation defensible is to represent $P[A^s > z | m, r]$ accurately. This probability is related to the scatter observed from empirical data at soil sites when fitting an attenuation equation. The problem with this procedure is that empirical attenuation equations use observations at multiple sites, usually on similar soil conditions, whereas we are after the probability that $A^s > z$ for one specific site.

An approximation to Approach 4 can be made by recognizing that soil response can be determined from the level of input motion and the magnitude and distance of the causative earthquake. Thus we can modify equation (6-1) to the following:

$$P[A^s > z] = \iiint P[A^s > z | m, r, a] f_{M,RIA}(m, r; a) f_A(a) dm dr da \quad (6-2)$$

$$P[A^s > z] = \iiint P[AF > \frac{z}{a} | m, r, a] f_{M,RIA}(m, r; a) f_A(a) dm dr da \quad (6-3)$$

where a is the amplitude of shaking on rock, for example the spectral acceleration at the same frequency as A^s , and $f_A(a)$ is derived from the hazard curve. We call this "Approach 3." The first equation above calculates $P[A^s > z]$ from the deaggregated rock hazard, i.e. from $[a, m, r]$ sets. The second equation is equivalent except that it defines soil response by an amplification factor:

$$AF = A^s / a \quad (6-4)$$

where AF is a random variable with a distribution that can potentially be a function of m and r as well as a .

Equation (6-1) can be written slightly differently by conditioning the first factor on a , as well as m and r , and using the AF form:

$$P[A^s > z] = \iiint P[AF > \frac{z}{a} | m, r, a] f_{AIM,R}(a; m, r) f_{M,R}(m, r) dm dr da \quad (6-5)$$

This formulation recognizes AF as being dependent on m , r and a and integrates over all m and r to calculate $P[A^s > z]$. In effect it is doing the PSHA on a rock-modified-to-soil attenuation equation. Bazzurro (1998) found this method to be an accurate way to calculate soil hazard.

Approach 3 can be approximated by recognizing that soil response is governed primarily by the level of rock motion and the magnitude of the event; given these two variables, distance does not have a significant effect. Thus:

$$P[A^s > z] = \iint P[A^s > z | m, a] f_{MA}(m; a) f_A(a) dm da \quad (6-6)$$

$$P[A^s > z] = \iint P[AF > \frac{z}{a} | m, a] f_{MA}(m; a) f_A(a) dm da \quad (6-7)$$

This is a variant of Approach 3, and is labeled, "Approach 3A." For application of this method we would need only the conditional magnitude distribution for relevant amplitudes of a .

Figure 6-1 represents Approaches 4 and 3 in graphical form. Part A of the figure shows the rock PSHA curve, and part B indicates soil amplitude A^s as a function of rock amplitudes A^R , for a given magnitude earthquake and for a soil that responds non-linearly to rock motion.

For this soil, Figure 6-1 shows that scatter in rock amplitude (for a given M and a) translates to scatter in soil amplitude from aleatory uncertainties, as illustrated by the dashed distributions in Figure 6-1B. These distributions are $P[A^s > z / m, a]$ in equation 6-6. When rock variability is included, the solid distribution in Figure 6-1B results. This is $P[A^s > z / m, r]$ in equation 6-1. Often the uncertainty in soil response is smaller than for rock because the slope of soil A^s vs. rock A^R is less than unity. This effect is seen in observations: empirical attenuation equations often show less scatter for soil data than for rock data. The non-linear soil response means that the distribution of soil amplitudes will be negatively skewed relative to the rock amplitudes, as illustrated in part B. A possible resulting soil hazard curve is shown in Figure 6-1C.

The translation of rock σ (from scatter) to a soil σ (from scatter) would take place as illustrated in Figure 6-1B if soil parameters were known perfectly. Of course, they aren't: knowing rock motion, even from a specified magnitude event, does not allow us to predict soil motion perfectly even if multiple sets of dynamic soil properties are available. This is illustrated in Figure 6-2B. Part of the variability is random (aleatory), coming from random incidence angles, interference of waves, and source effects. The remainder is epistemic uncertainty, i.e. we do not know precisely the dynamic soil characteristics, particularly at high amplitude levels. This uncertainty is represented by alternative possible soil amplification curves.

These combined uncertainties will lead to a distribution of soil response that is larger (the dashed curve in Figure 6-2B). The combined distribution may have smaller or larger σ than the rock distribution, depending on the amount of soil uncertainty and the degree of non-linearity (the slope of soil vs. rock response).

The bottom graph, Figure 6-2C, shows the seismic hazard curve for the three sets of soil properties. Depending on the degree of uncertainty in soil properties and the amount of site-specific soil data available, the range in soil PSHA curves (Figure 6-2C) may be wide or narrow.

If we are concentrating on calculating soil hazard at a specific annual probability p^* , we can simplify the calculations further by focusing on a particular rock amplitude a' and associated magnitude m' . The soil amplification factor AF can be computed at a' and m' , so that:

$$AF(a, m) = AF(a', m') \quad (6-8)$$

This removes the magnitude dependence of equation (6-7), simplifying it to:

$$P[A^s > z] = \int P[AF(a', m') > \frac{z}{a} | a] f_a(a) da \quad (6-9)$$

where the notation $P[AF(a', m') > z/a | a]$ means that the distribution of AF is calculated for a' and m' , and a is used to calculate $P[AF > z/a]$. This approach is labeled “Approach 3B,” and was proposed by Bazzurro (1998).

It would of course be possible to devise an intermediate approach between 3A and 3B, where AF is made a function of either m and a . Bazzurro (1998), for example, found AF for two saturated soil sites to depend on a but not m given a . Modeling one of these dependencies would be advised if Equation (6-9) proves to be too inaccurate for practical use.

Figure 6-3 illustrates how Approach 3B works. Rock amplitude a' is determined from the rock seismic hazard curves (part A). Entering part B at rock amplitude a' gives for each of the three possible sets of soil characteristics, a distribution of soil response A^s (the solid distributions in Figure 6-3B) that reflects random aleatory variabilities. Recognizing that the soil characteristics themselves are uncertain, we combine the solid distributions in Figure 6-3B to obtain the overall (dotted) distribution of A^s given a' . This is transformed to a distribution of amplification factor AF by dividing A^s by a' . Then equation (6-9) is used to calculate the soil hazard curve (graph C). This will be most accurate at annual probabilities near p' , as that is where AF has been calibrated.

Approaches Based on UHS Scaling: Approach 3B above prompts the idea of simply scaling the rock UHS to calculate a soil UHS. If soil uncertainties are small, or if we can account for them explicitly, we can estimate the soil UHS accurately, for a given rock UHS. This would certainly be the most straightforward, intuitive approach. We label the simplest scaling “Approach 1.”

Figure 6-4 visually illustrates how this works. At a chosen annual probability p' , the corresponding rock amplitude a' is chosen. For this a' and for a central magnitude m_m (obtained from deaggregation) the distribution of soil response is obtained, accounting for soil uncertainties. (The soil distribution in Figure 6-4B corresponds to the dotted distribution in Figure 6-3B). The mean of

this distribution for frequency f is used to construct a UHS for soil (part C). Note that the mean of the distribution may be different from the value obtained with a “best estimate” set of parameters. Figure 6-4 illustrates this process for one frequency, but in its simplest form Approach 1 is applied to all frequencies simultaneously.

Consideration of Multiple Frequencies. The discussion of Approach 1 implies that a single, broadband motion representing the rock UHS will be used to drive the soil calculations. It has been recognized that a broadbanded motion may be inaccurate in many applications (e.g. USNRC, 1997) and may in fact be unconservative. As an alternative, two earthquakes can be used: one that dominates at high frequencies (10 Hz) and another that dominates at low frequencies (1 Hz). Approach 1 can be cast in terms of $A^R = a_{10}$ and $A^R = a_1$, for 10 and 1 Hz, respectively. The amplification factor AF can be defined for all frequencies as the ratio of $A^S(f) / a_{10}$ and $A^S(f) / a_1$.

Using the amplitudes of 10 Hz and 1 Hz will simplify the analysis since, where magnitude values are required, they will be available from the rock PSHA results. The resulting soil UHS can be plotted and enveloped to obtain an overall UHS for soil. If more than two frequencies are necessary on rock to define specific events whose envelope matches the UHS, then these same frequencies can (and should) be used to calculate soil UHS. The use of two frequencies in this way is labeled “Approach 2A.”

A variant of this approach recognizes that the magnitudes of earthquakes, for a given rock amplitude, may have a strong effect on non-linear soil behavior (through the duration of shaking and long period effects). Figure 6-5A shows the magnitude deaggregation at rock amplitude a' ; this distribution can be discretized into three magnitudes m_L , m_m , and m_H . Then the rock amplitude a' can be translated into soil distributions for each magnitude, Figure 6-5B. These can be weighted (using weights derived from the deaggregation) to produce an overall distribution, the mean of which becomes one value on the soil UHS (Figure 6-5C). This is labeled “Approach 2B.” The soil’s (nonlinear) response to changing magnitudes is itself nonlinear: a one-unit magnitude increase hurts soil response more (drives it more nonlinear) than a one-unit magnitude decrease helps soil response. The result is that the mean soil amplitude considering M variability may be higher than if M variability is ignored, as illustrated in Figure 6-5B.

Summary. This subsection has presented five approaches to defining UHS on soil. Subsequent sections will explore some of these approaches with specific, real soil columns to make comparisons and inferences on the best procedures to use for a proposed site. These example cases implicitly assume that site-specific shear-wave velocities are available, and that dynamic soil properties (damping and modulus) can be estimated.

6.2 Development of WUS and CEUS Attenuation Relations

Regional- and site-(soil column) specific attenuation relations are required to evaluate the suitability of various approaches for developing probabilistic soil spectra that are consistent with the probabilistic control motions (rock outcrop spectra). Soil-column-specific attenuation relations (median spectra and uncertainties) were used to generate uniform hazard spectra at the soil surface while regional-specific rock profiles were used to develop attenuation relations for outcropping rock.

The soil uniform hazard spectra were then compared to soil motions generated by Approaches 1 and 2 (involving soil response with rock input motion). This process was applied to four actual soil sites with measured properties: Savannah River, South Carolina, and California strong motion recording sites Gilroy Array No. 2, Meloland, and Rinaldi. Each soil site was assumed to be located in the CEUS and WUS (Section 6.3) necessitating the development of appropriate attenuation relations and their uncertainties.

The process of developing site and region specific attenuation relations involved exercising the point source model (Appendix D) for a suite of magnitudes and distances and then regressing on the predicted ground motions. Regional- and site-specific elements were introduced through the selection of appropriate model parameters and their uncertainties. Parametric uncertainty about the median ground motion regression (which includes regression uncertainty) was estimated through multiple ground motion estimates at each magnitude and distance based on random model parameters. Total uncertainty was then estimated by adding modeling uncertainty (Appendix D) to the parametric and regression uncertainties. This process resulted in a regression equation for median ground motions (5% damped response spectra) as a function of magnitude and distance as well as estimates of the total uncertainty, both of which are required by probabilistic seismic hazard analyses. This process has been applied to a number of Department of Energy sites as well as many other commercial projects and forms the basis for a number of CEUS attenuation relations. As a result, the process is both mature and stable, undergoing the scrutiny of widespread application to engineered structures.

6.2.1 Point Source Model Parameters

Dependent parameters for the point-source model included source depth, stress drop ($\Delta\sigma$), $Q(f)$ model (deep crustal damping), kappa (shallow crustal damping), a crustal model, and a shallow profile along with nonlinear dynamic material properties parameterized through G/G_{\max} and hysteretic damping curves. Independent parameters were magnitude and distance, which were selected to cover the appropriate range in M and R in the hazard analyses. Three magnitudes were run (M 4.5 CEUS soil only, 5.5, 6.5, and 7.5) over the distance range of 1 to 400 km (Tables 6-2 and 6-3).

For the dependent parameters, base case (mean or median) values and their uncertainties are listed in Table 6-2 for the WUS and Table 6-3 for the CEUS. Source depth was based on region specific seismicity while $Q(f)$ [$Q(f) = Q_0 f^n$] models were based on inversions using the point-source model. WUS stress drops were based on inversions of the Abrahamson and Silva, 1997 empirical attenuation relation (Silva et al., 1997) and showed a magnitude dependency (EPRI, 1993; Atkinson and Silva, 1997). CEUS stress drops (Table 6-3) were assumed to follow the same magnitude scaling as WUS. The M 5.5 stress drop was set to 160 bars to correspond to Atkinson's (1993) value, which was based on high frequency spectral levels from CEUS earthquakes. In her database of CEUS earthquakes the mean magnitude was about 5.5. Interestingly, these stress drop values resulted in an average (over magnitude) difference of about a factor of two between CEUS (117 bars, Table 6-3) and WUS (65 bars, Table 6-2), in agreement with Hanks and Johnston's (1992) analyses of intensity data.

Kappa values were based on ground motion observations at hard rock sites in the CEUS (EPRI, 1993; Silva and Darragh, 1995) and soft rock sites in the WUS. The WUS kappa value of 0.03 sec

(Table 6-2) applied to the shallow portions of the Wald and Heaton (1994) crust (Table 6-4) and was adjusted to give a total kappa value of 0.04 sec for WUS rock (EPRI, 1993; Silva and Darragh, 1995; Silva et al., 1997; Boore and Joyner, 1997). The remaining kappa, 0.01 sec, was contributed by the shallow geotechnical portion of the profile, which had a shear-wave velocity of about 250 m/sec at the surface and increased roughly linearly to 1 km/sec at a depth of 30m, where it merged with the Wald and Heaton (1994) crustal model. The shallow geotechnical profile was based on shear-wave velocity measurements at strong motion sites classified as rock (Appendixes A and C; Silva et al., 1997). The profile was considered nonlinear to a depth of 150m (shear-wave velocity of 1 km/sec, Table 6-4) based on validations with recorded motions (Silva et al., 1997) and the damping for the shallow kappa contribution was taken from the rock damping curve at low strains. The crustal model is shown in Figure 6-6 along with the generic CEUS hard rock crustal model (Table 6-5).

The kappa value for the CEUS rock site was 0.006 sec (Table 6-3), significantly lower than the 0.04 sec value for the WUS rock site and was based on recordings (Section 2; EPRI, 1993). The variability in kappa $\sigma_n = 0.30$, was assumed to be the same in WUS and CEUS and was the observed variability in kappa values at rock sites in northern California that recorded the M 6.9 1989 Loma Prieta earthquake (EPRI, 1993). While this uncertainty of 0.3 for kappa may seem low to characterize both epistemic (uncertainty in the median value) and aleatory (uncertainty about the median value) variability in a site specific kappa value (Table 2-1), the point-source modeling uncertainty (Appendix D; Silva et al., 1997) already accommodates the effects of kappa variability. This arises because a fixed kappa value of 0.03 sec was used to characterize the linear rock damping at all rock sites in the validation exercises. As a result, site specific departures of kappa from the assumed value of 0.03 sec increased model deviations from recorded motions, and this resulted in larger estimates of model uncertainty. This also applied to shallow rock profiles (to a depth of a 300m [1,000 ft]) and soil profiles, both of which were randomized in developing the attenuation relations. While it is possible that the total variability in the attenuation relations was overestimated due to this probable double counting, validations are sparse for the CEUS (and are nonexistent for deep soil sites), and are sparse for M larger than about 7.0 in the WUS. As a result, assessment and partition of appropriate variability is not an unambiguous issue, particularly in the CEUS, and the approach taken here was to follow prudent design practice and not underestimate uncertainty.

The profile variability was taken over the top 300m to be as consistent as possible with the deepest soil profile (described in the next section), (Figure 6-6). Rock profile variability was incorporated using a profile randomization scheme that was based on an analysis of variance of over 500 measured profiles and has probabilistic models appropriate for WUS rock (both hard and soft) as well as soil conditions (EPRI, 1993; Silva et al., 1997). For WUS rock the soft rock model was used. For the CEUS profile, the WUS hard rock model was used, since there are few, if any, shallow geotechnical profiles with which to develop statistics on variability. Since the rock probabilistic model is only constrained to a depth of about 30m, only the top 30m of the rock profiles were randomized. To provide some consistency with the soil randomization, which included the entire soil column (typically 300m), a 270m thick layer was randomized in velocity using a σ_n of 0.3. This standard deviation is based on an analysis of variance of rock conditions beneath soil profiles. Figure 6-7 shows median and $\pm 1\sigma$ shear-wave velocity profiles for the WUS and CEUS rock sites. The profile variability models for rock were based on an analysis of variance of all rock profiles in the database and therefore are appropriate for generic applications. Site-specific applications would likely result in a

lower variability that reflects random (aleatory) variations over the dimensions of a foundation (or to a foundation dimension extending outside the footprint) as well as uncertainty in the mean or base case profile (epistemic). To develop these non-generic or small area models, multiple closely spaced holes are necessary. Such an analysis was undertaken at a deep soil site in the CEUS, and a footprint correlation model was developed by Gabriel Toro (Silva et al., 1997). However, similar data are not currently available for rock sites. The use of a generic statistical model for both WUS and CEUS rock sites therefore may also contribute to an overestimate of the variability in the rock outcrop attenuation relations.

To accommodate potential nonlinear response in the shallow portion (top 30m) of the soft rock profile (Table 6-4, Figures 6-6 and 6-7), the modulus reduction and hysteretic damping curves shown in Figure 6-8 were used. These curves were developed by modeling the rock site motions produced by a recently developed empirical attenuation relation (Abrahamson and Silva, 1997). The generic WUS rock profile (Figure 2-2) was used in developing the G/G_{max} and hysteretic damping curves and was validated by modeling the motions recorded at about 150 soft rock sites (Silva et al., 1997).

As with the soil material strain dependencies (Section 6.2.2), the rock G/G_{max} and hysteretic damping curves were randomized based on an analysis of variance of recent laboratory dynamic test results. To develop probabilistic models, multiple test results were analyzed and yielded standard errors (natural log) of 0.1 and 0.3 for G/G_{max} and hysteretic damping respectively, these values calculated at cyclic shear strains of 0.03%. These variabilities were appropriate for within-class (cohesionless or cohesive) uncertainties and were used to generate suites of random curves that follow the shapes of the base case G/G_{max} and hysteretic curves (EPRI, 1993). In the randomization process, upper and lower bounds of about $\pm 2 \sigma$ were used to prohibit physically implausible excursions (EPRI, 1993).

To model nonlinear response at the WUS rock site as well as the soil sites, RVT equivalent-linear analyses were performed (Appendix D). This process, the use of the simple point-source model coupled to RVT equivalent-linear site response, has been validated at about 500 sites for 17 earthquakes. This validation showed that the process results in an acceptably accurate characterization of strong ground motions for engineering design (Appendix D).

6.2.2 Soil Profiles And Nonlinear Properties

Four measured shear-wave velocity profiles (soil sites) were considered to be located at both the WUS and CEUS sites (Section 6.3). The soil profiles were placed on top of the rock crustal models (Wald and Heaton, 1994 for the WUS site; Table 6-4). The profiles selected include Savannah River (generic) South Carolina; Gilroy Arroyo site no. 2 in Northern California, which recorded the 1979 M 5.7 Coyote Lake, 1984 M 6.4 Morgan Hill, and 1989 M 6.9 Loma Prieta (and aftershocks) earthquakes; Meloland in the Imperial Valley, which recorded the 1979 M 6.5 Imperial Valley earthquake; and the Rinaldi substation in Southern California, which recorded the 1994 M 6.7 Northridge earthquake. All three California sites have recorded a maximum peak acceleration of at least 0.4g, with the Rinaldi site having a maximum peak horizontal acceleration of 0.84g (166.1 cm/sec peak velocity, Appendix A).

Base case shear-wave velocity profiles for the four sites are shown in Figure 6-9. The Rinaldi site, with a depth to 1 km/sec material of about 90m is comprised of cohesionless soils and is considered

a stiff site. Meloland is a “bottomless” soft profile consisting mainly of silty clays and silty sands with clay zones having a plasticity index (PI) less than about 20 but with some medium hard (MH) clays (PI \approx 40). The soil profile was truncated at a depth of 300m. The Savannah River generic site is a firm deep CEUS site modeled to a depth of about 300m (Figure 6-9). It is comprised of silty sands and low PI clays. To sample a site with gravelly soils, Gilroy was added. It is about 200m deep and consists of sands and silty sands with some thick gravelly zones. The low velocity zone at a depth of about 100m is comprised largely of gravels (EPRI, 1993).

As with the shallow (top 300m) rock profiles, the soil profiles were randomized using the same approach but with a soil statistical model appropriate for a footprint areal extent. The resulting median and $\pm 1 \sigma$ profiles are shown in Figure 6-10 for the Savannah River site. Compared to the rock site generic variability shown in Figure 6-7, the footprint soil site variability was significantly smaller. Part of the difference was caused by deep soil sites showing significantly smaller absolute variability than rock sites (EPRI, 1993; Silva et al., 1997). The remaining difference was attributed to variability over a limited area or similar depositional environment vs. generic conditions.

In addition to velocity and layer thickness variability, depth to basement material was also varied $\pm 5\%$ to accommodate changes that may occur over a site.

For the soil sites, three different sets of G/G_{max} and hysteretic damping curves were used. At the Gilroy site, validation exercises in modeling the Coyote Lake, Morgan Hill, and Loma Prieta earthquakes at a number of soil sites showed that the EPRI (1993) curves were appropriate for Bay Area soils (Figure 6-11). Similar modeling exercises at the Rinaldi (Northridge earthquake) and Meloland (Imperial Valley earthquake) sites, as well as other soil sites in the two areas, showed that the EPRI (1993) curves for cohesionless soils and the Vucetic and Dobry (1991) curves for cohesive soils resulted in too much nonlinearity (overdamping). As a result, revised sets of curves were developed for Southern California and Imperial Valley soils by modeling exercises at a number of soil sites (Silva et al., 1997). The revised sets of region specific curves are shown in Figure 6-12 for Southern California soils and Figure 6-13 for Imperial Valley soils. For reference, G/G_{max} and hysteretic damping curve recommendations from SHAKE (1992) and Vucetic and Dobry (1991) are shown in Figures 6-14 and 6-15. The revised curves generally reflect more linear response, particularly at depth. This may result from the maximum depth over which the profiles are considered nonlinear, which was taken to be 150m based on extensive validation exercises. The SHAKE (1992) and Vucetic and Dobry (1991) curves are independent of depth and may not have been intended to be implemented over such large depth ranges.

For the Savannah River generic site, the Rinaldi curves were used, as the soils at Savannah River are more similar in stiffness and grain size to southern California soils than to either northern California soils, more gravelly soils, or Imperial Valley soils. These soils are much softer (Figure 6-9) and contain more clays.

At the soil sites with depths exceeding 150m, profile damping was fixed at the low-strain value from the corresponding damping curves. The kappa values for the rock material was kept at 0.006 sec for CEUS sites and 0.03 sec for the WUS sites. For the WUS soil sites, the total kappa values were about 0.04 sec, similar to WUS rock and consistent with observations at low strains (Silva et al.,

1997). For the CEUS soil sites, this process resulted in total kappa values for the soil sites between about 0.01 and 0.02 sec, as the low strain kappa values for the soil columns was about 0.01 sec. This suggested different spectral shapes for the same soil profile located in the WUS and CEUS, particularly at low loading levels.

6.2.3 Attenuation Relations

The functional form used in the regression analyses accommodated both a magnitude saturation, due to both a magnitude-dependent stress drop and potential nonlinear response, and a magnitude-dependent, far-field attenuation (Tables 6-2 and 6-3):

$$\ln(y) = C_1 + C_2 M + (C_6 + C_7 M) \cdot \ln(R + e^{C_4}) + C_{10} (M - 6)^2 \quad (6-10),$$

where R is taken as the closest distance to the surface projection of the rupture (Boore et al., 1997). In arriving at this functional form, about 15 variations were used in regression analyses. This particular form resulted in an optimum combination of low sigma, accommodation of significant trends with M and R , stability over oscillator frequency (smoothness in spectral shape), and simplicity. The fictitious depth term, C_4 in Equation 6-10, appeared to be strongly related to nonlinear response, being nearly constant for CEUS rock (with a value near 3) and increasing strongly with frequency for WUS rock and for all four soil profiles from a value of about 2 at 0.2 Hz to about 3.5 at 10 Hz.

To illustrate the nature of the fits to the simulations (300 for each site) as well as the distribution about the regression lines, Figures 6-16 and 6-17 show peak accelerations M 7.5 for WUS and CEUS rock conditions. In general, the model captures the trends in the simulations for both rock site conditions. The variability about the regression for the CEUS (Figure 6-17) is larger than that for the WUS (Figure 6-16) reflecting the larger variability in stress drop and source depth (Tables 6-2 and 6-3) as well as shallow profile (Figure 6-7). The increase in variability at large distance for both WUS and CEUS resulted from the effects of variability in $Q(f)$ while the large variability at close distance for the CEUS resulted from the large range in source depth. The difference in the variability between WUS and CEUS rock site conditions for peak acceleration is significant, being about 0.64 for CEUS and 0.57 for WUS.

6.2.3.1 Attenuation Relations for WUS and CEUS Rock Site Conditions

Attenuation curves of peak acceleration for M 5.5, 6.5, and 7.5 for WUS and CEUS rock site conditions predicted by the regression equations are shown in Figures 6-18 and 6-19 respectively. Magnitude saturation at close distances is apparent in the jumps in peak acceleration as M increases. CEUS peak accelerations are close to the WUS at close distances and exceed the WUS at large distance. The WUS relation is generally consistent with empirical relations for comparable site conditions while the CEUS relation shows lower peak accelerations, particularly at large magnitude, than the (Toro et al., 1997; EPRI, 1993) relation. The difference results from the assumption of decreasing stress drop with increasing magnitude (Table 6-3). Toro et al. (1997) used a constant stress drop of 120 bars, perhaps resulting in motions that are too high at large magnitudes and somewhat low at small magnitudes.

To illustrate the resulting spectra for typical conditions, Figure 6-20 shows spectral accelerations (5% damping) at a distance of 10 km for magnitudes 5.5, 6.5, and 7.5 for WUS rock site conditions. Since the regression coefficients were not smoothed (Equation 6-10), some of the crustal resonances are present in the spectra. Shallow profile resonances were smoothed in the profile randomization, and the bump in the spectra near 0.5 Hz results from a deeper crustal velocity discontinuity (Figure 6-6). For M 6.5, Figure 6-21 shows median and $\pm 1 \sigma$ estimates of the WUS rock site spectra computed from the simulations. Comparison with M 6.5 spectra computed with the attenuation relations (Figure 6-20) shows the regression equations provide good estimates of median motions. Interestingly, the logarithmic standard deviation displayed in Figure 6-21 decreased at low frequency, which is opposite the trend in most empirical regressions (Abrahamson and Shedlock, 1997). The modeling uncertainty, however, increases with decreasing frequency (Appendix D) and, when combined with the parametric uncertainty, reverses the trend exhibited in Figure 6-21. Apparently neither the model nor regressions on recorded motions capture deterministic elements in the WUS strong ground motions at low frequency. Interesting, the empirical relation of Campbell (1997), when including depth to basement material ($V_s \approx 3$ km/sec) results in a largely frequency-independent sigma. Since the sigma is computed over all site conditions, the depth dependency suggests that the effects of deep sedimentary basins may not be fully captured in the other empirical relations, which neglect such a term.

For the CEUS rock site conditions, Figures 6-22 and 6-23 show corresponding plots. The CEUS spectra show the expected shift in peak to higher frequencies (near 30 Hz) as well as the result of larger uncertainty at high frequency (Figure 6-23).

Logarithmic uncertainties for both WUS and CEUS rock site conditions are shown in Figure 6-24. This sigma reflects variation about the median regression over the magnitude and distances listed in Tables 6-2 and 6-3. It includes only the variability in motions due to parametric variability as well as goodness-of-fit using the functional form shown in Equation 6-10. The difference between CEUS and WUS sigmas is about 30% at high frequency (PGA) but comparable at low frequency. As previously mentioned, the uncertainty for CEUS rock site conditions exceeds that for WUS because of the larger variability in stress drop and source depth (see Tables 6-2 and 6-3) and in the shallow (300m) part of the crustal models.

6.2.3.2 Attenuation Relations For WUS and CEUS Soil Site Conditions

This section illustrates the attenuation of peak accelerations and the magnitude dependence of response spectra at a distance of 10 km for the four soil profiles: Gilroy, Meloland, Rinaldi, and Savannah River Generic. For each profile results for both WUS and CEUS source and path conditions are presented.

Gilroy Profile

Figures 6-25 and 6-26 show peak acceleration attenuation and response spectra at 10 km, respectively, for profile Gilroy and for WUS conditions. For CEUS conditions, Figures 6-27 and 6-28 show corresponding plots. This site has the most nonlinear set of G/G_{max} and hysteretic damping curves (Figure 6-11), and these curves, contribute to the magnitude saturation shown at high frequency particularly for CEUS rock control motions. Nonlinearity in soil response also controls the large shift in the peak spectra to lower frequency as magnitude increases. The two low velocity

zones in the Gilroy profile at depths of about 30m and 100m (Figure 6-9) contribute to high strains as loading levels increase.

Meloland Profile

Figures 6-29 through 6-32 show the attenuation of peak acceleration and the magnitude dependence of spectra at 10 km for the Meloland profile. Although the G/G_{max} and hysteretic damping curves for the Imperial Valley (Figure 6-13) are more linear than the EPRI (1993) curves (Figure 6-11), the softer profile (Figure 6-9) results in saturation effects similar to Gilroy.

For the Meloland profile and both WUS and CEUS conditions, this saturation effect is very strong near 10 Hz (Figures 6-30 and 6-32). This trend indicates that the soils saturate in the levels of motions they can transmit as strains increase to high levels. This observation is not new, since soils are known to fail (lose shear strength) at very high loading levels and simply will not propagate waves with wavelengths shorter than about four times the width of the failed zone. However, early predictions on saturation of peak acceleration have routinely been exceeded, suggesting an incorrect assumption in the dynamic nonlinear properties of soils, particularly soft soils. The revised sets of G/G_{max} and hysteretic damping curves, based on modeling high levels of motions and recent laboratory testing (Figures 6-11 to 6-14), are believed to capture nonlinear properties reasonably well, suggesting that the degrees of saturation displayed in the spectra plots for profiles Gilroy and Meloland are appropriate for these sites. These results should be confirmed with nonlinear (effective stress) analyses with properties adjusted so that the nonlinear soil models produce the same G/G_{max} and hysteretic damping curves used in the equivalent-linear analyses. This is an important issue and may have significant impacts on probabilistic seismic hazard analyses since the uncertainties typically used in attenuation relations assume a lognormal distribution, symmetric about the median in log spectral ordinates. Saturation, on the other hand, suggests a lower probability for motions above the median than below (equivalent fractile levels) with the difference increasing with cyclic shear-strains.

Rinaldi Profile

The stiffest profile is Rinaldi (Figure 6-9). This site recorded a maximum peak acceleration of 0.84g during the M 6.7 Northridge earthquake. It is located at a rupture distance of 7.1 km updip from the Northridge earthquake rupture surface. These are high motions for a soil site, and model predictions result in high motions for both WUS and CEUS conditions (Figures 6-33 to 6-36). The WUS peak accelerations (Figure 6-33) agree reasonably well with the Northridge recordings (0.63g for average horizontal component (Appendix A)). For the CEUS, the maximum predicted peak acceleration for M 7.5 exceeds 1g out to about 10 km (Figure 6-35), indicating that stiff soil profiles have the capacity to amplify high frequency ground motions in the CEUS.

Another feature of interest includes comparing the WUS and CEUS Rinaldi soil spectra (Figures 6-34 and 6-36 respectively). The WUS Rinaldi spectra have distinctly different shapes than the corresponding CEUS Rinaldi spectra, showing peak spectral amplification at considerably lower frequencies. For stiff soils, as well as soft soil at the lower loading levels (Figures 6-30 and 6-32), the soil spectra preserve a significant degree of the spectral shift between the WUS and CEUS rock motions (Figures 6-20 and 6-22). This is a significant issue and illustrates that care must be exercised in scaling WUS soil motions to CEUS conditions. For soft soils such as Meloland and for high loading conditions, e.g. M 7.5, Figures 6-30 and 6-32 suggest that this process may be acceptable,

as the spectral shapes are similar for WUS and CEUS conditions. For M 5.5 however, the same figures show significantly different spectral shapes. These observations also indicate the difficulty in developing spectral shapes for generic soil site conditions.

Savannah River Profile

The generic Savannah River profile and the Meloland profile are the two deepest profiles analyzed (300m, Figure 6-9). The Savannah River profile is considered a firm soil. It has the highest shear-wave velocity at the surface, 400m/sec, with a broad soft zone extending from the near surface to a depth of about 70m. The attenuation of peak acceleration shown in Figures 6-37 and 6-39 indicate that this site is capable of transmitting high levels of high frequency motions, due largely to the assumed G/G_{\max} and hysteretic damping curves (Figure 6-12). For M 7.5, at a distance of 10 km, the spectral shapes are similar for WUS and CEUS conditions but differ significantly for M 5.5, showing a pattern similar to Meloland.

6.2.3.3 Uncertainty Estimates For Soil Sites

The uncertainties about the regression equations over all magnitudes and distances (Table 6-2 and 6-3) are shown in Figure 6-41 for WUS conditions and Figure 6-42 for CEUS conditions with the CEUS variability generally exceeding that of the WUS. These uncertainties result from the regression analyses and reflect parametric variability as well as goodness-of-fit provided by the regression functional form (Equation 6-10). They average about 0.5 (natural log units), lower than the corresponding sigmas for rock site conditions for frequencies above about 1 to 2 Hz (Figure 6-24). This reduction is likely due to the reduced profile variability, (compare Figures 6-7 and 6-10), and the effects of nonlinear response, which dampens variability in the control or input motions (EPRI, 1993). These variabilities are used in the generic site hazard analyses. Modeling (or model) uncertainty, Appendix D, has not been added to the parametric plus regression sigma for the hazard study as it is the same for all rock and soil sites. Total uncertainty, which includes the addition of modeling uncertainty (Appendix D), would be the appropriate uncertainty to use in applications to assess probabilistic hazard at a site for design purposes.

6.3 Seismic Hazard at CEUS and WUS Example Sites

6.3.1 Introduction

The purpose of testing soil amplification calculations is to ensure that methods of accounting for uncertainty in soil properties work in a variety of seismic hazard environments. To this end, we selected sites in both the central and eastern US (CEUS) and in the western US (WUS) that have high frequencies dominated by local sources of seismicity, and low frequencies dominated by more distant sources. In the CEUS the site was Columbia, South Carolina, which is about 130 km from the Charleston seismic zone (represented here by a fault). In the WUS we selected a site in the Mojave desert located about 30 km east of the San Andreas fault. Both sites are a good test of the soil amplification methodology, which uses one or a few events (magnitudes and distances) to calculate the effects of soil amplification, in order to accurately estimate uniform hazard spectra (UHS) on soil given the UHS on rock. It should be understood that the over-riding purpose here is not to make a perfectly accurate estimate of hazard at any one site, but to create several reasonable

hazard representations that test the alternative soil amplification methodologies under extreme conditions.

The four soil profiles examined in these seismic hazard test cases have been described in previous sections. They consist of a profile (no. 1) representative of the Savannah River site, a profile (no. 2) for Gilroy, California, array station no. 2, a profile (no. 3) for the Meloland site in the Imperial Valley in California, and the profile for the Rinaldi substation site, California. In both the CEUS and WUS, attenuation curves for each region reflect the properties of crustal rocks in that region as well as the local soil properties.

6.3.2 Seismic Hazard Environment, CEUS Example Site

Columbia, South Carolina was the site chosen as the example site in the CEUS. Its seismic hazard is affected by a local source and by the Charleston earthquake zone, represented here by a fictitious fault (see Figure 6-43).

Seismicity parameters of the two earthquake sources affecting Columbia were as follows. The local source consisted of a box surrounding Columbia, 220 km on a side, with a minimum magnitude M_{\min} of 4.5 (corresponding to $m_{Lg} = 5$, which is standard for CEUS seismic hazard assessments) and a maximum magnitude M_x of 6.5. The seismicity in the local source was taken to be exponentially distributed and spatially homogeneous, with a rate $\nu_0 = 1.13E-2$ and a b-value = 0.9. Both values came from the US Geological Survey assessment of seismicity for the national hazard maps, the rate being calculated as an average over the spatially-varying rate for the southeastern US derived by the USGS.

For the fictitious Charleston fault, earthquakes between $M=6.5$ and 7.8 were considered equally likely, that is a characteristic magnitude model was used between these two magnitudes with a rate of occurrence $\nu=1.54E-3$, meaning a mean recurrence period of 650 years. This is the rate used by the USGS for the Charleston fault, although they used a single characteristic magnitude of 7.3. We assumed a range of magnitudes for this test example to make the task of choosing a single (or a few) analysis earthquakes more challenging.

Contributions to hazard at Columbia. The Columbia site was selected because different earthquakes dominate the high and low frequency seismic hazard. This is illustrated in Figures 6-44 and 6-45, which show the contributions to hazard at Columbia for 10 Hz and 1 Hz spectral acceleration (SA). The ground motion attenuation equation used for these calculations was the CEUS rock curve. For 10 Hz SA, the local background source dominated at all ground motions levels, as illustrated in Figure 6-44. For 1 Hz SA the Charleston fault was dominant for annual frequencies around 10^{-3} to 10^{-5} (see Figure 6-45), which is the level at which seismic design motions are selected. The background source dominated at very low ground motions (because the recurrence rate in the background is higher than for the Charleston fault) and at high ground motions (because background earthquakes can occur very close to Columbia, generating high levels of shaking).

Figures 6-46 through 6-49 show the deaggregation of seismic hazard by magnitude, distance, and attenuation equation epsilon for 10 Hz and 1 Hz SA, respectively. This deaggregation was performed for 0.38g SA at 10 Hz, and 0.067g SA at 1 Hz, which are the levels corresponding to 10^{-4}

hazard. For 10 Hz (Figures 6-46 and 6-47), the large contribution of small local earthquakes ($M=4.5$ to 6.5 , $R \approx 20$ km) is evident. For 1 Hz (Figures 6-48 and 6-49), the dominance of large events from the Charleston fault ($M \approx 7.5$, $R \approx 130$ km) is clear. For both natural frequencies the ϵ values contributing to hazard are predominantly positive (see the bottom frame of Figures 6-46 and 6-48), mostly from 0 to 1.5 for 10 Hz and 1.0 to 1.7 for 1 Hz. This means that ground motions *higher* than the median dominate the hazard, which is typical at 10^{-4} ground motion levels.

Choices of deaggregation events. With these contributions to seismic hazard, the choices for deaggregation seismic events for Approach 2B were made as follows. The general approach was to use three magnitudes, one at the mean deaggregation event, one higher or lower representing the non-dominant source, and a third value representing the dominant source. Weights on the magnitudes were assigned so that the non-dominant source received its appropriate weight, and weights for the mean magnitude and dominant source were assigned so the mean of the three magnitudes equaled the mean magnitude calculated from deaggregation of the hazard.

For 10 Hz this worked as follows. The mean deaggregation magnitude was 5.6, a value of $M=7.7$ was chosen to represent the contribution from the Charleston fault (this is the most likely magnitude of that contribution—see the top plot of Figure 6-46), and a value of $M=4.6$ was chosen as the mode of the contributions from local magnitudes. The $M=7.7$ value received a weight of 0.12 (obtained from the deaggregation), and the other two values received weights of 0.25 and 0.63, assigned to give the correct mean of 5.6. In summary, the three seismic events and their weights were:

$M = 4.6$, $R=8$ km, weight=0.25,
 $M = 5.6$, $R=8$ km, weight=0.63,
 $M = 7.7$, $R=130$ km, weight=0.12,

where the distances were picked from Figure 6-47 to correspond to the magnitudes being represented.

For 1 Hz the choices were different. The mean deaggregation earthquake was 7.0 and a value of 7.6 was chosen to represent the Charleston earthquakes (see the top plot of Figure 6-48). The total contribution from the Charleston fault to the 10^{-4} hazard is 0.70. A third magnitude representing local earthquakes was assigned the remaining weight of 0.3, and the value of this magnitude was selected to be 5.8, which was calculated so that the mean magnitude of the distribution (5.8) was preserved. To summarize,

$M = 5.7$, $R=20$ km, weight=0.3,
 $M = 7.0$, $R=100$ km, weight=0.0,
 $M = 7.6$, $R=130$ km, weight=0.7.

This then represents the case of a bi-modal magnitude distribution where the mean magnitude has a low probability of contributing to exceedences of the 10^{-4} UHS.

For both of these derivations the single "design earthquake" was designated to be the central value, for use in Approach 2A.

6.3.3 Calculated spectra, CEUS

Rock motions. The seismic hazard calculations led to uniform hazard spectra (UHS) for rock conditions, for the Columbia site. In addition, the six deaggregation seismic events were used to calculate spectra. In this calculation the M and R value of each 10 Hz seismic event was used with the CEUS rock attenuation equation to calculate a spectrum; this spectrum was then scaled to the 10^{-4} UHS value at 10 Hz (0.38g) to create 3 deaggregation event spectra. This process was repeated for 1 Hz, except that the spectra were scaled to the 10^{-4} UHS value at 1 Hz (0.067g). This process created 6 spectra, and these are plotted in Figure 6-50 along with the UHS. This plot illustrates the range of spectral shapes used in the deaggregation events.

Soil motions. To calculate soil UHS, four alternative representations of the residual distribution for the four soil attenuation equations were investigated, as follows:

- Constant sigma, no truncation of residual distribution,
- Variable sigma, no truncation of residual distribution,
- Variable sigma, truncation of residual distribution at 1σ ,
- Variable sigma, truncation of residual distribution at $1.5 \times$ median.

The 1st alternative above is a standard assumption, particular for the CEUS. The 2nd alternative recognizes that the scatter around median predicted values of ground motion decreases with increasing amplitude, reflecting perhaps more homogeneous, repetitive characteristics of motion for large magnitude earthquakes. A variable sigma has been calculated for rock conditions in California from empirical data (Abrahamson and Silva, 1997; Campbell, 1997; Idriss, 1993; Sadigh et al, 1997) and the variation of sigma has generally been dependent only on magnitude. (Campbell, 1997, reports one equation where sigma varies with peak ground acceleration.) The 3rd and 4th alternatives recognize that the amplitudes of motion on soil will saturate because of non-linear response, thereby creating a ceiling on the soil amplitudes that can occur, even for large input rock motions. These last two alternatives investigate the effects on hazard of recognizing this saturation of soil response.

The values of sigma calculated for the four soil profiles (Savannah, Gilroy, Meloland and Rinaldi) are shown in Figures 6-51 through 6-54. Separate plots are shown for the soil profiles in the CEUS (top of each figure) and WUS (bottom of each figure). The standard deviation was calculated as a function of M and R , and curves are shown for six values of M and R as well as for a constant sigma (the first assumption listed above). Note that these standard deviations represent parametric variability and goodness-of-fit errors only, not modeling uncertainty.

The choice of constant or variable σ in the residual distribution does not make a large difference in the UHS for the CEUS rock site. This is illustrated in Figure 6-55. Rock motions remain largely linear, so there was no justification for truncation of the residual distribution. As a result, further comparisons with rock UHS are made with the variable σ spectrum.

The four alternatives for the soil residual distribution were used to calculate UHS for the Columbia site. These are shown in Figures 6-56 through 6-59, along with the rock UHS for comparison. The general observation from these figures is that the variable sigma UHS (alternative 2) indicates UHS similar to the constant sigma alternative (no. 1). The largest decrease in the UHS occurs when truncation is added (alternatives 3 and 4). Figures 6-56 through 6-59 show that truncating the residual distribution of soil response really limits the large amplitudes that can occur and reduces the calculated UHS.

6.3.4 Seismic Hazard Environment, WUS Example Site

A site in the Mojave desert of California was chosen as the example site for the WUS. This site, the nearby faults, and background seismicity points are illustrated in Figure 6-60.

Seismicity parameters for the faults and background points were selected following the USGS/CDMG interpretation for California. In this interpretation, major earthquakes ($M > 6.5$) are ascribed to faults and lower-level seismicity is ascribed to background points. The rate of activity of these background points, spaced at 0.1° longitude and latitude, is calculated based on a smoothed interpretation of historical seismicity. An exponential magnitude distribution with a $b=0.9$ is assigned to these points.

The seismicity model for the faults was taken to be that used by the USGS/CDMG in deriving seismic hazard maps for California. That is, each fault is assumed to produce a single characteristic magnitude with a specified annual frequency of occurrence. The characteristic magnitudes and associated frequencies were taken from the USGS/CDMG work.

Contributions to hazard at Mojave site. The Mojave site was selected because different sources of earthquakes dominate different natural frequency ranges of the ground motion spectrum. Figures 6-61 and 6-62 show the contribution of background sources and faults to the seismic hazard on rock at 10 Hz and 1 Hz, respectively. For 10 Hz the background sources dominate the hazard; for 1 Hz the San Andreas fault gives the largest contribution to hazard.

Figures 6-63 through 6-66 show the deaggregation of seismic hazard by magnitude, distance, and attenuation equation epsilon for 10 Hz and 1 Hz SA. This deaggregation was performed at 1.92g SA for 10 Hz and at 0.65g SA for 1 Hz, which are the levels corresponding to 10^{-4} hazard. For 10 Hz (Figures 6-63 and 6-64), the large contribution of the small background earthquakes ($M=5$ to 6.5, $R \sim 20$ km) is evident. For 1 Hz (Figures 6-65 and 6-66), the large events on distant faults produced most of the hazard.

Choices of deaggregation events. With the contributions to hazard shown in Figures 6-63 through 6-66, choices for the deaggregation seismic events were made in a manner identical to that for the CEUS. For 10 Hz the mean deaggregation magnitude was 6.1, and the resulting three seismic events and weights were as follows:

$M = 5.1, R=10$ km, weight=0.05,
 $M = 6.1, R=14$ km, weight=0.90,

$M = 7.8, R = 40 \text{ km}, \text{weight} = 0.05,$

where the distances were picked from Figure 6-64 to correspond to the magnitudes being represented.

For 1 Hz the choices for the three deaggregation seismic events were:

$M = 5.4, R = 10 \text{ km}, \text{weight} = 0.15,$

$M = 6.7, R = 18 \text{ km}, \text{weight} = 0.67,$

$M = 7.8, R = 30 \text{ km}, \text{weight} = 0.18.$

For both of these derivations the single "design earthquake" was designated to be the central value.

6.3.5 Calculated Spectra, WUS

Rock motions. The seismic hazard at the Mojave site led to UHS for rock conditions, and in addition six deaggregation seismic events were used to calculate spectra. Following the same procedure as for the Columbia site, the deaggregation spectra were scaled to the 10^{-4} UHS amplitude at 10 Hz and 1 Hz, as appropriate. These six spectra are shown in Figure 6-67, along with the 10^{-4} UHS spectrum.

The constant σ and variable σ attenuation residual distributions were examined for the Mojave site, as they were for the Columbia site. Again, little difference between the two assumptions was calculated, as shown in Figure 6-68, except between frequencies of 5 to 20 Hz, where the variable σ spectrum is up to 20% below the constant σ spectrum. The variable σ assumption was used for comparison purposes in the plots with soil UHS.

Soil motions. For soil hazard calculations, four soil attenuation equations were investigated, and for each, four alternatives on the residual distribution were examined (these are the same four alternatives used for CEUS soil calculations):

- Constant sigma, no truncation of residual distribution,
- Variable sigma, no truncation of residual distribution,
- Variable sigma, truncation of residual distribution at 1 sigma,
- Variable sigma, truncation of residual distribution at 1.5 x median.

This resulted in 16 different soil characteristics (four soils times four residual distribution alternatives). The 10^{-4} UHS for these 16 different characteristics are shown in Figures 6-69 through 6-72. As for the CEUS soils, the largest change in UHS occurs when truncation of the residual distribution is included.

6.4 Evaluation of Procedures to Develop Site-specific Soil Hazard Spectra

Section 6.1 presented a number of approaches to estimating site-specific soil spectra that are consistent with a specified hazard level and that accommodate uncertainties in soil properties. In

this section, comparisons are made among several of these approaches, and site-specific soil UHS are computed for the four soil profiles located in the WUS and CEUS (Section 6.3). The site-specific soil UHS presented in Section 6.3 reflect the desired hazard level with which to evaluate the various degrees of approximations using rock outcrop UHS and site response analyses. However, an issue exists in the soil UHS calculated with Approach 4 involving long return periods where the hazard may result from motions that significantly exceed the median ground shaking during earthquakes contributing to the hazard (see the epsilon distributions in Figures 6-46, 6-48, 6-63, and 6-65). Under these conditions the site-specific UHS may overestimate the hazard at high frequency, as the residual dispersion does not reflect the soils limited capacity to transmit high levels of motion (i.e. its non-linearity). This issue is discussed in the next Section.

6.4.1 Site-specific Soil UHS

The site-specific UHS were considered to represent “truth” in the context of the analyses of Section 6.1, as these spectra consist of amplitudes computed for the same probability of exceedence across structural frequency. However, as previously mentioned in Section 6.2, at high strains soil profiles tend to saturate, transmitting proportionally less high-frequency motion as loading levels increase. While this is reflected in the convolution analyses used to develop both the site-specific soil motions and the soil attenuation relations, the residual dispersion computed in a conventional (homoscedastic) regression analysis is a combination over all event (causative) conditions (all magnitudes and distances). As a consequence, for long return periods, much of the contribution to the soil UHS results from motions that significantly exceed median estimates for the magnitudes and distances dominating the hazard. These contributions are reflected in the deaggregation ϵ values (McGuire, 1995). This process can conceivably result in soil motions that imply control motions sufficiently high enough to fail the soil column. This apparent paradox, alluded to in Section 6.3, suggests that in the context of probabilistic seismic hazard analyses involving nonlinear site response, a magnitude- and distance-independent residual distribution may be inappropriate and can result in overly conservative soil motions. The “truth” or benchmark site-specific hazard level should then accommodate the appropriate (site-specific) amplitude dependencies in the residual dispersion as well as a distribution that accommodates negative skewness as depicted in Figure 6-2. Ongoing analyses of variance are intended to address this issue. These consist of developing an appropriate distribution for the residual dispersion about the regression as well as including potential amplitude or magnitude and distance dependencies in the standard error. Incorporating a residual dispersion in the development of the UHS that reflects an appropriate distribution of limiting values (perhaps a type II extreme value model) as well as conditional dependencies in the context of nonlinear response would provide a more appropriate benchmark or “truth” with which to evaluate the various approaches to developing hazard consistent soil spectra. While our current benchmark is limited in this respect because it uses a standard model of residual dispersion, it is consistent with current practice in the CEUS. WUS attenuation models do typically include a magnitude dependency in their standard errors (Abrahamson and Shedlock, 1997) resulting in a large decrease as magnitude increases for $M \geq 6.5$. However, the high frequency motions (≥ 5 Hz) are affected most by nonlinear saturation because of the contribution of low-magnitude ($M < 6.5$) close-in earthquakes. The magnitude dependency currently incorporated in WUS attenuation relations is not likely to resolve this issue, particularly since it is site independent, being applied at both rock and soil sites. As a result, we compare site-specific soil UHS with soil spectra computed using rock outcrop UHS and various approaches to conventional site

response analyses for a variety of profiles as well as different hazard environments. These comparisons provide valuable insights into potential degrees of conservatism implicit in soil site UHS computed using standard models of residual dispersion. These analyses will indicate the strain levels (degree of nonlinearity) that may require more sophisticated dispersion models.

6.4.2 Approaches To Developing Hazard-Consistent Site-specific Soil Motions Incorporating Profile Uncertainties

The conventional approach to developing site-specific soil motions involves convolutional analysis, either equivalent-linear or fully nonlinear, using rock outcrop control motions at the soil/rock transition zone. For “bottomless” profiles the “rock” control motions may be input at a sufficiently deep location such that soil amplification extends to the lowest frequency of interest, generally about 0.5 Hz. In the convolutional analyses, uncertainty in dynamic material properties is generally accommodated through parametric variations, either deterministically with upper-, mid-, and lower-range moduli or through a Monte Carlo approach using randomly generated properties with statistically based distributions. Uncertainties in soil properties and in model deficiencies (in the convolutional formulation) are accommodated by either smoothly enveloping the deterministic variations or selecting a fractile level, generally the mean, for the Monte Carlo approach. Both of these procedures appear to result in conservative spectral estimates since site variability is already accommodated in the variability associated with the attenuation relations used in developing the control (rock) motions. The approach using randomized material properties is preferred since the conservatism is quantified, provided the parameter distributions reflect a realistic assessment of how well the base case profile and nonlinear properties are known (epistemic uncertainty) and the variability over the site or footprint (aleatory uncertainty). A motivation for using the more conservative mean rather than median estimates, which acknowledges double counting site variability, is to accommodate a degree of model uncertainty in the convolutional formulation. Since this component of model uncertainty is currently unquantified, it is not possible to add it explicitly. It is, however, thought to be relatively small, based on validation exercises of the entire model (source, path and site, Appendix D). As a result, the possible double counting of site variability may be largely offset by neglecting the deficiencies in the convolutional formulation. For attenuation relations based solely on the validated stochastic point- or finite-source models (Appendix D; Silva et al., 1997) the inclusion of model uncertainty, accommodates the site model deficiencies for the vertically propagating shear-wave model using the equivalent-linear approximation.

The various approaches to developing hazard-consistent site-specific soil spectra include the following, in increasing order of accuracy (these approaches were described and illustrated in Section 6.1):

Approach 1: rock UHS used as control motions,

Approach 2A: develop transfer function for 1 Hz and 10 Hz design earthquakes, using a single magnitude for each frequency,

Approach 2B: develop transfer functions for 1 Hz and 10 Hz design earthquakes accommodating magnitude distributions,

Approach 3: approximations to UHS integrations (see Section 6.1 and Appendix J),

Approach 4: UHS computed using site-specific soil attenuation relations.

Approaches 1, 2A, 2B, and 4 are compared in the following sections, while Appendix J describes an evaluation of Approach 3 using different soil profiles and hazard environment. Approach 1 involves driving the soil column with the broad rock UHS spectrum and may result in unconservative high frequency motions, particularly in the context of equivalent-linear site response analyses. Additionally, the appropriate magnitude and time history duration are ambiguous using Approach 1 for hazard environments that do not result in strongly unimodal M and R deaggregation. Approach 2A recognizes that different earthquakes may dominate the high and low frequencies, and uses separate transfer functions for these events. This is the approach recommended by Regulatory Guide 1.165 (USNRC, 1997). Approach 2B requires some elucidation. In this approach, mean, high and low percentile magnitudes from deaggregation for each design earthquake (e.g., 1 Hz and 10 Hz, Section 6.3) are used to scale spectral shapes to the 1 Hz and 10 Hz rock UHS, and the resulting control motions are used to develop weighted mean transfer functions for each design earthquake. The transfer functions are then used to scale each design earthquake or are combined to scale the rock UHS. The use of a three-point magnitude distribution for each design earthquake accounts for non-linear effects caused by a wide range of magnitudes contributing to the hazard.

6.4.3 Control Motions

Figure 6-73 shows a comparison of the WUS and CEUS rock outcrop UHS. The effects of both the hazard environment (Section 6.3) and attenuations relations (Section 6.2) are evident, with the WUS motions generally exceeding the CEUS motions by a factor of five or more for frequencies below about 10 Hz. The scaled design earthquakes were presented earlier in Figures 6-50 and 6-67 for the CEUS and WUS respectively. The difference in the hazard environments between the WUS and CEUS is evident in the large differences in the 1 Hz and 10 Hz magnitude distributions (Section 6.3). The difference in magnitudes for the 1 Hz and 10 Hz design earthquakes is 1.3 units for the CEUS (Figure 6-72) and only 0.4 units for the WUS (Figure 6-73). The effects of magnitude distribution in the rock UHS on nonlinear soil response are much less an issue for WUS conditions than CEUS, at least for the example sites, which were chosen to maximize the differences at 1 and 10 Hz.

In the site response analyses, two additional issues are important: the degree of fit to the control motions (rock UHS and scaled design earthquake spectra computed using attenuation relations, Section 6.2) and the effect of control motion variability on median soil spectra. The first issue involves developing appropriate Fourier amplitude spectra for use in the RVT equivalent-linear soil analyses (Appendix D) that are consistent with target response spectra. To illustrate the RVT spectral matching process (Silva and Lee, 1987), Figure 6-74 compares a response spectrum computed using the CEUS attenuation relation (Section 6.2) for $M = 7.5$ and $R = 1$ km (target spectrum) to a spectrum resulting from spectral matching. The difference is less than a few percent over the entire frequency range.

The second issue involving the effect of control motion variability is of potential significance since the convolutional process uses a fixed or constant control motion while varying site properties. This

is not the process used in developing the attenuation relations where source, path, and site parameters were varied simultaneously. The implicit assumption involved in comparing results from these two different processes is that soil response is either independent or weakly dependent on control motion variability. To demonstrate any dependence, Figure 6-75 shows median and $\pm 1 \sigma$ spectral estimates for CEUS conditions at $M = 7.5$ and $R = 1$ km varying only site properties while Figure 6-76 shows results for varying source, path, and site parameters simultaneously (Section 6-2). Although the variability is significantly larger when source and path parameters variations are added ($\sigma_{ln PGA}$ increases from 0.17 to 0.44, a factor of about 2.6), the median spectra are nearly identical as illustrated in Figure 6-77.

In the following sections, the profiles are discussed in order of decreasing overall stiffness as reflected in Figure 6-9. Each section presents results for CEUS conditions followed by WUS conditions, contrasting relatively low and high loading conditions (Figure 6-71). Approaches 1, 2A, 2B, and 4 are compared along with the effects of truncating the deep profiles at depths of about 150m (500 ft) and 90m (300 ft). This comparison assesses the profile depth required in the site response analyses (as well as site characterization) to properly accommodate low frequency (0.5 Hz) soil motions.

There are a number of competing effects operating in the following analyses. The degree and extent of these analyses are intended to provide useful insights into issues that are significant in developing site-specific soil motions.

6.4.4 Example Case 1: Intermediate Depth Very Stiff Profile, Rinaldi

The Rinaldi profile is about 80m deep, is considered a very stiff soil, and has a column resonance near 2 Hz (Figure 6-9). All site properties, soil profile, depth to basement, and G/G_{max} and hysteretic damping curves, as well as their variabilities are the same (same probabilistic models) in these analyses as those used in the development of the site-specific attenuation relations (Section 6.2, Figures 6-9 and 6-12). This procedure was followed for all the profiles analyzed.

6.4.4.1 CEUS Conditions

To begin the approach comparisons, Figure 6-78 shows soil UHS computed using Approaches 1, 2B, and 4 for CEUS conditions. Approach 4 provides estimates of the UHS at the soil surface directly using the site-specific attenuation relation (Section 6.2) while Approach 1 simply uses the rock UHS as control motions. Approach 2B computes mean transfer functions for each design earthquake (based on 1 Hz and 10 Hz deaggregation) using the appropriate magnitude distribution for each earthquake. The two transfer functions are combined to scale the rock UHS or are used independently to scale the rock outcrop 1 Hz and 10 Hz design earthquakes to produce soil design earthquakes for cases where it may be desirable to perform two sets of design analyses. Figure 6-78 shows nearly the same motions for both Approaches 1 and 2B, both being conservative compared to the soil UHS. For a linear system, Approaches 1 and 2B should produce identical results and for the loading levels (Figure 6-71), profile stiffness (Figure 6-9), and nonlinear properties (Figure 6-12) used, this is nearly the case.

The median and $\pm 1 \sigma$ effective strains resulting from Approach 1 are shown in Figure 6-79. With median values generally less than about $10^{-2} \%$, little change in shear-wave velocity and hysteretic damping is expected (Figure 6-12) suggesting a nearly linear system. The apparent conservatism in Approaches 1 and 2B at frequencies exceeding 10 Hz shown in Figure 6-78 is about 20%. Near the fundamental column resonance at about 2 Hz and at low frequency (< 1 Hz) Approach 4 exceeds Approaches 1 and 2B by about 10%. Exceedence near a resonance is expected since there is a smoothing inherent to the regression process but the slight low-frequency underprediction and high-frequency exceedence are puzzling since the mean-to-median ratio resulting from profile variability is about 5% and the regression equations appear to provide a reasonable fit to the model predictions (Figures 6-16 and 6-17). Additionally, the RVT spectral matching process also appears to provide a good match to the target spectra, as Figure 6-74 suggests. While the degree of conservatism is larger than expected at high-frequency and requires further investigation along with the slight low-frequency underprediction, these results suggests that Approaches 1 and 2B are not likely to lead to unconservative spectral estimates for very stiff profiles under moderate loading conditions (peak rock outcrop acceleration of about 0.3g, Figure 6-73).

The transfer functions used to scale the rock outcrop spectra are shown in Figures 6-80 through 6-82. Figure 6-80 shows the ratio computed for the 1 Hz scaled design earthquake and Figure 6-81 the corresponding ratios for the 10 Hz design earthquake. Figure 6-82 compares the two (1 Hz and 10 Hz) mean ratios, the average of which is used to scale the rock outcrop UHS (Approach 2B). As expected, due to the largely linear response, little difference is seen between the ratios for frequencies below about 30 Hz, with about a 15% difference at peak acceleration (100 Hz). Approaches 1 and 2B are equivalent under these conditions (strain ranges and nonlinear properties).

For cases where multiple soil spectra are desired, Figure 6-83 compares 1 Hz and 10 Hz design earthquake soil motions (Approach 2A) with Approach 2B applied to the UHS along with Approach 1 results since they both reflect the use of rock UHS spectra. The 1 Hz and 10 Hz soil spectra are very close to the scaled rock UHS over the frequency ranges of the bounding criteria discussed in Section 5. At peak acceleration (near 100 Hz) Approach 2B applied to the rock UHS exceeds the 10 Hz soil motions by about 20%.

Figures 6-84 and 6-85 compare Approaches 1 and 2B using conventional deterministic profile variations. The deterministic variations reflect changes in the base case shear modulus of a factor of 2 and are shown in Figure 6-84. The mean and $\pm 1 \sigma$ spectra taken over the three spectra, reflecting base case and upper-and-lower-range profiles, are shown in Figure 6-85. The comparison in Figure 6-84 between the spectrum computed using the base case profile and the mean Approach 2B spectrum illustrates the effects of profile randomization, generally smoothing through the base case resonance peaks. With the exception of the fundamental resonance peak, Figure 6-84 suggests that an average of the three spectra (base case and upper- and lower-range profiles) may provide an acceptable soil spectrum. Figure 6-85 shows this comparison and confirms that a smoothed average of the three provides a reasonable estimate of design levels.

6.4.4.2 WUS Conditions

For the Rinaldi profile, Figures 6-86 to 6-93 show corresponding plots for WUS conditions. For this case, changes in the loading conditions (Figure 6-73) determined by the WUS hazard environment

as well as crustal structure resulted in distinctly different soil motions in both level and spectral shape. Figure 6-86 compares Approaches 1, 2B, and 4 and shows soil spectral shapes with peaks near 3 Hz compared to about 15 Hz for the same profile located in the CEUS (Figure 6-78). This difference results mainly from the difference in control motions, with a higher degree of nonlinearity for the WUS case contributing to the shift in peak spectral amplification to lower frequencies. For a deeper profile and a higher CEUS loading condition, the difference in spectral shapes between WUS and CEUS soil motions would diminish. However, a sufficient difference persists to conclude that the use of scaled broadband WUS deep soil motions is not appropriate for CEUS conditions.

At these higher loading levels in the WUS the high-frequency exceedence extends to about 0.5 Hz and neither Approaches 1 nor 2B are below the Approach 4 UHS. The effective strains for Approach 1 are shown in Figure 6-87 with a maximum in the median estimates of about $0.1 \pm 0.2\%$. This reflects a substantial change in dynamic material properties with material damping increasing to about 15% in the top 15m or so (Figure 6-12).

Exceedences of Approaches 1 and 2B over the soil UHS (Approach 4) spectra may actually not be as large as those depicted in Figure 6-86. The rock outcrop spectra are used as control motions for Approaches 1 and 2B and these contain amplification in the shallow portion of the soft rock profile (Figure 6-6). The very shallow portion of the WUS rock profile, with shear-wave velocities less than 1 km/sec, is not present in the soil motions used to develop the WUS soil attenuation relations (Section 6.2). In these cases, the soil profiles are placed on top of the Wald and Heaton (1994) crustal model. This crustal model has a surface shear-wave velocity of 1 km/sec (Table 6-4) and reflects baserock or base-of-soil conditions. The potential differences in soft rock outcropping and baserock outcropping motions are not accommodated in the WUS approach comparisons. These differences are quantified in Section 6.10 and result in about a 5% to 15% reduction in soil motions when using baserock outcropping, as opposed to surface, control motions. These results apply to all WUS approach comparisons, decreasing the difference between soil UHS (Approach 4) and Approaches 1 and 2B analyses.

For the WUS Rinaldi analyses, the accompanying transfer functions are shown in Figure 6-88 to 6-90 and show smaller resonances than the corresponding CEUS ratios (Figures 6-80 to 6-82). This is related to the differences in impedance contrast at the soil/rock boundary caused by the differences in shear-wave velocity between the top layers of the WUS and CEUS crustal models. For the CEUS, the shear-wave velocity is 2.83 km/sec while it is only 1 km/sec for WUS (Table 6-4 and 6-5). These values, along with the different densities, reflect a 84% larger impedance contrast for CEUS conditions giving rise to more energy trapped in the soil column, all other factors being the same. This effect naturally competes with the higher loading levels for WUS conditions in terms of inducing strains in the soil column. As with the CEUS ratios, little difference is seen in the 1 Hz and 10 Hz WUS ratios, suggesting largely linear response. However, in this case, the similarity in 1 Hz and 10 Hz ratios is driven largely by the similarity in 1 Hz and 10 Hz design earthquake scaled rock outcrop spectra (Figure 6-67). The similarity in the 1 Hz and 10 Hz control motions is reflected in Figure 6-91, which compares corresponding soil motions to Approaches 1 and 2B spectra. As with the CEUS, the 10 Hz spectrum controls at high-frequency (above about 3 Hz here) while the 1 Hz spectrum controls the low-frequencies.

Figures 6-92 and 6-93 compare deterministic profile variations and show that either the base case or mean (over deterministic profile variations) spectra provide motions comparable to those of Approach 2B. For very stiff profiles, these results and those of the previous section indicate that enveloping spectra based on conventional profile variations of twice and one half the base case shear moduli result in excessively conservative design motions. The implied velocity variation exceeds that typically associated with variability over a footprint or site area (Figure 6-10).

6.4.5 Example Case 2: Deep Stiff Profile, Gilroy 2

The Gilroy 2 profile is a deep stiff sandy to gravelly profile with a depth of about 180m (Figure 6-9) with a column resonance at about 1 Hz. Material nonlinearity for this site is modeled using the EPRI (1993) G/G_{max} and hysteretic damping curves (Figure 6-11). Gilroy 2 is located at a closest rupture distance of about 15 km from the 1989 M 6.9 Loma Prieta earthquake, and the site recorded an average horizontal component peak acceleration of about 35%g (Appendix A). The nearby hard California rock site Gilroy 1, about 2 km closer to the rupture, had a corresponding peak acceleration of about 50%g. Conversely, for the M 5.8 Coyote Lake earthquake, the Gilroy 2 site peak acceleration exceeded that of Gilroy 1 by about 100% (about 20% g and 10% g respectively). These two sites, with low level aftershocks recorded as well, provide compelling evidence for nonlinear response as well as validation of the nonlinear material strain dependencies (EPRI, 1993).

6.4.5.1 CEUS Conditions

As with the previous analyses, Figures 6-94 to 6-105 show approach comparisons, effective strains, and transfer functions. In this case and for subsequent profiles, the comparisons are augmented with additional comparisons for profiles truncated at about 150m (500 ft) and 90m (300 ft) to assess the extent of profile depth required to capture potential amplification effects at low frequency (0.5 Hz).

The comparisons of Approaches 1, 2B, and 4 shown in Figure 6-94 share features in common with the Rinaldi CEUS results (Figure 6-78) but with a smaller difference between the soil UHS and the spectra of Approaches 1 and 2B. A larger difference, however, exists between Approaches 1 and 2B at high frequency (> 10 Hz). This is the expected consequence of potential unconservatism at high frequencies resulting from driving the profile with a broad UHS (Approach 1). The larger difference in Approaches 1 and 2B for this site than for the Rinaldi profile is related to the more nonlinear material strain dependencies and softer profile. The effective strains are still relatively low, however, with median values less than about 0.05% (Figure 6-95).

The transfer functions, Figures 6-96 to 6-98, show larger effects than for Rinaldi, particularly for the 10 Hz design spectrum. The differences in the mean ratios, 1 Hz and 10 Hz shown in Figure 6-98, are still only significant at very high frequency, beyond about 30 Hz where they are up to about 30%. The difference between Approach 2B and the 10 Hz design soil spectrum (from Approach 2A) shown in Figure 6-99 is large above about 20 Hz, reflecting the tendency of Approach 1 to overdrive the soil column.

Comparisons of Approach 2B with deterministic profile variations are shown in Figures 6-100 and 6-101. As with the Rinaldi profile, enveloping is overly conservative. The mean spectrum from

Approach 1 (Figure 6-101) is lower than Approach 2B at the fundamental resonance near 1 Hz and at high frequency, above about 10 Hz.

To illustrate the effects of soil column truncation, Figures 6-102 to 6-105, show corresponding plots for column depths of 150m (500 ft) and 90m (300 ft) (Approach 2B reflects full column depth). For the profile truncated at 150m (full depth is about 180m), Figure 6-103 shows mean spectra (over deterministic profile variations) comparable to those in Figure 6-101 with the full profile, about 180m. Truncating to a depth of 90m (Figure 6-105), which is about half the original profile depth, results in slightly larger high frequency motion and lower motions at frequencies below the strain compatible fundamental resonance near 1 Hz (Figure 6-100). These results, strictly valid only for this profile, assumed material nonlinearity, and loading conditions suggest that at least 150m of profile is necessary to accommodate amplification effects frequencies of 0.5 Hz and above.

6.4.5.2 WUS Conditions

Figures 6-106 to 6-117 show the corresponding plots for the Gilroy 2 profile considering WUS conditions. For this case, the Gilroy 2 soil UHS (Approach 4) exceeds Approaches 1 and 2B but in this case by a larger amount (Figure 6-106). As discussed in Section 6.41, this feature likely results from the sigma or residual variability in the soil attenuation relations, which neglects the diminishing capacity of a soil column to transmit high frequency motions as the degree of nonlinearity (loading level) increases. As a result, the UHS computed for long return periods reflects sources generating rare, large earthquakes at close distances. High motions are then generated by sampling higher fractile levels. For these conditions, Approach 2B provides more reliable spectral estimates since it directly accommodates the soils amplification capacity. Additional verification will involve more accurately representing these site-specific soil capacities in models of the residual dispersion. The accompanying effective strains shown in Figure 6-107 are significantly larger as well, with shallow median values near 0.4%. For cases with effective strains larger than 1% over a depth range exceeding 10 to 20 feet, equivalent-linear results should be verified with corresponding nonlinear analyses. Sufficient care must be exercised with the nonlinear properties to ensure the nonlinear model matches the G/G_{max} and hysteretic damping curves. The transfer functions illustrated in Figures 6-108 to 6-110 show a stronger magnitude dependency than for the Rinaldi profile, a consequence of larger nonlinear effects (softer profile and more nonlinear material strain dependencies). The difference in the mean ratios for the 1 Hz and 10 Hz design earthquakes is only about 10% for frequencies 1 to 10 Hz range. As with the WUS Rinaldi results, Figure 6-111 shows that both the 1 Hz or 10 Hz soil design motions from Approach 2A closely reflect the Approach 2B spectrum.

For this case, the system is significantly nonlinear, (particularly for depths less than about 50m, see Figure 6-107), so the deterministic variation of two times the shear modulus (0.4 on shear-wave velocity) has a dramatic effect. Figure 6-112 shows shifts in the fundamental resonance of nearly a factor of ten (from about 3 Hz to 0.4 Hz) with a maximum range in spectral ordinates of nearly a factor of 8 around 3 Hz. These changes occur with a factor of 2 shift in overall stiffness (shear-wave velocity).

For systems well into nonlinear response, the range in conventional deterministic profile variations can result in dramatic differences in ground motions. Enveloping the deterministic range is generally quite conservative but, as with the Rinaldi profile and the CEUS Gilroy 2 results, leads to varying

degrees of conservatism with oscillator frequency. The mean spectrum over the three deterministic profile variations (Figure 6-113) shows some unconservatism near 1 Hz and may be inappropriate for both WUS and CEUS conditions near the column fundamental resonance. The trough in the -1σ (16th percentile) spectrum near 3 Hz is due to the large variability in the spectra from the three deterministic profile variations at 3 Hz (Figure 6-112) resulting in a sigma (normal) that is near the mean value of about 1g. The $+1 \sigma$ value is then near 3g and the -1σ spectrum then is about 0.05g. Truncating the profile at 150m (500 ft) and 90m (300 ft) show results (see Figures 6-114 through 6-117) similar to the full profile with some unconservatism in the 0.5 to 1.0 Hz range (Figures 6-116 and 6-117). These results suggest that fixed rules regarding required profile depths are going to be both elusive and conservative.

6.4.6 Example Case 3: Deep Firm Profile, Savannah River Generic

The Savannah River Generic profile (Figure 6-9) is very stiff near the surface, with a shear-wave velocity of about 400m/sec. It has a deep soft zone just below the surface extending to a depth of about 70m. Below that, the shear-wave velocity gradient is fairly steep and merges with the CEUS and WUS crustal models at about 300m (1,000 ft). The low-strain column resonance is at about 0.8 Hz. Nonlinearity is modeled through equivalent-linear G/G_{max} and hysteretic damping curves that are based on modeling strong ground motions in southern California at sites comprised of predominantly cohesionless soils. These are the same sets of curves that were used for the Rinaldi profile analyses (Figure 6-12).

6.4.6.1 CEUS Conditions

Following the patterns of the previous analyses, Figures 6-118 to 6-129 show comparisons of Approaches 1, 2B, and 4, effective strains, transfer functions, and the effects of profile truncation for the Savannah River Generic profile. For the relatively low strain CEUS motions, Figure 6-118 shows Approach 4 soil UHS comparable to the spectra of Approaches 1 and 2B. As with the Rinaldi and Gilroy 2 profiles, the Approach 1 spectrum falls below that of Approach 2B as well as Approach 4 for frequencies above about 10 Hz due to increased damping associated with the broadband control motions (rock outcrop UHS).

The effective strains shown in Figure 6-119 are relatively low, with median values below about 0.02 to 0.03%. The largest strains occur throughout the soft zone (Figure 6-9). With these strain values, modulus reduction is only about 0.8 to 0.9 and hysteretic damping ranges from about 2% to 4% (Figure 6-12). The combination of a firm profile and relatively linear G/G_{max} and hysteretic damping curves results in nearly linear response but with an increase in damping of about 50% in the soft zone.

The transfer functions shown in Figures 6-120 to 6-121 reflect the small degree of nonlinearity, showing small changes (about 20%) with earthquake magnitude. Differences in the mean ratios (Figure 6-122) are largest above 30 Hz (100 Hz reflects PGA scaling) and are about 20%. As with the previous CEUS cases, the 10 Hz design earthquake soil motion from Approach 2A compares favorably with Approach 2B for frequencies below about 20 Hz (Figure 6-123) but falls below at higher frequencies.

Comparisons of Approach 2B to deterministic soil variations shown in Figures 6-124 and 6-125 suggest that enveloping spectra for shear modulus variations of a factor of 2 will overestimate the effect of actual footprint variability (Figure 6-10), while a mean spectrum is unconservative, especially near the column resonance at about 0.5 Hz.

Profile truncation to 150m, Figures 6-126 and 6-127, shows results very similar to the original profile of about 300m depth. However, truncation at about 90m (300 ft) results in motions that are too low for frequencies below about 0.8 Hz (Figures 6-128 and 6-129). These results are similar to those of Gilroy 2 for CEUS conditions (Figures 6-112 to 6-117).

6.4.6.2 WUS Conditions

Figures 6-130 to 6-141 contain the results for the Savannah River Generic profile considering WUS hazard and rock conditions. In this case, even with the WUS higher loading conditions, Figure 6-130 shows that the Approach 4 soil UHS lies below those of Approaches 1 and 2B. Soil column saturation effects are insufficient to bring Approaches 1 and 2B spectra below the soil UHS at high frequency. A contributing factor may be related to the WUS Savannah River residual dispersion about the attenuation relation. It is among the lowest soil site sigmas overall (Figure 6-41) and is the lowest for frequencies exceeding about 1 Hz. A larger sigma would result in higher high frequency soil UHS.

The effective strains shown in Figure 6-131 show median values around 0.1 to nearly 0.2% throughout much of the profile with +1 σ values reaching 0.2%.

The transfer functions (Figures 6-132 to 6-134) show about the same magnitude dependency as the CEUS but extending to lower frequency. The difference in the mean ratios is generally less than about 5%. This latter similarity is again driven by the similarity in control motions (Figure 6-67).

Figure 6-135 shows the comparison of 1 and 10 Hz design events (Approach 2A) with Approaches 1 and 2B. In this application the envelope of spectra developed for Approach 2A would be below Approaches 1 and 2B, over much of the frequency range.

The effects of deterministic profile variations (Figures 6-136 and 6-137) show some exceedence of the base case profile spectrum for frequencies near 5 Hz, similar to the Rinaldi and Gilroy 2 profiles, again illustrating the effects of smooth (base case) vs. rough (randomized) profiles. In the context of nonlinear analyses, the median or mean spectrum computed with variation in soil properties is lower at high frequency than the spectrum computed from a mean or median profile. While the envelope of the deterministic profile variation spectra is overly conservative, Figure 6-137 suggests that the mean from Approach 1 may be unconservative at low frequency. Profile truncation to about 150m (500 ft) in Figures 6-138 and 6-139 shows results very similar to the full profile (305m, 1,000 ft) while truncation at 90m (300 ft), Figures 6-140 and 6-141, results in low motions at low frequency (below about 1 Hz). These results are similar to the CEUS conditions and to Gilroy 2 WUS and CEUS results as well. A tentative conclusion is that 150m of profile is adequate to reflect potential amplification for frequencies as low as about 1 Hz.

6.4.7 Example Case 4: Deep Soft Profile; Meloland

The Meloland Profile, located in the Imperial Valley of Southern California and Northern Mexico is the softest profile analyzed (Figure 6-9) and has a column frequency of about 0.5 Hz. While it is considered “bottomless” and extends kilometers in depth, it was truncated at a depth of 304m (1,000 ft) for these analyses. It is the location of a recently installed (Caltrans) vertical strong motion array and the nearby CDMG strong motion site recorded the M 6.5 1979 Imperial Valley earthquake at a rupture distance of 0.5 km (average horizontal component peak acceleration of about 0.3g). The modulus reduction and damping curves used are shown in Figure 6-13. They are based on modeling strong motions from the 1979 Imperial Valley earthquake recorded at Meloland and nearby sites (Silva et al., 1997) and reflect relatively weak strain dependencies.

6.4.7.1 CEUS Conditions

For the Meloland profile, the standard suite of comparisons are shown in Figures 6-142 to 6-153. For this soft profile, the soil UHS (Approach 4) exceeds spectra computed with Approach 1 for CEUS conditions (Figure 6-142). As explained previously in regard to Figures 6-83, 6-94, and 6-124, the Approach 2B spectrum exceeds the Approach 1 spectrum at high frequency (≥ 10 Hz). The effective strains are relatively small, as shown in Figure 6-143 yet the soil UHS exceeds Approach 1 motions. For this soft soil, magnitude differences in the transfer functions shown in Figure 6-145 for the 10 Hz design earthquake are large, reaching nearly a factor of 2 in total range near 10 Hz. The difference in mean ratios for the 1 Hz and 10 Hz design earthquake remains very small for frequencies below about 30 Hz but is important at peak acceleration (100 Hz), similar to the other profiles for CEUS conditions.

The comparison between Approaches 1 and 2B and the 1 Hz and 10 Hz design earthquake soil spectra (Approach 2A) is illustrated in Figure 6-147. As with the other profiles, Approach 1 and the 10 Hz soil Approach 2A design spectra fall below the Approach 2B spectra for frequencies above about 10 Hz. In this case, Approach 1, using the broad UHS rock spectrum, overdrives the soil column and is lower than the 10 Hz soil motion, which uses a rock shape reflecting a single magnitude. At lower frequencies, Approach 1 and the Approach 2A 1 Hz soil design spectrum are equivalent to the Approach 2B spectrum.

Deterministic profile variations shown in Figures 6-148 and 6-149 reflect the same results as the other profiles. Enveloping reflects overly conservative motions for footprint profile variations while the average is too low at some frequencies. Profile truncation to ~150m (~500 ft) adequately captures amplification at low frequency (to about 0.5 Hz) but the mean is low at high frequency ($\geq 8-10$ Hz) (Figures 6-150 and 6-151) relative to Approach 2B. Truncation at 90m (300 ft) does not adequately portray the profile amplification at low frequency (0.5 Hz), (this observation is similar to the other profiles) and is a bit low at higher frequencies as well.

6.4.7.2 WUS Conditions

Figures 6-154 to 6-165 show results for the Meloland profile considering WUS conditions. The comparison of Approaches 1, 2B, and 4 is illustrated in Figure 6-154 and shows the expected exceedence of the soil UHS (Approach 4) over the spectra of Approaches 1 and slightly for 2B as

well. The effective strains are large, with values significantly greater than for CEUS conditions. The median values are near 0.4% in the intermediate portion of the profile (compare Figures 6-107 and 6-155).

Magnitude dependencies in the transfer functions, Figures 6-156 and 6-157, are weak for the 1 Hz scaled design outcrop spectrum and strong for the corresponding 10 Hz spectrum, as they were for the Gilroy 2 and Savannah River Generic profiles (Figure 6-109 and 6-133). Because of the similarity in the 1 Hz and 10 Hz scaled rock outcrop spectra (Figure 6-173), the corresponding mean transfer functions are similar (Figure 6-158).

Comparisons of the 1 Hz and 10 Hz design earthquake soil spectra (Approach 2A) with those of Approaches 1 and 2B are shown in Figure 6-159. These results are similar to those of the other profiles and show expected similarity. With 0.6 magnitude difference between 1 Hz and 10 Hz contributions and at similar distances, the distinction between the shapes is not significant in site response.

The effects of deterministic profile variations are shown in Figure 6-160 and 6-161 and show results very similar to those of Gilroy 2 (Figures 6-112 and 6-113). There is a large variation in motions, a range of about a factor of 6 near 3 Hz for a factor of 2 range in shear-wave velocity. This is a strongly nonlinear system, due principally to the high loading level and low initial stiffness (its dynamic material strain dependencies are considered relatively linear). The combination of either a soft profile with relatively linear curves, as here, or a stiff profile and more nonlinear curves, such as Gilroy 2, results in a similar strong dependence on initial stiffness (variations in shear-moduli) under high loading conditions. The mean spectrum (over deterministic variations) is conservative for all frequencies (see Figure 6-161).

Truncating the profile to 150m (500 ft) also produces a mean spectrum that is very close to the full profile (304m) and compares favorably with that of Approach 2B for frequencies down to about 0.5 Hz (see Figures 6-162 and 6-163). It is, however, a bit high above the 2 Hz to 3 Hz frequency range (Figure 6-163). Truncation at 90m (300 ft) however, shows serious deficiencies at 1.0 Hz and below and larger motions above 2 to 3 Hz (see Figures 6-164 and 6-165).

6.4.8 Baserock Motions

Soft rock (WUS) shear-wave velocity profiles are characterized by steep shallow gradients (Figure 2-2) with median surface velocities in the 200 to 300m/sec range. Median and 1σ shear-wave velocity profiles based on measurements made at WUS strong motion recording sites classified as rock are shown in Figure 6-166. This strong velocity gradient results in large amplifications (source region to surface) at high frequency (Figure 2-3). At the base of soil profiles, due to more limited weathering, basement rock generally does not show such characteristics. Most boreholes that penetrate soil and into competent rock do not extend deep enough to fully characterize shear-wave velocities 15 to 30m into basement material. Nonetheless, most existing profiles suggest a large jump in velocity over a short depth range into baserock material. For WUS conditions, this jump or very steep gradient typically reflects a baserock shear-wave velocity ranging from about 1 to 2 km/sec over a depth range of several to tens of meters. The very shallow (top 30m or so) gradient shown in

Figure 6-166 is not typically present beneath soil profiles. As a result, the accompanying amplification present in motions recorded at soft rock sites may not be present in baserock motions that drive the soil column. Additionally, the variability of baserock motions, particularly for very deep profiles (> 150m), may also be significantly lower than rock outcrop motions due to a smaller variability in velocities, being less subject to weathering. While the issue of variability is currently not resolvable, the effects of the shallow soft rock velocity gradient on response spectra may be easily estimated.

6.4.8.1 Development of Outcrop-to-Basement Spectral Correction Factors

Two approaches are available to develop correction factors for conditioning soft rock (surface) motions to be more appropriate as base of soil control motions. An empirical approach that involves deconvolving strong motion recordings at soft rock sites with measured shear-wave velocities to base of soil velocities (1 to 2 km/sec) is currently underway as part of a PEER project (I.M. Idriss, personal communication, 1999). Another approach, implemented here, is analytical and involves point-source simulations (Appendix D) of motions at the surface of the soft rock profile (Figure 6-166) and progresses deeper (into higher velocities) in the profile by stripping off overlying materials. Taking ratios of motion at depth to surface motion results in depth- (velocity-) dependent correction factors. To provide statistical stability to the transfer functions or correction factors and to estimate their uncertainties, multiple simulations are run using the profile randomization scheme. The correction factors are then taken as ratios of median motions: depth as outcropping over surface. Potential nonlinearity is accommodated with equivalent-linear analyses using the rock G/G_{max} and hysteretic damping curves (Figure 6-8) and these parameters are also randomized.

An example of the motions (5% damped spectral acceleration) computed for $M = 6.5$ at a distance of 25 km is shown in Figure 6-167. The suite of spectra reflect median motions computed at the surface and at increasing depths in the soft rock profile, from 1.5m (5 ft) with a surface velocity of 305m/sec (1,000 ft/sec), to 386m (1,268 ft) with a corresponding "surface" velocity of 1,828m/sec (6,000 ft/sec). The decrease in spectral amplitudes begins below a depth of about 2m and progressively decreases in level and over a wider frequency range as more of the profile is stripped off. The resulting transfer functions are shown in Figure 6-168. These represent correction factors to be applied to surface motions to remove the effects of the shallow soft rock gradient to the same shear-wave velocity as that underlying a soil column. The factors range as low as about 0.5 near 3 Hz for a shear-wave velocity of about 1.9 km/sec (6,000 ft/sec), showing the large effects of the shallow gradient (Figure 6-166).

To assess the effects of potential nonlinearity on the correction factors, similar analyses were done for distances of 10 km (surface PGA \approx 0.3g) and 1 km (surface PGA \approx 0.5g). The resulting correction factors are shown in Figures 6-169 and 6-170 for distances of 10 km and 1 km respectively. The ratios actually increase, particularly at high frequency, because the surface (and shallow) motions decrease as the loading levels increase.

6.4.8.2 Effects Of Baserock Motions On The WUS Soil Motions

In developing the WUS soil attenuation relations (Section 6.2) the soil profiles were placed on top of the Wald and Heaton (1994) crustal model. This model has a surface shear-wave velocity of 1.0 km/sec implying a jump in velocity at the soil/rock interface (Figure 6-9). The attenuation relations

for WUS rock motions are appropriate for surface motions at an average soft rock site (Figure 6-6) and incorporate the shallow steep gradient shown in Figure 6-166. Since control motions for the WUS site response analyses are based on the soft rock attenuation relations, they incorporate near-surface amplification for velocities lower than 1 km/sec, not included in the simulations for the WUS soil attenuation relations. To assess the effects of using surface as opposed to baserock outcropping control motions, comparisons are made to the soil motions computed using Approach 1 with both sets of rock control motions.

The modified WUS rock outcrop UHS for baserock conditions is shown in Figure 6-171 compared to the original spectrum. The modified spectrum is appropriate for outcropping rock with a shear-wave velocity of about 1 km/sec (300 ft/sec) and is considered to reflect a much closer representation of control motions used in developing the soil attenuation relations. It was produced by multiplying the rock surface UHS (solid line in Figure 6-171) by the ratio computed for the velocity of 914m/sec and 0.5g surface peak acceleration (Figure 6-170). It shows a maximum reduction of about 20% in the 2 to 3 Hz range and 15% at peak acceleration. This corrected motion is then used as an outcropping control motion for an Approach 1 analysis.

For the Rinaldi profile, the results of using the modified motion as input to the soil column are shown in Figure 6-172. The solid line reflects Approach 1 soil spectra computed using the WUS UHS rock spectrum, and the dashed line shows the results using the modified control motion. The difference in soil spectra is about 10 to 15% over much of the bandwidth (11% at peak acceleration), nearly the same as the difference in control motions (Figure 6-171).

The Gilroy 2 profile is softer with more nonlinear dynamic material properties and shows less of a difference (10% at peak acceleration, Figure 6-173). The Savannah River Generic profile is softer still, but with more linear dynamic material properties than Gilroy 2. It has the same G/G_{max} and hysteretic damping curves as those used for the Rinaldi profile. Figure 6-174 shows nearly the same difference as Rinaldi (Figure 6-172), about 10 to 15% over much of the frequency range and 13% at peak acceleration. The softest profile, Meloland, also has the most linear dynamic material strain dependencies and shows a 10 to 15% reduction (Figure 6-175), 12% at peak acceleration.

In general, the soil motions computed using the more appropriate baserock motions in place of rock outcrop motions showed broadband reductions ranging from about 5 to 15%. The reductions depended upon initial profile stiffness as well as dynamic nonlinear properties and are generally somewhat less than the differences in control motions, rock outcrop vs. base rock or base of soil conditions. The correction factors have uncertainties associated with them, based on profile uncertainties (Figure 6-7), so fractiles other than the median may be used. As with the V/H ratios (Section 4.7), the correction factors may be implemented for ranges in rock outcrop peak acceleration values.

6.5 Conclusions and Recommendations

In the proceeding analyses three major issues were addressed in developing site-specific soil motions based on a rock outcrop UHS: (1) evaluation of procedures to develop hazard consistent soil spectra,

(2) assess minimum profile depth required to characterize soil motions in the frequency range of 0.2 to 5.0 Hz, and (3) assess the effects of baserock vs. rock outcrop control motions on soil spectra.

To address these issues, four deep profiles were analyzed reflecting a wide range in both overall stiffness (range in column frequency of 0.5 Hz to 2.0 Hz) and nonlinear dynamic material properties. To capture ranges in loading conditions of amplitude levels and spectral content, the four profiles were considered to be located in both the WUS (high hazard) and CEUS (moderate hazard) tectonic regions. Analyses consisted of comparisons of UHS computed directly for the soil sites using region- and site-specific soil attenuation relations with approaches that start from region-specific rock UHS and use traditional convolution analyses to produce site-specific soil motions.

Results of the analyses indicate that a conventional soil UHS can result in large high frequency motions. This is likely due to a combination of a symmetric (in log) uncertainty about median attenuation estimates, including the effects of profile saturation. However, the larger more significant effect is the inclusion of combinations of both high and low rock motions with large soil amplification. Such combinations are captured in the soil UHS by its very nature (aggregation of motions that exceed a given level) and are ignored in Approaches 1 and 2. As a result, at some exceedence level, Approaches 1 and 2 will become unconservative. Unfortunately, the exceedence level above which this occurs depends on the nonlinear properties of the soil column, range in loading levels, initial stiffness, and nonlinear dynamic material properties. Results presented herein suggest that for hazard levels up to 10^{-4} , Approach 2B results in adequately conservative soil motions, however, more work is clearly needed.

Further analyses showed that the conventional deterministic site property variation of a factor of 2 on shear modulus is too large for footprint variability. This variation results in overly conservative envelope motions and mean values that are unconservative at low-frequencies, near the column frequency of deep profiles. Profile truncation to about 150m (500 ft) provides soil motions that largely capture site amplifications for frequencies down to about 0.5 Hz. Truncation to about 90m (300 ft) will likely produce unconservative soil motions for frequencies below about 1 Hz.

The use of soft rock surface recordings as base-of-soil (baserock) control motions produces about 5% to 15% larger soil motions compared to correcting these rock motions to rock-soil interface motions. The degree of conservatism depends on frequency, shear-wave velocity at the base of the soil column, and level of rock motion. The effect is broadband, extending from about 0.3 Hz to 100 Hz (peak acceleration).

References

- Abrahamson, N.A and K.M. Shedlock (1997). "Overview." *Seis. Research Lett.*, 68(1), 9-23.
- Abrahamson, N.A. and W.J. Silva (1997). "Empirical response spectral attenuation relations for shallow crustal earthquakes." *Seism. Soc. Am.*, 68(1), 94-127.
- Atkinson, G.M and W.J. Silva (1997). "An empirical study of earthquake source spectra for California earthquakes." *Bull. Seism. Soc. Am.* 87(1), 97-113.

- Atkinson, G.M. (1993). "Source spectra for earthquakes in eastern North America." *Bull. Seism. Soc. Am.*, 83(6), 1778-1798.
- Bazzurro, Paolo (1998). Probabilistic Seismic Demand Analysis, Ph.D. Thesis, Supervised by C.A. Cornell, Stanford University, Palo Alto, CA.
- Bazzurro, P., C.A. Cornell and F. Pelli (1999). "Site- and soil-specific PSHA for nonlinear soil sites," Proc., 4th Earthq. Resist. Design Structures Conf. (ERES99), Catania, Italy, June 15-17.
- Boore, D.M, and W.B. Joyner (1997). "Site amplifications for generic rock sites." *Bull. Seism. Soc. Am.*, 87(2), 327-341.
- Boore, D.M., W.B. Joyner and T.E. Fumal (1997). "Equations for estimating horizontal response spectra and peak acceleration from Western North American earthquakes: A summary of recent work." *Seism. Res. Lett.* 68(1), 128-153.
- Campbell, K W. (1997). "Empirical near-source attenuation relationships for horizontal and vertical components of peak ground acceleration, peak ground velocity, and pseudo-absolute acceleration response spectra." *Seism. Soc. Am.*, 68(1), 154-176.
- Electric Power Research Institute (1993). "Guidelines for determining design basis ground motions." Electric Power Research Institute, Palo Alto, CA, Rept. EPRI TR-102293, vol. 1-5:
 vol. 1: Methodology and guidelines for estimating earthquake ground motion in eastern NA.
 vol. 2: Appendices for ground motion estimation.
 vol. 3: Appendices for field investigations.
 vol. 4: Appendices for laboratory investigations.
 vol. 5: Quantification of seismic source effects.
- Hanks, T.C. and A.C. Johnston (1992). "Common features of the excitation and propagation of strong ground motion for north American earthquakes." *Bull. Seism. Soc. Am.*, 82(1), 1-23.
- Idriss, I.M. (1993). "Procedures for selecting earthquake ground motions at rock sites," Nat. Inst. Of Stan. And Techn., Rept. NIST GCR 93-625.
- McGuire, R.K. (1995) "Probabilistic Seismic Hazard Analysis and Design Earthquakes: Closing the Loop," *Bulletin of the Seismological Society of America*, Vol. 85, No. 5, pp. 1275-1284, October.
- Sadigh, K., C-Y. Chang, J.A. Egan, F. Makdisi, and R.R. Youngs (1997). "Attenuation relationships for shallow crustal earthquakes based on California strong motion data." *Seism. Soc. Am.*, 68(1), 180-189.

- SHAKE (1992). "A computer program for conducting equivalent linear seismic response analyses of horizontally layered soil deposits." Sponsored by Structures Building and Fire Research Lab., Nat'l Institute of Standards and Technology, Gaithersburg, Maryland. Modifications by I. Idriss and J. Sun.
- Silva, W.J. and Lee, K. (1987). "WES RASCAL code for synthesizing earthquake ground motions." State-of-the-Art for Assessing Earthquake Hazards in the United States, Report 24, U.S. Army Engineers Waterways Experiment Station, Miscellaneous Paper S-73-1.
- Silva, W.J. and R. Darragh (1995). "Engineering characterization of earthquake strong ground motion recorded at rock sites." Palo Alto, Calif: Electric Power Research Institute, TR-102261.
- Silva, W.J., N.A. Abrahamson, G.R. Toro, and C.J. Costantino (1997). "Description and validation of the stochastic ground motion model." Report to Brookhaven National Laboratory, Associated Universities, Inc. Upton, New York, Contract 770573.
- Toro, G.R., N.A. Abrahamson, and J.F. Schneider (1997). "Model of strong ground motions from earthquakes in Central and Eastern North America: Best estimates and uncertainties." *Seismological Research Let.*, 68(1), 41-57.
- USNRC (1997). *Identification and characterization of seismic sources and determination of safe shutdown earthquake ground motion*, US Nuclear Regulatory Commission, Regulatory Guide 1.165, March.
- Vucetic, M. and R. Dobry (1991). "Effects of Soil Plasticity on Cyclic Response," *Journal of Geotechnical Engineering*, ASCE, 117(1), 89-107.
- Wald, D.J. and T.H. Heaton (1994). "A dislocation model of the 1994 Northridge, California, earthquake determined from strong ground motions." *U.S. Geological Survey*, Open-File Rpt. 94-278.

Table 6-1
Approaches for Developing Soil UHS

<u>Description</u>	<u>Frequencies Used</u>	<u>Integration</u>	<u>Label</u>
PSHA using site-specific soil attenuation	multiple	over m and r	Approach 4
Calculate soil hazard from rock hazard and m and r deaggregation	several	over a , and over m and r given a	Approach 3
Calculate soil hazard from rock hazard and m deaggregation	several	over a , and over m given a	Approach 3A
Calculate soil hazard using soil amplification for input amplitude a^* and magnitude m^*	one, e.g. PGA	over a only	Approach 3B
Scale rock UHS to soil UHS accounting for soil parameter uncertainty	two, e.g. 10 and 1 Hz	none	Approach 2A
Scale rock UHS to soil UHS accounting for soil parameter uncertainty and m deaggregation	two, e.g. 10 and 1 Hz	none	Approach 2B
Scale rock UHS to soil UHS using broadbanded input motion	none	none	Approach 1

Table 6-2
Parameters for WUS Rock Outcrop Simulations

M	5.5, 6.5, 7.5		
D(km)	1, 5, 10, 20, 50, 75, 100, 200, 400		
30 simulations for each M, R pair = 810 runs			
Randomly vary source depth, $\Delta\sigma$, kappa, Q_o , profile			
<u>Depth</u> , $\sigma_{\ln H} = 0.6$, \bar{H} ($M > 5$) = 8 km; Source, California Seismicity			
M	Lower Bound (km)	\bar{H} (km)	Upper Bound (km)
5.5	2	6	25
6.5	4	8	20
7.5	5	8	15
<u>$\Delta\sigma$</u> , $\sigma_{\ln\Delta\sigma} = 0.5$, Based on California earthquake inversions (Silva et al., 1997)			
M	$\Delta\sigma$ (bars)	AVG. $\Delta\sigma$ (bars) = 65	
5.5	85	Based on inversions of the A&S 97 relation (BNL, 1997)	
6.5	64		
7.5	50		
<u>$Q(s)$</u> , $\bar{Q}_o = 275$, <i>Southern California inversions</i> ; $\sigma_{\ln Q_o} = 0.4$, (Silva et al., 1997) $\eta = 0.60$, <i>Southern California inversions</i> ; $\sigma_\eta = 0$, (Silva et al., 1997) Varying Q_o only is sufficient, since $\pm 1 \sigma$ covers range of Southern California inversions from 1 to 20 Hz			
<u>Kappa</u> , $\bar{\kappa} = 0.03$ sec, $\sigma_{\ln \kappa} = 0.3$ (EPRI, 1997): linear zone ($V_s \geq 1$ km/sec)			
<u>Profile</u> , California soft rock: GEOMATRIX A + B over Wald and Heaton (1994) Los Angeles Crust, randomize to 30m ft			
Geometrical attenuation $R^{-(a+bM)}$, $a = 1.0296$, $b = -0.0422$ $R^{-(a+bM)/2}$, $R > 65$ km			
Based on inversions of the Abrahamson and Silva (1997) relation			

Table 6-3
Parameters for CEUS Rock Outcrop Simulations

M 5.5, 6.5, 7.5			
D(km) 1, 5, 10, 20, 50, 75, 100, 200, 400			
30 simulations = 810 runs			
Randomly vary source depth, $\Delta\sigma$, kappa, Q_0 , η , profile			
<u>Depth</u> , $\sigma_{\ln H} = 0.6$, \bar{H} ($M > 5$) = 10 km; Intraplate Seismicity (EPRI, 1993)			
M	Lower Bound (km)	\bar{H} (km)	Upper Bound (km)
5.5	3	8	30
6.5	4	10	30
7.5	5	12	30
<u>$\Delta\sigma$</u> , $\sigma_{\ln\Delta\sigma} = 0.7$ (EPRI, 1993)			
M	$\Delta\sigma$ (bars)	AVG. $\Delta\sigma$ (bars) = 122, Assumes M 5.5 = 160 bars (Atkinson, 1993) with magnitude scaling taken from WUS (Table 6- 2)	
5.5	160		
6.5	120		
7.5	95		
<p>$Q(s)$, $\bar{Q}_0 = 351$, <i>Saguenay inversions</i>; $\sigma_{\ln Q_0} = 0.4$, (Silva et al., 1997)</p> <p>$\eta = 0.84$, <i>Saguenay inversions</i>; $\sigma_\eta = 0$, (Silva et al., 1997)</p> <p>Varying Q_0 only is sufficient, since $\pm 1 \sigma$ covers range of CEUS inversions from 1 to 20 Hz</p>			
<u>Kappa</u> , $\bar{\kappa} = 0.006$ sec $\sigma_{\ln \kappa} = 0.3$, (EPRI, 1993)			
<u>Profile</u> , Midcontinent Crust (EPRI, 1993), randomize to 30m			
Geometrical attenuation $R^{-(a+bM)}$, $a = 1.0296$, $b = -0.0422$ $R^{-(a+bM)/2}$, $R > 100$ km			
Based on inversions of the Abrahamson and Silva (1997) relation			

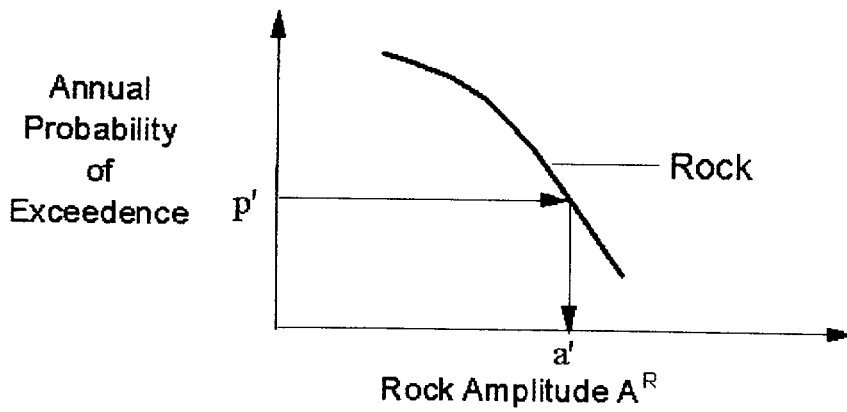
Table 6-4
Southern California Crustal Model**

Thickness (km)	V_s (km/sec)	Density (cgs)
0.0015239	0.24383	2.0
0.0024383	0.30478	2.0
0.0030479	0.42670	2.0
0.0042670	0.53337	2.0
0.0033526	0.63091	2.0
0.0042670	0.71624	2.0
0.0057909	0.83016	2.0
0.0067503	0.96617	2.0
0.5	1.0	2.1
1.5	2.0	2.3
2.5	3.2	2.5
23.0	3.6	2.6
5.0	3.9	2.9
	4.5	3.0

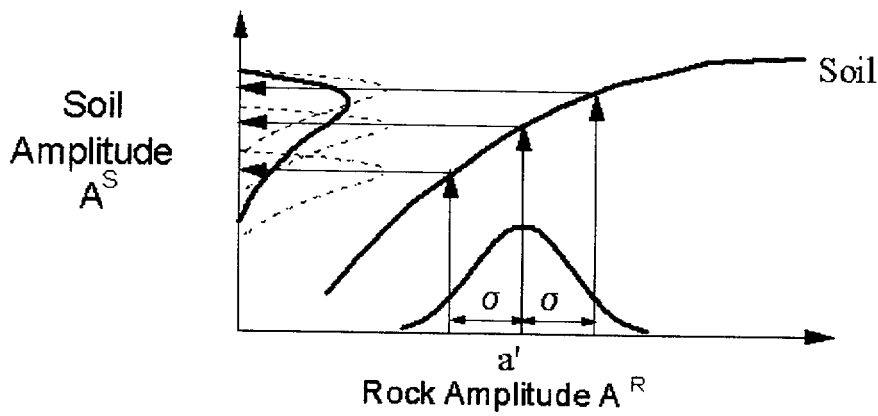
Table 6-5
CEUS Crustal Model (EPRI, 1993 Midcontinent)

Thickness (km)	V_s (km/sec)	Density (cgs)
1.0	2.830	2.52
11.0	3.520	2.71
28.0	3.750	2.78
	4.620	3.35

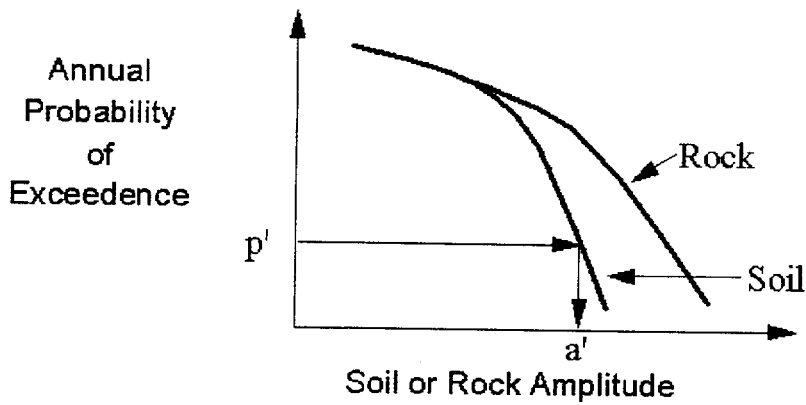
**Wald and Heaton, 1994 begins at $V_s = 1$ km/sec



A. Rock Seismic Hazard Curve

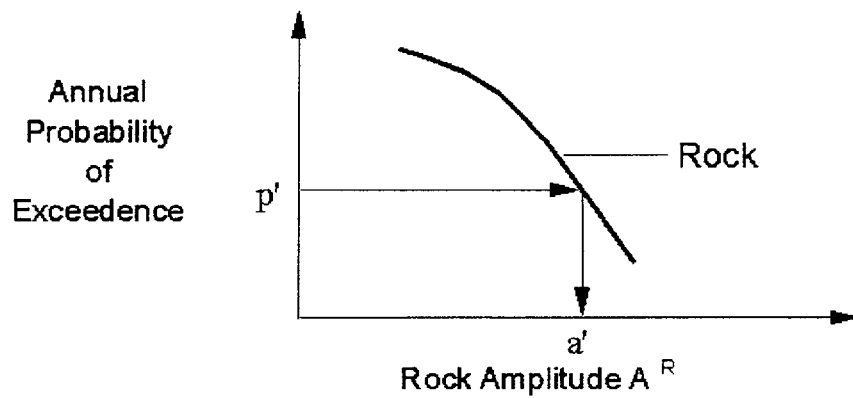


B. Soil Amplitude vs. Rock Amplitude, given M

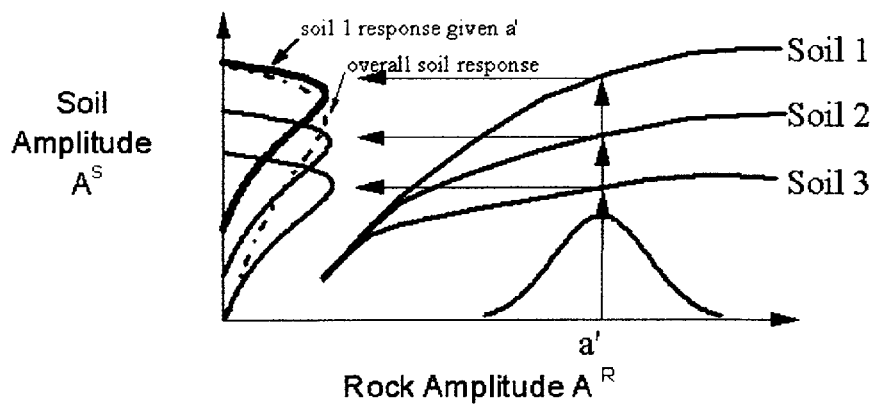


C. Soil Seismic Hazard Curves

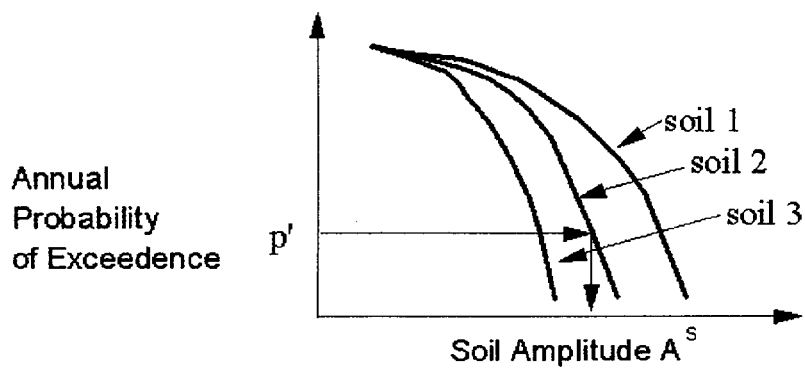
Figure 6-1. Integrations to calculate soil hazard, for known soil properties and aleatory variability on soil response.



A. Rock seismic hazard curve

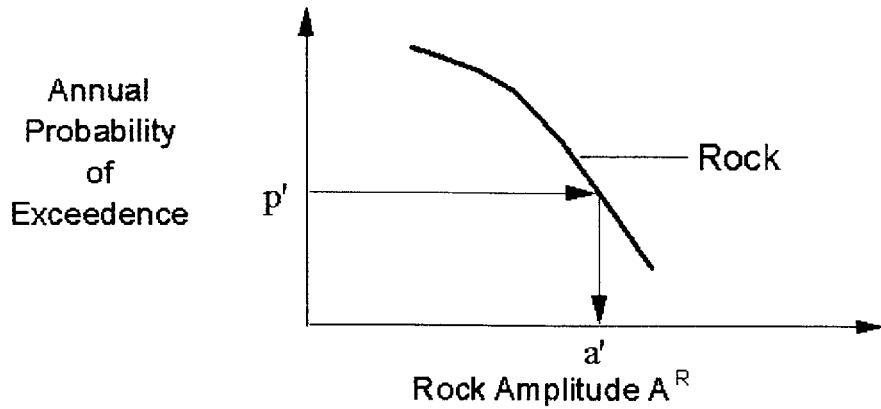


B. Soil amplitudes vs. rock for three sets of soil characteristics.

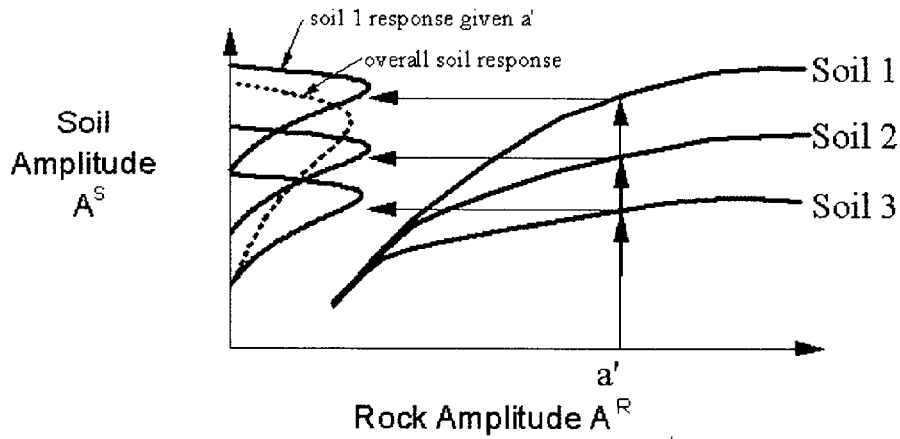


C. Soil seismic hazard curves

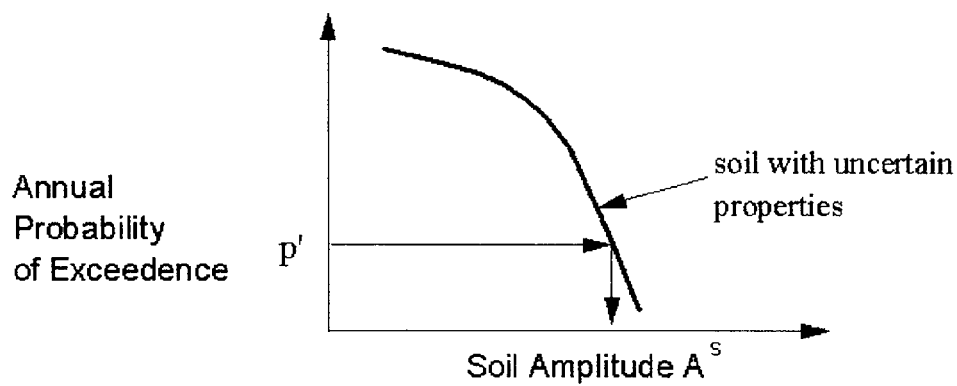
Figure 6-2: Integration to calculate soil hazard with uncertain soil properties.



A. Rock seismic hazard curve

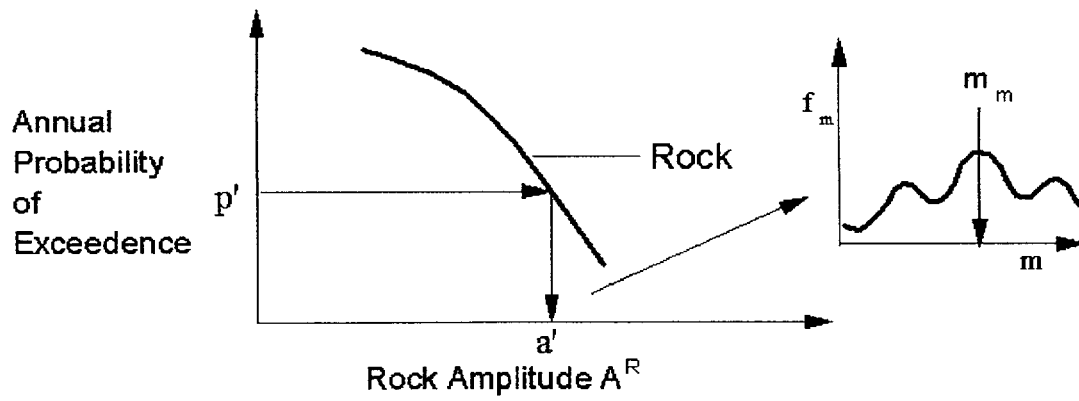


B. Soil amplitudes vs. rock for three sets of soil characteristics.

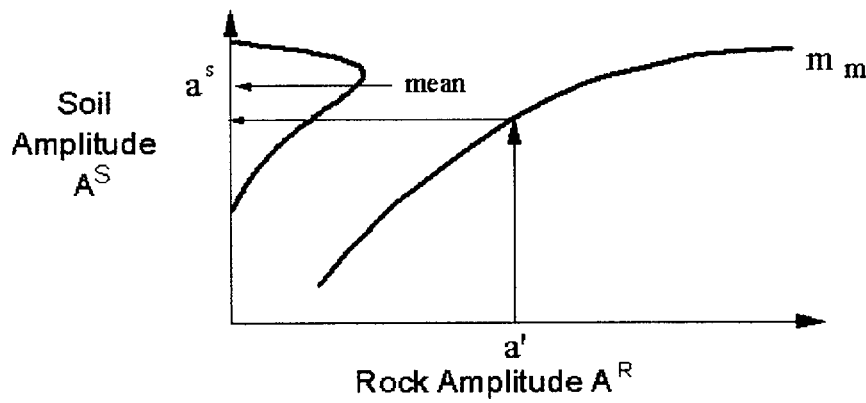


C. Soil seismic hazard curves

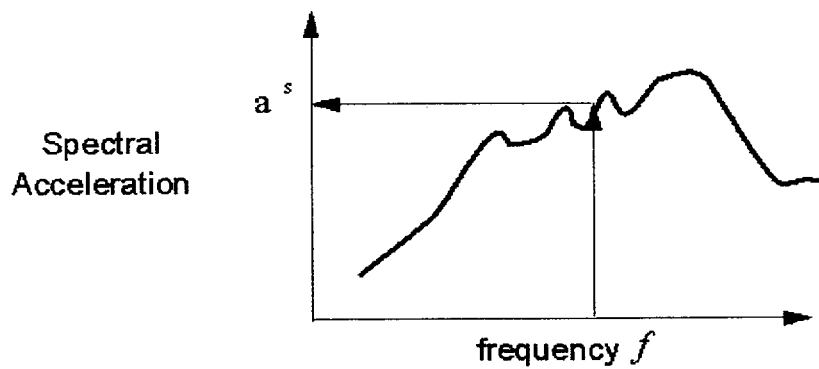
Figure 6-3: Integration to calculate soil hazard using distribution of AF at a' .



A. Rock Seismic Hazard Curve

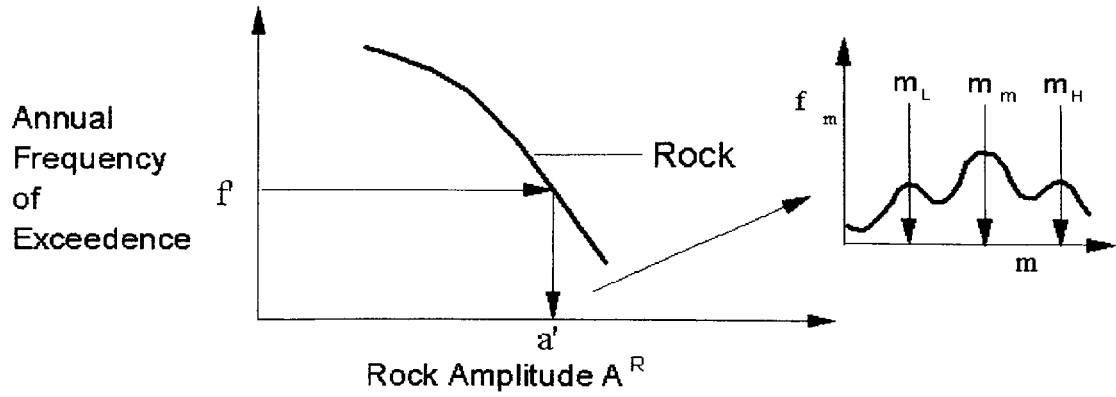


B. Soil Amplitude vs. Rock Amplitude, given a'

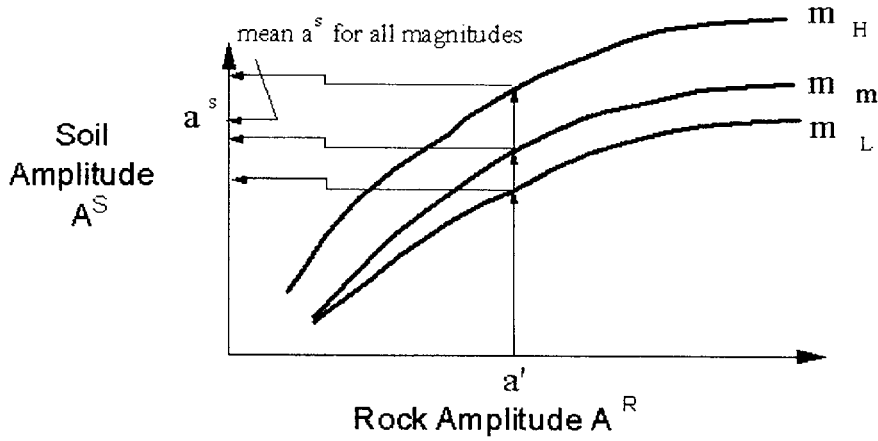


C. UHS on Soil

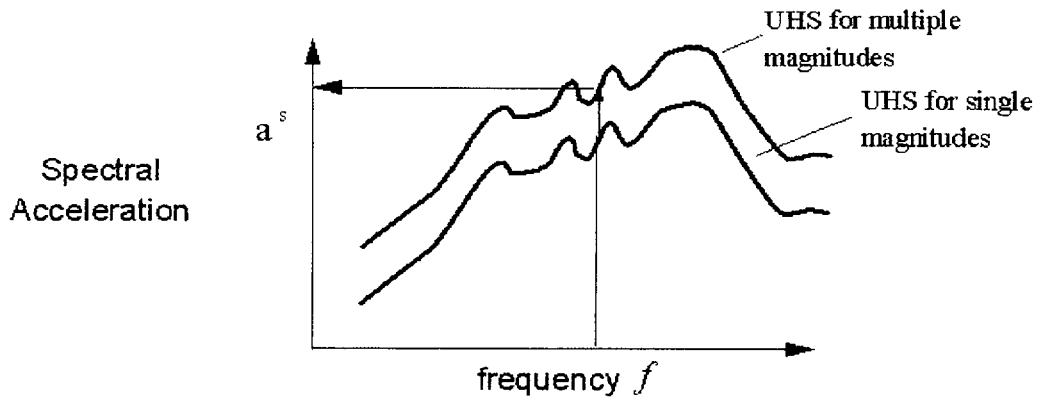
Figure 6-4: Scaling soil UHS from rock UHS, single magnitude.



A. Rock Seismic Hazard Curve

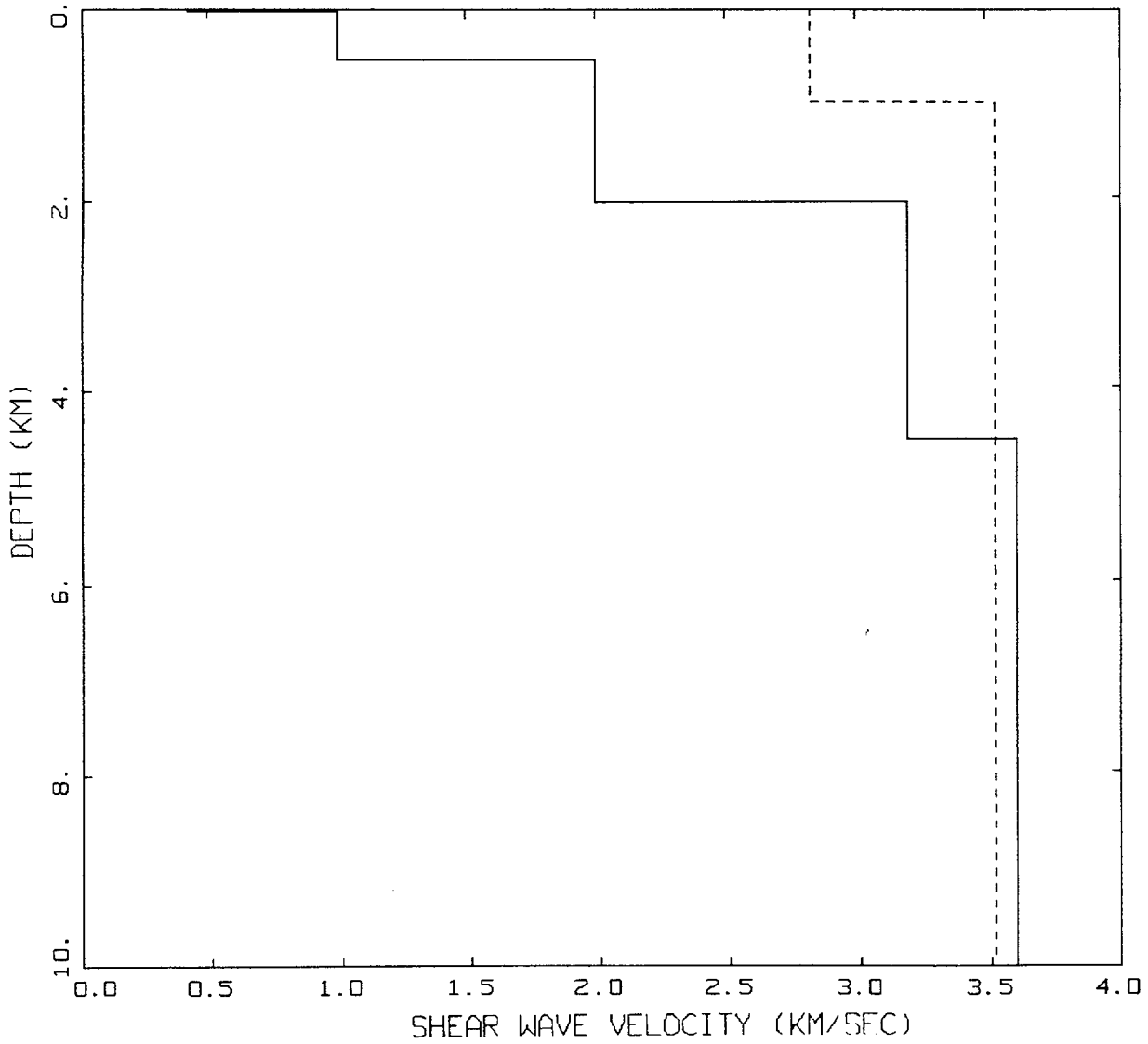


B. Soil Amplitude vs. Rock Amplitude, given a' , multiple magnitudes



C. UHS on Soil

Figure 6-5: Scaling soil UHS from rock UHS with magnitude dependence.



GENERIC WUS AND CEUS
CRUSTAL MODELS

LEGEND
 — WUS
 - - - CEUS

Figure 6-6. Comparison of generic shear-wave velocity profiles for WUS (Los Angeles) and CEUS crustal conditions.

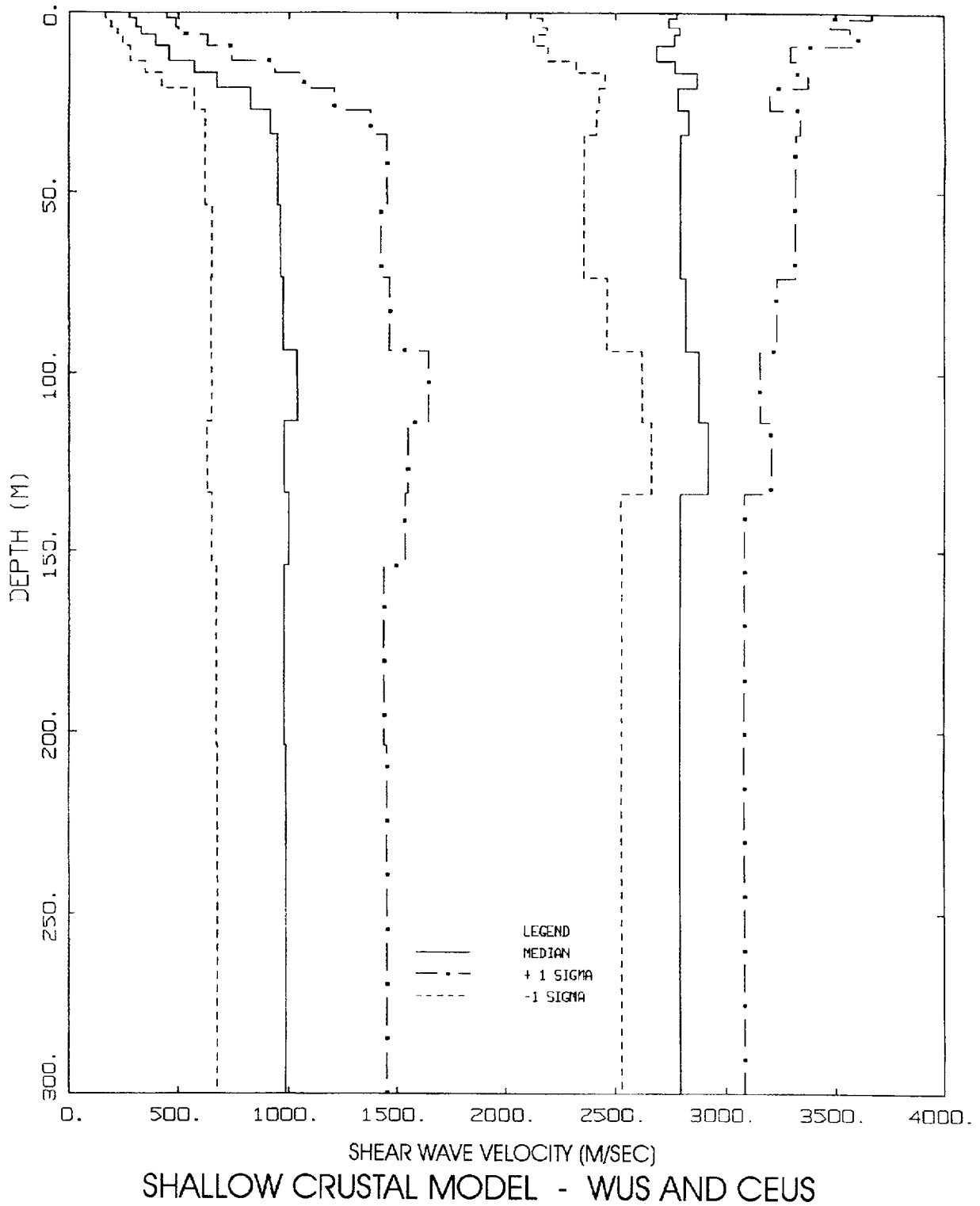
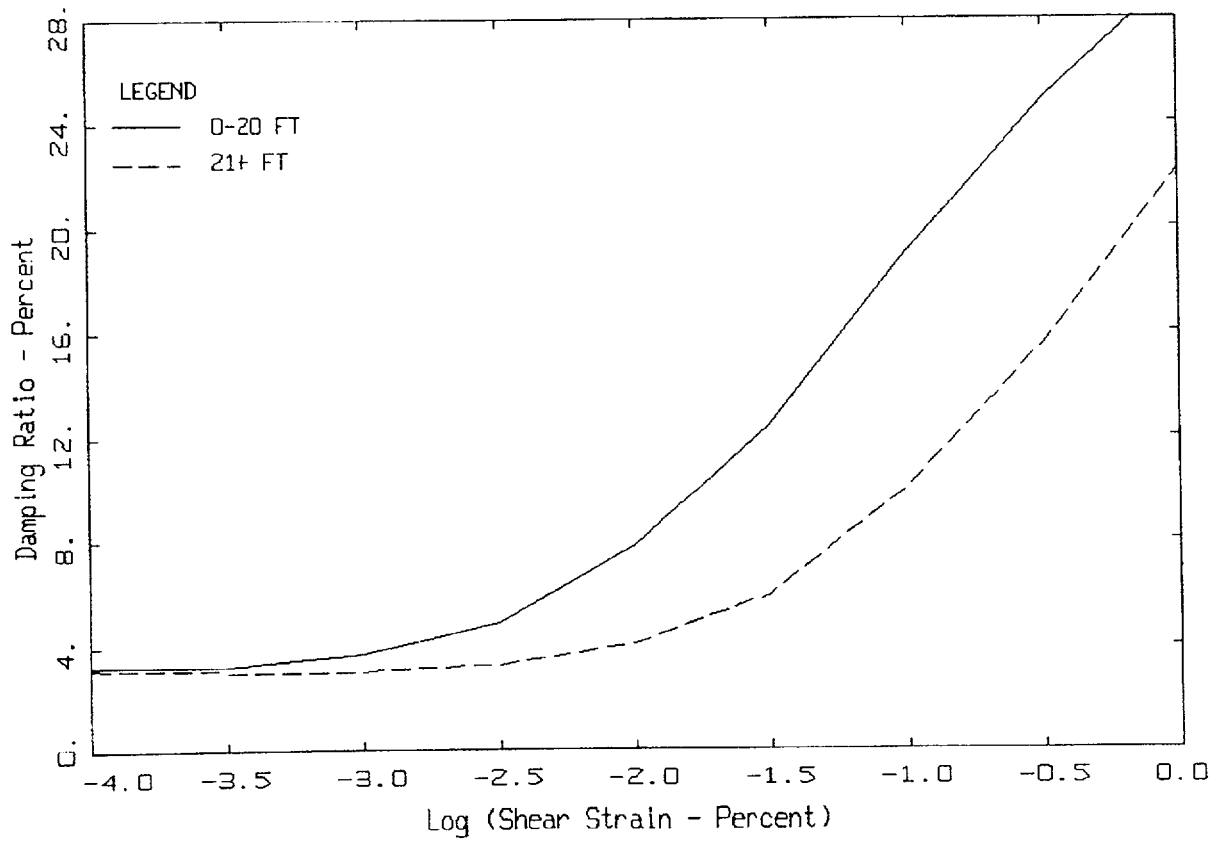
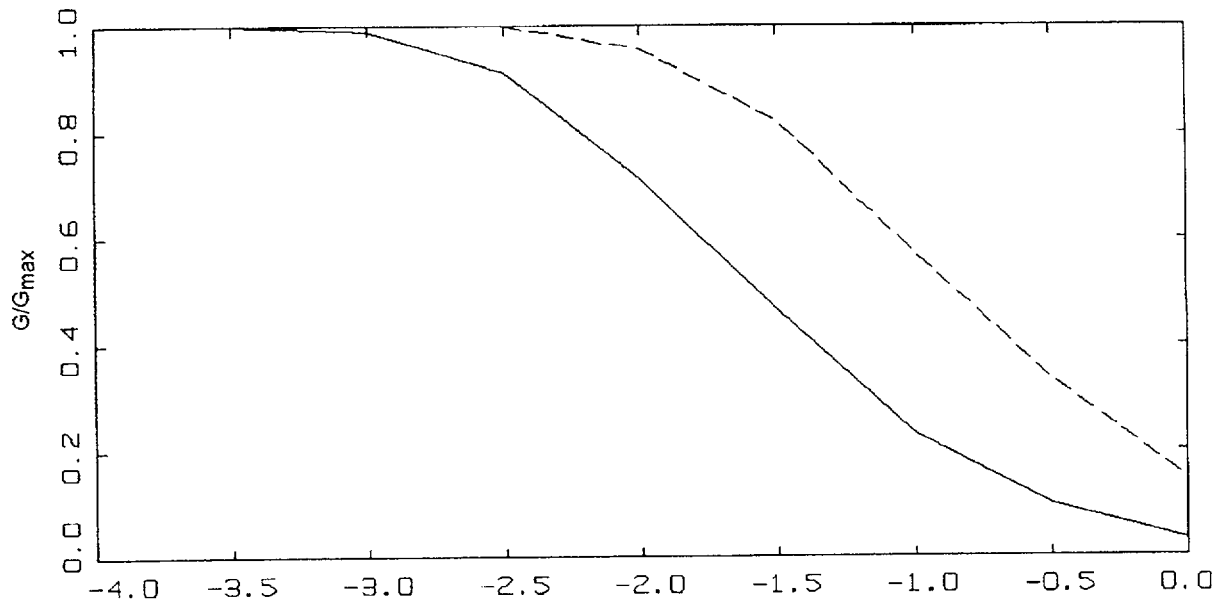
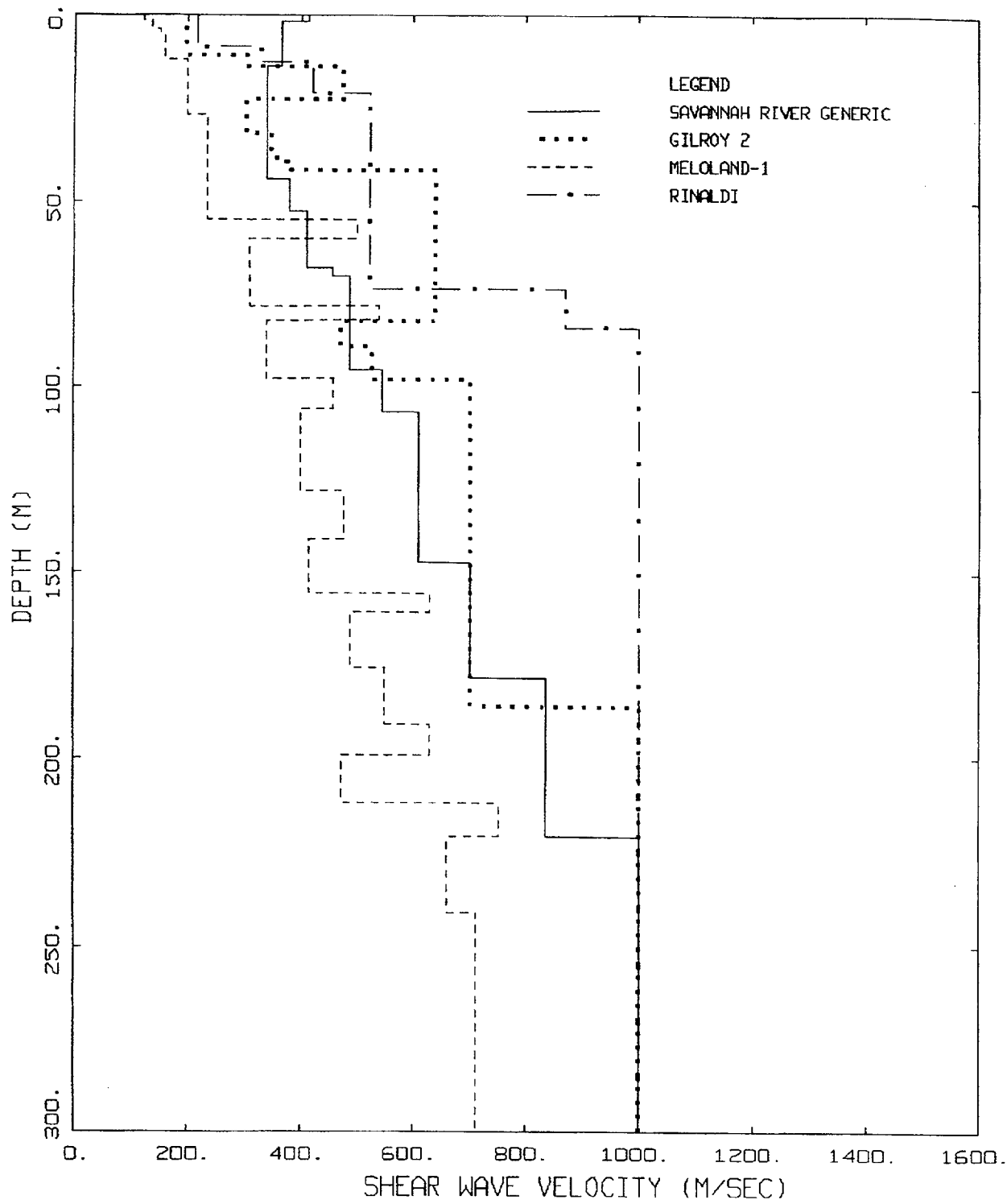


Figure 6-7. Variations in base case shallow crustal velocities. Solid lines are median estimates from a suite of randomly generated profiles (30) using base-case profiles (Figure 6-6) as input. Ranges reflect $\pm 1\sigma$ estimates.



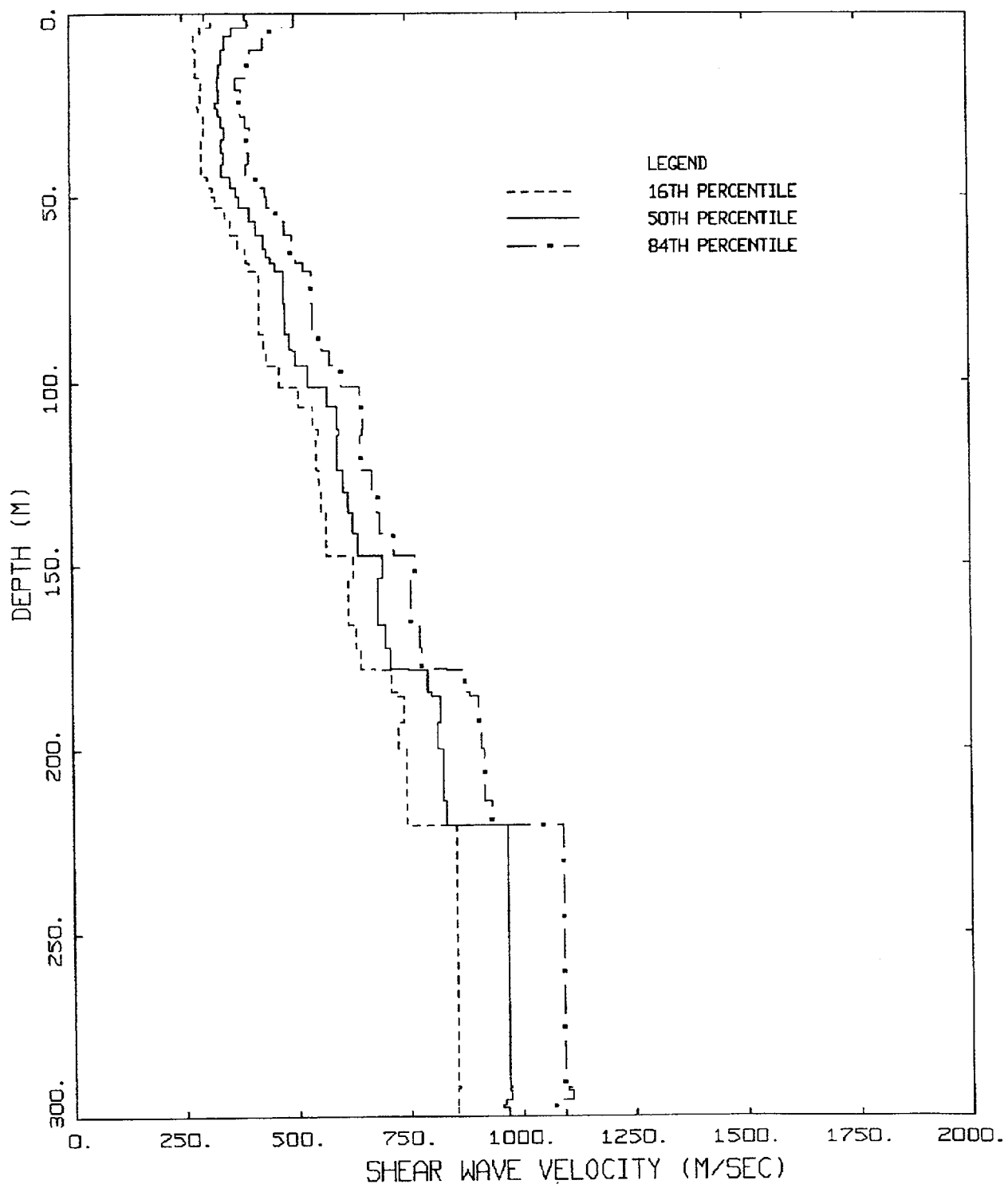
MODULUS REDUCTION AND DAMPING CURVES FOR ROCK

Figure 6-8. Generic G/G_{max} and hysteretic damping curves for soft rock.



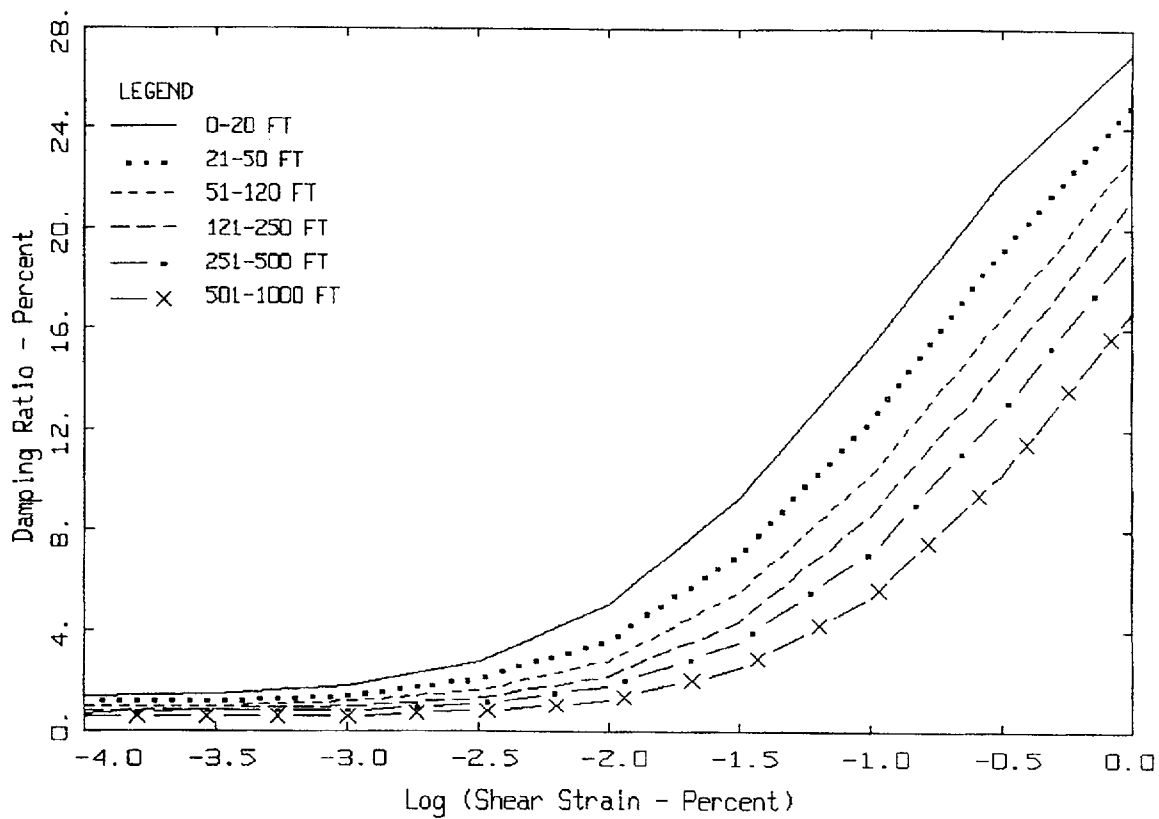
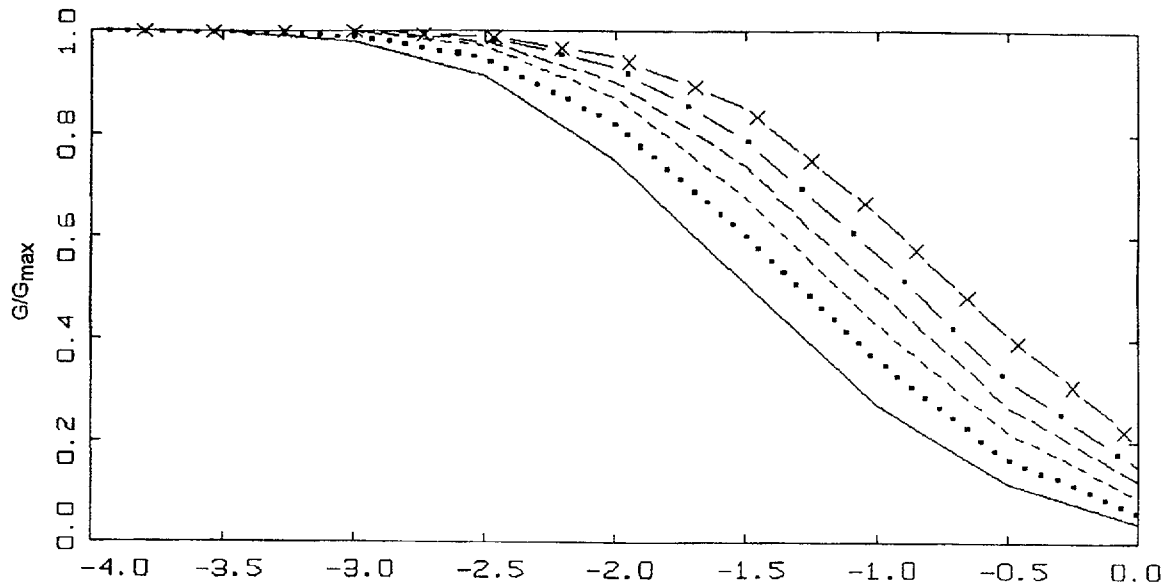
NRC, H_CON PROFILES

Figure 6-9. Base case shear-wave velocity profiles based on suspension logging measurements. Placed on top of Wald and Heaton (1994) crustal model (Table 6-4).



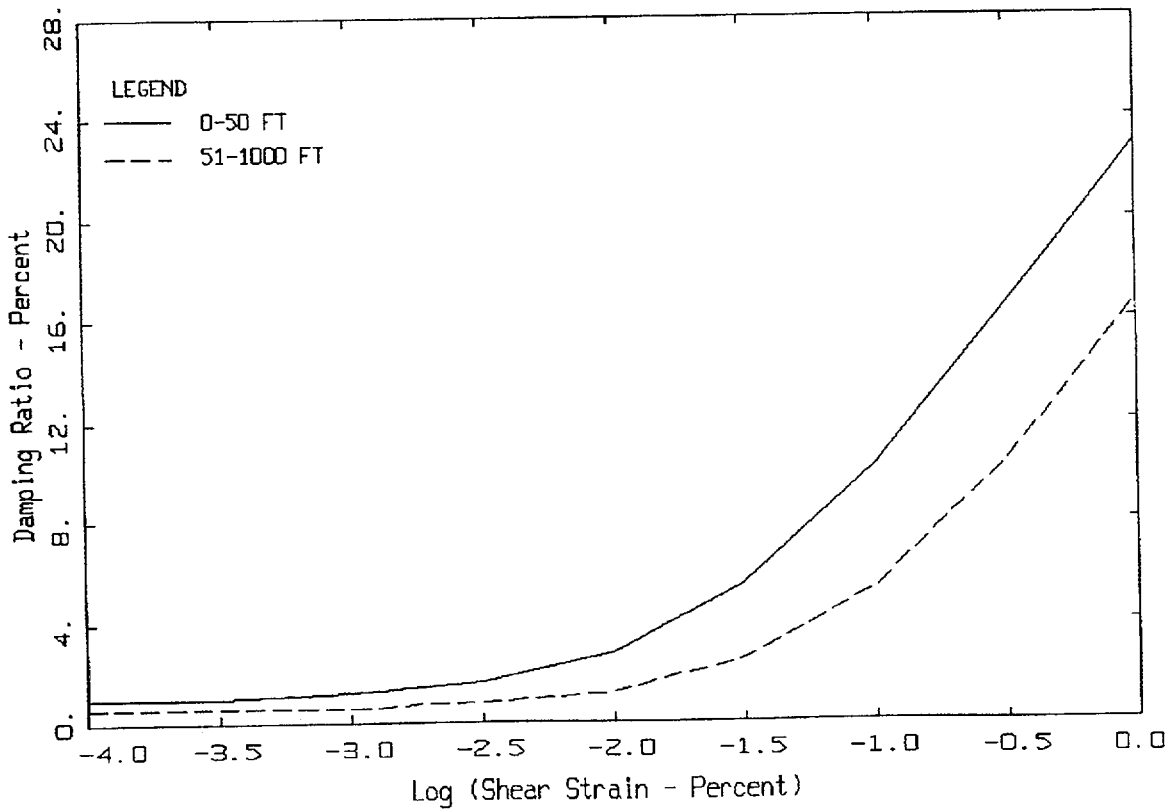
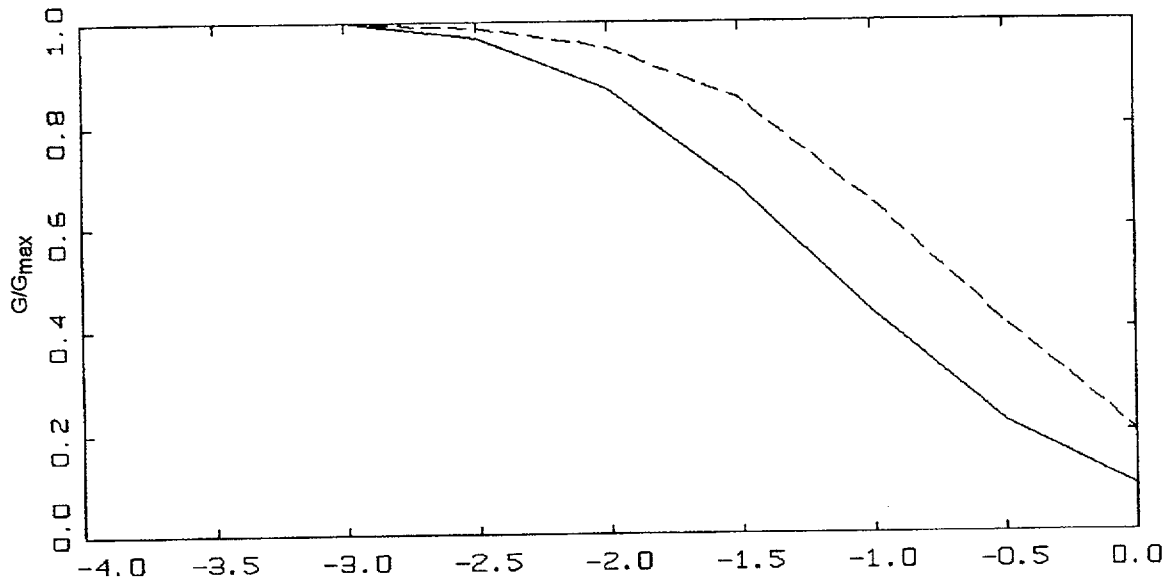
SAVANNAH RIVER GENERIC PROFILE

Figure 6-10. Variation in base case shear-wave velocity, generic Savannah River profile (Figure 6-9) based on thirty realizations. Median estimate along with $\pm\sigma$ values.



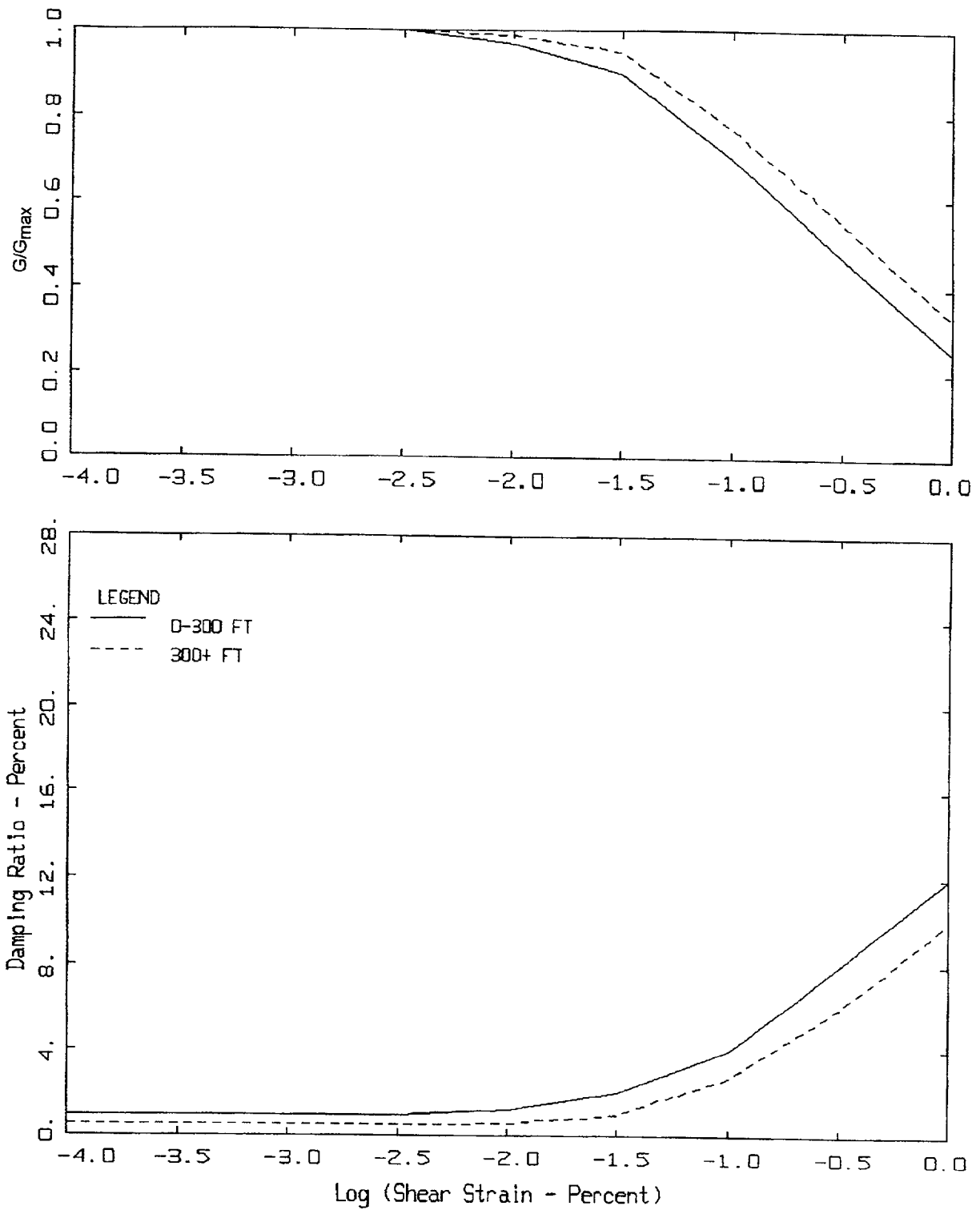
MODULUS REDUCTION AND DAMPING CURVES FOR COHESIONLESS SOILS

Figure 6-11. Generic G/G_{max} and hysteretic damping curves used for Northern California cohesionless soil site Gilroy 2 (EPRI, 1993).



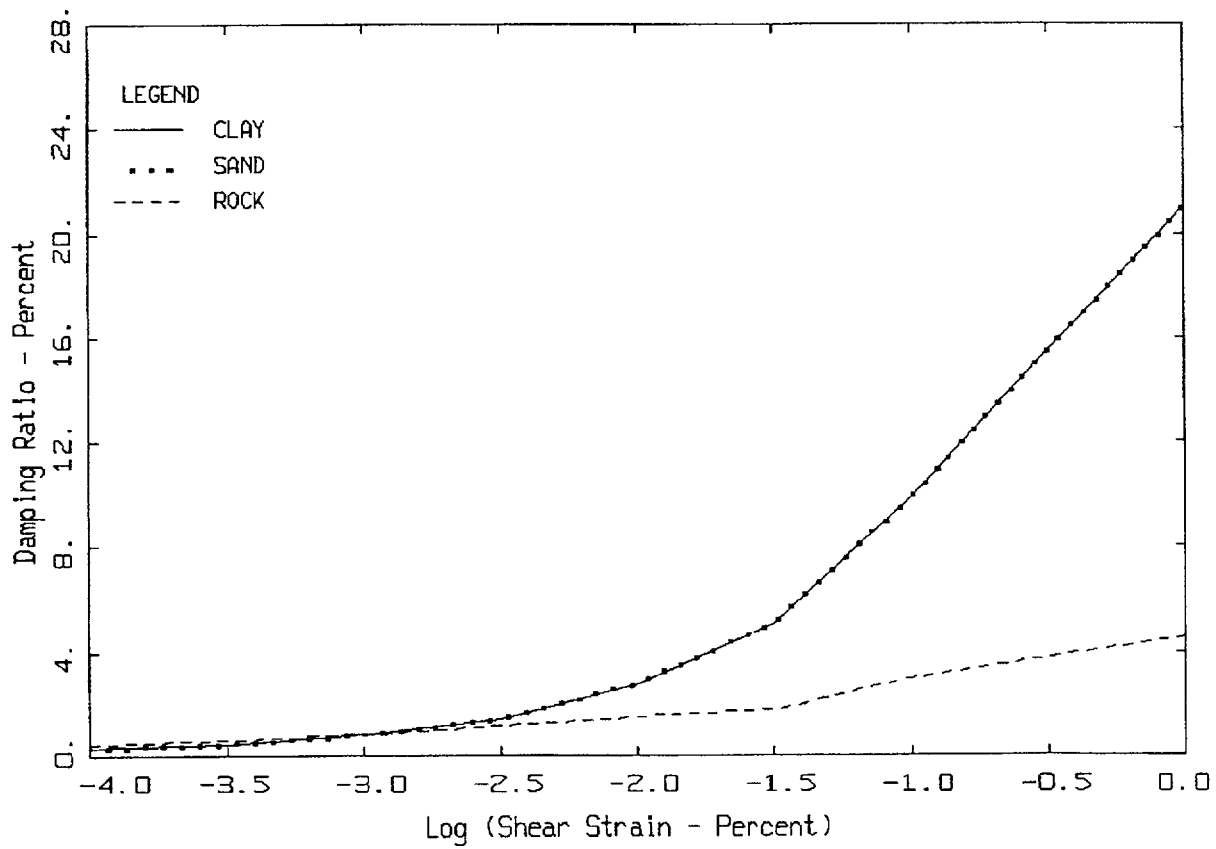
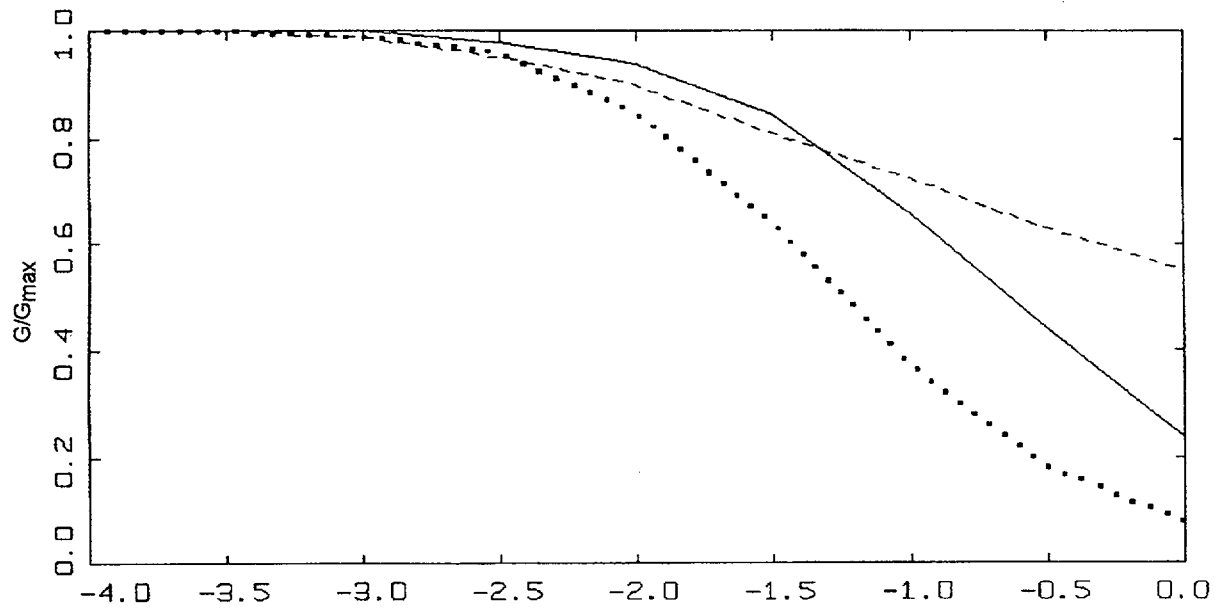
MODULUS REDUCTION AND DAMPING CURVES FOR COHESIONLESS SOILS

Figure 6-12. Generic G/G_{max} and hysteretic damping curves for Peninsular Range deep cohesionless soils. Used for soil sites Rinaldi and Savannah River Generic.



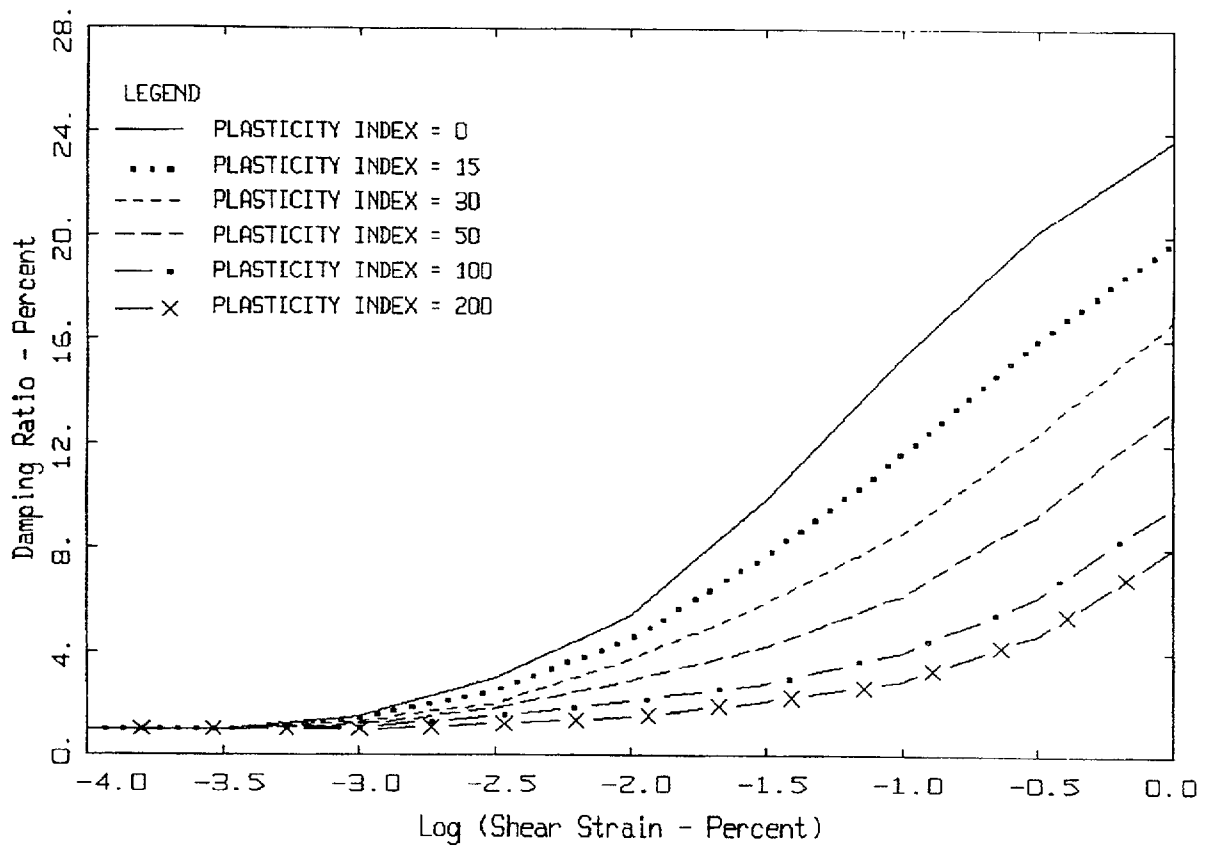
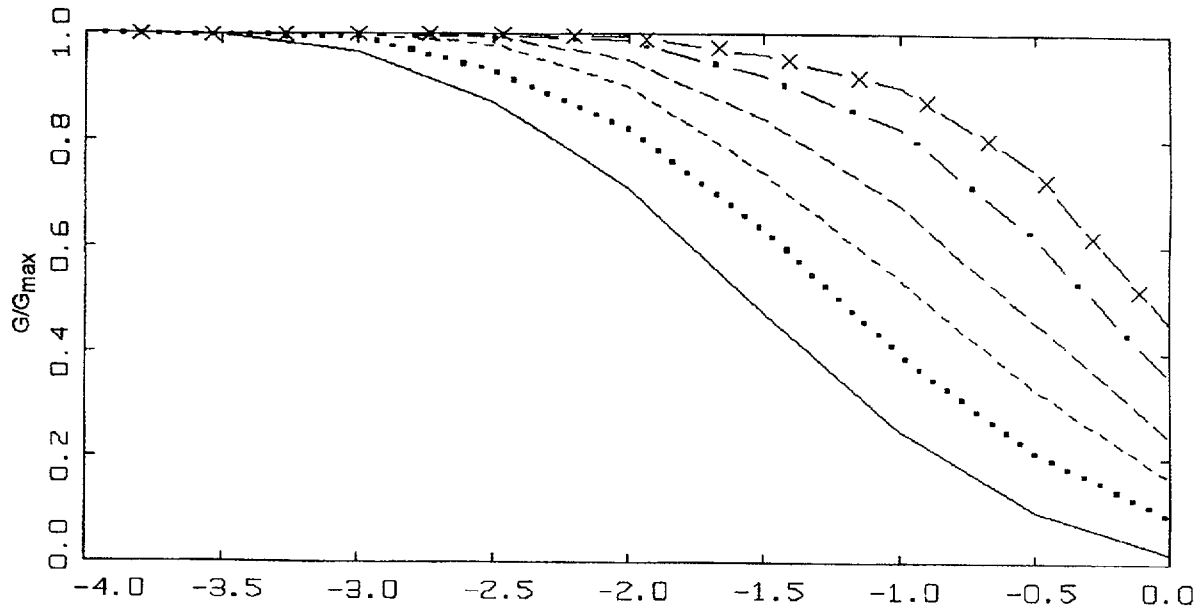
MODULUS REDUCTION AND DAMPING CURVES FOR EL CENTRO

Figure 6-13. Generic G/G_{max} and hysteretic damping curves for Imperial Valley soils. Used for soil site Meloland.



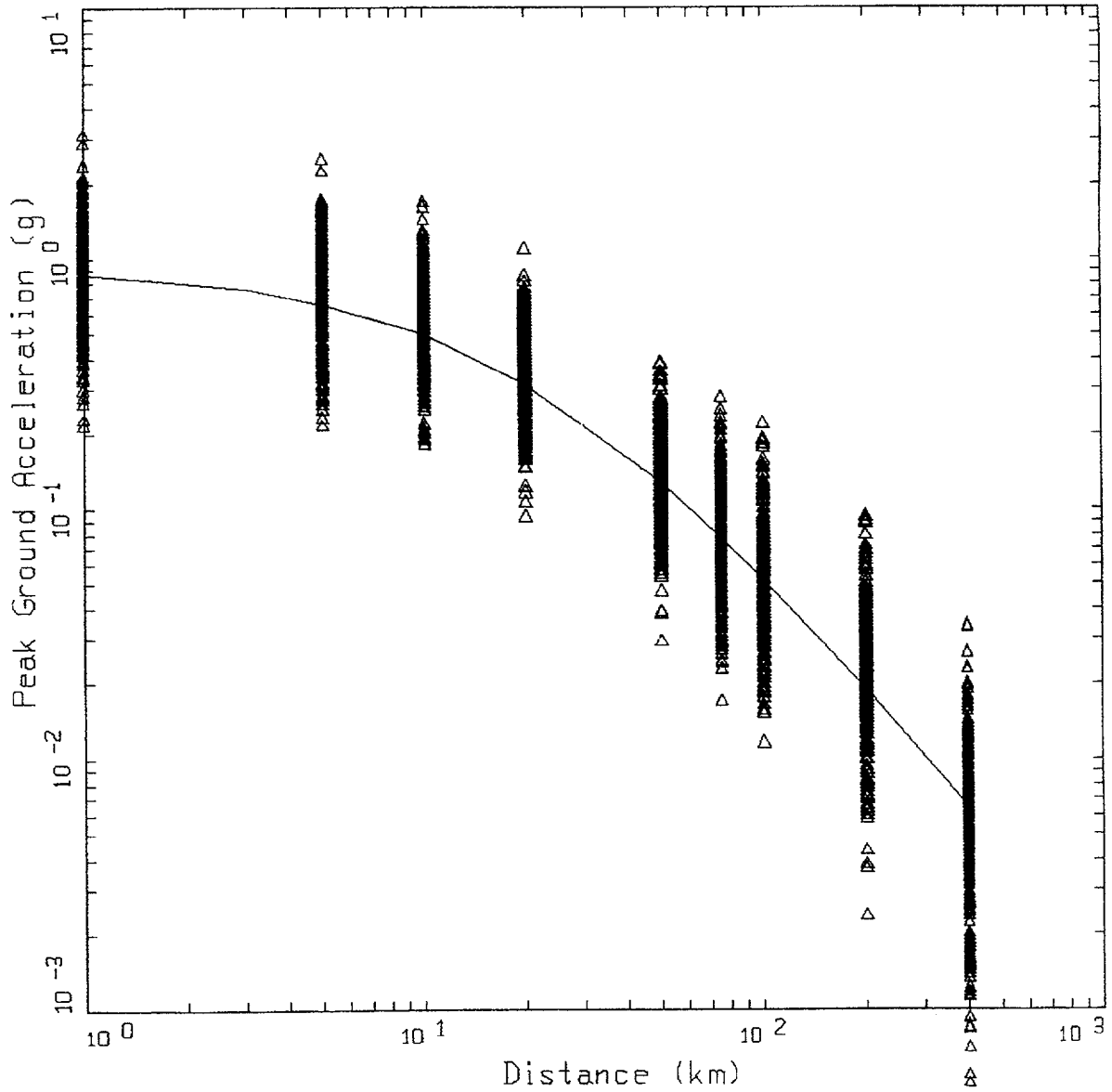
MODULUS REDUCTION AND DAMPING CURVES FROM SHAKE MANUAL

Figure 6-14. Generic G/G_{max} and hysteretic damping curves from SHAKE (Idriss and Sun, 1992).



VUCETIC/DOBRY MODULUS REDUCTION AND DAMPING CURVES

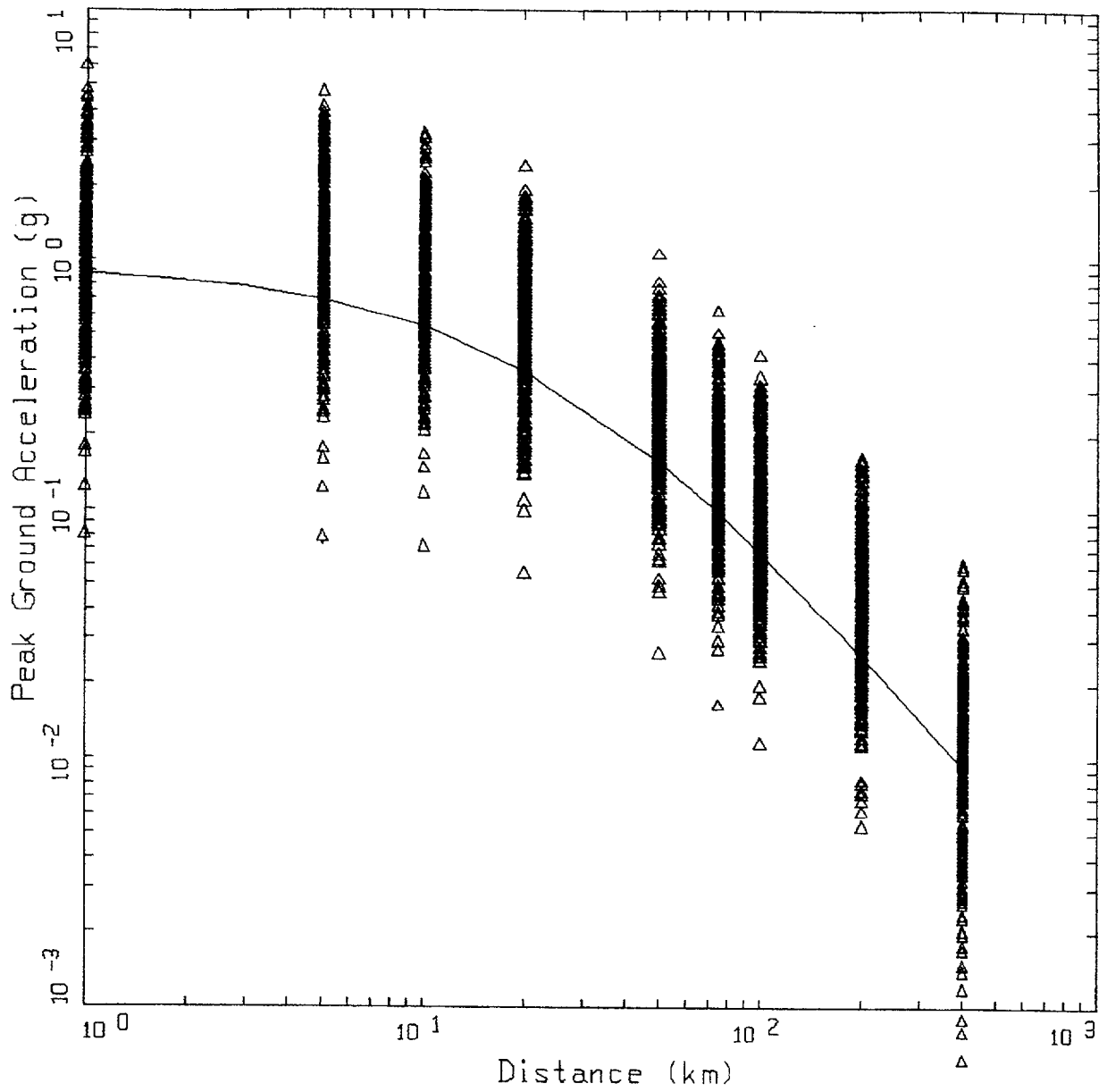
Figure 6-15. Generic G/G_{max} and hysteretic damping curves for cohesive soils (Vucetic and Dobry, 1991).



WUS ROCK
 M = 7.5

LEGEND
 Δ DATA: PGA
 — M=7.5, SIGMA=0.5655

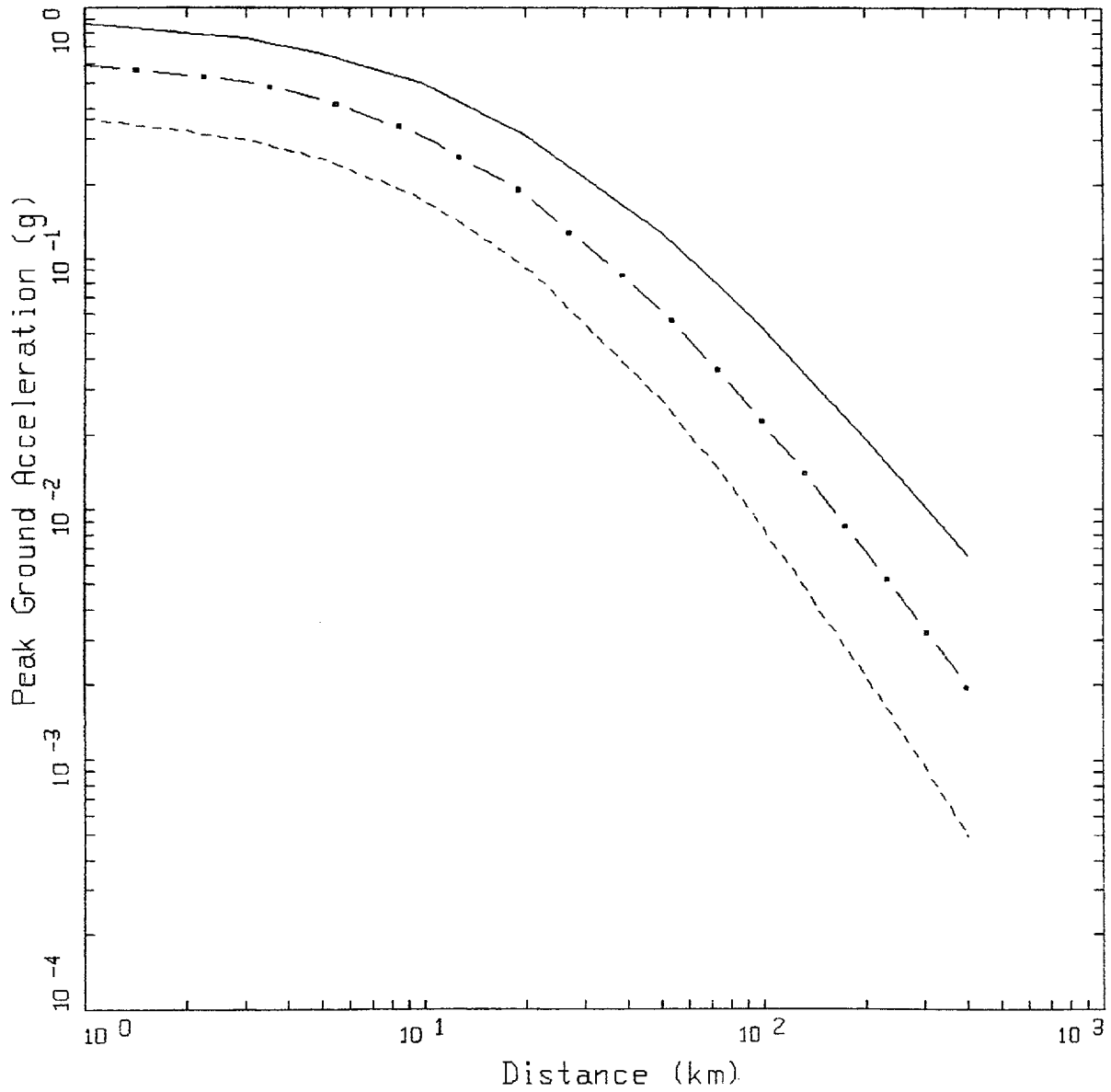
Figure 6-16. Peak acceleration estimates and regression fit at M 7.5 for WUS rock site conditions.



CEUS ROCK
 M = 7.5

LEGEND
 Δ DATA: PGA
 — M=7.5, SIGMA=0.6387

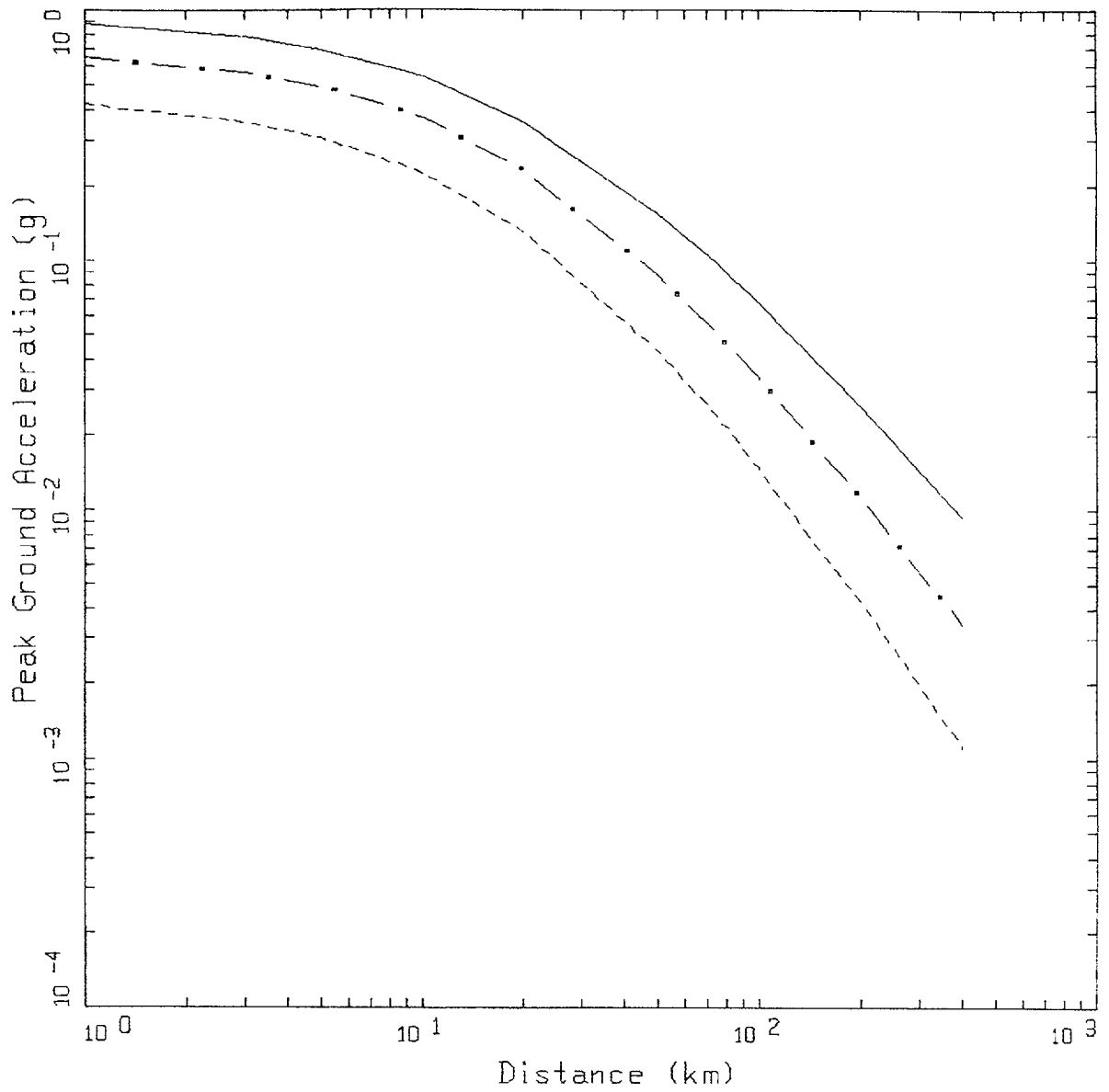
Figure 6-17. Peak acceleration estimates and regression fit at M7.5 for CEUS rock site conditions.



WUS ROCK

LEGEND
 ————— M=7.5, SIGMA=0.5655
 - · - M=6.5, SIGMA=0.5655
 - - - - M=5.5, SIGMA=0.5655

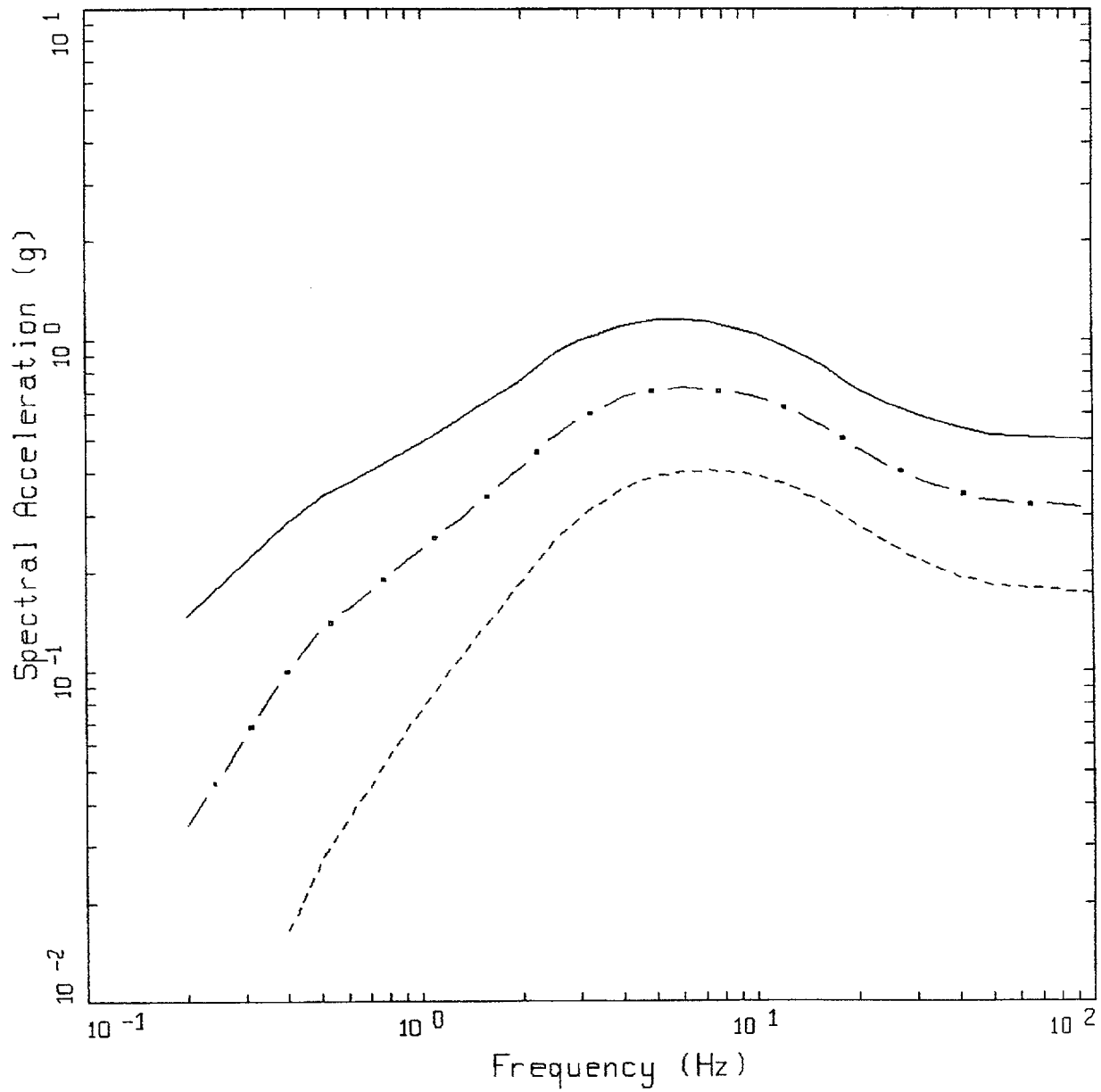
Figure 6-18. Attenuation of median peak horizontal acceleration at M 5.5, 6.5, and 7.5 for WUS rock site conditions.



CEUS ROCK

- LEGEND
- M=7.5, SIGMA=0.6387
 - ■ - M=6.5, SIGMA=0.6387
 - - - M=5.5, SIGMA=0.6387

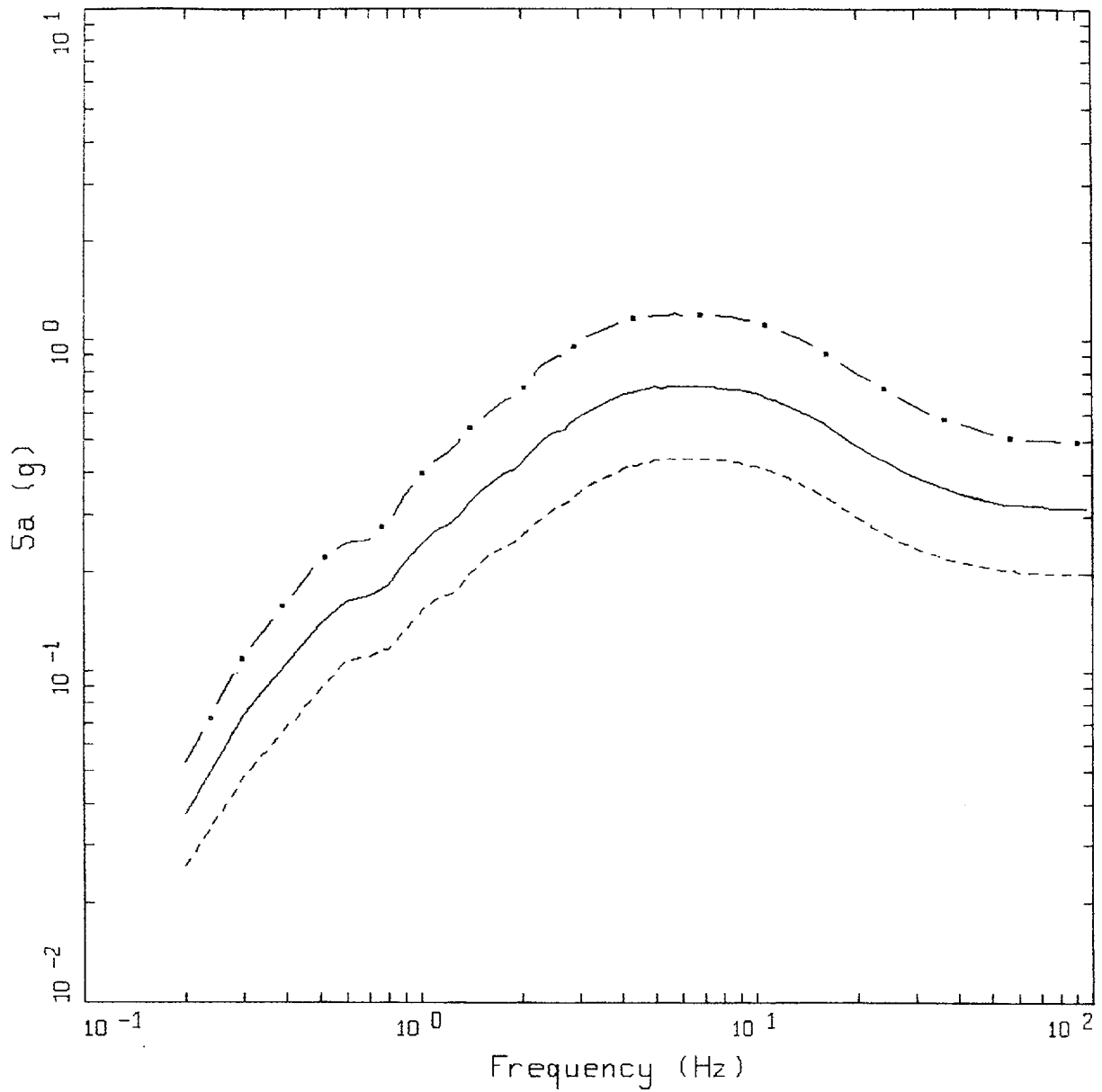
Figure 6-19. Attenuation of median peak horizontal acceleration at M 5.5, 6.5, and 7.5 for CEUS rock site conditions.



WUS ROCK
 DISTANCE=10 KM

LEGEND
 — M=7.5
 - · - M=6.5
 - - - M=5.5

Figure 6-20. Median response spectra (5% damping) at a distance of 10 km for magnitudes M 5.5, 6.5, and 7.5: WUS rock site.

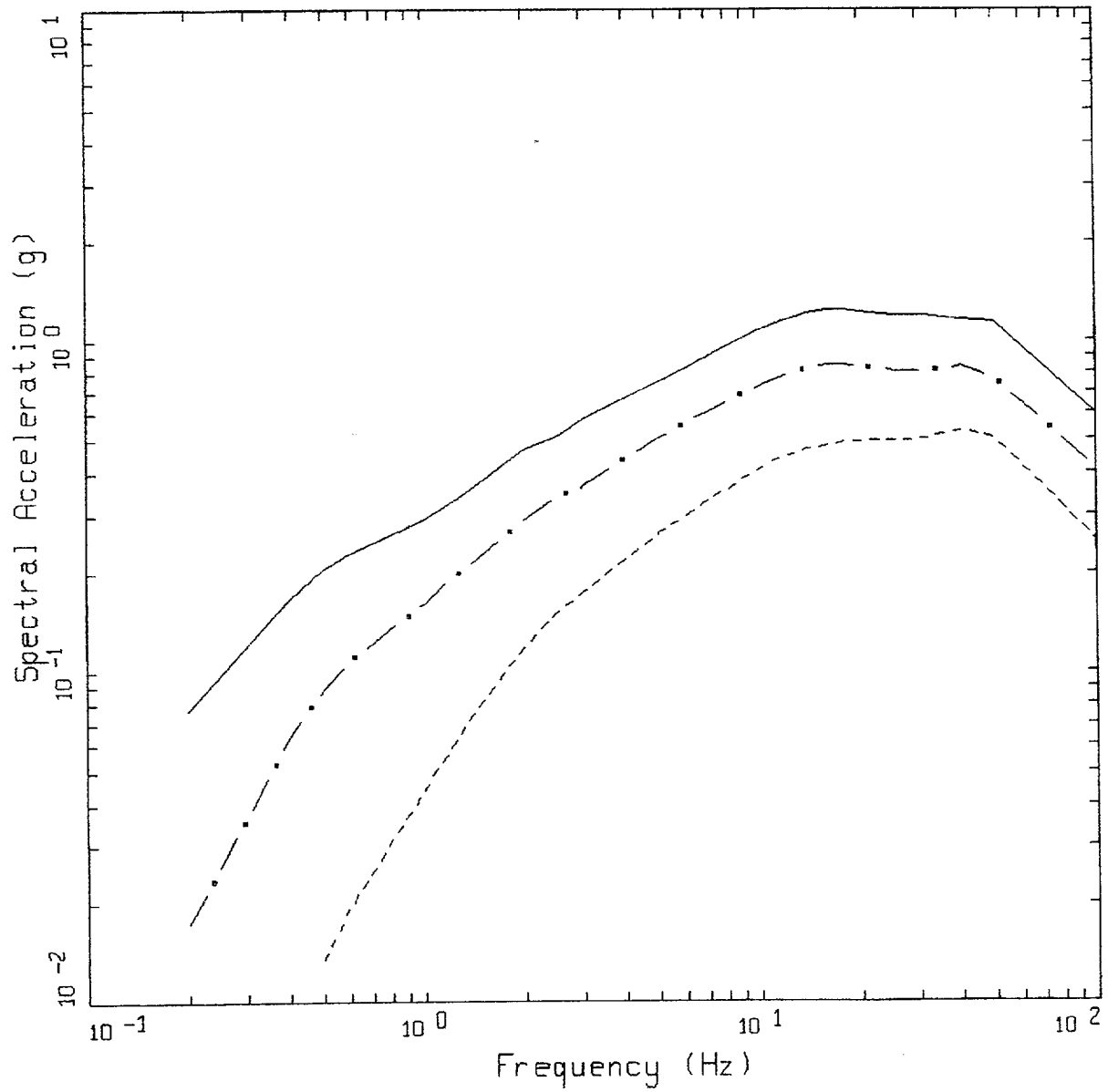


WUS ROCK
M=6.5, DISTANCE=10 KM

LEGEND

- • — 84TH PERCENTILE, PGA = 0.500 G
- 50TH PERCENTILE, PGA = 0.315 G
- - - 16TH PERCENTILE, PGA = 0.199 G

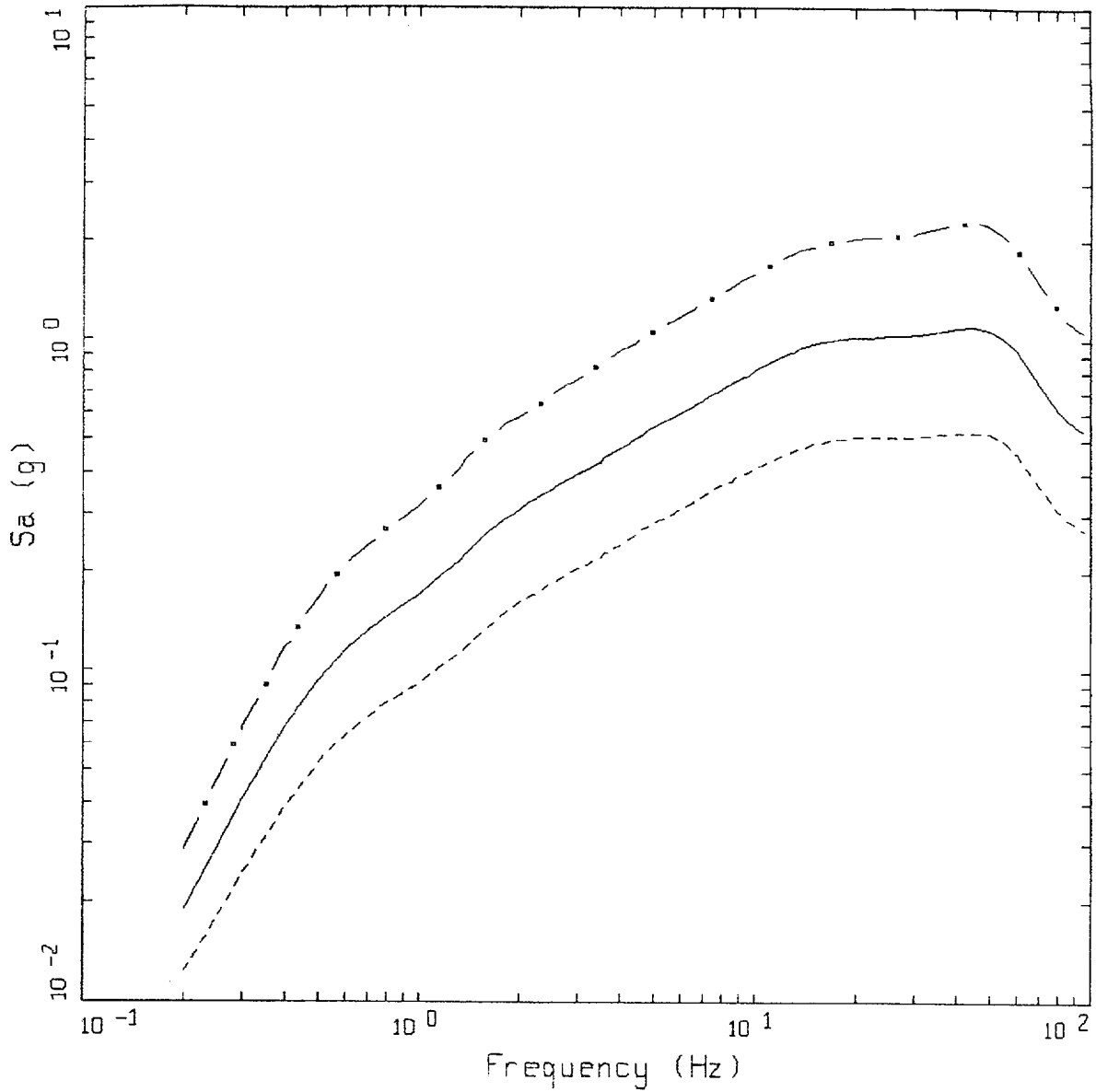
Figure 6-21. Response spectra (5% damping) at a distance of 10 km for M 6.5 showing median and $\pm 1\sigma$ estimates (parametric and regression uncertainty): WUS rock site.



CEUS ROCK
 DISTANCE = 10 KM

LEGEND
 — M=7.5
 - • - M=6.5
 - - - M=5.5

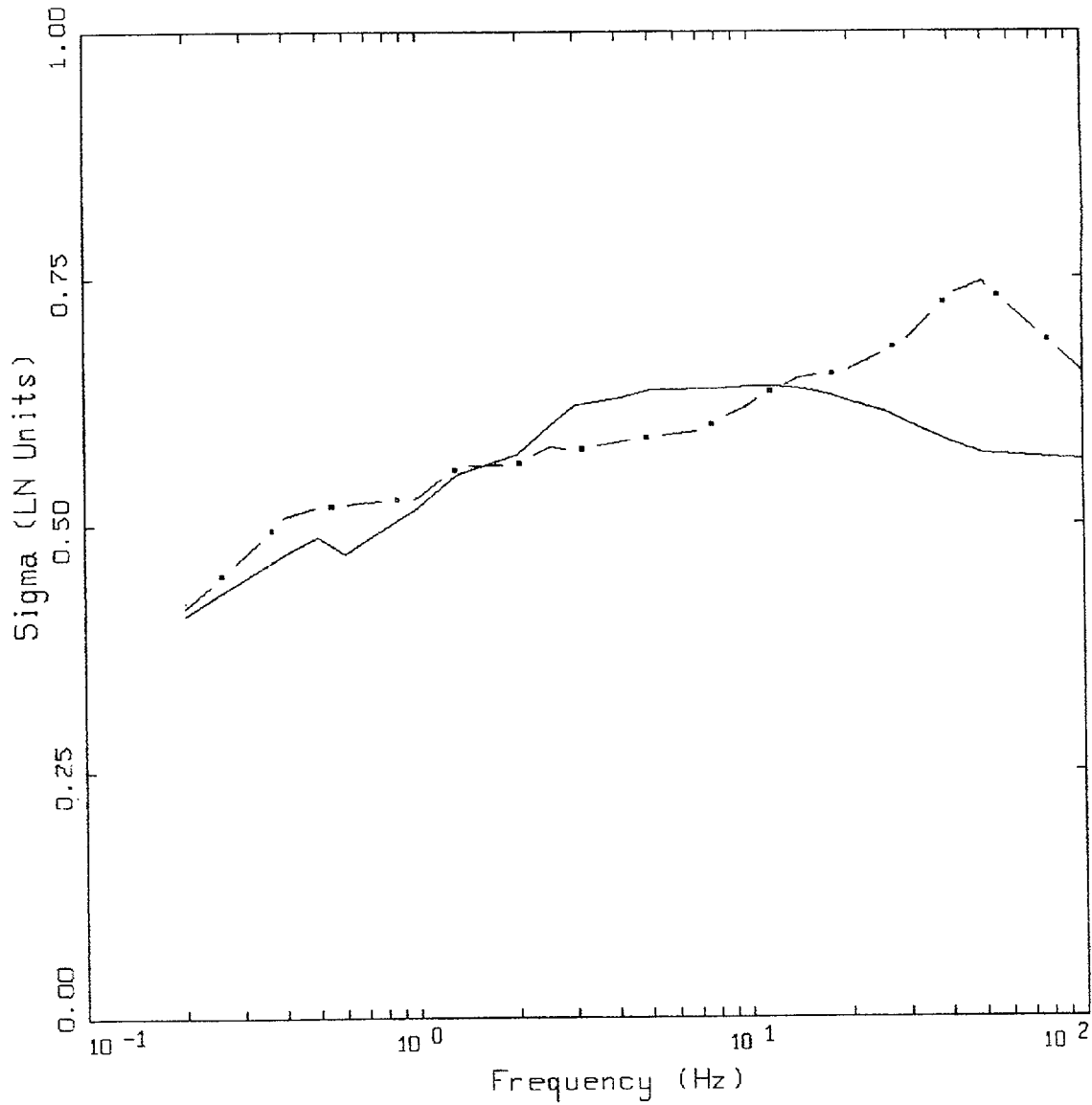
Figure 6-22. Median response spectra (5% damping) at a distance of 10 km for magnitudes M 5.5, 6.5, and 7.6: CEUS rock site.



CEUS ROCK
M=6.5, DISTANCE=10 KM

- LEGEND
- • — 84TH PERCENTILE, PGA = 1.033 G
 - 50TH PERCENTILE, PGA = 0.520 G
 - - - 16TH PERCENTILE, PGA = 0.262 G

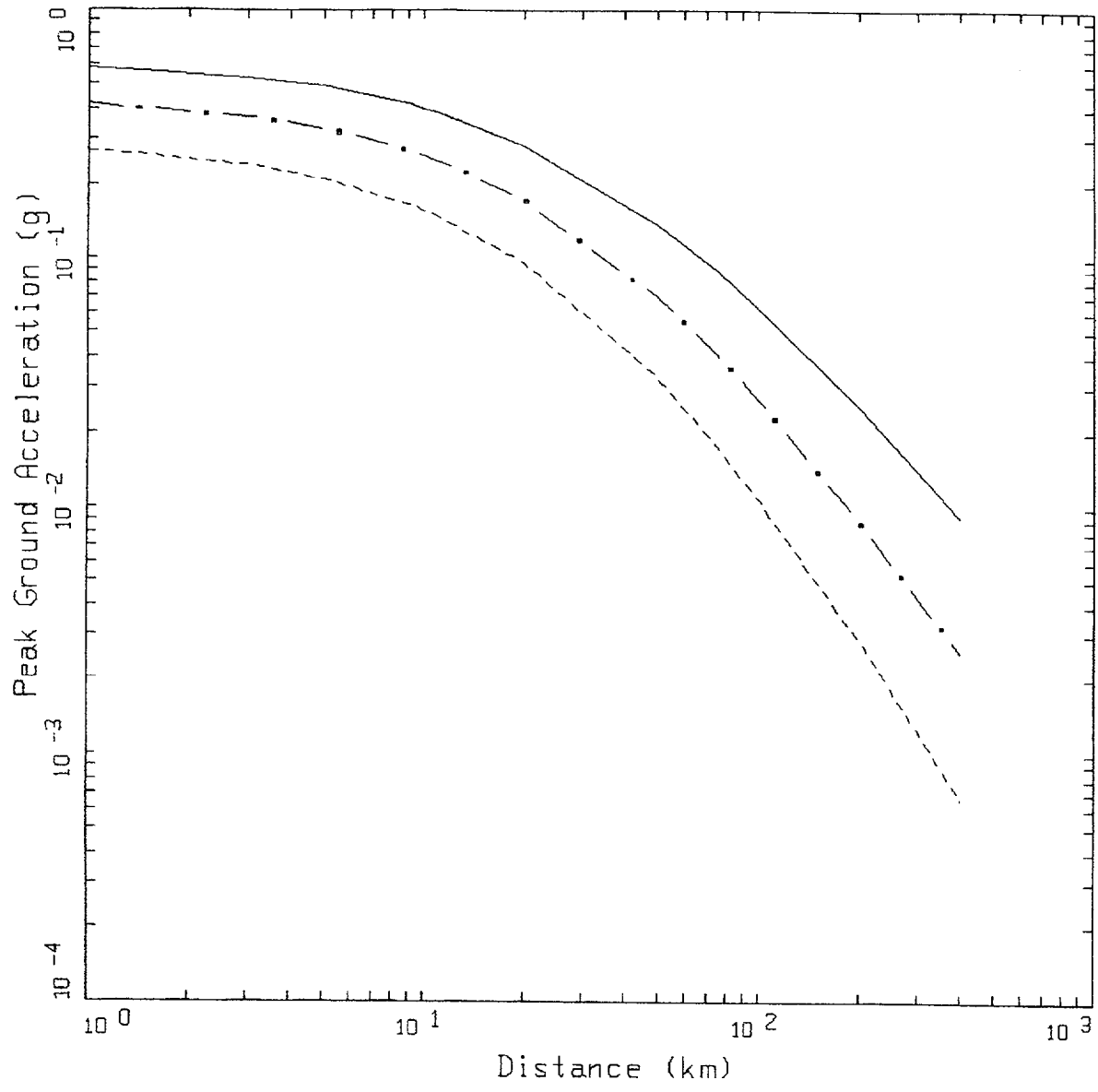
Figure 6-23. Response spectra (5% damping) at a distance of 10 km for M 6.5 showing median and $\pm 1\sigma$ estimates (parametric and regression uncertainty): CEUS rock site.



ROCK SITE VARIABILITY

——— WUS
 - . - CEUS

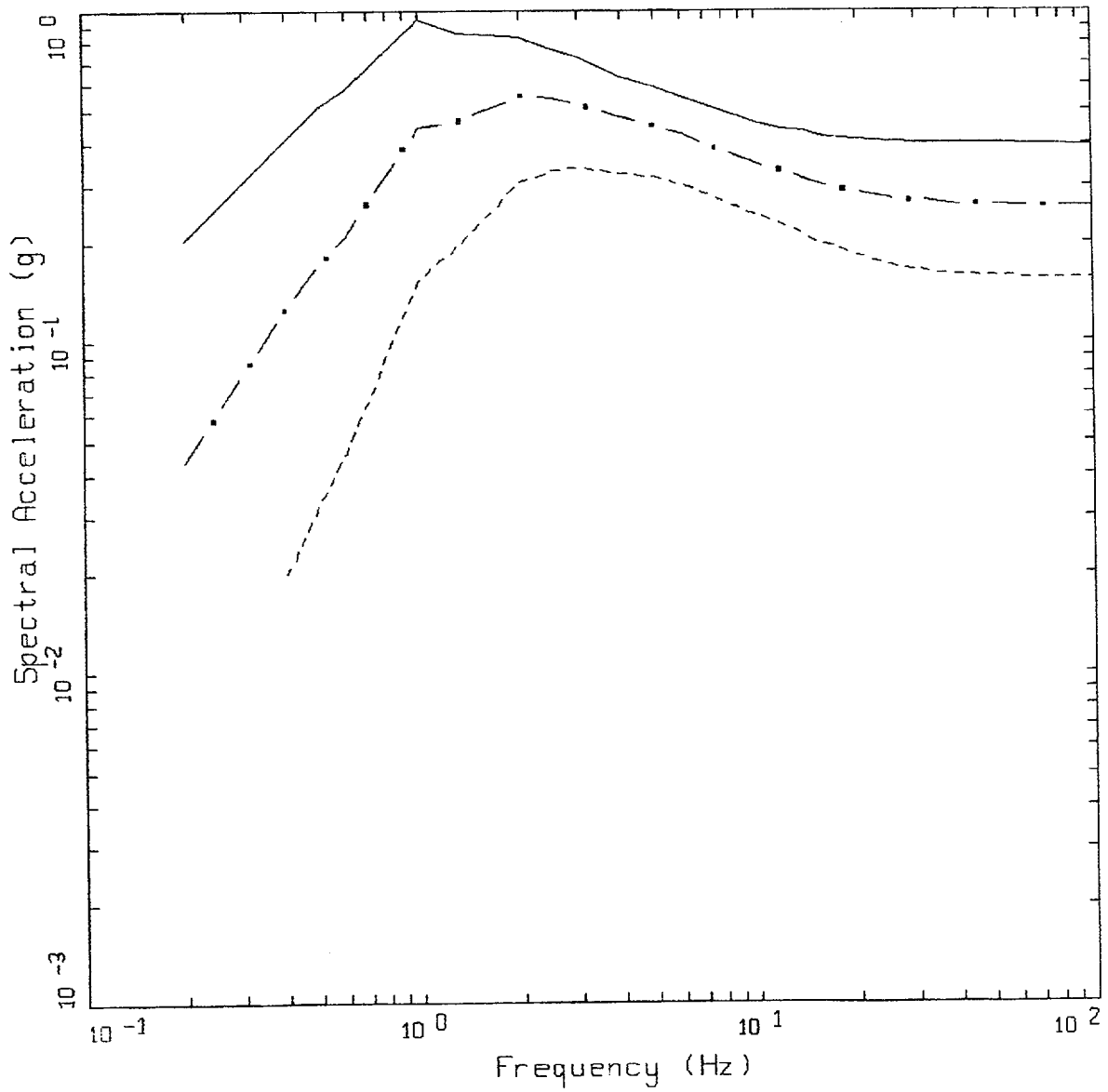
Figure 6-24. Variability in response spectral ordinates at WUS and CEUS rock sites resulting from parametric variability and regression fit over all magnitudes and distances (Tables 6-2 and 6-3).



NRC PT SOURCE WUS SOIL, GILROY2

- LEGEND
- M=7.5, SIGMA=0.4928
 - · - M=6.5, SIGMA=0.4928
 - - - M=5.5, SIGMA=0.4928

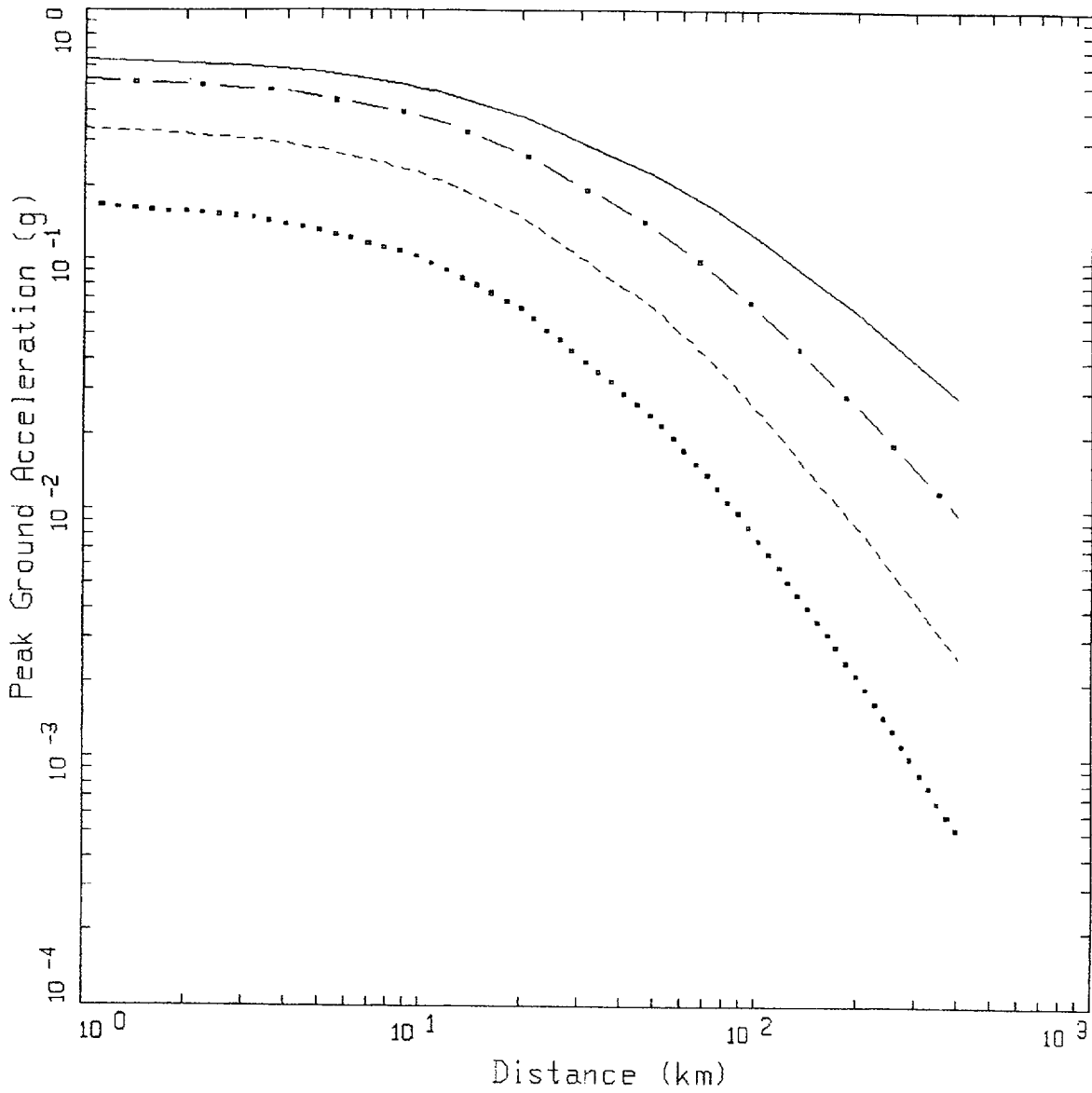
Figure 6-25. Attenuation of median peak horizontal acceleration at M 5.5, 6.5, and 7.5 for soil profile Gilroy 2 and WUS conditions.



WUS SOIL, GILROY 2
 DISTANCE=10 KM

LEGEND
 ————— M=7.5
 - · - M=6.5
 - - - M=5.5

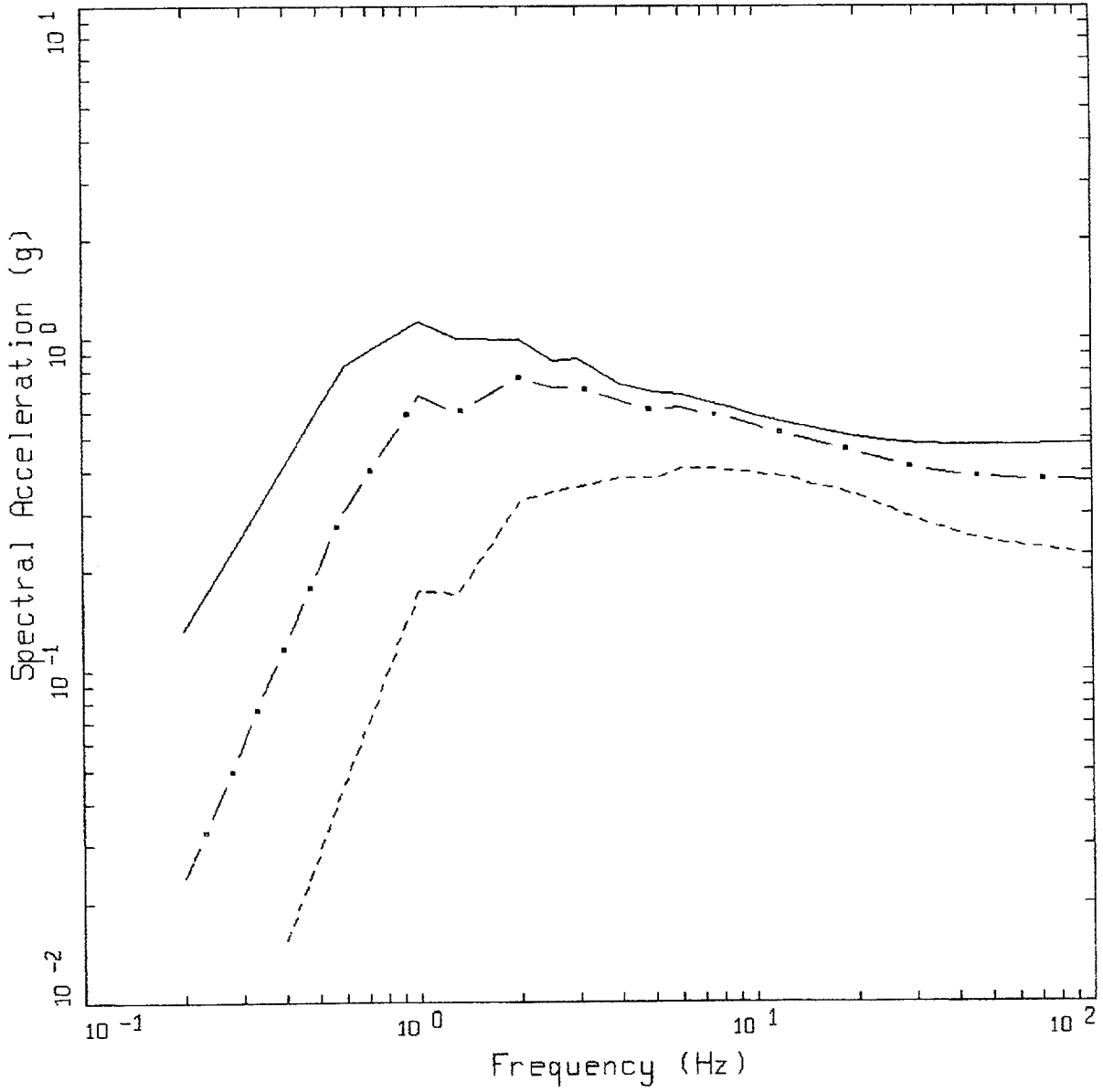
Figure 6-26. Median response spectra (5% damping) at a distance of 10 km for **M** 5.5, 6.5, and 7.5 for soil profile Gilroy 2 and WUS conditions.



CEUS SOIL, GILROY 2

- LEGEND
- M=7.5, SIGMA=0.4978
 - . - M=6.5, SIGMA=0.4978
 - - - M=5.5, SIGMA=0.4978
 - M=4.5, SIGMA=0.4978

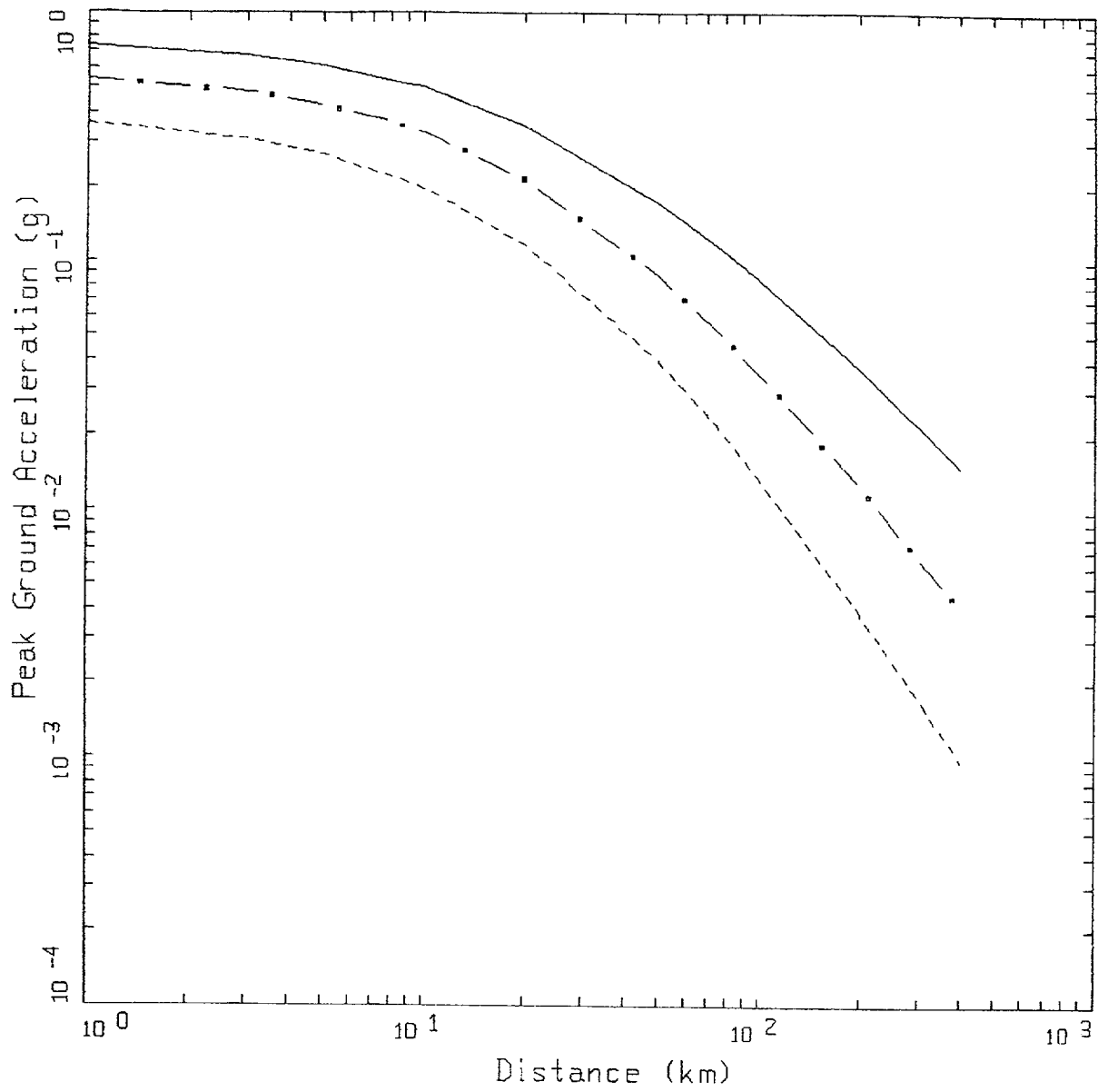
Figure 6-27. Attenuation of median peak horizontal acceleration at M 5.5, 6.5, and 7.5 for soil profile Gilroy 2 and CEUS conditions.



CEUS SOIL, GILROY 2
 DISTANCE=10 KM

LEGEND
 ————— M=7.5
 - . - . - . M=6.5
 - - - - - M=5.5

Figure 6-28. Median response spectra (5% damping) at a distance of 10 km for M 5.5, 6.5, and 7.5 for soil profile Gilroy 2 and CEUS conditions.



WUS SOIL, MELOLAND

- LEGEND
- M=7.5, SIGMA=0.4774
 - · - M=6.5, SIGMA=0.4774
 - - - M=5.5, SIGMA=0.4774

Figure 6-29. Attenuation of median peak horizontal acceleration at M 5.5, 6.5, and 7.5 for soil profile Meloland and WUS conditions.

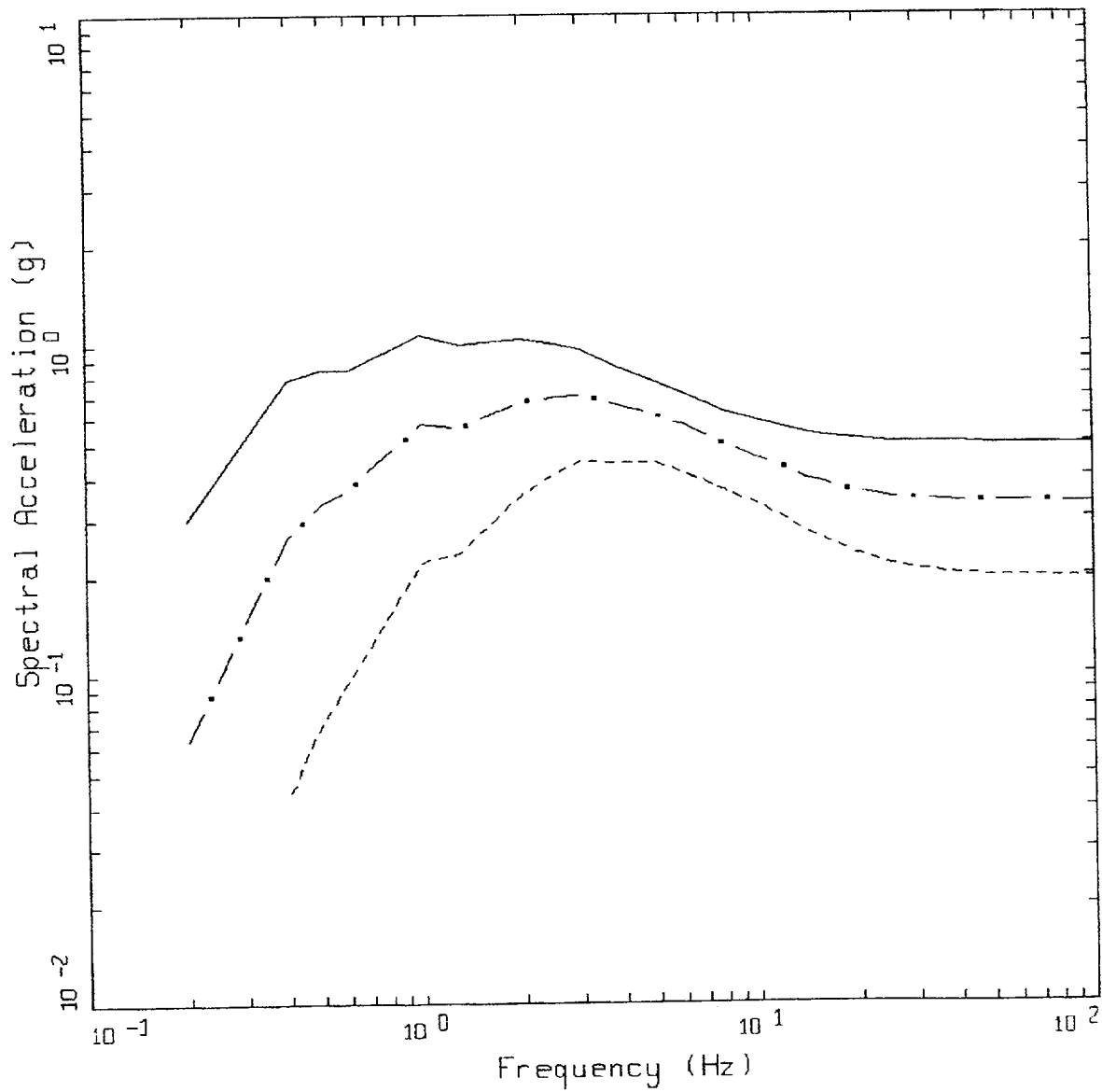
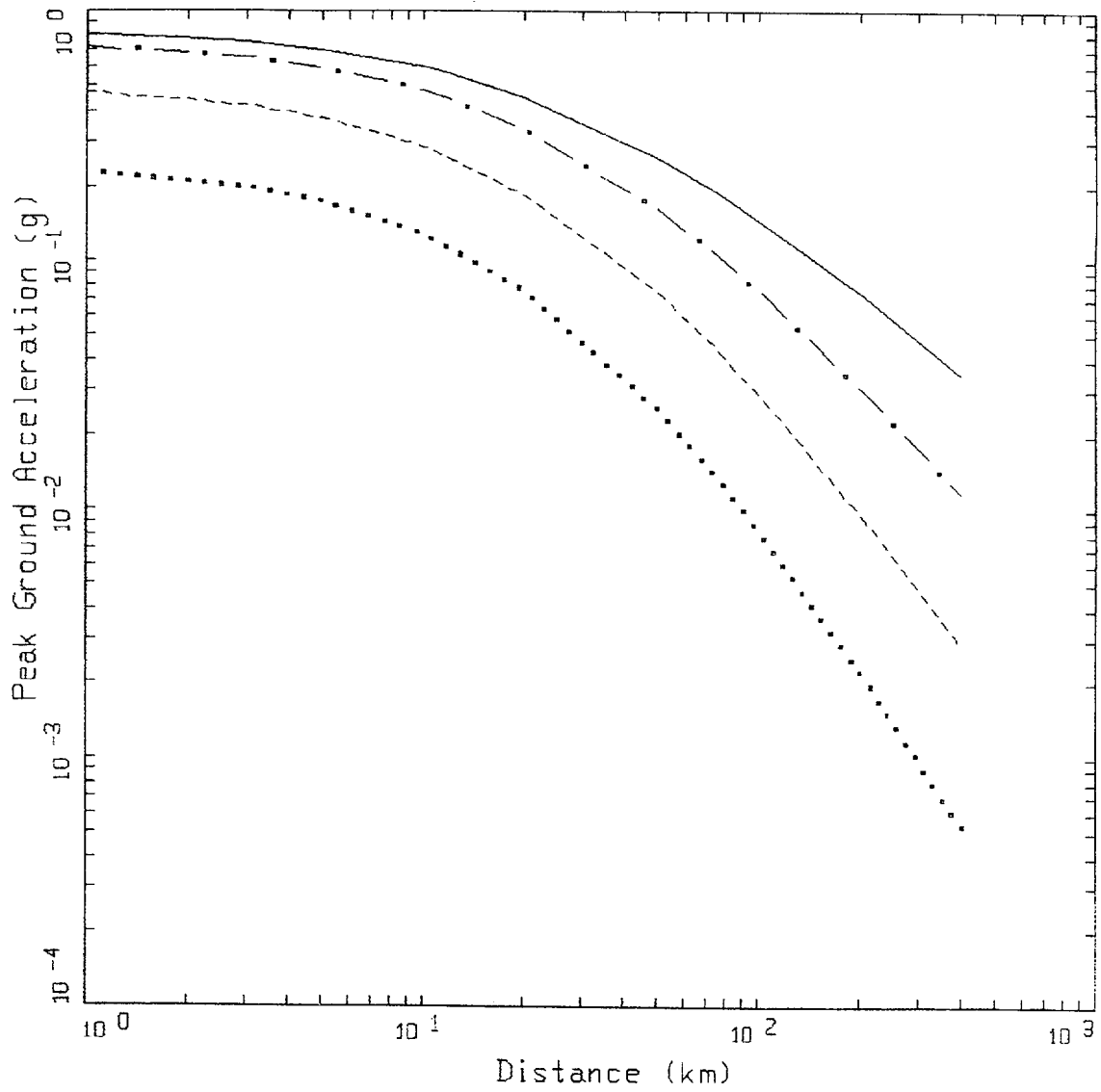


Figure 6-30. Median response spectra (5% damping) at a distance of 10 km for M 5.5, 6.5, and 7.5 for soil profile Meloland and WUS conditions.



CEUS SOIL, MELOLAND

LEGEND	
—	$M=7.5, \text{SIGMA}=0.5046$
- · -	$M=6.5, \text{SIGMA}=0.5046$
- - -	$M=5.5, \text{SIGMA}=0.5046$
· · ·	$M=4.5, \text{SIGMA}=0.5046$

Figure 6-31. Attenuation of median peak horizontal acceleration at M 5.5, 6.5, and 7.5 for soil profile Meloland and CEUS conditions.

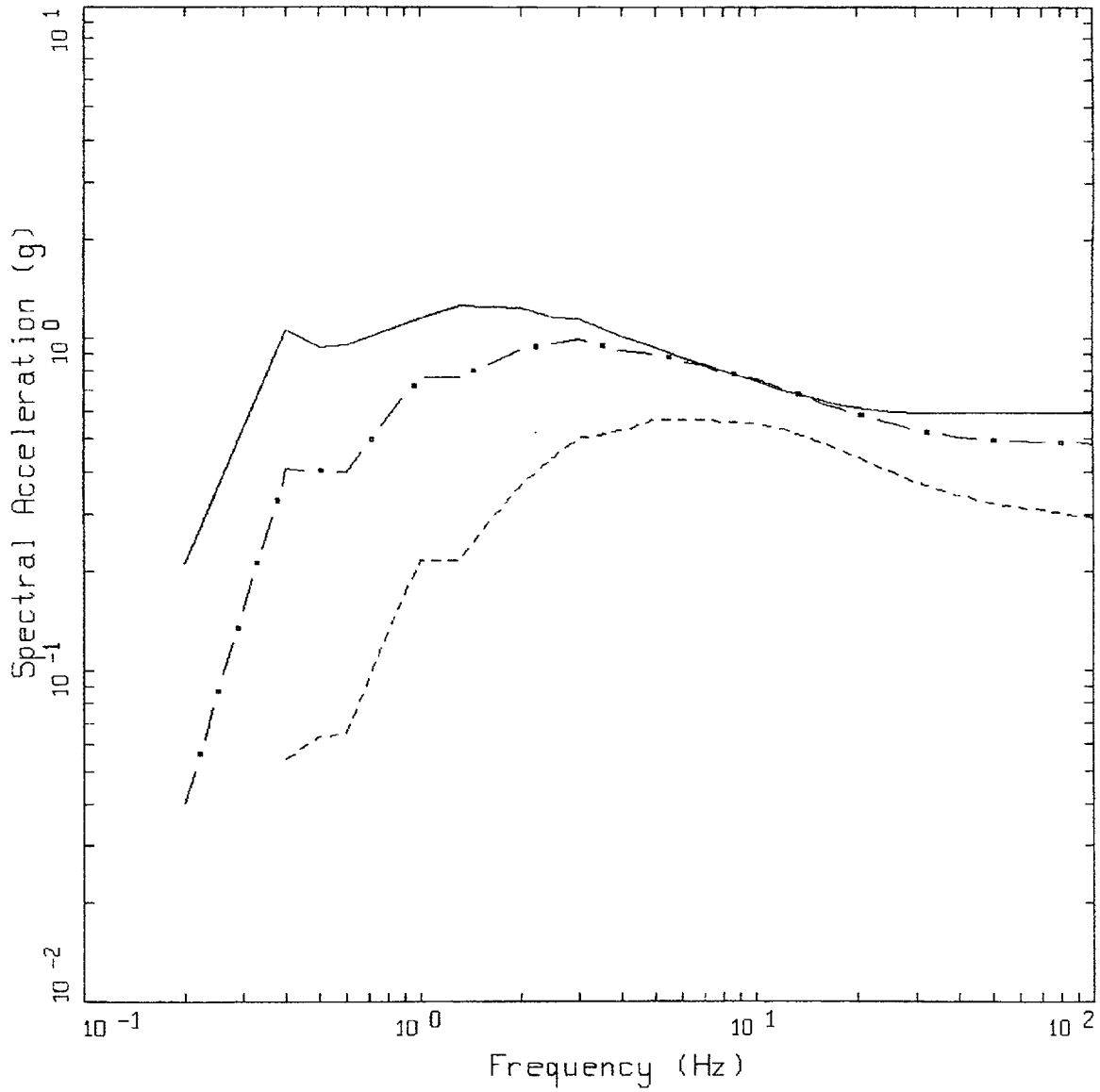
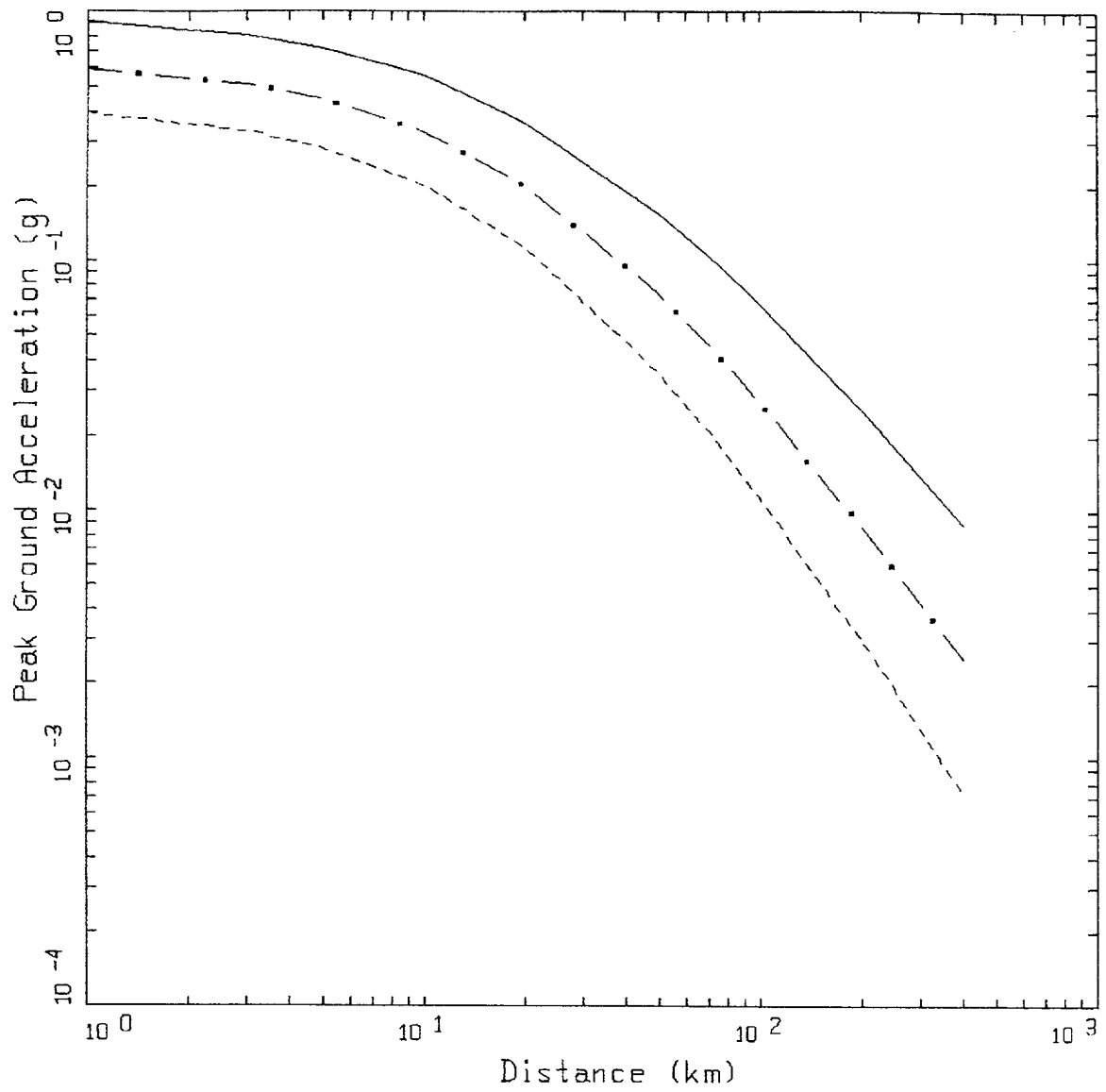


Figure 6-32. Median response spectra (5% damping) at a distance of 10 km for M 5.5, 6.5, and 7.5 for soil profile Meloland and CEUS conditions.

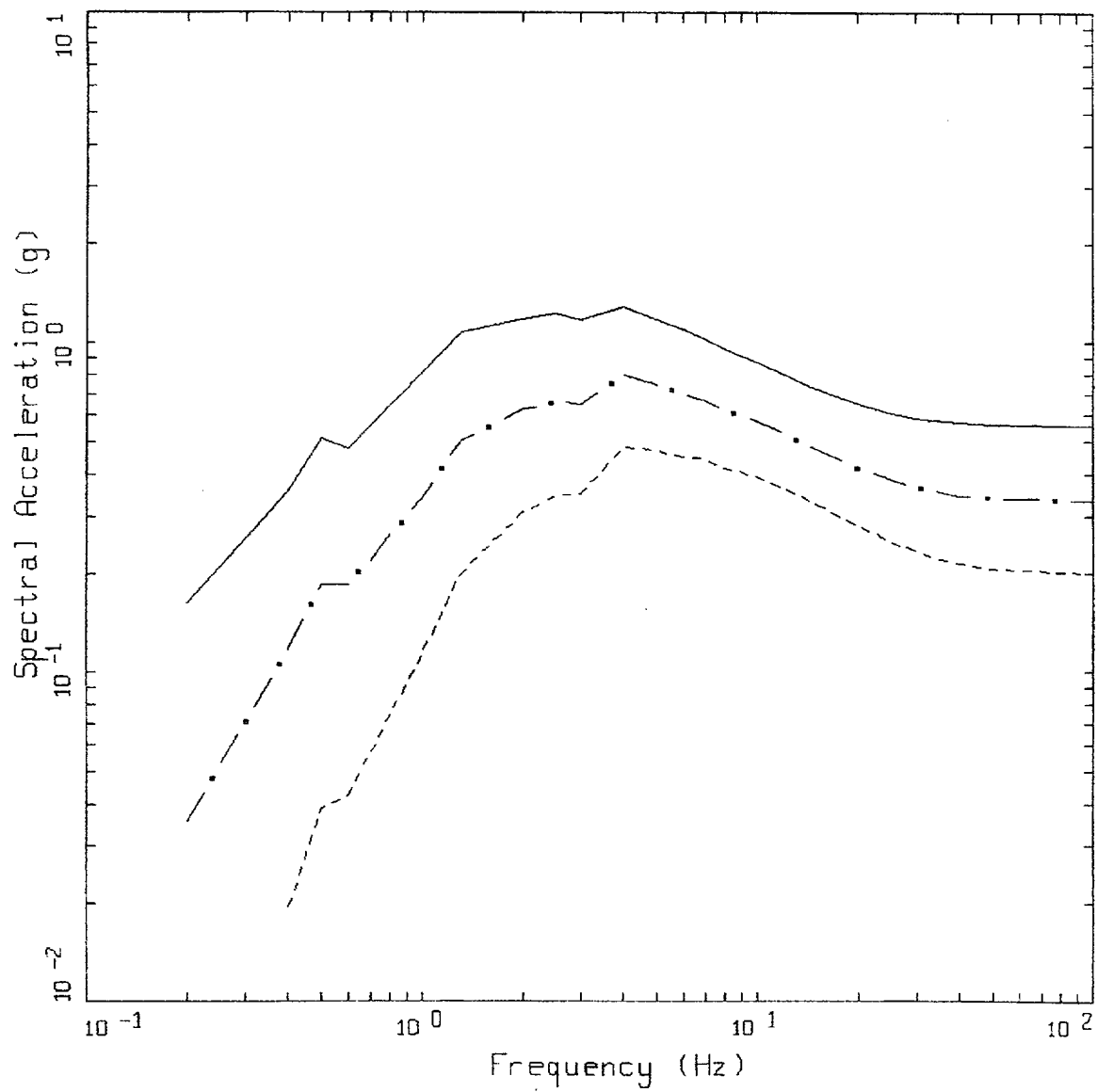


WUS SOIL, RINALDI

LEGEND

—	M=7.5, SIGMA=0.5320
- · -	M=6.5, SIGMA=0.5320
- - -	M=5.5, SIGMA=0.5320

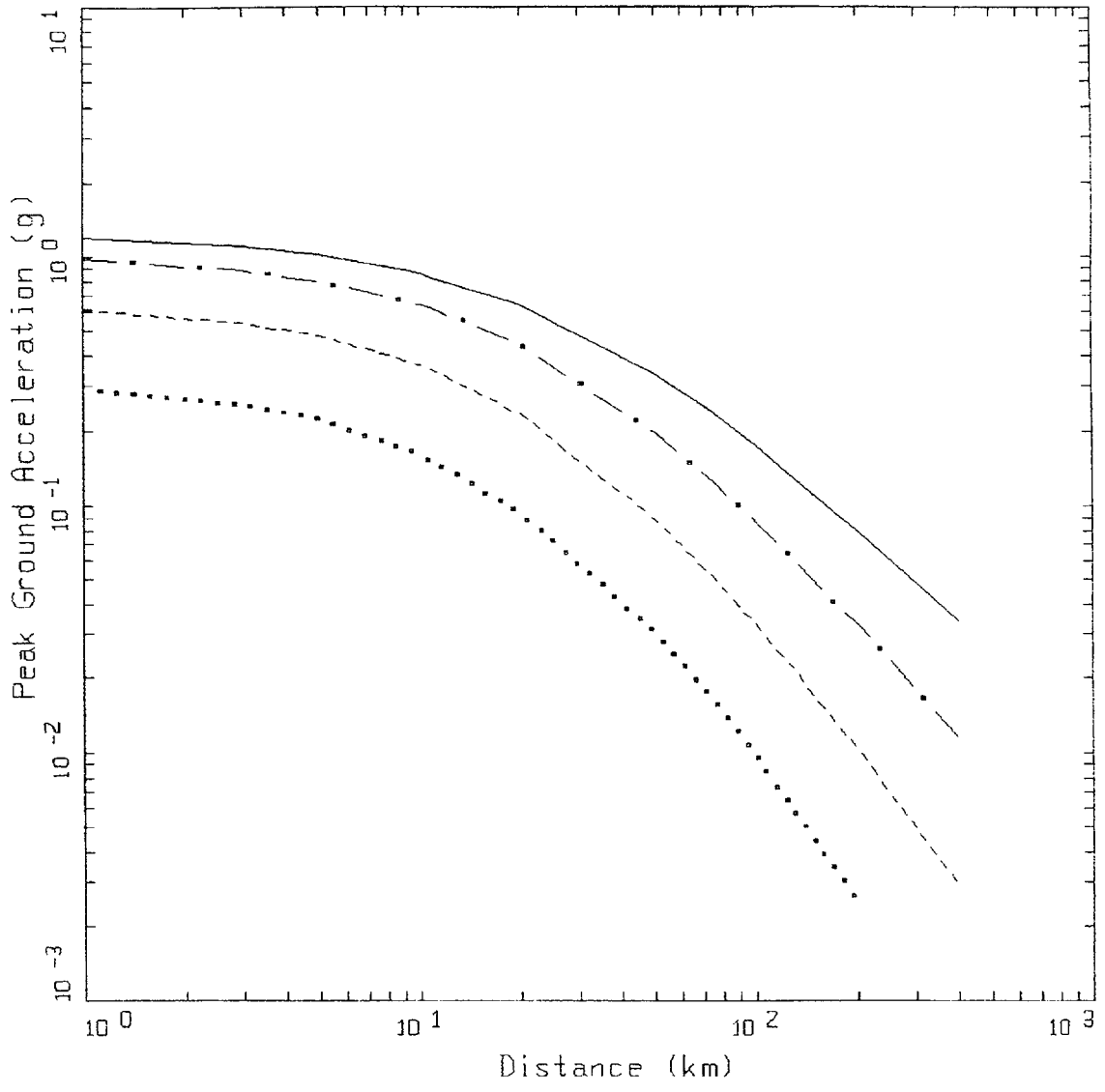
Figure 6-33. Attenuation of median peak horizontal acceleration at **M** 5.5, 6.5, and 7.5 for soil profile Rinaldi and WUS conditions.



WUS SOIL, RINALDI
 DISTANCE=10 KM

LEGEND
 — M=7.5
 - · - M=6.5
 - - - M=5.5

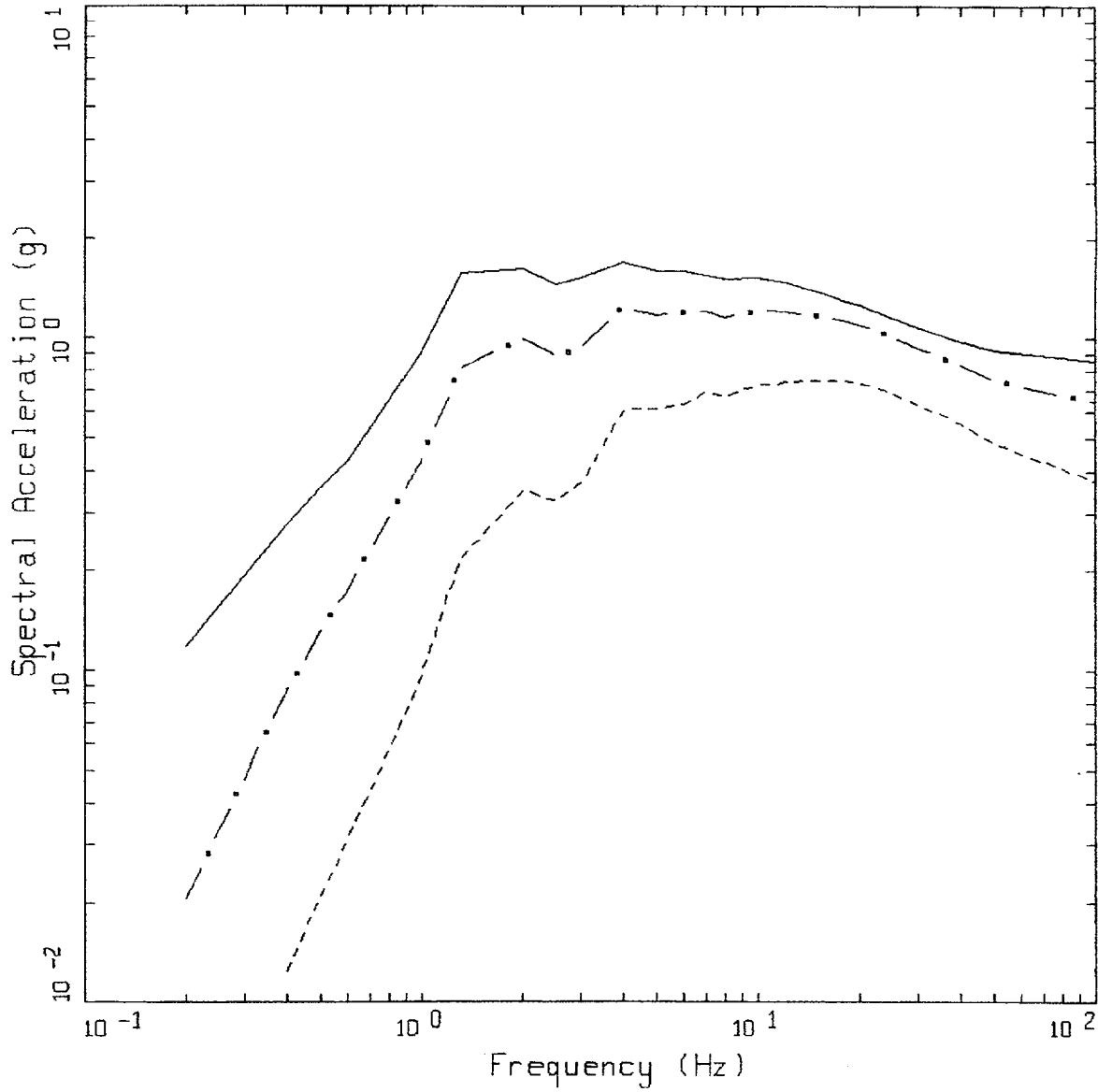
Figure 6-34. Median response spectra (5% damping) at a distance of 10 km for M 5.5, 6.5, and 7.5 for soil response Rinaldi and WUS conditions.



CEUS SOIL, RINALDI

- LEGEND
- M=7.5, SIGMA=0.5461
 - · - M=6.5, SIGMA=0.5461
 - - - M=5.5, SIGMA=0.5461
 - · · M=4.5, SIGMA=0.5461

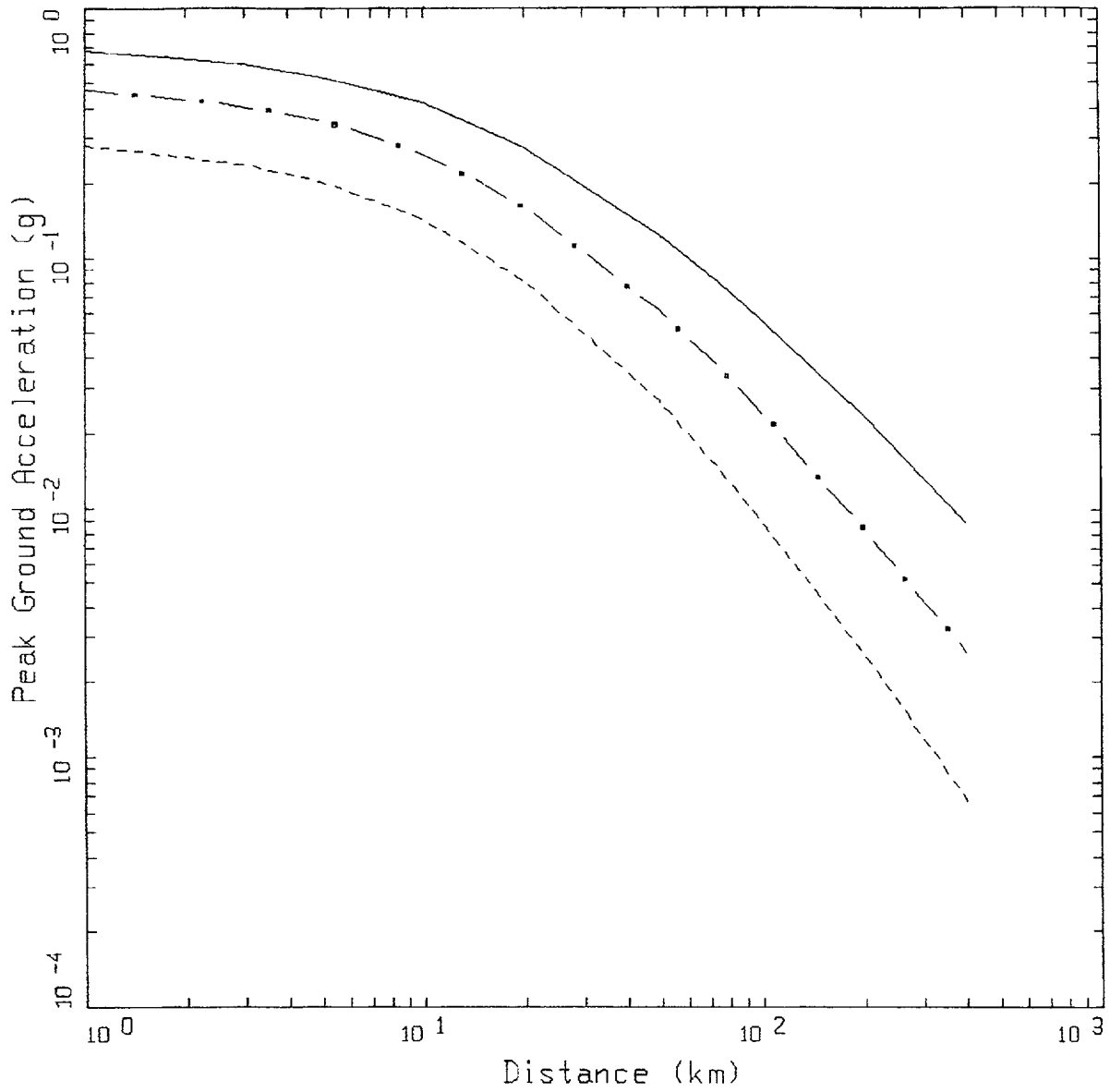
Figure 6-35. Attenuation of median peak horizontal acceleration at M 5.5, 6.5, and 7.5 for soil profile Rinaldi and CEUS conditions.



CEUS SOIL, RINALDI
 DISTANCE=10 KM

LEGEND
 — M=7.5
 - · - M=6.5
 - - - M=5.5

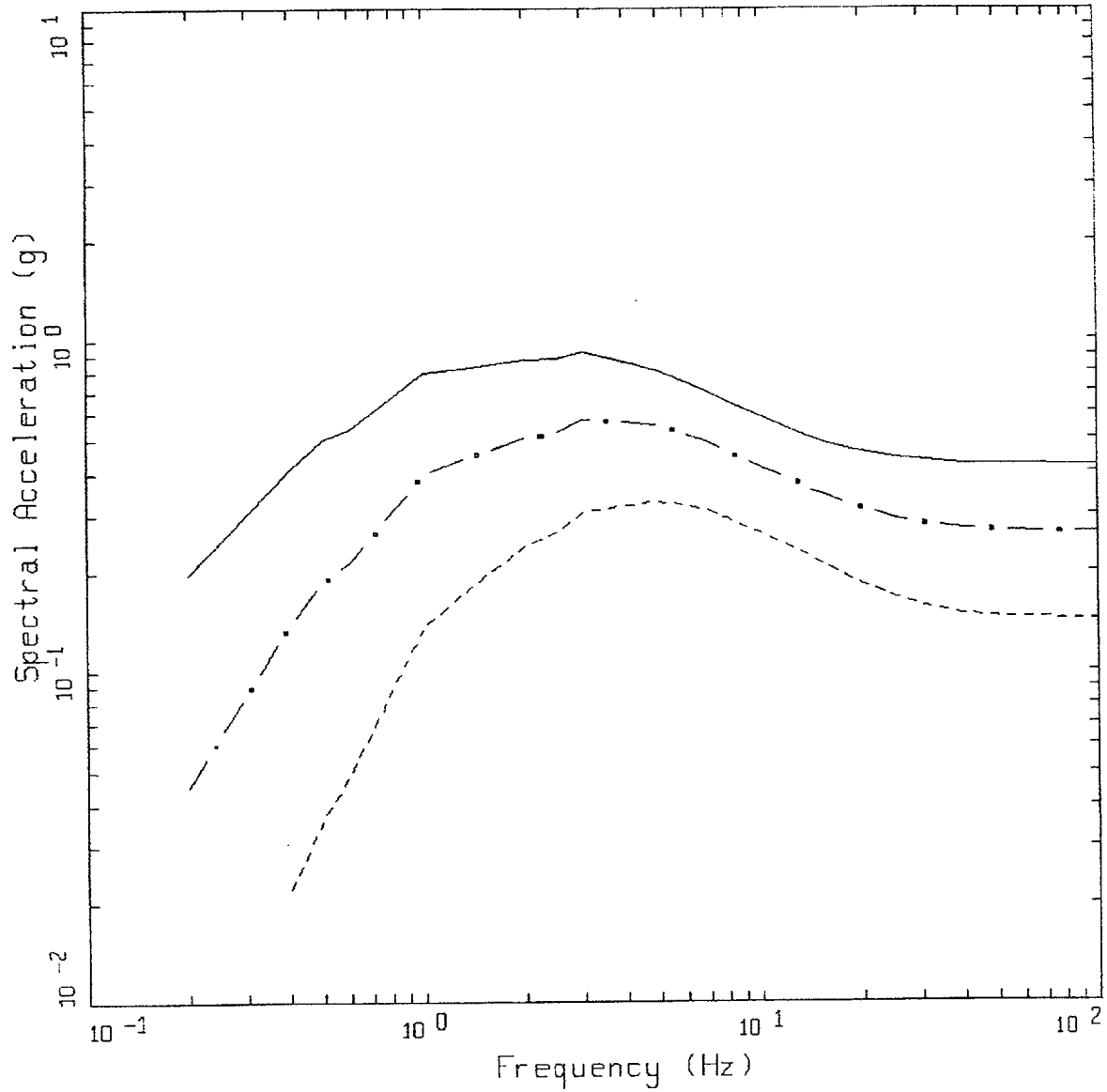
Figure 6-36. Median response spectra (5% damping) at a distance of 10 km for M 5.5, 6.5, and 7.5 for soil profile Rinaldi and CEUS conditions.



WUS SOIL, GENERIC SRS

- LEGEND
- M=7.5, SIGMA=0.4732
 - - - - - M=6.5, SIGMA=0.4732
 - - - - - M=5.5, SIGMA=0.4732

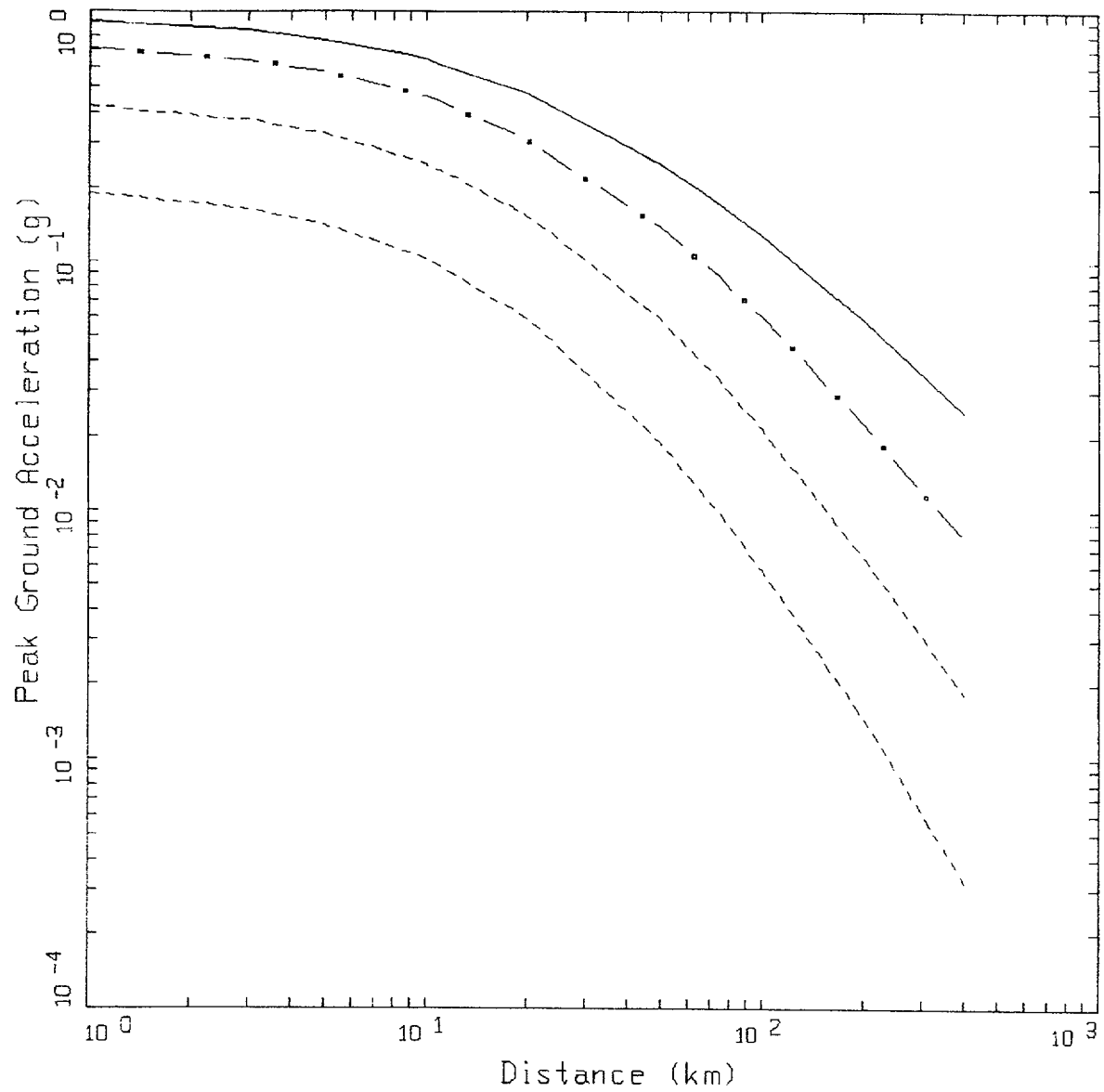
Figure 6-37. Attenuation of median peak horizontal acceleration at M 5.5, 6.5, and 7.5 for soil profile Savannah River Generic and WUS conditions.



WUS SOIL, GENERIC SRS
 DISTANCE=10 KM

LEGEND
 — M=7.5
 - · - M=6.5
 - - - M=5.5

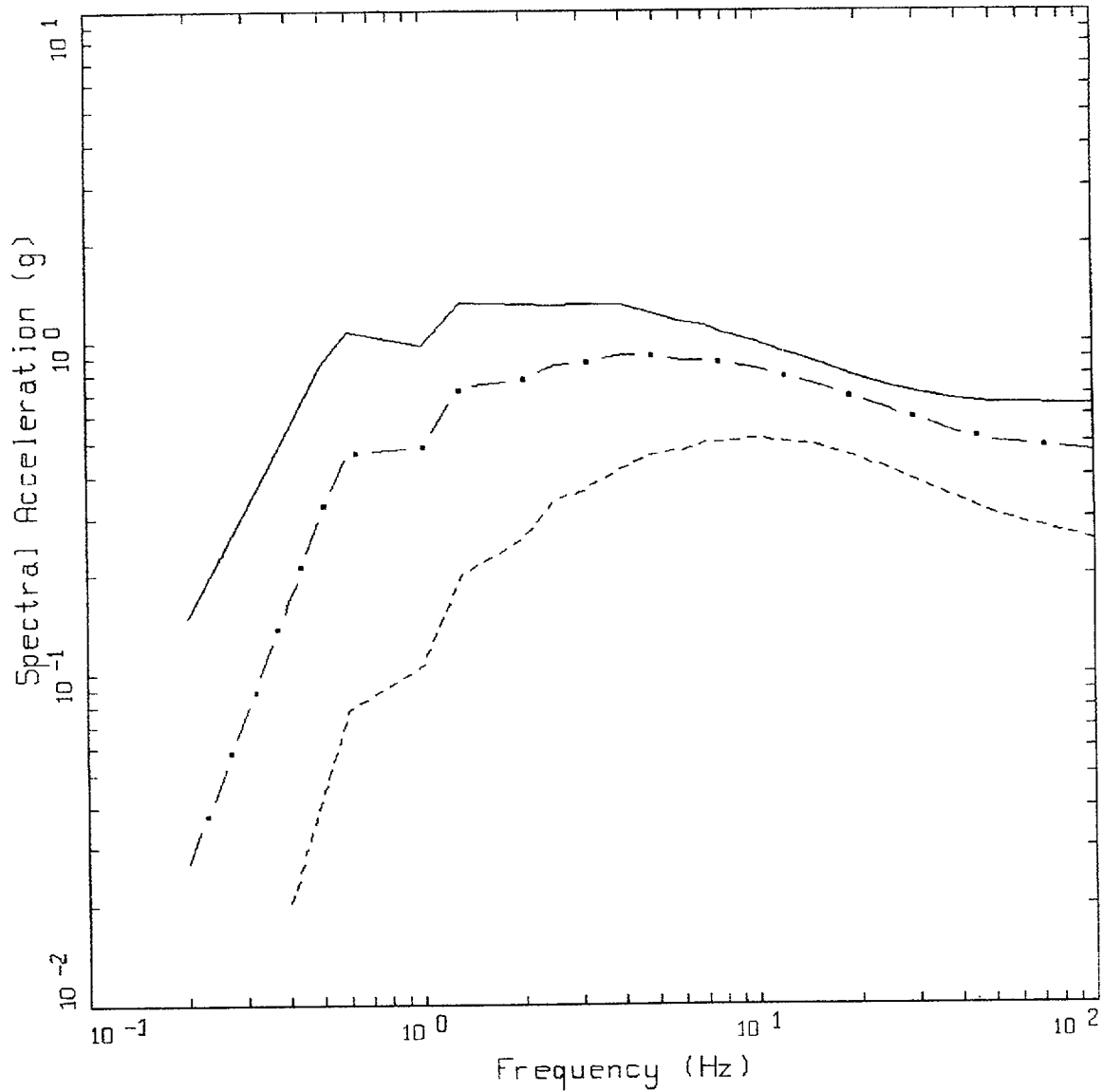
Figure 6-38. Median response spectra (5% damping) at a distance of 10 km for M 5.5, 6.5, and 7.5 for soil profile Savannah River Generic and WUS conditions.



CEUS SOIL, GENERIC SRS

- LEGEND
- M=7.5, SIGMA=0.5706
 - · — M=6.5, SIGMA=0.5706
 - - - - M=5.5, SIGMA=0.5706
 - · · · M=4.5, SIGMA=0.5706

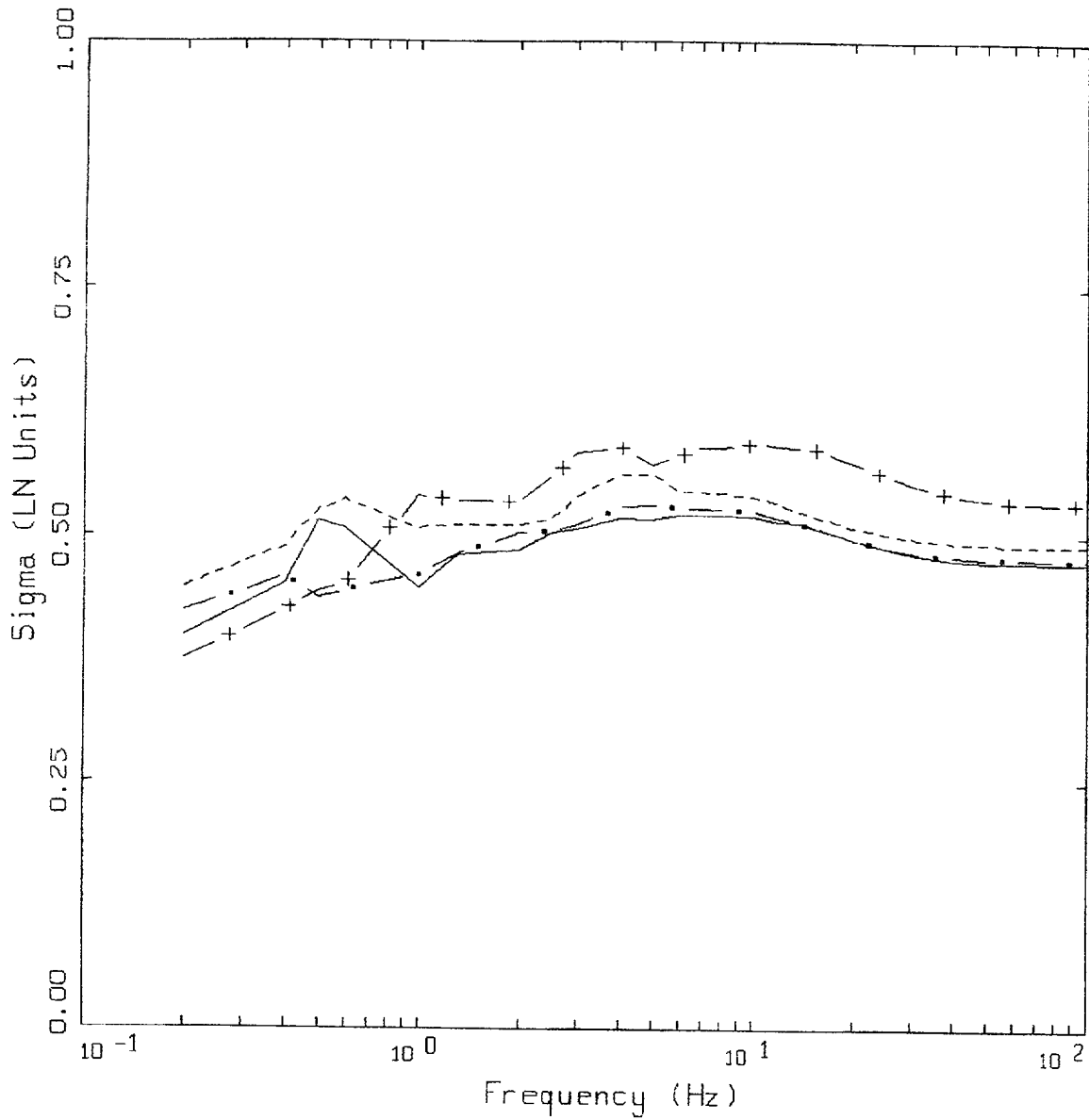
Figure 6-39. Attenuation of median peak horizontal acceleration at M 5.5, 6.5, and 7.5 for soil profile Savannah River Generic and CEUS conditions.



CEUS SOIL, GENERIC SRS
 DISTANCE=10 KM

LEGEND
 — M=7.5
 - · - M=6.5
 - - - M=5.5

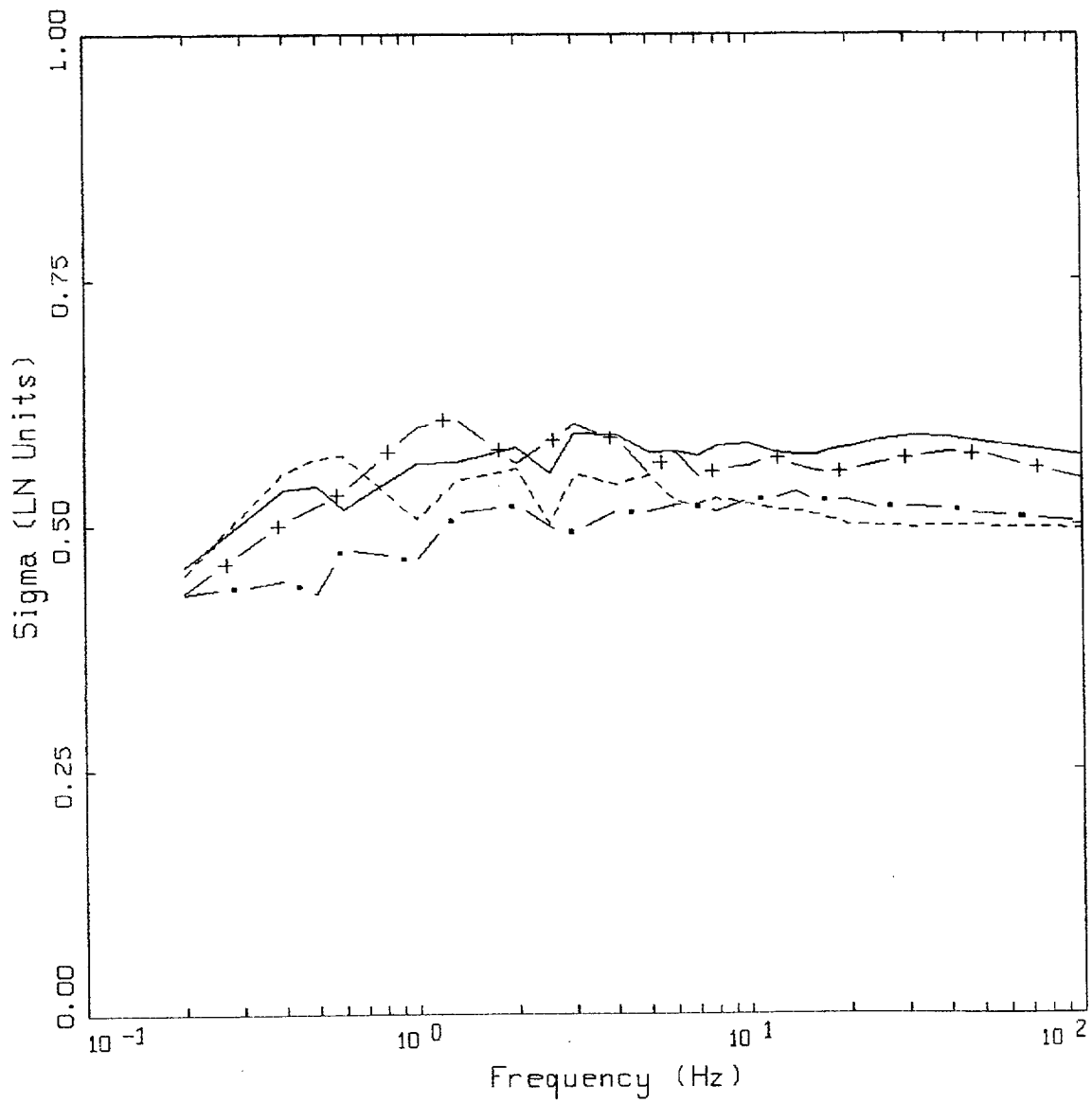
Figure 6-40. Median response spectra (5% damping) at a distance of 10 km for M 5.5, 6.5, and 7.5 for soil profile Savannah River Generic and CEUS conditions.



VARIABILITY, WUS SOIL

- LEGEND
- WUS SOIL (GILROY#2) SIGMA
 - . - WUS SOIL (MELOLAND) SIGMA
 - + - WUS SOIL (RINALDI) SIGMA
 - WUS SOIL (GENERIC SRS) SIGMA

Figure 6-41. Variability in response spectral ordinates for WUS soil sites resulting from parametric variability and regression fit over all magnitudes and distances (Table 6-2 and 6-3).



VARIABILITY, CEUS SOIL

- LEGEND
- CEUS SOIL (GILROY#2) SIGMA
 - . - CEUS SOIL (MELOLAND) SIGMA
 - + - CEUS SOIL (RINALDI) SIGMA
 - CEUS SOIL (GENERIC SRS) SIGMA

Figure 6-42. Variability in response spectral ordinates for CEUS soil sites resulting from parametric variability and regression fit over all magnitudes and distances (Tables 6-2 and 6-3).

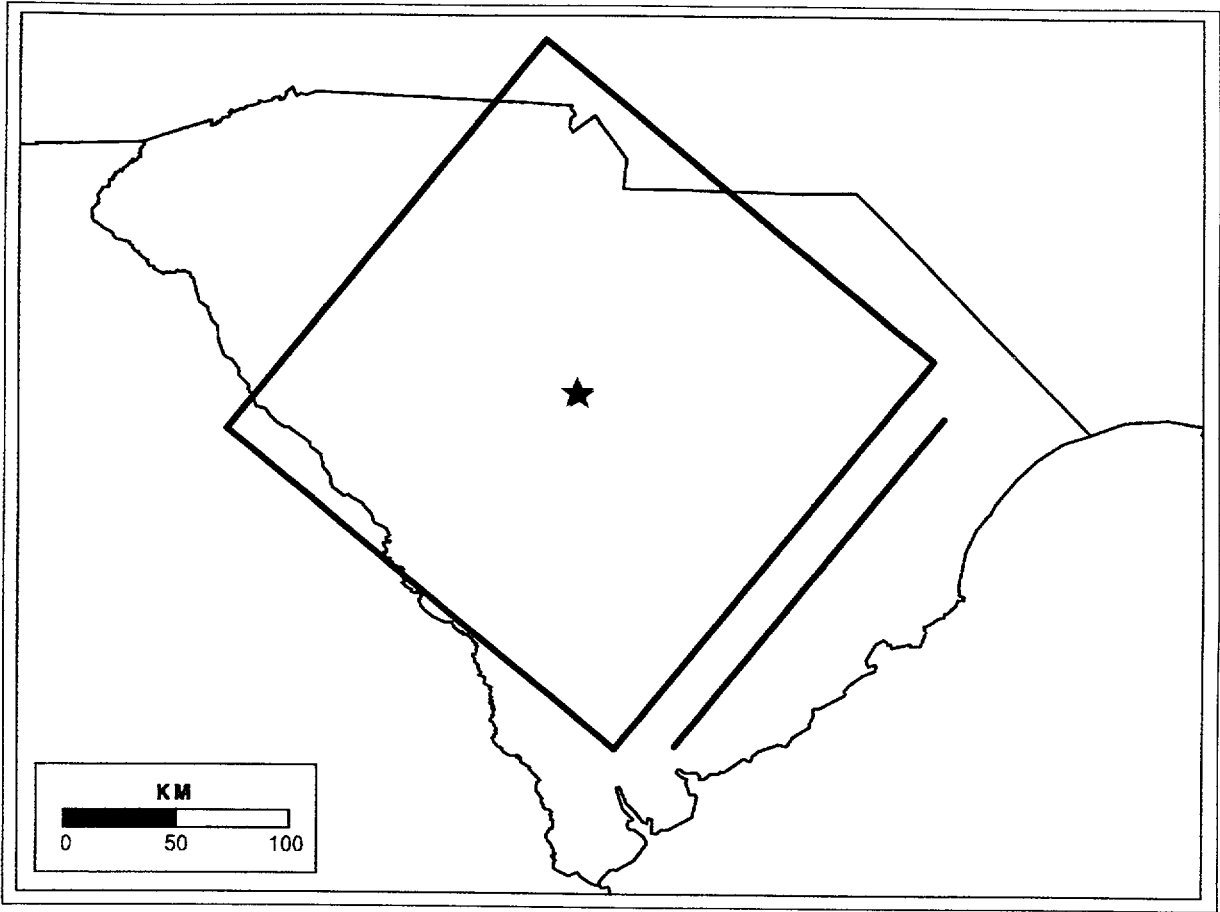


Figure 6-43. Configuration of background source and Charleston fault affecting CEUS example site (Columbia, South Carolina).

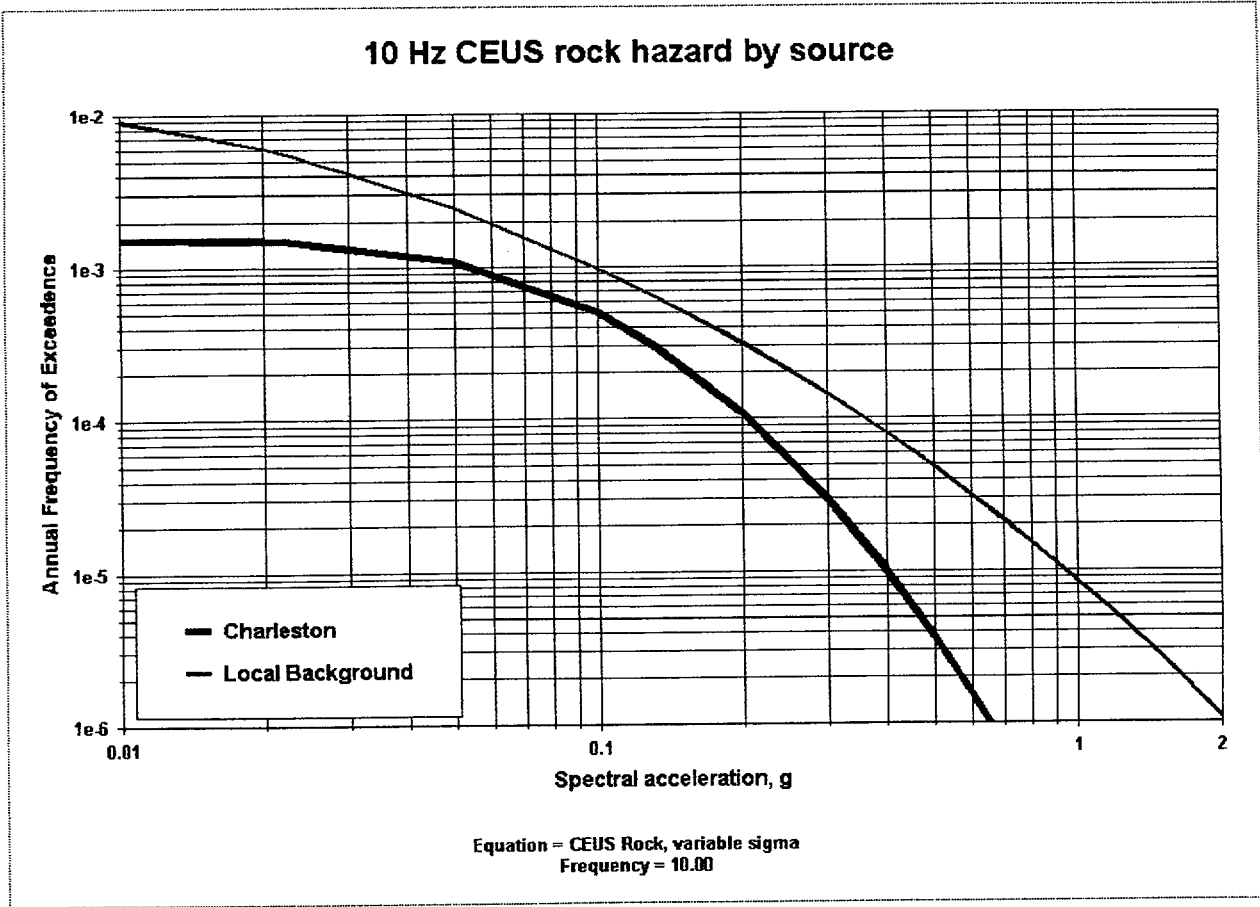


Figure 6-44. Contribution to seismic hazard by source for 10 Hz spectral acceleration, Columbia site.

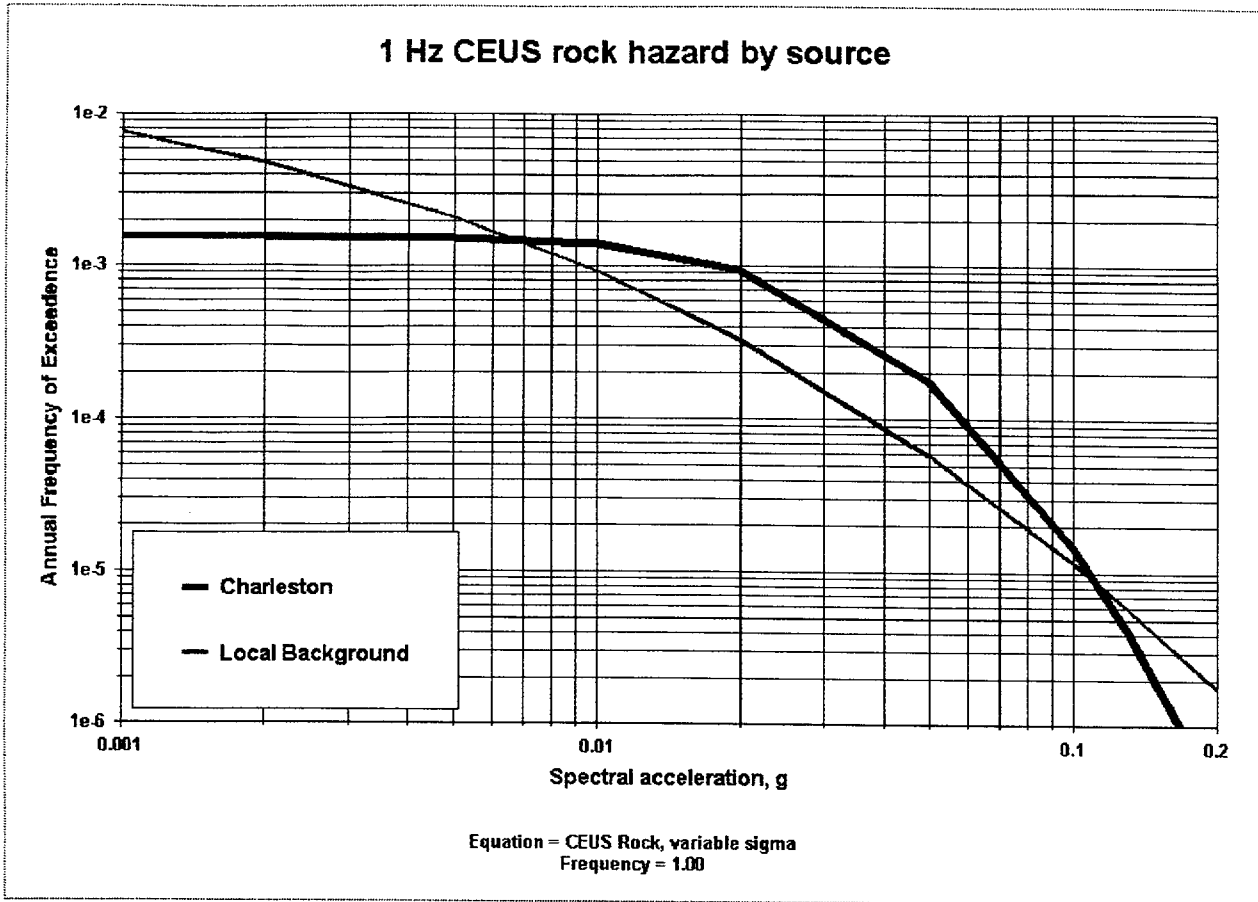


Figure 6-45. Contribution to seismic hazard by source for 1 Hz spectral acceleration, Columbia site.

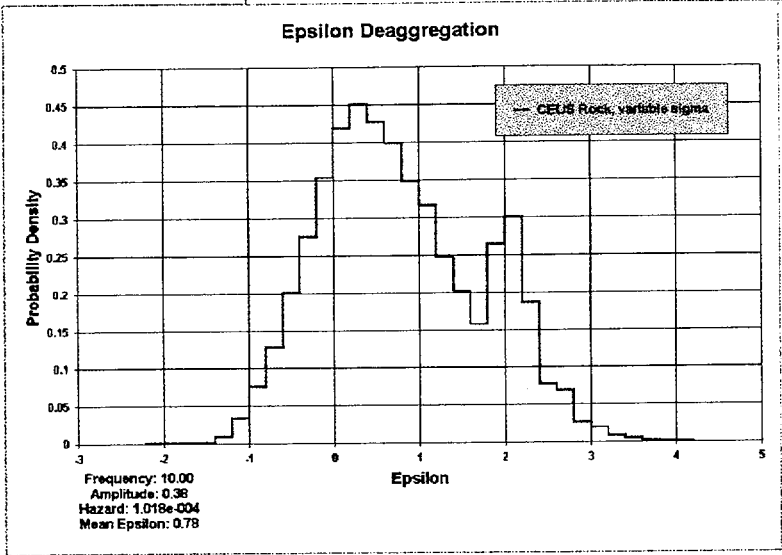
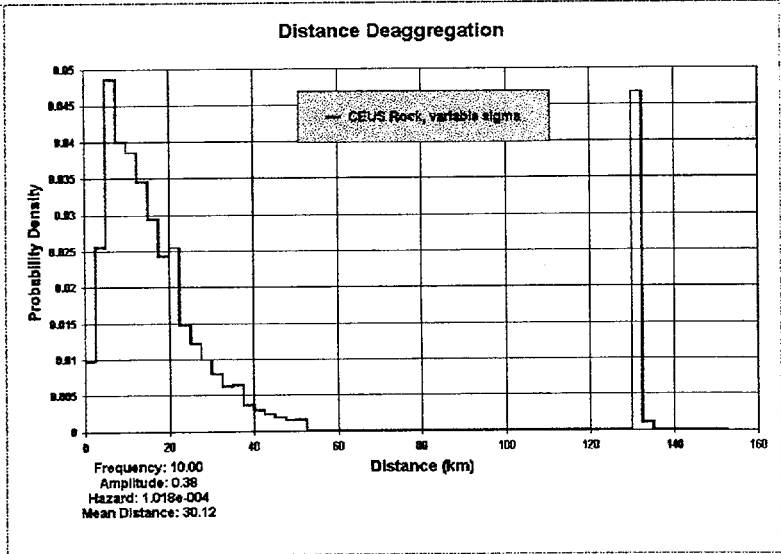
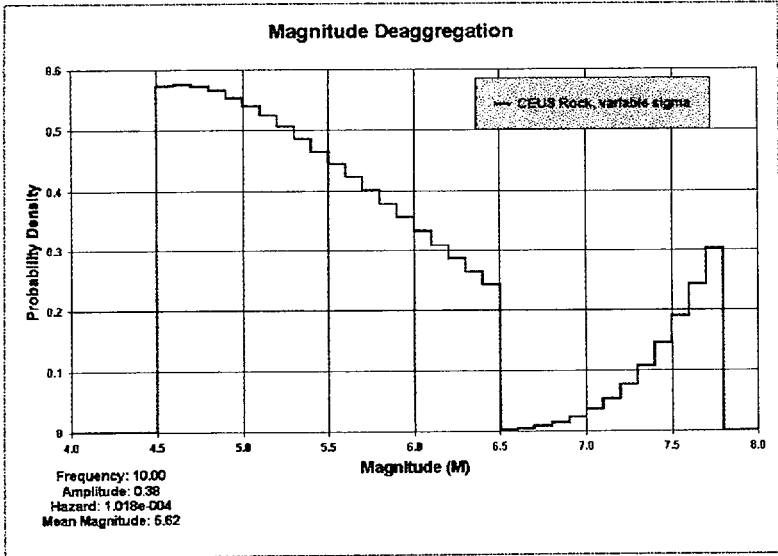


Figure 6-46. Deaggregation of seismic hazard by M, R, and a for 10 Hz SA at 0.38g, Columbia site.

CEUS 10 Hz magnitude-distance deaggregation

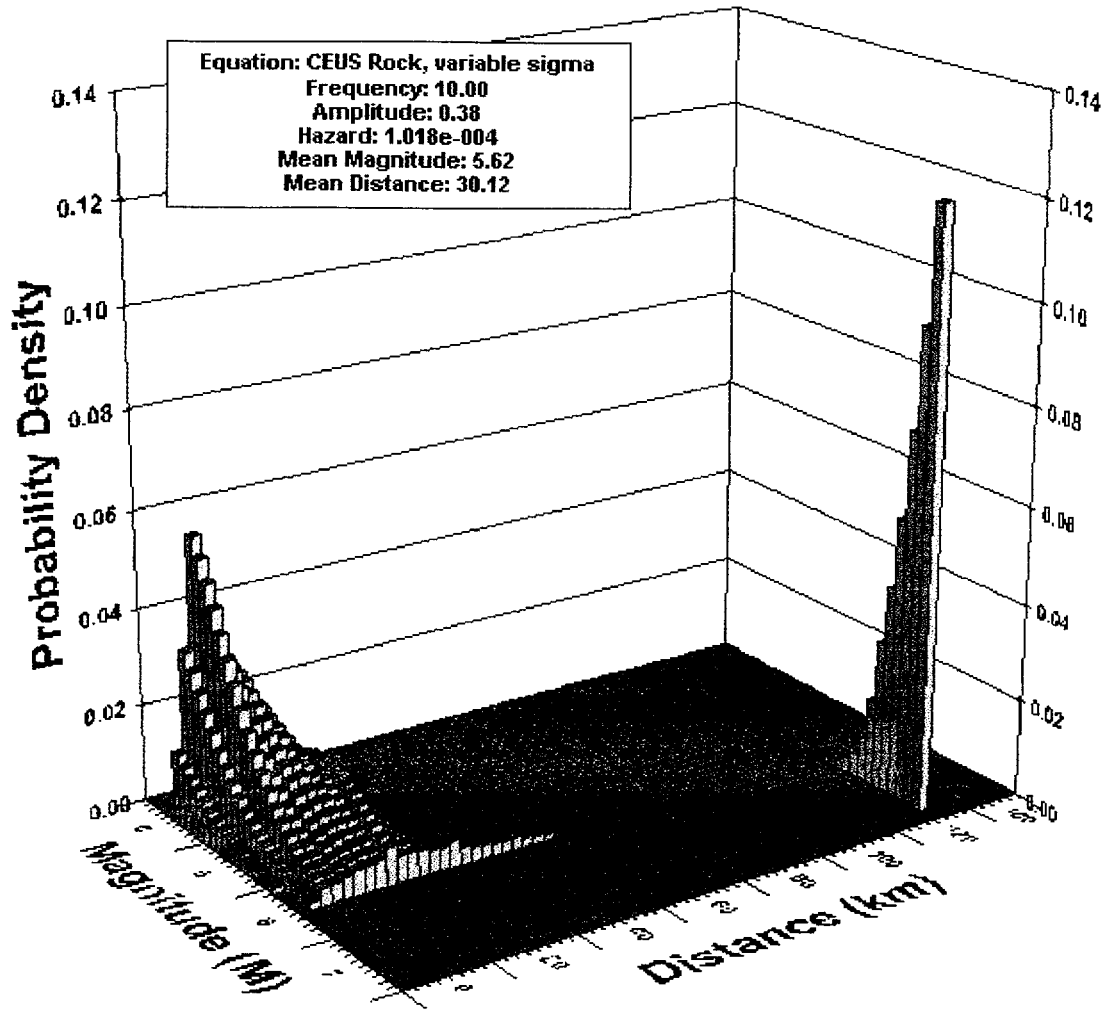


Figure 6-47. Deaggregation of seismic hazard by M and R for 10 Hz SA at 0.38g, Columbia site.

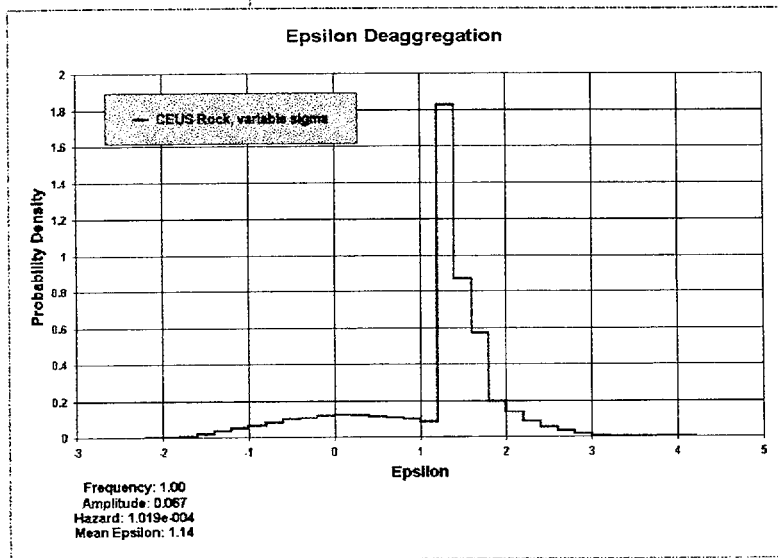
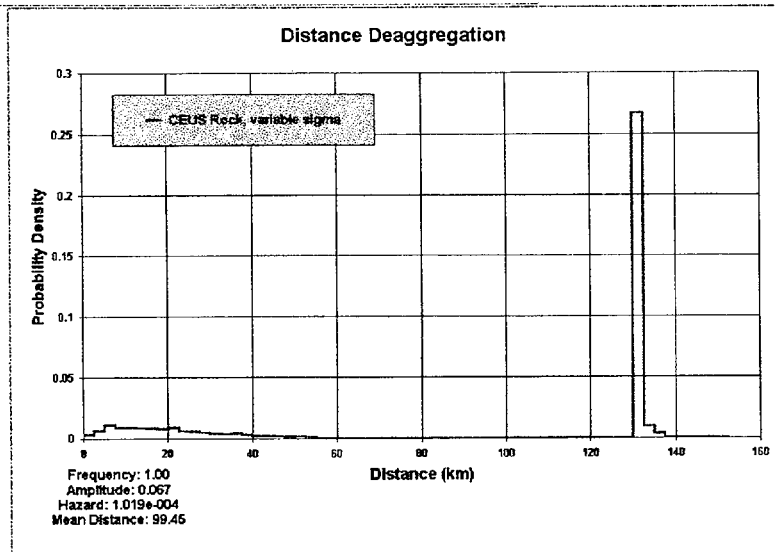
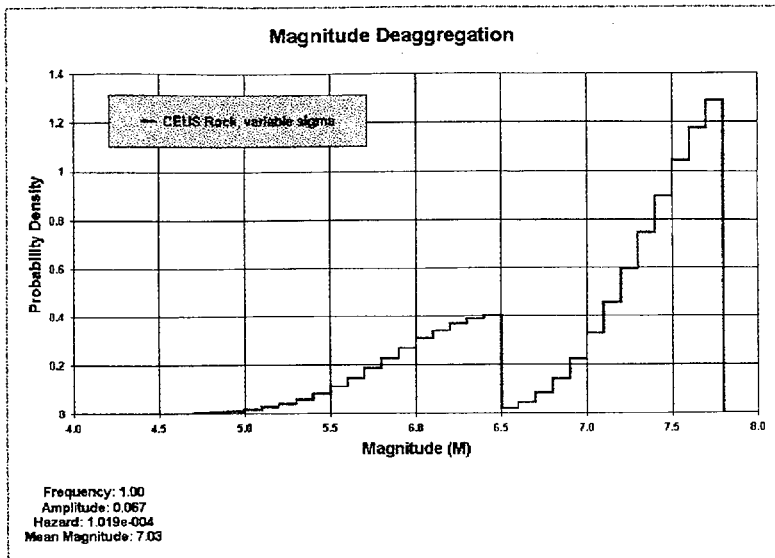


Figure 6-48: Deaggregation of seismic hazard by M, R, and a for 1 Hz SA at 0.067g, Columbia site.

CEUS 1 Hz magnitude-distance deaggregation

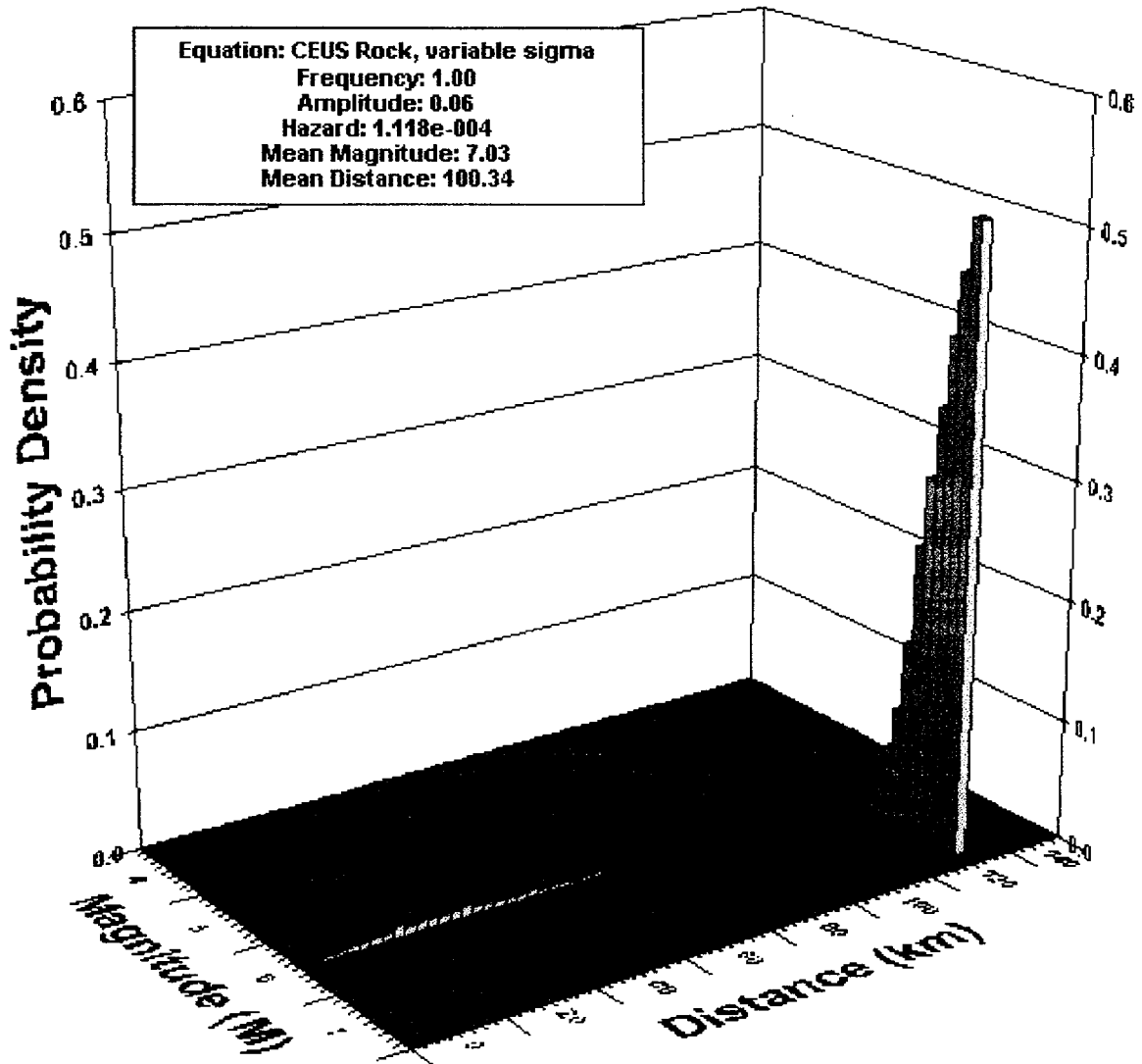


Figure 6-49. Deaggregation of seismic hazard by **M** and **R** for 1 Hz SA at 0.067g, Columbia site.

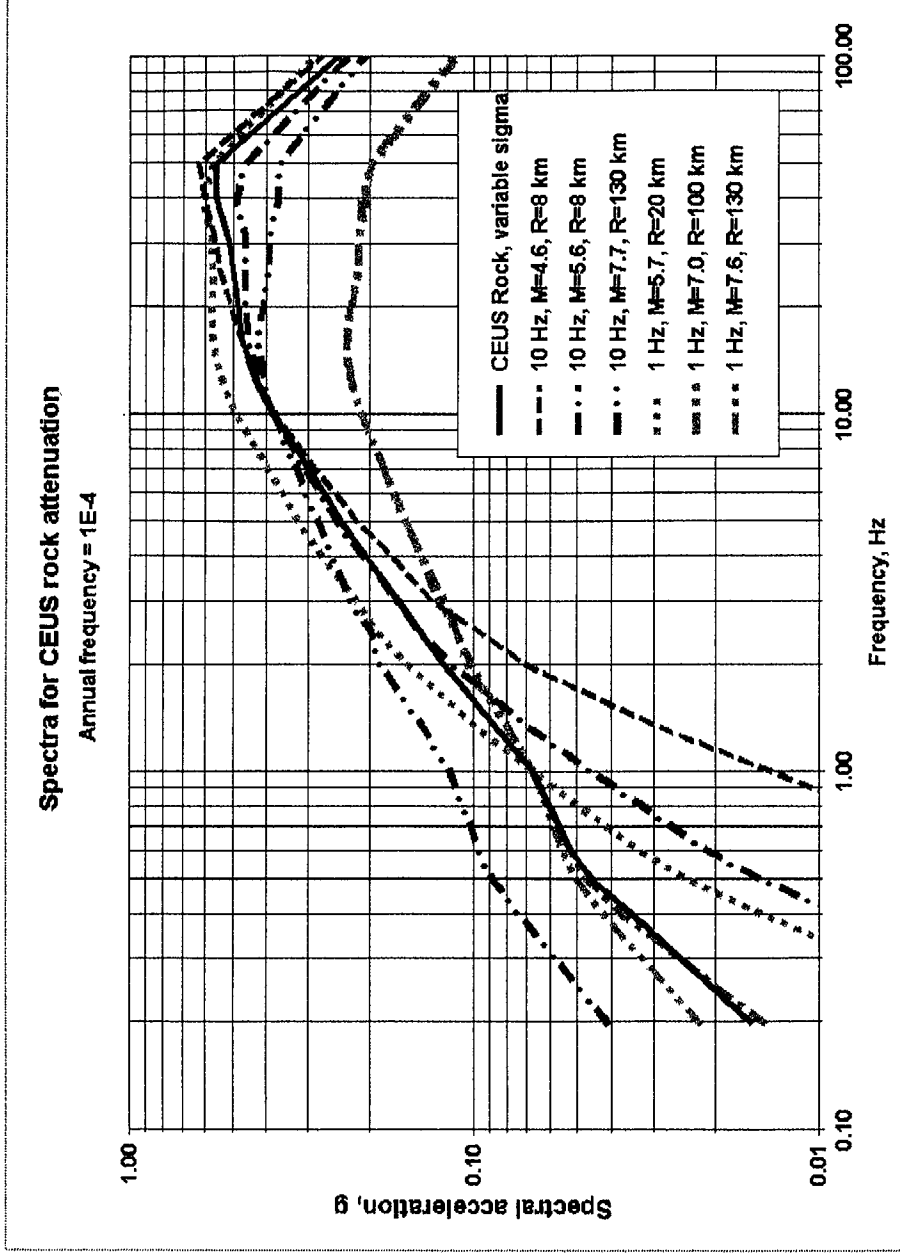
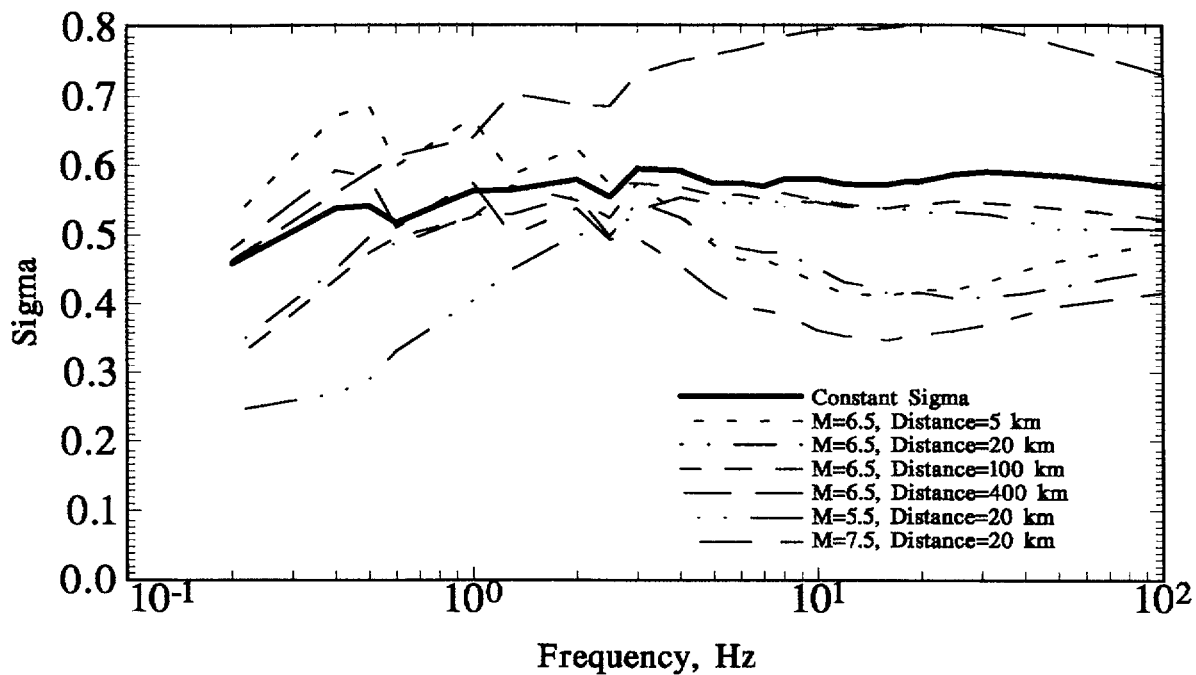


Figure 6-50. 10^{-4} UHS for rock, Columbia site, with spectra from deaggregation earthquakes.

Standard deviation of ln (SA), Savannah profile in CEUS



Standard deviation of ln (SA), Savannah profile in WUS

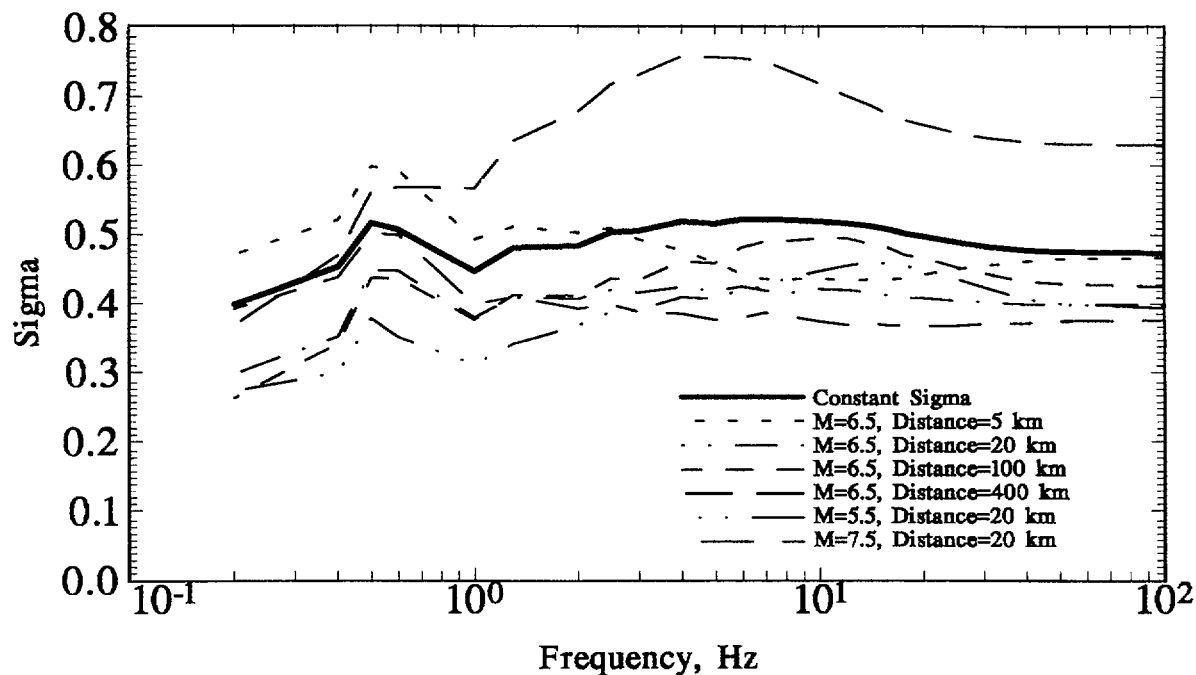


Figure 6-51. Variable σ and constant σ vs. frequency for Savannah profile.

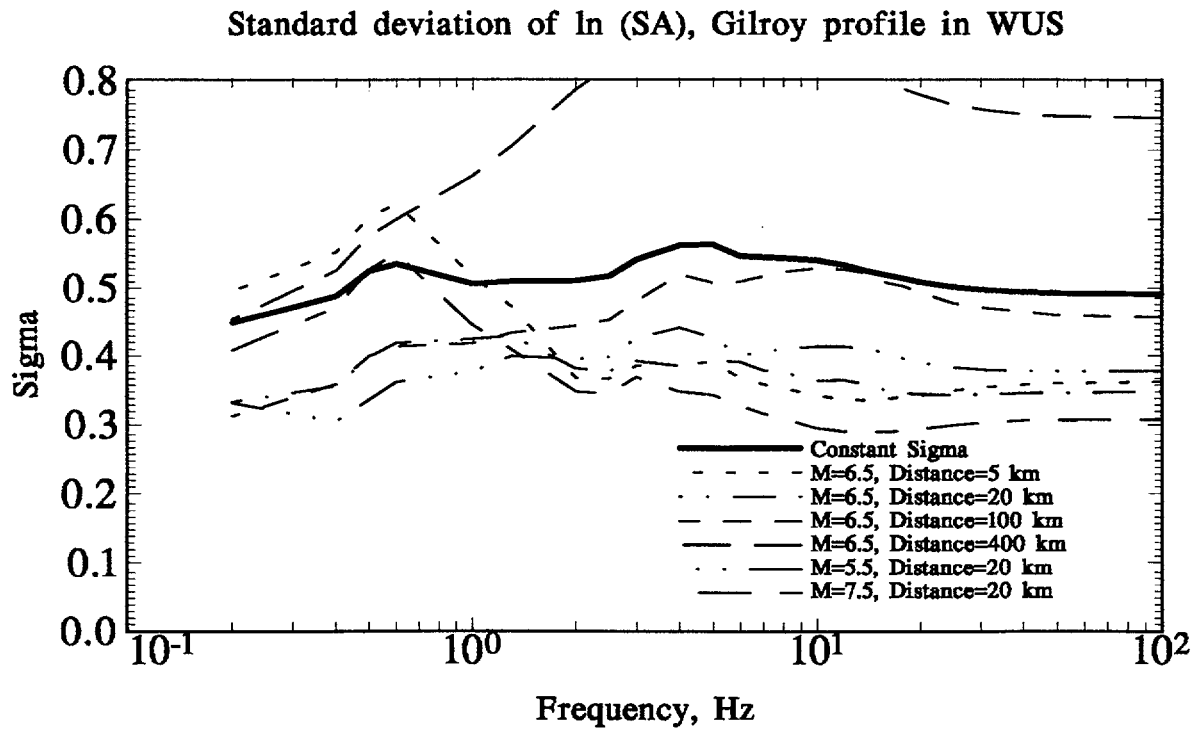
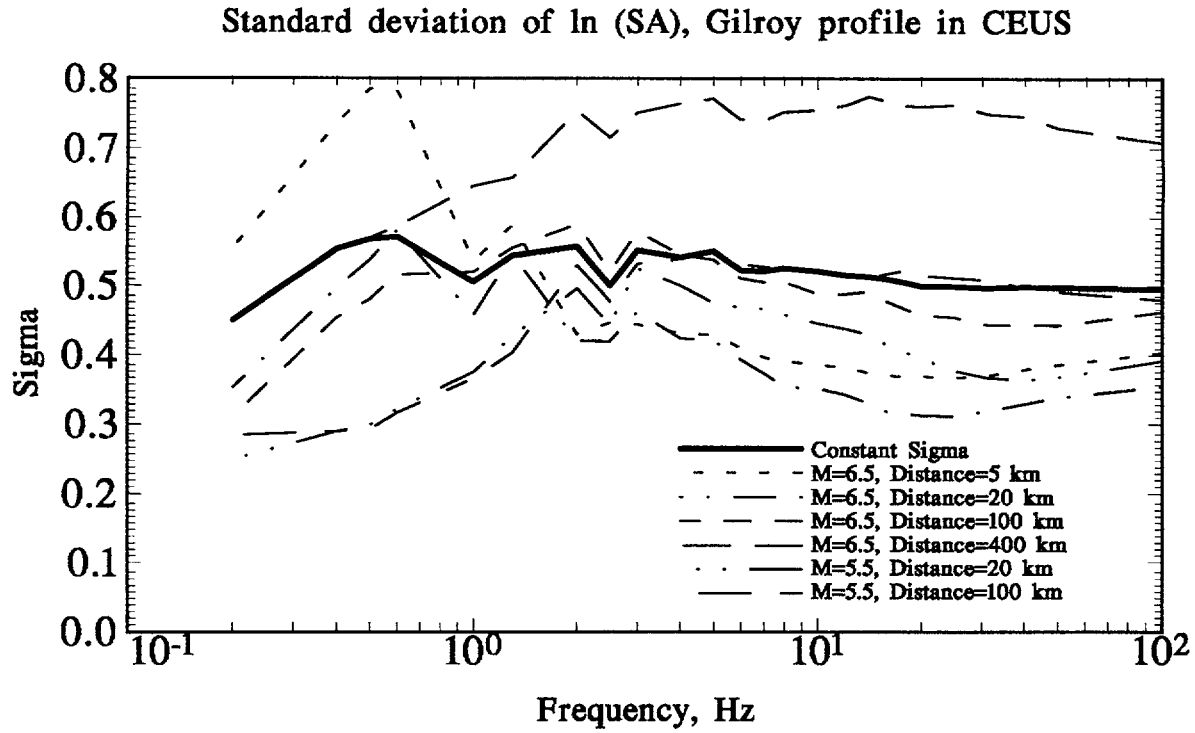
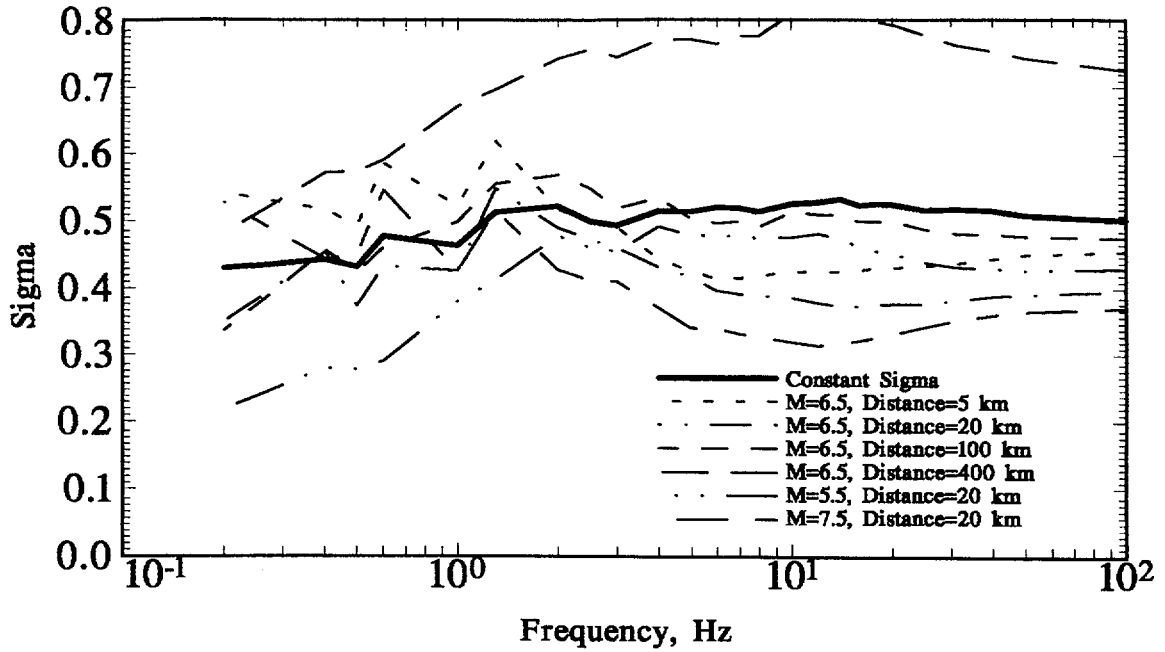


Figure 6-52. Variable σ and constant σ vs. frequency for Gilroy profile.

Standard deviation of $\ln(SA)$, Meloland profile in CEUS



Standard deviation of $\ln(SA)$, Meloland profile in WUS

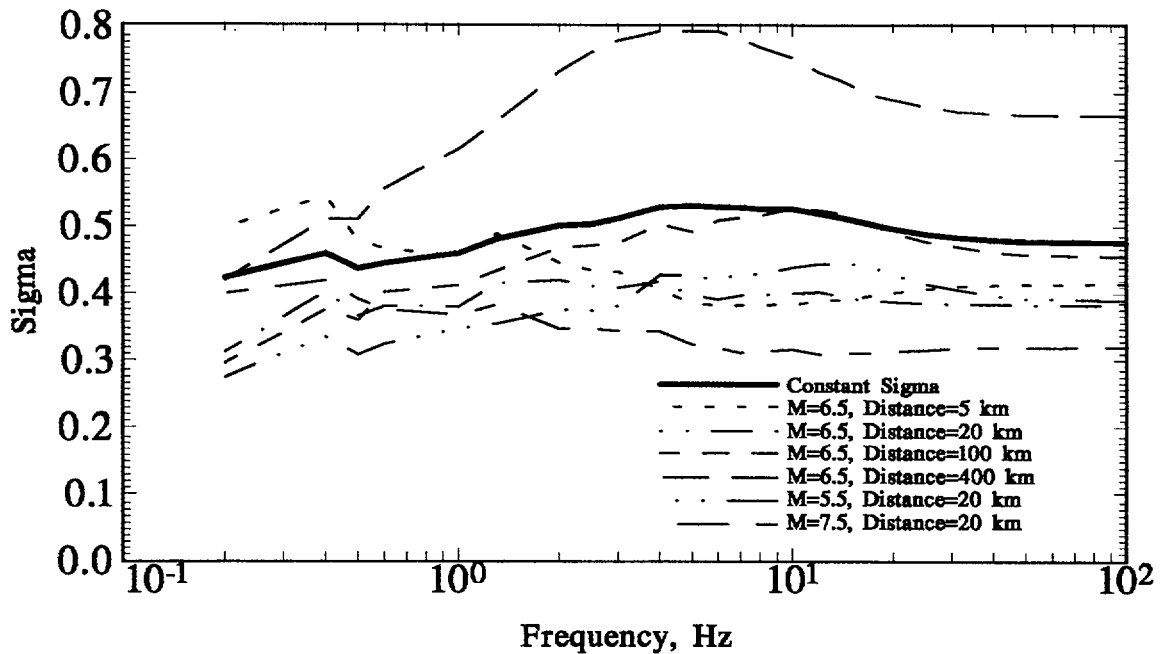
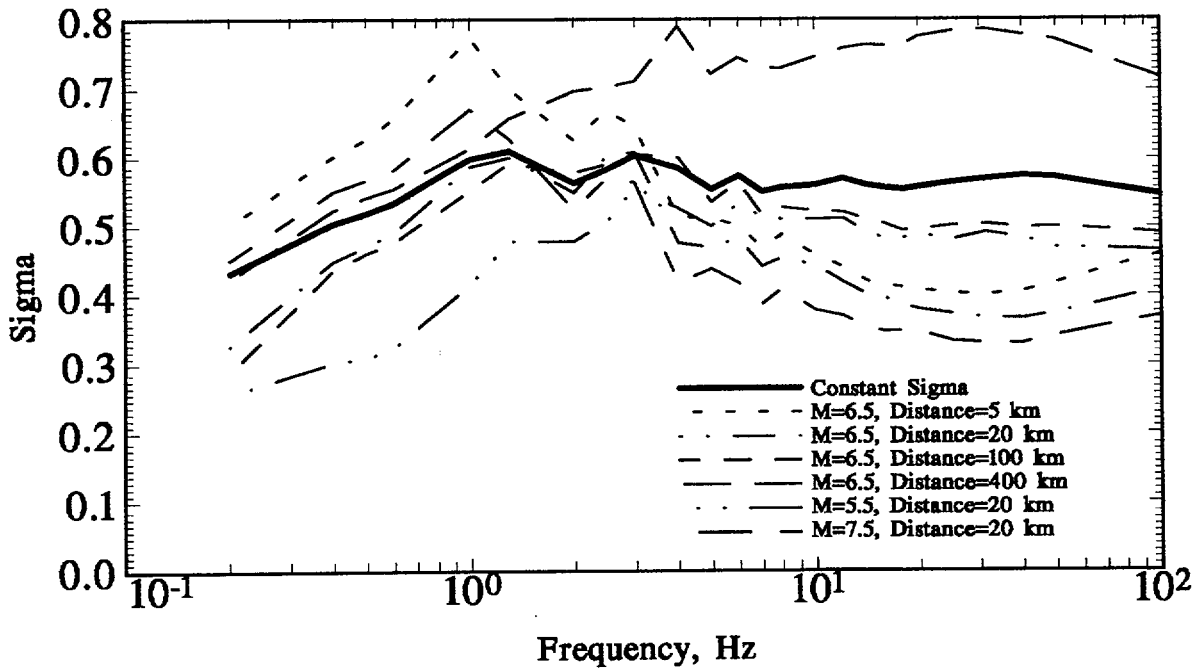


Figure 6-53. Variable σ and constant σ vs. frequency for Meloland profile.

Standard deviation of ln (SA), Rinaldi profile in CEUS



Standard deviation of ln (SA), Rinaldi profile in WUS

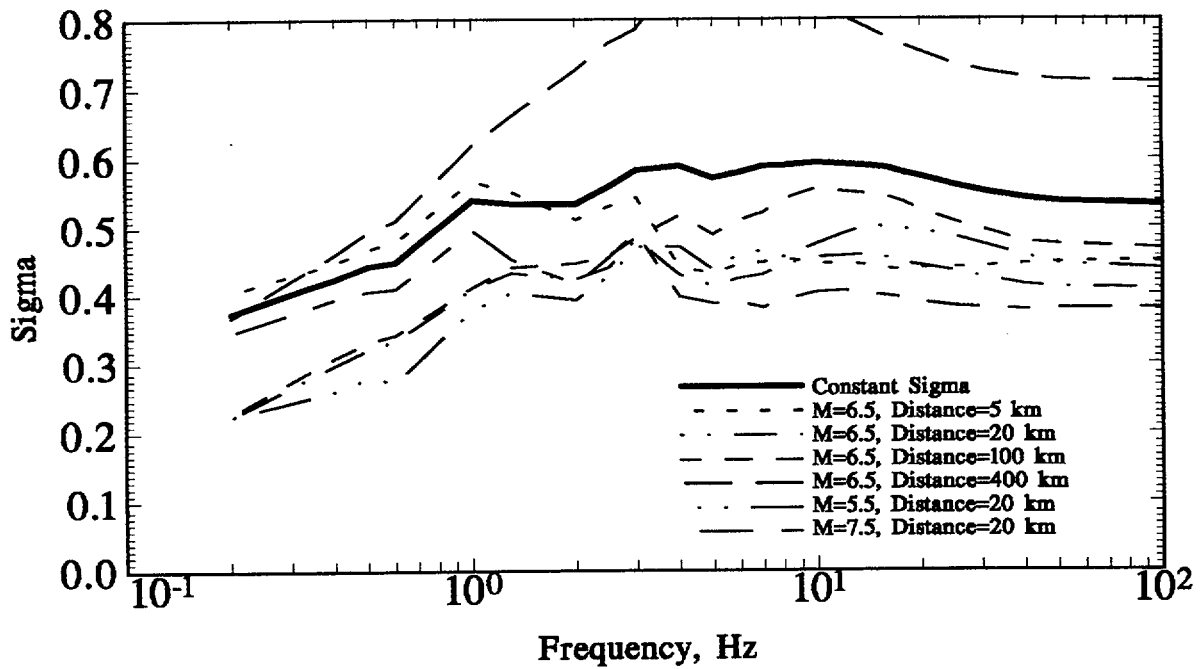


Figure 6-54. Variable σ and constant σ vs. frequency for Rinaldi profile.

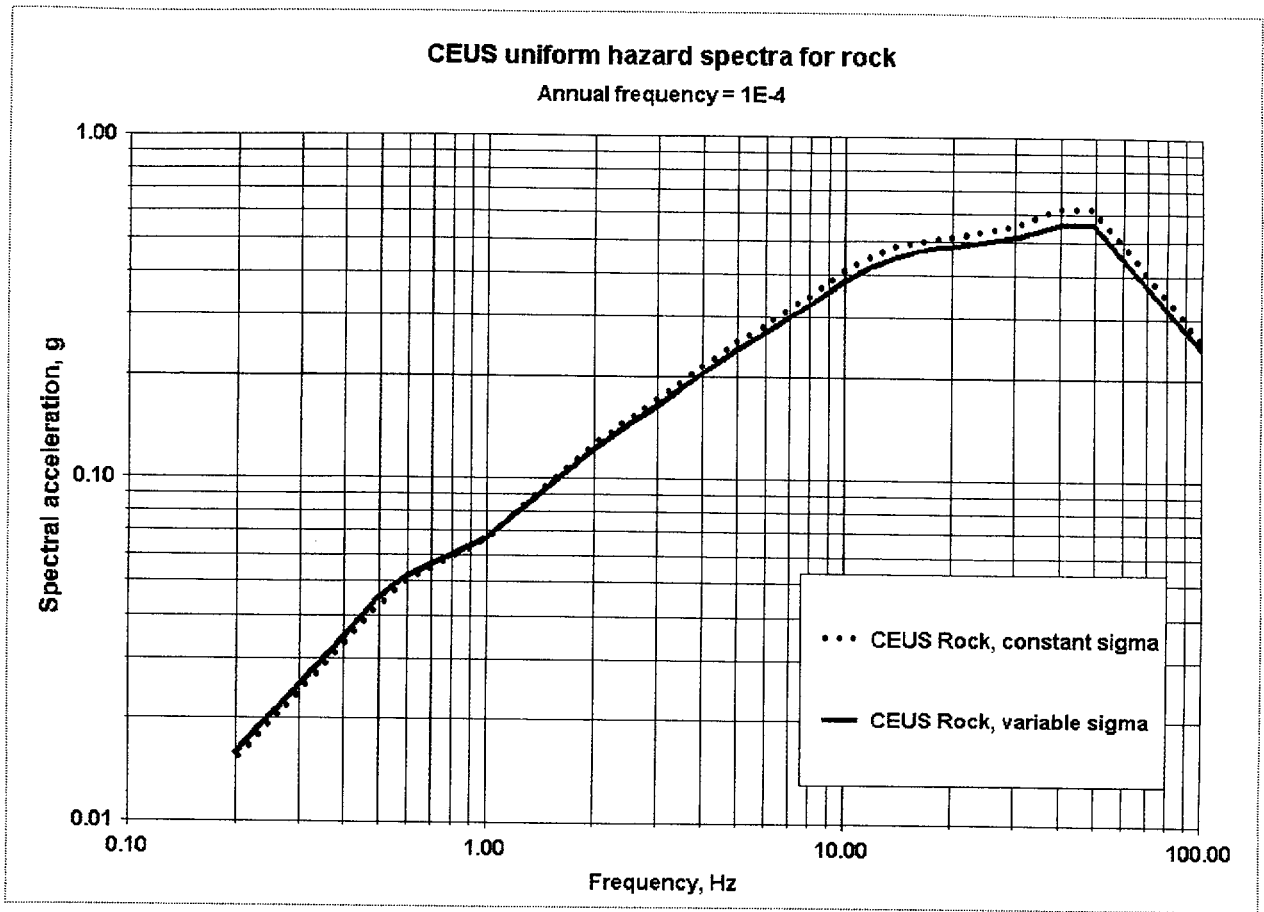


Figure 6-55: 10^{-4} UHS for rock, Columbia site, for constant σ and variable σ assumptions.

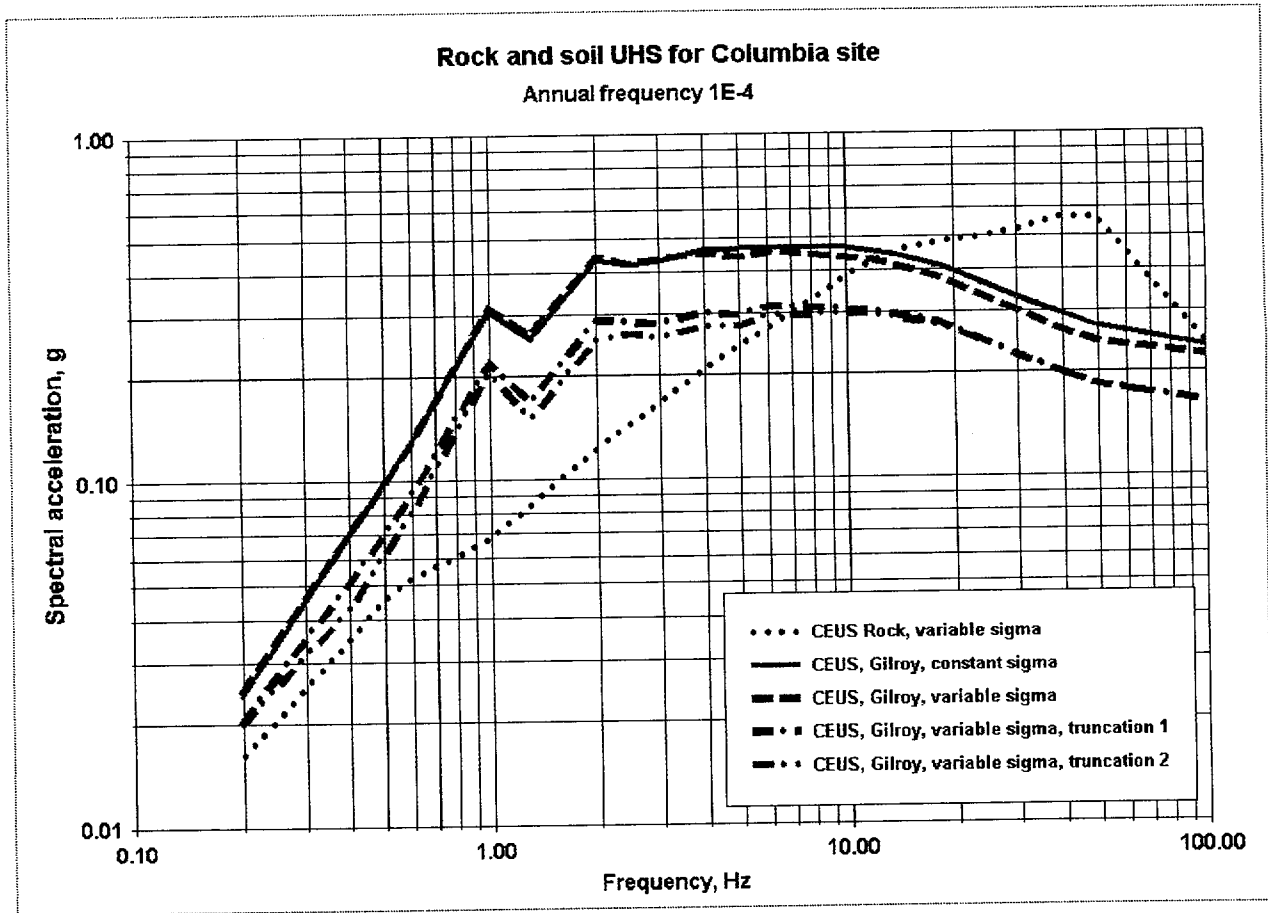


Figure 6-56. 10^{-4} UHS for CEUS rock and four soils, Gilroy profile.

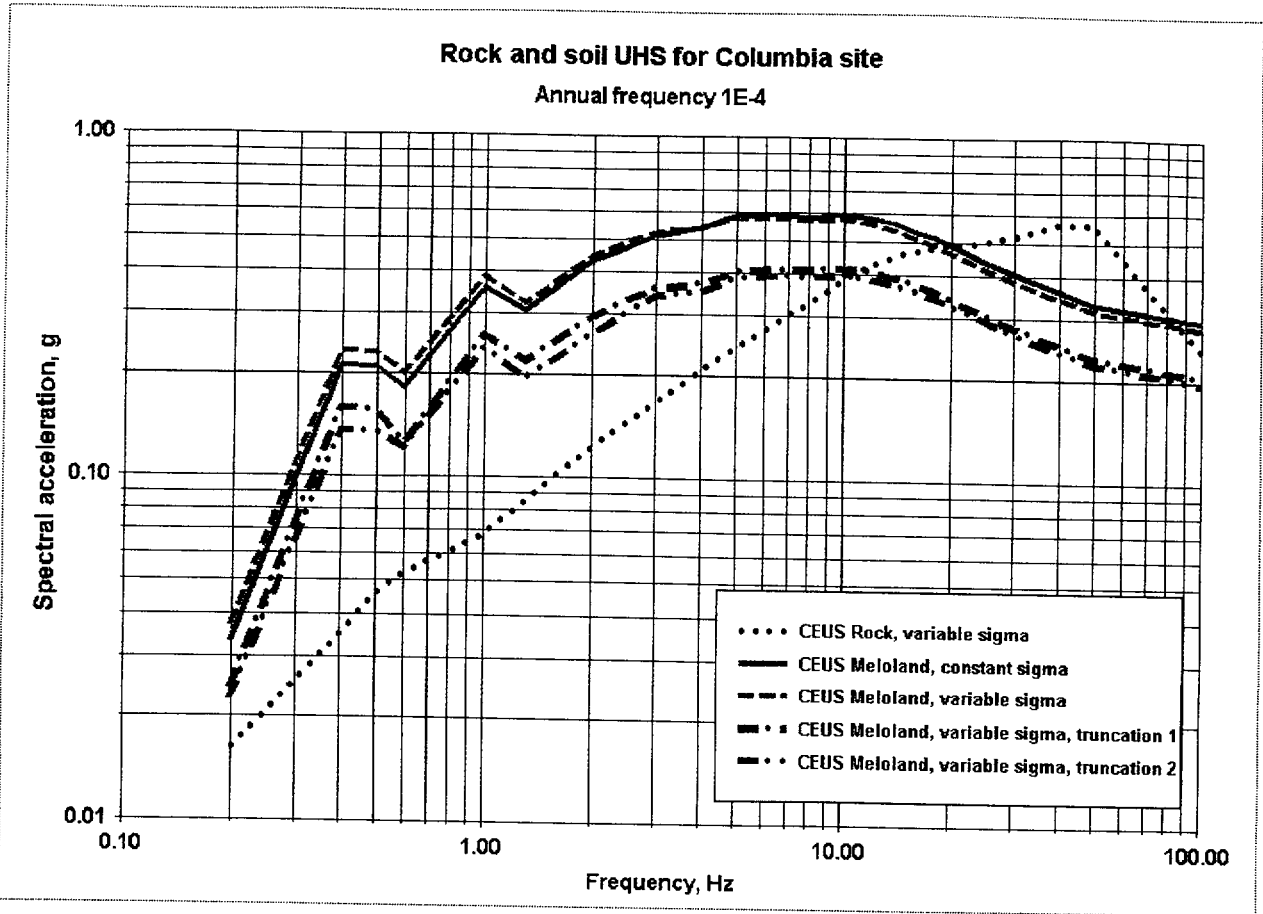


Figure 6-57. 10^{-4} UHS for CEUS rock and Meloland profile.

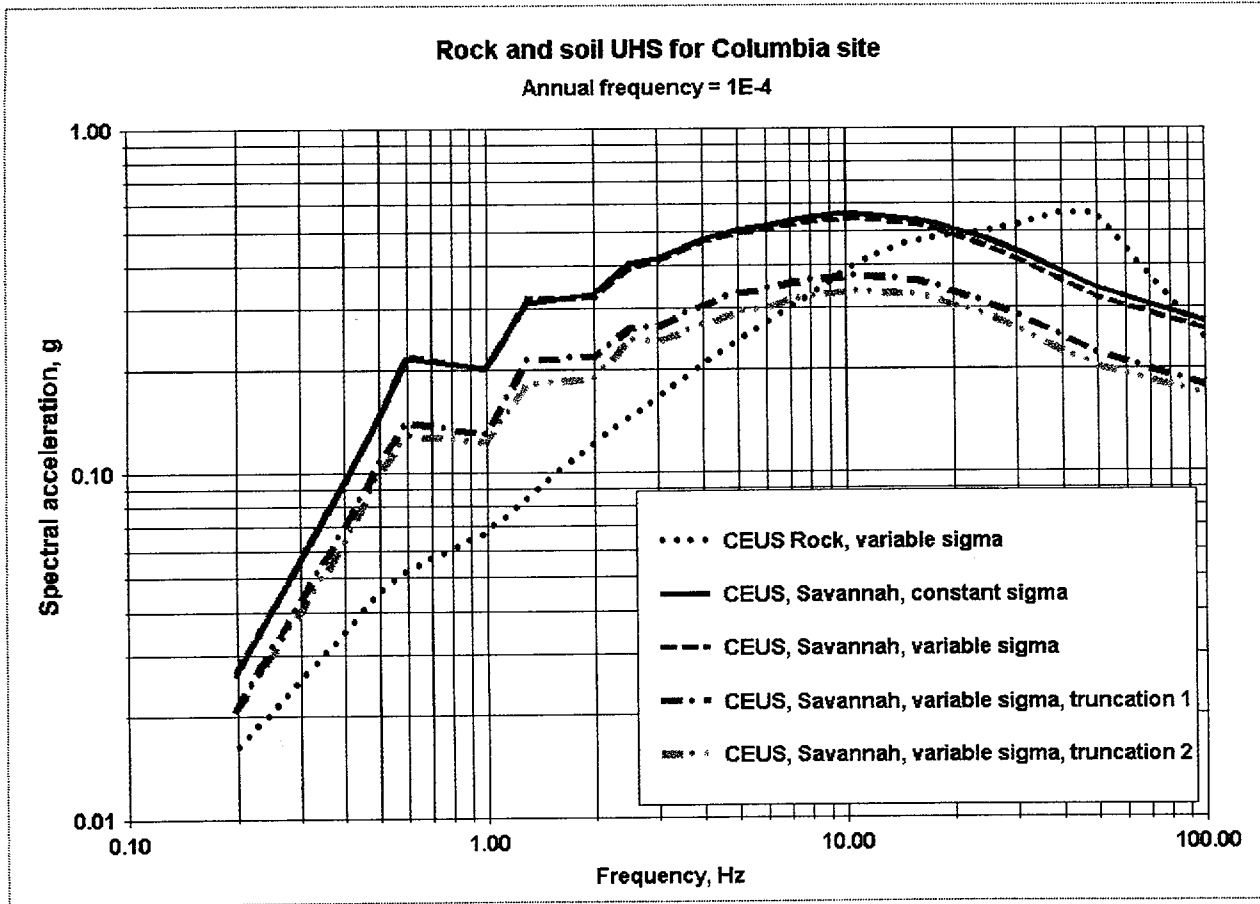


Figure 6-58. 10^{-4} UHS for CEUS rock and Savannah profile.

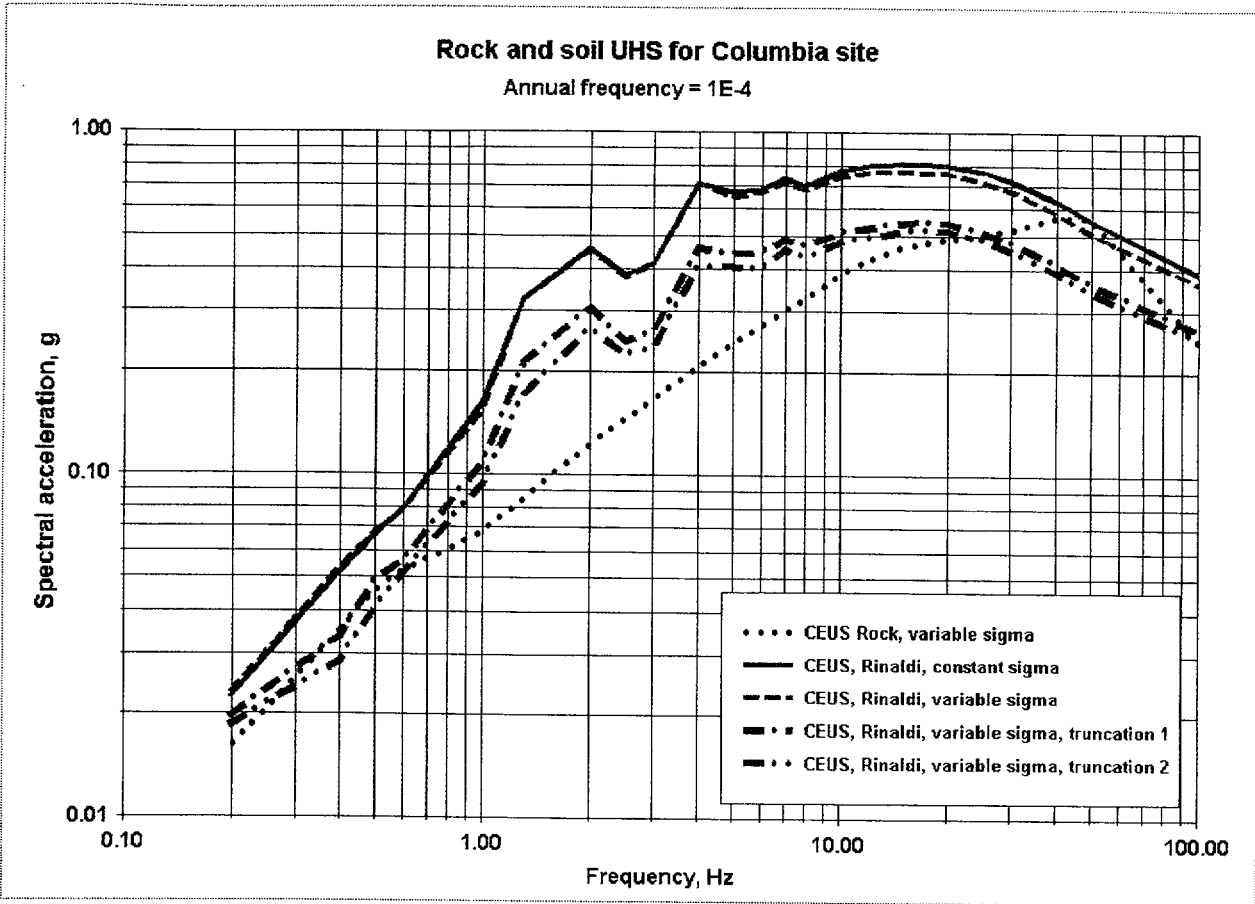


Figure 6-59. 10^{-4} UHS for CEUS rock and Rinaldi profile.

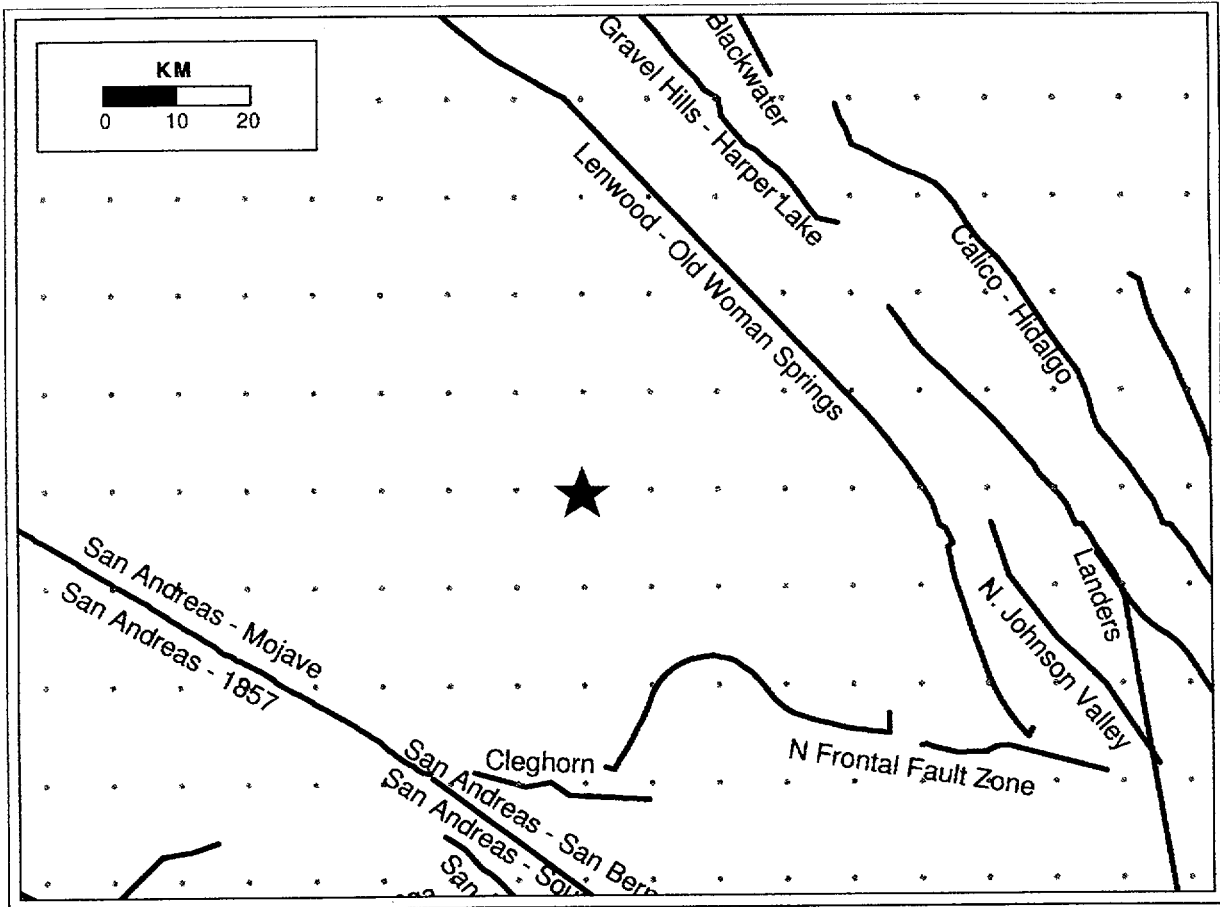


Figure 6-60. Configuration of background source and Mojave fault affecting WUS example site (Mojave, California).

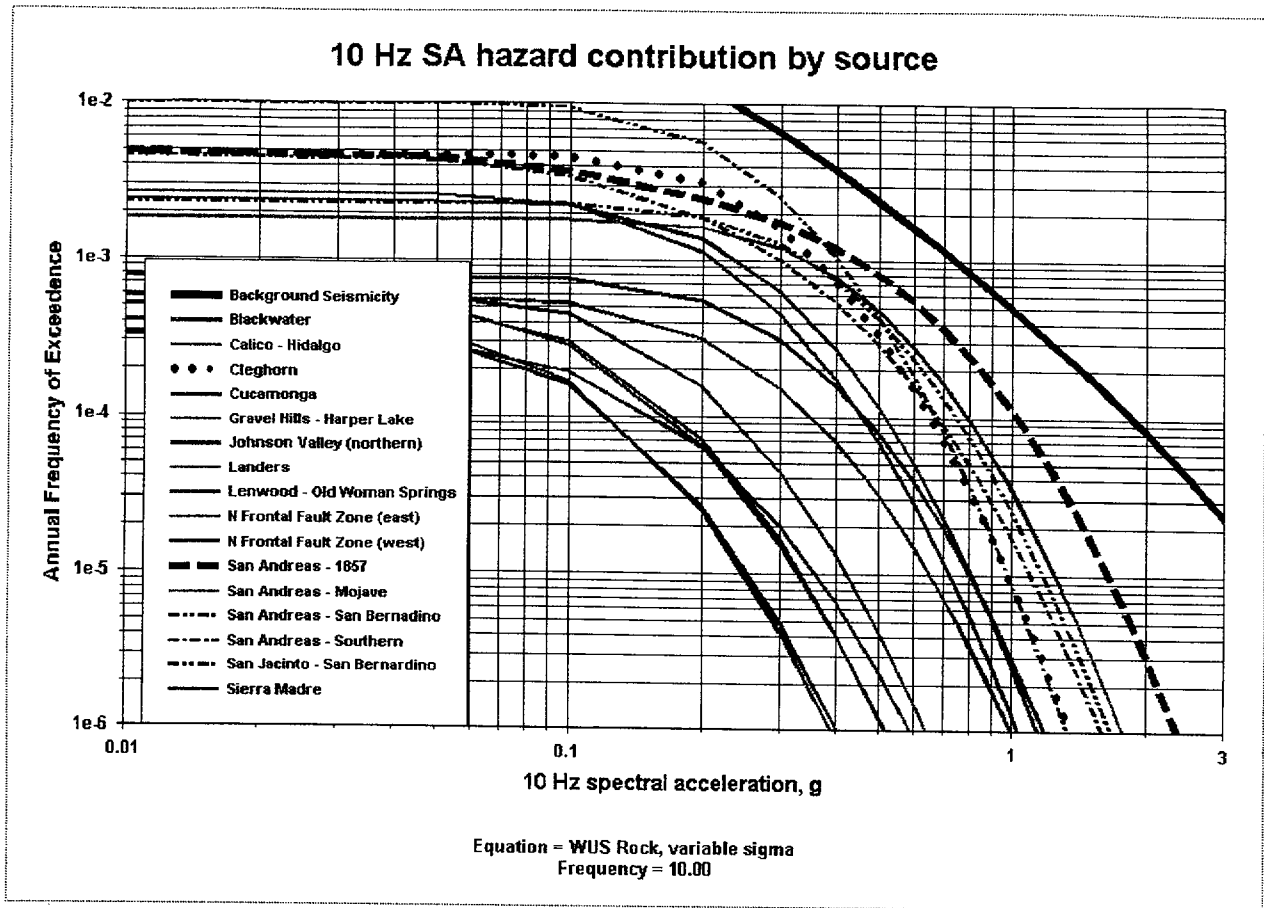


Figure 6-61. Contribution to seismic hazard by source for 10 Hz spectral acceleration, Mojave site.

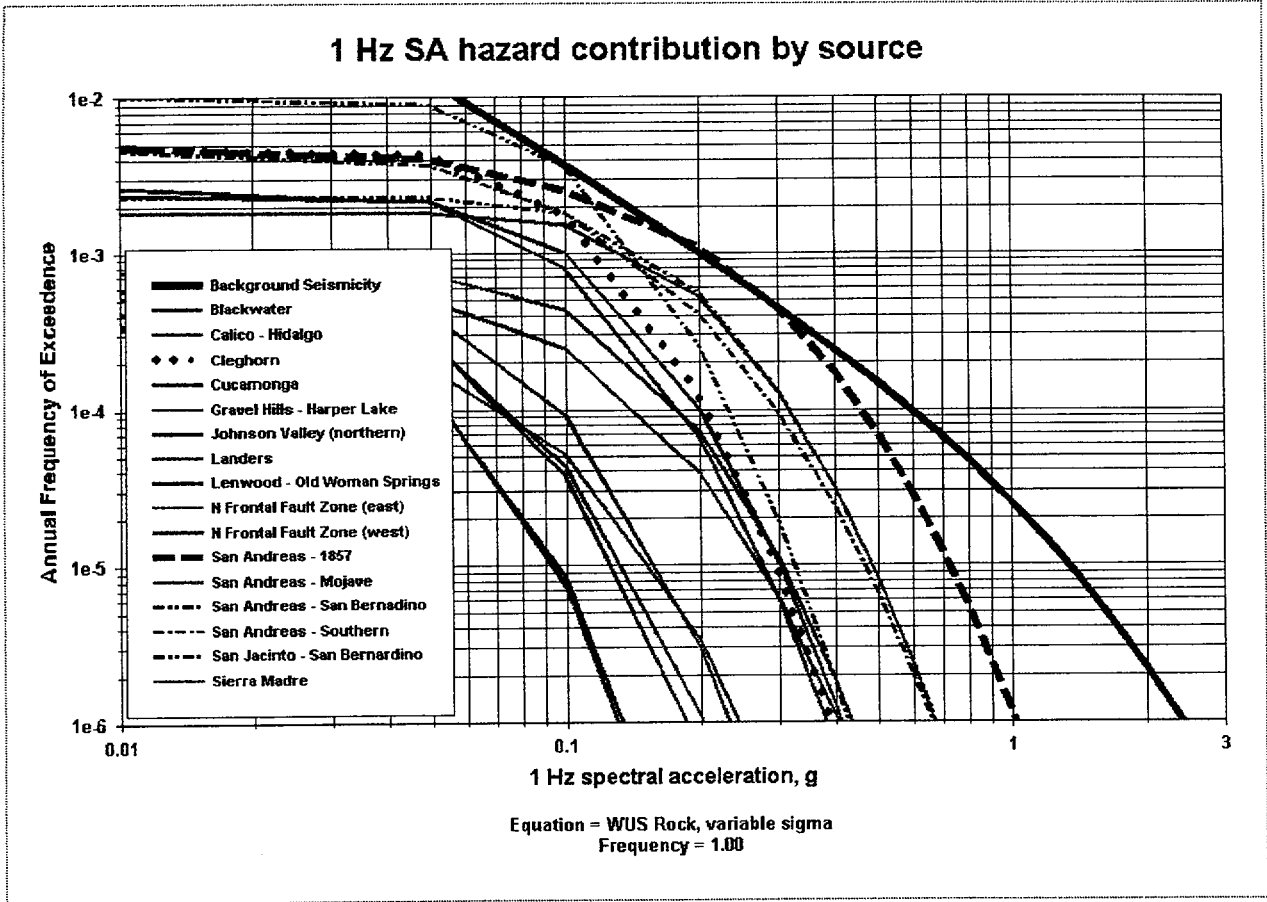


Figure 6-62. Contribution to seismic hazard by source for 1 Hz spectral acceleration, Mojave site.

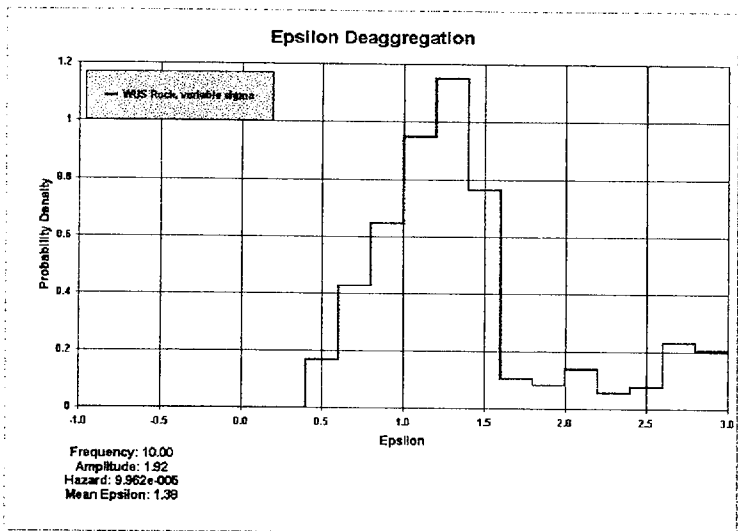
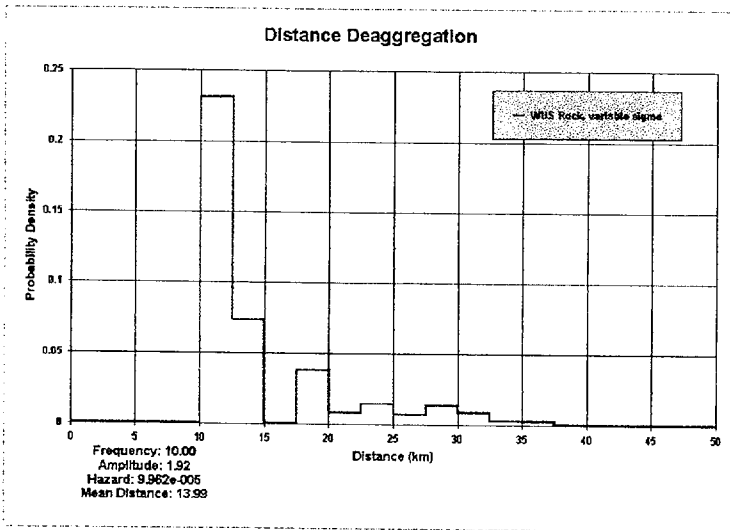
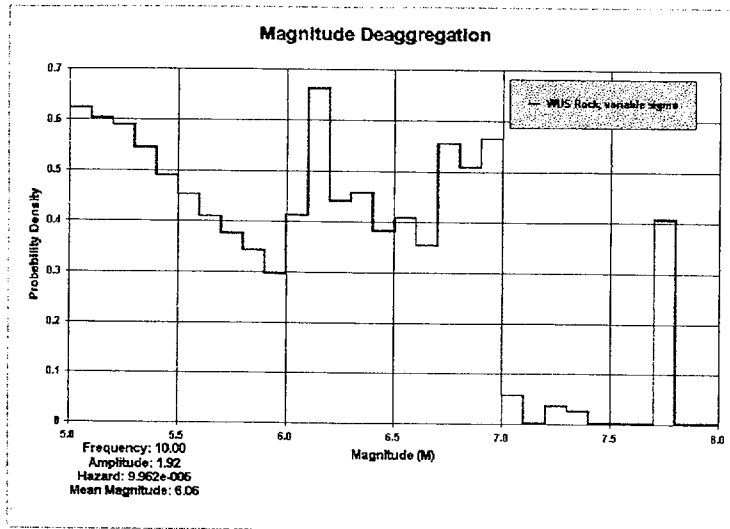


Figure 6-63. Deaggregation of seismicity hazard by M, R and ϵ for 10 Hz SA at 1.92g, Mojave site.

Magnitude-Distance Deaggregation

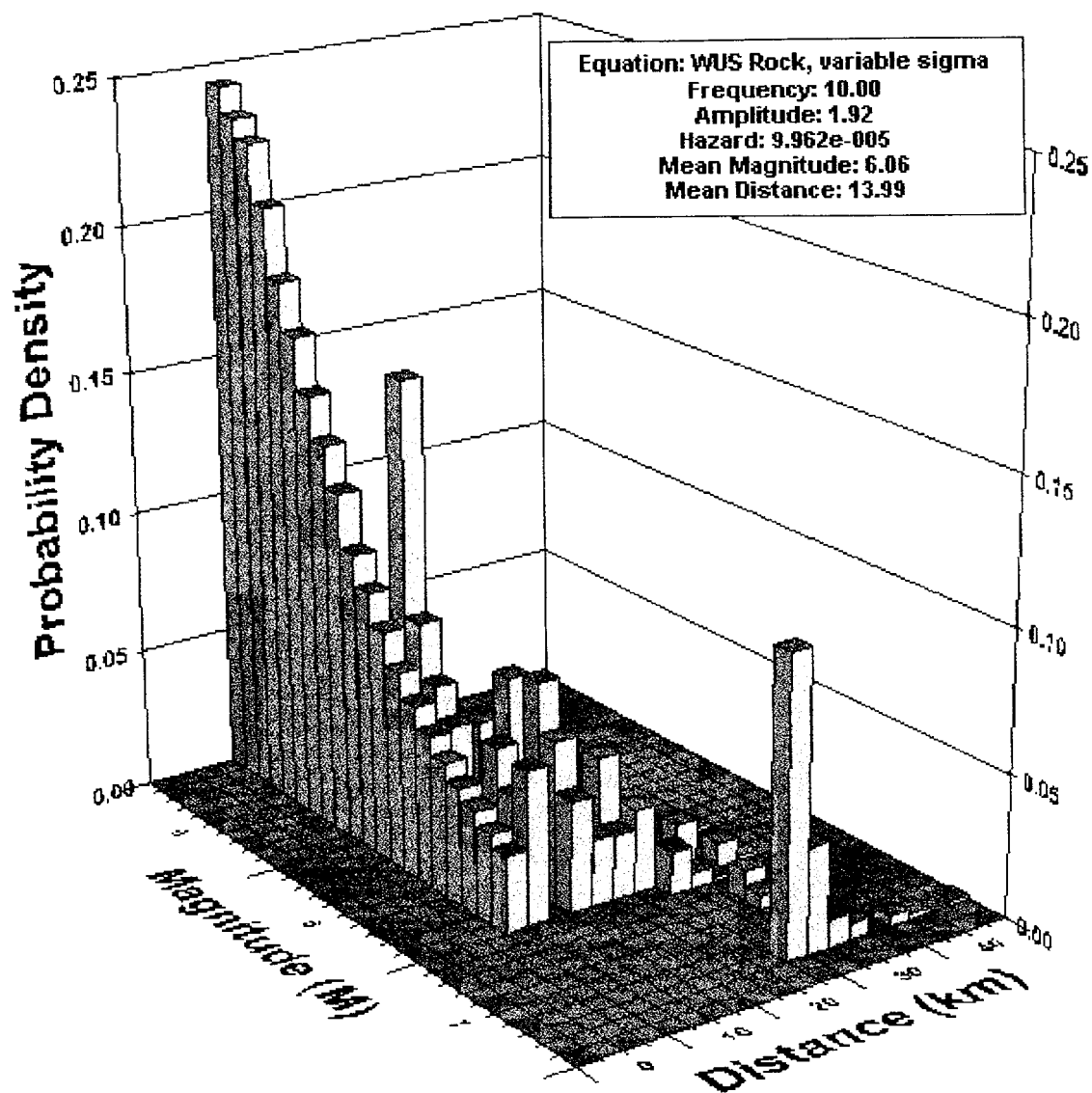


Figure 6-64. Deaggregation of seismic hazard by **M** and **R** for 10 Hz SA at 1.92g, Mojave site.

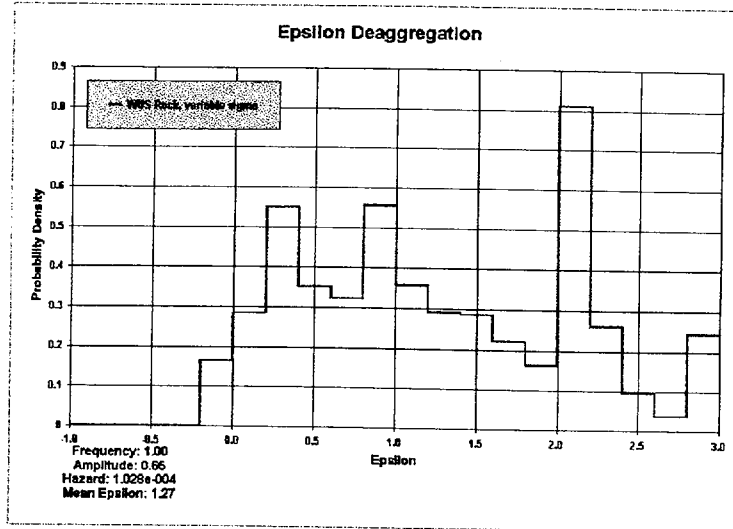
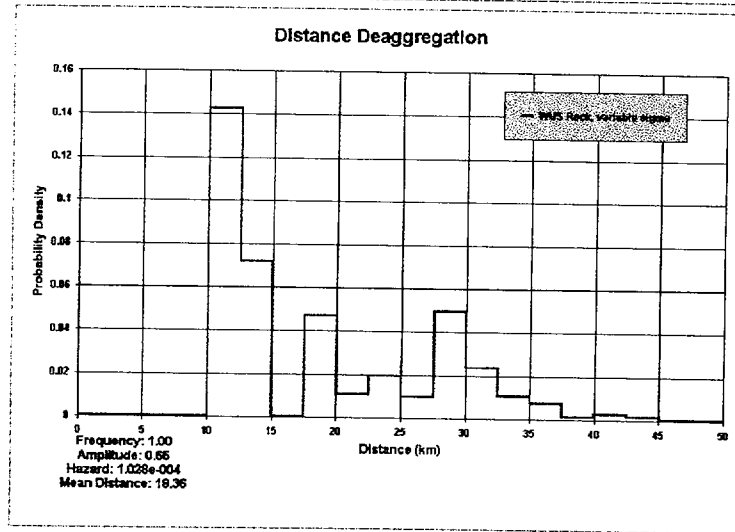
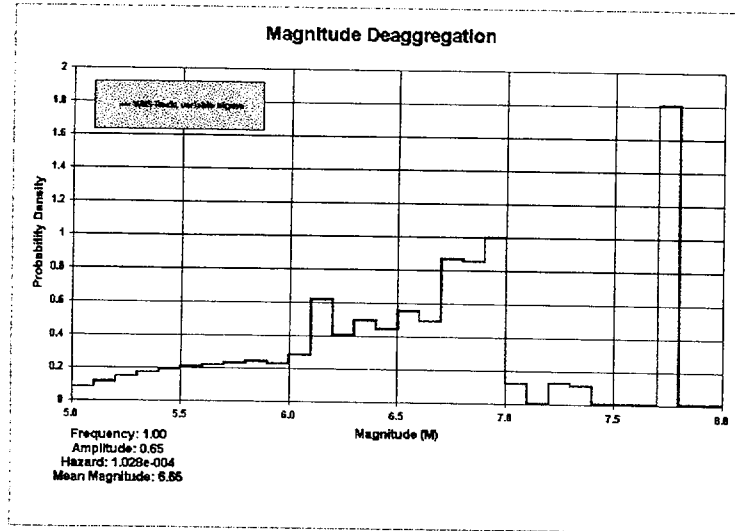


Figure 6-65. Deaggregation of seismic hazard by M , R and ϵ for 1 Hz SA at 0.65g, Mojave site.

Magnitude-Distance Deaggregation

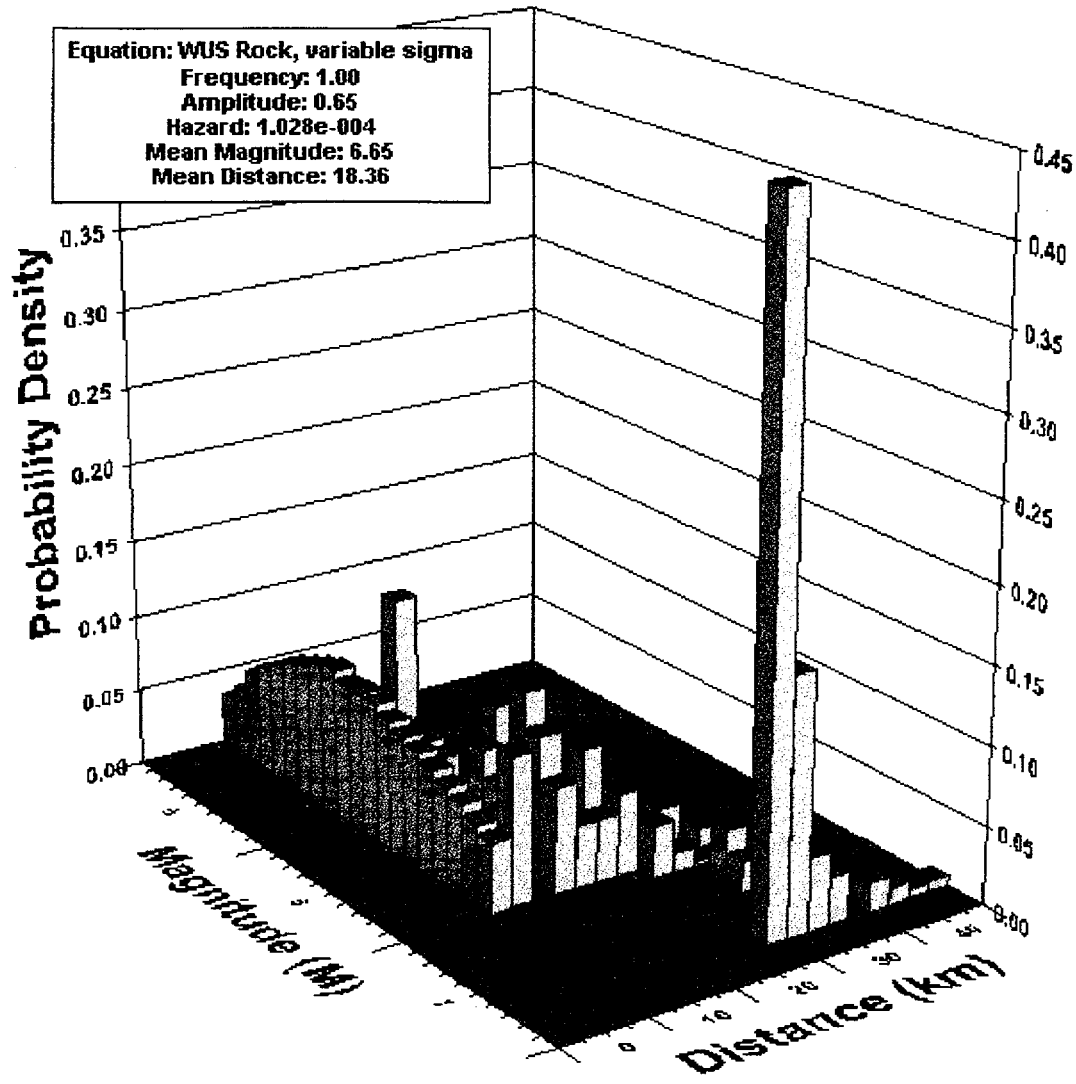


Figure 6-66: Deaggregation of seismic hazard by M and R for 1 Hz SA at 0.65g, Mojave site.

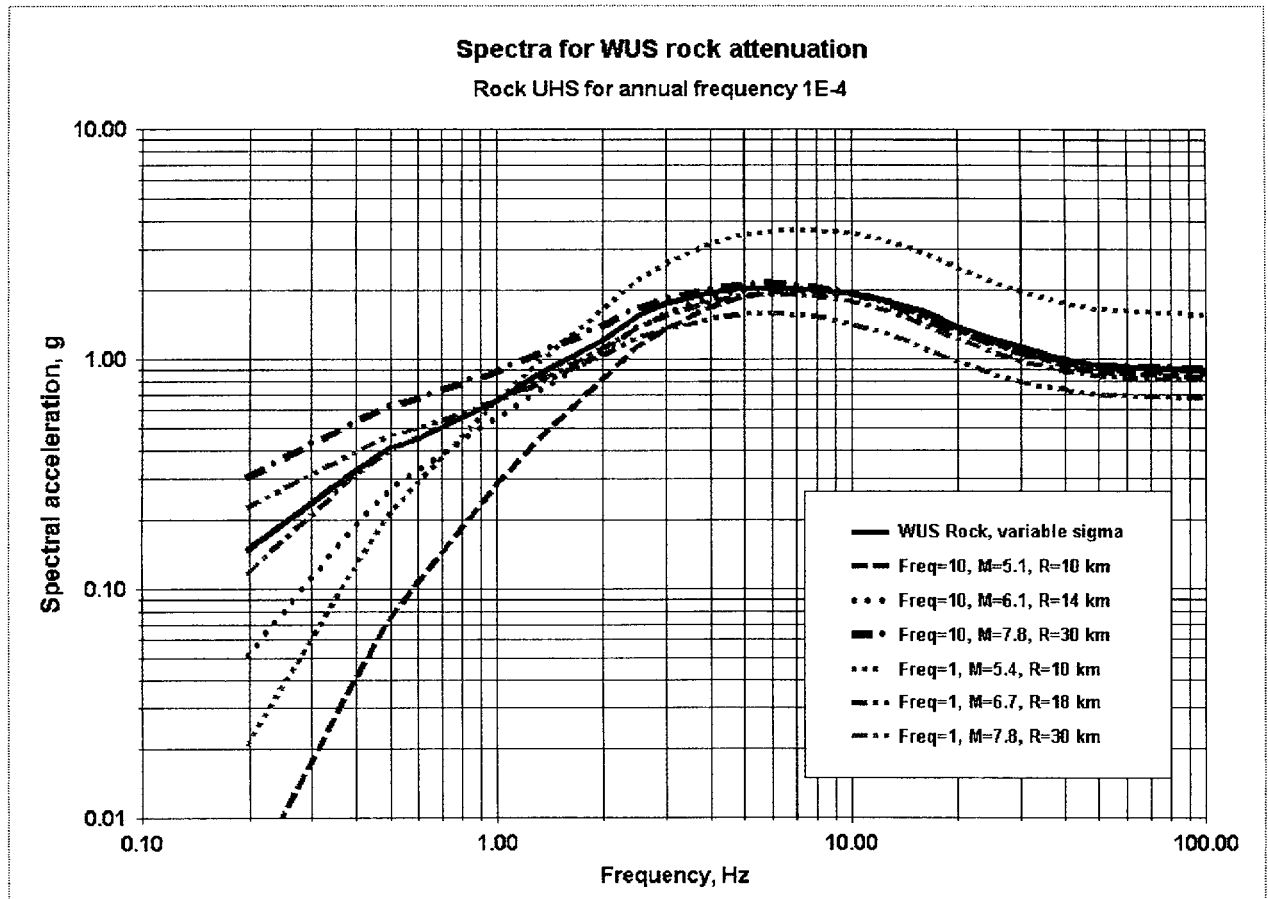


Figure 6-67: 10^{-4} UHS for rock, Columbia site, with spectra from deaggregation earthquakes.

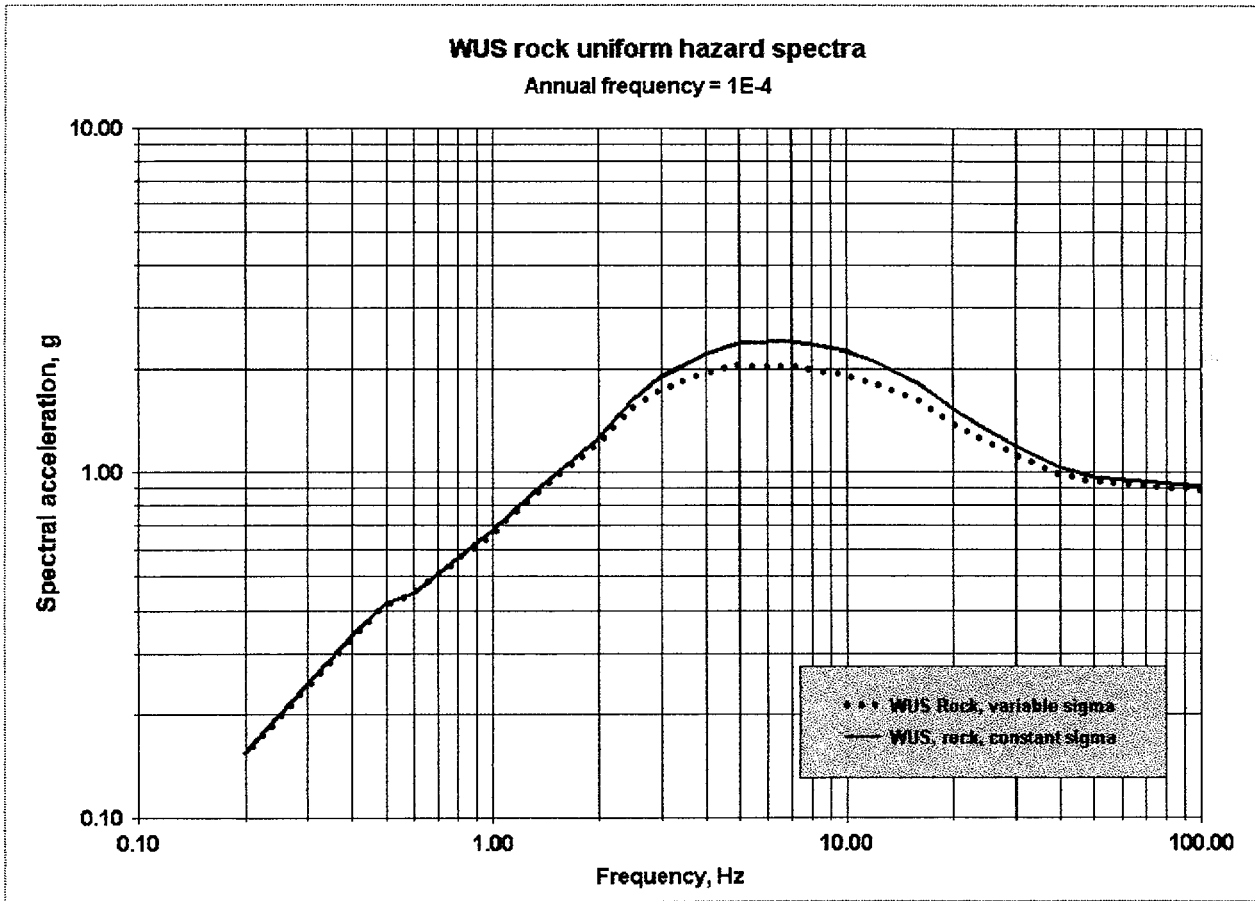


Figure 6-68: 10^{-4} UHS for rock, Mojave site, for constant σ and variable σ assumptions.

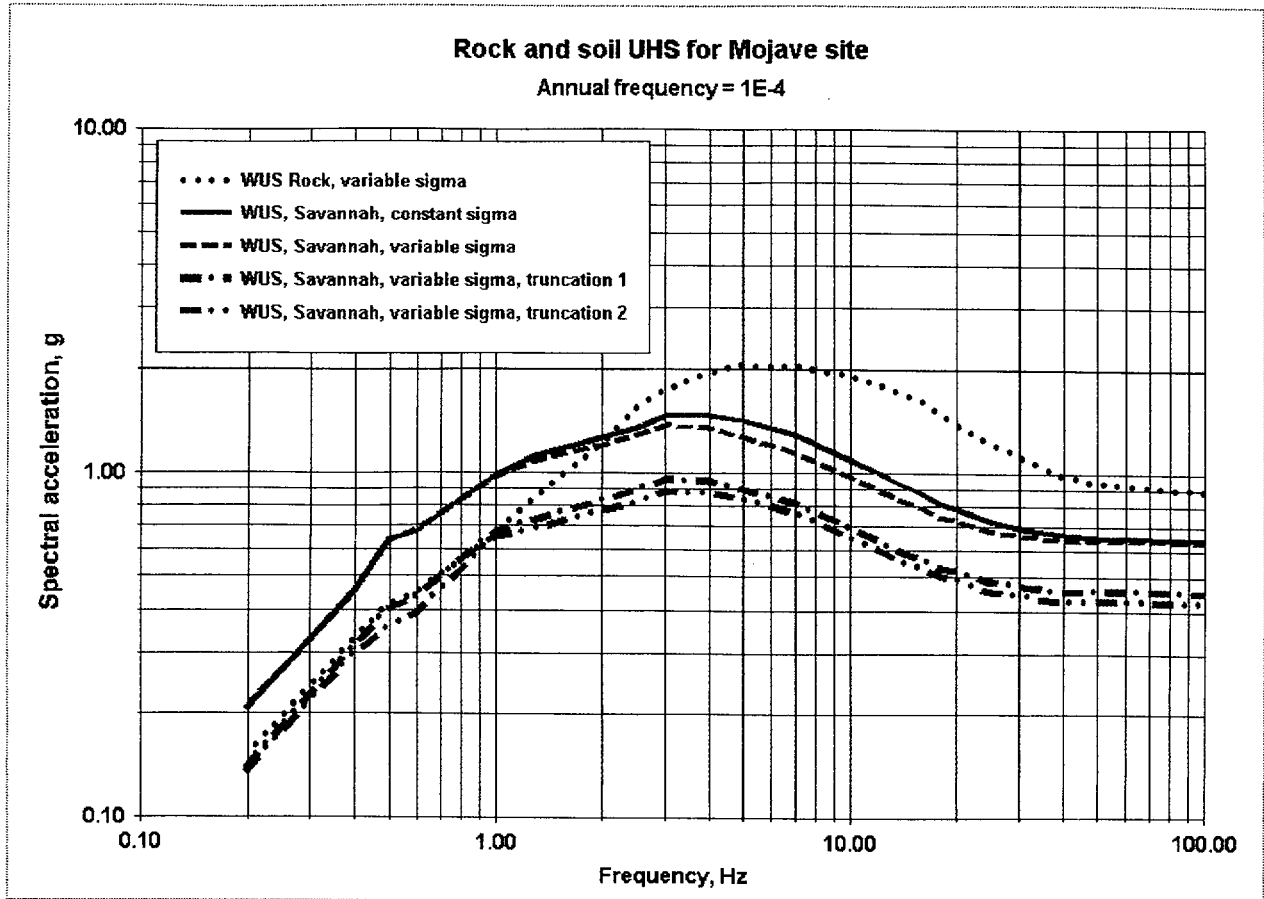


Figure 6-69: 10^{-4} UHS for WUS rock and Savannah site.

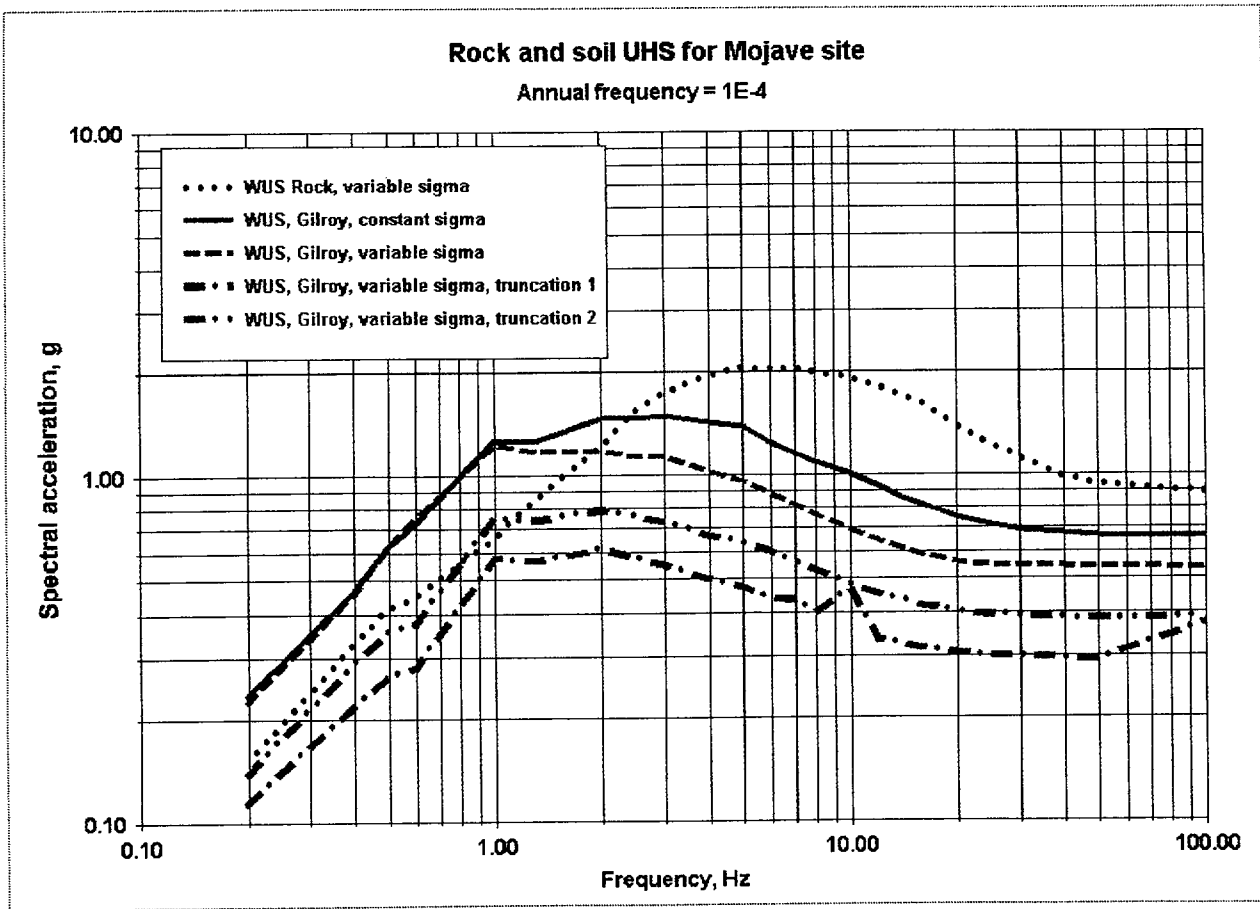


Figure 6-70: 10^{-4} UHS for WUS rock and Gilroy profile.

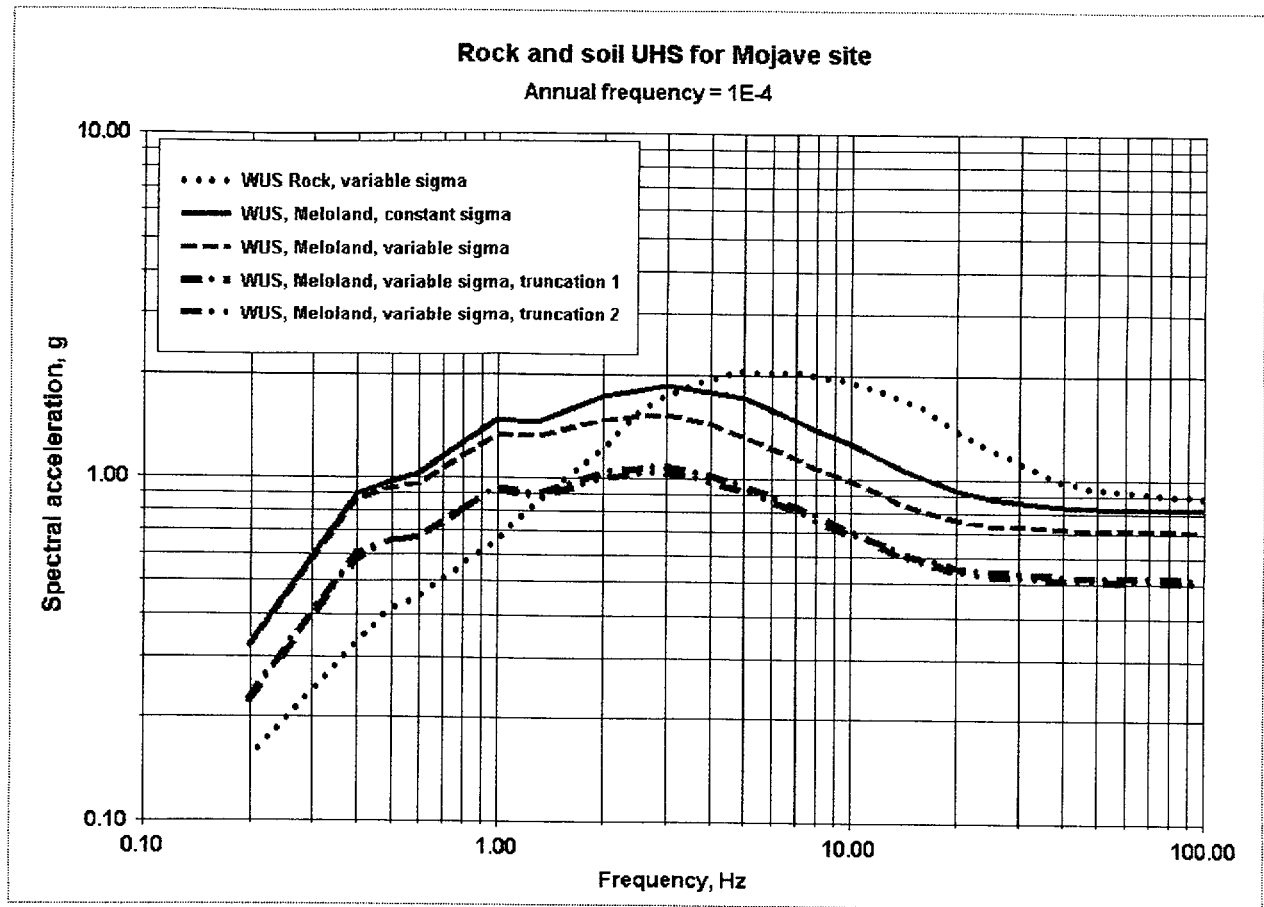


Figure 6-71: 10^{-4} UHS for WUS rock and Meloland profile.

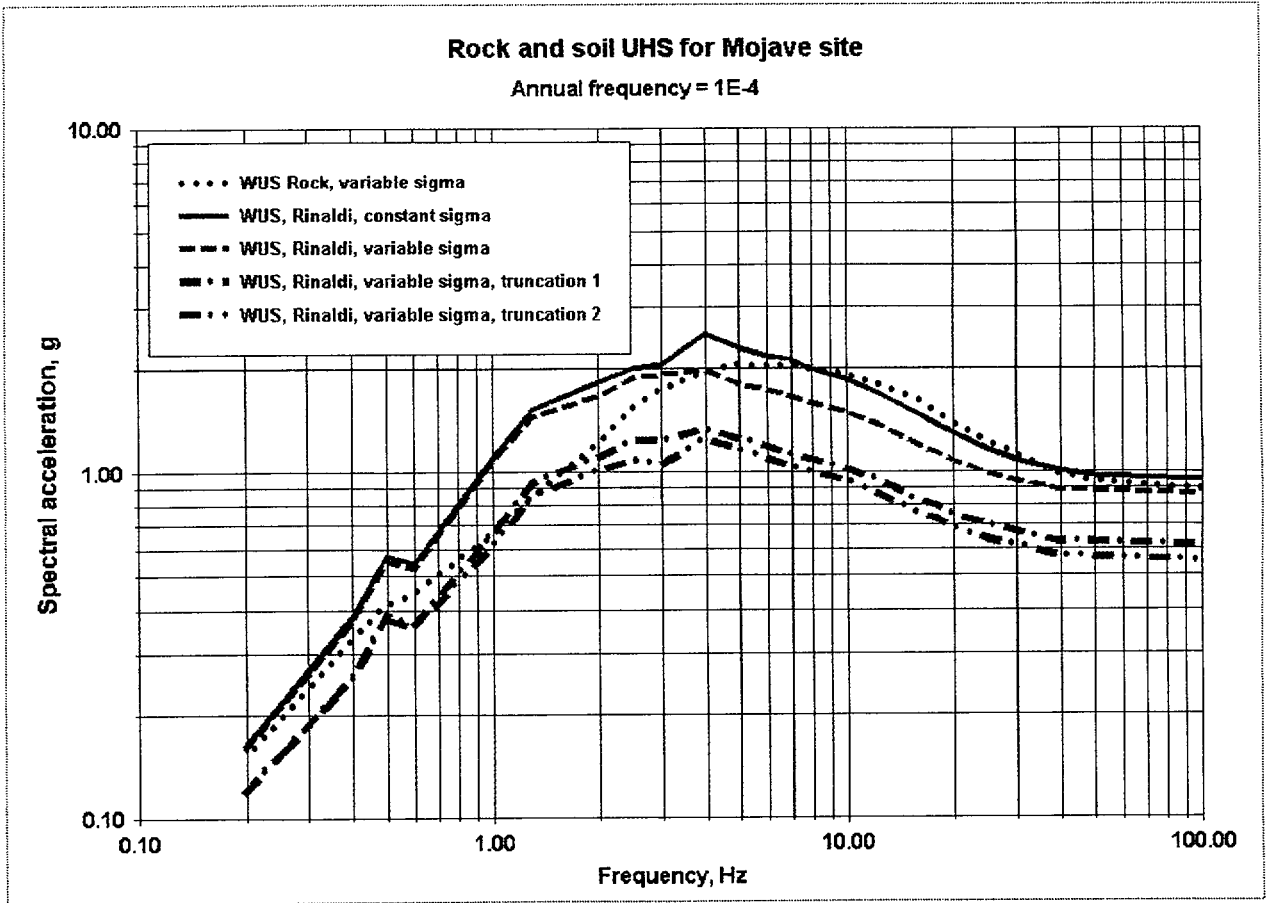


Figure 6-72: 10^{-4} UHS for WUS rock and Rinaldi profile.

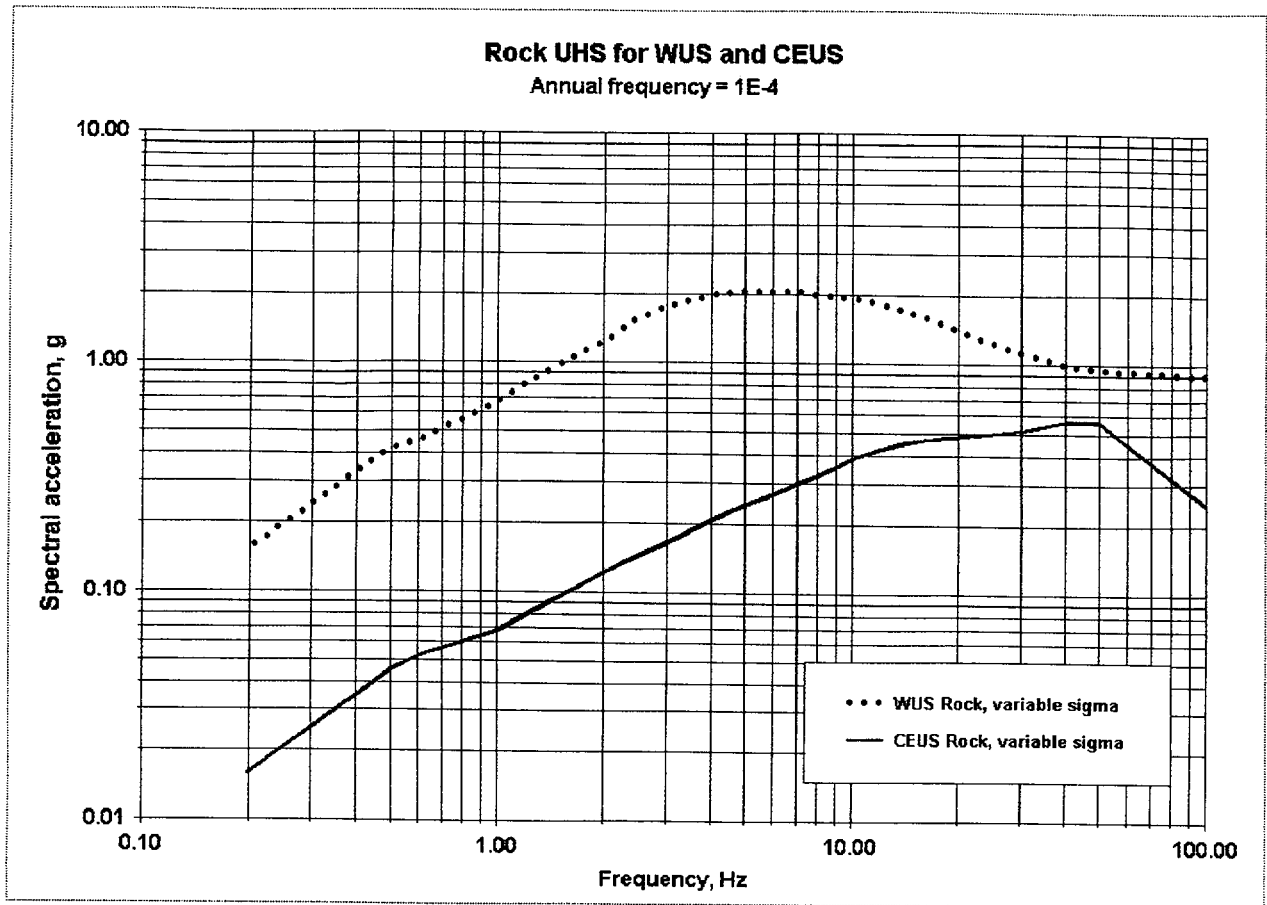
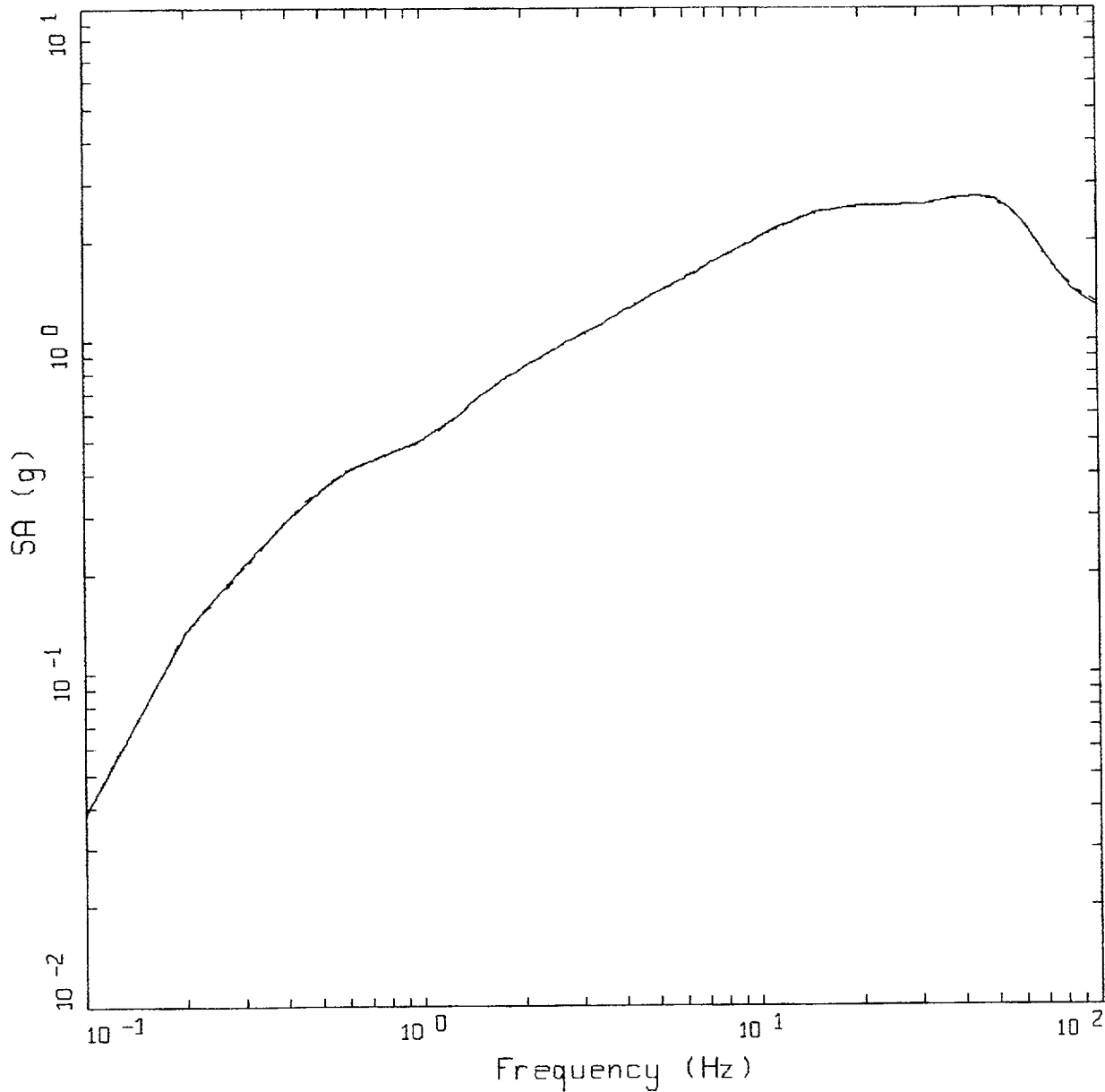


Figure 6-73. 10^{-4} UHS for CEUS site (Columbia) and WUS site (Mojave).

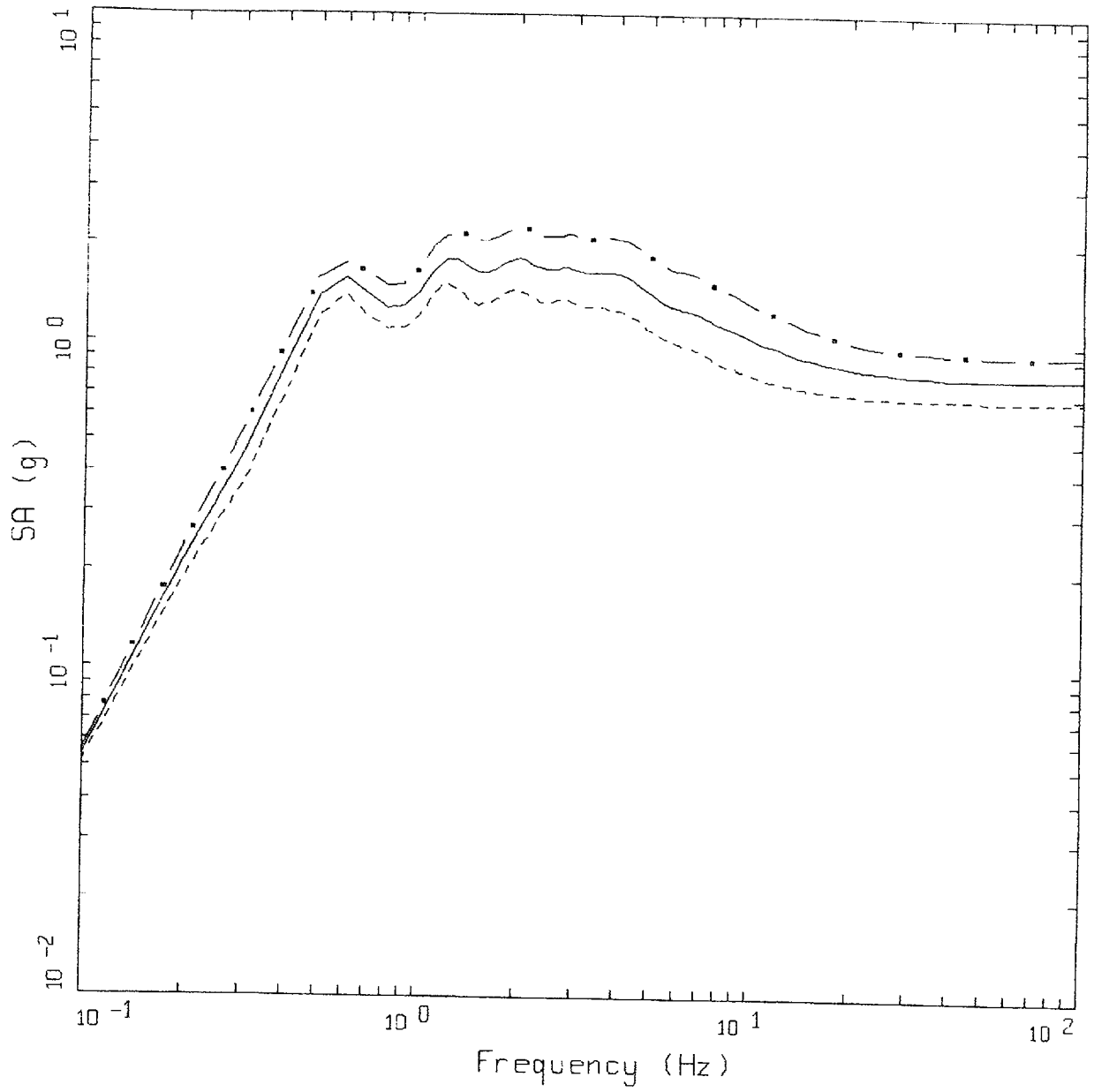


M = 7.5, D = 001 KM
 MATCH TO CEUS ROCK

LEGEND

- 5 %, TARGET; PGA = 1.271 G
- 5 %, SPECTRAL MATCH; PGA = 1.283 G

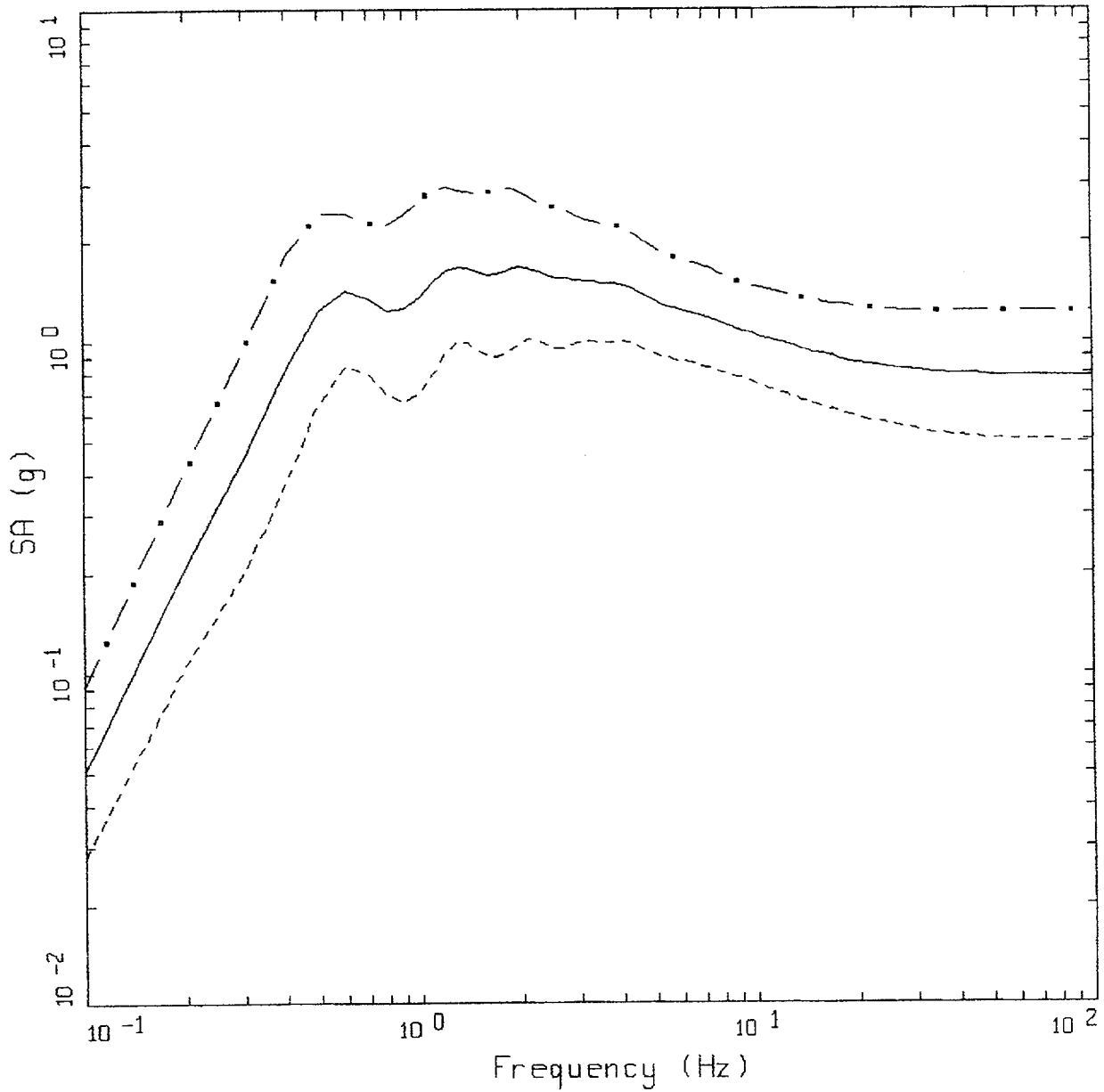
Figure 6-74. Comparison of spectral match (dotted line) to median spectrum computed for $M = 7.5$ at a distance of 1 km (solid line): CEUS rock outcrop.



CEUS, M = 7.5, D = 001 KM, H = 12 KM
 SD = 95 BARS, SAVANNAH GENERIC, SITE

- LEGEND
- · - 84TH PERCENTILE, PGA = 0.934 G
 - 50TH PERCENTILE, PGA = 0.801 G
 - - - 16TH PERCENTILE, PGA = 0.687 G

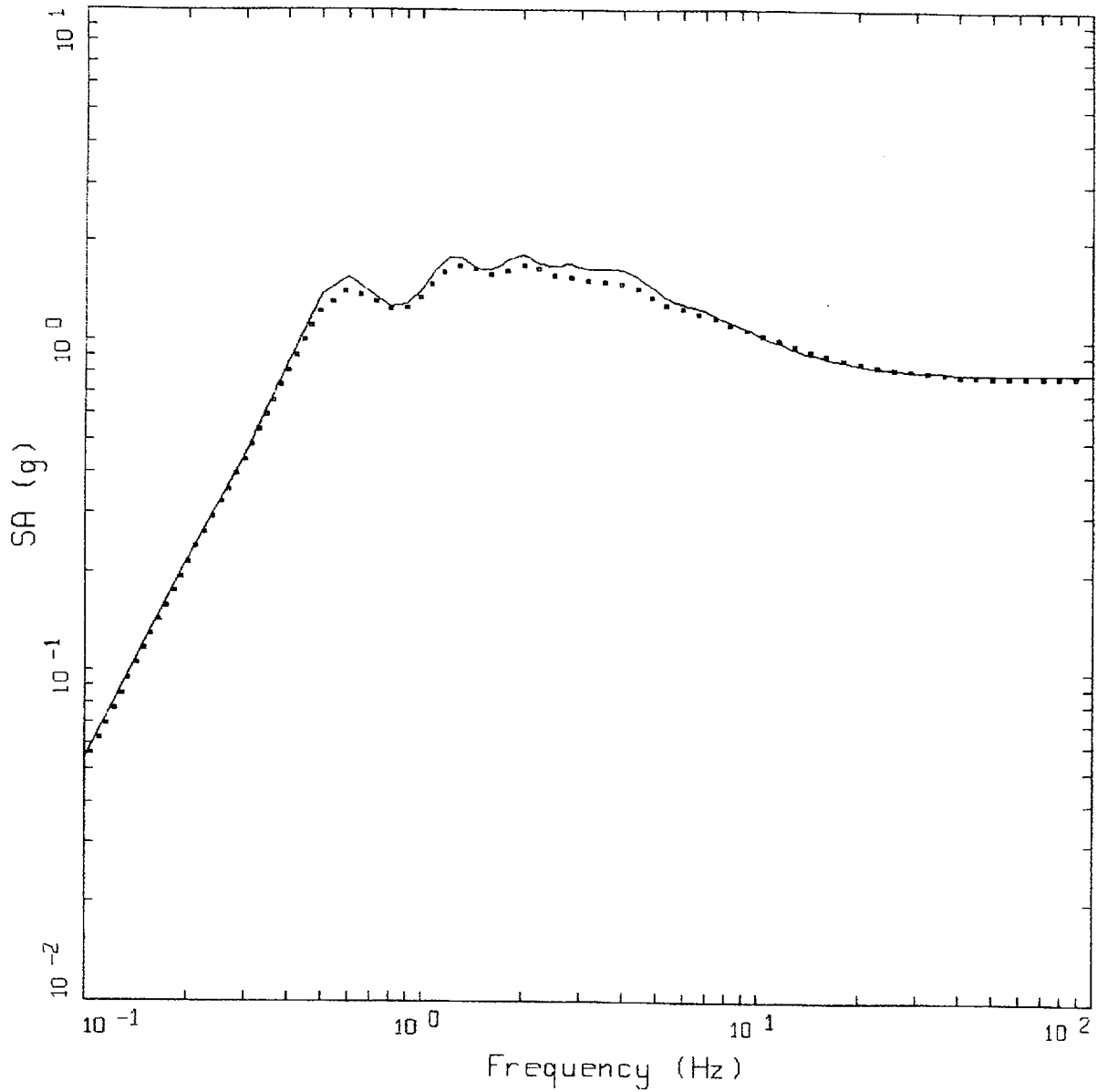
Figure 6-75. Median and $\pm\sigma$ spectra computed for $M = 7.5$ at a distance of 1 km using the Savannah River generic profile with site variations only (profile, G/G_{max} , and hysteretic damping): CEUS conditions.



CEUS, M = 7.5, D = 001 KM, H = 12 KM
 SD = 95 BARS, SAVANNAH GENERIC, SITE

- LEGEND
- · — 84TH PERCENTILE, PGA = 1.230 G
 - 50TH PERCENTILE, PGA = 0.782 G
 - 16TH PERCENTILE, PGA = 0.497 G

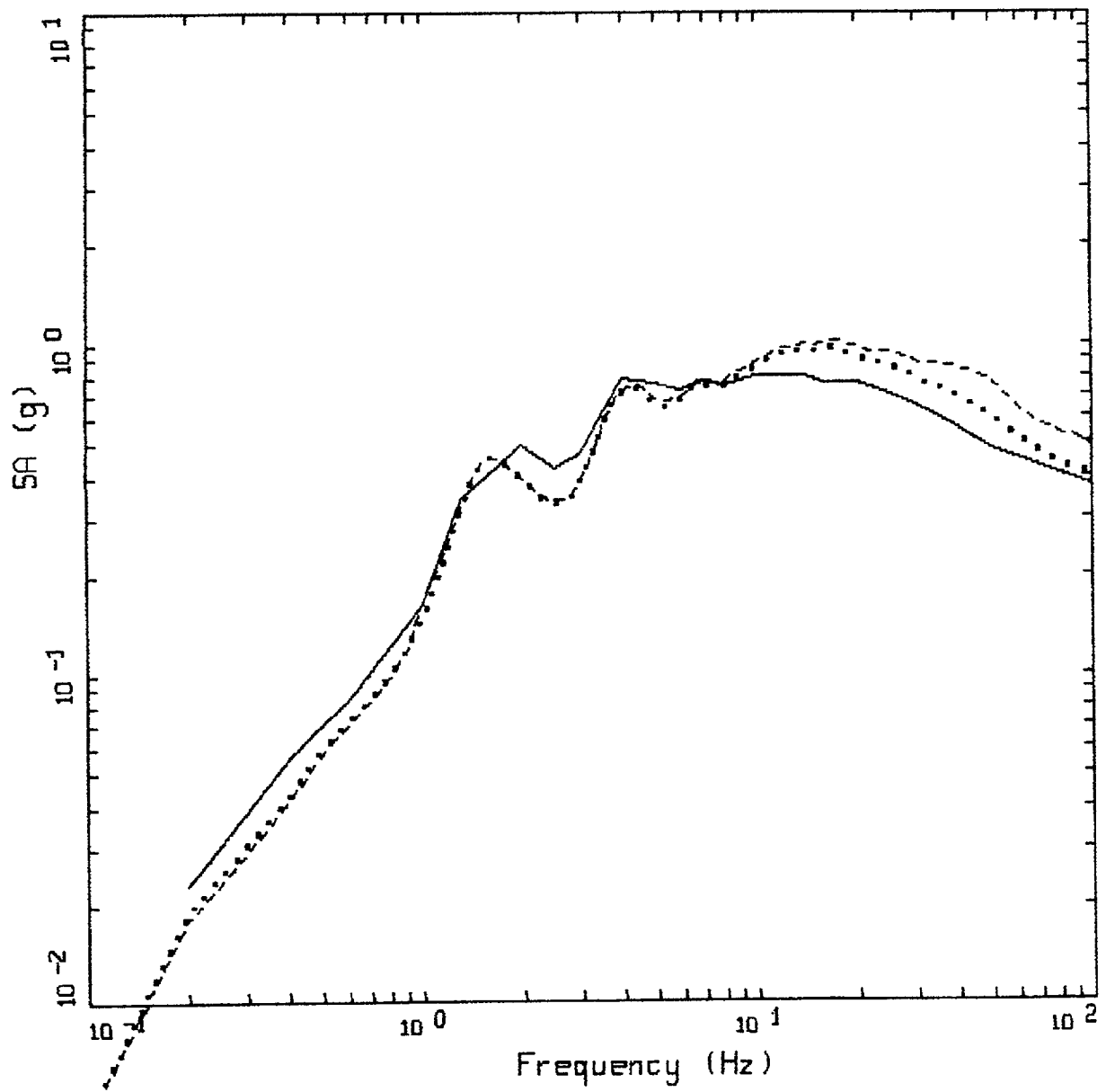
Figure 6-76. Median and $\pm\sigma$ spectra computed for $M=7.5$ at an epicentral distance of 12 km using the Savannah River Generic profile with source, path and site variations: CEUS conditions.



CEUS, M = 7.5, D = 001 KM, H = 12 KM
 SD = 95 BARS, SAVANNAH GENERIC

LEGEND
 — SITE; 50TH PERCENTILE, PGA = 0.801 G
 - - - S,P,S; 50TH PERCENTILE, PGA = 0.782 G

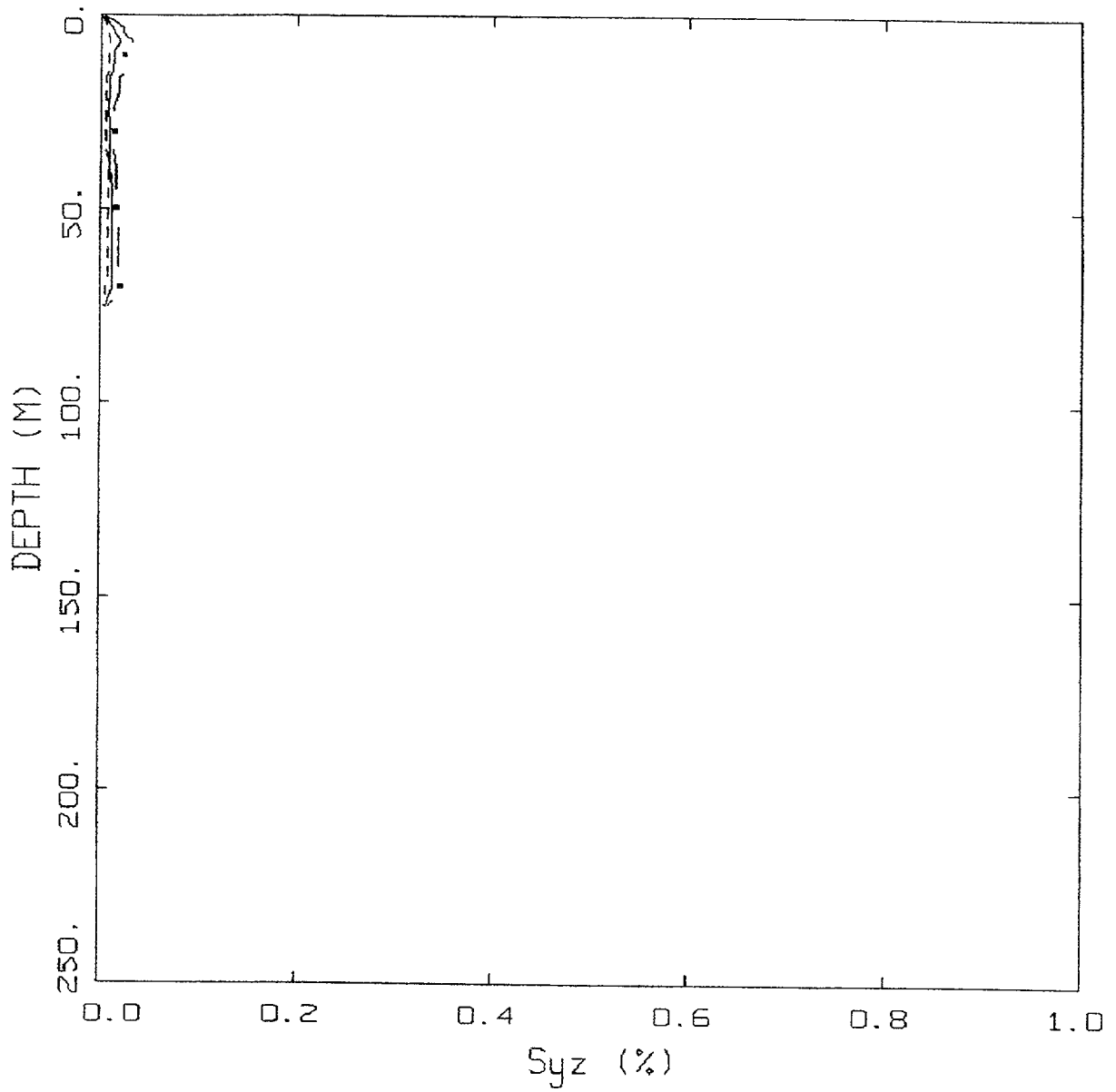
Figure 6-77. Comparison of median spectral estimates computed for $M=7.5$ at an epicentral distance of 1 km using the Savannah River Generic profile: varying site properties only (solid line) and varying source, path, and site properties (dashed line); CEUS conditions.



CEUS 10E-4 APPROACH COMPARISON, RI

- LEGEND
- APPROACH 4, 10⁻⁴ SOIL UNIFORM HAZARD SPECTRUM; PGA = 0.370 G
 - APPROACH 1, 10⁻⁴ ROCK CONTROL MOTION, MEAN PGA = 0.406 G
 - - - - APPROACH 2, 1 HZ AND 10 HZ DEAGGREGATION EQKS, MEAN PGA = 0.487 G

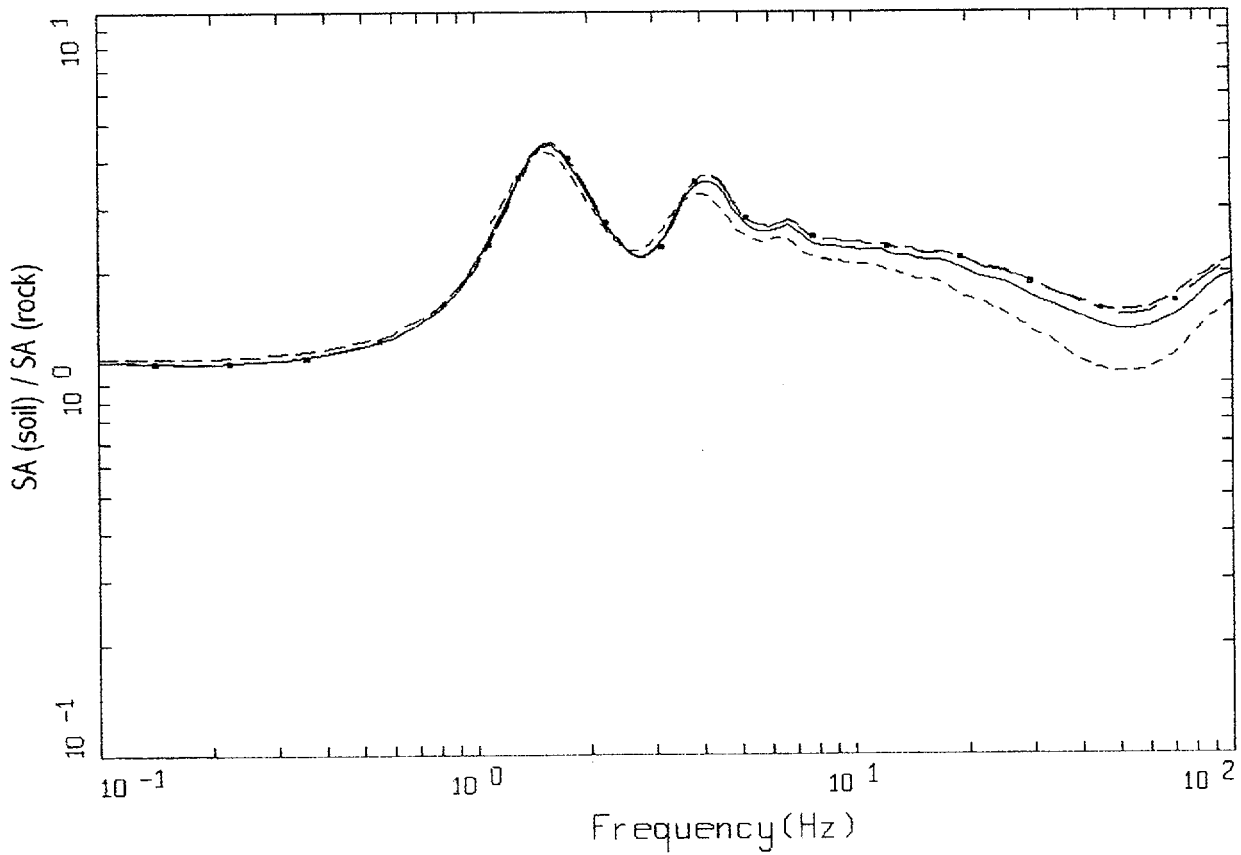
Figure 6-78. Comparison of Approaches 1, 2B, and 4 10⁻⁴ UHS on soil for profile Rinaldi: CEUS conditions.



CEUS, 10-4, RI
EFFECTIVE STRAINS (SYZ)

LEGEND
 - . - 84TH PERCENTILE
 — 50TH PERCENTILE
 - - - 16TH PERCENTILE

Figure 6-79. Median and $\pm\sigma$ effective strains for soil profile Rinaldi using Approach 1: CEUS conditions.

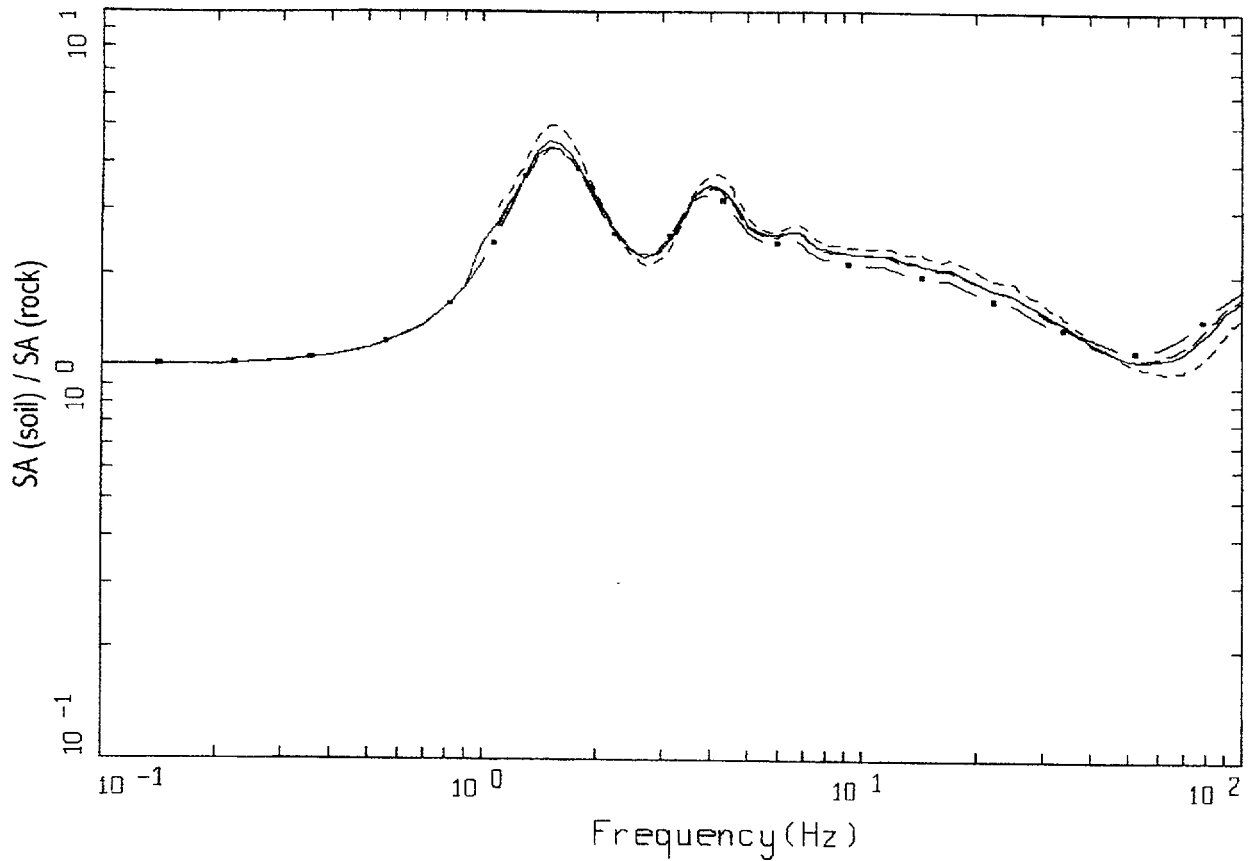


CEUS, 10E-4, 1HZ DESIGN, RI
 SURFACE MOTION, 1HZ TRANSFER FUNCTION
 WEIGHTS: ML=0.30, MM=0.00, MH=0.70

LEGEND

- ML = 5.7, D = 20 KM MEAN RATIO
- · - · - MM = 7.0, D = 100 KM, DESIGN MEAN RATIO
- · — MH = 7.6, D = 130 KM MEAN RATIO
- WEIGHTED MEAN RATIO

Figure 6-80. Comparison of transfer functions computed for the scaled 1 Hz design earthquake; soil profile Rinaldi, CEUS conditions.

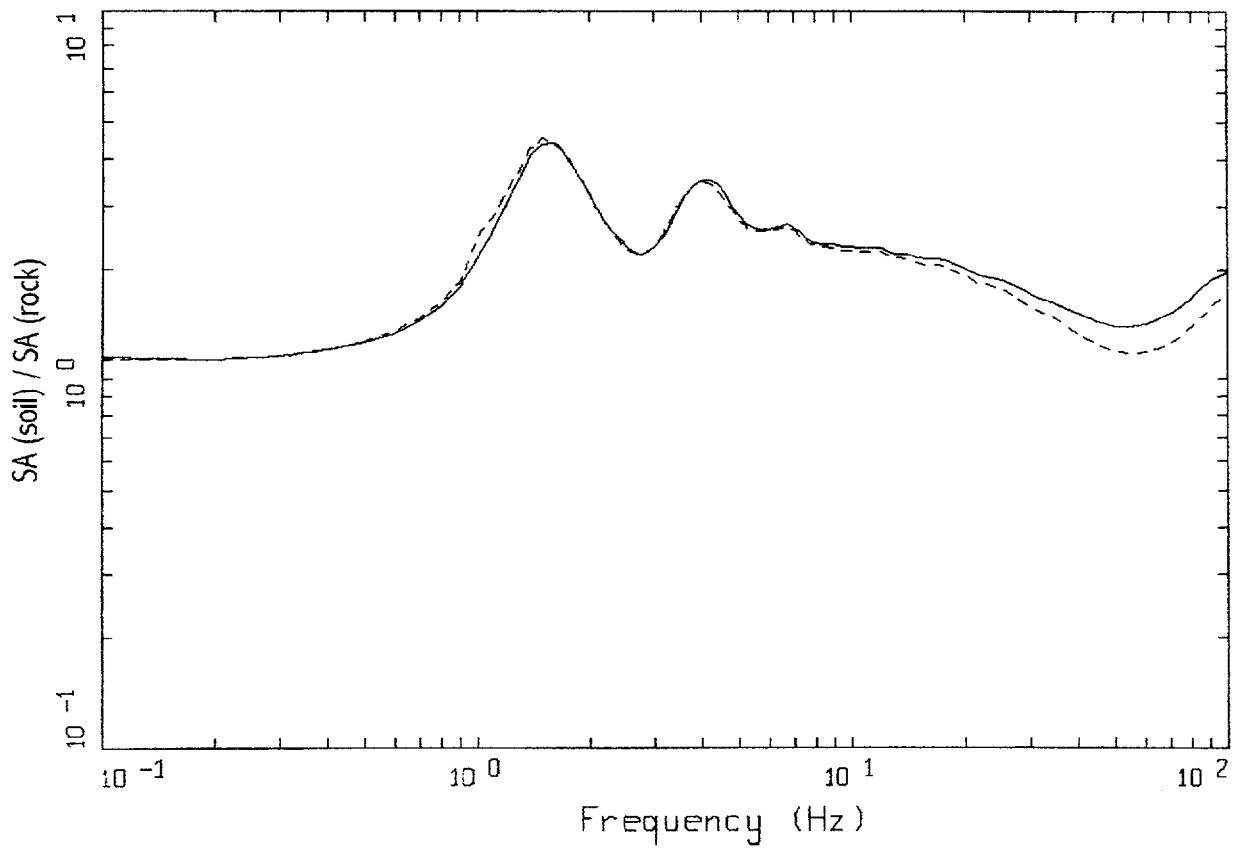


CEUS, 10E-4, 10HZ DESIGN, RI
 SURFACE MOTION, 10HZ TRANSFER FUNCTION
 WEIGHTS: ML=0.25, MM=0.53, MH=0.12

LEGEND

- ML = 4.6, D = 8 KM MEAN RATIO
- · - · - MM = 5.6, D = 8 KM, DESIGN MEAN RATIO
- · — MH = 7.7, D = 130 KM MEAN RATIO
- WEIGHTED MEAN RATIO

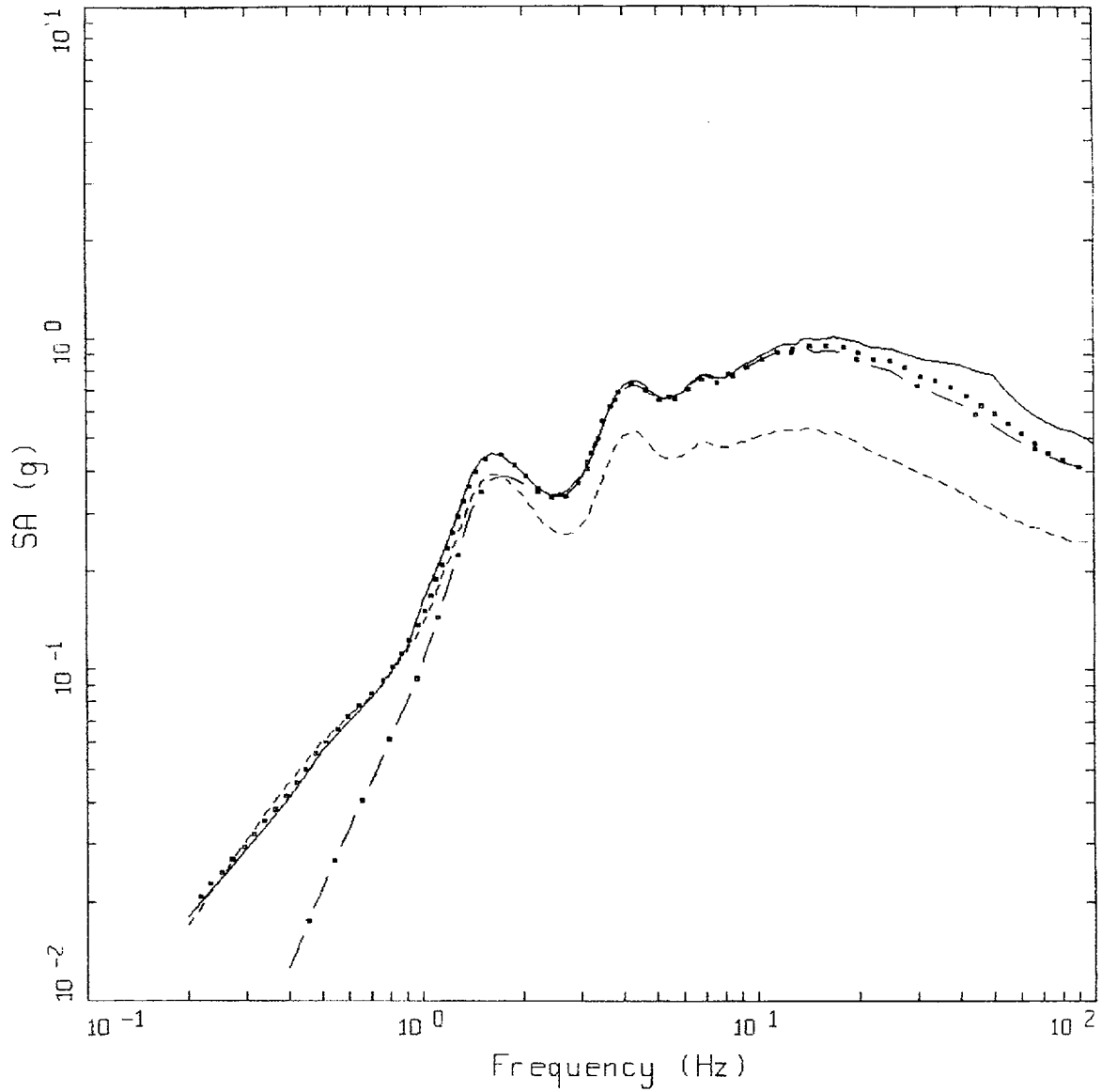
Figure 6-81. Comparison of transfer functions computed for the scaled 10 Hz design earthquake, soil profile Rinaldi, CEUS conditions.



CEUS, 10E-4, RI
TRANSFER FUNCTION

LEGEND
 ——— 1 HZ WEIGHTED MEAN RATIO; WEIGHTS:ML=0.30,MM=0.00,MH=0.70
 - - - - 10 HZ WEIGHTED MEAN RATIO; WEIGHTS:ML=0.25,MM=0.63,MH=0.12

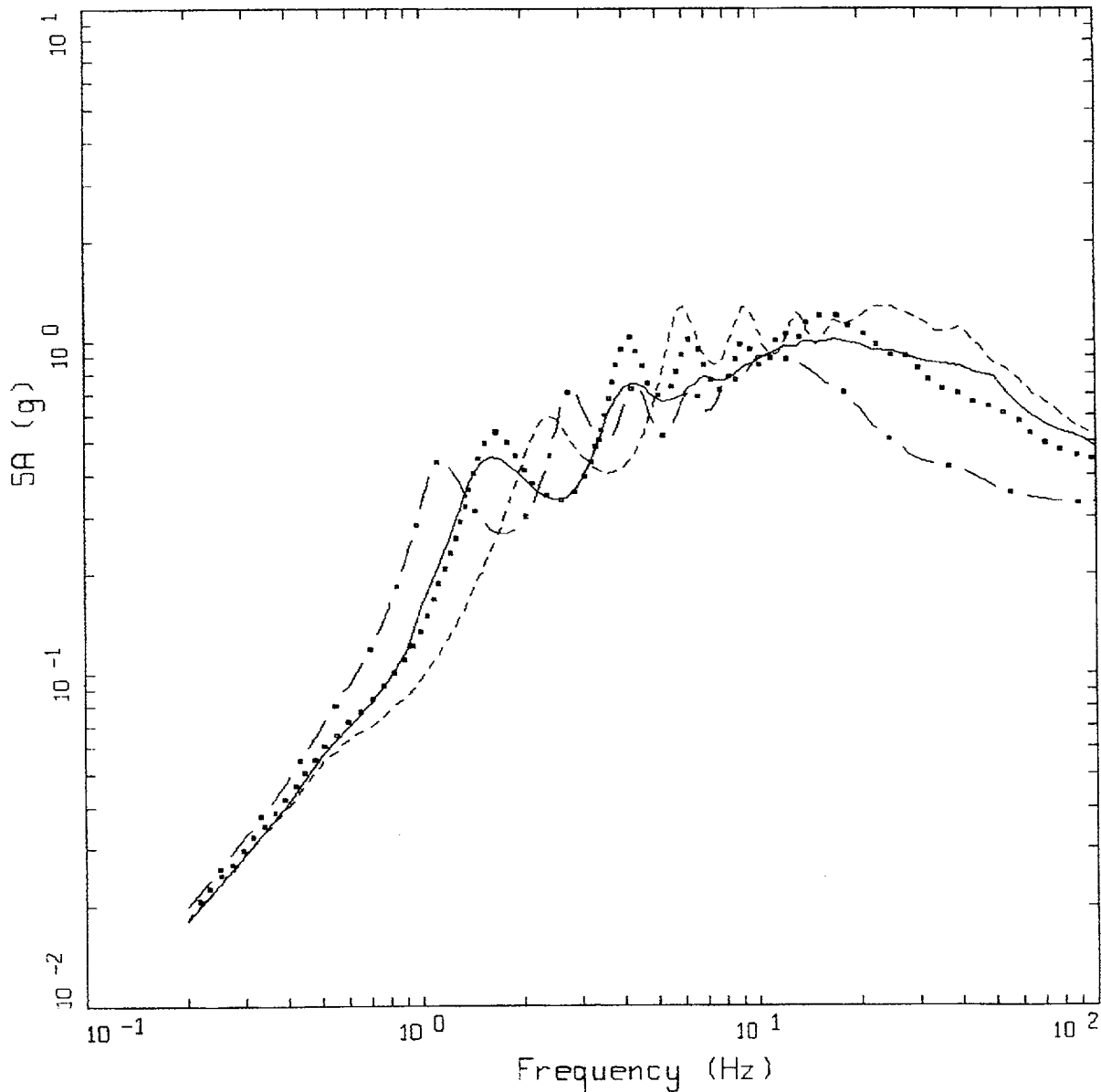
Figure 6-82. Comparison of mean transfer functions computed for the scaled 1 Hz and 10 Hz design earthquakes; soil profile Rinaldi, CEUS conditions.



CEUS, 10E-4 DESIGN SPECTRA, RI

- LEGEND
- APPROACH 2, 1 HZ AND 10 HZ DEAGGREGATION EQKS, MEAN PGA = 0.487 G
 - APPROACH 1, 10-4 ROCK CONTROL MOTION, MEAN PGA = 0.406 G
 - - - - 1 HZ MEAN; PGA = 0.243 G
 - • - • 10 HZ MEAN; PGA = 0.406 G

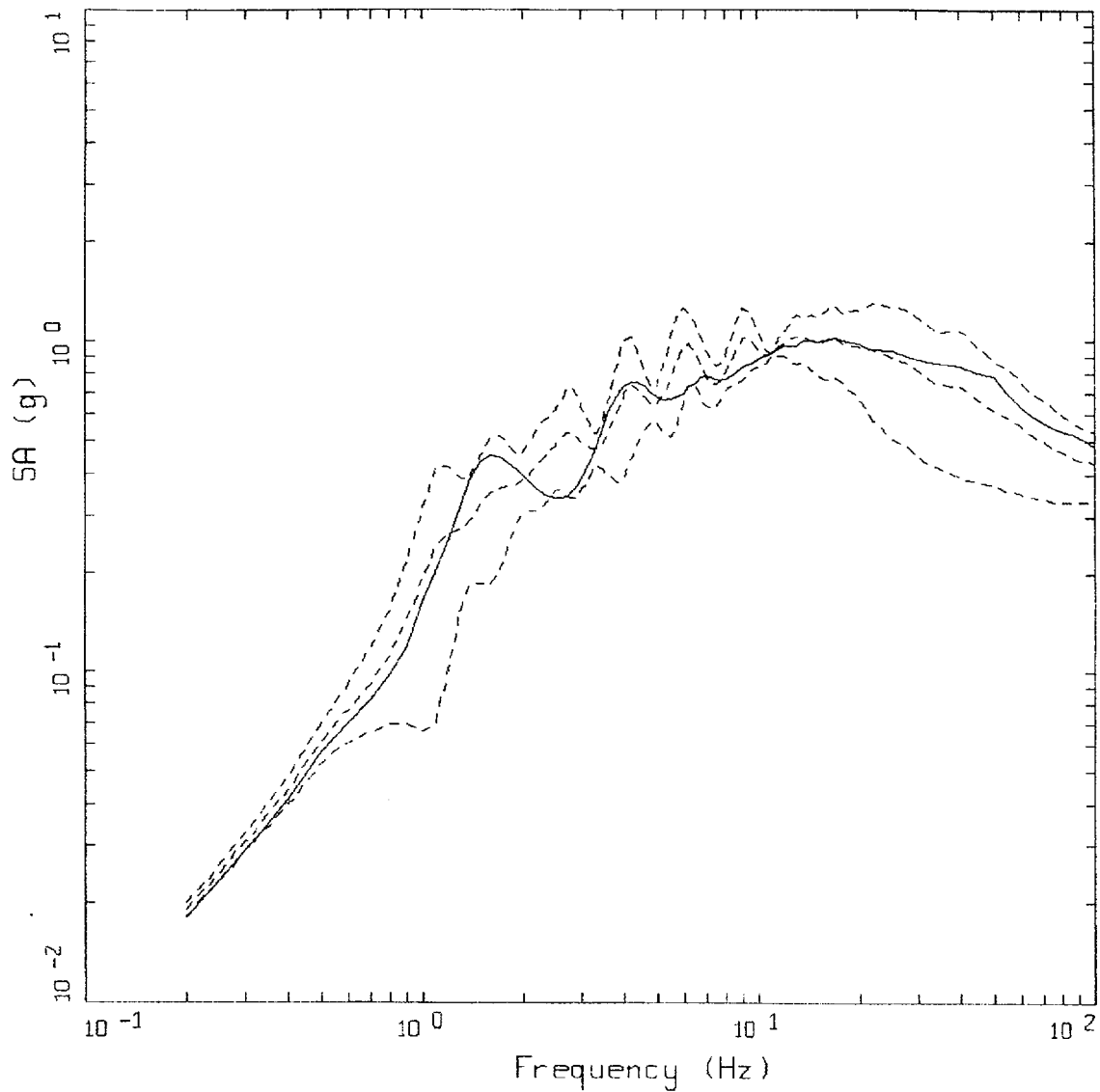
Figure 6-83. Comparison of soil spectra for Approaches 1, 2A, and 2B; soil profile Rinaldi, CEUS conditions.



CEUS 10E-4 APPROACH COMPARISON, RI

- LEGEND
- APPROACH 2, 1 HZ AND 10 HZ DEAGGREGATION EQKS, MEAN PGA = 0.487 G
 - APPROACH 1, 10-4 ROCK CONTROL MOTION, BASE CASE PGA = 0.445 G
 - APPROACH 1, 10-4 ROCK CONTROL MOTION, BASE CASE (UPPER) PGA = 0.528 G
 - . - - APPROACH 1, 10-4 ROCK CONTROL MOTION, BASE CASE (LOWER) PGA = 0.325 G

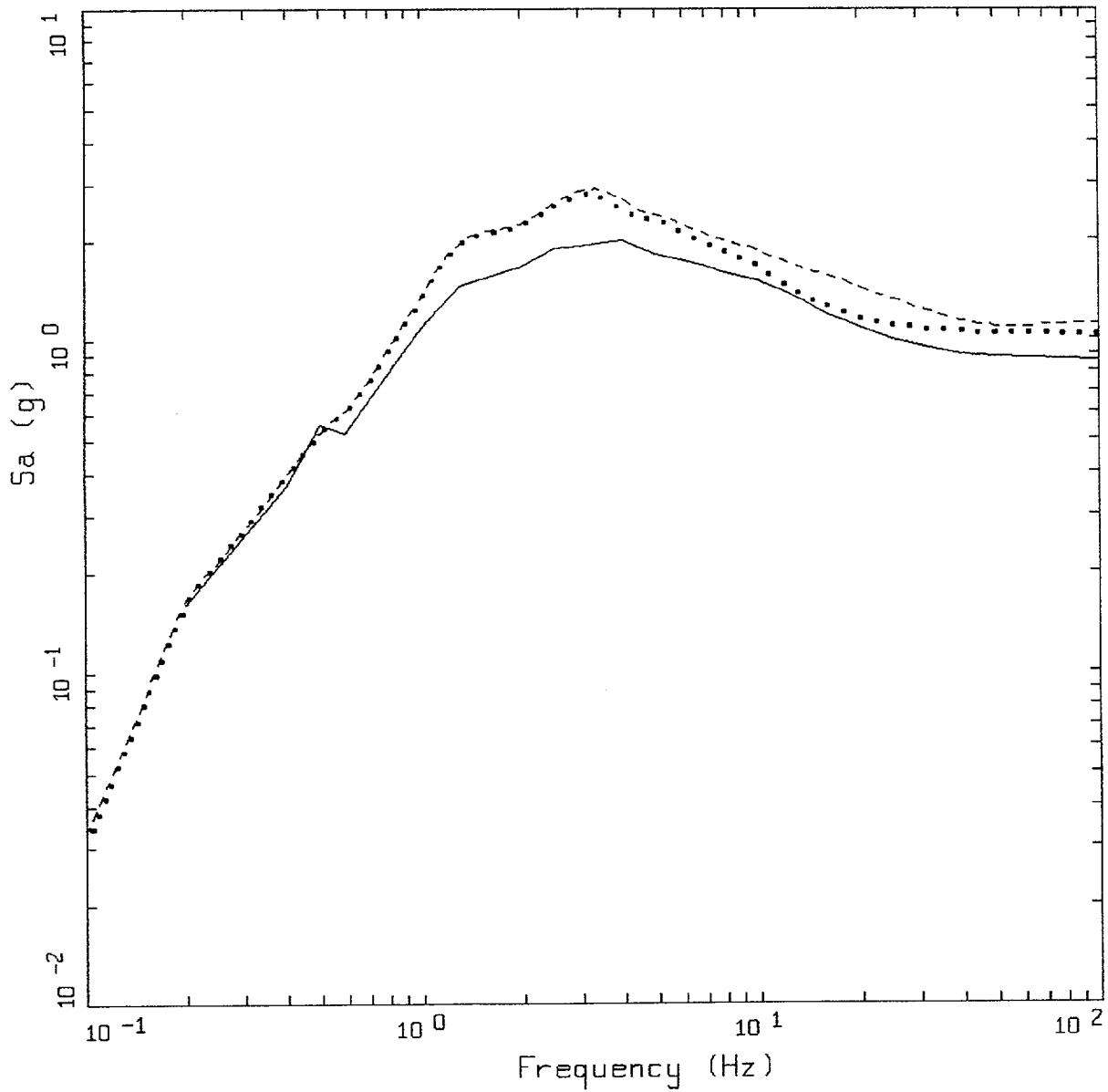
Figure 6-84. Comparison of soil spectra for Approach 2B with base case profile and deterministic profile variations (\pm factor of 2 on shear modulus); soil profile Rinaldi, CEUS conditions.



CEUS 1DE-4 APPROACH COMPARISON, RI

- LEGEND
- APPROACH 2, 1 HZ AND 10 HZ DEAGGREGATION EQKS, MEAN PGA = 0.487 G
 - APPROACH 1, 10-4 ROCK CONTROL MOTION, BASE CASE, 68TH PERCENTILE, PGA = 0.534 G
 - APPROACH 1, 10-4 ROCK CONTROL MOTION, BASE CASE, MEAN, PGA = 0.433 G
 - APPROACH 1, 10-4 ROCK CONTROL MOTION, BASE CASE, 32ND PERCENTILE, PGA = 0.331 G

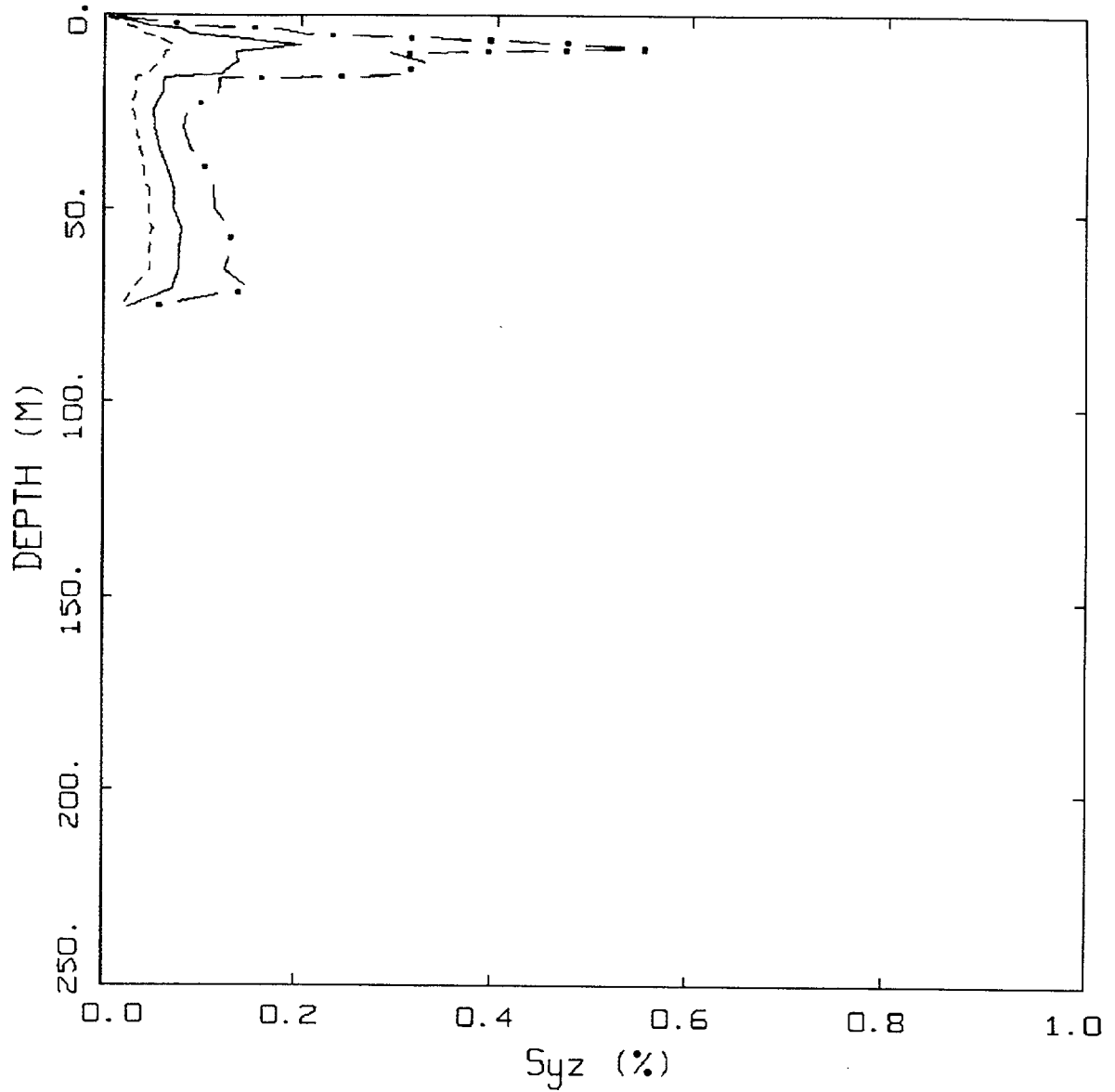
Figure 6-85. Comparison of soil spectra for Approach 2B with mean and $\pm 1\sigma$ variations of base case (\pm factor of 2 on shear modulus), soil profile Rinaldi, CEUS conditions.



WUS 10E-4 APPROACH COMPARISON, RI

- LEGEND
- APPROACH 4, 10⁻⁴ SOIL UNIFORM HAZARD SPECTRUM, PGA = 0.861 G
 - APPROACH 1, 10⁻⁴ ROCK CONTROL MOTION, MEAN PGA = 1.027 G
 - APPROACH 2, 1 HZ AND 10 HZ DEAGGREGATION EQKS, MEAN PGA = 1.114 G

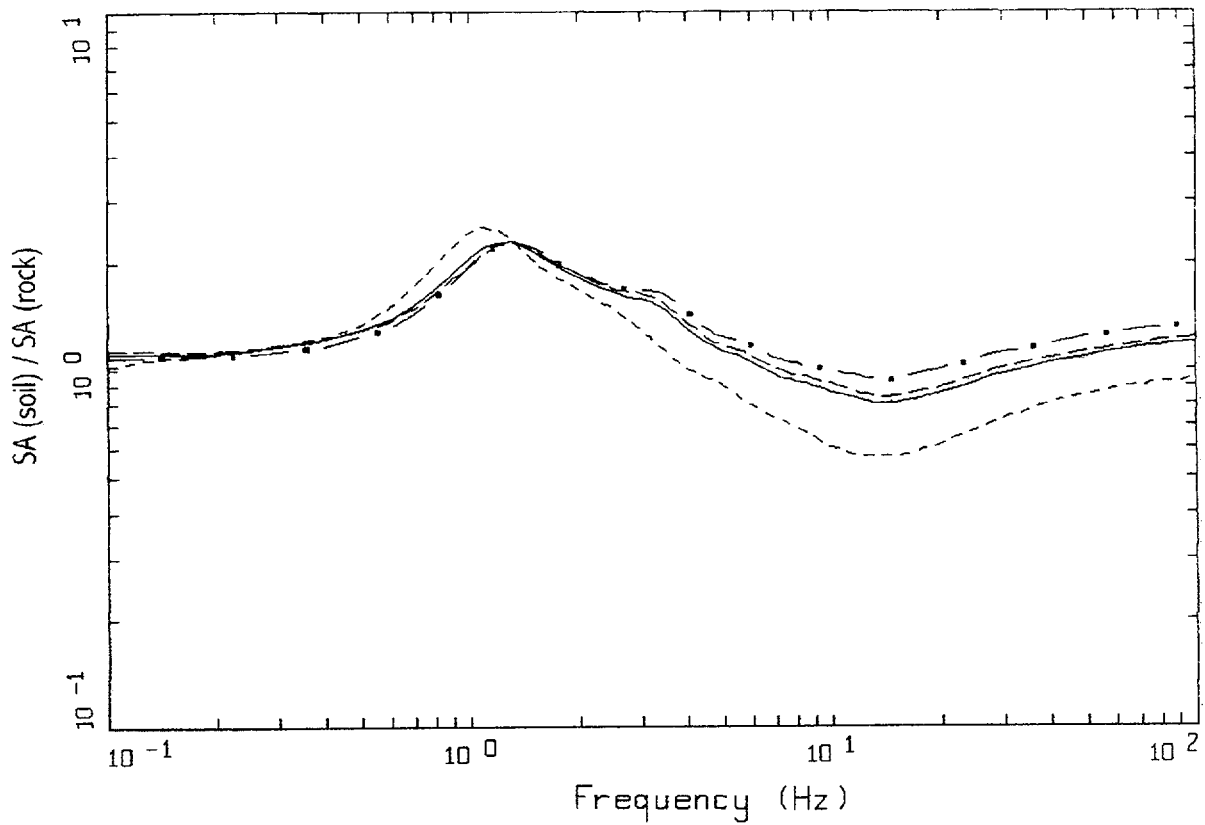
Figure 6-86. Comparison of Approaches 1, 2B, and 4 10⁻⁴ UHS on soil for profile Rinaldi: WUS conditions.



WUS, 10-4, RI
EFFECTIVE STRAINS (SYZ)

LEGEND
 - . - 84TH PERCENTILE
 — 50TH PERCENTILE
 - - - 16TH PERCENTILE

Figure 6-87. Median and $\pm 1 \sigma$ effective strains for soil profile Rinaldi using Approach 1: WUS conditions.

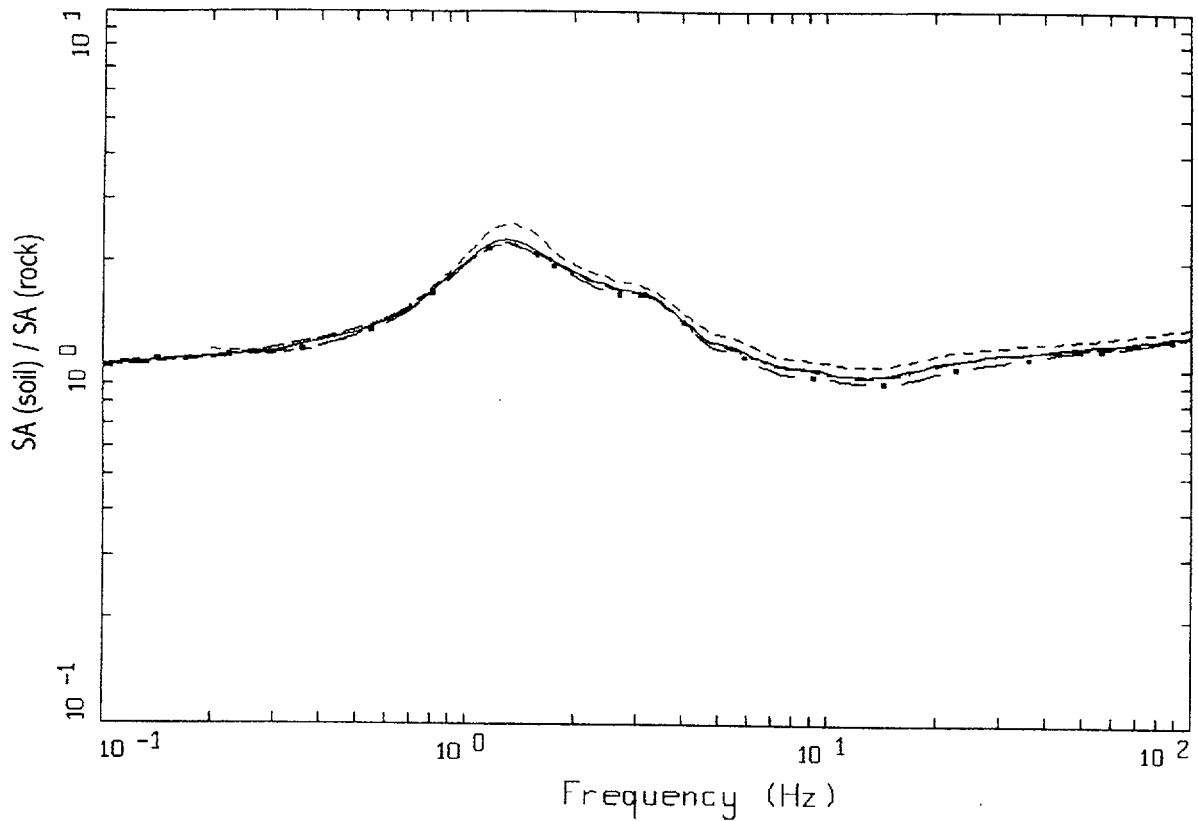


WUS, 10E-4, 1HZ DESIGN, RI
 SURFACE MOTION, 1HZ TRANSFER FUNCTION
 WEIGHTS: ML=0.24, MM=0.47, MH=0.29

LEGEND

- ML = 5.8, D = 10 KM MEAN RATIO
- . - . - MM = 6.9, D = 14 KM, DESIGN MEAN RATIO
- • — MH = 7.8, D = 40 KM MEAN RATIO
- WEIGHTED MEAN RATIO

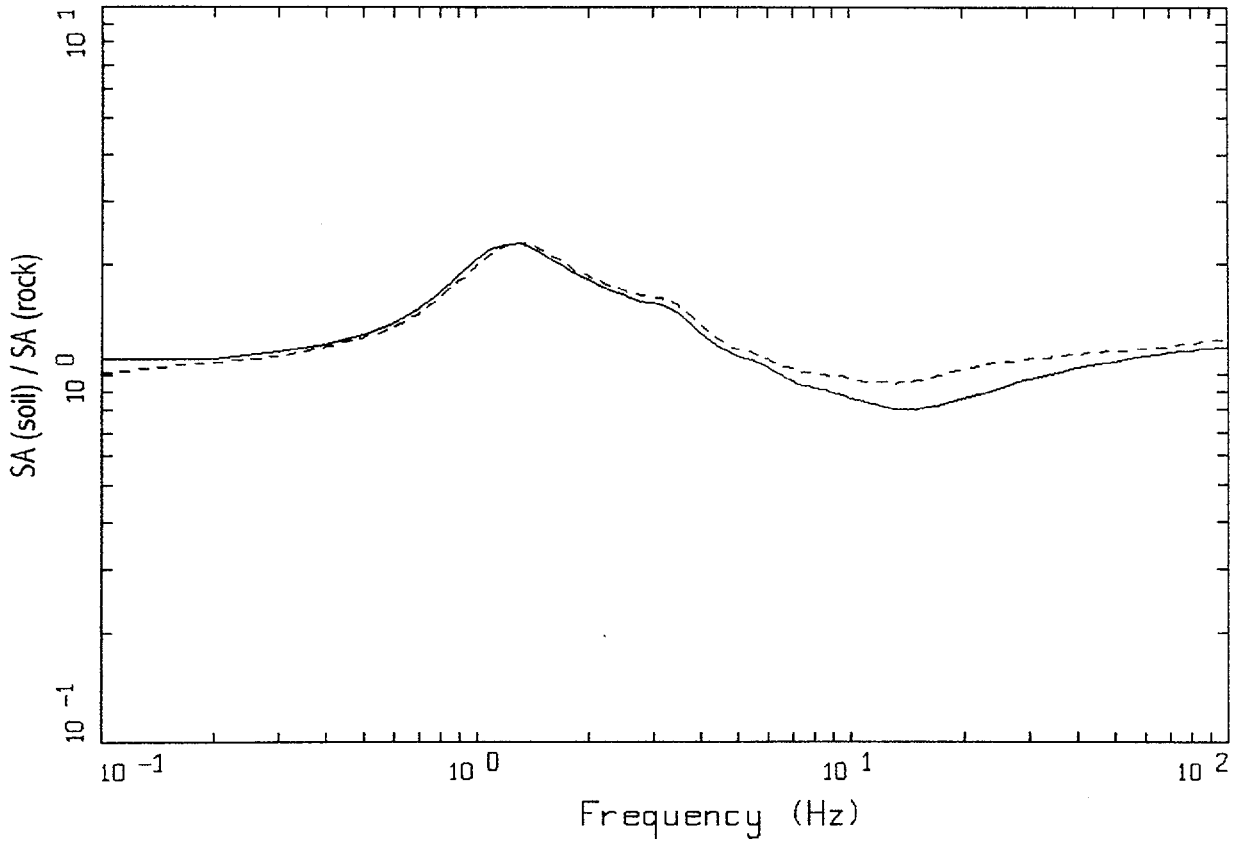
Figure 6-88. Comparison of transfer functions computed for the scaled 1 Hz design earthquake; soil profile Rinaldi, WUS conditions.



WUS, 10E-4, 10HZ DESIGN, RI
 SURFACE MOTION, 10HZ TRANSFER FUNCTION
 WEIGHTS: ML=0.20, MM=0.60, MH=0.20

LEGEND
 - - - - - ML = 5.1, D = 10 KM MEAN RATIO
 - · - · - MM = 6.1, D = 14 KM, DESIGN MEAN RATIO
 — · — MH = 7.8, D = 30 KM MEAN RATIO
 ——— WEIGHTED MEAN RATIO

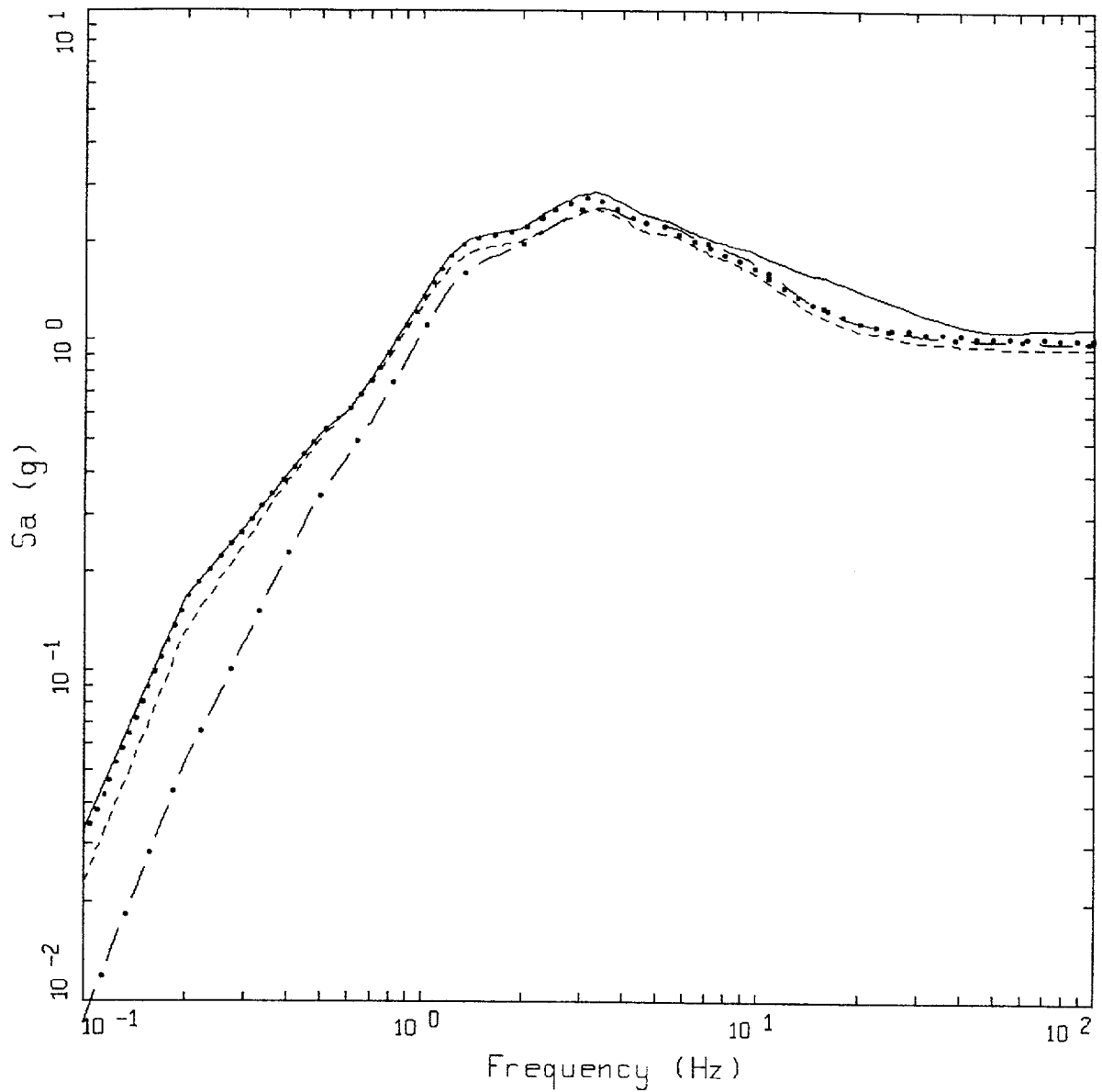
Figure 6-89. Comparison of transfer functions computed for the scaled 10 Hz design earthquake; soil profile Rinaldi, WUS conditions.



WUS, 10E-4, RI
AMPLIFICATION

LEGEND
 ——— 1 HZ WEIGHTED MEAN RATIO; WEIGHTS:ML=0.20,MM=0.60,MH=0.20
 - - - - 10 HZ WEIGHTED MEAN RATIO; WEIGHTS:ML=0.20,MM=0.60,MH=0.20

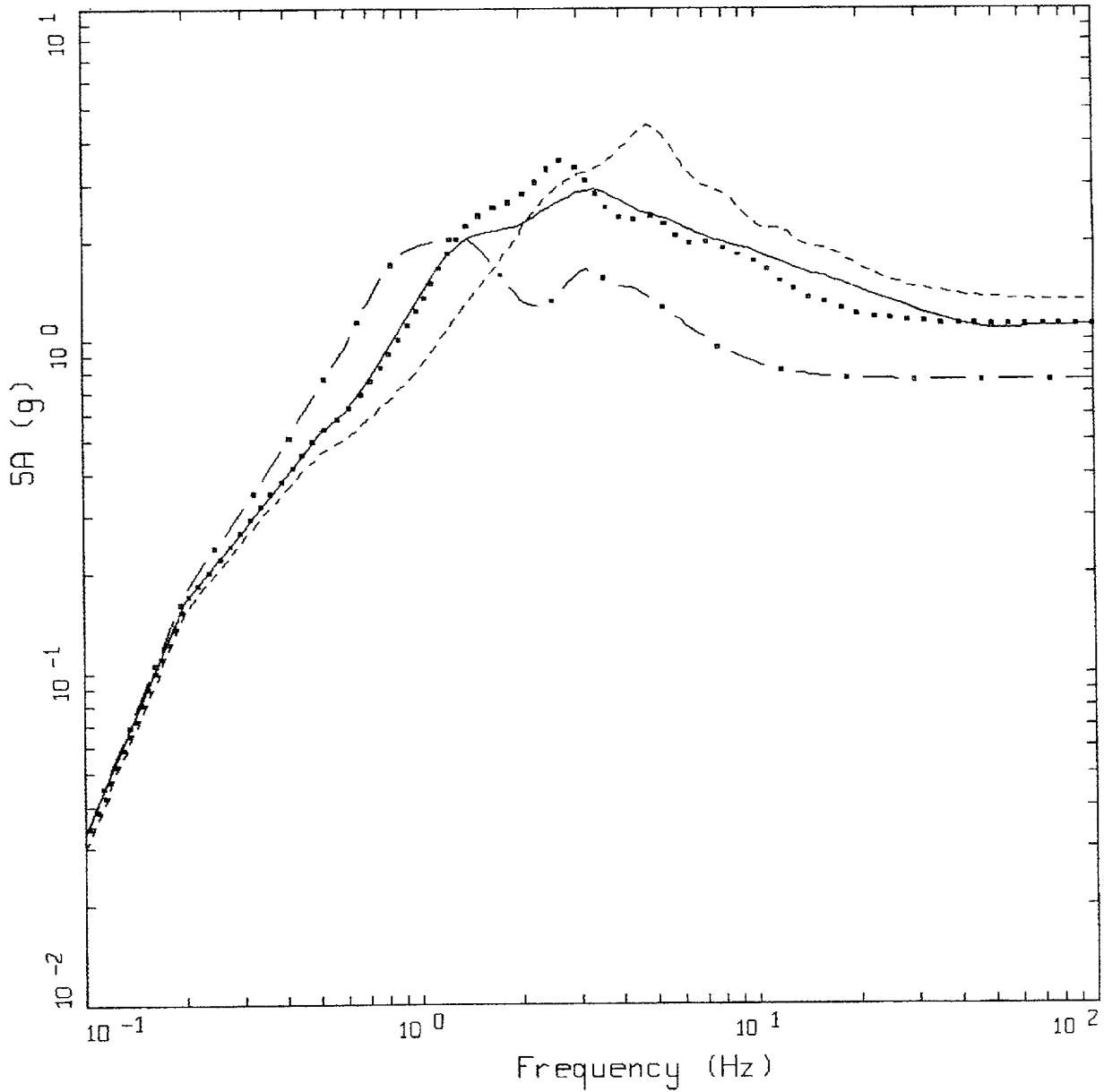
Figure 6-90. Comparison of mean transfer functions computed for the scaled 1 Hz and 10 Hz design earthquakes; soil profile Rinaldi, WUS conditions.



WUS, 10E-4 DESIGN SPECTRA, RI

- LEGEND
- APPROACH 2, 1 HZ AND 10 HZ DEAGGREGATION EQKS, MEAN PGA = 1.114 G
 - APPROACH 1, 10⁻⁴ ROCK CONTROL MOTION, MEAN PGA = 1.028 G
 - 1 HZ MEAN; PGA = 0.964 G
 - . - . 10 HZ MEAN; PGA = 1.003 G

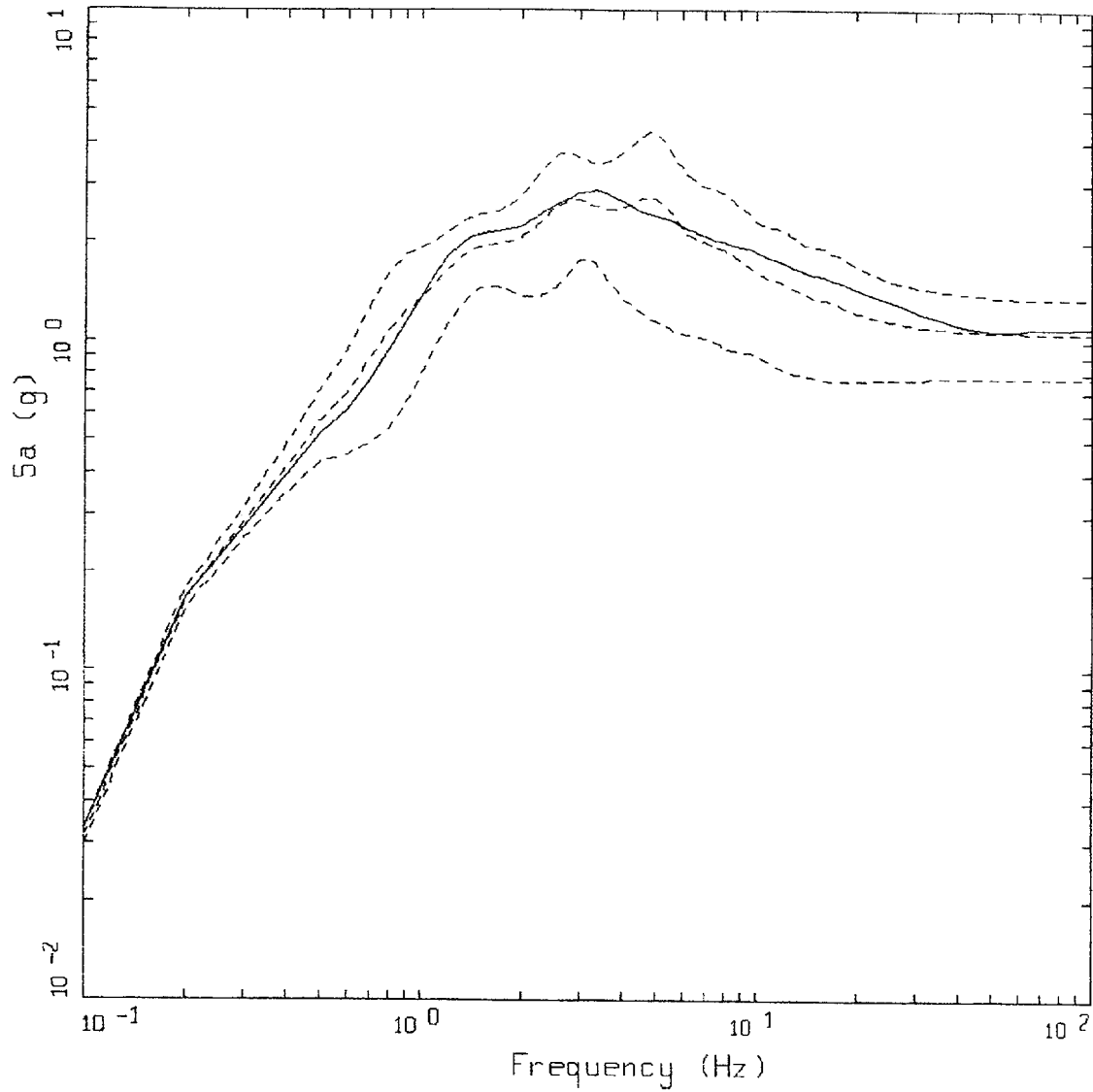
Figure 6-91. Comparison of soil spectra for Approaches 1, 2A, and 2B; soil profile Rinaldi, WUS conditions.



WUS 10E-4 APPROACH COMPARISON, RI

- LEGEND
- APPROACH 2, 1 HZ AND 10 HZ DEAGGREGATION EQKS, MEAN PGA = 1.114 G
 - APPROACH 1, 10-4 ROCK CONTROL MOTION, BASE CASE PGA = 1.132 G
 - APPROACH 1, 10-4 ROCK CONTROL MOTION, BASE CASE (UPPER) PGA = 1.101 G
 - . - . - APPROACH 1, 10-4 ROCK CONTROL MOTION, BASE CASE (LOWER) PGA = 0.756 G

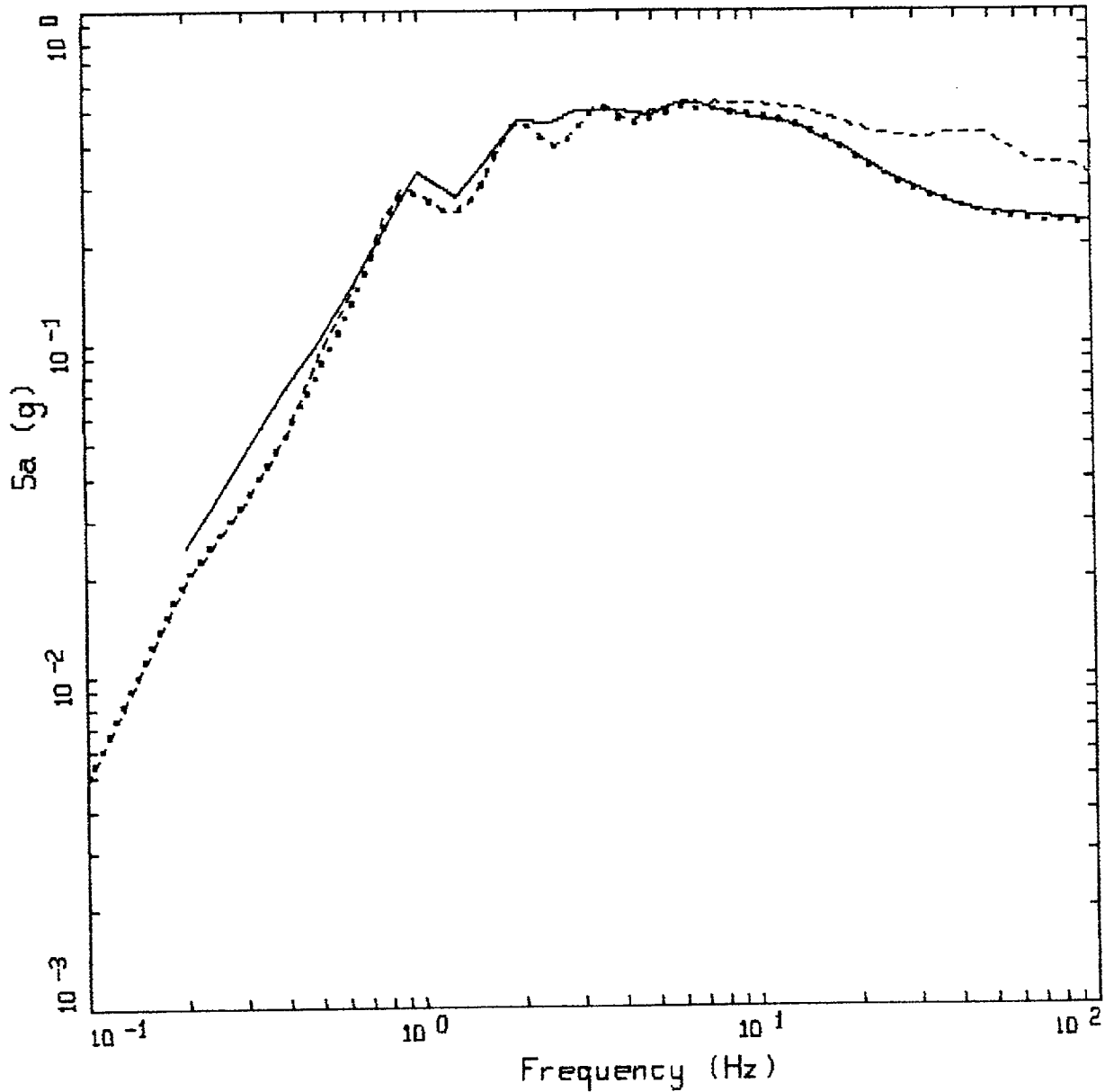
Figure 6-92. Comparison of soil spectra for Approach 2B with base case profile and deterministic profile variations (\pm factor of 2 on shear modulus); soil profile Rinaldi, WUS conditions.



WUS 10E-4 APPROACH COMPARISON, RI

- LEGEND
- APPROACH 2, 1 HZ AND 10 HZ DISAGGREGATION EQKS, MEAN PGA = 1.114 G
 - APPROACH 1, 10-4 ROCK CONTROL MOTION, BASE CASE, 84TH PERCENTILE, PGA = 1.342 G
 - - - - - APPROACH 1, 10-4 ROCK CONTROL MOTION, BASE CASE, MEAN, PGA = 1.060 G
 - · - · - APPROACH 1, 10-4 ROCK CONTROL MOTION, BASE CASE, 16TH PERCENTILE, PGA = 0.777 G

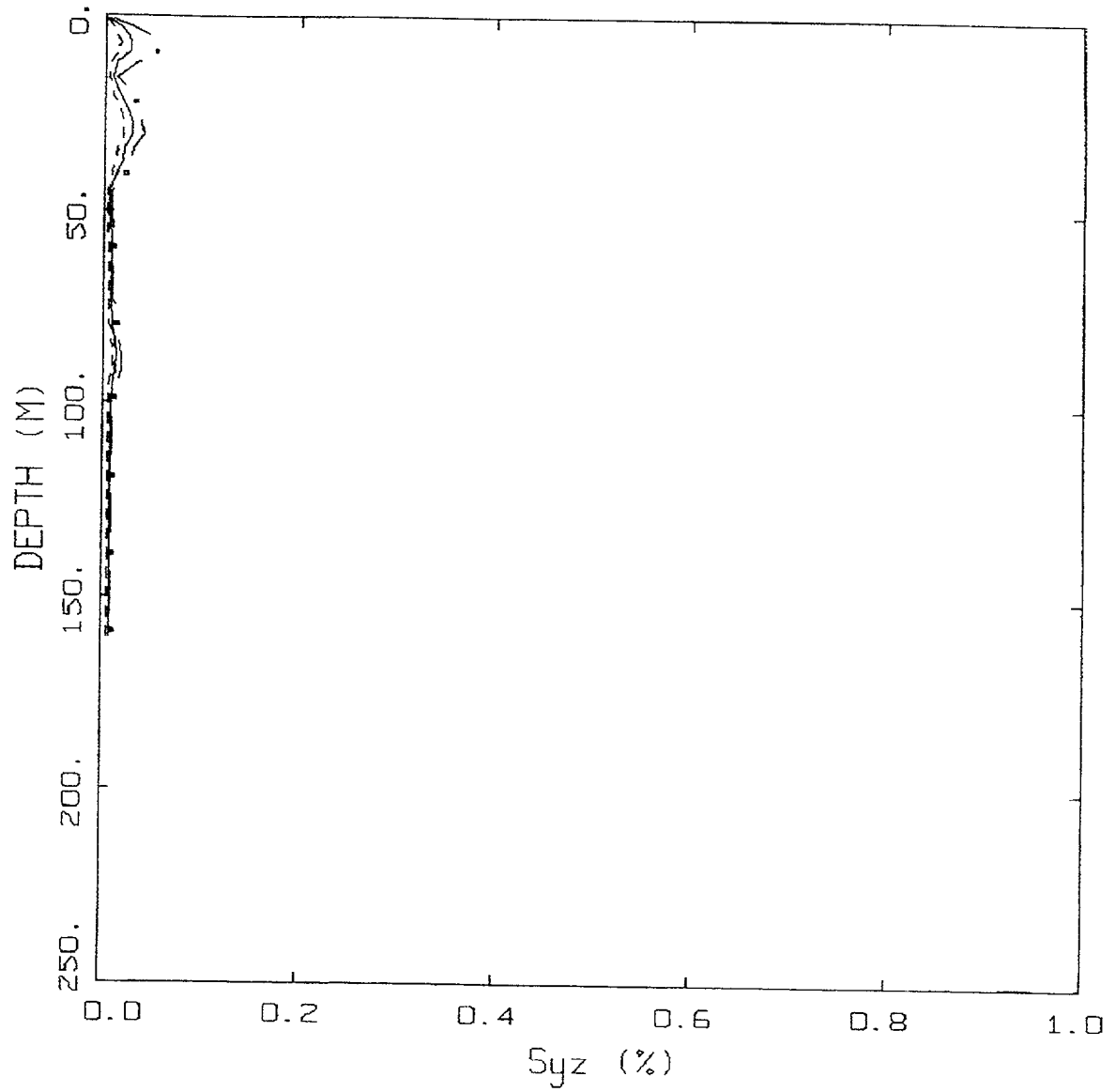
Figure 6-93. Comparison of soil spectra for Approach 2B with mean and $\pm 1\sigma$ variations of base case (\pm factor of 2 on shear modulus), soil profile Rinaldi, WUS conditions.



CEUS 10E-4 APPROACH COMPARISON, G2

- LEGEND
- APPROACH 4, 10⁻⁴ SOIL UNIFORM HAZARD SPECTRUM; PGA = 0.232 G
 - APPROACH 1, 10⁻⁴ ROCK CONTROL MOTION, MEAN PGA = 0.230 G
 - APPROACH 2, 1 HZ AND 10 HZ DEAGGREGATION EQS, MEAN PGA = 0.325 G

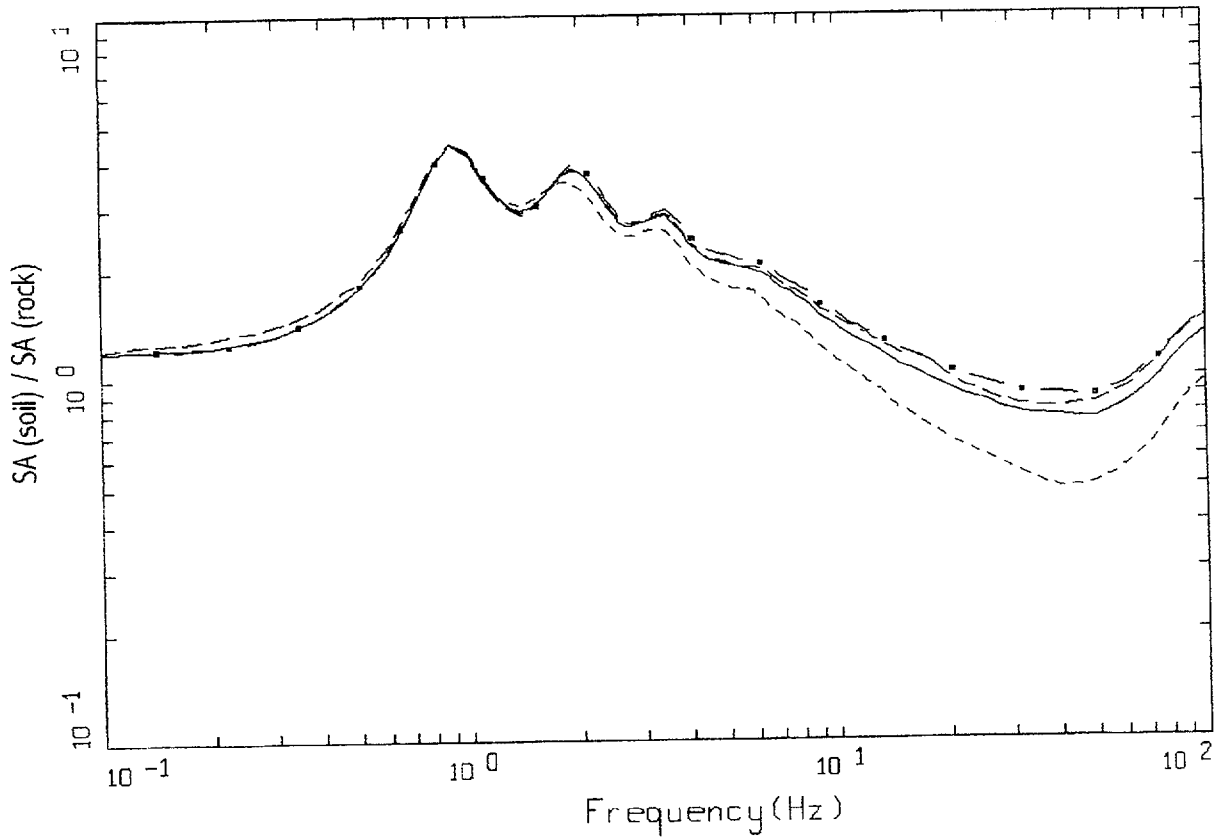
Figure 6-94. Comparison of Approaches 1, 2B, and 4 10⁻⁴ UHS on soil for profile Gilroy 2: CEUS conditions.



CEUS, 10-4, G2
 EFFECTIVE STRAINS (SYZ)

LEGEND
 - . - 84TH PERCENTILE
 ——— 50TH PERCENTILE
 - - - 16TH PERCENTILE

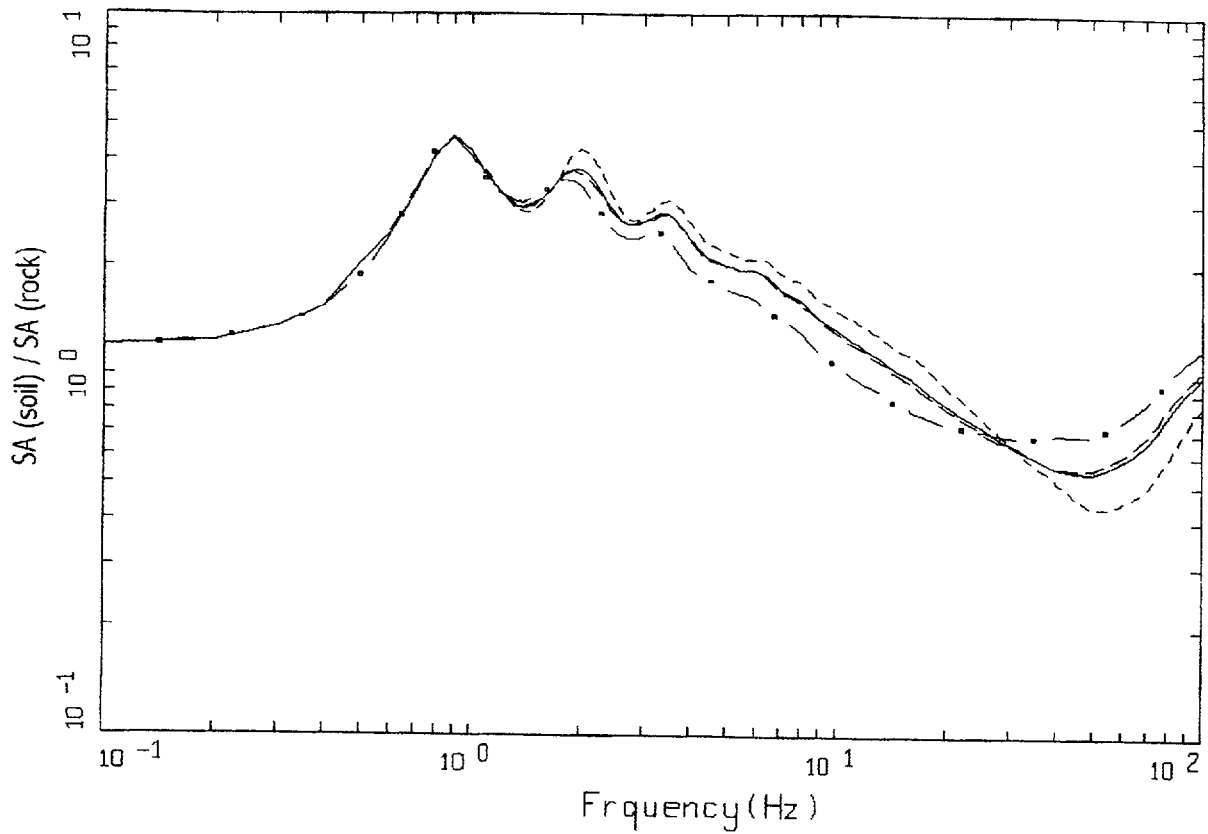
Figure 6-95. Median and $\pm 1 \sigma$ effective strains for soil profile Gilroy 2 using Approach 1: CEUS conditions.



CEUS, 10E-4, 1HZ DESIGN, G2
 SURFACE MOTION, 1HZ TRANSFER FUNCTION
 WEIGHTS: ML=0.30, MM=0.00, MH=0.70

LEGEND
 - - - - - ML = 5.7, D = 20 KM MEAN RATIO
 - · - · - MM = 7.0, D = 100 KM MEAN RATIO
 — · — MH = 7.7, D = 130 KM, DESIGN MEAN RATIO
 ——— WEIGHTED MEAN RATIO

Figure 6-96. Comparison of transfer functions computed for the scaled 1 Hz design earthquake, soil profile Gilroy 2, CEUS conditions.

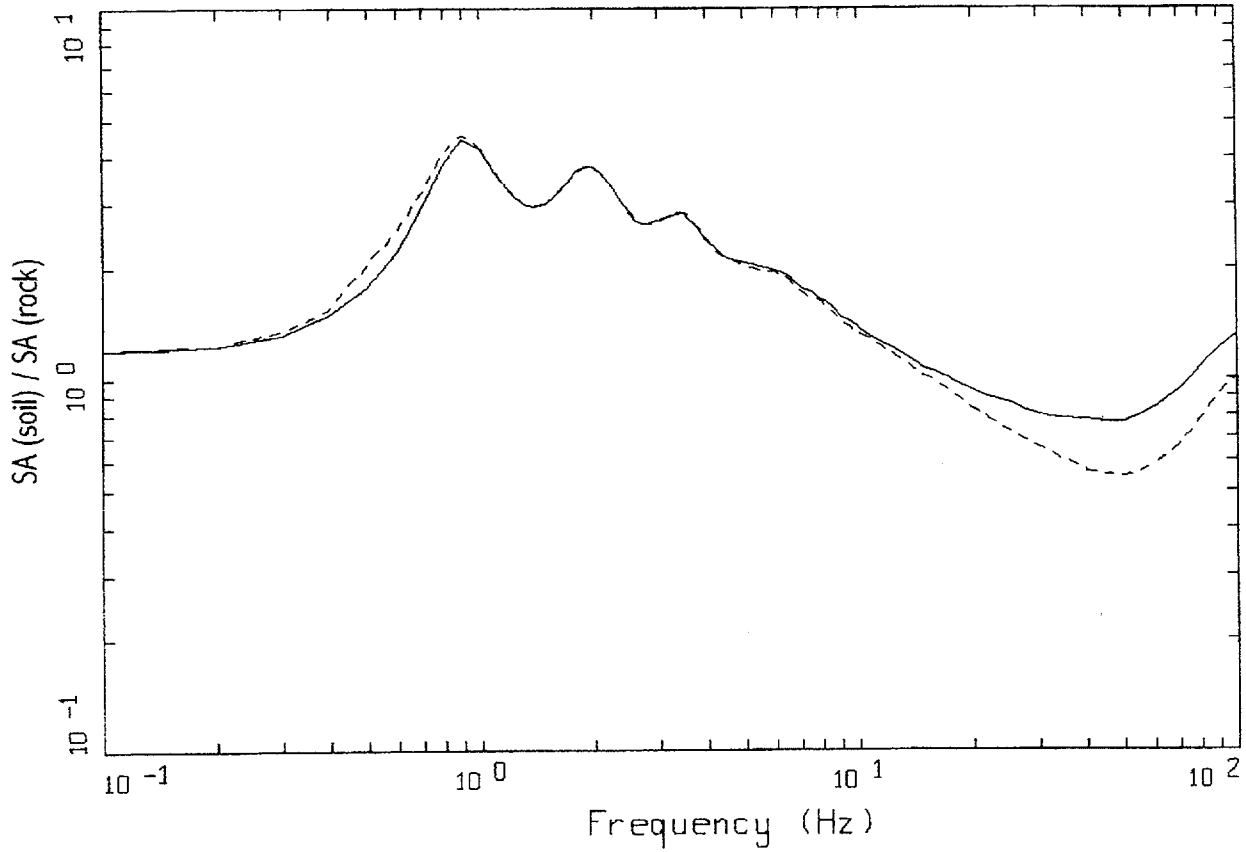


CEUS, 10E-4, 10HZ DESIGN, G2
 SURFACE MOTION, 10HZ TRANSFER FUNCTION
 WEIGHTS: ML=0.25, MM=0.63, MH=0.12

LEGEND

- ML = 4.6, D = 8 KM MEAN RATIO
- · - · - MM = 5.6, D = 8 KM, DESIGN MEAN RATIO
- · — MH = 7.7, D = 130 KM MEAN RATIO
- WEIGHTED MEAN RATIO

Figure 6-97. Comparison of transfer functions computed for the scaled 10 Hz design earthquake: soil profile Gilroy 2, CEUS conditions.

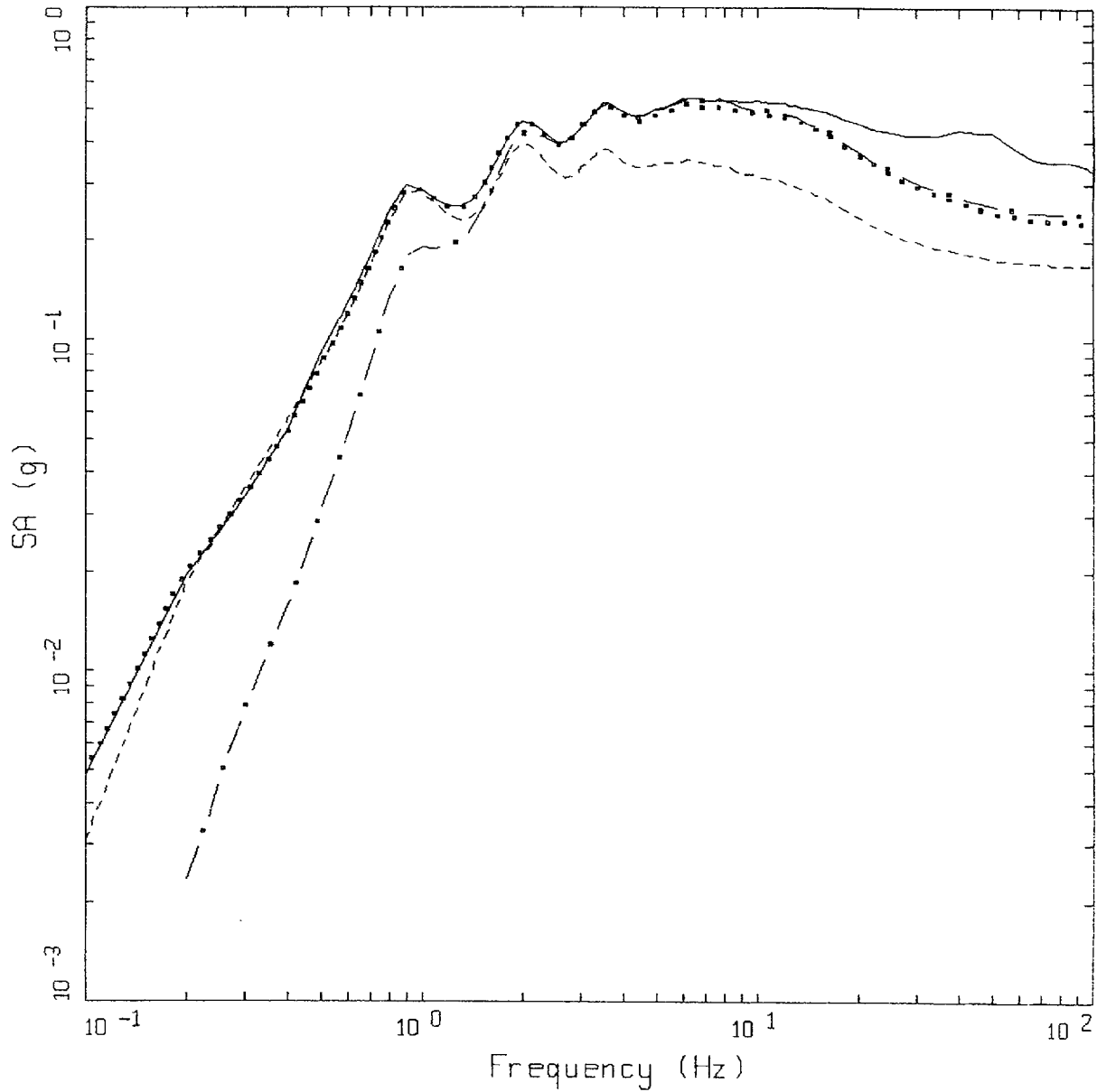


CEUS, 10E-4, G2
TRANSFER FUNCTION

LEGEND

- 1 HZ WEIGHTED MEAN RATIO; WEIGHTS: ML=0.30, MM=0.00, MH=0.70
- 10 HZ WEIGHTED MEAN RATIO; WEIGHTS: ML=0.25, MM=0.63, MH=0.12

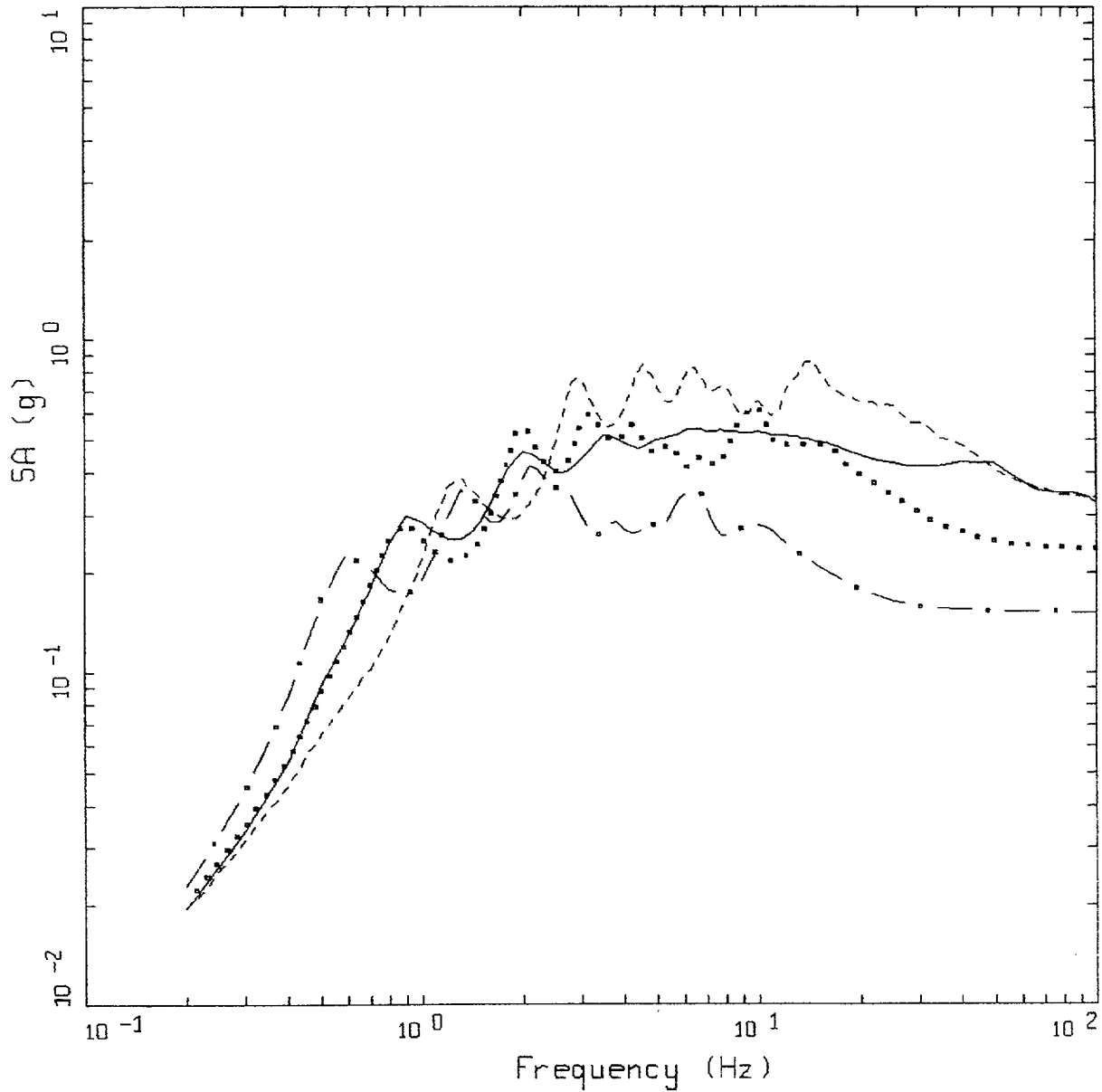
Figure 6-98. Comparison of mean transfer functions computed for the scaled 1 Hz and 10 Hz design earthquakes; soil profile Gilroy 2, CEUS conditions.



CEUS, 10E-4 DESIGN SPECTRA, GZ

- LEGEND
- APPROACH 2, 1 HZ AND 10 HZ DEAGGREGATION EQKS, MEAN PGA = 0.325 G
 - APPROACH 1, 10-4 ROCK CONTROL MOTION, MEAN PGA = 0.169 G
 - 1 HZ MEAN; PGA = 0.168 G
 - . - . 10 HZ MEAN; PGA = 0.241 G

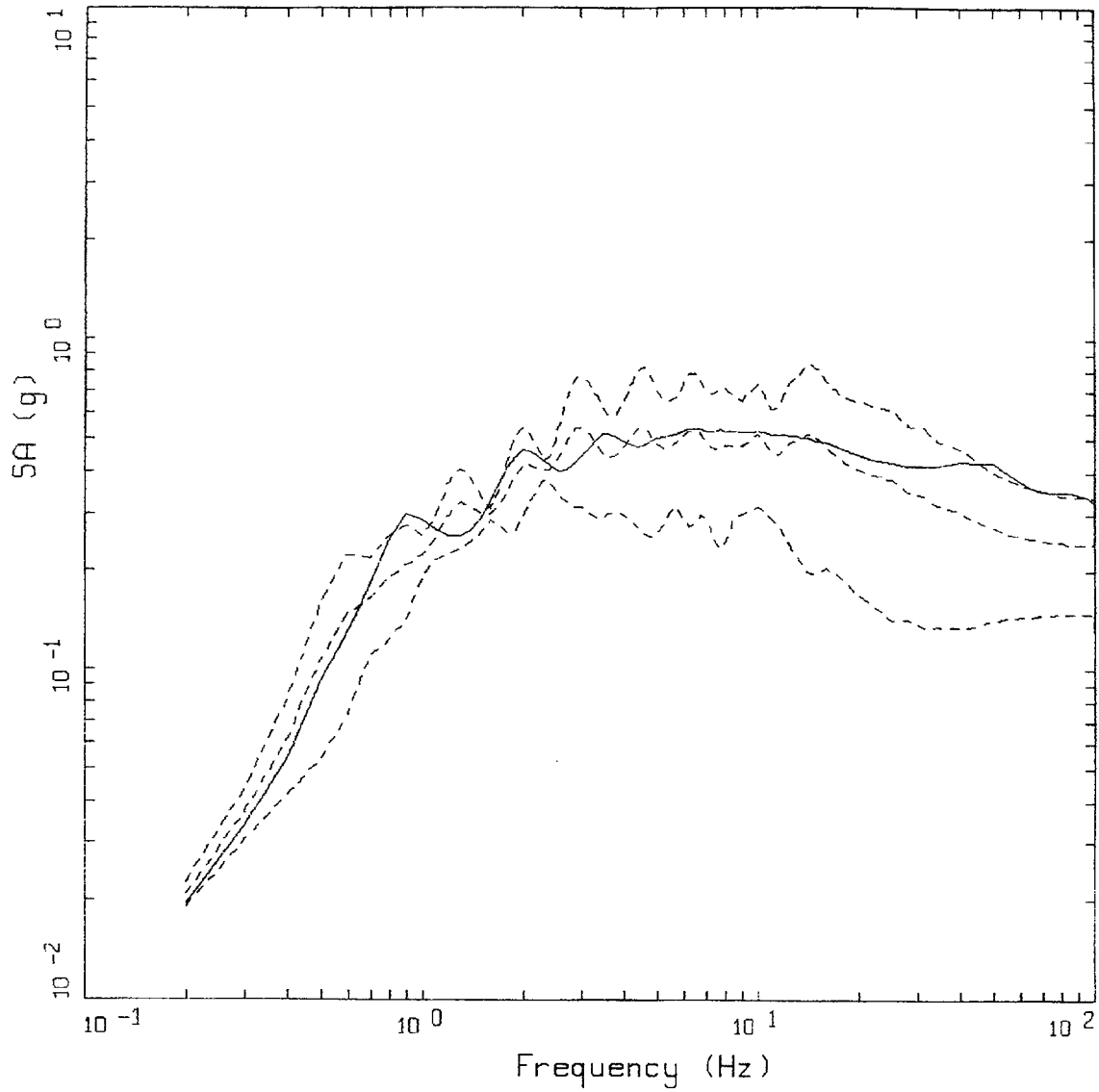
Figure 6-99. Comparison of soil spectra for Approaches 1, 2A, and 2B; soil profile Gilroy 2, CEUS conditions.



CEUS 10E-4 APPROACH COMPARISON, G2

- LEGEND
- APPROACH 2, 1 HZ AND 10 HZ DEAGGREGATION EQKS, MEAN PGA = 0.325 G
 - APPROACH 1, 10-4 ROCK CONTROL MOTION, BASE CASE PGA = 0.237 G
 - APPROACH 1, 10-4 ROCK CONTROL MOTION, BASE CASE (UPPER) PGA = 0.335 G
 - . - - APPROACH 1, 10-4 ROCK CONTROL MOTION, BASE CASE (LOWER) PGA = 0.152 G

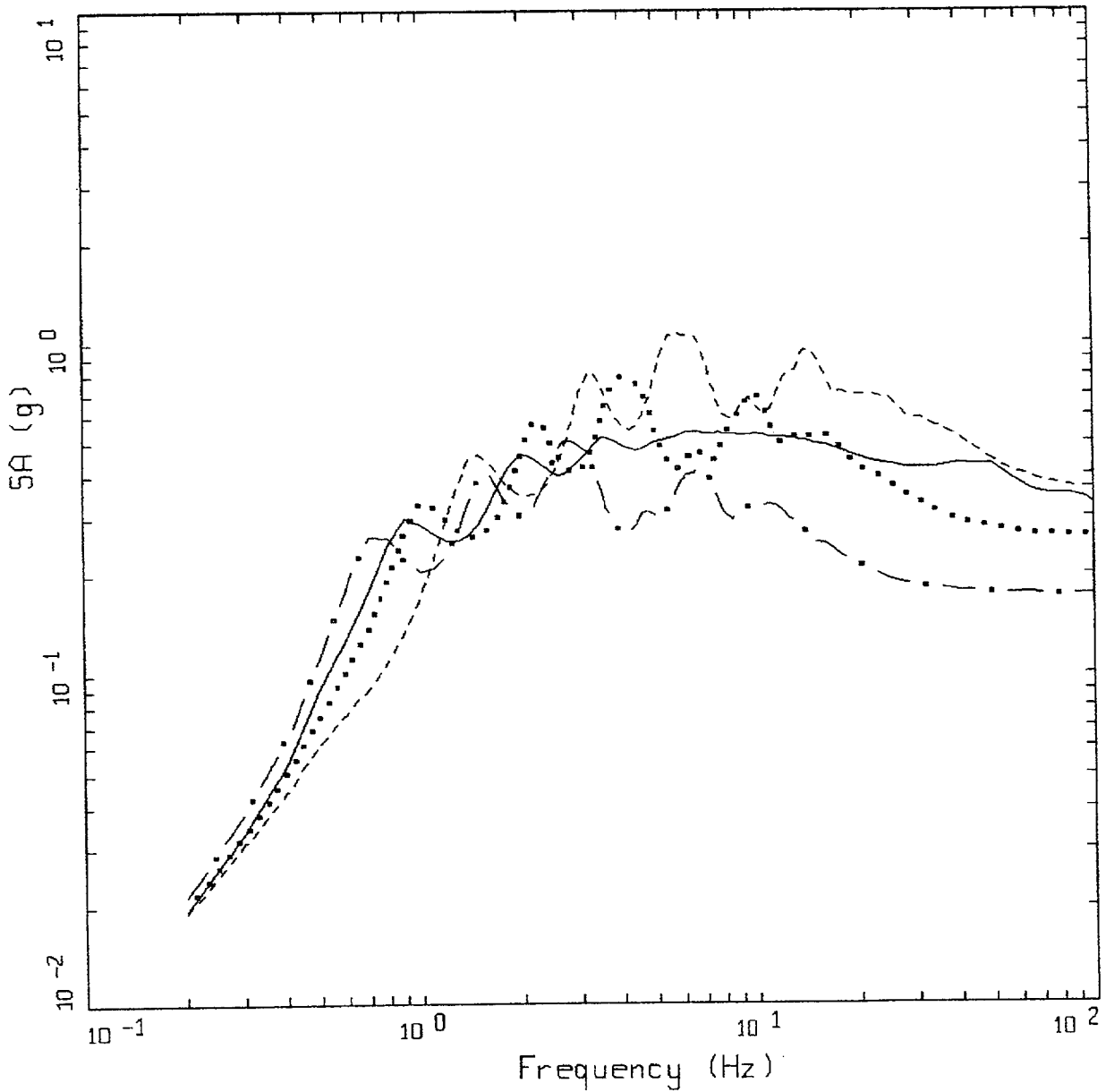
Figure 6-100. Comparison of soil spectra for Approach 2B with base case profile and deterministic profile variations (\pm factor of 2 on shear modulus); soil profile Gilroy 2, CEUS conditions.



CEUS 10E-4 APPROACH COMPARISON, G2

- LEGEND
- APPROACH 2, 1 HZ AND 10 HZ DEAGGREGATION EQKS, MEAN PGA = 0.325 G
 - APPROACH 1, 10-4 ROCK CONTROL MOTION, BASE CASE, 68TH PERCENTILE, PGA = 0.333 G
 - APPROACH 1, 10-4 ROCK CONTROL MOTION, BASE CASE, MEAN, PGA = 0.241 G
 - APPROACH 1, 10-4 ROCK CONTROL MOTION, BASE CASE, 32ND PERCENTILE, PGA = 0.150 G

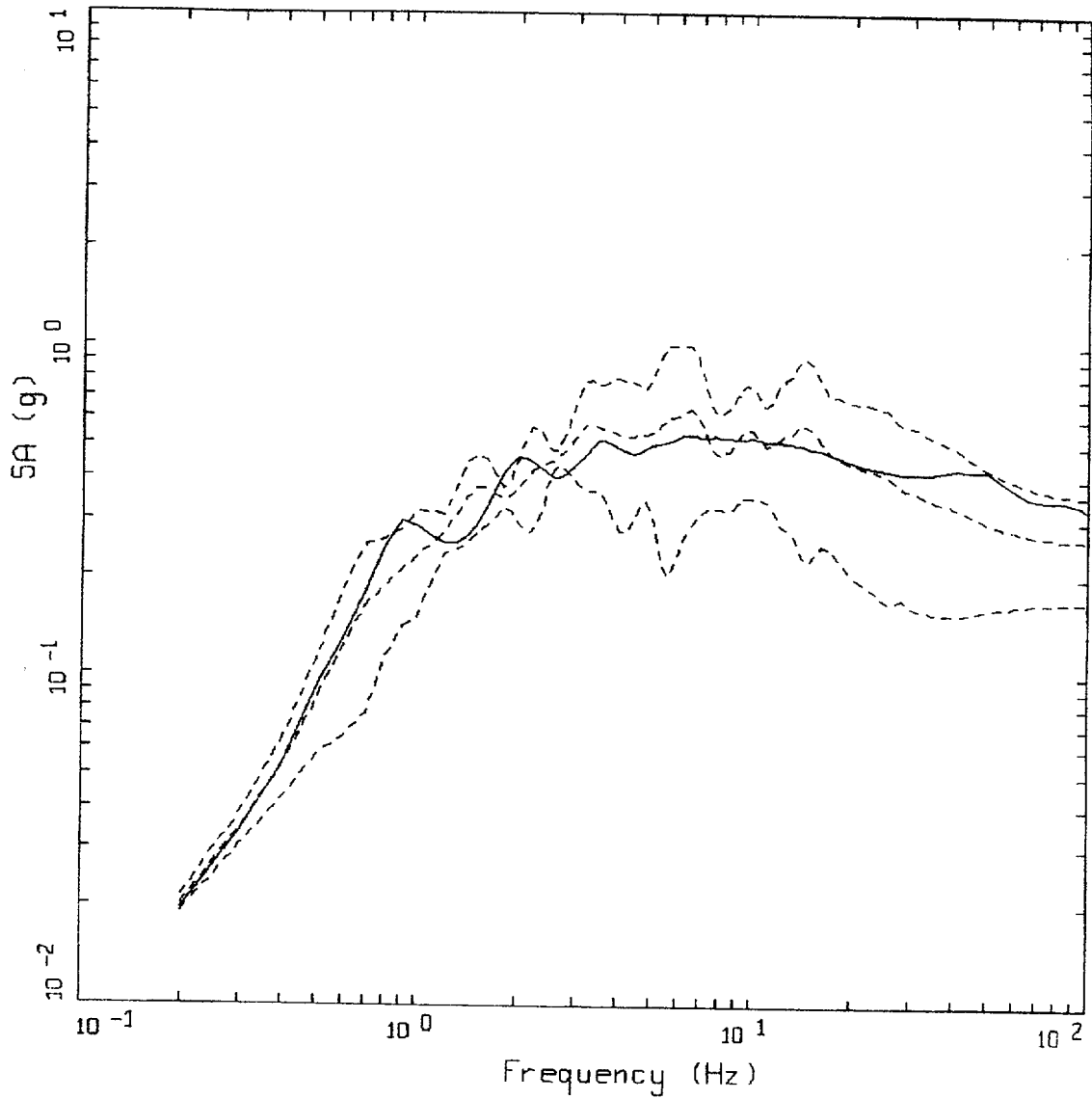
Figure 6-101. Comparison of soil spectra for Approach 2B with mean and $\pm 1\sigma$ variations of base case (\pm factor of 2 on shear modulus), soil profile Gilroy 2, CEUS conditions.



CEUS 10E-4 APPROACH COMPARISON, G2
 SOIL PROFILE TO 150 M (500 FT)

- LEGEND
- APPROACH 2, 1 HZ AND 10 HZ DEAGGREGATION EQKS, MEAN PGA = 0.325 G
 - APPROACH 1, 10-4 ROCK CONTROL MOTION, BASE CASE PGA = 0.259 G
 - APPROACH 1, 10-4 ROCK CONTROL MOTION, BASE CASE (UPPER) PGA = 0.361 G
 - . - . - . APPROACH 1, 10-4 ROCK CONTROL MOTION, BASE CASE (LOWER) PGA = 0.172 G

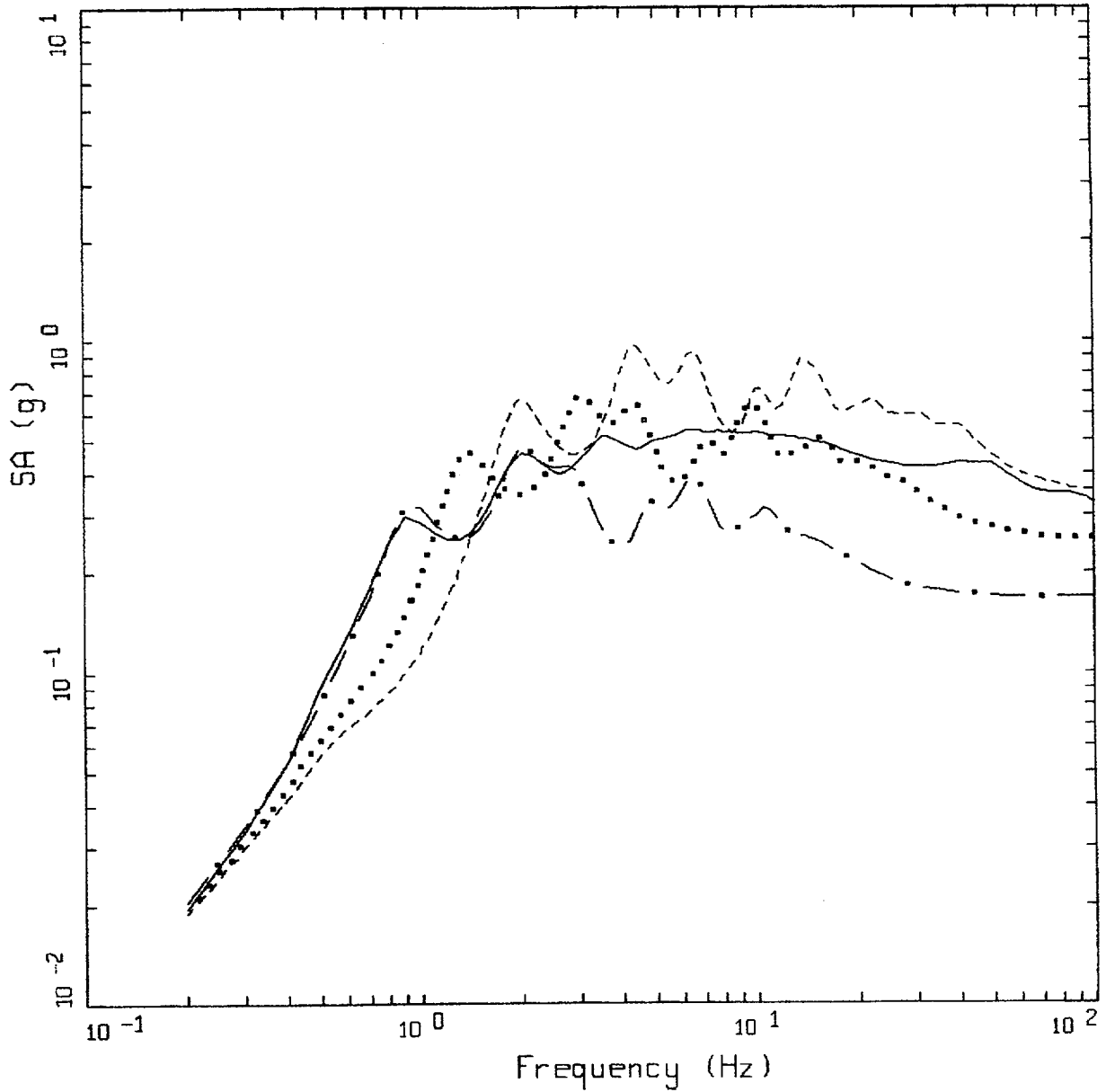
Figure 6-102. Comparison of soil spectra for Approach 2B (full profile) with base case profile and deterministic profile variations (\pm factor of 2 on shear modulus) with profile truncated at 150m; soil profile Gilroy 2, CEUS conditions.



CEUS 10E-4 APPROACH COMPARISON, G2
 SOIL PROFILE TO 150 M (500 FT)

- LEGEND
- APPROACH 2, 1 HZ AND 10 HZ DEAGGREGATION EQKS, MEAN PGA = 0.325 G
 - APPROACH 1, 10-4 ROCK CONTROL MOTION, BASE CASE, 68TH PERCENTILE, PGA = 0.358 G
 - APPROACH 1, 10-4 ROCK CONTROL MOTION, BASE CASE, MEAN, PGA = 0.264 G
 - APPROACH 1, 10-4 ROCK CONTROL MOTION, BASE CASE, 32ND PERCENTILE, PGA = 0.170 G

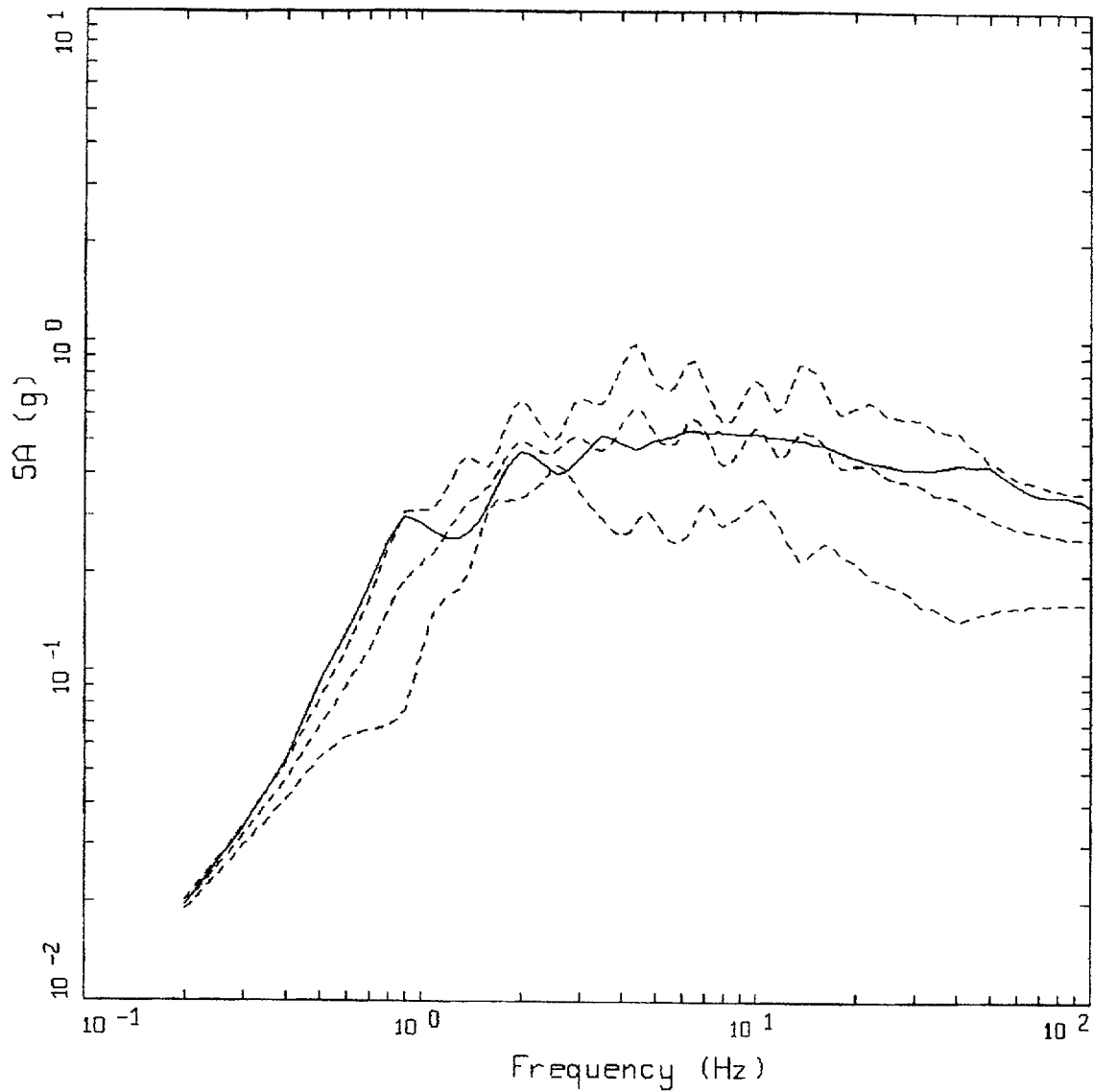
Figure 6-103. Comparison of soil spectra for Approach 2B (full profile) with mean and $\pm 1\sigma$ profile variations with profile truncated at 150m. Soil profile Gilroy 2, CEUS conditions.



CEUS 10E-4 APPROACH COMPARISON, G2
 SOIL PROFILE TO 90 M (300 FT)

- LEGEND
- APPROACH 2, 1 HZ AND 10 HZ DEAGGREGATION EQKS, MEAN PGA = 0.325 G
 - APPROACH 1, 10-4 ROCK CONTROL MOTION, BASE CASE PGA = 0.253 G
 - APPROACH 1, 10-4 ROCK CONTROL MOTION, BASE CASE (UPPER) PGA = 0.354 G
 - . - - APPROACH 1, 10-4 ROCK CONTROL MOTION, BASE CASE (LOWER) PGA = 0.167 G

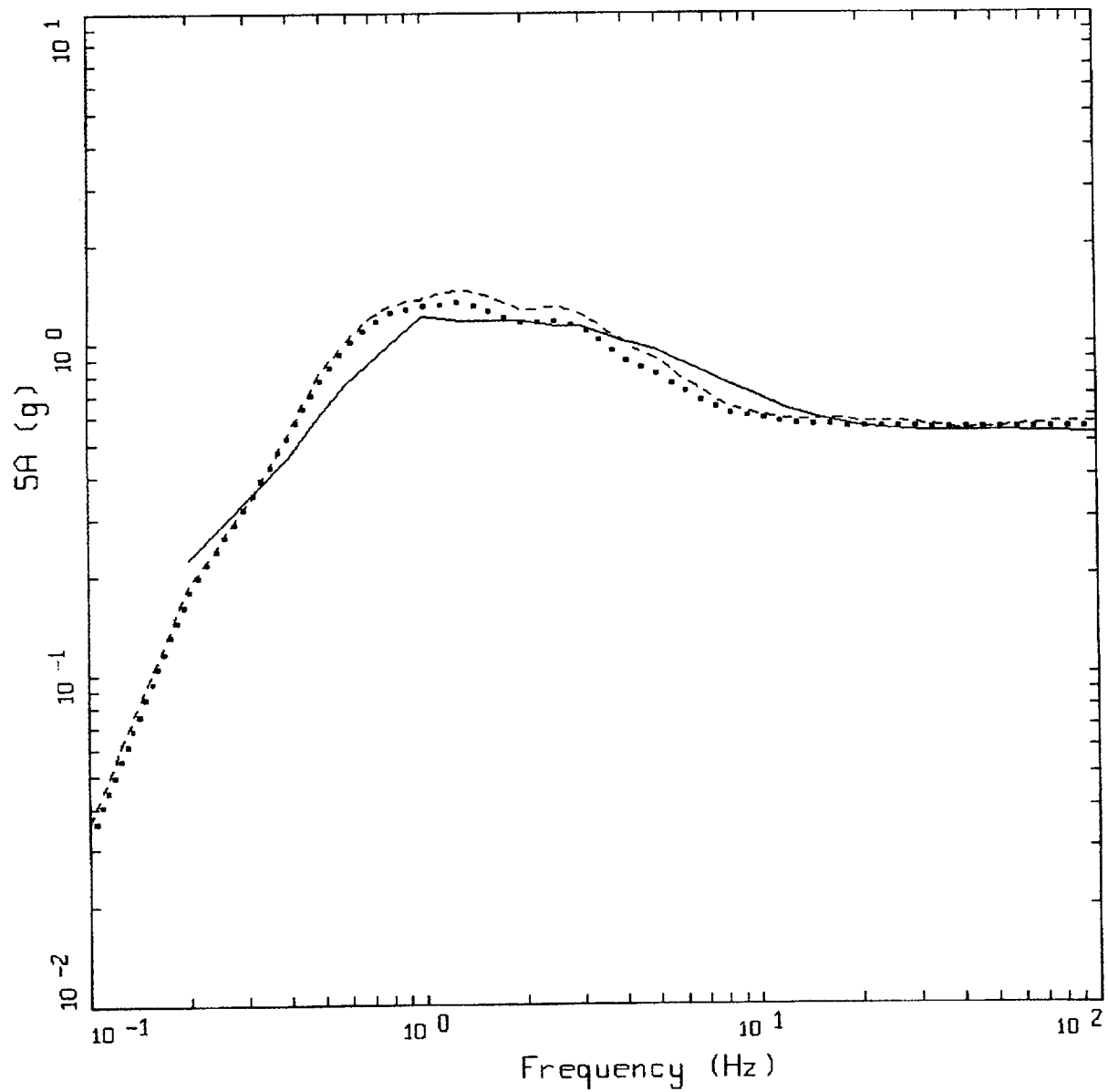
Figure 6-104. Comparison of soil spectra for Approach 2B (full profile) with base case profile and deterministic profile variations (\pm factor of 2 on shear modulus) with profile truncated at 90m; soil profile Gilroy 2, CEUS conditions.



CEUS 10E-4 APPROACH COMPARISON, GZ
 SOIL PROFILE TO 90 M (300 FT)

- LEGEND
- APPROACH 2, 1 HZ AND 10 HZ DEAGGREGATION EQKS, MEAN PGA = 0.325 G
 - - - - - APPROACH 1, 10-4 ROCK CONTROL MOTION, BASE CASE, 68TH PERCENTILE, PGA = 0.351 G
 - · - · - APPROACH 1, 10-4 ROCK CONTROL MOTION, BASE CASE, MEAN, PGA = 0.258 G
 - · · · · APPROACH 1, 10-4 ROCK CONTROL MOTION, BASE CASE, 32ND PERCENTILE, PGA = 0.165 G

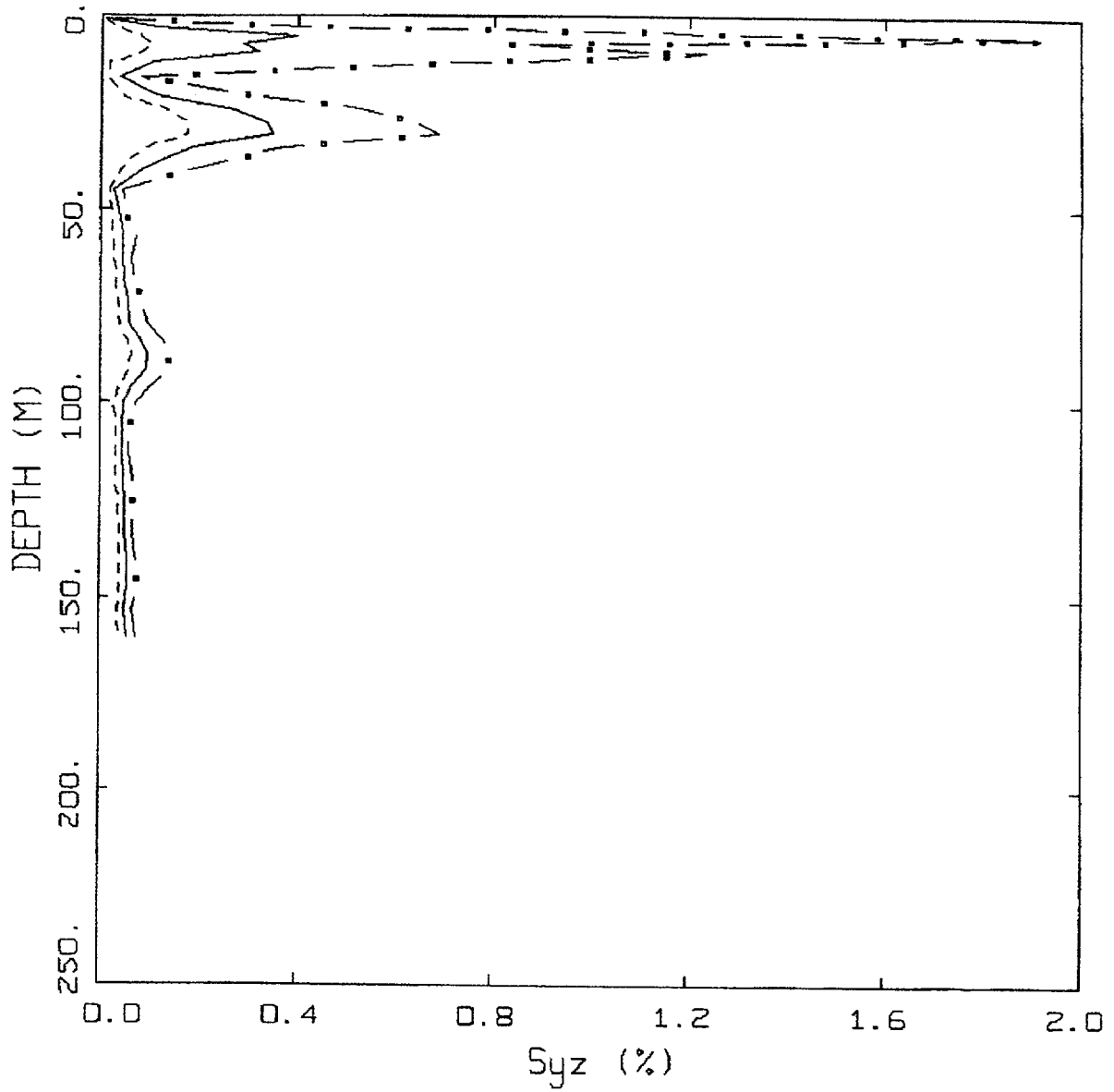
Figure 6-105. Comparison of soil spectra for Approach 2B (full profile) with mean and $\pm 1\sigma$ profile variations with profile truncated at 90m. Soil profile Gilroy 2, CEUS conditions.



WUS $10E-4$ APPROACH COMPARISON, G2

- LEGEND
- APPROACH 4, 10^{-4} SOIL UNIFORM HAZARD SPECTRUM, PGA = 0.532 G
 - APPROACH 1, 10^{-4} ROCK CONTROL MOTION, MEAN PGA = 0.550 G
 - APPROACH 2, 1 HZ AND 10 HZ DEAGGREGATION EQKS, MEAN PGA = 0.567 G

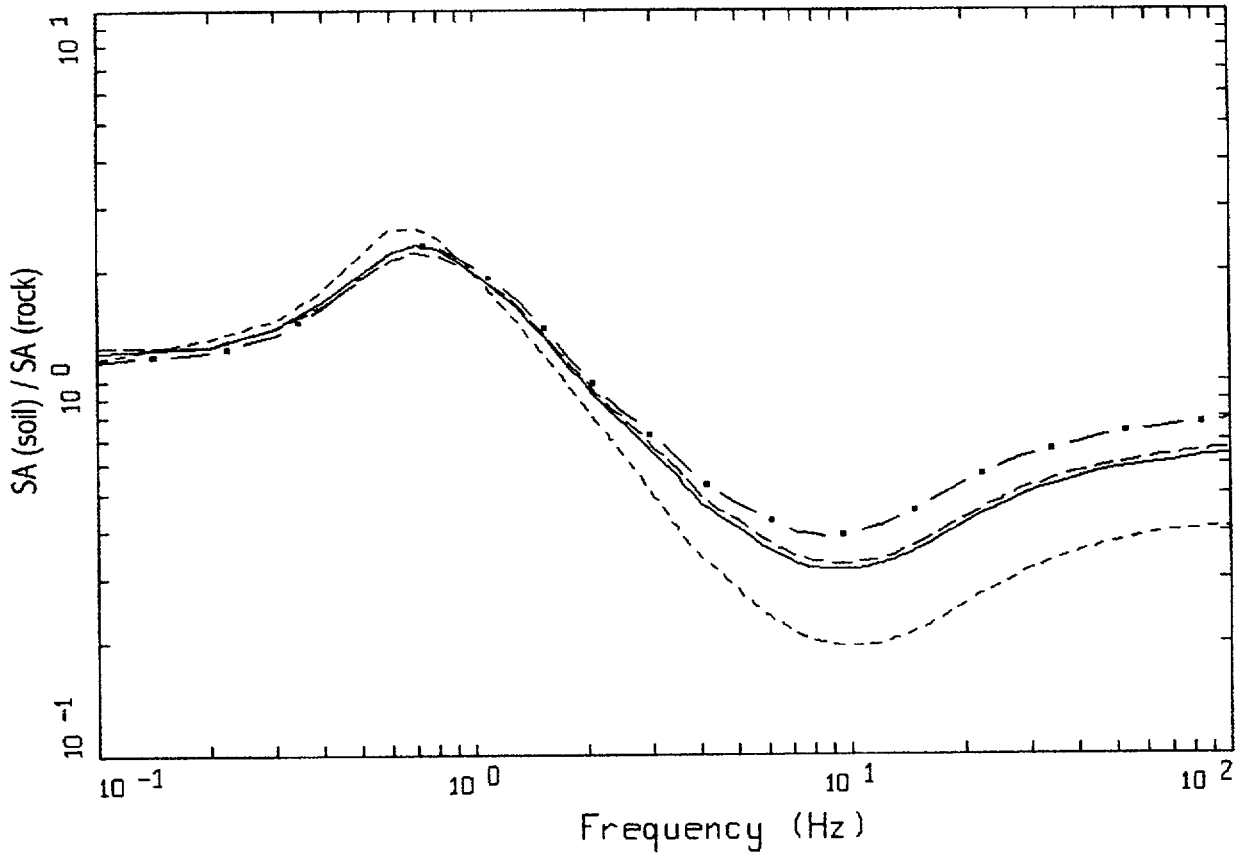
Figure 6-106. Comparison of Approaches 1, 2B, and 4 10^{-4} UHS on soil for profile Gilroy 2: WUS conditions.



WUS, 10-4, G2
 EFFECTIVE STRAINS (SYZ)

LEGEND
 - . - 84TH PERCENTILE
 ——— 50TH PERCENTILE
 - - - - 16TH PERCENTILE

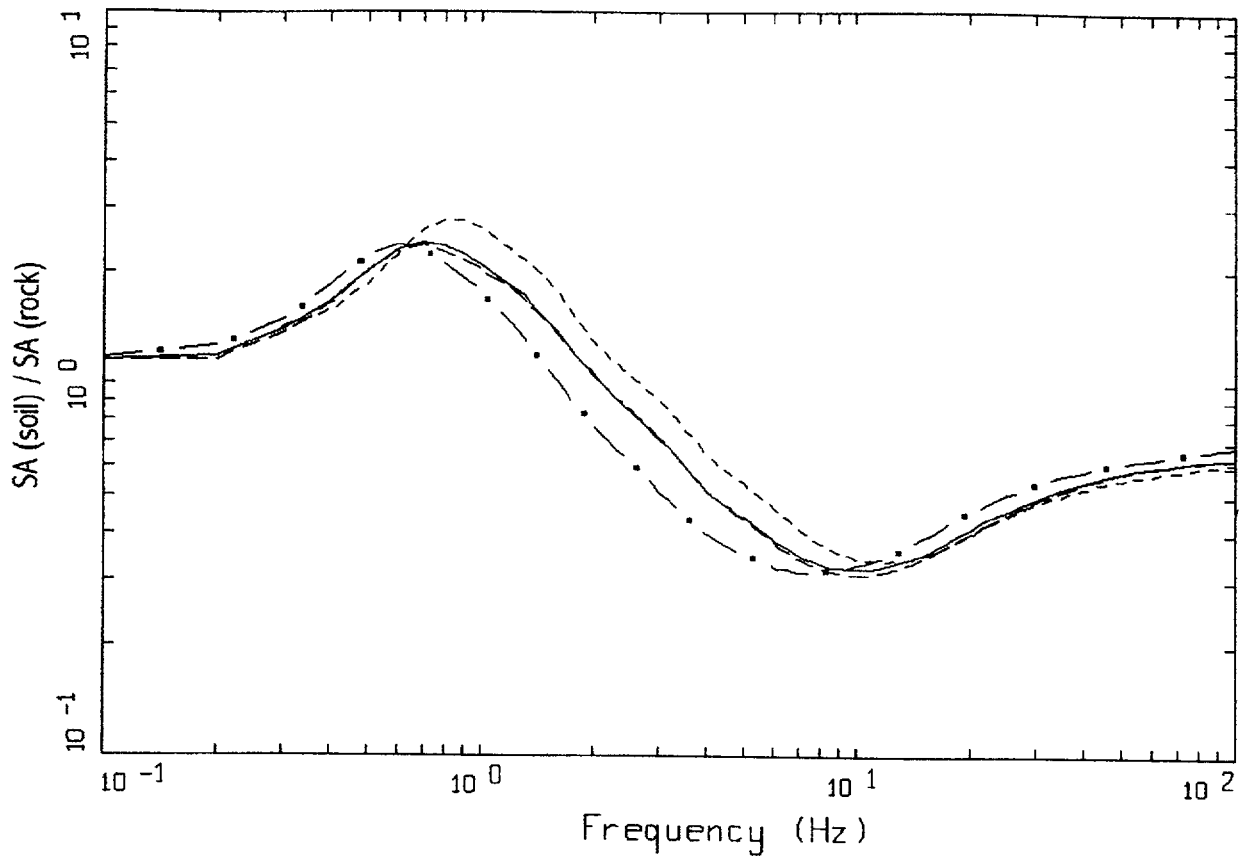
Figure 6-107. Median and $\pm 1\sigma$ effective strain for soil profile Gilroy 2 using Approach 1: WUS conditions.



WUS, 1DE-4, 1HZ DESIGN, G2
 SURFACE MOTION, 1HZ TRANSFER FUNCTION
 WEIGHTS: ML=0.20, MM=0.60, MH=0.20

- LEGEND
- ML = 5.4, D = 10 KM MEAN RATIO
 - . - . MM = 6.7, D = 18 KM, DESIGN MEAN RATIO
 - MH = 7.8, D = 30 KM MEAN RATIO
 - WEIGHTED MEAN RATIO

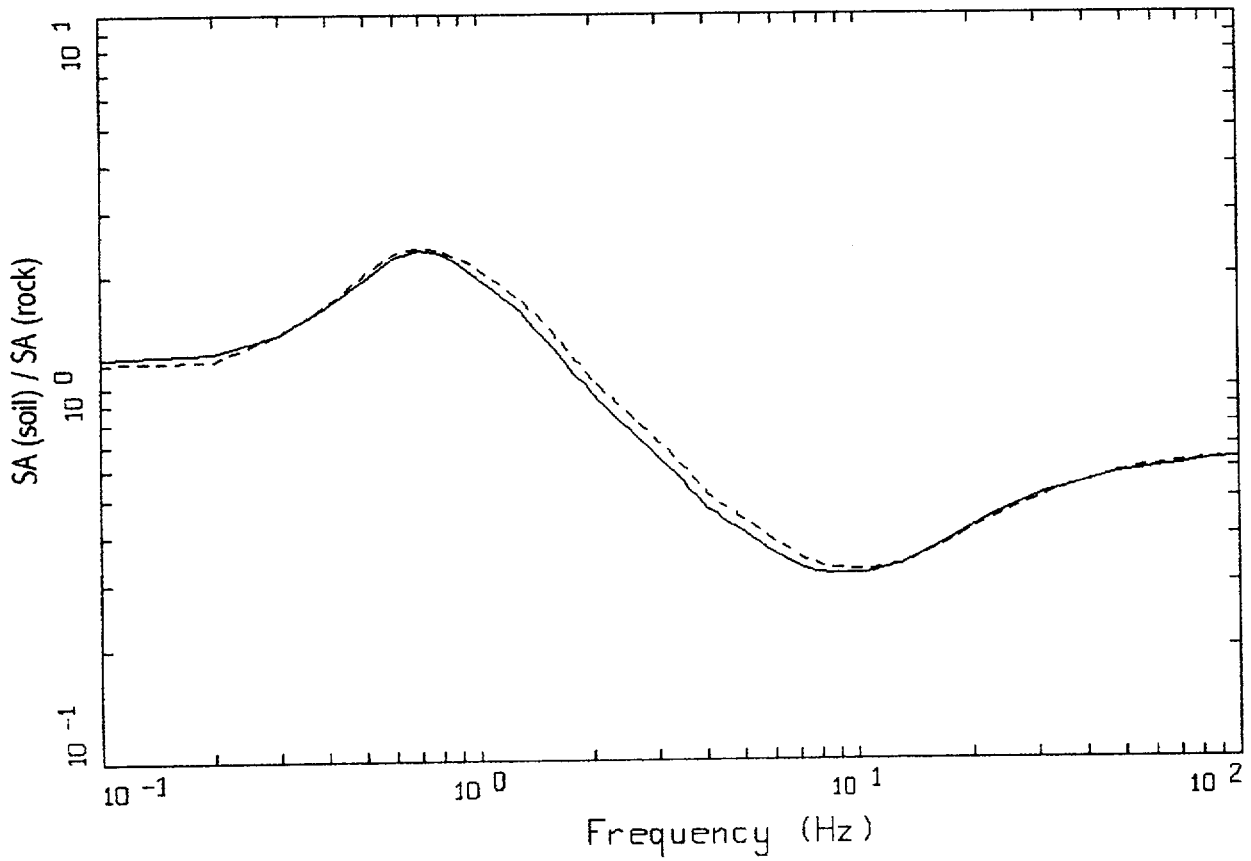
Figure 6-108. Comparison of transfer functions computed for the scaled 1 Hz design earthquake: soil profile Gilroy 2, WUS conditions.



WUS, 10E-4, 10HZ DESIGN, G2
 SURFACE MOTION, 10HZ TRANSFER FUNCTION
 WEIGHTS: ML=0.20, MM=0.60, MH=0.20

LEGEND
 - - - - - ML = 5.1, D = 10 KM MEAN RATIO
 - · - · - MM = 6.1, D = 14 KM, DESIGN MEAN RATIO
 — · — MH = 7.8, D = 30 KM MEAN RATIO
 ——— WEIGHTED MEAN RATIO

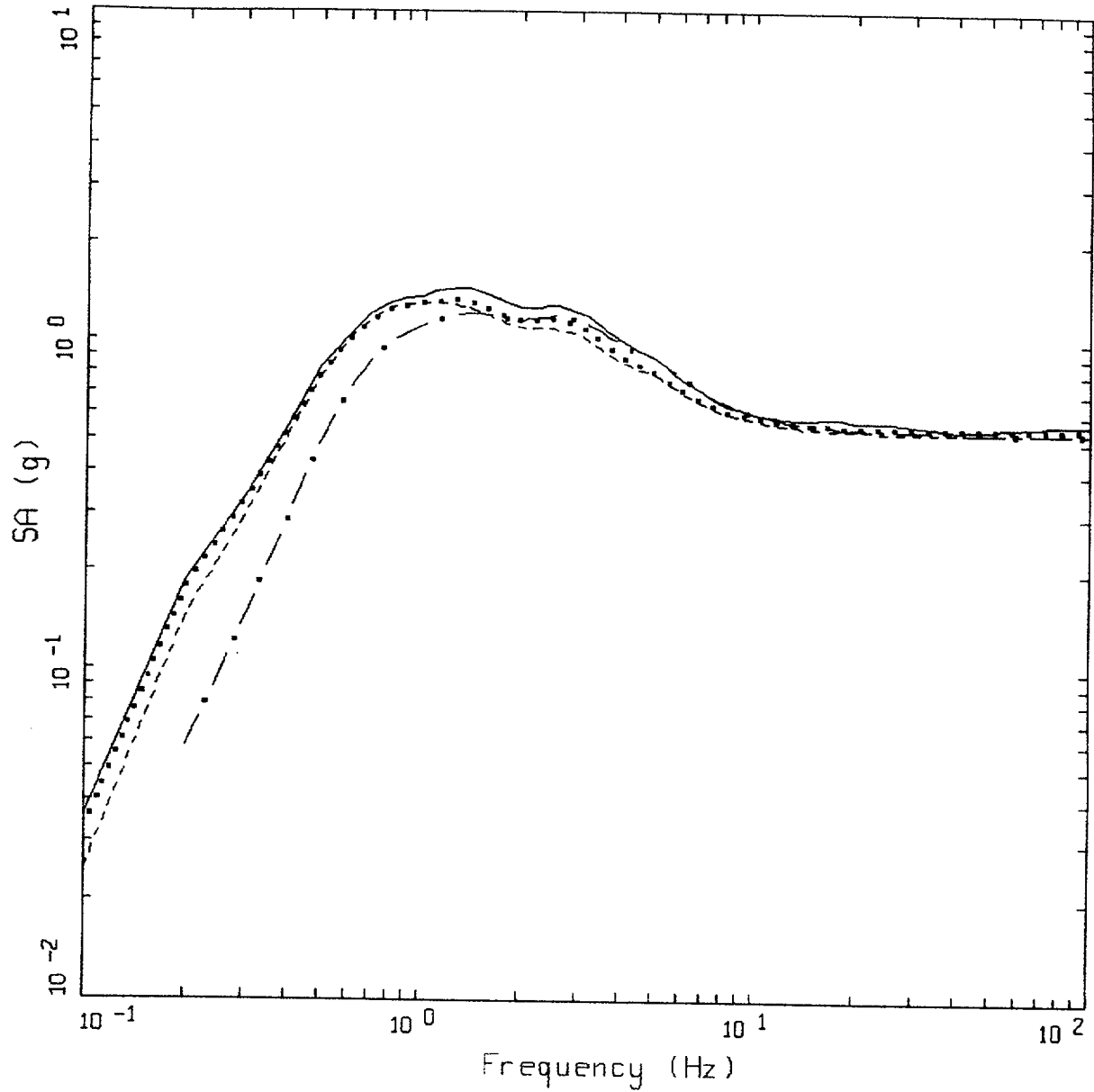
Figure 6-109. Comparison of transfer functions computed for the scaled 10 Hz design earthquake; soil profile Gilroy 2, WUS conditions.



WUS, $10E-4$, G2
AMPLIFICATION

LEGEND
 ——— 1 HZ WEIGHTED MEAN RATIO; WEIGHTS:ML=0.20,MM=0.60,MH=0.20
 - - - - 10 HZ WEIGHTED MEAN RATIO; WEIGHTS:ML=0.20,MM=0.60,MH=0.20

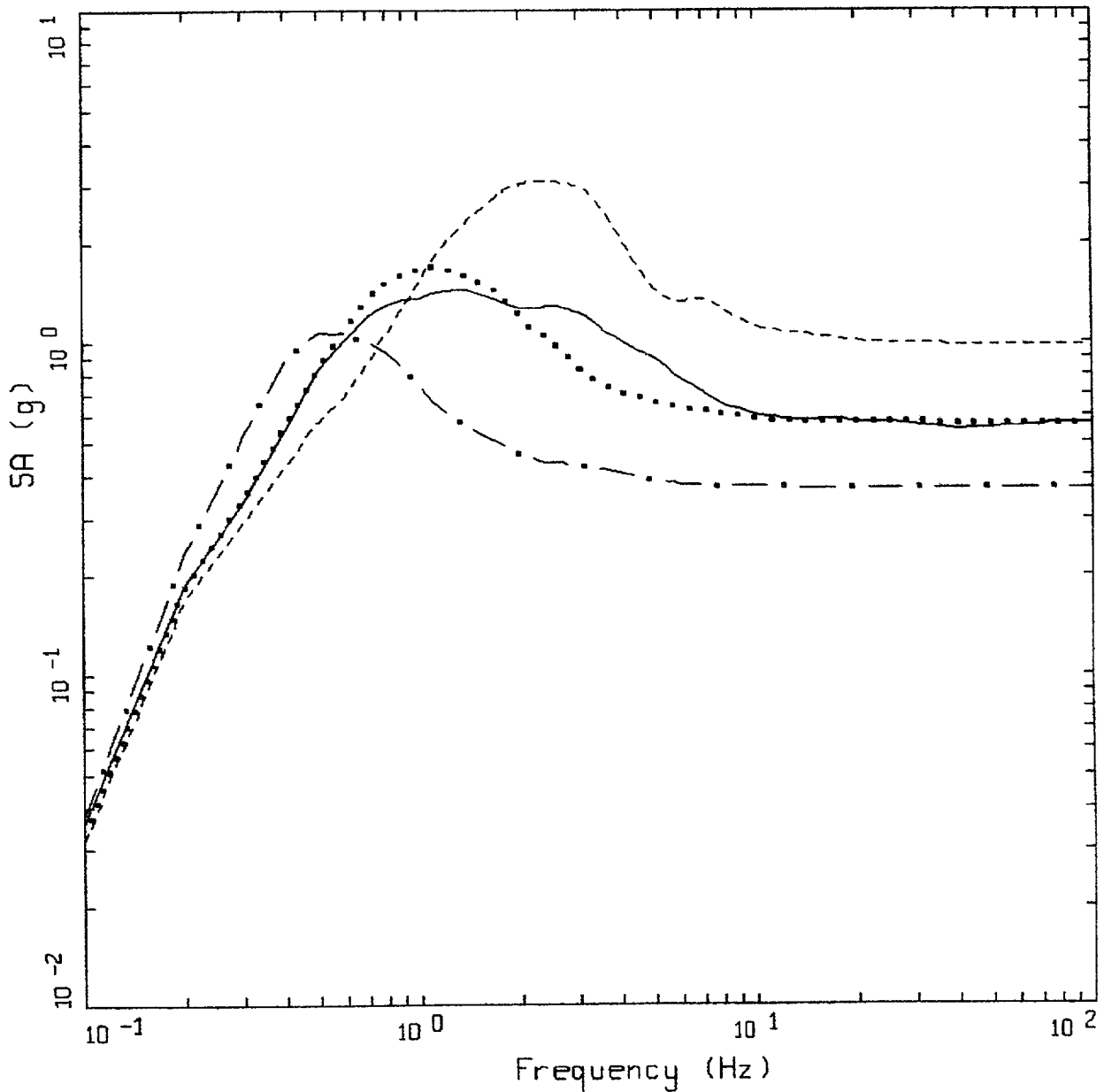
Figure 6-110. Comparison of mean transfer functions computed for the scaled 1 Hz and 10 Hz design earthquakes; soil profile Gilroy 2, WUS conditions.



WUS, 10E-4 DESIGN SPECTRA, GZ

- LEGEND
- APPROACH 2, 1 HZ AND 10 HZ DEAGGREGATION EQKS, MEAN PGA = 0.567 G
 - APPROACH 1, 10-4 ROCK CONTROL MOTION, MEAN PGA = 0.550 G
 - 1 HZ MEAN; PGA = 0.535 G
 - . - . 10 HZ MEAN; PGA = 0.539 G

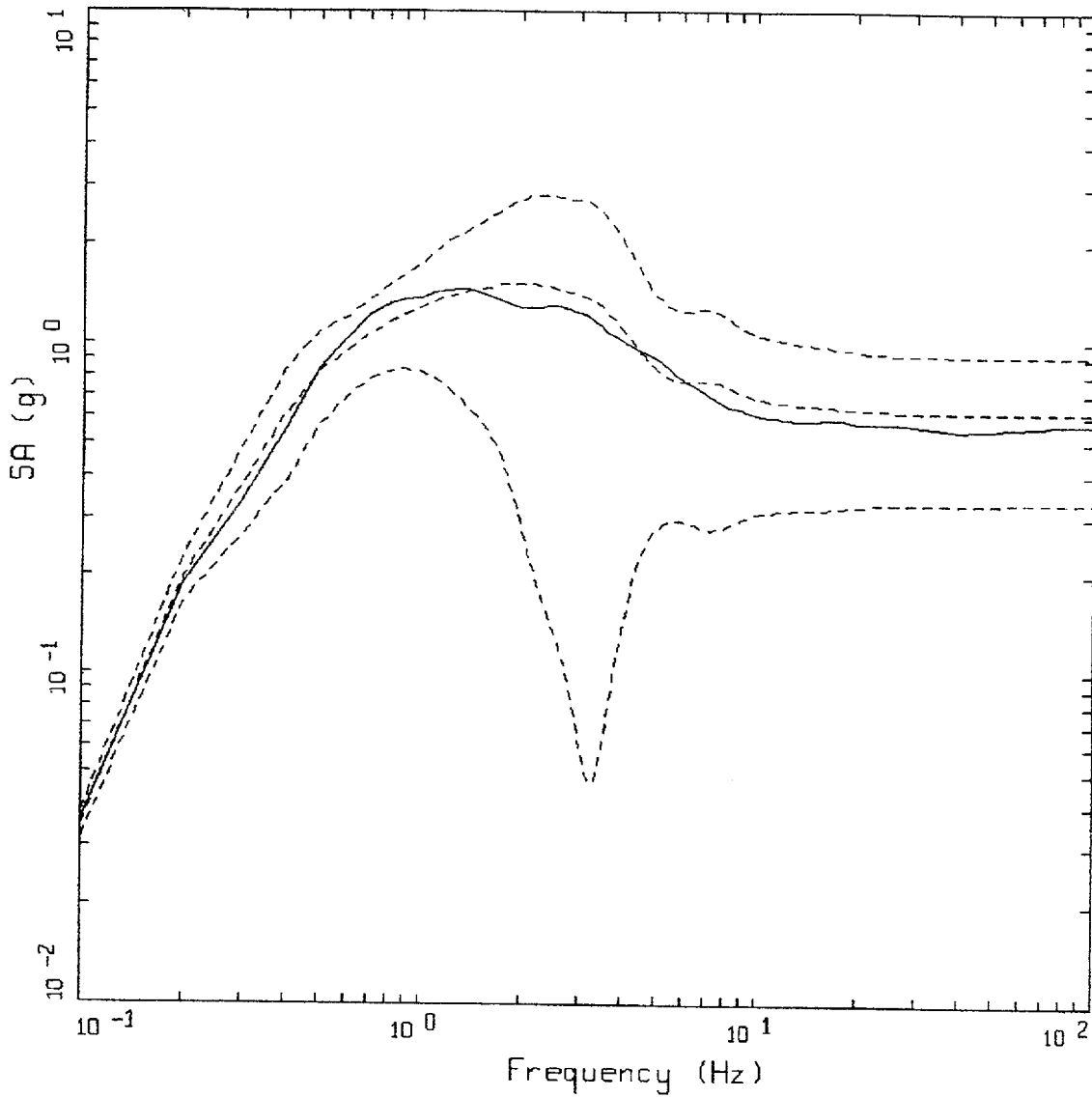
Figure 6-111. Comparison of soil spectra for Approaches 1, 2A, and 2B; soil profile Gilroy 2, WUS conditions.



WUS 10E-4 APPROACH COMPARISON, GZ

- LEGEND
- APPROACH 2, 1 HZ AND 10 HZ DEAGGREGATION EQKS, MEAN PGA = 0.567 G
 - APPROACH 1, 10⁻⁴ ROCK CONTROL MOTION, BASE CASE PGA = 0.571 G
 - APPROACH 1, 10⁻⁴ ROCK CONTROL MOTION, BASE CASE (UPPER) PGA = 0.978 G
 - · - APPROACH 1, 10⁻⁴ ROCK CONTROL MOTION, BASE CASE (LOWER) PGA = 0.368 G

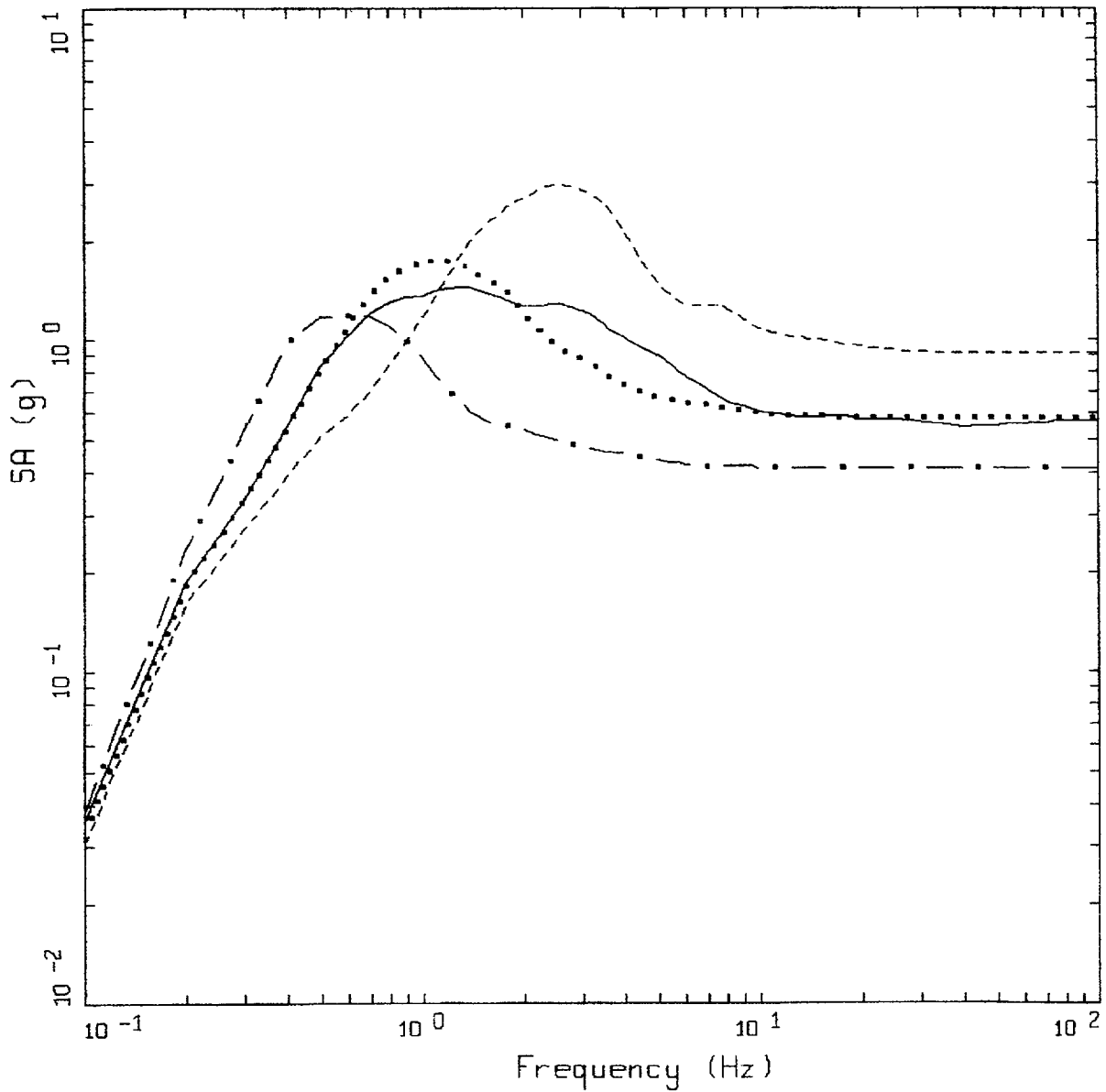
Figure 6-112. Comparison of soil spectra for Approach 2B with base case profile and deterministic profile variations (\pm factor of 2 on shear modulus); soil profile Gilroy 2, WUS conditions.



WUS 10E-4 APPROACH COMPARISON, GZ

- LEGEND
- APPROACH 2, 1 HZ AND 10 HZ DEAGGREGATION EQKS, MEAN PGA = 0.567 G
 - APPROACH 1, 10-4 ROCK CONTROL MOTION, BASE CASE, 84TH PERCENTILE, PGA = 0.912 G
 - APPROACH 1, 10-4 ROCK CONTROL MOTION, BASE CASE, MEAN, PGA = 0.621 G
 - APPROACH 1, 10-4 ROCK CONTROL MOTION, BASE CASE, 16TH PERCENTILE, PGA = 0.330 G

Figure 6-113. Comparison of soil spectra for Approach 2B with mean and $\pm 1\sigma$ variations of base case (\pm factor of 2 on shear modulus), soil profile Gilroy 2, WUS conditions.

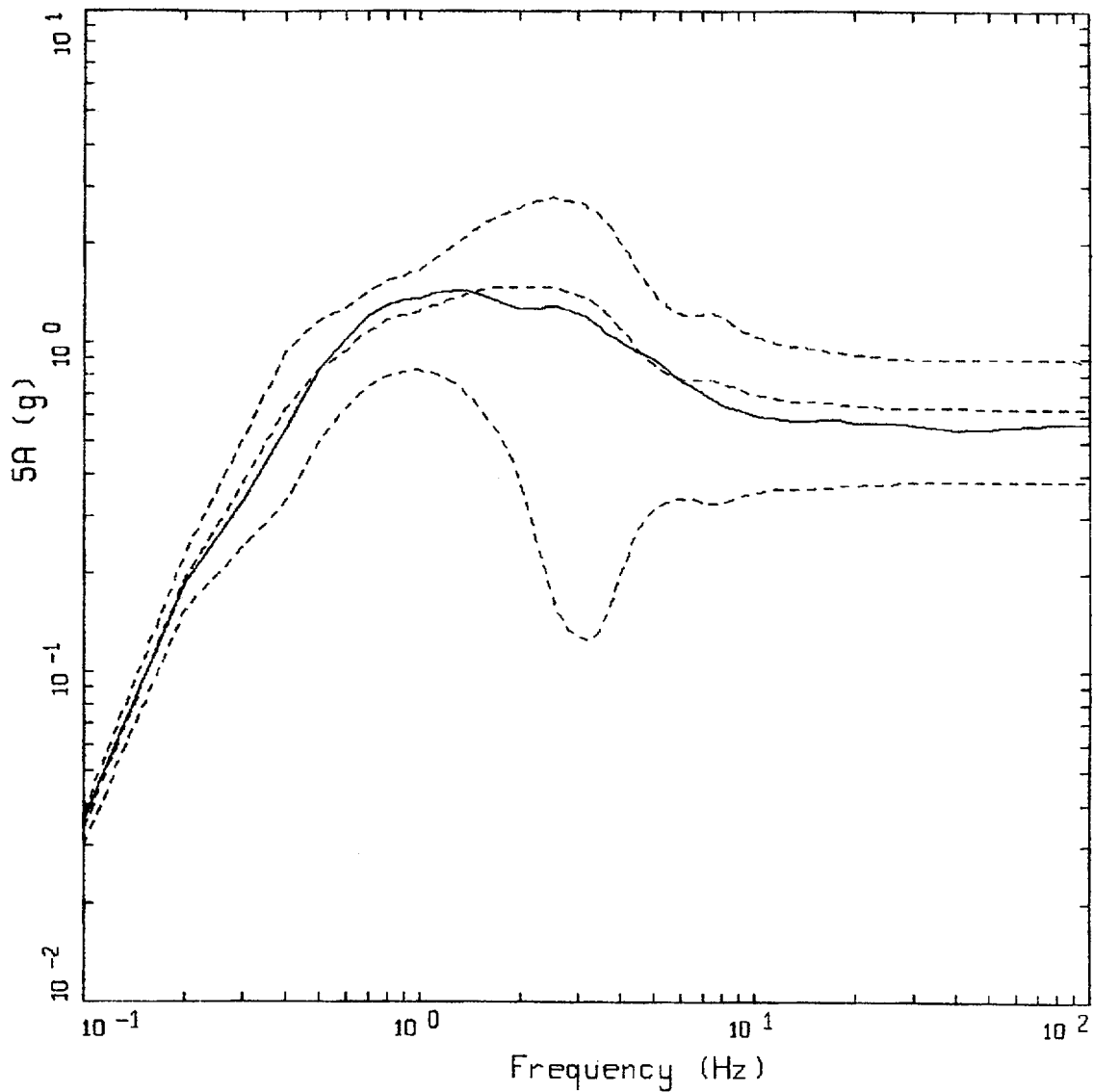


WUS 10E-4 APPROACH COMPARISON, G2
 SOIL PROFILE TO 150 M (500 FT)

LEGEND

- APPROACH 2, 1 HZ AND 10 HZ DEAGGREGATION EQKS, MEAN PGA = 0.567 G
- APPROACH 1, 10-4 ROCK CONTROL MOTION, BASE CASE PGA = 0.580 G
- APPROACH 1, 10-4 ROCK CONTROL MOTION, BASE CASE (UPPER) PGA = 0.908 G
- . - . APPROACH 1, 10-4 ROCK CONTROL MOTION, BASE CASE (LOWER) PGA = 0.411 G

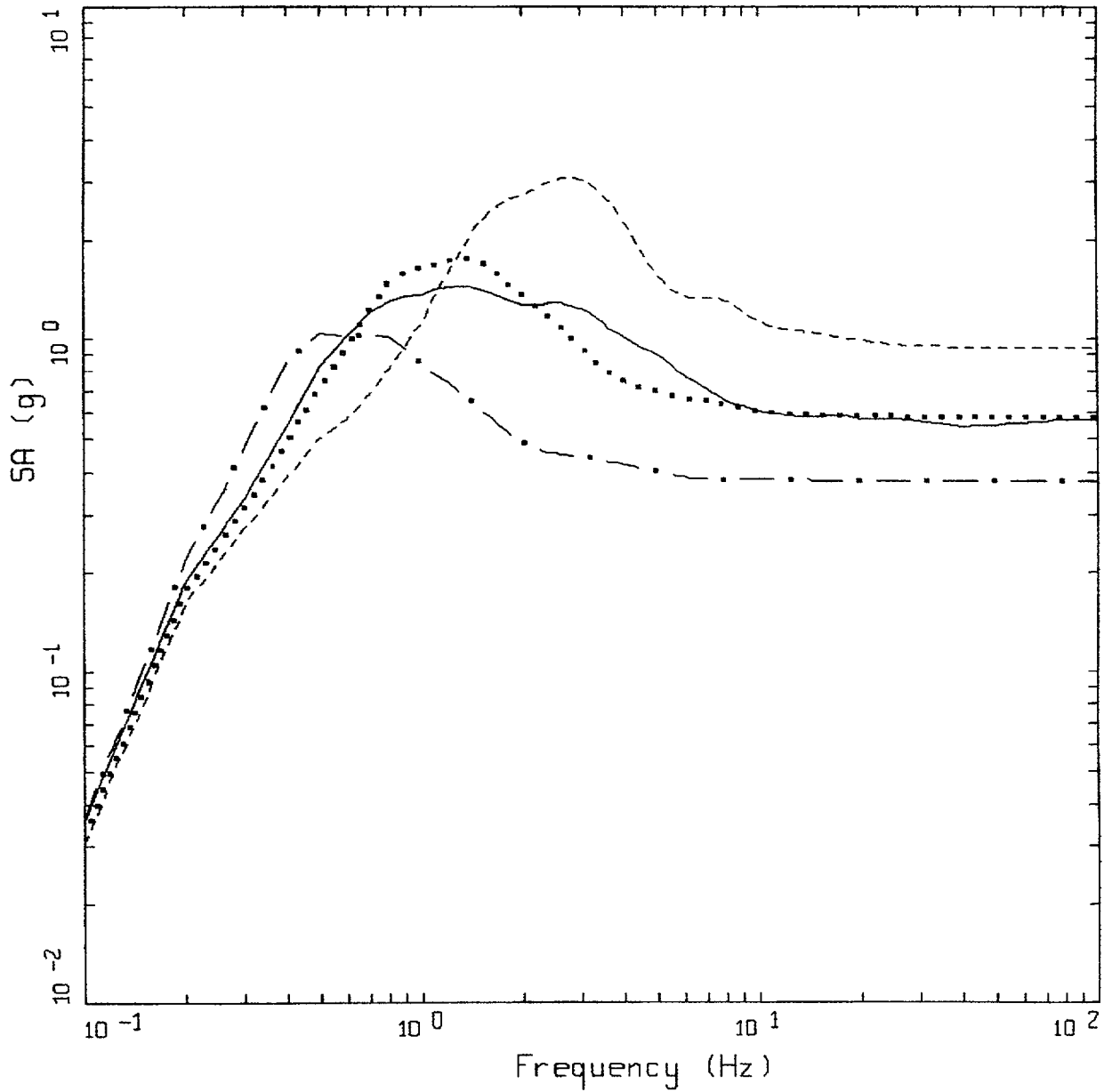
Figure 6-114. Comparison of soil spectra for Approach 2B (full profile) with base case profile and deterministic profile variations (\pm factor of 2 on shear modulus) with profile truncated at 150m; soil profile Gilroy 2, WUS conditions.



WUS 10E-4 APPROACH COMPARISON, GZ
 SOIL PROFILE TO 150 M (500 FT)

- LEGEND
- APPROACH 2, 1 HZ AND 10 HZ DEAGGREGATION EQKS, MEAN PGA = 0.567 G
 - APPROACH 1, 10-4 ROCK CONTROL MOTION, BASE CASE, 84TH PERCENTILE, PGA = 0.886 G
 - APPROACH 1, 10-4 ROCK CONTROL MOTION, BASE CASE, MEAN, PGA = 0.633 G
 - APPROACH 1, 10-4 ROCK CONTROL MOTION, BASE CASE, 16TH PERCENTILE, PGA = 0.380 G

Figure 6-115. Comparison of soil spectra for Approach 2B (full profile) with mean and $+1\sigma$ profile variations with profile truncated at 150m; soil profile Gilroy 2, WUS conditions.

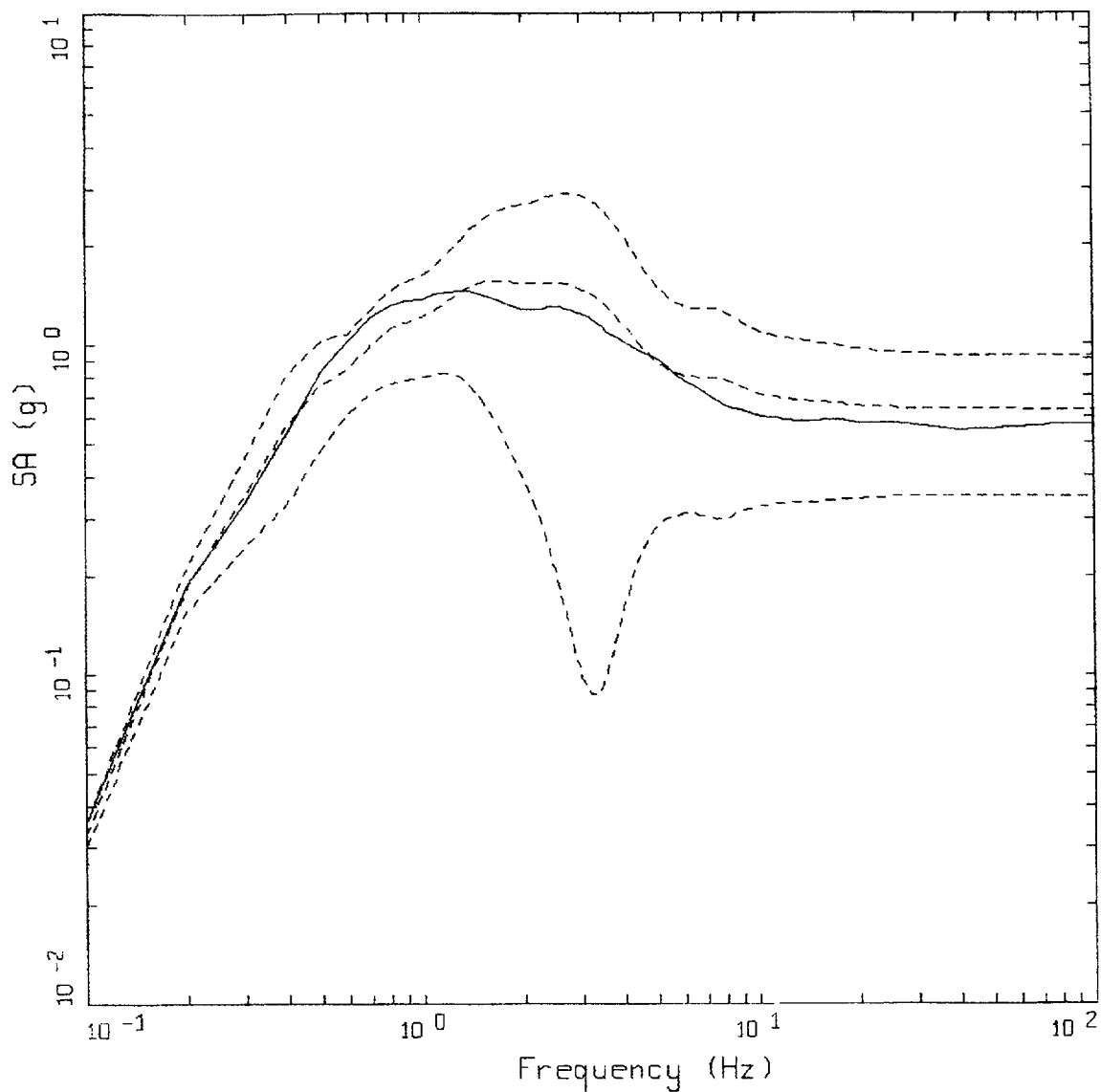


WUS 10E-4 APPROACH COMPARISON, GZ
 SOIL PROFILE TO 90 M (300 FT)

LEGEND

- APPROACH 2, 1 HZ AND 10 HZ DEAGGREGATION EQKS, MEAN PGA = 0.567 G
- APPROACH 1, 10-4 ROCK CONTROL MOTION, BASE CASE PGA = 0.583 G
- APPROACH 1, 10-4 ROCK CONTROL MOTION, BASE CASE (UPPER) PGA = 0.942 G
- . - . APPROACH 1, 10-4 ROCK CONTROL MOTION, BASE CASE (LOWER) PGA = 0.377 G

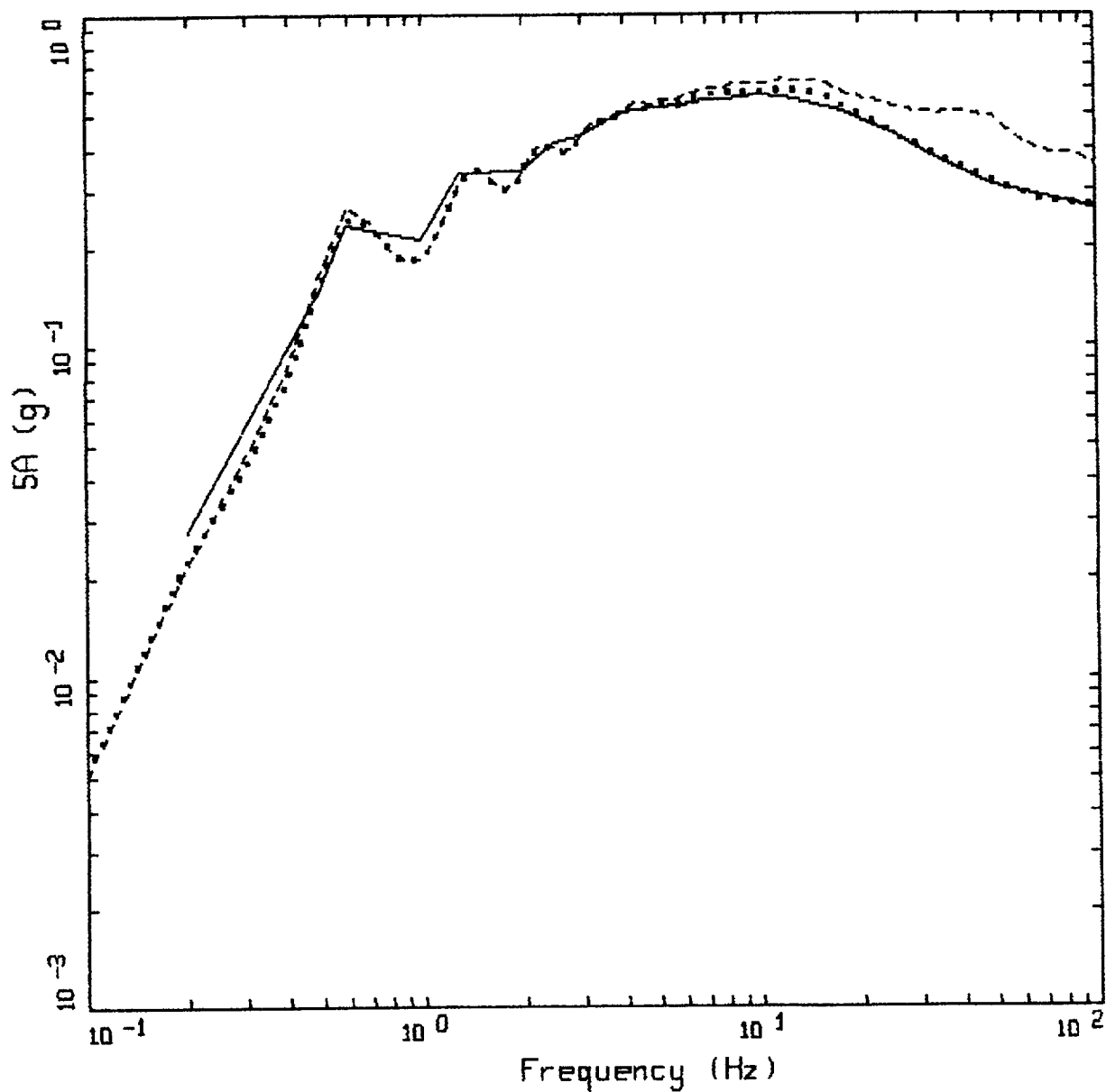
Figure 6-116. Comparison of soil spectra for Approach 2B (full profile) with base case profile and deterministic profile variations (\pm factor of 2 on shear modulus) with profile truncated at 90m; soil profile Gilroy 2, WUS conditions.



WUS 10E-4 APPROACH COMPARISON, GZ
 SOIL PROFILE TO 90M (300 FT)

- LEGEND
- APPROACH 2, 1 HZ AND 10 HZ DEAGGREGATION EQKS, MEAN PGA = 0.567 G
 - APPROACH 1, 10-4 ROCK CONTROL MOTION, BASE CASE, 84TH PERCENTILE, PGA = 0.920 G
 - APPROACH 1, 10-4 ROCK CONTROL MOTION, BASE CASE, MEAN, PGA = 0.634 G
 - APPROACH 1, 10-4 ROCK CONTROL MOTION, BASE CASE, 16TH PERCENTILE, PGA = 0.348 G

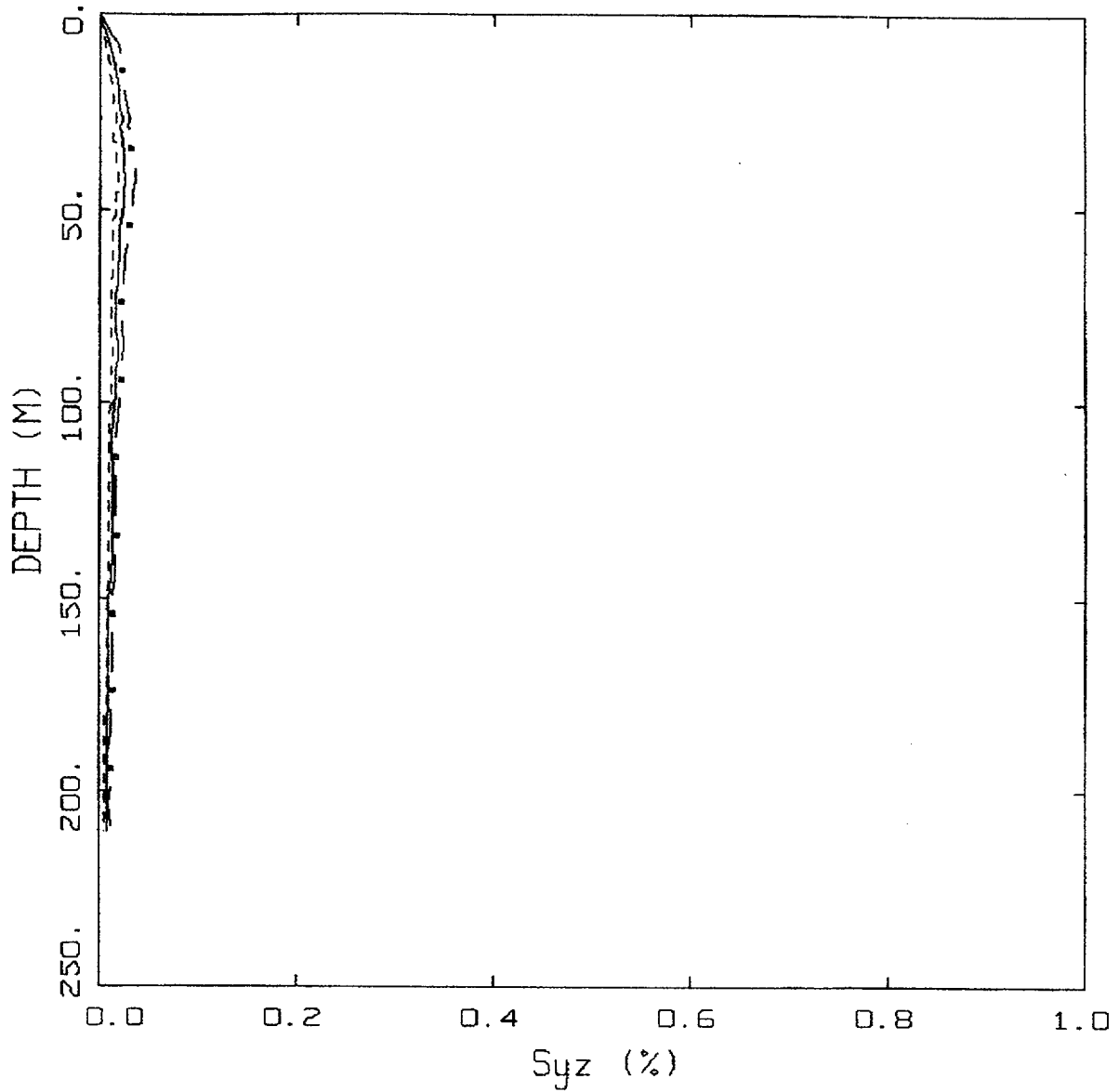
Figure 6-117. Comparison of soil spectra for Approach 2B (full profile) with mean and $\pm 1\sigma$ profile variations with profile truncated at 90m. Soil profile Gilroy 2, WUS conditions.



CEUS 10E-4 APPROACH COMPARISON, SR

- LEGEND
- APPROACH 4, 10⁻⁴ SOIL UNIFORM HAZARD SPECTRUM, PGA = 0.259 G
 - APPROACH 1, 10⁻⁴ ROCK CONTROL MOTION, MEAN PGA = 0.265 G
 - - - - APPROACH 2, 1 HZ AND 10 HZ DEAGGREGATION EQKS, MEAN PGA = 0.355 G

Figure 6-118. Comparison of Approaches 1, 2B, and 4, 10⁻⁴ UHS on soil for profile Savannah River Generic: CEUS conditions.

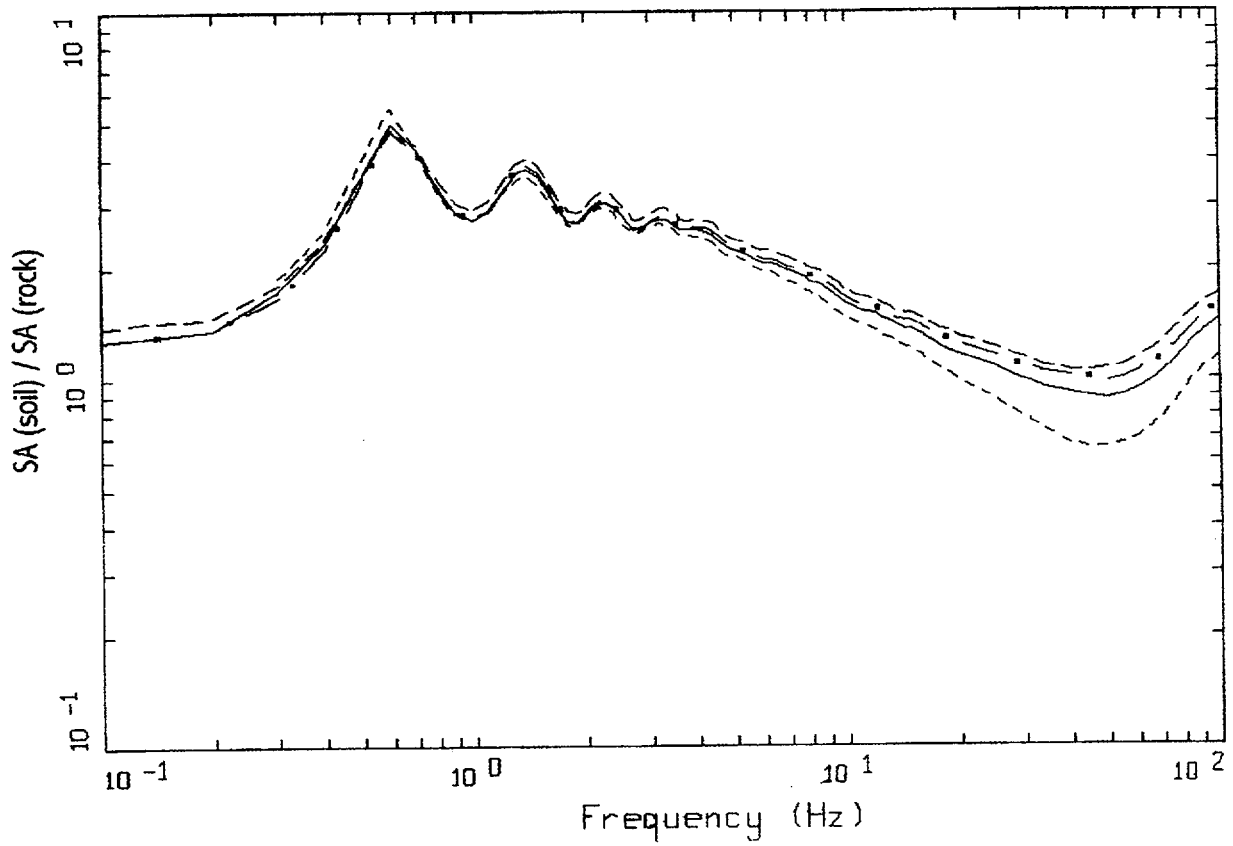


CEUS, 10-4, SR
EFFECTIVE STRAINS (SYZ)

LEGEND

- · — 84TH PERCENTILE
- 50TH PERCENTILE
- 16TH PERCENTILE

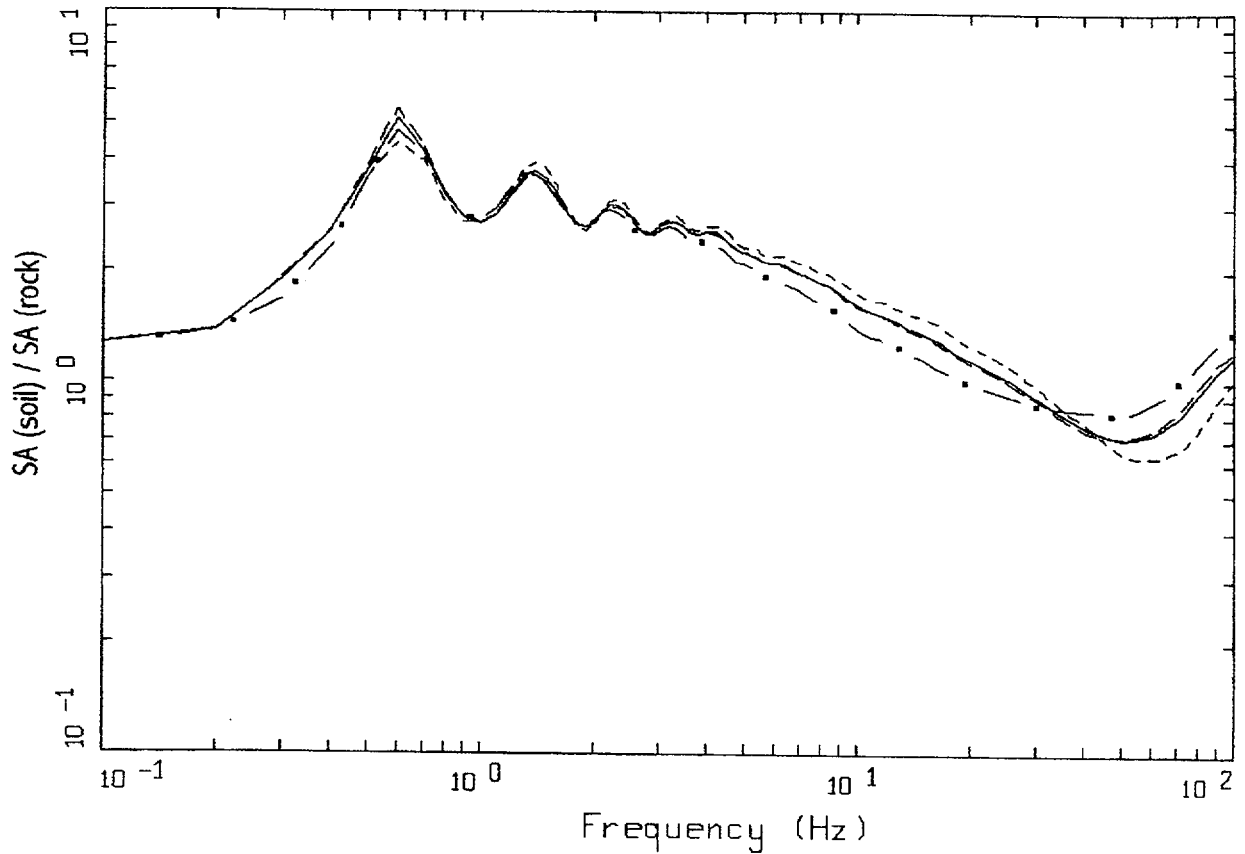
Figure 6-119. Median and $\pm 1\sigma$ effective strains for soil profile Savannah River Generic using Approach 1: CEUS conditions.



CEUS, 10E-4, 1HZ DESIGN, SR
 SURFACE MOTION, 1HZ TRANSFER FUNCTION
 WEIGHTS: ML=0.30, MM=0.00, MH=0.70

- LEGEND
- ML = 5.7, D = 20 KM MEAN RATIO
 - · - · - MM = 7.0, D = 100 KM, DESIGN MEAN RATIO
 - · — MH = 7.6, D = 130 KM MEAN RATIO
 - WEIGHTED MEAN RATIO

Figure 6-120. Comparison of transfer functions computed for the scaled 1 Hz design earthquake; soil profile Savannah River Generic, CEUS conditions.

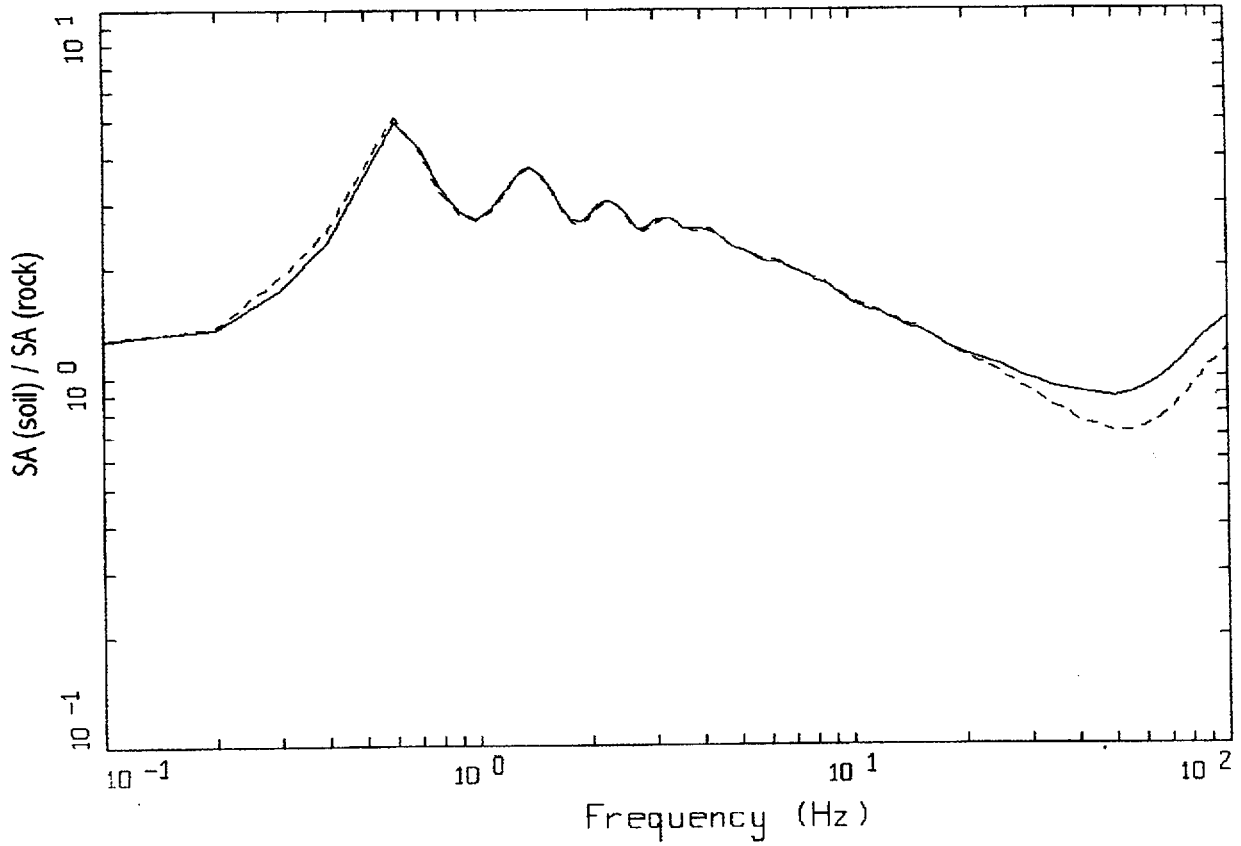


CEUS, 10E-4, 10HZ DESIGN, SR
 SURFACE MOTION, 10HZ TRANSFER FUNCTION
 WEIGHTS: ML=0.25, MM=0.63, MH=0.12

LEGEND

- ML = 4.6, D = 8 KM MEAN RATIO
- · - · - MM = 5.6, D = 8 KM, DESIGN MEAN RATIO
- · — MH = 7.7, D = 130 KM MEAN RATIO
- WEIGHTED MEAN RATIO

Figure 6-121. Comparison of transfer functions computed for the scaled 10 Hz design earthquake; soil profile Savannah River Generic, CEUS conditions.

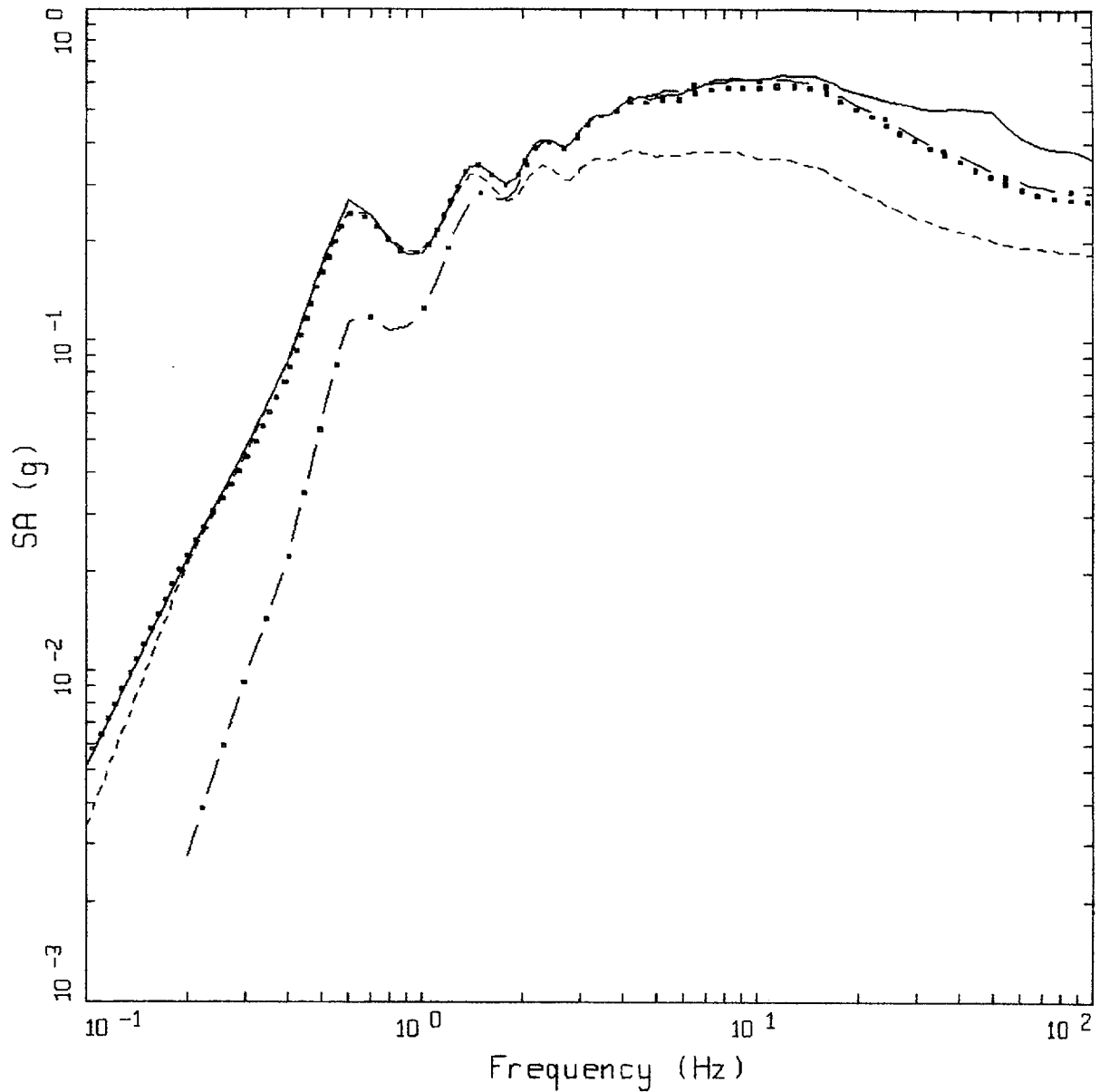


CEUS, 10E-4, SR
TRANSFER FUNCTION

LEGEND

- 1 HZ WEIGHTED MEAN RATIO; WEIGHTS: ML=0.30, MM=0.00, MH=0.70
- 10 HZ WEIGHTED MEAN RATIO; WEIGHTS: ML=0.25, MM=0.63, MH=0.12

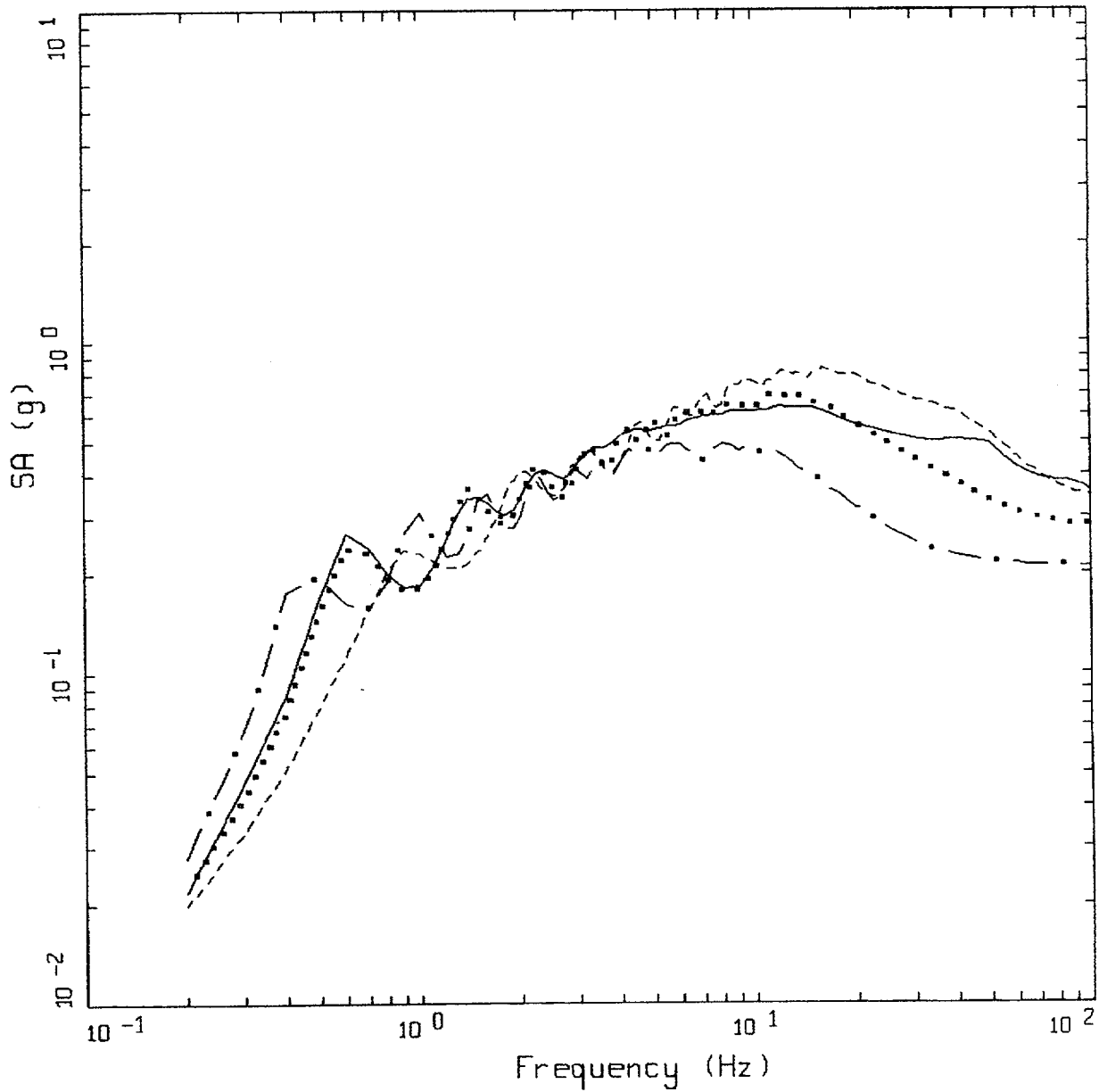
Figure 6-122. Comparison of mean transfer functions computed for the scaled 1 Hz and 10 Hz design earthquakes; soil profile Savannah River Generic, CEUS conditions.



CEUS, 10E-4 DESIGN SPECTRA, SR

- LEGEND
- APPROACH 2, 1 HZ AND 10 HZ DEAGGREGATION EQKS, MEAN PGA = 0.355 G
 - APPROACH 1, 10-4 ROCK CONTROL MOTION, MEAN PGA = 0.265 G
 - - - - 1 HZ MEAN; PGA = 0.185 G
 - . - . 10 HZ MEAN; PGA = 0.280 G

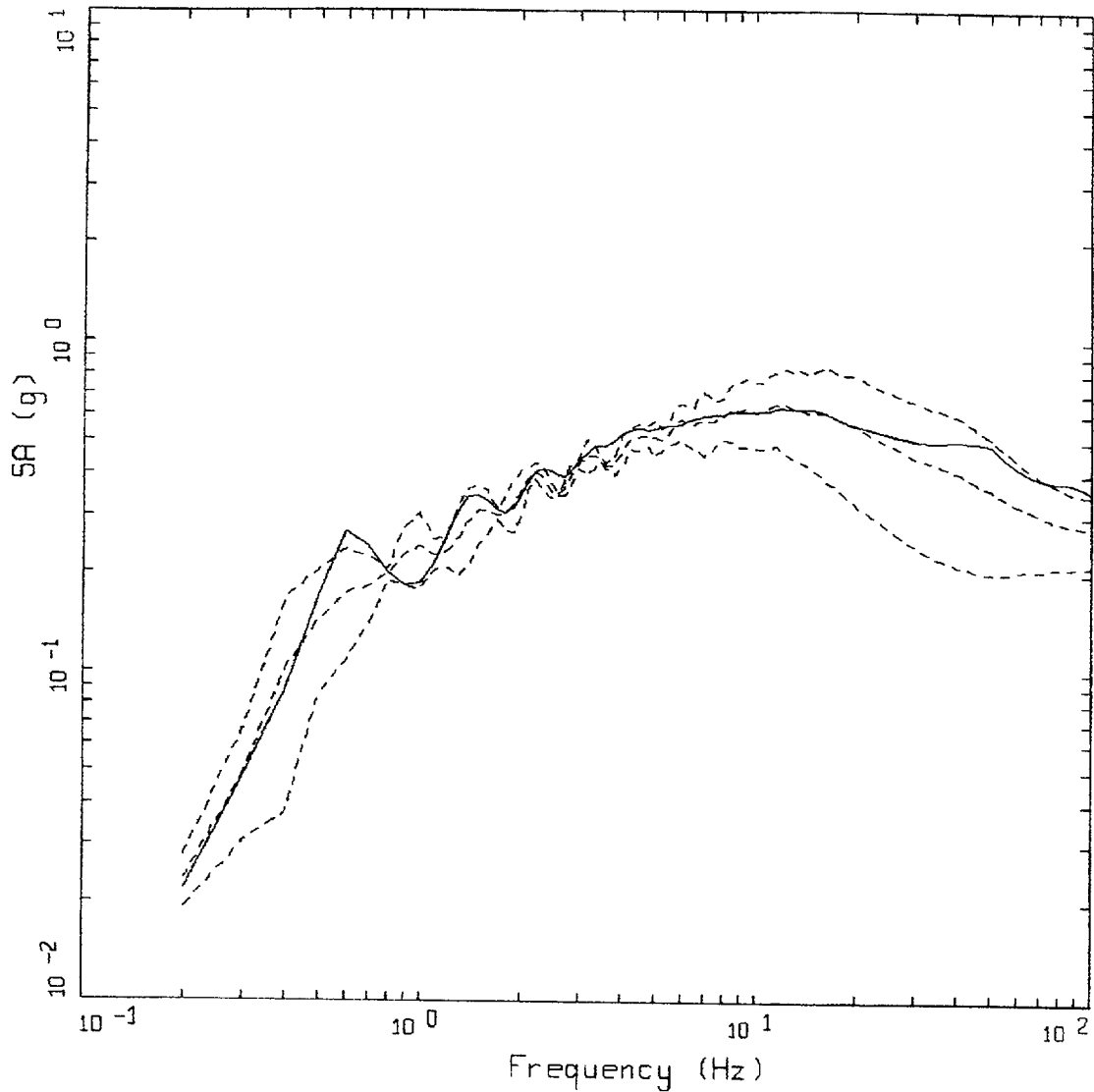
Figure 6-123. Comparison of soil spectra for Approaches 1, 2A, and 2B; soil profile Savannah River Generic, CEUS conditions.



CEUS 10E-4 APPROACH COMPARISON, SR

- LEGEND
- APPROACH 2, 1 HZ AND 10 HZ DEAGGREGATION EQKS, MEAN PGA = 0.355 G
 - APPROACH 1, 10-4 ROCK CONTROL MOTION, BASE CASE PGA = 0.280 G
 - APPROACH 1, 10-4 ROCK CONTROL MOTION, BASE CASE (UPPER) PGA = 0.344 G
 - . - . - APPROACH 1, 10-4 ROCK CONTROL MOTION, BASE CASE (LOWER) PGA = 0.210 G

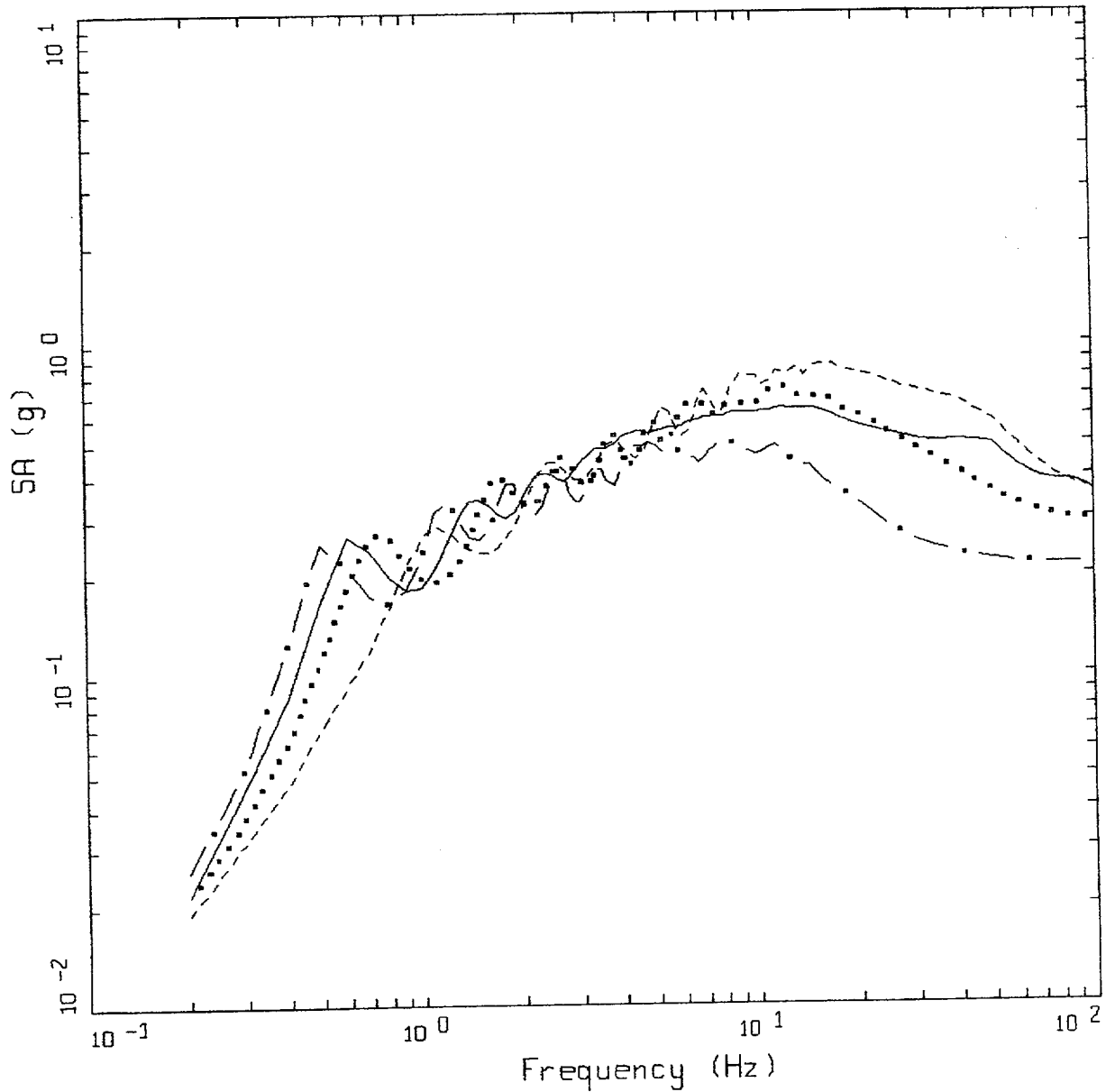
Figure 6-124. Comparison of soil spectra for Approach 2B with base case profile and deterministic profile variations (\pm factor of 2 on shear modulus); soil profile Savannah River Generic, CEUS conditions.



CEUS 10E-4 APPROACH COMPARISON, SR

- LEGEND
- APPROACH 2, 1 HZ AND 10 HZ DEAGGREGATION EQKS, MEAN PGA = 0.355 G
 - APPROACH 1, 10-4 ROCK CONTROL MOTION, BASE CASE, 68TH PERCENTILE, PGA = 0.346 G
 - · - · - APPROACH 1, 10-4 ROCK CONTROL MOTION, BASE CASE, MEAN, PGA = 0.278 G
 - APPROACH 1, 10-4 ROCK CONTROL MOTION, BASE CASE, 32ND PERCENTILE, PGA = 0.211 G

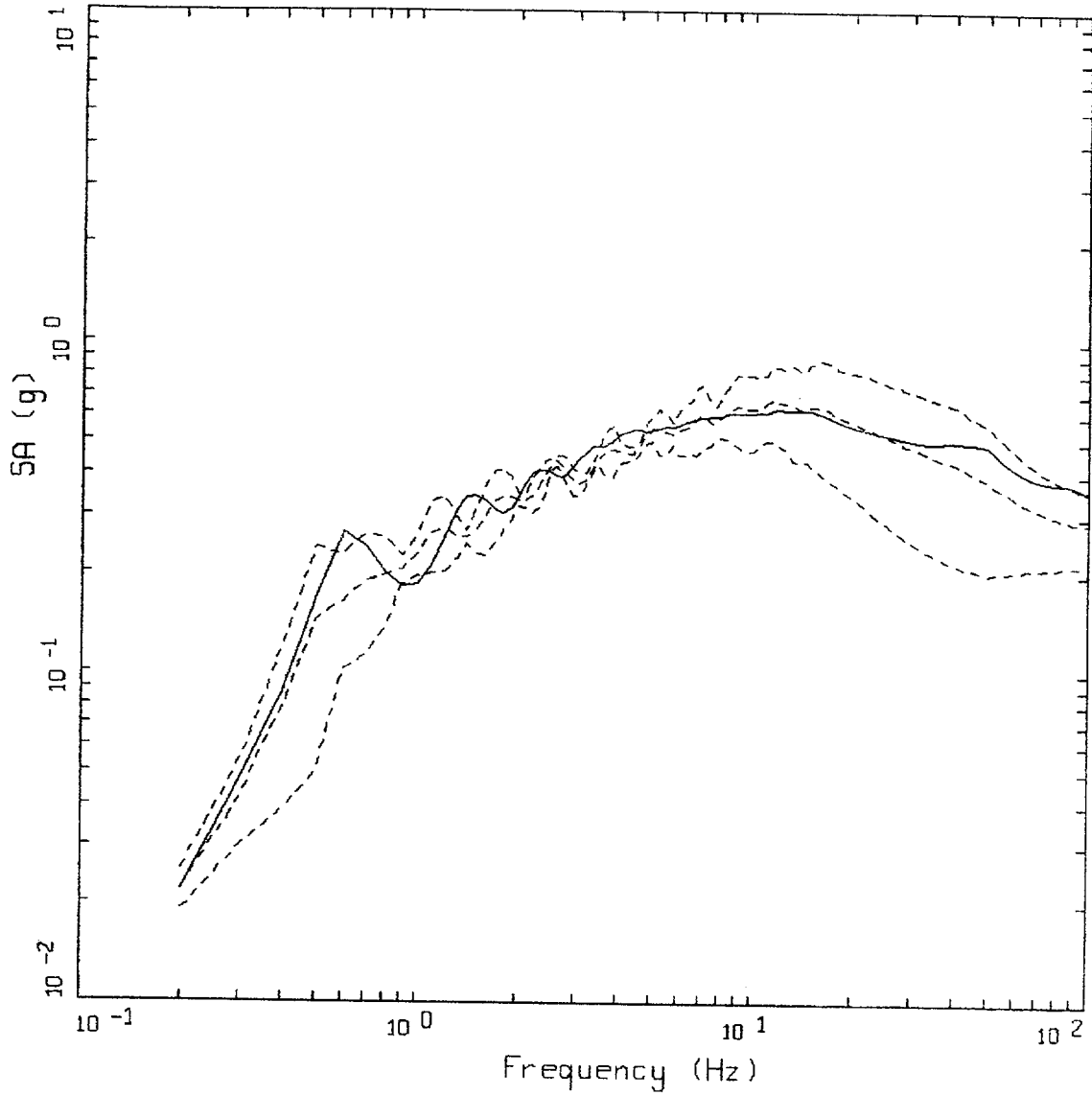
Figure 6-125. Comparison of soil spectra for Approach 2B with mean and $\pm 1\sigma$ variations of base case (\pm factor of 2 on shear modulus), soil profile Savannah River Generic, CEUS conditions.



CEUS 1DE-4 APPROACH COMPARISON, SR
SOIL PROFILE TO 150 M (500 FT)

- LEGEND
- APPROACH 2, 1 HZ AND 10 HZ DEAGGREGATION EQKS, MEAN PGA = 0.355 G
 - APPROACH 1, 10-4 ROCK CONTROL MOTION, BASE CASE PGA = 0.290 G
 - APPROACH 1, 10-4 ROCK CONTROL MOTION, BASE CASE (UPPER) PGA = 0.360 G
 - . - . APPROACH 1, 10-4 ROCK CONTROL MOTION, BASE CASE (LOWER) PGA = 0.213 G

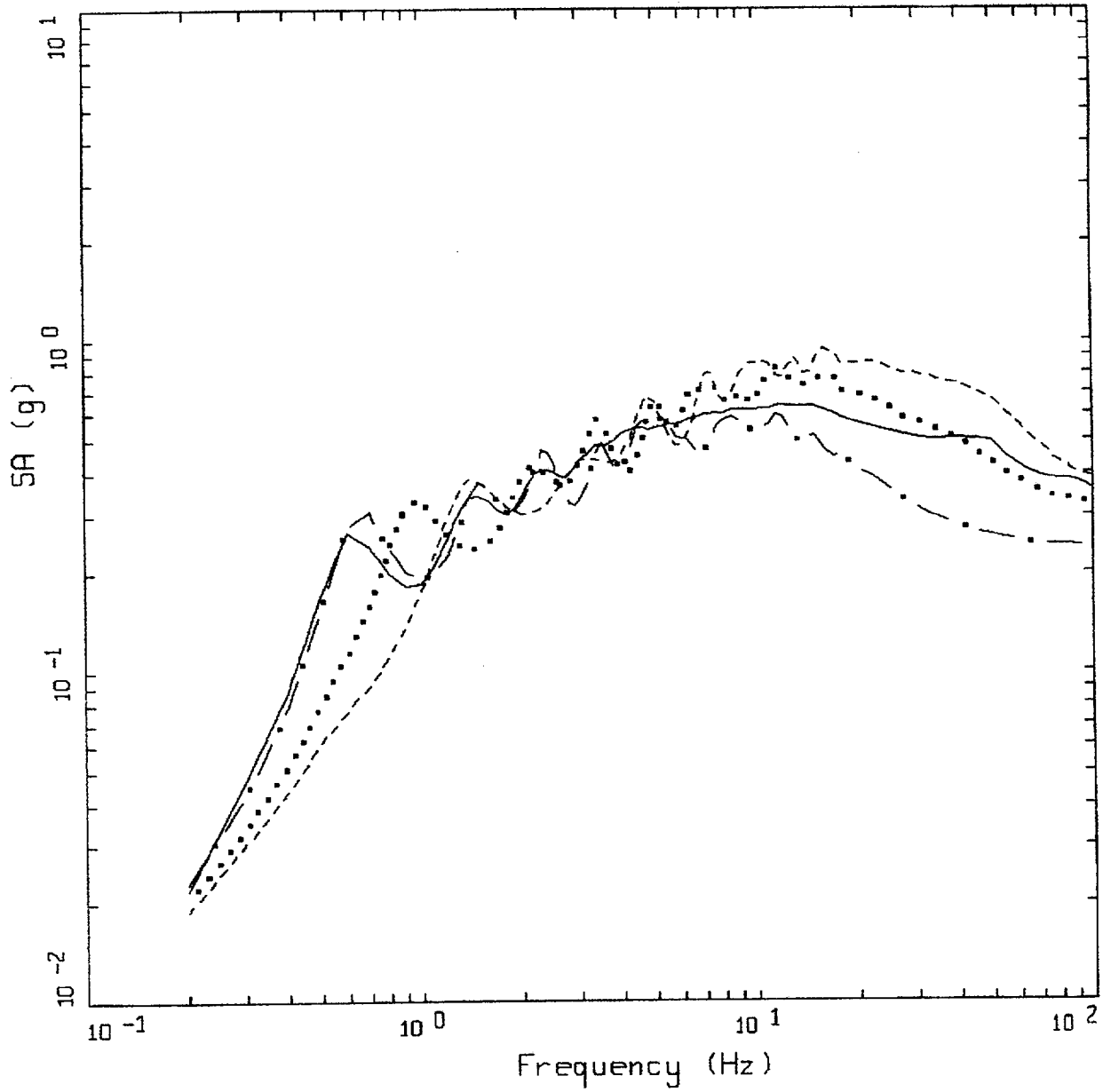
Figure 6-126. Comparison of soil spectra for Approach 2B (full profile) with base case profile and deterministic profile variations (\pm factor of 2 on shear modulus) with profile truncated at 150m; soil profile Savannah River Generic, CEUS conditions.



CEUS 10E-4 APPROACH COMPARISON, SR
SOIL PROFILE TO 150 M (500 FT)

- LEGEND
- APPROACH 2, 1 HZ AND 10 HZ DEAGGREGATION EQKS, MEAN PGA = 0.355 G
 - - - APPROACH 1, 10-4 ROCK CONTROL MOTION, BASE CASE, 68TH PERCENTILE, PGA = 0.361 G
 - · - APPROACH 1, 10-4 ROCK CONTROL MOTION, BASE CASE, MEAN, PGA = 0.288 G
 - · - APPROACH 1, 10-4 ROCK CONTROL MOTION, BASE CASE, 32ND PERCENTILE, PGA = 0.214 G

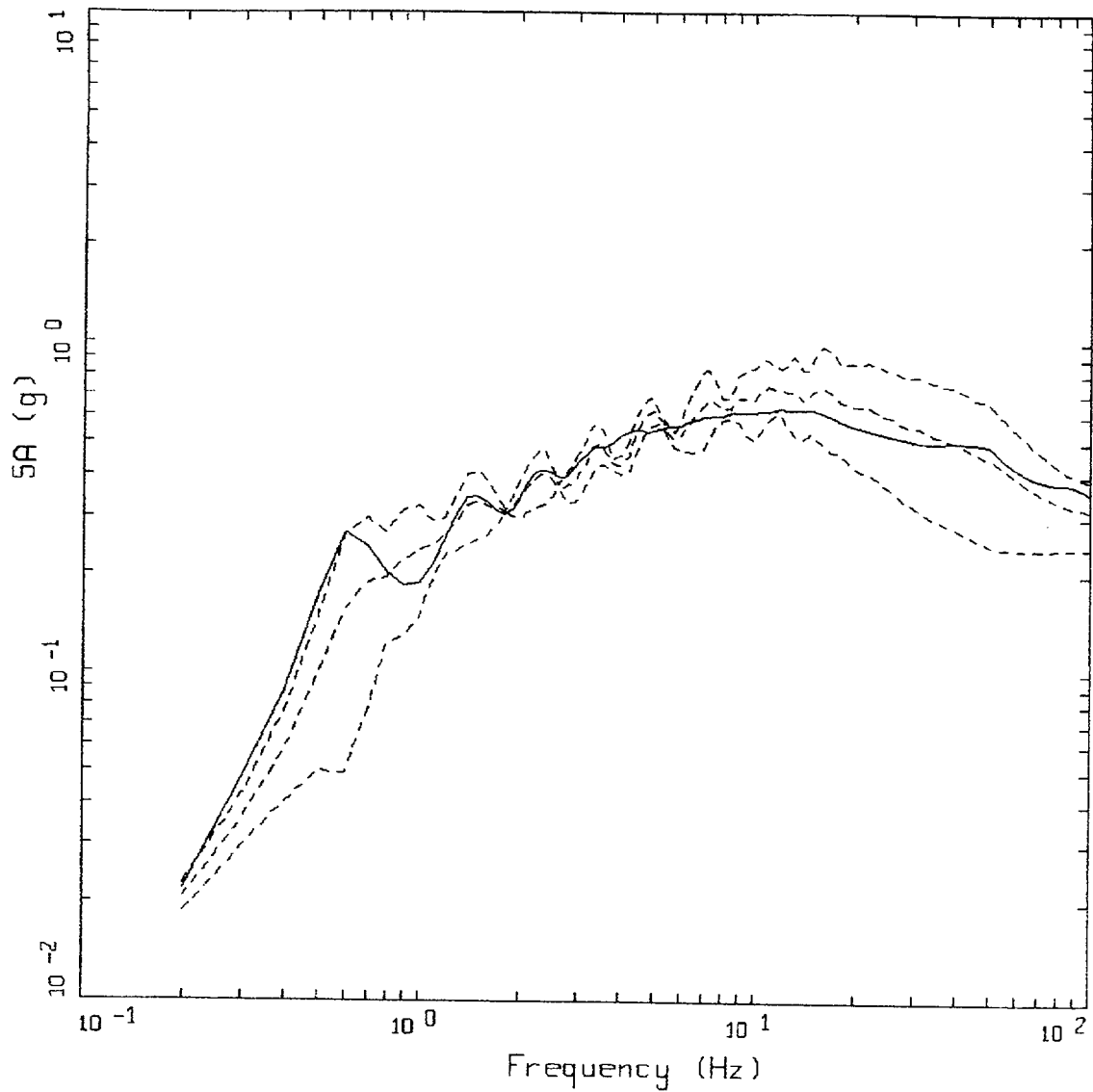
Figure 6-127. Comparison of soil spectra for Approach 2B (full profile) with mean and $\pm 1\sigma$ profile variations with profile truncated at 150m. Soil profile Savannah River Generic; CEUS conditions.



CEUS 10E-4 APPROACH COMPARISON, SR
SOIL PROFILE TO 90 M (300 FT)

- LEGEND
- APPROACH 2, 1 HZ AND 10 HZ DEAGGREGATION EQKS, MEAN PGA = 0.355 G
 - APPROACH 1, 10-4 ROCK CONTROL MOTION, BASE CASE PGA = 0.321 G
 - APPROACH 1, 10-4 ROCK CONTROL MOTION, BASE CASE (UPPER) PGA = 0.388 G
 - . - . - APPROACH 1, 10-4 ROCK CONTROL MOTION, BASE CASE (LOWER) PGA = 0.240 G

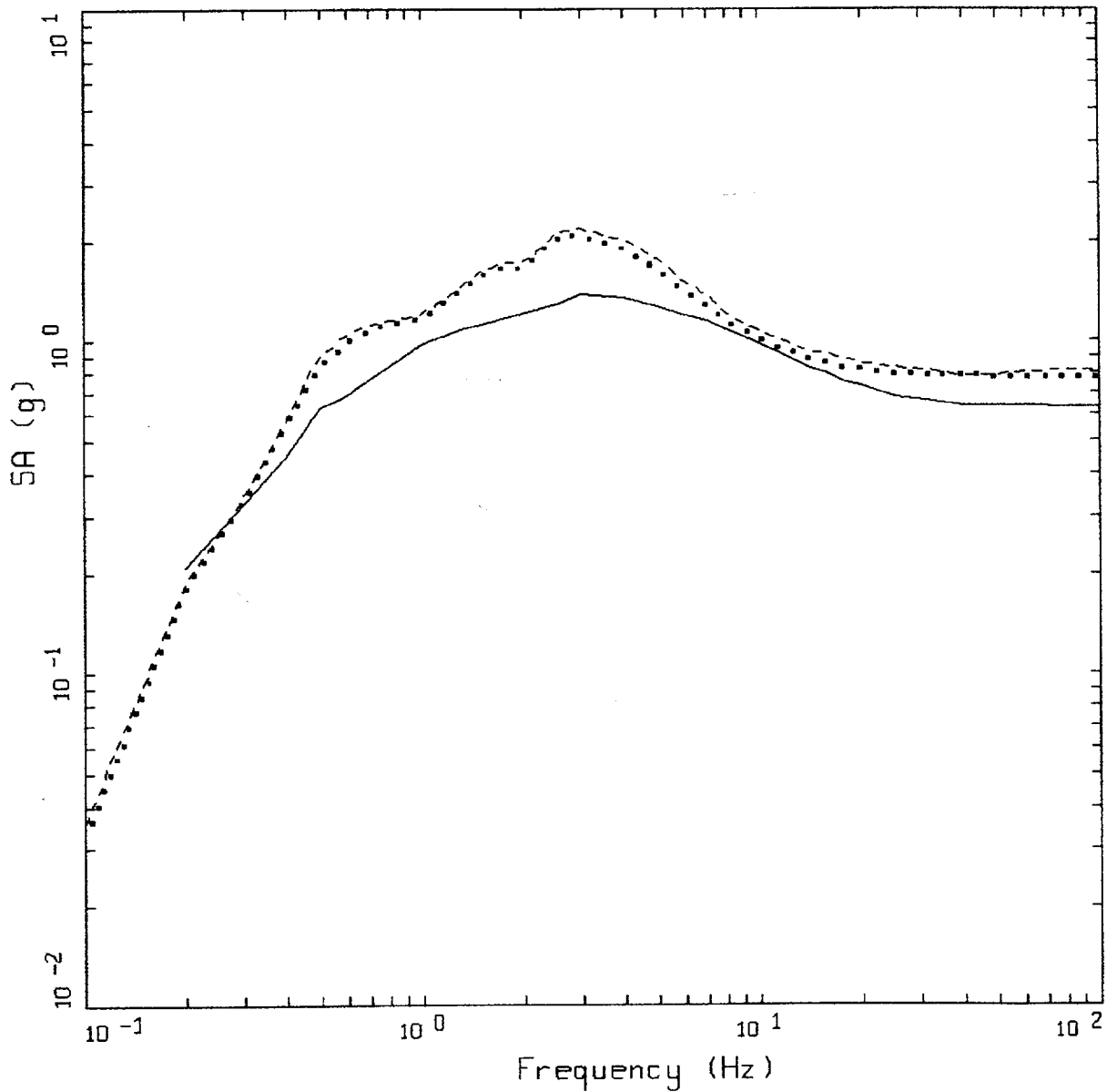
Figure 6-128. Comparison of soil spectra for Approach 2B (full profile) with base case profile and deterministic profile variations (\pm factor of 2 on shear modulus) with profile truncated at 90m; soil profile Savannah River Generic, CEUS conditions.



CEUS 10E-4 APPROACH COMPARISON, SR
SOIL PROFILE TO 90 M (300 FT)

- LEGEND
- APPROACH 2, 1 HZ AND 10 HZ DEAGGREGATION EQKS, MEAN PGA = 0.355 G
 - - - APPROACH 1, 10-4 ROCK CONTROL MOTION, BASE CASE, 68TH PERCENTILE, PGA = 0.390 G
 - - - APPROACH 1, 10-4 ROCK CONTROL MOTION, BASE CASE, MEAN, PGA = 0.316 G
 - . - APPROACH 1, 10-4 ROCK CONTROL MOTION, BASE CASE, 32ND PERCENTILE, PGA = 0.242 G

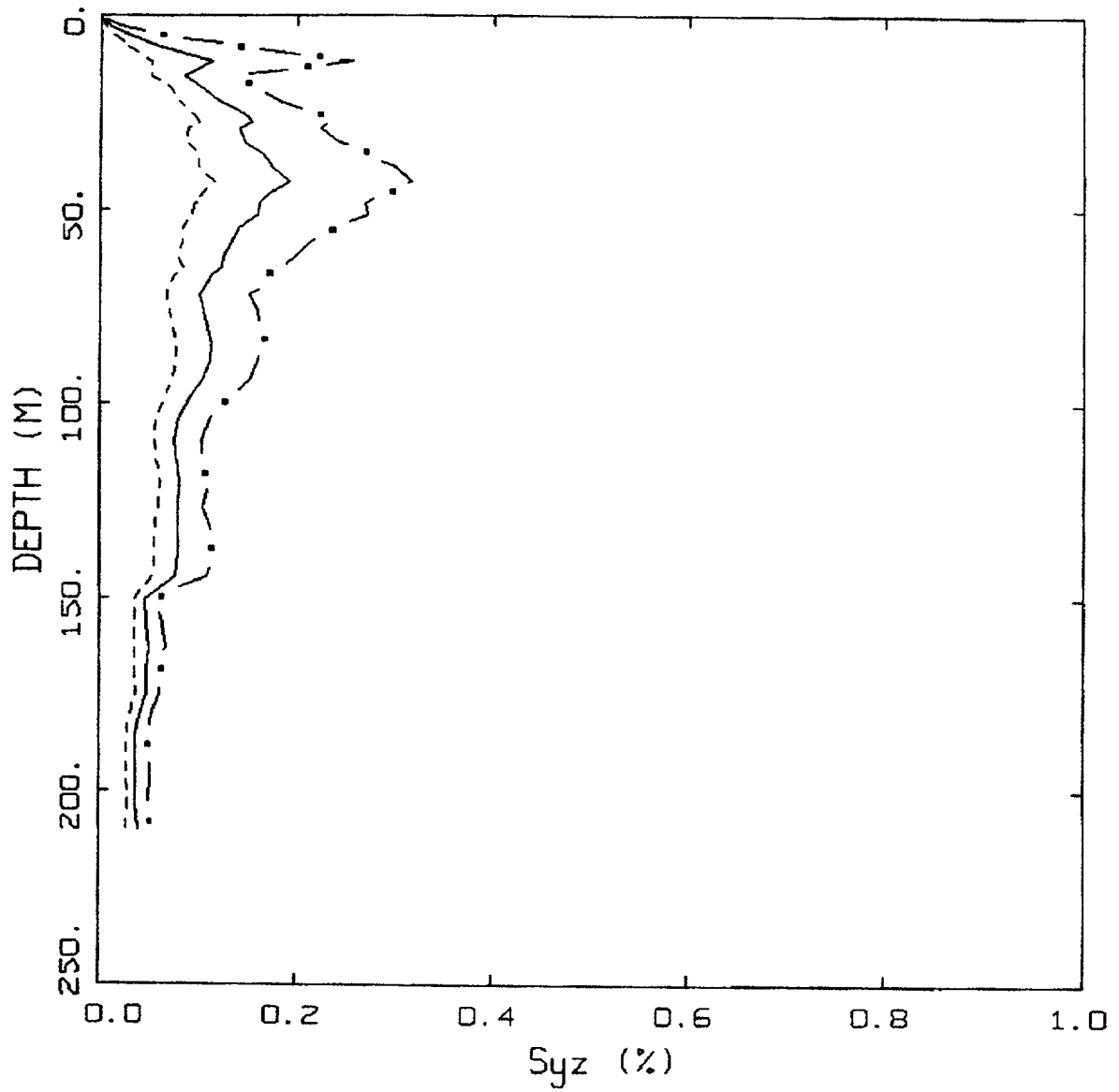
Figure 6-129. Comparison of soil spectra for Approach 2B (full profile) with mean and $\pm 1\sigma$ profile variations with profile truncated at 90m. Soil profile Savannah River Generic, CEUS conditions.



WUS $10E-4$ APPROACH COMPARISON, SR

- LEGEND
- APPROACH 4, 10^{-4} SOIL UNIFORM HAZARD SPECTRUM, PGA = 0.811 G
 - APPROACH 1, 10^{-4} ROCK CONTROL MOTION, MEAN PGA = 0.777 G
 - - - - APPROACH 2, 1 HZ AND 10 HZ DEAGGREGATION EQKS, MEAN PGA = 0.560 G

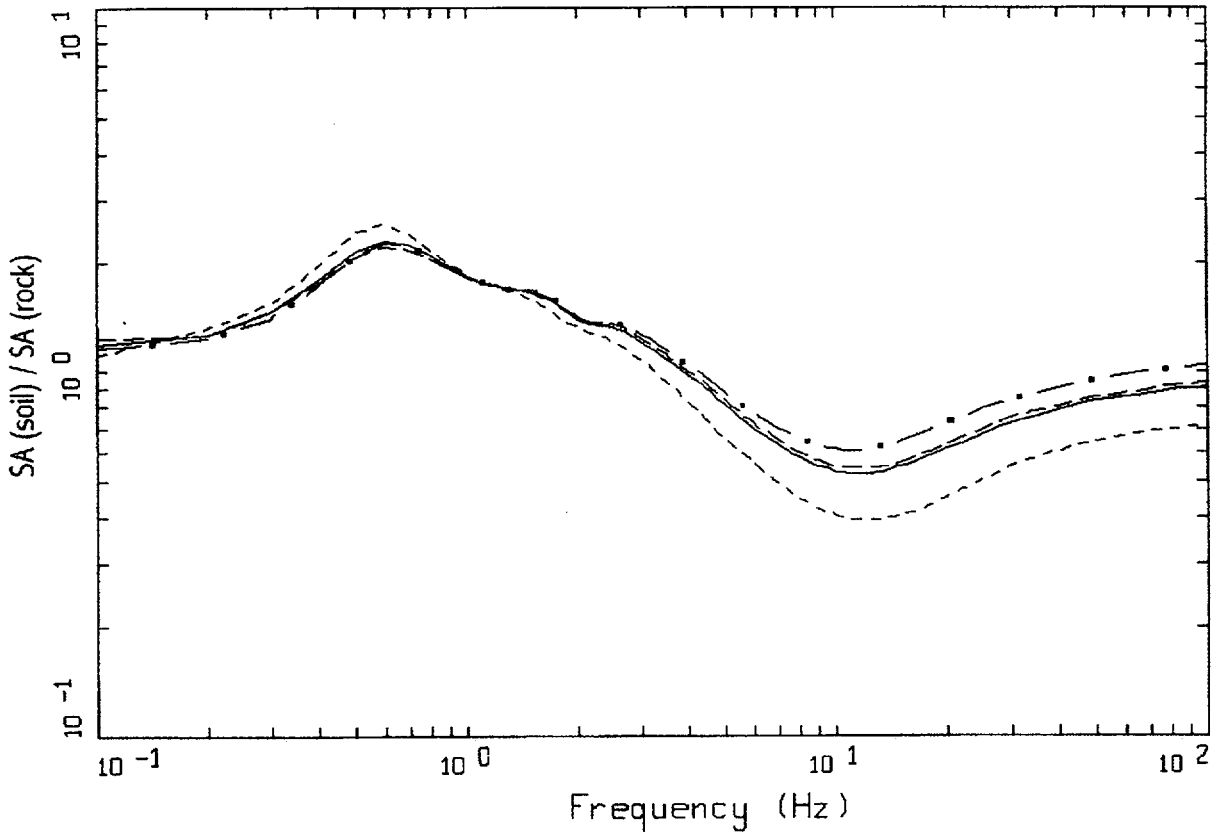
Figure 6-130. Comparison of Approaches 1, 2B, and 4 soil spectra for profile Savannah River Generic: WUS conditions.



WUS, 10⁻⁴, SR
EFFECTIVE STRAINS (SYZ)

LEGEND
 - . - 84TH PERCENTILE
 — 50TH PERCENTILE
 - - - 16TH PERCENTILE

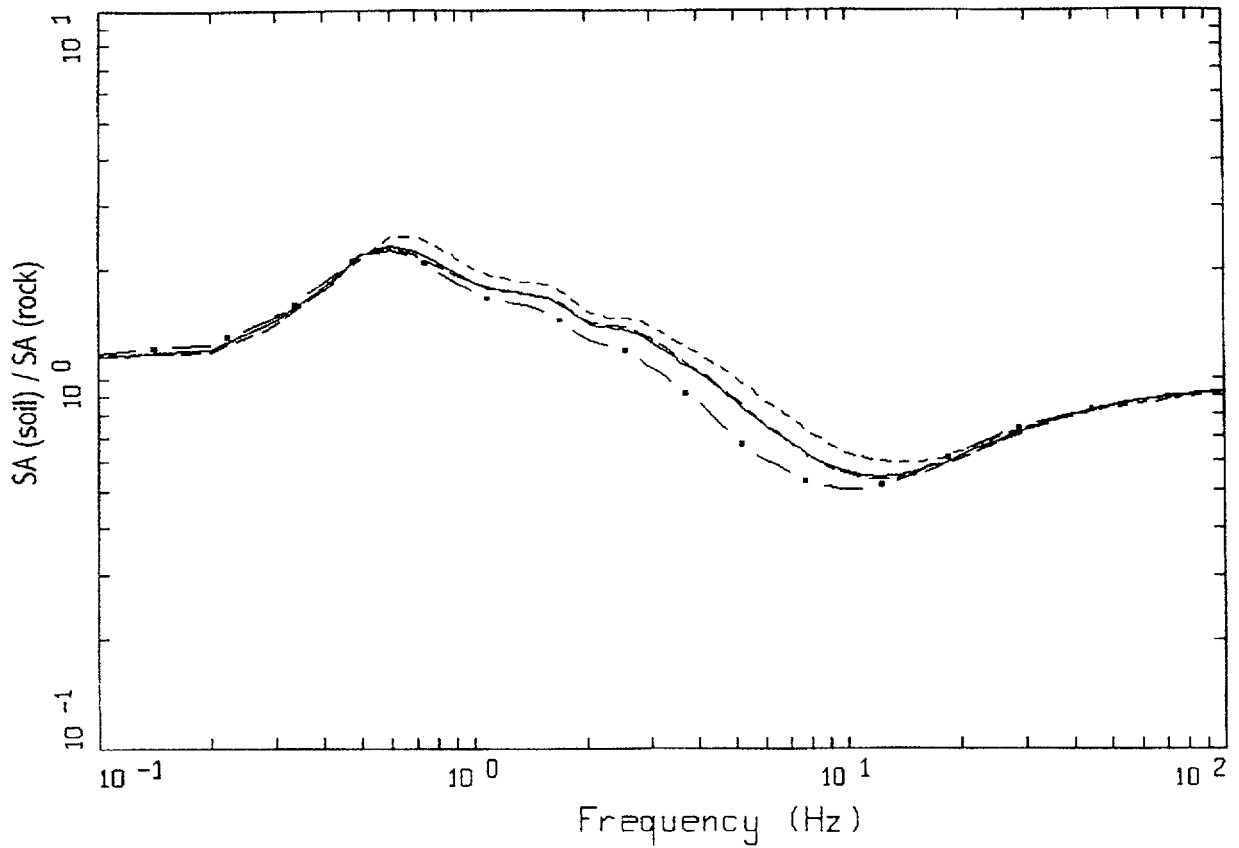
Figure 6-131. Median and $\pm 1\sigma$ effective strains for soil profile Savannah River Generic using Approach 1: WUS conditions.



WUS, 10E-4, 1HZ DESIGN, SR
 SURFACE MOTION, 1HZ TRANSFER FUNCTION
 WEIGHTS: ML=0.20, MM=0.60, MH=0.20

- LEGEND
- ML = 5.4, D = 10 KM MEAN RATIO
 - · - · - MM = 6.7, D = 18 KM, DESIGN MEAN RATIO
 - · — MH = 7.8, D = 30 KM MEAN RATIO
 - WEIGHTED MEAN RATIO

Figure 6-132. Comparison of transfer functions computed for the scaled 1 Hz design earthquake; soil profile Savannah River Generic, WUS conditions.

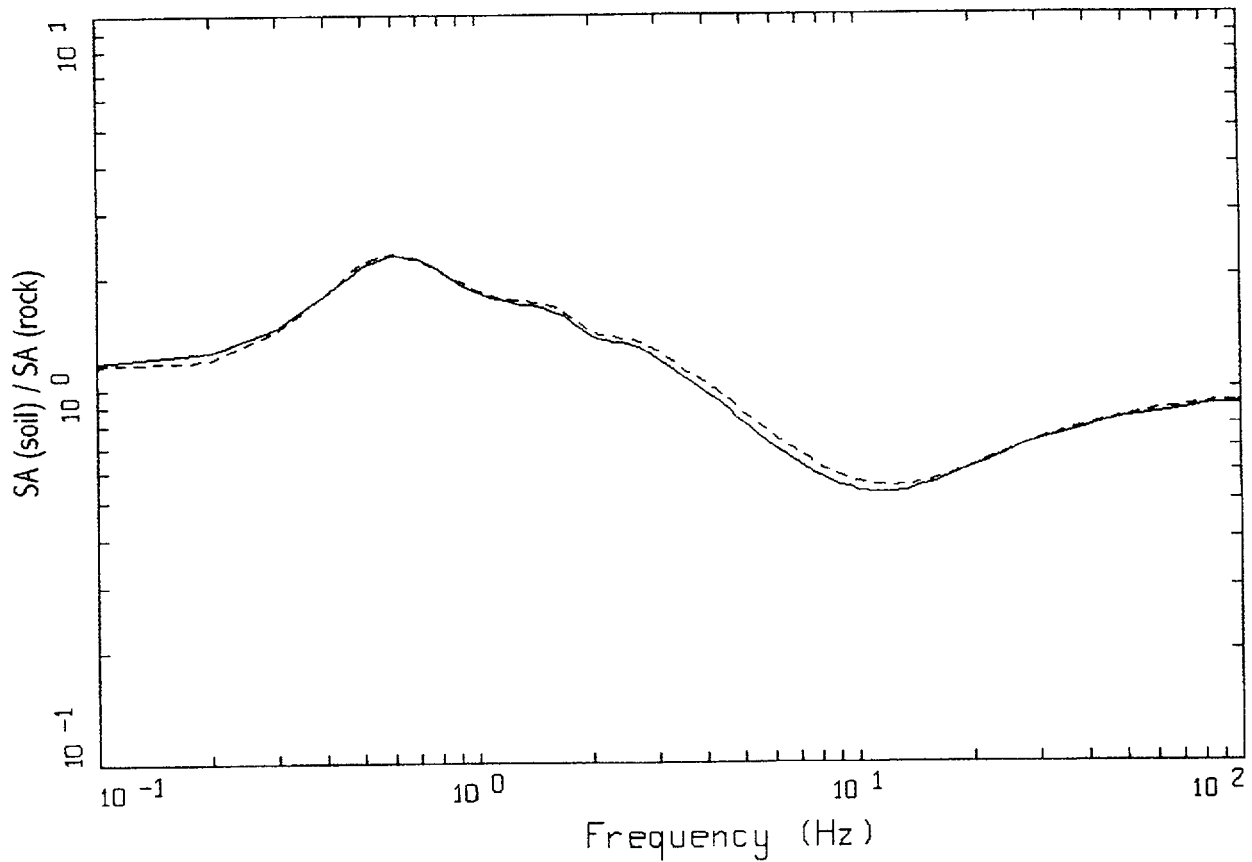


WUS, 10E-4, 10HZ DESIGN, SR
 SURFACE MOTION, 10HZ TRANSFER FUNCTION
 WEIGHTS: ML=0.20, MM=0.60, MH=0.20

LEGEND

- ML = 5.1, D = 10 KM MEAN RATIO
- . - . - . MM = 6.1, D = 14 KM, DESIGN MEAN RATIO
- • — MH = 7.8, D = 30 KM MEAN RATIO
- WEIGHTED MEAN RATIO

Figure 6-133. Comparison of transfer functions computed for the scaled 10 Hz design earthquake; soil profile Savannah River Generic, WUS conditions.

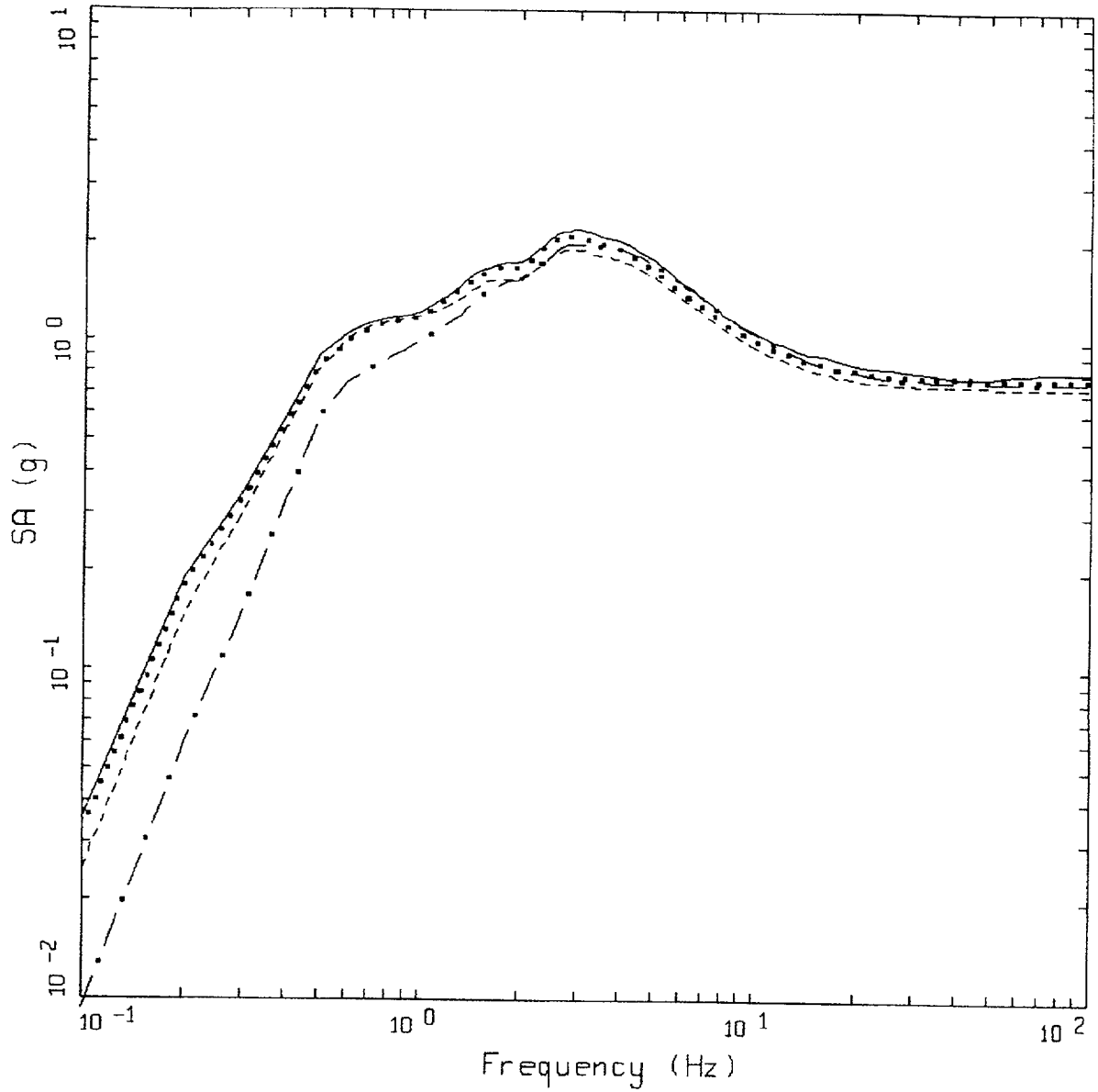


WUS, 10E-4, SR
AMPLIFICATION

LEGEND

- 1 HZ WEIGHTED MEAN RATIO; WEIGHTS:ML=0.20,MM=0.60,MH=0.20
- - - 10 HZ WEIGHTED MEAN RATIO; WEIGHTS:ML=0.20,MM=0.60,MH=0.20

Figure 6-134. Comparison of mean transfer functions computed for the scaled 1 Hz and 10 Hz design earthquakes; soil profile Savannah River Generic, WUS conditions.

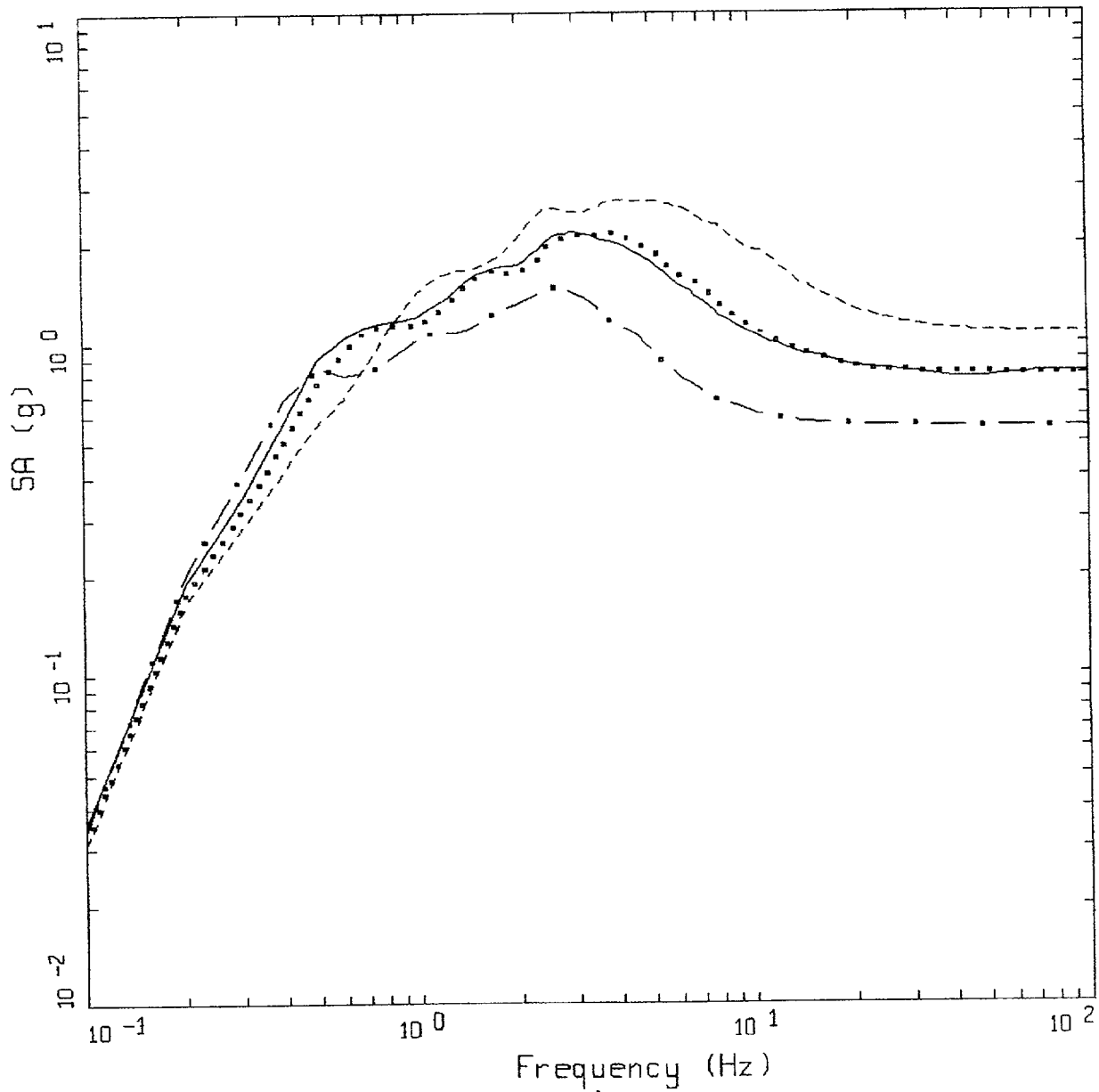


WUS, 10E-4 DESIGN SPECTRA, SR

LEGEND

- APPROACH 2, 1 HZ AND 10 HZ DEAGGREGATION EQKS, MEAN PGA = 0.811 G
- APPROACH 1, 10-4 ROCK CONTROL MOTION, MEAN PGA = 0.777 G
- - - - 1 HZ MEAN; PGA = 0.734 G
- . - . 10 HZ MEAN; PGA = 0.759 G

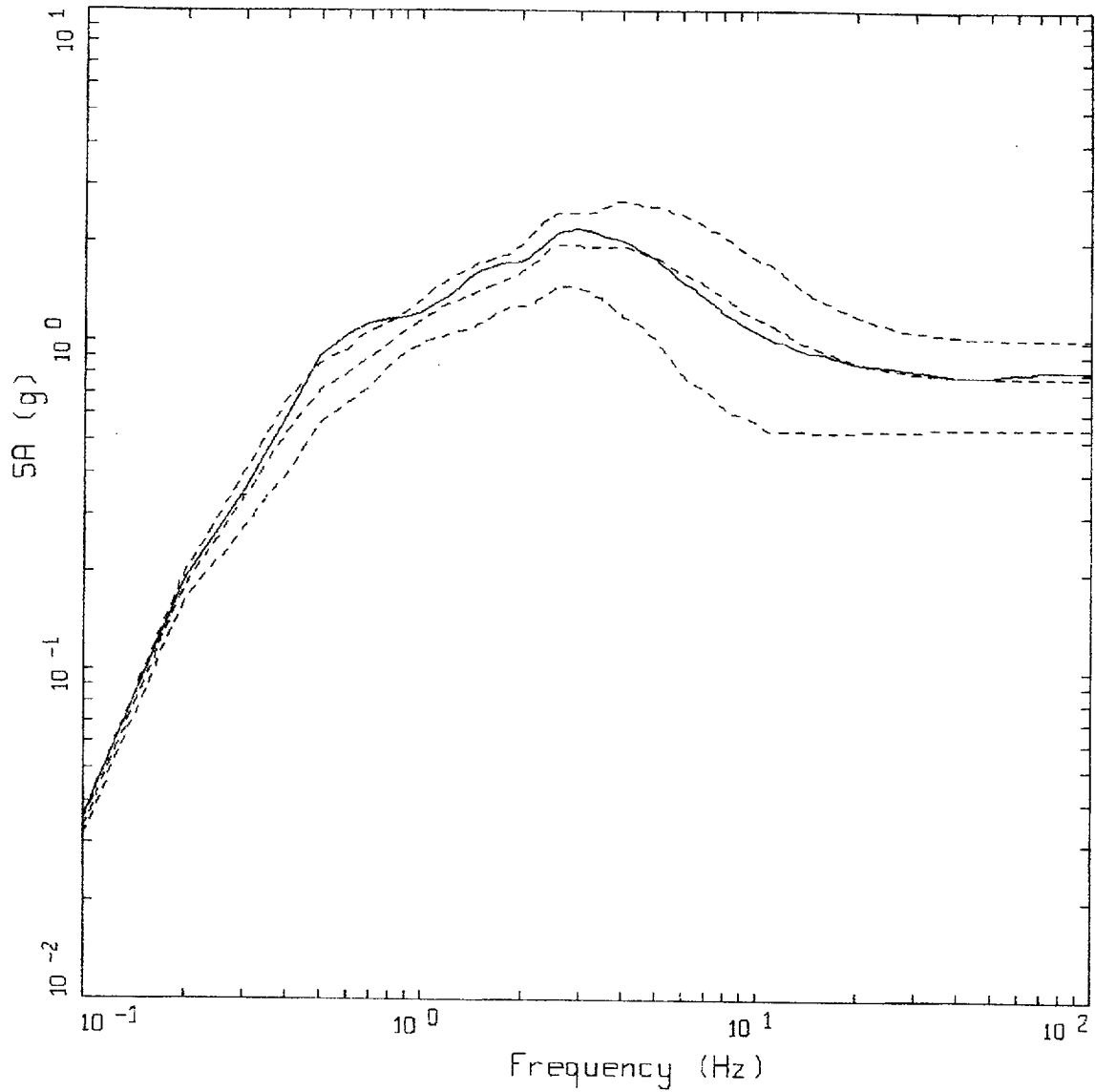
Figure 6-135. Comparison of soil spectra for Approaches 1, 2A, and 2B; soil profile Savannah River Generic, WUS conditions.



WUS 10E-4 APPROACH COMPARISON, SR

- LEGEND
- APPROACH 2, 1 HZ AND 10 HZ DEAGGREGATION EQKS, MEAN PGA = 0.811 G
 - APPROACH 1, 10-4 ROCK CONTROL MOTION, BASE CASE PGA = 0.805 G
 - APPROACH 1, 10-4 ROCK CONTROL MOTION, BASE CASE (UPPER) PGA = 1.070 G
 - . - . APPROACH 1, 10-4 ROCK CONTROL MOTION, BASE CASE (LOWER) PGA = 0.556 G

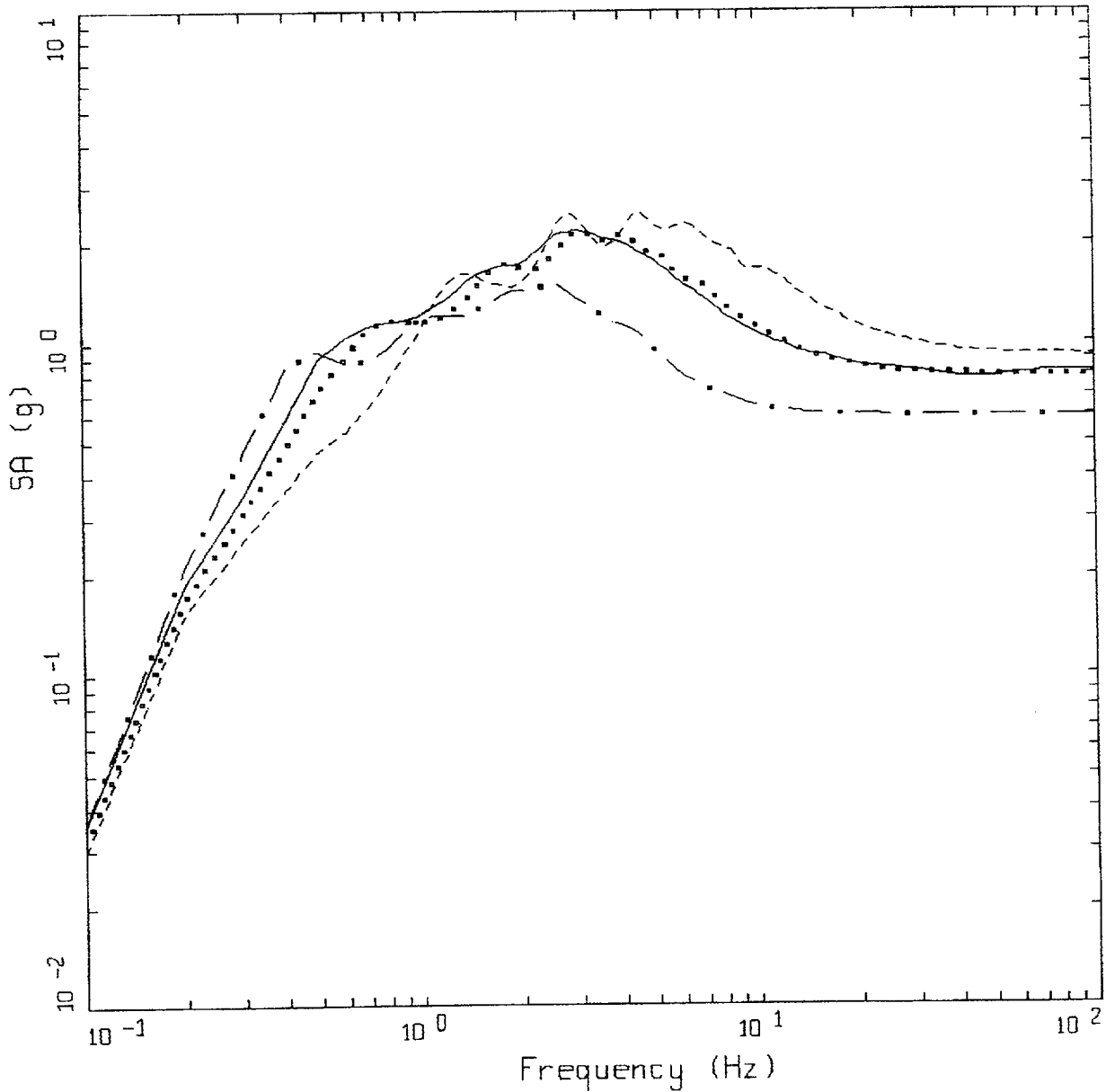
Figure 6-136. Comparison of soil spectra for Approach 2B with base case profile and deterministic profile variations (\pm factor of 2 on shear modulus); soil profile Savannah River Generic, WUS conditions.



WUS 10E-4 APPROACH COMPARISON, SR

- LEGEND
- APPROACH 2, 1 HZ AND 10 HZ DEAGGREGATION EQKS, MEAN PGA = 0.811 G
 - APPROACH 1, 10-4 ROCK CONTROL MOTION, BASE CASE, 84TH PERCENTILE, PGA = 1.006 G
 - - - - - APPROACH 1, 10-4 ROCK CONTROL MOTION, BASE CASE, MEAN, PGA = 0.774 G
 - · - · - APPROACH 1, 10-4 ROCK CONTROL MOTION, BASE CASE, 16TH PERCENTILE, PGA = 0.542 G

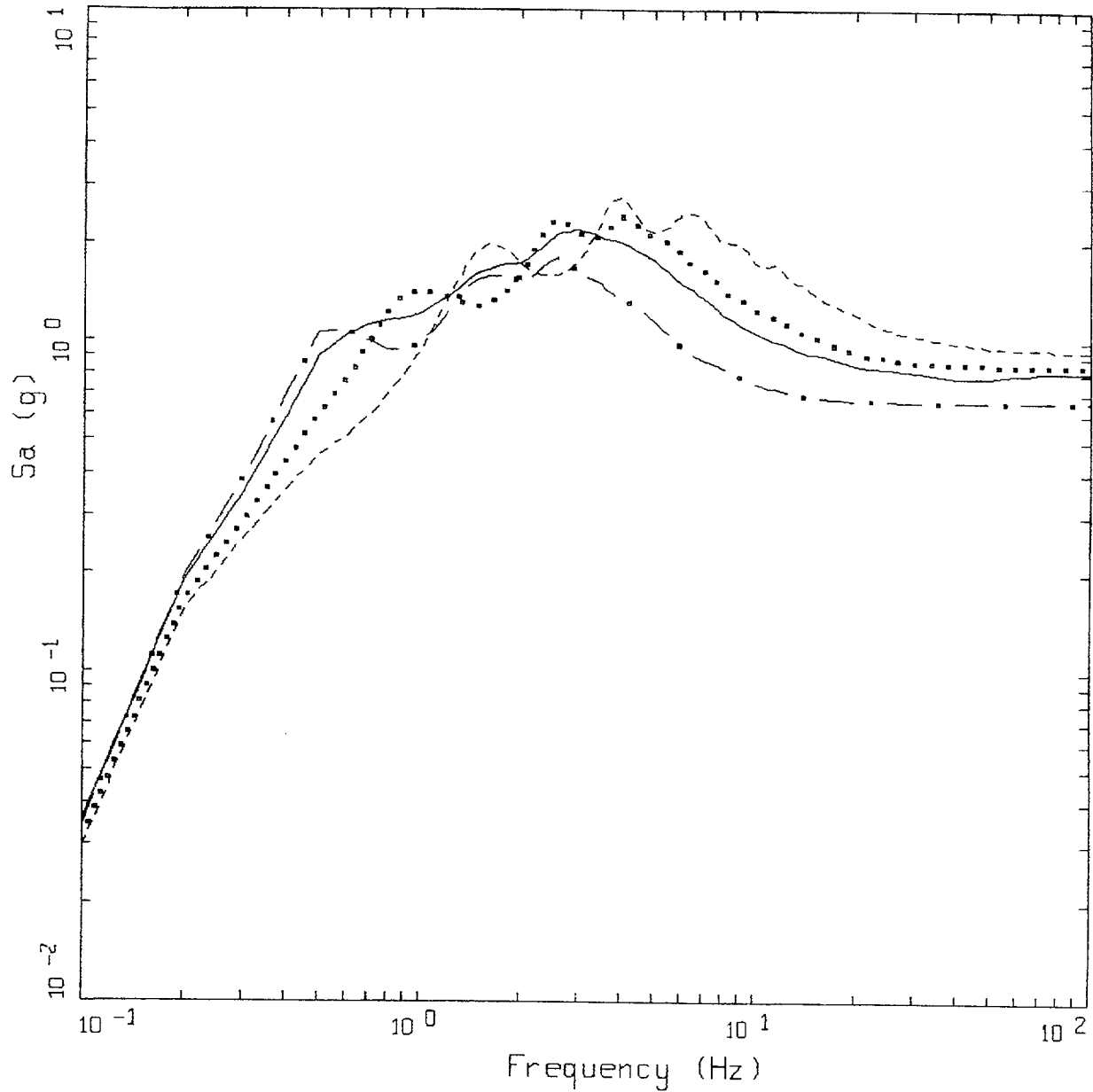
Figure 6-137. Comparison of soil spectra for Approach 2B with mean and $\pm 1\sigma$ variations of base case (\pm factor of 2 on shear modulus), soil profile Savannah River Generic, WUS conditions.



WUS 10E-4 APPROACH COMPARISON, SR
SOIL PROFILE TO 150 M (500 FT)

- LEGEND
- APPROACH 2, 1 HZ AND 10 HZ DEAGGREGATION EQKS, MEAN PGA = 0.811 G
 - APPROACH 1, 10-4 ROCK CONTROL MOTION, BASE CASE PGA = 0.793 G
 - APPROACH 1, 10-4 ROCK CONTROL MOTION, BASE CASE (UPPER) PGA = 0.916 G
 - . - . APPROACH 1, 10-4 ROCK CONTROL MOTION, BASE CASE (LOWER) PGA = 0.595 G

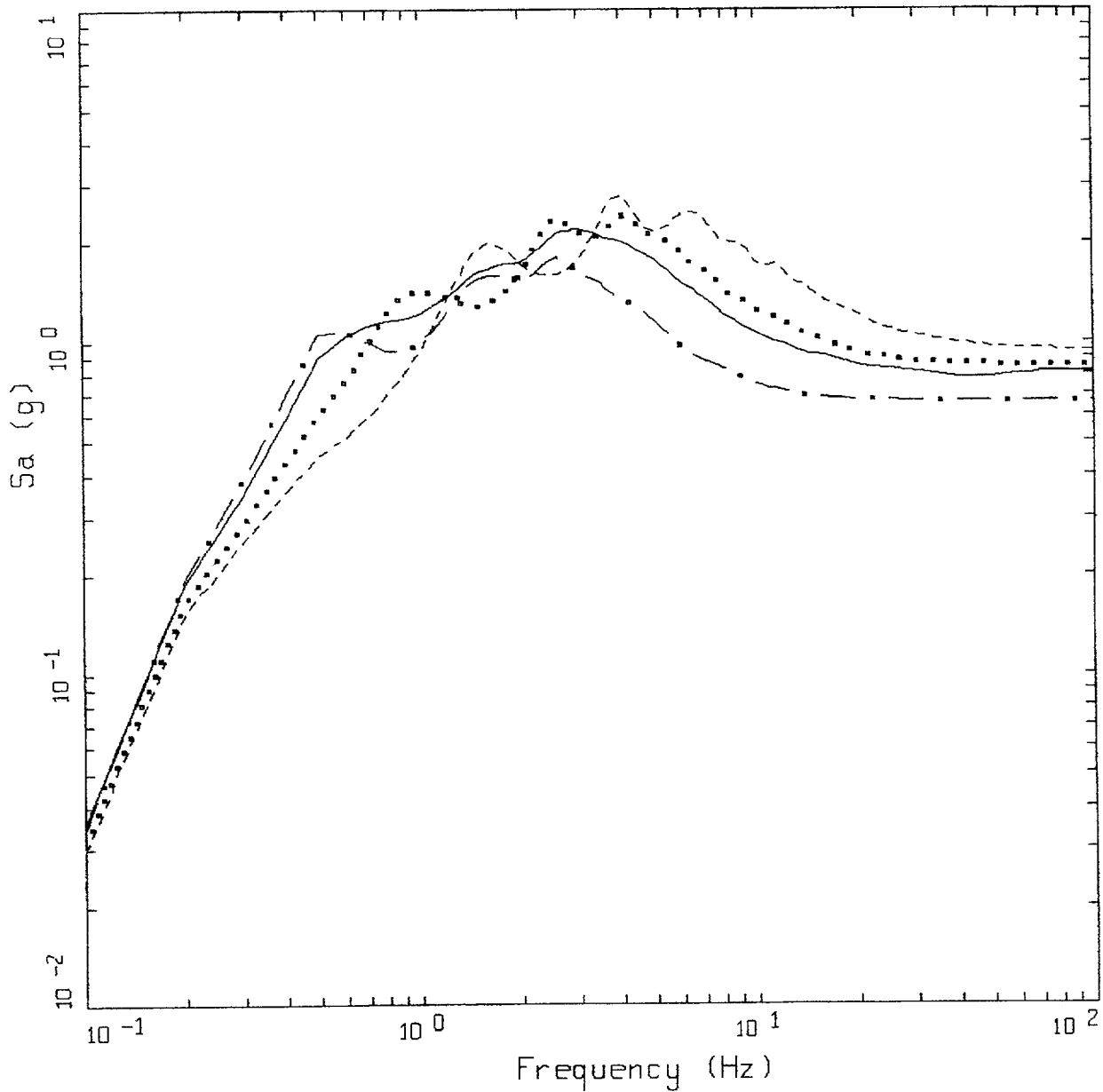
Figure 6-138. Comparison of soil spectra for Approach 2b (full profile) with base case profile and deterministic profile variations (\pm factor of 2 on shear modulus) with profile truncated at 150m; soil profile Savannah River Generic, WUS conditions.



WUS 10E-4 APPROACH COMPARISON, SR
 SOIL PROFILE TO 90 M (300 FT)

- LEGEND
- APPROACH 2, 1 HZ AND 10 HZ DEAGGREGATION EQKS, MEAN PGA = 0.811 G
 - APPROACH 1, 10-4 ROCK CONTROL MOTION, BASE CASE PGA = 0.851 G
 - APPROACH 1, 10-4 ROCK CONTROL MOTION, BASE CASE (UPPER) PGA = 0.946 G
 - . - . - APPROACH 1, 10-4 ROCK CONTROL MOTION, BASE CASE (LOWER) PGA = 0.659 G

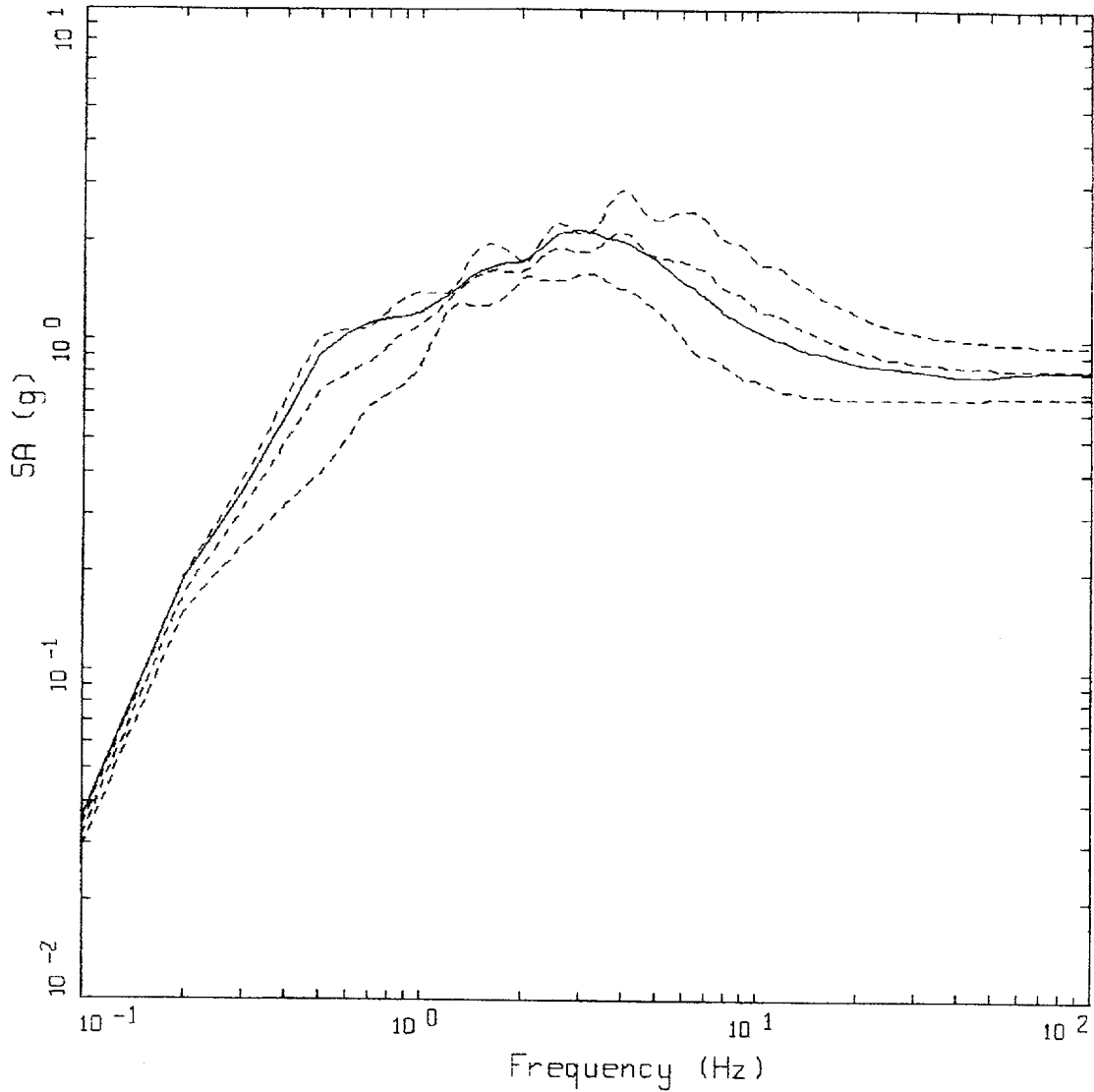
Figure 6-139. Comparison of soil spectra for Approach 2B (full profile) with mean and $\pm 1\sigma$ profile variation with profile truncated at 150m. Soil profile Savannah River Generic, WUS conditions.



WUS 10E-4 APPROACH COMPARISON, SR
SOIL PROFILE TO 90 M (300 FT)

- LEGEND
- APPROACH 2, 1 HZ AND 10 HZ DISAGGREGATION EQKS, MEAN PGA = 0.811 G
 - APPROACH 1, 10-4 ROCK CONTROL MOTION, BASE CASE PGA = 0.851 G
 - APPROACH 1, 10-4 ROCK CONTROL MOTION, BASE CASE (UPPER) PGA = 0.946 G
 - . - - APPROACH 1, 10-4 ROCK CONTROL MOTION, BASE CASE (LOWER) PGA = 0.659 G

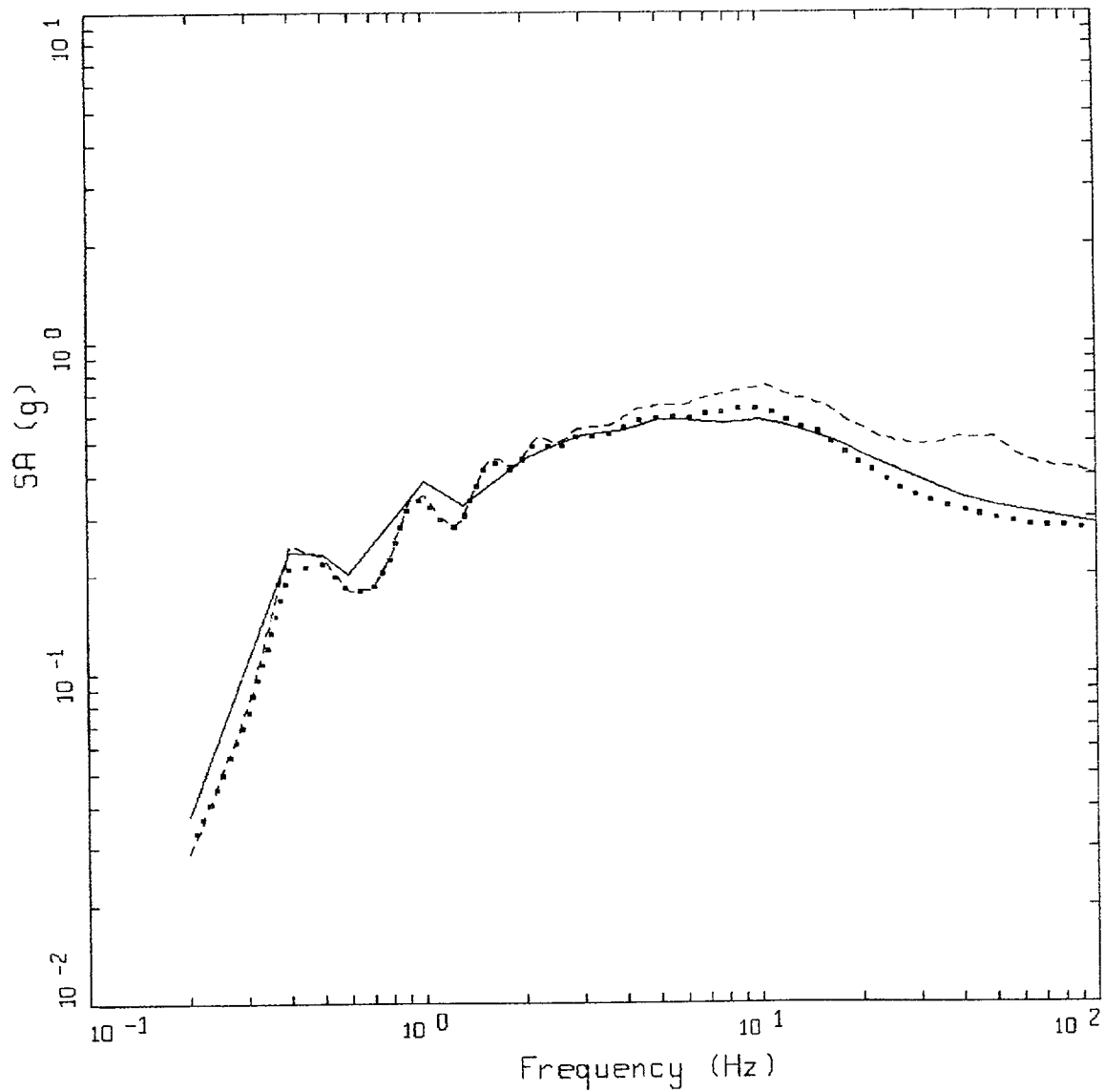
Figure 6-140. Comparison of soil spectra for Approach 2B (full profile) with base case profile and deterministic profile variations (\pm factor of 2 on shear modulus) with profile truncated at 90m; soil profile Savannah River Generic, WUS conditions.



WUS 10E-4 APPROACH COMPARISON, SR
SOIL PROFILE TO 90 M (300 FT)

- LEGEND
- APPROACH 2, 1 HZ AND 10 HZ DEAGGREGATION EQKS, MEAN PGA = 0.811 G
 - APPROACH 1, 10-4 ROCK CONTROL MOTION, BASE CASE, 84TH PERCENTILE, PGA = 0.965 G
 - APPROACH 1, 10-4 ROCK CONTROL MOTION, BASE CASE, MEAN, PGA = 0.819 G
 - APPROACH 1, 10-4 ROCK CONTROL MOTION, BASE CASE, 16TH PERCENTILE, PGA = 0.672 G

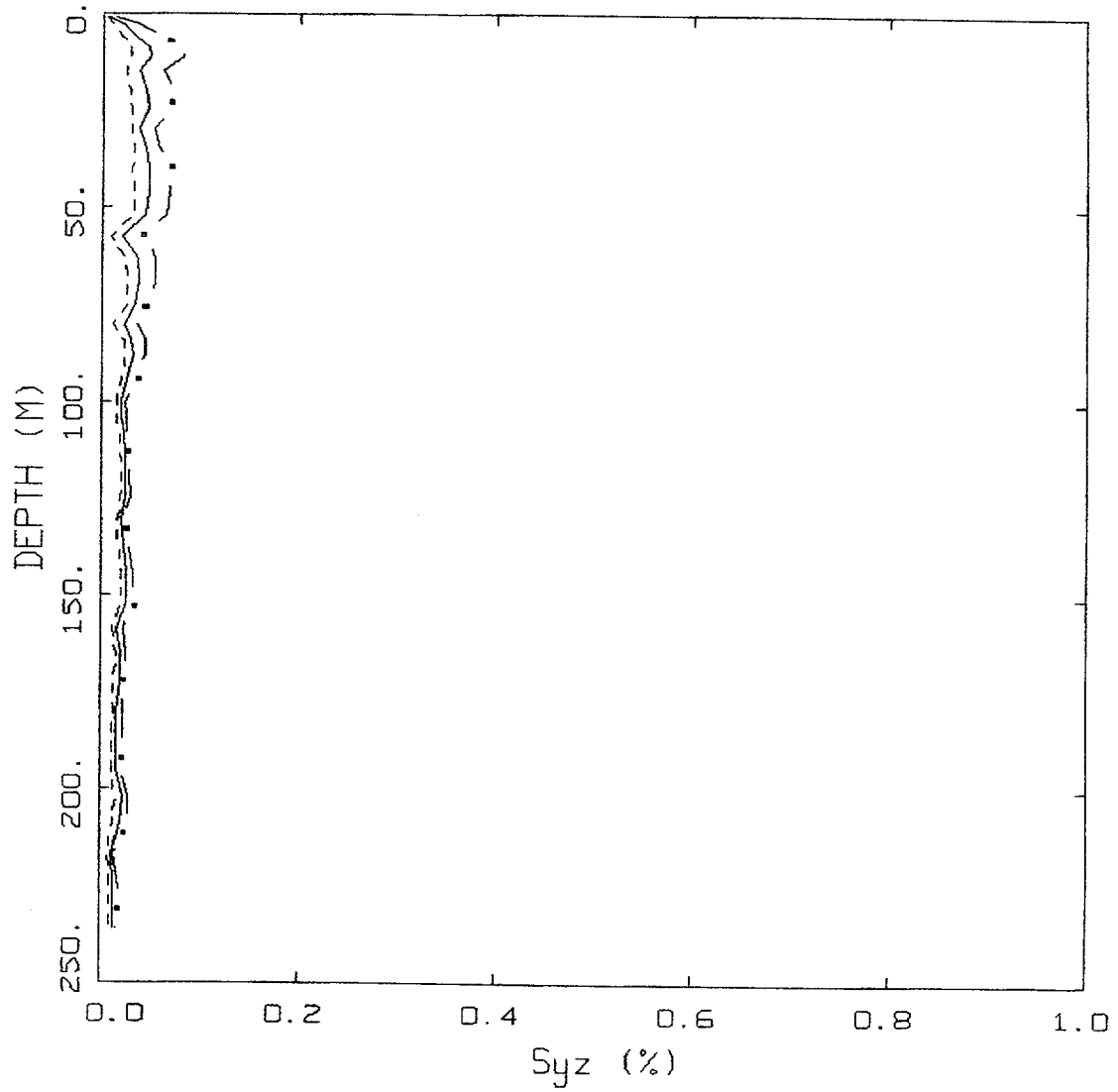
Figure 6-141. Comparison of soil spectra for Approach 2B (full profile) with mean and $\pm 1\sigma$ profile variations with profile truncated at 90m. Soil profile Savannah River Generic, WUS conditions.



CEUS 10E-4 APPROACH COMPARISON, IV

- LEGEND
- APPROACH 4, 10⁻⁴ SOIL UNIFORM HAZARD SPECTRUM; PGA = 0.284 G
 - APPROACH 1, 10⁻⁴ ROCK CONTROL MOTION, MEAN PGA = 0.276 G
 - APPROACH 2, 1 HZ AND 10 HZ DEAGGREGATION EQKS, MEAN PGA = 0.395 G

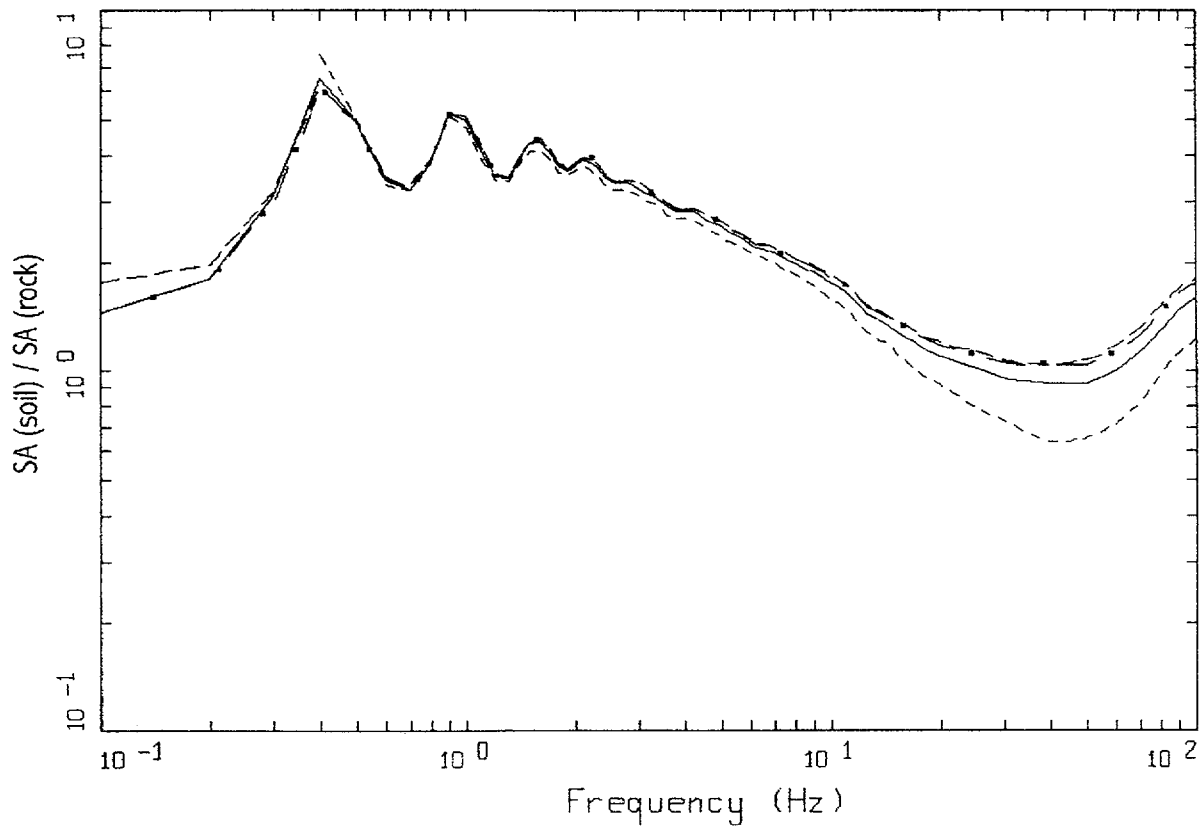
Figure 6-142. Comparison of Approaches 1, 2B, and 4 soil spectra for profile Meloland; CEUS conditions.



CEUS, 10-4, IV
EFFECTIVE STRAINS (SYZ)

LEGEND
 - · - 84TH PERCENTILE
 — 50TH PERCENTILE
 - - - 16TH PERCENTILE

Figure 6-143. Median and $\pm 1\sigma$ effective strains for soil profile Meloland using Approach 1: CEUS conditions.

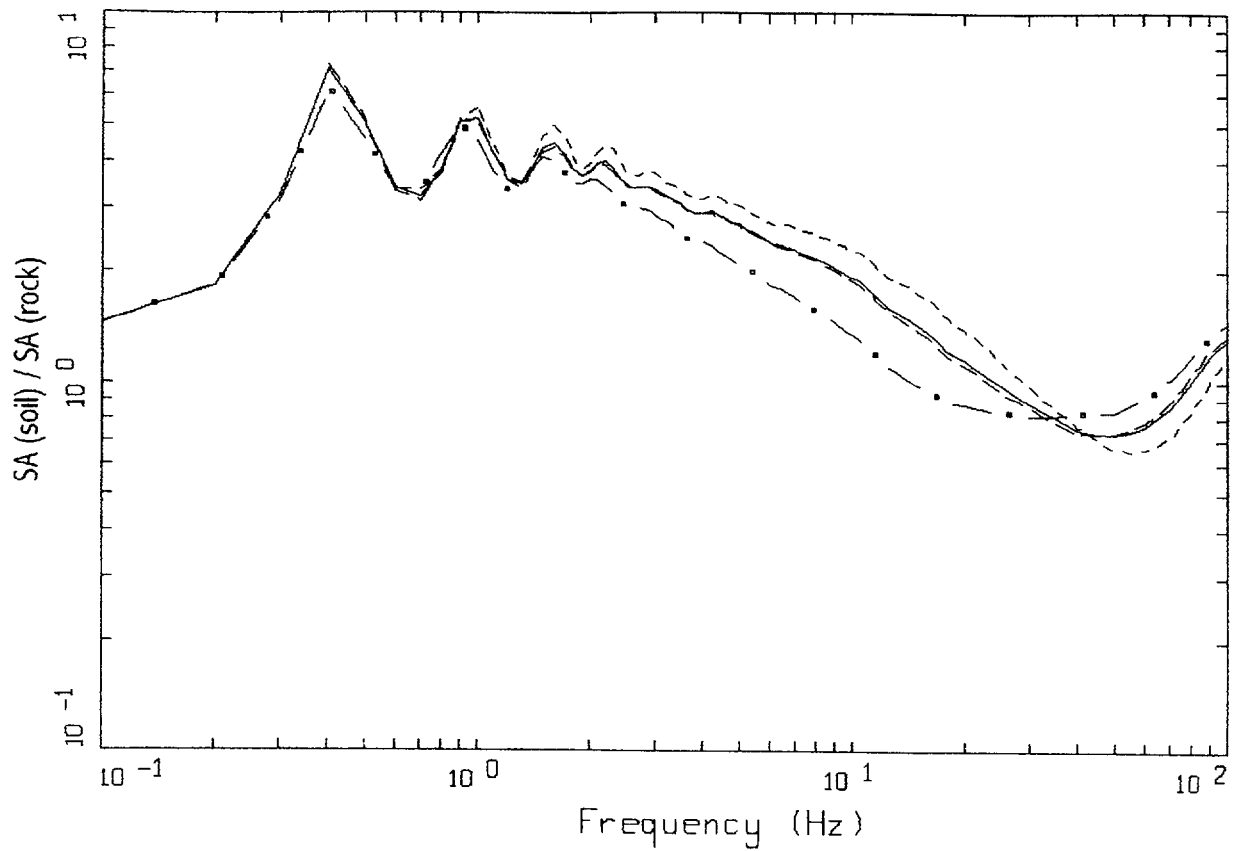


CEUS, 10E-4, 1HZ DESIGN, IV
 SURFACE MOTION, 1HZ TRANSFER FUNCTION
 WEIGHTS: ML=0.30, MM=0.00, MH=0.70

LEGEND

- ML = 5.7, D = 20 KM MEAN RATIO
- · - · - MM = 7.0, D = 100 KM, DESIGN MEAN RATIO
- · — MH = 7.6, D = 130 KM MEAN RATIO
- WEIGHTED MEAN RATIO

Figure 6-144. Comparison of transfer functions computed for the scaled 1 Hz design earthquake; soil profile Meloland, CEUS conditions.

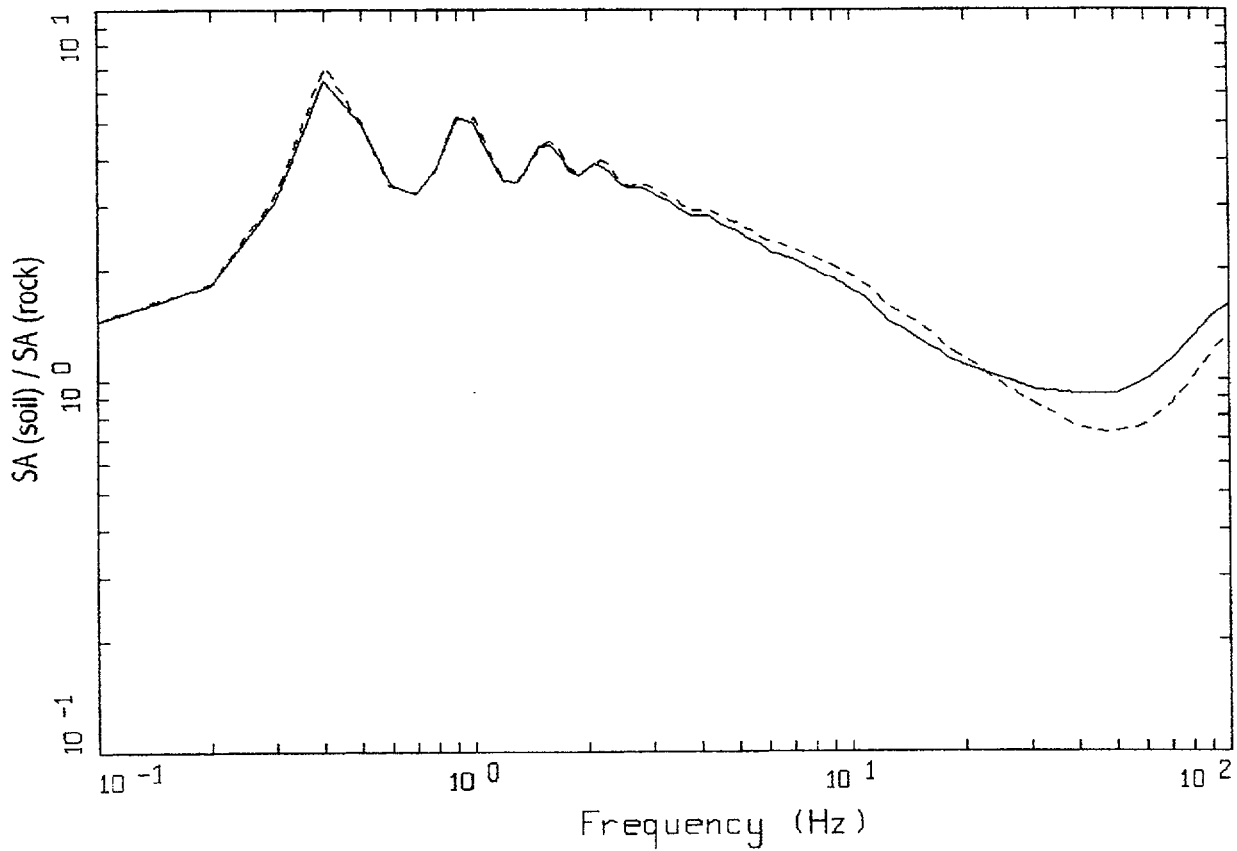


CEUS, 10E-4, 10HZ DESIGN, IV
 SURFACE MOTION, 10HZ TRANSFER FUNCTION
 WEIGHTS: ML=0.25, MM=0.63, MH=0.12

LEGEND

- ML = 4.6, D = 8 KM MEAN RATIO
- · - · - MM = 5.6, D = 8 KM, DESIGN MEAN RATIO
- · — MH = 7.7, D = 130 KM MEAN RATIO
- WEIGHTED MEAN RATIO

Figure 6-145. Comparison of transfer functions computed for the scaled 10 Hz design earthquake; soil profile Meloland, CEUS conditions.

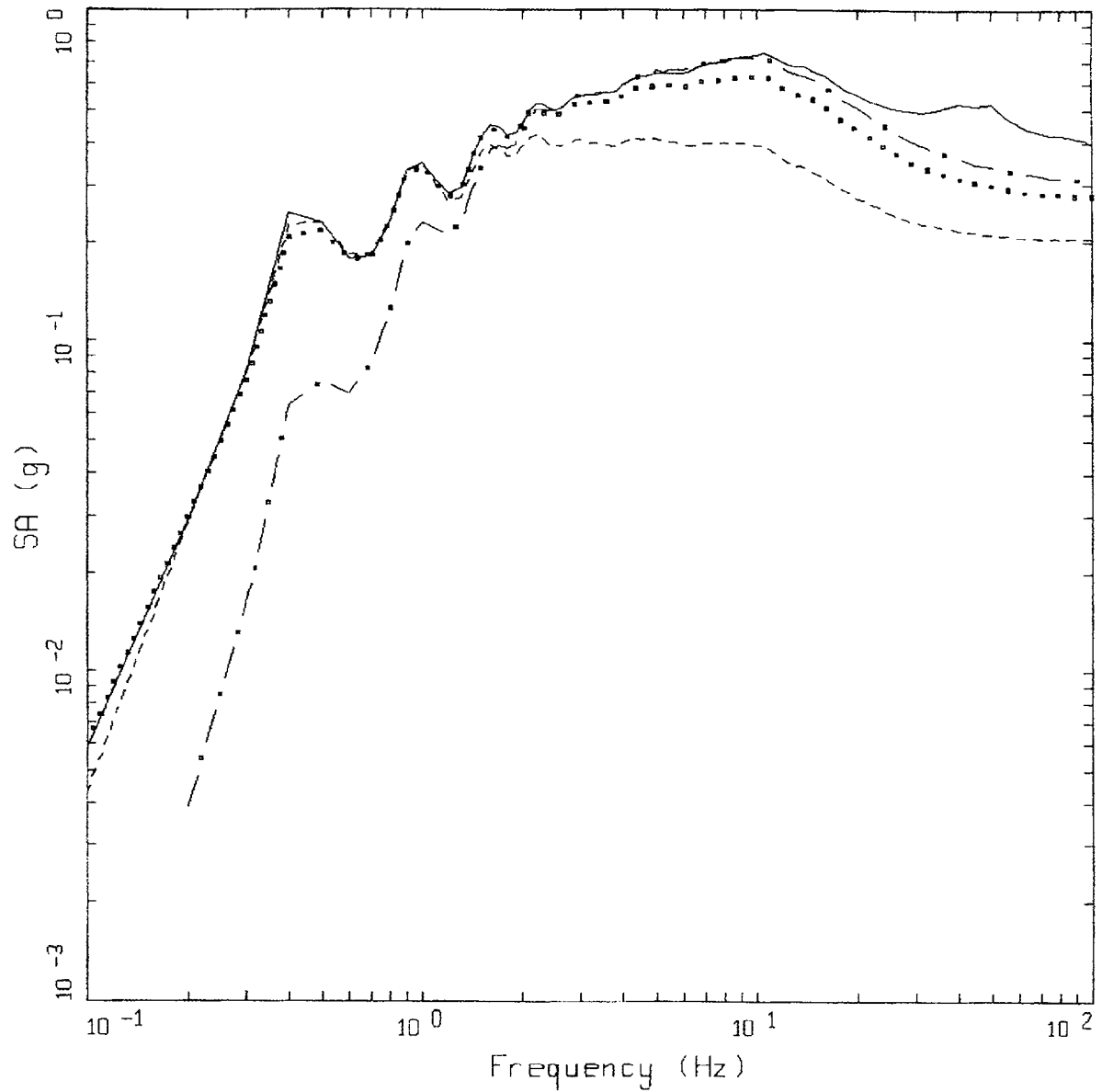


CEUS, 10E-4, IV
TRANSFER FUNCTION

LEGEND

- 1 HZ WEIGHTED MEAN RATIO; WEIGHTS:ML=0.30,MM=0.00,MH=0.70
- 10 HZ WEIGHTED MEAN RATIO; WEIGHTS:ML=0.25,MM=0.63,MH=0.12

Figure 6-146. Comparison of mean transfer functions computed for the scaled 1 Hz and 10 Hz design earthquakes; soil profile Meloland, CEUS conditions.

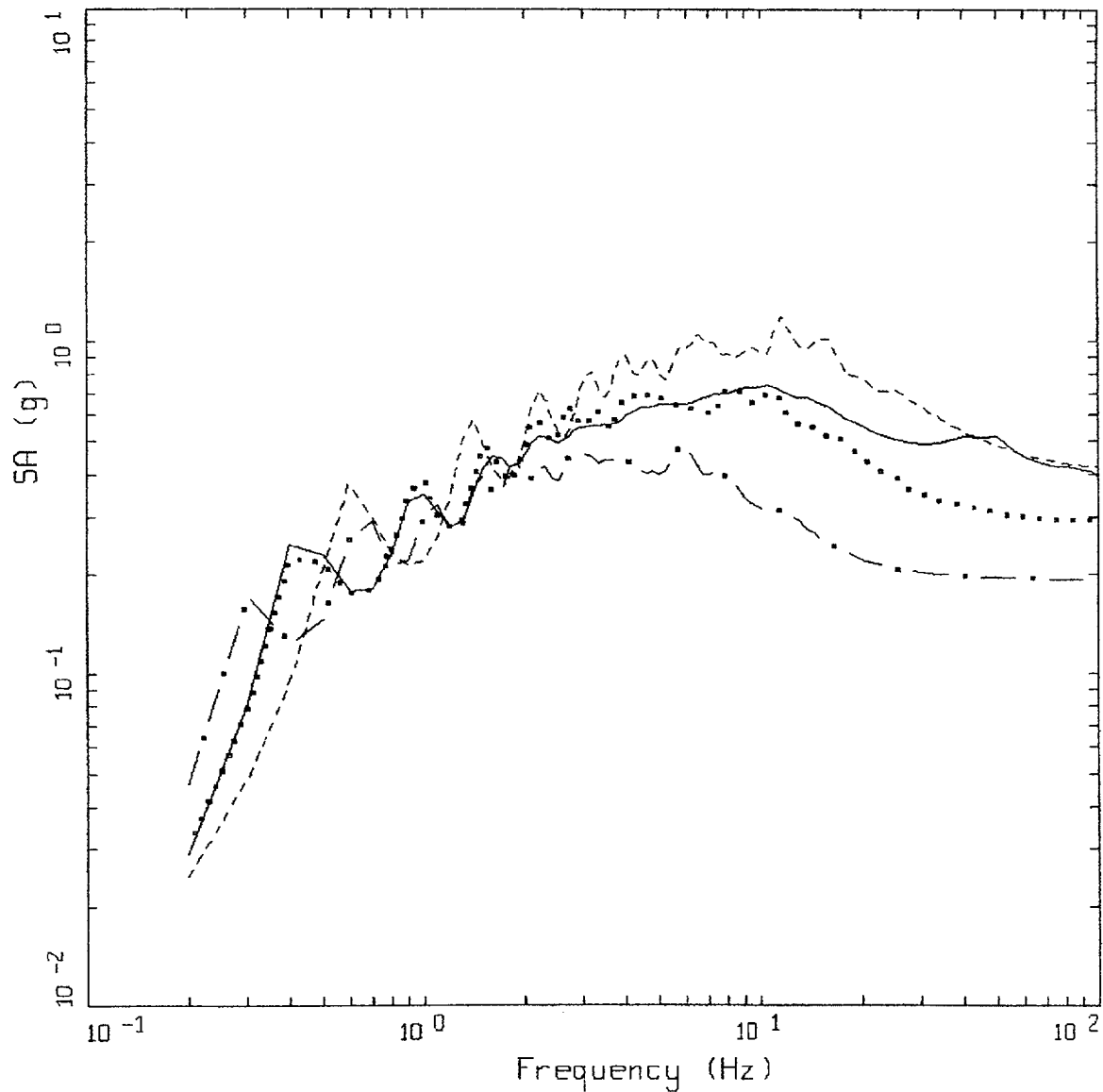


CEUS, 10E-4 DESIGN SPECTRA, IV

LEGEND

- APPROACH 2, 1 HZ AND 10 HZ DEAGGREGATION EQKS, MEAN PGA = 0.395 G
- APPROACH 1, 10-4 ROCK CONTROL MOTION, MEAN PGA = 0.276 G
- 1 HZ MEAN; PGA = 0.203 G
- . - . 10 HZ MEAN; PGA = 0.309 G

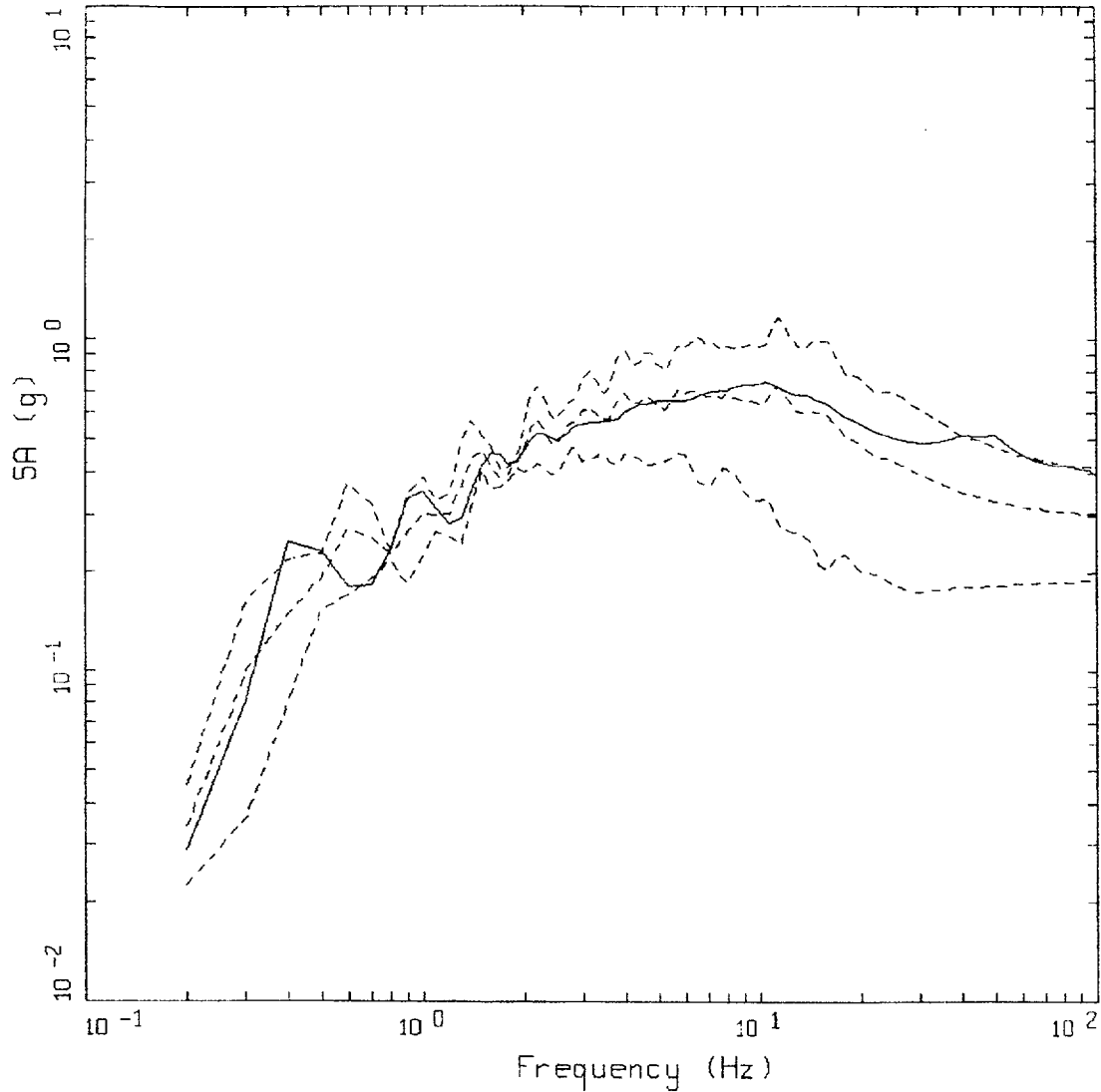
Figure 6-147. Comparison of soil spectra for Approaches 1, 2A, and 2B; soil profile Meloland, CEUS conditions.



CEUS 10E-4 APPROACH COMPARISON, IV

- LEGEND
- APPROACH 2, 1 HZ AND 10 HZ DEAGGREGATION EQKS, MEAN PGA = 0.395 G
 - APPROACH 1, 10-4 ROCK CONTROL MOTION, BASE CASE PGA = 0.291 G
 - - - - APPROACH 1, 10-4 ROCK CONTROL MOTION, BASE CASE (UPPER) PGA = 0.421 G
 - . - . APPROACH 1, 10-4 ROCK CONTROL MOTION, BASE CASE (LOWER) PGA = 0.193 G

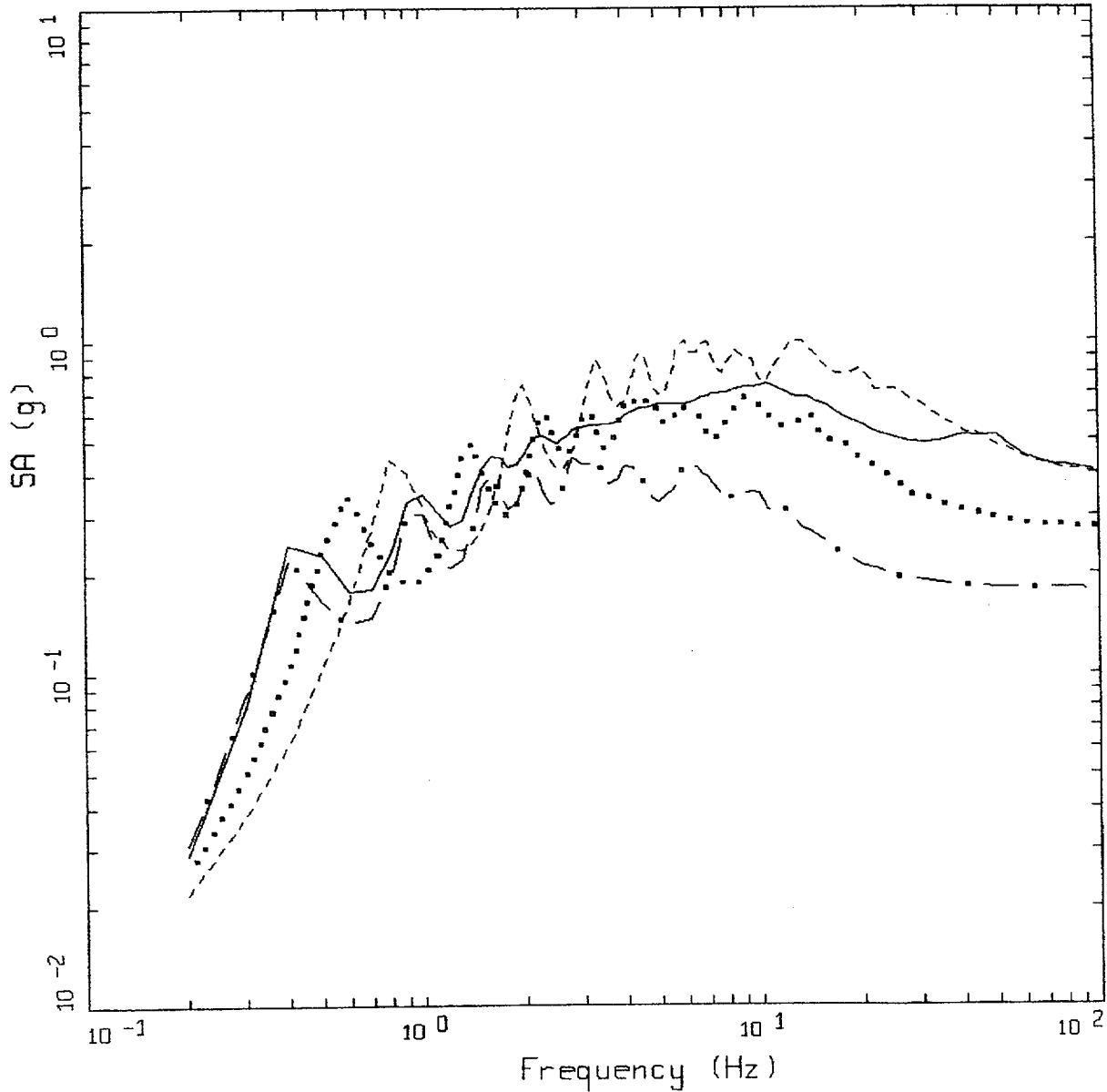
Figure 6-148. Comparison of soil spectra for Approach 2B with base case profile and deterministic profile variations (\pm factor of 2 on shear modulus); soil profile Meloland, CEUS conditions.



CEUS 10E-4 APPROACH COMPARISON, IV

- LEGEND
- APPROACH 2, 1 HZ AND 10 HZ DEAGGREGATION EQKS, MEAN PGA = 0.395 G
 - - - APPROACH 1, 10-4 ROCK CONTROL MOTION, BASE CASE, 84TH PERCENTILE, PGA = 0.416 G
 - · - APPROACH 1, 10-4 ROCK CONTROL MOTION, BASE CASE, MEAN, PGA = 0.301 G
 - · · APPROACH 1, 10-4 ROCK CONTROL MOTION, BASE CASE, 16TH PERCENTILE, PGA = 0.188 G

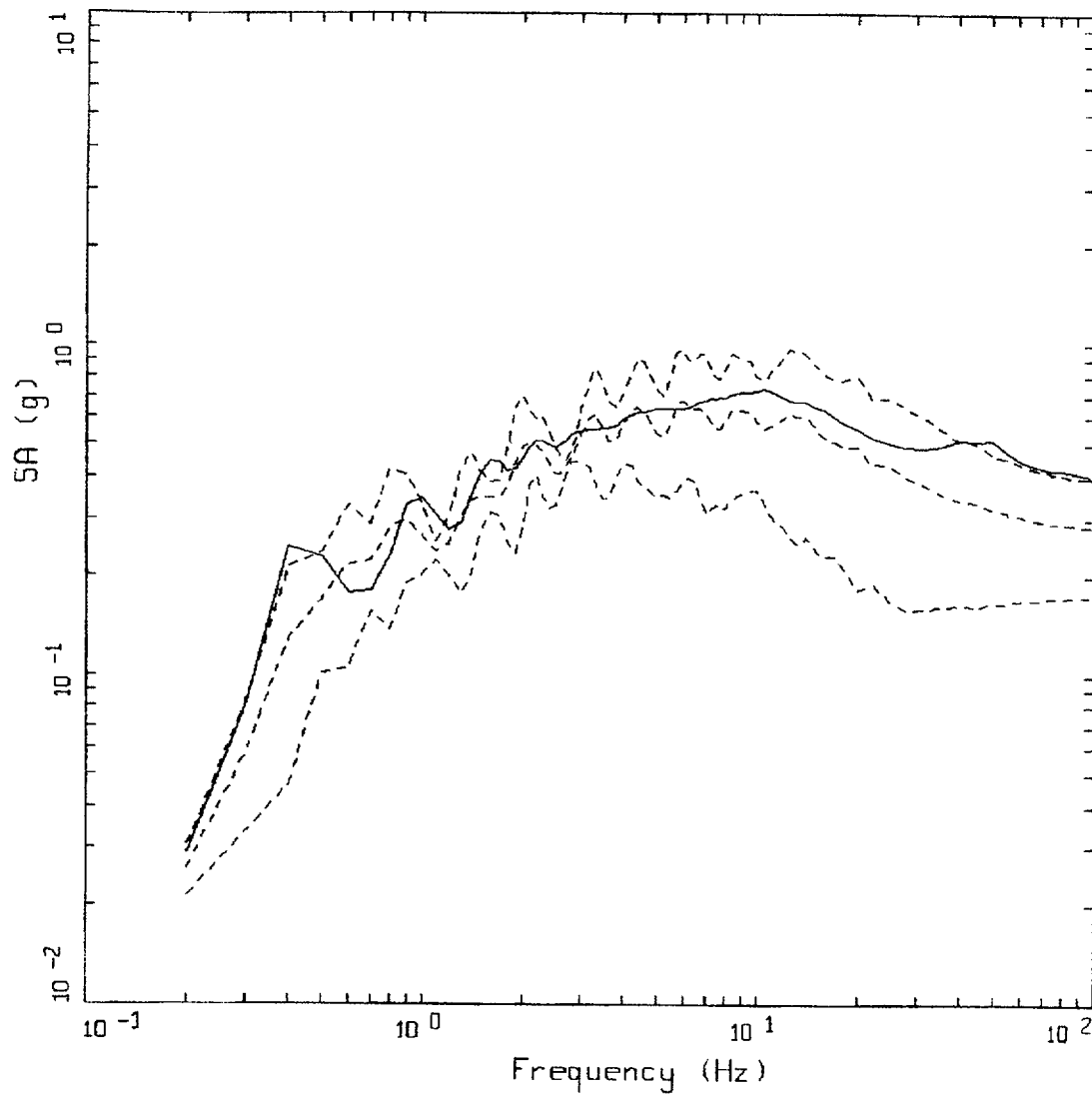
Figure 6-149. Comparison of soil spectra for Approach 2B with mean and $\pm 1\sigma$ variations of base case (\pm factor of 2 on shear modulus); soil profile Meloland, CEUS conditions.



CEUS 10E-4 APPROACH COMPARISON, IV
SOIL PROFILE TO 150 M (500 FT)

- LEGEND
- APPROACH 2, 1-HZ AND 10 HZ DEAGGREGATION EQKS, MEAN PGA = 0.395 G
 - APPROACH 1, 10-4 ROCK CONTROL MOTION, BASE CASE PGA = 0.275 G
 - APPROACH 1, 10-4 ROCK CONTROL MOTION, BASE CASE (UPPER) PGA = 0.400 G
 - . - - APPROACH 1, 10-4 ROCK CONTROL MOTION, BASE CASE (LOWER) PGA = 0.193 G

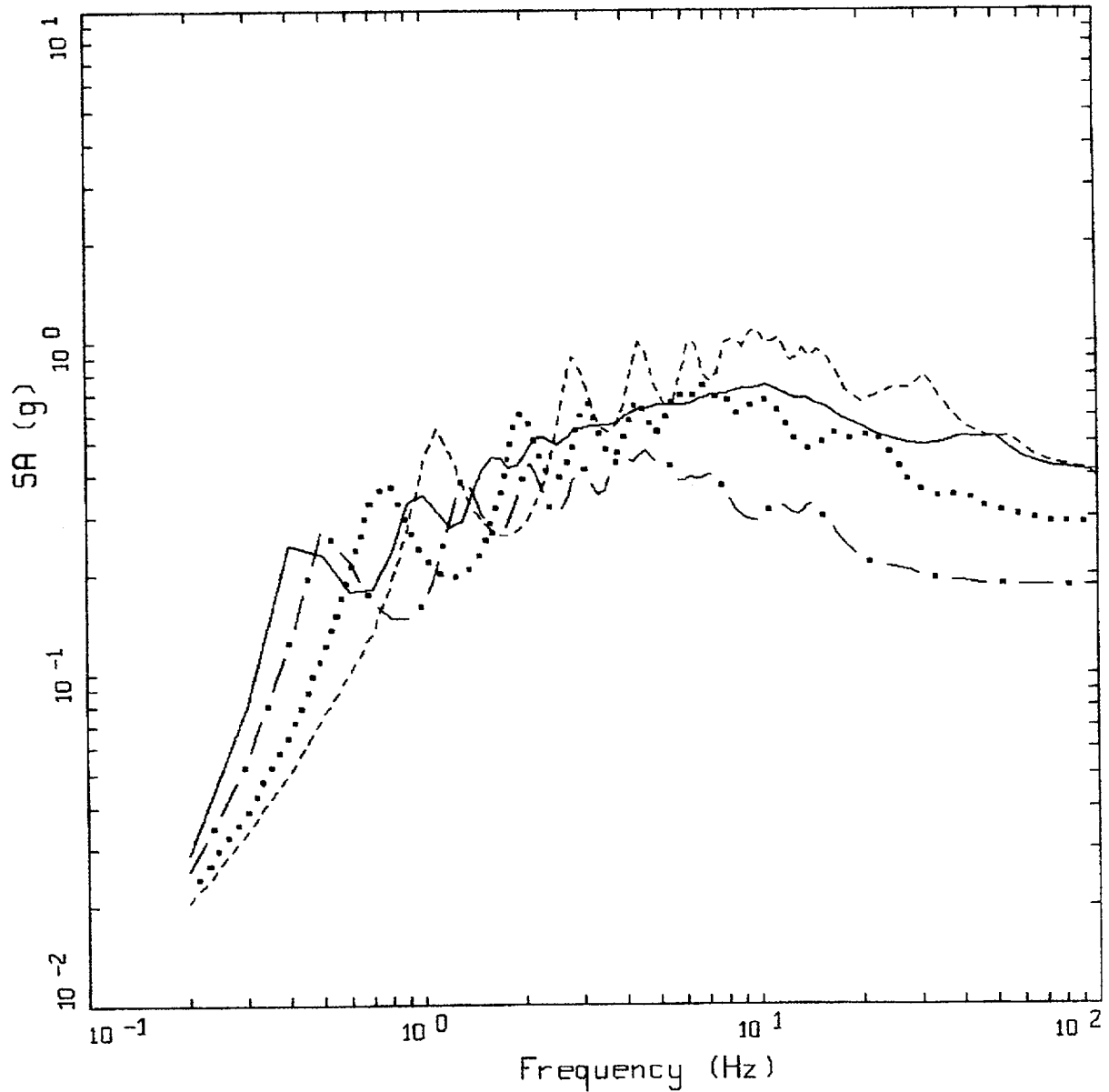
Figure 6-150. Comparison of soil spectra for Approach 2B (full profile) with base case profile and deterministic profile variations (\pm factor of 2 on shear modulus) with profile truncated at 150m; soil profile Meloland, CEUS conditions.



CEUS 10E-4 APPROACH COMPARISON, IV
 SOIL PROFILE TO 150 M (500 FT)

- LEGEND
- APPROACH 2, 1 HZ AND 10 HZ DEAGGREGATION EQKS, MEAN PGA = 0.395 G
 - APPROACH 1, 10-4 ROCK CONTROL MOTION, BASE CASE, 84TH PERCENTILE, PGA = 0.395 G
 - APPROACH 1, 10-4 ROCK CONTROL MOTION, BASE CASE, MEAN, PGA = 0.285 G
 - APPROACH 1, 10-4 ROCK CONTROL MOTION, BASE CASE, 16TH PERCENTILE, PGA = 0.174 G

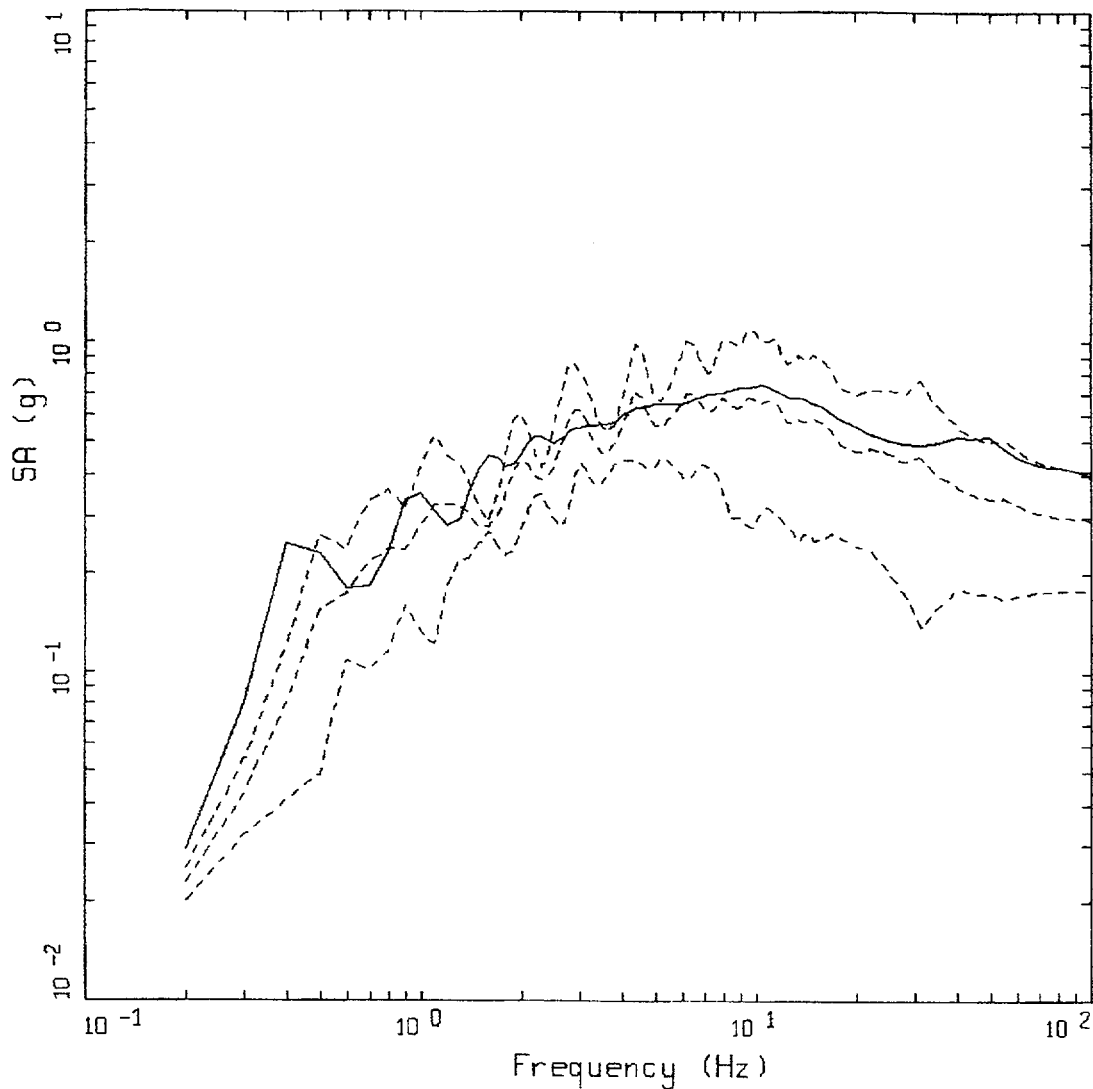
Figure 6-151. Comparison of soil spectra for Approach 2B (full profile) with mean and $\pm 1\sigma$ profile variations with profile truncated at 150m. Soil profile Meloland, CEUS conditions.



CEUS 10E-4 APPROACH COMPARISON, IV
SOIL PROFILE TO 90 M (300 FT)

- LEGEND
- APPROACH 2, 1 HZ AND 10 HZ DEAGGREGATION EQKS, MEAN PGA = 0.395 G
 - APPROACH 1, 10-4 ROCK CONTROL MOTION, BASE CASE PGA = 0.411 G
 - APPROACH 1, 10-4 ROCK CONTROL MOTION, BASE CASE (UPPER) PGA = 0.298 G
 - . - . - APPROACH 1, 10-4 ROCK CONTROL MOTION, BASE CASE (LOWER) PGA = 0.183 G

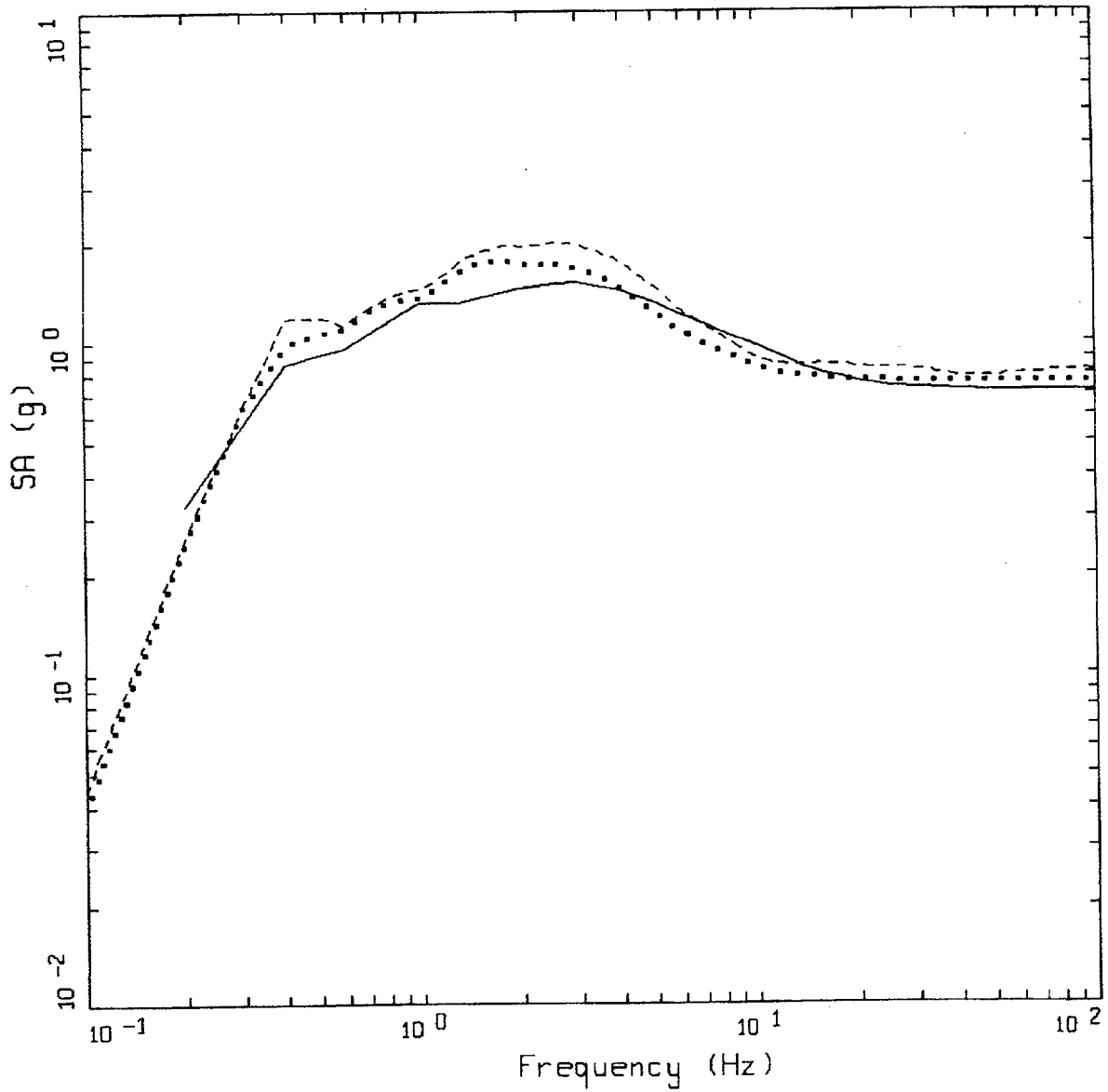
Figure 6-152. Comparison of soil spectra for Approach 2B (full profile) with base case profile and deterministic profile variations (\pm factor of 2 on shear modulus) with profile truncated at 90m; soil profile Meloland; CEUS conditions.



CEUS 10E-4 APPROACH COMPARISON, IV
 SOIL PROFILE TO 90 M (300 FT)

- LEGEND
- APPROACH 2, 1 HZ AND 10 HZ DEAGGREGATION EQKS, MEAN PGA = 0.395 G
 - APPROACH 1, 10-4 ROCK CONTROL MOTION, BASE CASE, 84TH PERCENTILE, PGA = 0.407 G
 - APPROACH 1, 10-4 ROCK CONTROL MOTION, BASE CASE, MEAN, PGA = 0.293 G
 - APPROACH 1, 10-4 ROCK CONTROL MOTION, BASE CASE, 16TH PERCENTILE, PGA = 0.179 G

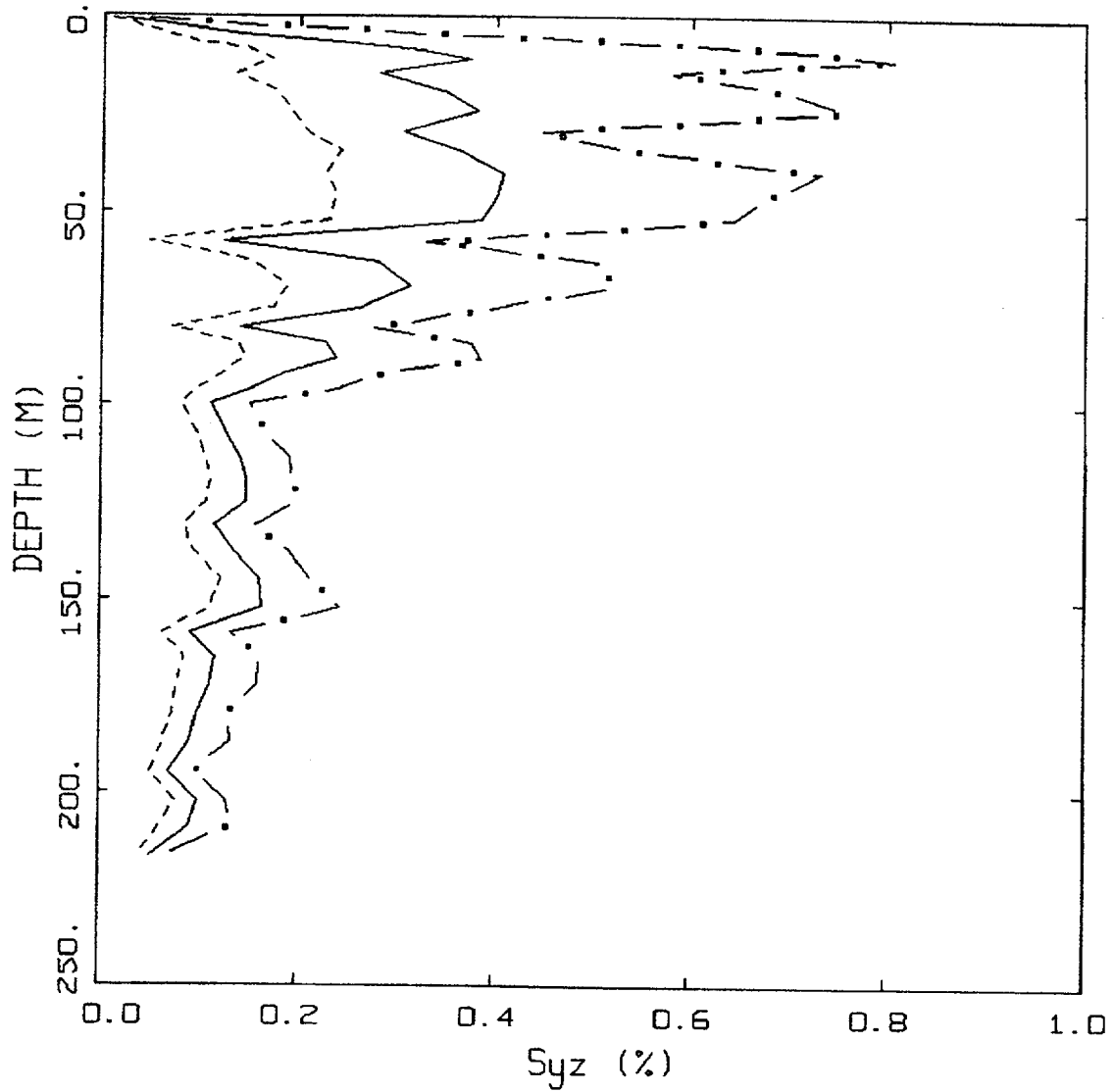
Figure 6-153. Comparison of soil spectra for Approach 2B (full profile) with mean and $\pm 1\sigma$ profile variations with profile truncated at 90m. Soil profile Meloland, CEUS conditions.



WUS 10E-4 APPROACH COMPARISON, IV

- LEGEND
- APPROACH 4, 10-4 SOIL UNIFORM HAZARD SPECTRUM, PGA = 0.704 G
 - APPROACH 1, 10-4 ROCK CONTROL MOTION, MEAN PGA = 0.755 G
 - - - - APPROACH 2, 1 HZ AND 10 HZ DEAGGREGATION EQKS, MEAN PGA = 0.817 G

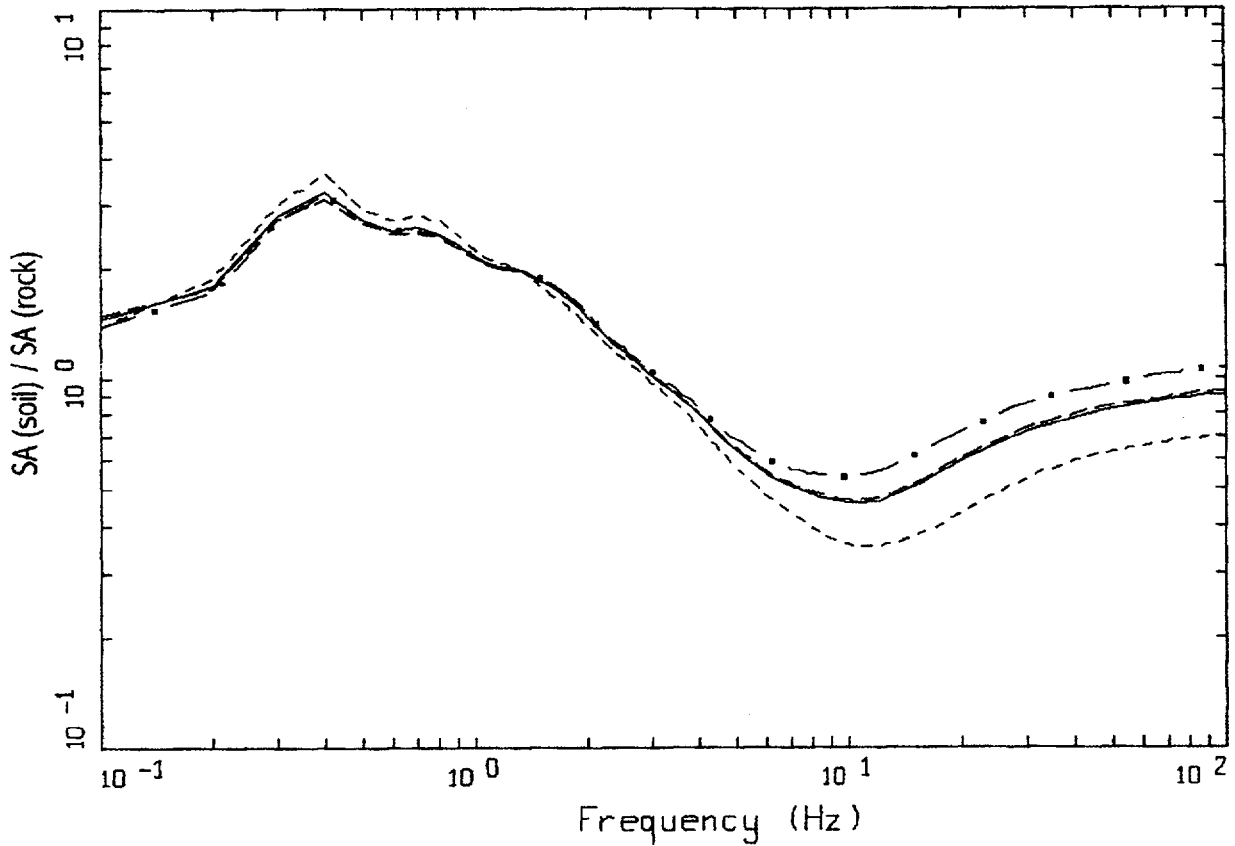
Figure 6-154. Comparison of Approaches 1, 2B, and 4 soil spectra for profile Meloland: WUS conditions.



WUS, 10-4, IV
EFFECTIVE STRAINS (SYZ)

LEGEND
 - . - 84TH PERCENTILE
 — 50TH PERCENTILE
 - - - 16TH PERCENTILE

Figure 6-155. Median and $\pm 1\sigma$ effective strains for soil profile Meloland using Approach 1 WUS conditions.

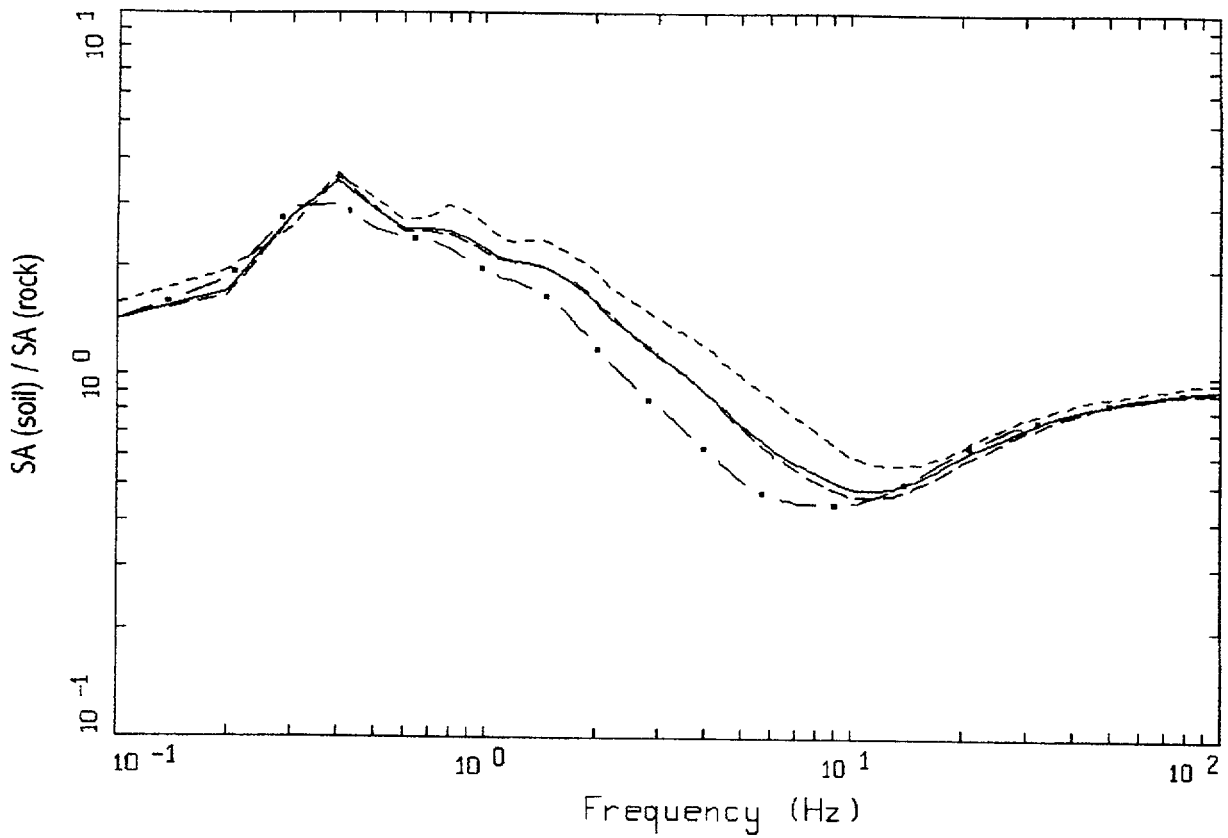


WUS, 10E-4, 1HZ DESIGN, IV PROFILE
 SURFACE MOTION, 1HZ TRANSFER FUNCTION
 WEIGHTS: ML=0.20, MM=0.60, MH=0.20

LEGEND

- ML = 5.4, D = 10 KM MEAN RATIO
- . - . - MM = 6.7, D = 18 KM, DESIGN MEAN RATIO
- • — MH = 7.8, D = 30 KM MEAN RATIO
- WEIGHTED MEAN RATIO

Figure 6-156. Comparison of transfer functions computed for the scaled 1 Hz design earthquake; soil profile Meloland, WUS conditions.

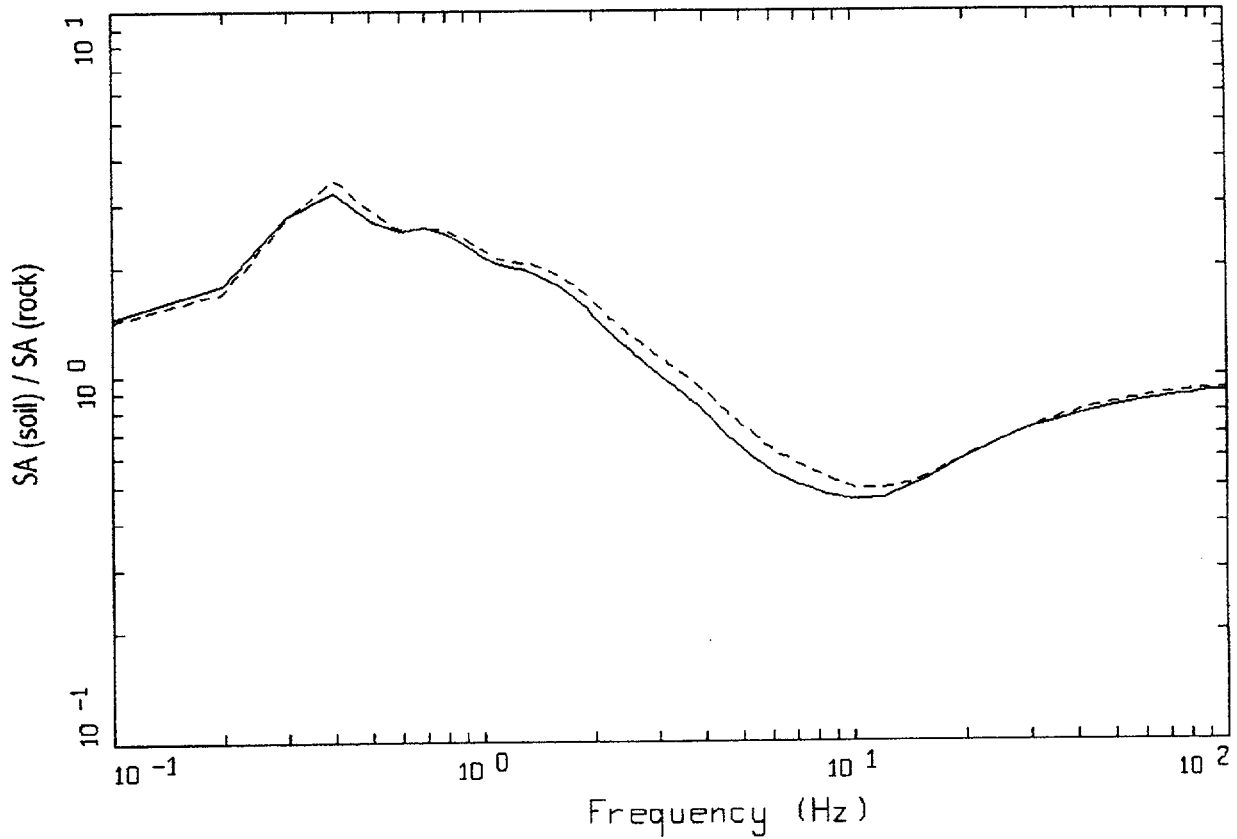


WUS, 10E-4, 10HZ DESIGN, IV PROFILE
 SURFACE MOTION, 10HZ TRANSFER FUNCTION
 WEIGHTS: ML=0.20, MM=0.60, MH=0.20

LEGEND

- ML = 5.1, D = 10 KM MEAN RATIO
- · - · - MM = 6.1, D = 14 KM, DESIGN MEAN RATIO
- · — MH = 7.8, D = 30 KM MEAN RATIO
- WEIGHTED MEAN RATIO

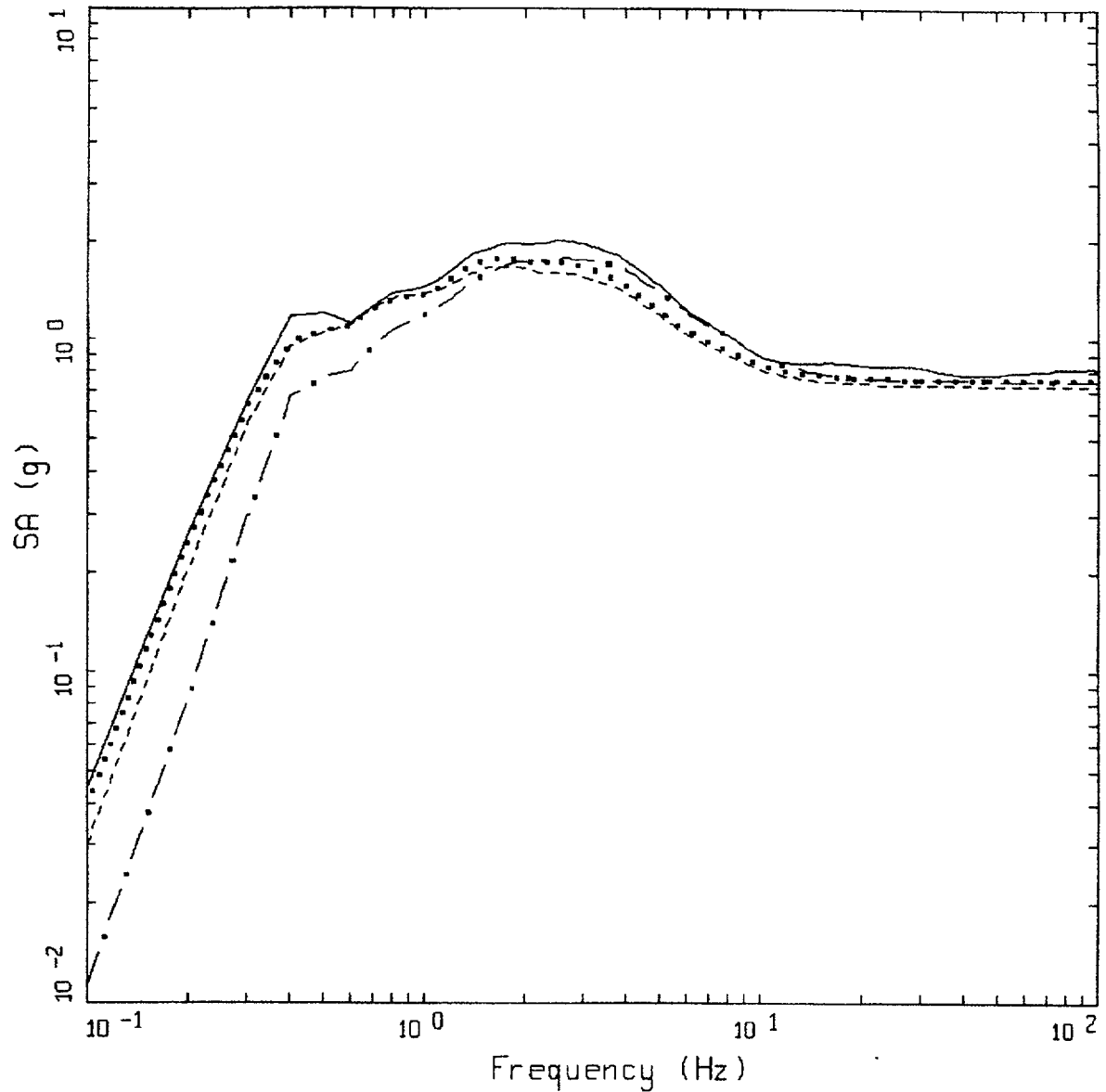
Figure 6-157. Comparison of transfer functions computed for the scaled 10 Hz design earthquake; soil profile Meloland, WUS conditions.



WUS, 10E-4, IV PROFILE
AMPLIFICATION

LEGEND
 ——— 1 HZ WEIGHTED MEAN RATIO; WEIGHTS:ML=0.20,MM=0.60,MH=0.20
 - - - - 10 HZ WEIGHTED MEAN RATIO; WEIGHTS:ML=0.20,MM=0.60,MH=0.20

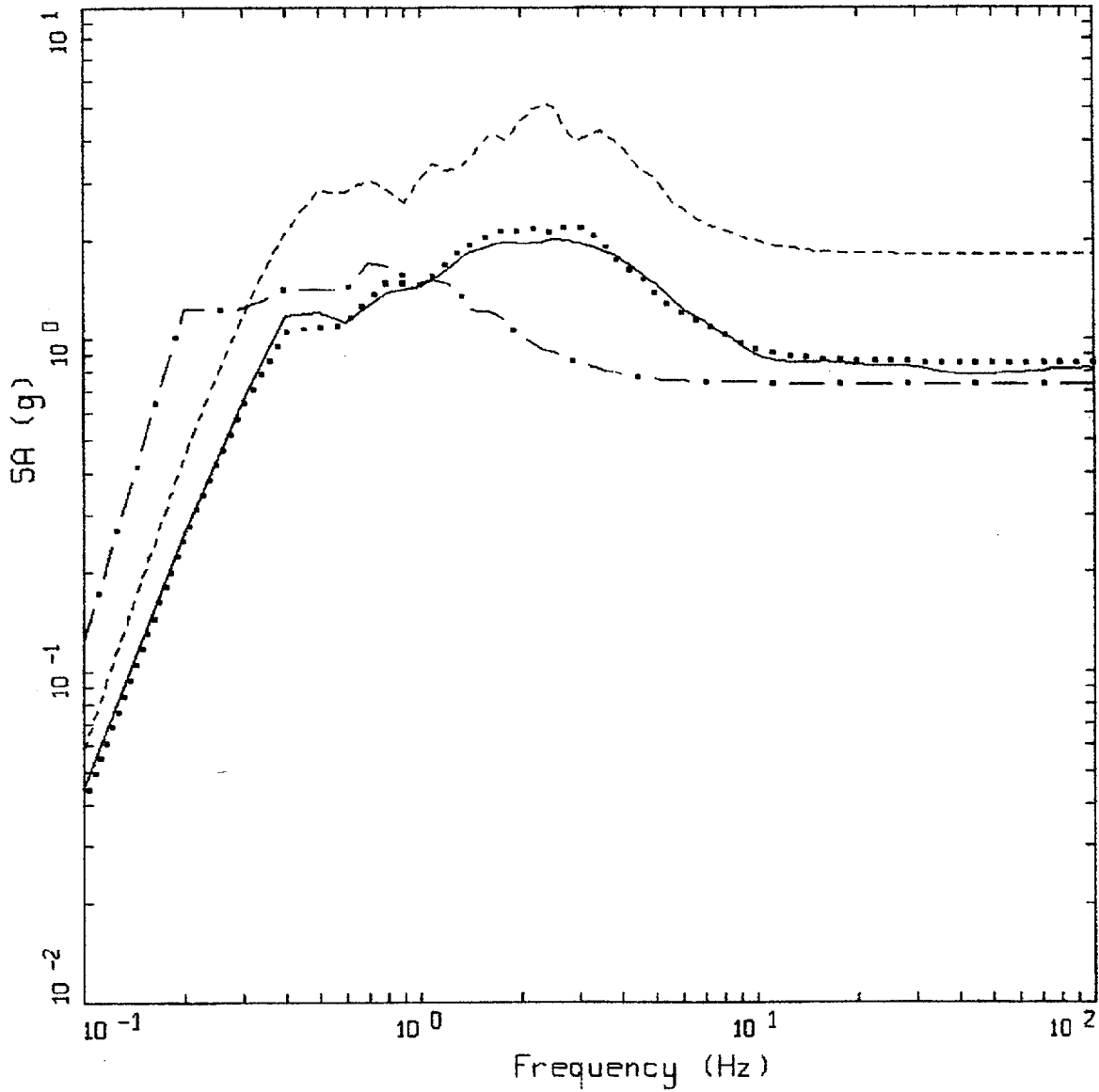
Figure 6-158. Comparison of mean transfer functions computed for the scaled 1 Hz and 10 Hz design earthquakes; soil profile Meloland, WUS conditions.



WUS, 10E-4 DESIGN SPECTRA, IV

- LEGEND
- APPROACH 2, 1 HZ AND 10 HZ DEAGGREGATION EQKS, MEAN PGA = 0.563 G
 - APPROACH 1, 10⁻⁴ ROCK CONTROL MOTION, MEAN PGA = 0.755 G
 - 1 HZ MEAN; PGA = 0.727 G
 - · - 10 HZ MEAN; PGA = 0.752 G

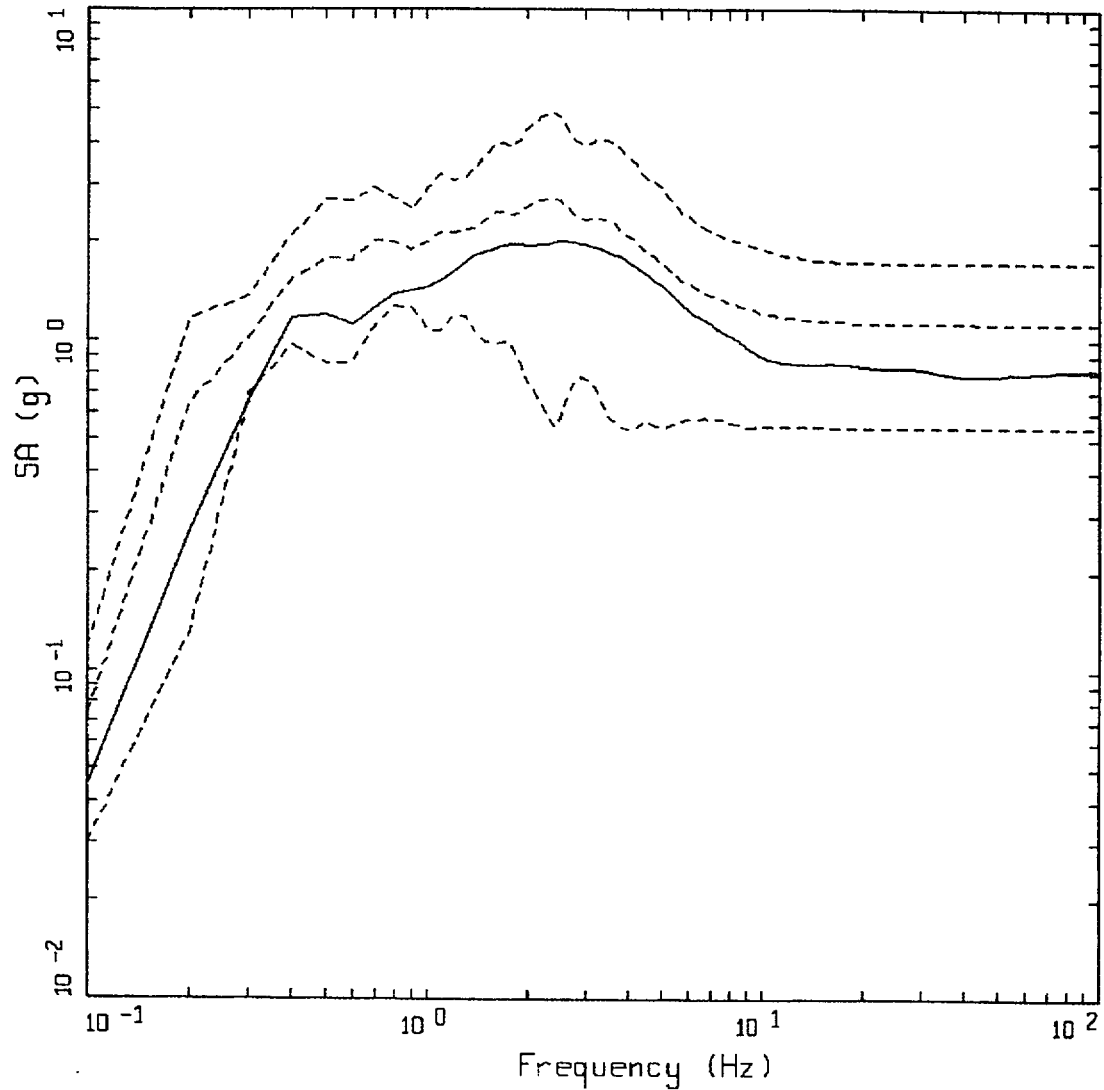
Figure 6-159. Comparison of soil spectra for Approaches 1, 2A, and 2B; soil profile Meloland, WUS conditions.



WUS 10E-4 APPROACH COMPARISON, IV

- LEGEND
- APPROACH 2, 1 HZ AND 10 HZ DEAGGREGATION EQKS, MEAN PGA = 0.817 G
 - APPROACH 1, 10-4 ROCK CONTROL MOTION, BASE CASE PGA = 0.851 G
 - APPROACH 1, 10-4 ROCK CONTROL MOTION, BASE CASE (UPPER) PGA = 2.804 G
 - . - . - APPROACH 1, 10-4 ROCK CONTROL MOTION, BASE CASE (LOWER) PGA = 0.733 G

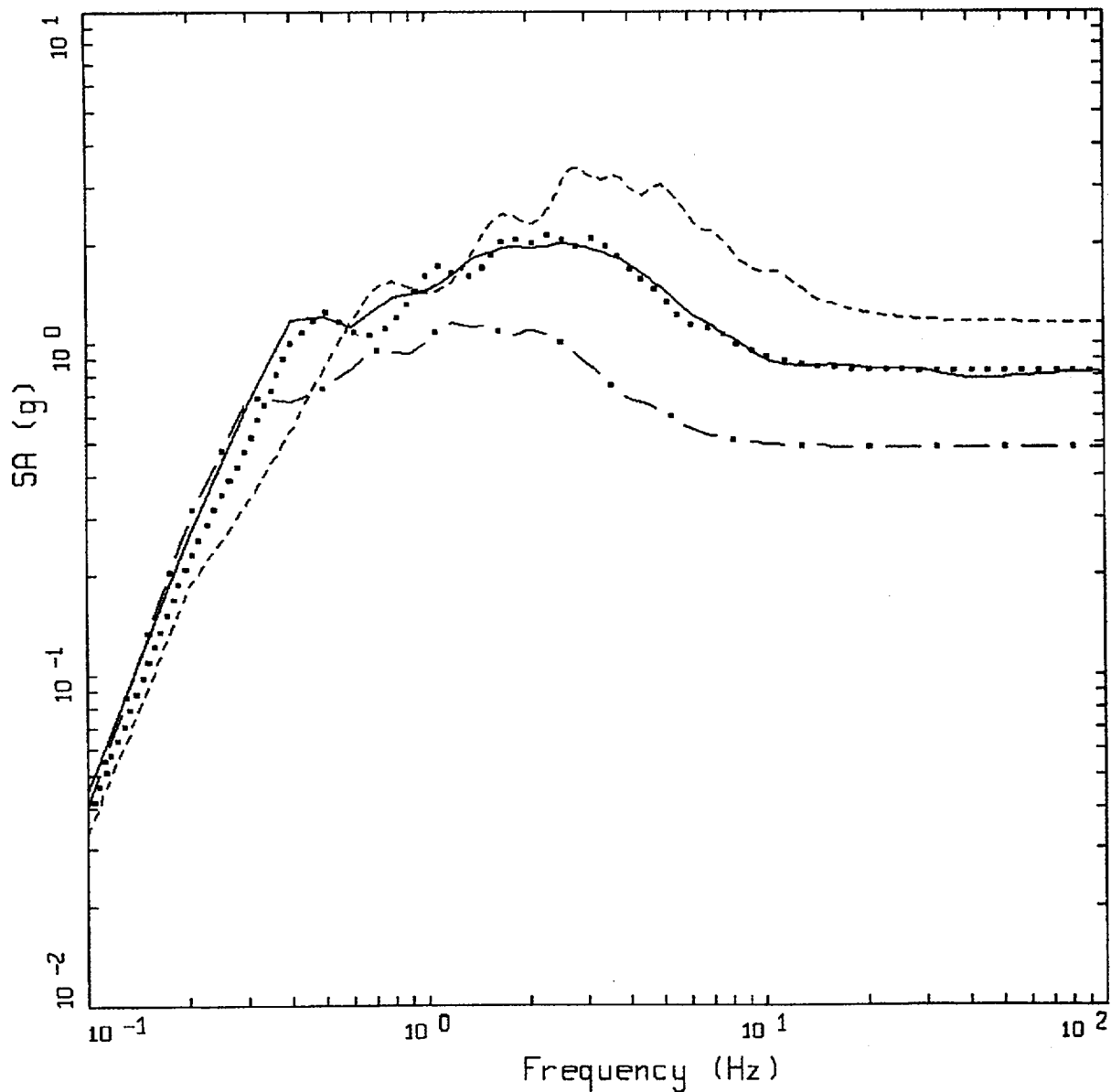
Figure 6-160. Comparison of soil spectra for Approach 2B with base case profile and deterministic profile variations (\pm factor of 2 on shear modulus); soil profile Meloland, WUS conditions.



WUS 10E-4 APPROACH COMPARISON, IV

- LEGEND
- APPROACH 2, 1 HZ AND 10 HZ DEAGGREGATION EQKS, MEAN PGA = 0.817 G
 - - - - APPROACH 1, 10-4 ROCK CONTROL MOTION, BASE CASE, 84TH PERCENTILE, PGA = 1.708 G
 - - - - APPROACH 1, 10-4 ROCK CONTROL MOTION, BASE CASE, MEAN, PGA = 1.126 G
 - - - - APPROACH 1, 10-4 ROCK CONTROL MOTION, BASE CASE, 16TH PERCENTILE, PGA = 0.544 G

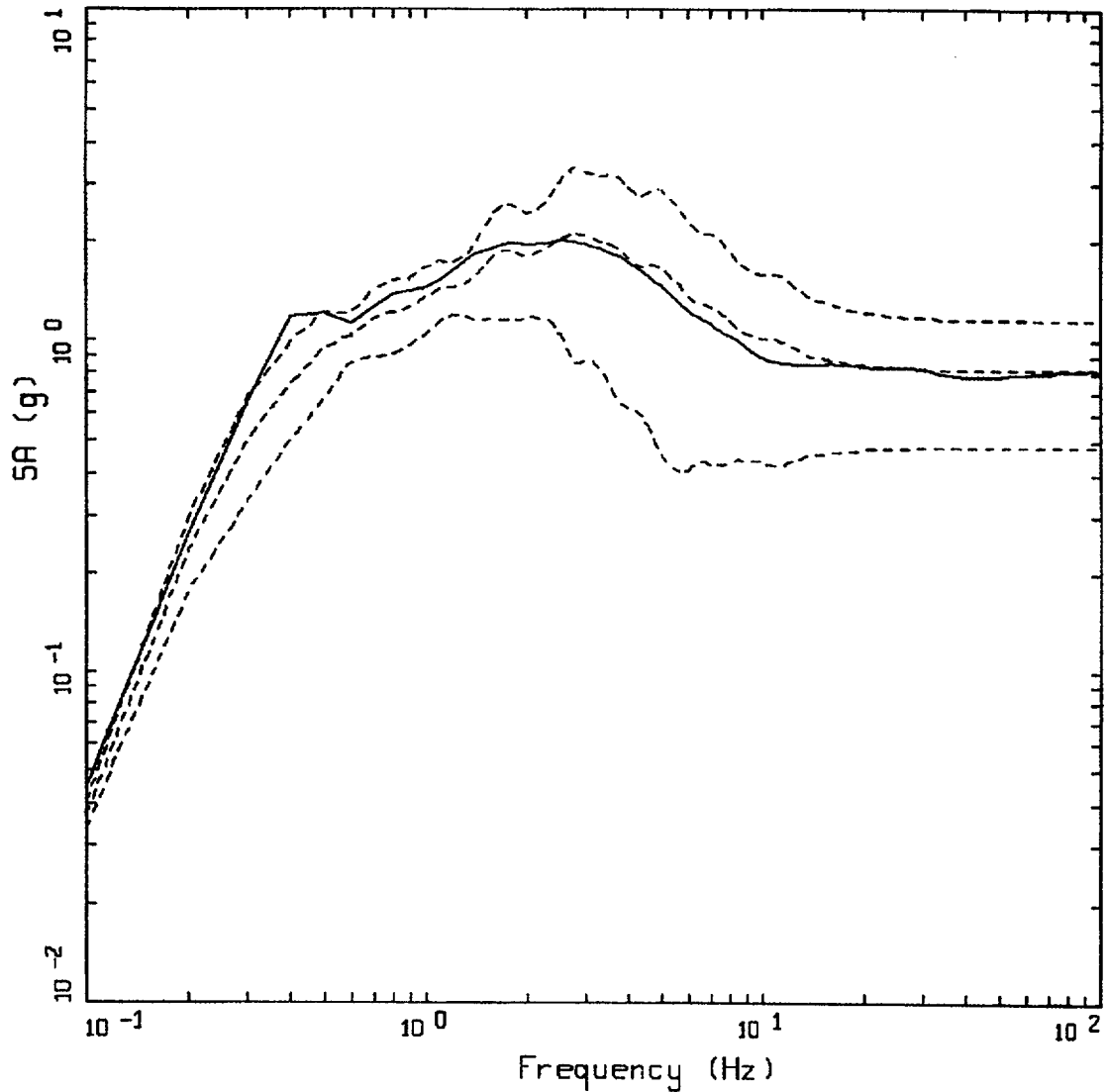
Figure 6-161. Comparison of soil spectra for Approach 2B with mean and $\pm 1\sigma$ variations of base case (\pm factor of 2 on shear modulus), soil profile Meloland, WUS conditions.



WUS 10E-4 APPROACH COMPARISON, IV
 SOIL PROFILE TO 150 M (500 FT)

- LEGEND
- APPROACH 2, 1 HZ AND 10 HZ DEAGGREGATION EQKS, MEAN PGA = 0.817 G
 - APPROACH 1, 10-4 ROCK CONTROL MOTION, BASE CASE PGA = 0.708 G
 - APPROACH 1, 10-4 ROCK CONTROL MOTION, BASE CASE (UPPER) PGA = 1.150 G
 - . - . APPROACH 1, 10-4 ROCK CONTROL MOTION, BASE CASE (LOWER) PGA = 0.733 G

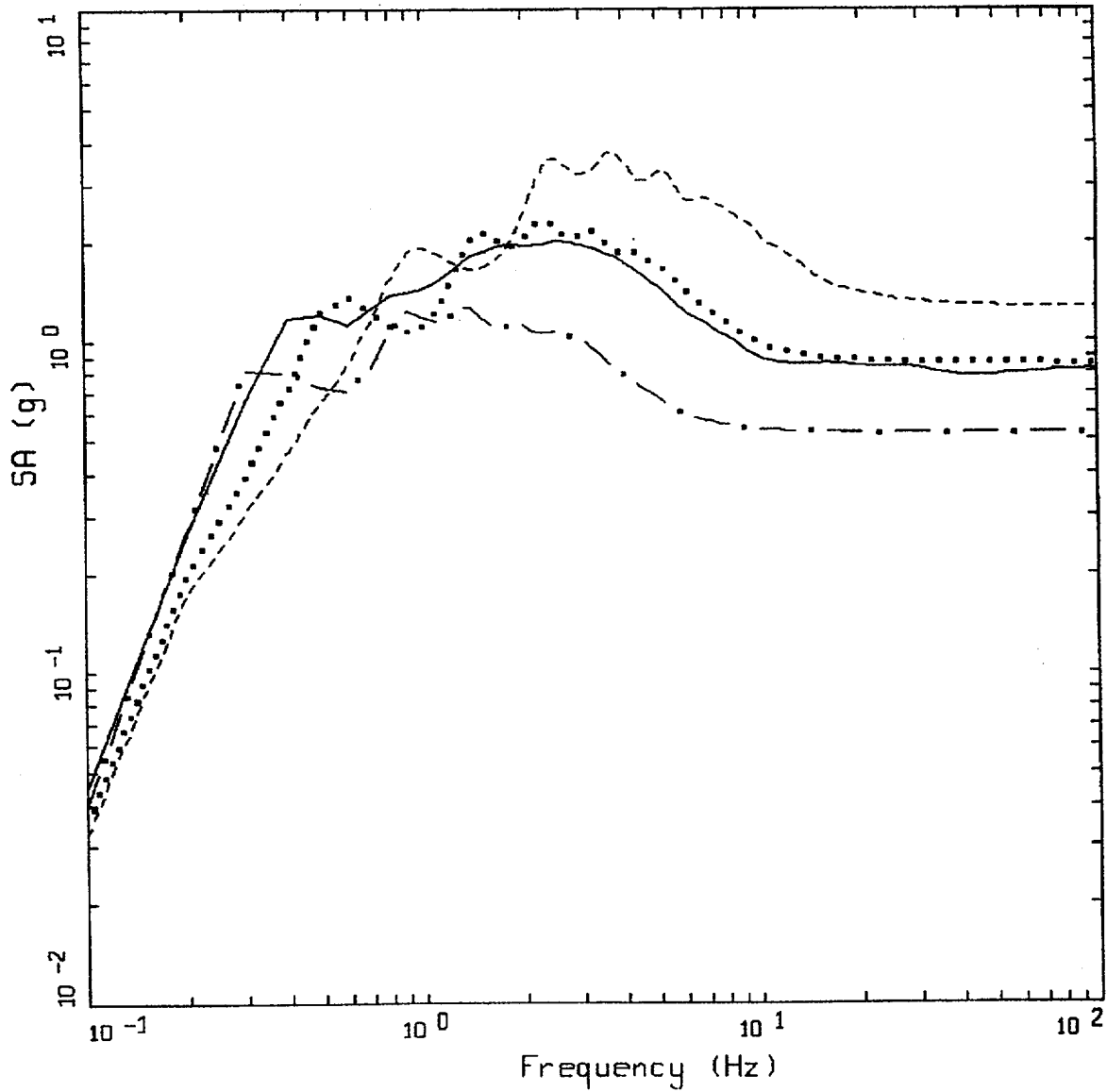
Figure 6-162. Comparison of soil spectra for Approach 2B (full profile) with base case profile and deterministic profile variations (\pm factor of 2 on shear modulus) with profile truncated at 150m; soil profile Meloland, WUS conditions.



WUS 10E-4 APPROACH COMPARISON, IV
 SOIL PROFILE TO 150 M (500 FT)

- LEGEND
- APPROACH 2, 1 HZ AND 10 HZ DEAGGREGATION EQKS, MEAN PGA = 0.817 G
 - - - APPROACH 1, 10-4 ROCK CONTROL MOTION, BASE CASE, 84TH PERCENTILE, PGA = 1.152 G
 - - - APPROACH 1, 10-4 ROCK CONTROL MOTION, BASE CASE, MEAN, PGA = 0.818 G
 - - - APPROACH 1, 10-4 ROCK CONTROL MOTION, BASE CASE, 16TH PERCENTILE, PGA = 0.483 G

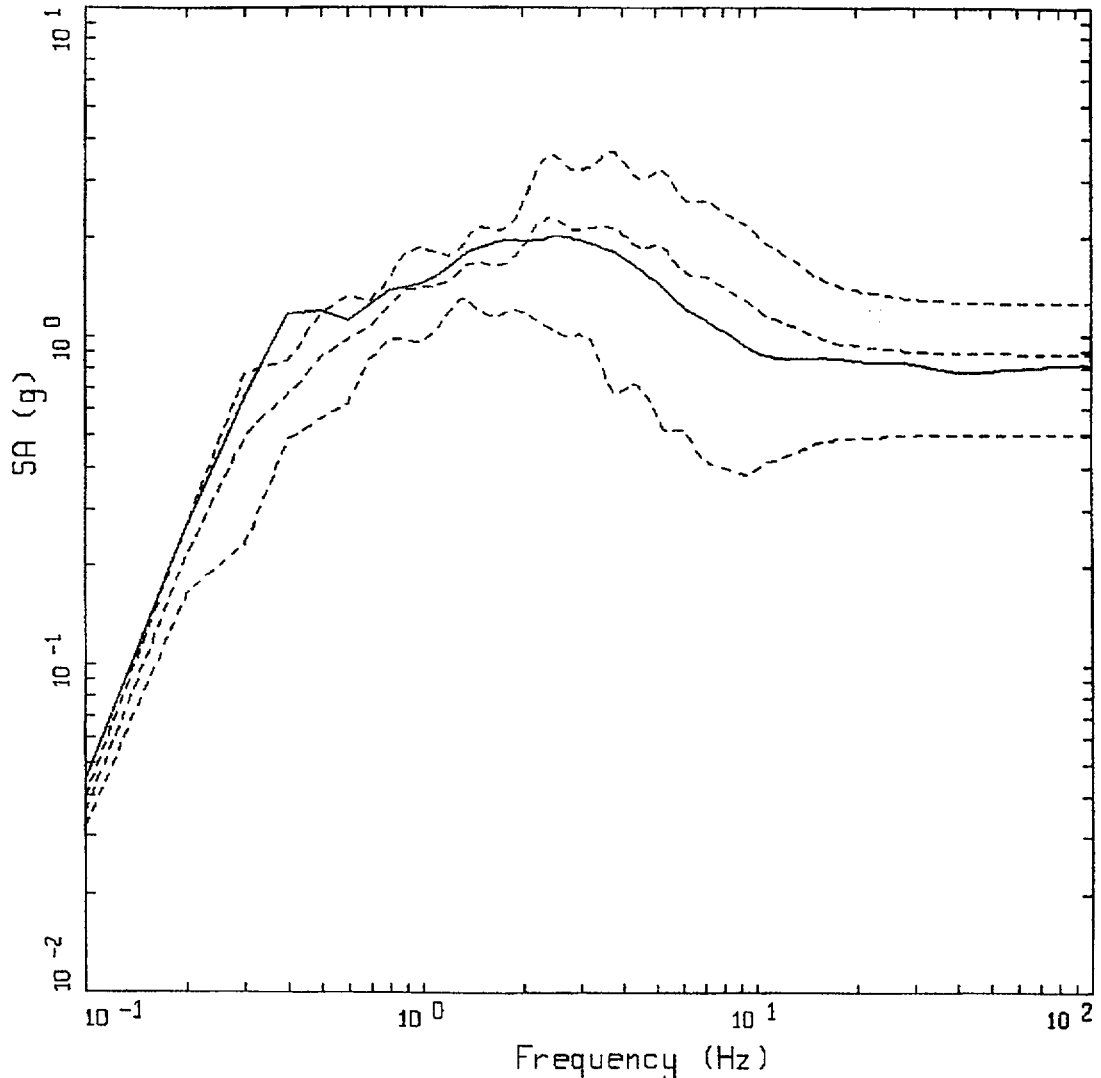
Figure 6-163. Comparison of soil spectra for Approach 2B (full profile) with mean and $\pm 1\sigma$ deterministic profile variations with profile truncated at 150m. Soil profile Meloland, WUS conditions.



WUS 10E-4 APPROACH COMPARISON, IV
 SOIL PROFILE TO 90 M (300 FT)

- LEGEND
- APPROACH 2, 1 HZ AND 10 HZ DEAGGREGATION EQKS, MEAN PGA = 0.817 G
 - APPROACH 1, 10-4 ROCK CONTROL MOTION, BASE CASE PGA = 0.855 G
 - APPROACH 1, 10-4 ROCK CONTROL MOTION, BASE CASE (UPPER) PGA = 1.150 G
 - . - . - . APPROACH 1, 10-4 ROCK CONTROL MOTION, BASE CASE (LOWER) PGA = 0.733 G

Figure 6-164. Comparison of soil spectra for Approach 2B (full profile) with base case profile and deterministic profile variations (\pm factor of 2 on shear modulus) with profile truncated at 90m; soil profile Meloland, WUS conditions.



WUS 10E-4 APPROACH COMPARISON, IV
 SOIL PROFILE TO 90 M (300 FT)

- LEGEND
- APPROACH 2, 1 HZ AND 10 HZ DEAGGREGATION EQKS, MEAN PGA = 0.817 G
 - - - - - APPROACH 1, 10-4 ROCK CONTROL MOTION, BASE CASE, 84TH PERCENTILE, PGA = 1.259 G
 - · - · - APPROACH 1, 10-4 ROCK CONTROL MOTION, BASE CASE, MEAN, PGA = 0.884 G
 - · · · · APPROACH 1, 10-4 ROCK CONTROL MOTION, BASE CASE, 16TH PERCENTILE, PGA = 0.508 G

Figure 6-165. Comparison of soil spectra for Approach 2B (full profile) with mean and $\pm 1\sigma$ profile variations with profile truncated at 90m. Soil profile Meloland, WUS conditions.

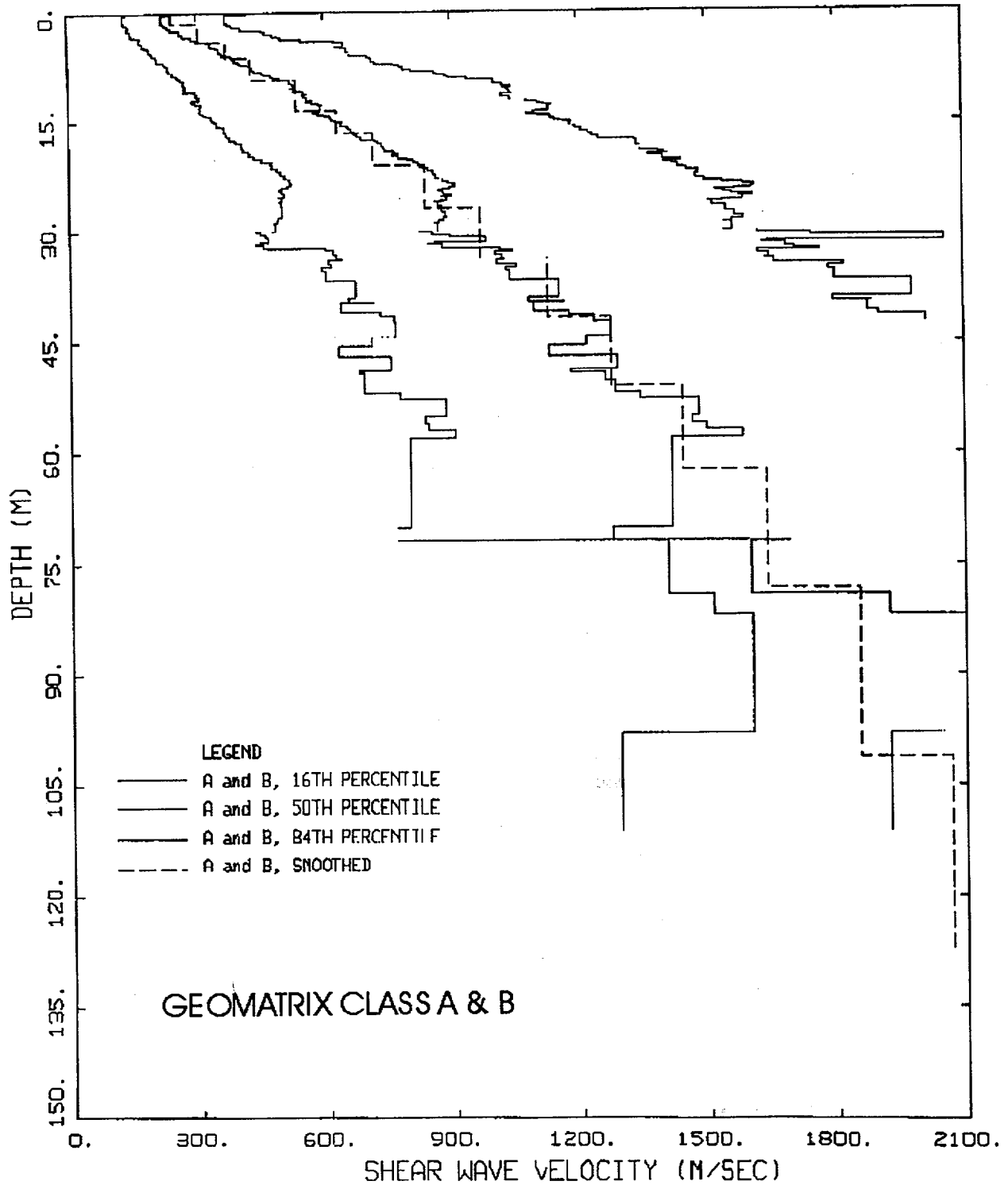
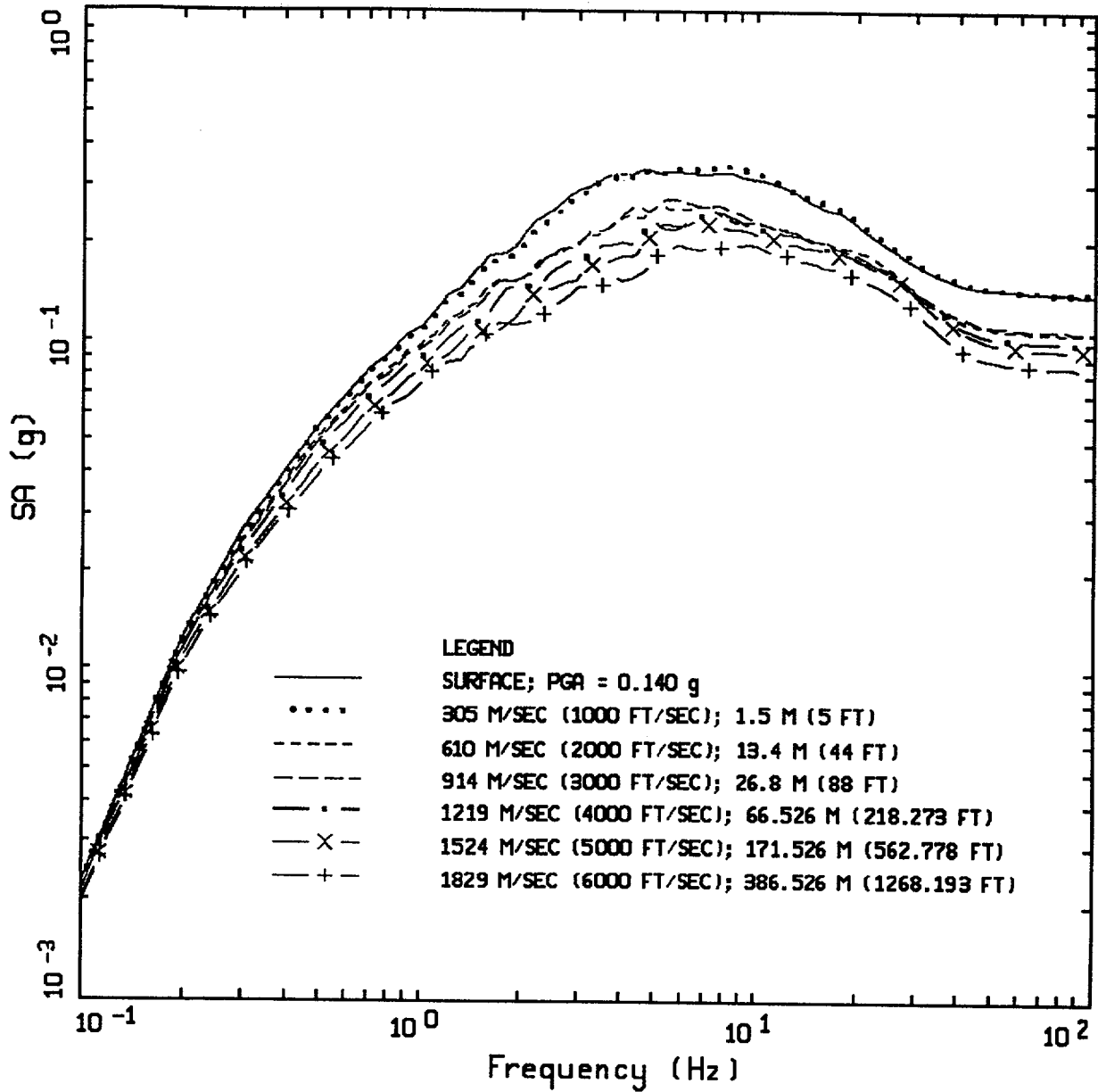
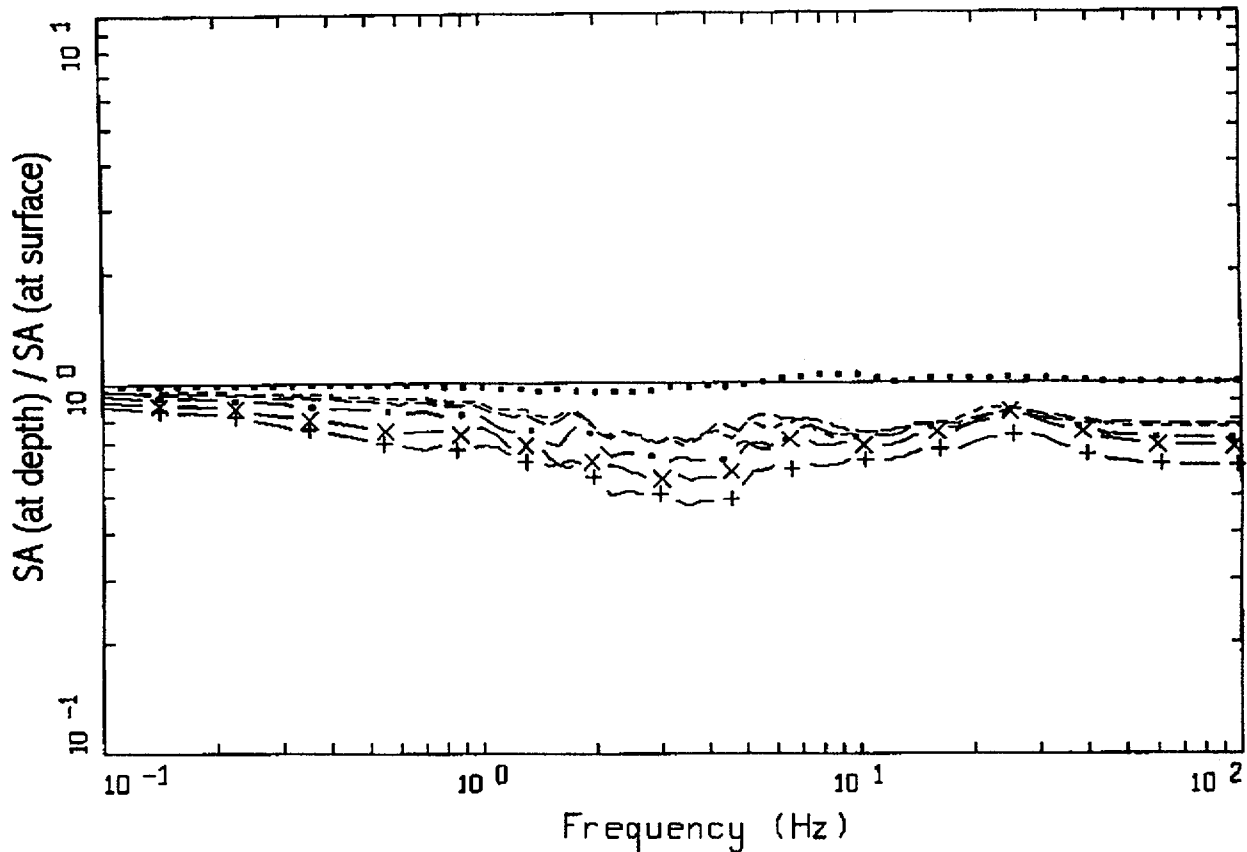


Figure 6-166. Median and $\pm 1\sigma$ shear-wave velocities based on measurements at WUS rock strong motion sites. Geomatrix categories A and B (Appendix A) assumed to reflect rock site conditions. Dashed line is smooth model used in analyses.



NRC, AVERAGE HORIZONTAL SPECTRA
M=6.5, D=25 KM, STRESS DROP = 55 BARS

Figure 6-167. Median WUS rock response spectra (5% damping) computed for $M = 6.5$ at a distance of 25 km using the soft rock profile (Figure 6-166) and the point source model (Appendix D). Suite of depths (shear-wave velocities) reflect depth to which overlying materials are removed.

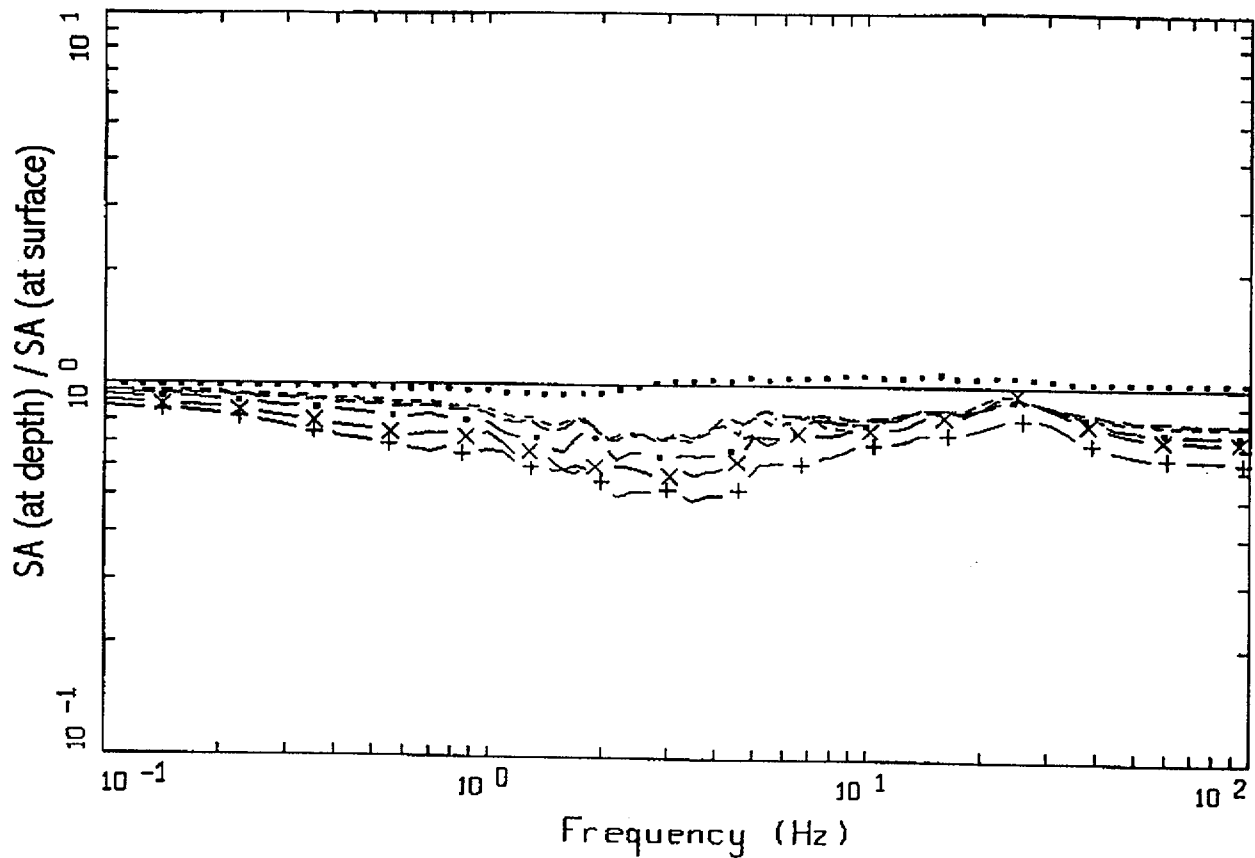


NRC, M=6.5, D=25 KM

LEGEND

- SURFACE RATIO OVER SURFACE; 0 M; PGA = 0.140 g
- 305 M/SEC (1000 FT/SEC) RATIO OVER SURFACE; 1.5 M (5 FT)
- 610 M/SEC (2000 FT/SEC) RATIO OVER SURFACE; 13.4 M (44 FT)
- 914 M/SEC (3000 FT/SEC) RATIO OVER SURFACE; 26.8 M (88 FT)
- . - 1219 M/SEC (4000 FT/SEC) RATIO OVER SURFACE; 66.526 M (218.273 FT)
- X - 1524 M/SEC (5000 FT/SEC) RATIO OVER SURFACE; 171.526 M (562.778 FT)
- + - 1829 M/SEC (6000 FT/SEC) RATIO OVER SURFACE; 386.526 M (1268.193 FT)

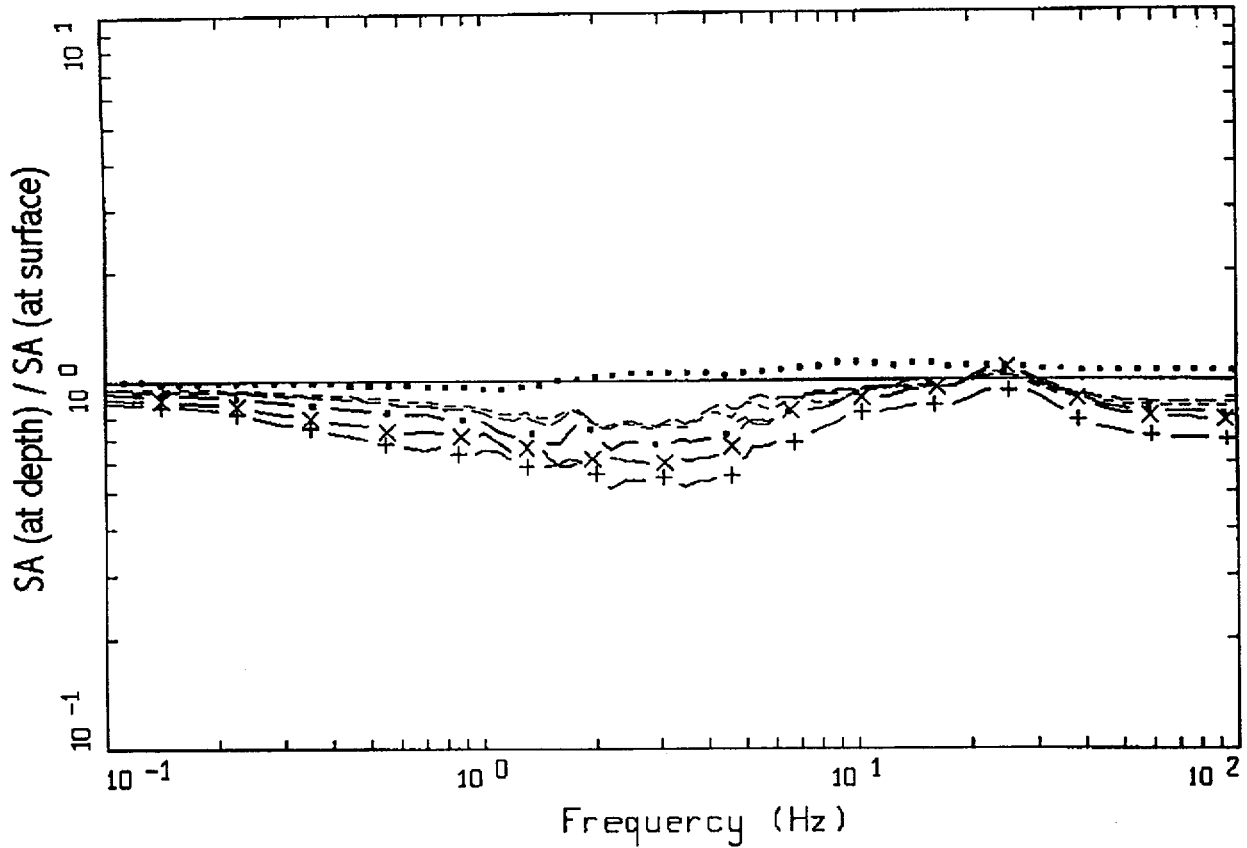
Figure 6-168. Depth-to-surface response spectral ratios (median estimates) computed for the suite of spectra shown on Figure 6-167.



NRC, M=6.5, D=10 KM

- LEGEND
- SURFACE RATIO OVER SURFACE; 0 FT; PGA = 0.306 g
 - 305 M/SEC (1000 FT/SEC) RATIO OVER SURFACE; 1.5 M (5 FT)
 - 610 M/SEC (2000 FT/SEC) RATIO OVER SURFACE; 13.4 M (44 FT)
 - 914 M/SEC (3000 FT/SEC) RATIO OVER SURFACE; 26.8 M (88 FT)
 - . - 1219 M/SEC (4000 FT/SEC) RATIO OVER SURFACE; 66.526 M (218.273 FT)
 - X - 1524 M/SEC (5000 FT/SEC) RATIO OVER SURFACE; 171.526 M (562.778 FT)
 - + - 1829 M/SEC (6000 FT/SEC) RATIO OVER SURFACE; 386.526 M (1268.193 FT)

Figure 6-169. Depth-to-surface response spectral ratios (median estimates) computed for M=6.5 at a distance of 10 km.

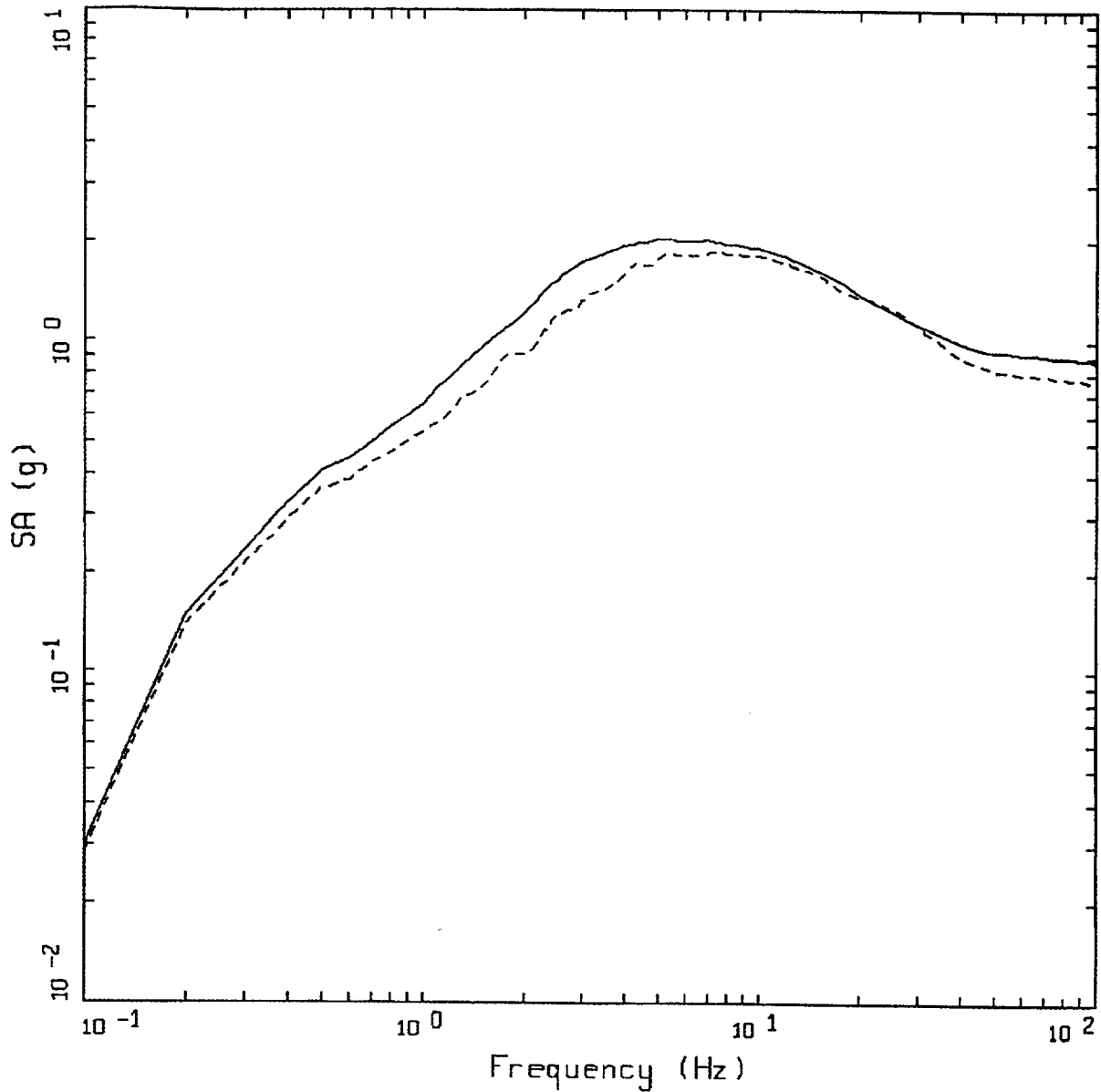


NRC, M=6.5, D=1 KM

LEGEND

- SURFACE RATIO OVER SURFACE; 0 M; PGA = 0.483 g
- 305 M/SEC (1000 FT/SEC) RATIO OVER SURFACE; 1.5 M (5 FT)
- 610 M/SEC (2000 FT/SEC) RATIO OVER SURFACE; 13.4 M (44 FT)
- 914 M/SEC (3000 FT/SEC) RATIO OVER SURFACE; 26.8 M (88 FT)
- • — 1219 M/SEC (4000 FT/SEC) RATIO OVER SURFACE; 66.526 M (218.273 FT)
- × — 1524 M/SEC (5000 FT/SEC) RATIO OVER SURFACE; 171.526 M (562.778 FT)
- + — 1829 M/SEC (6000 FT/SEC) RATIO OVER SURFACE; 386.526 M (1268.193 FT)

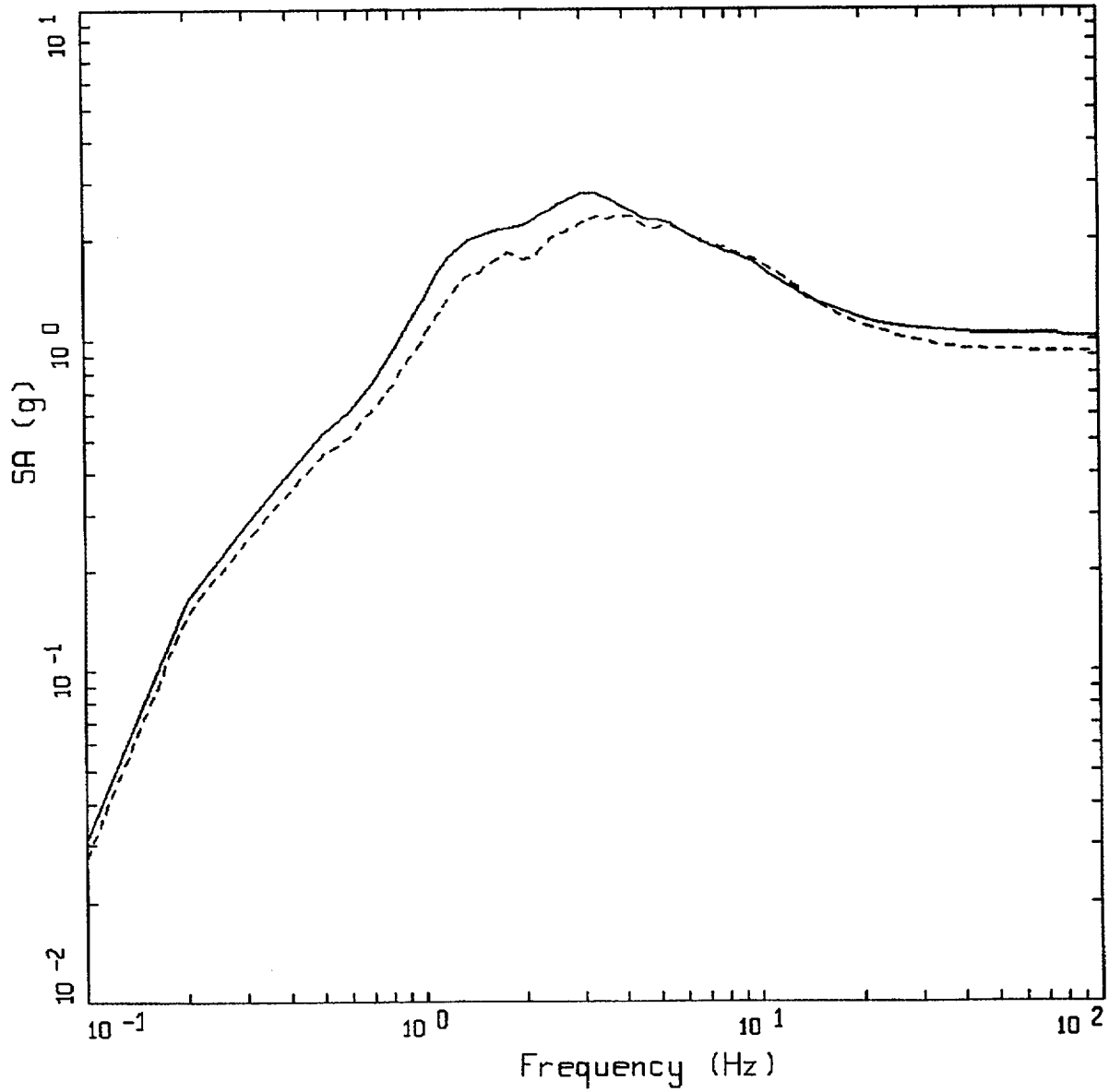
Figure 6-170. Depth-to-surface response spectral ratios (median estimates) computed for M=6.5 at a distance of 1 km.



ROCK OUTCROP SPECTRA

- LEGEND
- WUS ROCK UNIFORM HAZARD SPECTRA, PGA=0.884 g
 - - - MODIFIED ROCK UNIFORM HAZARD SPECTRA, PGA=0.767 g

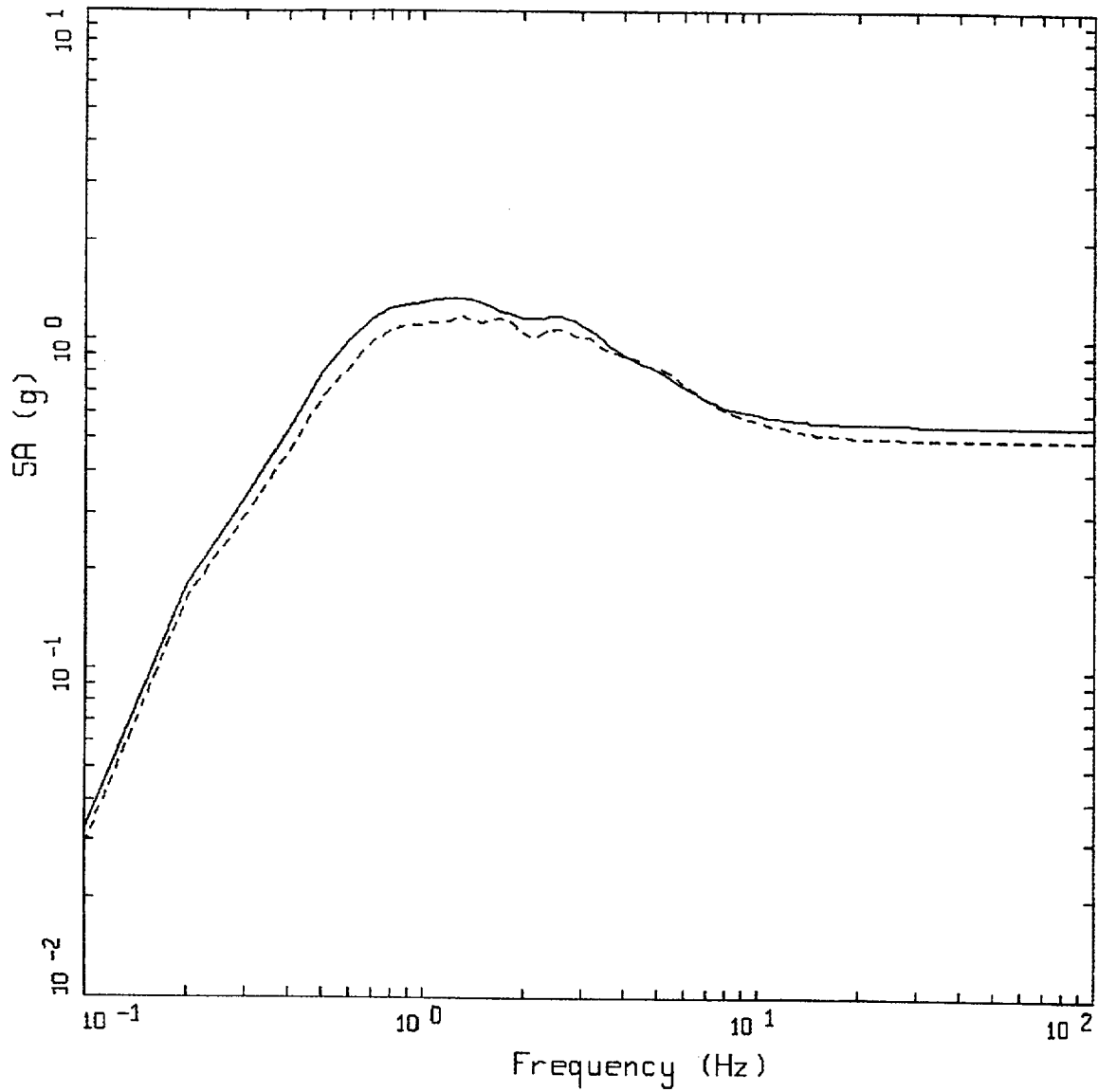
Figure 6-171. Comparison of WUS UHS at surface of rock site (solid line) and UHS at free surface with a shear-wave velocity of 914m/sec (3,000 ft/sec) using transfer function corresponding to surface acceleration of 0.483g (Figure 6-170). Modified spectrum represents modification of surface soft rock motions to base-of-soil motions.



CONTROL MOTION COMPARISON, RI

- LEGEND
- APPROACH 1, 10-4 ROCK CONTROL MOTION, MEAN PGA = 1.027 G
 - - - - - APPROACH 1, MODIFIED 10-4 ROCK CONTROL MOTION, MEAN PGA = 0.922 G

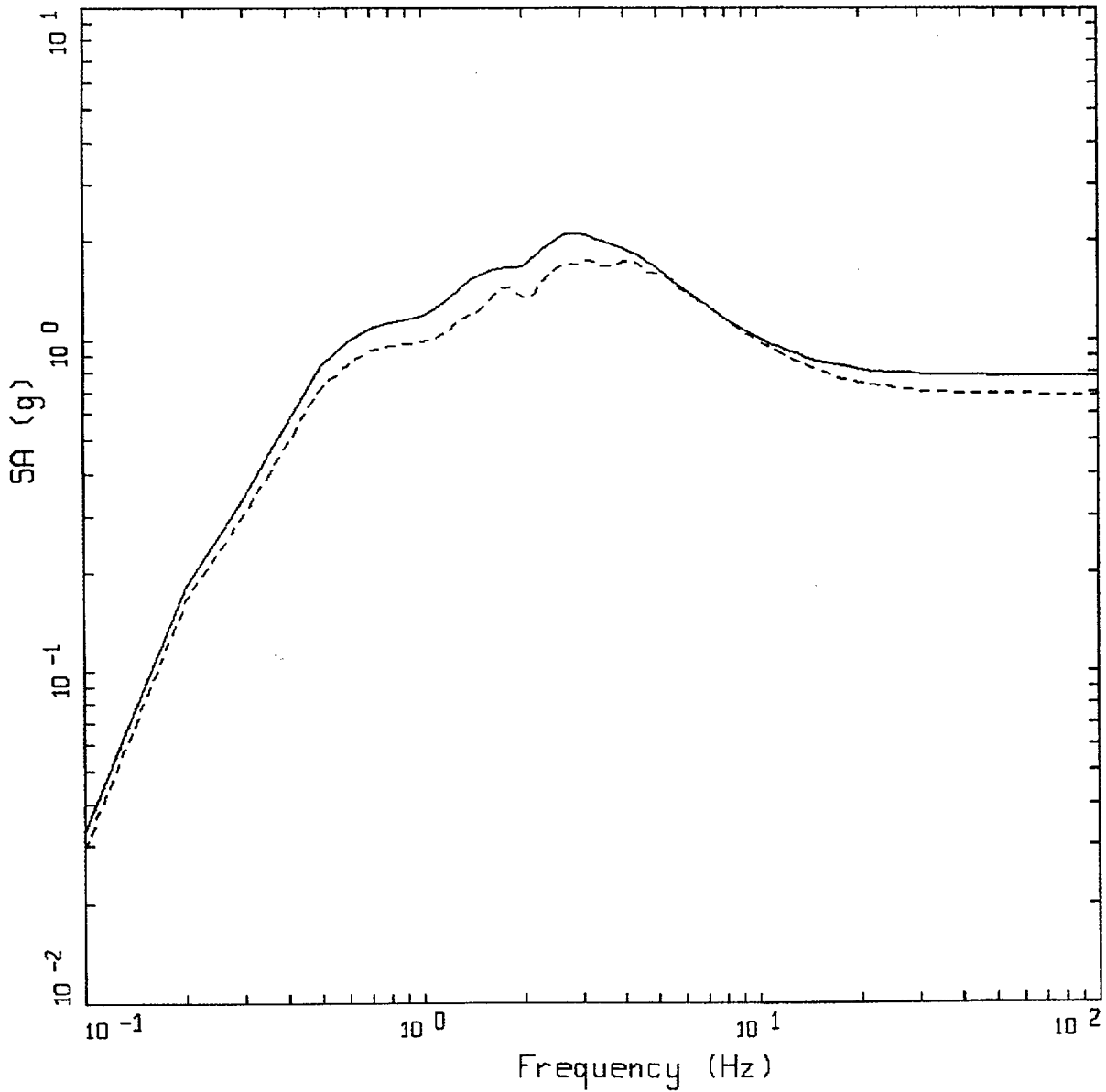
Figure 6-172. Comparison of WUS soil motions using rock UHS and modified rock (base-of-soil) UHS soil profile Rinaldi.



CONTROL MOTION COMPARISON, GZ

- LEGEND
- APPROACH 1, 10-4 ROCK CONTROL MOTION, MEAN PGA = 0.550 G
 - - - APPROACH 1, MODIFIED 10-4 ROCK CONTROL MOTION, MEAN PGA = 0.500 G

Figure 6-173. Comparison of WUS soil motions using rock UHS and modified rock (base-of-soil) UHS soil profile Gilroy 2.

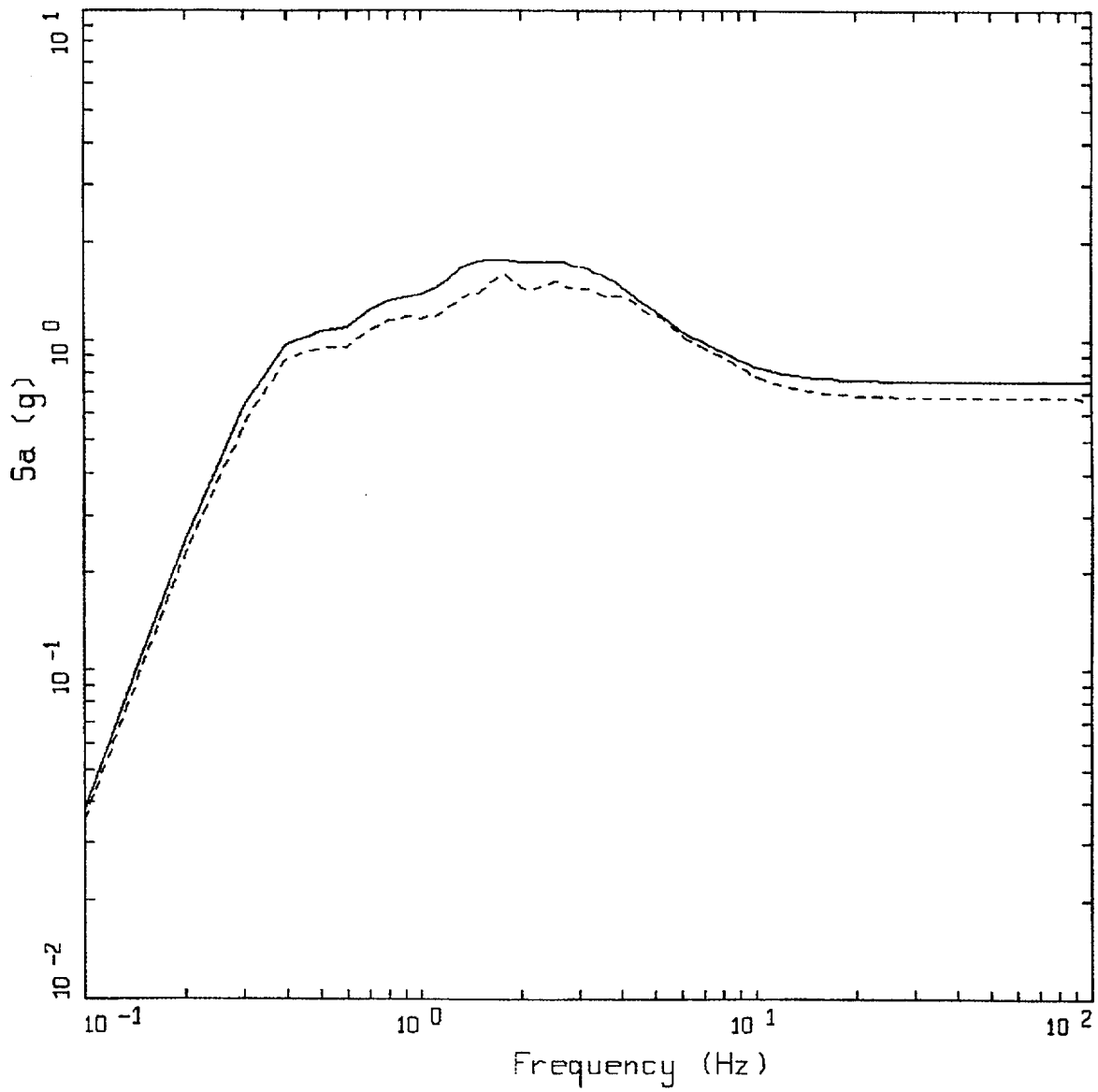


CONTROL MOTION COMPARISON, SR

LEGEND

- APPROACH 1, 10⁻⁴ ROCK CONTROL MOTION, MEAN PGA = 0.777 G
- APPROACH 1, MODIFIED 10⁻⁴ ROCK CONTROL MOTION, MEAN PGA = 0.686 G

Figure 6-174. Comparison of WUS soil motions using rock UHS and modified rock (base-of-soil) UHS soil profile Savannah River Generic.



CONTROL MOTION COMPARISON, IV

- LEGEND
- APPROACH 1, 10-4 ROCK CONTROL MOTION, MEAN PGA = 0.755 G
 - - - APPROACH 1, MODIFIED 10-4 ROCK CONTROL MOTION, MEAN PGA = 0.672 G

Figure 6-175. Comparison of WUS soil motions using rock UHS and modified rock (base-of-soil) UHS soil profile Meloland.

7 PROCEDURE FOR THE DEVELOPMENT OF RISK-CONSISTENT SPECTRA

7.1 Introduction

Within the general purpose of developing recommendations for earthquake ground motions is the specific goal of achieving consistency for different sites and site conditions. This raises the question of what is meant by "consistency," and over what range of sites and site conditions it is to be achieved. For the purposes of this project we mean by "consistency" that the ground motion recommendations result in facilities at different sites having about the same level of safety from earthquake-caused failures, no matter where they are located in the country. The achievement of consistency should be judged from highly seismic locations on the west coast of the US, to locations with the possibility of rare but large earthquakes on the east coast, to locations with low seismicity in the Midwest. The range of site conditions should span hard rock sites in the east, to soft rock sites in the west, to alluvium site conditions throughout the country that might reasonably be the foundation material for nuclear facilities (extremely soft soils being excluded).

It is a major effort to evaluate the seismic safety of an existing nuclear facility, and many studies have undertaken that task. It would be an even more daunting task to estimate the seismic safety of an unspecified facility whose specific features and redundancies have not yet been defined. For this reason we judge the seismic safety of a facility by the safety of its individual components, for which we have extensive experience from detailed seismic safety evaluations, and do not attempt to estimate the safety of an integrated facility as a whole.

Other parts of this project have derived ground motion spectral shapes and time histories for rock and soil sites, and have examined methods to scale ground motions to target spectra. Those results are to be used once the seismic hazard and a design spectrum are determined for a site, to obtain realistic spectral shapes for the controlling earthquakes and to derive time histories of motion for detailed analyses. The current recommendations (on risk- and hazard-consistent spectra) are to be used to determine the design spectra at a site, once the initial probabilistic seismic hazard results have been calculated.

Many factors affect seismic safety, of course. First is the level of seismic hazard, how frequently large earthquake ground motions might occur. Second is how that frequency of occurrence changes with ground motion amplitude, which is quantified as the "slope" of the hazard curves. This slope can depend on the natural period of a specific component as well as on the seismic environment. Presuming the hazard curves have been defined for rock conditions, which is the typical case, a third factor is how any local soils amplify or deamplify the ground motion, recognizing that this amplification (or deamplification) depends on the amplitude of the incoming rock motion. The fourth factor is the facilities components: how robust are they to seismic shaking and how certain (or uncertain) are we of that robustness?

The methods that follow account for the first, second and fourth factors, and lead to recommendations on deriving seismic design spectra that are consistent for a range of sites and seismic hazard conditions. While not all sites or conditions have been examined (it would be prohibitive in time and expense to do so), we are confident that the ranges of sites and conditions are

wide enough that our recommendations are solid. With respect to accounting for the effects of local soils, the results presented here are less conclusive and do point to the critical issues that need to be addressed, rather than to the resolution of those issues.

7.2 Methodology

7.2.1 Concepts and Goals for Seismic Risk Consistency Across Sites

The goal of achieving seismic risk consistency across sites is interpreted here as achieving the same levels of safety for the components of nuclear facilities to resist seismic shaking. Many studies of complete nuclear plants have been conducted in the US and overseas, but it would be difficult to interpret the results of those studies (even knowing the seismic design criteria) into a general recommendation for seismic components. Many components of plants have a seismic ruggedness that is well above that required by regulations, for various reasons, and interpreting the seismic safety of a plant as if all its components were designed to just meet the overall site seismic design criterion would be erroneous. Further, there is no target overall or seismic plant-level failure frequency that has been deemed acceptable by nuclear agencies. From these numerous studies of nuclear plant seismic safety has come a wealth of experience on individual component ruggedness to seismic shaking. Thus it more fruitful to examine the goal of seismic risk consistency on an individual component basis. What we can achieve is a recommendation on ground motion spectra that is robust on a relative basis from site to site, based on component responses. Thus we judge the degree of "seismic risk consistency" by evaluating the probability of failure of components for a range of sites and site conditions.

It is useful to first review the steps for specifying a required seismic capacity. This will introduce the nomenclature and clarify further discussions about design procedures and recommendations.

The development of design earthquakes and required capacities for components and equipment of nuclear power plants (NPP's) can be represented as three steps, as illustrated in Figure 7.1.

Step 1: Safe Shutdown Ground Motion. This step (illustrated in Figure 7.1 as 1A, 1B, and 1C) derives amplitudes of the Design Response Spectrum (DRS) in units of spectral acceleration (or its equivalent), either from a hazard curve (1A), from an attenuation equation for a given M and R (1B), or from a "standard" (or "site-specific") spectral shape (1C) anchored to a ground motion amplitude. The DRS is specified over a range of structural frequencies. (We deliberately use the term "DRS" here in place of "SSE" to emphasize that a *ground motion* is being specified from the hazard analysis, not an earthquake defined by a magnitude M and distance R. The dominant M and R may well be specified, but this would be information in support of a ground motion level.)

Step 2: Demand Analysis. This step translates the DRS ground motions into "demand" in terms of force on members, stress, etc., (step 2 in Figure 7.1) using for example dynamic structural analysis. In standard NPP design (as represented by ASCE [1986] 4-86 and USNRC Standard Review Plans) several factors contribute to conservatism in this step:

- Conservative damping values are used in estimating structural response.

- Multiple SSI analyses are performed and the envelope of these results is used, and
- any peaks in the response spectrum are broadened so that the structure at its natural frequency will be affected by those peaks.

These factors lead to a conservative estimate of demand for the given DRS. That is, when the Design Response Spectrum is specified at the 84% level (e.g. as illustrated in 1B or 1C in Figure 1), the calculated demand is also at about the 84% level, because of conservatisms in traditional demand calculations.

Step 3: Capacity Analysis. The required capacity of structural components is specified in terms of its fragility curve (illustrated as #3 of Figure 7.1). Here the fragility curve is a “composite” in the sense that it includes both randomness and uncertainty. As long as we are concerned only about mean or median risk numbers, we need not distinguish between randomness and uncertainty in the fragility curve. (This statement is true exactly for the mean and approximately for the median.) The High-Confidence of Low Probability of Failure (HCLPF) point on the fragility curve is a convenient point at which to specify the design capacity of a component. Traditionally, when randomness and uncertainty are segregated in component fragility analysis, the HCLPF corresponds to a 95% confidence (over uncertainty) of less than a 5% (over randomness) frequency of failure. When randomness and uncertainty are combined, this corresponds very closely to a 1% mean frequency of failure given the demand. Several points on the fragility curve of Figure 7.1 are identified: the HCLPF is indicated as the point at which there is a 1% frequency of failure for the given demand, CAP_{50} indicates the point at which there is 50% frequency of failure, and CAP_{10} indicates the point at which there is 10% frequency of failure. Here, “failure” is defined in terms of the performance level for that component, i.e. the component is affected to the extent that it cannot perform its intended function for the safety systems in which it participates.

Several terms are important. First, “seismic margin” applies to the product of conservatisms introduced in step 2 (for demand analysis) and in step 3 (capacity analysis). Also, herein β_R refers to the logarithmic standard deviation of response, and β_C to the logarithmic standard deviation of capacity. The combined logarithmic standard deviation β equals $\sqrt{\beta_R^2 + \beta_C^2}$, and this is the uncertainty measure used to characterize seismic fragility.

For typical codes (e.g. ASCE [1986] 4-86 and the USNRC Standard Review Plans) the design philosophy is to ensure that the calculated demand given the SSGM is at about the 84% level (this distribution being over uncertainties in response), so point 2 divided by point 2' in Figure 7.1 can be represented as $\exp(1.0 \beta_R)$, assuming a lognormal distribution. Also, typical design codes for civil structures and mechanical systems adopt several conservatisms to ensure a mean capacity well above the calculated demand, such as:

- Nominal capacities for members are chosen through the lowest data points,
- Strength reduction factors are used,
- Yield stresses are specified below average yield stress data,
- Load factors may be applied, and
- Ductility capacity in members above their yield strength may be present.

These conservatisms mean that, if CAP_{10} is the measure of capacity, the ratio of CAP_{10} /point 2 is typically 1.75 to 2.5. This ratio is illustrated with a value of 1.87 on Figure 7.1. For nuclear power plant design the factor of safety has typically been 1.25 to 1.5 (R.P. Kennedy, personal communication, 1997) on the HCLPF (point 3/point 2); this does not mean that nuclear plants have lower safety, just that the factor of safety is measured from a different point (the HCLPF vs CAP_{10}). Assuming a typical lognormal distribution for capacity (using β_C to represent logarithmic standard deviation), the ratio of CAP_{50} to the HCLPF is $\exp(2.32 \beta_C)$ because the HCLPF represents the 1% frequency of exceedence, by definition.

We understand a desire by the NRC to achieve a Factor of Safety of 1.67 from the calculated demand (point 2) to the HCLPF (point 3). Note that this does not, by itself, imply more stringent seismic criteria than what has been practiced in the past; other factors (in particular, the DRS) need to be specified to determine absolute seismic design levels. For a factor of safety of 1.67, the total seismic margin on capacity CAP_{50} (point 5/point 2) is

$$\begin{aligned} 1.67 \exp(1.0\beta_R + 2.32\beta_C) &\approx 1.67 \exp(2.32\sqrt{\beta_R^2 + \beta_C^2}) \\ &\approx 1.67 \exp(2.32\beta) \end{aligned} \quad (7.1)$$

The goal in developing risk-consistent spectra is to understand the relevant design codes and their implicit seismic margin, choose an appropriate DRS (perhaps scaled by some factor), and ensure that the resulting probability of component failure (represented by its mean or median) is acceptable. Factors that will influence the calculated probability of failure are:

1. The annual probability of exceedence that is chosen for the DRS, and whether this choice is a median or mean value (over uncertainties in seismic hazard)
2. The slope of the seismic hazard curve (annual probability of exceedence vs. ground motion)
3. The design seismic capacity (whether it is measured at the HCLPF, CAP_{10} , or some other value)
4. The uncertainty in response, β_R
5. The uncertainty in capacity, β_C .

With respect to item no. 1 above, we cannot make an independent recommendation, except to point out that if an acceptable failure frequency for components were adopted, a DRS could be designated (through its frequency of exceedence) to achieve that component failure frequency. With respect to mean vs. median hazard curves, there are advantages to using mean values, and these are reviewed below.

The slope of the hazard curve, item no. 2, can be taken into account through a very simple modification of the uniform hazard spectrum. This is demonstrated in Section 7.3.

The choice of where the seismic capacity is measured is not really a choice. Tradition has linked the HCLPF to the 1% frequency of failure level, and we are reluctant to recommend major changes to design codes and procedures to implement a new definition of seismic capacity, even though some advantages would accrue by doing so. Thus the recommendation will remain to use the HCLPF defined at 1% frequency of failure.

Items no. 4 and 5 above relate to uncertainties in facility response and component capacity under seismic shaking. These are not known before design, and it would be unworkable to require knowledge of a structure's or component's seismic response before it has been designed, in order to specify the seismic design requirement for it. Thus we pursue recommendations for a range of β factors, the range being consistent with past experience.

7.2.2 Factors Affecting Seismic Risk

Numerous factors affecting the evaluation of seismic risk, evaluated here as the probability of seismically induced failure of a component. This failure probability can be represented as:

$$P_F = \int_0^{\infty} H(a) \frac{dP_{F/a}}{da} da \quad (7.2)$$

where $H(a)$ is the hazard curve and $P_{F/a}$ is the probability of failure (the "fragility") given ground motion amplitude "a," which captures both response and capacity uncertainties (See Kennedy and Short, 1994, equation (5b) for further discussion.)

The integrand in equation (7.2) is represented in Figure 7.2, which is a re-drawing of the bottom illustration in Figure 7.1 with two changes. First, the component fragility is represented as a density function, not a cumulative function (this is $dP_{F/a}/da$ in equation (7.2)). Second, the abscissa of the plot has been translated back to ground motion amplitude units instead of demand units.

In words, equation (7.2) says that the total annual probability of failure equals the probability that the component fragility is "a," times the annual probability that "a" is exceeded, integrated over all values of "a." If we move the density function of component fragility to the right (increase its strength), P_F goes down. If we move it to the left, P_F goes up.

Several important effects of hazard curves and fragility curves on P_F have been investigated by Kennedy and Short (1994). These are illustrated here on separate figures.

The parameter β quantifies the uncertainty in the seismic fragility. For most equipment and components, β lies in the range 0.3 to 0.6. Figure 7.3 illustrates two seismic fragility distributions, C_1 with a small β and C_2 with a large β , both with the same CAP_{10} value. That is, the area under both the C_1 and C_2 curves below CAP_{10} is 10%. For DOE facilities, Kennedy and Short (1994) found that specifying the seismic fragility by CAP_{10} resulted in the P_F being insensitive to β . This means that the component with seismic fragility C_1 will have about the same failure probability P_F as the component with seismic fragility C_2 . This occurs, as illustrated in Figure 7.3, because over the important range

of amplitudes, sometimes $C_1 > C_2$ and sometimes $C_2 > C_1$, so that the total P_F is about the same. For other definitions of component capacity, e.g. the HCLPF, this insensitivity does not hold. That is, if the component capacity is defined at the HCLPF, P_F is sensitive to the β value of the component. This is illustrated in the next Section.

Another effect relates to the slope of the hazard curve. Figure 7.4 illustrates two hazard curves with different slopes, and these are quantified by K_H . K_H is the negative slope of the hazard curve on log-log scale; steeper curves have higher K_H values. Typical K_H values for U.S. plants range from 1.5 to 6. On the west coast K_H tends to be higher (steeper hazard curves) because plants are designed closer to the maximum magnitudes on faults and the hazard curve falls off faster with higher ground motions. For a specific site, K_H tends to be lower for low frequencies and higher for high frequencies.

The other parameter related to K_H that describes the hazard curve slope is A_R , and the two are related by

$$A_R = 10^{\frac{1}{K_H}} \quad \text{or} \quad K_H = \frac{1}{\log_{10} A_R} \quad (7.3)$$

A_R is the increase in ground motion corresponding to a factor of ten decrease in annual probability. As Figure 7.4 illustrates, $K_H=3.32$ corresponds to $A_R=2.0$ and $K_H=2.10$ corresponds to $A_R=3.0$.

Figure 7.5 compares two hazard curves with different slopes to a capacity curve. In this plot, the vertical axis is probability on a linear scale, so the hazard curves appear curved. If the hazard curves are equal at some annual probability (e.g. 10^{-4}) for a low-amplitude ground motion, the curve with the shallower slope (lower K_H , higher A_R) will cause a larger P_F . This is the case because, at all "a" values of interest, $H_2(a) > H_1(a)$.

This means that if we use the ground motion a associated with same annual probability of exceedence as the starting point for design, we must have a factor that makes the required capacity depend on the hazard curve slope, to achieve consistent P_F 's for all slopes. The alternative would be to assume a worst case (shallow) hazard curve slope; then the design for components at a site with a steeper hazard curve will be overly conservative. Or, one could specify a very high DRS and no conservatism in the response/capacity analysis, but this would significantly change current design practice and would not be easily accepted.

The quantitative effects of these sensitivities to β and slope are examined in Section 7.3 using actual sites and hazard curves from across the US.

7.2.3 Risk Equation

With some realistic assumptions on the shape of the hazard curve and the fragility curve, it is possible to derive a simple expression for P_F . This derivation has been done elsewhere (e.g. Sewell et al, 1990; 1996; Kennedy and Short, 1994), and is repeated here for completeness.

First we assume that the hazard curve $H(a)$ is linear on log-log scale, i.e.

$$H(a) = ka^{-K_H} \quad (7.4)$$

Actual hazard curves tend to get steeper at higher amplitudes, but over the important range of amplitudes for P_F calculations they can be approximated as linear on log-log scale.

Second we assume that component fragilities are lognormally distributed. This means that

$$P_{F/a} = \int_0^a \frac{1}{y\sqrt{2\pi\beta}} \exp\left\{-\frac{(\ln y - \overline{\ln y})^2}{2\beta^2}\right\} dy \quad (7.5)$$

where $\overline{\ln y} = \ln CAP_{50}$.

Substituting equations (7.4) and (7.5) into (7.2) gives

$$P_F = \int_0^\infty ka^{-K_H} \frac{1}{a\sqrt{2\pi\beta}} \exp\left\{-\frac{(\ln a - \overline{\ln a})^2}{2\beta^2}\right\} da \quad (7.6)$$

Transforming the integration variable a to variable $x = \ln a$ gives

$$P_F = \frac{k}{\sqrt{2\pi\beta}} \int_{-\infty}^\infty \exp\{-K_H x\} \exp\left\{-\frac{(x - \overline{\ln a})^2}{2\beta^2}\right\} dx \quad (7.7)$$

The integrand above is in the form

$$\exp\{cx\} Z(x) \quad (7.8)$$

where c is a constant and $Z(x)$ is the normal density function. The definite integral equation (7.7) can be solved by expansion or by published methods of integrating functions of normal probability distribution (e.g. Owens, 1980), yielding

$$P_F = kCAP_{50}^{-K_H} \exp\left\{\frac{1}{2}(K_H\beta)^2\right\} \quad (7.9)$$

This form, designated the "risk equation," was first derived by G. Toro during discussions with C.A. Cornell and published in Sewell et al. (1990, 1996). Expressing the hazard $H(a')$ at a ground motion level a' corresponding to the uniform hazard spectrum (UHS), using equation (7.4) gives:

$$H(a') = k(a')^{-K_H} \quad (7.10)$$

Solving for k and substituting into equation (7.9) gives:

$$P_F = H(a')^{K_H} CAP_{50}^{-K_H} \exp\left\{\frac{1}{2}(K_H\beta)^2\right\} \quad (7.11)$$

We can now derive a probability ratio R_p as the probability $H(a')$ that a' will be exceeded, divided by the probability of failure P_F :

$$R_p = H(a')/P_F \quad (7.12)$$

This ratio is usually much greater than unity because P_F is much less than the hazard at a' . R_p can be expressed as:

$$R_p = \left(\frac{CAP_{50}}{a'}\right)^{K_H} \exp\left\{-\frac{1}{2}(K_H\beta)^2\right\} \quad (7.13)$$

Instead of using CAP_{50} to designate capacity, we can use the HCLPF, where for a lognormal distribution the two are related by

$$HCLPF = CAP_{50} \exp\{-x_p\beta\} \quad (7.14)$$

where x_p is the number of standard deviates corresponding to the frequency of failure at the HCLPF, which is 2.326 for 1% frequency of failure. Also, we can express the required HCLPF in terms of a' times a factor of safety F_R :

$$HCLPF = a' \cdot F_R \quad (7.15)$$

Solving these last two equations for CAP_{50} and a' , and substituting into equation (7.13) gives:

$$R_p = F_R^{K_H} \exp\left\{x_p K_H \beta - \frac{1}{2}(K_H\beta)^2\right\} \quad (7.16)$$

This gives a simple means to calculate $P_F = H(a') / R_p$, given that the hazard associated with the DRS at (a') is known. The probability ratio R_p depends on the factor of safety F_R , the hazard curve slope K_H , and β of the fragility function; for the HCLPF defined at the 1% frequency of failure point, $x_p = 2.326$ as explained above.

Equation (7.16) also gives an easy way to compute the effect of hazard curve slope and fragility β on P_F for a specified hazard corresponding to a selected Uniform Hazard Spectrum (UHS). Stated another way, if we pick a UHS at each site with the same annual probability of exceedence, and define the required seismic capacity in terms of a HCLPF using equation (7.15), then equation (7.16) allows us to examine the *risk consistency* across sites for different hazard curve slopes K_H and fragility uncertainties β . The use of equation (7.16) in this way is demonstrated in Section 7.3.

A couple of points about the *distributions* of $H(a')$ and P_F are important. $H(a')$ is uncertain because of lack of knowledge in the earth sciences about earthquake sources, ground motions, etc. This uncertainty has been quantified by EPRI and LLNL at CEUS plant sites and by utilities at several WUS plant sites. If we use the mean of this distribution we will achieve a mean P_F for any set of design rules. The mean has the advantage that we can compute (and control) the mean P_F for multiple plants. That is, we have n plants and an average acceptable probability of component failure at these plants, we can achieve that by specifying a mean P_F at each plant. The disadvantage is that the mean is sensitive to low probability, high consequence assumptions in the seismic hazard analysis and is not as stable (from study to study) as the median.

If we use the *median* $H(a')$ we will achieve an *approximate median* P_F . The median has the advantage that it is more stable than the mean, but a target mean or median P_F for n plants cannot readily be translated to a required median P_F at each plant. So use of the median $H(a')$ leads to ill-constrained limits on P_F over multiple plants. For this reason the use of the mean $H(a)$ curve is recommended, although we show example results for both the mean and median in Section 7.3.

A final point is that R_p can be controlled by “deterministic acceptance criteria” associated with design codes and guides, and by a “scale factor” that moves the capacity up or down as a function of the hazard curve slope K_H , the desired P_F , or the desired R_p for a given $H(a)$. This scale factor is conveniently thought of as a scaling of the UHS to specify a DRS. The total factor of safety F_R , defined in terms of point 1 on Figure 7.1 relative to the HCLPF, would then be:

$$F_R = \alpha SF \quad (7.17)$$

where α is the conservatism achieved by design procedures (e.g. 1.67 on the HCLPF) and SF is the scale factor. The new design spectrum is then the UHS scaled by SF . To avoid confusion in terminology we label this scaled spectrum the “uniform reliability spectrum” (URS). We examine one useful form of SF in Section 7.3.

7.2.4 Accounting for Soil Amplification

We have assumed in the derivations of the previous sections that hazard curves are available for a site at critical natural periods, so that the slope of the hazard curves can be determined. For sites located on rock the hazard curve will be determined by a probabilistic seismic hazard analysis (PSHA) for that site’s rock conditions.

For sites with uniform soil conditions across the site, it may be possible to perform the PSHA using site-specific soil attenuation equations. In this case the soil PSHA results can be used directly. For other sites with varying soil conditions, or where some structures will be founded on soil and some on rock, it is likely that the PSHA will be performed for rock conditions, and that a translation to hazard curves at the soil surface will be necessary. In fact, multiple translations on a building-specific basis may be required if soil conditions vary from building to building.

The method of performing this translation to account for soil amplifications is important. Several factors complicate the analysis. First, a comprehensive PSHA includes uncertainties in rock hazard curves, and these must be translated into uncertainties in soil hazard curves. Second, there are always uncertainties in soil dynamic properties (e.g. shear wave velocity, stiffness, and damping characteristics), and these must be included. Third, soil response at high amplitudes will generally be non-linear. This is why the mean rock hazard curves cannot be simply translated to mean soil hazard curves; the distribution of hazard must be examined explicitly.

Section 6 describes several methods of translating rock hazard curves to soil hazard curves, incorporating the above effects. The methods are demonstrated for a range of site conditions. Final recommendations on simple ways of accounting for soil effects, so that the UHS on soil can easily be derived from a PSHA on rock, await further verification of accuracy using a wider range of rock attenuation equation assumptions..

7.3 Examples of Risk-consistent Spectral Amplitudes

As recommended here, risk consistency will be achieved by modifying design spectral amplitudes at two frequencies (10 and 1 Hz) and scaling ground motion spectral shapes (from the appropriate M and R) to those modified amplitudes. The scaling of spectral amplitudes will be done at all frequencies to generate a uniform reliability spectrum (URS) for comparison purposes. As an example, eleven sites are examined in this subsection, using 10 and 1 Hz spectral amplitudes and PGA, to show the risk consistency achieved for those parameters.

7.3.1 Example Sites

With the derivation of probability ratio R_p in Section 7.2, we can examine the risk-consistency of spectra for a range of sites with different hazard curve slopes and a range of fragility curve β 's. The hazard curve slopes K_H will in general vary from site to site and across natural frequencies at any single site.

To test several methods for uniform reliability spectra, we examined eleven sites and three ground motion measures at each site, as follows:

- | | |
|-----------------------------|---------------------------|
| 1. Arkansas plant, PGA | 6. Browns Ferry, SA 10 Hz |
| 2. Arkansas plant, SA 1Hz | 7. Davis Besse, PGA |
| 3. Arkansas plant, SA 10 Hz | 8. Davis Besse, SA 1 Hz |
| 4. Browns Ferry, PGA | 9. Davis Besse, SA 10 Hz |
| 5. Browns Ferry, SA 1 Hz | 10. Maine Yankee, PGA |

- | | |
|------------------------------|--------------------------|
| 11. Maine Yankee, SA 1 Hz | 23. Vogtle, SA 1 Hz |
| 12. Maine Yankee, SA 10 Hz | 24. Vogtle, SA 10 Hz |
| 13. Seabrook, PGA | 25. Zion, PGA |
| 14. Seabrook, SA 1 Hz | 26. Zion, SA 1 Hz |
| 15. Seabrook, SA 10 Hz | 27. Zion, SA 10 Hz |
| 16. Shearon Harris, PGA | 28. California, PGA |
| 17. Shearon Harris, SA 1 Hz | 29. California, SA 1 Hz |
| 18. Shearon Harris, SA 10 Hz | 30. California, SA 10 Hz |
| 19. Susquehanna, PGA | 31. Washington, PGA |
| 20. Susquehanna, SA 1 Hz | 32. Washington, SA 1 Hz |
| 21. Susquehanna, SA 10 Hz | 33. Washington, SA 10 Hz |
| 22. Vogtle, PGA | |

For the first 27 sets of results we used the LLNL hazard curves calculated for the USNRC (Sobel, 1994). For the "California" site, we calculated hazard at a site located near Santa Maria, California (120.5° W, 35.0° N), which has high frequencies dominated by nearby faults and long periods dominated by the more distant San Andreas fault. (A repeat of the 1857 earthquake dominates the long period hazard at this site.) For ground motion estimation the attenuation equation of Abrahamson and Silva (1997) was selected.

The last site examined was in Washington, located at 121°W and 46°N. This is in south-central Washington and also has high frequencies dominated by local earthquakes and low frequencies dominated by a large earthquake. In this case a large subduction zone earthquake controls the long-period hazard. We model this event using the assumptions of the US Geological Survey for the national seismic hazard maps. That is, an earthquake of $M \sim 9$ occurs in the subduction zone with rate 1/500 per year (credibility 1/3), or earthquakes of $M \sim 8$ to 9 occur with rate 1/110 per year (credibility 2/3). For both the California and Washington sites we model local earthquakes with the US Geological Survey gridded seismicity, as well as local faults for the California site.

The hazard curves for the eleven sites are compared in Figures 7.6, 7.7 and 7.8 for PGA, SA at 10 Hz, and SA at 1 Hz, respectively. The upper plot in each figure shows the raw hazard curves, the lower plot normalizes each curve by dividing the acceleration values by the acceleration at 10^{-4} annual probability. This shows that the site hazard curves encompass a range of slopes as well as amplitudes.

Prior to addressing issues of risk consistency, it is useful to examine graphically the details of a calculation of P_F . Figures 7.9 and 7.10 show the contributions to P_F by PGA level, where equation (7.2) has been used to evaluate P_F numerically. This calculation is for the Maine Yankee PGA hazard curve (taken from the LLNL study), shown at the top in both figures. The center plot in each figure shows a fragility curve, for $\beta = 0.3$ in Figure 7.9 and $\beta = 0.6$ in Figure 7.10. The bottom plot in each figure shows the contribution to P_F as a function of ground motion level. For both figures the HCLPF was arbitrarily chosen to be 0.375 g.

The β values of 0.3 and 0.6 were chosen to span the range of values observed for typical nuclear components and equipment (see Kennedy and Short, 1994). The observation from Figures 7.9 and

7.10 is that contributions to P_F come from a range of ground motion levels, from the HCLPF to two or three times the HCLPF.

As a general rule the main contributions come from ground motions at the HCLPF level, to ground motions associated with 0.1 times the hazard at the HCLPF. In Figures 7.9 and 7.10 these are ground motions with 10^{-4} to 10^{-5} annual frequency of exceedence. This rule of thumb was used to develop procedures described in subsequent sections, to estimate risks for a rate of sites and hazard characteristics.

7.3.2 Scaling Factor for Hazard Curve Slopes

As described in Section 7.2, it is convenient to adopt a scale factor SF , to scale the UHS to account for the site-specific (and natural period-specific) slope of the hazard curve. R.P. Kennedy (personal communication, 1997) has suggested the following scale factor:

$$SF = \max\{0.7, 0.35A_R^{1.2}\} \quad (7.18)$$

which was derived by back-figuring the scale factor that would give an approximately constant value of RP (equation 7.16) for a given value of α and range of β .

Recall that as A_R increases, the hazard curves become more shallow. Equation (7.18) indicates that for shallow hazard curves, SF increases, i.e. the design values become higher. With this definition, the URS can be thought of as:

$$URS = UHS \times SF \quad (7.19)$$

i.e. the URS is the UHS “corrected” for the slope of the hazard curve. For $A_R = 2.40$ (which corresponds to slope $K_H = 2.63$), $SF = 1$, i.e. the URS equals the UHS.

Another way to look at the design is through the total factor of safety F_R (see equation (7.17)). If the amount of conservatism in design codes and guides (sometimes referred to as the “deterministic acceptance criterion”) is 1.67, then the total factor of safety F_R is:

$$F_R = 1.67SF \quad (7.20)$$

The advantage of using a slope-dependent scale factor SF as defined in equation (7.18) is demonstrated in the next section.

It is useful to demonstrate the effect of SF on the UHS. Figure 7-11 shows the 10^{-4} UHS for the Columbia site described in Section 6, compared to the URS calculated by scaling the UHS at each frequency by SF . For the Columbia site, $SF > 1.0$ at high frequencies and < 1.0 at low frequencies. This low frequency result comes from the rapid fall-off of hazard between 10^{-4} and 10^{-5} (see Figure 6-45) from the Charleston fault. A site located in a region where the local zone dominates the low frequencies has a shallower hazard curve (see the “Local Background” curve in Figure 6-45). A more

typical case for the CEUS is shown in Figure 7-12, which was calculated for the Columbia site using only the hazard from the local background source. In this case the $URS > UHS$ at all frequencies. For the Mojave site, the hazard curve falls off steeply at all frequencies, so the $URS < UHS$ (see Figure 7-13). This is not surprising given the high rate of occurrence of earthquakes in the region.

7.3.3 Results for Example Sites

Calculations were made of the probability ratio R_p for the 33 site-parameter combinations listed in Section 7.3.1. This is an appropriate parameter to use because, if we start with the same hazard level $H(a')$ at all sites and all natural periods, and achieve a consistent R_p with our procedure, we will achieve a consistent probability of failure P_F .

With this background, Figure 7-14 shows R_p values for the 33 site-parameter combinations, calculated using the *mean* hazard curve for each site. For this plot R_p was calculated from the risk equation (eq. 7.16). The top plot in Figure 7-14 shows R_p when the design response spectrum (DRS) is taken to be *equal* to the UHS at the natural period of the parameter; the bottom plot shows R_p when the DRS is taken to be the $URS = UHS \times SF$, as in equation (7.19). The scale factor SF improves the consistency across sites and across parameters; results without SF vary from about 6 to 130 (a factor exceeding 20), but with SF they vary from about 15 to 45 (a factor of 3). This remaining factor of 3 is the effect of β . It would be inappropriate to define the URS on the basis of component response and capacity uncertainty. Options for choosing $H(a')$ and P_F for a range of β values are reviewed in Section 7.3.4.

Figure 7-15 shows how accurate the risk equation is, for the two definitions of DRS. An exact P_F was obtained by numerical convolution of the hazard curve and fragility curve, and the figures show the ratio of approximate P_F (from the risk equation) to exact P_F (by numerical convolution). A ratio of 1.0 would indicate perfect accuracy in the risk equation. For $DRS=UHS$ the risk equation is generally accurate (ratios of 1.0 to 1.3, with one exception for PGA at the California site); for the $DRS = URS = UHS \times SF$ the results are slightly less accurate (ratios of 1.0 to 1.38). Note that ratios > 1 are "conservative," i.e. the risk equation overestimates P_F . What this means is that, if we plot the "true" R_p (calculated from the numerical convolution), the results are not quite as consistent as shown in Figure 7-14 (bottom), which was prepared with the risk equation. This is shown in Figure 7-16 for the two definitions of the DRS. Values in Figure 7-16 (bottom) range from about 15 (for $\beta=0.3$) to 60 (for $\beta=0.6$). This is still more consistent than for the $DRS = UHS$, where the values range from 7 to 160 (Figure 7-16 [top]), a factor > 20 .

Figures 7-14 and 7-15 were prepared using the risk equation with the slope of the hazard curve defined from 10^{-4} to 10^{-5} hazard. Results were checked using the slope at other points on the hazard curve and were not as consistent as this slope. Therefore the slope from the target UHS to an annual probability of 0.1 times that at the target UHS is recommended for use in determining the slope-dependent scale factor SF.

All of the above results were calculated with *mean* hazard curves, so they correspond to *mean* P_F 's. Figures 7-17 and 7-18 show results (P_F values, and ratios of exact/approximate P_F) using the *median* hazard curves at each site. Because we are using a fragility curve that combines epistemic and

aleatory uncertainty, and the fractile hazard always monotonically increase in annual frequency at any ground motion, the median hazard curve gives the median P_F . [Correctly stated, this is actually an estimate of the “median (over hazard epistemic uncertainty) of the mean (over fragility epistemic uncertainty) P_F .”] But because the hazard epistemic uncertainty dominates, this is an accurate estimate of the median P_F . For these plots the UHS was taken to be the 10^{-5} ground motion from the median hazard curve, and the slope was calculated from 10^{-5} to 10^{-6} . Also, results are not shown for the California and Washington sites, as we did not extensively model uncertainties and generate a broad distribution of hazards at these sites to calculate a median.

Figure 7-17 (bottom) shows that selecting the $DRS = URS = UHS \times SF$ does about as well as for the mean hazard curve, but selecting the $DRS = UHS$ does not (see Figure 7-17 [top]). This is primarily a result of inaccuracy in the risk equation - see Figure 7-18 (top).

The conclusion from these comparisons is that the scale factor SF should be used to factor up the UHS to a URS, and the slope for the scale factor should be determined from the hazard level at the UHS to one-tenth that hazard level. In the examples above, the hazard level chosen was 10^{-4} and the slopes were determined from 10^{-4} to 10^{-5} .

A second conclusion is that the risk equation (eq. 7.16) accurately estimates R_p , the probability ratio between hazard and risk. It is not perfectly accurate because the hazard curves are not perfectly linear (in log-log space). But it can be used to quickly and accurately determine the hazard-to-risk ratio, for decision purposes as described in the next section.

7.3.4 Alternative Representations

Having demonstrated a method of achieving consistent R_p values across all sites and parameters for a given component fragility β , it is useful to review the alternatives available to specify seismic design. Ultimately the seismic ground motion criterion will be specified by a ground motion corresponding to a hazard level $H(a')$ determined at a specified annual probability of exceedence, by a scaling factor SF, and by a deterministic acceptance criterion α . These will lead to an implied probability of failure P_F . The parameters $H(a')$, SF, and α can be chosen in many ways, depending on the ultimate objective. However, it is our understanding that a value of $\alpha = 1.67$ is desired by the USNRC, and the previous section makes it clear that $SF = \max(0.7, A_R^{1.2})$ is our recommendation for the scaling factor.

One option is to specify $H(a')$ to be consistent with previous design levels. Regulatory Guide 1.165, for example, concludes that the median of the median hazard level for seismic design at 29 plants designed according to Regulatory Guide 1.60 is 10^{-5} per year. That is, half of the plants had a seismic design with a median hazard above this value, half had a design below this level. This conclusion could also be extended to the mean hazard, which would indicate a value of about 10^{-4} per year. Given these hazard levels, and given the above choices of α and SF, the associated P_F could be calculated.

An attractive alternative would be to specify an acceptable P_F , and then back-figure (using α and SF) the associated $H(a')$ required to achieve this P_F . This would have the advantage of allowing P_F for

seismic failures to be made consistent with other failures, for example, to ensure that seismic criteria are not overly conservative or unconservative with respect to other challenges to plant safety.

Recommending a method to select $H(a')$ or P_F is beyond the scope of the current project. However $H(a')$ and P_F are chosen, several other related issues need to be addressed as a part of the same decision process.

First is the choice of using the mean vs. median hazard curves. Advantages of using the mean hazard curves have been made above: a target mean probability of failure for components over n plants can be achieved by specifying a mean P_F at each plant, and this can be translated to a mean hazard curve. A target *median* probability of failure cannot be achieved by specifying a median P_F at each plant. On the other side, the calculated median hazard has been more consistent from study to study than the mean, although with communication and feedback this will probably not be the case for future studies. On balance we recommend that the mean P_F be used to derive requirements for a mean $H(a')$, to be used for design.

Second is the choice of which β value to use in calibrating the method. It would be less workable to specify the DRS to be dependent on the characteristics of individual components. Thus in specifying a design procedure (presuming the relationship between $H(a')$ and P_F is made explicit), a regulatory agency must decide whether to use an average β to pick $H(a')$ for a given P_F , or a worst-case β (i.e. a high value). Note that Kennedy and Short (1994) found that specifying the HCLPF in terms of the 10% frequency of failure point removed this sensitivity to β , but we do not recommend this re-definition of HCLPF — this would be too radical a change for designers to accept and adopt. Stated another way, if the $H(a')$ value is selected a priori, then a regulatory agency must decide whether the P_F for the *average* component (with an average β) is acceptable, or whether the P_F implied by the worst component (with the highest β) is acceptable.

Overall, our recommendation is that an average β be used, such as 0.45. This choice would result in less than a factor of 1.5 variation in P_F for a given $H(a')$ as a result of β -values different from a central value — see Figures 7-14 and 7-16. A variation of 1.5 is small, given other variabilities, particularly if a conservative α value of 1.67 is specified. The use of an average β value will avoid the compounding of additional conservatisms.

7.4 Summary

This section has demonstrated a method to scale UHS at a site to achieve approximately risk-consistent seismic design spectra (herein called “design response spectrum,” or DRS). The DRS is risk-consistent for sites and natural frequencies with a range of slopes on hazard curves, and is the recommended spectrum to use for scaling time histories for dynamic analysis. The consistency of this method has been demonstrated at eleven sites with different characteristics of seismic hazard across the US.

Several issues remain before a DRS method can be implemented. First, the annual frequency associated with the target UHS must be chosen, along with a selection of the mean or median UHS. Actually a better choice would be to select an acceptable seismically-induced mean annual frequency

of failure for components, and back-figure the mean UHS that will give this mean frequency. A second issue is whether an average or conservative β is used to model components. We recommend an average β of 0.45, so that a *mean* frequency of component failure is achieved, rather than a conservative value. This avoids undesirable compounding of conservatism.

With these issues resolved, the DRS can be determined from a probabilistic seismic hazard analysis at a site. The advantage will be more consistent seismic designs across the frequency range and across the US.

References

- Abrahamson, N.A. and W.J. Silva (1997). "Empirical response spectral attenuation relations for shallow crustal earthquakes." *Seism. Soc. Am.*, 68(1), 94-127.
- ASCE (1986). Seismic analysis of Safety-Related Nuclear Structures and Commentary on Standard for Seismic Analysis of Safety Related Nuclear Structures, Amer. Soc. Civil Engrs., New York, Rept. ASCE 4-86, Sept.
- Kennedy, R.P. and S.A. Short (1994). "Basis for seismic provisions of DOE-STD-1020." UCRL-CR-111478, prepared for US DOE, April.
- Owens, D.B. (1980) A Table of Normal Integrals. *Comm. Statist.-Simula. Computa.*, B9(4), 389-419.
- Sewell, R.T., G.R. Toro, and R.K. McGuire (1991). "Impact of Ground Motion Characterization on Conservatism and Variability in Seismic Risk Estimates," prepared for US NRC, May.
- Sewell, R.T., G.R. Toro, and R.K. McGuire (1996). "Impact of Ground Motion Characterization on Conservatism and Variability in Seismic Risk Estimates," US NRC, NUREG/CR-6467, July.
- Sobel, P. (1994). "Revised Livermore Seismic Hazard Estimates for Sixty-Nine Nuclear Power Plant Sites East of the Rocky Mountains," US NRC, April.

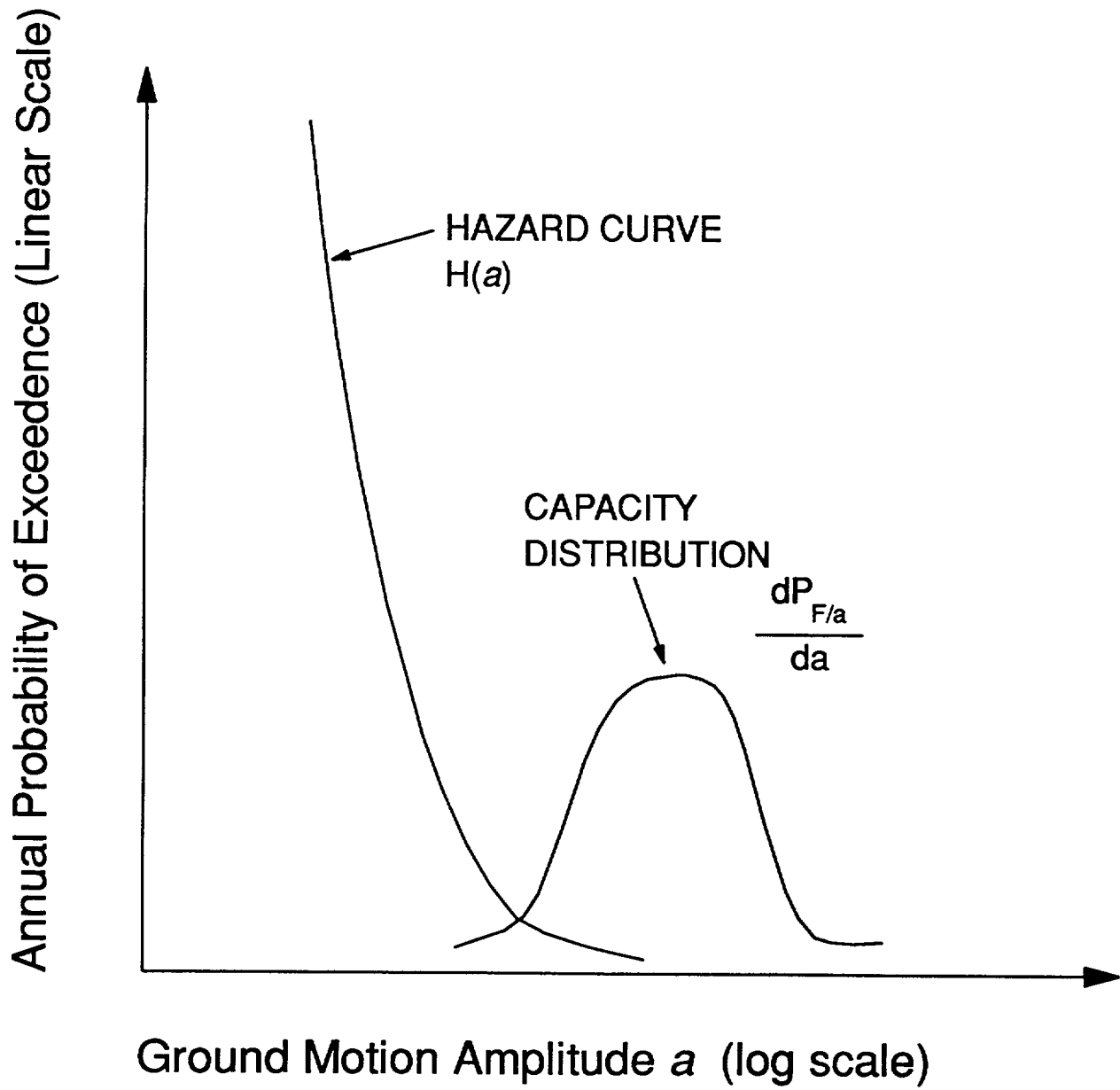


Figure 7-2. Graphical representation of curves for failure calculation.

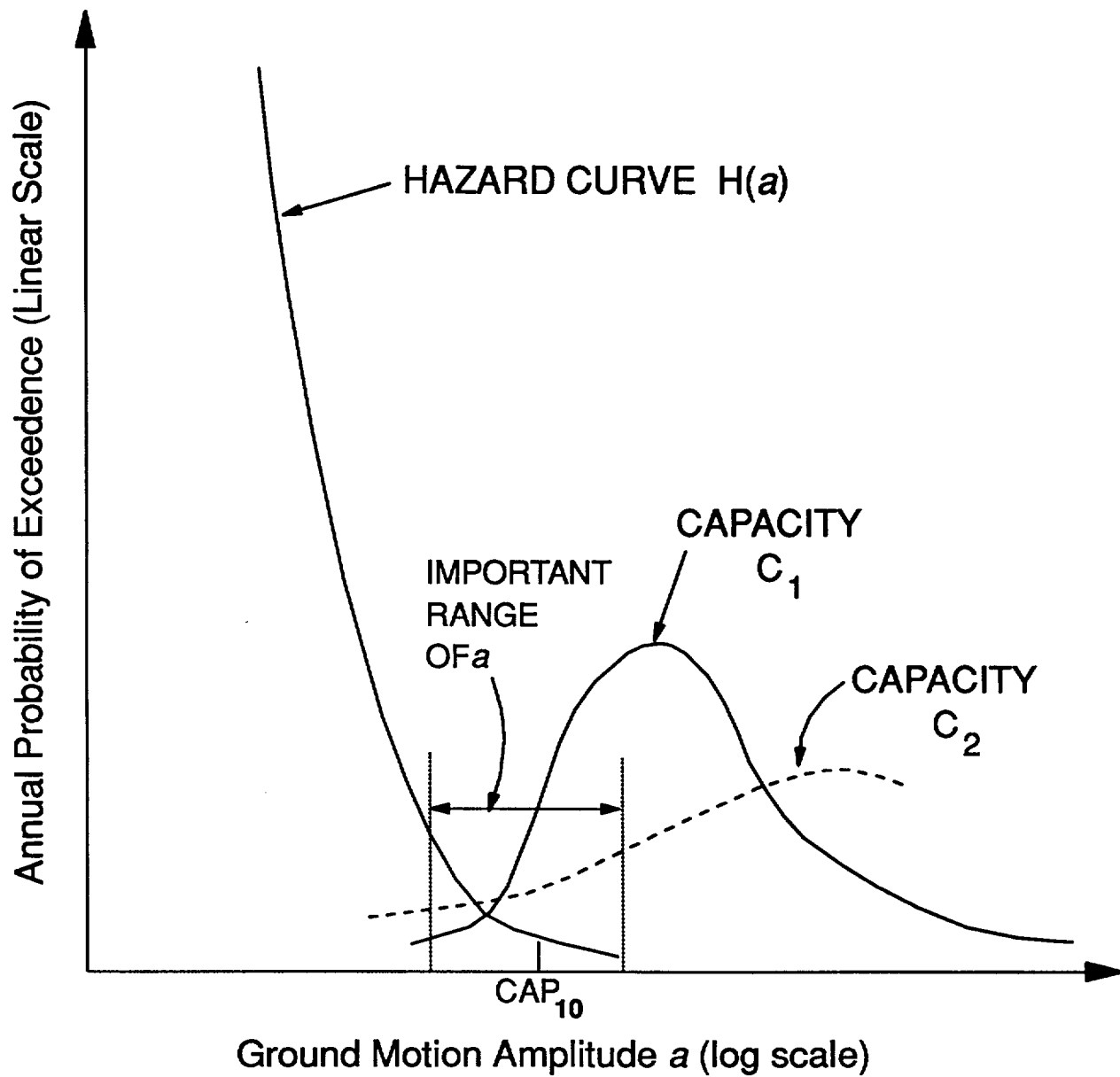


Figure 7-3. Alternative capacity distribution with same CAP_{10} .

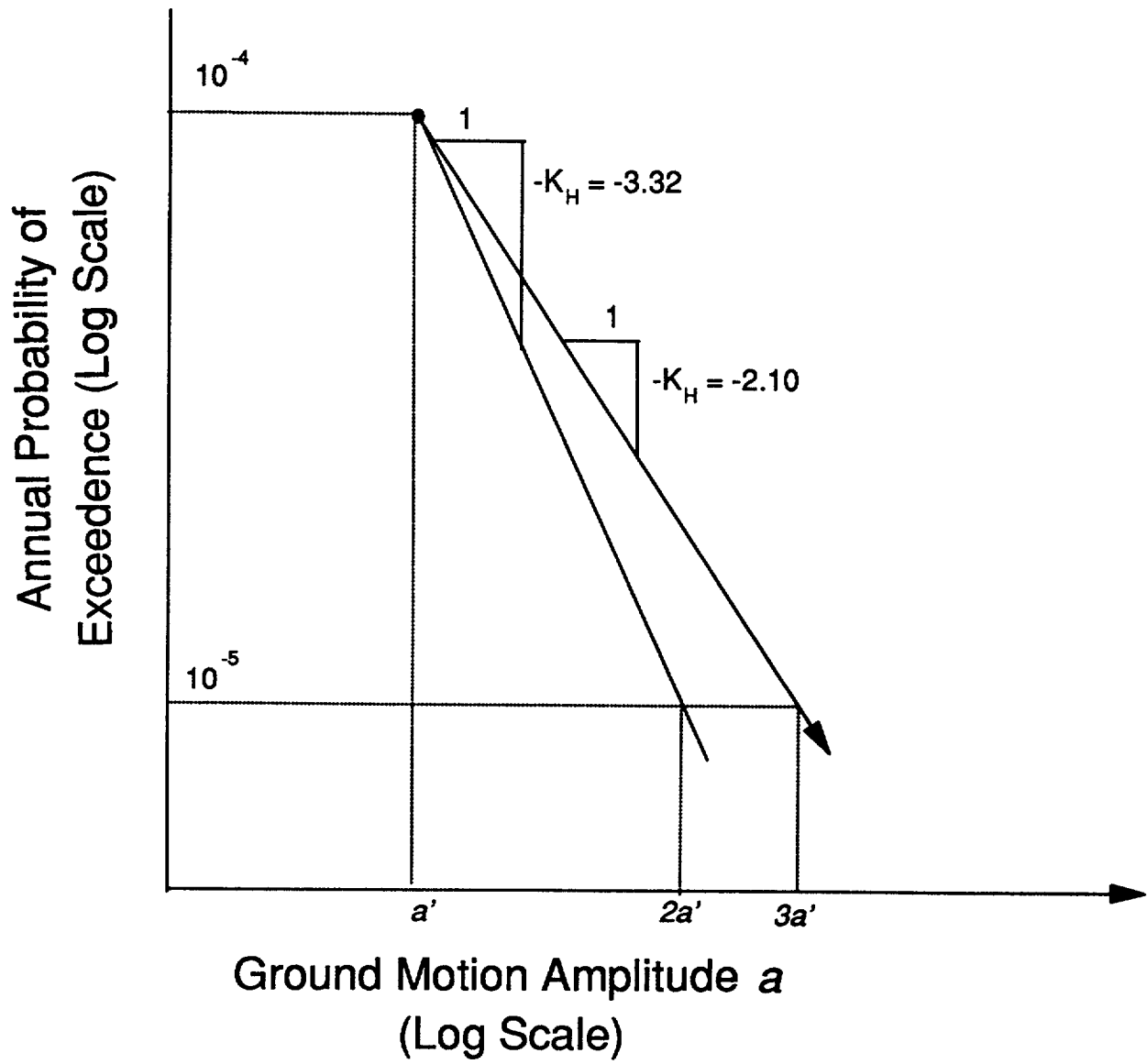


Figure 7-4. Hazard curve with different slopes.

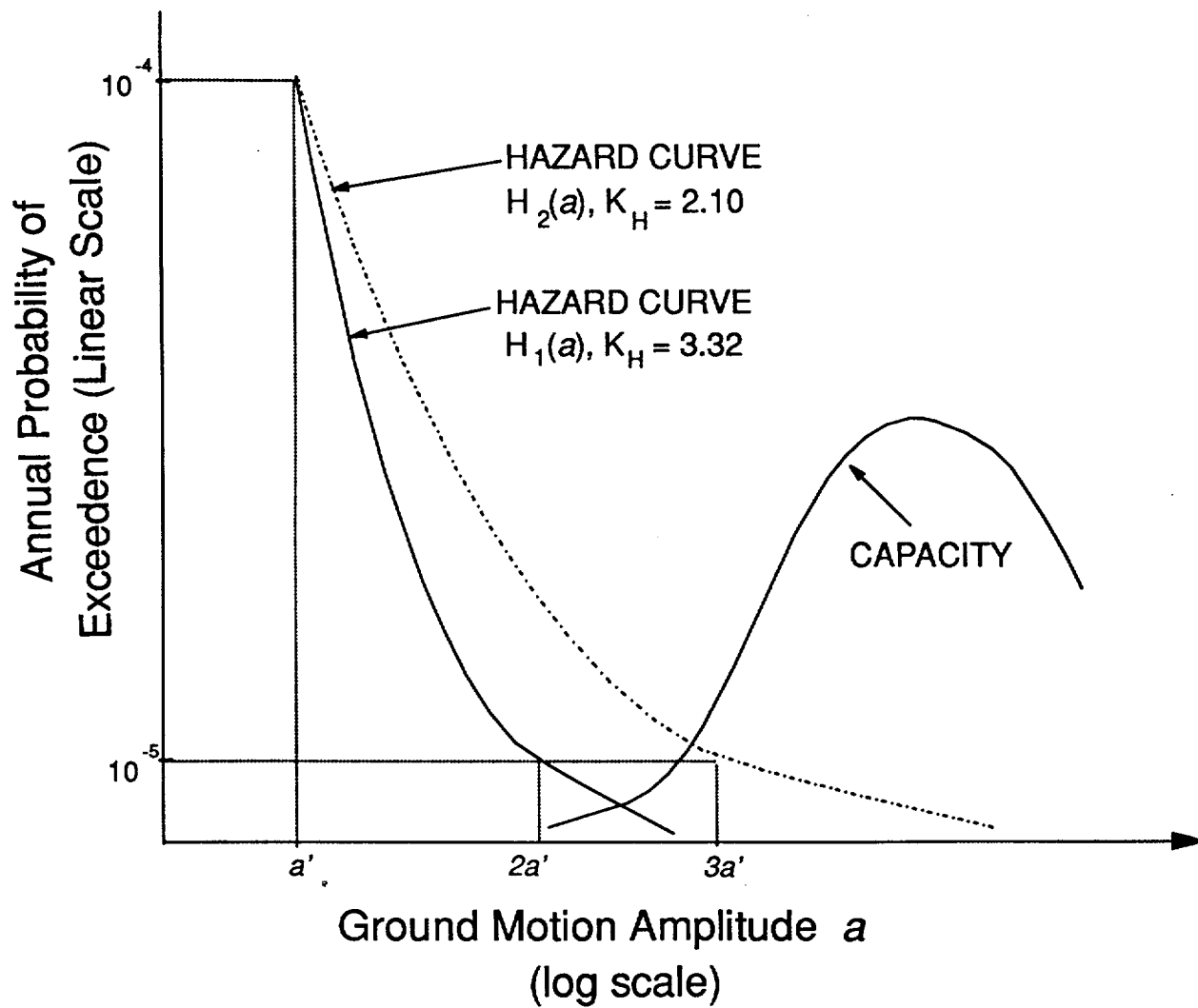


Figure 7-5. Comparison of hazard curves with different slopes to capacity curve.

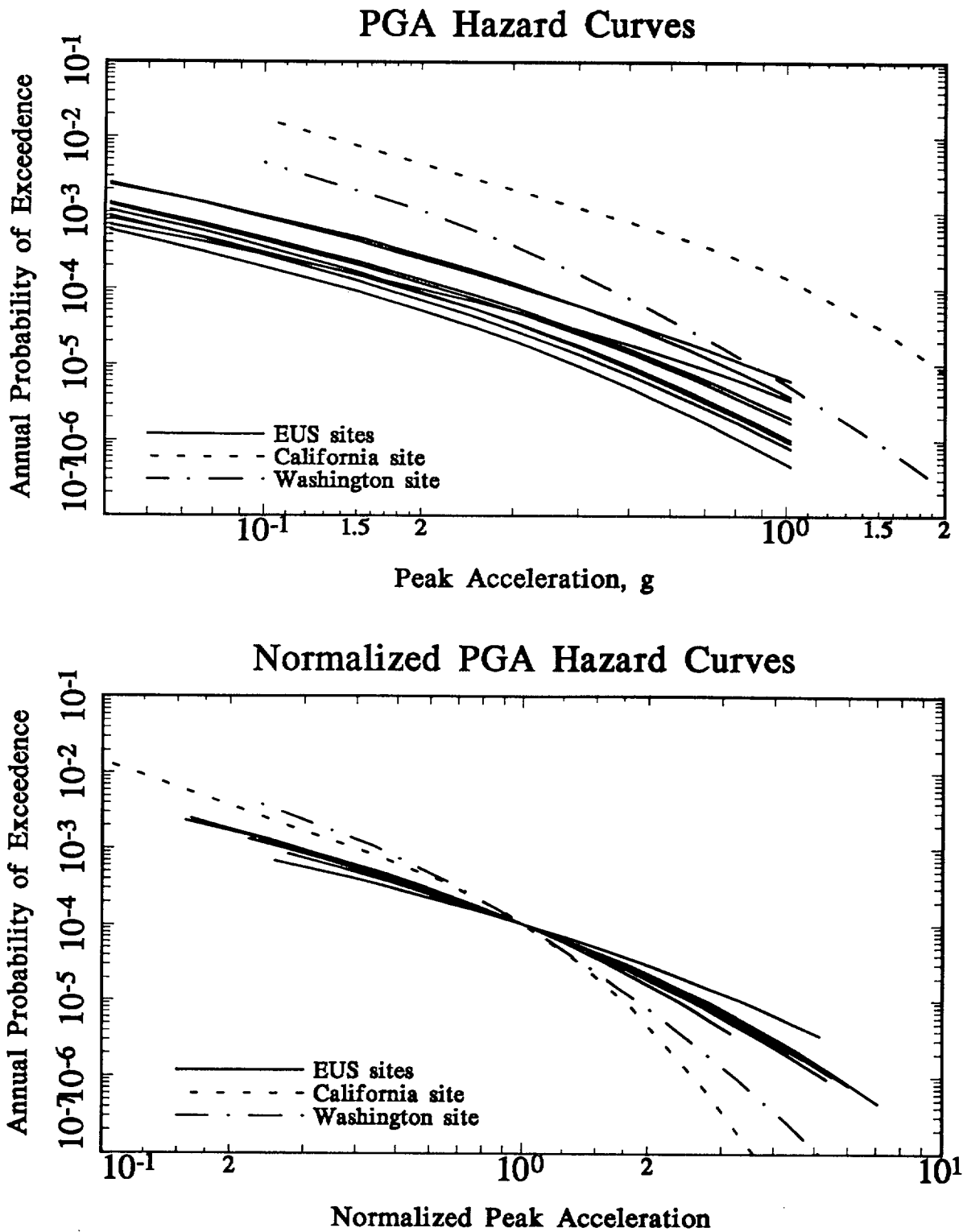


Figure 7-6. PGA hazard curves for the eleven test sites: (top) as calculated, (bottom) normalized by the acceleration value corresponding to 10^{-4} annual probability.

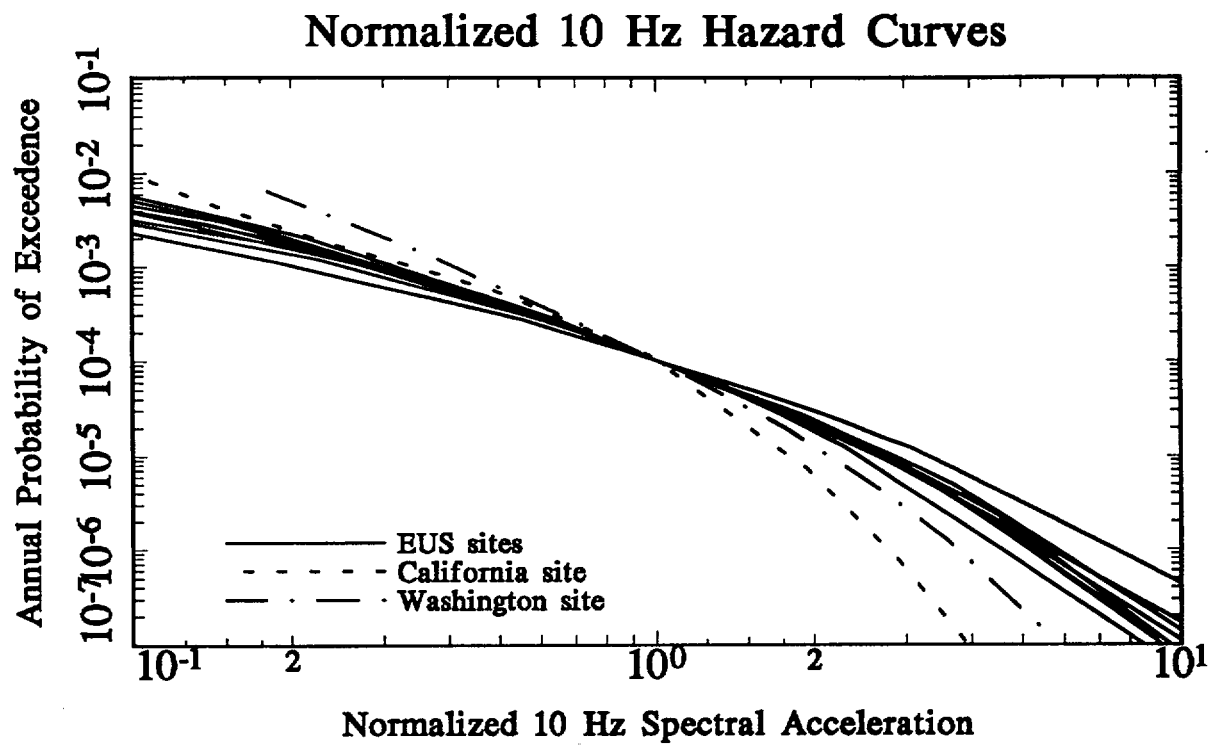
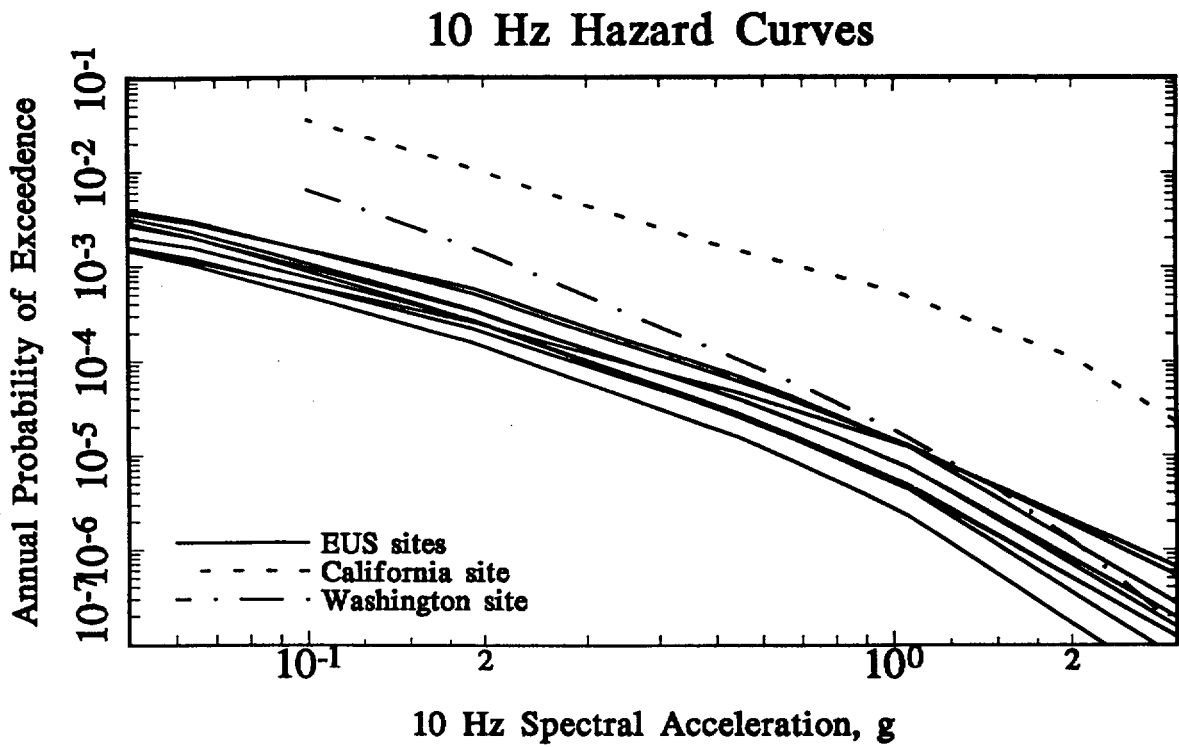


Figure 7-7. SA (10 Hz) hazard curves for the eleven test sites: (top) as calculated, (bottom) normalized by the acceleration value corresponding to 10^{-4} annual probability.

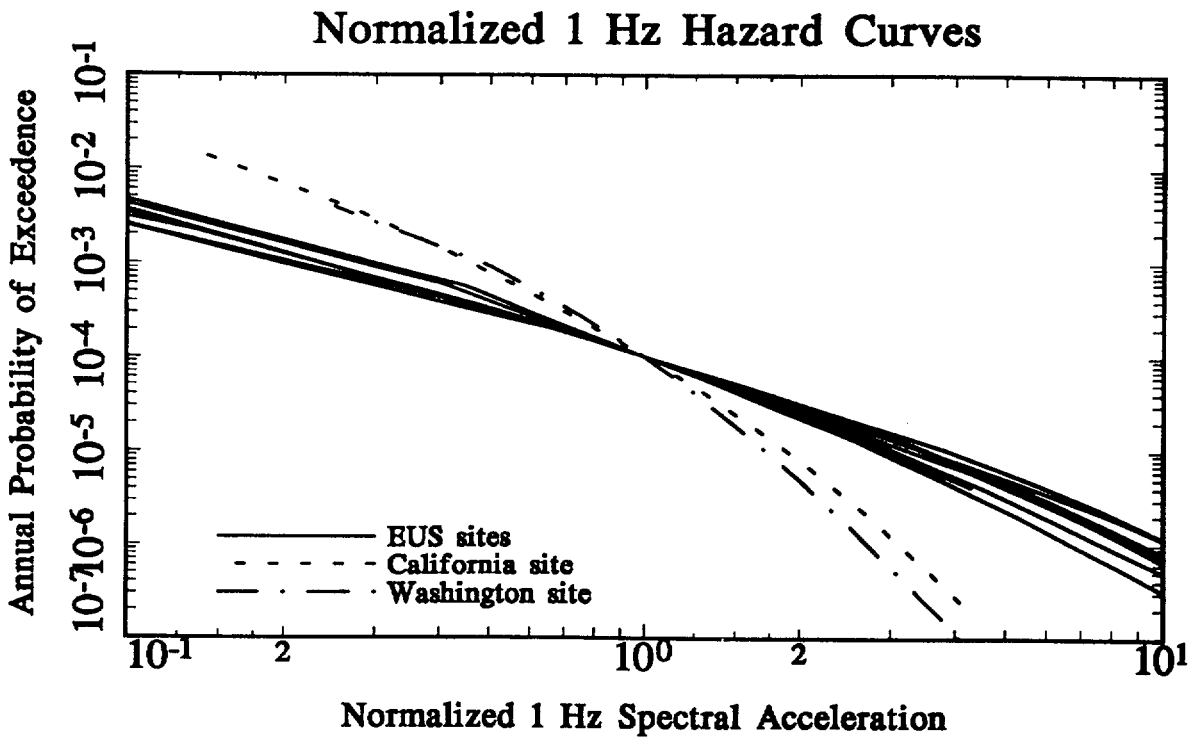
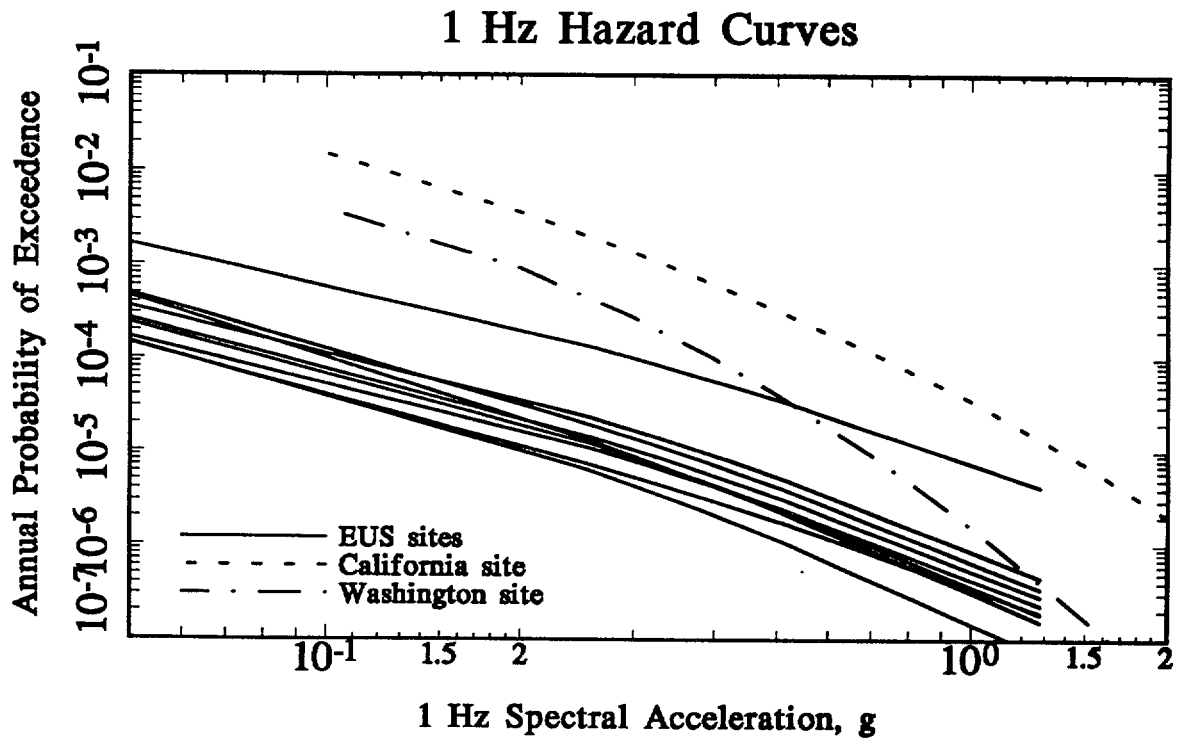


Figure 7-8. SA (1 Hz) hazard curves for the eleven test sites: (top) as calculated, (bottom) normalized by the acceleration value corresponding to 10^{-4} annual probability.

HCLPF = 0.375g, Beta = 0.3

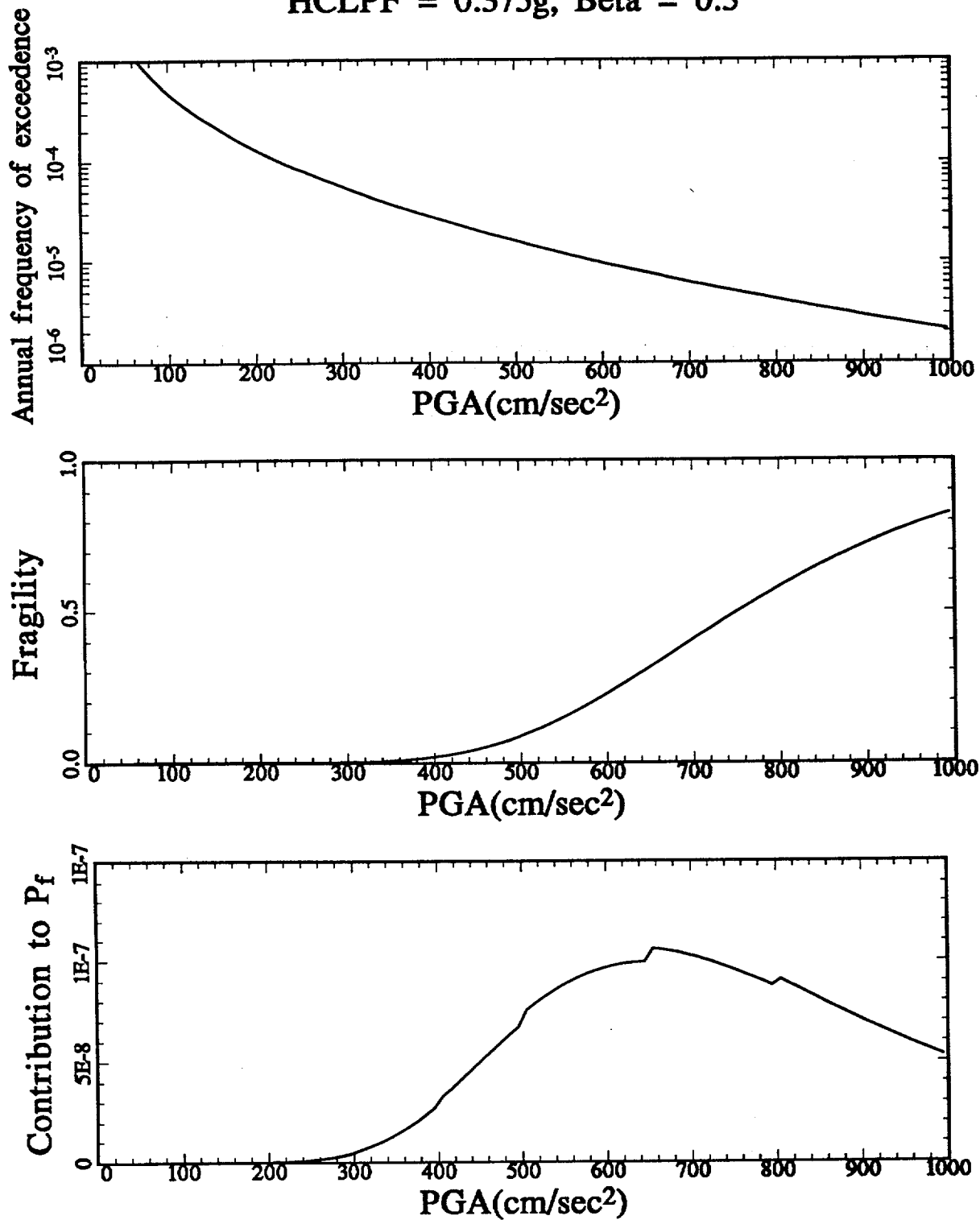


Figure 7-9. Maine Yankee PGA seismic hazard curve (top), fragility curve for $\beta = 0.3$ (middle), and contributions to P_F by PGA (bottom).

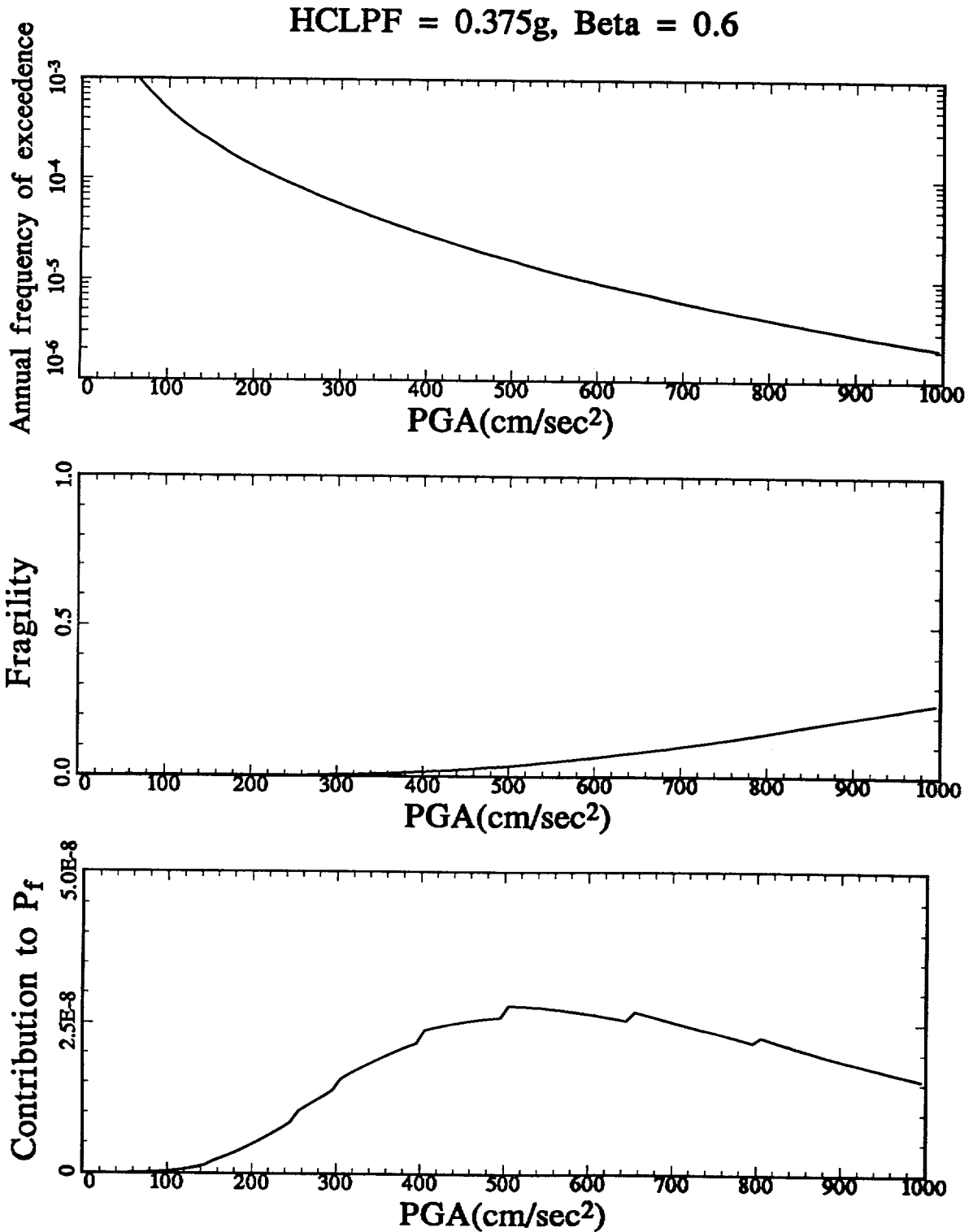


Figure 7-10. Maine Yankee PGA seismic hazard curve (top), fragility curve for $\beta = 0.6$ (middle), and contributions to P_F by PGA (bottom).

UHS and URS, Columbia site
Annual frequency = 1E-4

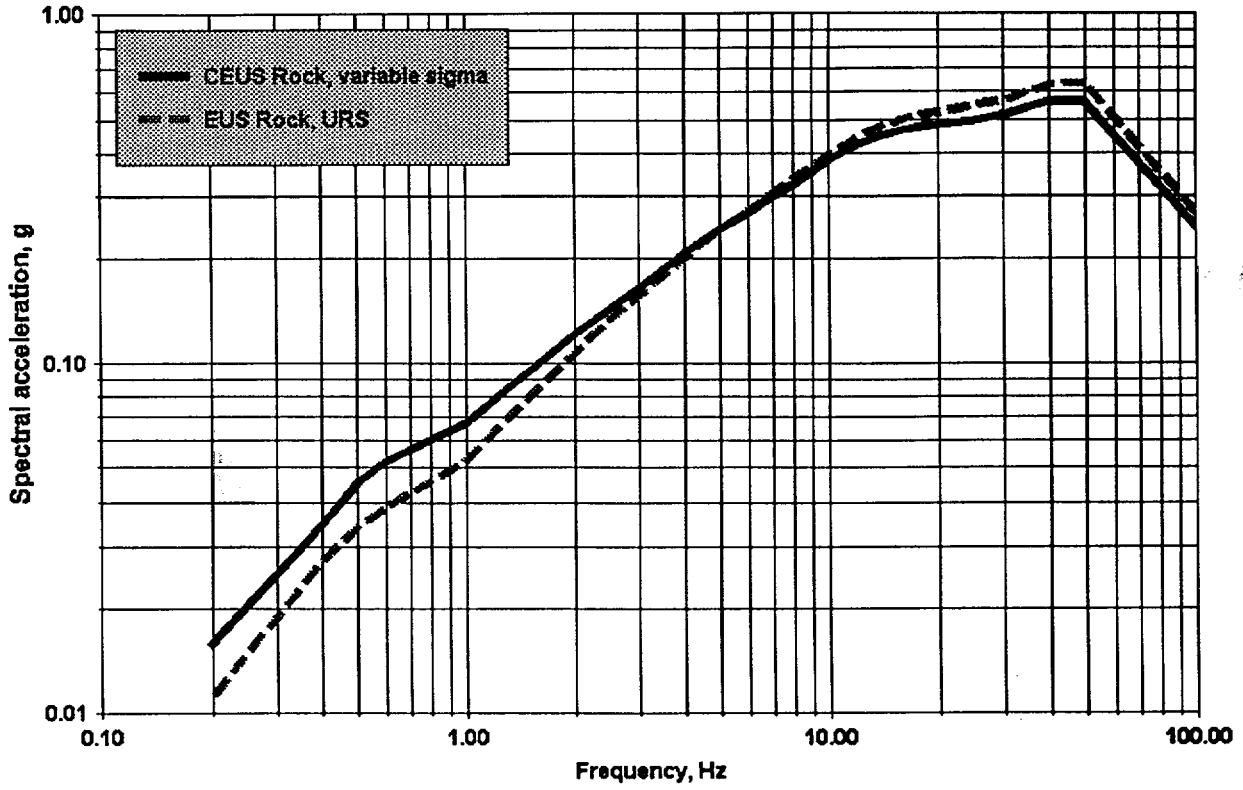


Figure 7-11. UHS for Columbia site, with URS calculated from seismic hazard analysis.

UHS and URS, Columbia site, local background only

Annual frequency = 1E-4

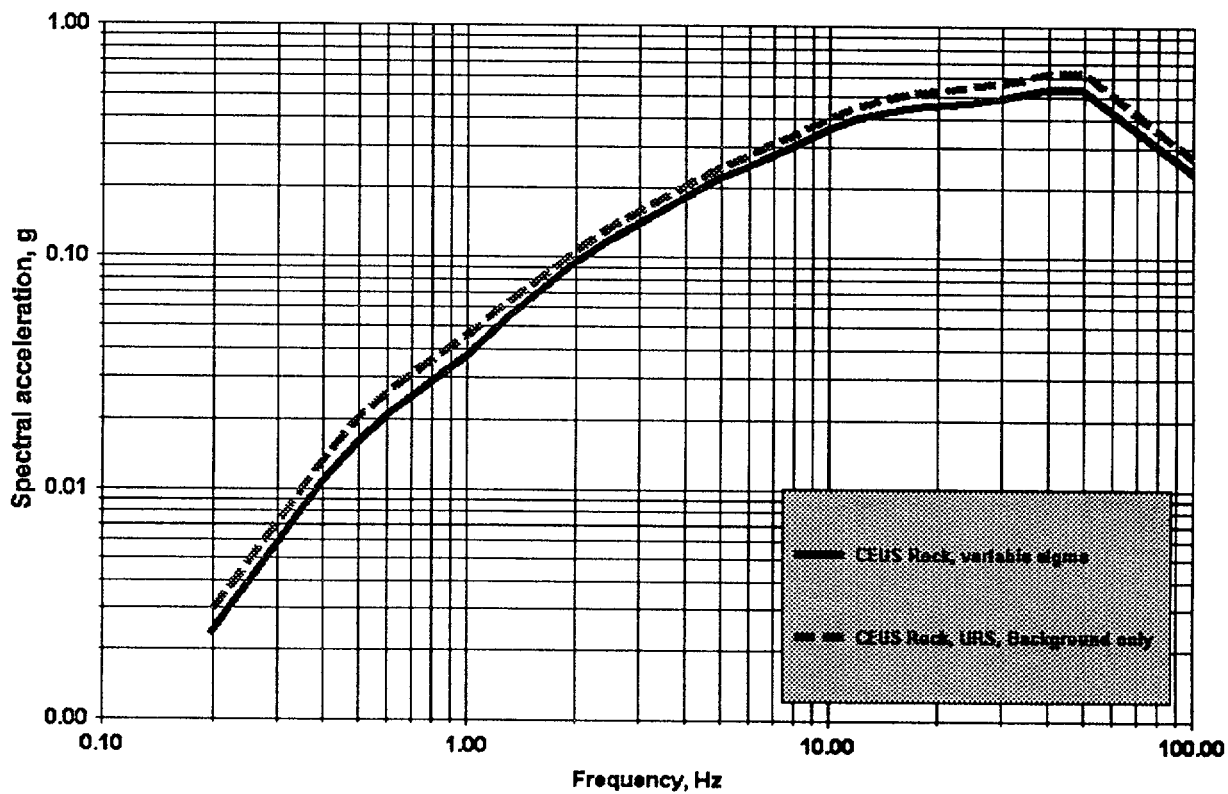


Figure 7-12. UHS for Columbia site, with URS calculated from seismic hazard analysis using background source only.

UHS and URS, Mojave site

Annual frequency = 1E-4

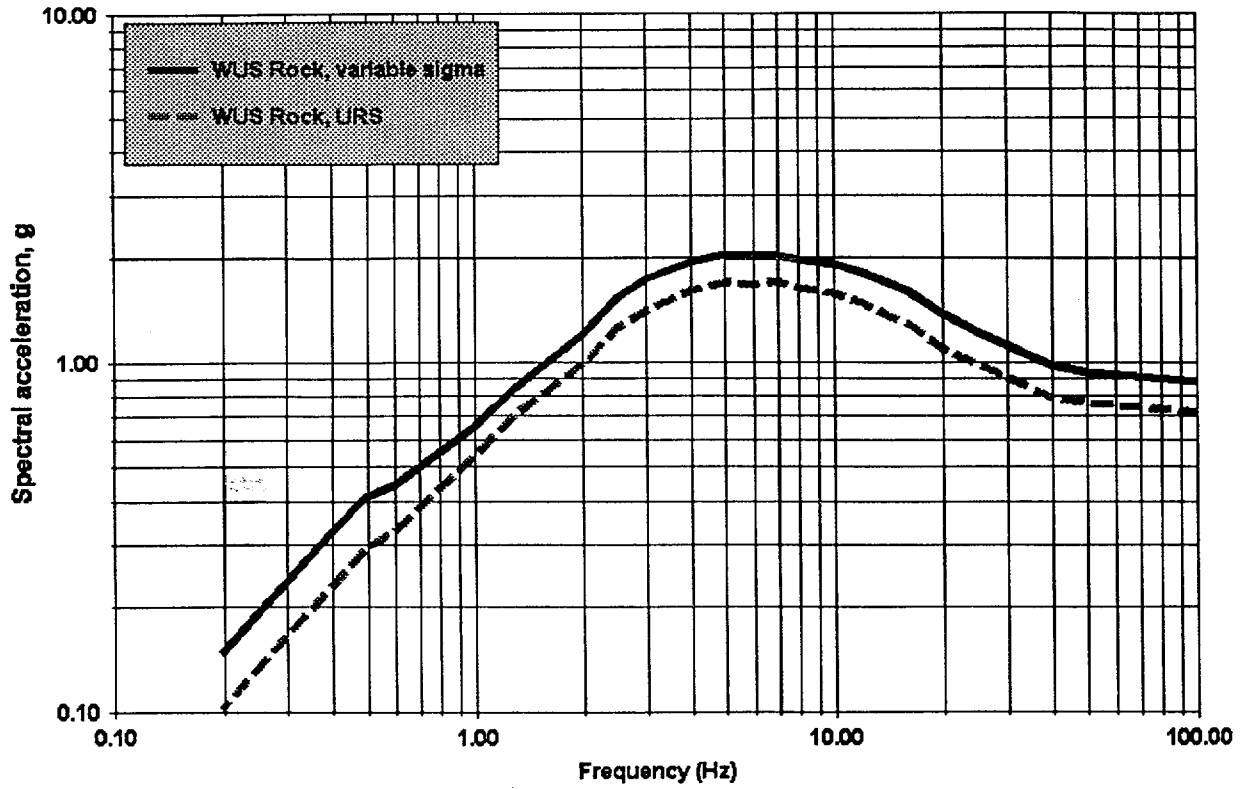
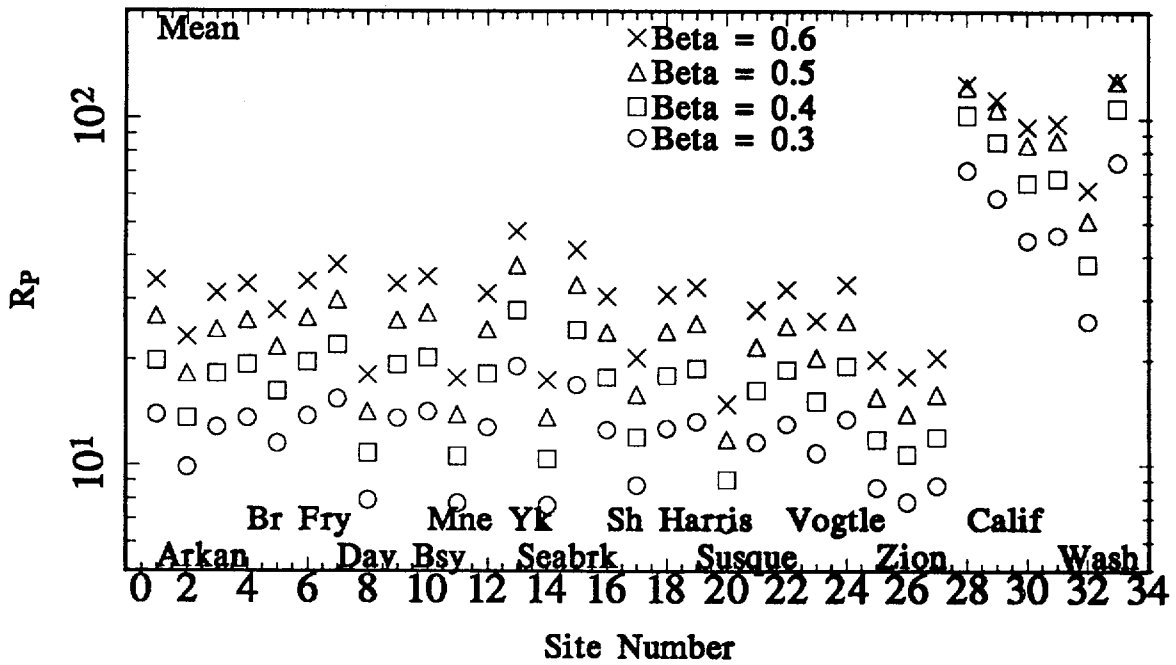


Figure 7-13. UHS for Mojave site with URS calculated from seismic hazard analysis.

HCLPF1 design using factor 1.67



HCLPF2 design using factor 1.67 x SF

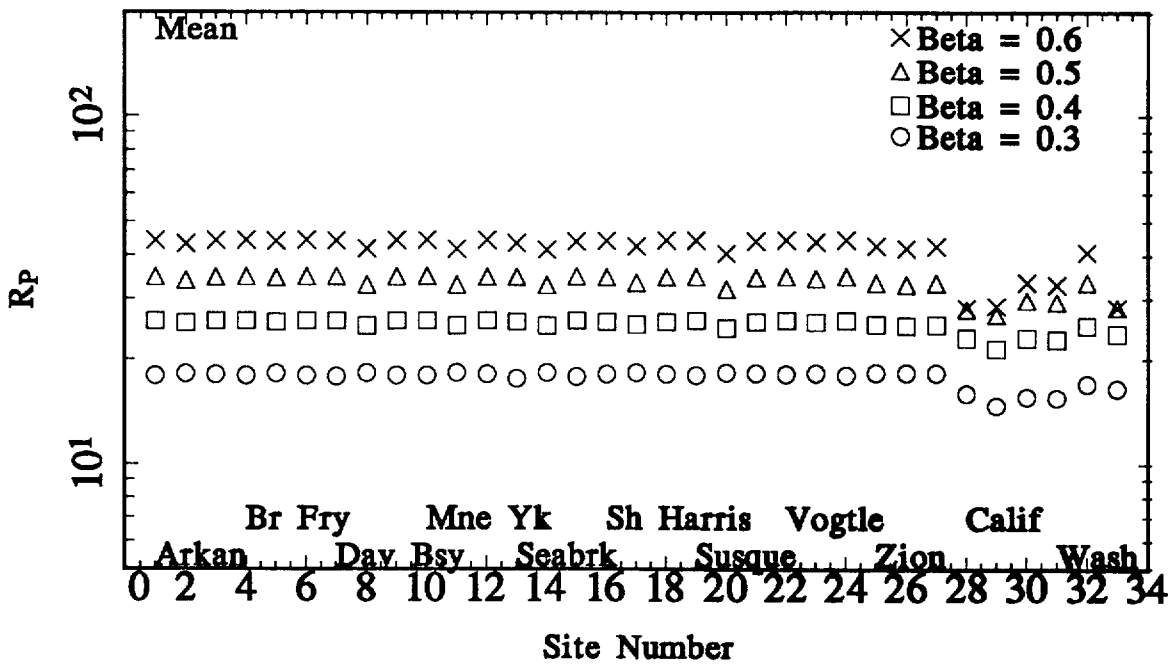
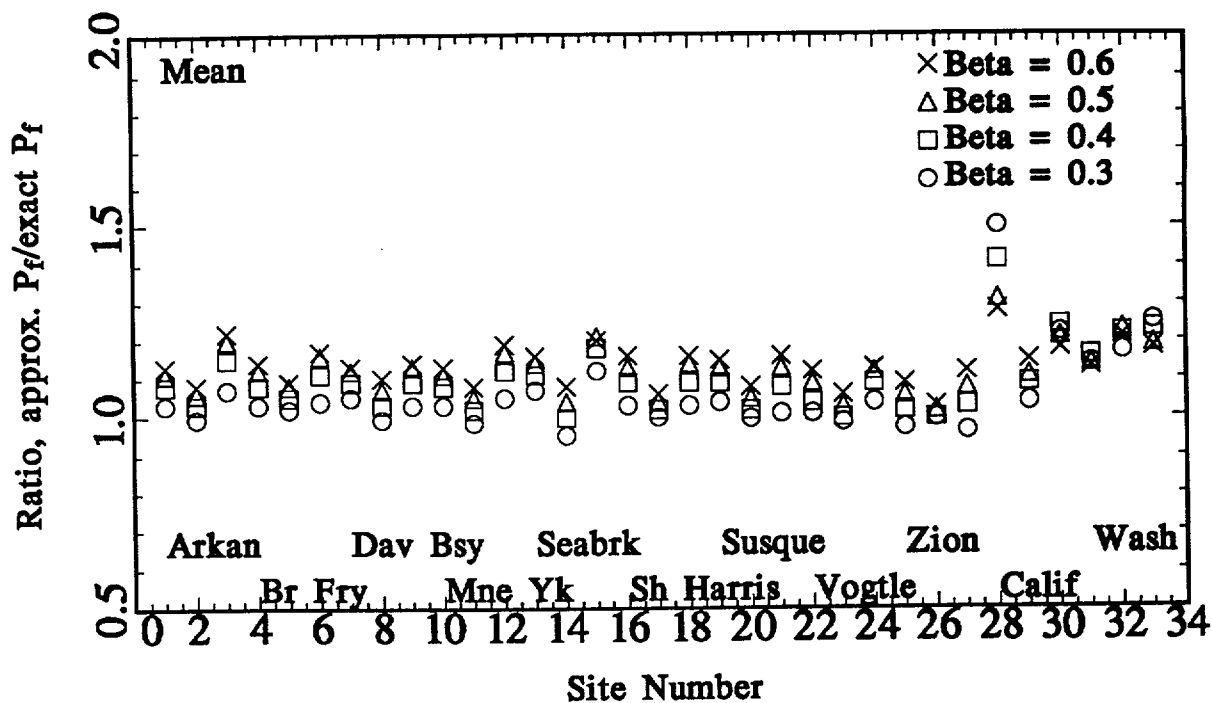


Figure 7-14. R_p calculated from risk equation for 11 test sites and 3 parameters, using $\alpha = 1.67$ (top) and using $\alpha = 1.67 \times SF$ (bottom).

HCLPF1 design using factor 1.67



HCLPF2 design using factor 1.67 x SF

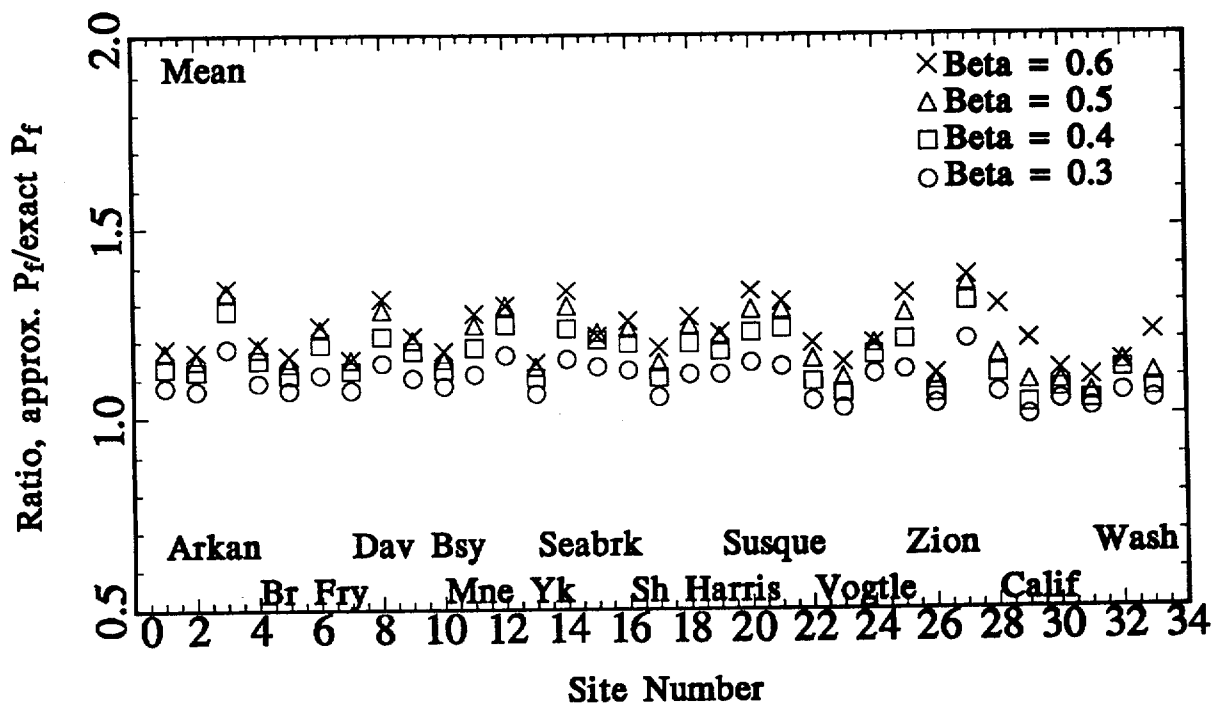
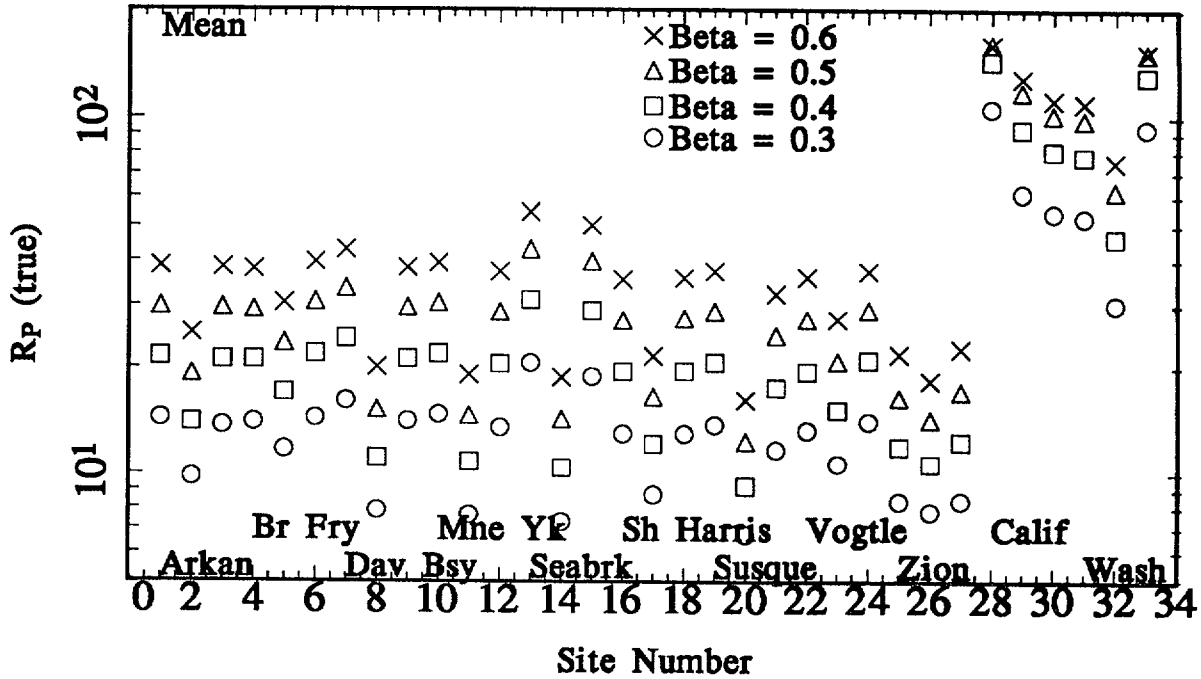


Figure 7-15. Ratio of approximate to exact P_f using $\alpha = 1.67$ (top), and using $\alpha = 1.67 \times SF$ (bottom).

HCLPF1 design using factor 1.67



HCLPF2 design using factor 1.67 x SF

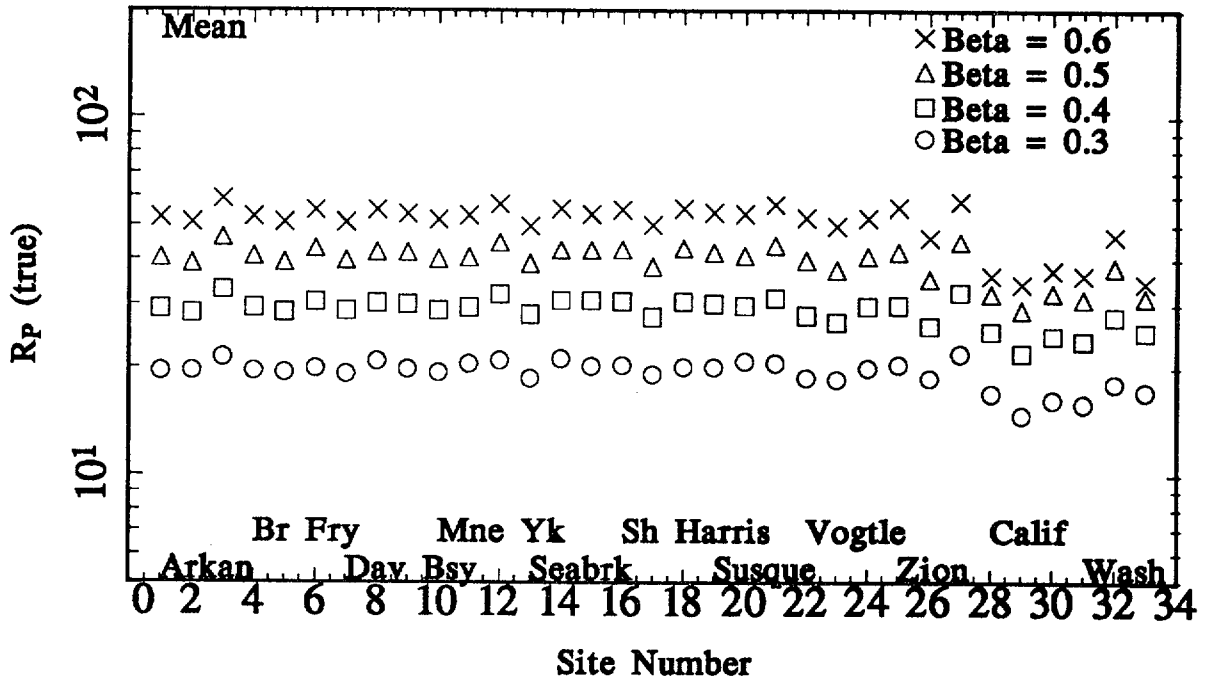
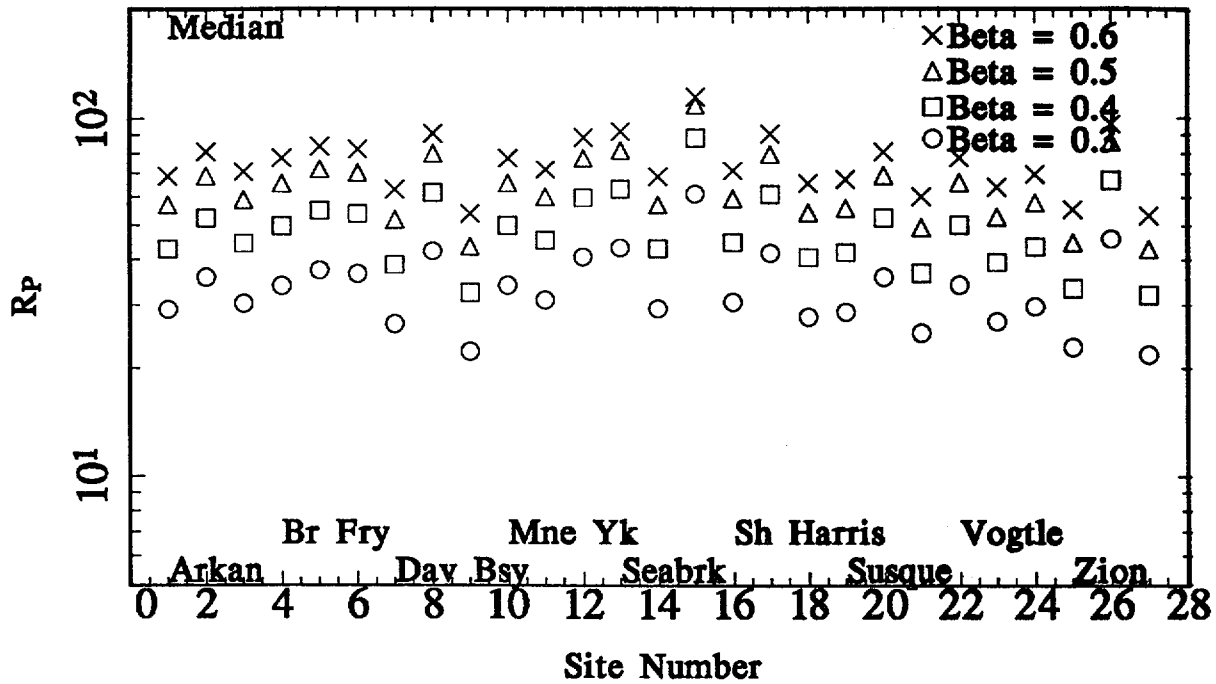


Figure 7-16. R_p calculated from direct integration for 11 test sites and 3 parameters, using $\alpha = 1.67$ (top) and using $\alpha = 1.67 \times SF$ (bottom).

HCLPF1 design using factor 1.67



HCLPF2 design using factor 1.67 x SF

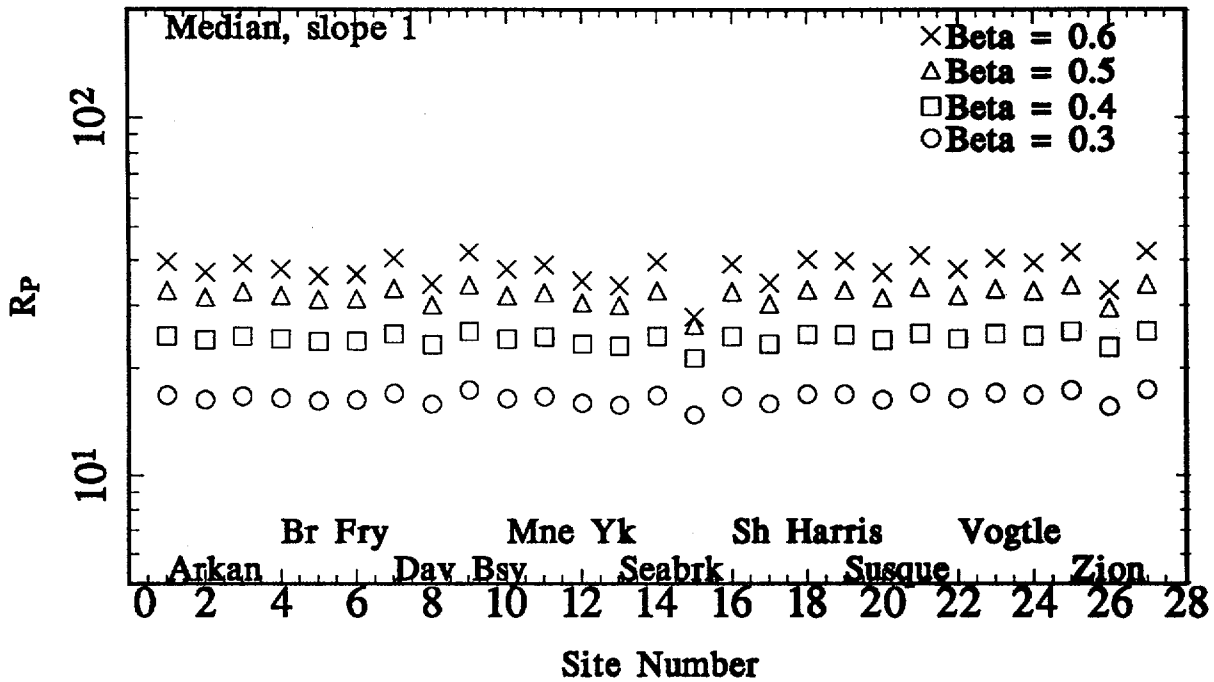


Figure 7-17. R_p calculated from direct integration for 11 test sites and 3 parameters, using median hazard curves.

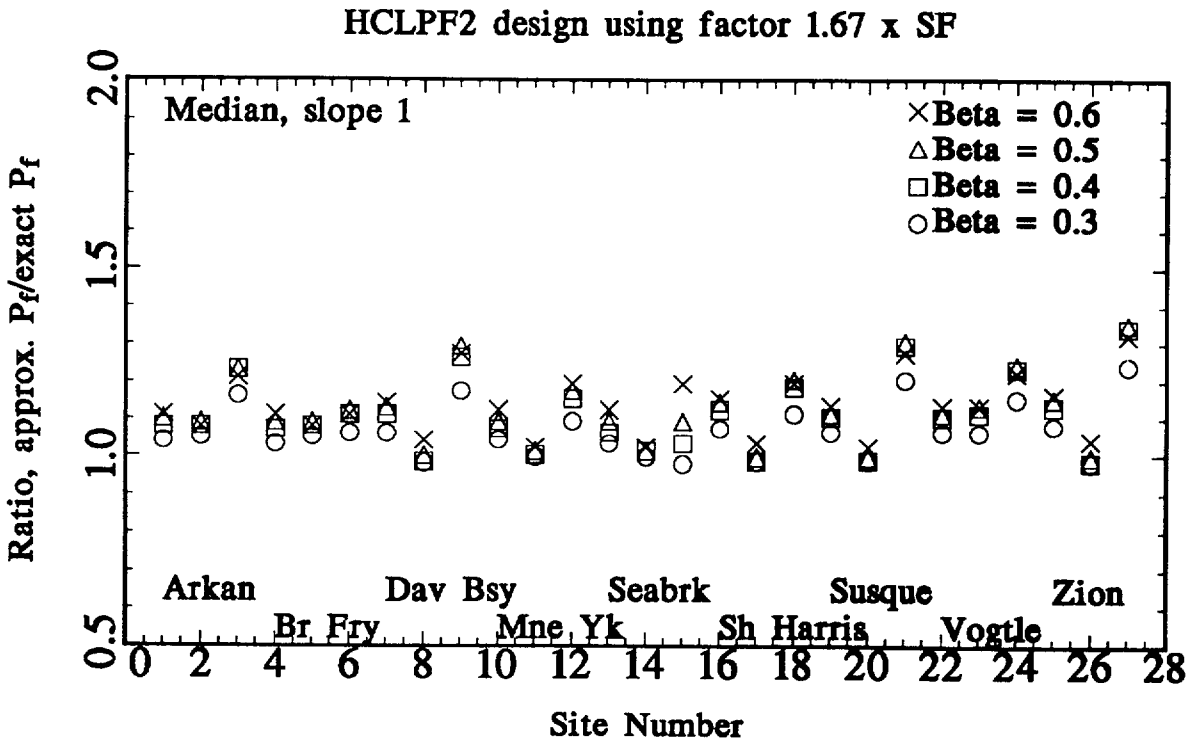
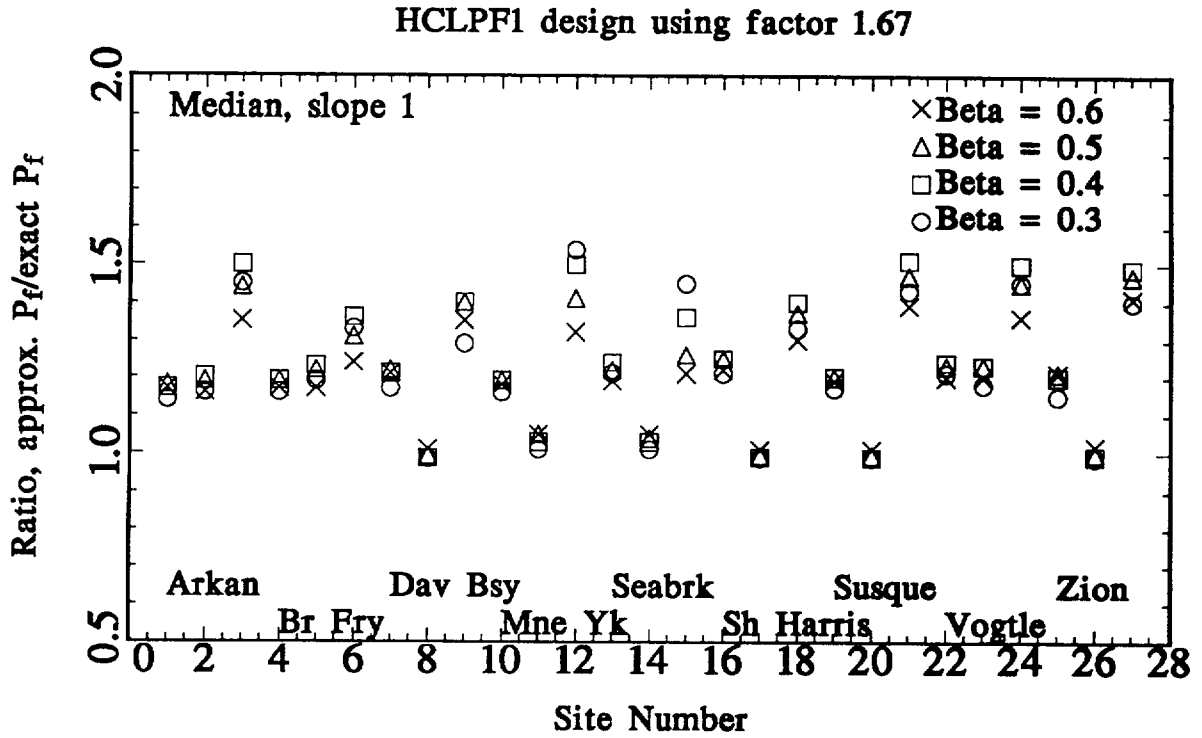


Figure 7-18. Ratio of approximate to exact P_f using $\alpha = 1.67$ (top) and using median hazard curves.

8. CONCLUSIONS AND RECOMMENDATIONS

8.1 Response Spectral Shapes

This report documents seismic response spectral shapes for design and analysis that were developed from empirical attenuation equations in the western US (WUS) and verified with observed data. These rock spectral shapes use continuous **M** and **R** scaling and are valid in the WUS for **M** in the range 4.75 to 8 and **R** in the range 0 to 200 km. For Cascadia subduction zone earthquakes the shapes are valid for **M** up to about 9 and distances to 300 km.

For the central and eastern US (CEUS), the WUS shapes were modified with a transfer function based on a random vibration model of strong ground motion that accounts for differences in source parameters, crustal damping, and near-surface damping. This transfer function was verified with observed data. CEUS rock spectral shapes are valid for **M** from 4.75 to 8 and **R** in the range 0 to 400 km.

These shapes will be scaled in design to a uniform hazard spectrum (UHS) at frequencies around 1 and 10 Hz. The frequency range of these shapes is 0.2 to 100 Hz, which allows the ratio of spectral acceleration to peak ground acceleration to reach nearly unity for hard rock conditions. For soft rock conditions this ratio will reach unity at 40-50 Hz.

The spectral shapes reflect median fractile estimates of spectral response. The shapes will be scaled to a UHS that reflects both epistemic and aleatory uncertainty, so further broadening or increasing the shapes by applying a higher fractile level is neither warranted nor justified.

Spectral shapes for soil conditions have not been developed because soil response depends strongly on the characteristics of the rock control motions and on the nonlinear dynamic soil properties. This is strongly site-dependent problem. The report includes examples of how to develop hazard-consistent soil spectra.

8.2 Time History Database

An important part of the project has been the development of a time history database for analysis. Recorded time histories of strong ground motion are archived for **M** and **R** bins that were selected to preserve significant differences in spectral composition and time domain characteristics such as duration. Each bin contains records reflecting ranges in **M** and **R**, and the report includes guidelines to make within-bin **M** and **R** adjustments for spectral matching.

In the WUS the bins are populated largely with recorded motions. Sparse bins were supplemented with scaled empirical records (from adjacent bins) and with a few direct finite-fault simulations. Since few records exist for the CEUS, motions in the database were created by modifying WUS motions to CEUS conditions. These motions are not as desirable as directly recorded data, and the database should be updated as new motions are recorded in the CEUS.

8.3 Development of Artificial Time Histories

This report makes recommendations on how to develop artificial time histories of motion that match target response spectra. The database of motions described above would be the starting point for this development. Artificial motions should be computed at 100 points per frequency decade between 0.2 and 50 Hz (or at the Nyquist frequency, if higher). The basis for comparison between one or a suite of artificial motions and the target spectrum is at frequencies between 0.2 and 25 Hz. The report includes rules for acceptability of the artificial motions based on under- or over-estimation of the target response spectrum at multiple frequencies.

There is no check required of the power spectral density function. However, the overall duration (5% to 75% Arias intensity) and ratios of PGV/PGA and $PGA \cdot PGD / PGV^2$ must be consistent with bin averages from the time history database.

The directional correlation between components of artificial motion (horizontal-to-horizontal and horizontal-to-vertical) should be checked. The lag-zero cross-correlation coefficient between two horizontal components, and between a vertical and a horizontal component, should not exceed 0.3. This will ensure that no significant reduction in directional response can be achieved by special orientation of the structure.

These recommendations are sufficient to ensure that no significant gaps in Fourier amplitude spectra or power spectral density function will occur for the generated artificial motions.

8.4 Hazard-consistent Spectra on Soil

We examined multiple methods of calculating uniform hazard spectra on soil that would give UHS consistent with rock motions. These applications were for four soil profiles assumed to be located at a CEUS and a WUS site. Both sites were chosen so that different sources contributed to the 10 and 1 Hz hazard, making the task of estimating soil response more challenging.

The most direct method to estimate UHS on soil is to develop a site-specific attenuation equation for motions at the soil surface, and to use this in a seismic hazard analysis. The disadvantage of the direct approach is that the seismic hazard analysis must be redone for each set of soil depths and parameters at a facility, and must be redone when additional properties are measured in the field or the lab (shear wave velocity, damping, stiffness). We examined two approximate approaches (and variants of these) that were based on a rock UHS at the site and that could be used to estimate an approximate soil UHS. Each approach relies on estimating a dominant M and R from the rock hazard, and driving the soil column with several motions scaled to the rock UHS with that M and R . We also examined an approach based on integrating over the rock hazard curve, converting the rock motion to soil motion and calculating seismic hazard for soil amplitudes.

A recommendation on the best method of estimating soil response awaits further comparisons to be made in a companion report on implementation of the methodology.

8.5 Risk-consistent Spectra

Spectra that are risk-consistent in terms of nuclear power plant component failure frequencies can be achieved by accounting for the slope of the hazard curves at each frequency. These slopes are important because they affect the frequency of higher ground motions, given a design that for example is keyed to the 10^{-4} UHS. We recommend modifying the rock UHS, based on the slope of the hazard from 10^{-4} to 10^{-5} , to achieve a "uniform reliability spectrum" (URS) for design that achieves consistent component failure frequencies.

The prescribed method of deriving the URS from the UHS is illustrated using three ground motion parameters (PGA and spectral acceleration at 10 and 1 Hz) at eleven nuclear plant sites across the US. The range of plant component failure frequencies is reduced from a factor of about 20 across all sites and parameters, to a factor of 3. This remaining factor results from different component failure uncertainties, and is not reducible within the context of current design procedures.

A specific recommendation for a UHS modification to achieve a URS depends on the hazard level chosen for design (the example used here is 10^{-4}) and on the deterministic level of conservatism associated with design codes and guides (the example used here is a factor of 1.67 on the design motion). With other hazard levels or deterministic levels, different forms of the modification factor would be recommended, but they would achieve the same degree of consistency as illustrated here.

APPENDIX A STRONG MOTION CATALOG (WUS)

The following catalog lists the WUS processed recordings for each earthquake and site condition.

PACIFIC ENGINEERING AND ANALYSIS STRONG-MOTION CATALOG (08/06/97)

No.	Earthquake Location, Mech, Dip (1)	Date & Time			Magnitude (2)				Station (3) No.	Station Description H/F	Closest Dist (km)(4)	Site Codes (5)	Filter Corners		PGA (g)	PGV (cm/s)	PGD (cm)
		YR	MODY	HRMN	M	ML	MS	OTH					HP (hz)	LP (hz)			
	Helena, Montana 00	1935	1031	1838	6.2	5.5	6.0	0.0	2022 99	Carroll College	8.0* 999.9	EZA -	0.20 0.20 0.20	15.0 15.0 15.0	0.102 0.150 0.173	7.3 5.8 16.5	2.29 1.00 2.37
0002	Helena, Montana 01	1935	1031	1918	0.0	0.0	0.0	0.0	2229 99	Helena Fed Bldg	36.7* 999.9	EAA -	0.50 1.00 0.50	20.0 20.0 20.0	0.012 0.047 0.041	0.3 0.7 0.7	0.57 0.23 0.45
0003	Humbolt Bay 99	1937	0207	0442	5.8	5.8	0.0	0.0	USGS 1023 99	Ferndale City Hall	73.7* 999.9	BQD -	0.60 0.50 0.30	10.0 10.0 10.0	0.019 0.044 0.038	1.2 2.6 3.2	0.12 0.30 0.45
0004	Imperial Valley 99	1938	0606	0242	0.0	0.0	0.0	5.0	USGS 117 99	El Centro Array #9	36.7* 999.9	BQD C	1.50 1.00 0.60	20.0 12.0 12.0	0.012 0.012 0.019	0.3 0.5 0.8	0.01 0.04 0.06
0005	Northwest Calif 99	1938	0912	0610	5.5	5.5	0.0	5.5	USGS 1023 99	Ferndale City Hall	55.0* 999.9	BQD -	0.30 0.50 0.20	15.0 11.0 11.0	0.030 0.134 0.097	1.4 7.2 5.4	0.14 0.58 0.78
0006	Imperial Valley 00	1940	0519	0437	7.0	0.0	7.2	0.0	USGS 117 00	El Centro Array #9	8.3 12.0	BQD C	0.20 0.20 0.20	15.0 15.0 15.0	0.205 0.313 0.215	10.7 29.8 30.2	9.16 13.32 23.91
0007	Northwest Calif 99	1941	0209	0945	0.0	0.0	0.0	6.6	USGS 1023 99	Ferndale City Hall	97.2* 999.9	BQD -	0.10 0.50 0.50	12.0 13.0 10.0	0.018 0.062 0.039	1.5 3.6 3.2	0.26 0.89 0.54
0008	Northern Calif 99	1941	1003	1614	0.0	0.0	0.0	6.4	USGS 1023 99	Ferndale City Hall	49.6* 999.9	BQD -	0.50 0.20 0.50	13.0 13.0 13.0	0.038 0.114 0.122	2.6 5.9 6.3	0.26 1.77 1.15
0009	Borrego 99	1942	1021	1622	0.0	0.0	0.0	6.5	USGS 117 99	El Centro Array #9	49.0* 999.9	BQD C	0.20 0.10 0.10	20.0 15.0 15.0	0.033 0.068 0.044	1.1 3.9 4.0	0.30 1.37 1.41
0010	Imperial Valley 99	1951	0124	0717	0.0	0.0	0.0	5.6	USGS 117 99	El Centro Array #9	28.5* 999.9	BQD C	0.40 0.40 0.15	20.0 13.0 12.0	0.013 0.029 0.030	0.6 2.4 2.9	0.14 0.39 0.92
0011	Northwest Calif 99	1951	1008	0411	5.8	0.0	0.0	0.0	USGS 1023 99	Ferndale City Hall	56.0* 999.9	BQD -	0.40 0.50 0.50	20.0 12.0 12.0	0.031 0.105 0.110	2.1 4.6 6.1	0.22 0.47 0.82
0012	Kern County 03	1952	0721	1153	7.4	0.0	7.7	0.0	USGS 135 99	LA - Hollywood Stor FF	120.5 107.0	IPD C	0.50 0.50 0.50	17.4 13.9 14.7	0.022 0.044 0.057	2.5 6.0 5.3	0.68 2.44 1.68
									USGS 135	LA - Hollywood Stor Lot	120.5	IPD	0.20 0.20	20.0 20.0	0.021 2.8	2.55	

A-2

No.	Earthquake Location, Mech, Dip (1)	Date & Time			Magnitude (2)				Station (3) No.	Description H/F	Closest Dist (km)(4)	Site Codes (5)	Filter Corners			PGA (g)	PGV (cm/s)	PGD (cm)	
		YR	MODY	HRMN	M	ML	MS	OTH					HP (hz)	LP (hz)					
										99			107.0	C	0.20	15.0	0.042	7.5	4.79
															0.20	13.0	0.058	6.2	1.86
									CDMG	80053	Pasadena - CIT Athenaeum	127.0	CQD	0.50	12.5	0.027	2.9	0.86	
										99		109.0	B	0.50	12.5	0.045	5.6	1.25	
														0.20	12.1	0.053	9.2	2.53	
									USGS	283	Santa Barbara Courthouse	87.0	CQD	0.50	12.3	0.041	4.4	1.27	
										99		85.0	B	0.50	14.3	0.087	12.1	2.81	
														0.50	13.2	0.127	15.5	4.06	
									USGS	1095	Taft Lincoln School	41.0	FQD	0.05	13.2	0.109	6.6	4.56	
										02		42.0	B	0.05	13.9	0.156	15.3	9.25	
														0.05	13.2	0.178	17.5	8.99	
0013	Northern Calif 99	1952	0922	1141	5.2	5.2	0.0	5.5	USGS	1023	Ferndale City Hall	39.3*	BQD	0.40	10.0	0.028	1.9	0.30	
										99		999.9	-	0.30	12.0	0.062	5.6	1.17	
														0.30	10.0	0.074	5.5	0.98	
0014	Southern Calif 99	1952	1122	0746	0.0	0.0	0.0	6.0	USGS	1083	San Luis Obispo	70.0*	CBB	0.20	13.0	0.028	2.4	0.74	
										99		999.9	-	0.20	13.0	0.036	2.8	0.93	
														0.50	13.0	0.054	3.3	0.55	
0015	Imperial Valley 99	1953	0614	0417	0.0	0.0	0.0	5.5	USGS	117	El Centro Array #9	28.5*	EQD	0.50	20.0	0.024	0.6	0.06	
										99		999.9	C	0.60	15.0	0.006	0.4	0.06	
														0.25	12.0	0.049	5.4	1.00	
0016	Central Calif 99	1954	0425	2033	0.0	0.0	0.0	5.3	USGS	1028	Hollister City Hall	28.0*	CHD	0.30	11.0	0.020	1.6	0.26	
										99		999.9	C	0.40	10.0	0.049	4.7	0.63	
														0.50	10.0	0.051	3.9	0.42	
0017	Northern Calif 99	1954	1221	1956	0.0	0.0	0.0	6.5	USGS	1023	Ferndale City Hall	31.5*	BQD	0.50	13.0	0.039	6.9	2.03	
										99		999.9	-	0.20	20.0	0.159	33.9	13.34	
														0.50	13.0	0.189	25.3	5.86	
0018	Imperial Valley 99	1955	1217	0607	0.0	0.0	0.0	5.4	USGS	117	El Centro Array #9	28.4*	EQD	0.60	15.0	0.028	0.9	0.07	
										99		999.9	C	0.23	12.0	0.056	4.0	0.79	
														0.20	15.0	0.042	3.7	0.70	
0019	El Alamo 99	1956	1217	1433	0.0	0.0	0.0	6.8	USGS	117	El Centro Array #9	130.0	EQD	0.50	20.0	0.014	1.7	0.77	
										99		999.9	C	0.10	15.0	0.033	4.1	2.89	
														0.10	15.0	0.052	6.6	4.93	
0020	San Francisco 02	1957	0322	1944	5.3	5.3	0.0	0.0	USGS	1117	Golden Gate Park	9.5*	IBA	0.30	25.0	0.047	1.1	0.18	
										02		8.0	A	0.80	20.0	0.095	3.9	0.19	
														0.30	20.0	0.112	4.6	0.43	
0021	Central Calif 99	1960	0120	0326	0.0	0.0	0.0	5.0	USGS	1028	Hollister City Hall	14.9*	CHD	0.40	12.0	0.027	1.7	0.25	
										99		999.9	C	0.40	11.0	0.041	2.2	0.38	
														0.50	11.0	0.063	3.6	0.60	
0022	Northern Calif	1960	0606	0117	5.7	5.7	0.0	5.7	USGS	1023	Ferndale City Hall	58.9*	BQD	0.30	15.0	0.016	0.9	0.17	

A-4

No.	Earthquake Location, Mech, Dip (1)	Date & Time			Magnitude (2)					Station (3)		Closest Dist (km)(4)	Site Codes (5)	Filter Corners				
		YR	MODY	HRMN	M	ML	MS	OTH	No.	Description H/F	HP (hz)			LP (hz)	PGA (g)	PGV (cm/s)	PGD (cm)	
												999.9	-	0.30	15.0	0.072	3.8	0.59
														0.40	15.0	0.065	3.0	0.35
0023	Hollister 99	1961	0409	0723	0.0	0.0	0.0	5.6	USGS	1028 99	Hollister City Hall	19.6* 999.9	CHD C	0.11 0.25 0.11	11.0 11.0 11.0	0.051 0.074 0.196	4.7 6.3 12.4	1.77 1.31 4.29
0024	Hollister 99	1961	0409	0725	0.0	0.0	0.0	5.5	USGS	1028 99	Hollister City Hall	12.6* 999.9	CHD C	0.30 0.40 0.30	13.0 12.0 11.0	0.049 0.072 0.075	3.0 4.9 9.7	0.53 0.71 1.75
0025	Parkfield 00	1966	0628	0426	6.1	6.1	0.0	0.0	CDMG	1013 00	Cholame #2	0.1 6.6	IHD C	0.20 0.20 -99.	20.0 10.0	0.255 0.476	13.7 75.1	3.79 22.49
									CDMG	1014 00	Cholame #5	5.3 9.3	IHC C	0.20 0.20 0.20	21.0 17.4 20.0	0.138 0.442 0.367	6.9 24.7 21.8	2.66 5.15 3.83
									CDMG	1015 00	Cholame #8	9.2 13.0	ABB C	0.20 0.20 0.20	24.0 20.0 20.0	0.116 0.246 0.273	4.3 10.2 11.3	1.48 3.60 3.20
									CDMG	1016 00	Cholame #12	14.7 17.3	IBB B	0.20 0.20 0.20	20.0 20.0 20.0	0.053 0.059 0.063	4.6 5.8 6.8	2.10 2.56 3.55
									USGS	1083 00	San Luis Obispo	60.0 63.6	CBB -	0.20 0.20 0.20	15.0 15.0 12.0	0.007 0.012 0.014	0.8 1.0 1.0	0.28 0.30 0.46
									CDMG	1438 00	Temblor pre-1969	9.9 16.1	IJA B	0.20 0.20 0.20	16.9 14.7 15.1	0.136 0.357 0.272	4.4 21.5 15.0	1.10 3.87 3.40
0026	Northern Calif 99	1967	1210	1206	5.6	5.6	0.0	5.8	USGS	1023 99	Ferndale City Hall	30.8* 999.9	BQD -	0.40 0.30 0.20	12.0 20.0 13.0	0.032 0.283 0.113	3.3 9.2 11.1	0.46 1.23 1.58
0027	Northern Calif 99	1967	1218	1725	0.0	0.0	0.0	5.2	USGS	1028 99	Hollister City Hall	45.0* 999.9	CHD C	0.50 0.30 0.30	15.0 15.0 15.0	0.011 0.013 0.013	0.5 2.0 1.0	0.09 0.37 0.27
0028	Borrego Mtn 00	1968	0409	0230	6.8	6.7	6.5	0.0	USGS	117 00	El Centro Array #9	46.0 45.0	BQD C	0.20 0.20 0.20	16.4 12.5 12.8	0.030 0.130 0.057	3.3 26.3 13.2	1.99 12.18 10.03
									USGS	135 00	LA - Hollywood Stor PE Lot	217.4 211.0	IPD C	0.20 0.20 0.10	30.0 13.0 13.0	0.005 0.012 0.011	1.1 2.9 2.3	1.10 1.30 2.33
									USGS	130 00	LB - Terminal Island	195.0 187.0	CCD C	0.10 0.10 0.10	20.0 15.0 15.0	0.005 0.010 0.009	1.6 2.8 3.0	1.76 2.53 5.46
									CDMG	475	Pasadena - Athenaeum	203.0	CQD	0.50	13.0	0.004	0.5	0.38

No.	Earthquake Location, Mech, Dip (1)	Date & Time			Magnitude (2)				Station (3)		Closest Dist (km)(4)	Site Codes (5)	Filter Corners			PGA (g)	PGV (cm/s)	PGD (cm)
		YR	MODY	HRMN	M	ML	MS	OTH	No.	Description H/F			HP (hz)	LP (hz)				
										00		B	0.50	13.0	0.007	1.4	0.82	
													0.50	13.0	0.009	1.8	0.64	
									SCE	280	San Onofre - So Cal Edison	ABB	0.20	15.0	0.062	1.9	0.50	
										00		-	0.10	20.0	0.041	3.7	1.72	
													0.20	20.0	0.045	3.7	1.30	
0029	Lyle Creek 03	1970	0912	1430	5.4	5.4	0.0	0.0	CDMG	24278	Castaic - Old Ridge Route	A-B	0.70	20.0	0.010	0.4	0.03	
										99		B	0.50	20.0	0.021	0.9	0.07	
													0.50	20.0	0.026	1.5	0.15	
									CDWR	111	Cedar Springs, Allen Ranch	AAA	-99.					
										99		A	0.60	15.0	0.071	1.8	0.11	
													1.10	20.0	0.050	1.2	0.06	
									CDWR	112	Cedar Springs Pumphouse	AAB	1.00	15.0	0.037	1.3	0.08	
										99		-	0.50	20.0	0.069	2.6	0.14	
													0.40	15.0	0.077	3.7	0.39	
									USGS	113	Colton, So Cal Edison	ACD	0.60	15.0	0.035	1.3	0.11	
										99		C	0.40	12.0	0.033	1.6	0.17	
													0.50	11.0	0.038	1.3	0.14	
									CDWR	620	Devil's Canyon	CAA	1.10	30.0	0.084	1.8	0.10	
										99		-	1.00	20.0	0.146	3.3	0.18	
													1.00	30.0	0.151	5.6	0.23	
									CDMG	125	Lake Hughes #1	APC	1.10	15.0	0.006	0.3	0.02	
										99		-	0.80	10.0	0.009	0.7	0.08	
													0.35	20.0	0.008	0.6	0.10	
									CDMG	24303	LA - Hollywood Stor FF	IPD	0.90	20.0	0.007	0.3	0.02	
										99		C	0.30	20.0	0.017	1.0	0.14	
													0.40	20.0	0.018	0.7	0.06	
									CDMG	278	Puddingstone Dam (Abutment)	IVB	0.35	20.0	0.014	0.7	0.12	
										99		-	0.50	20.0	0.018	0.9	0.09	
													0.50	20.0	0.019	0.9	0.12	
									LAFC	104	Santa Anita Dam	IGA	1.20	25.0	0.013	0.3	0.01	
										99		-	1.00	25.0	0.042	1.6	0.10	
													0.40	25.0	0.018	0.5	0.04	
									USGS	290	Wrightwood - 6074 Park Dr	BAB	0.60	40.0	0.078	2.3	0.25	
										99		B	0.60	20.0	0.162	10.1	1.02	
													0.70	30.0	0.200	10.5	0.62	
0030	San Fernando 02	1971	0209	1400	6.6	0.0	6.6	0.0		2	2516 Via Tejon PV	CBC	0.20	20.0	0.020	2.0	1.26	
										99		-	0.20	20.0	0.026	3.8	2.19	
													0.20	20.0	0.041	4.2	3.11	
									CIT	103	Anza Post Office	AAC	0.50	35.0	0.015	0.7	0.20	
										99		-	0.50	35.0	0.027	1.4	0.25	
													0.50	35.0	0.037	2.2	0.30	
									USGS	1004	Bakersfield - Harvey Aud	CCD	0.10	15.0	0.007	0.7	0.69	
										99		-	0.10	13.0	0.007	1.4	1.08	
													0.10	20.0	0.007	1.2	1.23	

No.	Earthquake Location, Mech, Dip (1)	Date & Time		Magnitude (2)				Station (3)		Closest Dist (km)(4)	Site Codes (5)	Filter Corners			PGA (g)	PGV (cm/s)	PGD (cm)
		YR	MODY	HRMN	M	ML	MS	OTH	No.			Description H/F	HP (hz)	LP (hz)			
								USGS	105 99	Borrego Springs Fire Sta	212.0 999.9	AAC -	0.10 0.10 0.10	30.0 23.0 30.0	0.005 0.009 0.009	1.2 1.2 1.2	1.13 1.22 0.90
								USGS	1 99	Buena Vista - Taft	118.0 999.9	AQD -	0.20 0.10 0.10	20.0 13.0 15.0	0.007 0.012 0.012	0.6 1.5 1.3	0.41 1.51 0.68
								ACOE	108 99	Carbon Canyon Dam	66.4 999.9	AMA -	0.50 0.50 0.50	35.0 35.0 35.0	0.043 0.070 0.071	1.6 2.7 3.9	0.93 1.27 0.85
								CDMG	24278 99	Castaic - Old Ridge Route	24.9 24.2	A-B B	0.50 0.50 0.50	35.0 35.0 35.0	0.171 0.324 0.268	6.5 15.6 25.9	1.28 2.31 4.67
								CDWR	111 99	Cedar Springs, Allen Ranch	86.6 999.9	AAA A	0.20 0.20 0.20	35.0 35.0 35.0	0.009 0.020 0.015	0.9 1.7 1.4	0.53 0.49 0.57
								CDWR	112 99	Cedar Springs - Pump	87.6 88.0	AAB -	0.10 0.10 0.10	20.0 20.0 20.0	0.012 0.027 0.025	0.8 2.0 2.9	0.30 0.31 0.40
								USGS	1013 99	Cholame-Shandon Array #2 @	219.0 999.9	IHD C	0.10 0.10 0.10	50.0 20.0 30.0	0.004 0.004 0.005	1.3 1.2 1.1	1.18 1.31 0.92
								USGS	1015 99	Cholame-Shandon Array #8	223.0 999.9	ABB C	-99. 0.10 0.10	23.0 23.0 15.0	0.005 0.006 0.023	1.0 1.6 1.1	0.75 0.97 0.16
								USGS	113 99	Colton - So Cal Edison @	89.6 91.0	ACD C	0.10 0.10 0.10	15.0 13.0 13.0	0.032 0.039 0.039	1.8 2.2 3.5	0.29 0.32 0.71
								CDMG	121 99	Fairmont Dam	29.1 999.9	AGA -	0.50 0.50 0.50	35.0 35.0 35.0	0.039 0.071 0.109	3.5 4.7 6.5	0.71 0.72 1.10
								USGS	998 99	Fort Tejon	64.1 64.0	AAB -	0.10 0.10 0.10	23.0 20.0 20.0	0.016 0.026 0.022	0.7 1.1 1.4	0.21 0.36 0.27
								CDWR	994 99	Gorman - Oso Pump Plant	48.1 46.7	EBC C	0.10 0.10 0.10	23.0 23.0 30.0	0.039 0.084 0.105	3.6 7.9 6.8	0.72 1.27 1.76
								CDMG	12331 99	Hemet Fire Station	136.0 999.9	AQD C	0.50 0.50 0.50	35.0 35.0 35.0	0.026 0.033 0.047	1.5 2.2 2.6	0.32 0.38 0.33
								ACOE	1035 99	Isabella Dam (Aux Abut)	113.0 999.9	AGA -	0.10 0.10 0.10	20.0 13.0 13.0	0.006 0.006 0.009	1.3 1.4 1.6	1.33 1.94 2.03
								USGS	135 99	LA - Hollywood Stor Lot	21.2 24.6	IPD C	0.50 0.20 0.20	35.0 35.0 35.0	0.136 0.210 0.174	4.3 18.9 14.9	1.52 12.40 6.25

No.	Earthquake Location, Mech, Dip (1)	Date & Time			Magnitude (2)				Station (3)		Closest Dist (km)(4)	Site Codes (5)	Filter Corners					
		YR	MODY	HRMN	M	ML	MS	OTH	No.	Description H/F			HP (hz)	LP (hz)	PGA (g)	PGV (cm/s)	PGD (cm)	
									CDMG	125 99	Lake Hughes #1	25.8 23.4	APC -	0.20 0.50	35.0 35.0	0.098 0.145	11.4 17.3	2.76 2.88
														0.50	35.0	0.110	14.0	1.93
									USGS	126 99	Lake Hughes #4	24.2 19.6	IGA C	0.50 0.50	35.0 35.0	0.164 0.192	6.4 5.6	0.93 0.92
														0.50	35.0	0.153	8.4	1.85
									USGS	127 99	Lake Hughes #9	23.5 20.2	AGA -	0.50 0.50	35.0 35.0	0.088 0.157	2.3 4.5	0.87 1.28
														0.50	35.0	0.134	3.9	1.12
									CDMG	128 99	Lake Hughes #12	20.3 17.0	AEB B	0.50 0.50	35.0 35.0	0.167 0.366	3.7 17.0	0.65 1.65
														0.50	35.0	0.283	12.7	2.97
									USGS	130 99	LB - Terminal Island	69.2 61.4	CCD C	0.10 0.10	50.0 20.0	0.017 0.029	3.9 9.6	3.03 8.25
														0.10	20.0	0.029	6.8	6.17
									CDWR	1041 99	Maricopa Array #1	115.0 999.9	IBB -	0.10 0.10	20.0 13.0	0.005 0.007	1.1 1.7	1.40 1.53
														0.10	20.0	0.011	2.4	2.33
									CDWR	1042 99	Maricopa Array #2	113.0 999.9	IBB -	0.20 0.10	20.0 20.0	0.007 0.009	0.7 1.3	0.22 1.03
														0.20	15.0	0.009	1.1	0.41
									CDWR	1043 99	Maricopa Array #3	113.0 999.9	IBB -	0.20 0.20	15.0 20.0	0.007 0.008	2.9 2.2	2.15 1.85
														0.10	20.0	0.010	2.0	2.16
									CDMG	279 02	Pacoima Dam	2.8 999.9	AMB -	0.10 0.10	35.0 35.0	0.699 1.226	56.5 112.5	18.25 35.50
														0.50	35.0	1.160	54.3	11.73
									USGS	262 99	Palmdale Fire Station	25.4 28.6	AQD B	-99. 0.50	35.0 35.0	0.121 0.151	12.3 8.1	2.65 1.85
														0.50	35.0	0.095	4.5	0.70
									CDMG	80053 99	Pasadena - CIT Athenaeum	31.7 25.7	CQD B	0.50 0.50	35.0 35.0	0.088 0.110	6.4 13.3	1.36 7.78
														0.20	35.0	0.110	13.3	7.78
									USGS	266 99	Pasadena - Old Seismo Lab	19.1 21.9	CGA -	0.50 0.50	35.0 35.0	0.090 0.089	4.4 5.3	1.40 0.86
														0.50	35.0	0.202	10.9	2.39
									CDWR	269 99	Pearblossom Pump	38.9 37.4	AGB B	0.20 0.20	35.0 35.0	0.050 0.102	2.1 4.7	0.95 1.53
														0.20	35.0	0.136	5.6	1.61
									CDMG	272 99	Port Hueneeme	63.0 62.0	BBD -	0.50 0.50	35.0 35.0	0.011 0.027	3.0 6.1	1.78 3.50
														0.50	35.0	0.025	3.9	2.65
									CDMG	278 99	Puddingstone Dam (Abut)	50.4 999.9	IVD -	0.50 0.50	35.0 35.0	0.036 0.074	1.6 4.0	0.51 0.76
														0.50	35.0	0.065	3.1	0.43

No.	Earthquake Location, Mech, Dip (1)	Date & Time			Magnitude (2)				Station (3) Description No. H/F	Closest Dist (km)(4)	Site Codes (5)	Filter Corners			PGA (g)	PGV (cm/s)	PGD (cm)	
		YR	MODY	HRMN	M	ML	MS	OTH				HP (hz)	LP (hz)					
									USGS	314 99	San Diego Gas & Electric	214.0 999.9	ABD -	0.10 0.10 0.10	33.0 30.0 30.0	0.003 0.006 0.004	1.0 1.5 1.2	0.90 1.16 1.00
									USGS	465 99	San Juan Capistrano	104.0 999.9	ABC -	0.50 0.50 0.50	35.0 35.0 35.0	0.021 0.046 0.035	2.0 3.3 3.7	0.67 1.05 0.79
									SCE	280 99	San Onofre - So Cal Edison	122.0 999.9	ABB -	0.10 0.10 0.20	23.0 20.0 20.0	0.011 0.013 0.016	0.8 1.7 1.8	0.77 0.74 0.63
									LAFC	104 99	Santa Anita Dam	27.0 999.9	IGA -	0.20 0.20 0.20	35.0 35.0 35.0	0.062 0.151 0.212	3.9 4.7 6.1	1.80 2.30 2.89
									CDMG	285 99	Santa Felita Dam (Outlet)	27.5 999.9	ABA -	0.10 0.10 0.10	20.0 20.0 13.0	0.065 0.148 0.152	4.1 9.4 6.5	2.36 7.02 3.46
									CDWR	1027 99	Tehachapi Pump	68.0 999.9	AAA -	0.20 0.20 0.20	35.0 35.0 35.0	0.045 0.053 0.025	1.7 2.0 1.0	0.28 0.37 0.13
									USGS	282 99	UCSB - Fluid Mech Lab	125.6 999.9	CPD -	0.20 0.20 0.20	30.0 30.0 30.0	0.011 0.017 0.017	1.3 2.7 3.0	0.73 1.41 1.29
									ACOE	287 99	Upland - San Antonio Dam	58.1 999.9	AAA B	0.50 0.50 0.50	35.0 35.0 35.0	0.032 0.058 0.079	1.3 2.9 3.5	0.54 0.55 0.50
									CDWR	1102 99	Wheeler Ridge - Ground	81.6 82.0	IBD C	0.10 0.10 0.10	30.0 23.0 23.0	0.014 0.027 0.031	1.4 2.0 1.7	1.46 1.47 1.23
									ACOE	289 99	Whittier Narrows Dam	45.1 999.9	IHD -	0.10 0.10 0.10	30.0 20.0 20.0	0.032 0.100 0.107	3.7 9.3 9.7	2.61 5.79 5.04
									USGS	290 99	Wrightwood - 6074 Park Dr	60.3 60.7	BAB B	0.20 0.20 0.20	40.0 30.0 30.0	0.028 0.061 0.044	1.6 2.6 3.3	0.78 0.47 0.68
0031	Point Mugu 02	1973	0221	1445	5.8	5.9	5.2	0.0	CDMG	272 99	Port Hueneme	25.0* 16.0	BBD C	0.15 0.20 0.20	30.0 25.0 30.0	0.047 0.112 0.083	2.2 14.8 4.6	0.39 2.59 0.80
0032	Hollister 00	1974	1128	2301	5.2	5.2	4.5	0.0	CDMG	47379 00	Gilroy Array #1	12.3* 10.0	IFA A	-99. 1.50 1.10	25.0 25.0 25.0	0.105 0.132 0.071	2.7 4.0 3.5	0.13 0.17 0.36
									USGS	1028 00	Hollister City Hall	11.1* 10.0	CHD C	0.30 0.40 0.40	20.0 15.0 11.0	0.071 0.089 0.177	3.5 6.2 10.3	0.36 0.56 1.25
									CDMG	1377 00	San Juan Bautista, 24 Polk St	11.4* 8.0	AQD B	1.00 0.80	20.0 20.0	0.046 0.049	1.5 2.2	0.10 0.17

A-9

No.	Earthquake Location, Mech, Dip (1)	Date & Time			Magnitude (2)				Station (3)		Closest Dist (km)(4)	Site Codes (5)	Filter Corners					
		YR	MODY	HRMN	M	ML	MS	OTH	No.	Description H/F			HP (hz)	LP (hz)	PGA (g)	PGV (cm/s)	PGD (cm)	
													0.40	15.0	0.130	7.3	0.64	
0033	Northern Calif 99	1975	0607	0846	5.2	5.2	5.7	0.0	CDMG	1249 99	Cape Mendocino, Petrolia	28.9* 999.9	IFA A	2.00 1.50	30.0 25.0	0.026 0.115	0.8 3.1	0.04 0.10
									USGS	1023 99	Ferndale City Hall	22.8* 999.9	BQD -	2.00 0.20	20.0 15.0	0.179 0.239	4.9 8.9	0.16 1.77
									CDMG	1398 99	Petrolia, General Store	29.9* 999.9	IMD -	0.40 1.00	15.0 35.0	0.038 0.041	2.7 1.8	0.28 0.10
									CDMG	1277 99	Shelter Cove, Sta A	59.2* 999.9	IBA -	0.45 -99.	25.0 30.0	0.156 0.131	8.6 7.8	0.92 0.55
									CDMG	1278 99	Shelter Cove, Sta B	60.2* 999.9	IBB -	1.00 -99.	20.0 30.0	0.032 0.081	1.5 2.3	0.11 0.10
													1.00 1.50	20.0 25.0	0.031 0.093	1.2 2.8	0.07 0.11	
0034	Oroville 01	1975	0801	2020	6.0	5.7	0.0	0.0	CDWR	1051 99	Oroville Seismograph Station	9.5* 8.0	AJA -	-99. 1.00	10.0 10.0	0.092 0.072	3.7 2.8	0.17 0.22
0035	Oroville 01	1975	0802	2022	5.0	5.1	0.0	0.0	CIT	1545 99	Oroville Airport	14.6* 999.9	ACD -	0.30 0.20	25.0 15.0	0.015 0.036	1.1 2.5	0.32 0.82
									CDMG	1546 99	Up & Down Cafe (OR1)	12.7* 999.9	ADD -	0.40 0.60	25.0 30.0	0.015 0.021	1.4 1.1	0.33 0.18
													0.70 0.20	25.0 20.0	0.034 0.030	1.1 2.9	0.15 0.72	
0036	Oroville 04	1975	0802	2059	4.4	5.2	0.0	0.0	CIT	1544 99	Medical Center	11.1* 999.9	ABB -	0.80 0.40	30.0 40.0	0.030 0.079	1.1 3.0	0.83 0.32
									CIT	1545 99	Oroville Airport	15.0* 999.9	ACD -	0.35 0.30	30.0 40.0	0.043 0.025	2.2 1.2	0.22 0.24
									CDMG	1546 99	Up & Down Cafe (OR1)	12.4* 999.9	ADD -	0.50 0.70	40.0 40.0	0.020 0.024	2.2 1.1	0.62 0.91
													0.35 0.40	30.0 30.0	0.065 0.050	1.1 2.5	0.14 0.43	
0037	Oroville 01	1975	0808	0700	4.7	4.9	0.0	0.0	CIT	1542 99	Broadbeck Residence	9.8* 999.9	ACC -	1.30 0.70	40.0 30.0	0.073 0.168	1.7 3.1	0.06 0.17
									CDMG	1550 99	Duffy Residence (OR5)	10.9* 999.9	ACD -	0.70 1.00	40.0 40.0	0.117 0.051	3.4 0.7	0.22 0.05
									CIT	1543 99	DWR Garage	6.5* 999.9	AAA -	0.80 5.00	40.0 50.0	0.085 0.106	2.0 0.7	0.20 0.01
													1.50	50.0	0.141	1.1	0.04	

A-10

No.	Earthquake Location, Mech, Dip (1)	Date & Time			Magnitude (2)				Station (3)		Closest Dist (km)(4)	Site Codes (5)	Filter Corners					
		YR	MODY	HRMN	M	ML	MS	OTH	No.	Description H/F			HP (hz)	LP (hz)	PGA (g)	PGV (cm/s)	PGD (cm)	
									CDMG	1493	Johnson Ranch	10.7*	AAB	3.00	40.0	0.209	1.8	0.02
										99		999.9	-	2.00	50.0	0.089	1.1	0.02
														1.00	45.0	0.191	3.9	0.10
									CDMG	1496	Nelson Ranch (OR7)	6.7*	ABB	1.00	40.0	0.095	1.6	0.05
										99		999.9	-	1.50	50.0	0.110	1.3	0.02
														1.00	40.0	0.088	1.3	0.05
									CIT	1545	Oroville Airport	11.7*	ACD	1.20	50.0	0.114	1.9	0.05
										99		999.9	-	0.80	50.0	0.072	1.1	0.07
														0.70	40.0	0.047	1.1	0.06
														0.35	30.0	0.065	2.4	0.27
									CDMG	1549	Pacific Heights Rd (OR4)	12.0*	ACD	0.80	40.0	0.042	1.0	0.09
										99		999.9	-	0.60	40.0	0.065	2.6	0.27
														1.00	40.0	0.069	2.1	0.11
									CDMG	1551	Summit Ave (OR6)	8.6*	AAA	1.50	40.0	0.059	0.8	0.02
										99		999.9	-	1.50	35.0	0.101	2.3	0.08
														1.30	35.0	0.081	1.2	0.04
									CDMG	1546	Up & Down Cafe (OR1)	13.3*	ADD	0.70	40.0	0.048	1.2	0.13
										99		999.9	-	0.50	40.0	0.152	3.9	0.20
														0.40	40.0	0.101	3.5	0.40
0038	Friuli, Italy 99	1976	0506	2000	6.5	6.2	6.5	0.0		8002	Barcis	49.7*	ABB	0.20	37.0	0.014	1.0	0.18
										99		999.9	-	0.20	30.0	0.029	1.3	0.53
														0.20	30.0	0.030	1.2	0.27
										8004	Codroipo	34.6*	ADD	0.10	30.0	0.035	5.9	3.33
										99		999.9	-	0.10	25.0	0.062	10.7	3.03
														0.10	25.0	0.090	8.5	3.09
										8005	Conegliano	73.7*	ADD	0.50	25.0	0.025	2.4	0.70
										99		999.9	-	0.50	20.0	0.049	3.5	0.76
														0.50	20.0	0.069	4.2	1.03
										8007	Feltre	97.1*	ABA	0.20	30.0	0.019	0.8	0.24
										99		999.9	-	0.20	30.0	0.033	1.5	0.26
														0.20	30.0	0.038	1.3	0.28
										8012	Tolmezzo	37.7*	ABB	0.10	45.0	0.268	10.7	2.50
										99		999.9	-	0.10	30.0	0.351	22.0	4.10
														0.10	30.0	0.315	30.8	5.10
0039	Gazli, USSR 02	1976	0517		6.8	0.0	7.3	0.0		9201	Karakyr	3.0*	AAA	0.50	38.0	1.264	54.2	30.15
										01		999.9	-	0.50	38.0	0.608	65.4	25.29
														0.50	38.0	0.718	71.6	23.71
0040	Friuli, Italy 99	1976	0911	1631	5.5	0.0	0.0	0.0		8023	Buia	13.6*	ABC	0.40	20.0	0.029	3.1	0.68
										99		999.9	-	0.20	12.0	0.041	6.2	1.18
														0.13	20.0	0.041	3.9	1.02
										8014	Forgaria Cornino	18.2*	ABB	0.60	20.0	0.046	3.1	0.22
										99		999.9	B	0.20	15.0	0.112	7.6	0.94
														0.30	20.0	0.093	8.4	0.68

A-11

No.	Earthquake Location, Mech, Dip (1)	Date & Time			Magnitude (2)				Station (3)		Closest Dist (km)(4)	Site Codes (5)	Filter Corners			PGA (g)	PGV (cm/s)	PGD (cm)	
		YR	MODY	HRMN	M	ML	MS	OTH	No.	Description H/F			HP (hz)	LP (hz)					
0041	Friuli, Italy 99	1976	0915	0315	0.0	6.1	0.0	0.0	8022	San Rocco	17.9*	ABA	0.40	15.0	0.013	1.8	0.34		
									99		999.9	-	0.20	15.0	0.029	2.3	0.48		
													0.40	20.0	0.072	4.3	0.90		
									8023	Buia	10.8*	ABC	0.50	48.0	0.074	6.5	1.58		
									99		999.9	-	0.50	30.0	0.110	10.2	2.22		
													0.50	33.0	0.091	10.6	1.61		
0042	Santa Barbara 03	1978	0813		6.0	5.1	6.0	0.0	USGS	106	Cachuma Dam Toe	36.6*	AAA	0.20	29.0	0.024	1.6	0.40	
										99		999.9	-	0.10	36.0	0.072	6.3	1.26	
														0.20	30.0	0.034	2.6	0.55	
										USGS	283	Santa Barbara Courthouse	14.0*	CQD	0.10	30.0	0.077	3.5	0.83
											01		0.0	B	0.10	26.0	0.102	7.4	1.80
														0.10	30.0	0.203	16.3	2.99	
0043	Tabas, Iran 02	1978	0916		7.4	7.7	7.4	0.0		69	Bajestan	121.2	--	0.05		0.029	5.7	6.16	
										99		999.9	-	0.02	15.0	0.094	7.6	10.77	
														0.02	15.0	0.067	5.7	10.03	
										70	Boshrooyeh	26.1	-C	0.06		0.085	11.6	8.36	
										99		999.9	-	0.04	20.0	0.107	13.7	10.50	
														0.04	20.0	0.089	18.0	18.27	
										9102	Dayhook	17.0*	ABA	0.10		0.183	12.0	4.97	
										01		999.9	-	0.10		0.328	20.6	12.56	
														0.10		0.406	26.5	8.75	
										71	Ferdows	94.4	-A	0.04		0.053	7.6	6.78	
										99		999.9	-	0.02	20.0	0.087	5.7	4.61	
														0.04	20.0	0.108	8.6	9.69	
72	Kashmar	199.1	--	0.05	20.0	0.026	7.4	6.78											
99		999.9	-	0.03	20.0	0.034	10.7	10.60											
				0.02	20.0	0.037	11.4	7.10											
73	Sedeh	164.5	--	0.02	20.0	0.013	6.1	11.61											
99		999.9	-	0.02	20.0	0.026	5.6	6.42											
				0.02	20.0	0.027	4.1	4.91											
				0.05		0.688	45.6	17.04											
				0.05		0.836	97.8	36.92											
				0.05		0.852	121.4	94.58											
0044	Coyote Lake	1979	0806	1705	5.7	5.7	5.6	0.0	CDMG	57217	Coyote Lake Dam (SW Abut)	3.2	IFA	0.30	30.0	0.121	6.4	0.67	

No.	Earthquake Location, Mech, Dip (1)	Date & Time			Magnitude (2)				Station (3)		Closest Dist (km)(4)	Site Codes (5)	Filter Corners			PGA (g)	PGV (cm/s)	PGD (cm)
		YR	MODY	HRMN	M	ML	MS	OTH	No.	Description H/F			HP (hz)	LP (hz)				
00									00		1.6	-	0.30	40.0	0.157	10.8	1.31	
									CDMG	47379	Gilroy Array #1	9.3	IFA	0.30	40.0	0.072	2.5	0.41
										00		9.1	A	0.30	40.0	0.103	3.4	0.48
									CDMG	47380	Gilroy Array #2	7.5	IQD	0.25	40.0	0.132	8.3	1.52
										00		7.4	C	0.20	40.0	0.211	10.9	2.29
									CDMG	47381	Gilroy Array #3	6.0	IHD	0.20	40.0	0.339	24.9	5.81
										00		5.3	C	0.30	40.0	0.160	5.2	1.26
									CDMG	57382	Gilroy Array #4	4.5	AHD	0.20	40.0	0.272	18.7	3.42
										00		3.7	C	0.15	40.0	0.228	28.8	4.87
									CDMG	57383	Gilroy Array #6	3.1	IKB	0.20	25.0	0.248	23.1	2.60
										00		1.2	B	0.12	25.0	0.271	26.3	4.78
									CDMG	57191	Halls Valley	31.2	IFC	0.10	30.0	0.146	12.8	3.92
										00		30.0	B	0.08	25.0	0.434	49.2	7.77
									CDMG	1377	San Juan Bautista	15.6	AQD	0.20	40.0	0.316	24.5	3.85
										00		17.9	B	0.50	20.0	0.027	1.3	0.13
									CDMG	1492	SJB Overpass, Bent 3 g.l.	17.2	DQD	0.30	15.0	0.039	2.2	0.27
										00		19.2	B	0.20	20.0	0.107	7.5	1.02
									CDMG	1492	SJB Overpass, Bent 5 g.l.	17.2	DQD	0.20	20.0	0.111	4.7	0.95
										00		19.2	B	0.20	20.0	0.108	7.6	0.95
									CDMG	1492	SJB Overpass, Bent 5 g.l.	17.2	DQD	0.20	20.0	0.107	7.5	1.02
										00		19.2	B	0.30	50.0	0.060	2.3	0.21
									CDMG	1492	SJB Overpass, Bent 5 g.l.	17.2	DQD	0.60	60.0	0.097	5.9	0.55
										00		19.2	B	0.23	60.0	0.124	7.6	1.07
									CDMG	1492	SJB Overpass, Bent 5 g.l.	17.2	DQD	0.30	50.0	0.036	2.2	0.23
										00		19.2	B	0.30	50.0	0.073	5.6	0.77
									CDMG	1492	SJB Overpass, Bent 5 g.l.	17.2	DQD	0.25	60.0	0.114	7.4	1.08
									CDMG	1492	SJB Overpass, Bent 5 g.l.	17.2	DQD	0.30	50.0	0.036	2.2	0.23
										00		19.2	B	0.30	50.0	0.073	5.6	0.77
									CDMG	1492	SJB Overpass, Bent 5 g.l.	17.2	DQD	0.25	60.0	0.114	7.4	1.08
0045	Imperial Valley 00	1979	1015	2316	6.5	6.6	6.9	0.0	UNAMUCSD	6616	Aeropuerto Mexicali	8.5	I-D	0.05		0.142	5.6	2.31
										00		1.4	C	0.05		0.327	42.8	10.10
									UNAM/UCSD	6618	Agrarias	12.9	IQD	0.05		0.260	24.9	3.81
										00		999.9	-	0.20		0.835	11.1	5.17
									USGS	5054	Bonds Corner	2.5	AQD	0.05		0.370	35.6	10.02
										00		2.6	C	0.10	40.0	0.221	42.4	11.70
									USGS	5054	Bonds Corner	2.5	AQD	0.10	40.0	0.425	12.2	4.02
										00		2.6	C	0.10	40.0	0.588	45.2	16.78
									USGS	5060	Brawley Airport	8.5	AQD	0.10	40.0	0.775	45.9	14.89
										00		8.5	C	0.10	40.0	0.146	8.4	3.49
									USGS	5053	Callexico Fire Station	10.6	AQD	0.10	40.0	0.160	35.9	22.44
										00		10.6	C	0.10	40.0	0.220	38.9	13.46
									USGS	5053	Callexico Fire Station	10.6	AQD	0.10	40.0	0.187	6.7	2.49
										00		10.6	C	0.10	40.0	0.275	21.2	9.02
									USGS	5061	Calipatria Fire Sta	23.8	BQD	0.20	40.0	0.202	16.0	9.20
										00		23.8	BQD	0.10	40.0	0.055	3.9	2.76

No.	Earthquake Location, Mech, Dip (1)		Date & Time				Magnitude (2)				Station (3)		Closest Dist (km)(4)	Site Codes (5)	Filter Corners			PGA (g)	PGV (cm/s)	PGD (cm)	
	YR	MODY	HRMN	M	ML	MS	OTH	No.	Description H/F	HP (hz)	LP (hz)										
												00			23.0	C	0.10	40.0	0.128	15.4	10.91
																	0.10	40.0	0.078	13.3	6.22
												UNAM/UCSD 6604	Cerro Prieto		26.5	AVA	0.10		0.212	6.8	3.29
												00			23.5	B	0.10		0.169	11.6	4.25
																	0.10		0.157	18.6	7.95
												UNAM/UCSD 6621	Chihuahua		28.7	IQD	0.05		0.218	5.1	1.28
												00			17.7	C	0.05		0.270	24.9	9.08
																	0.05		0.254	30.1	12.89
												USGS 5066	Coachella Canal #4		49.3	AQD	0.20	40.0	0.038	3.6	0.66
												00			49.0	C	0.20	40.0	0.115	12.5	2.33
																	0.20	40.0	0.128	15.6	2.95
												UNAM/UCSD 6622	Compuertas		32.6	IQD	0.20		0.075	2.9	0.98
												00			23.2	C	0.20		0.186	13.9	2.92
																	0.20		0.147	9.5	2.49
												UNAM/UCSD 6617	Cucapah		23.6	IQD	0.05		0.140	3.1	1.37
												00			12.9	C	0.05		0.309	36.3	10.44
																	-99.				
												UNAM/UCSD 6605	Delta		43.6	IQD	0.05		0.145	14.8	8.62
												00			32.7	C	0.05		0.238	26.0	12.06
																	0.05		0.351	33.0	19.02
												CDMG 5154	EC County Center FF		7.6	IDD	0.10	50.0	0.246	18.1	9.70
												00			7.6	C	0.10	40.0	0.213	37.5	15.98
																	0.10	35.0	0.235	68.8	39.35
												CDMG 5155	EC Meloland Overpass FF		0.5	IDD	0.10	50.0	0.248	28.9	8.36
												00			0.5	C	0.10	40.0	0.314	71.7	25.53
																	0.10	50.0	0.296	90.5	31.71
												USGS 5056	El Centro Array #1		15.5	AQD	0.10	40.0	0.056	3.8	2.14
												00			22.0	C	0.10	40.0	0.139	16.0	9.96
																	0.10	40.0	0.134	10.7	6.97
												USGS 5115	El Centro Array #2		10.4	IQD	0.10	40.0	0.110	7.6	5.14
												00			16.0	C	0.10	40.0	0.315	31.5	14.34
																	-99.				
												USGS 5057	El Centro Array #3		9.3	AQD	0.10	40.0	0.127	8.7	4.70
												00			999.9	D	0.10	40.0	0.266	46.8	18.92
																	0.10	40.0	0.221	39.9	23.31
												USGS 955	El Centro Array #4		4.2	IQD	0.10	40.0	0.248	16.0	10.66
												00			6.8	C	0.10	40.0	0.485	37.4	20.23
																	0.10	40.0	0.360	76.6	59.02
												USGS 952	El Centro Array #5		1.0	IQD	0.10	40.0	0.537	38.5	19.69
												00			4.0	C	0.10	40.0	0.519	46.9	35.35
																	0.10	40.0	0.379	90.5	63.03
												CDMG 942	El Centro Array #6		1.0	IQD	0.20	40.0	1.655	57.5	26.41
												00			1.3	C	0.10	40.0	0.410	64.9	27.69
																	0.10	40.0	0.439	109.8	65.89
												USGS 5028	El Centro Array #7		0.6	AQD	0.10	40.0	0.544	26.4	9.32

No.	Earthquake Location, Mech, Dip (1)	Date & Time			Magnitude (2)				Station (3)		Closest Dist (km)(4)	Site Codes (5)	Filter Corners					
		YR	MODY	HRMN	M	ML	MS	OTH	No.	Description H/F			HP (hz)	LP (hz)	PGA (g)	PGV (cm/s)	PGD (cm)	
										00		C	0.10	40.0	0.338	47.6	24.68	
													0.10	40.0	0.463	109.3	44.74	
									CDMG	958	El Centro Array #8	3.8	AQD	0.10	40.0	0.439	22.3	11.87
										00		C	0.10	40.0	0.602	54.3	32.32	
													0.10	40.0	0.454	49.1	35.59	
									USGS	412	El Centro Array #10	8.6	AQD	0.10	40.0	0.105	8.8	6.90
										00		C	0.10	40.0	0.171	47.5	31.10	
													0.10	40.0	0.224	41.0	19.38	
									USGS	5058	El Centro Array #11	12.6	AQD	0.10	40.0	0.140	11.1	6.82
										00		C	0.20	40.0	0.364	34.5	16.07	
													0.10	40.0	0.380	42.1	18.59	
									USGS	931	El Centro Array #12	18.2	IQD	0.10	40.0	0.066	6.7	5.31
										00		C	0.10	40.0	0.143	17.6	11.30	
													0.10	40.0	0.116	21.8	12.06	
									USGS	5059	El Centro Array #13	21.9	AQD	0.20	40.0	0.046	3.2	1.67
										00		C	0.20	40.0	0.117	14.7	7.33	
													0.20	40.0	0.139	13.0	5.84	
									USGS	5165	El Centro Differential Array	5.3	IQD	0.10	40.0	0.707	20.7	11.55
										00		C	0.10	40.0	0.352	71.2	45.80	
													0.10	40.0	0.480	40.8	14.04	
									USGS	5055	Holtville Post Office	7.5	AQD	0.10	40.0	0.230	9.9	5.69
										00		C	0.10	40.0	0.253	48.8	31.54	
													0.10	40.0	0.221	49.8	31.96	
									CDMG	724	Niland Fire Station	35.9	AQD	0.10	40.0	0.034	3.8	2.04
										00		C	0.10	30.0	0.109	11.9	6.88	
													0.10	40.0	0.069	8.3	5.26	
									USGS	5051	Parachute Test Site	14.2	AQD	0.10	40.0	0.159	6.8	4.76
										00		B	0.10	40.0	0.111	17.8	12.35	
													0.10	40.0	0.204	16.1	9.94	
									USGS	5052	Plaster City	31.7	AQD	0.10	40.0	0.026	2.4	0.98
										00		C	0.10	40.0	0.042	3.2	1.34	
													0.10	40.0	0.057	5.4	1.94	
									UNAM/UCSD	6619	SAHOP Casa Flores	11.1	I-C	0.20		0.379	9.2	1.53
										00		C	0.20		0.287	19.6	2.71	
													0.20		0.506	30.9	5.64	
									USGS	286	Superstition Mtn Camera	26.0	AGA	0.10	40.0	0.077	2.3	1.14
										00		B	0.10	40.0	0.109	5.2	2.21	
													0.10	40.0	0.195	8.8	2.78	
									UNAM/UCSD	6610	Victoria	54.1	IQD	0.05		0.059	1.6	0.68
										00		C	0.05		0.122	6.4	2.09	
													0.20		0.167	8.3	1.05	
									CDMG	5169	Westmorland Fire Sta	15.1	ADD	0.10	40.0	0.082	6.8	2.58
										00		C	0.10	40.0	0.074	21.2	16.59	
													0.10	40.0	0.110	21.9	10.00	
0046	Imperial Valley	1979	1015	2319	5.2	5.2	0.0	0.0	USGS	5054	Bonds Corner	15.6*	AQD	3.00	35.0	0.052	0.9	0.02

No.	Earthquake Location, Mech, Dip (1)	Date & Time			Magnitude (2)			Station (3)		Closest Dist (km)(4)	Site Codes (5)	Filter Corners			PGA (g)	PGV (cm/s)	PGD (cm)
		YR	MODY	HRMN	M	ML	MS	OTH	No.			Description H/F	HP (hz)	LP (hz)			
00								00		999.9	C	0.80	30.0	0.084	3.6	0.34	
								USGS	5060	27.0*	AQD	0.30	30.0	0.100	8.2	1.42	
									00	999.9	C	1.00	40.0	0.026	0.6	0.02	
								USGS	5053	15.0*	AQD	0.80	30.0	0.034	2.0	0.16	
									00	999.9	C	1.00	30.0	0.067	2.4	0.12	
									6605	15.0*	AQD	0.90	40.0	0.035	0.9	0.05	
									00	999.9	C	0.45	30.0	0.116	8.0	0.87	
									6605	52.1*	IQD	0.40	35.0	0.068	5.2	0.51	
									00	999.9	C	1.00	25.0	0.023	0.7	0.04	
								USGS	5056	26.1*	AQD	0.80	30.0	0.059	2.6	0.21	
									00	999.9	C	0.40	30.0	0.112	5.5	0.84	
								USGS	5115	20.3*	IQD	0.70	40.0	0.027	0.4	0.03	
									00	999.9	C	0.80	30.0	0.080	3.8	0.39	
								USGS	5057	17.9*	AQD	0.70	30.0	0.029	1.1	0.12	
									00	999.9	C	0.60	25.0	0.150	9.5	0.95	
								USGS	955	14.4*	IQD	1.00	40.0	0.072	3.3	0.23	
									00	999.9	C	0.60	40.0	0.031	0.6	0.07	
								USGS	952	13.8*	IQD	0.50	33.0	0.179	9.5	0.97	
									00	999.9	C	0.80	40.0	0.112	4.2	0.30	
								USGS	952	13.8*	IQD	0.60	40.0	0.097	1.2	0.13	
									00	999.9	C	0.50	40.0	0.262	8.8	0.64	
								USGS	952	13.8*	IQD	0.45	35.0	0.157	9.6	0.65	
									00	999.9	C	0.70	35.0	0.238	10.7	0.75	
								CDMG	942	13.1*	IQD	0.60	35.0	0.239	13.3	1.06	
									00	999.9	C	0.40	50.0	0.080	1.7	0.10	
								USGS	5028	13.1*	AQD	0.60	30.0	0.189	12.1	1.15	
									00	999.9	C	0.35	30.0	0.366	20.8	2.83	
								CDMG	958	13.6*	AQD	0.60	40.0	0.060	0.8	0.06	
									00	999.9	C	0.60	40.0	0.132	5.0	0.52	
								USGS	412	15.1*	AQD	0.40	40.0	0.192	12.2	1.00	
									00	999.9	C	0.60	50.0	0.067	1.1	0.08	
								USGS	5058	17.2*	AQD	0.70	45.0	0.120	5.6	0.35	
									00	999.9	C	0.60	45.0	0.145	9.1	0.87	
								USGS	5165	13.3*	IQD	0.60	35.0	0.021	0.4	0.06	
									00	999.9	C	1.00	30.0	0.066	3.2	0.25	
								USGS	5058	17.2*	AQD	0.50	30.0	0.037	2.9	0.44	
									00	999.9	C	0.60	40.0	0.055	1.3	0.08	
								USGS	5165	13.3*	IQD	0.70	35.0	0.124	7.3	0.74	
									00	999.9	C	0.45	30.0	0.173	11.1	1.02	
								USGS	5055	12.2*	AQD	0.60	40.0	0.097	1.6	0.08	
									00	999.9	C	0.60	30.0	0.169	10.1	0.82	
								USGS	5055	12.2*	AQD	0.70	30.0	0.135	6.7	0.41	
									00	999.9	C	0.80	40.0	0.044	1.0	0.08	

No.	Earthquake Location, Mech, Dip (1)	Date & Time			Magnitude (2)				Station (3) No.	Station Description H/F	Closest Dist (km)(4)	Site Codes (5)	Filter Corners			PGA (g)	PGV (cm/s)	PGD (cm)
		YR	MODY	HRMN	M	ML	MS	OTH					HP (hz)	LP (hz)				
										00	999.9	C	0.60 0.50	30.0 30.0	0.127 0.211	7.3 15.4	0.56 2.14	
0047	Imperial Valley 00	1979	1016	0658	0.0	5.5	0.0	0.0	CDMG	5169	Westmorland Fire Sta 00	11.2* 999.9	ADD C	1.00 0.25 0.70	50.0 40.0 40.0	0.115 0.171 0.089	2.0 11.0 4.7	0.15 2.83 0.62
0048	Livermore 00	1980	0124	1900	5.8	5.8	5.8	0.0	CDMG	67070	Antioch - 510 G St 00	20.3 20.8	ACD B	0.20 0.20 0.20	20.0 13.0 13.0	0.012 0.051 0.023	1.5 5.1 2.6	0.47 0.80 0.72
									CDWR	1265	Del Valle Dam (Toe) 00	12.9 999.9	ABB -	0.30 0.10 0.15	30.0 25.0 20.0	0.083 0.125 0.229	4.2 9.3 20.5	1.00 3.15 3.71
									CDMG	57064	Fremont - Mission San Jose 00	29.8 33.1	AMB B	0.13 0.30 0.30	13.0 13.0 20.0	0.027 0.044 0.055	2.3 4.4 3.9	0.55 0.85 0.93
									CDMG	58219	APEEL 3E Hayward CSUH 00	31.0 40.3	BKA B	0.23 0.20 0.20	25.0 25.0 25.0	0.020 0.072 0.057	1.1 4.1 2.7	0.20 0.75 0.40
									CDMG	57134	San Ramon Fire Station 00	21.7 16.7	ABB C	0.30 0.15 0.20	20.0 15.0 15.0	0.016 0.058 0.040	2.0 3.3 4.0	0.40 1.00 1.24
									CDMG	57187	San Ramon - Eastman Kodak 00	17.6 15.7	ABB C	0.40 0.08 0.20	30.0 20.0 20.0	0.042 0.154 0.076	2.8 18.9 6.1	0.45 6.13 1.69
									CDMG	57063	Tracy - Sewage Treatm Plant 00	37.3 28.5	BQC C	0.20 0.15 0.08	20.0 20.0 15.0	0.021 0.050 0.073	3.1 7.5 7.6	0.98 2.35 1.81
0049	Livermore 00	1980	0127	0233	5.4	5.4	5.5	0.0	CDMG	67070	Antioch - 510 G St 00	30.9 30.9	ACD B	0.30 0.20 0.30	15.0 15.0 12.0	0.015 0.112 0.050	0.8 5.8 2.7	0.11 0.62 0.32
									CDWR	1265	Del Valle Dam (Toe) 00	12.9 999.9	ABB -	0.30 0.40 0.30	30.0 25.0 20.0	0.028 0.043 0.041	0.8 1.8 2.8	0.13 0.14 0.33
									CDMG	57064	Fremont - Mission San Jose 00	29.8 29.0	AMB B	0.20 0.30 0.25	15.0 15.0 12.0	0.017 0.035 0.038	1.5 4.7 3.3	0.23 0.79 0.52
									CDMG	58219	APEEL 3E Hayward CSUH 00	31.0 37.8	BKA B	0.60 0.30 0.15	25.0 20.0 20.0	0.014 0.053 0.028	0.9 4.5 1.4	0.09 0.58 0.30
									CDMG	57T01	Livermore - Fagundas Ranch 00	3.6 4.0	ABB C	0.30 0.30 0.30	30.0 25.0 20.0	0.098 0.258 0.233	2.5 9.6 11.4	0.17 0.55 1.18
									CDMG	57T02	Livermore - Morgan Terr Park 00	8.0 10.1	ABA B	0.40 0.25	30.0 30.0	0.078 0.198	4.1 11.7	0.39 1.02

A-16

A-17

No.	Earthquake Location, Mech, Dip (1)	Date & Time			Magnitude (2)				Station (3)		Closest Dist (km)(4)	Site Codes (5)	Filter Corners			PGA (g)	PGV (cm/s)	PGD (cm)
		YR	MODY	HRMN	M	ML	MS	OTH	No.	Description H/F			HP (hz)	LP (hz)				
									CDMG	57187	San Ramon - Eastman Kodak	17.6	ABB	0.40	30.0	0.252	9.8	1.30
										00		17.7	C	0.30	30.0	0.037	4.0	0.50
									CDMG	57134	San Ramon Fire Station	21.7	ABB	0.20	25.0	0.301	19.1	2.82
										00		25.5	C	0.25	25.0	0.097	5.6	0.62
														0.40	20.0	0.022	1.5	0.21
														0.40	15.0	0.049	3.4	0.43
														0.30	15.0	0.059	4.2	0.46
0050	Anza (Horse Cany) 00	1980	0225	1047	4.9	0.0	4.7	0.0	USGS	5160	Anza Fire Station	12.1*	AHC	0.50	30.0	0.037	1.4	0.91
										00		12.1	A	0.25	25.0	0.065	3.3	0.36
														0.60	25.0	0.066	2.6	0.16
									USGS	5044	Anza - Pinyon Flat	13.0*	IGA	0.40	30.0	0.046	1.1	0.08
										00		12.0	A	0.40	30.0	0.110	2.5	0.11
														0.20	25.0	0.131	5.1	0.49
									USGS	5045	Anza - Terwilliger Valley	5.8*	I-A	2.00	30.0	0.068	1.7	0.06
										00		5.8	A	1.10	30.0	0.131	3.9	0.17
														1.30	30.0	0.081	1.7	0.06
									USGS	5049	Borrego Air Ranch	40.6*	AAA	0.90	40.0	0.014	0.6	0.06
										00		41.4	B	0.60	25.0	0.047	2.6	0.28
														0.70	25.0	0.036	1.2	0.10
									USGS	5047	Rancho De Anza	19.6*	IHC	0.60	40.0	0.052	1.6	0.12
										00		20.6	B	0.60	40.0	0.097	6.7	0.55
														0.50	35.0	0.092	6.0	0.45
0051	Mammoth Lakes 03	1980	0525	1634	6.3	6.1	6.1	0.0	CDMG	54099	Convict Creek	9.0*	AQD	0.20	41.0	0.388	20.5	5.93
										00		999.9	-	0.10	60.0	0.416	23.3	4.66
														0.10	50.0	0.442	23.1	5.42
									CDMG	54214	Long Valley dam (Upr L Abut)	15.5*	IVA	0.10	40.0	0.123	8.4	1.72
										00		999.9	-	0.10	57.0	0.430	23.6	7.52
														0.10	50.0	0.271	13.9	3.06
									CDMG	54301	Mammoth Lakes H. S.	14.0*	BVD	0.10	60.0	0.253	11.2	2.55
										00		999.9	-	0.50	44.0	0.321	15.7	1.57
														0.50	51.0	0.239	14.4	1.65
0052	Mammoth Lakes 00	1980	0525	1649	5.7	6.0	0.0	0.0	CDMG	54099	Convict Creek	16.3*	AQD	0.50	47.0	0.129	9.0	1.05
										00		999.9	-	0.50	35.0	0.160	11.3	1.95
														0.50	35.0	0.178	12.2	2.26
									CDMG	54214	Long Valley Dam (Upr L Abut)	24.3*	IVA	0.50	27.0	0.038	1.5	0.29
										00		999.9	-	0.50	40.0	0.194	5.1	0.65
														0.50	30.0	0.065	4.4	0.59
									CDMG	54301	Mammoth Lakes H. S.	14.2*	BVD	0.10	60.0	0.264	9.0	1.56
										00		999.9	-	0.50	50.0	0.441	22.5	2.28
														0.10	52.0	0.390	23.9	2.72
0053	Mammoth Lakes 00	1980	0525	1944	6.0	6.1	0.0	0.0	CDMG	54099	Convict Creek	17.4*	AQD	0.20	40.0	0.195	8.5	1.59
										00		999.9	-	0.08	30.0	0.219	18.5	4.87
														0.08	35.0	0.208	16.1	2.29

A-18

No.	Earthquake Location, Mech, Dip (1)	Date & Time			Magnitude (2)				Station (3) No.	Station (3) Description H/F	Closest Dist (km)(4)	Site Codes (5)	Filter Corners					
		YR	MODY	HRMN	M	ML	MS	OTH					HP (hz)	LP (hz)	PGA (g)	PGV (cm/s)	PGD (cm)	
0054	Mammoth Lakes 00	1980	0525	2035	5.7	5.7	0.0	0.0	CDMG	54214 00	Long Valley Dam (Downst)	19.7* 999.9	IVA -	0.30	40.0	0.078	4.4	0.42
														0.15	40.0	0.107	5.9	1.21
														0.20	35.0	0.070	5.5	1.33
														0.40	50.0	0.068	4.0	0.45
														0.35	50.0	0.104	6.6	1.06
														0.20	50.0	0.077	5.4	1.69
														0.35	35.0	0.119	4.3	0.53
														0.20	40.0	0.484	14.2	1.77
														0.10	40.0	0.188	10.8	3.28
														0.20	45.0	0.345	6.2	0.52
														0.20	35.0	0.380	13.3	1.16
														0.20	35.0	0.432	21.0	2.31
0055	Mammoth Lakes 00	1980	0526	1858	0.0	6.1	5.8	0.0	CDMG	54214 00	Long Valley Dam (Downst)	14.4* 999.9	IVA -	1.00	40.0	0.058	2.1	0.12
														0.50	30.0	0.089	5.0	0.59
														0.30	30.0	0.046	2.3	0.35
														0.30	40.0	0.141	5.0	0.36
														0.50	40.0	0.231	18.3	1.56
														0.30	40.0	0.185	8.0	0.93
														0.30	35.0	0.146	5.0	0.36
														0.50	40.0	0.245	18.5	1.56
														0.40	40.0	0.195	8.0	0.82
														0.50	40.0	0.050	3.8	0.46
														0.50	30.0	0.133	7.8	0.82
														0.20	31.0	0.099	3.8	0.41
0056	Mammoth Lakes 03	1980	0527	1451	6.0	6.2	6.0	0.0	CDMG	54214 00	Long Valley Dam (Upr L Abut)	17.5* 999.9	IVA -	0.50	30.0	0.027	1.2	0.22
														0.50	31.0	0.110	6.0	0.63
														0.50	23.0	0.071	6.3	0.65
														0.50	40.0	0.064	3.1	0.52
														0.50	38.0	0.109	7.0	0.98
														0.50	33.0	0.175	11.2	1.18
														0.20	50.0	0.084	3.0	0.77
														0.20	40.0	0.091	5.5	1.48
														0.20	40.0	0.114	5.3	1.41
														0.10	50.0	0.188	9.6	1.62
														0.10	40.0	0.266	19.1	1.74
														0.10	40.0	0.316	16.2	3.19
0057	Mammoth Lakes 00	1980	0527	1901	4.9	5.0	0.0	0.0	USGS	43 00	Fish & Game (FIS)	5.5* 999.9	IQD -	0.20	50.0	0.038	1.7	0.21
														0.20	50.0	0.103	4.2	0.37
														0.11	40.0	0.098	5.2	0.73
														0.20	51.0	0.408	33.9	6.41
														0.20	50.0	0.092	28.9	3.17
														0.20	51.0	0.408	33.9	6.41
									USC	3	Green Church	4.7*	IQD	0.80	30.0	0.079	2.2	0.19

No.	Earthquake Location, Mech, Dip (1)	Date & Time			Magnitude (2)				Station (3)		Closest Dist (km)(4)	Site Codes (5)	Filter Corners					
		YR	MODY	HRMN	M	ML	MS	OTH	No.	Description H/F			HP (hz)	LP (hz)	PGA (g)	PGV (cm/s)	PGD (cm)	
										00		-	0.25	25.0	0.167	10.7	1.05	
									USC	35	Long Valley Fire Sta	4.3*	ACC	0.30	30.0	0.170	12.1	1.06
										00		-	0.70	20.0	0.018	1.0	0.10	
													0.70	25.0	0.022	1.7	0.24	
													0.50	20.0	0.031	1.6	0.15	
									USC	36	Mammoth Elem School	8.7*	AAB	0.60	20.0	0.015	1.3	0.19
										00		-	0.80	20.0	0.050	2.8	0.26	
													0.60	15.0	0.078	5.0	0.30	
									USC	34	USC Cash Baugh Ranch	9.9*	AQD	0.45	20.0	0.025	1.9	0.22
										00		-	0.50	25.0	0.031	3.3	0.46	
													0.40	20.0	0.038	2.9	0.36	
									USC	37	USC McGee Creek Inn	1.8*	AAD	-99.				
										00		-	0.70	30.0	0.325	8.6	0.53	
													0.90	25.0	0.131	5.0	0.33	
0058	Mammoth Lakes 00	1980	0531	1516	4.9	5.1	0.0	0.0	USGS	41	Cashbaugh (CBR)	11.8*	IQD	0.40	80.0	0.093	4.1	0.22
										00		-	0.10	60.0	0.106	2.6	0.28	
													0.20	60.0	0.134	6.7	0.40	
									USGS	42	Convict Lakes (CON)	8.7*	IQB	1.00	70.0	0.114	2.0	0.12
										00		-	0.80	60.0	0.196	4.0	0.29	
													0.70	70.0	0.206	6.5	0.44	
									USGS	43	Fish & Game (FIS)	7.7*	IQD	0.60	60.0	0.081	3.3	0.27
										00		-	0.50	60.0	0.281	9.5	0.52	
													0.30	50.0	0.145	10.2	1.19	
									USGS	44	Hot Creek (HCF)	9.9*	IQD	0.35	100.0	0.049	1.8	0.20
										00		-	-99.					
													-99.					
									USC	35	Long Valley Fire Sta	8.9*	AAC	0.80	20.0	0.019	0.7	0.06
										00		-	0.60	20.0	0.026	1.2	0.17	
													0.50	20.0	0.031	1.5	0.12	
									USC	36	Mammoth Elem School	7.3*	AAB	0.45	30.0	0.045	1.5	0.29
										00		-	0.30	15.0	0.099	6.1	0.57	
													0.40	20.0	0.091	6.1	0.51	
									USC	40	USC Convict Lakes	9.1*	AAB	0.30	40.0	0.050	1.5	0.16
										00		-	0.50	30.0	0.164	6.0	0.48	
													0.80	30.0	0.141	2.9	0.20	
									USC	37	USC McGee Creek Inn	7.4*	AAD	0.50	30.0	0.179	3.6	0.12
										00		-	1.00	20.0	0.053	13.4	0.44	
													0.60	30.0	0.184	5.5	0.28	
0059	Victoria, Mexico 00	1980	0609	0328	0.0	6.1	6.4	0.0	UNAMUCSD	6604	Cerro Prieto	34.8*	AVA	0.20	62.5	0.304	12.1	4.9
										0	0	B	0.20	62.5	0.621	31.6	13.2	
													0.20	62.5	0.587	19.9	9.4	
									UN AM/UCSD	6621	Chihuahua	36.6*	IQD	0.20	23.0	0.098	5.5	2.6
										00		C	0.20	22.0	0.150	24.8	9.2	
													0.20	27.0	0.092	15.6	9.9	

No.	Earthquake Location, Mech, Dip (1)	Date & Time			Magnitude (2)				Station (3) No.	Station Description H/F	Closest Dist (km)(4)	Site Codes (5)	Filter Corners					
		YR	MODY	HRMN	M	ML	MS	OTH					HP (hz)	LP (hz)	PGA (g)	PGV (cm/s)	PGD (cm)	
									UN AM/UCSD	6617 00	Cucapah	41.9* 999.9	IQD C	0.20 0.20	49.0 44.0	0.067 0.092	10.9 13.1	5.1 5.6
									UN AM/UCSD	6619 00	SAHOP Casa Flores	58.3* 999.9	I-C C	0.50 0.20	62.5 28.0	0.047 0.101	2.4 7.8	0.5 2.6
									UN AM/UCSD	6624 00	Victoria Hospital Sotano	62.6* 999.9	-D -	0.50 0.20	62.5 26.0	0.024 0.045	1.9 5.2	0.6 2.5
														0.20	62.5	0.032	5.3	1.7
0060	Mammoth Lakes 00	1980	0611	0441	0.0	5.0	0.0	0.0	USGS	42 00	Convict Lakes (CON)	7.6* 999.9	IQB -	1.50 0.80	80.0 80.0	0.091 0.191	1.1 2.4	0.03 0.08
									USGS	43 00	Fish & Game (FIS)	11.2* 999.9	IQD -	1.50 0.90	70.0 60.0	0.183 0.061	2.2 1.6	0.05 0.07
									USC	3 00	Green Church	12.0* 999.9	IQD -	1.00 0.60	30.0 25.0	0.024 0.023	0.5 1.5	0.03 0.16
									USGS	44 00	Hot Creek (HCF)	12.8* 999.9	IQD -	0.60 0.60	80.0 60.0	0.022 0.065	0.5 1.3	0.05 0.05
									USC	35 00	Long Valley Fire Sta	14.2* 999.9	AAC -	0.50 0.60	50.0 20.0	0.099 0.015	1.5 0.4	0.10 0.06
									USC	36 00	Mammoth Elem School	12.3* 999.9	AAB -	0.60 0.50	20.0 13.0	0.006 0.012	0.3 0.6	0.03 0.06
									USGS	45 00	McGee Creek (MGE)	11.9* 999.9	IQC -	0.80 1.00	15.0 70.0	0.018 0.066	0.8 1.4	0.05 0.08
									USC	40 00	USC Convict Lakes	9.1* 999.9	AAB -	1.00 2.00	60.0 30.0	0.056 0.038	1.2 0.4	0.07 0.02
									USC	52 00	USC McGee Creek	11.1* 999.9	AAA -	1.00 0.70	40.0 35.0	0.090 0.078	0.8 1.6	0.03 0.10
														1.00	25.0	0.211	3.0	0.09
0061	Trinidad 99	1980	1108	1027	0.0	0.0	0.0	0.0	CDMG	1498 99	Rio Dell Overpass, E Ground	71.9* 999.9	APC B	0.10 0.10	35.0 45.0	0.050 0.163	4.1 9.0	4.06 9.02
									CDMG	1498 99	Rio Dell Overpass, FF	71.9* 999.9	IPC B	0.10 0.10	40.0 30.0	0.134 0.061	9.9 7.0	9.89 7.03
									CDMG	1498 99	Rio Dell Overpass, W Ground	71.9* 999.9	APC B	0.10 0.10	30.0 40.0	0.147 0.041	8.5 3.7	8.48 3.66
														0.10	40.0	0.150	9.1	9.09

A-21

No.	Earthquake Location, Mech, Dip (1)	Date & Time			Magnitude (2)				Station (3)		Closest Dist (km)(4)	Site Codes (5)	Filter Corners			PGA (g)	PGV (cm/s)	PGD (cm)
		YR	MODY	HRMN	M	ML	MS	OTH	No.	Description H/F			HP (hz)	LP (hz)				
													0.10	40.0	0.156	11.2	11.20	
0062	Taiwan SMART1(5) 02	1981	0129		0.0	6.3	5.7	0.0	25	SMART1 C00	21.0	IZD	0.20	25.0	0.043	1.7	0.40	
									99		999.9	-	0.50	25.0	0.096	6.0	0.91	
									26	SMART1 I06	21.0	IZD	0.20	25.0	0.114	13.4	1.93	
									99		999.9	-	0.50	25.0	0.032	1.3	0.28	
									27	SMART1 I12	21.0	IZD	0.50	25.0	0.090	4.2	0.81	
									99		999.9	-	0.50	25.0	0.077	9.8	1.50	
									27	SMART1 I12	21.0	IZD	0.20	25.0	0.060	2.0	0.46	
									99		999.9	-	0.10	25.0	0.140	5.1	1.20	
									28	SMART1 M01	21.0	IZD	0.10	25.0	0.113	12.5	2.14	
									99		999.9	-	0.10	25.0	0.095	2.4	0.35	
									29	SMART1 M07	21.0	IZD	0.10	25.0	0.082	4.8	1.00	
									99		999.9	-	0.10	25.0	0.178	15.9	2.19	
									29	SMART1 M07	21.0	IZD	0.20	25.0	0.050	1.5	0.34	
									99		999.9	-	0.10	25.0	0.111	5.6	0.86	
									30	SMART1 O01	21.0	IZD	0.10	25.0	0.109	10.9	1.74	
									99		999.9	-	0.20	25.0	0.032	1.3	0.35	
									30	SMART1 O01	21.0	IZD	0.20	25.0	0.089	6.4	0.91	
									99		999.9	-	0.20	25.0	0.115	13.7	2.23	
									31	SMART1 O07	21.0	IZD	0.20	25.0	0.028	1.9	0.42	
									99		999.9	-	0.10	25.0	0.086	6.9	0.92	
									31	SMART1 O07	21.0	IZD	0.20	25.0	0.080	11.7	2.18	
									99		999.9	-	0.10	25.0	0.080	11.7	2.18	
0063	Westmorland 00	1981	0426	1209	5.8	5.6	0.0	0.0	USGS	5060	Brawley Airport	22.0*	AQD	0.60	40.0	0.101	2.2	0.23
									00		999.9	C	0.15	40.0	0.169	12.7	3.09	
									CDMG	724	Niland Fire Station	19.4*	AQD	0.70	33.0	0.171	5.8	0.48
									00		999.9	C	0.30	33.0	0.126	2.9	0.47	
									USGS	5051	Parachute Test Site	24.1*	AQD	0.30	33.0	0.105	5.6	0.69
									00		999.9	B	0.35	35.0	0.176	6.6	0.80	
									USGS	5062	Salton Sea Wildlife Ref.	10.1*	AQD	0.10	30.0	0.157	11.2	1.78
									00		999.9	D	0.10	30.0	0.242	39.2	26.88	
									USGS	5062	Salton Sea Wildlife Ref.	10.1*	AQD	0.10	33.0	0.155	26.6	12.97
									00		999.9	D	0.25	50.0	0.214	4.8	1.08	
									USGS	286	Superstition Mtn Camera	26.5*	AGA	0.07	33.0	0.199	16.4	4.45
									00		999.9	B	0.08	33.0	0.176	12.3	2.33	
									USGS	286	Superstition Mtn Camera	26.5*	AGA	0.70	35.0	0.045	1.3	0.09
									00		999.9	B	0.70	30.0	0.071	3.6	0.24	
									CDMG	5169	Westmorland Fire Sta	13.3*	ADD	0.70	30.0	0.116	5.0	0.49
									00		999.9	C	0.90	40.0	0.838	10.4	0.46	
									CDMG	5169	Westmorland Fire Sta	13.3*	ADD	0.08	40.0	0.368	48.7	10.61
									00		999.9	C	0.05	40.0	0.496	34.4	10.89	
0064	Mammoth Lakes 99	1983	0107	0138	0.0	5.2	0.0	0.0	CDMG	54099	Convict Creek	9.5*	AQD	0.20	40.0	0.097	7.9	1.65
									99		999.9	-	0.15	30.0	0.165	14.4	2.05	
									99		999.9	-	0.15	30.0	0.153	18.7	2.88	

No.	Earthquake Location, Mech, Dip (1)	Date & Time			Magnitude (2)				Station (3) No.	Station Description H/F	Closest Dist (km)(4)	Site Codes (5)	Filter Corners										
		YR	MODY	HRMN	M	ML	MS	OTH					HP (hz)	LP (hz)	PGA (g)	PGV (cm/s)	PGD (cm)						
0065	Mammoth Lakes 99	1983	0107	0324	0.0	5.4	0.0	0.0	CDMG	54099	Convict Creek	10.8*	AQD	0.30	40.0	0.073	5.7	0.75					
										99		999.9	-	0.40	30.0	0.150	8.4	0.97					
														0.20	30.0	0.101	7.1	1.50					
0066	Coalinga 03	1983	0502	2342	6.4	6.7	6.5	0.0	CDMG	46314	Cantua Creek School	25.5	AHD	0.20	26.0	0.094	5.1	1.86					
										99		999.9	-	0.20	23.0	0.227	23.6	5.83					
														0.20	23.0	0.281	25.8	3.71					
														CDMG	36452	Parkfield - Cholame 1E	41.6	IHD	0.50	30.0	0.059	6.6	1.82
														99		999.9	-	0.20	20.0	0.090	10.8	2.66	
																		0.20	20.0	0.089	15.2	2.64	
														CDMG	36230	Parkfield - Cholame 2E	40.5	IJB	0.50	26.0	0.017	2.3	0.52
														99		999.9	-	0.50	23.0	0.026	2.9	0.62	
																		0.20	22.0	0.037	5.4	1.40	
														CDMG	36228	Parkfield - Cholame 2WA	42.8	IHD	0.20	23.0	0.044	5.1	1.39
														99		999.9	-	0.20	22.0	0.109	11.3	2.60	
																		0.20	26.0	0.114	9.6	1.79	
														CDMG	36450	Parkfield - Cholame 3E	38.4	IMA	0.20	26.0	0.024	3.0	0.60
														99		999.9	-	0.20	23.0	0.044	4.4	1.61	
																		0.20	22.0	0.056	6.5	1.75	
														CDMG	36410	Parkfield - Cholame 3W	43.9	IHC	0.20	27.0	0.034	4.5	1.46
														99		999.9	-	0.20	21.0	0.098	7.6	1.86	
								0.20	24.0	0.084	8.3	1.41											
				CDMG	36412	Parkfield - Cholame 4AW	46.0	IHC	0.50	33.0	0.022	2.0	0.50										
				99		999.9	-	0.20	21.0	0.047	5.0	0.90											
								0.20	20.0	0.078	8.0	1.32											
				CDMG	36411	Parkfield - Cholame 4W	44.7	IHC	0.20	30.0	0.041	3.5	0.87										
				99		999.9	-	0.20	21.0	0.136	11.3	1.79											
								0.20	23.0	0.136	9.1	1.42											
				CDMG	36227	Parkfield - Cholame 5W	47.3	IHC	0.50	30.0	0.034	2.3	1.14										
				99		999.9	C	0.20	22.0	0.147	10.8	1.07											
								0.20	22.0	0.131	10.0	1.28											
				CDMG	36451	Parkfield - Cholame 6W	49.0	IHC	0.20	30.0	0.037	3.2	0.62										
				99		999.9	-	0.50	21.0	0.126	11.0	1.34											
								0.20	28.0	0.102	9.9	1.26											
				CDMG	36226	Parkfield - Cholame 8W	50.7	IQD	0.20	27.0	0.024	3.3	0.90										
				99		999.9	C	0.20	23.0	0.098	8.6	1.53											
								0.50	21.0	0.100	8.0	1.25											
				CDMG	36229	Parkfield - Cholame 12W	55.2	IQD	0.20	30.0	0.023	3.0	1.08										
				99		999.9	-	0.20	23.0	0.040	4.2	1.01											
								0.20	21.0	0.053	5.5	1.57											
				CDMG	36407	Parkfield - Fault Zone 1	40.4	IHD	0.20	31.0	0.040	8.6	2.45										
				99		999.9	-	0.20	20.0	0.194	23.3	7.82											
								0.20	21.0	0.111	17.8	4.79											
				CDMG	36413	Parkfield - Fault Zone 2	37.9	IHD	0.50	33.0	0.039	3.8	0.94										
				99		999.9	-	0.20	22.0	0.116	22.7	6.05											

No.	Earthquake Location, Mech, Dip (1)	Date & Time			Magnitude (2)			Station (3)		Closest Dist (km)(4)	Site Codes (5)	Filter Corners			PGA (g)	PGV (cm/s)	PGD (cm)
		YR	MODY	HRMN	M	ML	MS	OTH	No.			Description H/F	HP (hz)	LP (hz)			
								CDMG	36408	Parkfield - Fault Zone 3	36.4	IHD	0.20	25.0	0.133	19.7	4.40
									99		999.9	-	0.10	31.0	0.049	6.0	2.32
													0.10	27.0	0.140	13.7	4.76
													0.10	22.0	0.164	24.5	4.94
								CDMG	36414	Parkfield - Fault Zone 4	34.3	IPB	0.20	30.0	0.046	6.2	2.29
									99		999.9	-	0.20	22.0	0.067	12.6	3.36
													0.20	28.0	0.120	20.4	4.43
								CDMG	36454	Parkfield - Fault Zone 6	32.8	IPB	0.20	31.0	0.026	5.0	1.74
									99		999.9	-	0.20	24.0	0.055	9.1	3.85
													0.20	24.0	0.056	11.6	3.19
								CDMG	36431	Parkfield - Fault Zone 7	31.0	IQC	0.20	31.0	0.054	7.8	1.88
									99		999.9	-	0.20	30.0	0.122	21.1	7.34
													0.20	30.0	0.119	14.9	3.36
								CDMG	36449	Parkfield - Fault Zone 8	29.6	IMB	0.20	29.0	0.054	4.9	1.66
									99		999.9	-	0.20	21.0	0.131	17.3	4.21
													0.20	27.0	0.116	14.2	1.71
								CDMG	36443	Parkfield - Fault Zone 9	31.9	IPB	0.20	30.0	0.026	3.8	1.61
									99		999.9	-	0.20	23.0	0.057	9.4	2.91
													0.20	28.0	0.050	8.9	2.46
								CDMG	36444	Parkfield - Fault Zone 10	30.4	IQD	0.20	26.0	0.043	5.8	2.57
									99		999.9	-	0.20	24.0	0.073	15.3	7.05
													0.20	21.0	0.131	16.1	3.15
								CDMG	36453	Parkfield - Fault Zone 11	28.4	IMB	0.20	28.0	0.042	4.8	1.80
									99		999.9	-	0.20	21.0	0.097	11.9	2.35
													0.20	28.0	0.087	6.6	1.83
								CDMG	36138	Parkfield - Fault Zone 12	29.5	IHC	0.20	27.0	0.070	7.9	2.10
									99		999.9	-	0.20	20.0	0.110	12.1	3.26
													0.20	20.0	0.112	14.6	5.69
								CDMG	36456	Parkfield - Fault Zone 14	29.9	IHC	0.10	30.0	0.097	11.4	4.13
									99		999.9	-	0.20	23.0	0.282	40.9	8.10
													0.10	23.0	0.274	28.3	5.10
								CDMG	36445	Parkfield - Fault Zone 15	29.9	IQB	0.20	24.0	0.084	10.4	2.08
									99		999.9	-	0.20	20.0	0.168	21.2	4.91
													0.20	22.0	0.117	14.1	2.94
								CDMG	36457	Parkfield - Fault Zone 16	28.1	IQC	0.20	30.0	0.061	6.5	1.92
									99		999.9	-	0.20	26.0	0.195	17.7	3.48
													0.20	27.0	0.122	12.0	1.83
								CDMG	36415	Parkfield - Gold Hill 1W	46.5	IHD	0.20	30.0	0.035	4.7	1.53
									99		999.9	-	0.20	24.0	0.119	16.7	4.54
													0.20	22.0	0.065	10.1	2.57
								CDMG	36421	Parkfield - Gold Hill 2E	32.3	IQD	0.20	32.0	0.035	3.3	0.90
									99		999.9	-	0.20	30.0	0.072	6.5	1.73
													0.20	30.0	0.076	7.6	1.40
								CDMG	36416	Parkfield - Gold Hill 2W	36.6	IPB	0.20	32.0	0.036	4.4	1.58
									99		999.9	-	0.20	21.0	0.083	11.4	3.72

No.	Earthquake Location, Mech, Dip (1)	Date & Time		Magnitude (2)				Station (3)		Closest Dist (km)(4)	Site Codes (5)	Filter Corners					
		YR	MODY	HRMN	M	ML	MS	OTH	No.			Description H/F	HP (hz)	LP (hz)	PGA (g)	PGV (cm/s)	PGD (cm)
												0.20	20.0	0.074	11.7	2.64	
								CDMG	36439	Parkfield - Gold Hill 3E	29.2	IQD	0.20	30.0	0.054	8.4	1.50
								99			999.9	-	0.20	26.0	0.094	11.0	2.87
													0.20	27.0	0.072	6.4	1.56
								CDMG	36420	Parkfield - Gold Hill 3W	38.8	IPB	0.20	36.0	0.067	7.5	1.77
								99			999.9	-	0.20	30.0	0.137	11.0	2.76
													0.20	30.0	0.122	9.0	1.74
								CDMG	36433	Parkfield - Gold Hill 4W	41.0	IPB	0.20	30.0	0.029	4.9	1.53
								99			999.9	-	0.20	31.0	0.056	8.1	2.28
													0.20	30.0	0.097	6.3	1.86
								CDMG	36434	Parkfield - Gold Hill 5W	43.7	IPB	0.20	30.0	0.034	3.9	1.53
								99			999.9	-	0.20	26.0	0.073	8.5	2.62
													0.20	30.0	0.054	5.9	1.55
								CDMG	36432	Parkfield - Gold Hill 6W	48.0	IPC	0.20	30.0	0.037	3.2	0.80
								99			999.9	-	0.20	30.0	0.059	8.2	1.55
													0.20	30.0	0.069	7.4	1.21
								CDMG	36422	Parkfield - Stone Corral 2E	34.4	IMA	0.20	35.0	0.033	4.0	1.65
								99			999.9	-	0.20	25.0	0.061	8.1	2.65
													0.20	30.0	0.095	7.1	1.75
								CDMG	36437	Parkfield - Stone Corral 3E	31.8	IMA	0.20	30.0	0.033	3.6	1.06
								99			999.9	-	0.20	23.0	0.151	8.7	2.92
													0.20	30.0	0.106	8.1	1.39
								CDMG	36438	Parkfield - Stone Corral 4E	29.6	IMA	0.20	26.0	0.030	3.0	0.89
								99			999.9	-	0.20	21.0	0.063	8.2	2.33
													0.20	22.0	0.072	6.7	1.39
								CDMG	36455	Parkfield - Vineyard Cany 1E	26.7	IQC	0.20	26.0	0.082	10.4	3.03
								99			999.9	-	0.20	24.0	0.167	20.9	5.03
													0.20	23.0	0.230	27.6	6.21
								CDMG	36448	Parkfield - Vineyard Cany 1W	29.5	IQC	0.50	28.0	0.068	6.1	1.49
								99			999.9	-	0.50	26.0	0.081	8.2	2.12
													0.50	23.0	0.087	11.1	2.41
								CDMG	36177	Parkfield - Vineyard Cany 2E	24.6	IFA	-99.				
								99			999.9	-	0.20	30.0	0.161	16.2	3.30
													-99.				
								CDMG	36447	Parkfield - Vineyard Cany 2W	30.7	IHC	0.20	40.0	0.057	5.2	1.54
								99			999.9	-	0.20	30.0	0.073	7.4	1.47
													0.20	30.0	0.083	6.9	1.22
								CDMG	36176	Parkfield - Vineyard Cany 3W	32.3	IPA	0.20	31.0	0.056	6.2	1.75
								99			999.9	-	0.20	30.0	0.098	11.8	2.95
													0.20	30.0	0.137	13.5	2.57
								CDMG	36446	Parkfield - Vineyard Cany 4W	34.6	IMB	0.20	30.0	0.024	2.8	0.64
								99			999.9	-	0.20	30.0	0.064	6.5	1.37
													0.20	27.0	0.046	4.2	0.95
								CDMG	36440	Parkfield - Vineyard Cany 5W	37.1	IHB	0.20	30.0	0.048	4.9	1.09
								99			999.9	-	0.20	21.0	0.062	6.9	1.47

No.	Earthquake Location, Mech, Dip (1)	Date & Time			Magnitude (2)				Station (3)		Closest Dist (km)(4)	Site Codes (5)	Filter Corners			PGA (g)	PGV (cm/s)	PGD (cm)
		YR	MODY	HRMN	M	ML	MS	OTH	No.	Description H/F			HP (hz)	LP (hz)				
														-99.				
									CDMG	36441	Parkfield - Vineyard Cany 6W	41.0	IPC	0.20	30.0	0.038	4.8	1.62
											999.9	-	0.20	25.0	0.054	9.5	2.76	
													0.20	27.0	0.076	5.4	1.82	
									USGS	1162	Pleasant Valley P.P. - bldg	8.5	AHD	0.20	30.0	0.206	12.3	2.53
											999.9	-	0.20	20.0	0.380	32.4	6.43	
													0.20	22.0	0.285	19.1	2.59	
									USGS	1162	Pleasant Valley P.P. - yard	8.5	AHD	0.20	31.0	0.353	16.1	2.35
											999.9	-	0.20	40.0	0.592	60.2	8.77	
													0.20	31.0	0.551	36.4	3.96	
									CDMG	46175	Slack Canyon	27.7	IGA	0.20	21.0	0.053	6.8	2.42
											999.9	-	0.20	21.0	0.166	16.1	4.19	
													0.20	21.0	0.153	13.3	2.72	
0067	Coalinga 02	1983	0509	0249	5.0	5.3	4.7	0.0	USGS	4	ALP (temp)	19.9*	IQD	0.30	35.0	0.018	1.0	0.09
											999.9	-	0.20	30.0	0.040	2.9	0.39	
													0.20	30.0	0.021	1.5	0.16	
									USGS	1607	Anticline Ridge Free-field	12.6*	IPA	2.00	30.0	0.250	4.3	0.11
											999.9	-	0.40	30.0	0.576	16.5	0.96	
													0.50	40.0	0.673	20.4	1.18	
									USGS	1607	Anticline Ridge Pad	12.6*	APA	0.60	45.0	0.380	8.1	0.22
											999.9	-	0.50	40.0	0.452	16.8	0.85	
													0.60	35.0	0.412	23.2	1.27	
									CDMG	46T05	Anticline Ridge - Palmer Ave	12.6*	APB	1.00	30.0	0.049	1.7	0.10
											999.9	-	0.35	25.0	0.292	12.1	0.78	
													0.40	25.0	0.216	9.2	0.64	
									USGS	1606	Burnett Construction	17.7*	AHD	0.40	30.0	0.077	2.0	0.15
											999.9	-	0.50	30.0	0.095	3.5	0.37	
													0.40	25.0	0.095	4.5	0.35	
									CDMG	46T04	CHP (temp)	16.7*	AHD	0.80	30.0	0.047	1.7	0.12
											999.9	-	0.40	25.0	0.145	5.2	0.47	
													0.50	20.0	0.114	6.0	0.33	
									CDMG	46T07	Harris Ranch - Hdqtrs (temp)	17.8*	AHD	0.70	20.0	0.071	1.8	0.10
											999.9	-	0.70	20.0	0.080	2.9	0.13	
													0.40	15.0	0.154	6.4	0.67	
									USGS	5	LLN (temp)	13.1*	IPA	0.40	50.0	0.059	2.2	0.18
											999.9	-	0.30	50.0	0.130	7.8	0.49	
													0.30	40.0	0.076	3.8	0.38	
									USGS	6	MIT (temp)	12.5*	IQD	0.40	50.0	0.158	3.8	0.30
											999.9	-	0.15	50.0	0.130	4.6	0.48	
													-99.					
									USGS	1604	Oil City	13.3*	APB	0.70	40.0	0.098	3.0	0.13
											999.9	-	0.50	30.0	0.250	9.3	0.71	
													0.70	30.0	0.284	9.3	0.39	
									USGS	1608	Oil Fields Fire Station	12.1*	APA	0.70	30.0	0.147	2.9	0.11
											999.9	-	0.70	30.0	0.247	7.9	0.34	

A-25

No.	Earthquake Location, Mech, Dip (1)	Date & Time			Magnitude (2)				Station (3)		Closest Dist (km)(4)	Site Codes (5)	Filter Corners					
		YR	MODY	HRMN	M	ML	MS	OTH	No.	Description H/F			HP (hz)	LP (hz)	PGA (g)	PGV (cm/s)	PGD (cm)	
									CDMG	46T06 99	Oil fields - Skunk Hollow	12.7* 999.9	APA -	0.60 1.00 0.50	30.0 35.0	0.178 0.082 0.313	5.0 1.7 9.3	0.26 0.07 0.41
									USGS	1609 99	Palmer Ave	12.7* 999.9	APB -	0.50 1.00 0.50	25.0 30.0 15.0	0.343 0.095 0.202	10.8 2.1 7.5	0.56 0.13 0.34
									USBR	1162 99	Pleasant Valley P.P. - yard	14.6* 999.9	AHD -	0.30 0.40 0.20	20.0 30.0 30.0	0.289 0.102 0.078	13.6 2.6 9.5	0.75 0.16 1.04
									USGS	7 99	SGT (temp)	14.1* 999.9	IZA -	0.50 0.30 0.10	25.0 50.0 60.0	0.220 0.071 0.139	9.3 2.7 5.8	0.50 0.15 0.70
									USGS	1605 99	Skunk Hollow	12.4* 999.9	APA -	0.10 0.70 0.30	60.0 35.0 25.0	0.244 0.077 0.171	7.4 1.9 6.1	0.68 0.12 0.49
									USGS	8 99	SUB (temp)	14.5* 999.9	IQD -	0.30 0.40 0.15	25.0 50.0 35.0	0.104 0.079 0.116	4.6 2.0 5.9	0.37 0.15 0.85
									CDMG	1703 99	Sulphur Baths (temp)	20.3* 999.9	APA -	0.10 0.50 0.60	40.0 20.0 15.0	0.216 0.005 0.008	12.2 0.3 0.5	1.42 0.06 0.04
									USGS	9 99	TRA (temp)	14.9* 999.9	IQD -	0.80 0.10 0.20	20.0 50.0 35.0	0.004 0.079 0.131	0.3 4.9 9.4	0.03 0.36 0.97
									USGS	10 99	VEW (temp)	12.6* 999.9	IPA -	0.20 0.08 0.05	30.0 60.0 60.0	0.088 0.065 0.146	6.9 1.5 8.7	0.70 0.19 1.09
									USGS	11 99	YUB (temp)	20.1* 999.9	IQD -	0.05 -99. 0.60	60.0 - 40.0	0.121 - 0.034	7.8 - 1.3	0.75 - 0.10
														0.40	40.0	0.022	0.9	0.07
0068	Coalinga 02	1983	0611	0309	5.3	5.2	5.4	0.0	USGS	1606 99	Burnett Construction	10.5* 999.9	AHD -	0.20 0.15 0.15	30.0 25.0 20.0	0.083 0.165 0.191	4.1 8.0 10.0	0.80 2.43 1.91
									CDMG	46T04 99	CHP (temp)	10.0* 999.9	AHD -	0.20 0.10 0.10	15.0 15.0 15.0	0.028 0.055 0.061	3.8 5.8 4.7	0.76 1.96 1.95
									CDMG	1703 99	Sulphur Baths (temp)	9.7* 999.9	APA -	0.20 0.20 0.20	20.0 20.0 20.0	0.034 0.044 0.037	3.5 5.1 4.5	1.47 2.29 1.64
0069	Coalinga 02	1983	0709	0740	5.2	5.4 (5.3)	4.9	0.0	USGS	1607 99	Anticline Ridge Free-Field	11.0* 999.9	IPA -	0.30 0.30 0.45	40.0 30.0 40.0	0.115 0.330 0.275	3.7 16.1 8.9	0.43 1.20 0.46
									USGS	1607	Anticline Ridge Pad	11.0*	APA	0.30	30.0	0.137	4.7	0.34

No.	Earthquake Location, Mech, Dip (1)	Date & Time			Magnitude (2)				Station (3)		Closest Dist (km)(4)	Site Codes (5)	Filter Corners						
		YR	MODY	HRMN	M	ML	MS	OTH	No.	Description H/F			HP (hz)	LP (hz)	PGA (g)	PGV (cm/s)	PGD (cm)		
										99			999.9	-	0.40	30.0	0.378	16.1	1.03
									USGS	1606	Burnett Construction	15.9*	AHD	0.40	30.0	0.261	9.2	0.53	
										99		999.9	-	0.50	30.0	0.119	6.6	0.50	
														0.40	30.0	0.149	7.7	0.52	
									CDMG	46T04	CHP (temp)	14.9*	AHD	0.45	30.0	0.079	2.4	0.22	
										99		999.9	-	0.30	25.0	0.204	8.0	0.62	
														0.30	25.0	0.171	5.4	0.38	
									USGS	1604	Oil City	10.0*	APB	0.40	30.0	0.210	4.6	0.29	
										99		999.9	-	0.20	30.0	0.387	13.8	1.59	
														0.20	30.0	0.370	12.4	0.89	
									USGS	1608	Oil Fields Fire Station - FF	11.9*	IPA	0.25	30.0	0.062	2.0	0.22	
										99		999.9	-	0.60	30.0	0.088	3.0	0.26	
														0.12	30.0	0.096	4.1	0.71	
									USGS	1608	Oil Fields Fire Stn - Pad	11.9*	APA	0.40	30.0	0.073	1.9	0.20	
										99		999.9	-	0.10	25.0	0.094	3.4	0.53	
														0.40	25.0	0.109	4.0	0.32	
									USGS	1609	Palmer Ave	14.0*	APB	0.60	25.0	0.073	2.1	0.10	
										99		999.9	-	0.60	20.0	0.109	3.2	0.24	
														0.50	20.0	0.211	7.0	0.43	
									USGS	1605	Skunk Hollow	12.6*	APA	0.50	30.0	0.161	3.1	0.19	
										99		999.9	-	0.40	30.0	0.187	6.4	0.32	
														0.30	20.0	0.141	6.2	0.37	
									CDMG	1703	Sulphur Baths (temp)	17.0*	APA	0.50	30.0	0.041	1.0	0.09	
										99		999.9	-	0.35	30.0	0.055	2.2	0.21	
														0.40	25.0	0.074	1.5	0.15	
									USGS	1651	Transmitter Hill	10.4*	APA	0.30	30.0	0.114	3.3	0.35	
										99		999.9	-	0.20	25.0	0.205	12.0	1.34	
														0.30	30.0	0.194	9.9	0.87	
0070	Coalinga 02	1983	0722	0239	5.8	6.0	5.7	0.0	USGS	1606	Burnett Construction	10.5	AHD	0.10	30.0	0.210	10.2	1.09	
						(5.9)				99		999.9	-	0.30	30.0	0.269	14.2	2.32	
														0.50	25.0	0.323	16.2	1.43	
									CDMG	46T04	CHP (temp)	10.0	AHD	0.30	30.0	0.204	7.1	1.10	
										99		999.9	-	0.40	30.0	0.324	14.4	1.39	
														0.30	30.0	0.605	20.7	2.32	
									USGS	1604	Oil City	8.2	APB	0.60	30.0	0.568	12.5	1.20	
										99		999.9	-	0.15	30.0	0.866	42.2	6.14	
														0.80	30.0	0.447	24.8	2.23	
									USGS	1608	Oil Fields Fire Station - FF	10.9	IPA	0.10	30.0	0.135	7.7	2.82	
										99		999.9	-	0.20	30.0	0.219	14.0	2.85	
														0.10	30.0	0.187	14.8	3.82	
									USGS	1608	Oil Fields Fire Station Pad	10.9	APA	0.10	30.0	0.152	8.5	3.19	
										99		999.9	-	0.05	30.0	0.217	18.1	2.90	
														0.08	25.0	0.210	14.8	4.38	
									USGS	1609	Palmer Ave	12.2	APB	0.20	25.0	0.201	6.9	1.35	

No.	Earthquake Location, Mech, Dip (1)	Date & Time			Magnitude (2)				Station (3)		Closest Dist (km)(4)	Site Codes (5)	Filter Corners					
		YR	MODY	HRMN	M	ML	MS	OTH	No.	Description H/F			HP (hz)	LP (hz)	PGA (g)	PGV (cm/s)	PGD (cm)	
										99	999.9	-	0.06	20.0	0.272	12.8	3.31	
									USBR	1162	Pleasant Valley P.P. - FF	17.4	AHD	0.09	20.0	0.290	21.5	3.31
										99	999.9	-	0.07	30.0	0.128	5.9	2.50	
													0.03	30.0	0.228	21.6	6.24	
									USBR	1162	Pleasant Valley P.P. - yard	17.4	AHD	0.10	30.0	0.408	18.9	5.64
										99	999.9	-	0.08	30.0	0.316	12.9	0.92	
									USGS	1605	Skunk Hollow	12.2	APA	0.10	30.0	0.602	34.8	8.06
										99	999.9	-	0.10	30.0	0.327	12.1	2.33	
									CDMG	1703	Sulphur Baths (temp)	9.7	APA	0.10	40.0	0.230	10.0	2.89
										99	999.9	-	0.07	30.0	0.375	16.4	6.23	
													0.10	30.0	0.233	18.9	2.65	
									USGS	1651	Transmitter Hill	9.2	APA	0.30	30.0	0.082	4.1	0.69
										99	999.9	-	0.30	25.0	0.141	5.5	0.79	
													0.30	25.0	0.127	6.3	0.66	
									CDMG	46T04	CHP (temp)	12.1*	AHD	0.10	40.0	0.394	11.0	3.60
										99	999.9	-	0.10	30.0	0.840	44.1	6.80	
													0.08	40.0	1.083	39.7	5.41	
0071	Coalinga 02	1983	0722	0343	4.9	5.0	0.0	0.0	CDMG	46T04	CHP (temp)	12.1*	AHD	0.70	30.0	0.118	3.1	0.17
										99	999.9	-	0.50	25.0	0.148	5.7	0.43	
													0.30	25.0	0.202	8.2	0.74	
									CDMG	1703	Sulphur Baths (temp)	13.7*	APA	0.20	20.0	0.029	1.1	0.17
										99	999.9	-	0.50	20.0	0.039	1.6	0.21	
													0.20	20.0	0.030	1.0	0.16	
0072	Coalinga 02	1983	0725	2231	5.2	5.3	5.1	0.0	CDMG	46T04	CHP (temp)	12.7*	AHD	0.30	40.0	0.332	8.4	0.61
						(5.1)				99	999.9	-	0.30	40.0	0.431	18.7	1.21	
													0.10	40.0	0.733	37.6	5.24	
									CDMG	1703	Sulphur Baths (temp)	14.7*	APA	0.40	30.0	0.139	6.5	0.32
										99	999.9	-	0.30	30.0	0.152	8.5	1.27	
													0.30	25.0	0.230	10.9	0.76	
0073	Trinidad offshore 99	1983	0824	1336	0.0	5.5	5.7	0.0	CDMG	1498	Rio Dell Overpass, E Ground	67.6*	APC	0.30	30.0	0.030	1.6	0.43
										99	999.9	B	0.15	30.0	0.194	8.5	0.82	
													0.30	30.0	0.145	6.4	4.93	
									CDMG	1498	Rio Dell Overpass, W Ground	67.6*	APC	0.50	40.0	0.033	1.8	1.62
										99	999.9	B	0.40	40.0	0.166	6.5	0.56	
													0.20	35.0	0.128	4.6	0.84	
0074	Coalinga 00	1983	0909	0916	5.3	5.3	5.4	0.0	CDMG	46T04	CHP (temp)	13.7*	AHD	0.80	30.0	0.030	0.8	0.07
										99	999.9	-	0.90	20.0	0.023	1.0	0.09	
													0.90	20.0	0.033	1.3	0.07	
									CDMG	1703	Sulphur Baths (temp)	18.4*	APA	0.80	20.0	0.016	0.6	0.04
										99	999.9	-	0.80	15.0	0.014	0.6	0.06	
													0.80	15.0	0.016	0.6	0.06	
0075	Taiwan SMART1(25)	1983	0921		0.0	6.8	6.5	0.0		25	SMART1 C00	83.0	IZD	-99.				

No.	Earthquake Location, Mech, Dip (1)	Date & Time			Magnitude (2)				Station (3)		Closest Dist (km)(4)	Site Codes (5)	Filter Corners								
		YR	MODY	HRMN	M	ML	MS	OTH	No.	Description H/F			HP (hz)	LP (hz)	PGA (g)	PGV (cm/s)	PGD (cm)				
03											999.9	-	0.20	25.0	0.028	4.2	0.91				
													0.20	25.0	0.028	3.5	1.16				
											32	SMART1 E01	83.0	IZD	0.50	25.0	0.013	1.8	0.31		
											99		999.9	-	0.20	25.0	0.028		0.96		
															0.20	25.0	0.028	4.1	0.71		
											33	SMART1 E02	83.0	IZD	0.10	25.0	0.005	0.5	0.20		
											99		999.9	-	0.10	25.0	0.020	1.4	0.30		
															0.10	25.0	0.022	2.2	0.41		
											62	SMART1 I01	83.0	IZD	0.10	25.0	0.008	1.5	0.40		
											99		999.9	-	0.10	25.0	0.023	3.9	0.87		
															0.10	25.0	0.037	4.6	0.85		
											61	SMART1 I07	83.0	IZD	0.10	25.0	0.009	1.4	0.43		
											99		999.9	-	0.10	25.0	0.035	3.8	0.79		
															0.10	25.0	0.032	4.0	0.97		
											28	SMART1 M01	83.0	IZD	0.10	25.0	0.005	0.8			
											99		999.9	-	0.10	25.0	0.020	2.7	0.67		
															0.10	25.0	0.039	5.0	0.82		
											60	SMART1 M06	83.0	IZD	0.10	25.0	0.010	1.7	0.40		
											99		999.9	-	0.10	25.0	0.021	2.8			
															0.10	25.0	0.031	4.3	1.10		
30	SMART1 O01	83.0	IZD	0.10	25.0	0.007	0.9														
99		999.9	-	0.50	25.0	0.028	3.2	0.52													
				0.10	25.0	0.027	2.8	0.69													
31	SMART1 O07	83.0	IZD	0.10	25.0	0.015	1.6														
99		999.9	-	0.10	25.0	0.025	4.2	1.42													
				0.10	25.0	0.026	3.3	1.10													
0076	Morgan Hill 00	1984	0424	2115	6.2	6.2	6.1	0.0	CDMG	57066	Agnews State Hospital 00	29.4	AQD	0.20	18.0	0.016	3.2	1.56			
												999.9	C	0.20	14.0	0.032	5.0	2.33			
														0.20	13.0	0.032	5.5	2.05			
												USGS	1652	Anderson Dam (Downstream) 00	2.6	AFD	0.10	45.0	0.204	9.8	1.81
														999.9	B	0.10	30.0	0.423	25.3	4.58	
																0.10	38.0	0.289	27.6	6.33	
												CDMG	58375	APEEL 1 - Redwood City 00	54.1	IQE	0.50	28.0	0.016	0.8	0.16
														999.9	D	0.20	21.0	0.046	3.4	0.66	
																0.20	23.0	0.068	3.9	0.63	
												USGS/CDMG	1180	APEEL 1B - Hayward 00	51.8	IHD	-99.				
														999.9	-	0.20	22.0	0.041	2.6	0.75	
																0.20	19.0	0.027	3.1	0.61	
												CDMG	47125	Capitola 00	38.1	AQC	0.20	35.0	0.045	2.1	0.39
														999.9	C	0.20	30.0	0.099	4.9	0.61	
																0.20	28.0	0.142	8.1	1.62	
												CDMG	57007	Corralitos 00	22.7	APB	0.20	27.0	0.040	4.0	0.54
		999.9	B	0.20	24.0	0.081	6.4	1.17													
				0.20	26.0	0.109	10.8	2.13													
CDMG	57217	Coyote Lake Dam (SW Abut)	0.1	IFA	0.10	50.0	0.388	15.6	2.65												

No.	Earthquake Location, Mech, Dip (1)	Date & Time			Magnitude (2)			Station (3)		Closest Dist (km)(4)	Site Codes (5)	Filter Corners			PGA (g)	PGV (cm/s)	PGD (cm)
		YR	MODY	HRMN	M	ML	MS	OTH	No.			Description H/F	HP (hz)	LP (hz)			
									00	999.9	-	0.10	39.0	0.711	51.6	12.00	
								CDMG	57064	Fremont - Mission San Jose		0.10	45.0	1.298	80.8	9.63	
									00	31.4	AMB	0.50	21.0	0.018	1.3	0.40	
									00	999.9	B	0.50	21.0	0.025	2.4	0.76	
												0.20	18.0	0.021	3.2	1.03	
								CDMG	47379	Gilroy Array #1		0.10	33.0	0.092	3.3	1.07	
									00	16.2	IFA	0.10	29.0	0.069	2.9	1.26	
									00	999.9	A	0.10	40.0	0.098	2.9	1.02	
								CDMG	47380	Gilroy Array #2		0.20	37.0	0.578	10.8	0.92	
									00	15.1	IQD	0.20	31.0	0.162	5.1	1.42	
									00	999.9	C	0.20	37.0	0.212	12.6	2.10	
								CDMG	47381	Gilroy Array #3		0.10	42.0	0.395	9.9	1.22	
									00	14.6	IHD	0.10	37.0	0.194	11.2	2.41	
									00	999.9	C	0.10	32.0	0.200	12.7	3.45	
								CDMG	57382	Gilroy Array #4		0.10	39.0	0.408	11.8	1.70	
									00	12.8	AHD	0.10	25.0	0.224	19.3	4.33	
									00	999.9	C	0.10	27.0	0.348	17.4	3.11	
								CDMG	57383	Gilroy Array #6		0.10	30.0	0.405	14.1	1.86	
									00	11.8	IKB	0.10	35.0	0.222	11.4	2.45	
									00	999.9	B	0.10	27.0	0.292	36.7	6.12	
								CDMG	57425	Gilroy Array #7		0.10	40.0	0.428	5.4	0.93	
									00	14.0	AHB	0.10	31.0	0.190	7.4	2.06	
									00	999.9	C	0.10	30.0	0.113	6.0	1.79	
								CDMG	47006	Gilroy Gavilan Coll.		0.50	42.0	0.081	2.3	0.41	
									00	16.2	AFB	0.10	30.0	0.114	3.6	0.87	
									00	999.9	B	0.10	30.0	0.095	2.9	0.93	
								CDMG	57191	Halls Valley		0.20	28.0	0.110	12.2	1.25	
									00	3.4	IFC	0.20	26.0	0.156	12.5	1.84	
									00	999.9	C	0.20	30.0	0.312	39.4	7.66	
								USGS	1028	Hollister City Hall		0.20	25.0	0.118	3.9	1.07	
									00	32.5	CHD	0.20	19.0	0.071	7.4	1.60	
									00	999.9	C	0.20	24.0	0.071	9.0	3.81	
								USGS	1656	Hollister Diff. Array		0.20	24.0	0.222	7.0	0.81	
									00	28.3	IQD	0.20	29.0	0.089	8.7	1.72	
									00	999.9	-	0.20	23.0	0.088	11.9	1.89	
								USGS	1656	Hollister Diff Array #1		0.10	35.0	0.213	6.2	0.90	
									00	28.3	IQD	0.20	33.0	0.095	9.7	1.53	
									00	999.9	-	0.20	30.0	0.088	11.6	1.76	
								USGS	1656	Hollister Diff Array #3		0.10	35.0	0.243	8.9	0.98	
									00	28.3	IQD	0.10	30.0	0.078	7.2	1.47	
									00	999.9	-	0.20	30.0	0.081	10.0	1.90	
								USGS	1656	Hollister Diff Array #4		0.10	35.0	0.282	9.8	1.03	
									00	28.3	IQD	0.10	30.0	0.098	10.3	1.68	
									00	999.9	-	0.20	30.0	0.092	10.2	1.90	
								USGS	1656	Hollister Diff Array #5		0.20	35.0	0.250	8.0	1.10	

No.	Earthquake Location, Mech, Dip (1)	Date & Time			Magnitude (2)				Station (3)		Closest Dist (km)(4)	Site Codes (5)	Filter Corners			PGA (g)	PGV (cm/s)	PGD (cm)
		YR	MODY	HRMN	M	ML	MS	OTH	No.	Description H/F			HP (hz)	LP (hz)				
										00	999.9	-	0.20	30.0	0.098	10.3	2.00	
													0.20	30.0	0.101	11.6	1.88	
									CDMG	56012	Los Banos	64.4	AHD	0.50	20.0	0.011	1.0	0.50
										00	999.9	C	0.50	18.0	0.051	5.8	1.75	
									CDMG	1377	San Juan Bautista	30.3	AQD	0.50	18.0	0.057	8.3	1.89
										00	999.9	B	0.10	21.0	0.052	2.7	1.35	
													0.10	21.0	0.044	4.3	1.73	
									USGS	1655	San Justo Dam (L Abut)	34.9	FPD	0.50	32.0	0.033	2.2	0.52
										00	999.9	-	0.20	29.0	0.081	6.5	2.59	
													0.20	30.0	0.070	5.1	1.86	
									USGS	1655	San Justo Dam (R Abut)	34.9	FPD	0.20	25.0	0.044	2.8	1.04
										00	999.9	-	0.20	24.0	0.078	7.0	3.07	
													0.20	23.0	0.060	5.8	2.16	
									CDMG	58235	Saratoga - WVC E Wall	28.7	AQD	-99.				
										00	999.9	-	0.50	30.0	0.098	4.6	0.61	
													-99.					
									CDMG	58235	Saratoga - WVC NE Corner	28.7	AQD	-99.				
										00	999.9	-	0.20	30.0	0.041	3.5	0.99	
													-99.					
									CDMG	58235	Saratoga - WVC SE Corner	28.7	AQD	-99.				
										00	999.9	-	0.50	30.0	0.045	3.1	0.88	
													-99.					
									CDMG	58223	SF Intern. Airport	71.2	AHD	0.50	32.0	0.018	0.8	0.28
										00	999.9	C	0.50	26.0	0.048	3.2	0.40	
													0.50	24.0	0.048	2.7	0.47	
									CDMG	58135	UCSC Lick Observatory	44.1	AKA	0.50	22.0	0.031	1.2	0.32
										00	999.9	E	0.50	21.0	0.039	2.0	0.29	
													0.50	22.0	0.076	3.6	0.62	
0077	Bishop (Rnd Val) 00	1984	1123	1912	5.8	5.5	5.7	0.0	USGS	1661	McGee Creek - Surface	19.0*	IQC	2.00	15.0	0.106	2.2	0.05
										00	999.9	-	1.50	40.0	0.088	1.8	0.07	
													1.00	40.0	0.128	2.2	0.07	
0078	Taiwan SMART1(33) 99	1985	0612		0.0	6.5	5.8	0.0		25	SMART1 C00	45.0	IZD	0.20	25.0	0.021	0.9	0.16
										99	999.9	-	0.20	25.0	0.083	3.9		
													0.20	25.0	0.051	3.1		
										62	SMART1 I01	45.0	IZD	0.50	25.0	0.025	0.9	0.15
										99	999.9	-	0.50	25.0	0.142	5.6	0.37	
													0.50	25.0	0.070	3.5	0.28	
										61	SMART1 I07	45.0	IZD	0.20	25.0	0.014	0.6	0.25
										99	999.9	-	0.20	25.0	0.055	2.8	0.41	
													0.20	25.0	0.040	2.2	0.29	
										28	SMART1 M01	45.0	IZD	0.20	25.0	0.015	0.6	
										99	999.9	-	0.20	25.0	0.031	2.0		
													0.20	25.0	0.052	2.3		

A-31

No.	Earthquake Location, Mech, Dip (1)	Date & Time			Magnitude (2)				Station (3) Description H/F	Closest Dist (km)(4)	Site Codes (5)	Filter Corners						
		YR	MODY	HRMN	M	ML	MS	OTH				HP (hz)	LP (hz)	PGA (g)	PGV (cm/s)	PGD (cm)		
									29	SMART1 M07	45.0	IZD	0.20	25.0	0.021	0.7	0.20	
									99		999.9	-	0.20	25.0	0.095	4.8	0.58	
													0.20	25.0	0.050	3.1	0.81	
									30	SMART1 O01	45.0	IZD	0.50	25.0	0.014	0.4		
									99		999.9	-	0.50	25.0	0.063	2.0	0.25	
													0.50	25.0	0.052	2.1	0.31	
									31	SMART1 O07	45.0	IZD	0.20	25.0	0.014	0.9		
									99		999.9	-	0.20	25.0	0.057	2.9	1.00	
													0.20	25.0	0.048	2.8	0.85	
0079	Nahanni, Canada 03	1985	1223		6.8	0.0	6.9	0.0										
									6097	Site 1	6.0	IZA	0.20	62.5	2.086	40.5	12.12	
									01		999.9	-	0.05	62.5	0.978	46.0	9.67	
													0.05	62.5	1.096	46.1	14.58	
									6098	Site 2	8.0	IZA	-99.					
									01		999.9	-	0.10	62.5	0.489	29.3	7.61	
													0.05	62.5	0.323	33.1	6.54	
									6099	Site 3	16.0	IZA	0.05	62.5	0.140	6.8	3.02	
									02		999.9	-	0.10	62.5	0.148	6.1	3.13	
													0.05	62.5	0.139	3.3	1.06	
0080	Hollister 00	1986	0126	1920	5.4	5.5	0.0	0.0	USGS	1656	Hollister Diff Array #1	16.9*	IQD	0.20	45.0	0.172	5.2	0.56
										00		999.9	-	0.10	45.0	0.101	9.3	1.95
														0.10	40.0	0.114	8.3	2.29
									USGS	1656	Hollister Diff Array #3	16.9*	IQD	0.30	40.0	0.124	5.0	0.51
										00		999.9	-	0.20	35.0	0.106	7.9	1.60
														0.40	40.0	0.104	9.2	1.41
									USGS	1656	Hollister Diff Array #4	16.9*	IQD	0.30	40.0	0.073	4.1	0.50
										00		999.9	-	0.10	35.0	0.102	9.0	1.91
														-99.				
									CDMG	47189	SAGO South - Surface	14.9*	IGB	0.30	20.0	0.053	3.4	0.53
										00		999.9	B	0.25	20.0	0.044	5.3	1.27
														0.15	15.0	0.090	9.3	1.70
0081	Mt. Lewis 99	1986	0331	1155	5.6	5.8	5.5	0.0	CDMG	57191	Halls Valley	15.5*	IFC	0.40	20.0	0.072	3.9	0.56
										99		999.9	C	0.30	20.0	0.140	8.5	1.65
														0.10	20.0	0.159	18.4	4.40
0082	Taiwan SMART1(40) 03	1986	0520		6.4	6.5	6.4	0.0		25	SMART1 C00	64.0	IZD	0.20	25.0	0.038	4.1	1.21
										99		999.9	-	0.20	25.0	0.172	33.0	6.94
														0.20	25.0	0.232	19.4	5.07
									32	SMART1 E01	64.0	IZD	0.20	25.0	0.046	4.9	1.15	
									99		999.9	-	0.20	25.0	0.203	36.5	7.60	
														0.20	25.0	0.183	15.1	3.06
									62	SMART1 I01	64.0	IZD	0.20	25.0	0.036	4.1	0.86	
									99		999.9	-	0.20	25.0	0.183	32.4	6.90	
														0.20	25.0	0.175	18.1	4.24
									61	SMART1 I07	64.0	IZD	0.20	25.0	0.041	3.7		

A-33

No.	Earthquake Location, Mech, Dip (1)	Date & Time			Magnitude (2)				Station (3)		Closest Dist (km)(4)	Site Codes (5)	Filter Corners			PGA (g)	PGV (cm/s)	PGD (cm)
		YR	MODY	HRMN	M	ML	MS	OTH	No.	Description H/F			HP (hz)	LP (hz)	PGA (g)			
											999.9	-	0.20	25.0	0.167	30.6	7.06	
													0.20	25.0	0.150	17.7	4.10	
									28	SMART1 M01	64.0	IZD	0.20	25.0	0.035	3.9	1.05	
									99		999.9	-	0.20	25.0	0.156	26.3	5.75	
													0.20	25.0	0.173	22.8	4.02	
									29	SMART1 M07	64.0	IZD	0.20	25.0	0.039	4.2	0.81	
									99		999.9	-	0.20	25.0	0.182	37.9	8.54	
													0.20	25.0	0.254	23.7	6.01	
									30	SMART1 O01	64.0	IZD	0.20	25.0	0.034	3.3	0.99	
									99		999.9	-	0.20	25.0	0.106	20.7	4.89	
													0.20	25.0	0.160	21.9	3.73	
									31	SMART1 O07	64.0	IZD	0.20	25.0	0.074	4.3	0.83	
									99		999.9	-	0.20	25.0	0.159	28.3	6.83	
													0.20	25.0	0.163	16.1	3.50	
0083	N. Palm Springs 03	1986	0708	0920	6.0	5.9	6.0	0.0	USGS	5224	Anza - Red Mountain	45.6	AGA	0.50	50.0	0.072	2.2	0.21
										99		999.9	A	0.30	35.0	0.104	5.2	0.62
														0.60	40.0	0.129	3.4	0.46
									USGS	5231	Anza - Tule Canyon	55.4	AGA	0.40	30.0	0.049	2.6	0.30
									99		999.9	B	0.30	30.0	0.110	6.5	0.71	
														0.35	35.0	0.095	7.5	0.71
									USGS	5160	Anza Fire Station	46.7	AHC	0.50	50.0	0.056	2.3	0.23
									99		999.9	A	0.50	40.0	0.099	5.8	0.29	
														0.60	30.0	0.067	4.0	0.50
									USGS	5073	Cabazon	16.3	AHD	0.20	45.0	0.363	7.4	0.84
									02		999.9	-	0.15	40.0	0.217	7.6	1.96	
														0.15	40.0	0.212	16.3	2.24
									CDOT	754	Colton Interchange - Vault	57.4	BHD	0.40	30.0	0.017	1.6	0.40
									99		999.9	-	0.40	30.0	0.042	3.5	0.59	
														0.40	30.0	0.065	4.1	0.43
									USGS	5157	Cranston Forest Station	35.3	AQB	0.70	45.0	0.118	4.0	0.55
									99		999.9	B	0.60	45.0	0.153	7.4	0.91	
														0.60	45.0	0.169	11.7	1.14
									CDMG	12149	Desert Hot Springs	8.0	AQD	-99.				
									01		999.9	B	0.50	46.0	0.331	29.5	5.69	
														0.50	40.0	0.271	15.7	3.61
									USGS	5069	Fun Valley	15.8	AHC	0.13	50.0	0.071	3.7	0.67
									99		999.9	B	0.21	35.0	0.129	6.4	1.06	
														0.25	40.0	0.119	10.6	1.38
									CDMG	12331	Hemet Fire Station	43.3	AQD	0.50	47.0	0.094	3.1	0.25
									99		999.9	C	0.50	35.0	0.144	4.9	0.73	
														0.50	31.0	0.132	4.9	0.38
									CDMG	23321	Hesperia	75.9	AQD	0.20	39.0	0.033	1.2	0.42
									99		999.9	B	0.20	25.0	0.041	2.3	0.70	
														0.20	30.0	0.037	1.7	0.91
									USGS	5043	Hurkey Creek Park	34.9	AQB	0.40	50.0	0.097	3.6	0.55

No.	Earthquake Location, Mech, Dip (1)	Date & Time		Magnitude (2)			Station (3)		Closest Dist (km)(4)	Site Codes (5)	Filter Corners					
		YR	MODY	HRMN	M	ML	MS	OTH			No.	Description H/F	HP (hz)	LP (hz)	PGA (g)	PGV (cm/s)
									999.9	B	0.60	50.0	0.240	7.4	0.45	
											0.50	50.0	0.187	9.1	0.89	
	CDMG							12026	Indio - Coachella Canal	45.7	IQD	0.50	40.0	0.054	1.8	0.62
								99		999.9	C	0.50	30.0	0.053	5.3	1.18
											0.50	33.0	0.050	3.2	1.23	
	USGS							5067	Indio	39.6	AHD	0.10	40.0	0.087	3.1	1.40
								99		999.9	-	0.10	35.0	0.064	6.6	2.21
											0.10	35.0	0.117	12.3	3.62	
	CDMG							22170	Joshua Tree	29.8	AGC	0.50	36.0	0.040	3.6	0.60
								99		999.9	B	0.50	30.0	0.052	3.7	0.75
											0.50	24.0	0.065	3.9	0.48	
	CDMG							707	Lake Mathews Dike Toe	73.7	AJA	2.00	40.0	0.039	0.5	0.02
								99		999.9	-	1.00	50.0	0.061	1.5	0.08
											1.00	35.0	0.046	0.8	0.03	
	CDMG							22T13	Landers Fire Station	38.2	AQD	0.50	40.0	0.055	2.4	0.42
								99		999.9	-	0.50	30.0	0.081	4.3	0.42
											0.50	30.0	0.098	4.6	0.53	
	USGS							5071	Morongo Valley	10.1	AHC	0.30	50.0	0.395	10.6	1.61
								01		999.9	B	0.08	50.0	0.218	31.4	8.51
											0.08	50.0	0.205	40.9	14.96	
	CDMG							13198	Murrieta Hot Springs	63.3	IGA	0.50	28.0	0.032	0.8	0.31
								99		999.9	A	0.50	40.0	0.053	1.8	0.30
											0.50	40.0	0.049	1.3	0.32	
	USGS							5070	North Palm Springs	8.2	AHD	0.40	40.0	0.435	12.1	1.16
								01		999.9	B	0.15	20.0	0.594	73.3	11.46
											0.23	30.0	0.694	33.8	3.88	
	CDMG							12025	Palm Springs Airport	16.6	IQD	-99.				
								99		999.9	C	0.20	50.0	0.158	12.4	2.30
											0.20	60.0	0.187	12.2	2.07	
	CDMG							12168	Puerta La Cruz	71.9	AQB	0.20	44.0	0.035	1.6	0.34
								99		999.9	B	0.20	38.0	0.075	2.4	0.27
											0.20	32.0	0.055	1.8	0.32	
	CDMG							5253	Rancho Cucamonga ff	82.8	IHD	-99.				
								99		999.9	-	0.20	40.0	0.021	1.3	0.33
											0.30	40.0	0.019	1.1	0.27	
	CDMG							13123	Riverside Airport	71.1	AQB	0.50	48.0	0.023	0.6	0.14
								99		999.9	B	0.50	40.0	0.051	1.2	0.14
											0.50	42.0	0.040	1.0	0.15	
	CDMG							12204	San Jacinto - Soboba	32.0	AGC	0.50	50.0	0.203	6.4	0.76
								99		999.9	B	0.50	48.0	0.250	9.6	1.14
											0.50	49.0	0.239	9.2	1.21	
	CDMG							12202	San Jacinto Vall. Cem	39.6	AQD	0.50	40.0	0.053	1.8	0.30
								99		999.9	C	0.20	38.0	0.069	3.1	0.99
											0.20	31.0	0.063	4.4	1.22	
	USGS							5230	Santa Rosa Mountain	43.8	AGA	1.00	50.0	0.051	1.5	0.10

A-35

No.	Earthquake Location, Mech, Dip (1)	Date & Time			Magnitude (2)				Station (3) No.	Station (3) Description H/F	Closest Dist (km)(4)	Site Codes (5)	Filter Corners						
		YR	MODY	HRMN	M	ML	MS	OTH					HP (hz)	LP (hz)	PGA (g)	PGV (cm/s)	PGD (cm)		
									99		999.9	-	1.50	60.0	0.102	2.2	0.10		
									CDMG	12206	Silent Valley - Poppet F	25.8	IGA	0.50	50.0	0.095	3.0	0.47	
										02		999.9	A	0.50	47.0	0.139	3.9	0.55	
														0.50	49.0	0.113	4.0	0.80	
									USGS	5038	Sunnymead	44.4	BHD	0.50	40.0	0.056	2.6	0.33	
										99		999.9	-	0.30	40.0	0.093	3.9	0.58	
														0.40	40.0	0.012	5.1	0.56	
									CDMG	13172	Temecula Fire Station	73.2	AQB	0.50	27.0	0.028	1.2	0.24	
										99		999.9	C	0.50	25.0	0.121	6.9	0.53	
														0.50	25.0	0.098	4.6	0.68	
									USGS	5072	Whitewater Trout Farm	7.3	AHC	0.50	40.0	0.471	13.4	1.02	
										01		999.9	A	0.10	40.0	0.492	34.7	6.38	
														0.15	45.0	0.612	31.5	4.58	
									CDMG	13199	Winchester Bergman Ran	57.6	AGA	0.50	48.0	0.072	1.6	0.25	
										99		999.9	A	0.50	42.0	0.070	1.9	0.19	
														0.50	50.0	0.093	1.8	0.29	
									CDMG	13201	Winchester Page Bros R	46.8	IQD	0.50	59.0	0.070	2.0	0.34	
										99		999.9	-	0.50	50.0	0.106	3.8	0.69	
														0.50	37.0	0.110	4.3	0.64	
	0084	Chalfant Valley	1986	0720	1429	0.0	5.9	0.0	0.0	CDMG	54100	Benton	27.0*	AQD	0.60	30.0	0.030	1.3	0.14
		00									00		999.9	-	0.30	30.0	0.061	3.0	0.57
														0.20	30.0	0.052	2.4	0.47	
									CDMG	54171	Bishop - LADWP South St	24.0*	AQD	0.10	40.0	0.049	3.3	0.96	
										00		999.9	-	0.11	20.0	0.129	8.5	2.38	
														0.10	20.0	0.094	8.6	3.05	
									CDMG	54424	Bishop - Paradise Lodge	18.4*	AVA	0.20	40.0	0.067	2.9	0.96	
										00		999.9	-	0.11	30.0	0.046	1.7	0.24	
														0.13	30.0	0.095	6.3	1.69	
									CDMG	54T03	Lake Crowley - Shehorn Res.	26.0*	AAB	0.70	30.0	0.029	0.9	0.06	
										00		999.9	-	0.16	30.0	0.051	2.2	0.54	
														0.16	25.0	0.031	1.8	0.53	
									CDMG	54428	Zack Brothers Ranch	11.0*	AAD	0.11	45.0	0.205	5.4	2.06	
										00		999.9	-	0.11	40.0	0.285	17.3	4.00	
														0.10	30.0	0.207	22.3	5.41	
	0085	Chalfant Valley	1986	0721	1442	6.2	6.3	6.0	0.0	CDMG	54100	Benton	37.2	AQD	0.50	30.0	0.127	6.8	1.53
		00									00		999.9	-	0.10	40.0	0.209	13.6	2.88
														0.20	33.0	0.177	15.7	3.12	
									CDMG	54171	Bishop - LADWP South St	9.2	AQD	0.10	40.0	0.140	6.7	2.25	
										00		999.9	-	0.10	40.0	0.248	19.2	7.04	
														0.10	30.0	0.175	19.4	6.72	
									CDMG	54424	Bishop - Paradise Lodge	23.0	AVA	0.10	50.0	0.127	5.9	1.41	
										00		999.9	-	0.20	30.0	0.165	4.9	2.17	
														0.10	40.0	0.161	12.4	3.26	

A-36

No.	Earthquake Location, Mech, Dip (1)	Date & Time			Magnitude (2)				Station (3) No.	Station Description H/F	Closest Dist (km)(4)	Site Codes (5)	Filter Corners					
		YR	MODY	HRMN	M	ML	MS	OTH					HP (hz)	LP (hz)	PGA (g)	PGV (cm/s)	PGD (cm)	
									CDMG	54099	Convict Creek	44.9	AQD	0.20	40.0	0.036	3.1	1.09
										00		999.9	-	0.10	30.0	0.060	4.0	1.57
														0.20	30.0	0.071	3.9	1.07
									CDMG	54T03	Lake Crowley - Shehorn Res.	36.0	AAB	0.50	40.0	0.085	3.2	0.49
										00		999.9	-	0.50	30.0	0.163	7.0	0.77
														0.50	30.0	0.091	5.5	1.61
									CDMG	54214	Long Valley Dam (Downstr)	33.4	IVA	0.10	50.0	0.047	3.4	1.01
										00		999.9	-	0.10	40.0	0.095	4.8	1.30
														0.10	40.0	0.056	6.4	2.58
									CDMG	54214	Long Valley Dam (L Abut)	33.4	IVA	0.10	43.0	0.075	3.3	1.45
										00		999.9	-	0.10	50.0	0.082	7.0	1.34
														0.10	50.0	0.074	7.9	3.06
									CDMG	54T04	Mammoth Lakes Sheriff Subst.	50.8	AVB	0.50	23.0	0.026	1.6	0.39
										00		999.9	-	0.50	20.0	0.042	2.2	0.42
														0.50	20.0	0.048	2.8	0.54
									USGS	1661	McGee Creek Surface	36.3	IQC	0.10	50.0	0.069	1.4	0.52
										00		999.9	-	0.10	50.0	0.078	2.3	0.65
														0.10	35.0	0.083	2.4	0.88
									CDMG	54101	Tinemaha Res. Free Field	40.6	AVA	0.50	30.0	0.023	1.7	0.54
										00		999.9	-	0.50	30.0	0.037	3.6	1.12
														0.50	30.0	0.037	6.3	1.21
									CDMG	54428	Zack Brothers Ranch	18.7	AAD	0.20	50.0	0.321	12.5	2.80
										00		999.9	-	0.10	33.0	0.447	36.9	7.01
														0.10	33.0	0.400	44.5	8.56
0086	Chalfant Valley 00	1986	0721	1451	0.0	5.6	0.0	0.0	CDMG	54171	Bishop - LADWP South St	14.0*	AQD	0.40	40.0	0.057	2.2	0.23
										00		999.9	-	0.23	25.0	0.106	4.9	0.53
														0.30	20.0	0.070	6.5	0.56
									CDMG	54424	Bishop - Paradise Lodge	14.0*	AVA	0.20	40.0	0.053	1.1	0.19
										00		999.9	-	0.20	30.0	0.037	1.9	0.34
														0.20	30.0	0.061	2.1	0.28
									CDMG	54428	Zack Brothers Ranch	20.0*	AAD	0.20	40.0	0.079	2.1	0.15
										00		999.9	-	0.13	35.0	0.143	7.4	0.67
														0.30	30.0	0.108	5.1	0.58
0087	Chalfant Valley 00	1986	0731	0722	0.0	5.8	0.0	0.0	CDMG	54171	Bishop - LADWP South St	13.0*	AQD	0.20	40.0	0.067	2.8	0.60
										00		999.9	-	0.10	20.0	0.120	10.4	2.71
														0.15	25.0	0.176	12.2	1.72
									CDMG	54428	Zack Brothers Ranch	21.0*	AAD	0.22	40.0	0.046	1.6	0.37
										00		999.9	-	0.13	30.0	0.064	4.1	0.91
														0.11	30.0	0.060	4.3	0.84
0088	Taiwan SMART1(45) 02	1986	1114		7.3	7.0	7.8	0.0		25	SMART1 C00	39.0	IZD	0.10	25.0	0.080	7.0	3.19
										99		999.9	-	0.10	25.0	0.122	29.4	9.74
														0.10	25.0	0.153	28.3	10.73
										32	SMART1 E01	39.0	IZD	0.10	25.0	0.075	6.9	3.47

No.	Earthquake Location, Mech, Dip (1)	Date & Time			Magnitude (2)				Station (3)		Closest Dist (km)(4)	Site Codes (5)	Filter Corners			PGD (cm)		
		YR	MODY	HRMN	M	ML	MS	OTH	No.	Description H/F			HP (hz)	LP (hz)	PGA (g)		PGV (cm/s)	
									99		999.9	-	0.10	25.0	0.159	2.5	8.26	
									33	SMART1 E02	39.0	IZD	0.10	25.0	0.052	5.5	3.03	
									99		999.9	-	0.10	25.0	0.136	13.7	5.84	
									62	SMART1 I01	39.0	IZD	0.10	25.0	0.143	12.5	6.07	
									99		999.9	-	0.10	25.0	0.132	30.5	9.05	
													0.10	25.0	0.141	29.8	10.34	
									61	SMART1 I07	39.0	IZD	0.10	25.0	0.089	6.9	3.22	
									99		999.9	-	0.10	25.0	0.118	23.3	10.69	
													0.10	25.0	0.122	27.0	9.64	
									28	SMART1 M01	39.0	IZD	0.10	25.0	0.078	6.1	2.26	
									99		999.9	-	0.10	25.0	0.119	27.0	8.91	
													0.10	25.0	0.141	21.8	9.93	
									29	SMART1 M07	39.0	IZD	0.20	25.0	0.106	8.6	3.19	
									99		999.9	-	0.10	25.0	0.156	26.8	9.09	
													0.20	25.0	0.160	22.5	7.62	
									30	SMART1 O01	39.0	IZD	0.10	25.0	0.063	6.3	3.31	
									99		999.9	-	0.10	25.0	0.126	21.8	9.66	
													0.10	25.0	0.174	21.2	7.90	
									63	SMART1 O02	39.0	IZD	0.10	25.0	0.062	7.0	4.66	
									99		999.9	-	0.10	25.0	0.160	20.4	9.90	
													0.10	25.0	0.242	26.2	11.56	
									64	SMART1 O04	39.0	IZD	0.10	25.0	0.081	7.2	2.95	
									99		999.9	-	0.10	25.0	0.126	31.9	9.11	
													0.10	25.0	0.163	25.3	9.84	
									65	SMART1 O06	39.0	IZD	0.10	25.0	0.079	7.0	2.44	
									99		999.9	-	0.10	25.0	0.171	24.5	8.91	
													0.10	25.0	0.190	22.8	8.65	
									31	SMART1 O07	39.0	IZD	0.10	25.0	0.106	8.7	2.36	
									99		999.9	-	0.10	25.0	0.154	19.4	8.17	
													0.10	25.0	0.164	23.2	11.13	
									66	SMART1 O08	39.0	IZD	0.10	25.0	0.105	9.2	4.18	
									99		999.9	-	0.10	25.0	0.142	24.5	9.33	
													0.10	25.0	0.163	30.1	13.21	
									67	SMART1 O10	39.0	IZD	0.10	25.0	0.062	6.2	3.82	
									99		999.9	-	0.10	25.0	0.148	24.2	9.97	
													0.10	25.0	0.116	26.8	10.08	
									68	SMART1 O12	39.0	IZD	0.20	25.0	0.065	6.1	1.99	
									99		999.9	-	0.10	25.0	0.139	24.5	8.82	
													0.10	25.0	0.159	23.3	10.61	
0089	Whittier Narrows 02	1987	1001	1442	6.0	5.9	5.7	0.0	CDMG	24461	Alhambra, Fremont Sch	13.2	AMD	0.40	50.0	0.190	5.5	0.84
									99		999.9	B	0.50	35.0	0.333	22.0	2.42	
													0.30	40.0	0.414	16.3	2.32	
								CDMG	24402	Altadena - Eaton Canyon	17.5	AQD	0.40	40.0	0.163	3.3	0.44	

No.	Earthquake Location, Mech, Dip (1)	Date & Time			Magnitude (2)				Station (3)		Closest Dist (km)(4)	Site Codes (5)	Filter Corners				
		YR	MODY	HRMN	M	ML	MS	OTH	No.	H/F			HP (hz)	LP (hz)	PGA (g)	PGV (cm/s)	PGD (cm)
										01	999.9	-	0.40	35.0	0.299	11.4	1.20
									USC	90088	24.4	-D	0.40	35.0	0.151	5.7	0.50
										99	999.9	C	0.60	25.0	0.062	1.8	0.10
													0.25	25.0	0.060	6.6	1.33
													0.50	25.0	0.055	3.4	0.63
									USC	90093	12.2	-D	0.28	25.0	0.229	6.2	0.56
										99	999.9	C	0.15	25.0	0.300	21.0	3.12
													0.38	25.0	0.163	6.8	0.73
									CDMG	24087	38.9	AQD	0.35	40.0	0.089	3.3	0.58
										99	999.9	-	0.40	30.0	0.093	5.4	0.55
													0.50	30.0	0.091	4.7	0.85
									USC	90069	11.9	-D	0.30	25.0	0.080	2.2	0.75
										99	999.9	B	0.13	25.0	0.127	8.6	2.50
													0.50	25.0	0.061	4.3	0.54
									USC	90094	9.8	-D	0.40	25.0	0.095	2.7	0.40
										99	999.9	C	0.25	25.0	0.219	18.9	2.54
													0.10	25.0	0.212	21.8	4.83
									USC	90014	27.2	-C	0.40	25.0	0.068	2.4	0.32
										99	999.9	B	0.35	25.0	0.089	5.1	0.53
													0.33	22.5	0.138	6.4	0.58
									USC	90013	30.3	-C	0.38	25.0	0.043	2.0	0.25
										99	999.9	C	0.33	25.0	0.104	6.5	0.58
													0.35	25.0	0.126	10.3	1.05
									USC	90061	25.5	-C	0.75	25.0	0.085	2.3	0.19
										99	999.9	B	0.40	25.0	0.126	4.6	0.61
													0.90	25.0	0.178	6.7	0.37
									USGS	951	23.3	IPD	0.50	40.0	0.094	3.1	0.22
										99	999.9	-	0.60	35.0	0.163	6.2	0.36
													0.60	40.0	0.313	14.5	0.77
									USGS	951	23.3	IPB	0.70	40.0	0.097	2.7	0.20
										99	999.9	-	0.50	40.0	0.118	6.2	0.60
													0.50	30.0	0.149	10.2	0.82
									USC	90087	17.9	-D	0.20	25.0	0.103	9.1	1.31
										99	999.9	C	0.16	25.0	0.115	7.1	1.21
													-99.				
									USC	90012	23.7	-D	0.35	25.0	0.105	3.2	0.53
										99	999.9	C	0.25	25.0	0.233	16.0	1.33
													0.30	25.0	0.190	11.6	1.16
									USC	90052	53.3	-B	0.40	25.0	0.023	1.6	0.15
										99	999.9	B	0.33	25.0	0.042	2.3	0.35
													0.45	25.0	0.025	1.2	0.13
									USC	90053	47.4	-D	0.35	25.0	0.055	1.9	0.30
										99	999.9	C	0.25	25.0	0.139	7.9	0.76
													0.28	25.0	0.116	8.1	1.13
									USC	90057	46.4	-D	0.40	25.0	0.073	1.9	0.26

No.	Earthquake Location, Mech, Dip (1)	Date & Time			Magnitude (2)				Station (3)		Closest Dist (km)(4)	Site Codes (5)	Filter Corners						
		YR	MODY	HRMN	M	ML	MS	OTH	No.	Description H/F			HP (hz)	LP (hz)	PGA (g)	PGV (cm/s)	PGD (cm)		
											999.9	C	0.38	25.0	0.109	7.5	0.49		
													0.23	22.5	0.103	7.0	0.85		
									USGS	108	Carbon Canyon Dam (L Abut)	26.8	AMA	0.80	45.0	0.058	2.4	0.13	
										99			999.9	-	0.80	40.0	0.200	6.5	0.51
													0.50	40.0	0.221	8.7	0.64		
									USC	90040	Carson - Catskill Ave #	28.1	-D	0.50	25.0	0.037	1.3	0.15	
										99			999.9	C	0.18	25.0	0.042	3.8	0.75
													0.55	25.0	0.059	2.4	0.32		
									USC	90081	Carson - Water St #	24.5	-D	0.50	25.0	0.046	2.0	0.23	
										99			999.9	C	0.20	25.0	0.104	9.0	1.91
													0.30	25.0	0.133	11.3	1.54		
									CDMG	24277	Castaic - Hasley Canyon	70.9	A-B	0.50	20.0	0.021	1.5	0.16	
										99			999.9	-	0.70	15.0	0.031	1.9	0.19
													0.50	15.0	0.035	2.6	0.31		
									CDMG	24278	Castaic - Old Ridge Route	78.3	A-B	1.00	23.0	0.026	1.1	0.08	
										99			999.9	B	0.80	15.0	0.071	4.4	0.40
													0.80	20.0	0.065	4.5	0.38		
									USC	90078	Compton - Castlegate St #	16.9	-D	0.50	25.0	0.167	3.3	0.19	
										99			999.9	C	0.09	25.0	0.332	27.1	5.04
													0.28	25.0	0.333	14.1	1.48		
									USC	90068	Covina - S Grand Ave #	17.1	-C	0.33	25.0	0.064	3.1	0.46	
										99			999.9	C	0.45	25.0	0.076	5.4	0.90
													0.40	25.0	0.068	4.1	0.62		
									USC	90070	Covina - W Badillo #	14.2	-D	0.50	25.0	0.082	2.9	0.22	
										99			999.9	C	0.28	25.0	0.134	7.7	1.33
													0.38	25.0	0.081	4.0	0.63		
									USC	90079	Downey - Birchdale #	56.8	-D	0.60	25.0	0.230	4.1	0.31	
										99			999.9	C	0.28	25.0	0.243	13.7	1.92
													0.15	25.0	0.299	37.8	4.95		
									CDMG	14368	Downey - Co Maint Bldg	18.3	AQD	1.00	40.0	0.177	3.3	0.23	
										99			999.9	-	0.20	30.0	0.221	28.8	3.95
													0.25	30.0	0.141	13.4	1.60		
									USC	90066	El Monte - Fairview Av #	9.8	-D	0.30	25.0	0.136	4.8	0.45	
										99			999.9	C	0.33	25.0	0.120	6.7	0.93
													0.13	25.0	0.228	15.0	4.06		
									CDMG	13122	Featherly Park - Maint	38.6	AMC	1.30	40.0	0.050	1.4	0.07	
										99			999.9	-	0.80	25.0	0.071	3.6	0.26
													0.90	25.0	0.087	5.1	0.33		
									USC	90002	Fountain Valley - Euclid #	35.0	-D	0.38	25.0	0.049	1.1	0.16	
										99			999.9	C	0.30	25.0	0.071	4.1	0.76
													0.30	25.0	0.062	6.0	1.75		
									USGS	709	Garvey Res. - Control Bldg	12.1	APB	0.70	40.0	0.362	9.9	0.75	
										01			999.9	-	0.15	40.0	0.384	15.8	2.49
													0.20	40.0	0.457	19.0	4.31		
									USC	90063	Glendale - Las Palmas #	19.0	-C	0.63	27.0	0.143	5.7	0.39	

No.	Earthquake Location, Mech, Dip (1)	Date & Time			Magnitude (2)			Station (3)		Closest Dist (km)(4)	Site Codes (5)	Filter Corners			PGA (g)	PGV (cm/s)	PGD (cm)
		YR	MODY	HRMN	M	ML	MS	OTH	No.			Description H/F	HP (hz)	LP (hz)			
									99	999.9	C	0.28	25.0	0.296	17.1	1.82	
								USC	90065	Glendora - N Oakbank #	69.7	-D	0.38	25.0	0.071	3.3	0.48
									99	999.9	B	0.35	25.0	0.092	3.4	0.50	
												0.23	25.0	0.110	5.0	0.81	
								USC	90073	Hacienda Heights - Colima #	10.5	-C	0.50	25.0	0.096	2.2	0.25
									99	999.9	C	0.23	25.0	0.195	8.6	0.84	
												0.45	25.0	0.201	6.3	0.62	
								CDMG	12331	Hemet Fire Station	105.0	AQD	1.00	30.0	0.027	0.9	0.07
									99	999.9	C	0.70	25.0	0.038	1.4	0.13	
												0.80	25.0	0.032	1.6	0.10	
								CDMG	13197	Huntington Beach - Lake St	42.8	AQD	0.22	30.0	0.027	1.3	0.26
									99	999.9	-	0.25	25.0	0.045	1.7	0.49	
												0.17	25.0	0.044	3.4	1.27	
								CDMG	14196	Inglewood - Union Oil	25.2	IQD	0.50	30.0	0.069	2.4	0.24
									99	999.9	-	0.60	40.0	0.299	8.9	0.78	
												0.25	40.0	0.247	18.1	1.92	
								CDMG	14403	LA - 116th St School	22.5	AQD	0.20	30.0	0.105	3.0	0.49
									99	999.9	-	0.20	30.0	0.294	17.6	1.97	
												0.20	30.0	0.396	21.0	1.75	
								CDMG	24157	LA - Baldwin Hills	27.0	IPB	0.40	35.0	0.114	4.0	0.37
									99	999.9	-	0.30	35.0	0.142	8.7	1.40	
												0.40	30.0	0.159	8.0	0.72	
								USC	90054	LA - Centinela St #	27.7	-D	0.33	25.0	0.032	1.2	0.27
									99	999.9	C	0.30	25.0	0.059	3.0	0.55	
												0.25	25.0	0.044	2.6	0.34	
								CDMG	24389	LA - Century City CC North	31.4	IQD	0.50	23.0	0.039	1.6	0.20
									99	999.9	-	0.60	30.0	0.078	3.1	0.34	
												0.35	30.0	0.111	6.2	0.70	
								CDMG	24390	LA - Century City CC South	31.3	IQD	0.40	30.0	0.021	1.7	0.25
									99	999.9	-	0.20	25.0	0.051	3.5	0.61	
												0.30	25.0	0.063	5.4	0.83	
								USC	90015	LA - Chalon Rd #	32.6	-B	1.00	25.0	0.019	0.7	0.07
									99	999.9	B	0.38	25.0	0.036	2.3	0.21	
												0.75	25.0	0.020	1.1	0.12	
								USC	90033	LA - Cypress Ave #	11.4	-C	0.40	25.0	0.084	2.9	0.29
									99	999.9	B	0.33	25.0	0.156	8.0	0.88	
												0.28	25.0	0.137	9.1	1.35	
								USC	90025	LA - E Vernon Ave #	10.8	-D	0.40	25.0	0.086	2.7	0.39
									99	999.9	C	0.18	25.0	0.146	12.8	1.43	
												0.16	25.0	0.175	8.8	1.37	
								USC	90034	LA - Fletcher Dr #	14.4	-D	0.30	25.0	0.103	7.6	1.03
									99	999.9	C	0.28	25.0	0.171	19.4	2.17	
												0.30	25.0	0.213	12.6	1.45	
								CDMG	24303	LA - Hollywood Stor FF	25.2	IPD	0.45	50.0	0.070	2.8	0.42

No.	Earthquake Location, Mech, Dip (1)	Date & Time			Magnitude (2)			Station (3)		Closest Dist (km)(4)	Site Codes (5)	Filter Corners			PGA (g)	PGV (cm/s)	PGD (cm)
		YR	MODY	HRMN	M	ML	MS	OTH	No.			Description H/F	HP (hz)	LP (hz)			
									99	999.9	C	0.40	25.0	0.221	9.0	1.43	
								USC	90016	28.5	-B	0.40	25.0	0.124	6.9	1.12	
									99	999.9	C	0.55	25.0	0.034	1.6	0.13	
									99	999.9	C	0.55	25.0	0.048	2.2	0.26	
								USC	90032	11.4	-C	0.40	25.0	0.053	3.0	0.29	
									99	999.9	B	0.55	25.0	0.169	5.7	0.47	
									99	999.9	B	0.30	25.0	0.151	7.9	1.10	
								USC	90021	16.6	-D	0.20	25.0	0.166	13.1	1.82	
									99	999.9	B	0.35	25.0	0.084	3.1	0.43	
									99	999.9	B	0.30	25.0	0.214	9.7	0.98	
									99	999.9	B	0.30	25.0	0.199	6.2	0.72	
								CDMG	24400	13.9	AQD	0.50	35.0	0.144	5.2	0.59	
									99	999.9	-	0.40	35.0	0.450	16.1	2.18	
									99	999.9	-	0.40	35.0	0.400	22.9	2.53	
								USC	90022	14.5	-D	0.30	25.0	0.122	3.5	0.29	
									99	999.9	C	0.35	25.0	0.191	8.6	0.75	
									99	999.9	C	0.28	25.0	0.149	8.0	1.19	
								USC	90091	20.8	-D	0.28	25.0	0.041	2.0	0.59	
									99	999.9	C	0.25	25.0	0.099	6.1	0.68	
									99	999.9	C	0.23	25.0	0.141	4.5	0.58	
								USC	90023	16.3	-D	0.30	25.0	0.077	2.8	0.45	
									99	999.9	C	0.30	25.0	0.198	19.5	2.49	
									99	999.9	C	0.20	25.0	0.151	8.7	1.51	
								USC	90017	24.6	-A	0.55	25.0	0.024	0.9	0.10	
									99	999.9	A	0.53	25.0	0.039	1.7	0.17	
									99	999.9	A	0.70	25.0	0.047	1.5	0.16	
								USC	90060	22.7	-C	0.38	25.0	0.090	2.8	0.40	
									99	999.9	C	0.40	25.0	0.134	11.7	1.18	
									99	999.9	C	0.30	25.0	0.141	10.9	1.69	
								USC	90074	13.5	-C	0.50	25.0	0.064	2.6	0.31	
									99	999.9	C	0.25	25.0	0.183	9.9	2.23	
									99	999.9	C	0.25	25.0	0.131	7.3	1.10	
								USC	90072	11.9	-D	0.45	25.0	0.076	2.5	0.19	
									99	999.9	C	0.18	25.0	0.143	6.2	1.04	
									99	999.9	C	0.50	21.5	0.118	5.9	0.42	
								CDMG	24271	74.7	APC	-99.					
									99	999.9	-	0.90	20.0	0.035	2.5	0.19	
									99	999.9	-	0.80	20.0	0.029	1.6	0.18	
								USC	90084	20.9	-D	0.30	25.0	0.126	3.4	0.55	
									99	999.9	C	0.30	25.0	0.277	28.5	4.52	
									99	999.9	C	0.30	25.0	0.178	11.8	2.13	
								CDMG	24526	69.5	IQC	1.30	35.0	0.027	0.8	0.03	
									99	999.9	-	0.80	25.0	0.067	2.5	0.16	
									99	999.9	-	0.60	25.0	0.071	2.8	0.17	
								USC	90045	25.1	-D	0.33	25.0	0.031	2.0	0.26	

No.	Earthquake Location, Mech, Dip (1)	Date & Time			Magnitude (2)				Station (3)		Closest Dist (km)(4)	Site Codes (5)	Filter Corners					
		YR	MODY	HRMN	M	ML	MS	OTH	No.	Description H/F			HP (hz)	LP (hz)	PGA (g)	PGV (cm/s)	PGD (cm)	
											999.9	C	0.35	25.0	0.066	5.3	0.89	
													0.38	25.0	0.053	5.3	0.71	
									CDMG	14395	LB - Harbor Admin FF	34.2	IQD	0.20	25.0	0.028	1.6	0.40
										99		999.9	-	0.60	30.0	0.058	4.1	0.63
														0.25	25.0	0.071	7.3	0.85
									USC	90080	LB - Orange Ave #	18.3	-D	0.55	25.0	0.136	3.4	0.38
										99		999.9	-	0.12	25.0	0.255	32.9	4.83
														0.28	25.0	0.149	10.3	1.36
									CDMG	14242	LB - R. Los Cerritos	26.0	IQD	0.70	35.0	0.084	2.8	0.21
										99		999.9	-	0.25	40.0	0.159	16.9	2.90
														0.50	35.0	0.194	17.2	2.21
									CDMG	14241	LB - Recreation Park	30.5	IQD	0.60	20.0	0.038	1.6	0.23
										02		999.9	-	0.20	30.0	0.058	3.1	0.80
														0.30	25.0	0.051	6.8	1.64
									CDMG	24055	Leona Valley #5 - Ritter	61.3	IQC	1.00	25.0	0.029	1.0	0.07
										99		999.9	-	0.80	25.0	0.047	2.1	0.14
														0.80	30.0	0.056	2.7	0.19
									CDMG	24309	Leona Valley #6	64.8	I-D	1.00	25.0	0.024	1.0	0.10
										99		999.9	-	1.00	25.0	0.036	1.6	0.10
														0.80	25.0	0.053	1.9	0.11
									USC	90050	Malibu - Las Flores Canyon #	46.3	-B	0.65	25.0	0.015	1.0	0.13
										99		999.9	B	0.65	25.0	0.065	2.3	0.14
														0.65	25.0	0.055	2.2	0.32
									CDMG	24396	Malibu - Point Dume Sch	65.3	AMB	0.35	30.0	0.029	1.9	0.15
										99		999.9	-	0.35	25.0	0.048	2.4	0.32
														0.60	20.0	0.040	2.0	0.18
									USC	90051	Malibu - W Pacific Cst Hwy #	60.0	-B	0.38	25.0	0.029	1.6	0.24
										99		999.9	B	0.40	25.0	0.038	2.5	0.28
														0.70	25.0	0.032	2.3	0.22
									USC	90046	Manhattan Beach - Manhattan #	28.9	-C	-99.				
										99		999.9	C	0.40	25.0	0.054	5.8	0.85
														-99.				
									USC	90062	Mill Creek, Angeles Nat For #	34.5	-B	0.70	25.0	0.040	1.6	0.10
										99		999.9	C	0.40	25.0	0.089	4.0	0.52
														0.63	25.0	0.071	3.3	0.32
									CDMG	24283	Moorpark - Fire Sta	27.1	AQD	1.00	25.0	0.019	1.0	0.08
										99		999.9	-	0.80	15.0	0.039	3.1	0.26
														0.50	15.0	0.042	2.5	0.26
									CDMG	24399	Mt Wilson - CIT Seis Sta	21.2	IGA	0.40	40.0	0.119	3.3	0.25
										01		999.9	-	0.60	40.0	0.123	3.3	0.37
														0.70	40.0	0.186	4.6	0.21
									USC	90009	N Hollywood - Coldwater Can #	30.8	-C	0.20	25.0	0.059	2.7	0.49
										99		999.9	B	0.20	25.0	0.116	6.2	0.97
														0.30	25.0	0.250	14.3	1.11
									CDMG	24279	Newhall - Fire Sta	55.2	AQD	1.00	25.0	0.038	1.0	0.09

No.	Earthquake Location, Mech, Dip (1)	Date & Time		Magnitude (2)				Station (3)		Closest Dist (km)(4)	Site Codes (5)	Filter Corners			PGA (g)	PGV (cm/s)	PGD (cm)
		YR	MODY	HRMN	M	ML	MS	OTH	No.			Description H/F	HP (hz)	LP (hz)			
									99	999.9	-	0.50	15.0	0.044	2.9	0.31	
								USC	90056	Newhall - W Pico Canyon #	57.1	-C	0.60	15.0	0.060	2.9	0.41
									99	999.9	-	0.30	25.0	0.035	1.7	0.17	
												0.28	25.0	0.088	5.6	0.47	
												0.38	25.0	0.055	3.9	0.32	
								USC	90003	Northridge - Saticoy St #	39.8	-D	0.25	25.0	0.084	2.4	0.41
									99	999.9	C	0.23	25.0	0.161	8.5	0.72	
												0.20	25.0	0.118	5.1	0.83	
								USGS	634	Norwalk - Imp Hwy, S Gmd	17.2	IHD	0.60	45.0	0.096	2.9	0.30
									02	999.9	-	0.15	40.0	0.107	8.4	1.40	
												0.15	45.0	0.248	20.7	4.21	
								USGS	697	Orange Co. Reservoir	23.0	APB	1.00	35.0	0.126	2.7	0.19
									99	999.9	-	0.40	30.0	0.185	10.2	0.96	
												0.30	30.0	0.198	6.1	0.74	
								USC	90049	Pacific Palisades - Sunset #	38.6	-B	0.28	25.0	0.035	1.3	0.25
									99	999.9	C	0.45	25.0	0.063	2.0	0.28	
												0.50	25.0	0.038	2.0	0.33	
								CDMG	24088	Pacoima Kagel Canyon	37.9	AMB	0.50	35.0	0.055	2.7	0.30
									99	999.9	-	0.35	20.0	0.166	6.2	0.68	
												0.45	20.0	0.164	6.8	0.87	
								USC	90005	Pacoima Kagel Canyon USC #	34.0	-D	0.53	25.0	0.076	4.0	0.57
									99	999.9	B	0.30	25.0	0.119	7.9	1.07	
												0.23	25.0	0.133	5.5	0.60	
								USC	90007	Panorama City - Roscoe #	33.0	-D	0.25	25.0	0.079	2.8	0.50
									99	999.9	B	0.25	23.5	0.105	7.2	0.81	
												0.20	25.0	0.108	7.2	1.48	
								CDMG	80046	Pasadena - Brown Gym	15.5	-QD	0.50	40.0	0.161	3.7	0.48
									99	999.9	-	0.35	30.0	0.165	13.2	2.09	
												0.35	30.0	0.149	9.1	1.24	
								CDMG	80053	Pasadena - CIT Athenaeum	15.4	CQD	0.50	30.0	0.125	4.8	0.44
									99	999.9	B	0.30	40.0	0.174	11.5	1.68	
												0.30	35.0	0.101	6.0	0.74	
								CDMG	80052	Pasadena - CIT Bridge Lab	15.5	-QD	0.70	40.0	0.132	3.6	0.28
									99	999.9	-	0.40	35.0	0.184	10.3	1.13	
												0.25	35.0	0.147	15.0	2.72	
								CDMG	80047	Pasadena - CIT Calif Blvd	15.5	AQD	0.30	40.0	0.171	7.0	0.58
									99	999.9	-	0.30	40.0	0.177	8.1	0.96	
												0.30	35.0	0.271	15.4	2.33	
								CDMG	80051	Pasadena - CIT Indust. Rel	15.5	BQD	0.50	40.0	0.184	5.5	0.45
									99	999.9	-	0.30	25.0	0.239	8.4	0.99	
												0.30	30.0	0.228	13.8	1.95	
								CDMG	80049	Pasadena - CIT Keck Lab	15.5	-QD	0.60	60.0	0.096	4.0	0.41
									99	999.9	-	0.40	35.0	0.152	5.1	0.60	
												0.25	35.0	0.188	14.1	2.63	
								CDMG	80054	Pasadena - CIT Kresge Lab	17.4	-QD	0.50	45.0	0.081	3.3	0.37

No.	Earthquake Location, Mech, Dip (1)	Date & Time			Magnitude (2)			Station (3)		Closest Dist (km)(4)	Site Codes (5)	Filter Corners			PGA (g)	PGV (cm/s)	PGD (cm)
		YR	MODY	HRMN	M	ML	MS	OTH	No.			Description H/F	HP (hz)	LP (hz)			
										999.9	-	0.40	40.0	0.112	8.0	0.99	
								CDMG	80048	Pasadena - CIT Lura St	15.5	AQD	0.43	50.0	0.236	5.0	0.61
									99		999.9	-	0.40	40.0	0.360	9.8	0.92
								CDMG	80050	Pasadena - CIT Mudd Lab	15.5	-QD	0.30	40.0	0.352	18.1	2.35
									99		999.9	-	0.40	30.0	0.134	3.9	0.36
								USC	90095	Pasadena - Old House Rd #	14.5	-C	0.30	35.0	0.163	15.1	2.23
									99		999.9	C	0.25	25.0	0.102	3.5	0.89
								USC	90047	Playa Del Rey - Saran #	28.8	-D	0.23	25.0	0.258	8.0	1.23
									99		999.9	E	0.35	25.0	0.018	1.2	0.22
								CDMG	23525	Pomona - 4th & Locust FF	28.8	IQD	0.40	25.0	0.025	2.5	0.47
									99		999.9	C	0.38	25.0	0.034	2.5	0.32
								CDMG	23497	Rancho Cucamonga - Law & J	44.3	IHD	0.80	40.0	0.055	1.3	0.13
									99		999.9	B	0.50	30.0	0.067	3.4	0.35
								USC	90044	Rancho Palos Verdes - Luconia #	37.7	-C	0.55	30.0	0.056	2.5	0.22
									99		999.9	C	0.60	50.0	0.060	1.5	0.18
								CDMG	13123	Riverside Airport	56.8	AQB	0.50	50.0	0.050	1.4	0.16
									99		999.9	B	0.45	21.5	0.017	0.9	0.11
								CDMG	24274	Rosamond - Goode Ranch	86.0	IQC	0.45	21.5	0.021	2.0	0.28
									99		999.9	-	0.53	25.0	0.021	1.6	0.24
								USC	90019	San Gabriel - E Grand Av #	9.0	-A	3.00	50.0	0.044	0.7	0.01
									99		999.9	A	1.70	35.0	0.050	1.4	0.05
								CDMG	24401	San Marino, SW Academy	14.7	AQD	2.00	45.0	0.047	1.4	0.04
									99		999.9	-	0.40	20.0	0.021	1.2	0.11
								USC	90077	Santa Fe Springs - E Joslin #	10.8	-D	0.50	20.0	0.065	3.2	0.31
									99		999.9	C	0.35	25.0	0.227	5.5	0.44
								CDMG	90048	Santa Monica - Second St #	32.6	-B	0.35	25.0	0.304	23.0	3.34
									99		999.9	B	0.35	25.0	0.199	11.0	1.04
								USC	90010	Studio City - Coldwater Can #	28.7	-D	0.60	40.0	0.142	5.4	0.74
									99		999.9	-	0.40	40.0	0.128	5.6	0.58
								USC	90006	Sun Valley - Roscoe Blvd #	32.6	-D	0.40	40.0	0.204	12.8	2.60
									99		999.9	C	0.25	25.0	0.206	6.7	1.03
								USC	90048	Santa Monica - Second St #	32.6	-B	0.35	25.0	0.426	38.1	3.54
									99		999.9	B	0.35	25.0	0.443	21.7	3.00
								USC	90010	Studio City - Coldwater Can #	28.7	-D	0.53	25.0	0.021	0.8	0.13
									99		999.9	C	0.53	25.0	0.033	2.7	0.28
								USC	90010	Studio City - Coldwater Can #	28.7	-D	0.28	25.0	0.034	4.1	0.60
									99		999.9	C	0.35	25.0	0.073	2.8	0.37
								USC	90006	Sun Valley - Roscoe Blvd #	32.6	-D	0.30	25.0	0.177	14.2	1.15
									99		999.9	-	0.30	25.0	0.231	13.7	1.14
								USC	90006	Sun Valley - Roscoe Blvd #	32.6	-D	0.25	25.0	0.093	3.9	0.43

A-44

A-45

No.	Earthquake Location, Mech, Dip (1)	Date & Time			Magnitude (2)				Station (3)		Closest Dist (km)(4)	Site Codes (5)	Filter Corners				
		YR	MODY	HRMN	M	ML	MS	OTH	No.	Description H/F			HP (hz)	LP (hz)	PGA (g)	PGV (cm/s)	PGD (cm)
										99	999.9	B	0.25	25.0	0.202	8.5	0.87
									USC	90008	29.3	-B	0.28	25.0	0.223	13.3	1.05
										99	999.9	B	0.35	25.0	0.043	2.3	0.41
													0.30	25.0	0.075	3.4	0.73
									USC	90058	27.5	-C	0.38	25.0	0.074	3.2	0.30
										99	999.9	B	0.30	25.0	0.072	3.5	0.50
													0.28	25.0	0.089	4.5	0.73
													0.28	25.0	0.072	4.0	0.59
									CDMG	24514	47.7	AQD	0.50	25.0	0.042	1.7	0.18
										99	999.9	C	0.35	20.0	0.065	4.4	0.67
													0.40	20.0	0.055	3.2	0.46
									USC	90001	38.6	-D	0.33	25.0	0.033	1.2	0.20
										99	999.9	B	0.25	25.0	0.051	4.2	0.65
													0.28	25.0	0.046	2.7	0.41
									CDMG	24436	43.0	A-B	0.70	40.0	0.248	5.9	0.31
										99	999.9	-	0.60	40.0	0.449	20.1	1.29
													0.60	40.0	0.644	22.9	1.68
									USC	90082	35.7	-D	0.28	25.0	0.021	1.2	0.32
										99	999.9	C	0.20	25.0	0.042	3.9	0.97
													0.28	25.0	0.041	3.1	0.97
									USC	90038	31.4	-E	0.40	25.0	0.025	1.2	0.26
										99	999.9	E	0.23	25.0	0.031	2.6	0.65
													0.28	25.0	0.051	2.4	0.48
									CDMG	24047	52.4	IBA	0.90	35.0	0.039	1.1	0.09
										99	999.9	-	1.00	25.0	0.060	2.1	0.12
													1.00	25.0	0.060	2.3	0.11
									USC	90090	30.1	-B	0.50	25.0	0.033	1.3	0.11
										99	999.9	B	0.70	25.0	0.046	1.4	0.13
													0.55	25.0	0.072	2.6	0.27
									USC	90071	10.5	-B	0.50	25.0	0.131	3.7	0.23
										99	999.9	C	0.23	25.0	0.137	10.6	1.84
													0.23	25.0	0.179	7.0	1.79
									USGS	289	12.3	IHD	0.55	50.0	0.505	7.1	0.31
										01	999.9	-	0.20	50.0	0.229	17.8	2.62
													0.40	40.0	0.316	12.0	1.36
0090	Whittier Narrows 03	1987	1004	1059	5.3	5.3	0.0	0.0	CDMG	24461	12.6*	AMD	0.50	40.0	0.082	2.9	0.26
										00	999.9	B	0.60	30.0	0.174	10.8	0.91
													0.50	40.0	0.178	8.9	0.87
									CDMG	24402	16.1*	AQD	0.50	30.0	0.122	3.4	0.28
										00	999.9	-	0.45	30.0	0.264	9.5	0.78
													0.30	30.0	0.199	10.2	0.81
									CDMG	14368	20.5*	AQD	0.80	40.0	0.048	1.2	0.14
										00	999.9	-	0.40	25.0	0.073	4.7	0.55
													0.60	30.0	0.065	5.4	0.58
									CMDG	14196	27.3*	IQD	1.00	30.0	0.031	1.9	0.12

A-46

No.	Earthquake Location, Mech, Dip (1)	Date & Time			Magnitude (2)				Station (3) No.	Description H/F	Closest Dist (km)(4)	Site Codes (5)	Filter Corners			PGA (g)	PGV (cm/s)	PGD (cm)
		YR	MODY	HRMN	M	ML	MS	OTH					HP (hz)	LP (hz)				
										00	999.9	-	0.40	30.0	0.110	6.9	0.93	
													0.40	30.0	0.157	9.2	0.98	
									CDMG	14403	24.6*	AQD	0.70	30.0	0.036	1.4	0.12	
										00	999.9	-	0.40	30.0	0.166	10.6	1.13	
													0.15	30.0	0.151	10.1	1.06	
									CDMG	24157	27.6*	IPB	0.80	35.0	0.040	2.5	0.19	
										00	999.9	-	0.30	30.0	0.065	6.2	1.08	
													0.30	30.0	0.134	11.2	1.07	
									CDMG	24303	24.5*	IPD	0.60	25.0	0.027	1.0	0.13	
										00	999.9	C	0.50	20.0	0.056	2.6	0.31	
													0.50	25.0	0.079	3.8	0.45	
									CDMG	24400	14.9*	AQD	0.45	35.0	0.098	3.7	0.35	
										00	999.9	-	0.55	25.0	0.374	14.5	0.98	
													0.30	30.0	0.261	24.0	2.57	
									CDMG	24399	20.4*	IGA	0.50	35.0	0.086	2.2	0.16	
										00	999.9	-	0.70	35.0	0.158	5.7	0.25	
													0.70	40.0	0.142	4.6	0.20	
									CDMG	24401	12.8*	AQD	0.60	40.0	0.079	2.7	0.26	
										00	999.9	-	0.50	40.0	0.156	7.8	1.02	
													0.30	50.0	0.212	12.9	1.51	
									CDMG	24436	42.7*	A-B	1.00	35.0	0.037	1.4	0.09	
										00	999.9	-	0.50	30.0	0.074	2.8	0.23	
													1.00	25.0	0.113	4.5	0.31	
0091	Superstn Hills (A) 00	1987	1124	0514	6.3	5.8	6.2	0.0	USGS	5210	24.7	IQD	0.20	50.0	0.186	4.6	2.2	
										00	999.9	-	0.20	50.0	0.132	12.7	7.3	
													0.20	50.0	0.134	13.4	5.2	
0092	Superstn Hills (B) 00	1987	1124	1316	6.7	0.0	6.6	0.0	USGS	5060	18.2	AQD	-99.					
										00	999.9	C	0.10	23.0	0.156	13.9	5.4	
													0.13	20.0	0.116	17.2	8.6	
									USGS	5061	28.3	BQD	-99.					
										00	999.9	C	0.23	20.0	0.180	15.5	3.3	
													0.23	18.0	0.247	14.6	3.1	
									CDMG	01335	13.9	AQD	0.10	47.0	0.128	8.4	4.9	
										00	999.9	C	0.10	40.0	0.358	46.4	17.5	
													0.10	38.0	0.258	40.9	20.2	
									USGS	temp	19.7	---	-99.					
										00	999.9	-	0.13	25.0	0.121	19.2	6.3	
													0.15	23.0	0.136	31.1	7.4	
									USGS	5051	0.7	AQD	-99.					
										00	999.9	B	0.06	20.0	0.455	112.0	52.8	
													0.12	23.0	0.377	43.9	15.2	
									USGS	5052	21.0	AQD	-99.					
										00	999.9	C	0.30	20.0	0.121	9.5	1.9	
													0.20	18.0	0.186	20.6	5.4	

No.	Earthquake Location, Mech, Dip (1)	Date & Time			Magnitude (2)				Station (3) Description No. H/F	Closest Dist (km)(4)	Site Codes (5)	Filter Corners						
		YR	MODY	HRMN	M	ML	MS	OTH				HP (hz)	LP (hz)	PGA (g)	PGV (cm/s)	PGD (cm)		
									USGS	temp 00	Poe Road (temp)	12.4 999.9	— -	-99. 0.20	23.0	0.446	35.7	8.8
									USGS	5062 00	Salton Sea Wildlife Refuge	27.1 999.9	AQD D	-99. 0.25	23.0	0.300	32.8	11.5
									USGS	286 00	Superstition Mtn.	4.3 999.9	AGA B	-99. 0.30	30.0	0.167	18.3	4.3
									CDMG	11369 00	Westmorland Fire Sta	13.3 999.9	ADD C	0.30 0.10	25.0	0.894	42.2	7.3
									USGS	5210 00	Wildlife Liquef. Array	24.4 999.9	IQD -	0.10 0.10	40.0	0.172	23.5	13.0
														0.10	40.0	0.211	31.0	20.3
														0.10	50.0	0.408	6.0	3.9
														0.10	40.0	0.181	29.9	19.9
														0.10	40.0	0.207	34.5	21.0
0093	Spitak, Armenia 03	1988	1207		6.8	0.0	7.0	0.0		12 99	Gukasian	30.0 999.9	A-A -	0.50 0.50	25.0	0.119	8.8	4.3
														0.50	25.0	0.199	28.6	9.8
														0.50	25.0	0.175	15.1	4.3
0094	Loma Prieta 03	1989	1018	0005	6.9	0.0	7.1	0.0	CDMG	57066 99	Agnews State Hospital	28.2 27.0	AQD C	0.20 0.20	42.0	0.093	8.3	4.43
														0.20	30.0	0.172	26.0	12.64
									BYU	0 99	Alameda Naval Air Stn Hanger 23	999.9 75.2	-E C	0.10 0.10	30.0	0.159	17.6	9.75
														0.10	00.0	0.061	4.7	2.20
														0.10	00.0	0.268	22.0	5.15
									USGS	1652 99	Anderson Dam (Downstream)	21.4 20.0	AFD B	0.20 0.20	48.0	0.209	42.5	14.07
														0.20	41.0	0.151	9.9	3.17
									USGS	1652 99	Anderson Dam (L. Abut)	21.4 20.0	AQA B	0.10 0.10	40.0	0.244	20.3	7.73
														0.20	40.0	0.240	18.4	6.73
									USGS	1002 99	APEEL 2 - Redwood City	47.9 999.9	IQD D	0.10 0.10	41.0	0.053	9.3	4.07
														0.10	41.0	0.064	12.2	11.87
									USGS	1002 99	APEEL 2 - Redwood City	47.9 999.9	IQD D	0.10 0.10	40.0	0.077	10.0	5.54
														0.10	40.0	0.083	9.5	3.15
									CDMG	58393 99	APEEL 2E Hayward Muir Sch	57.4 56.3	ABD C	0.20 0.20	22.0	0.274	53.6	12.68
														0.10	22.0	0.220	34.3	6.87
									CDMG	58219 99	APEEL 3E Hayward CSUH	57.1 56.0	ABA B	0.20 0.20	40.0	0.095	3.8	2.40
														0.20	25.0	0.139	11.5	5.65
									CDMG	58219 99	APEEL 3E Hayward CSUH	57.1 56.0	ABA B	0.20 0.20	38.0	0.047	4.2	3.33
														0.20	30.0	0.078	5.6	3.93
									CDMG	58378 99	APEEL 7 - Pulgas	47.7 46.5	IEA B	0.10 0.10	30.0	0.084	6.4	3.57
														0.10	30.0	0.061	6.2	3.08
									USGS	1161 99	APEEL 9 - Crystal Springs Res	46.9 46.4	IQA B	0.10 0.20	30.0	0.156	16.1	7.75
														0.10	22.0	0.088	15.7	8.41
														0.20	40.0	0.049	7.2	2.11
														0.20	40.0	0.113	15.6	5.78

No.	Earthquake Location, Mech, Dip (1)	Date & Time		Magnitude (2)				Station (3)		Closest Dist (km)(4)	Site Codes (5)	Filter Corners					
		YR	MODY	HRMN	M	ML	MS	OTH	No.			Description H/F	HP (hz)	LP (hz)	PGA (g)	PGV (cm/s)	PGD (cm)
												0.20	40.0	0.104	18.1	8.11	
								CDMG	58373	APEEL 10 - Skyline	47.8	I-A	0.10	30.0	0.037	8.0	3.71
								99			46.6	B	0.10	25.0	0.103	13.9	8.55
												0.10	20.0	0.088	24.0	7.35	
								CDMG	58262	Belmont - Envirotech	49.9	BFA	0.20	38.0	0.041	4.5	2.46
								99			48.7	B	0.20	22.0	0.108	11.8	3.30
												0.20	30.0	0.110	16.2	5.71	
								CDMG	58471	Berkeley LBL	83.6	-A	0.20	20.0	0.039	3.9	1.40
								99			999.9	B	0.20	20.0	0.057	9.2	1.78
												0.20	18.0	0.117	20.9	4.44	
								UCSC	13	BRAN	10.3	-A	0.10		0.507	17.9	4.17
								99			999.9	-	0.10		0.453	51.3	8.37
												0.10		0.501	44.6	4.86	
								CDMG	47125	Capitola	14.5	AQC	0.20	50.0	0.541	19.4	2.60
								99			8.6	C	0.20	48.0	0.529	36.5	9.11
												0.20	40.0	0.443	29.3	5.50	
								CDMG	57007	Corralitos	5.1	APB	0.20	32.0	0.455	17.7	7.11
								02			0.0	B	0.20	40.0	0.644	55.2	10.88
												0.20	40.0	0.479	45.2	11.37	
								CDMG	57504	Coyote Lake Dam (Downst)	22.3	IHD	0.10	30.0	0.095	9.9	4.51
								02			21.7	B	0.10	30.0	0.160	13.0	6.11
												0.10	29.0	0.179	22.6	13.20	
								CDMG	57217	Coyote Lake Dam (SW Abut)	21.8	IFA	0.10	50.0	0.076	8.6	3.21
								02			999.9	-	0.10	31.0	0.151	16.2	7.37
												0.10	33.0	0.484	39.7	15.17	
								USGS	1515	Foster City - 355 Menhaden	51.2	---	0.10	50.0	0.075	5.8	2.70
								99			999.9	-	0.10	28.0	0.107	20.6	8.05
												0.10	30.0	0.116	20.4	3.94	
								USGS	1686	Fremont - Emerson Court	43.4	AQB	0.10	38.0	0.067	8.6	6.37
								99			42.4	-	0.10	31.0	0.192	12.7	5.50
												0.10	32.0	0.141	12.9	8.37	
								CDMG	57064	Fremont - Mission San Jose	43.0	AMB	0.20	32.0	0.080	8.5	5.30
								99			42.0	B	0.20	24.0	0.124	11.5	5.43
												0.20	28.0	0.106	8.8	4.36	
								CDMG	47006	Gilroy - Gavilan Coll.	11.6	AFB	0.20	50.0	0.191	12.0	5.77
								99			10.9	B	0.20	45.0	0.357	28.6	6.35
												0.20	35.0	0.325	22.3	4.59	
								CDMG	57476	Gilroy - Historic Bldg.	12.7	BQD	0.20	52.0	0.149	11.1	6.03
								02			12.3	-	0.20	38.0	0.284	42.0	11.10
												0.20	40.0	0.241	24.0	3.66	
								CDMG	47379	Gilroy Array #1	11.2	IFA	0.20	52.0	0.209	14.0	5.59
								99			10.5	A	0.20	50.0	0.411	31.6	6.38
												0.20	50.0	0.473	33.9	8.03	
								CDMG	47380	Gilroy Array #2	12.7	IQD	0.20	40.0	0.294	14.6	4.66
								99			12.1	C	0.20	40.0	0.367	32.9	7.15

No.	Earthquake Location, Mech, Dip (1)	Date & Time			Magnitude (2)			Station (3)		Closest Dist (km)(4)	Site Codes (5)	Filter Corners			PGA (g)	PGV (cm/s)	PGD (cm)
		YR	MODY	HRMN	M	ML	MS	OTH	No.			Description H/F	HP (hz)	LP (hz)			
												0.20	31.0	0.322	39.1	12.07	
								CDMG	47381	Gilroy Array #3	14.4	IHD	0.10	50.0	0.338	15.5	7.03
									99		14.0	C	0.10	33.0	0.555	35.7	8.21
												0.10	40.0	0.367	44.7	19.25	
								CDMG	57382	Gilroy Array #4	16.1	AHD	0.20	42.0	0.159	14.6	5.10
									99		15.8	C	0.20	28.0	0.417	38.8	7.09
												0.20	30.0	0.212	37.9	10.08	
								CDMG	57383	Gilroy Array #6	19.9	IKB	0.20	32.0	0.101	9.5	4.10
									99		19.9	B	0.20	38.0	0.126	12.8	4.74
												0.20	31.0	0.170	14.2	3.79	
								CDMG	57425	Gilroy Array #7	24.2	AHB	0.20	48.0	0.115	5.6	2.87
									99		24.3	C	0.20	40.0	0.226	16.4	2.52
												0.20	35.0	0.323	16.6	3.26	
								USGS	1678	Golden Gate Bridge	85.1	-A	0.20	30.0	0.056	11.3	3.81
									99		999.9	B	0.20	22.0	0.233	38.1	11.45
												0.20	27.0	0.123	17.8	2.92	
								CDMG	57191	Halls Valley	31.6	IFC	0.20	28.0	0.056	8.4	4.07
									02		29.3	C	0.20	22.0	0.134	15.4	3.30
												0.20	22.0	0.103	13.5	5.46	
								CDMG	58498	Hayward - BART Sta	58.9	I-D	0.20	40.0	0.082	4.7	2.76
									99		57.7	B	0.20	31.0	0.159	15.1	3.72
												0.20	36.0	0.156	10.6	3.33	
								USGS	1028	Hollister City Hall	28.2	CHD	0.10	32.0	0.216	14.9	7.11
									99			C	0.10	29.0	0.247	38.5	17.83
												0.10	30.0	0.215	45.0	26.10	
								USGS	1656	Hollister Diff. Array	25.8	IQD	0.10	38.0	0.154	8.4	4.19
									99		999.9	-	0.10	40.0	0.269	43.9	18.48
												0.10	33.0	0.279	35.6	13.05	
								USGS	1032	Hollister - SAGO Vault	30.6	FGA	0.10	40.0	0.042	5.0	3.95
									99		29.9	A	0.10	32.0	0.036	7.1	4.55
												0.10	31.0	0.060	8.4	4.89	
								CDMG	47524	Hollister - South & Pine	28.8	IQD	0.10	31.0	0.197	15.1	7.06
									99		999.9	-	0.10	29.0	0.371	62.4	30.28
												0.10	23.0	0.177	29.1	18.13	
								UCSC	16	LGPC	6.1	-A	0.10		0.890	54.9	17.56
									99		999.9	-	0.10		0.563	94.8	41.18
												0.10		0.605	51.0	11.50	
								CDMG	47377	Monterey City Hall	44.8	CGA	0.20	32.0	0.032	2.7	0.92
									99		42.7	A	0.20	28.0	0.073	3.5	1.41
												0.20	22.0	0.063	5.8	2.89	
								CDMG	58224	Oakland - Title & Trust	77.4	BBD	0.20	49.0	0.148	6.8	1.81
									99		76.3	C	0.20	38.0	0.195	19.9	3.54
												0.20	44.0	0.244	36.1	7.20	
								CDMG	58264	Palo Alto - 1900 Embarc.	36.1	BQD	0.20	50.0	0.080	7.3	3.33
									99		34.8	-	0.20	32.0	0.204	22.0	11.67

No.	Earthquake Location, Mech, Dip (1)	Date & Time			Magnitude (2)			Station (3)		Closest Dist (km)(4)	Site Codes (5)	Filter Corners						
		YR	MODY	HRMN	M	ML	MS	OTH	No.			Description H/F	HP (hz)	LP (hz)	PGA (g)	PGV (cm/s)	PGD (cm)	
								USGS	1601	Palo Alto - SLAC Lab	36.3	AMA	0.20	30.0	0.213	39.6	17.13	
									99		35.0	C	0.20	40.0	0.090	10.2	2.82	
													0.20	28.0	0.194	37.5	9.96	
								CDMG	58338	Piedmont Jr High	78.3	I-A	0.20	32.0	0.278	29.3	9.72	
									99		77.2	A	0.20	27.0	0.084	8.2	2.94	
													0.20	28.0	0.071	9.1	3.35	
								CDMG	58043	Point Bonita	88.6	AFA	0.20	21.0	0.034	7.2	2.67	
									99		999.9	A	0.20	22.0	0.071	11.4	3.98	
													0.20	20.0	0.072	12.9	3.93	
								CDMG	58505	Richmond City Hall	93.1	I-D	0.20	30.0	0.032	4.4	1.27	
									99		999.9	C	0.20	25.0	0.124	17.3	2.59	
													0.20	29.0	0.106	14.2	3.91	
								CDMG	47189	SAGO South - Surface	34.7	IGB	0.10	29.0	0.060	7.8	5.86	
									99		34.1	B	0.10	25.0	0.073	10.5	6.40	
													0.10	30.0	0.067	9.6	6.42	
								CDMG	47179	Salinas - John & Work	32.6	AHD	0.10	42.0	0.101	6.7	2.38	
									99		31.4	C	0.10	30.0	0.091	10.7	8.56	
													0.10	28.0	0.112	15.7	7.87	
								CDMG	58065	Saratoga - Aloha Ave	13.0	AQD	0.10	58.0	0.389	26.9	15.15	
									99		11.7	B	0.10	38.0	0.512	41.2	16.21	
													0.10	50.0	0.324	42.6	27.53	
								CDMG	58235	Saratoga - W Valley Coll.	13.7	AQD	-99.					
									99		12.0	B	0.10	38.0	0.255	42.4	19.55	
													0.10	49.0	0.332	61.5	36.40	
								CDMG	58132	SF - Cliff House	84.4	CFA	0.20	29.0	0.062	7.7	2.38	
									99		999.9	-	0.20	22.0	0.075	10.8	4.35	
													0.20	28.0	0.108	19.8	5.06	
								CDMG	58130	SF - Diamond Heights	77.0	BBA	0.20	30.0	0.043	6.7	2.07	
									99		75.9	B	0.20	30.0	0.098	10.0	2.10	
													0.20	22.0	0.113	13.1	3.36	
								CDMG	58131	SF - Pacific Heights	81.6	BFA	0.20	24.0	0.031	6.0	2.87	
									99		80.5	A	0.20	22.0	0.061	12.8	3.45	
													0.20	20.0	0.047	9.2	2.92	
								CDMG	58222	SF - Presidio	83.1	IFA	0.10	31.0	0.058	11.7	4.07	
									99		999.9	-	0.10	32.0	0.099	12.9	4.32	
													0.10	32.0	0.200	32.4	5.86	
								CDMG	58151	SF - Rincon Hill	79.7	IFA	0.20	39.0	0.029	3.6	2.38	
									99		78.5	A	0.20	41.0	0.078	6.7	2.58	
													0.20	40.0	0.092	10.4	3.91	
								CDMG	58133	SF - Telegraph Hill	82.0	CFA	0.10	22.0	0.026	3.0	1.55	
									99		999.9	-	0.10	29.0	0.036	3.3	1.40	
													0.10	28.0	0.077	6.7	4.45	
								CDMG	58223	SF Intern. Airport	64.4	AHD	0.20	38.0	0.065	5.2	2.47	
									99		63.2	C	0.20	31.0	0.236	25.5	4.20	

No.	Earthquake Location, Mech, Dip (1)	Date & Time			Magnitude (2)				Station (3)		Closest Dist (km)(4)	Site Codes (5)	Filter Corners						
		YR	MODY	HRMN	M	ML	MS	OTH	No.	Description H/F			HP (hz)	LP (hz)	PGA (g)	PGV (cm/s)	PGD (cm)		
									CDMG	58539	So. San Francisco, Sierra Pt.	68.2	AFA	0.20	30.0	0.329	27.9	6.03	
										99		67.6	A	0.06	30.0	0.034	4.7	3.35	
														0.06	35.0	0.056	7.1	5.18	
									USGS	17	Stanford Park. Garage	36.3	—	-99.					
										99		999.9	-	0.10	70.0	0.254	38.5	15.89	
														-99.					
									USGS	1695	Sunnyvale - Colton Ave.	28.8	AHD	0.10	50.0	0.104	8.6	4.06	
										99		27.5	C	0.10	40.0	0.207	37.3	19.11	
														0.10	32.0	0.209	36.0	16.90	
									CDMG	58117	Treasure Island	82.9	B-D	0.10	21.0	0.016	1.2	1.44	
										99		999.9	D	0.10	28.0	0.100	15.6	4.41	
														0.10	30.0	0.159	32.8	11.52	
									UCSC	15	UCSC	18.1	-B	0.10		0.223	6.7	1.77	
										01		999.9	-	0.10		0.309	10.3	2.80	
														0.10		0.396	13.2	2.32	
									CDMG	58135	UCSC Lick Observatory	17.9	AKA	0.20	50.0	0.367	10.6	5.39	
										01		12.5	E	0.20	40.0	0.450	18.7	3.84	
														0.20	40.0	0.395	17.6	5.00	
									UCSC	14	WAHO	16.9	AQD	0.10		0.267	12.0	2.01	
										99		999.9	-	0.10		0.370	27.2	3.84	
														0.10		0.638	38.0	5.85	
									CDMG	58127	Woodside	39.9	APB	0.10	31.0	0.050	6.2	2.80	
										99		38.7	B	0.10	25.0	0.080	13.7	8.47	
														0.10	25.0	0.082	16.7	8.89	
									CDMG	58163	Yerba Buena Island	80.6	AFA	0.20	32.0	0.028	3.8	1.82	
										99		79.5	A	0.20	22.0	0.029	4.2	1.45	
														0.20	31.0	0.068	13.4	3.26	
0095	Georgia, USSR	1991	0615	0059	0.0	0.0	6.2	0.0		18	Ambralauri	73.7*	A-A	0.10		0.007	1.0	0.31	
	99									99		999.9	-	0.10		0.018	1.8	0.54	
														0.10		0.016	1.3	0.39	
										21	Baz	49.0*	A-D	0.10		0.016	1.4	0.39	
										99		999.9	-	0.10		0.033	2.2	0.40	
														0.10		0.038	2.0	0.35	
										19	Iri	36.4*	A-D	0.20		0.045	2.9	0.59	
										99		999.9	-	0.20		0.117	7.4	0.96	
														0.20		0.111	7.9	0.81	
										20	Oni	52.0*	A-D	0.20		0.018	1.2	0.32	
										99		999.9	-	0.20		0.075	3.1	0.40	
														0.20		0.046	2.6	0.44	
										22	Zem	56.9*	A-D	0.20		0.026	2.1	0.62	
										99		999.9	-	0.20		0.061	4.7	0.83	
														0.20		0.065	4.0	0.49	
0096	Erzincan, Turkey	1992	0313		6.9	0.0	0.0	0.0		95	Erzincan	2.0	-D	0.20		0.248	18.3	7.86	

A-52

No.	Earthquake Location, Mech, Dip (1)	Date & Time			Magnitude (2)				Station (3) Description No. H/F	Closest Dist (km)(4)	Site Codes (5)	Filter Corners						
		YR	MODY	HRMN	M	ML	MS	OTH				HP (hz)	LP (hz)	PGA (g)	PGV (cm/s)	PGD (cm)		
									99		C	0.10		0.515	83.9	27.35		
												0.10		0.496	64.3	22.78		
0097	Cape Mendocino 02	1992	0425	1806	7.1	0.0	7.1	0.0	CDMG	89005	Cape Mendocino # 01	8.5 999.9	IFA A	0.07 0.07	23.0 23.0	0.754 1.497	63.0 127.4	109.48 41.01
									CDMG	89509	Eureka - Myrtle & West # 99	44.6 35.8	IHD B	0.16 0.16	23.0 23.0	0.042 0.154	7.5 20.2	2.92 5.89
									CDMG	89486	Fortuna - Fortuna Blvd # 99	23.6 13.7	IQD B	0.07 0.07	23.0 23.0	0.049 0.116	5.8 30.0	3.72 27.59
									CDMG	89156	Petrolia # 01	9.5 0.0	IMD C	0.07 0.07	23.0 23.0	0.163 0.590	24.5 48.4	31.78 21.74
									CDMG	89324	Rio Dell Overpass - FF # 01	18.5 12.3	APC B	0.07 0.07	23.0 23.0	0.195 0.385	10.6 43.9	7.07 22.03
									CDMG	89530	Shelter Cove Airport # 99	33.8 32.6	IFB B	0.07 0.50	23.0 23.0	0.549 0.054	42.1 2.0	18.62 0.33
														0.229	7.1	0.39		
														0.50	23.0	0.189	6.6	0.57
0098	Landers 00	1992	0628	1158	7.3	0.0	7.4	0.0	CDMG	21081	Amboy # 99	69.2 68.3	AAB A	0.10 0.10	23.0 23.0	0.090 0.115	11.0 18.3	3.25 11.16
									USC	90088	Anaheim - W Ball # 99	134.0 999.9	-D C	0.20 0.13	25.0 25.0	0.146 0.047	20.0 10.8	7.38 5.91
									USC	90099	Arcadia - Arcadia Av # 99	137.1 999.9	-D C	0.12 0.20	25.0 25.0	0.035 0.031	10.5 6.1	4.01 2.91
									USC	90093	Arcadia - Campus Dr # 99	135.5 999.9	-D C	0.10 0.25	25.0 25.0	0.027 0.023	10.2 3.4	6.77 1.26
									CDMG	32075	Baker Fire Station # 99	88.5 88.3	A-D B	0.12 0.10	25.0 23.0	0.051 0.108	12.6 9.4	7.27 6.35
									USC	90069	Baldwin Park - N Holly # 99	131.6 999.9	-D B	0.10 0.15	23.0 25.0	0.106 0.028	11.0 8.7	7.96 5.03
									CDMG	23559	Barstow # 99	36.1 37.7	IQD B	0.12 0.07	25.0 23.0	0.026 0.066	7.4 7.7	5.04 4.38
									USC	90094	Bell Gardens - Jaboneria # 99	153.9 999.9	-D C	0.07 0.30	23.0 25.0	0.135 0.016	25.8 1.1	18.67 0.18
														0.036	4.7	1.48		
														0.18	25.0	0.044	10.5	4.74

No.	Earthquake Location, Mech, Dip (1)	Date & Time			Magnitude (2)				Station (3)		Closest Dist (km)(4)	Site Codes (5)	Filter Corners			PGA (g)	PGV (cm/s)	PGD (cm)
		YR	MODY	HRMN	M	ML	MS	OTH	No.	Description H/F			HP (hz)	LP (hz)				
									USC	90061	Big Tujunga, Angeles Nat F #	144.3	-C	0.30	25.0	0.015	2.8	0.98
										99		999.9	B	0.33	25.0	0.025	3.2	0.65
														0.30	25.0	0.025	3.4	0.69
									CDMG	33083	Boron Fire Station #	90.6	A-D	0.07	23.0	0.054	5.1	3.15
										99		92.4	B	0.07	23.0	0.119	12.9	9.14
														0.07	23.0	0.090	9.6	3.70
									USC	90087	Brea - S Flower Av #	136.5	-D	0.20	25.0	0.018	3.7	1.30
										99		999.9	C	0.13	25.0	0.036	11.0	6.15
														0.12	25.0	0.045	11.3	7.55
									USC	90086	Buena Park - La Palma #	148.6	-D	0.55	25.0	0.009	0.9	0.18
										99		999.9	C	0.18	25.0	0.045	11.5	4.81
														0.15	25.0	0.052	8.8	5.64
									USC	90012	Burbank - N Buena Vista #	162.1	-D	0.33	25.0	0.023	4.7	1.03
										99		999.9	C	0.25	25.0	0.049	7.2	2.18
														0.28	25.0	0.068	10.4	2.86
									USC	90052	Calabasas - N Las Virg #	194.1	-B	0.50	25.0	0.013	1.4	0.31
										99		999.9	B	0.28	25.0	0.018	2.8	0.81
														0.20	22.5	0.012	2.5	0.95
									USC	90004	Chatsworth - Devonshire #	176.8	-D	0.20	25.0	0.018	3.8	1.31
										99		999.9	C	0.23	25.0	0.031	4.2	1.50
														0.07	25.0	0.033	6.5	5.97
									USC	90078	Compton - Castlegate #	161.2	-D	1.25	25.0	0.020	0.8	0.07
										99		999.9	C	0.15	22.5	0.065	12.2	4.99
														0.15	25.0	0.063	13.1	4.05
									SCE	23	Coolwater	21.2	-D	0.10	30.0	0.174	9.9	4.01
										99		22.8	B	0.10	30.0	0.283	25.6	13.74
														0.10	30.0	0.417	42.3	13.76
									USC	90070	Covina - W Badillo #	128.3	-D	0.15	25.0	0.029	6.1	2.42
										99		999.9	C	0.13	25.0	0.057	15.8	9.60
														0.28	25.0	0.046	7.5	2.09
									CDMG	12149	Desert Hot Springs #	23.2	AQD	0.07	23.0	0.167	9.9	3.71
										99		22.5	B	0.07	23.0	0.171	20.2	13.87
														0.07	23.0	0.154	20.9	7.78
									CDMG	14368	Downey - Co Maint Bldg #	157.0	AQD	0.07	23.0	0.016	6.4	4.46
										99		999.9	-	0.07	23.0	0.051	18.3	24.03
														0.07	23.0	0.039	11.3	10.32
									USC	90067	Duarte - Mel Canyon Rd #	126.4	-B	0.28	25.0	0.019	4.0	1.14
										99		999.9	B	0.28	25.0	0.026	3.5	0.86
														0.30	25.0	0.017	2.8	1.05
									USC	90066	El Monte - Fairview Av #	136.1	-D	0.25	25.0	0.021	3.8	1.30
										99		999.9	C	0.09	25.0	0.037	11.8	9.40
														0.23	25.0	0.038	7.4	2.58
									CDMG	13122	Featherly Park #	121.9	AMC	0.16	23.0	0.026	2.2	1.25
										99		999.9	-	0.16	23.0	0.051	7.0	3.63
														0.16	23.0	0.052	4.6	2.66

No.	Earthquake Location, Mech, Dip (1)	Date & Time			Magnitude (2)				Station (3) Description No. H/F	Closest Dist (km)(4)	Site Codes (5)	Filter Corners						
		YR	MODY	HRMN	M	ML	MS	OTH				HP (hz)	LP (hz)	PGA (g)	PGV (cm/s)	PGD (cm)		
									CDMG	24577	Fort Irwin #	64.2	-D	0.07	23.0	0.056	5.6	3.90
										99		65.0	B	0.07	23.0	0.114	9.7	3.66
														0.07	23.0	0.122	16.4	21.81
									USC	90002	Fountain Valley - Euclid #	148.8	-D	0.90	25.0	0.014	1.0	0.11
										99		999.9	C	0.13	25.0	0.069	14.7	7.87
														0.13	25.0	0.058	10.3	4.70
									USC	90063	Glendale - Las Palmas #	147.9	-C	1.10	25.0	0.027	1.0	0.07
										99		999.9	C	0.30	25.0	0.044	6.4	1.07
														0.28	25.0	0.071	4.1	0.74
									USC	90065	Glendora - N Oakbank #	122.2	-D	0.38	25.0	0.030	2.8	0.60
										99		999.9	B	0.30	25.0	0.039	5.1	1.36
														0.28	25.0	0.063	9.9	2.79
									USC	90073	Hacienda Heights - Colima #	136.0	-C	0.20	25.0	0.027	2.9	1.11
										99		999.9	C	0.28	25.0	0.058	8.5	2.63
														0.25	25.0	0.046	5.7	1.31
									CDMG	12331	Hemet Fire Station #	69.5	AQD	0.16	23.0	0.063	3.0	1.60
										99		69.1	C	0.16	23.0	0.081	5.6	1.36
														0.16	23.0	0.097	5.7	2.27
									USC	90083	Huntington Bch - Waikiki #	153.3	-D	0.63	25.0	0.012	1.0	0.15
										99		999.9	C	0.14	25.0	0.056	9.5	5.09
														0.12	25.0	0.059	10.8	4.07
									CDMG	12026	Indio - Coachella Canal #	55.7	IQD	0.10	23.0	0.042	6.6	3.99
										99		54.9	C	0.10	23.0	0.104	9.6	5.05
														0.10	23.0	0.109	15.2	9.69
									CDMG	14196	Inglewood - Union Oil #	166.9	IQD	0.07	23.0	0.015	4.8	5.52
										99		999.9	-	0.07	23.0	0.043	15.7	19.03
														0.07	23.0	0.035	10.5	9.99
									CDMG	22170	Joshua Tree #	11.6	AGC	0.07	23.0	0.181	15.0	9.39
										99		11.3	B	0.07	23.0	0.274	27.5	9.82
														0.07	23.0	0.284	43.2	14.51
									CDMG	14403	LA - 116th St School #	164.0	AQD	0.07	23.0	0.013	5.2	4.36
										99		999.9	-	0.07	23.0	0.042	14.1	17.91
														0.07	23.0	0.042	12.1	13.75
									USC	90025	LA - E Vernon Av #	157.7	-D	0.38	25.0	0.019	2.2	0.61
										99		999.9	C	0.13	25.0	0.034	7.7	4.64
														0.18	25.0	0.039	8.9	4.24
									USC	90034	LA - Fletcher Dr #	152.3	-D	0.20	22.5	0.024	3.1	0.62
										99		999.9	C	0.28	25.0	0.045	6.2	1.48
														0.28	25.0	0.040	4.0	1.10
									USC	90032	LA - N Figueroa St #	148.7	-C	0.40	25.0	0.016	2.3	0.52
										99		999.9	B	0.35	25.0	0.030	3.6	1.09
														0.38	25.0	0.037	4.3	1.09
									USC	90021	LA - N Westmoreland	159.2	-D	0.53	25.0	0.016	1.9	0.38
										99		999.9	B	0.38	25.0	0.044	3.7	0.81
														0.25	25.0	0.036	3.9	1.31

No.	Earthquake Location, Mech, Dip (1)	Date & Time			Magnitude (2)			Station (3)		Closest Dist (km)(4)	Site Codes (5)	Filter Corners					
		YR	MODY	HRMN	M	ML	MS	OTH	No.			Description H/F	HP (hz)	LP (hz)	PGA (g)	PGV (cm/s)	PGD (cm)
								CDMG	24400	LA - Obregon Park #	151.4	AQD	0.07	23.0	0.020	4.1	3.72
									99		999.9	-	0.07	23.0	0.043	1	16.38
													0.07	23.0	0.065	7.6	5.83
								USC	90022	LA - S Grand Ave #	161.1	-D	0.40	25.0	0.014	1.9	0.51
									99		999.9	C	0.28	25.0	0.028	4.7	1.64
													0.18	25.0	0.035	6.6	2.88
								USC	90020	LA - W 15th St #	161.2	-C	0.30	25.0	0.015	3.3	1.02
									99		999.9	C	0.09	25.0	0.029	7.8	5.44
													0.30	25.0	0.036	6.3	1.89
								USC	90023	LA - W 70th St #	167.8	-D	0.35	25.0	0.014	1.8	0.56
									99		999.9	C	0.18	25.0	0.055	9.6	3.06
													0.20	25.0	0.049	11.3	3.93
								USC	90060	La Crescenta - New York #	147.9	-C	0.50	25.0	0.014	1.9	0.32
									99		999.9	C	0.40	25.0	0.024	2.7	0.56
													0.30	25.0	0.030	4.3	1.11
								USC	90074	La Habra - Briarcliff #	142.8	-C	0.53	25.0	0.026	2.2	0.44
									99		999.9	C	0.25	25.0	0.051	10.0	3.84
													0.23	25.0	0.053	9.5	3.04
								USC	90072	La Puente - Rimgrove Av #	132.0	-D	0.25	25.0	0.017	3.5	0.77
									99		999.9	C	0.13	25.0	0.035	8.3	4.39
													0.12	25.0	0.043	8.1	5.42
								USC	90084	Lakewood - Del Amo Blvd #	155.8	-D	0.50	25.0	0.016	1.7	0.35
									99		999.9	C	0.16	25.0	0.054	14.1	4.88
													0.15	25.0	0.050	12.8	5.14
								USC	90080	LB - Orange Av #	164.5	-D	0.50	25.0	0.019	1.6	0.30
									99		999.9	-	0.15	25.0	0.055	9.5	4.23
													0.15	25.0	0.061	11.1	4.40
								SCE	24	Lucerne #	1.1	A-A	0.00	60.0	0.805	41.2	43.88
									99		999.9	A	0.00	60.0	0.730	145.3	162.70
													0.00	60.0	0.797	32.3	39.40
								USGS	100	Mission Creek Fault	999.9	-	0.05		0.085	4.3	1.69
									99		27.8	B		0.126	6.8	2.31	
													0.05	0.125	23.0	24.44	
								USGS	5071	Morongo Valley	19.3	AHC			0.160	9.3	3.33
									99		17.7	B		0.188	16.6	9.45	
														0.140	20.2	6.33	
								USGS	5070	North Palm Springs	24.2	AHD			0.112	7.2	2.40
									99		27.7	B		0.136	11.0	4.97	
														0.134	14.5	5.57	
								USC	90003	Northridge - Saticoy St #	176.5	-D	0.20	25.0	0.017	4.5	1.69
									99		999.9	C	0.08	25.0	0.036	12.2	8.82
													0.07	25.0	0.036	15.9	17.06
								CDMG	12025	Palm Springs Airport #	37.5	IQD	0.07	23.0	0.108	6.8	3.08
									99		36.7	C	0.07	23.0	0.076	10.9	6.95
													0.07	23.0	0.089	13.8	5.29

No.	Earthquake Location, Mech, Dip (1)	Date & Time			Magnitude (2)			Station (3)		Closest Dist (km)(4)	Site Codes (5)	Filter Corners					
		YR	MODY	HRMN	M	ML	MS	OTH	No.			Description H/F	HP (hz)	LP (hz)	PGA (g)	PGV (cm/s)	PGD (cm)
								CDMG	23525	Pomona - 4th & Locust #	117.0	IQD	0.12	23.0	0.035	2.8	1.54
									99		117.6	C	0.12	23.0	0.067	12.8	6.95
													0.12	23.0	0.044	8.6	3.52
								CDMG	12168	Puerta La Cruz #	95.9	AQB	0.30	23.0	0.038	1.7	0.48
									99		93.1	B	0.30	23.0	0.047	2.0	0.41
													0.30	23.0	0.044	2.0	0.63
								CDMG	13123	Riverside Airport #	96.1	AQB	0.16	23.0	0.040	1.7	1.01
									99		96.2	B	0.16	23.0	0.043	3.0	1.62
													0.16	23.0	0.041	3.2	1.38
								CDMG	23542	San Bernardino-E & Hospitalit	80.5	-D	0.10	50.0	0.065	7.5	2.64
									99		79.9	C	0.10	50.0	0.078	19.8	10.49
													0.10	50.0	0.087	14.6	7.63
								USC	90019	San Gabriel - E Grand Av #	141.6	-A	0.16	22.5	0.022	6.3	2.97
									99		999.9	A	0.07	25.0	0.041	14.1	15.03
													0.13	25.0	0.036	9.6	6.03
								USC	90077	Santa Fe Springs - E Joslin #	150.4	-D	0.35	25.0	0.024	1.5	0.47
									99		999.9	C	0.18	25.0	0.060	5.9	2.67
													0.15	25.0	0.047	9.2	4.23
								CDMG	12206	Silent Valley - Poppet Flat #	51.7	IGA	0.12	23.0	0.038	3.2	2.08
									99		51.3	A	0.12	23.0	0.050	3.8	2.03
													0.12	23.0	0.040	5.1	3.88
								USC	90008	Sun Valley - Sunland #	162.6	-B	1.00	25.0	0.012	0.9	0.08
									99		999.9	B	0.33	25.0	0.027	2.6	0.71
													0.45	25.0	0.021	2.9	0.60
								USC	90006	Sun Valley - Roscoe Blvd #	167.8	-D	0.12	25.0	0.021	4.4	2.48
									99		999.9	B	0.07	25.0	0.039	18.1	18.27
													0.18	25.0	0.028	7.0	2.62
								USC	90058	Sunland - Mt Gleason Av #	151.1	-C	0.20	25.0	0.021	2.8	0.91
									99		999.9	B	0.33	25.0	0.029	5.3	1.40
													0.25	25.0	0.031	6.0	1.70
								CDMG	24436	Tarzana - Cedar Hill #	175.6	A-B	0.12	23.0	0.026	2.5	1.16
									99		999.9	-	0.12	23.0	0.066	9.5	5.83
													0.12	23.0	0.043	5.4	3.18
								USC	90089	Tustin - E Sycamore #	134.0	-D	0.28	25.0	0.017	3.3	0.97
									99		999.9	C	0.13	25.0	0.044	14.2	5.90
													0.23	25.0	0.046	6.6	2.11
								CDMG	22161	Twentynine Palms #	42.2	AGA	0.12	23.0	0.040	3.3	1.93
									99		41.9	A	0.12	23.0	0.080	3.7	2.34
													0.12	23.0	0.060	4.9	4.30
								USC	90090	Villa Park - Serrano Av #	131.4	-B	0.20	25.0	0.021	2.8	0.93
									99		999.9	B	0.11	25.0	0.028	8.0	5.32
													0.18	25.0	0.035	7.0	3.51
								USC	90071	West Covina - S Orange #	132.4	-B	0.25	25.0	0.023	5.7	2.38
									99		999.9	C	0.28	25.0	0.048	8.7	2.30
													0.13	25.0	0.048	15.1	12.06

No.	Earthquake Location, Mech, Dip (1)	Date & Time			Magnitude (2)				Station (3) No.	Description H/F	Closest Dist (km)(4)	Site Codes (5)	Filter Corners			PGD (cm)		
		YR	MODY	HRMN	M	ML	MS	OTH					HP (hz)	LP (hz)	PGA (g)		PGV (cm/s)	
								CDMG	22074	Yermo Fire Station #	24.9	AQD	0.07	23.0	0.136	12.9	4.82	
									99	1	26.3	C	0.07	23.0	0.245	51.5	43.81	
													0.07	23.0	0.152	29.7	24.69	
0099	Big Bear 99	1992	0628	1506	6.4	6.5	6.6	0.0	CDMG	23542	San Bernardino-E & Hospitality	999.9	-D	0.10	50.0	0.073	4.5	1.12
									99		999.9	C	0.10	50.0	0.092	13.8	3.53	
													0.10	50.0	0.101	11.9	3.35	
0100	Northridge 02	1994	0117	1231	6.7	6.6	6.7	0.0	CDMG	24461	Alhambra - Fremont School	35.7	AMD	0.12	25.0	0.046	4.6	1.12
									99		36.1	B	0.12	25.0	0.101	10.9	2.53	
													0.12	25.0	0.079	5.0	1.43	
								CDMG	25169	Anacapa Island #	71.2	--	0.30	23.0	0.013	0.8	0.25	
									99		68.2	-	0.30	23.0	0.067	3.2	0.47	
													0.30	23.0	0.037	1.8	0.25	
								USC	90088	Anaheim - W Ball Rd	71.1	-D	1.00	30.0	0.048	1.5	0.11	
									99		999.9	C	0.23	30.0	0.072	5.2	1.00	
													0.23	30.0	0.066	5.1	1.53	
								CDMG	24576	Anaverde Valley - City R #	38.4	-D	0.20	46.0	0.044	4.7	1.70	
									99		39.1	-	0.20	46.0	0.044	3.9	1.09	
													0.20	46.0	0.060	5.5	1.54	
								CDMG	24310	Antelope Buttes #	47.3	--	0.12	23.0	0.029	3.6	2.63	
									99		48.4	-	0.12	23.0	0.046	3.6	2.26	
													0.12	23.0	0.068	4.3	2.23	
								USC	90099	Arcadia - Arcadia Av	42.5	-D	0.50	30.0	0.092	4.0	0.56	
									99		40.6	C	0.25	30.0	0.104	7.3	1.59	
													0.30	30.0	0.083	10.2	1.61	
								USC	90093	Arcadia - Campus Dr.	44.2	-D	0.50	30.0	0.057	4.2	0.59	
									99		42.4	C	0.30	30.0	0.089	4.7	1.29	
													0.23	30.0	0.110	8.1	1.73	
								CDMG	24087	Arieta - Nordhoff Fire Sta #	9.2	AQD	0.12	23.0	0.552	18.4	8.83	
									99		3.9	-	0.12	23.0	0.344	40.6	15.04	
													0.12	23.0	0.308	23.2	10.75	
								USC	90069	Baldwin Park - N. Holly Ave	50.6	-D	0.70	30.0	0.045	1.7	0.23	
									99		49.0	B	0.20	30.0	0.090	3.9	1.19	
													0.23	30.0	0.123	8.2	1.33	
								USC	90094	Bell Gardens - Jaboneria	46.6	-D	0.13	30.0	0.049	3.5	1.88	
									99		42.5	C	0.13	30.0	0.098	7.4	3.50	
													0.13	30.0	0.068	7.6	2.46	
								USC	90014	Beverly Hills - 12520 Mulhol	20.8	-C	0.30	30.0	0.314	14.1	1.31	
									99		999.9	B	0.13	30.0	0.617	40.8	8.57	
													0.03	30.0	0.444	30.2	4.84	
								USC	90013	Beverly Hills - 14145 Mulhol	19.6	-C	0.40	30.0	0.326	16.9	2.56	
									99		999.9	C	0.13	30.0	0.416	59.0	13.14	
													0.20	30.0	0.516	62.8	11.08	
								USC	90061	Big Tujunga, Angeles Nat F	24.0	-C	0.30	30.0	0.172	3.8	0.56	
									99		21.9	B	0.30	30.0	0.163	8.1	0.83	

No.	Earthquake Location, Mech, Dip (1)	Date & Time		Magnitude (2)				Station (3)		Closest Dist (km)(4)	Site Codes (5)	Filter Corners					
		YR	MODY	HRMN	M	ML	MS	OTH	No.			H/F	HP (hz)	LP (hz)	PGA (g)	PGV (cm/s)	PGD (cm)
								USC	90087	Brea - S. Flower Ave.	67.3	-D	0.30	30.0	0.245	12.7	1.12
									99		65.0	C	0.40	30.0	0.037	2.0	0.30
													0.30	30.0	0.106	6.5	0.68
								VA	638	Brentwood V.A. Hospital	999.9	-D	0.30	30.0	0.108	9.1	1.39
									99		16.3	-	0.00	00.0	0.139	9.3	2.41
													0.00	00.0	0.187	23.7	5.42
								USC	90086	Buena Park - La Palma	64.6	-D	0.00	00.0	0.165	17.6	8.39
									99		999.9	C	0.80	30.0	0.034	1.5	0.11
													0.30	30.0	0.139	10.7	1.62
								USC	90059	Burbank - Howard Rd.	20.0	-B	0.30	30.0	0.095	8.1	1.60
									99		16.6	A	0.10	30.0	0.085	3.6	1.48
													0.10	30.0	0.120	9.5	2.25
								CDMG	25282	Camarillo	36.5	-	0.10	30.0	0.163	8.5	1.81
									99		0.0	-	0.10	25.0	0.050	4.5	1.28
													0.10	25.0	0.125	10.9	3.49
								USC	90053	Canoga Park - Topanga Can	15.8	-D	0.10	25.0	0.121	11.7	3.20
									99		999.9	C	0.10	30.0	0.489	14.2	5.50
													0.05	30.0	0.356	32.1	9.13
								USC	90057	Canyon Country - W Lost Cany	13.0	-D	0.05	30.0	0.420	60.8	20.17
									99		12.2	C	0.10	30.0	0.318	20.3	5.17
													0.05	30.0	0.410	43.0	11.75
													0.10	30.0	0.482	45.1	12.58
								USC	90040	Carson - Catskill Ave	53.0	-D	0.40	30.0	0.050	2.9	0.33
									99		49.2	C	0.20	30.0	0.087	8.0	1.50
													0.30	30.0	0.083	4.8	1.05
								USC	90081	Carson - Water St.	52.2	-D	0.70	30.0	0.041	2.3	0.25
									99		999.9	C	0.30	30.0	0.089	6.4	1.58
													0.30	30.0	0.086	8.0	1.92
								CDMG	24278	Castaic - Old Ridge Route #	22.6	A-B	0.12	23.0	0.217	12.4	1.94
									99		25.4	B	0.12	23.0	0.568	52.1	4.21
													0.12	23.0	0.514	52.2	2.41
								USC	90078	Compton - Castlegate St	49.6	-D	0.40	30.0	0.046	2.6	0.42
									99		45.2	C	0.10	30.0	0.088	6.8	3.41
													0.20	30.0	0.136	7.1	2.15
								USC	90068	Covina - S. Grand Ave.	60.2	-C	0.33	30.0	0.053	3.5	0.79
									99		999.9	C	0.13	30.0	0.066	7.1	1.94
													0.20	30.0	0.062	6.9	1.43
								USC	90070	Covina - W. Badillo	56.1	-D	0.30	30.0	0.043	2.9	0.70
									99		999.9	C	0.20	30.0	0.100	5.8	1.21
													0.20	30.0	0.079	7.0	1.62
								USC	90079	Downey - Birchdale	40.7	-D	0.30	30.0	0.058	3.4	0.64
									99		999.9	C	0.30	30.0	0.165	12.1	1.52
													0.30	30.0	0.171	8.1	1.52
								CDMG	14368	Downey - Co Maint Bldg #	47.6	AQD	0.20	23.0	0.146	3.9	0.27
									99		45.1	-	0.20	23.0	0.158	13.8	2.28

No.	Earthquake Location, Mech, Dip (1)	Date & Time			Magnitude (2)				Station (3)		Closest Dist (km)(4)	Site Codes (5)	Filter Corners					
		YR	MODY	HRMN	M	ML	MS	OTH	No.	Description H/F			HP (hz)	LP (hz)	PGA (g)	PGV (cm/s)	PGD (cm)	
									USC	90067	Duarte - Mel Canyon Rd.	51.6	-B	0.20	23.0	0.230	11.3	2.14
										99		50.2	B	0.90	30.0	0.046	2.2	0.17
														0.10	30.0	0.079	3.4	1.84
														0.30	30.0	0.028	2.4	0.46
									USC	90066	El Monte - Fairview Av	47.4	-D	0.20	30.0	0.059	2.8	1.36
										99		45.5	C	0.15	30.0	0.122	9.7	4.24
														0.30	30.0	0.163	8.8	1.88
									CDMG	24575	Elizabeth Lake #	37.2	-D	0.16	46.0	0.050	5.7	1.46
										99		37.6	-	0.16	46.0	0.155	7.3	2.70
														0.16	46.0	0.109	9.0	1.53
									CDMG	13122	Featherly Park - Pk Maint Bldg #	84.2	AMC	0.30	23.0	0.024	1.6	0.24
										99		82.5	-	0.30	23.0	0.104	7.7	0.81
														0.30	23.0	0.100	5.8	0.51
									USC	90085	Garden Grove - Santa Rita	68.9	-D	-99				
										99		999.9	C	0.30	30.0	0.104	8.7	2.10
														0.30	30.0	0.103	10.0	2.13
									USC	90063	Glendale - Las Palmas	25.4	-C	0.30	30.0	0.127	4.3	0.44
										99		22.9	C	0.13	30.0	0.357	12.3	1.94
														0.10	30.0	0.206	7.4	1.75
									USC	90065	Glendora - N. Oakbank	30.9	-D	0.50	30.0	0.051	3.6	0.58
										99		999.9	B	0.50	30.0	0.040	3.1	0.43
														0.10	30.0	0.092	4.9	1.75
									USC	90073	Hacienda Hts - Colima Rd	59.1	-C	0.40	30.0	0.041	2.2	0.35
										99		57.1	C	0.40	30.0	0.067	4.8	0.72
														0.40	30.0	0.056	3.2	0.87
									CDMG	13660	Hemet - Ryan Airfield #	144.1	-D	0.30	46.0	0.027	2.0	0.18
										99		145.9	-	0.30	46.0	0.064	4.5	0.66
														0.30	46.0	0.046	4.7	0.51
									USC	90018	Hollywood - Willoughby Ave	25.7	-D	0.20	30.0	0.142	9.0	3.40
										99		999.9	B	0.10	30.0	0.136	12.8	4.82
														0.13	30.0	0.245	33.5	6.28
									CDMG	13197	Huntington Beach - Lake St #	79.6	AQD	0.20	23.0	0.018	4.0	0.89
										99		68.9	-	0.20	23.0	0.091	10.1	1.13
														0.20	23.0	0.070	13.9	1.49
									USC	90083	Huntington Bch - Waikiki	57.4	-D	0.30	30.0	0.022	1.2	0.28
										99		999.9	C	0.20	30.0	0.086	5.0	1.63
														0.20	30.0	0.068	7.4	1.87
									CDMG	14196	Inglewood - Union Oil #	44.7	IQD	0.16	23.0	0.055	2.6	1.01
										99		40.0	-	0.16	23.0	0.091	7.1	2.25
														0.16	23.0	0.101	10.3	3.15
									USGS	0655	Jensen Filter Plant #	6.2	-D	0.30		0.400	34.1	8.89
										99		0.0	-	0.08		0.424	106.2	43.06
														0.20		0.593	99.3	24.00
									USGS	00000	LA Dam	2.6	-	0.13		0.424	19.5	8.71
										99		999.9	-	0.10		0.511	63.7	21.18

No.	Earthquake Location, Mech, Dip (1)	Date & Time		Magnitude (2)				Station (3)		Closest Dist (km)(4)	Site Codes (5)	Filter Corners			PGA (g)	PGV (cm/s)	PGD (cm)
		YR	MODY	HRMN	M	ML	MS	OTH	No.			Description H/F	HP (hz)	LP (hz)			
								CDMG	14403	LA - 116th St School #	41.9	AQD	0.12		0.349	50.8	15.11
									99		38.9	-	0.16	23.0	0.061	2.8	0.30
													0.16	23.0	0.208	10.3	2.67
								CDMG	24157	LA - Baldwin Hills #	31.3	IPB	0.16	23.0	0.133	13.5	2.83
									99		26.2	-	0.16	23.0	0.091	8.4	3.29
													0.16	23.0	0.239	14.9	6.17
								USC	90054	LA - Centinela St	30.9	-D	0.13	30.0	0.168	17.6	4.79
									99		999.9	C	0.13	30.0	0.109	10.6	3.76
													0.13	30.0	0.465	19.3	3.48
													0.20	30.0	0.322	22.9	5.47
								CDMG	24389	LA - Century City CC North #	25.7	IQD	0.14	23.0	0.116	8.7	3.47
									99		18.3	-	0.14	23.0	0.256	21.1	6.68
													0.14	23.0	0.222	25.2	5.70
								USC	90015	LA - Chalon Rd	23.7	-B	0.50	30.0	0.174	8.0	1.09
									99		999.9	B	0.30	30.0	0.225	16.6	3.39
													0.20	30.0	0.185	27.1	5.77
								CDMG	24592	LA - City Terrace #	37.0	-B	0.20	46.0	0.135	7.6	1.84
									99		35.4	-	0.20	46.0	0.263	12.8	2.89
													0.20	46.0	0.316	14.1	2.42
								USC	90033	LA - Cypress Ave	32.8	-C	0.30	30.0	0.085	3.1	0.44
									99		999.9	B	0.20	30.0	0.210	17.3	2.01
													0.13	30.0	0.149	10.0	2.23
								USC	90025	LA - E Vernon Ave	39.3	-D	0.20	30.0	0.063	3.4	1.21
									99		999.9	C	0.20	30.0	0.120	9.2	1.67
													0.10	30.0	0.153	10.1	1.79
								USC	90034	LA - Fletcher Dr	29.5	-D	0.30	30.0	0.109	6.9	1.20
									99		999.9	C	0.13	30.0	0.162	10.7	2.86
													0.15	30.0	0.240	26.2	3.60
								CDMG	24303	LA - Hollywood Stor FF #	25.5	IPD	0.20	23.0	0.139	9.2	2.30
									99		20.8	C	0.20	23.0	0.231	18.3	4.81
													0.20	23.0	0.358	27.5	3.04
								USC	90016	LA - N Faring Rd	23.9	-B	0.20	30.0	0.191	8.9	1.65
									99		999.9	C	0.13	30.0	0.273	15.8	3.29
													0.13	30.0	0.242	29.8	4.74
								USC	90032	LA - N. Figueroa St.	33.4	-C	0.40	30.0	0.097	4.3	0.78
									99		999.9	B	0.30	30.0	0.128	9.6	1.43
													0.30	30.0	0.174	9.1	1.28
								USC	90021	LA - N Westmoreland	29.0	-D	0.20	30.0	0.093	6.3	1.08
									99		999.9	B	0.20	30.0	0.401	20.9	2.29
													0.20	30.0	0.361	20.9	4.27
								CDMG	24400	LA - Obregon Park #	37.9	AQD	0.20	23.0	0.115	3.7	1.27
									99		35.9	-	0.60	23.0	0.355	16.7	1.43
													0.90	23.0	0.563	24.5	2.79
								CDMG	24612	LA - Pico & Sentous #	32.7	-D	0.20	46.0	0.065	5.3	1.69
									99		29.0	-	0.20	46.0	0.103	12.2	3.71

No.	Earthquake Location, Mech, Dip (1)	Date & Time			Magnitude (2)				Station (3)		Closest Dist (km)(4)	Site Codes (5)	Filter Corners					
		YR	MODY	HRMN	M	ML	MS	OTH	No.	Description H/F			HP (hz)	LP (hz)	PGA (g)	PGV (cm/s)	PGD (cm)	
									USC	90022	LA - S Grand Ave	36.9	-D	0.20	46.0	0.186	14.3	2.38
										99		999.9	C	0.30	30.0	0.094	3.8	0.68
														0.30	30.0	0.290	17.9	2.42
									USC	90096	LA - S. Vermont Ave	34.7	-D	0.30	30.0	0.264	20.4	1.88
										99		999.9	C	0.30	30.0	0.165	23.4	3.57
														0.30	30.0	0.164	10.7	1.83
									USC	90091	LA - Saturn St	30.0	-D	0.13	30.0	0.071	6.2	1.70
										99		23.2	C	0.10	30.0	0.097	7.7	2.12
														0.10	30.0	0.474	34.6	6.55
									CDMG	24611	LA - Temple & Hope #	32.3	-B	0.20	46.0	0.097	4.6	1.34
										99		29.5	-	0.20	46.0	0.126	13.9	3.15
														0.20	46.0	0.184	20.0	2.74
									CDMG	24605	LA - Univ. Hospital #	34.6	-B	0.20	46.0	0.119	6.4	1.37
										99		32.8	-	0.20	46.0	0.493	31.1	2.39
														0.20	46.0	0.214	10.8	2.37
									USC	90020	LA - W 15th St	32.4	-C	0.30	30.0	0.051	5.8	1.38
										99		999.9	C	0.13	30.0	0.104	11.6	5.73
														0.13	30.0	0.159	13.4	3.30
									USC	90017	LA - Wonderland Ave	22.7	-A	0.13	30.0	0.106	3.6	1.11
										99		999.9	A	0.13	30.0	0.112	8.7	1.79
														0.10	30.0	0.172	11.8	2.77
									CDMG	24688	LA - UCLA Grounds	14.9	-	0.08	25.0	0.265	10.2	3.08
										99		16.8	-	0.08	25.0	0.278	22.0	4.32
														0.08	25.0	0.474	22.2	7.38
									USC	90060	La Crescenta - New York	22.3	-C	0.13	30.0	0.106	3.9	0.87
										99		19.7	C	0.30	30.0	0.178	12.5	1.14
														0.10	30.0	0.159	11.3	3.00
									USC	90074	La Habra - Briarcliff	61.6	-C	0.40	30.0	0.056	2.6	0.37
										99		58.8	C	0.20	30.0	0.109	8.2	1.13
														0.20	30.0	0.206	12.3	1.23
									USC	90072	La Puente - 504 Ringrove Ave	58.9	-D	1.00	30.0	0.048	2.6	0.16
										99		57.1	C	0.80	30.0	0.109	7.9	0.70
														0.80	30.0	0.129	9.7	0.83
									CDMG	24271	Lake Hughes #1 #	36.3	APC	0.12	23.0	0.099	7.0	3.43
										99		37.7	-	0.12	23.0	0.087	9.4	3.70
														0.12	23.0	0.077	9.5	2.40
									CDMG	24469	Lake Hughes #4 - Camp Mend #	32.3	-B	0.12	23.0	0.053	4.1	3.05
										99		33.2	-	0.12	23.0	0.057	6.6	3.98
														0.12	23.0	0.084	6.2	2.27
									CDMG	24523	Lake Hughes #4B - Camp Mend #	32.3	-B	0.12	23.0	0.042	3.7	3.48
										99		34.1	-	0.12	23.0	0.036	3.2	2.21
														0.12	23.0	0.063	5.4	1.97
									USGS	127	Lake Hughes #9 #	26.8	AGA	0.08		0.079	3.6	3.56
										99		28.9	-	0.08		0.165	8.4	4.54

No.	Earthquake Location, Mech, Dip (1)	Date & Time			Magnitude (2)				Station (3) No. Description H/F	Closest Dist (km)(4)	Site Codes (5)	Filter Corners					
		YR	MODY	HRMN	M	ML	MS	OTH				HP (hz)	LP (hz)	PGA (g)	PGV (cm/s)	PGD (cm)	
												0.05	30.0	0.128	14.6	4.64	
								USC	90011	Montebello - Bluff Rd.	12.3	-D	0.20	30.0	0.076	2.8	0.48
									99		86.8	D	0.20	30.0	0.179	9.4	1.48
												0.10	30.0	0.128	5.9	2.25	
								CDMG	34093	Mojave - Hwys 14 & 58 #	85.7	--	0.30	23.0	0.027	1.8	0.30
									99		999.9	-	0.30	23.0	0.037	4.5	0.79
												0.30	23.0	0.053	4.1	0.47	
								CDMG	34237	Mojave - Oak Creek Canyon #	76.4	--	0.30	23.0	0.023	2.0	0.46
									99		78.5	-	0.30	23.0	0.050	3.1	0.52
												0.30	23.0	0.059	3.4	0.46	
								CDMG	24283	Moorpark - Fire Sta #	28.0	AQD	0.45	23.0	0.159	7.9	0.90
									99		18.8	-	0.16	23.0	0.193	20.2	4.79
												0.16	23.0	0.292	20.7	4.24	
								CDMG	23572	Mt Baldy - Elementary Sch #	71.5	-B	0.30	46.0	0.037	2.2	0.39
									99		74.0	-	0.30	46.0	0.080	3.8	0.56
												0.30	46.0	0.070	4.3	0.39	
								CDMG	24399	Mt Wilson - CIT Seis Sta #	36.1	IGA	0.08		0.087	3.6	0.58
									99		37.8	-	0.08		0.234	7.4	0.70
												0.08		0.134	5.8	0.45	
								USC	90009	N. Hollywood - Coldwater Can	14.6	-C	0.13	30.0	0.289	9.6	4.20
									99		8.3	B	0.10	30.0	0.298	25.0	6.46
												0.10	30.0	0.271	22.2	11.69	
								CDMG	24586	Neenach - Sacatara Ck #	53.2	-D	0.12	46.0	0.047	7.2	3.10
									99		55.5	-	0.12	46.0	0.056	10.0	6.48
												0.12	46.0	0.069	13.1	8.22	
								CDMG	24279	Newhall - Fire Sta #	7.1	AQD	0.12	23.0	0.548	31.5	16.27
									99		4.5	-	0.12	23.0	0.583	75.5	17.57
												0.12	23.0	0.590	97.2	38.05	
								USC	90056	Newhall - W. Pico Canyon Rd.	7.1	-C	0.05	30.0	0.290	37.2	13.29
									99		7.1	-	0.05	30.0	0.455	92.8	56.64
												0.10	30.0	0.325	67.4	16.11	
								CDMG	13160	Newport Bch - Irvine Ave. F.S. #	87.6	--	0.20	23.0	0.017	2.3	0.75
									99		85.3	-	0.20	23.0	0.041	4.1	1.29
												0.20	23.0	0.061	5.2	1.36	
								CDMG	13610	Newport Bch - Newp & Coast #	84.6	-B	0.17	46.0	0.021	2.2	0.66
									99		84.4	-	0.12	46.0	0.103	5.8	1.21
												0.12	46.0	0.085	6.3	1.34	
								USC	90003	Northridge - 17645 Satcoy St	13.3	-D	-99				
									99		0.1	C	0.10	30.0	0.368	28.9	8.44
												0.10	30.0	0.477	61.5	22.06	
								USC	90049	Pacific Palisades - Sunset Blvd	26.2	-B	0.10	30.0	0.179	14.7	3.98
									99		17.1	C	0.05	30.0	0.469	31.0	5.26
												0.05	30.0	0.197	14.9	5.62	
								CDMG	24207	Pacoima Dam (downstr) #	8.0	AMB	0.75	23.0	0.190	14.2	1.35
									99		999.9	-	0.16	23.0	0.415	45.6	5.06

No.	Earthquake Location, Mech, Dip (1)	Date & Time			Magnitude (2)				Station (3)		Closest Dist (km)(4)	Site Codes (5)	Filter Corners					
		YR	MODY	HRMN	M	ML	MS	OTH	No.	Description H/F			HP (hz)	LP (hz)	PGA (g)	PGV (cm/s)	PGD (cm)	
									CDMG	24207	Pacoima Dam (upper left) #	8.0	-A	0.16	23.0	0.434	31.3	4.80
										99		8.1	-	0.16	23.0	1.229	49.6	11.75
														0.16	23.0	1.585	55.7	6.06
									CDMG	24088	Pacoima Kagel Canyon #	8.2	AMB	0.20	23.0	0.169	15.1	4.14
										99		8.1	-	0.14	23.0	0.301	31.4	10.87
														0.14	23.0	0.433	51.5	7.21
									CDMG	24521	Palmdale - Hwy 14 & Palmdale #	43.6	-C	0.20	46.0	0.040	8.0	5.50
										99		43.3	-	0.20	46.0	0.061	14.8	7.18
														0.20	46.0	0.067	16.9	7.96
										0	Pardee - SCE	999.9	-	1.50	23.0	0.384	10.9	0.50
										99		999.9	-	0.50	20.0	0.657	75.2	13.16
														0.40	20.0	0.406	43.6	12.09
									USC	90095	Pasadena - N Sierra Madre	39.2	-C	0.40	30.0	0.141	8.4	0.57
										99		37.4	C	0.30	30.0	0.245	12.3	1.09
														0.20	30.0	0.174	9.6	1.53
									CDMG	23597	Phelan - Wilson Ranch #	86.1	-D	0.20	46.0	0.034	2.3	0.54
										99		89.2	-	0.20	46.0	0.047	5.0	1.00
														0.20	46.0	0.057	4.0	1.23
									USC	90047	Playa Del Rey - Saran	34.2	-D	0.10	30.0	0.055	8.4	4.33
										99		27.9	E	0.10	30.0	0.136	18.6	4.51
														0.10	30.0	0.076	13.8	6.88
									CDMG	25148	Point Mugu - Laguna Peak #	47.6	-A	0.30	23.0	0.067	3.4	0.47
										99		38.9	-	0.30	23.0	0.134	10.2	1.36
														0.30	23.0	0.223	19.1	1.87
									CDMG	24281	Port Hueneme - Naval Lab. #	54.3	-	0.14	23.0	0.037	2.3	1.17
										99		50.0	-	0.14	23.0	0.103	7.8	2.23
														0.14	23.0	0.086	7.7	3.08
									CDMG	23598	Rancho Cucamonga - Deer Can #	80.0	-A	0.30	46.0	0.025	2.2	0.40
										99		999.9	-	0.30	46.0	0.071	4.2	0.56
														0.30	46.0	0.051	5.9	0.78
									CDMG	14404	Rancho Palos Verdes - Hawth #	55.2	-A	0.30	23.0	0.043	1.8	0.39
										99		999.9	-	0.30	23.0	0.072	5.0	0.73
														0.30	23.0	0.054	3.5	0.98
									USC	90044	Rancho Palos Verdes - Luconia	57.4	-C	0.20	30.0	0.075	3.6	0.67
										99		999.9	C	0.30	30.0	0.167	9.9	0.87
														0.30	30.0	0.118	9.2	0.69
									DWP	77	Rinaldi Receiving Sta #	7.1	-C			0.852	50.7	11.65
										99		0.0	C			0.838	166.1	28.78
																0.472	73.0	19.76
									CDMG	13123	Riverside - Airport #	101.3	AQB	0.30	23.0	0.022	2.3	0.39
										99		100.4	B	0.30	23.0	0.059	2.7	0.28
														0.30	23.0	0.064	3.1	0.50
									CDMG	14405	Rolling Hills Est-Rancho Vista	46.6	-	0.15	25.0	0.041	2.4	0.44
										99		48.4	-	0.15	25.0	0.116	8.9	1.41

No.	Earthquake Location, Mech, Dip (1)	Date & Time		Magnitude (2)				Station (3) Description		Closest Dist (km)(4)	Site Codes (5)	Filter Corners						
		YR	MODY	HRMN	M	ML	MS	OTH	No.			H/F	HP (hz)	LP (hz)	PGA (g)	PGV (cm/s)	PGD (cm)	
								CDMG	24092	Rosamond - Airport #	65.0	—	0.15	25.0	0.106	5.8	1.17	
									99		65.5	-	0.30	23.0	0.023	1.4	0.36	
													0.30	23.0	0.075	4.7	0.43	
								CDMG	23672	San Bernardino - CSUSB Gr #	103.1	-D	0.30	46.0	0.039	3.5	0.75	
									99		105.7	-	0.30	46.0	0.021	1.5	0.25	
													0.30	46.0	0.034	2.8	0.31	
								CDMG	23542	San Bernardino - E & Hosp #	108.1	-D	0.20	46.0	0.069	4.0	0.77	
									99		110.4	C	0.20	46.0	0.044	2.6	0.51	
													0.20	46.0	0.085	5.9	0.97	
								USC	90019	San Gabriel - E. Grand Ave.	41.7	-A	0.10	30.0	0.096	6.5	1.34	
									99		39.5	A	0.13	30.0	0.073	3.7	1.49	
													0.10	30.0	0.141	9.6	2.21	
								CDMG	12673	San Jacinto - CDF Fire Sta #	146.5	-D	0.16	46.0	0.256	9.8	2.79	
									99		149.1	-	0.16	46.0	0.022	3.7	1.27	
													0.16	46.0	0.081	8.1	1.62	
								CDMG	24401	San Marino, SW Academy #	35.1	AQD	0.60	23.0	0.099	7.7	1.56	
									99		35.2	-	0.30	23.0	0.083	3.7	0.41	
													0.60	23.0	0.116	7.3	1.10	
								CDMG	14159	San Pedro - Palos Verdes #	59.9	—	0.30	23.0	0.150	7.4	0.75	
									99		56.7	-	0.30	23.0	0.070	3.0	0.30	
													0.30	23.0	0.101	5.6	0.59	
								CDMG	24644	Sandberg - Bald Mtn #	43.4	-B	0.30	23.0	0.095	6.6	1.02	
									99		999.9	-	0.12	46.0	0.044	6.4	3.66	
													0.12	46.0	0.091	12.2	4.73	
								CDMG	25091	Santa Barbara - UCSB Goleta #	111.3	—	0.12	46.0	0.098	8.9	4.61	
									99		109.3	-	0.20	23.0	0.039	2.9	0.74	
													0.20	23.0	0.078	7.0	1.46	
													0.20	23.0	0.069	6.7	1.57	
								USC	90077	Santa Fe Spr - E. Joslin	52.5	-D	0.40	30.0	0.052	2.6	0.32	
									99		48.9	C	0.30	30.0	0.135	9.5	1.13	
													0.30	30.0	0.123	7.0	0.96	
								CDMG	24538	Santa Monica City Hall #	27.6	-D	0.14	23.0	0.230	14.3	4.17	
									99		21.1	-	0.14	23.0	0.883	41.7	15.09	
													0.14	23.0	0.370	25.1	7.16	
								USGS	5108	Santa Susana Ground #	19.3	—	-99.					
									99		3.7	-	0.20		0.279	19.4	4.11	
														0.290	19.7	7.45		
								CDMG	14578	Seal Beach - Office Bldg #	64.9	-D	0.16	46.0	0.037	2.0	1.90	
									99		63.9	-	0.16	46.0	0.061	5.8	1.99	
													0.16	46.0	0.084	6.9	1.34	
								USGS	0637	Sepulveda VA #	8.9	-D	0.10		0.467	33.2	9.58	
									99		0.4	-	0.10		0.753	84.8	18.68	
													0.00		0.939	76.6	14.95	
								USC	90055	Simi Valley - Katherine Rd	14.6	-B	0.30	30.0	0.402	13.1	2.18	
									99		0.0	E	0.50	30.0	0.877	40.9	5.29	

No.	Earthquake Location, Mech, Dip (1)	Date & Time			Magnitude (2)			Station (3)		Closest Dist (km)(4)	Site Codes (5)	Filter Corners				
		YR	MODY	HRMN	M	ML	MS	OTH	No.			Description H/F	HP (hz)	LP (hz)	PGA (g)	PGV (cm/s)
												0.40	30.0	0.640	37.8	5.09
							MWD	78	Stone Canyon #	22.2	--	0.08		0.181	6.1	2.42
								99		999.9	-	0.03		0.252	28.0	3.14
												0.03		0.388	38.0	4.60
							USC	90006	Sun Valley - Roscoe Blvd	12.3	-D	0.10	30.0	0.306	12.5	5.00
								99		6.1	B	0.10	30.0	0.303	22.1	7.84
												0.10	30.0	0.443	38.2	10.04
							USC	90058	Sunland - Mt Gleason Ave	17.7	-C	0.10	30.0	0.193	11.6	2.35
								99		14.7	B	0.05	30.0	0.127	13.8	5.54
												0.05	30.0	0.157	14.5	4.29
							DWP	74	Sylmar - Converter Sta #	6.2	-D			0.586	34.6	25.44
								99		0.2	C			0.612	117.4	53.47
														0.897	102.8	46.99
							DWP	75	Sylmar - Converter Sta East #	6.1	-D			0.377	24.3	7.30
								99		0.0	C			0.828	117.5	34.22
														0.493	74.6	28.69
							CDMG	24514	Sylmar - Olive View Med FF #	6.4	AQD	0.12	23.0	0.535	19.1	8.54
								99		3.6	C	0.12	23.0	0.604	78.2	16.05
												0.12	23.0	0.843	129.6	32.68
							CDMG	24436	Tarzana, Cedar Hill #	17.5	A-B	0.10	23.0	1.048	75.4	20.05
								99		4.1	-	0.10	23.0	1.779	113.6	33.22
												0.10	23.0	0.990	77.6	30.45
							USC	90082	Terminal Island - S Seaside	60.0	-D	0.13	30.0	0.048	3.1	1.54
								99		56.7	C	0.13	30.0	0.133	13.7	2.68
												0.13	30.0	0.194	12.1	2.28
							USGS	5081	Topanga - Fire Sta #	23.4	--	0.10		0.199	10.5	3.10
								99		12.6	-	0.20		0.364	17.6	2.87
												0.30		0.266	12.9	1.34
							USC	90089	Tustin - E. Sycamore	85.9	-D	0.23	30.0	0.025	1.5	0.33
								99		999.9	C	0.30	30.0	0.070	4.0	0.76
												0.40	30.0	0.074	4.5	0.42
							CDMG	24047	Vasquez Rocks Park #	24.2	IBA	0.10		0.091	6.1	1.61
								99		24.0	-	0.00		0.151	18.5	2.92
												0.08		0.139	11.2	2.89
							CDMG	25340	Ventura - Harbor & California	55.5	--	0.10	25.0	0.025	5.1	3.12
								99		56.5	-	0.10	25.0	0.054	7.9	2.65
												0.10	25.0	0.075	12.0	3.87
							USC	90090	Villa Park - Serrano Ave	79.5	-B	0.30	30.0	0.027	2.5	0.37
								99		76.9	B	0.10	30.0	0.043	3.1	1.19
												0.10	30.0	0.045	3.8	2.00
							USC	90071	West Covina - S. Orange Ave	54.1	-B	0.20	30.0	0.049	2.7	0.95
								99		52.4	C	0.20	30.0	0.063	5.9	1.34
												0.10	30.0	0.067	5.8	2.65
							USC	90075	Whittier - S. Alta Dr	51.2	-B	0.40	30.0	0.024	1.6	0.34
								99		999.9	B	0.30	30.0	0.089	7.5	1.12

No.	Earthquake Location, Mech, Dip (1)	Date & Time			Magnitude (2)				Station (3)		Closest Dist (km)(4)	Site Codes (5)	Filter Corners			PGA (g)	PGV (cm/s)	PGD (cm)
		YR	MODY	HRMN	M	ML	MS	OTH	No.	Description H/F			HP (hz)	LP (hz)				
									CDMG	23590	Wrightwood - Jackson Flat #	68.4	-A	0.40	30.0	0.052	3.3	0.56
										99		67.7	-	0.24	46.0	0.034	5.8	1.32
														0.24	46.0	0.056	10.0	2.92
									CDMG	23573	Wrightwood - Nielson Ranch #	85.2	-	0.24	46.0	0.021	2.5	0.77
										99		84.5	-	0.24	46.0	0.042	5.8	2.29
														0.24	46.0	0.042	6.3	2.33
									CDMG	23574	Wrightwood - Swarthout #	71.9	-D	0.30	46.0	0.034	1.9	0.24
										99		74.7	-	0.30	46.0	0.047	3.7	0.49
														0.30	46.0	0.060	3.7	0.52
0101	Kobe 00	1995	0116	2046	6.9	0.0	0.0	0.0	CEOR	0	Abeno	23.8	-D	0.05	40.0	0.134	6.2	2.94
										99		999.9	C	0.05	40.0	0.222	20.7	9.11
														0.05	40.0	0.235	24.2	10.00
									CEOR	0	Amagasaki	10.2	-D	0.10	40.0	0.360	19.0	6.31
										99		999.9	D	0.10	40.0	0.301	54.3	23.75
														0.10	40.0	0.363	46.3	24.25
									CEOR	0	Chihaya	48.7	-A	0.05	40.0	0.080	2.5	1.77
										99		999.9	A	0.05	40.0	0.093	6.0	3.27
														0.08	40.0	0.108	4.7	1.24
										0	FUK	157.2	-D	0.05		0.010	1.7	0.67
										99		999.9	-	0.05		0.034	4.3	1.28
														0.05		0.042	5.3	2.08
									CEOR	0	Fukushima	16.8	-E	0.10	40.0	0.200	8.9	5.23
										99		999.9	D	0.08	40.0	0.178	36.3	13.37
														0.08	40.0	0.216	33.2	15.44
										0	HIK	94.2	-	0.05		0.039	3.3	0.92
										99		999.9	-	0.05		0.141	15.6	3.08
														0.05		0.148	15.4	1.96
									CUE	0	Kakogawa	26.4	-E	0.10		0.158	10.5	2.91
										99		999.9	D	0.10		0.251	18.7	5.83
														0.10		0.345	27.6	9.60
									CEOR	0	Kobe University	0.2	-A	0.20	30.0	0.380	20.2	6.48
										99		999.9	A	0.10	30.0	0.290	54.8	13.61
														0.10	30.0	0.310	34.2	7.14
										0	KJMA	0.6	-B	0.05		0.343	38.3	10.29
										99		999.9	B	0.05		0.821	81.3	17.68
														0.05		0.599	74.3	19.95
									CEOR	0	Morigawachi	23.4	-E	0.05	40.0	0.166	6.1	3.30
										99		999.9	D	0.05	40.0	0.214	26.3	11.99
														0.08	40.0	0.140	18.0	8.19
										0	MZH	69.4	-B	0.05		0.041	2.5	2.00
										99		999.9	-	0.05		0.070	4.4	1.54
														0.05		0.052	4.7	1.87
									CUE	0	Nishi-Akashi	11.1	-E	0.10	23.0	0.371	17.3	5.63
										99		999.9	D	0.10	23.0	0.509	37.3	9.52

- (2) M is moment magnitude, UNK = Magnitude type unknown. Missing magnitudes have the value of zero.
- (3) Station numbers were assigned where not available, using numbers 1-33 and 60-100.
 Records marked with a # were not processed by PE&A due to unavailability of uncorrected data
 Records marked with a @ did not have Fourier spectra computed because the noise levels were too high.
 H/F is the designation for the site being on the hanging wall (01) or foot wall (02), or unknown/not applicable (99).
- (4) Distances marked with a * are hypocentral instead of closest distances.
- (5) Site codes are from two sources: 1) Geomatrix (3 letter), 2) USGS (1 letter), described below.
- (6) This earthquake's recordings contain an aftershock in the data.

GEOMATRIX 3-LETTER SITE CLASSIFICATIONS

FIRST LETTER: Instrument housing

- I = Free-field instrument or instrument shelter. Instrument is located at or within several feet of the ground surface.
- A = One-story structure of lightweight construction. Instrument is located at the lowest level and within several feet of the ground surface.
- B = Two- to four-story structure of lightweight construction. Instrument is located at the lowest level and within several feet of the ground surface.
- C = Two- to four-story structure of lightweight construction. Instrument is located at the lowest level in a basement and below the ground surface.
- D = Five or more story structure of heavy construction. Instrument is located at the lowest level and within several feet of the ground surface.
- E = Five or more story structure of heavy construction. Instrument is located at the lowest level in a basement and below the ground surface.
- F = Structure housing instrument is buried below the ground surface, e.g., tunnel.
- G = Structure of light or heavyweight construction, instrument not at lowest level.
- H = Earth dam.
- I = Concrete Dam.

SECOND LETTER: Mapped local geology

Sedimentary or metasedimentary:

- H = Holocene (Recent) Quaternary (< 15000y bp).
- Q = Pleistocene Quaternary (< 2my bp).
- P = Pliocene Tertiary (< 6my bp).
- M = Miocene Tertiary (< 22my bp).
- O = Oligocene Tertiary (< 36my bp).
- E = Eocene Tertiary (< 58my bp).
- L = Paleocene Tertiary (< 63my bp).
- K = Cretaceous (< 145my bp).
- F = Franciscan Formation (Cretaceous/Late Jurassic).
- J = Jurassic (< 210my bp).
- T = Triassic (< 255my bp).
- Z = Permian or older (> 255my bp).

Igneous or meta-igneous:

- V = Volcanic (extrusive).
- N = Intrusive.
- G = Granitic.

THIRD LETTER: Geotechnical subsurface characteristics

- A = Rock. Instrument on rock ($V_s > 600$ mps) or < 5m of soil over rock.
- B = Shallow (stiff) soil. Instrument on/in soil profile up to 20m thick overlying rock.
- C = Deep narrow soil. Instrument on/in soil profile at least 20m thick overlying rock, in a narrow canyon or valley no more than several km wide.
- D = Deep broad soil. Instrument on/in soil profile at least 20m thick overlying rock, in a broad valley.
- E = Soft deep soil. Instrument on/in deep soil profile with average $V_s < 150$ mps.

USGS 1-LETTER CLASSIFICATIONS

Average shear-wave velocity to a depth of 30m is:

A = > 750 m/s

B = 360 - 750 m/s

C = 180 - 360 m/s

D = < 180 m/s

APPENDIX B CATALOG OF TIME HISTORIES FOR ANALYSES

The following tables (Table B-1 for WUS rock, Table B-2 for WUS soil, B-3 for CEUS rock, and B-4 for CEUS soil) list the selected three component recordings for each magnitude, distance, and duration bin for rock and soil site conditions. Sites are classified as rock or soil using the scheme of Geomatrix. Categories A or B are considered rock (ranging from hard California rock to very shallow soil) and categories C and D are considered soil (ranging from shallow or stiff to deep and firm). Site codes are described at the end of the catalog. Additional available source and site information (e.g. source mechanism, magnitude type, and hanging-wall/foot-wall site specification) are available in the general catalog (Appendix A). The explanation table for the general catalog (Appendix A) is shown at the end of Appendix A.

The time histories to be used for analysis are archived in a separate CD-ROM.

The tables are on the following pages:

Table B-1 (WUS rock)	B-2
Table B-2 (WUS soil)	B-23
Table B-3 (CEUS rock)	B-43
Table B-4 (CEUS soil)	B-63

TABLE B-1: WUS, ROCK
 NRC TIME HISTORY LIBRARY: WUS, ROCK, M = 5-6, D=0-50 km

No.	Earthquake	Date & Time					No.	Station	Closest Dist (km)	Site Codes		Filter Corners			PGV (g)	PGD (cm/s)	Dur (s)	Filename
		YR	MODY	HRMN	Mag	Own				Geom	USGS	HP (hz)	LP (hz)	PGA (g)				
0029	Lytile Creek	1970	0912	1430	5.4	CDWR	620	Devil's Canyon	21.9	CAA	-	1.10	30.00	.084	1.8	.10	1.1	DCFDWN
0029	Lytile Creek	1970	0912	1430	5.4	CDWR	620	Devil's Canyon	21.9	CAA	-	1.00	20.00	.146	3.3	.18	1.1	DCF090
0029	Lytile Creek	1970	0912	1430	5.4	CDWR	620	Devil's Canyon	21.9	CAA	-	1.00	30.00	.151	5.6	.23	1.2	DCF180
0029	Lytile Creek	1970	0912	1430	5.4	USGS	290	Wrightwood-6074 Park Dr	15.4	BAB	B	.60	40.00	.078	2.3	.25	2.0	WTWDWN
0029	Lytile Creek	1970	0912	1430	5.4	USGS	290	Wrightwood-6074 Park Dr	15.4	BAB	B	.60	20.00	.162	10.1	1.02	1.8	WTW115
0029	Lytile Creek	1970	0912	1430	5.4	USGS	290	Wrightwood-6074 Park Dr	15.4	BAB	B	.70	30.00	.200	10.5	.62	1.7	WTW205
0042	Fruili, Italy	1976	0911	1631	5.5		8022	San Rocco	17.9	ABA	-	.40	15.00	.013	1.8	.34	5.7	SRO-UP
0042	Fruili, Italy	1976	0911	1631	5.5		8022	San Rocco	17.9	ABA	-	.20	15.00	.029	2.3	.48	3.7	SRO-NS
0042	Fruili, Italy	1976	0911	1631	5.5		8022	San Rocco	17.9	ABA	-	.40	20.00	.072	4.3	.90	.8	SRO-WE
0045	Santa Barbara	1978	0813		6.0	USGS	106	Cachuma Dam Toe	36.6	AAA	-	.20	29.00	.024	1.6	.40	5.5	CAD-UP
0045	Santa Barbara	1978	0813		6.0	USGS	106	Cachuma Dam Toe	36.6	AAA	-	.10	36.00	.072	6.3	1.26	1.4	CAD250
0045	Santa Barbara	1978	0813		6.0	USGS	106	Cachuma Dam Toe	36.6	AAA	-	.20	30.00	.034	2.6	.55	3.4	CAD340
0054	Livermore	1980	0127	0233	5.4	CDMG	58219	APEEL 3E Hayward CSUH	31.0	AVA	B	.60	25.00	.014	.9	.09	5.2	B-A3E-UP
0054	Livermore	1980	0127	0233	5.4	CDMG	58219	APEEL 3E Hayward CSUH	31.0	AVA	B	.30	20.00	.053	4.5	.58	1.2	B-A3E146
0054	Livermore	1980	0127	0233	5.4	CDMG	58219	APEEL 3E Hayward CSUH	31.0	AVA	B	.15	20.00	.028	1.4	.30	3.9	B-A3E236
0054	Livermore	1980	0127	0233	5.4	CDMG	57187	San Ramon-Eastman Kodak	17.6	ABB	C	.30	30.00	.037	4.0	.50	7.0	B-KOD-UP
0054	Livermore	1980	0127	0233	5.4	CDMG	57187	San Ramon-Eastman Kodak	17.6	ABB	C	.20	25.00	.301	19.1	2.82	.7	B-KOD180
0054	Livermore	1980	0127	0233	5.4	CDMG	57187	San Ramon-Eastman Kodak	17.6	ABB	C	.25	25.00	.097	5.6	.62	5.8	B-KOD270
0065	Mammoth Lakes	1980	0611	0441	5.0	USC	40	USC Convict Lakes	9.1	AAB	-	1.00	40.00	.038	.4	.02	1.2	H-XCV-UP
0065	Mammoth Lakes	1980	0611	0441	5.0	USC	40	USC Convict Lakes	9.1	AAB	-	2.00	30.00	.030	.6	.02	1.7	H-XCV075
0065	Mammoth Lakes	1980	0611	0441	5.0	USC	40	USC Convict Lakes	9.1	AAB	-	2.00	30.00	.046	.6	.02	.8	H-XCV165
0079	Coalinga	1983	0709	0740	5.2	USGS	1607	Anticline Ridge Free-Field	11.0	IPA	-	.30	40.00	.115	3.7	.43	2.1	C-ATC-UP
0079	Coalinga	1983	0709	0740	5.2	USGS	1607	Anticline Ridge Free-Field	11.0	IPA	-	.30	30.00	.330	16.1	1.20	2.0	C-ATC270
0079	Coalinga	1983	0709	0740	5.2	USGS	1607	Anticline Ridge Free-Field	11.0	IPA	-	.45	40.00	.275	8.9	.46	1.8	C-ATC360
0079	Coalinga	1983	0709	0740	5.2	USGS	1607	Anticline Ridge Pad	11.0	APA	-	.30	30.00	.137	4.7	.34	2.1	C-ATP-UP
0079	Coalinga	1983	0709	0740	5.2	USGS	1607	Anticline Ridge Pad	11.0	APA	-	.40	30.00	.378	16.1	1.03	1.9	C-ATP270
0079	Coalinga	1983	0709	0740	5.2	USGS	1607	Anticline Ridge Pad	11.0	APA	-	.40	25.00	.261	9.2	.53	1.8	C-ATP360
0079	Coalinga	1983	0709	0740	5.2	USGS	1604	Oil City	10.0	APB	-	.40	30.00	.210	4.6	.29	2.7	C-OLC-UP
0079	Coalinga	1983	0709	0740	5.2	USGS	1604	Oil City	10.0	APB	-	.20	30.00	.387	13.8	1.59	1.7	C-OLC270
0079	Coalinga	1983	0709	0740	5.2	USGS	1604	Oil City	10.0	APB	-	.20	30.00	.370	12.4	.89	2.0	C-OLC360
0079	Coalinga	1983	0709	0740	5.2	USGS	1651	Transmitter Hill	10.4	APA	-	.30	30.00	.114	3.3	.35	3.0	C-TSM-UP
0079	Coalinga	1983	0709	0740	5.2	USGS	1651	Transmitter Hill	10.4	APA	-	.20	25.00	.205	12.0	1.34	2.2	C-TSM270

B-2

No.	Earthquake	Date & Time			Mag	Own	No.	Station	Closest Dist (km)	Site Codes		Filter Corners			PGV (g)	PGD (cm/s)	Dur (s)	Filename
		YR	MODY	HRMN						Geom	USGS	HP (hz)	LP (hz)	PGA (g)				
0079	Coalinga	1983	0709	0740	5.2	USGS	1651	Transmitter Hill	10.4	APA	-	.30	30.00	.194	9.9	.87	2.4	C-TSM360
0080	Coalinga	1983	0722	0239	5.8	USGS	1604	Oil City	8.2	APB	-	.60	30.00	.568	12.5	1.20	2.7	D-OLC-UP
0080	Coalinga	1983	0722	0239	5.8	USGS	1604	Oil City	8.2	APB	-	.15	30.00	.866	42.2	6.14	1.6	D-OLC270
0080	Coalinga	1983	0722	0239	5.8	USGS	1604	Oil City	8.2	APB	-	.80	30.00	.447	24.8	2.23	1.8	D-OLC360
0080	Coalinga	1983	0722	0239	5.8	USGS	1609	Palmer Ave	12.2	APB	-	.20	25.00	.201	6.9	1.35	3.5	D-PLM-UP
0080	Coalinga	1983	0722	0239	5.8	USGS	1609	Palmer Ave	12.2	APB	-	.06	20.00	.272	12.8	3.31	2.0	D-PLM270
0080	Coalinga	1983	0722	0239	5.8	USGS	1609	Palmer Ave	12.2	APB	-	.09	20.00	.290	21.5	3.31	1.8	D-PLM360
0103	N. Palm Springs	1986	0708	0920	6.0	USGS	5043	Hurkey Creek Park	34.9	AQB	B	.40	50.00	.097	3.6	.55	5.5	HCP-UP
0103	N. Palm Springs	1986	0708	0920	6.0	USGS	5043	Hurkey Creek Park	34.9	AQB	B	.60	50.00	.240	7.4	.45	2.4	HCP045
0103	N. Palm Springs	1986	0708	0920	6.0	USGS	5043	Hurkey Creek Park	34.9	AQB	B	.50	50.00	.187	9.1	.89	1.4	HCP135
0117	Whittier Narrows	1987	1001	1442	6.0	USGS	709	Garvey Res.-Control Bldg	12.1	APB	-	.70	40.00	.362	9.9	.75	2.6	A-GRV-UP
0117	Whittier Narrows	1987	1001	1442	6.0	USGS	709	Garvey Res.-Control Bldg	12.1	APB	-	.15	40.00	.384	15.8	2.49	2.5	A-GRV060
0117	Whittier Narrows	1987	1001	1442	6.0	USGS	709	Garvey Res.-Control Bldg	12.1	APB	-	.20	40.00	.457	19.0	4.31	2.1	A-GRV330

NRC TIME HISTORY LIBRARY: WUS, ROCK, M=5-6, D=50-100 km

No.	Earthquake	Date & Time			Mag	Own	No.	Station	Closest Dist (km)	Site Codes		Filter Corners		PGA (g)	PGV (g)	PGD (cm/s)	Dur (s)	Filename
		YR	MODY	HRMN						Geom	USGS	HP (hz)	LP (hz)					
0014	Southern Calif.	1952	1122	0746	6.0	USGS	1083	San Luis Obispo	70.0	CBB	-	.20	13.00	.028	2.4	.74	4.7	SLO-UP
0014	Southern Calif.	1952	1122	0746	6.0	USGS	1083	San Luis Obispo	70.0	CBB	-	.20	13.00	.036	2.8	.93	3.8	SLO234
0014	Southern Calif.	1952	1122	0746	6.0	USGS	1083	San Luis Obispo	70.0	CBB	-	.50	13.00	.054	3.3	.55	3.3	SLO324
0103	N. Palm Springs	1986	0708	0920	6.0	USGS	5231	Anza-Tule Canyon	55.4	AGA	B	.40	30.00	.049	2.6	.30	7.9	ATL-UP
0103	N. Palm Springs	1986	0708	0920	6.0	USGS	5231	Anza-Tule Canyon	55.4	AGA	B	.30	30.00	.110	6.5	.71	1.8	ATL270
0103	N. Palm Springs	1986	0708	0920	6.0	USGS	5231	Anza-Tule Canyon	55.4	AGA	B	.35	35.00	.095	7.5	.71	5.8	ATL360
0103	N. Palm Springs	1986	0708	0920	6.0	CDMG	707	Lake Mathews Dike Toe	73.7	AJA	-	2.00	40.00	.039	.5	.02	8.3	LMR-UP
0103	N. Palm Springs	1986	0708	0920	6.0	CDMG	707	Lake Mathews Dike Toe	73.7	AJA	-	1.00	50.00	.061	1.5	.08	3.4	LMR162
0103	N. Palm Springs	1986	0708	0920	6.0	CDMG	707	Lake Mathews Dike Toe	73.7	AJA	-	1.00	35.00	.046	.8	.03	6.4	LMR252
0103	N. Palm Springs	1986	0708	0920	6.0	CDMG	13198	Murrieta Hot Springs	63.3	IGA	A	.50	28.00	.032	.8	.31	5.8	H01-UP
0103	N. Palm Springs	1986	0708	0920	6.0	CDMG	13198	Murrieta Hot Springs	63.3	IGA	A	.50	40.00	.053	1.8	.30	5.0	H01000
0103	N. Palm Springs	1986	0708	0920	6.0	CDMG	13198	Murrieta Hot Springs	63.3	IGA	A	.50	40.00	.049	1.3	.32	2.7	H01090
0103	N. Palm Springs	1986	0708	0920	6.0	CDMG	12168	Puerta La Cruz	71.9	AQB	B	.20	44.00	.035	1.6	.34	10.8	PLC-UP
0103	N. Palm Springs	1986	0708	0920	6.0	CDMG	12168	Puerta La Cruz	71.9	AQB	B	.20	38.00	.075	2.4	.27	8.8	PLC258
0103	N. Palm Springs	1986	0708	0920	6.0	CDMG	12168	Puerta La Cruz	71.9	AQB	B	.20	32.00	.055	1.8	.32	9.0	PLC348
0103	N. Palm Springs	1986	0708	0920	6.0	CDMG	13123	Riverside Airport	71.2	AQB	B	.50	48.00	.023	.6	.14	10.6	RIV-UP
0103	N. Palm Springs	1986	0708	0920	6.0	CDMG	13123	Riverside Airport	71.2	AQB	B	.50	40.00	.051	1.2	.14	10.0	RIV180
0103	N. Palm Springs	1986	0708	0920	6.0	CDMG	13123	Riverside Airport	71.2	AQB	B	.50	42.00	.040	1.0	.15	6.8	RIV270
0103	N. Palm Springs	1986	0708	0920	6.0	CDMG	13172	Temecula Fire Station	73.2	AQB	C	.50	27.00	.028	1.2	.24	12.0	TSF-UP
0103	N. Palm Springs	1986	0708	0920	6.0	CDMG	13172	Temecula Fire Station	73.2	AQB	C	.50	25.00	.121	6.9	.53	1.5	TFS000
0103	N. Palm Springs	1986	0708	0920	6.0	CDMG	13172	Temecula Fire Station	73.2	AQB	C	.50	25.00	.098	4.6	.68	3.3	TFS090
0103	N. Palm Springs	1986	0708	0920	6.0	CDMG	13199	Winchester Bergman Ran	57.6	AGA	A	.50	48.00	.072	1.6	.25	3.2	H02-UP
0103	N. Palm Springs	1986	0708	0920	6.0	CDMG	13199	Winchester Bergman Ran	57.6	AGA	A	.50	42.00	.070	1.9	.19	3.9	H02000
0103	N. Palm Springs	1986	0708	0920	6.0	CDMG	13199	Winchester Bergman Ran	57.6	AGA	A	.50	50.00	.093	1.8	.29	3.1	H02090
0117	Whittier Narrows	1987	1001	1442	6.0	USC	90052	Calabasas - N Las Virg #	53.3	--B	B	.40	25.00	.023	1.6	.15	12.4	A-VIR-UP
0117	Whittier Narrows	1987	1001	1442	6.0	USC	90052	Calabasas - N Las Virg #	53.3	--B	B	.33	25.00	.042	2.3	.35	7.2	A-VIR200
0117	Whittier Narrows	1987	1001	1442	6.0	USC	90052	Calabasas - N Las Virg #	53.3	--B	B	.45	25.00	.025	1.2	.13	7.4	A-VIR290
0117	Whittier Narrows	1987	1001	1442	6.0	CDMG	24277	Castaio-Haaley Canyon	70.9	A-B	-	.50	20.00	.021	1.5	.16	11.9	A-CSH-UP
0117	Whittier Narrows	1987	1001	1442	6.0	CDMG	24277	Castaio-Haaley Canyon	70.9	A-B	-	.70	15.00	.031	1.9	.19	9.1	A-CSH000
0117	Whittier Narrows	1987	1001	1442	6.0	CDMG	24277	Castaio-Haaley Canyon	70.9	A-B	-	.50	15.00	.035	2.6	.31	7.3	A-CSH090
0117	Whittier Narrows	1987	1001	1442	6.0	CDMG	24278	Castaic - Old Ridge Route	78.3	A-B	B	1.00	23.00	.026	1.1	.08	12.3	A-ORR-UP
0117	Whittier Narrows	1987	1001	1442	6.0	CDMG	24278	Castaic - Old Ridge Route	78.3	A-B	B	.80	15.00	.071	4.4	.40	7.2	A-ORR000
0117	Whittier Narrows	1987	1001	1442	6.0	CDMG	24278	Castaic - Old Ridge Route	78.3	A-B	B	.80	20.00	.065	4.5	.38	6.4	A-ORR090
0117	Whittier Narrows	1987	1001	1442	6.0	CDMG	24396	Malibu-Point Dume Sch	65.3	AMB	B	.35	30.00	.029	1.9	.15	10.8	A-MAL-UP

B-4

No.	Earthquake	Date & Time			Mag	Own	No.	Station	Closest Dist (km)	Site Codes		Filter Corners		PGA (g)	PGV (g)	PGD (cm/s)	Dur (s)	Filename
		YR	MODY	HRMN						Geom	USGS	HP (hz)	LP (hz)					
0117	Whittier Narrows	1987	1001	1442	6.0	CDMG	24396	Malibu-Point Dume Sch	65.3	AMB	B	.35	25.00	.048	2.4	.32	5.5	A-MAL180
0117	Whittier Narrows	1987	1001	1442	6.0	CDMG	24396	Malibu-Point Dume Sch	65.3	AMB	B	.60	20.00	.040	2.0	.18	5.6	A-MAL270
0117	Whittier Narrows	1987	1001	1442	6.0	USC	90051	Malibu-W Pacific Coast Hwy #	60.0	--	B	.38	25.00	.029	1.6	.24	10.8	A-WPA-UP
0117	Whittier Narrows	1987	1001	1442	6.0	USC	90051	Malibu-W Pacific Coast Hwy #	60.0	--	B	.40	25.00	.038	2.5	.28	10.3	A-WPA060
0117	Whittier Narrows	1987	1001	1442	6.0	USC	90051	Malibu-W Pacific Coast Hwy #	60.0	--	B	.70	25.00	.032	2.3	.22	10.5	A-WPA150
0117	Whittier Narrows	1987	1001	1442	6.0	CDMG	13123	Riverside Airport	56.8	AQB	B	3.00	50.00	.044	.7	.01	8.3	A-RIV-UP
0117	Whittier Narrows	1987	1001	1442	6.0	CDMG	13123	Riverside Airport	56.8	AQB	B	1.70	35.00	.050	1.4	.05	7.0	A-RIV180
0117	Whittier Narrows	1987	1001	1442	6.0	CDMG	13123	Riverside Airport	56.8	AQB	B	2.00	45.00	.047	1.4	.04	4.9	A-RIV270
0117	Whittier Narrows	1987	1001	1442	6.0	CDMG	24047	Vasquez Rocks Park	52.4	IBA	B	.90	35.00	.039	1.1	.09	6.7	A-VAS-UP
0117	Whittier Narrows	1987	1001	1442	6.0	CDMG	24047	Vasquez Rocks Park	52.4	IBA	B	1.00	25.00	.060	2.1	.12	4.2	A-VAS000
0117	Whittier Narrows	1987	1001	1442	6.0	CDMG	24047	Vasquez Rocks Park	52.4	IBA	B	1.00	25.00	.060	2.3	.11	3.8	A-VAS090

NRC TIME HISTORY LIBRARY: WUS, ROCK, M=6-7, D=0-10 km

No.	Earthquake	Date & Time				Mag	Own	No.	Station	Closest Dist (km)	Site Codes		Filter Corners				Dur (s)	Filename
		YR	MODY	HRMN							Geom	USGS	HP (hz)	LP (hz)	PGA (g)	PGV (g)		
0001	Helena, Montana	1935	1031	1838	6.2		2022	Carroll College	8.0	EZA	-	.20	15.00	.102	7.3	2.29	1.1	A-HMCDWN
0001	Helena, Montana	1935	1031	1838	6.2		2022	Carroll College	8.0	EZA	-	.20	15.00	.150	5.8	1.00	1.3	A-HMC180
0001	Helena, Montana	1935	1031	1838	6.2		2022	Carroll College	8.0	EZA	-	.20	15.00	.173	16.5	2.37	1.1	A-HMC270
0025	Parkfield	1966	0628	0426	6.1	CDMG	1015	Cholame #8	9.2	ABB	C	.20	24.00	.116	4.3	1.48	4.0	C08DWN
0025	Parkfield	1966	0628	0426	6.1	CDMG	1015	Cholame #8	9.2	ABB	C	.20	20.00	.246	10.2	3.60	5.9	C08050
0025	Parkfield	1966	0628	0426	6.1	CDMG	1015	Cholame #8	9.2	ABB	C	.20	20.00	.273	11.3	3.20	3.7	C08320
0025	Parkfield	1966	0628	0426	6.1	CDMG	1438	Temblor pre-1969	9.9	LJA	B	.20	16.00	.136	4.4	1.10	3.2	TMBDWN
0025	Parkfield	1966	0628	0426	6.1	CDMG	1438	Temblor pre-1969	9.9	LJA	B	.20	14.00	.357	21.5	3.87	1.3	TMB205
0025	Parkfield	1966	0628	0426	6.1	CDMG	1438	Temblor pre-1969	9.9	LJA	B	.20	15.00	.272	15.0	3.40	1.3	TMB295
0030	San Fernando	1971	0209	1400	6.6	CDMG	279	Pacoima Dam	2.8	AMB	A	.10	35.00	.699	56.5	18.25	5.5	PULDWN
0030	San Fernando	1971	0209	1400	6.6	CDMG	279	Pacoima Dam	2.8	AMB	A	.10	35.00	1.226	112.5	35.50	5.4	PUL164
0030	San Fernando	1971	0209	1400	6.6	CDMG	279	Pacoima Dam	2.8	AMB	A	.50	35.00	1.160	54.3	11.73	5.8	PUL254
0041	Gazli, USSR	1976	0517		6.8		9201	Karakyr	3.0	AAA	-	.50	38.00	1.264	54.2	30.15	5.1	GAZ-UP
0041	Gazli, USSR	1976	0517		6.8		9201	Karakyr	3.0	AAA	-	.50	38.00	.608	65.4	25.29	4.5	GAZ000
0041	Gazli, USSR	1976	0517		6.8		9201	Karakyr	3.0	AAA	-	.50	38.00	.718	71.6	23.71	5.4	GAZ090
0090	Morgan Hill	1984	0424	2115	6.2	CDMG	57217	Coyote Lake Dam (SW Abut)	.1	IFA	-	.10	50.00	.388	15.6	2.65	3.0	CYC-UP
0090	Morgan Hill	1984	0424	2115	6.2	CDMG	57217	Coyote Lake Dam (SW Abut)	.1	IFA	-	.10	39.00	.711	51.6	12.00	3.0	CYC195
0090	Morgan Hill	1984	0424	2115	6.2	CDMG	57217	Coyote Lake Dam (SW Abut)	.1	IFA	-	.10	45.00	1.298	80.8	9.63	1.7	CYC285
0090	Morgan Hill	1984	0424	2115	6.2	CDMG	57383	Gilroy Array #6	11.8	IKB	B	.10	30.00	.405	14.1	1.86	.5	G06-UP
0090	Morgan Hill	1984	0424	2115	6.2	CDMG	57383	Gilroy Array #6	11.8	IKB	B	.10	35.00	.222	11.4	2.45	3.1	G06000
0090	Morgan Hill	1984	0424	2115	6.2	CDMG	57383	Gilroy Array #6	11.8	IKB	B	.10	27.00	.292	36.7	6.12	4.5	G06090
0117	Whittier Narrows	1987	1001	1442	6.0	USC	90019	San Gabriel - E Grand Ave #	9.0	--A	A	.35	25.00	.227	5.5	.44	2.5	A-GRN-UP
0117	Whittier Narrows	1987	1001	1442	6.0	USC	90019	San Gabriel - E Grand Ave #	9.0	--A	A	.35	25.00	.304	23.0	3.34	2.4	A-GRN180
0117	Whittier Narrows	1987	1001	1442	6.0	USC	90019	San Gabriel - E Grand Ave #	9.0	--A	A	.35	25.00	.199	11.0	1.04	2.8	A-GRN270
0122	Loma Prieta	1989	1018	0005	6.9	CDMG	57007	Corralitos	5.1	APB	B	.20	32.00	.455	17.7	7.11	3.5	CLS-UP
0122	Loma Prieta	1989	1018	0005	6.9	CDMG	57007	Corralitos	5.1	APB	B	.20	40.00	.644	55.2	10.88	3.4	CLS000
0122	Loma Prieta	1989	1018	0005	6.9	CDMG	57007	Corralitos	5.1	APB	B	.20	40.00	.479	45.2	11.37	4.6	CLS090
0122	Loma Prieta	1989	1018	0005	6.9	UCSC	16	LGPC	6.1	--A	-	.10		.890	54.9	17.56	4.5	LGP-UP
0122	Loma Prieta	1989	1018	0005	6.9	UCSC	16	LGPC	6.1	--A	-	.10		.563	94.8	41.18	5.5	LGP000
0122	Loma Prieta	1989	1018	0005	6.9	UCSC	16	LGPC	6.1	--A	-	.10		.605	51.0	11.50	5.5	LGP090
0131	Northridge	1994	0117	1231	6.7	CDMG	24207	Pacoima Dam (downstr) #	8.0	AGA	A	.75	23.00	.190	14.2	1.35	3.9	PAC-UP
0131	Northridge	1994	0117	1231	6.7	CDMG	24207	Pacoima Dam (downstr) #	8.0	AGA	A	.16	23.00	.415	45.6	5.06	.6	PAC175
0131	Northridge	1994	0117	1231	6.7	CDMG	24207	Pacoima Dam (downstr) #	8.0	AGA	A	.16	23.00	.434	31.3	4.80	2.0	PAC265

B-6

No.	Earthquake	Date & Time			Mag	Own	No.	Station	Closest Dist (km)	Site Codes		Filter Corners			PGV (g)	PGD (cm/s)	Dur (s)	Filename
		YR	MODY	HRMN						Geom	USGS	HP (hz)	LP (hz)	PGA (g)				
0131	Northridge	1994	0117	1231	6.7	CDMG	24207	Pacoima Dam (upper left) #	8.0	IGA	A	.16	23.00	1.229	49.6	11.75	3.0	PUL-UP
0131	Northridge	1994	0117	1231	6.7	CDMG	24207	Pacoima Dam (upper left) #	8.0	IGA	A	.16	23.00	1.585	55.7	6.06	2.5	PUL104
0131	Northridge	1994	0117	1231	6.7	CDMG	24207	Pacoima Dam (upper left) #	8.0	IGA	A	.16	23.00	1.285	103.9	23.80	3.8	PUL194
0131	Northridge	1994	0117	1231	6.7	CDMG	24088	Pacoima Kagel Canyon #	8.2	AMB	B	.20	23.00	.169	15.1	4.14	6.9	PKC-UP
0131	Northridge	1994	0117	1231	6.7	CDMG	24088	Pacoima Kagel Canyon #	8.2	AMB	B	.14	23.00	.301	31.4	10.87	5.7	PKC090
0131	Northridge	1994	0117	1231	6.7	CDMG	24088	Pacoima Kagel Canyon #	8.2	AMB	B	.14	23.00	.433	51.5	7.21	5.6	PKC360
0133	Kobe	1995	0116	2046	6.9	CEOR	99999	Kobe University	.2	--A	A	.20	30.00	.380	20.2	6.48	2.8	KBU-UP
0133	Kobe	1995	0116	2046	6.9	CEOR	99999	Kobe University	.2	--A	A	.10	30.00	.290	54.8	13.61	3.3	KBU000
0133	Kobe	1995	0116	2046	6.9	CEOR	99999	Kobe University	.2	--A	A	.10	30.00	.310	34.2	7.14	3.7	KBU090
0133	Kobe	1995	0116	2046	6.9		99999	KJMA	.6	--B	B	.05		.343	38.3	10.29	4.7	KJM-UP
0133	Kobe	1995	0116	2046	6.9		99999	KJMA	.6	--B	B	.05		.821	81.3	17.68	4.2	KJM000
0133	Kobe	1995	0116	2046	6.9		99999	KJMA	.6	--B	B	.05		.599	74.3	19.95	4.3	KJM090

NRC TIME HISTORY LIBRARY: WUS, ROCK, M=6-7, D=10-50 km

12-8

No.	Earthquake	Date & Time					Own	No.	Station	Closest Dist (km)	Site Codes		Filter Corners			Dur (s)	Filename	
		YR	MODY	HRMN	Mag						Geom	USGS	HP (hz)	LP (hz)	PGA (g)			PGV (g)
0030	San Fernando	1971	0209	1400	6.6	USGS	126	Lake Hughes #4	24.2	IGA	B	.50	35.00	.164	6.4	.93	4.1	L04DWN
0030	San Fernando	1971	0209	1400	6.6	USGS	126	Lake Hughes #4	24.2	IGA	B	.50	35.00	.192	5.6	.92	3.6	L04111
0030	San Fernando	1971	0209	1400	6.6	USGS	126	Lake Hughes #4	24.2	IGA	B	.50	35.00	.153	8.4	1.85	4.1	L04201
0030	San Fernando	1971	0209	1400	6.6	CDMG	285	Santa Felita Dam (Outlet)	27.5	ABA	-	.10	20.00	.065	4.1	2.36	8.9	FSD-UP
0030	San Fernando	1971	0209	1400	6.6	CDMG	285	Santa Felita Dam (Outlet)	27.5	ABA	-	.10	20.00	.148	9.4	7.02	7.4	FSD172
0030	San Fernando	1971	0209	1400	6.6	CDMG	285	Santa Felita Dam (Outlet)	27.5	ABA	-	.10	13.00	.152	6.5	3.46	5.0	FSD262
0050	Imperial Valley	1979	1015	2316	6.5	USGS	286	Superstition Mtn Camera	26.0	AGA	B	.10	40.00	.077	2.3	1.14	5.8	H-SUP-UP
0050	Imperial Valley	1979	1015	2316	6.5	USGS	286	Superstition Mtn Camera	26.0	AGA	B	.10	40.00	.109	5.2	2.21	6.3	H-SUP045
0050	Imperial Valley	1979	1015	2316	6.5	USGS	286	Superstition Mtn Camera	26.0	AGA	B	.10	40.00	.195	8.8	2.78	2.2	H-SUP135
0058	Mammoth Lakes	1980	0525	1944	6.0	CDMG	54214	Long Valley Dam (L. Abut)	19.7	IVA	-	.40	50.00	.068	4.0	.45	4.6	MLLVL-UP
0058	Mammoth Lakes	1980	0525	1944	6.0	CDMG	54214	Long Valley Dam (L. Abut)	19.7	IVA	-	.35	50.00	.104	6.6	1.06	4.2	MLLV000
0058	Mammoth Lakes	1980	0525	1944	6.0	CDMG	54214	Long Valley Dam (L. Abut)	19.7	IVA	-	.20	50.00	.077	5.4	1.69	4.8	MLLV090
0061	Mammoth Lakes	1980	0527	1451	6.0	CDMG	54424	Bishop-Paradise Lodge	43.7	AVA	-	.20	50.00	.084	3.0	.77	4.6	L-BPL-UP
0061	Mammoth Lakes	1980	0527	1451	6.0	CDMG	54424	Bishop-Paradise Lodge	43.7	AVA	-	.20	40.00	.091	5.5	1.48	4.9	L-BPL070
0061	Mammoth Lakes	1980	0527	1451	6.0	CDMG	54424	Bishop-Paradise Lodge	43.7	AVA	-	.20	40.00	.114	5.3	1.41	4.3	L-BPL160
0064	Victoria, Mexico	1980	0609	0328	6.1	UNAMUCSD	6604	Cerro Prieto	34.8	AVA	B	.20	62.00	.304	12.1	4.90	5.1	CPE-UP
0064	Victoria, Mexico	1980	0609	0328	6.1	UNAMUCSD	6604	Cerro Prieto	34.8	AVA	B	.20	62.00	.621	31.6	13.20	4.4	CPE045
0064	Victoria, Mexico	1980	0609	0328	6.1	UNAMUCSD	6604	Cerro Prieto	34.8	AVA	B	.20	62.00	.587	19.9	9.40	4.2	CPE315
0076	Coalinga	1983	0502	2342	6.4	CDMG	36453	Parkfield-Fault Zone 11	28.4	IMB	-	.20	28.00	.042	4.8	1.80	8.9	H-Z11-UP
0076	Coalinga	1983	0502	2342	6.4	CDMG	36453	Parkfield-Fault Zone 11	28.4	IMB	-	.20	21.00	.097	11.9	2.35	4.5	H-Z11000
0076	Coalinga	1983	0502	2342	6.4	CDMG	36453	Parkfield-Fault Zone 11	28.4	IMB	-	.20	28.00	.087	6.6	1.83	3.6	H-Z11090
0076	Coalinga	1983	0502	2342	6.4	CDMG	36420	Parkfield-Gold Hill 3W	38.8	IPB	-	.20	36.00	.067	7.5	1.77	9.0	H-PG3-UP
0076	Coalinga	1983	0502	2342	6.4	CDMG	36420	Parkfield-Gold Hill 3W	38.8	IPB	-	.20	30.00	.137	11.0	2.76	2.8	H-PG3000
0076	Coalinga	1983	0502	2342	6.4	CDMG	36420	Parkfield-Gold Hill 3W	38.8	IPB	-	.20	30.00	.122	9.0	1.74	3.8	H-PG3090
0076	Coalinga	1983	0502	2342	6.4	CDMG	36230	Parkfield-Cholame 2E	40.5	IJB	-	.50	26.00	.017	2.3	.52	12.1	H-TM2-UP
0076	Coalinga	1983	0502	2342	6.4	CDMG	36230	Parkfield-Cholame 2E	40.5	IJB	-	.50	23.00	.026	2.9	.62	8.8	H-TM2000
0076	Coalinga	1983	0502	2342	6.4	CDMG	36230	Parkfield-Cholame 2E	40.5	IJB	-	.50	22.00	.037	5.4	1.40	7.6	H-TM2090
0076	Coalinga	1983	0502	2342	6.4	CDMG	36446	Parkfield-Vineyard Cany 4W	34.6	IMB	-	.20	30.00	.024	2.8	.64	8.2	H-VC4-UP
0076	Coalinga	1983	0502	2342	6.4	CDMG	36446	Parkfield-Vineyard Cany 4W	34.6	IMB	-	.20	30.00	.064	6.5	1.37	4.3	H-VC4000
0076	Coalinga	1983	0502	2342	6.4	CDMG	36446	Parkfield-Vineyard Cany 4W	34.6	IMB	-	.20	27.00	.046	4.2	.95	5.9	H-VC4090
0090	Morgan Hill	1984	0424	2115	6.2	CDMG	57007	Corralitos	22.7	APB	B	.20	27.00	.040	4.0	.54	4.9	CLS-UP
0090	Morgan Hill	1984	0424	2115	6.2	CDMG	57007	Corralitos	22.7	APB	B	.20	24.00	.081	6.4	1.17	4.4	CLS220
0090	Morgan Hill	1984	0424	2115	6.2	CDMG	57007	Corralitos	22.7	APB	B	.20	26.00	.109	10.8	2.13	3.4	CLS310
0090	Morgan Hill	1984	0424	2115	6.2	CDMG	57383	Gilroy Array #6	11.8	IKB	B	.10	30.00	.405	14.1	1.86	.5	MHG06-UP

B-9

No.	Earthquake	Date & Time				Own	No.	Station	Closest Dist (km)	Site Codes		Filter Corners			PGD (cm/s)	Dur (s)	Filename	
		YR	MODY	HRMN	Mag					Geom	USGS	HP (hz)	LP (hz)	PGA (g)				PGV (g)
0090	Morgan Hill	1984	0424	2115	6.2	CDMG	57383	Gilroy Array #6	11.8	IKB	B	.10	35.00	.222	11.4	2.45	3.1	MHG06000
0090	Morgan Hill	1984	0424	2115	6.2	CDMG	57383	Gilroy Array #6	11.8	IKB	B	.10	27.00	.292	36.7	6.12	4.5	MHG06090
0090	Morgan Hill	1984	0424	2115	6.2	CDMG	47006	Gilroy - Gavilan Coll.	16.2	AFB	B	.50	42.00	.081	2.3	.41	3.6	GIL-UP
0090	Morgan Hill	1984	0424	2115	6.2	CDMG	47006	Gilroy - Gavilan Coll.	16.2	AFB	B	.10	30.00	.114	3.6	.87	5.0	GIL067
0090	Morgan Hill	1984	0424	2115	6.2	CDMG	47006	Gilroy - Gavilan Coll.	16.2	AFB	B	.10	30.00	.095	2.9	.93	4.7	GIL337
0103	N. Palm Springs	1986	0708	0920	6.0	USGS	5230	Santa Rosa Mountain	43.8	AGA	-	1.00	50.00	.051	1.5	.10	6.6	ARS-UP
0103	N. Palm Springs	1986	0708	0920	6.0	USGS	5230	Santa Rosa Mountain	43.8	AGA	-	1.50	60.00	.102	2.2	.10	6.0	ARS270
0103	N. Palm Springs	1986	0708	0920	6.0	USGS	5230	Santa Rosa Mountain	43.8	AGA	-	1.50	60.00	.103	2.2	.10	6.6	ARS360
0105	Chalfant Valley	1986	0721	1442	6.2	CDMG	54214	Long Valley Dam (L. Abut)	33.4	IVA	-	.10	43.00	.074	3.3	1.45	6.4	CVLVL-UP
0105	Chalfant Valley	1986	0721	1442	6.2	CDMG	54214	Long Valley Dam (L. Abut)	33.4	IVA	-	.10	50.00	.082	7.0	1.34	5.3	CVLV000
0105	Chalfant Valley	1986	0721	1442	6.2	CDMG	54214	Long Valley Dam (L. Abut)	33.4	IVA	-	.10	50.00	.071	7.9	3.06	7.9	CVLV090
0105	Chalfant Valley	1986	0721	1442	6.2	CDMG	54101	Tinemaha Res. Free Field	40.5	AVA	-	.50	30.00	.023	1.7	.54	11.3	A-TIN-UP
0105	Chalfant Valley	1986	0721	1442	6.2	CDMG	54101	Tinemaha Res. Free Field	40.5	AVA	-	.50	30.00	.037	3.6	1.12	6.7	A-TIN000
0105	Chalfant Valley	1986	0721	1442	6.2	CDMG	54101	Tinemaha Res. Free Field	40.5	AVA	-	.50	30.00	.037	6.3	1.21	5.6	A-TIN090
0117	Whittier Narrows	1987	1001	1442	6.0	USC	90015	LA-Chalon Rd #	32.6	--B	B	1.00	25.00	.019	.7	.07	5.1	A-CHL-UP
0117	Whittier Narrows	1987	1001	1442	6.0	USC	90015	LA-Chalon Rd #	32.6	--B	B	.38	25.00	.036	2.3	.21	3.5	A-CHL030
0117	Whittier Narrows	1987	1001	1442	6.0	USC	90015	LA-Chalon Rd #	32.6	--B	B	.75	25.00	.020	1.1	.12	5.6	A-CHL120
0117	Whittier Narrows	1987	1001	1442	6.0	USC	90016	LA-N Faring Rd #	28.5	--B	C	.55	25.00	.034	1.6	.13	6.1	A-FAR-UP
0117	Whittier Narrows	1987	1001	1442	6.0	USC	90016	LA-N Faring Rd #	28.5	--B	C	.55	25.00	.048	2.2	.26	4.4	A-FAR000
0117	Whittier Narrows	1987	1001	1442	6.0	USC	90016	LA-N Faring Rd #	28.5	--B	C	.40	25.00	.053	3.0	.29	4.1	A-FAR090
0117	Whittier Narrows	1987	1001	1442	6.0	USC	90050	Malibu-Las Flores Canyon #	46.3	--B	B	.65	25.00	.015	1.0	.13	4.4	A-LAS-UP
0117	Whittier Narrows	1987	1001	1442	6.0	USC	90050	Malibu-Las Flores Canyon #	46.3	--B	B	.65	25.00	.065	2.3	.14	3.3	A-LAS160
0117	Whittier Narrows	1987	1001	1442	6.0	USC	90050	Malibu-Las Flores Canyon #	46.3	--B	B	.65	25.00	.055	2.2	.32	3.5	A-LAS250
0117	Whittier Narrows	1987	1001	1442	6.0	CDMG	24088	Pacoima Kagel Canyon	37.9	AMB	B	.50	35.00	.055	2.7	.30	7.0	A-PKC-UP
0117	Whittier Narrows	1987	1001	1442	6.0	CDMG	24088	Pacoima Kagel Canyon	37.9	AMB	B	.35	20.00	.166	6.2	.68	3.7	A-PKC000
0117	Whittier Narrows	1987	1001	1442	6.0	CDMG	24088	Pacoima Kagel Canyon	37.9	AMB	B	.45	20.00	.164	6.8	.87	4.3	A-PKC090
0117	Whittier Narrows	1987	1001	1442	6.0	USC	90090	Villa Park-Serrano Ave #	30.0	--B	B	.50	25.00	.033	1.3	.11	8.9	A-SER-UP
0117	Whittier Narrows	1987	1001	1442	6.0	USC	90090	Villa Park-Serrano Ave #	30.0	--B	B	.70	25.00	.046	1.4	.13	6.4	A-SER000
0117	Whittier Narrows	1987	1001	1442	6.0	USC	90090	Villa Park-Serrano Ave #	30.0	--B	B	.55	25.00	.072	2.6	.27	5.5	A-SER270
0121	Spitak, Armenia	1988	1207	6.8			12	Gukasian	30.0	A-A	-	.50	25.00	.119	8.8	4.30	6.2	GUK-UP
0121	Spitak, Armenia	1988	1207	6.8			12	Gukasian	30.0	A-A	-	.50	25.00	.199	28.6	9.80	6.3	GUK000
0121	Spitak, Armenia	1988	1207	6.8			12	Gukasian	30.0	A-A	-	.50	25.00	.715	15.1	4.30	4.4	GUK090
0122	Loma Prieta	1989	1018	0005	6.9	CDMG	58262	Belmont-Envirotech	49.9	BFA	B	.20	38.00	.041	4.5	2.46	7.1	BES-UP
0122	Loma Prieta	1989	1018	0005	6.9	CDMG	58262	Belmont-Envirotech	49.9	BFA	B	.20	22.00	.108	11.8	3.30	4.7	BES000
0122	Loma Prieta	1989	1018	0005	6.9	CDMG	58262	Belmont-Envirotech	49.9	BFA	B	.20	30.00	.110	16.2	5.71	3.8	BES090

B-10

No.	Earthquake	Date & Time					Own	No.	Station	Closest Dist (km)	Site Codes		Filter Corners			Dur (s)	Filename	
		YR	MODY	HRMN	Mag						Geom	USGS	HP (hz)	LP (hz)	PGA (g)			PGV (g)
0122	Loma Prieta	1989	1018	0005	6.9	CDMG	57383	Gilroy Array #6	19.9	IKB	B	.20	32.00	.101	9.5	4.10	5.1	LPG06-UP
0122	Loma Prieta	1989	1018	0005	6.9	CDMG	57383	Gilroy Array #6	19.9	IKB	B	.20	38.00	.126	12.8	4.74	4.5	LPG06000
0122	Loma Prieta	1989	1018	0005	6.9	CDMG	57383	Gilroy Array #6	19.9	IKB	B	.20	31.00	.170	14.2	3.79	4.5	LPG06090
0122	Loma Prieta	1989	1018	0005	6.9	CDMG	47189	SAGO South - Surface	34.7	IGB	B	.10	29.00	.060	7.8	5.86	5.9	SG3-UP
0122	Loma Prieta	1989	1018	0005	6.9	CDMG	47189	SAGO South - Surface	34.7	IGB	B	.10	25.00	.073	10.5	6.40	5.4	SG3261
0122	Loma Prieta	1989	1018	0005	6.9	CDMG	47189	SAGO South - Surface	34.7	IGB	B	.10	30.00	.067	9.6	6.42	7.8	SG3351
0122	Loma Prieta	1989	1018	0005	6.9	CDMG	58127	Woodside	39.9	APB	B	.10	31.00	.050	6.2	2.80	6.5	WDS-UP
0122	Loma Prieta	1989	1018	0005	6.9	CDMG	58127	Woodside	39.9	APB	B	.10	25.00	.080	13.7	8.47	6.2	WDS000
0122	Loma Prieta	1989	1018	0005	6.9	CDMG	58127	Woodside	39.9	APB	B	.10	25.00	.082	16.7	8.89	6.3	WDS090
0131	Northridge	1994	0117	1231	6.7	USC	90059	Burbank - Howard Rd.	20.0	—B	B	.10	30.00	.085	3.6	1.48	7.0	HOW-UP
0131	Northridge	1994	0117	1231	6.7	USC	90059	Burbank - Howard Rd.	20.0	—B	B	.10	30.00	.120	9.5	2.25	5.9	HOW060
0131	Northridge	1994	0117	1231	6.7	USC	90059	Burbank-Howard Rd.	20.0	—B	B	.10	30.00	.163	8.5	1.81	5.1	HOW330
0131	Northridge	1994	0117	1231	6.7	USC	90015	LA - Chalon Rd	23.7	—B	B	.50	30.00	.174	8.0	1.09	5.8	CHL-UP
0131	Northridge	1994	0117	1231	6.7	USC	90015	LA - Chalon Rd	23.7	—B	B	.30	30.00	.225	16.6	3.39	5.7	CHL070
0131	Northridge	1994	0117	1231	6.7	USC	90015	LA - Chalon Rd	23.7	—B	B	.20	30.00	.185	27.1	5.77	5.0	CHL160
0131	Northridge	1994	0117	1231	6.7	USC	90016	LA - N Faring Rd	23.9	—B	C	.20	30.00	.191	8.9	1.65	5.9	FAR-UP
0131	Northridge	1994	0117	1231	6.7	USC	90016	LA - N Faring Rd	23.9	—B	C	.13	30.00	.273	15.8	3.29	4.8	FAR000
0131	Northridge	1994	0117	1231	6.7	USC	90016	LA - N Faring Rd	23.9	—B	C	.13	30.00	.242	29.8	4.74	5.8	FAR090
0131	Northridge	1994	0117	1231	6.7	CDMG	24605	LA-Univ Hospital #	34.6	IMA	B	.20	46.00	.119	6.4	1.37	7.6	UNI-UP
0131	Northridge	1994	0117	1231	6.7	CDMG	24605	LA-Univ Hospital #	34.6	IMA	B	.20	46.00	.493	31.1	2.39	5.6	UNI005
0131	Northridge	1994	0117	1231	6.7	CDMG	24605	LA-Univ Hospital #	34.6	IMA	B	.20	46.00	.214	10.8	2.37	6.7	UNI095

NRC TIME HISTORY LIBRARY: WUS, ROCK, M=6-7, D=50-100 km

No.	Earthquake	Date & Time				Mag	Own	No.	Station	Closest Dist (km)	Site Codes		Filter Corners			PGV (g)	PGD (cm/s)	Dur (s)	Filename
		YR	MODY	HRMN							Geom	USGS	HP (hz)	LP (hz)	PGA (g)				
0025	Parkfield	1966	0628	0426	6.1	USGS	1083	San Luis Obispo	60.0	CBB	-	.20	15.00	.007	.8	.28	5.3	SLO-UP	
0025	Parkfield	1966	0628	0426	6.1	USGS	1083	San Luis Obispo	60.0	CBB	-	.20	15.00	.012	1.0	.30	5.9	SLO234	
0025	Parkfield	1966	0628	0426	6.1	USGS	1083	San Luis Obispo	60.0	CBB	-	.20	12.00	.014	1.0	.46	6.3	SLO324	
0030	San Fernando	1971	0209	1400	6.6	CDWR	111	Cedar Springs, Allen Ranch	86.6	AAA	A	.20	35.00	.009	.9	.53	6.0	CSMDWN	
0030	San Fernando	1971	0209	1400	6.6	CDWR	111	Cedar Springs, Allen Ranch	86.6	AAA	A	.20	35.00	.020	1.7	.49	5.6	CSM095	
0030	San Fernando	1971	0209	1400	6.6	CDWR	111	Cedar Springs, Allen Ranch	86.6	AAA	A	.20	35.00	.015	1.4	.57	5.9	CSM185	
0030	San Fernando	1971	0209	1400	6.6	ACOE	287	Upland-San Antonio Dam	58.1	AAA	B	.50	35.00	.032	1.3	.54	7.0	SODDWN	
0030	San Fernando	1971	0209	1400	6.6	ACOE	287	Upland-San Antonio Dam	58.1	AAA	B	.50	35.00	.058	2.9	.55	7.1	SOD015	
0030	San Fernando	1971	0209	1400	6.6	ACOE	287	Upland-San Antonio Dam	58.1	AAA	B	.50	35.00	.079	3.5	.50	6.3	SOD285	
0117	Whittier Narrows	1987	1001	1442	6.0	USC	90052	Calabasas-N Las Virg#	53.3	--B	B	.40	25.00	.023	1.6	.15	12.4	A-VIR-UP	
0117	Whittier Narrows	1987	1001	1442	6.0	USC	90052	Calabasas-N Las Virg#	53.3	--B	B	.33	25.00	.042	2.3	.35	7.2	A-VIR200	
0117	Whittier Narrows	1987	1001	1442	6.0	USC	90052	Calabasas-N Las Virg#	53.3	--B	B	.45	25.00	.025	1.2	.13	7.4	A-VIR290	
0117	Whittier Narrows	1987	1001	1442	6.0	CDMG	24277	Castaic-Hasley Canyon	70.9	A-B	-	.50	20.00	.021	1.5	.16	11.9	A-CSH-UP	
0117	Whittier Narrows	1987	1001	1442	6.0	CDMG	24277	Castaic-Hasley Canyon	70.9	A-B	-	.70	15.00	.031	1.9	.19	9.1	A-CSH000	
0117	Whittier Narrows	1987	1001	1442	6.0	CDMG	24277	Castaic-Hasley Canyon	70.9	A-B	-	.50	15.00	.035	2.6	.31	7.3	A-CSH090	
0117	Whittier Narrows	1987	1001	1442	6.0	CDMG	24278	Castaic-Old Ridge Route	78.3	A-B	B	1.00	23.00	.026	1.1	.08	12.3	A-ORR-UP	
0117	Whittier Narrows	1987	1001	1442	6.0	CDMG	24278	Castaic-Old Ridge Route	78.3	A-B	B	.80	15.00	.071	4.4	.40	7.2	A-ORR000	
0117	Whittier Narrows	1987	1001	1442	6.0	CDMG	24278	Castaic-Old Ridge Route	78.3	A-B	B	.80	20.00	.065	4.5	.38	6.4	A-ORR090	
0117	Whittier Narrows	1987	1001	1442	6.0	CDMG	24396	Malibu-Point Dume Sch	65.3	AMB	B	.35	30.00	.029	1.9	.15	108	A-MAL-UP	
0117	Whittier Narrows	1987	1001	1442	6.0	CDMG	24396	Malibu-Point Dume Sch	65.3	AMB	B	.35	25.00	.048	2.4	.32	5.5	A-MAL180	
0117	Whittier Narrows	1987	1001	1442	6.0	CDMG	24396	Malibu-Point Dume Sch	65.3	AMB	B	.60	20.00	.040	2.0	.18	5.6	A-MAL270	
0117	Whittier Narrows	1987	1001	1442	6.0	CDMG	13123	Riverside Airport	56.8	AQB	B	3.00	50.00	.044	.7	.01	8.3	A-RIV-UP	
0117	Whittier Narrows	1987	1001	1442	6.0	CDMG	13123	Riverside Airport	56.8	AQB	B	1.70	35.00	.050	1.4	.05	7.0	A-RIV180	
0117	Whittier Narrows	1987	1001	1442	6.0	CDMG	13123	Riverside Airport	56.8	AQB	B	2.00	45.00	.047	1.4	.04	4.9	A-RIV270	
0124	Georgia, USSR	1991	0615	0059	6.2		18	Ambralauri	73.7	A-A	-	.10		.007	1.0	.31	13.9	AMB--Z	
0124	Georgia, USSR	1991	0615	0059	6.2		18	Ambralauri	73.7	A-A	-	.10		.018	1.8	.54	9.9	AMB--X	
0124	Georgia, USSR	1991	0615	0059	6.2		18	Ambralauri	73.7	A-A	-	.10		.016	1.3	.39	10.0	AMB--Y	
0131	Northridge	1994	0117	1231	6.7	USC	90067	Duarte-Mel Canyon Rd	51.6	--B	B	.90	30.00	.046	2.2	.17	7.8	MEL-UP	
0131	Northridge	1994	0117	1231	6.7	USC	90067	Duarte-Mel Canyon Rd	51.6	--B	B	.10	30.00	.079	3.4	1.84	8.3	MEL090	
0131	Northridge	1994	0117	1231	6.7	USC	90067	Duarte-Mel Canyon Rd	51.6	--B	B	.30	30.00	.028	2.4	.46	8.4	MEL180	
0131	Northridge	1994	0117	1231	6.7	CDMG	23598	Rancho Cucamonga - Deer Can #	80.0	IGA	A	.30	46.00	.025	2.2	.40	13.6	CUC-UP	
0131	Northridge	1994	0117	1231	6.7	CDMG	23598	Rancho Cucamonga - Deer Can #	80.0	IGA	A	.30	46.00	.071	4.2	.56	11.0	CUC090	
0131	Northridge	1994	0117	1231	6.7	CDMG	23598	Rancho Cucamonga - Deer Can #	80.0	IGA	A	.30	46.00	.051	5.9	.78	10.2	CUC180	
0131	Northridge	1994	0117	1231	6.7	CDMG	14404	Rancho Palos Verdes-Hawth#	55.2	AMA	A	.30	23.00	.043	1.8	.39	9.0	RAN-UP	

B-11

No.	Earthquake	Date & Time				Mag	Own	No.	Station	Closest Dist (km)	Site Codes		Filter Corners			PGV (g)	PGD (cm/s)	Dur (s)	Filename
		YR	MODY	HRMN							Geom	USGS	HP (hz)	LP (hz)	PGA (g)				
0131	Northridge	1994	0117	1231	6.7	CDMG	14404	Rancho Palos Verdes-Hawth#	55.2	AMA	A	.30	23.00	.072	5.0	.73	6.5	RAN000	
0131	Northridge	1994	0117	1231	6.7	CDMG	14404	Rancho Palos Verdes-Hawth#	55.2	AMA	A	.30	23.00	.054	3.5	.98	8.1	RAN090	
0131	Northridge	1994	0117	1231	6.7	USC	90090	Villa Park - Serrano Ave	79.5	--B	C	.30	30.00	.027	2.5	.37	14.8	SER-UP	
0131	Northridge	1994	0117	1231	6.7	USC	90090	Villa Park - Serrano Ave	79.5	--B	C	.10	30.00	.043	3.1	1.19	9.5	SER000	
0131	Northridge	1994	0117	1231	6.7	USC	90090	Villa Park - Serrano Ave	79.5	--B	C	.10	30.00	.045	3.8	2.00	8.1	SER270	
0131	Northridge	1994	0117	1231	6.7	USC	90071	West Covina - S Orange Ave	54.1	--B	C	.20	30.00	.049	2.7	.95	10.6	SOR-UP	
0131	Northridge	1994	0117	1231	6.7	USC	90071	West Covina - S Orange Ave	54.1	--B	C	.20	30.00	.063	5.9	1.34	10.7	SOR225	
0131	Northridge	1994	0117	1231	6.7	USC	90071	West Covina - S Orange Ave	54.1	--B	C	.10	30.00	.067	5.8	2.65	10.4	SOR315	
0131	Northridge	1994	0117	1231	6.7	CDMG	23590	Wrightwood-Jackson Flat #	68.4	I-A	A	.24	46.00	.034	5.8	1.32	13.9	WWJ-UP	
0131	Northridge	1994	0117	1231	6.7	CDMG	23590	Wrightwood-Jackson Flat #	68.4	I-A	A	.24	46.00	.056	10.0	2.92	7.3	WWJ090	
0131	Northridge	1994	0117	1231	6.7	CDMG	23590	Wrightwood-Jackson Flat #	68.4	I-A	A	.24	46.00	.037	7.0	2.84	10.0	WWJ180	

NRC TIME HISTORY LIBRARY: WUS, ROCK, M=6-7, D=100-200 km

No.	Earthquake	Date & Time			Mag	Own	No.	Station	Closest Dist (km)	Site Codes		Filter Corners			Dur (s)	Filename		
		YR	MODY	HRMN						Geom	USGS	HP (hz)	LP (hz)	PGA (g)			PGV (g)	PGD (cm/s)
0028	Borrego Mtn	1968	0409	0230	6.8	SCE	280	San Onofre-So. Cal. Edison	124.7	ABB	-	.20	15.00	.062	1.9	.50	19.1	A-SON-UP
0028	Borrego Mtn	1968	0409	0230	6.8	SCE	280	San Onofre-So. Cal. Edison	124.7	ABB	-	.10	20.00	.041	3.7	1.72	20.3	A-SON033
0028	Borrego Mtn	1968	0409	0230	6.8	SCE	280	San Onofre-So. Cal. Edison	124.7	ABB	-	.20	20.00	.045	3.7	1.30	20.1	A-SON303
0030	San Fernando	1971	0209	1400	6.6	ACOE	1035	Isabella Dam (Aux Abut)	113.0	AGA	-	.10	20.00	.006	1.3	1.33	23.0	ISDDWN
0030	San Fernando	1971	0209	1400	6.6	ACOE	1035	Isabella Dam (Aux Abut)	113.0	AGA	-	.10	13.00	.006	1.4	1.94	20.0	ISD014
0030	San Fernando	1971	0209	1400	6.6	ACOE	1035	Isabella Dam (Aux Abut)	113.0	AGA	-	.10	13.00	.009	1.6	2.03	19.3	ISD284
0030	San Fernando	1971	0209	1400	6.6	CDWR	1041	Maricopa Array #1	115.0	IBB	-	.10	20.00	.005	1.1	1.40	20.2	MA1DWN
0030	San Fernando	1971	0209	1400	6.6	CDWR	1041	Maricopa Array #1	115.0	IBB	-	.10	13.00	.007	1.7	1.53	16.5	MA1130
0030	San Fernando	1971	0209	1400	6.6	CDWR	1041	Maricopa Array #1	115.0	IBB	-	.10	20.00	.011	2.4	2.33	16.3	MA1220
0030	San Fernando	1971	0209	1400	6.6	CDWR	1042	Maricopa Array #2	113.0	IBB	-	.20	20.00	.007	.7	.22	13.0	MA2DWN
0030	San Fernando	1971	0209	1400	6.6	CDWR	1042	Maricopa Array #2	113.0	IBB	-	.10	20.00	.009	1.3	1.03	14.7	MA2130
0030	San Fernando	1971	0209	1400	6.6	CDWR	1042	Maricopa Array #2	113.0	IBB	-	.20	15.00	.009	1.1	.41	12.3	MA2220
0030	San Fernando	1971	0209	1400	6.6	CDWR	1043	Maricopa Array #3	113.0	IBB	-	.20	15.00	.007	2.9	2.15	11.9	MA3DWN
0030	San Fernando	1971	0209	1400	6.6	CDWR	1043	Maricopa Array #3	113.0	IBB	-	.20	20.00	.008	2.2	1.85	11.7	MA3130
0030	San Fernando	1971	0209	1400	6.6	CDWR	1043	Maricopa Array #3	113.0	IBB	-	.10	20.00	.010	2.0	2.16	14.4	MA3220
0030	San Fernando	1971	0209	1400	6.6	SCE	280	San Onofre-So Cal Edison	122.0	ABB	-	.10	23.00	.011	.8	.77	9.8	SONDWN
0030	San Fernando	1971	0209	1400	6.6	SCE	280	San Onofre-So Cal Edison	122.0	ABB	-	.10	20.00	.013	1.7	.74	12.7	SON033
0030	San Fernando	1971	0209	1400	6.6	SCE	280	San Onofre-So Cal Edison	122.0	ABB	-	.20	20.00	.016	1.8	.63	9.4	SON303
0030	San Fernando	1971	0209	1400	6.6	CDWR	111	Cedar Springs, Allen Ranch	86.6	AAA	A	.20	35.00	.009	.9	.53	6.0	CSMDWN
0030	San Fernando	1971	0209	1400	6.6	CDWR	111	Cedar Springs, Allen Ranch	86.6	AAA	A	.20	35.00	.020	1.7	.49	5.6	CSM095
0030	San Fernando	1971	0209	1400	6.6	CDWR	111	Cedar Springs, Allen Ranch	86.6	AAA	A	.20	35.00	.015	1.4	.57	5.9	CSM185
0030	San Fernando	1971	0209	1400	6.6	ACOE	287	Upland-San Antonio Dam	58.1	AAA	B	.50	35.00	.032	1.3	.54	7.0	SODDWN
0030	San Fernando	1971	0209	1400	6.6	ACOE	287	Upland-San Antonio Dam	58.1	AAA	B	.50	35.00	.058	2.9	.55	7.1	SOD015
0030	San Fernando	1971	0209	1400	6.6	ACOE	287	Upland-San Antonio Dam	58.1	AAA	B	.50	35.00	.079	3.5	.50	6.3	SOD285
0131	Northridge	1994	0117	1231	6.7	USC	90067	Duarte-Mel Canyon Rd	51.6	--B	B	.90	30.00	.046	2.2	.17	7.8	MEL-UP
0131	Northridge	1994	0117	1231	6.7	USC	90067	Duarte-Mel Canyon Rd	51.6	--B	B	.10	30.00	.079	3.4	1.84	8.3	MEL090
0131	Northridge	1994	0117	1231	6.7	USC	90067	Duarte-Mel Canyon Rd	51.6	--B	B	.30	30.00	.028	2.4	.46	8.4	MEL180
0131	Northridge	1994	0117	1231	6.7	CDMG	23598	Rancho Cucamonga-Deer Can#	80.0	IGA	A	.30	46.00	.025	2.2	.40	13.6	CUC-UP
0131	Northridge	1994	0117	1231	6.7	CDMG	23598	Rancho Cucamonga-Deer Can#	80.0	IGA	A	.30	46.00	.071	4.2	.56	11.0	CUC090
0131	Northridge	1994	0117	1231	6.7	CDMG	23598	Rancho Cucamonga-Deer Can#	80.0	IGA	A	.30	46.00	.051	5.9	.78	10.2	CUC180
0131	Northridge	1994	0117	1231	6.7	CDMG	14404	Rancho Palos Verdes-Hawth#	55.2	AMA	A	.30	23.00	.043	1.8	.39	9.0	RAN-UP
0131	Northridge	1994	0117	1231	6.7	CDMG	14404	Rancho Palos Verdes-Hawth#	55.2	AMA	A	.30	23.00	.072	5.0	.73	6.5	RAN000
0131	Northridge	1994	0117	1231	6.7	CDMG	14404	Rancho Palos Verdes-Hawth#	55.2	AMA	A	.30	23.00	.054	3.5	.98	8.1	RAN090
0131	Northridge	1994	0117	1231	6.7	CDMG	13123	Riverside Airport #	101.3	AQB	B	.30	23.00	.022	2.3	.39	7.4	RIV-UP

B-13

No.	Earthquake	Date & Time			Mag	Own	No.	Station	Closest Dist (km)	Site Codes		Filter Corners			PGV (g)	PGD (cm/s)	Dur (s)	Filename
		YR	MODY	HRMN						Geom	USGS	HP (hz)	LP (hz)	PGA (g)				
0131	Northridge	1994	0117	1231	6.7	CDMG	13123	Riverside Airport #	101.3	AQB	B	.30	23.00	.059	2.7	.28	6.4	RIV180
0131	Northridge	1994	0117	1231	6.7	CDMG	13123	Riverside Airport #	101.3	AQB	B	.30	23.00	.064	3.1	.50	6.2	RIV270
0131	Northridge	1994	0117	1231	6.7	USC	90090	Villa Park - Serrano Ave	79.5	--B	C	.30	30.00	.027	2.5	.37	14.8	SER-UP
0131	Northridge	1994	0117	1231	6.7	USC	90090	Villa Park - Serrano Ave	79.5	--B	C	.30	30.00	.043	3.1	1.19	9.5	SER000
0131	Northridge	1994	0117	1231	6.7	USC	90071	West Covina - S Orange Ave	54.1	--B	C	.30	30.00	.045	3.8	2.00	8.1	SER270
0131	Northridge	1994	0117	1231	6.7	USC	90071	West Covina - S Orange Ave	54.1	--B	C	.20	30.00	.049	2.7	.95	10.6	SOR-UP
0131	Northridge	1994	0117	1231	6.7	USC	90071	West Covina - S Orange Ave	54.1	--B	C	.20	30.00	.063	5.9	1.34	10.7	SOR225
0131	Northridge	1994	0117	1231	6.7	USC	90071	West Covina - S Orange Ave	54.1	--B	C	.10	30.00	.067	5.8	2.65	10.4	SOR315
0131	Northridge	1994	0117	1231	6.7	CDMG	23590	Wrightwood-Jackson Flat #	68.4	I-A	A	.24	46.00	.034	5.8	1.32	13.9	WWJ-UP
0131	Northridge	1994	0117	1231	6.7	CDMG	23590	Wrightwood-Jackson Flat #	68.4	I-A	A	.24	46.00	.056	10.0	2.92	7.3	WWJ090
0131	Northridge	1994	0117	1231	6.7	CDMG	23590	Wrightwood-Jackson Flat #	68.4	I-A	A	.24	46.00	.037	7.0	2.84	10.0	WWJ180

NRC TIME HISTORY LIBRARY: WUS, ROCK, M>7, D=0-10 km

No.	Earthquake	Date & Time			Mag	Own	No.	Station	Closest Dist (km)	Site Codes		Filter Corners			Dur (s)	Filename		
		YR	MODY	HRMN						Geom	USGS	HP (hz)	LP (hz)	PGA (g)			PGV (g)	PGD (cm/s)
0041	Gazli, USSR	1976	0517		6.8	9201	Karakyr	3.0	AAA	-	.50	38.00	1.264	54.2	30.15	5.1	GAZ-UP	
0041	Gazli, USSR	1976	0517		6.8	9201	Karakyr	3.0	AAA	-	.50	38.00	.608	65.4	25.29	4.5	GAZ000	
0041	Gazli, USSR	1976	0517		6.8	9201	Karakyr	3.0	AAA	-	.50	38.00	.718	71.6	23.71	5.4	GAZ090	
0122	Loma Prieta	1989	1018	0005	6.9	CDMG	57007	Corralitos	5.1	APB	B	.20	32.00	.455	17.7	7.11	3.5	CLS-UP
0122	Loma Prieta	1989	1018	0005	6.9	CDMG	57007	Corralitos	5.1	APB	B	.20	40.00	.644	55.2	1088	3.4	CLS000
0122	Loma Prieta	1989	1018	0005	6.9	CDMG	57007	Corralitos	5.1	APB	B	.20	40.00	.479	45.2	11.37	4.6	CLS090
0122	Loma Prieta	1989	1018	0005	6.9	UCSC	16	LGPC	6.1	--A	-	.10		.890	54.9	17.56	4.5	LGP-UP
0122	Loma Prieta	1989	1018	0005	6.9	UCSC	16	LGPC	6.1	--A	-	.10		.563	94.8	41.18	5.5	LGP000
0122	Loma Prieta	1989	1018	0005	6.9	UCSC	16	LGPC	6.1	--A	-	.10		.605	51.0	11.50	5.5	LGP090
0122	Loma Prieta	1989	1018	0005	6.9	UCSC	13	BRAN	10.3	--A	-	.10		.507	17.9	4.17	6.2	BRN-UP
0122	Loma Prieta	1989	1018	0005	6.9	UCSC	13	BRAN	10.3	--A	-	.10		.453	51.3	8.37	5.6	BRN000
0122	Loma Prieta	1989	1018	0005	6.9	UCSC	13	BRAN	10.3	--A	-	.10		.501	44.6	4.86	6.9	BRN090
0127	Cape Mendocino	1992	0425	1806	7.1	CDMG	89005	Cape Mendocino #	8.5	IFA	A	.07	23.00	.754	63.0	109.48	2.2	CPM-UP
0127	Cape Mendocino	1992	0425	1806	7.1	CDMG	89005	Cape Mendocino #	8.5	IFA	A	.07	23.00	1.497	127.4	41.01	2.5	CPM000
0127	Cape Mendocino	1992	0425	1806	7.1	CDMG	89005	Cape Mendocino #	8.5	IFA	A	.07	23.00	1.039	42.0	12.39	2.9	CPM090
0129	Landers	1992	0628	1158	7.3	SCE	24	Lucerne	1.1	A-A	A	.08	60.00	.818	45.9	22.23	7.4	LCN-UP
0129	Landers	1992	0628	1158	7.3	SCE	24	Lucerne	1.1	A-A	A	.08	60.00	.721	97.6	70.31	8.4	LNC260
0129	Landers	1992	0628	1158	7.3	SCE	24	Lucerne	1.1	A-A	A	.08	60.00	.785	31.9	16.42	8.4	LCN345
0133	Kobe	1995	0116	2046	6.9	CEOR	99999	Kobe University	.2	--A	A	.20	30.00	.380	20.2	6.48	2.8	KBU-UP
0133	Kobe	1995	0116	2046	6.9	CEOR	99999	Kobe University	.2	--A	A	.20	30.00	.290	54.8	13.61	3.3	KBU000
0133	Kobe	1995	0116	2046	6.9	CEOR	99999	Kobe University	.2	--A	A	.20	30.00	.310	34.2	7.14	3.7	KBU090
0133	Kobe	1995	0116	2046	6.9		99999	KJMA	.6	--B	B	.05		.343	38.3	10.29	4.7	KJM-UP
0133	Kobe	1995	0116	2046	6.9		99999	KJMA	.6	--B	B	.05		.821	81.3	17.68	4.2	KJM000
0133	Kobe	1995	0116	2046	6.9		99999	KJMA	.6	--B	B	.05		.599	74.3	19.95	4.3	KJM090
0141	Kocaeli, Turkey	1999	0817		7.4	ERD	99999	Izmit	7.7	--A	A	2.00	30.00	.149	11.9	4.99	8.4	IZT-UP
0141	Kocaeli, Turkey	1999	0817		7.4	ERD	99999	Izmit	7.7	--A	A	.10	30.00	.152	22.6	9.81	8.2	IZT180
0141	Kocaeli, Turkey	1999	0817		7.4	ERD	99999	Izmit	7.7	--A	A	.10	30.00	.220	29.8	17.12	6.3	IZT090
0142	Chi-Chi, Taiwan	1999	0920		7.6	CWB	99999	CHY080	6.9	---	B	.03	50.00	.724	49.0	27.82	5.9	CHY080-V
0142	Chi-Chi, Taiwan	1999	0920		7.6	CWB	99999	CHY080	6.9	---	B	.05	50.00	.902	102.4	33.97	5.7	CHY080-N
0142	Chi-Chi, Taiwan	1999	0920		7.6	CWB	99999	CHY080	6.9	---	B	.10	50.00	.968	107.5	18.60	7.0	CHY080-W
0142	Chi-Chi, Taiwan	1999	0920		7.6	CWB	99999	TCU087	3.1	--1	b	.02	30.00	.108	61.5	51.32	9.8	TCU087-V
0142	Chi-Chi, Taiwan	1999	0920		7.6	CWB	99999	TCU087	3.1	--1	b	.05	30.00	.122	37.1	25.54	16.1	TCU087-N
0142	Chi-Chi, Taiwan	1999	0920		7.6	CWB	99999	TCU087	3.1	--1	b	.02	30.00	.128	40.8	62.62	14.9	TCU087-W
0142	Chi-Chi, Taiwan	1999	0920		7.6	CWB	99999	TCU089	8.2	--1	b	.03	50.00	.191	22.3	24.36	18.0	TCU089-V

B-15

No.	Earthquake	Date & Time			Mag	Own	No.	Station	Closest Dist (km)	Site Codes		Filter Corners			PGV (g)	PGD (cm/s)	Dur (s)	Filename
		YR	MODY	HRMN						Geom	USGS	HP (hz)	LP (hz)	PGA (g)				
0142	Chi-Chi, Taiwan	1999	0920		7.6	CWB	99999	TCU089	8.2	--1	b	.04	50.00	.248	31.0	32.37	21.8	TCU089-N
0142	Chi-Chi, Taiwan	1999	0920		7.6	CWB	99999	TCU089	8.2	--1	b	.07	50.00	.333	30.9	18.48	19.3	TCU089-W
0142	Chi-Chi, Taiwan	1999	0920		7.6	CWB	99999	TCU120	8.1	--1	B	.03	50.00	.162	32.1	22.34	19.5	TCU120-V
0142	Chi-Chi, Taiwan	1999	0920		7.6	CWB	99999	TCU120	8.1	--1	B	.03	50.00	.192	36.9	33.30	21.7	TCU120-N
0142	Chi-Chi, Taiwan	1999	0920		7.6	CWB	99999	TCU120	8.1	--1	B	.02	50.00	.225	63.1	54.09	19.7	TCU120-W
0142	Chi-Chi, Taiwan	1999	0920		7.6	CWB	99999	TCU128	9.7	--1	B	.02	40.00	.097	46.0	34.77	18.1	TCU128-V
0142	Chi-Chi, Taiwan	1999	0920		7.6	CWB	99999	TCU128	9.7	--1	B	.05	30.00	.170	68.8	41.87	10.6	TCU128-N
0142	Chi-Chi, Taiwan	1999	0920		7.6	CWB	99999	TCU128	9.7	--1	B	.02	30.00	.139	73.0	90.62	13.5	TCU128-W
0142	Chi-Chi, Taiwan	1999	0920		7.6	CWB	99999	TCU136	8.9	----	B	.03	40.00	.123	27.3	30.19	17.6	TCU136-V
0142	Chi-Chi, Taiwan	1999	0920		7.6	CWB	99999	TCU136	8.9	----	B	.03	50.00	.171	55.8	66.48	17.4	TCU136-E
0142	Chi-Chi, Taiwan	1999	0920		7.6	CWB	99999	TCU136	8.9	----	B	.03	50.00	.177	47.5	44.82	19.2	TCU136-N

NRC TIME HISTORY LIBRARY: WUS, ROCK, M>7, D=10-50 km

No.	Earthquake	Date & Time				Mag	Own	No.	Station	Closest Dist (km)	Site Codes		Filter Corners			PGV (g)	PGD (cm/s)	Dur (s)	Filename
		YR	MODY	HRMN							Geom	USGS	HP (hz)	LP (hz)	PGA (g)				
0046	Tabas, Iran	1978	0916		7.4		9102	Dayhook	17.0	ABB	-	.10	.183	12.0	4.97	8.3	DAY-UP		
0046	Tabas, Iran	1978	0916		7.4		9102	Dayhook	17.0	ABB	-	.10	.328	20.6	12.56	6.7	DAY-LN		
0046	Tabas, Iran	1978	0916		7.4		9102	Dayhook	17.0	ABB	-	.10	.406	26.5	8.75	6.9	DAY-TR		
0127	Cape Mendocino	1992	0425	1806	7.1	CDMG	89530	Shelter Cove Airport #	33.8	IFB	B	.50	23.00	.054	2.0	.33	15.5	SHL-UP	
0127	Cape Mendocino	1992	0425	1806	7.1	CDMG	89530	Shelter Cove Airport #	33.8	IFB	B	.50	23.00	.229	7.1	.39	13.6	SHL000	
0127	Cape Mendocino	1992	0425	1806	7.1	CDMG	89530	Shelter Cove Airport #	33.8	IFB	B	.50	23.00	.189	6.6	.57	14.8	SHL090	
0129	Landers	1992	0628	1158	7.3	CDMG	22161	Twentynine Palms #	42.2	AGA	A	.12	23.00	.040	3.3	1.93	22.7	P-UP	
0129	Landers	1992	0628	1158	7.3	CDMG	22161	Twentynine Palms #	42.2	AGA	A	.12	23.00	.080	3.7	2.34	21.6	P000	
0129	Landers	1992	0628	1158	7.3	CDMG	22161	Twentynine Palms #	42.2	AGA	A	.12	23.00	.060	4.9	4.30	20.4	P090	
0141	Kocaeli, Turkey	1999	0817		7.4	KOERI	99999	Arcelik	17.0	--B	B	1.50	80.00	.086	2.6	.22	8.7	ARCDWN	
0141	Kocaeli, Turkey	1999	0817		7.4	KOERI	99999	Arcelik	17.0	--B	B	.80	70.00	.180	10.5	.90	7.7	ARC000	
0141	Kocaeli, Turkey	1999	0817		7.4	KOERI	99999	Arcelik	17.0	--B	B	.90	70.00	.108	6.2	.63	4.4	ARC090	
0141	Kocaeli, Turkey	1999	0817		7.4	ERD	9999	Gebze	17.0	--A	A	1.00	40.00	.151	6.3	.59	5.6	GBZ-UP	
0141	Kocaeli, Turkey	1999	0817		7.4	ERD	9999	Gebze	17.0	--A	A	.06	25.00	.244	50.3	42.74	5.3	GBZ000	
0141	Kocaeli, Turkey	1999	0817		7.4	ERD	9999	Gebze	17.0	--A	A	.08	30.00	.137	29.7	27.54	5.7	GBZ270	
0141	Kocaeli, Turkey	1999	0817		7.4	ERD	9999	Goy nuk	35.5	--B	-	.10	30.00	.114	11.5	7.59	6.6	GYN-UP	
0141	Kocaeli, Turkey	1999	0817		7.4	ERD	9999	Goy nuk	35.5	--B	-	.15	30.00	.132	8.8	3.05	5.5	GYN000	
0141	Kocaeli, Turkey	1999	0817		7.4	ERD	9999	Goy nuk	35.5	--B	-	.10	25.00	.119	10.5	3.94	4.4	GYN090	
0141	Kocaeli, Turkey	1999	0817		7.4	ERD	9999	Iz nik	29.7	--D	C	.30	30.00	.083	7.7	1.70	9.9	IZN-UP	
0141	Kocaeli, Turkey	1999	0817		7.4	ERD	9999	Iz nik	29.7	--D	C	.15	25.00	.103	16.5	7.00	12.7	IZN180	
0141	Kocaeli, Turkey	1999	0817		7.4	ERD	9999	Iz nik	29.7	--D	C	.07	25.00	.136	28.8	17.44	10.7	IZN090	
0142	Chi-Chi, Taiwan	1999	0920		7.6	CWB	99999	HWA056	48.7	----	A	.02	50.00	.062	7.1	10.35	10.7	HWA056-V	
0142	Chi-Chi, Taiwan	1999	0920		7.6	CWB	99999	HWA056	48.7	----	A	.03	50.00	.107	10.8	10.36	9.5	HWA056-N	
0142	Chi-Chi, Taiwan	1999	0920		7.6	CWB	99999	HWA056	48.7	----	A	.02	50.00	.107	11.7	17.64	9.2	HWA056-W	
0142	Chi-Chi, Taiwan	1999	0920		7.6	CWB	99999	TCU015	47.3	--1	B	.02	50.00	.068	17.2	14.85	19.1	TCU015-V	
0142	Chi-Chi, Taiwan	1999	0920		7.6	CWB	99999	TCU015	47.3	--1	B	.03	50.00	.114	29.5	24.14	12.7	TCU015-N	
0142	Chi-Chi, Taiwan	1999	0920		7.6	CWB	99999	TCU015	47.3	--1	B	.02	50.00	.119	49.8	49.79	15.7	TCU015-W	
0142	Chi-Chi, Taiwan	1999	0920		7.6	CWB	99999	TCU046	14.3	--1	A	.03	30.00	.104	32.3	37.74	9.5	TCU046-V	
0142	Chi-Chi, Taiwan	1999	0920		7.6	CWB	99999	TCU046	14.3	--1	A	.06	30.00	.116	30.9	23.18	10.8	TCU046-N	
0142	Chi-Chi, Taiwan	1999	0920		7.6	CWB	99999	TCU046	14.3	--1	A	.03	30.00	.133	39.8	37.37	11.5	TCU046-W	
0142	Chi-Chi, Taiwan	1999	0920		7.6	CWB	99999	TCU047	33.0	----	B	.02	50.00	.270	26.9	17.88	11.6	TCU047-V	
0142	Chi-Chi, Taiwan	1999	0920		7.6	CWB	99999	TCU047	33.0	----	B	.03	50.00	.413	40.2	22.22	9.8	TCU047-N	
0142	Chi-Chi, Taiwan	1999	0920		7.6	CWB	99999	TCU047	33.0	----	B	.02	50.00	.301	41.6	51.08	10.1	TCU047-W	
0142	Chi-Chi, Taiwan	1999	0920		7.6	CWB	99999	TCU095	43.4	--1	B	.02	50.00	.255	21.8	21.95	13.0	TCU095-V	

B-17

No.	Earthquake	YR	Date & Time			Own	No.	Station	Closest Dist (km)	Site Codes		Filter Corners			PGV (g)	PGD (cm/s)	Dur (s)	Filename
			MODY	HRMN	Mag					Geom	USGS	HP (hz)	LP (hz)	PGA (g)				
0142	Chi-Chi, Taiwan	1999	0920		7.6	CWB	99999	TCU095	43.4	--1	B	.04	50.00	.712	49.1	24.45	8.3	TCU095-N
0142	Chi-Chi, Taiwan	1999	0920		7.6	CWB	99999	TCU095	43.4	--1	B	.02	50.00	.378	62.0	51.75	8.3	TCU095-W
0143	Duzce, Turkey	1999	1112		7.1	ERD	99999	Bolu	16.0	--D	C	.05		.203	17.3	14.29	6.0	BOL-UP
0143	Duzce, Turkey	1999	1112		7.1	ERD	99999	Bolu	16.0	--D	C	.05		.728	56.4	23.07	2.6	BOL000
0143	Duzce, Turkey	1999	1112		7.1	ERD	99999	Bolu	16.0	--D	C	.05		.822	62.1	13.55	1.5	BOL090
0143	Duzce, Turkey	1999	1112		7.1	ERD	99999	Mudumu	34..6	--A	-	.08		.060	10.6	7.33	19.5	MDR-UP
0143	Duzce, Turkey	1999	1112		7.1	ERD	99999	Mudumu	34..6	--A	-	.08		.120	9.3	7.63	17.1	MDR000
0143	Duzce, Turkey	1999	1112		7.1	ERD	99999	Mudumu	34..6	--A	-	.08		.056	16.3	15.37	18.6	MDR090
0143	Duzce, Turkey	1999	1112		7.1	ERD	99999	Sakarya	42.7	--B	B	.05	40.00	.011	3.2	4.00	17.4	SKR-UP
0143	Duzce, Turkey	1999	1112		7.1	ERD	99999	Sakarya	42.7	--B	B	.05	40.00	.023	5.5	5.80	16.9	SKR180
0143	Duzce, Turkey	1999	1112		7.1	ERD	99999	Sakarya	42.7	--B	B	.05	40.00	.016	5.5	7.34	17.1	SKR090

NRC TIME HISTORY LIBRARY: WUS, ROCK, M>7, D=50-100 km

No.	Earthquake	Date & Time			Mag	Own	No.	Station	Closest Dist (km)	Site Codes		Filter Corners				Dur (s)	Filename	
		YR	MODY	HRMN						Geom	USGS	HP (hz)	LP (hz)	PGA (g)	PGV (g)			PGD (cm/s)
0046	Tabas, Iran	1978	0916		7.4	71	Ferdows	94.4	--A	-	.04	.053	7.6	6.78	21.9	FER-V1		
0046	Tabas, Iran	1978	0916		7.4	71	Ferdows	94.4	--A	-	.02	20.00	.087	5.7	4.61	16.6	FER-L1	
0046	Tabas, Iran	1978	0916		7.4	71	Ferdows	94.4	--A	-	.04	20.00	.108	8.6	9.69	20.5	FER-T1	
0129	Landers	1992	0628	1158	7.3	CDMG	21081	Amboy #	69.2	AAB	A	.10	23.00	.090	11.0	3.25	22.1	ABY-UP
0129	Landers	1992	0628	1158	7.3	CDMG	21081	Amboy #	69.2	AAB	A	.10	23.00	.115	18.3	11.16	17.7	ABY000
0129	Landers	1992	0628	1158	7.3	CDMG	21081	Amboy #	69.2	AAB	A	.10	23.00	.146	20.0	7.38	17.1	ABY090
0129	Landers	1992	0628	1158	7.3	CDMG	12168	Puerta La Cruz #	95.9	AQB	B	.30	23.00	.038	1.7	.48	26.3	PLC-UP
0129	Landers	1992	0628	1158	7.3	CDMG	12168	Puerta La Cruz #	95.9	AQB	B	.30	23.00	.047	2.0	.41	25.3	PLC000
0129	Landers	1992	0628	1158	7.3	CDMG	12168	Puerta La Cruz #	95.9	AQB	B	.30	23.00	.044	2.0	.63	24.3	PLC090
0129	Landers	1992	0628	1158	7.3	CDMG	13123	Riverside Airport #	96.1	AQB	B	.16	23.00	.040	1.7	1.01	21.8	RIV-UP
0129	Landers	1992	0628	1158	7.3	CDMG	13123	Riverside Airport #	96.1	AQB	B	.16	23.00	.043	3.0	1.62	18.6	RIV180
0129	Landers	1992	0628	1158	7.3	CDMG	13123	Riverside Airport #	96.1	AQB	B	.16	23.00	.041	3.2	1.38	16.6	RIV270
0129	Landers	1992	0628	1158	7.3	CDMG	12206	Silent Valley - Poppet Flat #	51.7	IGA	A	.12	23.00	.038	3.2	2.08	19.7	SIL-UP
0129	Landers	1992	0628	1158	7.3	CDMG	12206	Silent Valley - Poppet Flat #	51.7	IGA	A	.12	23.00	.050	3.8	2.03	20.3	SIL000
0129	Landers	1992	0628	1158	7.3	CDMG	12206	Silent Valley - Poppet Flat #	51.7	IGA	A	.12	23.00	.040	5.1	3.88	21.5	SIL090
0141	Kocaeli, Turkey	1999	0817		7.4	ITU	99999	Mecidiyekoy	62.3	--B	B	1.10	60.00	.028	1.3	.16	12.1	MCD-V
0141	Kocaeli, Turkey	1999	0817		7.4	ITU	99999	Mecidiyekoy	62.3	--B	B	.20	50.00	.053	3.8	1.49	10.7	MCD000
0141	Kocaeli, Turkey	1999	0817		7.4	ITU	99999	Mecidiyekoy	62.3	--B	B	.05	60.00	.068	8.8	10.11	10.0	MCD090
0142	Chi-Chi, Taiwan	1999	0920		7.6	CWB	99999	NSK	64.5	--1	A	.20	50.00	.034	5.1	1.12	11.5	NSK-V
0142	Chi-Chi, Taiwan	1999	0920		7.6	CWB	99999	NSK	64.5	--1	A	.02	30.00	.070	6.9	4.22	7.8	NSK-E
0142	Chi-Chi, Taiwan	1999	0920		7.6	CWB	99999	NSK	64.5	--1	A	.20	33.00	.065	5.1	1.20	11.7	NSK-N
0142	Chi-Chi, Taiwan	1999	0920		7.6	CWB	99999	TAP035	96.8	--1	A	.02	24.00	.028	7.6	9.01	18.6	TAP035-V
0142	Chi-Chi, Taiwan	1999	0920		7.6	CWB	99999	TAP035	96.8	--1	A	.02	24.00	.085	8.3	8.00	13.8	TAP035-N
0142	Chi-Chi, Taiwan	1999	0920		7.6	CWB	99999	TAP035	96.8	--1	A	.02	24.00	.067	8.4	12.78	15.1	TAP035-W
0142	Chi-Chi, Taiwan	1999	0920		7.6	CWB	99999	TAP036	95.6	--1	A	.02	30.00	.017	6.9	9.05	21.4	TAP036-V
0142	Chi-Chi, Taiwan	1999	0920		7.6	CWB	99999	TAP036	95.6	--1	A	.02	30.00	.039	6.1	5.83	14.9	TAP036-N
0142	Chi-Chi, Taiwan	1999	0920		7.6	CWB	99999	TAP036	95.6	--1	A	.02	20.00	.030	7.6	10.69	15.4	TAP036-W
0142	Chi-Chi, Taiwan	1999	0920		7.6	CWB	99999	TCU025	54.3	---	A	.05	50.00	.034	13.8	18.29	13.2	TCU025-V
0142	Chi-Chi, Taiwan	1999	0920		7.6	CWB	99999	TCU025	54.3	---	A	.05	50.00	.058	10.5	10.17	11.8	TCU025-N
0142	Chi-Chi, Taiwan	1999	0920		7.6	CWB	99999	TCU025	54.3	---	A	.05	50.00	.075	19.0	22.00	12.7	TCU025-W
0142	Chi-Chi, Taiwan	1999	0920		7.6	CWB	99999	ILA031	94.7	--1	A	.00	50.00	.030	7.3	9.75	17.1	ILA031-V
0142	Chi-Chi, Taiwan	1999	0920		7.6	CWB	99999	ILA031	94.7	--1	A	.00	30.00	.076	9.1	10.68	11.4	ILA031-N
0142	Chi-Chi, Taiwan	1999	0920		7.6	CWB	99999	ILA031	94.7	--1	A	.00	50.00	.057	10.0	9.94	11.6	ILA031-W
0142	Chi-Chi, Taiwan	1999	0920		7.6	CWB	99999	ILA051	90.3	---	A	.02	24.00	.024	8.4	10.13	18.9	ILA051-V

B-19

No.	Earthquake	Date & Time			Mag	Own	No.	Station	Closest Dist (km)	Site Codes		Filter Corners			PGV (g)	PGD (cm/s)	Dur (s)	Filename
		YR	MODY	HRMN						Geom	USGS	HP (hz)	LP (hz)	PGA (g)				
0142	Chi-Chi, Taiwan	1999	0920		7.6	CWB	99999	ILA051	90.3	----	A	.02	22.00	.033	7.3	9.19	19.8	ILA051-N
0142	Chi-Chi, Taiwan	1999	0920		7.6	CWB	99999	ILA051	90.3	----	A	.02	22.00	.080	12.3	9.66	11.6	ILA051-W
0142	Chi-Chi, Taiwan	1999	0920		7.6	CWB	99999	ILA063	71.6	----	A	.04	50.00	.031	7.3	9.45	14.7	ILA063-V
0142	Chi-Chi, Taiwan	1999	0920		7.6	CWB	99999	ILA063	71.6	----	A	.02	50.00	.091	8.1	12.98	13.7	ILA063-N
0142	Chi-Chi, Taiwan	1999	0920		7.6	CWB	99999	ILA063	71.6	----	A	.02	50.00	.082	12.6	8.81	13.0	ILA063-W
0142	Chi-Chi, Taiwan	1999	0920		7.6	CWB	99999	HWA023	57.0	--2	A	.03	50.00	.026	7.6	10.14	13.1	HWA023-V
0142	Chi-Chi, Taiwan	1999	0920		7.6	CWB	99999	HWA023	57.0	--2	A	.04	40.00	.037	6.6	9.03	9.5	HWA023-N
0142	Chi-Chi, Taiwan	1999	0920		7.6	CWB	99999	HWA023	57.0	--2	A	.04	40.00	.037	8.6	13.88	12.5	HWA023-W
0142	Chi-Chi, Taiwan	1999	0920		7.6	CWB	99999	HWA026	58.8	----	A	.02	50.00	.038	6.7	9.93	15.0	HWA026-V
0142	Chi-Chi, Taiwan	1999	0920		7.6	CWB	99999	HWA026	58.8	----	A	.03	50.00	.058	9.1	9.74	9.3	HWA026-N
0142	Chi-Chi, Taiwan	1999	0920		7.6	CWB	99999	HWA026	58.8	----	A	.02	50.00	.071	11.2	18.17	9.9	HWA026-W

NRC TIME HISTORY LIBRARY: WUS, ROCK, M>7, D=100-200 km

No.	Earthquake	Date & Time			Mag	Own	No.	Station	Closest Dist (km)	Site Codes		Filter Corners		PGA (g)	PGV (g)	PGD (cm/s)	Dur (s)	Filename
		YR	MODY	HRMN						Geom	USGS	HP (hz)	LP (hz)					
0046	Tabas, Iran	1978	0916		7.4		72	Kashmar	199.1	--B	-	.05	20.00	.026	7.4	6.78	17.2	KSH-V1
0046	Tabas, Iran	1978	0916		7.4		72	Kashmar	199.1	--B	-	.03	20.00	.034	10.7	10.60	16.8	KSH-L1
0046	Tabas, Iran	1978	0916		7.4		72	Kashmar	199.1	--B	-	.02	20.00	.037	11.4	7.10	15.9	KSH-T1
0129	Landers	1992	0628	1158	7.3	USC	90052	Calabasas-N Las Virg	194.1	--B	B	.50	25.00	.013	1.4	.31	27.5	VIR-UP
0129	Landers	1992	0628	1158	7.3	USC	90052	Calabasas-N Las Virg	194.1	--B	B	.28	25.00	.018	2.8	.81	20.9	VIR200
0129	Landers	1992	0628	1158	7.3	USC	90052	Calabasas-N Las Virg	194.1	--B	B	.20	22.00	.012	2.5	.95	20.8	VIR290
0129	Landers	1992	0628	1158	7.3	USC	90067	Duarte-Mel Canyon Rd #	126.4	--B	B	.28	25.00	.019	4.0	1.14	15.5	MEL-UP
0129	Landers	1992	0628	1158	7.3	USC	90067	Duarte-Mel Canyon Rd #	126.4	--B	B	.28	25.00	.026	3.5	.86	14.7	MEL090
0129	Landers	1992	0628	1158	7.3	USC	90067	Duarte-Mel Canyon Rd #	126.4	--B	B	.30	25.00	.017	2.8	1.05	15.5	MEL180
0129	Landers	1992	0628	1158	7.3	USC	90019	San Gabriel - E Grand Ave	141.6	--A	A	.16	22.00	.022	6.3	2.97	25.3	GRN-UP
0129	Landers	1992	0628	1158	7.3	USC	90019	San Gabriel - E Grand Ave	141.6	--A	A	.07	25.00	.041	14.1	15.03	20.9	GRN180
0129	Landers	1992	0628	1158	7.3	USC	90019	San Gabriel - E Grand Ave	141.6	--A	A	.13	25.00	.036	9.6	6.03	23.0	GRN270
0129	Landers	1992	0628	1158	7.3	USC	90008	Sun Valley - Sunland #	162.6	--B	B	1.00	25.00	.012	.9	.08	24.5	SUL-UP
0129	Landers	1992	0628	1158	7.3	USC	90008	Sun Valley - Sunland #	162.6	--B	B	.33	25.00	.027	2.6	.71	24.5	SUL230
0129	Landers	1992	0628	1158	7.3	USC	90008	Sun Valley - Sunland #	162.6	--B	B	.45	25.00	.021	2.9	.60	21.8	SUL320
0129	Landers	1992	0628	1158	7.3	USC	90090	Villa Park - Serrano Ave #	131.4	--B	B	.20	25.00	.021	2.8	.93	31.3	SER-UP
0129	Landers	1992	0628	1158	7.3	USC	90090	Villa Park - Serrano Ave #	131.4	--B	B	.11	25.00	.028	8.0	5.32	20.9	SER000
0129	Landers	1992	0628	1158	7.3	USC	90090	Villa Park - Serrano Ave #	131.4	--B	B	.18	25.00	.035	7.0	3.51	19.5	SER270
0142	Chi Chi, Taiwan	1999	0920		7.6	CWB	99999	PNG	114.2	--1	A	.40	30.00	.013	1.2	.21	26.8	PNG-V
0142	Chi Chi, Taiwan	1999	0920		7.6	CWB	99999	PNG	114.2	--1	A	.24	40.00	.028	1.6	.52	24.0	PNG-E
0142	Chi Chi, Taiwan	1999	0920		7.6	CWB	99999	PNG	114.2	--1	A	.22	30.00	.035	2.4	.75	22.4	PNG-N
0142	Chi Chi, Taiwan	1999	0920		7.6	CWB	99999	KAU078	102.8	--1	A	.03	50.00	.015	2.6	2.44	29.0	KAU078-V
0142	Chi Chi, Taiwan	1999	0920		7.6	CWB	99999	KAU078	102.8	--1	A	.02	50.00	.024	2.2	3.17	26.8	KAU078-N
0142	Chi Chi, Taiwan	1999	0920		7.6	CWB	99999	KAU078	102.8	--1	A	.02	50.00	.046	2.6	3.64	20.9	KAU078-W
0142	Chi Chi, Taiwan	1999	0920		7.6	CWB	99999	TAP059	125.9	--1	A	.02	20.00	.018	5.7	6.82	24.0	TAP059-V
0142	Chi Chi, Taiwan	1999	0920		7.6	CWB	99999	TAP059	125.9	--1	A	.02	30.00	.039	6.5	4.80	21.0	TAP059-N
0142	Chi Chi, Taiwan	1999	0920		7.6	CWB	99999	TAP059	125.9	--1	A	.00	15.00	.030	7.6	8.11	19.0	TAP059-W
0142	Chi Chi, Taiwan	1999	0920		7.6	CWB	99999	TAP060	128.4	--1	A	.02	24.00	.014	5.0	7.02	25.4	TAP060-V
0142	Chi Chi, Taiwan	1999	0920		7.6	CWB	99999	TAP060	128.4	--1	A	.02	20.00	.036	7.6	6.05	17.6	TAP060-N
0142	Chi Chi, Taiwan	1999	0920		7.6	CWB	99999	TAP060	128.4	--1	A	.00	20.00	.036	11.0	8.80	10.0	TAP060-W
0142	Chi Chi, Taiwan	1999	0920		7.6	CWB	99999	TAP067	104.2	--1	A	.03	20.00	.037	8.4	10.40	20.6	TAP067-V
0142	Chi Chi, Taiwan	1999	0920		7.6	CWB	99999	TAP067	104.2	--1	A	.02	20.00	.042	9.6	8.18	15.8	TAP067-N
0142	Chi Chi, Taiwan	1999	0920		7.6	CWB	99999	TAP067	104.2	--1	A	.02	20.00	.039	11.5	12.16	12.8	TAP067-W
0142	Chi Chi, Taiwan	1999	0920		7.6	CWB	99999	TAP069	135.3	--1	A	.04	20.00	.013	5.2	6.49	26.9	TAP069-V

B-21

No.	Earthquake	YR	Date & Time		Mag	Own	No.	Station	Closest Dist (km)	Site Codes		Filter Corners			PGV (g)	PGD (cm/s)	Dur (s)	Filename
			MODY	HRMN						Geom	USGS	HP (hz)	LP (hz)	PGA (g)				
0142	Chi Chi, Taiwan	1999	0920		7.6	CWB	99999	TAP069	135.3	--1	A	.05	20.00	.033	5.8	4.58	9.4	TAP069-N
0142	Chi Chi, Taiwan	1999	0920		7.6	CWB	99999	TAP069	135.3	--1	A	.04	20.00	.026	5.0	8.69	16.2	TAP069-W
0142	Chi Chi, Taiwan	1999	0920		7.6	CWB	99999	TAP072	110.0	--1	A	.03	30.00	.018	7.5	9.54	24.6	TAP072-V
0142	Chi Chi, Taiwan	1999	0920		7.6	CWB	99999	TAP072	110.0	--1	A	.04	30.00	.050	11.4	6.59	10.2	TAP072-N
0142	Chi Chi, Taiwan	1999	0920		7.6	CWB	99999	TAP072	110.0	--1	A	.03	50.00	.029	7.5	8.67	18.4	TAP072-W
0142	Chi Chi, Taiwan	1999	0920		7.6	CWB	99999	TAP075	118.4	---	A	.03	30.00	.024	6.3	8.90	22.3	TAP075-V
0142	Chi Chi, Taiwan	1999	0920		7.6	CWB	99999	TAP075	118.4	---	A	.02	50.00	.050	9.7	6.49	15.8	TAP075-N
0142	Chi Chi, Taiwan	1999	0920		7.6	CWB	99999	TAP075	118.4	---	A	.01	30.00	.083	10.3	11.98	12.3	TAP075-W
0142	Chi Chi, Taiwan	1999	0920		7.6	CWB	99999	TAP078	131.0	---	A	.03	33.00	.018	5.4	8.02	24.3	TAP078-V
0142	Chi Chi, Taiwan	1999	0920		7.6	CWB	99999	TAP078	131.0	---	A	.04	40.00	.042	8.6	5.60	13.3	TAP078-N
0142	Chi Chi, Taiwan	1999	0920		7.6	CWB	99999	TAP078	131.0	---	A	.02	40.00	.043	6.9	8.98	19.8	TAP078-W

TABLE B-2: WUS, SOIL
 NRC TIME HISTORY LIBRARY: WUS, SOIL, M=5-6, D=0-50 km

B-23

No.	Earthquake	Date & Time				Mag	Own	No.	Station	Closest Dist (km)	Site Codes		Filter Corners			Dur (s)	Filename	
		YR	MODY	HRMN							Geom	USGS	HP (hz)	LP (hz)	PGA (g)			PGV (g)
0026	Northern Calif	1967	1210	1206	5.6	USGS	1023	Ferndale City Hall	30.8	BQD	C	.40	12.00	.032	3.3	.46	8.7	C-FRN-UP
0026	Northern Calif	1967	1210	1206	5.6	USGS	1023	Ferndale City Hall	30.8	BQD	C	.30	20.00	.283	9.2	1.23	1.3	C-FRN224
0026	Northern Calif	1967	1210	1206	5.6	USGS	1023	Ferndale City Hall	30.8	BQD	C	.20	13.00	.113	11.1	1.58	6.0	C-FRN314
0058	Mammoth Lakes	1980	0525	1944	6.0	CDMG	54099	Convict Creek	17.4	AQD	-	.20	40.00	.195	8.5	1.58	3.3	A-CVK-UP
0058	Mammoth Lakes	1980	0525	1944	6.0	CDMG	54099	Convict Creek	17.4	AQD	-	.08	30.00	.219	18.5	4.87	2.8	A-CVK090
0058	Mammoth Lakes	1980	0525	1944	6.0	CDMG	54099	Convict Creek	17.4	AQD	-	.08	35.00	.208	16.1	2.29	2.1	A-CVK180
0074	Mammoth Lakes	1983	0107	0138	5.2	CDMG	54099	Convict Creek	9.5	AQD	-	.20	40.00	.097	7.9	1.65	3.9	F-CVK-UP
0074	Mammoth Lakes	1983	0107	0138	5.2	CDMG	54099	Convict Creek	9.5	AQD	-	.15	30.00	.165	14.4	2.05	2.8	F-CVK090
0074	Mammoth Lakes	1983	0107	0138	5.2	CDMG	54099	Convict Creek	9.5	AQD	-	.15	30.00	.153	18.7	2.88	1.9	F-CVK180
0077	Coalinga	1983	0509	0249	5.0	USGS	1606	Burnett Construction	17.7	AHD	-	.40	30.00	.077	2.0	.15	2.6	A-BNT-UP
0077	Coalinga	1983	0509	0249	5.0	USGS	1606	Burnett Construction	17.7	AHD	-	.50	30.00	.095	3.5	.37	3.6	A-BNT270
0077	Coalinga	1983	0509	0249	5.0	USGS	1606	Burnett Construction	17.7	AHD	-	.40	25.00	.095	4.5	.35	2.2	A-BNT360
0079	Coalinga	1983	0709	0740	5.2	CDMG	46T04	CHP (temp)	14.9	AHD	-	.45	30.00	.079	2.4	.22	3.7	C-CHP-UP
0079	Coalinga	1983	0709	0740	5.2	CDMG	46T04	CHP (temp)	14.9	AHD	-	.30	25.00	.204	8.0	.62	2.0	C-CHP000
0079	Coalinga	1983	0709	0740	5.2	CDMG	46T04	CHP (temp)	14.9	AHD	-	.30	25.00	.171	5.4	.38	2.2	C-CHP090
0103	N. Palm Springs	1986	0708	0920	6.0	USGS	5073	Cabazon	16.3	AHD	-	.20	45.00	.363	7.4	.84	2.0	CAB-UP
0103	N. Palm Springs	1986	0708	0920	6.0	USGS	5073	Cabazon	16.3	AHD	-	.15	40.00	.217	7.6	1.96	2.6	CAB180
0103	N. Palm Springs	1986	0708	0920	6.0	USGS	5073	Cabazon	16.3	AHD	-	.15	40.00	.212	16.3	2.24	1.5	CAB270
0103	N. Palm Springs	1986	0708	0920	6.0	USGS	5072	Whitewater Trout Farm	7.3	AHC	A	.50	40.00	.471	13.4	1.02	2.3	WWT-UP
0103	N. Palm Springs	1986	0708	0920	6.0	USGS	5072	Whitewater Trout Farm	7.3	AHC	A	.10	40.00	.492	34.7	6.38	1.7	WWT180
0103	N. Palm Springs	1986	0708	0920	6.0	USGS	5072	Whitewater Trout Farm	7.3	AHC	A	.15	45.00	.612	31.5	4.58	1.8	WWT270
0106	Chalfant Valley	1986	0721	1451	5.6	CDMG	54428	Zack Brothers Ranch	20.0	AAD	-	.20	40.00	.079	2.1	.15	3.9	C-ZAK-UP
0106	Chalfant Valley	1986	0721	1451	5.6	CDMG	54428	Zack Brothers Ranch	20.0	AAD	-	.13	35.00	.143	7.4	.67	1.5	C-ZAK270
0106	Chalfant Valley	1986	0721	1451	5.6	CDMG	54428	Zack Brothers Ranch	20.0	AAD	-	.30	30.00	.108	5.1	.58	3.6	C-ZAK360
0117	Whittier Narrows	1987	1001	1442	6.0	USGS	951	Brea Dam (Downstream)	23.3	IPD	-	.50	40.00	.094	3.1	.22	5.3	A-BRD-UP
0117	Whittier Narrows	1987	1001	1442	6.0	USGS	951	Brea Dam (Downstream)	23.3	IPD	-	.60	35.00	.163	6.2	.36	1.9	A-BRD040
0117	Whittier Narrows	1987	1001	1442	6.0	USGS	951	Brea Dam (Downstream)	23.3	IPD	-	.60	40.00	.313	14.5	.77	1.4	A-BRD130
0117	Whittier Narrows	1987	1001	1442	6.0	USC	90078	Compton - Castlegate St #	16.9	--D	C	.50	25.00	.167	3.3	.19	3.0	A-CAS-UP
0117	Whittier Narrows	1987	1001	1442	6.0	USC	90078	Compton - Castlegate St #	16.9	--D	C	.09	25.00	.332	27.1	5.04	1.8	A-CAS000
0117	Whittier Narrows	1987	1001	1442	6.0	USC	90078	Compton - Castlegate St #	16.9	--D	C	.28	25.00	.333	14.1	1.48	2.1	A-CAS270
0117	Whittier Narrows	1987	1001	1442	6.0	CDMG	14196	Inglewood-Union Oil	25.2	IQD	B	.50	30.00	.069	2.4	.24	5.9	A-ING-UP
0117	Whittier Narrows	1987	1001	1442	6.0	CDMG	14196	Inglewood-Union Oil	25.2	IQD	B	.60	40.00	.299	8.9	.78	1.6	A-ING000
0117	Whittier Narrows	1987	1001	1442	6.0	CDMG	14196	Inglewood-Union Oil	25.2	IQD	B	.25	40.00	.247	18.1	1.92	1.9	A-ING090

No.	Earthquake	Date & Time				Mag	Own	No.	Station	Closest Dist (km)	Site Codes Geom USGS	Filter Corners			PGA (g)	PGV (g)	PGD (cm/s)	Dur (s)	Filename
		YR	MODY	HRMN								HP (hz)	LP (hz)						
0117	Whittier Narrows	1987	1001	1442	6.0	USC	90072	La Puente - Ringrove Av #	11.9	--D	C	.45	25.00	.076	2.5	.19	4.0	A-RIM-UP	
0117	Whittier Narrows	1987	1001	1442	6.0	USC	90072	La Puente - Ringrove Av #	11.9	--D	C	.18	25.00	.143	6.2	1.04	3.8	A-RIM015	
0117	Whittier Narrows	1987	1001	1442	6.0	USC	90072	La Puente - Ringrove Av #	11.9	--D	C	.50	21.00	.118	5.9	.42	3.4	A-RIM105	
0117	Whittier Narrows	1987	1001	1442	6.0	CDMG	80047	Pasadena-CIT Calif Blvd	15.5	AQD	-	.30	40.00	.171	7.0	.58	2.8	A-CCB-UP	
0117	Whittier Narrows	1987	1001	1442	6.0	CDMG	80047	Pasadena-CIT Calif Blvd	15.5	AQD	-	.30	40.00	.177	8.1	.96	2.6	A-CCB270	
0117	Whittier Narrows	1987	1001	1442	6.0	CDMG	80047	Pasadena-CIT Calif Blvd	15.5	AQD	-	.30	35.00	.271	15.4	2.33	2.1	A-CCB360	
0117	Whittier Narrows	1987	1001	1442	6.0	CDMG	80049	Pasadena-CIT Keck Lab	15.5	-QD	-	.60	60.00	.096	4.0	.41	4.6	A-KEC-UP	
0117	Whittier Narrows	1987	1001	1442	6.0	CDMG	80049	Pasadena-CIT Keck Lab	15.5	-QD	-	.40	35.00	.152	5.1	.60	3.7	A-KEC270	
0117	Whittier Narrows	1987	1001	1442	6.0	CDMG	80049	Pasadena-CIT Keck Lab	15.5	-QD	-	.25	35.00	.188	14.1	2.63	2.6	A-KEC360	
0117	Whittier Narrows	1987	1001	1442	6.0	USGS	289	Whittier N. Dam upstream	12.3	IHD	-	.55	50.00	.505	7.1	.31	2.3	A-WHD-UP	
0117	Whittier Narrows	1987	1001	1442	6.0	USGS	289	Whittier N. Dam upstream	12.3	IHD	-	.20	50.00	.229	17.8	2.62	2.7	A-WHD062	
0117	Whittier Narrows	1987	1001	1442	6.0	USGS	289	Whittier N. Dam upstream	12.3	IHD	-	.40	40.00	.316	12.0	1.36	2.4	A-WHD152	

NRC TIME HISTORY LIBRARY: WUS, SOIL, M=5-6, D=50-100 km

B-25

No.	Earthquake	Date & Time					No.	Station	Closest Dist (km)	Site Codes		Filter Corners		PGV (g)	PGD (cm/s)	Dur (s)	Filename	
		YR	MODY	HRMN	Mag	Own				Geom	USGS	HP (hz)	LP (hz)					PGA (g)
0005	Northwest Calif	1938	0912	0610	5.5	USGS	1023	Ferndale City Hall	55.0	BQD	C	.30	15.00	.030	1.4	.14	7.3	A-FRNDWN
0005	Northwest Calif	1938	0912	0610	5.5	USGS	1023	Ferndale City Hall	55.0	BQD	C	.50	11.00	.134	7.2	.58	3.9	A-FRN045
0005	Northwest Calif	1938	0912	0610	5.5	USGS	1023	Ferndale City Hall	55.0	BQD	C	.20	11.00	.097	5.4	.78	4.2	A-FRN135
0011	Northwest Calif	1951	1008	0411	5.8	USGS	1023	Ferndale City Hall	56.0	BQD	C	.40	20.00	.031	2.1	.22	6.9	B-FRN-UP
0011	Northwest Calif	1951	1008	0411	5.8	USGS	1023	Ferndale City Hall	56.0	BQD	C	.50	12.00	.105	4.6	.47	5.8	B-FRN224
0011	Northwest Calif	1951	1008	0411	5.8	USGS	1023	Ferndale City Hall	56.0	BQD	C	.50	12.00	.110	6.1	.82	5.1	B-FRN314
0029	Lytle Creek	1970	0912	1430	5.4	CDMG	125	Lake Hughes #1	93.5	APC	B	1.10	15.00	.006	.3	.02	3.2	L01DWN
0029	Lytle Creek	1970	0912	1430	5.4	CDMG	125	Lake Hughes #1	93.5	APC	B	.80	10.00	.009	.7	.08	3.2	L01021
0029	Lytle Creek	1970	0912	1430	5.4	CDMG	125	Lake Hughes #1	93.5	APC	B	.35	20.00	.008	.6	.10	4.0	L01291
0029	Lytle Creek	1970	0912	1430	5.4	USGS	135	LA - Hollywood Stor FF	76.0	IPD	C	.90	20.00	.007	.3	.02	5.7	HOL-UP
0029	Lytle Creek	1970	0912	1430	5.4	USGS	135	LA - Hollywood Stor FF	76.0	IPD	C	.30	20.00	.017	1.0	.14	5.6	HOL090
0029	Lytle Creek	1970	0912	1430	5.4	USGS	135	LA - Hollywood Stor FF	76.0	IPD	C	.40	20.00	.018	.7	.06	4.4	HOL180
0051	Imperial Valley	1979	1015	2319	5.2	UNAMUCSD	6605	Delta	52.1	IQD	C	1.00	25.00	.023	.7	.04	5.8	DLTDWN
0051	Imperial Valley	1979	1015	2319	5.2	UNAMUCSD	6605	Delta	52.1	IQD	C	.80	25.00	.059	2.6	.21	4.0	A-DLT262
0051	Imperial Valley	1979	1015	2319	5.2	UNAMUCSD	6605	Delta	52.1	IQD	C	.40	30.00	.112	5.5	.84	2.6	A-DLT352
0084	Trinidad offshore	1983	0824	1336	5.5	CDMG	1498	Rio Dell Overpass, E Ground	67.6	APC	B	.30	30.00	.030	1.6	.43	9.5	RDE-UP
0084	Trinidad offshore	1983	0824	1336	5.5	CDMG	1498	Rio Dell Overpass, E Ground	67.6	APC	B	.15	30.00	.194	8.5	.82	3.1	RDE000
0084	Trinidad offshore	1983	0824	1336	5.5	CDMG	1498	Rio Dell Overpass, E Ground	67.6	APC	B	.30	30.00	.145	6.4	4.93	3.7	RDE270
0084	Trinidad offshore	1983	0824	1336	5.5	CDMG	1498	Rio Dell Overpass, W Ground	67.6	APC	B	.50	40.00	.033	1.8	1.62	9.2	RDW-UP
0084	Trinidad offshore	1983	0824	1336	5.5	CDMG	1498	Rio Dell Overpass, W Ground	67.6	APC	B	.40	40.00	.166	6.5	.56	3.3	RDW000
0084	Trinidad offshore	1983	0824	1336	5.5	CDMG	1498	Rio Dell Overpass, W Ground	67.6	APC	B	.20	35.00	.128	4.6	.84	3.3	RDW270
0103	N. Palm Springs	1986	0708	0920	6.0	CDOT	754	Colton Interchange-Vault	57.4	BHD	-	.40	30.00	.017	1.6	.40	10.8	CLI-UP
0103	N. Palm Springs	1986	0708	0920	6.0	CDOT	754	Colton Interchange-Vault	57.4	BHD	-	.40	30.00	.042	3.5	.59	5.1	CLI082
0103	N. Palm Springs	1986	0708	0920	6.0	CDOT	754	Colton Interchange-Vault	57.4	BHD	-	.40	30.00	.065	4.1	.43	3.8	CLI352
0103	N. Palm Springs	1986	0708	0920	6.0	CDMG	22T13	Landers Fire Station	38.2	AQD	-	.50	40.00	.055	2.4	.42	5.8	LDR-UP
0103	N. Palm Springs	1986	0708	0920	6.0	CDMG	22T13	Landers Fire Station	38.2	AQD	-	.50	30.00	.081	4.3	.42	3.9	LDR000
0103	N. Palm Springs	1986	0708	0920	6.0	CDMG	22T13	Landers Fire Station	38.2	AQD	-	.50	30.00	.098	4.6	.53	4.6	LDR090
0117	Whittier Narrows	1987	1001	1442	6.0	USC	90065	Glendora-N Oakbank #	69.7	--D	B	.38	25.00	.071	3.3	.48	5.2	A-OAK-UP
0117	Whittier Narrows	1987	1001	1442	6.0	USC	90065	Glendora-N Oakbank #	69.7	--D	B	.35	25.00	.092	3.4	.50	4.1	A-OAK080
0117	Whittier Narrows	1987	1001	1442	6.0	USC	90065	Glendora-N Oakbank #	69.7	--D	B	.23	25.00	.110	5.0	.81	4.1	A-OAK170
0117	Whittier Narrows	1987	1001	1442	6.0	CDMG	24526	Lancaster - Med Off FF	69.5	IQC	-	1.30	35.00	.027	.8	.03	9.2	A-LMD-UP
0117	Whittier Narrows	1987	1001	1442	6.0	CDMG	24526	Lancaster - Med Off FF	69.5	IQC	-	.80	25.00	.067	2.5	.16	5.5	A-LMD010
0117	Whittier Narrows	1987	1001	1442	6.0	CDMG	24526	Lancaster - Med Off FF	69.5	IQC	-	.60	25.00	.071	2.8	.17	5.1	A-LMD100

No.	Earthquake	Date & Time				Mag	Own	No.	Station	Closest Dist (km)	Site Codes		Filter Corners		PGA (g)	PGV (g)	PGD (cm/s)	Dur (s)	Filename
		YR	MODY	HRMN							Geom	USGS	HP (hz)	LP (hz)					
0117	Whittier Narrows	1987	1001	1442	6.0	CDMG	24309	Leona Valley #6	64.8	IHD	C	1.00	25.00	.036	1.6	.10	6.6	A-LV6000	
0117	Whittier Narrows	1987	1001	1442	6.0	CDMG	24309	Leona Valley #6	64.8	IHD	C	.80	25.00	.053	1.9	.11	6.4	A-LV6090	
0117	Whittier Narrows	1987	1001	1442	6.0	CDMG	24279	Newhall - Fire Sta	55.2	AQD	C	1.00	25.00	.038	1.0	.09	9.4	A-NWH-UP	
0117	Whittier Narrows	1987	1001	1442	6.0	CDMG	24279	Newhall - Fire Sta	55.2	AQD	C	.50	15.00	.044	2.9	.31	9.2	A-NWH180	
0117	Whittier Narrows	1987	1001	1442	6.0	CDMG	24279	Newhall - Fire Sta	55.2	AQD	C	.60	15.00	.060	2.9	.41	5.6	A-NWH270	
0117	Whittier Narrows	1987	1001	1442	6.0	USC	90056	Newhall - W Pico Canyon Rd. #	57.1	--C	B	.30	25.00	.035	1.7	.17	6.7	A-WPI-UP	
0117	Whittier Narrows	1987	1001	1442	6.0	USC	90056	Newhall - W Pico Canyon Rd. #	57.1	--C	B	.28	25.00	.088	5.6	.47	5.6	A-WPI046	
0117	Whittier Narrows	1987	1001	1442	6.0	USC	90056	Newhall - W Pico Canyon Rd. #	57.1	--C	B	.38	25.00	.055	3.9	.32	6.9	A-WPI316	
0117	Whittier Narrows	1987	1001	1442	6.0	CDMG	24274	Rosamond-Goode Ranch	86.0	IQC	-	.40	30.00	.021	1.2	.11	11.4	A-ROS-UP	
0117	Whittier Narrows	1987	1001	1442	6.0	CDMG	24274	Rosamond-Goode Ranch	86.0	IQC	-	.40	20.00	.070	3.8	.39	3.6	A-ROS000	
0117	Whittier Narrows	1987	1001	1442	6.0	CDMG	24274	Rosamond-Goode Ranch	86.0	IQC	-	.50	20.00	.065	3.2	.31	4.0	A-ROS090	

NRC TIME HISTORY LIBRARY: WUS, SOIL, M=6-7, D=0-10 km

B-27

No.	Earthquake	Date & Time				Mag	Own	No.	Station	Closest Dist (km)	Site Codes		Filter Corners			PGV (g)	PGD (cm/s)	Dur (s)	Filename
		YR	MODY	HRMN							Geom	USGS	HP (hz)	LP (hz)	PGA (g)				
0050	Imperial Valley	1979	1015	2316	6.5	USGS	5054	Bonds Corner	2.5	AQD	C	.10	40.00	.425	12.2	4.02	4.5	H-BCR-UP	
0050	Imperial Valley	1979	1015	2316	6.5	USGS	5054	Bonds Corner	2.5	AQD	C	.10	40.00	.588	45.2	16.78	6.1	H-BCR-140	
0050	Imperial Valley	1979	1015	2316	6.5	USGS	5054	Bonds Corner	2.5	AQD	C	.10	40.00	.775	45.9	14.89	4.7	H-BCR230	
0050	Imperial Valley	1979	1015	2316	6.5	USGS	5060	Brawley Airport	8.5	AQD	C	.10	40.00	.146	8.4	3.49	4.8	H-BRA-UP	
0050	Imperial Valley	1979	1015	2316	6.5	USGS	5060	Brawley Airport	8.5	AQD	C	.10	40.00	.160	35.9	22.44	5.2	H-BRA225	
0050	Imperial Valley	1979	1015	2316	6.5	USGS	5060	Brawley Airport	8.5	AQD	C	.10	40.00	.220	38.9	13.46	2.9	H-BRA315	
0050	Imperial Valley	1979	1015	2316	6.5	CDMG	5154	EC County Center FF	7.6	IDD	C	.10	50.00	.246	18.1	9.70	3.5	H-ECC-UP	
0050	Imperial Valley	1979	1015	2316	6.5	CDMG	5154	EC County Center FF	7.6	IDD	C	.10	40.00	.213	37.5	15.98	3.7	H-ECC002	
0050	Imperial Valley	1979	1015	2316	6.5	CDMG	5154	EC County Center FF	7.6	IDD	C	.10	35.00	.235	68.8	39.35	4.7	H-ECC092	
0050	Imperial Valley	1979	1015	2316	6.5	USGS	5057	El Centro Array #3	9.9	AQD	D	.10	40.00	.127	8.7	4.70	6.2	H-E03-UP	
0050	Imperial Valley	1979	1015	2316	6.5	USGS	5057	El Centro Array #3	9.9	AQD	D	.10	40.00	.266	46.8	18.92	4.3	H-E03140	
0050	Imperial Valley	1979	1015	2316	6.5	USGS	5057	El Centro Array #3	9.9	AQD	D	.10	40.00	.221	39.9	23.31	5.1	H-E03230	
0050	Imperial Valley	1979	1015	2316	6.5	USGS	952	El Centro Array #5	1.0	IQD	C	.10	40.00	.537	38.5	19.69	2.3	H-E05-UP	
0050	Imperial Valley	1979	1015	2316	6.5	USGS	952	El Centro Array #5	1.0	IQD	C	.10	40.00	.519	46.9	35.35	3.5	H-E05140	
0050	Imperial Valley	1979	1015	2316	6.5	USGS	952	El Centro Array #5	1.0	IQD	C	.10	40.00	.379	90.5	63.03	3.7	H-E05230	
0050	Imperial Valley	1979	1015	2316	6.5	CDMG	942	El Centro Array #6	1.0	IQD	C	.20	40.00	1.655	57.5	26.41	1.0	H-E06-UP	
0050	Imperial Valley	1979	1015	2316	6.5	CDMG	942	El Centro Array #6	1.0	IQD	C	.10	40.00	.410	64.9	27.69	5.3	H-E06140	
0050	Imperial Valley	1979	1015	2316	6.5	CDMG	942	El Centro Array #6	1.0	IQD	C	.10	40.00	.439	109.8	65.89	4.1	H-E06230	
0050	Imperial Valley	1979	1015	2316	6.5	USGS	5165	El Centro Differential Array	5.3	IQD	C	.10	40.00	.707	20.7	11.55	2.8	H-EDA-UP	
0050	Imperial Valley	1979	1015	2316	6.5	USGS	5165	El Centro Differential Array	5.3	IQD	C	.10	40.00	.352	71.2	45.80	3.7	H-EDA270	
0050	Imperial Valley	1979	1015	2316	6.5	USGS	5165	El Centro Differential Array	5.3	IQD	C	.10	40.00	.480	40.8	14.04	3.0	H-EDA360	
0050	Imperial Valley	1979	1015	2316	6.5	USGS	5055	Holtville Post Office	7.5	AQD	C	.10	40.00	.230	9.9	5.69	5.1	H-HVP-UP	
0050	Imperial Valley	1979	1015	2316	6.5	USGS	5055	Holtville Post Office	7.5	AQD	C	.10	40.00	.253	48.8	31.54	4.7	H-HVP225	
0050	Imperial Valley	1979	1015	2316	6.5	USGS	5055	Holtville Post Office	7.5	AQD	C	.10	40.00	.221	49.8	31.96	4.7	H-HVP315	
0056	Mammoth Lakes	1980	0525	1634	6.3	CDMG	54099	Convict Creek	9.0	AQD	-	.20	41.00	.388	20.5	5.93	6.0	I-CVK-UP	
0056	Mammoth Lakes	1980	0525	1634	6.3	CDMG	54099	Convict Creek	9.0	AQD	-	.10	60.00	.416	23.3	4.66	6.6	I-CVK090	
0056	Mammoth Lakes	1980	0525	1634	6.3	CDMG	54099	Convict Creek	9.0	AQD	-	.10	50.00	.442	23.1	5.42	7.1	I-CVK180	
0076	Coalinga	1983	0502	2342	6.4	USBR	1162	Pleasant Valley P.P. - yard	8.5	AHD	-	.20	31.00	.353	16.1	2.35	5.1	H-PVY-UP	
0076	Coalinga	1983	0502	2342	6.4	USBR	1162	Pleasant Valley P.P. - yard	8.5	AHD	-	.20	40.00	.592	60.2	8.77	4.1	H-PVY045	
0076	Coalinga	1983	0502	2342	6.4	USBR	1162	Pleasant Valley P.P. - yard	8.5	AHD	-	.20	31.00	.551	36.4	3.96	4.4	H-PVY135	
0105	Chalfant Valley	1986	0721	1442	6.2	CDMG	54171	Bisho-LADWP South St	9.2	AQD	-	.10	40.00	.140	6.7	2.25	5.1	A-LAD-UP	
0105	Chalfant Valley	1986	0721	1442	6.2	CDMG	54171	Bisho-LADWP South St	9.2	AQD	-	.10	40.00	.248	19.2	7.04	3.6	A-LAD180	
0105	Chalfant Valley	1986	0721	1442	6.2	CDMG	54171	Bisho-LADWP South St	9.2	AQD	-	.10	30.00	.175	19.4	6.72	3.1	A-LAD270	
0125	Erzican, Turkey	1992	0313		6.9		95	Erzincan	2.0	--D	C	.20		.248	18.3	7.86	5.4	ERZ-UP	

No.	Earthquake	Date & Time				Mag	Own	No.	Station	Closest Dist (km)	Site Codes		Filter Corners			Dur (s)	Filename
		YR	MODY	HRMN							Geom	USGS	HP (hz)	LP (hz)	PGA (g)		
0125	Erzican, Turkey	1992	0313		6.9		95	Erzincan	2.0	--D	C	.10	.515	83.9	27.35	1.5	ERZ-NS
0125	Erzican, Turkey	1992	0313		6.9		95	Erzincan	2.0	--D	C	.10	.496	64.3	22.78	2.0	ERZ-EW
0131	Northridge	1994	0117	1231	6.7	CDMG	24087	Arieta-Nordhoff Fire Sta #	9.2	AQD	C	.12 23.00	.552	18.4	8.83	6.5	ARL-UP
0131	Northridge	1994	0117	1231	6.7	CDMG	24087	Arieta-Nordhoff Fire Sta #	9.2	AQD	C	.12 23.00	.344	40.6	15.04	6.4	ARL090
0131	Northridge	1994	0117	1231	6.7	CDMG	24087	Arieta-Nordhoff Fire Sta #	9.2	AQD	C	.12 23.00	.308	23.2	10.75	5.7	ARL360
0131	Northridge	1994	0117	1231	6.7	USGS	0655	Jensen Filter Plant #	6.2	--D	B	.30	.400	34.1	8.89	5.2	JEN-UP
0131	Northridge	1994	0117	1231	6.7	USGS	0655	Jensen Filter Plant #	6.2	--D	B	.08	.424	106.2	43.06	4.0	JEN022
0131	Northridge	1994	0117	1231	6.7	USGS	0655	Jensen Filter Plant #	6.2	--D	B	.20	.593	99.3	24.00	3.1	JEN292
0131	Northridge	1994	0117	1231	6.7	USGS	0637	Sepulveda V A #	8.9	--D	B	.10	.467	33.2	9.58	5.6	SPV-UP
0131	Northridge	1994	0117	1231	6.7	USGS	0637	Sepulveda V A #	8.9	--D	B	.10	.753	84.8	18.68	4.5	SPV270
0131	Northridge	1994	0117	1231	6.7	USGS	0637	Sepulveda V A #	8.9	--D	B		.939	76.6	14.95	4.3	SPV360
0131	Northridge	1994	0117	1231	6.7	DWP	75	Sylmar-Converter Sta East #	6.1	--D	B		.377	24.3	7.30	3.6	SCE-UP
0131	Northridge	1994	0117	1231	6.7	DWP	75	Sylmar-Converter Sta East #	6.1	--D	B		.828	117.5	34.22	3.8	SCE018
0131	Northridge	1994	0117	1231	6.7	DWP	75	Sylmar-Converter Sta East #	6.1	--D	B		.493	74.6	28.69	3.4	SCE288
0133	Kobe	1995	0116	2046	6.9	CUE	99999	Takarazuka	1.2	--D	D	40.00	.433	34.8	12.38	1.5	TAZ-UP
0133	Kobe	1995	0116	2046	6.9	CUE	99999	Takarazuka	1.2	--D	D	40.00	.693	68.3	26.65	2.2	TAZ000
0133	Kobe	1995	0116	2046	6.9	CUE	99999	Takarazuka	1.2	--D	D	.13 33.00	.694	85.3	16.75	2.1	TAZ090
0133	Kobe	1995	0116	2046	6.9	CUE	99999	Takatori	.3	--E	D	.20	.272	16.0	4.47	7.5	TAK-UP
0133	Kobe	1995	0116	2046	6.9	CUE	99999	Takatori	.3	--E	D		.611	127.1	35.77	6.0	TAK000
0133	Kobe	1995	0116	2046	6.9	CUE	99999	Takatori	.3	--E	D		.616	120.7	32.72	4.8	TAK090

NRC TIME HISTORY LIBRARY: WUS, SOIL, M=6-7, D=10-50 km

No.	Earthquake	Date & Time					Mag	Own	No.	Station	Closest Dist (km)	Site Codes		Filter Corners			Dur (s)	Filename	
		YR	MODY	HRMN	Geom	USGS						HP (hz)	LP (hz)	PGA (g)	PGV (g)	PGD (cm/s)			
0030	San Fernando	1971	0209	1400	6.6	ACOE		289	Whittier Narrows Dam	45.1	IHD	-	.10	30.00	.032	3.7	2.61	9.8	WNDDWN
0030	San Fernando	1971	0209	1400	6.6	ACOE		289	Whittier Narrows Dam	45.1	IHD	-	.10	20.00	.100	9.3	5.79	6.8	WND143
0030	San Fernando	1971	0209	1400	6.6	ACOE		289	Whittier Narrows Dam	45.1	IHD	-	.10		.107	9.7	5.04	7.1	WND233
0050	Imperial Valley	1979	1015	2316	6.5	USGS		5053	Calexico Fire Station	10.6	AQD	C	.10	40.00	.187	6.7	2.49	6.5	H-CXO-UP
0050	Imperial Valley	1979	1015	2316	6.5	USGS		5053	Calexico Fire Station	10.6	AQD	C	.10	40.00	.275	21.2	9.02	5.8	H-CXO225
0050	Imperial Valley	1979	1015	2316	6.5	USGS		5053	Calexico Fire Station	10.6	AQD	C	.20	40.00	.202	16.0	9.20	7.2	H-CXO315
0050	Imperial Valley	1979	1015	2316	6.5	USGS		5056	El Centro Array #1	15.5	AQD	C	.10	40.00	.056	3.8	2.14	7.5	H-E01-UP
0050	Imperial Valley	1979	1015	2316	6.5	USGS		5056	El Centro Array #1	15.5	AQD	C	.10	40.00	.139	16.0	9.96	5.4	H-E01140
0050	Imperial Valley	1979	1015	2316	6.5	USGS		5056	El Centro Array #1	15.5	AQD	C	.10	40.00	.134	10.7	6.97	7.2	H-E01230
0071	Taiwan SMART1 (5)	1981	0129		6.3			29	SMART1 M07	21.0	IZD	-	.20	25.00	.050	1.5	.34	5.5	05M07DN
0071	Taiwan SMART1 (5)	1981	0129		6.3			29	SMART1 M07	21.0	IZD	-	.10	25.00	.111	5.6	.86	4.2	05M07EW
0071	Taiwan SMART1 (5)	1981	0129		6.3			29	SMART1 M07	21.0	IZD	-	.10	25.00	.109	10.9	1.74	4.3	05M07NS
0103	N. Palm Springs	1986	0708	0920	6.0	CDMG	22T13	Landers Fire Station	38.2	AQD	-	.50	40.00	.055	2.4	.42	5.8	LDR-UP	
0103	N. Palm Springs	1986	0708	0920	6.0	CDMG	22T13	Landers Fire Station	38.2	AQD	-	.50	30.00	.081	4.3	.42	3.9	LDR000	
0103	N. Palm Springs	1986	0708	0920	6.0	CDMG	22T13	Landers Fire Station	38.2	AQD	-	.50	30.00	.098	4.6	.53	4.6	LDR090	
0117	Whittier Narrows	1987	1001	1442	6.0	USC	90069	Baldwin Park - N Holly #	11.9	--D	C	.30	25.00	.080	2.2	.75	3.1	A-NHO-UP	
0117	Whittier Narrows	1987	1001	1442	6.0	USC	90069	Baldwin Park - N Holly #	11.9	--D	C	.13	25.00	.127	8.6	2.50	2.8	A-NHO180	
0117	Whittier Narrows	1987	1001	1442	6.0	USC	90069	Baldwin Park - N Holly #	11.9	--D	C	.50	25.00	.061	4.3	.54	6.9	A-NHO270	
0117	Whittier Narrows	1987	1001	1442	6.0	USC	90013	Beverly Hills-14145 Mulhol #	30.3	--C	C	.38	25.00	.043	2.0	.25	7.3	A-MUL-UP	
0117	Whittier Narrows	1987	1001	1442	6.0	USC	90013	Beverly Hills-14145 Mulhol #	30.3	--C	C	.33	25.00	.104	6.5	.58	5.7	A-MUL009	
0117	Whittier Narrows	1987	1001	1442	6.0	USC	90013	Beverly Hills-14145 Mulhol #	30.3	--C	C	.35	25.00	.126	10.3	1.05	3.4	A-MUL279	
0117	Whittier Narrows	1987	1001	1442	6.0	USC	90003	Northridge-17645 Saticoy St #	39.8	--D	C	.25	25.00	.084	2.4	.41	6.6	A-STC-UP	
0117	Whittier Narrows	1987	1001	1442	6.0	USC	90003	Northridge-17645 Saticoy St #	39.8	--D	C	.23	25.00	.161	8.5	.72	4.9	A-STC090	
0117	Whittier Narrows	1987	1001	1442	6.0	USC	90003	Northridge-17645 Saticoy St #	39.8	--D	C	.20	25.00	.118	5.1	.83	9.7	A-STC180	
0119	Superstition Hills (A)	1987	1124	0514	6.3	USGS	5210	Wildlife Liquef. Array	24.7	IQD	-	.20	50.00	.186	4.6	2.20	3.6	A-IVW-UP	
0119	Superstition Hills (A)	1987	1124	0514	6.3	USGS	5210	Wildlife Liquef. Array	24.7	IQD	-	.20	50.00	.132	12.7	7.30	7.1	A-IVW090	
0119	Superstition Hills (A)	1987	1124	0514	6.3	USGS	5210	Wildlife Liquef. Array	24.7	IQD	-	.20	50.00	.134	13.4	5.20	7.3	A-IVW360	
0122	Loma Prieta	1989	1018	0005	6.9	CDMG	58065	Saratoga - Aloha Ave	13.0	AQD	B	.10	58.00	.389	26.9	15.15	4.7	STG-UP	
0122	Loma Prieta	1989	1018	0005	6.9	CDMG	58065	Saratoga - Aloha Ave	13.0	AQD	B	.10	38.00	.512	41.2	16.21	3.7	STG000	
0122	Loma Prieta	1989	1018	0005	6.9	CDMG	58065	Saratoga - Aloha Ave	13.0	AQD	B	.10	50.00	.324	42.6	27.53	4.2	STG090	
0124	Georgia, USSR	1991	0615	0059	6.2			21	Baz	49.0	A-D	-	.10		.016	1.4	.39	11.6	BAZ-Z
0124	Georgia, USSR	1991	0615	0059	6.2			21	Baz	49.0	A-D	-	.10		.033	2.2	.40	7.2	BAZ-X
0124	Georgia, USSR	1991	0615	0059	6.2			21	Baz	49.0	A-D	-	.10		.038	2.0	.35	8.1	BAZ-Y
0131	Northridge	1994	0117	1231	6.7	USC	90063	Glendale - Las Palmas	25.4	--C	C	.30	30.00	.127	4.3	.44	7.2	GLP-UP	

B-29

No.	Earthquake	Date & Time					Mag	Own	No.	Station	Closest Dist (km)	Site Codes		Filter Corners			Dur (s)	Filename	
		YR	MODY	HRMN	Geom	USGS						HP (hz)	LP (hz)	PGA (g)	PGV (g)	PGD (cm/s)			
0131	Northridge	1994	0117	1231	6.7	USC	90063	Glendale - Las Palmas	25.4	--	C	C	.13	30.00	.357	12.3	1.94	6.2	GLP177
0131	Northridge	1994	0117	1231	6.7	USC	90063	Glendale - Las Palmas	25.4	--	C	C	.10	30.00	.206	7.4	1.75	6.2	GLP267
0131	Northridge	1994	0117	1231	6.7	CDMG	24389	LA - Century City CC North #	25.7	IQD	C	C	.14	23.00	.116	8.7	3.47	8.1	CCN-UP
0131	Northridge	1994	0117	1231	6.7	CDMG	24389	LA - Century City CC North #	25.7	IQD	C	C	.14	23.00	.256	21.1	6.68	7.0	CCN090
0131	Northridge	1994	0117	1231	6.7	CDMG	24389	LA - Century City CC North #	25.7	IQD	C	C	.14	23.00	.222	25.2	5.70	7.2	CCN360
0131	Northridge	1994	0117	1231	6.7	USC	90021	LA - N Westmoreland	29.0	--	D	B	.20	30.00	.093	6.3	1.08	8.1	WST-UP
0131	Northridge	1994	0117	1231	6.7	USC	90021	LA - N Westmoreland	29.0	--	D	B	.20	30.00	.401	20.9	2.29	5.3	WST000
0131	Northridge	1994	0117	1231	6.7	USC	90021	LA - N Westmoreland	29.0	--	D	B	.20	30.00	.361	20.9	4.27	5.7	WST270
0131	Northridge	1994	0117	1231	6.7	CDMG	24055	Leona Valley #5 - Ritter #	38.3	IQC	C	C	.20	23.00	.097	11.6	2.53	8.5	LV5-UP
0131	Northridge	1994	0117	1231	6.7	CDMG	24055	Leona Valley #5 - Ritter #	38.3	IQC	C	C	.20	23.00	.146	14.9	2.35	6.3	LV5000
0131	Northridge	1994	0117	1231	6.7	CDMG	24055	Leona Valley #5 - Ritter #	38.3	IQC	C	C	.20	23.00	.092	10.5	2.70	7.2	LV5090

NRC TIME HISTORY LIBRARY: WUS, SOIL, M=6-7, D=50-100 km

B-31

No.	Earthquake	Date & Time					No.	Station	Closest Dist (km)	Site Codes Geom USGS	Filter Corners				Dur (s)	Filename	
		YR	MODY	HRMN	Mag	Own					HP (hz)	LP (hz)	PGA (g)	PGV (g)			PGD (cm/s)
0030	San Fernando	1971	0209	1400	6.6	CDWR	1102	Wheeler Ridge - Ground	81.6	IBD C	.10	30.00	.014	1.4	1.46	12.8	WRP-UP
0030	San Fernando	1971	0209	1400	6.6	CDWR	1102	Wheeler Ridge - Ground	81.6	IBD C	.10	23.00	.027	2.0	1.47	7.2	WRP090
0030	San Fernando	1971	0209	1400	6.6	CDWR	1102	Wheeler Ridge - Ground	81.6	IBD C	.10	23.00	.031	1.7	1.23	6.2	WRP180
0086	TaiwanSMART1(25)	1983	0921		6.5		32	SMART1 E01	83.0	IZD -	.50	25.00	.013	1.8	.31	9.4	25E01DN
0086	TaiwanSMART1(25)	1983	0921		6.5		32	SMART1 E01	83.0	IZD -	.20	25.00	.028	.0	.96	8.3	25E01EW
0086	TaiwanSMART1(25)	1983	0921		6.5		32	SMART1 E01	83.0	IZD -	.20	25.00	.028	4.1	.71	6.1	25E01NS
0086	TaiwanSMART1(25)	1983	0921		6.5		61	SMART1 I07	83.0	IZD -	.10	25.00	.009	1.4	.43	11.4	25I07DN
0086	TaiwanSMART1(25)	1983	0921		6.5		61	SMART1 I07	83.0	IZD -	.10	25.00	.035	3.8	.79	5.6	25I07EW
0086	TaiwanSMART1(25)	1983	0921		6.5		61	SMART1 I07	83.0	IZD -	.10	25.00	.032	4.0	.97	8.6	25I07NS
0086	TaiwanSMART1(25)	1983	0921		6.5		60	SMART1 M06	83.0	IZD -	.10	25.00	.010	1.7	.40	7.7	25M06DN
0086	TaiwanSMART1(25)	1983	0921		6.5		60	SMART1 M06	83.0	IZD -	.10	25.00	.021	2.8	.00	6.9	25M06EW
0086	TaiwanSMART1(25)	1983	0921		6.5		60	SMART1 M06	83.0	IZD -	.10	25.00	.031	4.3	1.10	7.7	25M06NS
0090	Morgan Hill	1984	0424	2115	6.2	CDMG	56012	Los Banos	64.4	AHD C	.50	20.00	.011	1.0	.50	11.3	LBN-UP
0090	Morgan Hill	1984	0424	2115	6.2	CDMG	56012	Los Banos	64.4	AHD C	.50	18.00	.051	5.8	1.75	8.4	LBN090
0090	Morgan Hill	1984	0424	2115	6.2	CDMG	56012	Los Banos	64.4	AHD C	.50	18.00	.057	8.3	1.89	12.0	LBN180
0090	Morgan Hill	1984	0424	2115	6.2	CDMG	58223	SF Intern. Airport	71.2	AHD C	.50	32.00	.018	.8	.28	13.6	SFO-UP
0090	Morgan Hill	1984	0424	2115	6.2	CDMG	58223	SF Intern. Airport	71.2	AHD C	.50	26.00	.048	3.2	.40	11.0	SFO050
0090	Morgan Hill	1984	0424	2115	6.2	CDMG	58223	SF Intern. Airport	71.2	AHD C	.50	24.00	.048	2.7	.47	10.4	SFO320
0122	Loma Prieta	1989	1018	0005	6.9	CDMG	58498	Hayward - BART Sta	58.9	I-D B	.20	40.00	.082	4.7	2.76	10.5	HWB-UP
0122	Loma Prieta	1989	1018	0005	6.9	CDMG	58498	Hayward - BART Sta	58.9	I-D B	.20	31.00	.159	15.1	3.72	6.3	HWB220
0122	Loma Prieta	1989	1018	0005	6.9	CDMG	58498	Hayward - BART Sta	58.9	I-D B	.20	36.00	.156	10.6	3.33	6.6	HWB310
0124	Georgia, USSR	1991	0615	0059	6.2		20	Oni	52.0	A-D -	.20		.018	1.2	.32	11.7	ONI-Z
0124	Georgia, USSR	1991	0615	0059	6.2		20	Oni	52.0	A-D -	.20		.075	3.1	.40	6.6	ONI-X
0124	Georgia, USSR	1991	0615	0059	6.2		20	Oni	52.0	A-D -	.20		.046	2.6	.44	10.1	ONI-Y
0131	Northridge	1994	0117	1231	6.7	USC	90070	Covina-W Badillo	56.1	--D C	.30	30.00	.043	2.9	.70	11.7	BAD-UP
0131	Northridge	1994	0117	1231	6.7	USC	90070	Covina-W Badillo	56.1	--D C	.20	30.00	.100	5.8	1.21	8.6	BAD000
0131	Northridge	1994	0117	1231	6.7	USC	90070	Covina-W Badillo	56.1	--D C	.20	30.00	.079	7.0	1.62	7.8	BAD270
0131	Northridge	1994	0117	1231	6.7	CDMG	13197	Huntington Beach - Lake St #	79.6	AQD C	.20	23.00	.018	4.0	.89	18.2	HNT-UP
0131	Northridge	1994	0117	1231	6.7	CDMG	13197	Huntington Beach - Lake St #	79.6	AQD C	.20	23.00	.091	10.1	1.13	11.3	HNT000
0131	Northridge	1994	0117	1231	6.7	CDMG	13197	Huntington Beach - Lake St #	79.6	AQD C	.20	23.00	.070	13.9	1.49	10.8	HNT090
0131	Northridge	1994	0117	1231	6.7	USC	90083	Huntington Beach - Waikiki	57.4	--D C	.30	30.00	.022	1.2	.28	15.2	WAI-UP
0131	Northridge	1994	0117	1231	6.7	USC	90083	Huntington Beach - Waikiki	57.4	--D C	.20	30.00	.086	5.0	1.63	12.1	WAI200
0131	Northridge	1994	0117	1231	6.7	USC	90083	Huntington Beach - Waikiki	57.4	--D C	.20	30.00	.068	7.4	1.87	10.6	WAI290
0131	Northridge	1994	0117	1231	6.7	USC	90072	La Fuente - Rimgrove Av	58.9	--D C	1.00	30.00	.048	2.6	.16	7.2	RIM-UP

No.	Earthquake	Date & Time					Own	No.	Station	Closest Dist (km)	Site Codes		Filter Corners			PGV (g)	PGD (cm/s)	Dur (s)	Filename
		YR	MODY	HRMN	Mag						Geom	USGS	HP (hz)	LP (hz)	PGA (g)				
0131	Northridge	1994	0117	1231	6.7	USC	90072	La Puente - Ringrove Av	58.9	--D	C	.80	30.00	.109	7.9	.70	7.0	RIM015	
0131	Northridge	1994	0117	1231	6.7	USC	90072	La Puente - Ringrove Av	58.9	--D	C	.80	30.00	.129	9.7	.83	7.0	RIM105	
0131	Northridge	1994	0117	1231	6.7	USC	90084	Lakewood - Del Amo Blvd	59.3	--D	C	.80	30.00	.058	1.6	.18	7.8	DEL-UP	
0131	Northridge	1994	0117	1231	6.7	USC	90084	Lakewood - Del Amo Blvd	59.3	--D	C	.13	30.00	.137	11.2	1.98	11.0	DEL000	
0131	Northridge	1994	0117	1231	6.7	USC	90084	Lakewood - Del Amo Blvd	59.3	--D	C	.20	30.00	.123	10.4	2.86	11.3	DEL090	
0131	Northridge	1994	0117	1231	6.7	CDMG	24586	Neenach - Sacatara Ck #	53.2	IHD	B	.12	46.00	.047	7.2	3.10	25.9	NEE-UP	
0131	Northridge	1994	0117	1231	6.7	CDMG	24586	Neenach - Sacatara Ck #	53.2	IHD	B	.12	46.00	.056	10.0	6.48	11.5	NEE090	
0131	Northridge	1994	0117	1231	6.7	CDMG	24586	Neenach - Sacatara Ck #	53.2	IHD	B	.12	46.00	.069	13.1	8.22	13.1	NEE180	
0131	Northridge	1994	0117	1231	6.7	CDMG	14578	Seal Beach - Office Bldg #	64.9	IQD	B	.16	46.00	.037	2.0	1.90	13.9	SEA-UP	
0131	Northridge	1994	0117	1231	6.7	CDMG	14578	Seal Beach - Office Bldg #	64.9	IQD	B	.16	46.00	.061	5.8	1.99	12.3	SEA000	
0131	Northridge	1994	0117	1231	6.7	CDMG	14578	Seal Beach - Office Bldg #	64.9	IQD	B	.16	46.00	.084	6.9	1.34	9.0	SEA090	

NRC TIME HISTORY LIBRARY: WUS, SOIL, M=6-7, D=100-200 km

No.	Earthquake	Date & Time				Mag	Own	No.	Station	Closest Dist (km)	Site Codes Geom USGS	Filter Corners			PGV (g)	PGD (cm/s)	Dur (s)	Filename
		YR	MODY	HRMN								HP (hz)	LP (hz)	PGA (g)				
0019	El Alamo	1956	1217	1433	6.8	USGS	117	El Centro Array #9	130.0	EQD C	.50	20.00	.014	1.7	.77	24.8	ELC-UP	
0019	El Alamo	1956	1217	1433	6.8	USGS	117	El Centro Array #9	130.0	EQD C	.10	15.00	.033	4.1	2.89	23.0	ELC180	
0019	El Alamo	1956	1217	1433	6.8	USGS	117	El Centro Array #9	130.0	EQD C	.10	15.00	.052	6.6	4.93	17.3	ELC270	
0028	Borrego Mtn	1968	0409	0203	6.8	USGS	130	LB - Terminal Island	195.0	CCD C	.10	20.00	.005	1.6	1.76	31.9	A-TLI-UP	
0028	Borrego Mtn	1968	0409	0203	6.8	USGS	130	LB - Terminal Island	195.0	CCD C	.10	15.00	.010	2.8	2.53	32.8	A-TLI249	
0028	Borrego Mtn	1968	0409	0203	6.8	USGS	130	LB - Terminal Island	195.0	CCD C	.10	15.00	.009	3.0	5.46	28.6	A-TLI339	
0030	San Fernando	1971	0209	1400	6.6	CIT	103	Anza Post Office	169.0	AAC -	.50	35.00	.015	.7	.20	10.9	AZPDWN	
0030	San Fernando	1971	0209	1400	6.6	CIT	103	Anza Post Office	169.0	AAC -	.50	35.00	.027	1.4	.25	8.1	AZP045	
0030	San Fernando	1971	0209	1400	6.6	CIT	103	Anza Post Office	169.0	AAC -	.50	35.00	.037	2.2	.30	6.2	AZP315	
0030	San Fernando	1971	0209	1400	6.6	USGS	1004	Bakersfield - Harvey Aud	120.0	CCD -	.10	15.00	.007	.7	.69	18.6	BFA-UP	
0030	San Fernando	1971	0209	1400	6.6	USGS	1004	Bakersfield - Harvey Aud	120.0	CCD -	.10	13.00	.007	1.4	1.08	24.0	BFA180	
0030	San Fernando	1971	0209	1400	6.6	USGS	1004	Bakersfield - Harvey Aud	120.0	CCD -	.10	20.00	.007	1.2	1.23	21.3	BFA270	
0030	San Fernando	1971	0209	1400	6.6	USGS	1	Buena Vista - Taft	118.0	AQD -	.20	20.00	.007	.6	.41	11.5	BVPDWN	
0030	San Fernando	1971	0209	1400	6.6	USGS	1	Buena Vista - Taft	118.0	AQD -	.10	13.00	.012	1.5	1.51	13.2	BVP090	
0030	San Fernando	1971	0209	1400	6.6	USGS	1	Buena Vista - Taft	118.0	AQD -	.10	15.00	.012	1.3	.68	13.6	BVP180	
0030	San Fernando	1971	0209	1400	6.6	CDMG	12331	Hemet Fire Station	136.0	AQD C	.50	35.00	.026	1.5	.32	7.3	H05DWN	
0030	San Fernando	1971	0209	1400	6.6	CDMG	12331	Hemet Fire Station	136.0	AQD C	.50	35.00	.033	2.2	.38	7.2	H05135	
0030	San Fernando	1971	0209	1400	6.6	CDMG	12331	Hemet Fire Station	136.0	AQD C	.50	35.00	.047	2.6	.33	7.5	H05225	
0030	San Fernando	1971	0209	1400	6.6	USGS	465	San Juan Capistrano	104.0	ABC -	.50	35.00	.021	2.0	.67	18.9	SJCDWN	
0030	San Fernando	1971	0209	1400	6.6	USGS	465	San Juan Capistrano	104.0	ABC -	.50	35.00	.046	3.3	1.05	12.6	SJC033	
0030	San Fernando	1971	0209	1400	6.6	USGS	465	San Juan Capistrano	104.0	ABC -	.50	35.00	.035	3.7	.79	12.5	SJC303	
0030	San Fernando	1971	0209	1400	6.6	USGS	282	UCSB-Fluid Mech Lab	125.6	CPD -	.20	30.00	.011	1.3	.73	13.4	SBF-UP	
0030	San Fernando	1971	0209	1400	6.6	USGS	282	UCSB-Fluid Mech Lab	125.6	CPD -	.20	30.00	.017	2.7	1.41	13.7	SBF042	
0030	San Fernando	1971	0209	1400	6.6	USGS	282	UCSB-Fluid Mech Lab	125.6	CPD -	.20	30.00	.017	3.0	1.29	14.8	SBF132	
0117	Whittier Narrows	1987	1001	1442	6.0	CDMG	12331	Hemet Fire Station	105.0	AQD C	1.00	30.00	.027	.9	.07	14.0	A-H05-UP	
0117	Whittier Narrows	1987	1001	1442	6.0	CDMG	12331	Hemet Fire Station	105.0	AQD C	.70	25.00	.038	1.4	.13	11.3	A-H05270	
0117	Whittier Narrows	1987	1001	1442	6.0	CDMG	12331	Hemet Fire Station	105.0	AQD C	.80	25.00	.032	1.6	.10	9.2	A-H05360	
0131	Northridge	1994	0117	1231	6.7	CDMG	13660	Hemet - Ryan Airfield #	144.1	IHD -	.30	46.00	.027	2.0	.18	18.2	HEM-UP	
0131	Northridge	1994	0117	1231	6.7	CDMG	13660	Hemet - Ryan Airfield #	144.1	IHD -	.30	46.00	.064	4.5	.66	11.3	HEM000	
0131	Northridge	1994	0117	1231	6.7	CDMG	13660	Hemet - Ryan Airfield #	144.1	IHD -	.30	46.00	.046	4.7	.51	10.9	HEM090	
0131	Northridge	1994	0117	1231	6.7	CDMG	23672	San Bernardino - CSUSB Gr #	103.1	IHD -	.30	46.00	.021	1.5	.25	15.6	BER-UP	
0131	Northridge	1994	0117	1231	6.7	CDMG	23672	San Bernardino - CSUSB Gr #	103.1	IHD -	.30	46.00	.034	2.8	.31	9.7	BER000	
0131	Northridge	1994	0117	1231	6.7	CDMG	23672	San Bernardino - CSUSB Gr #	103.1	IHD -	.30	46.00	.069	4.0	.77	7.7	BER090	
0131	Northridge	1994	0117	1231	6.7	CDMG	23542	San Bernardino - E&Hospitality#	108.1	IHD C	.20	46.00	.044	2.6	.51	17.3	HOS-UP	

B-33

No.	Earthquake	Date & Time				Mag	Own	No.	Station	Closest Dist (km)	Site Codes		Filter Corners			PGV (g)	PGD (cm/s)	Dur (s)	Filename
		YR	MODY	HRMN							Geom	USGS	HP (hz)	LP (hz)	PGA (g)				
0131	Northridge	1994	0117	1231	6.7	CDMG	23542	San Bernandino - E&Hospitality#	108.1	IHD	C	.20	46.00	.085	5.9	.97	9.1	HOS090	
0131	Northridge	1994	0117	1231	6.7	CDMG	23542	San Bernandino - E&Hospitality#	108.1	IHD	C	.20	46.00	.096	6.5	1.34	9.4	HOS180	
0131	Northridge	1994	0117	1231	6.7	CDMG	12673	San Jacinto - CDF Fire Sta #	146.5	IHD	-	.16	46.00	.022	3.7	1.27	24.6	CDF-UP	
0131	Northridge	1994	0117	1231	6.7	CDMG	12673	San Jacinto - CDF Fire Sta #	146.5	IHD	-	.16	46.00	.081	8.1	1.62	12.0	CDF000	
0131	Northridge	1994	0117	1231	6.7	CDMG	12673	San Jacinto - CDF Fire Sta #	146.5	IHD	-	.16	46.00	.099	7.7	1.56	8.1	CDF090	
0131	Northridge	1994	0117	1231	6.7	CDMG	25091	Santa Barbara-UCSB Goleta #	111.3	AHD	-	.20	23.00	.039	2.9	.74	9.3	SBG-UP	
0131	Northridge	1994	0117	1231	6.7	CDMG	25091	Santa Barbara-UCSB Goleta #	111.3	AHD	-	.20	23.00	.078	7.0	1.46	10.8	SBG000	
0131	Northridge	1994	0117	1231	6.7	CDMG	25091	Santa Barbara-UCSB Goleta #	111.3	AHD	-	.20	23.00	.069	6.7	1.57	13.9	SBG090	
0133	Kobe	1995	0116	2046	6.9		99999	FUK	157.2	--D	-	.05		.010	1.7	.67	28.2	FUK-UP	
0133	Kobe	1995	0116	2046	6.9		99999	FUK	157.2	--D	-	.05		.034	4.3	1.28	23.2	FUK000	
0133	Kobe	1995	0116	2046	6.9		99999	FUK	157.2	--D	-	.05		.042	5.3	2.08	23.8	FUK090	

NRC TIME HISTORY LIBRARY: WUS, SOIL, M>7, D=0-10 km

No.	Earthquake	Date & Time				Mag	Own	No.	Station	Closest Dist (km)	Site Codes Geom USGS	Filter Corners			PGV (g)	PGD (cm/s)	Dur (s)	Filename
		YR	MODY	HRMN								HP (hz)	LP (hz)	PGA (g)				
0006	Imperial Valley	1940	0519	0437	7.0	USGS	117	El Centro Array #9	8.3	EQD C	.20	15.00	.205	10.7	9.16	7.6	I-ELC-UP	
0006	Imperial Valley	1940	0519	0437	7.0	USGS	117	El Centro Array #9	8.3	EQD C	.20	15.00	.313	29.8	13.32	11.3	I-ELC180	
0006	Imperial Valley	1940	0519	0437	7.0	USGS	117	El Centro Array #9	8.3	EQD C	.20	15.00	.215	30.2	23.91	16.9	I-ELC270	
0046	Tabas, Iran	1978	0916		7.4		9101	Tabas	3.0	ABC -	.05		.688	45.6	17.04	9.5	TAB-UP	
0046	Tabas, Iran	1978	0916		7.4		9101	Tabas	3.0	ABC -	.05		.836	97.8	36.92	8.3	TAB-LN	
0046	Tabas, Iran	1978	0916		7.4		9101	Tabas	3.0	ABC -	.05		.852	121.4	94.58	7.5	TAB-TR	
0125	Erzican, Turkey	1992	0313		6.9		95	Erzincan	2.0	--D C	.20		.248	18.3	7.86	5.4	ERZ-UP	
0125	Erzican, Turkey	1992	0313		6.9		95	Erzincan	2.0	--D C	.10		.515	83.9	27.35	1.5	ERZ-NS	
0125	Erzican, Turkey	1992	0313		6.9		95	Erzincan	2.0	--D C	.10		.496	64.3	22.78	2.0	ERZ-EW	
0127	Cape Mendocino	1992	0425	1806	7.1	CDMG	89156	Petrolia #	9.5	IMD C	.07	23.00	.163	24.5	31.78	5.8	PET-UP	
0127	Cape Mendocino	1992	0425	1806	7.1	CDMG	89156	Petrolia #	9.5	IMD C	.07	23.00	.590	48.4	21.74	6.5	PET000	
0127	Cape Mendocino	1992	0425	1806	7.1	CDMG	89156	Petrolia #	9.5	IMD C	.07	23.00	.662	89.7	29.55	2.7	PET090	
0133	Kobe	1995	0116	2046	6.9	CUE	99999	Takarazuka	1.2	--D D	.00	40.00	.433	34.8	12.38	1.5	TAZ-UP	
0133	Kobe	1995	0116	2046	6.9	CUE	99999	Takarazuka	1.2	--D D	.00	40.00	.693	68.3	26.65	2.2	TAZ000	
0133	Kobe	1995	0116	2046	6.9	CUE	99999	Takarazuka	1.2	--D D	.13	33.00	.694	85.3	16.75	2.1	TAZ090	
0133	Kobe	1995	0116	2046	6.9	CUE	99999	Takatori	.3	--E D	.20		.272	16.0	4.47	7.5	TAK-UP	
0133	Kobe	1995	0116	2046	6.9	CUE	99999	Takatori	.3	--E D			.611	127.1	35.77	6.0	TAK000	
0133	Kobe	1995	0116	2046	6.9	CUE	99999	Takatori	.3	--E D			.616	120.7	32.72	4.8	TAK090	
0141	Kocaeli, Turkey	1999	0817		7.4	KOERI	99999	Yarimca	4.4	B-D C			.242	30.8	29.55	6.5	YPT-UP	
0141	Kocaeli, Turkey	1999	0817		7.4	KOERI	99999	Yarimca	4.4	B-D C	.10	80.00	.292	62.3	44.91	6.0	YPT270	
0141	Kocaeli, Turkey	1999	0817		7.4	KOERI	99999	Yarimca	4.4	B-D C	.10	80.00	.340	68.2	35.86	6.4	YPT000	
0142	Chi-Chi, Taiwan	1999	0920		7.6	CWB	99999	CHY024	9.0	--1 C	.03	50.00	.152	44.8	34.80	15.5	CHY024-V	
0142	Chi-Chi, Taiwan	1999	0920		7.6	CWB	99999	CHY024	9.0	--1 C	.02	50.00	.175	48.9	31.04	13.7	CHY024-N	
0142	Chi-Chi, Taiwan	1999	0920		7.6	CWB	99999	CHY024	9.0	--1 C	.02	50.00	.278	52.9	43.62	11.5	CHY024-W	
0142	Chi-Chi, Taiwan	1999	0920		7.6	CWB	99999	TCU049	4.4	--2 C	.02	50.00	.171	26.1	21.82	12.5	TCU049-V	
0142	Chi-Chi, Taiwan	1999	0920		7.6	CWB	99999	TCU049	4.4	--2 C	.02	30.00	.251	61.2	51.29	16.5	TCU049-N	
0142	Chi-Chi, Taiwan	1999	0920		7.6	CWB	99999	TCU049	4.4	--2 C	.02	50.00	.293	47.9	65.28	17.6	TCU049-W	
0142	Chi-Chi, Taiwan	1999	0920		7.6	CWB	99999	TCU051	8.2	--- C	.03	50.00	.114	34.6	24.56	17.3	TCU051-V	
0142	Chi-Chi, Taiwan	1999	0920		7.6	CWB	99999	TCU051	8.2	--- C	.03	50.00	.225	38.4	56.52	20.0	TCU051-N	
0142	Chi-Chi, Taiwan	1999	0920		7.6	CWB	99999	TCU051	8.2	--- C	.03	50.00	.186	49.3	70.26	17.4	TCU051-W	
0142	Chi-Chi, Taiwan	1999	0920		7.6	CWB	99999	TCU052	.2	--1 c	.04	50.00	.241	110.5	163.51	6.2	TCU052-V	
0142	Chi-Chi, Taiwan	1999	0920		7.6	CWB	99999	TCU052	.2	--1 c	.04	50.00	.419	118.4	246.15	5.8	TCU052-N	
0142	Chi-Chi, Taiwan	1999	0920		7.6	CWB	99999	TCU052	.2	--1 c	.04	50.00	.348	159.0	184.42	6.3	TCU052-W	
0142	Chi-Chi, Taiwan	1999	0920		7.6	CWB	99999	TCU060	9.4	--2 C	.02	50.00	.086	27.5	24.81	16.2	TCU060-V	

B-35

No.	Earthquake	Date & Time				Mag	Own	No.	Station	Closest Dist (km)	Site Codes		Filter Corners			PGV (g)	PGD (cm/s)	Dur (s)	Filename
		YR	MODY	HRMN							Geom	USGS	HP (hz)	LP (hz)	PGA (g)				
0142	Chi-Chi, Taiwan	1999	0920		7.6	CWB	99999	TCU060	9.4	--2	C	.03	50.00	.106	45.3	45.56	20.3	TCU060-N	
0142	Chi-Chi, Taiwan	1999	0920		7.6	CWB	99999	TCU060	9.4	--2	C	.03	50.00	.201	36.3	51.89	17.6	TCU060-W	
0142	Chi-Chi, Taiwan	1999	0920		7.6	CWB	99999	TCU067	.3	--1	C	.04	50.00	.225	42.7	28.48	10.6	TCU067-V	
0142	Chi-Chi, Taiwan	1999	0920		7.6	CWB	99999	TCU067	.3	--1	C	.03	50.00	.325	66.6	45.95	7.6	TCU067-N	
0142	Chi-Chi, Taiwan	1999	0920		7.6	CWB	99999	TCU067	.3	--1	C	.02	50.00	.503	79.5	93.09	11.0	TCU067-W	
0142	Chi-Chi, Taiwan	1999	0920		7.6	CWB	99999	TCU068	1.0	--1	C	.02	50.00	.486	187.3	266.55	2.0	TCU068-V	
0142	Chi-Chi, Taiwan	1999	0920		7.6	CWB	99999	TCU068	1.0	--1	C	.02	50.00	.462	263.1	430.00	7.6	TCU068-N	
0142	Chi-Chi, Taiwan	1999	0920		7.6	CWB	99999	TCU068	1.0	--1	C	.03	50.00	.566	176.6	324.11	6.4	TCU068-W	
0142	Chi-Chi, Taiwan	1999	0920		7.6	CWB	99999	TCU072	7.3	--1	C	.05	50.00	.279	35.8	27.28	14.6	TCU072-V	
0142	Chi-Chi, Taiwan	1999	0920		7.6	CWB	99999	TCU072	7.3	--1	C	.05	50.00	.400	56.3	41.28	15.5	TCU072-N	
0142	Chi-Chi, Taiwan	1999	0920		7.6	CWB	99999	TCU072	7.3	--1	C	.05	50.00	.489	71.7	38.64	14.0	TCU072-W	
0142	Chi-Chi, Taiwan	1999	0920		7.6	CWB	99999	TCU076	1.9	--2	C	.02	50.00	.281	34.1	17.39	16.5	TCU075-V	
0142	Chi-Chi, Taiwan	1999	0920		7.6	CWB	99999	TCU076	1.9	--2	C	.05	50.00	.416	64.2	35.37	16.5	TCU076-N	
0142	Chi-Chi, Taiwan	1999	0920		7.6	CWB	99999	TCU076	1.9	--2	C	.10	50.00	.303	62.6	31.47	17.5	TCU076-W	
0142	Chi-Chi, Taiwan	1999	0920		7.6	CWB	99999	TCU082	5.7	--2	C	.04	50.00	.131	40.8	25.50	15.2	TCU082-V	
0142	Chi-Chi, Taiwan	1999	0920		7.6	CWB	99999	TCU082	5.7	--2	C	.04	50.00	.192	40.5	53.79	19.5	TCU082-N	
0142	Chi-Chi, Taiwan	1999	0920		7.6	CWB	99999	TCU082	5.7	--2	C	.02	50.00	.223	58.4	71.47	17.9	TCU082-W	
0142	Chi-Chi, Taiwan	1999	0920		7.6	CWB	99999	TCU101	2.9	--2	C	.03	50.00	.169	55.2	39.19	15.7	TCU101-V	
0142	Chi-Chi, Taiwan	1999	0920		7.6	CWB	99999	TCU101	2.9	--2	C	.04	50.00	.251	49.4	35.12	16.9	TCU101-N	
0142	Chi-Chi, Taiwan	1999	0920		7.6	CWB	99999	TCU101	2.9	--2	C	.01	50.00	.202	67.9	75.36	16.5	TCU101-W	
0142	Chi-Chi, Taiwan	1999	0920		7.6	CWB	99999	TCU102	1.7	--2	C	.02	50.00	.189	56.2	48.74	11.0	TCU102-V	
0142	Chi-Chi, Taiwan	1999	0920		7.6	CWB	99999	TCU102	1.7	--2	C	.05	50.00	.169	77.1	44.87	15.2	TCU102-N	
0142	Chi-Chi, Taiwan	1999	0920		7.6	CWB	99999	TCU102	1.7	--2	C	.04	50.00	.298	112.4	89.19	13.1	TCU102-W	
0142	Chi-Chi, Taiwan	1999	0920		7.6	CWB	99999	TCU128	9.7	--1	B	.02	40.00	.097	46.0	34.77	18.1	TCU128-V	
0142	Chi-Chi, Taiwan	1999	0920		7.6	CWB	99999	TCU128	9.7	--1	B	.05	30.00	.170	68.8	41.87	10.6	TCU128-N	
0142	Chi-Chi, Taiwan	1999	0920		7.6	CWB	99999	TCU128	9.7	--1	B	.02	30.00	.139	73.0	90.62	13.5	TCU128-W	
0143	Duzce, Turkey	1999	1112		7.1	ERD	99999	Duzce	6.7	--D	C	.06	50.00	.357	22.6	19.40	11.5	DZC-UP	
0143	Duzce, Turkey	1999	1112		7.1	ERD	99999	Duzce	6.7	--D	C	.06	50.00	.348	60.0	42.09	14.4	DZC180	
0143	Duzce, Turkey	1999	1112		7.1	ERD	99999	Duzce	6.7	--D	C	.08	50.00	.535	83.5	51.59	13.8	DZC270	

NRC TIME HISTORY LIBRARY: WUS, SOIL, M>7, D=10-50 km

No.	Earthquake	Date & Time			Mag	Own	No.	Station	Closest Dist (km)	Site Codes		Filter Corners			Dur (s)	Filename			
		YR	MODY	HRMN						Geom	USGS	HP (hz)	LP (hz)	PGA (g)			PGV (g)	PGD (cm/s)	
0046	Tabas, Iran	1978	0916		7.4	70	Boshrooyeh	26.1	--	C	-	.06	.084	11.6	8.36	15.8	BOS-V1		
0046	Tabas, Iran	1978	0916		7.4	70	Boshrooyeh	26.1	--	C	-	.04	20.00	.107	13.7	10.50	14.7	BOS-L1	
0046	Tabas, Iran	1978	0916		7.4	70	Boshrooyeh	26.1	--	C	-	.04	20.00	.089	18.0	18.27	14.8	BOS-T1	
0113	Taiwan SMART1(45)	1986	1114		7.3	62	SMART1 I01	39.0	IZD	-	-	.10	25.00	.075	7.1	4.22	10.8	45I01DN	
0113	Taiwan SMART1(45)	1986	1114		7.3	62	SMART1 I01	39.0	IZD	-	-	.10	25.00	.132	30.5	9.05	10.4	45I01EW	
0113	Taiwan SMART1(45)	1986	1114		7.3	62	SMART1 I01	39.0	IZD	-	-	.10	25.00	.141	29.8	10.34	12.7	45I01NS	
0113	Taiwan SMART1(45)	1986	1114		7.3	29	SMART1 M07	39.0	IZD	-	-	.20	25.00	.106	8.6	3.19	10.0	45M07DN	
0113	Taiwan SMART1(45)	1986	1114		7.3	29	SMART1 M07	39.0	IZD	-	-	.10	25.00	.156	26.8	9.09	9.9	45M07EW	
0113	Taiwan SMART1(45)	1986	1114		7.3	29	SMART1 M07	39.0	IZD	-	-	.20	25.00	.160	22.5	7.62	9.4	45M07NS	
0113	Taiwan SMART1(45)	1986	1114		7.3	66	SMART1 O08	39.0	IZD	-	-	.10	25.00	.105	9.2	4.18	11.1	45O08DN	
0113	Taiwan SMART1(45)	1986	1114		7.3	66	SMART1 O08	39.0	IZD	-	-	.10	25.00	.142	24.5	9.33	12.8	45O08EW	
0113	Taiwan SMART1(45)	1986	1114		7.3	66	SMART1 O08	39.0	IZD	-	-	.10	25.00	.163	30.1	13.21	10.4	45O08NS	
0129	Landers	1992	0628	1158	7.3	CDMG	12025	Palm Springs Airport #	37.5	IQD	C	.07	23.00	.108	6.8	3.08	22.8	PSA-UP	
0129	Landers	1992	0628	1158	7.3	CDMG	12025	Palm Springs Airport #	37.5	IQD	C	.07	23.00	.076	10.9	6.95	25.5	PSA000	
0129	Landers	1992	0628	1158	7.3	CDMG	12025	Palm Springs Airport #	37.5	IQD	C	.07	23.00	.089	13.8	5.29	26.2	PSA090	
0129	Landers	1992	0628	1158	7.3	CDMG	22074	Yermo Fire Station #	24.9	AQD	C	.07	23.00	.136	12.9	4.82	13.4	YER-UP	
0129	Landers	1992	0628	1158	7.3	CDMG	22074	Yermo Fire Station #	24.9	AQD	C	.07	23.00	.245	51.5	43.81	7.1	YER270	
0129	Landers	1992	0628	1158	7.3	CDMG	22074	Yermo Fire Station #	24.9	AQD	C	.07	23.00	.152	29.7	24.69	10.9	YER360	
0141	Kocaeli, Turkey	1999	0817		7.4	ERD	99999	Duzce	14.2	--	D	C	.08	20.00	.229	20.4	17.01	2.9	DZC-UP
0141	Kocaeli, Turkey	1999	0817		7.4	ERD	99999	Duzce	14.2	--	D	C	.00	20.00	.312	58.8	44.11	3.0	DZC180
0141	Kocaeli, Turkey	1999	0817		7.4	ERD	99999	Duzce	14.2	--	D	C	.08	15.00	.358	46.4	17.61	1.8	DZC270
0142	Chi-Chi, Taiwan	1999	0920		7.6	CWB	99999	WGK	11.1	--	2	C	.06	33.00	.180	25.0	16.28	11.0	WGK-V
0142	Chi-Chi, Taiwan	1999	0920		7.6	CWB	99999	WGK	11.1	--	2	C	.07	50.00	.334	69.0	35.70	13.3	WGK-E
0142	Chi-Chi, Taiwan	1999	0920		7.6	CWB	99999	WGK	11.1	--	2	C	.06	50.00	.484	74.4	66.92	10.2	WGK-N
0142	Chi-Chi, Taiwan	1999	0920		7.6	CWB	99999	CHY036	20.3	--	2	C	.04	50.00	.104	11.3	10.18	17.3	CHY036-V
0142	Chi-Chi, Taiwan	1999	0920		7.6	CWB	99999	CHY036	20.3	--	2	C	.03	50.00	.207	41.4	34.17	12.3	CHY036-N
0142	Chi-Chi, Taiwan	1999	0920		7.6	CWB	99999	CHY036	20.3	--	2	C	.05	50.00	.294	38.9	21.19	8.7	CHY036-W
0142	Chi-Chi, Taiwan	1999	0920		7.6	CWB	99999	CHY101	11.1	--	2	C	.04	50.00	.165	28.0	19.73	13.0	CHY101-V
0142	Chi-Chi, Taiwan	1999	0920		7.6	CWB	99999	CHY101	11.1	--	2	C	.04	50.00	.440	115.0	68.75	10.3	CHY101-N
0142	Chi-Chi, Taiwan	1999	0920		7.6	CWB	99999	CHY101	11.1	--	2	C	.04	50.00	.353	70.6	45.28	13.5	CHY101-W
0142	Chi-Chi, Taiwan	1999	0920		7.6	CWB	99999	HWA006	44.0	--	2	C	.03	50.00	.063	6.9	6.81	14.3	HWA006-V
0142	Chi-Chi, Taiwan	1999	0920		7.6	CWB	99999	HWA006	44.0	--	2	C	.06	50.00	.089	9.2	6.11	9.3	HWA006-E
0142	Chi-Chi, Taiwan	1999	0920		7.6	CWB	99999	HWA006	44.0	--	2	C	.06	50.00	.083	7.3	5.89	10.0	HWA006-N
0142	Chi-Chi, Taiwan	1999	0920		7.6	CWB	99999	HWA030	46.3	--	2	C	.02	50.00	.049	8.2	11.65	12.5	HWA030-V

B-37

No.	Earthquake	Date & Time			Mag	Own	No.	Station	Closest Dist (km)	Site Codes		Filter Corners					Dur (s)	Filename
		YR	MODY	HRMN						Geom	USGS	HP (hz)	LP (hz)	PGA (g)	PGV (g)	PGD (cm/s)		
0142	Chi-Chi, Taiwan	1999	0920		7.6	CWB	99999	HWA030	46.3	--2	C	.02	50.00	.079	13.8	8.48	10.6	HWA030-N
0142	Chi-Chi, Taiwan	1999	0920		7.6	CWB	99999	HWA030	46.3	--2	C	.02	50.00	.070	11.0	19.95	9.5	HWA030-W
0142	Chi-Chi, Taiwan	1999	0920		7.6	CWB	99999	HWA035	45.8	--2	C	.02	50.00	.054	7.5	9.60	12.1	HWA035-V
0142	Chi-Chi, Taiwan	1999	0920		7.6	CWB	99999	HWA035	45.8	--2	C	.02	50.00	.074	7.5	8.88	10.1	HWA035-N
0142	Chi-Chi, Taiwan	1999	0920		7.6	CWB	99999	HWA035	45.8	--2	C	.02	50.00	.078	11.9	16.89	11.4	HWA035-W
0142	Chi-Chi, Taiwan	1999	0920		7.6	CWB	99999	TCU038	22.4	--2	C	.02	50.00	.067	34.6	28.80	19.2	TCU038-V
0142	Chi-Chi, Taiwan	1999	0920		7.6	CWB	99999	TCU038	22.4	--2	C	.05	20.00	.168	44.9	43.60	13.1	TCU038-N
0142	Chi-Chi, Taiwan	1999	0920		7.6	CWB	99999	TCU038	22.4	--2	C	.02	50.00	.141	48.9	64.17	15.9	TCU038-W
0142	Chi-Chi, Taiwan	1999	0920		7.6	CWB	99999	TCU042	23.3	--2	C	.02	50.00	.086	19.7	24.09	16.0	TCU042-V
0142	Chi-Chi, Taiwan	1999	0920		7.6	CWB	99999	TCU042	23.3	--2	C	.05	50.00	.199	39.3	23.86	14.8	TCU042-N
0142	Chi-Chi, Taiwan	1999	0920		7.6	CWB	99999	TCU042	23.3	--2	C	.02	50.00	.246	44.8	46.91	12.7	TCU042-W

NRC TIME HISTORY LIBRARY: WUS, SOIL, M>7, D=50-100 km

No.	Earthquake	Date & Time			Mag	Own	No.	Station	Closest Dist (km)	Site Codes Geom USGS	Filter Corners				Dur (s)	Filename	
		YR	MODY	HRMN							HP (hz)	LP (hz)	PGA (g)	PGV (g)			PGD (cm/s)
0129	Landers	1992	0628	1158	7.3	CDMG	12331	Hemet Fire Station #	69.5	AQD C	.16	23.00	.063	3.0	1.60	23.9	H05-UP
0129	Landers	1992	0628	1158	7.3	CDMG	12331	Hemet Fire Station #	69.5	AQD C	.16	23.00	.081	5.6	1.36	22.6	H05000
0129	Landers	1992	0628	1158	7.3	CDMG	12331	Hemet Fire Station #	69.5	AQD C	.16	23.00	.097	5.7	2.27	21.3	H05090
0129	Landers	1992	0628	1158	7.3	CDMG	12026	Indio - Coachella Canal #	55.7	IQD C	.10	23.00	.042	6.6	3.99	29.5	IND-UP
0129	Landers	1992	0628	1158	7.3	CDMG	12026	Indio - Coachella Canal #	55.7	IQD C	.10	23.00	.104	9.6	5.05	25.2	IND000
0129	Landers	1992	0628	1158	7.3	CDMG	12026	Indio - Coachella Canal #	55.7	IQD C	.10	23.00	.109	15.2	9.69	25.1	IND090
0129	Landers	1992	0628	1158	7.3	CDMG	23542	San Bernardino-E &Hospitality	80.5	--D C	.10	50.00	.065	7.5	2.64	25.0	HOS-UP
0129	Landers	1992	0628	1158	7.3	CDMG	23542	San Bernardino-E &Hospitality	80.5	--D C	.10	50.00	.078	19.8	10.49	20.3	HOS090
0129	Landers	1992	0628	1158	7.3	CDMG	23542	San Bernardino-E &Hospitality	80.5	--D C	.10	50.00	.087	14.6	7.63	20.6	HOS180
0141	Kocaeli, Turkey	1999	0817		7.4	ERD	99999	Cekmece	76.1	--D C	.60	20.00	.046	3.4	.34	5.8	CEK-UP
0141	Kocaeli, Turkey	1999	0817		7.4	ERD	99999	Cekmece	76.1	--D C	.30	20.00	.114	12.1	1.41	5.2	CEK000
0141	Kocaeli, Turkey	1999	0817		7.4	ERD	99999	Cekmece	76.1	--D C	.40	20.00	.105	6.4	.84	5.7	CEK270
0142	Chi-Chi, Taiwan	1999	0920		7.6	CWB	99999	TTN	94.3	--2 C	.30	12.00	.013	2.7	.86	28.5	TTN-V
0142	Chi-Chi, Taiwan	1999	0920		7.6	CWB	99999	TTN	94.3	--2 C	.10	12.00	.031	9.7	6.80	24.1	TTN-E
0142	Chi-Chi, Taiwan	1999	0920		7.6	CWB	99999	TTN	94.3	--2 C	.11	12.00	.023	6.2	2.80	21.5	TTN-N
0142	Chi-Chi, Taiwan	1999	0920		7.6	CWB	99999	CHY078	82.4	--2 C	.03	24.00	.021	5.3	6.40	29.0	CHY078-V
0142	Chi-Chi, Taiwan	1999	0920		7.6	CWB	99999	CHY078	82.4	--2 C	.03	24.00	.045	9.6	7.93	26.5	CHY078-N
0142	Chi-Chi, Taiwan	1999	0920		7.6	CWB	99999	CHY078	82.4	--2 C	.03	20.00	.093	14.2	7.16	20.5	CHY078-W
0142	Chi-Chi, Taiwan	1999	0920		7.6	CWB	99999	HWA011	56.7	--2 C	.02	40.00	.039	10.0	10.86	19.0	HWA011-V
0142	Chi-Chi, Taiwan	1999	0920		7.6	CWB	99999	HWA011	56.7	--2 C	.02	30.00	.102	22.0	13.76	13.3	HWA011-N
0142	Chi-Chi, Taiwan	1999	0920		7.6	CWB	99999	HWA011	56.7	--2 C	.02	30.00	.089	21.3	26.83	11.5	HWA011-W
0142	Chi-Chi, Taiwan	1999	0920		7.6	CWB	99999	HWA013	57.4	--2 C	.02	50.00	.064	8.3	11.31	19.0	HWA013-V
0142	Chi-Chi, Taiwan	1999	0920		7.6	CWB	99999	HWA013	57.4	--2 C	.02	50.00	.118	22.0	11.63	11.8	HWA013-N
0142	Chi-Chi, Taiwan	1999	0920		7.6	CWB	99999	HWA013	57.4	--2 C	.02	50.00	.142	31.2	27.00	13.4	HWA013-W
0142	Chi-Chi, Taiwan	1999	0920		7.6	CWB	99999	HWA041	50.0	---- C	.02	30.00	.044	9.5	5.58	23.2	HWA041-V
0142	Chi-Chi, Taiwan	1999	0920		7.6	CWB	99999	HWA041	50.0	---- C	.02	30.00	.082	18.9	7.48	19.8	HWA041-N
0142	Chi-Chi, Taiwan	1999	0920		7.6	CWB	99999	HWA041	50.0	---- C	.02	30.00	.080	11.6	7.47	21.2	HWA041-W
0142	Chi-Chi, Taiwan	1999	0920		7.6	CWB	99999	ILA064	83.4	---- C	.02	50.00	.050	8.8	9.46	15.4	ILA064-V
0142	Chi-Chi, Taiwan	1999	0920		7.6	CWB	99999	ILA064	83.4	---- C	.02	50.00	.072	7.6	16.60	13.9	ILA064-N
0142	Chi-Chi, Taiwan	1999	0920		7.6	CWB	99999	ILA064	83.4	---- C	.02	40.00	.062	9.0	7.97	13.8	ILA064-W
0142	Chi-Chi, Taiwan	1999	0920		7.6	CWB	99999	TCU017	52.2	--2 C	.02	50.00	.050	15.6	16.36	24.3	TCU017-V
0142	Chi-Chi, Taiwan	1999	0920		7.6	CWB	99999	TCU017	52.2	--2 C	.02	50.00	.121	31.9	32.55	11.1	TCU017-N
0142	Chi-Chi, Taiwan	1999	0920		7.6	CWB	99999	TCU017	52.2	--2 C	.02	33.00	.088	42.7	49.82	15.1	TCU017-W
0142	Chi-Chi, Taiwan	1999	0920		7.6	CWB	99999	TTN001	57.6	--2 C	.03	30.00	.041	8.7	6.61	22.7	TTN001-V

B-39

No.	Earthquake	Date & Time		Mag	Own	No.	Station	Closest Dist (km)	Site Codes		Filter Corners			PGV (g)	PGD (cm/s)	Dur (s)	Filename
		YR	MODY HRMN						Geom	USGS	HP (hz)	LP (hz)	PGA (g)				
0142	Chi-Chi, Taiwan	1999	0920	7.6	CWB	99999	TTN001	57.6	--2	C	.03	30.00	.094	14.4	7.38	17.1	TTN001-E
0142	Chi-Chi, Taiwan	1999	0920	7.6	CWB	99999	TTN001	57.6	--2	C	.03	30.00	.063	9.3	5.91	22.2	TTN001-N
0142	Chi-Chi, Taiwan	1999	0920	7.6	CWB	99999	TTN010	95.2	--2	C	.03	14.00	.010	3.0	4.13	34.2	TTN010-V
0142	Chi-Chi, Taiwan	1999	0920	7.6	CWB	99999	TTN010	95.2	--2	C	.03	14.00	.029	7.4	3.95	25.8	TTN010-N
0142	Chi-Chi, Taiwan	1999	0920	7.6	CWB	99999	TTN010	95.2	--2	C	.02	14.00	.019	7.8	9.13	25.4	TTN010-W
0142	Chi-Chi, Taiwan	1999	0920	7.6	CWB	99999	TTN020	57.6	--2	C	.02	30.00	.023	4.8	4.13	28.8	TTN020-V
0142	Chi-Chi, Taiwan	1999	0920	7.6	CWB	99999	TTN020	57.6	--2	C	.02	23.00	.030	7.5	6.44	22.6	TTN020-N
0142	Chi-Chi, Taiwan	1999	0920	7.6	CWB	99999	TTN020	57.6	--2	C	.02	23.00	.035	9.0	9.49	23.4	TTN023-W
0142	Chi-Chi, Taiwan	1999	0920	7.6	CWB	99999	TTN023	63.2	---	C	.03	30.00	.028	6.4	5.21	28.7	TTN023-V
0142	Chi-Chi, Taiwan	1999	0920	7.6	CWB	99999	TTN023	63.2	---	C	.02	30.00	.067	12.0	5.61	29.3	TTN023-N
0142	Chi-Chi, Taiwan	1999	0920	7.6	CWB	99999	TTN023	63.2	---	C	.02	30.00	.044	9.8	7.68	25.6	TTN023-W

NRC TIME HISTORY LIBRARY: WUS, SOIL, M>7, D=100-200 km

B-41

No.	Earthquake	Date & Time			Mag	Own	No.	Station	Closest Dist (km)	Site Codes		Filter Corners			PGV (g)	PGD (cm/s)	Dur (s)	Filename
		YR	MODY	HRMN						Geom	USGS	HP (hz)	LP (hz)	PGA (g)				
012	Kern County	1952	0721	1153	7.4	USGS	135	LA - Hollywood Stor FF	120.5	IPD	C	.20	20.00	.021	2.8	2.55	21.2	PEL-UP
012	Kern County	1952	0721	1153	7.4	USGS	135	LA - Hollywood Stor FF	120.5	IPD	C	.20	15.00	.042	7.5	4.79	18.4	PEL090
012	Kern County	1952	0721	1153	7.4	USGS	135	LA - Hollywood Stor FF	120.5	IPD	C	.20	13.00	.058	6.2	1.86	16.9	PEL180
0046	Tabas, Iran	1978	0916		7.4		69	Bajestan	121.2	--C	-	.05		.029	5.7	6.16	23.9	BAJ-V1
0046	Tabas, Iran	1978	0916		7.4		69	Bajestan	121.2	--C	-	.02	15.00	.094	7.6	10.77	20.4	BAJ-L1
0046	Tabas, Iran	1978	0916		7.4		69	Bajestan	121.2	--C	-	.02	15.00	.067	5.7	10.03	21.3	BAJ-T1
0046	Tabas, Iran	1978	0916		7.4		73	Sedeh	164.5	--D	-	.02	20.00	.013	6.1	11.61	24.7	SED-V1
0046	Tabas, Iran	1978	0916		7.4		73	Sedeh	164.5	--D	-	.02	20.00	.026	5.6	6.42	22.4	SED-L1
0046	Tabas, Iran	1978	0916		7.4		73	Sedeh	164.5	--D	-	.02	20.00	.027	4.1	4.91	21.8	SED-T1
0129	Landers	1992	0628	1158	7.3	USC	90094	Bell Gardens - Jaboneria #	153.9	--D	C	.65	25.00	.016	1.1	.18	24.3	JAB-UP
0129	Landers	1992	0628	1158	7.3	USC	90094	Bell Gardens - Jaboneria #	153.9	--D	C	.30	25.00	.036	4.7	1.48	19.8	JAB220
0129	Landers	1992	0628	1158	7.3	USC	90094	Bell Gardens - Jaboneria #	153.9	--D	C	.18	25.00	.044	10.5	4.74	16.1	JAB310
0129	Landers	1992	0628	1158	7.3	USC	90012	Burbank - N Buena Vista #	162.1	--D	C	.33	25.00	.023	4.7	1.03	27.6	BUE-UP
0129	Landers	1992	0628	1158	7.3	USC	90012	Burbank - N Buena Vista #	162.1	--D	C	.25	25.00	.049	7.2	2.18	23.4	BUE250
0129	Landers	1992	0628	1158	7.3	USC	90012	Burbank - N Buena Vista #	162.1	--D	C	.28	25.00	.068	10.4	2.86	19.7	BUE340
0129	Landers	1992	0628	1158	7.3	USC	90002	Fountain Valley - Euclid #	148.8	--D	C	.90	25.00	.014	1.0	.11	26.3	EUC-UP
0129	Landers	1992	0628	1158	7.3	USC	90002	Fountain Valley - Euclid #	148.8	--D	C	.13	25.00	.069	14.7	7.87	21.3	EUC022
0129	Landers	1992	0628	1158	7.3	USC	90002	Fountain Valley - Euclid #	148.8	--D	C	.13	25.00	.058	10.3	4.70	17.6	EUC292
0129	Landers	1992	0628	1158	7.3	USC	90025	LA - E Vernon Ave #	157.7	--D	C	.38	25.00	.019	2.2	.61	25.6	VER-UP
0129	Landers	1992	0628	1158	7.3	USC	90025	LA - E Vernon Ave #	157.7	--D	C	.13	25.00	.034	7.7	4.64	17.9	VER090
0129	Landers	1992	0628	1158	7.3	USC	90025	LA - E Vernon Ave #	157.7	--D	C	.18	25.00	.039	8.9	4.24	19.3	VER180
0129	Landers	1992	0628	1158	7.3	USC	90080	LB - Orange Ave #	164.5	--D	C	.50	25.00	.019	1.6	.30	24.5	OR2-UP
0129	Landers	1992	0628	1158	7.3	USC	90080	LB - Orange Ave #	164.5	--D	C	.15	25.00	3055	9.5	4.23	20.7	OR2010
0129	Landers	1992	0628	1158	7.3	USC	90080	LB - Orange Ave #	164.5	--D	C	.15	25.00	.061	11.1	4.40	20.2	OR2280
0129	Landers	1992	0628	1158	7.3	USC	90077	Sante Fe Springs - E Joslin #	150.4	--D	C	.35	25.00	.024	1.5	.47	22.6	EJS-UP
0129	Landers	1992	0628	1158	7.3	USC	90077	Sante Fe Springs - E Joslin #	150.4	--D	C	.18	25.00	.060	5.9	2.67	18.4	EJS030
0129	Landers	1992	0628	1158	7.3	USC	90077	Sante Fe Springs - E Joslin #	150.4	--D	C	.15	25.00	.047	9.2	4.23	17.1	EJS120
0142	Chi-Chi, Taiwan	1999	0920		7.6	CWB	99999	SGL	105.0	--2	C	.20	8.00	.008	2.4	.78	28.9	SGL-V
0142	Chi-Chi, Taiwan	1999	0920		7.6	CWB	99999	SGL	105.0	--2	C	.10	14.00	.038	7.7	3.74	24.2	SGL-E
0142	Chi-Chi, Taiwan	1999	0920		7.6	CWB	99999	SGL	105.0	--2	C	.20	14.00	.029	6.0	2.36	24.1	SGL-N
0142	Chi-Chi, Taiwan	1999	0920		7.6	CWB	99999	ILA002	109.1	----	C	.02	30.00	.022	6.7	9.01	20.5	ILA002-V
0142	Chi-Chi, Taiwan	1999	0920		7.6	CWB	99999	ILA002	109.1	----	C	.04	24.00	.073	10.7	7.70	18.0	ILA002-N
0142	Chi-Chi, Taiwan	1999	0920		7.6	CWB	99999	ILA002	109.1	----	C	.02	24.00	.048	10.2	9.47	15.0	ILA002-W
0142	Chi-Chi, Taiwan	1999	0920		7.6	CWB	99999	TAP024	100.2	--2	C	.02	50.00	.023	7.9	9.62	26.8	TAP024-V

No.	Earthquake	Date & Time			Mag	Own	No.	Station	Closest Dist (km)	Site Codes		Filter Corners				Dur (s)	Filename	
		YR	MODY	HRMN						Geom	USGS	HP (hz)	LP (hz)	PGA (g)	PGV (g)			PGD (cm/s)
0142	Chi-Chi, Taiwan	1999	0920		7.6	CWB	99999	TAP024	100.2	--2	C	.02	50.00	.075	20.2	11.49	14.8	TAP024-S
0142	Chi-Chi, Taiwan	1999	0920		7.6	CWB	99999	TAP024	100.2	--2	C	.02	50.00	.062	14.6	21.11	18.1	TAP024-W
0142	Chi-Chi, Taiwan	1999	0920		7.6	CWB	99999	TAP046	127.2	--1	C	.02	30.00	.018	4.5	6.17	25.8	TAP046-V
0142	Chi-Chi, Taiwan	1999	0920		7.6	CWB	99999	TAP046	127.2	--1	C	.02	30.00	.054	6.6	4.93	18.4	TAP046-N
0142	Chi-Chi, Taiwan	1999	0920		7.6	CWB	99999	TAP046	127.2	--1	C	.02	24.00	.084	12.6	7.08	18.4	TAP046-W
0142	Chi-Chi, Taiwan	1999	0920		7.6	CWB	99999	TAP084	127.7	----	C	.03	40.00	.012	5.5	7.73	25.7	TAP084-V
0142	Chi-Chi, Taiwan	1999	0920		7.6	CWB	99999	TAP084	127.7	----	C	.02	40.00	.032	5.5	5.15	25.6	TAP084-N
0142	Chi-Chi, Taiwan	1999	0920		7.6	CWB	99999	TAP084	127.7	----	C	.02	40.00	.035	6.9	10.30	17.6	TAP084-W
0142	Chi-Chi, Taiwan	1999	0920		7.6	CWB	99999	TTN003	108.1	----	C	.02	20.00	.013	2.1	3.11	31.2	TTN003-V
0142	Chi-Chi, Taiwan	1999	0920		7.6	CWB	99999	TTN003	108.1	---	C	.03	20.00	.018	3.0	2.18	25.7	TTN003-N
0142	Chi-Chi, Taiwan	1999	0920		7.6	CWB	99999	TTN003	108.1	---	C	.03	20.00	.023	3.3	4.17	24.6	TTN003-W

TABLE B-3: CEUS, ROCK
NRC TIME HISTORY LIBRARY: CEUS, ROCK, M=4.5-6, D=0-50 km

No.	Earthquake	Date & Time		Mag	Own	No.	Station	Closest Dist (km)	Site Codes		Filter Corners			Dur (s)	Filename			
		YR	MODY						HRM N	Geom	USGS	HP (hz)	LP (hz)			PGA (g)	PGV (g)	PGD (cm/s)
0029	Lytle Creek	1970	0912	1430	5.4	CDWR	620	Devil's Canyon	21.9	CAA	-	1.10	30.00	.205	2.7	.16	.8	DCFDWN
0029	Lytle Creek	1970	0912	1430	5.4	CDWR	620	Devil's Canyon	21.9	CAA	-	1.00	20.00	.295	4.3	.16	.8	CDF090
0029	Lytle Creek	1970	0912	1430	5.4	CDWR	620	Devil's Canyon	21.9	CAA	-	1.00	30.00	.286	6.0	.20	1.2	DCF180
0029	Lytle Creek	1970	0912	1430	5.4	USGS	290	Wrightwood - 6074 Park Dr	15.4	BAB	B	.60	40.00	.158	3.3	.34	1.9	WTWDWN
0029	Lytle Creek	1970	0912	1430	5.4	USGS	290	Wrightwood - 6074 Park Dr	15.4	BAB	B	.60	20.00	.245	8.4	.90	1.6	WTW115
0029	Lytle Creek	1970	0912	1430	5.4	USGS	290	Wrightwood - 6074 Park Dr	15.4	BAB	B	.70	30.00	.317	11.0	.53	1.7	WTW205
0042	Fruili, Italy	1976	0911	1631	5.5		8022	San Rocco	17.9	ABA	-	.40	15.00	.023	2.3	.42	6.8	SRO-UP
0042	Fruili, Italy	1976	0911	1631	5.5		8022	San Rocco	17.9	ABA	-	.20	15.00	.044	1.9	.48	9.3	SRO-NS
0042	Fruili, Italy	1976	0911	1631	5.5		8022	San Rocco	17.9	ABA	-	.40	20.00	.086	3.6	.61	9.7	SRO-WE
0045	Santa Barbara	1978	0813		6.0	USGS	106	Cachuma Dam Toe	36.6	AAA	-	.20	29.00	.041	2.3	.41	5.1	CAD-UP
0045	Santa Barbara	1978	0813		6.0	USGS	106	Cachuma Dam Toe	36.6	AAA	-	.10	36.00	.120	4.8	.96	2.5	CAD250
0045	Santa Barbara	1978	0813		6.0	USGS	106	Cachuma Dam Toe	36.6	AAA	-	.20	30.00	.067	2.3	.38	2.8	CAD340
0054	Livermore	1980	0127	0233	5.4	CDMG	58219	APEEL 3E Hayward CSUH	31.0	AVA	B	.60	25.00	.023	1.2	.12	6.0	B-A3E-UP
0054	Livermore	1980	0127	0233	5.4	CDMG	58219	APEEL 3E Hayward CSUH	31.0	AVA	B	.30	20.00	.082	4.1	.44	8.5	B-A3E146
0054	Livermore	1980	0127	0233	5.4	CDMG	58219	APEEL 3E Hayward CSUH	31.0	AVA	B	.15	20.00	.043	1.4	.21	7.2	B-A3E236
0054	Livermore	1980	0127	0233	5.4	CDMG	57187	San Ramon - Eastman Kodak	17.6	ABB	C	.30	30.00	.058	5.4	.62	8.1	B-KOD-UP
0054	Livermore	1980	0127	0233	5.4	CDMG	57187	San Ramon - Eastman Kodak	17.6	ABB	C	.20	25.00	.340	16.3	2.05	8.9	B-KOD180
0054	Livermore	1980	0127	0233	5.4	CDMG	57187	San Ramon - Eastman Kodak	17.6	ABB	C	.25	25.00	.181	4.6	.45	10.3	B-KOD270
0045	Santa Barbara	1978	0813		6.0	USGS	106	Cachuma Dam Toe	36.6	AAA	-	.20	29.00	.041	2.3	.41	5.1	CAD-UP
0045	Santa Barbara	1978	0813		6.0	USGS	106	Cachuma Dam Toe	36.6	AAA	-	.10	36.00	.120	4.8	.96	2.5	CAD250
0045	Santa Barbara	1978	0813		6.0	USGS	106	Cachuma Dam Toe	36.6	AAA	-	.20	30.00	.067	2.3	.38	2.8	CAD340
0054	Livermore	1980	0127	0233	5.4	CDMG	58219	APEEL 3E Hayward CSUH	31.0	AVA	B	.60	25.00	.012	.1	.12	6.0	B-A3E-UP
0054	Livermore	1980	0127	0233	5.4	CDMG	58219	APEEL 3E Hayward CSUH	31.0	AVA	B	.30	20.00	.082	4.1	.44	8.5	B-A3E146
0054	Livermore	1980	0127	0233	5.4	CDMG	58219	APEEL 3E Hayward CSUH	31.0	AVA	B	.15	20.00	.043	1.4	.21	7.2	B-A3E236
0054	Livermore	1980	0127	0233	5.4	CDMG	57187	San Ramon - Eastman Kodak	17.6	ABB	C	.30	30.00	.058	5.4	.62	8.1	B-KOD-UP
0054	Livermore	1980	0127	0233	5.4	CDMG	57187	San Ramon - Eastman Kodak	17.6	ABB	C	.20	25.00	.340	16.3	2.05	8.9	B-KOD180
0054	Livermore	1980	0127	0233	5.4	CDMG	57187	San Ramon - Eastman Kodak	17.6	ABB	C	.25	25.00	.181	4.6	.45	10.3	B-KOD270
0065	Mammoth Lakes	1980	0611	0441	5.0	USC	40	USC Convict Lakes	9.1	AAB	-	1.00	40.00	.104	.5	.02	2.1	H-XCV-UP
0065	Mammoth Lakes	1980	0611	0441	5.0	USC	40	USC Convict Lakes	9.1	AAB	-	2.00	30.00	.060	.7	.02	1.9	H-XCV075
0065	Mammoth Lakes	1980	0611	0441	5.0	USC	40	USC Convict Lakes	9.1	AAB	-	2.00	30.00	.111	1.0	.02	1.4	H-XCV165
0079	Coalinga	1983	0709	0740	5.2	USGS	1607	Anticline Ridge Free-Field	11.0	IPA	-	.30	40.00	.215	4.9	.59	2.0	C-ATC-UP
0079	Coalinga	1983	0709	0740	5.2	USGS	1607	Anticline Ridge Free-Field	11.0	IPA	-	.30	30.00	.660	14.2	1.00	1.6	C-ATC270
0079	Coalinga	1983	0709	0740	5.2	USGS	1607	Anticline Ridge Free-Field	11.0	IPA	-	.45	40.00	.716	10.3	.38	1.5	C-ATC360

B-43

B-44

No.	Earthquake	Date & Time			Mag	Own	No.	Station	Closest Dist (km)	Site Codes		Filter Corners			Dur (s)	Filename		
		YR	MODY	HRM N						Geom	USGS	HP (hz)	LP (hz)	PGA (g)			PGV (g)	PGD (cm/s)
0079	Coalinga	1983	0709	0740	5.2	USGS	1607	Anticline Ridge Pad	11.0	APA	-	.30	30.00	.290	6.7	.48	1.8	C-ATP-UP
0079	Coalinga	1983	0709	0740	5.2	USGS	1607	Anticline Ridge Pad	11.0	APA	-	.40	30.00	.943	14.6	.93	1.2	C-ATP270
0079	Coalinga	1983	0709	0740	5.2	USGS	1607	Anticline Ridge Pad	11.0	APA	-	.40	25.00	.556	9.9	.45	1.6	C-ATP360
0079	Coalinga	1983	0709	0740	5.2	USGS	1604	Oil City	10.0	APB	-	.40	30.00	.408	6.1	.32	2.3	C-OLC-UP
0079	Coalinga	1983	0709	0740	5.2	USGS	1604	Oil City	10.0	APB	-	.20	30.00	.702	15.0	1.30	1.6	C-OLC270
0079	Coalinga	1983	0709	0740	5.2	USGS	1604	Oil City	10.0	APB	-	.20	30.00	.647	10.8	.59	2.0	C-OLC360
0079	Coalinga	1983	0709	0740	5.2	USGS	1651	Transmitter Hill	10.4	APA	-	.30	30.00	.219	4.7	.39	3.2	C-TSM-UP
0079	Coalinga	1983	0709	0740	5.2	USGS	1651	Transmitter Hill	10.4	APA	-	.20	25.00	.368	10.6	.92	2.7	C-TSM270
0079	Coalinga	1983	0709	0740	5.2	USGS	1651	Transmitter Hill	10.4	APA	-	.30	30.00	.338	8.6	.70	3.0	C-TSM360
0079	Coalinga	1983	0709	0740	5.2	USGS	1604	Oil City	8.2	APB	-	.60	30.00	1.046	21.2	1.78	2.1	D-OLC-UP
0079	Coalinga	1983	0709	0740	5.2	USGS	1604	Oil City	8.2	APB	-	.15	30.00	1.586	40.8	5.14	1.8	D-OLC270
0079	Coalinga	1983	0709	0740	5.2	USGS	1604	Oil City	8.2	APB	-	.80	30.00	.720	20.9	1.68	1.7	D-OLC360
0080	Coalinga	1983	0722	0239	5.8	USGS	1609	Palmer Ave	12.2	APB	-	.20	25.00	.413	9.6	1.67	3.4	D-PLM-UP
0080	Coalinga	1983	0722	0239	5.8	USGS	1609	Palmer Ave	12.2	APB	-	.06	20.00	.477	14.3	1.52	3.2	D-PLM270
0080	Coalinga	1983	0722	0239	5.8	USGS	1609	Palmer Ave	12.2	APB	-	.09	20.00	.509	20.7	1.88	2.8	D-PLM360
0103	N. Palm Springs	1986	0708	0920	6.0	USGS	5043	Hurkey Creek Park	34.9	AQB	B	.40	50.00	.192	5.0	.74	5.4	HCP-UP
0103	N. Palm Springs	1986	0708	0920	6.0	USGS	5043	Hurkey Creek Park	34.9	AQB	B	.60	50.00	.509	6.5	.44	6.8	HCP045
0103	N. Palm Springs	1986	0708	0920	6.0	USGS	5043	Hurkey Creek Park	34.9	AQB	B	.50	50.00	.292	8.1	.70	6.5	HCP135
0017	Whittier Narrows	1987	1001	1442	6.0	USGS	709	Garvey Res. - Control Bldg.	12.1	APB	-	.70	40.00	.844	14.0	1.04	2.4	A-GRV-UP
0017	Whittier Narrows	1987	1001	1442	6.0	USGS	709	Garvey Res. - Control Bldg.	12.1	APB	-	.15	40.00	.556	15.1	1.56	3.3	A-GRV060
0017	Whittier Narrows	1987	1001	1442	6.0	USGS	709	Garvey Res. - Control Bldg.	12.1	APB	-	.20	40.00	.796	17.9	2.20	2.4	A-GRV330

NRC TIME HISTORY LIBRARY: CEUS, ROCK, M=4.5-6, D=50-100 km

No.	Earthquake	Date & Time			Mag	Own	No.	Station	Closest Dist (km)	Site Codes Geom USGS	Filter Corners		PGA (g)	PGV (g)	PGD (cm/s)	Dur (s)	Filename	
		YR	MODY	HRMN							HP (hz)	LP (hz)						
0014	Southern Calif	1952	1122	0746	6.0	USGS	1083	San Luis Obispo	70.0	CBB	-	.20	13.00	.055	2.3	.59	3.2	SLO-UP
0014	Southern Calif	1952	1122	0746	6.0	USGS	1083	San Luis Obispo	70.0	CBB	-	.20	13.00	.073	2.7	.54	3.0	SLO234
0014	Southern Calif	1952	1122	0746	6.0	USGS	1083	San Luis Obispo	70.0	CBB	-	.50	13.00	.109	2.8	.40	2.7	SLO324
0103	N. Palm Springs	1986	0708	0920	6.0	USGS	5231	Anza - Tule Canyon	55.4	AGA	B	.40	30.00	.121	3.5	.41	8.0	ATL-UP
0103	N. Palm Springs	1986	0708	0920	6.0	USGS	5231	Anza - Tule Canyon	55.4	AGA	B	.30	30.00	.209	6.3	.55	8.8	ATL270
0103	N. Palm Springs	1986	0708	0920	6.0	USGS	5231	Anza - Tule Canyon	55.4	AGA	B	.35	35.00	.156	7.4	.52	8.6	ATL360
0103	N. Palm Springs	1986	0708	0920	6.0	CDMG	707	Lake Mathews Dike Toe	73.7	AJA	-	2.00	40.00	.122	1.0	.02	8.7	LMR-UP
0103	N. Palm Springs	1986	0708	0920	6.0	CDMG	707	Lake Mathews Dike Toe	73.7	AJA	-	1.00	50.00	.130	2.1	.08	7.5	LMR162
0103	N. Palm Springs	1986	0708	0920	6.0	CDMG	707	Lake Mathews Dike Toe	73.7	AJA	-	1.00	35.00	.120	1.6	.03	7.8	LMR252
0103	N. Palm Springs	1986	0708	0920	6.0	CDMG	13198	Murrieta Hot Springs	63.3	IGA	A	.50	28.00	.066	1.7	.24	9.1	H01-UP
0103	N. Palm Springs	1986	0708	0920	6.0	CDMG	13198	Murrieta Hot Springs	63.3	IGA	A	.50	40.00	.109	2.1	.21	7.7	H01000
0103	N. Palm Springs	1986	0708	0920	6.0	CDMG	13198	Murrieta Hot Springs	63.3	IGA	A	.50	40.00	.099	2.1	.17	6.6	H01090
0103	N. Palm Springs	1986	0708	0920	6.0	CDMG	12168	Puerta La Cruz	71.9	AQB	B	.20	44.00	.078	2.3	.27	10.2	PLC-UP
0103	N. Palm Springs	1986	0708	0920	6.0	CDMG	12168	Puerta La Cruz	71.9	AQB	B	.20	38.00	.144	2.8	.17	11.2	PLC258
0103	N. Palm Springs	1986	0708	0920	6.0	CDMG	12168	Puerta La Cruz	71.9	AQB	B	.20	32.00	.121	1.9	.18	11.2	PLC348
0103	N. Palm Springs	1986	0708	0920	6.0	CDMG	13123	Riverside Airport	71.1	AQB	B	.50	48.00	.061	1.0	.15	10.8	RIV-UP
0103	N. Palm Springs	1986	0708	0920	6.0	CDMG	13123	Riverside Airport	71.1	AQB	B	.50	40.00	.123	1.3	.11	11.9	RIV180
0103	N. Palm Springs	1986	0708	0920	6.0	CDMG	13123	Riverside Airport	71.1	AQB	B	.50	42.00	.099	1.2	.09	9.8	RIV270
0103	N. Palm Springs	1986	0708	0920	6.0	CDMG	13172	Temecula Fire Station	73.2	AQB	C	.50	27.00	.079	1.7	.25	9.0	TFS-UP
0103	N. Palm Springs	1986	0708	0920	6.0	CDMG	13172	Temecula Fire Station	73.2	AQB	C	.50	25.00	.228	5.9	.47	8.8	TFS000
0103	N. Palm Springs	1986	0708	0920	6.0	CDMG	13172	Temecula Fire Station	73.2	AQB	C	.50	25.00	.164	4.8	.59	10.0	TFS090
0048	Saguenay	1988	1123	0911	4.5	Ms	0	ECTN: A54	99.4	-AA	-	.20	30.00	.001	.0	.00	22.9	A54-Z
0048	Saguenay	1988	1123	0911	4.5	Ms	0	ECTN: A54	99.4	-AA	-	.20	30.00	.001	.0	.00	18.9	A54-N
0048	Saguenay	1988	1123	0911	4.5	Ms	0	ECTN: A54	99.4	-AA	-	.40	30.00	.001	.0	.00	15.6	A54-E
0049	Saguenay	1988	1125	2346	5.9		0	ECTN: A54	91.4	-AA	-	.40	25.00	.014	.3	.04	18.9	1125A54Z
0049	Saguenay	1988	1125	2346	5.9		0	ECTN: A54	91.4	-AA	-	.33	22.00	.015	.3	.05	13.0	1125A54E
0049	Saguenay	1988	1125	2346	5.9		0	ECTN: A54	91.4	-AA	-	.40	23.00	.014	.3	.05	16.6	1125A54N
0049	Saguenay	1988	1125	2346	5.9		0	ECTN: A61	91.9	-AA	-	.50	30.00	.014	.3	.04	18.3	1125A61Z
0049	Saguenay	1988	1125	2346	5.9		0	ECTN: A61	91.9	-AA	-	.40	20.00	.014	.3	.04	20.6	1125A61E
0049	Saguenay	1988	1125	2346	5.9		0	ECTN: A61	91.9	-AA	-	.60	23.00	.014	.4	.05	18.6	1125A61N
0049	Saguenay	1988	1125	2346	5.9		0	BCTN: A64	99.1	-AA	-	.80	20.00	.014	.4	.03	19.4	1125A64Z
0049	Saguenay	1988	1125	2346	5.9		0	BCTN: A64	99.1	-AA	-	.40	22.00	.014	.3	.05	23.7	1125A64E
0049	Saguenay	1988	1125	2346	5.9		0	BCTN: A64	99.1	-AA	-	.90	25.00	.013	.4	.03	16.0	1125A64N
0049	Saguenay	1988	1125	2346	5.9		8	GSC Site 8 - La Malbaie, Que	97.5	ABA	-	.20	30.00	.066	1.7	.12	22.7	1125S08V

B-45

No.	Earthquake	Date & Time				Own	No.	Station	Closest Dist (km)	Site Codes		Filter Corners			PGV (g)	PGD (cm/s)	Dur (s)	Filename
		YR	MODY	HRMN	Mag					Geom	USGS	HP (hz)	LP (hz)	PGA (g)				
0049	Saguenay	1988	1125	2346	5.9		8	GSC Site 8 - La Malbaie, Que	97.5	ABA	-	.25	.00	.134	4.6	.48	10.4	1125S08L
0049	Saguenay	1988	1125	2346	5.9		8	GSC Site 8 - La Malbaie, Que	97.5	ABA	-	.25	30.00	.058	1.4	.13	21.0	1125S08T
0049	Saguenay	1988	1125	2346	5.9		16	GSC Site 16 - Chicoutimi-Nord	51.9	CAA	-	.40	.00	.101	2.1	.10	24.2	1125S16V
0049	Saguenay	1988	1125	2346	5.9		16	GSC Site 16 - Chicoutimi-Nord	51.9	CAA	-	.60	.00	.109	1.8	.07	19.1	1125S16L
0049	Saguenay	1988	1125	2346	5.9		16	GSC Site 16 - Chicoutimi-Nord	51.9	CAA	-	.40	.00	.130	2.7	.14	21.7	1125S16T
0049	Saguenay	1988	1125	2346	5.9		17	GSC Site 17 - St-Andre-Du-Lac	70.3	IAA	-	.70	.00	.042	.8	.03	25.9	1125S17V
0049	Saguenay	1988	1125	2346	5.9		17	GSC Site 17 - St-Andre-Du-Lac	70.3	IAA	-	.70	.00	.169	1.6	.08	14.9	1125S17L
0049	Saguenay	1988	1125	2346	5.9		17	GSC Site 17 - St-Andre-Du-Lac	70.3	IAA	-	.50	.00	.096	1.1	.04	17.8	1125S17T
0049	Saguenay	1988	1125	2346	5.9		20	GSC Site 20 - Les Eboulements	95.0	IAA	-	.50	.00	.237	5.1	.25	33.5	1125S20V
0049	Saguenay	1988	1125	2346	5.9		20	GSC Site 20 - Les Eboulements	95.0	IAA	-	.40	.00	.148	3.8	.33	11.6	1125S20L
0049	Saguenay	1988	1125	2346	5.9		20	GSC Site 20 - Les Eboulements	95.0	IAA	-	.40	45.00	.104	2.5	.22	29.0	1125S20T

NRC TIME HISTORY LIBRARY: CEUS, ROCK, M=6-7, D=0-10 km

No.	Earthquake	Date & Time				Mag	Own	No.	Station	Closest Dist (km)	Site Codes		Filter Corners			PGV (g)	PGD (cm/s)	Dur (s)	Filename
		YR	MODY	HRMN							Geom	USGS	HP (hz)	LP (hz)	PGA (g)				
0001	Helena, Montana	1935	1031	1838	6.2		2022	Carroll College	8.0	EZA	-	.20	15.00	.271	13.9	3.50	A-HMCDWN		
0001	Helena, Montana	1935	1031	1838	6.2		2022	Carroll College	8.0	EZA	-	.20	15.00	.400	8.9	.91	A-HMC180		
0001	Helena, Montana	1935	1031	1838	6.2		2022	Carroll College	8.0	EZA	-	.20	15.00	.436	19.2	2.45	A-HMC270		
0025	Parkfield	1966	0628	0426	6.1	CDMG	1015	Cholame #8	9.2	ABB	C	.20	24.00	.391	10.3	2.35	C08DWN		
0025	Parkfield	1966	0628	0426	6.1	CDMG	1015	Cholame #8	9.2	ABB	C	.20	20.00	.592	12.4	3.71	C08050		
0025	Parkfield	1966	0628	0426	6.1	CDMG	1015	Cholame #8	9.2	ABB	C	.20	20.00	.541	12.4	2.59	C08320		
0025	Parkfield	1966	0628	0426	6.1	CDMG	1438	Tembler pre-1969	9.9	IJA	B	.20	16.00	.412	7.6	2.23	TMBDWN		
0025	Parkfield	1966	0628	0426	6.1	CDMG	1438	Tembler pre-1969	9.9	IJA	B	.20	14.00	.989	21.2	2.40	TMB205		
0025	Parkfield	1966	0628	0426	6.1	CDMG	1438	Tembler pre-1969	9.9	IJA	B	.20	15.00	.689	18.8	3.31	TMB295		
0030	San Fernando	1971	0209	1400	6.6	CDMG	279	Pacoima Dam	2.8	AMB	A	.10	35.00	2.509	83.1	30.37	PCDDWN		
0030	San Fernando	1971	0209	1400	6.6	CDMG	279	Pacoima Dam	2.8	AMB	A	.10	35.00	3.033	86.3	28.57	PCD164		
0030	San Fernando	1971	0209	1400	6.6	CDMG	279	Pacoima Dam	2.8	AMB	A	.50	35.00	3.199	53.1	9.86	PCD254		
0041	Gazli, USSR	1976	0517		6.8		9201	Karakyr	3.0	AAA	-	.50	38.00	3.888	165.1	40.63	GAZ-UP		
0041	Gazli, USSR	1976	0517		6.8		9201	Karakyr	3.0	AAA	-	.50	38.00	1.760	62.5	24.10	GAZ000		
0041	Gazli, USSR	1976	0517		6.8		9201	Karakyr	3.0	AAA	-	.50	38.00	2.349	67.0	29.5	GAZ090		
0090	Morgan Hill	1984	0424	2115	6.2	CDMG	57127	Coyote Lake Dam (SW Abut)	.1	IFA	-	.10	50.00	1.164	30.1	5.28	CYC-UP		
0090	Morgan Hill	1984	0424	2115	6.2	CDMG	57127	Coyote Lake Dam (SW Abut)	.1	IFA	-	.10	39.00	1.608	43.9	9.92	CYC195		
0090	Morgan Hill	1984	0424	2115	6.2	CDMG	57127	Coyote Lake Dam (SW Abut)	.1	IFA	-	.10	45.00	3.372	79.4	10.81	CYC285		
0090	Morgan Hill	1984	0424	2115	6.2	CDMG	57383	Gilroy Array #6	11.8	IKB	B	.10	30.00	.927	22.6	2.77	G06-UP		
0090	Morgan Hill	1984	0424	2115	6.2	CDMG	57383	Gilroy Array #6	11.8	IKB	B	.10	35.00	.465	12.3	2.22	G06000		
0090	Morgan Hill	1984	0424	2115	6.2	CDMG	57383	Gilroy Array #6	11.8	IKB	B	.10	27.00	.608	36.2	6.69	G06090		
0117	Whittier Narrows	1987	1001	1442	6.0	USC	90019	San Gabriel - E Grand Ave #	9.0	--A	A	.35	25.00	.785	10.2	.92	A-GRN-UP		
0117	Whittier Narrows	1987	1001	1442	6.0	USC	90019	San Gabriel - E Grand Ave #	9.0	--A	A	.35	25.00	.731	30.5	3.04	A-GRN180		
0117	Whittier Narrows	1987	1001	1442	6.0	USC	90019	San Gabriel - E Grand Ave #	9.0	--A	A	.35	25.00	.534	11.7	.92	A-GRN270		
0122	Loma Prieta	1989	1018	0005	6.9	CDMG	57007	Corralitos	5.1	APB	B	.20	32.00	1.300	28.8	9.34	CLS-UP		
0122	Loma Prieta	1989	1018	0005	6.9	CDMG	57007	Corralitos	5.1	APB	B	.20	40.00	1.328	57.4	7.22	CLS000		
0122	Loma Prieta	1989	1018	0005	6.9	CDMG	57007	Corralitos	5.1	APB	B	.20	40.00	1.080	49.4	7.43	CLS090		
0122	Loma Prieta	1989	1018	0005	6.9	UCSC	16	LGPC	6.1	--A	-	.10	.00	1.758	69.5	29.72	LGP-UP		
0122	Loma Prieta	1989	1018	0005	6.9	UCSC	16	LGPC	6.1	--A	-	.10	.00	1.647	99.9	43.46	LGP000		
0122	Loma Prieta	1989	1018	0005	6.9	UCSC	16	LGPC	6.1	--A	-	.10	.00	1.518	52.1	12.18	LGP090		
0131	Northridge	1994	0117	1231	6.7	CDMG	24207	Pacoima Dam (downst) #	8.0	AGA	A	.75	23.00	.591	24.7	2.45	PAC-UP		
0131	Northridge	1994	0117	1231	6.7	CDMG	24207	Pacoima Dam (downst) #	8.0	AGA	A	.16	23.00	1.381	44.0	5.94	PAC175		
0131	Northridge	1994	0117	1231	6.7	CDMG	24207	Pacoima Dam (downst) #	8.0	AGA	A	.16	23.00	1.264	31.1	6.39	PAC265		
0131	Northridge	1994	0117	1231	6.7	CDMG	24207	Pacoima Dam (upper left) #	8.0	IGA	A	.16	23.00	4.253	103.2	13.24	PUL-UP		

B-47

No.	Earthquake	Date & Time			Mag	Own	No.	Station	Closest Dist (km)	Site Codes		Filter Corners			PGD (cm/s)	Dur (s)	Filename
		YR	MODY	HRMN						Geom	USGS	HP (hz)	LP (hz)	PGA (g)			
0131	Northridge	1994	0117	1231	6.7	CDMG	24207	Pacoima Dam (upper left) #	8.0	IGA	A	.16	23.00	3.942	65.0	6.12	PUL104
0131	Northridge	1994	0117	1231	6.7	CDMG	24207	Pacoima Dam (upper left) #	8.0	IGA	A	.16	23.00	3.592	87.0	15.32	PUL194
0131	Northridge	1994	0117	1231	6.7	CDMG	24088	Pacoima Kagel Canyon #	8.2	AMB	B	.20	23.00	.559	23.7	9.84	PKC-UP
0131	Northridge	1994	0117	1231	6.7	CDMG	24088	Pacoima Kagel Canyon #	8.2	AMB	B	.14	23.00	.752	34.3	11.48	PKC090
0131	Northridge	1994	0117	1231	6.7	CDMG	24088	Pacoima Kagel Canyon #	8.2	AMB	B	.14	23.00	.978	48.5	8.38	PKC360
0131	Northridge	1994	0117	1231	6.7		99999	KJMA	.6	--	B	.05	.00	1.137	70.7	17.19	KJM-UP
0131	Northridge	1994	0117	1231	6.7		99999	KJMA	.6	--	B	.05	.00	2.124	88.8	18.65	KJM000
0131	Northridge	1994	0117	1231	6.7		99999	KJMA	.6	--	B	.05	.00	1.757	80.4	17.71	KJM090
0004	Gazli, USSR	1976	0517		6.8		9201	Karakyr	3.0	AAA	-	.00	.03	1.260	454.0	230.10	E_GAZ-UP
0004	Gazli, USSR	1976	0517		6.8		9201	Karakyr	3.0	AAA	-	.00	.03	.600	865.0	425.20	E_GAZ000
0004	Gazli, USSR	1976	0517		6.8		9201	Karakyr	3.0	AAA	-	.00	.03	.710	871.0	623.70	E_GAZ090
0041	Nahanni	1985	1223	0516	6.8		6097	NW TERR, CANADA: MACKENZIE, ST1	6.0	IZA	-	.20	62.00	2.086	40.5	12.12	S1-UP
0041	Nahanni	1985	1223	0516	6.8		6097	NW TERR, CANADA: MACKENZIE, ST1	6.0	IZA	-	.05	62.00	.978	46.0	9.67	S1010
0041	Nahanni	1985	1223	0516	6.8		6097	NW TERR, CANADA: MACKENZIE, ST1	6.0	IZA	-	.05	62.00	1.096	46.1	14.58	S1280

NRC TIME HISTORY LIBRARY: CEUS, ROCK, M=6-7, D=10-50 km

No.	Earthquake	Date & Time			Ma g	Own	No.	Station	Closest Dist (km)	Site Codes		Filter Corners			Dur (s)	Filename		
		YR	MODY	HRMN						Geom	USGS	HP (hz)	LP (hz)	PGA (g)			PGV (g)	PGD (cm/s)
0030	San Fernando	1971	0209	1400	6.6	USGS	126	Lake Hughes #4	24.2	IGA	B	.50	35.00	.386	9.6	1.78	5.0	L04DWN
0030	San Fernando	1971	0209	1400	6.6	USGS	126	Lake Hughes #4	24.2	IGA	B	.50	35.00	.488	8.3	1.17	6.1	L04111
0030	San Fernando	1971	0209	1400	6.6	USGS	126	Lake Hughes #4	24.2	IGA	B	.50	35.00	.418	12.4	1.40	6.3	L04201
0030	San Fernando	1971	0209	1400	6.6	CDMG	285	Santa Felita Dam (Outlet)	27.5	ABA	-	.10	20.00	.161	8.0	3.75	8.3	FSD-UP
0030	San Fernando	1971	0209	1400	6.6	CDMG	285	Santa Felita Dam (Outlet)	27.5	ABA	-	.10	20.00	.344	9.1	6.28	7.3	FSD172
0030	San Fernando	1971	0209	1400	6.6	CDMG	285	Santa Felita Dam (Outlet)	27.5	ABA	-	.10	13.00	.370	8.5	2.87	6.5	FSD262
0050	Imperial Valley	1979	1015	2316	6.5	USGS	286	Superstition Mtn Camera	26.0	AGA	B	.10	40.00	.190	3.7	1.57	5.8	H-SUP-UP
0050	Imperial Valley	1979	1015	2316	6.5	USGS	286	Superstition Mtn Camera	26.0	AGA	B	.10	40.00	.229	6.2	1.86	6.1	H-SUP045
0050	Imperial Valley	1979	1015	2316	6.5	USGS	286	Superstition Mtn Camera	26.0	AGA	B	.10	40.00	.533	9.2	2.50	5.7	H-SUP135
0058	Mammoth Lakes	1980	0525	1944	6.0	CDMG	54214	Long Valley Dam (L Abut)	19.7	IVA	-	.40	50.00	.178	6.6	.79	5.3	A-LVL-UP
0058	Mammoth Lakes	1980	0525	1944	6.0	CDMG	54214	Long Valley Dam (L Abut)	19.7	IVA	-	.35	50.00	.230	8.1	.93	6.7	A-LVL000
0058	Mammoth Lakes	1980	0525	1944	6.0	CDMG	54214	Long Valley Dam (L Abut)	19.7	IVA	-	.20	50.00	.129	5.8	2.19	6.5	A-LVL090
0061	Mammoth Lakes	1980	0527	1451	6.0	CDMG	54424	Bishop - Paradise Lodge	43.7	AVA	-	.20	50.00	.248	6.3	1.40	4.9	L-BPL-UP
0061	Mammoth Lakes	1980	0527	1451	6.0	CDMG	54424	Bishop - Paradise Lodge	43.7	AVA	-	.20	40.00	.195	6.7	1.90	5.4	L-BPL070
0061	Mammoth Lakes	1980	0527	1451	6.0	CDMG	54424	Bishop - Paradise Lodge	43.7	AVA	-	.20	40.00	.263	6.3	1.71	5.8	L-BPL160
0064	Victoria, Mexico	1980	0609	0328	6.1	UNAMUCSD	6604	Cerro Prieto	34.8	AVA	B	.20	62.00	.819	20.8	8.49	5.3	CPE-UP
0064	Victoria, Mexico	1980	0609	0328	6.1	UNAMUCSD	6604	Cerro Prieto	34.8	AVA	B	.20	62.00	2.070	46.3	19.77	3.8	CPE045
0064	Victoria, Mexico	1980	0609	0328	6.1	UNAMUCSD	6604	Cerro Prieto	34.8	AVA	B	.20	62.00	1.623	23.6	9.49	4.5	CPE315
0076	Coalinga	1983	0502	2342	6.4	CDMG	36453	Parkfield - Fault Zone 11	28.4	IMB	-	.20	28.00	.115	8.7	3.90	12.5	H-Z11-UP
0076	Coalinga	1983	0502	2342	6.4	CDMG	36453	Parkfield - Fault Zone 11	28.4	IMB	-	.20	21.00	.187	11.1	3.63	19.3	H-Z11000
0076	Coalinga	1983	0502	2342	6.4	CDMG	36453	Parkfield - Fault Zone 11	28.4	IMB	-	.20	28.00	.167	7.4	1.40	18.8	H-Z11090
0076	Coalinga	1983	0502	2342	6.4	CDMG	36420	Parkfield - Gold Hill 3W	38.8	IPB	-	.20	36.00	.175	10.9	3.20	14.1	H-PG3-UP
0076	Coalinga	1983	0502	2342	6.4	CDMG	36420	Parkfield - Gold Hill 3W	38.8	IPB	-	.20	30.00	.246	11.9	2.91	17.4	H-PG3000
0076	Coalinga	1983	0502	2342	6.4	CDMG	36420	Parkfield - Gold Hill 3W	38.8	IPB	-	.20	30.00	.219	9.4	1.67	14.6	H-PG3090
0076	Coalinga	1983	0502	2342	6.4	CDMG	36230	Parkfield - Cholame 2E	40.5	UJB	-	.50	26.00	.040	3.7	.93	12.7	H-TM2-UP
0076	Coalinga	1983	0502	2342	6.4	CDMG	36230	Parkfield - Cholame 2E	40.5	UJB	-	.50	23.00	.053	3.0	.69	13.0	H-TM2000
0076	Coalinga	1983	0502	2342	6.4	CDMG	36230	Parkfield - Cholame 2E	40.5	UJB	-	.50	22.00	.081	5.2	1.77	14.4	H-TM2090
0076	Coalinga	1983	0502	2342	6.4	CDMG	36446	Parkfield - Vineyard Cany 4W	34.6	IMB	-	.20	30.00	.057	5.1	1.03	10.1	H-VC4-UP
0076	Coalinga	1983	0502	2342	6.4	CDMG	36446	Parkfield - Vineyard Cany 4W	34.6	IMB	-	.20	30.00	.108	6.6	1.35	12.7	H-VC4000
0076	Coalinga	1983	0502	2342	6.4	CDMG	36446	Parkfield - Vineyard Cany 4W	34.6	IMB	-	.20	27.00	.085	5.2	.94	13.1	H-VC4090
0090	Morgan Hill	1984	0424	2115	6.2	CDMG	57007	Corralitos	22.7	APB	B	.20	27.00	.080	7.2	1.01	6.5	CLS-UP
0090	Morgan Hill	1984	0424	2115	6.2	CDMG	57007	Corralitos	22.7	APB	B	.20	24.00	.155	7.5	1.14	14.3	CLS220
0090	Morgan Hill	1984	0424	2115	6.2	CDMG	57007	Corralitos	22.7	APB	B	.20	26.00	.206	13.5	1.33	15.1	CLS310
0090	Morgan Hill	1984	0424	2115	6.2	CDMG	57383	Gilroy Array #6	11.8	IKB	B	.10	30.00	.901	21.2	2.55	2.8	G06-UP

B-49

No.	Earthquake	Date & Time			Ma g	Own	No.	Station	Closest Dist (km)	Site Codes		Filter Corners			PGV (g)	PGD (cm/s)	Dur (s)	Filename
		YR	MODY	HRMN						Geom	USGS	HP (hz)	LP (hz)	PGA (g)				
0090	Morgan Hill	1984	0424	2115	6.2	CDMG	57383	Gilroy Array #6	11.8	IKB	B	.10	35.00	.455	12.5	2.38	3.0	G06000
0090	Morgan Hill	1984	0424	2115	6.2	CDMG	57383	Gilroy Array #6	11.8	IKB	B	.10	27.00	.613	39.0	7.18	5.4	G06090
0090	Morgan Hill	1984	0424	2115	6.2	CDMG	47006	Gilroy - Gavilian Coll.	16.2	AFB	B	.50	42.00	.161	3.5	.55	5.7	GIL-UP
0090	Morgan Hill	1984	0424	2115	6.2	CDMG	47006	Gilroy - Gavilian Coll.	16.2	AFB	B	.10	30.00	.276	5.2	.83	7.1	GIL067
0090	Morgan Hill	1984	0424	2115	6.2	CDMG	47006	Gilroy - Gavilian Coll.	16.2	AFB	B	.10	30.00	.196	3.6	.97	10.3	GIL337
0103	N. Palm Springs	1986	0708	0920	6.0	USGS	5230	Santa Rosa Mountain	43.8	AGA	-	1.00	50.00	.121	2.5	.17	6.5	ARS-UP
0103	N. Palm Springs	1986	0708	0920	6.0	USGS	5230	Santa Rosa Mountain	43.8	AGA	-	1.50	60.00	.286	4.0	.13	6.5	ARS270
0103	N. Palm Springs	1986	0708	0920	6.0	USGS	5230	Santa Rosa Mountain	43.8	AGA	-	1.50	60.00	.303	2.9	.13	6.5	ARS360
0041	Nahanni	1985	1223	0516	6.8	Ms	6099	NW TERR, CANADA: MACKENZIE, ST3	16.0	IZA	-	.05	62.00	.140	6.8	3.02	6.8	S3-UP
0041	Nahanni	1985	1223	0516	6.8	Ms	6099	NW TERR, CANADA: MACKENZIE, ST3	16.0	IZA	-	.10	62.00	.148	6.1	3.13	6.8	S3270
0041	Nahanni	1985	1223	0516	6.8	Ms	6099	NW TERR, CANADA: MACKENZIE, ST3	16.0	IZA	-	.05	62.00	.139	3.3	1.06	7.3	S3360

NRC TIME HISTORY LIBRARY: CEUS, ROCK, M=6-7, D=50-100 km

B-51

No.	Earthquake	Date & Time				Mag	Own	No.	Station	Closest Dist (km)	Site Codes Geom USGS	Filter Corners			PGV (g)	PGD (cm/s)	Dur (s)	Filename
		YR	MODY	HRMN								HP (hz)	LP (hz)	PGA (g)				
0025	Parkfield	1966	0628	0426	6.1	USGS	1083	San Luis Obispo	60.0	CBB	-	.20	15.00	.020	1.1	.45	5.4	SLO-UP
0025	Parkfield	1966	0628	0426	6.1	USGS	1083	San Luis Obispo	60.0	CBB	-	.20	15.00	.033	1.0	.29	5.8	SLO234
0025	Parkfield	1966	0628	0426	6.1	USGS	1083	San Luis Obispo	60.0	CBB	-	.20	12.00	.030	1.0	.40	5.8	SLO324
0030	San Fernando	1971	0209	1400	6.6	CDWR	111	Cedar Springs, Allen Ranch	86.6	AAA	A	.20	35.00	.026	1.8	.62	6.5	CSMDWN
0030	San Fernando	1971	0209	1400	6.6	CDWR	111	Cedar Springs, Allen Ranch	86.6	AAA	A	.20	35.00	.050	1.9	.39	6.0	CSM095
0030	San Fernando	1971	0209	1400	6.6	CDWR	111	Cedar Springs, Allen Ranch	86.6	AAA	A	.20	35.00	.035	1.2	.51	6.7	CSM185
0030	San Fernando	1971	0209	1400	6.6	ACOE	287	Upland - San Antonio Dam	58.1	AAA	B	.50	35.00	.098	2.1	.69	8.8	SODDWN
0030	San Fernando	1971	0209	1400	6.6	ACOE	287	Upland - San Antonio Dam	58.1	AAA	B	.50	35.00	.159	3.0	.46	8.9	SOD015
0030	San Fernando	1971	0209	1400	6.6	ACOE	287	Upland - San Antonio Dam	58.1	AAA	B	.50	35.00	.185	4.2	.46	9.4	SOD285
0117	Whittier Narrows	1987	1001	1442	6.0	USC	90052	Calabasas - N Las Virg #	53.3	--B	B	.40	25.00	.086	2.7	.27	12.2	A-VIR-UP
0117	Whittier Narrows	1987	1001	1442	6.0	USC	90052	Calabasas - N Las Virg #	53.3	--B	B		25.00	.119	2.8	.29	11.4	A-VIR200
0117	Whittier Narrows	1987	1001	1442	6.0	USC	90052	Calabasas - N Las Virg #	53.3	--B	B		25.00	.075	1.5	.15	11.7	A-VIR290
0117	Whittier Narrows	1987	1001	1442	6.0	CDMG	24277	Castaic - Hasley Canyon	70.9	A-B	-	.50	20.00	.048	2.9	.32	13.5	A-CSH-UP
0117	Whittier Narrows	1987	1001	1442	6.0	CDMG	24277	Castaic - Hasley Canyon	70.9	A-B	-	.70	15.00	.063	2.3	.20	15.9	A-CSH000
0117	Whittier Narrows	1987	1001	1442	6.0	CDMG	24277	Castaic - Hasley Canyon	70.9	A-B	-	.50	15.00	.072	2.5	.40	17.0	A-CSH090
0117	Whittier Narrows	1987	1001	1442	6.0	CDMG	24278	Castaic - Old Ridge Route	78.3	A-B	B	1.00	23.00	.067	2.0	.15	15.2	A-ORR-UP
0117	Whittier Narrows	1987	1001	1442	6.0	CDMG	24278	Castaic - Old Ridge Route	78.3	A-B	B	.80	15.00	.127	5.1	.43	20.1	A-ORR000
0117	Whittier Narrows	1987	1001	1442	6.0	CDMG	24278	Castaic - Old Ridge Route	78.3	A-B	B	.80	20.00	.111	4.6	.41	21.6	A-ORR090
0117	Whittier Narrows	1987	1001	1442	6.0	CDMG	24396	Malibu - Point Dume Sch	65.3	AMB	B	.35	30.00	.080	3.3	.26	13.1	A-MAL-UP
0117	Whittier Narrows	1987	1001	1442	6.0	CDMG	24396	Malibu - Point Dume Sch	65.3	AMB	B	.35	25.00	.102	3.2	.30	16.4	A-MAL180
0117	Whittier Narrows	1987	1001	1442	6.0	CDMG	24396	Malibu - Point Dume Sch	65.3	AMB	B	.60	20.00	.085	2.5	.20	17.7	A-MAL270
0117	Whittier Narrows	1987	1001	1442	6.0	CDMG	13123	Riverside Airport	56.8	AQB	B	3.00	50.00	.124	1.4	.03	10.8	A-RIV-UP
0117	Whittier Narrows	1987	1001	1442	6.0	CDMG	13123	Riverside Airport	56.8	AQB	B	1.70	35.00	.148	2.0	.06	9.9	A-RIV180
0117	Whittier Narrows	1987	1001	1442	6.0	CDMG	13123	Riverside Airport	56.8	AQB	B	2.00	45.00	.133	2.3	.06	8.6	A-RIV270
0124	Georgia, USSR	1991	0615	0059	6.2		18	Ambralauri	73.7	A-A	-	.10	.00	.018	1.7	.55	15.8	AMB-Z
0124	Georgia, USSR	1991	0615	0059	6.2		18	Ambralauri	73.7	A-A	-	.10	.00	.035	1.9	.57	16.4	AMB-X
0124	Georgia, USSR	1991	0615	0059	6.2		18	Ambralauri	73.7	A-A	-	.10	.00	.035	1.5	.34	17.0	AMB-Y
0131	Northridge	1994	0117	1231	6.7	USC	90067	Duarte - Mel Canyon Rd.	51.6	--B	B	.90	30.00	.158	4.3	.29	12.9	MEL-UP
0131	Northridge	1994	0117	1231	6.7	USC	90067	Duarte - Mel Canyon Rd.	51.6	--B	B	.10	30.00	.154	5.0	1.63	13.5	MEL090
0131	Northridge	1994	0117	1231	6.7	USC	90067	Duarte - Mel Canyon Rd.	51.6	--B	B	.30	30.00	.066	2.8	.39	11.9	MEL180
0131	Northridge	1994	0117	1231	6.7	CDMG	23598	Rancho Cucamonga - Deer Can#	80.0	IGA	A	.30	46.00	.068	4.4	.67	17.8	CUC-UP
0131	Northridge	1994	0117	1231	6.7	CDMG	23598	Rancho Cucamonga - Deer Can#	80.0	IGA	A	.30	46.00	.149	4.4	.66	17.6	CUC090
0131	Northridge	1994	0117	1231	6.7	CDMG	23598	Rancho Cucamonga - Deer Can#	80.0	IGA	A	.30	46.00	.100	6.5	.82	18.4	CUC180
0131	Northridge	1994	0117	1231	6.7	CDMG	14404	Rancho Palos Verdes - Hawth#	55.2	AMA	A	.30	23.00	.160	3.7	.67	9.8	RAN-UP

No.	Earthquake	Date & Time			Mag	Own	No.	Station	Closest Dist (km)	Site Codes		Filter Corners			PGV (g)	PGD (cm/s)	Dur (s)	Filename
		YR	MODY	HRMN						Geom	USGS	HP (hz)	LP (hz)	PGA (g)				
0131	Northridge	1994	0117	1231	6.7	CDMG	14404	Rancho Palos Verdes - Hawth#	55.2	AMA	A	.30	23.00	.198	5.0	.64	11.9	RAN000
0131	Northridge	1994	0117	1231	6.7	CDMG	14404	Rancho Palos Verdes - Hawth#	55.2	AMA	A	.30	23.00	.157	4.4	.87	10.8	RAN090
0131	Northridge	1994	0117	1231	6.7	USC	90090	Villa Park - Serrano Ave	79.5	--B	C	.30	30.00	.075	3.7	.78	14.7	SER-UP
0131	Northridge	1994	0117	1231	6.7	USC	90090	Villa Park - Serrano Ave	79.5	--B	C	.10	30.00	.102	3.4	1.06	15.3	SER000
0131	Northridge	1994	0117	1231	6.7	USC	90090	Villa Park - Serrano Ave	79.5	--B	C	.10	30.00	.103	4.3	1.26	14.2	SER270
0131	Northridge	1994	0117	1231	6.7	USC	90071	West Covina - S Orange Ave	54.1	--B	C	.20	30.00	.192	4.1	1.63	11.5	SOR-UP
0131	Northridge	1994	0117	1231	6.7	USC	90071	West Covina - S Orange Ave	54.1	--B	C	.20	30.00	.151	7.1	1.25	16.9	SOR315
0131	Northridge	1994	0117	1231	6.7	USC	90071	West Covina - S Orange Ave	54.1	--B	C	.10	30.00	.172	5.7	3.03	14.3	SOR315
0131	Northridge	1994	0117	1231	6.7	CDMG	23590	Wrightwood - Jackson Flat #	68.4	I-A	A	.24	46.00	.087	4.8	.60	25.0	WWJ-UP
0131	Northridge	1994	0117	1231	6.7	CDMG	23590	Wrightwood - Jackson Flat #	68.4	I-A	A	.24	46.00	.114	5.5	.82	25.0	WWJ090
0131	Northridge	1994	0117	1231	6.7	CDMG	23590	Wrightwood - Jackson Flat #	68.4	I-A	A	.24	46.00	.082	3.7	.91	24.6	WWJ180

NRC TIME HISTORY LIBRARY: CEUS, ROCK, M=6-7, D=100-200 km

No.	Earthquake	Date & Time				Mag	Own	No.	Station	Closest Dist (km)	Site Codes		Filter Corners			Dur (s)	Filename	
		YR	MODY	HRMN	Geom						USGS	HP (hz)	LP (hz)	PGA (g)	PGV (g)			PGD (cm/s)
0028	Borrogo Mtn	1968	0409	0230	6.8	SCE	280	San Onofre - So Cal Edison	124.7	ABB	-	.20	15.00	.167	3.9	1.11	19.3	A-SON-UP
0028	Borrogo Mtn	1968	0409	0230	6.8	SCE	280	San Onofre - So Cal Edison	124.7	ABB	-	.10	20.00	.108	3.6	1.52	19.7	A-SON033
0028	Borrogo Mtn	1968	0409	0230	6.8	SCE	280	San Onofre - So Cal Edison	124.7	ABB	-	.20	20.00	.103	4.4	1.31	19.1	A-SON303
0030	San Fernando	1971	0209	1400	6.6	ACOE	1035	Isabella Dam (Aux Abut)	113.0	AGA	-	.10	20.00	.020	1.6	1.32	19.5	ISDDWN
0030	San Fernando	1971	0209	1400	6.6	ACOE	1035	Isabella Dam (Aux Abut)	113.0	AGA	-	.10	13.00	.017	1.1	.89	21.0	ISD014
0030	San Fernando	1971	0209	1400	6.6	ACOE	1035	Isabella Dam (Aux Abut)	113.0	AGA	-	.10	13.00	.021	1.3	1.03	21.6	ISD284
0030	San Fernando	1971	0209	1400	6.6	CDWR	1041	Maricopa Array #1	115.0	IBB	-	.10	20.00	.017	1.6	1.06	19.1	MA1DWN
0030	San Fernando	1971	0209	1400	6.6	CDWR	1041	Maricopa Array #1	115.0	IBB	-	.10	13.00	.016	1.7	.80	14.9	MA1130
0030	San Fernando	1971	0209	1400	6.6	CDWR	1041	Maricopa Array #1	115.0	IBB	-	.10	20.00	.030	2.1	1.53	17.4	MA1220
0030	San Fernando	1971	0209	1400	6.6	CDWR	1042	Maricopa Array #2	113.0	IBB	-	.20	20.00	.024	1.2	.32	13.6	MA2DWN
0030	San Fernando	1971	0209	1400	6.6	CDWR	1042	Maricopa Array #2	113.0	IBB	-	.10	20.00	.027	1.8	.92	12.9	MA2130
0030	San Fernando	1971	0209	1400	6.6	CDWR	1042	Maricopa Array #2	113.0	IBB	-	.20	15.00	.019	1.1	.43	12.9	MA2220
0030	San Fernando	1971	0209	1400	6.6	CDWR	1043	Maricopa Array #3	113.0	IBB	-	.20	15.00	.024	2.8	3.01	11.1	MA3DWN
0030	San Fernando	1971	0209	1400	6.6	CDWR	1043	Maricopa Array #3	113.0	IBB	-	.20	20.00	.023	1.9	1.16	10.1	MA3130
0030	San Fernando	1971	0209	1400	6.6	CDWR	1043	Maricopa Array #3	113.0	IBB	-	.10	20.00	.021	1.6	1.52	10.5	MA3220
0030	San Fernando	1971	0209	1400	6.6	SCE	280	San Onofre - So Cal Edison	122.0	ABB	-	.10	23.00	.046	1.8	.77	9.2	SONDWN
0030	San Fernando	1971	0209	1400	6.6	SCE	280	San Onofre - So Cal Edison	122.0	ABB	-	.10	20.00	.039	1.6	.78	9.7	SON033
0030	San Fernando	1971	0209	1400	6.6	SCE	280	San Onofre - So Cal Edison	122.0	ABB	-	.20	20.00	.039	1.9	.66	10.0	SON303
0030	San Fernando	1971	0209	1400	6.6	CDWR	111	Cedar Springs, Allen Ranch	86.6	AAA	A	.20	35.00	.037	1.9	.62	6.7	CSMDWN
0030	San Fernando	1971	0209	1400	6.6	CDWR	111	Cedar Springs, Allen Ranch	86.6	AAA	A	.20	35.00	.064	2.1	.40	6.0	CSM095
0030	San Fernando	1971	0209	1400	6.6	CDWR	111	Cedar Springs, Allen Ranch	86.6	AAA	A	.20	35.00	.044	1.3	.51	6.6	CSM185
0030	San Fernando	1971	0209	1400	6.6	ACOE	287	Upland - San Antonio Dam	58.1	AAA	B	.50	35.00	.137	2.5	.70	8.8	SODDWN
0030	San Fernando	1971	0209	1400	6.6	ACOE	287	Upland - San Antonio Dam	58.1	AAA	B	.50	35.00	.198	3.6	.43	8.5	SOD015
0030	San Fernando	1971	0209	1400	6.6	ACOE	287	Upland - San Antonio Dam	58.1	AAA	B	.50	35.00	.228	4.9	.48	9.1	SOD285
0131	Northridge	1994	0117	1231	6.7	USC	90067	Duarte - Mel Canyon Rd.	51.6	--B	B	.90	30.00	.212	5.1	.33	13.2	MEL-UP
0131	Northridge	1994	0117	1231	6.7	USC	90067	Duarte - Mel Canyon Rd.	51.6	--B	B	.10	30.00	.193	5.6	1.58	13.1	MEL090
0131	Northridge	1994	0117	1231	6.7	USC	90067	Duarte - Mel Canyon Rd.	51.6	--B	B	.30	30.00	.080	3.1	.42	11.3	MEL180
0131	Northridge	1994	0117	1231	6.7	CDMG	23598	Rancho Cucamonga - Deer Can #	80.0	IGA	A	.30	46.00	.091	4.9	.71	17.7	CUC-UP
0131	Northridge	1994	0117	1231	6.7	CDMG	23598	Rancho Cucamonga - Deer Can #	80.0	IGA	A	.30	46.00	.179	4.9	.71	17.3	CUC090
0131	Northridge	1994	0117	1231	6.7	CDMG	23598	Rancho Cucamonga - Deer Can #	80.0	IGA	A	.30	46.00	.121	7.3	.86	17.7	CUC180
0131	Northridge	1994	0117	1231	6.7	CDMG	14404	Rancho Palos Verdes - Hawth #	55.2	AMA	A	.30	23.00	.216	4.3	.69	9.9	RAN-UP
0131	Northridge	1994	0117	1231	6.7	CDMG	14404	Rancho Palos Verdes - Hawth #	55.2	AMA	A	.30	23.00	.240	5.9	.67	11.9	RAN000
0131	Northridge	1994	0117	1231	6.7	CDMG	14404	Rancho Palos Verdes - Hawth #	55.2	AMA	A	.30	23.00	.187	5.0	.89	10.8	RAN090
0131	Northridge	1994	0117	1231	6.7	CDMG	13123	Riverside Airport #	101.3	AQB	B	.30	23.00	.110	3.5	.74	9.0	RIV-UP

B-53

No.	Earthquake	Date & Time				Mag	Own	No.	Station	Closest Dist (km)	Site Codes		Filter Corners			PGA (g)	PGV (g)	PGD (cm/s)	Dur (s)	Filename
		YR	MODY	HRMN							Geom	USGS	HP (hz)	LP (hz)						
0131	Northridge	1994	0117	1231	6.7	CDMG	13123	Riverside Airport #	101.3	AQB	B	.30	23.00	.179	4.4	.36	9.0	RIV180		
0131	Northridge	1994	0117	1231	6.7	CDMG	13123	Riverside Airport #	101.3	AQB	B	.30	23.00	.261	3.9	.55	7.6	RIV270		
0131	Northridge	1994	0117	1231	6.7	USC	90090	Villa Park - Serrano Ave	79.5	--B	C	.30	30.00	.100	4.0	.81	15.0	SER-UP		
0131	Northridge	1994	0117	1231	6.7	USC	90090	Villa Park - Serrano Ave	79.5	--B	C	.10	30.00	.123	4.0	1.06	15.0	SER000		
0131	Northridge	1994	0117	1231	6.7	USC	90090	Villa Park - Serrano Ave	79.5	--B	C	.10	30.00	.123	4.8	1.28	13.8	SER270		
0131	Northridge	1994	0117	1231	6.7	USC	90071	West Covina - S Orange Ave	54.1	--B	C	.20	30.00	.263	4.5	1.67	11.5	SOR-UP		
0131	Northridge	1994	0117	1231	6.7	USC	90071	West Covina - S Orange Ave	54.1	--B	C	.20	30.00	.187	7.9	1.27	16.0	SOR225		
0131	Northridge	1994	0117	1231	6.7	USC	90071	West Covina - S Orange Ave	54.1	--B	C	.10	30.00	.208	6.9	3.07	13.6	SOR315		
0131	Northridge	1994	0117	1231	6.7	CDMG	23590	Wrightwood - Jackson Flat #	68.4	I-A	A	.24	46.00	.141	5.4	1.05	4.4	WWJ-UP		
0131	Northridge	1994	0117	1231	6.7	CDMG	23590	Wrightwood - Jackson Flat #	68.4	I-A	A	.24	46.00	.159	16.5	.93	3.7	WWJ090		
0131	Northridge	1994	0117	1231	6.7	CDMG	23590	Wrightwood - Jackson Flat #	68.4	I-A	A	.24	46.00	.116	4.8	1.02	4.2	WWJ180		

NRC TIME HISTORY LIBRARY: CEUS, ROCK, M>7, D=0-10 km

No.	Earthquake	Date & Time			Mag	Own	No.	Station	Closest Dist (km)	Site Codes		Filter Corners			Dur (s)	Filename		
		YR	MODY	HRMN						Geom	USGS	HP (hz)	LP (hz)	PGA (g)			PGV (g)	PGD (cm/s)
0041	Gazli, USSR	1976	0517		6.8	9201	Karakyr	3.0	AAA	-	.50	38.00	3.578	169.6	47.24	6.0	GAZ-UP	
0041	Gazli, USSR	1976	0517		6.8	9201	Karakyr	3.0	AAA	-	.50	38.00	1.766	67.2	27.24	5.3	GAZ000	
0041	Gazli, USSR	1976	0517		6.8	9201	Karakyr	3.0	AAA	-	.50	38.00	1.790	71.3	32.71	7.0	GAZ090	
0122	Loma Prieta	1989	1018	0005	6.9	CDMG	57007	Corralitos	5.1	APB	B	.20	32.00	1.189	28.1	11.96	3.7	CLS-UP
0122	Loma Prieta	1989	1018	0005	6.9	CDMG	57007	Corralitos	5.1	APB	B	.20	40.00	1.301	56.1	8.43	3.7	CLS000
0122	Loma Prieta	1989	1018	0005	6.9	CDMG	57007	Corralitos	5.1	APB	B	.20	40.00	1.207	52.1	10.20	3.7	CLC090
0122	Loma Prieta	1989	1018	0005	6.9	USCS	16	LGPC	6.1	--A	-	.10	.00	1.626	73.5	33.44	4.5	LGP-UP
0122	Loma Prieta	1989	1018	0005	6.9	USCS	16	LGPC	6.1	--A	-	.10	.00	1.642	110.1	48.24	5.1	LGP000
0122	Loma Prieta	1989	1018	0005	6.9	USCS	16	LGPC	6.1	--A	-	.10	.00	1.645	53.4	13.66	5.5	LGP090
0122	Loma Prieta	1989	1018	0005	6.9	USCS	13	BRAN	10.3	--A	-	.10	.00	1.022	34.4	9.16	7.1	BRN-UP
0122	Loma Prieta	1989	1018	0005	6.9	USCS	13	BRAN	10.3	--A	-	.10	.00	1.296	54.6	8.15	7.2	BRN000
0122	Loma Prieta	1989	1018	0005	6.9	USCS	13	BRAN	10.3	--A	-	.10	.00	1.236	40.2	7.08	8.6	BRN090
0127	Cape Mendocino	1992	0425	1806	7.1	CDMG	89005	Cape Mendocino #	8.5	IFA	A	.07	23.00	2.143	157.6	104.61	1.7	CPM-UP
0127	Cape Mendocino	1992	0425	1806	7.1	CDMG	89005	Cape Mendocino #	8.5	IFA	A	.07	23.00	4.721	127.3	30.88	3.1	CPM000
0127	Cape Mendocino	1992	0425	1806	7.1	CDMG	89005	Cape Mendocino #	8.5	IFA	A	.07	23.00	3.242	85.1	14.88	.6	CPM090
0129	Landers	1992	0628	1158	7.3	SCE	24	Lucerne #	1.1	A-A	A	.00	60.00	2.184	80.7	40.72	9.7	LCN-UP
0129	Landers	1992	0628	1158	7.3	SCE	24	Lucerne #	1.1	A-A	A	.00	60.00	1.844	117.9	71.19	10.0	LCN260
0129	Landers	1992	0628	1158	7.3	SCE	24	Lucerne #	1.1	A-A	A	.00	60.00	2.249	36.9	18.40	10.9	LCN345
0133	Kobe	1995	0116	2046	6.9	CEOR	99999	Kobe University	.2	--A	A	.20	30.00	1.017	38.1	14.53	3.3	KBU-UP
0133	Kobe	1995	0116	2046	6.9	CEOR	99999	Kobe University	.2	--A	A	.10	30.00	.596	53.7	14.94	4.1	KBU000
0133	Kobe	1995	0116	2046	6.9	CEOR	99999	Kobe University	.2	--A	A	.10	30.00	.713	36.4	11.92	5.3	KBU090
0133	Kobe	1995	0116	2046	6.9		99999	KJMA	.6	--B	B	.05	.00	1.067	67.9	18.11	5.6	KJM-UP
0133	Kobe	1995	0116	2046	6.9		99999	KJMA	.6	--B	B	.05	.00	1.924	87.3	19.50	6.1	KJM000
0133	Kobe	1995	0116	2046	6.9		99999	KJMA	.6	--B	B	.05	.00	1.559	81.1	19.12	5.7	KJM090
0141	Kocaeli, Turkey	1999	0817		7.4	ERD	99999	Izmit	7.7	--A	A	2.00	30.00	.363	24.0	11.55	9.6	IZT-UP
0141	Kocaeli, Turkey	1999	0817		7.4	ERD	99999	Izmit	7.7	--A	A	.10	30.00	.401	41.8	14.39	10.1	IZT180
0141	Kocaeli, Turkey	1999	0817		7.4	ERD	99999	Izmit	7.7	--A	A	.10	30.00	.349	26.0	10.58	10.1	IZT090
0142	Chi-Chi, Taiwan	1999	0920		7.6	CWB	99999	CHY080	6.9	---	B	.03	50.00	1.622	98.8	41.93	6.9	CHY080-V
0142	Chi-Chi, Taiwan	1999	0920		7.6	CWB	99999	CHY080	6.9	---	B	.05	50.00	2.113	121.3	34.68	7.1	CHY080-N
0142	Chi-Chi, Taiwan	1999	0920		7.6	CWB	99999	CHY080	6.9	---	B	.10	50.00	2.752	125.4	23.04	7.9	CHY080-W
0142	Chi-Chi, Taiwan	1999	0920		7.6	CWB	99999	TCU087	3.1	--1	b	.02	30.00	.226	116.5	95.34	17.6	TCU087-V
0142	Chi-Chi, Taiwan	1999	0920		7.6	CWB	99999	TCU087	3.1	--1	b	.05	30.00	.209	42.2	29.50	31.8	TCU087-N
0142	Chi-Chi, Taiwan	1999	0920		7.6	CWB	99999	TCU087	3.1	--1	b	.02	30.00	.248	36.6	30.87	33.9	TCU087-W
0142	Chi-Chi, Taiwan	1999	0920		7.6	CWB	99999	TCU089	8.2	--1	b	.03	50.00	.431	41.4	23.19	23.9	TCU089-V

B-55

No.	Earthquake	Date & Time			Mag	Own	No.	Station	Closest Dist (km)	Site Codes		Filter Corners				Dur (s)	Filename	
		YR	MODY	HRMN						Geom	USGS	HP (hz)	LP (hz)	PGA (g)	PGV (g)			PGD (cm/s)
0142	Chi-Chi, Taiwan	1999	0920		7.6	CWB	99999	TCU089	8.2	--1	b	.04	50.00	.440	29.8	17.94	22.5	TCU089-N
0142	Chi-Chi, Taiwan	1999	0920		7.6	CWB	99999	TCU089	8.2	--1	b	.07	50.00	.660	36.8	18.47	21.6	TCU089-W
0142	Chi-Chi, Taiwan	1999	0920		7.6	CWB	99999	TCU120	8.1	--1	B	.03	50.00	.403	74.2	44.57	22.1	TCU120-V
0142	Chi-Chi, Taiwan	1999	0920		7.6	CWB	99999	TCU120	8.1	--1	B	.03	50.00	.379	44.1	32.94	24.2	TCU120-N
0142	Chi-Chi, Taiwan	1999	0920		7.6	CWB	99999	TCU120	8.1	--1	B	.02	50.00	.480	61.2	32.60	23.9	TCU120-W
0142	Chi-Chi, Taiwan	1999	0920		7.6	CWB	99999	TCU128	9.7	--1	B	.02	40.00	.265	103.8	80.72	25.1	TCU128-V
0142	Chi-Chi, Taiwan	1999	0920		7.6	CWB	99999	TCU128	9.7	--1	B	.05	30.00	.305	81.2	52.89	29.9	TCU128-N
0142	Chi-Chi, Taiwan	1999	0920		7.6	CWB	99999	TCU128	9.7	--1	B	.02	30.00	.266	63.4	61.33	35.7	TCU128-W
0142	Chi-Chi, Taiwan	1999	0920		7.6	CWB	99999	TCU136	8.9	---	B	.03	40.00	.262	65.6	48.69	22.9	TCU136-V
0142	Chi-Chi, Taiwan	1999	0920		7.6	CWB	99999	TCU136	8.9	---	B	.03	50.00	.284	54.7	46.26	22.1	TCU136-E
0142	Chi-Chi, Taiwan	1999	0920		7.6	CWB	99999	TCU136	8.9	---	B	.03	50.00	.302	38.5	42.42	22.9	TCU136-N

NRC TIME HISTORY LIBRARY: CEUS, ROCK, M>7, D=10-50 km

No.	Earthquake	Date & Time			Mag	Own	No.	Station	Closest Dist (km)	Site Codes		Filter Corners			PGD (cm/s)	Dur (s)	Filename	
		YR	MODY	HRMN						Geom	USGS	HP (hz)	LP (hz)	PGA (g)				PGV (g)
0046	Tabas, Iran	1978	0916		7.4	9102	Dayhook	17.0	ABB	-	.10	.00	.538	21.7	9.75	8.3	DAY-UP	
0046	Tabas, Iran	1978	0916		7.4	9102	Dayhook	17.0	ABB	-	.10	.00	.993	19.9	6.93	8.8	DAY-LN	
0046	Tabas, Iran	1978	0916		7.4	9102	Dayhook	17.0	ABB	-	.10	.00	.947	32.1	9.75	9.7	DAY-TR	
0127	Cape Mendocino	1992	0425	1806	7.1	CDMG	89530	Shelter Cove Airport #	33.8	IFB	B	.50	23.00	.182	3.9	.33	15.2	SHL-UP
0127	Cape Mendocino	1992	0425	1806	7.1	CDMG	89530	Shelter Cove Airport #	33.8	IFB	B	.50	23.00	.648	8.9	.44	14.4	SHL000
0127	Cape Mendocino	1992	0425	1806	7.1	CDMG	89530	Shelter Cove Airport #	33.8	IFB	B	.50	23.00	.585	9.2	.63	14.6	SHL090
0129	Landers	1992	0628	1158	7.3	CDMG	22161	Twentynine Palms #	42.2	AGA	A	.12	23.00	.125	4.8	4.26	21.3	29P-UP
0129	Landers	1992	0628	1158	7.3	CDMG	22161	Twentynine Palms #	42.2	AGA	A	.12	23.00	.207	5.4	2.67	20.4	29P000
0129	Landers	1992	0628	1158	7.3	CDMG	22161	Twentynine Palms #	42.2	AGA	A	.12	23.00	.180	4.6	4.38	20.2	29P090
0141	Kocaeli, Turkey	1999	0817		7.4	KOERI	99999	Arcelik	17.0	--B	B	1.50	80.00	.174	11.2	1.67	11.4	ARCDWN
0141	Kocaeli, Turkey	1999	0817		7.4	KOERI	99999	Arcelik	17.0	--B	B	.80	70.00	.298	23.7	4.23	10.4	ARC000
0141	Kocaeli, Turkey	1999	0817		7.4	KOERI	99999	Arcelik	17.0	--B	B	.90	70.00	.209	14.8	3.77	9.1	ARC090
0141	Kocaeli, Turkey	1999	0817		7.4	ERD	99999	Gebze	17.0	--A	A	1.00	40.00	.405	11.3	1.01	5.9	GBZ-UP
0141	Kocaeli, Turkey	1999	0817		7.4	ERD	99999	Gebze	17.0	--A	A	.06	25.00	.454	19.0	37.50	7.3	GBZ000
0141	Kocaeli, Turkey	1999	0817		7.4	ERD	99999	Gebze	17.0	--A	A	.08	30.00	.340	35.2	26.63	6.4	GBZ270
0141	Kocaeli, Turkey	1999	0817		7.4	ERD	99999	Goynuuk	35.5	--B	-	.10	30.00	.247	20.7	5.64	8.1	GYN-UP
0141	Kocaeli, Turkey	1999	0817		7.4	ERD	99999	Goynuuk	35.5	--B	-	.15	30.00	.313	10.7	3.01	8.3	GYN000
0141	Kocaeli, Turkey	1999	0817		7.4	ERD	99999	Goynuuk	35.5	--B	-	.10	25.00	.278	13.0	4.72	8.2	GYN090
0141	Kocaeli, Turkey	1999	0817		7.4	ERD	99999	Iznik	29.7	--D	C	.30	30.00	.219	14.9	3.54	9.3	IZN-UP
0141	Kocaeli, Turkey	1999	0817		7.4	ERD	99999	Iznik	29.7	--D	C	.15	25.00	.239	33.5	14.42	14.5	IZN180
0141	Kocaeli, Turkey	1999	0817		7.4	ERD	99999	Iznik	29.7	--D	C	.07	25.00	.175	22.3	8.59	13.8	IZN090
0142	Chi-Chi, Taiwan	1999	0920		7.6	CWB	99999	HWA056	48.7	---	A	.02	50.00	.120	11.4	8.20	15.6	HWA056-V
0142	Chi-Chi, Taiwan	1999	0920		7.6	CWB	99999	HWA056	48.7	---	A	.03	50.00	.203	9.6	5.74	12.3	HWA056-N
0142	Chi-Chi, Taiwan	1999	0920		7.6	CWB	99999	HWA056	48.7	---	A	.02	50.00	.207	6.9	5.94	14.0	HWA056-W
0142	Chi-Chi, Taiwan	1999	0920		7.6	CWB	99999	TCU015	47.3	--1	B	.02	50.00	.135	27.1	24.34	31.6	TCU015-V
0142	Chi-Chi, Taiwan	1999	0920		7.6	CWB	99999	TCU015	47.3	--1	B	.03	50.00	.218	28.3	22.42	22.4	TCU015-N
0142	Chi-Chi, Taiwan	1999	0920		7.6	CWB	99999	TCU015	47.3	--1	B	.02	50.00	.185	40.4	41.66	26.7	TCU015-W
0142	Chi-Chi, Taiwan	1999	0920		7.6	CWB	99999	TCU046	14.3	--1	A	.03	30.00	.240	67.4	57.28	24.4	TCU046-V
0142	Chi-Chi, Taiwan	1999	0920		7.6	CWB	99999	TCU046	14.3	--1	A	.06	30.00	.224	32.9	20.62	25.0	TCU046-N
0142	Chi-Chi, Taiwan	1999	0920		7.6	CWB	99999	TCU046	14.3	--1	A	.03	30.00	.336	33.3	38.09	18.8	TCU046-W
0142	Chi-Chi, Taiwan	1999	0920		7.6	CWB	99999	TCU047	33.0	---	B	.02	50.00	.566	47.7	24.42	16.3	TCU047-V
0142	Chi-Chi, Taiwan	1999	0920		7.6	CWB	99999	TCU047	33.0	---	B	.03	50.00	1.168	32.5	19.83	10.8	TCU047-N
0142	Chi-Chi, Taiwan	1999	0920		7.6	CWB	99999	TCU047	33.0	---	B	.02	50.00	.700	58.9	29.69	12.9	TCU047-W
0142	Chi-Chi, Taiwan	1999	0920		7.6	CWB	99999	TCU095	43.4	--1	B	.02	50.00	.463	49.3	37.53	16.2	TCU095-V

B-57

No.	Earthquake	Date & Time			Mag	Own	No.	Station	Closest Dist (km)	Site Codes		Filter Corners			PGV (g)	PGD (cm/s)	Dur (s)	Filename
		YR	MODY	HRMN						Geom	USGS	HP (hz)	LP (hz)	PGA (g)				
0142	Chi-Chi, Taiwan	1999	0920		7.6	CWB	99999	TCU095	43.4	--1	B	.04	50.00	1.700	57.1	20.85	14.7	TCU095-N
0142	Chi-Chi, Taiwan	1999	0920		7.6	CWB	99999	TCU095	43.4	--1	B	.02	50.00	.782	42.4	40.06	14.0	TCU095-W
0143	Duzce, Turkey	1999	1112		7.1	ERD	99999	Bolu	16.0	--D	C	.05	.00	.470	31.5	19.34	6.5	BOL-UP
0143	Duzce, Turkey	1999	1112		7.1	ERD	99999	Bolu	16.0	--D	C	.05	.00	1.645	69.7	17.73	4.5	BOL000
0143	Duzce, Turkey	1999	1112		7.1	ERD	99999	Bolu	16.0	--D	C	.05	.00	1.765	72.8	15.32	6.4	BOL090
0143	Duzce, Turkey	1999	1112		7.1	ERD	99999	Mudurnu	34.6	--A	-	.08	.00	.132	19.7	13.62	11.9	MDR-UP
0143	Duzce, Turkey	1999	1112		7.1	ERD	99999	Mudurnu	34.6	--A	-	.08	.00	.201	9.9	8.56	15.5	MDR000
0143	Duzce, Turkey	1999	1112		7.1	ERD	99999	Mudurnu	34.6	--A	-	.08	.00	.123	17.2	14.98	13.8	MDR090
0143	Duzce, Turkey	1999	1112		7.1	ERD	99999	Sakarya	42.7	--B	B	.05	40.00	.025	5.3	6.09	18.9	SKR-UP
0143	Duzce, Turkey	1999	1112		7.1	ERD	99999	Sakarya	42.7	--B	B	.05	40.00	.055	5.5	4.76	17.4	SKR180
0143	Duzce, Turkey	1999	1112		7.1	ERD	99999	Sakarya	42.7	--B	B	.05	40.00	.037	5.7	5.90	16.4	SKR090

NRC TIME HISTORY LIBRARY: CEUS, ROCK, M>7, D=50-100 km

No.	Earthquake	Date & Time				Mag	Own	No.	Station	Closest Dist (km)	Site Codes		Filter Corners				Dur (s)	Filename	
		YR	MODY	HRMN							Geom	USGS	HP (hz)	LP (hz)	PGA (g)	PGV (g)			PGD (cm/s)
0049	Tabas, Iran	1978	0916		7.4		71	Ferdows	94.4	--	A	-	.04	.189	11.7	9.82	21.2	FER-V1	
0049	Tabas, Iran	1978	0916		7.4		71	Ferdows	94.4	--	A	-	.02	20.00	.277	6.7	3.06	19.3	FER-L1
0049	Tabas, Iran	1978	0916		7.4		71	Ferdows	94.4	--	A	-	.04	20.00	.358	9.7	6.32	23.2	FER-T1
0129	Landers	1992	0628	1158	7.3	CDMG	21081	Amboy #	69.2	AAB	A	.10	23.00	.315	18.7	5.90	21.7	ABY-UP	
0129	Landers	1992	0628	1158	7.3	CDMG	21081	Amboy #	69.2	AAB	A	.10	23.00	.370	19.3	9.79	18.0	ABY000	
0129	Landers	1992	0628	1158	7.3	CDMG	21081	Amboy #	69.2	AAB	A	.10	23.00	.434	22.3	9.22	19.6	ABY090	
0129	Landers	1992	0628	1158	7.3	CDMG	12168	Puerta La Cruz #	95.9	AQB	B	.30	23.00	.173	3.1	.84	26.9	PLC-UP	
0129	Landers	1992	0628	1158	7.3	CDMG	12168	Puerta La Cruz #	95.9	AQB	B	.30	23.00	.160	2.1	.49	27.4	PLC000	
0129	Landers	1992	0628	1158	7.3	CDMG	12168	Puerta La Cruz #	95.9	AQB	B	.30	23.00	.163	2.5	.58	26.8	PLC090	
0129	Landers	1992	0628	1158	7.3	CDMG	13123	Riverside Airport #	96.1	AQB	B	.16	23.00	.157	3.0	1.57	22.6	RIV-UP	
0129	Landers	1992	0628	1158	7.3	CDMG	13123	Riverside Airport #	96.1	AQB	B	.16	23.00	.133	4.2	1.75	19.8	RIV180	
0129	Landers	1992	0628	1158	7.3	CDMG	13123	Riverside Airport #	96.1	AQB	B	.16	23.00	.151	4.6	1.48	18.0	RIV270	
0129	Landers	1992	0628	1158	7.3	CDMG	12206	Silent Valley - Poppet Flat #	51.7	IGA	A	.12	23.00	.134	5.0	3.01	19.2	SIL-UP	
0129	Landers	1992	0628	1158	7.3	CDMG	12206	Silent Valley - Poppet Flat #	51.7	IGA	A	.12	23.00	.153	4.5	2.47	18.8	SIL000	
0129	Landers	1992	0628	1158	7.3	CDMG	12206	Silent Valley - Poppet Flat #	51.7	IGA	A	.12	23.00	.138	5.2	4.04	19.9	SIL090	
0141	Kocaeli, Turkey	1999	0817		7.4	ITU	99999	Mecidiyekoy	62.3	--	B	B	1.10	60.00	.084	2.4	.26	14.8	MCD-V
0141	Kocaeli, Turkey	1999	0817		7.4	ITU	99999	Mecidiyekoy	62.3	--	B	B	.20	50.00	.129	5.0	1.79	14.2	MCD000
0141	Kocaeli, Turkey	1999	0817		7.4	ITU	99999	Mecidiyekoy	62.3	--	B	B	.05	60.00	.132	8.9	8.15	15.6	MCD090
0142	Chi-Chi, Taiwan	1999	0920		7.6	CWB	99999	NSK	64.5	--	1	A	.20	50.00	.081	8.3	2.52	14.2	NSK-V
0142	Chi-Chi, Taiwan	1999	0920		7.6	CWB	99999	NSK	64.5	--	1	A	.02	30.00	.126	8.3	1.90	14.4	NSK-E
0142	Chi-Chi, Taiwan	1999	0920		7.6	CWB	99999	NSK	64.5	--	1	A	.20	33.00	.118	5.7	1.37	14.4	NSK-N
0142	Chi-Chi, Taiwan	1999	0920		7.6	CWB	99999	TAP035	96.8	--	1	A	.02	24.00	.072	10.9	12.31	34.3	TAP035-V
0142	Chi-Chi, Taiwan	1999	0920		7.6	CWB	99999	TAP035	96.8	--	1	A	.02	24.00	.218	9.8	5.19	33.9	TAP035-N
0142	Chi-Chi, Taiwan	1999	0920		7.6	CWB	99999	TAP035	96.8	--	1	A	.02	24.00	.115	9.2	5.53	36.8	TAP035-W
0142	Chi-Chi, Taiwan	1999	0920		7.6	CWB	99999	TAP036	95.6	--	1	A	.02	30.00	.049	10.0	11.13	23.5	TAP036-V
0142	Chi-Chi, Taiwan	1999	0920		7.6	CWB	99999	TAP036	95.6	--	1	A		30.00	.072	6.5	5.41	19.5	TAP036-N
0142	Chi-Chi, Taiwan	1999	0920		7.6	CWB	99999	TAP036	95.6	--	1	A	.02	20.00	.048	5.7	5.84	20.4	TAP036-W
0142	Chi-Chi, Taiwan	1999	0920		7.6	CWB	99999	TCU025	54.3	---		A	.05	50.00	.086	23.5	21.45	15.2	TCU025-V
0142	Chi-Chi, Taiwan	1999	0920		7.6	CWB	99999	TCU025	54.3	---		A	.05	50.00	.118	9.7	6.71	15.3	TCU025-N
0142	Chi-Chi, Taiwan	1999	0920		7.6	CWB	99999	TCU025	54.3	---		A	.03	50.00	.143	14.2	13.37	14.7	TCU025-W
0142	Chi-Chi, Taiwan	1999	0920		7.6	CWB	99999	ILA031	94.7	--	1	A		50.00	.073	7.8	8.46	29.9	ILA031-V
0142	Chi-Chi, Taiwan	1999	0920		7.6	CWB	99999	ILA031	94.7	--	1	A		30.00	.154	6.5	4.61	25.6	ILA031-N
0142	Chi-Chi, Taiwan	1999	0920		7.6	CWB	99999	ILA031	94.7	--	1	A		50.00	.115	6.3	5.16	20.5	ILA031-W
0142	Chi-Chi, Taiwan	1999	0920		7.6	CWB	99999	ILA051	90.3	---		A	.02	24.00	.059	11.0	12.40	36.0	ILA051-V

B-59

No.	Earthquake	Date & Time		Mag	Own	No.	Station	Closest Dist (km)	Site Codes		Filter Corners			PGV (g)	PGD (cm/s)	Dur (s)	Filename
		YR	MODY						HRMN	Geom	USGS	HP (hz)	LP (hz)				
0142	Chi-Chi, Taiwan	1999	0920	7.6	CWB	99999	ILA051	90.3	----	A	.02	22.00	.064	7.4	5.12	38.3	ILA051-N
0142	Chi-Chi, Taiwan	1999	0920	7.6	CWB	99999	ILA051	90.3	----	A	.02	22.00	.151	14.1	7.98	39.6	ILA051-W
0142	Chi-Chi, Taiwan	1999	0920	7.6	CWB	99999	ILA063	71.6	----	A	.04	50.00	.122	11.2	11.31	15.6	ILA063-V
0142	Chi-Chi, Taiwan	1999	0920	7.6	CWB	99999	ILA063	71.6	----	A	.02	50.00	.221	9.3	7.43	15.3	ILA063-N
0142	Chi-Chi, Taiwan	1999	0920	7.6	CWB	99999	ILA063	71.6	----	A	.02	50.00	.226	10.5	6.52	15.9	ILA063-W
0142	Chi-Chi, Taiwan	1999	0920	7.6	CWB	99999	HWA023	57.0	--2	A	.03	50.00	.076	9.7	8.31	18.0	HWA023-V
0142	Chi-Chi, Taiwan	1999	0920	7.6	CWB	99999	HWA023	57.0	--2	A	.04	40.00	.072	8.9	5.40	22.6	HWA023-N
0142	Chi-Chi, Taiwan	1999	0920	7.6	CWB	99999	HWA023	57.0	--2	A	.04	40.00	.073	6.1	4.19	22.7	HWA023-W
0142	Chi-Chi, Taiwan	1999	0920	7.6	CWB	99999	HWA026	58.8	----	A	.02	50.00	.110	9.1	6.98	26.2	HWA026-V
0142	Chi-Chi, Taiwan	1999	0920	7.6	CWB	99999	HWA026	58.8	----	A	.03	50.00	.135	8.2	5.00	15.0	HWA026-N
0142	Chi-Chi, Taiwan	1999	0920	7.6	CWB	99999	HWA026	58.8	----	A	.02	50.00	.202	7.4	4.75	17.0	HWA026-W

NRC TIME HISTORY LIBRARY: CEUS, ROCK, M>7, D=100-200 km

No.	Earthquake	Date & Time				Mag	Own	No.	Station	Closest Dist (km)	Site Codes		Filter Corners			Dur (s)	Filename	
		YR	MODY	HRMN							Geom	USGS	HP (hz)	LP (hz)	PGA (g)			PGV (g)
0046	Tabas, Iran	1978	0916		7.4		72	Kashmar	199.1	--B	-	.05	20.00	.120	12.1	7.94	17.5	KSH-V1
0046	Tabas, Iran	1978	0916		7.4		72	Kashmar	199.1	--B	-	.03	20.00	.144	10.4	7.01	17.6	KSH-L1
0046	Tabas, Iran	1978	0916		7.4		72	Kashmar	199.1	--B	-	.02	20.00	.135	10.4	6.11	16.5	KSH-T1
0129	Landers	1992	0628	1158	7.3	USC	90052	Calabasas - N Las Virg #	194.1	--B	B	.50	25.00	.065	3.0	.62	27.9	VIR-UP
0129	Landers	1992	0628	1158	7.3	USC	90052	Calabasas - N Las Virg #	194.1	--B	B	.28	25.00	.062	3.3	1.13	27.7	VIR200
0129	Landers	1992	0628	1158	7.3	USC	90052	Calabasas - N Las Virg #	194.1	--B	B	.20	22.00	.038	3.1	1.10	25.1	VIR290
0129	Landers	1992	0628	1158	7.3	USC	90067	Duarte - Mel Canyon Rd #	126.4	--B	B	.28	25.00	.084	7.7	2.54	17.5	MEL-UP
0129	Landers	1992	0628	1158	7.3	USC	90067	Duarte - Mel Canyon Rd #	126.4	--B	B	.28	25.00	.091	4.5	1.37	17.0	MEL090
0129	Landers	1992	0628	1158	7.3	USC	90067	Duarte - Mel Canyon Rd #	126.4	--B	B	.30	25.00	.062	3.9	1.40	18.2	MEL180
0129	Landers	1992	0628	1158	7.3	USC	90019	San Gabriel - E Grand Ave	141.6	--A	A	.16	22.00	.100	11.7	6.66	25.7	GRN-UP
0129	Landers	1992	0628	1158	7.3	USC	90019	San Gabriel - E Grand Ave	141.6	--A	A	.07	25.00	.145	13.4	14.21	26.4	GRN180
0129	Landers	1992	0628	1158	7.3	USC	90019	San Gabriel - E Grand Ave	141.6	--A	A	.13	25.00	.123	10.6	6.41	27.0	GRN270
0129	Landers	1992	0628	1158	7.3	USC	90008	Sun Valley - Sunland #	162.6	--B	B	1.00	25.00	.067	2.0	.18	23.8	SUL-UP
0129	Landers	1992	0628	1158	7.3	USC	90008	Sun Valley - Sunland #	162.6	--B	B	.33	25.00	.094	3.7	.79	26.0	SUL230
0129	Landers	1992	0628	1158	7.3	USC	90008	Sun Valley - Sunland #	162.6	--B	B	.45	25.00	.076	3.9	.66	25.4	SUL320
0129	Landers	1992	0628	1158	7.3	USC	90090	Villa Park - Serrano Ave #	131.4	--B	B	.20	25.00	.103	6.3	1.71	29.8	SER-UP
0129	Landers	1992	0628	1158	7.3	USC	90090	Villa Park - Serrano Ave #	131.4	--B	B	.11	25.00	.095	8.6	6.85	31.7	SER000
0129	Landers	1992	0628	1158	7.3	USC	90090	Villa Park - Serrano Ave #	131.4	--B	B	.18	25.00	.121	8.9	3.32	26.7	SER270
0142	Chi-Chi, Taiwan	1999	0920		7.6	CWB	99999	PNG	114.2	--1	A	.40	30.00	.047	2.4	.39	32.4	PNG-V
0142	Chi-Chi, Taiwan	1999	0920		7.6	CWB	99999	PNG	114.2	--1	A	.24	40.00	.112	2.6	.59	29.9	PNG-E
0142	Chi-Chi, Taiwan	1999	0920		7.6	CWB	99999	PNG	114.2	--1	A	.22	30.00	.110	3.5	.86	31.1	PNG-N
0142	Chi-Chi, Taiwan	1999	0920		7.6	CWB	99999	KAU078	102.8	--1	A	.03	50.00	.046	4.0	3.45	32.1	KAU078-V
0142	Chi-Chi, Taiwan	1999	0920		7.6	CWB	99999	KAU078	102.8	--1	A	.02	50.00	.066	2.2	1.54	30.3	KAU078-N
0142	Chi-Chi, Taiwan	1999	0920		7.6	CWB	99999	KAU078	102.8	--1	A	.02	50.00	.114	3.7	1.05	25.4	KAU078-W
0142	Chi-Chi, Taiwan	1999	0920		7.6	CWB	99999	TAP059	125.9	--1	A	.02	20.00	.053	9.6	8.61	35.6	TAP059-V
0142	Chi-Chi, Taiwan	1999	0920		7.6	CWB	99999	TAP059	125.9	--1	A	.02	30.00	.094	6.1	4.23	37.4	TAP059-N
0142	Chi-Chi, Taiwan	1999	0920		7.6	CWB	99999	TAP059	125.9	--1	A		15.00	.069	9.1	4.92	32.0	TAP059W
0142	Chi-Chi, Taiwan	1999	0920		7.6	CWB	99999	TAP060	128.4	--1	A	.02	24.00	.040	8.1	6.83	39.7	TAP060-V
0142	Chi-Chi, Taiwan	1999	0920		7.6	CWB	99999	TAP060	128.4	--1	A	.02	20.00	.091	8.8	4.32	37.7	TAP060-N
0142	Chi-Chi, Taiwan	1999	0920		7.6	CWB	99999	TAP060	128.4	--1	A		20.00	.076	12.1	4.47	37.0	TAP060-W
0142	Chi-Chi, Taiwan	1999	0920		7.6	CWB	99999	TAP067	104.2	--1	A	.03	20.00	.114	13.9	12.64	40.8	TAP067-V
0142	Chi-Chi, Taiwan	1999	0920		7.6	CWB	99999	TAP067	104.2	--1	A	.02	20.00	.091	11.0	5.63	39.3	TAP067-N
0142	Chi-Chi, Taiwan	1999	0920		7.6	CWB	99999	TAP067	104.2	--1	A	.02	20.00	.089	12.0	7.39	38.2	TAP067-W
0142	Chi-Chi, Taiwan	1999	0920		7.6	CWB	99999	TAP069	135.3	--1	A	.04	20.00	.063	5.8	4.25	37.8	TAP069-V

B-61

No.	Earthquake	Date & Time		Mag	Own	No.	Station	Closest Dist (km)	Site Codes		Filter Corners			PGV (g)	PGD (cm/s)	Dur (s)	Filename
		YR	MODY HRMN						Geom	USGS	HP (hz)	LP (hz)	PGA (g)				
0142	Chi-Chi, Taiwan	1999	0920	7.6	CWB	99999	TAP069	135.3	--1	A	.05	20.00	.072	5.5	3.60	35.6	TAP069-N
0142	Chi-Chi, Taiwan	1999	0920	7.6	CWB	99999	TAP069	135.3	--1	A	.04	20.00	.063	5.8	4.25	35.6	TAP069-W
0142	Chi-Chi, Taiwan	1999	0920	7.6	CWB	99999	TAP072	110.0	---	A	.03	30.00	.081	10.5	10.90	28.7	TAP072-V
0142	Chi-Chi, Taiwan	1999	0920	7.6	CWB	99999	TAP072	110.0	---	A	.04	30.00	.163	11.7	5.02	21.9	TAP072-N
0142	Chi-Chi, Taiwan	1999	0920	7.6	CWB	99999	TAP072	110.0	---	A	.03	50.00	.067	10.3	5.40	23.0	TAP072-W
0142	Chi-Chi, Taiwan	1999	0920	7.6	CWB	99999	TAP075	118.4	---	A	.03	30.00	.110	10.8	9.85	28.2	TAP075-V
0142	Chi-Chi, Taiwan	1999	0920	7.6	CWB	99999	TAP075	118.4	---	A	.02	50.00	.171	11.1	4.74	24.9	TAP075-N
0142	Chi-Chi, Taiwan	1999	0920	7.6	CWB	99999	TAP075	118.4	---	A	.01	30.00	.205	11.4	5.38	24.9	TAP075-W
0142	Chi-Chi, Taiwan	1999	0920	7.6	CWB	99999	TAP078	131.0	---	A	.03	33.00	.063	8.6	8.30	30.5	TAP078-V
0142	Chi-Chi, Taiwan	1999	0920	7.6	CWB	99999	TAP078	131.0	---	A	.04	40.00	.088	13.0	5.55	25.8	TAP078-N
0142	Chi-Chi, Taiwan	1999	0920	7.6	CWB	99999	TAP078	131.0	---	A	.02	40.00	.094	10.7	4.98	30.1	TAP078-W

TABLE B-4: CEUS, SOIL
 NRC TIME HISTORY LIBRARY: CEUS, SOIL, M=4.5-6, D=0-50 km

No.	Earthquake	Date & Time				Mag	Own	No.	Station	Closest Dist (km)	Site Codes		Filter Corners				Dur (s)	Filename
		YR	MODY	HRMN							Geom	USGS	HP (hz)	LP (hz)	PGA (g)	PGV (g)		
0026	Northern Calif.	1967	1210	1206	5.6	USGS	1023	Ferndale City Hall	30.8	BQD	C	.40	12.00	.061	5.5	.59	7.0	C-FRN-UP
0026	Northern Calif.	1967	1210	1206	5.6	USGS	1023	Ferndale City Hall	30.8	BQD	C	.30	20.00	.611	13.4	1.17	1.1	C-FRN224
0026	Northern Calif.	1967	1210	1206	5.6	USGS	1023	Ferndale City Hall	30.8	BQD	C	.20	13.00	.250	14.3	1.41	3.6	C-FRN314
0058	Mammoth Lakes	1980	0525	1944	6.0	CDMG	54099	Convict Creek	17.4	AQD	-	.20	40.00	.544	14.5	2.37	2.7	A-CVK-UP
0058	Mammoth Lakes	1980	0525	1944	6.0	CDMG	54099	Convict Creek	17.4	AQD	-	.08	30.00	.365	24.0	3.50	2.8	A-CVK090
0058	Mammoth Lakes	1980	0525	1944	6.0	CDMG	54099	Convict Creek	17.4	AQD	-	.08	35.00	.454	17.8	2.54	3.4	A-CVK180
0074	Mammoth Lakes	1983	0107	0138	5.2	CDMG	54099	Convict Creek	9.5	AQD	-	.20	40.00	.201	15.6	1.91	3.1	F-CVK-UP
0074	Mammoth Lakes	1983	0107	0138	5.2	CDMG	54099	Convict Creek	9.5	AQD	-	.15	30.00	.281	19.3	2.18	1.8	F-CVK090
0074	Mammoth Lakes	1983	0107	0138	5.2	CDMG	54099	Convict Creek	9.5	AQD	-	.15	30.00	.280	22.9	3.22	1.3	F-CVK180
0077	Coalinga	1983	0509	0249	5.0	USGS	1606	Burnett Construction	17.7	AHD	-	.40	30.00	.202	4.3	.21	2.6	A-BNT-UP
0077	Coalinga	1983	0509	0249	5.0	USGS	1606	Burnett Construction	17.7	AHD	-	.50	30.00	.183	5.4	.41	3.0	A-BNT270
0077	Coalinga	1983	0509	0249	5.0	USGS	1606	Burnett Construction	17.7	AHD	-	.40	25.00	.178	6.8	.42	3.2	A-BNT360
0079	Coalinga	1983	0709	0740	5.2	CDMG	46T04	CHP (temp)	14.9	AHD	-	.45	30.00	.195	4.3	.31	3.4	C-CHP-UP
0079	Coalinga	1983	0709	0740	5.2	CDMG	46T04	CHP (temp)	14.9	AHD	-	.30	25.00	.382	12.1	.68	1.8	C-CHP000
0079	Coalinga	1983	0709	0740	5.2	CDMG	46T04	CHP (temp)	14.9	AHD	-	.30	25.00	.369	8.7	.33	2.1	C-CHP090
0103	N. Palm Springs	1986	0708	0920	6.0	USGS	5073	Cabazon	16.3	AHD	-	.20	45.00	.982	13.5	1.18	2.2	CAB-UP
0103	N. Palm Springs	1986	0708	0920	6.0	USGS	5073	Cabazon	16.3	AHD	-	.15	40.00	.494	9.7	1.74	2.7	CAB180
0103	N. Palm Springs	1986	0708	0920	6.0	USGS	5073	Cabazon	16.3	AHD	-	.15	40.00	.405	18.6	2.65	1.6	CAB270
0103	N. Palm Springs	1986	0708	0920	6.0	USGS	5072	Whitewater Trout Farm	7.3	AHC	A	.50	40.00	1.252	25.4	1.53	2.3	WWT-UP
0103	N. Palm Springs	1986	0708	0920	6.0	USGS	5072	Whitewater Trout Farm	7.3	AHC	A	.10	40.00	.882	45.3	5.30	1.7	WWT180
0103	N. Palm Springs	1986	0708	0920	6.0	USGS	5072	Whitewater Trout Farm	7.3	AHC	A	.15	45.00	1.217	44.3	3.97	2.0	WWT270
0106	Chalfant Valley	1986	0721	1451	5.6	CDMG	54428	Zack Brothers Ranch	20.0	AAD	-	.20	40.00	.216	4.3	.22	3.3	C-ZAK-UP
0106	Chalfant Valley	1986	0721	1451	5.6	CDMG	54428	Zack Brothers Ranch	20.0	AAD	-	.13	35.00	.338	12.0	.80	2.3	C-ZAK270
0106	Chalfant Valley	1986	0721	1451	5.6	CDMG	54428	Zack Brothers Ranch	20.0	AAD	-	.30	30.00	.243	7.8	.57	3.9	C-ZAK360
0117	Whittier Narrows	1987	1001	1442	6.0	USGS	951	Brea Dam (Downstream)	23.3	IPD	-	.50	40.00	.249	6.4	.37	5.4	A-BRD-UP
0117	Whittier Narrows	1987	1001	1442	6.0	USGS	951	Brea Dam (Downstream)	23.3	IPD	-	.60	35.00	.343	10.0	.43	3.3	A-BRD040
0117	Whittier Narrows	1987	1001	1442	6.0	USGS	951	Brea Dam (Downstream)	23.3	IPD	-	.60	40.00	.590	24.1	1.17	3.2	A-BRD130
0117	Whittier Narrows	1987	1001	1442	6.0	USC	90078	Compton - Castlegate St #	16.9	--D	C	.50	25.00	.446	7.2	.26	3.1	A-CAS-UP
0117	Whittier Narrows	1987	1001	1442	6.0	USC	90078	Compton - Castlegate St #	16.9	--D	C	.09	25.00	.635	32.0	4.70	2.4	A-CAS000
0117	Whittier Narrows	1987	1001	1442	6.0	USC	90078	Compton - Castlegate St #	16.9	--D	C	.28	25.00	.718	19.0	1.85	2.6	A-CAS270
0117	Whittier Narrows	1987	1001	1442	6.0	CDMG	14196	Inglewood - Union Oil	25.2	IQD	B	.50	30.00	.197	5.1	.39	5.3	A-ING-UP
0117	Whittier Narrows	1987	1001	1442	6.0	CDMG	14196	Inglewood - Union Oil	25.2	IQD	B	.60	40.00	.597	13.6	.92	2.1	A-ING000
0117	Whittier Narrows	1987	1001	1442	6.0	CDMG	14196	Inglewood - Union Oil	25.2	IQD	B	.25	40.00	.517	25.9	2.48	1.8	A-ING090

B-63

No.	Earthquake	Date & Time					Mag	Own	No.	Station	Closest Dist (km)	Site Codes		Filter Corners			Dur (s)	Filename	
		YR	MODY	HRMN	Geom	USGS						HP (hz)	LP (hz)	PGA (g)	PGV (g)	PGD (cm/s)			
0117	Whittier Narrows	1987	1001	1442	6.0	USC		90072	La Puente - Ringrove Av #	11.9	--D	C	.45	25.00	.197	5.2	.24	3.9	A-RIM-UP
0117	Whittier Narrows	1987	1001	1442	6.0	USC		90072	La Puente - Ringrove Av #	11.9	--D	C	.18	25.00	.336	8.1	1.09	4.5	A-RIM015
0117	Whittier Narrows	1987	1001	1442	6.0	USC		90072	La Puente - Ringrove Av #	11.9	--D	C	.50	21.00	.271	8.9	.46	2.5	A-RIM105
0117	Whittier Narrows	1987	1001	1442	6.0	CDMG		80047	Pasadena - CIT Calif Blvd	15.5	AQD	-	.30	40.00	.468	12.2	.93	2.8	A-CCB-UP
0117	Whittier Narrows	1987	1001	1442	6.0	CDMG		80047	Pasadena - CIT Calif Blvd	15.5	AQD	-	.30	40.00	.303	11.7	1.21	3.3	A-CCB270
0117	Whittier Narrows	1987	1001	1442	6.0	CDMG		80047	Pasadena - CIT Calif Blvd	15.5	AQD	-	.30	35.00	.477	20.6	3.05	2.9	A-CCB360
0117	Whittier Narrows	1987	1001	1442	6.0	CDMG		80049	Pasadena - CIT Keck Lab	15.5	-QD	-	.60	60.00	.230	7.6	.60	4.0	A-KEC-UP
0117	Whittier Narrows	1987	1001	1442	6.0	CDMG		80049	Pasadena - CIT Keck Lab	15.5	-QD	-	.40	35.00	.294	7.2	.80	3.4	A-KEC270
0117	Whittier Narrows	1987	1001	1442	6.0	CDMG		80049	Pasadena - CIT Keck Lab	15.5	-QD	-	.25	35.00	.345	19.2	2.63	2.7	A-KEC360
0052	New Madrid, MO	1989	0427	1647	4.7			0	Ridgely, Tennessee	39.9	IDD	-	.50	70.00	.110	.1	.00	12.0	RDG-UP
0052	New Madrid, MO	1989	0427	1647	4.7			0	Ridgely, Tennessee	39.9	IDD	-	.40	60.00	.007	.2	.01	15.0	RDG007
0052	New Madrid, MO	1989	0427	1647	4.7			0	Ridgely, Tennessee	39.9	IDD	-	.30	60.00	.009	.2	.02	13.0	RDG097

NRC TIME HISTORY LIBRARY: CEUS, SOIL, M=4.5-6, D=50-100 km

B-65

Date & Time							Closest Site Codes Filter Corners											
No.	Earthquake	YR	MODY	HRMN	Mag	Own	No.	Station	Dist (km)	Geom	USGS	HP (hz)	LP (hz)	PGA (g)	PGV (g)	PGD (cm/s)	Dur (s)	Filename
0005	Northwest Calif	1938	0912	0610	5.5	USGS	1023	Ferndale City Hall	55.0	BQD	C	.30	15.00	.074	2.9	.18	5.9	A-FRNDWN
0005	Northwest Calif	1938	0912	0610	5.5	USGS	1023	Ferndale City Hall	55.0	BQD	C	.50	11.00	.329	13.2	.66	3.4	A-FRN045
0005	Northwest Calif	1938	0912	0610	5.5	USGS	1023	Ferndale City Hall	55.0	BQD	C	.20	11.00	.236	7.8	.90	3.2	A-FRN135
0011	Northwest Calif	1951	1008	0411	5.8	USGS	1023	Ferndale City Hall	56.0	BQD	C	.40	20.00	.084	3.3	.28	6.5	B-FRN-UP
0011	Northwest Calif	1951	1008	0411	5.8	USGS	1023	Ferndale City Hall	56.0	BQD	C	.50	12.00	.233	9.5	.59	3.5	B-FRN224
0011	Northwest Calif	1951	1008	0411	5.8	USGS	1023	Ferndale City Hall	56.0	BQD	C	.50	12.00	.234	9.7	1.05	3.8	B-FRN314
0029	Lytle Creek	1970	0912	1430	5.4	CDMG	125	Lake Hughes #1	93.5	APC	B	1.10	15.00	.016	.5	.03	3.0	L01DWN
0029	Lytle Creek	1970	0912	1430	5.4	CDMG	125	Lake Hughes #1	93.5	APC	B	.80	10.00	.026	1.1	.09	2.9	L01021
0029	Lytle Creek	1970	0912	1430	5.4	CDMG	125	Lake Hughes #1	93.5	APC	B	.35	20.00	.022	.9	.12	3.5	L01291
0029	Lytle Creek	1970	0912	1430	5.4	USGS	135	LA - Hollywood Stor FF	76.0	IPD	C	.90	20.00	.018	.5	.03	5.9	HOL-UP
0029	Lytle Creek	1970	0912	1430	5.4	USGS	135	LA - Hollywood Stor FF	76.0	IPD	C	.30	20.00	.050	1.8	.13	4.9	HOL090
0029	Lytle Creek	1970	0912	1430	5.4	USGS	135	LA - Hollywood Stor FF	76.0	IPD	C	.40	20.00	.049	1.3	.07	4.1	HOL180
0051	Imperial Valley	1979	1015	2319	5.2	UNAMUCSD	6605	Delta	52.1	IQD	C	1.00	25.00	.058	1.2	.06	7.3	A-DLTDWN
0051	Imperial Valley	1979	1015	2319	5.2	UNAMUCSD	6605	Delta	52.1	IQD	C	.80	25.00	.183	4.5	.27	3.7	A-DLT262
0051	Imperial Valley	1979	1015	2319	5.2	UNAMUCSD	6605	Delta	52.1	IQD	C	.40	25.00	.264	10.5	.75	2.2	A-DLT352
0084	Trinidad offshore	1983	0824	1336	5.5	CDMG	1498	Rio Dell Overpass, E Ground	67.6	APC	B	.30	30.00	.069	2.7	.26	8.8	RDE-UP
0084	Trinidad offshore	1983	0824	1336	5.5	CDMG	1498	Rio Dell Overpass, E Ground	67.6	APC	B	.15	30.00	.571	18.2	.78	3.3	RDE000
0084	Trinidad offshore	1983	0824	1336	5.5	CDMG	1498	Rio Dell Overpass, E Ground	67.6	APC	B	.30	30.00	.354	11.8	.82	6.0	RDE270
0084	Trinidad offshore	1983	0824	1336	5.5	CDMG	1498	Rio Dell Overpass, W Ground	67.6	APC	B	.50	40.00	.081	2.5	.22	8.4	RDW-UP
0084	Trinidad offshore	1983	0824	1336	5.5	CDMG	1498	Rio Dell Overpass, W Ground	67.6	APC	B	.40	40.00	.409	10.4	.69	5.6	RDW000
0084	Trinidad offshore	1983	0824	1336	5.5	CDMG	1498	Rio Dell Overpass, W Ground	67.6	APC	B	.20	35.00	.375	9.3	.62	5.8	RDW270
0103	N. Palm Springs	1986	0708	0920	6.0	CDOT	754	Colton Interchange - Vault	57.4	BHD	-	.40	30.00	.043	1.9	.40	9.9	CLI-UP
0103	N. Palm Springs	1986	0708	0920	6.0	CDOT	754	Colton Interchange - Vault	57.4	BHD	-	.40	30.00	.093	5.2	.54	8.8	CLI082
0103	N. Palm Springs	1986	0708	0920	6.0	CDOT	754	Colton Interchange - Vault	57.4	BHD	-	.40	30.00	.119	7.0	.63	9.0	CLI352
0103	N. Palm Springs	1986	0708	0920	6.0	CDMG	22T13	Landers Fire Station	38.2	AQD	-	.50	40.00	.134	4.7	.27	5.4	LDR-UP
0103	N. Palm Springs	1986	0708	0920	6.0	CDMG	22T13	Landers Fire Station	38.2	AQD	-	.50	30.00	.197	7.6	.57	5.1	LDR000
0103	N. Palm Springs	1986	0708	0920	6.0	CDMG	22T13	Landers Fire Station	38.2	AQD	-	.50	30.00	.295	7.2	.63	4.4	LDR090
0117	Whittier Narrows	1987	1001	1442	6.0	USC	90065	Glendora - N Oakbank #	69.7	--D	B	.38	25.00	.212	5.2	.45	5.0	A-OAK-UP
0117	Whittier Narrows	1987	1001	1442	6.0	USC	90065	Glendora - N Oakbank #	69.7	--D	B	.35	25.00	.289	5.4	.68	4.1	A-OAK080
0117	Whittier Narrows	1987	1001	1442	6.0	USC	90065	Glendora - N Oakbank #	69.7	--D	B	.23	25.00	.342	7.7	.82	3.6	A-OAK170
0117	Whittier Narrows	1987	1001	1442	6.0	CDMG	24526	Lancaster - Med Off FF	69.5	IQC	-	1.30	35.00	.080	1.9	.05	8.2	A-LMD-UP
0117	Whittier Narrows	1987	1001	1442	6.0	CDMG	24526	Lancaster - Med Off FF	69.5	IQC	-	.80	25.00	.150	5.0	.26	7.9	A-LMD010
0117	Whittier Narrows	1987	1001	1442	6.0	CDMG	24526	Lancaster - Med Off FF	69.5	IQC	-	.60	25.00	.193	4.5	.26	10.2	A-LMD100
0117	Whittier Narrows	1987	1001	1442	6.0	CDMG	24309	Leona Valley #6	64.8	IHD	C	1.00	25.00	.054	1.6	.12	7.8	A-LV6-UP

No.	Earthquake	Date & Time				Own	No.	Station	Closest Dist (km)	Site Codes		Filter Corners			PGV (g)	PGD (cm/s)	Dur (s)	Filename
		YR	MODY	HRMN	Mag					Geom	USGS	HP (hz)	LP (hz)	PGA (g)				
0117	Whittier Narrows	1987	1001	1442	6.0	CDMG	24309	Leona Valley #6	64.8	IHD	C	1.00	25.00	.109	3.0	.15	6.8	A-LV6000
0117	Whittier Narrows	1987	1001	1442	6.0	CDMG	24309	Leona Valley #6	64.8	IHD	C	.80	25.00	.134	3.8	.18	7.5	A-LV6090
0117	Whittier Narrows	1987	1001	1442	6.0	CDMG	24279	Newhall - Fire Sta	55.2	AQD	C	1.00	25.00	.077	1.7	.12	9.1	A-NWH-UP
0117	Whittier Narrows	1987	1001	1442	6.0	CDMG	24279	Newhall - Fire Sta	55.2	AQD	C	.50	15.00	.104	4.5	.41	9.0	A-NWH180
0117	Whittier Narrows	1987	1001	1442	6.0	CDMG	24279	Newhall - Fire Sta	55.2	AQD	C	.60	15.00	.146	4.3	.54	6.5	A-NWH270
0049	Saguenay	1988	1125	2346	5.9		7	GSC Site 7 - Baie-St-Paul, Que	95.6	CBC	-	.40		.122	2.6	.28	19.1	1125S07V
0049	Saguenay	1988	1125	2346	5.9		7	GSC Site 7 - Baie-St-Paul, Que	95.6	CBC	-	.30	40.00	.122	4.7	.51	17.2	1125S07L
0049	Saguenay	1988	1125	2346	5.9		7	GSC Site 7 - Baie-St-Paul, Que	95.6	CBC	-	.10	30.00	.173	5.7	.66	16.0	1125S07T
0052	New Madrid, MO	1989	0427	1647	4.7		0	Hornbeak, TN	56.7	IDD	-	.40	70.00	.003	.6	.00	15.9	HRN-UP
0052	New Madrid, MO	1989	0427	1647	4.7		0	Hornbeak, TN	56.7	IDD	-	.40	60.00	.005	.8	.01	12.8	HRN000
0052	New Madrid, MO	1989	0427	1647	4.7		0	Hornbeak, TN	56.7	IDD	-	.40	60.00	.005	1.0	.01	15.0	HRN090

NRC TIME HISTORY LIBRARY: CEUS, SOIL, M=6-7, D=0-10 km

No.	Earthquake	Date & Time					No.	Station	Closest Dist (km)	Site Codes		Filter Corners					Dur (s)	Filename
		YR	MODY	HRMN	Mag	Own				Geom	USGS	HP (hz)	LP (hz)	PGA (g)	PGV (g)	PGD (cm/s)		
0050	Imperial Valley	1979	1015	2316	6.5	USGS	5054	Bonds Corner	2.5	AQD	C	.10	40.00	1.055	18.3	4.23	4.7	H-BCR-UP
0050	Imperial Valley	1979	1015	2316	6.5	USGS	5054	Bonds Corner	2.5	AQD	C	.10	40.00	.745	59.6	12.09	4.9	H-BCR140
0050	Imperial Valley	1979	1015	2316	6.5	USGS	5054	Bonds Corner	2.5	AQD	C	.10	40.00	1.120	56.9	12.59	4.1	H-BCR230
0050	Imperial Valley	1979	1015	2316	6.5	USGS	5060	Brawley Airport	8.5	AQD	C	.10	40.00	.347	14.2	3.92	5.2	H-BRA-UP
0050	Imperial Valley	1979	1015	2316	6.5	USGS	5060	Brawley Airport	8.5	AQD	C	.10	40.00	.223	35.5	17.93	5.2	H-BRA225
0050	Imperial Valley	1979	1015	2316	6.5	USGS	5060	Brawley Airport	8.5	AQD	C	.10	40.00	.398	34.1	11.74	2.7	H-BRA315
0050	Imperial Valley	1979	1015	2316	6.5	CDMG	5154	EC County Center FF	7.6	IDD	C	.10	50.00	.531	21.7	9.22	3.8	H-ECC-UP
0050	Imperial Valley	1979	1015	2316	6.5	CDMG	5154	EC County Center FF	7.6	IDD	C	.10	40.00	.312	49.5	12.99	3.9	H-ECC002
0050	Imperial Valley	1979	1015	2316	6.5	CDMG	5154	EC County Center FF	7.6	IDD	C	.10	35.00	.386	57.8	31.89	5.0	H-ECC092
0050	Imperial Valley	1979	1015	2316	6.5	USGS	5057	El Centro Array #3	9.3	AQD	D	.10	40.00	.306	10.6	6.75	6.1	H-E03-UP
0050	Imperial Valley	1979	1015	2316	6.5	USGS	5057	El Centro Array #3	9.3	AQD	D	.10	40.00	.419	44.0	17.37	4.7	H-E03140
0050	Imperial Valley	1979	1015	2316	6.5	USGS	5057	El Centro Array #3	9.3	AQD	D	.10	40.00	.314	34.9	20.27	5.3	H-E03230
0050	Imperial Valley	1979	1015	2316	6.5	USGS	952	El Centro Array #5	1.0	IQD	C	.10	40.00	1.370	40.0	14.91	2.4	H-E05-UP
0050	Imperial Valley	1979	1015	2316	6.5	USGS	952	El Centro Array #5	1.0	IQD	C	.10	40.00	.804	52.3	26.67	4.0	H-E05140
0050	Imperial Valley	1979	1015	2316	6.5	USGS	952	El Centro Array #5	1.0	IQD	C	.10	40.00	.542	106.6	52.23	3.8	H-E-5230
0050	Imperial Valley	1979	1015	2316	6.5	CDMG	942	El Centro Array #6	1.0	IQD	C	.20	40.00	3.990	128.3	21.73	1.7	H-E06-UP
0050	Imperial Valley	1979	1015	2316	6.5	CDMG	942	El Centro Array #6	1.0	IQD	C	.10	40.00	.635	65.8	32.84	5.2	H-E06140
0050	Imperial Valley	1979	1015	2316	6.5	CDMG	942	El Centro Array #6	1.0	IQD	C	.10	40.00	.580	93.5	56.78	4.8	H-E06230
0050	Imperial Valley	1979	1015	2316	6.5	USGS	5165	El Centro Differential Array	5.3	IQD	C	.10	40.00	1.630	29.4	15.66	3.1	H-EDA-UP
0050	Imperial Valley	1979	1015	2316	6.5	USGS	5165	El Centro Differential Array	5.3	IQD	C	.10	40.00	.581	54.7	35.73	3.8	H-EDA270
0050	Imperial Valley	1979	1015	2316	6.5	USGS	5165	El Centro Differential Array	5.3	IQD	C	.10	40.00	.621	59.7	20.49	4.5	H-EDA360
0050	Imperial Valley	1979	1015	2316	6.5	USGS	5055	Holtville Post Office	7.5	AQD	C	.10	40.00	.530	14.4	6.93	5.3	H-HVP-UP
0050	Imperial Valley	1979	1015	2316	6.5	USGS	5055	Holtville Post Office	7.5	AQD	C	.10	40.00	.367	53.0	24.34	5.1	H-HVP225
0050	Imperial Valley	1979	1015	2316	6.5	USGS	5055	Holtville Post Office	7.5	AQD	C	.10	40.00	.368	42.1	24.61	4.7	H-HVP315
0056	Mammoth Lakes	1980	0525	1634	6.3	CDMG	54099	Convict Creek	9.0	AQD	-	.20	41.00	.933	31.6	6.62	5.7	I-CVK-UP
0056	Mammoth Lakes	1980	0525	1634	6.3	CDMG	54099	Convict Creek	9.0	AQD	-	.10	60.00	.586	27.1	5.99	6.6	I-CVK090
0056	Mammoth Lakes	1980	0525	1634	6.3	CDMG	54099	Convict Creek	9.0	AQD	-	.10	50.00	.675	24.6	7.59	7.2	I-CVK180
0076	Coalinga	1983	0502	2342	6.4	USBR	1162	Pleasant Valley P.P. - yard	8.5	AHD	-	.20	31.00	.697	28.0	2.84	4.7	H-PVY-UP
0076	Coalinga	1983	0502	2342	6.4	USBR	1162	Pleasant Valley P.P. - yard	8.5	AHD	-	.20	40.00	.968	68.3	8.56	4.1	H-PVY045
0076	Coalinga	1983	0502	2342	6.4	USBR	1162	Pleasant Valley P.P. - yard	8.5	AHD	-	.20	31.00	.761	39.9	4.84	4.5	H-PVY135
0105	Chalfant Valley	1986	0721	1442	6.2	CDMG	54171	Bishop - LADWP South St	9.2	AQD	-	.10	40.00	.303	11.3	3.18	4.3	A-LAD-UP
0105	Chalfant Valley	1986	0721	1442	6.2	CDMG	54171	Bishop - LADWP South St	9.2	AQD	-	.10	40.00	.403	24.5	8.00	3.7	A-LAD180
0105	Chalfant Valley	1986	0721	1442	6.2	CDMG	54171	Bishop - LADWP South St	9.2	AQD	-	.10	30.00	.235	23.1	5.14	3.9	A-LAD270

B-67

B-68

No.	Earthquake	Date & Time				Mag	Own	No.	Station	Closest Dist (km)	Site Codes		Filter Corners			PGV (g)	PGD (cm/s)	Dur (s)	Filename
		YR	MODY	HRMN							Geom	USGS	HP (hz)	LP (hz)	PGA (g)				
0125	Erzican, Turkey	1992	0313		6.9		95	Erzincan	2.0	--D	C	.20	.490	22.2	10.01	5.2	ERZ-UP		
0125	Erzican, Turkey	1992	0313		6.9		95	Erzincan	2.0	--D	C	.10	.707	105.9	27.25	1.9	ERZ-NS		
0125	Erzican, Turkey	1992	0313		6.9		95	Erzincan	2.0	--D	C	.10	.765	72.1	22.49	2.3	ERZ-EW		
0131	Northridge	1994	0117	1231	6.7	CDMG	24087	Arleta - Nordhoff Fire Sta #	9.2	AQD	C	.12	23.00	1.288	30.4	9.57	5.4	ARL-UP	
0131	Northridge	1994	0117	1231	6.7	CDMG	24087	Arleta - Nordhoff Fire Sta #	9.2	AQD	C	.12	23.00	.545	45.6	10.24	6.5	ARL090	
0131	Northridge	1994	0117	1231	6.7	CDMG	24087	Arleta - Nordhoff Fire Sta #	9.2	AQD	C	.12	23.00	.477	35.0	9.90	5.7	ARL360	
0131	Northridge	1994	0117	1231	6.7	USGS	0655	Jensen Filter Plant #	6.2	--D	B	.30	.979	43.6	13.76	4.7	JEN-UP		
0131	Northridge	1994	0117	1231	6.7	USGS	0655	Jensen Filter Plant #	6.2	--D	B	.08	.599	96.2	40.72	4.0	JEN022		
0131	Northridge	1994	0117	1231	6.7	USGS	0655	Jensen Filter Plant #	6.2	--D	B	.20	.891	132.6	33.07	3.1	JEN292		
0131	Northridge	1994	0117	1231	6.7	USGS	0637	Sepulveda VA #	8.9	--D	B	.10	1.211	48.0	11.03	5.5	SPV-UP		
0131	Northridge	1994	0117	1231	6.7	USGS	0637	Sepulveda VA #	8.9	--D	B	.10	1.088	107.0	14.46	4.5	SPV270		
0131	Northridge	1994	0117	1231	6.7	USGS	0637	Sepulveda VA #	8.9	--D	B		1.552	78.8	16.49	4.3	SPV360		
0131	Northridge	1994	0117	1231	6.7	DWP	75	Sylmar - Converter Sta East #	6.1	--D	B		.804	32.5	9.14	3.7	SCE-UP		
0131	Northridge	1994	0117	1231	6.7	DWP	75	Sylmar - Converter Sta East #	6.1	--D	B		1.251	108.2	36.53	3.8	SCE018		
0131	Northridge	1994	0117	1231	6.7	DWP	75	Sylmar - Converter Sta East #	6.1	--D	B		.616	86.3	21.40	3.6	SCE288		
0133	Kobe	1995	0116	2046	6.9	CUE	99999	Takarazuka	1.2	--D	D		40.00	1.072	60.6	10.06	2.1	TAZ-UP	
0133	Kobe	1995	0116	2046	6.9	CUE	99999	Takarazuka	1.2	--D	D		40.00	.881	83.6	25.97	2.1	TAZ000	
0133	Kobe	1995	0116	2046	6.9	CUE	99999	Takarazuka	1.2	--D	D	.13	33.00	1.007	89.0	20.11	2.1	TAZ090	
0133	Kobe	1995	0116	2046	6.9	CUE	99999	Takatori	.3	--E	D	.20	.636	22.8	6.74	7.4	TAK-UP		
0133	Kobe	1995	0116	2046	6.9	CUE	99999	Takatori	.3	--E	D		.768	146.4	39.15	5.4	TAK000		
0133	Kobe	1995	0116	2046	6.9	CUE	99999	Takatori	.3	--E	D		1.052	113.8	35.42	4.5	TAK090		

NRC TIME HISTORY LIBRARY: CEUS, SOIL, M=6-7, D=10-50 km

B-69

No.	Earthquake	Date & Time			Mag	Own	No.	Station	Closest Dist (km)	Site Codes Geom USGS	Filter Corners				Dur (s)	Filename		
		YR	MODY	HRM N							HP (hz)	LP (hz)	PGA (g)	PGV (g)			PGD (cm/s)	
0030	San Fernando	1971	0209	1400	6.6	ACOE	289	Whittier Narrows Dam	45.1	IHD	-	.10	30.00	.082	5.1	3.71	8.0	WNDDWN
0030	San Fernando	1971	0209	1400	6.6	ACOE	289	Whittier Narrows Dam	45.1	IHD	-	.10	20.00	.197	9.9	5.44	6.7	WND143
0030	San Fernando	1971	0209	1400	6.6	ACOE	289	Whittier Narrows Dam	45.1	IHD	-	.10	20.00	.212	13.2	5.34	6.8	WND233
0050	Imperial Valley	1979	1015	2316	6.5	USGS	5053	Calexico Fire Station	10.6	AQD	C	.10	40.00	.477	12.0	3.55	6.6	H-CXO-UP
0050	Imperial Valley	1979	1015	2316	6.5	USGS	5053	Calexico Fire Station	10.6	AQD	C	.10	40.00	.513	30.5	9.20	6.5	H-CXO225
0050	Imperial Valley	1979	1015	2316	6.5	USGS	5053	Calexico Fire Station	10.6	AQD	C	.20	40.00	.349	25.9	8.05	7.1	H-CXO315
0050	Imperial Valley	1979	1015	2316	6.5	USGS	5056	El Centro Array #1	15.5	AQD	C	.10	40.00	.164	5.1	2.39	7.5	H-E01-UP
0050	Imperial Valley	1979	1015	2316	6.5	USGS	5056	El Centro Array #1	15.5	AQD	C	.10	40.00	.280	19.0	6.41	5.4	H-E01140
0050	Imperial Valley	1979	1015	2316	6.5	USGS	5056	El Centro Array #1	15.5	AQD	C	.10	40.00	.277	11.3	5.44	7.0	H-E01230
0071	Taiwan SMART1(5)	1981	0129		6.3		29	SMART1 M07	21.0	IZD	-	.20	25.00	.129	3.1	.49	6.1	05M07DN
0071	Taiwan SMART1(5)	1981	0129		6.3		29	SMART1 M07	21.0	IZD	-	.10	25.00	.206	10.5	1.16	6.4	05M07EW
0071	Taiwan SMART1(5)	1981	0129		6.3		29	SMART1 M07	21.0	IZD	-	.10	25.00	.222	13.9	2.30	5.4	05M07NS
0103	N. Palm Springs	1986	0708	0920	6.0	CDMG	22T13	Landers Fire Station	38.2	AQD	-	.50	40.00	.147	5.6	.42	5.7	LDR-UP
0103	N. Palm Springs	1986	0708	0920	6.0	CDMG	22T13	Landers Fire Station	38.2	AQD	-	.50	30.00	.162	7.3	.65	4.8	LDR000
0103	N. Palm Springs	1986	0708	0920	6.0	CDMG	22T13	Landers Fire Station	38.2	AQD	-	.50	30.00	.221	6.3	.71	4.1	LDR090
0117	Whittier Narrows	1987	1001	1442	6.0	USC	90069	Baldwin Park - N Holly #	11.9	--D	C	.30	25.00	.235	4.9	.74	2.7	A-NHO-UP
0117	Whittier Narrows	1987	1001	1442	6.0	USC	90069	Baldwin Park - N Holly #	11.9	--D	C	.13	25.00	.288	13.8	2.47	2.2	A-NHO180
0117	Whittier Narrows	1987	1001	1442	6.0	USC	90069	Baldwin Park - N Holly #	11.9	--D	C	.50	25.00	.136	6.8	.80	6.6	A-NHO270
0117	Whittier Narrows	1987	1001	1442	6.0	USC	90013	Beverly Hills - 14145 Mulhol #	30.3	--C	C	.38	25.00	.121	3.8	.42	7.0	A-MUL-UP
0117	Whittier Narrows	1987	1001	1442	6.0	USC	90013	Beverly Hills - 14145 Mulhol #	30.3	--C	C	.33	25.00	.274	10.2	.82	9.0	A-MUL009
0117	Whittier Narrows	1987	1001	1442	6.0	USC	90013	Beverly Hills - 14145 Mulhol #	30.3	--C	C	.35	25.00	.240	15.8	1.60	4.1	A-MUL279
0117	Whittier Narrows	1987	1001	1442	6.0	USC	90003	Northridge - 17645 Saticoy St #	39.8	--D	C	.25	25.00	.214	4.6	.44	6.3	A-STC-UP
0117	Whittier Narrows	1987	1001	1442	6.0	USC	90003	Northridge - 17645 Saticoy St #	39.8	--D	C	.23	25.00	.412	11.5	1.00	3.4	A-STC090
0117	Whittier Narrows	1987	1001	1442	6.0	USC	90003	Northridge - 17645 Saticoy St #	39.8	--D	C	.20	25.00	.277	7.0	.86	7.8	A-STC180
0119	Superstn Hills (A)	1987	1124	0514	6.3	USGS	5210	Wildlife Liquef. Array	24.7	IQD	-	.20	50.00	.475	8.1	2.30	3.2	A-IVW-UP
0119	Superstn Hills (A)	1987	1124	0514	6.3	USGS	5210	Wildlife Liquef. Array	24.7	IQD	-	.20	50.00	.262	19.1	8.07	7.0	A-IVW090
0119	Superstn Hills (A)	1987	1124	0514	6.3	USGS	5210	Wildlife Liquef. Array	24.7	IQD	-	.20	50.00	.260	15.6	5.16	7.1	A-IVW360
0122	Loma Prieta	1989	1018	0005	6.9	CDMG	58065	Saratoga - Aloha Ave	13.0	AQD	B	.10	58.00	.958	42.7	15.62	4.4	STG-UP
0122	Loma Prieta	1989	1018	0005	6.9	CDMG	58065	Saratoga - Aloha Ave	13.0	AQD	B	.10	38.00	.929	62.0	14.45	4.3	STG000
0122	Loma Prieta	1989	1018	0005	6.9	CDMG	58065	Saratoga - Aloha Ave	13.0	AQD	B	.10	50.00	.670	53.7	26.59	4.3	STG090
0124	Georgia, USSR	1991	0615	0059	6.2			Baz	49.0	A-D	-	.10		.042	3.0	.58	10.1	BAZ-Z
0124	Georgia, USSR	1991	0615	0059	6.2			Baz	49.0	A-D	-	.10		.066	3.0	.42	11.0	BAZ-X
0124	Georgia, USSR	1991	0615	0059	6.2			Baz	49.0	A-D	-	.10		.079	3.1	.45	9.6	BAZ-Y

No.	Earthquake	Date & Time				Mag	Own	No.	Station	Closest Dist (km)	Site Codes		Filter Corners			PGV (g)	PGD (cm/s)	Dur (s)	Filename
		YR	MODY	HRM N							Geom	USGS	HP (hz)	LP (hz)	PGA (g)				
0131	Northridge	1994	0117	1231	6.7	USC	90063	Glendale - Las Palmas	25.4	--	C C	.30	30.00	.338	10.7	.62	8.0	GLP-UP	
0131	Northridge	1994	0117	1231	6.7	USC	90063	Glendale - Las Palmas	25.4	--	C C	.13	30.00	.774	20.8	2.47	6.5	GLP177	
0131	Northridge	1994	0117	1231	6.7	USC	90063	Glendale - Las Palmas	25.4	--	C C	.10	30.00	.460	13.4	1.71	6.4	GLP267	
0131	Northridge	1994	0117	1231	6.7	CDMG	24389	LA - Century City CC North #	25.7	IQD	C	.14	23.00	.283	13.0	4.52	7.9	CCN-UP	
0131	Northridge	1994	0117	1231	6.7	CDMG	24389	LA - Century City CC North #	25.7	IQD	C	.14	23.00	.503	32.1	8.57	7.1	CCN090	
0131	Northridge	1994	0117	1231	6.7	CDMG	24389	LA - Century City CC North #	25.7	IQD	C	.14	23.00	.432	38.1	6.48	7.1	CCN360	
0131	Northridge	1994	0117	1231	6.7	USC	90021	LA - N Westmoreland	29.0	--	D B	.20	30.00	.263	10.8	1.69	8.1	WST-UP	
0131	Northridge	1994	0117	1231	6.7	USC	90021	LA - N Westmoreland	29.0	--	D B	.20	30.00	.853	37.5	3.65	5.8	WST000	
0131	Northridge	1994	0117	1231	6.7	USC	90021	LA - N Westmoreland	29.0	--	D B	.20	30.00	.609	37.6	5.09	5.8	WST270	
0131	Northridge	1994	0117	1231	6.7	CDMG	24055	Leona Valley #5 - Ritter #	38.3	IQC	C	.20	23.00	.215	21.9	3.64	8.5	LV5-UP	
0131	Northridge	1994	0117	1231	6.7	CDMG	24055	Leona Valley #5 - Ritter #	38.3	IQC	C	.20	23.00	.297	26.3	3.40	7.4	LV5000	
0131	Northridge	1994	0117	1231	6.7	CDMG	24055	Leona Valley #5 - Ritter #	38.3	IQC	C	.20	23.00	.191	17.3	3.80	8.5	LV5090	

NRC TIME HISTORY LIBRARY: CEUS, SOIL, M=6-7, D=50-100 km

B-71

No.	Earthquake	Date & Time					Own	No.	Station	Closest Dist (km)	Site Codes		Filter Corners			Dur (s)	Filename	
		YR	MODY	HRMN	Mag						Geom	USGS	HP (hz)	LP (hz)	PGA (g)			PGV (g)
0030	San Fernando	1971	0209	1400	6.6	CDWR	1102	Wheeler Ridge - Ground	81.6	IBD	C	.10	30.00	.043	1.9	1.24	9.5	WRP-UP
0030	San Fernando	1971	0209	1400	6.6	CDWR	1102	Wheeler Ridge - Ground	81.6	IBD	C	.10	23.00	.063	2.5	.88	7.0	WRP090
0030	San Fernando	1971	0209	1400	6.6	CDWR	1102	Wheeler Ridge - Ground	81.6	IBD	C	.10	23.00	.097	1.9	.69	3.7	WRP180
0086	Taiwan SMART1 (25)	1983	0921		6.5		32	SMART1 E01	83.0	IZD	-	.50	25.00	.034	2.6	.43	10.3	25E01DN
0086	Taiwan SMART1 (25)	1983	0921		6.5		32	SMART1 E01	83.0	IZD	-	.20	25.00	.065	5.0	.97	7.2	25E01EW
0086	Taiwan SMART1 (25)	1983	0921		6.5		32	SMART1 E01	83.0	IZD	-	.20	25.00	.071	6.6	.97	7.4	25E01NS
0086	Taiwan SMART1 (25)	1983	0921		6.5		61	SMART1 I07	83.0	IZD	-	.10	25.00	.021	1.9	.39	10.2	25I07DN
0086	Taiwan SMART1 (25)	1983	0921		6.5		61	SMART1 I07	83.0	IZD	-	.10	25.00	.086	6.0	1.04	8.0	25I07EW
0086	Taiwan SMART1 (25)	1983	0921		6.5		61	SMART1 I07	83.0	IZD	-	.10	25.00	.072	5.9	1.37	8.5	25I07NS
0086	Taiwan SMART1 (25)	1983	0921		6.5		60	SMART1 M06	83.0	IZD	-	.10	25.00	.025	2.3	.54	8.1	25M06DN
0086	Taiwan SMART1 (25)	1983	0921		6.5		60	SMART1 M06	83.0	IZD	-	.10	25.00	.050	4.6	.79	6.7	25M06EW
0086	Taiwan SMART1 (25)	1983	0921		6.5		60	SMART1 M06	83.0	IZD	-	.10	25.00	.075	6.3	1.36	6.8	25M06NS
0090	Morgan Hill	1984	0424	2115	6.2	CDMG	56012	Los Banos	64.4	AHD	C	.50	20.00	.025	2.1	.45	10.7	LBN-UP
0090	Morgan Hill	1984	0424	2115	6.2	CDMG	56012	Los Banos	64.4	AHD	C	.50	18.00	.108	7.8	2.01	12.2	LBN090
0090	Morgan Hill	1984	0424	2115	6.2	CDMG	56012	Los Banos	64.4	AHD	C	.50	18.00	.124	9.7	1.98	16.7	LBN180
0090	Morgan Hill	1984	0424	2115	6.2	CDMG	58223	SF Intern. Airport	71.2	AHD	C	.50	32.00	.050	1.4	.33	12.9	SFO-UP
0090	Morgan Hill	1984	0424	2115	6.2	CDMG	58223	SF Intern. Airport	71.2	AHD	C	.50	26.00	.109	4.8	.46	11.3	SFO050
0090	Morgan Hill	1984	0424	2115	6.2	CDMG	58223	SF Intern. Airport	71.2	AHD	C	.50	24.00	.113	5.4	.68	12.6	SFO320
0122	Loma Prieta	1989	1018	0005	6.9	CDMG	58498	Hayward - BART Sta	58.9	I-D	B	.20	40.00	.234	7.4	3.14	10.6	HWB-UP
0122	Loma Prieta	1989	1018	0005	6.9	CDMG	58498	Hayward - BART Sta	58.9	I-D	B	.20	31.00	.449	28.4	3.59	8.5	HWB220
0122	Loma Prieta	1989	1018	0005	6.9	CDMG	58498	Hayward - BART Sta	58.9	I-D	B	.20	36.00	.380	16.7	2.68	9.7	HWB310
0124	Georgia, USSR	1991	0615	0059	6.2		20	Oni	52.0	A-D	-	.20		.049	2.4	.38	12.2	ONI-Z
0124	Georgia, USSR	1991	0615	0059	6.2		20	Oni	52.0	A-D	-	.20		.171	6.2	.49	11.0	ONI-X
0124	Georgia, USSR	1991	0615	0059	6.2		20	Oni	52.0	A-D	-	.20		.116	5.0	.50	11.0	ONI-Y
0131	Northridge	1994	0117	1231	6.7	USC	90070	Covina - W Badillo	56.1	--D	C	.30	30.00	.120	5.2	1.00	10.6	BAD-UP
0131	Northridge	1994	0117	1231	6.7	USC	90070	Covina - W Badillo	56.1	--D	C	.20	30.00	.242	11.1	1.23	10.2	BAD000
0131	Northridge	1994	0117	1231	6.7	USC	90070	Covina - W Badillo	56.1	--D	C	.20	30.00	.206	10.9	1.79	8.3	BAD270
0131	Northridge	1994	0117	1231	6.7	CDMG	13197	Huntington Beach - Lake St #	79.6	AQD	C	.20	23.00	.059	2.8	.90	15.8	HNT-UP
0131	Northridge	1994	0117	1231	6.7	CDMG	13197	Huntington Beach - Lake St #	79.6	AQD	C	.20	23.00	.222	10.0	1.20	12.6	HNT000
0131	Northridge	1994	0117	1231	6.7	CDMG	13197	Huntington Beach - Lake St #	79.6	AQD	C	.20	23.00	.199	8.5	1.78	11.1	HNT090
0131	Northridge	1994	0117	1231	6.7	USC	90083	Huntington Bch - Waikiki	57.4	--D	C	.30	30.00	.057	2.4	.41	13.9	WAI-UP
0131	Northridge	1994	0117	1231	6.7	USC	90083	Huntington Bch - Waikiki	57.4	--D	C	.20	30.00	.217	8.9	1.65	11.4	WAI200
0131	Northridge	1994	0117	1231	6.7	USC	90083	Huntington Bch - Waikiki	57.4	--D	C	.20	30.00	.189	9.6	2.37	11.2	WAI290
0131	Northridge	1994	0117	1231	6.7	USC	90072	La Puente - Rimgrove Av	58.9	--D	C	1.00	30.00	.143	5.6	.36	9.1	RIM-UP

No.	Earthquake	Date & Time					Own	No.	Station	Closest Dist (km)	Site Codes		Filter Corners				Dur (s)	Filename
		YR	MODY	HRMN	Mag						Geom	USGS	HP (hz)	LP (hz)	PGA (g)	PGV (g)		
0131	Northridge	1994	0117	1231	6.7	USC	90072	La Puente - Ringrove Av	58.9	--	D C	.80	30.00	.280	13.5	1.10	8.2	RIM015
0131	Northridge	1994	0117	1231	6.7	USC	90072	La Puente - Ringrove Av	58.9	--	D C	.80	30.00	.294	15.1	1.23	8.8	RIM105
0131	Northridge	1994	0117	1231	6.7	USC	90084	Lakewood - Del Amo Blvd	59.3	--	D C	.80	30.00	.173	3.6	.28	7.8	DEL-UP
0131	Northridge	1994	0117	1231	6.7	USC	90084	Lakewood - Del Amo Blvd	59.3	--	D C	.13	30.00	.377	20.1	2.13	9.3	DELO00
0131	Northridge	1994	0117	1231	6.7	USC	90084	Lakewood - Del Amo Blvd	59.3	--	D C	.20	30.00	.273	14.1	3.12	9.7	DELO90
0131	Northridge	1994	0117	1231	6.7	CDMG	24586	Neenach - Sacatara Ck #	53.2	IHD	B	.12	46.00	.122	10.7	4.17	16.1	NEE-UP
0131	Northridge	1994	0117	1231	6.7	CDMG	24586	Neenach - Sacatara Ck #	53.2	IHD	B	.12	46.00	.124	11.6	5.96	14.8	NEE090
0131	Northridge	1994	0117	1231	6.7	CDMG	24586	Neenach - Sacatara Ck #	53.2	IHD	B	.12	46.00	.139	16.4	5.49	16.3	NEE180
0131	Northridge	1994	0117	1231	6.7	CDMG	14578	Seal Beach - Office Bldg #	64.9	IQD	B	.16	46.00	.108	3.3	.57	14.3	SEA-UP
0131	Northridge	1994	0117	1231	6.7	CDMG	14578	Seal Beach - Office Bldg #	64.9	IQD	B	.16	46.00	.150	7.4	1.92	13.7	SEA000
0131	Northridge	1994	0117	1231	6.7	CDMG	14578	Seal Beach - Office Bldg #	64.9	IQD	B	.16	46.00	.234	13.6	1.89	11.7	SEA090

NRC TIME HISTORY LIBRARY: CEUS, SOIL, M=6-7, D=100-200 km

No.	Earthquake	Date & Time				Mag	Own	No.	Station	Closest Dist (km)	Site Codes		Filter Corners			PGV (g)	PGD (cm/s)	Dur (s)	Filename
		YR	MODY	HRMN							Geom	USGS	HP (hz)	LP (hz)	PGA (g)				
0019	El Alamo	1956	1217	1433	6.8	USGS	117	El Centro Array #9	130.0	EQD	C	.50	20.00	.063	1.9	.90	11.9	ELC-UP	
0019	El Alamo	1956	1217	1433	6.8	USGS	117	El Centro Array #9	130.0	EQD	C	.10	15.00	.094	6.4	2.24	14.6	ELC180	
0019	El Alamo	1956	1217	1433	6.8	USGS	117	El Centro Array #9	130.0	EQD	C	.10	15.00	.166	10.0	3.61	13.0	ELC270	
0028	Borrogo Mtn	1968	0409	0230	6.8	USGS	130	LB - Terminal Island	195.0	CCD	C	.10	20.00	.016	1.7	1.23	24.9	A-TLI-UP	
0028	Borrogo Mtn	1968	0409	0230	6.8	USGS	130	LB - Terminal Island	195.0	CCD	C	.10	15.00	.026	3.0	1.44	28.9	A-TLI249	
0028	Borrogo Mtn	1968	0409	0230	6.8	USGS	130	LB - Terminal Island	195.0	CCD	C	.10	15.00	.022	3.5	1.80	28.0	A-TI339	
0030	San Fernando	1971	0209	1400	6.6	CIT	103	Anza Post Office	169.0	AAC	-	.50	35.00	.078	1.6	.28	11.8	AZPDWN	
0030	San Fernando	1971	0209	1400	6.6	CIT	103	Anza Post Office	169.0	AAC	-	.50	35.00	.085	2.5	.29	10.4	AZP045	
0030	San Fernando	1971	0209	1400	6.6	CIT	103	Anza Post Office	169.0	AAC	-	.50	35.00	.117	4.1	.41	7.3	AZP315	
0030	San Fernando	1971	0209	1400	6.6	USGS	1004	Bakersfield - Harvey Aud	120.0	CCD	-	.10	15.00	.021	1.1	.50	13.0	BFA-UP	
0030	San Fernando	1971	0209	1400	6.6	USGS	1004	Bakersfield - Harvey Aud	120.0	CCD	-	.10	13.00	.021	1.8	1.14	16.2	BFA180	
0030	San Fernando	1971	0209	1400	6.6	USGS	1004	Bakersfield - Harvey Aud	120.0	CCD	-	.10	20.00	.020	1.6	.86	16.8	BFA270	
0030	San Fernando	1971	0209	1400	6.6	USGS	1	Buena Vista - Taft	118.0	AQD	-	.20	20.00	.025	.9	.39	10.5	BVPDWN	
0030	San Fernando	1971	0209	1400	6.6	USGS	1	Buena Vista - Taft	118.0	AQD	-	.10	13.00	.030	1.9	1.04	12.1	BVP090	
0030	San Fernando	1971	0209	1400	6.6	USGS	1	Buena Vista - Taft	118.0	AQD	-	.10	15.00	.035	1.9	.52	14.4	BVP180	
0030	San Fernando	1971	0209	1400	6.6	CDMG	12331	Hemet Fire Station	136.0	AQD	C	.50	35.00	.112	3.5	.39	7.3	H05DWN	
0030	San Fernando	1971	0209	1400	6.6	CDMG	12331	Hemet Fire Station	136.0	AQD	C	.50	35.00	.125	5.0	.43	6.4	H05135	
0030	San Fernando	1971	0209	1400	6.6	CDMG	12331	Hemet Fire Station	136.0	AQD	C	.50	35.00	.185	5.4	.46	7.4	H05225	
0030	San Fernando	1971	0209	1400	6.6	USGS	465	San Juan Capistrano	104.0	ABC	-	.50	35.00	.077	3.5	.69	17.6	SJCDWN	
0030	San Fernando	1971	0209	1400	6.6	USGS	465	San Juan Capistrano	104.0	ABC	-	.50	35.00	.126	6.1	1.00	12.6	SJC033	
0030	San Fernando	1971	0209	1400	6.6	USGS	465	San Juan Capistrano	104.0	ABC	-	.50	35.00	.125	5.6	.91	12.1	SJC303	
0030	San Fernando	1971	0209	1400	6.6	USGS	282	UCSB - Fluid Mech Lab	125.6	CPD	-	.20	30.00	.037	2.1	1.10	14.3	SBF-UP	
0030	San Fernando	1971	0209	1400	6.6	USGS	282	UCSB - Fluid Mech Lab	125.6	CPD	-	.20	30.00	.052	4.3	.96	13.3	SBF042	
0030	San Fernando	1971	0209	1400	6.6	USGS	282	UCSB - Fluid Mech Lab	125.6	CPD	-	.20	30.00	.053	4.6	1.31	14.5	SBF132	
0117	Whittier Narrows	1987	1001	1442	6.0	CDMG	12331	Hemet Fire Station	105.0	AQD	C	1.00	30.00	.118	2.8	.14	14.1	A-H05-UP	
0117	Whittier Narrows	1987	1001	1442	6.0	CDMG	12331	Hemet Fire Station	105.0	AQD	C	.70	25.00	.121	3.9	.22	11.6	A-H05270	
0117	Whittier Narrows	1987	1001	1442	6.0	CDMG	12331	Hemet Fire Station	105.0	AQD	C	.80	25.00	.126	3.9	.18	8.7	A-H05360	
0131	Northridge	1994	0117	1231	6.7	CDMG	13660	Hemet - Ryan Airfield #	144.1	IHD	-	.30	46.00	.084	4.6	.36	21.6	HEM-UP	
0131	Northridge	1994	0117	1231	6.7	CDMG	13660	Hemet - Ryan Airfield #	144.1	IHD	-	.30	46.00	.179	9.8	.98	22.2	HEM000	
0131	Northridge	1994	0117	1231	6.7	CDMG	13660	Hemet - Ryan Airfield #	144.1	IHD	-	.30	46.00	.136	8.2	.90	21.9	HEM090	
0131	Northridge	1994	0117	1231	6.7	CDMG	23672	San Bernadino - CSUSB Gr #	103.1	IHD	-	.30	46.00	.066	3.2	.44	16.6	BER-UP	
0131	Northridge	1994	0117	1231	6.7	CDMG	23672	San Bernadino - CSUSB Gr #	103.1	IHD	-	.30	46.00	.114	5.6	.52	16.0	BER000	
0131	Northridge	1994	0117	1231	6.7	CDMG	23672	San Bernadino - CSUSB Gr #	103.1	IHD	-	.30	46.00	.225	7.8	1.00	15.9	BER090	
0131	Northridge	1994	0117	1231	6.7	CDMG	23542	San Bernadino - E&Hospitality#	108.1	IHD	C	.20	46.00	.145	5.9	.66	18.6	HOS-UP	

B-73

No.	Earthquake	Date & Time					Mag	Own	No.	Station	Closest Dist (km)	Site Codes		Filter Corners			Dur (s)	Filename	
		YR	MODY	HRMN	Geom	USGS						HP (hz)	LP (hz)	PGA (g)	PGV (g)	PGD (cm/s)			
0131	Northridge	1994	0117	1231	6.7	CDMG		23542	San Bernadino - E&Hospitality#	108.1	IHD	C	.20	46.00	.230	12.0	1.36	17.3	HOS090
0131	Northridge	1994	0117	1231	6.7	CDMG		23542	San Bernadino - E&Hospitality#	108.1	IHD	C	.20	46.00	.263	14.5	1.47	17.9	HOS180
0131	Northridge	1994	0117	1231	6.7	CDMG		12673	San Jacinto - CDF Fire Sta #	146.5	IHD	-	.16	46.00	.080	5.8	1.43	24.0	CDF-UP
0131	Northridge	1994	0117	1231	6.7	CDMG		12673	San Jacinto - CDF Fire Sta #	146.5	IHD	-	.16	46.00	.197	14.9	1.93	22.3	CDF000
0131	Northridge	1994	0117	1231	6.7	CDMG		12673	San Jacinto - CDF Fire Sta #	146.5	IHD	-	.16	46.00	.233	14.4	2.02	20.8	CDF090
0131	Northridge	1994	0117	1231	6.7	CDMG		25091	Santa Barbara - UCSB Goleta #	111.3	AHD	-	.20	23.00	.137	6.7	1.17	8.1	SBG-UP
0131	Northridge	1994	0117	1231	6.7	CDMG		25091	Santa Barbara - UCSB Goleta #	111.3	AHD	-	.20	23.00	.272	11.1	1.50	9.8	SBG000
0131	Northridge	1994	0117	1231	6.7	CDMG		25091	Santa Barbara - UCSB Goleta #	111.3	AHD	-	.20	23.00	.189	11.8	1.91	10.8	SBG090
0133	Kobe	1995	0116	2046	6.9			99999	FUK	157.2	--D	-	.05		.040	2.5	.69	26.4	FUK-UP
0133	Kobe	1995	0116	2046	6.9			99999	FUK	157.2	--D	-	.05		.098	7.6	1.35	24.9	FUK000
0133	Kobe	1995	0116	2046	6.9			99999	FUK	157.2	--D	-	.05		.119	8.9	1.61	29.8	FUK090

NRC TIME HISTORY LIBRARY: CEUS, SOIL, M>7, D=0-10 km

No.	Earthquake	Date & Time			Mag	Own	No.	Station	Closest Dist (km)	Site Codes		Filter Corners			Dur (s)	Filename		
		YR	MODY	HRMN						Geom	USGS	HP (hz)	LP (hz)	PGA (g)			PGV (g)	PGD (cm/s)
0006	Imperial Valley	1940	0519	0437	7.0	USGS	117	El Centro Array #9	8.3	EQD	C	.20	15.00	.379	14.3	5.89	7.9	I-ELC-UP
0006	Imperial Valley	1940	0519	0437	7.0	USGS	117	El Centro Array #9	8.3	EQD	C	.20	15.00	.371	32.7	7.75	13.1	I-ELC180
0006	Imperial Valley	1940	0519	0437	7.0	USGS	117	El Centro Array #9	8.3	EQD	C	.20	15.00	.221	24.8	11.85	16.9	I-ELC270
0046	Tabas, Iran	1978	0916		7.4		9101	Tabas	3.0	ABC	-	.05		1.312	53.9	15.62	10.2	TAB-UP
0046	Tabas, Iran	1978	0916		7.4		9101	Tabas	3.0	ABC	-	.05		.937	89.6	33.62	9.6	TAB-LN
0046	Tabas, Iran	1978	0916		7.4		9101	Tabas	3.0	ABC	-	.05		1.087	109.7	83.21	8.7	TAB-TR
0125	Erzican, Turkey	1992	0313		6.9		95	Erzincan	2.0	--D	C	.20		.445	22.9	10.31	5.2	ERZ-UP
0125	Erzican, Turkey	1992	0313		6.9		95	Erzincan	2.0	--D	C	.10		.579	86.0	23.90	1.9	ERZ-NS
0125	Erzican, Turkey	1992	0313		6.9		95	Erzincan	2.0	--D	C	.10		.619	59.3	19.06	2.3	ERZ-EW
0127	Cape Mendocino	1992	0425	1806	7.1	CDMG	89156	Petrolia #	9.5	IMD	C	.07	23.00	.329	29.8	17.63	5.4	PET-UP
0127	Cape Mendocino	1992	0425	1806	7.1	CDMG	89156	Petrolia #	9.5	IMD	C	.07	23.00	.630	46.4	11.05	6.5	PET000
0127	Cape Mendocino	1992	0425	1806	7.1	CDMG	89156	Petrolia #	9.5	IMD	C	.07	23.00	.789	93.5	20.07	2.0	PET090
0133	Kobe	1995	0116	2046	6.9	CUE	99999	Takarazuka	1.2	--D	D		40.00	.975	54.5	8.95	2.1	TAZ-UP
0133	Kobe	1995	0116	2046	6.9	CUE	99999	Takarazuka	1.2	--D	D		40.00	.700	67.4	20.51	2.2	TAZ000
0133	Kobe	1995	0116	2046	6.9	CUE	99999	Takarazuka	1.2	--D	D	.13	33.00	.783	72.9	16.83	2.1	TAZ090
0133	Kobe	1995	0116	2046	6.9	CUE	99999	Takatori	.3	--E	D	.20		.578	22.2	6.27	7.5	TAK-UP
0133	Kobe	1995	0116	2046	6.9	CUE	99999	Takatori	.3	--E	D			.606	116.7	31.37	5.4	TAK000
0133	Kobe	1995	0116	2046	6.9	CUE	99999	Takatori	.3	--E	D			.807	93.6	28.81	4.6	TAK090
0141	Kocaeli, Turkey	1999	0817		7.4	KOERI	99999	Yarimca	4.4	B-D	C			.463	99.8	97.19	7.8	YPT-UP
0141	Kocaeli, Turkey	1999	0817		7.4	KOERI	99999	Yarimca	4.4	B-D	C	.10	80.00	.271	93.1	97.91	11.5	YPT000
0141	Kocaeli, Turkey	1999	0817		7.4	KOERI	99999	Yarimca	4.4	B-D	C	.10	80.00	.358	65.8	34.69	6.6	YPT270
0142	Chi-Chi, Taiwan	1999	0920		7.6	CWB	99999	CHY024	9.0	--1	C	.03	50.00	.290	62.7	45.65	16.1	CHY024-V
0142	Chi-Chi, Taiwan	1999	0920		7.6	CWB	99999	CHY024	9.0	--1	C	.02	50.00	.237	45.4	28.57	17.2	CHY024-N
0142	Chi-Chi, Taiwan	1999	0920		7.6	CWB	99999	CHY024	9.0	--1	C	.02	50.00	.335	47.2	32.06	13.7	CHY024-W
0142	Chi-Chi, Taiwan	1999	0920		7.6	CWB	99999	TCU049	4.4	--2	C	.02	50.00	.313	32.5	25.56	16.3	TCU049-V
0142	Chi-Chi, Taiwan	1999	0920		7.6	CWB	99999	TCU049	4.4	--2	C	.02	30.00	.305	45.8	29.53	18.0	TCU049-N
0142	Chi-Chi, Taiwan	1999	0920		7.6	CWB	99999	TCU049	4.4	--2	C	.02	50.00	.330	45.0	28.21	20.7	TCU049-W
0142	Chi-Chi, Taiwan	1999	0920		7.6	CWB	99999	TCU051	8.2	--2	C	.03	50.00	.224	43.4	39.92	20.1	TCU051-V
0142	Chi-Chi, Taiwan	1999	0920		7.6	CWB	99999	TCU051	8.2	--2	C	.03	50.00	.235	29.3	33.47	20.3	TCU051-N
0142	Chi-Chi, Taiwan	1999	0920		7.6	CWB	99999	TCU051	8.2	--2	C	.03	50.00	.215	33.5	27.11	20.5	TCU051-W
0142	Chi-Chi, Taiwan	1999	0920		7.6	CWB	99999	TCU052	.2	--1	c	.04	50.00	.483	109.4	111.62	10.2	TCU052-V
0142	Chi-Chi, Taiwan	1999	0920		7.6	CWB	99999	TCU052	.2	--1	c	.04	50.00	.545	127.4	85.41	5.2	TCU052-N
0142	Chi-Chi, Taiwan	1999	0920		7.6	CWB	99999	TCU052	.2	--1	c	.04	50.00	.411	104.1	92.75	11.9	TCU052-W
0142	Chi-Chi, Taiwan	1999	0920		7.6	CWB	99999	TCU060	9.4	--2	C	.02	50.00	.193	43.8	27.27	19.0	TCU060-V

B-75

No.	Earthquake	Date & Time			Mag	Own	No.	Station	Closest Dist (km)	Site Codes		Filter Corners					Dur (s)	Filename
		YR	MODY	HRMN						Geom	USGS	HP (hz)	LP (hz)	PGA (g)	PGV (g)	PGD (cm/s)		
0142	Chi-Chi, Taiwan	1999	0920		7.6	CWB	99999	TCU060	9.4	--2	C	.03	50.00	.122	31.9	30.02	22.7	TCU060-N
0142	Chi-Chi, Taiwan	1999	0920		7.6	CWB	99999	TCU060	9.4	--2	C	.03	50.00	.189	24.7	20.88	22.1	TCU060-W
0142	Chi-Chi, Taiwan	1999	0920		7.6	CWB	99999	TCU067	.3	--1	C	.04	50.00	.426	48.2	31.85	14.1	TCU067-V
0142	Chi-Chi, Taiwan	1999	0920		7.6	CWB	99999	TCU067	.3	--1	C	.03	50.00	.378	55.4	24.24	12.2	TCU067-N
0142	Chi-Chi, Taiwan	1999	0920		7.6	CWB	99999	TCU067	.3	--1	C	.02	50.00	.563	79.6	39.10	13.4	TCU067-W
0142	Chi-Chi, Taiwan	1999	0920		7.6	CWB	99999	TCU068	1.0	--1	C	.02	50.00	.831	188.4	158.96	5.9	TCU068-V
0142	Chi-Chi, Taiwan	1999	0920		7.6	CWB	99999	TCU068	1.0	--1	C	.02	50.00	.669	124.2	155.74	12.4	TCU068-N
0142	Chi-Chi, Taiwan	1999	0920		7.6	CWB	99999	TCU068	1.0	--1	C	.03	50.00	.713	112.9	106.46	7.2	TCU068-W
0142	Chi-Chi, Taiwan	1999	0920		7.6	CWB	99999	TCU072	7.3	--1	C	.05	50.00	.489	40.3	22.03	15.7	TCU072-V
0142	Chi-Chi, Taiwan	1999	0920		7.6	CWB	99999	TCU072	7.3	--1	C	.05	50.00	.487	52.4	20.23	16.8	TCU072-N
0142	Chi-Chi, Taiwan	1999	0920		7.6	CWB	99999	TCU072	7.3	--1	C	.05	50.00	.530	53.0	16.83	14.4	TCU072-W
0142	Chi-Chi, Taiwan	1999	0920		7.6	CWB	99999	TCU076	1.9	--2	C	.02	50.00	.456	37.4	21.35	17.5	TCU076-V
0142	Chi-Chi, Taiwan	1999	0920		7.6	CWB	99999	TCU076	1.9	--2	C	.05	50.00	.425	56.5	20.78	18.7	TCU076-N
0142	Chi-Chi, Taiwan	1999	0920		7.6	CWB	99999	TCU076	1.9	--2	C	.10	50.00	.327	41.4	23.41	20.3	TCU076-W
0142	Chi-Chi, Taiwan	1999	0920		7.6	CWB	99999	TCU082	5.7	--2	C	.04	50.00	.261	55.2	37.42	18.3	TCU082-V
0142	Chi-Chi, Taiwan	1999	0920		7.6	CWB	99999	TCU082	5.7	--2	C	.04	50.00	.193	49.9	27.88	19.6	TCU082-N
0142	Chi-Chi, Taiwan	1999	0920		7.6	CWB	99999	TCU082	5.7	--2	C	.02	50.00	.224	45.1	36.79	20.6	TCU082-W
0142	Chi-Chi, Taiwan	1999	0920		7.6	CWB	99999	TCU101	2.9	--2	C	.03	50.00	.348	61.7	42.80	14.9	TCU101-V
0142	Chi-Chi, Taiwan	1999	0920		7.6	CWB	99999	TCU101	2.9	--2	C	.04	50.00	.238	41.4	28.89	18.4	TCU101-N
0142	Chi-Chi, Taiwan	1999	0920		7.6	CWB	99999	TCU101	2.9	--2	C	.04	50.00	.246	42.0	34.21	18.0	TCU101-W
0142	Chi-Chi, Taiwan	1999	0920		7.6	CWB	99999	TCU102	1.7	--2	C	.02	50.00	.269	66.2	46.55	13.9	TCU102-V
0142	Chi-Chi, Taiwan	1999	0920		7.6	CWB	99999	TCU102	1.7	--2	C	.05	50.00	.205	73.5	38.80	17.8	TCU102-N
0142	Chi-Chi, Taiwan	1999	0920		7.6	CWB	99999	TCU102	1.7	--2	C	.04	50.00	.288	73.3	48.19	16.9	TCU102-W
0142	Chi-Chi, Taiwan	1999	0920		7.6	CWB	99999	TCU128	9.7	--1	B	.02	40.00	.197	71.2	56.35	17.8	TCU128-V
0142	Chi-Chi, Taiwan	1999	0920		7.6	CWB	99999	TCU128	9.7	--1	B	.05	30.00	.172	65.5	42.12	14.2	TCU128-N
0142	Chi-Chi, Taiwan	1999	0920		7.6	CWB	99999	TCU128	9.7	--1	B	.02	30.00	.138	52.2	48.52	17.3	TCU128-W
0143	Duzce, Turkey	1999	1112		7.1	ERD	99999	Duzce	6.7	--D	C	.06	50.00	.702	29.5	26.84	5.9	DZC-UP
0143	Duzce, Turkey	1999	1112		7.1	ERD	99999	Duzce	6.7	--D	C	.06	50.00	.364	59.5	35.20	6.0	DZC180
0143	Duzce, Turkey	1999	1112		7.1	ERD	99999	Duzce	6.7	--D	C	.08	50.00	.549	68.8	42.83	6.1	DZC270

NRC TIME HISTORY LIBRARY: CEUS, SOIL, M>7, D=10-50 km

No.	Earthquake	Date & Time			Mag	Own	No.	Station	Closest Dist (km)	Site Codes		Filter Corners			Dur (s)	Filename	
		YR	MODY	HRMN						Geom	USGS	HP (hz)	LP (hz)	PGA (g)			PGV (g)
0046	Tabas, Iran	1978	0916		7.4	70	Boshrooyeh	26.1	--C	-	.06		.233	15.3	11.19	16.5	BOS-V1
0046	Tabas, Iran	1978	0916		7.4	70	Boshrooyeh	26.1	--C	-	.04	20.00	.167	15.6	9.17	17.6	BOS-L1
0046	Tabas, Iran	1978	0916		7.4	70	Boshrooyeh	26.1	--C	-	.04	20.00	.138	22.3	9.71	17.0	BOS-T1
0113	Taiwan SMART1 (45)	1986	1114		7.3	62	SMART1 IO1	39.0	IZD	-	.10	25.00	.209	12.8	5.65	12.2	IO1DN
0113	Taiwan SMART1 (45)	1986	1114		7.3	62	SMART1 IO1	39.0	IZD	-	.10	25.00	.204	28.9	9.30	10.9	IO1EW
0113	Taiwan SMART1 (45)	1986	1114		7.3	62	SMART1 IO1	39.0	IZD	-	.10	25.00	.214	33.3	11.09	13.3	IO1NS
0113	Taiwan SMART1 (45)	1986	1114		7.3	29	SMART1 M07	39.0	IZD	-	.20	25.00	.261	12.8	5.74	10.8	M07DN
0113	Taiwan SMART1 (45)	1986	1114		7.3	29	SMART1 M07	39.0	IZD	-	.10	25.00	.259	25.2	8.54	9.9	45M07EW
0113	Taiwan SMART1 (45)	1986	1114		7.3	29	SMART1 M07	39.0	IZD	-	.20	25.00	.246	30.3	10.86	11.1	45M07NS
0113	Taiwan SMART1 (45)	1986	1114		7.3	66	SMART1 O08	39.0	IZD	-	.10	25.00	.283	15.7	6.01	10.9	45O08DN
0113	Taiwan SMART1 (45)	1986	1114		7.3	66	SMART1 O08	39.0	IZD	-	.10	25.00	.207	25.3	8.35	11.9	45O08EW
0113	Taiwan SMART1 (45)	1986	1114		7.3	66	SMART1 O08	39.0	IZD	-	.10	25.00	.233	34.7	12.73	10.8	45O08NS
0129	Landers	1992	0628	1158	7.3	CDMG	12025 Palm Springs Airport #	37.5	IQD	C	.07	23.00	.296	12.1	4.63	23.8	PSA-UP
0129	Landers	1992	0628	1158	7.3	CDMG	12025 Palm Springs Airport #	37.5	IQD	C	.07	23.00	.120	13.7	4.48	26.4	PSA000
0129	Landers	1992	0628	1158	7.3	CDMG	12025 Palm Springs Airport #	37.5	IQD	C	.07	23.00	.142	17.5	5.38	27.3	PSA090
0129	Landers	1992	0628	1158	7.3	CDMG	22074 Yermo Fire Station #	24.9	AQD	C	.07	23.00	.383	16.1	10.25	13.4	YER-UP
0129	Landers	1992	0628	1158	7.3	CDMG	22074 Yermo Fire Station #	24.9	AQD	C	.07	23.00	.323	43.9	32.94	10.1	YER270
0129	Landers	1992	0628	1158	7.3	CDMG	22074 Yermo Fire Station #	24.9	AQD	C	.07	23.00	.224	31.0	20.13	12.7	YER360
0141	Kocaeli, Turkey	1999	0817		7.4	ERD	99999 Duzce	14.2	--D	C	.08	20.00	.613	31.3	24.23	3.4	DZC-UP
0141	Kocaeli, Turkey	1999	0817		7.4	ERD	99999 Duzce	14.2	--D	C		20.00	.452	66.4	41.49	5.0	DZC180
0141	Kocaeli, Turkey	1999	0817		7.4	ERD	99999 Duzce	14.2	--D	C	.08	15.00	.508	60.5	17.43	2.1	DZC270
0142	Chi-Chi, Taiwan	1999	0920		7.6	CWB	99999 WGK	11.1	--2	C	.06	33.00	.456	28.6	19.46	12.3	WGK-V
0142	Chi-Chi, Taiwan	1999	0920		7.6	CWB	99999 WGK	11.1	--2	C	.07	50.00	.479	48.4	25.76	14.0	WGK-E
0142	Chi-Chi, Taiwan	1999	0920		7.6	CWB	99999 WGK	11.1	--2	C	.06	50.00	.617	85.3	44.87	15.2	WGK-N
0142	Chi-Chi, Taiwan	1999	0920		7.6	CWB	99999 CHY036	20.3	--2	C	.04	50.00	.243	16.4	16.00	19.0	CHY036-V
0142	Chi-Chi, Taiwan	1999	0920		7.6	CWB	99999 CHY036	20.3	--2	C	.03	50.00	.295	50.6	38.46	14.0	CH036-N
0142	Chi-Chi, Taiwan	1999	0920		7.6	CWB	99999 CHY036	20.3	--2	C	.05	50.00	.455	42.2	21.49	13.0	CHY036-W
0142	Chi-Chi, Taiwan	1999	0920		7.6	CWB	99999 CHY101	11.1	--2	C	.04	50.00	.365	50.0	36.20	12.5	CHY101-V
0142	Chi-Chi, Taiwan	1999	0920		7.6	CWB	99999 CHY101	11.1	--2	C	.04	50.00	.661	101.6	77.96	12.9	CHY101-N
0142	Chi-Chi, Taiwan	1999	0920		7.6	CWB	99999 CHY101	11.1	--2	C	.03	50.00	.483	78.9	44.15	14.3	CHY101-W
0142	Chi-Chi, Taiwan	1999	0920		7.6	CWB	99999 HWA006	44.0	--2	C	.03	50.00	.162	9.8	6.59	15.5	HWA006-V
0142	Chi-Chi, Taiwan	1999	0920		7.6	CWB	99999 HWA006	44.0	--2	C	.06	50.00	.129	9.0	4.09	14.8	HWA006-E
0142	Chi-Chi, Taiwan	1999	0920		7.6	CWB	99999 HWA006	44.0	--2	C	.06	50.00	.105	10.3	3.02	15.5	HWA006-N
0142	Chi-Chi, Taiwan	1999	0920		7.6	CWB	99999 HWA030	46.3	--2	C	.02	50.00	.098	12.4	7.85	16.3	HWA030-V

B-77

No.	Earthquake	Date & Time				Own	No.	Station	Closest Dist (km)	Site Codes		Filter Corners			PGV (g)	PGD (cm/s)	Dur (s)	Filename
		YR	MODY	HRMN	Mag					Geom	USGS	HP (hz)	LP (hz)	PGA (g)				
0142	Chi-Chi, Taiwan	1999	0920		7.6	CWB	99999	HWA030	46.3	--2	C	.02	50.00	.101	14.1	2.62	14.0	HWA030-N
0142	Chi-Chi, Taiwan	1999	0920		7.6	CWB	99999	HWA030	46.3	--2	C	.02	50.00	.099	11.8	4.16	12.6	HWA030-W
0142	Chi-Chi, Taiwan	1999	0920		7.6	CWB	99999	HWA035	45.8	--2	C	.02	50.00	.139	11.5	6.23	15.0	HWA035-V
0142	Chi-Chi, Taiwan	1999	0920		7.6	CWB	99999	HWA035	45.8	--2	C	.02	50.00	.102	8.9	3.80	13.2	HWA035-N
0142	Chi-Chi, Taiwan	1999	0920		7.6	CWB	99999	HWA035	45.8	--2	C	.02	50.00	.115	8.8	4.46	14.6	HWA035-W
0142	Chi-Chi, Taiwan	1999	0920		7.6	CWB	99999	TCU038	22.4	--2	C	.02	5.00	.158	50.5	42.72	21.1	TCU038-V
0142	Chi-Chi, Taiwan	1999	0920		7.6	CWB	99999	TCU038	22.4	--2	C	.05	20.00	.233	60.8	37.69	18.6	TCU038-N
0142	Chi-Chi, Taiwan	1999	0920		7.6	CWB	99999	TCU038	22.4	--2	C	.02	50.00	.197	50.0	46.26	18.9	TCU038-W
0142	Chi-Chi, Taiwan	1999	0920		7.6	CWB	99999	TCU042	23.3	--2	C	.02	50.00	.195	44.8	34.52	19.3	TCU042-V
0142	Chi-Chi, Taiwan	1999	0920		7.6	CWB	99999	TCU042	23.3	--2	C	.05	50.00	.241	45.2	30.48	19.4	TCU042-N
0142	Chi-Chi, Taiwan	1999	0920		7.6	CWB	99999	TCU042	23.3	--2	C	.02	50.00	.352	38.9	42.94	16.0	TCU042-W

NRC TIME HISTORY LIBRARY: CEUS, SOIL, M>7, D=50-100 km

B-79

No.	Earthquake	Date & Time			Mag	Own	No.	Station	Closest Dist (km)	Site Codes		Filter Corners					Dur (s)	Filename
		YR	MODY	HRMN						Geom	USGS	HP (hz)	LP (hz)	PGA (g)	PGV (g)	PGD (cm/s)		
0129	Landers	1992	0628	1158	7.3	CDMG	12331	Hemet Fire Station #	69.5	AQD	C	.16	23.00	.224	5.1	2.15	22.6	H05-UP
0129	Landers	1992	0628	1158	7.3	CDMG	12331	Hemet Fire Station #	69.5	AQD	C	.16	23.00	.178	7.3	1.36	22.4	H05000
0129	Landers	1992	0628	1158	7.3	CDMG	12331	Hemet Fire Station #	69.5	AQD	C	.16	23.00	.186	7.2	2.38	21.0	H05090
0129	Landers	1992	0628	1158	7.3	CDMG	12026	Indio - Coachella Canal #	55.7	IQD	C	.10	23.00	.134	9.4	5.18	25.3	IND-UP
0129	Landers	1992	0628	1158	7.3	CDMG	12026	Indio - Coachella Canal #	55.7	IQD	C	.10	23.00	.186	12.3	4.05	25.5	IND000
0129	Landers	1992	0628	1158	7.3	CDMG	12026	Indio - Coachella Canal #	55.7	IQD	C	.10	23.00	.181	19.4	7.62	27.0	IND090
0129	Landers	1992	0628	1158	7.3	CDMG	23542	San Bernadino - E & Hospitality	80.5	--D	C	.10	50.00	.157	13.5	3.25	25.2	HOS-UP
0129	Landers	1992	0628	1158	7.3	CDMG	23542	San Bernadino - E & Hospitality	80.5	--D	C	.10	50.00	.145	27.4	11.55	21.6	HOS090
0129	Landers	1992	0628	1158	7.3	CDMG	23542	San Bernadino - E & Hospitality	80.5	--D	C	.10	50.00	.153	15.9	8.58	22.4	HOS180
0141	Kocaeli, Turkey	1999	0817		7.4	ERD	99999	Cekmece	76.1	--D	C	.60	20.00	.137	6.4	.57	4.7	CEK-UP
0141	Kocaeli, Turkey	1999	0817		7.4	ERD	99999	Cekmece	76.1	--D	C	.30	20.00	.215	18.9	1.66	4.4	CEK000
0141	Kocaeli, Turkey	1999	0817		7.4	ERD	99999	Cekmece	76.1	--D	C	.40	20.00	.208	9.5	1.18	5.8	CEK270
0142	Chi-Chi-Taiwan	1999	0920		7.6	CWB	99999	TTN	94.3	--2	C	.30	12.00	.030	3.9	1.17	35.4	TTN-V
0142	Chi-Chi-Taiwan	1999	0920		7.6	CWB	99999	TTN	94.3	--2	C	.10	12.00	.041	11.6	6.26	30.7	TTN-E
0142	Chi-Chi-Taiwan	1999	0920		7.6	CWB	99999	TTN	94.3	--2	C	.11	12.00	.035	7.6	2.49	31.3	TTN-N
0142	Chi-Chi-Taiwan	1999	0920		7.6	CWB	99999	CHY078	82.4	--2	C	.03	24.00	.062	6.3	6.59	32.5	CHY078-V
0142	Chi-Chi-Taiwan	1999	0920		7.6	CWB	99999	CHY078	82.4	--2	C	.03	24.00	.076	10.3	5.83	31.7	CHY078-N
0142	Chi-Chi-Taiwan	1999	0920		7.6	CWB	99999	CHY078	82.4	--2	C	.03	20.00	.164	13.4	3.72	32.5	CHY078-W
0142	Chi-Chi-Taiwan	1999	0920		7.6	CWB	99999	HWA011	56.7	--2	C	.02	40.00	.100	13.1	7.19	19.6	HWA011-V
0142	Chi-Chi-Taiwan	1999	0920		7.6	CWB	99999	HWA011	56.7	--2	C	.02	30.00	.154	26.2	9.42	23.7	HWA011-N
0142	Chi-Chi-Taiwan	1999	0920		7.6	CWB	99999	HWA011	56.7	--2	C	.02	30.00	.142	19.4	8.12	16.9	HWA011-W
0142	Chi-Chi-Taiwan	1999	0920		7.6	CWB	99999	HWA013	57.4	--2	C	.02	50.00	.149	12.0	7.69	18.9	HWA013-V
0142	Chi-Chi-Taiwan	1999	0920		7.6	CWB	99999	HWA013	57.4	--2	C	.02	50.00	.225	28.9	8.82	15.3	HWA013-N
0142	Chi-Chi-Taiwan	1999	0920		7.6	CWB	99999	HWA013	57.4	--2	C	.02	50.00	.211	34.3	9.34	15.1	HWA013-W
0142	Chi-Chi-Taiwan	1999	0920		7.6	CWB	99999	HWA041	50.0	----	C	.02	30.00	.106	15.3	9.39	30.0	HWA041-V
0142	Chi-Chi-Taiwan	1999	0920		7.6	CWB	99999	HWA041	50.0	----	C	.02	30.00	.135	19.1	6.40	25.9	HWA041-N
0142	Chi-Chi-Taiwan	1999	0920		7.6	CWB	99999	HWA041	50.0	----	C	.02	30.00	.119	16.4	6.48	28.9	HWA041-W
0142	Chi-Chi-Taiwan	1999	0920		7.6	CWB	99999	ILA064	83.4	----	C	.02	50.00	.125	8.4	7.03	19.9	ILA064-V
0142	Chi-Chi-Taiwan	1999	0920		7.6	CWB	99999	ILA064	83.4	----	C	.02	50.00	.123	9.9	4.74	17.2	ILA064-N
0142	Chi-Chi-Taiwan	1999	0920		7.6	CWB	99999	ILA064	83.4	----	C	.02	40.00	.116	10.4	3.93	16.7	ILA064-W
0142	Chi-Chi-Taiwan	1999	0920		7.6	CWB	99999	TCU017	52.2	--2	C	.02	50.00	.115	22.9	21.52	20.8	TCU017-V
0142	Chi-Chi-Taiwan	1999	0920		7.6	CWB	99999	TCU017	52.2	--2	C	.02	50.00	.161	33.5	27.01	16.8	TCU017-N
0142	Chi-Chi-Taiwan	1999	0920		7.6	CWB	99999	TCU017	52.2	--2	C	.02	33.00	.157	30.3	37.93	17.3	TCU017-W
0142	Chi-Chi-Taiwan	1999	0920		7.6	CWB	99999	TTN001	57.6	--2	C	.03	30.00	.096	13.6	10.82	24.1	TTN001-V

No.	Earthquake	Date & Time			Mag	Own	No.	Station	Closest Dist (km)	Site Codes		Filter Corners			PGV (g)	PGD (cm/s)	Dur (s)	Filename
		YR	MODY	HRMN						Geom	USGS	HP (hz)	LP (hz)	PGA (g)				
0142	Chi-Chi-Taiwan	1999	0920		7.6	CWB	99999	TTN001	57.6	--2	C	.03	30.00	.145	22.1	6.74	23.8	TTN001-E
0142	Chi-Chi-Taiwan	1999	0920		7.6	CWB	99999	TTN001	57.6	--2	C	.03	30.00	.116	14.1	4.11	25.2	TTN001-N
0142	Chi-Chi-Taiwan	1999	0920		7.6	CWB	99999	TTN010	95.2	--2	C	.03	14.00	.029	3.9	3.60	35.0	TTN010-V
0142	Chi-Chi-Taiwan	1999	0920		7.6	CWB	99999	TTN010	95.2	--2	C	.03	14.00	.047	7.3	3.51	34.4	TTN010-N
0142	Chi-Chi-Taiwan	1999	0920		7.6	CWB	99999	TTN010	95.2	--2	C	.02	14.00	.038	7.9	5.24	31.6	TTN010-W
0142	Chi-Chi-Taiwan	1999	0920		7.6	CWB	99999	TTN020	57.6	--2	C	.02	30.00	.047	8.8	5.36	34.6	TTN020-V
0142	Chi-Chi-Taiwan	1999	0920		7.6	CWB	99999	TTN020	57.6	--2	C	.02	23.00	.048	7.9	5.45	27.4	TTN020-N
0142	Chi-Chi-Taiwan	1999	0920		7.6	CWB	99999	TTN020	57.6	--2	C	.02	23.00	.065	10.2	7.31	31.9	TTN020-W
0142	Chi-Chi-Taiwan	1999	0920		7.6	CWB	99999	TTN023	63.2	---	C	.03	30.00	.059	8.5	4.18	32.5	TTN023-V
0142	Chi-Chi-Taiwan	1999	0920		7.6	CWB	99999	TTN023	63.2	---	C	.02	30.00	.104	16.1	4.50	36.8	TTN023-N
0142	Chi-Chi-Taiwan	1999	0920		7.6	CWB	99999	TTN023	63.2	---	C	.02	30.00	.073	12.5	6.69	31.5	TTN023-W

NRC TIME HISTORY LIBRARY: CEUS, SOIL, M>7, D=100-200 km

B-81

No.	Earthquake	Date & Time				Mag	Own	No.	Station	Closest Dist (km)	Site Codes		Filter Corners			Dur (s)	Filename	
		YR	MODY	HRMN							Geom	USGS	HP (hz)	LP (hz)	PGA (g)			PGV (g)
0012	Kern County	1952	0721	1153	7.4	USGS	135	LA - Hollywood Stor FF	120.5	IPD	C	.20	20.00	.069	4.6	1.76	17.6	PEL-UP
0012	Kern County	1952	0721	1153	7.4	USGS	135	LA - Hollywood Stor FF	120.5	IPD	C	.20	15.00	.123	11.1	3.76	20.5	PEL090
0012	Kern County	1952	0721	1153	7.4	USGS	135	LA - Hollywood Stor FF	120.5	IPD	C	.20	13.00	.131	8.7	1.98	19.7	PEL180
0046	Tabas, Iran	1978	0916		7.4		69	Bajestan	121.2	--C	-	.05		.141	6.7	6.50	23.7	BAJ-V1
0046	Tabas, Iran	1978	0916		7.4		69	Bajestan	121.2	--C	-	.02	15.00	.246	7.8	5.06	21.8	BAJ-L1
0046	Tabas, Iran	1978	0916		7.4		69	Bajestan	121.2	--C	-	.02	15.00	.157	6.0	4.59	22.3	BAJ-T1
0046	Tabas, Iran	1978	0916		7.4		73	Sedeh	164.5	--D	-	.02	20.00	.057	6.8	8.20	21.6	SED-V1
0046	Tabas, Iran	1978	0916		7.4		73	Sedeh	164.5	--D	-	.02	20.00	.072	4.6	3.02	22.4	SED-L1
0046	Tabas, Iran	1978	0916		7.4		73	Sedeh	164.5	--D	-	.02	20.00	.078	4.9	2.71	22.2	SED-T1
0129	Landers	1992	0628	1158	7.3	USC	90094	Bell Gardens - Jaboneria #	153.9	--D	C	.65	25.00	.054	2.1	.27	23.8	JAB-UP
0129	Landers	1992	0628	1158	7.3	USC	90094	Bell Gardens - Jaboneria #	153.9	--D	C	.30	25.00	.101	5.7	1.34	24.3	JAB220
0129	Landers	1992	0628	1158	7.3	USC	90094	Bell Gardens - Jaboneria #	153.9	--D	C	.18	25.00	.097	13.3	4.27	22.2	JAB310
0129	Landers	1992	0628	1158	7.3	USC	90012	Burbank - N Buena Vista #	162.1	--D	C	.33	25.00	.102	6.6	1.50	26.8	BUE-UP
0129	Landers	1992	0628	1158	7.3	USC	90012	Burbank - N Buena Vista #	162.1	--D	C	.25	25.00	.118	8.9	2.45	25.7	BUE250
0129	Landers	1992	0628	1158	7.3	USC	90012	Burbank - N Buena Vista #	162.1	--D	C	.28	25.00	.185	14.2	3.30	25.4	BUE340
0129	Landers	1992	0628	1158	7.3	USC	90002	Fountain Valley - Euclid #	148.8	--D	C	.90	25.00	.067	2.2	.20	23.9	EUC-UP
0129	Landers	1992	0628	1158	7.3	USC	90002	Fountain Valley - Euclid #	148.8	--D	C	.13	25.00	.162	21.4	8.78	26.7	EUC022
0129	Landers	1992	0628	1158	7.3	USC	90002	Fountain Valley - Euclid #	148.8	--D	C	.13	25.00	.137	18.9	4.40	24.8	EUC292
0129	Landers	1992	0628	1158	7.3	USC	90025	LA - E Vernon Ave #	157.7	--D	C	.38	25.00	.083	4.1	.99	23.7	VER-UP
0129	Landers	1992	0628	1158	7.3	USC	90025	LA - E Vernon Ave #	157.7	--D	C	.13	25.00	.076	10.4	5.03	23.8	VER090
0129	Landers	1992	0628	1158	7.3	USC	90025	LA - E Vernon Ave #	157.7	--D	C	.18	25.00	.093	9.7	4.41	22.6	VER180
0129	Landers	1992	0628	1158	7.3	USC	90080	LB - Orange Ave #	164.5	--D	C	.50	25.00	.080	2.6	.38	24.2	OR2-UP
0129	Landers	1992	0628	1158	7.3	USC	90080	LB - Orange Ave #	164.5	--D	C	.15	25.00	.137	10.8	4.39	25.5	OR2010
0129	Landers	1992	0628	1158	7.3	USC	90080	LB - Orange Ave #	164.5	--D	C	.15	25.00	.155	14.3	5.49	24.7	OR2280
0129	Landers	1992	0628	1158	7.3	USC	90077	Santa Fe Springs - E Jostlin #	150.4	--D	C	.35	25.00	.105	3.9	.71	23.2	EJS-UP
0129	Landers	1992	0628	1158	7.3	USC	90077	Santa Fe Springs - E Jostlin #	150.4	--D	C	.18	25.00	.120	10.3	2.60	25.2	EJS030
0129	Landers	1992	0628	1158	7.3	USC	90077	Santa Fe Springs - E Jostlin #	150.4	--D	C	.15	25.00	.115	10.7	3.81	24.3	EJS120
0142	Chi-Chi, Taiwan	1999	0920		7.6	CWB	99999	SGL	105.0	--2	C	.20	8.00	.026	3.6	1.22	26.3	SGL-V
0142	Chi-Chi, Taiwan	1999	0920		7.6	CWB	99999	SGL	105.0	--2	C	.10	14.00	.066	8.8	2.94	26.9	SGL-E
0142	Chi-Chi, Taiwan	1999	0920		7.6	CWB	99999	SGL	105.0	--2	C	.20	14.00	.062	8.7	2.17	27.7	SGL-N
0142	Chi-Chi, Taiwan	1999	0920		7.6	CWB	99999	ILA002	109.1	----	C	.02	30.00	.070	9.4	7.74	27.5	ILA002-V
0142	Chi-Chi, Taiwan	1999	0920		7.6	CWB	99999	ILA002	109.1	----	C	.04	24.00	.160	12.9	5.16	22.2	ILA002-N
0142	Chi-Chi, Taiwan	1999	0920		7.6	CWB	99999	ILA002	109.1	----	C	.02	24.00	.098	12.2	5.70	23.2	ILA002-W

No.	Earthquake	Date & Time				Mag	Own	No.	Station	Closest Dist (km)	Site Codes Geom USGS	Filter Corners			PGV (g)	PGD (cm/s)	Dur (s)	Filename
		YR	MODY	HRMN								HP (hz)	LP (hz)	PGA (g)				
0142	Chi-Chi, Taiwan	1999	0920		7.6	CWB	99999	TAP024	100.2	--2	C	.02	50.00	.097	12.2	10.00	24.8	TAP024-V
0142	Chi-Chi, Taiwan	1999	0920		7.6	CWB	99999	TAP024	100.2	--2	C	.02	50.00	.130	22.3	7.33	20.9	TAP024-S
0142	Chi-Chi, Taiwan	1999	0920		7.6	CWB	99999	TAP024	100.2	--2	C	.02	50.00	.123	16.6	11.61	21.1	TAP024-W
0142	Chi-Chi, Taiwan	1999	0920		7.6	CWB	99999	TAP046	127.2	--1	C	.02	30.00	.058	4.6	5.82	23.7	TAP046-V
0142	Chi-Chi, Taiwan	1999	0920		7.6	CWB	99999	TAP046	127.2	--1	C	.02	30.00	.114	8.4	3.60	21.9	TAP046-N
0142	Chi-Chi, Taiwan	1999	0920		7.6	CWB	99999	TAP046	127.2	--1	C	.02	24.00	.181	13.7	5.75	21.8	TAP046-W
0142	Chi-Chi, Taiwan	1999	0920		7.6	CWB	99999	TAP084	127.7	----	C	.03	40.00	.045	7.0	7.14	28.5	TAP084-V
0142	Chi-Chi, Taiwan	1999	0920		7.6	CWB	99999	TAP084	127.7	----	C	.02	40.00	.059	6.0	3.65	30.1	TAP084-N
0142	Chi-Chi, Taiwan	1999	0920		7.6	CWB	99999	TAP084	127.7	----	C	.02	40.00	.064	8.6	2.96	24.8	TAP084-W
0142	Chi-Chi, Taiwan	1999	0920		7.6	CWB	99999	TTN003	108.1	----	C	.02	20.00	.056	3.9	2.53	28.5	TTN003-V
0142	Chi-Chi, Taiwan	1999	0920		7.6	CWB	99999	TTN003	108.1	----	C	.03	20.00	.036	3.4	2.10	32.0	TTN003-N
0142	Chi-Chi, Taiwan	1999	0920		7.6	CWB	99999	TTN003	108.1	----	C	.03	20.00	.047	4.8	1.88	33.1	TTN003-W

Notes:

1. M is moment magnitude
2. Station numbers were assigned where not available, using numbers 1-33 and 60-100.
3. Distances marked with a * are hypocentral instead of closest distances.
4. Site codes are from two sources: 1) Geomatrix (3 letter), 2) USGS (1 letter), described below.

5. GEOMATRIX 3-LETTER SITE CLASSIFICATIONS:

FIRST LETTER: Instrument housing

I = Free-field instrument or instrument shelter. Instrument is located at or within several feet of the ground surface.

A = One-story structure of lightweight construction. Instrument is located at the lowest level and within several feet of the ground surface.

B = Two- to four-story structure of lightweight construction. Instrument is located at the lowest level and within several feet of the ground surface.

C = Two- to four-story structure of lightweight construction. Instrument is located at the lowest level in a basement and below the ground surface.

D = Five or more story structure of heavy construction. Instrument is located at the lowest level and within several feet of the ground surface.

E = Five or more story structure of heavy construction. Instrument is located at the lowest level in a basement and below the ground surface.

F = Structure housing instrument is buried below the ground surface, e.g. tunnel.

G = Structure of light or heavyweight construction, instrument not at lowest level.

H = Earth dam.

I = Concrete Dam.

SECOND LETTER: Mapped local geology

Sedimentary or metasedimentary:

H = Holocene (Recent) Quaternary (< 15000y bp).

Q = Pleistocene Quaternary (< 2my bp).

P = Pliocene Tertiary (< 6my bp).

M = Miocene Tertiary (< 22my bp).

O = Oligocene Tertiary (< 36my bp).

E = Eocene Tertiary (< 58my bp).

L = Paleocene Tertiary (< 63my bp).

K = Cretaceous (< 145my bp).

F = Franciscan Formation (Cretaceous/Late Jurassic).

J = Jurassic (< 210my bp).

T = Triassic (< 255my bp).

Z = Permian or older (> 255my bp).

Igneous or meta-igneous:

V = Volcanic (extrusive).

N = Intrusive.

G = Granitic.

THIRD LETTER: Geotechnical subsurface characteristics

A = Rock. Instrument on rock ($V_s > 600$ mps) or < 5m of soil over rock.

B = Shallow (stiff) soil. Instrument on/in soil profile up to 20m thick overlying rock.

C = Deep narrow soil. Instrument on/in soil profile at least 20m thick overlying rock, in a narrow canyon or valley no more than several km wide.

D = Deep broad soil. Instrument on/in soil profile at least 20m thick overlying rock, in a broad valley.

E = Soft deep soil. Instrument on/in deep soil profile with average $V_s < 150$ mps.

6. USGS 1-LETTER SITE CLASSIFICATIONS

Average shear-wave velocity to a depth of 30m is:

A = > 750 m/s

B = 360 - 750 m/s

C = 180 - 360 m/s

D = < 180 m/s

**APPENDIX C WUS STATISTICAL RESPONSE SPECTRAL SHAPES (SA/PGA,
5% DAMPING) FOR ROCK AND DEEP SOIL SITE CONDITIONS**

This Appendix contains bin average (median) statistical response spectral shapes computed using the WUS strong motion catalog (Appendix A). Table C-1 lists the *M* and *R* bins, average parameters, and number of recordings comprising each average shape. Although not used in developing the revised spectral shapes (Section 4) due to potential diluting of near-fault effects, statistical shapes were computed for a 0 to 50 km distance bin and are shown here for completeness. Horizontal component shapes for rock and deep soil are followed by vertical component shapes for both rock and deep soil site conditions.

For each component, response spectra are computed in a bandwidth that extends to 1.25 (or 1/1.25) of filter corner frequencies (Appendix A). This primarily affects the low frequencies and results in an increased variability as frequency decreases due to loss of records.

Table C-1 WUS STATISTICAL SHAPE BINS (HORIZONTAL COMPONENT)								
<u>Magnitude Bins (M)</u>								
<u>Range</u>				<u>Bin Center</u>				
5 - 6				5.5				
6 - 7				6.5				
7+				7.5				
Distance Bin (km)	\bar{M}	\bar{R} (km)	Number of spectra	PGA** (g), σ_{ln}	PGV** (cm/sec), σ_{ln}	PGD** (cm), σ_{ln}	$\frac{PGV^{**}}{PGA}$ ($\frac{cm/sec}{g}$) σ_{ln}	$\frac{PGA \cdot PGD^{**}}{PGV^2}$ σ_{ln}
0 - 10, rock	5.54	7.91	30	0.18, 0.91	8.14, 1.14	0.80, 1.60	44.50, 0.58	2.17, 0.28
	6.53	5.75	32	0.44, 0.76	32.65, 0.93	6.22, 1.26	73.51, 0.40	2.54, 0.42
	7.27	4.20	6	0.93, 0.26	81.73, 0.25	47.42, 0.66	87.94, 0.39	6.47, 0.60
0 - 10, soil	5.76	7.80	24	0.26, 0.65	18.57, 0.56	3.11, 0.46	70.72, 0.33	2.32, 0.35
	6.46	6.00	77	0.38, 0.43	46.88, 0.59	14.79, 0.89	122.00, 0.44	2.54, 0.41
	7.05	8.90	4	0.40, 0.62	44.46, 0.56	21.27, 0.25	110.42, 0.07	4.25, 0.24
10 - 50, rock	5.57	21.80	180	0.11, 0.87	5.08, 0.85	0.54, 1.04	46.96, 0.37	2.24, 0.38
	6.43	30.28	238	0.13, 0.73	8.81, 0.76	1.96, 1.01	70.41, 0.49	3.09, 0.54
	7.27	31.00	6	0.17, 0.85	8.80, 0.88	2.50, 1.56	50.59, 0.37	5.51, 0.90
10 - 50, soil	5.69	21.82	378	0.11, 0.73	6.63, 0.77	0.87, 0.94	59.88, 0.34	2.16, 0.33
	6.35	28.27	542	0.14, 0.63	10.77, 0.74	2.25, 1.04	78.77, 0.41	2.57, 0.41
	7.29	33.46	56	0.16, 0.35	22.38, 0.38	10.46, 0.39	141.17, 0.36	3.25, 0.56

Table C-1
WUS STATISTICAL SHAPE BINS (HORIZONTAL COMPONENT)

<u>Magnitude Bins (M)</u>								
				<u>Bin Center</u>				
				5.5				
				6.5				
				7.5				
Distance Bin (km)	<u>Range</u>							
	\bar{M}	\bar{R} (km)	Number of spectra	PGA** (g), σ_{ln}	PGV** (cm/sec), σ_{ln}	PGD** (cm), σ_{ln}	$\frac{PGV^{**}}{PGA}$ ($\frac{cm/sec}{g}$) σ_{ln}	$\frac{PGA \cdot PGD^{**}}{PGV^2}$ σ_{ln}
50 - 100, rock	5.91	64.27	34	0.05, 0.40	2.22, 0.53	0.21, 0.83	41.16, 0.43	2.24, 0.57
	6.51	70.35	102	0.06, 0.51	3.87, 0.82	0.79, 1.23	69.89, 0.56	2.88, 0.56
	7.32	81.46	10	0.06, 0.52	5.16, 0.87	2.64, 1.17	80.63, 0.45	6.23, 0.50
50 - 100, soil	5.80	67.22	42	0.06, 0.80	3.12, 0.78	0.38, 0.92	53.20, 0.23	2.28, 0.49
	6.49	67.34	158	0.07, 0.67	6.23, 0.78	1.26, 0.99	88.00, 0.42	2.26, 0.44
	7.31	79.57	14	0.10, 0.12	11.24, 0.34	5.42, 0.60	111.37, 0.35	4.24, 0.50
100 - 200, rock	5.4	107.80	2	0.02, ----	1.16, ----	0.10, ----	49.72, ----	1.74, ----
	6.64	114.57	14	0.02, 0.86	2.03, 0.38	1.09, 0.68	132.54, 0.59	3.98, 0.27
	7.30	152.01	14	0.03, 0.47	5.55, 0.66	2.43, 1.06	184.16, 0.35	2.34, 0.31
100 - 200, soil	6.0	105.00	2	0.03, ----	1.50, ----	0.11, ----	49.92, ----	1.74, ----
	6.64	132.97	28	0.03, 0.78	3.05, 0.58	0.89, 0.97	98.24, 0.53	2.90, 0.42
	7.31	147.07	88	0.04, 0.25	8.09, 0.39	3.50, 0.76	188.64, 0.36	2.25, 0.29

Table C-1
WUS STATISTICAL SHAPE BINS (HORIZONTAL COMPONENT)

<u>Magnitude Bins (M)</u>								
				<u>Bin Center</u>				
				5.5				
				6.5				
				7.5				
				5.5				
				6.5				
				7.5				
Distance Bin (km)	\bar{M}	\bar{R} (km)	Number of spectra	PGA** (g), σ_{ln}	PGV** (cm/sec), σ_{ln}	PGD** (cm), σ_{ln}	$\frac{PGV^{**}}{PGA}$ ($\frac{cm/sec}{g}$) σ_{ln}	$\frac{PGA \cdot PGD^{**}}{PGV^2}$ σ_{ln}
0 - 50, rock	5.57	19.91	208	0.12, 0.89	5.39, 0.91	0.57, 1.14	46.73, 0.40	2.22, 0.37
	6.44	27.39	270	0.15, 0.84	10.27, 0.89	2.24, 1.10	70.77, 0.48	3.02, 0.53
	7.27	17.60	12	0.40, 1.07	26.82, 1.35	10.89, 1.94	66.70, 0.46	5.97, 0.69
soil	5.69	21.10	398	0.12, 0.75	7.02, 0.79	0.93, 0.97	60.48, 0.34	2.16, 0.33
	6.37	25.50	619	0.16, 0.70	12.93, 0.87	2.85, 1.20	83.17, 0.44	2.57, 0.41
	7.27	31.82	60	0.17, 0.42	23.43, 0.42	10.97, 0.42	138.87, 0.36	3.30, 0.55

C-4

** Median values

Table C-2
WUS STATISTICAL SHAPE BINS (VERTICAL COMPONENT)

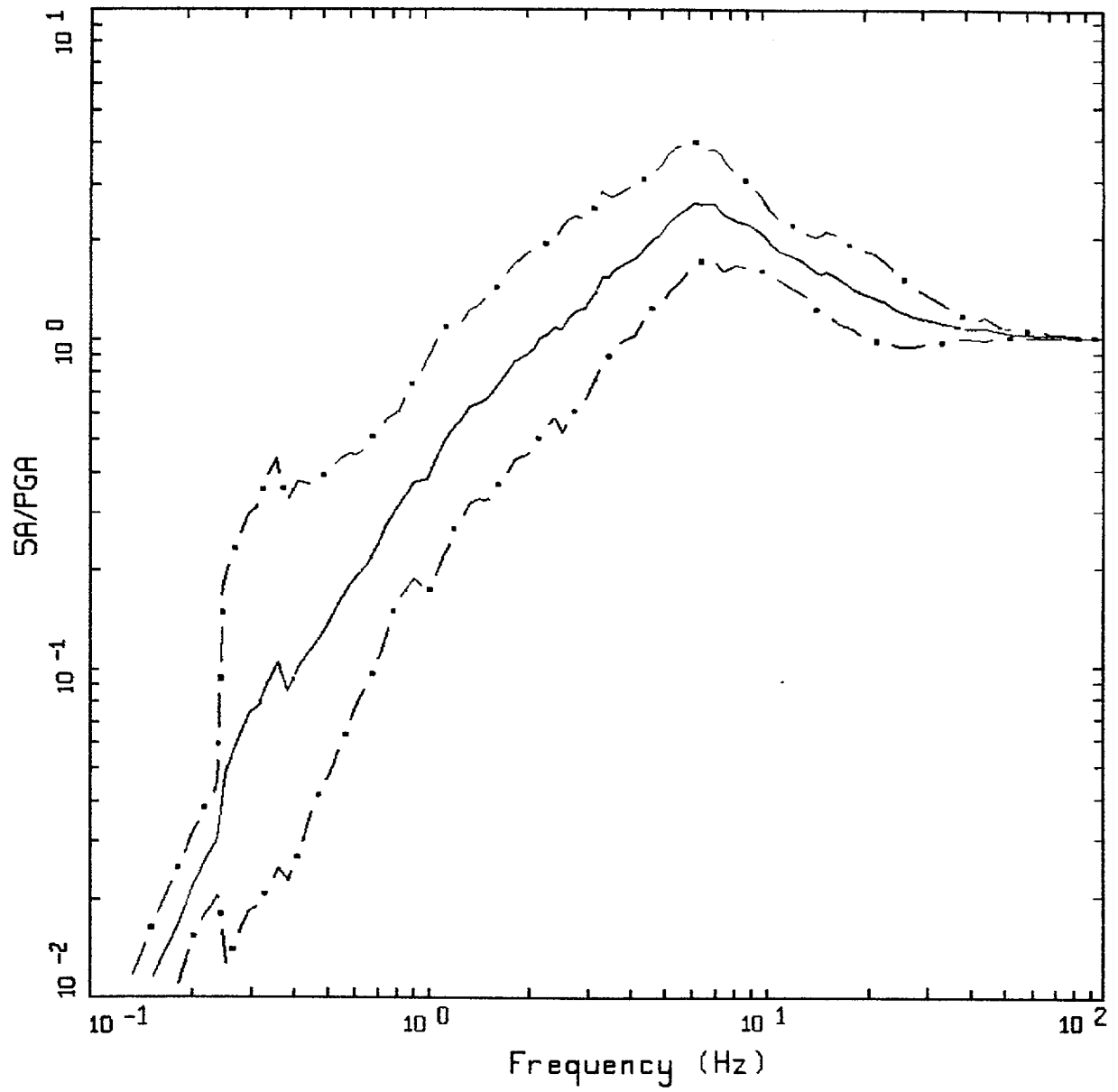
<u>Magnitude Bins (M)</u>								
<u>Range</u> 5 - 6 6 - 7 7+				<u>Bin Center</u> 5.5 6.5 7.5				
Distance Bin (km)	\bar{M}	\bar{R} (km)	Number of spectra	PGA** (g), σ_{ln}	PGV** (cm/sec), σ_{ln}	PGD** (cm), σ_{ln}	$\frac{PGV^{**}}{PGA} \left(\frac{cm/sec}{g} \right)$, σ_{ln}	$\frac{PGA \cdot PGD^{**}}{PGV^2}$, σ_{ln}
0 - 10, rock	5.54	7.91	14	0.11, 0.83	3.55, 1.00	0.41, 1.54	31.80, 0.67	3.59, 0.50
	6.53	5.75	14	0.34, 0.85	17.67, 0.95	4.48, 1.25	52.19, 0.44	4.76, 0.62
	7.27	4.20	3	0.75, 0.08	49.10, 0.22	43.42, 0.93	65.69, 0.25	13.20, 0.75
0 - 10, soil	5.76	7.80	11	0.18, 0.84	6.68, 0.50	0.95, 0.56	37.89, 0.56	3.68, 0.48
	6.46	6.00	37	0.30, 0.66	15.84, 0.69	5.19, 1.03	52.89, 0.40	6.07, 0.66
	7.05	8.90	2	0.18, 0.16	16.19, 0.59	17.06, 0.88	88.57, 0.75	11.67, 0.45
10 - 50, rock	5.57	21.80	87	0.06, 0.86	2.25, 0.74	0.22, 0.98	31.17, 0.46	2.57, 0.49
	6.43	30.28	119	0.07, 0.80	4.33, 0.72	1.05, 1.11	60.29, 0.58	3.95, 0.61
	7.27	31.00	3	0.07, 0.81	4.30, 0.92	1.47, 1.38	58.52, 0.41	5.73, 0.24
10 - 50, soil	5.69	21.82	188	0.07, 0.80	2.40, 0.76	0.28, 1.00	35.78, 0.46	3.20, 0.49
	6.35	28.27	263	0.08, 0.79	4.22, 0.74	0.92, 1.07	50.69, 0.56	4.06, 0.61
	7.29	33.46	28	0.09, 0.41	7.83, 0.25	3.66, 0.37	86.35, 0.28	5.30, 0.34

Magnitude Bins (M)								
Distance Bin (km)	Range			Bin Center				
	\bar{M}	\bar{R} (km)	Number of spectra	PGA** (g), σ_{ln}	PGV** (cm/sec), σ_{ln}	PGD** (cm), σ_{ln}	$\frac{PGV^{**}}{PGA} \left(\frac{cm/sec}{g} \right)$, σ_{ln}	$\frac{PGA \cdot PGD^{**}}{PGV^2}$, σ_{ln}
50 - 100, rock	5.91	64.27	15	0.03, 0.33	1.25, 0.49	0.14, 1.10	38.32, 0.58	2.95, 0.80
	6.51	70.35	51	0.03, 0.50	2.02, 0.75	0.52, 1.30	68.36, 0.66	3.66, 0.71
	7.32	81.46	5	0.05, 0.37	3.78, 0.86	1.86, 1.03	77.56, 0.56	6.22, 0.63
50 - 100, soil	5.80	67.22	19	0.03, 0.77	1.18, 0.66	0.14, 1.16	44.26, 0.38	2.63, 0.68
	6.49	67.34	74	0.03, 0.71	2.11, 0.57	0.48, 0.99	70.52, 0.56	3.02, 0.69
	7.31	76.57	7	0.05, 0.18	5.11, 0.30	2.65, 0.45	96.26, 0.36	5.29, 0.54
100 - 200, rock	5.4	107.80	1	0.01, ----	0.40, ----	0.03, ----	40.00, ----	1.84, ----
	6.64	114.57	7	0.01, 0.90	1.39, 0.54	0.75, 0.81	124.36, 0.86	4.24, 0.78
	7.30	152.01	7	0.02, 0.29	2.77, 0.72	0.80, 1.25	147.89, 0.51	1.92, 0.47
100 - 200, soil	6.0	105.00	1	0.03, ----	0.90, ----	0.07, ----	33.33, ----	2.29, ----
	6.64	132.97	14	0.02, 0.63	1.42, 0.52	0.46, 0.85	91.78, 0.59	3.42, 0.56
	7.31	147.07	44	0.02, 0.28	2.55, 0.52	0.76, 1.04	135.47, 0.53	2.15, 0.45
0 - 50, rock	5.57	19.91	100	0.07, 0.88	2.39, 0.79	0.24, 1.09	36.56, 0.49	2.69, 0.51
	6.44	27.39	133	0.08, 0.93	5.02, 0.86	1.22, 1.21	59.38, 0.56	4.03, 0.61
	7.27	17.60	6	0.23, 1.37	14.52, 1.46	7.98, 2.13	62.00, 0.31	8.70, 0.68

Magnitude Bins (M)								
Range				Bin Center				
5 - 6				5.5				
6 - 7				6.5				
7+				7.5				
Distance Bin (km)	\bar{M}	\bar{R} (km)	Number of spectra	PGA** (g), σ_{ln}	PGV** (cm/sec), σ_{ln}	PGD** (cm), σ_{ln}	$\frac{PGV^{**}}{PGA} \left(\frac{cm/sec}{g} \right)$, σ_{ln}	$\frac{PGA \cdot PGD^{**}}{PGV^2}$, σ_{ln}
0 - 50, soil	5.69	21.10	197	0.07, 0.83	2.52, 0.78	0.30, 1.02	36.65, 0.46	3.24, 0.49
	6.37	25.50	300	0.10, 0.88	4.96, 0.86	1.14, 1.21	50.95, 0.54	4.27, 0.63
	7.27	31.82	30	0.10, 0.44	8.22, 0.32	4.05, 0.55	86.50, 0.31	5.58, 0.39

C-7

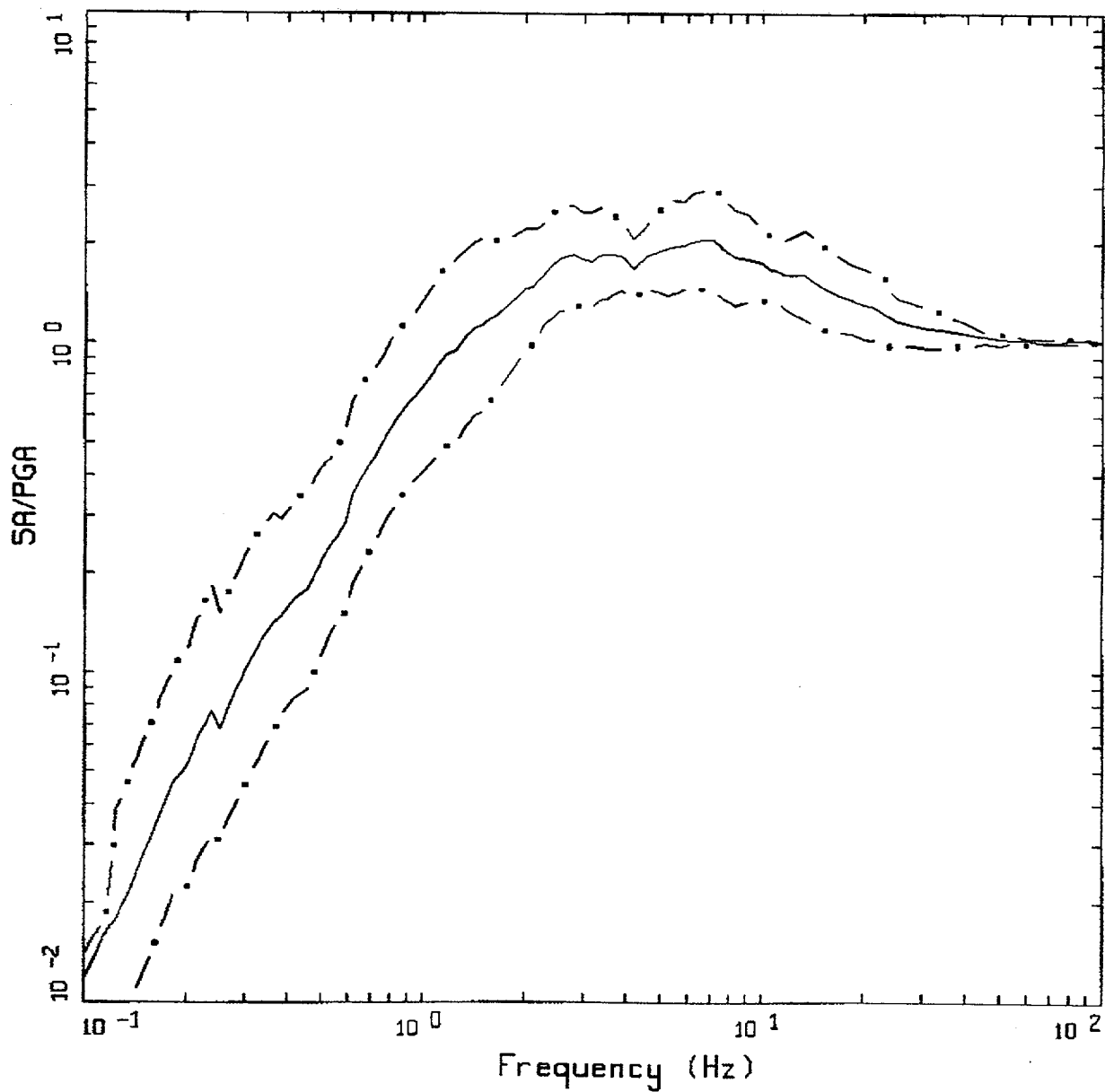
** Median values



AVERAGE HORIZONTAL SPECTRA
 M=5.5 (5.0-6.0), R=0-10 KM, ROCK
 AVERAGE M = 5.54, AVERAGE DISTANCE = 7.91 KM

LEGEND
 ————— 50TH PERCENTILE
 - . - . 16TH PERCENTILE
 - . . - 84TH PERCENTILE

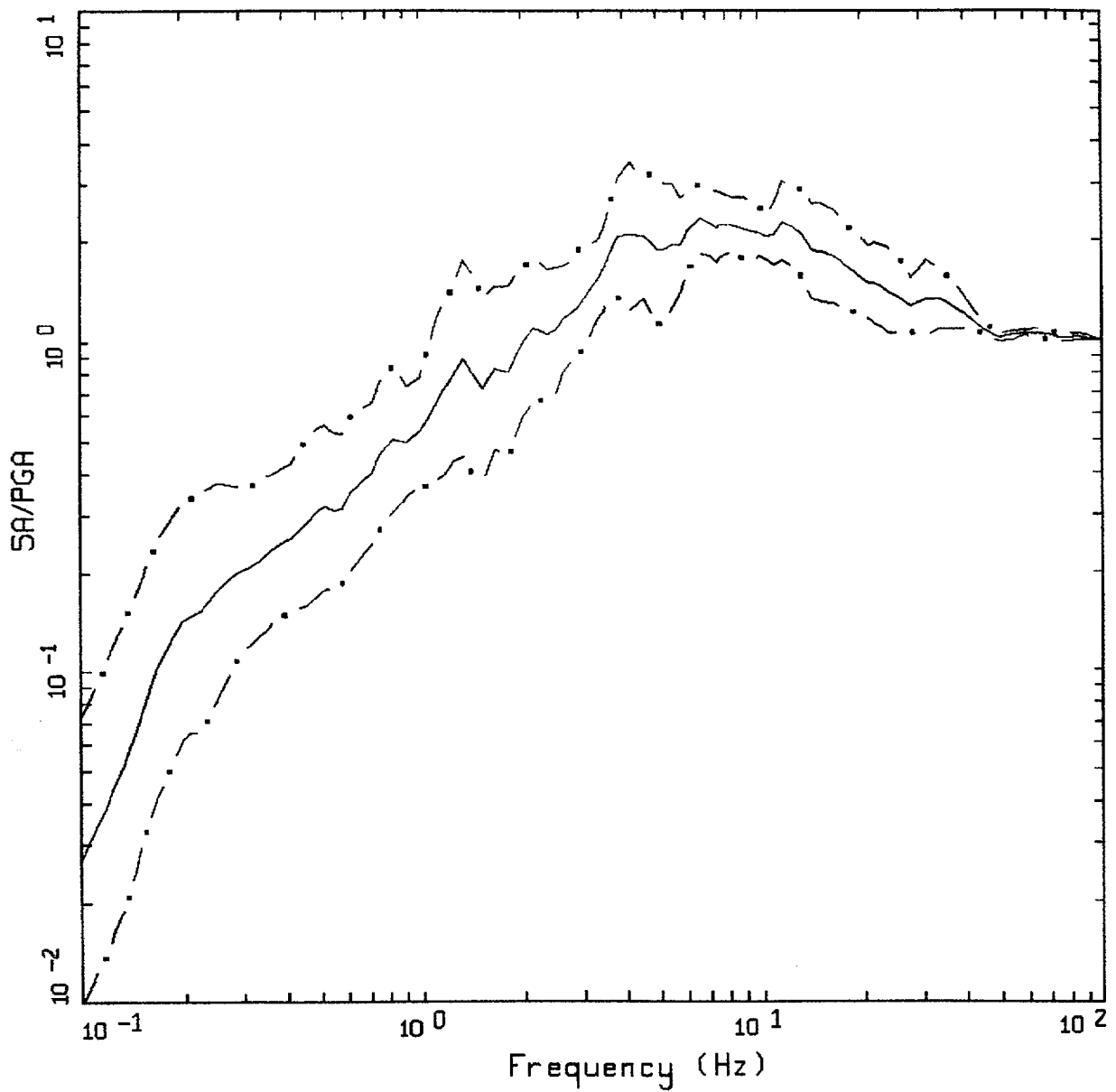
Figure C-1. Median $\pm 1 \sigma$ spectral shapes for $M \approx 5.5$, $R = 0-10$ km, horizontal WUS rock.



AVERAGE HORIZONTAL SPECTRA
 M=6.5 (6.0-7.0), R=0-10 KM, ROCK
 AVERAGE M = 6.53, AVERAGE DISTANCE = 5.75 KM

LEGEND
 ————— 50TH PERCENTILE
 - . - . 16TH PERCENTILE
 - . - . 84TH PERCENTILE

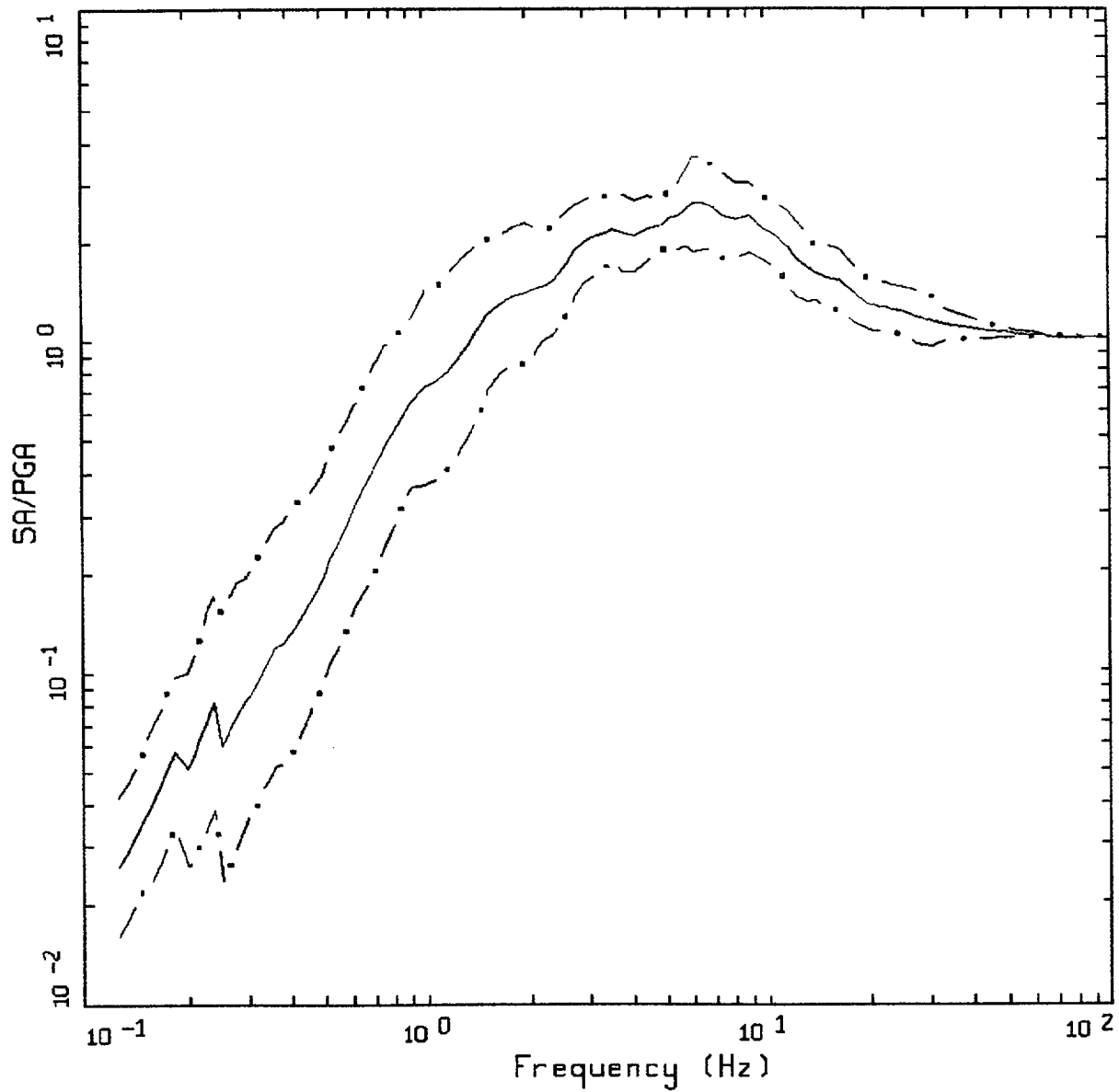
Figure C-2. Median $\pm 1 \sigma$ spectral shapes for $M = 6.5$, $R = 0-10$ km, horizontal WUS rock.



AVERAGE HORIZONTAL SPECTRA
 M=7.5 (7.0-7.0+), R=0-10 KM, ROCK
 AVERAGE M = 7.27, AVERAGE DISTANCE = 4.20 KM

LEGEND
 ————— 50TH PERCENTILE
 - . - 16TH PERCENTILE
 - . . 84TH PERCENTILE

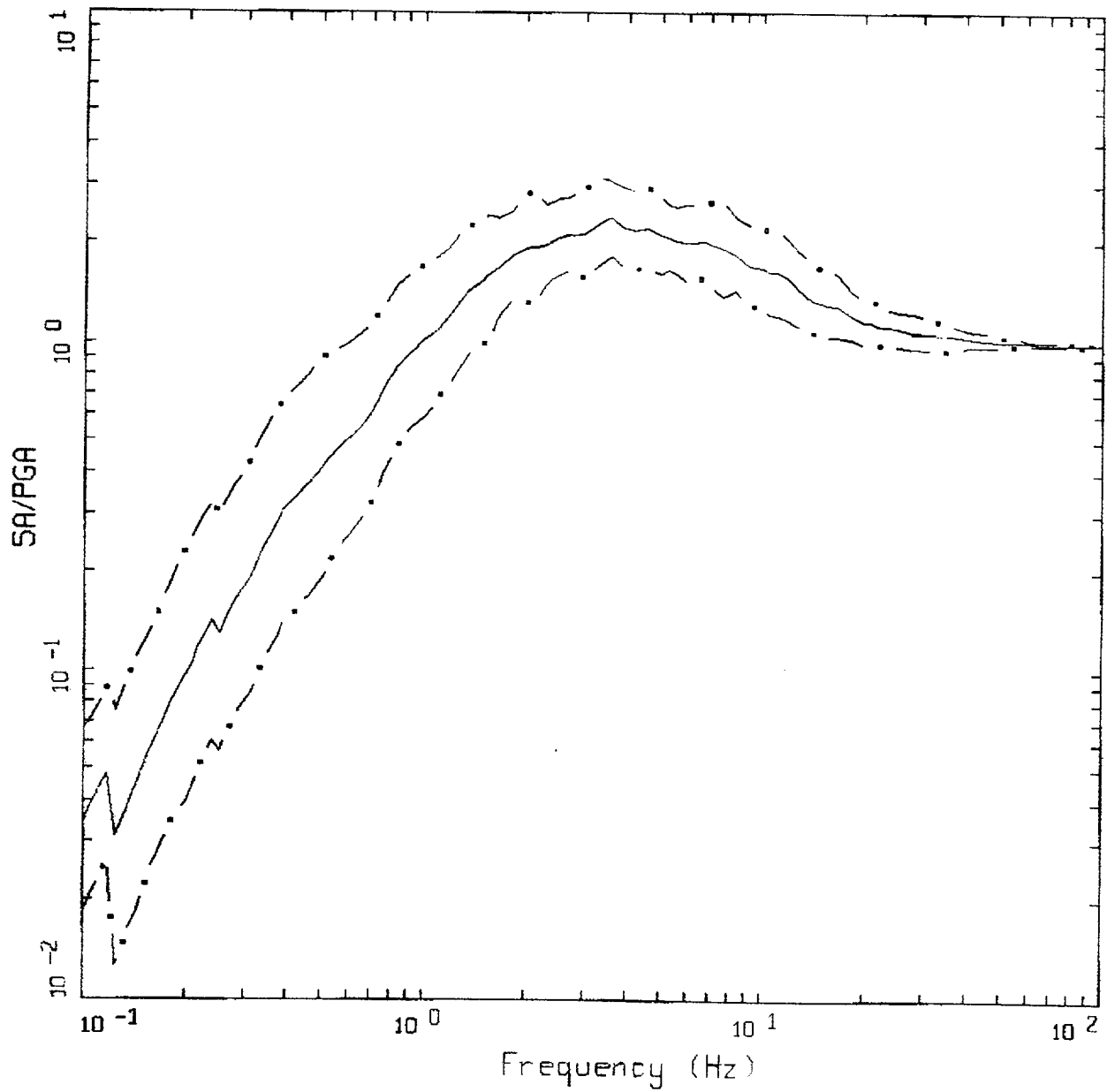
Figure C-3. Median $\pm 1 \sigma$ spectral shapes for $M \approx 7.5$, $R = 0-10$ km, horizontal WUS rock.



AVERAGE HORIZONTAL SPECTRA
 M=5.5 (5.0-6.0), R=0-10 KM, SOIL
 AVERAGE M = 5.76, AVERAGE DISTANCE = 7.80 KM

LEGEND
 ————— 50TH PERCENTILE
 - . - - 16TH PERCENTILE
 - . - - 84TH PERCENTILE

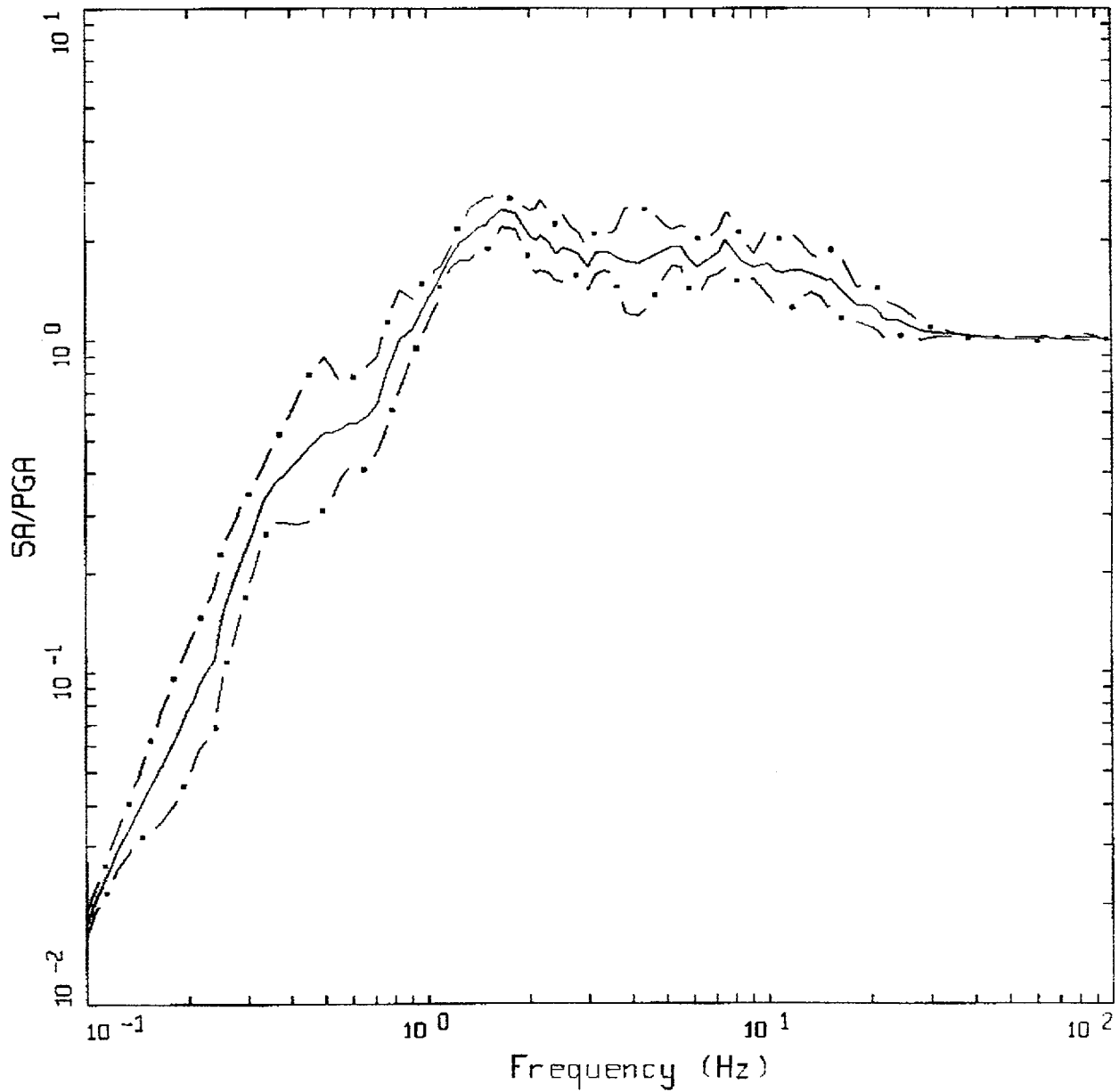
Figure C-4. Median $\pm 1 \sigma$ spectral shapes for $M = 5.5$, $R = 0-10$ km, horizontal WUS soil.



AVERAGE HORIZONTAL SPECTRA
 $M=6.5$ (6.0-7.0), $R=0-10$ KM, SOIL
 AVERAGE $M = 6.46$, AVERAGE DISTANCE = 6.00 KM

LEGEND
 — 50TH PERCENTILE
 - · - 16TH PERCENTILE
 - · - 84TH PERCENTILE

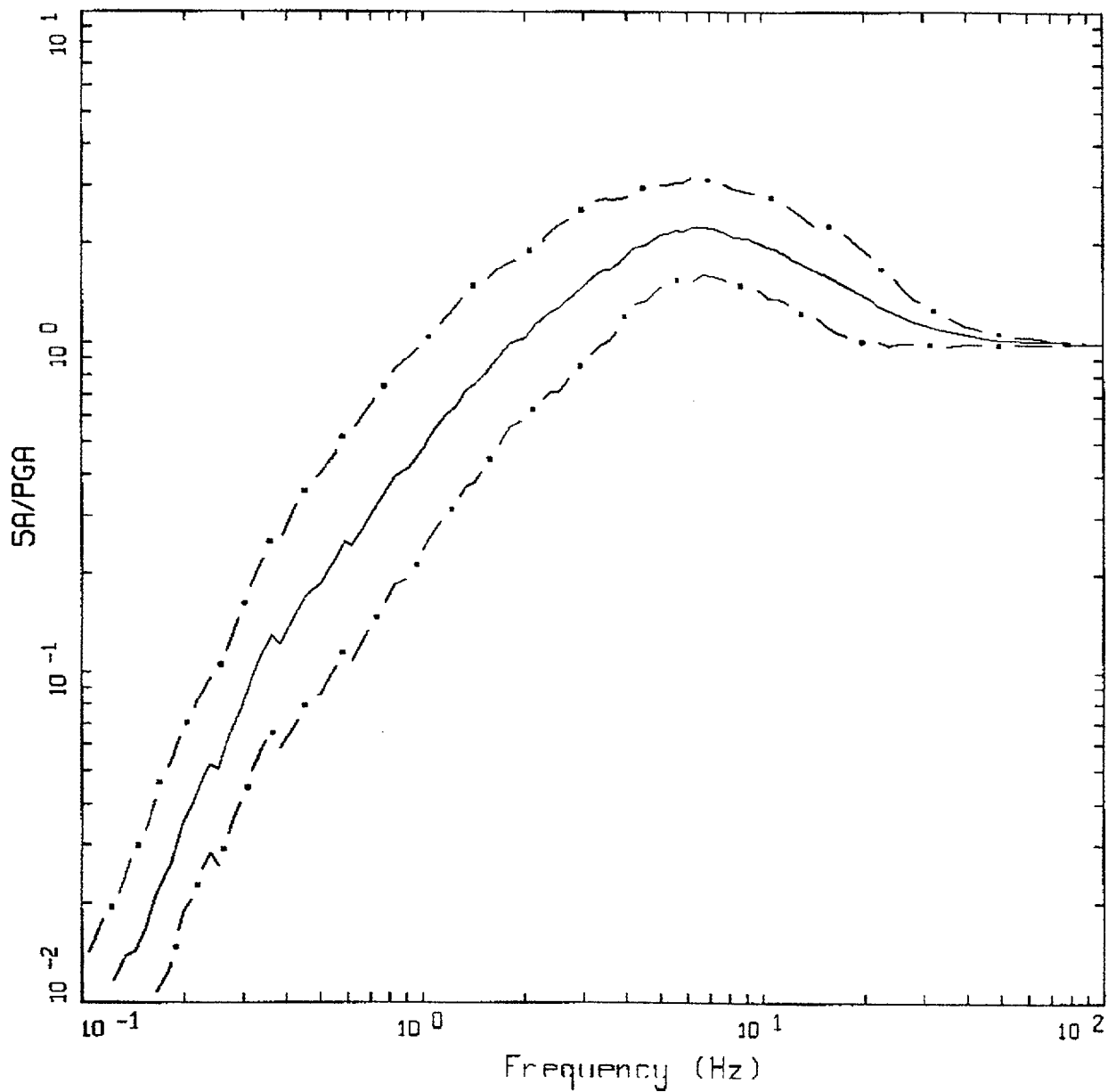
Figure C-5. Median $\pm 1 \sigma$ spectral shapes for $M = 6.5$, $R = 0-10$ km, horizontal WUS soil.



AVERAGE HORIZONTAL SPECTRA
 M=7.5 (7.0-7.0+), R=0-10 KM, SOIL
 AVERAGE M = 7.05, AVERAGE DISTANCE = 8.90 KM

LEGEND
 ————— 50TH PERCENTILE
 - - - - - 16TH PERCENTILE
 - . - . - 84TH PERCENTILE

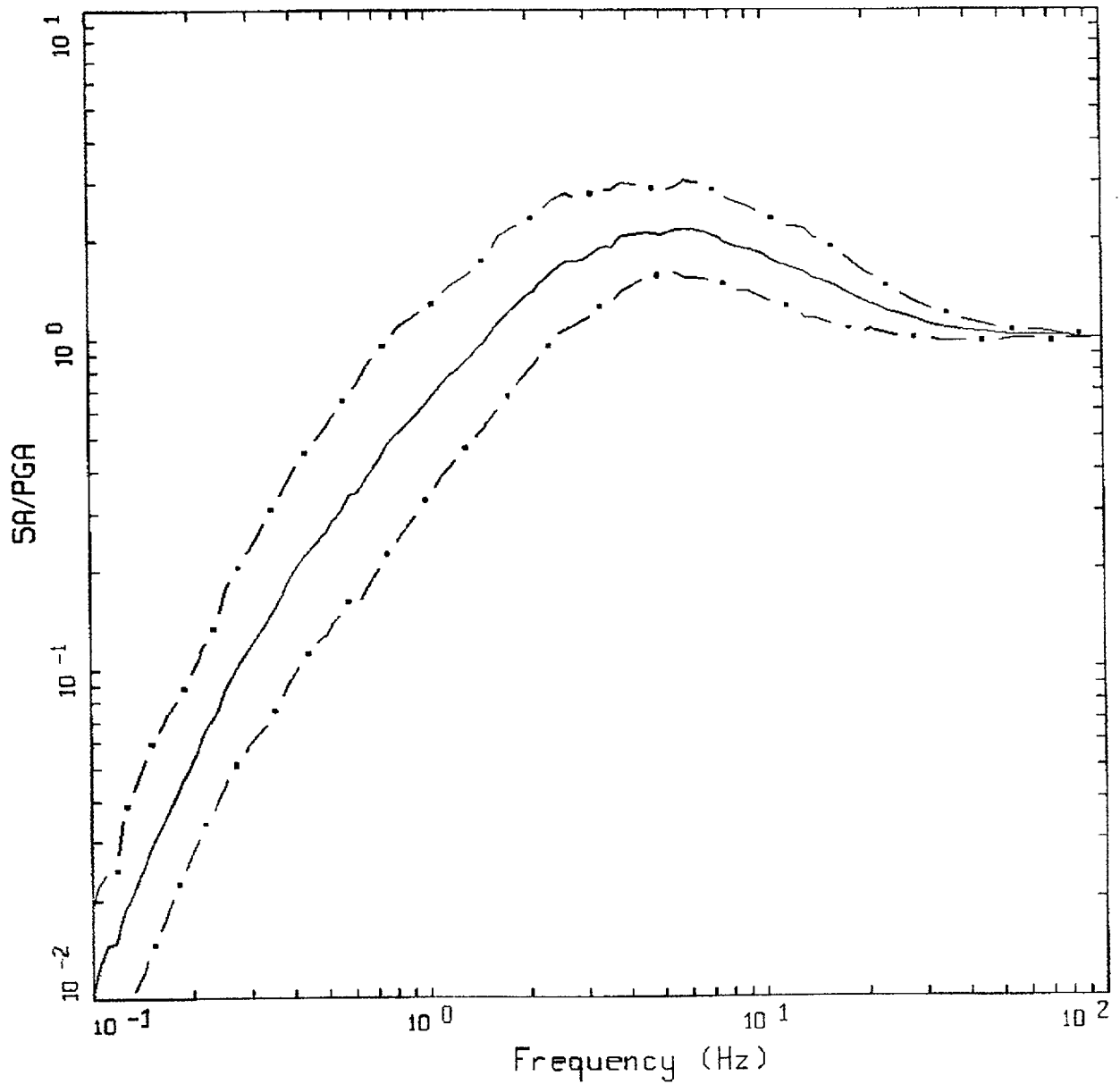
Figure C-6. Median $\pm 1 \sigma$ spectral shapes for $M \approx 7.5$, $R = 0-10$ km, horizontal WUS soil.



AVERAGE HORIZONTAL SPECTRA
 M=5.5 (5.0-6.0), R=10-50 KM, ROCK
 AVERAGE M = 5.57, AVERAGE DISTANCE = 21.80 KM

LEGEND
 ————— 50TH PERCENTILE
 - . - . 16TH PERCENTILE
 - . . - 84TH PERCENTILE

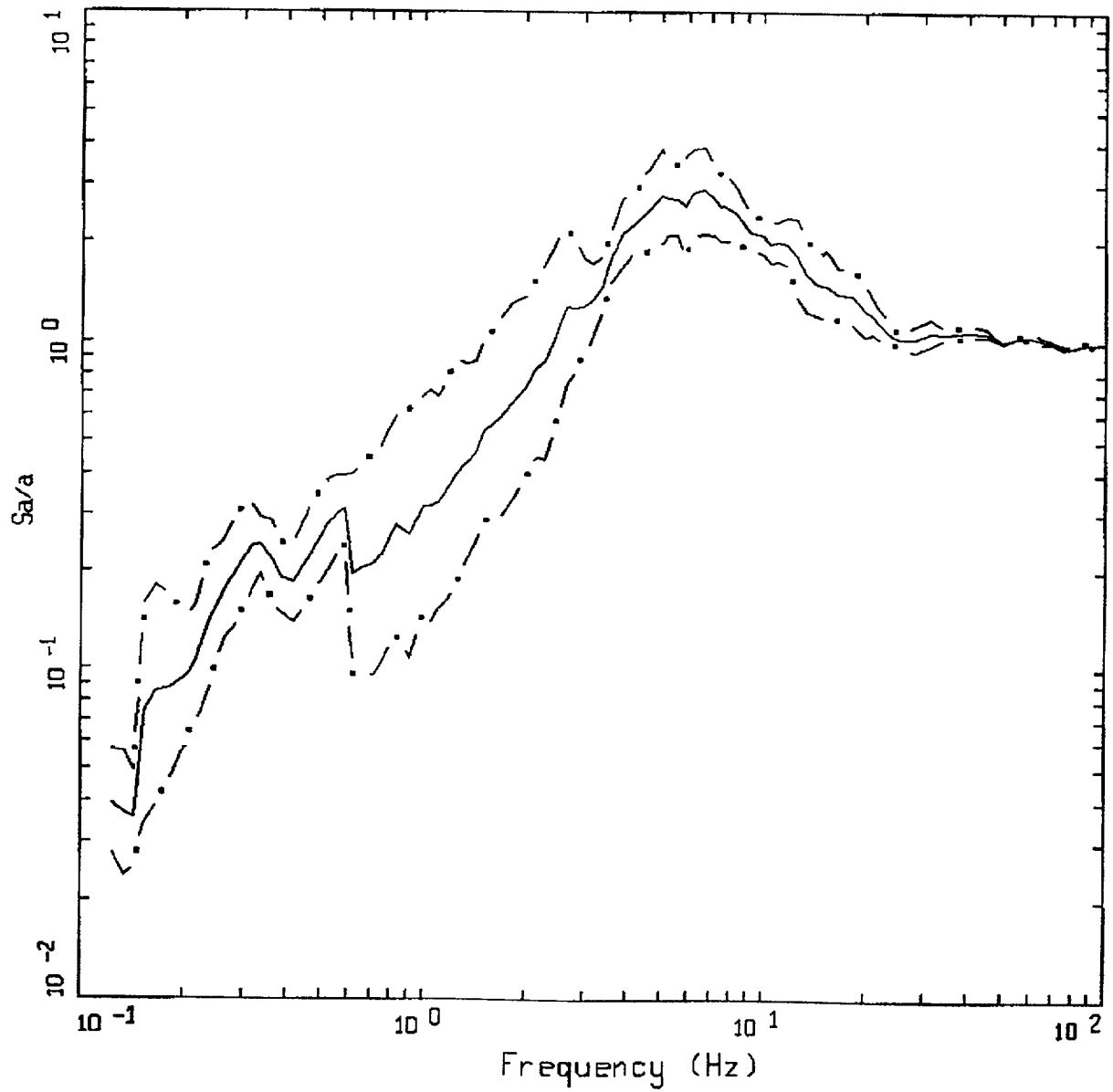
Figure C-7. Median $\pm 1 \sigma$ spectral shapes for $M \approx 5.5$, $R = 10-50$ km, horizontal WUS rock.



AVERAGE HORIZONTAL SPECTRA
 M=6.5 (6.0-7.0), R=10-50 KM, ROCK
 AVERAGE M = 6.43, AVERAGE DISTANCE = 30.28 KM

LEGEND
 — 50TH PERCENTILE
 - · - 16TH PERCENTILE
 - · · - 84TH PERCENTILE

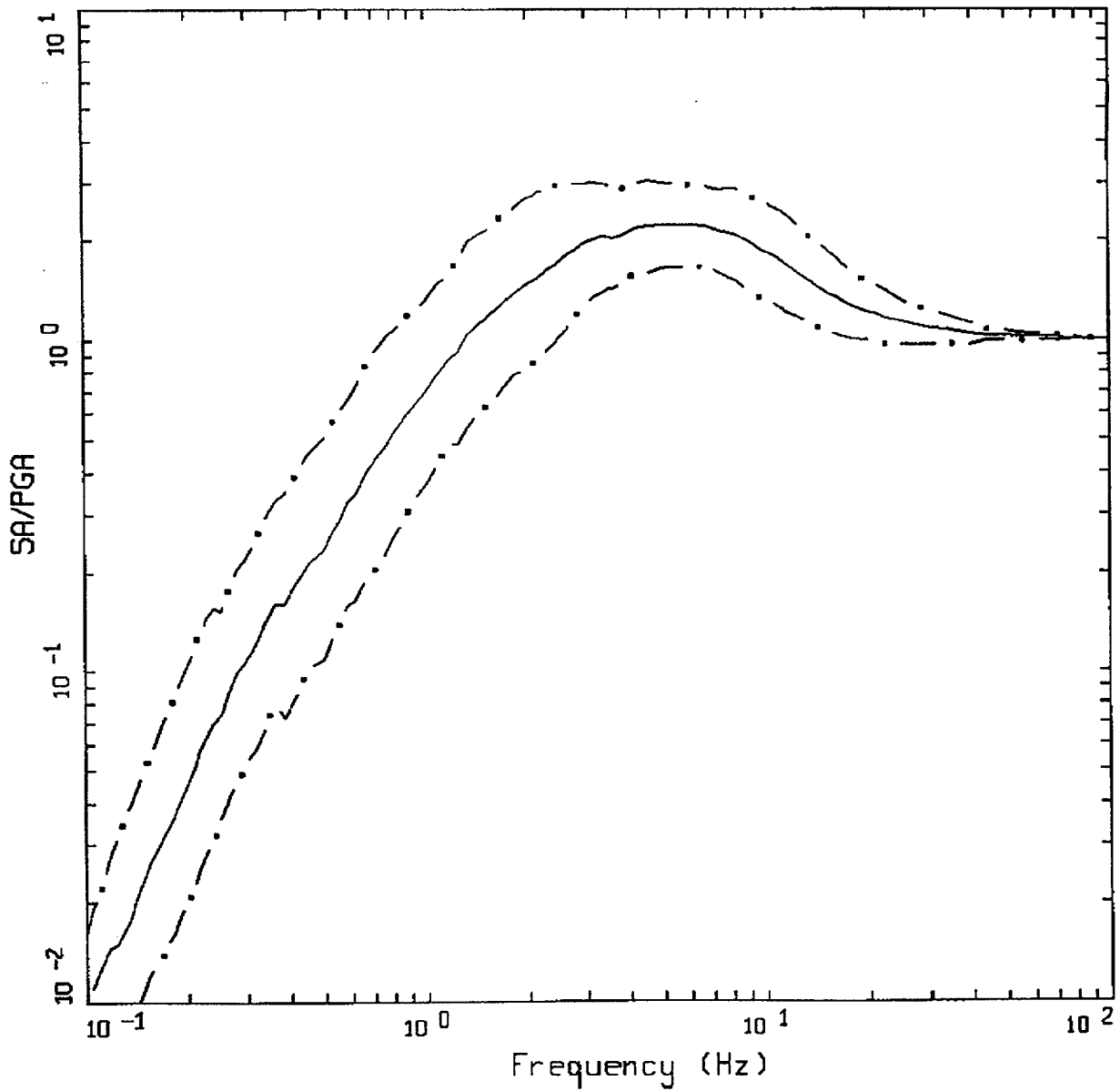
Figure C-8. Median $\pm 1 \sigma$ spectral shapes for $M \approx 6.5$, $R = 10-50$ km, horizontal WUS rock.



AVERAGE HORIZONTAL SPECTRA
 M=7.5 (7.0-7.0+), R=10-50 KM, ROCK
 AVERAGE M = 7.27, AVERAGE DISTANCE = 31.00 KM

LEGEND
 ————— 50TH PERCENTILE
 - · - · 16TH PERCENTILE
 - · · - 84TH PERCENTILE

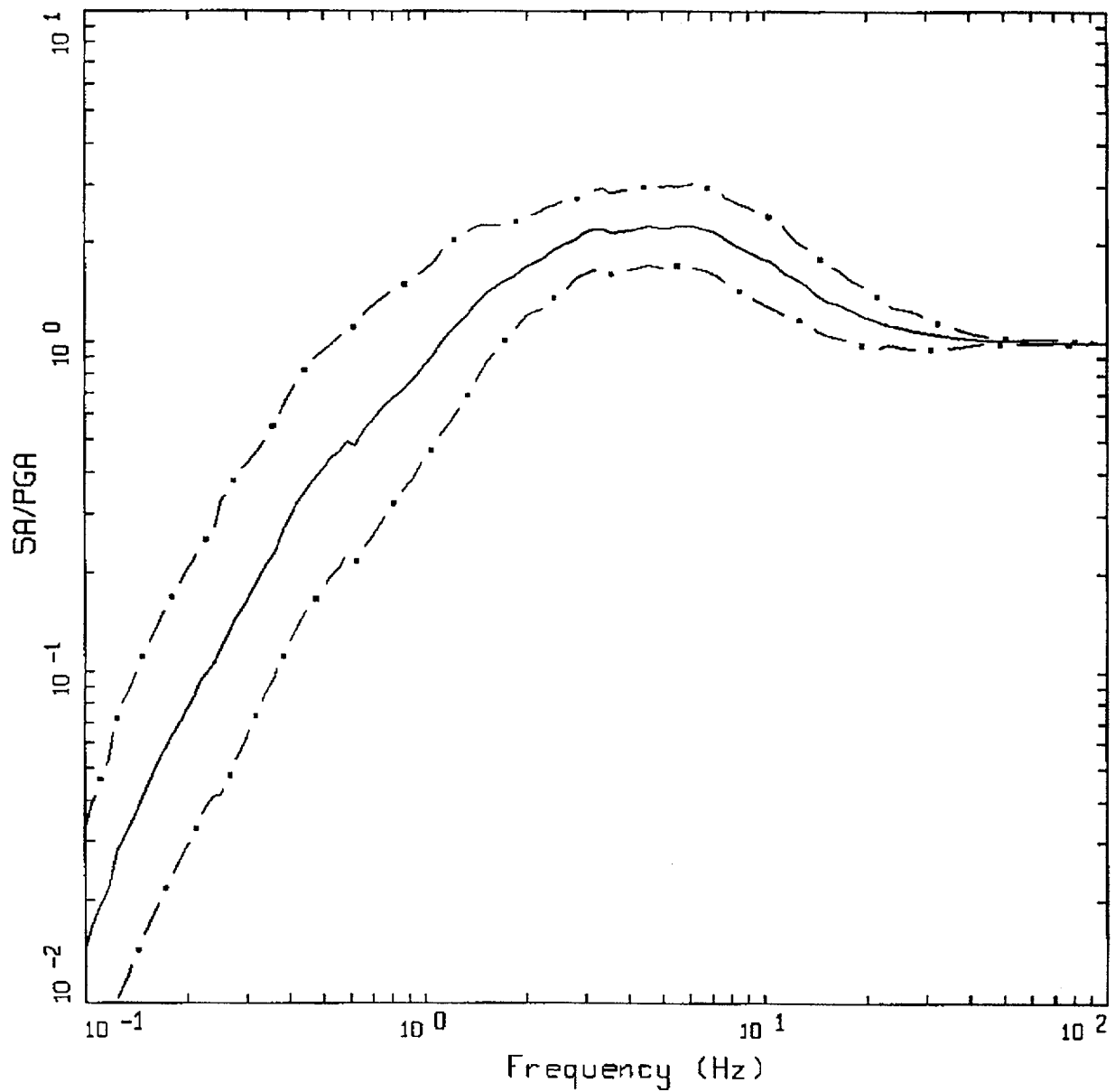
Figure C-9. Median $\pm 1 \sigma$ spectral shapes for $M \approx 7.5$, $R = 10-50$ km, horizontal WUS rock.



AVERAGE HORIZONTAL SPECTRA
 M=5.5 (5.0-6.0), R=10-50 KM, SOIL
 AVERAGE M = 5.69, AVERAGE DISTANCE = 21.82 KM

LEGEND
 — 50TH PERCENTILE
 - - - 16TH PERCENTILE
 - . - 84TH PERCENTILE

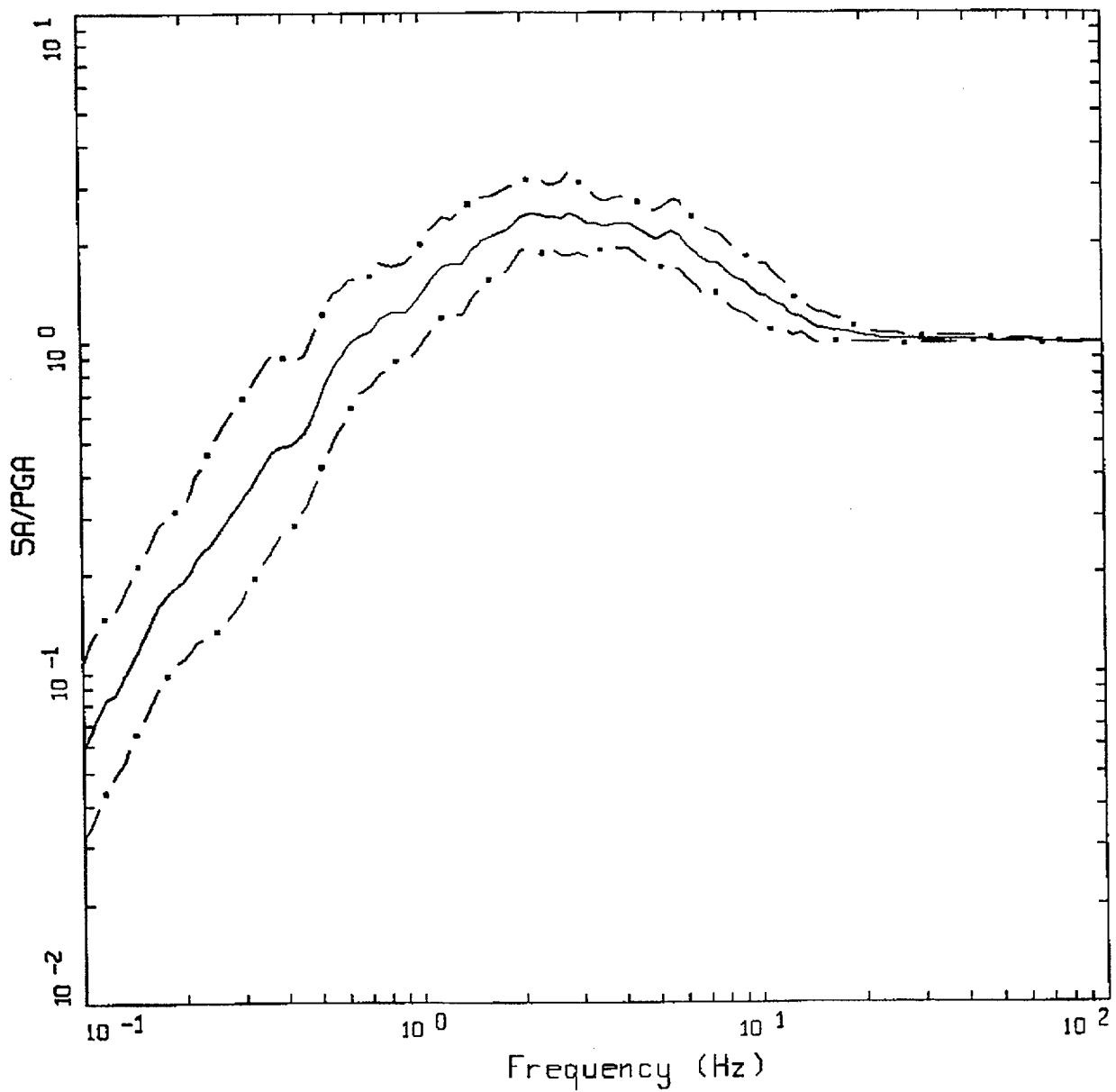
Figure C-10. Median $\pm 1 \sigma$ spectral shapes for $M \approx 5.5$, $R = 10-50$ km, horizontal WUS soil.



AVERAGE HORIZONTAL SPECTRA
 M=6.5 (6.0-7.0), R=10-50 KM, SOIL
 AVERAGE M = 6.35, AVERAGE DISTANCE = 28.27 KM

LEGEND
 ————— 50TH PERCENTILE
 - . - . 16TH PERCENTILE
 - . - . 84TH PERCENTILE

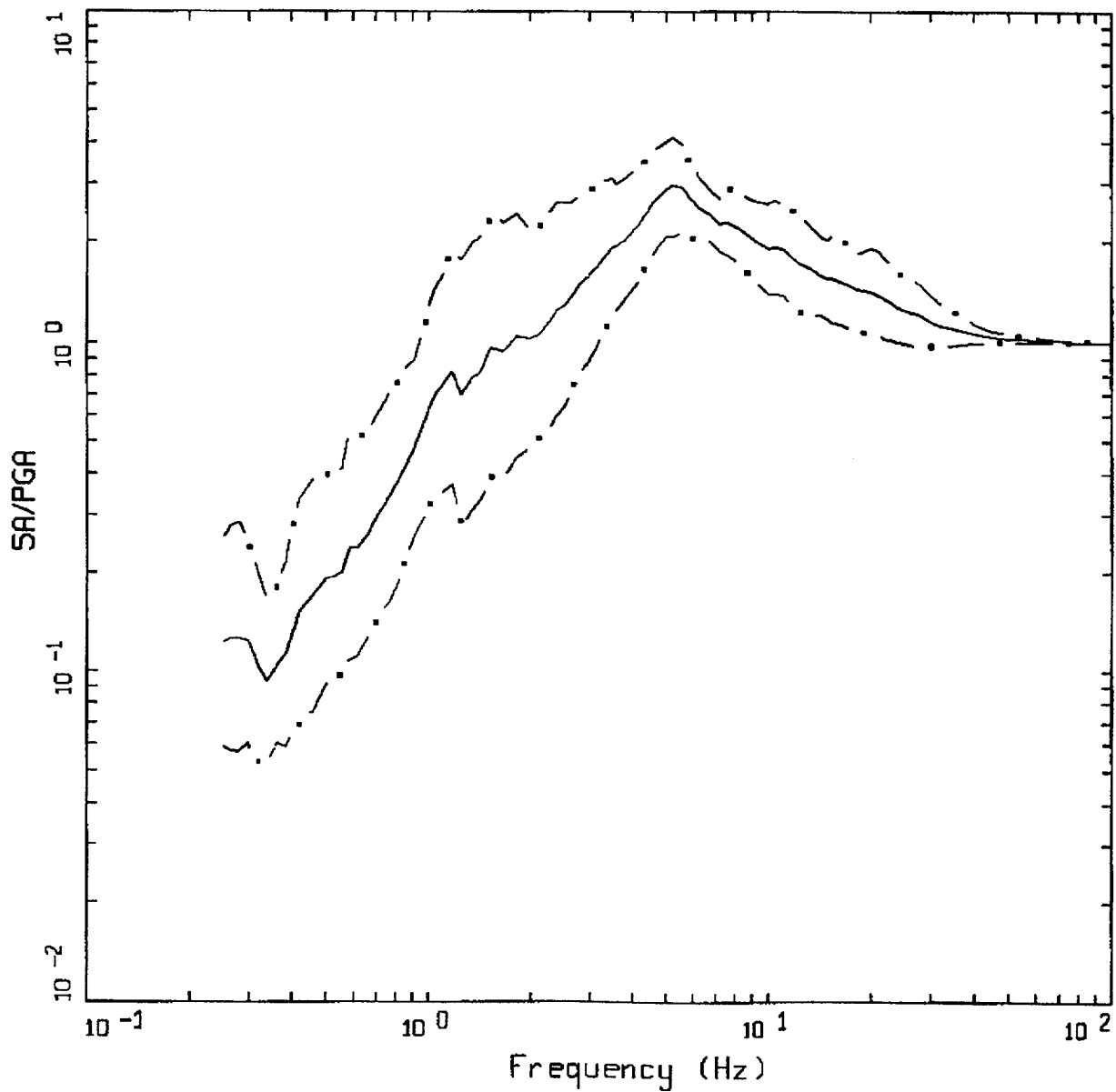
Figure C-11. Median $\pm 1 \sigma$ spectral shapes for $M \approx 6.5$, $R = 10-50$ km, horizontal WUS soil.



AVERAGE HORIZONTAL SPECTRA
 M=7.5 (7.0-7.0+), R=10-50 KM, SOIL
 AVERAGE M = 7.29, AVERAGE DISTANCE = 33.46 KM

LEGEND
 ————— 50TH PERCENTILE
 - - - - - 16TH PERCENTILE
 - . - . - 84TH PERCENTILE

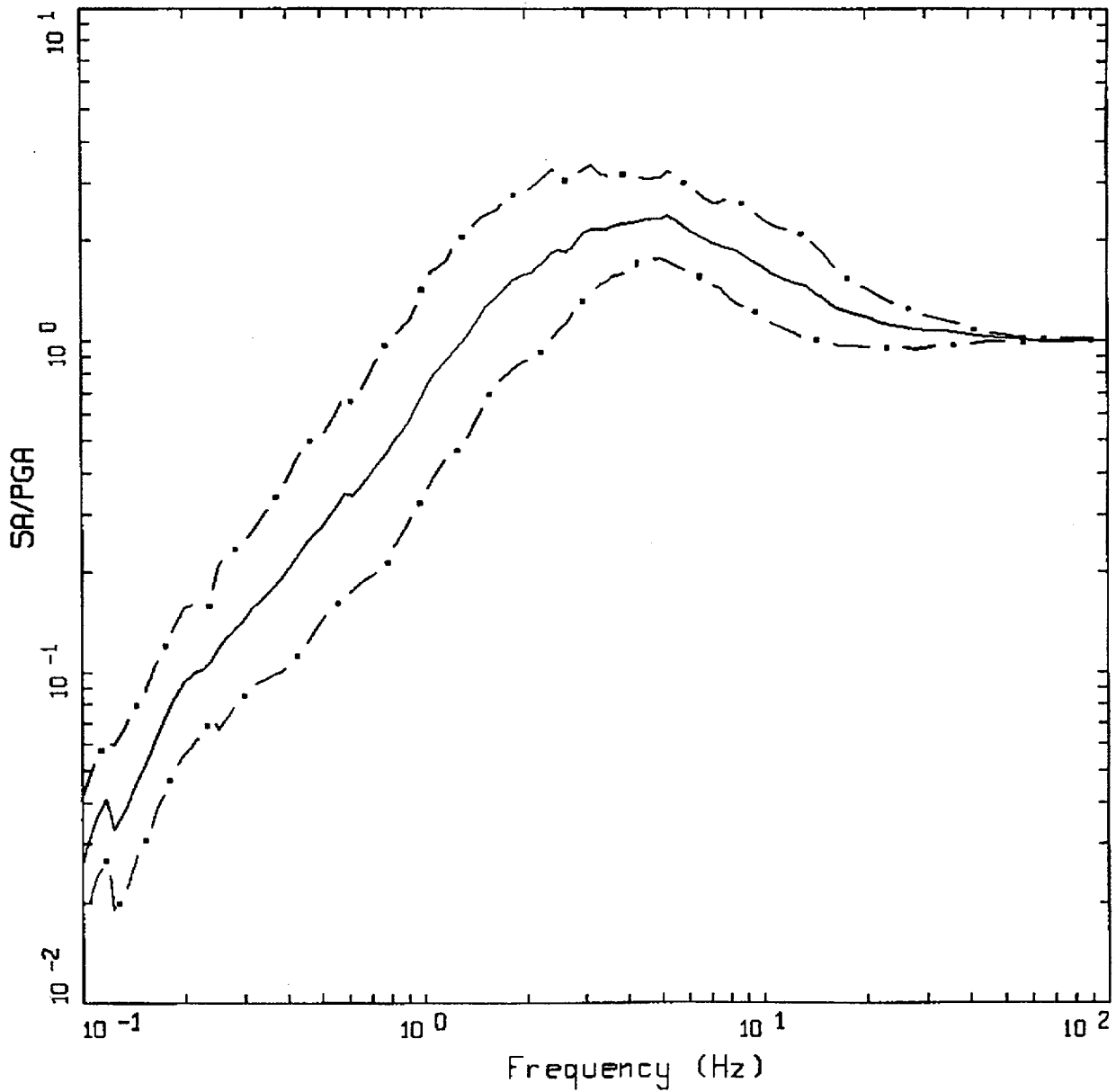
Figure C-12. Median $\pm 1 \sigma$ spectral shapes for $M \approx 7.5$, $R = 10-50$ km, horizontal WUS soil.



AVERAGE HORIZONTAL SPECTRA
 M=5.5 (5.0-6.0), R=50-100 KM, ROCK
 AVERAGE M = 5.91, AVERAGE DISTANCE = 64.27 KM

LEGEND
 ————— 50TH PERCENTILE
 - . - - 16TH PERCENTILE
 - . . - 84TH PERCENTILE

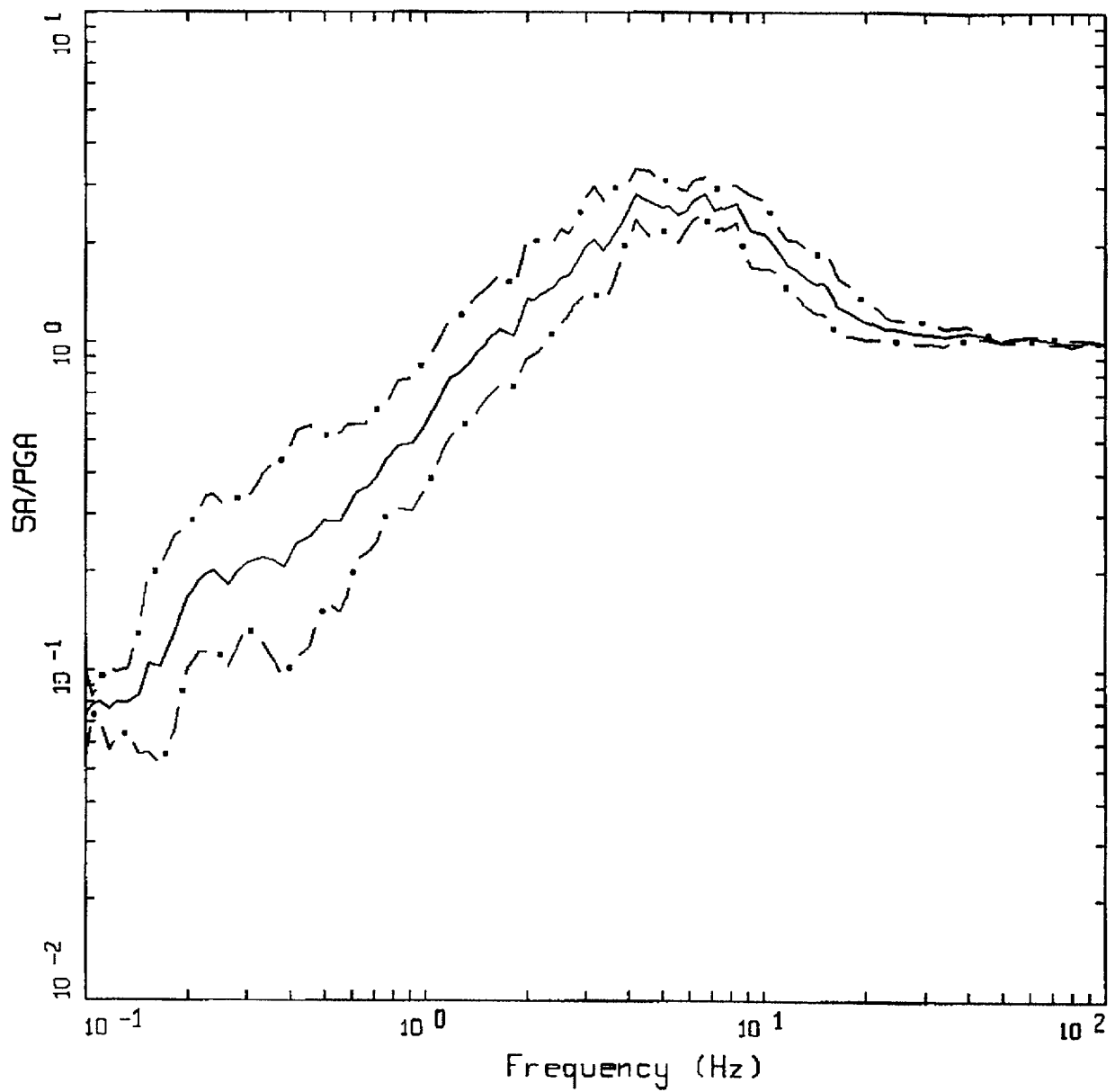
Figure C-13. Median $\pm 1 \sigma$ spectral shapes for $M \approx 5.5$, $R = 50-100$ km, horizontal, WUS rock.



AVERAGE HORIZONTAL SPECTRA
 M=6.5 (6.0-7.0), R=50-100 KM, ROCK
 AVERAGE M = 6.51, AVERAGE DISTANCE = 70.35 KM

LEGEND
 ——— 50TH PERCENTILE
 - - - 16TH PERCENTILE
 - · - 84TH PERCENTILE

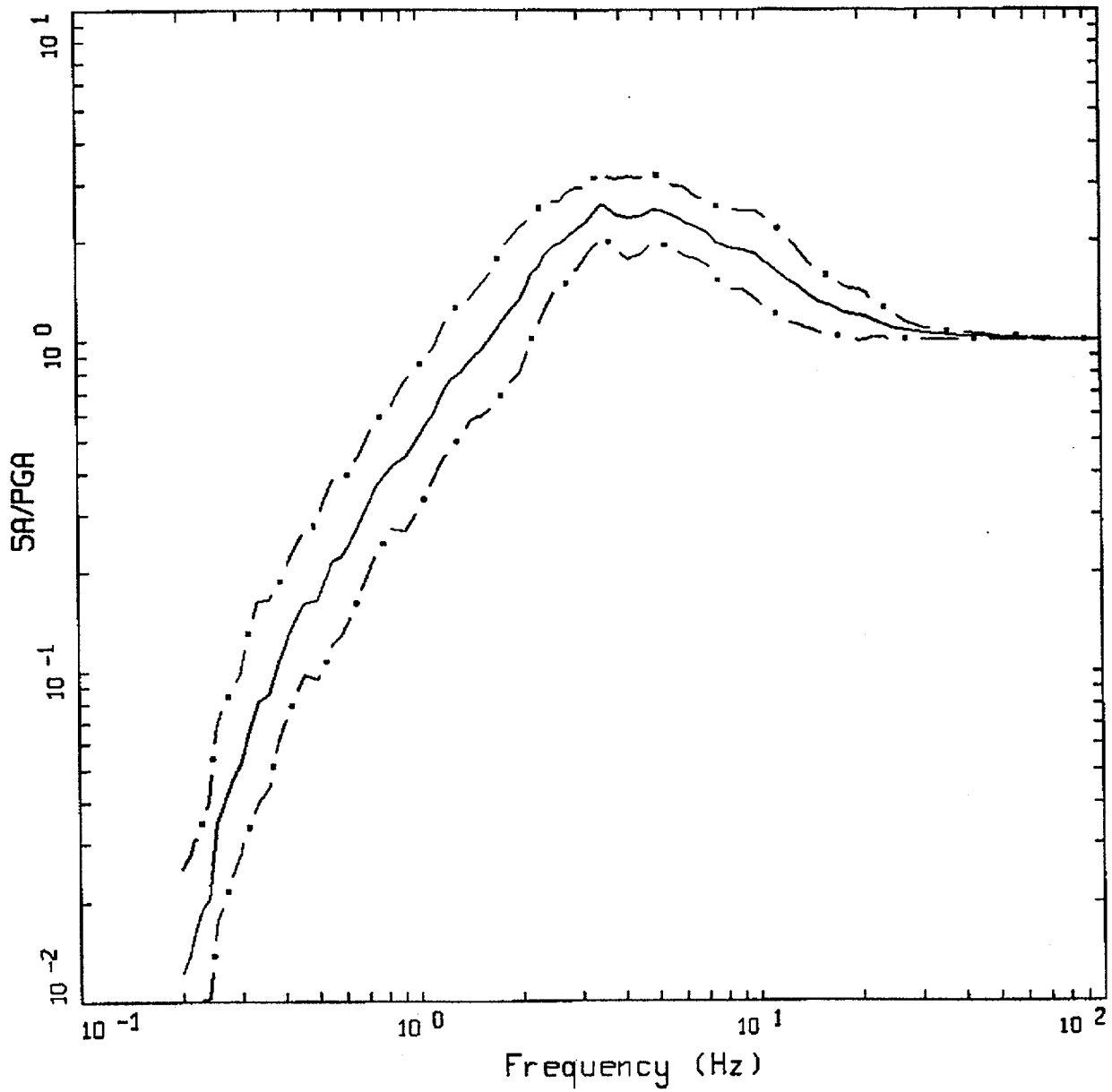
Figure C-14. Median $\pm 1 \sigma$ spectral shapes for $M \approx 6.5$, $R = 50-100$ km, horizontal, WUS rock.



AVERAGE HORIZONTAL SPECTRA
 M=7.5 (7.0-7.0+), R=50-100 KM, ROCK
 AVERAGE M = 7.32, AVERAGE DISTANCE = 81.46 KM

LEGEND
 — 50TH PERCENTILE
 - · - 16TH PERCENTILE
 - · - 84TH PERCENTILE

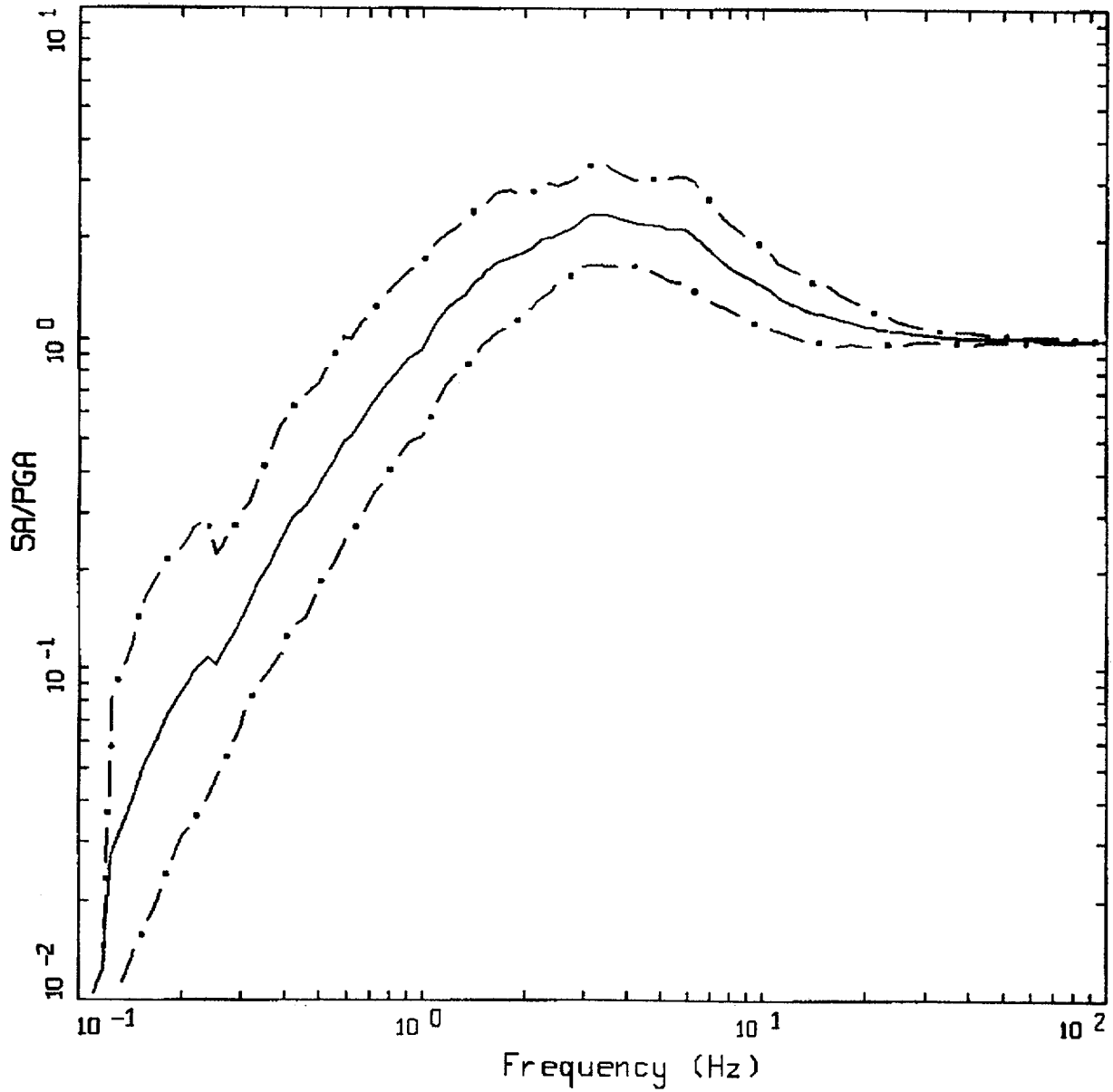
Figure C-15. Median $\pm 1 \sigma$ spectral shapes for $M \approx 7.5$, $R = 50-100$ km, horizontal, WUS rock.



AVERAGE HORIZONTAL SPECTRA
 M=5.5 (5.0-6.0), R=50-100 KM, SOIL
 AVERAGE M = 5.80, AVERAGE DISTANCE = 67.22 KM

LEGEND
 ————— 50TH PERCENTILE
 - . - - 16TH PERCENTILE
 - . - - 84TH PERCENTILE

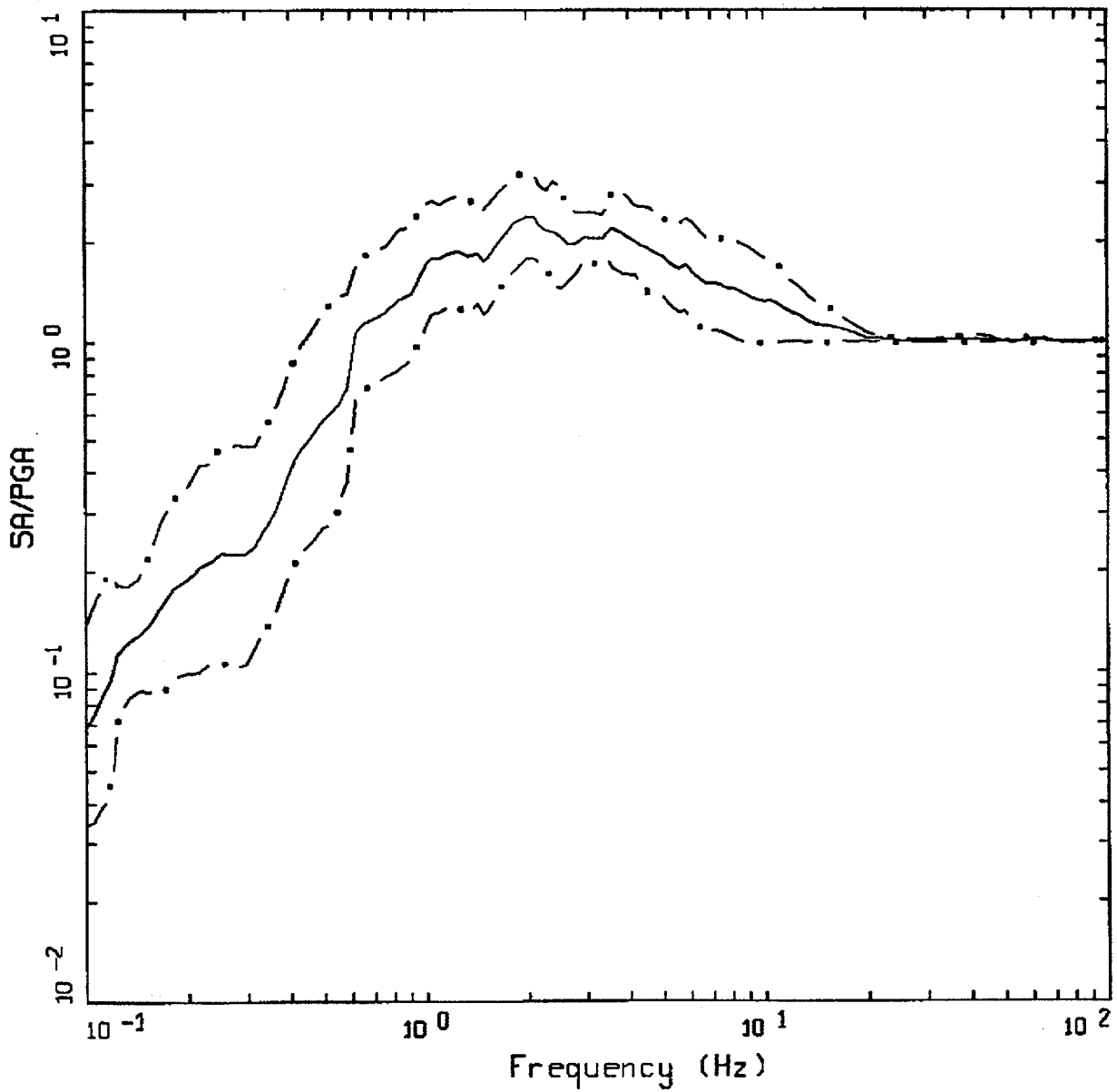
Figure C-16. Median $\pm 1 \sigma$ spectral shapes for $M \sim 5.5$, $R = 50-100$ km, horizontal, WUS soil.



AVERAGE HORIZONTAL SPECTRA
 M=6.5 (6.0-7.0), R=50-100 KM, SOIL
 AVERAGE M = 6.49, AVERAGE DISTANCE = 67.34 KM

LEGEND
 — 50TH PERCENTILE
 - - - 16TH PERCENTILE
 - . - 84TH PERCENTILE

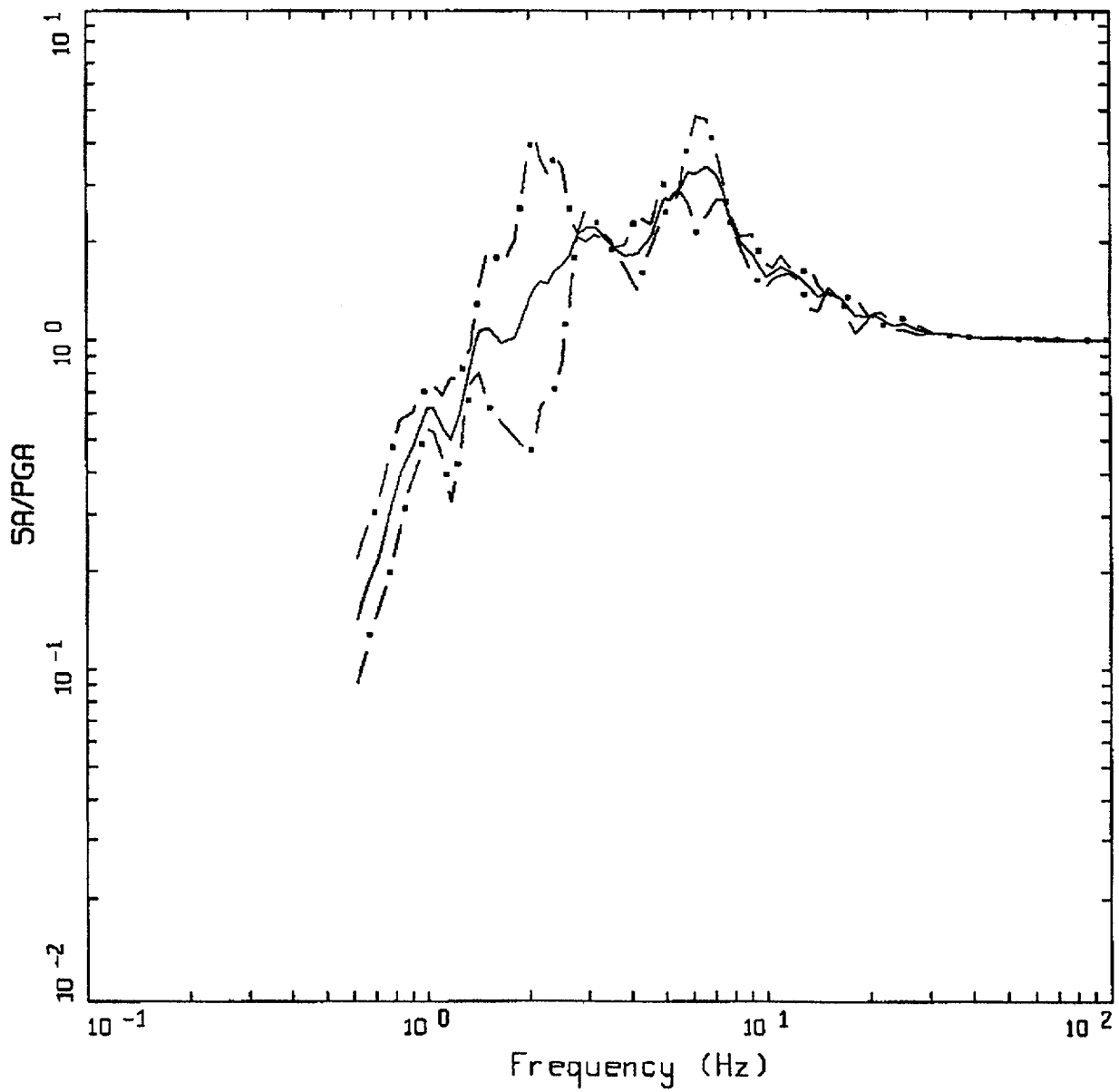
Figure C-17. Median $\pm 1 \sigma$ spectral shapes for $M = 6.5$, $R = 50-100$ km, horizontal, WUS soil.



AVERAGE HORIZONTAL SPECTRA
 M=7.5 (7.0-7.0+), R=50-100 KM, SOIL
 AVERAGE M = 7.31, AVERAGE DISTANCE = 76.57 KM

LEGEND
 — 50TH PERCENTILE
 - - 16TH PERCENTILE
 - . - 84TH PERCENTILE

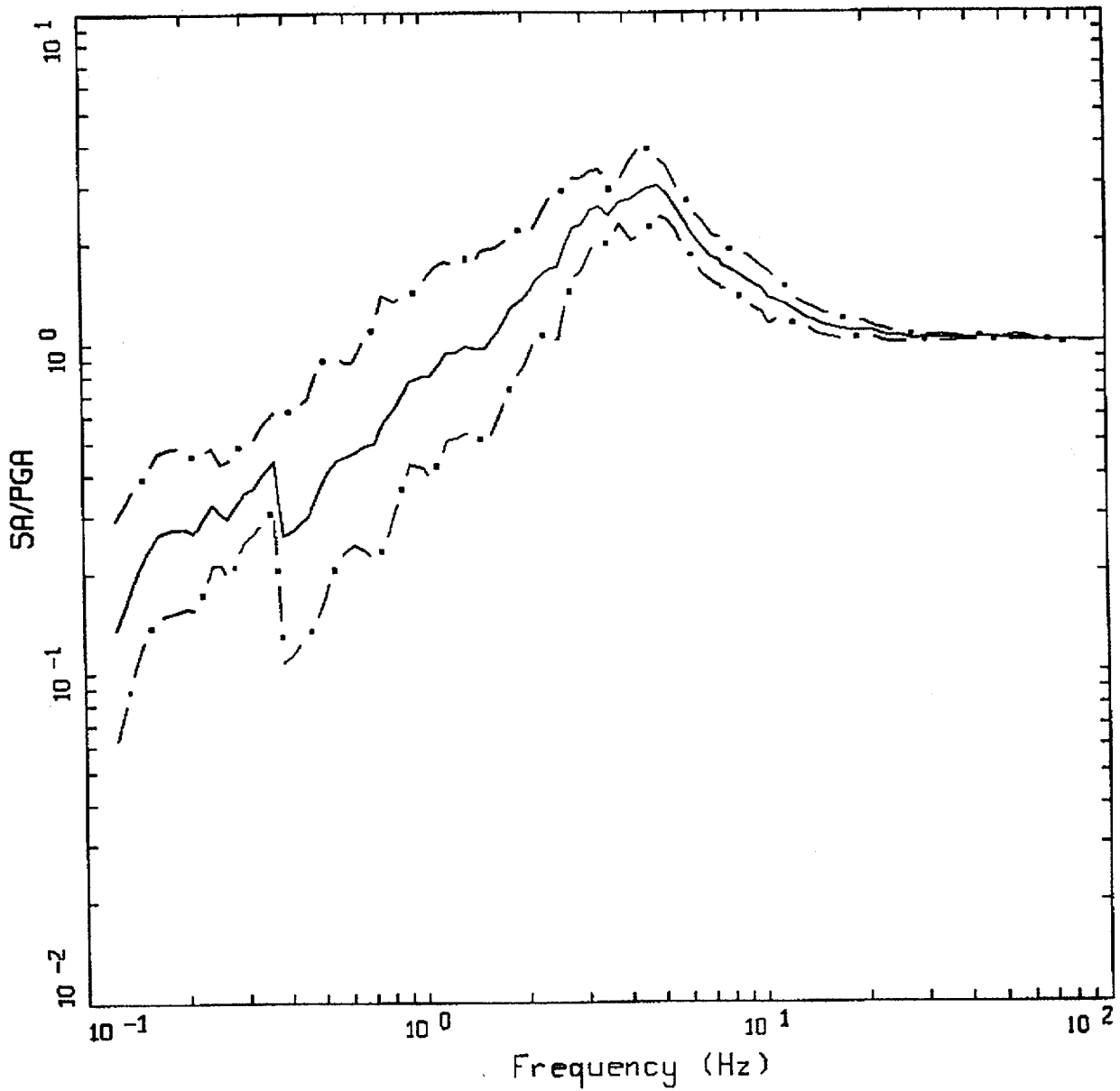
Figure C-18. Median $\pm 1 \sigma$ spectral shapes for $M = 7.5$, $R = 50-100$ km, horizontal, WUS soil.



AVERAGE HORIZONTAL SPECTRA
 M=5.5 (5.0-6.0), R=100-200 KM, ROCK
 AVERAGE M = 5.40, AVERAGE DISTANCE = 107.80 KM

LEGEND
 ————— 50TH PERCENTILE
 - - - - - 16TH PERCENTILE
 - . - . - 84TH PERCENTILE

Figure C-19. Median $\pm 1 \sigma$ spectral shapes for $M \approx 5.5$, $R = 100-200$ km, horizontal, WUS rock.



AVERAGE HORIZONTAL SPECTRA
 M=6.5 (6.0-7.0), R=100-200 KM, ROCK
 AVERAGE M = 6.64, AVERAGE DISTANCE = 114.57 KM

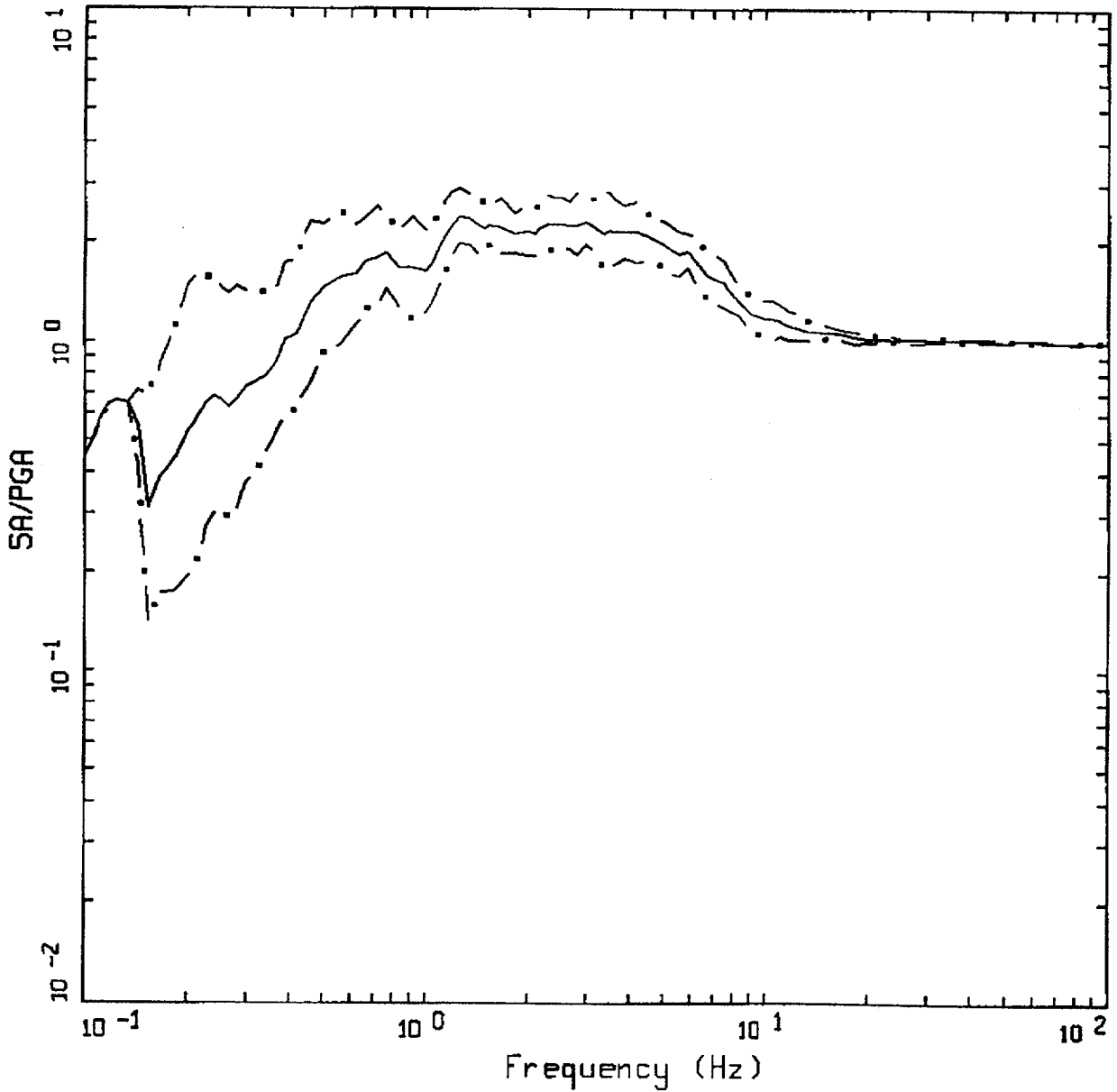
LEGEND

— 50TH PERCENTILE

- . - 16TH PERCENTILE

- . - 84TH PERCENTILE

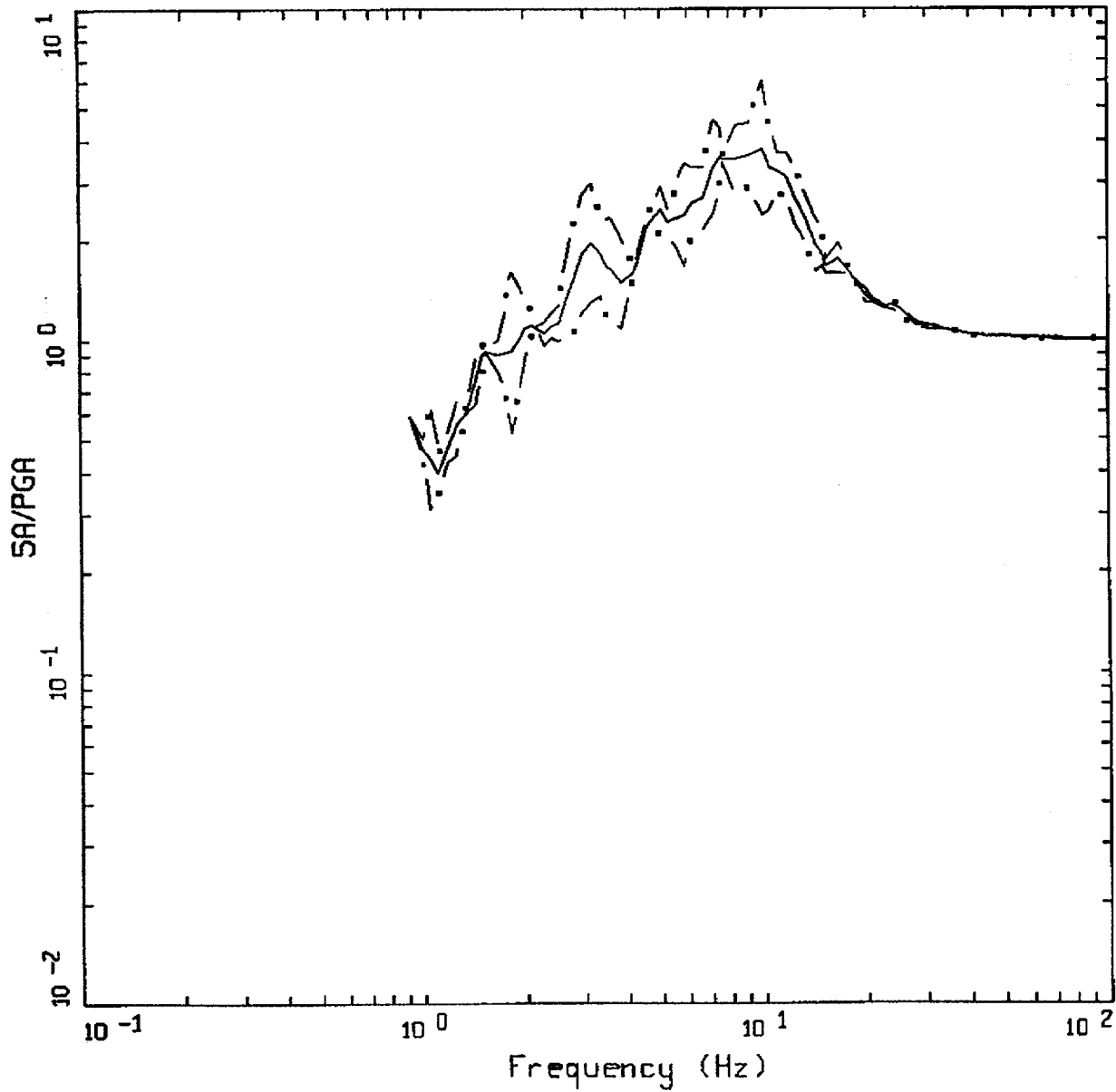
Figure C-20. Median $\pm 1 \sigma$ spectral shapes for $M \approx 6.5$, $R = 100-200$ km, horizontal, WUS rock.



AVERAGE HORIZONTAL SPECTRA
 M=7.5 (7.0-7.0+), R=100-200 KM, ROCK
 AVERAGE M = 7.30, AVERAGE DISTANCE = 152.01 KM

LEGEND
 — 50TH PERCENTILE
 - · - 16TH PERCENTILE
 - · · - 84TH PERCENTILE

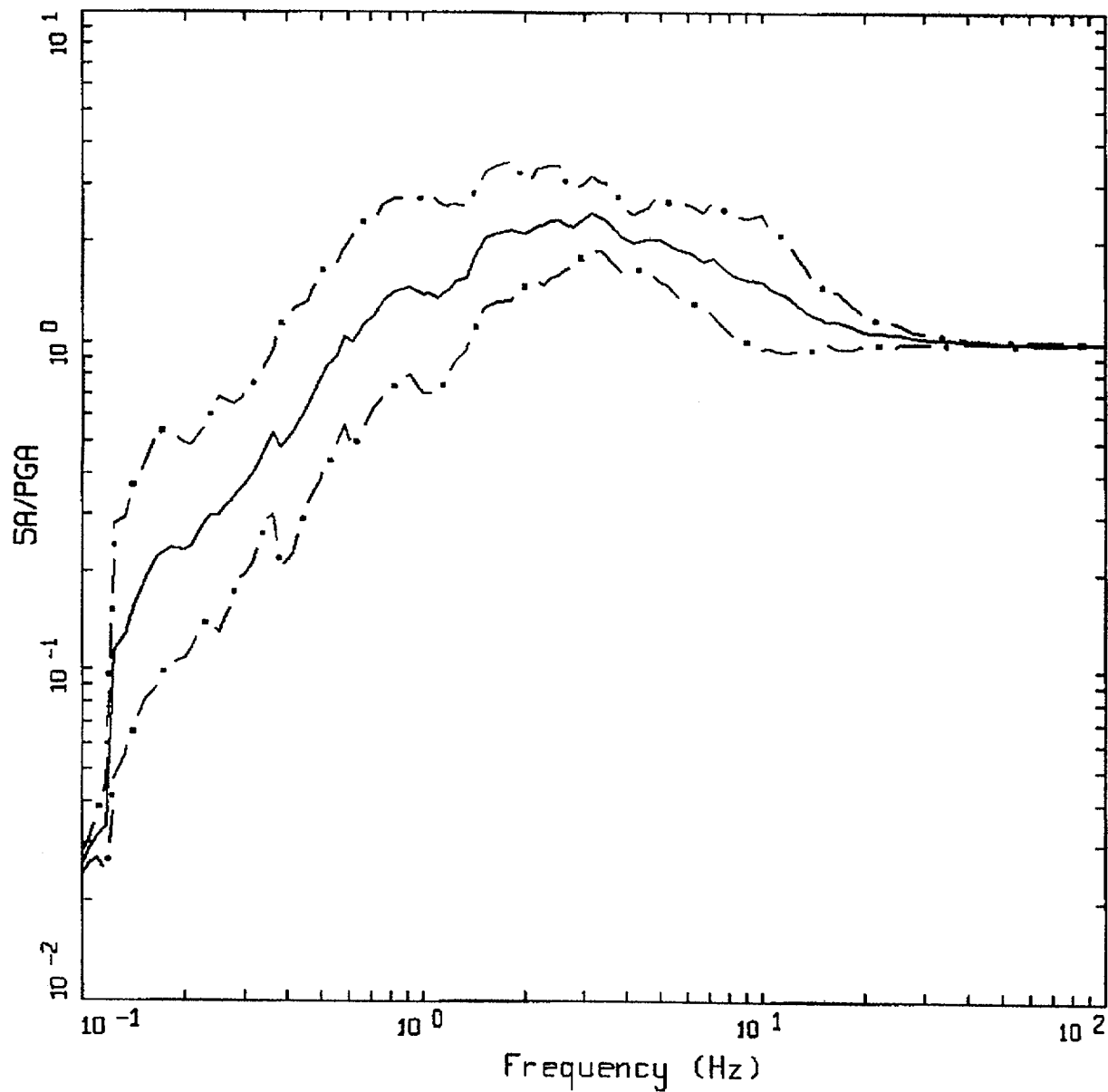
Figure C-21. Median $\pm 1 \sigma$ spectral shapes for $M \approx 7.5$, $R = 100-200$ km, horizontal, WUS rock.



AVERAGE HORIZONTAL SPECTRA
 M=5.5 (5.0-6.0), R=100-200 KM, SOIL
 AVERAGE M = 6.0, AVERAGE DISTANCE = 105.00 KM

LEGEND
 ————— 50TH PERCENTILE
 - - - - - 16TH PERCENTILE
 - . - . - 84TH PERCENTILE

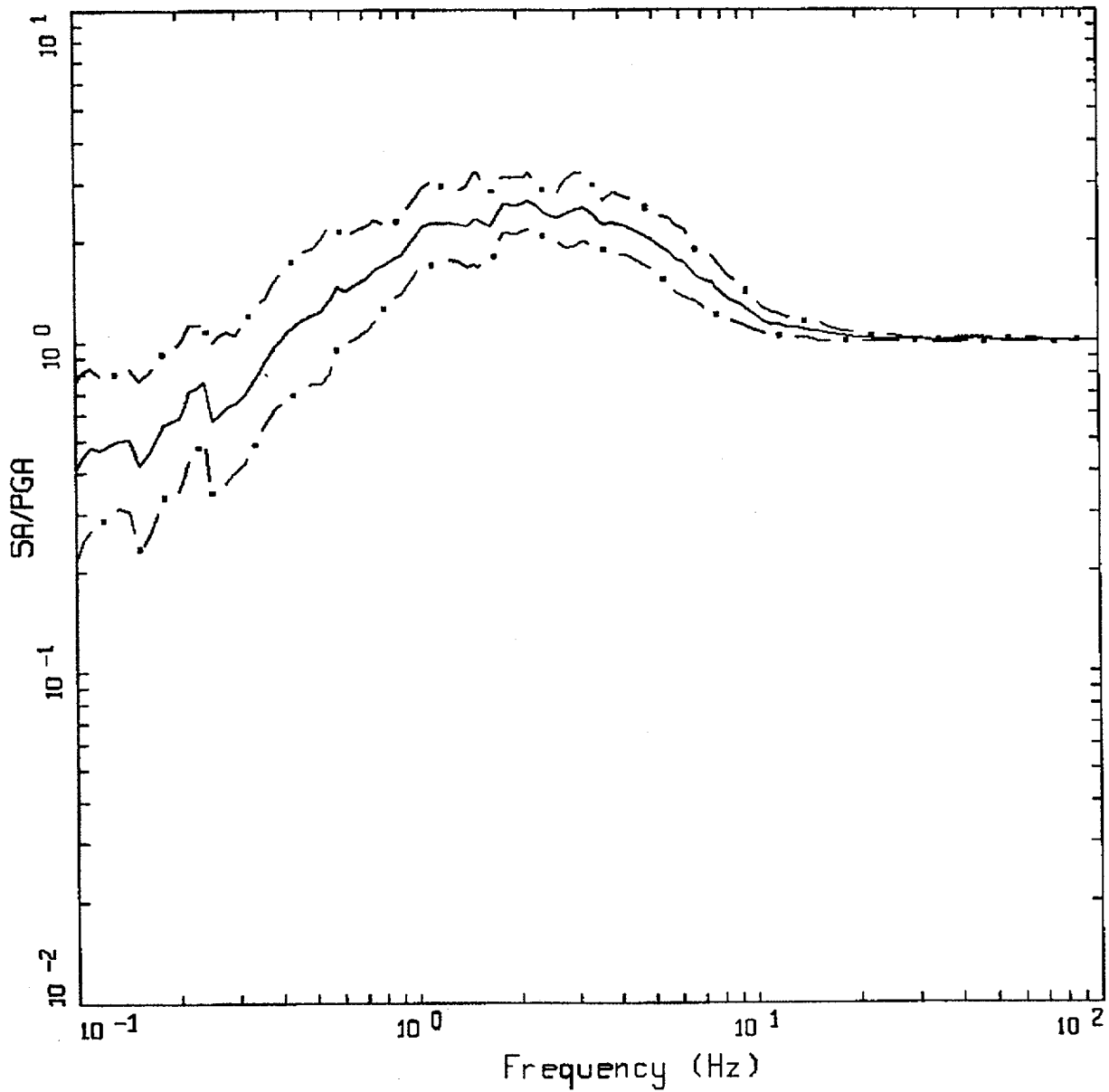
Figure C-22. Median $\pm 1 \sigma$ spectral shapes for M = 5.5, R = 100-200 km, horizontal, WUS soil.



AVERAGE HORIZONTAL SPECTRA
 M=6.5 (6.0-7.0), R=100-200 KM, SOIL
 AVERAGE M = 6.64, AVERAGE DISTANCE = 132.97 KM

LEGEND
 ————— 50TH PERCENTILE
 - - - - - 16TH PERCENTILE
 - . - . - 84TH PERCENTILE

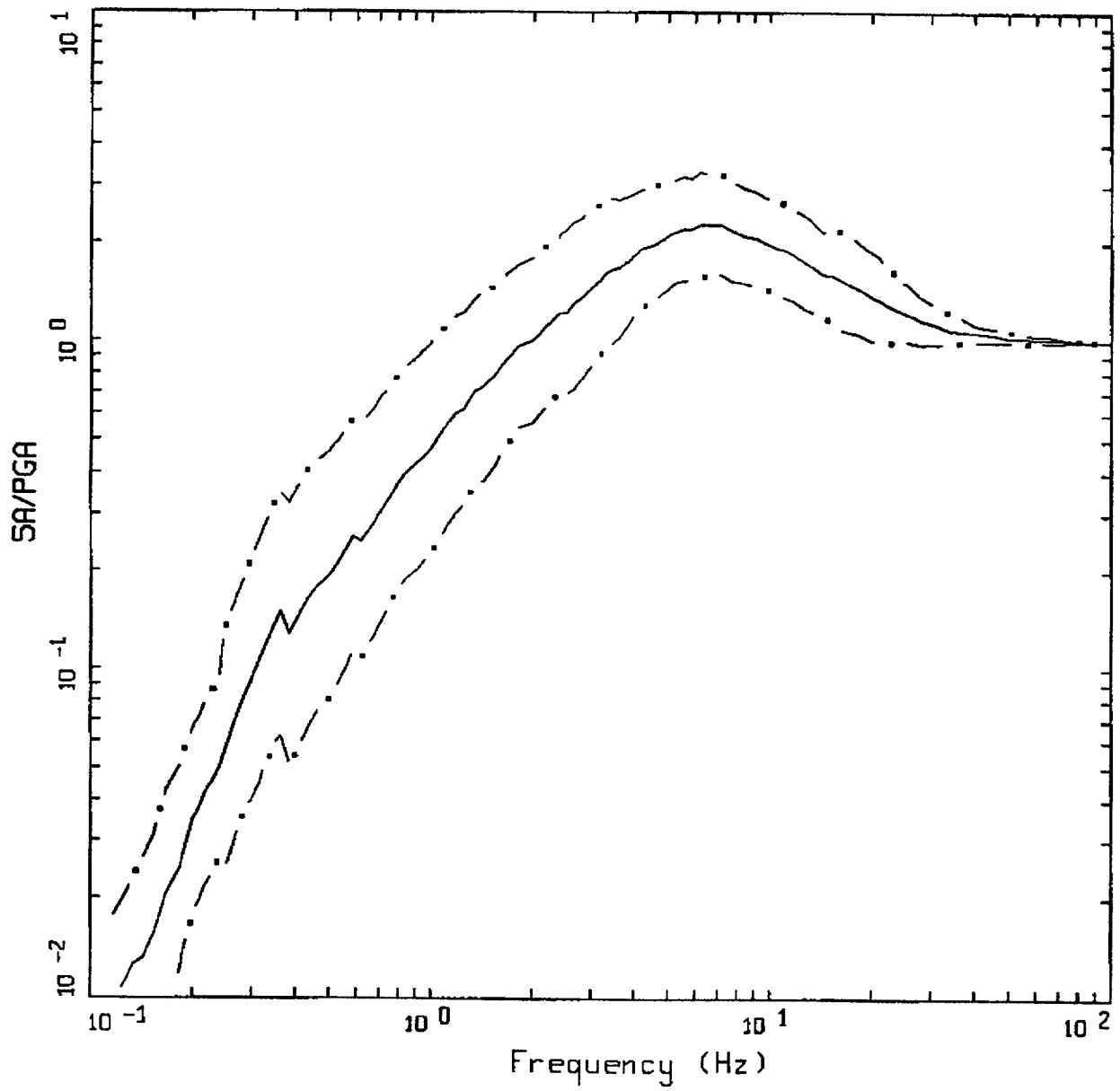
Figure C-23. Median $\pm 1 \sigma$ spectral shapes for $M \approx 6.5$, $R = 100-200$ km, horizontal, WUS soil.



AVERAGE HORIZONTAL SPECTRA
 M=7.5 (7.0-7.0+), R=100-200 KM, SOIL
 AVERAGE M = 7.31, AVERAGE DISTANCE = 147.07 KM

LEGEND
 ——— 50TH PERCENTILE
 - . - 16TH PERCENTILE
 - . - 84TH PERCENTILE

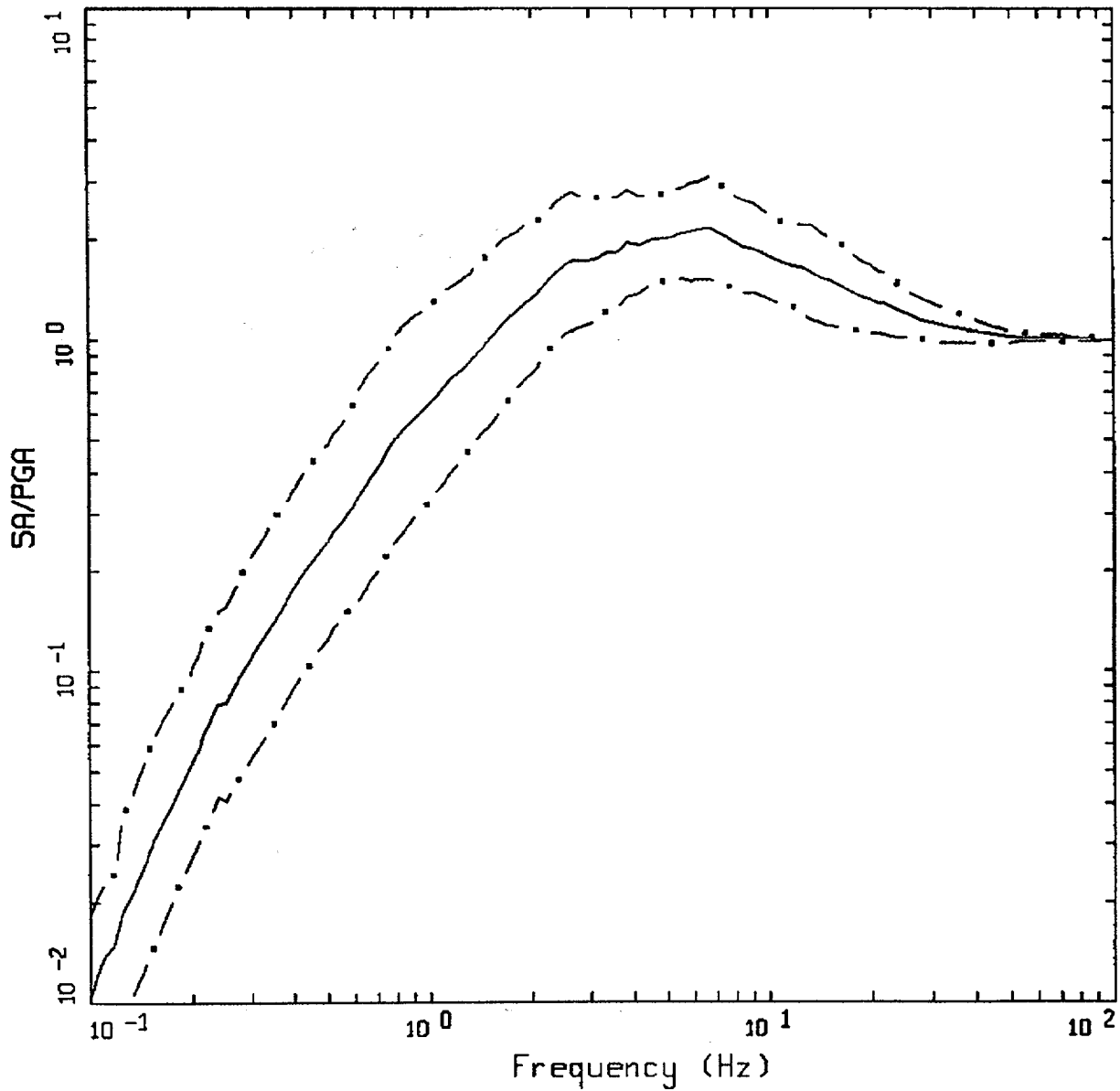
Figure C-24. Median $\pm 1 \sigma$ spectral shapes for $M \approx 7.5$, $R = 100-200$ km, horizontal, WUS soil.



AVERAGE HORIZONTAL SPECTRA
 M=5.5 (5.0-6.0), R=0-50 KM, ROCK
 AVERAGE M = 5.57, AVERAGE DISTANCE = 19.91 KM

LEGEND
 ——— 50TH PERCENTILE
 - . - 16TH PERCENTILE
 - . - 84TH PERCENTILE

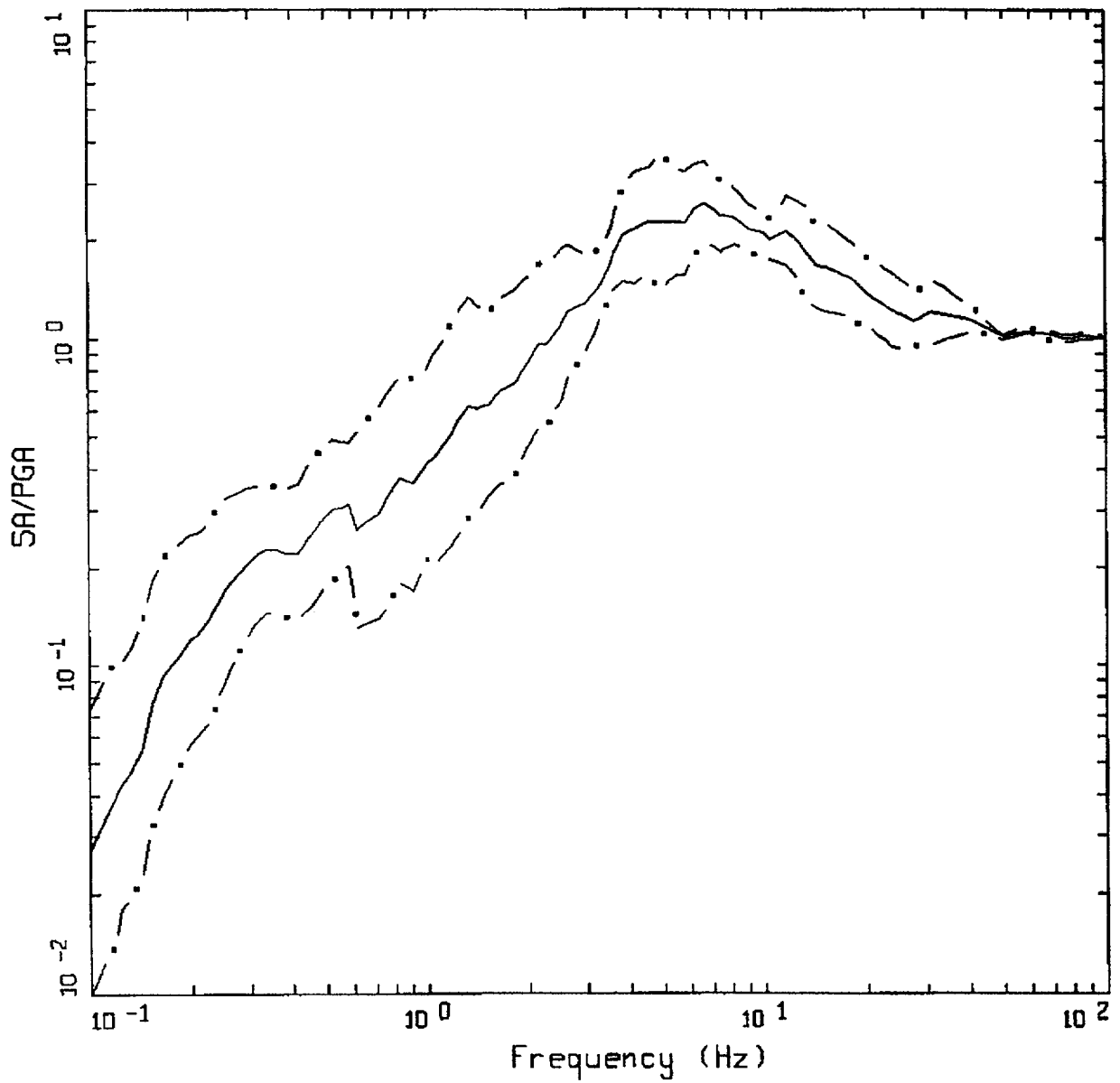
Figure C-25. Median $\pm 1 \sigma$ spectral shapes for $M \approx 5.5$, $R = 0-50$ km, horizontal, WUS rock.



AVERAGE HORIZONTAL SPECTRA
 M=6.5 (6.0-7.0), R=0-50 KM, ROCK
 AVERAGE M = 6.44, AVERAGE DISTANCE = 27.39 KM

LEGEND
 ——— 50TH PERCENTILE
 - - - 16TH PERCENTILE
 - . - 84TH PERCENTILE

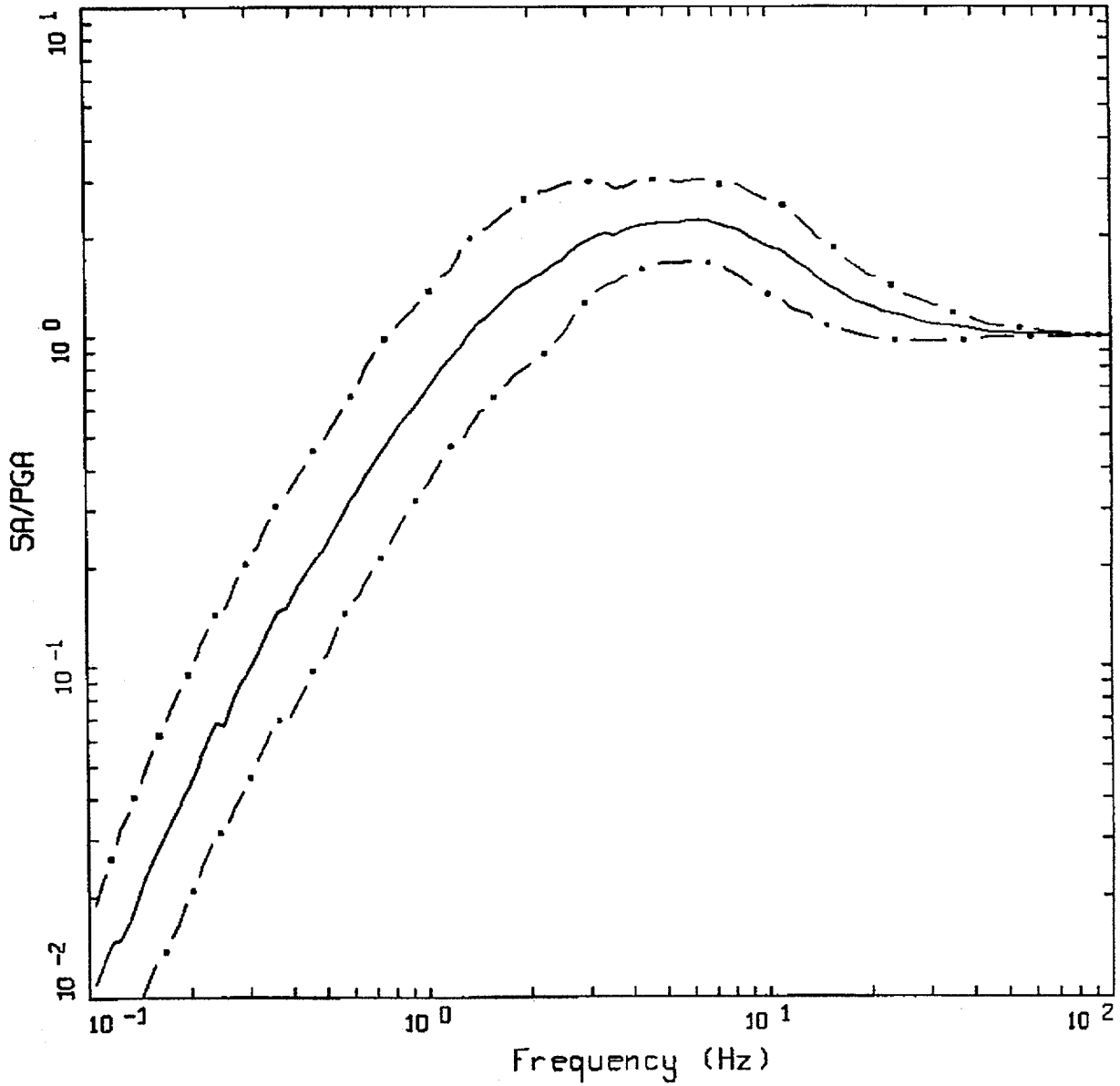
Figure C-26. Median $\pm 1 \sigma$ spectral shapes for M \approx 6.5, R = 0-50 km, horizontal, WUS rock.



AVERAGE HORIZONTAL SPECTRA
 M=7.5 (7.0-7.0+), R=0-50 KM, ROCK
 AVERAGE M = 7.27, AVERAGE DISTANCE = 17.60 KM

LEGEND
 ————— 50TH PERCENTILE
 - . - . 16TH PERCENTILE
 - . . - 84TH PERCENTILE

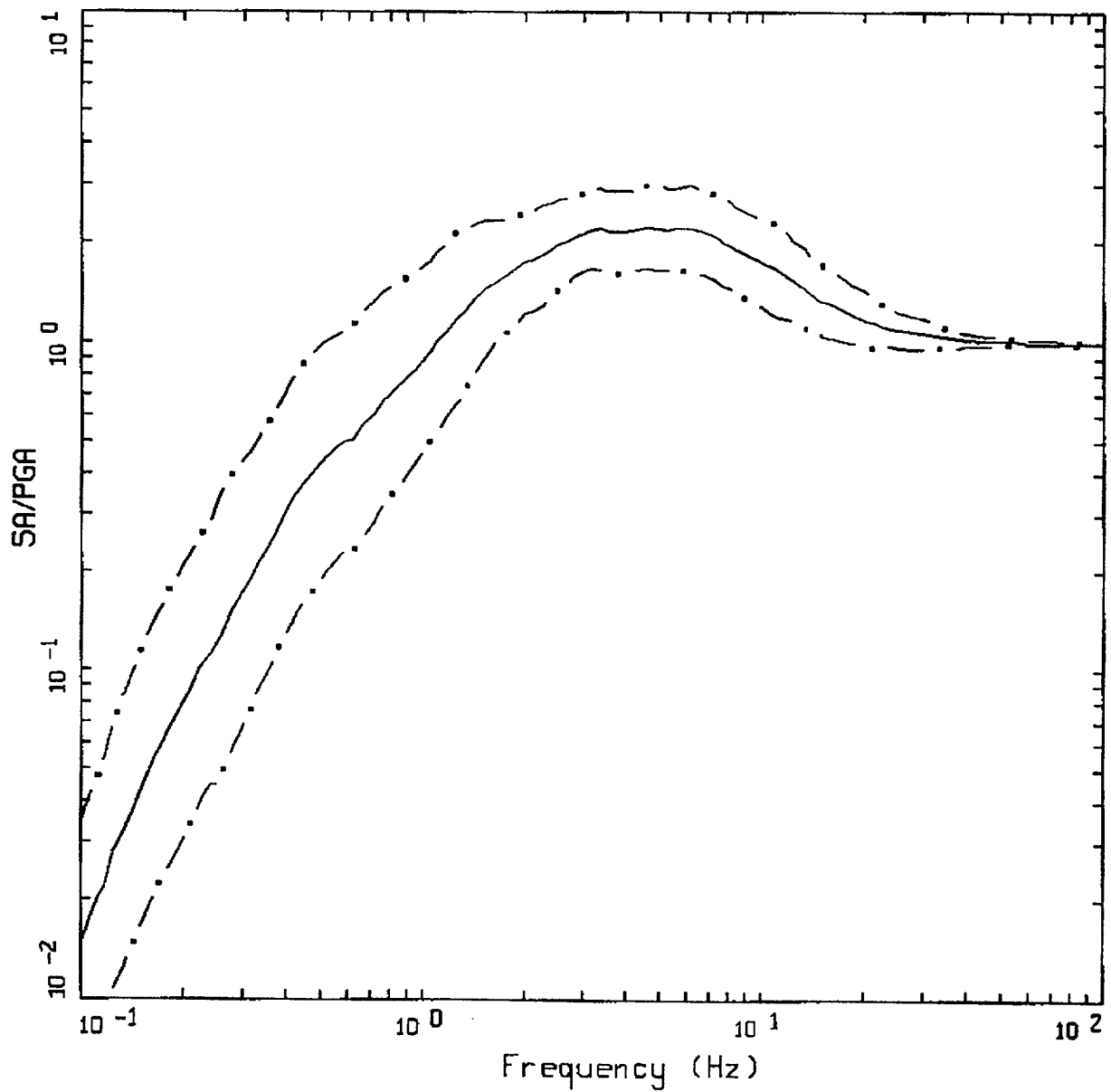
Figure C-27. Median $\pm 1 \sigma$ spectral shapes for M = 7.5, R = 0-50 km, horizontal, WUS rock.



AVERAGE HORIZONTAL SPECTRA
 M=5.5 (5.0-6.0), R=0-50 KM, SOIL
 AVERAGE M = 5.69, AVERAGE DISTANCE = 21.10 KM

LEGEND
 ————— 50TH PERCENTILE
 - - - - - 16TH PERCENTILE
 - . - . - 84TH PERCENTILE

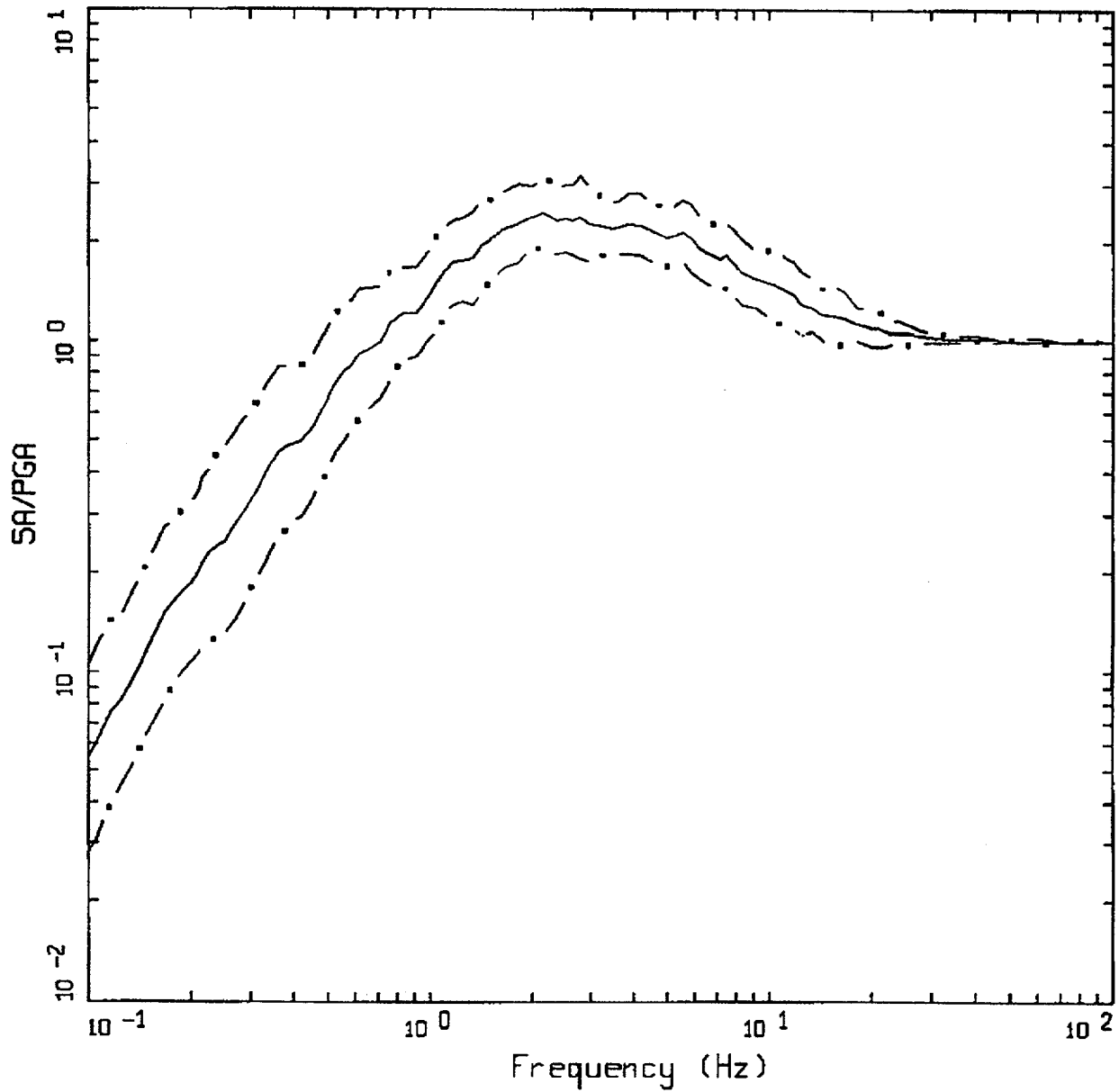
Figure C-28. Median $\pm 1 \sigma$ spectral shapes for $M \approx 5.5$, $R = 0-50$ km, horizontal, WUS soil.



AVERAGE HORIZONTAL SPECTRA
 M=6.5 (6.0-7.0), R=0-50 KM, SOIL
 AVERAGE M = 6.37, AVERAGE DISTANCE = 25.50 KM

LEGEND
 — 50TH PERCENTILE
 - • - 16TH PERCENTILE
 - • - 84TH PERCENTILE

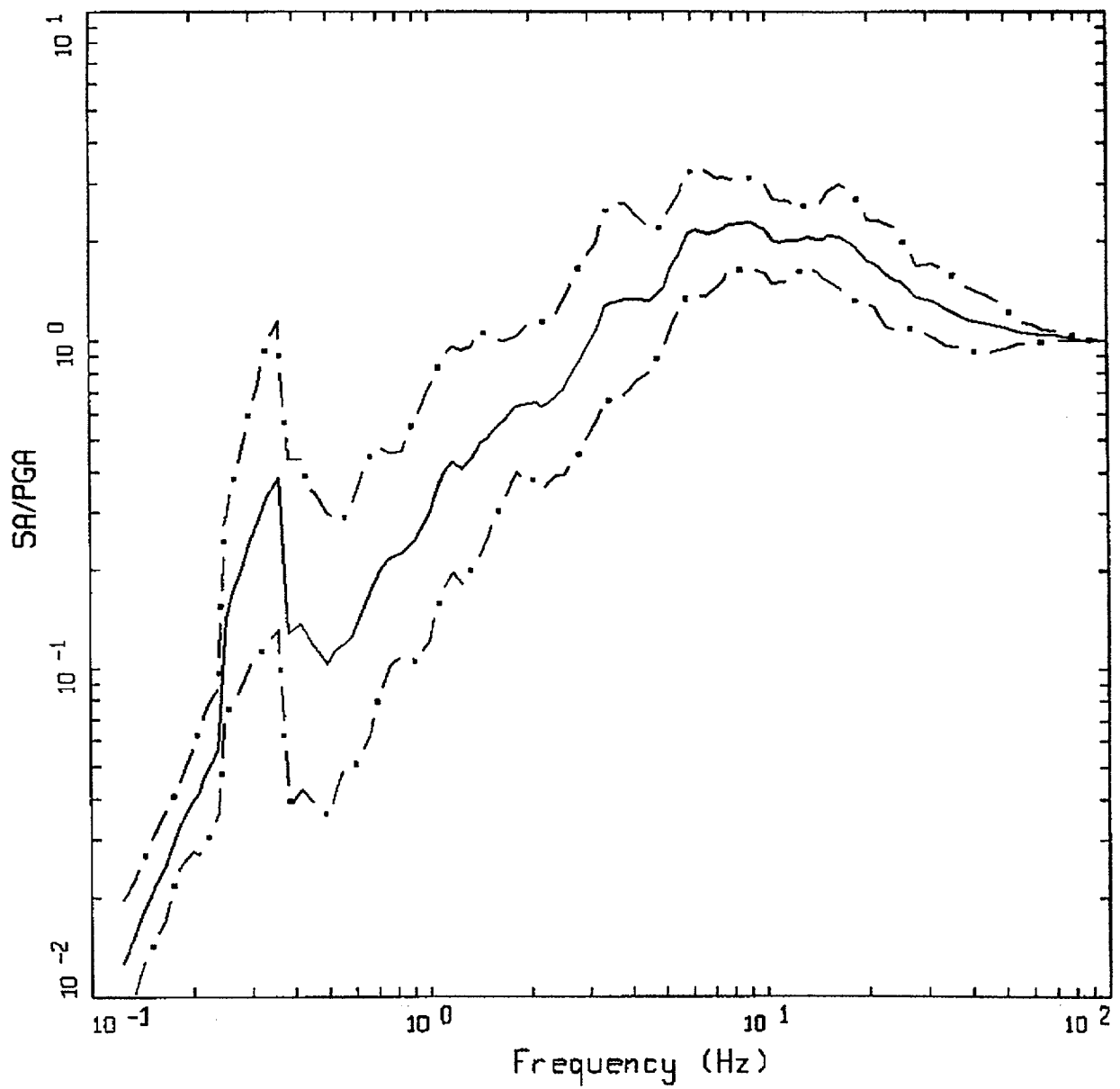
Figure C-29. Median $\pm 1 \sigma$ spectral shapes for $M = 6.5$, $R = 0-50$ km, horizontal, WUS soil.



AVERAGE HORIZONTAL SPECTRA
 M=7.5 (7.0-7.0+), R=0-50 KM, SOIL
 AVERAGE M = 7.27, AVERAGE DISTANCE = 31.82 KM

LEGEND
 ————— 50TH PERCENTILE
 - . - . 16TH PERCENTILE
 - . - . 84TH PERCENTILE

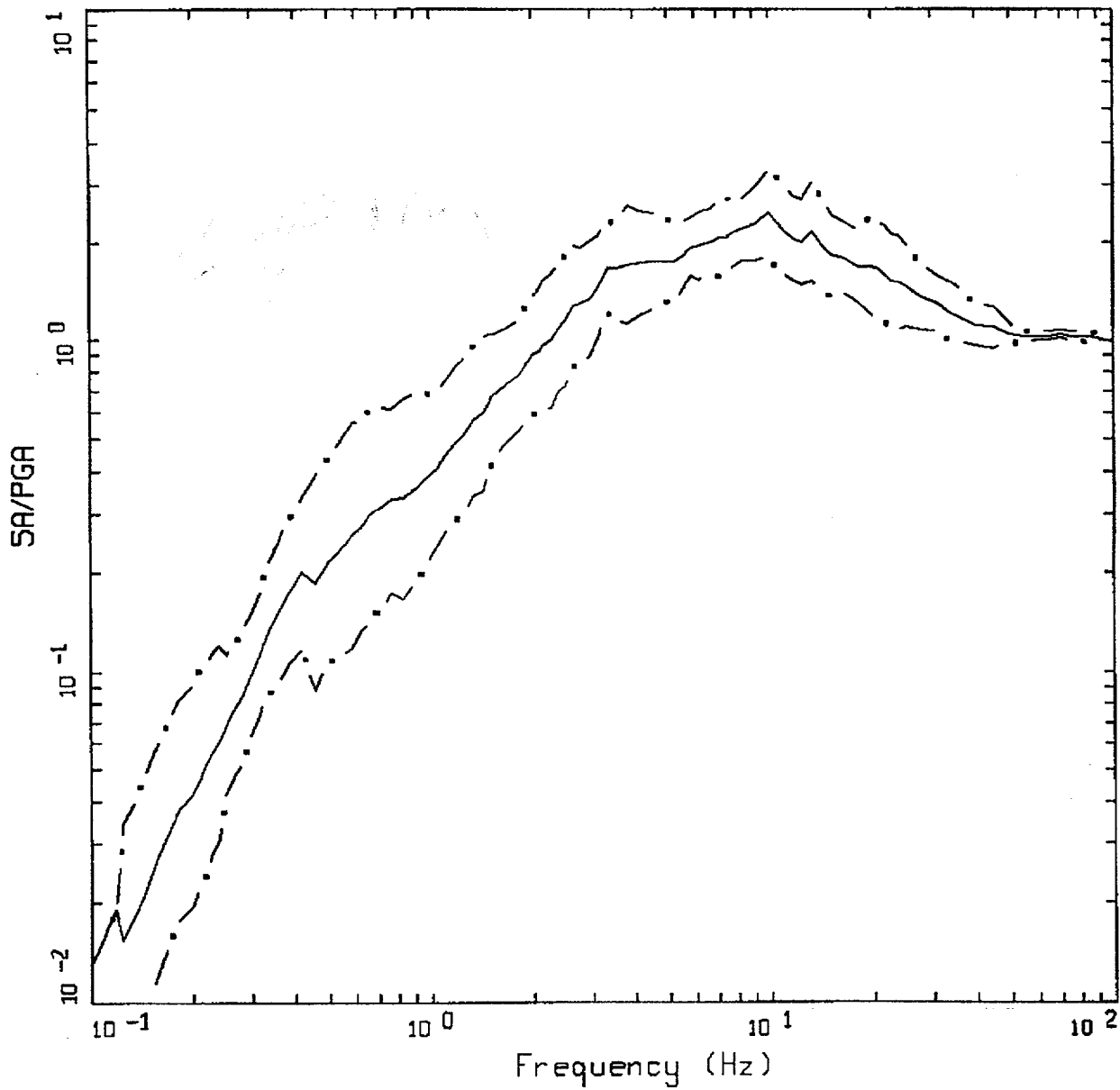
Figure C-30. Median $\pm 1 \sigma$ spectral shapes for $M = 7.5$, $R = 0-50$ km, horizontal, WUS soil.



AVERAGE VERTICAL SPECTRA
 M=5.5 (5.0-6.0), R=0-10 KM, ROCK
 AVERAGE M = 5.54, AVERAGE DISTANCE = 7.91 KM

LEGEND
 ——— 50TH PERCENTILE
 - - - 16TH PERCENTILE
 - . - 84TH PERCENTILE

Figure C-31. Median $\pm 1 \sigma$ spectral shapes for $M \approx 5.5$, $R = 0-10$ km, vertical, WUS rock.



AVERAGE VERTICAL SPECTRA
 M=6.5 (6.0-7.0), R=0-10 KM, ROCK
 AVERAGE M = 6.53, AVERAGE DISTANCE = 5.75 KM

LEGEND
 ——— 50TH PERCENTILE
 - · - 16TH PERCENTILE
 - · · 84TH PERCENTILE

Figure C-32. Median $\pm 1 \sigma$ spectral shapes for $M \approx 6.5$, $R = 0-10$ km, vertical, WUS rock.

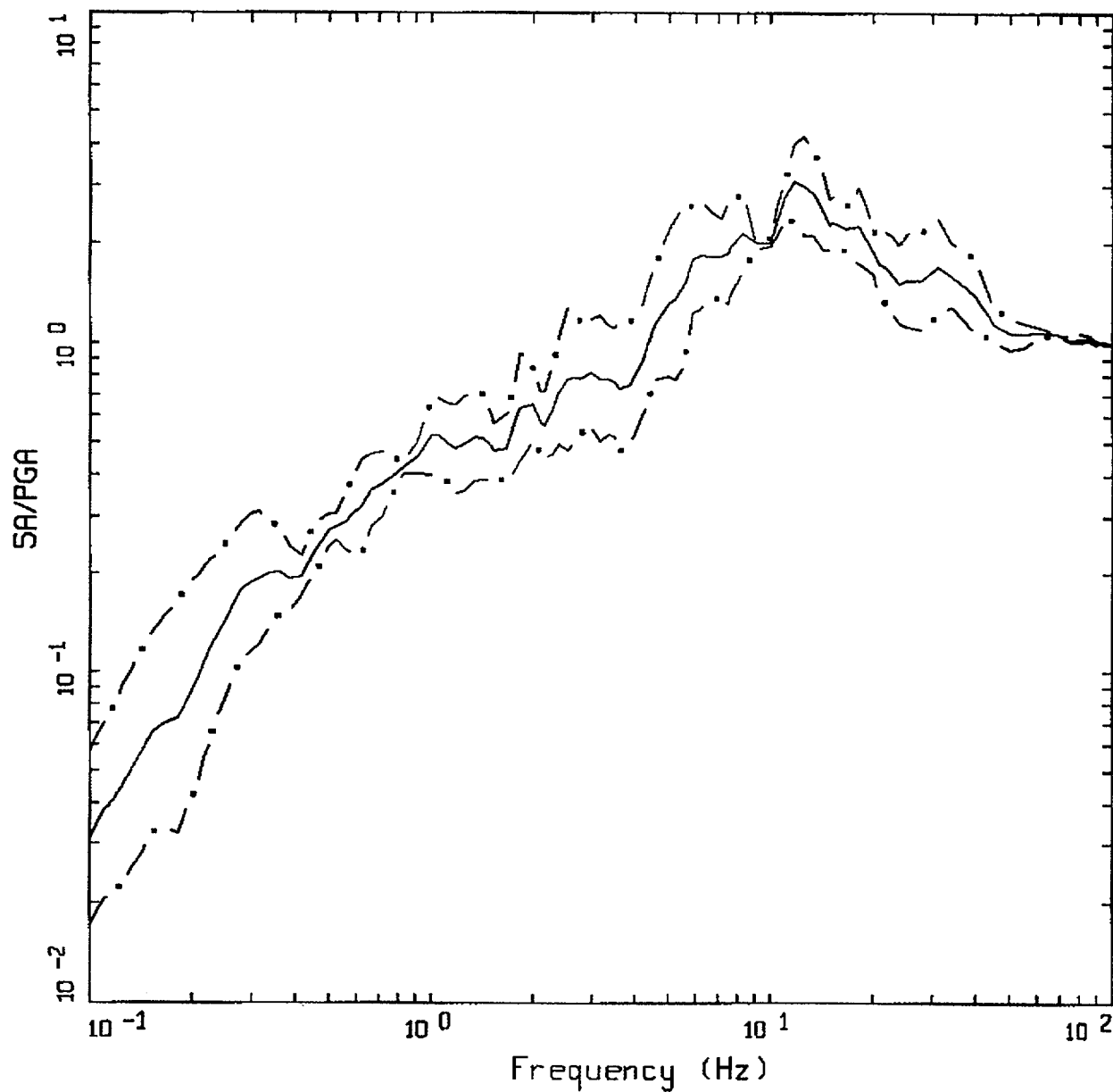
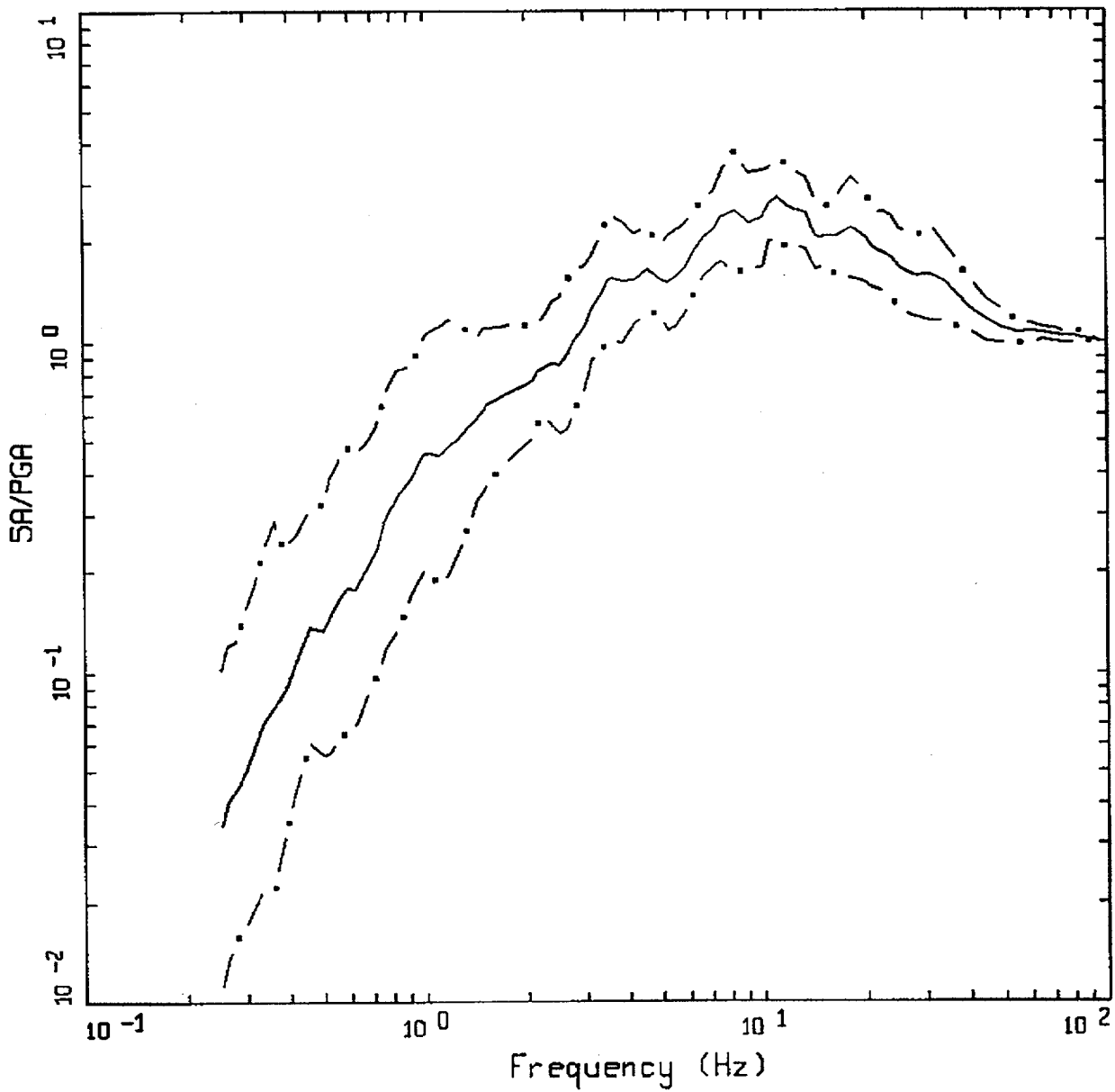


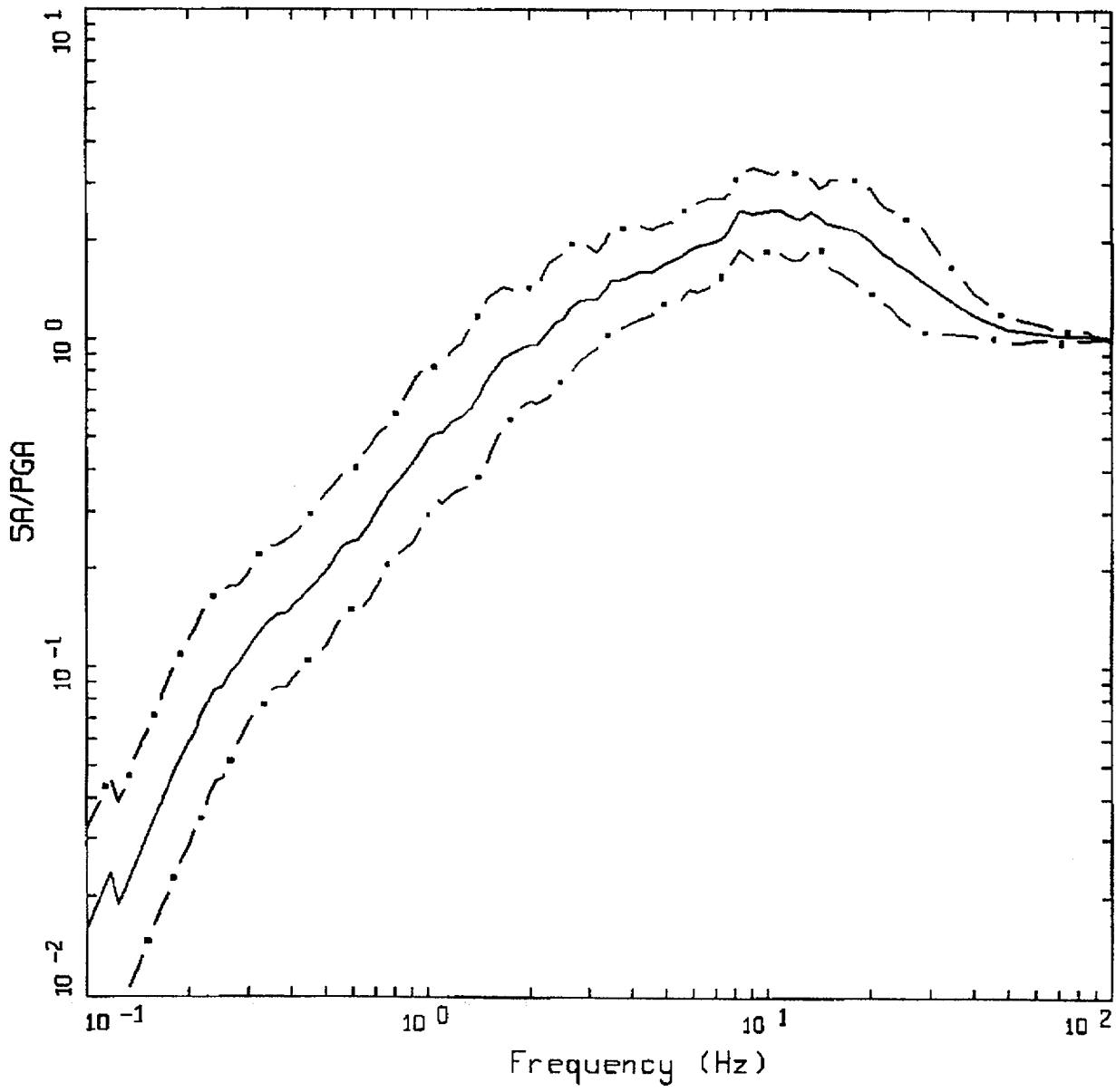
Figure C-33. Median $\pm 1 \sigma$ spectral shapes for $M \approx 7.5$, $R = 0-10$ km, vertical, WUS rock.



AVERAGE VERTICAL SPECTRA
 M=5.5 (5.0-6.0), R=0-10 KM, SOIL
 AVERAGE M = 5.76, AVERAGE DISTANCE = 7.80 KM

LEGEND
 — 50TH PERCENTILE
 - - - 16TH PERCENTILE
 - . - 84TH PERCENTILE

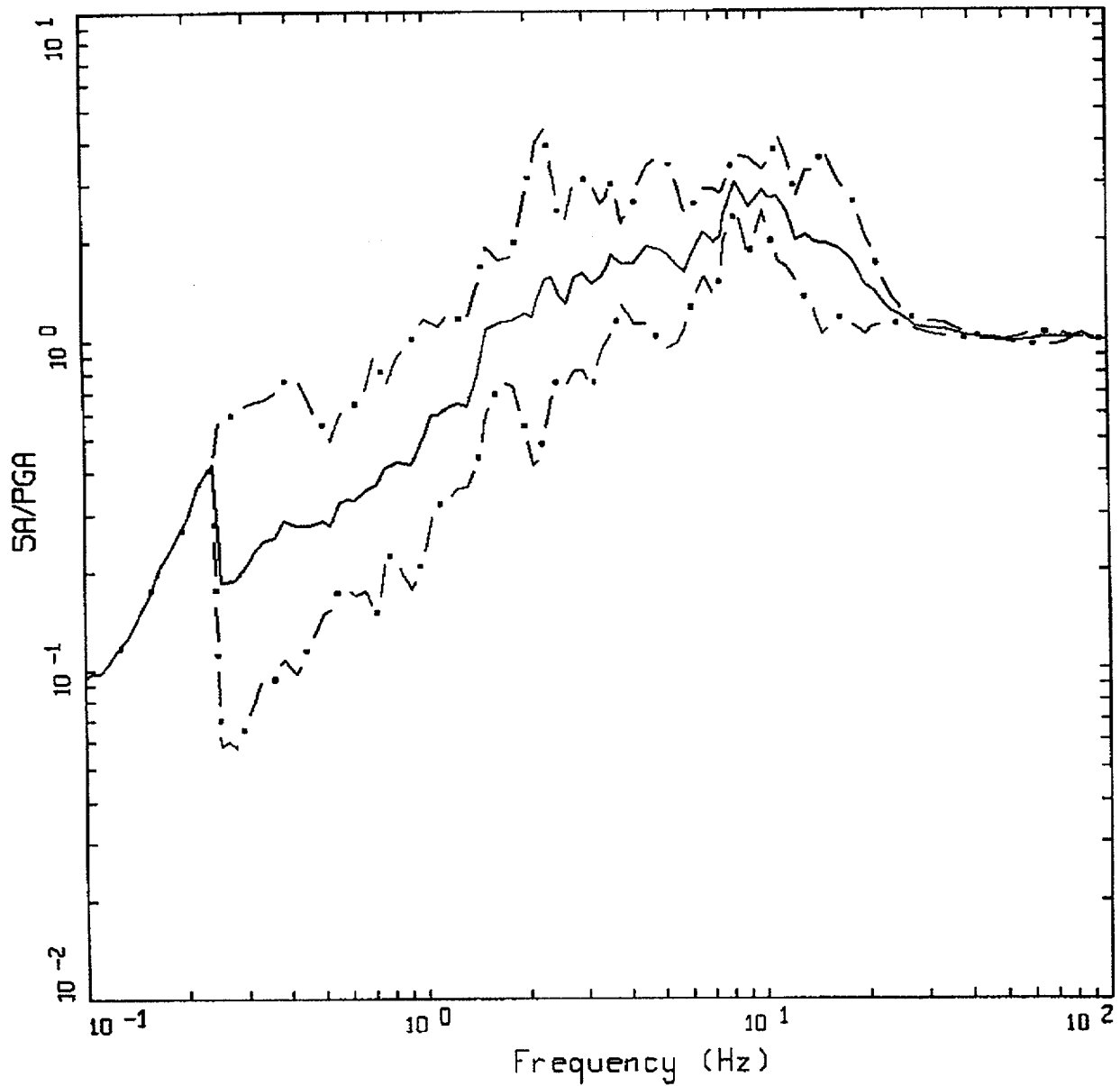
Figure C-34. Median $\pm 1 \sigma$ spectral shapes for $M \approx 5.5$, $R = 0-10$ km, vertical, WUS soil.



AVERAGE VERTICAL SPECTRA
 M=6.5 (6.0-7.0), R=0-10 KM, SOIL
 AVERAGE M = 6.46, AVERAGE DISTANCE = 6.00 KM

LEGEND
 ————— 50TH PERCENTILE
 - . - 16TH PERCENTILE
 - . . - 84TH PERCENTILE

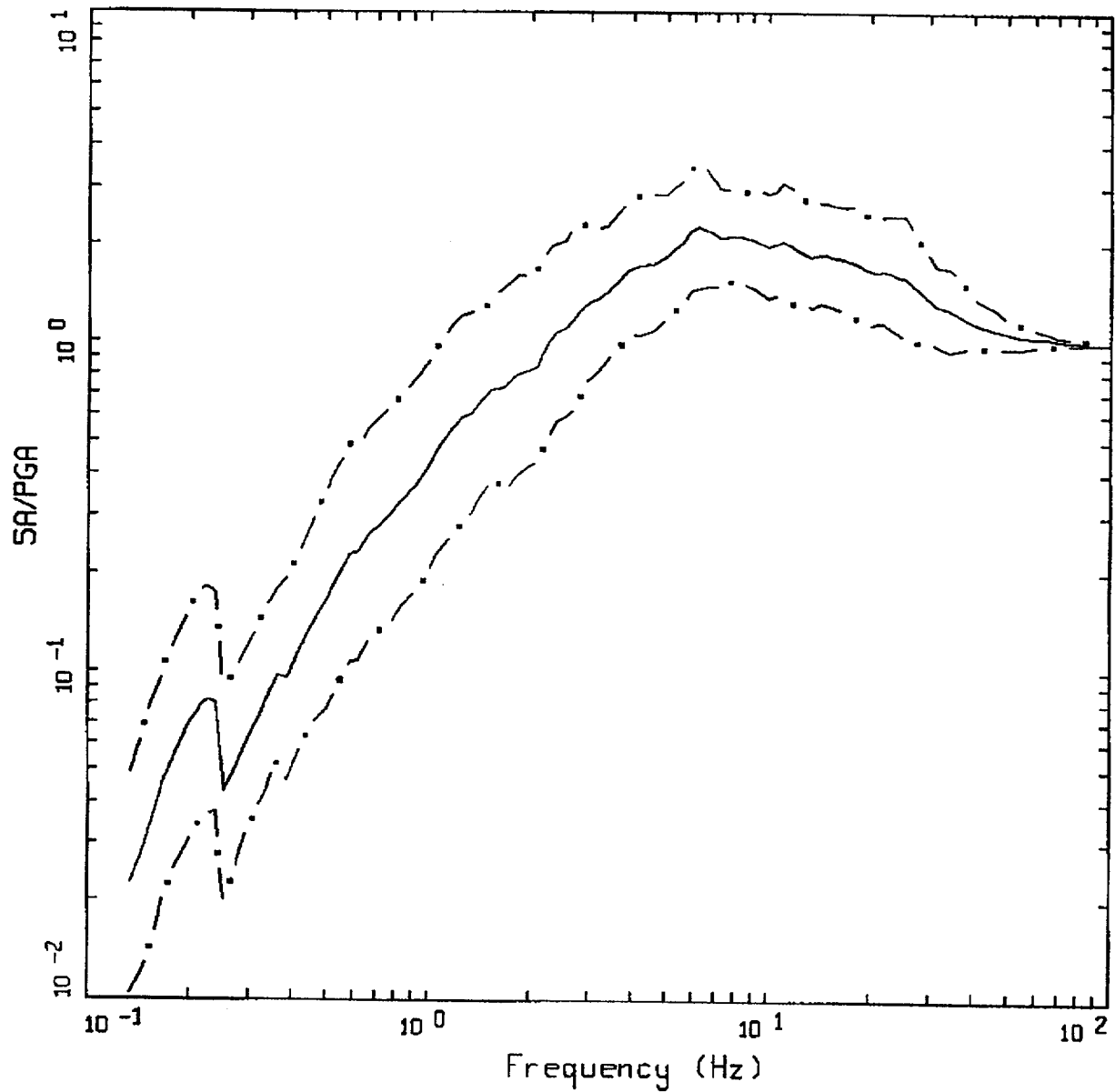
Figure C-35. Median $\pm 1 \sigma$ spectral shapes for $M \approx 6.5$, $R = 0-10$ km, vertical, WUS soil.



AVERAGE VERTICAL SPECTRA
 M=7.5 (7.0-7.0+), R=0-10 KM, SOIL
 AVERAGE M = 7.05, AVERAGE DISTANCE = 8.90 KM

LEGEND
 ————— 50TH PERCENTILE
 - . - . 16TH PERCENTILE
 - . . - 84TH PERCENTILE

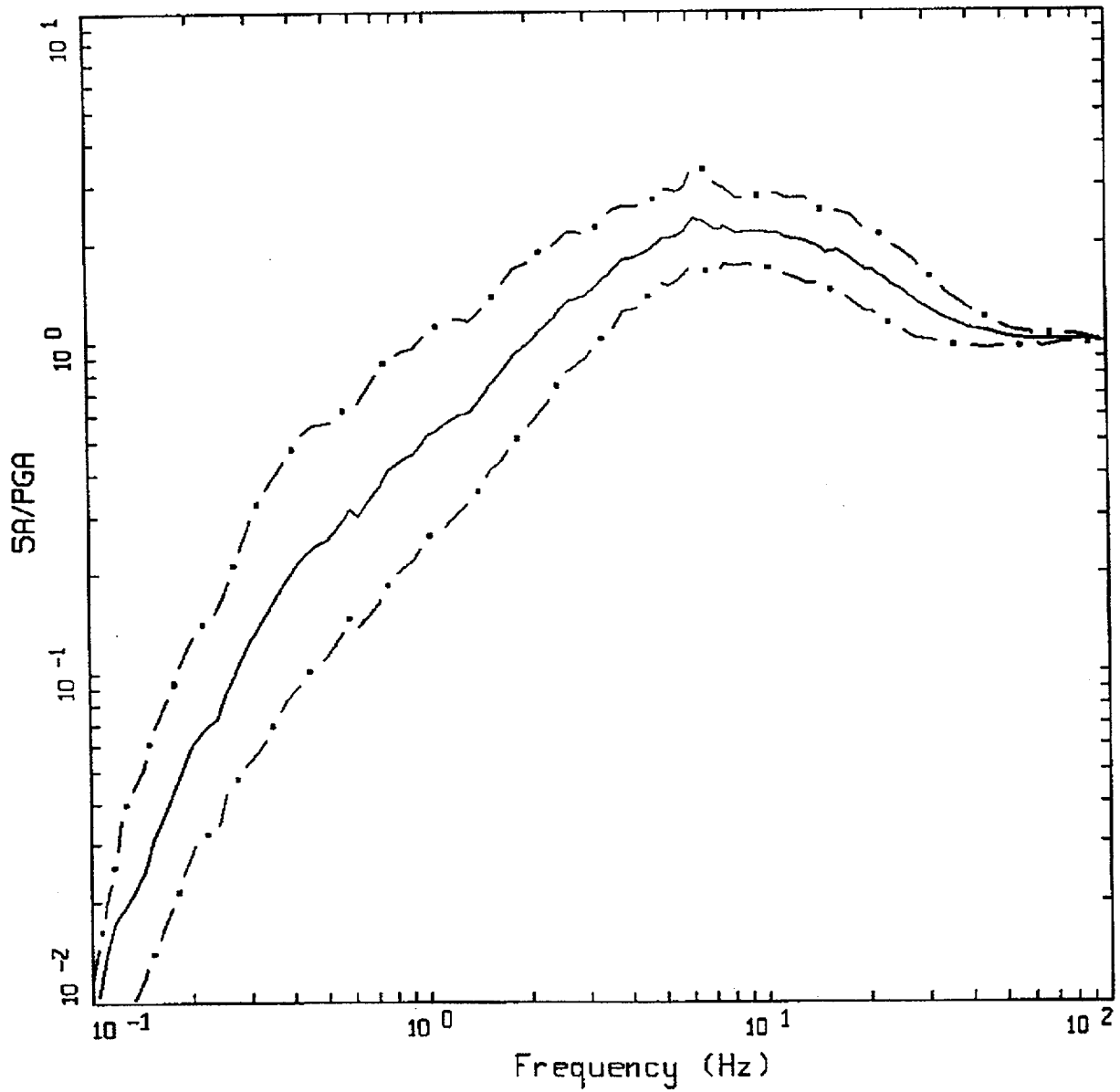
Figure C-36. Median $\pm 1 \sigma$ spectral shapes for $M \approx 7.5$, $R = 0-10$ km, vertical, WUS soil.



AVERAGE VERTICAL SPECTRA
 M=5.5 (5.0-6.0), R=10-50 KM, ROCK
 AVERAGE M = 5.57, AVERAGE DISTANCE = 21.80 KM

LEGEND
 ————— 50TH PERCENTILE
 - - - - - 16TH PERCENTILE
 - . - . - 84TH PERCENTILE

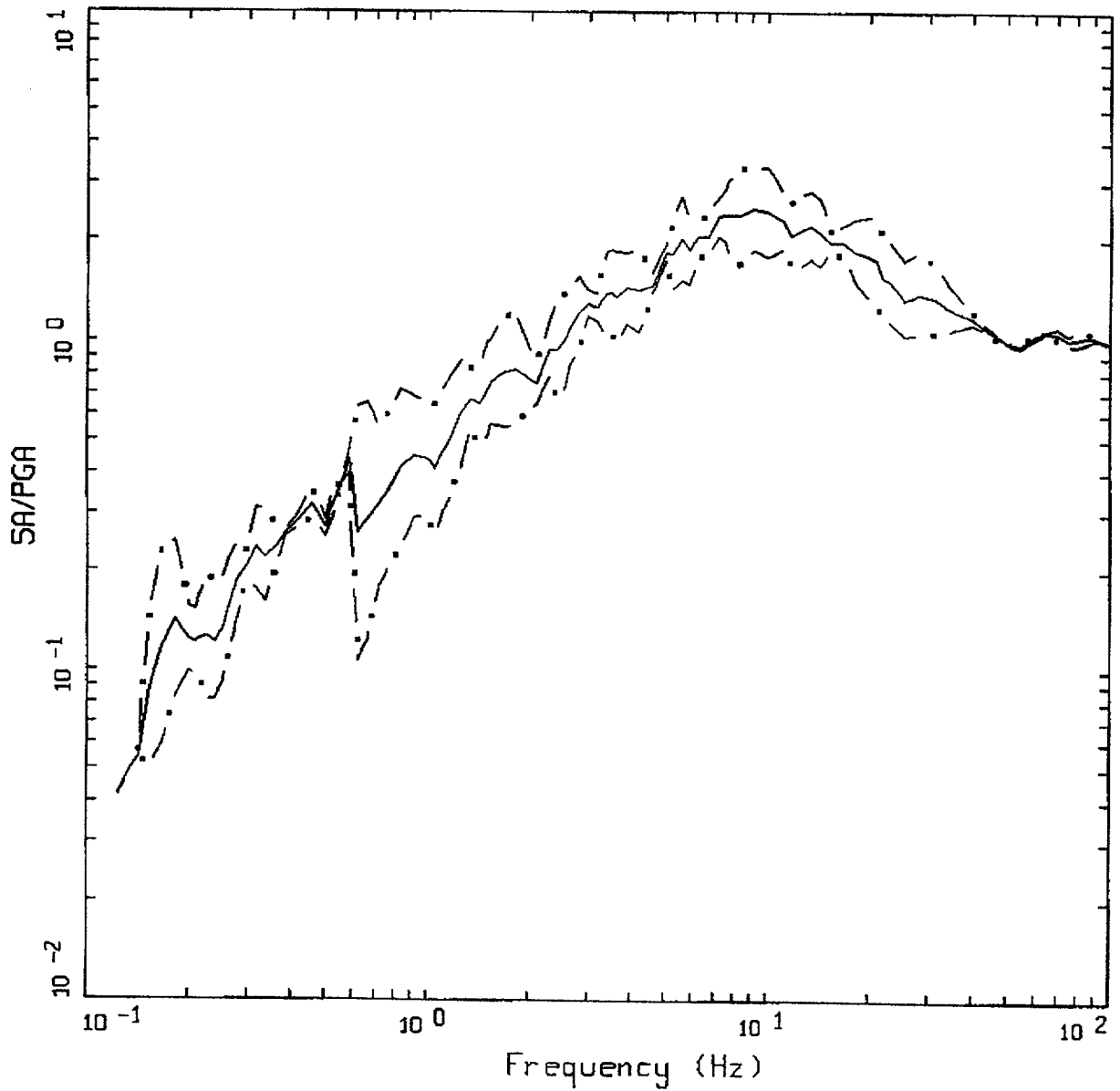
Figure C-37. Median $\pm 1 \sigma$ spectral shapes for $M \approx 5.5$, $R = 10-50$ km, vertical, WUS rock.



AVERAGE VERTICAL SPECTRA
 M=6.5 (6.0-7.0), R=10-50 KM, ROCK
 AVERAGE M = 6.43, AVERAGE DISTANCE = 30.28 KM

- LEGEND
- 50TH PERCENTILE
 - · - 16TH PERCENTILE
 - · · - 84TH PERCENTILE

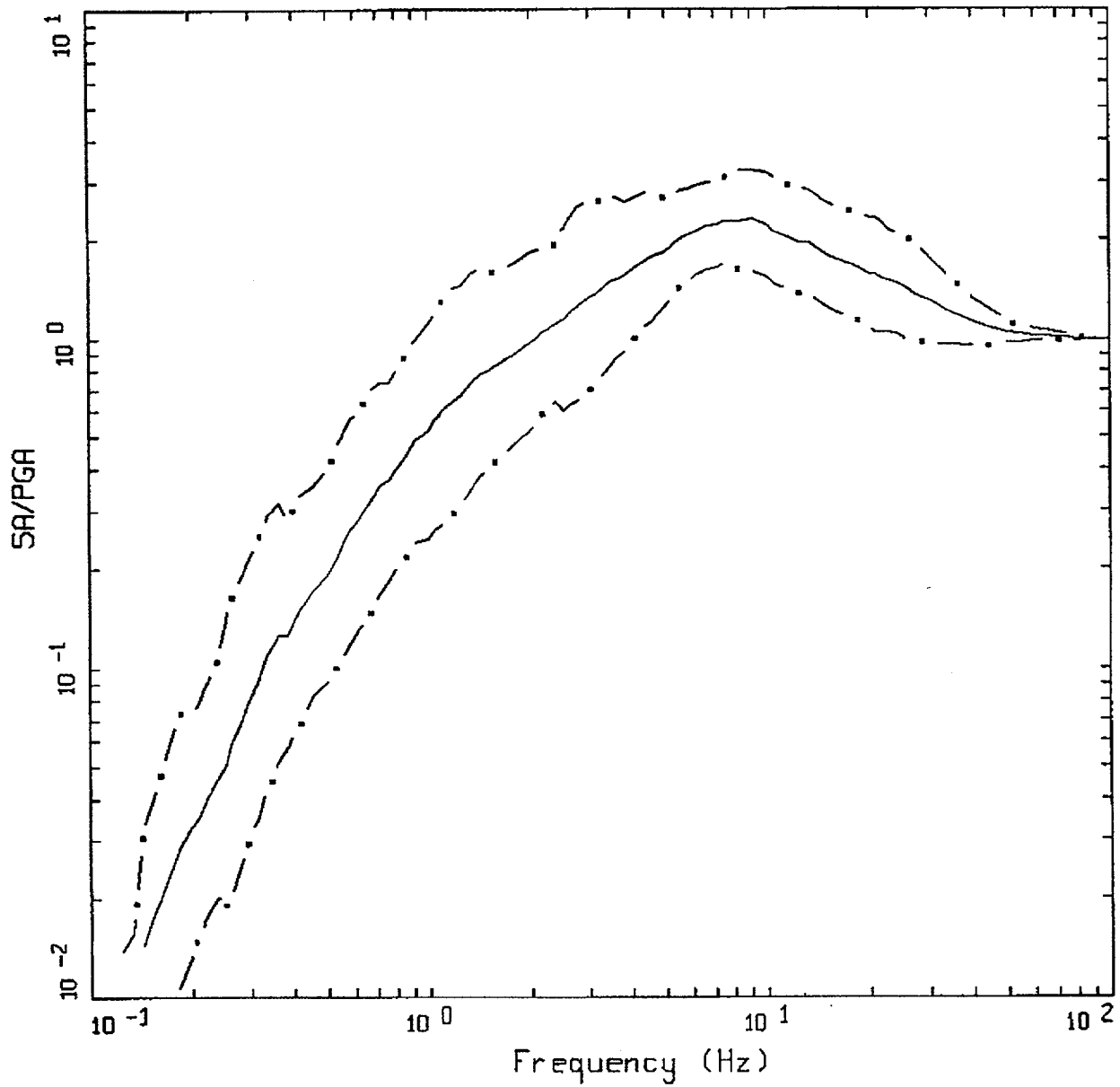
Figure C-38. Median $\pm 1 \sigma$ spectral shapes for $M \approx 6.5$, $R = 10-50$ km, vertical, WUS rock.



AVERAGE VERTICAL SPECTRA
 M=7.5 (7.0-7.0+), R=10-50 KM, ROCK
 AVERAGE M = 7.27, AVERAGE DISTANCE = 31.00 KM

LEGEND
 — 50TH PERCENTILE
 - · - 16TH PERCENTILE
 - · - 84TH PERCENTILE

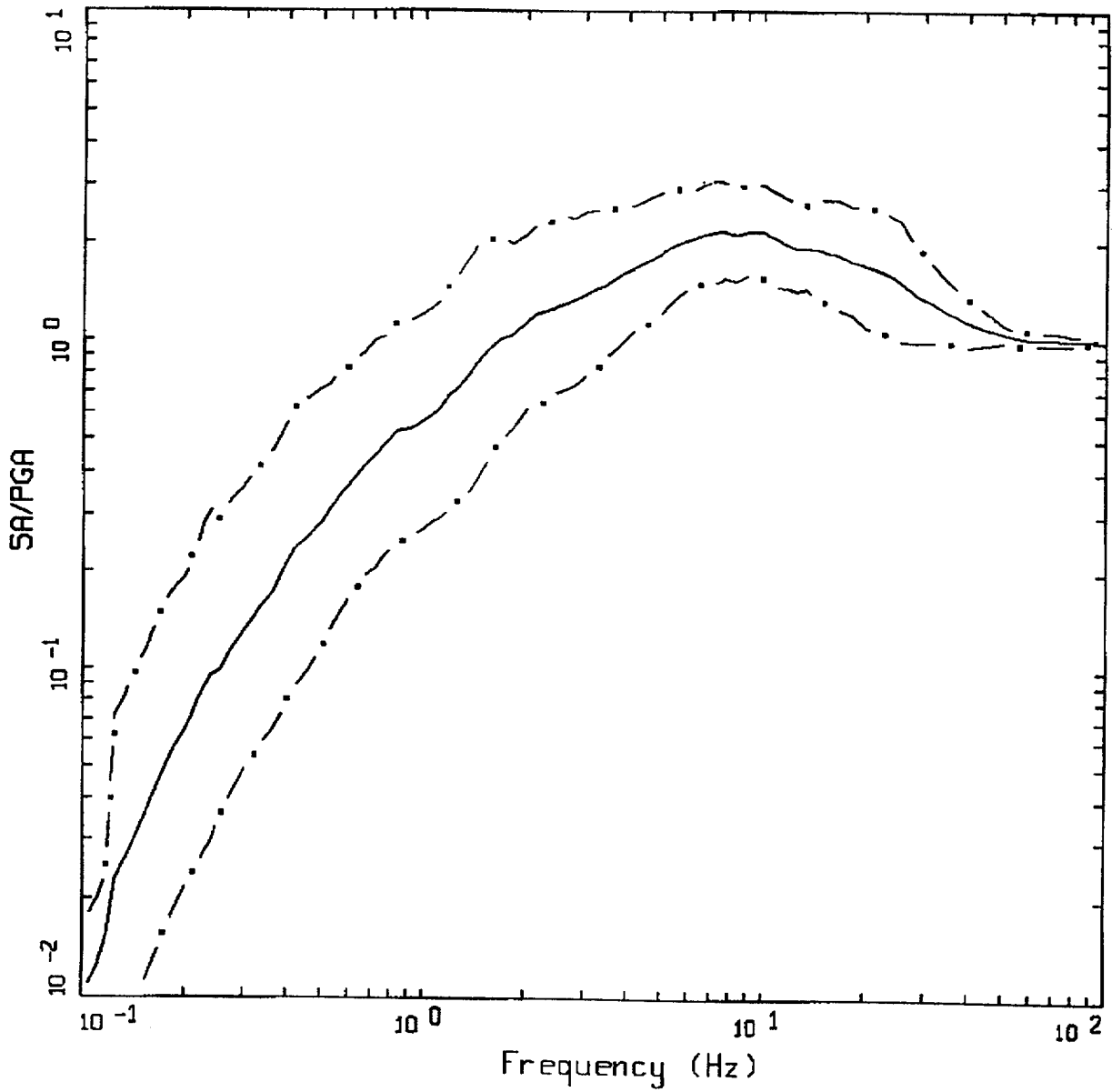
Figure C-39. Median $\pm 1 \sigma$ spectral shapes for $M \approx 7.5$, $R = 10-50$ km, vertical, WUS rock.



AVERAGE VERTICAL SPECTRA
 M=5.5 (5.0-6.0), R=10-50 KM, SOIL
 AVERAGE M = 5.69, AVERAGE DISTANCE = 21.82 KM

LEGEND
 ————— 50TH PERCENTILE
 - . - - 16TH PERCENTILE
 - . - - 84TH PERCENTILE

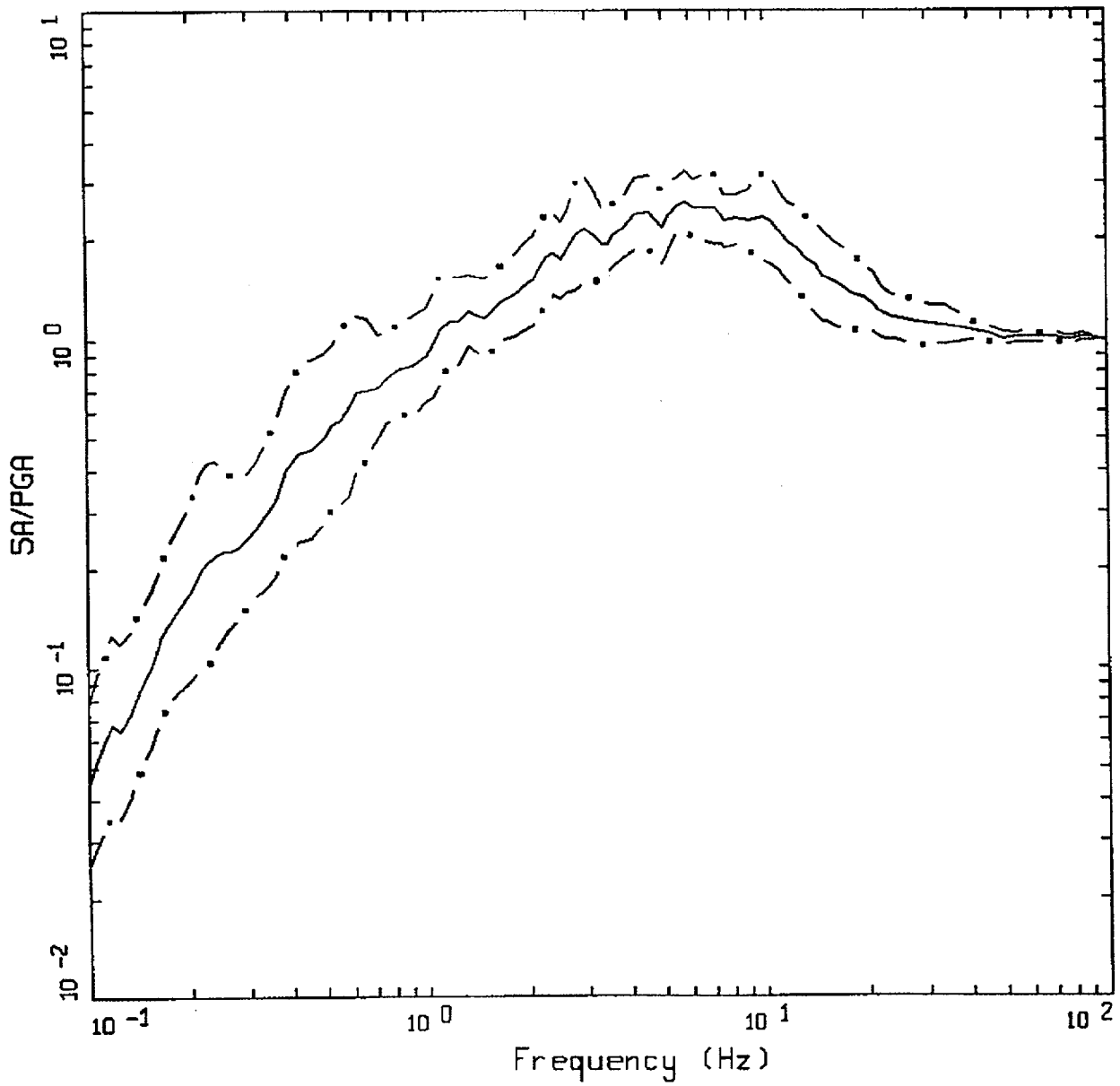
Figure C-40. Median $\pm 1 \sigma$ spectral shapes for $M \approx 5.5$, $R = 10-50$ km, vertical, WUS soil.



AVERAGE VERTICAL SPECTRA
 M=6.5 (6.0-7.0), R=10-50 KM, SOIL
 AVERAGE M = 6.35, AVERAGE DISTANCE = 28.27 KM

LEGEND
 ————— 50TH PERCENTILE
 - . - . 16TH PERCENTILE
 - . - . 84TH PERCENTILE

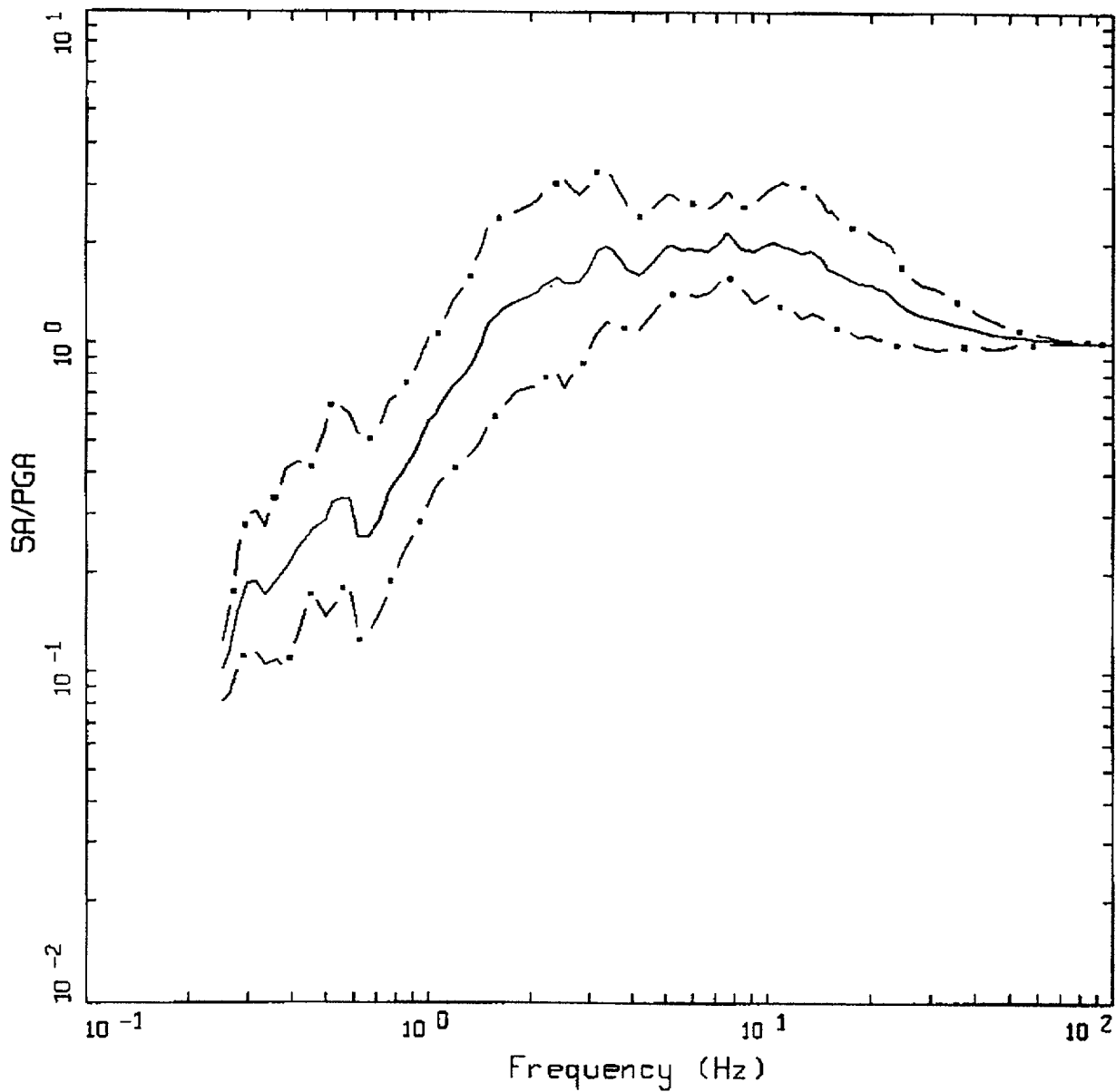
Figure C-41. Median $\pm 1 \sigma$ spectral shapes for $M = 6.5$, $R = 10-50$ km, vertical, WUS soil.



AVERAGE VERTICAL SPECTRA
 M=7.5 (7.0-7.0+), R=10-50 KM, SOIL
 AVERAGE M = 7.29, AVERAGE DISTANCE = 33.46 KM

LEGEND
 — 50TH PERCENTILE
 - - - 16TH PERCENTILE
 - . - 84TH PERCENTILE

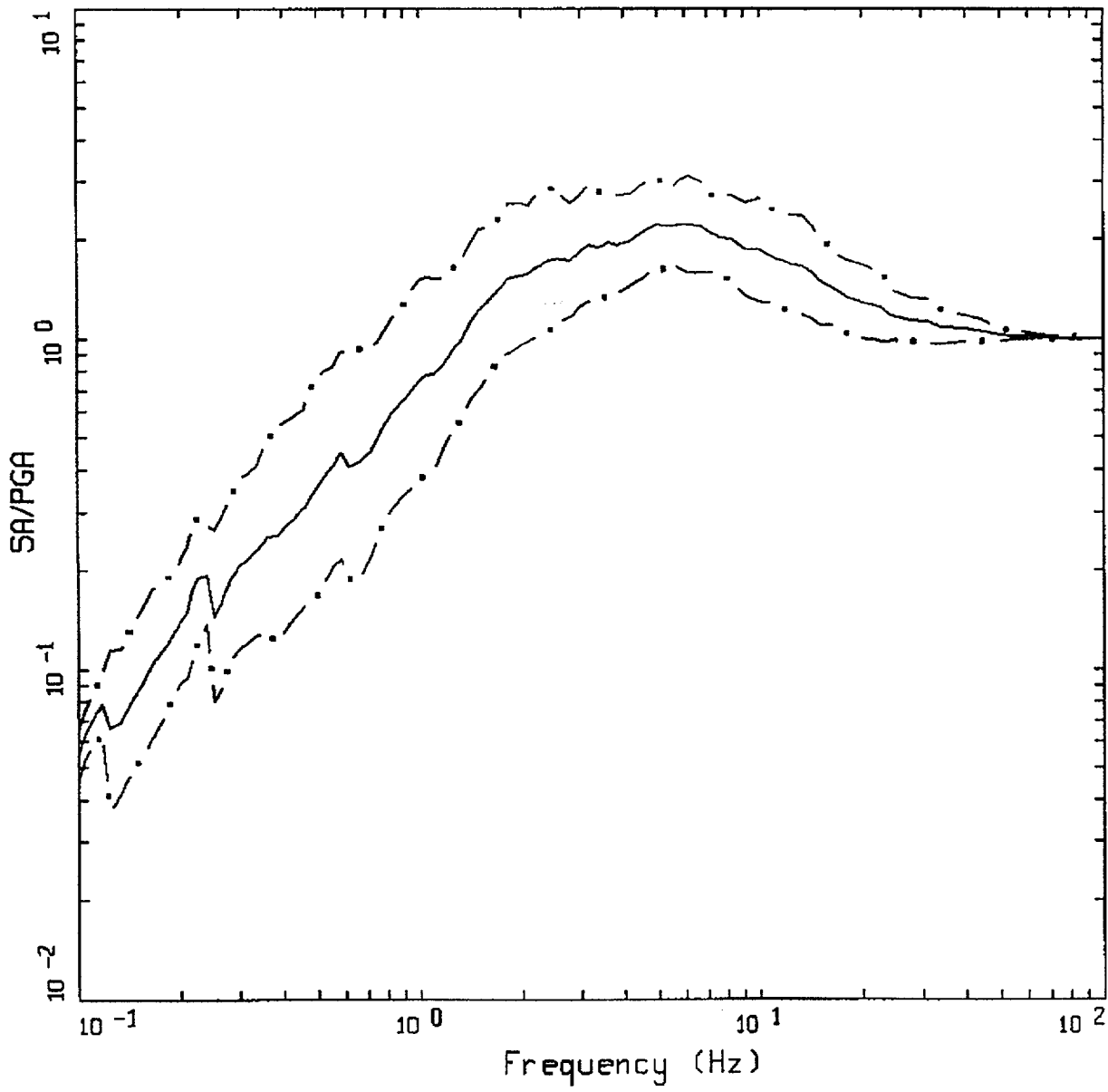
Figure C-42. Median $\pm 1 \sigma$ spectral shapes for $M \approx 7.5$, $R = 10-50$ km, vertical, WUS soil.



AVERAGE VERTICAL SPECTRA
 M=5.5 (5.0-6.0), R=50-100 KM, ROCK
 AVERAGE M = 5.91, AVERAGE DISTANCE = 64.27 KM

LEGEND
 ————— 50TH PERCENTILE
 - . - - 16TH PERCENTILE
 - . - - 84TH PERCENTILE

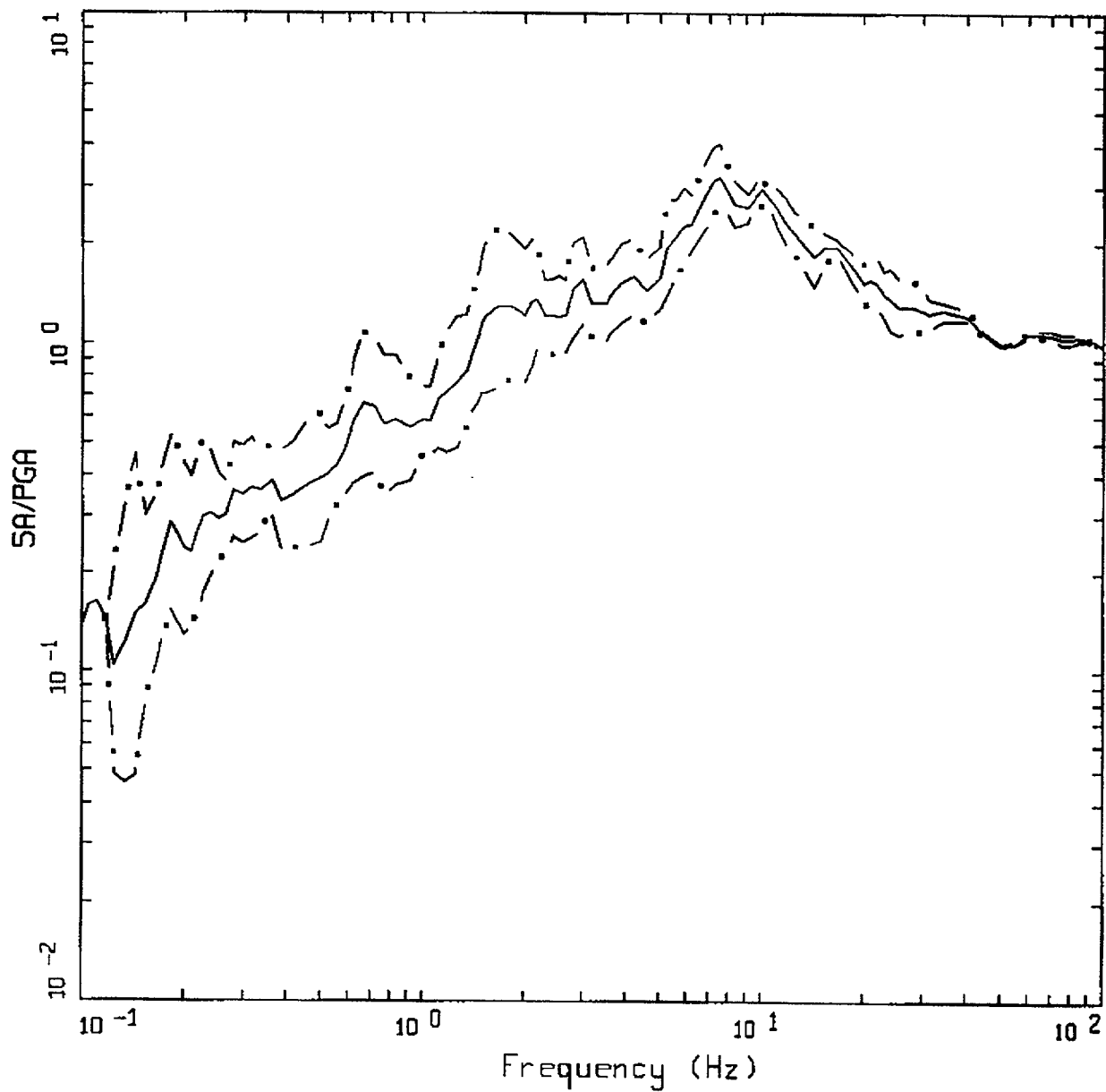
Figure C-43. Median $\pm 1 \sigma$ spectral shapes for $M \approx 5.5$, $R = 50-100$ km, vertical, WUS rock.



AVERAGE VERTICAL SPECTRA
 M=6.5 (6.0-7.0), R=50-100 KM, ROCK
 AVERAGE M = 6.51, AVERAGE DISTANCE = 70.35 KM

- LEGEND
- 50TH PERCENTILE
 - . - 16TH PERCENTILE
 - . - 84TH PERCENTILE

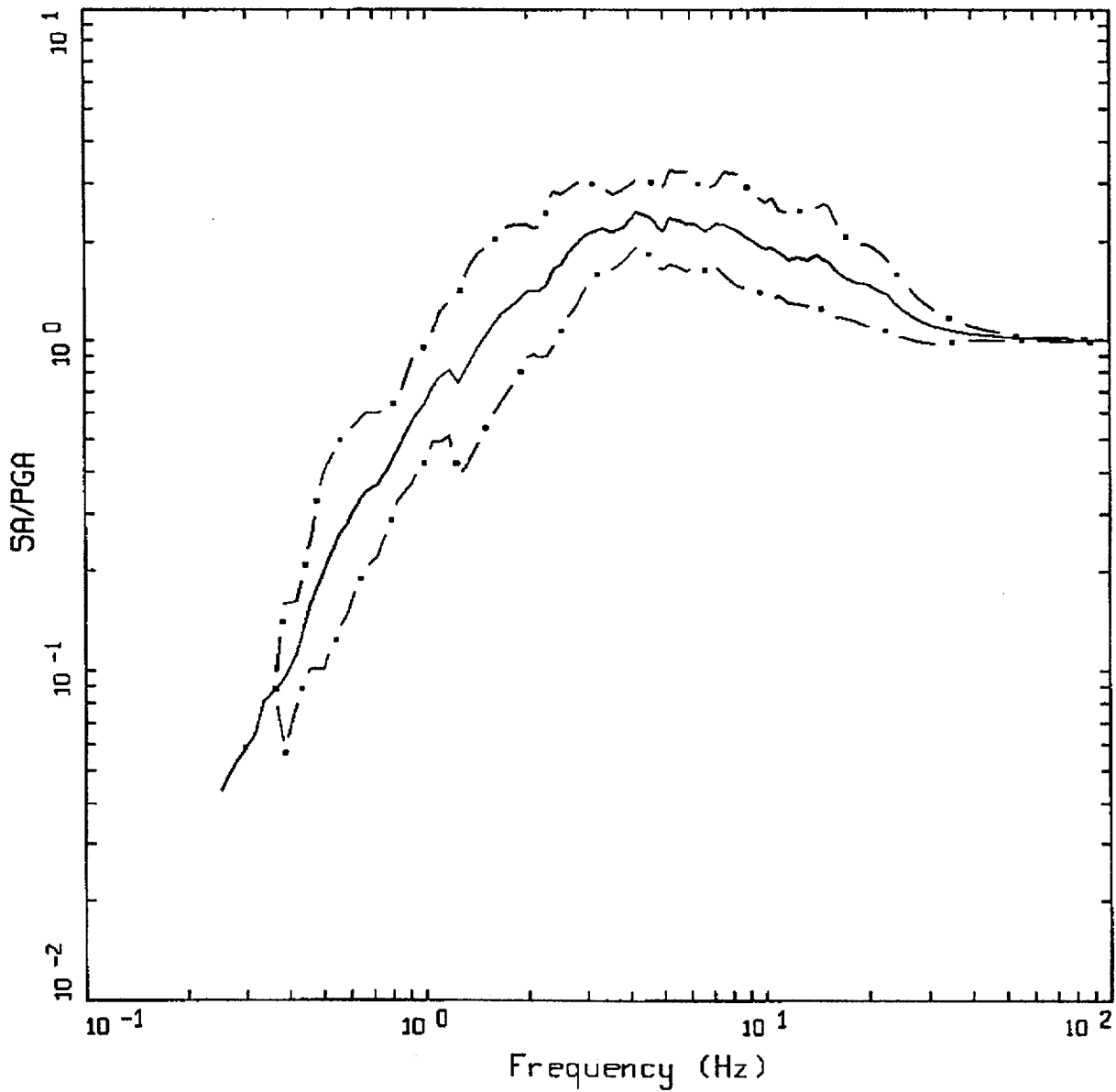
Figure C-44. Median $\pm 1 \sigma$ spectral shapes for $M \approx 6.5$, $R = 50-100$ km, vertical, WUS rock.



AVERAGE VERTICAL SPECTRA
 M=7.5 (7.0-7.0+), R=50-100 KM, ROCK
 AVERAGE M = 7.32, AVERAGE DISTANCE = 81.46 KM

LEGEND
 — 50TH PERCENTILE
 - - - 16TH PERCENTILE
 - . - 84TH PERCENTILE

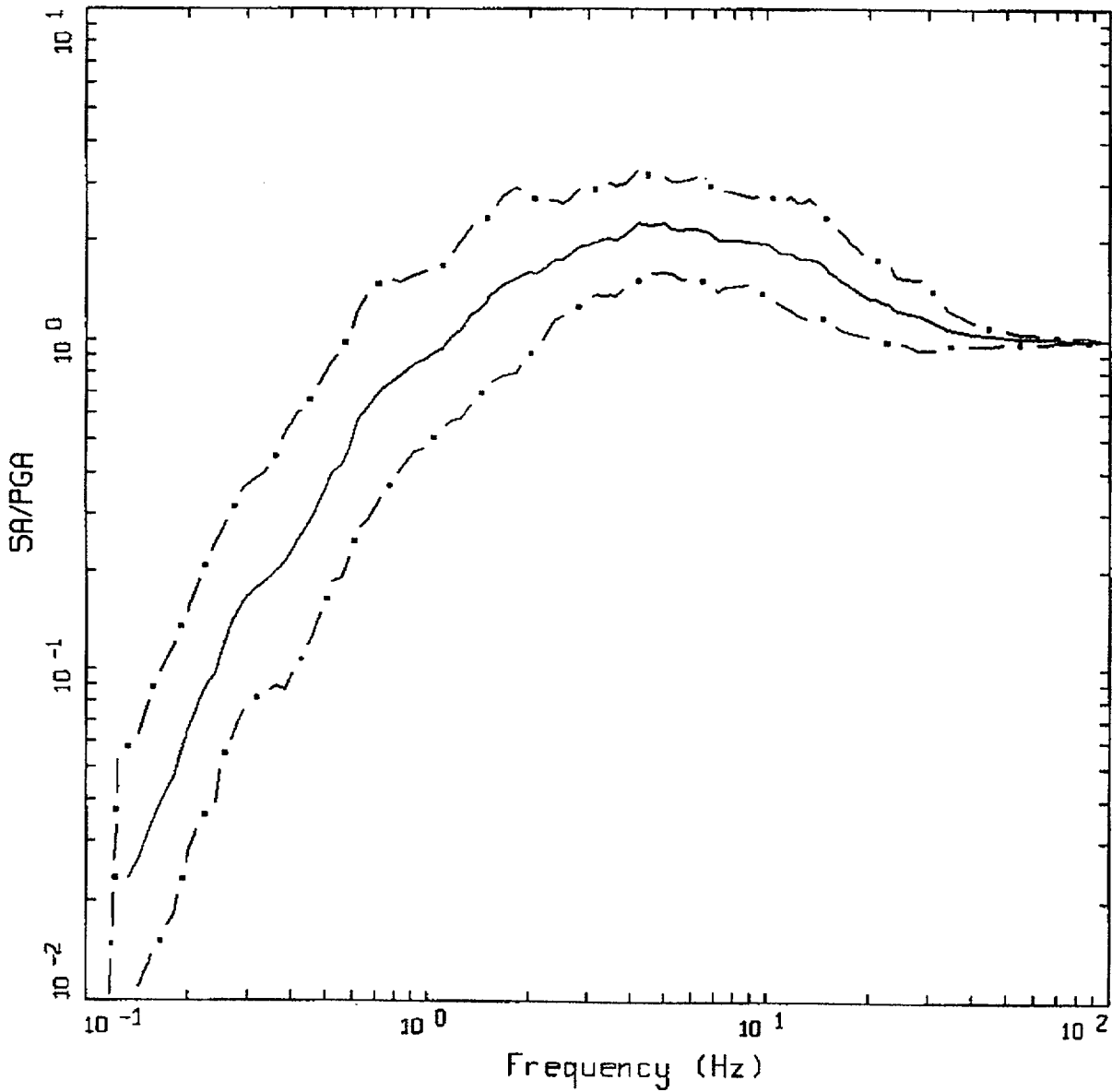
Figure C-45. Median $\pm 1 \sigma$ spectral shapes for $M \approx 7.5$, $R = 50-100$ km, vertical, WUS rock.



AVERAGE VERTICAL SPECTRA
 M=5.5 (5.0-6.0), R=50-100 KM, SOIL
 AVERAGE M = 5.80, AVERAGE DISTANCE = 67.22 KM

LEGEND
 ————— 50TH PERCENTILE
 - - - - - 16TH PERCENTILE
 - . - . - 84TH PERCENTILE

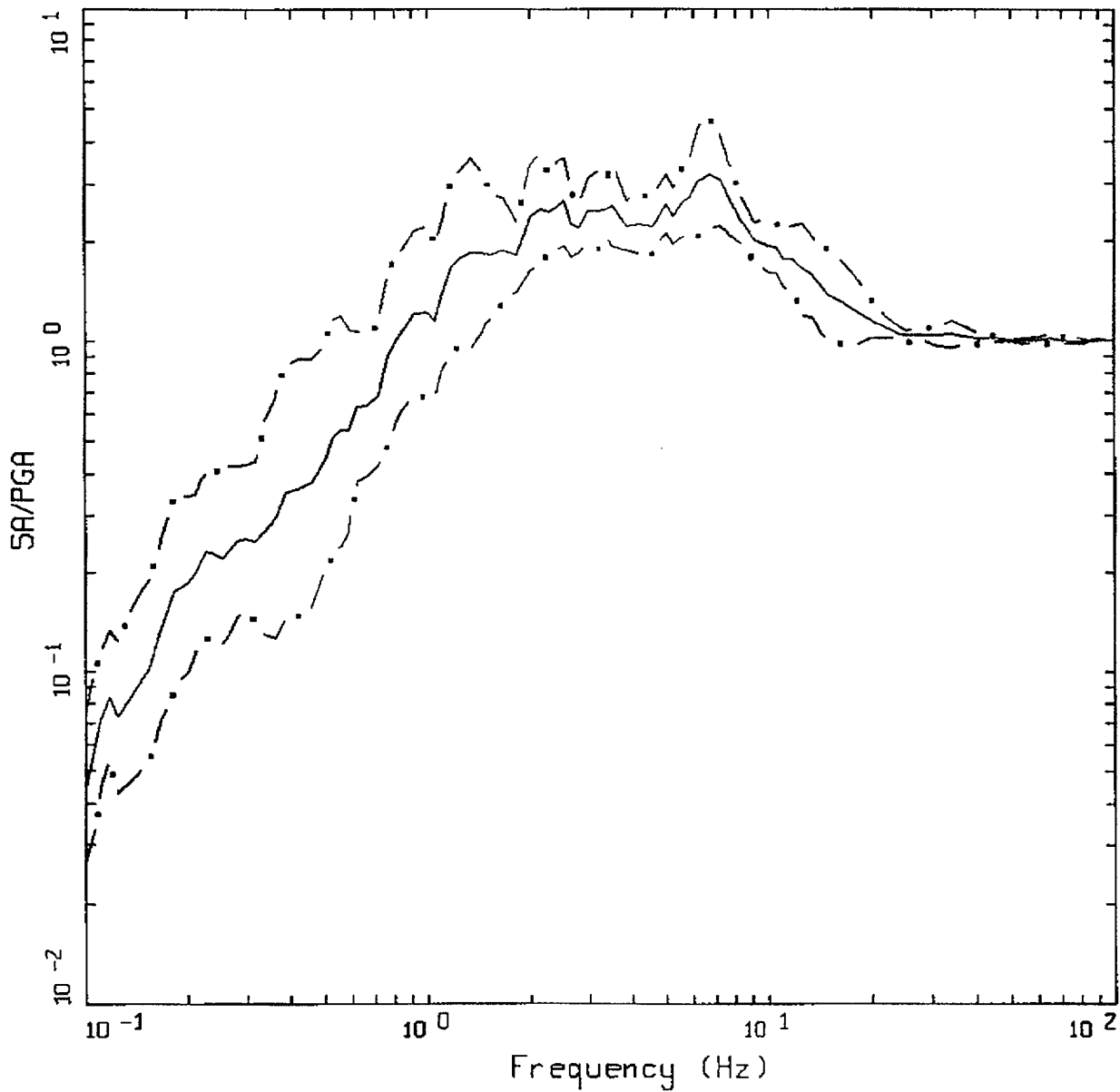
Figure C-46. Median $\pm 1 \sigma$ spectral shapes for $M \approx 5.5$, $R = 50-100$ km, vertical, WUS soil.



AVERAGE VERTICAL SPECTRA
 M=6.5 (6.0-7.0), R=50-100 KM, SOIL
 AVERAGE M = 6.49, AVERAGE DISTANCE = 67.34 KM

LEGEND
 ————— 50TH PERCENTILE
 - · - · 16TH PERCENTILE
 - · - · 84TH PERCENTILE

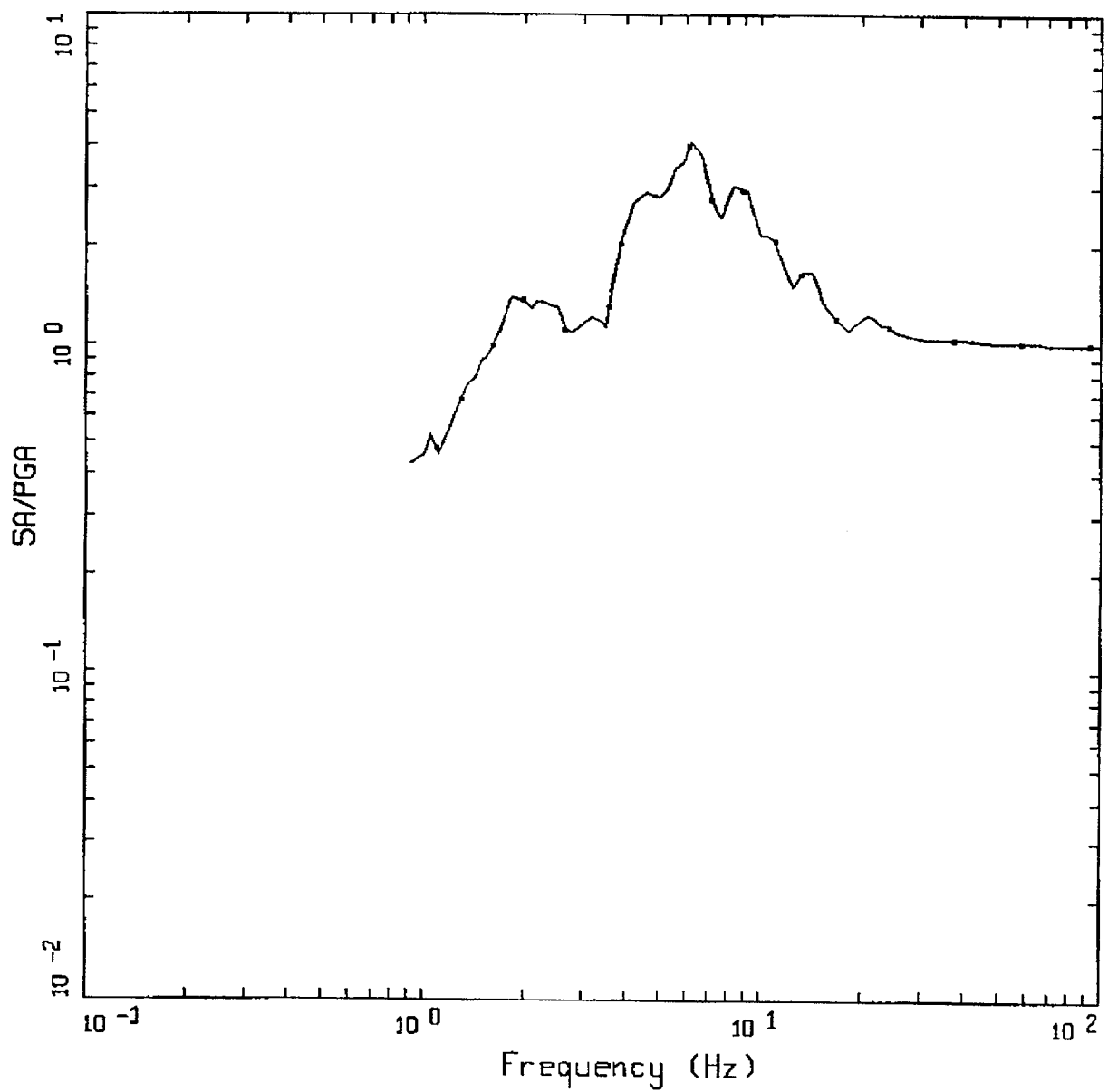
Figure C-47. Median $\pm 1 \sigma$ spectral shapes for $M = 6.5$, $R = 50-100$ km, vertical, WUS soil.



AVERAGE VERTICAL SPECTRA
 M=7.5 (7.0-7.0+), R=50-100 KM, SOIL
 AVERAGE M = 7.31, AVERAGE DISTANCE = 76.57 KM

LEGEND
 — 50TH PERCENTILE
 - - - 16TH PERCENTILE
 - . - 84TH PERCENTILE

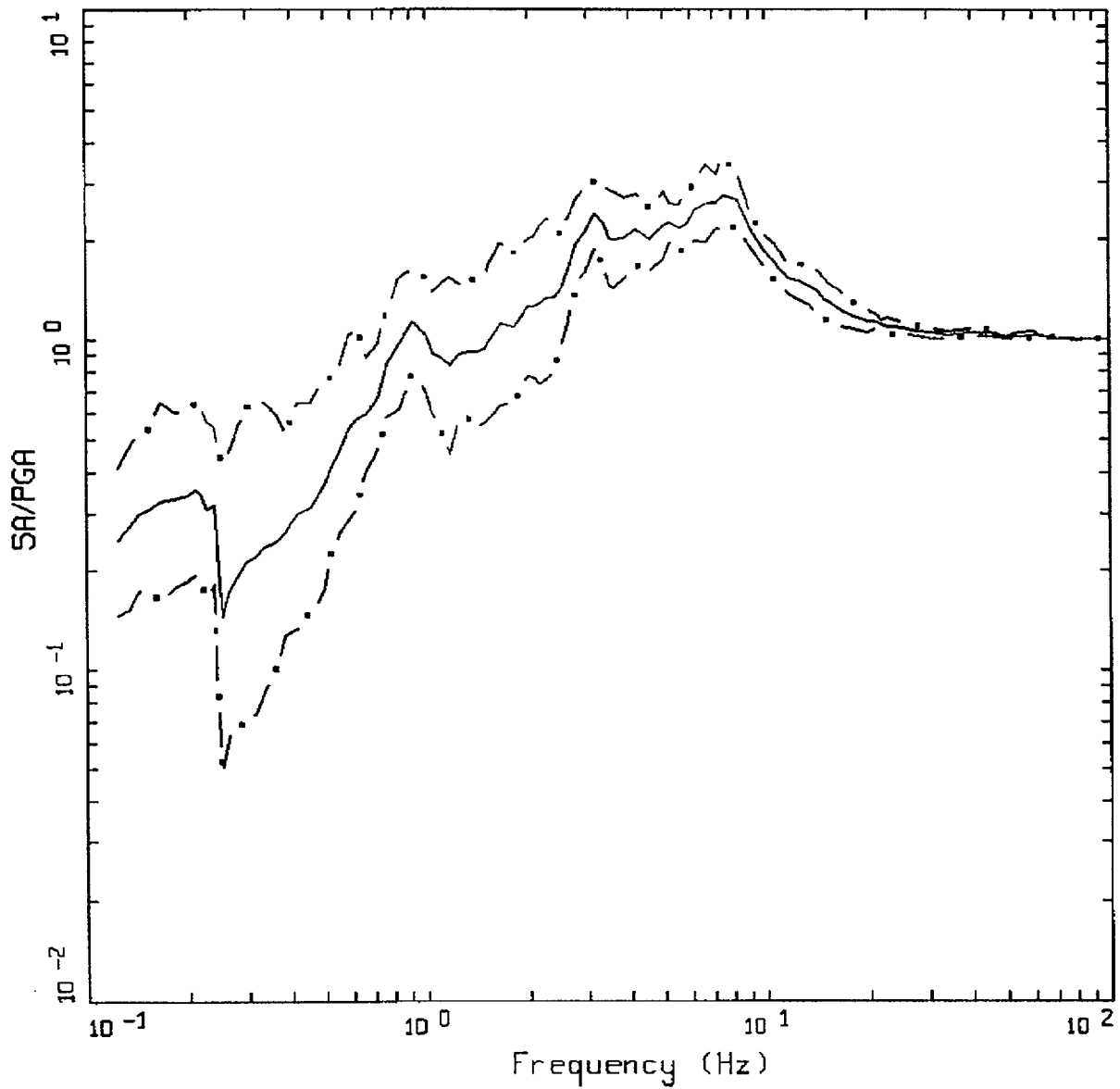
Figure C-48. Median $\pm 1 \sigma$ spectral shapes for $M \approx 7.5$, $R = 50-100$ km, vertical, WUS soil.



AVERAGE VERTICAL SPECTRA
 M=5.5 (5.0-6.0), R=100-200 KM, ROCK
 AVERAGE M = 5.40, AVERAGE DISTANCE = 107.80 KM

LEGEND
 ————— 50TH PERCENTILE
 - - - - - 16TH PERCENTILE
 - . - . - 84TH PERCENTILE

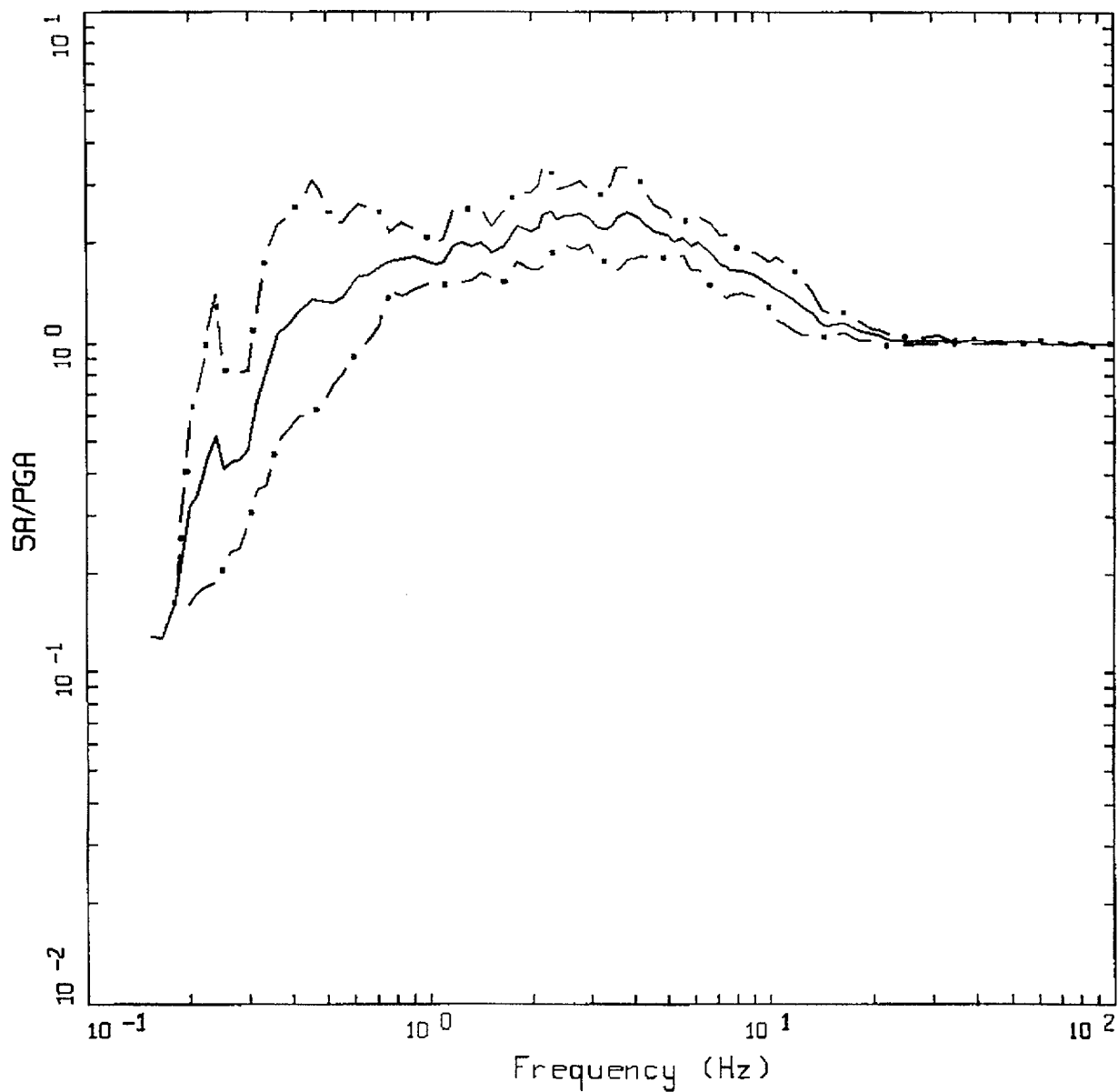
Figure C-49. Median $\pm 1 \sigma$ spectral shapes for $M \approx 5.5$, $R = 100-200$ km, vertical, WUS rock.



AVERAGE VERTICAL SPECTRA
 M=6.5 (6.0-7.0), R=100-200 KM, ROCK
 AVERAGE M = 6.64, AVERAGE DISTANCE = 114.57 KM

LEGEND
 ——— 50TH PERCENTILE
 - - - 16TH PERCENTILE
 - . - 84TH PERCENTILE

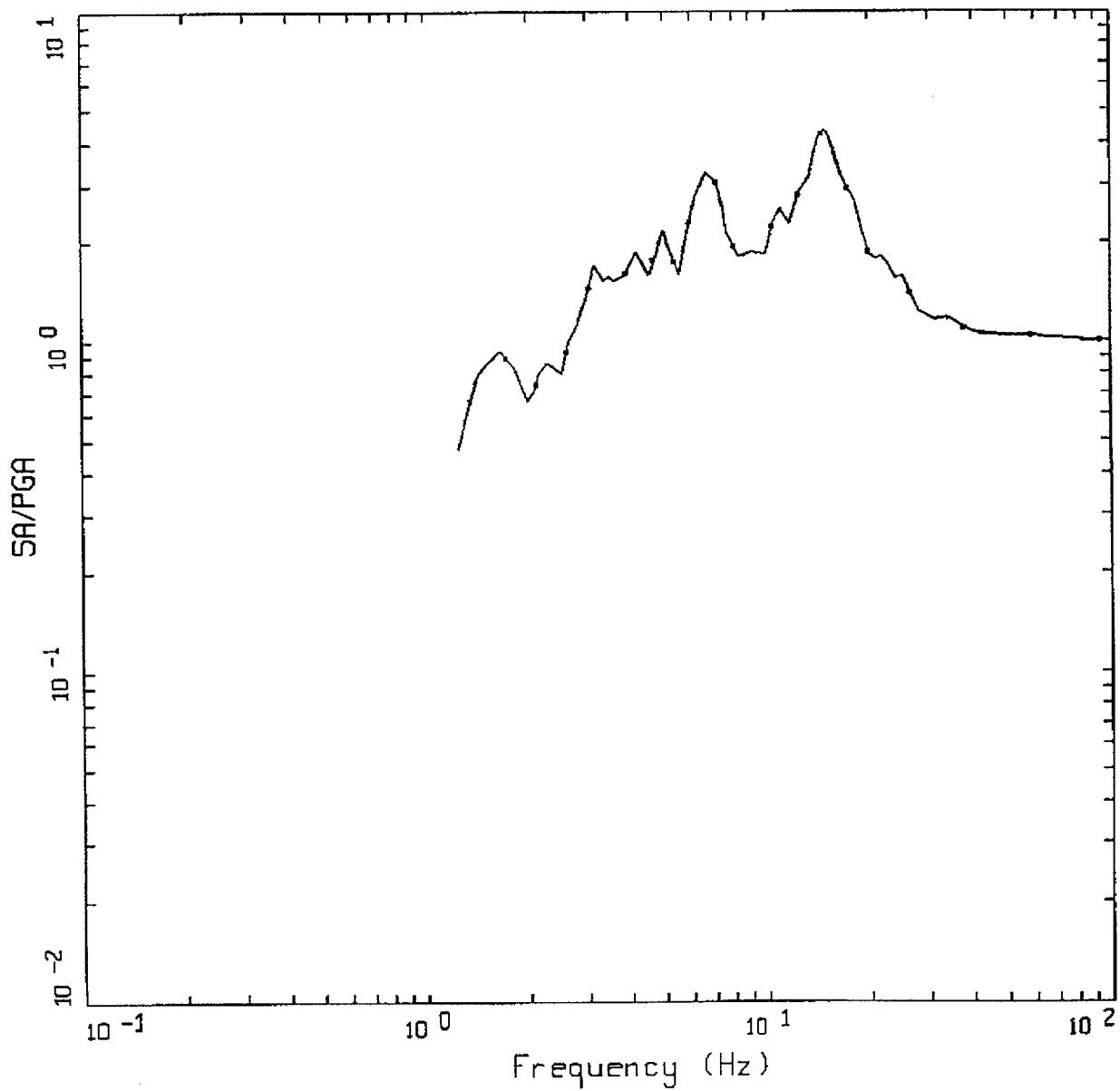
Figure C-50. Median $\pm 1 \sigma$ spectral shapes for $M \approx 6.5$, $R = 100-200$ km, vertical, WUS rock.



AVERAGE VERTICAL SPECTRA
 M=7.5 (7.0-7.0+), R=100-200 KM, ROCK
 AVERAGE M = 7.30, AVERAGE DISTANCE = 152.01 KM

LEGEND
 ————— 50TH PERCENTILE
 - - - - - 16TH PERCENTILE
 - . - . - 84TH PERCENTILE

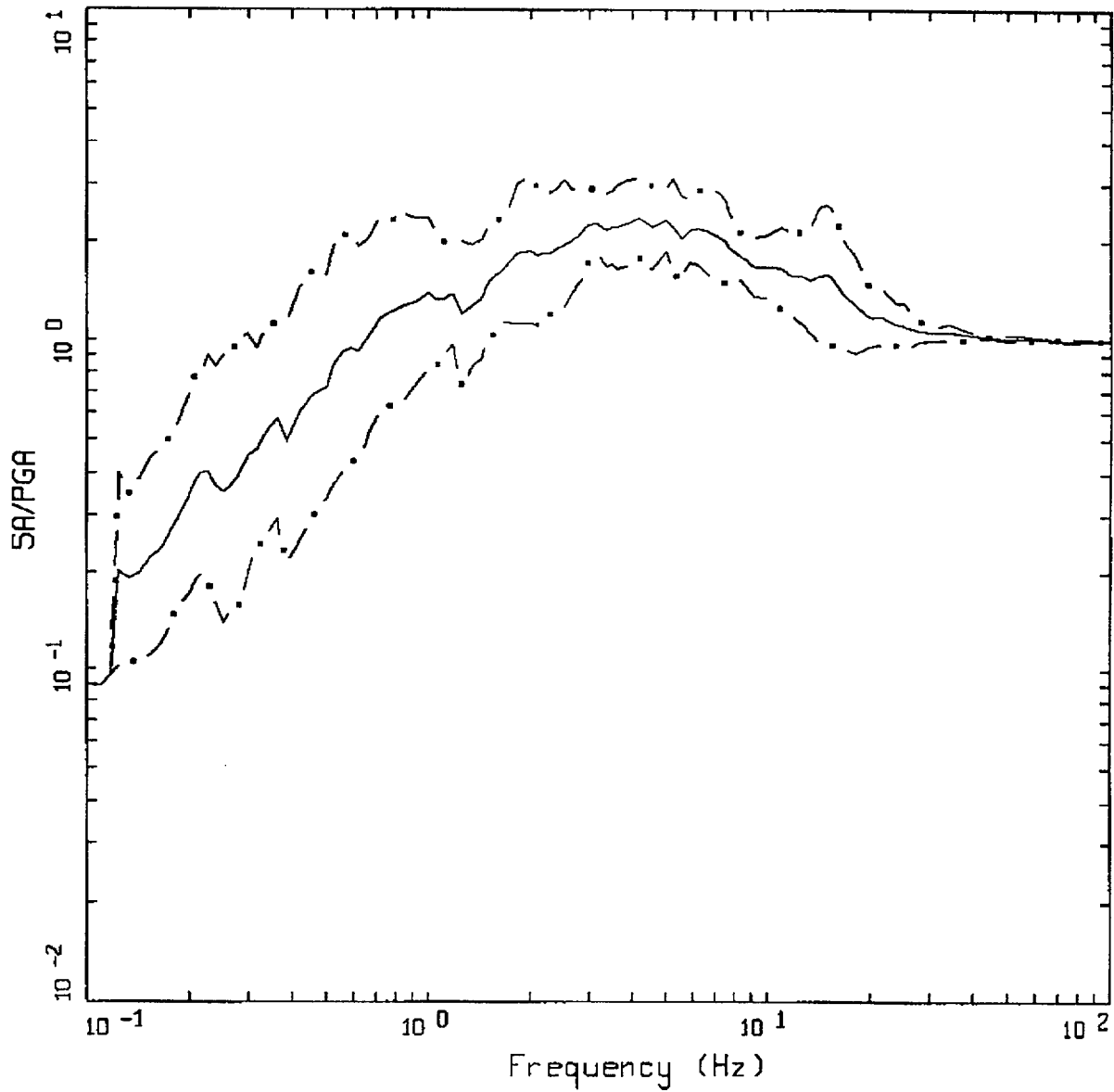
Figure C-51. Median $\pm 1 \sigma$ spectral shapes for $M \approx 7.5$, $R = 100-200$ km, vertical, WUS rock.



AVERAGE VERTICAL SPECTRA
 M=5.5 (5.0-6.0), R=100-200 KM, SOIL
 AVERAGE M = 6.0, AVERAGE DISTANCE = 105.00 KM

- LEGEND
- 50TH PERCENTILE
 - . - 16TH PERCENTILE
 - . . 84TH PERCENTILE

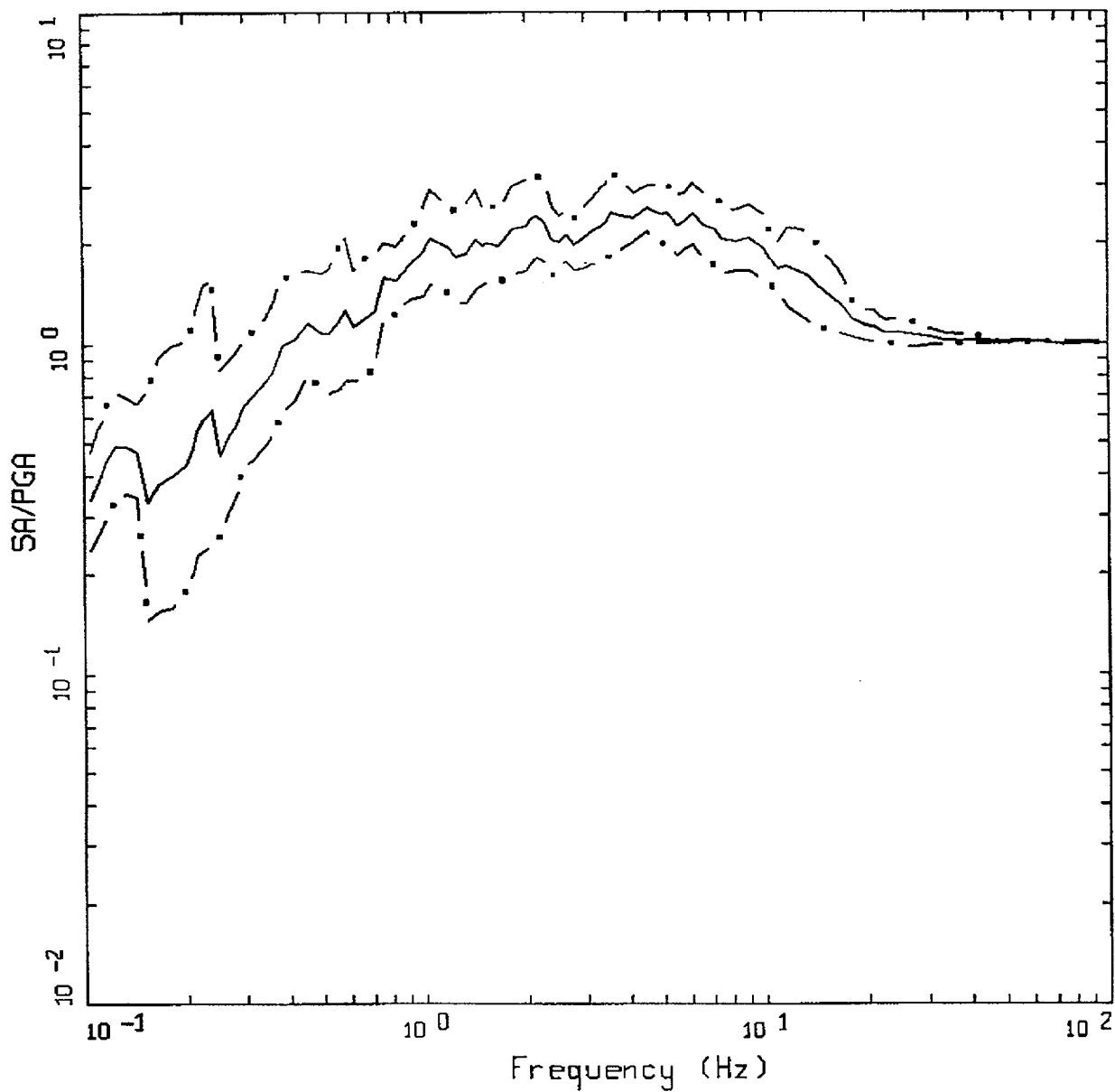
Figure C-52. Median $\pm 1 \sigma$ spectral shapes for $M \approx 5.5$, $R = 100-200$ km, vertical, WUS soil.



AVERAGE VERTICAL SPECTRA
 M=6.5 (6.0-7.0), R=100-200 KM, SOIL
 AVERAGE M = 6.64, AVERAGE DISTANCE = 132.97 KM

LEGEND
 — 50TH PERCENTILE
 - · - 16TH PERCENTILE
 - · - 84TH PERCENTILE

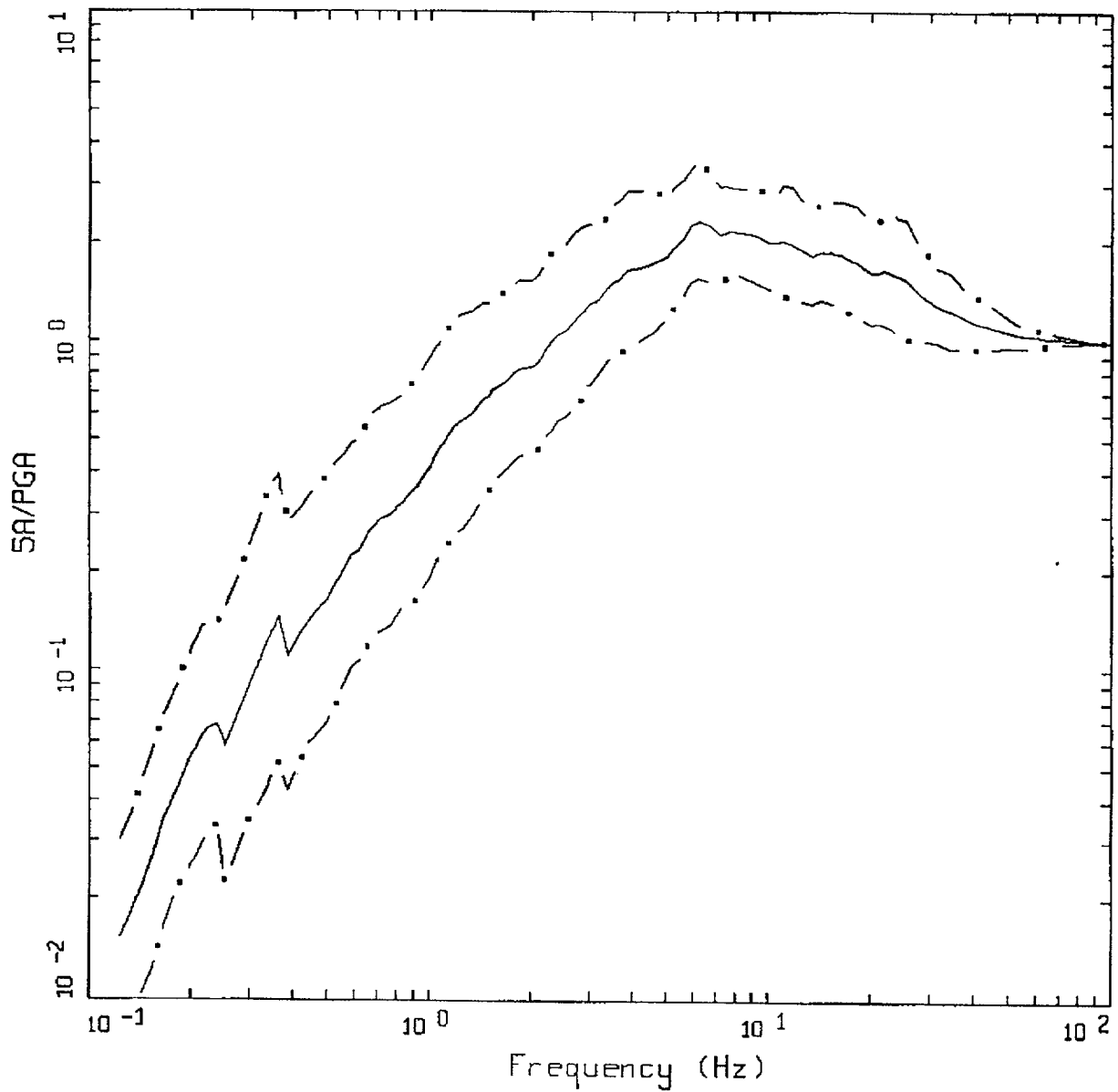
Figure C-53. Median $\pm 1 \sigma$ spectral shapes for $M \approx 6.5$, $R = 100-200$ km, vertical, WUS soil.



AVERAGE VERTICAL SPECTRA
 M=7.5 (7.0-7.0+), R=100-200 KM, SOIL
 AVERAGE M = 7.31, AVERAGE DISTANCE = 147.07 KM

LEGEND
 — 50TH PERCENTILE
 - - - 15TH PERCENTILE
 - . - 84TH PERCENTILE

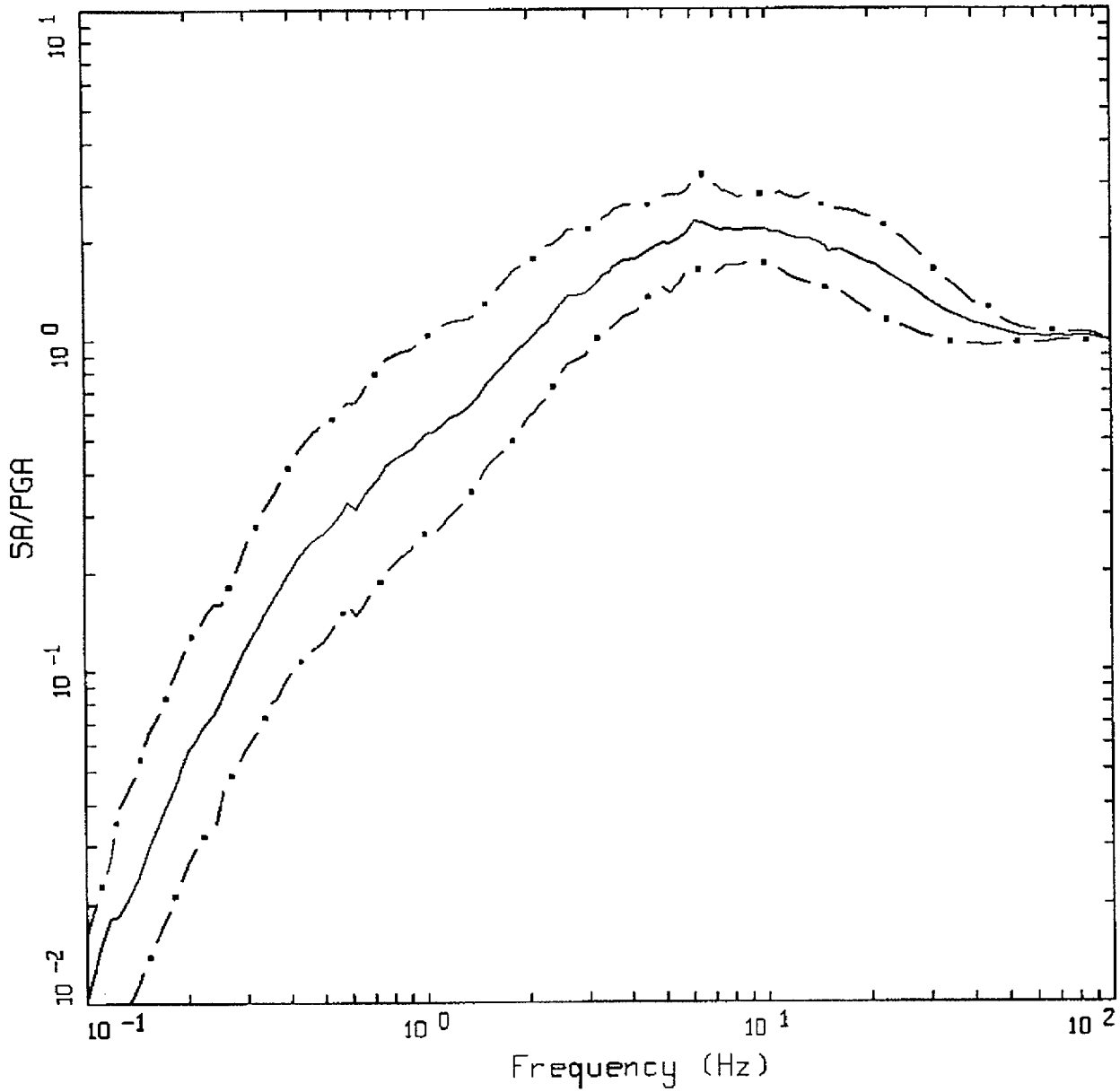
Figure C-54. Median $\pm 1 \sigma$ spectral shapes for $M \approx 7.5$, $R = 100-200$ km, vertical, WUS soil.



AVERAGE VERTICAL SPECTRA
 M=5.5 (5.0-6.0), R=0-50 KM, ROCK
 AVERAGE M = 5.57, AVERAGE DISTANCE = 19.91 KM

LEGEND
 ————— 50TH PERCENTILE
 - - - - - 16TH PERCENTILE
 - . - . - 84TH PERCENTILE

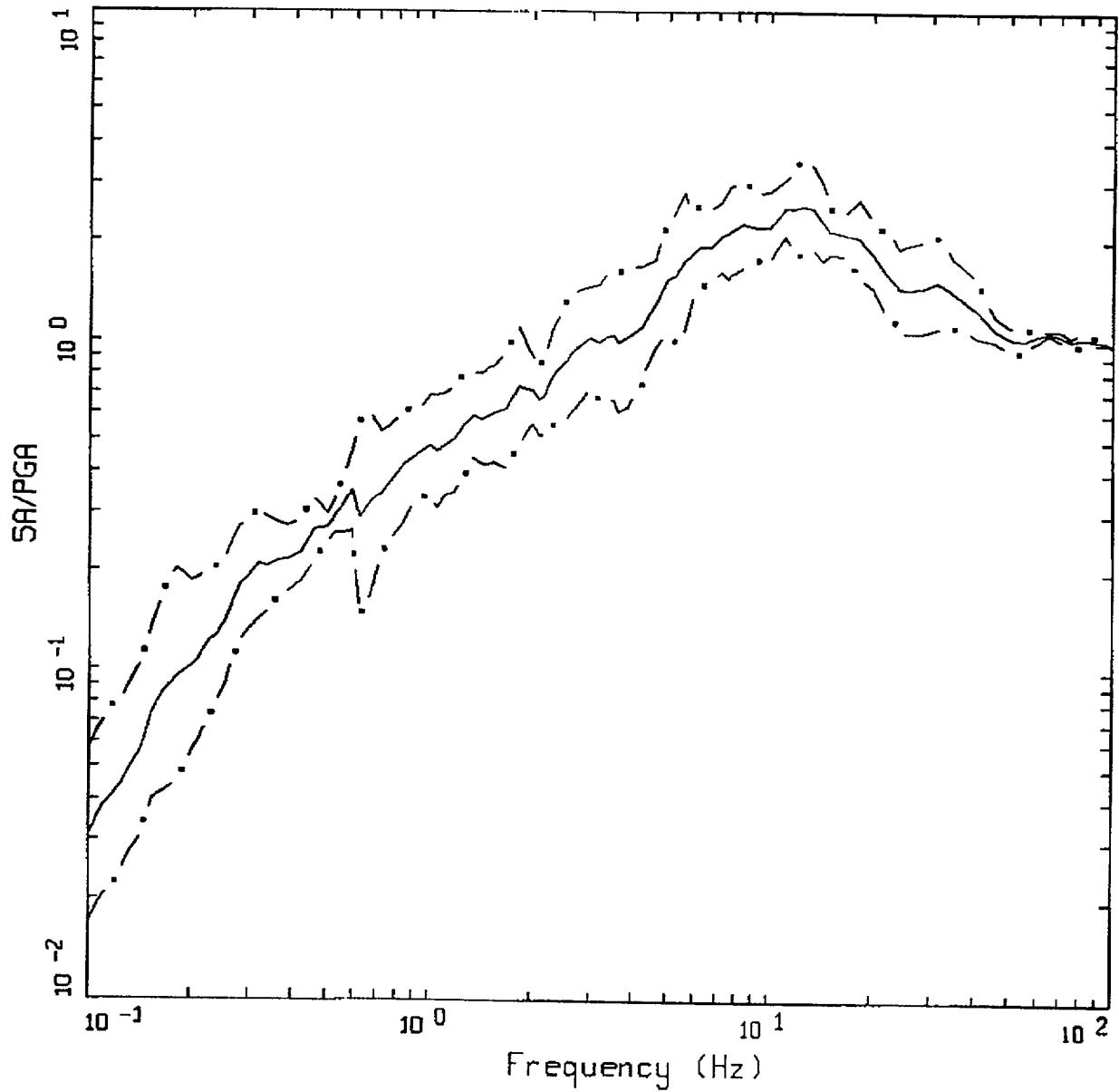
Figure C-55. Median $\pm 1 \sigma$ spectral shapes for $M \approx 5.5$, $R = 0-50$ km, vertical, WUS rock.



AVERAGE VERTICAL SPECTRA
 M=6.5 (6.0-7.0), R=0-50 KM, ROCK
 AVERAGE M = 6.44, AVERAGE DISTANCE = 27.39 KM

LEGEND
 ————— 50TH PERCENTILE
 - . - . 16TH PERCENTILE
 - . - . 84TH PERCENTILE

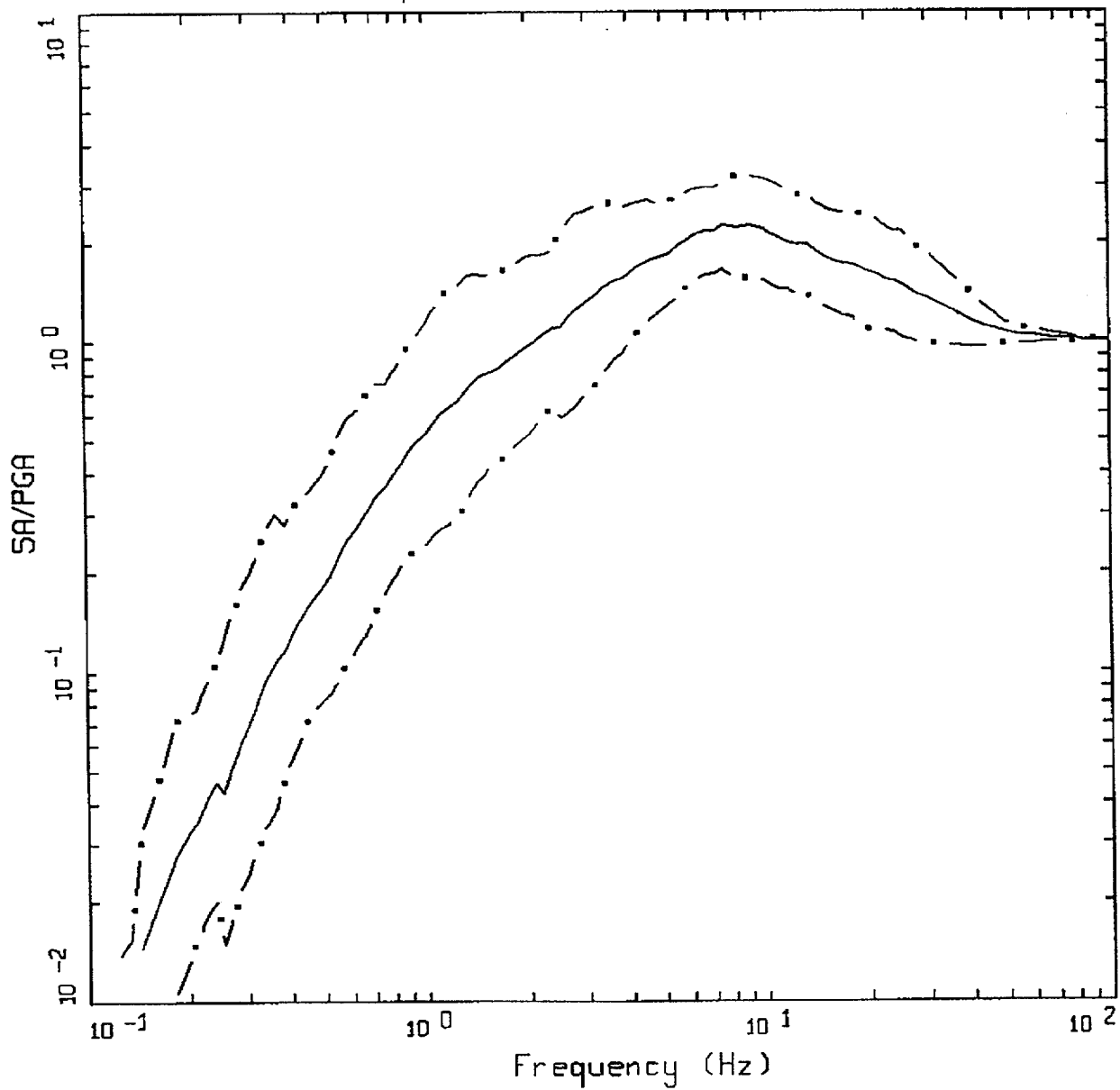
Figure C-56. Median $\pm 1 \sigma$ spectral shapes for $M \approx 6.5$, $R = 0-50$ km, vertical, WUS rock.



AVERAGE VERTICAL SPECTRA
 M=7.5 (7.0-7.0+), R=0-50 KM, ROCK
 AVERAGE M = 7.27, AVERAGE DISTANCE = 17.60 KM

LEGEND
 ————— 50TH PERCENTILE
 - - - - - 16TH PERCENTILE
 - . - . - 84TH PERCENTILE

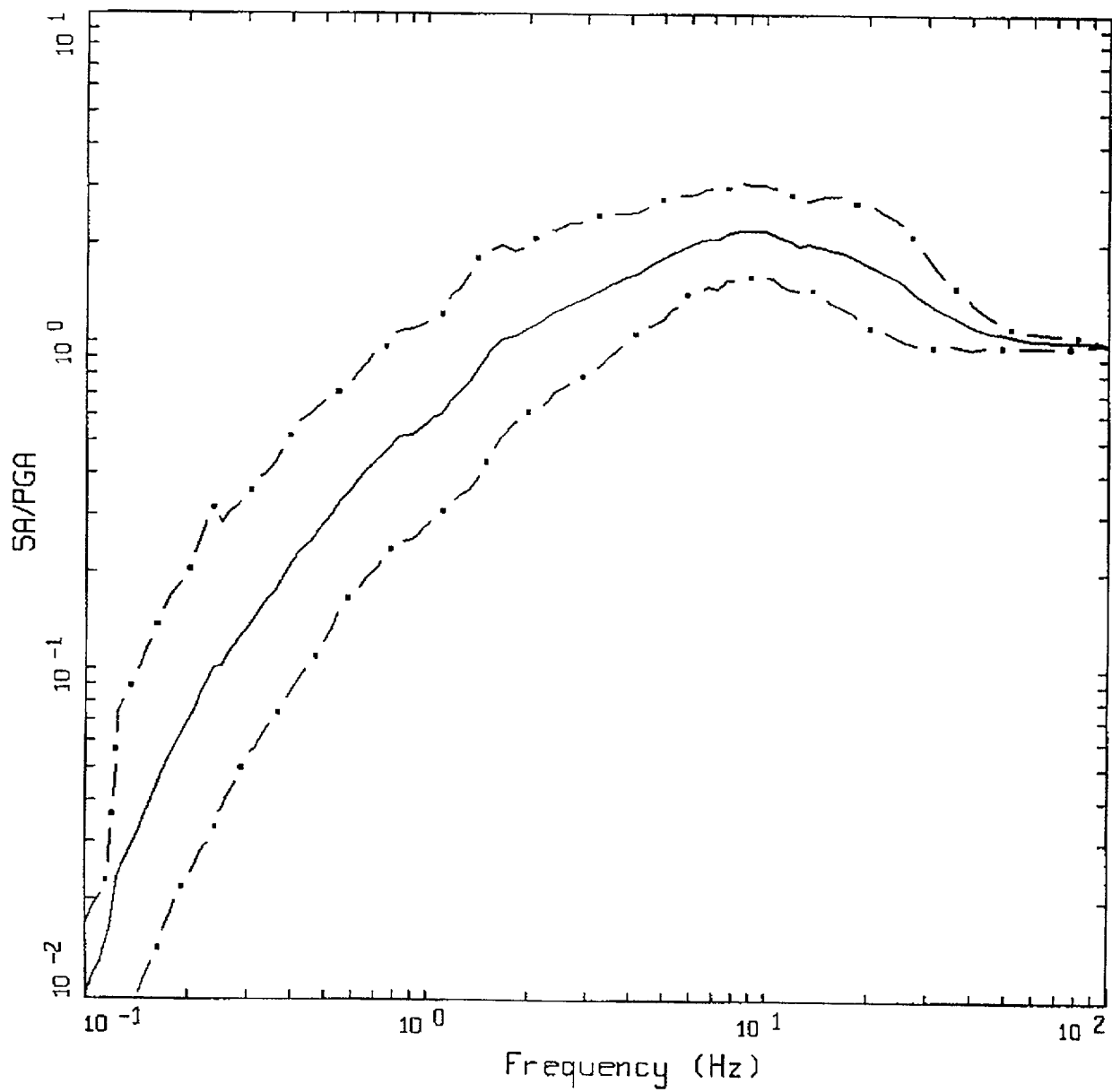
Figure C-57. Median $\pm 1 \sigma$ spectral shapes for $M \approx 7.5$, $R = 0-50$ km, vertical, WUS rock.



AVERAGE VERTICAL SPECTRA
 M=5.5 (5.0-6.0), R=0-50 KM, SOIL
 AVERAGE M = 5.69, AVERAGE DISTANCE = 21.10 KM

LEGEND
 ————— 50TH PERCENTILE
 - . - . 16TH PERCENTILE
 - . - . 84TH PERCENTILE

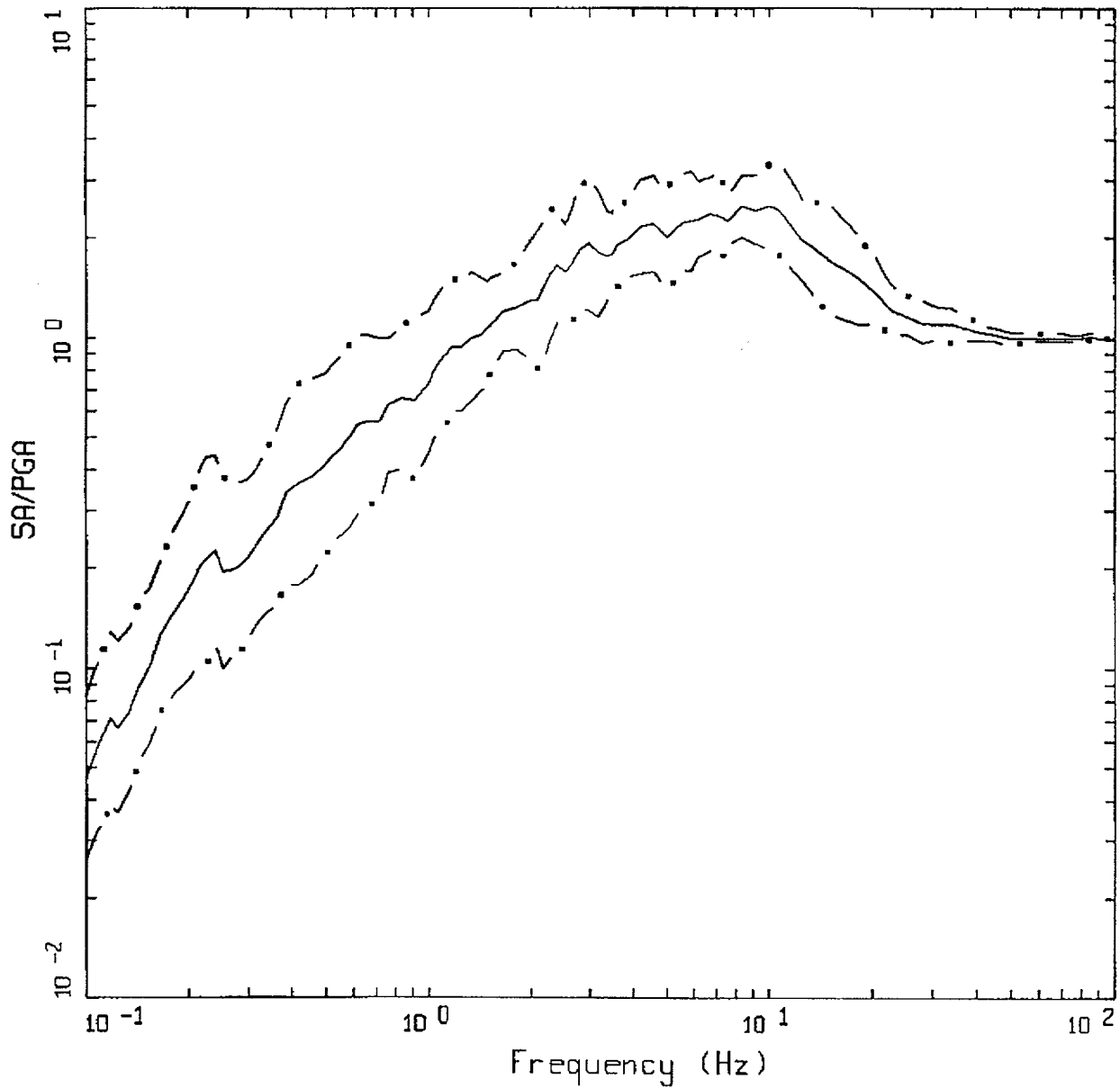
Figure C-58. Median $\pm 1 \sigma$ spectral shapes for $M \approx 5.5$, $R = 0-50$ km, vertical, WUS soil.



AVERAGE VERTICAL SPECTRA
 M=6.5 (6.0-7.0), R=0-50 KM, SOIL
 AVERAGE M = 6.37, AVERAGE DISTANCE = 25.50 KM

LEGEND
 ————— 50TH PERCENTILE
 - . - 16TH PERCENTILE
 - . . - 84TH PERCENTILE

Figure C-59. Median $\pm 1 \sigma$ spectral shapes for $M \approx 6.5$, $R = 0-50$ km, vertical, WUS soil.



AVERAGE VERTICAL SPECTRA
 M=7.5 (7.0-7.0+), R=0-50 KM, SOIL
 AVERAGE M = 7.27, AVERAGE DISTANCE = 31.82 KM

LEGEND
 — 50TH PERCENTILE
 - • - 16TH PERCENTILE
 - • - 84TH PERCENTILE

Figure C-60. Median $\pm 1 \sigma$ spectral shapes for $M \approx 7.5$, $R = 0-50$ km, vertical, WUS soil.

APPENDIX D STOCHASTIC POINT SOURCE GROUND MOTION MODEL

D.1 Background

The stochastic point source model may be termed a spectral model in that it fundamentally describes the Fourier amplitude spectral density at the surface of a half-space (Hanks and McGuire, 1981). The model uses a Brune (1970, 1971) omega-squared description of the earthquake source Fourier amplitude spectral density. This model is easily the most widely used and qualitatively validated source description available. Seismic sources ranging from $M = -6$ (hydrofracture) to $M = 8$ have been interpreted in terms of the Brune omega-squared model in dozens of papers over the last 30 years. The general conclusion is that it provides a reasonable and consistent representation of crustal sources, particularly for tectonically active regions such as plate margins. A unique phase spectrum can be associated with the Brune source amplitude spectrum to produce a complex spectrum that can be propagated using either exact or approximate (1-, 2- or 3-D) wave propagation algorithms to produce single or multiple component time histories. In this context the model is not stochastic, it is decidedly deterministic and as exact and rigorous as one chooses. A two-dimensional array of such point sources may be appropriately located on a fault surface (area) and fired with suitable delays to simulate rupture propagation on an extended rupture plane. As with the single-point source, any degree of rigor may be used in the wave propagation algorithm to produce multiple-component or average horizontal-component time histories. The result is a kinematic¹ finite-source model that has as its basis a source time history defined as a Brune pulse whose Fourier amplitude spectrum follows an omega-squared model. This finite-fault model would be very similar to that used in published inversions for slip models if the 1-D propagation were treated using a reflectivity algorithm (Aki and Richards, 1980). This algorithm is a complete solution to the wave equation from static offsets (near-field terms) to an arbitrarily selected high frequency cutoff (generally 1-2 Hz).

Alternatively, to model the wave propagation more accurately, recordings of small earthquakes at the site of interest (with source locations distributed along the fault of interest) may be used as empirical Green functions (Hartzell, 1978). To model the design earthquake, the empirical Green's functions are delayed and summed in a manner to simulate rupture propagation (Hartzell, 1978). Provided (a) sufficient small earthquakes are recorded at the site of interest, (b) the source locations adequately cover the expected rupture surface, and (c) sufficient low frequency energy is present in the Green's functions, this would be the most appropriate procedure to use if nonlinear site response is not an issue. With this approach the wave propagation is, in principle, exactly represented from each Green's function source to the site. However, nonlinear site response is not treated unless Green's function motions are recorded at a nearby rock outcrop with dynamic material properties similar to the rock underlying the soils at the site, or recordings are made at depth within the site soil column. These motions may then be used as input to either total or effective stress site response codes to model nonlinear effects. Important issues associated with this approach include the availability of an appropriate nearby (1 to 2 km) rock outcrop and, for the downhole recordings, the necessity to

¹Kinematic source model is one whose slip (displacement) is defined (imposed) while in a dynamic source model forces (stress) are defined (see Aki and Richards 1980 for a complete description).

remove all downgoing energy from the at-depth soil recordings. The downgoing energy must be removed from the downhole Green's functions (recordings) prior to generating the control motions (summing) as only the upgoing wavefields are used as input to the nonlinear site response analyses. Removal of the downgoing energy from each recording requires multiple site response analyses that model uncertainty in the Green's functions resulting from uncertainty in dynamic material properties and from the numerical site response model used to separate the upgoing and downgoing wavefields.

To alleviate these difficulties one can use recordings widely distributed in azimuth at close distances to a small earthquake and correct the recordings back to the source by removing wave propagation effects using a simple approximation (say $1/R$ or generalized rays plus a constant for crustal amplification and radiation pattern), to obtain an empirical source function. This source function can be used to replace the Brune pulse to introduce some natural (although source, path, and site specific) variation into the dislocation time history. If this is coupled to an approximate wave propagation algorithm (asymptotic ray theory) that includes the direct rays and those that have undergone a single reflection, the result is the empirical source function method (EPRI, 1993). Combining the reflectivity propagation (which is generally limited to frequencies $\leq 1-2$ Hz due to computational demands) with the empirical source function approach (appropriate for frequencies ≥ 1 Hz; EPRI, 1993) results in a broad band simulation procedure. This method is strictly deterministic at low frequencies (where an analytical source function is used) and incorporates some natural variation at high frequencies through the use of an empirical source function (Somerville et al., 1995).

All of these techniques are fundamentally similar, well founded in seismic source and wave propagation physics, and importantly, they are *all* approximate. Simply put, all models are inexact and the single essential element in selecting a model is to incorporate the appropriate degree of rigor, commensurate with uncertainties and variabilities in crustal structure and site effects, through extensive validation exercises. It is generally felt that more complicated models produce more accurate results. However, the implication that is often overlooked is that more sophisticated models require an increased number of parameters that must be specified. This is not too serious a consequence in modeling past earthquakes since a reasonable range in parameter space can be explored to give the "best" results. For future predictions, however, this increased rigor may carry undesirable baggage in increased parametric variability (Roblee et al., 1996). The effects of lack of knowledge (epistemic uncertainty; EPRI, 1993) regarding parameter values for future occurrences results in uncertainty or variability in ground motion predictions. It may easily be the case that a very simple model such as the point source model can have comparable, or even smaller, total variability (modeling plus parametric) than a much more rigorous model with an increased number of parameters (EPRI, 1993). What is desired in a model is sufficient sophistication that it captures the dominant and stable features of source, distance, and site dependencies observed in strong ground motions. It is these considerations that led to the development of the stochastic point source model and, in part, leads to the stochastic element of the models.

The stochastic nature of the point source RVT model is simply the assumption made about the character of ground motion time histories that permits stable estimates of peak parameters (e.g. acceleration, velocity, strain, stress, oscillator response) to be made without computing detailed time histories (Hanks and McGuire, 1981; Boore, 1983). This process uses random vibration theory to relate a time domain peak value to the time history root-mean-square (RMS) value (Boore, 1983).

An important assumption is that the process is normally distributed random noise and stationary (its statistics do not change with time) over its duration. A visual examination of any time history quickly reveals that this is clearly not the case: time histories (acceleration, velocity, stress, strain, oscillator) start, build up, and then diminish with time. However, during the critical strong-motion part of the shaking, the assumption is accurate enough to permit the approach to work surprisingly well, as numerous comparisons with recorded motions and both qualitative and quantitative validations have shown (Hanks and McGuire, 1981; Boore, 1983, 1986; McGuire et al., 1984; Boore and Atkinson, 1987, Silva and Lee, 1987; Toro and McGuire, 1987; Silva et al., 1990; EPRI, 1993; Schneider et al., 1993; Silva and Darragh, 1995). Corrections to RVT are available to accommodate different distributions as well as non-stationarity and are usually applied to the estimation of peak oscillator response in the calculated response spectra (Boore and Joyner, 1984; Toro, 1985).

D.2 Point Source Model Description

The conventional stochastic ground motion model uses an ω -squared source model (Brune, 1970, 1971) with a single-corner frequency and a constant stress drop (Boore, 1983; Atkinson, 1984). Random vibration theory is used to relate RMS (root-mean-square) values to peak values of acceleration (Boore, 1983), and oscillator response (Boore and Joyner, 1984; Toro, 1985; Silva and Lee, 1987) computed from the power spectra to expected peak time domain values (Boore, 1983).

The shape of the Fourier amplitude spectrum of acceleration $FA(f)$, is given by

$$FA(f) = C \frac{f^2}{1 + \left(\frac{f}{f_0}\right)^2} \frac{M_0}{R} P(f) A(f) e^{-\frac{\pi f R}{\beta_0 Q(f)}} \quad (D-1)$$

where

$$C = \left(\frac{1}{\rho_0 \beta_0^3}\right) \cdot (2) \cdot (0.55) \cdot \left(\frac{1}{\sqrt{2}}\right) \cdot \pi.$$

- M_0 = seismic moment,
- R = hypocentral distance,
- β_0 = shear-wave velocity at the source,
- ρ_0 = crustal density at the source
- $Q(f)$ = frequency dependent quality factor (crustal damping),
- $A(f)$ = crustal amplification,
- $P(f)$ = high-frequency truncation filter,
- f_0 = source corner frequency.

C is a constant that contains source region density (ρ_0) and shear-wave velocity (β_0) terms and accounts for the free-surface effect (factor of 2), the source radiation pattern averaged over a sphere (0.55) (Boore, 1986), and the partition of energy into two horizontal components ($1/\sqrt{2}$).

Source scaling is provided by specifying two independent parameters, the seismic moment (M_0) and the high-frequency stress parameter or stress drop ($\Delta\sigma$). The seismic moment is related to magnitude through the definition of moment magnitude M by the relation

$$\log M_0 = 1.5 M + 16.05 \quad (\text{Hanks and Kanamori, 1979}) \quad (\text{D-2})$$

The stress drop ($\Delta\sigma$) relates the corner frequency f_0 to M_0 through the relation

$$f_0 = \beta_0 (\Delta\sigma/8.44 M_0)^{1/3} \quad (\text{Brune; 1970, 1971}) \quad (\text{D-3})$$

The stress drop is sometimes referred to as the high frequency stress parameter (Boore, 1983) (or simply the stress parameter) since it directly scales the Fourier amplitude spectrum for frequencies above the corner frequency (Silva, 1991; Silva and Darragh 1995). High (> 1 Hz) frequency model predictions are very sensitive to this parameter (Silva, 1991; EPRI, 1993) and the interpretation of it being a stress drop or simply a scaling parameter depends upon how well real earthquake sources (on average) obey the omega-squared scaling (Equation D-3) and how well they are fit by the single-corner-frequency model. If earthquakes truly have single-corner-frequency omega-squared sources, the stress drop in Equation D-3 is a physical parameter and its values have a physical interpretation of the forces (stresses) accelerating the relative slip across the rupture surface. High stress drop sources result from a smaller fault rupture area (for the same M) than low stress drop sources (Brune, 1970). Less physically, stress drop can be viewed as simply a high frequency scaling or fitting parameter.

The spectral shape of the single-corner-frequency ω -squared source model is then described by the two free parameters M_0 and $\Delta\sigma$. The corner frequency increases with the shear-wave velocity and with increasing stress drop, both of which may be region dependent.

Crustal amplification accounts for the increase in wave amplitude as seismic energy travels through lower-velocity crustal materials from the source to the surface. The amplification depends on average crustal and near surface shear-wave velocity and density (Boore, 1986).

The $P(f)$ filter in equation (D-1) is used in an attempt to model the observation that acceleration spectral density appears to fall off rapidly beyond some region- or site-dependent maximum frequency (Hanks, 1982; Silva and Darragh, 1995). This observed phenomenon truncates the high frequency portion of the spectrum and is responsible for the band-limited nature of the stochastic model. The band limits are the source corner frequency at low frequency and the high frequency spectral attenuation. This spectral fall-off at high frequency has been attributed to near-site attenuation (Hanks, 1982; Anderson and Hough, 1984) or to source processes (Papageorgiou and Aki, 1983) and perhaps results from both effects. In the Anderson and Hough (1984) attenuation model, adopted here, the form of the $P(f)$ filter is taken as

$$P(f, r) = e^{-\pi\kappa(r)f} \quad (\text{D-4})$$

($\kappa(r)$ in Equation D-4 is a site- and distance-dependent parameter that represents the effect of intrinsic attenuation upon the wavefield as it propagates through the crust from source to receiver.

$\kappa(r)$ depends on epicentral distance (r) and on both the shear-wave velocity (β) and quality factor (Q_s) averaged over a depth of H beneath the site (Hough et al., 1988;). At zero epicentral distance $\kappa(0)$ is given by

$$\kappa(0) = \frac{H}{\bar{\beta} \bar{Q}_s} \quad (D-5)$$

and is referred to as simply κ .

The bars in Equation D-5 represents an average of β and Q_s over a depth H . The value of κ at zero epicentral distance is attributed to attenuation in the very shallow crust directly below the site (Hough and Anderson, 1988; Silva and Darragh, 1995). The intrinsic attenuation along this part of the path is not thought to be frequency dependent and is modeled as a frequency independent, (although site- and crustal-region dependent) constant value of κ (Hough et al., 1988; Rovelli et al., 1988). This zero epicentral distance κ is the model implemented in this study.

The crustal path attenuation from the source to just below the site is modeled with the frequency-dependent quality factor $Q(f)$. Thus the distance component of the original $\kappa(r)$ (Equation D-4) is accommodated by $Q(f)$ and R in the last term of Equation D-1:

$$\kappa(r) = \frac{H}{\bar{\beta} \bar{Q}_s} + \frac{R}{\beta_0 Q(f)} \quad (D-6)$$

The Fourier amplitude spectrum, $FA(f)$, given by Equation D-1 represents the stochastic ground motion model employing a Brune source spectrum that is characterized by a single corner frequency. It is a point source and models direct shear-waves in a homogeneous half-space (with effects of a velocity gradient captured by the $A(f)$ filter, Equation D-1). For horizontal motions, vertically propagating shear-waves are assumed. Validations using incident inclined SH-waves accompanied with raytracing to find appropriate incidence angles leaving the source showed little reduction in uncertainty compared to results using vertically propagating shear-waves. For vertical motions, P/SV propagators are used in addition to raytracing to model incident inclined plane waves (Appendix K and EPRI, 1993). This approach has been validated with recordings from the 1989 M 6.9 Loma Prieta earthquake (EPRI, 1993).

Equation D-1 represents an elegant ground motion model that accommodates source and wave propagation physics as well as propagation path and site effects with an attractive simplicity. The model is appropriate for an engineering characterization of ground motion since it captures the general features of strong ground motion in terms of peak acceleration and spectral composition with a minimum of free parameters (Boore, 1983; McGuire et al., 1984; Boore, 1986; Silva and Green, 1988; Silva et al., 1988; Schneider et al., 1993; Silva and Darragh, 1995). An additional important aspect of the stochastic model employing a simple source description is that the region-dependent parameters may be evaluated by observations of small local or regional earthquakes. Region-specific seismic hazard evaluations can then be made for areas with sparse strong motion data with relatively simple spectral analyses of weak motion (Silva, 1992).

In order to compute peak time-domain values, i.e. peak acceleration and oscillator response, RVT is used to relate RMS computations to peak value estimates. Boore (1983) and Boore and Joyner (1984) present an excellent development of the RVT methodology as applied to the stochastic ground motion model. The procedure involves computing the RMS value by integrating the power spectrum from zero frequency to the Nyquist frequency and applying Parseval's relation. Extreme value theory is then used to estimate the expected ratio of the peak value to the RMS value of a specified duration of the stochastic time history. The duration is generally taken as the inverse of the source corner frequency plus a term that increases with distance (Boore, 1983).

Factors that affect strong ground motions such as surface topography, finite and propagating seismic sources, laterally varying near-surface velocity and Q gradients, and random inhomogeneities along the propagation path are not included in the model. While some or all of these factors are generally present in any observation of ground motion and may exert controlling influences in some cases, the simple stochastic point source model appears to be robust in predicting median or average properties of ground motion (Boore 1983, 1986; Schneider et al., 1993; Silva, 1993). For this reason it represents a powerful predictive and interpretative tool for engineering characterization of strong ground motion.

D.3 Site Effects Model

To model soil and soft rock response, an RVT-based equivalent-linear approach is used by propagating either the point source outcrop power spectral density through a one-dimensional column. RVT is used to predict peak time domain values of shear-strain based upon the shear-strain power spectrum. In this sense, the procedure is analogous to the program SHAKE (Schnabel et al., 1972) except that peak shear strains in SHAKE are measured in the time domain. The purely frequency domain approach obviates a time domain control motion and, perhaps just as significantly, eliminates the need for a suite of analyses based on different input motions. This arises because each time domain analysis may be viewed as one realization of a random process. In this case, several realizations of the random process must be sampled to have a statistically stable estimate of site response. The realizations are usually performed by employing different control motions whose response spectrum matches a specified target. In the frequency-domain approach, the estimates of peak shear strains and oscillator response are, as a result of the RVT, fundamentally probabilistic in nature. Stable estimates of site response can then be rapidly computed permitting statistically significant estimates of uncertainties based on parametric variations.

The parameters that influence computed response include the shear-wave velocity profile and the strain dependencies of both the shear modulus and shear-wave damping.

D.4 Partition and Assessment of Ground Motion Variability

An essential requirement of any numerical modeling approach, particularly one that is implemented in the process of defining design ground motions, is a quantitative assessment of prediction accuracy. This means that one must characterize the variability associated with model predictions. For a ground motion model, prediction variability is comprised of two components: modeling variability and parametric variability. Modeling variability is a measure of how well the model works (how

accurately it predicts ground motions) when specific parameter values are known. Modeling variability is measured by misfits of model predictions to recorded motions through validation exercises and results from unaccounted components in the source, path, and site models (e.g. a point source cannot model the effects of directivity, and linear site response cannot accommodate nonlinear effects). Parametric variability results from a range of values for model parameters (i.e. slip distribution, soil profile, G/G_{\max} and hysteretic damping curves). It is the sensitivity of a model to a range of values for model parameters. The total variability, modeling plus parametric, represents the variance associated with the ground motion prediction and, because it is a necessary component in estimating fractile levels, may be regarded as important as median predictions.

Both the modeling and parametric variabilities may have components of randomness and uncertainty. Table D-1 summarizes the four components of total variability in the context of ground motion predictions. Uncertainty is that portion of both modeling and parametric variability that, in principle, can be reduced as additional information becomes available, whereas randomness represents the intrinsic or irreducible component of variability for a given model or parameter. Randomness is that component of variability that is intrinsic or irreducible *for a given model*. The uncertainty component reflects a lack of knowledge and may be reduced as more data are analyzed. For example, in the point source model, stress drop is generally taken to be independent of source mechanism and tectonic region, and is found to have a standard error of about 0.7 (natural log) (EPRI, 1993). This variation or uncertainty plus randomness in $\Delta\sigma$ results in a variability in ground motion predictions for future earthquakes. If, for example, it is found that normal faulting earthquakes have generally lower stress drops than strike-slip events, which are, in turn, lower than reverse mechanism events, perhaps much of the variability in $\Delta\sigma$ may be reduced. In extensional regimes, where normal faulting earthquakes are most likely to occur, this new information may provide a reduction in variability (uncertainty component) for stress drop, say to 0.3 or 0.4 resulting in less ground motion variation due to a lack of knowledge of the mean stress drop. There is, however, a component of this stress drop variability that can *never* be reduced in the context of the Brune model. This results simply from the heterogeneity of the earthquake dynamics, which is not accounted for in the model and which results in the randomness component of parametric variability in stress drop. A more sophisticated model may be able to accommodate or model more accurately the source dynamics but, at the expense of a larger number of parameters and increased parametric uncertainty (i.e. finite-fault with slip model and nucleation point as unknown parameters for future earthquakes). That is, more complex models typically seek to reduce modeling randomness by more closely modeling physical phenomena. However, such models often require more comprehensive sets of observed data to constrain additional model parameters, which generally leads to increased parametric variability. If the increased parametric variability is primarily in the form of uncertainty, it is possible to reduce total variability, but only at the additional expense of constraining the additional parameters. Therefore, existing knowledge and/or available resources may limit the ability of more complex models to reduce total variability.

The distinction of randomness and uncertainty is model driven and somewhat arbitrary. The allocation is only important in the context of probabilistic seismic hazard analyses, because uncertainty is treated using alternative hypotheses in logic trees while randomness is integrated over in the hazard calculation (Cornell, 1968). For example, the uncertainty component in stress drop may be treated by using a discrete representation of the stress drop distribution and assigning weights and

specific values. A reasonable three point approximation to a normal distribution is given by weights of 0.2, 0.6, 0.2 for 5%, mean, and 95% values of stress drop respectively. If the distribution of uncertainty in stress drop were such that the 5%, mean, and 95% values were 50, 100, and 200 bars respectively, the stress drop values would be 50 and 200 bars with weights of 0.2, and 100 bars with a weight of 0.6. The randomness component in stress drop variability would then be formally integrated over in the hazard calculation.

D.4.1 Assessment of Modeling Variability

Modeling variability (uncertainty plus randomness) is usually evaluated by comparing response spectra computed from recordings to predicted spectra. The modeling variability is defined as the standard error of the residuals of the log of the average horizontal component (or vertical component) response spectra. The residual is defined as the difference of the logarithms of the observed average 5% damped acceleration response spectra and the predicted response spectra. At each period, the residuals are squared and summed over the total number of sites for one or all earthquakes modeled. Dividing the resultant sum by the number of sites (provided they are statistically independent) results in an estimate of the model variance. Any model bias (average offset) that exists may be estimated in the process (Abrahamson et al., 1990; EPRI, 1993) and used to correct (lower) the variance (and to adjust the median as well). In this approach, the modeling variability can be separated into randomness and uncertainty where the bias-corrected variability represents randomness and the total variability represents randomness plus uncertainty. The uncertainty is captured in the model bias as this may be reduced in the future by refining the model. The remaining variability (randomness) remains irreducible for *this* model. In computing the variance and bias estimates only the frequency range between processing filters at each site (minimum of the 2 components) is used. The causal butterworth filter corners are listed for each site (and component) in the Strong Motion Catalogue (Appendix B).

D.4.2 Assessment of Parametric Variability

Parametric variability, or the variation in ground motion predictions due to uncertainty and randomness in model parameters is difficult to assess. Formally it is straightforward: a Monte Carlo approach may be used with each parameter randomly sampled about its mean (or median) value either individually for sensitivity analyses (Silva, 1992; Roblee et al., 1996) or in combination to estimate the total parametric variability (Silva, 1992; EPRI, 1993). In reality, however, there are two complicating factors.

The first factor involves the specific parameters kept fixed with all earthquakes, paths, and sites when computing the modeling variability. These parameters are then implicitly included in modeling variability provided the data sample a sufficiently wide range in source, path, and site conditions. The parameters that are varied during the assessment of modeling variation should have a degree of uncertainty and randomness associated with them for the next earthquake. Any ground motion prediction should then have a variation reflecting this lack of knowledge and randomness in the free parameters.

An important adjunct to fixed and free parameters is the issue of parameters that may vary but by fixed rules. For example, source rise time is magnitude dependent and is specified by an empirical relation (Silva et al., 1997) in the stochastic finite-source model. In evaluating the modeling variability with different magnitude earthquakes, rise time is varied, but because it follows a strict rule, any variability associated with rise time variation is counted as modeling variability. This is strictly true only if the sample of earthquakes has adequately spanned the space of magnitude, source mechanism, and other factors that may affect rise time. Also, the earthquake to be modeled must be within that validation space. As a result, the validation or assessment of model variation should be done on as large a number of earthquakes of varying sizes and mechanisms as possible.

The second, more obvious factor in assessing parametric variability is a knowledge of the appropriate distributions for the parameters (assuming correct values for median or mean estimates are known). In general, for the stochastic models, median parameter values and uncertainties are based, to the extent possible, on evaluating the parameters derived from previous earthquakes (Silva, 1992; EPRI, 1993).

The parametric variability is site, path, and source dependent and must be evaluated for each application (Roblee et al., 1996). For example, at large source-to-site distances, crustal path damping may control short-period motions. At close distances to a large fault, both the site and finite-source (asperity location and nucleation point) may dominate, and depending upon site characteristics, the source or site may control different frequency ranges (Silva, 1992; Roblee et al., 1996).

In combining modeling and parametric variance, independence is assumed (covariance is zero) and the variances are simply added to give the total variance.

$$\sigma^2_T = \sigma^2_M + \sigma^2_P \quad (D-7),$$

where

σ^2_M = modeling variance,

σ^2_P = parametric variance.

D.4.3 Model Bias And Variance Estimates For The Point Source Model

Results presented here are from a validation exercise sponsored by the Department of Energy. It was begun in 1994 and completed in 1997 (Silva et al., 1997) and included the stochastic finite-source model as well. In this exercise, regional crustal models (for each earthquake) were used along with generic rock and soil profiles (one each) and generic (region specific) G/G_{max} and hysteric damping curves. Region and earthquake specific inversions were done for $Q(f)$ models and point source stress drops. Bias and variance estimates were computed over 16 earthquakes, 503 sites, reflecting the magnitude range of M 5.3 (Imperial Valley aftershock) to M 7.4 and a site distance range of 1 to 218 km (460 km for CEUS). CEUS data include both the Saguenay and Nahanni earthquakes. This

²Strong ground motions are generally considered to be log normally distributed.

represents a comprehensive data set and provides a statistically robust assessment of prediction accuracy for the point source model.

Model bias and variability estimates are shown in Figures D-1, D-2, and D-3. Over all the sites, Figure D-1, the bias is slightly positive for frequencies greater than about 10 Hz and is near zero from about 10 Hz to 1 Hz. Below 1 Hz, a stable point source overprediction is reflected in the negative bias. The analyses are considered reliable down to about 0.3 Hz where the model shows about a 40% overprediction.

The model variability is low, about 0.5 above about 3 to 4 Hz and increases with decreasing frequency to near 1 at 0.3 Hz. Above 1 Hz, there is little difference between the total variability (uncertainty plus randomness) and randomness (bias corrected variability) reflecting the near zero bias estimates. Below 1 Hz there is considerable uncertainty contributing to the total variability suggesting that the model can be measurably improved, as its predictions tend to be consistently high at very low frequencies (≤ 1 Hz). This stable misfit may be interpreted as the presence of a second corner frequency for WNA sources (Atkinson and Silva, 1997).

For the soil sites, Figure D-2 shows a slight improvement at 1 Hz and above in both the bias and variability estimates. This indicates that the rock sites must reflect the converse and Figure D-3 does show larger bias and variability estimates than the results for all the sites. Soil sites are modeled more accurately than rock sites. This suggests that strong ground motions at rock sites are more variable than motions at soil sites and that the model is not capturing the increased site-to-site variation. This is consistent with the trend seen in the individual earthquake analyses: soil sites are modeled more accurately than rock sites because they have less intra-event variability. The larger rock site bias above 20 Hz suggests a small stable underprediction possibly from the use of a single smooth rock profile rather than randomizing the profile and using a mean spectrum.

In general, for frequencies of about 1 Hz and higher, the point source bias estimates are small (near zero) and the variabilities range from about 0.5 to 0.6. These estimates are low considering that high frequency ground motion variance decreases with increasing magnitude, particularly above M 6.5 (Youngs et al., 1995), and these validations are based on a data set comprised of several earthquakes with M less than M 6.5 (288 of 513 sites). Because generic site parameters were used, the model variability (mean = 0) contains the total uncertainty and randomness contribution for the site. The parametric variability due to uncertainty and randomness in site parameters: shear-wave velocity, profile depth, G/G_{\max} and hysteretic damping curves need not be added to the model variability estimates. It is useful to perform parametric variations to assess site parameter sensitivities on the ground motions, but only source and path damping $Q(f)$ parametric variabilities require assessment on a site-specific basis for addition to the model variability. The uncertainty and randomness for the point source is contained in the stress drop for the single-corner frequency model as well as source depth. For applications to the CEUS, additional uncertainty may be appropriate to accommodate the likelihood of a double corner source, that is, to include epistemic uncertainty in the shape of the source spectrum. Alternatively, composite source spectra could be used based on weighted averages of the single- and double-corner models.

References

- Abrahamson, N.A., P.G. Somerville, and C.A. Cornell (1990). "Uncertainty in numerical strong motion predictions" *Proc. Fourth U.S. Nat. Conf. Earth. Engin.*, Palm Springs, CA., 1, 407-416.
- Aki, K. and P. G. Richards. (1980). "*Quantitative seismology.*" W. H. Freeman and Co., San Francisco, California.
- Anderson, J. G. and S. E. Hough (1984). "A Model for the Shape of the Fourier Amplitude Spectrum of Acceleration at High Frequencies." *Bull. Seism. Soc. Am.*, 74(5), 1969-1993.
- Atkinson, G.M and W.J. Silva (1997). "An empirical study of earthquake source spectra for California earthquakes." *Bull. Seism. Soc. Am.* 87(1), 97-113.
- Atkinson, G.M. (1984). "Attenuation of strong ground motion in Canada from a random vibrations approach." *Bull. Seism. Soc. Am.*, 74(5), 2629-2653.
- Boore, D.M., and G.M. Atkinson (1987). "Stochastic prediction of ground motion and spectral response parameters at hard-rock sites in eastern North America." *Bull. Seism. Soc. Am.*, 77(2), 440-467.
- Boore, D.M. and W.B. Joyner (1984). "A note on the use of random vibration theory to predict peak amplitudes of transient signals." *Bull. Seism. Soc. Am.*, 74, 2035-2039.
- Boore, D.M. (1986). "Short-period P- and S-wave radiation from large earthquakes: implications for spectral scaling relations." *Bull. Seism. Soc. Am.*, 76(1) 43-64.
- Boore, D.M. (1983). "Stochastic simulation of high-frequency ground motions based on seismological models of the radiated spectra." *Bull. Seism. Soc. Am.*, 73(6), 1865-1894.
- Brune, J.N. (1971). "Correction." *J. Geophys. Res.* 76, 5002.
- Brune, J.N. (1970). "Tectonic stress and the spectra of seismic shear waves from earthquakes." *J. Geophys. Res.* 75, 4997-5009.
- Electric Power Research Institute (1993). "Guidelines for determining design basis ground motions." Palo Alto, Calif: Electric Power Research Institute, vol. 1-5, EPRI TR-102293.
vol. 1: Methodology and guidelines for estimating earthquake ground motion in eastern North America.
vol. 2: Appendices for ground motion estimation.
vol. 3: Appendices for field investigations.
vol. 4: Appendices for laboratory investigations.
vol. 5: Quantification of seismic source effects.

- Hanks, T.C. (1982). " f_{max} ," *Bull. Seism. Soc. Am.*, 72, 1867-1879.
- Hanks, T.C., and R.K. McGuire (1981). "The character of high-frequency strong ground motion." *Bull. Seism. Soc. Am.*, 71(6), 2071-2095.
- Hanks, T.C., and H. Kanamori (1979). "A moment magnitude scale." *J. Geophys. Res.*, 84, 2348-2350.
- Hartzell, S.H. (1978). "Earthquake aftershocks as Green's functions." *Geophys. Res. Letters*, 5, 1-4.
- McGuire, R. K., A. M. Becker, and N. C. Donovan (1984). "Spectral Estimates of Seismic Shear Waves." *Bull. Seism. Soc. Am.*, 74(4), 1427-1440.
- Hough, S. E. and J. G. Anderson (1988). "High-Frequency Spectra Observed at Anza, California: Implications for Q Structure." *Bull. Seism. Soc. Am.*, 78(2), 692-707.
- Hough, S.E., J.G. Anderson, J. Brune, F. Vernon III, J. Berger, J. Fletcher, L. Haar, T. Hanks, and L. Baker (1988). "Attenuation near Anza, California." *Bull. Seism. Soc. Am.*, 78(2), 672-691.
- Papageorgiou, A.S., and K. Aki (1983). "A specific barrier model for the quantitative description of inhomogeneous faulting and the prediction of strong ground motion, part I, Description of the model." *Bull. Seism. Soc. Am.*, 73(4), 693-722.
- Roblee, C.J., W.J. Silva, G.R. Toro and N. Abrahamson (1996). "Variability in site-specific seismic ground-motion design predictions." in press.
- Rovelli, A., O. Bonamassa, M. Cocco, M. Di Bona and S. Mazza (1988). "Scaling laws and spectral parameters of the ground motion in active extensional areas in Italy." *Bull. Seism. Soc. Am.*, 78(2), 530-560.
- Schneider, J.F., W.J. Silva, and C.L. Stark (1993). "Ground motion model for the 1989 M 6.9 Loma Prieta earthquake including effects of source, path and site." *Earthquake Spectra*, 9(2), 251-287.
- Silva, W.J., N. Abrahamson, G. Toro, C. Costantino (1997). "Description and validation of the stochastic ground motion model." Submitted to Brookhaven National Laboratory, Associated Universities, Inc. Upton, New York.
- Silva, W.J., and R. Darragh (1995). "Engineering characterization of earthquake strong ground motion recorded at rock sites." Palo Alto, Calif:Electric Power Research Institute.
- Silva, W.J. (1993) "Factors controlling strong ground motions and their associated uncertainties." *Seismic and Dynamic Analysis and Design Considerations for High Level Nuclear Waste Repositories*, ASCE 132-161.

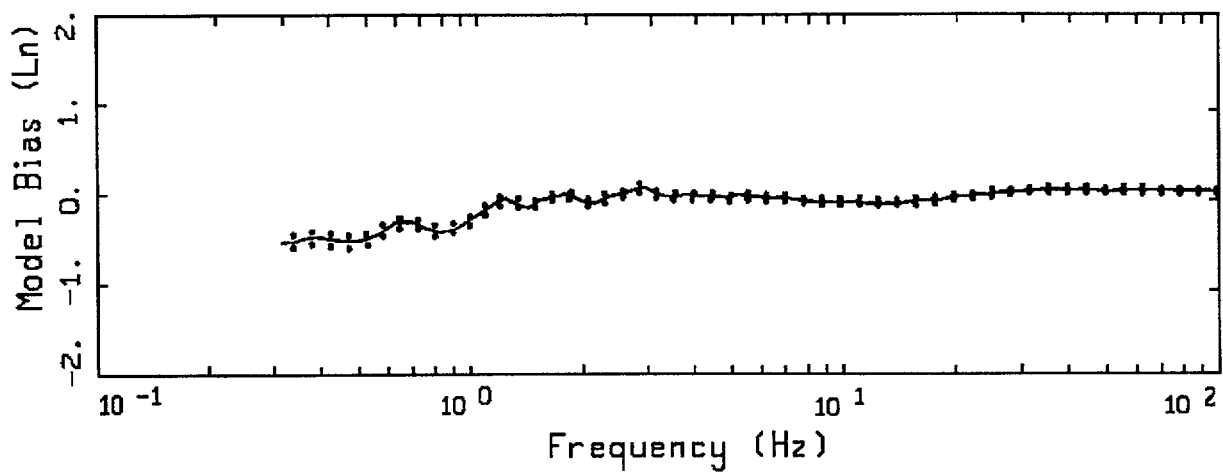
- Silva, W.J. (1992). "Factors controlling strong ground motions and their associated uncertainties." *Dynamic Analysis and Design Considerations for High Level Nuclear Waste Repositories*, ASCE 132-161.
- Silva, W.J. (1991). "Global characteristics and site geometry." Chapter 6 in *Proceedings: NSF/EPRI Workshop on Dynamic Soil Properties and Site Characterization*. Palo Alto, Calif.: Electric Power Research Institute, NP-7337.
- Silva, W. J., R. Darragh, C. Stark, I. Wong, J. C. Stepp, J. Schneider, and S-J. Chiou (1990). "A Methodology to Estimate Design Response Spectra in the Near-Source Region of Large Earthquakes Using the Band-Limited-White-Noise Ground Motion Model". *Procee. of the Fourth U.S. Conf. on Earthquake Engineering*, Palm Springs, California. 1, 487-494.
- Silva, W.J., T. Turcotte, and Y. Moriwaki (1988). "Soil Response to Earthquake Ground Motion," Palo Alto, CA: EPRI, RP 2556-07.
- Silva, W. J. and R. K. Green (1988). "Magnitude and Distance Scaling of Response Spectral Shapes for Rock Sites with Applications to North American Environments." In *Proceedings: Workshop on Estimation of Ground Motion in the Eastern United States*, EPRI NP-5875, Electric Power Research Institute.
- Silva, W.J. and K. Lee (1987). "WES RASCAL code for synthesizing earthquake ground motions." State-of-the-Art for Assessing Earthquake Hazards in the United States, Report 24, U.S. Army Engineers Waterways Experiment Station, Miscellaneous Paper S-73-1.
- Toro, G. R. and R. K. McGuire (1987). "An Investigation into Earthquake Ground Motion Characteristics in Eastern North America." *Bull. Seism. Soc. Am.*, 77(2), 468-489.
- Toro, G. R. (1985). "Stochastic Model Estimates of Strong Ground Motion." In *Seismic Hazard Methodology for Nuclear Facilities in the Eastern United States*, Appendix B, R. K. McGuire, ed., Electric Power Research Institute, Project P101-29.
- Youngs, R.R., N.A. Abrahamson, F. Makdisi, and K. Sadigh (1995). "Magnitude dependent dispersion in peak ground acceleration." *Bull. Seism. Soc. Am.*, 85(1), 1161-1176.

Table D-1

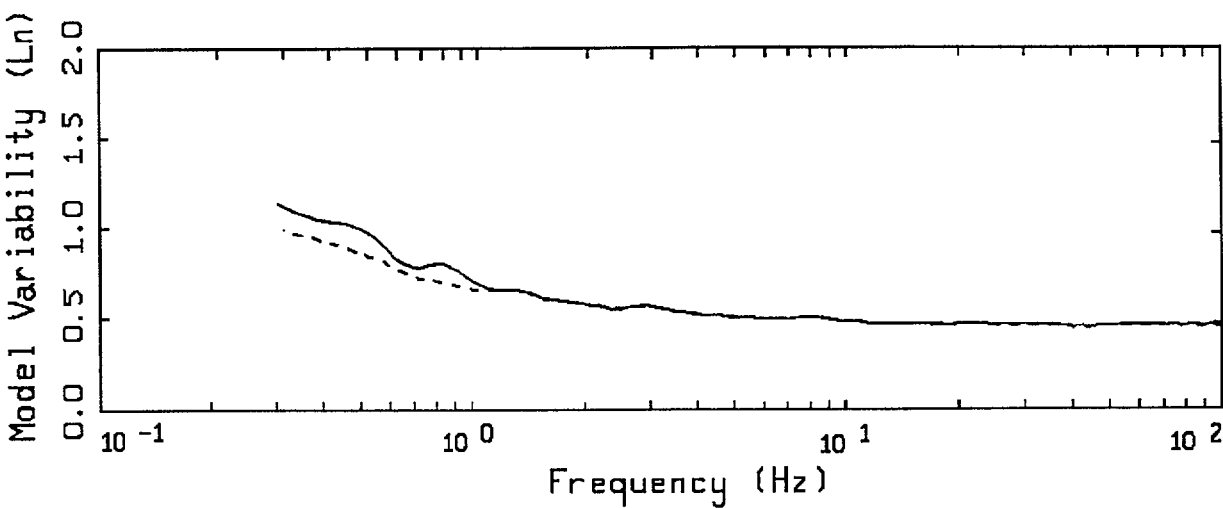
CONTRIBUTIONS TO TOTAL VARIABILITY
IN GROUND MOTION MODELS

	Modeling Variability	Parametric Variability
<p>Uncertainty <i>(also Epistemic Uncertainty)</i></p>	<p><u>Modeling Uncertainty:</u> Variability in predicted motions resulting from particular model assumptions, simplifications and/or fixed parameter values. <i>Can be reduced by adjusting or "calibrating" model to better fit observed earthquake response.</i></p>	<p><u>Parametric Uncertainty:</u> Variability in predicted motions resulting from incomplete data needed to characterize parameters. <i>Can be reduced by collection of additional information which better constrains parameters</i></p>
<p>Randomness <i>(also Aleatory Uncertainty)</i></p>	<p><u>Modeling Randomness:</u> Variability in predicted motions resulting from discrepancies between model and actual complex physical processes. <i>Cannot be reduced for a given model form.</i></p>	<p><u>Parametric Randomness:</u> Variability in predicted motions resulting from inherent randomness of parameter values. <i>Cannot be reduced a priori* by collection of additional information.</i></p>

* Some parameters (e.g. source characteristics) may be well defined after an earthquake.



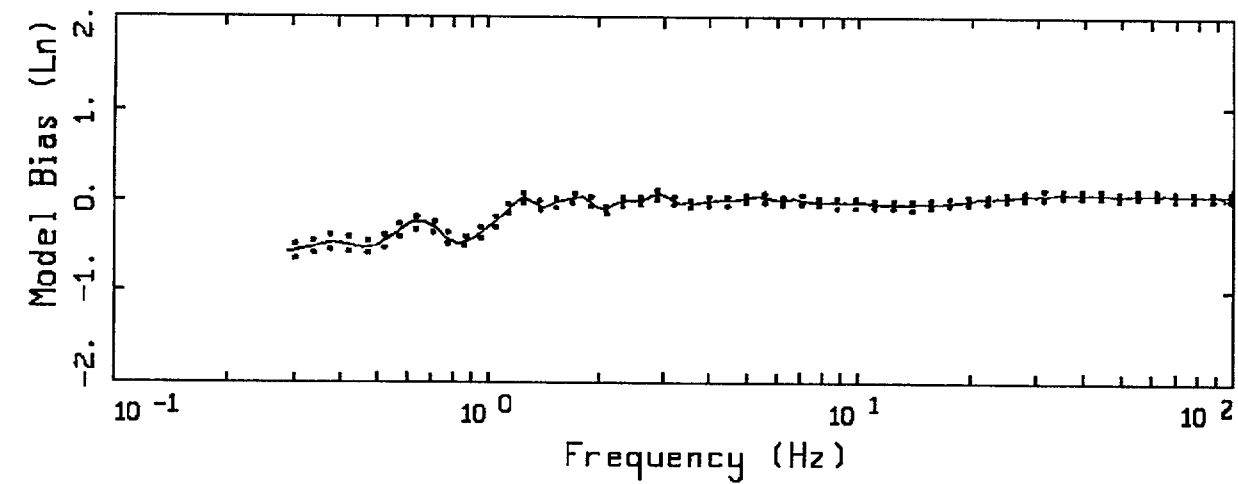
LEGEND
 ——— MODELING BIAS
 90% CONFIDENCE INTERVAL OF MODELING BIAS
 90% CONFIDENCE INTERVAL OF MODELING BIAS



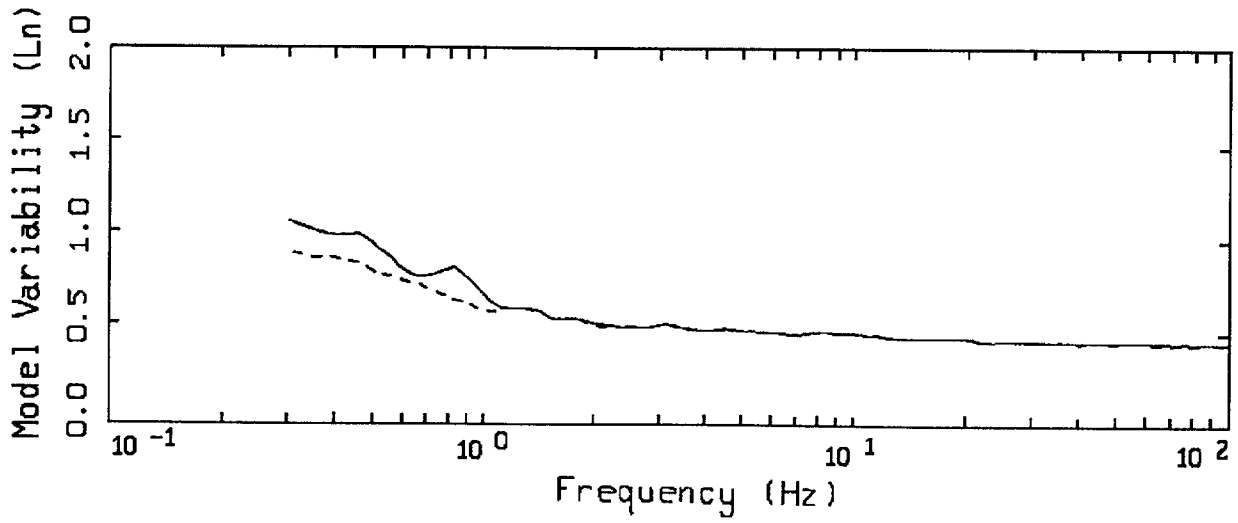
LEGEND
 ——— MEAN=0.0
 - - - - BIAS CORRECTED

16 EARTHQUAKES POINT-SOURCE
 NONLINEAR, ALL 503 SITES

Figure D-1. Model bias and variability estimates for all earthquakes computed over all 503 sites for the point-source model.



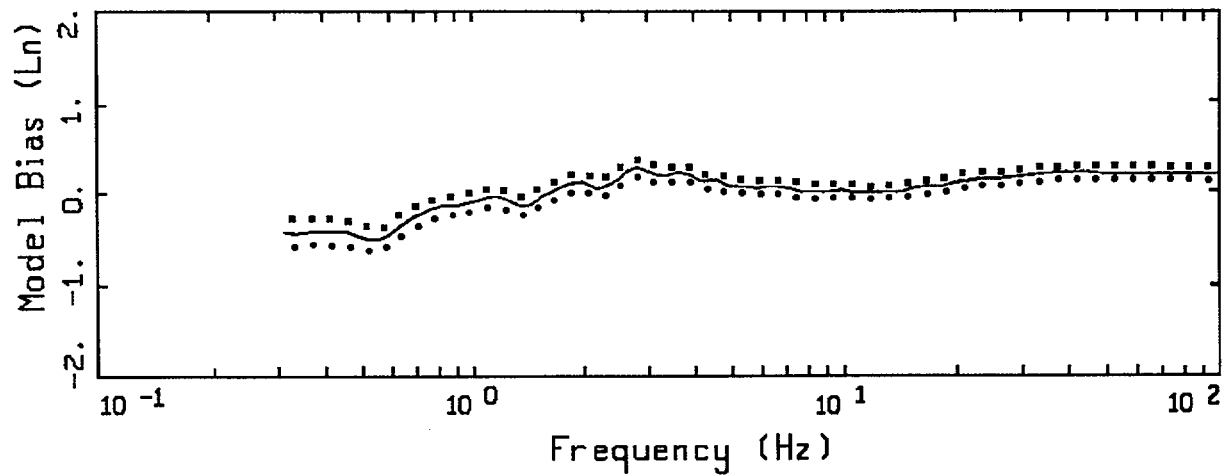
LEGEND
 — MODELING BIAS
 90% CONFIDENCE INTERVAL OF MODELING BIAS
 90% CONFIDENCE INTERVAL OF MODELING BIAS



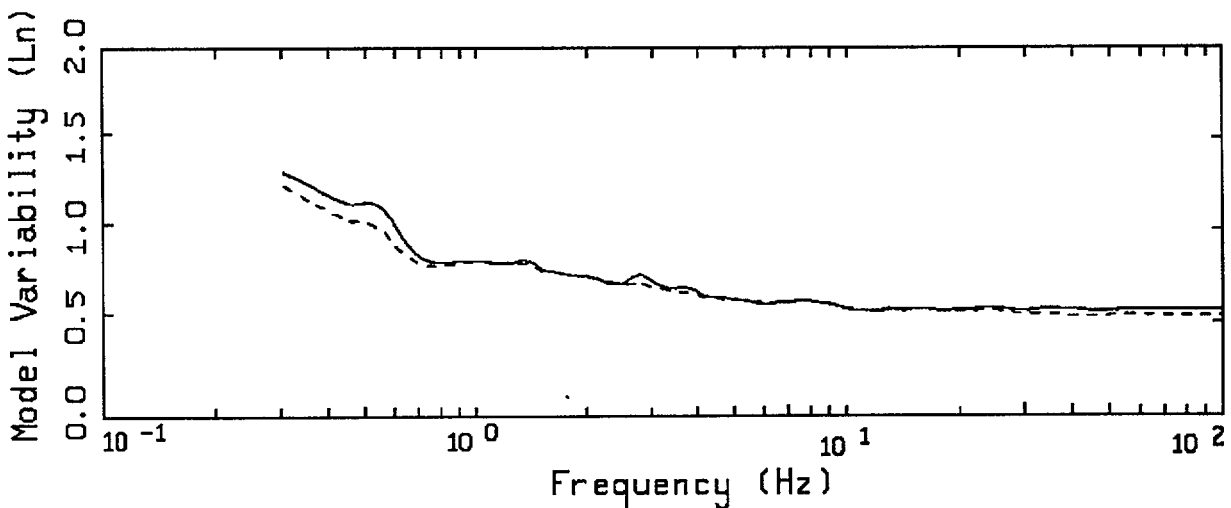
LEGEND
 — MEAN=0.0
 - - - BIAS CORRECTED

16 EARTHQUAKES POINT-SOURCE
 NONLINEAR, ALL 344 SOIL SITES

Figure D-2. Model bias and variability estimates for all earthquakes computed over all 344 soil sites for the point-source model.



LEGEND
 — MODELING BIAS
 90% CONFIDENCE INTERVAL OF MODELING BIAS
 90% CONFIDENCE INTERVAL OF MODELING BIAS



LEGEND
 — MEAN=0.0
 - - - - - BIAS CORRECTED

16 EARTHQUAKES POINT-SOURCE
 NONLINEAR, ALL 159 ROCK SITES

Figure D-3. Model bias and variability estimates for all earthquakes computed over all 159 rock sites for the point-source model.

APPENDIX E FOURIER AMPLITUDE SPECTRA FOR WUS EMPIRICAL MOTIONS

Notation: D1RM55HV

D1	Distance Bin 1 (0 - 10 km)
R	Rock Site
S	Soil Site
M55	Magnitude Bin 5 - 6
H	Horizontal
V	Vertical
AMPAVGH	Average Value Horizontal Records
AMPAVGV	Average Value Vertical Records

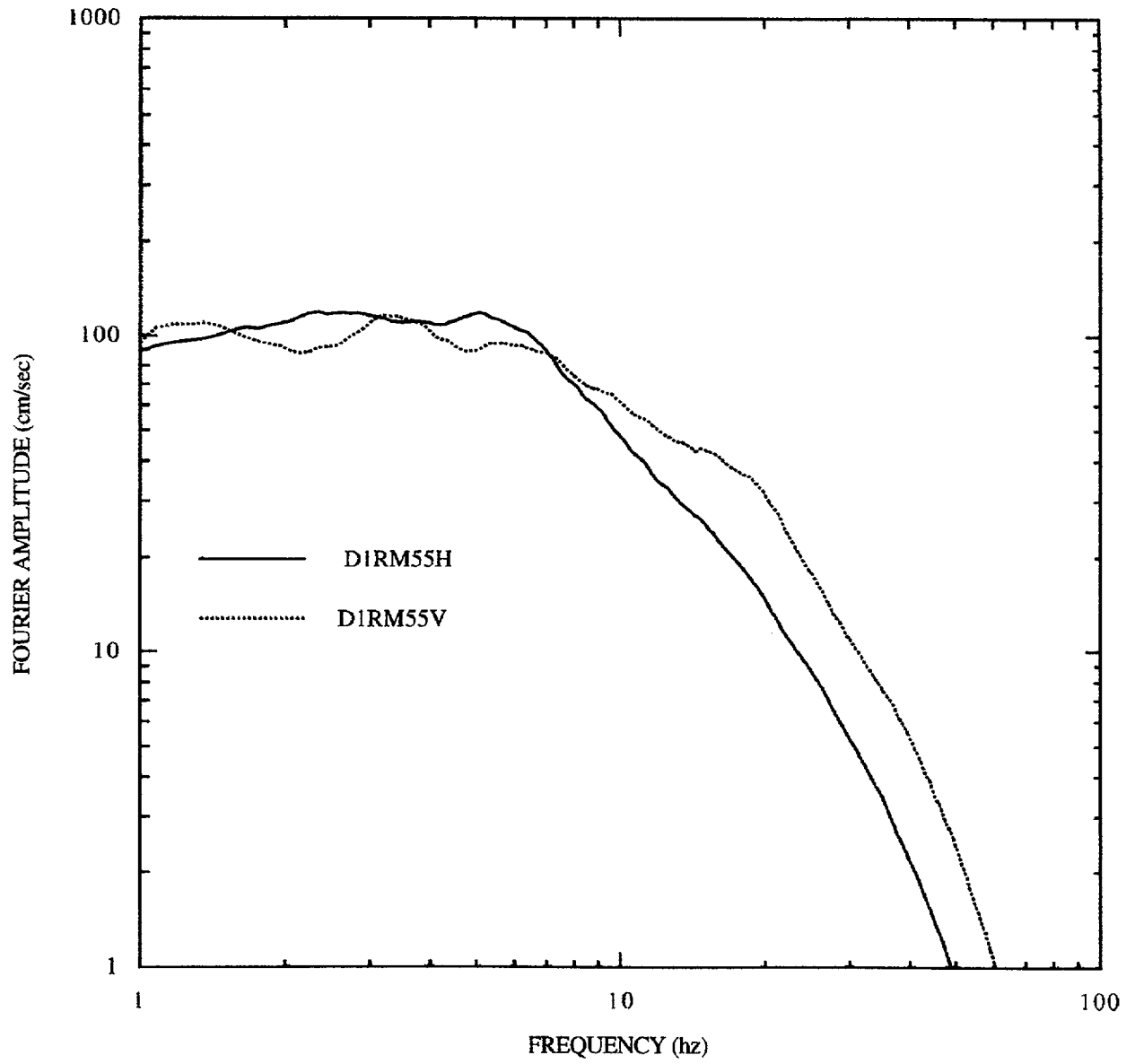


Figure E-1. Mean Fourier spectra for distance 0-10km, rock sites, M5-6

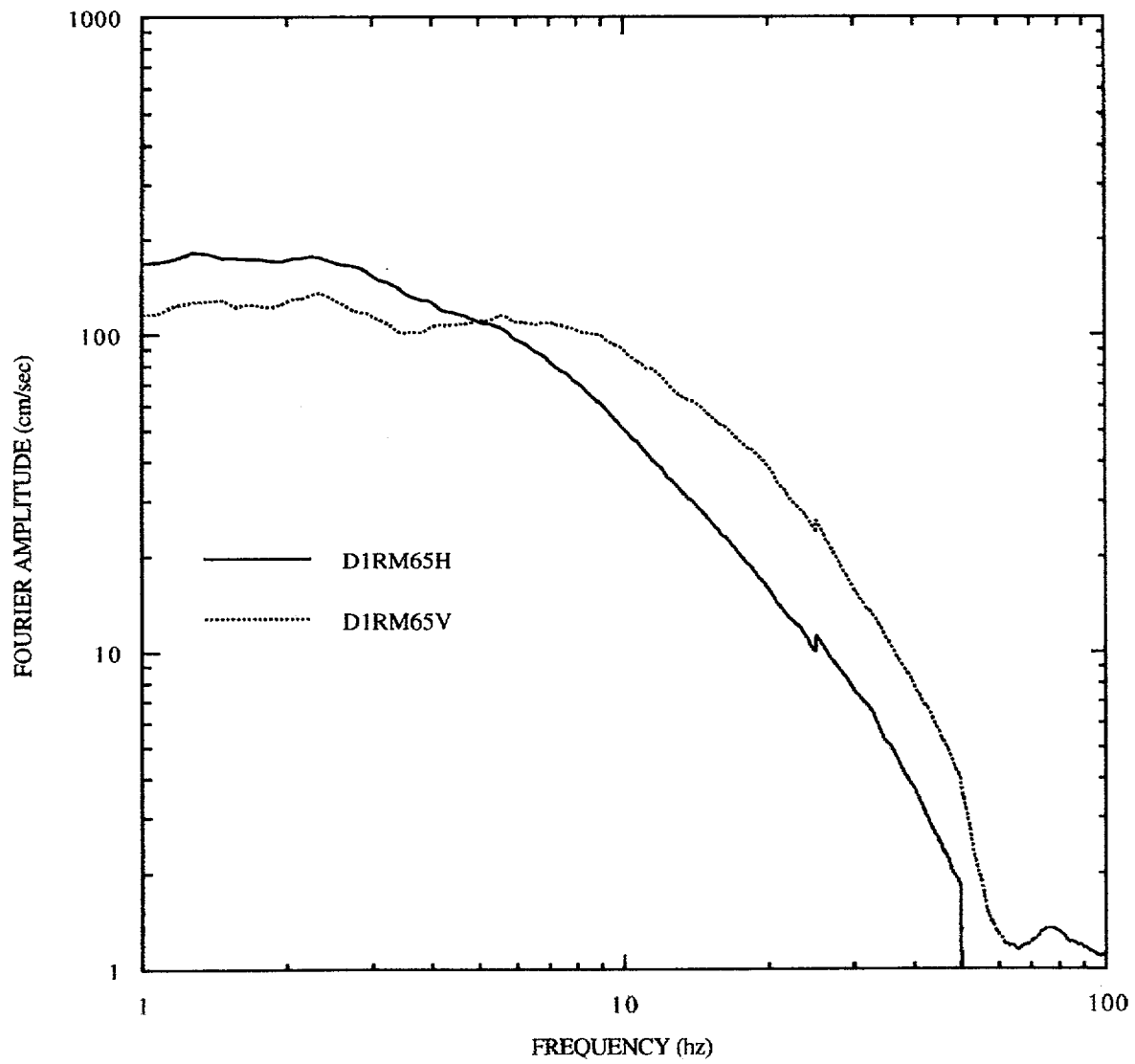


Figure E-2. Mean Fourier spectra for distance 0-10km, rock sites, M6-7

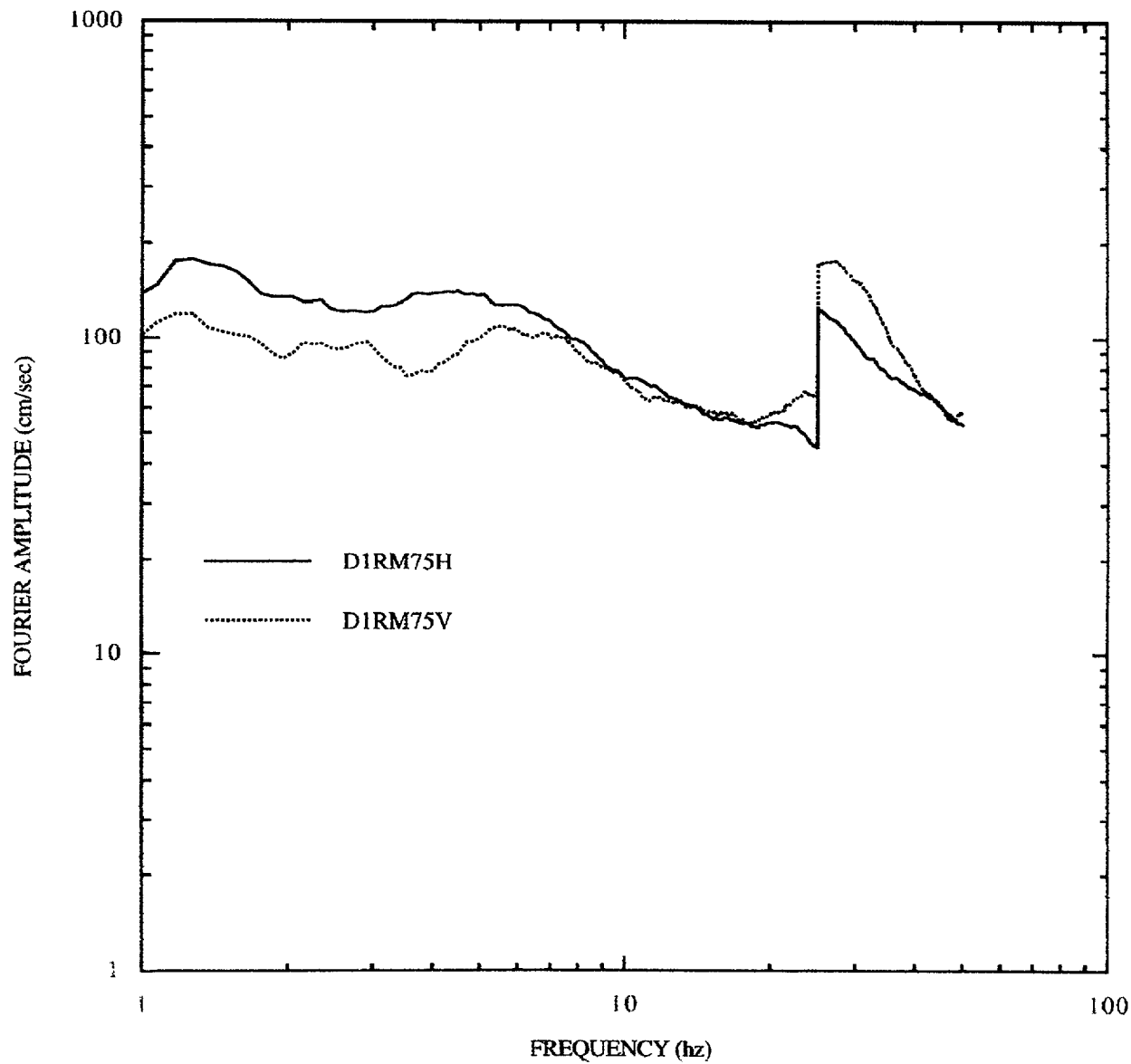


Figure E-3. Mean Fourier spectra for distance 0-10 km, rock sites, M7+. Note: discontinuity at 25 Hz is caused by few records available above that frequency.

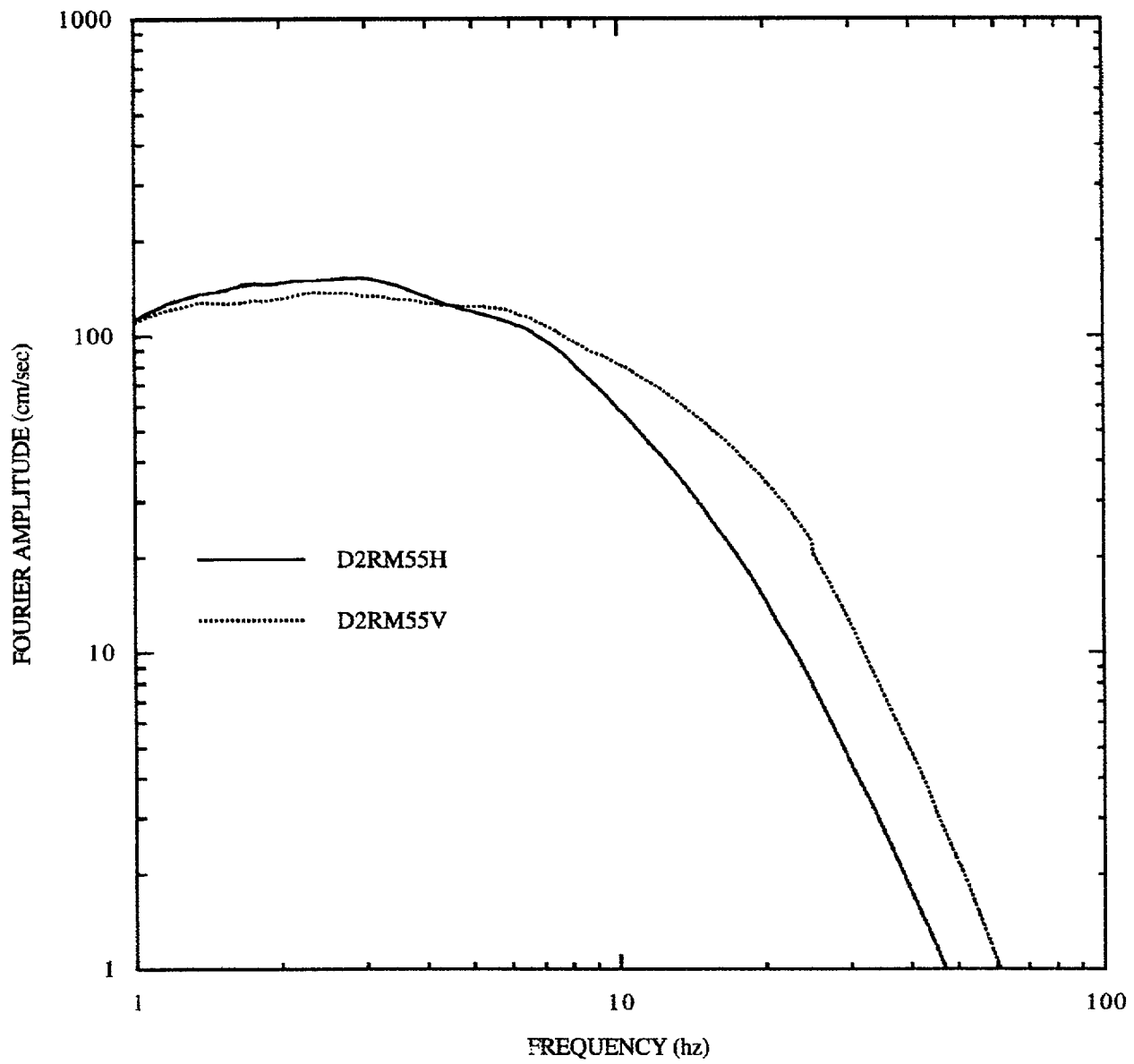


Figure E-4. Mean Fourier spectra for distance 10-50km, rock sites, M5-6

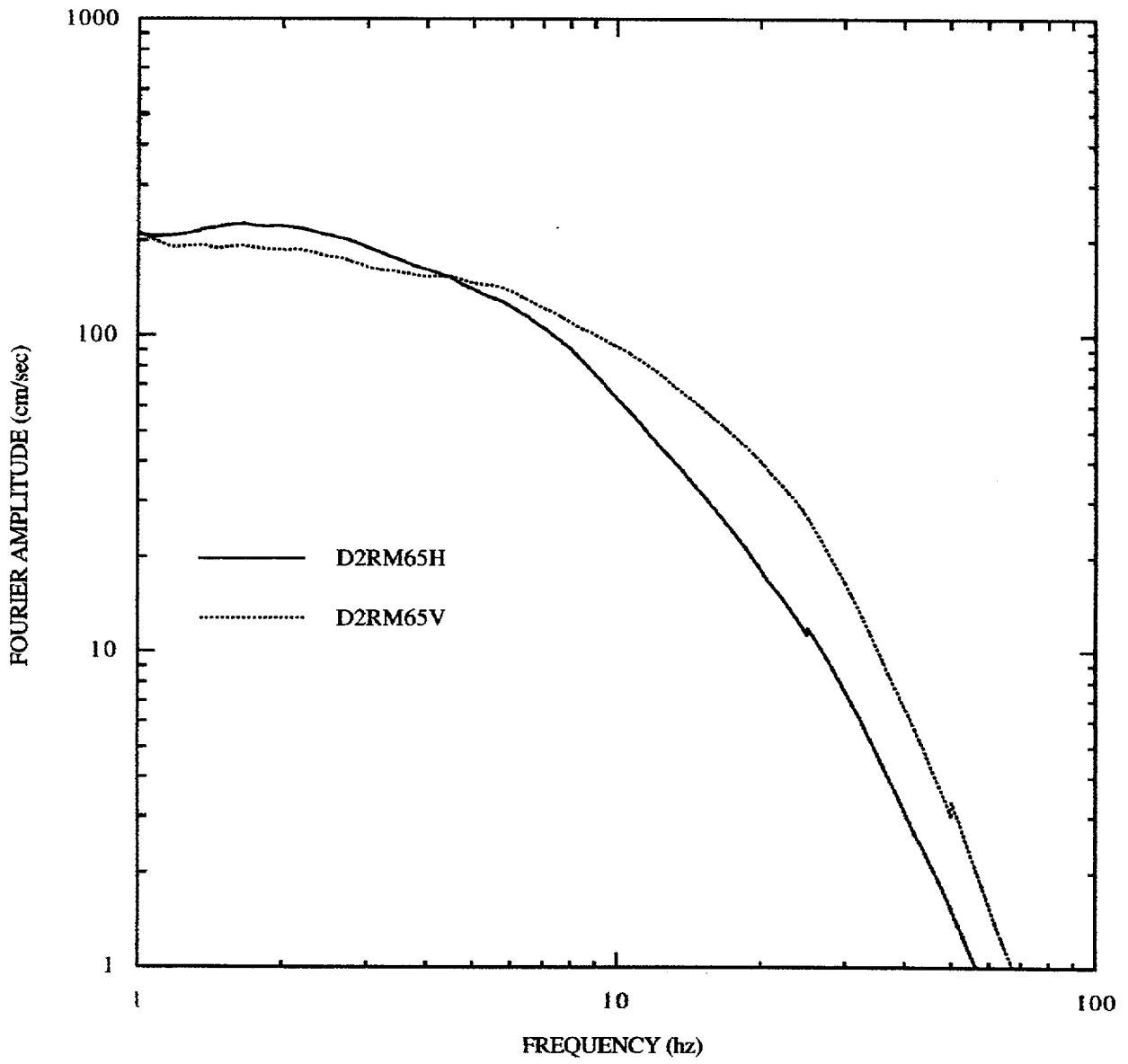


Figure E-5. Mean Fourier spectra for distance 10-50km, rock sites, M6-7.

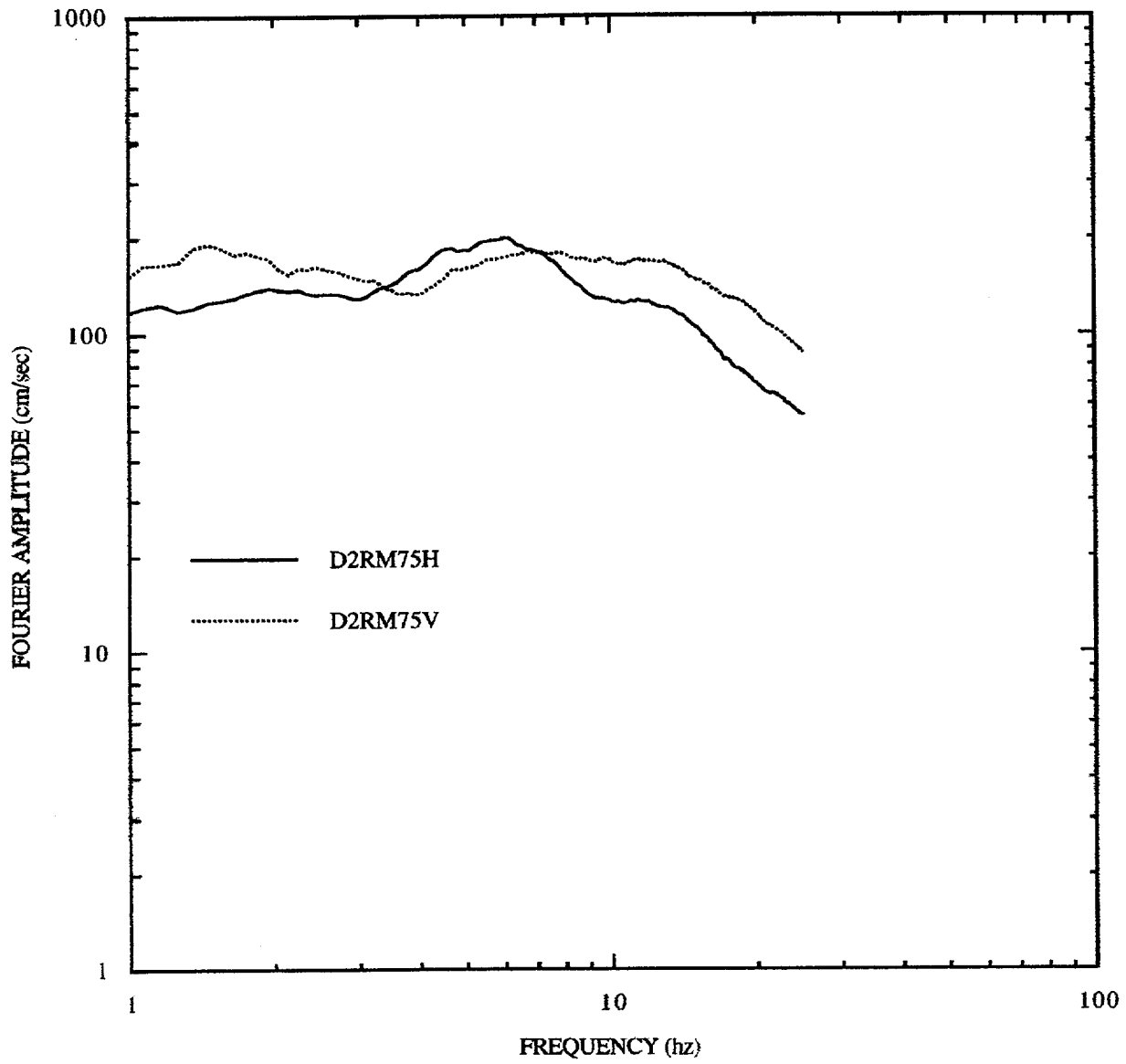


Figure E-6. Mean Fourier spectra for distance 10-50km, rock sites, M7+.

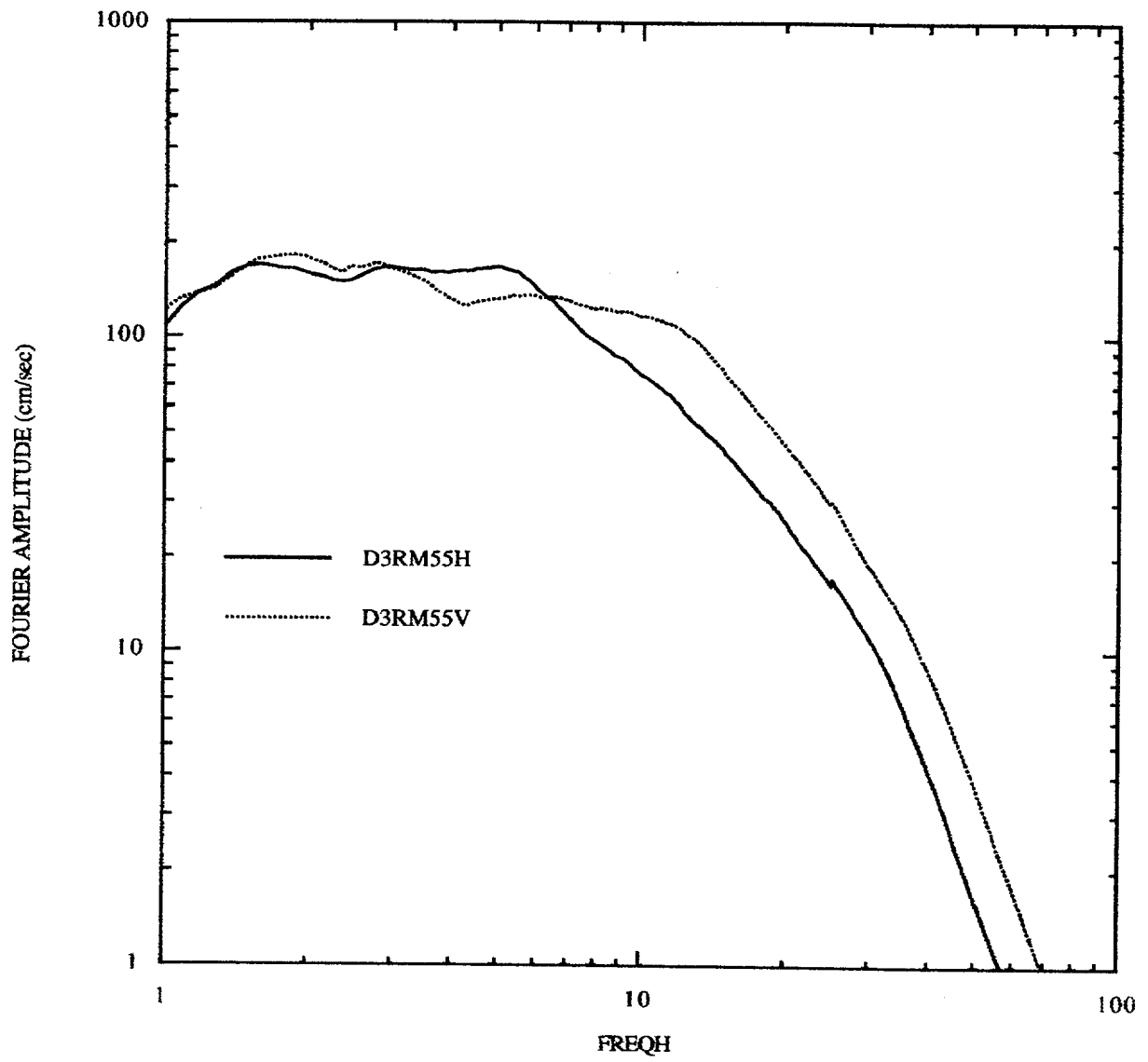


Figure E-7. Mean Fourier spectra for distance 50-100 km, rock sites, M5-6.

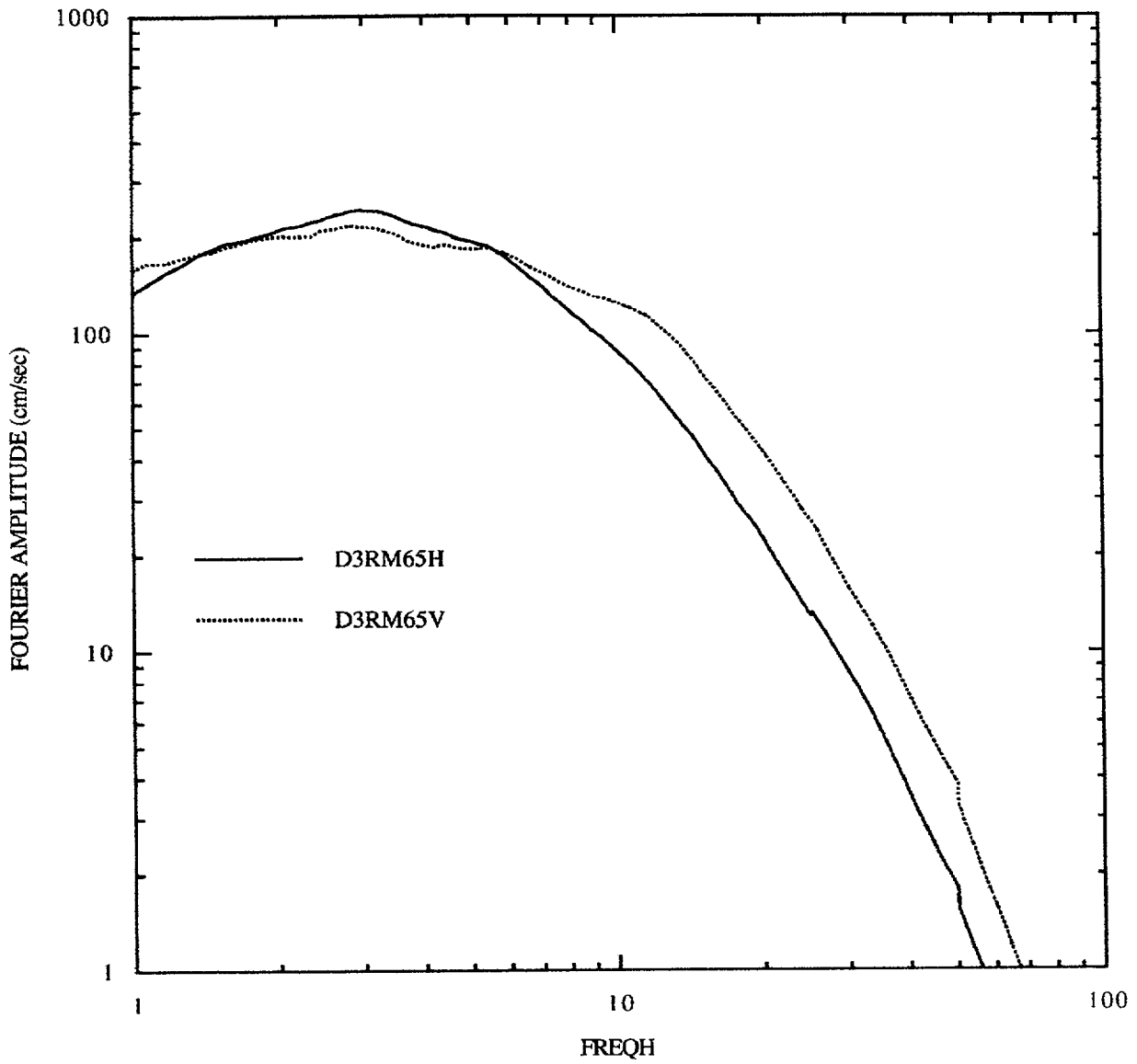


Figure E-8. Mean Fourier spectra for distance 50-100 km, rock sites, M6-7.

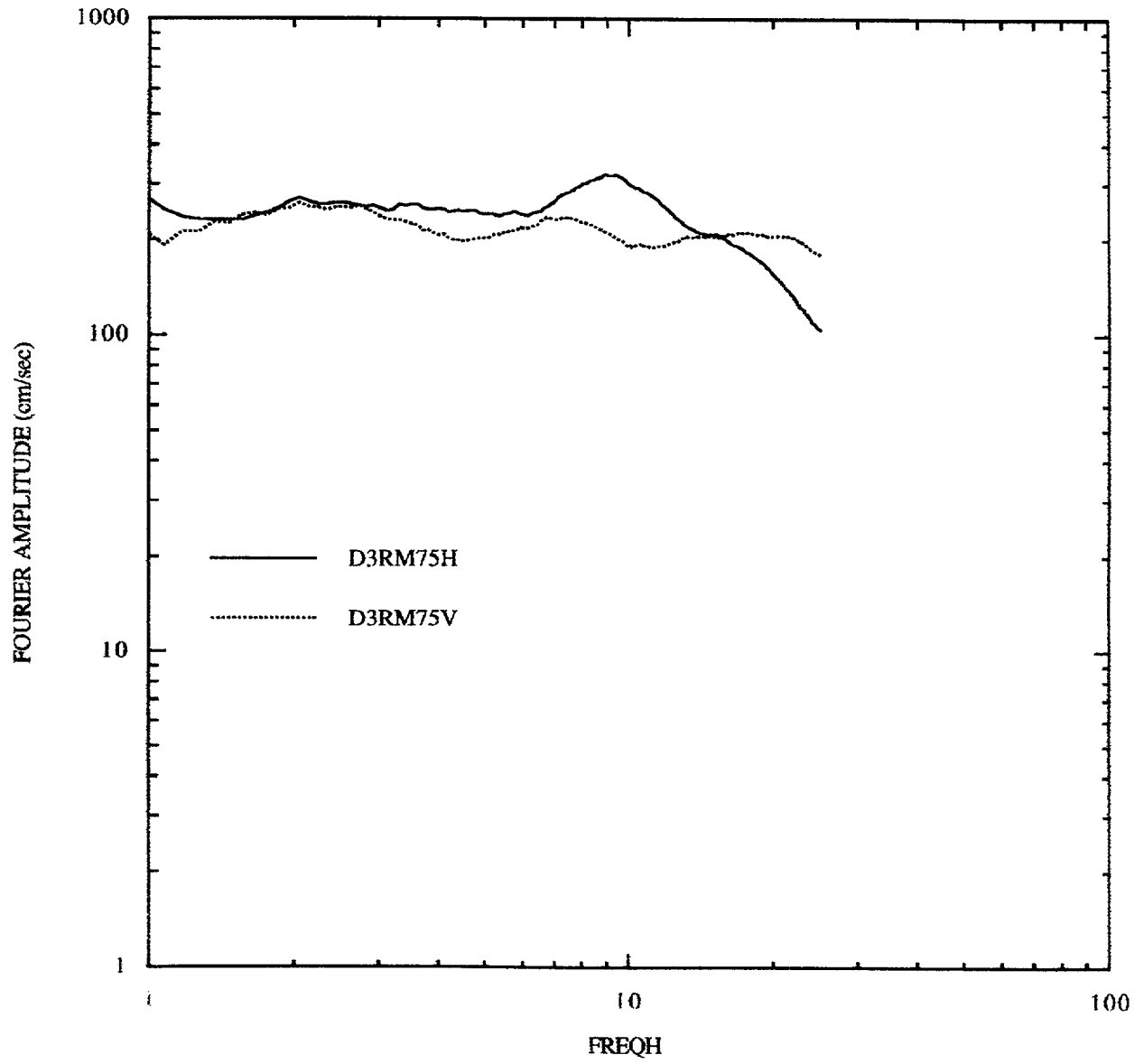


Figure E-9. Mean Fourier spectra for distance 50-100 km, rock sites, M7+.

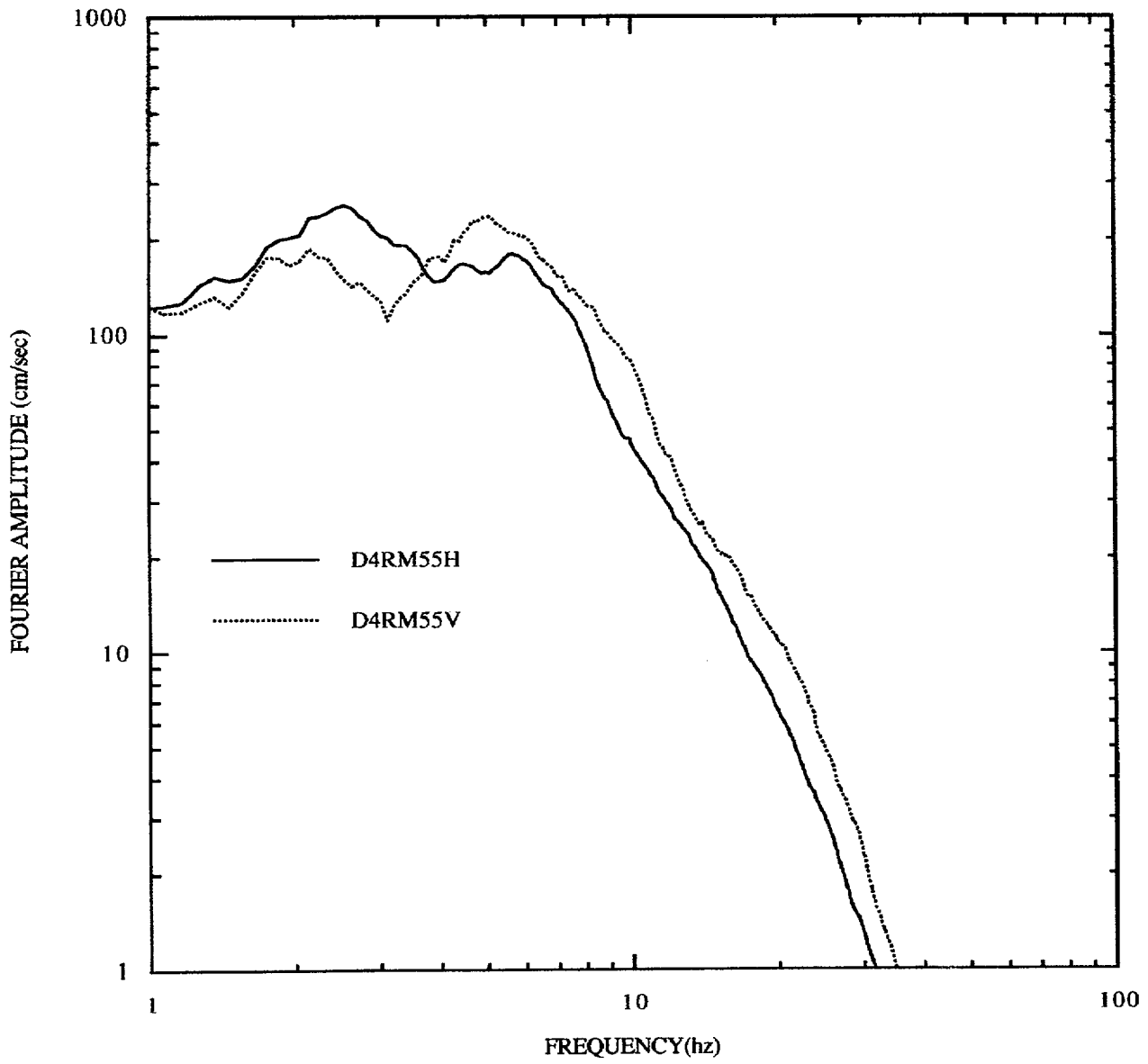


Figure E-10. Mean Fourier spectra for distance 100-200 km, rock sites, M5-6.

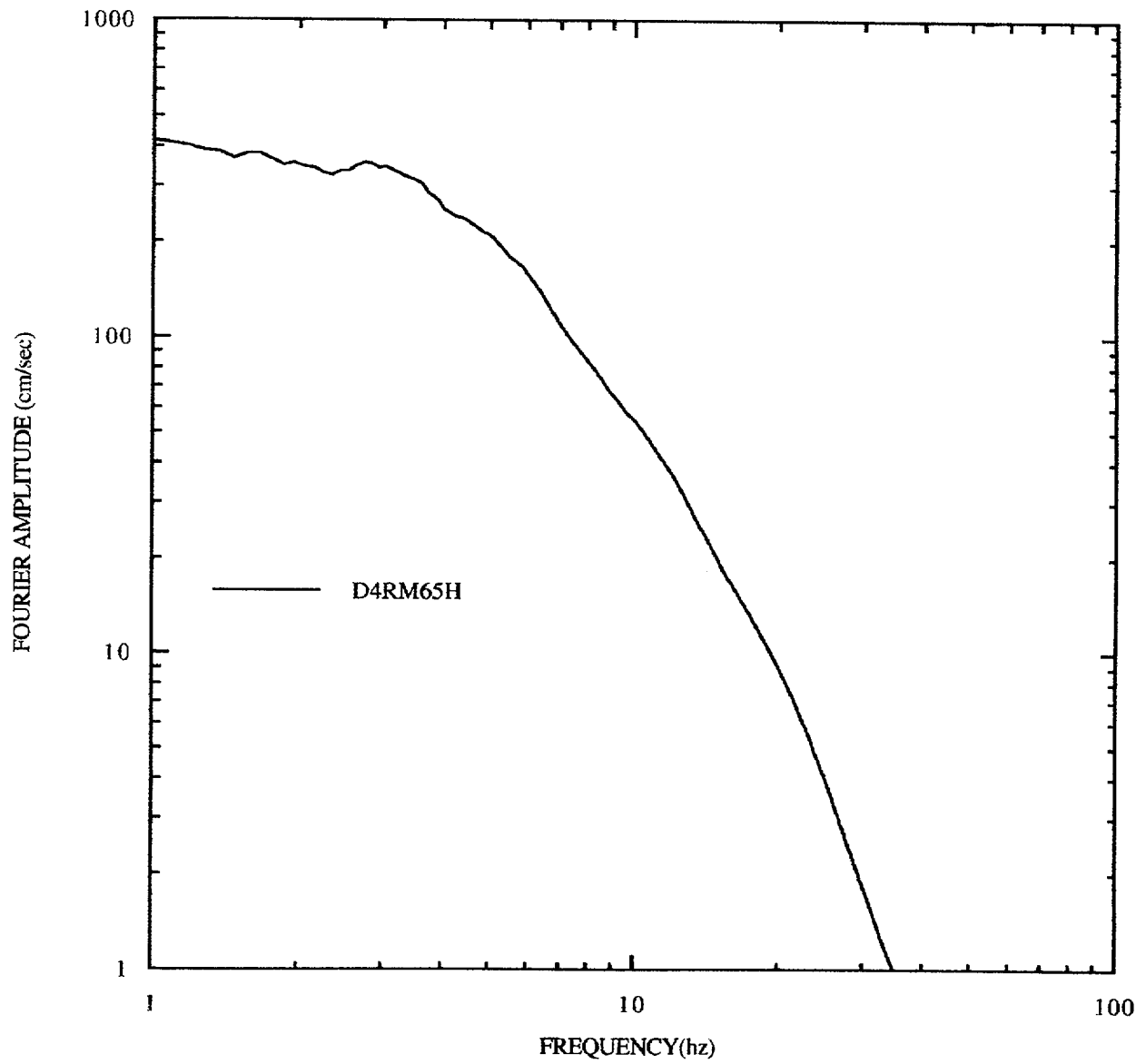


Figure E-11. Mean Fourier spectra for distance 100-200 km, rock sites, M6-7.

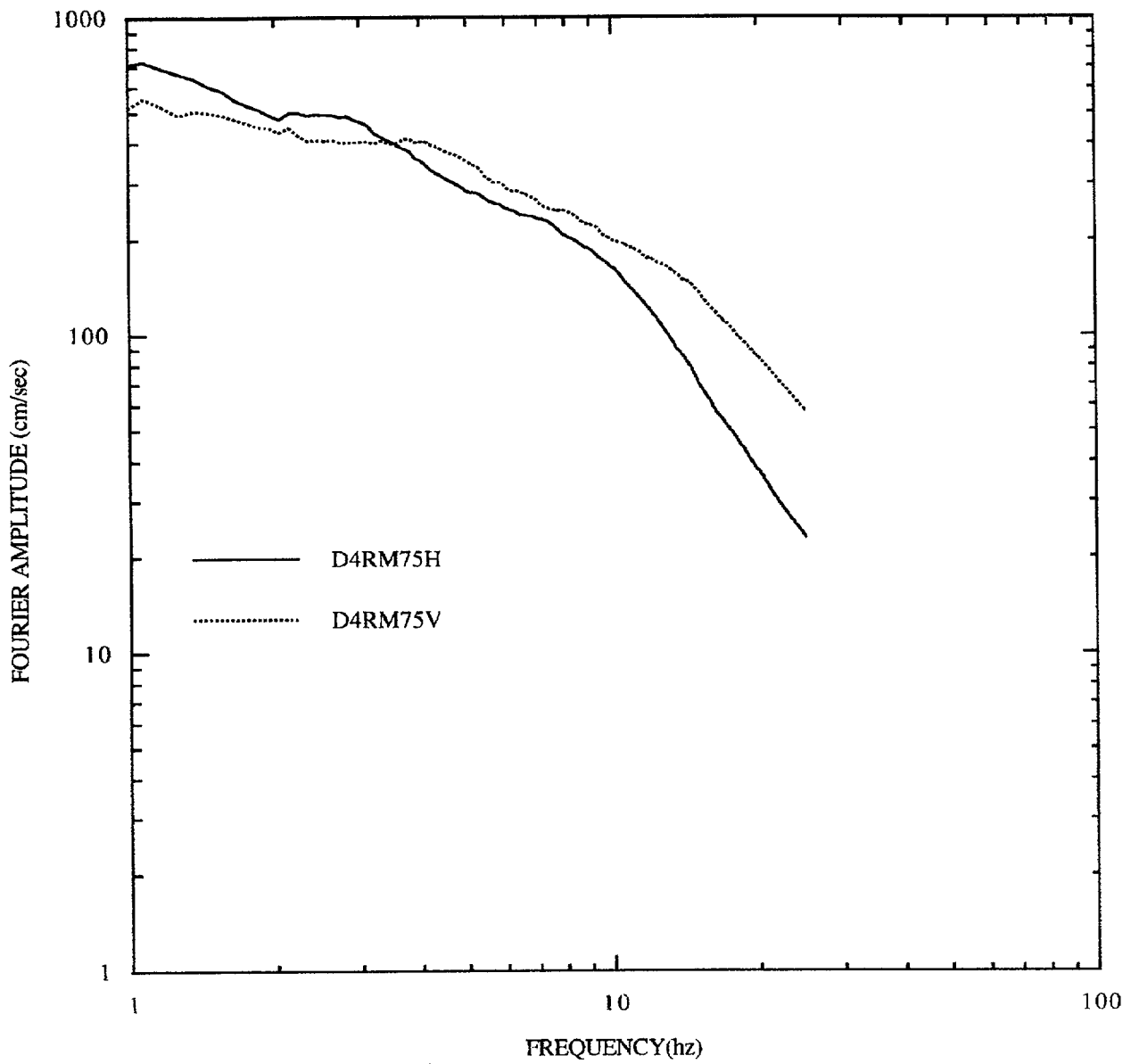


Figure E-12. Mean Fourier spectra for distance 10-200 km, rock sites, M7+.

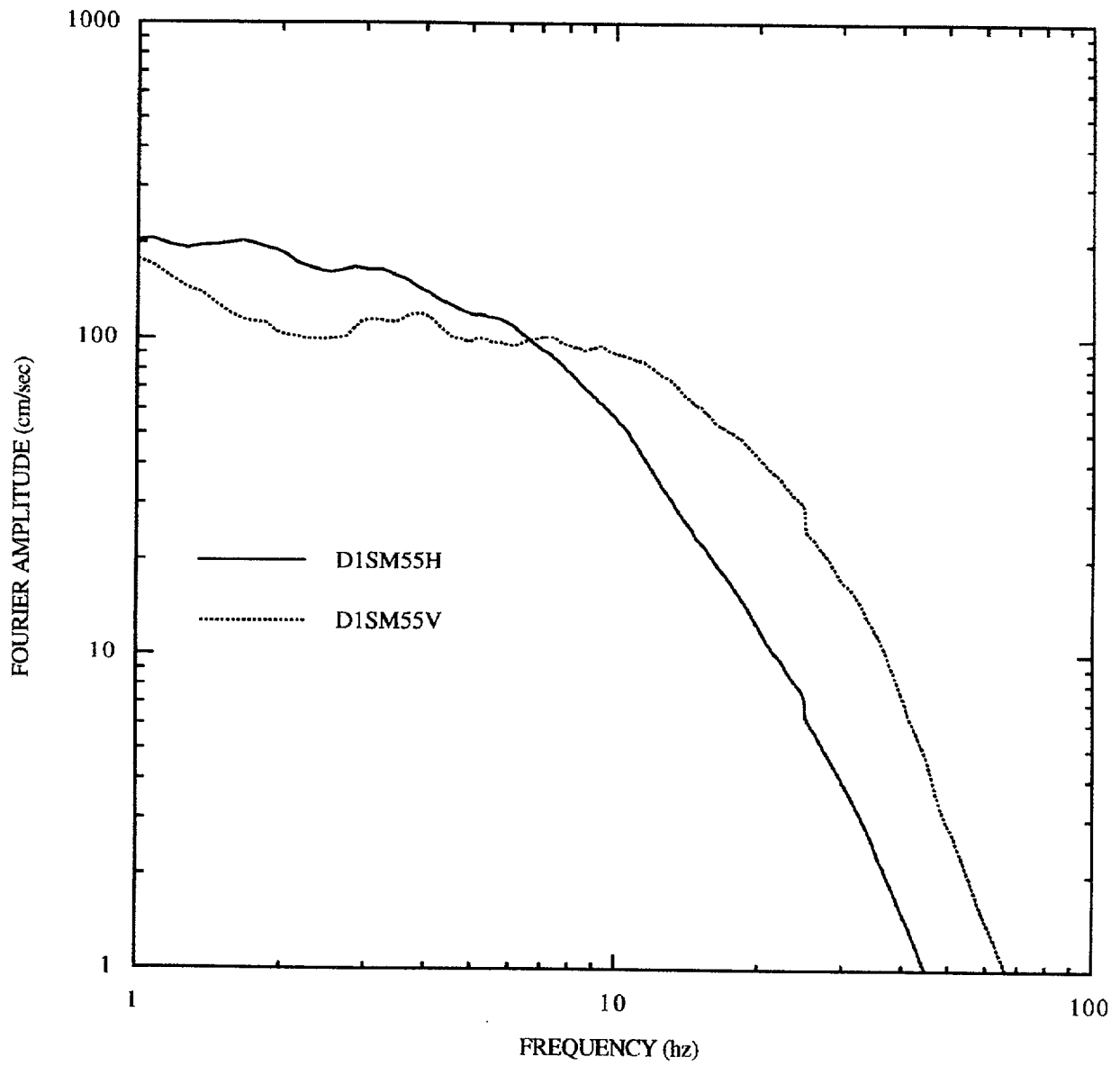


Figure E-13. Mean Fourier spectra for distance 0-10 km, soil sites, M5-6.

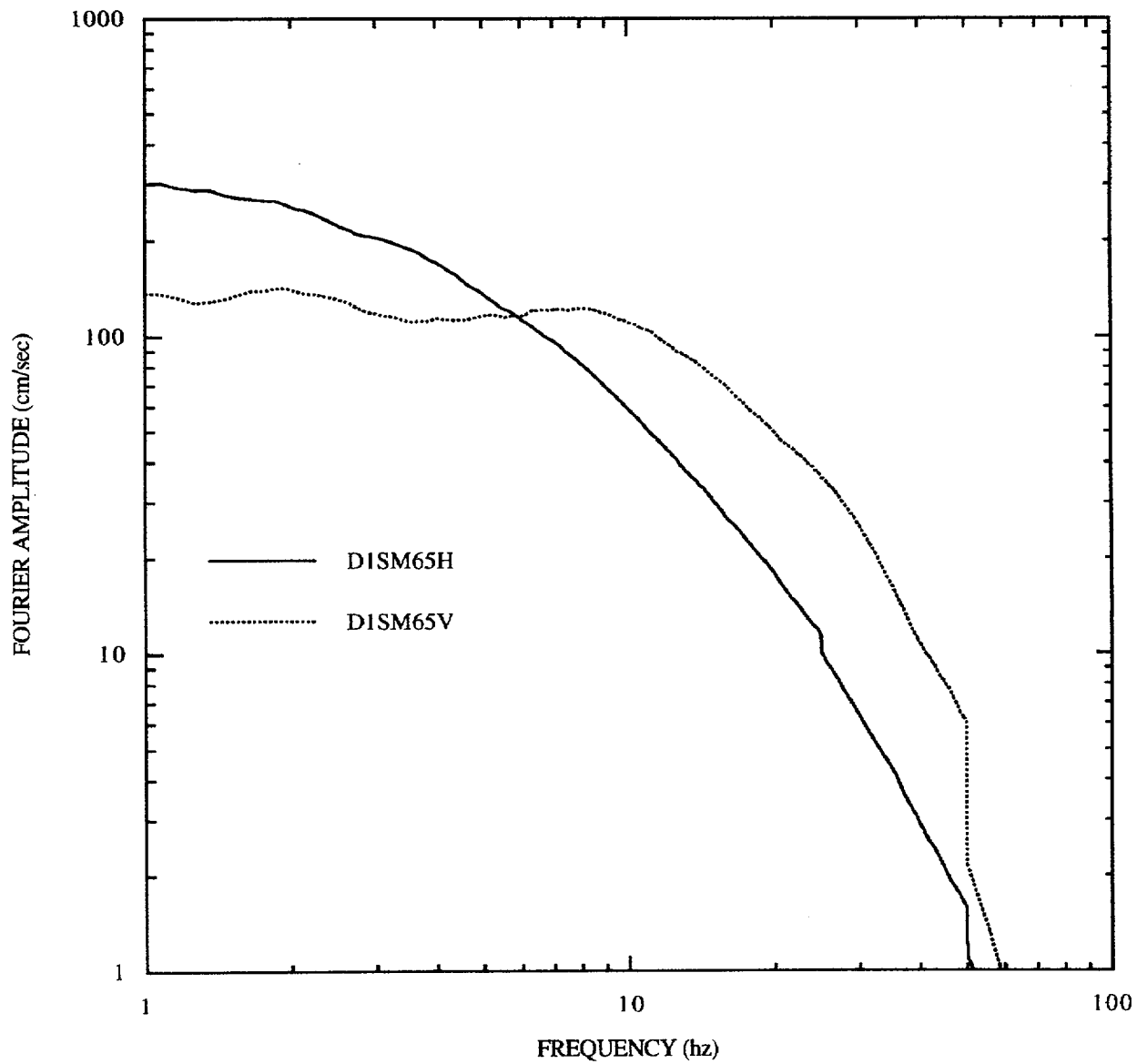


Figure E-14. Mean Fourier spectra for distance 0-10 km, soil sites, M 6-7.

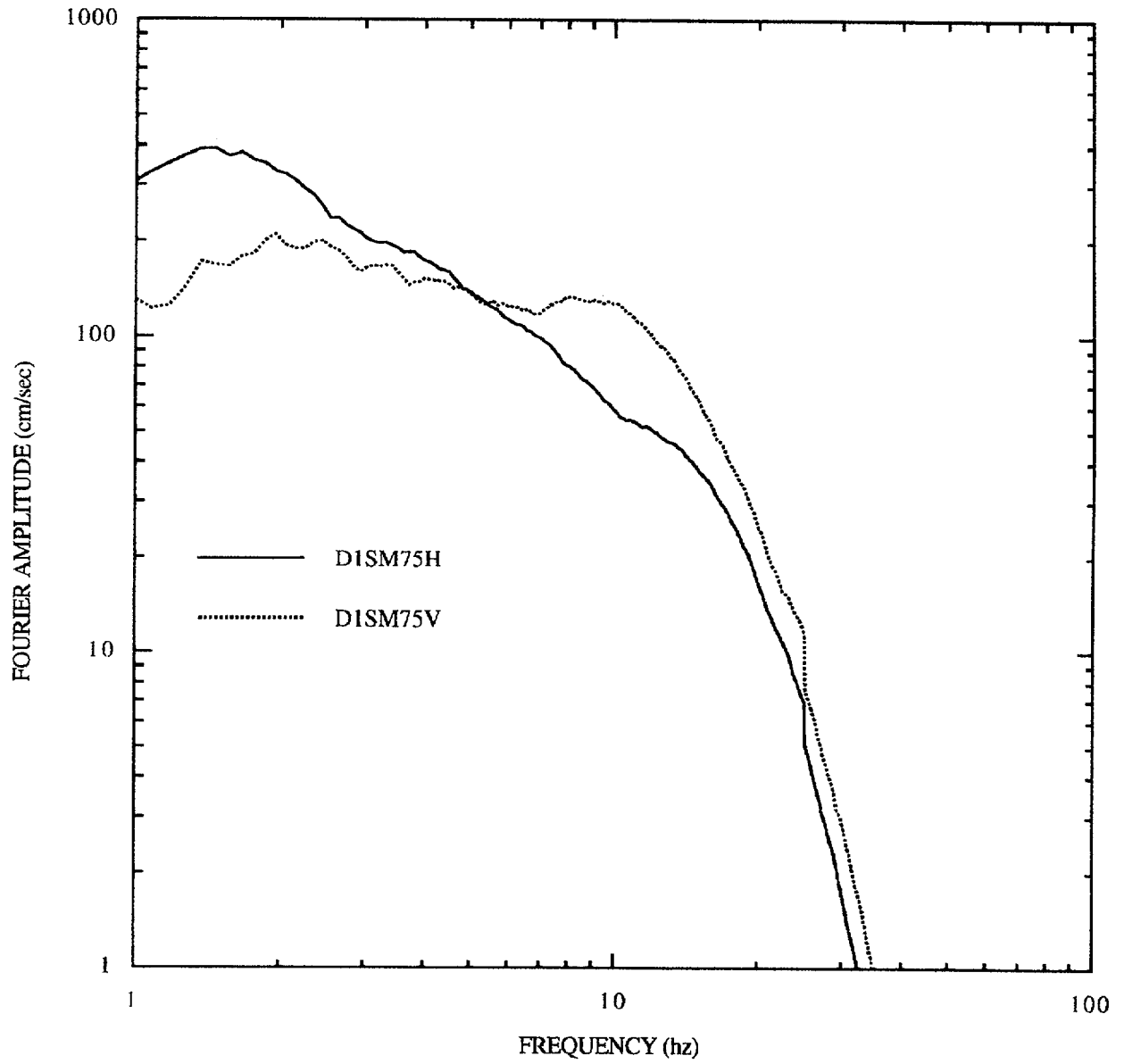


Figure E-15. Mean Fourier spectra for distance 0-10 km, soil sites, M 7+.

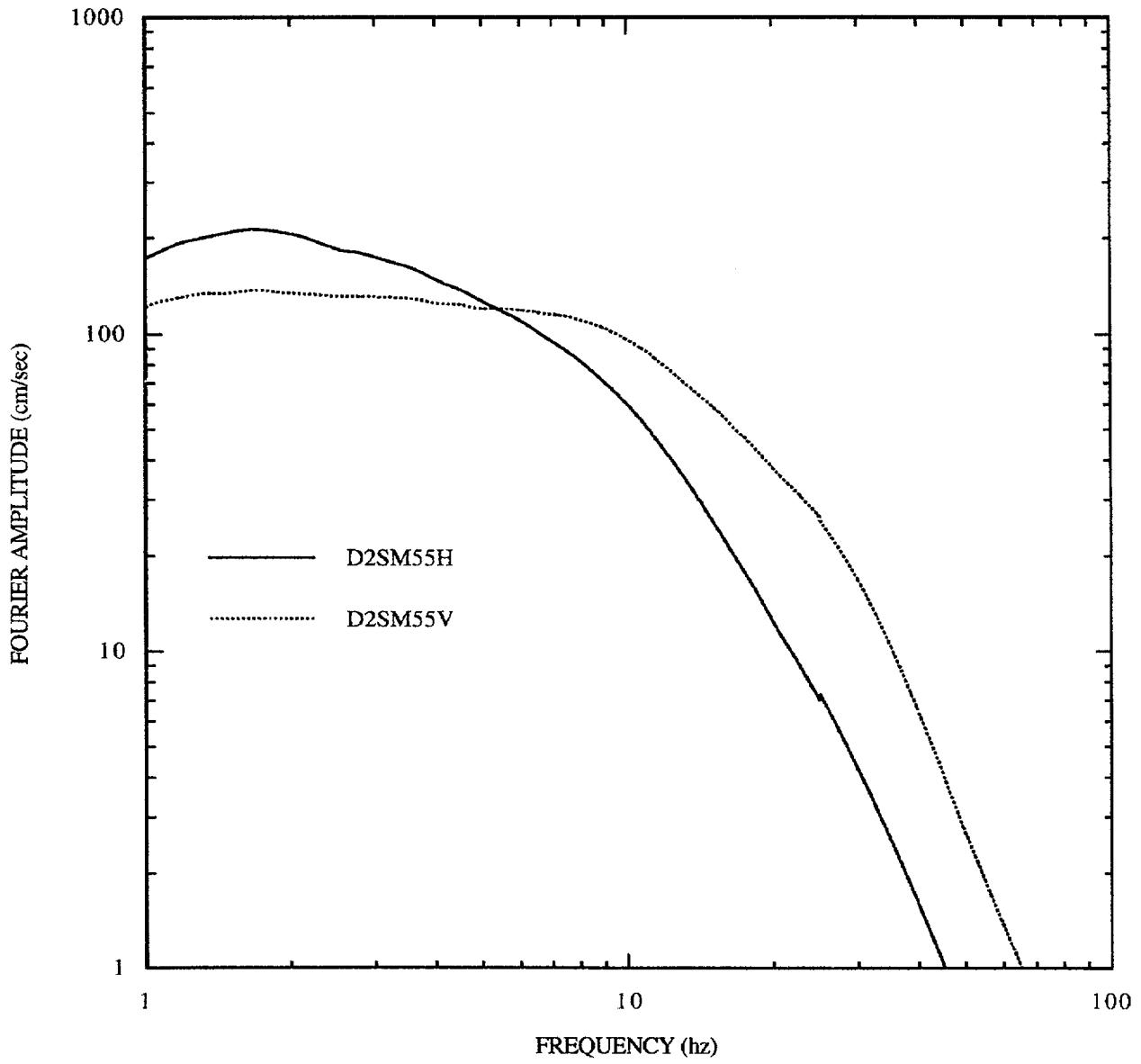


Figure E-16. Mean Fourier spectra for distance 10-50 km, soil sites, M 5-6.

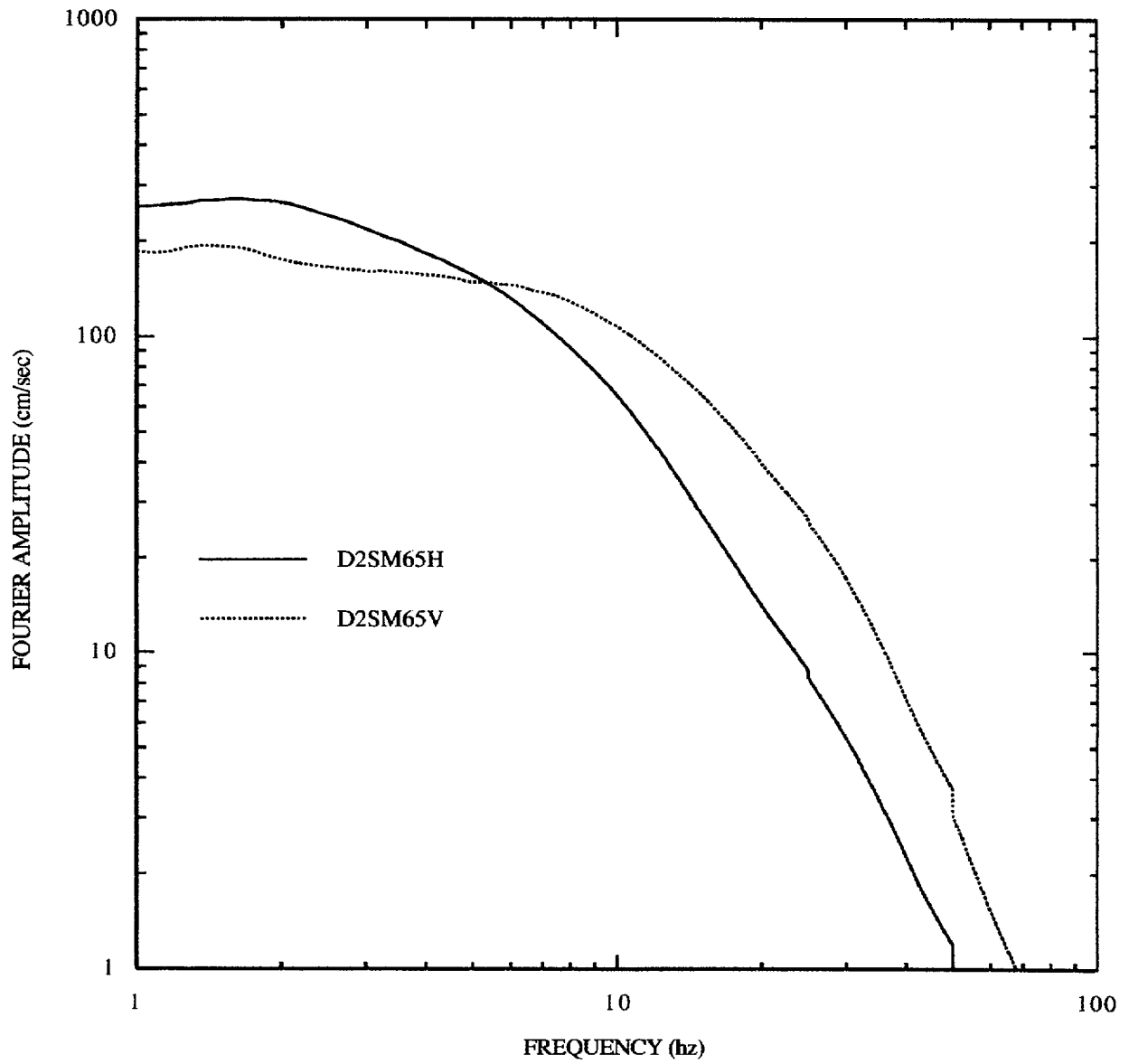


Figure E-17. Mean Fourier spectra for distance 10-50 km, soil sites, M 6-7.

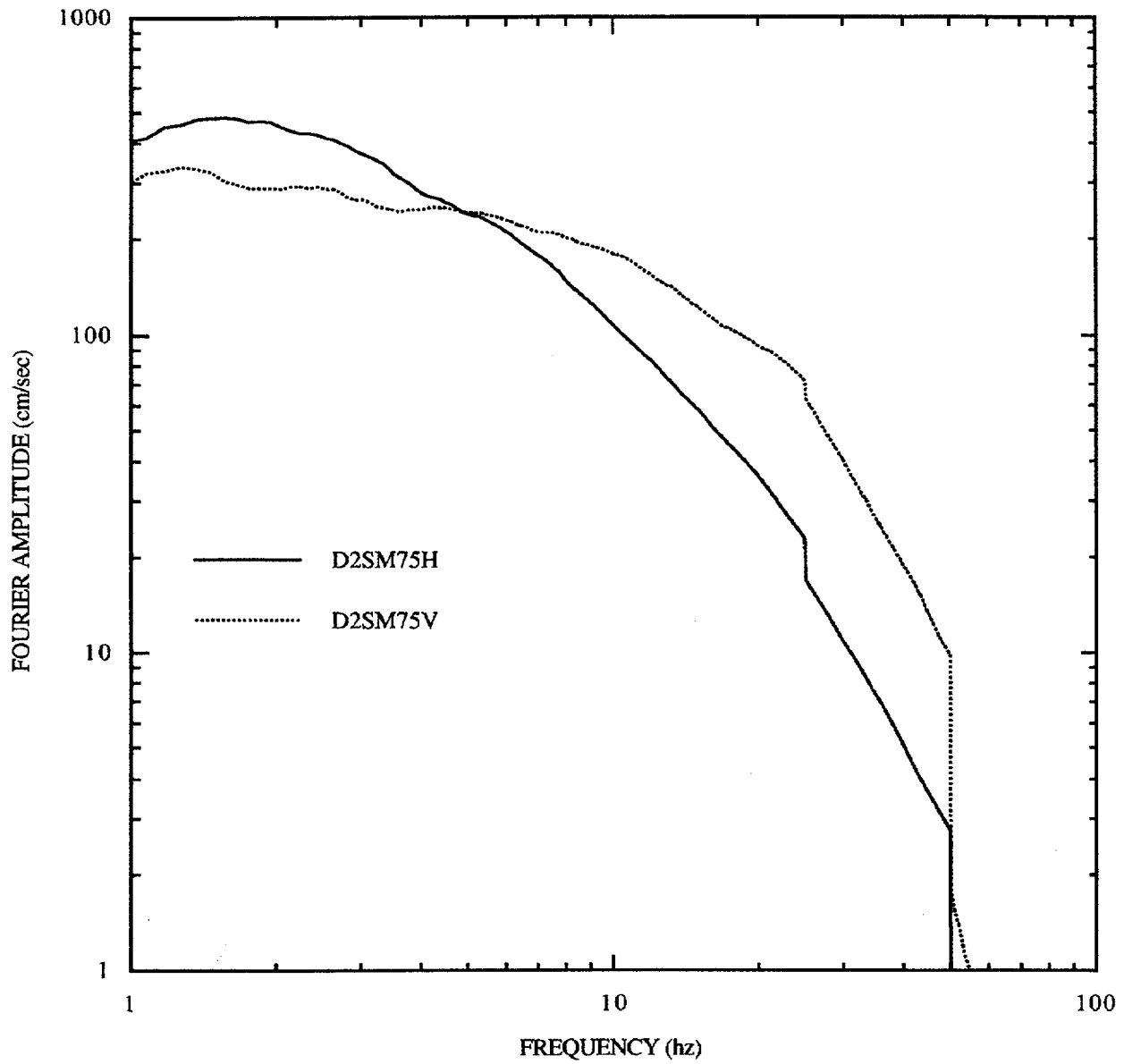


Figure E-18. Mean Fourier spectra for distance 10-50 km, soil sites, M 7+. Note: discontinuity at 25 Hz is caused by few records available above that frequency.

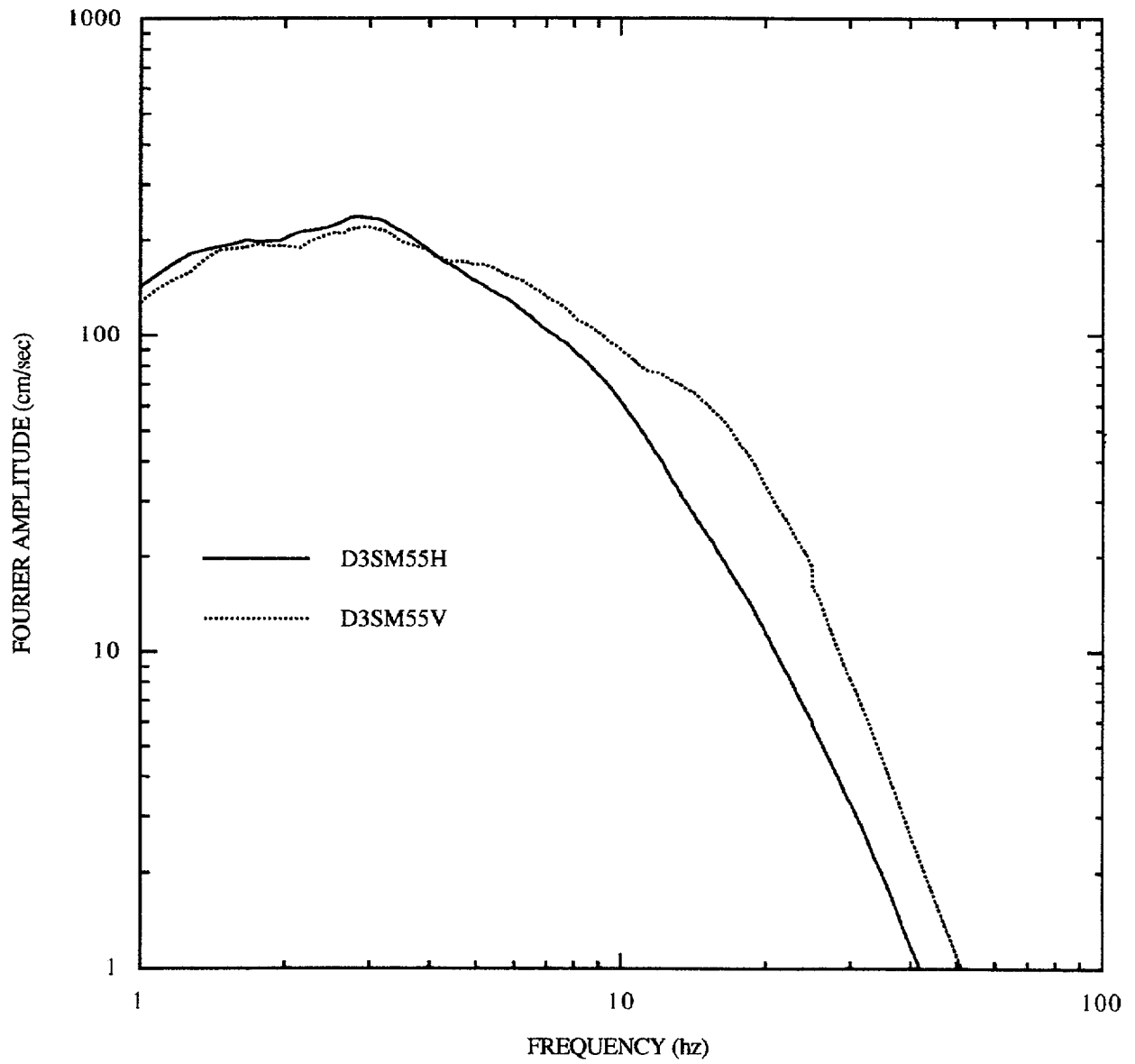


Figure E-19. Mean Fourier spectra for distance 50-100 km, soil sites, M 5-6.

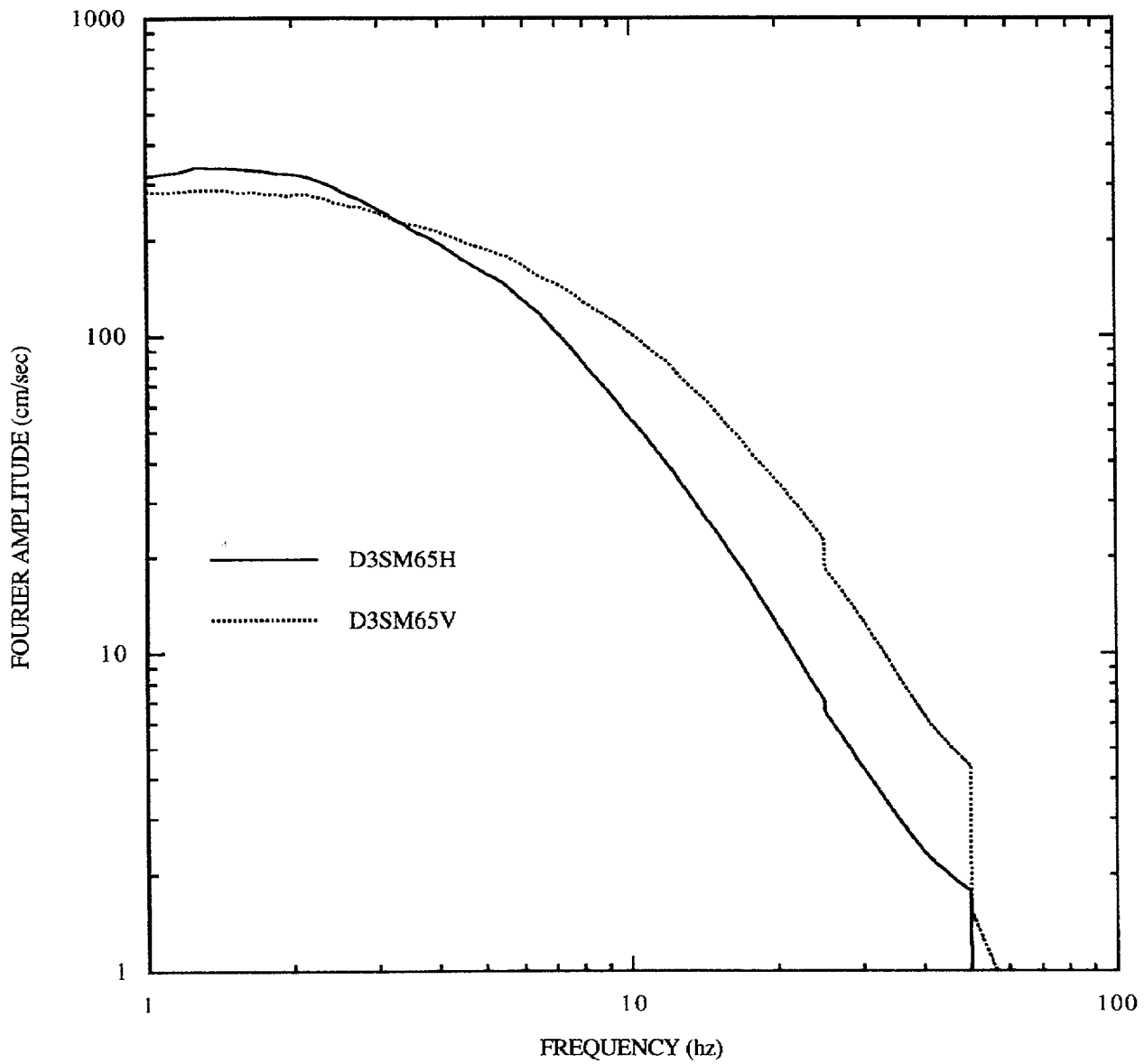


Figure E-20. Mean Fourier spectra for distance 50-100 km, soil sites, M 6-7. Note: discontinuity at 50 Hz is caused by few records available above that frequency.

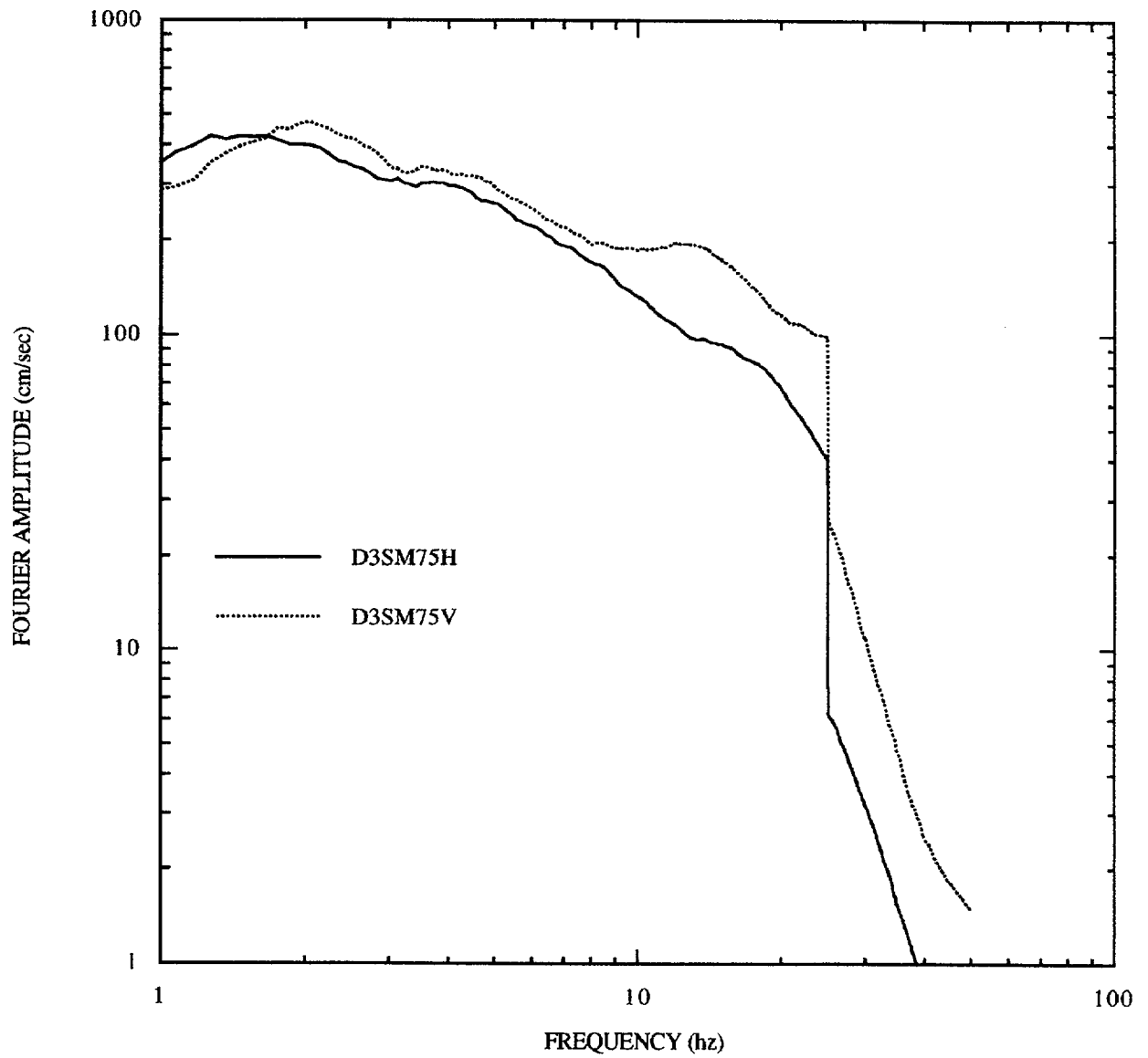


Figure E-21. Mean Fourier spectra for distance 50-100 km, soil sites, M 7+. Note: discontinuity at 25 Hz is caused by few records available above that frequency.

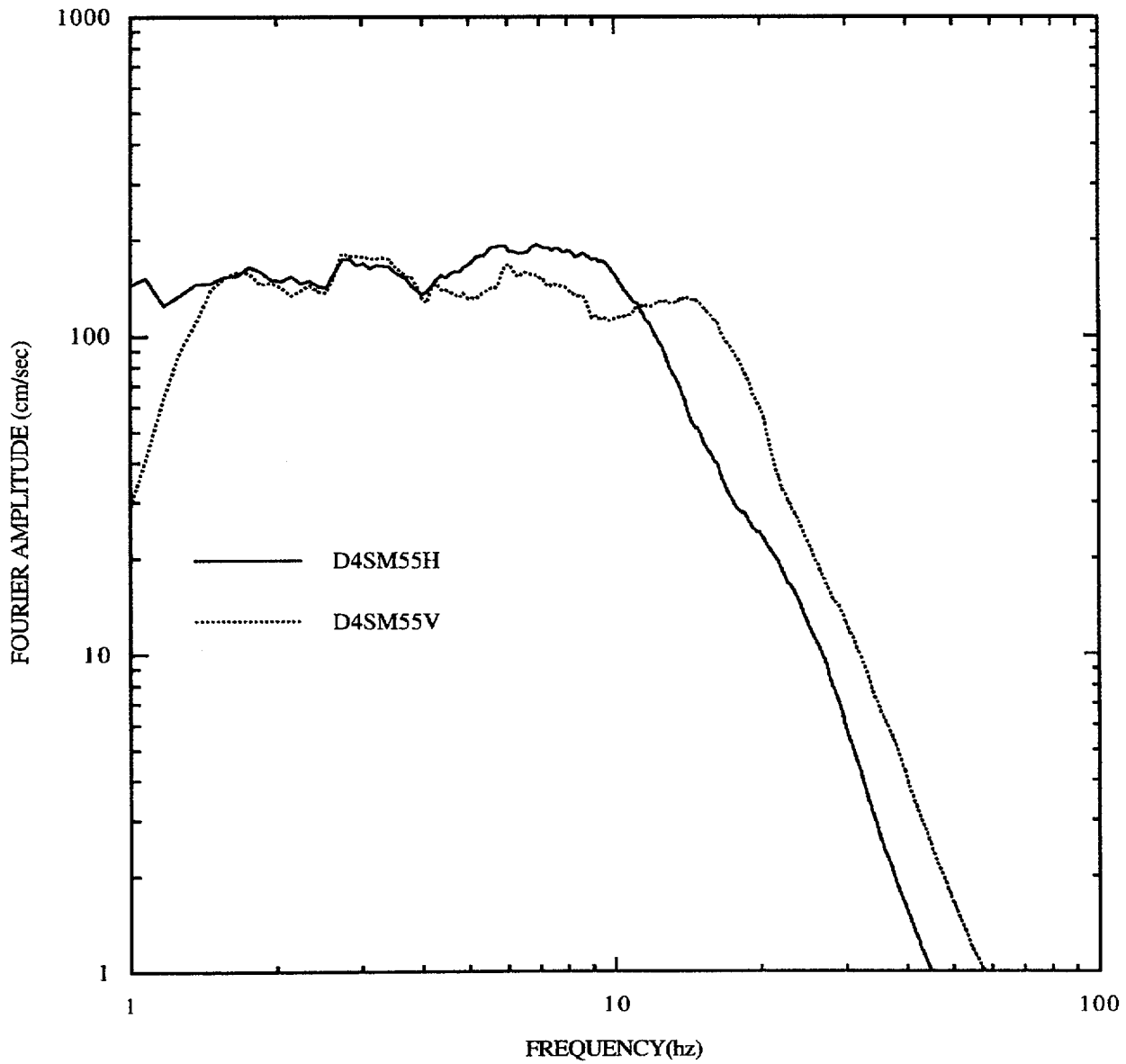


Figure E-22. Mean Fourier spectra for distance 100-200 km, soil sites, M 5-6.

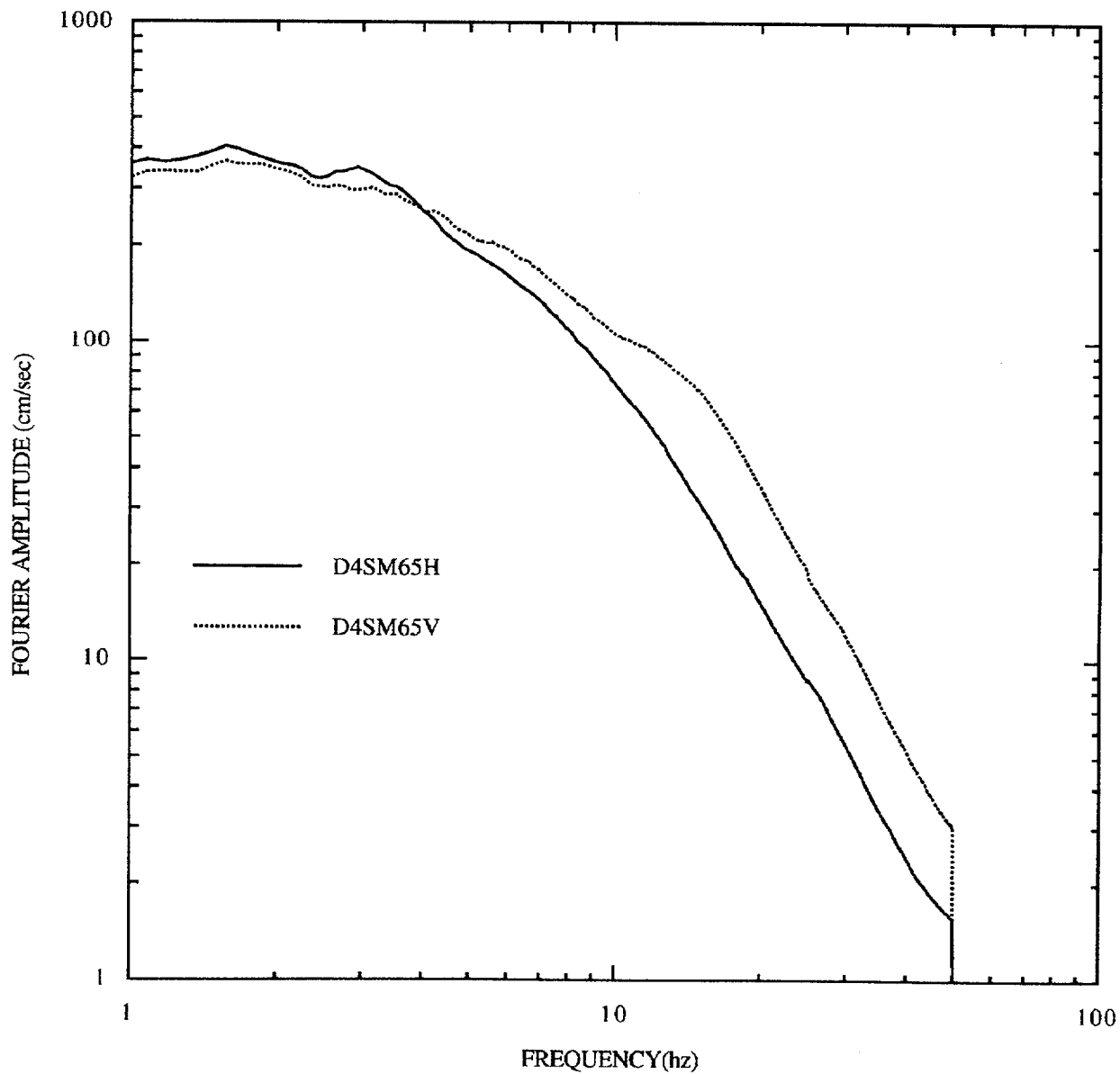


Figure E-23. Mean Fourier spectra for distance 100-200 km, soil sites, M 6-7. Note: discontinuity at 50 Hz is caused by few records available above that frequency.

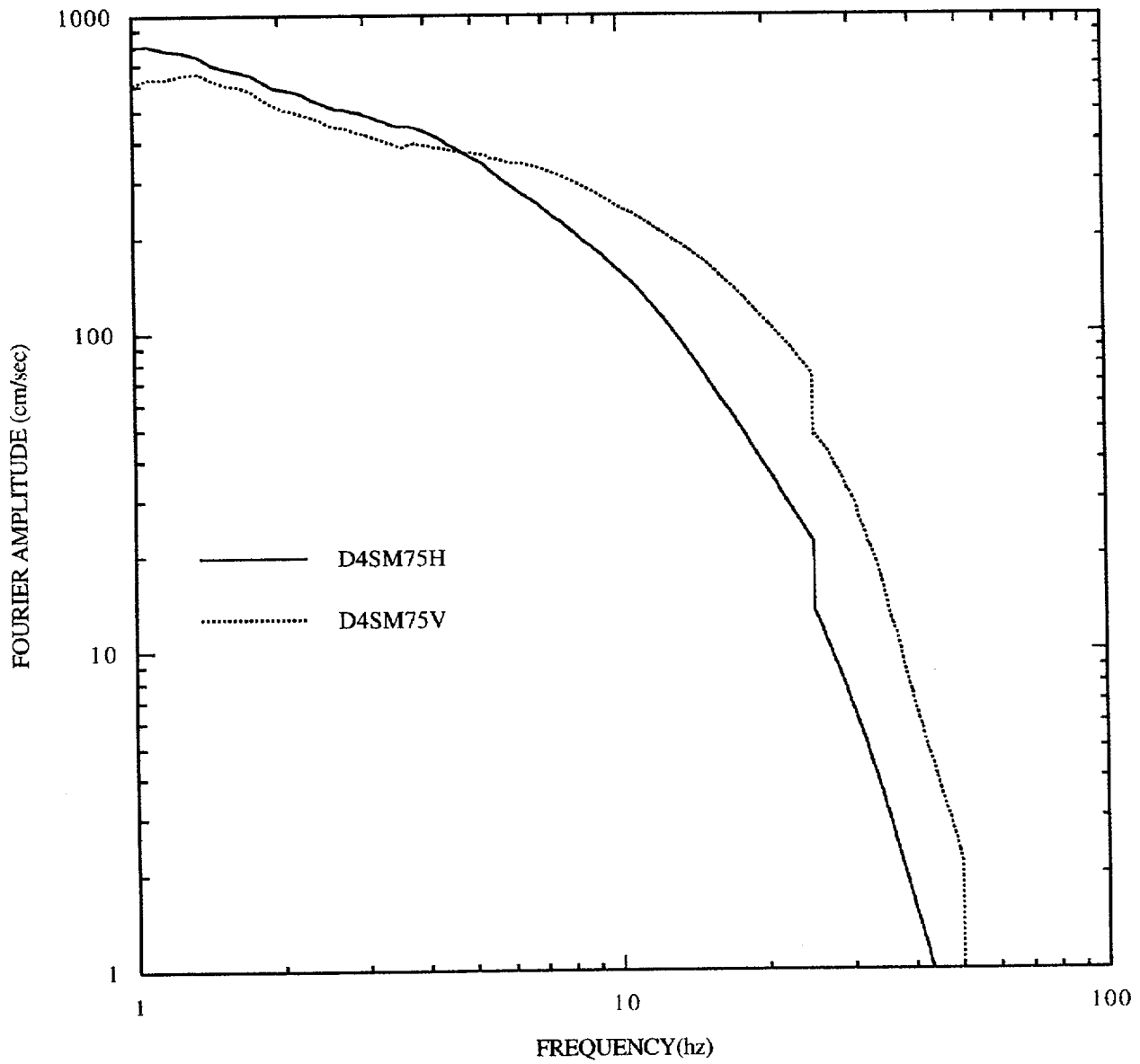


Figure E-24. Mean Fourier spectra for distance 100-200 km, soil sites, M 7+.
 Note: discontinuity at 25 and 50 Hz is caused by few records available above that frequency.

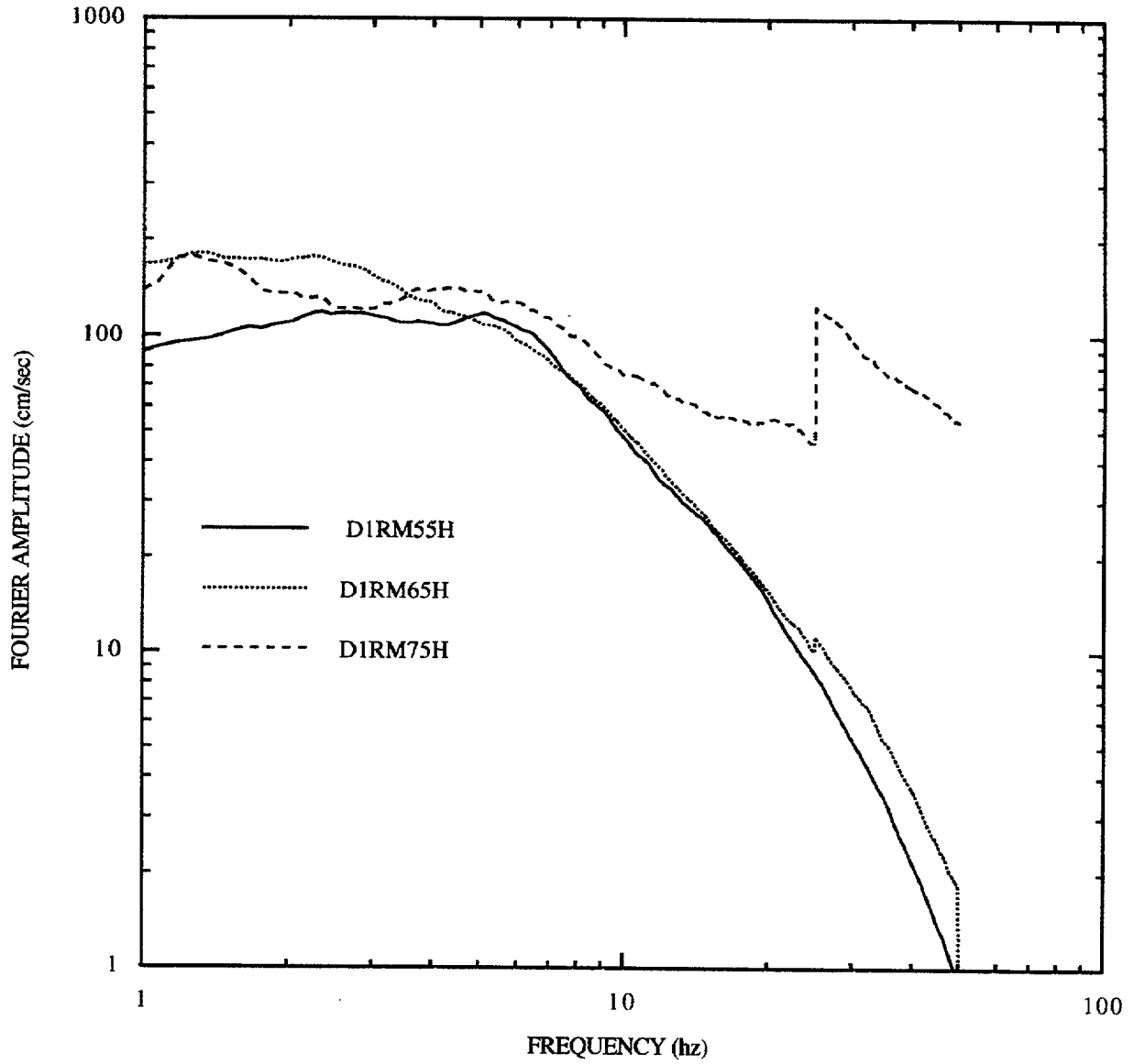


Figure E-25. Mean Fourier spectra for distance 0-10 km, rock sites, horizontal motions.
 Note: discontinuity at 25 and 50 Hz is caused by few records available above that frequency.

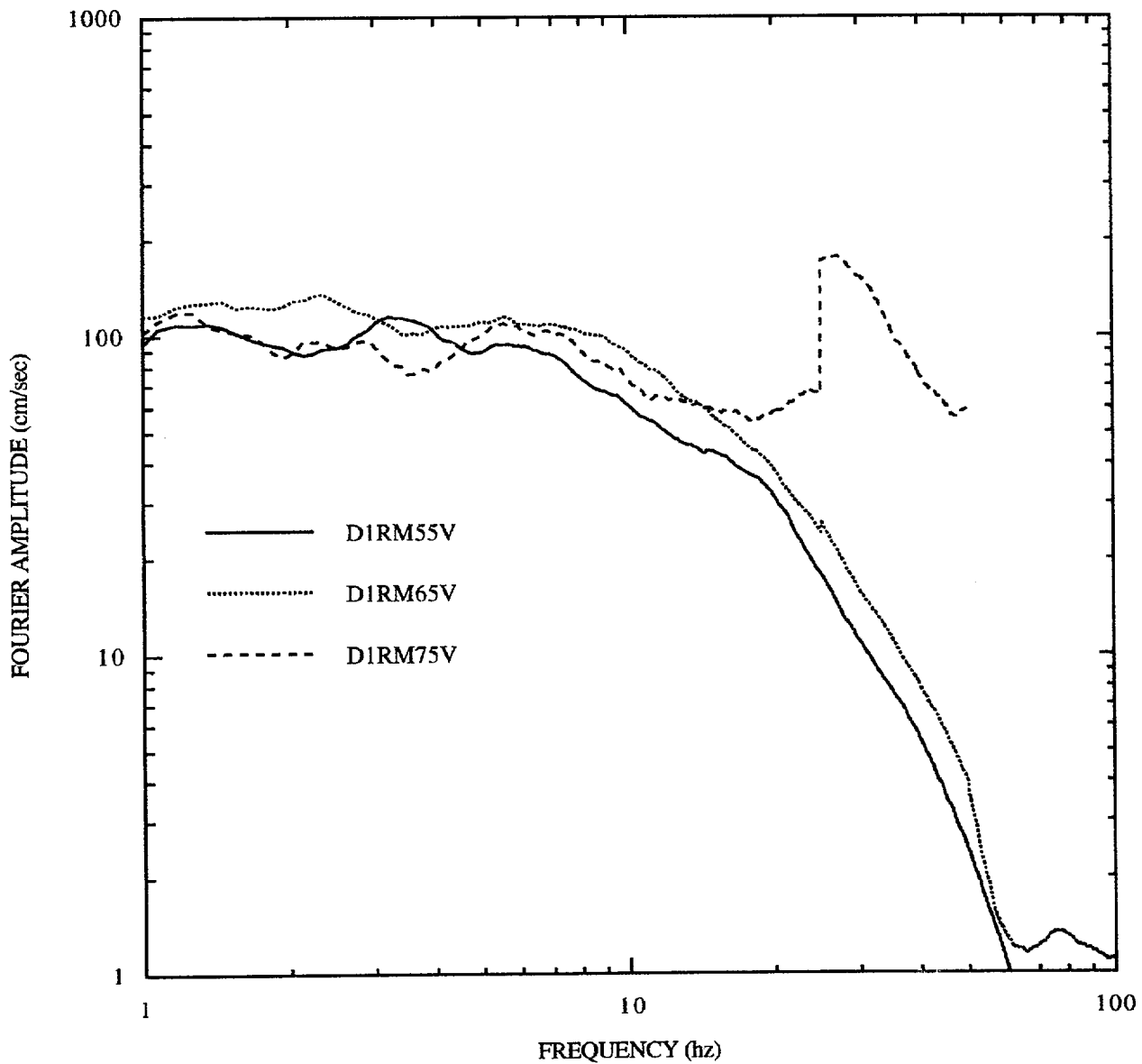


Figure E-26. Mean Fourier spectra for distance 0-10 km, rock sites, vertical motions. Note: discontinuity at 25 Hz is caused by few records available above that frequency.

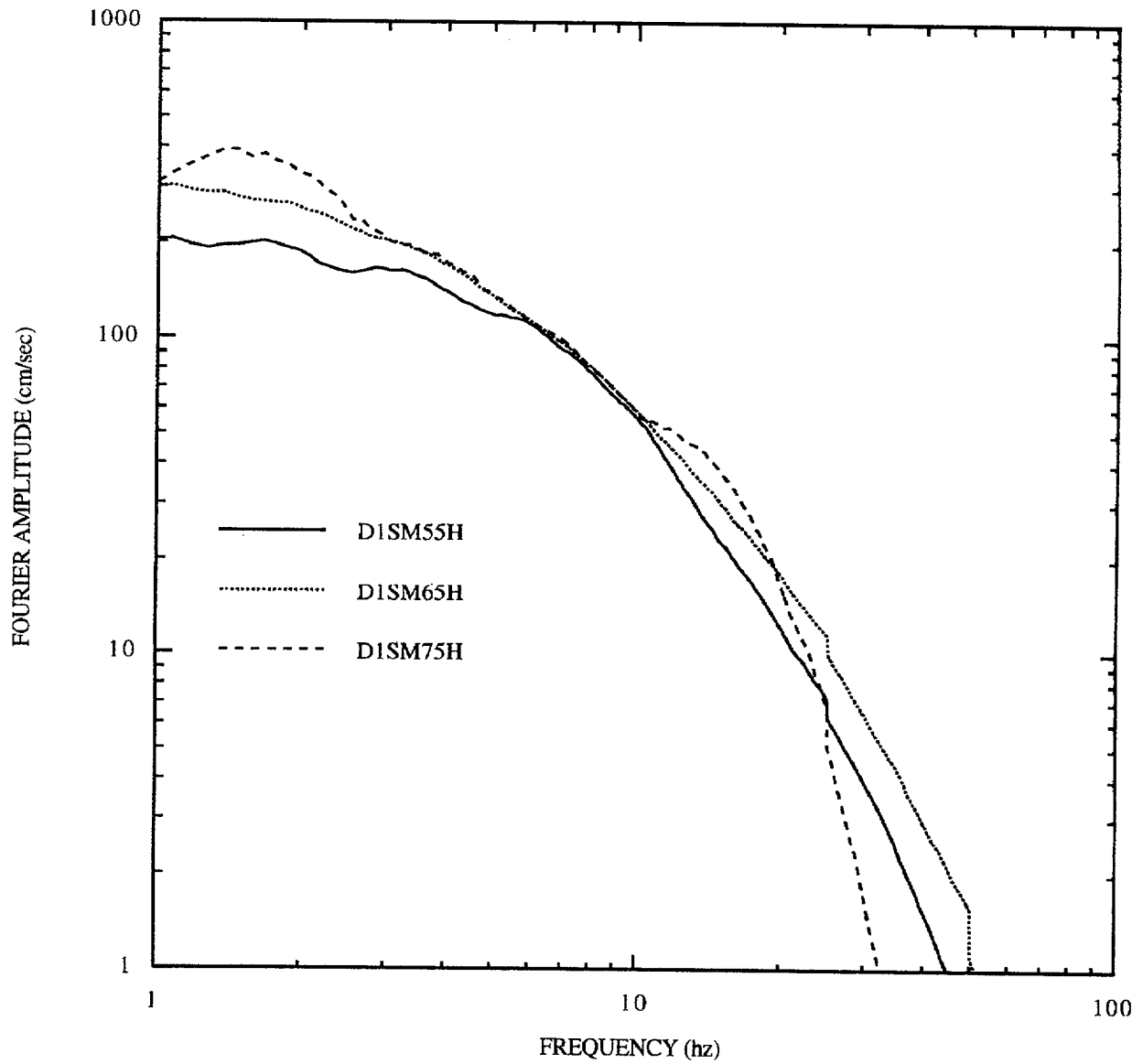


Figure E-27. Mean Fourier spectra for distance 0-10 km, soil sites, horizontal motions.
 Note: discontinuity at 25 and 50 Hz is caused by few records available above that frequency.

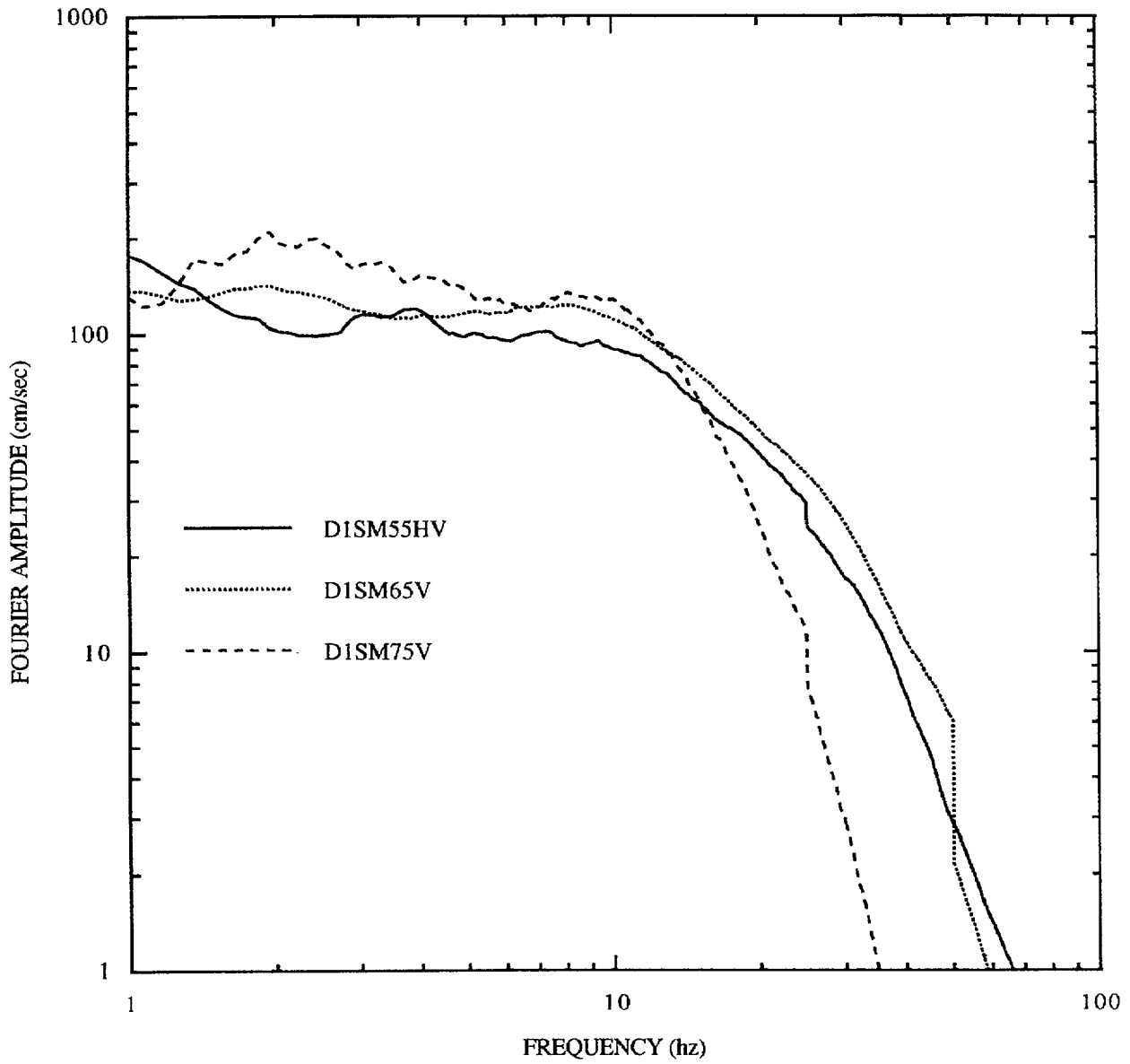


Figure E-28. Mean Fourier spectra for distance 0-10 km, soil sites, vertical motions.
 Note: discontinuity at 25 and 50 Hz is caused by few records available above that frequency.

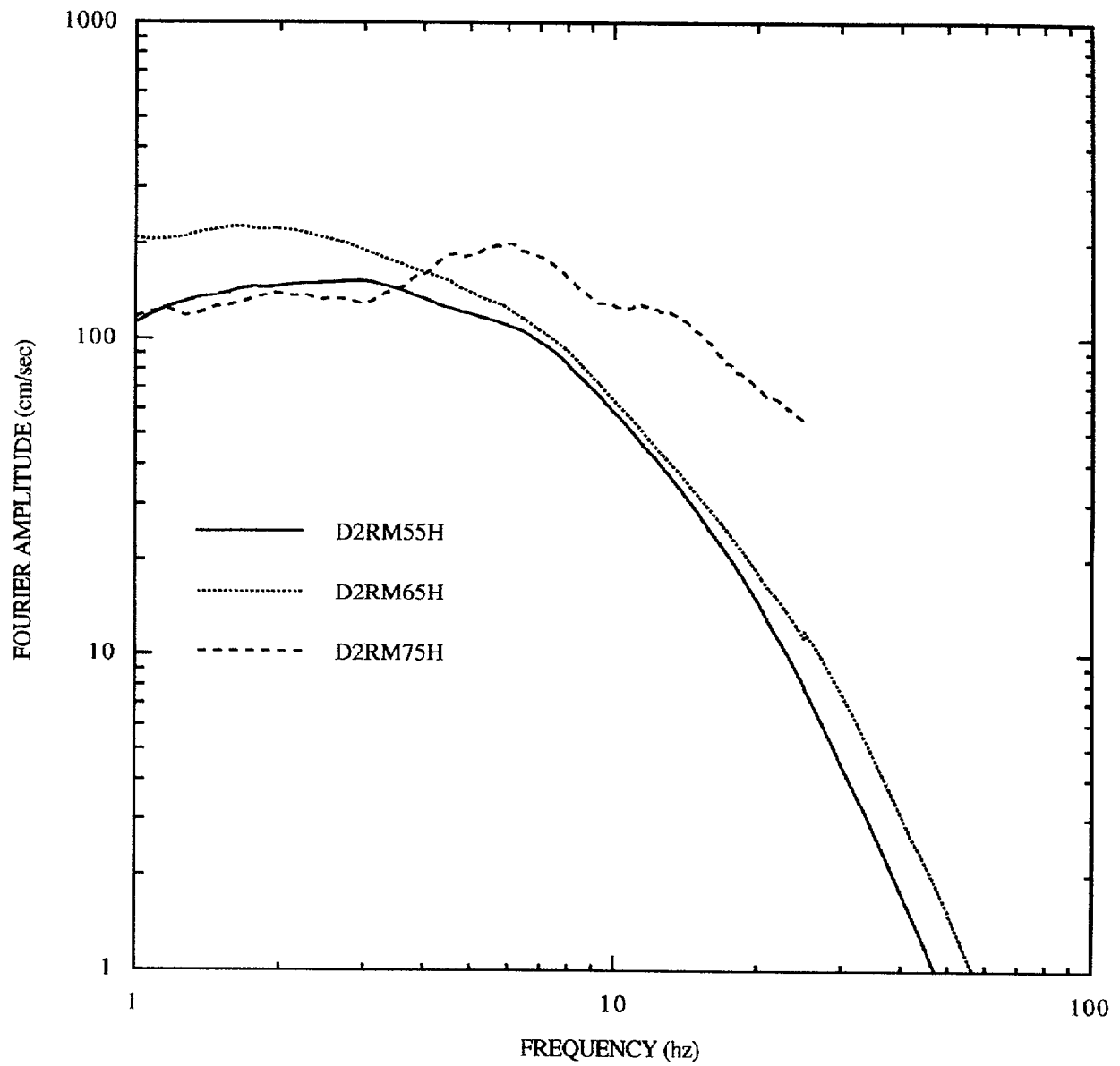


Figure E-29. Mean Fourier spectra for distance 10-50 km, rock sites, horizontal motions.

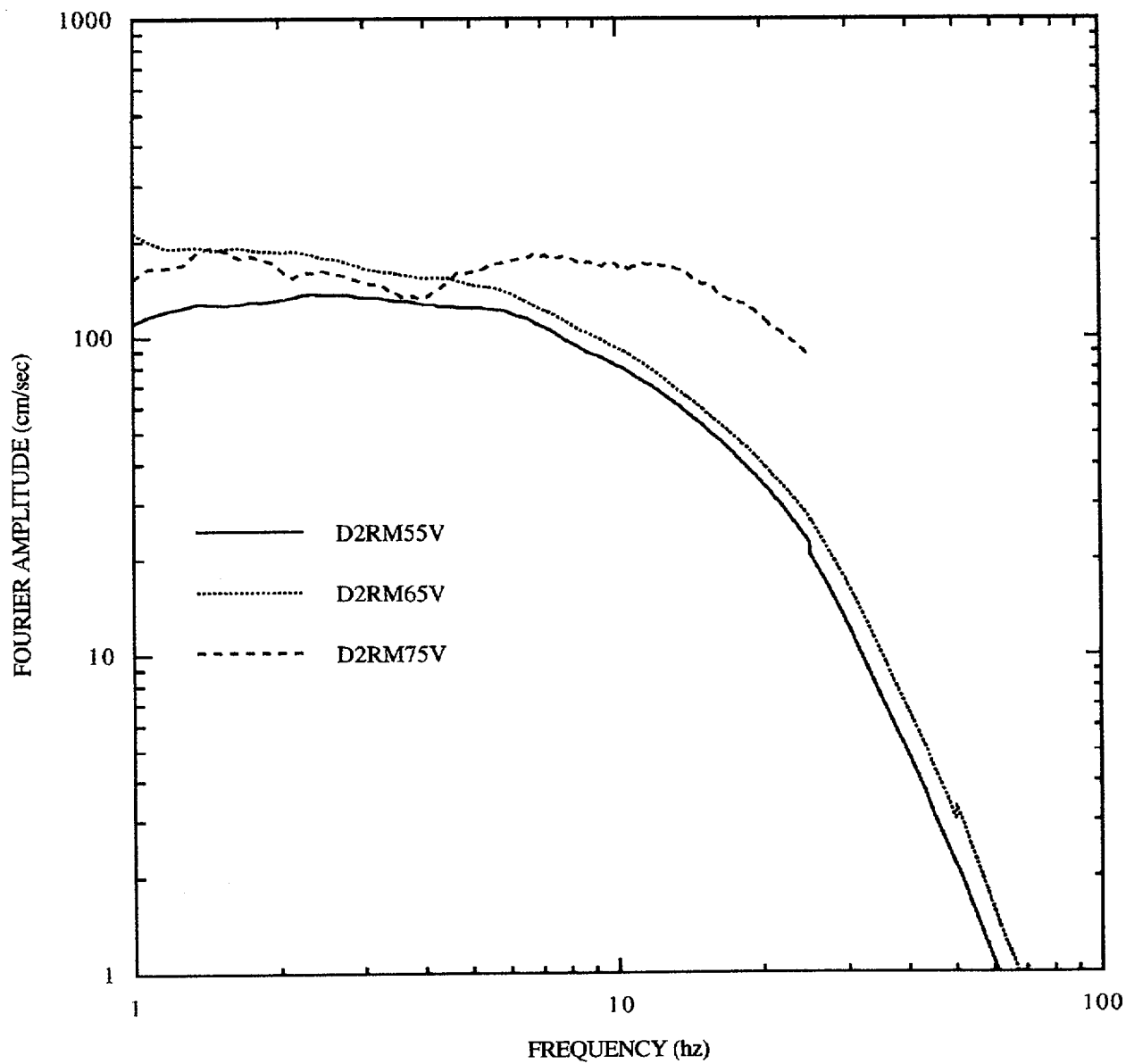


Figure E-30. Mean Fourier spectra for distance 10-50 km, rock sites, vertical motions.

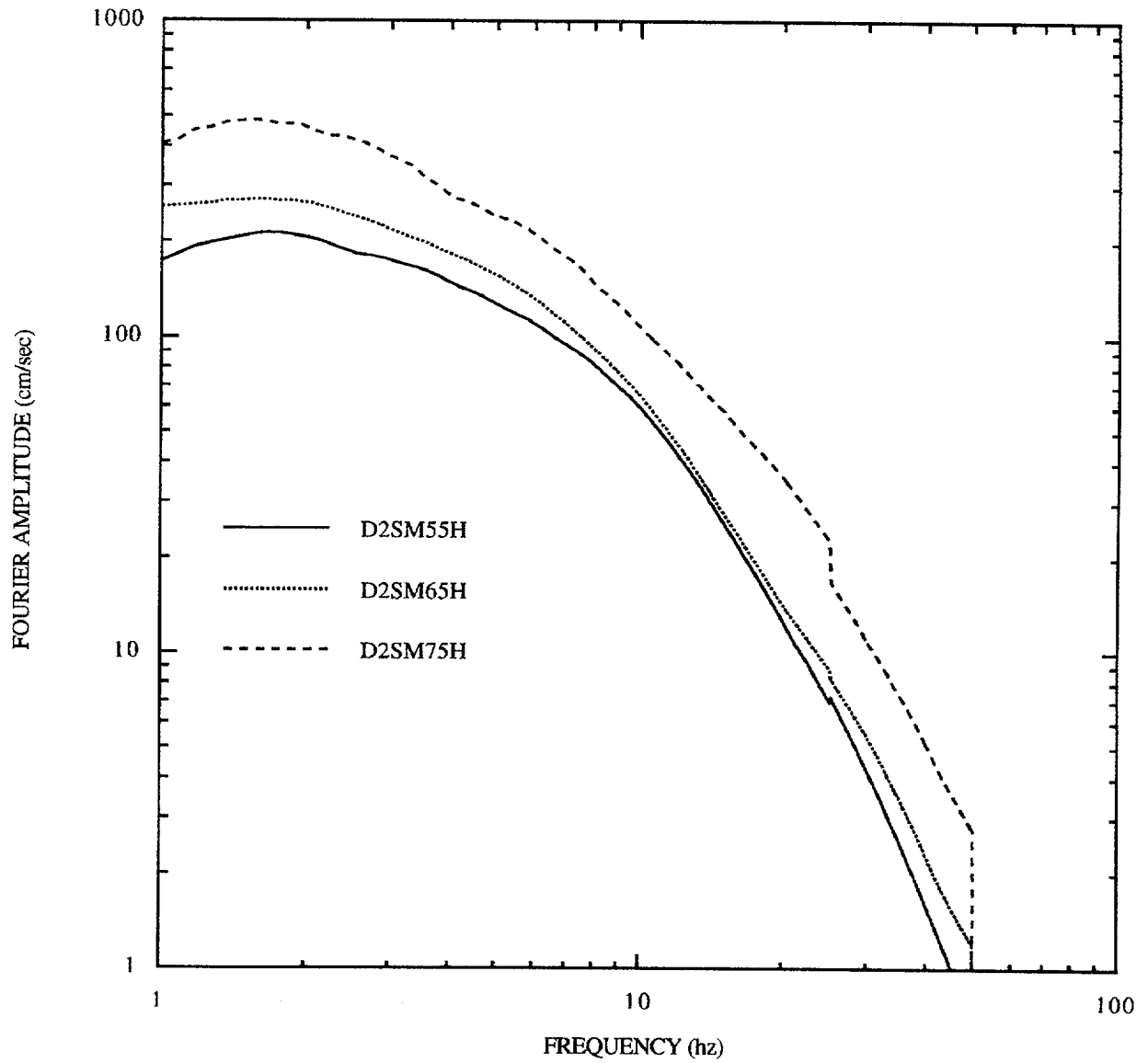


Figure E-31. Mean Fourier spectra for distance 10-50 km, soil sites, horizontal motions.
 Note: discontinuity at 25 and 50 Hz is caused by few records available above that frequency.

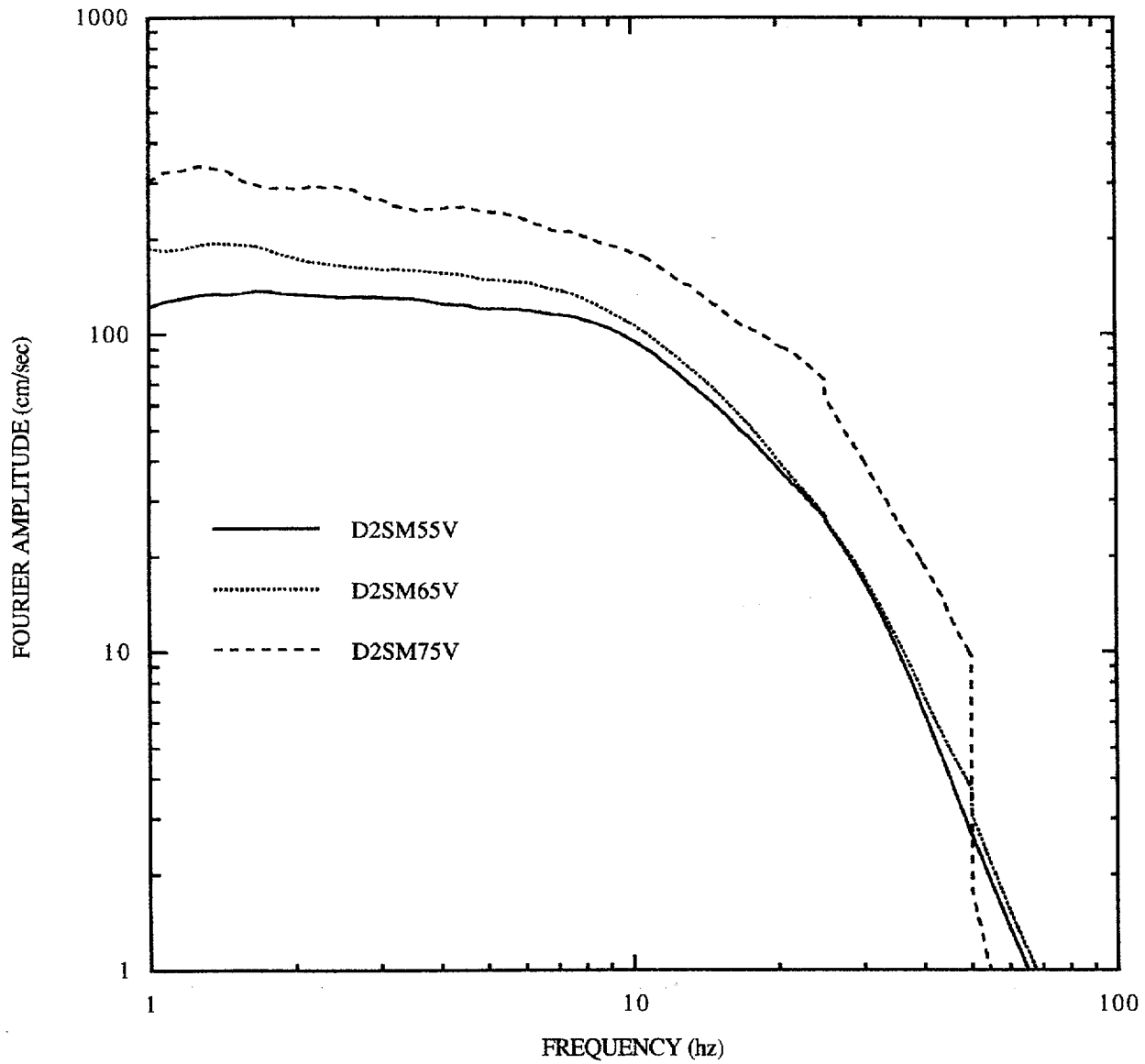


Figure E-32. Mean Fourier spectra for distance 10-50 km, soil sites, vertical motions.
 Note: discontinuity at 25 and 50 Hz is caused by few records available above that frequency.

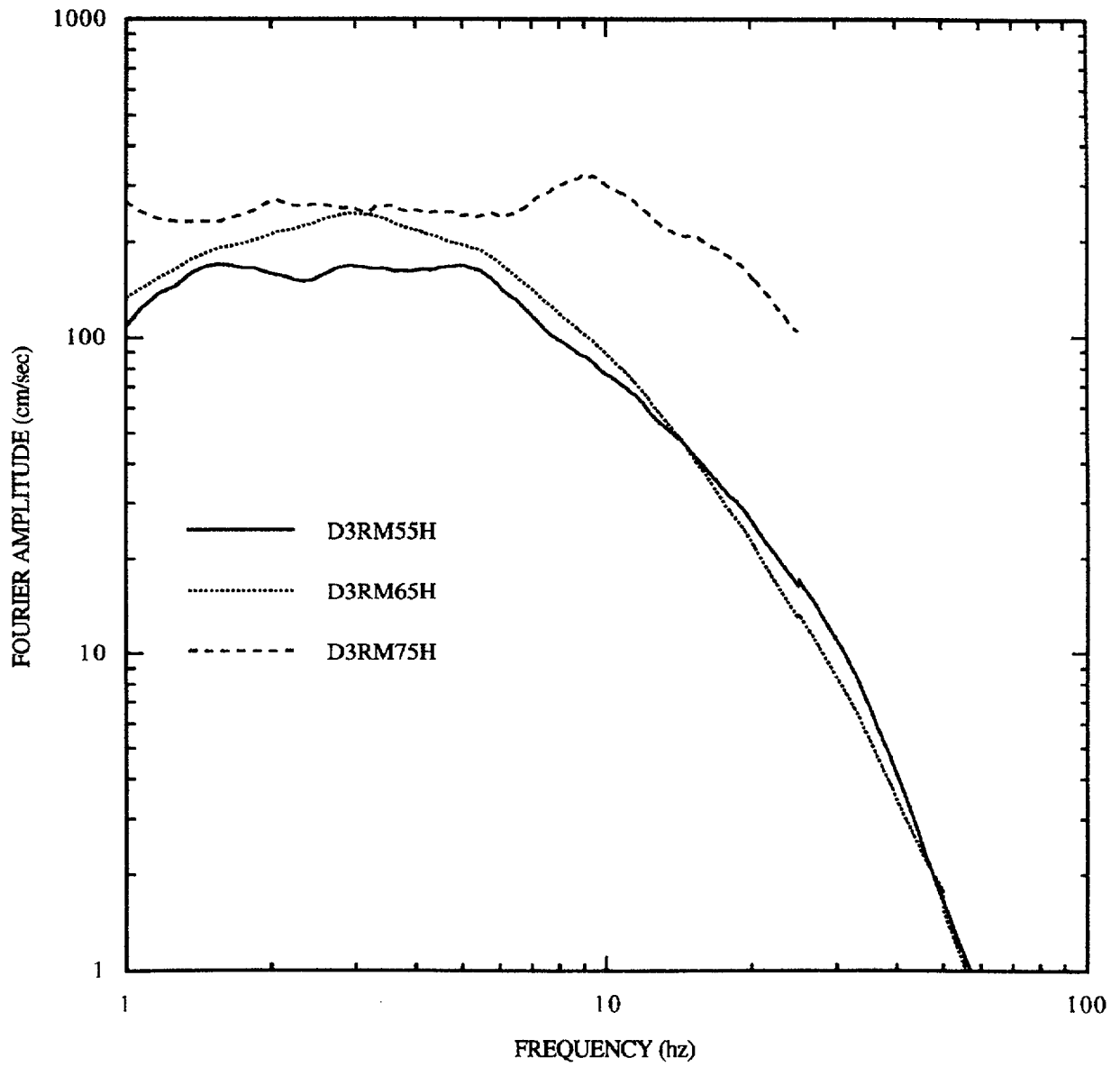


Figure E-33. Mean Fourier spectra for distance 50-100 km, rock sites, horizontal motions.

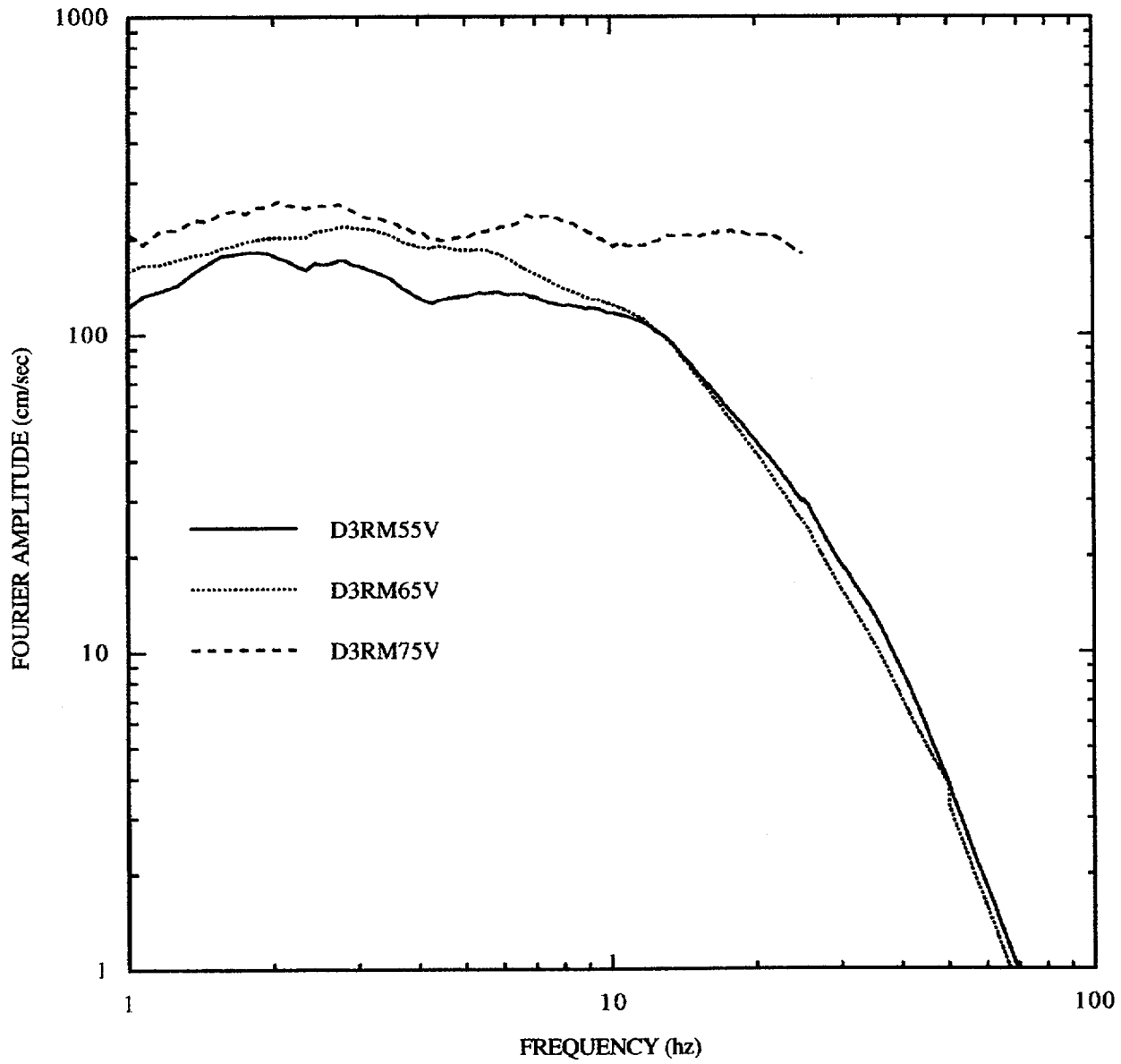


Figure E-34. Mean Fourier spectra for distance 50-100 km, rock sites, vertical motions.

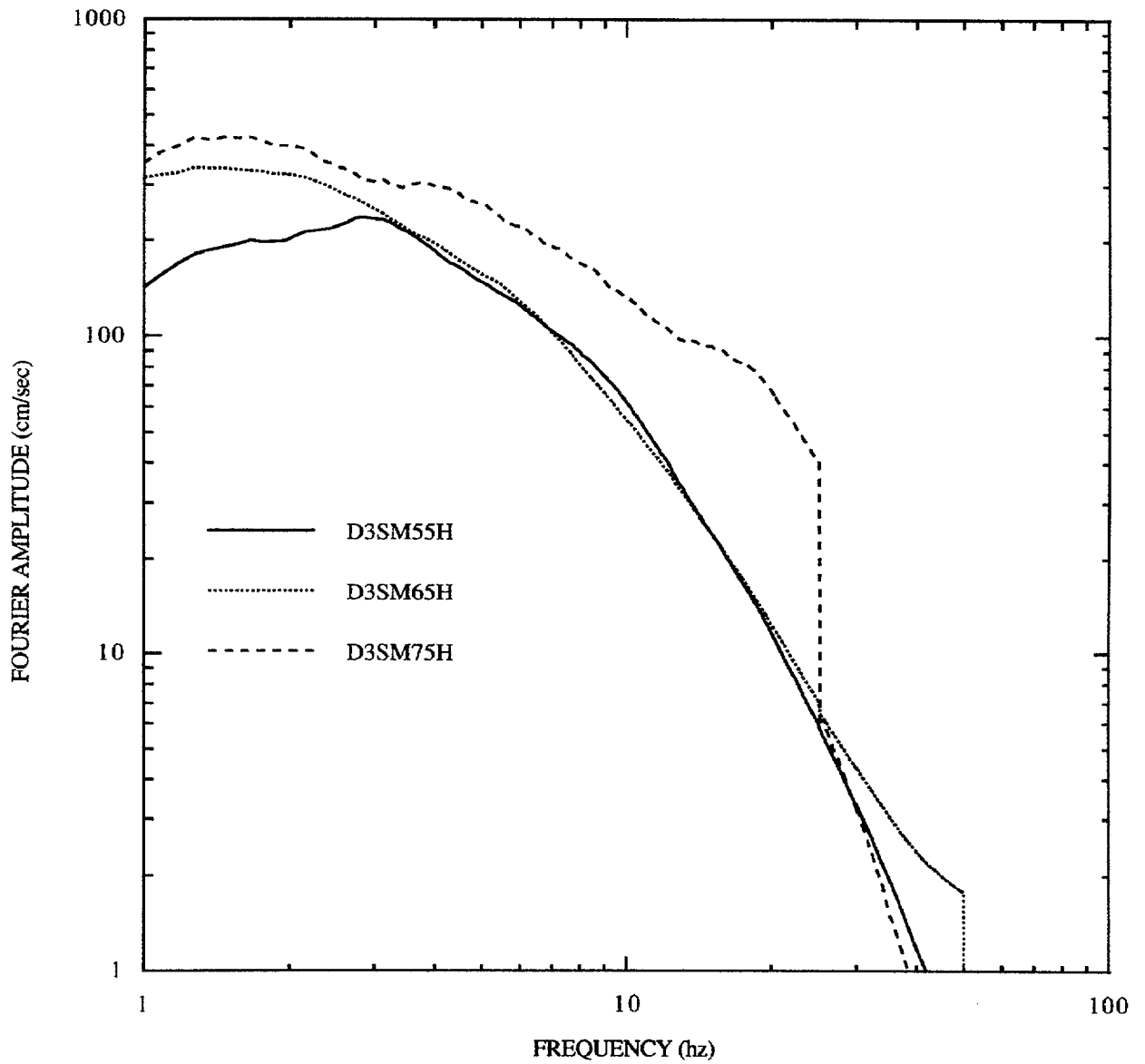


Figure E-35. Mean Fourier spectra for distance 50-100 km, soil sites, horizontal motions.
 Note: discontinuity at 25 and 50 Hz is caused by few records available above that frequency.

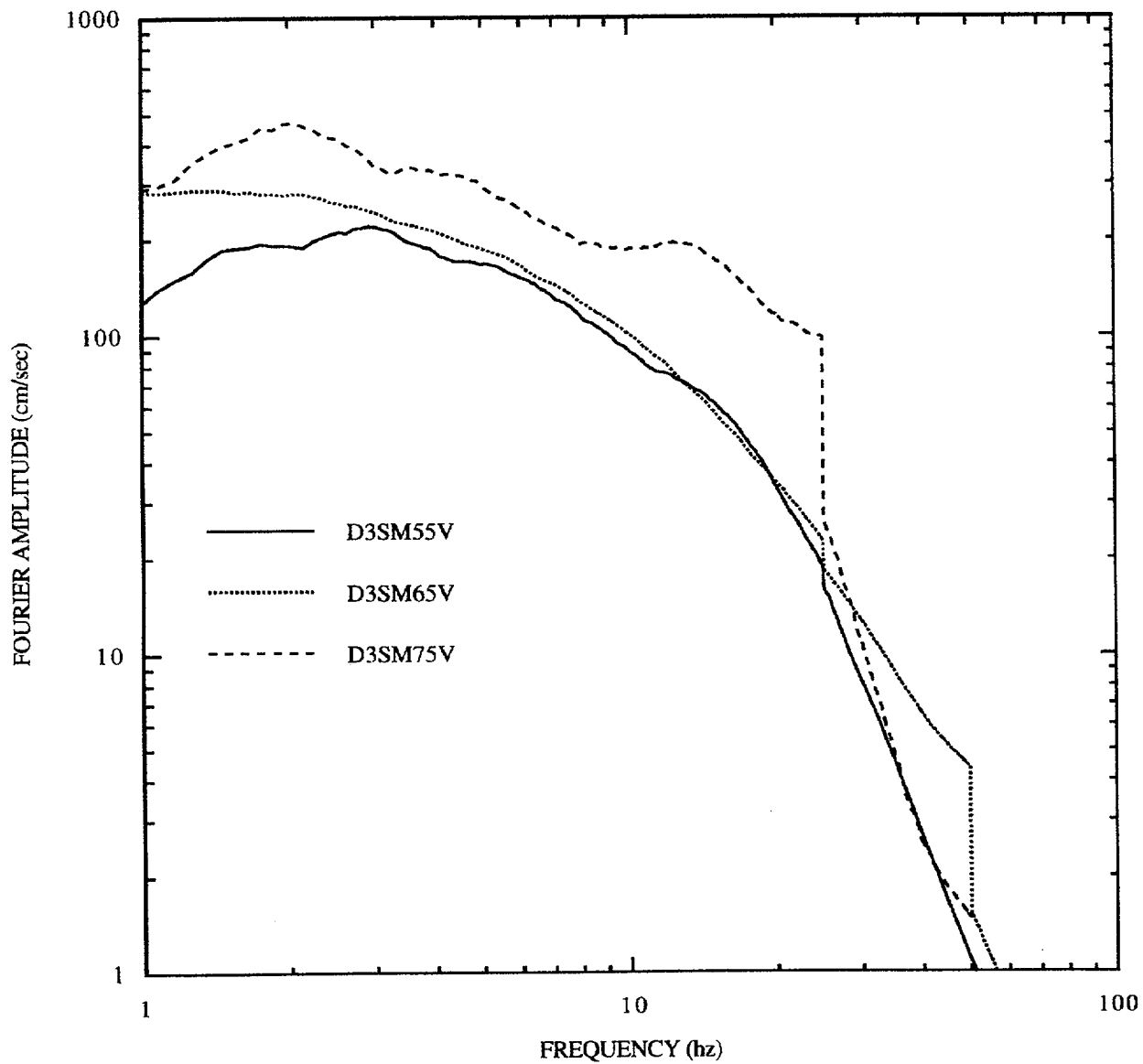


Figure E-36. Mean Fourier spectra for distance 50-100 km, rock sites, vertical motions.
 Note: discontinuity at 25 and 50 Hz is caused by few records available above that frequency.

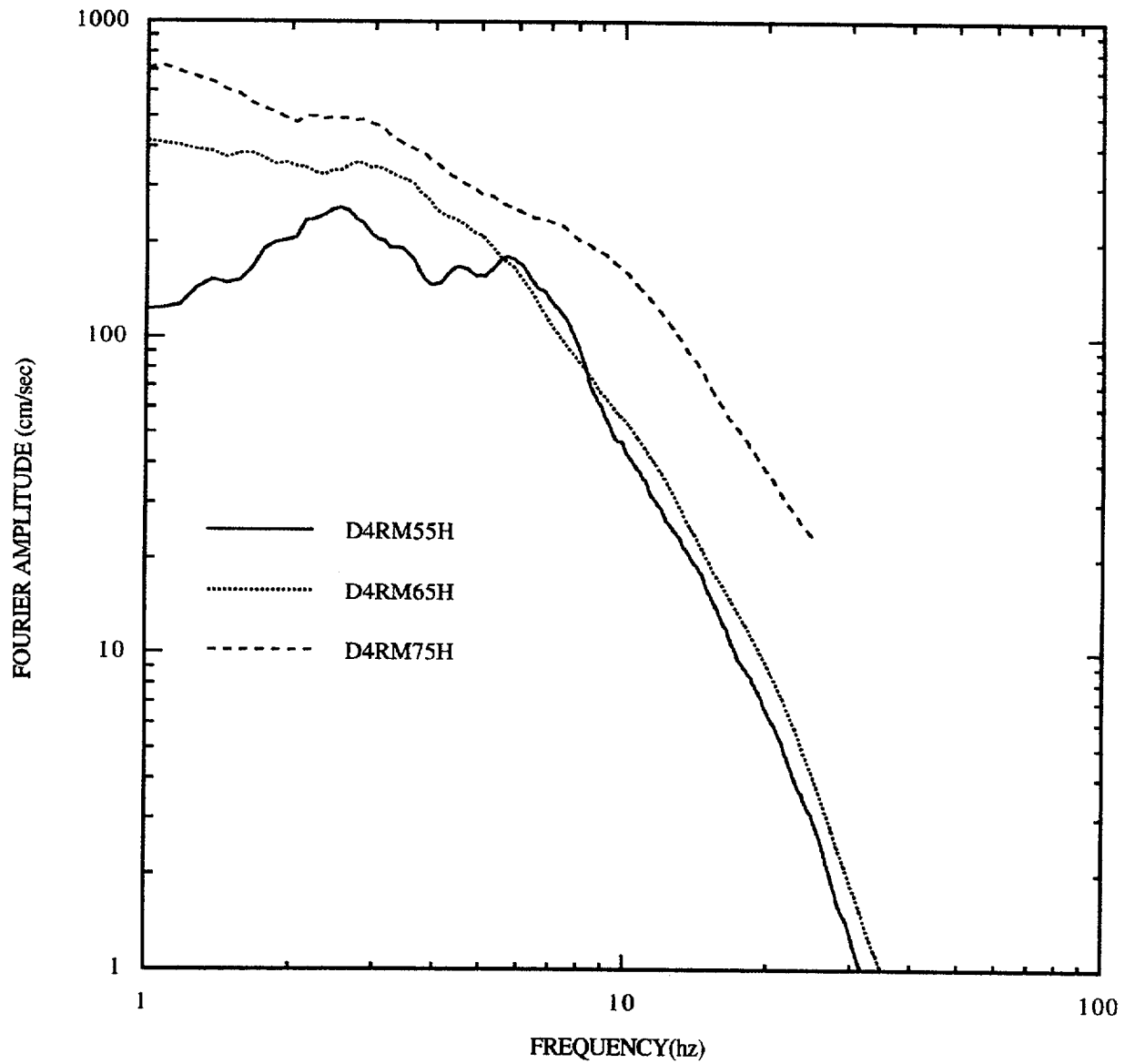


Figure E-37. Mean Fourier spectra for distance 100-200 km, rock sites, horizontal motions.

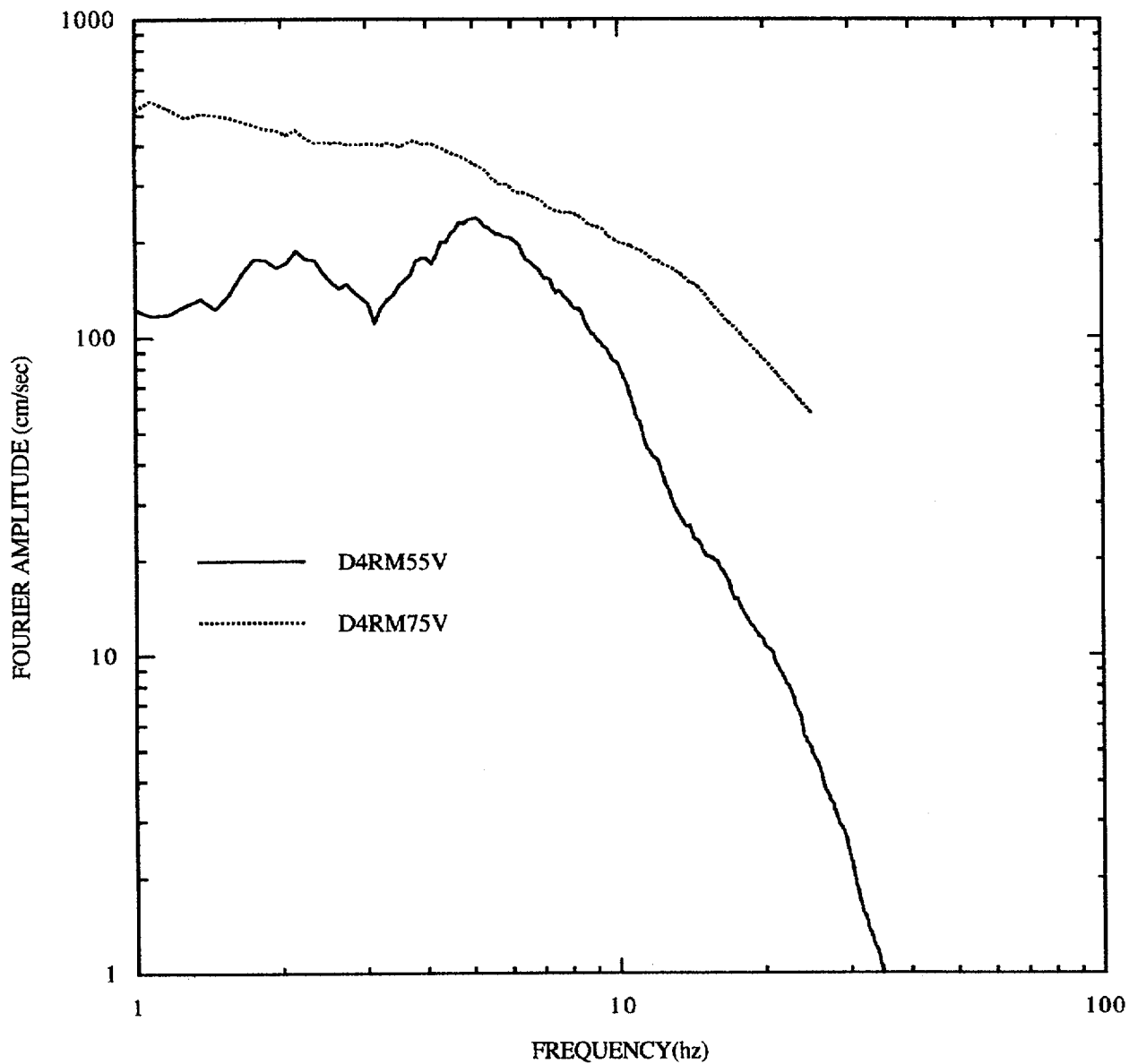


Figure E-38. Mean Fourier spectra for distance 100-200 km, rock sites, vertical motions.

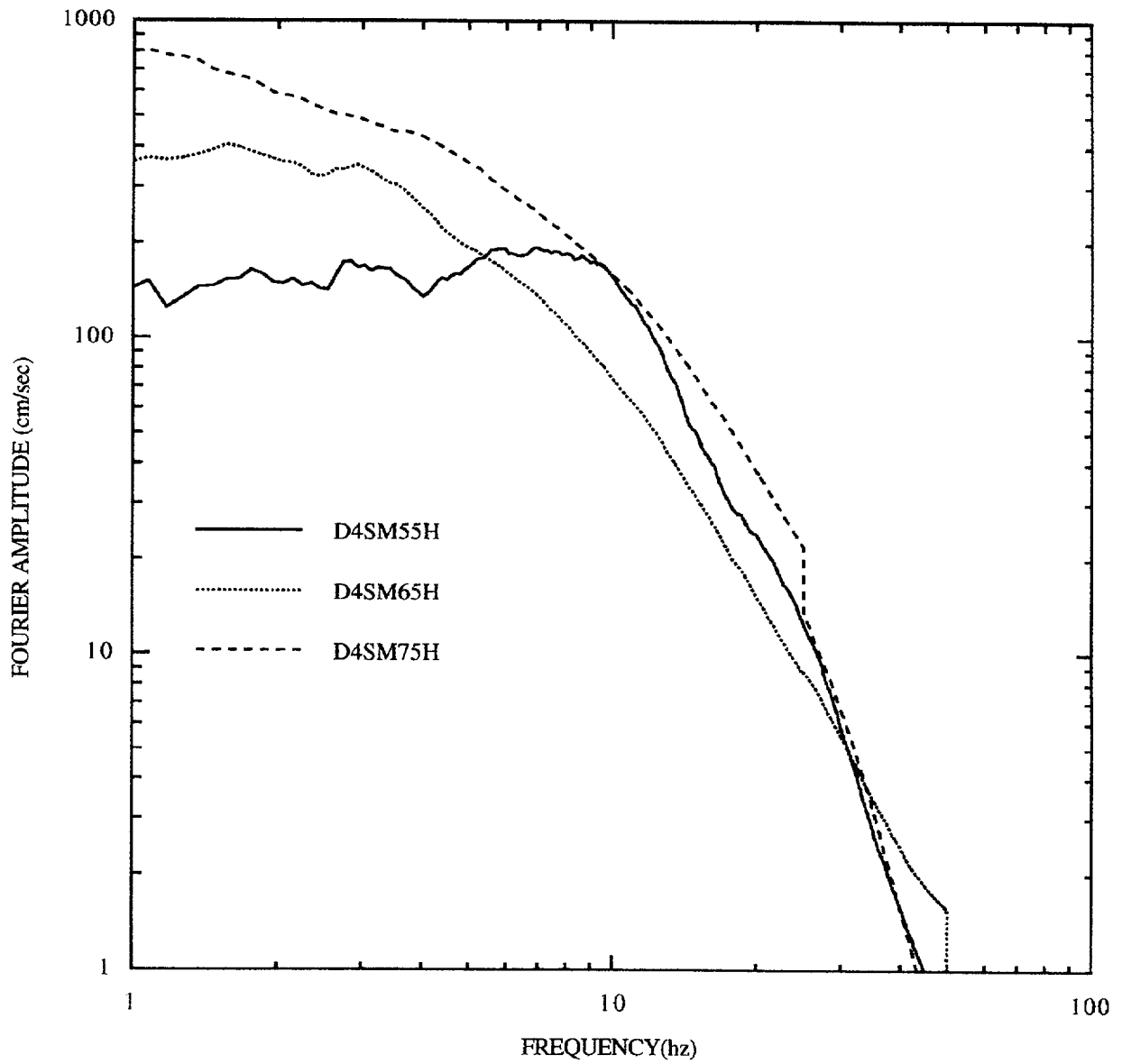


Figure E-39. Mean Fourier spectra for distance 100-200 km, soil sites, horizontal motions. Note: discontinuity at 25 and 50 Hz is caused by few records available above that frequency.

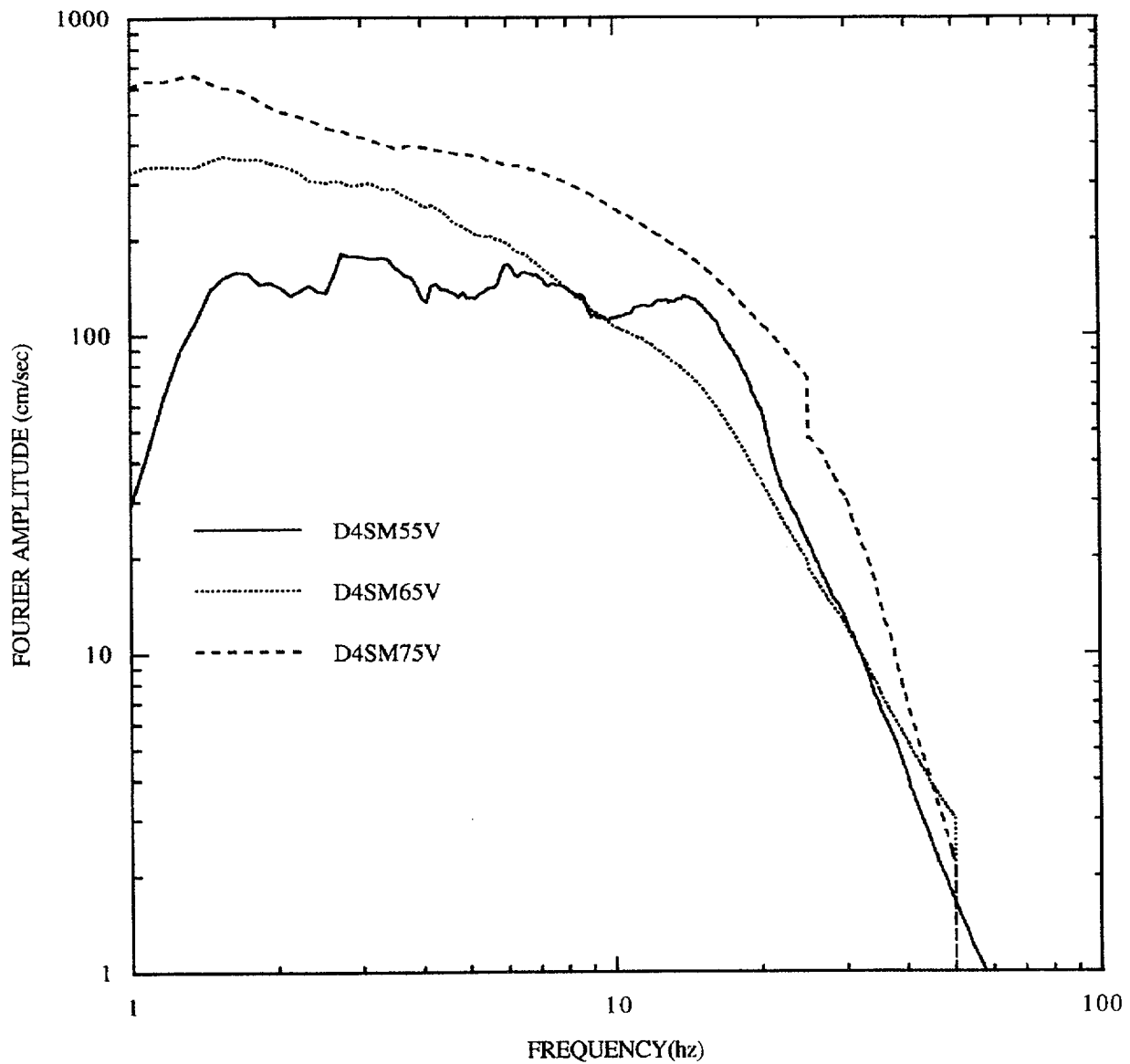


Figure E-40. Mean Fourier spectra for distance 100-200 km, soil sites, vertical motions.
 Note: discontinuity at 25 and 50 Hz is caused by few records available above that frequency.

APPENDIX F PLOTS OF EMPIRICAL DATA FROM WUS RECORDS

	Figures
1. Peak scaled velocity and displacement parameters from WUS empirical motions	F-1 to F-12
2. Bin duration parameters from WUS time histories	
Arias intensity 5% - 75%	F-13 to F-16
Arias intensity 5% - 95%	F-17 to F-20
3. Average component correlations between horizontal pairs in WUS empirical data base for acceleration, velocity, and displacement records	F-21 to F-26
4. Comparison of component correlations between vertical and horizontal pairs in WUS empirical data base for acceleration, velocity, and displacement records	F-27 to F-32

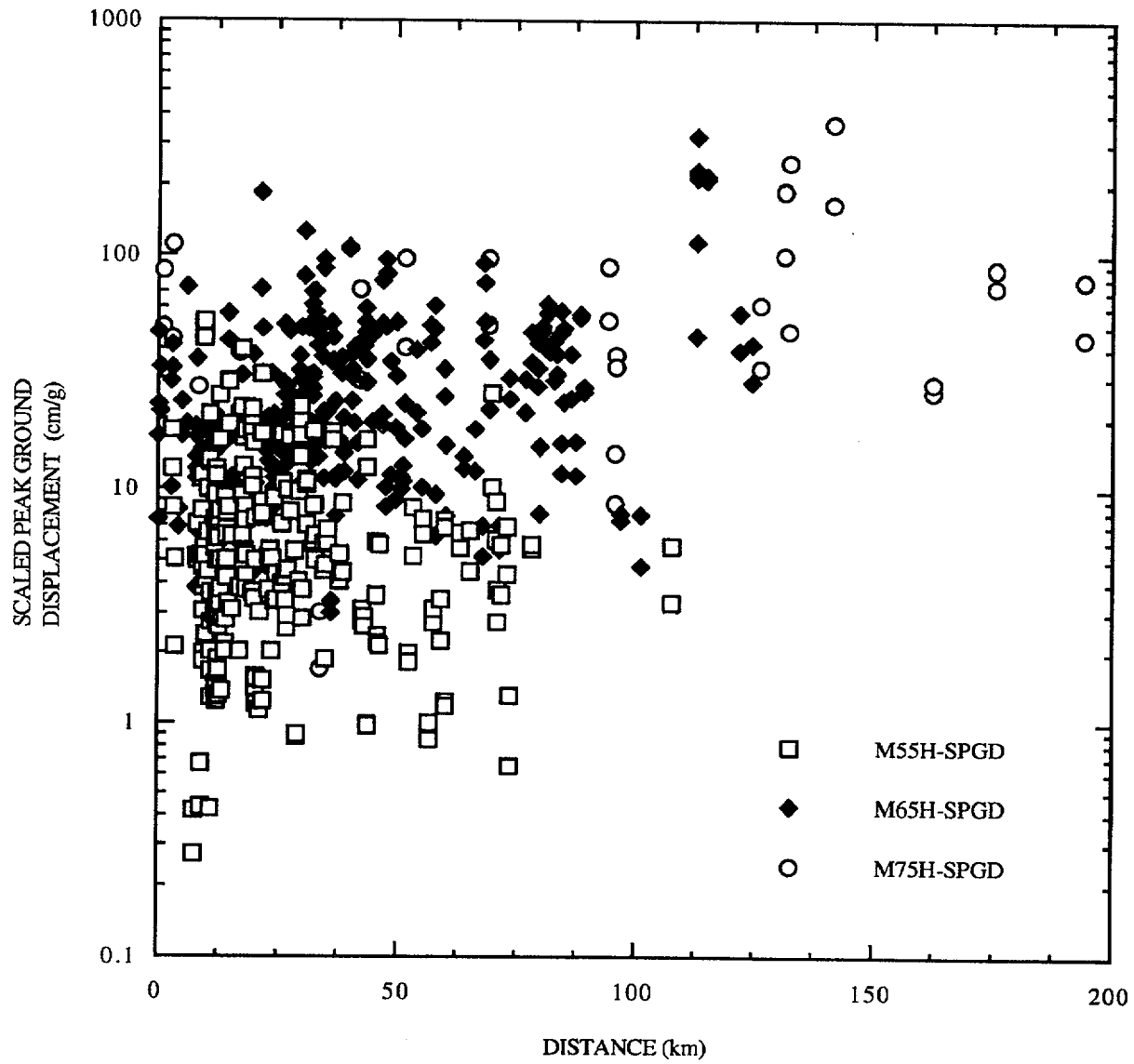


Figure F-1. PGD/PGA (cm/g) for horizontal motion, rock sites

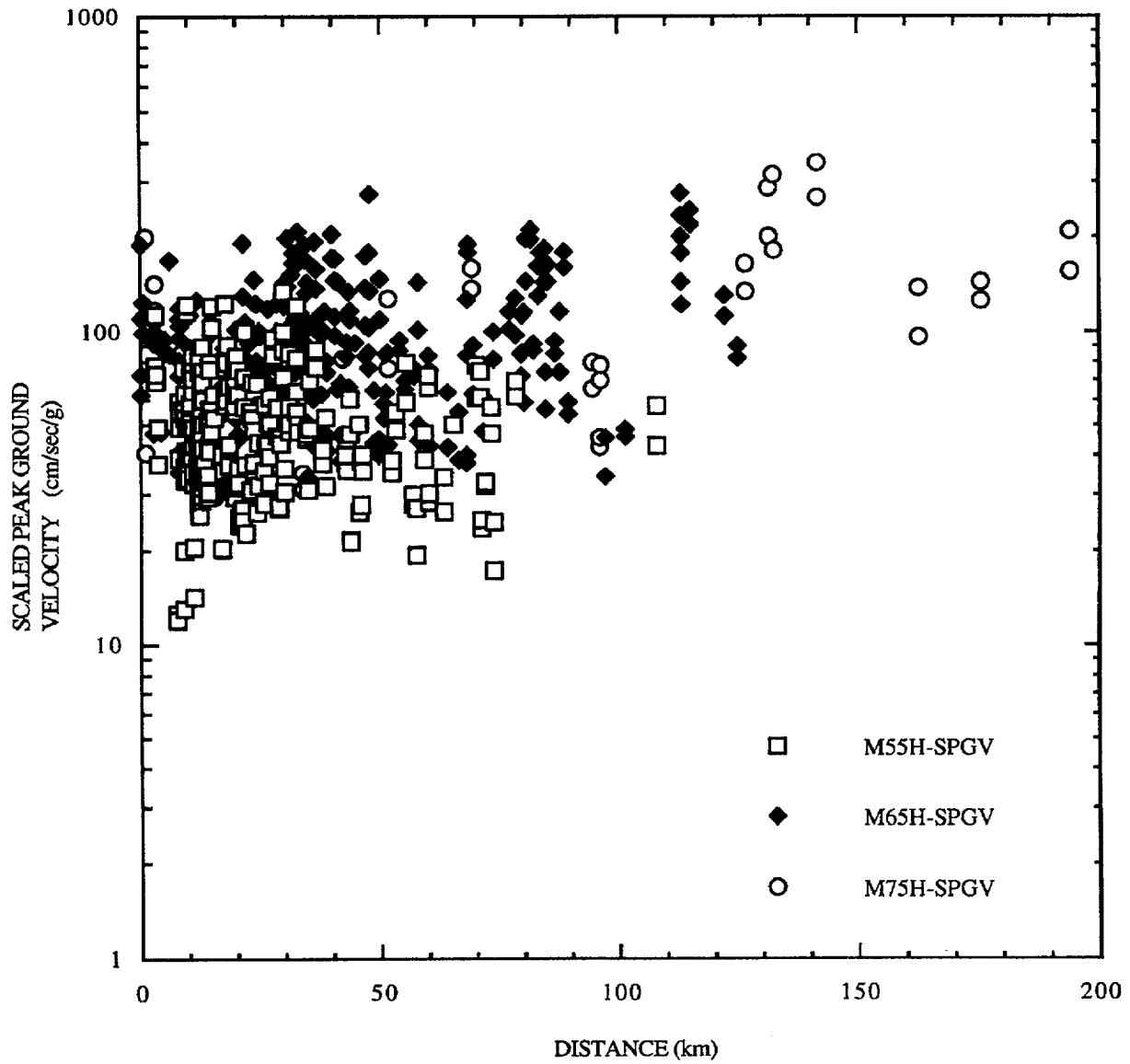


Figure F-2. PGV/PGA (cm/s/g) for horizontal motion, rock sites.

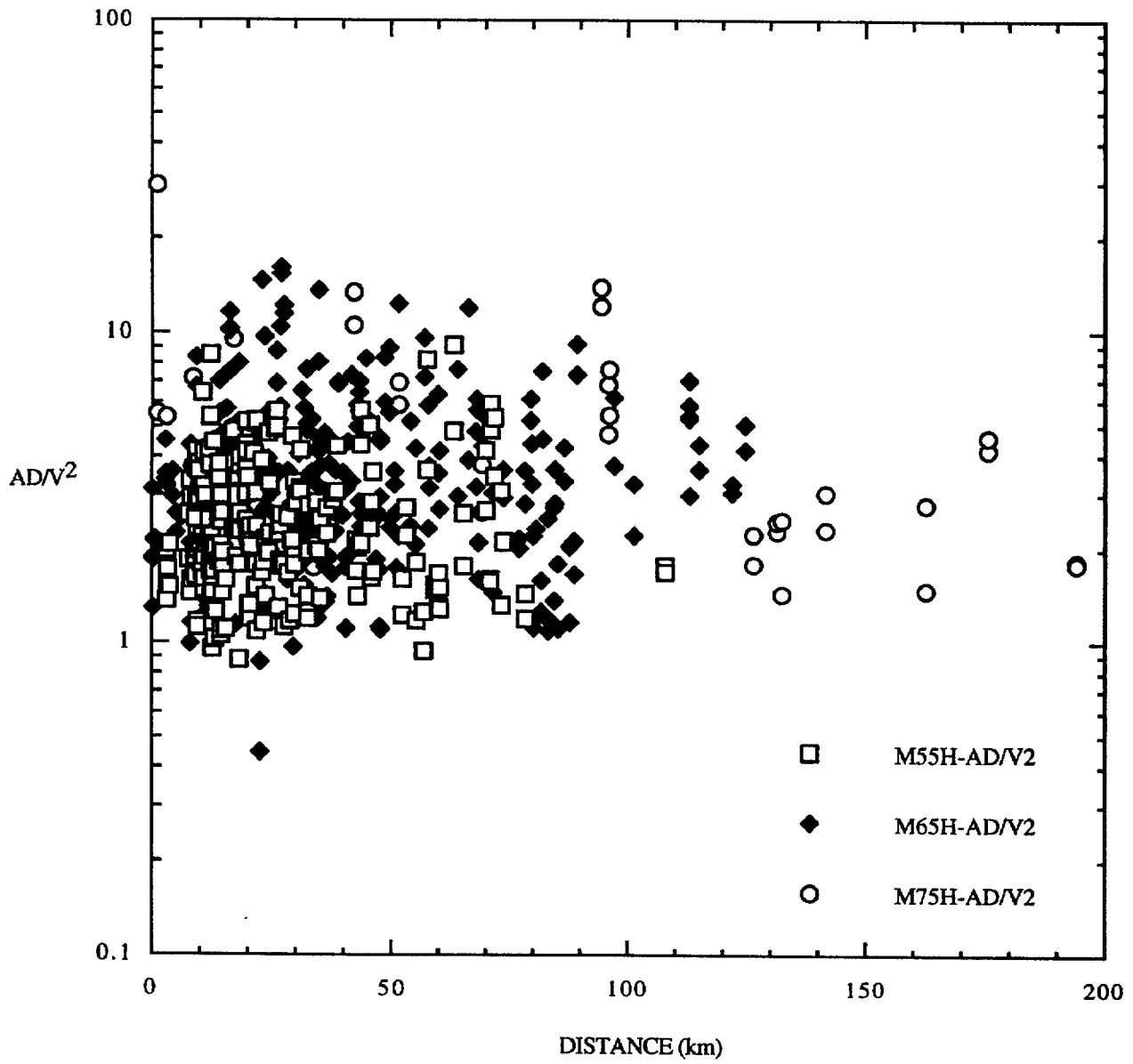


Figure F-3. $PGA \cdot PGA / PGV^2$ for horizontal motion, rock sites.

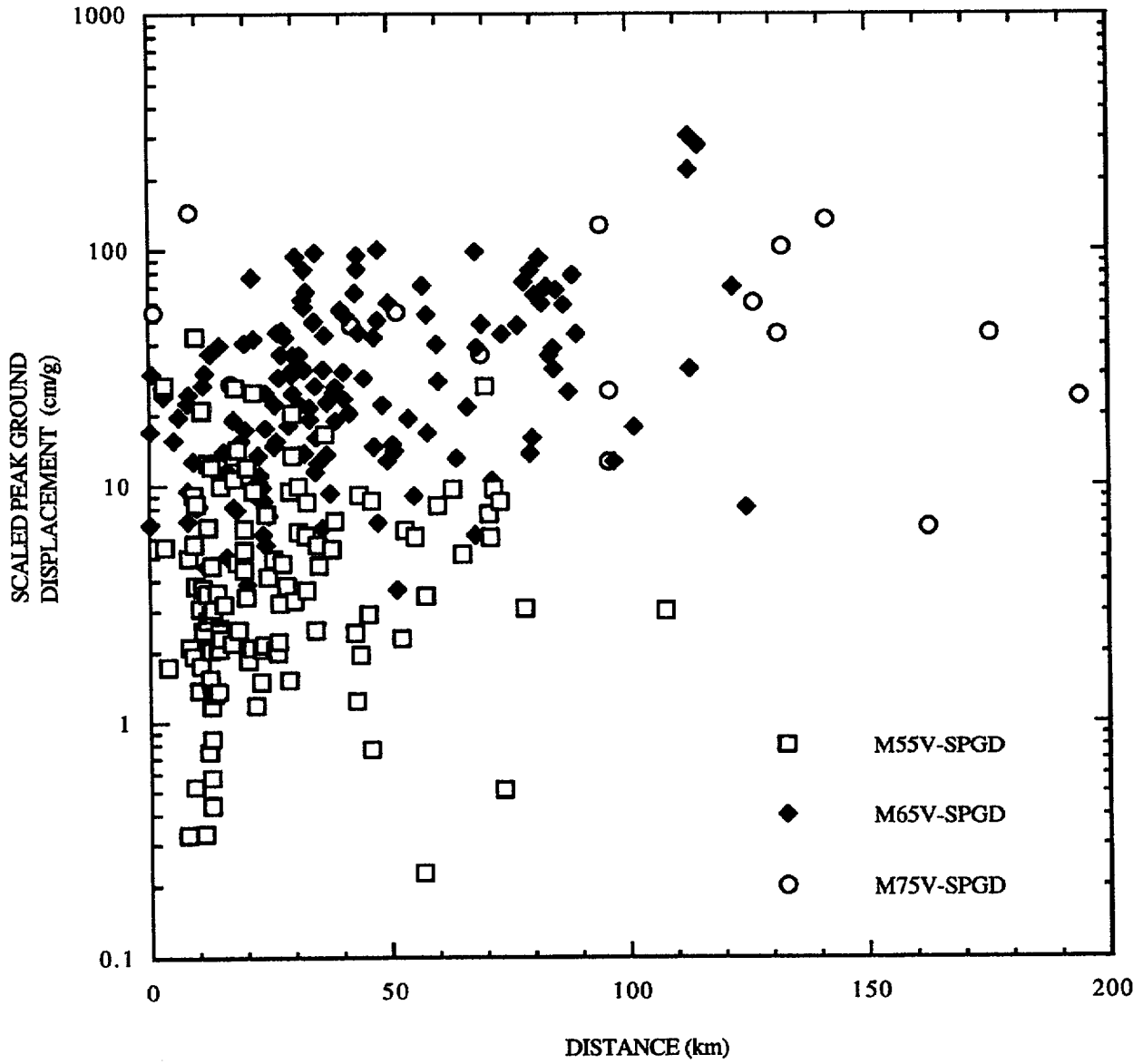


Figure F-4. PGD/PGA (cm/g) for vertical motion, rock sites.

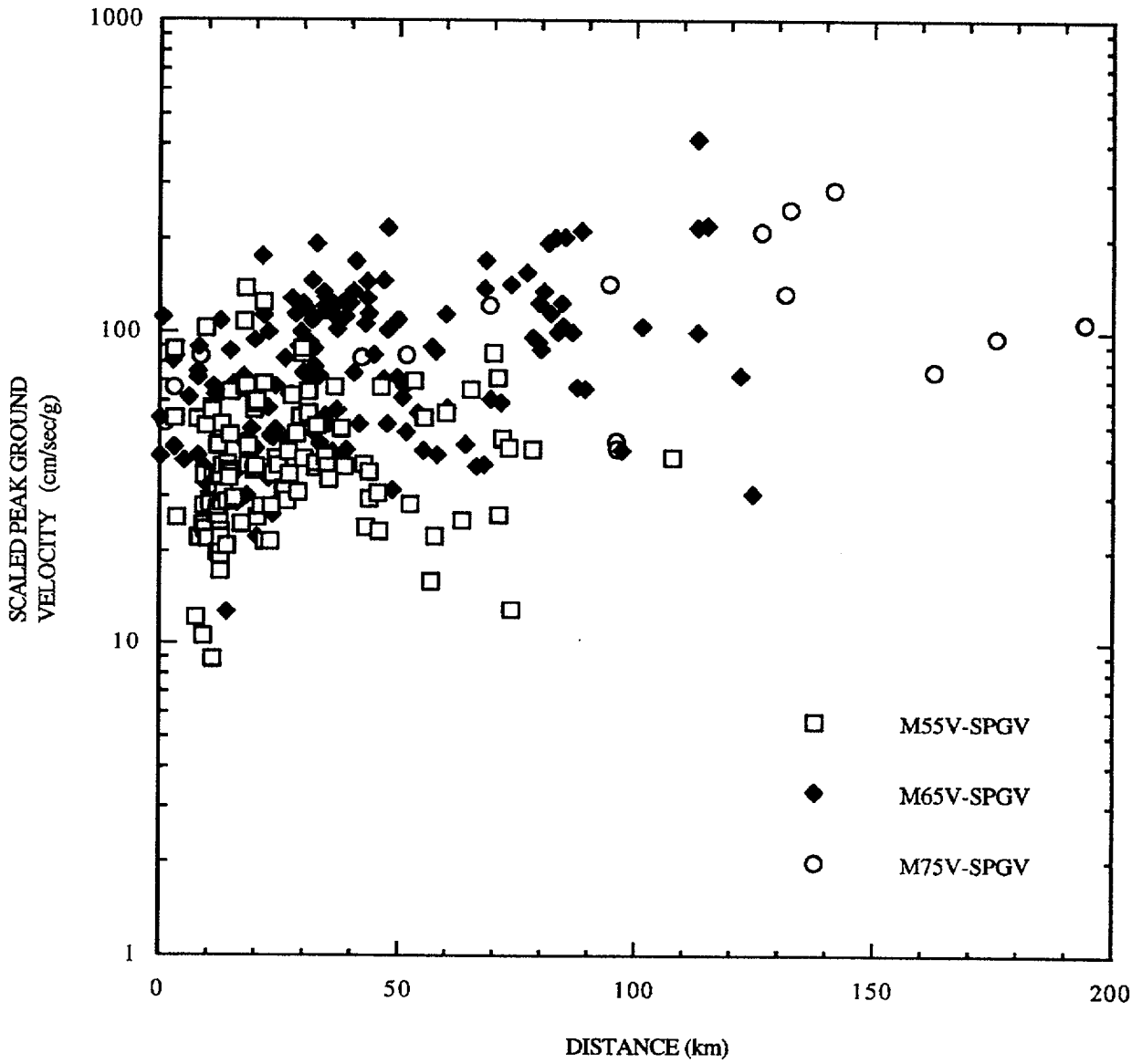


Figure F-5. PGV/PGA (cm/s/g) for vertical motion, rock sites.

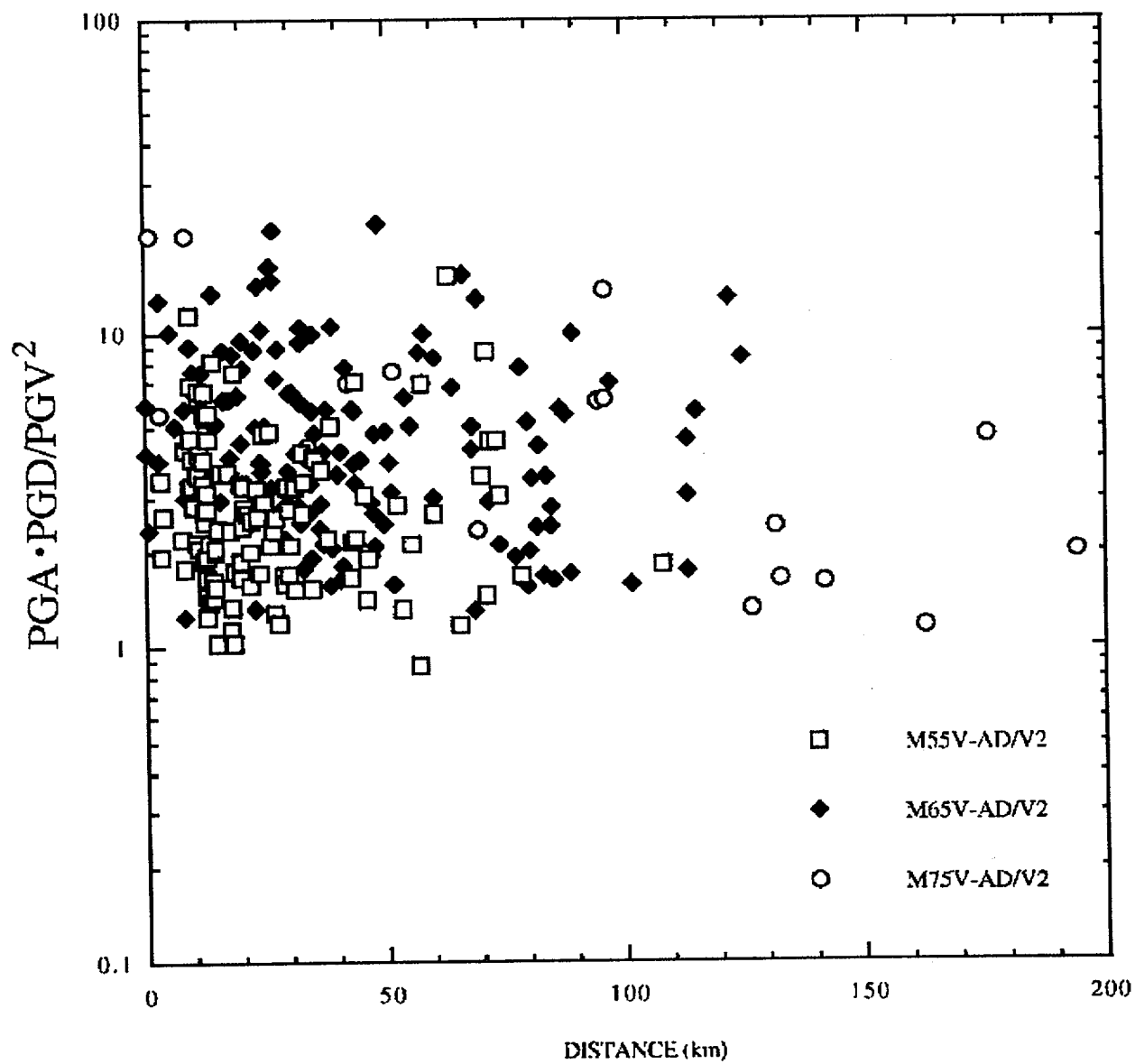


Figure F-6. $PGA \cdot PGD / PGV^2$ for vertical motion, rock sites.

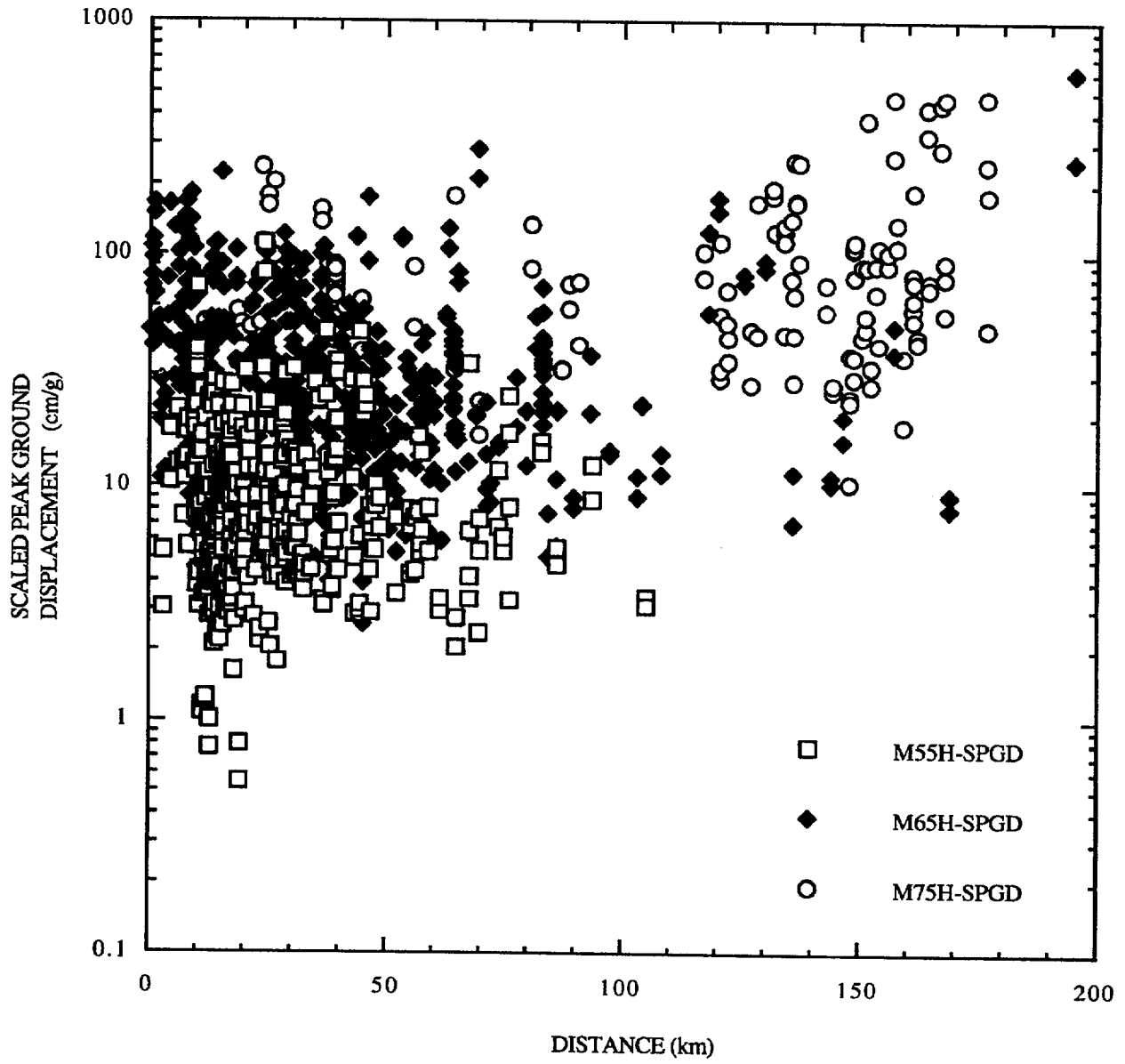


Figure F-7. PGD/PGA (cm/g) for horizontal motion, soil sites.

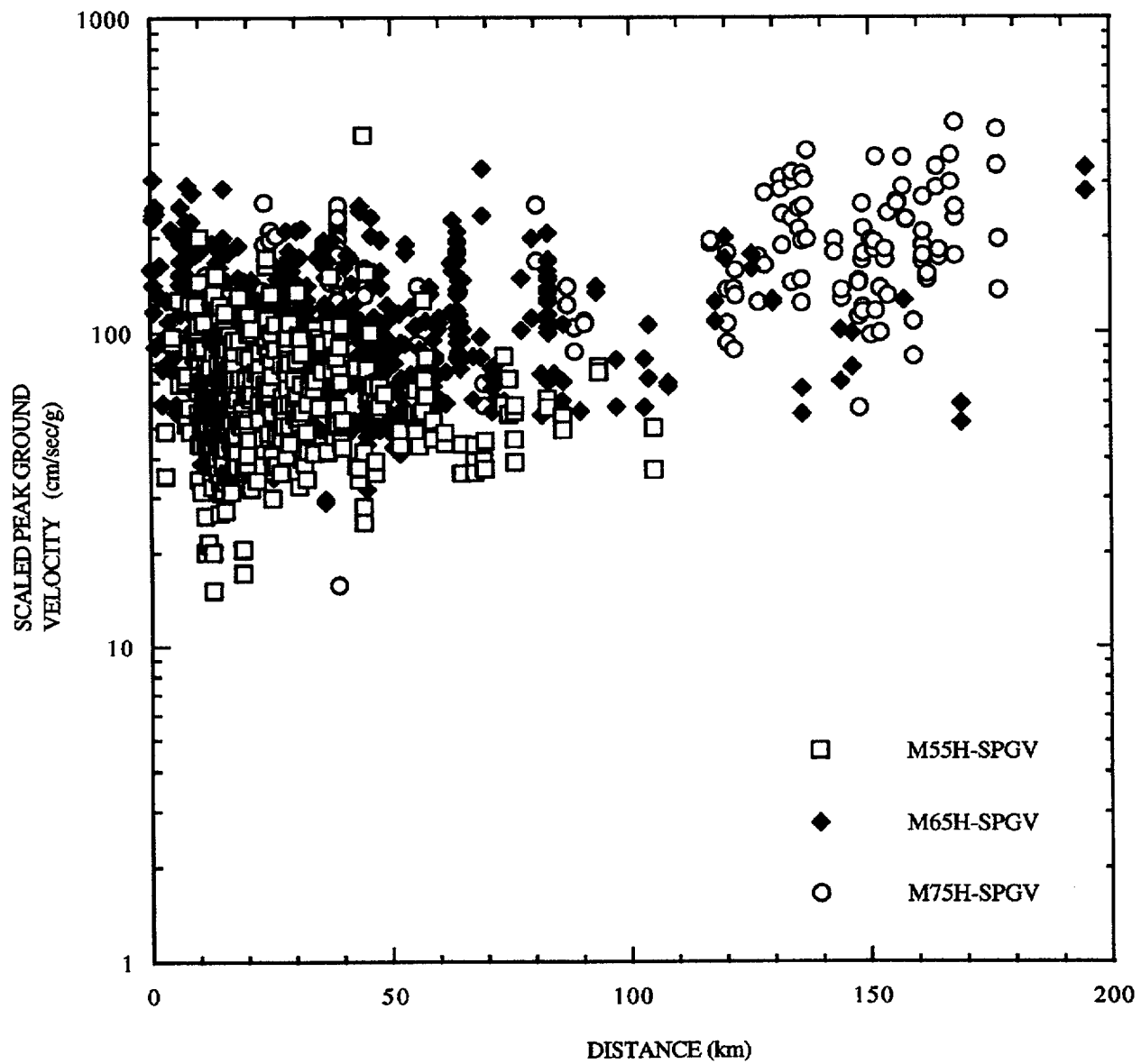


Figure F-8. PGV/PGA (cm/s/g) for horizontal motion, soil sites.

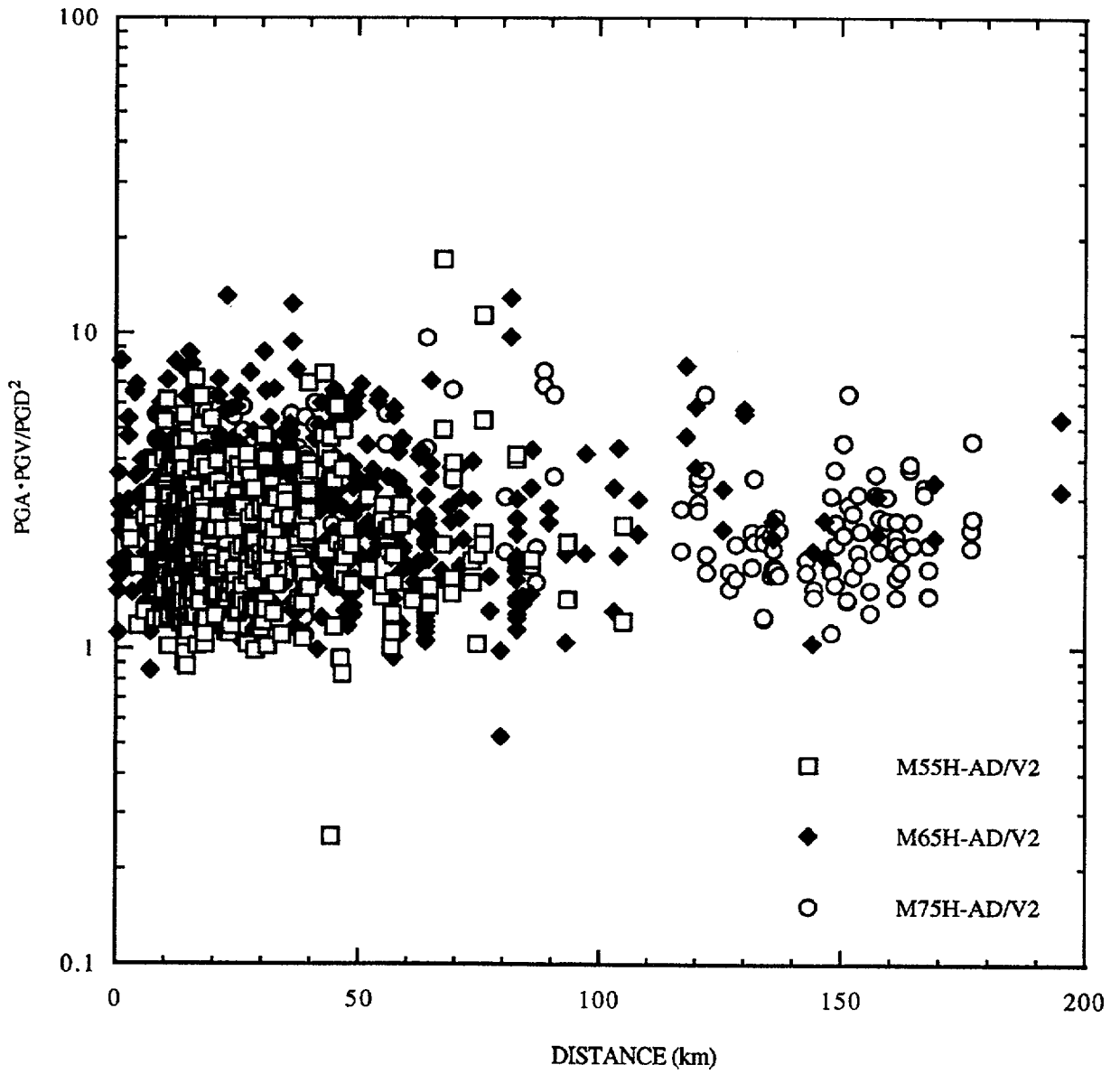


Figure F-9. $PGA \cdot PGD / PGV^2$ for horizontal motion, soil sites.

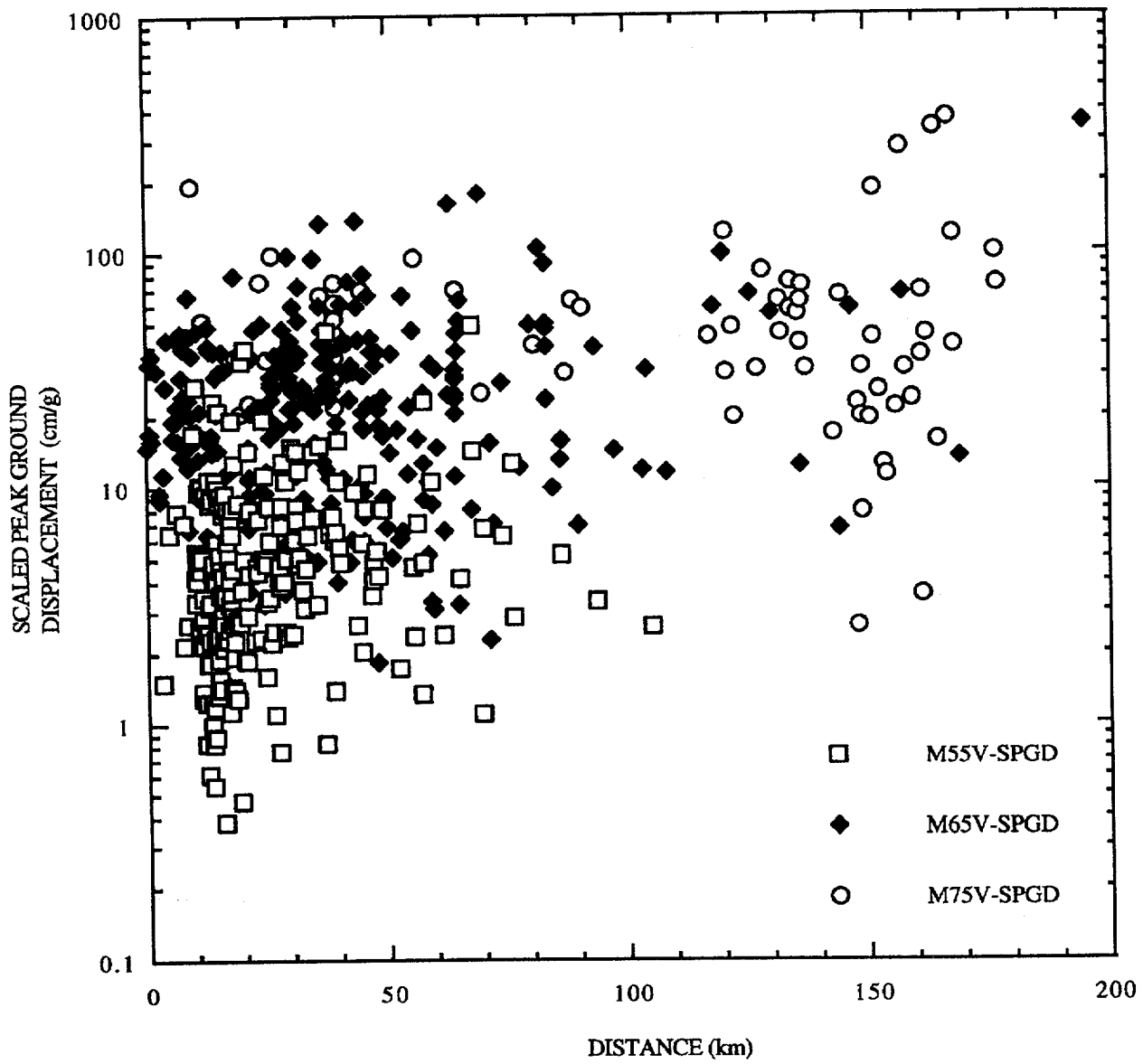


Figure F-10. PGD/PGA (cm/g) for vertical motions, soil sites.

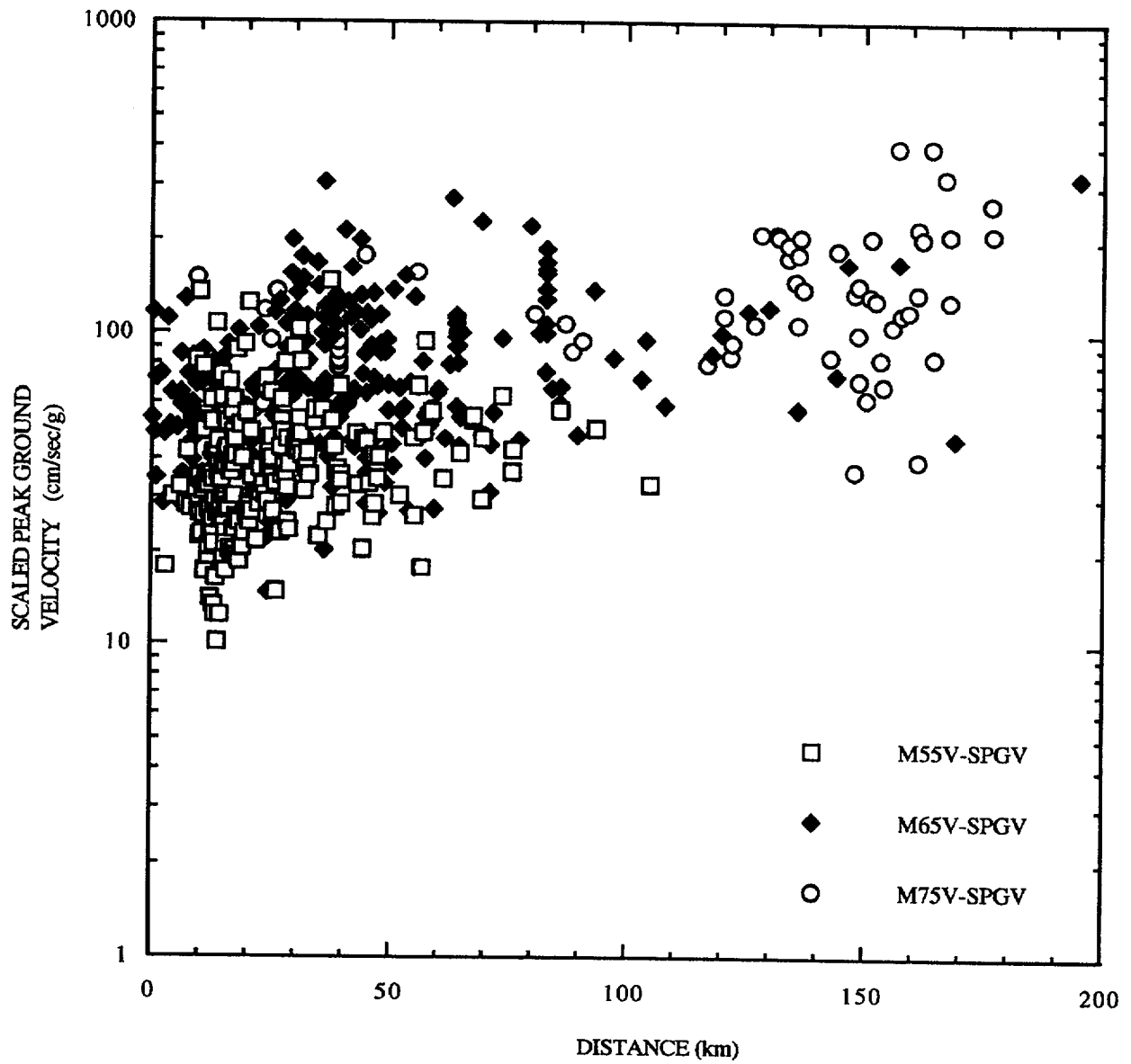


Figure F-11. PGV/PGA (cm/s/g) for vertical motion, soil sites.

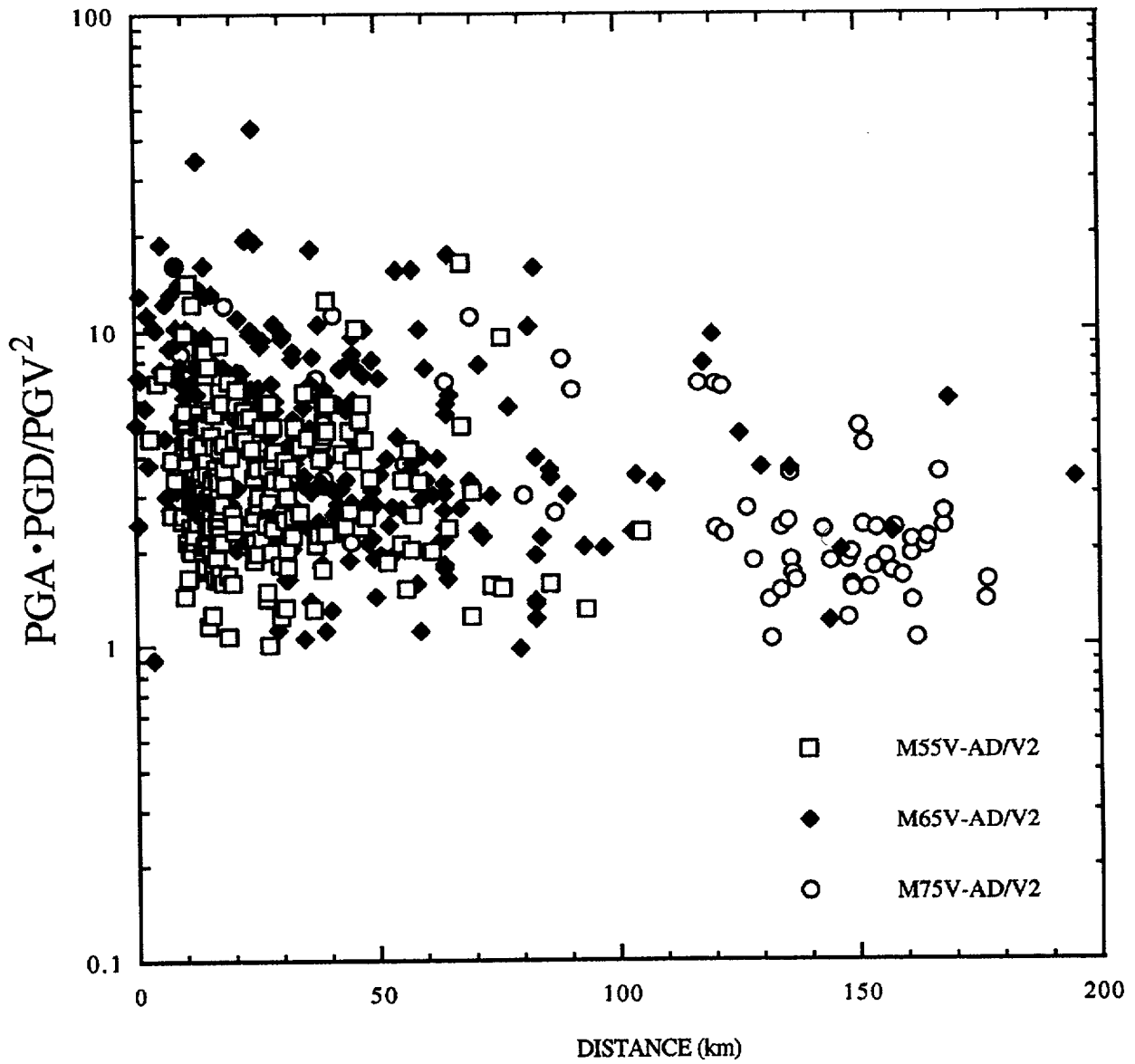


Figure F-12. $PGA \cdot PGD / PGV^2$ for vertical motion, soil sites.

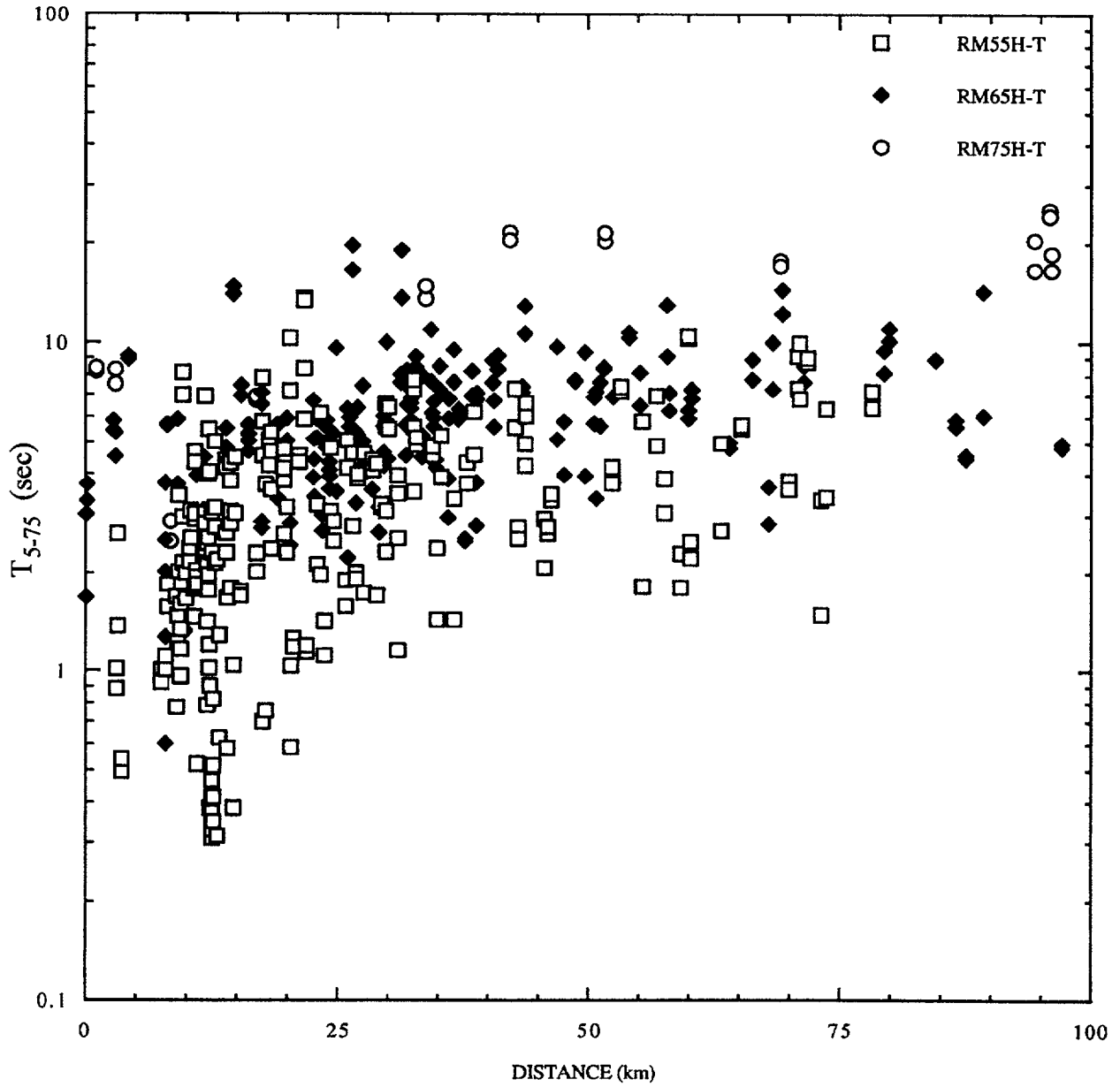


Figure F-13. Duration calculated as 5%-75% of Arias intensity, rock sites, horizontal motion.

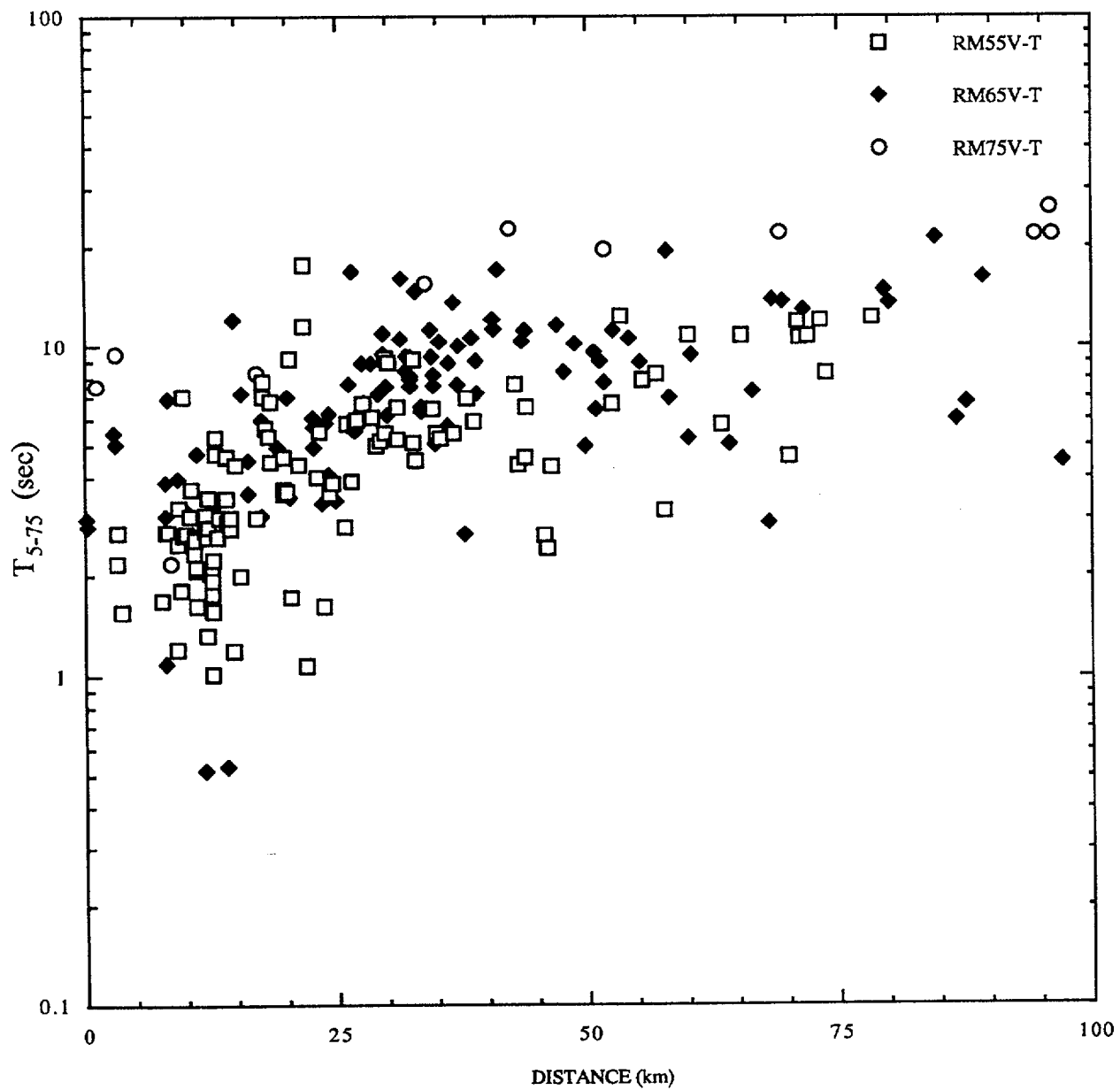


Figure F-14. Duration calculated as 5-75% of Arias intensity, rock sites, vertical motion.

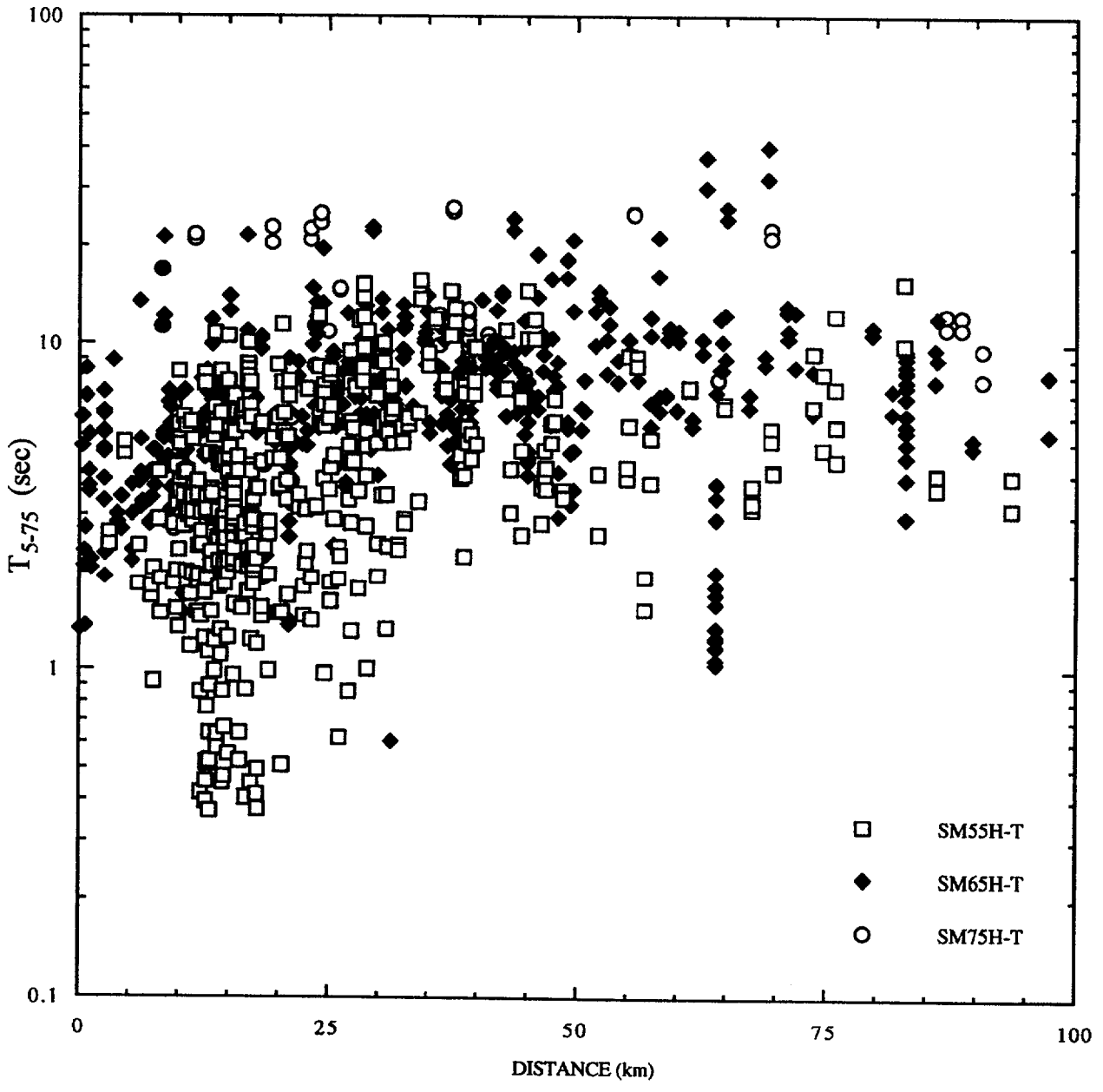


Figure F-15. Duration calculated as 5-75% of Arias intensity, soil sites, horizontal motion.

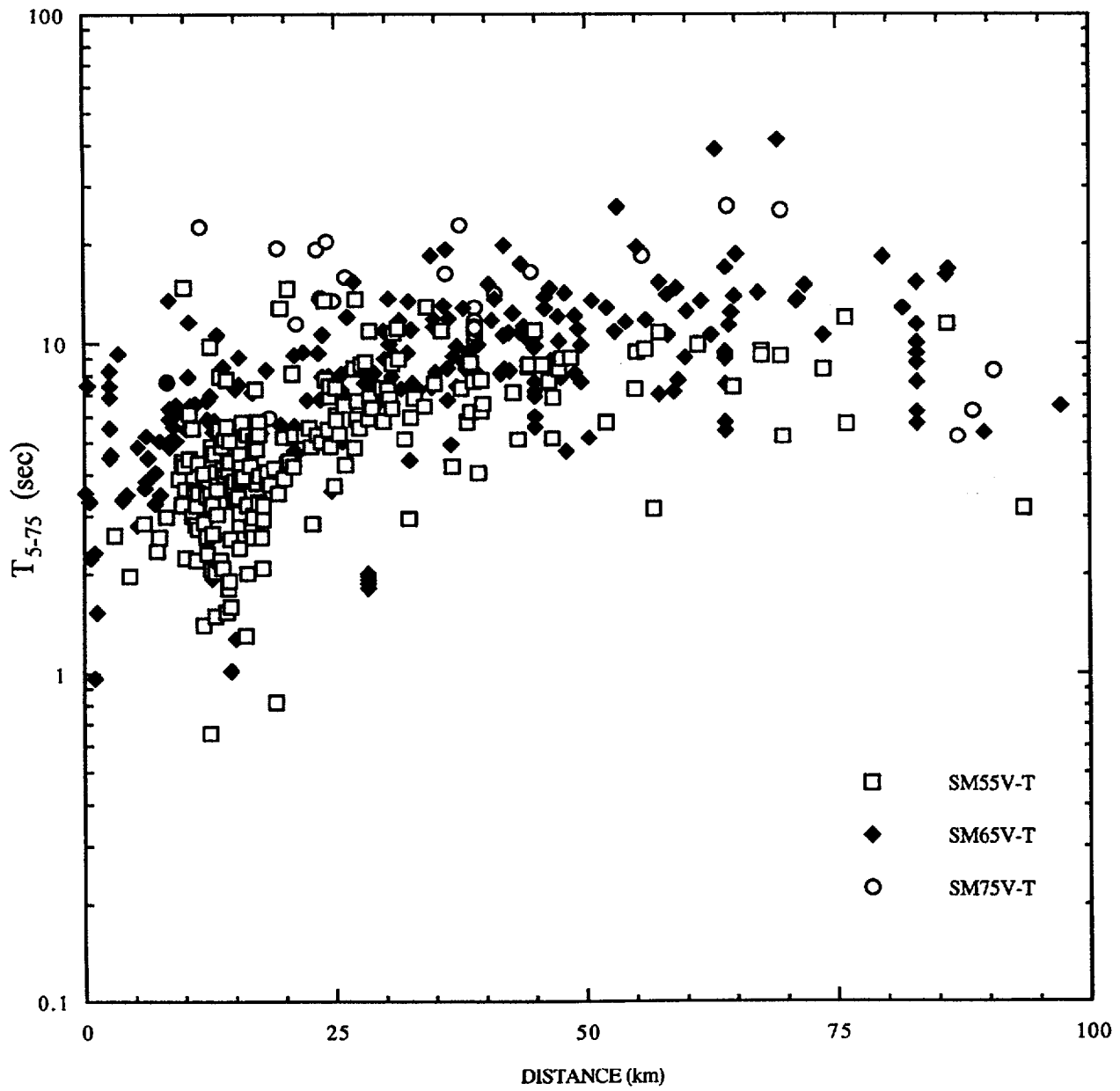


Figure F-16. Duration calculated as 5-75% of Arias intensity, soil sites, vertical motion.

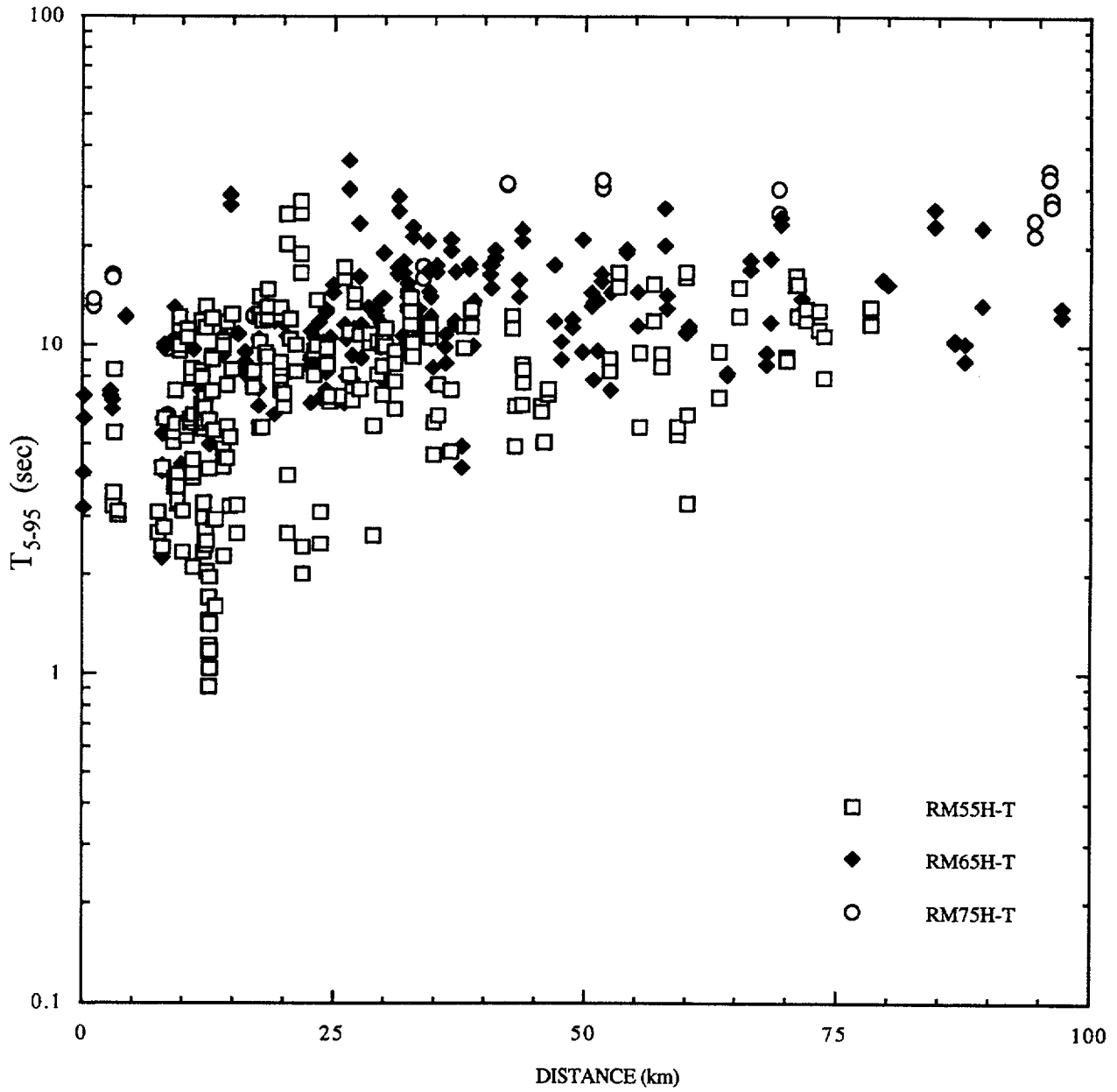


Figure F-17. Duration calculated as 5-95% of Arias intensity, rock sites, horizontal motion.

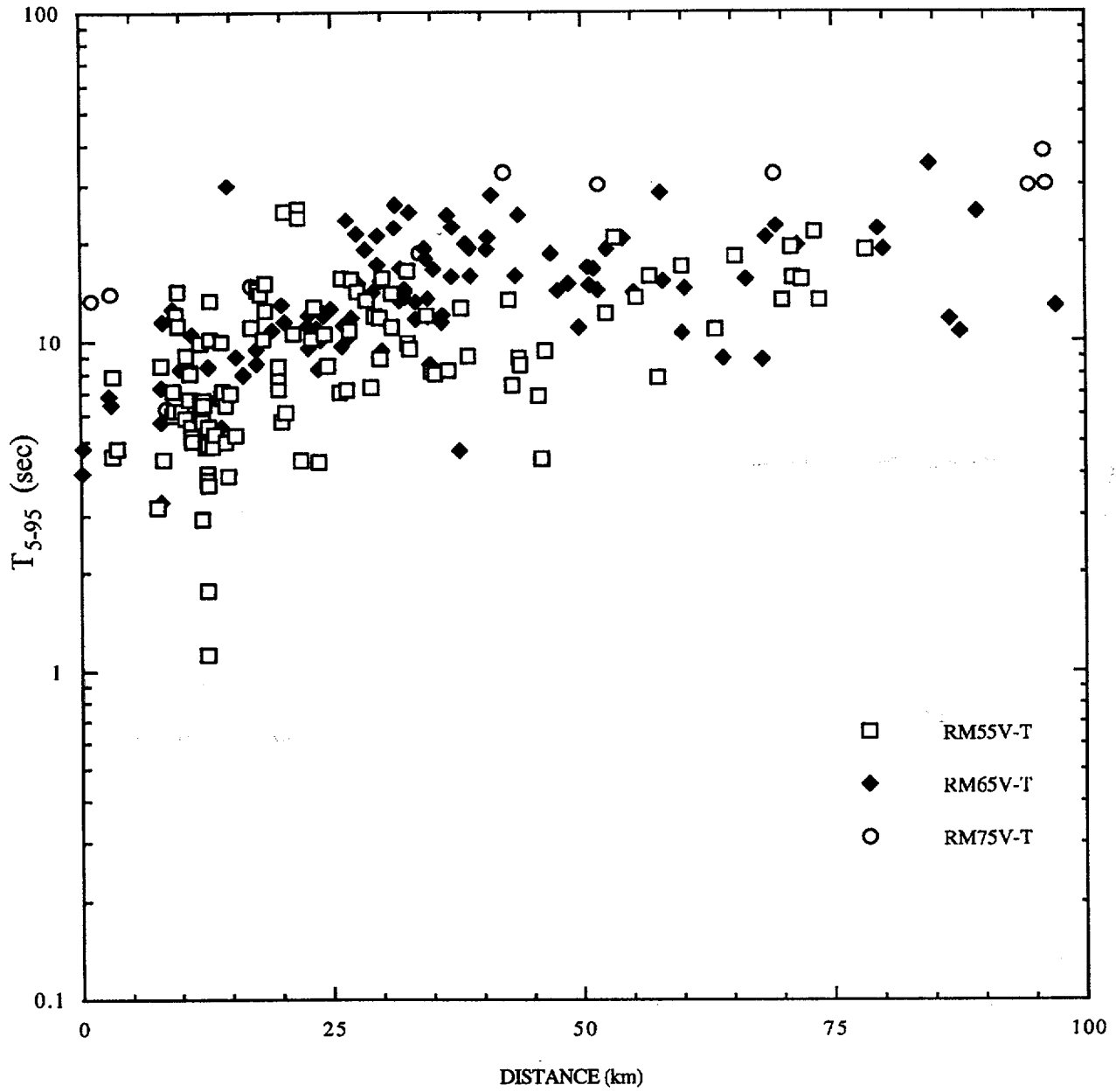


Figure F-18. Duration calculated as 5-95% of Arias intensity, rock sites, vertical motion.

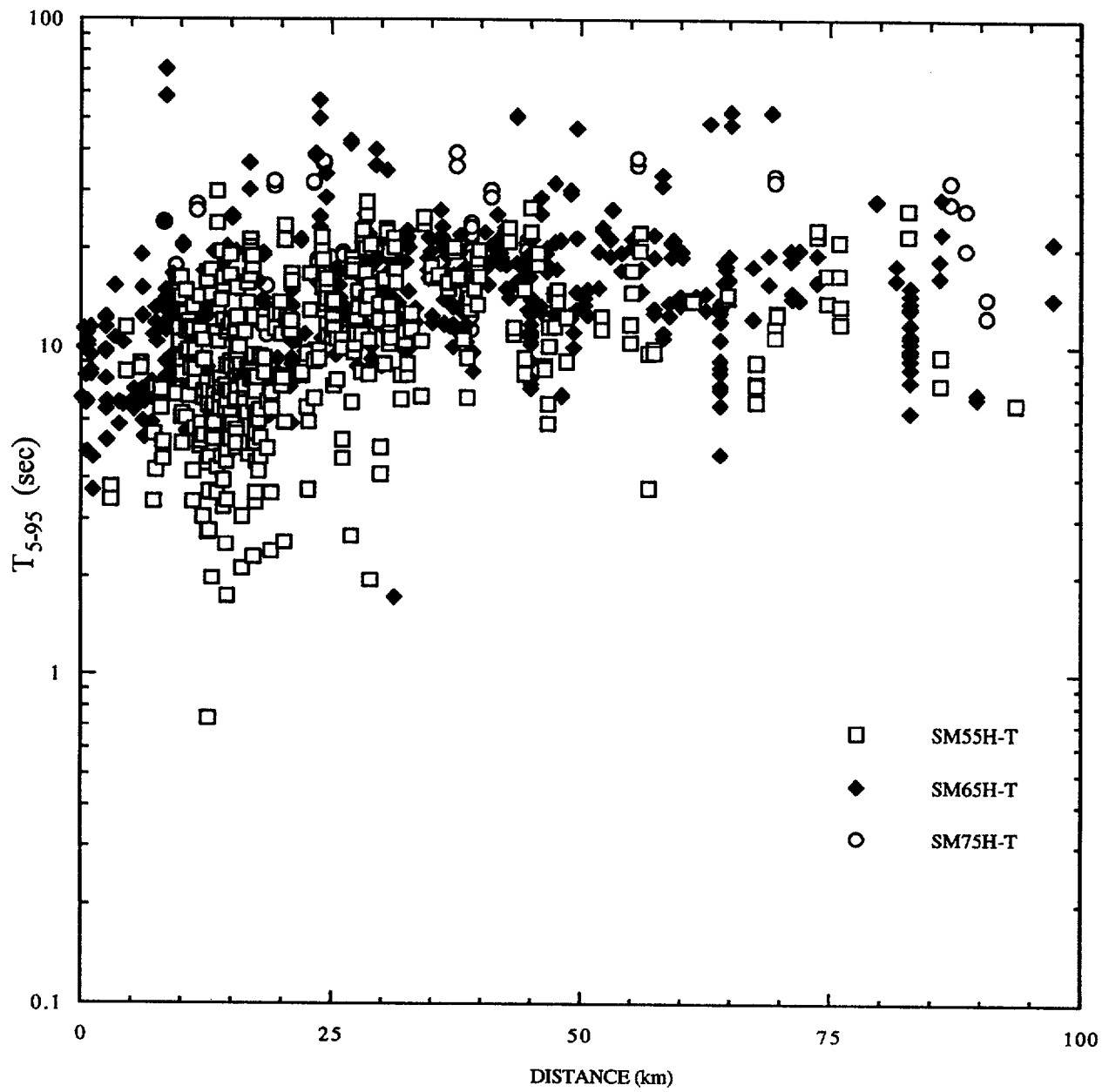


Figure F-19. Duration calculated as 5-95% of Arias intensity, soil sites, horizontal motion.

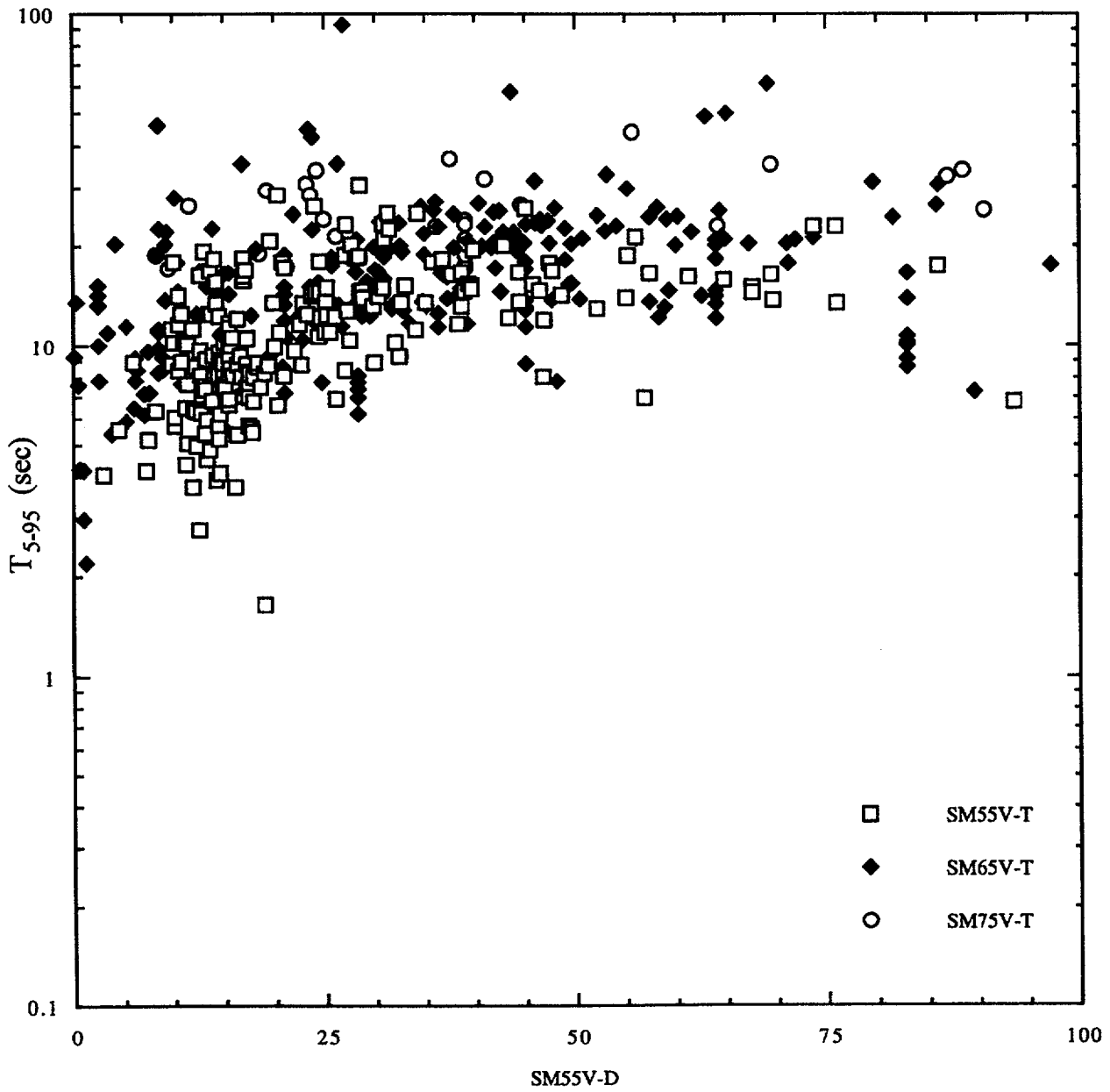


Figure F-20. Duration calculated as 5-95% of Arias intensity, soil sites, vertical motion.

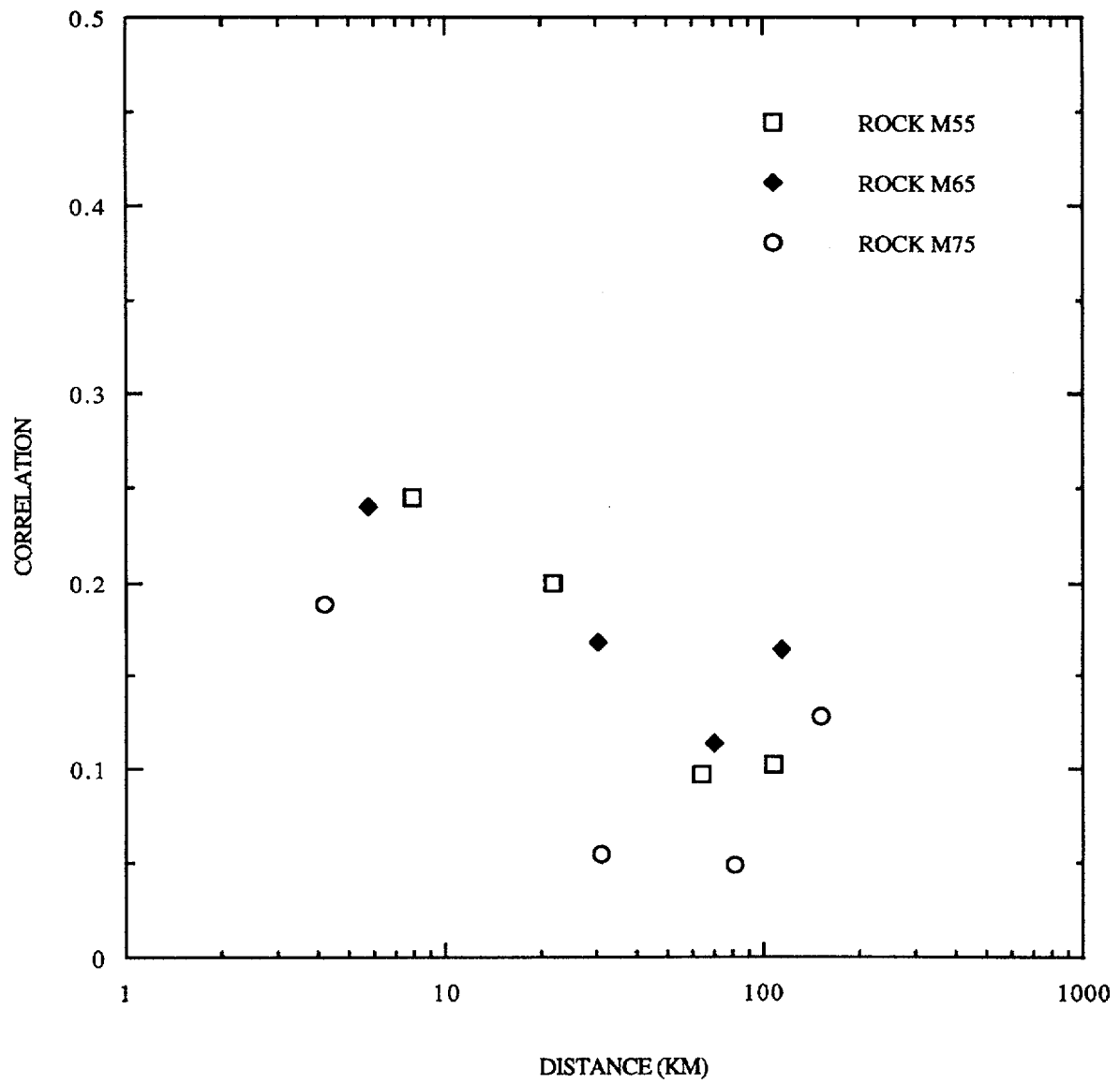


Figure F-21. Correlations of H1/H2 acceleration pairs, WUS rock sites.

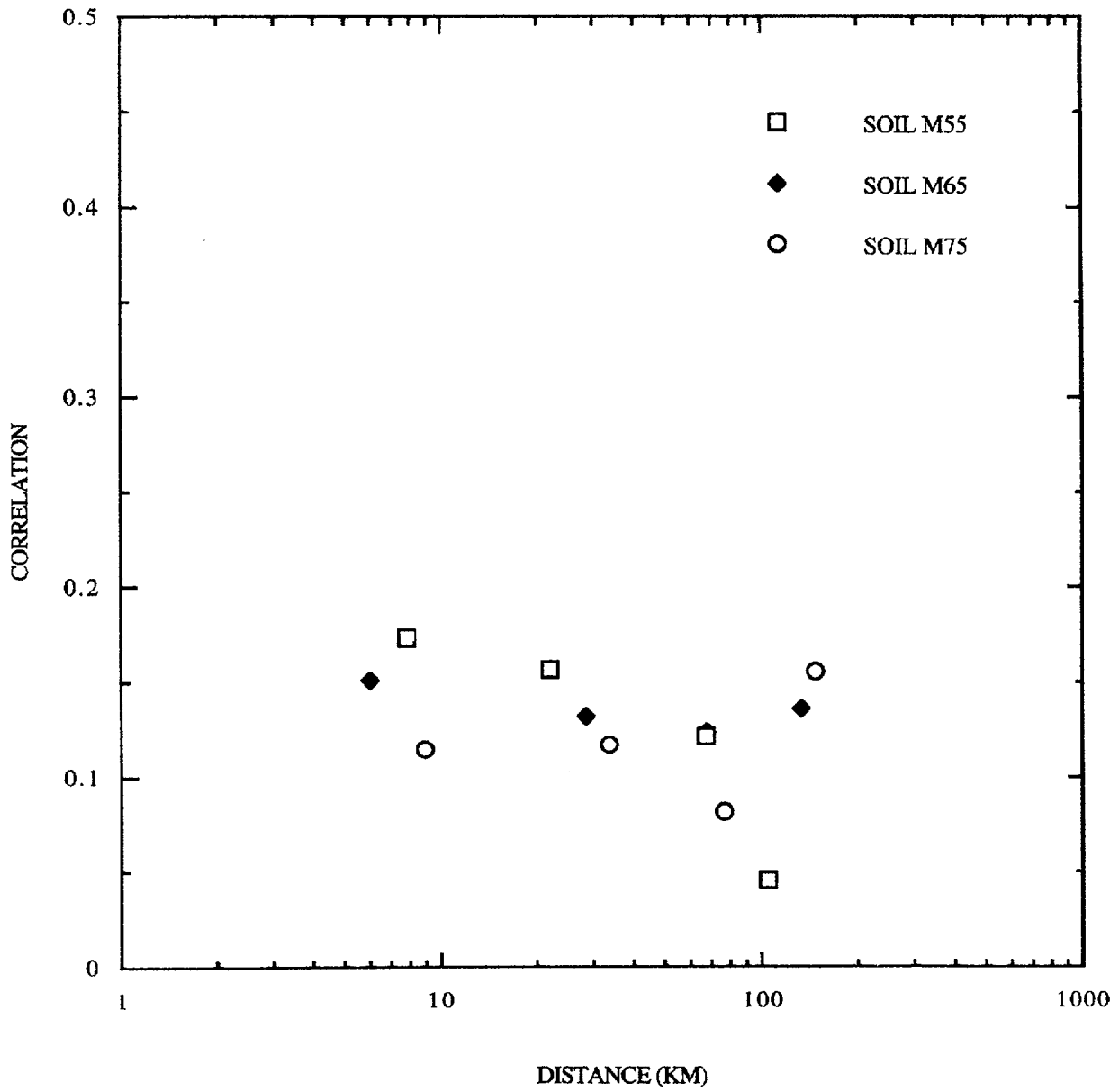


Figure F-22. Correlations of H1/H2 acceleration pairs, WUS soil sites.

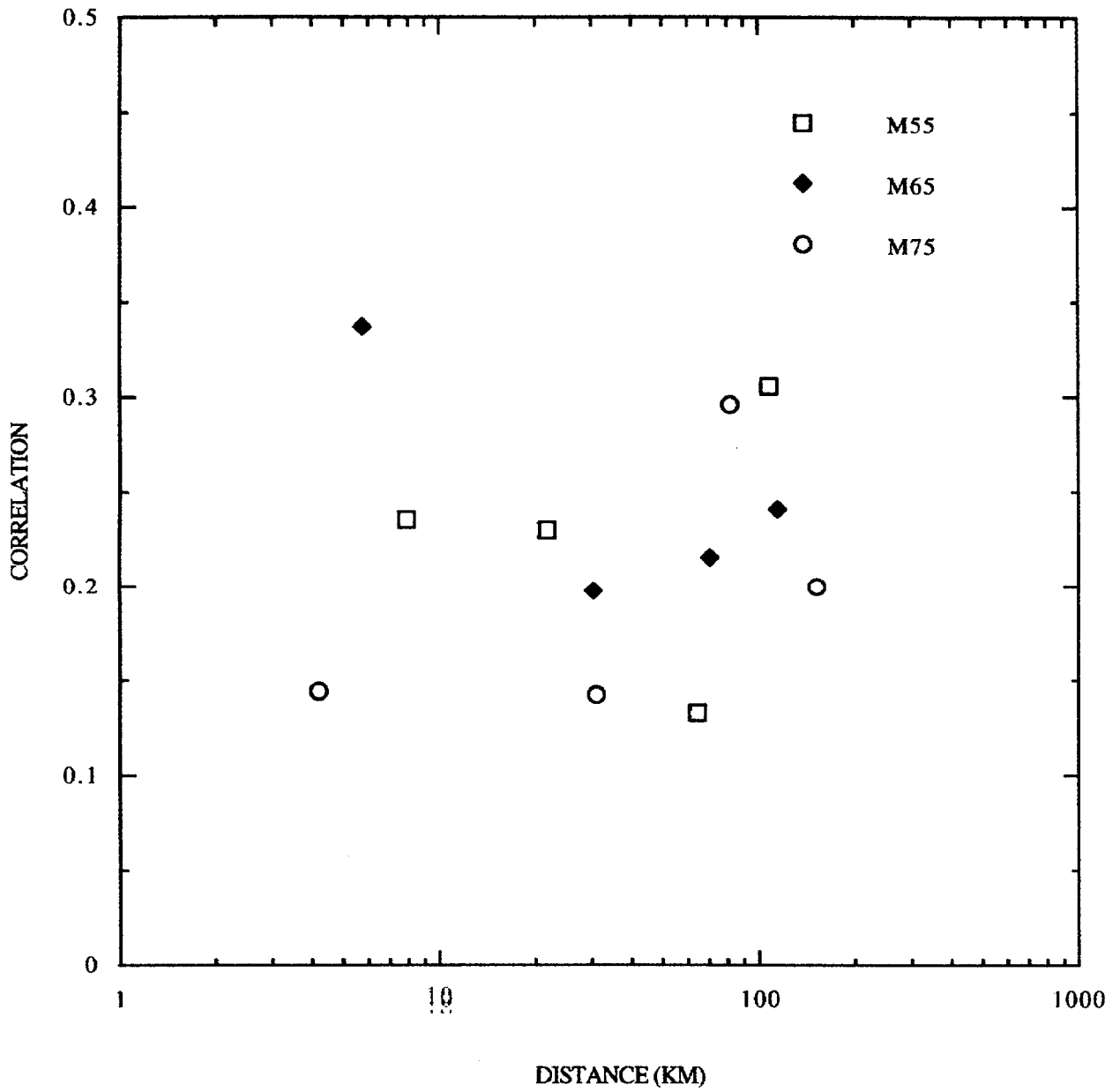


Figure F-23. Correlations of H1/H2 velocity pairs, WUS rock sites.

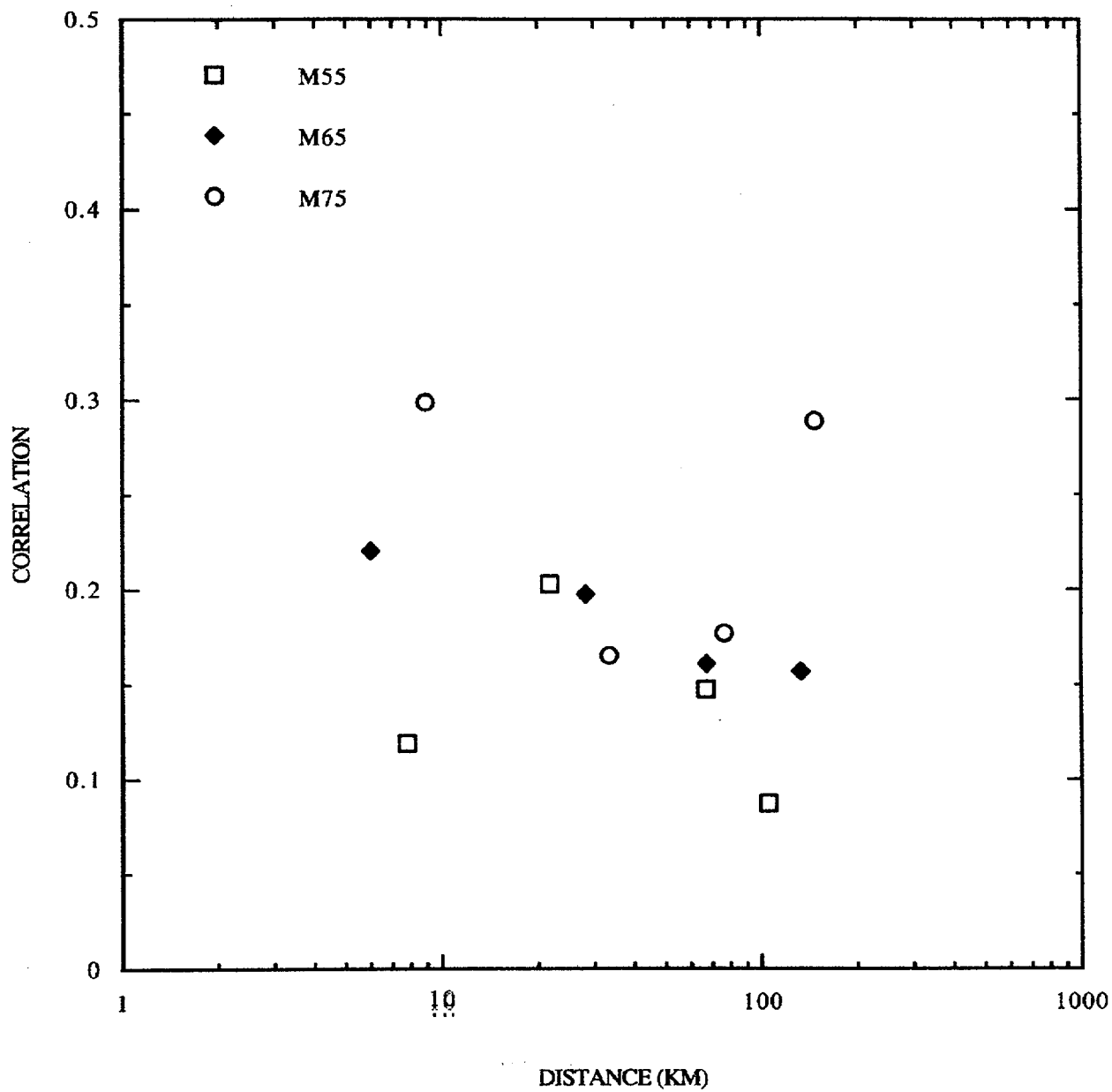


Figure F-24. Correlations of H1/H2 velocity pairs, WUS soil sites.

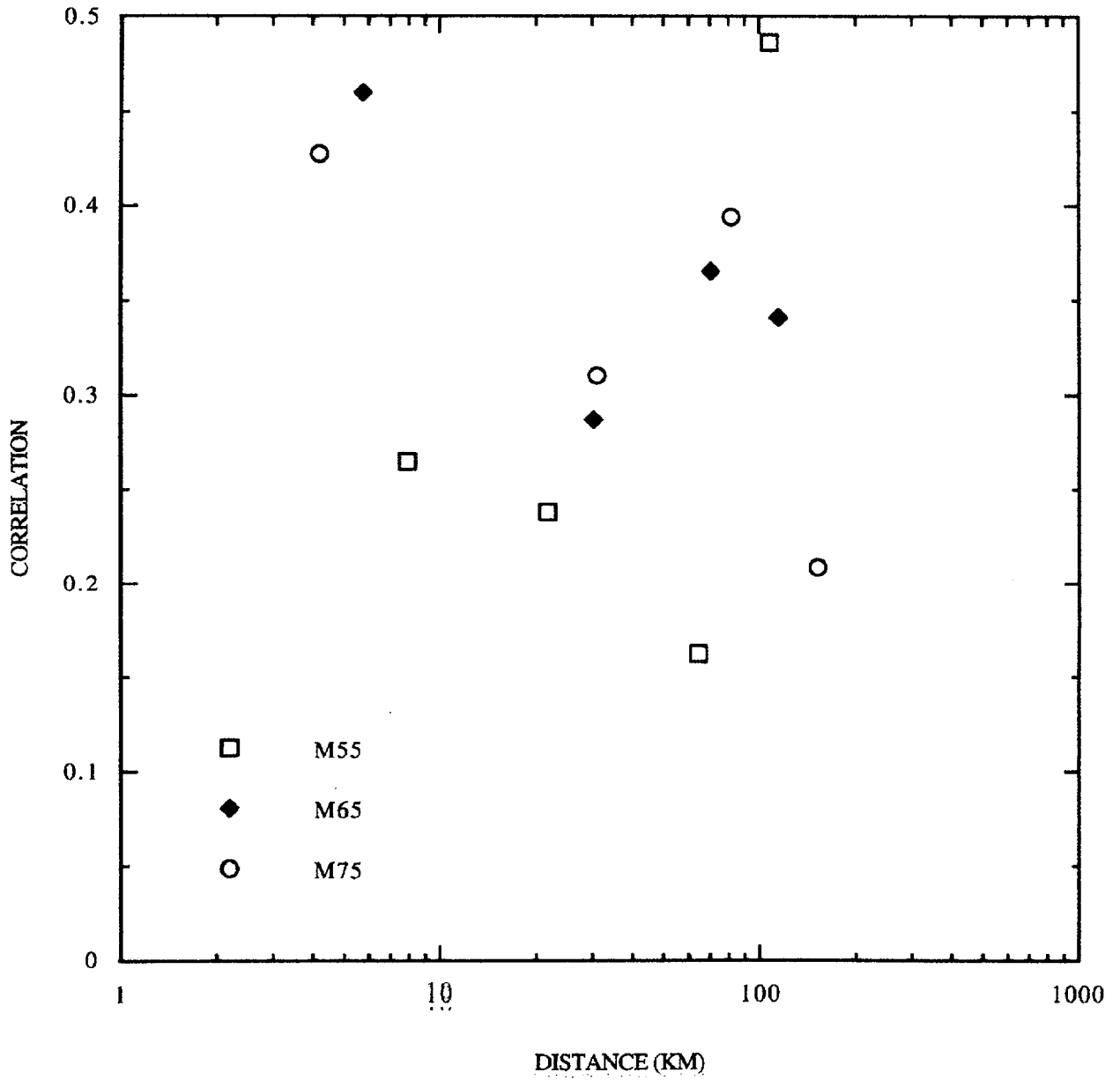


Figure F-25. Correlations of H1/H2 displacement pairs, WUS rock sites.

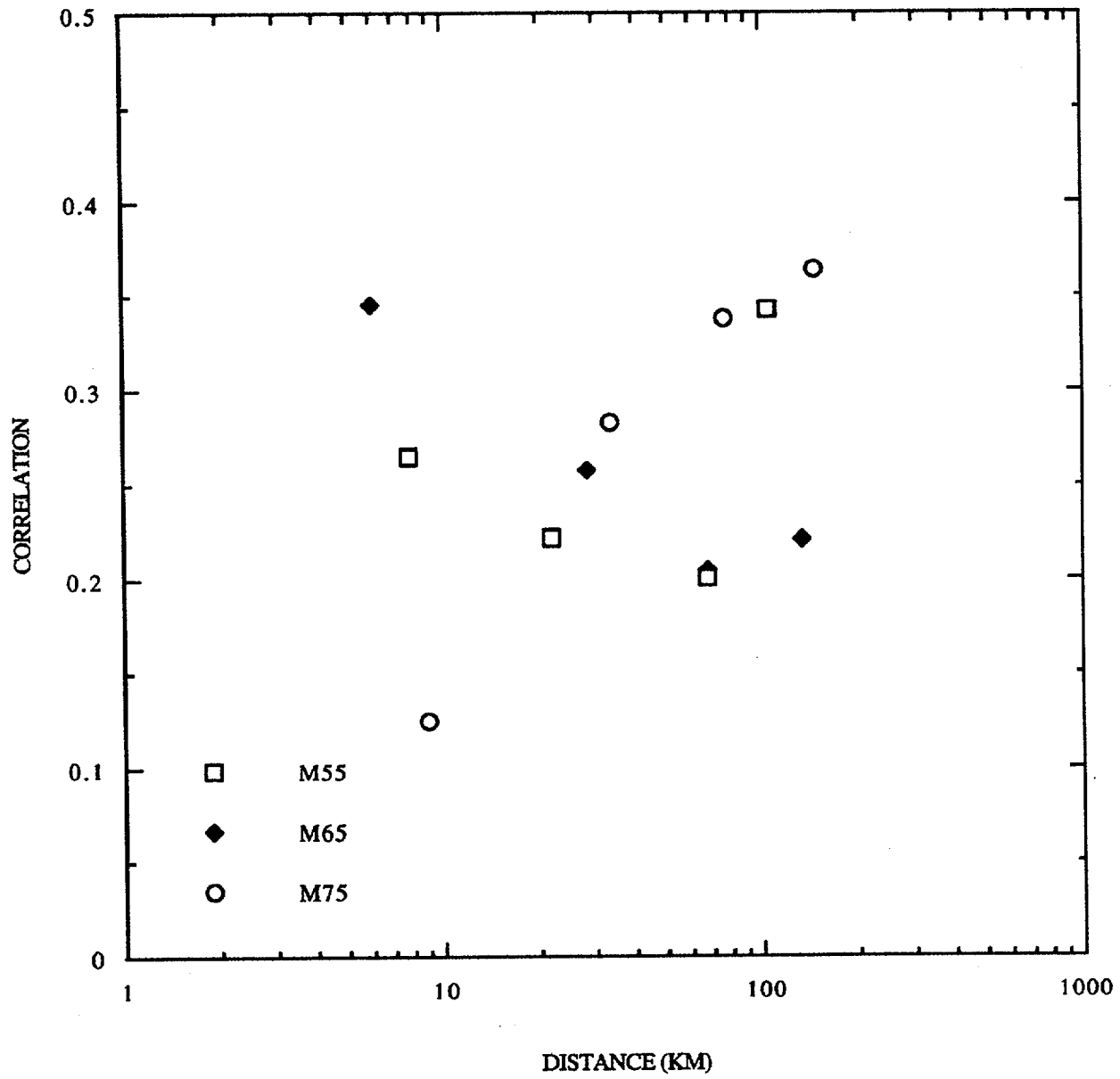


Figure F-26. Correlations of H1/H2 displacement pairs, WUS soil sites.

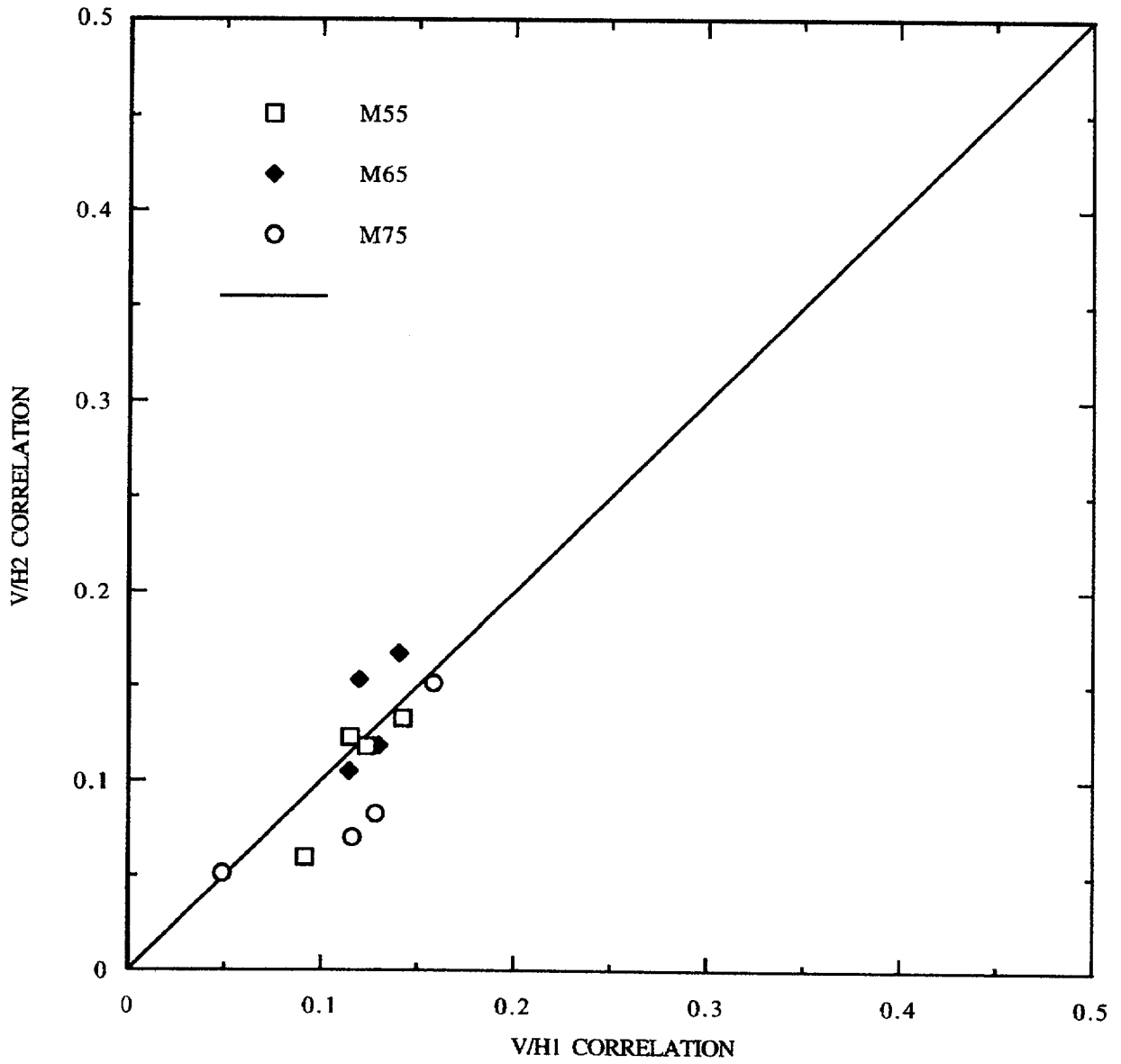


Figure F-27. Comparison of correlations of vertical/horizontal acceleration pairs at WUS rock sites.

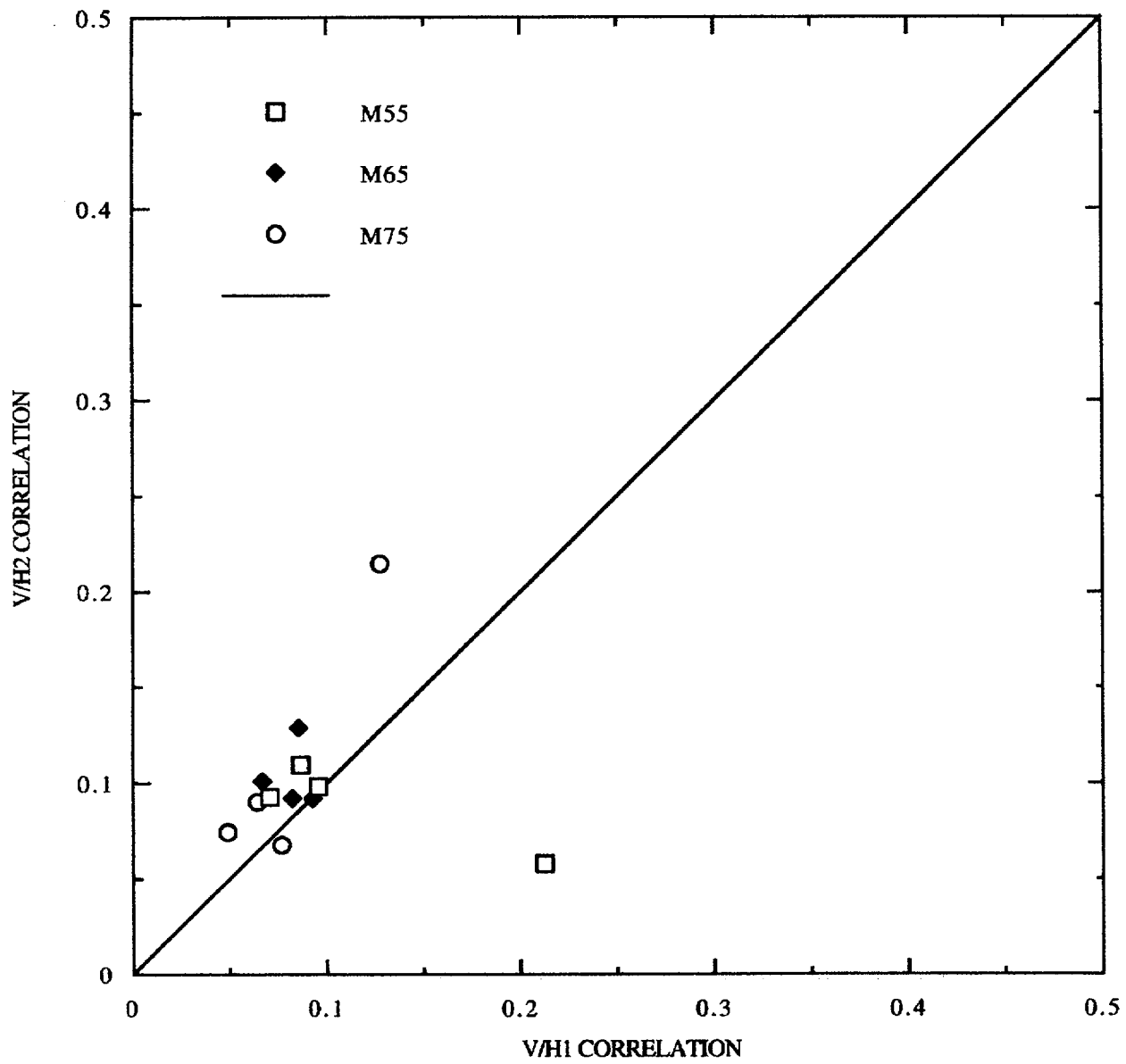


Figure F-28. Comparison of correlations of vertical/horizontal acceleration pairs at WUS soil sites.

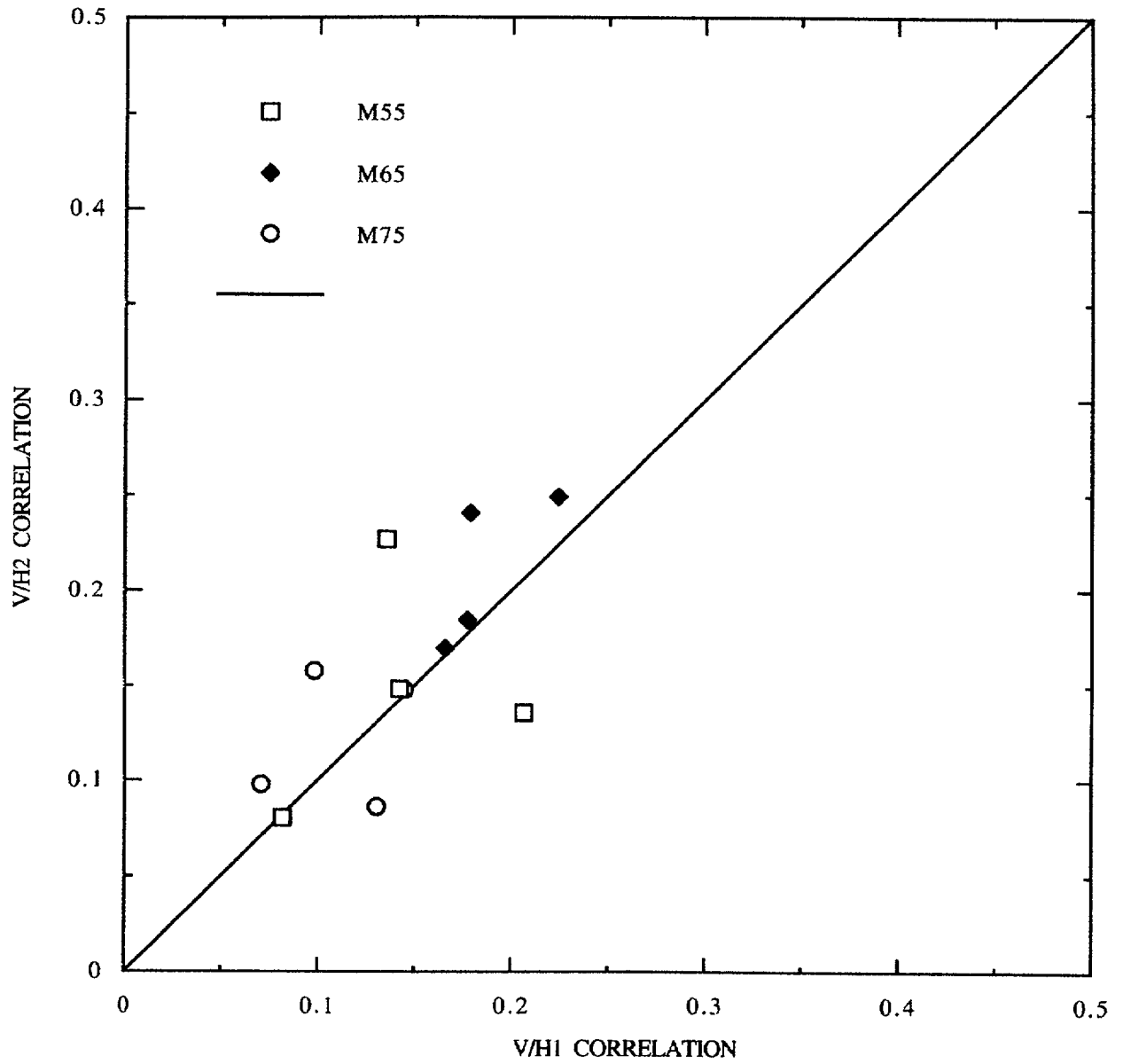


Figure F-29. Comparison of correlations of vertical/horizontal velocity pairs at WUS rock sites.

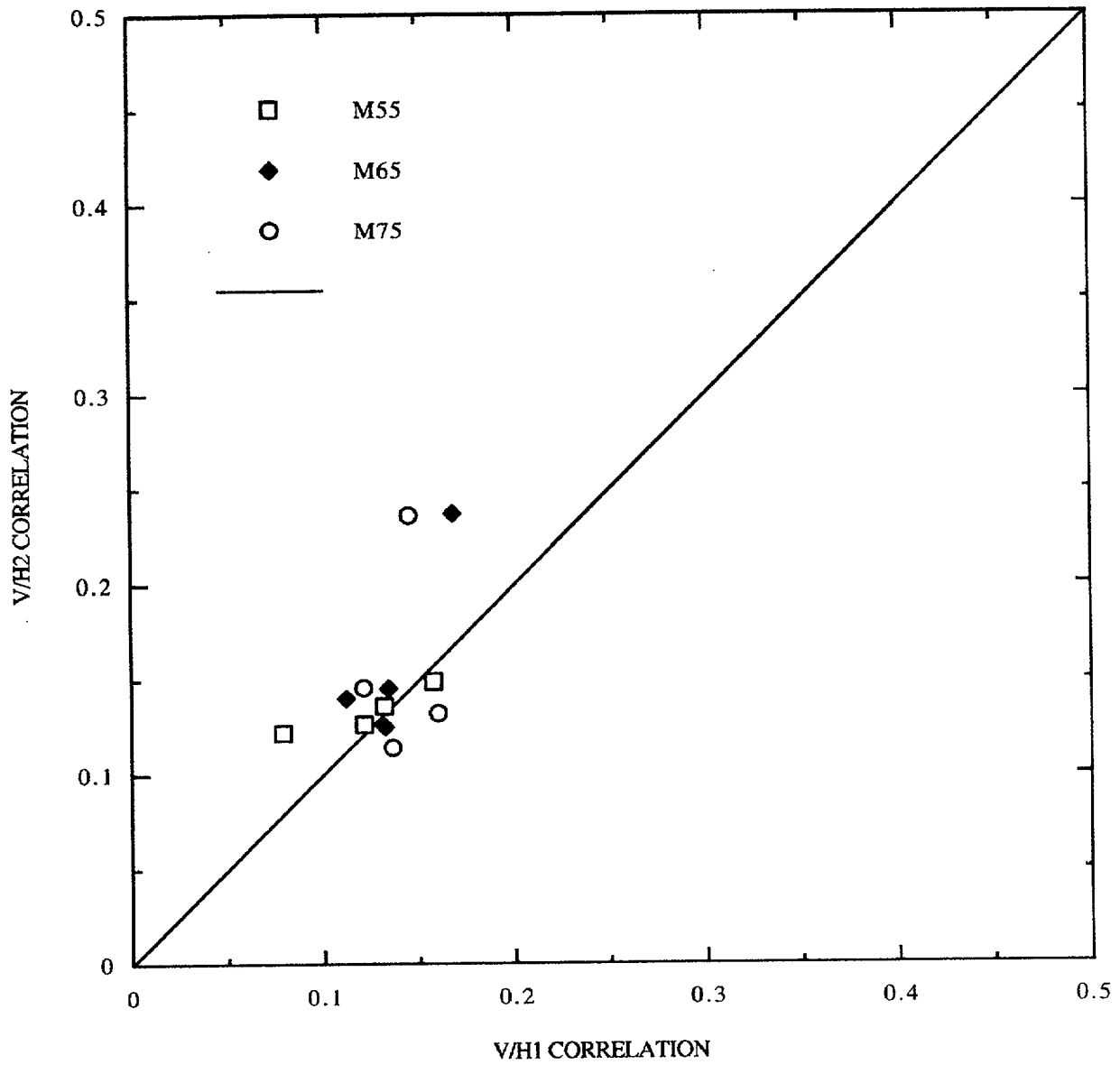


Figure F-30. Comparison of correlations of vertical/horizontal velocity pairs at WUS soil sites.

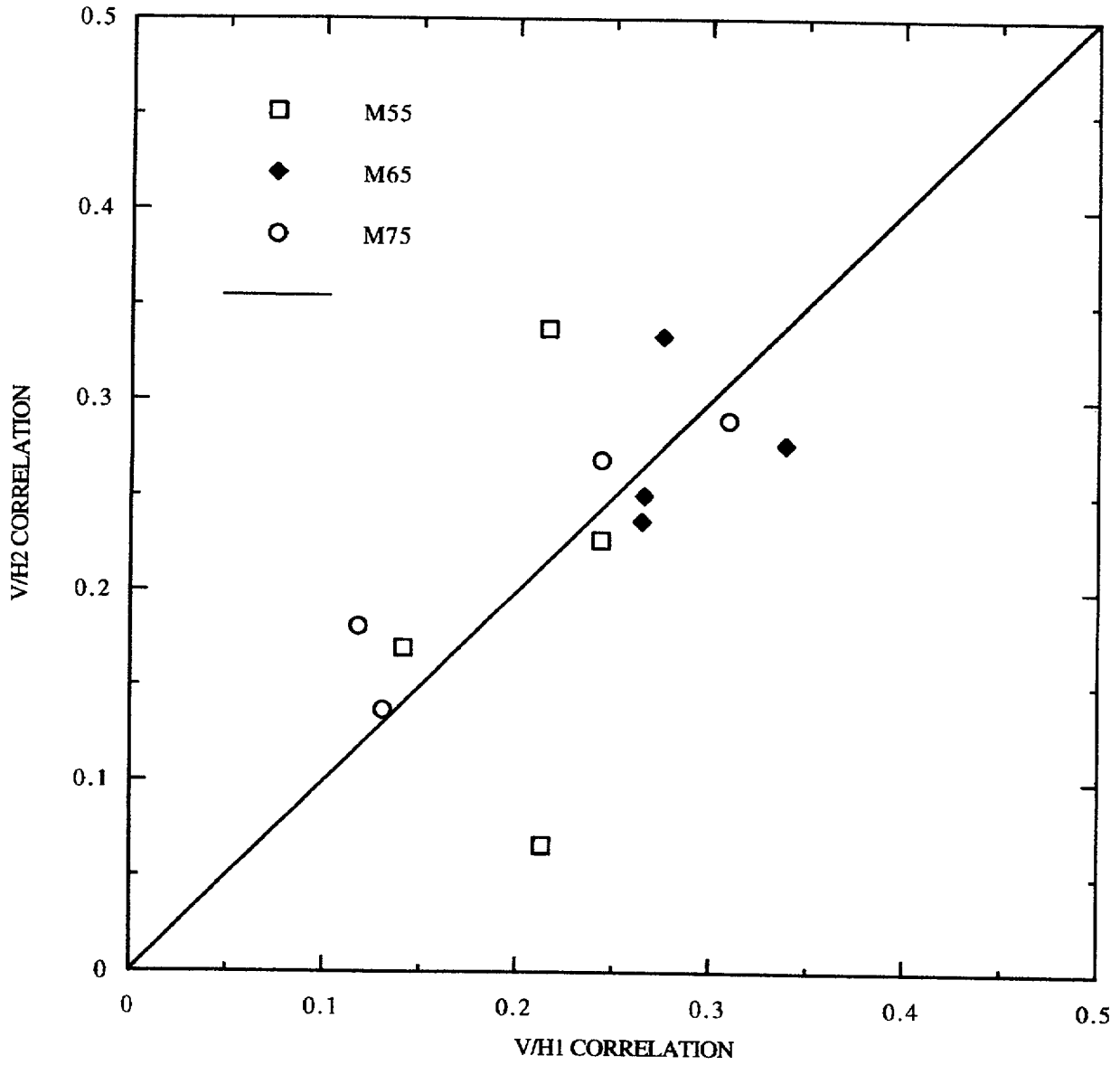


Figure F-31. Comparison of correlations of vertical/horizontal displacement pairs at WUS rock sites.

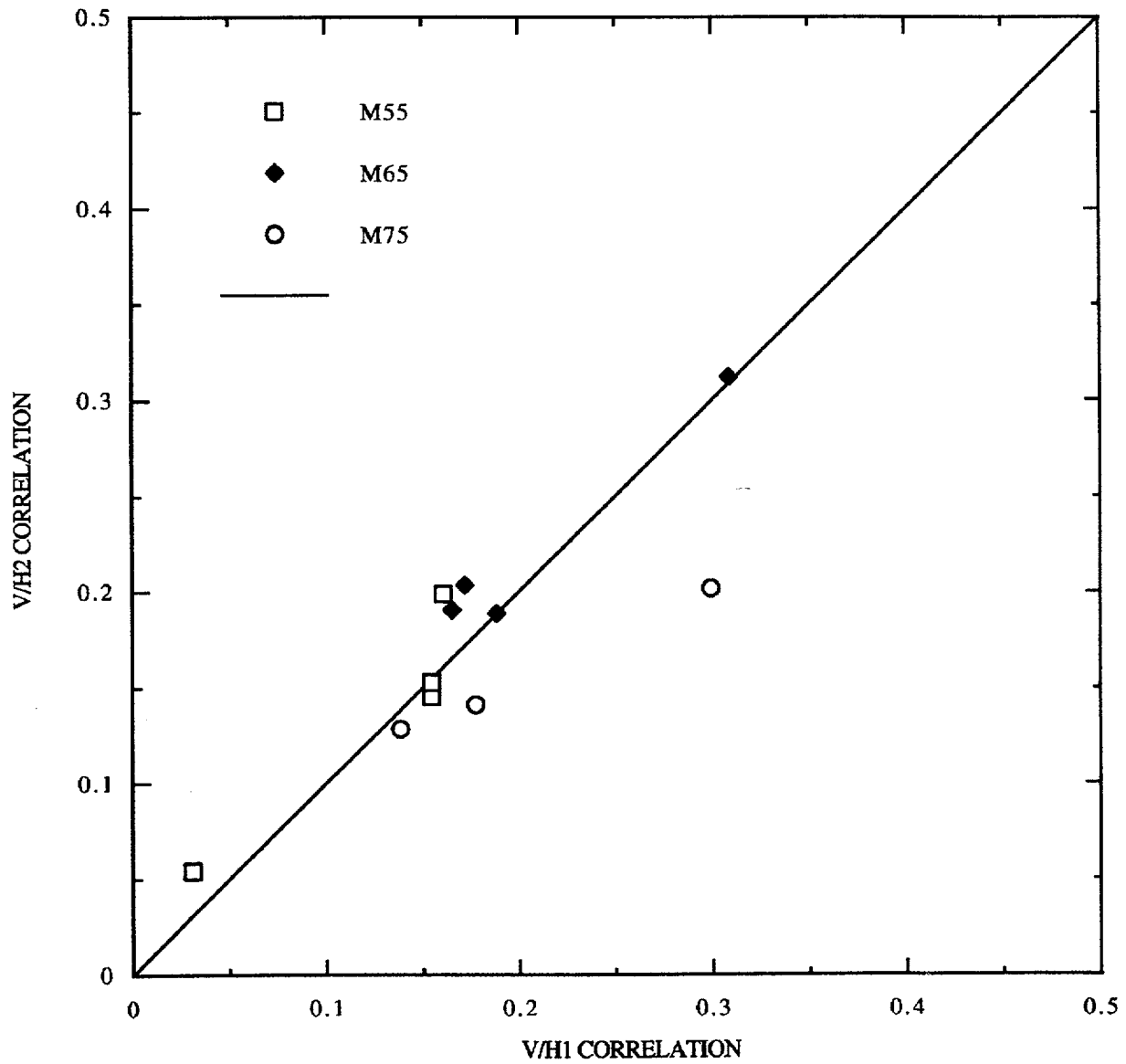


Figure F-32. Comparison of correlations of vertical/horizontal displacement pairs at WUS soil sites.

APPENDIX G

PLOTS OF ARIAS INTENSITY AND CUMULATIVE ABSOLUTE VELOCITY FROM WUS RECORDS

Notation: R55H
S55V

R	Rock Site
S	Soil Site
M55	Magnitude Bin 5 - 6
H	Horizontal records
V	Vertical records

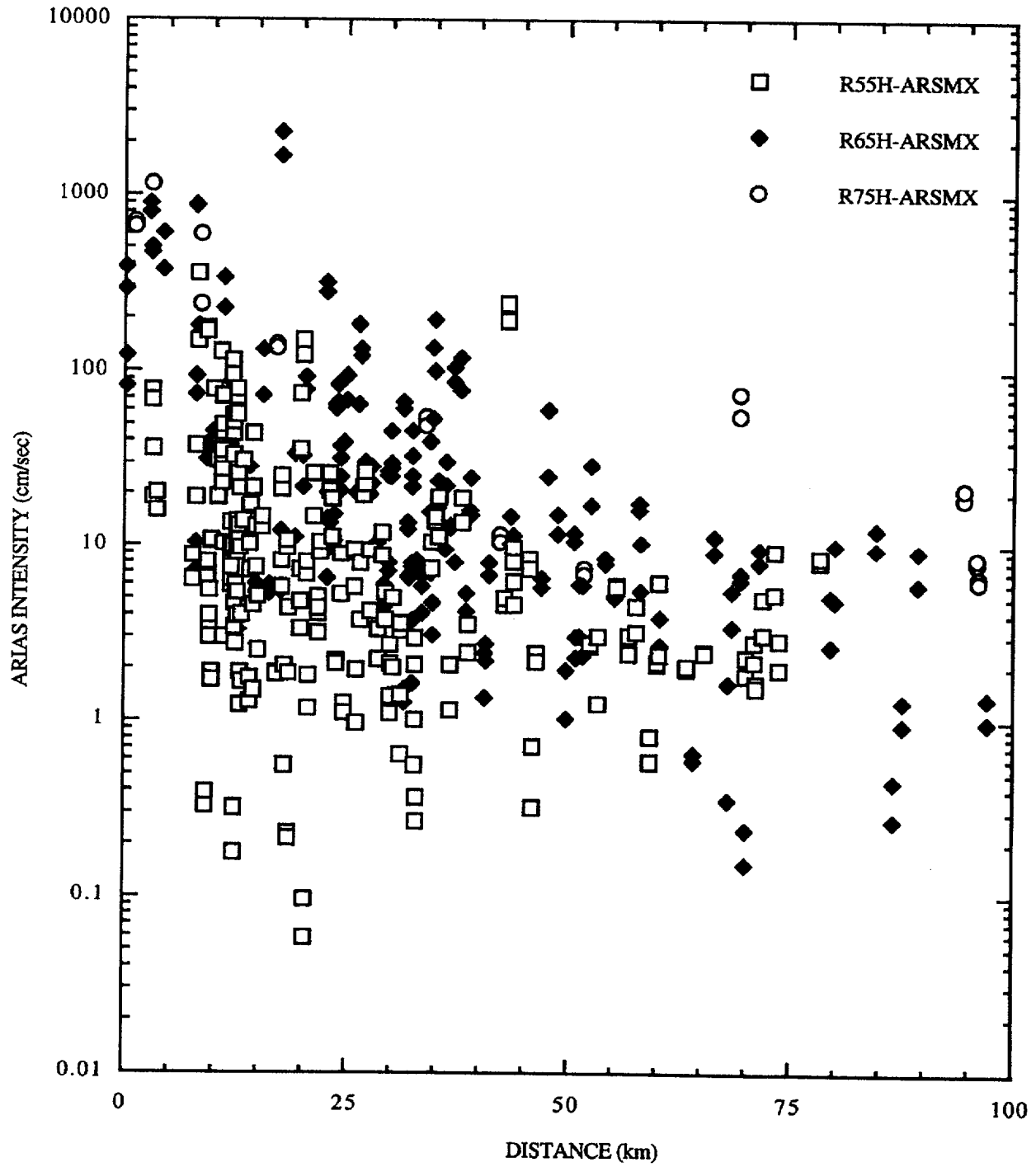


Figure G-1. Arias intensity, WUS horizontal motions, rock sites.

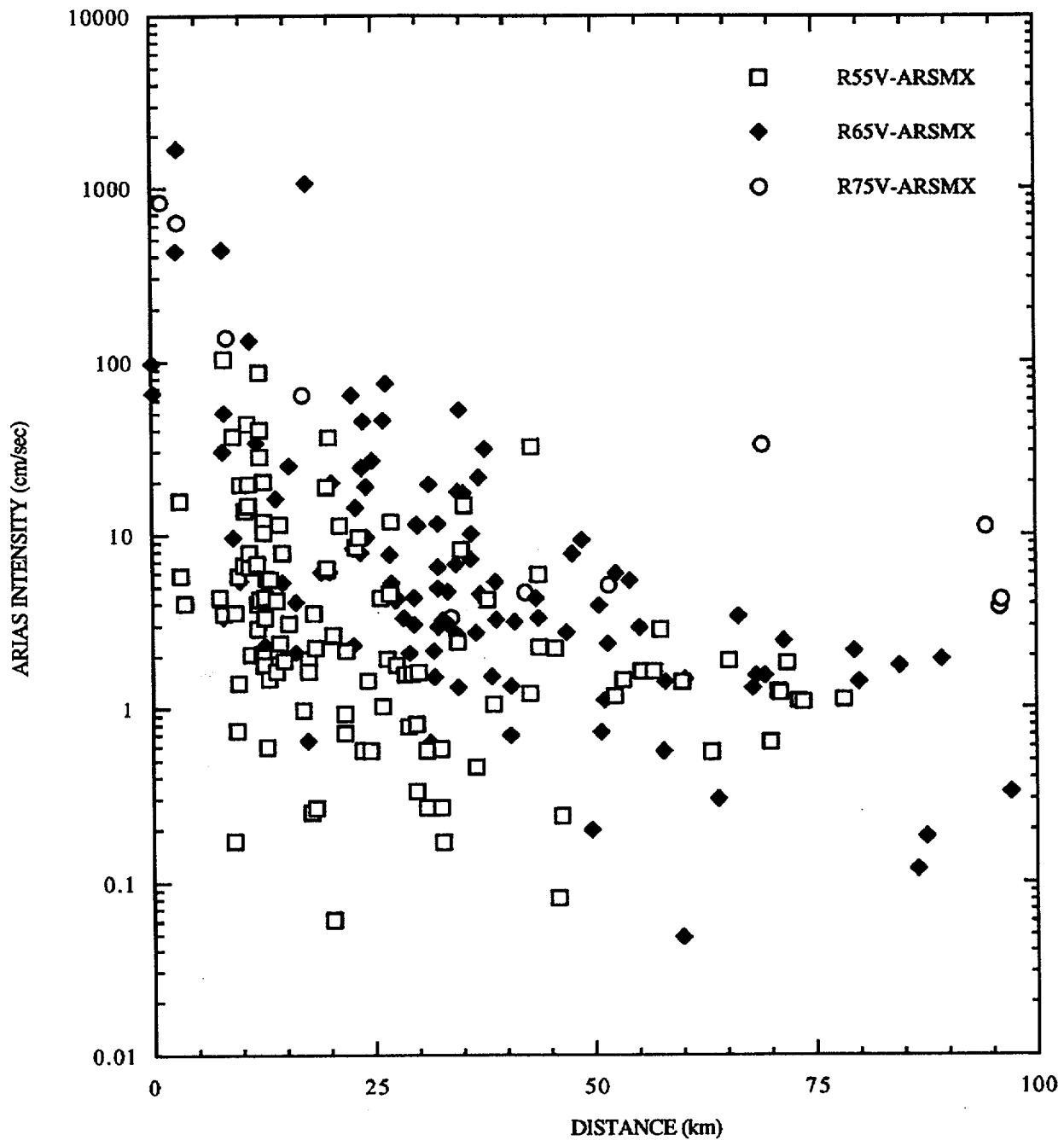


Figure G-2. Arias intensity, WUS vertical motions, rock sites.

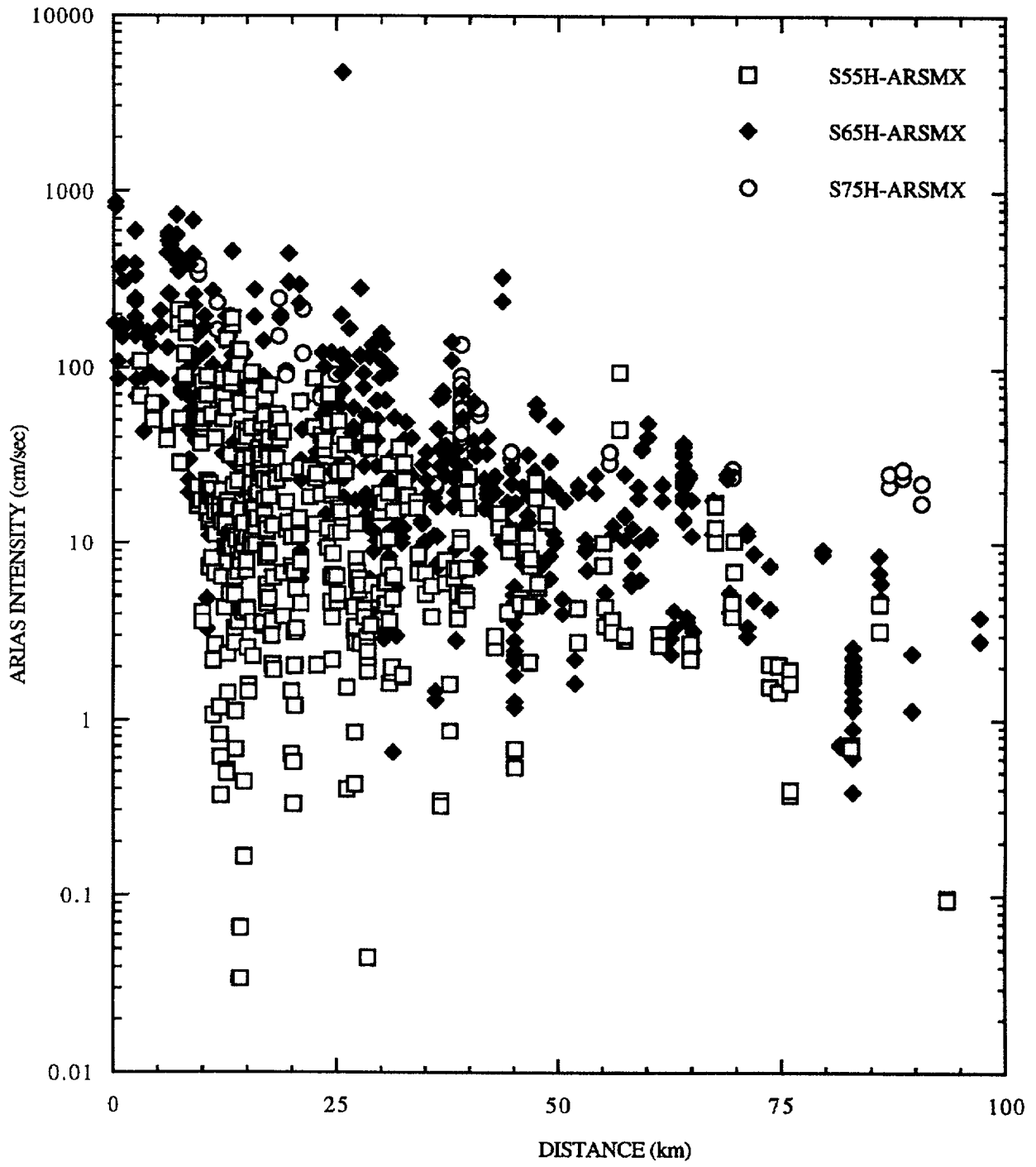


Figure G-3. Arias intensity, WUS horizontal motions, soil sites.

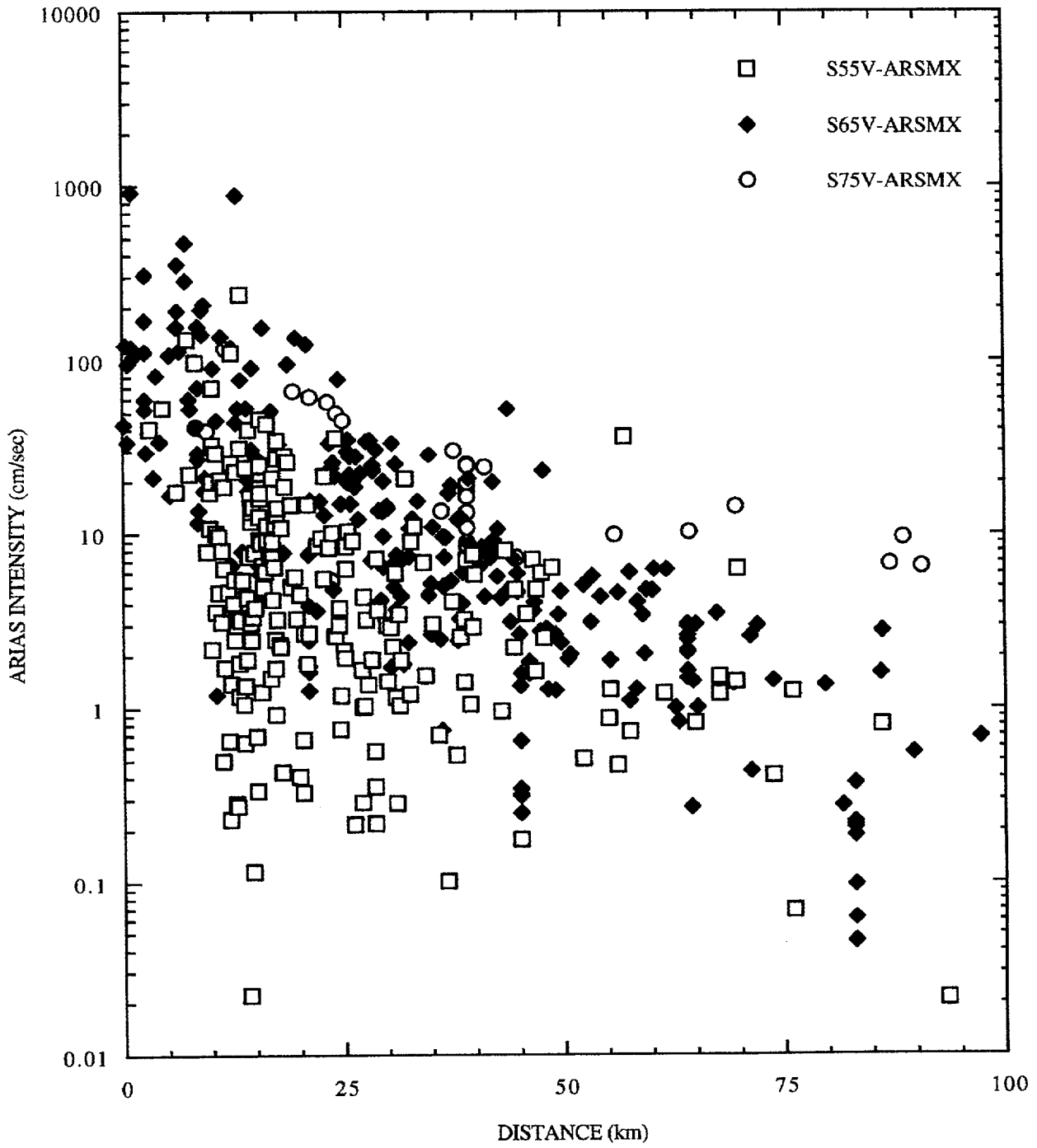


Figure G-4. Arias intensity, WUS vertical motions, soil sites.

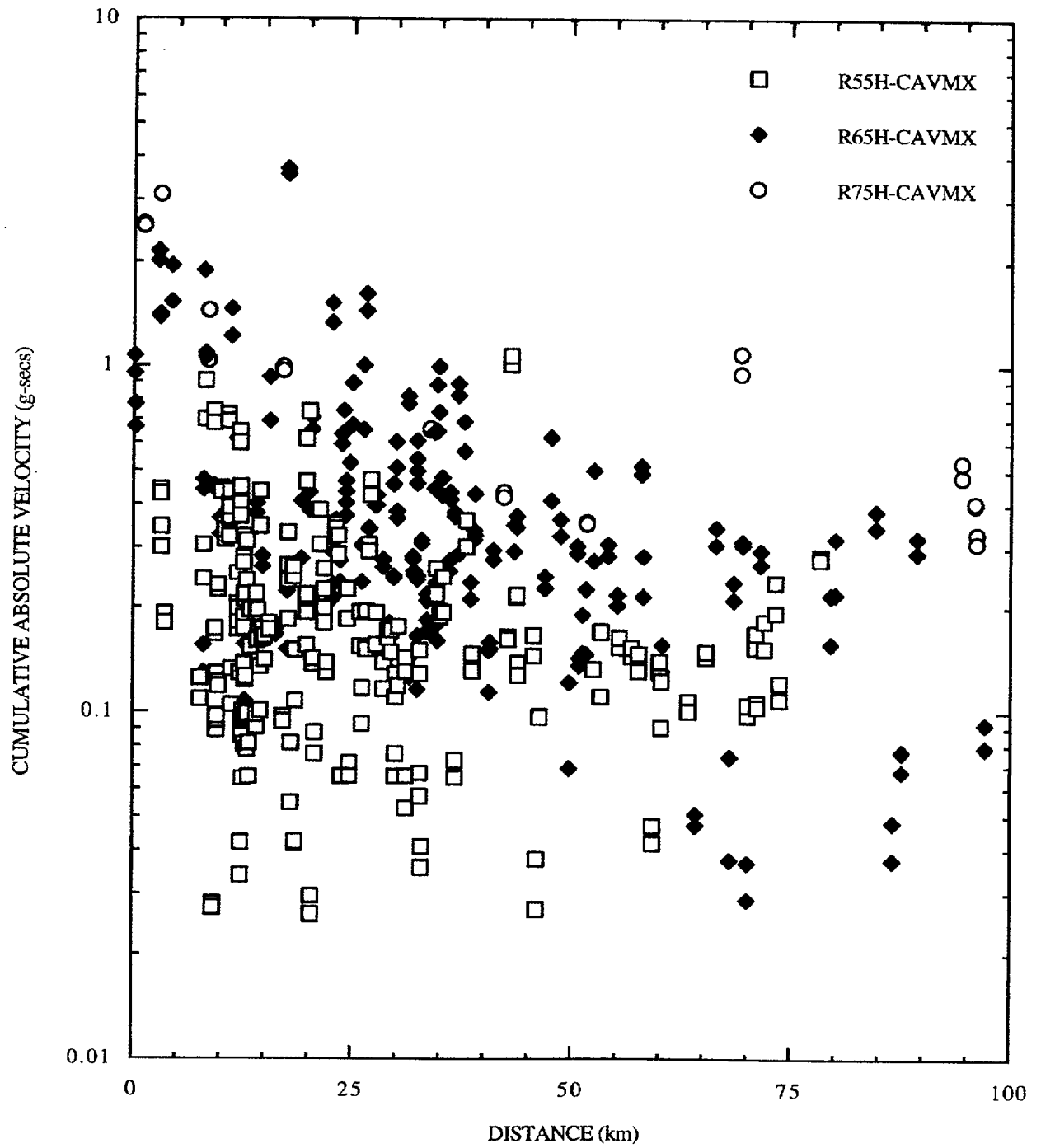
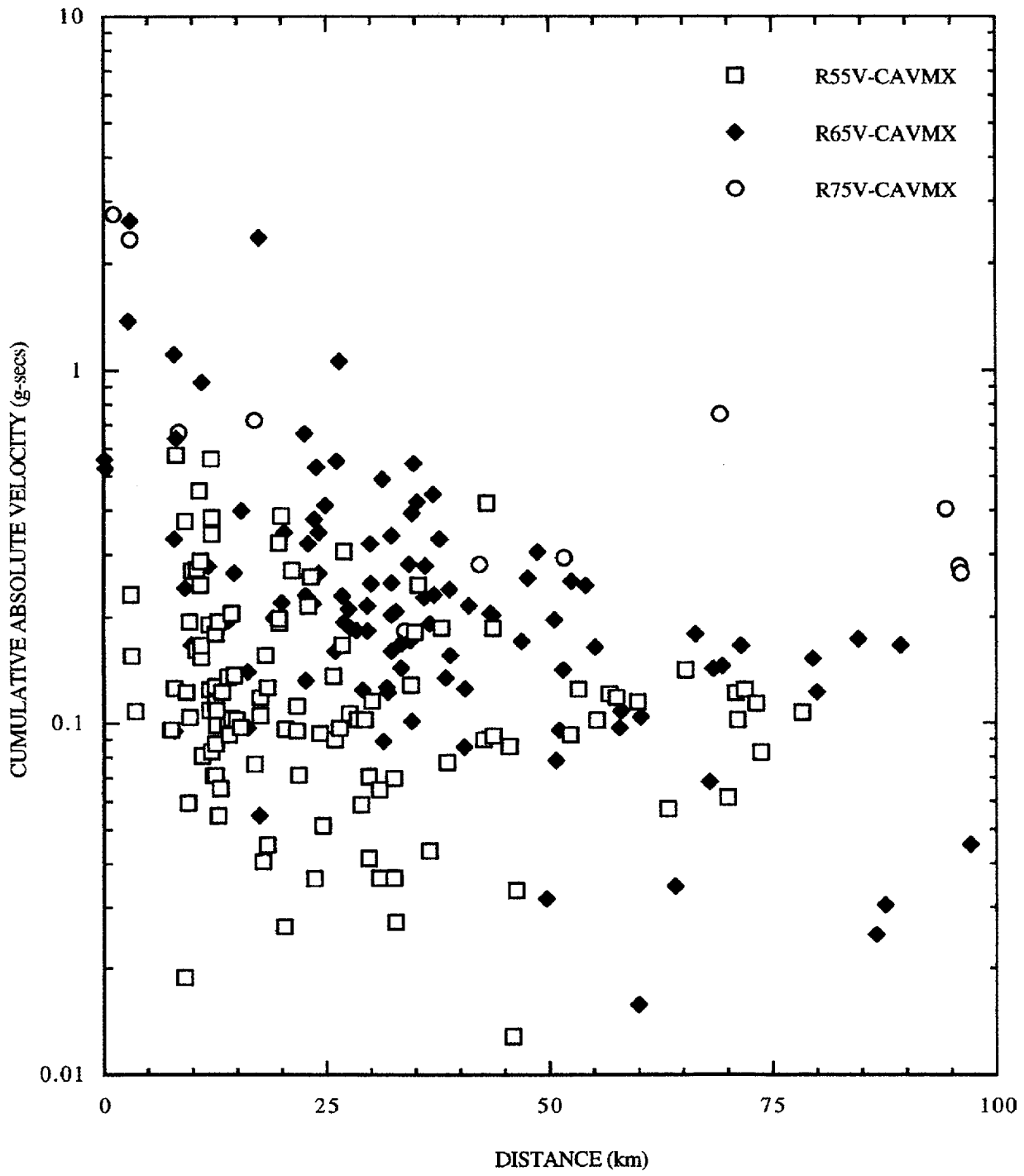


Figure G-5. CAV, WUS horizontal motions, rock sites.



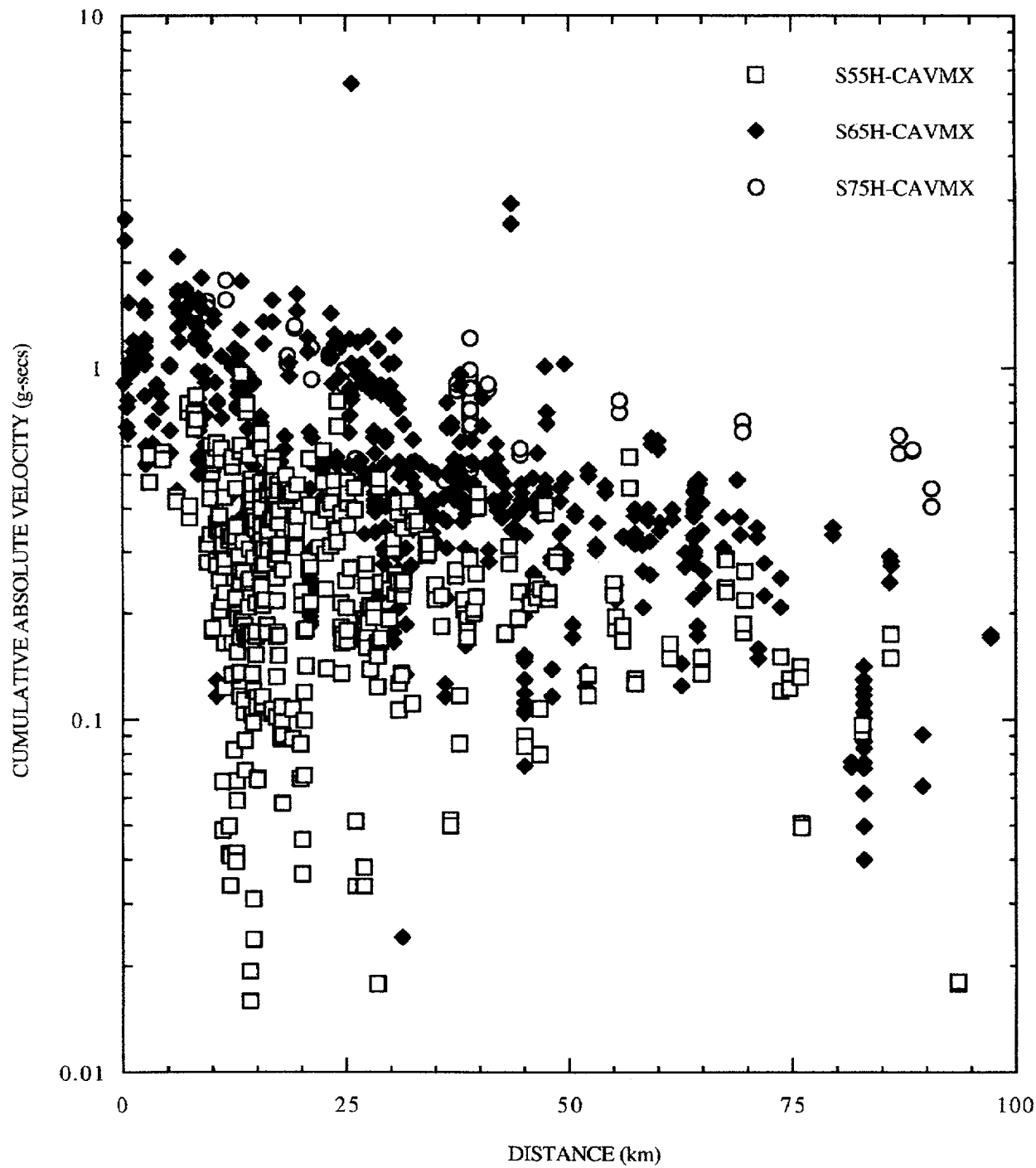


Figure G-7. CAV, WUS horizontal motions, soil sites.

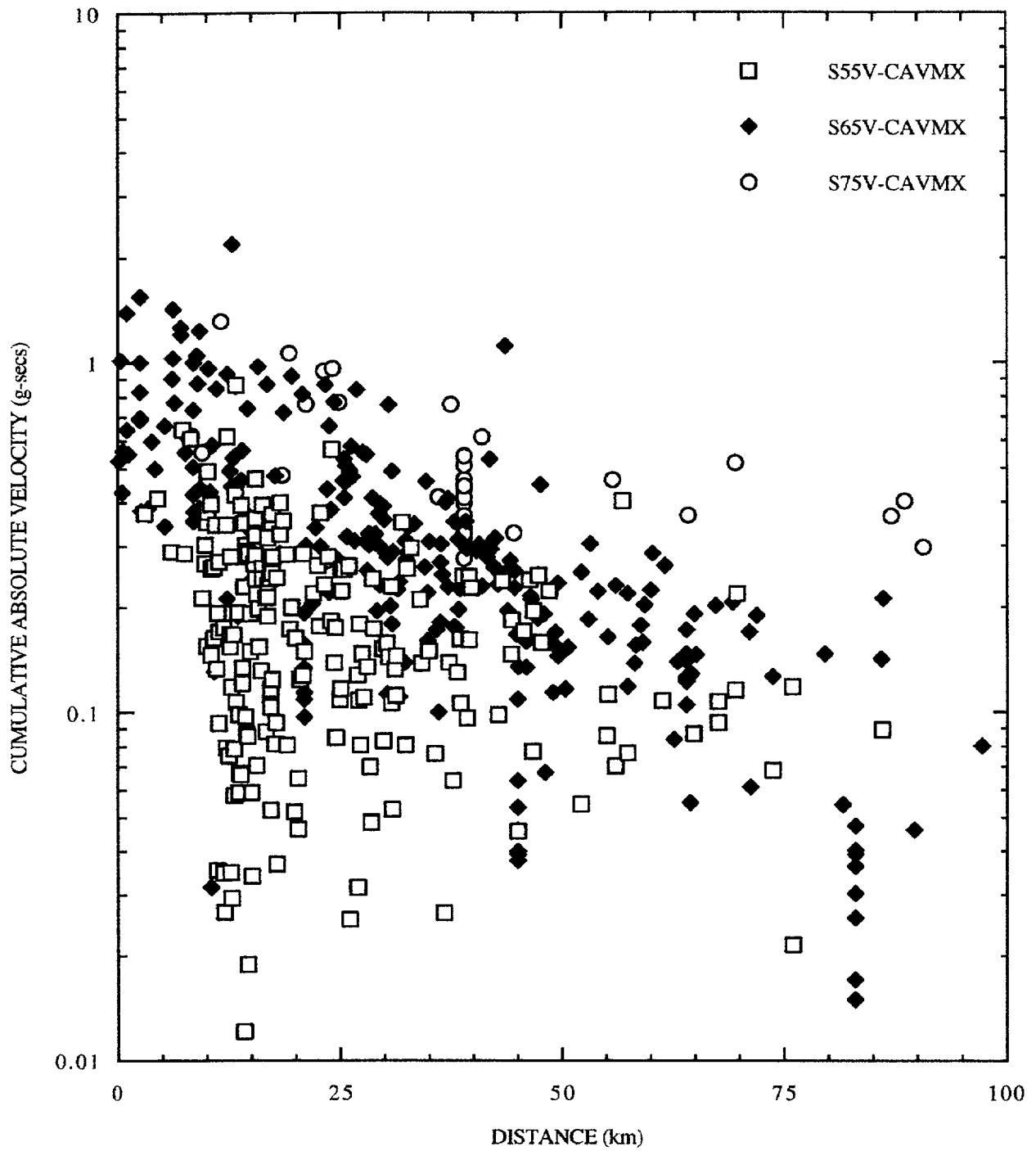


Figure G-8. CAV, WUS vertical motions, soil sites.

APPENDIX H DURATION RELATIONS FOR WUS STRONG GROUND MOTION (MODIFIED FROM ABRAHAMSON AND SILVA, 1997)

H.1 Introduction

Although the duration is an important characteristics of strong ground motion, there has been much less effort for developing empirical models of duration than there has been for developing empirical models of response spectra attenuation relations. Part of the difficulty has been that there are several different definitions of duration that have been used in previous studies. As a result, while duration is well understood in a qualitative sense, there is a wide range of quantitative duration estimates for the same set of recordings.

The definition of duration used here is based on the normalized Arias intensity of acceleration because this is the measure of duration that is most appropriate for the RVT models. The normalized Arias intensity is defined as

$$I(t) = \frac{\int_0^t a^2(\tau) d\tau}{\int_0^{\infty} a^2(\tau) d\tau} \quad (\text{H-1})$$

where $a(\tau)$ is the acceleration time history and the normalized intensity, $I(t)$, ranges from 0 to 1. The duration is defined as the time history interval between which $I(t)$ reaches two values. That is, given $I(t)$, we then develop the inverse relation for $t(I)$. The duration, $T_{I_1-I_2}$, is given by

$$T_{I_1-I_2} = t(I_2) - t(I_1) \quad (\text{H-2})$$

For example, if $I_1=0.05$ and $I_2=0.75$, then $D_{I_1-I_2}$ is the duration of the 5-75% normalized Arias intensity.

H.2 Approach

A two-step approach is used to develop the empirical model for duration. In the first step, a model is developed describing the magnitude, distance, and site dependence of duration for the 5-75% normalized Arias intensity (T_{5-75}). In the second step, a model is developed describing the ratio of the duration at other normalized Arias intensity levels (e.g. 5-95%) relative to the 5-75% duration. Together, these two models provide a description of the magnitude, distance, and site dependence of the duration for a range of normalized Arias intensities.

T₅₋₇₅ Model

In the first step, the model is developed for T₅₋₇₅. Previous studies have found that at short distances on rock sites, T₅₋₇₅ is similar to the source duration, which is approximately by 1/f_c, where f_c is the corner frequency of the earthquake. That is, for short distances at rock sites:

$$T_{5-75} = \frac{1}{f_c(M_o, \Delta\sigma)} \quad (\text{H-3})$$

where

$$f_c(M_o, \Delta\sigma) = 4.9 \cdot 10^6 \beta \left(\frac{\Delta\sigma}{M_o} \right)^{1/3} \quad (\text{H-4})$$

and β is the shear wave velocity at the source (in km / s), Δσ is the stress drop (in bars), and M_o is the moment (in dyne-cm).

At larger distances, the duration increases due to complexities in wave propagation (scattering and 3-D effects). At soil sites, the duration is typically larger than at rock sites. The distance dependence and site dependence are considered to be additive to the source duration. This leads to a model of the form:

$$T_{5-75} = \frac{1}{f_c(M_o, \Delta\sigma)} + t_1(r) + t_2(S, r) \quad (\text{H-5})$$

where t₁(r) is the distance dependence on rock and t₂(S, r) is a site dependence that allows for coupling of the site and distance dependence.

The magnitude dependence of the duration is determined by the magnitude dependence of the corner frequency, f_c, which in turn is determined by the magnitude dependence of the moment and stress-drop. The moment is related to magnitude by

$$\log_{10} M_o = 1.5 M + 16.05 \quad (\text{H-6})$$

The magnitude dependence of the stress drop is estimated as part of the regression analysis.

Previous studies have found that the distance dependence of duration on rock, f₁(r), is approximately proportional to distance. The distance dependence of T₅₋₇₅ is shown in Figures H-1a and H-1b for the horizontal component and in Figures H-2a and H-2b for the vertical component. These data also indicate that the duration increases approximately linearly with distance at large distances. At short distances the duration is approximately independent of distance. This leads to a piecewise continuous form for t₁(r):

$$t_1(r) = \begin{cases} 0 & \text{for } r \leq r_c \\ d_2(r-r_c) & \text{for } r > r_c \end{cases} \quad (\text{H-7})$$

where r_c is a cutoff distance determined by the regression analysis.

For the site dependence, $t_2(S, r)$, a constant is used for short distances. A distance dependence of the site effect is also considered, leading to the following model:

$$t_2(r) = \begin{cases} d_1 S & \text{for } r \leq r_c \\ \{d_1 + d_3(r - r_c)\} S & \text{for } r > r_c \end{cases} \quad (\text{H-8})$$

where S is the site term coefficient and is equal to zero for rock sites and 1 for soil sites. In preliminary evaluations the regression analyses were performed with and without the d_3 term. The d_3 term did not significantly improve the fit so this term was not used further. Also, the distribution of observed residuals was positively skewed (Figure H-3a-b). The hypothesis that the duration residuals are normally distributed can be rejected with greater than 95% confidence. The skewed distribution of residuals is consistent with a lognormal distribution.

The resulting model for mean log duration is

$$\text{Ln}(T_{5-75}) = \text{Ln} \left[\frac{\left(\frac{\Delta\sigma(M)}{10^{1.5M+16.05}} \right)^{-1/3}}{4.9 \cdot 10^6 \beta} + Sd_1 + d_2(r - r_c) \right] \text{ for } r \geq r_c \quad (\text{H-9a})$$

and

$$\text{Ln}(T_{5-75}) = \text{Ln} \left[\frac{\left(\frac{\Delta\sigma(M)}{10^{1.5M+16.05}} \right)^{-1/3}}{4.9 \cdot 10^6 \beta} + Sd_1 \right] \text{ for } r < r_c \quad (\text{H-9b})$$

In the regression analysis, β was fixed at 3.2 km/s.

In the initial regression, the stress drop term (Eq. H-9a, H-9b) was treated as a constant for all magnitudes. The r_c term was not well resolved by the data and ranged from 5 to 15 km, so its value was set at 10 km. The remaining coefficients estimated from the initial regression are listed in Table H-1. The distributions of the residuals shown in Figures H-4a and H-4b indicate that a lognormal distribution is appropriate; the hypothesis that the duration residuals are lognormally distributed cannot be rejected with 40% confidence.

It is important to note that the "duration" stress drop given in Table H-1 is a ground motion parameter with units of bars that lead to the appropriate duration under the assumption that the 5-75% normalized Arias intensity is given by a source duration equal to $1/f_c$. It is by definition different from the static stress drop or RMS stress drop.

When fixing other coefficients fixed to their values from Table I-1; the value of $\Delta\sigma$ varies with magnitude. The estimated stress drop for the individual magnitude bins are shown in Figures H-5a and H-5b, for horizontal and vertical components respectively. The standard errors of the mean estimates are also shown. An exponential form of the magnitude dependence of $\Delta\sigma$ was selected because it is consistent with the trend in the estimates shown in Figures H-5a and H-5b and because it is consistent with the exponential magnitude dependence of seismic moment. (For short distances on rock, the magnitude dependence of the log duration reduces to a linear function in magnitude if an exponential magnitude dependence of $\Delta\sigma$ is used.) The magnitude dependence of $\Delta\sigma$ is modeled by

$$\Delta\sigma(M) = \exp\{b_1 + b_2(M-6)\} \quad (\text{H-10})$$

Substituting this form for $\Delta\sigma(M)$ in Eq (H-9), the regression analysis was repeated holding the remaining coefficients fixed to their values from the initial regression (from Table H-1). The estimates of the coefficients are listed in Table H-2. The solid curves in Figures H-5a and H-5b show the resulting model for duration stress drop. The magnitude dependence of $\Delta\sigma$ found here (increasing duration stress drop with increasing magnitude) indicates that the magnitude dependence of the duration is weaker than implied by constant stress drop scaling.

The residuals were computed for separate, unit magnitude bins to evaluate the fit. The residuals for the horizontal and vertical duration (T_{5-75}) are shown as a function of distance in Figures H-6a and H-7a, for M6.5-7.0. (Data for other magnitude ranges are similar.)

The resulting magnitude and distance dependence of the model for the 5-75% duration is shown in Figures H-8a through H-8d.

Duration for Other Ranges

The second part of the duration regression evaluates the shape of the normalized Arias intensity so that the duration at the other ranges can be estimated. For each record, the duration values were normalized by the T_{5-75} value for that record. The mean normalized durations for the average horizontal component are shown in Figures H-9 and H-10 for different distance ranges (given $6.5 < M < 7.0$) and magnitude ranges (given $30 < R < 60$), respectively. Curves for other magnitudes, distances, and vertical components are similar. The normalized duration does not show a significant systematic dependence on either magnitude or distance, so a magnitude- and distance- independent functional form is used. Several alternative forms were evaluated and the following power relations was found to provide a good fit to the mean:

$$\ln\left(\frac{T_{5-I}}{T_{5-75}}\right) = e_1 + e_2 \ln\left(\frac{I-5}{1-.01I}\right) + e_3 \left(\ln\left(\frac{I-5}{1-.01I}\right)\right)^2 \quad (\text{H-11})$$

where I is the percentage of the normalized Arias intensity defining the duration. The coefficients were estimated using ordinary least-squares and are listed in Table H-3. The mean predicted relation is compared to the mean of the data in Figures H-12a and H-12b for the horizontal and vertical components, respectively.

H.3 Duration Model

Combining the two models, the resulting duration model is given by

$$\text{Ln } (T_{5-l}) = \text{Ln} \left[\left(\frac{\Delta\sigma(M)}{10^{1.5M+16.05}} \right)^{-1/3} + Sd_1 + d_2(r - r_c) \right] + \ln \left(\frac{T_{5-l}}{T_{5-75}} \right) \quad (\text{H-12a})$$

for $r \geq r_c$ and by

$$\text{Ln } (T_{5-l}) = \text{Ln} \left[\left(\frac{\Delta\sigma(M)}{10^{1.5M+16.05}} \right)^{-1/3} + Sd_1 \right] + \ln \left(\frac{T_{5-l}}{T_{5-75}} \right) \quad (\text{H-12b})$$

for $r < r_c$.

The standard error is computed from this combined model to estimate the total standard error directly (not a combination of the standard error of the two parts of the model). The standard errors are plotted in Figure H-12 and are listed in Table H-4.

H.4 Model Predictions

The model predictions for the horizontal duration for a distance of 30 km are shown in Figure H-13 for rock and Figure H-14 for soil. Similar plots of the model predictions for the vertical component are shown in Figures H-15 and H-16.

References

- Abrahamson, N.A. and W. J. Silva (1997), "Empirical ground motion models," Appendix in Silva et al. (1997).
- Silva, W.J., N. Abrahamson, G. Toro, C. Costantino (1997). "Description and validation of the stochastic ground motion model." Report to Brookhaven National Laboratory, Associated Universities, Inc. Upton, New York, Contract 77053.

Table H-1
 INITIAL REGRESSION ESTIMATES OF COEFFICIENTS
 FOR $T_{5.75}$ USING $\Delta\sigma$ INDEPENDENT OF MAGNITUDE

Coefficient	Horizontal	Vertical
d_1	0.805 0.130	1.076 0.155
d_2	0.063 0.006	0.107 0.008
$\Delta\sigma$	230 34	152 23
r_c	10*	10*
β	3.2*	3.2*

* fixed values

Table H-2
 REGRESSION ESTIMATES OF COEFFICIENTS
 FOR $T_{5.75}$ USING MAGNITUDE DEPENDENT $\Delta\sigma$

Coefficient	Horizontal	Vertical
d_1	0.805*	1.076*
d_2	0.063*	0.107*
b_1	5.204 0.105	4.61**
b_2	0.851 0.146	1.536**
r_c	10*	10*
β	3.2*	3.2*
Standard Error	0.55	0.46

* fixed values

**standard deviations not reported

Table H-3
REGRESSION ESTIMATES FOR THE NORMALIZED DURATION

Coefficient	Horizontal		Vertical	
e_1	-0.532	0.005	-0.466	0.009
e_2	0.552	0.002	0.540	0.005
e_3	-0.0262	0.0013	-0.0537	0.0026

Table H-4
STANDARD ERROR FOR DURATION (EQ. H-12a,b)

I	Horizontal	Vertical
10%	0.843	0.915
15%	0.759	0.841
20%	0.713	0.788
25%	0.691	0.742
30%	0.674	0.703
35%	0.660	0.666
40%	0.646	0.630
45%	0.636	0.609
50%	0.628	0.583
55%	0.616	0.555
60%	0.605	0.535
65%	0.594	0.519
70%	0.582	0.500
75%	0.565	0.478
80%	0.545	0.462
90%	0.510	0.443
95%	0.493	0.449

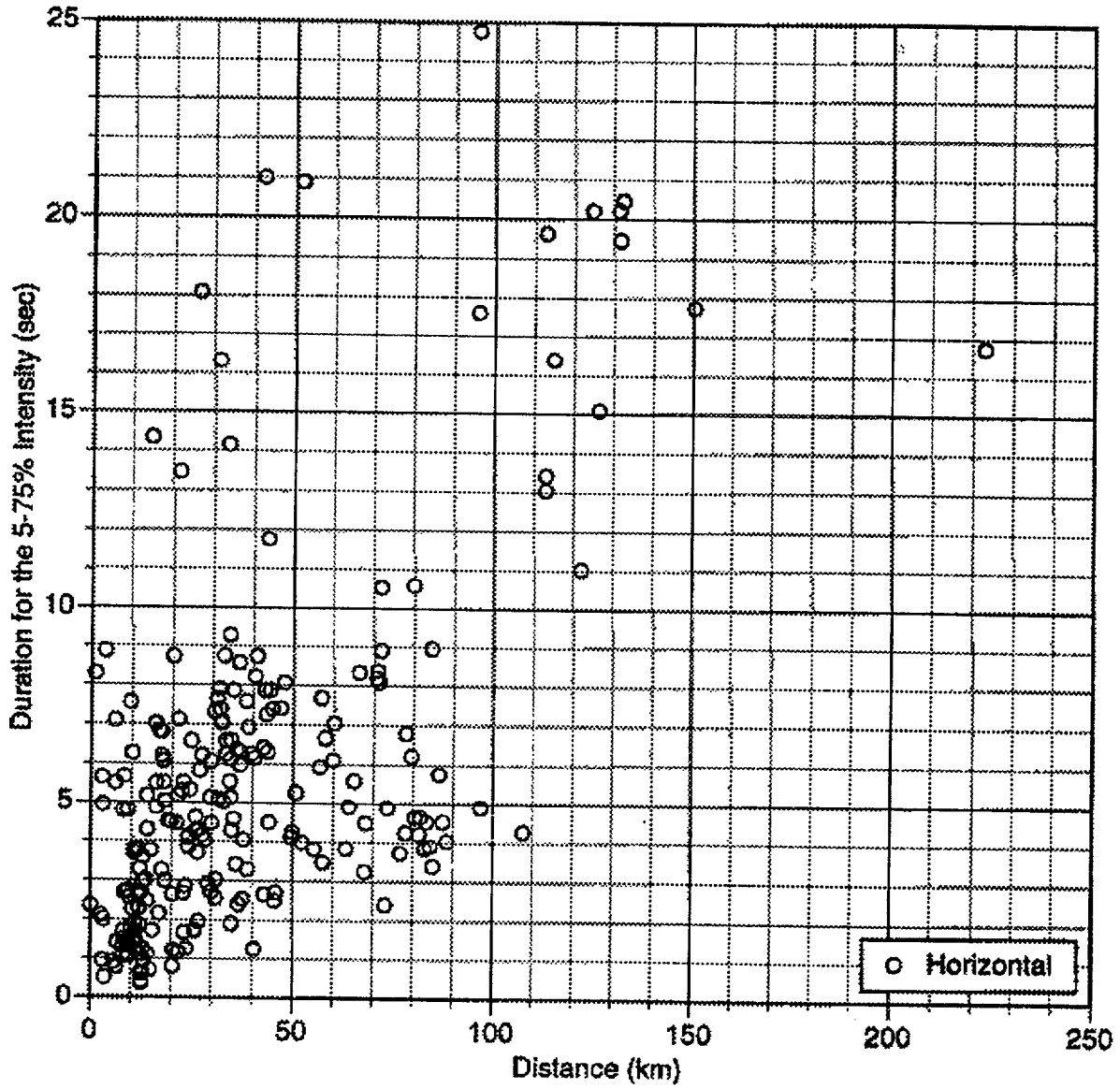


Figure H-1a. Distance dependence of the horizontal duration for the 5-75% intensity for rock site conditions.

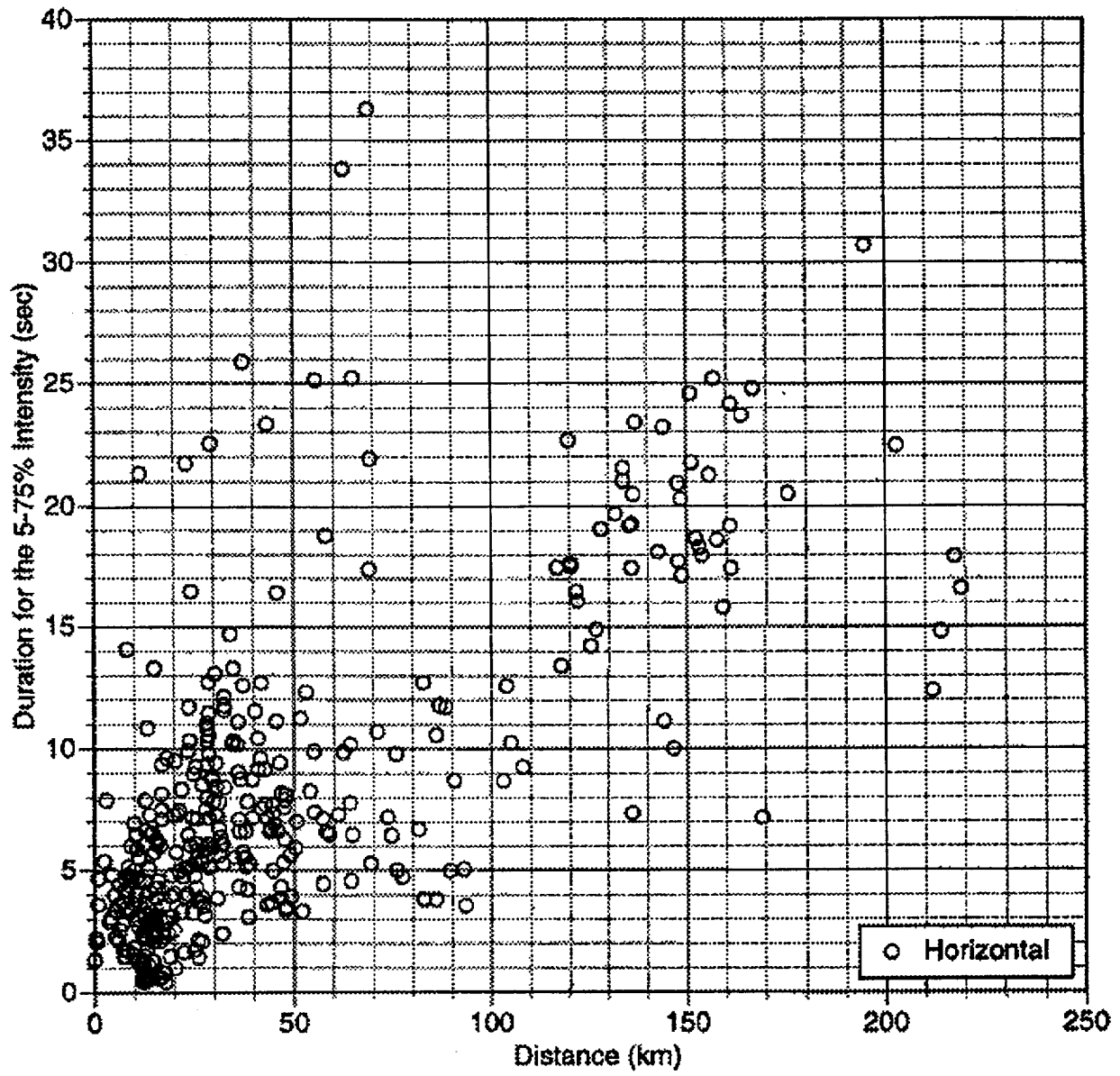


Figure H-1b. Distance dependence of the horizontal duration for the 5-75% intensity for soil site conditions.

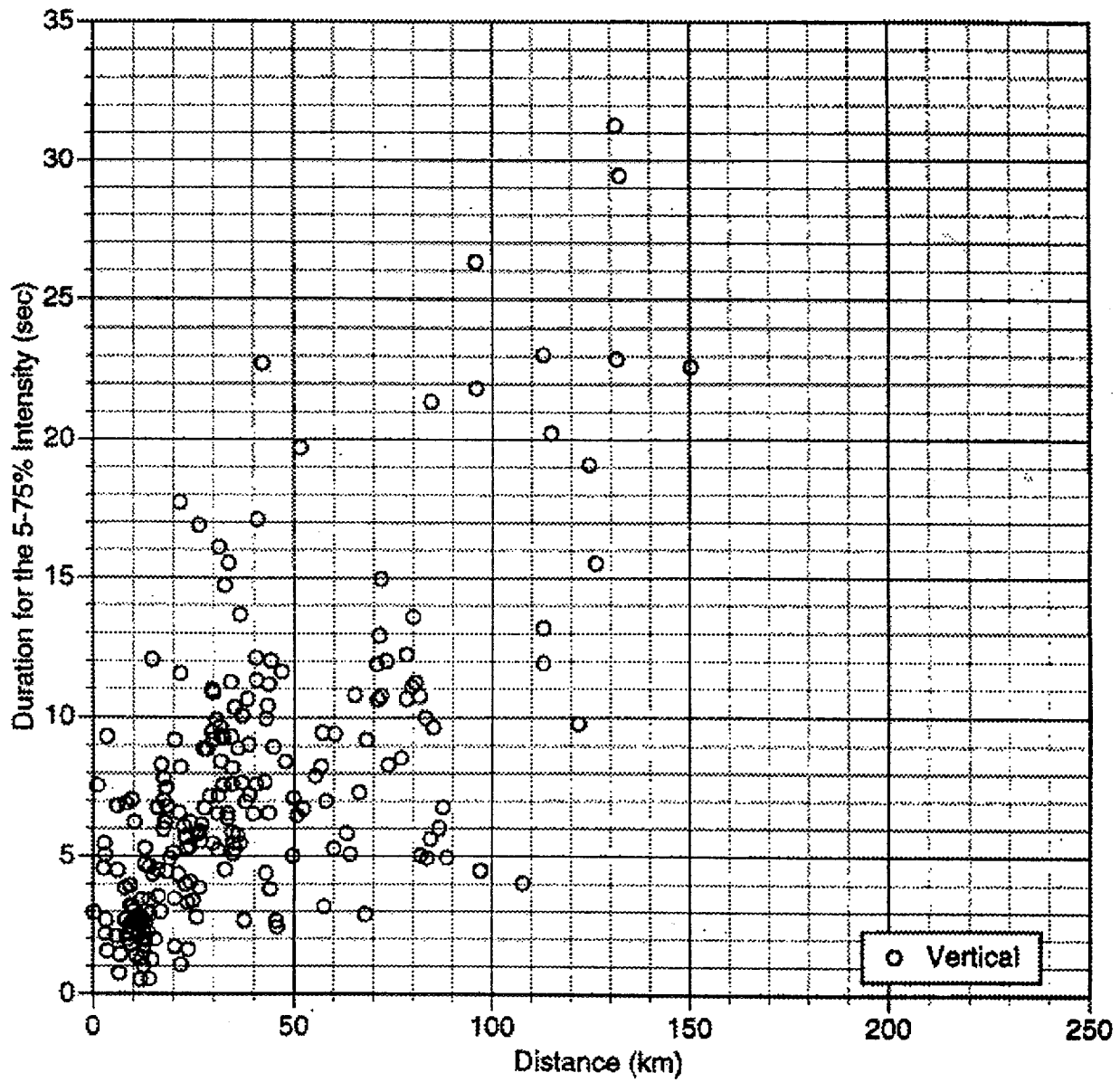


Figure H-2a. Distance dependence of the vertical duration for the 5-75% intensity for rock site conditions.

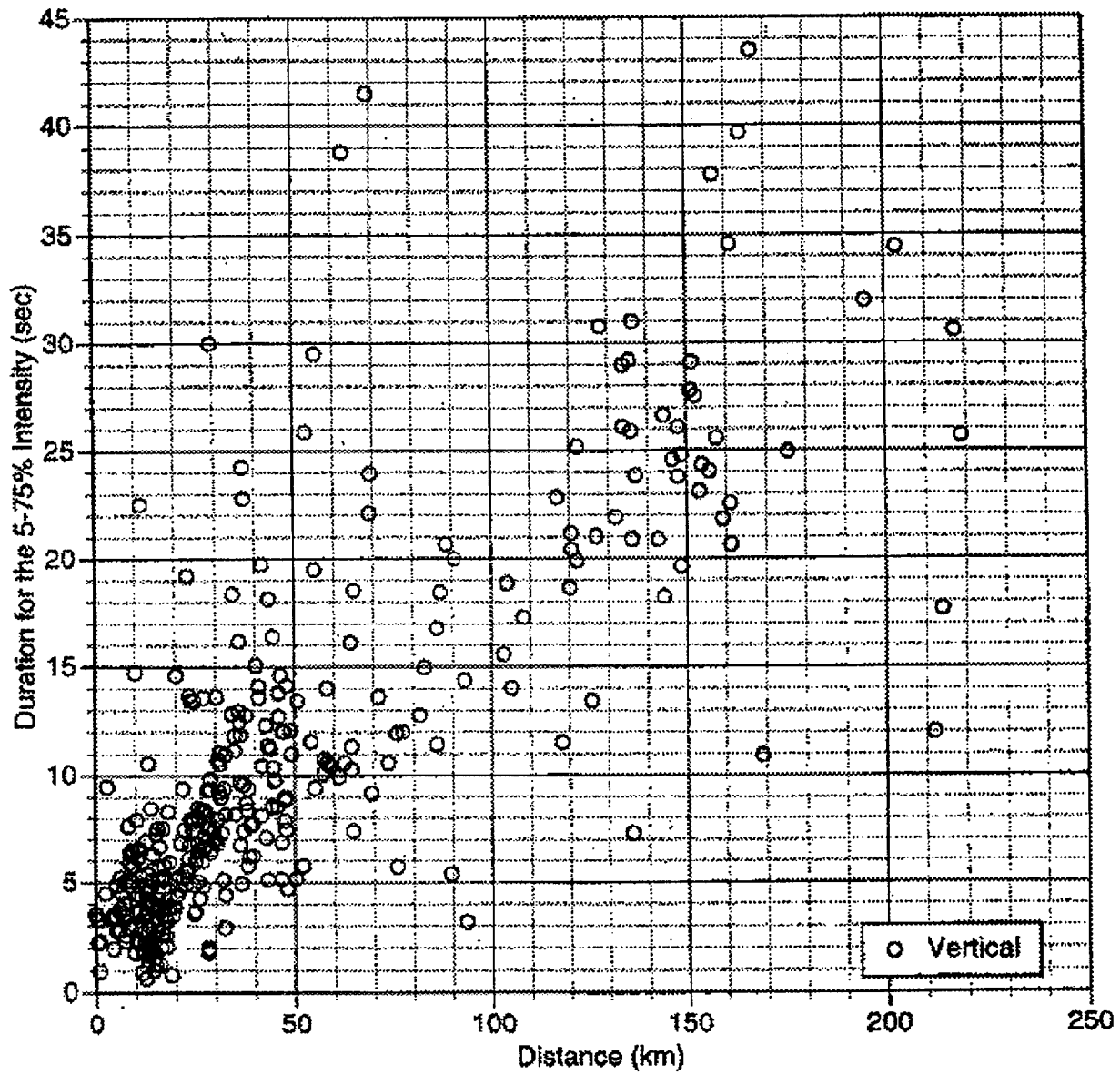


Figure H-2b. Distance dependence of the vertical duration for the 5-75% intensity for soil site conditions.

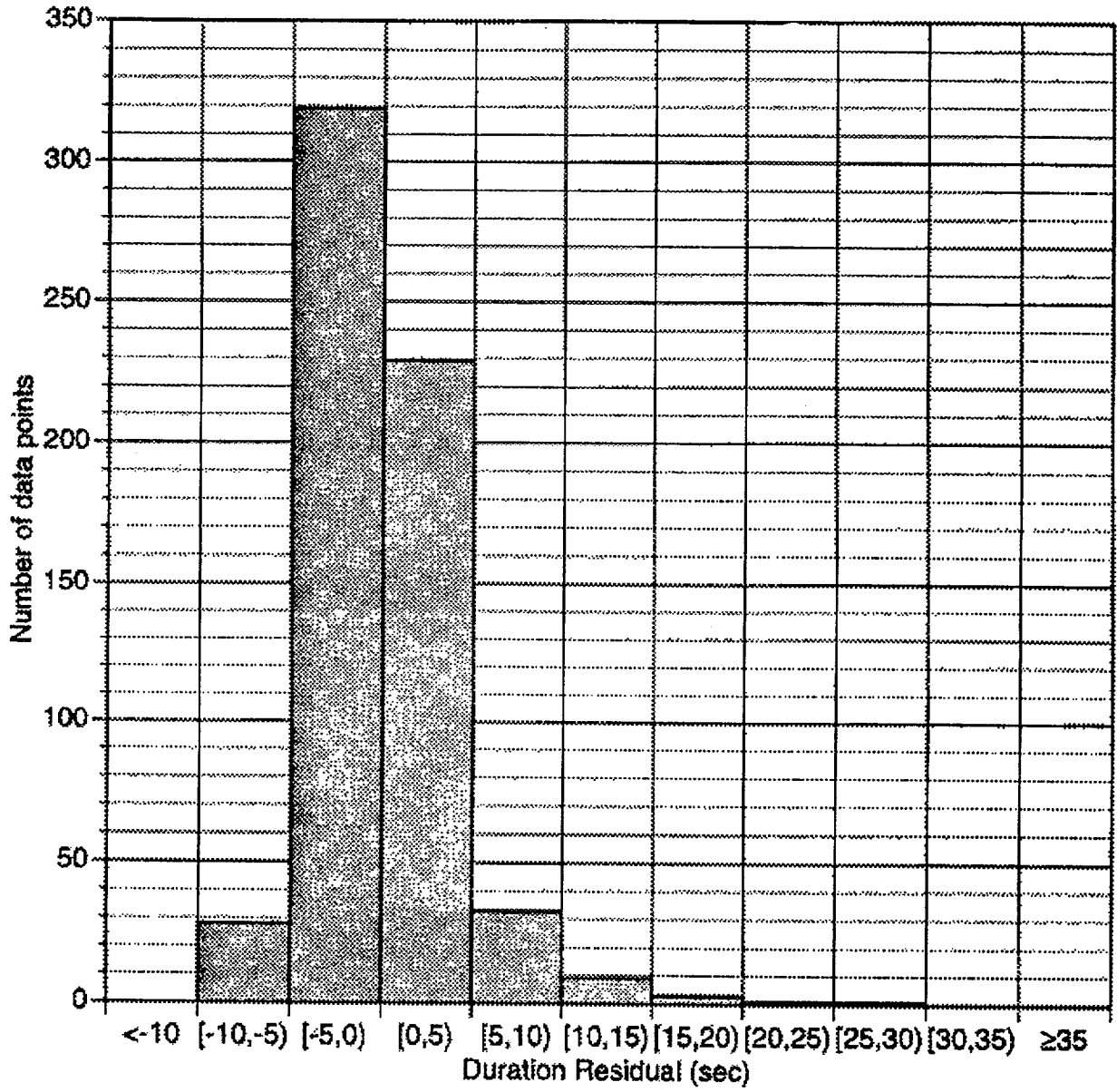


Figure H-3a. Distribution of the horizontal 5-75% intensity model (Equation H-9).

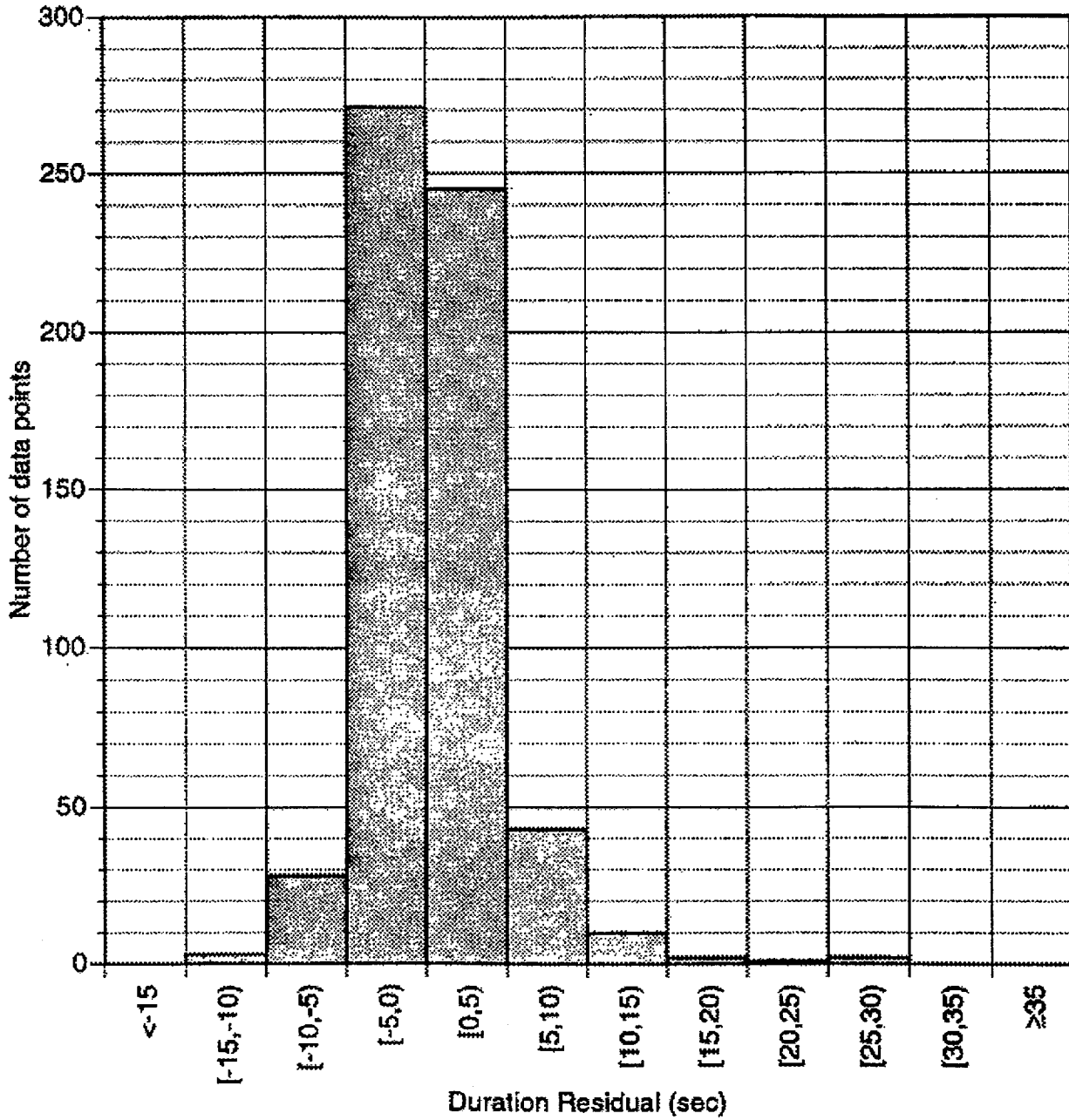


Figure H-3b. Distribution of the vertical 5-75% intensity model (Equation H-9).

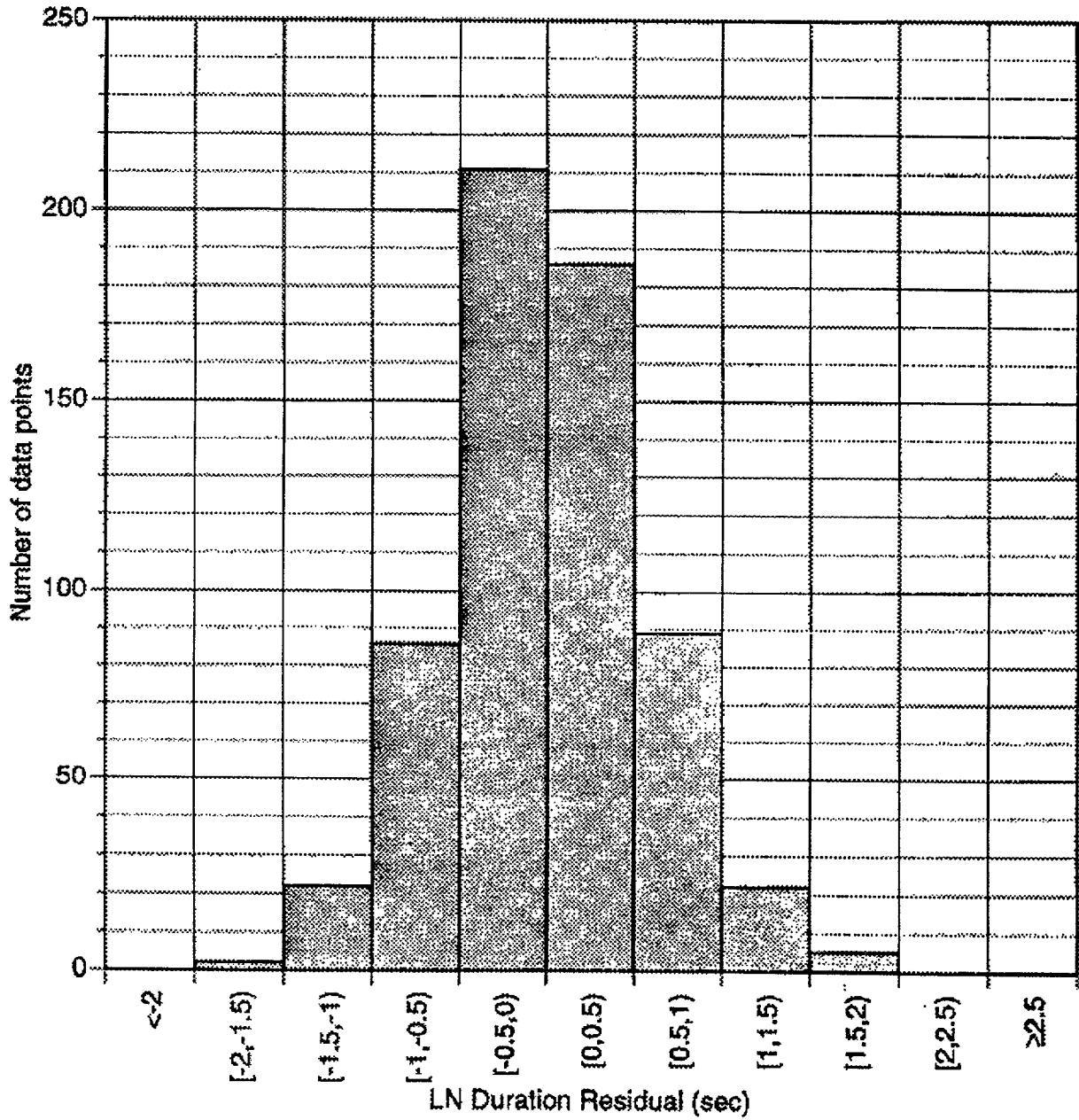


Figure H-4a. Distribution of the horizontal 5-75% intensity model (Equation H-9).

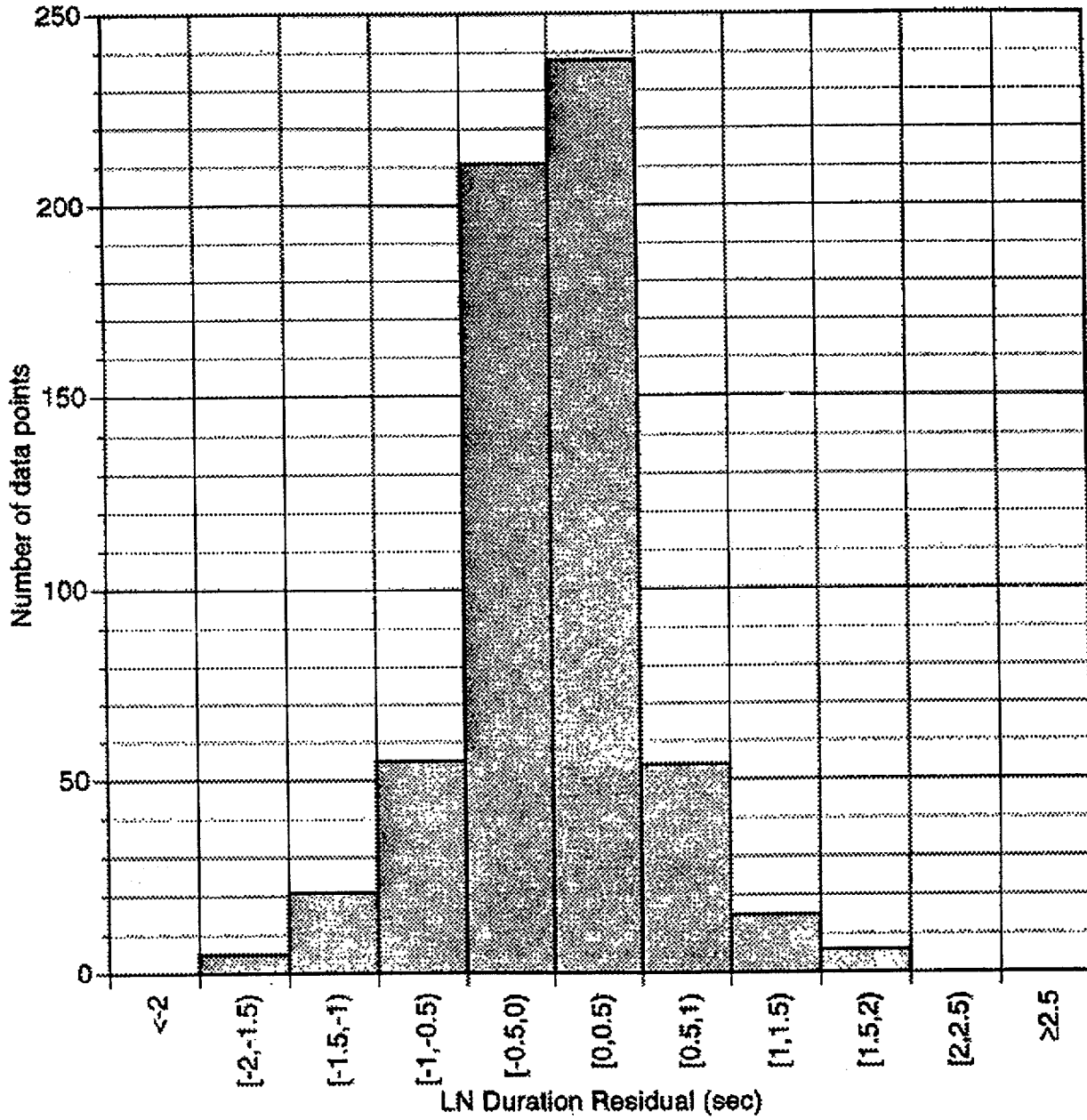


Figure H-4b. Distribution of the vertical 5-75% intensity model (Equation H-9).

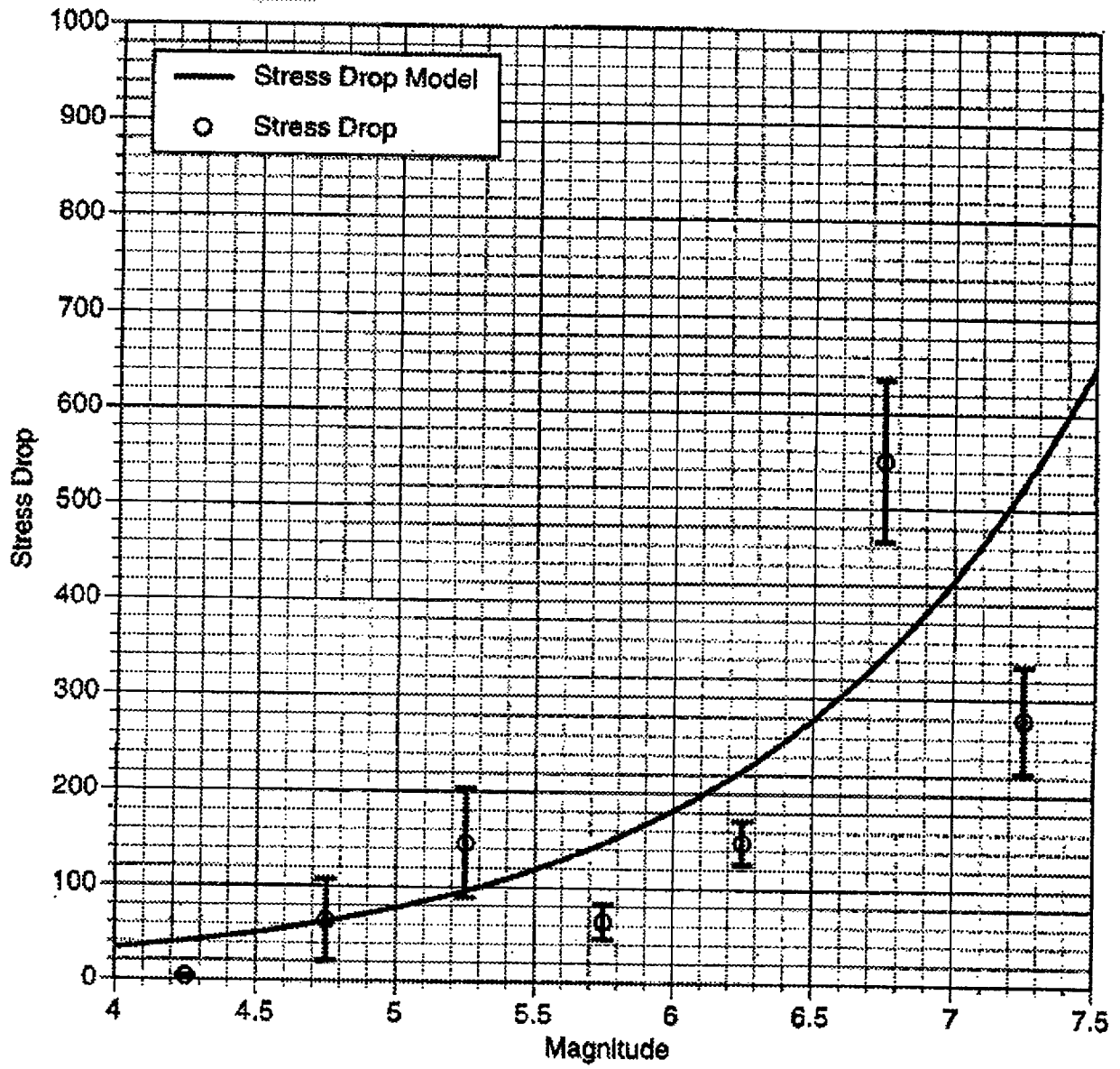


Figure H-5a. Stress drop estimates and model for the horizontal component.

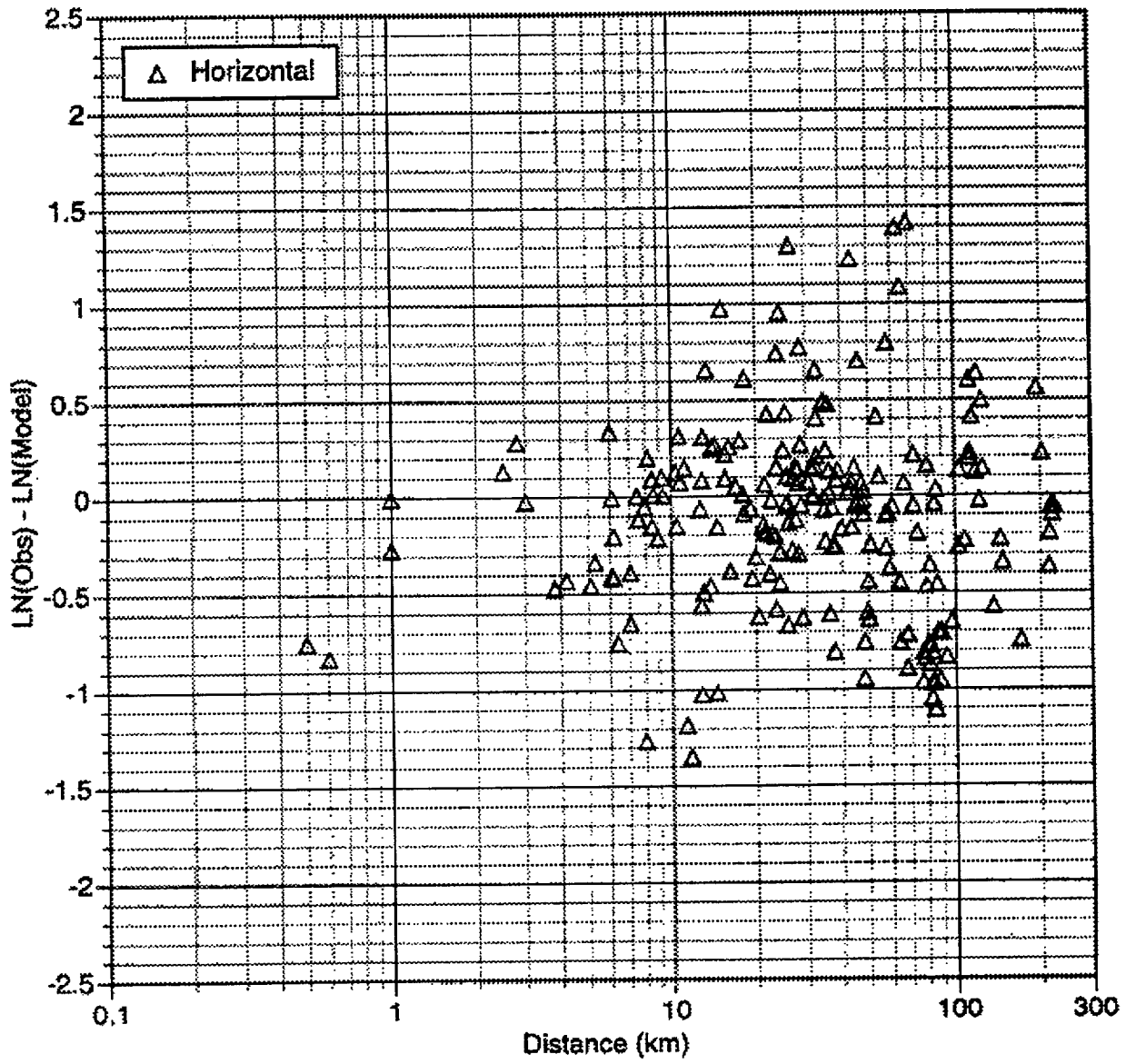


Figure H-6. Horizontal residuals for magnitudes between $6.5 < M < 7.0$.

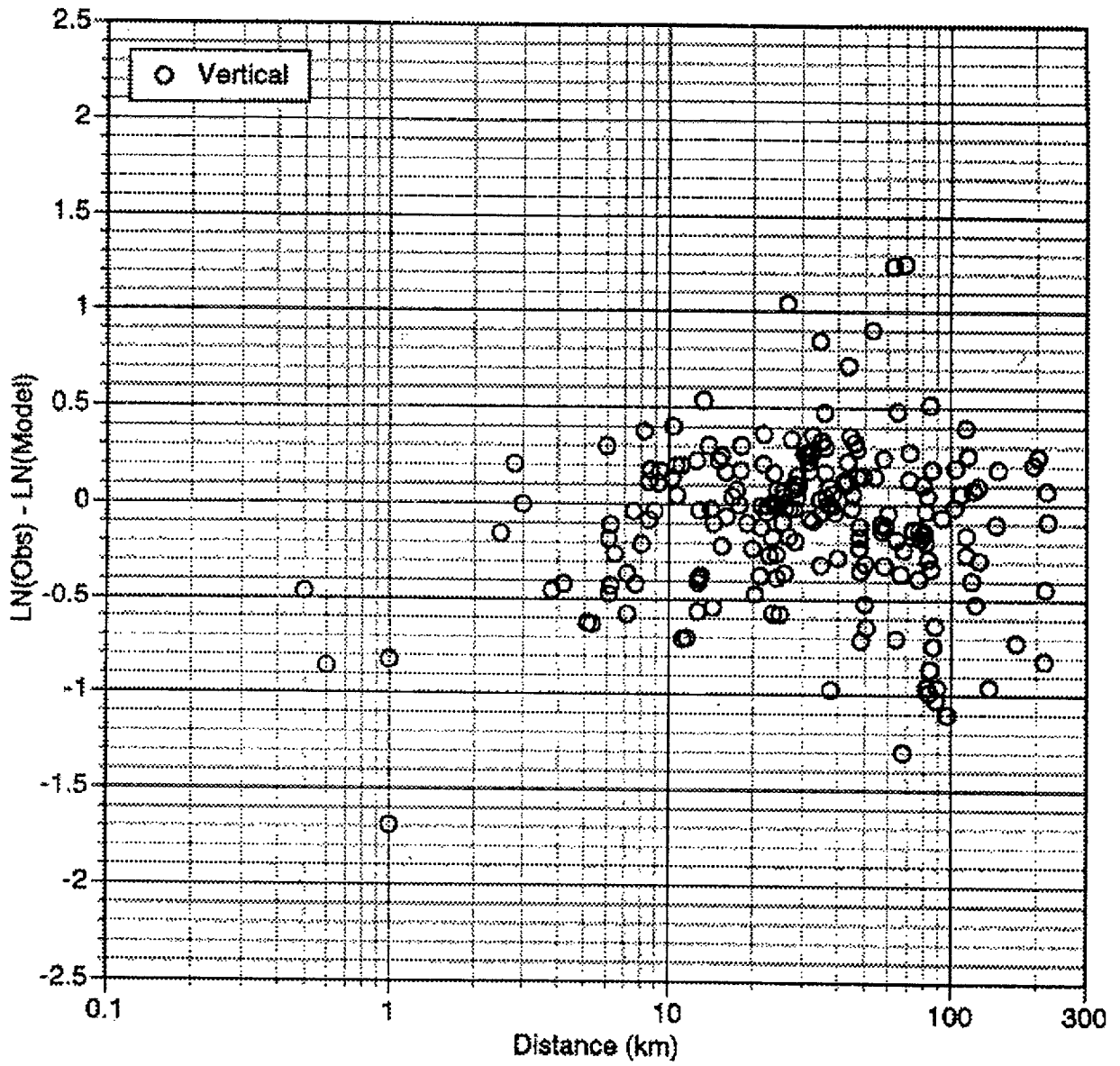


Figure H-7. Vertical residuals for magnitudes between $6.5 < M < 7.0$.

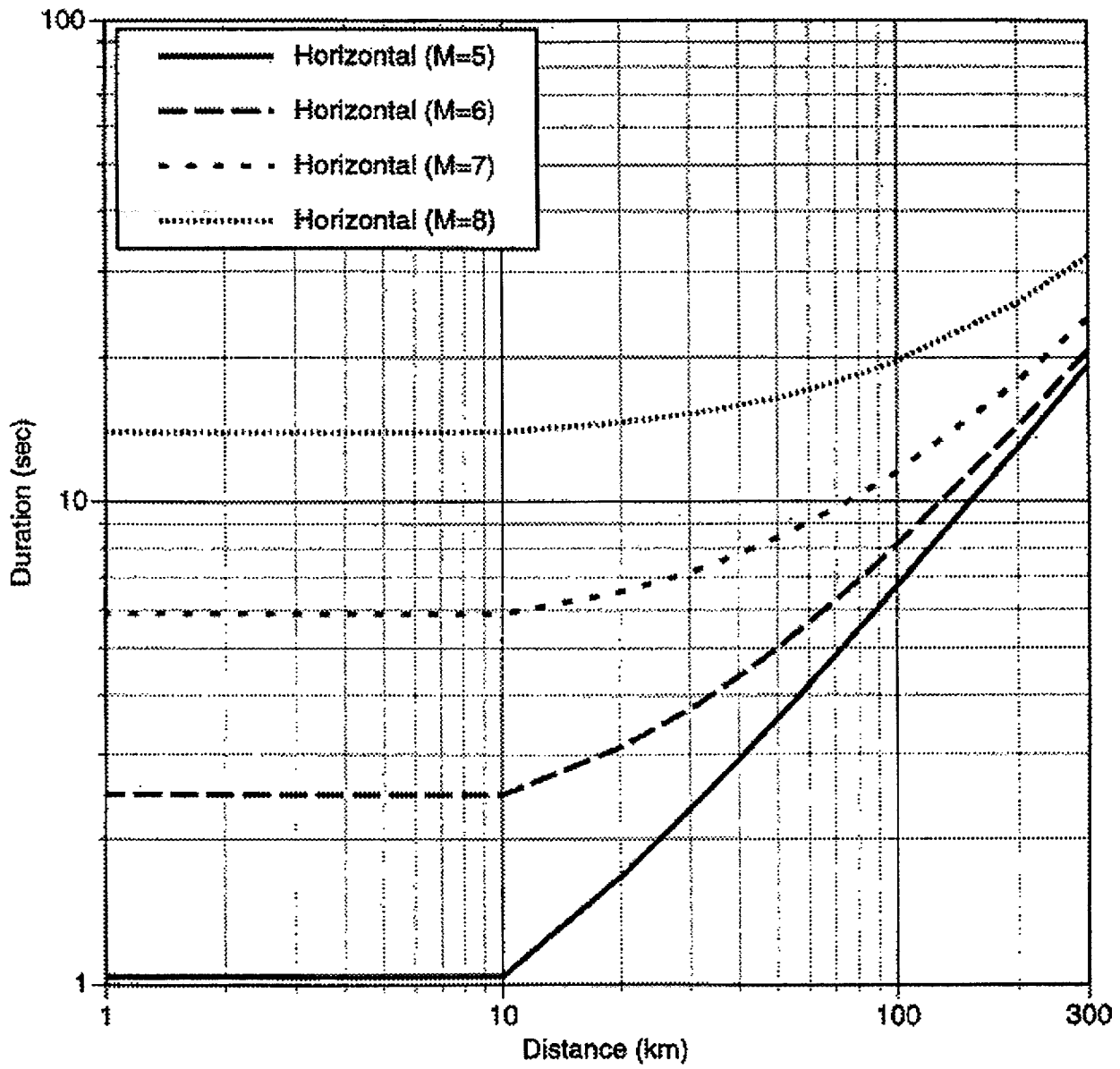


Figure H-8a. Horizontal 5-75% intensity duration model for rock site conditions.

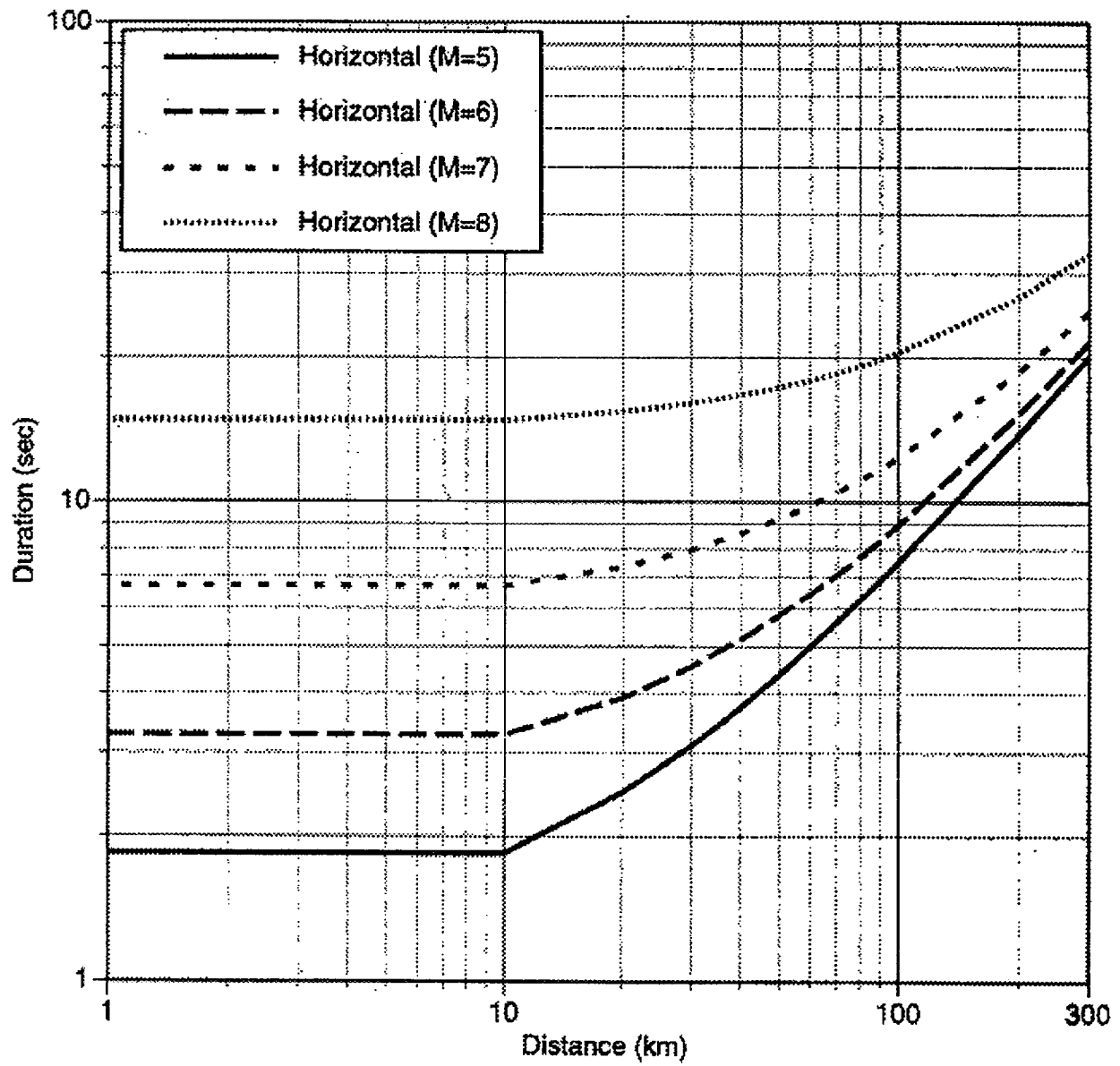


Figure H-8b. Horizontal 5-75% intensity duration model for soil site conditions.

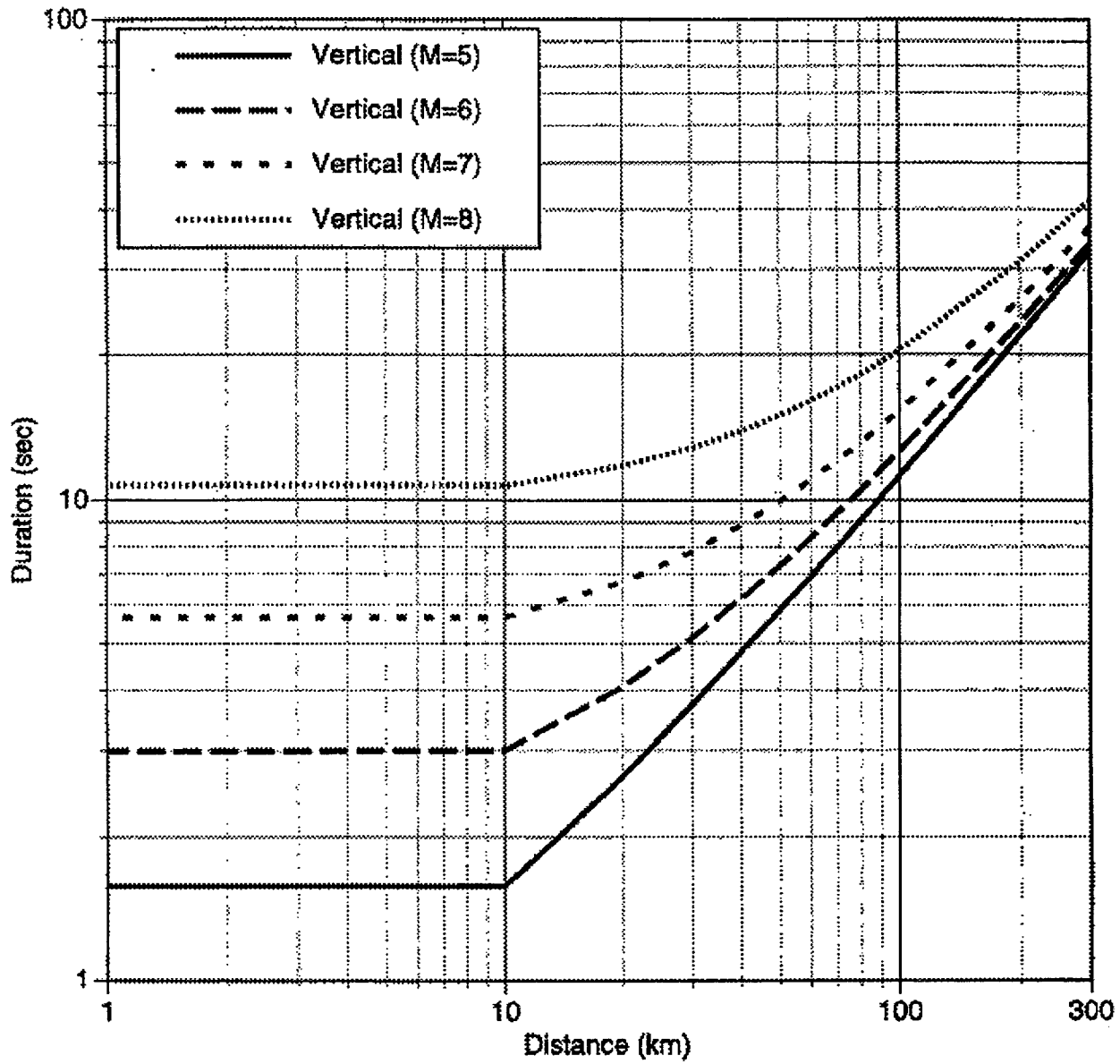


Figure H-8c. Vertical 5-75% intensity duration model for rock site conditions.

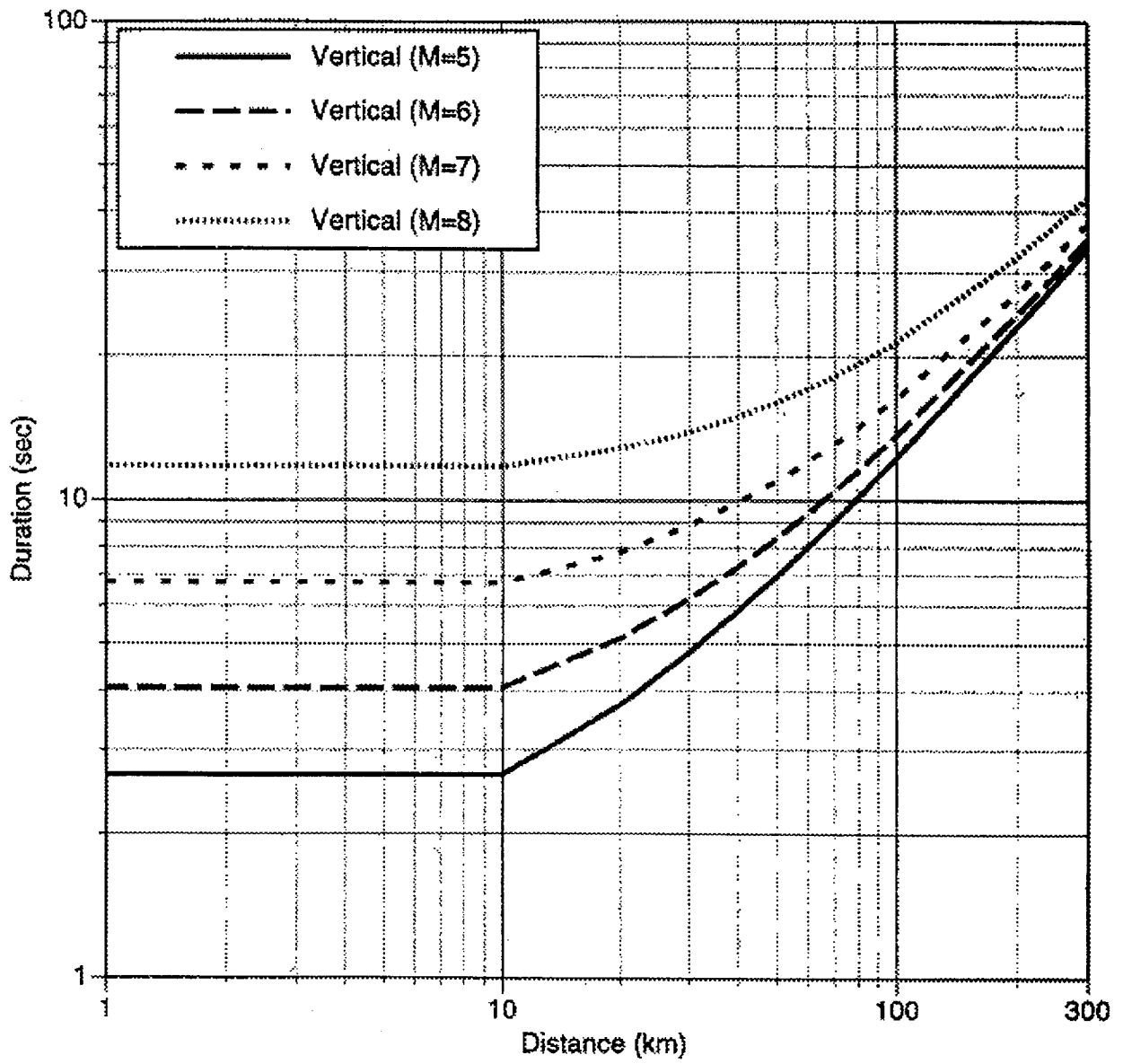


Figure H-8d. Vertical 5-75% intensity duration model for soil site conditions.

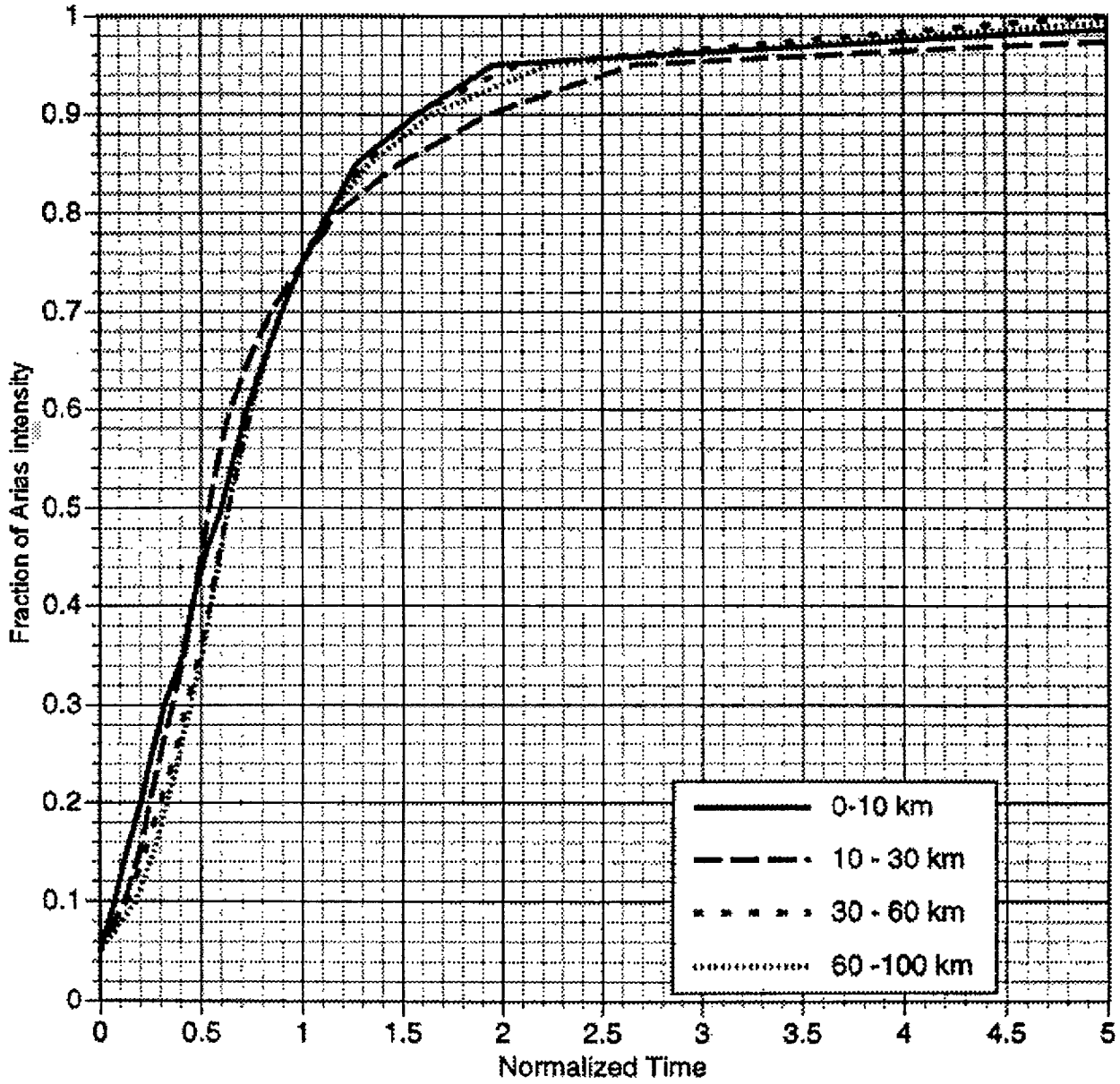


Figure H-9. Mean normalized durations averaged over distance bins for the horizontal component for rock site conditions and $6.5 < M < 7.0$.

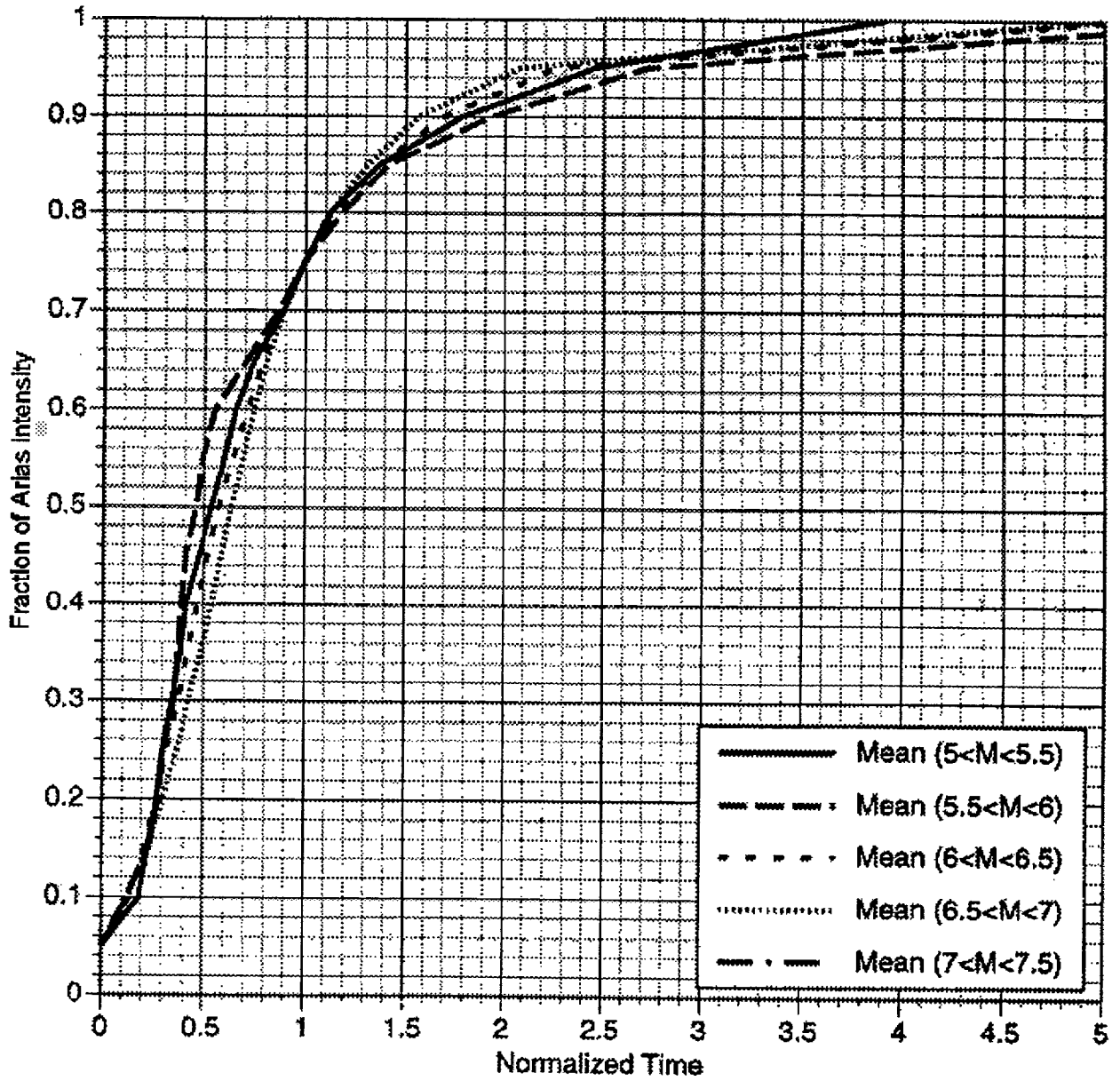


Figure H-10. Mean normalized durations averaged over magnitude bins for the horizontal component for rock site conditions and distance = 30-60 km.

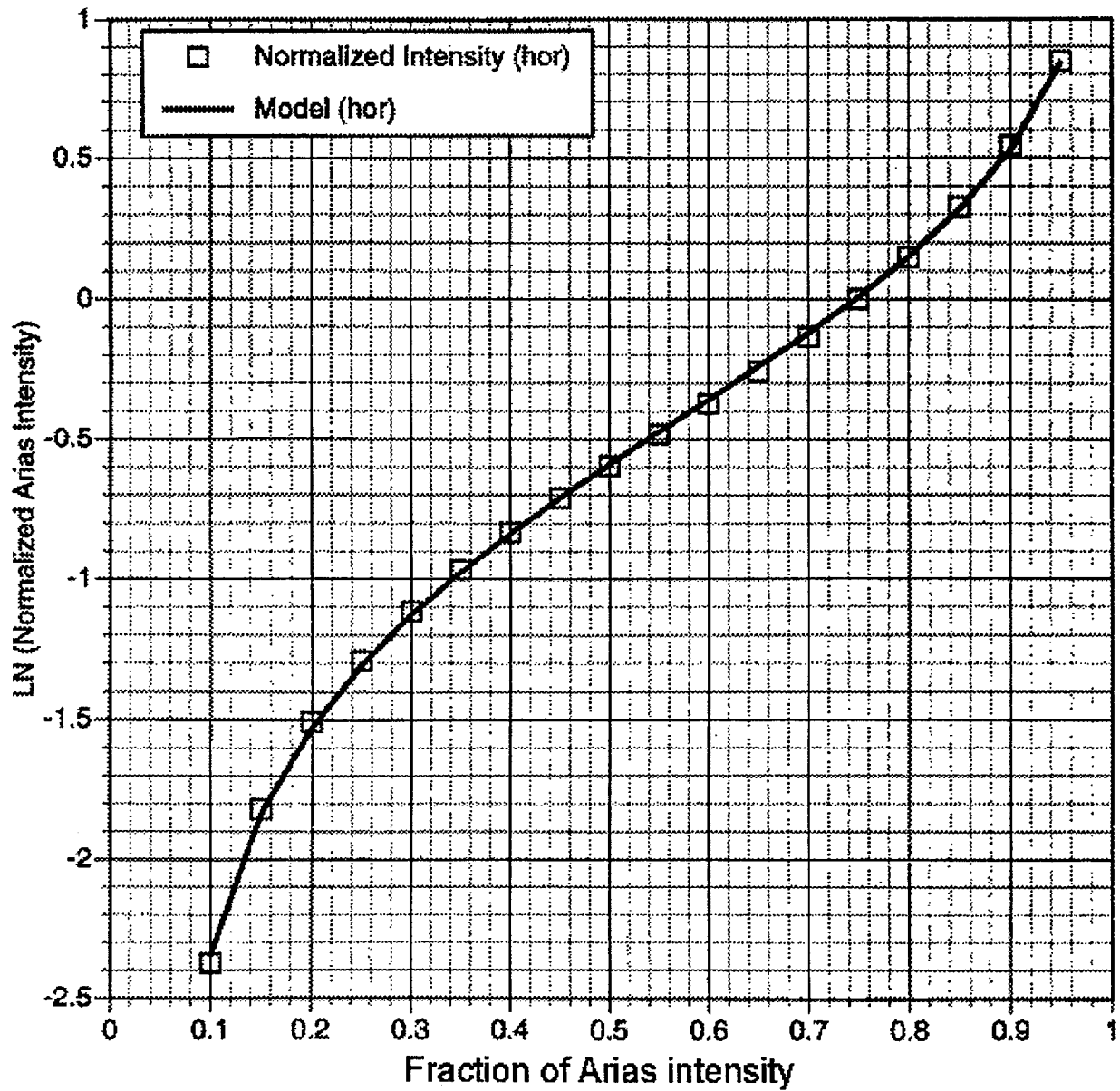


Figure H-11a. Mean predicted model (Equation H-11) compared to the mean of the data for the horizontal component.

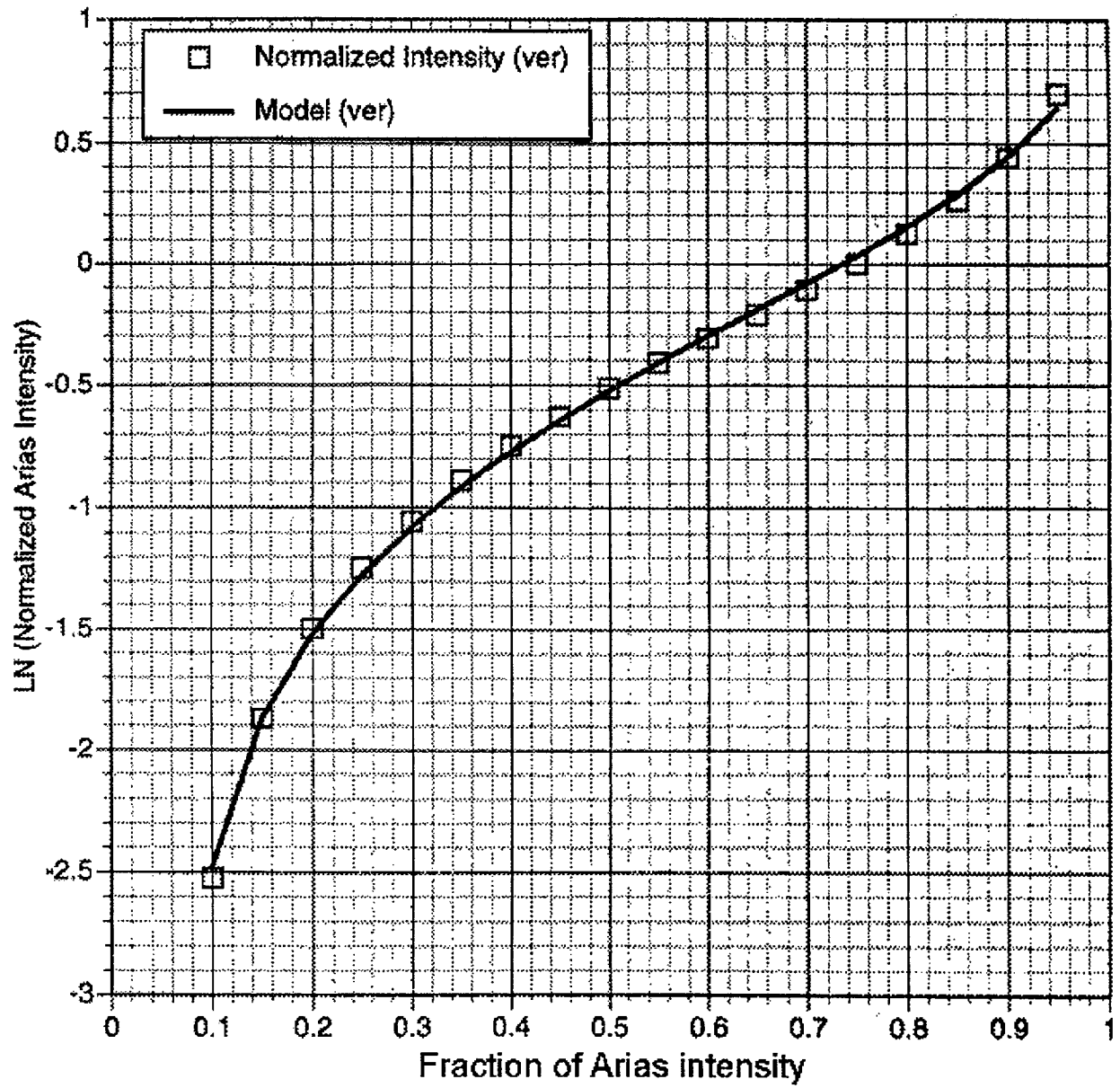


Figure H-11b. Mean predicted model (Equation H-11) compared to the mean of the data for the vertical component.

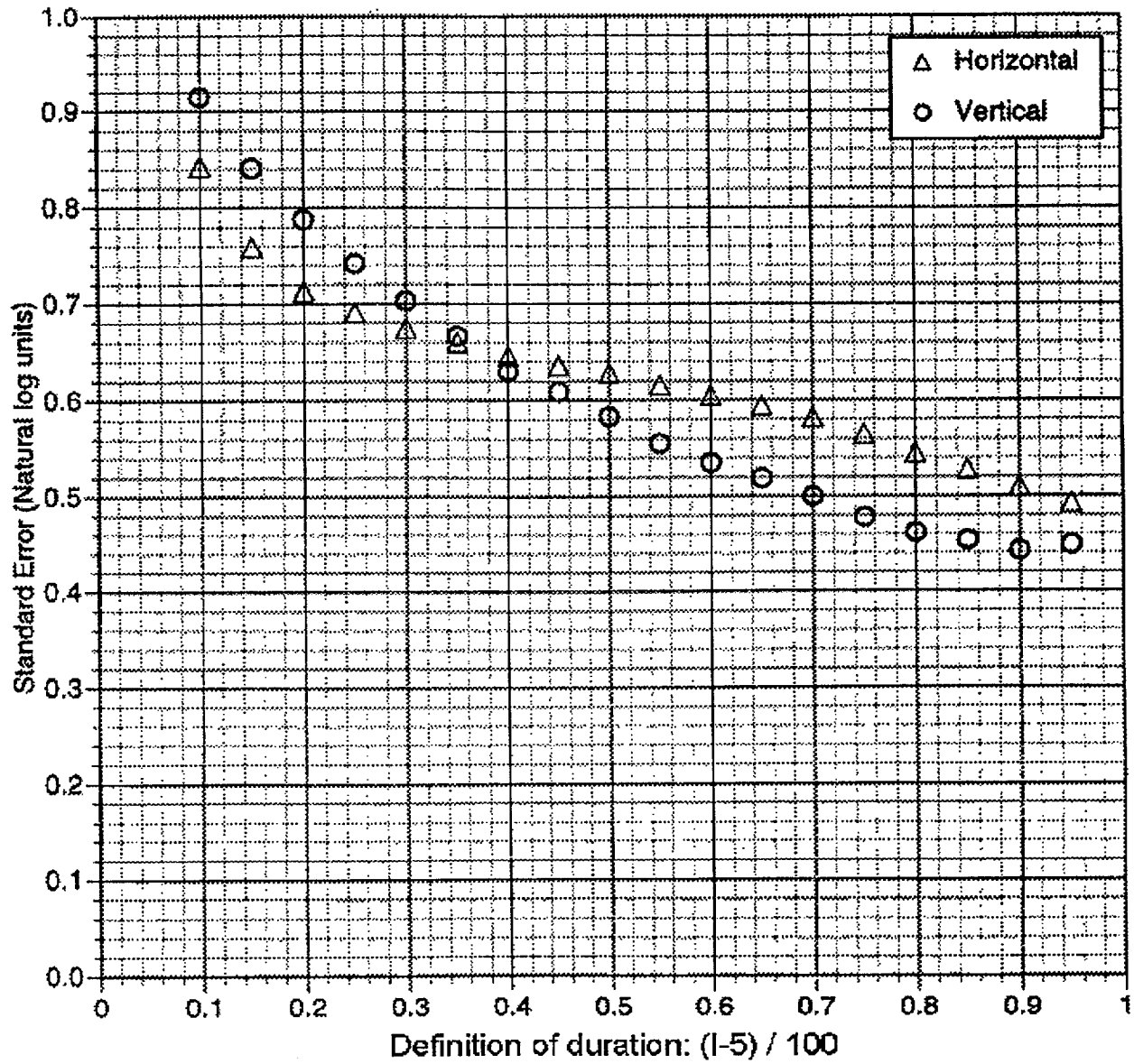


Figure H-12. Standard errors for the horizontal and vertical duration models.

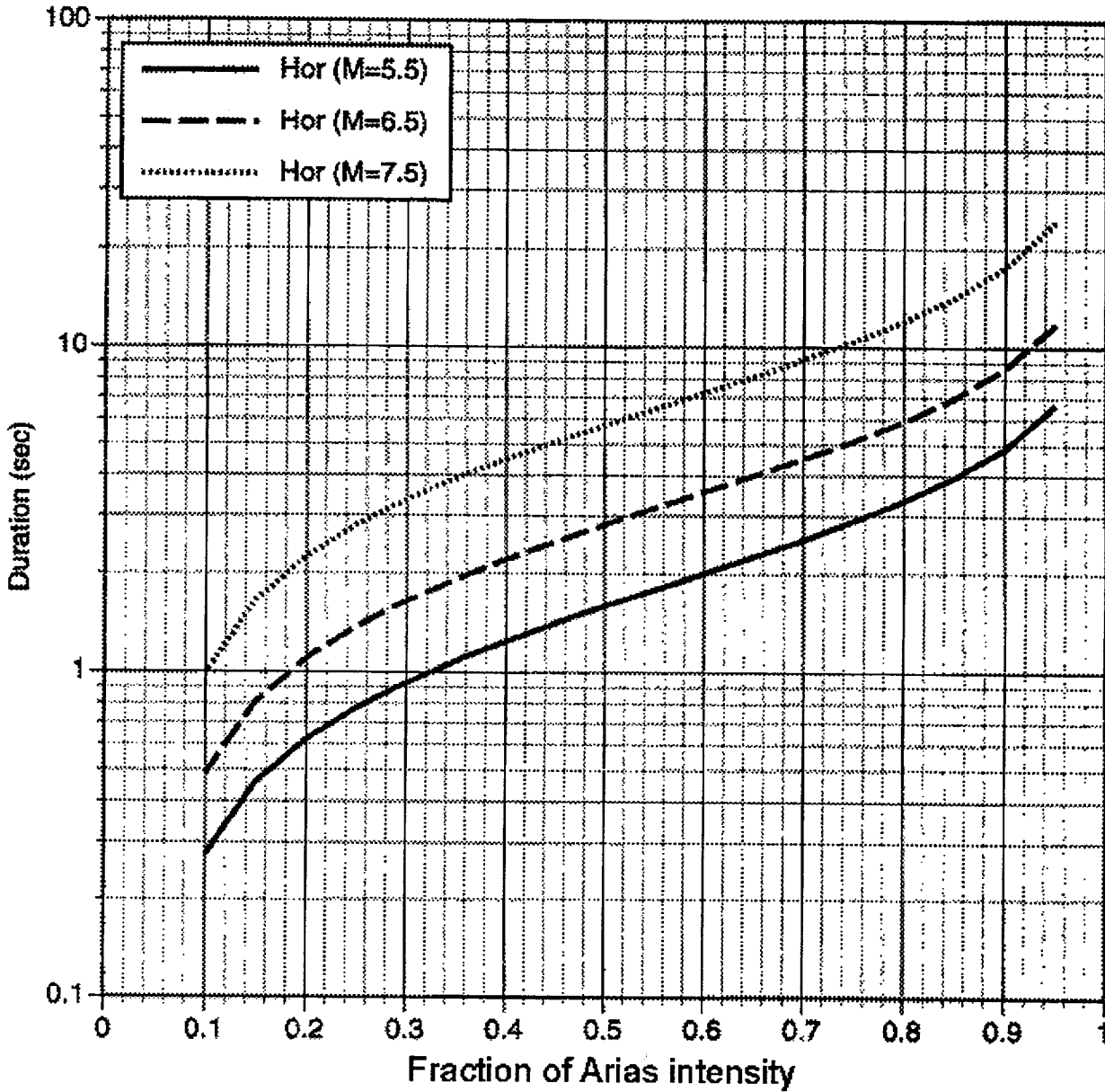


Figure H-13. Duration model for horizontal component for rock site conditions and distance of 30 km.

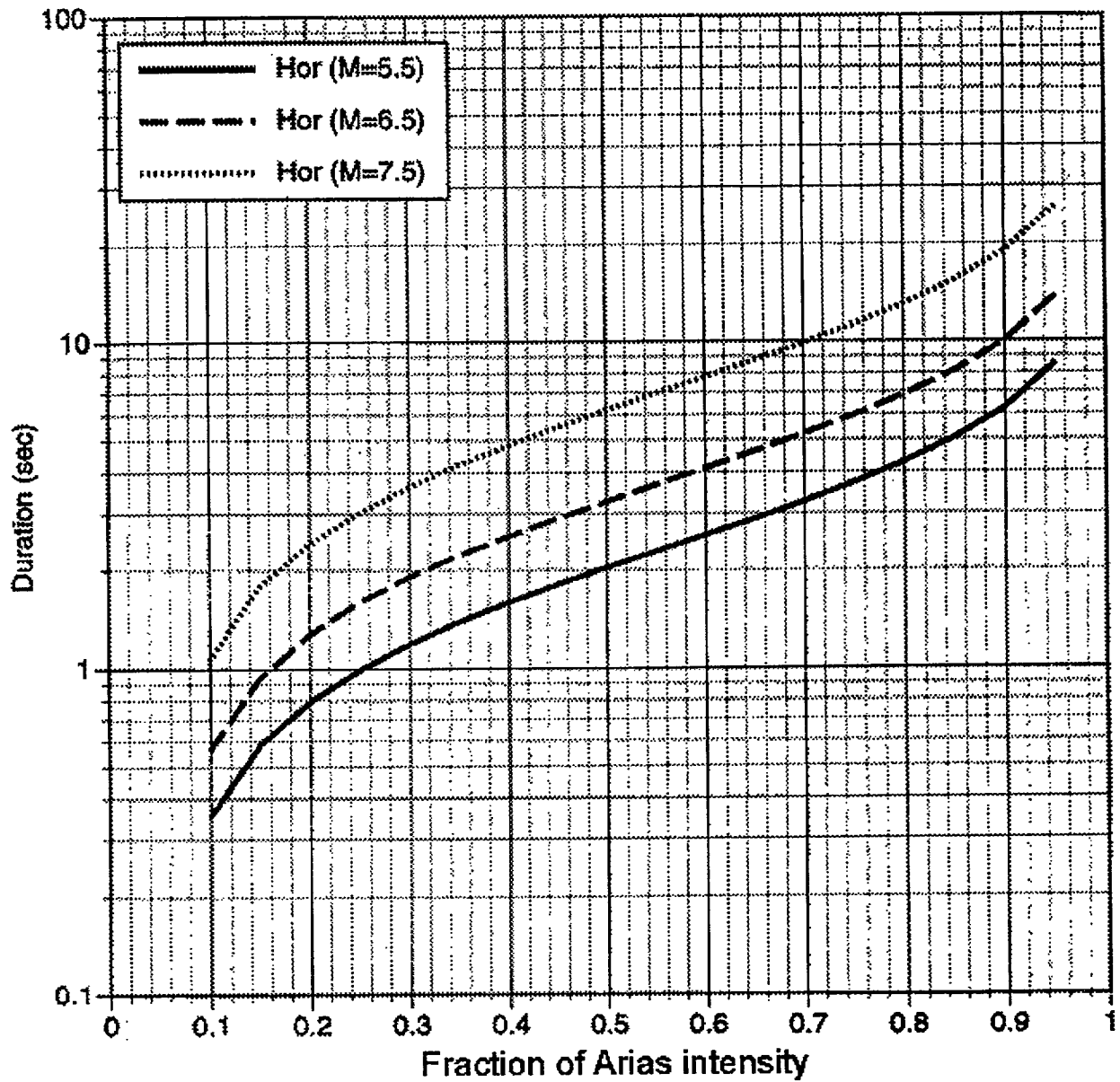


Figure H-14. Duration model for horizontal component for soil site conditions and distance of 30 km.

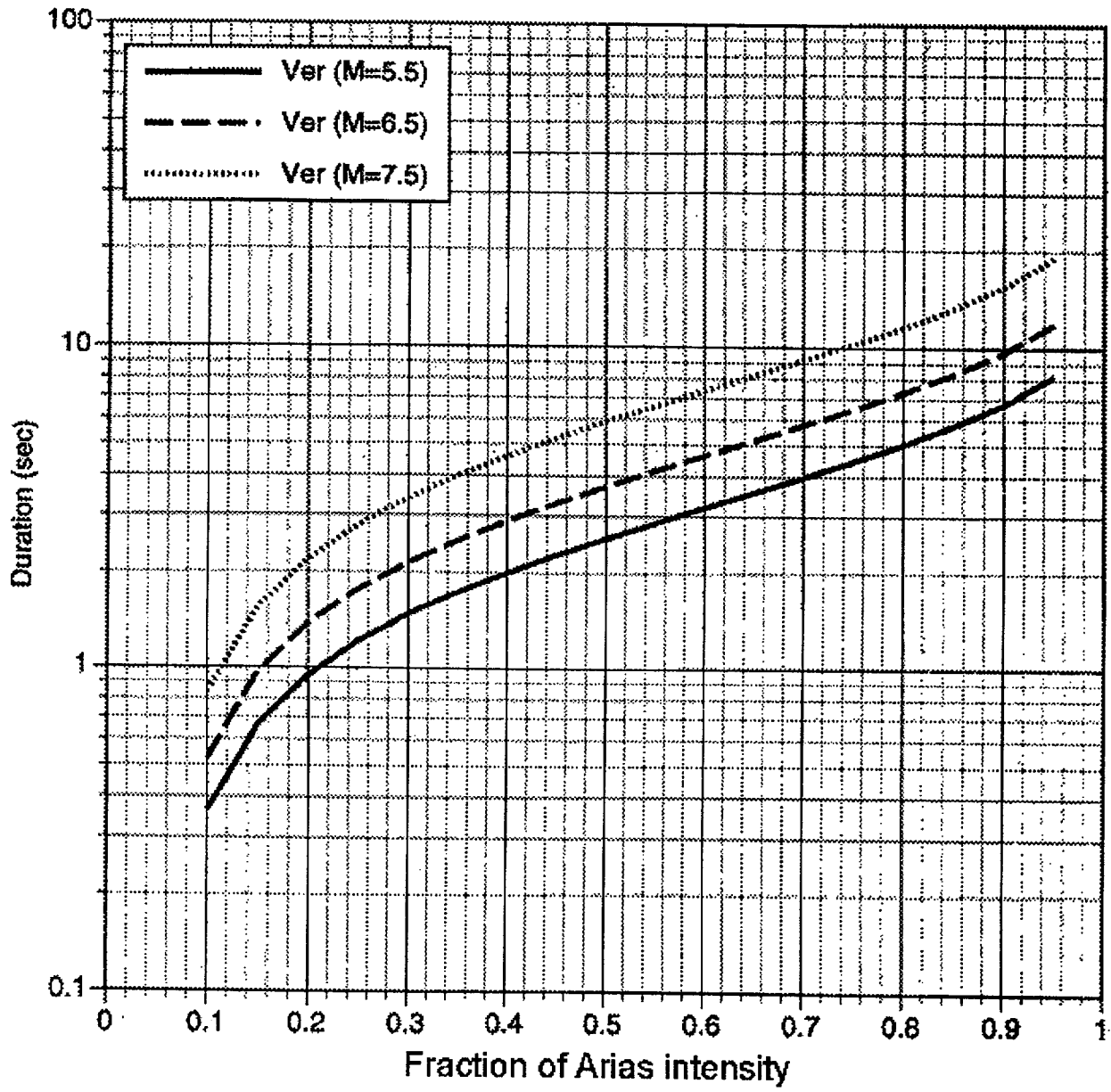


Figure H-15. Duration model for vertical component for rock site conditions and distance of 30 km.

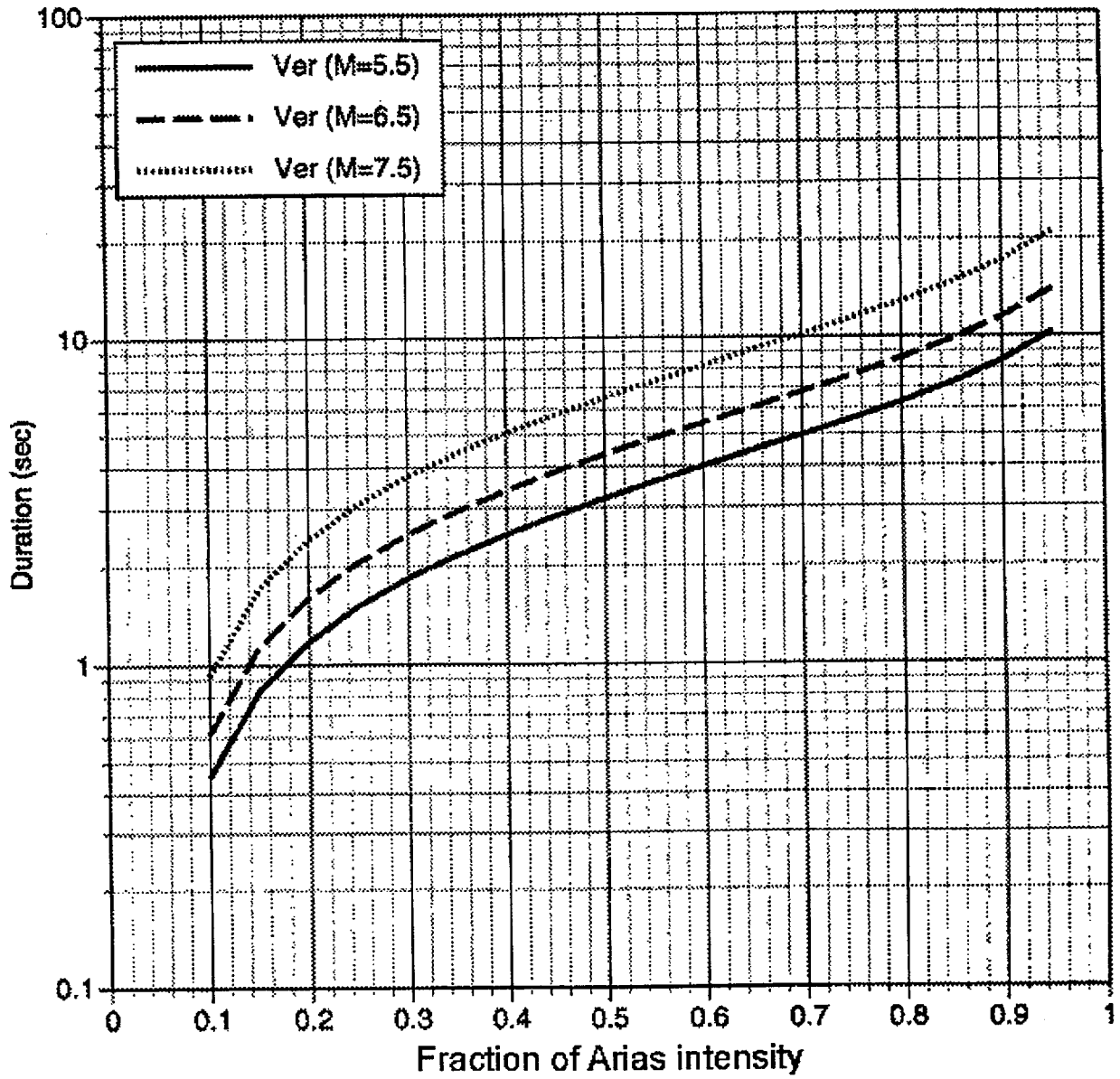


Figure H-16. Duration model for vertical component for soil site conditions and distance of 30 km.

APPENDIX I SITE- AND SOIL-SPECIFIC PSHA FOR NONLINEAR SOIL SITES^a

^a Bazzurro, P., Cornell, C.A., and F. Pelli (1999). "Site- and Soil-specific PSHA for Nonlinear Soil Sites", Proceedings of 2nd International Symposium on Earthquake Resistant Engineering Structures – ERES99, Published by WIT Press, Southampton, UK, Paper No. 27214, 15-17 June, Catania, Italy

I.1 Introduction

The probabilistic site amplification of ground motions has been extensively studied by others.^{5,10,4} The procedure proposed here, however, is fully probabilistic since it includes the variability both in the ground motion and in the soil parameters at the site. Moreover, the soil nonlinear response is evaluated by driving real rock ground motions through a finite element model of the column using a program capable of predicting the pore water pressure build-up and dissipation. In practical applications this method can use a small number of records/runs, as few as ten or less, which is a big advantage if resources and/or "appropriate" records for a site are a major constraint. Results suggest, in fact, that sufficient accuracy is achieved without running many records at many magnitude and distance pairs. This implies that real accelerograms rather than simulated ones can often be used. Two case studies involving both a sandy and clayey soil deposit are discussed here.

I.2 Methodology

For brevity, this section describes only the main features of the methodology. More details can be found in Bazzurro and Cornell.² The effect of the soil on the intensity of the ground motion at the surface is studied in terms of a site-specific, frequency-dependent amplification function, $AF(f)$, where f is a generic oscillator frequency:

$$AF(f) = \frac{S_a^s(f)}{S_a^r(f)} \quad (1)$$

where $S_a^s(f)$ and $S_a^r(f)$ are the 5%-damped spectral acceleration values at the soil surface and at the bedrock, respectively.

The behavior of $AF(f)$ for multiple ground motion records has shown that $S_a^r(f)$ is the most effective predictor variable for estimating $AF(f)$ (at the same frequency f) among different bedrock ground motion parameters, such as magnitude, M , source-to-site distance, R , Peak Ground Acceleration, PGA_r , and spectral acceleration values, $S_a^r(f_{sc})$, at the initial resonant frequency, f_{sc} , of the soil column. Furthermore, results showed that once the $S_a^r(f)$ value of a record at the bedrock is known, the additional knowledge of M and R , which implicitly define its average response spectrum shape, do not appreciably improve the estimation of $AF(f)$ at the same frequency f . In other words, $AF(f)$ conditioned on $S_a^r(f)$ is virtually independent on M and R (see Fig. 4 to come).

The proposed method for computing surface hazard curves for $Z = S_a^s(f)$ convolves the site-specific rock hazard curves for $X = S_a^r(f)$, which may be exogenously provided, with the $Y = AF(f)$ estimates obtained through nonlinear dynamic analyses of the soil. Bazzurro and Cornell² describe also a different but equally effective approach which requires performing a PSHA for the site with

$$P[Z > z] = G_z(z) = \sum_{\text{all } x_j} G_{YX} \left(\frac{z}{x} | X = x_j \right) P[X = x_j]$$

where $G_w(w)$ is the complementary cumulative distribution function (CCDF) of any random variable, W (e.g., $G_z(z)$ is the sought hazard curve for $S_a^s(f)$, i.e., the annual probability of exceeding level z), and $P[X = x_j] = p_X(x_j)$ is the probability that the rock input level is x_j . The latter can be approximately derived by differentiating the rock hazard curve in “discrete” or numerical form. G_{YX} is the CCDF of $AF(f)$, conditional on a rock level amplitude x_j .

Assuming lognormality of Y given X , the G_{YX} is given by:

$$G_{YX} \left(\frac{z}{x} | x_j \right) = \hat{\Phi} \left(\frac{\ln \left[\frac{z}{x} \right] - \ln[\hat{m}_{YX}(x)]}{\sigma_{\ln YX}} \right)$$

in which $\hat{\Phi}(\cdot)$ is the widely tabulated complementary standard Gaussian CDF. Estimates of the distribution parameters of Y , (i.e., the conditional median of Y , \hat{m}_{YX} , and the conditional standard deviation of natural logarithm of Y , $\sigma_{\ln YX}$) can be found by driving a suite of n rock ground motion records through a sample of soil column representations (recall that the soil properties are uncertain) and then regressing, for each frequency f , the values of $\ln Y$ on $\ln X$.

For the two case studies presented later the values of $\sigma_{\ln YX}$ were found to be between 0.2 and 0.35 for *all* oscillator frequencies, f , of interest, and to be virtually independent of the level x_j . When the dependence of $AF(f)$ on $S_a^r(f)$ was *not* considered the $\sigma_{\ln Y}$ values increased from 0.2 to 0.3 (at f around 0.25Hz to 0.5Hz) to 0.6 to 0.7 (at f around 10Hz) and then decreased to approximately 0.5 at infinite f (i.e., PGA).

This reduction in dispersion translates into requiring a smaller number of runs to attain the same accuracy, ζ , in the estimate of the median $AF(f)$. The number of records, n , needed to keep the standard error, σ_{YX} , of the regression line within a specified ζ is given by $n = [\sigma_{YX}/\zeta]^2$. To achieve $\zeta = 10\%$ only ten analyses are sufficient.

I.3 Applications

I.3.1 Ground Motion Database

For validating the procedure, we used a large database of 78 free-field surface rock strong ground motions from 28 different earthquakes that occurred worldwide between 1966 and 1995. It is emphasized again, however, that in real applications only about 10 records would be needed. The magnitude range is between $M5$ and $M7.4$, while the shortest distances to the rupture are between 0km and 142km. Approximately 40% of such accelerograms were recorded during three earthquakes: the Loma Prieta (1989), Landers (1992), and Northridge (1994) events in California. This concentration, however, does not statistically affect the results of the amplification analyses. In the amplification study we chose at random one horizontal component of each recording (Fig. 1). The PGA, values range from 0.01g to 1.5g. These seismograms, which contain “true” signal up to a

period of at least 5 seconds, were applied directly at the base of the soil column without any prior deconvolution. This assumption, which implies same rock outcrop and bedrock motions, is known to underestimate the motion at the column base above a site-dependent f value usually around 2Hz.⁸ Deconvolution was not performed because a possible underestimation of the amplification at high f is not crucial for the majority of longer period structures (e.g, taller buildings, bridges, offshore platforms, etc.) which may warrant a detailed soil amplification study like the one proposed here.

I.3.2 Soil Amplification Software and Soil Modeling

The computer program adopted for computing the soil site effects is a modified version of the finite element program SUMDES,⁶ which is based on the effective stress principle, vectored motion, transient pore fluid movement, and generalized material stiffness formulation. Unlike SHAKE,⁷ SUMDES is capable of predicting the pore pressure build-up and dissipation and can adequately describe liquefaction and cyclic mobility phenomena. We used a inelastic constitutive reduced-order bounding surface model which is a special version of the hypoplasticity model with fewer material parameters. The boundary conditions (i.e., elastic base) were chosen to accommodate the rock-outcrop nature of the input.

Both soil deposits are located in the Mediterranean Sea. The sandy deposit consists of sands and gravels with occasional presence of cobbles. The relative density is between 60 and 80% and the total unit weight is 20kN/m³. The behavior of this sand under undrained shear is dilative and the effect of pore pressure build-up and cyclic mobility can be relevant. This effect tends to soften the soil by increasing the shear strain level at which dilation occurs. The clayey deposit is cohesive (silts and clays) and soft with both normally and overconsolidated layers. The shear modulus at small strain levels, G_{max} , was established based on both shear wave velocity, V_s , measurements and on correlations between the cone (CPT) tip resistance and V_s . The G/G_{max} versus shear strain curves were obtained from Li *et al.*.⁶

In both cases, a soil column of 100m was modeled using 100 elements of one meter of thickness each. The median V_s increases from 80m/sec below the mudline to 400m/sec at 100m of depth. The variability in the soil properties was included through a Monte Carlo approach by randomly varying the coefficient of permeability (π_0), the shear and the compression viscous damping ratios at 1Hz (ξ_s and ξ_c), the coefficient of lateral earth pressure at rest (K_0), the coefficient, G_0 , which defines the elastic shear modulus G_{max} at very low strain levels, the friction angle, Φ_0 , and the shear strain value, $\gamma_{64\%}$, at 64% of G_{max} . The seven basic RVs above were considered lognormally distributed with σ_{lnRV} equal to 0.25 for ξ_s , ξ_c , K_0 and G_0 ; to 0.1 for Φ_0 ; to 0.35 for $\gamma_{64\%}$, and to 0.7 for π_0 . A distribution truncation at $2\sigma_{lnRV}$ was included to prevent unrealistic parameter values.

The spatial correlation among layers was characterized by a first-order auto-regressive model,⁹ with lag-one correlation coefficient equal to 0.58. The thickness of each layer is not considered random. *Within each layer* perfect positive correlation is assumed for Φ_0 , G_0 and $\gamma_{64\%}$ and all three are considered to be perfectly negatively correlated with both ξ_s and ξ_c . K_0 and Φ_0 are assumed to be independent of all other RVs.

I.3.3 Amplification Study Results

For both soil deposits, each one of the 78 records was driven through a different realization of the soil column. The 78 amplification functions are displayed in Fig. 2. The two wide peaks (at $f_{sc}=0.8\text{Hz}$ and 2Hz) identify the first two soil resonant frequencies. At f_{sc} the two soil columns amplify on average more than three and four times the spectral acceleration at the bedrock, $S_a^r(f_{sc})$, while PGA_r is amplified on average by 40% and 100%.

$AF(f)$ displays a large variability particularly in the high frequency range (see solid lines in Fig. 4 to come). Some of the records induce a highly nonlinear behavior in the soil deposit with associated large deformations and the corresponding $AF(f)$ do not exhibit the peaks mentioned above.

On the other hand, other records have $AF(f)$ well above one for the entire frequency range. This discrepancy is due to the difference both in intensities of the input ground motions and in the “strengths” of different realizations of the soil column. When the intensity increases (i.e., increasing values of M , PGA_r , and $S_a^r(f)$, and decreasing values of R) the $AF(f)$ tends to diminish in amplitude and to flatten out, and f_{sc} systematically decreases towards lower f values. The dependence of $AF(f)$ on $S_a^r(f)$ (i.e., locally at the same frequency, f) can be appreciated from Fig. 3. The negative correlation is statistically significant at frequencies around f_{sc} and above. It is emphasized that nonlinear soil responses at frequencies above 2Hz have been recently observed.³

Fig. 4 shows the predictive power of different combinations of four bedrock ground motion intensity measures (M , R , $S_a^r(f)$, and PGA_r) in terms of the standard error of estimation, $\sigma_{\ln AF(f)}$. For comparison, we included the unconditional $\sigma_{\ln AF(f)}$ curve, which describes the total variation in $AF(f)$ from Fig. 2 when no regression is done. The similarities between the two sites is remarkable. M and R , even when coupled with PGA_r , yield a higher error than $S_a^r(f)$ alone.

Hence to predict $AF(f)$ it is more informative to know $S_a^r(f)$ than M , R and PGA_r . When $S_a^r(f)$ is already included in the regression function the extra explanatory power provided by M (which carries information about the spectral shape) is negligible (compare 3rd and 4th model). In different words, $AF(f)$ conditional on $S_a^r(f)$ is virtually independent of M . The most important consequence, however, is that, given the low values of $\sigma_{\ln AF(f) | \ln S_a^r(f)}$, the median $AF(f)$ can be estimated within 10% for all frequencies with the knowledge of $S_a^r(f)$ from only ten response analyses. Although record selection with no attention to M and R is always to be discouraged, these results show that there is no apparent predictive benefit in keeping the explicit dependence of M and R . During the selection more care should be devoted to ensure a wide range of $S_a^r(f)$ for f values of interest rather than in selecting records with the most appropriate M and R values for the region around the site. Finally results not shown here for brevity,² indicate that the portion of $\sigma_{\ln AF(f)}$ due to the uncertainty in the soil properties is of secondary importance with respect to that due to record-to-record variability.

I.3.4 PSHA Results

The two soil deposits were assumed to be located in the Santa Barbara Channel (SBC) (Fig. 5), Southern California, for which a seismotectonic model was readily available. The site hazard was

readily available. The site hazard was computed both by a conventional PSHA approach with the Abrahamson and Silva¹ attenuation law for generic soil conditions, and by the proposed convolution method applied to both soil deposits. The latter method makes use of the rock hazard curves found using the same attenuation relation¹. The median $AF(f)$ in Fig 3 and the $\sigma_{\ln AF(f)}$ values in Fig 4 were used to estimate $S_a^s(f)$. The UHS displayed in Fig. 6 show that using a generic soil attenuation law may lead to severe underestimation of the hazard for $S_a^s(f)$ below approximately $f=2\text{Hz}$ at low MRP values. The hazard at high frequencies (here above 2Hz) is overestimated by the predictive equation for generic soil conditions especially at high MRP values. The gap at high frequencies between the UHS found by convolution and by conventional PSHA, however, may be partly due to the application of rock outcrop motions directly to the column base. These differences in hazard prediction are due to the significant nonlinear response (Fig. 3) of the two soil columns considered in this study.

I.4 Summary and Conclusions

Two applications of a practical soil- and site-specific PSHA method have been presented in this paper. Soil surface hazard estimates more precise than those provided by attenuation equations for generic soil conditions can be found by explicitly considering the nonlinear behavior of the deposit via an amplification function. The dynamic behavior of the soil at all oscillator frequencies can be accurately predicted with as few as ten ground motions which may be selected without particular attention to specific scenario events (i.e., M and R pairs) representing the hazard at the site. Each record is run through a different characterization of the soil column to account for uncertainty in the soil parameters. This effect is minor.

References

- Abrahamson, N.A., W.J. Silva, "Empirical Response Spectra Attenuation Relations for Shallow Crustal Earthquakes," *Seism. Res. Lett.*, 68 (1), pp. 94-127, 1997.
- Bazzurro, P., C.A. Cornell, "Efficient PSHA for Nonlinear Soil Sites with Uncertain Properties," submitted to *Journ. Of Geotech. And Geoenvironmental Engineering*, ASCE, 1999.
- Beresnev, I.A, G.M. Atkinson, P.A. Johnson, E.H. Field, "Stochastic Finite-Fault Modeling of Ground Motions from the 1994 Northridge, California, Earthquake," *II. Widespread Nonlinear Response at Soil Sites*, *BSSA*, 88(6), pp 1402-1410, 1998.
- Electric Power Research Institute (EPRI), "Guidelines for Site Specific Ground Motions," Rept. TR-102293, Vol. 1-5, Palo Alto, CA, November 1993.
- Faccioli, E., "A Stochastic Approach to Soil Amplification," *BSSA*, 66(4), pp. 1277-1291, 1976.
- Li, X.S., Z.L. Wang, C.K. Shen, "SUMDES - A Nonlinear procedure for Response Analysis of Horizontally-layered Sites Subjected to Multi-directional Earthquake Loading," Dept. of Civil Engineering, University of California, Davis, March 1992.

- Schnabel, P., H.B. Seed, J. Lysmer, "Modification of Seismograph Records for Effect of Local Soil Conditions," *B.S.S.A.*, 62, pp. 1649-1664, 1972.
- Steidl, J.H., A.G. Tumarkin, R.J. Archuleta, "What is a Reference Site?", *B.S.S.A.*, 86(6), pp. 1733-1748, 1996.
- Toro, G. "Probabilistic model of soil-profile Variability-Guidelines for Determining Design Basis Ground Motions," ed. J.F. Schneider, Electric Power Research Institute, EPRI TR-102293, Vol. 2, App. 6A, 1993.
- Whitman, R.V., J.N. Protonotarios, "Inelastic Response to Site-modified Ground Motions," *Journal of the Geotechnical Engineering Division*, ASCE, 103 (10), pp. 1037-1053, 1977.

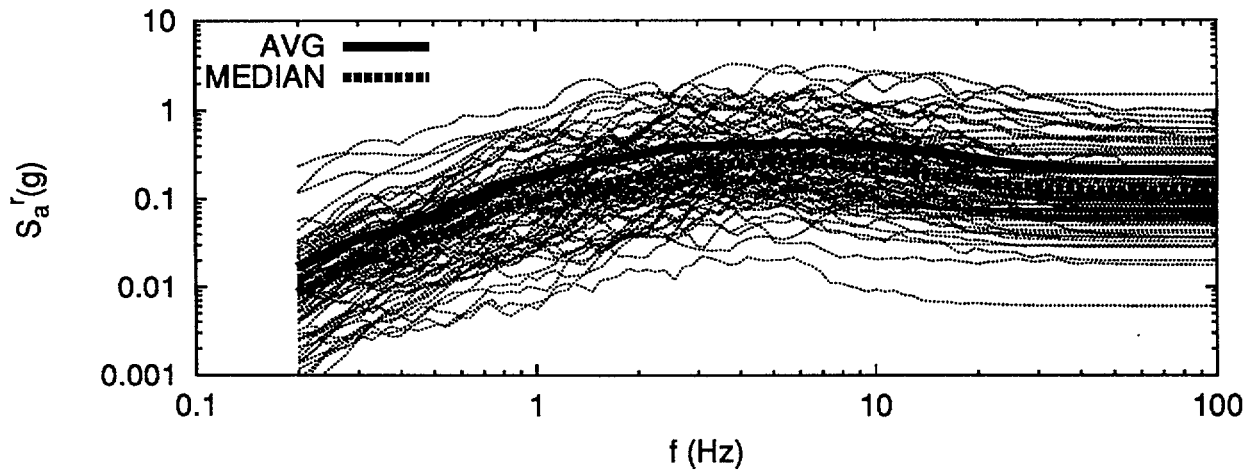


Figure I-1: Response spectra for 5% of damping of the selected records.

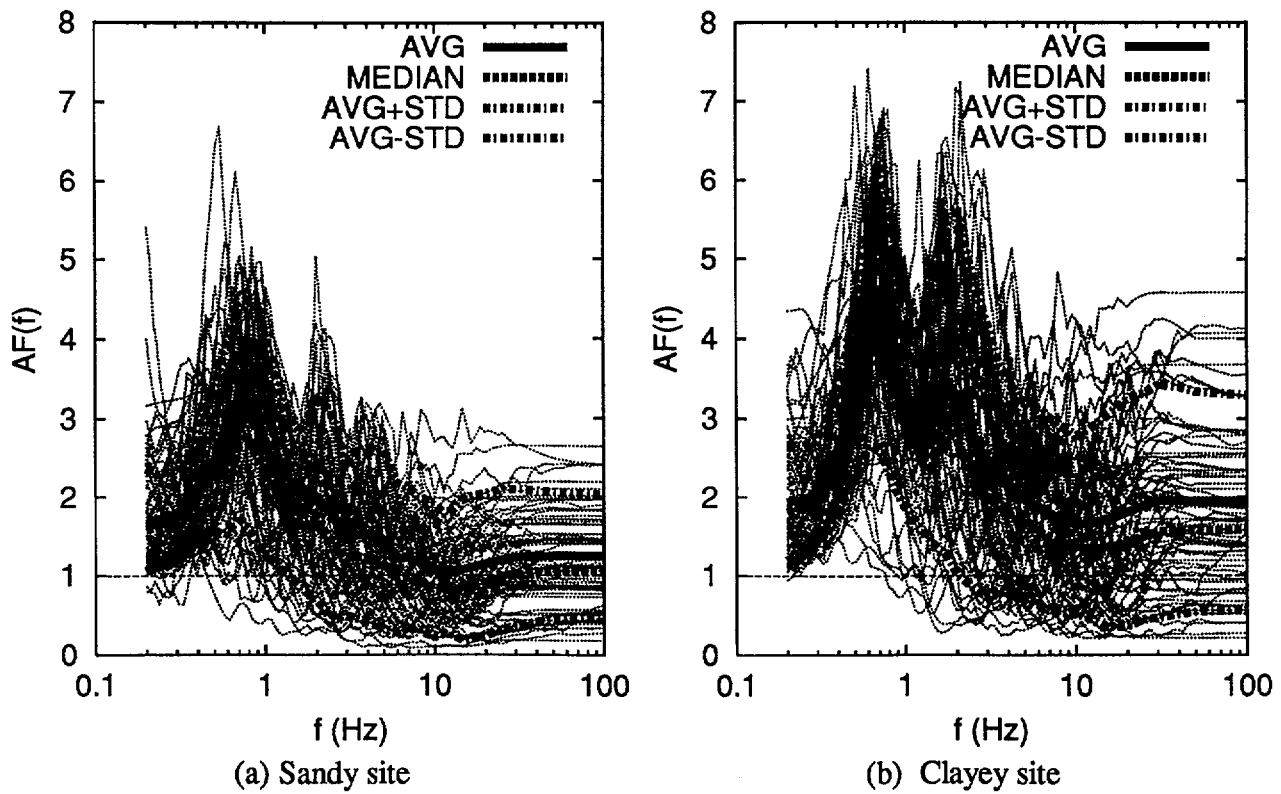
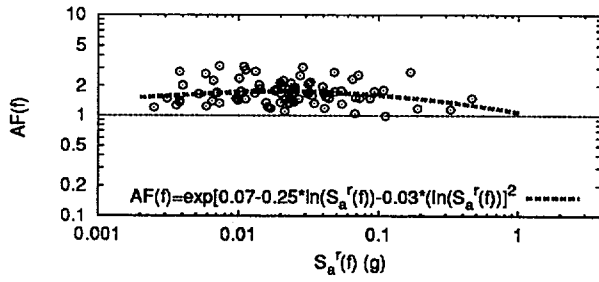
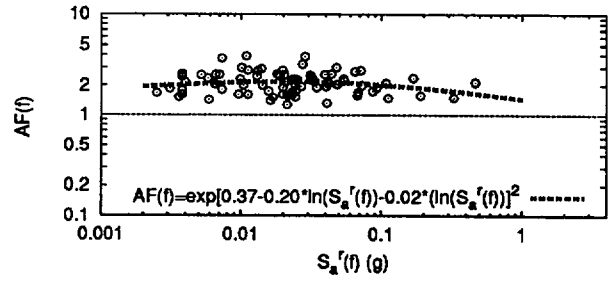


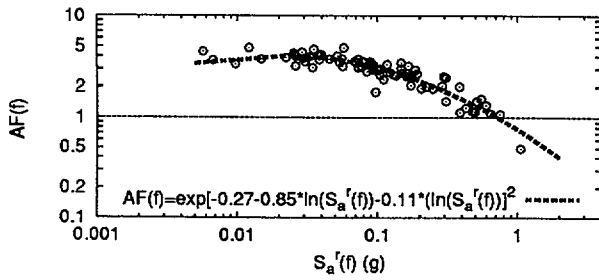
Figure I-2: Amplification function for both soil deposits.



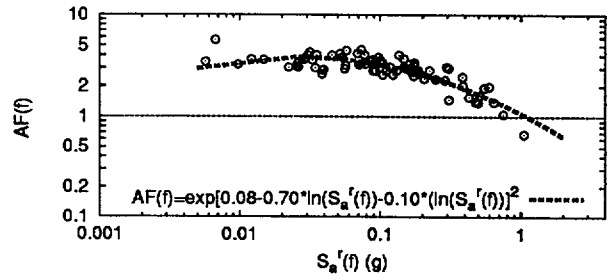
(a) Sand: $f=0.33\text{Hz}$



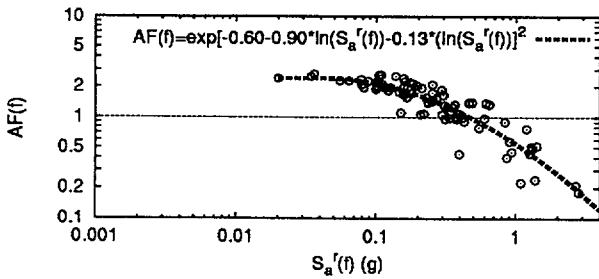
(b) Clay: $f=0.33\text{Hz}$



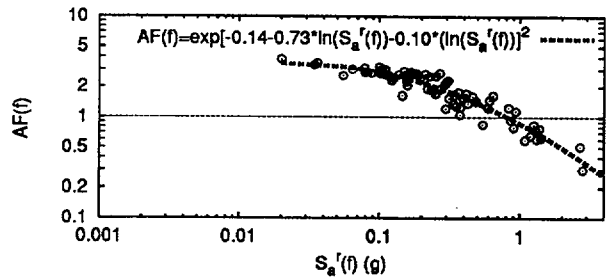
(c) Sand: $f=1.0\text{Hz}$



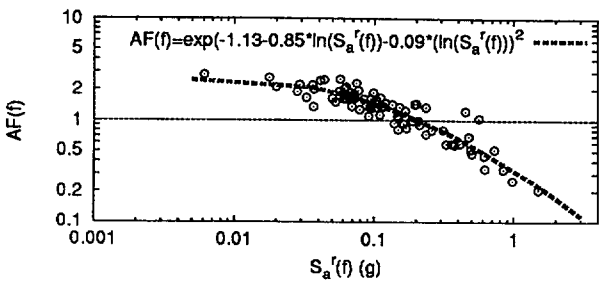
(d) Clay: $f=1.0\text{Hz}$



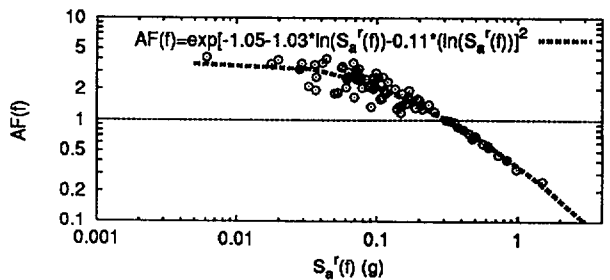
(e) Sand: $f=5.0\text{Hz}$



(f) Clay: $f=5.0\text{Hz}$



(g) Sand: PGA_r (100Hz)



(h) Clay: PGA_r (100Hz)

Figure I-3: Regression of $AF(f)$ on $S_a^r(f)$ at different f values for both soil deposits.

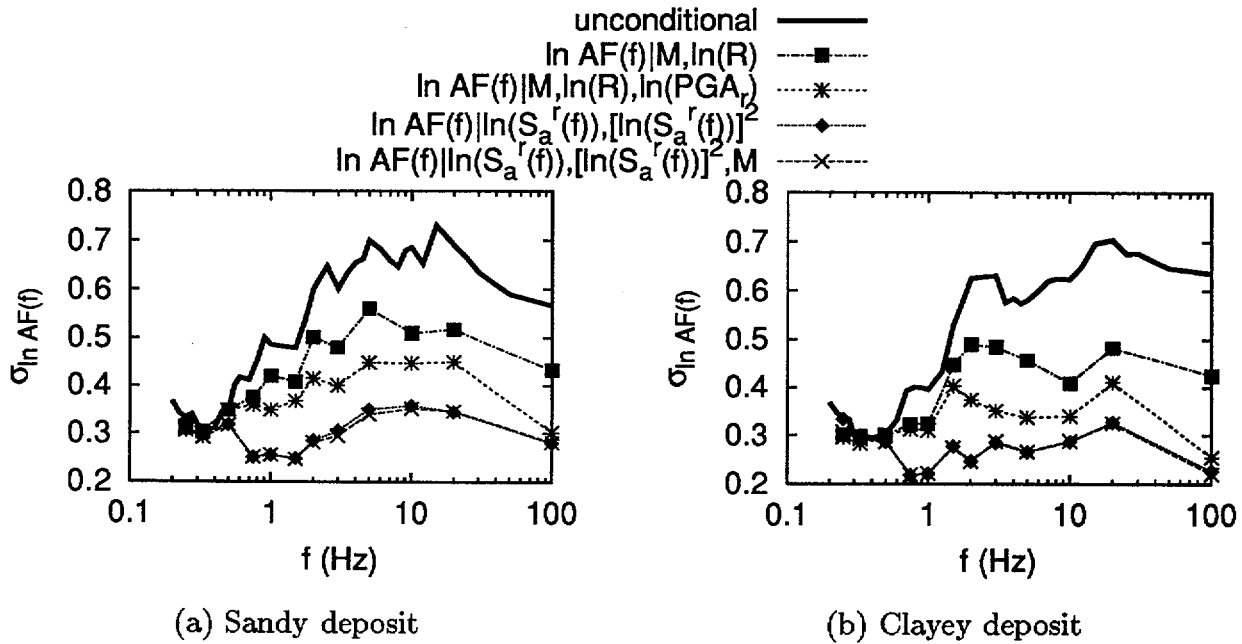


Figure I-4: Regression of $AF(f)$, on M , R , $S_a^r(f)$, and PGA_r .

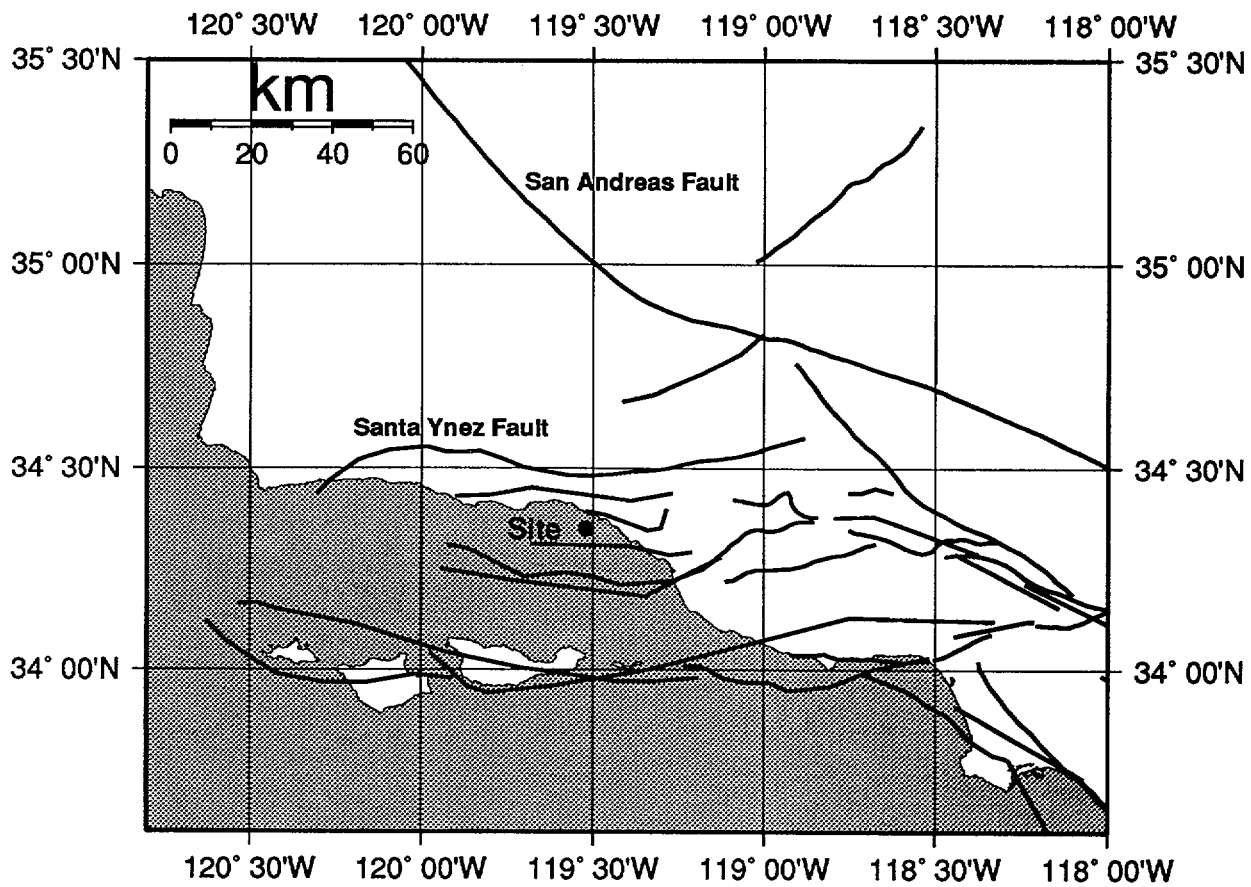
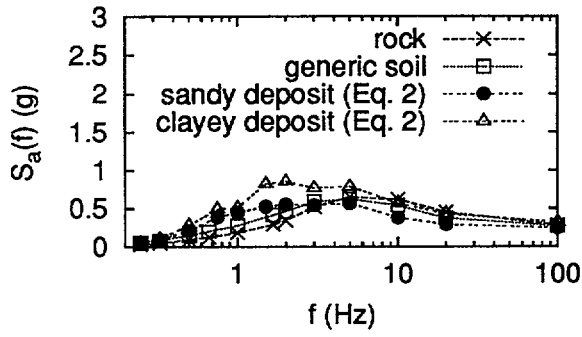
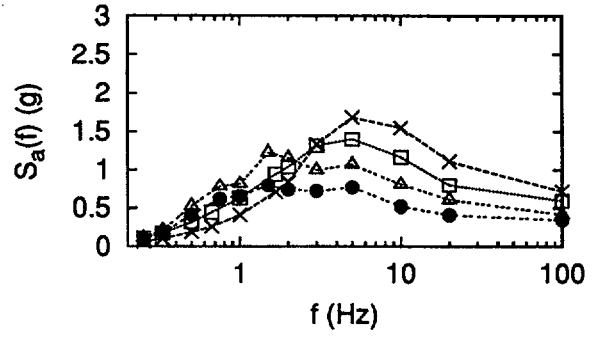


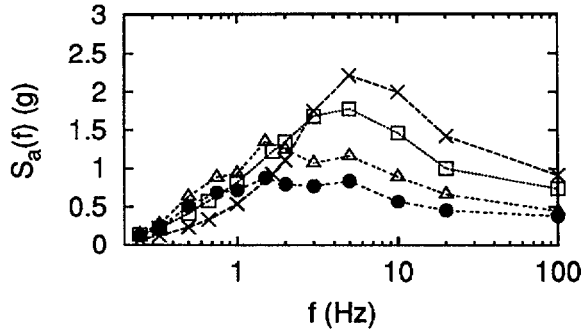
Figure I-5: Location of the site in the Santa Barbara Channel.



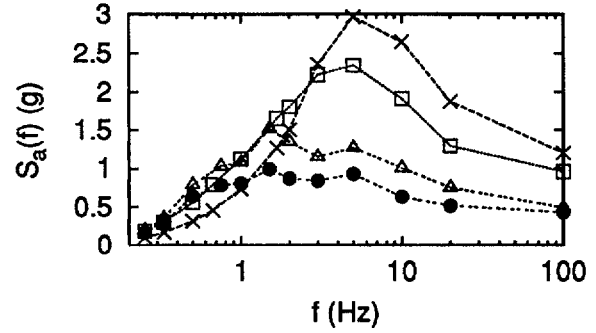
(a) PE=50%/50yrs (MRP=72yrs)



(b) PE=10%/50yrs (MRP=475yrs)



(c) PE=5%/50yrs (MRP=975yrs)



(d) PE=2%/50yrs (MRP=2475yrs)

Figure I-6: Uniform Hazard Spectra (UHS) for the SBC site. (PE=Probability of Exceedence; MRP=Mean Return Period.)

APPENDIX J CHARACTERISTICS OF VERTICAL STRONG GROUND MOTIONS FOR APPLICATIONS TO ENGINEERING DESIGN

J.1 Introduction

In the near-source region (distance $R \leq 10$ to 15 km) of large earthquakes, the characteristics of strong ground motions change in stable and predictable ways. Durations become significantly shorter (Chang et al., 1996; Abrahamson and Silva, 1997), velocity and displacement time histories increase significantly in amplitude and become more pulse-like (depending upon rupture directivity effects), long period fault normal motions show a stable increase over fault parallel motions (Somerville et al., 1997), and short period vertical motions can exceed horizontal motions (Niazi and Bozorgnia, 1991; Bozorgnia et al., 1995) at both rock and soil sites (EPRI, 1993).

For vertical motions, the trends indicated above imply that the commonly adopted vertical-to-horizontal response spectral ratio of 2/3 (Newmark and Hall, 1978) may be significantly exceeded at short periods in the near-source distance range. The increase in near-source strong motion recordings at both rock and soil sites aid in constraining empirical attenuation relationships and provide direct empirical estimation of statistical spectral shapes for vertical and horizontal components. These data also make it possible to examine the dependencies of the vertical-to-horizontal response spectral ratio (V/H) on magnitude, distance, and site conditions.

An additional, important use of these data is to examine similarities and differences in the characteristics of the time histories between vertical and horizontal motions. For design motions, the relative phasing between horizontal and vertical motions can be an important issue, leading to different structural analyses and design decisions depending on whether or not significant energy is expected to occur both vertically and horizontally at nearly the same time.

J.2 Effects of Site Conditions on the Characteristics of Vertical and Horizontal Strong Ground Motions

The Geomatrix categorization criterion listed in Table J-1 is used to broadly classify strong motion recording sites into rock or soil. While the distinction between rock and soil is becoming less clear for Western United States (WUS) sites as more rock sites are drilled and velocities determined (EPRI, 1993; BNL, 1997), this largely qualitative classification scheme captures significant and stable differences in strong ground motions (Sadigh et al., 1997; Abrahamson and Silva, 1997; BNL, 1997).

J.3 Generic Rock and Soil Site Velocity Profiles

To demonstrate the compression- and shear-wave velocity profiles implied by the rock and soil categories (Table J-1), Figures J-1 and J-2 show median (lognormal distribution) and 1σ velocity profiles computed for the two categories. The velocity profiles were computed from measured (downhole or crosshole) velocities at strong motion sites classified as Geomatrix A or B (Figure J-1) or C or D (Figure J-2). For the generic rock site, a strong velocity gradient is seen in the top 150 ft, with low near-surface shear- and compression-wave velocities (V_s and V_p , respectively) being

approximately 800 ft/sec and 1,600 ft/sec. The shear-wave velocity value of about 800 ft/sec departs significantly from the classically assumed value of about 2,500 ft/sec which is not reached, on average, until a depth of about 70 to 100 ft. With such low near- surface velocities, these rock sites can be expected to show some nonlinear effects under very high loading conditions (BNL, 1997).

The absolute variability of both the shear- and compression-wave velocities is high (COV 0.5 to 0.6) and there is little to suggest the presence of the water table at a compression-wave velocity of about 5,000 ft/sec. Contrasting the rock site profiles in Figure J-1 with those of the soil in Figure J-2, significant differences are immediately apparent. Interestingly, over the top 50 ft or so, the compression-wave velocities are very similar for both the rock and soil sites. For the soil site, the much lower shear-wave velocities imply a significantly higher Poisson's ratio, reflecting a larger V_p/V_s ratio for soil than for rock. Additionally for the soil site, the effect of the water table on the compression-wave velocity is apparent in the nearly constant velocity of the fluid phase at about 5,000 ft/sec at depths from around 100 ft to 250 ft. Beyond about 250 ft, the compression-wave velocity of the skeleton material exceeds that of the fluid phase, increasing V_p with depth.

The velocity variability at the soil sites is much less in absolute variation but similar to that of the rock sites in a relative sense ($\sigma_v \approx 0.4$ to 0.5). The lower absolute variability suggests that strong ground motions are less variable at soil than at rock sites.

To contrast the dynamic material properties between rock and soil sites further, Figures J-3 and J-4 show Poisson's ratios computed from the compression- and shear-wave velocity profiles. The $+1 \sigma$ values of Poisson's ratio greater than 0.5 are non-physical and result from a higher shallow ratio combined with a large variability. The higher variability in dynamic material properties for the rock versus the soil sites is reflected in the larger variation in Poisson's ratio for the rock site (Figure J-3 versus Figure J-4). Rock sites have lower overall Poisson's ratios, and they increase with depth to about 70 ft, remain nearly constant to a depth of about 200 ft, and then decrease to a value near 0.25 at a depth of 500 ft. Interestingly, Poisson's ratio for the soil sites (Figure J-4) show a similar trend but shifted nearly a constant amount to a depth of about 350 ft. Beyond about 350 ft, Poisson's ratio for the soil sites decreases less rapidly than for rock sites, remaining at a value of around 0.4 to a depth of 500 ft.

The dashed lines on Figures J-3 and J-4 represent smooth Poisson's ratio models and are shown in Figure J-5 for the generic rock and soil sites. The similar patterns and nearly constant shift to a depth of about 350 ft are quite apparent in the smooth models.

The differences in Poisson's ratio as well as the overall velocities between the rock and soil sites may have important implications for the differences in vertical and horizontal motions. At rock sites, even though the shallow shear-wave velocities are low, the steep velocity gradient results in shear-wave velocities exceeding 2,000 to 3,000 ft/sec at depths of 50 to 70 ft. As a result, for the same level of input motion, nonlinear effects are expected to be much less pronounced than at a corresponding soil site and are expected to be confined to the top 50 to 100 ft. The higher rock velocities and shallower potentially nonlinear zone will also tend to confine nonlinear effects to higher frequencies (BNL, 1997). If vertical motions are more linear than horizontal, perhaps because of lower strains for inclined SV-waves and contributions of P-waves, the magnitude dependence of the V/H ratio would

be expected to be less at rock sites than at soil sites. As earthquake magnitude increases, the higher loading levels induce more nonlinearity in the horizontal motions at soil sites than the rock sites. The vertical motions, remaining relatively linear, simply scale up and broaden in spectral content as magnitude increases. As a result, the magnitude scaling of the V/H ratios should be inversely proportional to the profile stiffness, and should be significantly larger for soil than for rock.

In addition to the effects of overall stiffness, the large jump in Poisson's ratio at the soil/rock interface (or steep gradient) at soil sites (Figure J-5) will have an important impact on incoming wavefields. For a generic California deep crustal model, the average shear- and compression-wave velocities at the surface are about 3,500 to 4,500 ft/sec and 6,500 to 8,000 ft/sec, respectively (BNL, 1997). For a deep generic soil site, Figure J-2 shows shear- and compression-wave velocities at a depth of 500 ft of about 2,000 ft/sec and 6,500 ft/sec respectively. Transition to rock at this depth then would likely involve a very steep shear-wave velocity gradient with a factor of 2 or more jump in velocity. For the compression wave, the transition is much less pronounced, a factor of only 1.0 to 1.2 on average. This consequence of the drop in Poisson's ratio between soil and rock, manifested as a large jump in shear-wave velocity, tends to refract (bend) incident shear-waves much more severely than incident compression-waves. In passing through the rock/soil transition zone, the incident shear-waves will become much more vertical than the incident compression-waves. For incident SV-waves, this will have the effect of converting vertical motions to horizontal motions while the compression-waves largely remain inclined until depths of 100 to 200 ft where they are amplified and refracted (bent to a more vertical incidence) by the shallow compression-wave gradient (Figure J-2).

Since earthquake sources emit much larger shear-wave amplitudes than compression-wave amplitudes, by the ratio of the source-region velocities cubed ($(V_p/V_s)^3 \approx 5$), incident inclined SV-waves may be expected to dominate vertical motions at close distances. At large distances, the SV-wave is beyond its critical angle and does not propagate to the surface very effectively (Kawase and Aki, 1990). At a source depth of 8 km and a generic California crustal model (Figure J-3), the SV-wave critical angle for geometrical ray theory occurs at an epicentral distance of about 5 km for a point-source. Crustal heterogeneity and source finiteness (vertical extent) tend to extend this distance somewhat. Also, geometrical ray theory is appropriate for high frequencies, and low frequency energy tend to be refracted less by the shallow velocity gradients, also resulting in extending the distance to the SV-wave critical angle. However, even considering these effects, the SV-wave is not likely to dominate the vertical component of rock motion at distances exceeding 10 to 20 km.

At soil sites, because of the large change in shear-wave velocity at the base of the profile and the accompanying wave refraction, compression-waves may be expected to dominate the vertical motions at near as well as far distances. Additionally, because of the large compression-wave velocity gradient from the surface to depths of about 100 to 200 ft, short period compression waves will be amplified, which will result in large short period vertical motions.

J.4 Short-Period Time Domain Characteristics of Vertical Motions

A series of plots from the CDMG initial earthquake data reports illustrate the effects of site conditions on acceleration time histories for vertical and horizontal components. These plots show all three components for each site in a convenient format for illustrative purposes.

As an illustration of close-in rock sites, Figure J-6 shows three component acceleration time histories at the Pacoima Dam (Downstream) and Corralitos sites for the 1994 M 6.7 Northridge and 1989 M 6.9 Loma Prieta earthquakes. Both sites are located about 8 km from the fault and both sets of records show very similar motions on the horizontal and vertical components. Structures founded on rock conditions at close distances may then be expected to experience simultaneous horizontal and vertical demands at similar levels and over a fairly broad period range.

For close-in soil sites, Figure J-7 shows distinctly different features in the Sylmar County Hospital and Arleta records for the Northridge earthquake. These soil sites are close-in recordings at fault distances of 6.1 km for Sylmar and 9.2 km for Arleta. Unlike the rock site recordings, the soil site records show strong short-period motion arriving significantly before the large horizontal motions. Structures founded on deep soil can be expected to experience vertical and horizontal demands significantly different from those on rock conditions. The vertical demands at close-in soil sites can be characterized as out-of-phase with the dominant horizontal motions and of much higher frequencies. The largest short period motions on the vertical component may arrive before those of the horizontal and will be larger than the short period horizontal motions. During the passage of the dominant horizontal component motions, the vertical demands on a structure could be characterized as random high-frequency chatter that may exceed 1g at short periods. This is markedly different from the vertical motions at close-in rock sites, which tend to show strong low-frequency coherence with the horizontal motions. (Further illustrations of this coherence are presented in the next section.)

For the more distant sites, Figure J-8 shows some interesting features across the Gilroy array for motions during the 1989 Loma Prieta earthquake. Rock sites Gilroy 6 and 7, at fault distances of 19.9 and 24.2 km respectively, show features similar to those at the close-in soil site: earlier arriving and high-frequency vertical motions out-of-phase with the dominant horizontal motions. At rock site Gilroy 1 however, at a fault distance of 11.2 km, the vertical motions display early arriving high frequency energy as well as low-frequency energy coherent with the dominant horizontal motions. A possible explanation for this behavior is that this site, at a fault distance of about 11 km, is in the transition region from close-in to more distant rock site characteristics.

An interesting and apparent contradiction to the expected close-in rock site characteristics are the recordings at Pacoima Kugel Canyon for the Northridge earthquake (Figure J-9). This rock site is at a fault distance of 8.2 km, about the same distance as the Pacoima Downstream site (Figure J-6), but displays soil site characteristics on the vertical component: early arriving high frequency energy and out-of-phase motions with the horizontal components. As part of a recent, Caltrans/NSF/EPRI-sponsored project to Resolve Site Response Issues associated with the Northridge Earthquake (ROSRINE project), the Pacoima Kugel Canyon site has recently been drilled and logged, as have been other sites. Based on the shear-wave velocity logging, the site is misclassified. With shear-wave velocities of just under 2,000 ft/sec from about 100 ft to the bottom of the hole at about 300 ft, the site is closer to a stiff soil than rock (Figures J-1 and J-2). This is not entirely unexpected, the site being underlain by the Saugus formation, a typically soft Los Angeles area sandstone.

For the distant ($R \geq 10$ to 15 km) soil sites, Figure J-10 shows the remaining sites across the Gilroy array that recorded the Loma Prieta earthquake. Site Gilroy 2 is at fault distance of 10.7 km and sites 3 and 4 are at fault distances of 14.4 and 16.1 km respectively. As with the close-in soil sites (Figure

J-7) and the distant rock sites (Figure J-8), the vertical motions show high-frequency early arriving energy and little coherence with the dominant horizontal motions.

These acceleration time history plots illustrate general trends in short period vertical and horizontal motions. For rock sites at close distances ($R \leq 10$ to 15 km) the plots show dominant SV motion on the vertical component with phasing similar to the horizontal components. At soil sites, compression-waves dominate the vertical motions, showing earlier-arriving and larger higher frequency energy content. For more distant sites, compressional-wave energy tends to dominate the vertical component at both rock and soil sites.

J.5 Response Spectral Characteristics of Vertical Motions

In order to illustrate the distance and site dependencies of vertical motions in more detail, over a broad frequency period range, Figures J-11 to J-18 show 5% damped pseudo-absolute acceleration response spectra and acceleration, velocity, and displacement time histories for selected sites. Cases examined are close-in and distant rock and soil sites. Acceleration, velocity, and displacement time histories are plotted to show that at close-in soil sites and at more distant rock and soil sites, long period coherence exists between vertical and horizontal components. This results in the dominant long period motions being “in-phase” in the sense that the largest long period motions occur at nearly the same time on both the vertical and horizontal components.

For the close-in rock site, Figure J-11 shows response spectra computed for the vertical and two horizontal component records at the Southern California Edison Lucerne site from the 1992 M 7.2 Landers earthquake. The fault distance is about 2 km and the vertical component slightly exceeds the horizontal components at periods shorter than about 0.1 sec. At long periods, beyond about 1 sec, the vertical is comparable to the smaller of the horizontal components, the fault-parallel motion. The period range of nearly constant spectral acceleration in the horizontal components, about 2 to 5 sec, is likely due to the effects of directivity.

The corresponding time histories are shown in Figure J-12 and reveal strong coherence among components. The maximum velocity and displacement of the vertical component exceed those of the fault-parallel component (labeled “345”). The maximum vertical displacement is about 15 cm (6 inches) occurring over a 2 sec period of time during which the fault-normal direction (labeled “260”) moved about 60 cm (2 ft).

For the close-in soil site, Figures J-13 and J-14 show the response spectra and time histories at the Arleta site for the 1994 Northridge earthquake. The fault distance is 9.2 km and the vertical component greatly exceeds the horizontal components at periods shorter than about 0.2 sec. Beyond about 2 sec, as with the rock site Lucerne, the vertical component becomes comparable to the horizontals. The time histories are shown in Figure J-14 and indicate long period coherence and out-of-phase short period energy (as noted previously in Figure J-7).

For the more distant sites, Figures J-15 and J-16 show response spectra and time histories for the Gilroy array no. 6 rock site and Figures J-17 and J-18 show corresponding plots for the Gilroy array no. 4 soil site. These motions occurred during the 1989 Loma Prieta and the fault distances are 16.1

and 19.9 km for sites 4 and 6 respectively. For both sites, the short period vertical motions relative to the corresponding horizontal motions are significantly lower, as compared to the close-in sites. Interestingly, as with the close-in sites, the long period vertical motions approach the horizontal motions for periods beyond about 2 to 4 sec. This feature is not predicted by either empirical or numerical modeling and suggests that vertical motions are associated with high variability.

The corresponding time histories, Figures J-16 and J-18, show the usual pattern: early arriving short period energy on the verticals that is out-of-phase with the horizontal motions, and longer period motions that are more in-phase between the components.

J.6 Magnitude, Site, and Distance Dependencies of Horizontal and Vertical Component Response Spectral Shapes

To examine empirically the role of possible site nonlinearity in the V/H ratios, statistical spectral shapes (SA/PGA) were computed for magnitude bins centered on M 5.5 and M 6.5 for both rock and soil sites. The magnitude bins are one unit wide (M 5.5 = M 5 - 6, M 6.5 = M 6 - 7 for soil, M 6.5 = M 6-7+, for rock) to include enough records to produce smooth and stable shapes.

The distance range was truncated at 50 km to avoid the effects of distance dependencies on the shapes. Records were selected from a strong motion database that includes available strong motion data for $M \geq 4.5$. For this application, only earthquakes occurring in tectonically active regions were selected (the 1995 M 6.9 Kobe earthquake is included).

To examine the effects of the level of motion on the vertical and horizontal component spectral shapes, two distance bins were selected: 0 to 10 km and 10 to 50 km. For M 5.5 rock sites, Figure J-19 shows the horizontal and vertical statistical shapes. To assess nonlinear effects, Figure J-19 shows shapes computed for the two distance bins: 0 to 10 km and 10 to 50 km. The vertical spectral shapes (dashed lines) show more short period energy than the horizontal shapes (solid and dotted lines) and about the same level of maximum spectral amplification. The vertical shapes have a maximum spectral amplification near 0.1 sec whereas the shapes for the horizontal component peak near 0.2 sec. This difference is likely due to differences in damping, with the vertical component showing significantly less damping than the horizontal. The lack of any significant distance dependency in this shift in peak spectral amplification between the vertical and horizontal components suggests that the difference in damping exists in the shallow portion of the path and that the sites behave in a linear manner. The shallow crustal damping is thought to occur in the top 1 to 2 km of the crust (Anderson and Hough 1984; Silva and Darragh, 1995) and is generally modeled as a frequency independent exponential damping term with a damping parameter termed kappa:

$$\kappa = \frac{H}{\bar{V}_s \bar{Q}}, \quad \bar{Q} = \frac{1}{2 \bar{\eta}} \quad (\text{J-1})$$

where H is the depth of the damping zone (1 to 2 km), \bar{V}_s and \bar{Q} are the average shear-wave velocity and quality factor over the depth H , and $\bar{\eta}$ is the corresponding damping ratio (decimal).

Response spectral shapes depend strongly on kappa, shifting to shorter periods as kappa decreases (Silva and Darragh, 1995). To illustrate this effect, Figure J-20 shows response spectral shapes computed using a simple point-source model with kappa values ranging from 0.006 sec to 0.160 sec. The shift in shape with kappa is easily seen and a peak near 0.2 sec is consistent with a kappa value of about 0.04 sec while a factor of two shift in the peak to about 0.1 sec corresponds to a similar shift in kappa value to about 0.02 sec. Interestingly, the factor of 2 shift in kappa for the verticals ($\kappa_V \approx \kappa_H/2$; EPRI, 1993) was also found by Anderson (1991) in a detailed analysis of vertical and horizontal motions recorded at rock sites and may be a result of the contribution of compressional waves to vertical strong ground motions. The kappa or shallow crustal damping effect is the likely mechanism controlling the large shift in spectral shapes between soft rock WUS spectral shapes and hard rock CEUS spectral shapes (Silva and Darragh, 1995) and will impact hard rock vertical spectral shapes as well as horizontal shapes.

To continue the shape comparison for rock sites, Figure J-21 shows horizontal and vertical shapes computed for **M 6.5 (M 6.0 - 7+)** at the two distance ranges: 0 to 10 km and 10 to 50 km. As with the **M 5.5** shapes, there is a distinct shift in the peak amplification frequency between vertical and horizontal spectra of nearly 2. Also there does not appear to be a strong distance or amplitude effect on either the vertical or horizontal shapes suggesting largely linear response at these ground motion levels.

To consider soil sites, Figures J-22 and J-23 show the vertical and horizontal response spectral shapes for **M 5.5 (M 5.0 - 6.0)** and **M 6.5 (M 6.0 - 7+)** earthquakes. As with the **M 5.0** rock shapes, there is about a factor of two difference in the periods of maximum spectral amplification between the vertical (near 0.1 sec) and horizontal shapes (near 0.2 sec). Also there is no appreciable and stable shift in either the vertical or horizontal shapes with distance (0 - 10 km or 10 - 50 km) reflecting largely linear response. Similar periods of peak amplification between rock and soil of about 0.2 sec for the horizontal and 0.1 sec for the vertical suggests similar low strain damping values at both rock and soil sites.

For the **M 6.5 (M 6.0 - 7+)** soil records, shown in Figure J-23, the horizontal shapes show a well-defined and broad-band shift between 10 to 50 km and 0 to 10 km. The horizontal shape for 10 to 50 km peaks near 0.2 sec whereas the shape for 0 to 10 km peaks near 0.3 sec, crosses the 10 to 50 km shape at that period, remains above the 10-50 km shape out to nearly 10 sec. These characteristics are very similar to those shown in Figure J-20 which illustrated the effects of kappa on response spectral shapes. The Figure J-23 results suggest nonlinear response resulting in an overall increase in kappa from about 0.04 sec (linear soil response) to about 0.06 to 0.08 sec at the higher amplitude levels.

For the vertical component in Figure J-23, a slight shift appears to be present between the shapes computed for the 0 to 10 km and 10 to 50 km bins but the shift is in the wrong direction and is not stable with period, crossing at about 0.1 and again near 2.0 sec. This is likely due to a sampling problem with too few sites contributing to the close-in (0 to 10 km) shapes.

The analyses of response spectral shapes reveals several features of interest: (1) a consistent shift in shapes between vertical and horizontal components at both rock and soil sites indicating lower shallow crustal damping for vertical components by about a factor of about 2, (2) similar low-strain damping values for rock and soil sites, and 3) horizontal component soil shapes that show nonlinear response characterized by a stable and broad-band shift in shape to longer periods at higher amplitude levels. These features are important factors in understanding the effects of magnitude, distance, and site condition on vertical-to-horizontal response spectral ratios.

J.7 Empirical and Numerical Model Estimates of the Vertical-to-Horizontal Response Spectral Ratios

A combination of empirical attenuation relations and numerical modeling is used to estimate vertical-to-horizontal ratios as functions of magnitude, distance, and site conditions. While the empirical relations are reasonably well constrained for WUS (or other tectonically active regions), little data exist for $M > 5.0$ for CEUS conditions at distances of interest ($R \leq 20$ km).

The only large magnitude earthquake considered representative of the CEUS that generated close-in strong motion records is the M 6.8 1985 Nahanni earthquake. Strong motions were recorded at three sites, all hard rock and all within 20 km of the source. This earthquake, along with smaller magnitude CEUS hard rock recordings, clearly show significantly different spectral content between WUS and CEUS horizontal rock motions. This feature is illustrated in Figure J-24, which compares WUS and CEUS horizontal component rock site response spectral shapes for M around 6.5 and 4.0. The difference in short period spectral content between WUS and CEUS is significant and consistent between different magnitude earthquakes and is attributed to differences in shallow crustal damping or kappa values (Silva and Darragh, 1995). For CEUS rock site vertical components, an open question exists as to whether they show a shift to even shorter periods than the horizontal components (see Figure J-21 for WUS rock). The effective bandwidth of current recordings is not capable of resolving this issue, however if similar physical mechanisms control the motions at WUS and CEUS rock sites, some degree of shift would be expected and should be reflected in estimates of CEUS V/H ground motion ratios.

These differences in rock site spectral content have implications for soil motions since WUS and CEUS control motions (at depth), would be expected to have differences in spectral content, given the differences for rock outcrop motions. The differences in WUS and CEUS control motion spectral content may not result in significantly different deep soil horizontal motions due to the effects of material damping and nonlinearity. However, vertical component soil motions, if response remains largely linear in compression (constrained modulus), may have very high short period levels at close distances to large magnitude earthquakes (EPRI, 1993).

J.8 Applications to WUS Rock and Deep Soil Sites

For rock sites, the recommended V/H ratios reflect the average of Sadigh et al. (1997) and Abrahamson and Silva (1997) empirical relations, while for soil, because Sadigh et al. (1997) do not present a relationship for the vertical component, only the Abrahamson and Silva (1997) relation is used. Figure J-25 shows empirical vertical and horizontal spectra (5% damping) for M 6.5 at a

distance of 5 km for both rock and soil site conditions. A shift of the peak response of the vertical spectra to shorter periods than the horizontal is present showing a crossing in spectral levels at short periods. At this close distance ($R = 5$ km), response spectral ratios (V/H) exceed 1 at short periods and drop significantly at longer periods.

To examine the distance dependency of the V/H ratio for WUS, Figure J-26 shows empirical V/H ratios computed for both rock and soil sites. As expected, from the earlier examination of response spectra at individual sites (Figures J-11, J-13, J-15, and J-17), the maximum rock site V/H ratios are lower than the corresponding ratios for soil sites. For the rock sites, the distance dependency is considerably less than that for soil, a maximum of about 1.5 in the distance range 1 to 40 km. The larger distance dependence in the V/H ratios for soil sites may be due to nonlinear response of the soils: as distance increases, relatively less damping occurs in the soil column.

To examine the magnitude dependency of the V/H ratios, Figure J-27 shows empirical V/H ratios for rock and soil sites computed for distances of 1 and 20 km. The magnitude dependence of the V/H ratios is stronger for soil sites than for rock sites, again possibly reflecting effects of nonlinearity. Additionally, the magnitude dependence decreases with increasing distance for both rock and soil sites. For rock sites, this may be an artifact of the magnitude saturation built into the empirical relations, being different for rock and soil sites.

These empirical V/H ratios are reasonably well constrained and can provide the basis for developing smooth design ratios for WUS rock and deep moderately stiff soils. For applications to design motions, strong consideration should be given to adequate conservatism, which should reflect the higher uncertainty in vertical motions compared to horizontal motions, particularly for close distances to large magnitude ($M \geq 7$) earthquakes.

J.9 Applications to CEUS Rock and Deep Soil Sites

Based on the comparisons of the spectral content between WUS and CEUS rock site spectral shapes shown in Figure J-24, differences in rock (and possibly soil) V/H ratios are expected between the two tectonic regions (EPRI, 1993).

As previously discussed, due to the paucity of recordings ($M \geq 5$, $R \leq 50$ km) reflecting CEUS conditions, some form of modeling is necessary to assess the appropriateness of WUS V/H ratios for engineering design applications.

J.10 Computational Model

To model vertical motions, inclined P-SV waves from the stochastic point-source ground motion model (EPRI, 1993) are assumed and the P-SV propagators of Silva (1976) are used to model the crust and soil response to inclined P-SV wavefields. The angle of incidence at the top of the source layer is computed by two-point ray tracing through the crust and soil column (if present) assuming incident compression-waves.

To model soil response, a soil column is placed on top of the crustal structure and the incident inclined P-SV wavefield is propagated to the surface where the vertical (or radial) motions are computed.

J.11 Treatment of Soil Response for Vertical Motions

Commonly, equivalent-linear site response analyses for vertical motions have used strain-iterated shear moduli from a horizontal motion analysis to adjust the compression-wave velocities assuming either a strain-independent Poisson's ratio or bulk modulus. Some fraction (generally 30% to 100%) of the strain-iterated shear-wave damping is used to model the compression-wave damping, and a linear analyses is performed for vertically propagating compression waves using the horizontal control motions scaled by some factor near 2/3.

The equivalent-linear approach implicitly assumes some coupling between horizontal and vertical motions. This is necessitated by the lack of well determined M/M_{\max} (constrained modulus over maximum constrained modulus) and damping curves for the constrained modulus. Ideally the strain dependency of the constrained modulus should be determined independently of the shear modulus. Also, the conventional approach assumes vertically-propagating compression waves and not inclined P-SV waves. Additionally, the use of some fraction of the horizontal control motion is an approximation and does not reflect the generally greater high-frequency content of vertical component motions at rock sites due to lower kappa values (EPRI, 1993).

Alternatively, fully nonlinear analyses can be made using two- or three-component control motions (Costantino, 1967; 1969; Li et al., 1992; EPRI, 1993). These nonlinear analyses require two- or three-dimensional soil models that describe plastic flow and yielding and the accompanying volume changes as well as coupling between vertical and horizontal motions through Poisson's effect. These analyses are important to examine expected dependencies of computed motions on material properties and may have applications to the study of soil compaction, deformation, slope stability, and component coupling. However, the models are very sophisticated and require specification of many parameters, at least some of which are poorly understood.

In the current implementation of the equivalent-linear approach to estimate vertical to horizontal response spectral ratios, the horizontal component analyses are performed for vertically propagating shear waves using an equivalent-linear random vibration theory (RVT) methodology coupled to the point-source stochastic ground motion model (EPRI, 1993; Schneider et al., 1993). To compute the vertical motions, a linear analysis is performed for incident inclined P-SV waves using low-strain, compression- and shear-wave velocities derived from the generic shear- and compression-wave velocity profiles (Figures J-1 and J-2). Compression-wave damping is assumed to be equal to the low strain shear-wave damping (Johnson and Silva, 1981). The horizontal component and vertical component analyses are assumed to be independent.

These approximations (linear analysis for the vertical component, and uncoupled vertical and horizontal components) have been checked by comparing results of fully nonlinear analyses at soil sites Gilroy 2 and Treasure Island to recorded vertical and horizontal motions from the 1989 Loma Prieta earthquake (EPRI, 1993). The nonlinear analyses indicate that little coupling exists between

the vertical and horizontal motions for the ranges in control motions analyzed (maximum about 0.5g). These assumptions will, if anything, result in conservative estimates of vertical motions since a higher degree of coupling implies degradation of constrained modulus and an accompanying increase in compression-wave damping.

The point-source computational model has been validated for horizontal motions with the Loma Prieta earthquake by comparing recorded motions with model predictions (Schneider et al., 1993) and more recently with 14 additional earthquakes (M 5.0 - 7.4) at about 500 sites (BNL, 1997). For vertical motions, current validation includes comparisons of recorded motions to model predictions for the 1989 M 6.9 Loma Prieta earthquake (20 rock and 16 soil sites), 1992 M 7.2 Landers earthquake (3 rock and 9 soil sites), and the 1994 M 6.7 Northridge earthquake (16 rock and 56 soil sites). The variability of vertical motions is not modeled as well as horizontal motions because observed vertical motions show more variation than the horizontal and the model is not able to capture the increased variability. The larger standard error associated with vertical motions is reflected in empirical relations (Abrahamson and Silva, 1997).

As an example of the comparison of model predictions to recorded motions, Figure J-28 shows recorded and computed vertical and horizontal motions for the M 7.2 Landers earthquake at the rock* site Lucerne ($R \approx 2$ km). The simple point-source, using the generic shallow rock profile with equivalent-linear analyses for the horizontal component and a linear analysis for the vertical appears to capture the general features of the recorded motions.

To generate V/H ratios based on numerical modeling, the shallow generic profiles (Figures J-1 and J-2) were placed on top of the generic California crust (Figure J-29). For equivalent-linear analyses, recently developed rock and cohesionless soil modulus curves (G/G_{max}) and hysteretic damping curves (BNL, 1997) were used. The point-source stress drop was 60 bars, based on inversions of the Abrahamson and Silva (1997) empirical attenuation (BNL, 1997), and the source depth was taken as 8 km (equivalent to the value used in the inversions).

Figures J-30 and J-31 compare simulated V/H ratios to empirical ratios for rock and soil sites for M 6.5, the best constrained magnitude for the empirical relations. In general the model captures the overall shapes and trends with distance of the empirical ratios but shows a stronger close-in distance effect. This strong distance effect is controlled by the incidence angle (top of source layer) increasing rapidly with increasing epicentral distance. As previously mentioned, crustal heterogeneity as well as source finiteness would tend to weaken this distance dependence. For the point-source model, crustal randomization to simulate uncertainty and randomness in the crustal structure would reduce the near-source distance dependency making it similar to the empirical. However, the simple point-source model, as implemented here, captures the general trends of the WUS empirical rock and soil V/H ratios well enough to provide guidance in assessing the appropriateness of applying WUS ratios to CEUS conditions.

*The Lucerne site is actually a shallow (15 ft) soil over very hard rock (unweathered granite).

To generate V/H ratios for the CEUS, a generic midcontinent crustal model was used (EPRI, 1993). The CEUS crustal model is considered appropriate for hard rock sites in the CEUS east of the Rocky Mountains with the possible exception of the Gulf Coast region. This region has a crustal structure somewhat intermediate between the WUS and the CEUS (EPRI, 1993). The large difference between the two generic crustal models shown in Figure J-31 gives rise to significantly different short-period strong ground motion characteristics at close-in distances (as depicted in Figure J-24) as well as different rates of attenuation with distance. These differences may be expected to impact the V/H ratios as well. For the WUS ratios, both the empirical and numerical model results showed that the stiffer profile (rock versus soil) resulted in lower short period (≤ 0.3 sec) V/H ratios but larger long period ratios. For the hard rock CEUS crust, this trend is also expected, resulting in a lower maximum V/H ratio with perhaps a higher long period level. Because of the lower horizontal and vertical kappa values for the CEUS crust, the peak in the V/H ratio may be expected to occur at much shorter periods than in the CEUS rock ratios. These expected trends are reflected in the model prediction shown in Figure J-32 (top plot). Oscillations in the model V/H ratios are due to resonances in the vertical and horizontal spectra. These would be reduced if the profile were randomized and median spectra used in the V/H ratios. For CEUS hard rock sites, the peak V/H ratio is significantly lower and at a shorter period than soft rock sites and the long period level is higher as well. This difference between WUS and CEUS in the period range of 0.1 to 1.0 sec was also found by Atkinson and Boore (1997) in an empirical analysis of the H/V ratio of Fourier amplitude spectra at large distances ($R \geq 20$ km) in Western and Eastern Canada.

For deep soil sites, Figure J-32 (bottom) plot) suggests that the V/H ratio may be significantly higher in the CEUS than in WUS. This results primarily from nonlinear soil response in the horizontal component as well as assuming linear response for the verticals. The factors contributing to the higher degree of nonlinear response for the CEUS soil ratios are the higher levels of high frequency energy in the control motions (Figure J-24), the larger overall motions due to the higher stress drop (100 bars for CEUS and 60 bars for WUS), and the large jump in shear-wave velocity from the base of the soil to the top layer of the CEUS crust (Figure J-31). These results suggest that for both rock and soil CEUS V/H ratios, it is probably inappropriate to adopt WUS ratios for design purposes. A similar conclusion was reached in the EPRI (1993) project to estimate strong ground motion in the CEUS. In that project, design V/H ratios were developed for CEUS rock and stiff soil conditions based primarily on model simulations.

It should be emphasized that only a single and very simple model, which involves many assumptions, has been implemented here. However, the results may provide a useful contribution to developing design V/H ratios for CEUS conditions. Naturally, the most satisfying approach is to make use of multiple well-validated models to assess the range in uncertainty in the CEUS V/H ratios.

J.12 Conclusions

Characteristics of vertical and horizontal component strong ground motions have been examined to reveal general trends that may be of significance to structural analyses. Recordings at both rock and deep soil sites representative of WUS showed distinctly different behavior of vertical motions at rock and soil sites at close source distances ($R \leq 10$ to 15 km). At rock sites, the largest motions tend to occur on all three components at nearly the same time and "in-phase" motion is present on

acceleration, velocity, and displacement time histories. Vertical component response spectra can exceed those of the horizontal components at short periods (≤ 0.1 sec) by moderate amounts (20% on average) and at very close fault distances ($R \leq 5$ km).

At soil sites, short period (≤ 0.2 sec) vertical motions occur earlier in acceleration time histories than the largest motions on the horizontal components and are not in phase. For intermediate-to-long periods, however, near-source soil site velocity and displacement time histories are “in-phase”, showing the dominant motion occurring at about the same time. At close source distances ($R \leq 5$ km) short period (≤ 0.1 sec) vertical motions may exceed horizontal motions by a factor of 2.

Analyses of vertical and horizontal component statistical response spectral shapes for both rock and soil sites at varying magnitudes and distances show significantly less damping at both rock and soil sites for vertical motions. These analyses also suggest that vertical motions are largely linear at both rock and soil sites. Horizontal motions, on the other hand show a broad-band shift in spectral shape to longer periods consistent with an increase in damping due to nonlinear site response, for earthquakes of M 6.0 to 7.0+ and at source distances within 10 km.

Response spectral V/H ratios were computed from median WUS empirical horizontal and vertical component response spectra at rock and soil sites for a suite of distances (Figure J-26). These empirical V/H ratios may be used to obtain ratios for applications to structural design for WUS conditions.

Nonlinear response in horizontal motions coupled with largely linear response for vertical motions at WUS soil sites is expected to result in larger V/H ratios and a stronger magnitude dependency for soil sites compared to rock sites at close distances. This trend is seen in V/H ratios computed using empirical attenuation relations, and at least part of this effect is attributable to nonlinear response involving horizontal motions at soil sites.

To estimate V/H ratios for CEUS hard rock and deep soil conditions, a simple point-source model is used to predict both rock and soil horizontal and vertical motions. The model treats vertical motions as inclined P-SV waves with a linear analysis and horizontal motions as vertically incident shear-waves using equivalent-linear analyses. Model predictions for WUS V/H ratios show generally favorable agreement with empirical V/H ratios. Application of the simple model to CEUS show generally higher V/H ratios for hard rock sites compared to soft rock sites at long periods (> 0.3 sec). At short periods, the peak in the V/H ratio is shifted from about 0.07 sec for soft rock to about 0.013 sec for hard rock. This shift results from the lower shallow crustal damping at the hard rock site.

For soil sites, the CEUS V/H ratio is predicted to be significantly larger than the corresponding WUS ratio. This is attributed to higher levels of nonlinear soil response for the horizontal motions caused by CEUS rock control motions being richer in short period energy, higher overall levels of control motions caused by higher CEUS stress drops (100 bars compared to 60 bars), and a larger impedance contrast at the base of the soil column. Because of the simplicity of the model and the number of significant assumptions, use of multiple well validated models is recommended in developing design V/H ratios for the CEUS.

A general conclusion is that the conventional V/H factor of 2/3 is not appropriate at CEUS rock and soil sites and may only be appropriate for WUS sites at periods longer than about 0.3 sec and for distances beyond about 50 km.

References

- Abrahamson, N.A. and W.J. Silva (1997). "Empirical response spectral attenuation relations for shallow crustal earthquakes." *Seism. Soc. Am.*, 68(1), 94-127.
- Anderson, J.G. (1991). "A preliminary descriptive model for the distance dependence of the spectral decay parameter in southern California." *Bull. Seism. Soc. Am.*, 81(6), 2186-2193.
- Anderson, J. G. and S. E. Hough (1984). "A Model for the Shape of the Fourier Amplitude Spectrum of Acceleration at High Frequencies." *Bull. Seism. Soc. Am.*, 74(5), 1969-1993.
- Atkinson, G.M. and D.M. Boore (1997). "Some comparisons between recent ground-motion relations." *Seism. Res. Lett.* 68(1), 24-40.
- Bozorgnia, Y., M. Niazi, and K.W. Campbell (1995). "Characteristics of free-field vertical ground motion during the Northridge earthquake." *Earthquake Spectra*, 11(4), 515-525.
- Brookhaven National Laboratory (1997). "Description and validation of the stochastic ground motion model." Submitted to Brookhaven National Laboratory, Associated Universities, Inc. Upton, New York.
- Chang, S.W., J.D. Bray and R.B. Seed (1996). "Engineering implications of ground motions from the Northridge earthquake." *Bull. Seism. Soc. Am.*, 86(1B), S270-S288.
- Costantino, C.J. (1967). "Finite element approach to wave propagation problems." *J. Engin. Mechanics Div. Amer. Soc. Civil Engrs.*, vol. 93
- Costantino, J.C. (1969). "Two dimensional wave propagation through nonlinear media." *J. Comput. Physics*, vol. 4.
- Electric Power Research Institute (1993). "Guidelines for determining design basis ground motions." Palo Alto, Calif: Electric Power Research Institute, vol. 1-5, EPRI TR-102293.
- Johnson, L.R. and W.J. Silva (1981). "The effects of unconsolidated sediments upon the ground motion during local earthquakes." *Bull. Seism. Soc. Am.*, 71, 127-142.
- Li, X.S., Z.L. Wang, and C.K. Shen (1992). SUMDES: A nonlinear procedure for response analysis of horizontally-layered sites subjected to multi-directional earthquake loading. Dept. of Civil Eng. Univ. of Calif., Davis.

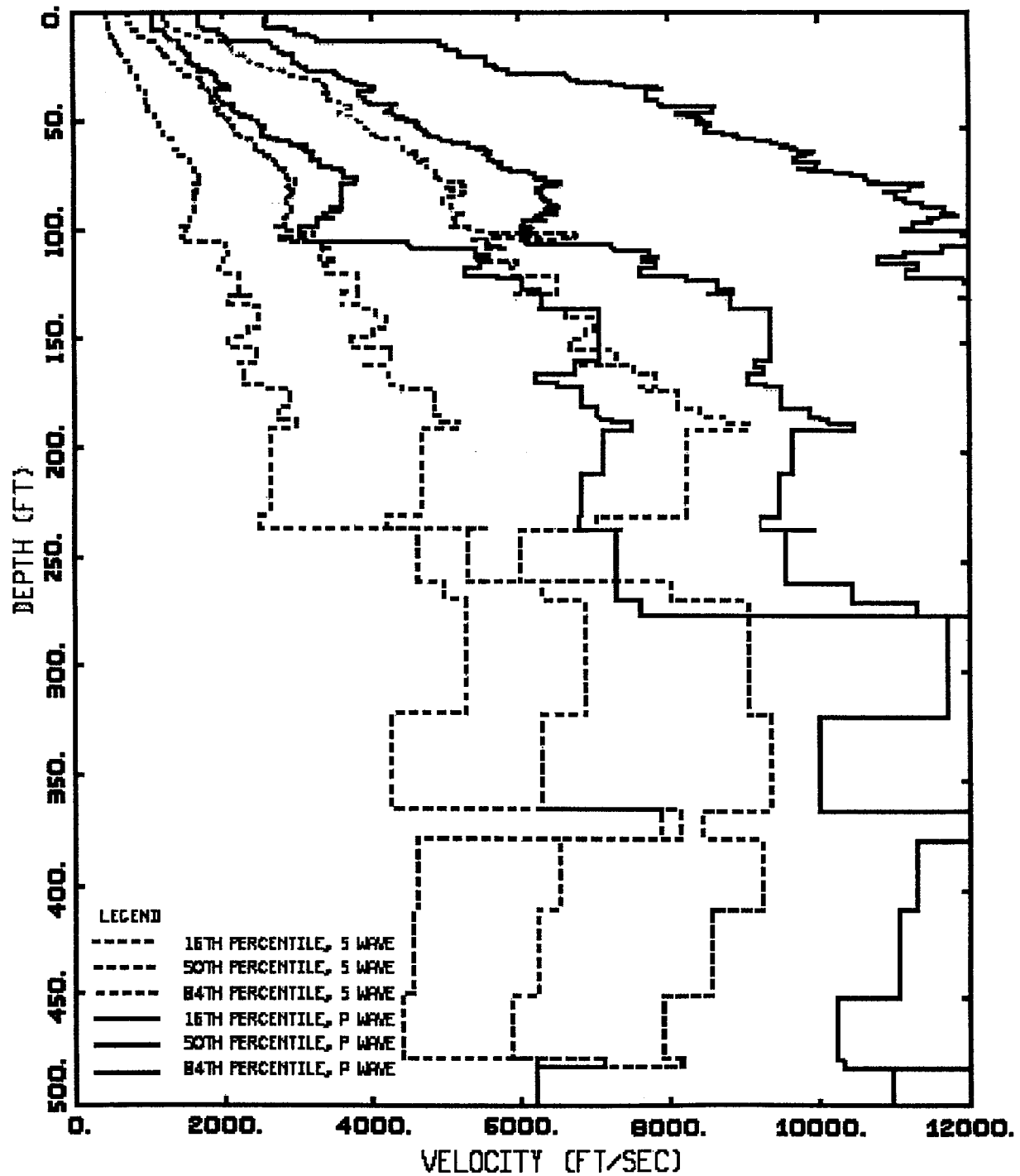
- Niazi, M. and Y. Bozorgnia (1991). "Behavior of near-source peak horizontal and vertical ground motions over smart-1, array, Taiwan." *Bull. Seism. Soc. Am.*, 81(3), 715-732.
- Newmark, N.M. and W.J. Hall (1978). "Development of criteria for seismic review of selected nuclear power plants." NUREG/CR-0098, Nuclear Regulatory Commission.
- Kawase, H. and K. Aki (1990). "Topography effect at the critical SV-wave incidence: possible explanation of damage pattern by the Whittier Narrows, California, earthquake of 1 October 1987." *Bull. Seism. Soc. Am.*, 80(1), 1-30.
- Sadigh, C.-Y. Chang, J.A. Egan, F. Makdisi, and R.R. Youngs (1997). "Attenuation relationships for shallow crustal earthquakes based on California strong motion data." *Seism. Soc. Am.*, 68(1), 180-189.
- Schneider, J.F., W.J. Silva, and C.L. Stark (1993). "Ground motion model for the 1989 M 6.9 Loma Prieta earthquake including effects of source, path and site." *Earthquake Spectra*, 9(2), 251-287.
- Silva, W.J. and R. Darragh (1995). "Engineering characterization of earthquake strong ground motion recorded at rock sites." Palo Alto, Calif:Electric Power Research Institute, TR-102261.
- Silva, W.J. (1976). "Body Waves in a Layered Anelastic solid." *Bull. Seism. Soc. Am.*, 66(5), 1539-1554.
- Somerville, P.G., N.F. Smith, R.W. Graves, and N.A. Abrahamson (1997). "Modification of empirical strong ground motion attenuation relations to include the amplitude and duration effects of rupture directivity." *Seism. Res. Lett.*, 68(1), 199-222.
- Wald, D.J., and T.H. Heaton (1994). "Spatial and temporal distribution of slip for the 1992 Landers, California, earthquake." *Bull. Seism. Soc. Amer.*, 84(3), 668-691.

Table J-1

GEOMATRIX CONSULTANTS
STRONG-MOTION RECORDING STATIONS
CLASSIFICATION SYSTEM

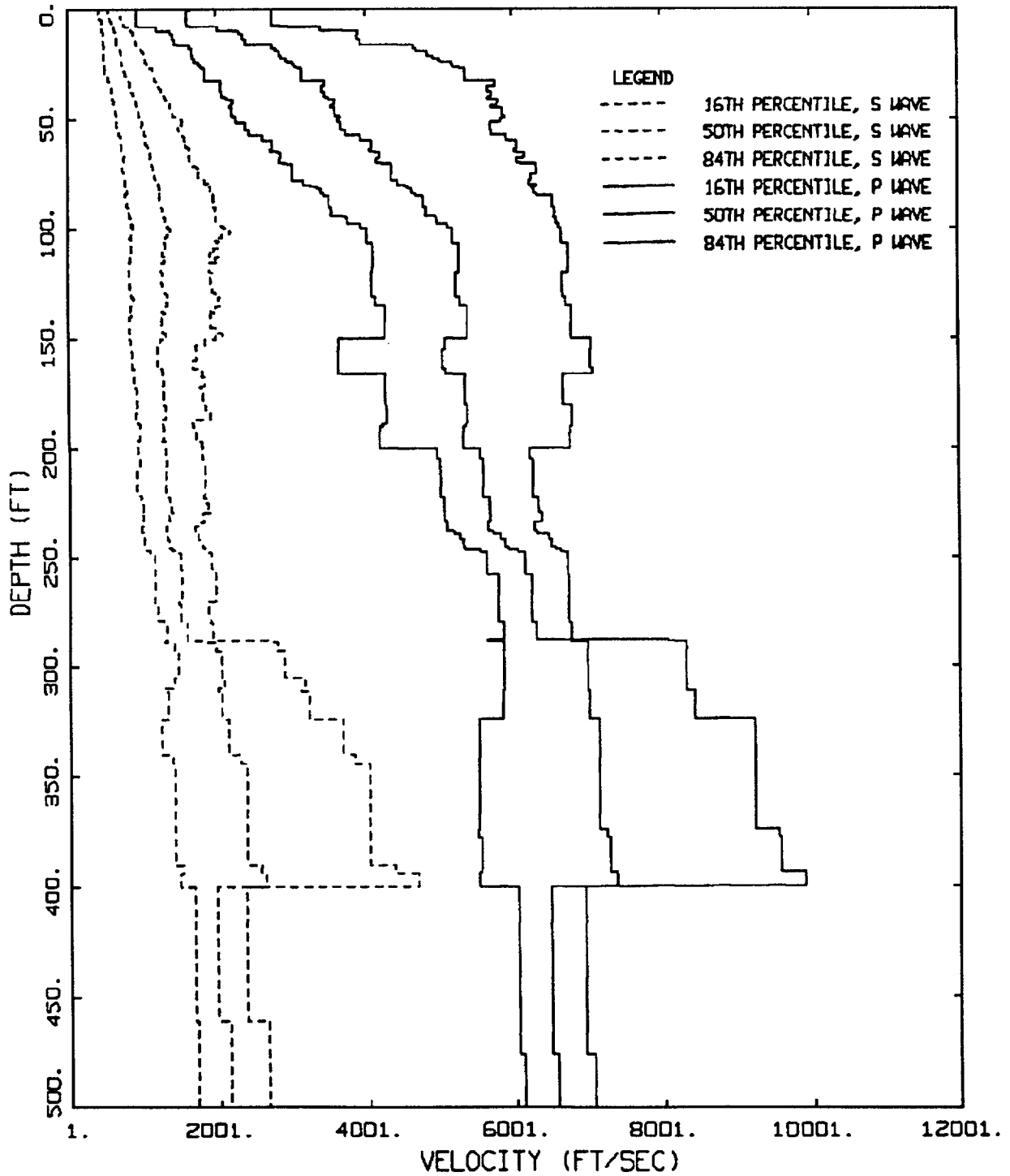
Geotechnical Subsurface Characteristics

<u>Designation</u>	<u>Description</u>
A	Rock. Instrument is founded on rock material ($V_s > 600$ mps (1969 ft/sec) or a very thin veneer (less than 5m (16 ft)) of soil overlying rock material.
B	Shallow (stiff) soil. Instrument is founded in/on a soil profile up to 20m (66 ft) thick overlying rock material, typically in a narrow canyon, near a valley edge, or on a hillside.
C	Deep narrow soil. Instrument is founded in/on a soil profile at least 20m (66 ft) thick overlying rock material in a narrow canyon or valley no more than several kilometers wide.
D	Deep broad soil. Instrument is founded in/on a soil profile at least 20m (66 ft) thick overlying rock material in a broad canyon or valley.
E	Soft deep soil. Instrument is founded in/on a deep soil profile that exhibits low average shear-wave velocity ($V_s < 150$ mps (492 ft/sec)).



GEOMATRIX SITE CLASS A & B

Figure J-1. Median and $\pm \sigma$ compression- and shear-wave velocity profiles for Geomatrix site class A plus B (soft rock, table J-1).



GEOMATRIX SITE CLASS C & D

Figure J-2. Median and $\pm 1 \sigma$ compression- and shear-wave velocity profiles for Geomatrix site class C plus D (deep soil, Table J-1).

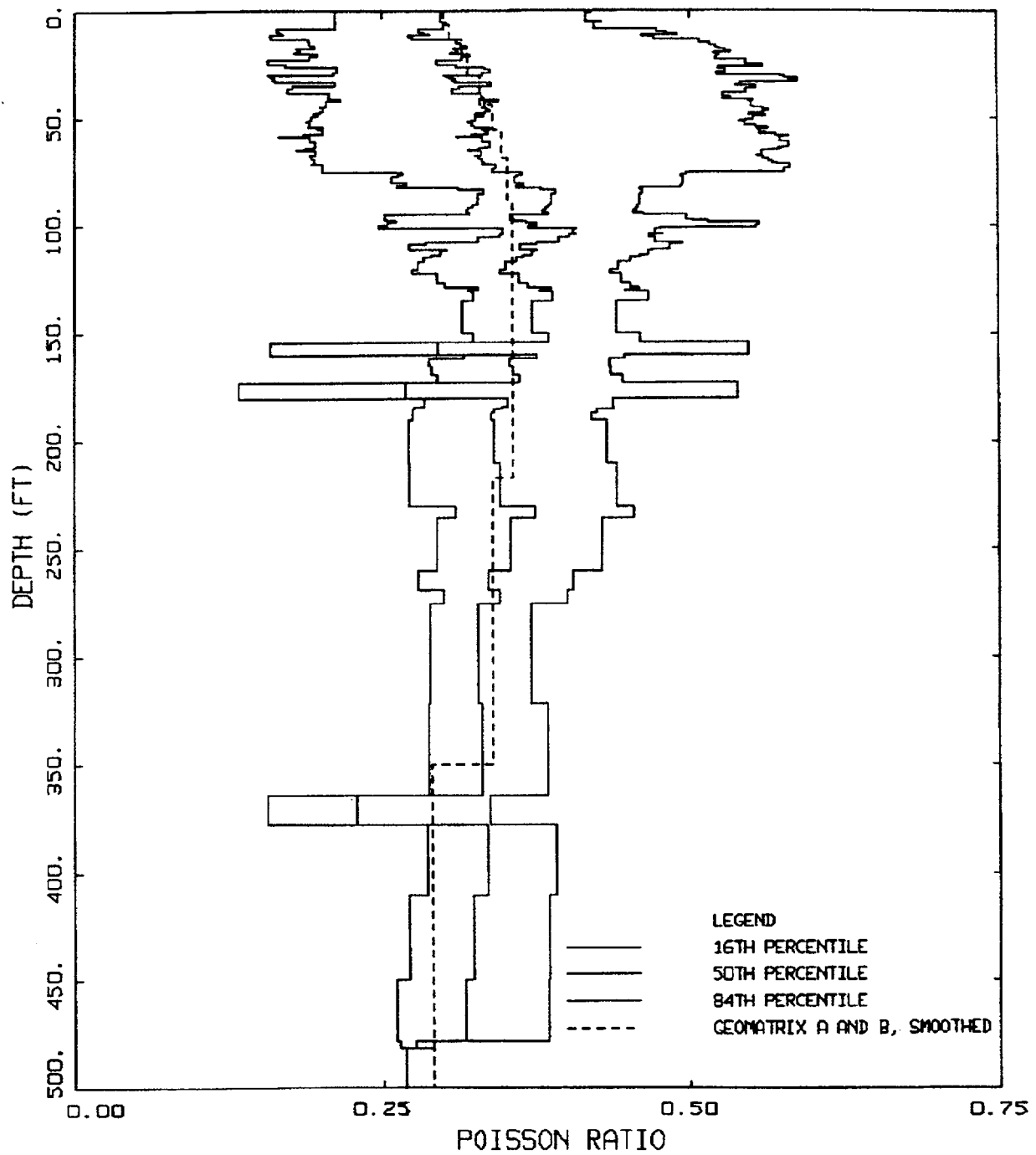
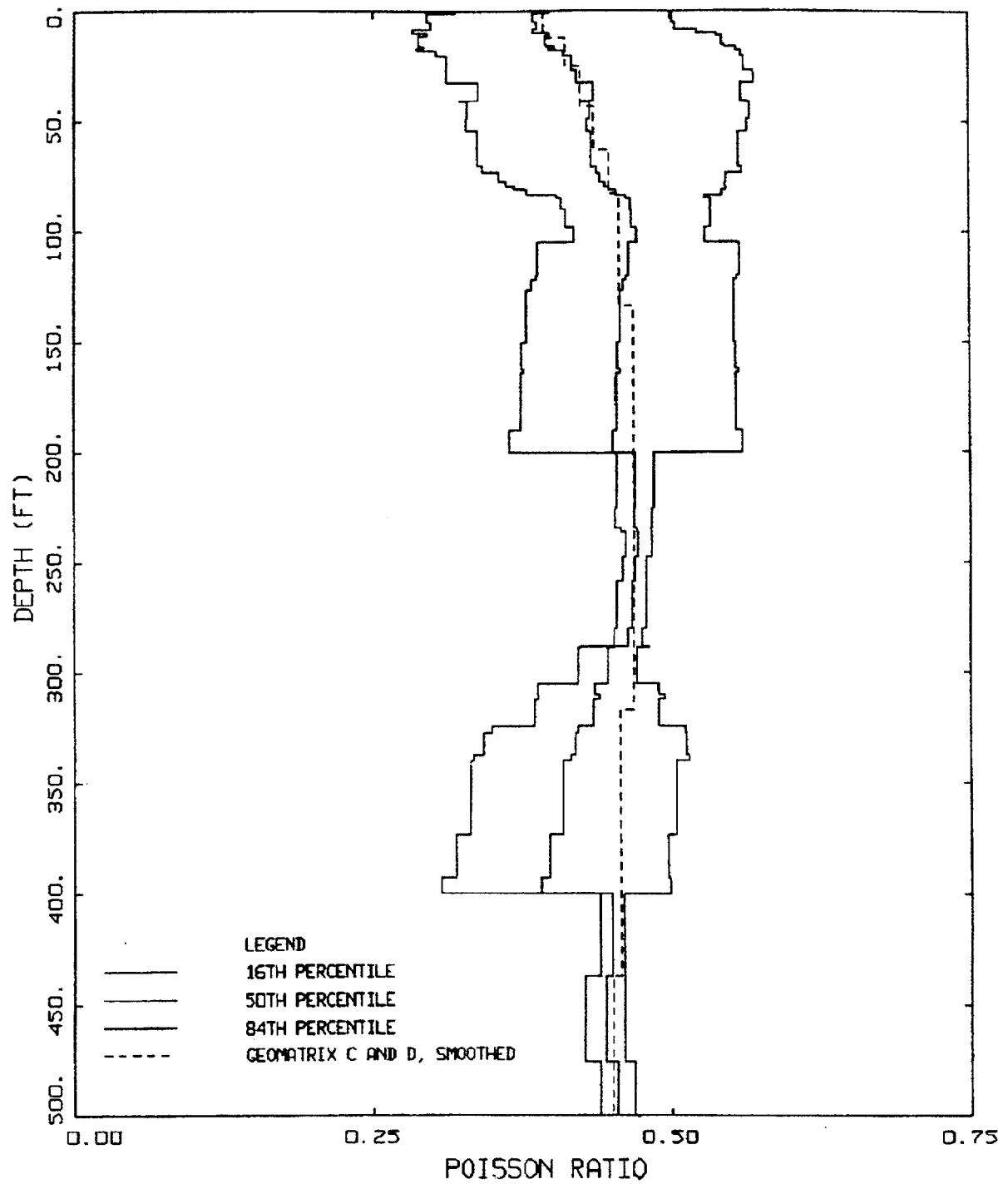
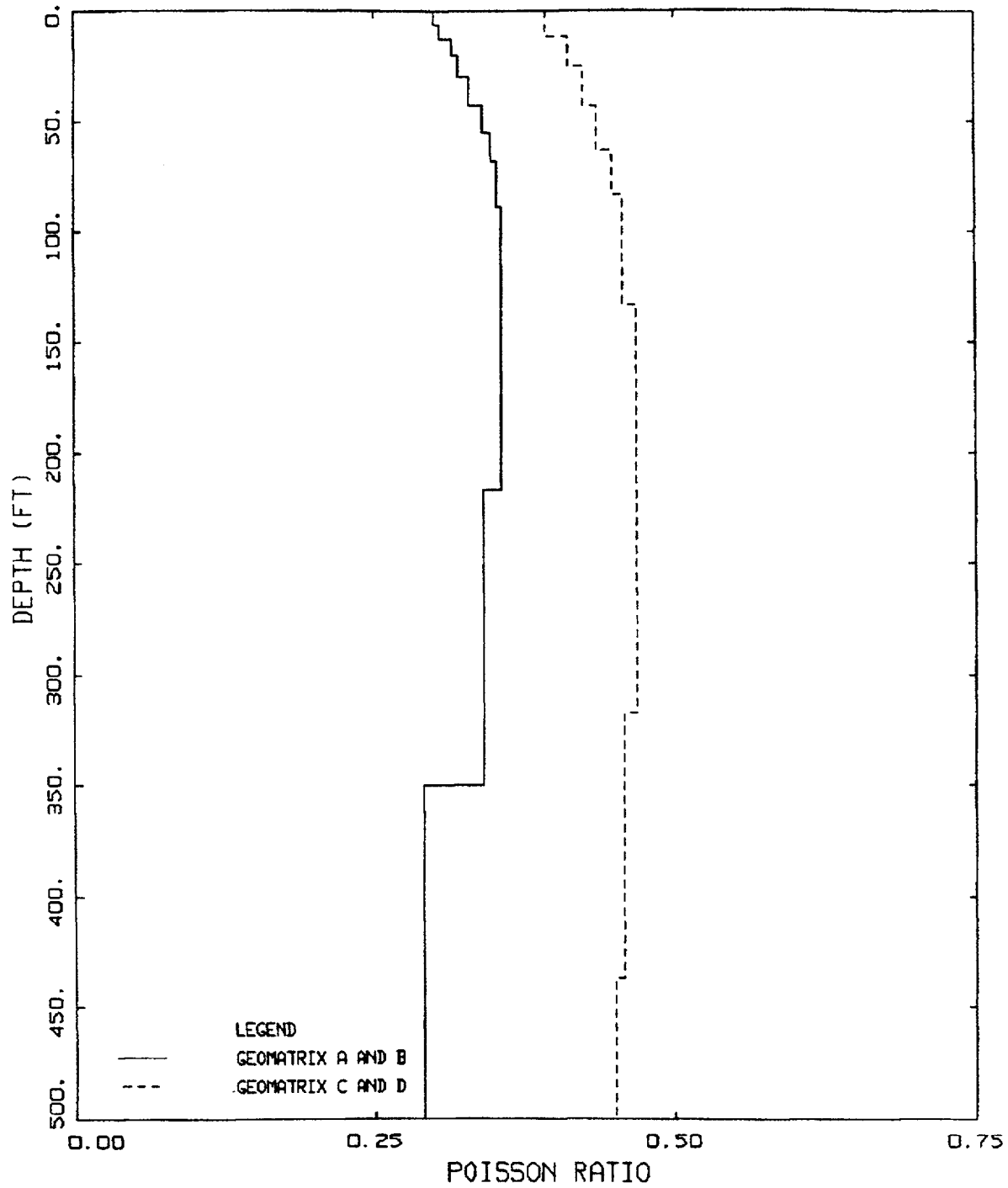


Figure J-3. Median and $\pm 1 \sigma$ Poisson's ratio profiles for Geomatrix site class A plus B (soft rock, Table J-1).



POISSON'S RATIO
GEOMATRIX C AND D

Figure J-4. Median and $\pm 1 \sigma$ Poisson's ratio profiles for Geomatrix site class C plus D (deep soil, Table J-1).



POISSON'S RATIO
 ROCK AND SOIL

Figure J-5. Poisson's ratio profiles for Geomatrix site class A plus B and C plus D (soft rock, Table J-1).

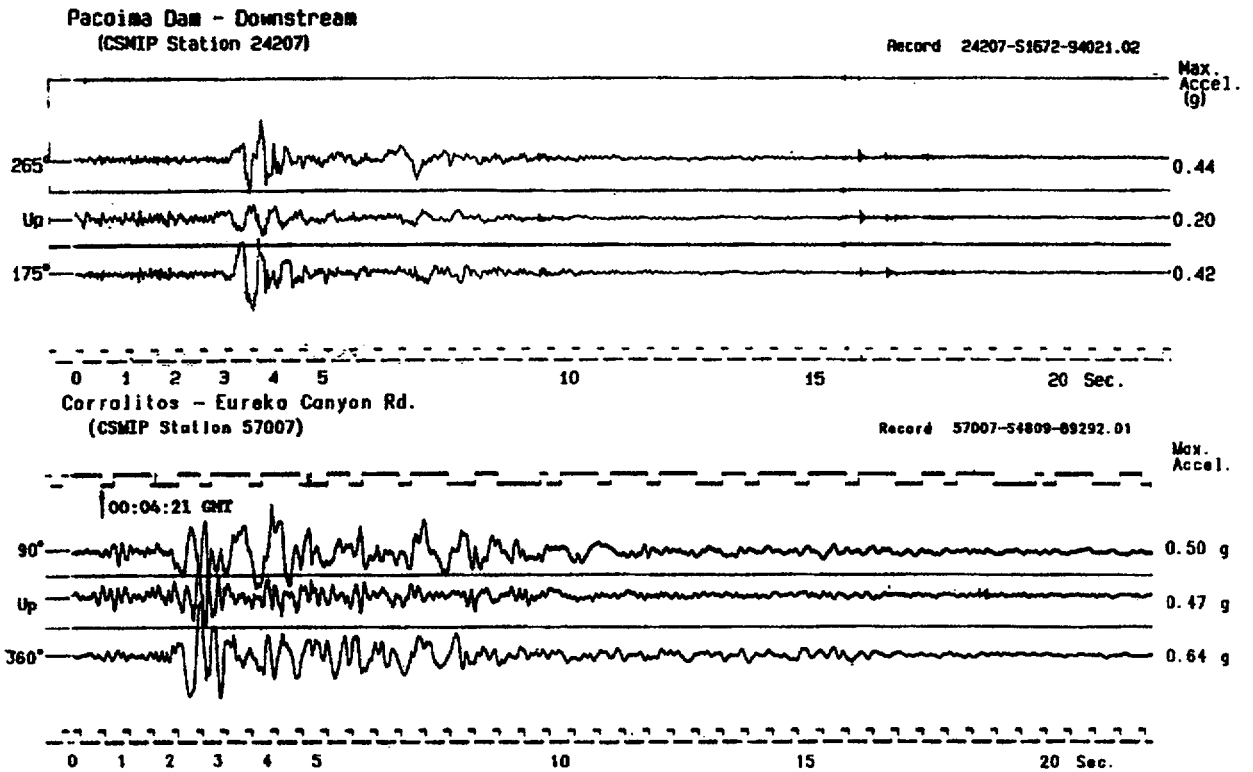


Figure J-6. Horizontal and vertical component acceleration time histories recorded at rock sites Pacoima Downstream for the 1994 M 6.7 Northridge earthquake (top) and Corralitos for the 1989 M 6.9 Loma Prieta earthquake (bottom). (Source: CDMG initial data reports).

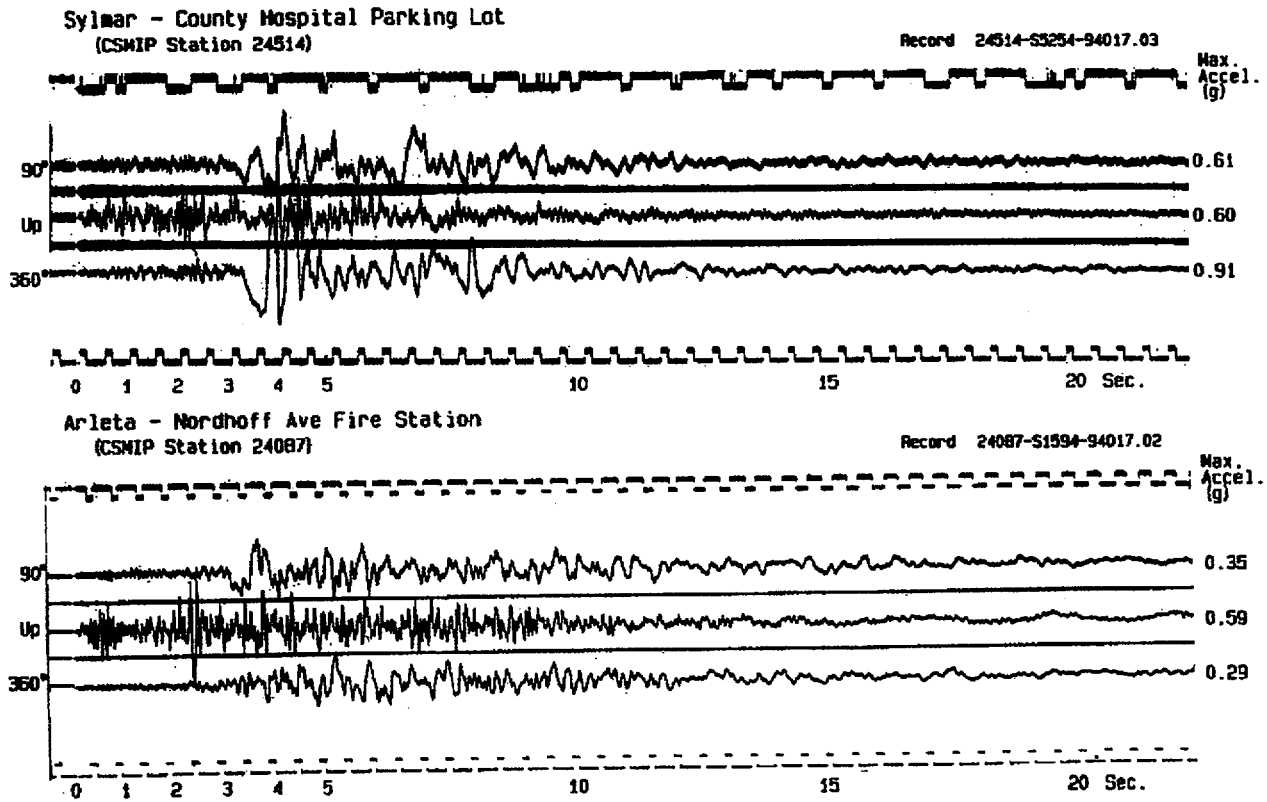


Figure J-7. Horizontal and vertical component acceleration time histories recorded at soil sites Sylmar (top) and Arleta (bottom) for the 1994 M 6.7 Northridge earthquake. (Source: CDMG initial data reports).

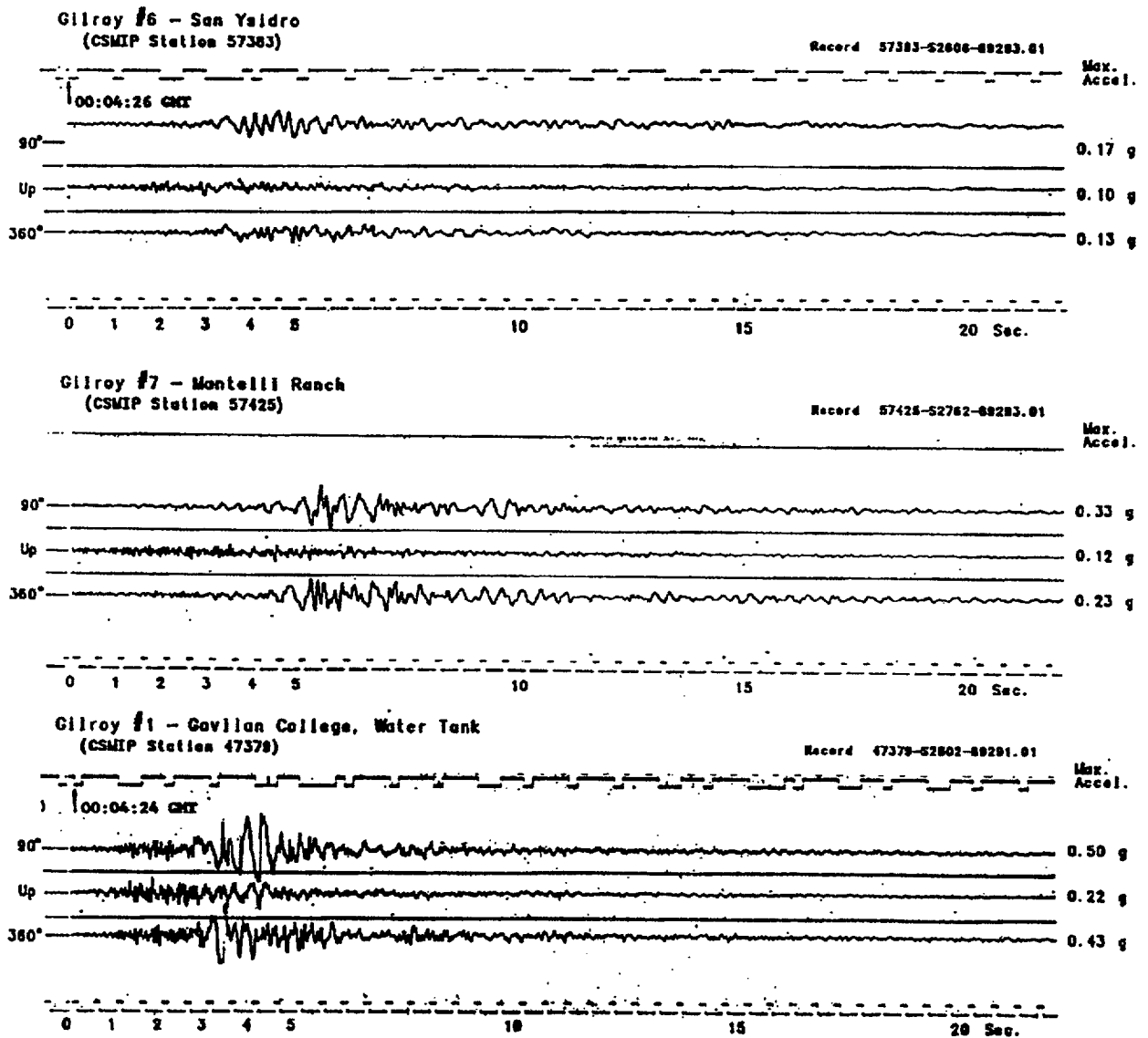


Figure J-8. Horizontal and vertical component acceleration time histories recorded at rock sites Gilroy 6, 7, and 1 (top, middle, and bottom) for the 1989 M 6.9 Loma Prieta earthquake. (Source: CDMG initial data reports)

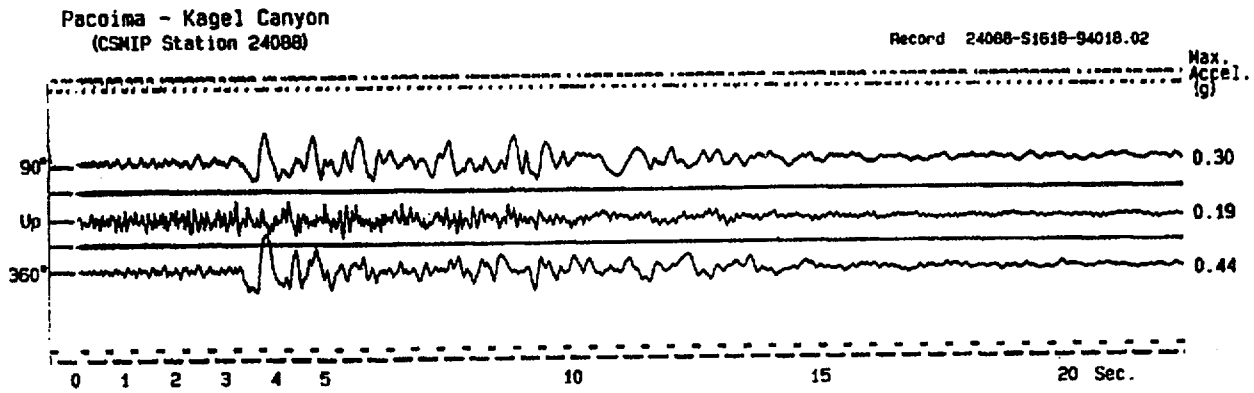


Figure J-9. Horizontal and vertical component acceleration time histories recorded at “rock” site Pacoima Kagel for the 1994 M 6.7 Northridge earthquake. (Source: CDMG initial data reports)

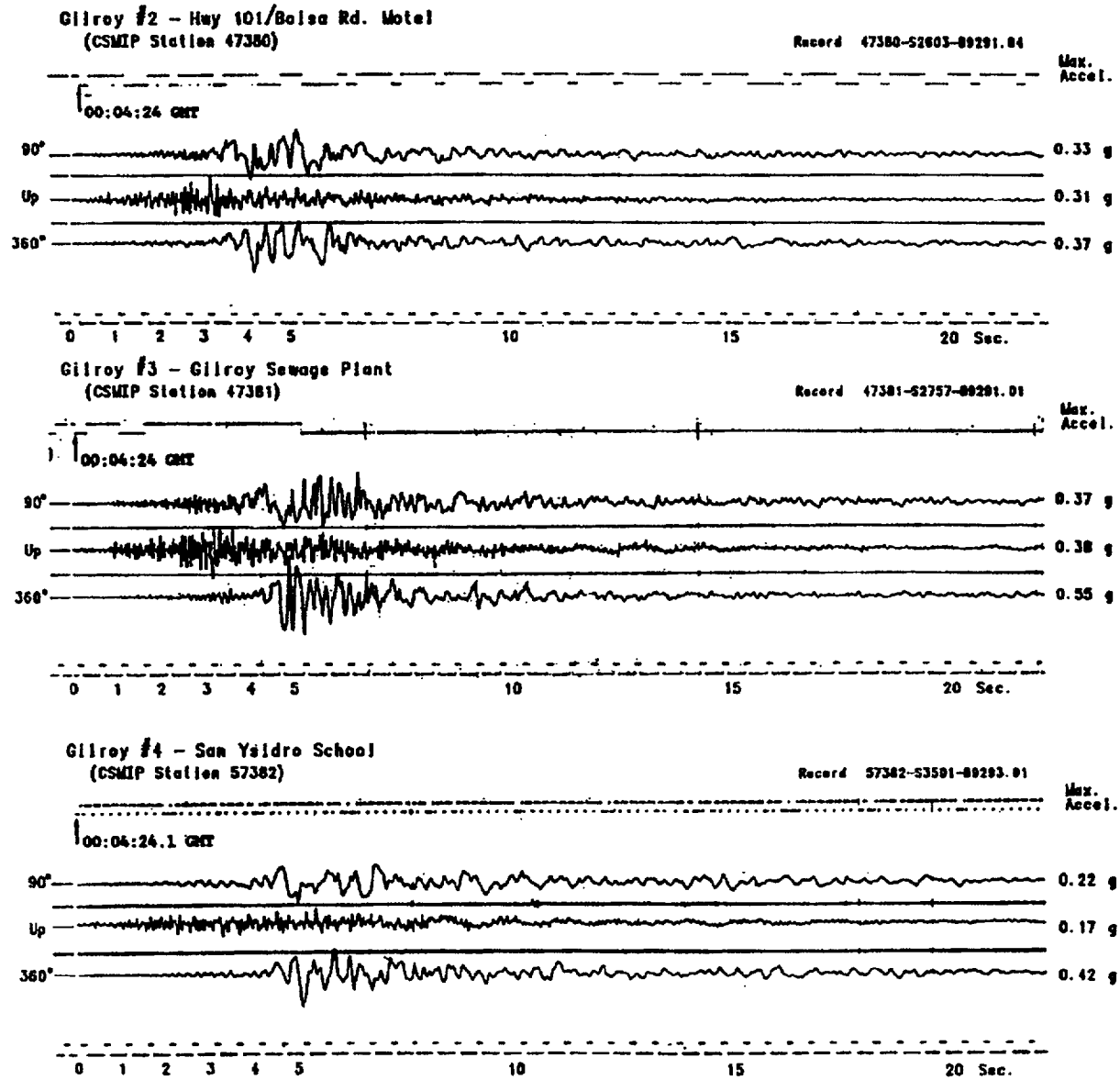
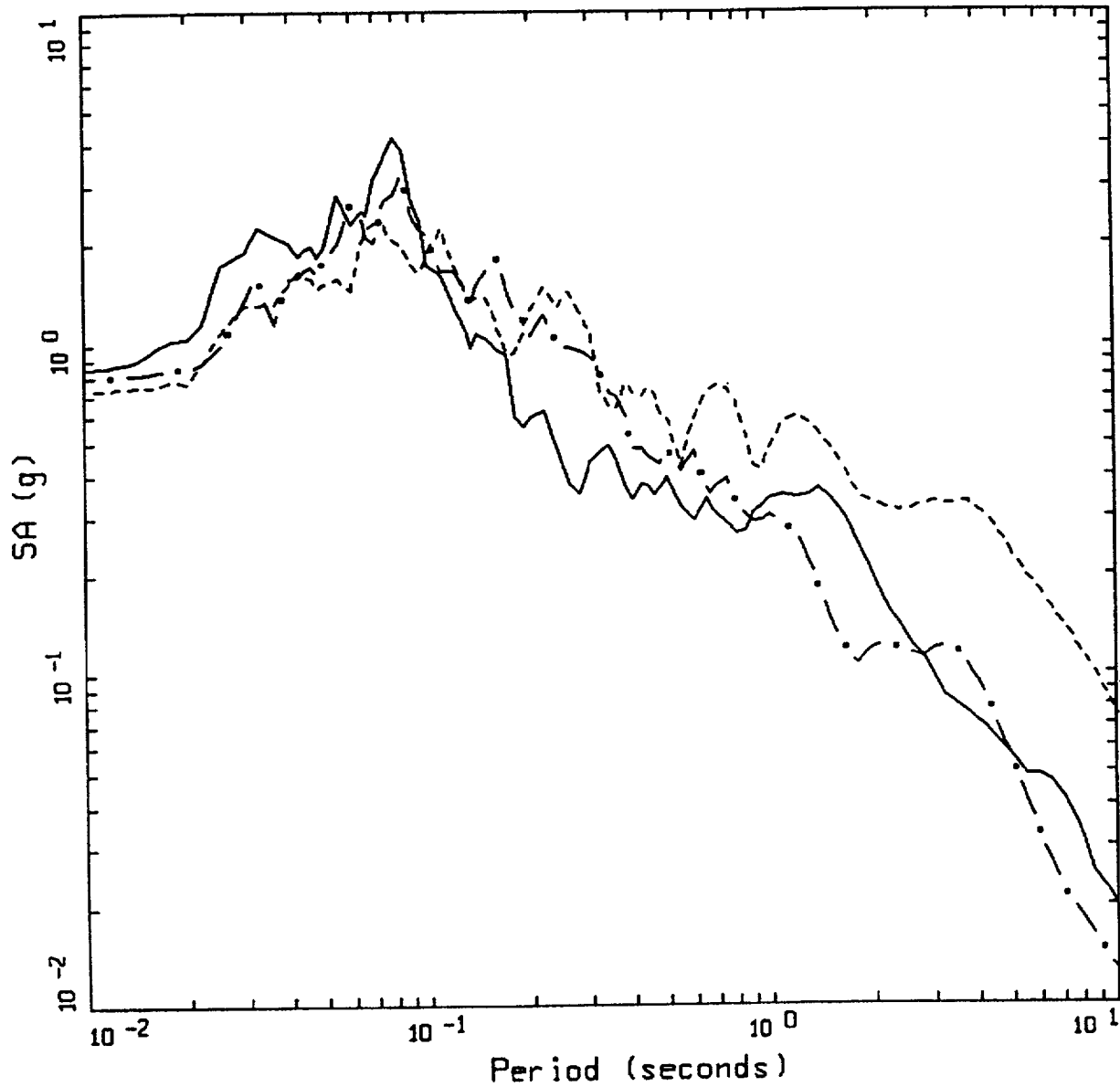


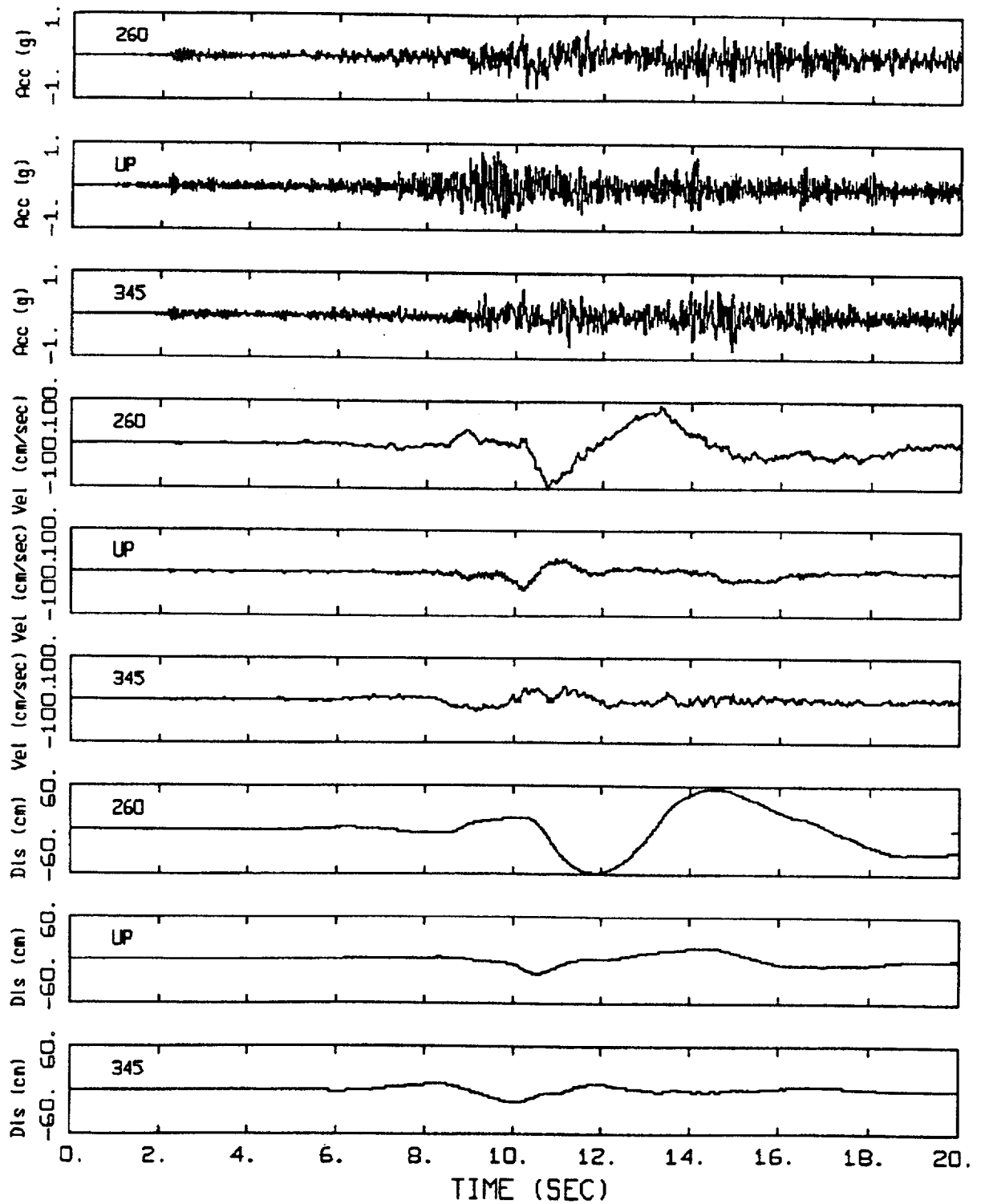
Figure J-10. Horizontal and vertical component acceleration time histories recorded at soil sites Gilroy 2, 3, and 4 (top, middle, and bottom) for the 1989 M 6.9 Loma Prieta earthquake. (Source: CDMG initial data reports)



LANDERS 06/28/92 1158
 LUCERNE

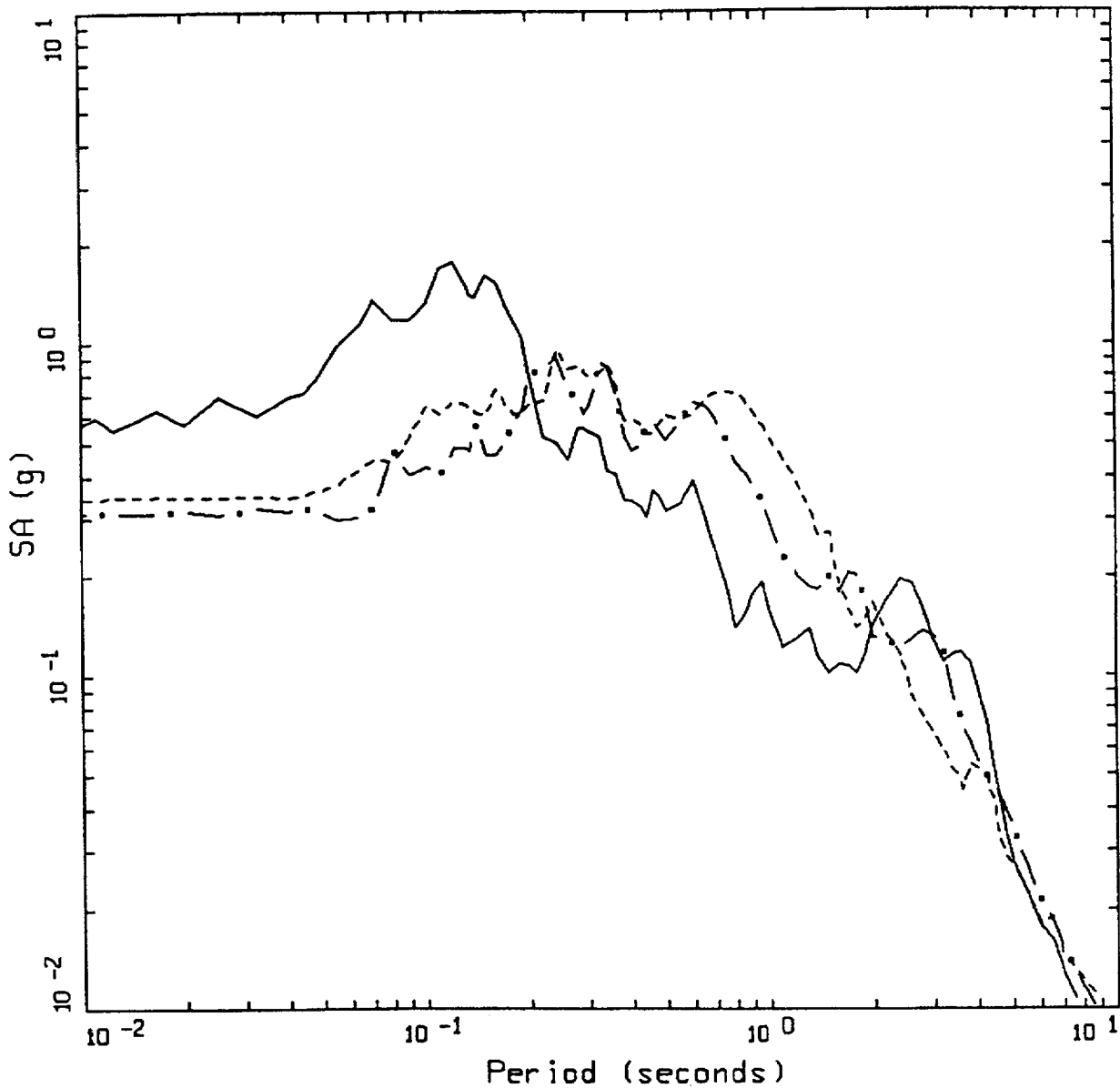
- LEGEND
- 5 %, IWAN & PE&A-CORRECTED DATA, COMP UP
 - - - 5 %, IWAN & PE&A-CORRECTED DATA, COMP 260
 - . - 5 %, IWAN & PE&A-CORRECTED DATA, COMP 345

Figure J-11. 5% damped psuedo absolute response spectra at the SCE rock site Lucerne for the 1992 M 7.2 Landers earthquake. Fault distance is about 2 km.



LANDERS 06/28/92 1158, LUCERNE

Figure J-12. Acceleration, velocity, and displacement time histories at the SCE rock site Lucerne for the 1992 M 7.2 Landers earthquake. Fault distance is about 2 km.

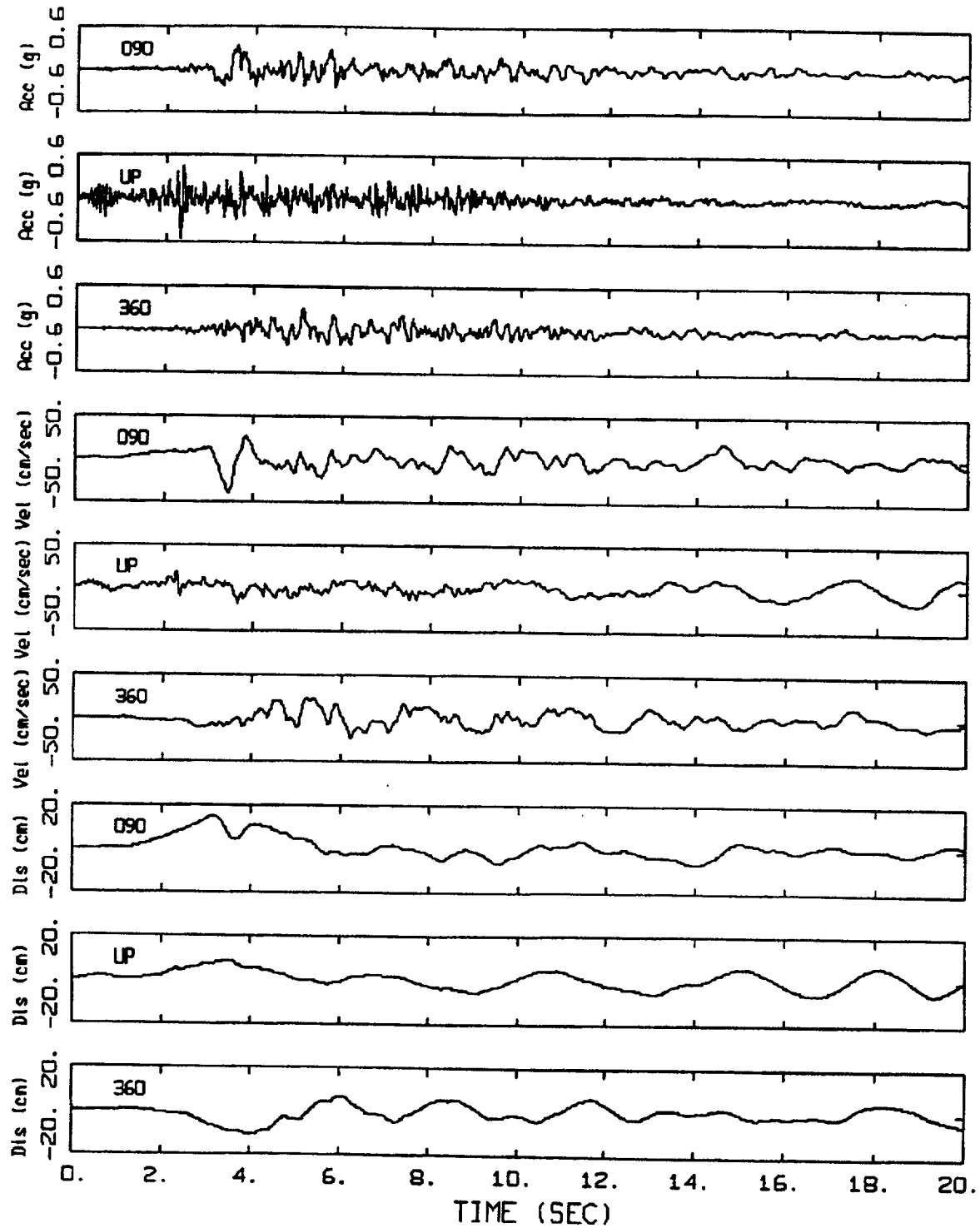


NORTHRIDGE 01/17/94 1231
 ARLETA - NORDHOFF FIRE STA

LEGEND

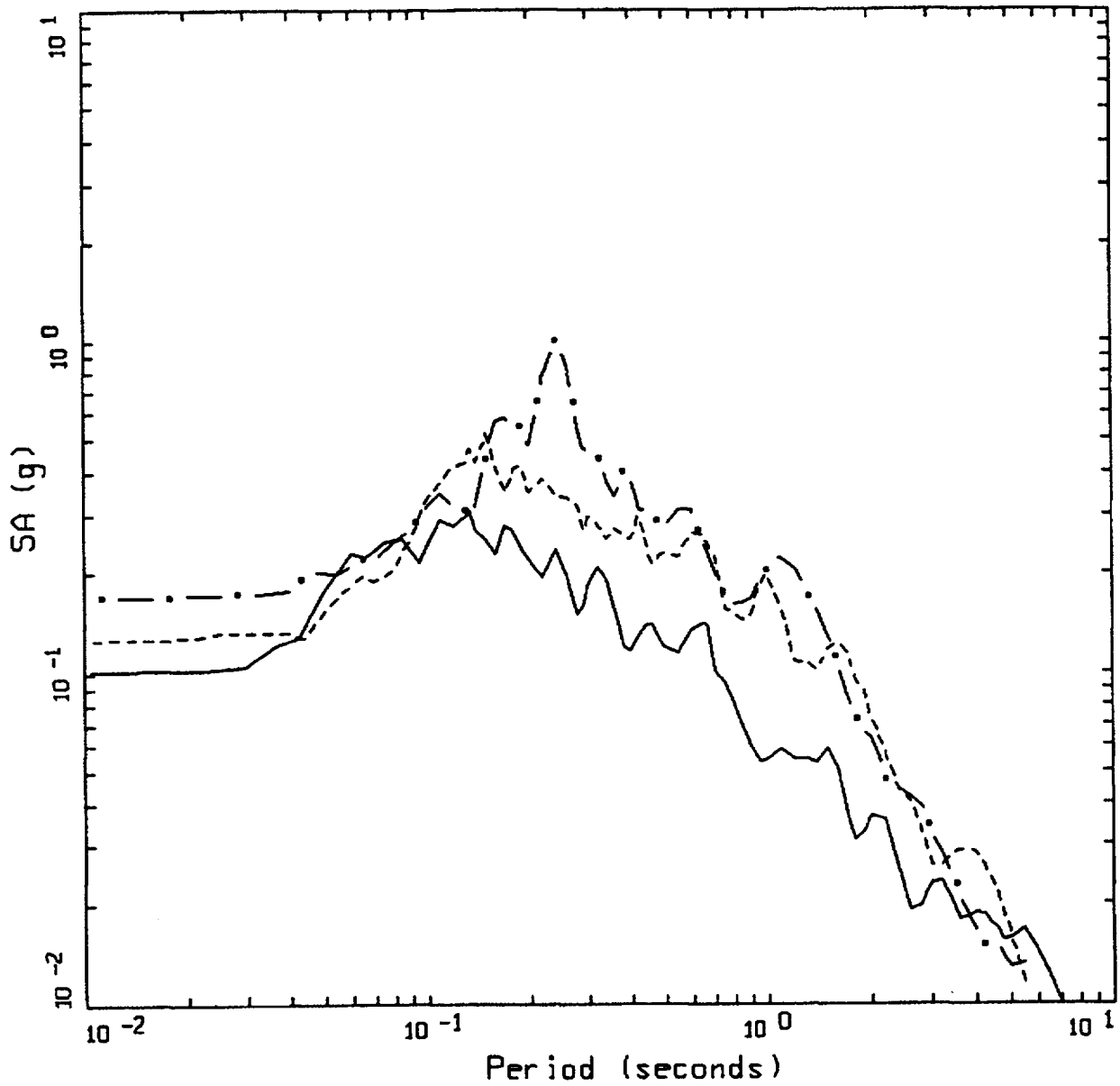
- 5 %, CDMG & PE&A-CORRECTED DATA, COMP UP
- - - 5 %, CDMG & PE&A-CORRECTED DATA, COMP 090
- · - 5 %, CDMG & PE&A-CORRECTED DATA, COMP 360

Figure J-13. 5% damped psuedo absolute response spectra at the soil site Arleta for the 1994 M 6.7 Northridge earthquake. Fault distance is about 9 km.



NORTHRIDGE 01/17/94 1231, ARLETA - NORDHOFF FIRE STA

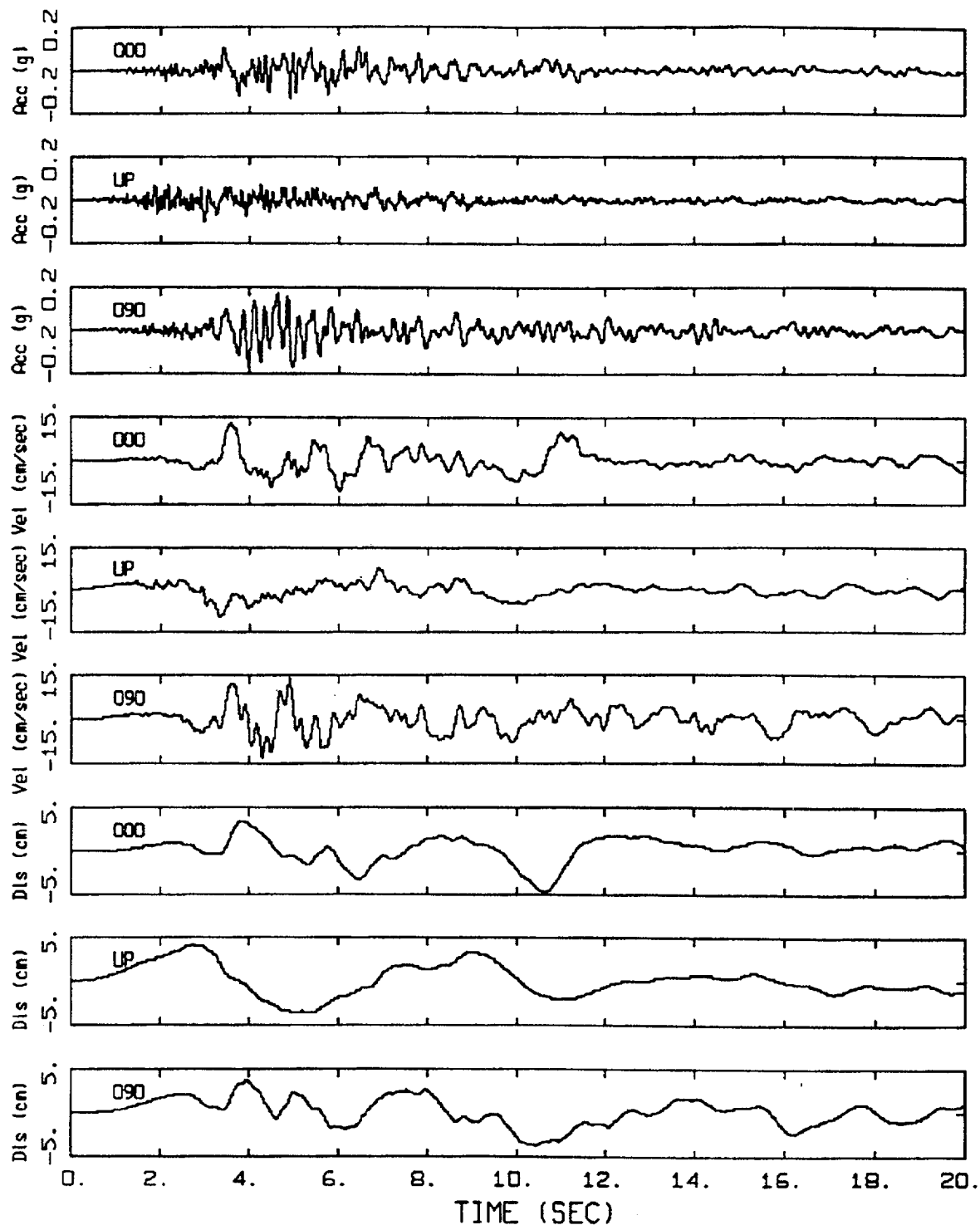
Figure J-14. Acceleration, velocity, and displacement time histories at the soil site Arleta for the 1994 M 6.7 Northridge earthquake. Fault distance is about 9 km.



LOMA PRIETA 10/18/89 0004
 GILROY ARRAY #6

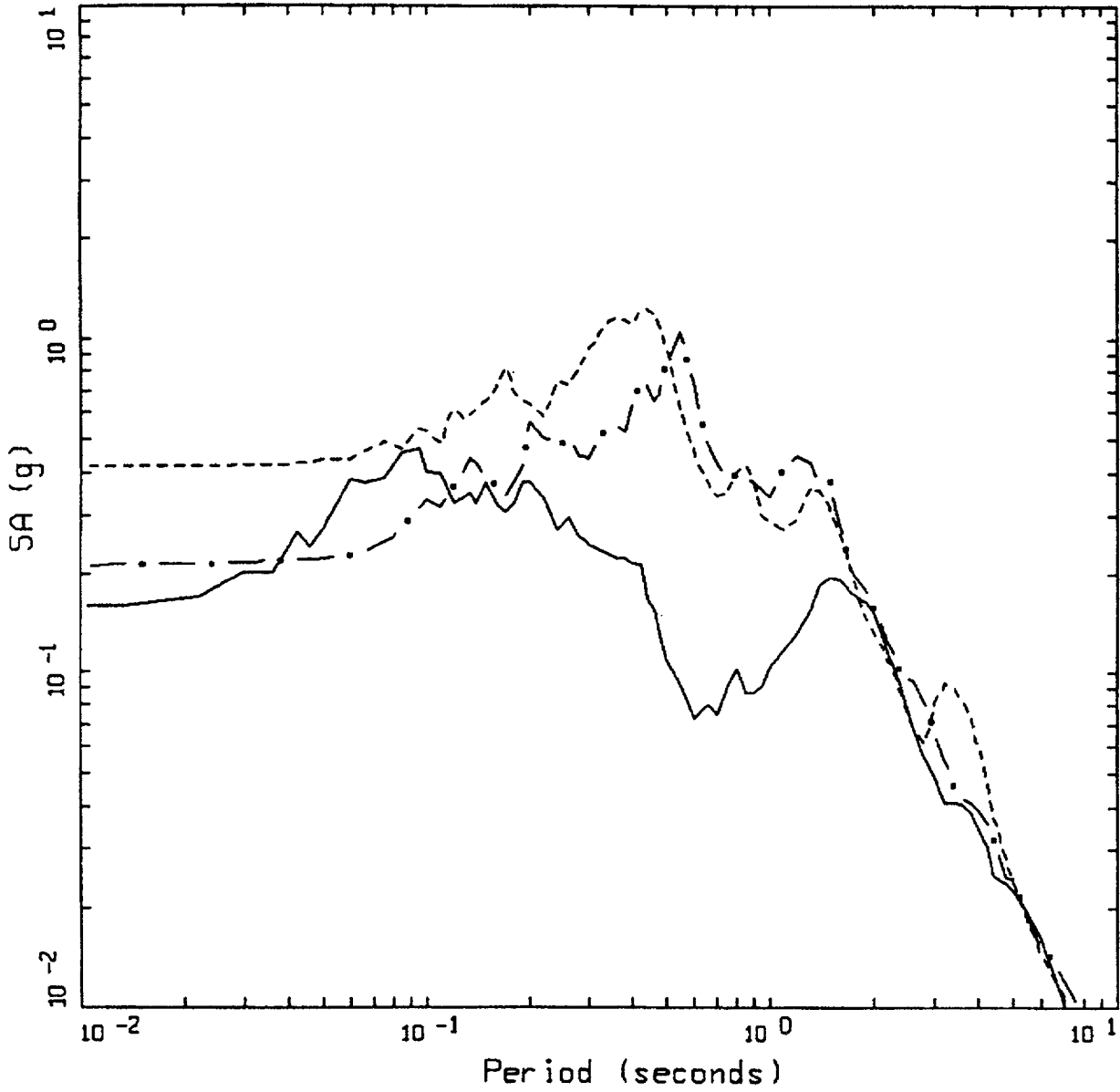
- LEGEND
- 5 %, PE&A-CORRECTED DATA, COMP 1P
 - - - 5 %, PE&A-CORRECTED DATA, COMP 000
 - . - 5 %, PE&A-CORRECTED DATA, COMP 090

Figure J-15. 5% damped pseudo absolute response spectra at the rock site Gilroy 6 for the 1989 M 6.9 Loma Prieta earthquake. Fault distance is about 19 km.



LOMA PRIETA 10/18/89 0004, GILROY ARRAY #6

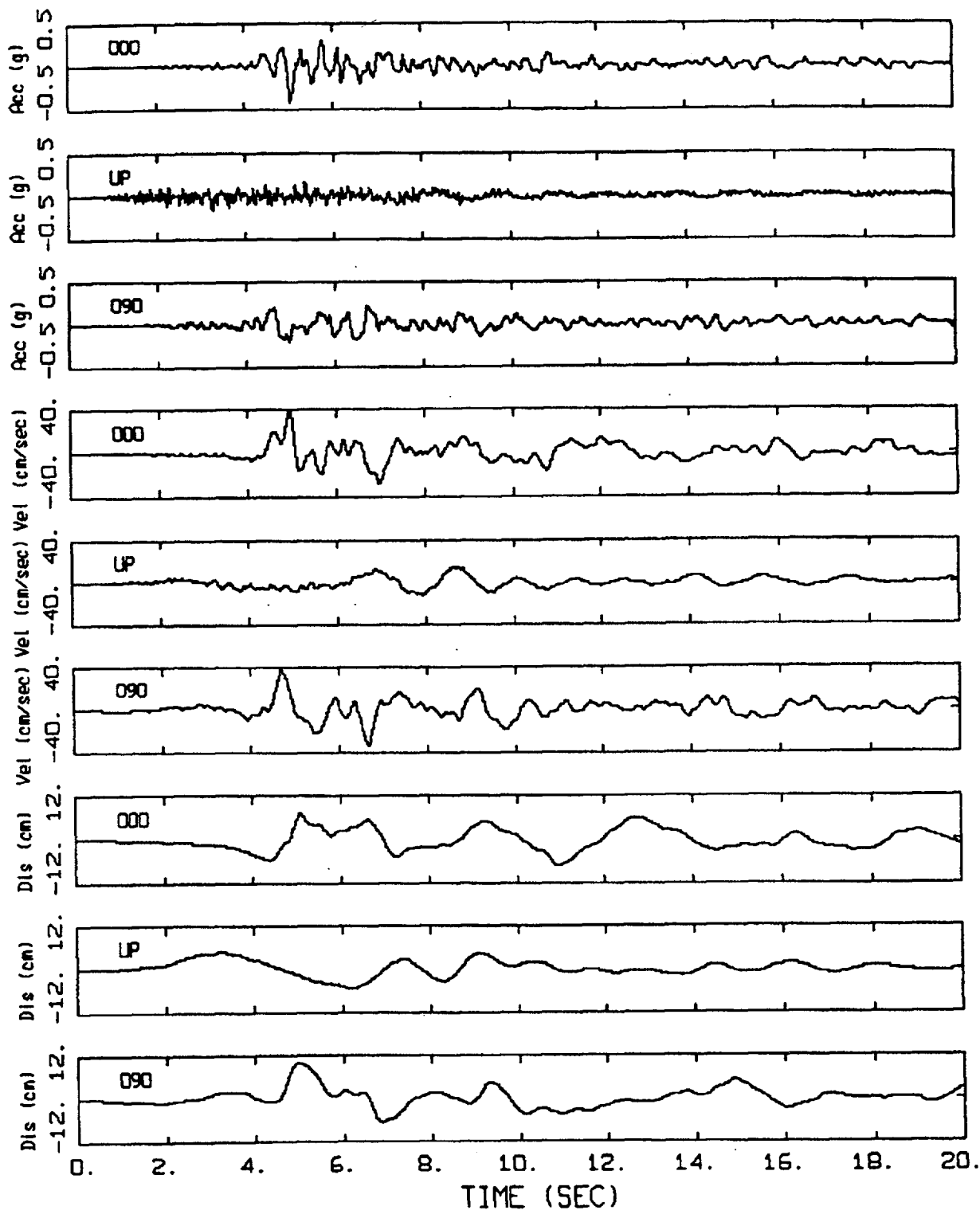
Figure J-16. Acceleration, velocity, and displacement time histories at the rock site Gilroy 6 for the 1989 M 6.9 Loma Prieta earthquake. Fault distance is about 19 km.



LOMA PRIETA 10/18/89 0004
 GILROY ARRAY #4

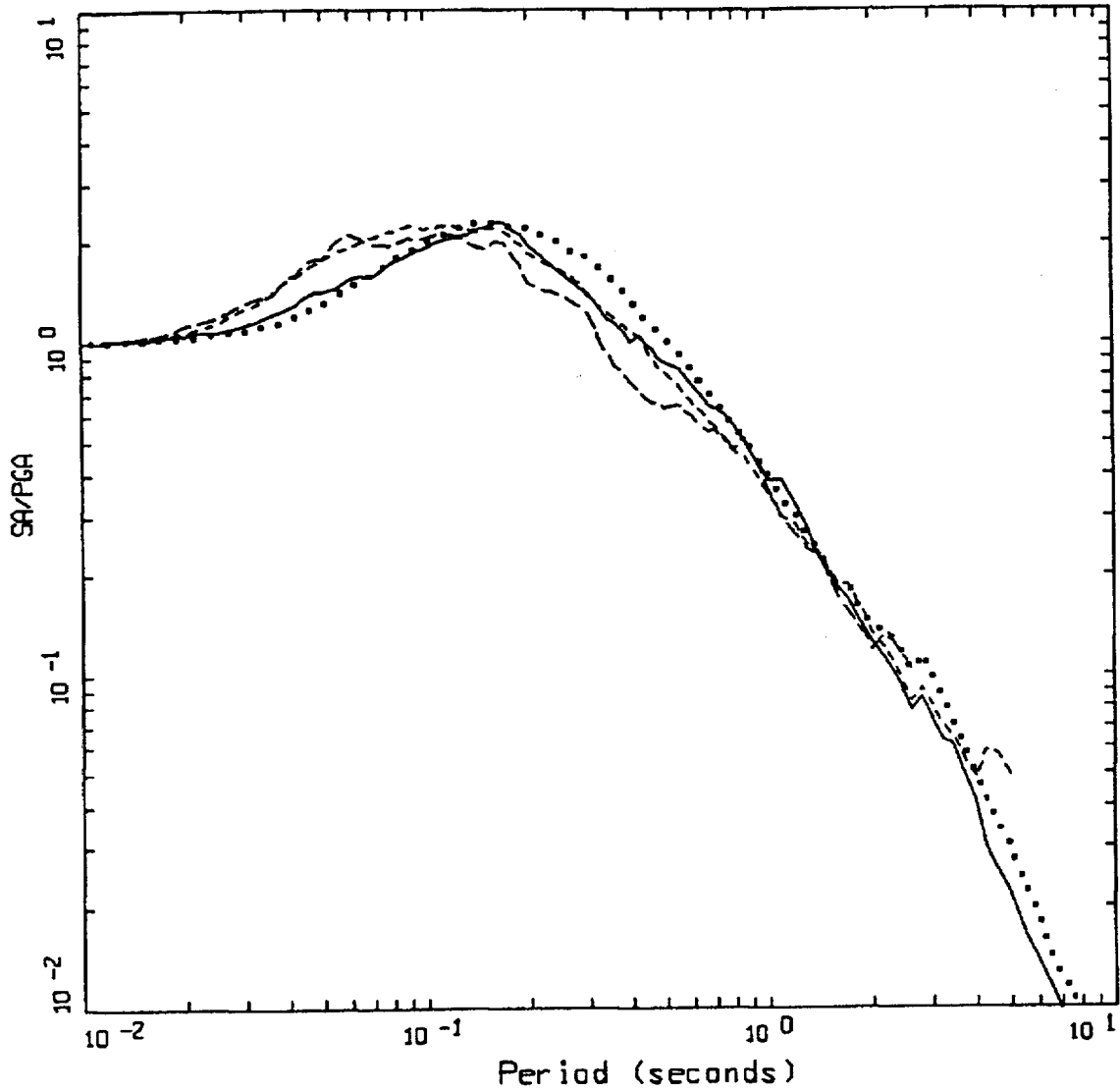
- LEGEND
- 5 %, PE&A-CORRECTED DATA, COMP UP
 - - - 5 %, PE&A-CORRECTED DATA, COMP 000
 - . - 5 %, PE&A-CORRECTED DATA, COMP 090

Figure J-17. 5% damped pseudo absolute response spectra at the soil site Gilroy 4 for the 1989 M 6.9 Loma Prieta earthquake. Fault distance is about 16 km.



LOMA PRIETA 10/18/89 DDD4, GILROY ARRAY #4

Figure J-18. Acceleration, velocity, and displacement time histories at the soil site Gilroy 4 for the 1989 M 6.9 Loma Prieta earthquake. Fault distance is about 16 km.



MEDIAN SPECTRAL SHAPES
M=5.5 (5.0-6.0), ROCK

- LEGEND
- HORIZONTAL, M=5.51 (5.0-6.0), D=7.84 KM (0-10 KM), AVG PGA = 0.179 G, 28 REC.
 - HORIZONTAL, M=5.59 (5.0-6.0), D=21.70 KM (10-50 KM), AVG PGA = 0.108 G, 182 REC.
 - VERTICAL, M=5.51 (5.0-6.0), D=7.84 KM (0-10 KM), AVG PGA = 0.124 G, 13 REC.
 - · - · - VERTICAL, M=5.59 (5.0-6.0), D=21.70 KM (10-50 KM), AVG PGA = 0.067 G, 88 REC.

Figure J-19. Median statistical response spectral shapes (5% damping) computed from WUS data recorded at rock sites in the magnitude range of M 5 to M 6. Rupture distances range from 0 to 10 km and 10 to 50 km.

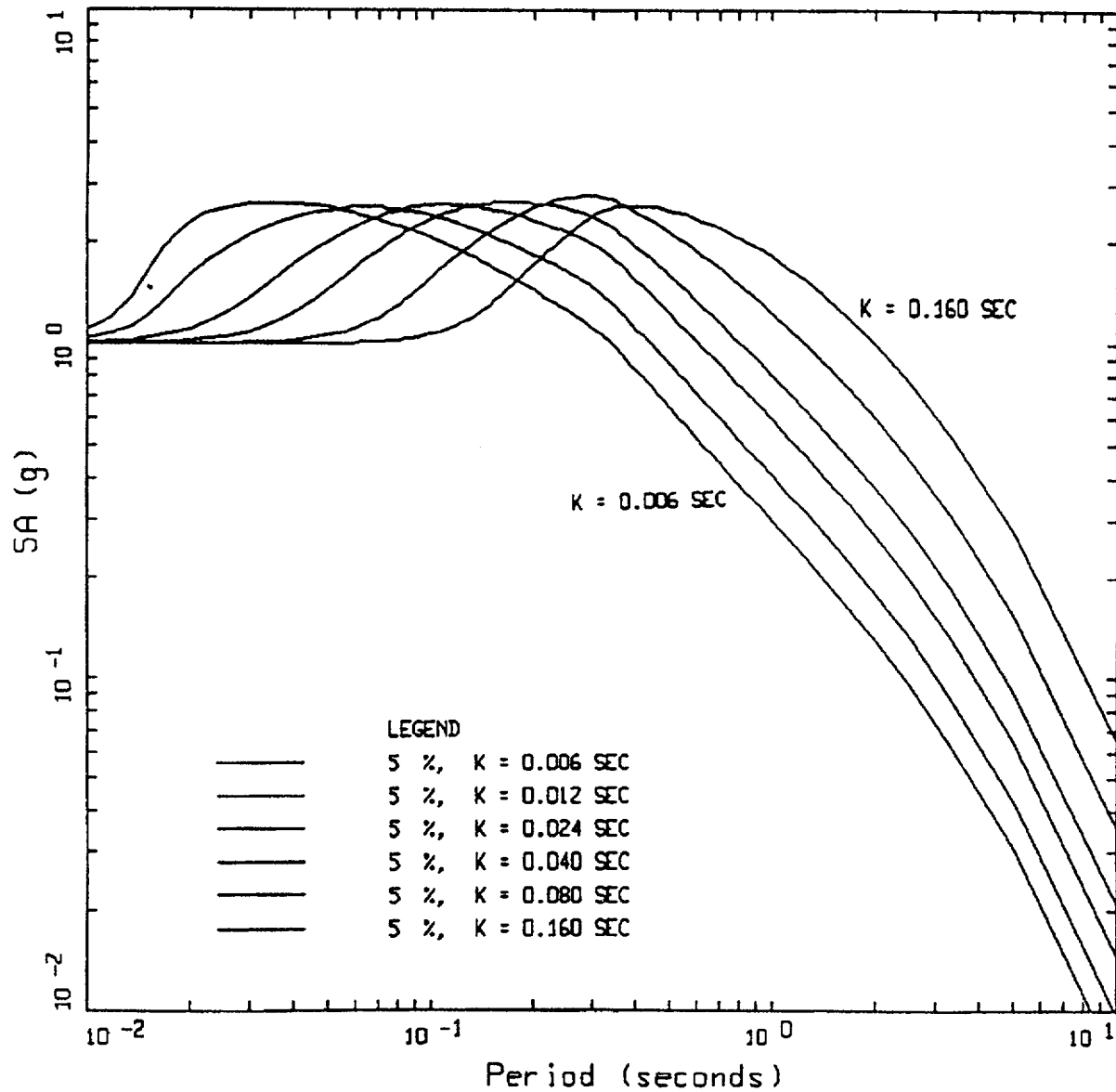
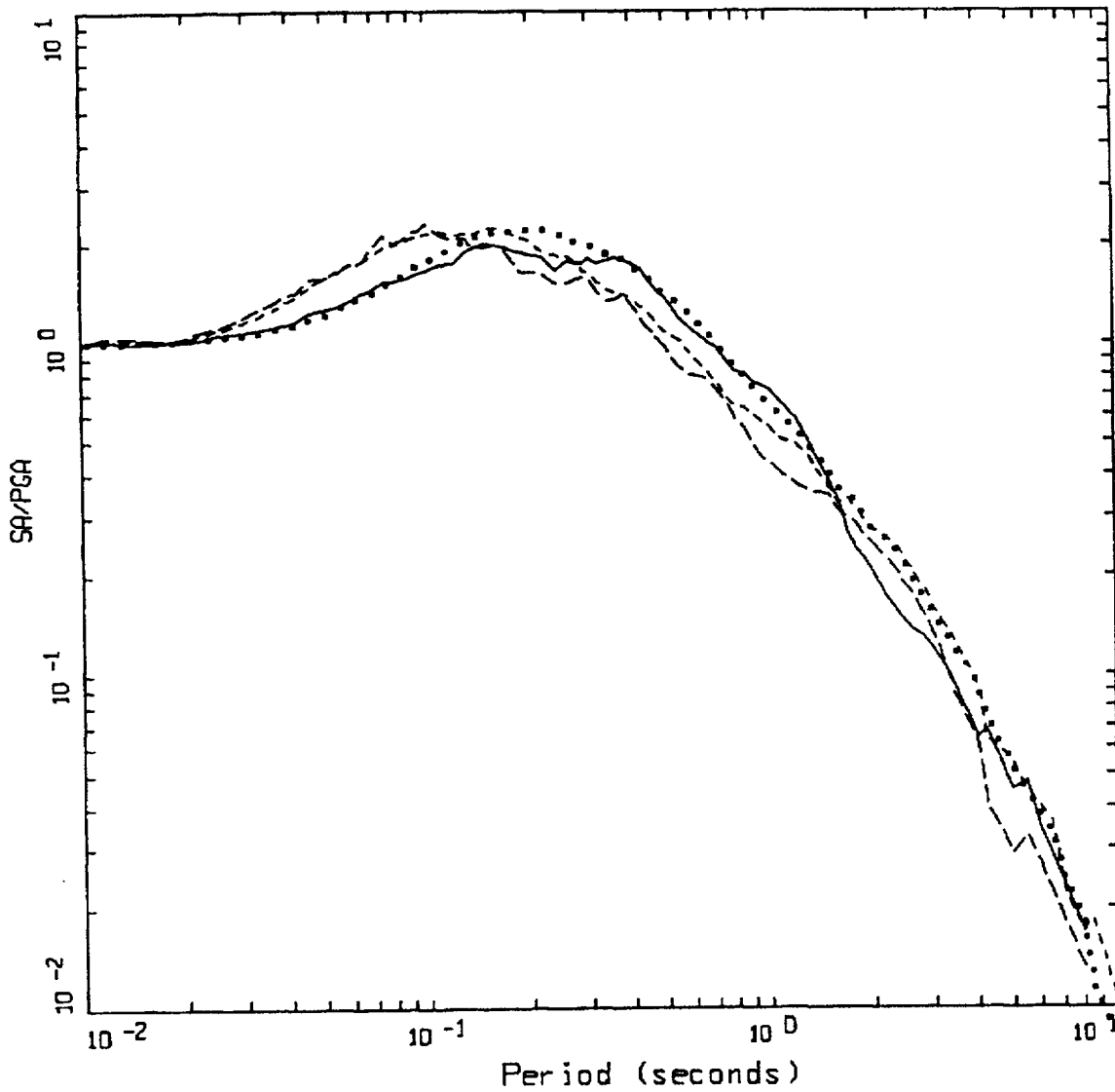


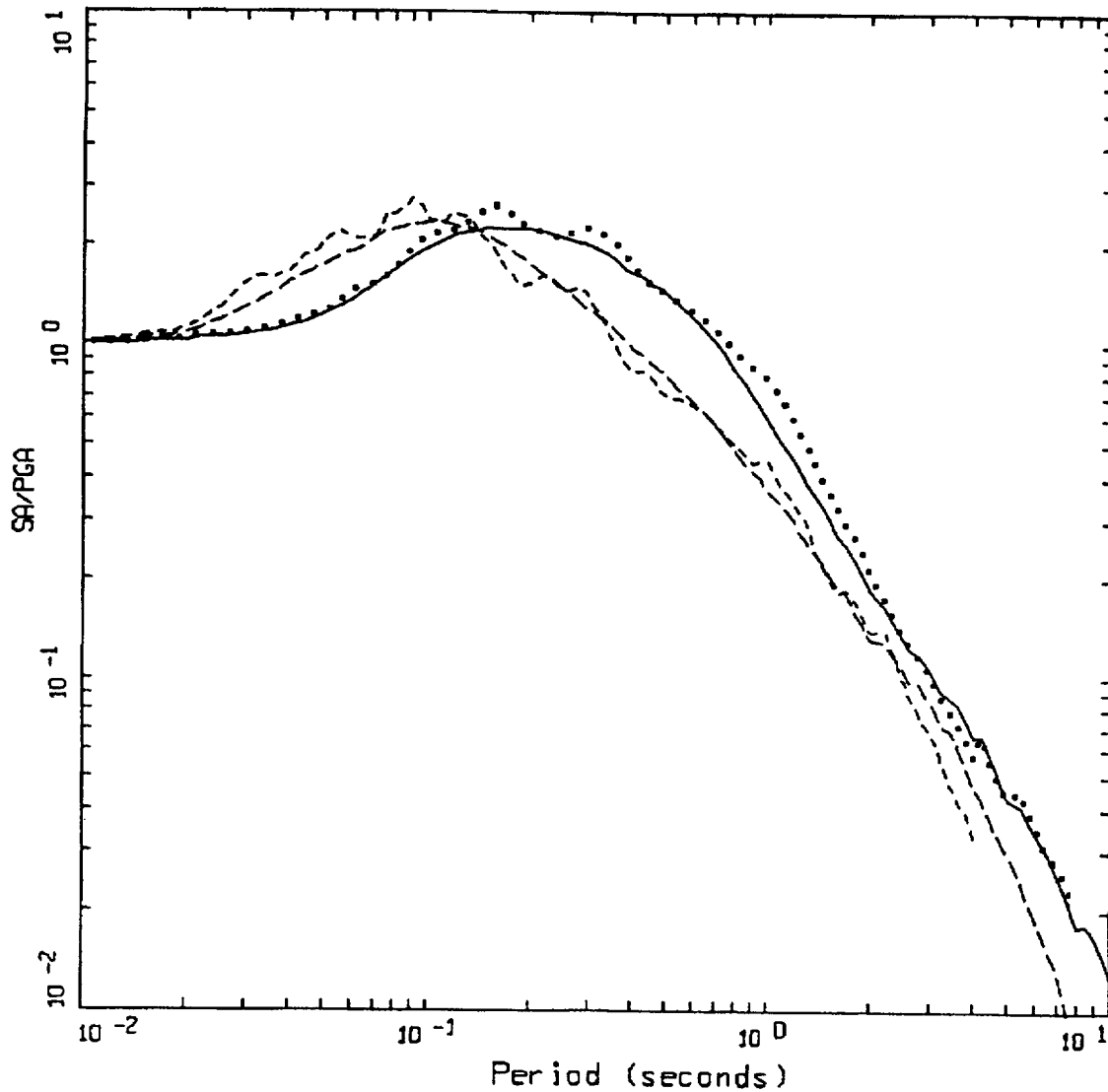
Figure J-20. The effects of kappa on 5% damped response spectral shapes computed for a M 6.5 earthquake at 10 km using WNA parameters. As kappa increases, the peak shifts to longer periods and remains essentially constant in amplitude.



MEDIAN SPECTRAL SHAPES
M=6.5 (6.0-7+), ROCK

- LEGEND
- HORIZONTAL, M=6.52 (6.0-7+), D=6.09 KM (0-10 KM), AVG PGA = 0.456 G, 28 REC.
 - HORIZONTAL, M=6.36 (6.0-7+), D=26.47 KM (10-50 KM), AVG PGA = 0.124 G, 206 REC.
 - - - - - VERTICAL, M=6.52 (6.0-7+), D=6.09 KM (0-10 KM), AVG PGA = 0.457 G, 11 REC.
 - · - · - VERTICAL, M=6.36 (6.0-7+), D=26.47 KM (10-50 KM), AVG PGA = 0.074 G, 103 REC.

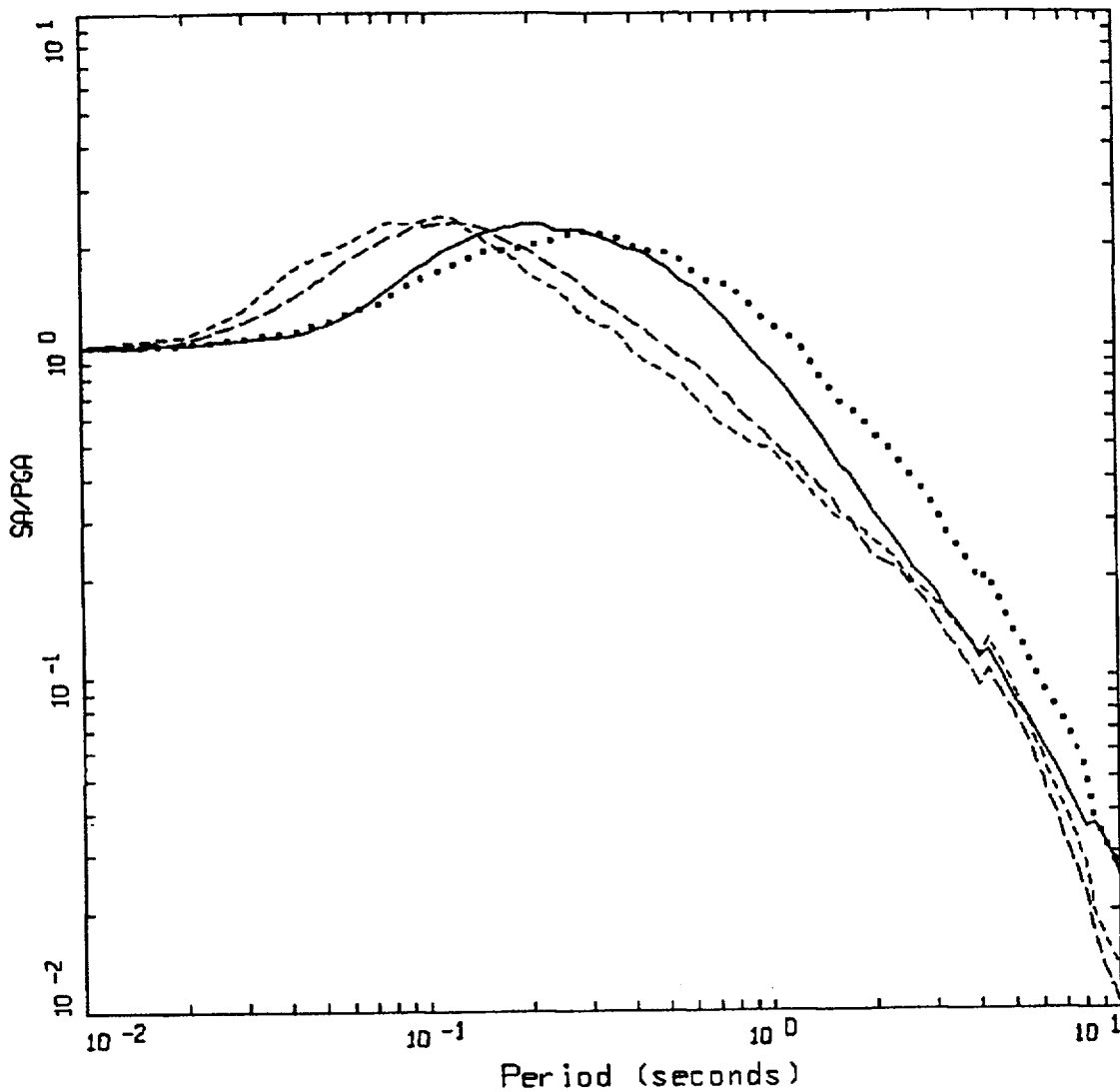
Figure J-21. Median statistical response spectral shapes (5% damping) computed from WUS data recorded at rock sites in the magnitude range of M 6 to M 7+. Rupture distances range from 0 to 10 km and 10 to 50 km.



MEDIAN SPECTRAL SHAPES
M=5.5 (5.0-6.0), SOIL

- LEGEND
- HORIZONTAL, M=5.76 (5.0-6.0), D=7.80 KM (0-10 KM), AVG PGA = 0.263 G, 24 REC.
 - HORIZONTAL, M=5.69 (5.0-6.0), D=22.06 KM (10-50 KM), AVG PGA = 0.110 G, 370 REC.
 - VERTICAL, M=5.76 (5.0-6.0), D=7.80 KM (0-10 KM), AVG PGA = 0.204 G, 11 REC.
 - · - · - VERTICAL, M=5.69 (5.0-6.0), D=22.06 KM (10-50 KM), AVG PGA = 0.069 G, 184 REC.

Figure J-22. Median statistical response spectral shapes (5% damping) computed from WUS data recorded at soil sites in the magnitude range of M 5 to M 6. Rupture distances range from 0 to 10 km and 10 to 50 km.



MEDIAN SPECTRAL SHAPES
M=6.5 (6.0-7.0), SOIL

- LEGEND
- HORIZONTAL, M=6.51 (6.0-7.0), D=5.56 KM (0-10 KM), AVG PGA = 0.381 G, 87 REC.
 - HORIZONTAL, M=6.33 (6.0-7.0), D=28.49 KM (10-50 KM), AVG PGA = 0.136 G, 505 REC.
 - VERTICAL, M=6.51 (6.0-7.0), D=5.56 KM (0-10 KM), AVG PGA = 0.315 G, 42 REC.
 - · - · - VERTICAL, M=6.33 (6.0-7.0), D=28.49 KM (10-50 KM), AVG PGA = 0.089 G, 247 REC.

Figure J-23. Median statistical response spectral shapes (5% damping) computed from WUS data recorded at soil sites in the magnitude range of M 6 to M 7+. Rupture distances range from 0 to 10 km and 10 to 50 km.

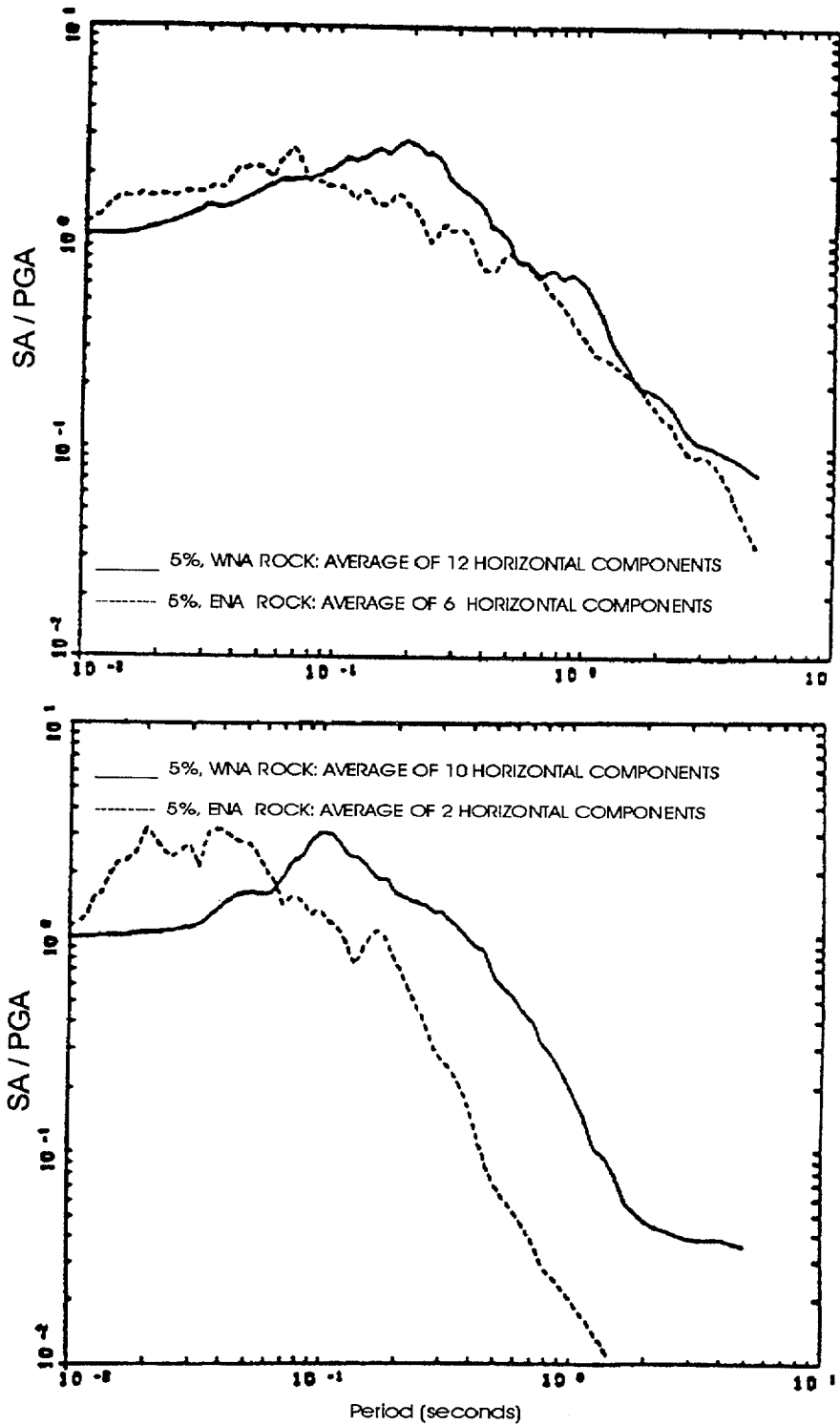
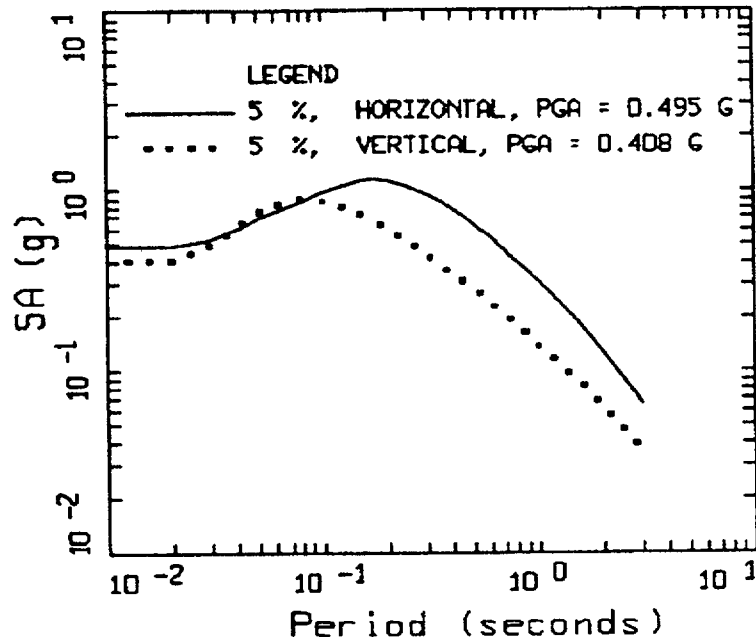
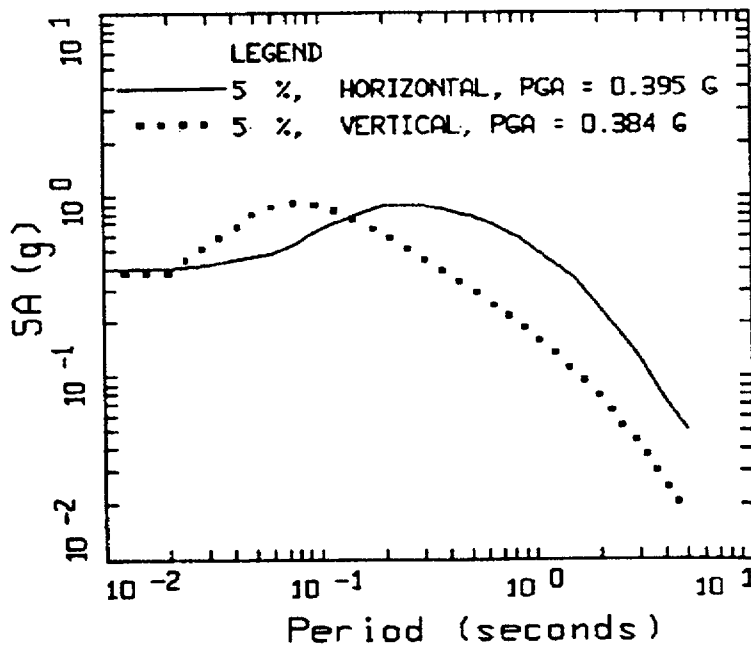


Figure J-24. Average 5% damping response spectral shapes (SA/PGA) computed from motions recorded on rock sites at close distances to $M = 6.4$ earthquakes (top figure) and $M = 4.0$ earthquakes (bottom figure). In each figure the solid line corresponds to motions recorded in WNA, dashed line to motions recorded in ENA.



M = 6.5, ROCK
 D = 5 KM



M = 6.5, SOIL
 D = 5 KM

Figure J-25. Median empirical response spectra (5% damped) computed at rock and soil sites for M 6.5 at fault distance of 5 km.

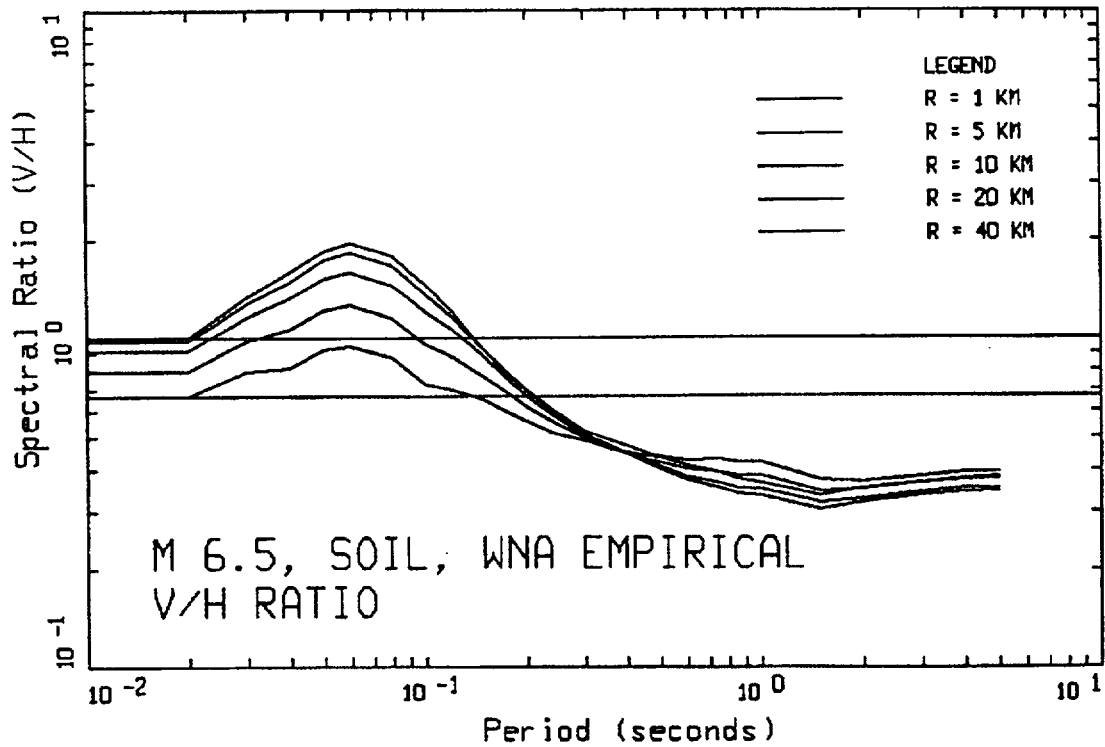
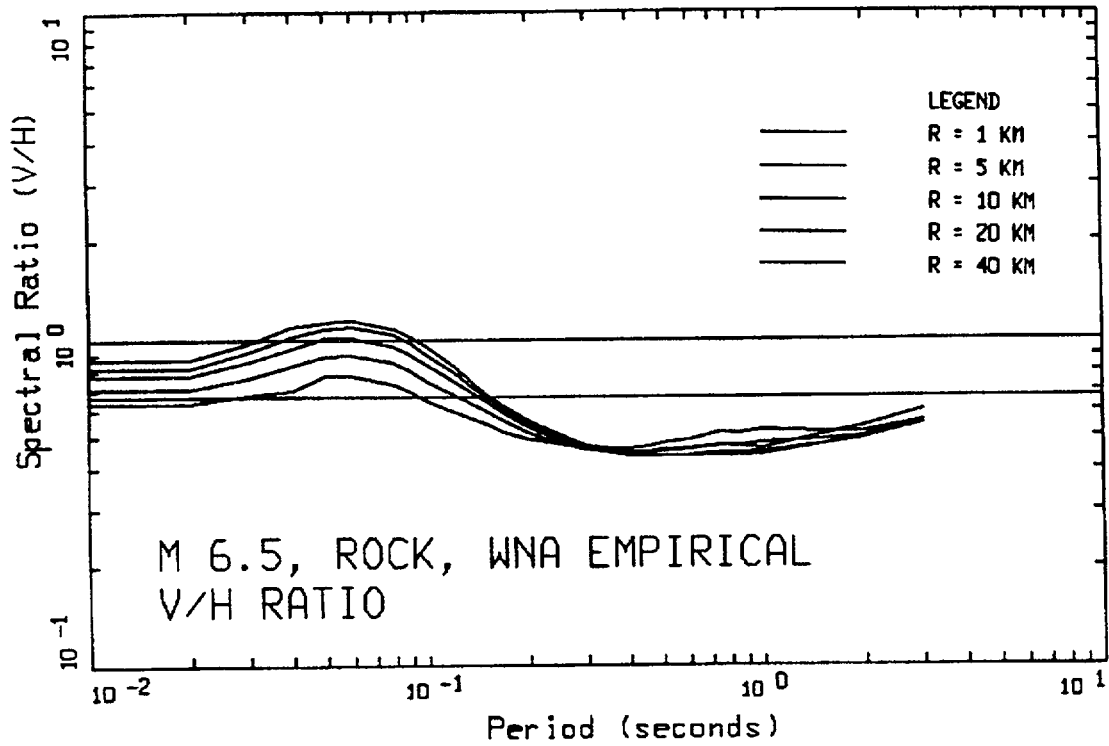


Figure J-26. Distance to fault dependency of response spectral ratios (V/H) for M 6.5 at rock and soil sites. Line at 0.66 indicates the constant ratio of 2/3. The R=1 km line is the highest on each plot at 0.05 sec.

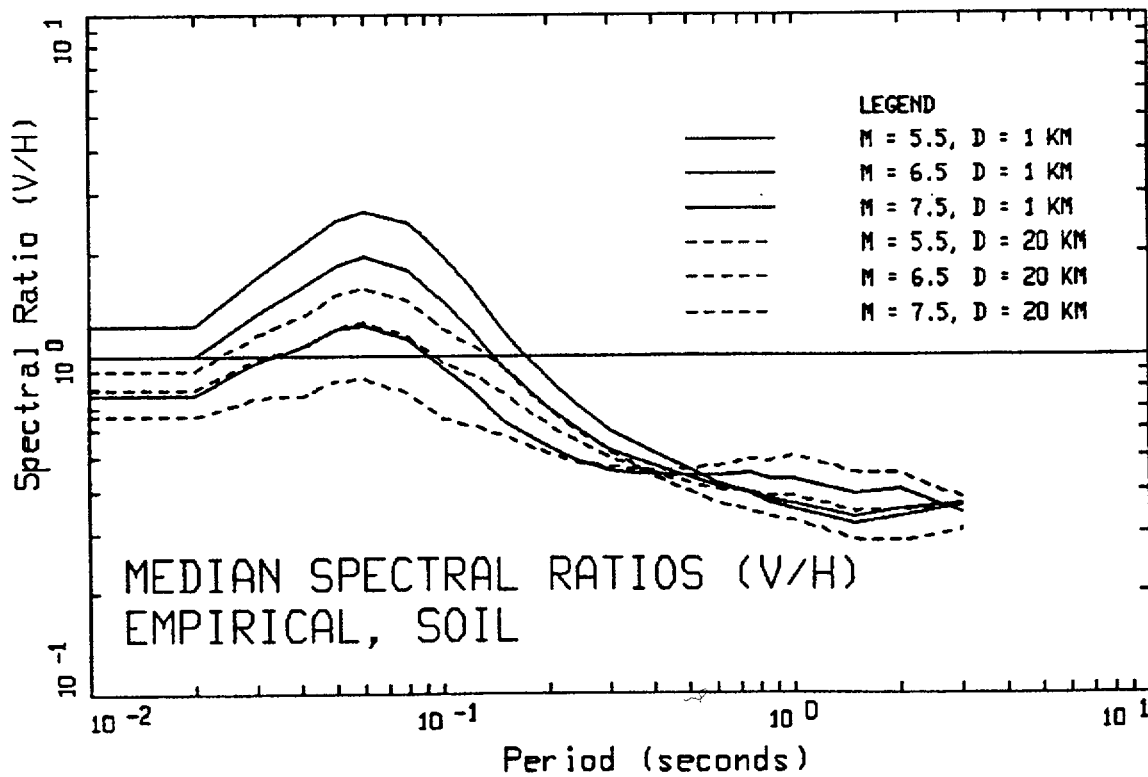
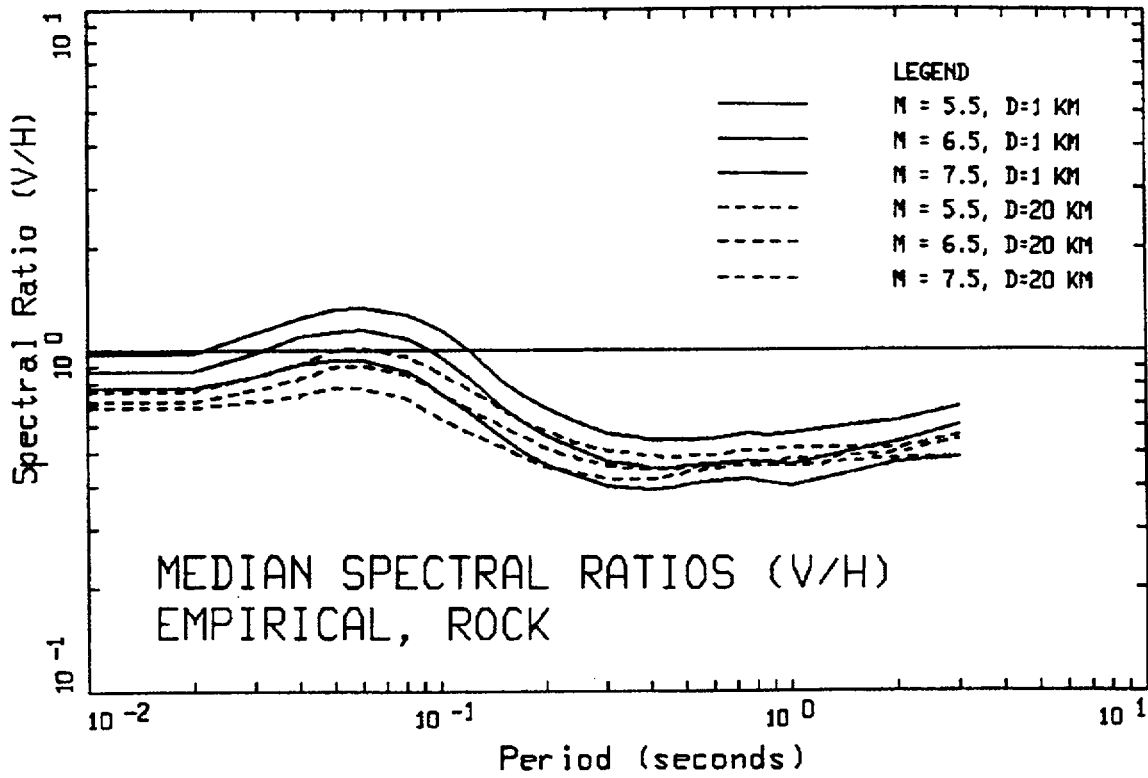
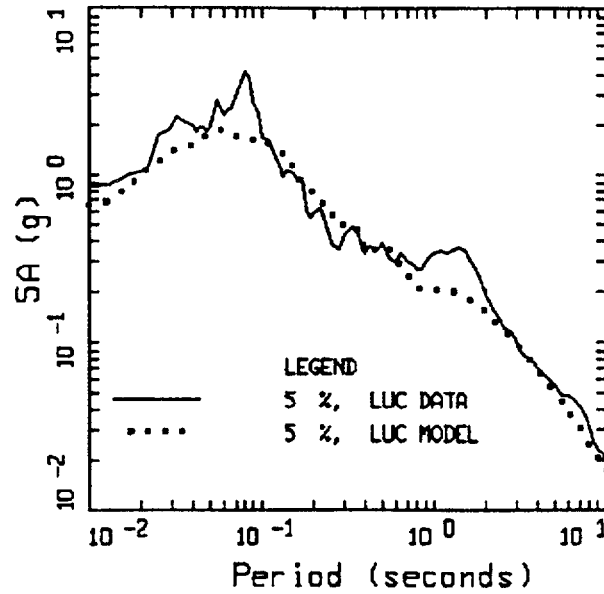
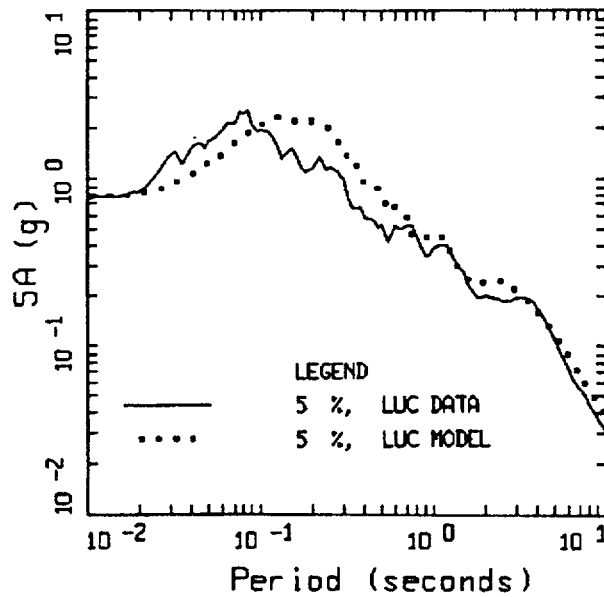


Figure J-27. Magnitude dependency of response spectral ratios (V/H) at fault distances 1 and 20 km. M 7.5 shows the highest amplification at 0.05 sec., M 5.5 shows the lowest.

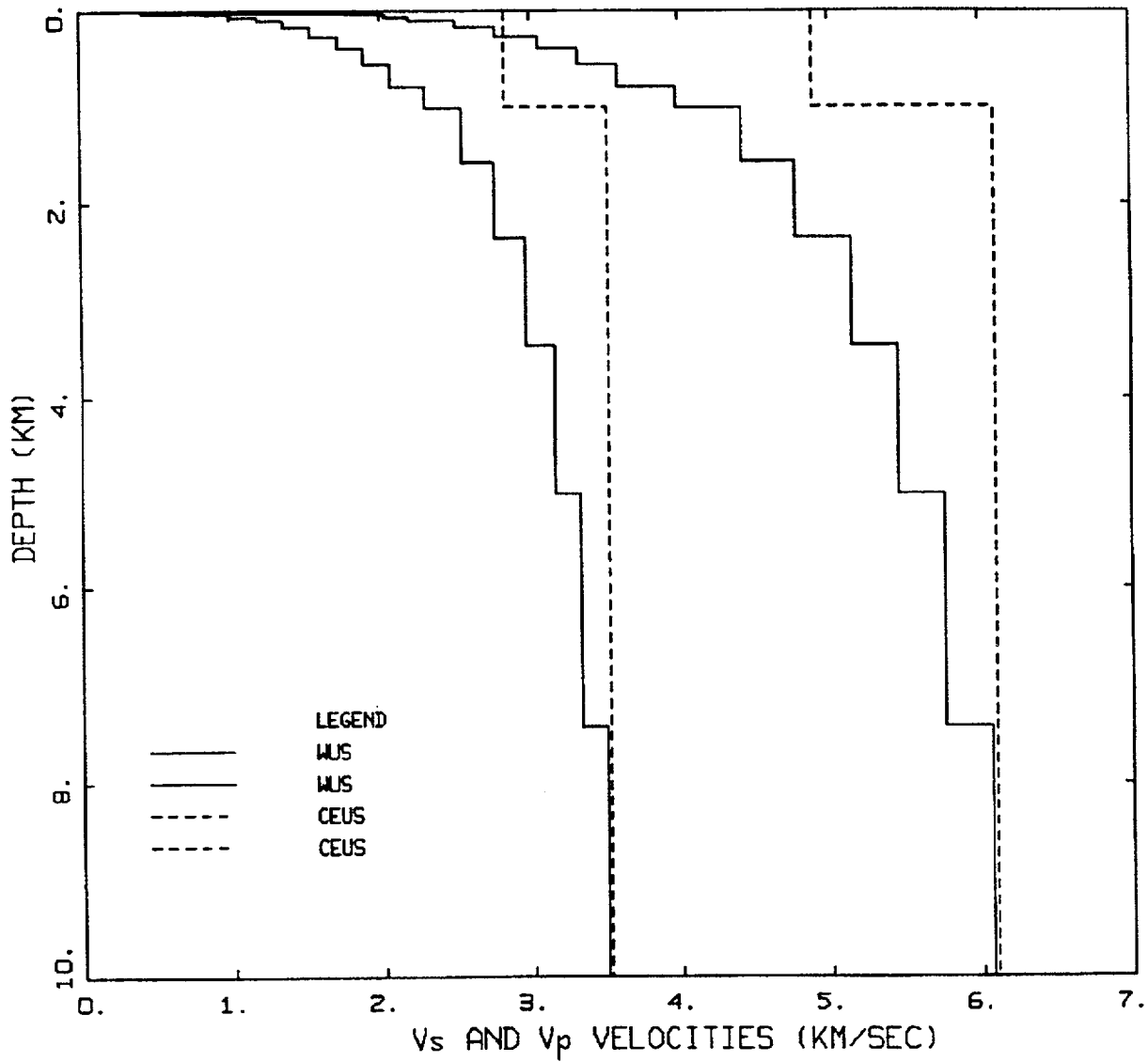


LANDERS, VERTICAL
LUC



LANDERS, HORIZONTAL
LUC

Figure J-28. Comparison of simulations to recorded motions for vertical and horizontal (average) components at the SCE rock site Lucerne for the 1992 M 7.2 Landers earthquake. The site is at a fault distance of about 2 km. A point-source model is used with the generic rock compression- and shear-wave velocity profiles (Figure J-1) over the regional crustal model (Wald and Heaton, 1994).



GENERIC WUS AND CEUS
CRUSTAL MODELS

Figure J-29. Comparison of generic compression- and shear-wave velocity profiles for WUS and CEUS crustal conditions.

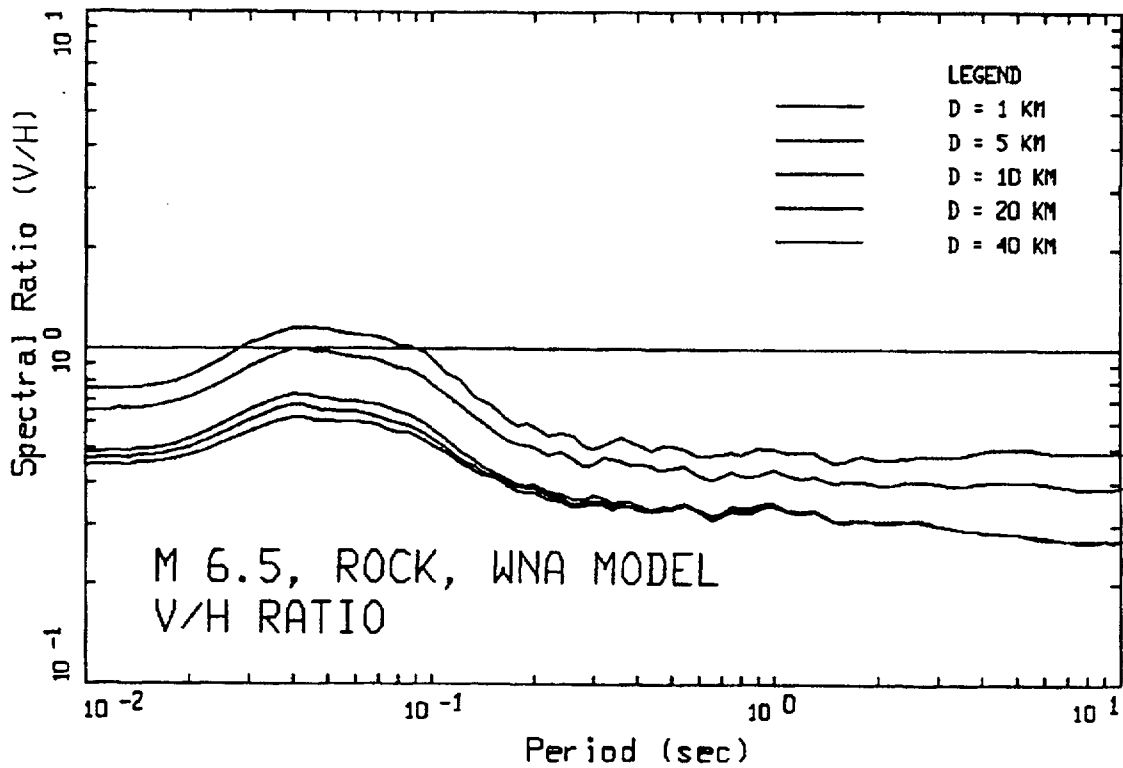
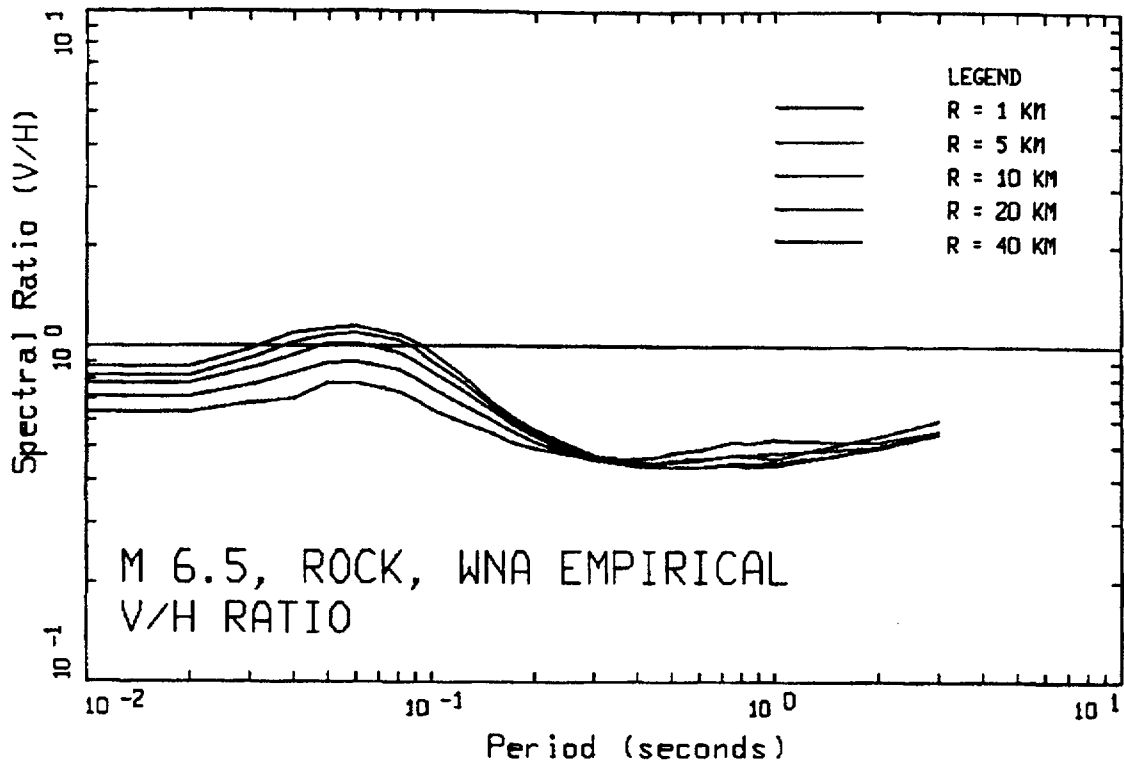


Figure J-30. Comparison of empirical and model response spectral ratios (V/H) at rock sites for M 6.5. The R=1 km line is the highest on each plot at 0.05 sec.

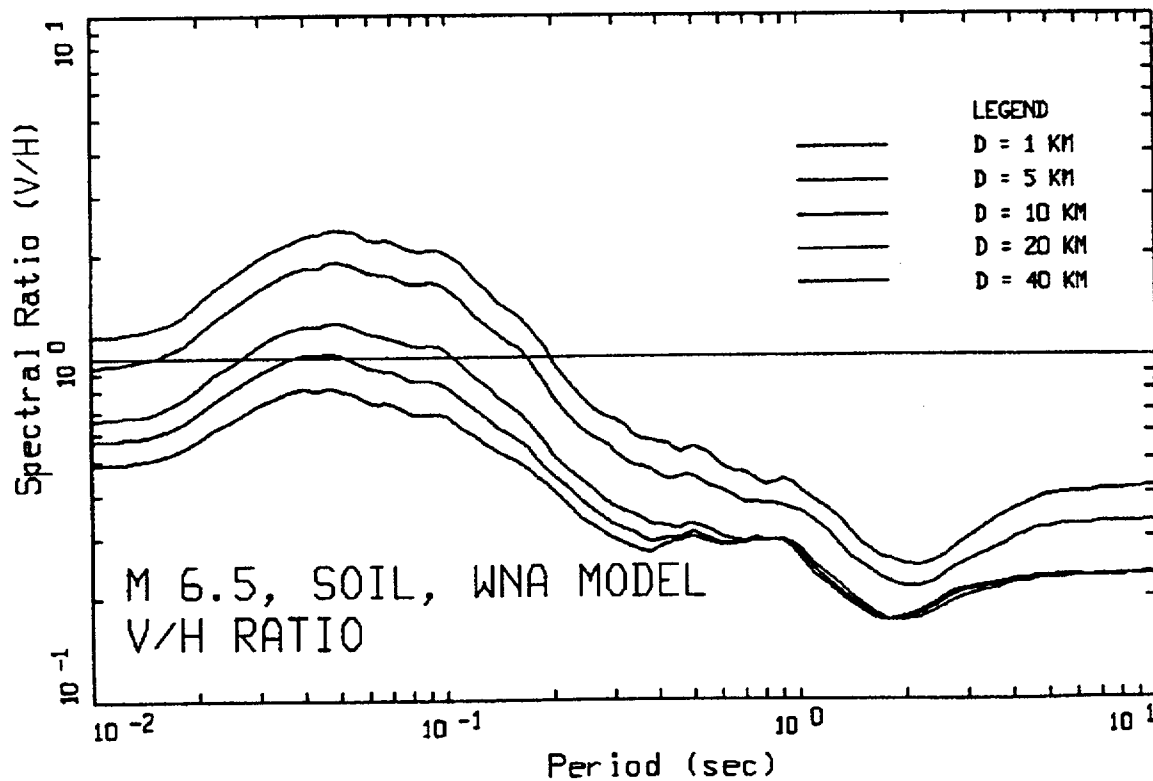
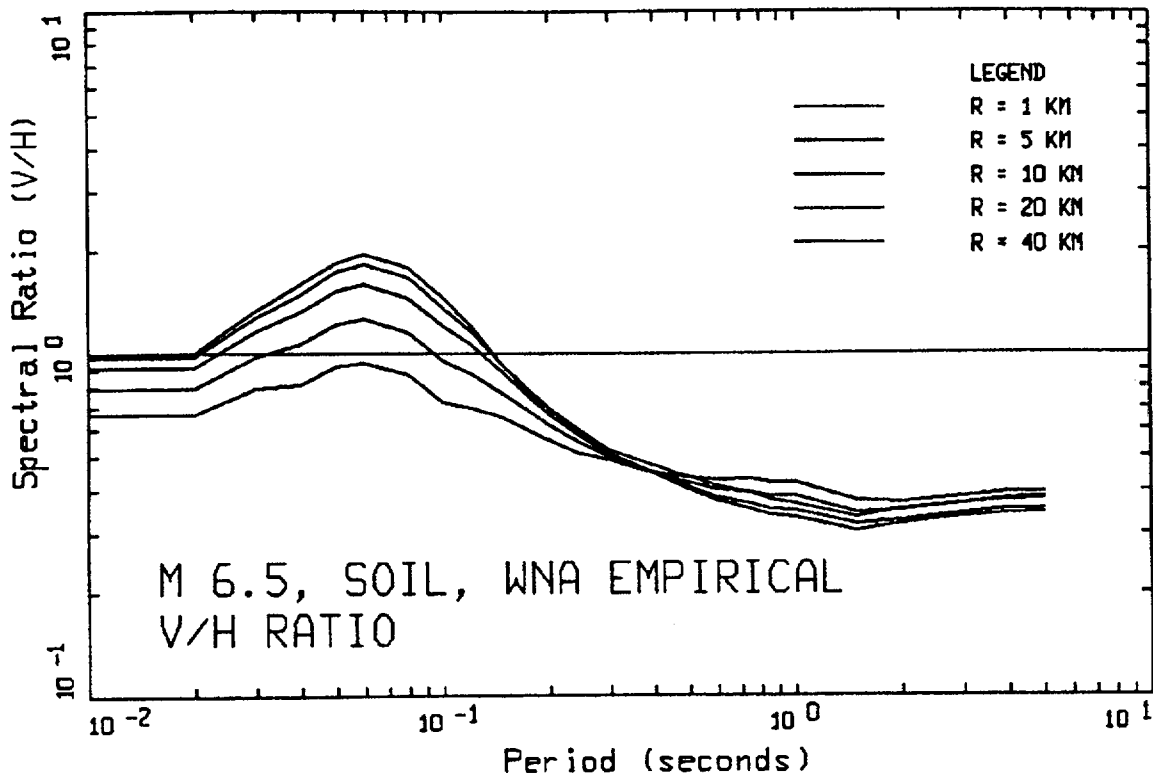


Figure J-31. Comparison of empirical and model response spectral ratios (V/H) at soil sites for M 6.5. The R=1 km line is the highest on each plot at 0.05 sec.

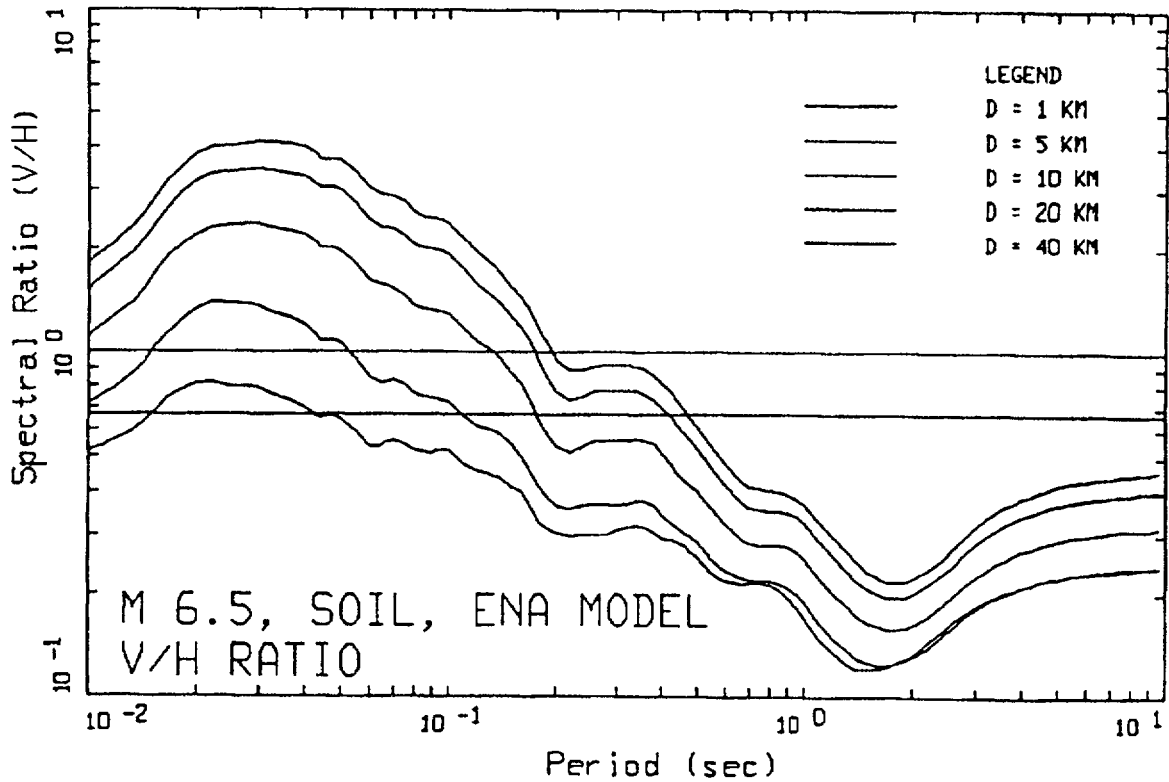
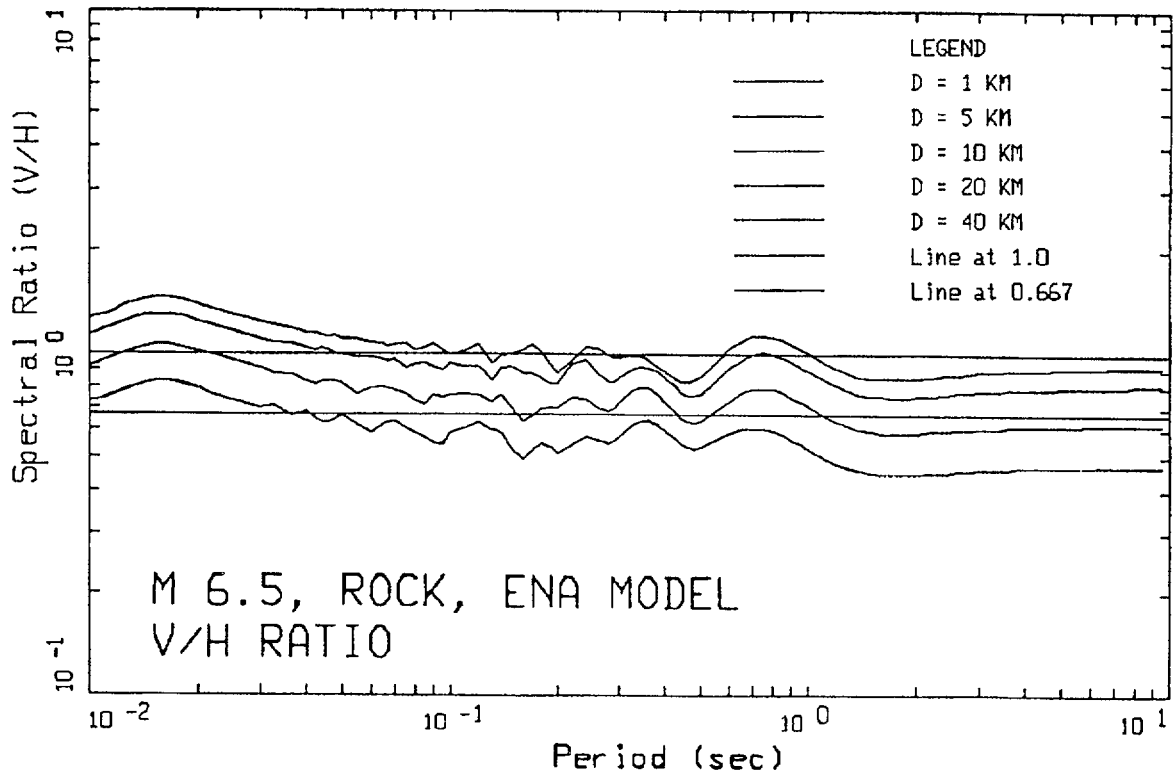


Figure J-32. Response spectral ratios (V/H) computed for CEUS rock and soil sites for M 6.5 at a suite of distances. The CEUS crustal model (Figure J-29) is used for rock sites with the generic soil profile (Figure J-2) placed on top to model soil sites.

APPENDIX K COMPARISON OF WUS RECOMMENDED RESPONSE SPECTRAL SHAPES TO RECORDINGS OF THE CHI-CHI, TAIWAN AND TURKEY EARTHQUAKES

The recent September 20, 1999, M 7.6 Chi-Chi, Taiwan and August 17, 1999, M 7.4 Kocaeli and November 12, 1999, M 7.1 Duzce, Turkey earthquakes resulted in over 400 strong motion recordings, greatly increasing the number of data available for large earthquakes. While the number of rock sites is fewer than 400 (a total of 214) and site conditions are not as well determined as most WUS and CEUS sites, the available data reflect a unique opportunity to evaluate the recommended spectral shapes. Although neither Turkey nor Taiwan are within the conterminous US, they both reflect active tectonics and are expected to have ground motions due from shallow crustal sources with similar characteristics to WUS, those being soft rock conditions and a dominantly single-corner frequency source spectrum (Atkinson and Silva; 1997, 2000).

To provide a basis for comparing the Taiwan and Turkey statistical response spectral shapes to the recommended shapes, the data were parceled into the standard distance bins (see Section 4): 0 to 10 km, 10 to 50 km, 50 to 100 km, 100 to 200 km, and 0 to 50 km. Tables K-1 and K-2 indicate bin statistics from the Chi-Chi and Turkey earthquakes, respectively, and Table K-3 lists the bin statistics for the combined data set. The tables show significantly larger motions for the Chi-Chi earthquake than for the Turkey earthquakes. Part of this likely results from the differences in magnitude and source mechanism (thrust versus strike slip, Abrahamson and Silva, 1997) but examination of PGV, PGV/PGA, and $PGA \cdot PGD / PGV^2$ suggests large differences in absolute motion over a wide frequency range.

For the combined data set (Chi-chi and Turkey earthquakes), Figures K-1 to K-5 compare the statistical shapes to the recommended spectral shapes computed for the bin average magnitudes and distances. Records are weighted such that each earthquake has equal weight in the bin shapes. The figures show a difference in shapes between the statistical and the recommended shapes, with the recommended shapes higher at high frequency and generally lower at low frequency. At the largest distance bin, 100 to 200 km, Figure K-4 shows a very large frequency shift. In this case the recommended shape peak is near 3 Hz while the peak in the statistical shape is shifted to 1 to 2 Hz. These trends suggest the effects of shallow crustal damping, (κ) within about 50 km and a combination of κ and deep crustal damping ($Q(f)$) beyond 50 km (Silva and Green, 1989; Silva and Darragh, 1995; McGuire et al., 2000). To see this more clearly, Figure K-6 shows the effects of κ on response spectral shapes computed for M 6.5 (McGuire et al., 2000). The shift in shape to lower frequency as κ increases is evident. Figure K-6 shows that for large κ values (about 0.04, the value for soft WUS rock [(Silva and Darragh, 1995; McGuire et al., 2000)], a factor of two increase in κ results in a frequency shift of nearly a factor of two. For sites within 50 km, Figure K-5 shows a slight shift to lower frequency for the combined data set, suggesting a small increase in κ over that for WUS. However, Figure K-4 (100 to 200 km) shows a dramatic frequency shift, nearly a factor of two. Since this distance bin is populated entirely by Chi-Chi data, the shift in spectral shape suggests major differences in κ and $Q(f)$ between Taiwan and WUS.

To see this more clearly, Figures K-7 to K-11 show spectral comparisons for the Chi-Chi earthquake only, and Figures K-12 to K-15 show comparisons for the Turkey earthquakes only. For the Chi-Chi earthquake sufficient data are available for each bin to adequately define stable shapes (Table K-2). For the Turkey earthquakes (Table K-3) only the 10 to 50 km and 0 to 50 km bins have sufficient data from which to discern trends.

For the Chi-Chi earthquake, Figures K-7 to K-9 and Figure K-11 (0 to 50 km) show about a 30% shift in the spectra to lower frequency relative to WUS. From Figure K-6 this shift suggests an increase in κ of about 20 to 30% over the soft rock WUS value of about 0.04 sec (Silva and Darragh, 1995; McGuire et al., 2000) to about 0.05 sec. Figure K-10, which plots the 100 to 200 km bin, shows a larger shift, about a factor of two, suggesting a much lower $Q(f)$ for Taiwan than WUS (Silva and Green, 1989).

Data from recent Turkey earthquakes that have sufficiently populated bins show shapes generally consistent with the WUS empirical (recommended) shapes. These shapes are illustrated in Figure K-13 for the 10 to 50 km bin, and in Figure K-15 for the 0 to 50 km bin.

Results of these comparisons indicate that Turkey data appear to be representative of WUS soft rock conditions. However, because of possibly higher crustal damping in Taiwan, care should be taken in decisions to include the Chi-Chi data with the WUS data set, or alternatively, to use WUS empirical relations for applications in Taiwan as larger crustal damping will result in lower absolute levels at high frequency (Section 3). Analyses of the larger aftershock data will likely resolve the issue of crustal damping (κ and $Q(f)$). Both the Chi-Chi and Turkey data sets are considered appropriate for use as inputs to scaling or spectral matching procedures, so they are included in the time history analysis data set.

REFERENCES

- Abrahamson, N.A. and Silva, W.J. (1997). "Empirical response spectral attenuation relations for shallow crustal earthquakes." *Seism. Res. Lett.*, 68(1), 94-127.
- Atkinson, G.M and W.J. Silva (1997). "An empirical study of earthquake source spectra for California earthquakes." *Bull. Seism. Soc. Am.* 87(1), 97-113.
- Atkinson, G.M and W.J. Silva (2000). "Stochastic modeling of California ground motions." *Bull. Seism. Soc. Am.* 90(2), 255-274.
- Silva, W.J. and R. Darragh (1995). "Engineering characterization of earthquake strong ground motion recorded at rock sites." Palo Alto, Calif: Electric Power Research Institute, TR-102261.
- Silva, W.J., and Green, R.K. (1989). "Magnitude and distance scaling of response spectral shapes for rock sites with applications to North American tectonic environment." *Earthquake Spectra*, 5(3), 591-624.

Table K-1
WUS STATISTICAL SHAPE BINS
CHI CHI

<u>Magnitude Bins (M)</u>								
				<u>Bin Center</u>				
				5.5				
				6.5				
				7.5				
		<u>Range</u>						
		5 - 6						
		6 - 7						
		7+						
Distance Bin (km)	\bar{M}	\bar{D} (km)	Number of Spectra	PGA ¹ (g), σ_{ln}	PGV*(cm/sec), σ_{ln}	PGD*(cm), σ_{ln}	$\frac{PGV^*}{PGA}$ ($\frac{cm/sec}{g}$), σ_{ln}	$\frac{PGA \cdot PGD^*}{PGV^2}$, σ_{ln}
0 - 10, rock	7.60	4.93	20	0.42, 0.55	61.92, 0.50	37.56, 0.83	145.87, 0.49	4.08, 0.39
10 - 50, rock	7.60	33.42	38	0.14, 0.90	20.49, 0.81	13.87, 0.82	143.71, 0.52	4.62, 0.54
50 - 100, rock	7.60	76.29	116	0.05, 0.47	8.68, 0.59	7.81, 0.80	162.08, 0.39	5.44, 0.45
100 - 200, rock	7.60	126.8 5	40	0.03, 0.66	6.19, 0.63	5.60, 0.80	218.66, 0.37	4.06, 0.30
0 - 50, rock	7.60	24.08	56	0.20, 0.94	29.37, 0.90	19.88, 0.96	146.30, 0.51	4.54, 0.48

K-3

¹Median values

Table K-2
WUS STATISTICAL SHAPE BINS
TURKEY

<u>Magnitude Bins (M)</u>								
				<u>Bin Center</u>				
				5.5				
				6.5				
				7.5				
Distance Bin (km)	<u>Range</u>		Number of Spectra	PGA ¹ (g), σ_{in}	PGV*(cm/sec), σ_{in}	PGD*(cm), σ_{in}	$\frac{PGV^*}{PGA}$ ($\frac{cm/sec}{g}$), σ_{in}	$\frac{PGA \cdot PGD^*}{PGV^2}$, σ_{in}
	\bar{M}	\bar{D} (km)						
0 - 10, rock	7.40	5.50	3	0.26, 0.51	45.42, 0.79	30.23, 1.20	173.22, 0.28	3.77, 0.12
10 - 50, rock	7.27	27.50	14	0.12, 1.09	15.94, 0.87	7.42, 1.24	128.21, 0.61	3.56, 0.42
50 - 100, rock	7.40	62.30	2	0.06, ----	5.79, ----	3.88, ----	96.49, ----	6.81, ----
100 - 200, rock	-----	-----	-----	-----	-----	-----	-----	-----
0 - 50, rock	7.30	22.61	17	0.15, 1.02	20.11, 0.93	10.14, 1.31	137.07, 0.55	3.60, 0.37

¹Median values

Table K-3
WUS STATISTICAL SHAPE BINS
CHI CHI AND TURKEY

<u>Magnitude Bins (M)</u>								
				<u>Bin Center</u>				
				5.5				
				6.5				
				7.5				
		<u>Range</u>						
		5 - 6						
		6 - 7						
		7+						
Distance Bin (km)	\bar{M}	\bar{D} (km)	Number of Spectra	PGA ² (g), σ_{ln}	PGV*(cm/sec), σ_{ln}	PGD*(cm), σ_{ln}	$\frac{PGV^*}{PGA} (\frac{cm/sec}{g})$, σ_{ln}	$\frac{PGA \cdot PGD^*}{PGV^2}$, σ_{ln}
0 - 10, rock	7.57	5.03	23	0.39, 0.56	58.80, 0.52	36.22, 0.83	150.10, 0.45	4.02, 0.36
10 - 50, rock	7.51	31.82	52	0.14, 0.93	19.15, 0.82	11.72, 0.97	139.36, 0.54	4.31, 0.52
50 - 100, rock	7.60	76.05	118	0.05, 0.47	8.62, 0.59	7.72, 0.80	160.66, 0.39	5.46, 0.45
100 - 200, rock	7.60	126.85	40	0.03, 0.66	6.19, 0.63	5.60, 0.80	218.66, 0.37	4.06, 0.30
0 - 50, rock	7.53	23.72	73	0.19, 0.96	26.79, 0.91	16.88, 1.07	144.00, 0.51	4.29, 0.46

K-5

²Median values

Table K-4

CHI-CHI, TAIWAN AND TURKEY STRONG-MOTION CATALOG (09/05/00)

Earthquake No. Location, Mech. Dip (1)	Date & Time		Magnitude (2)				Station (3)		Closest Dist (km)(4)	Site Codes (5)	Comp.	Filter HP (hz)	Corners LP (hz)	PGA (g)	PGV (cm/s)	PGD (cm)	
	YEAR	MOD Y M	ML	MS	OTH	No.	Description H/F										
0141 Kocaeli, Turkey 00	1999	0817	7.4	0.0	7.8	6.7	KOERI	99999	Arcelik	17.0	--B	UP	1.50	80.0	0.086	2.6	0.22
								99		17.0	-	000	0.80	70.0	0.180	10.5	0.90
											270	0.90	70.0	0.108	6.2	0.63	
							ERD	99999	Cekmece	76.1	--D	UP	0.60	20.0	0.046	3.4	0.34
								99		76.1	-	000	0.30	20.0	0.114	12.1	1.41
											270	0.40	20.0	0.105	6.4	0.84	
							ERD	99999	Duzce	14.2	--D	UP	0.08	20.0	0.229	20.4	17.01
								99		14.2	-	180	0.312	20.0	0.312	58.8	44.11
											270	0.08	15.0	0.358	46.4	17.61	
							ERD	99999	Eregli	999.9	--	UP	1.00	20.0	0.047	2.9	0.21
								99		999.9	-	180	0.40	20.0	0.121	13.3	2.75
											090	0.40	20.0	0.090	10.2	1.23	
							ERD	99999	Gebze	17.0	--B	UP	1.00	40.0	0.151	6.3	0.59
								99		17.0	-	000	0.06	25.0	0.244	50.3	42.74
											270	0.08	30.0	0.137	29.7	27.54	
							ERD	99999	Goy nuk	35.5	--B	UP	0.10	30.0	0.114	11.5	7.59
								99		35.5	-	000	0.15	30.0	0.132	8.8	3.05
											090	0.10	25.0	0.119	10.5	3.94	
							ERD	99999	Izmit	7.7	--B	UP	2.00	30.0	0.149	11.9	4.99
								99		7.7	-	180	0.10	30.0	0.152	22.6	9.81
											090	0.10	30.0	0.220	29.8	17.12	
							ERD	99999	Iz nik	29.7	--B	UP	0.30	30.0	0.083	7.7	1.70
								99		29.7	-	180	0.15	25.0	0.103	16.5	7.00
											090	0.07	25.0	0.136	28.8	17.44	
ITU	99999	Mecidiyekoy	62.3	--B	UP	1.10	60.0	0.028	1.3	0.16							
	99		62.3	-	000	0.20	50.0	0.053	3.8	1.49							
				270	0.05	60.0	0.068	8.83	10.11								
ERD	99999	Sakarya	3.3	--B	UP			0.259	41.84	31.32							
	99		3.3	-	XXX	-99.											
				090	0.04	40.0	0.376	79.5	70.52								
ERD	99999	Tekirdag	999.9	--A	UP	0.10	20.0	0.011	1.2	0.74							

Table K-4

CHI-CHI, TAIWAN AND TURKEY STRONG-MOTION CATALOG (09/05/00)

Earthquake No. Location, Mech. Dip (1)	Date & Time			Magnitude (2)			Station (3)		Closest Dist (km)(4)	Site Codes (5)	Comp.	Filter HP (hz)	Corners LP (hz)	PGA (g)	PGV (cm/s)	PGD (cm)	
	YEAR	Y	M	ML	MS	OTH	No.	Description H/F									
									999.9	-	180	0.60	30.0	0.033	2.6	0.35	
											090	0.10	30.0	0.035	2.8	1.29	
							KOERI	99999	Yarimca	4.4	B-D	UP		0.242	30.8	29.55	
								99		4.4	-	000	0.10	80.0	0.292	62.3	44.91
											270	0.1	80.0	0.340	68.2	35.86	
0142 Chi-Chi, Taiwan 02	1999	0920	7.6	7.3	7.6	0.0	CWB	99999	ALS	15.29	-1	V	0.14	40.0	0.073	14.2	6.13
								99		12.27	A	E	0.10	30.0	0.183	39.3	10.37
												N	0.14	40.0	0.163	21.9	8.64
							CWB	99999	ESL	44.94	-1	V	0.04	50.0	0.057	7.4	7.33
								99		40.24	C	E	0.15	25.0	0.068	6.2	2.31
												N	0.05	25.0	0.077	7.9	5.55
							CWB	99999	NST	36.95	-1	V	0.06	24.0	0.108	17.5	11.82
								99		36.95	A	E	0.03	50.0	0.309	22.7	21.38
												N	0.05	50.0	0.388	26.9	16.05
							CWB	99999	STY	52.06	-1	V	0.10	30.0	0.018	2.7	1.94
								99		50.58	A	E	0.10	30.0	0.033	4.8	2.29
												N	0.1	30.0	0.040	4.0	1.98
							CWB	99999	WNT	1.18	-1	V	0.05	50.0	0.311	34.2	17.06
								02		1.18	C	E	0.03	50.0	0.958	68.8	31.11
												N	0.05	50.0	0.626	42.0	18.83
							CWB	99999	WSF	45.71	-1	V	0.05	30.0	0.035	6.9	5.36
								99		45.71	D	E	0.06	50.0	0.066	14.8	12.72
												N	0.05	30.0	0.073	11.1	8.92
							CWB	99999	CHK	67.90	-1	V	0.40	20.0	0.016	2.4	0.45
								99		64.88	C	E	0.20	20.0	0.040	5.1	1.34
												N	0.14	20.0	0.051	7.1	2.13
							CWB	99999	ENA	77.75	-1	V	0.20	30.0	0.046	6.2	1.61
								99		75.14	A	E	0.30	30.0	0.070	5.9	0.90
												N	0.30	22.0	0.060	5.1	1.18
							CWB	99999	ILA027	94.73	-1	V	0.03	20.0	0.022	5.6	6.17
								99		92.59	C	E	0.06	20.0	0.101	17.8	8.02
												N	0.10	20.0	0.062	14.4	9.16

Table K-4

CHI-CHI, TAIWAN AND TURKEY STRONG-MOTION CATALOG (09/05/00)

Earthquake No. Location, Mech. Dip (1)	Date & Time MOD YEAR Y M			Magnitude (2) ML MS OTH			Station (3) No. Description H/F		Closest Dist (km)(4)	Site Codes (5)	Comp.	Filter HP (hz)	Corners LP (hz)	PGA (g)	PGV (cm/s)	PGD (cm)		
							CWB	99999	ILA032	95.77	-1	V	0.33	20.0	0.025	2.6	0.80	
								99		92.59		C	E	0.03	20.0	0.056	11.7	5.05
												N	0.13	20.0	0.049	8.6	2.09	
							CWB	99999	ILA035	104.77	-1	V	0.20	20.0	0.011	2.1	0.61	
								99		103.19		C	E	0.05	20.0	0.070	10.5	5.51
												N	0.13	20.0	0.052	9.9	3.32	
							CWB	99999	ILA039	97.56	-1	V	0.20	14.0	0.020	3.2	1.18	
								99		95.76		C	E	0.03	20.0	0.058	12.1	13.71
												N	0.15	20.0	0.062	12.1	4.66	
							CWB	99999	ILA043	88.86	--	V	0.30	30.0	0.034	2.9	0.59	
								99		86.58		A	E	0.40	20.0	0.063	5.2	0.61
												N	0.30	14.0	0.052	5.8	1.06	
							CWB	99999	NCU	78.90	-1	V	0.05	12.0	0.036	8.1	6.19	
								99		78.90		B	E	0.04	20.0	0.075	16.7	19.86
												N	0.10	20.0	0.086	16.1	8.36	
							CWB	99999	NSK	64.51	-1	V	0.20	50.0	0.034	5.1	1.12	
								99		63.95		A	E	0.02	30.0	0.070	6.9	4.22
												N	0.20	33.0	0.065	5.1	1.20	
							CWB	99999	PNG	114.21	-1	V	0.40	30.0	0.013	1.2	0.21	
								99		114.21		A	E	0.24	40.0	0.028	1.6	0.52
												N	0.22	30.0	0.035	2.4	0.75	
							CWB	99999	SSD	99.30	-1	V	0.30	20.0	0.014	1.5	0.35	
								99		98.47		C	E	0.20	20.0	0.018	1.7	0.48
												N	0.30	20.0	0.026	1.6	0.27	
							CWB	99999	TAW	136.58	-1	V	0.10	14.0	0.003	0.6	0.27	
								99		135.11		C	E	0.40	14.0	0.005	0.7	0.18
												N	0.20	14.0	0.007	0.9	0.30	
							CWB	99999	TAP042	108.19	-1	V	0.02	30.0	0.025	9.2	8.73	
								99		108.19		B	N	0.02	30.0	0.100	15.5	11.46
												W	0.02	30.0	0.085	19.1	19.06	
							CWB	99999	TCU018	63.81	-1	V		50.0	0.032	18.7	17.55	
								99		63.81		C	N	0.02	30.0	0.057	22.3	28.27

Table K-4

CHI-CHI, TAIWAN AND TURKEY STRONG-MOTION CATALOG (09/05/00)

Earthquake No. Location, Mech. Dip (1)	Date & Time MOD YEAR Y M			Magnitude (2) ML MS OTH			Station (3) No. Description H/F		Closest Dist (km)(4)	Site Codes (5)	Comp.	Filter HP (hz)	Corners LP (hz)	PGA (g)	PGV (cm/s)	PGD (cm)	
											W	0.02	30.0	0.054	34.5	52.36	
							CWB	99999	KAU082	183.97	--	V	0.02	12.0	0.009	2.8	2.60
							99			182.87	A	N	0.02	15.0	0.019	4.8	4.58
												W	0.02	12.0	0.017	7.8	6.77
							CWB	99999	TAP059	125.93	--1	V	0.02	20.0	0.018	5.7	6.82
							99			125.89	A	N	0.02	30.0	0.039	6.5	4.80
												W		15.0	0.030	7.6	8.11
							CWB	99999	TAP060	128.49	--1	V	0.02	24.0	0.014	5.0	7.02
							99			128.41	A	N	0.02	20.0	0.036	7.6	6.05
												W		20.0	0.036	11.0	8.80
							CWB	99999	TAP035	96.88	--1	V	0.02	24.0	0.028	7.6	9.01
							99			96.68	A	N	0.02	24.0	0.085	8.3	8.00
												W	0.02	24.0	0.067	8.4	12.78
							CWB	99999	TCU096	51.96	--1	V	0.02	50.0	0.037	15.0	14.59
							99			51.96	C	N	0.04	40.0	0.107	27.0	26.11
												W	0.02	22.0	0.059	39.5	41.34
							CWB	99999	TCU007	88.39	--1	V	0.03	30.0	0.028	8.5	9.98
							99			88.39	B	N	0.02	20.0	0.071	18.0	15.45
												W	0.02	22.0	0.060	23.6	37.22
							CWB	99999	TCU025	54.36	---	V	0.05	50.0	0.034	13.8	18.29
							99			54.36	A	N	0.05	50.0	0.058	10.5	10.17
												W	0.03	50.0	0.075	19.0	22.00
							CWB	99999	ILA046	91.45	--1	V	0.04	40.0	0.028	8.0	11.80
							99			89.23	C	N	0.04	40.0	0.055	9.8	7.66
												W	0.04	40.0	0.068	13.3	10.59
							CWB	99999	TCU014	92.42	--1	V	0.03	22.0	0.018	6.2	8.05
							99			92.42	B	N	0.02	25.0	0.075	13.5	15.04
												W	0.02	20.0	0.058	24.2	37.42
							CWB	99999	TCU015	47.35	--1	V	0.02	50.0	0.068	17.2	14.85
							99			47.35	B	N	0.03	50.0	0.114	29.5	24.14
												W	0.02	50.0	0.119	49.8	49.79
							CWB	99999	TAP043	93.73	--1	V	0.02	20.0	0.026	8.4	9.53

Table K-4

CHI-CHI, TAIWAN AND TURKEY STRONG-MOTION CATALOG (09/05/00)

Earthquake No. Location, Mech. Dip (1)	Date & Time			Magnitude (2)			Station (3)		Closest Dist (km)(4)	Site Codes (5)	Comp.	Filter HP (hz)	Corners LP (hz)	PGA (g)	PGV (cm/s)	PGD (cm)	
	YEAR	Y	M	ML	MS	OTH	No.	Description H/F									
									99								
									93.73	C	N	0.02	20.0	0.082	17.3	13.10	
											W	0.02	20.0	0.065	18.4	2.61	
							CWB	99999	TAP032	98.79	--1	V	0.02	50.0	0.059	9.6	8.76
								99	98.79	C	N	0.03	50.0	0.115	18.0	11.46	
											W	0.02	40.0	0.107	24.2	21.13	
							CWB	99999	KAU034	122.84	--1	V	0.02	12.0	0.009	2.3	3.08
								99	121.84	A	N	0.04	12.0	0.009	2.1	2.42	
											W	0.05	14.0	0.009	2.1	2.56	
							CWB	99999	TCU026	54.61	--1	V	0.02	50.0	0.061	17.1	18.12
								99	54.61	B	N	0.02	50.0	0.091	27.5	29.95	
											W	0.02	50.0	0.120	39.4	43.09	
							CWB	99999	ILA036	101.55	--1	V	0.03	30.0	0.026	12.8	9.59
								99	99.79	C	N	0.05	40.0	0.068	17.0	8.86	
											W	0.04	30.0	0.055	15.2	10.41	
							CWB	99999	KAU038	157.43	--1	V	0.03	20.0	0.006	2.0	2.69
								99	156.16	B	N	0.03	15.0	0.010	2.4	2.56	
											W	0.30	12.0	0.007	1.2	0.39	
							CWB	99999	KAU018	87.76	--1	V	0.02	20.0	0.016	6.2	5.41
								99	87.71	A	N	0.02	22.0	0.026	7.9	6.97	
											W	0.02	20.0	0.035	6.2	7.12	
							CWB	99999	TAP053	98.33	--	V	0.03	20.0	0.035	10.4	9.77
								99	98.24	A	N	0.03	20.0	0.086	12.2	7.62	
											W	0.02	24.0	0.082	11.3	15.70	
							CWB	99999	TAP046	127.26	--1	V	0.02	30.0	0.018	4.5	6.17
								99	126.99	C	N	0.02	30.0	0.054	6.6	4.93	
											W	0.02	24.0	0.084	12.6	7.08	
							CWB	99999	TAP052	99.92	--	V	0.03	50.0	0.039	8.2	10.24
								99	99.92	B	N	0.02	50.0	0.127	23.6	14.06	
											W	0.02	30.0	0.066	16.6	25.29	
							CWB	99999	KAU007	117.13	--1	V	0.02	20.0	0.014	6.8	5.13
								99	117.13	C	N	0.02	20.0	0.024	9.0	9.31	
											W	0.04	15.0	0.025	7.4	6.92	

Table K-4

CHI-CHI, TAIWAN AND TURKEY STRONG-MOTION CATALOG (09/05/00)

Earthquake No. Location, Mech. Dip (1)	Date & Time MOD YEAR Y M			Magnitude (2) ML MS OTH			Station (3) No. Description H/F		Closest Dist (km)(4)	Site Codes (5)	Comp.	Filter HP (hz)	Corners LP (hz)	PGA (g)	PGV (cm/s)	PGD (cm)	
	YEAR	Y	M	ML	MS	OTH	No.	Description									
							CWB	99999	CHY063	78.12	--1	V	0.03	24.0	0.025	5.3	5.42
							99			78.12	B	N	0.03	24.0	0.068	9.4	8.27
												W	0.02	22.0	0.060	7.9	6.92
							CWB	99999	TCU009	80.14	--1	V	0.02	30.0	0.022	11.8	11.19
							99			80.14	C	N	0.02	30.0	0.069	19.5	24.70
												W	0.02	30.0	0.070	26.5	41.45
							CWB	99999	KAU012	92.08	--1	V	0.03	20.0	0.022	7.7	7.48
							99			92.08	C	N		20.0	0.047	9.8	10.83
												W	0.05	20.0	0.086	9.9	7.82
							CWB	99999	TCU006	71.05	--1	V	0.02	22.0	0.036	15.2	14.26
							99			71.05	B	N	0.02	17.0	0.081	19.3	21.23
												W	0.02	20.0	0.057	36.2	56.14
							CWB	99999	CHY065	90.23	--1	V	0.02	50.0	0.031	5.1	7.56
							99			90.23	C	N	0.03	40.0	0.097	12.5	8.25
												W	0.02	33.0	0.118	15.8	8.44
							CWB	99999	TCU011	76.22	--1	V	0.03	30.0	0.031	9.3	14.51
							99			76.22	C	N	0.03	30.0	0.074	24.6	14.39
												W		30.0	0.065	24.6	32.14
							CWB	99999	TAP086	101.12	--	V	0.02	22.0	0.034	8.0	9.62
							99			100.93	A	N	0.02	30.0	0.050	7.9	5.70
												W	0.02	22.0	0.038	8.5	11.86
							CWB	99999	TAP036	95.60	--1	V	0.02	30.0	0.017	6.9	9.15
							99			95.33	A	N		30.0	0.039	6.1	5.83
												W	0.02	20.0	0.030	7.6	10.69
							CWB	99999	TAP034	98.81	--1	V	0.02	30.0	0.023	9.3	9.57
							99			98.69	C	N	0.02	30.0	0.066	12.6	6.79
												W	0.02	30.0	0.055	9.8	14.06
							CWB	99999	TCU092	96.44	--	V	0.02	30.0	0.028	10.3	10.11
							99			96.44	B	N	0.02	24.0	0.066	17.2	15.60
												W	0.02	20.0	0.086	23.0	36.91
							CWB	99999	TCU008	83.68	--1	V	0.02	30.0	0.025	9.6	9.64
							99			83.68	B	N	0.02	30.0	0.062	17.5	13.38

Table K-4

CHI-CHI, TAIWAN AND TURKEY STRONG-MOTION CATALOG (09/05/00)

Earthquake No. Location, Mech. Dip (1)	Date & Time MOD YEAR Y M			Magnitude (2) ML MS OTH			Station (3) No. Description H/F		Closest Dist (km)(4)	Site Codes (5)	Comp.	Filter HP (hz)	Corners LP (hz)	PGA (g)	PGV (cm/s)	PGD (cm)	
											W	0.02	30.0	0.071	29.8	42.50	
							CWB	99999	KAU040	154.59	--1	V	0.02	18.0	0.007	1.8	1.99
							99			153.29	C	N		10.0	0.008	2.1	3.20
												W	0.04	12.0	0.008	2.2	2.67
							CWB	99999	ILA031	94.77	--1	V		50.0	0.030	7.3	9.75
							99			92.63	A	N		30.0	0.076	9.1	10.68
												W		50.0	0.057	10.0	9.94
							CWB	99999	TCU010	80.42	--1	V	0.02	20.0	0.026	13.7	12.95
							99			80.42	B	N	0.02	20.0	0.074	19.3	23.89
												W	0.03	20.0	0.088	31.8	46.68
							CWB	99999	KAU078	102.85	--1	V	0.03	50.0	0.015	2.6	2.44
							99			101.92	C	N	0.02	50.0	0.024	2.2	3.17
												W	0.02	50.0	0.046	2.6	3.64
							CWB	99999	KAU077	97.20	--1	V	0.03	20.0	0.012	3.4	3.01
							99			95.65	A	N	0.03	20.0	0.023	2.5	3.76
												W	0.02	20.0	0.022	3.2	2.68
							CWB	99999	TAP069	135.31	--1	V	0.04	20.0	0.013	5.2	6.49
							99			133.93	A	N	0.05	20.0	0.033	5.8	4.58
												W	0.04	20.0	0.026	5.0	8.69
							CWB	99999	TTN024	70.58	--1	V	0.03	30.0	0.022	4.0	3.35
							99			67.69	A	N	0.02	30.0	0.027	3.9	3.50
												W	0.02	20.0	0.030	3.8	5.32
							CWB	99999	TTN018	86.15	--2	V	0.02	20.0	0.014	2.9	3.17
							99			83.80	A	N	0.02	20.0	0.024	4.1	3.55
												W	0.02	20.0	0.035	3.8	5.56
							CWB	99999	TTN027	87.62	--1	V	0.03	22.0	0.015	3.6	2.64
							99			85.31	B	N	0.03	30.0	0.039	6.1	3.68
												W	0.03	20.0	0.031	6.6	5.69
							CWB	99999	ILA050	77.75	--1	V	0.02	40.0	0.055	8.6	8.92
							99			75.14	A	N		40.0	0.064	9.9	16.41
												W	0.04	40.0	0.065	7.3	6.69
							CWB	99999	TAP065	130.91	--1	V	0.03	20.0	0.013	5.6	6.37

Table K-4

CHI-CHI, TAIWAN AND TURKEY STRONG-MOTION CATALOG (09/05/00)

Earthquake No. Location, Mech. Dip (1)	Date & Time			Magnitude (2)			Station (3)		Closest Dist (km)(4)	Site Codes (5)	Comp.	Filter HP (hz)	Corners LP (hz)	PGA (g)	PGV (cm/s)	PGD (cm)		
	YEAR	Y	M	ML	MS	OTH	No.	Description H/F										
									99									
									130.75	A	N	0.04	20.0	0.023	7.7	5.28		
											W	0.03	18.0	0.040	9.9	6.98		
							CWB	99999	TTN028	90.63	--1	V	0.03	20.0	0.016	3.0	3.14	
								99	88.39	A	N	0.02	20.0	0.016	3.1	2.79		
											W	0.02	18.0	0.019	3.2	4.93		
							CWB	99999	KAU051	139.70	--1	V	0.03	12.0	0.007	3.3	3.60	
								99	138.52	A	N	0.02	22.0	0.008	2.9	2.69		
											W	0.10	14.0	0.009	2.4	2.12		
							CWB	99999	KAU069	83.58	--1	V	0.03	24.0	0.019	2.2	3.05	
								99	82.75	A	N	0.10	30.0	0.036	3.1	0.859		
											W	0.02	22.0	0.039	3.3	3.69		
							CWB	99999	ILA051	90.37	---	V	0.02	24.0	0.024	8.4	10.13	
								99	88.49	A	N	0.02	22.0	0.033	7.3	9.19		
											W	0.02	22.0	0.080	12.3	9.66		
							CWB	99999	TCU085	64.51	--1	V	0.03	50.0	0.042	9.4	12.32	
								99	63.95	A	N		40.0	0.054	6.4	7.38		
											W		40.0	0.063	7.5	13.88		
							CWB	99999	TTN036	90.48	--1	V	0.02	14.0	0.018	8.4	6.97	
								99	88.24	B	N	0.02	12.0	0.030	6.8	4.79		
											W	0.02	12.0	0.025	7.6	8.65		
							CWB	99999	TTN016	136.58	--1	V	0.03	14.0	0.006	2.5	2.80	
								99	135.11	C	N	0.03	14.0	0.010	2.6	4.05		
											W	0.04	14.0	0.009	2.9	3.38		
							CWB	99999	KAU083	123.04	--1	V	0.02	14.0	0.011	4.9	4.97	
								99	122.87	D	N	0.02	14.0	0.024	8.4	5.81		
											W	0.02	14.0	0.030	8.9	7.18		
							CWB	99999	HWA022	71.45	--1	V		30.0	0.040	7.9	7.62	
								99	68.60	A	N		30.0	0.082	11.0	17.16		
											W	0.02	30.0	0.123	12.0	11.01		
							CWB	99999	TTN025	81.68	--1	V	0.02	30.0	0.024	3.7	3.11	
								99	79.19	C	N	0.02	30.0	0.050	5.0	2.60		
											W	0.02	30.0	0.034	3.9	5.08		

Table K-4

CHI-CHI, TAIWAN AND TURKEY STRONG-MOTION CATALOG (09/05/00)

Earthquake No. Location, Mech. Dip (1)	Date & Time			Magnitude (2)			Station (3)		Closest Dist (km)(4)	Site Codes (5)	Comp.	Filter HP (hz)	Corners LP (hz)	PGA (g)	PGV (cm/s)	PGD (cm)	
	YEAR	Y	M	ML	MS	OTH	No.	Description H/E									
							CWB	99999	TAP067	104.27	--1	V	0.03	20.0	0.037	8.4	10.40
								99		104.11	A	N	0.02	20.0	0.042	9.6	8.18
												W	0.02	20.0	0.039	11.5	12.16
							CWB	99999	TAP066	117.50	--1	V	0.02	22.0	0.022	4.1	6.23
								99		117.50	B	N	0.03	20.0	0.074	12.7	7.78
												W	0.02	22.0	0.050	9.1	15.81
							CWB	99999	ILA052	96.68	--1	V	0.04	24.0	0.017	6.4	8.32
								99		94.59	A	N	0.04	22.0	0.039	5.7	9.33
												W	0.04	22.0	0.027	7.3	9.66
							CWB	99999	TTN026	81.76	--1	V	0.03	22.0	0.014	3.2	3.22
								99		79.28	A	N	0.02	20.0	0.040	4.1	2.88
												W	0.02	20.0	0.027	4.2	5.63
							CWB	99999	KAU057	121.39	---	V	0.50	24.0	0.010	1.0	0.27
								99		121.39	A	N	0.03	20.0	0.016	4.6	5.55
												W	0.02	20.0	0.017	6.0	11.22
							CWB	99999	TCU083	78.90	--1	V	0.02	30.0	0.034	9.4	11.66
								99		78.90	B	N	0.02	20.0	0.111	23.6	13.27
												W	0.02	20.0	0.089	31.9	48.44
							CWB	99999	CHY006	14.93	---	V	0.03	50.0	0.202	25.0	11.63
								99		14.93	C	E	0.03	50.0	0.364	55.4	25.59
												N	0.03	50.0	0.345	42.8	15.18
							CWB	99999	CHY010	25.39	---	V	0.03	20.0	0.125	10.6	5.16
								99		25.39	C	E	0.02	20.0	0.227	19.2	7.26
												N	0.03	50.0	0.173	21.9	11.07
							CWB	99999	CHY014	41.49	---	V	0.03	40.0	0.101	11.5	5.16
								99		41.46	C	E	0.02	50.0	0.229	24.3	6.21
												N	0.03	50.0	0.263	21.9	6.57
							CWB	99999	CHY019	57.08	---	V	0.03	40.0	0.024	4.6	5.02
								99		57.08	C	E	0.02	50.0	0.052	6.3	6.66
												N	0.03	50.0	0.064	6.4	4.22
							CWB	99999	CHY022	71.64	--1	V	0.03	30.0	0.024	3.9	5.79
								99		71.64	A	E	0.00	40.0	0.065	6.9	7.12

Table K-4

CHI-CHI, TAIWAN AND TURKEY STRONG-MOTION CATALOG (09/05/00)

Earthquake No. Location, Mech. Dip (1)	Date & Time		Magnitude (2)			Station (3)		Closest Dist (km)(4)	Site Codes (5)	Comp.	Filter HP (hz)	Corners LP (hz)	PGA (g)	PGV (cm/s)	PGD (cm)	
	YEAR	Y	M	ML	MS	OTH	No.									Description H/F
										N	0.03	40.0	0.044	5.1	5.47	
						CWB	99999	CHY034	20.23	---	V	0.03	30.0	0.091	15.0	8.37
							99		20.23	C	E	0.03	30.0	0.248	38.8	11.46
										N	0.03	30.0	0.310	48.5	16.54	
						CWB	99999	CHY047	29.36	---	V	0.03	50.0	0.086	15.4	8.55
							99		29.36	C	E	0.03	50.0	0.168	21.1	10.27
										N	0.03	50.0	0.186	22.2	13.65	
						CWB	99999	CHY052	45.00	-1	V	0.03	40.0	0.039	6.6	5.45
							99		45.00	A	E	0.03	50.0	0.086	9.6	6.91
										N	0.03	50.0	0.154	12.1	9.40	
						CWB	99999	HWA002	53.85	---	V	0.03	40.0	0.033	7.0	7.18
							99		49.99	C	E	0.06	20.0	0.049	6.1	4.58
										N	0.06	40.0	0.094	11.9	6.80	
						CWB	99999	HWA003	56.07	-2	V	0.00	30.0	0.053	9.3	5.34
							99		52.38	A	E	0.04	20.0	0.050	10.5	5.45
										N	0.00	20.0	0.138	19.1	8.92	
						CWB	99999	HWA046	59.26	---	V	0.03	40.0	0.049	5.7	8.73
							99		55.78	A	E	0.02	50.0	0.076	9.8	18.09
										N	0.02	50.0	0.087	9.0	14.01	
						CWB	99999	KAU001	54.58	---	V	0.02	30.0	0.041	5.9	6.65
							99		54.21	A	E	0.03	30.0	0.043	5.4	3.68
										N	0.03	30.0	0.022	5.9	6.21	
						CWB	99999	TTN040	55.01	---	V	0.03	30.0	0.021	4.1	5.13
							99		51.25	A	E	0.03	33.0	0.030	7.2	7.37
										N	0.04	30.0	0.032	5.4	4.39	
						CWB	99999	TTN041	54.16	---	V	0.03	30.0	0.041	4.7	4.39
							99		50.33	A	E	0.03	40.0	0.079	6.8	6.50
										N	0.03	40.0	0.066	4.6	4.02	
						CWB	99999	ILA007	95.52	-1	V	0.03	30.0	0.036	6.7	10.54
							99		93.40	A	N	0.02	30.0	0.089	10.6	12.90
										W	0.02	30.0	0.062	9.5	9.27	
						CWB	99999	ILA008	96.54	-1	V	0.03	30.0	0.037	9.2	11.36

Table K-4

CHI-CHI, TAIWAN AND TURKEY STRONG-MOTION CATALOG (09/05/00)

Earthquake No. Location, Mech. Dip (1)	Date & Time MOD			Magnitude (2)			Station (3)		Closest Dist (km)(4)	Site Codes (5)	Comp.	Filter HP (hz)	Corners LP (hz)	PGA (g)	PGV (cm/s)	PGD (cm)		
	YEAR	Y	M	ML	MS	OTH	No.	Description H/F										
							CWB	99999	TAP078	131.02	---	V	0.03	33.0	0.018	5.4	8.02	
							99			130.29	A	N	0.04	40.0	0.042	8.6	5.60	
												W	0.02	40.0	0.043	6.9	8.98	
							CWB	99999	TAP081	135.55	---	V	0.03	20.0	0.012	6.0	8.01	
							99			134.22	A	N	0.02	20.0	0.021	4.9	5.44	
												W	0.02	50.0	0.031	7.9	8.78	
							CWB	99999	TTN002	76.01	-1	V	0.03	20.0	0.016	5.2	4.77	
							99			73.33	A	N	0.03	20.0	0.026	5.4	4.57	
												W	0.03	20.0	0.026	5.4	6.40	
							CWB	99999	TTN004	77.41	-1	V	0.04	20.0	0.026	3.9	4.07	
							99			74.78	C	N	0.04	20.0	0.046	8.3	4.57	
												W	0.03	20.0	0.039	7.4	5.69	
							CWB	99999	TTN042	72.62	---	V	0.03	20.0	0.019	5.4	5.05	
							99			69.82	A	N	0.03	20.0	0.059	5.9	4.55	
												W	0.03	22.0	0.059	5.4	5.97	
							CWB	99999	TTN044	68.22	---	V	0.03	22.0	0.033	6.0	4.44	
							99			65.23	B	N	0.02	22.0	0.055	10.2	6.66	
												W	0.03	30.0	0.048	9.7	7.12	
							CWB	99999	TTN046	74.49	---	V	0.03	22.0	0.020	5.0	5.04	
							99			71.76	A	N	0.03	22.0	0.067	7.4	3.18	
												W	0.03	20.0	0.113	11.2	6.13	
							CWB	99999	TTN047	74.90	---	V	-99.					
							99			82.51	B	N	0.03	20.0	0.027	5.7	4.78	
												W	0.03	20.0	0.026	6.2	6.44	
							CWB	99999	TCU078	7.50	-1	V	0.02	50.0	0.176	18.8	14.19	
							01			0.00	B	N	0.15	50.0	0.292	29.8	9.17	
												W	0.04	50.0	0.444	39.2	31.24	
							CWB	99999	TCU089	8.22	-1	V	0.03	50.0	0.191	22.3	24.36	
							01			0.00	B	N	0.04	50.0	0.248	31.0	32.37	
												W	0.07	50.0	0.333	30.9	18.48	
							CWB	99999	TCU079	10.04	-1	V	0.03	50.0	0.388	25.3	12.59	
							01			0.01	B	N	0.07	50.0	0.393	48.8	13.78	

Table K-4

CHI-CHI, TAIWAN AND TURKEY STRONG-MOTION CATALOG (09/05/00)

Earthquake No. Location, Mech. Dip (1)	Date & Time MOD		Magnitude (2)			Station (3)		Closest Dist (km)(4)	Site Codes (5)	Comp.	Filter HP (hz)	Corners LP (hz)	PGA (g)	PGV (cm/s)	PGD (cm)	
	YEAR	Y	M	ML	MS	OTH	No.									Description H/F
										W	0.20	50.0	0.742	61.2	11.11	
						CWB	99999	TCU084	10.39	-1	V	0.09	50.0	0.340	25.3	11.94
							01		0.01	B	N	0.10	50.0	0.417	45.6	21.27
										W	0.20	30.0	1.157	114.7	31.43	
						CWB	99999	TCU071	4.94	-1	V	0.10	50.0	0.449	34.8	31.32
							01		1.01	B	N	0.04	50.0	0.655	69.4	49.06
										W	0.20	50.0	0.567	44.4	13.76	
						CWB	99999	TCU072	7.36	-1	V	0.05	50.0	0.279	35.8	27.28
							99		0.24	B	N	0.05	50.0	0.400	56.3	41.28
										W	0.05	50.0	0.488	71.7	38.64	
						CWB	99999	CHY024	9.06	-1	V	0.03	50.0	0.152	44.8	34.80
							02		9.06	D	N	0.02	50.0	0.175	48.9	31.04
										W	0.02	50.0	0.278	52.9	43.62	
						CWB	99999	TCU120	8.10	-1	V	0.03	50.0	0.162	32.1	22.34
							02		8.10	C	N	0.03	50.0	0.192	36.9	33.30
										W	0.02	50.0	0.225	63.1	54.09	
						CWB	99999	TCU065	0.98	-1	V	0.02	50.0	0.272	77.0	53.70
							02		0.98	B	N	0.06	50.0	0.603	78.8	60.74
										W	0.03	50.0	0.814	126.2	92.57	
						CWB	99999	TCU067	0.33	-1	V	0.04	50.0	0.225	42.7	28.48
							02		0.33	B	N	0.03	50.0	0.325	66.6	45.95
										W	0.02	50.0	0.503	79.5	93.09	
						CWB	99999	CHY080	6.95	--	V	0.03	50.0	0.724	49.0	27.82
							99		6.79	B	N	0.05	50.0	0.902	102.4	3.97
										W	0.10	50.0	0.968	107.5	18.60	
						CWB	99999	CHY028	7.31	-1	V	0.04	50.0	0.337	36.4	13.56
							02		7.31	C	N	0.10	50.0	0.821	67.0	23.28
										W	0.12	50.0	0.653	72.8	14.68	
						CWB	99999	TCU109	13.09	-1	V	0.03	50.0	0.137	26.6	20.27
							02		13.09	C	N	0.04	50.0	0.155	53.1	34.74
										W	0.05	50.0	0.156	50.8	46.49	
						CWB	99999	TCU107	20.35	-2	V	0.03	50.0	0.088	27.8	21.70

Table K-4

CHI-CHI, TAIWAN AND TURKEY STRONG-MOTION CATALOG (09/05/00)

Earthquake No. Location, Mech. Dip (1)	Date & Time MOD		Magnitude (2)			Station (3)		Closest Dist (km)(4)	Site Codes (5)	Comp.	Filter HP (hz)	Corners LP (hz)	PGA (g)	PGV (cm/s)	PGD (cm)	
	YEAR	Y	M	ML	MS	OTH	No.									Description H/F
							02	20.35	C	N	0.03	50.0	0.158	47.4	32.79	
										W	0.03	50.0	0.124	36.8	39.81	
						CWB	99999	TCU052	0.24	-1	V	0.04	50.0	0.241	110.5	163.51
							01	0.06	B	N	0.04	50.0	0.419	118.4	246.15	
										W	0.04	50.0	0.348	159.0	184.42	
						CWB	99999	CHY074	82.49	-1	V	0.03	40.0	0.094	15.6	9.40
							99	82.49	B	N	0.02	40.0	0.158	23.6	11.74	
										W	0.02	40.0	0.234	28.1	19.04	
						CWB	99999	TCU056	11.11	-1	V	0.05	50.0	0.115	41.4	27.07
							02	11.11	D	N	0.03	50.0	0.134	42.9	54.55	
										W	0.04	40.0	0.134	42.5	50.77	
						CWB	99999	CHY029	15.28	-1	V	0.04	50.0	0.155	18.7	9.82
							02	15.28	C	N	0.03	50.0	0.238	35.2	29.10	
										W	0.03	50.0	0.277	30.3	14.73	
						CWB	99999	TCU048	14.38	-1	V	0.04	50.0	0.098	20.8	21.64
							02	14.38	C	N	0.04	50.0	0.184	48.3	53.55	
										W	0.02	50.0	0.123	32.6	52.18	
						CWB	99999	TCU113	31.49	-1	V	0.03	50.0	0.077	16.0	17.03
							02	31.49	E	N	0.03	50.0	0.074	23.4	27.12	
										W	0.04	50.0	0.070	27.8	22.21	
						CWB	99999	CHY035	18.12	-1	V	0.08	50.0	0.099	14.4	5.99
							99	180.12	C	N	0.04	50.0	0.246	37.6	16.86	
										W	0.04	40.0	0.252	45.6	12.03	
						CWB	99999	TCU104	13.64	--	V	0.03	50.0	0.083	23.3	20.60
							02	13.64	B	N	0.03	50.0	0.085	47.2	52.70	
										W	0.03	50.0	0.106	36.6	51.97	
						CWB	99999	TCU070	19.10	--	V	0.03	50.0	0.085	31.0	30.93
							02	19.10	B	N	0.03	50.0	0.169	62.3	56.67	
										W	0.02	50.0	0.255	52.1	48.09	
						CWB	99999	TCU068	1.09	-1	V	0.02	50.0	0.486	187.3	266.55
							01	0.50	D	N	0.02	50.0	0.462	263.1	430.00	
										W	0.03	50.0	0.566	176.6	324.11	

Table K-4

CHI-CHI, TAIWAN AND TURKEY STRONG-MOTION CATALOG (09/05/00)

Earthquake No. Location, Mech. Dip (1)	Date & Time MOD		Magnitude (2)			Station (3)		Closest Dist (km)(4)	Site Codes (5)	Comp.	Filter HP (hz)	Corners LP (hz)	PGA (g)	PGV (cm/s)	PGD (cm)	
	YEAR	Y	M	ML	MS	OTH	No.									Description H/F
						CWB	99999	TCU105	18.10	--	V	0.02	40.0	0.064	21.4	18.40
							02		18.10	C	N	0.03	30.0	0.129	38.9	45.59
										W		0.03	40.0	0.112	34.6	48.59
						CWB	99999	TCU103	4.01	-1	V	0.02	50.0	0.149	64.3	42.36
							99		4.01	C	N	0.05	50.0	0.162	26.8	15.97
										W		0.02	50.0	0.134	61.9	87.54
						CWB	99999	CHY041	25.96	-1	V	0.03	50.0	0.123	9.8	6.37
							99		25.96	D	N	0.03	50.0	0.639	39.5	11.25
										W		0.04	50.0	0.302	20.4	8.62
						CWB	99999	TCU059	17.84	--	V	0.05	40.0	0.057	18.6	12.06
							99		17.84	C	N	0.03	30.0	0.172	56.2	53.52
										W		0.03	30.0	0.165	59.4	63.65
						CWB	99999	TCU087	3.18	-1	V	0.02	30.0	0.108	61.5	51.32
							99		3.18	B	N	0.05	30.0	0.122	37.1	25.54
										W		0.02	30.0	0.128	40.8	62.62
						CWB	99999	CHY046	29.49	-1	V	0.03	50.0	0.079	8.6	6.21
							99		29.49	C	N	0.04	50.0	0.182	21.0	11.90
										W		0.03	50.0	0.142	20.6	10.28
						CWB	99999	CHY042	34.91	-1	V	0.04	30.0	0.061	9.0	4.72
							99		34.90	B	N	0.03	30.0	0.067	12.3	7.97
										W		0.06	30.0	0.099	15.5	6.50
						CWB	99999	CHY087	34.46	-1	V	0.03	40.0	0.056	6.4	5.77
							99		34.46	D	N	0.03	50.0	0.126	11.9	8.11
										W		0.02	50.0	0.136	10.2	7.18
						CWB	99999	CHY086	35.43	-1	V	0.04	30.0	0.050	8.2	4.78
							99		35.41	B	N	0.03	30.0	0.204	17.8	7.89
										W		0.10	30.0	0.115	14.2	6.66
						CWB	99999	TCU128	9.70	-1	V	0.02	40.0	0.097	46.0	34.77
							99		9.70	D	N	0.05	30.0	0.170	68.8	41.87
										W		0.02	30.0	0.139	73.0	90.62
						CWB	99999	HWA020	44.94	-1	V	0.02	50.0	0.056	8.0	12.44
							99		40.24	D	N	0.02	50.0	0.069	7.9	8.80

Table K-4

CHI-CHI, TAIWAN AND TURKEY STRONG-MOTION CATALOG (09/05/00)

Earthquake No. Location, Mech. Dip (1)	Date & Time MOD YEAR Y M			Magnitude (2) ML MS OTH			Station (3) No. Description H/F		Closest Dist (km)(4)	Site Codes (5)	Comp.	Filter HP (hz)	Corners LP (hz)	PGA (g)	PGV (cm/s)	PGD (cm)	
											W	0.02	50.0	0.061	10.3	18.07	
							CWB	99999	KAU054	40.50	-1	V	0.03	50.0	0.030	5.9	4.66
								99		39.64	B	N	0.03	50.0	0.080	5.2	3.56
												W	0.04	50.0	0.085	8.5	6.00
							CWB	99999	TCU036	16.69	-1	V	0.02	40.0	0.064	23.9	22.50
								99		16.69	D	N	0.02	40.0	0.131	50.2	42.17
												W	0.02	20.0	0.139	59.6	63.60
							CWB	99999	TCU046	14.34	-1	V	0.03	30.0	0.104	32.3	37.74
								99		14.34	D	N	0.06	30.0	0.116	30.9	23.18
												W	0.03	30.0	0.133	39.8	37.37
							CWB	99999	CHY088	42.82	-1	V	0.04	40.0	0.040	7.4	4.93
								99		42.82	D	N	0.04	33.0	0.216	20.5	14.21
												W	0.04	33.0	0.144	21.0	8.06
							CWB	99999	HWA038	42.91	-2	V	0.02	33.0	0.041	5.5	5.25
								99		37.97	C	N	0.03	30.0	0.059	7.4	7.51
												W	0.04	30.0	0.035	8.8	4.97
							CWB	99999	TCU039	16.70	-1	V	0.02	50.0	0.136	50.7	45.98
								99		16.70	C	N	0.02	50.0	0.145	54.0	44.54
												W	0.02	50.0	0.206	50.0	76.78
							CWB	99999	CHY102	46.17	-1	V	0.03	30.0	0.025	6.5	5.06
								99		45.99	B	N	0.03	33.0	0.050	6.3	4.15
												W	0.04	30.0	0.044	7.1	5.35
							CWB	99999	CHY081	47.74	-1	V	0.03	30.0	0.025	7.2	4.86
								99		47.74	B	N	0.03	30.0	0.045	9.8	7.66
												W	0.02	30.0	0.052	11.0	7.18
							CWB	99999	HWA024	44.32	-2	V	0.03	40.0	0.025	4.5	5.43
								99		39.55	B	N	0.03	30.0	0.024	4.8	5.02
												W	0.03	30.0	0.023	7.5	7.36
							CWB	99999	HWA017	53.91	-1	V	0.03	50.0	0.049	9.4	11.67
								99		50.06	D	N	0.02	50.0	0.084	9.4	7.23
												W	0.02	50.0	0.082	10.8	21.83
							CWB	99999	HWA043	54.90	-1	V	0.02	40.0	0.031	10.2	9.99

Table K-4

CHI-CHI, TAIWAN AND TURKEY STRONG-MOTION CATALOG (09/05/00)

Earthquake No. Location, Mech. Dip (1)	Date & Time MOD YEAR Y M			Magnitude (2) ML MS OTH			Station (3) No. Description H/F		Closest Dist (km)(4)	Site Codes (5)	Comp.	Filter HP (hz)	Corners LP (hz)	PGA (g)	PGV (cm/s)	PGD (cm)
							99		51.13	D	N	0.02	40.0	0.070	7.7	9.31
											W	0.05	40.0	0.056	8.9	7.04
	CWB	99999					99999	CHY050	50.07	-1	V	0.03	50.0	0.028	4.9	5.29
							99		50.07	B	N	0.03	50.0	0.069	8.3	7.73
											W	0.04	50.0	0.106	9.8	4.51
	CWB	99999					99999	TCU045	24.06	---	V	0.02	50.0	0.361	21.4	22.95
							99		24.06	B	N	0.04	50.0	0.512	39.0	14.34
											W	0.02	50.0	0.474	36.7	50.66
	CWB	99999					99999	HWA016	54.73	-1	V	0.02	50.0	0.053	10.1	10.39
							99		50.95	D	N	0.05	50.0	0.080	12.7	5.65
											W	0.05	50.0	0.102	13.3	12.88
	CWB	99999					99999	KAU050	52.06	-1	V	0.02	30.0	0.023	5.2	4.13
							99		50.58	B	N	0.03	40.0	0.040	6.4	3.28
											W	0.02	30.0	0.042	5.2	6.98
	CWB	99999					99999	TCU029	24.71	-1	V	0.02	50.0	0.063	23.2	26.81
							99		24.71	D	N	0.04	50.0	0.200	54.0	40.19
											W	0.03	50.0	0.166	38.6	44.57
	CWB	99999					99999	TCU031	26.78	-1	V	0.02	30.0	0.065	26.8	29.00
							99		26.78	C	N	0.02	30.0	0.122	43.4	31.11
											W	0.02	20.0	0.110	51.1	47.95
	CWB	99999					99999	HWA056	48.75	---	V	0.02	50.0	0.062	7.1	10.35
							99		44.46	B	N	0.03	50.0	0.107	10.8	10.36
											W	0.02	50.0	0.107	11.7	17.64
	CWB	99999					99999	CHY079	54.97	---	V	0.03	25.0	0.029	5.2	4.77
							99		54.96	B	N	0.03	23.0	0.050	6.7	4.18
											W	0.02	30.0	0.043	5.6	5.62
	CWB	99999					99999	HWA023	57.06	-2	V	0.03	50.0	0.026	7.6	10.14
							99		53.44	B	N	0.04	40.0	0.037	6.6	9.03
											W	0.04	40.0	0.037	8.6	13.88
	CWB	99999					99999	TCU047	33.01	---	V	0.02	50.0	0.270	26.9	17.88
							99		33.01	B	N	0.03	50.0	0.413	40.2	22.22
											W	0.02	50.0	0.301	41.6	51.08

Table K-4

CHI-CHI, TAIWAN AND TURKEY STRONG-MOTION CATALOG (09/05/00)

Earthquake No. Location, Mech. Dip (1)	Date & Time MOD			Magnitude (2)			Station (3)		Closest Dist (km)(4)	Site Codes (5)	Comp.	Filter HP (hz)	Corners LP (hz)	PGA (g)	PGV (cm/s)	PGD (cm)	
	YEAR	Y	M	ML	MS	OTH	No.	Description H/F									
							CWB	99999	TTN031	57.00	--1	V	0.03	40.0	0.043	14.2	5.59
							99			53.38	D	N	0.03	50.0	0.086	12.8	7.83
												W	0.03	30.0	0.074	13.3	6.66
							CWB	99999	TCU034	32.97	--1	V	0.02	50.0	0.074	12.9	14.93
							99			32.97	B	N	0.04	50.0	0.108	23.1	21.66
												W	0.02	50.0	0.250	42.1	46.07
							CWB	99999	HWA026	58.80	—	V	0.02	50.0	0.038	6.7	9.93
							99			55.30	B	N	0.03	50.0	0.058	9.1	9.74
												W	0.02	50.0	0.071	11.2	18.17
							CWB	99999	CHY057	62.81	--1	V	0.03	30.0	0.022	5.2	5.10
							99			62.81	D	N	0.03	30.0	0.056	6.2	4.90
												W	0.02	30.0	0.038	7.1	6.10
							CWB	99999	CHY062	64.07	--1	V	0.04	50.0	0.019	4.1	4.77
							99			64.07	D	N	0.18	50.0	0.053	4.7	2.09
												W	0.20	15.0	0.053	4.5	1.60
							CWB	99999	TTN032	59.11	--1	V	0.02	40.0	0.030	7.1	5.95
							99			55.62	B	N	0.02	40.0	0.078	12.6	6.60
												W	0.03	40.0	0.053	10.0	5.53
							CWB	99999	TCU033	38.19	--1	V	0.03	50.0	0.079	15.6	15.15
							99			38.19	D	N	0.03	50.0	0.180	24.5	21.00
												W	0.02	50.0	0.156	47.2	51.72
							CWB	99999	CHY061	66.91	--1	V	0.04	30.0	0.021	4.5	4.54
							99			66.89	B	N	0.07	30.0	0.042	3.7	3.13
												W	0.02	30.0	0.029	6.0	6.04
							CWB	99999	TTN033	61.68	--1	V	0.02	22.0	0.018	5.5	4.81
							99			58.34	D	N	0.02	30.0	0.040	7.0	4.63
												W	0.03	30.0	0.031	6.4	5.83
							CWB	99999	TCU095	43.44	--1	V	0.02	50.0	0.255	21.8	21.95
							99			43.44	D	N	0.04	50.0	0.712	49.1	24.45
												W	0.02	50.0	0.378	62.0	51.75
							CWB	99999	TCU098	45.02	--1	V	0.02	50.0	0.050	14.8	14.36
							99			45.02	D	N	0.03	50.0	0.107	34.9	25.1

Table K-4

CHI-CHI, TAIWAN AND TURKEY STRONG-MOTION CATALOG (09/05/00)

Earthquake No. Location, Mech. Dip (1)	Date & Time MOD		Magnitude (2)				Station (3)		Closest Dist (km)(4)	Site Codes (5)	Comp.	Filter HP (hz)	Corners LP (hz)	PGA (g)	PGV (cm/s)	PGD (cm)
	YEAR	Y	M	ML	MS	OTH	No.	Description H/F								
											W	0.02	50.0	0.100	42.0	51.93
0143 Duzce, Turkey 00	1999	1112	7.1	7.2	7.3	6.5	ERD	99999 99	Bolu 16.0 16.0	-B -	UP 000 090	0.05 0.05 0.05		0.203 0.728 0.822	17.3 56.4 62.1	14.29 23.07 13.55
							ERD	99999 99	Duzce 6.7 6.7	-D -	UP 180 270	0.06 0.06 0.08	50.0 50.0 50.0	0.357 0.348 0.535	22.6 60.0 83.5	19.40 42.09 51.59
							ERD	99999 99	Mudurnu 34.6 34.6	-A -	UP 000 090	0.08 0.08 0.08		0.060 0.120 0.056	10.6 9.3 16.3	7.33 7.63 15.37
							ERD	99999 99	Sakarya 42.7 42.7	-B -	UP 180 090	0.05 0.05 0.05	40.0 40.0 40.0	0.011 0.023 0.016	3.2 5.5 5.5	4.00 5.80 7.34

K-24

Notes:

- (1) Source mechanism: 00 = strike slip, 01 = normal, 02 = reverse, 03 = reverse-oblique, 04 = normal-oblique, 99 = unknown.
Dip is the dip of rupture surface.
- (2) M is moment magnitude, UNK = Magnitude type unknown. Missing magnitudes have the value of zero.
- (3) Station numbers were assigned as 99999 where not available.
H/F is the designation for the site being on the hanging wall (01) or foot wall (02), or unknown/not applicable (99).
- (4) Distances are closest distances. Values of 999.9 indicate unknown distances.
Second distance is to the surface projection of the fault plane (i.e., JB Distance).
- (5) Site codes definitions are from three sources: 1) Geomatrix (3 letter), 2) USGS (1 letter), 3) CWB (1 number), described below.

GEOMATRIX 3-LETTER SITE CLASSIFICATIONS

FIRST LETTER: Instrument housing

- = Unknown

I = Free-field instrument or instrument shelter. Instrument is located at or within several feet of the ground surface.

A = One-story structure of lightweight construction. Instrument is located at the lowest level and within several feet of the ground surface.

B = Two- to four-story structure of lightweight construction. Instrument is located at the lowest level and within several feet of the ground surface.

- C = Two- to four-story structure of lightweight construction. Instrument is located at the lowest level in a basement and below the ground surface.
- D = Five or more story structure of heavy construction. Instrument is located at the lowest level and within several feet of the ground surface.
- E = Five or more story structure of heavy construction. Instrument is located at the lowest level in a basement and below the ground surface.
- F = Structure housing instrument is buried below the ground surface, eg. tunnel.
- G = Structure of light or heavyweight construction, instrument not at lowest level.
- H = Earth dam.
- I = Concrete Dam

SECOND LETTER: Mapped local geology

Sedimentary or metasedimentary:

- = Unknown
 - H = Holocene (Recent) Quaternary (< 15000y bp).
 - Q = Pleistocene Quaternary (< 2my bp).
 - P = Pliocene Tertiary (< 6my bp).
 - M = Miocene Tertiary (< 22my bp).
 - O = Oligocene Tertiary (< 36my bp).
 - E = Eocene Tertiary (< 58my bp).
 - L = Paleocene Tertiary (< 63my bp).
 - K = Cretaceous (< 145my bp).
 - F = Franciscan Formation (Cretaceous/Late Jurassic).
 - J = Jurassic (< 210my bp).
 - T = Triassic (<255my bp).
 - Z = Permian or older (> 255my bp).
- Igneous or meta-igneous:
- V = Volcanic (extrusive).
 - N = Intrusive.
 - G = Granitic.

THIRD LETTER: Geotechnical subsurface characteristics for the Turkey earthquakes

- A = Rock. Instrument on rock ($V_s > 600$ mps) or < 5m of soil over rock.
- B = Shallow (stiff) soil. Instrument on/in soil profile up to 20m thick overlying rock.
- C = Deep narrow soil. Instrument on/in soil profile at least 20m thick overlying rock, in a narrow canyon or valley no more than several km wide.
- D = Deep broad soil. Instrument on/in soil profile at least 20m thick overlying rock, in a broad valley.
- E = Soft deep soil. Instrument on/in deep soil profile with average $V_s < 150$ mps.
- = Unknown

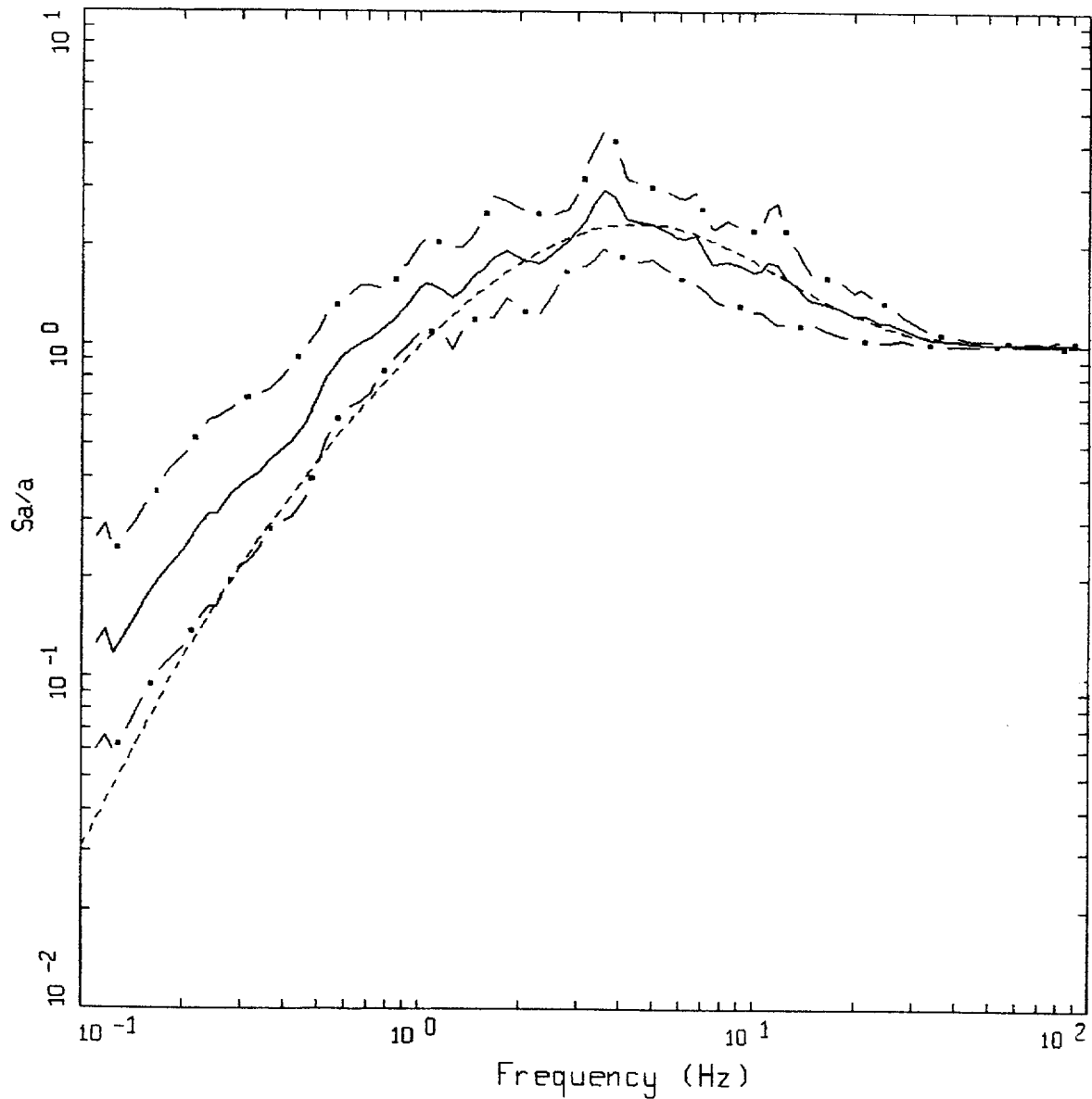
THIRD LETTER: Geotechnical subsurface characteristics for the Chi-Chi, Taiwan earthquake from the Central Weather Bureau of Taiwan.

- 1 = Hard site.
- 2 = Medium site.
- 3 = Soft soil site.
- = Unknown

USGS 1-LETTER SITE CLASSIFICATIONS

Average shear-wave velocity to a depth of 30m is:

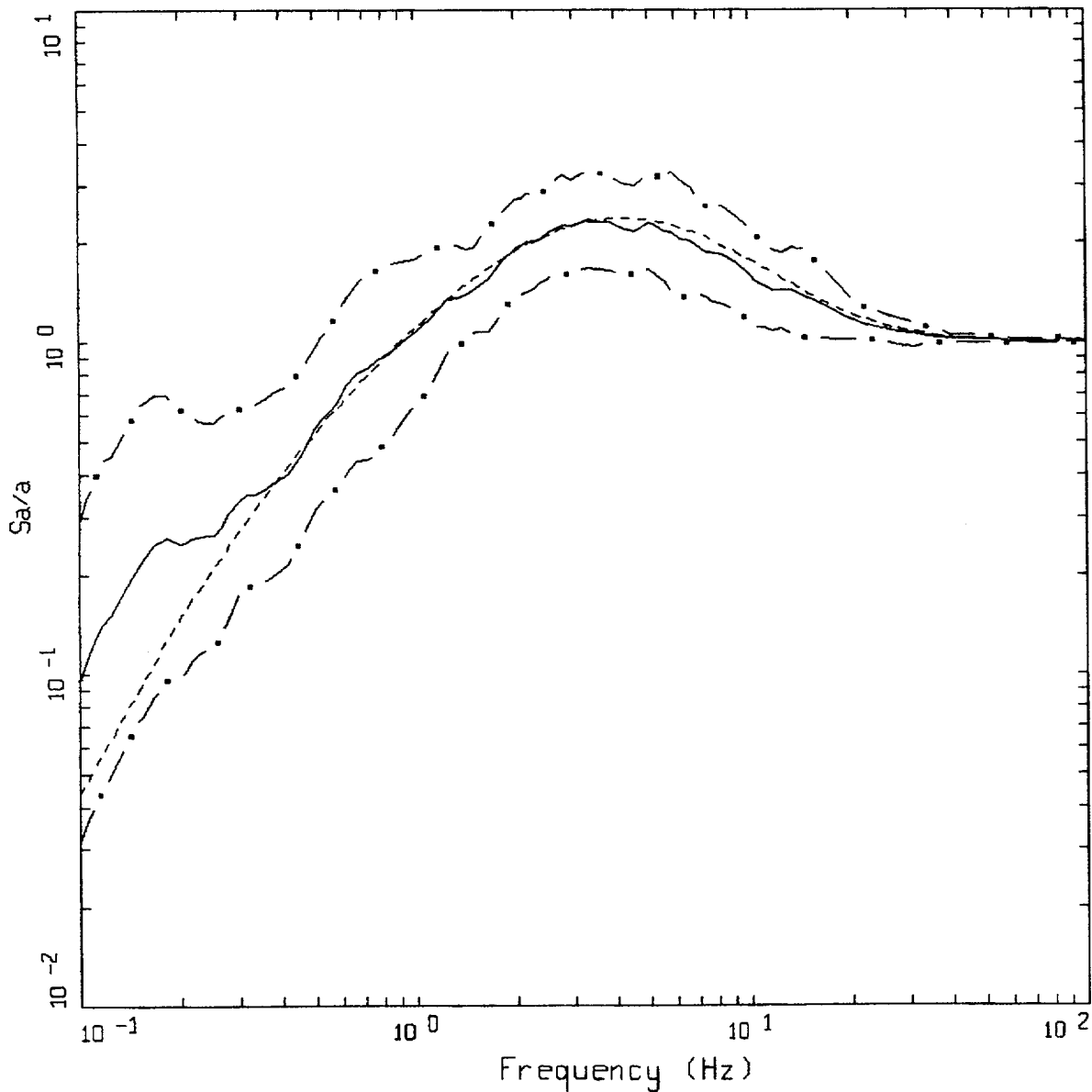
- A = > 750 m/s
- B = 360 - 750 m/s
- C = 180 - 360 m/s
- D = < 180 m/s



AVERAGE HORIZONTAL SPECTRA: CHI-CHI, TURKEY
 M=7.5 (7.0-7.0+), R=0-10 KM, ROCK
 AVERAGE M = 7.57, AVERAGE DISTANCE = 5.03 KM

- LEGEND
- 50TH PERCENTILE
 - · - 16TH PERCENTILE
 - - - 84TH PERCENTILE
 - · · · · RECOMMENDED SHAPE; M = 7.57, D = 5 KM

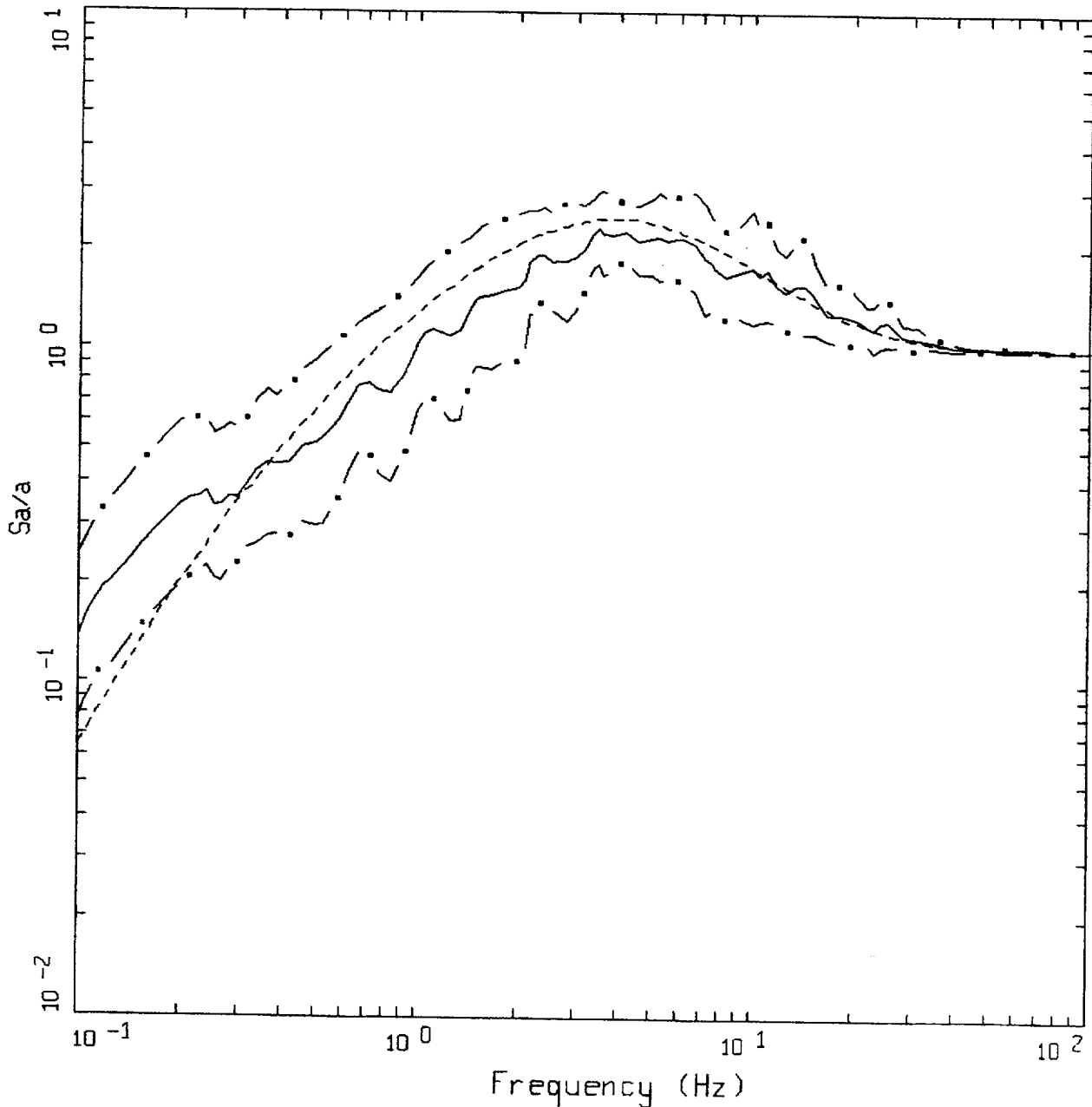
Figure K-1. Comparison of statistical response spectral shapes computed for the Chi Chi, Taiwan and Turkey earthquakes with recommended shape: bin M 7+ and D = 0 to 10 km.



AVERAGE HORIZONTAL SPECTRA: CHI-CHI, TURKEY
 M=7.5 (7.0-7.0+), R=10-50 KM, ROCK
 AVERAGE M = 7.51, AVERAGE DISTANCE = 31.82 KM

- LEGEND
- 50TH PERCENTILE
 - · - 16TH PERCENTILE
 - · - 84TH PERCENTILE
 - - - - RECOMMENDED SHAPE; M = 7.51, D = 32 KM

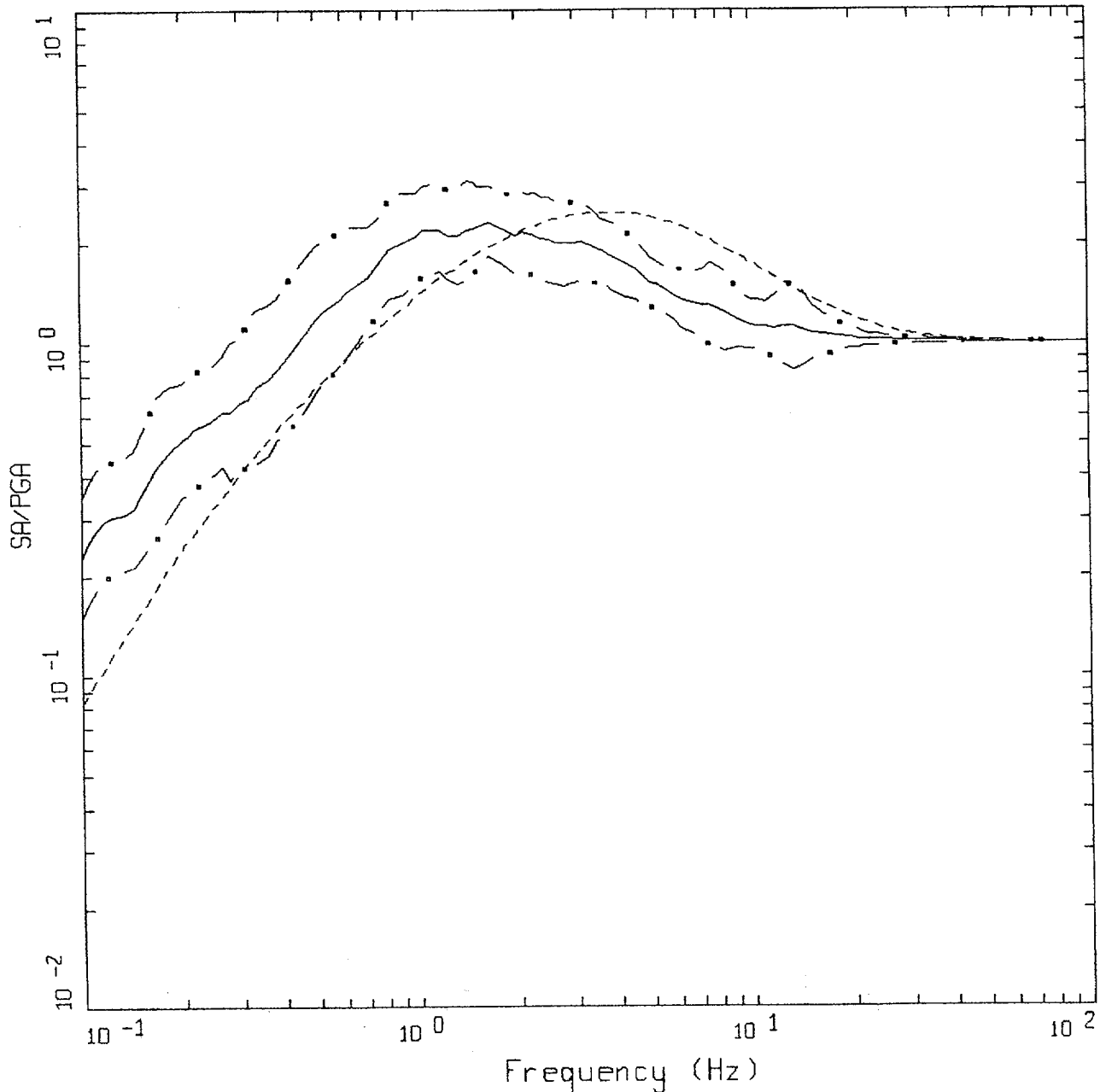
Figure K-2. Comparison of statistical response spectral shapes computed for the Chi Chi, Taiwan, and Turkey earthquakes with recommended shape: bin M 7+ and D =10 to 50 km.



AVERAGE HORIZONTAL SPECTRA: CHI-CHI, TURKEY
 M=7.5 (7.0-7.0+), R=50-100 KM, ROCK
 AVERAGE M = 7.60, AVERAGE DISTANCE = 76.05 KM

- LEGEND
- 50TH PERCENTILE
 - . - 16TH PERCENTILE
 - . - 84TH PERCENTILE
 - - - RECOMMENDED SHAPE; M = 7.60, D = 76 KM

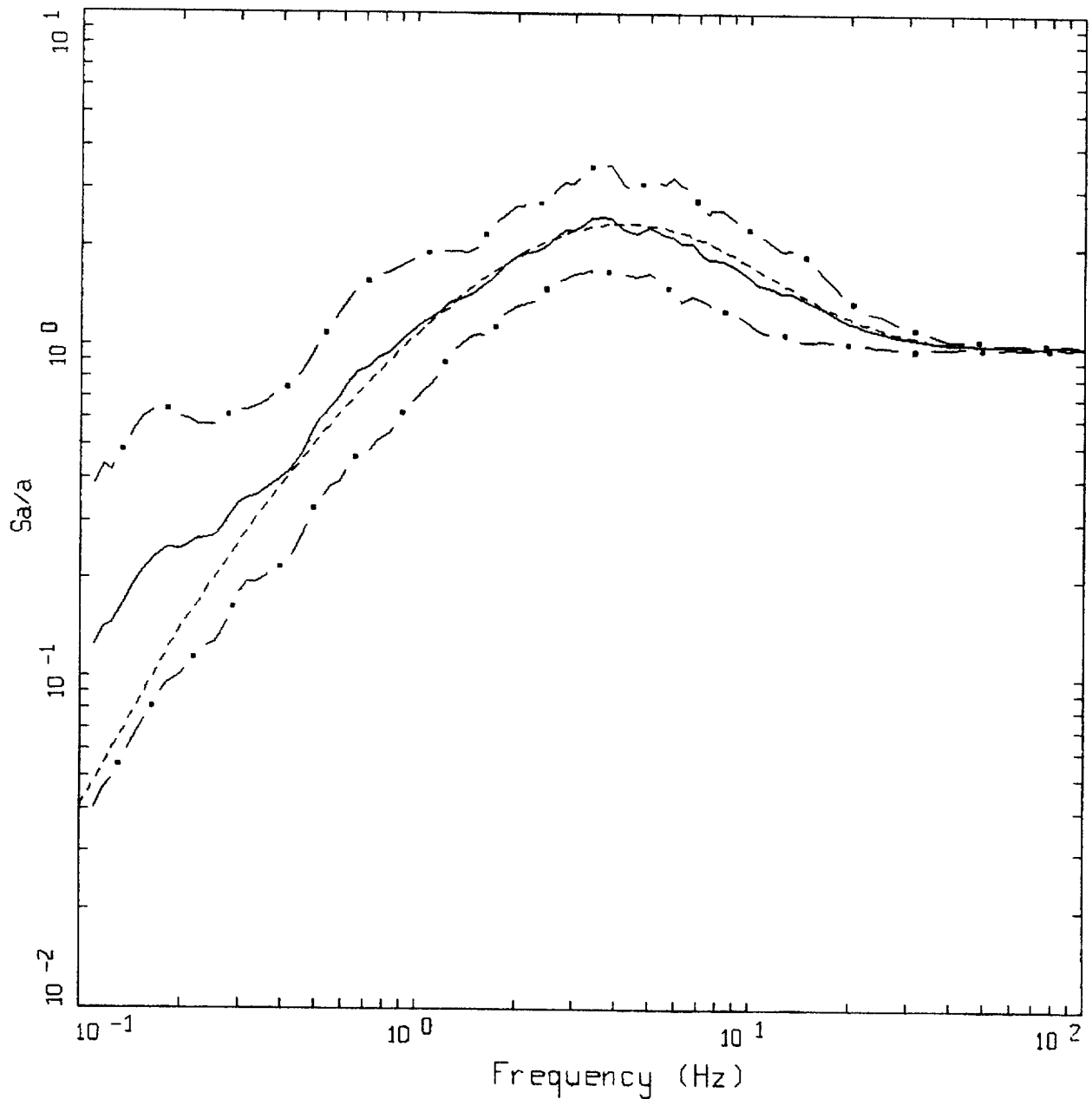
Figure K-3. Comparison of statistical response spectral shapes computed for the Chi Chi, Taiwan and Turkey earthquakes with recommended shape: bin M 7+ and D = 50 to 100 km.



AVERAGE HORIZONTAL SPECTRA: CHI-CHI, TURKEY
 M=7.5 (7.0-7.0+), R=100-200 KM, ROCK
 AVERAGE M = 7.60, AVERAGE DISTANCE = 126.85 KM

- LEGEND
- 50TH PERCENTILE
 - . - 16TH PERCENTILE
 - . - 84TH PERCENTILE
 - - - - RECOMMENDED SHAPE; M = 7.60, D = 127 KM

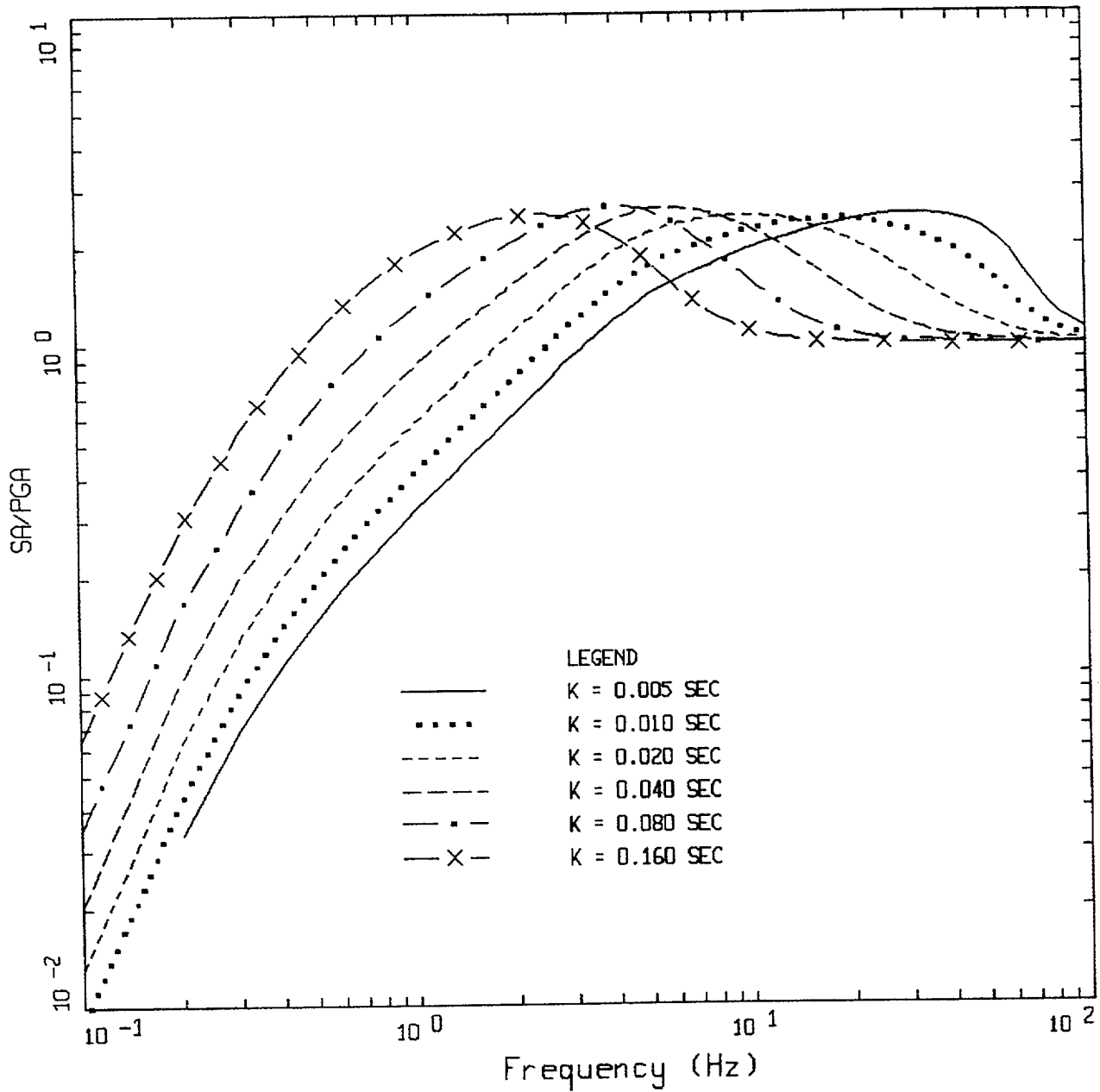
Figure K-4. Comparison of statistical response spectral shapes computed for the Chi Chi, Taiwan and Turkey earthquakes with recommended shape: bin M 7+ and D = 100 to 200 km.



AVERAGE HORIZONTAL SPECTRA: CHI-CHI, TURKEY
 M=7.5 (7.0-7.0+), R=0-50 KM, ROCK
 AVERAGE M = 7.53, AVERAGE DISTANCE = 23.72 KM

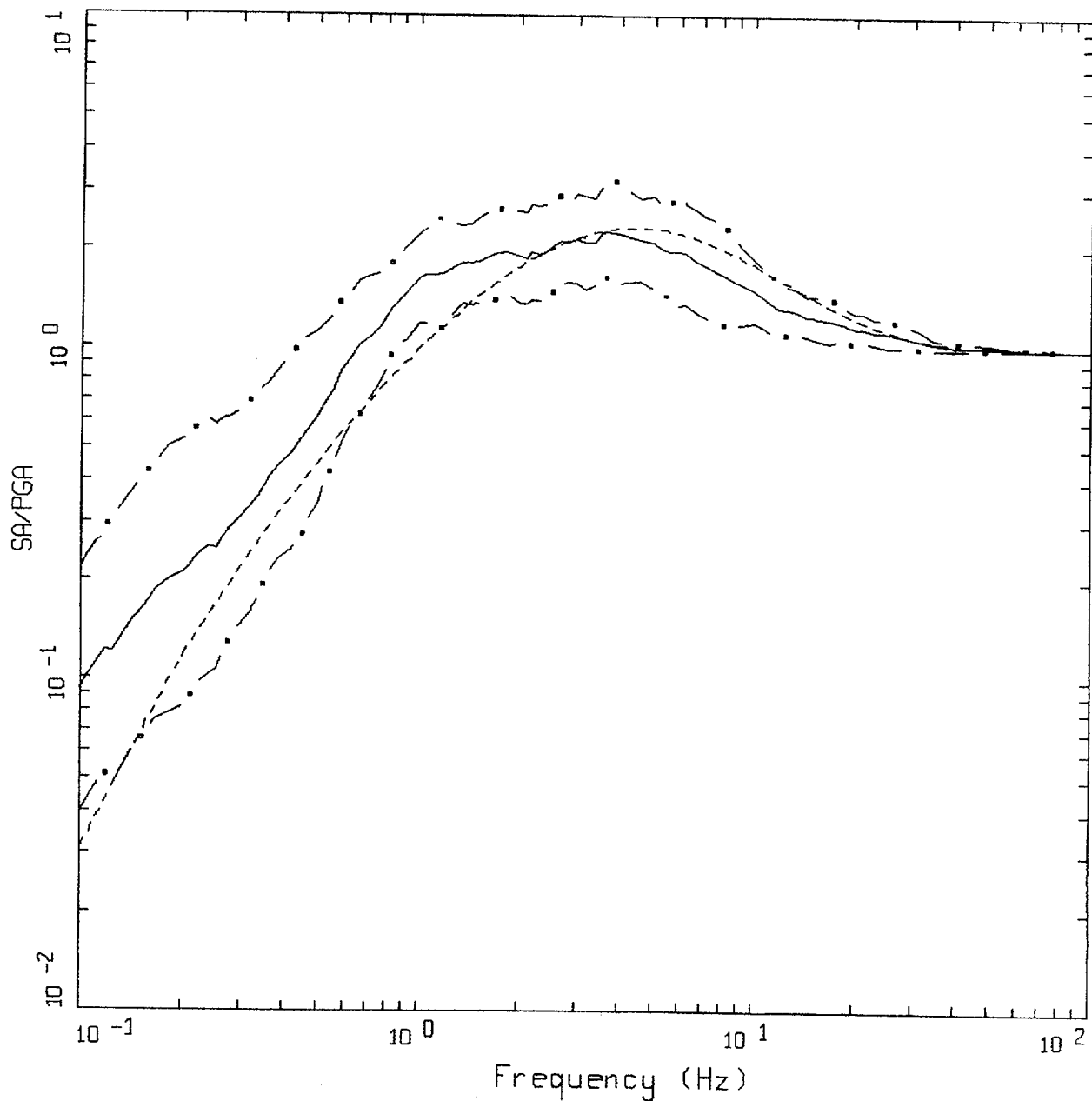
LEGEND
 ————— 50TH PERCENTILE
 - . - . 16TH PERCENTILE
 - . - . 84TH PERCENTILE
 - - - - - RECOMMENDED SHAPE; M = 7.53, D = 23 KM

Figure K-5. Comparison of statistical response spectral shapes computed for the Chi Chi, Taiwan and Turkey earthquakes with recommended shape: bin M 7+ and D = 0 to 50 km.



ROCK
 BASE CASE, WUS, 1-CORNER SOURCE MODEL
 M = 6.5, D = 25 KM, STRESS DROP = 65 BARS

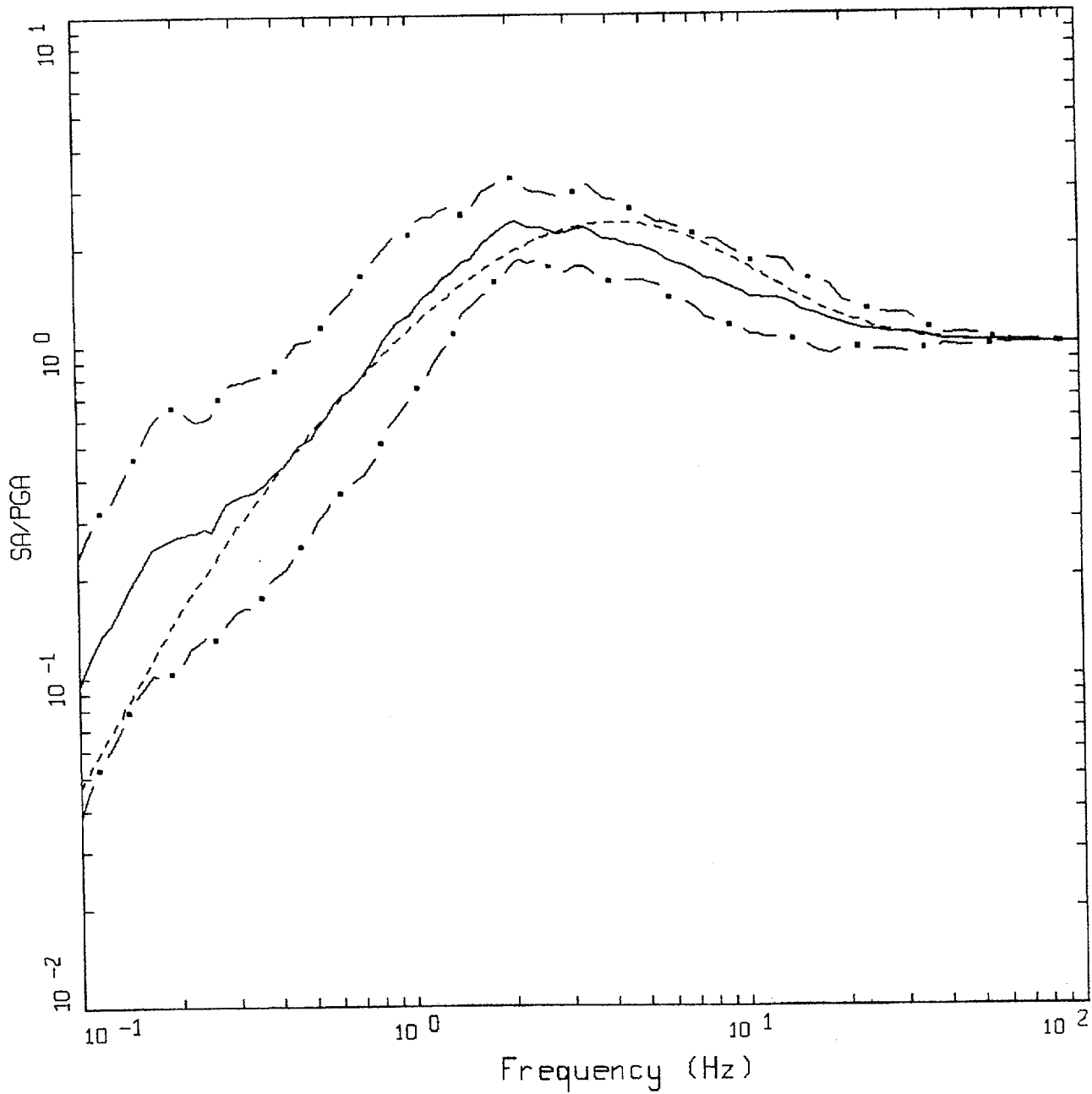
Figure K-6. Response spectral shapes computed for M 6.5 at a distance of 25 km for a suite of kappa values using WUS parameters.



AVERAGE HORIZONTAL SPECTRA: CHI-CHI
 M=7.5 (7.0-7.0+), R=0-10 KM, ROCK
 AVERAGE M = 7.60, AVERAGE DISTANCE = 4.93 KM

LEGEND
 ————— 50TH PERCENTILE
 - . - - 16TH PERCENTILE
 - . - - 84TH PERCENTILE
 - - - - - RECOMMENDED SHAPE; M = 7.60, D = 5 KM

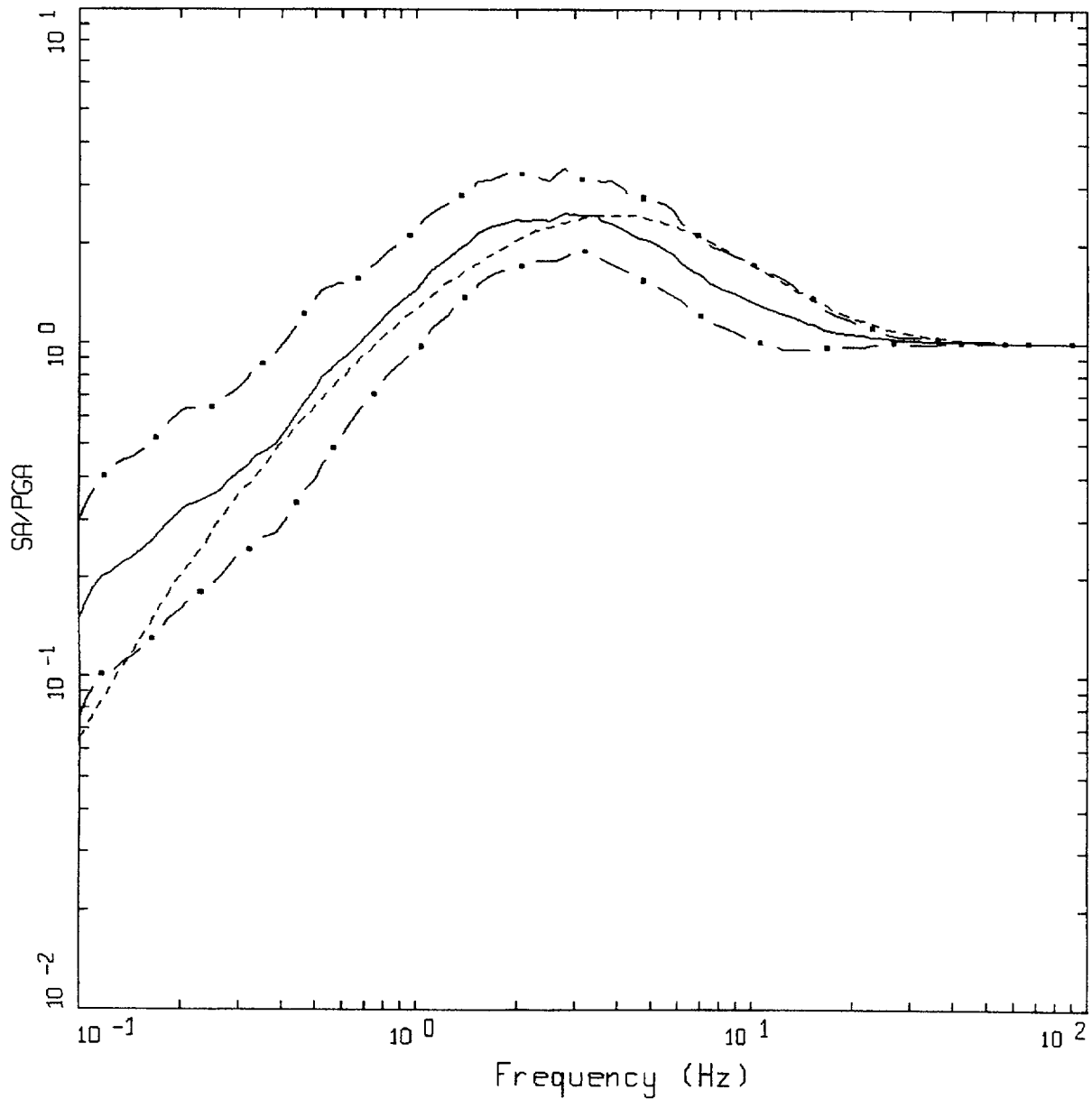
Figure K-7. Comparison of statistical response spectral shapes computed for the Chi Chi, Taiwan earthquake with recommended shape: bin M 7+ and D = 0 to 10 km.



AVERAGE HORIZONTAL SPECTRA: CHI-CHI
 M=7.5 (7.0-7.0+), R=10-50 KM, ROCK
 AVERAGE M = 7.60, AVERAGE DISTANCE = 33.42 KM

- LEGEND
- 50TH PERCENTILE
 - · - 16TH PERCENTILE
 - · - 84TH PERCENTILE
 - - - RECOMMENDED SHAPE; M = 7.60, D = 33 KM

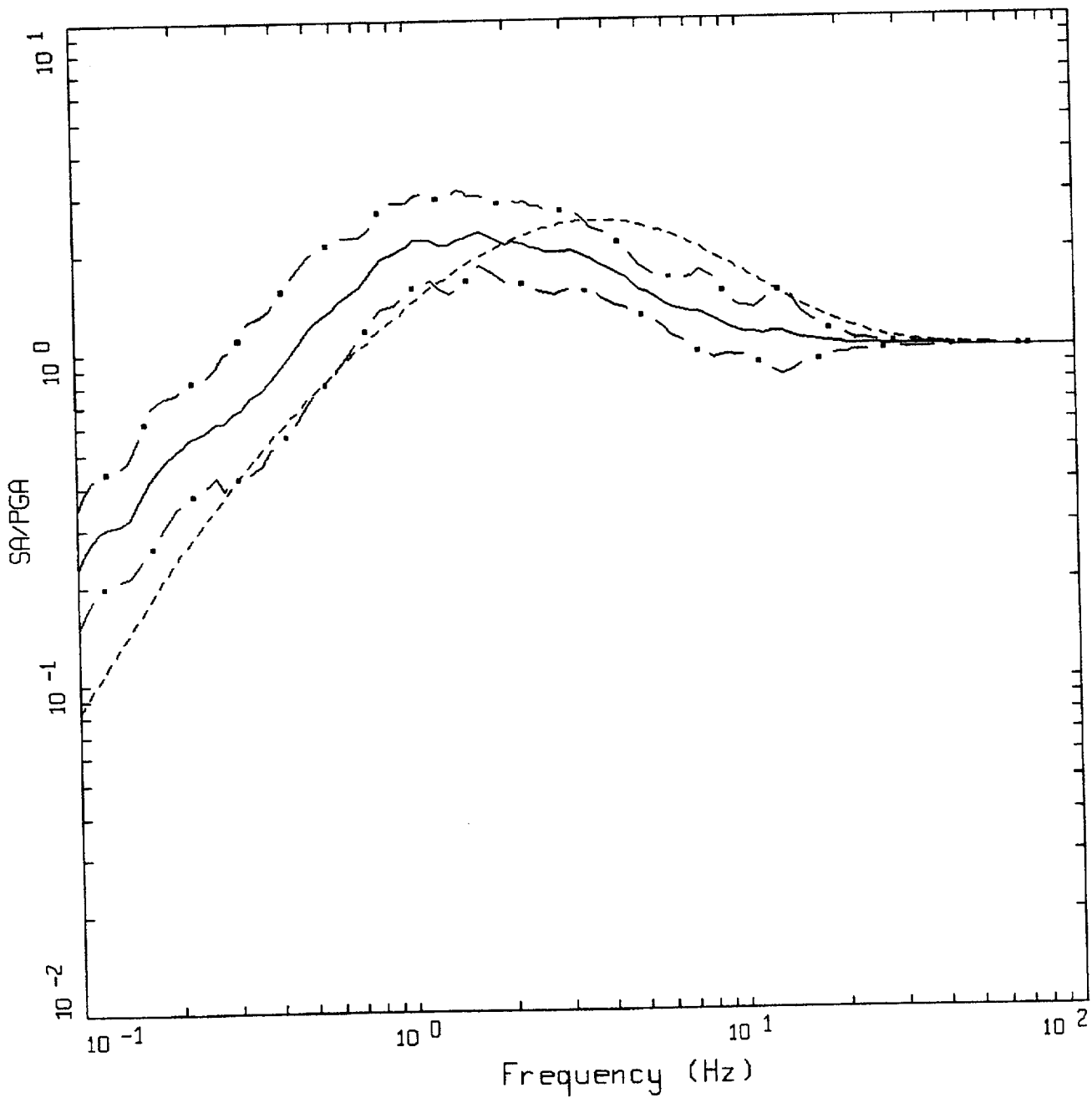
Figure K-8. Comparison of statistical response spectral shapes computed for the Chi Chi, Taiwan earthquake with recommended shape: bin M 7+ and D = 10 to 50 km.



AVERAGE HORIZONTAL SPECTRA: CHI-CHI
 M=7.5 (7.0-7.0+), R=50-100 KM, ROCK
 AVERAGE M = 7.60, AVERAGE DISTANCE = 76.29 KM

- LEGEND
- 50TH PERCENTILE
 - - - 16TH PERCENTILE
 - . - 84TH PERCENTILE
 - RECOMMENDED SHAPE; M = 7.60, D = 76 KM

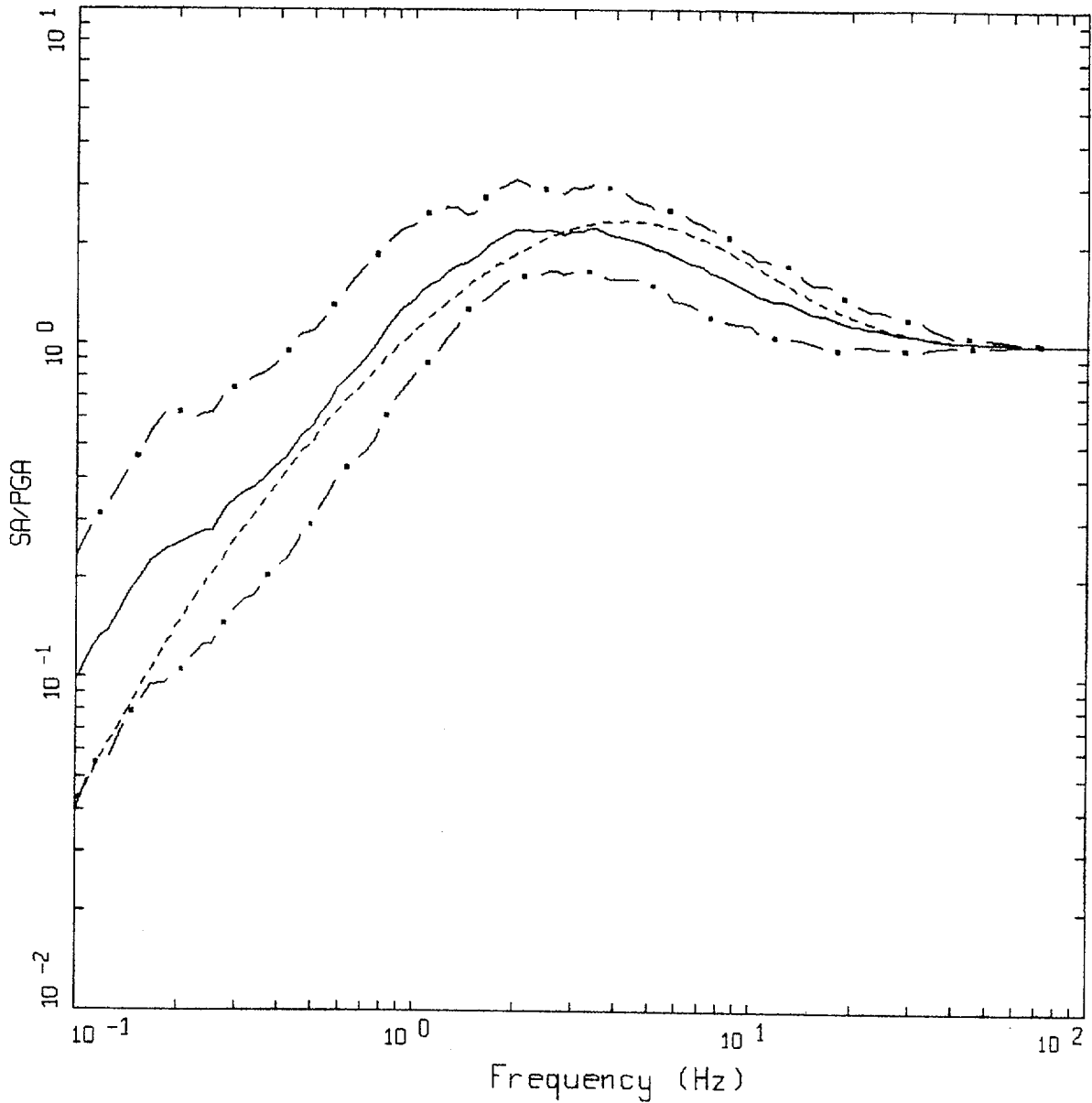
Figure K-9. Comparison of statistical response spectral shapes computed for the Chi Chi, Taiwan earthquake with recommended shape: bin M 7+ and D = 50 to 100 km.



AVERAGE HORIZONTAL SPECTRA: CHI-CHI
 M=7.5 (7.0-7.0+), R=100-200 KM, ROCK
 AVERAGE M = 7.60, AVERAGE DISTANCE = 126.85 KM

- LEGEND
- 50TH PERCENTILE
 - · - 16TH PERCENTILE
 - · - 84TH PERCENTILE
 - - - - RECOMMENDED SHAPE; M = 7.60, D = 127 KM

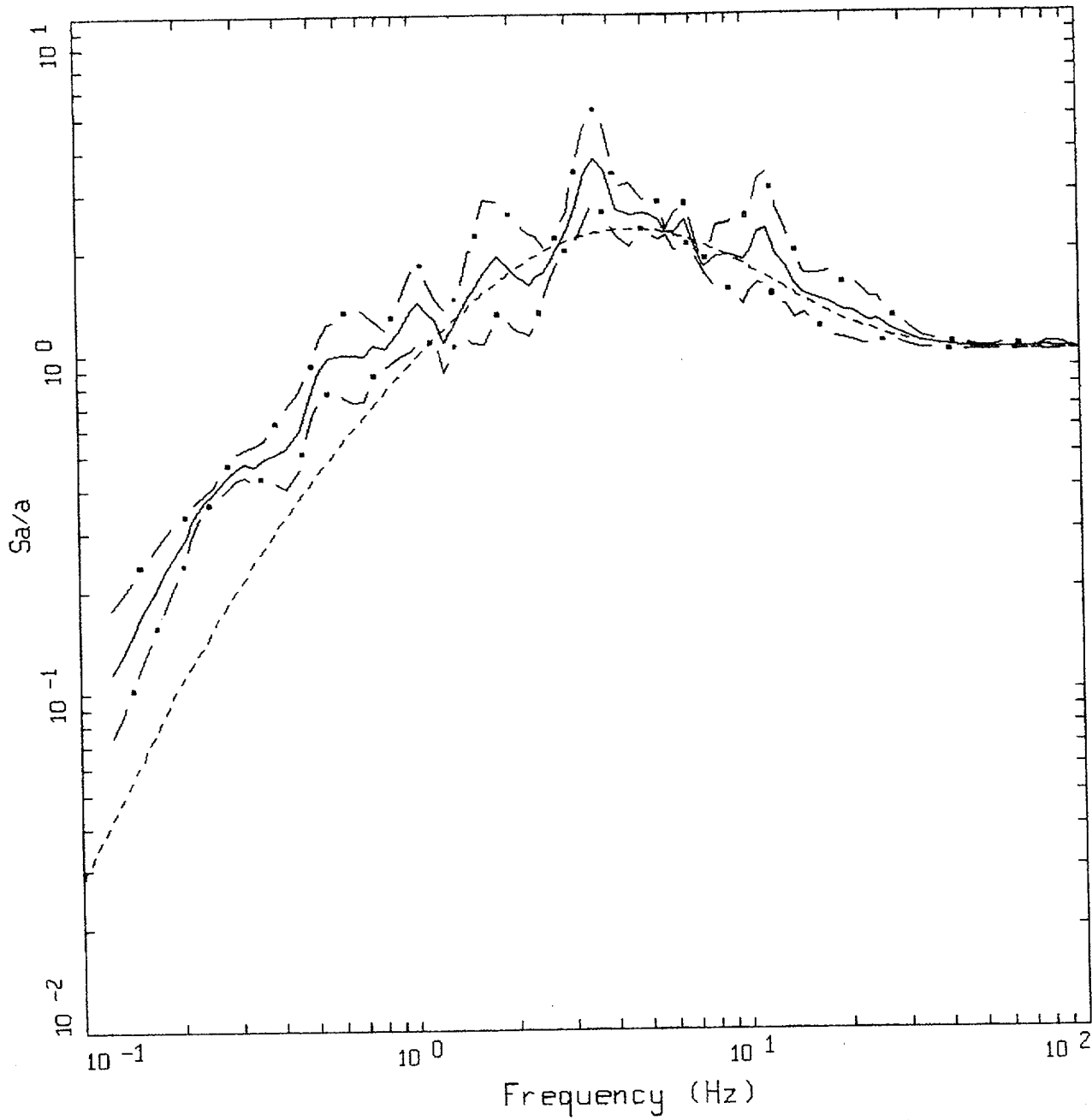
Figure K-10. Comparison of statistical response spectral shapes computed for the Chi Chi, Taiwan earthquake with recommended shape: bin M 7+ and D = 100 to 200 km.



AVERAGE HORIZONTAL SPECTRA: CHI-CHI
 M=7.5 (7.0-7.0+), R=0-50 KM, ROCK
 AVERAGE M = 7.60, AVERAGE DISTANCE = 24.08 KM

LEGEND
 ————— 50TH PERCENTILE
 - . - . 16TH PERCENTILE
 - - - - 84TH PERCENTILE
 RECOMMENDED SHAPE; M = 7.60, D = 24 KM

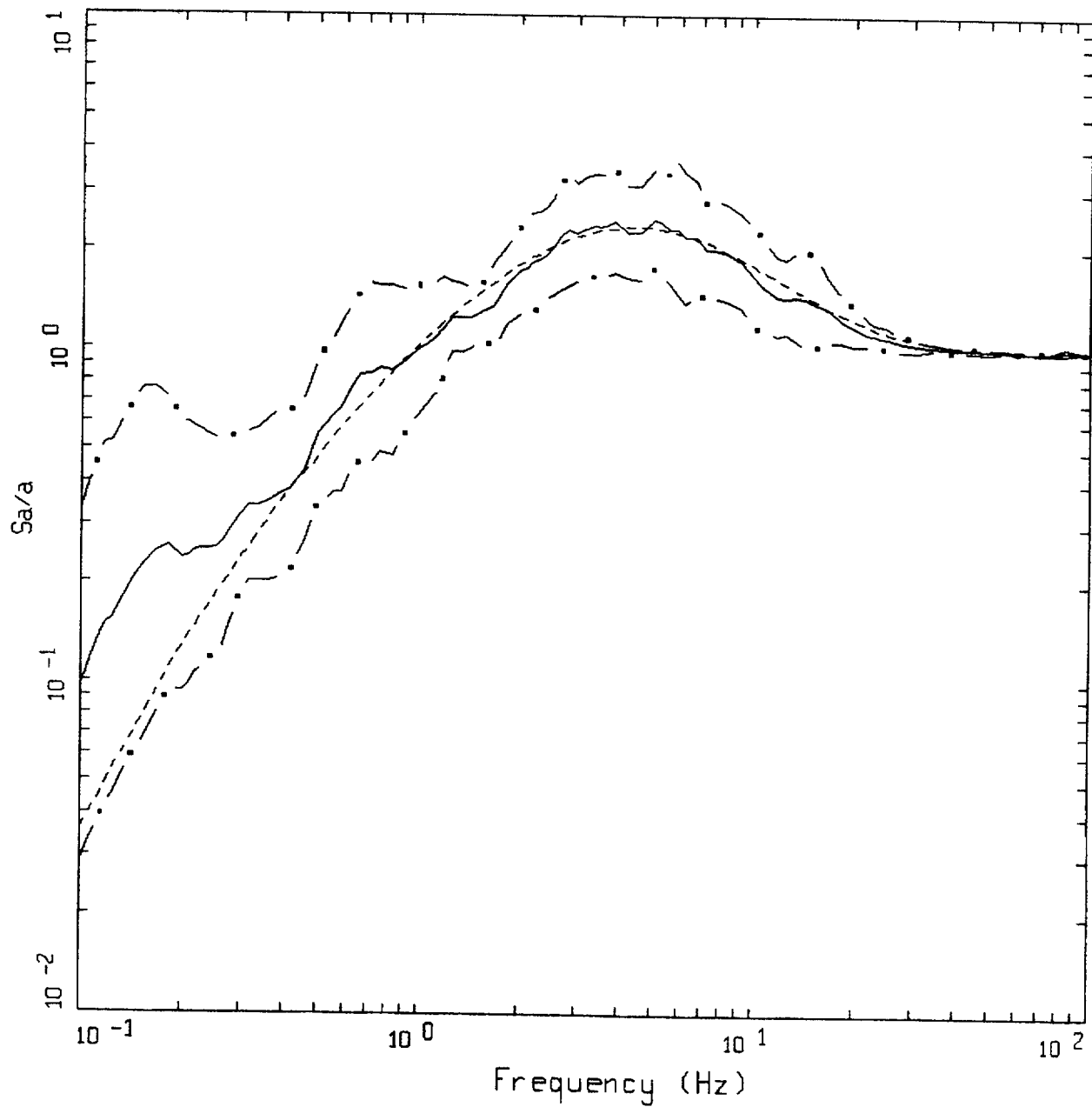
Figure K-11. Comparison of statistical response spectral shapes computed for the Chi Chi, Taiwan earthquake with recommended shape: bin M 7+ and D = 0 to 50 km.



AVERAGE HORIZONTAL SPECTRA: TURKEY
 M=7.5 (7.0-7.0+), R=0-10 KM, ROCK
 AVERAGE M = 7.40, AVERAGE DISTANCE = 5.50 KM

- LEGEND
- 50TH PERCENTILE
 - · - · 16TH PERCENTILE
 - · - · 84TH PERCENTILE
 - RECOMMENDED SHAPE; M = 7.40, D = 5.5 KM

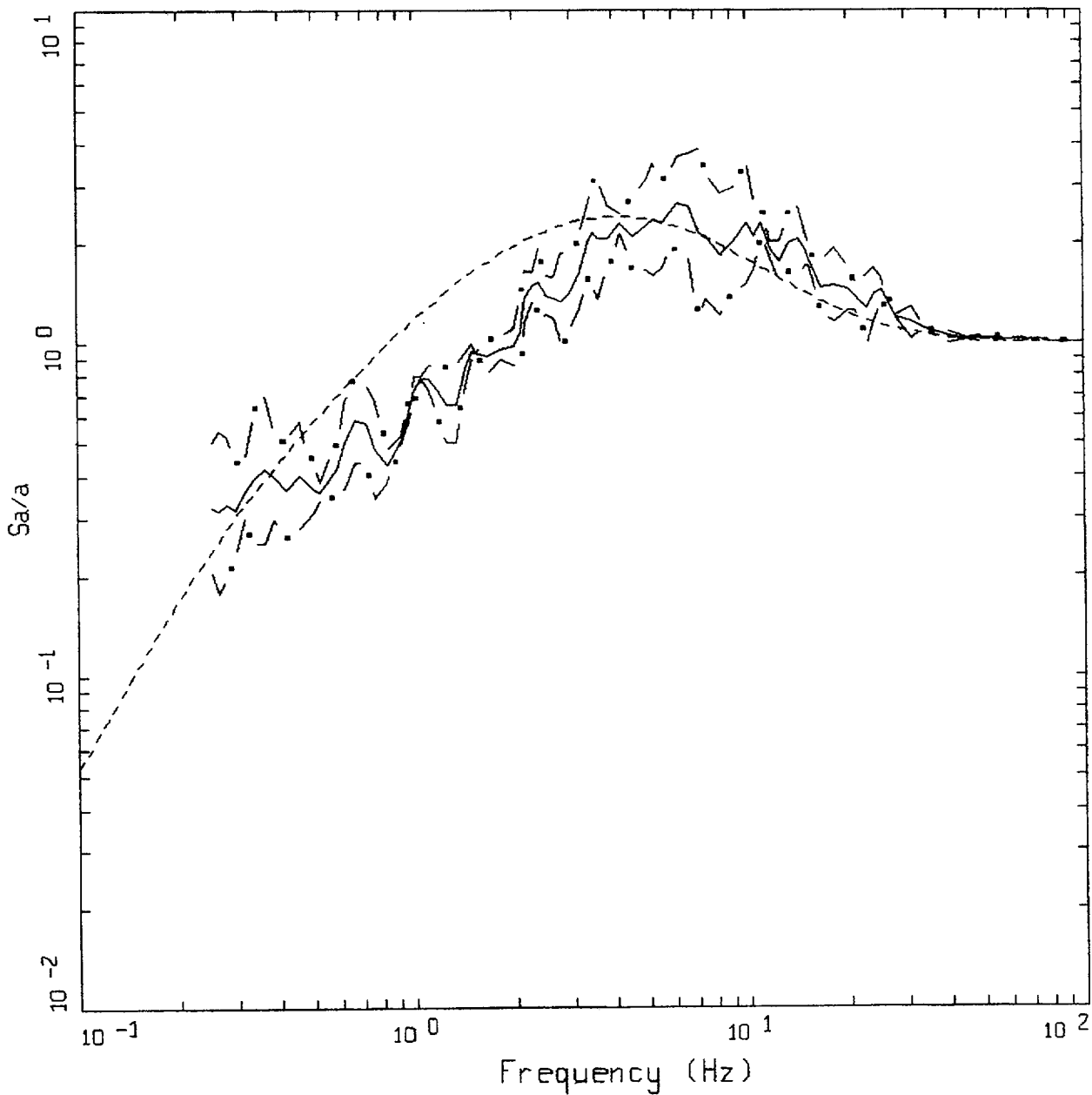
Figure K-12. Comparison of statistical response spectral shapes computed for the Turkey earthquakes with recommended shape: bin M 7+ and D = 0 to 10 km.



AVERAGE HORIZONTAL SPECTRA: TURKEY
 M=7.5 (7.0-7.0+), R=10-50 KM, ROCK
 AVERAGE M = 7.27, AVERAGE DISTANCE = 27.50 KM

- LEGEND
- 50TH PERCENTILE
 - . - 16TH PERCENTILE
 - . - 84TH PERCENTILE
 - - - RECOMMENDED SHAPE; M = 7.27, D = 27.5 KM

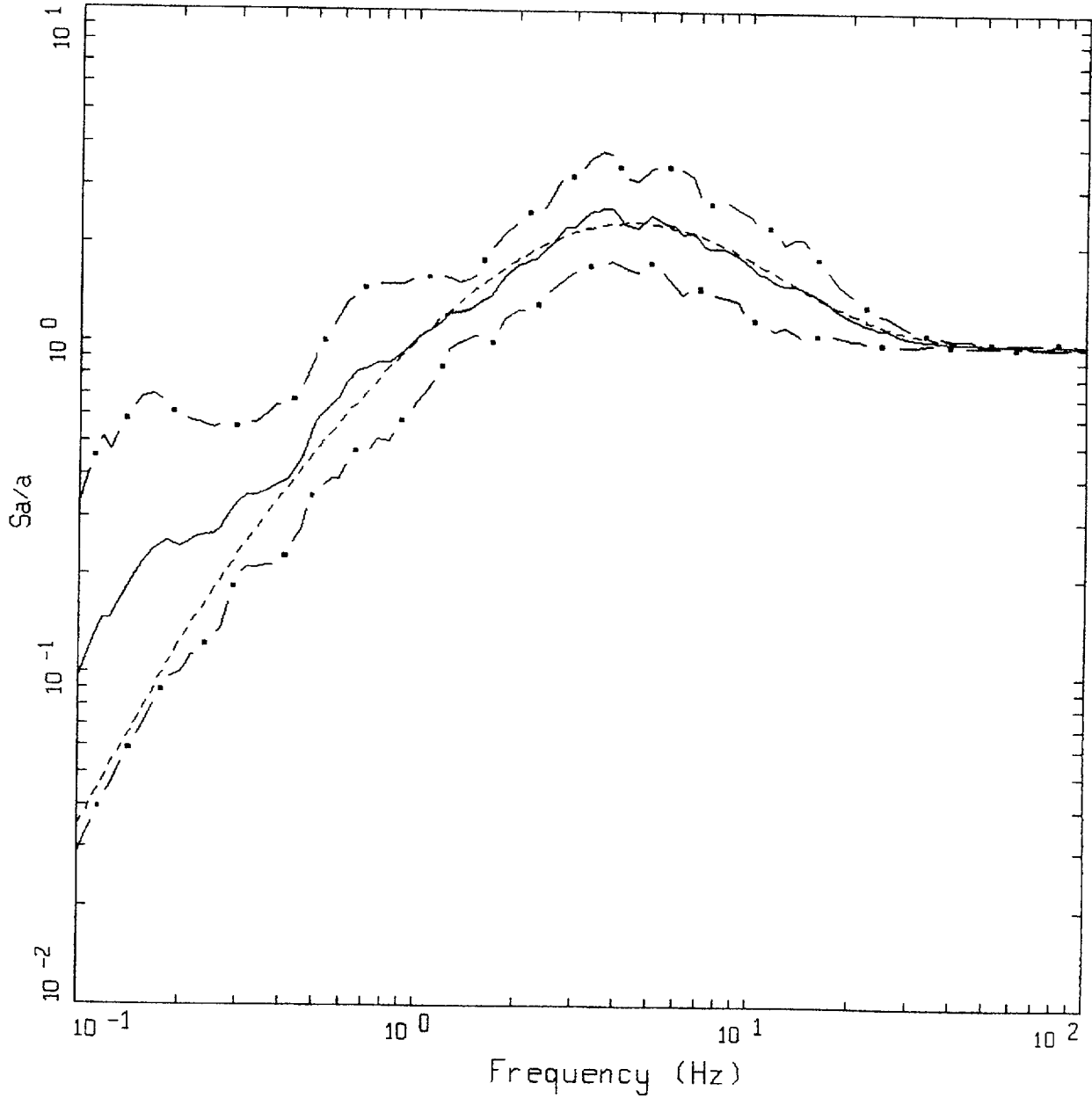
Figure K-13. Comparison of statistical response spectral shapes computed for the Turkey earthquakes with recommended shape: bin M 7+ and D = 10 to 50 km.



AVERAGE HORIZONTAL SPECTRA: TURKEY
 M=7.5 (7.0-7.0+), R=50-100 KM, ROCK
 AVERAGE M = 7.40, AVERAGE DISTANCE = 62.30 KM

- LEGEND
- 50TH PERCENTILE
 - · - 16TH PERCENTILE
 - · - 84TH PERCENTILE
 - RECOMMENDED SHAPE; M = 7.40, D = 62 KM

Figure K-14. Comparison of statistical response spectral shapes computed for the Turkey earthquakes with recommended shape: bin M 7+ and D = 50 to 100 km.



AVERAGE HORIZONTAL SPECTRA: TURKEY
 M=7.5 (7.0-7.0+), R=0-50 KM, ROCK
 AVERAGE M = 7.30, AVERAGE DISTANCE = 22.61 KM

- LEGEND
- 50TH PERCENTILE
 - . - 16TH PERCENTILE
 - . - 84TH PERCENTILE
 - - - - RECOMMENDED SHAPE; M = 7.30, D = 23 KM

Figure K-15. Comparison of statistical response spectral shapes computed for the Turkey earthquakes with recommended shape: bin M 7+ and D = 0 to 50 km.

BIBLIOGRAPHIC DATA SHEET

(See instructions on the reverse)

1. REPORT NUMBER
(Assigned by NRC, Add Vol., Supp., Rev.,
and Addendum Numbers, if any.)

NUREG/CR-6728

2. TITLE AND SUBTITLE

Technical Basis for Revision of Regulatory Guidance on Design Ground Motions: Hazard- and Risk-consistent Ground Motion Spectra Guidelines

3. DATE REPORT PUBLISHED

MONTH	YEAR
October	2001

4. FIN OR GRANT NUMBER

W6248

5. AUTHOR(S)

(1) R.K. McGuire, (2) W.J. Silva, and (3) C.J. Costantino

6. TYPE OF REPORT

Technical

7. PERIOD COVERED (Inclusive Dates)

04/1996 - 03/2001

8. PERFORMING ORGANIZATION - NAME AND ADDRESS (If NRC, provide Division, Office or Region, U.S. Nuclear Regulatory Commission, and mailing address; if contractor, provide name and mailing address.)

- (1) Risk Engineering, Inc., 4155 Darley Avenue, Suite A, Boulder, CO 80305
- (2) Pacific Engineering & Analysis, 311 Pomona Avenue, El Cerrito, CA 94530
- (3) Carl J. Costantino, 4 Rockingham Road, Spring Valley, NY 10977

9. SPONSORING ORGANIZATION - NAME AND ADDRESS (If NRC, type "Same as above"; if contractor, provide NRC Division, Office or Region, U.S. Nuclear Regulatory Commission, and mailing address.)

Division of Engineering Technology
Office of Nuclear Regulatory Research
U.S. Nuclear Regulatory Commission
Washington, DC 20555-0001

10. SUPPLEMENTARY NOTES

R.M. Kenneally, NRC Project Manager

11. ABSTRACT (200 words or less)

Recommendations for seismic design ground motions for nuclear facilities require a consistency with both observed strong motion data and with seismological theory on the characteristics of strong shaking. A database of recorded time histories forms the foundation of empirical recommendations for spectral shapes. For the central and eastern US (CEUS), a well-validated, simple model of strong motion allows quantification of the difference between western US (WUS) and CEUS motions. For design recommendations, the uniform hazard spectrum (UHS) is modified by a scale factor to a Uniform Reliability Spectrum (URS). Spectral shapes are scaled to the 10 Hz and 1 Hz URS amplitudes. We recommend criteria to match artificial motions to the target (scaled) spectra. We demonstrate the procedures for developing design spectra for rock conditions and for four soil profiles in the WUS and in the CEUS, using as example sites at a location in the Mojave desert, California, and Columbia, South Carolina. Results indicate that the URS, as calculated here, provides reliability-consistent designs over a range of site locations and structural frequencies.

12. KEY WORDS/DESCRIPTORS (List words or phrases that will assist researchers in locating the report.)

Seismic Effects
Regulatory Guides
Design Ground Motion
Response Spectra for Seismic Design

13. AVAILABILITY STATEMENT

unlimited

14. SECURITY CLASSIFICATION

(This Page)

unclassified

(This Report)

unclassified

15. NUMBER OF PAGES

16. PRICE



Federal Recycling Program

**UNITED STATES
NUCLEAR REGULATORY COMMISSION
WASHINGTON, DC 20555-0001**

OFFICIAL BUSINESS
PENALTY FOR PRIVATE USE, \$300